

ASTES

# Advances in Science, Technology & Engineering Systems Journal



VOLUME 5-ISSUE 2 | MAR-APR 2020

[www.astesj.com](http://www.astesj.com)

ISSN: 2415-6698

## EDITORIAL BOARD

### Editor-in-Chief

**Prof. Passerini Kazmerski**  
University of Chicago, USA

### Editorial Board Members

**Prof. Rehan Ullah Khan**  
Qassim University, Saudi  
Arabia

**Prof. María Jesús Espinosa**  
Universidad Tecnológica  
Metropolitana, Mexico

**Dr. Hongbo Du**  
Prairie View A&M University, USA

**Dr. Nguyen Tung Linh**  
Electric Power University,  
Vietnam

**Tariq Kamal**  
University of Nottingham, UK  
  
Sakarya University, Turkey

**Dr. Mohmaed Abdel Fattah  
Ashabrawy**  
Prince Sattam bin Abdulaziz  
University, Saudi Arabia

**Mohamed Mohamed Abdel-  
Daim**  
Suez Canal University, Egypt

**Dr. Omeje Maxwell**  
Covenant University, Nigeria

**Prof. Majida Ali Abed Meshari**  
Tikrit University Campus, Iraq

**Dr. Heba Afify**  
MTI university, Cairo, Egypt

### Regional Editors

**Dr. Hung-Wei Wu**  
Kun Shan University, Taiwan

**Dr. Maryam Asghari**  
Shahid Ashrafi Esfahani, Iran

**Dr. Shakir Ali**  
Aligarh Muslim University, India

**Dr. Ahmet Kayabasi**  
Karamanoglu Mehmetbey  
University, Turkey

**Dr. Ebubekir Altuntas**  
Gaziosmanpasa University,  
Turkey

**Dr. Sabry Ali Abdallah El-Naggar**  
Tanta University, Egypt

**Aamir Nawaz**  
Gomal University, Pakistan

**Dr. Gomathi Periasamy**  
Mekelle University, Ethiopia

**Dr. Walid Wafik Mohamed Badawy**  
National Organization for Drug Control  
and Research, Egypt

**Dr. Abhishek Shukla**  
R.D. Engineering College,  
India

**Abdullah El-Bayoumi**  
Cairo University, Egypt

**Ayham Hassan Abazid**  
Jordan university of science and  
technology, Jordan



## Editorial

**A**dvances in Science, Technology and Engineering Systems Journal (ASTESJ) is an online-only journal dedicated to publishing significant advances covering all aspects of technology relevant to the physical science and engineering communities. The journal regularly publishes articles covering specific topics of interest.

Current Issue features key papers related to multidisciplinary domains involving complex system stemming from numerous disciplines; this is exactly how this journal differs from other interdisciplinary and multidisciplinary engineering journals. This issue contains 99 accepted papers in Computer Science and Artificial Intelligence domain.

**Editor-in-chief**

*Prof. Passerini Kazmersk*

# ADVANCES IN SCIENCE, TECHNOLOGY AND ENGINEERING SYSTEMS JOURNAL

Volume 5 Issue 2

March-April 2020

## CONTENTS

<i>A New Distributed Reinforcement Learning Approach for Multiagent Cooperation Using Team-mate Modeling and Joint Action Generalization</i> Wiem Zemzem, Ines Hosni	01
<i>Productify News Article Classification Model with Sagemaker</i> Johannes Linden, Xutao Wang, Stefan Forsstrom, Tingting Zhang	13
<i>Distributed Linear Summing in Wireless Sensor Networks with Implemented Stopping Criteria</i> Martin Kenyeres, Jozef Kenyeres	19
<i>Ontological and Epistemological Issues of Studying the Development of Uzbekistan in the Context of Globalization from the Point of View of The Paradigm of Civilizations</i> Djurayeva Nigora Avazovna	28
<i>Design and Validation of a Meter Band Rate in OpenFlow and OpenDaylight for Optimizing QoS</i> Mohamed Saleh Al Breiki, Suiping Zhou, Yuan Roger Luo	35
<i>Improvement of the Natural Self-Timed Circuit Tolerance to Short-Term Soft Errors</i> Yuri Afanasyevich Stepchenkov, Anton Nikolaevich Kamenskih, Yuri Georgievich Diachenko, Yuri Vladimirovich Rogdestvenski, Denis Yuryevich Diachenko	44
<i>Performance Evaluation and Examination of Data Transfer: A Review of Parallel Migration in Cloud Storage</i> Mimouna Alkhonaini, Hoda El-Sayed	57
<i>A Regenerative Energy Recovery System for Electric Vehicles Charging A Battery at A Low Speed</i> Wonseok Yeo, Sungchul Jung, Seungtaik Kim, Keonho Park, Jongsun Ko	64
<i>In Body Antenna for Monitoring and Controlling Pacemaker</i> Sourav Sinha, Ta-Seen Reaz Niloy, Raja Rashidul Hasan, Md. Abdur Rahman	74
<i>Attacks Classification and a Novel IDS for Detecting Jamming Attack in WBAN</i> Asmae Bengag, Amina Bengag, Omar Moussaoui	80



<i>New Solution Implementation to Protect Encryption Keys Inside the Database Management System</i>	87
Karim El bouchti, Soumia Ziti, Fouzia Omary, Nassim Kharmoum	
<i>Review on Outliers Identification Methods for Univariate Circular Biological Data</i>	95
Siti Zanariah Satari, Ku Muhammad Naim Ku Khalif	
<i>New Color Image Encryption for Medical Images Based on Three Dimensional Generalized Chaotic Cat Map and Combined Cellular Automata</i>	104
Un Sook Choi, Sung Jin Cho, Sung Won Kang	
<i>Model of Automatic Parking House</i>	111
Radek Guráš, Miroslav Mahdal	
<i>Analysis of Cyberattacks in Public Organizations in Latin America</i>	116
Segundo Moisés Toapanta Toapanta, José David López Cobeña, Luis Enrique Mafla Gallegos	
<i>Lead Bioaccumulation in Root and Aerial Part of Natural and Cultivated Pastures in Highly Contaminated Soils in Central Andes of Peru</i>	126
Jorge Castro Bedriñana, Doris Chirinos Peinado, Richard Peñaloza-Fernández	
<i>Big Data Analytics using Deep LSTM Networks: A Case Study for Weather Prediction</i>	133
Shweta Mittal, Om Prakash Sangwan	
<i>The Acquiring Process of Entrepreneurship Competencies in Realist Airbrush Art</i>	138
Bayu Rahmat Setiadi, Suparmin, Slamet Priyanto, Henny Pratiwi, Sugiyono	
<i>Dynamic Behavior of Multi-Story Concrete Buildings Based on Non-Linear Pushover &amp; Time History Analyses</i>	143
Sherif Gamal Abd-Elhamid, Reham Mohamed Galal Ebrahim El-Tahawy, Mohamed Nour El-Din Fayed	
<i>Transfer Learning and Fine Tuning in Breast Mammogram Abnormalities Classification on CBIS-DDSM Database</i>	154
Lenin G. Falconi, Maria Perez, Wilbert G. Aguilar, Aura Conci	
<i>Satisfaction of Old Graduates of Zootechnical Engineering for Improvement of Educational Quality at the UNCP</i>	166
Jorge Castro-Bedriñana, Doris Chirinos-Peinado, Felipe Zenteno-Vigo, Gianfranco Castro-Chirinos	
<i>The Implementation of Smart Farming Application Based on the Microcontroller and Automatic Sprinkler Irrigation System of Agricultural Land</i>	174
Ery Muchyar Hasiri, Asniati, Mohamad Arif Suryawan, Rasmuin	

<i>An Algorithm to Improve Data Accuracy of PMs Concentration Measured with IoT Devices</i>	180
Mihaela Balanescu, George Suciu, Marius-Alexandru Dobrea, Cristina Balaceanu, Radu-loan Ciobanu, Ciprian Dobre, Andrei-Cristian Birdici, Andreea Badicu, Iulia Oprea, Adrian Pasat	
<i>Hybrid Solar Thermal/Electricity Automated Oven</i>	188
Ajah Onu Victor, Emenike Ejiogu	
<i>A Study on the Effects of Combining Different Features for the Recognition of Handwritten Bangla Characters</i>	197
Halima Begum, Muhammed Mazharul Islam	
<i>Control of Electrostatic Suspension System Using Pulse Width Modulation</i>	204
The Truyen Le	
<i>System of Sequential D-Optimal Identification for Dynamic Objects in Real-Time Scale</i>	211
Fatuev Victor, Mishin Anton	
<i>Enhancing an SDN Architecture with DoS Attack Detection Mechanisms</i>	215
Ranyelson Neres Carvalho, Lucas R. Costa, Jacir Luiz Bordim, Eduardo Adilo Pelinson Alchieri	
<i>A Psychovisual Optimization of Wavelet Foveation-Based Image Coding and Quality Assessment Based on Human Quality Criteria</i>	225
Abderrahim Bajit, Mohammed Nahid, Ahmed Tamtaoui, Mohammed Benbrahim	
<i>A Framework for Plans Permeable Breakwater Eco-Friendly Building Identification and Characteristics Materials Construction Study Case at Demak Village</i>	235
Denny Nugroho Sugianto, Sugeng Widada, Anindya Wirastriya, Aris Ismanto, Retno Hartati, Widianingsih, Agus Indarjo, Suripin	
<i>Implementing an AGV System to Transport Finished Goods to the Warehouse</i>	241
Nuno Correia, Leonor Teixeira, Ana Luísa Ramos	
<i>Safety in Industry 4.0: The Multi-Purpose Applications of Augmented Reality in Digital Factories</i>	248
Lorenzo Damiani, Roberto Revetria, Emanuele Morra	
<i>Analyzing Job Tenure Factors in Private and Public Companies in Albania by Using Cox Proportional Hazards Model</i>	254
Lule Basha, Eralda Gjika, Llukan Puka	
<i>The Effectiveness of Personality-Based Gamification Model for Foreign Vocabulary Online Learning</i>	261
Hasung Kang, Gede Putra Kusuma	



<i>Optimization of Low Temperature Differential Stirling Engine Regenerator Design</i>	272
Hind El Hassani, Nour- Eddine Boutammachte, Sanae El Hassani	
<i>Electronic Steering of the Vehicle Axle with Force Feedback</i>	280
Tomas Pawlenka, Jaromir Skuta, Jiri Kulhanek	
<i>A Systematic Literature Review of Vessel Anomaly Behavior Detection Methods Based on Automatic Identification System (AIS) and another Sensor Fusion</i>	287
Nova Muhammad Ferlansyah, Suharjito	
<i>Scapy Scripting to Automate Testing of Networking Middleboxes</i>	293
Dr. Minal Moharir, Karthik Bhat Adyathimar, Dr. Shobha G, Vishal Soni	
<i>The Adventure of BipBop: An Android App Pathfinding Adventure Game</i>	299
Gredion Prajena, Jeklin Harefa, Andry Chowanda, Alexander, Maskat, Kamal Rahman, Muhammad Naufal Fadhil	
<i>Evolutionary Quantum Technology: The Future with Holographic Plasma Voxel</i>	305
Yogi Udjaja	
<i>A Sustainable Multi-layered Open Data Processing Model for Agriculture: IoT Based Case Study Using Semantic Web for Hazelnut Fields</i>	309
?ahin AYDIN, Mehmet Nafiz AYDIN	
<i>Methodology for Assessing Synchronization Conditions in Telecommunication Devices</i>	320
Juliy Boiko, Ilya Pyatin, Oleksander Eromenko, Oleg Barabash	
<i>Extending Movable Surfaces with Touch Interaction Using the VirtualTablet: An Extended View</i>	328
Adrian H. Hoppe, Felix Marek, Florian van de Camp, Rainer Stiefelhagen	
<i>Mutual Reduction in the Coupling of the MIMO Antenna Network Applied to the Broadband Transmission</i>	338
Chafai Abdelhamid, Hedi Sakli	
<i>Antenna Radiation Performance Enhancement Using Metamaterial Filter for Vehicle to Vehicle Communications Applications</i>	344
Marwa DAGHARI, Hedi SAKLI	
<i>Shear Strength of Unreinforced Masonry Walls Retrofitted with CFRP</i>	351
Sanaa El Malyh, Azzeddine Bouyahyaoui, Toufik Cherradi, Ancuta Rotaru, Petru Mihai	

<i>In-Plane Shear Behavior of Unreinforced Masonry Walls Strengthened with Fiber Reinforced Polymer Composites</i>	360
Sanaa El Malyh, Azzeddine Bouyahyaoui, Toufik Cherradi, Ancuta Rotaru, Petru Mihai	
<i>Territorial Sales Redesign Using Geotechnical Tools</i>	368
Diana Sánchez-Partida, Moises Ernesto Sánchez-Castro, José-Luis Martínez-Flores, Patricia Cano-Olivos, Martin Straka	
<i>Wilson-Hilferty-type approximation for Poisson Random Variable</i>	377
Paolo Giammatteo, Tania Di Mascio	
<i>A Critical Analysis of Usability and Learning Methods on an Augmented Reality Application for Zoology Education</i>	384
Diego Iquirá-Becerra, Michael Flores-Conislla, Juan Deyby Carlos-Chullo, Briseida Sotelo-Castro, Claudia Payalich-Quispe, Carlo Corrales-Delgado	
<i>Hybrid Autogyro: Model and Longitudinal Control for Wind Gust Energy Conversion Using Autorotation</i>	393
Jonathan Flores Santiago, Sergio Salazar Cruz, Rogelio Lozano Leal	
<i>Using Metaheuristics-Based Methods to Provide Sustainable Market Solutions, Suitable to Consumer Needs</i>	399
Ricardo Simões Santos, António João Pina da Costa Feliciano Abreu, Joaquim José Rodrigues Monteiro	
<i>A Comparative Analysis of ARIMA and Feed-Forward Neural Network Prognostic Model for Bull Services</i>	411
Jude B. Rola, Cherry Lyn C. Sta. Romana, Larmie S. Feliscuzo, Ivy Fe M. Lopez, Cherry N. Rola	
<i>A Comprehensive Study of Privacy Preserving Techniques in Cloud Computing Environment</i>	419
Bayan O Al-Amri, Mohammed A. AlZain, Jehad Al-Amri, Mohammed Baz, Mehedi Masud	
<i>Optimal Flow Analysis of a Unified Energy System with Effects of P2G</i>	425
Haseeb Yar Hiraj, Wenping Qin, Muhammad Abbas, Muhammad Zeeshan Adil	
<i>Author Identification for Marathi Language</i>	432
C. Namrata Mahender, Ramesh Ram Naik, Maheshkumar Bhujangrao Landge	
<i>Pyrolysis of Beech Wood in A Continuous Drop Tube Reactor in Comparison to A Batch Reactor</i>	441
Chetna Mohabeer, Nourelhouda Boukaous, Antoinette Maarawi, Lokmane Abdelouahed, Abdeslam-Hassen Meniai, Mustapha Chikhi, Bechara Taouk	



- Promoting Continuous Professional Development Among Academics from A Vocational College by Using A Practical Workshop Based on Arduino Technology* 452  
Arthur James Swart, Pierre Eduard Hertzog
- The Usability Evaluation of Academic Progress Information System (SIsKA-NG)* 460  
Gede Indrawan, I Made Agus Oka Gunawan, Sariyasa
- Comparison Analysis between Mobile Banking and Mobile Payment as Determinant Factors of Customer Privacy* 469  
Yakob Utama Chandra, Bahtiar Saleh Abbas, Agung Trisetyarso, Wayan Suparta, Chul-Ho Kang
- Object Classifications by Image Super-Resolution Preprocessing for Convolutional Neural Networks* 476  
Bokyoon Na, Geoffrey C Fox
- Interaction Model and Respect of Rules to Enhance Collaborative Brainstorming Results* 484  
Thierry Gidel, Andrea Tucker, Shigeru Fujita, Claude Moulin, Kenji Sugawara, Takuo Suganuma, Yuki Kaeri6, Norio Shiratori
- Design of Interactive Aids for Children's Teeth Cleaning Habits* 494  
Cheng Chuko, Fang-Lin Chao, Hsin-Yu Tsai
- Alternative Braking Method for Small Scaled-Wind Turbines Connected DC Green House with Analogical Experiment on Blade Destruction* 500  
Anupa Koswatta, Famaraz Alsharif, Yasushi Shiroma, Mahdi Khosravy, Shiro Tamaki, Junji Tamura
- On the Ensemble of Recurrent Neural Network for Air Pollution Forecasting: Issues and Challenges* 512  
Ola Surakhi, Sami Serhan, Imad Salah
- A Simple Modelling Tool for Fast Combined Simulation of Interconnections, Inter-Symbol Interference and Equalization in High-Speed Serial Interfaces for Chip-to-Chip Communications* 527  
Davide Menin, Thomas Bernardi, Alessio Cortiula, Martino Dazzi, Alessio De Pr, Mattia Marcon, Marco Scapol, Andrea Bandiziol, Francesco Brandonisio, Andrea Cristofoli, Werner Grollitsch, Roberto Nonis, Pierpaolo Palestri
- Understanding Human Perception of Vibrotactile Feedback in Walking and Running Tasks* 537  
Emel Demircan, Elliot Recinos, I-Hung Khoo, Sharon Teng, Will Wu
- The Capacity Factor of Renewable Energy Power Plants During Electric Power Peak Times in Jeju Island* 545  
Gaemyoung Lee, Zulmandakh Otgongerel, Ankhzaya Baatarbileg

- Approach to Combine an Ontology-Based on Payment System with Neural Network for Transaction Fraud Detection* 551  
Ahmed EL Orche, Mohamed Bahaj
- Minimizing the Cleaning Cost in Flash Based Storage Sub-Systems by Proliferating the Valid Data Copying Process* 561  
Hisyamuddin Kasim, Amir Rizaan Abdul Rahiman, Nor Asilah Wati Abdul Hamid, Thinagaran Perumal
- Securing Hybrid SDN-based Geographic Routing Protocol using a Distributed Trust Model* 567  
Lylia Alouache, Mohamed Maachaoui, Rachid Chelouah
- An ISO 25010 Based Quality Model for ERP Systems* 578  
Emmanuel Peters, George Kwamina Aggrey
- Combination of Salient Object Detection and Image Matching for Object Instance Recognition* 584  
Evan Kristia Wigati, Gede Putra Kusuma, Yesun Utomo
- Statistical Aspects of the Environment of Albanian Students Who Were Admitted to Higher Public Education Institutions in the Year 2014* 592  
Feruze Shakaj, Markela Muça, Klodiana Bani
- Analysis of Two-Dimensional Electron Gas Formation in InGaAs-Based HEMTs* 597  
Itsuki Takagi, Takuma Kato, Hirohisa Taguchi
- HDR Image Tone Mapping Approach Using Multiresolution and Piecewise Linear Perceptual Quantization* 606  
Quoc Thai Pham, Ba Chien Thai
- Determinants of Students' Actual use of the Learning Management System (LMS): An Empirical Analysis of a Research Model* 614  
Charles Buabeng-Andoh, Charles Baah
- Commercialization Process of Disruptive Innovations in Corporate Ventures and Spinoff Companies: A Comparison* 621  
Javier Nieto Cubero, Saheed Adebayo Gbadegeshin, Carolina Consolación Segura
- Activerest: Design of A Graphical Interface for the Remote use of Continuous and Holistic Care Providers* 635  
Nuno Martins, Jéssica Campos, Ricardo Simoes
- Evaluation of Vapor Jet Refrigeration Cycle Driven by Solar Thermal Energy for Air Conditioning Applications: Case Study* 646  
Ishaq Sider, Khaled Sider



<i>On the use of Triple Graph Grammars for Model Composition</i>	653
Hatime Bencharqui, Younes Moubachir, Adil Anwar	
<i>A Resolution-Reconfigurable Asynchronous SAR ADC with Segmented and Non-Binary Weighted Capacitance DACs</i>	665
Chih-Hsuan Lin, Kuei-Ann Wen	
<i>Analysis of Vulnerabilities, Risks and Threats in the Process of Quota Allocation for the State University of Ecuador</i>	673
Segundo Moisés Toapanta Toapanta, Andrés Aurelio García Henríquez, Luis Enrique Mafla Gallegos	
<i>Classification of Timber Load on Trucks</i>	683
Jan Sikora, David Fojtík	
<i>ROS Based Multimode Control of Wheeled Robot</i>	688
Rajesh Kannan Megalingam, Santosh Tantravahi, Hemanth Sai Surya Kumar Tammana, Nagasai Thokala, Hari Sudarshan Rahul Puram, Naveen Samudrala	
<i>Neural Network-based Efficient Measurement Method on Upside Down Orientation of a Digital Document</i>	697
Yeji Shin, Youngone Cho, Hyun Wook Kang, Jin-Gu Kang, Jin-Woo Jung	
<i>Evaluation of Mini-Hydro Power for Off Grid Electrification in Rural/Isolated Areas in Africa</i>	703
Ogbuefi Uche Chinweoke, Ene Princewill Chigozie, Kenneth Chijioke Chike	
<i>Seismic Performance of Infilled Reinforced Concrete Buildings</i>	711
Miloud Mouzzoun, Abdelkader Cherrabi	
<i>Comparison of the RC-Triggered MOSFET-Based ESD Clamp Circuits for an Ultra-low Power Sensor System</i>	718
Chih-Hsuan Lin, Kuei-Ann Wen	
<i>Towards Enterprise Technical Architecture for the Implementation of the South African NHI</i>	724
Farirai Chitsa, Tiko Iyamu	
<i>Face Recognition on Low Resolution Face Image With TBE-CNN Architecture</i>	730
Suharjito, Atria Dika Puspita	
<i>Review on Smart Electronic Nose Coupled with Artificial Intelligence for Air Quality Monitoring</i>	739
Rabeb Faleh, Souhir Bedoui, Abdennaceur Kachouri	
<i>A Comprehensive Survey on Image Modality based Computerized Dry Eye Disease Detection Techniques</i>	748
Aditi Haresh Vyas, Mayuri A. Mehta	

- Actigraph Analysis of Elderly Dementia Patients During Phototherapy Using Non-Linear Analysis* 757  
Fumiya Kinoshita, Yuki Mukumoto, Keiko Teranishi, Hideaki Touyama
- Analysis of the Blockchain for Adoption in Electronic Commerce Management in Ecuador* 762  
Segundo Moisés Toapanta Toapanta, Daniela Monserrate Moreira Gamboa, Luis Enrique Mafla Gallegos
- Legal Regulation as Driver for Sustainable Development of Nigeria's Solid Mineral Sector* 769  
Isaac Onyeyirichukwu Chukwuma, Benjamin Onoriode Mukoro, Fidelis Odinakachukwu Alaefule, Gertrude Chinelo Ugwuja, Emmanuel Kalu Agbaeze, Ifeanyi Leo Madu
- Mobile Based for Basic English Learning Assessment with Augmented Reality* 774  
Zuhri Syarifudin, Suharjito
- A Novel Quantum No-Key Protocol for Many Bits Transfer with Error Correction Codes* 781  
Duc Manh Nguyen, Sunghwan Kim
- Low Carbon Sustainable Building Material: Maximizing Slag Potentials for Improved Lime Mortar Mechanical Properties* 786  
Sule Adeniyi Olaniyan

# A New Distributed Reinforcement Learning Approach for Multi-agent Cooperation Using Team-mate Modeling and Joint Action Generalization

Wiem Zemzem<sup>1</sup>, Ines Hosni<sup>2\*</sup>

<sup>1</sup>Department of Information Systems, College of Computer and Information Sciences, Jouf University, Sakaka, Saudi Arabia, [wzemzem@ju.edu.sa](mailto:wzemzem@ju.edu.sa)

<sup>2</sup>Department of Information Systems, College of Computer and Information Sciences, Jouf University, Sakaka, Saudi Arabia, [itabbakh@ju.edu.sa](mailto:itabbakh@ju.edu.sa)

## ARTICLE INFO

Article history:

Received: 02 January, 2020

Accepted: 22 February, 2020

Online: 09 March, 2020

Keywords:

Distributed reinforcement learning

The curse of dimensionality

Cooperative learning

Dynamic environments

Avoiding collisions

## ABSTRACT

This paper focuses on the issue of distributed reinforcement learning (RL) for decision-making in cooperative multi-agent systems. Although this problem has been a topic of interest to many researchers, results obtained from these works aren't sufficient and several difficulties have not yet been resolved, such as, the curse of dimensionality and the multi-agent coordination problem. These issues are aggravated exponentially as the number of agents or states increases, resulting in large memory requirement, slowness in learning speed, coordination failure and even no system convergence. As a solution, a new distributed RL algorithm, called the ThMLA-JAG method, is proposed here. Its main idea is to decompose the coordination of all agents into several two-agent coordination and to use a team-mate model for managing other agents' experiences. Validation tests on a pursuit game show that the proposed method overcomes the aforementioned limitations and is a good alternative to RL methods when dealing with cooperative learning in dynamics environments while avoiding collisions with obstacles and other learners.

## 1 Introduction

Reinforcement Learning (RL) focuses on the question of an agent learning by interacting with its environment and analyzing the effects of these interactions and has been successfully applied in many single-agent systems [1, 2]. Throughout RL, the learning takes place iteratively and is carried out through trials and errors, making it a safe tool to deal with complex and uncertain environments [3].

Given RL properties, a growing interest was developing these last years in order to extend reinforcement learning to multi-agent systems (MASs). MASs are applied to a wide variety of domains including robotic teams [4, 5], air traffic management [6] and product delivery [7].

We are specifically interested in distributed cooperative mobile robots, Where multiple cooperative robots can perform tasks faster and more efficiently than a single robot. The decentralized point of view provides many potential benefits

such as speed-up, scalability and robustness [8, 9]. Cooperative systems means that the agents (robots) share common interests (e.g., the same reward function), thus the increase in individual's benefit also leads to the increase of the benefits of the whole group[10, 11].

In recent years, an increasing number of researches have shown interest in extending reinforcement learning (RL) to MASs in the powerful framework of Markov games (MG, also known as stochastic games, SG), and many promising multi-agent reinforcement learning (MARL) algorithms have been proposed [10][12]-[13]. These methods can be divided into two big categories: the case of independent learners (ILs) where each agent only knows its own actions [13] and the case of joint actions learners (JALs) where each agent collects information about their own choice of action as well as the choices of other agents [14].

Many algorithms derived from these both IALs and JALs can learn the coordinated optimal joint behaviors and provide cer-

\*Corresponding Author: Ines Hosni, Dept. of Information Systems, College of Computer and Information Sciences, Jouf University, Sakaka, Saudi Arabia, [itabbakh@ju.edu.sa](mailto:itabbakh@ju.edu.sa)

tain convergence guarantees as well but in simple cooperative games (matrix games, few players, not fully stochastic environment, etc). However, they fail when the domain becomes more complex [15, 16], especially when the number of agents or state spaces increases, resulting in large memory requirement, slowness in learning speed and then more challenging coordination.

As JALs offer good coordination results but suffer from the curse of dimensionality, a new kind of distributed multi-agent reinforcement learning algorithm, called the ThMLA-JAG (Three Model Learning Architecture based on Joint Action Generalization) method, is proposed here. The main idea is to decompose the coordination of all JALs into several two-agent coordinations. Validation tests which are realized on a pursuit problem show that an overall coordination of the multi-agent system is ensured by the new method as well as a great reduction of the amount of information managed by each learner, which considerably accelerates the learning process.

To the best of our knowledge, this is the first distributed MARL system that decompose the multi-agents learning process into several two-agents learning systems. The system is decentralized in the sense that learned parameters are split among the agents: each agent learns by interacting with its environment and observing the results of all agents' displacements. Hence no direct communication is required into learning agents, a communication that can be expensive or insufficient because of bad synchronization and/or limited communication range [17]. As such, the proposed approach is different from methods that learn when such communication is necessary [9][18]-[19]. We particularly show that the system remains effective even when agents' information are distorted due to frequent environmental changes.

The rest of the paper is arranged as follows. In section 2, we introduce some basic reinforcement learning concepts. In section 3, two existing RL methods on which our proposed approach is based are presented. Section 4 is dedicated to present the ThMLA-JAG method. Several experiences are conducted in section 5 showing the efficiency of our proposals. Some concluding remarks and future works are discussed in section 6.

## 2 Reinforcement learning

Markov Decision Processes (MDPs) are often used to model single-agent problems. MDPs [20] are suitable for studying a wide range of optimization problems that have been solved by dynamic programming and reinforcement learning. They are used to model scenarios where an agent has to determine how to behave based on the current state's observation.

More precisely, a Markov model is defined as a 4-tuple  $(S, A, T, R)$ , where  $S$  is a discrete set of environmental states,  $A$  is a discrete set of agent actions,  $R : S \times A \rightarrow \mathfrak{R}$  is a reward function and  $T : S \times A \rightarrow \Pi(S)$  is a state transition function ( $\Pi(S)$  is a probability distribution over  $S$ ). We write  $T(s, a, s')$  as the probability of making a transition from  $s$  to

$s'$  taking action  $a$ . The action-value function  $Q^*(s, a)$  is defined as the expected infinite discounted sum of rewards that the agent will gain if it chooses the action  $a$  in the state  $s$  and follows the optimal policy. Given  $Q^*(s, a)$  for all state/action pairs, the optimal policy  $\pi^*$  will be developed as the mapping from states to actions such that the future reward is maximized [1].

One of the most relevant advances in reinforcement learning was the development of the Qlearning algorithm, an off-policy TD (temporal-difference) control algorithm [15, 21]. Q-learning is especially used when the model (T and R) are unknown. It directly maps states to actions by using a Q function updated as in (1):

$$Q(s_t, a_t) = (1 - \alpha_t) \times Q(s_{t-1}, a_{t-1}) + \alpha_t \times [r_t + \gamma \times \max_{a'_t \in A} Q(s'_t, a'_t)] \quad (1)$$

where,

- $(1 - \alpha_t) \times Q(s_{t-1}, a_{t-1})$ : the previous estimation,
- $\alpha_t \times [r_t + \gamma \times \max_{a'_t \in A} Q(s'_t, a'_t)]$ : the new experience,
- $\alpha \in [0, 1]$  is the learning rate and  $\gamma \in [0, 1]$  is the discount factor.

Despite its multiple successful results in single agent cases, Qlearning can't be directly applied to multi-agent systems. In fact, learning becomes a much more complex task when moving from a single agent to a multi-agent setting. One problem is the lack of the single agent framework's convergence hypotheses. For instance, the environment is no longer static from a single-agent perspective due to many agents working on it: this is a commonly cited source of multi-agent learning systems difficulties [22]. Another issue is the communication between agents: How to ensure a relevant information exchange for effective learning [23]?, and finally the problem of multi-agent coordination in order to ensure a coherent joint behavior.

In what follows, several MAL methods derived from Qlearning are presented and classified according to the state/action definition.

### 2.1 Individual state / individual action

Many researchers are interested on extending Qlearning to distributed MAS using cooperative ILs. They aim to design multiple agents capable of performing tasks faster and more reliably than a single agent. Examples include PA (Policy Averaging) [24], EC (Experience Counting) [25], D-DCM-Multi-Q (Distributed Dynamic Correlation Matrix based MultiQ) [17], CMRL-MRMT (Cooperative Multi-agent learning approach based on the Most Recently Modified Transitions) [26] and CBG-LRVS [27]. Here, each entry of the Qfunction is relative to the individual state/action pair of the agent itself like in the case of single-agent learning and a direct communication is used to share information between different learners. These methods use also the assumption that all learners can

be in the same state at the same time which eliminates the coordination problem. So, these methods succeed to establish a cooperative learning but become inapplicable when considering the collision between learners, like the case in reality of mobile and autonomous robotic systems.

## 2.2 Joint state / individual action

To better address the coordination problem, many other learning algorithms have been proposed in literature while keeping collisions between learners, like, decentralized Qlearning [23], distributed Qlearning [15], WoLF PHC [22], Implicit coordination [28], Recursive FMQ [16] and Hysteritic learners [29].

In such methods, agents are fully cooperative which means that they all receive the same reward and are non-communicative that are unable to observe the actions of other agents. These methods are based on Markov games, i.e, each learner updates its Qvalues using joint states ( relatives to all agents and even other elements presenting in the environment) and individual actions ( specific to the agent itself). Their performances can greatly vary between successful and unsuccessful coordination of agents.

As explained in [13], no one of those algorithms fully resolves the coordination problem. Complications arise from the need of balance between exploration and exploitation to ensure efficiency like in single RL algorithms. But the exploration of an agent induces noise in received rewards of the group and can destabilize the learned policies of other ILs.

To sort out this problem, called the alter-exploration problem, many parameters, which the convergence relies on, are introduced. So, the main drawbacks of these methods are that parameter tuning is difficult and that when the number of agent increases, the difficulty of coordination increases and the alter-exploration problem outweighs. The learning velocity is also highly affected when altering the number of agents and/or the environment size due to the use of joint states.

## 2.3 Joint state / joint action

Given ILs' limitations, methods using JALs are much more used for stochastic games[14]. They can provide distributed learning while avoiding collisions between agents. They solve ILs' problems since the whole system's state is considered by each learner, i.e, the Qvalues are updated using joint states and joint actions. However, JALs suffer from combinatorial explosion of the size of the state-action space with the number of agents, as the value of joint actions is learnt by each agent, contrary to ILs that ensure a state space size independent of the number of agents.

As an example, TM-LM-ASM (team-mate model- learning model- Action Selection Model) [30] is a JAL method that combines traditional Q-learning with a team-mate modeling mechanism. To do that, each learner has to memorize a table Q storing all possible joint states/actions pairs and a table P storing all possible joint states/actions pairs except its own action. The Q table is used by the learning model as simi-

lar as the Qlearning method and the P table is used by the teammate model to estimate the behaviors strategies of other agents. Then, the strategy used by the learner to select an action is done by the action selection module using both the P and Q tables.

Experiments done on a pursuit game [30] using two predators and one moving prey show the effectiveness of the TM-LM-ASM method and that it ensures a global coordination without the need of a direct communication between different members. However, obtained results are limited to two-agent systems. A problem of state space explosion can be obviously detected when increasing the number of agents because of the use of joint states and joint actions. As an example, let's consider the case of  $N_{agents}$  agents able to execute  $N_{actions}$  actions in an  $L \times L$  grid world. If the state of every agent is relative to its position in the grid, every learner has to store a table Q containing  $(L^2 \cdot N_{actions})^{N_{agents}}$  entries and a table P having  $\frac{(L^2 \cdot N_{actions})^{N_{agents}}}{N_{actions}}$  entries, without forgetting the significant number of possible team-mates actions' combinations to consider when updating the table P and when choosing the next action to execute, that's:  $N_{actions}^{N_{agents}-1}$  possible actions' combinations.

If we examine the case of 4 agents which can make 5 actions in a  $10 \times 10$  grid world, we obtain:

- $625 \cdot 10^8$  entries of the table Q,
- $125 \cdot 10^8$  entries of the table P,
- 125 possible combinations of team-mates' actions in every state.

As it is mentioned in the theoretical convergence of the Qlearning algorithm [15], an optimal policy is only achieved if every state action pair has often been performed infinitely. For the above described example, we can see that a first visit of each state/action pair isn't obvious and requires a long time. The amount of memory needed for storing the tables P and Q is also significant. A huge computing power is thus required so that all possible combinations of team-mates' actions can be taken into account and this is at every learning step (during the updates of P and Q and when choosing actions).

## 2.4 Learning by pair of agents

To solve the state space explosion problem along with ensuring a satisfactory multi-agent coordination, Lawson and Mairesse [18] propose a new method inspired by both ILs and JALs approaches. The main idea is to learn a joint Q-function of two agents and to generalize it to any number of agents.

Considering a system of  $N_{agents}$  agents, at any learning step, each agent has to communicate with its  $(N_{agents} - 1)$  teammate agents, update its  $(N_{agents} - 1)$  Q-tables of two agents and then identify the next joint action to follow. Note that the same joint action must be chosen by all the learners. Additional computations are then required. Indeed, the most promising joint action is not directly determined from a joint

table Q, as in the case of joint actions learners, but it needs the evaluation of the sum of  $(N_{agents} - 1)$  values of Q. Also,  $(N_{agents} - 1)$  updates of Q are done instead of one update of the joint table. However, this increase in required computing power is widely compensated by the advantages that present this method compared with the approaches using ILs or JALs, namely:

- By learning through agents' pairs as the JAG method, a huge reduction in the number of state/action pairs is ensured which leads to the acceleration of the system convergence. As illustrated in Table 1, these memory savings widen with the increase of the environment size and/or the number of agents.
- Contrary to independent agents, a global coordination is provided by the JAG method because this method evaluates all possible joint actions of every pair of agents and chooses the global joint action (of the whole multi-agent system) after maximizing the Qvalue of each of these pairs. This is based on the assumption that a global coordination is ensured by coordinating each couple of agents, provided that the policy obtained for two agents is optimal.

Several experiences are made by Lawson and Mairesse [18] on the problem of the navigation of a group of agents in a discrete and dynamic environment so that each of them reaches its destination as quickly as possible while avoiding obstacles and other agents. The results of these experiences confirm the aforesaid advantages, namely an acceleration of learning with a global coordination as in the case of JALs.

However, the distribution of learning does not facilitate the task but results in an identical treatment of the same information by all the agents. More precisely, in every iteration, agents communicate their new states and rewards to all their team-mates. As a consequence, each of them updates the Q-entries of all agents' couples and executes the JAG procedure to choose the next joint action. Another communication is then necessary to make sure that the same joint action is chosen by all learners. Thus, the JAG method seems to be less expensive by adopting a centralized architecture: only one agent is responsible for updating information and for choosing actions and informs other agents of their corresponding actions. Conversely, every agent executes its own action and informs the central entity of its new state and the resulted reward.

### 3 Proposed reinforcement learning algorithm

As explained earlier, the JAG method [18] ensures a global coordination while using independent learners but needs a centralized process to make sure that all agents choose the same joint action at each learning step, whereas the TM-LM-ASM method [30] is a full distributed learning approach that also provides a global coordination but employs joint action learners which make it unsuitable for systems considering many

agents and/or large state spaces.

Our objective is to develop a new intermediate approach between TM-LM-ASM and JAG. The main idea is to generalize the TM-LM-ASM architecture which is learned by two agents to a larger number of agents while using the JAG decomposition instead of joint state-action pairs. The new proposed approach is called ThMLA-JAG (a Three-Model Learning Architecture using Joint Action Generalization).

According to the ThMLA-JAG method, the multi-agent coordination process is divided into several two-agents learning tasks. Assuming that the system contains  $N_{agents}$  agents, each agent must memorize  $(N_{agents} - 1)$  P-Tables of two agents for the team-mates' model and  $(N_{agents} - 1)$  Q-Tables of two agents for the learning model.

#### 3.1 The team-mates' model

Consider a system of N learning agents in a joint state  $s = (s_1, \dots, s_{N_{agents}})$ . At a learning step  $t$ , a learning agent  $i$  under consideration executes an action  $a_i^*$  and observes its partners' actions  $(a_1^*, \dots, a_{i-1}^*, a_{i+1}^*, \dots, a_N^*)$ , the new obtained state  $s' = (s'_1, \dots, s'_{N_{agents}})$  and the resulted reward  $r$ . Then, it updates  $(N_{agents} - 1)$  P-tables concerning each partner  $j$  for each action  $a_j$  that can be tried by this agent  $j$  in the experimented state  $s = (s_i, s_j)$ . The table  $P_{ij}$  concerning the pair of agents  $(i, j)$  can be updated using (2), similarly to the TM-LM-ASM method when is applied to two-agent systems.

$$P_{ij.t}(s, a_i) = \begin{cases} P_{ij.(t-1)}(s, a_j) + \beta^{T-t+1} \sum_{a_t \in A_j - \{a_j\}} P_{ij.(t-1)}(s, a_t), & a_j = a^* \\ (1 - \beta^{T-t+1})P_{ij.(t-1)}(s, a_j), & elsewhere \end{cases} \quad (2)$$

where,  $\beta \in [0, 1]$  is the learning rate that determines the effect of previous action distribution, and  $T$  is the number of iterations needed for the task completion.  $s$  and  $s'$  are joint states that present the instantaneous positions of agents  $(i, j)$  in the environment.

#### 3.2 The learning model

Similar to the JAG method,  $(N_{agents} - 1)$  updates are made by each learner at each learning step. Each update concerns an entry of one of the  $(N_{agents} - 1)$  Q-tables that are saved by this learner and is relative to one of its partner.

If we consider that the transition  $(s_i, a_i) \rightarrow s'_i$  had been executed by a learner  $i$  while another learner  $j$  executed the transition  $(s_j, a_j) \rightarrow s'_j$ , the table  $Q_{ij}$  corresponding to the pair  $(i, j)$  with the joint state  $s = (s_i, s_j)$  and the joint action  $a = (a_i, a_j)$  can be updated using (3), as when applying the TM-LM-ASM method for two agents.

$$Q_{ij}(s, a_i, a_j) = (1 - \alpha) Q_{ij}(s, a_i, a_j) + \alpha \left( r + \gamma \max_{a' \in A_i} Q_{ij}(s', a'_i, a'_j) \right) \quad (3)$$

Table 1: Comparison of the Q size following the joint and the JAG method. Note that  $N_{agents}$  agents evolve in an  $L \times L$  grid world by executing  $N_{actions}$  possible actions and the state of each agent corresponds to its position in the grid

$N_{agents}$	$N_{actions}$	L	Size of Q using TM-LM-ASM	the JAG method	
				Size of Q for two agents	Total size of all agents' Q
N	A	L	$(L^2 \times A)^N$	$(L^2 \times A)^2$	$(L^2 \times A)^{(N-1)}$
4	4	5	$10^8$	$10^4$	$6 \cdot 10^4$
		10	$2.56 \cdot 10^{10}$	$1.6 \cdot 10^5$	$9.6 \cdot 10^5$
		50	$10^{16}$	$10^8$	$6 \cdot 10^8$
8	4	5	$10^{16}$	$10^4$	$28 \cdot 10^4$
		10	$6.5536 \cdot 10^{20}$	$1.6 \cdot 10^5$	$44.8 \cdot 10^5$
		50	$10^{32}$	$10^8$	$28 \cdot 10^8$

where,

$$a'_j = \operatorname{argmax}_{b \in A_j} P_{ij}(s', b)$$

Thus, the team-mate model is exploited by the learning model. More precisely, the best move in the next state  $s'$  relies on the next action  $a'_i$  of the agent  $i$  under consideration and the next action  $a'_j$  of its partner  $j$ . Given that the Q function of this later isn't known by agent  $i$ , a prediction of its action is done using the memorized team-mate model. For the examined agent, the action that should be preferably executed in the next state is determined by the exploitation of its Q function.

### 3.3 The action selection model

For a better selection of the next action to execute, a generalization of the action selection model proposed by Zhou and Shen [30] for 2 agents to N agents ( $N \geq 2$ ) is possible by exploiting all stored P-tables and Q-tables of the learner. To this end, for each agent  $i$  having  $(N_{agents} - 1)$  team-mates and staying at a joint state  $s = (s_1, \dots, s_i, \dots, s_{N_{agents}})$ , the action  $a_i^*$  to be executed in that state  $s$  can be selected by using (4):

$$a_i^* = \operatorname{argmax}_{a_i \in A_i} V(a_i | a_1^*, \dots, a_{i-1}^*, a_{i+1}^*, \dots, a_{N_{agents}}^*) \quad (4)$$

where,  $(a_1^*, \dots, a_{i-1}^*, a_{i+1}^*, \dots, a_{N_{agents}}^*)$  are predicted by agent  $i$  as the next actions to be executed by its partners in the joint state  $s$ ,  $A_i$  is the set of possible actions of agent  $i$  and  $V(a_i | a_1^*, \dots, a_{i-1}^*, a_{i+1}^*, \dots, a_{N_{agents}}^*)$  is the conditional expectation value of action  $a_i^*$  of agent  $i$  when it considers the team-mates' model:

For all  $a_i \in A_i$ ,  $V(a_i | a_1^*, \dots, a_{i-1}^*, a_{i+1}^*, \dots, a_{N_{agents}}^*)$  is calculated using (5):

$$V(a_i | A_1, \dots, A_{i-1}, A_{i+1}, \dots, A_{N_{agents}}) = \sum_{j=1, j \neq i}^{N_{agents}} \sum_{a_k \in A_j} P_{ij}((s_i, s_j), a_k) Q_{ij}((s_i, s_j), a_i, a_k) \quad (5)$$

where,  $(s_i, s_j)$  is the actual state of agent  $i$  and its team-mate  $j$  and  $A_j$  is the set of all possible actions of agent  $j$ . Here, all possible actions of team-mates are equally considered

and there's no prediction of any particular joint action. This can be explained by the fact that, for each pair of agents  $(i, j)$ ,  $P_{ij}$  and  $Q_{ij}$  have initially the same values for all state/action pairs. As the learning progresses or new circumstances take place (such as collisions or environmental changes), a particular set of state/action pairs will become favoured as a result of the increase of their corresponding  $P_{ij}$  and  $Q_{ij}$  values. Therefore, different values  $V$  will be attributed to each action  $a_i$  of agent  $i$ . Then, a greedy choice following (4), allows the agent  $i$  to select the most promising action  $a_i^*$  in the current state  $s$ .

### 3.4 Improving multi-agent coordination

When updating a table  $Q_{ij}$  related to the team-mate  $j$ , the learner  $i$  has to predict the most promising joint action  $(a'_i, a'_j)$  in the next state. As described in (3), its own action  $a'_i$  is that maximizing  $Q_{ij}$  in that state. However, our proposition assumes that each agent has  $(N_{agents} - 1)$  Q-tables corresponding to its  $(N_{agents} - 1)$  partners and all these Q-tables will be exploited during the choice of the action to be really executed. Thus, by referring to the unique table  $Q_{ij}$  when predicting a possible next action, the predicted action will not necessary reflect the one which will be really experimented in the next state. As a result, the learner can continuously oscillate between two consecutive states if those states are updated according to a predicted state different from that really visited. For that, it would be better to predict the action maximizing the next state using the maximum amount of information, explicitly, all the Q-tables and P-tables which have been stored by the learner. Thus, the updated version of (3) is shown by (6):

$$Q_{ij}(s, a_i, a_j) = (1 - \alpha) Q_{ij}(s, a_i, a_j) + \alpha (r' + \gamma Q_{ij}(s', a'_i, a'_j)) \quad (6)$$

where,  $a'_j$  is identified as before in (4) and  $a_i^*$  is calculated using the predefined action selection model of (4): it is the same strategy used for real actions' selection. This modification in the update of the Q-function will be further justified in the experimental section.

### 3.5 The proposed learning algorithm

A possible extension of the algorithm proposed by Lawson and Mairesse [18] for a system having more than two agents is presented by algorithm 1 and illustrated in Figure 1. Note that all agents are learning synchronously, specifically:

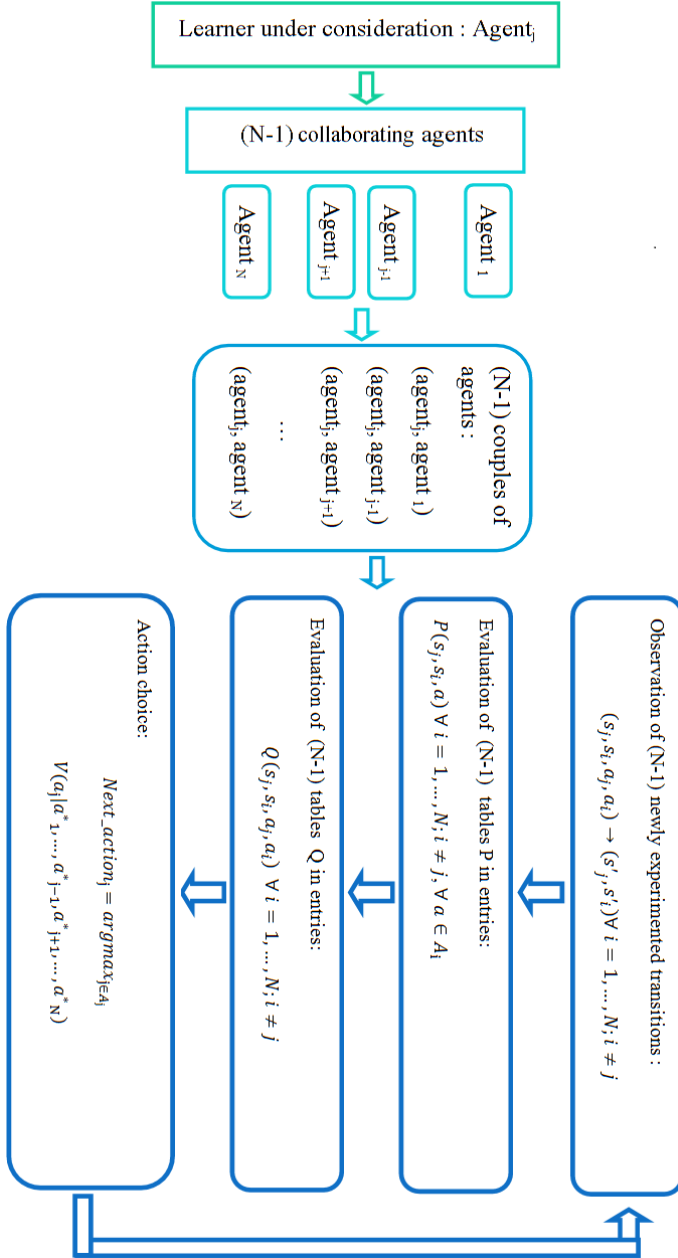


Figure 1: The ThMLA-JAG learning architecture

- Initialize learning (the steps 1,...,14 of algorithm 1),
- Select the action, execute it and observe the result (the steps 17,...,20 of algorithm 1),
- Update P-table (the step 22 of algorithm 1),
- Update Q-table (the step 23 of algorithm 1). Two alternatives of updating a Q-table will be compared in the experimental section: (3) and (6),

- Test the end of learning or the release of a new episode (the steps 25 and 26 of algorithm 1),
- Go to a new iteration in the same episode (the steps 27 and 28 of algorithm 1).

It should also be noted that the reward is defined by pair of agents in accordance with the learning architecture, i.e, every two agents receive a specific reward that describes the result of their own displacement. In what follows, we are going to examine two test cases:

- In the first case (S1: a temporary dynamic environment), the prey is temporary moving and each predator should be able to build an optimal path from its starting position to that target while avoiding obstacles, other predators and the prey as well as to correct this path after each environmental change. An episode ends if the prey is captured or that it exceeds 1000 iterations. Initially, the environment is in the form of Figure 2. After 1200 episodes, the prey moves to a new position as shown in Figure 2-b.

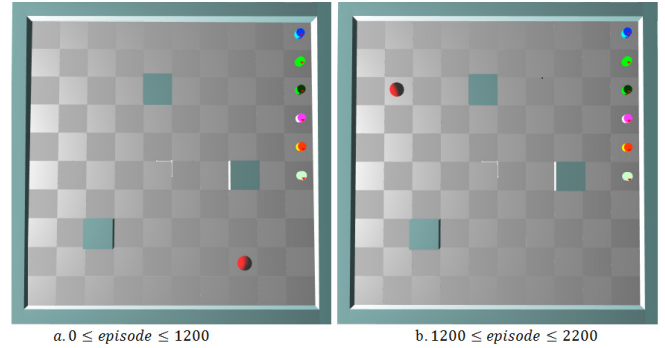


Figure 2: The testing environment of S1

Figure 3 describes the environment used to test this scenario. Once an episode is ended, agents are relocated on the right extremity of the labyrinth and a new trial begins. Because collisions between agents aren't permitted and in order to test a system containing more than four agents, we suppose that the prey is captured if each hunter is in one of its eight neighboring cells including corners. Figure 3-a describes a possible capture position.

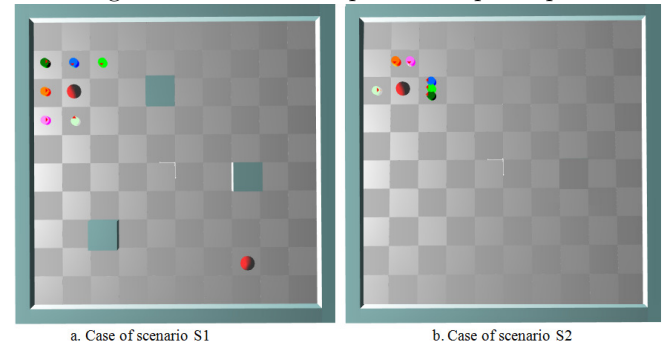


Figure 3: Example of capture position

- In the second case ( S2: a highly dynamic environment), agents move in a frequently dynamic environment and



**Algorithm 1** Algorithm ThMLA-JAG**Require:**

$N$ : the total number of agents

$S = \{(s_i, s_j); i, j = 1 \dots N\}$  is the set of possible states for all agents' pairs  $(i, j)$

$A_i$  is the set of possible actions of agent  $i$

**Ensure:**

**for** agent:  $i = 1 \dots N$  **do**

**for** *team - mate* $_i$  :  $j = 1 \dots N, j \neq i$  **do**

**for**  $s = (s_i, s_j) \in S \times S$  **do**

**for**  $a = (a_i, a_j) \in A_i \times A_j$  **do**

$Q_{ij} \leftarrow \frac{1}{|A_i| \cdot |A_j|}$

$P_{ij} \leftarrow \frac{1}{|A_j|}$

**end for**

**end for**

**end for**

**end for**

**while** learning in progress **do**

**for** agent  $i = 1 \dots N$  **do**

$t \leftarrow 0$ , initialize its own current state  $s_{i,t}$

**end for**

**for** each learning step **do**

**for** agent  $i = 1 \dots N$  **do**

      Observe the current joint state  $s_t = (s_{1,t}, s_{2,t}, \dots, s_{N,t})$

      Choose an action  $a_{i,t}$  following equation(4)

      Execute  $a_{i,t}$  and observe the actions being simultaneously executed by other team-mates

**for** *team - mate* $_i$  :  $j = 1 \dots N, j \neq i$  **do**

        Determine the new state  $s_{t+1} = (s_{i,t+1}, s_{j,t+1})$  and the corresponding reward  $r_{t+1} = r_{ij}$

        Update  $P_{ij}(s_{i,t}, s_{j,t}, a_j)$  following equation (2), for all  $a_j \in A_j$

        Update  $Q_{ij}(s_{i,t}, s_{j,t}, a_{i,t}, a_{j,t})$  following equation (3) or equation (6) , where  $a_{j,t}$  is the simultaneous action of agent  $j$

**end for**

**if** the new state  $s_{t+1}$  is the goal state **then**

        The episode is ended, go to 11

**else**  $\{s_{t+1} \neq \text{goal\_state}\}$

$t \leftarrow t + 1$ , go to 15

**end if**

**end for**

**end for**

**end while**

devoid of obstacles. At each stage of learning, the prey has a probability equal to 0.2 to remain motionless or to move towards vertically or horizontally neighboring cells. As to hunters, they can share the same position except the one containing the prey. These agents are initially in random positions. They move according to 5 above-mentioned actions in a synchronized way until they catch the prey or their current episode exceeds 1000 iterations. Once an episode is ended, these agents are relocated at new random positions and a new episode begins. The prey is captured when all hunters are positioned in the vertically and/or horizontally neighboring cells of that prey.

In the rest of the paper, the term agent refers to only a predator (a learner). Some experiences are conducted while vary-

ing the number of agents. The results reported below are obtained by average results of 30 experiments where each one contains 2200 episodes.

### 3.6 Communication between agents

Communication between the different agents must be ensured by an autonomous multi-agent network system which aims to exchange data between the different nodes while meeting and maintaining certain communication performance requirements (coordination, synchronization of messages and cooperation). As wireless technology has led to consider a new era for robotics, where robots are networked and work in cooperation with sensors and actuators, we have defined a wireless communication allowing the different agents to work in cooperation, and to exchange data locally in a multi-agent system.

A wireless access point is used to operate in the command link of a mobile agent. The link will carry data signals for the other agents.

### 3.7 Parameter setting

As most RL methods, the major problems met during the implementation of the ThMLA-JAG algorithm (algorithm 1) are essentially the initialization of its parameters. To do it, several values had been experimented and the best configuration was then adopted to test the above-mentioned test cases. As a result, the same distribution of rewards is used in both scenarios, namely:

- a penalty of 0.9 is attributed to every agent striking an obstacle and/or to every couple of colliding agents,
- a reward of 3 is received by every couple of agents having captured the prey,
- a reward of -0.05 is given to every agent moving to a new state without neither colliding nor capturing the prey.

Concerning the other parameters, they are initialized as follows:

- the learning rates  $\alpha = 0.8$  and  $\beta = 0.8$ ,
- the update factor  $\gamma = 0.9$ ,
- the Qvalues (values of Q-table) are set to 0.04,
- the Pvalues (values of P-table) are set to 0.2,

Finally, the ThMLA-JAG method is tested in scenarios S1 and S2 while comparing both possibilities of update of the table Q, that are:

- according to (3) where the Qtable concerning one teammate is only updated according to the information saved by the current learner about this latter. In this case, the learning method to be tested is indicated by ThMLA-JAG1,
- according to (6) where the Qtable concerning one teammate is updated according to all information saved by the current learner, including those concerning other team-mates. Here, the variant to be tested is denoted by ThMLA-JAG2.

### 3.8 Memory savings

According to the ThMLA-JAG method and regardless of the manner in which the Q-tables are updated, a lot of saving in memory is ensured comparing to the TM-LM-ASM method (a JAL method) as well as the Hysteritic Qlearning method (an IL method) and this is all the more important as the number of agents increases. Table 2 illustrates this result.

### 3.9 Computation savings

In addition to memory savings, important computation savings are provided by the ThMLA-JAG1 method and are described in Table 3. Note that a  $P_{entry}$  (respt. a  $Q_{entry}$ ) designates an entry in the table P (respt. Q).

### 3.10 Comparing the two variants of ThMLA-JAG

In this section, we will compare ThMLA-JAG1 and ThMLA-JAG2 using 4-agent systems in both test cases S1 and S2.

#### 3.10.1 Testing S1

As noted by Figure 4 and Table 4, both ThMLA-JAG1 and ThMLA-JAG2 lead to the system convergence before and after the environmental change. Figure 4-a shows the number of iterations needed for each episode over time while Figure 4-b describes the number of collisions in each learning episode.

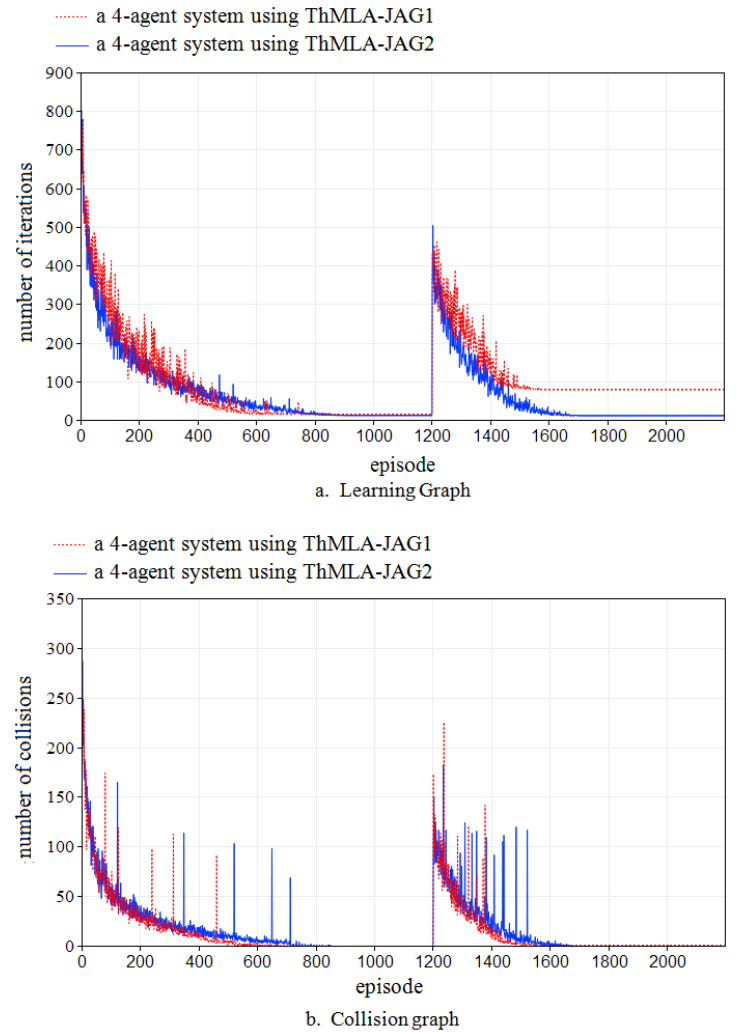


Figure 4: Testing the S1 scenario with a four-agent system (average of 30 experiences)

We can see that in both environments, the agents succeed to catch the prey without colliding with each other or with obstacles and this is after some iterations (about 850

Table 2: Variation of the saved information’s size according to the adopted method and the number of learners ( $|S| = 361$  and  $|A| = 5$ )

Learning method	$N_{Agents}$	Size of tables P	Size of tables Q
Hysteritic Q	N		$ S ^N \cdot  A $
	2		651605
	4		84917815205
	8		1442207067838105838405
TM-LM-ASM	N	$ S ^N \cdot  A ^{N-1}$	$ S ^N \cdot  A ^N$
	2	651605	3258025
	4	2122945380125	10614726900625
	8	22534485434970403725078125	112672427174852018625390625
ThMLA-JAG	N	$(N - 1) S ^2 \cdot  A $	$(N - 1) S ^2 \cdot  A ^2$
	2	651605	3258025
	4	1954815	9774075
	8	14561235	22806175

episodes in the first environmental form and 450 episodes after moving the target). On another hand, when updating a Q-table by only using the information of the corresponding team-mate (ThMLA-JAG1), the number of collisions is less than by exploiting the information of all other team-mates (ThMLA-JAG2). This is because with ThMLA-JAG2, the action resulting previous collisions is more likely to be chosen again, especially if these collisions concerned only some members of the multi-agent system.

On the contrary, the learning following ThMLA-JAG1 is much slower than that using ThMLA-JAG2. Figure 4-a and Table 4 show this result. Using ThMLA-JAG1, the first episodes are longer and the adaptation to the new environmental form requires more iterations than ThMLA-JAG2. Moreover, after displacing the target, the agents following ThMLA-JAG1 risk to not find a path leading to the new position of the target. Some experiences considering the ThMLA-JAG1 method are ended without a successful adaptation to the new environmental form. This explains the reason why the average length of the constructed path is equal to 80 steps in case of ThMLA-JAG1 and only 12 steps with ThMLA-JAG2. Besides, by observing the curves of collisions of ThMLA-JAG1 (Figure 4-b), we notice the existence of few collisions even after the system convergence. These collisions are related to failed experiences. The weakness of ThMLA-JAG1 is caused by the difference that can happen between the predicted action when updating the Qvalue and that will be really chosen using the adopted policy. This difference can block the learner between consecutive states. As the updates of Q no longer depend on recent movements, the Qvalues will remain invariants after some updates and the agent can’t modify or correct it.

### 3.10.2 Testing S2

The same remains true with the scenario S2. Figure 5 describes the number of captures done each 1000 episodes by considering two systems of 4 learning agents following

ThMLA-JAG1 and ThMLA-JAG2, respectively. Results show that the number of captures after the system convergence are much more important and stable by considering ThMLA-JAG2: After  $16 \cdot 10^4$  iterations, the number of captures is slightly changing in the case of ThMLA-JAG2 due to the movement of the prey but is significantly degrading in the case of ThMLA-JAG1. This difference in learning performance lies in the fact that, with ThMLA-JAG2, the Q-update is more in line with the adopted PEE, contrary to ThMLA-JAG1 where the system fails to converge to a final solution because the saved information can be considerably distorted by the movement of the prey which can occurs at every stage of learning.

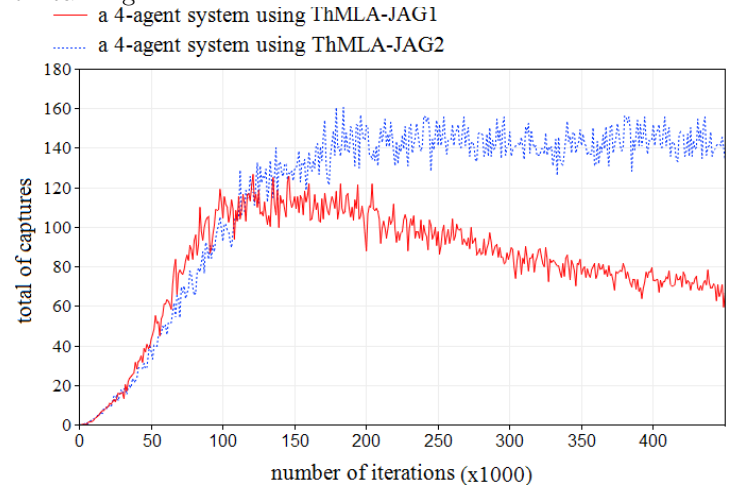


Figure 5: Variation of captures in function of the used learning method with the test case S2 (average of 30 experiences)

### 3.11 Effect of increasing the number of agents on the learning performance

In this section, we aim to evaluate the ThMLA-JAG2 method in both cases S1 and S2 while varying the number of agents from 2 to 6.

Table 3: Operations made by each learner at each learning iteration with  $|A| = 5$

	Operations	$N_{agents}$	TM-LM-ASM	ThMLA-JAG1	ThMLA-JAG2
team-mate model	Number of P-entries to update at each learning step	N	$ A ^{N-1}$	$(N - 1) \cdot  A $	$(N - 1) \cdot  A $
		2	5	5	5
		4	125	15	15
		8	78125	35	35
Action selection Model	Calculate $V(a_i)$ for every possible action $a_i$ of the current learner $i$ by performing $k$ sum of $(P_{entry} \cdot Q_{entry})$ where $k$	N	$ A ^{(N-1)}$	$(N - 1) \cdot  A $	$(N - 1) \cdot  A $
		2	5	5	5
		4	125	15	15
		8	78125	35	35
Learning model	is equal to Number of Q-entries to update at each learning step	N	1	(N-1)	(N-1)
		2	1	1	1
		4	1	3	3
		8	1	7	7
	Number of P-entries to be browsed to predict the possible next action of all team-mates	N	$ A ^{N-1}$	$(N - 1) \cdot  A $	$(N - 1) \cdot  A $
		2	5	5	5
		4	125	15	15
		8	78125	35	35

3.11.1 Case of T1

From Figure 6, we can see that the multi-agent system converges to a near optimal and collision free path and this is regardless of the number of agents.

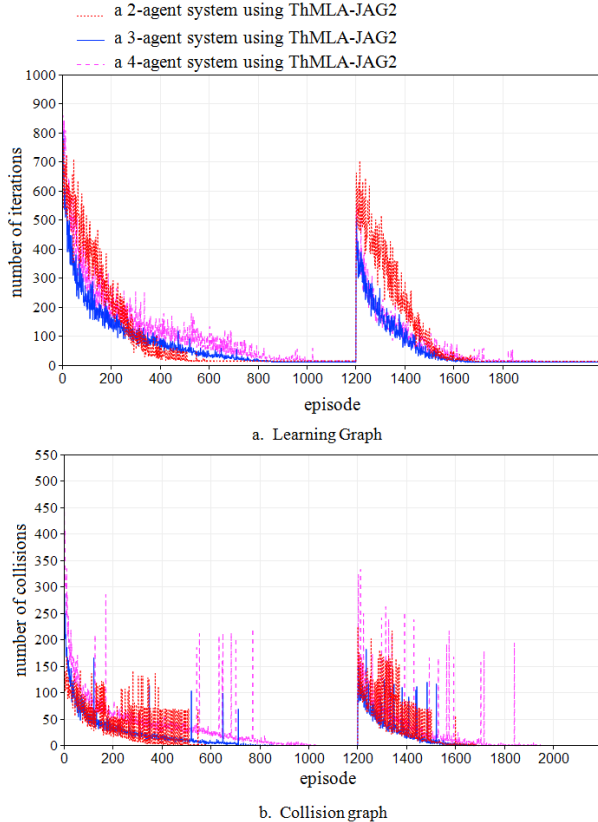


Figure 6: Effect of increasing the number of agents on the ThMLA-JAG2 method in the case of S1 (average of 30 experiences)

Likewise, agents succeed to adapt to the new environmental form once the prey is moved and the learning time isn't considerably delayed by the addition of new agents as well. As shown by Table 5, the 4-agent system needs more episodes to converge than the 2-agent system but a smaller number of iterations and collisions. As for the 6-agent system, the learning is slightly slower than the other cases.

3.11.2 Case of S2

Promising results are also obtained in case of S2. Figure 7 shows the number of captures done each 1000 episodes by considering three systems containing 2, 4 and 6 agents and using the ThMLA-JAG2 method. The results prove that the learning is accelerated by adding new agents.

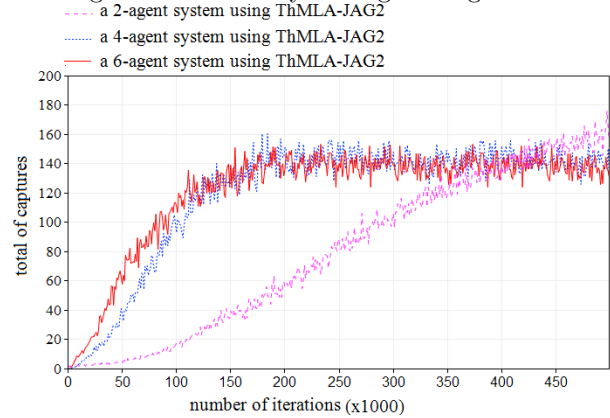


Figure 7: Variation of captures in function of the number of agents in the case of S2 (average of 30 experiences)

- From the beginning of learning to the  $15 \cdot 10^{4th}$  iteration, the number of captures done each 1000 episodes increases over time and is all the more important as

Table 4: Comparing ThMLA-JAG1 and ThMLA-JAG2 in the case of S1 with a four-agent system (average of 30 experiences)

		ThMLA-JAG1	ThMLA-JAG2
Episodes [0-1200[	Total of iterations $\in [0 - 800]$	100596	94001
	Total of collisions $\in [0 - 800]$	19080	22017
	Length of the path after convergence	<b>16</b>	<b>13</b>
Episodes [1200-2200[	Total of iterations $\in [1200 - 1850]$	90144	52693
	Total of collisions $\in [1200 - 1850]$	10781	13541
	Length of the path after convergence	<b>80</b>	<b>12</b>

Table 5: Impact of varying agents' number on the performance of ThMLA-JAG2 in the case of S1 (average of 30 experiences)

Episodes	Number of learners	2	4	6
[0-1200]	Episodes for convergence	583	850	1028
	Iterations for convergence	114382	94786	140343
	Total of collisions before convergence	24776	22051	43991
	Total of collisions after convergence	0	0	0
[1200-2200]	Episodes for convergence	1694	1658	1948
	Iterations for convergence	97795	50326	62682
	Total of collisions before convergence	21047	13533	23205
	Total of collisions after convergence	0	0	0

agents are more numerous.

- From the  $15 \cdot 10^{4th}$  to the  $42 \cdot 10^{4th}$  iteration, the number of captures further increases in case of 2-agent systems and converges to approximately 140 captures every 1000 episodes in the case of 4-agents and 6-agents systems with low oscillations due to the movements of the prey.

## 4 Conclusion

In this paper, we have studied the problem of cooperative learning with avoiding collisions between agents. For that, a new learning method, called ThMLA-JAG, has been proposed. Using this method, a global coordination is ensured between agents as well as a great reduction in the amount of stored information and the learning computations with regard to classic joint RL methods. This is effectively due to the decomposition of learning into pairs of agents. By this decomposition, the learning process is considerably accelerated and the problem of the states' space explosion is partially resolved.

This research is still in its early stages. Experimental results so far point to the fact that the proposed method is a good alternative to RL algorithms when dealing with distributed decision making in cooperative multi-agent systems. However, all conducted tests on the ThMLA-JAG method are restricted to small environments with a limited number of agents. We expect to further improve our work by expanding

it with the ability to solve more complex scenarios. Possible test cases include more agents, several targets, as well as continuous state spaces. Such complex elements typically describe real-world applications.

Furthermore, all agents in our current Markov game model can observe the global state space, while in reality this may not be feasible. More research into how agents can still efficiently collaborate when only partial state information is available would be worthwhile. In addition, the study of fully competitive MARL methods is also a good focus for next researches.

## Acknowledgements

This research received no specific grant from any funding agency in the public, commercial or not-for-profit sectors.

## References

- [1] R. Sutton, A. Barto, Reinforcement Learning: An Introduction, IEEE Transactions on Neural Networks 9 (5) (1998) 1054–1054. doi:10.1109/TNN.1998.712192.
- [2] W. Zemzem, M. Tagina, A New Approach for Reinforcement Learning in non Stationary Environment Navigation Tasks, International Review on Computers and Software 7 (5) (2012) 134–143.
- [3] W. Zemzem, M. Tagina, A novel exploration/exploitation policy accelerating learning in both stationary and non stationary envi-

- ronment navigation tasks, *International Journal of Computer and Electrical Engineering* 7 (3) (2015) 149–158.
- [4] M. Wu, W.-H. Cao, J. Peng, J.-H. She, X. Chen, Balanced reactive-deliberative architecture for multi-agent system for simulation league of RoboCup, *International Journal of Control, Automation and Systems* 7 (6) (2009) 945–955. doi:10.1007/s12555-009-0611-z.
- [5] L. Parker, C. Touzet, F. Fernandez, Techniques for learning in multi-robot teams, *Robot Teams: From Diversity to Polymorphism*. AK Peters.
- [6] K. Tumer, A. Agogino, Improving Air Traffic Management with a Learning Multiagent System, *IEEE Intelligent Systems* 24 (1) (2009) 18–21. doi:10.1109/MIS.2009.10.
- [7] S. Proper, P. Tadepalli, Solving multiagent assignment Markov decision processes, in: *Proceedings of The 8th International Conference on Autonomous Agents and Multiagent Systems*, A.C.M, Budapest, Hungary, 2009, pp. 681–688.
- [8] P. Stone, M. Veloso, Multiagent systems: a survey from a machine learning perspective, *Autonomous Robots* 8 (3) (2000) 345–383. doi:10.1023/A:1008942012299.
- [9] Y. Cai, Intelligent Multi-robot Cooperation for Target Searching and Foraging Tasks in Completely Unknown Environments, Ph.D. thesis, University of Guelph (2013).
- [10] C. Claus, C. Boutilier, The dynamics of reinforcement learning in cooperative multiagent systems, in: *Proceedings of the National Conference on Artificial Intelligence*, 1998, pp. 746–752.
- [11] X. Chen, G. Chen, W. Cao, M. Wu, Cooperative learning with joint state value approximation for multi-agent systems, *Journal of Control Theory and Applications* 11 (2) (2013) 149–155. doi:10.1007/s11768-013-1141-z.
- [12] J. Hao, D. Huang, Y. Cai, H.-f. Leung, The dynamics of reinforcement social learning in networked cooperative multiagent systems, *Engineering Applications of Artificial Intelligence* 58 (2017) 111–122. doi:10.1016/J.ENGAPPAI.2016.11.008.
- [13] L. Matignon, G. J. Laurent, N. Le, Independent reinforcement learners in cooperative Markov games: a survey regarding coordination problems, *Knowledge Engineering Review* 27 (1) (2012) 1–31. doi:10.1017/S026988891200057>.
- [14] E. Yang, D. Gu, Multiagent reinforcement learning for multi-robot systems: A survey, *Tech. rep.*, 2004 (2004).
- [15] C. Watkins, P. Dayan, Q-learning, *Machine Learning* 8 (1992) 279–292.
- [16] L. Matignon, G. Laurent, N. L. Fort-Piat, A study of FMQ heuristic in cooperative multi-agent games, in: *In The 7th International Conference on Autonomous Agents and Multiagent Systems. Workshop 10: Multi-Agent Sequential Decision Making in Uncertain Multi-Agent Domains*, aamas’ 08, Vol. 1, 2008, pp. 77–91.
- [17] H. Guo, Y. Meng, Distributed Reinforcement Learning for Coordinate Multi-Robot Foraging, *Journal of Intelligent and Robotic Systems* 60 (3-4) (2010) 531–551. doi:10.1007/s10846-010-9429-4.
- [18] J.-Y. Lawson, F. Mairesse, Apprentissage de la coordination dans les systèmes multi-agents, Master’s thesis, Catholic University of Louvain (2004).
- [19] W. Zemzem, M. Tagina, M. Tagina, Multi-agent Coordination using Reinforcement Learning with a Relay Agent, in: *Proceedings of the 19th International Conference on Enterprise Information Systems*, SCITEPRESS - Science and Technology Publications, 2017, pp. 537–545. doi:10.5220/0006327305370545.
- [20] M. L. Puterman, *Markov Decision Processes: Discrete Stochastic Dynamic Programming* (1994). doi:10.1080/00401706.1995.10484354.
- [21] K. Tuyls, G. Weiss, Multiagent Learning: Basics, Challenges, and Prospects, *AI Magazine* 33 (3) (2012) 41. doi:10.1609/aimag.v33i3.2426.
- [22] M. Bowling, M. Veloso, Multiagent learning using a variable learning rate, *Artificial Intelligence* 136 (2) (2002) 215–250. doi:10.1016/S0004-3702(02)00121-2.
- [23] M. Tan, Multi-Agent Reinforcement Learning: Independent vs. Cooperative Agents, in: *In Proceedings of the Tenth International Conference on Machine Learning*, 1993, pp. 330–337.
- [24] M. Tan, Multi-agent reinforcement learning: independent vs. cooperative agents, in: *the tenth international conference on machine learning*, Morgan Kaufmann Publishers Inc., 1997, pp. 330–337.
- [25] B. Cunningham, Y. Cao, Non-reciprocating Sharing Methods in Cooperative Q-Learning Environments, in: *2012 IEEE/WIC/ACM International Conferences on Web Intelligence and Intelligent Agent Technology*, IEEE, 2012, pp. 212–219. doi:10.1109/WI-IAT.2012.28.
- [26] W. Zemzem, M. Tagina, Cooperative multi-agent learning in a large dynamic environment, in: *Lecture Notes in Computer Science*, Springer, 2015, Ch. MDAI, pp. 155–166.
- [27] W. Zemzem, M. Tagina, Cooperative multi-agent reinforcement learning in a large stationary environment, in: *2017 IEEE/ACIS 16th International Conference on Computer and Information Science (ICIS)*, IEEE, 2017, pp. 365–371. doi:10.1109/ICIS.2017.7960020.
- [28] M. Lauer, M. Riedmiller, Reinforcement Learning for Stochastic Cooperative Multi-Agent Systems, in: *Ithe 3rd International Joint Conference on Autonomous Agents and Multi Agent systems*, IEEE Computer Society, New York, USA, 2004, pp. 1516–1517. doi:10.1109/AAMAS.2004.226.
- [29] L. Matignon, G. J. Laurent, N. L. Fort-Piat, Hysteretic q-learning :an algorithm for decentralized reinforcement learning in cooperative multi-agent teams, in: *2007 IEEE/RSJ International Conference on Intelligent Robots and Systems*, IEEE, 2007, pp. 64–69. doi:10.1109/IRoS.2007.4399095.
- [30] P. Zhou, H. Shen, Multi-agent cooperation by reinforcement learning with teammate modeling and reward allotment, *8th International Conference on Fuzzy Systems and Knowledge Discovery*, FSKD 2011 2 (4) (2011) 1316–1319. doi:10.1109/FSKD.2011.6019729.

# Productify News Article Classification Model with Sagemaker

Johannes Lindén\*, Xutao Wang, Stefan Forsström, Tingting Zhang

Mid. Sweden University, Department of Information Systems and Technology (IST), 851 70, Sweden

---

## ARTICLE INFO

Article history:  
Received: 29 May, 2019  
Accepted: 09 July, 2019  
Online: 09 March, 2020

---

Keywords:  
Machine learning  
Data mining  
Big data  
News events  
Journalists  
Editors  
Text analysis  
Natural language processing  
NLP  
Paragraph vectors

---

## ABSTRACT

News companies have a need to automate and make the process of writing about popular and new events more effective. Current technologies involve robotic programs that fill in values in templates and website listeners that notify editors when changes are made so that the editor can read up on the source change on the actual website. Editors can provide news faster and better if directly provided with abstracts of the external sources and categorical meta-data that supports what the text is about. To make categorical meta-data a reality an auto-categorization model was created and optimized for Swedish articles written by local news journalists. The problem was that it was not scale-able enough to use out of the box. Instead of having this local model that could make good predictions of the text documents, the model is to be deployed in the cloud and an API interface is created. The API can be accessed from the tools where the articles is being written and therefore these services can automatically assign categories to the articles once the journalist is done writing it. To allow scale-ability to several thousands of simultaneously categorized articles and at the same time improving the workflow of deploying new models easier the API is uploaded to Sagemaker where several models are trained and once an improved model is found that model will be used in production in such a way that the system organically adapts to new written articles. An evaluation of Sagemaker API was done and it was concluded that the complexity of this solution was polynomial.

## 1 Introduction

Modelling data with machine learning algorithms has shown to give promising results in various of areas, for example image processing and robotics. The areas are growing and machine learning becomes more advanced for every day. Natural language processing is one area that is difficult and requires larger and deeper networks to perform. The larger a network is the more computational power is required to compute a prediction. For a system in production the speed and memory usage could be fatal to the incoming requests of the application. This article addresses the difficulties to take such a system from the model produced by the algorithm to a productified version utilized by a product or users in real time. The response time, memory consumption and computational power are of importance when these types of models will be available with minimal waiting- and downtime. This article addresses one way to scale the application to handle all requests from the user base of a media company distributed over 22 regions in Sweden and reasons behind

possibilities to scale up to the entire Sweden user base of local news production line.

In a longer run the focus is also to use the categories metadata point in other products such as improving article personalization algorithms, data analytic of supply and demand of article categories. This article is an extension from Linden et al presented at Fedcsis conference 2018 [1]. The auto-categorization prediction accuracy are improved by parameter optimization since the last article and are now at 80 % and that is the underlying reason why the system is ready for an production environment. The classification model will categorize articles into different news topics and reply with a given confidence for each category. The while the journalists writes their articles in they would like to have categories in or close to real time.

## 2 Related Work

The novelty of this research, that concerns productification, is the idea to take the auto-categorization neural network

---

\*Johannes Lindén, Holmgatan 10 Sundsall Sweden, 010-142 80 69 & johannes.linden@miun.se



model from its experimental phases all the way to a use case where it brings value. Several research projects has been done for managing and supporting big data pipelines, where live data needs to be processed by several organizations (for example analysis and business intelligence) [2]-[3]. The auto-categorization model predictions needs a similar automatic data pipeline to uphold the load of each prediction and at the same time allow analysis of the result that will be brought back to the model in a feedback loop. Blaiszik et al made a scalable service that manages machine learning models through a structured API [4]. Blaiszik is using docker containers to wrap the model logic into an environment with controlled variables. This research approach is similar to Blaiszik but instead of using containers for only the models the idea is to have one container for the service as well. Cloud based services such as AWS Sagemaker or IBM's Watson has benefits as well as flaws explained in detail by Hummer et al that builds their own cloud service for training machine learning models [5]. According to Hummer's research it is essential for the AI expert to focus on the model itself and care less about the pipeline and how to set it up properly but Hummer also mentions the importance of having the settings available to tweak the service for special needs. For simplicity this research are using Sagemaker to deploy models in production since there is knowledge about other AWS services available and having all systems in the same cloud has other benefits of latency and authorization flexibility. An evaluation investigation in signal processing was issued that was written by Massimo Ravasi and Marco Mattavelli where they motivated the importance of the system complexity and the partitioning of hardware and software evaluation [6].

As for the auto-categorization model itself Payne et al have made an evaluation of their SVM classification algorithm which yields promising results in performance [7]. The model used in this research utilizes a bigger neural network to comprehend a larger problem domain. Rather than only focusing on a domain concerning digital archives it is focused on local news which could be very specific to each region of the country but could also be very general where regions have common information needs of local news.

### 3 Approach and Model

The proposed four step model in previous research that predicts categories of arbitrary text paragraphs are going to be the main model in this research that will conduct scalability experiments and propose a system structure of this machine learning model. See Figure 1 for an overview of previous implementation.

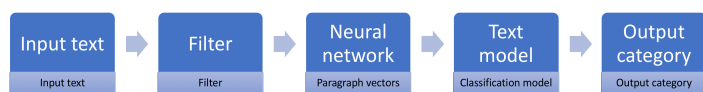


Figure 1: An overview of the model

The input is the algorithm parameters  $\theta$  and a single

document  $D$ , which is interpreted as a sequence of words  $w_1, w_2, \dots, w_n$ . The output of the model is a set of category probabilities  $c_1, c_2, \dots, c_i, \dots, c_m$  computed by 1.

$$c_i = P(\text{ith category} | D, \theta) \approx P(\text{ith category} | D) \quad (1)$$

In this research the model are used for example as shown in Figure 2, the article shown to the left in a web-browser will request a category from the trained auto-categorization model and retrieve a list of probable categories.

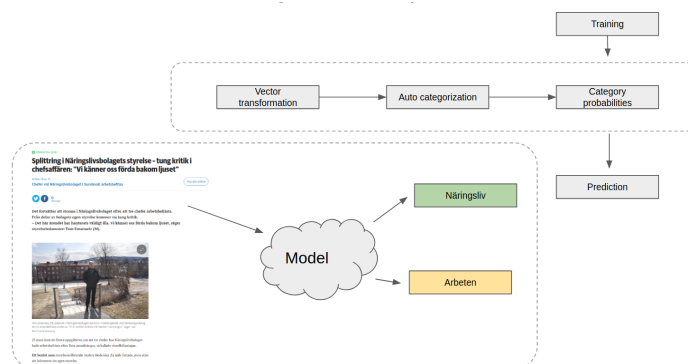


Figure 2: Auto-categorization in a real case scenario. While a user navigates to a article page the category of that particular article is determined based on the body/text within it.

The algorithm takes an unstructured sequence of words forming a text paragraph as input. Language of this model is Swedish and even though the text length could be of any length the articles that has been evaluated has the length between 5 to 600 words in the first step of Figure 1. Text paragraphs are filtered before training to not include articles with only links or empty texts since these articles are not describing what the article is about. Within an text paragraph some additional modifications is done which is step two in Figure 1. Non-alphabetic characters, exclamation and question marks are replaced by full stops. XML tags and its attributes are removed. Some additional optional modifications are left in the settings file to be turned on or off while using the system. Such modifications include Named Entity Recognition (NER) substitution of locations, organizations, names and time units, another modification are Part-of-speech (POS) tagger and Dependency parser which will filter out certain types of tagged words and leaf nodes [8]. POS and Dependency parser chosen in this research where Google SyntaxNet [9, 10]. Out of the resources mentioned in Nilson et al, we selected a treebank made by Jan Einarsson's project, which is well documented [11]-[12]. The other steps in Figure 1 are described in the following sections.

#### 3.1 Paragraph Vectors

The third step in Figure 1 is a constructed one layered neural network model that will transform the filtered text paragraphs from previous step into vectors. The paragraph vectors are unique vectors that maps the paragraph to a high dimensional vector space. A softmax activation function



makes sure that the elements are within the interval -1 to 1. The vectors are constructed in such a way that it is possible to relate a paragraph from the distance between another paragraph. The relation of two paragraphs can be obtained by computing the cosine similarity which will give a positive value when the documents are sharing similar contexts, a value close to zero when no relatedness could be found, and a negative number when the paragraphs appears in in opposite contexts [13]. The vectors can also use common subtraction and additions operations in case other related context will be retrieved, as shown in 2.

$$king - man + woman = queen \quad (2)$$

The paragraph vectors context awareness contains information about what makes a document category as shown in previous research [1]. The paragraph vectors are as before computed using the PV-DM algorithm which is an extension of the known word2vec algorithm bag of words (WV-BOW) [1, 14].

Experiments previously conducted showed that the PV-DBOW paragraph algorithm is reliable when implemented by the distributed memory vector concatenated with the distributed bag of words vector described by Mikolov et al [13].

### 3.2 Text Model

The paragraph representation vectors is input to the fourth step where the auto-categorization takes place. The categorization algorithms we proposed in previous research experiments where decision trees, random forest, multi layer perception and long-short term memory (LSTM). The one outperformed the others where the LSTM model which are used in this extended paper with the possibility to exchange to another model at any time through a settings parameter in the system. The output is the category belonging probabilities for each considered category described in 1. The LSTM model has a time parameter that each time sequence are used for a vector transformed sentence in the paragraph. Figure 3 shows the LSTM input format, each colored line is a sentence which are fed in per time-slot in the model for training .

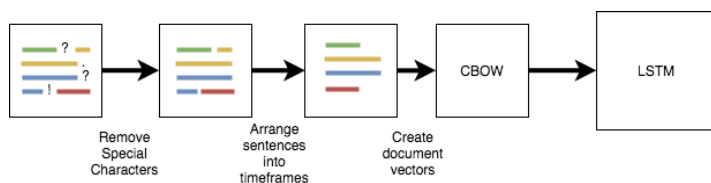


Figure 3: The input vector of the LSTM algorithm is shown above. It first applies the filter layer conditions, then divides the document into sentences to be used as input data for the CBOW algorithm that produces the document vectors.

LSTM models are based on the principles of recurrent neural networks (RNN). A RNN is constructed like a neural network with an input, hidden layers and a output layer. The RNN-cell can be visualised as shown in Figure 4. The activation function of an RNN is usually the *tanh* function.

For each iteration, the model is trained by backpropagation through the network. The purpose of RNN is to have a short-term memory that remembers previous neurons. One of the first and simple constructions of RNN is the recurrent neural network language Model (RNN-LM). The hidden layer of an RNN-LM algorithm remembers the neurons one time-step back in the training history [15].

For different use-cases there are different variations of RNNs. Andrej Karpathy summarises the different networks that are used into different mappings [16]. One-to-one mapping is the original algorithm, for example the RNN-LM algorithm. One-to-many mapping when there is one input and several RNNs connecting to several outputs. This mapping can, for example be, used for image prediction with one image and several words that predict the image. Many-to-one mapping is where there are several inputs mapping to one output, this mapping can for example be used for classification. Many-to-many mapping is what Karpathy describes as two different mappings: one mapping that maps to an equal number of input and output RNNs (N-N), and another mapping that maps to a different number of inputs and outputs (N-M). The N-N mapping can, for example, be used to predict video sequences over time, while N-M mapping can be used for translation problems.

LSTM networks are a special case of RNN that tends to solve a problem in the original RNN. The long-term memory in RNN (the gradient descent) exponentially diverges to infinity or converges to zero in many cases and LSTM introduces an additional memory cell and forget parts of the information and therefore avoiding more cases of vanishing gradients. LSTM networks introduce three sigmoid layers and certain gates that only let parts of the information through to compensate for the vanishing gradient. The first sigmoid layer determines what information that is important from the previous LSTM-cell, the second sigmoid layer determines what information is important from the *tanh* layer in the current cell and the third sigmoid layer determines what information will be passed to the next LSTM-cell. The gates that open or close based on the input from the previous LSTM-cell either remove or add information to a cell state that is also passed through to the next LSTM-cell. The third sigmoid layer extracts a piece of information from the cell state to the output value [17, 18].

### 3.3 Output Category

Output category is the last, fifth, step of the model which determines the output categories. This step interprets the output of the categorization model and limits the categories to suggest via a threshold of the category probability. If the probability is higher than the average probability of seen paragraphs the category are recommended and sent to output of the model. Before the categories that will be replied is returned from the auto-categorization model the probabilities are normalized according to 3.

$$\frac{value - min(value)}{max(value) - min(value)} \quad (3)$$

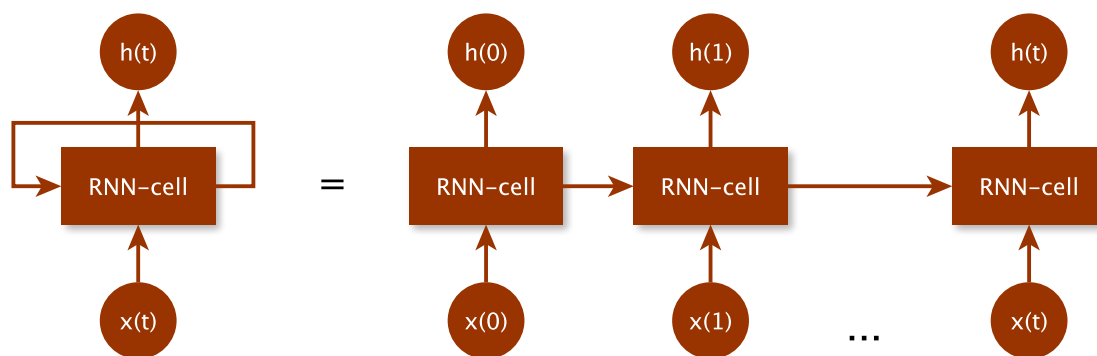


Figure 4: A recurrent neural network cell. The cell to the left is the general notation of the hidden layer in an RNN model. The right unfolded version is the representative of the RNN with a short-term length of  $t$ .

## 4 Architecture

The architectural approach consists of the system, the data pipeline and the neural network model. For making the auto-categorization available to use on texts written by the journalists all three pieces has to be in place. The procedure should be close to real time and this was accomplished by a system that could easily be scaled up to bigger machines with load distributed support for the user prediction requests. Figure 5 shows an overview of the system.

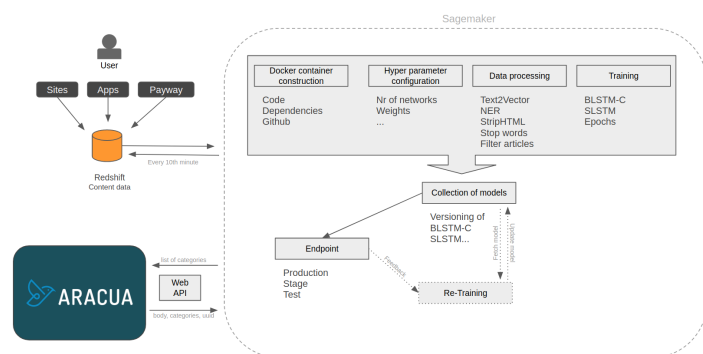


Figure 5: Architectural overview of production environment.

Aracua is the name of the system the journalists are writing their articles in, this system will request categories given the text of the article. Each categorization request is stored together with the previous category for further live evaluation purposes. The requests are stored in a AWS Redshift cluster to compare the final categories of each article with the suggested ones along the way while the journalists are writing the article [19]. In Redshift other services models will have access to the auto-categorized categories to be used for example in personalization purposes. This section will further describe the deployment process of the model.

### 4.1 System

A Ngnix server was used for the system that can handle requests and reply the the model prediction of categories. The

server instantiates python flask applications on demand when the load is high and one instance cannot keep up the clients requests as illustrated in Figure 6.

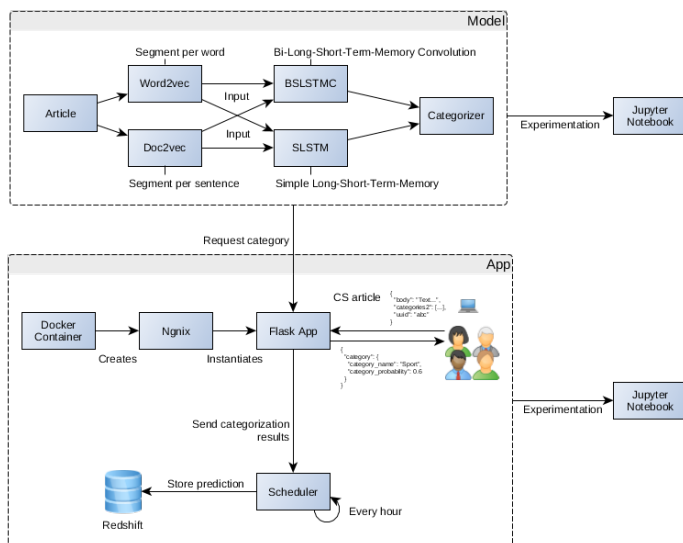


Figure 6: Architecture of the server system.

All runs inside a docker container to make it easy to increase the memory and processing power on an AWS EC2 instance if needed [20]. Each time a client requests categories for an article the user also sends the current categories on the article so that in a later step it is possible to evaluate an article over time as it is being worked on.

The predictions and articles are temporarily stored in memory to speed up the replies for the same article. A scheduled task is triggered every 10 minute or when number of articles in memory are larger than 1000 documents. The scheduler dumps these articles in memory to a persistent database where evaluation will be performed. The model is parameterized so that depending on the settings different models are being used for the prediction see Section 4.3.

### 4.2 Data pipeline

The system gets article contents that are being written by journalists from Aracua and stores them in a database. The articles are distributed on various of different places depending on the product that will use them. The auto-categorization product retrieves all articles and trains its models on these articles as described in Section 3. Each model that is trained is stored separately so that it is easy to switch models in production. A retraining process is started in production to dynamically improve the model for the articles. There are not only models for each environment (development, staging and production) but also models for different versions and improved models as the time progresses.

### 4.3 Neural network model

The parameters that is used to train the model are stored in a configuration file. The configuration file contains what model structures that are going to be used, how long the training will take in terms of number of epochs, layer sizes pre-processing steps to be done, where the data is taken from and model stored to. Currently the following setup shown in Table 1 is used since it was shown to be the best one in previous experiments.

Table 1: Neural network model parameters

Param	Value
Layer size	3
LSTM timestep size	200
Document vector size	1000
Pre-processing steps	NER, StripHTML, Filter stop words, Part-of-speech

### 4.4 Hardware specifics

The evaluation conducted in this research is performed on an AWS Graviton Processor with two 64-bit Arm cores. The processor is capped at 2.3 GHz clock frequency, the memory is 16 GB and high network speed according to AWS specifications [21]. The computer used corresponds to the specification of "ml.m4.xlarge" in Amazon Instance specifications[21].

## 5 Results

Figure 5 and 6 shows the resulting production system and how it works. The main result is that this system is used by thousands of journalists all over Sweden. Additional results of this extended article is to provide evaluation metrics of the system in terms of responsiveness to the journalists. Figure 7 shows how long the response time is in average given the number of clients trying to access the system at the same time.

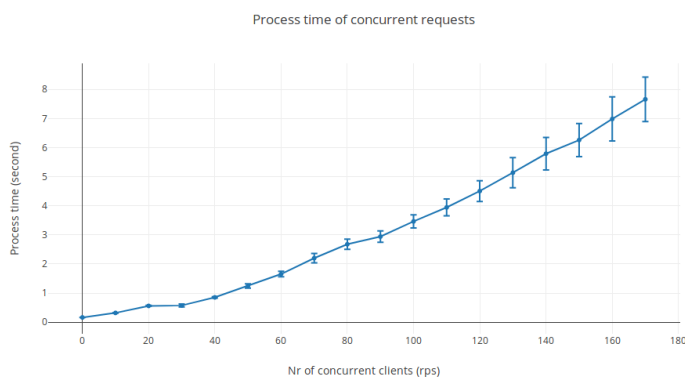


Figure 7: Process time of concurrent requests with standard deviation.

By analysing the number of characters an article body consists of when categorizing it is possible to say how much implications long articles have on the system, the resulting analysis can be seen in Figure 8.

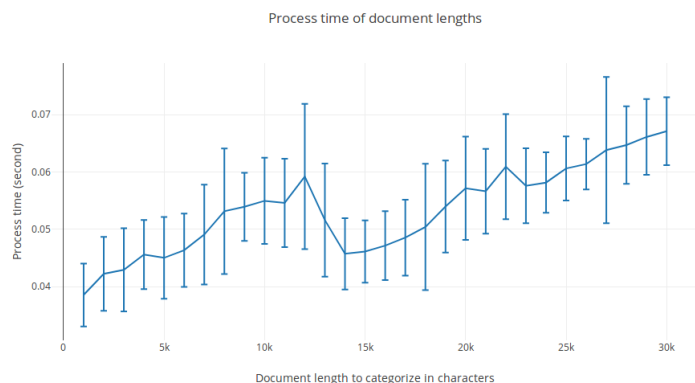


Figure 8: Process time of document lengths with standard deviation.

The training process is the process that initially takes the longest time of all in this research. Training a model with all articles of the categories in question takes up to 2.2 hours using a document vector embedding size of 600 elements as shown in Figure 9.

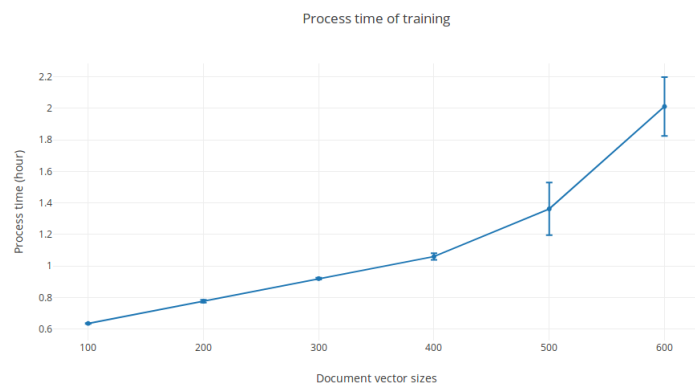


Figure 9: Process time of training with standard deviation.

## 6 Conclusion

In this article a proposition for a productification of a categorization algorithm that through a web API serves journalists with automatically categorized texts in their writing tool. The main question was if the performance of such model could be serving a large amount of users in their daily work and in that case how many users can it handle. It can be concluded that the number of concurrent requests have somewhat a linear time complexity but could potentially be exponential of higher orders for larger number of clients. Analysing the article length it can be interpreted to have an impact of the process time but would not be a problem for journalists since it is rare that they write long articles. Around 15 000 characters seem to be a good number of characters to have in an article. Training performance is growing with polynomial complexity and could be a risk as more categories are introduced and larger vector embedding needs to be considered. Future work for this project will be to include more categories with more complex algorithms which will use a wisdom of the many approach.

## References

- [1] Johannes Lindén, Stefan Forsström, and Tingting Zhang. Evaluating combinations of classification algorithms and paragraph vectors for news article classification, 2018.
- [2] Ryan Chard, Kyle Chard, Jason Alt, Dilworth Y Parkinson, Steve Tuecke, and Ian Foster. Ripple: Home automation for research data management. In *2017 IEEE 37th International Conference on Distributed Computing Systems Workshops (ICDCSW)*, pages 389–394. IEEE, 2017.
- [3] Jack Deslippe, Abdelilah Essiari, Simon J Patton, Taghrid Samak, Craig E Tull, Alexander Hexemer, Dinesh Kumar, Dilworth Parkinson, and Polite Stewart. Workflow management for real-time analysis of lightsource experiments. In *2014 9th Workshop on Workflows in Support of Large-Scale Science*, pages 31–40. IEEE, 2014.
- [4] Ben Blaiszik, Kyle Chard, Ryan Chard, Ian Foster, and Logan Ward. Data automation at light sources. In *AIP Conference Proceedings*, volume 2054, page 020003. AIP Publishing, 2019.
- [5] Waldemar Hummer, Vinod Muthusamy, Thomas Rausch, Parijat Dube, and Kaoutar El Maghraoui. Modelops: Cloud-based lifecycle management for reliable and trusted ai.
- [6] Massimo Ravasi and Marco Mattavelli. High-level algorithmic complexity evaluation for system design. *Journal of Systems Architecture*, 48(13-15):403–427, 2003.
- [7] Nathaniel Payne and Jason R Baron. Auto-categorization methods for digital archives. In *2017 IEEE International Conference on Big Data (Big Data)*, pages 2288–2298. IEEE, 2017.
- [8] Atro Voutilainen. Part-of-speech tagging. *The Oxford handbook of computational linguistics*, pages 219–232, 2003.
- [9] Daniel Andor, Chris Alberti, David Weiss, Aliaksei Severyn, Alessandro Presta, Kuzman Ganchev, Slav Petrov, and Michael Collins. Globally normalized transition-based neural networks. *arXiv preprint arXiv:1603.06042*, 2016.
- [10] Chris Alberti, Daniel Andor, Ivan Bogatyy, Michael Collins, Dan Gillick, Lingpeng Kong, Terry Koo, Ji Ma, Mark Omernick, Slav Petrov, et al. Syntaxnet models for the conll 2017 shared task. *arXiv preprint arXiv:1703.04929*, 2017.
- [11] Jens Nilsson and Johan Hall. *Reconstruction of the Swedish Treebank Talbanken*. Matematiska och systemtekniska institutionen, 2005.
- [12] Jan Einarsson. *Talbankens talsprkskonkordans*. 1976.
- [13] Quoc V Le and Tomas Mikolov. Distributed Representations of Sentences and Documents. In *ICML*, volume 14, pages 1188–1196, 2014.
- [14] Johannes Lindén. Understand and Utilise Unformatted Text Documents by Natural Language Processing algorithm. 46(0), 2017.
- [15] Tomáš Mikolov, Stefan Kombrink, Lukáš Burget, Jan Černocky, and Sanjeev Khudanpur. Extensions of recurrent neural network language model. In *Acoustics, Speech and Signal Processing (ICASSP), 2011 IEEE International Conference on*, pages 5528–5531. IEEE, 2011.
- [16] Andrej Karpathy. The unreasonable effectiveness of recurrent neural networks. *Andrej Karpathy blog*, 2015.
- [17] Christopher Olah. Understanding lstm networks. *GITHUB blog, posted on August, 27:2015*, 2015.
- [18] Martin Sundermeyer, Ralf Schlüter, and Hermann Ney. LSTM Neural Networks for Language Modeling. In *Interspeech*, pages 194–197, 2012.
- [19] Joseph Baron and Sanjay Kotecha. Storage options in the aws cloud. *Amazon Web Services, Washington DC, Tech. Rep*, 2013.
- [20] Gideon Juve, Ewa Deelman, Karan Vahi, Gaurang Mehta, Bruce Beriman, Benjamin P Berman, and Phil Maechling. Scientific workflow applications on amazon ec2. In *2009 5th IEEE international conference on e-science workshops*, pages 59–66. IEEE, 2009.
- [21] Amazon Co. Amazon SageMaker Instance Types - Amazon Web Services (AWS). <https://aws.amazon.com/sagemaker/pricing/instance-types/>.

# Distributed Linear Summing in Wireless Sensor Networks with Implemented Stopping Criteria

Martin Kenyeres<sup>\*1</sup>, Jozef Kenyeres<sup>2</sup>

<sup>1</sup>Institute of Informatics, Slovak Academy of Sciences, Dubravská cesta 9, 845 07 Bratislava 45, Slovak Republic

<sup>2</sup>Sipwise GmbH, Europaring F15, 2345 Brunn am Gebirge, Austria

## ARTICLE INFO

Article history:

Received: 04 January, 2020

Accepted: 31 January, 2020

Online: 09 March, 2020

Keywords:

Distributed summing

Average consensus

Wireless sensor networks

## ABSTRACT

Many real-life applications based on the wireless sensor networks are equipped with data aggregation mechanisms for suppressing or even overcoming negative environmental effects and data redundancy. In this paper, we present an extended analysis of the linear average consensus algorithm for distributed summing with bounded execution over wireless sensor networks. We compare a centralized and a fully-distributed stopping criterion proposed for the wireless sensor networks with a varied initial configuration over random geometric graphs with 200 vertices in order to identify the optimal initial configuration of both analyzed stopping criteria and the algorithm as well as finding out which stopping criterion ensures higher performance of the examined algorithm in terms of the estimation precision and the convergence rate expressed as the iteration number for the consensus.

## 1 Introduction

This paper is an extension of work originally presented in the conference Proceedings of the IEEE 17th World Symposium on Applied Machine Intelligence and Informatics, (SAMI 2019) [1].

### 1.1 Wireless Sensor Networks

Wireless sensor networks (WSNs), a technology operating in an unattended ad-hoc mode, may be formed by hundreds to thousands autonomous sensor nodes<sup>1</sup>, example shown in Figure 1, to gather information from the adjacent environment and to detect certain events of interest over the monitored area (e.g., buildings, homes, forests, oceans, mountains, etc.) [2–5]. Over the past years, this technology has found the application in many different areas, e.g., disaster detection, industrial monitoring, health assistance, military surveillance, etc. [6]. Therefore, the design of the sensor nodes has to be adapted to environmental conditions (e.g., the sensor nodes for underground operation have an increased transmission power whereby noisy channel attenuations can be overcome) [3]. However, as these sensor nodes are simple and low-cost devices, they suffer from limited energy capacity and computation capabilities, resulting in decreased robustness to potential threats such as radiations, pressure, temperature, attacks, etc. [7–9]. Thus, many of the real-life WSN-based applications are equipped with data aggregation mechanisms

for suppressing or even overcoming the impacts of these negative factors on the operation of WSNs. Moreover, data aggregation can eliminate highly correlated and duplicated information as well [8].

### 1.2 Data Aggregation

In general, data aggregation poses any process in which data from multiple sources is transformed into a summary form for further statistical processing or analyzing. The data aggregation mechanisms are designed to process measured information from multiple independent sensor nodes in order to provide a greater quality of service (QoS) [8]. Xiao et al. define two categories of the data aggregation mechanisms, namely [9]:

- Centralized
- Distributed

In the centralized data aggregation schemes, the sensor nodes transmit their measured information to a fusion center either directly or by multi-hop communication. In the second scenario, each sensor node has to establish and update the table with routing information, which is not a too effective way to deliver information to a fusion center over mobile networks and networks with limited energy sources such as WSNs [9]. Therefore, the distributed schemes

<sup>\*</sup>Corresponding author: Martin Kenyeres, E-mail: martin.kenyeres@savba.sk

<sup>1</sup>see Figure 1 for an example



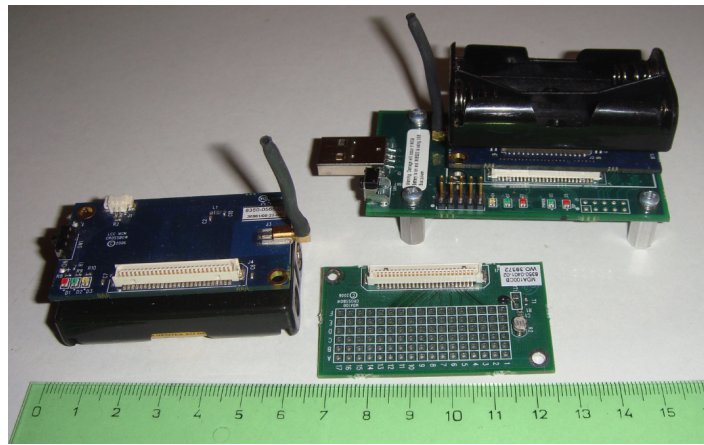


Figure 1: Example of WSNs – Memsic's classroom kit (Source: Reprinted from [13])

are more frequently applied nowadays [10–13]. In these schemes, the adjacent sensor nodes communicate with each other and update their states according to the collected data [14]. Thus, a fusion center is not necessary for data aggregation as well as the sensor nodes know only local information whereby data aggregation is significantly simplified. In [15], Jesus et al. divide distributed aggregation schemes into three groups in terms of the communication perspective:

- *Structured*
- *Unstructured*
- *Hybrid*

*Structured algorithms* are dependent on network topologies and routing algorithms and therefore are not appropriate for mobile systems. Moreover, a single point of failure (e.g., a dead node, a link failure) can have a fatal impact on a whole system, especially in sparsely connected topologies such as tree-based structures. The next category, *Unstructured algorithms*, is independent of network topology and structure unlike the first category, and thus, network topology does not have to be predefined. These algorithms are characterized by simplicity, high scalability, high robustness, etc. The last category, i.e., *Hybrid algorithms*, utilizes strengths and suppress weaknesses of the previous approaches by their combination.

In terms of the computation perspective, the distributed data aggregation mechanisms can be classified as follows [15]:

- *Computation of decomposable functions*
- *Computation of complex functions*
- *Counting*

As mentioned earlier, we focus our attention on linear consensus-based algorithms for distributed summing, which can be classified as unstructured algorithms for computation of decomposable functions. These algorithms have significantly attracted the attention of the academy recently [16–18]. In [19], Gutierrez-Gutierrez et al. define two categories of these algorithms, namely:

- *Deterministic*

- *Stochastic*

From this set of the algorithms, we choose deterministic linear average consensus (referred to as AC), characterized by a variable mixing parameter  $\epsilon$ , for distributed summing [20].

A properly configured stopping criterion can significantly optimize data aggregation over WSNs; therefore, its implementation is an essential complement for distributed data aggregation mechanisms. As mentioned above, we assume that the execution of the examined algorithm is bounded by a stopping criterion in our analyzes.

### 1.3 Summary of Contribution

In this paper, we analyze AC for distributed summing whose execution is bounded by a stopping criterion. We vary its initial configuration and the configuration of the analyzed stopping criteria (we examine a centralized and a fully-distributed one) in order to identify which configurations ensure the highest performance of the examined algorithm and in order to compare the analyzed stopping criteria in terms of the precision and the convergence rate. As mentioned earlier, a properly configured stopping criterion and algorithm optimize data aggregation, thereby saving energy, reducing the computation/the communication requirements, prolonging the network lifetime, etc.

In this paragraph we clarify the novelty of the presented paper in a comparison with the existing work presented in [1]: In [1], we analyze AC bounded by the fully-distributed stopping criterion defined in [13] - we vary the mixing parameter and the parameters of the implemented stopping criterion in order to identify the best-performing initial configurations of both the algorithm and the stopping criterion. In that paper, the inner states are multiplied by the network size before AC begins. In this paper, we compare these results with the scenario when the inner states are multiplied after AC is completed. The goal of this contribution is to identify when it is the most optimal to carry this multiplication out in terms of the precision and the convergence rate expressed as the iteration number for the consensus achievement. Furthermore, we also analyze the performance of the centralized stopping criterion from [6] and compare it with the results from [1] and the results from the

extended analysis presented in this paper in order to identify which stopping criterion achieves higher performance.

#### 1.4 Paper Organization

The paper is organized as follows: Section 2 is concerned with theoretical insight into the topic, i.e., we provide a mathematical model of AC and WSNs, the convergence conditions, and an explanation of the analyzed stopping criteria. Section 3 deals with the applied methodology and the used metrics for performance evaluation. Section 4 consists of the experimentally obtained results and a consecutive discussion. Conclusions are presented in Section 5.

## 2 Theoretical Background

The primary purpose of AC is to estimate the arithmetic mean from all the initial states. However, it can fulfill also other functionalities - in this paper, we analyze AC for distributed summing, i.e., the sum from all the initial states is estimated. In this case, the information about the network size  $n$  is necessary to be known by each sensor node, and the inner states have to be multiplied by this value, otherwise, the arithmetic mean is estimated instead of the sum [1].

### 2.1 Model of AC for Distributed Summing in WSNs

We model WSNs as simple finite graphs determined by the vertex and the edge sets, i.e.,  $G = (\mathbf{V}, \mathbf{E})$  [20]. The vertex set  $\mathbf{V}$  is formed by all the graph vertices, which represent the sensor nodes in a network, i.e.,  $\mathbf{V} = \{v_1, v_2, \dots, v_n\}$ . The graph order is equal to the number of the sensor nodes in a network, and so,  $|\mathbf{V}| = n$ . Two vertices  $v_i$  and  $v_j$  are adjacent when they are connected to one another by an edge, i.e.,  $e_{ij} \in \mathbf{E}$ .

In AC, each vertex  $v_i$  stores and update its inner state  $x_i(k)$ <sup>2</sup>, represented by a scalar value - the inner states are initiated by for example a local measurement. After the initialization, the inner states asymptotically converge to the arithmetic mean from all the initial inner states by being updated at each iteration, as described in 1, [21]:

$$\mathbf{x}(k+1) = \mathbf{W} \times \mathbf{x}(k) \quad (1)$$

Here,  $\mathbf{x}(k)$  is a variant column vector gathering all the inner states at the corresponding iteration, and  $\mathbf{W}$  poses the weight matrix, affecting many aspects of the algorithm such as the convergence rate of the algorithm, the initial configuration, meeting/violating the convergence conditions, etc. [22]. As already stated, the inner states asymptotically converge to the estimated aggregate function, which can be expressed using 2, [21]:

$$\lim_{k \rightarrow \infty} \mathbf{x}(k) = \lim_{k \rightarrow \infty} \mathbf{W}^k \times \mathbf{x}(0) = \frac{1}{n} \cdot \mathbf{1} \times \mathbf{1}^T \times \mathbf{x}(0) \quad (2)$$

Here,  $\mathbf{1}$  represents a column all-ones vector formed by  $n$  elements. The algorithm works correctly iff the limit from (2) exists, which

is ensured by meeting these convergence conditions described by 3–5, [21], [23, 24]:

$$\mathbf{1}^T \times \mathbf{W} = \mathbf{1}^T \quad (3)$$

$$\mathbf{W} \times \mathbf{1} = \mathbf{1}, \quad (4)$$

$$\rho\left(\mathbf{W} - \frac{1}{n} \cdot \mathbf{1} \times \mathbf{1}^T\right) < 1 \quad (5)$$

Here,  $\rho(\cdot)$  represents the spectral radius of the corresponding vector/matrix, which is the largest eigenvalue in the modulus, i.e. 6, [22]

$$\rho(\cdot) = \max\{|\lambda_i(\cdot)|\} \quad (6)$$

One of the ways to configure the weight matrix  $\mathbf{W}$  is to allocate a constant value<sup>3</sup> to all the edges in a graph. Such a matrix is referred to as the Peron Matrix and is defined by 7, [25]:

$$[W]_{ij} = \begin{cases} \epsilon, & \text{if } e_{ij} \in \mathbf{E} \\ 1 - d_i \cdot \epsilon, & \text{if } i = j \\ 0, & \text{otherwise} \end{cases} \quad (7)$$

Here,  $d_i$  is the degree of the corresponding vertex, i.e., the number of its neighbors. As discussed in [23], the convergence of the algorithm is ensured in each non-bipartite non-regular graph when the mixing parameter  $\epsilon$  is selected from the interval described in 8:

$$0 < \epsilon \leq \frac{1}{d_{max}} \quad (8)$$

Here,  $d_{max}$  is the degree of the best-connected vertex in a graph, so it can be represented using 9:

$$d_{max} = \max_i \{d_i\} \quad (9)$$

### 2.2 Analyzed Stopping Criteria

In this subsection, we introduce the implemented stopping criteria for bounding the execution of AC.

The first analyzed stopping criterion is proposed in [13] and poses a fully-distributed approach, i.e., no global information is necessary for its proper functioning. It is determined by two constants, namely *accuracy* and *counter threshold*, which are the same for each sensor node and preset before AC begins. Moreover, each sensor node has its own *counter*, which is initiated with "0" at each node. The principle of the stopping criterion is based on the calculation of the finite difference between the inner states at two consecutive iterations. If the finite difference is smaller than *accuracy*, the corresponding sensor node increments its *counter* by "1". If not, *counter* is reset<sup>4</sup> regardless of its current value. When the finite difference is smaller than *accuracy* more times<sup>5</sup> in a row, the algorithm is completed at the corresponding sensor node. Thus, this sensor node does not participate in AC and update its inner state any longer.

The other implemented stopping criterion from [6] is a centralized approach, i.e., it requires global information for its proper functioning. This stopping criterion is determined by only one constant *accuracy*, which is preset and the same for each sensor node again. Its principle lies in comparing the maximum and the

<sup>2</sup>Here,  $k$  is the label of an iteration, and  $k = 0$  represents the initial inner state

<sup>3</sup>referred to as the mixing parameter  $\epsilon$

<sup>4</sup>i.e., set to "0"

<sup>5</sup>equal to the value of *counter threshold*

minimum from all the inner states with *accuracy*. The algorithm is globally stopped at the first iteration when the difference between the maximum and the minimum is smaller than the value of *accuracy*. Thus, the algorithm is executed until the condition described by 10 is met:

$$| \max\{\mathbf{x}(k)\} - \min\{\mathbf{x}(k)\} | < \textit{accuracy} \quad (10)$$

### 3 Applied Methodology

In this section, we introduce the applied methodology and the used metrics for performance evaluation.

As mentioned earlier, AC described by the Perron Matrix meets all three convergence conditions in non-bipartite non-regular graphs when its mixing parameter  $\epsilon$  takes a value from the interval (8). Thus, we select these four initial configurations for evaluation:

$$\bullet \epsilon = \left\{ 0.25 \cdot \frac{1}{d_{\max}}, 0.5 \cdot \frac{1}{d_{\max}}, 0.75 \cdot \frac{1}{d_{\max}}, \frac{1}{d_{\max}} \right\}$$

These values are furthermore abbreviated as  $\epsilon = \{ 0.25, 0.5, 0.75, 1 \}$ . As it is not likely that real-life WSNs are bipartite regular graphs [21], we omit these critical topologies from our analyzes.

As mentioned above, we bound the execution of AC by the stopping criteria from [6, 13]. In Section 2.1, it is stated that the fully-distributed stopping criterion from [13] is determined by two preset constants, whose values take these following values in our analyzes:<sup>6</sup>

- *accuracy* =  $\{ 10^{-2}, 10^{-4}, 10^{-5}, 10^{-6} \}$
- *counter threshold* =  $\{ 3, 5, 7, 10, 20, 40, 60, 80, 100 \}$

Moreover, as mentioned earlier in this paper, we compare two scenarios related to this stopping criterion: either the initial inner states or the final estimates are multiplied by the network size  $n$ .

Furthermore, the performance achieved with the implemented stopping criterion from [13] is compared to MSE and the convergence rate when the centralized stopping criterion from [6] is implemented. As stated in the previous section, it is determined by *accuracy*, which takes the same values as the examined fully-distributed approach, i.e.:

$$\bullet \textit{accuracy} = \{ 10^{-2}, 10^{-4}, 10^{-5}, 10^{-6} \}$$

In this paper, AC is analyzed over RGGs of dense connectivity<sup>7</sup>. We generate 30 RGGs with unique topologies that are formed by 200 vertices each. A representative of the generated graphs is shown in Figure 2.

In our analyzes, each vertex initiates its inner states with a randomly generated scalar value of the standard Gaussian distribution, describe by 11:

$$x_i(0) \sim N(0, 1), \text{ for } \forall v_i \in \mathbf{V} \quad (11)$$

To evaluate the performance of the algorithm, we apply two metrics for this purpose, namely the mean square error (MSE) and the

convergence rate expressed as the iteration number necessary for the consensus achievement. In all the presented figures, we show MSE/the convergence rate averaged over 30 RGGs.

The first metric, MSE, is applied for precision evaluation of the final estimates and is defined in 12, [26]:

$$\text{MSE} = \frac{1}{n} \cdot \sum_{i=1}^n \left( x_i(k_i) - \mathbf{1}^T \times \frac{\mathbf{x}(0)}{n} \right)^2 \quad (12)$$

Here,  $k_i$  is the label of the iteration when the algorithm is completed at each vertex. The other metric, i.e., the number of the iterations, is applied in order to identify how long the algorithm has to be executed until the consensus upon the sum of all the initial inner states is achieved.

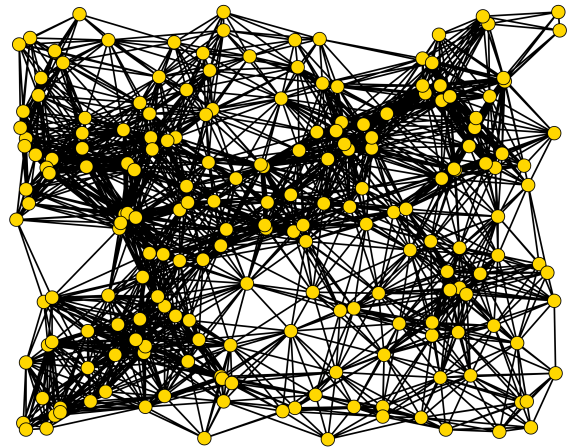


Figure 2: Representative of generated RGGs

## 4 Experiments and Discussion

In this section, we present the results obtained in Matlab2016a and Matlab2018b and discuss the character of the depicted functions and observable phenomena.

In the first experiment, we analyze the precision of the final estimates quantified by MSE when AC is bounded by the stopping criterion presented in [13]. As already mentioned, we examine two scenarios: either the initial states (i.e., before AC begins – referred to as scenario 1) or the final estimates (i.e., after AC is completed – referred to as scenario 2) are multiplied by the network size  $n$ . From the results shown in Figure 3 and 4, we can observe in both examined scenarios that a decrease in the value of *accuracy* (see (a), (b), (c), and (d) in both figures for the results achieved for different values of *accuracy*) and an increase in the value of *counter threshold* ensure that MSE is smaller for each analyzed mixing parameter  $\epsilon$ . Moreover, it can be seen that also an increase in the value of the mixing parameter  $\epsilon$  results in a decrease in MSE for each *accuracy* and *counter threshold*. Furthermore, in scenario 2, we can see that

<sup>6</sup>the values  $10^{-1}, 10^{-3}$  are omitted in order to ensure good readability of the paper

<sup>7</sup>in [1], also an analysis of AC for distributed summing in sparsely connected RGGs is provided, but it is not extended in this paper in order to achieve better readability of the paper



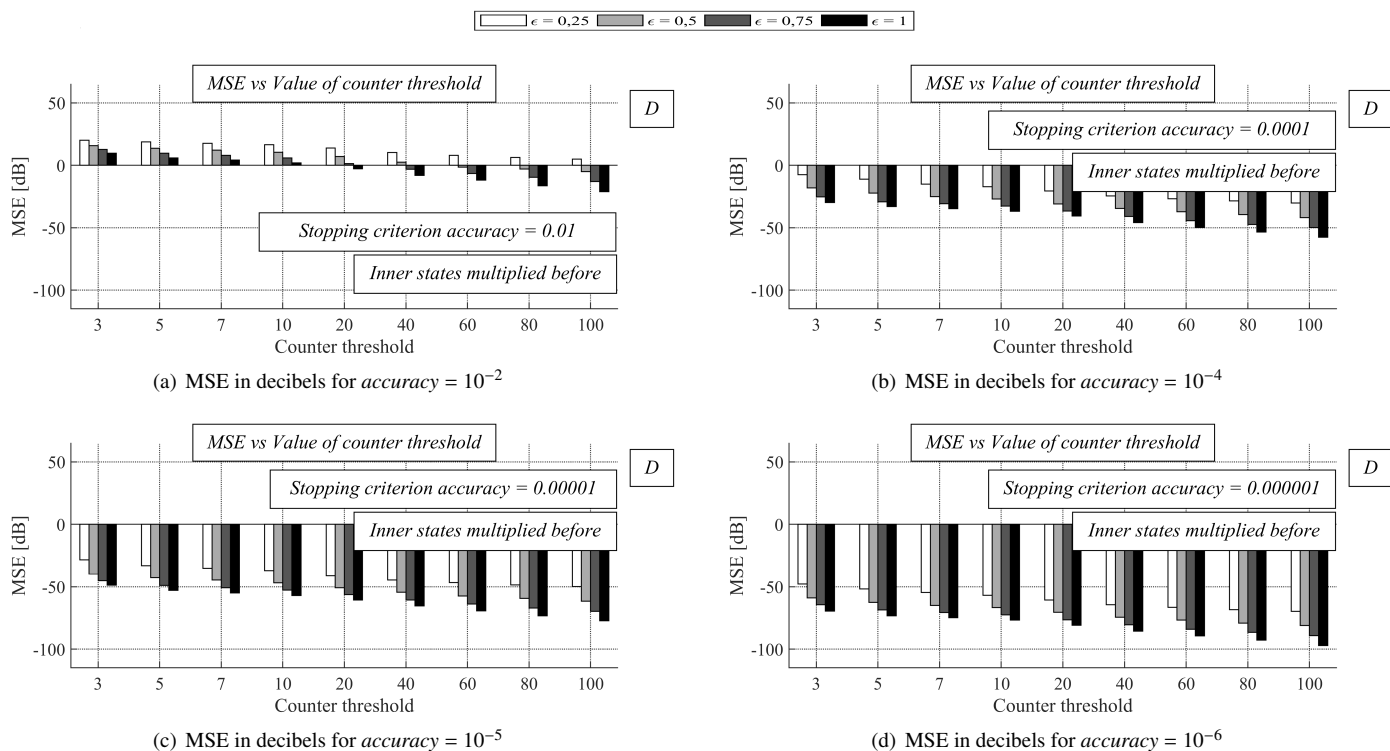


Figure 3: MSE [dB] averaged over 30 dense RGGs – fully-distributed approach is implemented, initial inner states are multiplied by network size

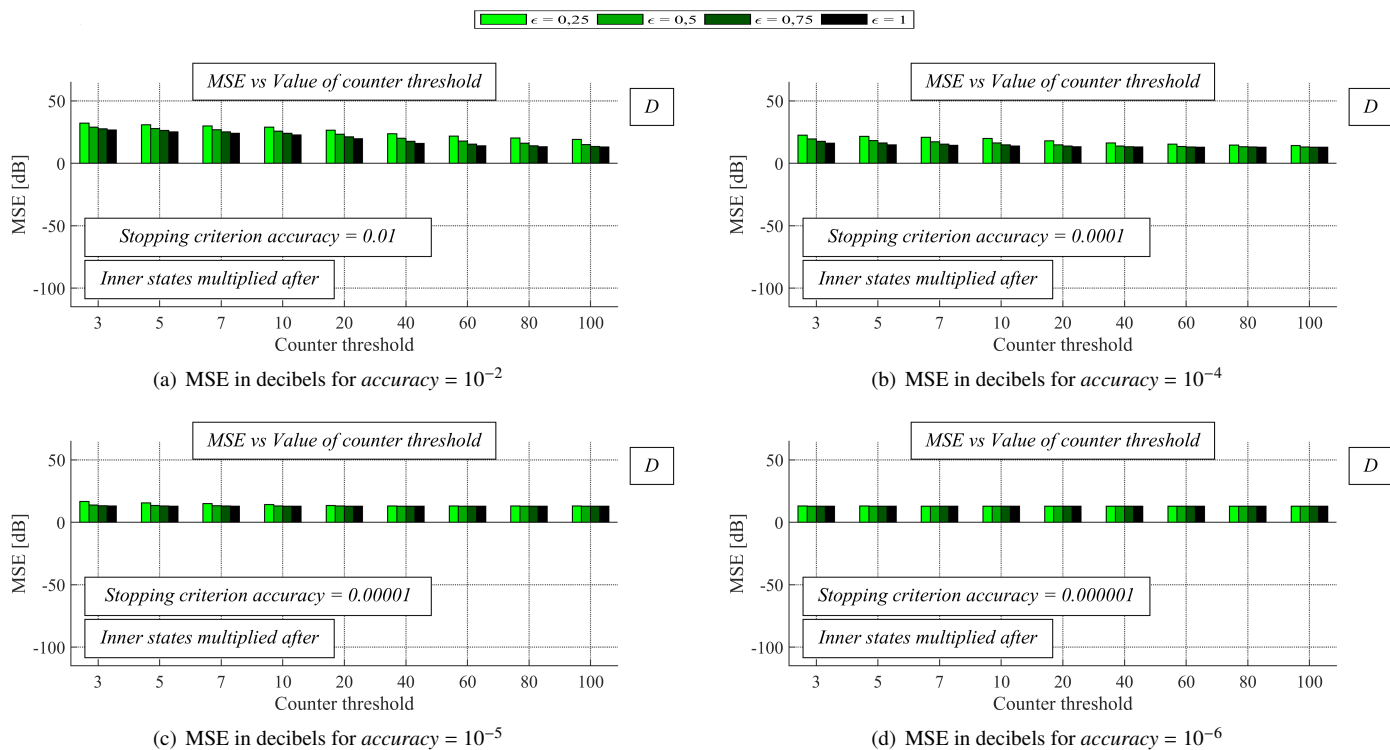


Figure 4: MSE [dB] averaged over 30 dense RGGs – fully-distributed approach is implemented, final estimates are multiplied by network size

the precision of the final estimates is much smaller than in scenario 1, and a decrease in *accuracy* (see (a), (b), (c), and (d)) and an increase in *counter threshold* have a significantly smaller impact on an increase in the precision compared to scenario 1.

In the next experiment, we analyze the convergence rate expressed as the number of the iterations for the consensus achievement in both scenarios again. From the presented results in Figure 5 and 6, it can be seen that a decrease in the values of *accuracy* (see (a), (b), (c), and (d)) and an increase in the values of *counter threshold* result in a deceleration of the algorithm (i.e., AC requires more iterations to be completed) for each examined mixing parameter  $\epsilon$  in both analyzed scenarios. Again, it is seen that AC with a larger mixing parameter  $\epsilon$  achieves a higher performance like in the previous analyzes. However, unlike the previous analysis, AC in scenario 2 outperforms AC in scenario 1 for each value of both *accuracy* and *counter threshold*, and therefore, multiplying the initial states with the network size  $n$  ensures higher precision of the final estimates, but a higher convergence rate is achieved in scenario 2.

In the last experiment, we test AC with the centralized stopping criterion from [6]. In Figure 7 and 8, we depict MSE and the convergence rate expressed as the number of the iteration for the consensus for same *accuracy* as in the previous two experiments. From Figure 7, it can be observed that a decrease in *accuracy* (see (a), (b), (c), and (d)) results in a decrease in MSE, and so, the precision of the final estimates is increased. Compared to the analysed fully-distributed approach, we can see that the value of the mixing parameter  $\epsilon$  has only a marginal impact on MSE regardless of *accuracy* of the stopping criterion (in fact, increasing  $\epsilon$  ensures a small increase in the performance). Regarding the convergence rate, a higher value of the mixing parameter  $\epsilon$  ensures a higher convergence rate just like in the

previous analyzes. Also, it is seen that a decrease in *accuracy* (see (a), (b), (c), and (d)) results in a lower convergence rate; therefore, more iterations are necessary for AC to be completed.

In the two following paragraphs, we turn our attention to a comparison of the centralized and the fully-distributed stopping criterion, which are analyzed in the previous parts - in all the comparisons, the results achieved for  $\epsilon = 1$  are examined (i.e., the results achieved by the best performing initial configuration). From Figure 3, Figure 4, and Figure 7, where the precision of the final estimates is analyzed, we can see that a decrease in *accuracy* (see (a), (b), (c), and (d)) results in a decrease in MSE in all three cases. Also, it is seen that the value of the mixing parameter  $\epsilon$  has only a marginal impact on MSE when the centralized stopping criterion is applied in contrast to the fully-distributed approach. In addition, in Figure 4, it is seen that the value of the mixing parameter  $\epsilon$  less affects the precision of the final estimates for lower values of *accuracy* and higher values of *counter threshold*. Furthermore, in the first case, when AC is bounded by the fully-distributed stopping criterion in scenario 1, MSE is from the range  $\langle -97.12 \text{ dB} - 9.63 \text{ dB} \rangle$ , meanwhile, in scenario 2, MSE takes the values from this interval  $\langle 12.95 \text{ dB} - 26.67 \text{ dB} \rangle$ . In the third case, when the centralized stopping criterion is implemented, the values of MSE are from  $\langle -131.80 \text{ dB} - -52.07 \text{ dB} \rangle$ . Therefore, the centralized stopping criterion significantly outperforms the fully-distributed approach in terms of the estimation precision. Even though this approach achieves a significantly higher performance according to the MSE-metric, it is less appropriate for real-life implementations since it requires time-variant global information – the maximum and the minimum from all the current inner states at each iteration.

In terms of the convergence rate expressed as the number of

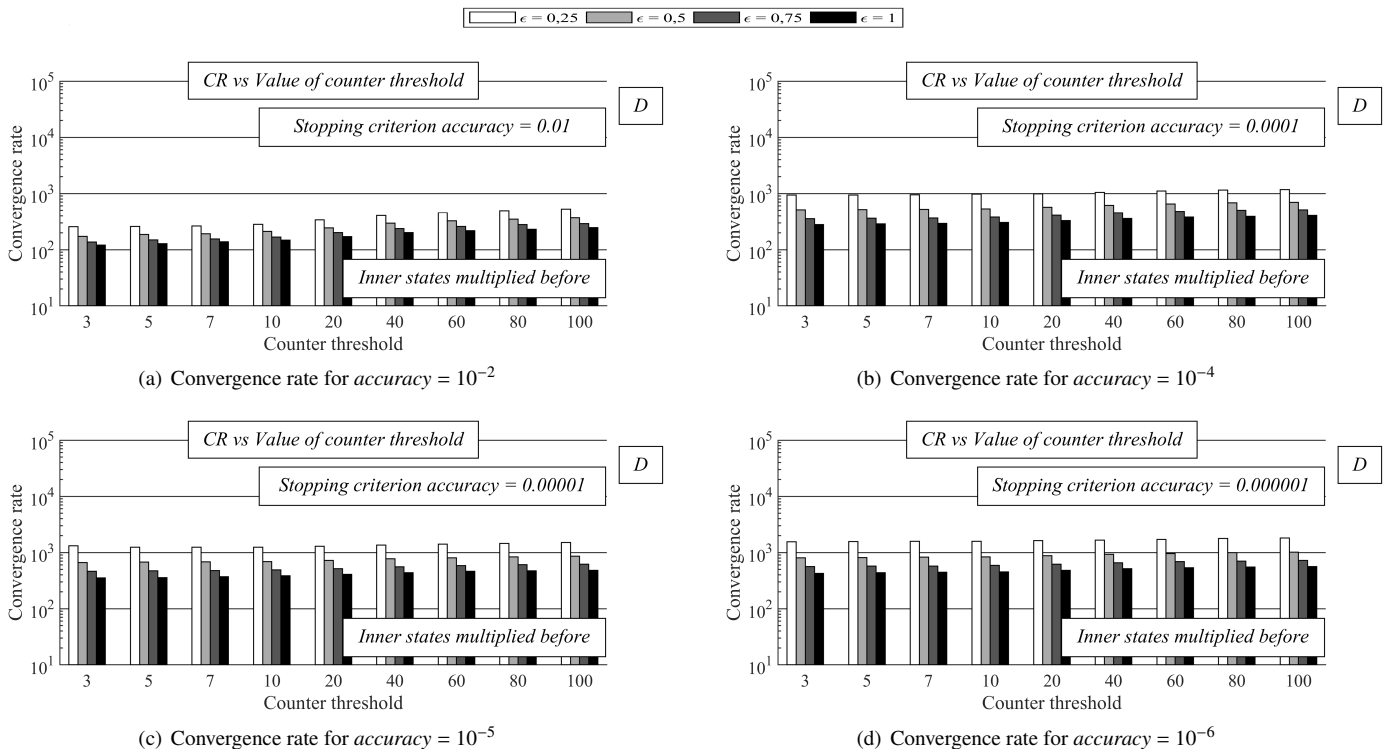


Figure 5: Convergence rate averaged over 30 dense RGGs – fully-distributed approach is implemented, initial inner states are multiplied by network size

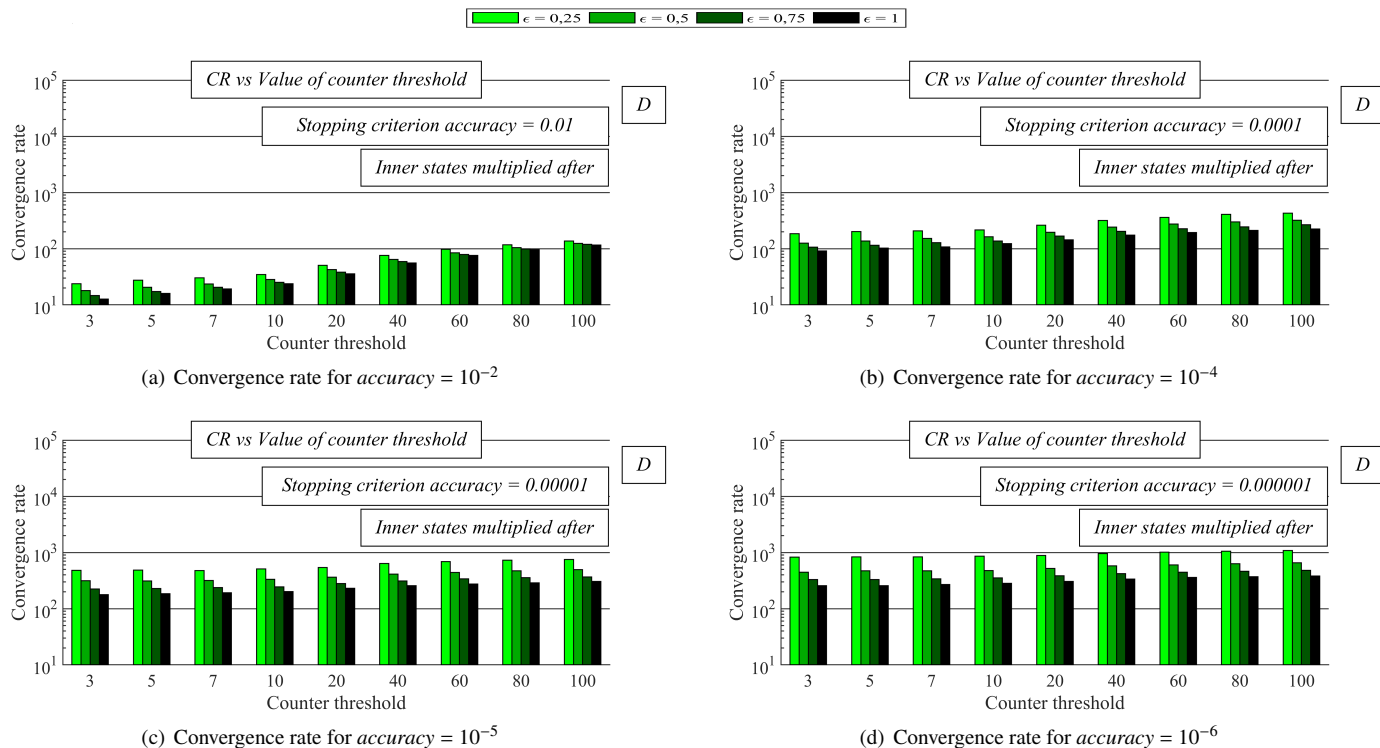


Figure 6: Convergence rate averaged over 30 dense RGGs – fully-distributed approach is implemented, final estimates are multiplied by network size

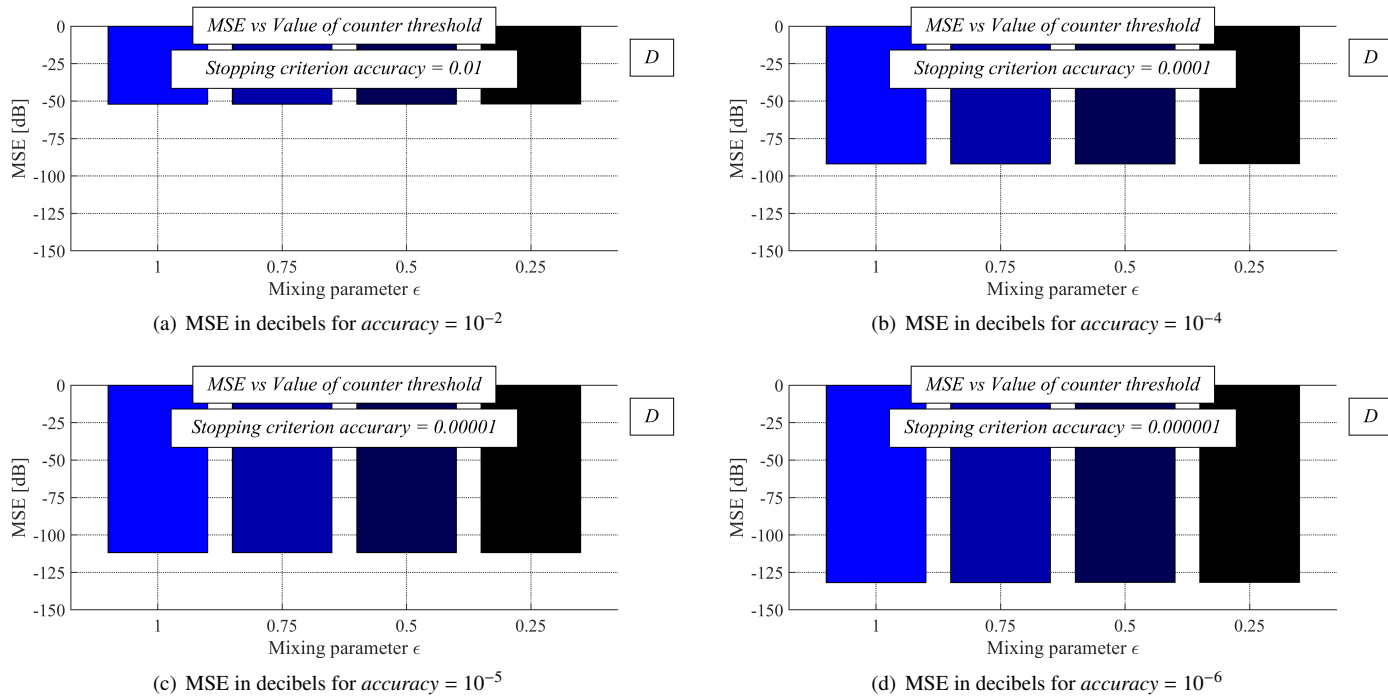


Figure 7: MSE [dB] averaged over 30 dense RGGs – centralized approach is implemented

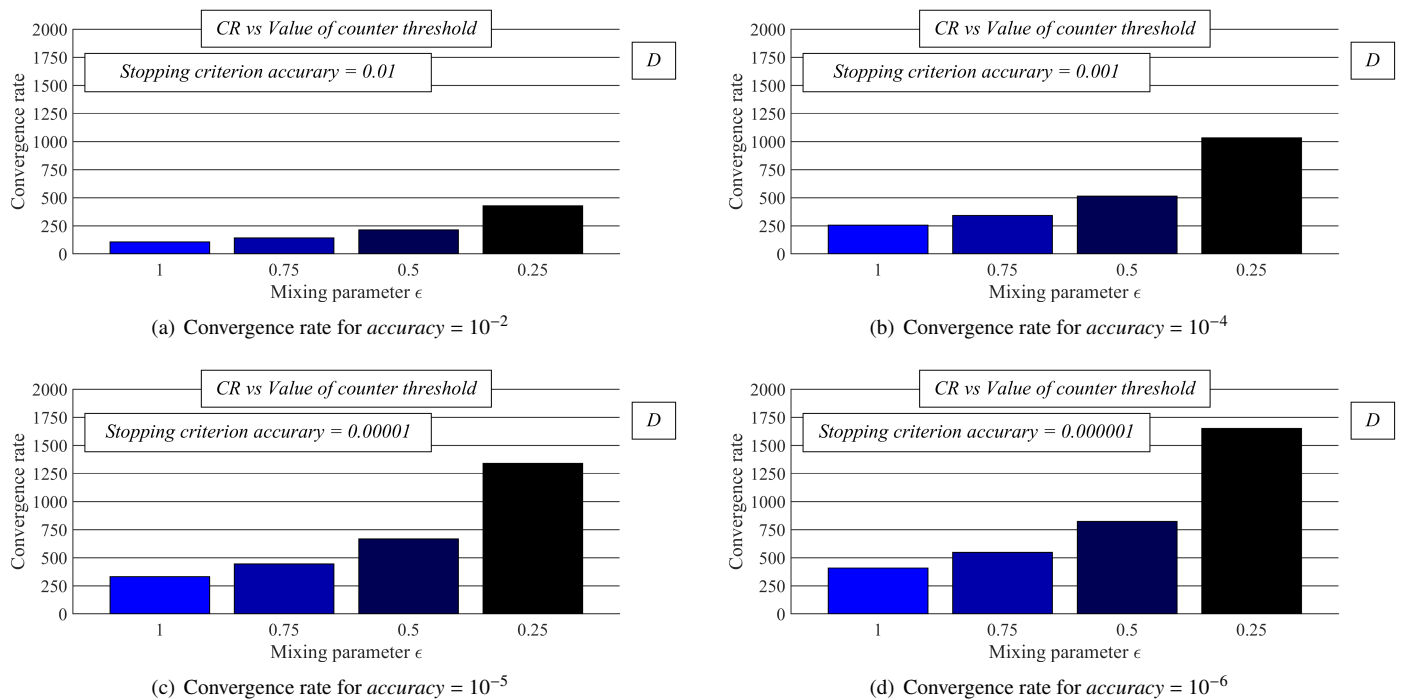


Figure 8: Convergence rate averaged over 30 dense RGGs – centralized approach is implemented

the iterations necessary for the consensus achievement (the results from Figure 5, Figure 6, and Figure 8 are compared), we can see that a decrease in *accuracy* (whereby a higher precision is achieved – see (a), (b), (c), and (d)) causes a deceleration of the algorithm in all three cases again. In the case, when AC is bounded by the fully-distributed stopping criterion in scenario 1, the convergence rate is from  $\langle 121 - 560.4 \rangle$ . In scenario 2, the convergence is from the following interval  $\langle 12.63 - 383.1 \rangle$ , and, in the third case, when the centralized stopping criterion is implemented, the convergence rate takes the following values  $\langle 105.9 - 408.50 \rangle$ . So, it is seen that the highest convergence rate is achieved by the fully-distributed stopping criterion when the final estimates are multiplied by the network size  $n$ .

## 5 Conclusion

In this paper, we address AC for distributed summing whose execution is bounded by either a centralized or a fully-distributed stopping criterion. The results from our experiments show that decreasing *accuracy* ensures a higher precision of the final estimates but at a cost of a deceleration of the algorithm regardless of the applied stopping criterion. The precision of the final estimates can be improved also by increasing *counter threshold* when the fully-distributed stopping criterion is implemented. Moreover, it is proven that an increase in the mixing parameter  $\epsilon$  optimizes the algorithm in terms of both the precision and the convergence when AC is bounded by the fully-distributed stopping criterion. In the case of the implementation of the centralized one, the value of  $\epsilon$  has only a marginal impact on the precision of the final estimates, however, its higher values ensure a higher convergence rate like in the case of the fully-distributed stopping criterion. The fully-distributed stopping

criterion achieves a higher precision when the initial inner states are multiplied by the network size  $n$  instead of the final estimates. However, on the other hand, multiplying the final estimates with  $n$  results in a higher convergence rate. Furthermore, it is proven that the centralized stopping criterion achieves higher performance in terms of the precision, however, this approach is less suitable for real-life implementations because it requires the information about the maximum and the minimum from all the current inner states at each iteration for its proper operating. The fastest is AC with the fully-distributed stopping criterion when the final estimates are multiplied by the network size  $n$ . On the other hand, in this case, the precision of the final estimates is significantly lower.

## Acknowledgment

This work was supported by the VEGA agency under the contract No. 2/0155/19 and by COST: Improving Applicability of Nature-Inspired Optimisation by Joining Theory and Practice (ImAppNIO) CA 15140. Since 2019, Martin Kenyeres has been a holder of the Stefan Schwarz Supporting Fund.

## References

- [1] M. Kenyeres, J. Kenyeres, I. Budinska, "Distributed linear summing in wireless sensor networks" in IEEE 17th World Symposium on Applied Machine Intelligence and Informatics (SAMI 2019), Herlany, Slovakia, 2019. <https://doi.org/10.1109/SAMI.2019.8782782>
- [2] H. Yetgin, K. T. K. Cheung, M. El-Hajjar, L. Hanzo, "A survey of network lifetime maximization techniques in wireless sensor networks" IEEE Commun. Surv. Tutor., **19**(2), 828–854, 2017. <https://doi.org/10.1109/COMST.2017.2650979>

- [3] B. Rashid, M. H. Rehmani, "Applications of wireless sensor networks for urban areas: a survey" *J. Netw. Comput. Appl.*, **60**, 192–219, 2016. <https://doi.org/10.1016/j.jnca.2015.09.008>
- [4] T. Qiu, A. Zhao, F. Xia, W. Si, D. O. Wu, "ROSE: robustness strategy for scale-free wireless sensor networks" *IEEE/ACM Trans. Netw.*, **25**(5), 2944–2959, 2017. <https://doi.org/10.1109/TNET.2017.2713530>
- [5] B. Krishnamachari, D. Estrin, S. B. Wicker, "The impact of data aggregation in wireless sensor networks" in 22nd International Conference on Distributed Computing Systems Workshops (ICDCSW 2002), Vienna, Austria, 2002. <https://doi.org/10.1109/ICDCSW.2002.1030829>
- [6] M. Kenyeres, J. Kenyeres, V. Skorpil, "The distributed convergence classifier using the finite difference" *Radioengineering*, **25**(1), 148–155, 2016. <https://doi.org/10.13164/re.2016.0148>
- [7] Y. Liu, M. Dong, K. Ota, A. Liu, "ActiveTrust: secure and trustable routing in wireless sensor networks" *IEEE Trans. Inf. Forensics Secur.*, **11**(9), 2013–2027, 2016. <https://doi.org/10.1109/TIFS.2016.2570740>
- [8] D. Izadi, J. H. Abawajy, S. Ghanavati, T. Herawan, "A data fusion method in wireless sensor networks," *Sensors*, **15**(2), 2964–2979, 2015. <https://doi.org/10.3390/s150202964>
- [9] L. Xiao, S. Boyd, S. Lall, "A scheme for robust distributed sensor fusion based on average consensus" in 4th International Symposium on Information Processing in Sensor Networks (IPSN 2005), Los Angeles, CA, USA, 2005.
- [10] G. Stamatescu, I. Stamatescu, D. Popescu, "Consensus-based data aggregation for wireless sensor networks" *Control. Eng. App. Inf.*, **19**(2), 43–50, 2017.
- [11] A. K. Idrees, W. L. Al-Yassen, M. A. Taam, O. Zahwe, "Distributed data aggregation based modified K-means technique for energy conservation in periodic wireless sensor networks" in 2018 IEEE Middle East and North Africa Communications Conference (MENACOMM 2018), Jounieh, Lebanon, 2018. <https://doi.org/10.1109/MENACOMM.2018.8371007>
- [12] Q. Chen, H. Gao, Z. Cai, L. Cheng, J. Li, "Distributed low-latency data aggregation for duty-cycle wireless sensor networks" *IEEE/ACM Trans. Netw.*, **26**(5), 2347–2360, 2018. <https://doi.org/10.1109/TNET.2018.2868943>
- [13] M. Kenyeres, J. Kenyeres, M. Rupp, P. Farkas, "WSN implementation of the average consensus algorithm" in 17th European Wireless Conference 2011 (EW 2011), Vienna, Austria, 2011.
- [14] D. Merezeanu, M. Nicolae, "Consensus control of discrete-time multi-agent systems," *U. Politeh. Buch. Ser. A*, **79**(1), 167–174, 2017. <https://doi.org/10.1109/TNET.2018.2868943>
- [15] P. Jesus, C. Baquero, P. S. Almeida, "A survey of distributed data aggregation algorithms" *IEEE Commun. Surv. Tutor.*, **17**(1), 381–404, 2015. <https://doi.org/10.1109/COMST.2014.2354398>
- [16] A. Olshevsky, "Linear time average consensus and distributed optimization on fixed graphs" *SIAM J. Control. Optim.*, **55**(6), 3990–4014, 2017. <https://doi.org/10.1137/16M1076629>
- [17] G. Oliva, R. Setola, C. N. Hadjicostis, "Distributed finite-time average-consensus with limited computational and storage capability" *IEEE Trans. Control. Netw. Syst.*, **4**(2), 380–391, 2017. <https://doi.org/10.1137/16M1076629>
- [18] L. Faramondi, R. Setola, G. Oliva, "Performance and robustness of discrete and finite time average consensus algorithms" *Int. J. Syst. Sci.*, **49**(12), 2704–2724, 2018. <https://doi.org/10.1080/00207721.2018.1510059>
- [19] J. Gutierrez-Gutierrez, M. Zarraga-Rodriguez, X. Insausti, "Analysis of known linear distributed average consensus algorithms on cycles and paths" *Sensors*, **18**(4), 1–25, 2018. <https://doi.org/10.3390/s18040968>
- [20] T. C. Aysal, B. N. Oreshkin, M. J. Coates, "Accelerated distributed average consensus via localized node state prediction" *IEEE Trans. Signal Process.*, **57**(4), 1563–1576, 2009. <https://doi.org/10.1109/TSP.2008.2010376>
- [21] V. Schwarz, G. Hannak, G. Matz, "On the convergence of average consensus with generalized Metropolis-Hasting weights" in 2014 IEEE International Conference on Acoustics, Speech, and Signal Processing (ICASSP 2014), Florence, Italy, 2014. <https://doi.org/10.1109/ICASSP.2014.6854643>
- [22] L. Xiao, S. Boyd, "Fast linear iterations for distributed averaging" *Syst. Control. Lett.*, **53**(1), 65–78, 2004. <https://doi.org/10.1016/j.sysconle.2004.02.022>
- [23] N. E. Manitara, C. N. Hadjicostis, "Distributed stopping for average consensus in directed graphs via a randomized event-triggered strategy" in 6th International Symposium on Communications, Control and Signal Processing (ISCCSP 2014), Athens, Greece, 2014. <https://doi.org/10.1109/ISCCSP.2014.6877918>
- [24] S. V. Macua, C. M. Leon, J. S. Romero, S. S. Pereira, J. Zazo, A. Pages-Zamora, R. Lopez-Valcarce, S. Zazo, "How to implement doubly-stochastic matrices for consensus-based distributed algorithms" in 2014 IEEE 8th Sensor Array and Multichannel Signal Processing Workshop (SAM 2014), A Coruna, Spain, 2014. <https://doi.org/10.1109/SAM.2014.6882409>
- [25] V. Schwarz, G. Matz, "Nonlinear average consensus based on weight morphing" in IEEE International Conference on Acoustics, Speech, and Signal Processing (ICASSP 2012), Kyoto, Japan, 2012. <https://doi.org/10.1109/ICASSP.2012.6288578>
- [26] S. S. Pereira, A. Pages-Zamora, "Mean square convergence of consensus algorithms in random WSNs" *IEEE Trans. Signal Process.*, **58**(5), 2866–2874, 2010. <https://doi.org/10.1109/TSP.2010.2043140>

## Ontological and Epistemological Issues of Studying the Development of Uzbekistan in the Context of Globalization from the Point of View of the Paradigm of Civilizations

Djurayeva Nigora Avazovna\*

National University of Uzbekistan named after Mirzo Ulugbek, Tashkent Uzbekistan Doctoral student of the faculty of Social sciences, the Department of Philosophy and Logic, 702506, Uzbekistan

### ARTICLE INFO

Article history:

Received: 19 August, 2019

Accepted: 05 February, 2020

Online: 09 March, 2020

Keywords:

Uzbekistan

Paradigm of civilizations

Ontology

The factors of development of the paradigm of civilizations

Strategy of development

Culture

Synergetic Approach

Geographical Factor

Space

Time

Value Factor

Modernization

### ABSTRACT

In this scientific work, the basic synergetic principles of the development of the paradigm of civilizations are substantiated, an assessment of the time boundaries within which civilizations exist, the features of their own path of development of Uzbek culture are revealed. It is especially drawn attention to the sociocultural codes of civilization, a combination of which identifies the essence of Uzbek civilization. However, gives the reasons for the threat of the existence of civilizations and the prospects for their further development. The problem of the paradigm of civilizations interested many inquisitive minds of mankind, philosophical schools and trends. Its origins can be found in antiquity and in the Middle Ages. Dosocrats, Plato, Aristotle, Stoics, Epicureans, Neoplatonists, Thomas Aquinas, al-Farabi, Ibn Sina developed problems of society and history within the framework of the classical metaphysical and dialectical-idealistic tradition. It is believed that the modern form and meaning of the term civilization in some cases preserves what was put into circulation, first of all, by the French and English enlighteners in the second half of the 18th century, who proposed a universal scheme for the development of mankind - savagery, barbarism, civilization and focused on the search for the source of the development of society, the driving forces of history: V. Voltaire, J. Kondors, A. Turgot. This problem has not been developed in Uzbekistan from a philosophical point of view, in particular, that part of it that deals with ontological and epistemological aspects. In connection with the study, dialectical, formal-logical, historical-morphological methods were used, as well as comparative analysis methods.

## 1. Introduction

The changes taking place in modern Uzbekistan, the search for a new socio-economic orientation, have highlighted the question of its civilization and ways of its further development. Speaking without exaggeration, "civilization" is one of the main categories of philosophy, and in particular the part that deals with its ontological and epistemological aspects of its development, in addition, it is obvious that this category is one of the significant phenomena of social reality. Each civilization has a number of distinctive properties that have a huge impact on its history, political and socio-economic structure. The disclosure of their own characteristics is extremely relevant for modern Uzbekistan. It is important to analyze the prospects for the development of Uzbekistan in the context of inter-civilization relations against the backdrop of global changes in the world.

## 2. Explanation of thematic literature

It is important to note that the analysis of the formation of the concept of "civilization" appears on the pages of the works of the Marquis de Mirabeau, "Friend of men or a treatise on population" and "Friend of women, or a treatise on civilization"; in Ferguson's work, "An Essay on the History of Civil Society," where civilization is interpreted as the highest stage in the development of society compared to barbarism[1]. S. Montesquieu in his work "On the Spirit of Laws" identifies two stages in the life of mankind and explains the need for a transition to a civilized existence. For S. Montesquieu, civilization is a society where they are engaged in agriculture, live in cities, have money and have a civil code of laws [2].

The contrast of civilization and culture marked the thoughts of N. A. Berdyaev, A. Toynbee, O. Spengler [3]-[5].

\* Djurayeva Nigora Avazovna, nigoradjurayeva@mail.ru



In the works of M.A. Barg, N.Ya. Bromley, K. Marx, L. Morgan, F. Engels, civilization is considered as the level of development of society "based on the upward movement" arising in the course of the dialectical interaction of material productive forces and production relations [6]-[8].

Coverage of the cultural and historical foundations of civilization is given in the works of M. Weber, N. Ya. Danilevsky, P. Sorokin, A. Toynbee.

On the basis of this material, a number of modern Russian scientists: B.Erasov, L.Novikova, L.Reisner - reveal the significance of the civilizational structure of society, based on the general principles of organizing people's lives.

### **3. Materials and methods**

In connection with the study, dialectical, formal-logical, historical-morphological methods were used, as well as comparative analysis methods.

### **4. Analysis and results**

The paradigm of civilization is a manifestation of the aggregate set of knowledge that affirms the specific system of its construction and shows the optimal mechanism of its existence, but it is relative.

When analyzing the ontological-epistemological problems of studying the development of Uzbekistan in the context of globalization from the point of view of the paradigm of civilizations, it is important to pay attention to the fact that the main content of the last decade of the twentieth century was the search for a new paradigm of world structure, which also affected Uzbekistan. In the inter-paradigmatic decade, the theory of modernization was again in demand. Nevertheless, it should be noted that there could be no universal scheme or model of modernization. There are no ready-made, the same for all cultures and civilizations programs for the reconstruction of society. Modernization is a modern stage of the socio-historical, ontological-epistemological processes that exclude a single and linear development path.

It is the presence of political independence as a prerequisite for the development of an independent civilization that can be considered another principle for the formation of a paradigm of civilizations. There is not a single civilization that would achieve a high degree of maturity without political independence. Without it, the emerging civilization turns into a tool that serves the interests and goals of others.

Modernization, by contrast, strengthens national cultures that are becoming more modern and less western. Peoples and generations are changing, scenes of historical life are moving, social orders are changing, civilizations are alternating, but the thread of historical development is not interrupted. And generation after generation preserves the cultural stock that managed to survive in the stormy historical ocean. Modernization is turning into a panacea, miracles are expected from it, all hopes for a bright future for the Uzbek sociocultural system are associated with it. On the one hand, in the conditions of an unprecedented technological breakthrough made recently by leading Western countries, as well as Asian states that are gaining strength, a bet on modernization is not only desirable, but also necessary. However, it is important to emphasize that

modernization, like any other socio-cultural process, does not take place on its own, its effective implementation is preceded by a number of preparatory measures, the main of which is the determination of the goals and objectives of modernization, the ways and means of its implementation, sociocultural and civilizational consequences of modernization transformations.

Globalization, the new openness of the world is a challenge, but a positive challenge that we must be able to use in order not to stay on the sidelines among the laggards. Our task is not to fence ourselves off from globalization processes, but to develop a comprehensive strategy for adapting to new processes and phenomena that is beneficial for society and the country [9].

Today in Uzbekistan, the problems of stabilization and reform of various spheres of human activity are being solved based on our own development model, and our own programmatic approaches have been developed. The sociocultural features of Uzbek modernization are it catching up, fragmented, incomplete nature. In Uzbekistan, the Head of State Sh.Mirziyoyev developed an Action Strategy for 2017-2021, the purpose of which is to radically increase the effectiveness of the reforms, create conditions to ensure the comprehensive and accelerated development of the state and society, modernize the country and liberalize all spheres of life. In particular, five priority areas of the country's development have been identified:

- Improving state and social construction;
- Ensuring the rule of law and further reform of the judicial system;
- Development and liberalization of the economy;
- Development of the social sphere;
- Ensuring security, interethnic harmony and religious tolerance, implementing a balanced, mutually beneficial and constructive foreign policy.

The own path of our republic is based on the centuries-old experience of developed countries, as well as on the comprehensive consideration of the national historical heritage, lifestyle, traditions and mentality of the people of Uzbekistan.

It is important to note that the implementation of the Action Strategy will be a powerful impetus for the progressive movement of the Republic of Uzbekistan along the path of reforming and modernizing the country, building a legal and democratic state with a developed market economy, a strong civil society, ensuring the rule of law, security and the rule of law, inviolability of state borders, and interethnic consent and religious tolerance in society.

In the ontological-epistemological study of the paradigms of civilizations in general, as well as the development of Uzbekistan in the context of globalization, the role of the synergetic approach in philosophy is important. The specificity of the synergetic approach to the study of the development of the paradigm of civilization lies in such a modeling of the dynamics of civilization processes that takes into account the interconnectedness of ordered and chaotic states of the system, the variability of the ways of its development and the fundamental inevitability of the prognostic horizon, which is usually very close to the current state of the system. The value-semantic content penetrates into the synergetic approach mainly under the guise of improving the adaptive abilities of society to its increasing capabilities. The synergetic approach allows you to integrate various theories of civilization, in conceptual terms it can be used as one of the hermeneutics of the process of world-historical development of

civilization, and in terms of modeling civilization processes lasting several decades, it significantly complements already known concepts, changing the very structure of the study.

It is necessary to pay attention to the fact that from the point of view of development, every civilization or culture has its own hidden code, which includes a set of rules or principles that permeate all its inherent types of activity[6]. For example, the basic principles of industrial civilization have become standardization, specialization, synchronization, concentration, maximization and centralization. Moreover, at the heart of civilization are three types of backbone ties:

- spatial, extending to the features of the natural environment, landscape, which can also be called a geographical factor in the development of the paradigm of civilizations;
- temporary, forming a community of historical being, traditions, widely understood culture, language.
- social, cementing super ethnic community through the formation of comparable value-normative mechanisms, subjective awareness of community, self-identification of people.

Sociocultural codes, a combination of which identifies the essence of Uzbek civilization, its difference from others, can be attributed to:

1. Historical heritage, which is a temporary backbone link. Due to its unique geographical location, Uzbekistan has rich historical roots. The territory of the country became an eyewitness and experienced the change of many cultures and religions during various periods of the region's development, from the conquests of Alexander the Great to the campaigns of Genghis Khan. The formation of the Uzbek nationality is closely connected with the ancient peoples of Central Asia - Sogdians, Bactrians, Sako-Massageti and other tribes that for centuries inhabited the Central Asian rivers Amu Darya and Syr Darya and neighboring areas. Here were the centers of many powerful empires, such as the empire of Amir Temur. However, the name itself - the Uzbeks - was established only in the late 15th - early 16th centuries with the advent of the Sheibanid dynasty in Maverannahr, but the very concept of "Uzbek" was not used as a separate historically cultural type. Only in the Soviet period did this concept begin to be used in the context of statehood. Such a bright period of historical development largely explains the accumulated great spiritual and cultural potential.
2. National tolerance based on the Asian nature of peoples is a feature inextricably linked with the previous one. Uzbekistan, which has absorbed tribes and nationalities, has retained them as much as it received. Dozens of nationalities and nationalities live here, including residents of the Central Asian region: Uzbeks, Karakalpaks, Tajiks, Turkmens, Kazakhs, Kyrgyz, Uighurs, Dungans; Western and Eastern Slavs: Russians, Ukrainians, Belarusians, Poles; the numerous diasporas in Uzbekistan are Koreans, Iranians, Armenians, Georgians, Azerbaijanis, Tatars, Bashkirs, Germans, Jews, Lithuanians, Greeks, Turks and many other nationalities. Such ethnic diversity is due to various historical events. Many representatives of the indigenous peoples of the Union republics of the USSR were evacuated to Uzbekistan during the Second World

War (Russians, Tatars, Armenians, Belarusians, Ukrainians, Germans, Jews, etc.). Representatives of individual nations were deported from places of permanent residence during the years of Stalinist repression (Koreans, Crimean Tatars, Chechens and others).

3. Tolerance. Scientific sources indicate that Uzbekistan is one of the most ancient places in the world where the first religious views and ideas arose. This is eloquently evidenced by the ancient burial places in the Teshik-Tash caves, the bas-relief finds of Faez and Kara-Tepa, the finds in Dalverzintepa and Sogdiana, the records of Darius the first on the Behistun rock, as well as the results of studies conducted jointly with French and Japanese archaeologists. Since ancient times, Zoroastrianism, Buddhism, Judaism existed in our region, which then turned into complex ideological systems. On the eve of the Arab offensive and the emergence of the religion of Islam in the region, Nestorian Christianity penetrated here from Syria through Iran and took an important position. At the beginning of the VI century, a Nestorian bishop served in Samarkand, and in the VIII century - Nestorian Metropolitan. In addition, in ancient times, the population professing Christianity lived on the territory of the present Tashkent and Khorezm regions. In the X century A.Hanafi's school emerged in the territory of the modern Uzbekistan region, which is distinguished by its tolerance that has formed at the moment, this was not an accidental phenomenon. The culture of Uzbekistan, which absorbed the best achievements of the past, had, in turn, a tangible impact not only on the subsequent development of Islamic culture, but also on the Western Renaissance, on the development of principles of tolerance on a global scale. With the spread of Islam in Uzbekistan, a meaningful dominant of the spiritual space of the state is being established. Apparently, it should be agreed that it was Islam as a cultural dominant that formed the basis of the civilizational development of the Uzbek people and largely extent formed the national spirit of society, the metaphysical reality existing in Uzbekistan. Over the years of independence of Uzbekistan, religious education has risen to a qualitatively new level. Today, we can confidently say that we have formed a complete system of religious education, which includes the Tashkent Islamic Institute, ten specialized secondary Islamic educational institutions (madrassas), Orthodox and Protestant seminaries. The cooperation, commonwealth, interethnic harmony and religious tolerance that have existed for centuries between the peoples of our region acquired a peculiar content during the years of independence. This also confirms the same attitude on the territory of our multinational and multiconfessional country to every citizen of our state, regardless of race, nation, religion and mother tongue.
4. Spirituality. Uzbekistan is characterized by a special spiritual disposition, characterized by the predominance of the heart over will, contemplation over analysis, conscience over reason, prudence and practical sobriety, freedom and will overpower and coercion, compassion over personal gain and self-interest. These features, in their totality incomprehensible to representatives of other civilizations, have led to a special spiritual depth, which is



reflected in our music, painting, literature, culture as a whole.

5. Collectivism. The dominance of collectivism as a value is confirmed by all cross-country comparative studies. The whole history of the development of our civilization - this is the history of the survival of peoples in natural and climatic conditions, the development of uninhabited spaces, the protection of borders, the vital need for mutual assistance, in collective work - have shaped community, collectivism as a hallmark of mentality.
6. The Uzbek language. For the development and functioning of civilization, the functions of language as a means of consolidating the community, a means of ensuring social interaction, and a means of accumulating and transmitting social experience are especially significant.

In historical terms, the civilizational activity of society contributes to the formation of national languages in the course of a series of convergent-divergent processes: the growth of social integration leads to the strengthening of the speech unity of society, and the increasing differentiation of social life determines the internal differentiation and enrichment of the language system, and the expansion of its communicative functions. Historically important is the emergence of nation-states and urban settlements that support centripetal forces in society and ensure social stability - one of the main prerequisites for creating a national language.

The ability to communicate is one of the factors satisfying human needs and is the paradigm foundation of civilizational existence. Language is not just a means for exchanging thoughts, but also a kind of spiritual authority, which reflects the nature and history of the people, their spiritual traits, mentality, and temperament. It is with the help of language that cultural values are exchanged, the spiritual integration of civilization takes place. Thanks to the emergence of alphabetical writing and a single language, knowledge takes shape and becomes more accessible, accumulates and takes shape in the form of scientific theories of knowledge, develops common moral standards that contribute to the process of self-identification and the growth of national self-awareness. We can agree that "civilization is the largest" "we" "... that breaks up into a huge number of smaller ones: identification with a country, region, with a local community" [10].

M.Barg believes that "the emergence of civilization became possible after the advent of writing" [6]. The development of writing and number systems is becoming necessary in administrative affairs of complex political systems, in the management of large lands and in commercial affairs. The introduction of writing to replace mnemonic methods had revolutionary consequences, since it was used to satisfy a wide range of new society needs. It was used to write laws, record cosmological knowledge, dynastic stories, to register transactions, as well as to write magic formulas, which was of no small importance in early civilizations. Writing refers to the functionally significant criteria of civilization. Subsequently, writing acts as an objective form of self-awareness.

In particular, with the help of writing, a person got the opportunity to communicate with people who are far beyond the reach of his voice, to control vast populated territories. In addition, writing allowed a person to go beyond the present. Thanks to it, the opportunity was opened not only to know the past, but also to turn to the future. As Giddens notes, writing, "expands the boundaries of spatio-temporal distance and creates a perspective

of the past, in which the reflective comprehension of newfound knowledge can be separated from the established tradition" [11].

It should be noted that the concept of "civilization" in the singular and today retains its significance when we discuss the problems of global civilization that affect all of humanity. These are, first, the problems of environmental and nuclear safety, the preservation of humanity, the fight against epidemics and others. Turning to the problems of civilization gradually leads to the formation in science of various directions or approaches that are important for a thorough understanding of the studied sociocultural phenomenon of civilization.

As mentioned above, from the point of view of synergetics, the development of the paradigm of civilizations is based on system-forming connections, some of which are called spatial, they form the geographical factor of the paradigm. Social laws, the way of life of peoples, their social system, mores correspond to physical conditions, climate, soil properties, geographical location of the country. The political system of the state, the form of government also depends on the territorial size of the state. L.Mechnikov in the work "Civilization and the Great Historic Rivers" carefully traces the connection between the distribution of mountains and rivers, and so on with the development of countries and nationalities. He writes: "Is it possible to create any generalization of the cultural and historical meanings of the geographical environment in all their diversity ... work on the discovery of a formula that encompasses in general terms those hidden relationships that bring together and link each phase of social evolution, each period of history humanity with a certain state of the geographical environment" [12]. Representatives of the geographical approach note that primary civilizations arose in an ecologically favorable subtropical climate. Consequently, favorable natural and climatic conditions, the availability of water resources allowed mankind to move to a productive economy. Moving to the subtropics, as well as territorial expansion, has a direct impact on the occupation of the population, and determines its economic and economic base. The uniqueness of natural conditions affects the psychology of the population, the nature of culture, contributing to the formation of its specificity and identity.

Bearing in mind the arguments of the proponents of a geographical approach, we agree that for a comprehensive explanation of the concept of "civilization", the geographical factor is important. In our opinion, the geographical factor has a huge impact on the development of the paradigm of civilizations, but it cannot be considered absolute, since civilization is not only a territorial space formed as a result of the influence of the climatic conditions of a particular region. The natural environment for civilization is that element that must first be understood and then overcome. Accordingly, the development of civilization will depend on the innovative activity of society as a response to the challenge of nature. Uzbekistan is the largest state in Central Asia. In the past, the country had a very favorable location for trade, being on the ancient Silk Road from Europe to the Far East. If we consider the geography of Uzbekistan in general, it can be noted that the vast majority of the territory are deserts and mountains, valleys and lowlands occupy only a small part. At the same time, almost 80 percent of Uzbekistan is the Kyzylkum desert. The southeastern and northeastern parts are represented by mountainous terrain, the elements of which are the foothills and lower mountains of the Tien Shan system. Due to the hot and dry climate, the predominance of mountain and desert

landscapes in Uzbekistan, residents settled unevenly across the territory. The population is concentrated mainly in oases. In the desert regions of the republic, the population density is very low. For example, in Karakalpakstan and the Navoi region, there are only 7-9 people per square kilometer of the territory, while in the most densely populated region of Uzbekistan - the Ferghana Valley - about 500 people per square kilometer. This is the highest indicator of population density not only among the CIS countries, but also one of the highest in the world.

There is one more systemically important factor in the framework of the synergistic approach to the development of the paradigm of civilizations - axiological, whose supporters in the study of the paradigm of civilizations consider values to be the basis for dividing into different civilizations, which are defined as the expression of the general attitudes of their time. Values determine not only spiritual culture, but also material, therefore, cover all aspects of society. Values pervade the whole life of society, form people's attitude to the world, faith and turn into conscious or unconscious psychological attitudes. We can say that values to a greater extent influence the creation of a national-ethnic community, where value guidelines are formed in the process of cultural development. Values provide an opportunity for a qualitative change in society, both in the spiritual and social spheres. Here, it should be concluded that in the value sphere there is a curious phenomenon: with the advent of new urgent problems and new values corresponding to these problems, the old attitudes are partially revised and are gradually being rebuilt in the spirit of the times. For example, quite radical changes in the value sphere were accompanied by industrial revolutions in the West and in the East. This suggests that the value systems of various civilizations in the future will come closer to certain limits as the field of general problems and common moral norms expand. Already today, the main principle of the new positioning of values in various civilizations is the desire to avoid the risk of environmental catastrophe and exacerbation of global problems. However, fundamental civilizational values persist.

In Uzbekistan, these values include the followings:

- Vital values: the right to life and procreation, the preservation of health, the integrity of the person, as indicated in the Basic Law of the state;
- Environmental values: clean soil, water, air, the adequacy of basic resources.
- Primary civil rights: protection of unlawful violence and coercion, freedom of movement, inviolability of the home, freedom of conscience, speech, assembly, association.
- Universal political and legal values: independence of the court, freedom and independence of the press, various forms of citizen participation in political life
- Universal socio-economic values: the right of everyone to self-sufficiency, the right to work and others.

All of the listed values serve as the basis for the implementation, firstly, of civilizational values proper, related to the peculiarities of the lifestyle and thinking of each civilization, and secondly, of national values associated with the characteristic features of each of the peoples included in this civilization. The recognition of universal civilizational values, aimed at protecting civilizational and national values, as leading and defining, today constitutes the minimum platform that is necessary for consensus in the dialogue of cultures.

When considering the most significant approaches to understanding the essence of civilization, it should be noted that the above descriptions and definitions are characteristic of a comprehensive understanding of civilization as a complex, developed society in which both economic factors and the social system, as the moral principles of the regulation of relations, are important, and the political structure, both practical knowledge and aesthetic ideals. We define civilization as a societal cultural-historical system, uniting at the superethnic level a population with a common self-identification, organically connected with a specific natural and spatial environment.

It is also important to note that the process of development of the paradigm of civilization on a macro-chronological scale is represented by the concepts of "moral synergetics". The study of the paradigm of civilization from the standpoint of self-development of the method of material production focuses on the alternation of the regular stages of its evolution and transition periods containing alternative paths of civilizational development. "Moral" synergetics, however, emphasizes that the transition of mankind from a natural state to a civilized one and the subsequent development of civilization were mainly associated with the creation, selection and subsequent consolidation of the most effective mechanisms for maintaining the sociocultural integrity of society[6].

Some researchers of the development of civilizations have identified attractors that draw it into the lumen of cultural and historical life. So, for example, N.Danilevsky acted as an attractor with an original national idea, Spengler - "prasybol", for Toynbee - God, for Kreber - style, for McNeill - text, for S.Huntington - culture. It can be said that in the globalizing conditions of development for Uzbekistan, such attractors of development as the national idea, symbolism, religion, language and writing, original culture and millennia-old traditions are important and there are.

However, the trajectory of civilization is not limited to the upward movement, it also includes a number of other phases. In the initial phase of the formation of civilization, its slow growth occurs. It is being replaced by a phase of accelerated, exponential growth. In this phase, the trajectory of civilization rises most rapidly. However, accelerated growth cannot continue continuously. Encountering internal and external restrictions, it is inevitably accompanied by an increase in contradictions. The growth of such contradictions indicates that civilization has entered the critical zone of its development. It is during this period that she faces a challenge from the environment. The challenge requires the resolution of urgent contradictions, and depending on how successful the answer is, various paths for the further development of civilization are possible.

The critical zone is, in fact, a region of bifurcations where the branching of the trajectory of civilization takes place. Moreover, in our opinion, three main ways of its further changes are possible. Firstly, civilization may fail, which, as a rule, is accompanied by the collapse of the previous structure, a decrease in the level of complexity and a transition to another, much lower trajectory of movement. Secondly, civilization can go through its entire life cycle, including a period of upward changes, a "plateau" and a downward phase of movement. Finally, a third option is possible, in which, having found an adequate response to the environmental challenge, having overcome the ascending section in its development, having passed the "plateau", civilization can again

continue the upward movement. In the development of civilization, not only its breakdown may arise, but also its disintegration, or transformation. The era of the breakdown should be considered complete when, as a result of the promotion of this mechanism, a return to the modification of the nucleus or at least the forcible introduction of new stagnation is no longer possible. This border is conditional, and then the same processes of breakdown unfold in the collapse of civilization or transformation into other civilizations.

## 5. Result and Discussions

In this regard, it is also important to emphasize the threats that threaten the existence of civilizations and cultures:

- the “tension” generated by the conflict of the “organic” social needs of man and the abstract social requirements of civilization;
- the inability of society to find ways of sociocultural adaptation to its own growing opportunities;
- inconsistencies in the development of the economic, social and informational subsystems of civilization.
- from the excess pressure exerted by it on human nature and the environment, the mismatch between the demographic and sociocultural spheres of the development of civilization.

As modern mankind has approached the threshold of permissible anthropogenic pressure on the biosphere, relations between society and the environment have become sources of civilizational conflicts. New natural restrictions require a change in the development strategy of mankind in general and individual civilizations in particular. The Moiseev are offered two key directions for changing this strategy, which do not go beyond the circle of recipes outlined earlier by the Club of Rome: technical and technological re-equipment of mankind and the adoption of a new morality, both of which are dependent on the “environmental imperative” [13]. Synergetics has established that stabilization of a nonequilibrium state is possible only due to an increase in entropy in other systems, an increase in chaos at lower hierarchical levels of being. Consequently, environmental and man-made crises in relation to the development of the paradigm of civilization do not have an eventual but an attributive status. And if the technological and economic progress of civilization is not accompanied by a corresponding improvement in the institutions of sociocultural integration, then no technology for adapting society to the environment will help him overcome the barrier of another ecological crisis.

In the future, the development of civilization:

- will lead to the creation of an ecumenical system;
- needs to expand its own technical basis;
- will be determined mainly by innovations in the information subsystem.
- can lead to the creation of the noosphere, when the causal relationship between nature and civilization will reverse and civilization will become a factor in the development of nature.

## 6. Conclusion

Making a conclusion, it is important emphasize that in the present work, the idea of the uniqueness of each civilization and

culture is developed, and this does not allow building their hierarchy, gradation “above” and “below”. Social norms, values, factors, principles of organization, social institutions of one civilization are not standard for others. The features and results of modernization process are always determined by the previous development and predetermined by the cultural, historical, social features of the country. The modernization process is determined by history, which means a conceptual limitation of the mass of possible solutions at each stage of development. The unlimited borrowing of foreign cultural values, institutions leads to the loss of certainty, the loss of one's own path of development, degradation and destruction of the system, and the violation of the intrasystem determinism of values.

Uzbek society is a special world, civilization, therefore, it is necessary to analyze it, exploring the corresponding phenomena and categories inherent in it. It is a special social organism, distinctively isolated from other societies and having common spiritual sources and foundations, common territory, common economic and geopolitical space.

## References

- [1] Benvenist E. General Linguistics. Civilization. Word history. –M., 1974. [https://platona.net/load/knigi\\_po\\_filosofii/filosofija\\_jazyka/benvenist\\_ehmi\\_l\\_obshhaja\\_lingvistika\\_pod\\_red\\_ju\\_s\\_stepanova\\_izd\\_1974\\_g/32-1-0-708.-P.448](https://platona.net/load/knigi_po_filosofii/filosofija_jazyka/benvenist_ehmi_l_obshhaja_lingvistika_pod_red_ju_s_stepanova_izd_1974_g/32-1-0-708.-P.448).
- [2] Montesquieu S. On the spirit of laws // Elect. production - M., 1955. –P.357. URL: [http://www.civisbook.ru/files/File/Monteskye.O\\_dukhe.pdf](http://www.civisbook.ru/files/File/Monteskye.O_dukhe.pdf)
- [3] Berdyaev N.A. The philosophy of free spirit. –M., 1994; ISBN 5-250-02453-X. DOI: 10.24045/conf.2017.1.16
- [4] Toynbee A. Comprehension of history. –M., 1991; ISBN: 978-5-8112-3798-2. DOI: [https://doi.org/10.14258/izvasu\(2015\)3.2-39](https://doi.org/10.14258/izvasu(2015)3.2-39)
- [5] Spengler O. Sunset of Europe. –M., 1993. DOI: 10.17805/zpu.2016.1.2. –P.663.
- [6] Barg M.A. A civilizational approach to history: a tribute to conjuncture or a requirement of science? // Civilizations. –M., 1993. –Vyp.2 ; P.46. <https://cyberleninka.ru/article/n/ponyatie-tsvivilizatsionnyy-podhod-v-otechestvennoy-istoriografii-na-rubezhe-xx-xxi-vekov-1>
- [7] Barg M.A. Eras and ideas. –M., 1987 ; [https://imwerden.de/pdf/barg\\_epokhi\\_i\\_idei\\_1987.pdf](https://imwerden.de/pdf/barg_epokhi_i_idei_1987.pdf) -P.348.
- [8] Bromley N.Ya. To the question of the relationship between the concepts of “civilization” and “formation” // Civilization. –M., 1992. –Vyp. one.;
- [9] Karaganov S.A. Chances and threats of the new world // Russia in global politics. 2003. No2. –P.13-14. [https://globalaffairs.ru/number/n\\_771](https://globalaffairs.ru/number/n_771)
- [10] Orlova I.B. Civilization paradigm in the study of the socio-historical process. Dis. On the co. Uch. Step. Doc. –M., 1999. –P.167.
- [11] Morgan L. Ancient society. –L., 1934; –P.104. [http://www.pseudology.org/Sex/MorganLG\\_DrevneeObshestvo2.pdf](http://www.pseudology.org/Sex/MorganLG_DrevneeObshestvo2.pdf)
- [12] Mechnikov L.I. Civilization and the great historical rivers. –M., 1995. –P.81. ISBN: 978-5-8112-5112-4 <https://cyberleninka.ru/article/n/tsvivilizatsiya-i-velikie-istoricheskie-reki-geograficheskaya-teoriya-progressa-i-sotsialnogo-razvitiya>
- [13] Moiseev N.N. Modern anthropogenesis and civilizational faults // Problems of Philosophy. -1995. -№1. P.6, 24 ;
- [14] Weber M. Selected Works. –M., 1990 ; ISBN 5-01-001584-6 –P.808. [https://www.gumer.info/bibliotek\\_Buks/Sociolog/vebizbr/index.php](https://www.gumer.info/bibliotek_Buks/Sociolog/vebizbr/index.php)
- [15] Condorcet J. Sketch of the historical picture of the progress of the human mind. –M., 1936 ;
- [16] Erasov B.S. Culture, Religion, and Civilization in the East: Essays on the General Theory. –M., 1990; ISBN 5-02-017165-4. –P.205. <https://search.rsl.ru/ru/record/01001569098>
- [17] A new post-industrial wave in the West. Anthology / ed. V.L. Inozemtsev. –M. : Academia, 1999. –P.104. ISBN 5-87444-067-4. [http://iir-mp.narod.ru/books/inozemcev/page\\_1003.html](http://iir-mp.narod.ru/books/inozemcev/page_1003.html) -P.640.
- [18] Novikova L.I. Civilization and culture in the historical process // Questions of philosophy. -1982. -№10 ; Novikova L.I. Civilization as an idea and as an explanatory principle of the historical process // Civilizations. -M., 1992. –Vyp.1 ;

- [19] Peccechi A. Human qualities. –M .: Progress, 1985. –P. 312.  
<https://www.twirpx.com/file/359138/>
- [20] Reisner L.I. Civilization and the way of communication. –M., 1993. ISBN 5-02-017681-8 . <https://search.rsl.ru/record/01001676355> –P.304.
- [21] Ruzavin G.I. Self-organization and organization in the development of society// Questions of philosophy. -1995.-№8 10.7256/2306-0158.2013.4.581 URL:  
[https://nbpublish.com/library\\_read\\_article.php?id=581](https://nbpublish.com/library_read_article.php?id=581). -P.71.



## Design and Validation of a Meter Band Rate in OpenFlow and OpenDaylight for Optimizing QoS

Mohamed Saleh Al Breiki\*, Suiping Zhou, Yuan Roger Luo

Department of Computer Science, Middlesex University, NW4 4BT, United Kingdom

### ARTICLE INFO

Article history:

Received: 15 October, 2019

Accepted: 01 February, 2020

Online: 09 March, 2020

Keywords:

Cloud Computing

Meter Band Rate

Network Function Virtualization

OpenDaylight

OpenFlow

Quality of Service

Software Defined Networks

### ABSTRACT

Technological developments in the Internet and communications have created a vastly complex and dynamic context with diverse heterogeneous networks and fast growth of mobile devices and multimedia. As the Internet becomes the primary mode of communication for many organisations there is requirement to enhance quality of service (QoS) from heterogeneous systems and networks. Traditional networks such as TETRA have become increasingly incapable of addressing the demand for media rich, bandwidth intensive traffic flows and applications. Mission-critical multimedia over new generation mobile networks face QoS constraints. This research explores a novel solution for quality of service performance for streaming mission-critical video data in OpenFlow SDN networks. A Meter Band Rate Evaluation (MBE) mechanism is advanced that improves the native QoS capability of OpenFlow and OpenDaylight. The MBE is a physical component added to the OpenFlow meter table to evaluate and dynamically adjust traffic rates and allows the traffic volume to be specified relative to other traffic in the network. Its design and development are presented, and the mechanism is verified through a simulated experiment in an SDN testbed. The results identified that QoS performance experienced a significant percentage increase when the MBE was active. These findings contribute a novel Meter Band Rate Evaluation mechanism that extends the native capability of OpenFlow and OpenDaylight to enhance the efficiency of QoS provision.

### 1. Introduction

Software Defined Networking (SDN) has received increasing attention as a new approach implementing new and innovative cloud-based architectures capable of integrating quality of service (QoS) enhancing end-to-end video performance. QoS dimensions of SDN and Network Function Virtualization (NFV) have the potential to address reliability and the quality of mission-critical applications over hybrid networks including 4G, 5G, Terrestrial Trunked Radio (TETRA) [1]. SDN is a novel technology designed to be dynamic and flexible to modern computing contexts by offering improved network management features [2] and enhanced network control for cloud computing [3].

The context of this research is UAE law enforcement in which there has been a growing dependence on mobile real-time video communications. TETRA networks have become increasingly incapable of addressing the demand for media rich, bandwidth intensive traffic flows and applications [4]. Modern policing like all areas of society is engaged in intensive sharing of different forms of real-time data and media across a diverse range of devices

and platforms that form a critical part of its operations [5]. This context underlines the need to enlarge policing capabilities through the adoption of commercial mobile broadband and wireless networks and leveraging of cloud computing and SDN and NFV technologies to map multimedia applications over heterogeneous underlying networks. The programmability and the abstraction of the control plane from the forward and data plane is a key aspect of SDN's design [6,7]. This enables a single software control programme to control the data plane of numerous network elements [8] and enables greater and more flexible control and management of network components.

This paper contributes a novel Meter Band Rate Evaluation mechanism that extends the native capability of OpenFlow and OpenDaylight to enhance the efficiency of QoS provision. This research experiments with and analyses the implementation of an integrated set of technologies (SDN OpenDaylight controller, OpenFlow protocol and OpenQoS) over a centralized cloud platform using real-time video to 4G mobile devices. The primary goal of this research is to evaluate and validate the application of SDN and OpenFlow in realizing QoS for real-time video data transfer in a hybrid cloud computing context. A key objective is to

\*Mohamed Saleh Al Breiki, +1 646 580 6284, ma2634@live.mdx.ac.uk

monitor QoS parameters and evaluate the SDN-based architecture in optimizing QoS performance. This paper presents a novel QoS mechanism that expands capabilities by incorporating a new meter band rate component. The experiment results in this paper verify the performance of this mechanism. This contributes a new mechanism and demonstrates the potential to expand the features of OpenDaylight SDN controller to realize more optimized QoS for real-time video traffic over heterogeneous networks. Thus this research represents a novel QoS mechanism that advances existing QoS capabilities of OpenFlow and OpenDaylight.

## 2. Related Work

Multiple studies have focused on improving quality of service (QoS) by means of leveraging the network control components of SDN by focusing software solutions at the switch level. This allows for transparency of network resource interfaces in alignment with application requirements.

Quality of service concerns the extent to which applications receive expected service quality relative to their level of mission-criticalness [1,9]. Hakiri and Berthou [1] indicate that QoS provision lacks this responsiveness to guarantee the required service level. The design of the OpenFlow protocol allows the SDN controller to access and modify flow data at the switch level for all devices thereby connecting the control and data planes [10]. OpenFlow flexibility allows for data to be automatically directed with minimal disruption achieved by decoupling the forwarding layer from the control layers [11] which manages data flows and creates or updates rules for devices in the network [12].

Changes in hardware are not required by employing OpenFlow and vendors do not need to open systems to support it provided a small number of widely used interfaces are available to the control plane [13]. Any system that integrates the protocol is capable of controlling the switch behaviour of any devices in the Openflow network. Directives allow ISPs to deploy SDN to guarantee quality of service of streaming services alongside traditional network services [13].

The significant potential to manage QoS within the OpenFlow protocol has generated multiple studies focused on addressing QoS issues at network level. A key attribute of OpenFlow is the focus of QoS to address specifically different parameters such as delay, throughput and jitter [14] as a result of the control of packet and flow level activity. This granularity permits users of OpenFlow to specify how individual flows are to be managed in accordance with Integrated Services (IntServ) and open standards definitions [15]. Individual flows can also be amalgamated into classes by users. OpenFlow grants access to a set of programming tools which enable the generation and recycling of virtual flows or slices. Thus the user can stipulate how network resources including routers, switches and queues are allocated to different slices with different priorities [15].

In [2], the author proposes an SDN-based solution to ensure network-wide QoS based on multi-paths routing that utilizes OpenFlow's queue support to maximize the efficiency of resources in line with the network user requirements and minimizing excess provisioning. The solution focuses guaranteeing end-to-end QoS for individual data flows and the efficient management of open virtual switches (OVSs). The OVS configuration is recalculated in

response to new network demands or as users progress on to new nodes in order to minimize the utilization of OVSs in the network.

In an attempt to guarantee bandwidth end-to-end Tomovic et al. [16] advance an explicit QoS guarantee as in IntServ by incorporating controls for admission and reserving bandwidth in OpenFlow. This commences by transmitting the bandwidth requirements of a QoS flow initiating a Constrained Shortest Path computation by the controller in which the required bandwidth is used as a limiter. The technique uses the available unreserved bandwidth as the link weight ensuring that the reserved flows are allocated to bandwidth that has been reserved. The flow is rejected where the bandwidth is not available for end-end path. Furthermore, there is intermittent checking by the controller of all links associated with the QoS flow, with utilization greater than 80% resulting in the re-routing of best-effort flow to an alternative path with lower utilization.

To maintain QoS in real-time video streaming in SDN Liang and Shen [17] introduce a new SDN-based routing approach that is capable of dynamically routing deployment across layers of Scalable Video Coding (SVC) accounting for bandwidth and different QoS parameters: delay, and packet loss. SDN research by Celenioglu and Mantar [18] advanced a routing and resource control approach for enhancing QoS that takes into account pre-defined paths and reservation of resources between network segments. By improving routing scalability and decreasing admission time the solution provides QoS guarantees to stationary nodes.

Research into Openflow by Egilmez et al. [11] contributed an OpenQos controlled solution that concentrated on achieving end-to-end QoS which secures an optimal path for the service delivery of application traffic that prioritize multimedia traffic [19]. Flows for data, video and voice are categorized and subject to different algorithms either shortest routing for data or dynamic routing to guarantee QoS.

In a new approach [8] multiple issues are identified: the requirement for each node device to configure the same information; need for manual configuration of all ports of each forwarding device which can be error-prone and time-consuming; and the incapacity of legacy networks to make a distinction between the different resource requirements of voice and data network traffic. Data traffic requires more bandwidth while voice is associated with small packets and delay sensitivity. Achieving QoS in SDN is predicated on two key steps of marking packets for the data plane and management at the control plane. The network is made up of multiple virtual networks whose resources and requirements are autonomously monitored and managed [8].

To enhance QoS some research has focused on an extension of OpenFlow. The purpose of research by Lu et al. [20] was to provide a solution for QoS using conventional flow control techniques and maximizing flow. A QoS slice method and forwarding mechanism is advanced nevertheless the study does not address the issue of supporting QoS in OpenFlow natively. Other studies undertaken in this field do not examine the constraints associated with QoS by OpenFlow [8, 21, 22, 23]. Bhattacharya and Das [24] propose that a module is embedded to minimize any communication latency between switch and controller by means of caching flows nevertheless a QoS mechanism for the data plane is not advanced.

Examining the utilization of DiffServ and multipath QoS routing in OpenFlow Jinyao et al. [25] propose HiQoS as a method to guarantee QoS. In HiQoS traffic is classified into three groups of best effort data stream, low delay interactive multimedia and high throughput video streaming. The switches forward the different categories of traffic into three preconfigured queues with fixed rates that effectively divides bandwidth. Flow paths are determined by employing existing bandwidth usage as weight and flows from the same category of traffic are able to utilize different paths. While the method distinguishes low delay traffic as a distinct category it fails to account for delays in relay-time and calculates routes using existing bandwidth information. The assumption is that greater utilization in terms of bandwidth and queue leads to greater delay. Therefore HiQoS aims to guarantee bandwidth for categories of traffic rather than providing guarantees at flow level [25].

### **3. Problem Formulation**

While cloud networking solutions based on SDN have specific performance, scalability and flexibility advantages, they are nevertheless limited to supporting specific kinds of network environments and lack more precise control of network paths for attaining objectives such as traffic prioritization or rapid failover [11]. QoS mechanisms including Differentiated Services (DiffServ), IntServ and Multiprotocol Label Switching (MPLS), are subject to numerous limitations in respect of level of flexibility and integration in different systems. The potential of SDN is associated with the ability to extend the diversity and targeting of resource provision so that it better aligns with specific application of QoS requirements [26]. One component of this is a suite of tools that facilitate distributed and collaborative management to achieve better classification of data flows in accordance with traffic characteristics.

The OpenDaylight SDN controller based on the OpenFlow protocol is widely used and has been embraced by vendors worldwide. OpenFlow is a key component within SDN as it controls switches through signalling between switches, guarantees the provision of QoS and is significant in respect of the best effort paradigm. The major benefit of the protocol is backwards compatibility and its ability to be integrated within current network infrastructures and legacy flow-enabled network devices with minimal changes in design. Outlining the present capabilities of OpenFlow's support for QoS in SDN assists understanding of the problem. Currently support is provided using two approaches of either DiffServ or per-flow QoS. Using Per-port Queue, a queue for a flow in a flow-entry can be specified within OpenFlow so that in the event of a match decision is allocated for each queue. Every single queue is configurable with properties, governing the treatment of packets within the queue. OpenFlow's per-flow queue attribute is utilized for the definition of per-flow QoS by means of a per-flow meter table in which single or multiple flows can be attached. The role of meters is to determine packet rate and control that rate. There is also the possibility to attach single flows to multiple meter tables on the condition that different tables are utilized. Within a single table each flow may be assigned to only one meter table. The combination of per-flow queues and meter tables can enable the implementation of DiffServ.

There are a number of drawbacks and areas in which QoS in OpenFlow (versions 1.1-1.5.1.) could be improved. Simple queuing mechanisms such as min-rate and max-rate provide limited support for QoS and queues cannot be configured inside OpenFlow. Only rudimentary support for DiffServ (for example, DSCP Remark) is available. Moreover when using queue, QoS is solely permitted at egress. Lastly, most switches do not support optional meters. The simplicity of the queuing mechanisms engenders two key problems for QoS. Firstly the per-port queue allows the available bandwidth to be sliced into a number of queues and to specify certain properties for each queue of min-rate, max-rate and others. However this action fails to guarantee that the bandwidth available is efficiently utilized. Furthermore over-provisioning to avoid low QoS during congestion may be needed, resulting from the specification of minimum bandwidth for traffic. Behavior is reliant on the particular hardware implemented and is therefore not able to be predicted. A second QoS issue is the restricted scalability entailed by the simple queuing mechanisms. For all traffic, there is a flow-entry requirement to specify which it belongs to however switches have a limitation in the number of flow-entries. For a large network, every switch needs flow-entry and queue configuration for all traffic in the network. Furthermore, OpenFlow's inability to allow for queues to be configured implies that dynamic changes cannot be made. This results from the nature of the SDN controller which is not able to be utilized to configure queues and therefore other mechanisms including OVSDB, OF-Config, or cli must be deployed. These however do not work in the fast path. Consequently end-to-end QoS implementation is challenging using this approach. The basic support provided for DiffServ such as DSCP Remark is a further key issue undermining QoS. Fields are adjustable by means of meter tables nevertheless meters complement rather than replace queues and are unable to surmount the limitations associated with them. Within a packet meters have the capacity to alter certain fields but do not provide support for the comprehensive operation of all kinds of per-hop-behavior (PHB). Illustrating this point, different queuing mechanisms such as strict priority queuing (SPQ) or weighted fair queuing (WFQ) are not able to be applied as solutions for a PHB. In addition there are feasibility issues in applying mechanisms such as Call Admission Control (CAC) when using meters. By permitting QoS at the single point of egress only the use of queues is problematic as there is a distinct advantage in the ability to drop traffic at the point of ingress that safeguards switch resources, when possible, for other traffic. Meters can support this however possess a limited capability for QoS as previously outlined. The prevailing absence of switch support for meters underlines a lack of guarantee that support will be provided by OpenFlow switches.

### **4. Experimental Study**

This research applied an experimental approach in order to test and analyse video streaming quality of service performance under different experimental conditions. This comprised the establishment of an SDN based network testbed based on OpenDaylight SDN controller and OpenFlow 1.3 and utilizing the Mininet emulator to undertake several tests. The testbed was implemented in line with the system parameter and mechanisms indicated and detailed in Figure 1 and Table 1 that specify the key software versions utilized during the implementation.



Table 1: Software versions utilized in implementation

Software	Description
Python 2.7.14	Programming language
Linux	Host OS
Open vSwitch 2.5	Virtual multilayer switch with OpenFlow support
Ubuntu 16.04	Virtual machines
Yang UI	User interface for OpenDaylight
Mobile Phone Samsung 4/4G Client smartphone device	
Networks	WiFi (WLAN), 3G, 4G, SDN Controlled
OpenDaylight Controller	SDN framework
Mininet 2.2.1	Network topology environment

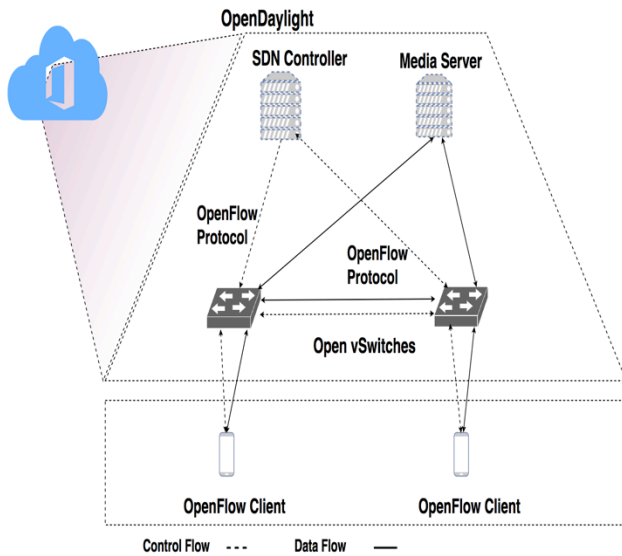


Figure 1: OpenFlow-based SDN network testbed

OpenDaylight Controller (ODL) was utilized as the implementation framework subsequent to assessment of different controllers. Key benefits are associated with ODL in terms of: regular updating relative to other controllers; support for all versions of OpenFlow; necessary features to allow for the implementation of a traffic engineering platform in SDN, and possession of several existing modules able to be used with customized applications. Firstly a series of experiments were undertaken to assess QoS performance for existing SDN/OpenFlow capabilities in a high traffic environment utilizing two distinct sets of experimental conditions. The experiment allowed for detection and analysis of issues associated with QoS and the constraints of SDN/OpenFlow that can be addressed in the following stage of research. The tests provided benchmarks for different QoS metrics of delay, packet delay variance (jitter), packet loss and throughput.

### 5. Meter Band Rate Design

The design of the Meter Band Rate algorithm is focused on enhancing the native capability of OpenFlow at the switch level. The design of the proposed mechanism is outlined in this section and an overview of MBR model and components is represented in

Figure 2. The evaluator represents the novel component of this design based on a band rate description language (BRDL) for analysing required dynamic states for the mechanism. The BRDL facilitates classification of network traffic. For instance, if there are  $i = 1 \dots c$  types of classes in a network with priority of types as follows,  $1 > 2 > \dots > c$  such that the network is sliced into  $c$  classes. The BRDL syntax enables the specification of slices relative to others within the network:

$$\text{rate}(x) = \{\text{MAX}-\} \{\text{rate}(y)-\} \dots \{\text{rate\_const}\} \quad (1)$$

Where, MAX is the total available capacity,  $\text{rate}(x)$  specifies rate of this traffic class,  $\text{rate}(y)$  specifies rate of any other traffic class and  $\text{rate\_const}$  is any constant. Bandwidth reservation is controlled by  $\text{rate\_const}$  and avoids the need for explicit assignments of services to meters. In the case of different types of traffic, for instance voice or data flows, the data traffic needs only to be configured with meter and assigned the necessary bandwidth for voice traffic to  $\text{rate\_const}$ . To exemplify the value of this consider two types of flows in the network of voice traffic and iSCSI traffic. Voice flow has a fixed rate and therefore can be assigned a constant rate. Therefore, only  $\text{rate\_const}$  part will be applied:

$$\text{rate}(\text{voice}) = \text{rate\_const\_voice} \quad (2)$$

Then, iSCSI traffic is assigned  $\text{rate}(y) = \text{rate}(\text{voice})$  is set and the  $\text{rate\_const}$  component is not required. Therefore,

$$\text{rate}(\text{iSCSI}) = \text{MAX} - \text{rate}(\text{voice}) \quad (3)$$

Using this approach, the MBR invocation is either DROP or ALLOW. The benefit of the BRDL is in overcoming the limitation of meters and per-port queues by adding constant max-rate and min-rate limiting features. Further this optimizes traffic flow in terms of throughput and simultaneously guaranteeing QoS requirements of each individual slice. The SDN controller assigns all flows with OpenFlow meter at the install stage with unique  $\text{meter\_id}$  identifier associated with local switch for each flow entry. This action is dependent on the supported meter band type:

1. OFPMBT\_DROP
2. OFPMBT\_DSCP\_REMARK
3. OFPMBT\_EXPERIMENTER

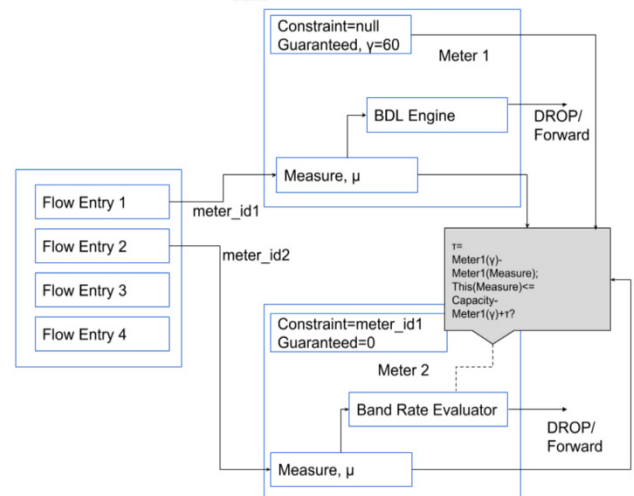


Figure 2: Meter Band Rate model



The OFPMBT\_EXPERIMENTER indicates the band rate evaluator in this model. OpenFlow meter bands comprise three bands: type, rate, burst and counters. *Constraint* and *guaranteed rate* extends the meter band to enforce priorities. The *constraint* records the priority of meter\_id's supplied by band description language given in Equation (1). Thus the *constraint* list of "band rate evaluator" is determined from  $rate(y)$  and  $rate\_const$  of BRDL. The *guaranteed rate* specifies the bandwidth guarantee for this meter. The *measure* field reflects the measured data rate by the meter. The above values can be specified in KBPS or packets per second as set in meter flags.

Figure 2 depicts the flow-entries associated with meters. Flow 1 is associated with Meter 1 having meter id "meter\_id1" and Flow 2 is associated with Meter 2 having meter id "meter\_id2". The *band rate evaluator logic* is given in the following section. Thus all incoming packets are associated with a meter flow entry at the ingress port. Figure 3 depicts meter evaluation to determine the band rate to drop the packet, so that where the evaluated rate is higher than the existing rate, the packet is passed.

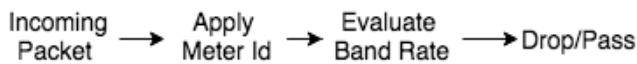


Figure 3: Applying Meter Band Rate Evaluator to all packets

Figure 4 illustrates the evaluation process that treats guaranteed and measure components as *superior constraints*. The evaluator meter uses the *guaranteed* and *measure* parameters of the meters specified in the *constraint* field. Parameters of "higher priority" or "superior" meters, are considered *superior constraints*. The constraint meter list is used to identify superior constraints. Step 1 - the measure field is subtracted from the guaranteed field of each meter in the constraint list, which yields the available bandwidth of each constraint meter; Step 2 - available bandwidths are totalled; Step 3 - the band rate evaluator adds the guaranteed fields and deducts the result from the total port capacity; Step 4 - the results from step 2 and step 3 are totalled. The result from the step 4 is compared with the measure field; if higher, the packet is allowed to pass. In respect of compilation of the band description language into the constraint list used by band rate evaluator three types of traffic are specified: voice, video and data. The data rates of these traffic types in band description language can be expressed as:

$$\begin{aligned}
 \text{rate}(\text{voice}) &= 32\text{Kbps (const)} \\
 \text{rate}(\text{video}) &= 1\text{Mbps} \\
 \text{rate}(\text{data}) &= \text{MAX} - \text{rate}(\text{video}) - 32\text{Kbps}
 \end{aligned}$$

The  $rate\_const$  (=32Kbps) is used in expressing rate (data). Meters will not be required for voice traffic. Thus, there are two meters: meter\_video and meter\_data. The Constraint and Guaranteed fields of these meters are as follows:

$$\begin{aligned}
 \text{meter\_video: } &\{\text{constraint} = \text{null, guaranteed} = 1\text{Mbps}\} \\
 \text{meter\_data: } &\{\text{constraint} = \text{meter\_video, 32Kbps}\}
 \end{aligned}$$

The proposed design focuses on the limitations of OpenFlow to provide a flexible and optimum QoS solution. Currently there

are two instruments inside OpenFlow to harness traffic behavior, namely per-port-queues and meters. Both queues and meters have their own limitations in terms of versatility and efficiency.

To address these shortcomings the following components have been incorporated in the proposed solution:

- 1) Band description language (BDL)
- 2) Band rate evaluator (BRE)
- 3) Constraint list
- 4) Guaranteed rate

The band description language (BDL) is a logical component of the design which allows the network administrator to specify desired QoS behavior in a flexible and efficient manner. A major limitation of OpenFlow queues is that they only allow for simple QoS behavior such as max-rate limit. This means that rate limited traffic will face restriction despite the availability of free capacity in the network. In this solution, BDL allows the traffic volume to be specified relative to other traffic in the network. As a result, there is no unnecessary bandwidth restriction for any traffic.

The inability to be provisioned in the fast path is another limitation of the queue-based approach. Consequently, the SDN controller is unable to update the queues in real time to reflect network demand. The proposed design solves this issue firstly by making BDL capable of specifying per-flow bandwidth in terms of other flows. Therefore, flow rates are automatically adjusted to network demand. Secondly, OpenFlow meters are used to implement the solution. Meters in OpenFlow can be configured in the fast path, therefore the QoS settings can be updated in real time by the SDN controller in the solution.

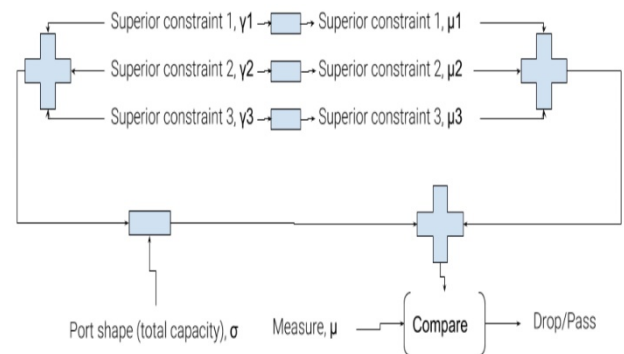


Figure 4: Evaluator process

The band rate evaluator (BRE) is a physical component added to the OpenFlow meter table. Presently, in OpenFlow, band rates can be specified as static constants. When the traffic rate reaches one of these band rates, OpenFlow meter will execute a certain action (e.g. dropping the packet, or modifying certain protocol header fields in the packet). This static meter bands feature can be useful for simple rate limiting but is unable to adjust to dynamic network demand. It is theoretically possible to periodically update these static band rates by the SDN controller. However, in practice the traffic rate is too fast for the SDN controller to be able to continuously update meter band rates, even in a small network. In

this solution therefore BRE is used to dynamically adjust traffic rates based on the BDL.

The constraint list is another physical component of the proposed design. As discussed, the BDL and BRE allow traffic rates to be specified relative to other flows. The constraint list is responsible for storing information in relation to which traffic rates are dependent upon which other traffic. The constraint list is designed to be understood by the BRE whereas the BDL is intended for use by humans and the SDN controller. The QoS rules specified in BDL are processed by the SDN controller to create the constraint list. Once the constraint list is generated, the SDN controller will install it into the SDN switch.

The guaranteed rate is the final physical component of the proposed solution. This allows reservation of a virtually dedicated amount of traffic for a flow. Use of the term ‘virtually dedicated’ signifies that this operation is not a dumb reservation as performed by min-rate limiters in OpenFlow queues. In OpenFlow queues, reserved bandwidth by a min-rate limiter will be unavailable to other traffic when the flow for which bandwidth is reserved has a lower rate than reserved bandwidth. This means that the reserved bandwidth will be wasted most of the time. In this design the BRE will mitigate this problem by allowing the bandwidth specified by the guaranteed rate for a certain flow to be re-used by other traffic as long as there is some free bandwidth unused by the owner of the guaranteed bandwidth. The guaranteed rate can be left unspecified for any flow as long as it is not mentioned in the constraint list of another flow. This can be useful for best effort traffic which requires least priority. For other traffic which has more priority compared to other traffic the guaranteed rate must be given.

## 6. Meter Band Rate Evaluator Implementation

The Meter Band Rate Evaluator outlined earlier was deployed in OpenFlow Software Switch 1.3. The module ofsoftswitch13 was modified to integrate the mechanism to implement the Meter Band Rate Evaluator. Table 2 depicts the key components and core functions of the Meter Band Rate Evaluator algorithm developed for this implementation. Several modifications were made to the OFLIB. All messages in OpenFlow share common header containing information message type where the default struct for each message allows for two actions: marshalling (packing) and unmarshalling (unpacking). These functions enable Ofl-messages transmission of new modifications through wire format. In Ofl-struct.h the meter\_configuration was modified with statistical function adding to the number of fields to perform metering monitoring of parent free tokens. A flag in meter configuration was added to facilitate enabling or disabling of the band evaluation engine. Oflib-messages were modified to allow for band evaluation engine to be set to enabled/disabled states. The central part of the algorithm is deployed in meter\_entry.c of the udatapath component to enable parent monitoring support and to apply entries. The Meter Table is responsible for QoS operations and was adapted with fields to define new actions.

The meter table performs the main processing of packets in accordance with the band meter design. Meter\_table.c was modified to activate the evaluation engine and increase the structure size from 16 to 20. Finally, the BEEFLAGS within the utilities/dpctl component was modified to enable tracking and

debugging and query of Flow Table state in OpenFlow switches which avoids the requirement for debugging at the controller level.

Table 2: MBE core algorithm

Packet Handling at Meter
Input: <i>packet, monitoringPeriod</i> Output: <i>decision</i>
WHILE <i>parent</i> ← <i>nextParent</i> DO IF <i>free(parent)</i> < <i>free</i> <i>free</i> ← <i>free</i> + <i>free(parent)</i> ENDIF ENDWHILE
<i>elapsedTime</i> ← <i>currentTime</i> - <i>startTime</i>
IF <i>elapsedTime</i> = <i>monitoringPeriod</i> <i>totalFree</i> ← <i>free</i> <i>startTime</i> ← <i>currentTime</i> ENDIF
IF <i>available(meter)</i> > <i>size(packet)</i> <i>decision</i> ← ALLOW <i>available(meter)</i> ← <i>available(meter)</i> - <i>size(packet)</i>
ELSIF <i>free</i> > <i>size(packet)</i> <i>decision</i> ← ALLOW <i>free</i> ← <i>free</i> - <i>size(packet)</i>
ELSE <i>decision</i> ← DROP
ENDIF

## 7. Results

Two rounds of testing were undertaken with and without the Meter Band Rate Evaluator (MBE). Initial tests conducted without the MBE provided a benchmark for performance and gathered and analysed QoS data for four parameters of delay, jitter, packet loss and throughput under conditions simulating a congested environment. The second stage of testing was undertaken after the MBE had been installed and configured in order to evaluate the capacity of the novel solution to improve QoS performance. The tests undertaken in the first experiment were replicated under the same environmental conditions for periods of 4.3 minutes.

For the four QoS parameters the results showed that there was a marked improvement when the MBE was applied. The figures chart the comparison between the benchmark tests and those for the MBE. Figure 5 reveals significant optimization in delay performance with a reduction in delay time over the period of 260 seconds. In the first round of tests delay ranged on average between 500-1100ms in comparison to results with the MBE enabled of between 80-360ms. Average delay with the MBE disabled was 546.7ms compared to 206.6ms with the MBE.

For the remaining three QoS performance measures the positive impact of the MBE was evident and provides support for the solution to optimize QoS performance within OpenFlow. Analysis of the data for jitter performance as shown in Figure 6

indicates that in comparison application of the MBE significantly reduced jitter to a median average of 1430 compared to 1906.5 without the MBE. Similarly there was a substantial minimization of packet loss when the MBE was active as shown in Figure 7, indicating a consistent average of under 5% across all tests, compared to between 5-15% when the MBE was inactive. The median average PLR was 2.1% when the MBE was enabled compared to a figure of 8.3% when disabled.

Results also revealed significant optimization of throughput performance, a key QoS performance measure for ensuring the quality of video. As shown in Figure 8 when the MBE is active there is a significant increase in throughput of more than 4000 packets/sec and rising to 9000 packets/sec, a markedly higher figure than when the MBE is inactive. Results without the MBE show that packets/sec varied between 300-4000 packets/sec.

As Table 3 shows for all QoS parameters there was a significant percentage change in performance when the MBE was active. For delay, results reveal an average reduction of 94% reflecting the substantial impact of MBE on performance for this measure. A mean percentage reduction in excess of 800% for jitter is indicated, and when extreme values are accounted for a 32% median average decrease in jitter is shown.

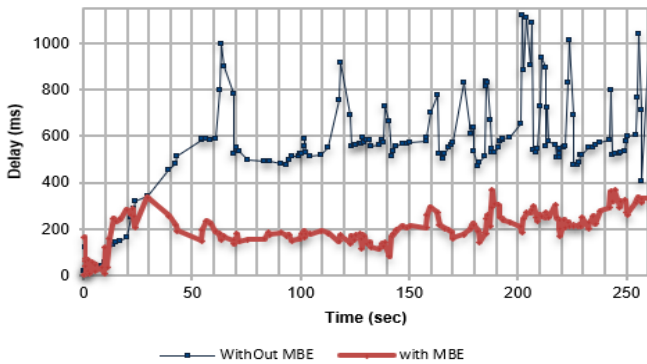


Figure 5: Delay performance with MBE

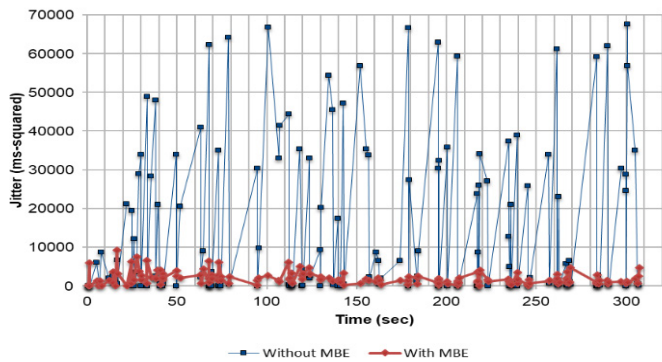


Figure 6: Jitter performance with MBE

Table 3: Percentage change in QoS measures with Meter Band Rate Evaluator

	Delay	Jitter	Packet Loss	Throughput
Mean % Change	-94.16	-866.45	-285.32	200.20
Median % Change	-96.27	-32.76	-325.83	189.49

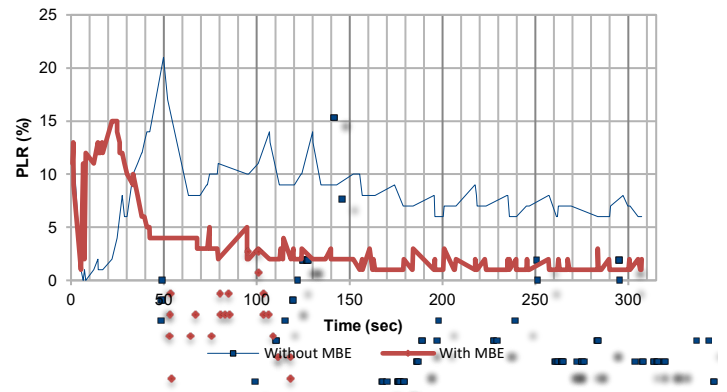


Figure 7: Packet loss ratio performance with MBE

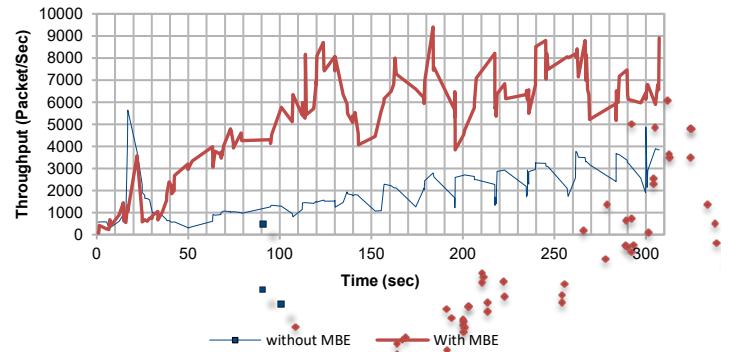


Figure 8: Throughput with MBE

In relation to ratio of packet loss the mean average decrease was 285% and median average decrease of 325%. Lastly, throughput under MBE increased by 200% for the mean average and 189% for the median. Based on the metrics tested these results provide substantial validation and support for the ability of the MBE to improve the native capability of OpenFlow QoS performance.

## 8. Discussion of Findings

This research explored application of an SDN-based mechanism to enhance QoS for real-time end-to-end video transmission. The solution centres on the development of a Meter Band Rate Evaluator (MBE) mechanism employing a new band rate description language that extends the capabilities of OpenFlow and OpenDaylight to support QoS. This solution was designed and subject to experiments in a Mininet test environment which revealed significant improvements in level of QoS performance across multiple parameters: jitter, throughput, delay, packet loss. This contribution addresses the limitations of existing methodologies to guarantee QoS performance, either through marking data-plane packets and management at the control plane automatic manager for monitoring requirements of virtual networks [8] or slice and forward methods [20]. The findings of this study demonstrate potential to address the limitations of QoS in OpenFlow’s native features and protocol to support QoS [8, 21, 22, 23]. Bhattacharya and Das [24] introduce an embedded module to reduce communication latency between switch and controller by caching flows, however a data plane QoS mechanism is not proposed.



The mechanism applies a hierarchical approach in classifying traffic classes providing higher positions of priority for mission-critical types of data. This provides flexibility for defining relative QoS relationship between different classes of traffic. The meter band rate determines the point of application using constant 32-bit values specified either in packets/sec or kb/s which can be updated by OFPT\_METER\_MOD message. This constant inhibits the application of a more dynamic and QoS responsive approach because it fails to account for the co-existence of flows within the wider networks. This solution addresses this issue by specifying band rates of slices relative to multiple slices in the wider network. The issue of constant rate limiting in existing meters and per-port queues is addressed. Furthermore, the results validate performance of this new mechanism to provide higher levels of QoS across the four parameters measured.

In comparison with other solutions in the literature this design offers some distinct contributions. Civanlar et al. [27] aim to provide QoS guarantee to video services similar to the proposed architecture in this solution, however their work is limited to selecting best route for QoS traffic. Minimal detail is provided on how to prioritize the QoS traffic in the SDN infrastructure layer, except for the assumption that QoS traffic can have the right to disrupt non-QoS traffic when they are placed on the same route. The primary focus of this work is on overall best path selection therefore how traffic is processed at each hop is not considered. Contrastingly the proposed solution in this paper focuses on this area and provides per-hop processing with the help of the four physical components.

In [28] video traffic is divided into two classes (lossless and lossy) accompanied by two types of routing algorithms generating different types of flows. The number of traffic classes is shown to have significant impact on overall video performance. From this it can be concluded that there is an advantage to flexibility in the number of classes that can be implemented. The proposed algorithm is flexible enough to accommodate any number of traffic classes as in BDL there is no limitation to the number of meters. Therefore, the network administrator is free to design the system with his or her preferred number of classes.

In advancing OpenQoS Egilmez et al. [29] extend the OpenFlow controller to provide QoS for multimedia traffic. In this architecture the call admission process is relied on to block incoming traffic when there is insufficient resource available in the network to guarantee the requested QoS. However, this could deny admission to voice traffic although possible to guarantee QoS for this type of traffic at the expense of quality for non-priority traffic. The protocol proposed here does not suffer from this limitation of OpenQoS as there is no call admission process. QoS is guaranteed by using OpenFlow meters and the band evaluation engine.

Certain limitations are acknowledged in relation to the proposed solution. The maintenance of network state information is increasingly complex under the dynamic character of the network topology and changing route behaviour. Established routing paths can be disrupted even while data is being transferred entailing, for QoS, necessary maintenance and development of paths in ad hoc networks that have minimal routing overhead and delay [30]. Mobile nodes may further be constrained by limited power supply in comparison with the nodes of wired networks.

Ensuring QoS could mean that, as a result of overheads, more power is used that rapidly drains that available to the node [30]. Scalability of this solution may also be impacted by the computational cost associated with the centralized algorithm in SDN. As networks become larger in size, they become more expensive and difficult to maintain requiring greater storage and more powerful infrastructure [31]. Finally increased computational time on systems in the network can impact negatively on the energy consumption of user devices [31].

## 9. Conclusion

These findings contribute a novel Meter Band Rate Evaluation mechanism that extends the native capability of OpenFlow and OpenDaylight to enhance the efficiency of QoS provision. The focus of this research was on addressing constant rate limiting with existing QoS mechanisms by extending the capability of OpenFlow to support efficient QoS provision. The introduction of a Meter Band Rate mechanism extends knowledge and suggests new possibilities in developing the existing capabilities of OpenFlow and OpenDaylight to support QoS. Experiment results indicated a significant increase in video streaming and multimedia traffic for multiple QoS parameters and point to the scope of the meter band rate mechanism for optimization of QoS in OpenFlow. The evaluator represents the novel component of the design based on a band rate description language (BRDL) for analysing required dynamic states. This allows specification of desired QoS behavior in a flexible and efficient manner and there is no unnecessary bandwidth restriction for any traffic. Further research in this area may subject the mechanisms to further testing and validation across more complex networking scenarios and hybrid networks. In addition, this may address a comprehensive range of optimization strategies to establish performance and validation in relation to load balancing, energy-consumption, controllability of network flow, safe updating or network security.

## Conflict of Interest

The authors declare no conflict of interest.

## Acknowledgment

The research has been supported and sponsored by the Ministry of Interior in the United Arab Emirates as part of an international research programme.

## References

- [1] A. Hakiri, and P. Berthou, "Leveraging SDN for the 5G networks: Trends, prospects and challenges," 2015, <http://arxiv.org/abs/1506.02876>
- [2] D.L.C Dutra, M. Bagaa, T. Taleb, and K. Samdanis, "Ensuring end-to-end QoS based on multi-paths routing using SDN technology," in GLOBECOM IEEE Global Comms Conf., 2017, pp. 1-6.
- [3] M. Banikazemi, D. Olshefski, A. Shaikh, J. Tracey, and G. Wang, "Meridian: An SDN platform for cloud network services," IEEE Comm. Magazine, vol 51, pp. 120-127, 2013.
- [4] J. Dunlop, D. Girma, and J. Irvine, Digital Mobile Communications and the TETRA System, John Wiley & Sons, 2013.
- [5] R. Blom, P. de Bruin, J. Eman, M. Folke, H. Hannu, M. Näslund, M. Stålnacke, and P. Synnergren, "Public safety communication using commercial cellular technology," in IEEE Next Gen Mobile Applications, Services and Technologies, NGMAST'08., 2008, pp. 291-296.
- [6] M. Jammal, T. Singh, A. Shami, R. Asal, and Y. Li, "Software defined networking: State of the art and research challenges," Computer Networks, vol 72, pp.74-98, 2014.

- [7] O. Coker, and S. Azodolmolky, *Software-Defined Networking with OpenFlow*, Packt Publishing, 2017.
- [8] J. Shi, and S.H. Chung, "A traffic-aware quality-of-service control mechanism for software-defined networking-based virtualized networks," *Int. J. Dist. Sensor Networks*, vol 13, pp.1-13, 2017.
- [9] J. Huang, P.J. Wan, and D.Z. Du, "Criticality-and QoS-based multi-resource negotiation and adaptation," *Real-Time Systems*, vol 15, pp. 249-273, 1998.
- [10] T. Reza, *Learning OpenDaylight: A Gateway to SDN (Software Defined Networking) and NFV (Network Functions Virtualization) Ecosystem*, Packt Publishing Ltd, 2017.
- [11] H.E. Egilmez, S. Civanlar, and A.M Tekalp, "An optimization framework for QoS-enabled adaptive video streaming over OpenFlow networks," *IEEE Trans.on Multimedia*, vol 15, pp. 710–715, 2013.
- [12] M. Sisov, "Building a software-defined networking system with OpenDaylight controller", BSc Thesis, Inf. Techn., Helsinki Metro. Uni. of Applied Sciences, 2016.
- [13] I. Trajkovska, P. Aeschlimann, C. Marti, T.M. Bohnert, and J. Salvachúa, "SDN enabled QoS provision for online streaming services in residential ISP networks," in *IEEE International Conference on Consumer Electronics-Taiwan (ICCE-TW)*, pp. 33-34, 2014.
- [14] S. Jivorasetkul, M. Shimamura, and K. Iida, "End-to-end header compression over software-defined networks: A low latency network architecture," in *4th Int Conf on Intell. Networking and Collab. Sys., (INCoS)*, pp. 493–494, 2012.
- [15] F. Hu, Q. Hao, and K. Bao, K, "A survey on software-defined network and openflow: From concept to implementation," *IEEE Comm. Sur. & Tutor.*, vol 16, pp. 2181-2206, 2014.
- [16] S. Tomovic, N. Prasad, and I. Radusinovic. "SDN control framework for QoS provisioning,". *Telecomms Forum Telfor (TELFOR)*, 22nd. IEEE. pp. 111–114, 2014.
- [17] W.E. Liang, and C.A. Shen, "A high performance media server and QoS routing for SVC streaming based on Software-Defined Networking," in *Int. Conf. on Comput., Networking and Comm., (ICNC)*, pp. 556-560, 2017.
- [18] M.R. Celenlioglu, and H.A. Mantar, "An SDN based intra-domain routing and resource management model," in *IEEE Int. Conf. on Cloud Eng.*, pp. 347-352, 2015.
- [19] A Mirchev, "Survey of concepts for QoS improvements via SDN," in *Future Internet (FI) and Innovative Internet Technologies and Mobile Communications (IITM)*, Summer Semester, Munich, Germany, pp. 33-39, 2015.
- [20] Y. Lu, B. Fu, X. Xi, Z. Zhang, and H. Wu, "An SDN-based flow control mechanism for guaranteeing QoS and maximizing throughput," *Wireless Personal Comm.*, vol 97, pp.417-442, 2017.
- [21] D. D'souza, K.P. Sundharan, S. Lokanath, V. Mittal, L. Perigo, and R. Hagens, *Improving QoS in a Software-Defined Network*, University of Colorado, 2016.
- [22] R. Thenmozhi, T. Preethi, S. Sadhana, V. Shruthi, and B. Yuvarani, "Integrating multimedia services over software defined networking," *Int. Res. J. Eng. and Tech (IRJET)*, vol. 4, 2017.
- [23] L. Han, S. Sun, B. Joo, X. Jin, and S. Han, "QoS-aware routing mechanism in OpenFlow-enabled wireless multimedia sensor networks," *Int. J. Dist. Sensor Networks*, vol 12, p.9378120, 2016.
- [24] B. Bhattacharya, and D. Das, "QoS enhancement using embedded agent in OpenFlow based SDN node," in *Elect., Comp. and Comm Techn. (ICECCT)*, *IEEE Int. Conf. on*, pp. 1-5, 2015.
- [25] Y. Jinyao, Z. Hailong, S. Qianjun, L. Bo, and G. Xiao, "HiQoS: An SDN-based multipath QoS solution," in *Comms, China*, pp. 123–133, 2015.
- [26] I.F. Akyildiz, S.C. Lin, and P. Wang, "Wireless software-defined networks (W-SDNs) and network function virtualization (NFV) for 5G cellular systems: An overview and qualitative evaluation," *Computer Networks*, vol 93, pp.66-79, 2015.
- [27] S. Civanlar, M. Parlakisik, A.M. Tekalp, B. Gorkemli, B. Kaytaz, E Onem, "A qos-enabled openflow environment for scalable video streaming," in *IEEE Globecom Workshops*, pp. 351-356, 2010.
- [28] H.E. Egilmez, B. Gorkemli, A.M. Tekalp, and S. Civanlar, "Scalable video streaming over OpenFlow networks: An optimization framework for QoS routing," in *2011 18th IEEE International Conference on Image Processing*, pp. 2241-2244, 2011.
- [29] H.E. Egilmez, S.T. Dane, K.T. Bagci, and A.M.. Tekalp, "OpenQoS: An OpenFlow controller design for multimedia delivery with end-to-end Quality of Service over Software-Defined Networks,". in *Proceedings of The 2012 Asia Pacific Signal and Information Processing Association Annual Summit and Conference*, pp. 1-8, 2012.
- [30] N. Kumar, "Mobile ad hoc network: issue and challenges related to QoS and solutions," *Int. J. Eng. Technol. Sci. Res*, vol 4, pp.415-419, 2017.
- [31] M. Masip-Bruina, J. Yannuzzib, A. Domingo-Pascuala, M. Fonteb, E. Curadob, F. Monteirob, "Research challenges in QoS routing," *Comp. Comms*, vol 29, pp.563-581, 2006.

## Improvement of the Natural Self-Timed Circuit Tolerance to Short-Term Soft Errors

Yuri Afanasyevich Stepchenkov<sup>\*1</sup>, Anton Nikolaevich Kamenskih<sup>2</sup>, Yuri Georgievich Diachenko<sup>1</sup>, Yuri Vladimirovich Rogdestvenski<sup>1</sup>, Denis Yuryevich Diachenko<sup>1</sup>

<sup>1</sup>Department of architectural and schematic basis of the innovative computational systems, Institute of Informatics Problems, Federal Research Center "Computer Science and Control" of the Russian Academy of Sciences (IPI FRC CSC RAS), Moscow, 119333, Russian Federation

<sup>2</sup>Department of Automation and remote control, Perm National Research Polytechnic University, Perm, Russian Federation

### ARTICLE INFO

Article history:  
Received: 15 October, 2019  
Accepted: 01 February, 2020  
Online: 09 March, 2020

Keywords:  
Self-timed circuit  
Soft error tolerance  
Indication  
Dual-rail  
Anti-spacer  
DICE-approach

### ABSTRACT

The paper discusses the features of the implementation and functioning of digital self-timed circuits. They have a naturally high tolerance to short-term single soft errors caused by various factors, such as nuclear particles, radiation, and others. Combinational self-timed circuits using dual-rail coding of signals are naturally immune to 91% of typical soft errors classified in the paper. The remaining critical soft errors are related to the state of the dual-rail signal, opposite to the spacer and forbidden in traditional dual-rail coding of signals. Paper proposes to consider this state as the second spacer and to indicate it as a spacer to increase the self-timed circuit tolerance to soft errors. Together with an improved indication of the self-timed pipeline, this provides masking of 100% of the considered typical soft errors in combinational self-timed circuits. Due to internal feedback, self-timed latches and flip-flops are less protected from soft errors, as are synchronous memory cells. But thanks to their indication and the input and output signals generation discipline, they are also immune to 89% of typical soft errors. Usage of the self-timed latches and flip-flops with dual-rail coding of information outputs increases the tolerance of self-timed latches and flip-flops to soft errors by 2%. Application of the DICE-like approach to circuitry and layout design of sequential self-timed circuits provide an increase in their tolerance to the single soft errors up to the level of 100%.

## 1. Introduction

The failure-tolerance of digital integrated circuits depends, firstly, on their complexity and aging mechanisms of their components, and secondly, on the impact of a number of the destabilizing factors (noise on power and signal nets, radiation, heavy charged particles (HCP), protons, neutrons traveling through the semiconductor bulk, and others). The first type of factors leads to catastrophic failures of the CMOS integrated circuits. The second type of factors can also lead to catastrophic failures as the latch-up effect. Still, much more often, they cause short-term soft errors.

This paper discusses the natural properties of self-timed (ST) circuits, providing their high tolerance to soft errors, and proposes

methods for increasing this tolerance. It is an extension of work initially presented in the 10th IEEE International Conference on Dependable Systems, Services, and Technologies, DESSERT'2019 [1].

The Single Event Transient (SET) of the digital cell (which in combinational CMOS circuits is a short-term event) is the most common [2]. A change of the memory cell state (Single Event Upset, SEU) is also possible. If the last event occurs in the memory cell storage phase, it becomes permanent rather than short-term. The duration of the failure depends on the cause of it. In this article, we consider failures caused by the passage of a nuclear particle. Depending on the particle's energy, they last up to units of nanoseconds [3].

\* Yuri Afanasyevich Stepchenkov, Ystepchenkov@ipiran.ru  
[www.astesj.com](http://www.astesj.com)  
<https://dx.doi.org/10.25046/aj050206>

There are various circuitry methods for protection against soft errors. For example, Dual Data Stream Logic memory cells [4], two-phase logic cells [5], Dual Interlocked Storage Cell [6], combinational parts duplication [7], doubling each transistor in a schematic circuit [8], detection and fault isolation [9], applying additional gates [10], and so on. These solutions use the doubled or redundant implementation of circuit logical functions. There are many known techniques for improving the fault tolerance of synchronous and asynchronous circuits, for example, [11, 12], and even at the circuit synthesis level, for example, [13].

ST circuits [14 – 18] are alternative to synchronous circuits. They are initially hardware redundant, as the failure-resistant synchronous circuits are. The first reason for such redundancy is the usage of redundant code, which is mainly dual-rail one with a spacer. Secondly, ST circuits indicate the outputs of all their cells and implement a two-phase operation discipline. Such a circuit provides an increased soft-error tolerance in comparison with synchronous and even asynchronous counterparts.

The purpose of this paper is to evaluate the natural ST circuit tolerance to soft errors and suggest ways to increase it. The ST circuits analyzed in the paper belong to the quasi delay insensitive (QDI) class. They use dual-rail coding of the information signals and two-phase operation. They indicate the switching completion of all fired cells of the ST circuit in both phases of its operation. The articles and studies known to us do not contain, to our knowledge, the results of a quantitative analysis of QDI circuit tolerance to soft errors. The results of this analysis presented here are the main contribution of the paper.

The scientific novelty of this paper consists of two ideas.

The first idea is to indicate a usually forbidden state of the dual-rail signal, which is opposite to its spacer, as the correct spacer. As a result, this forbidden state becomes non-critical and does not corrupt processed data.

Another idea is to use RS-latches and RS-flip-flops with dual-rail output with spacer for storing any data. They improve ST sequential circuit tolerance to soft errors.

## 2. Features of ST circuits

Dual-rail coding replaces each information signal  $X$  with a dual-rail signal (DRS)  $\{X, XB\}$ . Usually, DRS has two working states (“01” and “10”) and one spacer. Spacer can be either zero (“00”) or a unit (“11”). The state opposite to spacer, called “anti-spacer” (AS), is prohibited in traditional ST circuits. Considering AS never appears, the classic ST indication interprets it as a valid working state (VWS). So, when it appears, for example, as a result of SET, it propagates along the circuit and corrupts data.

In addition to DRS, the ST circuits use single-rail signals – indication signals and control ones. Indication signals are generated by indication subcircuits and acknowledge the completion of the ST circuit switching into a working or spacer phase. Indication subcircuits consist of C-elements or hysteretic triggers (H-triggers) [16]. They regulate the interaction between ST parts of a total ST circuit. Therefore, we have to consider the impact of soft errors on the operation of the ST circuits with DRS and single-rail signals, which are internal and output signals for

this circuit. The inputs of this ST circuit are always the output signals of some other one.

Request-acknowledge procedure for units connected by information signals (handshake procedure) accompanies a two-phase operation discipline. Each ST circuit allows switching sources of its inputs to a working (or spacer) phase only itself completes turning to a spacer (or working) phase [16]. Therefore, the ST circuit discipline masks a short-term soft error, which duration is less than the time for forming a new working state at the ST circuit outputs. Therefore, soft error criticality for the ST circuit operation depends on the time when the failure occurs within the operation cycle of the ST circuit. However, in high-performance digital ST circuits, the time factor ceases to play a decisive role.

ST sequential circuits (STSC) consist of bistable cells (BSC), which are analogs of synchronous RS-latches with cross-connections. BSC outputs form a signal having two static working states and one dynamic transit state through which the BSC passes when switching between static working states. At the absence of soft errors, its outputs at any time are in the working state (“10” or “01”) or transit state (“00” for the BSC on NOR cells or “11” for the BSC on NAND cells). The inverse state of the transit state (let's call it “anti-transit state,” ATS) never occurs during regular operation.

A soft error occurred in an STSC can lead to irreversible consequences if it causes switching BSC to an opposite working state. In contrast to the combinational circuit, BSC has positive feedback due to cross-connections. Therefore, when BSC inputs are inactive, a soft error in one half of BSC can force switching its second half as well. As a result, the BSC latches an invalid working state (IWS) and can't return itself to a VWS.

The difference between STSCs and combinational ST circuits also lies in their indication. STSC indication checks if BSC outputs and its inputs match in a working phase. Therefore, not all soft errors are critical.

As a result of soft errors in the source circuit, the following conditions may appear on the DRS inputs of the combinational ST circuit, not corresponded to the ST signal discipline:

- AS at one or more DRS inputs in a working or spacer phase,
- A spacer at one or more DRS inputs in a working phase,
- A working state at one or more DRS inputs in a spacer phase,
- IWS at one or more DRS inputs in a working phase.

Their duration depends on the time of natural or forced elimination of both factors:

- Soft error cause (e.g., the noise on communication wires and power stripes),
- Physical effects of the failures (e.g., an ionization current of the excess carriers injected by the traveled particles or radiation in a semiconductor bulk).



Traditional ST methodology considers AS is a prohibited state: it can never appear during the regular ST circuit operation. Therefore, the traditional ST circuit indicators do not expect it during both phases of its operation. However, a soft error can lead to the appearance of an AS state that violates the fundamental DRS generation discipline. The AS can propagate along the data processing path if one does not mask or stop it.

In a working phase, a DRS source can switch to VWS or AS, when AS appears at its inputs. For example, DRS with zero spacer, described by a pair of logical functions:

$$Y = A + B,$$

$$YB = AB * BB,$$

switches either to the AS  $\{Y=YB=1\}$  at  $\{B=0, BB=1\}$ , or to the expected working state  $\{Y=1, YB=0\}$  at  $B=1, BB=0$ , when the AS  $\{A=YB=1\}$  appears at the inputs.

Premature switching one or more DRS inputs to the spacer in the working phase does not lead to negative functional consequences. In the worst case, the internal signals and ST circuit outputs can, after switching to the working state, again return to the spacer for a time corresponding to the soft error duration. At this, data remains uncorrupted, and the indication output does not “rattle.” But some cells in the circuit can switch three times during the working phase. Initially, they switch to the expected working state before the failure, and then back to the spacer at the soft error, and again to the expected working state after the failure ends. Collector (e.g., H-trigger or C-element) combined these failure cell indicators can also switch three times during the ST circuit operation phase.

Premature switching DRS back to the working state during the transition to the spacer phase does not cause any negative functional consequences if it corresponds to the working state in the previous working phase. Otherwise, there is a possibility of switching ST circuit outputs to an IWS, after they have already switched to the current working state acknowledged by their indicator. (Remind of that in ST circuits, the previous unit does not turn to a spacer until the subsequent unit completes switching to a working phase.)

IWS in the working phase is the least probable. It involves the simultaneous switching of both DRS parts to an opposite value, i.e., the simultaneous appearance of failure in two different logical cells driving this DRS. However, such a soft error is the most dangerous for the ST circuit operation, as the circuit actively reads and processes its input data. The circuit may, in turn, generate an IWS at its outputs.

The traditional ST circuit indicator does not mask critical soft errors of BSC outputs and the accompanying control signals, which are information and indication outputs of the STSC. So, such errors can corrupt processed data and disturb the handshake between ST units.

### 3. Soft errors classification in ST circuits

Let's consider the ST circuit as a functionally complete ST unit having DRS inputs and outputs and an indication output. An external source generates DRS inputs. The indication output

acknowledges the completion of switching ST circuit into the current phase. Let's assume that the ST circuit working phase lasts for the time indication output acknowledges the completion of switching this ST circuit into the spacer. Conversely, the ST circuit spacer phase corresponds to the working state of its indication output. Then the DRS can be both in a working state and in a spacer state for some time in each ST circuit phase.

In this regard, we propose a classification of all typical soft errors in the ST circuits, shown in Figure 1. All encountered observed effects can occur in both a working phase and a spacer phase of the ST circuit. A working state into which the DRS turns because of soft error may be either the expected VWS or IWS.

An ionization pulse current generated in a semiconductor body by HCP, proton, or neutron with high enough energy is one of the typical physical soft error causes. The effective track diameter of the particle traveled through the semiconductor and induced the electron-hole pairs does not exceed one micrometer (<https://habr.com/post/189066> (in Russian)). In 65-nm and below CMOS process, this corresponds to the area covering the drains and sources of the homogeneous or complementary transistors in a few logical cells. Figure 2 shows a 65-nm layout fragment, including four NOR2 cells. The plan is symmetrical. CMOS n-transistors occupy the center; p-type transistors are located at left and right. Dotted circles A1 - A4 show the effective track diameter possible positions.

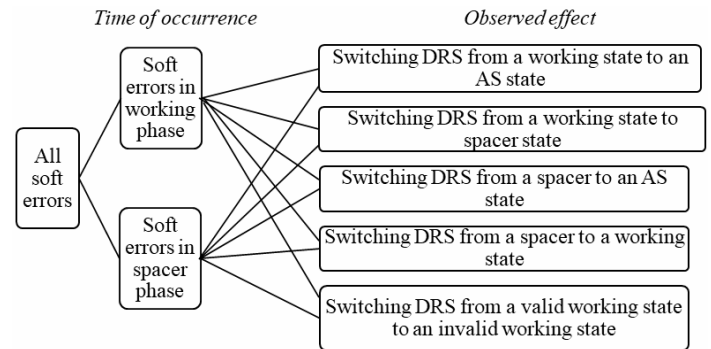


Figure 1 – Classification of the soft errors in combinational ST circuits

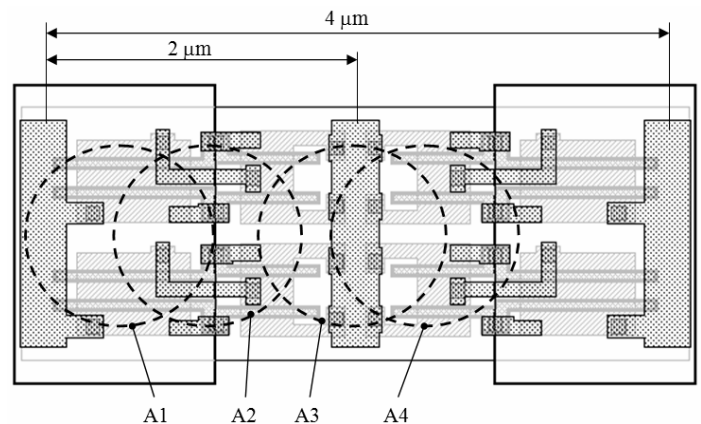


Figure 2 – Effective track diameters of the particles in the 65-nm layout

One particle cannot selectively hit, for example, only n-type transistors in one cell and only p-type transistors in another cell. It always impacts either the homogeneous transistor drains (A1, A3, A4), or the complementary transistor drains (A2) in one or



several adjacent cells at the same time. Consequently, the particles affect the structure of adjacent cells symmetrically.

Thus, one traveling particle can cause ionization currents in several adjacent cells. These currents have the same direction in all impacted cells. Therefore, the potential changes at the outputs of adjacent cells have the same polarity. In the layouts with lower design rules, the effective track diameter of the impacting particle further covers the transistor drains of both types in several adjacent cells.

If the logical cells driving DRS are forcibly placed close enough to each other on a layout, the impact of particle is symmetrical. It does not cause switching these cell outputs in opposite directions. Consequently, in the CMOS ST circuits manufactured by the 65-nm process and below, existing VWS practically never turns to IWS because of any soft error.

The ST circuit response to soft errors depends on the circuit type: combinational or sequential.

The STSC consists of one (latch) or two (flip-flop) consecutive BSC, an indication subcircuit, and BSC outputs convertors into a DRS (optional). The variety of the STSCs [19] makes difficulties for analyzing all their types in one paper. So, let's consider an STSC tolerance to soft errors by the example of ST RS-flip-flop (RSFF) shown in Figure 3. It has a DRS input {R, S} with a unit spacer, reset input (Rst), BSC output {Q, QB} with a zero-transition state (Q=QB=0), indication output (I), and consists of BSC-1, BSC-2, and indicator. BSC-1 has a unit transit state (U=UB=1).

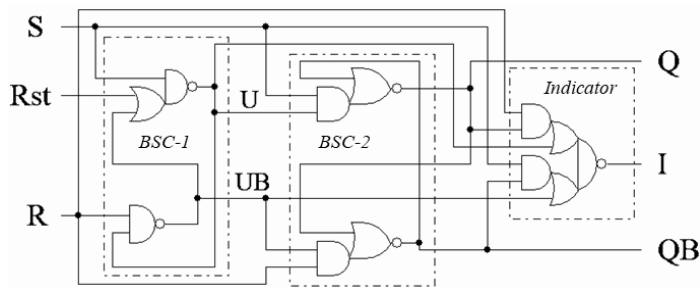


Figure 3 – ST RS-flip-flop

Figure 4 shows a classification of possible typical soft errors in ST RSFF. It includes soft errors that occur in both BSC and the indicator. For the reasons discussed above, soft error cannot lead to simultaneous switching both parts of BSC in opposite directions. Therefore, the possible occurrence of IWS is not a soft error directly. Still, it can happen as a result of the BSC transit state and the spacer at the input {R, S}.

The ST RSFF current phase is a working one if the DRS {R, S} is in the spacer. In the working phase, the RSFF information output {Q, QB} updates its state. The input {R, S} working phase corresponds to the ST RSFF spacer phase. In the spacer phase, the BSC-1 updates its state, and the BSC-2 stores its state. Note that ATS in BSC-1 causes the BSC-2 to store its state.

Let's examine the possible soft errors in combinational ST circuits and RSFFs in more detail and evaluate the probability of data corruption in the ST circuit due to them. In the first approximation, we consider the possible cases in each analyzed

situation to be equally probable. Let's call the reason, caused the soft error, by the term "bug."

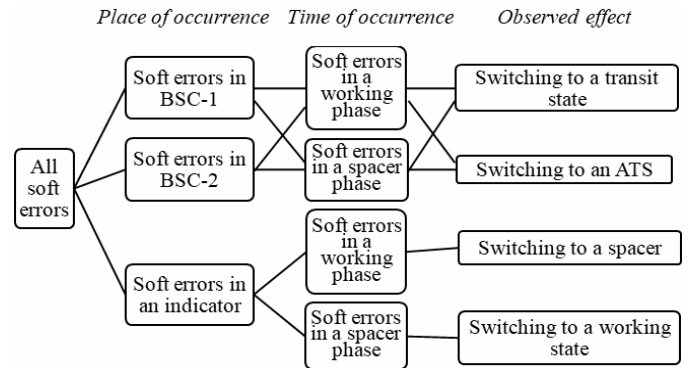


Figure 4 – Classification of the soft errors in the ST RS-flip-flops

#### 4. Soft error cases in combinational ST circuits

According to the classification of soft errors given in Section 3 in Figure 1, the following types of soft errors are possible in a combinational ST circuit:

- 4.1. Switching DRS from VWS to an AS in a working phase;
- 4.2. Switching DRS from VWS to a spacer in a working phase;
- 4.3. Switching DRS from a spacer to an AS in a working phase;
- 4.4. Switching DRS from a spacer to a working state in a working phase;
- 4.5. Switching DRS from VWS to an AS in a spacer phase;
- 4.6. Switching DRS from VWS to a spacer in a spacer phase;
- 4.7. Switching DRS from a spacer to an AS in a spacer phase;
- 4.8. Switching the DRS from a spacer to a working state in a spacer phase.

Let's assume that any of the situations 4.1 - 4.8 may appear because of a single bug with a probability of 1/8. Let's estimate the likelihood of these soft errors corrupt data processed in the ST circuit. Corrupting data is precisely the critical situation. In other cases, a bug only leads to an additional delay in the ST circuit operation.

*Case 4.1.* ST circuits consider AS is a working state. Therefore, AS does not prevent the indication output of this ST circuit from switching to the working value and thereby initiating turning this ST circuit to the spacer phase. But AS actually contains a corrupted information bit. This ST circuit functioning logic does not mask AS with a probability of  $P_{4.1.1} = 0.5$ . AS appears at its output and then passes to the following ST circuits inputs. In the first approximation, we assume that, with a probability of  $P_{4.1.2} = 0.5$ , AS at the inputs of subsequent circuits corrupts their information outputs and leads to a critical error. Then the likelihood that situation 4.1 corrupts data equals to:

$$P_{4.1} = P_{4.1.1} \cdot P_{4.1.2} = 0.25.$$

*Case 4.2.* Switching DRS from VWS to a spacer in a working phase means that the DRS has already turned to the VWS, but a

bug caused it to switch back to the spacer. The ST circuit indication output can already acknowledge switching DRS into VWS. Since the indication subcircuit consists of triggers (i.e., C-elements or H-triggers), the indication output does not return to the spacer. With some probability, the DRS spacer causes switching of one or more DRS outputs of this ST circuit into the spacer. Subsequent ST circuits cannot complete their switch to a working phase due to the spacer on their inputs. They expect the appearance of a working state on all their significant inputs and prohibit the switching of this ST circuit into the spacer. This situation is not critical.

*Case 4.3.* This case means that a bug forces turning DRS to the AS instead of VWS. Similar to situation 4.1, the probability that situation 4.3 becomes critical equals  $P_{4.3} = 0.25$ .

*Case 4.4.* Switching DRS from a spacer to a working state in a working phase means that a bug caused a premature DRS transition to the working state. If this working state matches the expected VWS, the situation is not critical. However, with a probability of  $P_{4.4.1} = 0.5$ , this working state is IWS. As we noted earlier, the bug cannot affect both parts of DRS in opposite directions. Therefore, in this situation, a soft error appears on only one DRS part. Then the second DRS part switches to a working value under the influence of the working state of ST circuit inputs. As a result, a fail DRS turns to AS. Similar to situation 4.1, the probability that situation 4.4 becomes critical equals

$$P_{4.4} = P_{4.4.1} \cdot P_{4.1} = 0.125.$$

*Case 4.5.* The ST circuit has already completed the switch to a working phase. With a probability of  $P_{4.5.1} = 0.5$ , the functional logic of this ST circuit does not mask AS. AS appears at the output of this ST circuit, and then passes to the following ST circuit inputs. With a probability of  $P_{4.5.2} = 0.5$ , the ST circuit output receivers have not yet switched to a working state, and AS takes part in the generation of their outputs. Then the probability that situation 4.5 becomes critical equals to:

$$P_{4.5} = P_{4.5.1} \cdot P_{4.5.2} \cdot P_{4.1} = 0.0625.$$

*Case 4.6.* The ST circuit already completely switched to a working phase, and this soft error means a premature spacer. With some probability, the functional logic of this ST circuit does not mask the premature spacer. It appears at the output of this ST circuit. If these output receivers have not yet switched to a working state, a premature spacer can lock this switching. ST receivers suspend their work in anticipation of a working state on the failed inputs. They do not allow the inputs of this ST circuit in which a soft error occurred to switch to a spacer. This situation is not critical.

*Case 4.7.* The ST circuit has completed switching to a working phase, and DRS in which the soft error occurred has already turned to a spacer. The ST circuit output receivers also completed the switch to a working phase. AS can pause the switching this ST circuit to a spacer for the bug duration but is not critical.

*Case 4.8.* The ST circuit and its output receivers completed switching to the working phase, and DRS, in which the soft error occurred, has already turned to a spacer. The working state is

premature. It can pause the switching this ST circuit to a spacer for the bug duration but is not critical.

Thus, only the soft errors in cases 4.1, 4.3, 4.4, and 4.5 are critical for the combinational ST circuit operation. The total probability of corrupting data processed in the ST circuits, because of soft errors classified in Section 3, equals to:

$$P_4 = (1/8) \cdot (P_{4.1} + P_{4.3} + P_{4.4} + P_{4.5}) = 0.0859375 \approx 8.6\%.$$

The soft errors that appeared in the indication subcircuit of the ST circuits are not critical. They can only cause an additional delay in the switching circuit from one phase to another.

## 5. Soft error cases in RSFFs

According to the classification of soft errors in the RSFFs in Figure 4, the following their types are possible:

- 5.1. Switching BSC-1 to a transit state in a working phase;
- 5.2. Switching BSC-1 to an ATS in a working phase;
- 5.3. Switching BSC-1 to a transit state in a spacer phase;
- 5.4. Switching BSC-1 to an ATS in a spacer phase;
- 5.5. Switching BSC-2 to a transit state in a working phase;
- 5.6. Switching BSC-2 to an ATS in a working phase;
- 5.7. Switching BSC-2 to a transit state in a spacer phase;
- 5.8. Switching BSC-2 to an ATS in a spacer phase;
- 5.9. Switching indicator to a spacer in a working phase;
- 5.10. Switching indicator to a working state in a spacer phase.

Let's assume that any of the cases 5.1 - 5.10 may appear because of a single bug with a probability of 1/10. Let's estimate the likelihood that these soft errors become critical and corrupt processed data.

*Case 5.1.* In a working phase of the ST RS-flip-flop,  $Rst = 0$ ,  $R = S = 1$ . Suppose that before the soft error, the state of BSC-1 was ( $U = 0$ ,  $UB = 1$ ). The BSC-1 can switch to a transit state in the RSFF working phase in two situations:

- 5.1.1 Bug affects a logical level of a single BSC-1 output.
- 5.1.2. The bug affects the logical levels of both BSC-1 outputs.

In situation 5.1.1, the transit state of BSC-1 ( $U = UB = 1$ ) turns to IWS ( $U = 1$ ,  $UB = 0$ ) as the bug affects only the output U of BSC-1. As a result, BSC-1 stores IWS. The spacer  $R = S = 1$  causes an immediate rewriting of this IWS to BSC-2 and corrupts an information bit stored in the RSFF and presented at its output. Data corruption, not only in the RSFF but also in the subsequent data processing path, occurs in the following cases:

- With a probability of  $P_{5.1.1.1} = 0.5$ , the input  $\{R, S\}$  remains in the spacer until switching BSC-1 into IWS and writing IWS to BSC-2. With a likelihood of  $P_{5.1.1.2} = 0.5$ , IWS at the output  $\{Q, QB\}$  corrupts the data in the RSFF output receivers,

- With a probability of  $P_{5.1.1.3} = 0.5$ , the input  $\{R, S\}$  has time to switch to a new VWS before writing IWS from BSC-1 to BSC-2. Still, the new VWS with a probability of  $P_{5.1.1.4} = 0.5$  is opposite

to the IWS stored in BSC-1 and does not prevent writing IWS to BSC-2. In this case, BSC-1 returns to the transit state and supports the indicator working value. With a probability of  $P_{5.1.1.5} = 0.5$ , IWS at the output  $\{Q, QB\}$  corrupts the data in the RSFF output receivers.

In situation 5.1.2, the bug does not allow BSC-1 to switch from the transit state to the IWS. At  $R = S = 1$ , BSC-2 turns to its transit state ( $Q = QB = 0$ ), which traditional ST circuits consider as a spacer, and the RSFF remains in the working phase. There are two ways of situation evolution:

- With a probability of  $P_{5.1.2.1} = 0.5$ , the RSFF output receivers complete switching to a working phase, despite the transit state of the RSFF output. Together with the RSFF indicator, they initiate the DRS  $\{R, S\}$  transition to a new VWS. With a probability of  $P_{5.1.2.2} = 0.5$ , BSC-1 is still in transit state. Then the VWS at RSFF input is written to BSC-2 as IWS. Still, the RSFF indicator remains in a working value and suspends the ST circuit operation until the bug ends. When bug ends, BSC-1 turns to VWS and toggles the RSFF indicator to a spacer. IWS in BSC-2 does not prevent the ST circuit from completing a transition to a spacer and initiating the switching of the RSFF input  $\{R, S\}$  to a spacer ( $R = S = 1$ ), which rewrites VWS from BSC-1 to BSC-2. ST circuit continues operation with correct data;

- With a probability of  $P_{5.1.2.3} = 0.5$ , the RSFF output receivers do not complete switching to a working phase because of the RSFF output transit state. The ST circuit pauses while waiting for the RSFF working state. The DRS  $\{R, S\}$  remains in a spacer. At the bug end, the BSC-1 state becomes metastable. With a probability of  $P_{5.1.2.4} = 0.5$ , BSC-1 switches to IWS. The spacer  $R = S = 1$  causes an immediate rewriting IWS to BSC-2. ST circuit continues to work with corrupted data.

The total data corruption probability in case 5.1 equals to:

$$P_{5.1} = 0.5 \cdot (P_{5.1.1.1} \cdot P_{5.1.1.2} + P_{5.1.1.3} \cdot P_{5.1.1.4} \cdot P_{5.1.1.5}) + 0.5 \cdot (P_{5.1.2.3} \cdot P_{5.1.2.4}) = 0.3125.$$

Case 5.2. BSC-1 can switch to ATS ( $U = UB = 0$ ) in an RSFF working phase also in two situations:

5.2.1 The bug affects a logical level of a single BSC-1 output.

5.2.2. The bug affects the logical levels of both BSC-1 outputs.

Suppose that before the bug, the state of BSC-1 was ( $U = 0$ ,  $UB = 1$ ). ATS in BSC-1 appears due to a failed switching UB from the logical 1 level to logical 0 level. In a working phase of ST RS-flip-flop,  $Rst = 0$ ,  $R = S = 1$ , and BSC-2 stores VWS. ATS in BSC-1 does not damage the BSC-2 state, but ATS is not stable.

In situation 5.2.1, at the spacer  $R = S = 1$ , BSC-1 turns to IWS ( $U = 1$ ,  $UB = 0$ ), that is written to BSC-2, corrupting the data in the RSFF output receivers with a probability of  $P_{5.2.1.1} = 0.5$ .

In situation 5.2.2, at the spacer  $R = S = 1$ , BSC-1 remains in ATS until the bug end. With a probability of  $P_{5.2.2.1} = 0.5$ , the RSFF output receivers do not have time to switch into a working phase. So, they do not allow DRS  $\{R, S\}$  source to turn the RSFF inputs into a new VWS before the bug ends. At the bug end, BSC-1 is in a metastable state. With a probability of  $P_{5.2.2.2} = 0.5$ , it turns to a working state opposite to BSC-2 state, which is written to

BSC-2, corrupting the data in the RSFF output receivers with a probability of  $P_{5.2.2.3} = 0.5$ .

The data corruption probability in case 5.2 equals to:

$$P_{5.2} = 0.5 \cdot P_{5.2.1.1} + 0.5 \cdot (P_{5.2.2.1} \cdot P_{5.2.2.2} \cdot P_{5.2.2.3}) = 0.3125.$$

Case 5.3. BSC-1 can switch to a transit state ( $U = UB = 1$ ) in an RSFF spacer phase in two situations:

5.3.1. The bug affects a logical level of a single BSC-1 output.

5.3.2. The bug affects the logical levels of both BSC-1 outputs.

In situation 5.3.1, BSC-1 may switch from the transit state to IWS. Let, for example,  $R = Rst = 0$ ,  $S = 1$ ,  $U = 0$ ,  $UB = 1$ . BSC-1 output  $U$  switches to  $U = 1$  because of the bug. With a probability of  $P_{5.3.1.1} = 0.5$ , the RSFF and its output receivers have already completed the transition to a spacer and initiated switching DRS  $\{R, S\}$  to a spacer. BSC-1 remains in transit state until input  $R$  switches to a spacer value ( $R = 1$ ). With a probability of  $P_{5.3.1.2} = 0.5$ , the bug does not end by this time, and BSC-1 switches from the transit state to IWS ( $U = 1$ ,  $UB = 0$ ). IWS is written from BSC-1 to BSC-2 since  $R = S = 1$  and appears at the RSFF output. With a probability of  $P_{5.3.1.3} = 0.5$ , IWS corrupts the data in the RSFF output receivers.

In situation 5.3.2, BSC-1 may also switch from transit state to IWS. Let, for example,  $R = Rst = 0$ ,  $S = 1$ ,  $U = 0$ ,  $UB = 1$ . The bug switches BSC-1 output  $U$  to  $U = 1$  and reinforces  $UB=1$  value. With a probability of  $P_{5.3.2.1} = 0.5$ , the RSFF and its output receivers have already completed the transition to a spacer and initiated switching DRS  $\{R, S\}$  to a spacer. The BSC-1 remains in transit state until input  $R$  switches to the spacer value ( $R = 1$ ). With a probability of  $P_{5.3.2.2} = 0.5$ , the bug does not end by this time, but BSC-1 cannot switch from the transit state to any working state because the bug forces the logical 1 level at both BSC-1 outputs. As a result, upon bug completion, BSC-1 is in a metastable state. With a probability of  $P_{5.3.2.3} = 0.5$ , it switches to the working state opposite to that of BSC-2. BSC-2 turns into this state. With a probability of  $P_{5.3.2.4} = 0.5$ , it corrupts data in the RSFF output receivers.

The total data corruption probability in case 5.3 equals to:

$$P_{5.3} = 0.5 \cdot (P_{5.3.1.1} \cdot P_{5.3.1.2} \cdot P_{5.3.1.3}) + 0.5 \cdot (P_{5.3.2.1} \cdot P_{5.3.2.2} \cdot P_{5.3.2.3} \cdot P_{5.3.2.4}) = 0.09375.$$

Case 5.4. BSC-1 can switch to ATS ( $U = UB = 0$ ) in the RSFF spacer phase also in two situations:

5.4.1. The bug affects a logical level of a single BSC-1 output.

5.4.2. The bug affects the logical levels of both BSC-1 outputs.

In situation 5.4.1, BSC-1 switches from ATS to IWS. Let, for example,  $R = Rst = 0$ ,  $S = 1$ ,  $U = 0$ ,  $UB = 1$  before the bug. The output  $UB$  of BSC-1 switches to  $UB = 0$  because of the bug. Since the bug did not affect the  $U$  node, condition  $UB = Rst = 0$  causes switching  $U$  from logical 0 to logical 1 level, and BSC-1 turns to IWS ( $U = 1$ ,  $UB = 0$ ). The following writing IWS to BSC-2 turns indicator to a working value  $I = 0$ . Two directions of further evolution are possible:



- With a probability of  $P_{5.4.1.1} = 0.5$ , the RSFF and its output receivers have already completed the transition to a spacer and initiated switching DRS  $\{R, S\}$  to a spacer. With a probability of  $P_{5.4.1.2} = 0.5$ , BSC-1 remains in the IWS until the input R switches to a spacer value ( $R = 1$ ). The RSFF input spacer writes the IWS from BSC-1 to BSC-2, which with a probability of  $P_{5.4.1.3} = 0.5$  corrupts data in the RSFF output receivers;

- With a probability of  $P_{5.4.1.3} = 0.5$ , the RSFF and its output receivers do not have time to switch to a spacer. Input  $\{R, S\}$  remains in VWS until the bug end. At the bug end, BSC-1 switches to VWS, the RSFF indicator acknowledges the RSFF spacer state, and the ST circuit continues operation with the correct data.

In the situation, 5.4.2 BSC-1 can also switch from ATS to IWS. Let, for example,  $R = Rst = 0, S = 1, U = 0, UB = 1$  before the bug. Bug switches the output UB of BSC-1 to  $UB = 0$  and reinforce the value  $U = 0$ . BSC-1 remains in ATS and provides storage of VWS in BSC-2. The indicator acknowledges the RSFF spacer state. With a probability of  $P_{5.4.2.1} = 0.5$ , the RSFF output receivers complete the transition to a spacer and initiate switching DRS  $\{R, S\}$  to a spacer. With a probability of  $P_{5.4.2.2} = 0.5$ , BSC-1 remains in ATS until the input R switches to a spacer value ( $R = 1$ ). Until the bug end, BSC-1 cannot switch from ATS to any working state, because the bug holds logical 0 levels at both outputs of BSC-1. At the bug end, BSC-1 enters a metastable state, which with a probability of  $P_{5.4.2.3} = 0.5$ , switches into the working state opposite to the initial VWS of DRS input  $\{R, S\}$ . BSC-2 turns to this IWS, and with a probability of  $P_{5.4.2.4} = 0.5$ , corrupts data in the RSFF output receivers.

The total data corruption probability in case 5.4 equals to:

$$P_{5.4} = 0.5 \cdot (P_{5.4.1.1} \cdot P_{5.4.1.2} \cdot P_{5.4.1.3}) + 0.5 \cdot (P_{5.4.2.1} \cdot P_{5.4.2.2} \cdot P_{5.4.2.3} \cdot P_{5.4.2.4}) = 0.09375.$$

*Case 5.5.* In a working phase of an RSFF,  $Rst = 0, R = S = 1$ . Suppose that before a bug, the states of the BSCs were ( $U = 0, UB = 1$ ), and ( $Q = 1, QB = 0$ ). BSC-2 can switch to a transit state in the RSFF working phase in two situations:

5.5.1. The bug affects a logical level of a single BSC-2 output.

5.5.2. The bug affects the logical levels of both BSC-2 outputs.

In situation 5.5.1, the transit state of BSC-2 ( $Q = QB = 0$ ) switches the RSFF indicator to a spacer. Further situation evolution is possible in two directions:

- With a probability of  $P_{5.5.1.1} = 0.5$ , the RSFF output receivers complete switching into a working phase and initiate the transition of DRS  $\{R, S\}$  to a new VWS. A spacer value of the RSFF indicator remains until the bug ends. If a new VWS appears before the bug end, it supports the spacer value of the RSFF indicator, and the ST circuit continues regular operation. If the bug ends before the new input VWS, a condition  $R = S = 1$  causes writing VWS from BSC-1 to BSC-2. It does not corrupt data in the RSFF output receivers;

- With a probability of  $P_{5.5.1.2} = 0.5$ , the RSFF output receivers do not complete switching into a working phase and do not initiate the transition of DRS  $\{R, S\}$  to a new VWS. The receivers

consider the RSFF output transit state as a spacer. ST circuit pauses with its operation. At the bug end, the spacer  $R = S = 1$  forces writing VWS from BSC-1 to BSC-2. BSC-2 restores its VWS, and the ST circuit continues regular operation with correct data.

Situation 5.5.2 is similar to the situation 5.5.1 and also cannot cause any data corruption. So, the total data corruption probability in case 5.5 equals  $P_{5.5} = 0$ .

*Case 5.6.* Let  $Rst = 0, R = S = 1, U = 0, UB = 1, Q = 1, QB = 0$  in the ST RS-flip-flop working phase. BSC-2 can switch to ATS in two situations:

5.6.1. The bug affects only a logical level of QB output.

5.6.2. The bug affects the logical levels of both BSC-2 outputs.

In situation 5.6.1, ATS ( $Q = QB = 1$ ) in BSC-2 forces switching BSC-2 to IWS ( $Q = 0, QB = 1$ ) due to cross-connections. The RSFF indicator turns to a spacer value  $I = 1$  and prevents the RSFF output receivers from using the  $\{Q, QB\}$  state.

With a probability of  $P_{5.6.1.1} = 0.5$ , the RSFF output receivers do not complete the switch to a working phase. They do not allow the RSFF input  $\{R, S\}$  source to initiate the transition of DRS  $\{R, S\}$  to a new VWS. At the bug end, the spacer  $R = S = 1$  forces writing VWS from BSC-1 to BSC-2. BSC-2 restores its VWS, the RSFF indicator switches to a working value, and the ST circuit continues regular operation with correct data.

With a probability of  $P_{5.6.1.2} = 0.5$ , the RSFF output receivers have time to complete the switching to a working phase and allow the RSFF input  $\{R, S\}$  source to initiate the transition of DRS  $\{R, S\}$  to a new VWS. With a probability of  $P_{5.6.1.3} = 0.5$ , IWS at the output  $\{Q, QB\}$  during the switching RSFF indicator from a working value to a spacer has time to corrupt data in subsequent ST circuits. With a probability of  $P_{5.6.1.4} = 0.5$ , DRS  $\{R, S\}$  has time to switch to the new VWS before the bug ends. The RSFF indicator remains in the spacer and not allow for restoring corrupted data.

In situation 5.6.2, the ATS in BSC-2 ( $Q = QB = 1$ ) does not switch into any working state, because of the bug forces logical 1 level on both BSC-2 outputs. The RSFF indicator remains in a working value  $I = 0$  and allows the RSFF output receivers to use the  $\{Q, QB\}$  state. With a probability of  $P_{5.6.2.1} = 0.5$ , ATS at the output  $\{Q, QB\}$  corrupts data in the receivers of this output, since they consider it is a working state. With a probability of  $P_{5.6.2.2} = 0.5$ , the RSFF output receivers complete switching to a working phase. They initiate the transition of DRS  $\{R, S\}$  to a new VWS, which occurs, with a probability of  $P_{5.6.2.3} = 0.5$ , before the bug ends. The RSFF indicator switches to a spacer  $I = 1$  and prohibits restoring corrupted data.

The total data corruption probability in case 5.6 equals to:

$$P_{5.6} = 0.5 \cdot (P_{5.6.1.2} \cdot P_{5.6.1.3} \cdot P_{5.6.1.4}) + 0.5 \cdot (P_{5.6.2.1} \cdot P_{5.6.2.2} \cdot P_{5.6.2.3}) = 0.125.$$

*Case 5.7.* Let's suppose that in the ST RS-flip-flop spacer phase,  $Rst = 0, R = 1, S = 0, U = 1, UB = 0$ , and before the bug, BSC-2 state was ( $Q = 0, QB = 1$ ). In a spacer phase, the BSC-1 static state and the RSFF inputs do not affect the BSC-2 state.

BSC-2 can switch to the transit state ( $Q = QB = 0$ ) in the RSFF spacer phase in two situations:

- 5.7.1. The bug affects only a logical level of QB output.
- 5.7.2. The bug affects the logical levels of both BSC-2 outputs.

In situation 5.7.1, the transit state of BSC-2 ( $Q = QB = 0$ ) turns to IWS ( $Q = 1, QB = 0$ ) due to cross-connections, since the bug does not affect the logical level of Q. But the indicator remains in a spacer, and following the handshake discipline, the RSFF output receivers do not use IWS at the output of this RSFF. The RSFF indicator and its output receivers initiate the transition of DRS  $\{R, S\}$  to a spacer.

With a probability of  $P_{5.7.1.1} = 0.5$ , VWS in BSC-1 does not correspond to the BSC-2 state, as in the case under consideration. Since bug only affects QB, the condition ( $S = U = 1$ ) causes switching output Q to  $Q = 0$ . BSC-2 turns back to the transit state considered as a spacer by subsequent ST circuits. The indicator remains in a spacer value  $I = 1$ . The RSFF output receivers do not complete switching to a working phase and do not allow the RSFF input  $\{R, S\}$  source to initiate the transition of DRS  $\{R, S\}$  to a new VWS. At the bug end, the QB output switches to  $QB = 1$ , and BSC-2 turns to the expected VWS. The ST circuit continues regular operation with correct data.

If the states of BSC-1 and BSC-2 coincide, then after the DRS  $\{R, S\}$  transition to a spacer, the ST circuit continues regular operation with uncorrupted data.

In situation 5.7.2, the transit state of BSC-2 ( $Q = QB = 0$ ) does not switch into a working state, since the bug forces the logical level of both RSFF outputs. But the indicator also remains in a spacer. Following the handshake discipline, the RSFF output receivers switch to a spacer. Together with the RSFF indicator, they initiate the transition of DRS  $\{R, S\}$  to the spacer. Upon bug completion and switching DRS  $\{R, S\}$  to the spacer, BSC-2 turns to the state of BSC-1, and the ST circuit continues regular operation with correct data.

The total data corruption probability in case 5.7 equals to  $P_{5.7} = 0$ .

*Case 5.8.* Let's suppose that in the ST RS-flip-flop spacer phase,  $Rst = 0, R = 1, S = 0, U = 1, UB = 0$ , and BSC-2 state is ( $Q = 0, QB = 1$ ) before the bug. BSC-2 can switch to ATS in two situations:

- 5.8.1. The bug affects only a logical level of Q output.
- 5.8.2. The bug affects the logical levels of both BSC-2 outputs.

In situation 5.8.1, ATS in BSC-2 ( $Q = QB = 1$ ) causes switching BSC-2 into IWS ( $Q = 1, QB = 0$ ) due to cross-connections. The indicator is in a spacer value  $I = 1$  regardless of the BSC-2 state. It prevents the RSFF output receivers from using the state  $\{Q, QB\}$ . The RSFF output receivers complete switching to a spacer and allow the RSFF input  $\{R, S\}$  source to initiate the transition of DRS  $\{R, S\}$  to a spacer.

With a probability of  $P_{5.8.1.1} = 0.5$ , DRS  $\{R, S\}$  has time to switch to the spacer ( $R = S = 1$ ) before the bug ends. With a probability of  $P_{5.8.1.2} = 0.5$ , VWS in BSC-1 does not correspond to the BSC-2 state, as in the case under consideration. Since the bug

forces logical 1 level at the output Q, condition ( $S = U = 1$ ) cannot switch the output Q to  $Q = 0$ . BSC-2 remains in IWS, but the RSFF indicator does not turn to a working value  $I = 0$ . It does not allow the RSFF output receivers to use the  $\{Q, QB\}$  state before the bug ends, and BSC-2 turns into VSC stored in BSC-1. Only then the RSFF indicator switches to a working value  $I = 0$  and allow the RSFF output receivers to use the state  $\{Q, QB\}$ . The ST circuit continues regular operation with correct data. If, after switching DRS  $\{R, S\}$  to the spacer, the VWS in BSC-1 coincides BSC-2 state, the ST circuit also continues to work with the correct data.

With a probability of  $P_{5.8.1.3} = 0.5$ , DRS  $\{R, S\}$  does not have time to switch to the spacer ( $R = S = 1$ ) before the bug ends. The input  $\{R, S\}$  working state, and VWS in BSC-1 prevent writing to the BSC-2. At the bug end, BSC-2 continues to store IWS. Still, due to the spacer value of the RSFF indicator, the RSFF output receivers do not use it, and their data remains uncorrupted.

In situation 5.8.2, ATS in BSC-2 ( $Q = QB = 1$ ) does not cause the BSC-2 to switch into any working state, because of the bug forces logical 1 level on both outputs of BSC-2. The RSFF indicator remains in a spacer value  $I = 1$  and prevents the RSFF output receivers from using ATS. The RSFF output receivers complete switching to the spacer and allow the RSFF input  $\{R, S\}$  source to initiate the transition of DRS  $\{R, S\}$  to a spacer.

With a probability of  $P_{5.8.2.1} = 0.5$ , DRS  $\{R, S\}$  has time to switch to the spacer ( $R = S = 1$ ) before the bug ends. Because of ongoing bug, BSC-2 does not turn into VWS stored in BSC-1. ATS at the output  $\{Q, QB\}$  causes switching the RSFF indicator to a working value  $I = 0$ , which allows the RSFF output receivers to use the ATS as a working state. With a probability of  $P_{5.8.2.2} = 0.5$ , the ATS corrupts data in the RSFF output receivers.

With a probability of  $P_{5.8.2.3} = 0.5$ , DRS  $\{R, S\}$  does not have time to switch to the spacer ( $R = S = 1$ ) before the bug ends. The input  $\{R, S\}$  working state, and VWS in BSC-1 prevent writing to BSC-2. After the bug ends, BSC-2 is in a metastable state, which switches to an arbitrary working state. But due to the spacer value of the RSFF indicator, the output  $\{Q, QB\}$  working state is not used by the RSFF output receivers, and their data remains uncorrupted.

The total data corruption probability in case 5.8 equals to:

$$P_{5.8} = 0.5 \cdot (P_{5.8.2.1} \cdot P_{5.8.2.2}) = 0.125.$$

*Case 5.9.* It suggests the indicator has switched to the working value but returned to the spacer because of the bug. In this case, BSC-1 and BSC-2 store VWS. Since the data inside and at the RSFF information output do not change, a failed switching indicator to the spacer, in the worst case, only pauses the ST circuit regular operation. When the bug ends, the RSFF indicator returns to the working value, and the ST circuit continues the correct operation.

The total data corruption probability in case 5.9 equals to  $P_{5.9} = 0$ .

*Case 5.10.* It assumes the indicator has switched to the spacer but returned to the working state because of the bug. In this case, BSC-1 and BSC-2 store VWS. Similarly, to case 5.9, when the

bug ends, the RSFF indicator returns to the spacer, and the ST circuit continues the correct operation.

The total data corruption probability in case 5.10 equals to  $P_{5.10} = 0$ .

The reasoning given above for the specific values of the inputs, outputs, and internal state of the ST RS-flip-flop in cases 5.1 - 5.8 is also valid for any other initial conditions.

Thus, only the soft errors in the ST RS-flip-flop in cases 5.1 - 5.4, 5.6, and 5.8 are critical for the ST circuit functioning. The total data corruption probability because of a single soft error in the ST RS-flip-flop equals to:

$$P_5 = (1/10) \cdot (P_{5.1} + P_{5.2} + P_{5.3} + P_{5.4} + P_{5.6} + P_{5.8}) = 0.10625.$$

Failure analysis for other types of STSCs gives a similar result. We do not cite it due to the limited volume of the paper.

### 6. Masking critical failures in ST circuits

#### 6.1 Masking soft errors in ST combinational circuits

The following two methods, being used simultaneously, can improve soft error tolerance of the ST circuit:

- masking AS state,
- improvements in the ST pipeline indication.

The first method uses the fail-safe DRS discipline, considering AS is the second spacer [1], as shown in Table 1. Two spacers inside the same circuit were used earlier in secure dual-rail logic [20] and NCL circuits [11]. There they were formed by the different DRS sources and provided increased security for data encoding [20] or reduced power consumption [11]. We propose to indicate the AS as a valid second spacer of the same DRS.

Table 1: Fail-safe DRS discipline in ST circuits

S.No	Synchronous signal X	ST signal		State
		X	XB	
1	0	0	1	bit 0
2	1	1	0	bit 1
3	-	0	0	spacer 0
4	-	1	1	spacer 1

XNOR, or “equivalence” cell, indicates two DRS spacers (“00” and “11”). Figure 5 shows two XNOR implementations suitable for use in QDI circuits. The circuit in Figure 5(a) [21] is convenient for implementation with a standard cell library. The circuit in Fig. 1(b) has the least possible transistor number.

The two-phase discipline of the ST circuit operation and the requirement of a mandatory indication of each DRS mask a mixed spacer-working state at the circuit inputs. Indeed, the DRS consistently switches from spacer to a working state and back to spacer state. The indicator acknowledges the completion of this switching to each state. The indicator also acknowledges the incorrect switching DRS to a state that does not correspond to the ST circuit operation phase. As a result, the indicator does not

correspond to an expected one in the current phase of the ST circuit. An indication subcircuit detects and localizes this case.

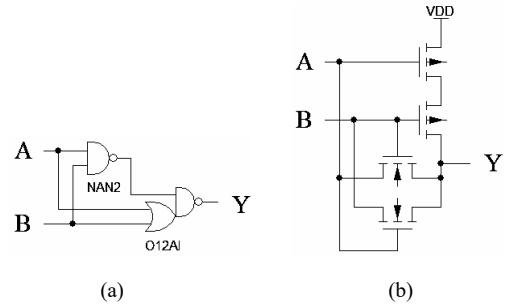


Figure 5 – XNOR implementation: on standard cells (a) and pass CMOS transistors (b)

Thus, the usage of a double spacer allows one to mask all soft errors causing the AS appearance in combinational ST circuits, namely, cases 4.1, 4.3, 4.4, and 4.5 in Section 4.

As a result, with the indication subcircuit slight complication providing AS indication as a spacer, the combinational ST circuits mask soft errors in all cases analyzed in Section 4. An improved method for controlling the phases of the output register during pipeline implementation of the ST circuit retains this advantage within the framework of the general ST circuit.

Figure 6 shows a circuit of an optimized ST pipeline utilized in the Fused Multiply-Add (FMA) project [22]. The logic and register parts implement the pipeline stage. LI\* and RI\* blocks compress the logical part and register bitwise indicators in each pipeline stage into one total indication signal, respectively. The output signals of the LI\* and RI\* blocks indicate the completion of the switching of all cells in the pipeline stage, “fired” by the stage inputs in the current operation phase.

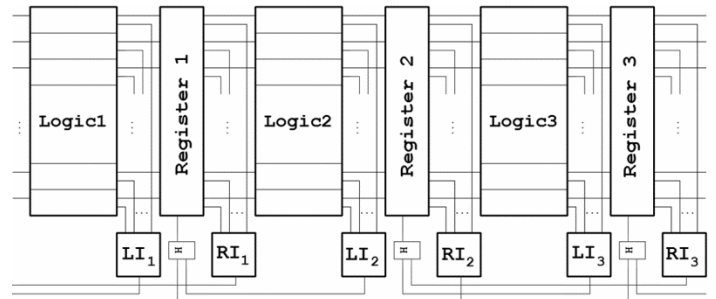


Figure 6 – Traditional ST pipeline

H-trigger [16] collects the outputs of the blocks  $LI_{k+1}$  and  $RI_{k+1}$ , forming a control signal for the output register of the k-th pipeline stage within the ST pipeline handshake discipline. The k-th stage output register, in turn, forms the working state and the spacer of the logical part inputs of the (k+1)-th pipeline stage.

The H-trigger is a static analog of the Muller C-element [16], traditionally used for ST circuit indication. Figure 7 shows the two-input H-trigger CMOS circuit. Unlike the C-element, the H-trigger does not contain a “weak” inverter, and due to this, it has better noise immunity. Table 2 represents the truth table of the two-input H-trigger. If the states of the inputs I0 and I1 are equal, then output Q turns to the same state. Otherwise, output Q stores its state.

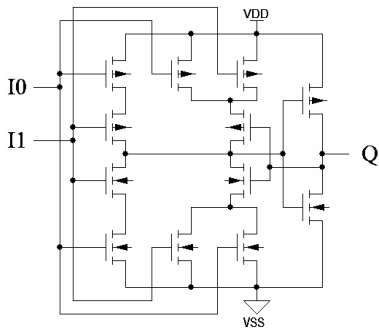


Figure 7 – CMOS circuit of the two-input H-trigger

Table 2: Truth table of the two-input H-trigger

S.No	Inputs		Output, Q <sup>+</sup>
	I0	I1	
1	0	0	0
2	1	0	Q
3	0	1	Q
4	1	1	1

Note that the pipeline control circuit in Figure 6 is correct only if the logic block of the current pipeline stage indicates all previous pipeline stage register outputs. Otherwise, the H-trigger controlling the k-th stage register must have a third input connected to this register indication output.

Figure 8(a) shows a one register bit implementation, where the DRS inputs  $\{X_j, XB_j\}$  have a unit spacer. It consists of two H-triggers. Due to this, it stores both the working and spacer states of DRS inputs  $\{X_j, XB_j\}$ , while ensuring an indication of all its inputs and outputs. Ph input is a total phase control signal for all register bits. When the k-th pipeline stage combinational part switches to a spacer phase, its output register, for some time, is in the working phase and provides the k-th stage outputs to the (k+1)-th stage inputs.

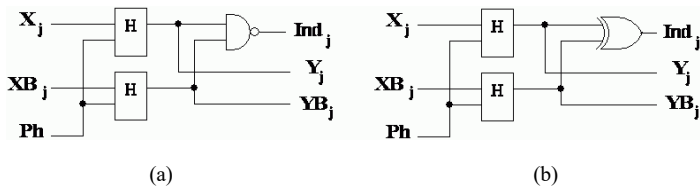


Figure 8 – ST register bit: traditional (a) and soft error resisted (b)

The indicators of the combinational part and the register of the (k+1)-th stage acknowledge their switching to the working phase. Then the H-trigger combining them forms the spacer value of the general register control signal Ph. Only after this, the register becomes insensitive to the working state changes of the inputs  $\{X_j, XB_j\}$ . Therefore, for some time, any working state change at the output of the k-th stage combinational part is stored in its output register and transferred to the (k+1)-th pipeline stage inputs.

The register bit circuit complication, as shown in Figure 8 (b), increases its tolerance to soft errors. Then register indicates the AS state of the  $\{Y_j, YB_j\}$  output as a spacer.

Table 3 displays the data corruption probabilities for the cases discussed in Section 4 in the classical combinational ST circuit

and the ST circuit using the proposed circuit techniques increasing soft error tolerance. The last row shows the total data corruption probability in combinational ST circuits because of soft errors analyzed in Section 4, taking into account the equal likelihood of their occurrence.

Table 3: Data corruption probabilities in classical and improved combinational ST circuit

Soft error case	Classical ST circuit	Improved ST circuit
4.1	0.25	0
4.2	0	0
4.3	0.25	0
4.4	0.125	0
4.5	0.125	0
4.6	0	0
4.7	0	0
4.8	0	0
Total	8.6%	0%

Thus, classical ST combinational circuits mask soft errors classified in Section 3 in 91.4% of their occurrence cases. AS indication as a spacer and the bit implementation of the pipeline stage output register by the circuit in Figure 8(b) mask the remaining 8.6% of soft error cases in the combinational ST circuit that are not masked by the classical ST circuits properties and their interaction discipline.

Remind, we consider the soft errors that occur too close to the ST circuit current phase end or having a too long duration. So, the ST circuit two-phase discipline cannot mask them. In synchronous circuits, critical soft errors having no time to disappear before the active clock edge arrives. They can only be masked by using fail-safe coding or through special circuitry techniques that increase the hardware complexity.

### 6.2 Masking soft errors in STSCs

The usage of ST RSFFs with DRS information outputs [19] and circuitry methods improving the failure-tolerance of memory circuits (for example, LTMR [23], DICE [24, Figure 3]) allow for essential increasing the STSC soft error tolerance.

Combinational ST circuits use DRS inputs, while the RSFF information outputs in Figure 3 form a signal without spacer. The RSFF with DRS information input  $\{R, S\}$  and output  $\{QP, QPB\}$ , shown in Figure 9, resolves this problem.

The RSFFs with DRS information output write the BSC-2 state to their information outputs only in the working phase of the BSC-2 and only when its state corresponds to the BSC-1 state. The inputs of the RSFF shown in Figure 9 have a unit spacer ( $R = S = 1$ ), which forces writing BSC-1 state to BSC-2. Indicator value  $I = 0$  acknowledges this write successful completion and allows for switching DRS outputs (QP, QPB) to a working state corresponding to the BSC-2 state. The working state at the RSFF information inputs ( $\{R = 0, S = 1\}$  or  $\{R = 1, S = 0\}$ ) causes switching the RSFF indication output to  $I = 1$  and forces turning DRS output to the spacer ( $QP = QPB = 0$ ). Therefore, any change in the BSC-2 state in this phase does not affect the RSFF output state.



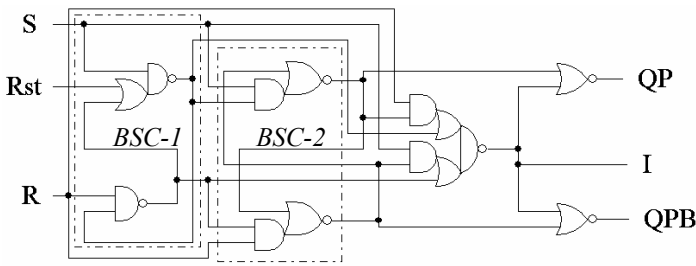


Figure 9 – ST RS-flip-flop with DRS input and output

The indication output spacer value  $I = 1$  or ATS in BSC-2 force the spacer at the {QP, QPB} output of the RSFF in Figure 9. As a result, the data corruption probabilities  $P_{5.6.2.1}$  and  $P_{5.8.2.2}$  for ATS at {QP, QPB} output become zero. Then the probabilities of cases 5.6 and 5.8 from Section 5 become equal to  $P_{5.6} = 0.0625$  and  $P_{5.8} = 0$ , and the total data corruption likelihood because of the soft error in the RSFF shown in Figure 9 decreases to  $P_5 = 0.0875 \approx 8.8\%$ .

DICE (Dual Interlocked Cell) is a particular circuitry method for protecting RAM cells and a sequential logic against soft errors. First, it doubles hardware, using cross-connections to control the gates of p- and n-type transistors in the symmetric parts of the circuit. Second, it assumes spacing the corresponding layout fragments to avoid a simultaneous impact on them the same particle. Figure 10 shows an example of a dice-style synchronous D-latch [24, Figure 3].

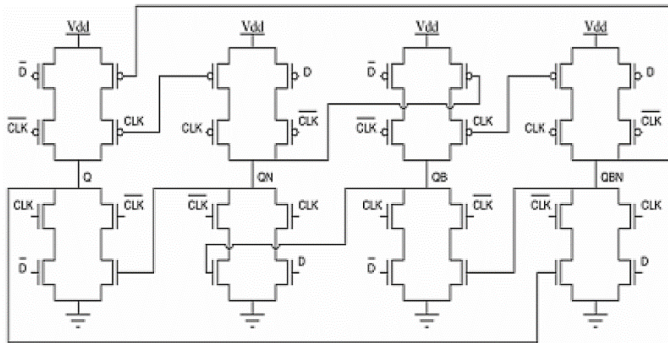


Figure 10 – Synchronous DICE-style D-latch

LTMR (Localized Triple Modular Redundancy) is a method of local majoring applied at the level of individual logical cells. Figure 11 demonstrates an example of a synchronous LTMR flip-flop [23].

The LTMR method surpasses the DICE approach in protecting high-performance synchronous circuits against single failures. It masks failure in the assumption that the failure occurs only in one of the three parts of the circuit and does not corrupt the result of data processing. Unlike LTMR, DICE prevents writing incorrect state to the sequential cell and provides a self-healing of the circuit after the end of the failure. But writing the correct state to the sequential cell requires a time exceeding the duration of the failure. Therefore, the effectiveness of the DICE method drops, as the clock frequency increases.

The DICE method has lower hardware complexity comparing to LTMR one. So, it is preferable for use in the failure-resisted STSCs since they are inherently more complex than synchronous

counterparts because of the dual-rail discipline and obligatory indication. In STSCs, LTMR method usage leads to a manifold complexity increase not only in the STSC's functional part but also in its indication subcircuit. As a result, not only the time parameters and energy consumption deteriorate, but also the reliability characteristics (for example, the average time between failures).

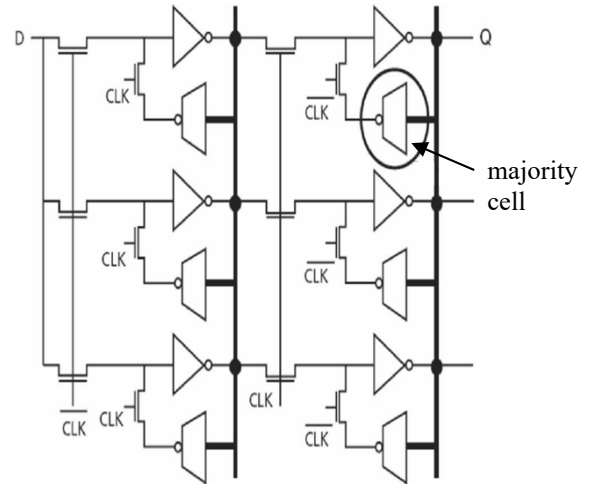
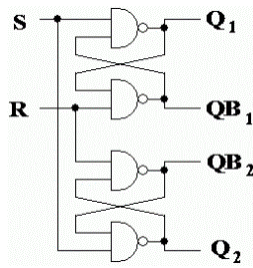


Figure 11 – Synchronous LTMR flip-flop

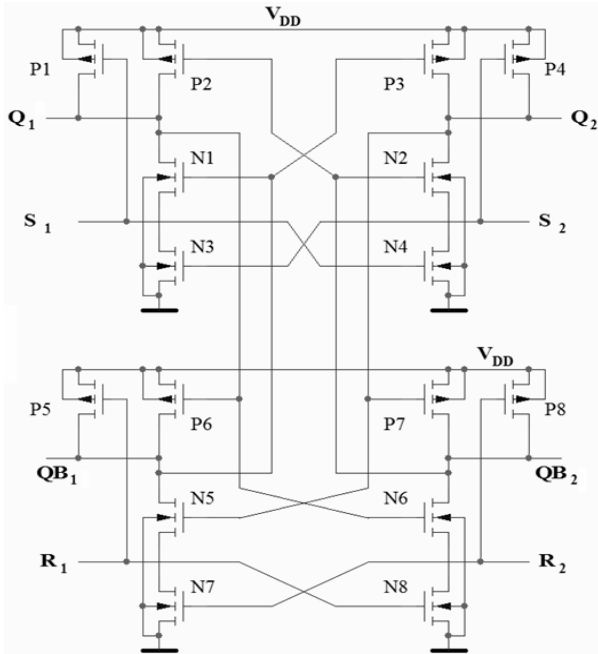
STSCs specificity makes it easy enough to adapt the DICE method for increasing their soft error tolerance. Figure 12(a) represents the synchronous simplified RS-latch circuit on NAND2 cells, which implements a DICE-like approach. The NAND2 cells are spaced a sufficient distance in a layout to minimize the probability of several particles impact them simultaneously.

Figure 12(b) shows a real DICE-style RS-latch circuit implementation [25]. Signals in the pairs  $\{S_1, S_2\}$ , and  $\{R_1, R_2\}$  are logically equivalent and correspond to the S and R inputs in Figure 12(a). They are also spaced in the layout, as the increase in parasitic capacitance between them contributes to a growth in the sequential cell failure-tolerance [25]. Figure 12(b) demonstrates the real connections of the internal nodes of the circuit with the gates of transistors. Such the circuit successfully resists against the effects of a single particle in any submicron CMOS process.

However, an analysis shows that a significant difference in the time of switching its homogeneous inputs into the active state leads to the short-circuit current in the RS-latch. Let, for example, the RS-latch state in Figure 12(b) is  $R_1=R_2=S_1=S_2=1$ ,  $Q_1=Q_2=1$ ,  $QB_1=QB_2=0$ , and  $(R_1, R_2)$  inputs switch to logic-zero state ( $R_1 \rightarrow 0, R_2 \rightarrow 0$ ),  $R_2$  input does this later than  $R_1$ . Switching  $R_1 \rightarrow 0$  results in unlocking the transistor P5, turning the node  $QB_1 \rightarrow 1$ , and unlocking the transistor N1. Since transistor N3 is already open ( $S_2=1$ ), node  $QB_1$  connects to the power supply through transistor P2 and to the ground through a chain of open transistors N1 and N3. Short-circuit current flows between the power and ground buses. It stops only after switching  $R_2 \rightarrow 0$  and charging  $QB_2$  node to a high potential, sufficient to close P2 transistor. Therefore, the  $R_1$  and  $R_2$ ,  $S_1$ , and  $S_2$  nets should be paired with symmetry when implementing the RS-latch layout, so that the signal propagation delays along them are not too different.



(a)



(b)

Figure 12 – DICE-style RS-latch: schematic view (a) and CMOS circuit (b)

Using the DICE-like approach to implement STSCs also improves their failure-tolerance while complying with specific layout design rules. BSC built on the DICE-style RS-latch (Figure 12(a)) has two times more outputs than a conventional BSC. The DICE approach leads to doubling an STSC functional part. The principles of the ST circuits require an indication of all STSC inputs and outputs. Therefore, an increase in the number of outputs of the functional part also complicates the indication subcircuit.

Figure 13 shows a conventional ST RS-latch circuit, which information input is the DRS with a unit spacer. At the same time, the OAI22 cell implements an indication subcircuit. Figure 14 demonstrates the DICE implementation of the same latch. The indication subcircuit is more complex, as it should indicate all outputs in the ST circuit, but does not double.

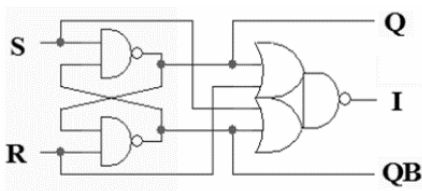


Figure 13 – Conventional ST RS-latch

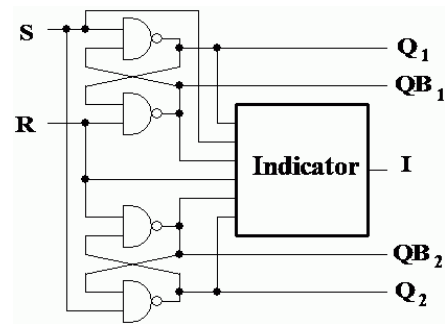


Figure 14 – DICE-style ST RS-latch

Figures 3 and 15 demonstrate a similar conversion of the original RS-flip-flop. The conventional ST RS-flip-flop shown in Figure 3 has two BSCs. In contrast, the failure-resisted DICE implementation shown in Figure 15 has duplicated BSCs. The indicator of the DICE implementation also is complicated but not doubled.

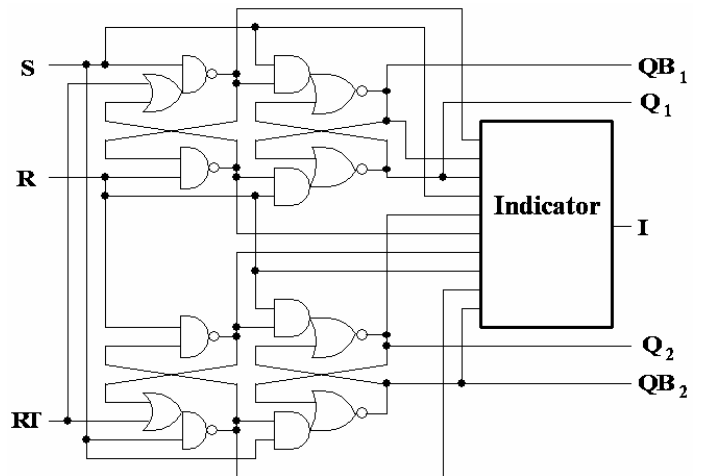


Figure 15 – DICE-style ST RSFF

Table 4: Data corruption probabilities in classical and advanced ST RSFF

Soft error case	Classical ST RSFF	Advanced ST RSFF	
		with DRS output	DICE-style
5.1	0.3125	0.3125	0
5.2	0.3125	0.3125	0
5.3	0.09375	0.09375	0
5.4	0.09375	0.09375	0
5.5	0	0	0
5.6	0.125	0.0625	0
5.7	0	0	0
5.8	0.125	0	0
5.9	0	0	0
5.10	0	0	0
Total	10.6%	8.8%	0%

Table 4 displays the data corruption probabilities in the ST circuit because of the soft errors, classified in Section 3 and analyzed in Section 5, for the ST RSFF implemented by the classical circuit (Figure 3), the circuit with DRS output (Figure 9), and DICE-style circuit. The last row shows the total data corruption probability because of soft errors in the RSFF

discussed in Section 5, taking into account the equal probabilities of their occurrence.

Thus, STSCs, unlike synchronous standard sequential cells and memory cells, mask 89.4% of soft errors analyzed in Section 5 due to their properties. The use of the ST RS-flip-flops with a DRS information output increases the tolerance to the soft errors discussed in Section 5, up to 91.2%. As in synchronous circuits, the DICE-style technique makes STSCs insensitive to remaining critical failures.

## 7. Conclusions

Due to using dual-rail code with spacer, two-phase operation discipline, and mandatory indication, ST circuits mask most of the short-term soft errors without any changes in their circuitry. Classical ST circuit implementations guarantee the high level of masking soft faults classified in Section 3: 91.4% in combinational ST circuits and 89.4% in ST sequential circuits.

The indication of prohibited DRS state that is opposite to the spacer state, as the second spacer masks remained classified soft errors in the combinational ST circuits.

The increase of the ST sequential circuits tolerance to the soft errors analyzed in Section 5 up to 91.2% is achieved by using ST RS-flip-flops with a dual-rail information output. DICE-style approach for implementing ST sequential circuits provides an additional increase of their tolerance to discussed soft errors up to 100%.

Thanks to ST circuit ability to mask most of the soft errors due to their features and their ability to maintain functional performance in a wide range of operating conditions, ST circuits are a promising basis for designing failure-resisted digital hardware.

## Conflict of Interest

The authors declare no conflict of interest.

## Acknowledgment

We would like to acknowledge the help of Dr. Alexander Kushnerov in discussing and preparing the paper. The study was funded by a grant from the Russian Science Foundation (Project № 19-11-00334).

## References

- [1] Y. A. Stephenkov, A. N. Kamenskih, Y. G. Diachenko, Y. V. Rogdestvenski, D. Y. Diachenko, "Fault-Tolerance of Self-Timed Circuits" in 2019 10th International Conference on Dependable Systems, Services, and Technologies (DESSERT), Leeds, United Kingdom, 2019. <https://doi.org/10.1109/DESSERT.2019.8770047>
- [2] A. I. Chumakov, "Forecasting local radiation effects in IC under the influence of the outer space factors" *Microelectronics*, 39(2), 85-90, 2010 (article in Russian with an abstract in English)
- [3] P. Eaton, J. Benedetto, D. Mavis, K. Avery, M. Sibley, M. Gadlage, T. Turflinger, "Single event transient pulse width measurements using a variable temporal latch technique" *IEEE Trans. Nucl. Sci.*, 51(6), 3365-3368, 2004. <https://doi.org/10.1109/TNS.2004.840020>
- [4] B. Wiseman, "Design and Testing of SEU/SEL Immune Memory and Logic Circuits in a Commercial CMOS Process" in *IEEE Radiation Effects Data Workshop*, 1994, 51-55. <https://doi.org/10.1109/REDW.1994.633039>
- [5] S. I. Ol'chev, V. Y. Stenin, "CMOS logic elements with increased failure resistance to single-event upsets" *Russian Microelectronics*, 40(3), 156-169, 2011. <https://doi.org/10.1134/S106373971103005X> (article in Russian with an abstract in English)
- [6] J. E. Knudsen, L. T. Clark, "An area and power-efficient radiation hardened by design flip-flop" *IEEE Trans. on Nucl. Sci.*, 53(6), 3392-3399, 2006. <https://doi.org/10.1109/TNS.2006.886199>
- [7] Y. Monnet, M. Renaudin, R. Leveugle, "Hardening techniques against transient faults for asynchronous circuits" in 11th IEEE International Conference: On-Line Testing Symposium, IOLTS 2005. <https://doi.org/10.1109/IOLTS.2005.30>
- [8] S. F. Tyurin, A. N. Kamenskih, "Research into the reservation of logic functions at transistor level" In a world of scientific discoveries, 10(58), 232-247, 2014. <https://doi.org/10.12731/wsd-2014-10-18> (article in Russian with an abstract in English).
- [9] C. LaFrieda, R. Manohar, "Fault Detection and Isolation Techniques for Quasi Delay-Insensitive Circuits" in *International Conference on Dependable Systems and Networks*, 2004. <https://doi.org/10.1109/DSN.2004.1311875>
- [10] A. Balasubramanian, B. L. Bhuvu, J. D. Black, L. W. Massengill, "RHBD techniques for mitigating effects of single-event hits using guard-gates" *IEEE Trans. on Nucl. Sci.*, 52(6), 2531-2535, 2005. <https://doi.org/10.1109/TNS.2005.860719>
- [11] M. T. Moreira, G. Trojan, F. G. Moraes, N. L. V. Calazans, "Spatially distributed dual-spacer null convention logic design" *Journal of Low Power Electronics*, 10(3), 313-320, 2014. <https://doi.org/10.1166/jolpe.2014.1332>
- [12] S. A. Aketi, S. G. H. Cheng, J. Mekiey, P. A. Beerel, "SERAD: Soft Error Resilient Asynchronous Design using a Bundled Data Protocol," arXiv:2001.04039 [cs.AR]. <http://https://arxiv.org/abs/2001.04039v1>
- [13] A. Taubin, A. Kondratyev, J. Cortadella, L. Lavagno, "Behavioral Transformations to Increase Noise Immunity in Asynchronous Specifications," in *International Symposium on Advanced Research in Asynchronous Circuits and Systems*, 1999. <https://doi.org/10.1109/ASYNC.1999.761521>
- [14] D. Muller, W. Bartky, "A theory of asynchronous circuits" *Annals of computation laboratory of Harvard University*, V.29, 204-243, 1959.
- [15] K. M. Fant, S. A. Brandt, "NULL Convention Logic: a Complete and Consistent Logic for Asynchronous Digital Circuit Synthesis" in *International Conference on Application-Specific Systems, Architectures, and Processors*, 1996. <https://doi.org/10.1109/ASAP.1996.542821>
- [16] M. Kishinevsky, A. Kondratyev, A. Taubin, V. Varshavsky, *Concurrent Hardware: The Theory and Practice of Self-timed Design*, J. Wiley, 1994.
- [17] Y. A. Stephenkov, Y. G. Diachenko, V. S. Petrukhin, A. V. Filin, "The price of realizing the unique properties of self-timed circuits" *Systems and means of informatics*, 9, 261-292, 1999. (article in Russian with an abstract in English)
- [18] Y. A. Stephenkov, Y. G. Diachenko, G. A. Gorelkin, "Self-Timed circuits are the Microelectronics Future" *Radio-electronic issue*, 2, 153-184, 2011 (article in Russian with an abstract in English).
- [19] Ю. А. Степченков, А. Н. Денисов, Ю. Г. Дьяченко, Ф. И. Гринфельд, О. П. Филимонов, Н. В. Морозов, Д. Ю. Степченков, Л. П. Плеханов, Библиотека функциональных ячеек для проектирования самосинхронных полужаказных БМК микросхем серий 5503/5507, Техносфера, 2017. ISBN 978-5-94836-332-5 (in Russian).
- [20] D. Shang, A. Yakovlev, A. Koelmans, D. Sokolov, A. Bystrov, "Registers for Phase Difference Based Logic" *IEEE Trans. Very Large Scale Integration (VLSI) Systems*, 15(6), 720-724, 2007. <https://doi.org/10.1109/TVLSI.2007.898772>
- [21] Y.-C. Rhee, "Exclusive-OR and/or Exclusive-NOR Circuits Including Output Switches and Related Methods," US Patent No. 7,312,634 B2, 2007
- [22] Y. Stepchenkov, Y. Rogdestvenski, Y. Diachenko, D. Stepchenkov, Y. Shikunov, "Energy Efficient Speed-Independent 64-bit Fused Multiply-Add Unit" in 2019 IEEE Conference of Russian Young Researchers in Electrical and Electronic Engineering (EIConRus2019), 2019. <https://doi.org/10.1109/EIConRus.2019.8657207>
- [23] M. Berg, "Revisiting Dual Interlocked Storage Cell (DICE) Single Event Upset (SEU) Sensitivity" in *Microelectronics Reliability & Qualification Work Meeting (MRQW) 2013 and HiREV Industry Day*, El Segundo, CA, December 10-12, 2013.
- [24] T. Lakshmiavaraprasad, M. Sivakumar, B. K. V. Prasad, S. A. Inthiyaz, "Nanoscale CMOS technology for hardened latch with efficient design" *International Journal of Electronics and Communication Engineering*, 5(3), 343-349, 2012. ISSN 0974-2166
- [25] Y. V. Katunin, V. Y. Stenin, P. V. Stepanov, "Simulation of trigger two-phase CMOS logic cell characteristics, taking into account the separation of charge at the effects of individual nuclear particles" *Microelectronics*, 43(2), 104-117, 2014. <https://doi.org/10.7868/S0544126914020069> (article in Russian with an abstract in English)

## Performance Evaluation and Examination of Data Transfer: A Review of Parallel Migration in Cloud Storage

Mimouna Alkhonaini\*, Hoda El-Sayed

Department of Computer Science, Bowie State University, 20715, USA

### ARTICLE INFO

Article history:

Received: 05 November, 2019

Accepted: 21 February, 2020

Online: 09 March, 2020

Keywords:

Parallel

Transfer

Cloud

### ABSTRACT

Recent years have seen a continued pattern of development in the cloud computing field. Numerous approaches to maximize file transfer capacity are still completely standing for use on cloud computing storage; however, they do not maximize the advantage of data migration scalability and elasticity in cloud storage. One potential problem is that elasticity takes time; however, the scalability attributes that have not been fully exploited include multicore chips and parallelization that can further be leveraged to enhance the overall data transfer performance and efficiency. In that regard, considerable effort has been directed to multiprocessors. Such systems involve a plurality of processors or functioning units capable of independent operation to process separate tasks in parallel. Nevertheless, the penalization is complicated when a task requires several resources or signals to proceed with meaningful computation. Thus, accommodating equitable priority among tasks further complicates operations. In this paper, we propose a parallel server to cloud storage transfer system in which parallelism method can only be utilized in case of transferring a large number of files and applied in order to increase the transfer throughput. The data is transmitted into several chunks via TCP network within the same period slot in a single data path which indicates dataflow on parallelism. Our target in this system is that increasing number of processors and the problem size will simultaneously maintain the efficiency of the data transfer system. The proposed model is based on the combination of dynamic segmentation, CRS, AES, and hashing. In summary, the proposed model shows the potential to enhance the performance by increasing the data transferability. The performance of the proposed model will be measured with the help of comparing the average execution time with the number of processors and speedup of the entire parallel system.

### 1. Introduction

The cloud computing involves the provision of on-demand computing services to the customers. These services are similar to the usual services that can be obtained by using the physical computing equipment such as storage devices, servers, networking and many more. As the realization of the benefits of cloud computing come to light, many businesses, companies, organizations, and institutions are switching to the cloud services.

Cloud services are provided by the cloud service providers (CSP) who are responsible for manning all the infrastructures, software, and the platforms to which the customers subscribe. Performance remains a significant concern for the consumers who are still struggling with the decision of moving to the cloud. Though there are many significant standards in cloud computing, the primary standard is on the data migration performance from the non-cloud infrastructure to the cloud. This paper is an extension of the work which was initially published and presented in IEEE 20th International Conference on High-Performance Computing and Communications [1].

\*Mimouna Alkhonaini, COSC Department, 14000 Jericho Park Road, Bowie, MD 20715, 301-860-3964 & alkhonainim0522@student.bowiestate.edu

[www.astesj.com](http://www.astesj.com)

<https://dx.doi.org/10.25046/aj050207>



Typically, a multiprocessor includes a variety of computational units, a memory, a control, and at least one I/O processor. The functions of a job are initiated and processed, sometimes being moved from one computational unit to another. In the course of such operations, tasks must be synchronized and, in this regard, a function may require data from another function supplied through the I/O processor [2]. Under such circumstances, there is an issue in increasing number of processors against problem size.

The features of parallelism have been known since Babbage's effort to construct a mechanistic computer [3]. Industrial and academic researchers have studied every imaginable aspect of parallel computation. A system becomes slower due to combined cumbersome computation processes, therefore, there is a need of using parallel computing to improve and provide high levels of execution performance efficiency. Moreover, this research also provides the design and validation of the analytic performance of the parallel migration to enhance the speed of the system.

Related studies in the fields of data migration via parallelism have gained focus over the past few years. However, most of the proposed studies only get the standpoint of either a cloud provider or cloud consumers, not both. In the present work, the proposed scheme shall concentrate on allowing the cloud provider and also the consumer to accomplish data migration efficiently by exploiting potential improvements found in consumer PC multicore chips. Moreover, future cloud storage environments will be primarily designed and built on top of multicore technology.

In this paper, we propose a parallel migration system that can be made cost-optimal by adjusting the number of processors and the problem size. The parallel migration is achieved by dynamic distribution for the combination of file slicing, cryptography, fault tolerance, and hashing.

The remaining paper is structured in a manner that section 2 presents the related works in this field. Section 3 defines and models how the proposed system achieves parallel migration by dynamic distribution. Section 4 shows the experimental outcome and section 5 concludes the paper with some future remarks.

## 2. Related Works

In this section, we discuss some of the approaches related to the data migration parallelism as well as increasing file transfer bandwidth.

HTTP, SFTP, and SCP are the standard data migration communication protocols for point-to-point transfer. In terms of elasticity, the improvement is based on the work of [4] that helps to scale down the repetitive data migration through developing "checksum comparison" and the work presented in [5] prevents resource conflict by distinguishing "back-pressure". However, still, these approaches have thus far to capitalize on cloud elasticity. In our method, we aim at matching the amount of resources allocated to data transfer in parallel mode with the amount of resources it actually requires, avoiding over-provisioning or under-provisioning.

In terms of connection speed, the existing odd source to odd end target data migration speed is usually limited by either cloud provider settings or limits set by the hardware of physical connection. Though, one of the solutions to prevent these restrictions and to expand data migration throughput is to perform data migration from multiple servers concurrently. Even though, BTorrent [6] illustrates that this is rational but processing this data

involvement procedure (As It Is) is far from appropriate "for a one-time point-to-point" migration. However, our parallelization data migration combines data segmentation and erasure code, AES, and hash with developing parallel migration capacity and minimizing data transfer delay.

Multiple data transmission develops the processor's total bandwidth; however, it is limited because the "bottleneck" lies in the specific cloud processor's bandwidth. One more comparable system is the parallel transfer where files are prearranged through several input/output processors to minimize storage bottleneck, which allows transmission across several TCP connections concurrently. Another similar system can be applied in cloud storage, but the overheads to rearranged files across numerous storages should be considered in order to improve the file transmission performance. In our parallelization model, provisional buffer is created on the cloud machine, and these buffers are indicted to as the 'holes'. As the buffer hole is fully occupied, it is then taken away from the list. The entries of these buffer-holes are then tested with the descriptor-list to confirm if the buffer-hole which has been loaded by the arriving segment is rejected [1].

In [7], multi-hop and multi-path which are two optimization techniques to increase the performance of file transmission across WAN are briefly discovered. In multi-hop path splitting, throughput was improved by exchanging direct connection between start and end point via multi-hopping. On other hand, multi-path technique includes slicing data at the start point and sending it through various overlapping paths. Chunking and rebuilding data theoretically cause data corruption, damage or failure. Thus, our proposed model takes into consideration fault-protection by applying several Reed-Solomon (RS) code values along with the data sizes to supplementary explore the impact of different values.

The authors in [8] propose a cloud-based data management system targeted for big data science applications running across large and high geographical environment sites which shows expectable data transfer management performance in terms of cost and time. The system automatically implements and adjusts performance designs for the cloud platform structure for enhancing data and efficient schedule of the transfer process. Though, it shows a poor execution performance when compared with our proposed parallelization model.

Another similar approach [9] is the parallel data transfer where data are lined across several intermediate nodes that are spawned in order to avoid the bandwidth limitation, but the overheads to reallocated data across multiple nodes in source DC and destination DC have to be taken into attention for performance improvement on the file transfer.

## 3. Server to Cloud Parallel Data Transfer Modelling

### 3.1. General Concept of the Model

In this section, we define the outline of our server-to-cloud parallel transfer conception and formulate an arithmetic model constructed on the proposed parallel migration concept. In the rest of the paper, we then cover the server-to-cloud parallel migration task as parallel data transfer.

Figure 1 represents the construction overview of our parallel migration model. The process starts with the data as the input, the data is then segmented into chunks, every segmented data is

encrypted. Encrypted chunks are migrated to the cloud and then decrypted. The decrypted chunks are then compared against the un-encrypted segments on the local server. If they don't match, the process is taken back to the segmentation stage. If they match, the segments are then re-assembled and saved on the cloud server. We then end the process.

The following is the arrangement of status for a single file transmission from server to cloud storage.

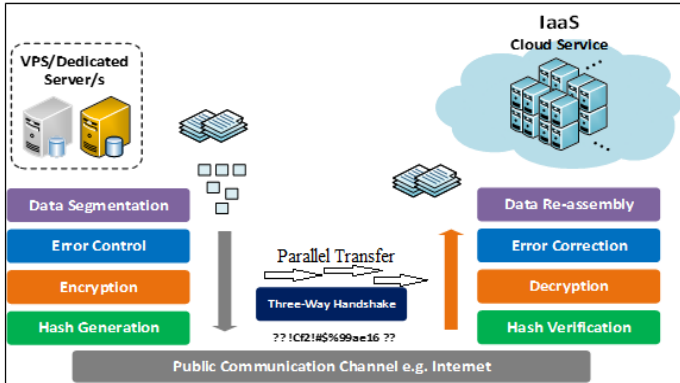


Figure 1: Overview of parallel transfer mechanism

- **Data Segmentation [10]:** Data segmentations split-up the bigger data units into smaller controllable data slices. In our data segmentation, we will be using an algorithm that will take the shortest time possible to segment larger volumes of data packets, while optimizing the memory efficiency of the working machines. In this algorithm, the system scans the data packets to find the size of the whole data to be segmented. The total data size is then used as a base for the determination of how many segments should be generated from the original data. Data size levels are then predefined to allow the categorization how a given data set belonging to a given size group is segmented. The categorizing of data based on the whole data size ensures that we have larger data size, the right segmentation size will be obtained in order to make the process faster. The data will then be split into smaller equal sized chunks of 4MB each. The chunks are assigned a sequence number each, according to the order in which they are segmented. If we have a larger volume of data, then more instances of segmentations will be initiated to make sure that less time is taken to process the whole data. The number of segmentation instances is dictated by the size of whole data.
- **Error control:** The end-to-end transmission of data from the server to the destination storage encompasses many steps which can be subjected to errors leading to data loss. Error control ensures that any error that occurs during the transmission of the data is detected and addressed. Reliable data transmission implements error detection and correction. Error correction enables a system to detect and correct both the bit-level and packet-level errors. There are two types of errors that can occur during the data transmission: single-bit error, in which only one-bit changes from 0 to 1 and vice versa and burst error where two or more bits change from 0 to 1 and vice versa. Burst-error is known as the packet-level error which results in duplication or re-ordering of the data. We are using the checksum method for error control which is applied at the upper-layer, and it uses the concept of redundancy. There are

two operations which are being performed in checksum technique: Checksum-generator on the server side and Checksum-checker on the cloud side while the local server makes use of the checksum-generator. The following is the procedure for the checksum generation:

- The data segments are sub-segmented into equal n-bits.
- This is followed by adding together the sub-segments with the usage of 1's compliment.
- The data segment is re-complimented to become a checksum.
- It is then sent alongside the data-unit.
- **Encryption:** The system uses an Advanced Encryption System (AES) with the RSA key-exchange. The symmetric encryption technique requires a proper key exchange to maintain the security of communication and minimize the risk of eavesdropping during the key exchange phase. RSA-2048 is then used for key exchange. The main reason for not choosing RSA for encryption is that it needs more processing power and is slower than the mighty AES.
- **Hash generation:** Hash functions are one-way which means that it is impossible to revert from the generated values to the initial values. The hash function is used in our system to enhance the confidentiality of the data (message). We are using the secure hashing algorithm (SHA) which was modeled after MD4 and its proposal was made by NIST to offer a more secure hash standard (SHS). This will produce a 160 bits hash value.
- **Three-way handshake initialization:** Three-way handshake is a flow control technique which allows the communicating devices to initiate the communication platform. In Figure 2, the local server will initiate the three-way handshake by sending the cloud server a SYN (synchronization) message. This is a way of asking the cloud server if it is ready to communicate. The recipient, which is the cloud server sends back a SYN/ACK message to the local server telling it that it is ready for the communication. The local server then sends an ACK (Acknowledgement), and the connection between the two sides is established. The data is then transmitted.

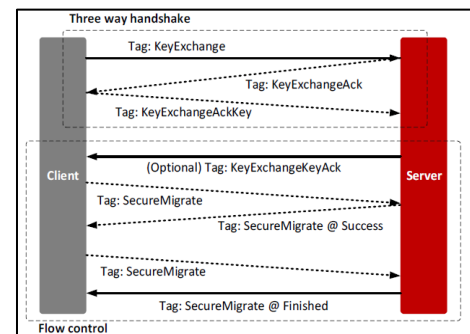


Figure 2: Three-way handshake initialization.

- **Hash verification:** Hash checks for the integrity of the message. The cloud server receives a segment and runs SHA algorithm over it, if it matches, then we increment the number of received healthy segments by one, we ignore (discard) the rest of the segments which do not match. The system waits until receiving other segments (we know the total number of segments sender



is going to send for us) and see how many of them are healthy (their integrity can be verified).

- **Decryption:** With the Cipher Block Chaining decryption, application of the inverse-cipher function to the first cipher-text block results into an output-block which passes through the XOR operation with the initialization-vector to allow the recovery of the first plaintext block. The inverse-cipher function is also applicable to the second cipher-text block which provides the output-block which is then XORed with the first cipher-text block for the recovery of the second plaintext block. Generally, the recovery of any plaintext block (except the first plain-text), the inverse cipher-function applies to the corresponding cipher-text block, and the output-block is XORed with the prior cipher-text block.
- **Error correction:** Error correction allows the cloud server which receives the data to reconstruct the original data in the event that it was corrupted during transmission. Error correction is implemented using the hamming code. Hamming code is a single-bit error correction method that uses the redundant bits. The redundant bits are included on the original data and their arrangement is in such a way that any different and incorrect bits will lead to the production of various error results. The corrupted bits are then identified and upon the identification of the corrupted bits, the cloud server which receives the data is capable of reversing its values hence, correcting the errors. Hamming code applies to any data length and makes use of the relationship between the data and the redundancy-bits. **Checksum-checker:** The cloud server makes use of the checksum-checker. The following is the procedure for the checksum checker:

- The cloud server which receives the data-unit will divide the received data-unit into equal sub-segments.
- All the sub-segments are then added together using the 1's compliment.
- The outcome is complimented again. If the final result is found to be zero, the system accepts the data while when it is found to be 1, the data should be rejected and considered to have errors.
- **Reassembling of data [11]:** After all the data segments have arrived and each segment is verified, an algorithm to arrange the segments in order according to their sequence numbers will be used. This ensures that the data segments will be ordered back to their original state before being segmented on the local server [12]. In Figure 3, the flowchart diagram shows how the model receives the segment and allocates the buffer space for each segment. There are more segments in the buffer, by comparing the size of the segment with the size of the space available in the buffer, the segment is taken back. If there are no more data in the buffer, then the data unit is identified, and the data unit is bound to the context. It will then check if it is occupied by a different data unit. The bound data is then updated, and the segment is inserted into the data unit. The number of segments is then checked, if there are any remaining segments, they will return back to step one. If there are no remaining segments, then the header will be updated and the data unit will be transmitted. The numbering sequence plays a crucial role as it is the sequence number used to arrange back the data to its original state [13]. The size of the unencrypted segments on the source server is furthermore tested and

matched with the size of the corresponding decrypted segments on the destination server. Re-assembling of data segments will only take place after all the previous stages have been successfully completed.

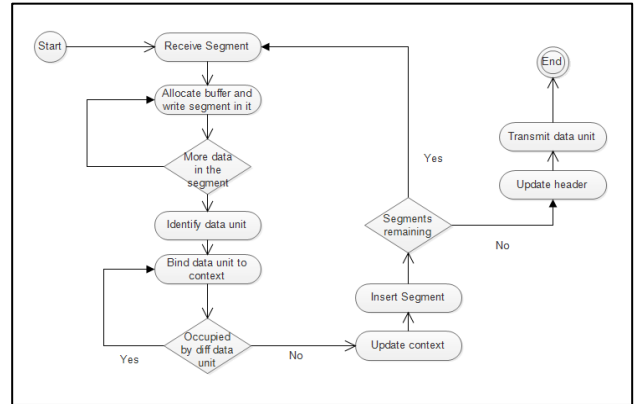


Figure 3: Reassembling of segments.

### 3.2. Parallel Transfer Algorithm

Server user may perhaps definitely benefit from the rapid growth of multicore systems. The physical server typically holds several regular data centers or computer storage, where commodity high-performance multicore bunches are employed. Our migration algorithm designed for one direction data flow which begins at the server storage and ends at the cloud storage. Algorithm 1 shows the parallel-serial transmission which starts from a master processor acting as a management system. The aim of the master processor is to reach the final output by collecting the necessary information from the slave processors. In our migration algorithm, we will assume that the data is ready for transfer after the four stages: data chunks, error control/correction, encryption/decryption with AES-256 and SHA-256 algorithm which is identified as the significant component of the integrity process. The transfer process will start by taking the ready data list, FList, and divides it between the slave processors. Correspondingly, each slave processor would obtain blocks of FList. We use single program multiple data (SPMD) algorithm where there is a single instruction that each processor performs, but on various data. Each slave processor would establish its secure channel, port, and buffer. Each slave processor will then send its FList to the cloud buffer before the storage stage. The final task of the slave processor is to update its FList by removing the sent chunks from the list. This procedure would reflect to have a higher bandwidth transmission capacity. Finally, the master processor receives the FList from all the slave processors and takes the re-transmission decision. If the FList size=0, it means that all the data chunks have been sent successfully. However, if FList size!=0, it means that the master processor will request for the re-transmission of the missing chunks by the method explained in [1]. The master processor would close the connection after all the re-transmission requests. At this phase, the cloud buffer is full of the data that need to be checked for integrity, verified and re-build to be stored.

### 3.3. Time Factor of Parallel Transfer

The performance of the proposed model will be evaluated by computing the average of execution time, the number of processors, and the speedup ratio.

**Algorithm 1** Parallel Migration Algorithm

```

Input: FinalChunksList FList
1: procedure ALLOCATESBLOCKTOEACHPROCESSOR
2:   P ← Number of processors
3:   if Processor 0 then           ▷ Processor 0 is the root
4:     Scan FList size
5:     Establish Secure Connection (3-way handshake )
6:     Divide the FList into x by y blocks   ▷ Matrix
7:     for i ← 0, x - 1 do
8:       for j ← 0, y - 1 do
9:         Send block (i, j) to processor (i+j) mod P
10:      end for
11:    end for
12:  end if
13: end procedure
14: procedure EACHPROCESSORTRANSMISSION
15:   (Note that RS,AES25,SHA5126 is applied on FList)
16:   Receive FList blocks from the root
17:   S ← Scan block size
18:   for index ← 0, S - 1 do
19:     Initiate the TCP
20:     Transfer the block
21:     Remove the block (FList[index])
22:   end for
23:   Return FList
24: end procedure
25: if Processor 0 then
26:   if FList Non Empty then
27:     while NotAllFListsSent do
28:       send the next FList
29:     end while
30:   else Close Connections
31:   end if
32: end if
    
```

**3.3.1 Data Distribution Time (Segmentation+ CRS+ AES + HashGen)**

Divided into four actions, file chunking, encoding, encryption, and hash generation. In order to minimize the delay between individual execution time, transferring has to be started directly after the segmentation when the exact chunk is ready, without waiting for the overall segments process to be completed. Server execution time can also be minimized by manipulating the chunk size and sequence when the network resource is unutilized.

**3.3.2 Parallel Data Migration Time**

This time factor indicates the transfer from local server to buffers in the cloud storage. In order to increase the throughput of this phase, the parallelism method can be applied only if the transmission files are of a large number. Processor 0 would act as the root and starts to define the number of the chunks and divide them among the slave processors. As a result, each slave processor would collect a block of chunks. Later, they would establish their connections and send their chunk lists to the cloud buffers. The control would then be passed to TCP in order to finalize the transmission task.

**3.3.3 Data Amalgamation Time (HashVerify +AES +CRS +Re-Assembling)**

In this time factor, the file reassembling is the prime task. It also involves the migration from the cloud buffers to the destination storages. This step also contains massive disk operations such as the writing process.

**3.4. Model and Evaluation of Parallel Migration**

The parallel performance was analyzed by displaying speedup rate and throughput to illustrate the parallel model profit. The

speedup of parallel operations on P processors is defined as the following [14]:

$$S_p = \frac{T_1}{T_p} \tag{1}$$

Where  $T_1$  is the sequential execution time using one processor,  $T_p$  is the parallel execution time using P processors, p and 1 are indexes as written in equation 1. While Sequential Transfer Time equation ( $T_1$ ) is:

$$T_1 = \frac{D_s}{t_e} \tag{2}$$

Where  $D_s$  is data size in MB,  $t_e$  is transfer speed in MB/s. Parallel Transfer Time ( $T_p$ ) = data distribution time in the server + transfer time + data amalgamation time in the cloud. Hence, the speedup rate is acquired as below:

$$S_p = \frac{\frac{D_s/t_e}{T_p}}{D_s/t_e + D_s(1/P)/t_e}$$

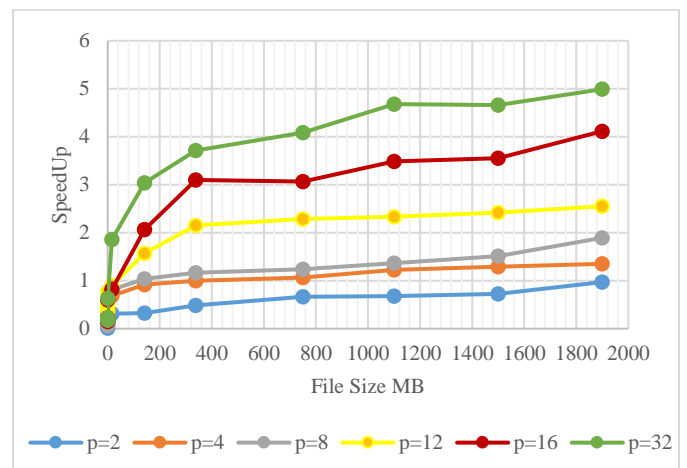


Figure 4: Speedup model for parallel transfer, where p is the number of processors.

It can be noticed that the smaller file transfer size (not many of small and large files together), a minimum number of parallel processors are required to accomplish a speedup. However, when trying to parallelize the transfer, there is no prediction of when the packet loss rate would begin to increase exponentially which causes a critical overhead. Thus, smaller file sizes do not benefit from the parallelization. Therefore, Figure 4 shows that the speedup rate is steep for the file size of below 4MB.

For a larger data transfer size, the speedup rate grows as the number of parallel processors are increased. However, performance gains are hardly worth when each subsequent increase in processors number brings a lesser performance profit contrasted to the previous increment.

**4. Experimental Evaluation**

This section shows the performance evaluation for our parallel migration system on an Infrastructure as a Service (IaaS) cloud environment.

4.1. Experiment Setup

We carry out these experiments on two separate VMs (VM hardware were identical) hosted on Cray XC40 within two locations: Oregon and Amsterdam. Linux Operating System in various cores with 8 GB of memory was assembled on the VMs. All the encryption /decryption stages are constructed with the help of python cryptography 2.1.4.

Our experiment concentrates on migrating a single file from the server to cloud storage. The model is designed in such a way that each part of the system is pluggable. Thus, replacing an encryption algorithm will not affect the selection of the coding algorithm. We have chosen numerous file sizes, starting from .05 MB to 1900MB and RS parameters (k, m) in range of (1 ≤ m ≤ k and k ≤ 256, where m=parity) in order to evaluate the transfer rate. For coding layer, we employed PyECLib source on GitHub (1.5.0) module with liberasurecode source on GitHub (1.5.0) as Interface to erasure back-ends for Reed-Solomon coding.

4.2. Preliminary test

To evaluate the actual performance, we first examined the performance of our algorithm by measuring the execution time in the server (source) and cloud storage (destination) processes for a data, depending on the file size and variability of RS parameters k and m.

In Table 1 below, we showed the average operating time for the source and destination for each process. It is quite apparent that the source average is mainly estimated by the slicing process because it involves additional parameters and computations than the other internal operations.

Table 1: Average execution time in the source/destination.

OPERATIONS	TIME (ms)	SUM
CRS Coding	691.99	1,089.74
AES Encryption	116.78	
SHA Hash	280.97	
SHA Verify	277.39	487.55
AES Decryption	119.53	
CRS Decoding	90.63	

The throughput define as that is the amount sum of processed data that execute in a period of time (processed data /second) [15]. It is concluded as the following relation:

$$P_n = \frac{W}{T_p} \quad (3)$$

Where W is indicated as the workload, T<sub>p</sub> as the execution time required to accomplish the calculation using P processors [16], p is index as written in equation (3). From equation 3, the throughput for each location is shown in the Table 2. Table 2 depicts the comparison between the average throughputs of transmitting many file sizes between Oregon and Amsterdam locations. The transfer throughput gained for Oregon and Amsterdam is ~.9, .7 MB/ms respectively. The range of throughput achieved when transferring the file is astonishingly large. It was observed that the throughput

rate does not follow a certain way; the variation seems to arise randomly.

Table 2: Locations Transfer Throughput.

File sizes	Oregon TO	Amsterdam
	Amsterdam	TO Oregon
0.05	0.005101482	0.001007
0.10	0.009208418	0.001696
0.55	0.038767525	0.008251
1.00	0.019112421	0.011328
17.00	0.041170096	0.073851
142.00	0.086551034	0.263185
339.00	0.093888415	0.333905
750.00	0.107918311	0.442913
1,100.00	0.102385909	0.468758
1,500.00	0.109188015	0.502546
1,900.00	0.114588619	0.579061

4.3. Result

Figure 5 and Figure 6 are linearly dependent features and are just shown for further clarification. It is verifiable that by choosing bigger fault tolerance rate in the coding stage (smaller k in proportion to m) the final transfer time increases rapidly. It is shown that transferring bigger files with no-error tolerance (k =m) added in the coding stage, the system will exhibit the best performance, especially in case of bigger file sizes. Choosing k such that it covers 10-15% error correction without the need for data retransmission in smaller file sizes less than 24MB, the impact on transmission time is noticeably less than the profit it brings.

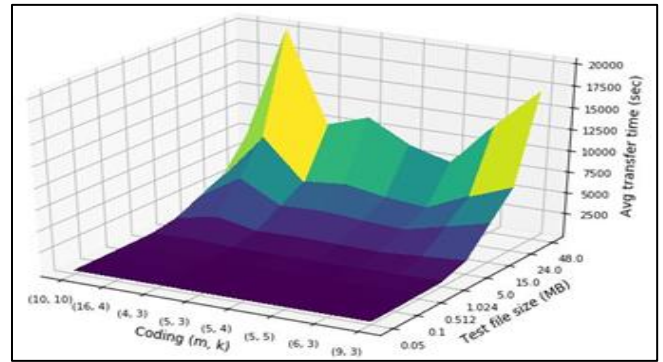


Figure 5: Average execution time in source side.

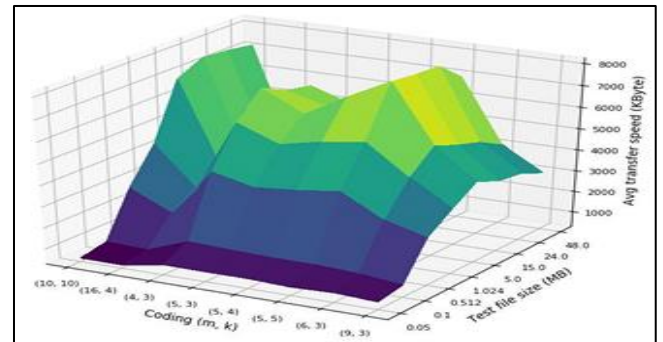


Figure 6: Average execution time in destination.

In Figure 7, we portray a 2D graph of the speedup rate against data size for a different number of processors. It can be noted that analogous to our model, speedup cannot be obtained for the data migration that is below 0.5GB by using 2, 4, 8, and 16 parallel processors. The overall note is steady with our approach, the speedup is extremely poor for small file size, but increases for bigger file size.

Although the speedup rate is not computed yet in the real environment, we found an independent argument that can be used in our model to compute the speedup in the real environment. Based on our observation, the independent argument is close to 0.47. Hence, we are certain about the fact that when the count of parallel processors is greater than 8 and the data size is bigger than 1GB, the speedup will be achieved.

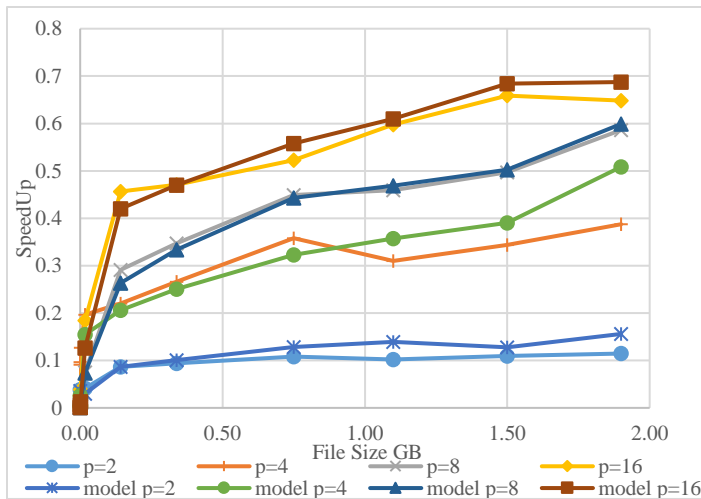


Figure 7: Comparing actual speedup and our model for parallel transfer, where p is the number of processors.

## 5. Conclusion and Future Work

This paper concentrated on explaining and exhibiting a parallel design for data transmission in cloud environment. First, we demonstrated the proposed model. Next, we presented the implementation and evaluation of the proposed model. Though our parallel transfer model shows a prospect to enhance the performance, however, our implementation exposed that there is an independent argument that should be considered. This study also suggests that there are overhead factors that can affect the parallel transfer performance, such as initialization, chunking the data file, and transfer time. Thus, those overhead effects should be investigated in order to reach maximum performance. In brief, we should consider the computation of hardware power and processors I/O's speed that is assigned by the CSP to design the parallel migration model.

### Conflict of Interest

The authors declare no conflict of interest.

### References

[1] M. Alkhonaini and H. El-Sayed, "Optimizing Performance in Migrating Data between Non-cloud Infrastructure and Cloud Using Parallel Computing," *2018 IEEE 20th International Conference on High Performance Computing and Communications (HPCC)*, Exeter, United Kingdom, 2018, pp. 725-732.

[2] Hesham El-Rewini, Hesham H. Ali, and Ted Lewis. 1995. Task Scheduling in Multiprocessing Systems. *Computer* 28, 12 (December 1995), 27-37. DOI: <https://doi.org/10.1109/2.476197>

[3] S. Razdan, *Fundamentals of Parallel Computing*. New Delhi: Alpha Science International, 2014.

[4] "rsync(1) - Linux man page." [Online]. <http://linux.die.net/man/1/rsync>. 2015.

[5] H. Pucha, M. Kaminsky, D. G. Andersen, and M. A. Kozuch, "Adaptive File Transfers for Diverse Environments," in *USENIX 2008 Annual Technical Conference on Annual Technical Conference*, Berkeley, CA, USA, 2008, pp. 157-170.

[6] Bram Cohen, "The BitTorrent Protocol Specification." [Online]. [http://www.bittorrent.org/beps/bep\\_0003.html](http://www.bittorrent.org/beps/bep_0003.html). 2015.

[7] G. Khanna et al., "Multi-hop Path Splitting and Multi-pathing Optimizations for Data Transfers over Shared Wide-area Networks Using gridFTP," in *Proceedings of the 17th International Symposium on High Performance Distributed Computing*, New York, NY, USA, 2008, pp. 225-226.

[8] R. Tudoran, A. Costan, R. Wang, L. Bouge, and G. Antoniu, "Bridging Data in the Clouds: An Environment-Aware System for Geographically Distributed Data Transfers," in *Cluster, Cloud and Grid Computing (CCGrid)*, 2014 14th IEEE/ACM International Symposium on, 2014, pp. 92-101.

[9] C. B. M. Lek, O. B. Yaik and L. S. Yue, "Cloud-to-cloud parallel data transfer via spawning intermediate nodes," *TENCON 2017 - 2017 IEEE Region 10 Conference*, Penang, 2017, pp. 657-661. doi: 10.1109/TENCON.2017.8227943

[10] M. Alkhonaini and H. El-Sayed, "Minimizing Delay Recovery in Migrating Data between Physical Server and Cloud Computing Using Reed-Solomon Code," *2018 IEEE 20th International Conference on High Performance Computing and Communications (HPCC)*, Exeter, United Kingdom, 2018, pp. 718-724.

[11] M. Alkhonaini and H. El-Sayed, "Migrating Data Between Physical Server and Cloud: Improving Accuracy and Data Integrity," *2018 17th IEEE International Conference On Trust, Security And Privacy In Computing And Communications/ 12th IEEE International Conference On Big Data Science And Engineering (TrustCom/BigDataSE)*, New York, NY, 2018, pp. 1570-1574. doi: 10.1109/TrustCom/BigDataSE.2018.00226.

[12] "Sequence data submission and accession numbers", *FEBS Letters*, vol. 360, no. 3, pp. 322-322, 1995.

[13] C. Diot and F. Gagnon, "Impact of out-of-sequence processing on the performance of data transmission", *Computer Networks*, vol. 31, no. 5, pp. 475-492, 1999.

[14] Roosta, S. " *Parallel Processing and Parallel Algorithms: Theory and Computation* ", ISBN: 0-387-98716-9, Springer Verlag, 2000.

[15] Kermarrec, A.; Bougé, L. and Priol, T. "Euro-Par 2007 Parallel Processing ", 13th International Euro-Par Conference: Lecture Notes in Computer Science, ISBN 978-3-540-74465-8, Vol. 4641, 2007.

[16] Hwang, K. and Xu, Z. (1998). *Scalable Parallel computing*. New York: McGraw-Hill.



## A Regenerative Energy Recovery System for Electric Vehicles Charging A Battery at A Low Speed

Wonseok Yeo, Sungchul Jung, Seungtaik Kim, Keonho Park, Jongsun Ko\*

*Dankook University, Electronics and Electrical Engineering, Institute, KS009, Republic of Korea*

### ARTICLE INFO

*Article history:*

*Received: 04 December, 2019*

*Accepted: 01 February, 2020*

*Online: 09 March, 2020*

*Keywords:*

*Regenerative Energy*

*Energy Recovery*

*Battery*

*Electric Vehicle*

*L-C Resonance*

*Permanent magnet synchronous motor*

### ABSTRACT

*In this paper, a regenerative energy recovery system for electric vehicles charging a battery at a low speed is proposed. When a permanent magnet synchronous motor driving the electric vehicles is driven by a generator, the generated voltage is controlled to rise or drop by using the L-C resonance circuit. As the circuit only has three capacitors and three IGBTs, the proposed system is very simple. A resonance frequency is found through frequency analysis of the L-C resonance circuit; furthermore, using the resonance effect, a generated voltage control algorithm is proposed. PI duty control in the algorithm raises the generated voltage and reverse PI duty control in the algorithm reduces the generated voltage. The results of simulations and experiments confirm that a remodeled electric vehicle by the proposed system is charged to the driving battery. The results also demonstrate that a small energy storage capacity, which is a disadvantage of the electric vehicle, is largely compensated without increasing the complexity of the electric vehicle.*

### 1. Introduction

Due to emitting zero greenhouse gas, electric vehicles (EVs) are completely eco-friendly [1]. In addition, heat loss of a motor in EVs is very low as compared to that of internal combustion engines, so a high driving efficiency can be expected. Accordingly, the interest in the EVs that can solve the problems of internal combustion engine cars has been increasing worldwide. However, energy storage capacity of batteries, energy storage devices of EVs, is significantly smaller as compared to that of internal combustion engines [1,2]. Therefore, commercialization of EVs requires that EVs have efficient use and management of energy.

The main components of an EV include inverter, cluster, battery, driving motors, and battery management system (BMS) (see Figure 1). Due to the characteristics of the EVs, the most driving motor is a permanent magnet synchronous motor (PMSM) which has a high starting torque and a high efficiency [3,4]. To briefly describe each component, the battery is an energy storage device for driving EVs, while the BMS protects the battery and is a system for efficient energy use and charging [5]. The inverter converts DC voltage into AC voltage, while the PMSM generates driving force by using the converted AC voltage. When the PMSM operates as a generator, back EMF of the PMSM is converted from AC voltage to DC voltage through freewheeling diodes of the inverter [5].

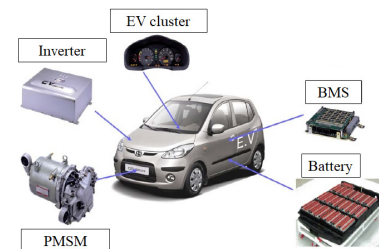


Figure 1: Main components of EVs

The PMSM may be operated as the generator when driving downhill or in coasting operation. The generated electrical energy can be used in two ways. Firstly, a method commonly called a dynamic braking consumes electric energy with resistances mounted in the EVs or eddy currents. However, a disadvantage of this method is an increase of heat inside, because electric energy dissipates into heat energy [6-8]. Secondly, a method called the regenerative energy recovery returns the generated electrical energy to the power supply system [6]. Therefore, the small energy storage capacity, which is the disadvantage of the EVs, can be compensated by using a regenerative energy recovery system (RERS) [5].

The conventional RERS recovers small energy. It increases the complexity of the EV system by using a DC/DC converter to charge the regenerative energy into supercapacitors. [5,6,9]. In

\*Corresponding Author: Jongsun Ko, Email: [jsko@dankook.ac.kr](mailto:jsko@dankook.ac.kr)

addition, a maximum energy recovery switching scheme is developed [6]. This system is charging supercapacitors using switches at the bottom of the inverter. At present, several RERS studies are underway.

In this paper, a very simple new RERS charged in a driving battery with a high capacity and a high nominal voltage through a L-C resonance circuit in EVs is proposed. As the circuit has only three capacitors and three IGBTs, the proposed system is simple. The proposed system is then analyzed by simulations using Matlab Simulink and experiments using a remodeled commercial EV.

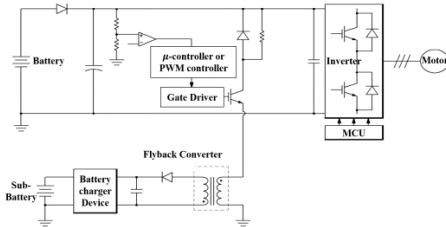


Figure 2: Regenerative energy control device for the motor driving system (Korean Patent)

## 2. Conventional RERS

An example of the RERS is shown in Figure 2. The battery on the upper side is used for the driving motor on the right. The flyback DC/DC converter is used to reduce the generated voltage of the motor [5]. The reduced voltage charges a sub-battery of a low capacity and a low nominal voltage. There are three disadvantages to this method. Firstly, it can be used only when the generated voltage is higher than chargeable voltage. Secondly, it cannot be used in the EV without the sub-battery. Thirdly, the regenerative power is small and has a small braking force, because it is charged in the sub-battery of a low capacity.

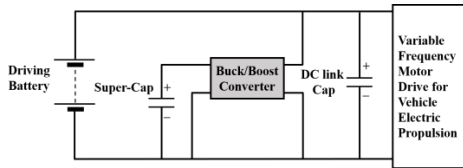


Figure 3: RERS using a supercapacitor

An example of the RERS using the supercapacitors is shown in Figure 3 [10]. When braking, the energy is charged in the supercapacitor using the buck converter and, when driving, the energy is discharged in the supercapacitor using the boost converter. Depending on the type of the RERS, the energy stored in the supercapacitor is either used directly for driving or is charged by the battery [6,10,11]. The use of DC/DC converters increases the complexity of the EV.

On the other hand, the proposed system has two advantages over the system shown in Figure 2. The first advantage is that even if the generated voltage is lower than the chargeable voltage, charging is possible by controlling the voltage through the L-C resonance control technology. Furthermore, the second advantage is that sufficient regenerative energy can be obtained because the proposed system is charging the driving battery instead of the sub-battery. Compared to the system in Figure 3, the proposed system is advantageous in the EV complexity due to its simple hardware configuration.

## 3. Proposed RERS Analysis

### 3.1. Simple Hardware Structure

Figure 4 shows a conceptual diagram of the proposed RERS. As shown in Figure 4, since the DC link voltage is short-circuited with the driving battery, the driving battery is charged only when the DC link voltage is upper than the driving battery. However, if the DC link voltage is higher than the maximum voltage of the driving battery, the BMS disconnects the driving battery to protect the battery. Therefore, the driving battery can be charged only when magnitude of the DC link voltage is within a certain range depending on the driving battery condition. In order to control DC link voltage, capacitors of  $C_1, C_2, C_3$  are used to generate resonance in a circuit consisting of inductors and resistors of the PMSM, and a resonance rate is changed by three IGBTs above the capacitors [5]. For the purpose of three-phase equilibrium, the capacitance of  $C_1, C_2, C_3$  is selected equally even in the resonance.

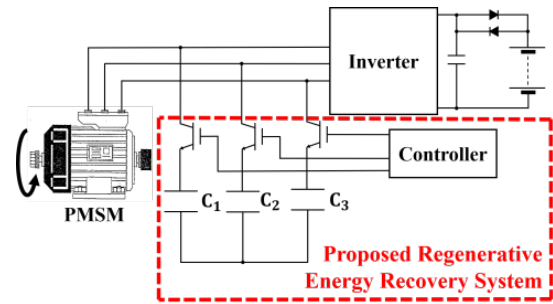


Figure 4: Conceptual diagram of the proposed system

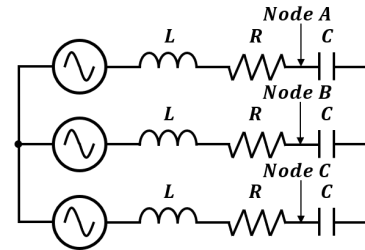


Figure 5: PMSM equivalent circuit for L-C resonance

### 3.2. Resonance Frequency Analysis

Figure 5 shows a PMSM equivalent circuit for L-C resonance. The L and the R are equivalent phase leakage inductance and resistance of the PMSM, and voltage sources are a three-phase voltage source generated by the PMSM. The DC link voltage varies in proportion to the voltage of nodes A, B, and C. The resonance is caused by using the capacitors in each phase for varying the voltages at nodes A, B, and C. As the circuit is a balanced three-phase circuit, the nodes A, B, and C all have same equivalent impedance. The equivalent impedance of each node is obtained as shown in Equation (1).

$$\begin{aligned}
 Z &= (j\omega L + R) \parallel \left( \frac{1}{j\omega C} + \alpha \parallel \alpha \right) \\
 &= \frac{R(C^2 R^2 \omega^2 + C^2 L^2 \omega^4 - 2CL\omega^2 + 3)}{3\{C^2 R^2 \omega^2 + (CL\omega^2 - 1)^2\}} \\
 &+ j \frac{\{CR^2(CL\omega^2 - 2) + L(CL\omega^2 - 3)(CL\omega^2 - 1)\}\omega}{3\{C^2 R^2 \omega^2 + (CL\omega^2 - 1)^2\}}
 \end{aligned} \tag{1}$$



with:

$$\alpha = j\omega L + R + \frac{1}{j\omega C}$$

where  $\omega$  is an electrical angular frequency. The frequency at which the imaginary part of the impedance is zero and the voltage response is the largest is a resonance frequency. There are five solutions where the imaginary part becomes zero, because degree of  $\omega$  is five. The solutions are shown in Equation (2).

$$\omega = 0$$

$$\omega = \pm \sqrt{\frac{-R^2C + 4L - \sqrt{R^4C^2 + 4L^2}}{2L^2C}} \quad (2)$$

$$\omega = \pm \sqrt{\frac{4L - CR^2 + \sqrt{R^4C^2 + 4L^2}}{2L^2C}}$$

The electrical angular frequency is always higher than zero, unless the EV is stopped; furthermore, assuming Equation (3),

$$R^2C \approx 0 \quad (3)$$

the solutions which cause the imaginary part to be zero are as follows (see Equation (4)):

$$\omega \approx \frac{1}{\sqrt{LC}}, \sqrt{\frac{3}{LC}} \quad (4)$$

Among the two frequencies, the frequency with a larger voltage response is the resonance frequency. The resonance frequency is selected considering the vehicle's main speed, wheel radius, gear ratio, number of poles [5]. The speed of the motor is 1km/h and the electric frequency of the motor to match the resonance frequency is :  $f_c = 1\text{km}/1\text{h} * 1\text{h}/3600\text{sec} * 1000\text{m}/1\text{km} * 1/2\pi r * \text{poles}/2 * \text{gear ratio}$ . The capacitance is calculated from this electric frequency( $f_c$ ) and equation (4) [5]. In order to achieve the resonance effect frequently, it is advantageous to match the main driving speed of the vehicle with the resonance frequency.

### 3.3. Generated Voltage Control Algorithm

A flow chart of the generated voltage control algorithm is shown in Figure 6. The flow chart shows a method of controlling the DC link voltage to the suitable voltage for the driving battery charging according to the condition of the DC link voltage. If there is no a wide gap between the DC link voltage  $V_{DC}$  and flag voltage  $V_{flag}$ , voltage control is possible by the resonance rate. Therefore, the  $V_{DC}$  is compared with the minimum controllable voltage  $V_{c.min}$  and the maximum controllable voltage  $V_{c.max}$ . If the  $V_{DC}$  is between the  $V_{c.min}$  and the  $V_{c.max}$ , compare with the  $V_{flag}$ . If the  $V_{DC}$  is higher, a reverse PI duty control is performed. A pulse width modulation of 1kHz is then generated through a pulse generator and used as IGBT gate input signals. There are the three IGBTs in the proposed RERS in Figure 4. In the opposite case, the PI duty control is performed.

The reverse PI duty control in the proposed system sets P gain and I gain to negative values, and the PI duty control sets P gain and I gain to positive values. Therefore, the PI duty control

increases the duty, as the difference of DC link voltage at the reference voltage increases, and the reverse PI duty control decreases the duty. The adjusted duty increases or decreases the DC link voltage to match the reference voltage.

If the reference voltage of the PI duty control  $V_{ref(PI)}$  and the reference voltage of the reverse PI duty control  $V_{ref(RPI)}$  are equal to  $V_{flag}$ , the ripple of the  $V_{DC}$  makes comparison between  $V_{DC}$  and  $V_{flag}$  very difficult. Therefore, the  $V_{ref(RPI)}$  is set above the  $V_{flag}$  and below the battery maximum voltage and the  $V_{ref(PI)}$  is set below the  $V_{flag}$ .

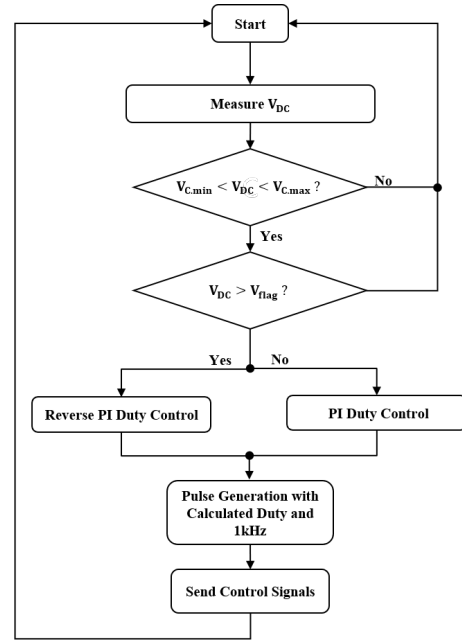


Figure 6: Flow chart

## 4. Simulations

Three simulations have been performed. First, a simulation of frequency response has been performed. Characteristic of frequency response is that the equivalent circuit of a PMSM's stator is taken into account. The second simulation has been performed to verify the generated voltage control algorithm. The characteristic to verify the generated voltage control algorithm is that the DC link voltage response is fast because of low inertia, low viscous friction and short battery response time. Using this fast response, the proposed system algorithm is verified. The third simulation has been performed taking into account the remodeled commercial EV. The characteristics considered the EV are that the DC link voltage response is slow, because the EV has high inertia, high viscous friction, and long battery response time.

### 4.1. Frequency Response of Equivalent Circuit

Table 1: 3kW PMSM Parameters Used for the Remodeled Commercial EV

Parameter	Value	Unit
Rated Power	3	<i>kW</i>
Rated Current	17.2	$A_{rms}$
Rated Speed	3000	<i>rpm</i>
Rated Torque	9.54	<i>Nm</i>
Stator Phase Resistance	0.102	$\Omega$
Stator Phase Inductance	1.22	<i>mH</i>
Poles	8	-
Inertia	0.28	<i>kgm<sup>2</sup></i>
Viscous friction	0.026	<i>Nms</i>

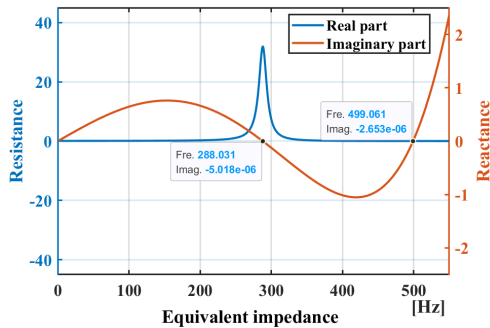


Figure 7: Frequency response of PMSM equivalent circuit for L-C resonance

The simulator for the frequency response with the capacitors and without the capacitors is shown in Figure 8. If capacitors in a red box in Figure 8 is removed, the simulator is a common 3-phase rectifier circuit. The opposite case is the L-C resonance circuit. This simulator can find the resonance frequency, which is either 288Hz or 499Hz, and also shows the resonance effect.

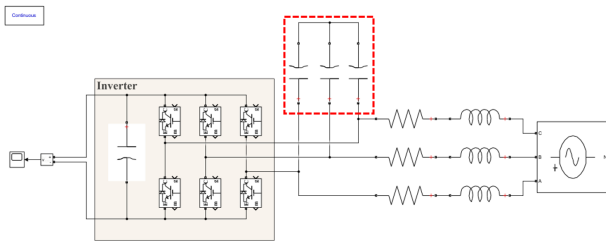


Figure 8: Simulator for frequency response

In this simulation, the DC link voltage for frequency is shown in Figure 9. The frequency of the highest voltage response is 288Hz in the L-C resonance circuit. Therefore, the resonance frequency is 288Hz. From 1Hz to 416Hz, the DC link voltage of the circuit with the capacitors is higher than the DC link voltage of the circuit without capacitors. In addition, after 416Hz, the DC link voltage of the circuit with the capacitors is lower than the DC link voltage of the circuit without the capacitors. In PMSM, generated voltage is generally proportional to frequency. When the frequency and generated voltage are low, the generated voltage can be raised using the L-C resonance circuit [5]. In contrast, when the frequency is high, and the generated voltage is high, the generated voltage can be reduced using the L-C resonance circuit. In this way, it is possible to control voltage, since the resonance rate is changed when the capacitors and the IGBTs switching duty are adjusted.

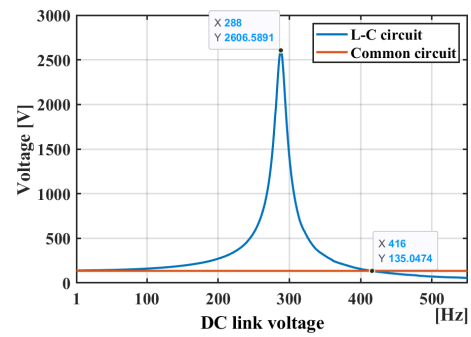


Figure 9: Simulation results of frequency response

#### 4.2. Generated Voltage Control Algorithm Verification

The simulator to verify the generated voltage control algorithm is shown in Figure 10. The parameters used in this simulator are shown Table 2. Due to the high back EMF of the PMSM, RCD snubber is used to reduce the switching stress of the IGBTs. Due to the small inductance of 4.5kW PMSM, voltage rise using resonance is low at the desired speed. To maximize the voltage rise, the inductance (15mH) is added in front of the capacitance (1.25mF).

Table 2: Parameters Used in the Algorithm Verification

Item	Parameter	Value	Unit
PMSM	Rated Power	4.5	<i>kW</i>
	Rated Current	17.9	$A_{rms}$
	Rated Speed	2000	<i>rpm</i>
	Rated Torque	21.5	<i>Nm</i>
	Stator Phase Resistance	0.2	$\Omega$
	Stator Phase Inductance	2.625	<i>mH</i>
	Poles	6	-
	Inertia	0.00369	<i>kgm<sup>2</sup></i>
	Viscous friction	10	$\mu Nms$
Driving Battery	Initial SoC	84	%
	Rated Power	3	<i>kW</i>
	Rated Voltage	295	<i>V</i>
	Maximum Voltage	340	<i>V</i>
	Minimum Voltage	224	<i>V</i>
	Response Time	30	<i>sec</i>
	Proposed System	Phase Capacitance	1.25
Phase Inductance		15	<i>mH</i>
Snubber Resistance		500	$\Omega$
Snubber Capacitance		4.7	<i>nF</i>
$V_{flag}$		332	<i>V</i>
$V_{c,min}$		280	<i>V</i>
$V_{c,max}$		400	<i>V</i>
$V_{ref(RPI)}$	335	<i>V</i>	
$V_{ref(PI)}$	330	<i>V</i>	

Simulation results without the algorithm are shown in Figure 11, while simulation results with the algorithm are shown in Figure 12. The torque input from 0 to 15 seconds is -5Nm, and torque input from 15 to 30 seconds is -10Nm. A flag in Figures 11 and 12 is a variable for distinguishing the control (1 : reverse PI duty control, 2 : PI duty control, 3 : no control). In a voltage waveform

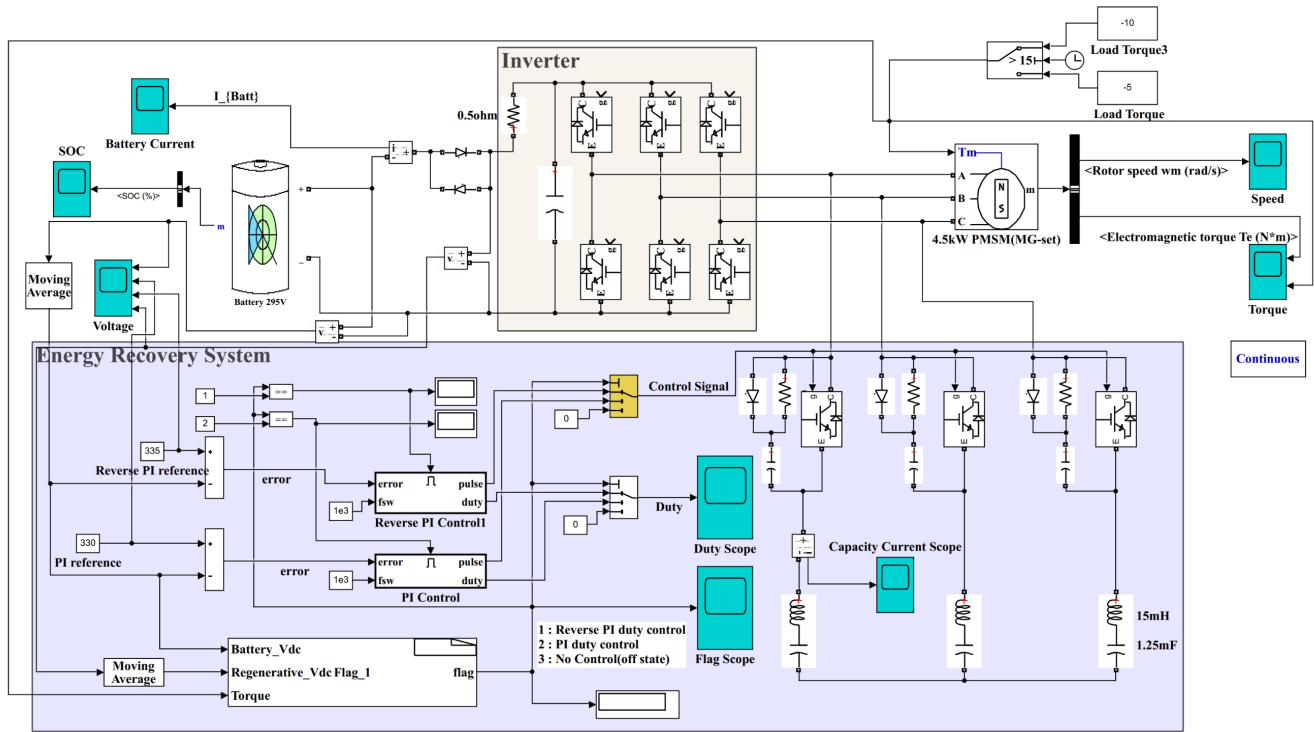


Figure 10: Simulator for the generated voltage control algorithm verification

of Figure 12 from 0 to 15 seconds, the PI duty control (flag 2) is performed, because the  $V_{DC}$  is lower than the  $V_{flag}$ . In order to raise the generated voltage, the duty ratio of the PI duty controller steady state output is 1. The voltage and current waveforms in Figure 12 are higher than those in Figure 11. In the voltage waveform of Figure 12 from 15 to 30 seconds, the reverse PI duty control (flag 2) is performed, because  $V_{DC}$  is higher than  $V_{flag}$ . The resonance rate is changed by the reverse PI duty control so that  $V_{DC}$  is controlled to  $V_{ref}(RPI)$  in voltage in Figure 12. On the other hand, in the voltage in Figure 11, the battery voltage  $V_{batt}$  rises above the battery maximum voltage. In the EV, when the battery voltage rises above the battery maximum voltage, the BMS disconnects the DC link capacitor from the battery. Therefore, battery charge current  $I_{BC}$  does not flow when EVs are applied. Because  $V_{batt}$  in Figure 12 does not exceed the battery maximum voltage, the battery charge current  $I_{BC}$  flows when the proposed system is applied to the EVs.

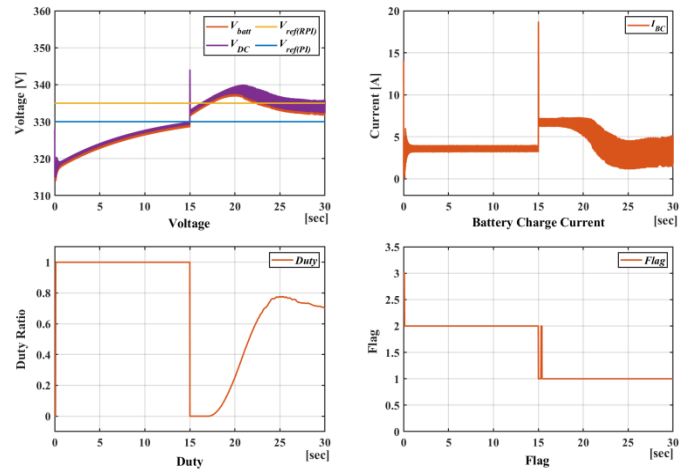


Figure 12: Simulation results without the voltage control algorithm on torque variation

### 4.3. Energy Recovery Rate Considered the Remodeled EV

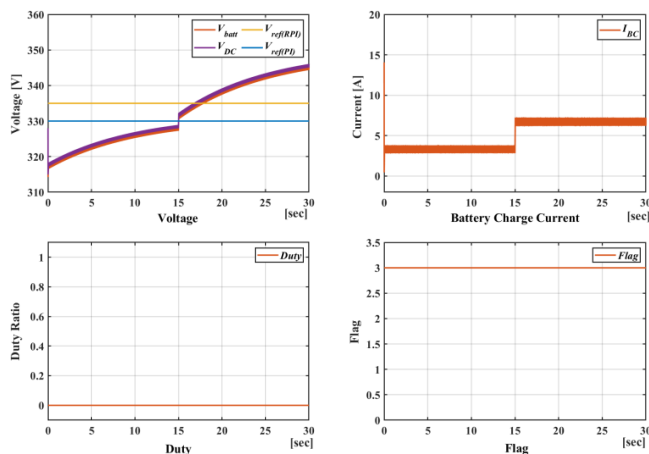


Figure 11: Simulation results without the voltage control algorithm on torque variation  
[www.astesj.com](http://www.astesj.com)

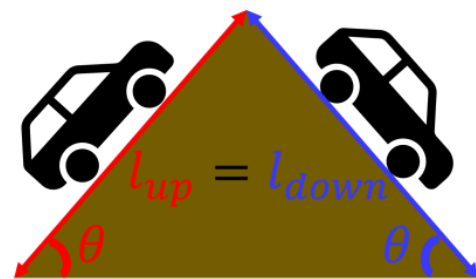


Figure 13: Road environment measured by the energy recovery rate

An energy recovery rate  $\eta$  is defined by Equation (5).  $E_{BC}$  is battery charge energy, and  $E_{BD}$  is battery discharge energy.

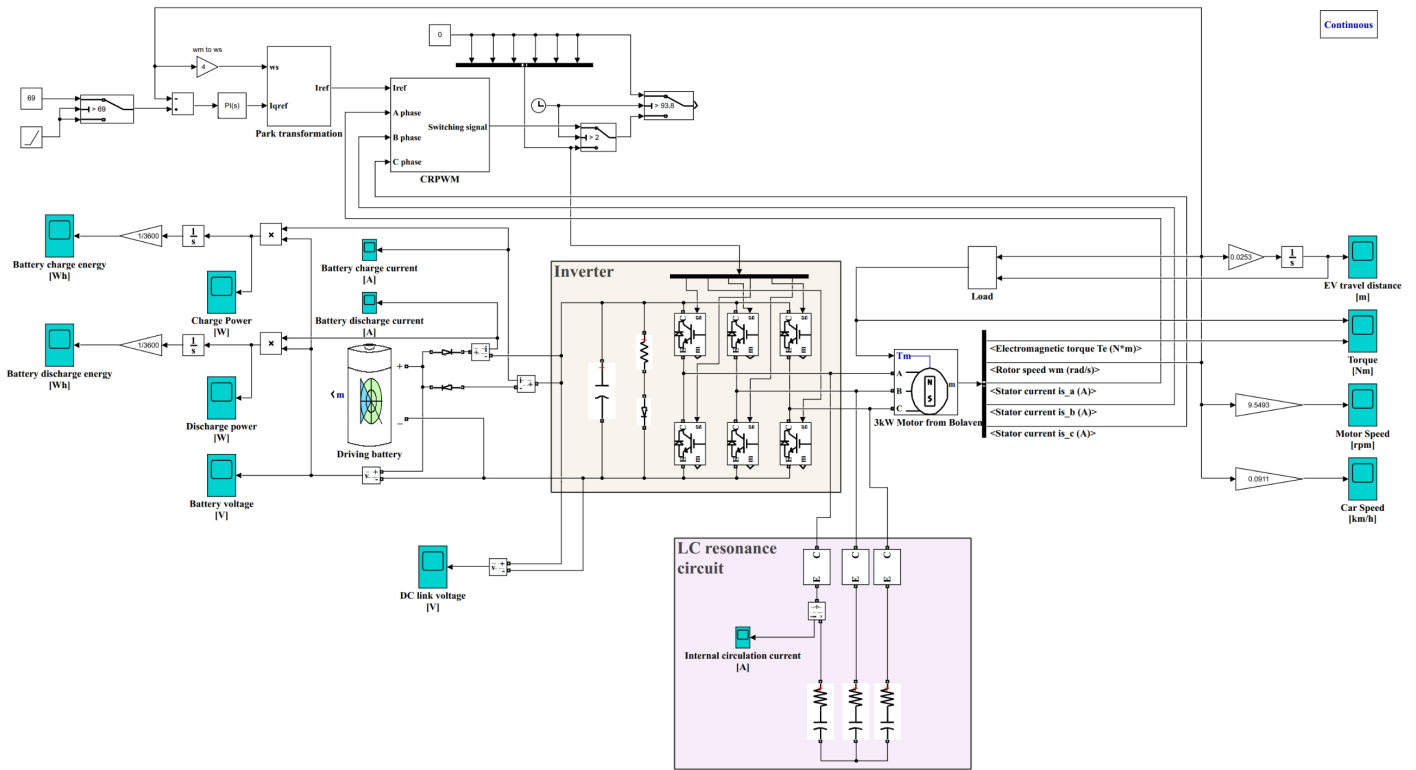


Figure 14: Simulator considered the remodeled commercial EV

$$\eta = \frac{E_{BC}}{E_{BD}} \times 100 \quad (5)$$

Measurement road environment is a road with the same travel distance and the same slope as shown in Figure 13. Since the EV input by the slope is the force of  $mg\sin(\theta)$ , this torque is put into the mechanical input of the PMSM in the simulation.

Travel distance of the EV  $D_{EV}$  is calculated using Equation (6). When the EV moved 150m, PMSM is stopped so that the same travel distance is obtained.

$$D_{EV} = \int (\omega_m \times \frac{1}{2\pi G} \times 2\pi r) dt \quad (6)$$

A  $\omega_m$  is the speed of the PMSM (rad/s), the G is the gear ratio and r is the wheel radius of the EV.

Table 3: Parameters of the Remodeled Commercial EV

Item	Parameter	Value	Unit
Driving Battery	Initial SoC	10.5	%
	Rated Power	3	kW
	Rated Voltage	295	V
	Maximum Voltage	340	V
	Minimum Voltage	224	V
	Response Time	500	sec
Proposed System	Phase Capacitance	250	$\mu F$
Power Transmission Device	Gear	9.3	—
Road Environment	Torque	13.5	Nm
	Distance	150	m
	Wheel Radius	0.235	m

A simulator considered the remodeled commercial EV is shown in Figure 14. Applying the environment in Figure 13, the parameters in Tables 1 and 3 to this simulator, the 3kW PMSM cannot run the high speed needed for the reverse PI duty control. For that reason, only the PI duty control has been performed. Also, due to the slow DC link voltage response, the duty of the PI duty control output is 100%. Therefore, the three IGBTs of the proposed system are replaced by shorting a emitter and a collector. The three IGBTs are short-circuited only in the downhill condition where the PMSM can act as a generator. The resistance of the L-C resonance circuit is equivalent to lead resistance, which is very small. The PMSM is driven by speed control in the uphill condition.

Two simulations considered the remodeled commercial EV have been performed. Firstly, to see change in the generated voltage, existence and non-existence of the proposed system have been simulated after removing the driving battery. Secondly, to see change in the energy recovery rate, existence and nonexistence of the proposed system have been simulated after installing the battery.

The generated DC link voltage and the remodeled EV travel distance after the proposed system is removed are shown in Figure 15 (a). Before connecting the battery, the simulation results in the capacitor model without the battery to see the controllability with the voltage that can be charged to the battery through the proposed system. The generated DC link voltage and the remodeled EV travel distance after the proposed system is installed are shown in Figure 15 (b). The remodeled EV travels the same distance of 150m, but the DC link voltage in Figure 15 (b) nearly doubles as compared to the DC link voltage in Figure 15 (a). The DC link voltage in Figure 15 (a) is always lower than the minimum voltage of the driving battery, so the battery cannot be charged. However,

the DC link voltage in Figure 15 (b) can be charged, because there is a section higher than the minimum voltage of the driving battery. At brake points in Figure 15 (a) and Figure 15 (b), a mechanical brake is activated, after which the DC link voltage is reduced.

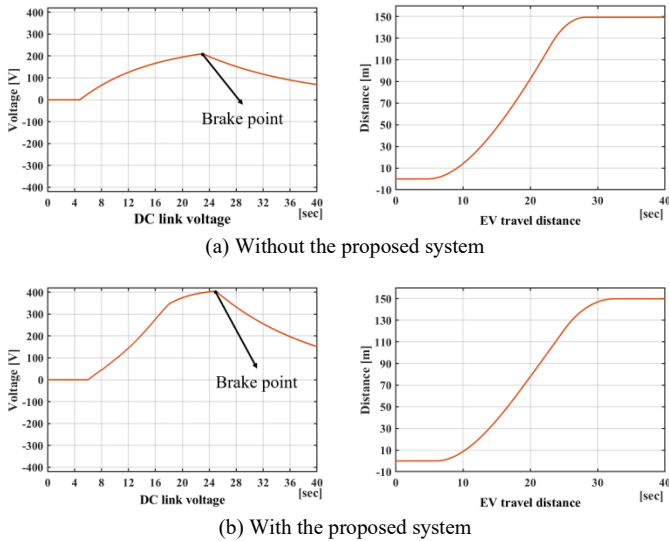


Figure 15: Downhill simulation results without the driving Battery

Battery voltage, discharge current, discharge energy, and the remodeled EV travel distance in the driving uphill condition are shown in Figure 16. In this condition, the driving battery is discharged. 32.8689Wh is consumed while traveling 150m. As the driving battery's energy is consumed, the battery voltage in Figure 16 decreases. The battery discharge current in Figure 16 is displayed because the remodeled EV is initially driven at the accelerated speed, while the remodeled EV is driven at the constant speed after 18 seconds.

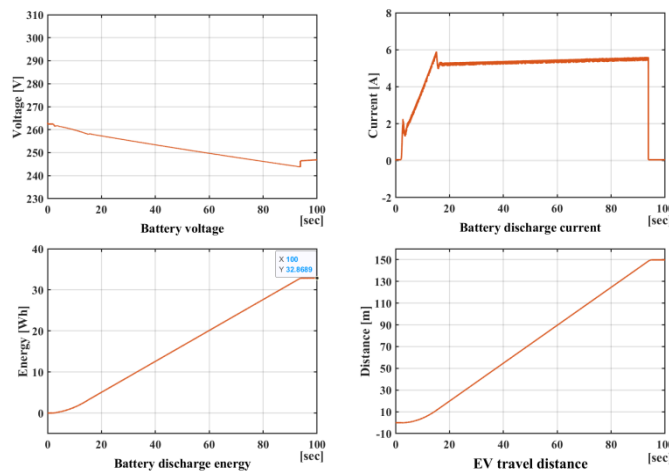
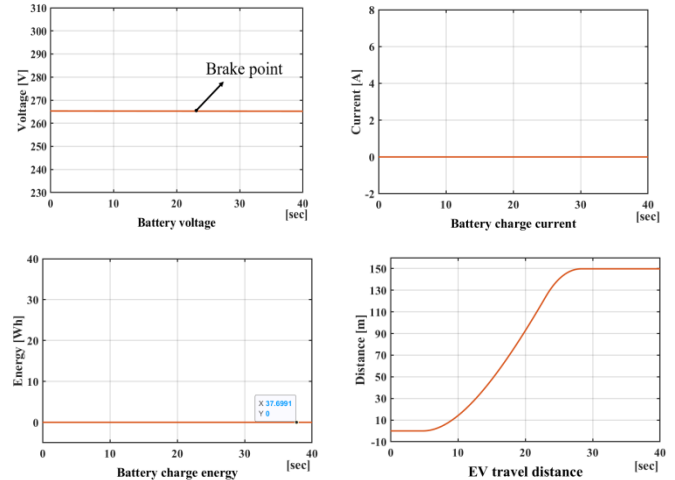


Figure 16: Uphill simulation results with the driving battery

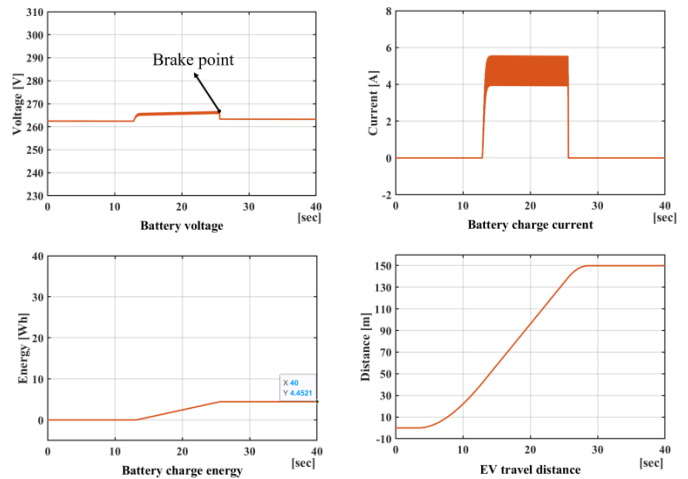
Battery voltage, charge current, charge energy, and the remodeled EV travel distance in the driving downhill condition without the proposed system are shown in Figure 17 (a). Although the remodeled EV traveled 150m, the energy is not recovered, as the generated voltage is lower than the battery voltage.

Battery voltage, charge current, charge energy and remodeled EV travel distance in the driving downhill condition with the

proposed system are shown in Figure 17 (b). While the remodeled EV traveled 150m, the energy is recovered because the generated voltage is lower than the battery voltage. Therefore, the battery voltage and the charge current raise. At the brake point, the mechanical brake is activated, after which the battery stops charging. The charged energy in the battery is 4.451Wh. The energy recovery rate is computed to 13.54% using Equation (5).



(a) Without the proposed system



(b) With the proposed system

Figure 17: Downhill simulation results with the driving battery

Battery voltage, charge current, charge energy, and the remodeled EV travel distance in the driving downhill condition without the proposed system are shown in Figure 17 (a). Although the remodeled EV traveled 150m, the energy is not recovered, as the generated voltage is lower than the battery voltage.

Battery voltage, charge current, charge energy and remodeled EV travel distance in the driving downhill condition with the proposed system are shown in Figure 17 (b). While the remodeled EV traveled 150m, the energy is recovered because the generated voltage is lower than the battery voltage. Therefore, the battery voltage and the charge current raise. At the brake point, the mechanical brake is activated, after which the battery stops charging. The charged energy in the battery is 4.451Wh. The energy recovery rate is computed to 13.54% using Equation (5).



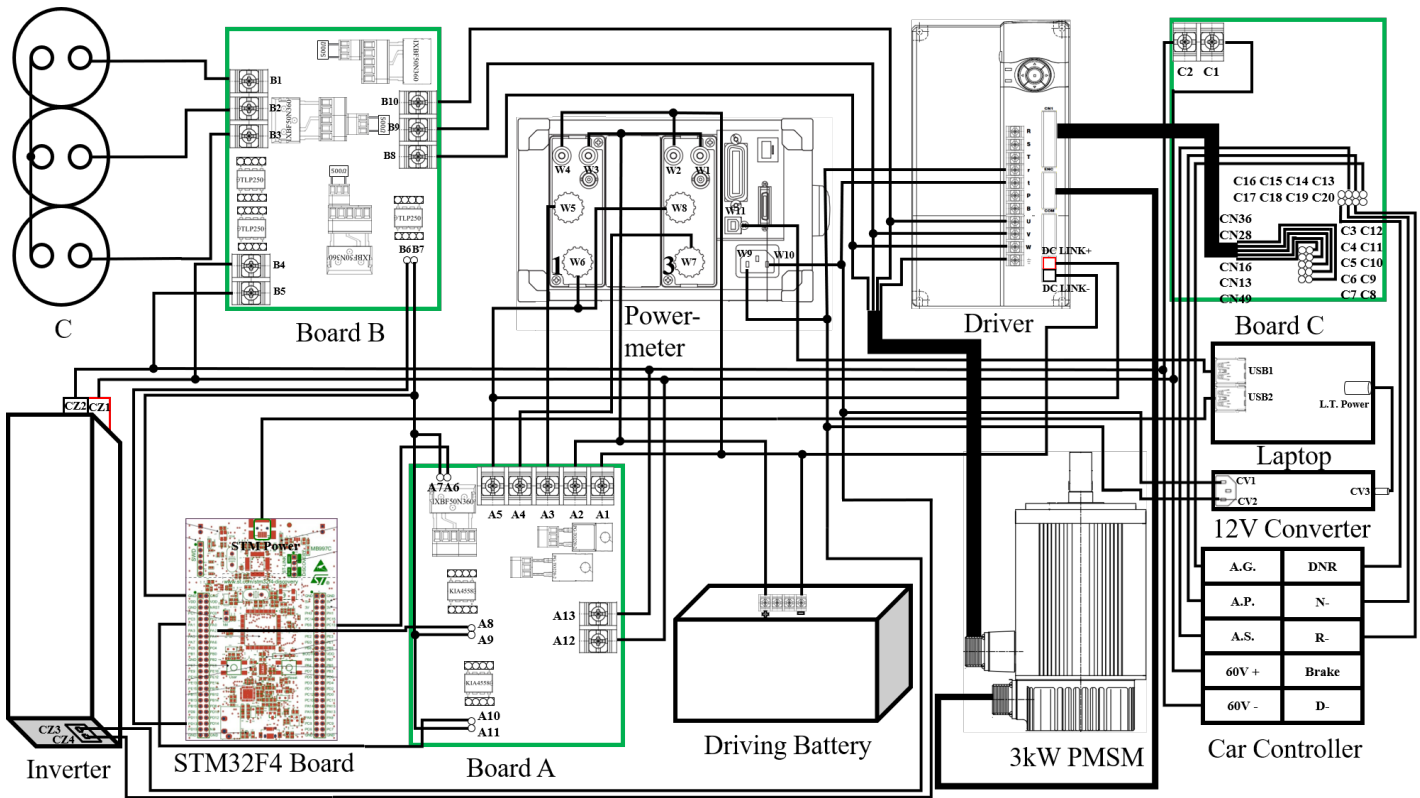


Figure 19: Connection diagram of the remodeled commercial EV

## 5. Experiment

A small commercial EV has been replaced with the 3kW PMSM, motor driver, gear and driving battery; then the proposed system has been installed in a small commercial EV. Interior and exterior of the remodeled commercial EV are shown in Figure 18. The upper left is a front part of the remodeled EV, while the upper right is a picture of installing the replaced 3kW PMSM. The bottom left shows equipment installed in a back seat of the remodeled EV. This equipment includes a board C for connecting the remodeled EV, motor driver, board A and B for the proposed system, inverter for driving the motor driver, laptop, power meter, and so on. In the bottom right, there are the power meter and laptop for measuring the energy recovery rate, and three capacitors of the proposed system.

A wiring diagram of the equipment has mounted on the remodeled EV is shown in Figure 19. A car controller, which send signals from the remodeled EV, has been connected to the motor driver via the board C.

A map and road at the experimental site place in Figure 13 are shown in Figure 20. Two experiments have been performed. First, to see the change in the generated voltage, existence and nonexistence of the proposed system have been experimented with after removing the driving battery. Second, to see the change in the battery charge energy, existence and nonexistence of the proposed system have been experimented with after installing the driving battery. The parameters used in the experiments are shown in Tables 1 and 3.



Figure 18: The remodeled commercial EV

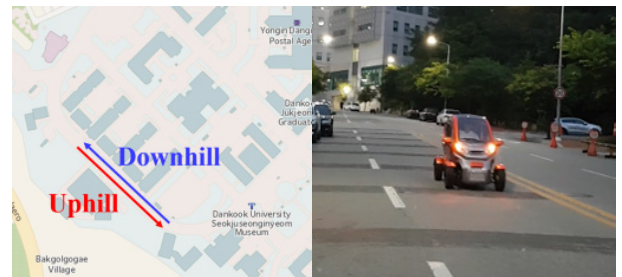
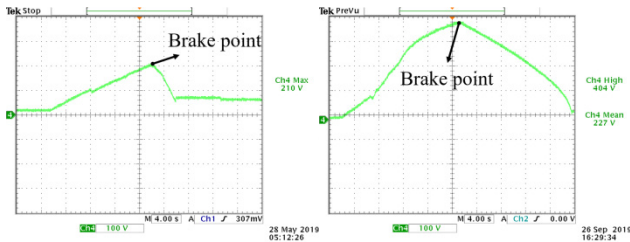


Figure 20: Map and road of the experiment place

In downhill experiments, the low slope of the road cannot output the high speed needed for the reverse PI duty control. For that reason, only the PI duty control has been performed in the experiments. Also, due to the slow DC link voltage response, the duty of the PI duty control output is 100%. Therefore, the three IGBTs of the proposed system have been replaced by shorting a emitter and a collector.

5.1. Energy Recovery Rate Considered the Remodeled EV

Figure 21 shows experimental results without the driving battery. Figure 21 (a) shows DC link voltage without the proposed system and (b) shows DC link voltage with the proposed system. Comparing the (a) and (b) in Figure 21, the DC link voltage almost doubled. The driving battery cannot be charged in Figure 21 (a), because the DC link voltage is always lower than the minimum voltage of the driving battery. However, the DC link voltage in Figure 21 (b) can be charged, because there is a section higher than the minimum voltage of the driving battery. At brake points in Figure 21 (a) and (b), the mechanical brake is activated, after which the DC link voltage is reduced.



(a) Without the proposed system (b) With the proposed system

Figure 21: DC link voltage of downhill experiment without the driving battery

Battery voltage, discharge current, discharge power, and discharge energy in the driving uphill condition are shown in Figure 22. As much as the driver activates the accelerator, the battery discharge current and discharge power is shown. 32.878Wh is consumed while traveling 150m. As the driving battery's energy is consumed, the battery voltage is reduced.

The results on the driving downhill condition without the proposed system are shown in Figure 23 (a). Since the generated DC link voltage is lower than the battery voltage, the energy is hardly recovered.

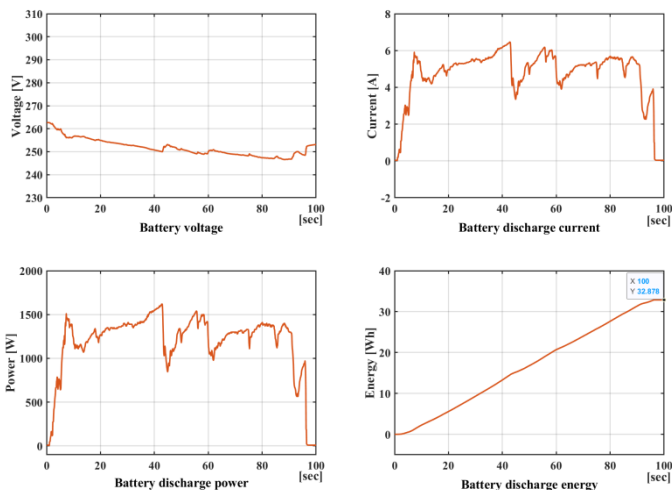
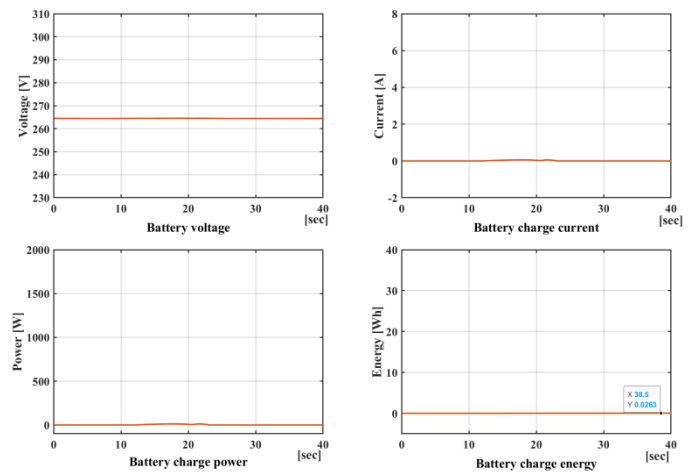


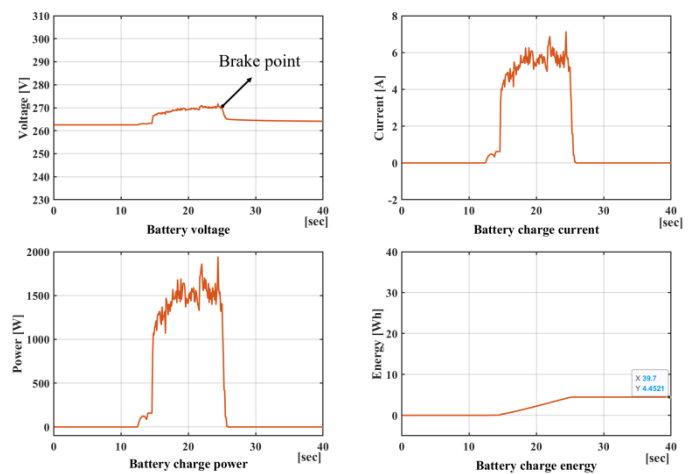
Figure 22: Uphill experiment results with the driving battery

Experimental results for the driving downhill condition with the proposed system are shown in Figure 23 (b). The generated DC link voltage is higher than the battery voltage. Therefore, the energy is charged to the battery, increasing the battery voltage and charge current and showing the charge power in Figure 23 (b). At the brake point in Figure 23 (b), the mechanical brake is activated,

after which the generated voltage reduces, and the battery charge stops. The charge energy in the battery is 4.4521Wh. The energy recovery rate is computed to 13.54% using Equation (5). This result complements the small energy storage capacity of the EVs, increasing travel distance on a single charge.



(a) Without the proposed system



(b) With the proposed system

Figure 23: Downhill experiment results with the driving battery

6. Conclusion

In this paper, a very simple new RERS was proposed to complement the EVs with a low energy storage capacity. The conventional RERS uses DC/DC converters to increase the complexity of the EV or has a small recovery area. The proposed system does not increase the complexity of the EVs, as the hardware is very simple. Furthermore, the recovered energy is large, because the generated voltage is controlled to the optimal level for the driving battery.

Three major analyses were performed. Firstly, the proposed system was analyzed. The results of this analysis showed that the circuit is very simple, and resonance frequency was formulated. Secondly, the simulation of the proposed system was performed, which allowed us to test the formulated resonance frequency and the generated voltage control algorithm. In addition, the energy recovery rate amounted to 13.54% in the simulation considering

the remodeled commercial EV. Third, the using the remodeled commercial EV was performed. In the experiment, the energy recovery rate amounted to 13.54%. The results showed that the proposed system can very simply significantly compensate for the small energy storage capacity, which is a disadvantage of the EVs.

### Acknowledgments

The present research was supported by the research fund of Dankook University in 2020.

### References

- [1] C. C. Chan, "The State of the Art of Electric, Hybrid, and Fuel Cell Vehicles," in *Proceedings of the IEEE*, vol. 95, no. 4, pp. 704-718, Apr. 2007. <https://doi.org/10.1109/JPROC.2007.892489>
- [2] C. Zheng, W. Li and Q. Liang, "An Energy Management Strategy of Hybrid Energy Storage Systems for Electric Vehicle Applications," in *IEEE Transactions on Sustainable Energy*, vol. 9, no. 4, pp. 1880-1888, Oct. 2018. <https://doi.org/10.1109/TSTE.2018.2818259>
- [3] G. Pellegrino, A. Vagati, B. Boazzo and P. Guglielmi, "Comparison of Induction and PM Synchronous Motor Drives for EV Application Including Design Examples," in *IEEE Transactions on Industry Applications*, vol. 48, no. 6, pp. 2322-2332, Nov. 2012. <https://doi.org/10.1109/TIA.2012.2227092>
- [4] J. Nerg, M. Rilla, V. Ruuskanen, J. Pyrhönen and S. Ruotsalainen, "Direct-Driven Interior Magnet Permanent-Magnet Synchronous Motors for a Full Electric Sports Car," in *IEEE Transactions on Industrial Electronics*, vol. 61, no. 8, pp. 4286-4294, Aug. 2014. DOI:10.1109/TIE.2013.2248340
- [5] K. Park, S. Jung, S. Kim and J. Ko, "Generated Voltage Control of EV PMSM for Maximizing Energy Recovery Rate using Switched Resonant L-C," 2019 14th Annual Conference System of Systems Engineering (SoSE), Anchorage, AK, USA, May 2019, pp. 195-199. <https://doi.org/10.1109/SYSE.2019.8753832>
- [6] R. E. Hellmund, "Regenerative Braking of Electric Vehicles," in *Transactions of the American Institute of Electrical Engineers*, vol. XXXVI, pp. 1-78, Jan. 1917. <https://doi.org/10.1109/T-AIEE.1917.4765458>
- [7] Sung-Chul Jung, In-Sik Yoon, and Jong-Sun Ko, "Electromagnetic Retarder's Power Recovery Device and Voltage Control," in *The Transactions of Korean Institute of Power Electronics*, vol. 21, no.5, pp. 396-403, Oct. 2016.
- [8] Sung-Chul Jung, Jong-Sun Ko, "A Study on Electromagnetic Retarders Power Recovery System and Regenerating Voltage Control," in *The Transactions of The Korean Institute of Electrical Engineers*, vol. 66, no. 8, pp. 1207-1214, Aug. 2017.
- [9] P. J. Grbovic, P. Delarue, P. Le Moigne and P. Bartholomeus, "The Ultracapacitor-Based Regenerative Controlled Electric Drives With Power-Smoothing Capability," in *IEEE Transactions on Industrial Electronics*, vol. 59, no. 12, pp. 4511-4522, Dec. 2012. <https://doi.org/10.1109/TIE.2011.2181129>
- [10] S. Lu, K. A. Corzine and M. Ferdowsi, "A New Battery/Ultracapacitor Energy Storage System Design and Its Motor Drive Integration for Hybrid Electric Vehicles," in *IEEE Transactions on Vehicular Technology*, vol. 56, no. 4, pp. 1516-1523, July 2007. <https://doi.org/10.1109/TVT.2007.896971>
- [11] J. Cao and A. Emadi, "A New Battery/UltraCapacitor Hybrid Energy Storage System for Electric, Hybrid, and Plug-In Hybrid Electric Vehicles," in *IEEE Transactions on Power Electronics*, vol. 27, no. 1, pp. 122-132, Jan. 2012. <https://doi.org/10.1109/TPEL.2011.2151206>

## In Body Antenna for Monitoring and Controlling Pacemaker

Sourav Sinha\*, Ta-Seen Reaz Niloy, Raja Rashidul Hasan, Md. Abdur Rahman

Department of Electrical & Electronic Engineering, American International University-Bangladesh (AIUB), Dhaka-1229, Bangladesh

### ARTICLE INFO

Article history:

Received: 13 December, 2019

Accepted: 05 February, 2020

Online: 09 March, 2020

Keywords:

Pacemaker

Wireless monitoring

Micro-strip antenna

Perfect Electric Conductor

Specific Absorption Rate

2/3 muscle-equivalent phantom

Wideband

Directivity

Rogers

### ABSTRACT

This paper is an extension of work originally presented in 2019 International Conference on Automation, Computational and Technology Management (ICACTM). A micro-strip patch in-body designed antenna is constructed on pacemaker to monitor and control the pacemaker wirelessly. The antenna is intended for ISM (Industrial, Scientific, and Medical) band (2.4 GHz to 2.48 GHz). A perfect electric conductor (PEC) is considered as pacemaker body and used as the ground of the propounded antenna having dimensions  $40 \times 30 \times 10 \text{ mm}^3$ . The patch material is chosen Copper having dimensions  $35 \times 22 \times 0.1 \text{ mm}^3$  and covered up with substrate material Rogers R03010 (loss tangent  $\delta = 0.0035$  and dielectric constant,  $\epsilon_r = 10.2$ ) with thickness of 1.55 mm to make it compatible in human body. The designed antenna is placed and analyzed in 2/3 muscle equivalent phantom by changing the depth of the antenna. Results disclose that operating frequency is 2.464 GHz with reflection coefficient -28.37 dB. The antenna maintains frequency range from 1.8075 GHz to 3.445 GHz, which represents wide bandwidth of 1.6375 GHz. To ensure the human body safety, specific absorption rate is analyzed and found 0.937 W/Kg for 10g tissue at operating frequency, which makes it biocompatible. The surface current distribution, Voltage Standing Wave Ratio, Current density, far-field radiation characteristics, radiation efficiency, and total efficiency are investigated to analyze the effect and performance of the designed antenna. CST Microwave Studio is used for simulation and analysis the parameters of the antenna.

## 1. Introduction

Nowadays in our modern scenario, heart attack is very familiar disease caused by loss of blood supply. It appears when the heart is beating too rapidly or when the body is not receiving enough blood [1]. A small electrical medical device called artificial implantable pacemaker provides an electrical pulse to the heart with proper intensity by the electrodes [2]. The main objective of pacemaker is to regulate irregular heartbeats (known as arrhythmias) at normal rate. Many organizations come up with distinctive features, such as wireless communication and monitoring assistance [3]. This monitoring and controlling system is extremely relevant because it decreases the amount of eye to eye visits with doctors, as well as the physical and mental stress of patients. Since it can communicate wirelessly, there is no need to cut the skin, which can prevent infection from a germ in a medical diagnosis, but the antenna is needed to transmit the data wirelessly.

A micro-strip patch antenna's geometric shape contains a shedding layer on first part of the dielectric substrate with a ground

plane on the next. Radiating element can be square, circular, semicircular, triangular etc. [4]. In present days, a number of antenna design have been proposed on several researches for the different applications. With many advantages, this antenna can communicate with others wireless system spontaneously [5, 6]. Easy to manufacture, lightweight, low profile, low cost, replaceable and high efficiency is such advances. The popularity of patch antenna in microwave communication is raised nowadays that requires semispherical coverage. Safety of a patient with a compact size, as well as wider bandwidth and radiation efficiency is the main concern to design an antenna [7, 8]. Various types of antenna have been developed, e.g. meander line, monopole, and loop antenna for wireless monitoring [9, 10].

ISM or Industrial, Scientific and Medical band (2.4 GHz - 2.4835 GHz) and MICS or Medical Implant Communication System band (402 MHz to 405 MHz) specified for bio-suitable antenna by U.S. Federal Communications Commission and European Radio communications Committee (ERC) in wireless medical telemetry service (WMITS) [11]. ISM band has shorter wavelength due to its high frequency area range apart from MICS

\*Sourav Sinha, +8801711190232, [souravsinha272@gmail.com](mailto:souravsinha272@gmail.com)

[www.astesj.com](http://www.astesj.com)

<https://dx.doi.org/10.25046/aj050209>



band has wider wavelength due to its smaller frequency. Therefore, ISM band is extra reasonable than MICS to design an antenna on pacemaker [12].

In this article, a design of bio-implantable micro-strip patch antenna is propounded for monitoring and controlling pacemaker, which operates at ISM band. The pacemaker with the antenna placed inside 2/3 muscle equivalent phantom, then the characteristics are analyzed. The performance is also analyzed by changing depth of the pacemaker in 2/3 muscle equivalent phantom. The pacemaker box considered as box of PEC (perfect electric conductor) as well as ground of the proposed antenna [13]. Rogers R03010 ( $\epsilon_r = 10.2$ ) covers the antenna from all the side can also called superstrate and substrate of the antenna for its flexibility and durability characteristics [14]. All the characteristics of the propounded antenna observed in CST microwave studio and discussed in this article.

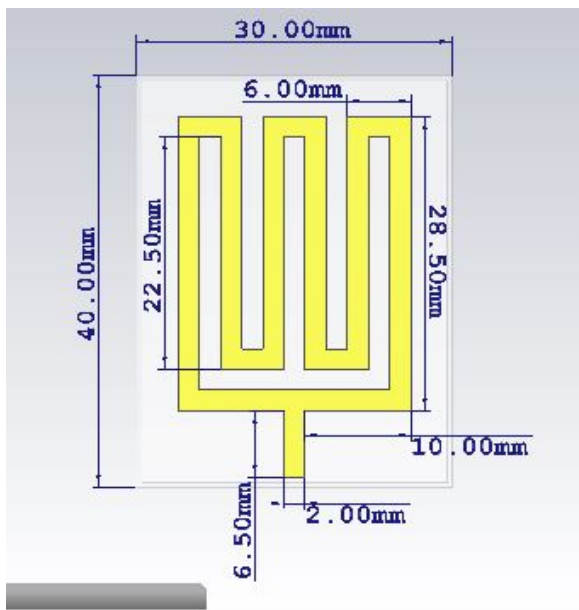


Figure 1: Propounded micro-strip patch antenna front view with dimension.

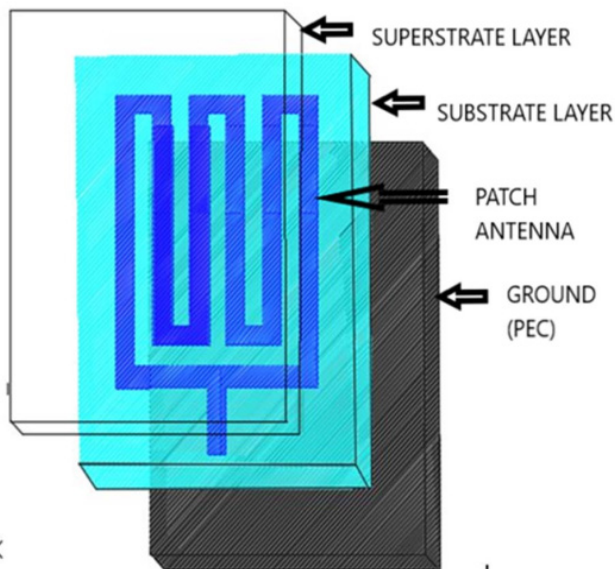


Figure 2: Antenna Structure

## 2. Structure and Design Method

### 2.1. Design of Antenna

The propounded micro-strip patch antenna has the length 35 mm and width 22 mm respectively, which overcome the most challenging issues - biocompatibility and size. The designed antenna is consisting superstrate, patch, substrate, and ground. Copper is chosen for patch with 0.1 mm of thickness. The pacemaker box is built with PEC or perfect electric conductor with thickness of 0.1 mm from all sides and it acts as ground of the antenna. The substrate and superstrate are made with Rogers R03010 that covers full patch material with 1.55 mm thickness.

The geometrical front view of antenna shows all the dimensions of patch, which are placed in Figure 1. The patch is located in the middle of the superstrate and substrate with 35 x 22 x 0.1 mm<sup>3</sup> to reduce the effects of a high conductive human tissue as well as to avoid shortening the antenna [12-15]. Having 6.5 mm length and 2 mm width, feed line is also shown. All the dimensions are organized in Table 1.

Table 1: The Antenna Parameters

Antenna Part	Material	Parameter	Value (mm)
Superstrate	Rogers	Length	40
		Width	30
		Thickness	1.55
Patch	Copper	Length	35
		Width	22
		Thickness	0.1
Substrate	Rogers	Length	40
		Width	30
		Thickness	1.55
Ground	PEC	Length	40
		Width	30
		Thickness	0.1

### 2.2. Design of Pacemaker Casing

Figure 3 shows casing of Pacemaker and the location of the antenna with waveguide port. The antenna patch covers with substrate and superstrate is placed on the top surface of the antenna. The waveguide port is connected underneath the feed line from where the power of input is given. The red part states the port of the waveguide as shown in Figure 3. Dimensions of the pacemaker case are tabulated in Table 2.

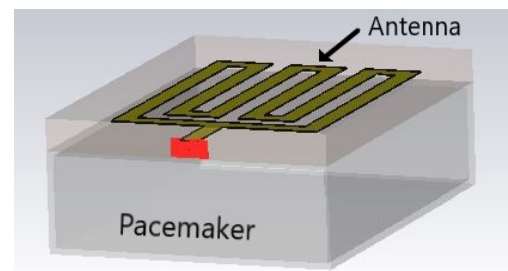


Figure 3: Antenna with Pacemaker Case Showing Waveguide Port



Table 2: Pacemaker Case Dimension

Name of Parameters	Value (mm)
Pacemaker Length	30
Pacemaker Width	40
Pacemaker Thickness	10
Pacemaker Case Thickness	0.1

2.3. Structure of Body Phantom

As shown in Figure 4, the pacemaker with surfaced antenna is placed inside the 2/3 muscle-equivalent phantom. The interval between antenna and the phantom’s surface is denoted with “d” and it varies depending on gender and age.

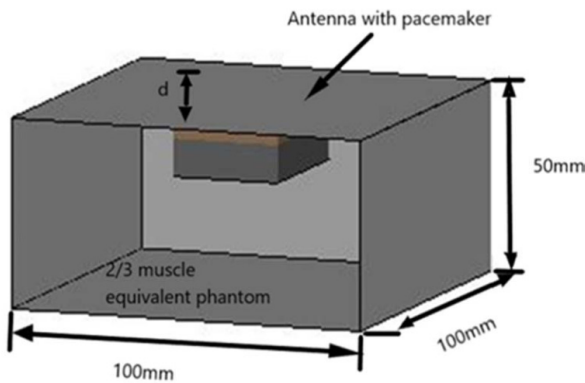


Figure 4: 2/3 muscle-equivalent phantom model pacemaker inside

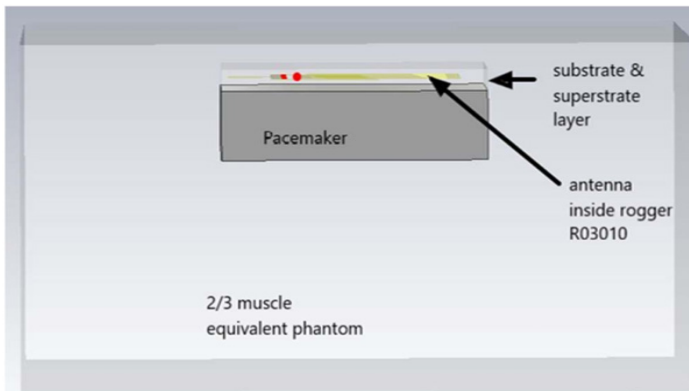


Figure 5: Cross sectional view of 2/3 muscle phantom with pacemaker inside.

Cross sectional view of the designed antenna with pacemaker inside the 2/3 muscle equivalent phantom is shown in Figure 5. The positioning pattern of pacemaker is clearly described.

3. Characteristics Analysis of Designed Antenna

3.1. Reflection coefficient or  $S_{11}$  parameter

Reflection coefficient or  $S_{11}$  parameter measures the quantity of power that radiated or reflected from an antenna [16]. The return loss is noticed after implanting the proposed antenna inside 2/3 muscle equivalent phantom model at resonant frequency. In Figure 6, the X-axis is in GHz range, which represents the frequency and the Y-axis is in dB scale, which constitutes the return loss. The resonant frequency or operating frequency of the propounded antenna is found 2.464 GHz, which is in ISM band and that turns

the antenna into biocompatible and also return loss of -28.369 dB that indicates better performance by maximum radiation of the antenna [14]. The bandwidth of the propounded antenna is observed 1.6375 GHz (1.8075 GHz to 3.445 GHz) by sketching a linear line in -10 dB, which is enough sufficient to implant on human body [14].

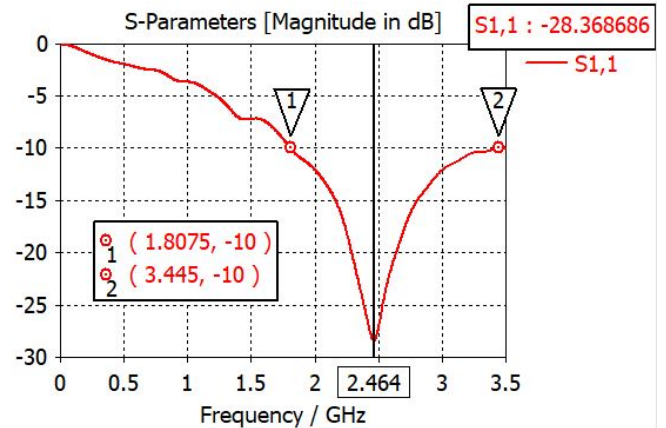


Figure 6: Return loss ( $S_{11}$  parameter) of the antenna inside 2/3 muscle equivalent phantom model.

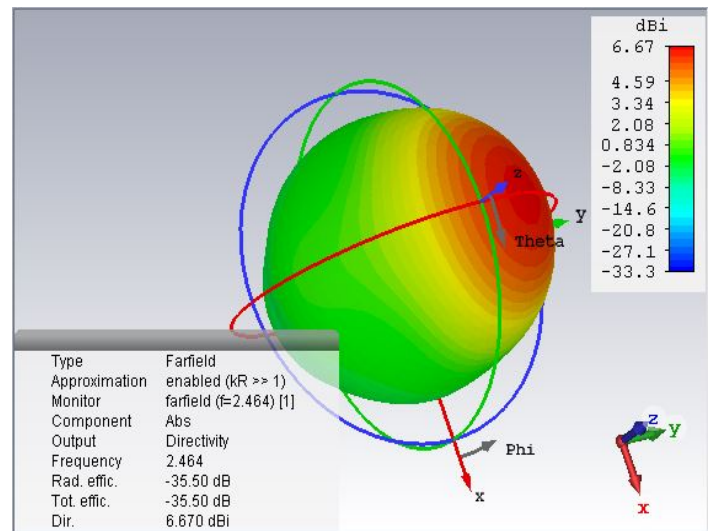
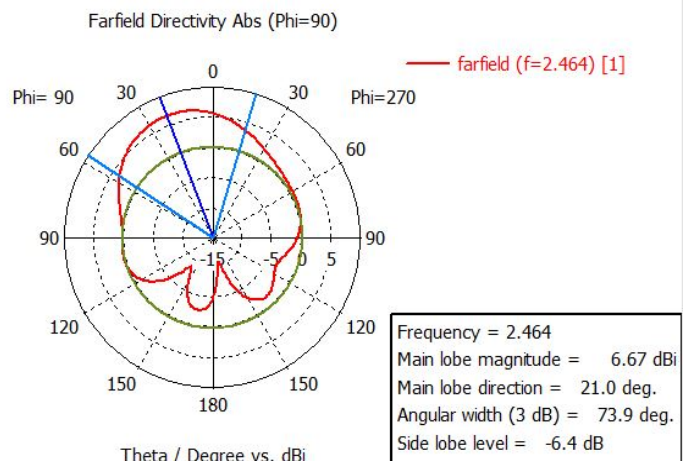


Figure 7: Far-field radiation pattern view (3D) of the propounded antenna inside 2/3 muscle equivalent phantom model.



### 3.2. Far-field radiation pattern

The radiation characteristics of the proposed antenna is explained in Figure 7. As the antenna is designed for monitoring and controlling pacemaker so unidirectional directivity is maintained to get the best values because pacemaker is a static device inside human body. Various parameters such as the directivity, total efficiency and the radiation efficiency is got 6.67 dBi, -35.5 dB and -35.5 dB respectively at the resonance frequency of 2.464 GHz and represented the radiation characteristics of the designed antenna. Figure 8 is displayed the far-field radiation pattern's polar view of the proposed antenna with main lobe magnitude 6.67 dBi.

### 3.3. Voltage standing wave ratio or VSWR

The voltage standing wave ratio is a function of the coefficient of reflection and of the intensity reflected from antenna [16]. For better performance, VSWR should be in between 1 to 2. In Figure 9, the X-axis is in GHz range, which represents the frequency and the Y-axis is ratio, which represents VSWR. In addition, it founds 1.08 at resonance frequency 2.464 GHz.

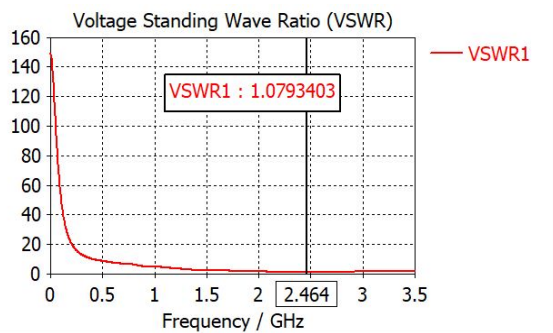


Figure 9: Voltage standing wave ratio (VSWR) of the antenna inside 2/3 muscle equivalent phantom model.

### 3.4. Specific Absorption Rate (SAR)

SAR is measured by the radiation of the surrounding tissue [17] that is used for safety purpose. According to FCC, in 10g tissue and 1mW input power, SAR must be less than 2 W/Kg to ensure higher safety [18, 19]. From Figure 10, Maximum Specific Absorption Rate (SAR) for the proposed antenna is noticed 0.937 W/kg at operating frequency for 10g tissue.

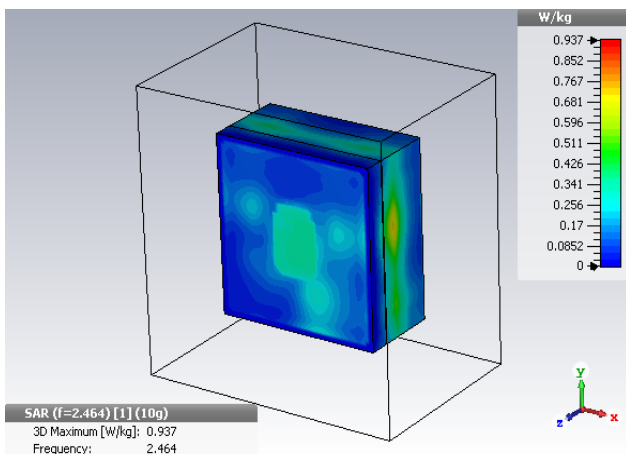


Figure 10: SAR distribution of the propounded antenna for 10g tissue in 1mW of input power.

### 3.5. Current density

Figure 11 shows the current density (abs) of the antenna at resonance 2.464 GHz. In addition, the current magnitude is not same in every position of the antenna patch. The current density in patch lies between 1017 A/m<sup>2</sup> to 1176 A/m<sup>2</sup>. In addition, the maximum current density is found 5851 A/m<sup>2</sup>.

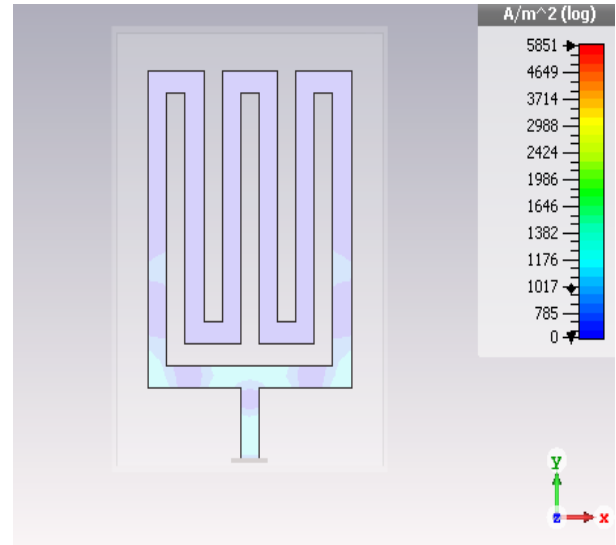


Figure 11: Current density of the designed antenna at 2.464 GHz.

### 3.6. Surface current distribution

The surface current distribution of the designed antenna at resonance frequency 2.464GHz is shown on Figure 12. The maximum current is found 52.5 A/m in design while the peck current on patch is found about 14.3 A/m. Figure 12 is also clearly described that the current is high on the lower edges which close to feeding point and low on the upper edges.

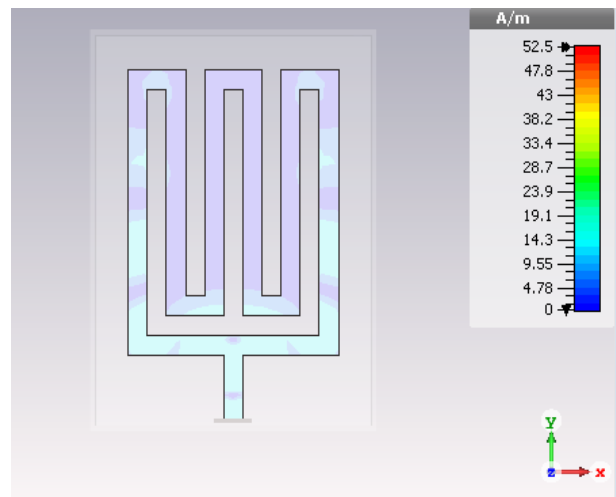


Figure 12: Surface current distribution of the designed antenna at 2.464 GHz.

## 4. Comparison Analysis

### 4.1. For various depth

Depending on the gender and age, the depth of the pacemaker is varied and analyzed. The depth defines the distance between the phantom surface and the superstrate surface. As shown in Figure

13, the reflection coefficient or  $S_{11}$  and the operating frequency is slightly shifted with the change of depth (d). Table 3 is shown the total changelog for different depth of pacemaker.

Table 4: Changelog with different materials

Patch	Substrate	$S_{11}$	Directivity	VSWR	SAR
Copper	FR-4	-28.37	6.67 dBi	1.07934	0.937
Copper	Roger	-28.36	6.67 dBi	1.07937	0.937
Gold	FR-4	-28.35	6.67 dBi	1.07946	0.937
Gold	Roger	-28.35	6.67 dBi	1.07946	0.937

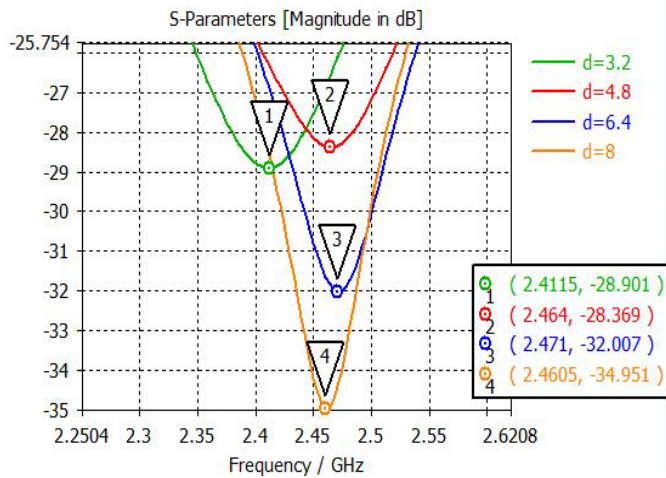


Figure 13: Return loss or  $S_{11}$  parameter of the antenna for various depth

Table 3: Changelog with different depth

Position	Depth (mm)	Operating Frequency	$S_{11}$
1	3.2	2.4115	-28.901
2	4.8	2.464	-28.369
3	6.4	2.471	-32.007
4	8	2.4605	-34.951

4.2. By changing material

The designed antenna parameters are also analyzed with two patch materials Copper, Gold and two substrate-superstrate materials Roger and FR-4 variations. As shown in Figure 14, the resonance is found 2.464 GHz frequency for all possible combinations and return loss or  $S_{11}$  parameters are almost same in the variations. Table 4 displays all the parameters findings by changing the materials.

5. Conclusion

In this article, a micro-strip patch antenna is proposed for monitoring and controlling pacemaker. Biocompatibility have been checked by embedded the propounded antenna with pacemaker inside 2/3 muscle equivalent phantom. The depth is varied and analyzed to ensure same characteristics for any gender and any age’s people.  $S_{11}$  or reflection coefficient is found -28.37 and the resonance frequency is found 2.464 GHz for 4.8 mm depth. Pacemaker is one of the vital device nowadays for heart patients, especially for arrhythmias patients. Any kind of interruption in working of pacemaker can turn a patient into death. Therefore, monitoring and controlling pacemaker is become most important issue for pacemaker holders. In conclusion, according to the antenna performance, the propounded antenna is biocompatible and applicable for medical application with proper output.

References

- [1] R. R. Hasan, M. A. Rahman, S. Sinha, M. N. Uddin, T. R. Niloy, "In Body Antenna for Monitoring Pacemaker" in 2019 International Conference on Automation, Computational and Technology Management (ICACTM), London, United Kingdom, 2019. doi: 10.1109/ICACTM.2019.8776836
- [2] Y. Hao, Y. Li, D. Liao, L. Yang, "Seven times replacement of permanent cardiac pacemaker in 33 years to maintain adequate heart rate: a case report" Annals of translational medicine, 3(21), 2015. doi: 10.3978/j.issn.2305-5839.2015.11.35
- [3] P. Soontornpipit, C. M. Furse, Y. C. Chung, "Miniaturized biocompatible microstrip antenna using genetic algorithm," IEEE Transactions on Antennas and Propagation, 53(6), 1939-1945, 2005. doi: 10.1109/TAP.2005.848461
- [4] H. Werfelli, K. Tayari, M. Chaoui, M. Lahiani, H. Ghariani, "Design of rectangular microstrip patch antenna" in 2016 2nd International Conference on Advanced Technologies for Signal and Image Processing (ATSIP), Monastir, 2016. doi: 10.1109/ATSIP.2016.7523197
- [5] C. Liu, Y. Guo, H. Sun, S. Xiao, "Design and Safety Considerations of an Implantable Rectenna for Far-Field Wireless Power Transfer" IEEE Transactions on Antennas and Propagation, 62(11), 5798-5806, 2014. doi: 10.1109/TAP.2014.2352363
- [6] S. Gollakota, H. Hassanieh, B. Ransford, D. Katabi, K. Fu, "They can hear your heartbeats: non-invasive security for implantable medical devices" Proc. ACM SIGCOMM 2011, 41(4), 2-13, 2011. doi: 10.1145/2018436.2018438
- [7] W. El Hajj, C. Person, J. Wiart, "A Novel Investigation of a Broadband Integrated Inverted-F Antenna Design; Application for Wearable Antenna" IEEE Transactions on Antennas and Propagation, 62(7), 3843-3846, 2014. doi: 10.1109/TAP.2014.2318061
- [8] Z. Duan, Y. Guo, M. Je, D. Kwong, "Design and in Vitro Test of a Differentially Fed Dual-Band Implantable Antenna Operating at MICS and ISM Bands" IEEE Transactions on Antennas and Propagation, 62(5), 2430-2439, 2014. doi: 10.1109/TAP.2014.2309130
- [9] J. Kim and Y. Rahmat-Samii, "Implanted antennas inside a human body: simulations, designs, and characterizations" IEEE Transactions on Microwave Theory and Techniques, 52(8), 1934-1943, 2004. doi: 10.1109/TMTT.2004.832018
- [10] P. Soontornpipit, C. M. Furse, Y. C. Chung, "Design of implantable microstrip antenna for communication with medical implants" IEEE Transactions on Microwave Theory and Techniques, 52(8), 1944-1951, 2004. doi: 10.1109/TMTT.2004.831976
- [11] K. S. Nikita, Handbook of Biomedical Telemetry, IEEE press, 2014.
- [12] H. Usui, M. Takahashi, K. Ito, "Radiation characteristics of an implanted cavity slot antenna into the human body" in 2006 IEEE Antennas and

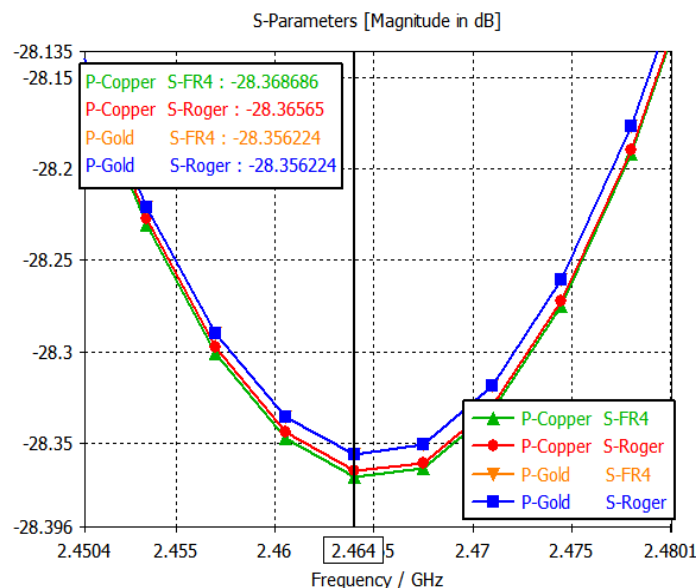


Figure 14: Return loss or  $S_{11}$  parameter of the antenna for different material.

Propagation Society International Symposium, Albuquerque, NM, 2006.  
doi: 10.1109/APS.2006.1710726

- [13] T. Houzen, M. Takahashi, K. Saito, K. Ito, "Implanted Planar Inverted F-Antenna for Cardiac Pacemaker System" in 2008 International Workshop on Antenna Technology: Small Antennas and Novel Metamaterials, Chiba, 2008. doi: 10.1109/IWAT.2008.4511351
- [14] M. Islam, R.R. Hasan, M. Haque, S. Ahmad, K. Mazed, M. Islam, "In-Body Antenna for Wireless Capsule Endoscopy at MICS Band" in Computing Conference 2018, London, United Kingdom, 2018. doi: 10.1007/978-3-030-01177-2\_59
- [15] S. Sinha, R. R. Hasan, M. A. Rahman, M. T. Ali, M. N. Uddin, "Antenna Design for Biotelemetry System" in 2019 International Conference on Robotics, Electrical and Signal Processing Techniques (ICREST), Dhaka, Bangladesh, 2019. doi: 10.1109/ICREST.2019.8644307
- [16] R. R. Hasan, M. A. H. Shanto, S. Howlader, S. Jahan, "A novel design and miniaturization of a scalp implantable circular patch antenna at ISM band for biomedical application" in 2017 Intelligent Systems Conference (IntelliSys), London, United Kingdom, 2017. doi: 10.1109/IntelliSys.2017.8324286
- [17] N. A. Islam, F. Arifin, "Performance analysis of a miniaturized implantable PIFA antenna for WBAN at ISM band" in 2016 3rd International Conference on Electrical Engineering and Information Communication Technology (ICEEICT), Dhaka, 2016. doi: 10.1109/CEEICT.2016.7873145
- [18] E. Safety, S. C. Committee, N. Radiation, I. S. Board, "IEEE Recommended Practice for Measurements and Computations of Radio Frequency Electromagnetic Fields With Respect to Human Exposure to Such Fields 100 kHz –300 GHz" Measurement, 2002, 2008.
- [19] J. H. Bernhardt, "The New ICNIRP Guidelines: Criteria, Restrictions, and Dosimetric Needs" Radio Frequency Radiation Dosimetry and Its Relationship to the Biological Effects of Electromagnetic Fields. NATO Science Series (Series 3: High Technology), 82, 2000. doi: 10.1007/978-94-011-4191-8\_56



## Attacks Classification and a Novel IDS for Detecting Jamming Attack in WBAN

Asmae Bengag\*, Amina Bengag, Omar Moussaoui

*Applied Mathematics, Signal Processing and Computer Science Laboratory, ESTO, University Mohamed Ier Oujda, Morocco*

### ARTICLE INFO

Article history:

Received: 01 January, 2020

Accepted: 16 February, 2020

Online: 09 March, 2020

Keywords:

WBAN

Medical Sensors

Jamming attack

IDS

Parameters Network

ZigBee

OMNET++

Castalia 3

### ABSTRACT

*Wireless Body Area Network (WBAN) aims to monitor patient's health remotely, by using mini medical sensors that are attached on the human body to collect important data via the wireless network. However, this type of communication is very vulnerable to various types of attacks, poses serious problems to the individual's life who wears the nodes. In this paper, we present a new classification of the most dangerous attacks based on different criteria, which gives us a clear vision of how attacks affect a WBAN system. Moreover, this classification will help us to specify the strength and the weakness of each attack in order to facilitate the development of a new intrusion detection system (IDS). In the second part of this work, we develop a novel IDS for detecting three types of jamming attacks in WBAN. The proposed methodology is based on the network parameters as an indicator to differentiate the normal case from the abnormal case like false alert or attack state. Through simulation analysis that was applied on Castalia platform by using OMNET++ as a simulator, proves that the proposed IDS have a great effect for detecting the presence of jamming attack in the network.*

## 1. Introduction

In the last two decades, wireless body area network (WBAN) has attracted huge number of researchers. WBAN is a network consisted of several types of medical sensors; each one has its own debit and functionality. These sensors facilitate the supervision of the patient's health and intervene as quickly as possible in emergencies.

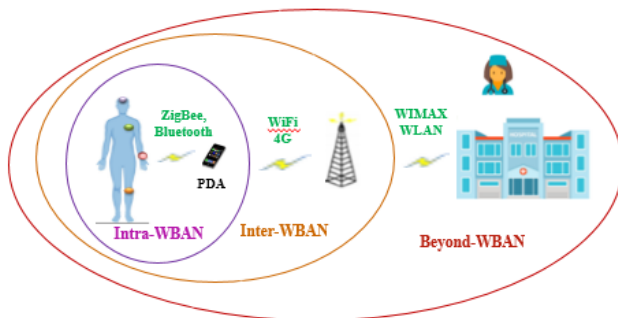


Figure 1 : Communication architecture of WBAN

The medical sensors are attached on the human body for collecting the biomedical parameters as the activity of muscles, brain or heart rate. Then, this information will be transmitted to the

personal device assistant (PDA). Finally, the data will be received by the medical team via a wireless mode, as shown in Figure 1.

Actually, the communication is done by three levels [1]:

- Level 1: 'Intra-WBAN communication' that contains different devices especially medical sensors and the coordinator node or PDA. The communication between these nodes could be based on Bluetooth (802.15.1) or ZigBee (802.15.4). In fact, the main goal of PDA is to ensure a communication between sensors, and informs the final user as doctor or patient via an external gateway [2].

- Level 2: is named an 'Inter WBAN communication' that concerns a communication between the PDA and one or more access points (APs) via WiFi, to interconnect WBAN network with several networks [3].

- Level 3: called a 'Beyond-WBAN communication' in which the communication is between a various access points and medical server (hospital, nurse etc.) using for instance Internet or mobile networks.

However, the communication used in WBAN system is not reliable one hundred percent, because the wireless communication deployed on open radio frequencies with various attacks and different cases of anomalies. Furthermore, several attacks threat

\*Asmae Bengag, asmaebengag@gmail.com



the security aspects like availability, which makes the medical nodes not able to send or transmit any information especially in the case of emergency. Besides, other attacks affect the integrity that can modify the data transmitted during the transmission and other ones threaten the confidentiality aspect that could access sensitive data [4].

One of the most important challenges to secure the WBAN system is by using a robust mechanism to detect an attack in this kind of networks. Hence, we started our work by studying the impact of the most dangerous attacks in WBAN, by classifying them according to various criteria. Then, we focused on the Denial of Service (DoS) jamming attack that disturbs wireless communication by affecting the physical and MAC layers. In fact, we have developed a new IDS technique to detect jamming attacks that based on four important network parameters: packet delivery ratio (PDR), energy consumption amount (ECA), received signal strength indication (RSSI) and bad packet ratio (BPR).

The rest of this paper is organized as follows: in section II, we describe the previous different classification attacks works, and the various IDS mechanisms for detecting jamming on the network. Then in section III, we present our attacks classification in WBAN according to various measures. The steps of our IDS algorithm, the simulations scenarios and the results are discussed in section IV. Finally, our work is concluded in section V.

## **2. Related Work**

In order to propose a new classification of attacks in WBAN, we are based on several previous works. In fact, each work is based on different measures and applied on specific technology such as MANET, WSN or WBAN.

In [5] authors proposed a classification attacks that applied in MANETs and based on six attributes: legitimacy of attacking node (external or internal node), the number of nodes participating as an attacker (singleton or collision attack), MANETs vulnerabilities utilized by the attack, the network resources exploited by the attacking node/s, the targeted victim and compromised security service of attack.

Another taxonomy proposed by Wu et al. in [6] that is applied in network and computer, which based on three dimensions: (i) the source of attack (local or remote); (ii) the techniques dimension that mean the all-possible techniques adopted by the attackers; and (iii) the results of attack. However, the weakness of this work is the less information about the type of target.

In [7], the authors present various attacks get into IEEE 802.15.4 and classifying them into three categories: (i) the radio jamming that is an attack created the problems of denial of service in the physical layer; (ii) the message manipulation attacks for injecting false information into the node network; and (iii) the last one is the steganography attacks. However, the weakness of this classification is the lack of other important measures as security aspects and position of attack in the network that will be presented in our classification.

In [8] authors classified attacks according MAC Layer basing on the functionality of the mac layer. They are presented two classification, the first one concerns the MAC layer as Guaranteed

Time Slot (GTS) attack, and the second one based on MAC layer protocol rules.

The OSI model is important measure to identify problems of security in each layer; this work is proposed by Pooja et al. [9] and applied in MANET. Nonetheless, this classification is based on just one criterion and it is not enough to have a robust security solution.

All the above-mentioned classification has some limits that make them inappropriate to specify all types of attacks because they not consider some important metrics. Basically, in our classification, we are based on the important and clear metrics especially in WBAN as attack position basing on the communication architecture of WBAN and the attack functionality.

In this second part, we give an overview about the detection mechanisms that have been studied to detect jamming attack in a wireless network.

Fuzzy Inference System (FIS) is a technique proposed by Reyes et al. [4] that built in Matlab tool using the following metrics as input values: CCA, BPR, RSS and PDR. In order, detecting the link loss in wireless networks, these parameters will be used to calculate the values of the Jamming index (JI). The idea of this method is good, but it has a complicated calculation that makes sensor nodes consume more energy. In addition, it does not differentiate the types of jamming present in the network.

In [10] proposed a technique for identifying the following jamming types: constant, random, reactive and deceiving. The methodology is based on SS (Signal Strength) and PDR (Packet Delivery Ratio), to determine the normal cases from the jamming attack cases. However, the method could consider that the sensor is under a jamming attack but there is no attack in the network. For instance, in the case where the receptor sensor has a problem to respond with an ACK packet to the transmitter, we found that the transmitter node has a high SS level, and the PDR value is low. Hence, there is confusion between jamming scenario and affected node.

In [11], the author improved an IDS that includes Signal Strength (SS) and Packet Delivery Rate (PDR) to define the presence of jamming attack. On the other hand, they are used also Packet Send Rate (PSR), to distinguish different types of jamming attacks in WSN.

In [12] proposed jamming detection technique for WSN that called physical layer jamming identification using PDR and RSSI parameter. This method used only some nodes as monitor in the network that have residual energy. Nevertheless, for monitoring the entire network, the method needs to implement various monitor nodes.

By comparing our proposed methodology with the previous works, we are focused on four important network parameters PDR, ECA, RSSI and ECA that will be presented in the section 4. By using these parameters based on a simple technique that consume a less energy compared to the above-mentioned techniques. Moreover, these parameters have a good effect to differentiate the normal case and false alerts for the jamming attacks. Our intrusion detection system allows also us to identify three types of jamming

attacks (constant jamming, reactive jamming and deceptive jamming) that are applied in the WBAN system.

### 3. Classification of attacks in WBAN

In this section, we describe our classification that based on previous attack taxonomies and other metrics, which adopt in wireless body area networks. Our taxonomy is based on six important criteria as follow:

- Attack impacts: are the results or the effects of attack action in the network.
- Security aspects: for having a robust system, we must take into consideration the fundamental security requirements in the medical application [13], such as data integrity, availability, data confidentiality, data freshness and authentication.
- OSI model: we can also classify attacks by the layers of the OSI model.
- Communication architecture of the WBAN: attack could place in different levels of the architecture of WBAN, either in the first level that directly threatens the medical sensors, level 2 or level 3 as exposed in the Table 1.
- Attack position in the network: we can distinguish two types of attack position, as internal attack that is a part of the network action, or as an external attack that is not a part of the system [5], like sniffing and man in the middle.

- Interruption act: the attack could be active by modifying or damaging the transmitted message to the receiver, and disrupting the communication [9]. Further, the passive attack threatens the confidentiality aspect by collecting the data in the network without perturbing the communication [5].

Thus, the Table 1 presents the different attacks classified according to our taxonomy that are cited above.

This attack classification facilitates us to understand and identify the operation or strategy of each attack in the network. Furthermore, it helps us to find a robust mechanism to detect jamming attack in WBAN that will present in the next section.

### 4. A novel detecting jamming attack

Jamming attack is among one of the attacks that blocks and disrupts the communication between nodes, by sending illegitimate signals, in order to make the system unavailable. In other words, this attack generates interference, which makes the medical sensors consume a lot of energy, and involves the collision between them [14].

As we present in the previous section, jamming attack threatens the physical layer that transmit a signal to create interference. Besides, data link layer could be under jammer node that does not respect the mechanism of its MAC protocol.

Table 1 Attacks classification in WBAN system

Attacks	Attack impacts	Security aspects	OSI model	Communication architecture of the WBAN	Attack position in the network	Interruption act
Tampering	Extracting cryptographic keys from the captured node [15]	Confidentiality Integrity data	Physical	Intra-WBAN	External	Active
Jamming	Disruption of communication by sending radio waves at a same frequency in the wireless network.	Availability	Physical Data Link	Intra and Inter WBAN	External	Active
Sybil	Obstruct the operation of routing protocols by operating multiple fake identities.	Confidentiality Integrity data	Network Data link	Intra, Inter and Beyond WBAN	Internal / External	Active
Hello floods	Blocking communication by sending broadcasts HELLO packets with high transmission.	Availability Confidentiality	Network	Inter and Beyond WBAN	External	Active
Selective forwarding	Delete some packets and refuse the transmission of data.	Availability, Confidentiality	Network	Inter and Beyond WBAN	External	Active
Flooding	Exhaust the energy of sensor and saturate the network.	Availability	Network Transport	Inter and Beyond WBAN	External	Active

4.1. Proposed methodology

In this section, we present our proposed methodology for identifying and detecting the presence of jamming attacks in WBAN system.

Our proposed algorithm has the ability to detect the presence of a jamming attack, and then identify which type it is. In fact, there are many types of jamming attack, but in our work, we mainly focus on three of them, constant jamming, deceptive jamming and reactive jamming.

Indeed, there are a lot of cases that resemble as jamming attack in the network namely false alerts, for example problems caused by a low energy or collision in the nodes, which reduce the quality of the IDS. In order, to have good IDS defending a malicious activities jamming in WBAN system, we are based on four important network parameters as a performance metrics that are mentioned in Table 2.

Table 2 : The network settings used

Parameters	Definition
PDR (Packet Delivery Ratio)	The authors of [10][16] defined the PDR as the ratio of the packets successfully sent by the node, to the total sent packets.
ECA (Energy Consumption Amount)	Amount of energy consumed in a specified time [4].
BPR (Bad Packet Ratio)	BPR is a ratio of the failed packets received by a node [16].
RSSI (Received Signal Strength Indication)	RSSI is defined as a power content of the received radio signal at the receiver [4].

The diagram in Figure 3 shows the essential algorithm steps of the proposed IDS, which describes how our mechanism defend the remaining or not of jamming, and differentiate which types are on WBAN. As first step, we assume that the WBAN system is operating normally, without jamming attack or any problems. Then, each receiver sensors medical are calculated the thresholds of the network parameters PDRth, ECAtH, BPRth and RSSIth. After that, for observing if there are any problems on the WBAN, the initial parameters (PDRth, ECAtH, BPRth and RSSIth) are compared with the current values.

For mentioning the presence of jammer node and specify its type, one of the conditions will be launched an alert, and we can conclude that the node is under jamming attack. For the constant jamming, could be generated interferences between nodes sensors, by sending continually a random bits or signals in the wireless network [4], and forces the legitimate nodes to stay in listening mode, which cause a higher energy consumption. That is why the PDR and BPR values are lower than the normal case, and the ECA and RSSI parameters are higher.

In the case where the legitimate node is under the deceptive jamming, the latter sends data regularly to the channel that resembles legal, in order to deceive each node. Hence, we could be found that the PDR value is lower than the PDRth, and for the BPR, RSSI and ECA values are higher than their thresholds.

Furthermore, to identify a reactive radio jammer when the legitimate node sends the packet RTS, then the attack starts to transmit data and makes the communication medium busy. Thence, the legitimate node will consume a modest rate of energy. However, the value of the PDR input parameter very lower, whereas the BPR and RSSI values are higher than the normal values and the packet delivery ratio is very lower.

4.2. Simulation and results

4.2.1. Simulation parameters

We have made two main scenarios, in the first one we are simulated a WBAN system in normal case without malicious node, the studied scenario covers three types of medical sensors (EMG, ECG and EEG) are attached on human body. More specifically, the wireless communication protocol used between legitimate sensors and PDA is ZigBee (802.15.4 MAC), and CC2420 Radio used as a radio model as shown in Figure 2.

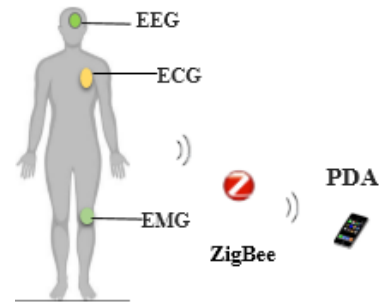


Figure 2: Simulation of WBAN in normal case

Simulation parameters, used in this case, are listed in Table 3.

Table 3 : Simulation parameters for WBAN without jamming

Used parameters	Values
Nodes	4 (3 medical sensors and 1 PDA)
Simulation time	300s (second)
MAC protocol type	ZigBee (Basic802154)
End simulation	End of the simulation

After that, we are simulated a WBAN system under a jammer node, as shown in Figure 4, in order to understand the impacts of jamming attack in the WBAN system and specially the MAC layer and the network parameters to compare with the normal case.

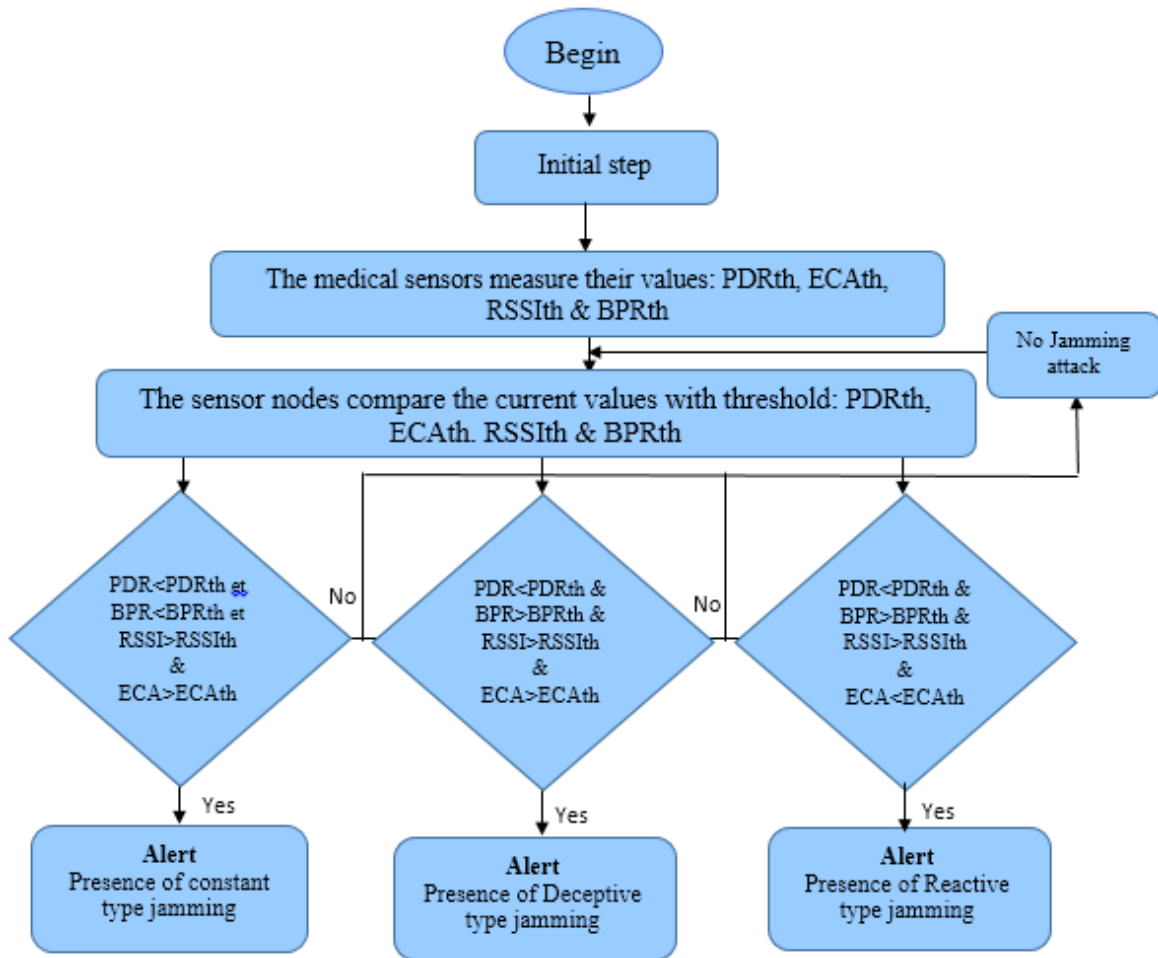


Figure 3 : Proposed mechanism for detecting different types of jamming attacks

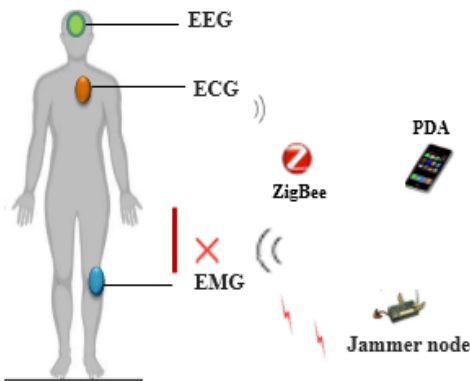


Figure 4: The scenario of WBAN with jamming attack

Table 4: Simulation parameters for jammer node

Used parameters	Values
Number of jammer nodes	1
Simulation time	300s (second)
MAC protocol	BypassMAC
Constant Data Payload	2000
End simulation	End of the simulation

As mentioned in Table 4, we are chosen the BypassMAC as MAC protocol for the jammer node, because as we explained before the jamming attack interrupts the communication between the nodes, and makes them not able to access the channel, by perturbing the MAC protocol mechanism.

#### 4.2.1. Simulation results and discussion

In this section, we measure the performance of our proposed approach jamming detection in WBAN, by calculating the network parameters in both cases without and with jammer node.

As shown in Figure 5 and Figure 6, when the legitimate node is under Jamming, the PDR value is very lower than the normal case, and the signal indicator is higher (-63,43 dBm). Moreover, in the normal case, the PDR parameter is higher and the RSSI is lower (-90 dBm). When the node (1) is near to the node (2) who is under jamming, we found that the node (1) could be also affected by the attack.

When the medical sensor (node 1) is under jamming, it consumes a lot of energy comparing with normal case (ECAtH) as shown in the Figure 7.



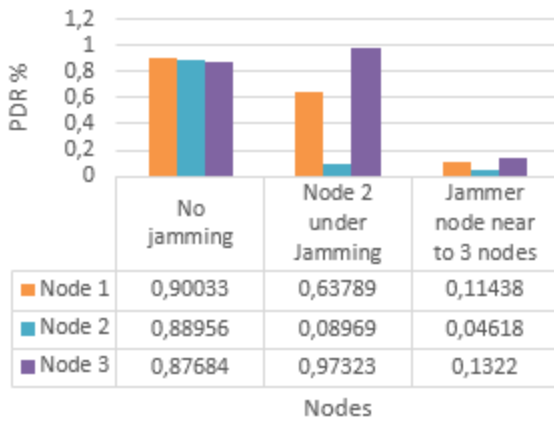


Figure 5: Packet delivery ratio values per node in WBAN (with and without jamming)

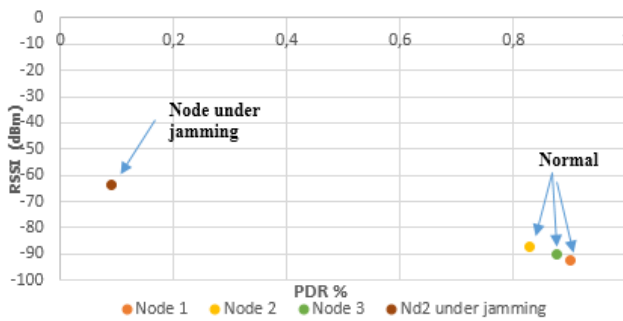


Figure 6: RSSI and PDR values in WBAN

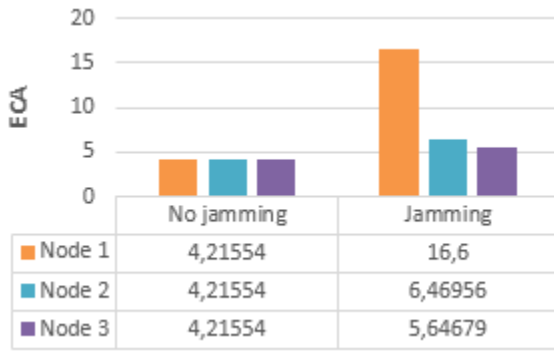


Figure 7: ECA parameter values in WBAN

Therefore, we can notice from these results that the used network parameters PDR, ECA, BPR and RSSI are very useful and have a great effect for identifying the presence of jamming attack in the WBAN system.

### 5. Conclusion and future work

In the recent years, many studies are interested to ameliorate and secure the healthcare industry. This paper is divided into two main parts. The first one presents our new classification of attacks in WBAN. The second one concerns a new IDS to detect three types of jamming attacks.

Thanks to our classification based on various measures, the researchers could have a deep view that helps them to understand

the different attacks in order to propose a robust solution security for defending attacks in the WBAN system.

Our novel Jamming Intrusion Detection System was implemented on the medical sensors, which is based on four fundamental network parameters: PDR, RSSI, ECA and BPR. Indeed, by using a simple technique, based on these parameters, the jamming attack could identify three types of jamming as constant, deceptive and reactive. Furthermore, our mechanism detects these attacks without consuming a lot of energy. However, according to the best of our knowledge, the most of proposed techniques have some limits as consuming a lot of energy because of complex calculation techniques, detecting false alerts due to a less of parameters, and other IDS do not specify types of jamming. Our simulation carried out in two main scenarios, the first one is with jamming and the second one is without jamming, which is done with the popular WBAN’s simulator tools OMNET++ and Castalia. According to the results of simulation, our method proves that the used parameters have good effects to detect the presence of jamming with less false alerts.

For future works, we aim to improve our proposed IDS by using Fuzzy Logic to make our mechanism more robust in order to increase detection and decrease the false alerts.

### Acknowledgment

This research is performed inside the MATSI Lab., ESTO, University Mohammed First, Oujda (Morocco).

### References

- [1] Y. Qu, G. Zheng, H. Ma, X. Wang, B. Ji, and H. Wu, “A survey of routing protocols in WBAN for healthcare applications,” *Sensors (Switzerland)*, vol. 19, no. 7, 2019.
- [2] H. Fouad, “Continuous Health-monitoring for early Detection of Patient by Web Telemedicine System,” pp. 76–83, 2001.
- [3] S. Movassaghi, A. Mehran, J. Lipman, D. Smith, and A. Jamalipour, “Wireless Body Area Networks: A Survey,” *IEEE Commun. Surv. TUTORIALS*, vol. 16, pp. 1658–1686, 2014.
- [4] H. I. Reyes and N. Kaabouch, “Jamming and Lost Link Detection in Wireless Networks with Fuzzy Logic,” *Int. J. Sci. Eng. Res.*, vol. 4, no. 2, pp. 1–7, 2013.
- [5] N. A. Noureldien, “A novel taxonomy of MANET attacks,” *Proc. 2015 Int. Conf. Electr. Inf. Technol. ICEIT 2015*, pp. 109–113, 2015.
- [6] Z. Wu, Y. Ou, and Y. Liu, “A taxonomy of network and computer attacks based on responses,” *Proc. - 2011 Int. Conf. Inf. Technol. Comput. Eng. Manag. Sci. ICM 2011*, vol. 1, pp. 26–29, 2011.
- [7] Y. M. Amin, A. T. Abdel-hamid, and S. Member, “Classification and analysis of IEEE 802.15.4 PHY layer attacks,” *2016 Int. Conf. Sel. Top. Mob. Wirel. Netw.*, pp. 74–79, 2016.
- [8] Y. M. Amin, A. T. Abdel-hamid, and S. Member, “Classification and Analysis of IEEE 802.15.4 MAC Layer Attacks,” pp. 74–79, 2016.
- [9] P. Chahal, “Comparative Analysis of Various Attacks on MANET,” vol. 111, no. 12, pp. 42–46, 2015.
- [10] W. Xu, W. Trappe, Y. Zhang, and T. Wood, “The feasibility of launching and detecting jamming attacks in wireless networks,” p. 46, 2005.
- [11] B. Yu and L. Y. Zhang, “An improved detection method for different types of jamming attacks in wireless networks,” *2014 2nd Int. Conf. Syst. Informatics, ICSAI 2014*, no. Icsai, pp. 553–558, 2015.
- [12] V. C. Manju and K. M. Sasi, “Detection of jamming style DoS attack in Wireless Sensor Network,” *Proc. 2012 2nd IEEE Int. Conf. Parallel, Distrib. Grid Comput. PDGC 2012*, pp. 563–567, 2012.
- [13] M. Messai, “Classification of Attacks in Wireless Sensor Networks,” *Icta*, no. April 2014, pp. 23–24, 2014.
- [14] C. Del-Valle-Soto, L. J. Valdivia, and J. C. Rosas-Caro, “Novel detection methods for securing wireless sensor network performance under intrusion jamming,” *CONIELECOMP 2019 - 2019 Int. Conf. Electron. Commun. Comput.*, pp. 1–8, 2019.
- [15] B. Kiruthika, S. Abinaya, R. Ezhilarasie, and A. Umamakeswari, “Security



attacks and its countermeasures in wireless sensor networks - A survey," *Res. J. Pharm. Biol. Chem. Sci.*, vol. 6, no. 3, pp. 1374–1387, 2015.

- [16] M. Çakiroğlu and A. T. Özcerit, "Design and evaluation of a query-based jamming detection algorithm for wireless sensor networks," *Turkish J. Electr. Eng. Comput. Sci.*, vol. 19, no. 1, pp. 1–19, 2011.

## **New Solution Implementation to Protect Encryption Keys Inside the Database Management System**

Karim El bouchti\*, Soumia Ziti, Fouzia Omary, Nassim Kharmoum

*Faculty of Sciences, Mohammed V University in Rabat, Intelligent Processing Systems & Security (IPSS) Team, Morocco*

---

### **ARTICLE INFO**

*Article history:*

*Received: 31 December, 2019*

*Accepted: 13 February, 2020*

*Online: 09 March, 2020*

---

*Keywords:*

*Encryption keys protection*

*Database encryption*

*Database security*

*keys protection in Databases*

---

---

### **ABSTRACT**

*Due to the attacks' growth on sensitive databases by deploying advanced tools, beyond access control and authentication mechanisms, the database encryption remains a useful and effective way to ensure robust security of data stored within it. Any database encryption solution is based on a specific encryption model that determines how data is encrypted inside it. A relevant database encryption model must necessarily adopt a strong security policy of data encryption keys. It determines how these keys are generated, stored, and protected. In this work, we will implement an original solution that protects the encryption keys when encrypting data occurred at the Database Management System level. Our solution suggests protecting the keys by their encryption with other ones named Master Keys, which are generated according to the encryption granularity defined by the database encryption model. The proposed solution protects the keys of two database encryption models: at the level of the columns and the level of tables.*

---

### **1. Introduction**

Database (DB) level encryption is a way to encrypt and decrypt data within the Database Management System (DBMS) using keys held by the DB server [1]. In fact, this encryption model offers major advantages, in particular, those related to the security of the encryption keys against external attacks performed outside the information system [2, 3]. Though the probability of the administrator attack is not negligible, he owns large privileges on DB. Hence, he can attack the DB directly, via a collaboration with a malicious external attacker (disclosure of the administrator account for example), or with an internal attacker such as a legitimate user [4, 5, 6]. Obviously, the DB administrator has the ability to perform all these attacks without leaving any traces [7, 8].

Data encryption at the DBMS level is based fundamentally on its specific encryption model. The management of encryption keys within this model is a crucial point, it defines the ways how keys are generated, stored, and protected [9, 10]. Actually, keys values, how users access them, and where they are stored are the ultimate goal of any attacker. Therefore, it should be necessary to establish a protection policy for encryption keys to minimizing their exposure face of malicious attackers. Indeed, many solutions have

been developed in order to resolve this problem. For instance, the keys protection solutions implemented at DBMSs such as Oracle, Ms SQL Server and My SQL are mainly based on the use of "Wallets", Hardware Security Module (HSM) and "Security server" [11-14]. In fact, each one of these solutions has advantages and major limits, as have already explained in more detail in our previous work [8, 15].

Several studies proposed several solutions to protect DB encryption keys either in DB encryption models or separate solutions of keys protection [16, 17]. The authors of [16] proposed a model to protect encryption keys based on a concept of distributed keys representation. The first key part stored in the DB, and the other part is obtained by converting the user password. Elovici et al. presented a special DB encryption model that permits to protect keys using "Wallet" mechanism [17], although Itimar et al. used asymmetric key encryption [18]. The authors of [19] suggested a solution called "Server-HSM" which merges an HSM and a security server into a module called "HW Security Module" that might be integrated into a DB server. This module manages user privileges and protects keys with their encryption. El bouchti et al. presented a full package of encryption keys protection models inside the DBMS. Their method allows encrypting keys with master keys generated according to encryption granularity adopted by the DBMS encryption model [15]. Sesay et al. in their proposed

---

\* Karim El bouchti, Email: [elbouchtikarim@gmail.com](mailto:elbouchtikarim@gmail.com)

DB encryption model suggested protecting keys by the use of a particular way. In fact, they generate the encryption keys from a unique master key (Km) generated and stored in a tamper-proof controller [20].

Notwithstanding several DB security studies for improving the concept of encryption keys protection within DBMS, more investigations are required to develop, improve, and provide more security and flexibility to keys protection. Then, as discussed in our previous work presented in [7, 10, 15], most of the proposed solutions have their advantages and disadvantages. However, to our knowledge, a trusted and simple solution concretized by a real implementation, and adapted to more than one DB encryption model has not yet been proposed.

In this context, the present work aims to implement two solutions proposed in our previous work [15] to protect DB encryption keys. Our solutions protect encryption keys when encryption granularity adopted by the DBMS is fixed at the column level or the entire table level. They consist of encrypting the DB encryption keys of tables and columns using Km, generated by deploying two models. We consider that the main original features of our solution are its reliability and its principle. It does not require any control or management of key protection by a DB or security administrator as well as it resists strongly against attacks performed by administrators.

The present work will be structured as follows: section two presents the proposed models of Km and the common objects of the implementation of each model. It also explains how our Km models work with DB encryption models that we will implement. Section three explains the implementation and discusses the provided results. Finally, our article ends with a conclusion.

## 2. Definition of the proposed solution

In this section, we will define two models (1 and 2) of the Km generation that protects, respectively, the columns and tables keys. We will also describe the role of the common objects that have used between the two models' implementation and how those models work in an encryption/decryption process.

### 2.1. Proposed models of Km

The generation of the Km follows the two different models below:

- The Km (C) key used to protect the encryption keys of the DB columns. It is generated by the DBMS according to the model defined below:

$$Km(C) = H(\text{Table\_name} || \text{Column\_name}) \quad (1)$$

- The Km (T) key utilized to protect the encryption keys of the DB tables. It is generated by the DBMS according to the model defined below:

$$Km(T) = H(\text{Table\_name} || \text{Database\_name}) \quad (2)$$

In order to concretize the functioning and the response of the models (1) and (2), we have designed and implemented two models of DB encryption (A) and (B) having, respectively, two encryption levels: column and table. The functioning of each Km generation model is associated with the execution of a DB encryption model, as shown in Table 1.

Table 1: The generation model of Km and the DB encryption model associated

Km generation model	Associated DB encryption model
Model (1): Km generation model for protecting encryption keys of columns	Model (A): DB encryption model at the column level
Model (2): Km generation model for protecting encryption keys of tables	Model (B): DB encryption model at table level

### 2.2. The common objects of each model implementation

The creation of elements below is common for the implementation of the models (1) and (2).

MYTABLE\_ENCRYPT\_OBJET: This DB table contains records of: i) the names of the objects on which encryption has defined, ii) the used encrypt algorithms, and iii) the encryption of the encryption keys using Km. It has the following structure:

```
MYTABLE_ENCRYPT_OBJET (K_OBJECT_NAME,
K_ENCRYPT_ALGO, K_KEY)
```

TEST\_MANAGEMENT: This DB table contains the records of: i) the names of the objects on which encryption has defined, ii) the used encrypt algorithms, iii) the object encryption keys, and iv) the Km of each object name. In fact, TEST\_MANAGEMENT table is not implemented in the real working case of our solution. Nevertheless, its main role is to illustrate the results of the creation of both encryption keys and the Km. The table has the following structure:

```
TEST_MANAGEMENT (C1_OBJECT, C2_ALGO, C3_KEY,
C4_MASTERKEY)
```

where:

C1\_OBJECT, K\_OBJECT\_NAME: the object on which we have defined encryption;

C2\_ALGO, K\_ENCRYPT\_ALGO: the algorithm used for encryption;

C3\_KEY: the encryption key;

C4\_MASTERKEY: the generated Km;

K\_KEY: the encrypting result of encryption keys using Km.

The Md5 hash function: it is used to create the encryption keys and the Km while implementing all models.

The AES256 algorithm: it is the algorithm used to encrypt / decrypt the data.

**Note:** The term “Objet” signifies the column and table names.

2.3. Principle of the encryption/decryption process

An encryption/decryption process in the model (A) follows the defined steps below:

When a user sends a query to be executed, the DBMS generates the Km for each column on which encryption is defined. The DBMS decrypts, using the generated Km, a value from the K\_KEY column belonging to MYTABLE\_ENCRYPT\_OBJET table and which corresponds to the column desired to be encrypted or decrypted. This process generates the real encryption key of column that will encrypt (in the case of an inserting or updating query) or decrypt (in the case of a consulting query) the data.

The encryption/decryption process in the model (B) follows similar operations. In this case, the DBMS generates a single Km in response to the user's query since the encryption is defined on the entire table.

2.4. Case study: the dosimetric monitoring of agents

A real case study has chosen to illustrate the models' implementation results.

Let have a database named "ORCL10G" of a nuclear power plant intended to manage the dosimetric monitoring of agents working under ionizing radiation. The "agent" table stores the accumulation of the different types of doses received by each agent during the period of his work within the plant. We assume that all the data in the "agent" table are sensitive since the dose values are considered in the nuclear field as medical secret. The table "agent" has the following structure:

```
agent (idf_agent, name_agt, Dose_interne_agt,
Dose_superficielle_agt, Dose_profonde_agt, Catégorie_agt)
```

3. Implementation of the proposed models

In this section, we will present the implementation of the models (1) and (2) generating Km as well as the corresponding DB encryption models (A) and (B).

3.1. Implementation of the model (1)

In order to create the "agent" table and defining encryption on all its sensitive columns, we have used the following SQL syntax:

```
Create table agent (idf_agent varchar2(100) encrypt using
AES256, name_agt varchar2(100) encrypt using AES256,
Dose_interne_agt varchar2(100) encrypt using AES256,
Dose_superficielle_agt varchar2(100) encrypt using AES256,
Dose_profonde_agt varchar2(100) encrypt using AES256,
Catégorie_agt varchar2(100) encrypt using AES256);
```

The "Algo1" algorithm supports the execution task of this statement; it creates the "agent" table and defines encryption on its columns using the AES256 algorithm. In fact, the data column will be encrypted/decrypted with six keys Kc which will be protected by six masters key Km (C). In addition, the "Algo1" generates and stores the encryption keys of the columns (Kc) and the master keys (Km (C)) within MYTABLE\_ENCRYPT\_OBJET and TEST\_MANAGEMENT according to the models defined below:

```
/* The model of the encryption key used in the model (A)*/
Kc = H (Column_name)
/* The Km generation model of a column */
Km (C) = H (Table_name || Column_name)
```

Algorithm1: Process managed by Algo1.

```
Algo1
Input: Sensitive_column_query
Output: Created_sensitive_column_query

Begin
Loop
Decompose (Sensitive_column_query);
Sensitive_column_name := Extract (Sensitive_column
_query);
Kc:= Kc_Generator (Sensitive_column_name);
Km (C):= Km_Generator (Sensitive_column_name, Table
_name) ;
End loop;
Insert into TEST_MANAGEMENT values
(Sensitive_column_name , Used_algo, Kc, Km (C));
Insert into MYTABLE_ENCRYPT_OBJET values
(Sensitive_column_name , Used_algo, Encrypt_AES256 (Km
(C), Kc ));
Execute (Sensitive_column_query) ;
End;
```

The execution of the "Algo1" algorithm generates the following records:

Table 2: Records created in the TEST\_MANAGEMENT table in the model (1).

C1_OBJECT	2_ALGO	C3_KEY	C4_MASTERKEY
idf_agent	AES256	46D18AC7BD06518B5A33C650CA760D9C	36EE05BA4ACDEC7D1C07D16FCDDCC9CBF
name_agt	AES256	4BF0A8B1EB8CA12C2912ED25E4D4BDC5	F8422E273F1957702DE160662923C0EA
Dose_interne_agt	AES256	C8FE8472457B1A9436EE90E6D022178F	452C55A53935CF7056CE1C293FE8D4FC
Dose_superficielle_agt	AES256	1FD82F97BE7BA2565D7FDD4BD6A91179	44BB0C031437DB46B641257337C7C458
Dose_profonde_agt	AES256	F67D1D0A822D37E3AC03D69C94A38994	8D71448C964377D9F0E539B3FB230133
Catégorie_agt	AES256	822E1CDA2CFA7B1EF36B90523E337682	FE30063A2D96A6DB6059CE708103BD5F

Table 3: Records created in the MYTABLE\_ENCRYPT\_OBJET table in the model (1).

K_OBJECT_NAME	K_ENCRYPT_ALGO	K_KEY
idf_agent	AES256	12BB4076B53A907324D42AFB9B0501006A93E1F347EC05536A7115E4554 CD8D06662D1EEEAC1CA8D71BC2A33EFD7810B
name_agt	AES256	90F4D05F7C5A11A5752E8AB1354BE82D797BFE16051F78DD7018A60856 49A709515637DB88472F14509DB73FC76E6B0C
Dose_interne_agt	AES256	6B40D18BF99C712F4F4034E8A11AF73FC8B422CCC218AF595FD06EB4 E4AE4BB3E8D5D0CCA9BE57434FCD690A577D05D0
Dose_superficielle_agt	AES256	5F03CF21D034BFFBA1FEA4BD5CEA43A15A32E8C9F4FDE591AF842995B BD30FF53CC25849363BCF54B8FC2E28FD7FF7A7
Dose_profonde_agt	AES256	3A468DD545A12883543199A45202E4CE3AAA4D006CE4453BFC380377423 C24C3FA85A1BF68F31F6E011C062C5E19D2AE
Catégorie_agt	AES256	34FEFD552E0D63C4A99281FC1B0A8189D5B527EDC303E9AB760B35C1A2 28C1F7B0EFDAAF26B7E3F507297D351E64FFE9

Table 4: The "agent" table before encryption.

idf_agent	name_agt	Dose_interne_agt	Dose_superficielle_agt	Dose_profonde_agt	Catégorie_agt
1000	Azzaoui	10	15	25	A
1001	Rachidi	8	11	12	A
1002	Kharmoum	16	05	14	A
1003	Sajid	14	66	65	B

Table 5: The "agent" table after encryption.

idf_agent	name_agt	Dose_interne_agt	Dose_superficielle_agt	Dose_profonde_agt	Catégorie_agt
5754957F70316A9C02 01002A8CBFE412	745A2F1FF2BDAD322 6910989994A7287	B5063DD0A036503D0 2F11B63DF1B12B1	FDBD02C08C389AE7 583F8211E428B2A7	D694729051643896225 89DA79E580A60	D1D88EDED1CF67BF 3AB34261052FF335
A6776D65772F8F4992 D8AFC2A2B387C9	1C65506D1F8AA015B 5B98765133E9782	5C6ABEA8480996813 19175A05C4B1AB5	BD706EE5E149EBDC E6796457E944FB81	BECBC7C7B6BD0B0E 12CF1AD549E22682	D1D88EDED1CF67BF 3AB34261052FF335
AFBFEA3BC5FCD283 96E974016169DF5D	67BC01E3BF672D7BF 568ACC3A582ECB8	B8C892229BBB1E395 1290107C524B12A	125180FAB503F868E DC55F42D0BB34CB	A8A68F1B4D1D3DD0F 398AFED4A54A0A5	D1D88EDED1CF67BF 3AB34261052FF335
14DB0A7462832F494E AC7C8D12A09FC6	7A1FBFCD0E02BC191 0055CF76279F21A	23BF97F16393EC6A8 4B93FF4F9EB74AA	293A72927BD5C9760 450FFFF14CEC693	A2B800E15CAFD3AFA 9A22FB0A4C257B8	5315BF4B7B530AA72 9AC1CDCB53F4C8B

In order to test model (1), the "Algo2" algorithm represents the functioning of Model (A). It supports the data encryption inserted by a user. Tables 4 and 5 show the result of inserting four lines in the "agent" table before and after the encryption.

Algorithm 2: The DB encryption using the model (1) and (A).

```

Algo2
CREATE OR REPLACE TRIGGER Insert_Model_A
BEFORE INSERT ON agent
FOR EACH ROW
DECLARE
    
```

```

Kc1 varchar2(100);
Kc2 varchar2(100);
Kc3 varchar2(100);
Kc4 varchar2(100);
Kc5 varchar2(100);
Kc6 varchar2(100);

BEGIN

/*Generating Km and seeking Kc for each column from
MYTABLE_ENCRYPT_OBJET*/
    
```



```
Kc1:= Search_Encrypt_Key ('idf_agent');
Kc2:= Search_Encrypt_Key ('name_agt');
Kc3:= Search_Encrypt_Key ('Dose_interne_agt');
Kc4:= Search_Encrypt_Key ('Dose_superficielle_agt');
Kc5:= Search_Encrypt_Key ('Dose_profonde_agt');
Kc6:= Search_Encrypt_Key ('Catégorie_agt');

/* Inserting in table "agent"*/

INSERT INTO agent VALUES (Encrypt_AES256
(Kc1, :new.idf_agent), Encrypt_AES256
(Kc2, :new.name_agt, Encrypt_AES256
(Kc3, :new.Dose_interne_agt), Encrypt_AES256
(Kc4, :new.Dose_superficielle_agt), Encrypt_AES256
(Kc5, :new.Dose_profonde_agt), Encrypt_AES256
(Kc6, :new.Catégorie_agt));
End ;
```

```
Decompose (Sensitive_table_query) ;
Sensitive_table_name:= Extract (Sensitive_table_query);
KT:= KT_Generator (Sensitive_table_name);
Km(T):= Km_Generator (Sensitive_table_name, Database_name);
Insert into TEST_MANAGEMENT values
(Sensitive_table_name, Used_algo, KT, Km(T));
Insert into MYTABLE_ENCRYPT_OBJET values
(Sensitive_table_name, Used_algo, Encrypt_AES256
(Km(T), KT));
Execute (Sensitive_table_query);
End ;
```

3.2. Implementation of the model (2)

To implement model (2), we define encryption on the "agent" table level using the following SQL syntax:

Create table agent encrypt using AES256 (idf\_agent varchar2(100), name\_agt varchar2(100), Dose\_interne\_agt varchar2(100), Dose\_superficielle\_agt varchar2(100), Dose\_profonde\_agt varchar2(100), Catégorie\_agt varchar2(100));

The "Algo3" algorithm supports the execution of this instruction. It creates the "agent" table and defines encryption on all its data using the algorithm AES256. In this case, the data are encrypted/decrypted with a single key K<sub>T</sub>, which will be protected by a single master key K<sub>m</sub> (T). The "Algo3" algorithm generates and stores K<sub>T</sub> and K<sub>m</sub> (T) also in MYTABLE\_ENCRYPT\_OBJET and TEST\_MANAGEMENT according to the models defined below:

```
/* The model of the encryption key used in the model (B)*/
KT= H (Table_name)
/* The Km generation model of a table */
Km (T) = H (Table_name || Database_name)
```

Algorithm 3: Process managed by Algo3.

Algo3
Input: Sensitive_table_query Output: Created_sensitive_table_query
Begin

Table 6: Records created in the TEST\_MANAGEMENT table in the model (2).

C1_OBJECT	C2_ALGO	C3_KEY	C4_MASTERKEY
agent	AES256	B33AED8F3134996703DC39F9A7C95783	697C371A913425CF202D15F143D2DAF0

Table 7: Records created in the MYTABLE\_ENCRYPT\_OBJET table in the model (2).

K_OBJECT_NAME	K_ENCRYPT_ALGO	K_KEY
agent	AES256	736079082547466884631FC41910AB5770A6962367465EC1CB9526A 864367916929D05016D02B96D9B55511854D3AB13

The execution of the "Algo3" algorithm generates the following records:

The "Algo4" algorithm represents the functioning of the model (B). It supports the data encryption inserted by a user. The tables 8 and 9 show the result of inserting four rows in the "agent" table before and after the encryption.

Algorithm 4: The DB encryption using model (2) and (B).

```
Algo4
CREATE OR REPLACE TRIGGER Insert_Model_2
BEFORE INSERT ON agent
FOR EACH ROW
DECLARE
KT varchar2(100);
BEGIN

/* Generating Km and seeking KT for each column from
MYTABLE_ENCRYPT_OBJET*/

KT :=Search_Ecrypt_Key( 'agent');

/* Inserting in table "agent"*/

INSERT INTO agent VALUES (Encrypt_AES256
(KT,:new.idf_agent), Encrypt_AES256 (KT,:new.name_agt),
Encrypt_AES256 (KT,:new.Dose_interne_agt),
Encrypt_AES256 (KT,:new.Dose_superficielle_agt),
Encrypt_AES256 (KT,:new.Dose_profonde_agt),
Encrypt_AES256 (KT,:new.Catégorie_agt));
End ;
```

Table 8: The "agent" table before encryption.

idf_agent	name_agt	Dose_interne_agt	Dose_superficielle_agt	Dose_profonde_agt	Catégorie_agt
1000	Azzaoui	25	25	25	A
1001	Rachidi	8	11	12	A
1002	Kharmoum	16	05	14	A
1003	Sajid	14	66	65	B

Table 9: The "agent" table after encryption.

idf_agent	name_agt	Dose_interne_agt	Dose_superficielle_agt	Dose_profonde_agt	Catégorie_agt
3F843D72B4CF6AF3B FEDD0F8A73A46DB	03377847D26334CDA6 65F815335C87F9	7012CB55124F226FA2 E530E0D8133F14	7012CB55124F226FA2 E530E0D8133F14	7012CB55124F226FA2 E530E0D8133F14	91B5BD099938E4CE4 DF76529F6740B8A
2D80DCE15D394B765 94AD5E18F3405BE	0B71021170A841DAE 0CB4641C08076CD	0C04B7B8C2A594ED2 D6CE2FCD9EE91FD	52516FBF14B5DB600 CF294F47153C168	CF92FB85EF0E373795 F9C4D57D66ECF1	91B5BD099938E4CE4 DF76529F6740B8A
4CDDFEF4428E61343 AD6C823FF1860A4	DA45B069E89AC7BE4 C2B69EE232EB1A4	0F8913B9B06C772A68 8E9489B13A1124	5C9D1E8240D88EAD 7072C8B7673AB4C1	CC2CCB3C2994CE129 59B9C9B66F478A5	91B5BD099938E4CE4 DF76529F6740B8A
CA80281E0ADB105C E371803DD3F575E	EE6099C500334279227 AFA5C27E199FB	CC2CCB3C2994CE129 59B9C9B66F478A5	9B07E13AC87C52956 2187B81CFCD6B2B	EC2F5721D81D6CACE 4C6EA7B9B49ED52	72621DFBF38C674D9 BA24509BDA41160

### 3.3. Results and discussion

This section introduces data discussion and analysis based on the findings obtained by implementing the two Km models. They are summarized as follow:

- The proposed solutions are more practical than the conventional ones, primarily the Wallet, HSM, and the security server, where their disadvantages have explained and revealed in [15]. Our solutions optimize perfectly additional costs to protect the keys either in terms of hardware acquisition (case of HSM and security server) or in human resources (the administrator of the security server).
- The Wallet solution used in Oracle TDE generates Km, which protects encryption keys, and stores it within the Wallet. Here, it is necessary to create the Wallet and its password as well as a secured location (such as backup systems) to store the password whenever the Km is newly created. This operation is mandatory before starting the process of data encryption/decryption inside DBMS [11]. It is worthy to mention that the backup system is a critic component of the Wallet concept. In this vein, the protection concept of encryption keys based on the proposed models (1) and (2) is similar to the Wallet solution in terms of Km generation within the DBMS. However, with our concept, the Km creation does not require any Wallet creation to store Km or secured location to store the password.
- The proposed solution does not require any protection management of the encryption keys by a security administrator, DB administrator or another trusted collaborator, as discussed in [15]. Hence, none of them knew about the generation of Km or its location. The probability of attacking keys is almost impossible, even if the attacker arrives to consult table

MYTABLE\_ENCRYPT\_OBJET stored in the DB dictionary.

- The proposed solution does not define the place where storing Km. Km generation is performed automatically while defining encryption on a sensitive object (column or table), precisely during the creation by the DB administrator. Obtaining a value of Km by attackers (administrators, internal or external attackers) is almost an impossible operation.
- It is important to notice that the new concept we have proposed and implemented enhances the security of encryption keys. In fact, compared to the Oracle TDE Column Encryption solution that uses a single master key to protect all the column keys, the model (1) generates several Km to protect each column key. The number of Km generated is equal to the number of sensitive columns. For example, if a DB contains 20 sensitive columns to encrypt, we need 20 keys to encrypt data and 20 Km to protect them.
- Our solution can work with any DB encryption models, obviously with those implementing encryption granularities at the level of columns and tables. It is well adapted to free license DBMSs.
- In the model (1) implementation, we focused on to protect 6 encryption keys of the following columns (idf\_agent, name\_agt, Dose\_interne\_agt, Dose\_superficielle\_agt, Dose\_profonde\_agt, Catégorie\_agt). Each column key is protected by encrypting it with its own Km generated by the model (1). This protection was tested by the implementation of the model (A). Table 4 shows the encryption test results of the 6 columns of the "agent" table deploying the model (1). Likewise, in the model (2) implementation, one encryption key of the table "agent" has protected with a single Km generated using this model. Then, this protection was tested using the model (B). Table

8 represents the result obtained of encrypting table "agent" by deploying the model (2).

- The results presented in tables 2 and 3 shows the keys generation when the "agent" table is created by the administrator. In table 2, the columns C3\_KEY and C4\_MASTERKEY represents, respectively, the encryption key generated of each column and its associated Km. In table 3, the column K\_KEY, belongs to MYTABLE\_ENCRYPT\_OBJET table, represents the encryption of each column key of the table "agent" using its associate Km.
- In table 6, the columns C3\_KEY and C4\_MASTERKEY represents, respectively, the key generated to encrypt the entire table and its Km. The value of the column K\_KEY in table 7 represents the encryption of the encryption key using its associate Km. Both tables show the keys generation when the "agent" table is created by the administrator.
- As described earlier, tables 4, 5, 8, and 9 show the result of inserting rows in the "agent" table before and after the encryption. The encryption results showed that our solution works perfectly, either when encrypting or decrypting data. Actually, the encryption process via model (A) or (B) requires the generation of Km through model (1) or (2), respectively. Each value of generated Km is used to extract, from K\_KEY column, the real encryption /decryption key. The process of data decryption follows the same operations.
- Finally, both proposed model works inside DBMS are summarized according to the algorithm flowchart described below:

Let's consider a sensitive table A

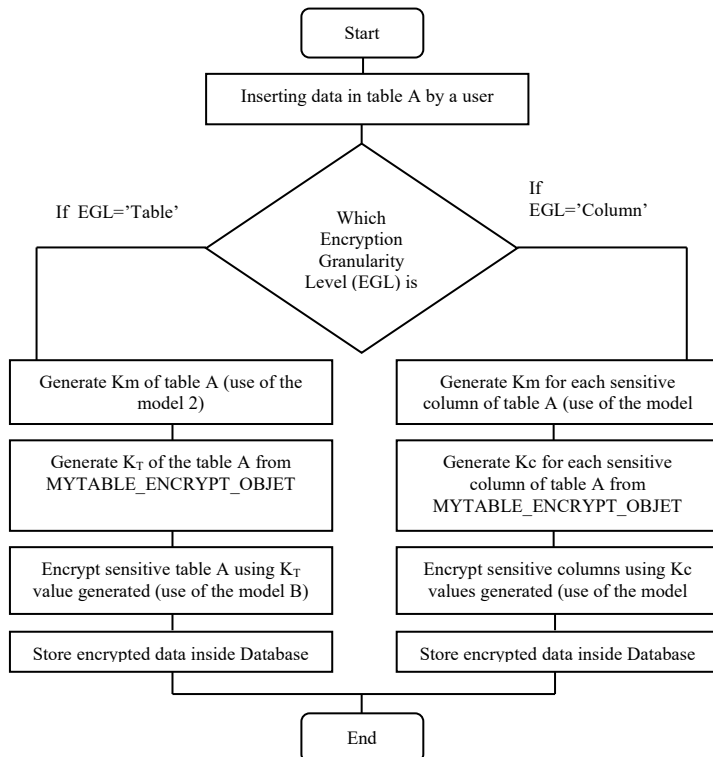


Figure 1: Algorithm flowchart specifying the both proposed models.

## Conclusion:

Besides the conventional mechanisms deployed to secure sensitive DB (network protection, authentication, and access control), data encryption at DBMS level is a strong way that reinforces the defense in depth of the sensitive data. This process is strongly linked to the protection of the encryption keys on which they depend on two main factors: the location where the keys are stored and users who have access to them.

Our contribution in this article is to implement two solutions that secure encryption keys within the DBMS. These solutions are original and well adapted to any encryption model inside a DBMS. The solution's purpose is to protect DB keys by their encryption using a master key generated when defining encryption on a table or column. In forthcoming works, we aim to develop a solution that covers the protection of encryption keys when encryption is done on Tablespace.

## Conflict of Interest

This manuscript has not been published and is not under consideration for publication elsewhere. We have no conflicts of interest to disclose.

## Acknowledgment

I would like to express my appreciation to all my professors, whom they helped and guided me to realize this work.

## References

- [1] E. Shmueli, R. Vaisenberg, Y. Elovici, C. Glezer, "Database encryption: an overview of contemporary challenges and design considerations" ACM SIGMOD Record, New York, NY, USA, 2010. DOI: 10.1145/1815933.1815940
- [2] Hashim, Hassan B, "Challenges and Security Vulnerabilities to Impact on Database Systems" Al-Mustansiriyah Journal of Science 29(2), 117-125,2018. DOI: <http://doi.org/10.23851/mjs.v29i2.332>
- [3] S. Jacob, "Protection cryptographique des bases de données: conception et cryptanalyse," Ph.DThesis, Université Pierre et Marie Curie-Paris VI, 2005.
- [4] A.M.Mostafa, F.A. Almutairi, M.M. Hassan, "False alarm reduction scheme for database intrusion detection system" Journal of Theoretical & Applied Information Technology., 96(10), 2816-2825. ISSN: 1992-8645
- [5] I. Homoliak, J.Guarnizo, Y.Elovici, M.Ochoa, "Insight into insiders and it: A survey of insider threat taxonomies, analysis, modeling, and countermeasures" ACM Computing Surveys, New York, NY, USA 2019. <https://doi.org/0000001.0000001>
- [6] Deepicata. N. Soni, "Database Security: Threats and Security Techniques" International Journal of Advanced Research in Computer Science and Software Engineering., 5(5), 621-624, 2015. ISSN: 2277 128X
- [7] K. El bouchti, S.Ziti, Y.Ghazali, N.Kharmoum, "Sécurité des Bases de Données : Menaces principales et solution de chiffrement existantes", in Proceedings of the JDSIRT Conference Information Systems, Networks Telecommunications, Meckness, Morocco, 2018.
- [8] K. El bouchti, N. Kharmoum, S. Ziti, F. Omary, "A new approach to prevent internal attacks on Database encryption keys" Proceedings of the International Conference Scientific Days Applied Sciences, Larache, Morocco, 2019
- [9] E. Shmueli, R. Vaisenberg, E. Gudes, Y. Elovici, "Implementing a database encryption solution, design and implementation issues" Computers & security, 44, 33-50, 2014. DOI: [ORG/10.1016/J.COSE.2014.03.011](https://doi.org/10.1016/J.COSE.2014.03.011)
- [10] K. El Bouchti, S. Ziti, F. Omary, N. Kharmoum, "A New Database Encryption Model Based on Encryption Classes" Journal of Computer Science., 15(6), 844.854, 2019. DOI: [10.3844/jcssp.2019.844.854](https://doi.org/10.3844/jcssp.2019.844.854)
- [11] Oracle (2016), Oracle® Database Advanced Security Administrator's Guide 11g Release 2 (11.2)[online] Technical Document:
- [12] S. Mukherjee, "Popular SQL Server Database Encryption Choices" International Journal of Computer Science and Engineering, arXiv preprint arXiv: 1901.03179, 2018. ISSN: 2231 – 2803
- [13] MySQL Server Documentation. MySQL 5.7 Reference Manual Online
- [14] A. K. Maurya , A.Singh, U.Dubey, S.Pandey, U. N.Tripathi, "Protection of Data Stored in Transparent Database System using Encryption" Journal of

Computer and Mathematical Sciences., 10(1), 190-196, 2019. ISSN 2319-8133.

- [15] K. El bouchti, S.ZITI, F.OMARY, "A new approach to protect encryption keys in Database Management System", Proceedings of the International Conference Modern Intelligent Systems Concepts, Rabat, Morocco, 2018.
- [16] V.V.Galushka, A.R.Aydinyan, O.L.Tsvetkova, V.A.Fathi, D.V.Fathi, "System of end-to-end symmetric database encryption" In International Conference Information Technologies in Business and Industry, 2018. Doi :10.1088/1742-6596/1015/4/042003.
- [17] Elovici, Y., Vaisenberg, R., & Shmueli, E. (2018). U.S. Patent No. 9,934,388. Washington, DC: U.S. Patent and Trademark Office.
- [18] Itamar, E., & Rotem, A. (2018). U.S. Patent Application No. 15/570,775.
- [19] L.Bouganim, Y.Guo, Database encryption. In Encyclopedia of Cryptography and Security, Springer US, 2011
- [20] S.Sesay, Z. Yang, J.Chen, D. Xu, "A secure database encryption scheme" In Consumer Communications and Networking Conference, CCNC. 2005 Second IEEE, Las Vegas, NV, USA, 2015. DOI: 10.1109/CCNC.2005.1405142

## Review on Outliers Identification Methods for Univariate Circular Biological Data

Siti Zanariah Satari\*, Ku Muhammad Naim Ku Khalif

Centre for Mathematical Sciences, Universiti Malaysia Pahang, 26300 Gambang, Kuantan, Pahang, Malaysia

### ARTICLE INFO

Article history:

Received: 01 January, 2020

Accepted: 22 February, 2020

Online: 09 March, 2020

Keywords:

Biological Data

Outliers

Circular Data

Abnormality

### ABSTRACT

Circular data are common in biological studies which are involved angle and direction measurements. An outlier in circular biological data mostly related to the abnormality of the data set. The existence of outliers may affect the final outcome of a data analysis. Thus, an outliers' identification method is essential in circular biological data to determine the stage of abnormality for the sample that has been studied. Past studies were mostly focusing on detecting outliers for multivariate circular biological data. However, identifying outlier for univariate data is more essential in the abnormality stage investigation. In this study, outliers' identification methods for univariate circular biological data have been reviewed. The strength and weaknesses of the methods are investigated and discussed.

## 1. Introduction

Biology involves the studies on living organism evolution, growth, function, dissemination or advancement. Biological research currently covers a variety of fields of experimental biology; including biochemistry, bioinformatics, biotechnology, biomedicine, genetics, genomics, molecular biology, neuroscience and system biology. Biological data that related to angle and direction measurement is classified as circular biological data. This paper investigates the wide use of biomedical and ecological circular data from biological branches. For example, biomedical data involving circular values are bone structure measurement [1] and heart rhythm analysis [2]. While ecological circular data involve animal mobility such as bison trails shaped [3] and movement of intertidal gastropods [4]. Due to circular characteristic, circular biological data requires special care and a suitable circular distribution model is needed. Specific outliers' detection method also need to be used to get accurate and precise results during analysis. An extreme outlier may affect the result especially on modeling and forecasting purposes [5]. An outlier in circular biological data mostly related to the abnormality of the data set which may affect the final finding of the analysis and lead to erroneous in decision making. For example, in biopharmaceuticals especially for vaccines research, drug productions will effected by outliers that can cause of the false acceptance or rejection of a bad or good drug [6].

While in phylogenomic studies, errors during orthology detection, may cause a systematic error which can effect

Siti Zanariah Satari, Centre for Mathematical Sciences, Universiti Malaysia Pahang, +60197699240, zanariah@ump.edu.my

[www.astesj.com](http://www.astesj.com)

<https://dx.doi.org/10.25046/aj050212>

regulation of biological process that need to be taken [7]. Therefore, outliers can cause misdirecting factual outcomes and estimation of parameters which are may not bring precise forecasts. There is a great deal of difficulties in outliers detection with the expanding complexity, size and assortment of biological datasets. Thus, a lot of study has been done to identify outliers in biological data, but most of them for circular regression model. For example on eye dataset of glaucoma patient [8,9], on circadian data taken from systolic blood pressure reading [10] and on angular of protein chain shapes [11]. Hence, there is a need to explore more outliers' detection technique for univariate circular biological data. Identifying outlier for univariate data is more essential in the abnormality stage investigation [6,7]. Also, previous study shows that, most data are from environmental study such as wind direction [12] and direction of sandstone [13]. Therefore, the aim of this paper is to review outliers' identification methods for univariate biological circular data. The strength and weaknesses of the methods are reviewed and discussed to highlight the similarity and differences of each method. Besides that, the trend of univariate circular biological data types that has been used and its distribution models also been investigated.

## 2. Circular Biological Data

In biological study, there are two types of directional data represented either in two or three dimensions. It is called circular data for the two dimensions. Circular data can be represented as measurements in the clockwise or anti-clockwise direction, and can be measured in degrees ( $0^\circ$ ,  $360^\circ$ ), or radians ( $0$ ,  $2\pi$ ).



Meanwhile, it's defined as spherical data for the three dimensions where the data is measured as points on a unit sphere's surface by two angles, such as the points measured by longitude and latitude on the surface of the earth [14]. There are a lot of biological circular data. There are few examples in ecology studies such as the vanishing angle of the pigeon after release [14], the homing ability of the frog [15,16], and the direction of the sea star after removal from the natural habitat [15].

In addition, there are also many angles involved in molecular research. For example, protein structure shape that determines by dihedral angle sequence [17], protein structure pairing angles [18,19], protein angle formation [11], and protein structure prediction [18]. Biomedical also includes some circular data such as heart rhythm analyst [2], corneal shape anomaly after cataract surgery [19], psoriasis observation of psoriatic plaque segmentation in skin images [20], and angular measurement of craniofacial disease (angel of jaw) [21]. Circular statistics and vector strength were used in the analysis of heart rhythm by measuring angular histogram in the R-wave vector to analyze ECG-waves. Circular linear analysis was used in Psoriasis by applying circular copula model means.

### 3. Univariate Circular Model for Biological Data

There are few types of univariate circular distribution such as Uniform distribution, Cardioid distribution, a triangular distribution, Circular Normal (CN) distribution, off set normal distribution, Wrapped Normal (WN) distribution, Wrapped Cauchy (WC) distribution, general Wrapped Stable (WS) distribution, variations of CN distribution, a Circular Beta Model and Asymmetric Circular distributions. The most commonly used circular distribution for circular biological data is Circular Normal (CN) distribution or called as von Mises distribution which can be found in many literatures [22,23,24]. The probability density function of the Von Mises distribution is given by

$$f_{vm}(\theta; \mu, \kappa) = \frac{1}{2\pi I_0(\kappa)} \exp\{\kappa \cos(\theta - \mu)\} \quad (1)$$

$$0 \leq \theta < 2\pi, \kappa \geq 0, 0 \leq \mu < 2\pi,$$

where

$$I_0(\kappa) = \frac{1}{2\pi} \int_0^{2\pi} \exp\{\kappa \cos(\theta)\} d\theta. \quad (2)$$

The mean direction is stated as  $\mu$  parameter. The concentration parameter  $\kappa$ , influences the concentrated distribution around the mean direction. The larger values of  $\kappa$  will show the result of the distribution which is more closely grouped around the mean direction. The von Mises distribution is continuous on the circle and is the circular analogue of a linear normal distribution. For example, in biological studies, [25] used frog data following a von Mises distribution and identifying outliers in the data. Meanwhile, [26] suggested that circular data could be tested by considering the probability ratio test for slippage location in a von Mises distribution or the probability ratio test for slippage concentration in a Fisher distribution by [27].

Also, [28] used von Mises distribution to propose a new definition of truncated probability distribution for univariate and bivariate circular data which is applied to protein chains for angular values. Besides, [15] used von Mises distribution for

adjusting and detecting outliers of the sea star directions using robust circular distance. In other hand, some researcher used other probability distribution such as by mixing a wrapped stable distribution with a circular uniform distribution in identifying outliers. For example, [14] used Symmetric Wrapped Stable (SWS) and Circular Uniformity (CU) to analyse the distribution of pigeon's vanishing angles data.

### 4. Outlier Identification in Circular Biological Data

Outliers are data that do not appear as normal with the remaining data in the same set. An outlier may be data that is novel, new, anomalous, abnormal, strange or noise. Circular biological data contains two types of outliers, including any analytical or biological data [29]. During the analytical process, analytical outliers consist of one or more abnormal values among all the samples. Thus, the researcher needs to determine whether the outliers need to be removed or adjusted. While, the biological outliers occur when the sample value tends to be extremely higher or lower than other sample values [30]. Many researchers did a lot of studies to identify outliers for biological circular data. [15] have suggested two main ways to deal with this problem which are outliers either can be deleted or adjusted. Besides that, robust statistical methods also can be used to detect outliers. However, it has been used only in the circular regression model that is applied to environmental data in particular for wind direction data [31], not for biological data. Therefore, it is very important to choose suitable methods of identifying outliers in circular data for proper data handling. Graphical and numerical methods are the most common tools used in investigating the existence of outliers in circular data. Thus, all those methods have been reviewed intensively in the next section.

### 5. Outlier Identification for Univariate Circular Biological Data

There are several graphical techniques used to detect outliers in univariate circular biological data. The summary of all the graphical methods in identifying outliers for univariate circular biological data is shown in Table 1. There are three common types of graphical techniques such are P-P Plot, Q-Q Plot and Circular Boxplot. As example, [14] used the P-P Plot and Q-Q plot to identify outliers in the pigeons vanishing angles after been released. Meanwhile, [32] used the Q-Q plot to identify outliers in the sea star movement directions after they were displaced from their natural habitat. The P-P Plot is simple and easy to obtain by finding the best-fitting circular normal distribution model but it need supplement from numerical test. The Q-Q plot is obtained by calculating the sample quartiles, but the technique was harder to get accurate result especially for outlier that situated too close to the other sample values. Meanwhile, [24] and [33] proposed Circular Boxplot which is modification from the normal boxplot. The technique is applied to the frog's directions data. Homing ability of northern cricket frog, *Acris Crepitans* has been taken from [34]. The proposed method (Circular Boxplot) performed better when both value of  $\kappa$  and the sample size are larger.

Table 2 to Table 4 show few numerical methods for identifying outliers of univariate circular biological data particularly for ecological data which are frog, sea star and pigeon movement. From the tables, it can be seen that the homing ability

Table 1: Review on Outliers Identification in Univariate Circular Biological Data Using Graphical Methods

Biological Data (Ecological Data)	Model Distribution	Outliers Identification Methods	Strength	Weakness	Analysis tool	References
Pigeons- Vanishing angles of pigeons released	Circular Normal (CN) or Von Mises (VM) model	P-P Plot	Simple graphical way to detect outlier and easier to obtain by finding the best-fitting CN distribution, and then plot it.	Need to support by numerical test for a more accurate result.	Statistical package: SPlus	[14]
		Q-Q Plot	Approximate plot is obtained by calculating the sample quantiles.	It is harder to get the result especially for outlier that situated too close to the other sample values.		
Sea stars directions - after they were displaced from their natural habitat	Von Mises (VM) model	Q-Q Plot	The extra feature of the Q-Q plot is that may reveal an outlying value.	The type of plot may very vary even when the hypothesized model is appropriate to the data, therefore need to supplement by numerical test.	Not Mention	[32]
Frog - homing ability of the northern cricket frog, <i>Acris Crepitans</i>	Von Mises (VM) model	Circular Boxplot	Performs better when both the sample size and value of $\kappa$ are greater.  It advisable to use different values of resistant constant $\nu$ for identifying possible outliers in the circular variable.	Overlapping lower and upper fences may occur.	Statistical package: SPlus	[24, 33]

of northern cricket frog data has been widely used to illustrate the capability of the proposed numerical methods. As example in 1980, [27] proposed four test statistics, namely L, C, D, and M' Statistic to identify a single outlier in univariate circular data, particularly for the frog data (refer Table 2). It was found for small samples sizes that; it is better to use the C and D statistics. However, no single statistic was recommended to detect multiple outliers, and typical methods are only successful in detecting a single outlier at one time. Furthermore, there was no discussion on how to identify an outlier when the sample size is large.

One Spurious Observation which is introduced by [25], also been implied to the frog data to present more than one outlier by using the posterior probabilities of sets of  $m$  spurious observations (refer Table 2). However, this technique is too sensitive to small data. Later, [16, 24, 35] intensively done research on the frog data and proposed few methods for identifying outliers in univariate circular data (refer Table 2 and Table 3). The authors proposed

three methods which are *A* Statistic, *Chord* Statistic and An Alternative Test of Discordance.

Firstly, [35] introduced A Statistic which is based on the summation of the circular distances from the point of interest to all other points. It performed well in large sample sizes and provide an alternative test of discordancy in circular sample, especially with the known problem of finding the estimate of the concentration parameter  $\kappa$ , using maximum likelihood method. Secondly, [24] proposed *Chord* Statistic which is more simpler and easier to interpret. This method is based on the summation of the chords' length between the circular observations which is using circular distance as parameter. Finally, [16] proposed a discordance test which is based on the circular distance between sample points. The test is called as An Alternative Test of Discordance. This test can be applied to detect possible outliers in both univariate and bivariate data. All simulations and tests done by [16, 24, 35] were using SPlus Statistical Package.

On the other hand, [23] used R Statistical Package to detect outliers in the frog data (refer Table 3). The authors introduced triple measure of robustness which is called a Robust Circular Distance Statistic (*RCDu*). A high probability of outliers detected, and low rates of masking and swamping are always considered as the good robustness properties for any outlier detection methods. *RCDu* successfully detect outliers with high levels of contamination in large univariate circular biological data.

Table 4 shows the review of the outliers identification methods for the sea star movement directions, vanishing pigeon’s angles and Jander’s ant orientation. Two methods have been introduced for sea star data that apply to the von Mises (VM) distribution model. Firstly, [32] proposed  $M_n$  Statistic (based on resultant length) which is adapted from [27]. The method suitable for small sample size and for single outlier. Secondly, [15] proposed a method based on circular distance between circular data points and circular mean direction by adjusting the outlier. The procedures provided results of the mean resultant length as close as the results of the clean data and minimize *MCD* (Mean Circular Distance) with low and high contamination levels.

Few other methods have been introduced by [14]. The authors proposed Likelihood Ratio Testing (*LRT*) Statistic and Locally Most Powerful Invariant (*LMPI*) Statistic which are applied to vanishing angles of pigeons once released. The results show that, *LRT* has best performance when location parameter  $\mu_1$  value is moderate. While *LMPI* has best performance when location parameter  $\mu_1$  value is small. It shows the same result when the ant orientation data have been applied to *LMPI* [36]. Two types of statistical package have been applied to *LMPI* which are SPlus and DDSTAP Statistical package developed by [37].

In addition, Table 5 shows the studies in identifying outliers for biomedical circular data. Only one research that used von Mises distribution model which is study on eye data set of glaucoma patients. [38] proposed  $G_a$  Statistic, which is based on the spacing theory. Other studies have been done on eye and circadian rhythm data set but for Multiple Circular Regression (MCR) model. [10] using DMCEs Statistic to analyse circadian

data base on systolic blood pressure. The DMCEs Statistic performed well when the sample size  $n$  and the value of concentration parameter  $\kappa$  are large. Other statistics called DFBETAc Statistic and COVRATIO Statistic are introduced by [8, 9] applying to the eye data set. It is shown that, DFBETAc Statistic performed well and more accurate when parameters estimation become smaller after removing the outliers.

### 6. Discussion

Currently, review on circular biological data shows that, most of the data are from ecological area of study. Only one biomedical data has been found recently that using univariate circular distribution model. While the other biomedical study involves multiple regression analyses for example eye data of glaucoma patients [8,9], and on circadian data which take from systolic blood pressure reading [10]. Hence, we believe there is a need to explore more on univariate circular data related to human being especially in biomedical research and health informatics since identifying outlier for univariate data is crucial in the abnormality stage investigation.

Outlier identification obviously becoming more important for identifying of abnormality or error in circular biological data. From the review tables, numerical techniques more frequently used compared to graphical techniques. Although graphical technique more interesting and simpler to calculate, the results still need to be supplement by numerical technique to get adequate and precise results. The graphical techniques also have disadvantage when the sample size and value of  $\kappa$  are smaller. It is shown that, a lot of new technique has been evolving from Mardia (M) Statistic by [39]. More new procedures have been proposed, mainly calculated based on circular distance between circular observations such as *A* Statistic [35], *Chord* Statistic [24] and An Alternative Test of Discordance [16]. It shows that, those proposed statistic performed well compared to *C*, *D*, *L* and *M'* Statistics and can be applied to both univariate and bivariate data for large sample size. The SPlus Statistical Package become the most popular analysis tools that has been used for a lot of proposed techniques.

Table 2: Review on Outliers Identification in Univariate Circular Biological Data Using Numerical Method

Biological Data (Ecological Data)	Model Distribution	Outliers Identification Methods	Strength	Weakness	Analysis tools	References
Frog - homing ability of the northern cricket frog, <i>Acris crepitans</i> .	Von Mises (VM) model	<p><i>L</i> Statistic (<i>LRT</i> Statistic): based on maximum likelihood ratio.</p> <p><i>C</i> Statistic: based on sample mean resultant length.</p> <p><i>D</i> Statistic: based on relative arc lengths.</p> <p><i>M'</i> Statistic: adaptation from</p>	<p>For large values of <math>\kappa</math>, <i>M</i> Statistic is better and formed asymptotic distribution.</p> <p>Small sample size better to use <i>C</i> and <i>D</i> statistics.</p> <p><i>D</i> statistic is easier to calculate than <i>C</i> Statistic.</p>	There was no discussion on how to identify an outlier when the sample size is large and when it has multiple outliers.	Not Mention	[27]

		Mardia Statistic.	(M)					
Frog - homing ability of the northern cricket frog, <i>Acris Crepitans</i> .	Von Mises (VM) model	One spurious observation		Proposed method may indicate whether the data implies the presence of more than one spurious observation using the subsequent probabilities of sets of $m$ spurious observations.	Too sensitive to small data, most of the result detect more than one spurious observation, therefore need to be validate more.	Not Mention	[25]	
				Extremely potent method in identifying outliers for small samples.				
Frog - homing ability of the northern cricket frog, <i>Acris Crepitans</i> .	Von Mises (VM) model	$A$ Statistic: based on the summation of circular distances between circular observations.		Perform well in detecting outlier especially for sample size of 10 and above.  An alternative test of discordance in the circular sample using the maximum likelihood method, especially with the known of estimated $\kappa$	The result not accurate when sample size is small.	Statistical package: SPlus	[35]	

Table 3: Review on Outliers Identification in Univariate Circular Biological Data Using Numerical Method

Biological Data (Ecological Data)	Model Distribution	Outliers Identification Methods	Strength	Weakness	Analysis tools	References
Frog - homing ability of the northern cricket frog, <i>Acris Crepitans</i> .	Von Mises (VM) model	$A$ Statistic: based on the summation of circular distances between circular data.  $Chord$ Statistic: based on the summation of the chords' length between the circular observations.	$A$ and $Chord$ statistics have similar performance but perform better than the other tests (C, D, M tests) of discordancy in a circular data set.  The proposed statistics are simple and easy to interpret by practitioners.	The test not been done for small $\kappa$ . All the successful test presented only done by a large $\kappa$ .	Statistical package: SPlus	[24]
Frog - homing ability of the northern cricket frog, <i>Acris Crepitans</i> .	Von Mises (VM) model	<i>An alternative test of discordance</i> : proposed based on the circular distance between sample points.	It enables users to detect outliers in univariate and bivariate data.  It can be used for large sample sizes.	The propose method did not evaluate their statistic by comparing with others any statistical measures.	Statistical package: SPlus	[16]

Frog - homing ability of the northern cricket frog, <i>Acris Crepitans</i> .	Von Mises (VM) model	A Robust Circular Distance ( $RCDu$ ) Statistic.	<p>Triple measures of robustness to evaluate the proposed method:</p> <ul style="list-style-type: none"> <li>• Proportion of outliers detected.</li> <li>• Rate of masking.</li> <li>• Rate of swamping.</li> </ul> <p>A high proportion of outliers detected, and low masking and swamping rates, are always considered to be good robustness properties for any outlier detection statistic.</p> <p>Able to detect outliers in data with a high level of contamination.</p> <p>Successful in detecting outliers in a large data set.</p>	The performance of the $RCDu$ statistic is relatively low for small values of $\kappa$ because the circular data is more widely distributed around the circumference of the circle for low values of the $\kappa$ .	Statistical package: R codes	[23]
--	----------------------	--	--	---	------------------------------	------

Table 4: Review on Outliers Identification in Univariate Circular Biological Data Using Numerical Method

Biological Data (Ecological Data)	Model Distribution	Outliers Identification Methods	Strength	Weakness	Analysis tools	References
Sea stars - after they were displaced from their natural habitat.	Von Mises (VM) model	$M_n$ Statistic: based on resultant lengths -adaptation from [22]	$M_n$ performed better than Q-Q plot, suitable for small sample size and for a single outlier.	Cannot detect multiple outliers and not suitable for large sample sizes.	Not Mention	[32]
Sea stars - after they were displaced from their natural habitat.	Von Mises (VM) model	<i>Adjust Outlier</i> : based on circular distance between the circular data points and the circular mean direction	<p>The procedure decreases the bias of both the circular mean and the <math>\kappa</math> values.</p> <p>The procedure provides results of the mean resulting length as close as clean data results and minimizes <math>MCD</math> (Mean Circular Distance) with low and high contamination levels.</p> <p>Successful for various sample sizes.</p>	The performance not yet been tested with other methods such as $L, C, D$ statistics.	Not Mention	[15]
Pigeons-Vanishing angles of pigeons once released.	Symmetric Wrapped Stable (SWS) and Circular Uniformity	Locally Most Powerful Invariant ( $LMPI$ ) Statistic	<p>Applied this test in two cases:</p> <p>1. When location parameter <math>\mu; \mu_0, \mu_1</math>, and <math>\kappa</math> are all known.</p>	Did not propose a way to test circular data if $\kappa$ is unknown.	Statistical package: SPlus	[14]



(CU) mixture model				2. When only $\kappa$ is known. Best performing when small values of $\mu_1$ .			
		Likelihood Ratio Testing Statistic	Ratio ( <i>LRT</i> )	The LRT performs best for moderate values of $\mu_1$ .	Very computation-intensive and hard to apply as they can't be written in any closed form. The exact LRT statistic distribution is intractable.		
Jander's ant data - orientation of ants towards a black target when released in a round arena.	SWS-CU mixture model	Locally Powerful ( <i>LMPI</i> )	Most Invariant Statistic	Easy to obtain and, as is seen, enjoy nice properties, namely monotonicity of the power function and consistency.	Small departures from the null hypotheses are difficult to detect while large departures can be easily detected by any reasonable test.	Statistical package: DDSTAP by [37]	[36]

Table 5: Review on Outliers Identification in Circular Biological Data Using Biomedical Data

Biological Data (Biomedical Data)	Model Distribution	Outliers Identification Methods	Strength	Weakness	Analysis tools	References
Eye data set obtained from a glaucoma patient.	Von Mises (VM) model (for univariate circular data)	$G_a$ Statistic: based on the spacing theory in circular data	Identification of a patch of two outliers in the data successfully.  Expected to improve performance when using a robust approach that warrants further investigation.	Application for multiple outliers is difficult.  The swamping rates are relatively high in identifying error as outliers.	Statistical package: SPlus	[38]
Eye data set obtained from a glaucoma patient.	Multiple Circular Regression (MCR) model	<i>COVRATIO</i> Statistic: determinant of the covariance matrix	Clearly favorable and are showing good performance in identifying outliers in <i>MCR</i> model, even though it was extended from a linear regression model.	Detect one single outlier at one time.	Not Mention	[9]
Eye data set obtained from a glaucoma patient.	Multiple Circular Regression (MCR) model	<i>DFBETAc</i> Statistic (extended from <i>DFBETAS</i> Statistic): based on row deletion approach	Performed well and more accurate when parameters estimation become smaller after removing the outliers.	Regression model needs to refit in order to get accurate parameter estimations.	Not mention	[8]

Circadian data	DM Regression model	Circular	$DMCEs$ based on row deletion approach	statistic: Good when $\kappa$ value is large. Performs better for larger sample size.	Performance not much clearly small $\kappa$ and when sample size is small.	Not Mention	[10]
----------------	---------------------	----------	--	---	--	-------------	------

## 7. Conclusion

In conclusion, outliers detection method for univariate circular biological data has been transform a lot. The graphical techniques are good in detecting outliers when both the sample size,  $n$  and the value of concentration parameter,  $\kappa$  are larger. Meanwhile, the numerical techniques that based on the maximum likelihood ratio, mean resultant length, arc lengths, circular distances and chord lengths as its mainly parameters have been used to identify outliers for univariate circular biological data. Circular distance was widely used, and few methods has been proposed either to detect, adjust or remove the outliers. However, the numerical method mostly focused on identifying a single outlier at one time only. Other techniques such as clustering has been used recently for detecting outliers in circular regression models [22,40,41]. Hence, clustering also can be as one other alternative that can be explored to detect outliers in univariate circular biological data.

Currently, most of the outliers detection methods proposed in literature have been applied to study animal orientation data that follows Von Mises Distribution Model. Only few studies on outliers detection for biomedical data such as using spacing theory [38], and row deletion approach [8,10] are used. Therefore, more modern approaches can be explored to identify outliers in circular biological data especially in biomedical study such as 3D analysis [21], computer simulation and statistical modeling [42]. Finally, analysis tools that mostly used for univariate circular biological data analysis are SPlus and R Codes statistical packages. Thus, we can explore other analysis tools such as Python and MatLab, since circular package can also be found in both tools.

## Acknowledgment

Authors would like to thank all the associate editors and referees for their thorough reading and valuable suggestions which led to the improvement of this paper. The Universiti Malaysia Pahang is acknowledged for the financial support received for this study (RDU190363).

## References

- [1] H. Oulhaj, M. Rziza, A. Amine, H. Toumi, E. Lespessailles, R. Jennane, E. M. Hassouni, "Trabecular bone characterization using circular parametric models" *Biomed. Signal Proces*, 33, 411–421, 2017. <https://doi.org/10.1016/j.bspc.2016.10.009>
- [2] J-D. Janßen, T. Schanze, "Analysis and classification of ECG-waves and rhythms using circular statistics and vector strength" *Current Directions in Biomedical Engineering*, 3(2): 91–94, 2017. <https://doi.org/10.1515/cdbme-2017-0020>
- [3] L. Rivest, T. Duchesne, "A general angular regression model for the analysis of data on animal movement in ecology" *Appl. Statist.*, 65, 445–463, 2016. <https://doi.org/10.1111/rssc.12124>
- [4] N. I. Fisher, A. J. Lee, "Regression Models for an Angular Response" *Biometrics*, 48, 665, 1992. <https://doi.org/10.2307/2532334>
- [5] I. B. Mohamed, A. Rambli, N. Khaliddin, A. Ibrahim, "A New Discordancy Test in Circular Data Using Spacings Theory" *Commun. Stat. Simulat.*, 45, 2904–2916, 2015. <https://doi.org/10.1080/03610918.2014.932799>
- [6] P. Sondag, L. Zeng, B. Yu, R. Rousseau, B. Boulanger, H. Yang, S. Novick, "Effect of a statistical outlier in potency bioassays" *Pharm. Stat.*, 17, 701–709, 2018. <https://doi.org/10.1002/pst.1893>
- [7] J. F. Walker, J. W. Brown, S. A. Smith, "Analyzing Contentious Relationships and Outlier Genes in Phylogenomics" *Syst. Biol.*, 67(5), 916–924, 2018. <https://doi.org/10.1093/sysbio/syy043>
- [8] N. A. Alkasadi, A. H. M. Abuzaid, S. Ibrahim, M. I. Yusoff, "Outliers Detection in Multiple Circular Regression Model via DFBETAc Statistic" *Int. J. Appl. Eng. Res.*, 13(11), 9083–9090, 2018.
- [9] N. A. Alkasadi, S. Ibrahim, M. F. Ramli, M. I. Yusoff, "A comparative study of outlier detection procedures in multiple circular regression" *AIP Conf. Proc.*, 1775, 2016. <https://doi.org/10.1063/1.4965152>
- [10] A. Rambli, A. H. M. Abuzaid, I. B. Mohamed, A. G. Hussin, "Procedure for Detecting Outliers in a Circular Regression Model" *PLoS One*, 11(4), 2016. <https://doi.org/10.1371/journal.pone.0153074>
- [11] K. V. Mardia, C. C. Taylor, G. K. Subramaniam, "Protein Bioinformatics and Mixtures of Bivariate von Mises Distributions for Angular Data" *Biometrics*, 63(2), 505–512, 2007. <https://doi.org/10.1111/j.1541-0420.2006.00682.x>
- [12] A. Rambli, S. Ibrahim, M. I. Abdullah, A. G. Hussin, I. Mohamed, "On Discordance Test for the Wrapped Normal Data" *Sains Malaysiana*, 41(6), 769–778, 2012.
- [13] A. SenGupta, A. K. Laha, "Theory & Methods: The Slippage Problem for the Circular Normal Distribution" *Aust. N. Z. J. Stat.*, 43(4), 461–471, 2001. <https://doi.org/10.1111/1467-842X.00194>
- [14] S. R. Jammalamadaka, A. SenGupta, *Topics in Circular Statistics*, World Scientific, 2001.
- [15] E. A. Mahmood, S. Rana, A. G. Hussin, H. Midi, "Adjusting Outliers in Univariate Circular Data" *Pertanika J. Sci. Technol.*, 25(4), 1147–1158, 2017.
- [16] A. H. Abuzaid, A. G. Hussin, A. Rambli, I. Mohamed, "Statistics for a New Test of Discordance in Circular Data" *Commun. Stat. Simul. Comput.*, 41(10), 1882–1890, 2012. <https://doi.org/10.1080/03610918.2011.624239>
- [17] M. D. Marzio, S. Fensore, A. Panzera, C. C. Taylor, "Circular local likelihood" *Test*, 27, 921–945, 2018. doi:10.1007/s11749-017-0576-9
- [18] S. Kim, A. SenGupta, "Multivariate-multiple circular regression" *J. Stat. Comput. Simul.*, 87(7), 1277–1291, 2017. <https://doi.org/10.1080/00949655.2016.1261292>
- [19] J. Jha, A. Biswas, "Circular-circular regression model with a spike at zero" *Stat. Med.*, 37(1), 71–81, 2018. <https://doi.org/10.1002/sim.7496>
- [20] A. Roy, A. Pal, U. Garain, "JCLMM: A finite mixture model for clustering of circular-linear data and its application to psoriatic plaque segmentation" *Pattern Recogn.*, 66, 160–173, 2017. <https://doi.org/10.1016/j.patcog.2016.12.016>
- [21] H. A. Hasan, M. K. Alam, A. Yusof, S. Matsuda, M. Shoumura, N. Osuga, "Accuracy of Three Dimensional CT Craniofacial Measurements Using Mimics and InVesalius Software Programs" *J. Hard Tissue Biol.*, 25, 219–224, 2016. <https://doi.org/10.2485/jhtb.25.219>
- [22] S. Z. Satari, "Parameter Estimation and Outlier Detection for some Types of Circular Model," Ph.D Thesis, University of Malaya, 2015.
- [23] E. A. Mahmood, S. Rana, H. Midi, A. G. Hussin, "Detection of Outliers in Univariate Circular Data using Robust Circular Distance" *Journal of Modern Applied Statistical Methods*, 16(2), 418–438, 2017. doi: 10.22237/jmasm/1509495720
- [24] A. H. Abuzaid "Some Problems of Outliers in Circular Data," Ph.D Thesis, University of Malaya, 2010.
- [25] P. Bagchi, I. Guttman, "Spuriousity and outliers in directional data" *J. Appl. Stat.*, 17(3), 341–350, 1990. <https://doi.org/10.1080/02664769000000006>
- [26] K. V. Mardia, P. E. Jupp, *Directional Statistics*, John Wiley and Son, 2000.
- [27] D. Collett, "Outliers in Circular Data" *J. Appl. Stat.*, 29(1), 50–57, 1980. <https://doi.org/10.2307/2346410>
- [28] P. Fernandez-Gonzalez, C. Bielza, P. Larrañaga, "Univariate and bivariate truncated von Mises distributions" *Progress in Artificial Intelligence*, 6(2), 171–180, 2017. <https://doi.org/10.1007/s13748-016-0109-x>
- [29] L. Zhang, J. J. Zhang, R. J. Kubiak, H. Yang, "Statistical methods and tool for cut point analysis in immunogenicity assays" *J. Immunol. Methods*, 389, 79–87, 2013. <https://doi.org/10.1016/j.jim.2012.12.008>
- [30] R. J. Kubiak, J. Zhang, P. Ren, H. Yang, L. K. Roskos, "Excessive outlier removal may result in cut points that are not suitable for immunogenicity

- assessments” *J. Immunol.*, 463, 105–111, 2018. <https://doi.org/10.1016/j.jim.2018.10.001>
- [31] S. Rana, E. A. Mahmood, H. Midi, A. G. Hussin, “Robust Detection of Outliers in Both Response and Explanatory Variables of the Simple Circular Regression Model” *J. Math. Sci.*, 10(3), 399–414, 2016.
- [32] N. I. Fisher, *Statistical analysis of circular data*, Cambridge: Cambridge University Press, 1993.
- [33] A. H. Abuzaid, I. B. Mohamed, A. G. Hussin, “Boxplot for circular variables” *Comput. Stat.*, 27, 381–392, 2012. <https://doi.org/10.1007/s00180-011-0261-5>
- [34] D. E. Ferguson, H. F. Landreth, J. P. McKeown, “Sun compass orientation of the northern cricket frog, *Acris crepitans*” *Anim. Behav.*, 15(1), 45-53, 1967. [https://doi.org/10.1016/S0003-3472\(67\)80009-5](https://doi.org/10.1016/S0003-3472(67)80009-5)
- [35] A. H. Abuzaid, I. B. Mohamed, A. G. Hussin, “A New Test of Discordancy in Circular Data” *Commun. Stat. Simul. Comput.*, 38(4), 682–691, 2009. <https://doi.org/10.1080/03610910802627048>
- [36] A. Sengupta, C. Pal, “ On optimal tests for isotropy against the symmetric wrapped stable-circular uniform mixture family” *J. Appl. Stat.*, 28(1), 129–143, 2001. <https://doi.org/10.1080/02664760120011653>
- [37] A. SenGupta, DDSTAPD Statistical package for the analysis of directional data, Applied Statistics Division Calcutta: Indian Statistical Institute, 1998b.
- [38] I. B. Mohamed, A. Rambli, N. Khaliddin, A. I. N. Ibrahim, “New Discordancy Test in Circular Data Using Spacings Theory” *Commun. Stat-Simul C*, 45(8), 2904–2916, 2016. <https://doi.org/10.1080/03610918.2014.932799>
- [39] K. V. Mardia, “Statistics of Directional Data”, *J. R. Statist. Soc.*, 37(3), 349–393, 1975. <https://doi.org/10.1111/j.2517-6161.1975.tb01550.x>
- [40] N. F. M. Di, S.Z. Satari, R. Zakaria “Outlier Detection In Circular Regression Model Using Minimum Spanning Tree Method” *J. Phys. Conf. Ser.* 1366 012102, 2019. <https://doi.org/10.1088/1742-6596/1366/1/012102>
- [41] S.Z. Satari, N. F. M. Di, R. Zakaria. “Single-linkage Method to Detect Multiple Outliers with Different Outlier Scenarios in Circular Regression Model” *AIP Conference Proceedings* 2059, 020003, 2019. <https://doi.org/10.1063/1.5085946>
- [42] J. Jin, *Evaluation System for Craniosynostosis Surgeries with Computer Simulation and Statistical Modelling*, The University of Western Ontario, 2016.

## New Color Image Encryption for Medical Images Based on Three Dimensional Generalized Chaotic Cat Map and Combined Cellular Automata

Un Sook Choi<sup>1</sup>, Sung Jin Cho<sup>2,\*</sup>, Sung Won Kang<sup>2</sup>

<sup>1</sup>Department of Information and Communications Engineering, Tongmyong University, Busan, South Korea

<sup>2</sup>Department of Applied Mathematics, Pukyong National University, Busan, South Korea

### ARTICLE INFO

Article history:

Received: 13 December, 2019

Accepted: 05 February, 2020

Online: 09 March, 2020

Keywords:

Image Encryption

Chaotic Cat Map

Combined Cellular Automata

Medical Image Encryption

PRNG

Group Cellular Automata

### ABSTRACT

Medical images are transmitted via the Internet or the hospital intranet which include many important information about the patient's personal information. Medical image encryption is a technology that can effectively protect the information contained in these medical images. In this paper, we give a secure and trusty Combined Cellular Automata (CoCA) based medical image encryption algorithm. CoCA is made up of a nonlinear CA and a linear 90/150 maximum length CA, and three dimensional generalized chaotic map. The proposed algorithm consists of two phases. The first phase encryption process that changes pixel values of a given image using two CoCAs. The second phase is to change the position of each pixel in the image encrypted using the three dimensional generalized chaotic cat map that can change with effect the position of pixels not only in two dimensions horizontally and vertically but also in color plane three colored channels simultaneously. We show the stability and high reliability of the given color medical image cryptosystem through detailed analysis and various statistical experimental tests.

## 1. Introduction

With the development of internet communication technology, the amount of transmission of various types of multimedia data including images is increasing. This trend is also true for medical data. Medical diagnostic images are transmitted over wired and wireless networks. These medical images are transmitted via the Internet or the hospital intranet which include many important information about the patient's personal information. However, current hospital intranet lacks reliable security equipment. In addition, on the Internet, not only malicious manipulation of information by malicious attackers, but also leakage of information on unauthorized third parties is very serious. Medical image encryption is an effective technique that can protect not only medical images but also important personal information of patients from these various attacks.

Some existing traditional encryption techniques, such as International Data Encryption Algorithm (IDE), AES and DES are well suited for text data security, but not for bulk data encryption such as digital images. This is because images have inherent properties with large data sizes, high redundancy, and strong imagery correlation.

Since chaos function is ergodic and sensitive to initial conditions and parameters, it is a powerful function that can effectively encrypt various types of data. These chaotic functions are easy to implement with microprocessors and personal computers [1]. Therefore, the chaos map-based encryption algorithm is suitable for mass multimedia data encryption because it can design a fast encryption system at low cost.

Recently, methods of medical image encryption based on chaotic function have been studied by many researchers [2-10]. Mao et al. proposed a cryptographic algorithm that not only maintains a high level of security but also speeds up image encryption using a map that extends the Baker map in three dimensions [2]. In [3], Dai and Wang proposed logistic maps and Chebyshev maps based a medical image encryption. They overcame the problem that logistic maps-based cryptographic systems are inadequate for medical image cryptography because of their low key space and low security. Wang et al. designed a color image cryptographic system that used the chaotic function to simultaneously encrypt the three colored components of the given image and allow these components to affect each other [4]. Fu et al. proposed an alternative bit shuffling algorithm in which pixel value mixing effects can be contributed by the replacement and the permutation process. That chaotic based algorithm reached

\*Sung Jin Cho, e-mail: [sjcho@pknu.ac.kr](mailto:sjcho@pknu.ac.kr)

[www.astesj.com](http://www.astesj.com)

<https://dx.doi.org/10.25046/aj050213>

existing cryptographic security levels with fewer rounds of performance [5]. Zhang and Luo proposed chaotic CA based an image encryption algorithm [6]. The algorithm proposed by them was used a two dimensional logistic function to encrypt images and then applies two dimensional CA on the initial encrypted image. In [7], Nandi et al. noted that the unique and powerful nature of CA is the ease of hardware implementation and the large number of rules that apply to the CA, making it impossible for an attacker to find a combination of rules that is the key to extracting the original information. So they proposed a CA-based cryptographic algorithm to substitute pixel values of original image. However, this method needs to be supplemented because it is weak to noise and data loss that may occur for image transmission.

Jeong et al. gave an encryption algorithm for medical image. They used a maximum length one-dimensional CA with complemented rules and a modified chaotic cat map. They changed pixel values of the given image using a nonlinear key sequence generated by a one-dimensional CA with complemented rules. And then they changed pixel positions of the image with pixel value changed using the modified chaotic map. However, the modified chaotic maps they designed have an unmaintained weakness of the image size required by the chaotic cat map [8]. Therefore, there is a need to overcome the weaknesses of the modified two-dimensional chaos function in [8] and to efficiently encrypt color images. In order to enhance security, a PRNG that can generate a nonlinear key sequence is required.

In this paper, we design CoCA for medical image encryption. CoCA is made up of a nonlinear CA and a linear 90/150 maximum length CA. And we give a secure and trusty encryption scheme based on CoCA and three dimensional generalized chaotic map. The proposed algorithm consists of two phases. The first phase encryption process that changes pixel values of a given image using two CoCAs. The second phase is to change the position of each pixel in the image encrypted using the three dimensional generalized chaotic cat map that can change with effect the position of pixels not only in two dimensions horizontally and vertically but also in color plane three colored channels simultaneously. We show the stability and high reliability of the given color medical image cryptosystem through detailed analysis and various statistical experimental tests.

## 2. Preliminaries

### 2.1. Cellular Automata

Von Neumann [11] introduced CA at first and Wolfram [12] developed CA. CA is very important mathematically for modelling complex behavior. CA is composed of an array of basic memory called cells, and its state is updated to the following state depending on the state of neighboring cells of radius 1 including itself. These CAs are classified into one-dimensional CA, two-dimensional CA, and the like according to the arrangement of the cells. In addition, according to the number of cells that affect when one cell of the CA is updated to the following state, it is classified as 3-neighbor CA, 5-neighbor CA, 9-neighbor CA. And it is classified into NBKA, PBKA, and IBKA according to boundary condition of both ends of CA. The CA used in this paper is an NBKA. The CA used in this paper is the simplest CA that is the 1-D 2-state 3-neighbor NBKA.

The state transition function  $f$ , which decides the following state of the cell, is a mapping in which the domain is  $\{000, 001, 010, \dots, 111\}$  and the airspace is  $\{0,1\}$ .  $f$  is expressed as follows.

$$w_j^{t+1} = f(w_{j-1}^t, w_j^t, w_{j+1}^t) \tag{1}$$

, where  $w_j^t$  is the  $j$ th cell state of CA at the time  $t$ . As shown in Table 1, the CA transition rule is a decimal representation of the numerical value of the following state determined according to the state of the current neighbor. For example, if the following state function value for  $\{111, 110, 101, \dots, 010, 000\}$  is '01010010', the converted value is 82, so the given transition rule is 82. Table 1 shows the transition rule numbers of the state transition function according to the following state of the cell with respect to the state of the current neighbor cells.

Table 1: The Transition Rule Number according to the Following State of the Cell

Nbd state	111	110	101	100	011	010	001	000	RN.
Following state	0	0	0	1	1	1	1	0	30
	0	1	0	1	1	0	0	1	90
	1	0	0	0	1	1	0	1	141
	1	0	0	1	0	1	1	0	150
	1	0	1	0	1	1	0	0	172

When the state transition function is expressed as a Boolean function, a rule consisting only of XOR logic is called a linear rule, and a rule consisting of XOR logic and XNOR logic is called a complemented rule. And rules that include OR and AND logic are called nonlinear rules. In Table 2, rules 30, 141, and 172 are nonlinear rules, and rules 90 and 150 are linear rules. A CA having a linear rule applied to all cells of a CA is called a linear CA, and a CA to which a nonlinear rule is applied is called a nonlinear CA. The linear CA can express a function for obtaining the following state as a matrix, which is called the state transition matrix  $T_n$ .

Table 2: The Boolean functions for Rules 30, 90, 141, 150 and 172

RN	Boolean functions
30	$w_i^{t+1} = w_{i-1}^t \oplus (w_i^t + w_{i+1}^t)$
90	$w_i^{t+1} = w_{i-1}^t \oplus w_{i+1}^t$
141	$w_i^{t+1} = w_i^t \cdot w_{i+1}^t \oplus w_{i-1}^t \cdot w_{i+1}^t \oplus w_{i-1}^t \oplus w_{i+1}^t \oplus 1$
150	$w_i^{t+1} = w_{i-1}^t \oplus w_i^t \oplus w_{i+1}^t$
172	$w_i^{t+1} = w_i^t + w_{i-1}^t \cdot w_{i+1}^t$

From now on we use a CA using only the transition rules 90 and 150 which is called 90/150 CA.  $T_n$  of the 90/150 CA is as following [13, 14] :

$$T_n = (t_{ij})_{n \times n} = \begin{cases} 1, & i - j = 1, i - j = -1 \\ d_i, & i = j \\ 0, & \text{otherwise} \end{cases} \tag{2}$$

The linear CA  $C$  can express a function for obtaining the following state as a matrix  $T_n$ . We call  $T_n$  the state transition matrix of  $C$ . The CA applicable to the cryptographic algorithm must be reversible and decryptable. This reversible CA must be unique to the previous state for a given state. Therefore, the inverse of  $T$  must exist. This means that the determinant of  $T$  must not be zero. If  $W^t$  is the current state of  $C$  and  $W^{t+1}$  is the following state of  $W^t$ , then  $W^{t+1}$  can be obtained by  $T_n$  and  $W^t$  as follows [15] :



$$W^{t+1} = T_n W^t \quad (2)$$

By (2), the state  $W^{t+k}$  satisfies the following equation :

$$W^{t+k} = T^k W^t \quad (3)$$

An  $n$ -cell reversible CA  $C$  is referred to as Maximum Length CA (MLCA) when the minimum  $p$  satisfying  $T_n^p = I_n$  for  $T_n$  of  $C$  is  $2^n - 1$ , where  $I_n$  is the  $n \times n$  identity matrix. For example, a four-cell CA with transition rules  $\langle 90, 150, 90, 150 \rangle$  is MLCA with period 15.

### 2.2. Three Dimensional Generalized Chaotic Map

For a metric space  $X$  with metric  $d$ , a function  $F: X \rightarrow X$  that satisfies the following is said to be sensitive to initial conditions:

if there is a  $\delta > 0$  such that for every  $x \in X$  and  $\varepsilon > 0$  there exists  $y \in X$  with  $d(x, y) < \varepsilon$  and  $d(F^k(x), F^k(y)) > \delta$  for  $k \in \mathbb{N}$  [16].

Chaos is associated with randomness, disorder, and entropy. Arnold Cat Map is a simple function proposed by Russian mathematician Arnold that can randomly transform the composition of image pixels. This transformation causes the image to be very complicated when this transformation is repeated by changing the position of the pixels without changing the size of the image. This function is represented by a two-dimensional matrix

$$\begin{pmatrix} 1 & 1 \\ 1 & 2 \end{pmatrix} \quad (4)$$

and has been applied to various algorithms to protect images. Chen et al. generalized (4) using parameters as shown in (5) [17].

$$\begin{pmatrix} 1 & a \\ b & 1 + ab \end{pmatrix} \quad (5)$$

Jeong et al. designed an encryption algorithm for medical color image using the map modified (5) [8]. However, (5) only changes the pixel position of the gray image because it can change the pixel position of the two-dimensional image. Therefore, in order to effectively protect color images, methods of extending from the 2-D chaotic cat map to a 3-D chaotic cat map have been proposed [17, 18]. A 3-D chaotic cat map is gotten by the following operations using the  $3 \times 3$  identity matrix:

$$c_j \leftarrow a_{ij} \cdot c_i + c_j, r_j \leftarrow b_{ij} \cdot r_i + r_j \quad (6)$$

, where  $a_{ij}, b_{ij} \in \mathbb{N}$ ,  $i = 1, 2, j = 1, 2, 3$  and  $i \neq j$ . Using (6), we obtain  $L_1$  for  $i = 1, j = 2, 3$ .

$$L_1 = \begin{pmatrix} 1 & a_{12} & a_{13} \\ b_{12} & a_{12}b_{12} + 1 & a_{13}b_{12} \\ b_{13} & a_{12}b_{13} & a_{13}b_{13} + 1 \end{pmatrix} \quad (7)$$

Similarly using (6) we get  $L_2$  for  $i = 2, j = 1, 3$ , when. The three dimensional generalized chaotic cat map is as follows:

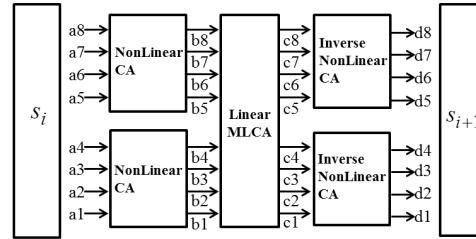
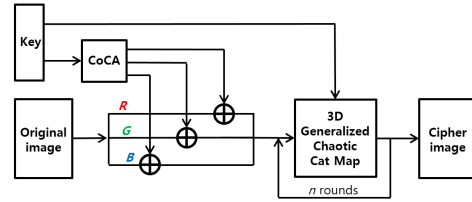
$$L = L_2 L_1 \quad (8)$$

Since  $\det(L_i) = 1$  for each  $L_i (i = 1, 2)$ ,  $\det(L) = 1$ .

### 3. Proposed Algorithm

Now we design an algorithm for encrypting medical images. Figure 1 shows a block diagram of the proposed algorithm. The medical image encryption algorithm proposed in this paper

consists of two phases. The proposed algorithm consists of alternate and shuffling phases, and the pixel shuffling phase repeats  $n$  rounds to increase the security level of the encryption system.



#### 3.1. Substitution Phase

To generate an effective key image we design an effective PRNG. This PRNG is constructed as shown in Figure 2 by the combination of nonlinear reversible CA  $C_1$  and linear maximum length CA  $C_2$ . This PRNG is called CoCA. When  $S_0$ , a shared key, is the initial value of CoCA, the following state  $S_1$  is  $S_1 = C_1^{-1}C_2C_1(S_0)$ . And  $S_2 = C_1^{-1}C_2^2C_1(S_0)$ . Therefore,  $S_n$  obtained by repeatedly applying CoCA  $n$  times to  $S_0$  satisfies  $S_n = C_1^{-1}C_2^nC_1(S_0)$ . Therefore, even if  $C_1$  is not an MLCA, if  $C_2$  is an MLCA, the CoCA becomes a nonlinear MLCA. The algorithm proposed in this paper generates key images using two CoCAs  $G_1$  and  $G_2$ . The  $(i, j)$  pixel of the key image generated by  $G_1$  and  $G_2$  is represented  $K_{i,j}$ .  $K_{i,j}$  can be expressed as (9):

$$K_{i,j} = G_2^i(G_1^j(S_0)) \quad (1 \leq i, j \leq 256) \quad (9)$$

c \ r	1	2	3	4	5	.....	253	254	255	256
1	96	109	57	61	47	.....	203	208	112	34
2	217	50	91	121	166	.....	141	111	11	111
3	182	105	233	82	239	.....	63	29	4	139
4	52	105	43	68	84	.....	43	194	66	98
5	155	155	89	75	176	.....	146	13	79	230
...	...	...	...	...	...	...	...	...	...	...
253	194	66	98	207	0	.....	36	36	6	41
254	109	187	47	148	63	.....	75	54	203	22
255	22	160	207	134	9	.....	25	18	246	178
256	146	13	79	230	224	.....	82	239	244	210

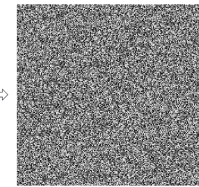


Figure 3 shows the procedure of generating a key image from two CoCAs. This process divides the shared key value 8 bits  $S_0$  in half and performs state transitions through 4 cell nonlinear reversible CA  $C_1$ , and then combines them into 8 bits again. The combined 8-bit values are once again transitioned using 8-cell linear MLCA  $C_2$ . This transitioned result is then divided in half and converted to the final state by  $C_1^{-1}$  the inverse of  $C_1$  to produce pixel values. First, each pixel of the first row of the key image is a

key sequence generated using  $G_1$ , and pixels of each column of the key image are generated by  $G_2$  using the pixel value generated by  $G_1$  as the initial value.

### 3.2. Shuffling Phase

The result of the XOR combining of the key image generated by two CoCAs and the original image is very effective because it results in the randomly changing the pixel value of the given image. However, if the encrypted image is damaged by unexpected noise or deliberate deletion attacks in the process of transmitting the digital image, the damaged part remains completely lost when the encrypted image is decrypted. Therefore, in order to design a cryptographic algorithm that is resistant to such attacks, in this paper, the final cryptographic image is generated by mixing the pixel positions of the image encrypted by the key image using a generalized 3-D chaotic cat map. Each pixel in the image has a gray level value from 1 to 255 for the R, G, and B components. Therefore, the total number of bits required to represent a color image of size  $M \times M$  is  $M \times M \times 3 \times 8$ . Each pixel position of a color image can be represented by (row, column, color component). In the image shuffling phase, we use the  $L$  in (8) to change not only the position of the rows and columns of pixels but also the positions of the components of R, G, and B using a generalized 3-D chaotic cat map. Mathematically, the pixel shuffling phase is represented by (10).

$$\begin{pmatrix} x_{n+1} \\ y_{n+1} \\ z_{n+1} \end{pmatrix} = L \begin{pmatrix} x_n \\ y_n \\ z_n \end{pmatrix} \quad (10)$$

In (10), if each row of  $L$  is  $L(r_i) (i = 1, 2, 3)$ , then  $x_{n+1} = L(r_1)(x_n, y_n, z_n)^T \bmod M$ ,  $y_{n+1} = L(r_2)(x_n, y_n, z_n)^T \bmod M$ ,  $z_{n+1} = L(r_3)(x_n, y_n, z_n)^T \bmod 3$ , where  $M$  is the multiple of 3.

### 3.3. Color Medical Image Encryption Algorithm

Table 3 shows a color medical image encryption algorithm Col\_Medi\_Encryp\_Algorithm. This algorithm is a color image encryption algorithm that merges the encryption phases proposed in sections 3.1 and 3.2.

Table 3: Col\_Medi\_Encryp\_Algorithm

---

**Function 1** : CoCA state transition  
**Def** CoCA(*Image*, *rule\_table.nonlinear*, *rule\_table.MLCA*, *Rule\_table.Inverse*)  
**For** (*i, j, k*) in *Image\_Index*(*row*, *column*, *color*)  
    *a* = *rule\_table.nonlinear*(*Image*[*i, j, k*] // 16)  
    *b* = *rule\_table.nonlinear*(*Image*[*i, j, k*] % 16)  
    *Image*[*i, j, k*] = *a*\*16 + *b*  
    *number* = *key.MLCA*  
**For** (*i, j, k*) in *Image\_Index*(*row*, *column*, *color*)  
    *Key\_Image*[*i, j, k*] = ((*number* ^ *rule\_table.MLCA*) ⊕ (*number* // 2) ⊕ (*number* \* 2)) mod 256  
*Image* = *Image* ⊕ *Key\_Image* mod 256  
**For** (*i, j, k*) in *Image\_Index*(*row*, *column*, *color*)  
    *a* = *rule\_table.Inverse*(*Image*[*i, j, k*] // 16)  
    *b* = *rule\_table.Inverse*(*Image*[*i, j, k*] % 16)  
    *CoCAed\_Image*[*i, j, k*] = *a*\*16 + *b*  
**Return** *CoCAed\_Image*

---



---

**Function 2** : 3D generalized chaotic cat mapping  
**Def** 3D\_Chaotic\_cat\_map(*Image*, *cat\_map\_matrix*, *times*)  
**Construct** (*Index\_list*(*row*, *column*, *color*) of *Image*)  
**For** *i* from 1 to *times*:  
    *cat\_mapped\_Index\_list* = *matrix\_vector\_multiply*(*cat\_map\_matrix*, *Index\_list*(*row*, *column*, *color*) of *Image*)  
**For** (*i, j, k*) in *Image\_Index*(*row*, *column*, *color*)  
    *Cat\_mapping\_Image*[*i, j, k*] = *Image*[*cat\_mapped\_Index\_list*(*i, j, k*)]  
**Return** *Cat\_mapping\_Image*

---

**Algorithm** : Col\_Medi\_Encryp\_Algorithm  
**Input** : *Image*, *rule\_table.nonlinear*, *rule\_table.MLCA*, *Rule\_table.Inverse*, *cat\_map\_matrix*, *times*  
**Output** : *Encrypted\_Image*  
*Encrypted\_Image* = CoCA(*Image*, *rule\_table.nonlinear*, *rule\_table.MLCA*, *key.MLCA*, *rule\_table.Inverse*)  
*Image* = 3D\_Chaotic\_cat\_map(*Image*, *cat\_map\_matrix*, *times*)

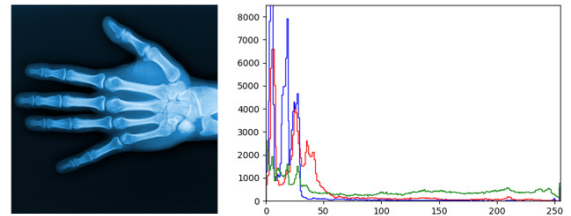
---

### 3.4. Key Scheming

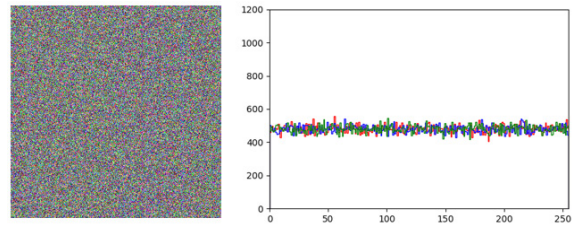
The variables that can be used as keys are: (1) Transition rules and initial values, which are the components of the two CoCAs require for the generation of a key image in the substitution phase. (2) Parameters of the proposed chaotic cat map used in the shuffling phase of mixing pixel positions.

## 4. Safety analysis of the proposed system

By the proposed cryptosystem we present the performance results in this section. Since medical images often have a high color bias, it must be shown whether the results are suitable for such images. Medical X-ray images were adopted as basic images suitable for such safety analysis.



(a) Original image and histogram



(b) Encrypted image and histogram

Figure 4: The histograms of the original image and the encrypted image

Table 4: Entropy and Comparison Analysis of Methods

Methods	Entropy
Proposed Algorithm	7.99837
Wang et al. [19]	7.99763
Wu et al. [20]	7.99722

4.1. Histogram Analysis

Figure 4- (a) shows the original medical image and histogram used to perform encryption. Most of the given medical images occupy black, and the original image actually has a very high bias at pixel value zero.

Figure 4- (b) shows the image and histogram that encrypted the original image using the proposed encryption system. Although the original medical image is a high deflection image, the pixel values of the encrypted image are very evenly distributed. This means that the distribution of colors is spread evenly according to the result of the encryption system. This proves to be safe for traditional statistical methods.

4.2. Information Entropy Analysis

A cryptographic image with high uncertainty means it is safe from accidental information attacks. In other words, the encrypted image must have a high degree of uncertainty with respect to information analysis. High uncertainty can be expressed through information entropy. Information entropy is as shown in (11).

$$H(m) = \sum_{i=0}^{2^n-1} p(m_i) \log_2(1/p(m_i)) \quad (11)$$

Where  $m$  is the information source and  $p(m)$  is the probability for finding the original value for each bit. Table 4 shows the information entropy of the encrypted image obtained by the proposed encryption system. In addition, the information entropy of cryptographic images obtained through several other cryptographic systems is also shown. In an 8-bit RGB format image, the closer to 8, the higher the uncertainty. According to Table 4, it is shown that the proposed cryptosystem, like the previously proposed cryptosystems, provides high uncertainty in the cryptographic image.

4.3. Correlation Coefficient Analysis

Correlation coefficients between pixel values indicate how distributed the image is in a particular color. The correlation coefficient is expressed as in (12) below:

$$\rho_{xy} = cov(x, y) / \sqrt{D(x)D(y)} \quad (12)$$

where  $x$  and  $y$  represent the values of two different positions in the RGB color space. In the correlation coefficient analysis, two positions are examined by randomly extracting two adjacent pixels horizontally, vertically, and diagonally. We examined random 2500 pairs of pixel values for each color channel of the image for correlation coefficient analysis. After repeating this test 400 times, the mean of all the extracted correlation coefficients was examined.

Table 5: Correlation Coefficients of an original image and an encrypted image

Methods	Horizontal	Vertical	Diagonal
Original image	0.9785	0.9730	0.9543
Proposed Algorithm	0.0019	0.0048	-0.0048
Zhang et al. [21]	0.0035	0.0037	0.0023

We provide the results of the correlation coefficient analysis obtained in the above-mentioned method in Table 5. Correlation coefficient analysis results are for the original image, the encrypted image using the proposed encryption, and the encrypted image

based on previous studies. The value obtained according to (12) is distributed from -1 to 1. The closer to 1, the higher the correlation coefficient, which means that adjacent pixels have almost the same value. The correlation coefficients of the original image are close to 1 in either direction. This means that pixel values in adjacent locations almost always have a similar color. Closer to zero means that there is almost no correlation. The correlation coefficient of the encrypted image using the proposed encryption system is very close to zero in all directions.

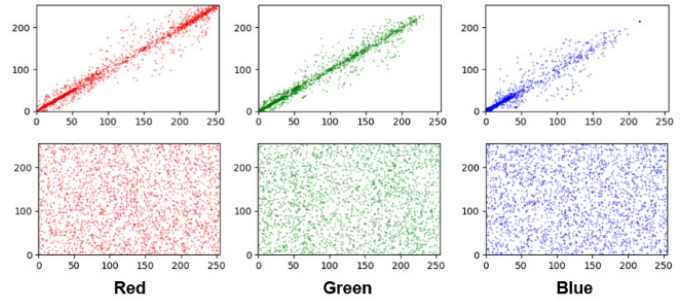


Figure 5: Scatter plots of horizontal direction of each color channels of the plain image and cipher image

The encrypted image indicates that it has different values at any adjacent positions, and it is difficult to find out what the original image is by color analysis. Figure 5 shows a scatter plot in the horizontal direction for each color channel in the normal and password images. It can be seen from the figure that the proposed encrypted image has little correlation between adjacent pixels.

4.4. Sensitive Analysis

An adversary can make a differential attack by analyzing different encrypted images obtained from a single key. Therefore, the slightest change of the image in the cryptosystem should cause a huge change as a whole. Analysis of these changes is called sensitivity analysis, and there are two well-known methods: The number of changing pixel rate (NPCR)

and the unified averaged changed intensity (UACI). NPCR and UACI for analyzing the proposed encryption algorithm are defined as the following (13) and (14):

$$NPCR_{RGB} = \frac{\sum_{i,j} D_{RGB}(i,j)}{W \times H} \times 100(\%) \quad (13)$$

$$UACI_{RGB} = \frac{\sum_{i,j} |C_{RGB}(i,j) - C'_{RGB}(i,j)|}{W \times H \times 255} \times 100(\%) \quad (14)$$

where  $W \times H$  represent the size of the plain image. In (14),  $C(i, j)$  denotes a difference between pixel values of the  $i$ th rows and the  $j$ th columns of an image, and  $C_{RGB}(i, j)$  and  $C'_{RGB}(i, j)$  are of an original image and an encrypted image, respectively. In (13),  $D_{RGB}(i, j) = 0$ , if  $C_{RGB}(i, j) = C'_{RGB}(i, j)$ , and  $D_{RGB}(i, j) = 1$ , if  $C_{RGB}(i, j) \neq C'_{RGB}(i, j)$ .

Table 6: NPCR and UACI of encrypted images of different Images due to a small difference

Color	NPCR (%)	UACI (%)
R	99.6347	33.6082
G	99.6404	33.6748
B	99.61445	33.5853



NPCR and UACI of medical cryptographic color images through the proposed cryptographic system are provided in Table 6. The NPCR of over 99% indicates that the microscopic image changes almost entirely. In cryptography, about 33% of the UACI indicates that the distribution of differences in pixel values is even. Figure 6 shows encrypted images with different 1 bit of original image data.

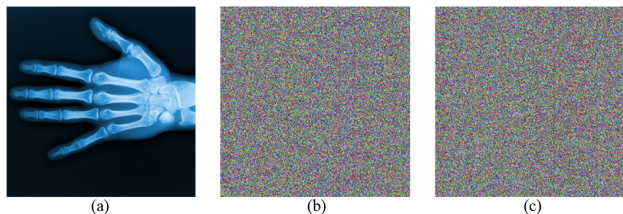


Figure 6: Encrypted images with different 1 bit of original image data

#### 4.5. Key Space Analysis

The number of available keys determines the size of the key space. To create a key image, we need two CoCAs consisting of a nonlinear CA and a 90/150 MLCA. In 8-cell CA, the number of rules is the number of cases applicable to each cell, which is  $2^8$ . the number of rules that can be used for two CoCAs is  $2^{8 \times 16} \cdot 2^{8 \times 16} = 2^{256}$ . The number of keys required for the initial value is  $2^{8 \times 3} = 2^{24}$ . We can control the variables a and b for the pixel shuffling process of the 3D cat map, and the number of variables is  $N^{12}$  where N is the size of one direction of the image to be shuffled. If  $N = 256$ , the key space size is  $2^{256+24+136} = 2^{416}$  in the proposed encryption scheme. Therefore, the proposed medical cryptography algorithm has a sufficiently large key space that the information eavesdropper cannot launch brute force attacks.

#### 4.6. Restore for data corruption

Data stored in the database may be damaged by abnormal external interference. Image encryption algorithms must be able to resist these abnormalities. Experiments are conducted to test the resistance to noise and data loss. Figure 7 shows that even when abnormal data corruption occurs in an encrypted image, the original image is sufficiently resilient to be identified.

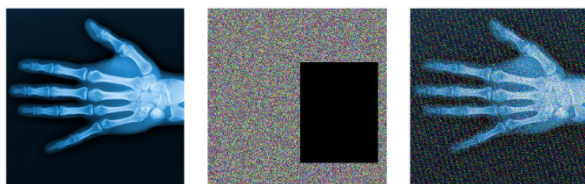


Figure 7: Restoration of damaged cipher image

### 5. Conclusion

In this paper, we proposed a safe and reliable color medical image algorithm based on CoCAs and three dimensional generalized chaotic cat map. The proposed algorithm had a very large key space and improved the nonlinearity of the key stream generated by using CoCAs. In addition, in the pixel shuffling phase of the encrypted image, the pixel positions of the image were changed together with the R, G, and B planes simultaneously, and thus we implemented a cryptosystem having a very strong resistance to noise and data loss. The detailed analysis of the

encrypted images obtained by the proposed algorithm showed the high security and stability of the new medical color image encryption system. In the future, we will study high-speed image encryption suitable for encrypting large-capacity images and study various CA-based PRNG designs.

#### Acknowledgment

This paper is the revised and expanded version of a paper entitled “Color Medical Image Encryption using 3D Chaotic Cat Map and NCA” presented at 2019 10th IFIP International Conference on New Technologies, Mobility and Security (NTMS), Canary island, Spain, 24-26 June 2019. And this research was supported by the Tongmyong University Research Grants 2018(2018A046).

#### References

- [1] X. Wang, L. Liu and Y. Zhang, “A novel chaotic block image encryption algorithm based on dynamic random growth technique,” *Opt. Laser Eng.*, **66**, 10-18, 2015 <https://doi.org/10.1016/j.optlaseng.2014.08.005>
- [2] Y.B. Mao, G.R. Chen, S.G. Lian, “A novel fast image encryption scheme based on 3D chaotic baker maps,” *Int. J. Bifurcation Chaos*, **14**(10), 3613-3624, 2004. <https://doi.org/10.1142/S021812740401151X>
- [3] Y. Dai, X. Wang, “Medical image encryption based on a composition of logistic maps and Chebyshev maps”, in 2012 IEEE International Conference on Information and Automation, Shenyang, China, 210-214, 2012. <http://doi.org/10.1109/ICInfA.2012.6246810>
- [4] X. Wang, L. Teng, X. Qin, “A novel color image encryption algorithm based on chaos,” *Signal Process.*, **92**(4), 1101-1108, 2012. <https://doi.org/10.1016/j.sigpro.2011.10.023>
- [5] C. Fu, W. Meng, Y. Zhan, Z. Zhu, F.C.M. Lau, C.K. Tse, H. Mae, “An efficient and secure medical image protection scheme based on chaotic maps,” *Comput. Biol. Med.*, **43**(8), 1000-1010, 2013. <https://doi.org/10.1016/j.combiomed.2013.05.005>
- [6] S. Zhang and H. Luo, “The Research of Image Encryption Algorithm Based on Chaos Cellular Automata,” *J. Multimedia*, **7**(1), 66-73, 2012. <https://doi.org/10.4304/jmm.7.1.66-73>
- [7] S. Nandi, S. Chakraborty, S. Roy, W.B.A. Karaa, S. Nath, N. Dey, “1-D Group Cellular Automata Based Image Encryption Technique,” in 2014 IEEE International Conference on Control, Instrumentation, Communication and Computational Technologies (ICCICCT), Kanyakumari, India, 521-526, 2014. <https://doi.org/10.1109/ICCICCT.2014.6993017>
- [8] H.S. Jeong, K.C. Park, S.J. Cho, S.T. Kim, “Color medical image encryption using two-dimensional chaotic map and C-MLCA,” in 2018 10th International Conference on Ubiquitous and Future Networks (ICUFN), Prague, Czech Republic, 801-804, 2018. <https://doi.org/10.1109/ICUFN.2018.8437025>
- [9] R.Enayatifar, H.J. Sadaei, A.H. Abdullah, M. Lee and I.F. Isnin, “A novel chaotic based image encryption using a hybrid model of deoxyribonucleic acid and cellular automata,” *Opt. Laser Eng.*, **71**(8), 33-41, 2015. <https://doi.org/10.1016/j.optlaseng.2015.03.007>
- [10] Y. Zhou, L. Bao, C.L.P. Chen, “A new 1D chaotic system for image encryption,” *Signal Process.*, **97**, 172-182, 2014. <https://doi.org/10.1016/j.sigpro.2013.10.034>
- [11] J.V. Neumann, *Theory of Self Reproducing Automata*, University of Illinois, Urbana, 1966.
- [12] S. Wolfram, “Computation theory of cellular automata”, *COMMUN MATH PHYS*, **96**(1), 15-57, 1984. <https://doi.org/10.1201/9780429494093-4>
- [13] S.J. Cho, U.S. Choi, H.D. Kim, Y.H. Hwang, J.G. Kim and S.H. Heo, “New synthesis of one-dimensional 90/150 linear hybrid group cellular automata,” *IEEE Trans. Comput-Aided Design Integr. Circuits Syst.*, **26**(9), 1720-1724, 2007. <https://doi.org/10.1109/TCAD.2007.895784>
- [14] U.S. Choi, S.J. Cho, H.D. Kim, J.G. Kim, “Analysis of 90/150 CA corresponding to the power of irreducible polynomials,” *J. Cell. Autom.*, **14**(5-6), 417-433, 2019.
- [15] P.P. Chaudhuri, D.R. Chowdhury, S. Nandi and S. Chatterjee, *Additive cellular automata, Theory and applications*, vol. 1, Los Alamitos; California; IEEE Computer Society Press, 1997.
- [16] B. Hasselblatt, A. Katok, *A First Course in Dynamics: With a Panorama of Recent Developments*, Cambridge University Press, 2003.
- [17] G. Chen, Y. Mao and C.K. Chui, “A symmetric image encryption scheme based on 3D chaotic cat maps,” *Chaos Solitons Fractals*, **21**(3), 749-761, 2004. <https://doi.org/10.1016/j.chaos.2003.12.022>
- [18] U.S. Choi, S.J. Cho, J.G. Kim, S.W. Kang, H.D. Kim, S.T. Kim, “Color Image Encryption Based on PC-MLCA and 3-D Chaotic Cat Map,” in 2019

IEEE 4th International Conference on Computer and Communication Systems (ICCCS), Singapore, 2019. <http://doi.org/10.1109/CCOMS.2019.8821691>

- [19] X. Wang, Y. Zhao, H. Zhang, K. Guo, "A novel color image encryption scheme using alternate chaotic mapping structure," *Opt. Laser Eng.*, **82**, 79-86, 2016. <https://doi.org/10.1016/j.optlaseng.2015.12.006>
- [20] X. Wu, H. Kan, J. Kurths, "A new color image encryption scheme based on DNA sequences and multiple improved 1D chaotic maps," *Appl. Soft Comput.*, **37**, 24-39, 2015. <https://doi.org/10.1016/j.asoc.2015.08.008>
- [21] L. Zhang, Z. Zhu, B. Yang, W. Liu, H. Zhu, M. Zou, "Cryptanalysis and improvement of an efficient and secure medical image protection scheme," *Math. Probl. Eng.*, **2015**(2), 1-11, 2015. <https://doi.org/10.1155/2015/913476>



## Model of Automatic Parking House

Radek Guráš\*, Miroslav Mahdal

Department of Control Systems and Instrumentation, VSB – Technical University of Ostrava, Ostrava, Czech Republic

---

### ARTICLE INFO

Article history:

Received: 13 December, 2019

Accepted: 05 February, 2020

Online: 09 March, 2020

---

Keywords:

Automatic Parking House

Vehicle Parking

Storage Mechanism

---

---

### ABSTRACT

This article deals with the issue of parking houses, storage mechanisms and how to control them. A laboratory model of a multi-storey underground automatic parking house was designed and created for this purpose, which is used to test a new innovative way of storing cars and specialized approaches to driving actuators. The model is based on an aluminum profile frame to which a newly made linear two-stage dual-sided telescopic mechanism and a two-axis positioning mechanism is attached. The emphasis is placed on the smooth movement of all axes which limits shocks caused by mechanism speed change while moving to a defined position.

---

## 1. Introduction

This paper is an extension of work originally presented in International Carpathian Control Conference 2019 [1] which deals with the design of whole automated parking house and new solution of car storing.

Automatic parking systems offer modern, sophisticated and intelligent car parking solutions in places where there is a lack of parking space for many vehicles. In such places as city centers, airports, hotels, housing estates, etc. it is possible to use parking houses, which will increase the parking area by the number of floors, whether in the above-ground or underground variant. This solution can be further improved by using an automated system with many advantages over the classic solution.

To demonstrate the functioning of a possible solution of such an automatic parking system, a model of an automatic parking house of the underground structure was created on the principle of a two-axis motion device with a dual-sided sliding telescopic storage mechanism. This solution brings a new perspective on the design of the storage mechanism and develops the widely used principles of automatic car parking, e.g. in [2-4].

The control of this model is provided by a distributed control system consisting of Arduino units in two levels. Arduino Nano microcontroller boards form the zero-order level together with the power modules for control of step and dc motors and represent the analogy of real intelligent systems such as intelligent frequency

inverters. The Arduino Mega forms the top level, which represents the master control board of the model. Both levels communicate with each other via UART. The higher level is also ready for connection to the visualization software.

## 2. Description of Construction

For the purposes of this project, a model of a parking house was designed as physical support for the following solution of the control system and its software. In terms of the optimal ratio between price, size and assembly, the dimensions were chosen so that the device was able to work with 1:24 scale car models.

Some components, particularly the propulsion system, do not entirely match the overall proportions of the parking house model, but they have been used for the fact that they are standard, standardized components whose price is many times lower than the price of atypical prototypes made bespoke.

### 2.1. Design of the storage mechanism

The basic element of each automated parking house is the mechanism that transports cars from the entry area to the individual storage positions. The most commonly used principle is the transfer of a car on a pallet that the individual carriage systems of the garage convey between themselves. However, in this work, the principle used for transferring the car from the static to the moving part of the system is based on mutually passing support bars (see Figure 1), which support the wheels of the car and during their mutual pass the wheel is transferred from the bars with larger pitch to ones with smaller pitch and vice versa. Based on this principle, a storage mechanism has been developed that functions as a

---

\*Radek Guráš, Department of Control Systems and Instrumentation, VSB – Technical University of Ostrava, Ostrava, Czech Republic, radek.guras@vsb.cz

telescopic sliding dual-sided system with a support element mounted on the second stage of the telescopic device. In this way, the mechanism is able to eject the support element by more than one length of the retracted state, thus enabling the vehicle to be moved to the storage position without the support element being physically disconnected from the storage mechanism.

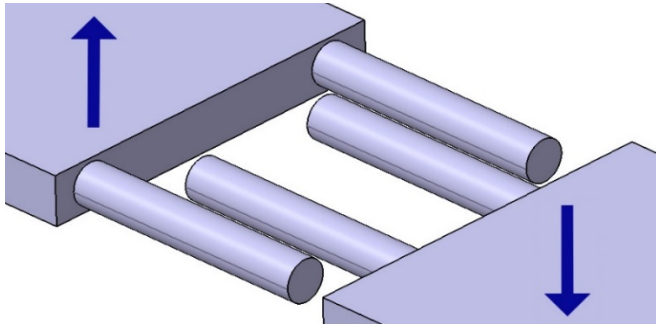


Figure 1: Mutually passing support bars

The storage mechanism (see Figure 2) consists of three basic parts, designed for a linear extension, symmetrically on both sides. The parts were made according to their design from ABS plastic by the 3D printing method based on the requirements for the range of motion, stiffness, and specific dimensions. To measure the deflection of the telescopic structure, a simple strength analysis with a load of 0.5 kg was performed, resulting in maximum stress (according to the HMM hypothesis) of 1.731 MPa and the maximum deflection of the first stage endpoint of 0.66 mm at the maximum assumed load. It has to be emphasized that during the analysis the assembly was considered as a solid body and the properties of 3D printed plastic undoubtedly differed from other manufacturing technologies.

The first telescopic stage drive is realized by a Microcon stepper motor of type SX17-1005LQCEF. This motor has a standardized NEMA 17 flange size, static torque of 0.52 Nm at a rated current of 1 A. The motor movement is transmitted over the pulley by a toothed belt of GT2 type mounted on the opposite end of the first stage slider from the underside.

For the second stage drive, the RC nano-servomechanism was used. It was modified so that the feedback was removed, and the motor is used as a conventional high-speed DC motor with a high ratio gear train due to its small mounting dimensions. The motor is mounted on a second stage moving part and its rotary motion is converted to linear by a pinion and a toothed rack running through the middle of the second stage.

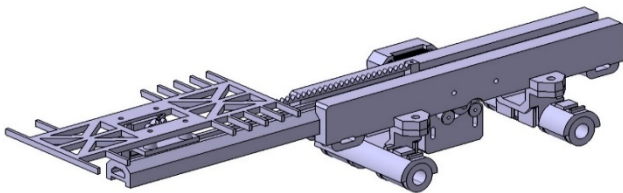


Figure 2: The storage mechanism

### 2.2. Design of the two-axis motion system

The main system enabling the storage mechanism to move in the handling space is a two-axis system (see Figure 3), capable of

moving the car in the vertical axis between the floors and horizontally between the storage boxes within the floor. For this model, the mechanism was designed combining two basic principles: the industrial storage crane and the 3D printer's motion system. Microcon SX17-1005LQCEF and SX17-1003LQCEF stepper motors were chosen to drive both axes. Due to many atypical parts, the method of 3D print was selected to create them. A toothed belt of GT2 type was selected for the transmission of the movement on a horizontal axis. On the vertical axis, due to the requirement for safe stopping of motion in the event of power failure, the trapezoidal screw was used - even at the cost of slower motion.



Figure 3: The motion system

### 2.3. Design of a frame

As a main load-bearing structure of the entire parking house, a design of a frame made of aluminum modular profiles with dimensions 30 x 30 mm was created (see Figure 4). This solution has been chosen especially with regard to the easy attachment of all parts into the profile grooves.

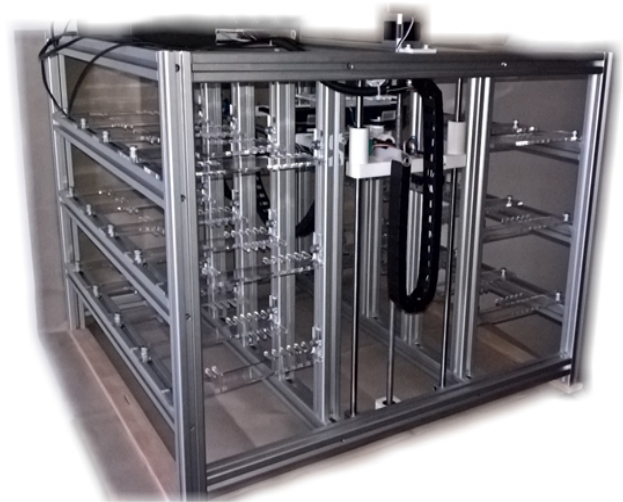


Figure 4: The parking house model frame

## 3. Realization of the Model

The construction of the parking house model for automatic parking of cars was realized on the basis of a previous design.

### 3.1. Motion system

The axes are formed by hardened; polished guide rods attached to the base frame. Linear ball bearings embedded in 3D printed carrier parts allow easy motion along the guide rods. Torque transmission of the motors is realized via a flexible coupling, a trapezoidal motion screw and a trapezoidal nut on the horizontal axis and over the pulley and a toothed belt as a drive of the storage mechanism.

The trapezoidal screw of the specific parameters meets the self-locking condition, so even in the event of a power outage or other failure, it will ensure a safe stop of the vertical movement of the mechanism. For verification, the conditions of self-locking in equations (1) and (2) are used.

$$\varphi' = \tan^{-1} \left( \frac{f_z}{\cos \frac{\alpha}{2}} \right) = 8.82^\circ \quad (1)$$

$$\psi \leq \varphi' \quad (2)$$

where  $\psi$  is the pitch angle (here from the manufacturer  $4^\circ 07'$ ),  $\varphi'$  reduced friction angle of the thread,  $f_z$  for steel – steel 0.15 and the angle of the thread profile  $\alpha$  for a trapezoidal thread is  $30^\circ$ .

### 3.2. Storage mechanism

The most important and the most complex part of the whole model - the storage system (see Figure 5) was made using the 3D printing method as an assembly consisting of three main carrying parts and many other supporting elements.

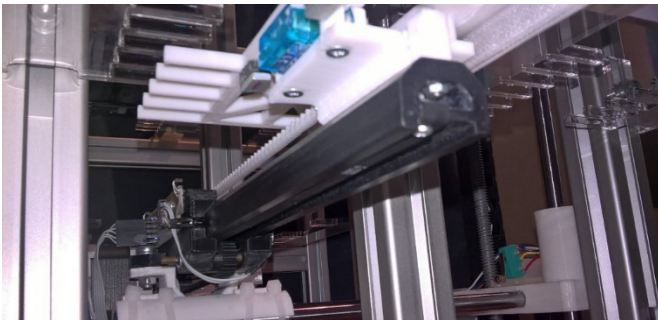


Figure 5: Extruded telescopic mechanism

The main carrier, printed on a 3D printer, has an inner groove for the middle carrying part - the first stage of the telescopic mechanism. Also, there are two smooth pulleys mounted on the underside, through which the toothed belt passes to drive the first telescopic stage. Through the holes on the side of the main carrier, it is possible to mount the stepper motor to drive the first stage.

The second carrier - the first telescopic stage - has such a profile that passes as tightly as possible through the groove in the base part. Also, it has another shaped groove for guiding the moving carriage - the second telescopic stage.

A toothed pinion, made by 3D print, is attached to the output shaft of the second stage motor, transferring motion to the toothed

rack, which is solidly connected to the first stage of the telescopic mechanism and passes through the middle of the second stage.

### 3.3. Static parking spaces

Static parking spaces were made of plexiglass parts cut by a laser (see Figure 6). Ladder shelves have been created, which always in pairs form a parking space for one car. One of their ends was heat-bent at a right angle so that it could be then attached to the main frame of the model.

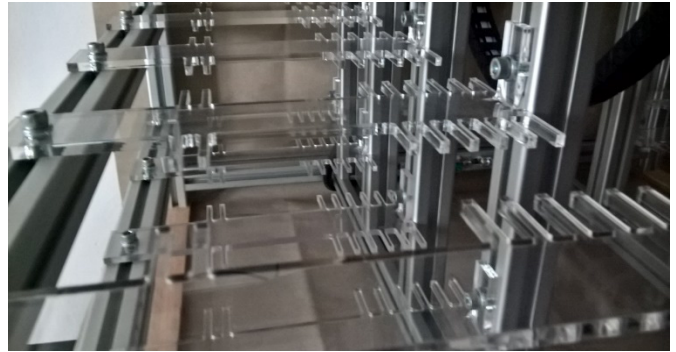


Figure 6: Parking spaces

### 3.4. Sensors

Several types of sensors were used to build the model. The main purpose of these sensors is to define end positions, homing positions, pullout position control and parking space occupancy detection.

For these purposes, sensors of the following types were used:

- Mechanical end stops (homing, handling space definition)
- Hall sensors (determining the position of the second stage of the telescopic mechanism)
- Optical IR gates (homing of the first stage of the telescopic mechanism, incremental sensors)
- Reflective IR sensors (parking space occupancy detection)

For easier processing of signals from occupancy detection sensors, the PCB was used, with sensitivity tuning and conversion to serial signal using a shift register of “parallel in – serial out“ type (see Figure 7).

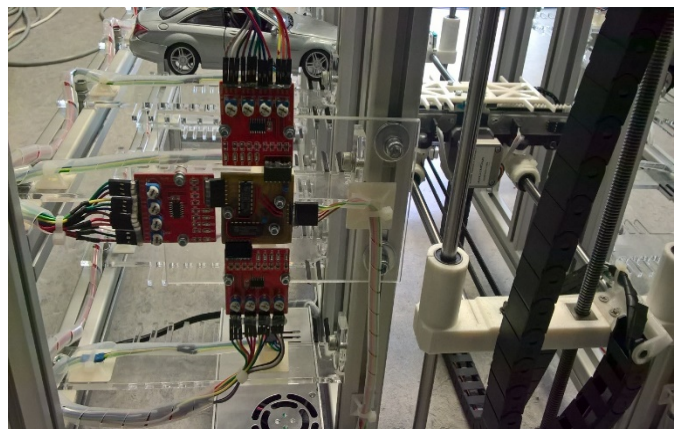


Figure 7: Signal conversion boards



All cabling has been run in power chains in places of motion to prevent cables from entering the moving parts of the system.

#### 4. Model Control

A multilevel system (see Figure 8) has been designed to control the model, consisting of a master controller, build on the Arduino Mega 2560 microcontroller board, which provides data acquisition, communication with the user and with superior control level, and mainly management of three subsystems controlling the movement of each axis of the model. These subsystems are built on the Arduino Nano microcontroller boards, which in combination with the Pololu DRV8825 power stepper motor driver and with the L298N H-bridge for driving DC motor, is an analog of a real intelligent control system, such as an intelligent frequency converter.

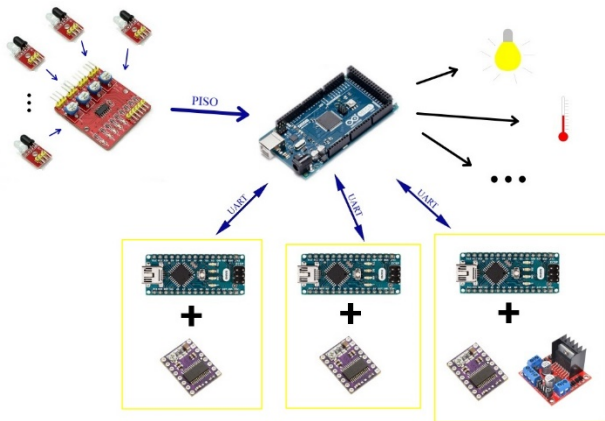


Figure 8: Control system diagram

The UART hardware communication device was used for serial communication between the mainboard and the subsystems.

The DC motor is controlled by a bridge driver by switching the respective inputs which control the power components of the driver and the speed of motion is given by the input PWM modulated enable signal.

##### 4.1. Stepper motor control

A separate chapter in the control algorithm is controlling stepper motors using the Pololu DRV8825 stepper motor driver. This driver switches the individual phases of the motor, eventually provides micro-stepping, depending on the DIR and STEP input signals, where one determines the direction of motion and the other responds to the starting edge of the pulse by performing one step of the motor.

Control pulses for the driver are generated by the microcontroller of the respective axis using the timer interrupt handler. This, depending on the desired time gap between pulses, generates an interrupt flag, triggering the service subroutine, switching the respective outputs and calculates the requested pause time. The longer the pause is, the slower the motor moves.

To ensure the smoothness of the engine's acceleration and deceleration, and to prevent step loss due to a rapid transition from idle to maximum speed, an algorithm was developed to accelerate

and decelerate the engine according to the ramp function. Some of these principles can be also found in the online articles (D. Austin, *Generate stepper-motor speed profiles in real time*, Atmel, *Linear speed control of stepper motor*) or in [5].

The time between control pulses can be calculated using the following formula (3)

$$c_n = c_0 (\sqrt{n+1} - \sqrt{n}) \quad (3)$$

where  $c_0$  is the initial pulse pause length,  $c_n$  is the length of  $n^{\text{th}}$  pulse pause and  $n$  is the calculation step. This way the ramp function is calculated until the motor speed reaches the maximum value.

Since the calculation of the two square roots is very demanding for the microcontroller processor and does not meet the requirement for the shortest possible interrupt service subroutine time. It is useful to replace the previous formula with Taylor series (4) with a certain, not so significant inaccuracy, and calculate the pause between steps from the previous value according to

$$c_n = c_{n-1} - \frac{2c_{n-1}}{4n+1} \quad (4)$$

This measure reduces the calculation to only division of two numbers that is considerably faster than the square root calculation. In order to further accelerate the calculation, measures have been introduced replacing the more demanding division of decimal numbers by dividing integers into two phases. Firstly, the integer is divided normally and then the modulo division is used to obtain the remainder of the division, which in the next step is added to the divider to reduce the inaccuracy of the calculation [6].

##### 4.2. Homing

Movement of motional parts to the default, home position called "homing" is accomplished by a series of algorithms, each controlled by the respective combination of the microcontroller and the power driver.

The horizontal and vertical axes travel to its home limit switch at a reduced speed, and after activation, it will leave enough to switch off the switch again. The algorithm also considers the situation when it is necessary to get into the home position after a non-standard situation, when one of the limit switches is active at the beginning of the process, especially when the home switch is active. In this case, the switch will firstly move from the switch and then the homing will start.

The first stage of the storage mechanism performs homing by means of two optical gates located at the end of the base part of the mechanism. If the two gates are not interrupted, the slider moves in small increments in the direction of the uninterrupted sensor. At the moment of its deactivation, a predefined deviation from the default value is corrected.

The second stage firstly "moves back" to the nearest Hall sensor in the given direction and then moves forward to its home

sensor. If the stage moves back even to the outer sensor, it is assumed that the starting position is already verified with enough space behind it.

## **5. Conclusion**

During a realization of this project, a model of an underground parking house for parking cars, driven by stepper and DC motors, and designed with suitable position sensors, end position sensors, and sensors of occupied parking space, was designed and built. Many 3D prints have been used to produce many atypical parts. The individual parking positions are made of plexiglass ladder shelves. Vehicle storage is performed by a dual-sided sliding telescopic storage mechanism specially designed for this model, operating on the principle of passing support bars.

Next, a multi-level control system based on Arduino microcontroller boards was designed so that one of them serves as a master controller of the model and others formed intelligent drivers for the individual motion axes of the model. All of these individual boards have been programmed and interconnected by the UART communication device.

This project brings a new perspective on car manipulation and storing and allows further development of algorithms for optimal automatic parking.

## **Conflict of Interest**

The authors declare no conflict of interest.

## **Acknowledgment**

This work was supported by the European Regional Development Fund in the Research Centre of Advanced Mechatronic Systems project, CZ.02.1.01/0.0/0.0/16\_019/0000867 within the Operational Programme Research, Development and Education and the project SP2020/57 Research and Development of Advanced Methods in the Area of Machines and Process Control supported by the Ministry of Education, Youth and Sports.

## **References**

- [1] R. Guráš, M. Mahdal, "Parking house action subsystem control," in Proceedings of 2019 20th International Carpathian Control Conference (ICCC), Krakow-Wieliczka, Poland, 2019, doi: 10.1109/CarpathianCC.2019.8765989
- [2] U. Maheswari, D. Aswini, G. Murtugudde, B. Karthiga, "Automatic car parking system" Int. J. Pure Appl. Math. (Online), Vol. 120, No. 6, 2018. ISSN: 1314-3395
- [3] I. L. J. Hamelink, The Mechanical Parking Guide, CreateSpace Independent Publishing Platform, 2011, ISBN 1-466-43786-3
- [4] A. Mathijssen, A. J. Pretorius, "Verified Design of an Automated Parking Garage" in Formal Methods: Applications and Technology: 11th International Workshop, FMICS 2006 and 5th International Workshop PDMC 2006, Bonn, Germany, 2006, doi: 10.1007/978-3-540-70952-7\_11
- [5] P. Novák, Mobilní roboty: pohony, senzory, řízení, Praha: BEN - technická literatura, 2005, ISBN 80-7300-141-1
- [6] J. Czebe, J. Škuta, "Usage of single-chip computers for control MIMO systems," in Proceedings of 2017 18th International Carpathian Control Conference (ICCC), Sinaia, Romania, 2017, doi: 10.1109/CarpathianCC.2017.7970428



## Analysis of Cyberattacks in Public Organizations in Latin America

Segundo Moisés Toapanta Toapanta<sup>\*1</sup>, José David López Cobeña<sup>1</sup>, Luis Enrique Mafla Gallegos<sup>2</sup>

<sup>1</sup> Department of Computer Science, Universidad Politécnica Salesiana (UPS), Guayaquil, 010102, Ecuador

<sup>2</sup> Faculty of Systems Engineering, Escuela Politécnica Nacional (EPN), Quito, 17-01-2759, Ecuador

---

### ARTICLE INFO

*Article history:*

*Received: 21 November, 2019*

*Accepted: 25 February, 2020*

*Online: 09 March, 2020*

---

*Keywords:*

*Cybersecurity*

*Cyberattack*

*Public Organization*

*Denial of Service*

*Minimize the attack*

---

---

### ABSTRACT

*It was analyzed certain information about cyberattacks in Latin America and methods to counteract the aggressions that affect services, data and infrastructure. The problem is the cyberattack on information networks where there is interdependence between processes, people and devices within public organizations with the negative consequence of denial of services. The objective is to propose a protection model against cyberattacks in public organizations in Latin America to minimize the denial of public services. It was applied the deductive method and exploration to examine the information of cited articles. It resulted a General Model of Protection against Attacks, a Prototype of a network, a Algorithm in flowchart to minimize the attack arrival and a Formula of probability of attack arrival. It was concluded that in order to maintain the continuity of services and activities of public organizations, secure platforms must be in place to monitor and minimize possible attacks; our proposal has an attack detection accuracy of 87.49%.*

---

### 1. Introduction

Today national and sectional governments use desktop applications, web applications, mobile applications and social networks to improve public services to citizens; ICT help public and private organizations serve their taxpayers and customers respectively, such as time reduction in processes, zero documentation, reservation of shifts, digital tax returns.

The advancement of technology brings with it threats that materialize in damage to infrastructure and services provided by public organizations; the most common types of attacks are social engineering and network attack. There are specific attacks such as: integrity attacks, sparse sensor attacks, false data injection attacks, fake-acknowledge attack, denial-of-service attacks and replay attacks[1].

The cyberattack maliciously update a system, the attacking software tries to destroy the environment; the antithesis of this is cyber security that is protection of information, hardware, software and services against vandalism[2].

Countries like Ecuador, Chile, Brazil, Colombia and Mexico are updating their laws to guarantee privacy, protect data[3] some countries consider cybercrimes in their laws such as Argentina,

---

<sup>\*</sup>Segundo Moisés Toapanta Toapanta, & Email: [stoapanta@ups.edu.ec](mailto:stoapanta@ups.edu.ec)

Bolivia, Costa Rica, Guatemala, Mexico, Paraguay and Peru; other countries generate specific laws: Brazil, Chile, Colombia and Venezuela; Ecuador uses its civil and commercial law in criminal sanctions; Uruguay has a Law on Protection of Copyright[4]. Countries such as United States, China and Israel are pioneers in the application of technological advances in national defense.

Formulation of the research problem: How cyberattack can be minimized to an information network where there is interdependence between processes, people and devices within public organizations; and there are exposed servers that provide services with the possibility of denial of services. The following hypothesis:

Why is an approach to cyberattacks necessary in public organizations in Latin America?

The objective is to propose a protection model against cyberattacks in public organizations in Latin America to minimize the denial of public services.

This research is motivated by the need to analyze and identify cyberattacks in public organizations in Latin America; review mechanisms that serve to minimize the denial of public services; Obtain a model for the identification of vulnerabilities that threaten the provision of services; propose a mechanism that can be used in

areas such as: education, aerospace, electricity networks, water services, telephony, financial, transportation, communication, business, attention, risk control or infrastructure; avoid the loss of taxpayers, credibility, time and other resources of a public organization, in addition to certifying the availability of services and keep a critical service located on an application server enabled.

The articles reviewed and related cyberattacks in Latin America are: Are We Ready in Latin America and the Caribbean[5], Cyber Risks and Information Security in Latin America & Caribbean Trends [6], Data Breach Investigations Report[7], A cyber-attack on communication link in distributed systems and detection scheme based on H-infinity filtering [8], Cyber-Attack Features for Detecting Cyber Threat Incidents from Online News [9], A Novel Approach for Classification and Detection of DOS Attacks [10], Analysis of efficient processes for optimization in a distributed database [11], Biometric Systems Approach Applied to a Conceptual Model to Mitigate the Integrity of the Information [12], Cyberattacks on Devices Threaten Data and Patients [13], Assessing Mission Impact of Cyberattacks: Toward a Model-Driven Paradigm [14], A survey of iot-enabled cyberattacks: Assessing attack paths to critical infrastructures and services [15], Attacklets: Modeling high dimensionality in real world cyberattacks [16], Cyberattack Prediction Through Public Text Analysis and Mini-Theories [17], Deep learning approach for cyberattack detection [18], Cyberattack detection in mobile cloud computing: A deep learning approach [19], Adaptation of the neural network model to the identification of the cyberattacks type 'denial of service'[20], Cybercriminals, cyberattacks and cybercrime [21], Resource efficiency, privacy and security by design [22], A survey of similarities in banking malware behaviours [23], A new strategy for improving cyber-attacks evaluation in the context of Tallinn Manual[24], Evaluating practitioner cyber-security attack graph configuration preferences [25], Correlating human traits and cyber security behavior intentions [26], Record route IP traceback: Combating DoS attacks and the variants [27], Evaluating the applicability of the double system lens model to the analysis of phishing email judgments [28], Enhancing security behaviour by supporting the user [29], An Algorithm for Moderating DoS Attack in Web based Application [30], Impact of a DDoS attack on computer systems [31], How Secure are Web Servers? [32], Detection of DoS/DDoS attack against HTTP servers using naive Bayesian [33], Detection of DoS attack and Zero Day Threat with SIEM [34], A Framework for Making Effective Responses to Cyberattacks [35], Attack detection/prevention system against cyberattack in industrial control systems [36], Is the responsabilization of the cyber security risk reasonable and judicious? [37], A visualization cybersecurity method based on features' dissimilarity [38], Automatic security policy enforcement in computer systems [39], Defending Against Web Application Attacks: Approaches, Challenges and Implications [40], Statistical Application Fingerprinting for DDoS Attack Mitigation [41], Detecting lateral spear phishing attacks in organisations [42], A Survey on Distributed Denial of Service (DDoS) Attacks in SDN and Cloud [43], BWManager: Mitigating Denial of Service Attacks in Software-Defined Networks Through Bandwidth Prediction [44].

It is applied the deductive method and exploration to examine the information of cited articles.

The results are: A General Model of Protection against Attacks, a Prototype of a network, a Algorithm in flowchart to minimize the attack arrival and a Formula of probability of attack arrival.

It is concluded that in order to maintain the continuity of services and activities of public organizations, secure platforms must be in place to monitor and minimize possible attacks; our proposal has an attack detection accuracy of 87.49%.

## **2. Materials and Methods**

In a first instance in Materials, works of attacks carried out in Latin America and global level were reviewed. In the second instance in Methods, elements are presented to put together a proposal to minimize attacks such as Ranking, Types and tendencies of attacks, general steps of attack and scope.

### *2.1. Materials*

In 2016 the Organization of American States and the Inter-American Development Bank produced a cybersecurity report from 32 countries in Latin America and the Caribbean; for each country they reviewed 5 dimensions such as policies and strategies, culture and society, education, legal framework and technology; 49 indicators distributed in 5 dimensions were applied; 5 maturity levels were also reviewed as initial, format, established, strategic and dynamic; It is reported that Brazil, Colombia, Jamaica, Panama, Trinidad and Uruguay adopted cybersecurity strategies [5]. For 2019, Deloitte Touche Tohmatsu Limited presented a report on cyber risks in Latin America and the Caribbean, the public, financial, manufacturing, communications, services, oil and other areas were reviewed; the results compare Latin America against Colombia; Latin America is 9% more important than Colombia in cyber security; Latin America has 5% more protection than Colombia in security level; Latin America has 9% less protection than Colombia in Denial of Services attacks [6].

For 2019, Verizon presented a report that determined that: victims were from the public, health, financial and business sectors; the tactics used were hacking, social engineering, malware, casual, misuse; the actors of the attacks were foreign, internal actors, partners, third parties, criminal organizations and governments; the main attack was Denial of Services[7]. The authors defined a management architecture in a distributed topology, there are physical areas interconnected through software links and they provide data to each monitoring center; for the detection scheme the input data of the areas are filtered before applying the anomaly detection process; by hiding the attack vector effect and not being a data entry, the attack is detected, the time that intervals are 20 seconds [8].

The authors proposed a model that has three phases: preprocessing, identification and classification; in the first phase the news is filtered to leave simple text to analyze; in the second phase the characteristics of the attack are validated with other investigations and the extracted text is stored in a dictionary; the third phase uses statistics to create a probabilistic model and identify the data; the classification algorithm is under construction [9]. The authors proposed a web application for classification and detection of attacks; they have two classifiers, the first one works with a list of malicious communications and the second one works with a tree decision; they also have a package to analyze user data and warn in case of an attack; in the accuracy tests the minimum was 77.77% and the maximum 93.33% [10].

The authors carried out a descriptive evaluation of works in security and processing of distributed databases; they described fourteen articles on scales of 1 to 5; in addition, they grouped the works in processing, concurrence, consultations, fragmentation, communication, consistency and load[11]. The authors proposed a biometric system model to increase the level of information security, the model manage security by fingerprint access, iris, facial recognition; this data is stored in a database [12].

The authors conducted a questionnaire for three cybersecurity professionals; the questions dealt with threats in the health industry, attacks on medical devices, device certification, laboratory evaluation, advances in research; one researcher concluded that the risks are adherent and real when connecting to a network, you should consider mitigating the risks [13]. The authors described the characteristics of an attack evaluation model; this model has several fronts: organization, processes, motivations of the attacker, individual or group attacks and architectures; they affirm that defense against attacks depends on the systematic and quantitative evaluation of the business [14].

The authors modeled a cyberattack where they identified the attacker, the devices, characteristics of the attack, vulnerabilities of the devices, the connection paths between the devices and the data warehouse; the attack model was applied to company infrastructure, an electric power network, a transport system, a medical system and smart home; they concluded that weaknesses and limitations are characteristic of fragile security [15]. With historical data from 1971 to 2017; the authors modeled a cyberattack that executes several actions, uses several user attributes, several data sets simulating people or groups, several states of actors; one of the objectives is the classification of attacks, which serves to determine securities; Attacks are stored and serve as feedback for self-learning [16].

The authors proposed that unused sources of information can be used for the prediction and preparation of cyberattacks found in extensive texts on the web; ontological knowledge is used about the attacks demonstrated that their technique of event extraction and detection of named entities showed a large scale of cyberattack prediction [17]. To mitigate the cyber security problem in IoT environments by shortening the detection time; The authors proposed a DFEL deep learning framework that reduced detection time by 57.75% over other traditional machine learning algorithms [18].

An important point to exist attacks today are mobile devices; the authors proposed a deep learning framework to detect cyber threats in the mobile cloud; its detection accuracy was 97.11% compared to other machine learning approaches[19]. The authors suggested increasing the coefficient values of a reduced quadratic learning error in a neural network; they improved the accuracy of the deviations of the safety parameters in the area of their minimum values [20].

The massive increase in cyberattacks determines that system security is quite vulnerable; the authors proposed that by hardening security at all levels, these attacks can be prevented and if omitted, critical and non-critical infrastructure would be compromised[21]. The authors proposed a prototype that performs a renewing analysis of the connections associated with the resources, the validity, cybersecurity, data protection and data privacy arguments; the model is a set of policies that seeks to increase storage and data security; in the tests they obtained the 2%, 5%,

8% and 15% reuse rate in first, second, third and fourth scenarios respectively [22].

The authors reviewed the attack by malware in the banking sector, where criminal groups steal information; they used an analysis framework for decomposition, control flow study and instruction review; they concluded that there is a need to understand malware tactics at a high level [23]. The authors carried out a cyberattack evaluation model, based on a normative scheme of the United Nations "force use" letters of 1945; some parameters are difficulty, speed, causes, number of operations, identification of consequences, relations between operations and permitted acts; their strategy is in a new calculation to measure the criteria, where they combined algorithms and new grouping of reasons to obtain a destruction value [24].

The authors proposed a graphic visual syntax configuration to effectively present the attacks; in tests the precondition attribute is 38.5%, the flow of events is 32.6% and exploit is 28.8%; Precondition is more significant, and the exploit attribute is less significant in decision making [25]. The authors related human characteristics to cybersecurity behavior; they conducted a survey of 369 people from a public university; the results were: 5.2% of security intention of the device, 16.8% of security intention of the users, 22.8% of intention of conscience, 12.6% of intention to update; they concluded that their work helps to understand populations in safety behavior [26].

The authors studied the denial of services and their variants, they proposed a probabilistic package marking design to forecast routes from the attacker to the victims, this allows the victim to delegate their protection to the ISP; in the tests they carried out between 100 and 5000 DDoS attacks with averages between 20 and 11 packages respectively, where the design takes 21.42 milliseconds to 18.5 seconds to obtain the route; they concluded that their design requires fewer packages to obtain attack routes and lower bandwidth consumption [27]. The authors designed a double lens model to assess human judgments in the mails; in the tests they obtained performance values 0.923 units indicates that the model has a good work to adjust environment and criteria; the knowledge value was 1 unit, indicates a good level in the fields; Other values found are: lack of details of the signer is 0.542, without logos is 0.400 and URL hyperlinks is 0.349; they concluded that their work is a first step to apply judgments to the phishing environment [28].

The authors studied the maintenance and accompaniment in user safety; the experiment on social networks was with 60 participants in 5 scenarios; the e-commerce experiment evaluated the generation of passwords to classify security elections; password security control is less than 0.01 units; the control in the times of the change of password is 0.11 units; suggestion control is 0.17 units [29].

### *2.1.1. Related Jobs*

The authors proposed an algorithm with monitoring, detection and mitigation; in the first phase the IP addresses are identified against a block list to prevent the message from passing; in the second phase the number of applications is verified; in the third phase a threshold value is used according to a behavior; The algorithm identifies the type of attack, there is no evidence of the algorithm[30]. An attack tree was used to identify actions and tools against threats; review of system security behavior, review of attack indicators, selection of profiles of attackers and victims; the

results obtained and evaluated the costs of attacks, benefits, impacts, possibilities and skills [31].

The authors evaluated DoS HTTP vulnerabilities in Apache, IIS, Nginx and Lighttpd through the GET and POST methods; in the POST interval tests it is 88% less likely than GET; in slow message attack POST is 87% lower probability than GET; in real traffic POST is 99% less than GET; they concluded that their proposal has precision to detect attacks [32]. The authors proposed architecture that uses Bayes theorem probability to detect attacks on servers; the central package captures and analyzes network traffic, malicious traffic is stored; in the detection tests the minimum accuracy is 96.61% [33].

To detect DoS attack on the server, the authors proposed to work with the server's Log, network characteristics, connection time, packets and addresses; uses a rule implementation which verifies against the records, alarms are notified to the administrator and saved; this process works permanently [34]. The authors described 2 potential risks, defending themselves with a weak system or defending themselves with greater intensity in direct attacks on the attackers [35].

The authors studied the location of vulnerability and attacks on programmable controllers, they created a set of rules to see the start or stop of attacks; they proposed an algorithm in three phases: attack, observation and detection; the tests were descriptive, there are no numerical data, they concluded that security is not yet a priority in organizations [36]. The authors compared the risks in individual security and government security; at the government level they proposed deterrence, rules, location, recovery, remediation; there is no numerical data in tests; they suggested a hierarchical approach where governments take a more dynamic role, provide resources, have police authority and prevention units [37].

To increase intelligent phishing identification, the authors proposed a technique to detect websites and deliver early alerts; the authors applied a formula to rule out redundant characteristics, the values are global score and average score; they evaluated 30 characteristics and reduced to 6; its accuracy is 93% in the classification [38]. The authors proposed a technique for complying with computer policies through the formal relationship and the assessment of security settings; they proposed a formula with conjunction and disjunction; they implemented a prototype, there are no measurement values in the tests [39].

The authors described the validation problems when entering applications, these are entry doors for attackers with different attack targets; the authors created an exploitation model to understand code injection attacks, the algorithm uses common attack steps to identify exploitation routes [40].

The authors created a model for monitoring and detecting traffic behavior in a network; the package, flow and traffic anomalies are measured, also incorporated flow statistics to compare against real traffic; the model has a flow level and a package level; they use algorithms based on histograms, entropy calculation, normal profiles, flow and attacks; the authors state that their model is accurate between 97% and 100% [41].

The authors adopted a technique to detect false positives and true positives in the arrival of emails, they are given a score to take actions on the mail; in the tests they obtained a false positive rate of 0.88% and a true positive rate of 86.69%; the accuracy of the model was 98.79%; they stated that their research serves as an

improvement in identifying a higher rate of true positives and a lower rate of false positives [42].

The authors described the concept of cloud computing, the DDoS attack and how it acts on the application layer, control layer and data layer; they deliver the guidelines to detect the attack through resource sharing accesses, highlighted the reasons, software tools to mitigate the attacks; described the attacks of other investigations [43].

The authors proposed an architecture to mitigate DoS attacks, consisting of six components with their detailed description; it also uses an algorithm as a priority manager, a queue management algorithm and a time algorithm; the tests were carried out in 100s with a speed of 500 packages / s they concluded that the architecture is effective by increasing the attack rate [44].

Related works dealt with cyberattacks and against subtracted through: phases, algorithms, threat reviews, indicators to measure attacks, types of attacks, threat identification; others detect attacks, defined rules or alarms, security risks, forms of deterrence, early warning delivery, redundancy reduction, policy compliance.

## 2.2. Methods

### 2.2.1. Ranking

According to Internet Crime Report 2018 [45], it received 351,936 complaints with losses of \$2.7 Billion, has a ranking of 20 countries of which: the first place is India with 4556 victims; the seventh place is Brazil with 605 victims; the eighth place is Mexico with 591 victims; the tenth place is Philippines with 511 victims, the twentieth place is Japan with 311 victims. The type of crime Government Impersonation has 10,978 victims and cost \$64,211,765; Denial of Service/TDoS has 1,799 victims and cost \$2,052,340. In this ranking United States is excluded because the 2018 report has an analysis dedicated to this last country.

Figure 1 shows information obtained from [6] and [7]; according to Deloitte, the public sector in Latin America had 6% attacks and according to Verizon, the public sector worldwide had attacks of 16%; the highest percentages are Financial and Small Business where 44.7% and 43% of Deloitte and Verizon respectively. In the tactics used to the organizations we see that 69% are perpetrated outside the organization according to Verizon and 70% of the organizations affirm that they have no effectiveness in response to these cyberattack events according to Deloitte.

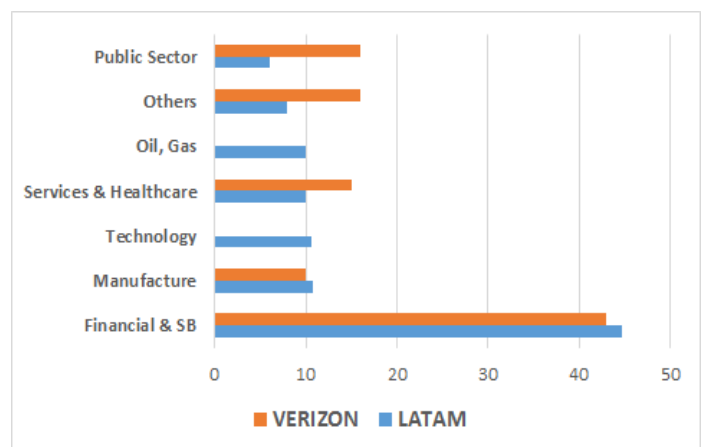


Figure 1 – Victims by sectors.



There are different types of cyberattacks some are: Defacement, Denial of Service, Account Hijacking, Malware and Virus, Phishing, SQL injection, Targeted Attack Unauthorized Access, Unknown Attacks and Zero Day [46].

The trends of cyber-attacks are: Root kit, BotNet, Scareware, SQL Injection, Phishing, Kido, Advanced Persistent Threat, Code Injection, HTML Injection [2].

Reference [30] puts DoS with 37% and Brute Force 25%; there are 2 types of DoS attacks: a) DoS is an attack executed by a single device (multiple requests) to a victim; b) DDoS is an attack executed by many devices distributed to same victim; the victim can be a server, service or infrastructure.

Attacks DoS can be separated into the layers of OSI model: on layer 3 Network that carries Packets there are UDP reflection attacks; on layer 4 Transport that carries Segments are given attacks SYN floods; on layer 6 Presentation that carries data attacks are given SSL abuse; on layer 7 Application that carries data are given attacks HTTP floods, floods of DNS queries.

In [30] 37% of the attacks were due to DoS, it is a type of cyberattack that happens more frequently and causes the interruption of the services offered by public organizations; attacks on the public sector: in [6] it was 6% in Latin America and in [7] it was 16% globally.

2.2.2. Comparison table of references

The different proposals reviewed obtained the methods that the authors used to estimate the detection, identification, conduct and analysis of cyber attacks, they propose to protect any of the following resources: information, physical network, infrastructure, applications or computer services.

Table 1 shows the proposals that protect computing resources, according to the information in the references there are a variety of protection methods, each proposal aims to protect only one resource at a time.

Table 1: Comparison of proposal.

Reference	Method	Protect	Accuracy
[1]	Detection estimates	Physical network	Residual evaluation > 0
[2]	Steps to use the internet	Information	Only algorithm
[8]	Filtering H-infinity	Communication links	Residual signal > 0
[9]	Identification of badges	Websites	Only algorithm
[10]	List and decision tree	Web server	77.77%
[12]	Biometric system	Information	Only algorithm
[13]	Cyberattacks	Questionnaire	No evaluation
[15], [16]	Attack models	Information	Descriptive results
[17]	Entity Detection	Information	Only algorithm

[18]	Learning Framework	Hardware connected to IoT	Detection greater than 57.55%
[19]	Learning Framework	Mobile cloud	97.11%
[20]	Cyberattacks identification DoS	Physical network	Only algorithm
[22]	Connection analysis	Data centers	Reuse 15%
[23]	Framework analysis	Bank information	Only algorithm
[24]	Cyberattack evaluation model	Information	Criteria calculation
[25]	Attack tree	Information	Precondition is 38.5%
[26]	Safety behavior	Information	Security intensity 5.2% to 22.8%
[27]	Probabilistic design	Services	Route in 18.5s
[28]	Dual lens model	Mails	Performance 92.3%
[30]	Identification of types of attacks	Web application	Only algorithm
[31]	Impact of attacks	Computer systems	94.80%
[32]	Stopping training and testing	Web server	87.00%
[33]	Odds and capture package	HTTP server	96.61%
[34]	Verification of rules	Web server	Only algorithm
[35]	Risk Classification	Infrastructure	Only Procedure
[36]	Set of rules	Systems	Only algorithm
[37]	Deterrence	Information	Only algorithm
[38]	Phishing identification	User data	93% predictive accuracy
[39]	Security policy framework	Information	Prototype

The information of the materials and of Table 1, was used to propose the scopes and also certain characteristics were adopted from the references to propose results.

2.2.3. Scope for the proposal

- Propose a General Model of Protection against Attacks
- Propose general security axes
- Propose a Prototype of a Network to minimize the attack called Denial of Services DoS, the main service of a Public Organization is Service to Citizens
- An algorithm expressed in a flowchart to prevent and minimize attacks that corrupt operations, functions, availability of services that are provided through websites, applications and database; without degrading the functionality of services
- Service servers are inside DMZ
- To access the data services from internet, a 3-layer model is used



- To access the data services from intranet, a 2-layer model is used

2.2.4. Methodology to generate results

General Model: To propose a protection model, the following elements were taken from the references: the qualitative criteria of cyberattack were considered [24]; user behavior was considered for access control [29]; the criteria of levels of responsibility were adopted [37]; the application of security policies was considered [39]; [31] and the [36] use of phases for attack and response detection was considered.

General prototype of a Network: Models, network architecture and services that protect information from the following references [11], [14], [30] and [39] were considered; Server protection was decided as they do in [32], [33] and [34] to continue providing services offered by an organization through its applications.

Algorithm: The Packet Sniffing Sensor[10] was adopted for unusual traffic analysis; of [36] we adopt the use of phases in the proposed algorithm, the scanning and monitoring of traffic.

Formula: The poisson distribution facilitates the event of occurrence of events that occur in a given interval, this formula was adopted and the number of requests, the time interval in seconds and the attack per unit of time are taken as variables.

3. Results

The information and systems are critical assets, this research tries to minimize cyberattacks and that do not materialize in damages, in addition to increasing the levels of continuity of services and activities of public organization.

The following results were obtained:

- General Model of Protection against Attacks
- Prototype of a network
- Algorithm in flowchart to minimize the attack arrival
- Formula of probability of attack arrival

	IDENTIFY	PROTECT	DETECT	RECOVER AND RESPOND
<b>BASIC</b>	<ul style="list-style-type: none"> <li>• VULNERABILITIES</li> <li>• ORGANIZATION SERVICES</li> </ul>	<ul style="list-style-type: none"> <li>• ACCESS CONTROL</li> <li>• NETWORKS</li> <li>• CONNECTIONS</li> </ul>	<ul style="list-style-type: none"> <li>• MONITORING</li> </ul>	<ul style="list-style-type: none"> <li>• RECOVERY PLAN</li> <li>• EXECUTE CONTINGENCY PLAN</li> </ul>
<b>STANDARD</b>	<ul style="list-style-type: none"> <li>• CERTIFICATION OF HARDWARE AND SOFTWARE</li> <li>• PROCESS IMPROVEMENT</li> <li>• HUMAN FACTORS</li> <li>• PROTECTION SOFTWARE</li> </ul>	<ul style="list-style-type: none"> <li>• BACKUPS</li> <li>• PRIVACY</li> </ul>	<ul style="list-style-type: none"> <li>• ANOMALIES</li> <li>• LONG PROCESSES</li> </ul>	<ul style="list-style-type: none"> <li>• ORGANIZATION INFORMATION</li> <li>• RECOVERY SCHEDULE</li> <li>• ADMINISTRATION OF THE ACCIDENT</li> <li>• CONTINUITY OF SERVICE</li> </ul>
<b>OPTIMIZED</b>	<ul style="list-style-type: none"> <li>• POLITICS AND PROCEDURES</li> <li>• ROLES AND RESPONSIBILITIES</li> <li>• CRITICAL APPLICATIONS</li> <li>• CRITICAL INFORMATION</li> </ul>	<ul style="list-style-type: none"> <li>• CRITICAL APPLICATIONS</li> <li>• CRITICAL INFORMATION</li> <li>• APPLY AUDITS</li> </ul>	<ul style="list-style-type: none"> <li>• TRAFFIC ANALYSIS</li> <li>• SHARED INFORMATION</li> </ul>	<ul style="list-style-type: none"> <li>• LEGAL ACTIONS</li> <li>• MAINTENANCE PLAN</li> <li>• NEW STRATEGIES</li> <li>• ACCIDENT REPORT</li> </ul>

Figure 2: General Model of Protection against Attacks.

3.1. General Model of Protection against Attacks

According to what is specified in the methods section, a protection model was defined to minimize attacks and protect information, it was segmented into three levels; the basic level has the essential measures in to secure the information; the standard level has the measures that every organization must have to increase the level of security of the organization; the optimized level has robust measures against cyberattacks. Figure 2 presents the tasks of each model process.

The model describes vertically the scope of each level that can be applied in a small, medium or large organization in order to prevent or mitigate these attacks; only one level can be applied at a time that allows to control the security of the information in the processes, systems and infrastructure depending on the organization for its economy and development; horizontally there are the phases to identify, protect, detect and recover when there is a threat of attack in the organization; These phases should be applied progressively until reaching the optimum level to ensure the information security of organizations.

3.2. Prototype of a Network

In accordance with what is specified in the methods section, a general prototype of a network was proposed to control the arrival of abnormal requests that are hidden in other legitimate requests and want to reach web servers, applications, mail or transfers; implementing security layers such as ACL that control access to our network allows us to have these levels of greater security; as observed in the following network proposal, it is desired to limit and control access to the network obtaining a high degree of security preventing one of the modalities of denial of service attacks that arrive from the internet or the organization's intranet.

Figure 3 submit the prototype proposal separating in a DMZ the servers that provide services with the local network of the organization, for the security of the database servers a firewall will be used who will control the access by port and IP requirement.

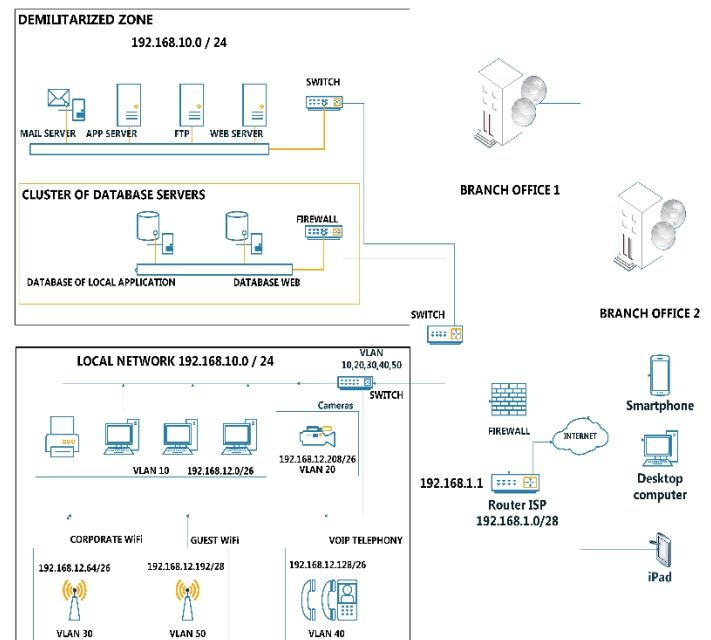


Figure 3: Prototype of a network.

Specifications of proposed network:

Router: 2 WAN interfaces, 2 LAN ports, Link redundancy protocol, Routing protocol

Firewall: UTM policy compliance (Unified Threat Management), 8 LAN ports, 1 WAN port, UTM requirements (statistic, risk threats, security policies by heuristic analysis), manageable by SNMP

Switch: layer 2 manageable by SNMP, with VLAN management, 24 ports, security management MAC

Through the firewall the separation of traffic towards the DMZ and LAN is defined

VLANs are defined in switch, the ports are from the trunk mode to firewall and VLAN is brought to firewall; ports are defined in access mode; VLAN is interconnected in the firewall and security policies are defined by application, port and physical interface or logical interface; each subnet is defined in a different VLAN to separate the traffic flows.

Phase 1, Traffic analysis: The analysis was focused on unusual traffic to detect anomalies with adoption of Packet Sniffing Sensor.

Phase 2, Traffic filtering: Packet filtering controls access to network by analyzing incoming, outgoing or transferring packets.

Phase 3, Passage of legitimate traffic: To identify all illegitimate IP packets and pass legitimate IP packets, after phase 2 there may be malicious traffic.

Figure 4 expresses the algorithm in flowchart, then the steps of each phase are recorded.

The algorithm must be applied before entering the DMZ, as a greater protection of services that the organization provides to citizens.

Algorithm:

Star

Phase 1: Traffic analysis

Monitor total traffic, web traffic, mail traffic, file transfer, traffic infrastructure, remote control, other UDP and TCP traffic.

Phase 2: Traffic filtering

Obtain the source IP address of package

Obtain the Access Control Entry

Compare the direction with those of ACE sequentially If it matches IP address with ACE entry then allow the packet else deny the packet

Phase 3: Passage of legitimate traffic

About traffic, check the characteristics of:

Time of permanence

Sources of non-frequent locations

One website per session

New users

End

### 3.4. Formula of probability of attack arrival

To obtain a formula of probability and arrival of the attack it was proposed to adopt the Poisson Distribution because it specializes in the probability of occurrence of abnormal or rare events, number of results occur in an interval, probability that more than one result occurs in a range is insignificant.

Equation (1) determines the average rate of requests in a time interval

$$\lambda = \frac{\text{requests}}{\text{time}} \quad (1)$$

Here:

$\lambda$  = average request rate

requests = number of requests

time = time interval in seconds

Equation (2) is Poisson distribution that offers continuity in the requests, the probability of a request is the same in all intervals and the arrival of one request does not affect the others.

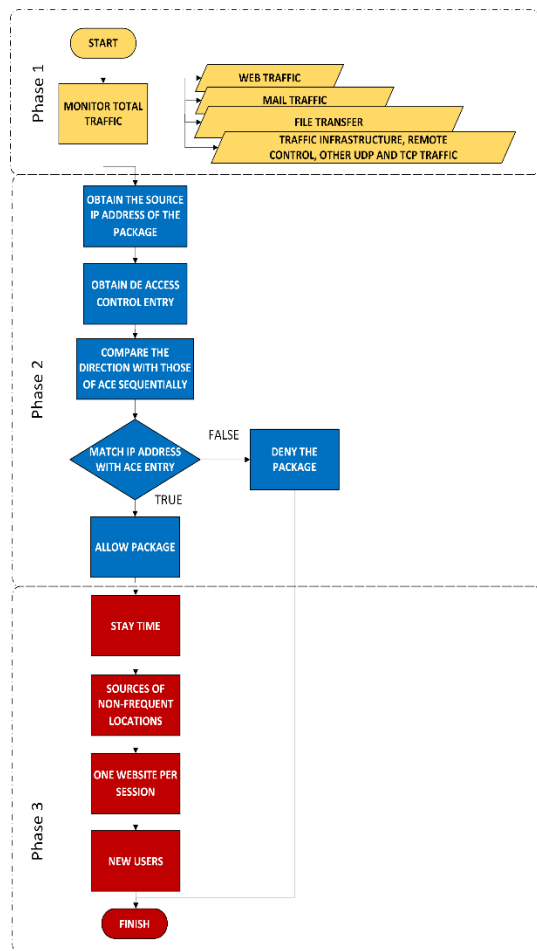


Figure 4: Proposed algorithm expressed in flowchart.

### 3.3. Algorithm in flowchart to minimize the attack arrival

The sequence of steps that the flowchart technique uses to obtain the algorithm specified in methods is expressed. To help minimize an attack due to the amount of traffic to network, the following algorithm was proposed, which has three phases:

Description of the phases:

$$P(k) = \frac{\lambda^k e^{-\lambda}}{k!} \quad (2)$$

Here:

$e = 2.7182818$

$k =$  attacks per unit of time

Description of the method used:

The parameter  $\lambda$  is taken because the client platforms make a number of requests for services in a time interval to server; the requests are the demand to some platform that provides services. The parameters  $k$  are the false requests to server in a unit of time, these requests are also demands towards the offering platform. With this formula we obtain a rate of occurrence of legitimate and not legitimate requests addressed to server.

The simulation was given in a time interval of 60 seconds, Figure 5 shows the taking of four numbers of applications (600, 900, 1200, 2400) where the average rates are ( $\lambda = 10, \lambda = 15, \lambda = 20, \lambda = 40$ ); for each  $\lambda$  there are 20 attack attempts ( $k = 1, 2, 4 \dots 40$ ). The intersection of attack attempts on the X-axis with the average rates generates the probability of arrival of the attack on the Y-axis.

In cases that  $\lambda=10$  and number of requests is 600, when the number of attacks is 10 the attack arrival is 12.51%; when the number of attacks is 20 the attack arrival is 0.19%; when the number of attacks is 30 the attack arrival is 0.000017%.

In cases that  $\lambda=20$  and number of requests is 1200, when the numbers of attacks is 10 the attack arrival is 0.581631%; when the number of attacks is 20 the attack arrival is 8.88%; when the number of attacks is 30 the attack arrival is 0.834354%; when the number of attacks is 40 the attack arrival is 0.002778%.

In cases that  $\lambda=40$  and number of requests is 2400, when the number of attacks is 10 the attack arrival is 0.000001%; when the number of attacks is 20 the attack arrival is 0.0192%; when the number of attacks is 30 the attack arrival is 1.84%; when the number of attacks is 40 the attack arrival is 6.29%.

when the number of requests is higher the percentage of attack arrival drops because it would already be within the system; another behavior is to have high requests and high number of attacks, here the attack success is also high.

From the simulation, the highest attack arrival value was 12.51%, it was deduced that the proposal has an attack detection accuracy is 87.49%.

In the model when the average request rate rises, the number of requests to the server and the number of attacks decreases the probability of arrival of the attack to the server; the number of attacks is inversely proportional to the arrival of attacks; in other words by increasing attacks on the server, the model increases its efficiency.

#### 4. Discussion

- This proposal is a model to minimize the cyberattack in public organizations of countries with similar cultures in Latin America; there is still a need to mature and increase security levels against denial of service attacks, at the moment it is 51%[6].
- The proposed research is related to the results with the following references: in [8] a management and monitoring architecture was defined through software to filter attacks; in [9] an algorithm of classification of the characteristics in the attacks was used; in [21] security levels were defined to prevent attacks; in [22] a set of policies for storage and data security was applied; in [27] a package registration procedure was used to minimize the denial of service in the network; in [29] the application of security policy and user control was used; in [30] an attack mitigation algorithm was used when entering ip addresses and invalid requests; in [32] the detection of attacks in the request and delivery messages was analyzed; in [33] and [34] they defined an architecture to detect attacks on the server and analysis of network traffic; in [37] analyzed a responsibility approach and rules to minimize individual and community risks; in [39] a security policy was applied to computer equipment.
- As exceptions there are issues that should be improved as Cyber Threat Socialization, Threat Tracking, Threat Intelligence and processes to manage attacks and incidents.

As theoretical consequences of this proposal are the denial of attacks, greater protection and security, which are set out below:

Attacks: With the proposed model through identification, defense, identification and recovery, it is intended to apply levels against attack regardless of the size of the organization; the hardware named in the network architecture minimizes the possible denial of services; The algorithm proposed in phases monitors the information or requests that are intended to damage the services.

Protection: The model proposed gives a higher level of defense against attacks that can be executed, faster and more effective reaction; network proposal is a hardware standard that many organizations can implement to protect the services delivered to

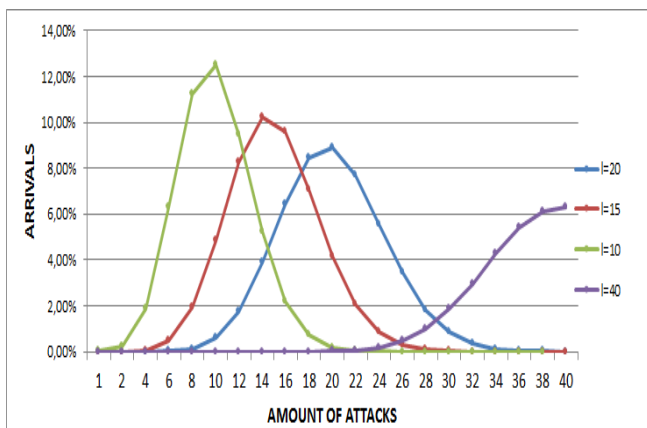


Figure 5: Probability of attack arrival.

It was observed that in a period of 60 seconds in the requests made to server; with low number of requests the percentage of attack arrival is low; when the number of requests grows there are also more hidden attacks that would be successful in their arrival;

citizens; The algorithm performs the analysis, filtering and passing of requests or legitimate information towards the services.

Security: The model provides confidence against attacks to apply in organizations with little or a lot of plant personnel, the activities of the model are independent of the infrastructure of an organization; the network proposal also gives confidence for the characteristics of the equipment to be used; The formula applied to calculate the effectiveness of the algorithm demonstrates a low arrival of attacks.

## 5. Future work and conclusions

As future work, a common policy model is foreseen to increase the security of digital services and prevent cyberattacks in public organizations.

- It was concluded that in order to maintain the continuity of services and activities of public organizations, secure platforms must be in place to monitor and minimize possible attacks; our proposal has an attack detection accuracy of 87.49%.
- ICTs allow the efficient delivery of public services, it is important to adopt a security strategy for normal performance of infrastructure and services of public organizations.
- Cyberattacks can have consequences on strategic, general and specific objectives; in order to meet social objectives, computer services are used, and it is necessary to be prepared for a possible attack.

## Conflict of Interest

The authors declare no conflict of interest.

## Acknowledgment

The authors thanks to Universidad Politécnica Salesiana del Ecuador, to the research group of the Guayaquil Headquarters "Computing, Security and Information Technology for a Globalized World" (CSITGW) created according to resolution 142-06-2017-07-19 and Secretaría de Educación Superior, Ciencia, Tecnología e Innovación (Senescyt).

## References

[1] Y. Guan and X. Ge, "Distributed Attack Detection and Secure Estimation of Networked Cyber-Physical Systems Against False Data Injection Attacks and Jamming Attacks," *IEEE Trans. Signal Inf. Process. over Networks*, vol. 4, no. 1, pp. 48–59, 2018.

[2] S. Gupta, S. Vashisht, and D. Singh, "A CANVASS on cyber security attacks and countermeasures," *2016 1st Int. Conf. Innov. Challenges Cyber Secur. ICICCS 2016*, no. Iciccs, pp. 31–35, 2016.

[3] H. S. Castro, "The right to privacy and state intervention in the digital age," *Publ. Univ. Netw. Hum. Rights Democr. Lat. Am.*, pp. 73–93, 2015.

[4] G. A. Bustamante, J. R. Rivera, and S. S. Cañas, "Cyber defense as part of the South American integration agenda," *Línea Sur*, vol. 9, no. March 2016, pp. 100–116, 2015.

[5] Organization of American States, "Are We Ready in Latin America and the Caribbean," p. 193, 2016.

[6] Deloitte, "Cyber Risks and Information Security in Latin America & Caribbean Trends," *Risk Advis.*, 2019.

[7] Verizon, "2019 Data Breach Investigations Report," *Verizon Bus. J.*, vol. 2018, no. 1, pp. 1–60, 2018.

[8] F. Ahmadloo and F. R. Salmasi, "A cyber-attack on communication link in distributed systems and detection scheme based on H-infinity filtering,"

*Proc. IEEE Int. Conf. Ind. Technol.*, pp. 698–703, 2017.

[9] M. S. Abdullah, A. Zainal, M. A. Maarof, and M. Nizam Kassim, "Cyber-Attack Features for Detecting Cyber Threat Incidents from Online News," *Proc. 2018 Cyber Resil. Conf. CRC 2018*, pp. 1–4, 2019.

[10] P. J. Shinde and M. Chatterjee, "A Novel Approach for Classification and Detection of DOS Attacks," *Biomed. Res.*, vol. 2016, pp. S22–S30, 2016.

[11] S. M. T. Toapanta, L. E. M. Gallegos, F. G. M. Quimi, and J. A. O. Trejo, "Analysis of efficient processes for optimization in a distributed database," *CITS 2018 - 2018 Int. Conf. Comput. Inf. Telecommun. Syst.*, pp. 1–4, 2018.

[12] S. M. T. Toapanta, M. A. M. Anchundia, L. E. G. Mafia, and J. A. T. Orizaga, "Biometric systems approach applied to a conceptual model to mitigate the integrity of the information," *CITS 2018 - 2018 Int. Conf. Comput. Inf. Telecommun. Syst.*, 2018.

[13] L. Mertz, "Cyberattacks on Devices Threaten Data and Patients: Cybersecurity Risks Come with the Territory. Three Experts Explain What You Need to Know," *IEEE Pulse*, vol. 9, no. 3, pp. 25–28, 2018.

[14] A. Kott, J. Ludwig, and M. Lange, "Assessing Mission Impact of Cyberattacks: Toward a Model-Driven Paradigm," *IEEE Secur. Priv.*, vol. 15, no. 5, pp. 65–74, 2017.

[15] I. Stelios, P. Kotzanikolaou, M. Psarakis, C. Alcaraz, and J. Lopez, "A survey of iot-enabled cyberattacks: Assessing attack paths to critical infrastructures and services," *IEEE Commun. Surv. Tutorials*, vol. 20, no. 4, pp. 3453–3495, 2018.

[16] C. G. Akcora, J. Z. Bakdash, Y. R. Gel, M. Kantarcioglu, L. R. Marusich, and B. Thuraisingham, "Attacklets: Modeling high dimensionality in real world cyberattacks," *2018 IEEE Int. Conf. Intell. Secur. Informatics, ISI 2018*, pp. 55–57, 2018.

[17] I. Perera, J. Hwang, K. Bayas, B. Dorr, and Y. Wilks, "Cyberattack Prediction Through Public Text Analysis and Mini-Theories," *Proc. - 2018 IEEE Int. Conf. Big Data, Big Data 2018*, pp. 3001–3010, 2019.

[18] Y. Zhou, M. Han, L. Liu, J. S. He, and Y. Wang, "Deep learning approach for cyberattack detection," *INFOCOM 2018 - IEEE Conf. Comput. Commun. Work.*, pp. 262–267, 2018.

[19] K. K. Nguyen, D. T. Hoang, D. Niyato, P. Wang, D. Nguyen, and E. Dutkiewicz, "Cyberattack detection in mobile cloud computing: A deep learning approach," *IEEE Wirel. Commun. Netw. Conf. WCNC*, vol. 2018-April, pp. 1–6, 2018.

[20] O. Oksiuk, L. Tereikovska, and I. Tereikovskiy, "Adaptation of the neural network model to the identification of the cyberattacks type 'denial of service,'" *14th Int. Conf. Adv. Trends Radioelectron. Telecommun. Comput. Eng. TCSET 2018 - Proc.*, vol. 2018-April, pp. 502–505, 2018.

[21] R. Sabillon, V. Cavaller, J. Cano, and J. Serra-Ruiz, "Cybercriminals, cyberattacks and cybercrime," *2016 IEEE Int. Conf. Cybercrime Comput. Forensic, ICCCF 2016*, pp. 1–9, 2016.

[22] D. Polverini, F. Ardente, I. Sanchez, F. Mathieux, P. Tecchio, and L. Beslay, "Resource efficiency, privacy and security by design: A first experience on enterprise servers and data storage products triggered by a policy process," *Comput. Secur.*, vol. 76, pp. 295–310, 2018.

[23] P. Black, I. Gondal, and R. Layton, "A survey of similarities in banking malware behaviours," *Comput. Secur.*, vol. 77, pp. 756–772, 2018.

[24] K. Pipyros, C. Thraskias, L. Mitrou, D. Gritzalis, and T. Apostolopoulos, "A new strategy for improving cyber-attacks evaluation in the context of Tallinn Manual," *Comput. Secur.*, vol. 74, pp. 371–383, 2018.

[25] H. S. Lallie, K. Debattista, and J. Bal, "Evaluating practitioner cyber-security attack graph configuration preferences," *Comput. Secur.*, vol. 79, pp. 117–131, 2018.

[26] M. Gratian, S. Bandi, M. Cukier, J. Dykstra, and A. Ginther, "Correlating human traits and cyber security behavior intentions," *Comput. Secur.*, vol. 73, pp. 345–358, 2018.

[27] A. Y. Nur and M. E. Tozal, "Record route IP traceback: Combating DoS attacks and the variants," *Comput. Secur.*, vol. 72, pp. 13–25, 2018.

[28] K. A. Molinaro and M. L. Bolton, "Evaluating the applicability of the double system lens model to the analysis of phishing email judgments," *Comput. Secur.*, vol. 77, pp. 128–137, 2018.

[29] S. Furnell, W. Khern-am-nuai, R. Esmael, W. Yang, and N. Li, "Enhancing security behaviour by supporting the user," *Comput. Secur.*, vol. 75, pp. 1–9, 2018.

[30] D. S. N. Mary and A. T. Begum, "An Algorithm for Moderating DoS Attack in Web based Application," pp. 26–31, 2017.

[31] R. Maciel, J. Araujo, J. Dantas, C. Melo, E. Guedes, and P. Maciel, "Impact of a DDoS attack on computer systems: An approach based on an attack tree model," *12th Annu. IEEE Int. Syst. Conf. SysCon 2018 - Proc.*, pp. 1–8, 2018.

[32] N. Tripathi, N. Hubballi, and Y. Singh, "How Secure are Web Servers? An empirical study of Slow HTTP DoS attacks and detection," *Proc. - 2016 11th*



*Int. Conf. Availability, Reliab. Secur. ARES 2016*, pp. 454–463, 2016.

- [33] V. Katkar, A. Zinjade, S. Dalvi, T. Bafna, and R. Mahajan, "Detection of DoS/DDoS attack against HTTP servers using naive Bayesian," *Proc. - 1st Int. Conf. Comput. Commun. Control Autom. ICCUBE 2015*, pp. 280–285, 2015.
- [34] Sornalakshmi.K, "Detection of DoS attack and Zero Day Threat with SIEM," pp. 1–7, 2017.
- [35] N. E. Herald and M. W. David, "A Framework for Making Effective Responses to Cyberattacks," *Proc. - 2018 IEEE Int. Conf. Big Data, Big Data 2018*, pp. 4798–4805, 2019.
- [36] E. N. Yılmaz and S. Gönen, "Attack detection/prevention system against cyber attack in industrial control systems," *Comput. Secur.*, vol. 77, pp. 94–105, 2018.
- [37] K. Renaud, S. Flowerday, M. Warkentin, P. Cockshott, and C. Orgeron, "Is the responsabilization of the cyber security risk reasonable and judicious?," *Comput. Secur.*, vol. 78, pp. 198–211, 2018.
- [38] R. AlShboul, F. Thabtah, N. Abdelhamid, and M. Al-diabat, "A visualization cybersecurity method based on features' dissimilarity," *Comput. Secur.*, vol. 77, pp. 289–303, 2018.
- [39] K. Adi, L. Hamza, and L. Pene, "Automatic security policy enforcement in computer systems," *Comput. Secur.*, vol. 73, pp. 156–171, 2018.
- [40] D. Mitropoulos, P. Louridas, M. Polychronakis, and A. D. Keromytis, "Defending Against Web Application Attacks: Approaches, Challenges and Implications," *IEEE Trans. Dependable Secur. Comput.*, vol. 16, no. 2, pp. 188–203, 2019.
- [41] M. E. Ahmed, S. Ullah, and H. Kim, "Statistical Application Fingerprinting for DDoS Attack Mitigation," *IEEE Trans. Inf. Forensics Secur.*, vol. 14, no. 6, pp. 1471–1484, 2019.
- [42] A. Bhadane and S. B. Mane, "Detecting lateral spear phishing attacks in organisations," *IET Inf. Secur.*, vol. 13, no. 2, pp. 133–140, 2019.
- [43] S. Dong, K. Abbas, and R. Jain, "A Survey on Distributed Denial of Service (DDoS) Attacks in SDN and Cloud Computing Environments," *IEEE Access*, vol. 7, pp. 80813–80828, 2019.
- [44] G. Aranda et al., "BWManager: Mitigating Denial of Service Attacks in Software-Defined Networks Through Bandwidth Prediction," *IEEE Trans. Netw. Serv. Manag.*, vol. 15, no. 4, pp. 1235–1248, 2018.
- [45] FBI, "FBI 2018 Internet Crime Report," pp. 1–28, 2018.
- [46] S. Pournouri, S. Zargari, and B. Akhgar, "An Investigation of Using Classification Techniques in Prediction of Type of Targets in Cyber Attacks," *Proc. 12th Int. Conf. Glob. Secur. Saf. Sustain. ICGS3 2019*, pp. 202–212, 2019.



## Lead Bioaccumulation in Root and Aerial Part of Natural and Cultivated Pastures in Highly Contaminated Soils in Central Andes of Peru

Jorge Castro Bedriñana<sup>\*1</sup>, Doris Chirinos Peinado<sup>1</sup>, Richard Peñaloza-Fernández<sup>2</sup>

<sup>1</sup>Universidad Nacional del Centro del Perú (UNCP), Huancayo, Peru

<sup>2</sup>Universidad Nacional Agraria La Molina, Peru

### ARTICLE INFO

Article history:

Received: 21 November, 2019

Accepted: 25 February, 2020

Online: 09 March, 2020

Keywords:

Heavy metals

Smelting

Soil

Pastures

Transfer factor

Particulate material

### ABSTRACT

Lead concentration on surface soil (0-20 cm), root and aerial part of natural and cultivated pastures were evaluated, in the rainy season (March 2018), collected in 20 sites of a rural community located 20 km from the La Oroya metallurgical complex, which has been emitting to the environment particulate material with heavy metals since 1922. Lead concentration was determined by flame atomic absorption spectrometry. The data was statistically processed in SPSS 23. Lead levels in the soil, root and aerial part of the cultivated pastures were  $224.75 \pm 39.41$ ,  $169.13 \pm 58.79$  and  $20.73 \pm 2.52$  mg / kg ( $p < 0.01$ ). In natural pastures values were  $210.87a \pm 40.37$ ,  $184.36b \pm 52.66$  and  $19.47c \pm 3.12$  mg / kg ( $p < 0.01$ ). There are no differences between cultivated and natural pastures. Lead transfer factor from soil to root of cultivated and natural pastures was 0.75 and 0.87. Lead transfer factor value from soil to aerial part of cultivated and natural pastures was 0.092 in both. High lead content in soil and aerial part of the pastures used as food for high Andean cattle is a public health problem; livestock products produced in these soils would not be fit for human consumption.

### 1. Introduction

The important mining activity for Peru [1] involves the emission of particulate matter (PM) loaded with heavy metals, which are transported by air [2] and deposited in water and soil, then transferred to pastures, causing adverse effects on animals and human health [3-6].

Lead soil contamination affects its quality, destroys the power of self-purification through biological regeneration, decreases the normal growth of soil microorganisms, alters biodiversity and decreases crop yields [7].

Due to the long half-life and high potential for bioaccumulation, lead is available to grass roots causing damage to the same plant [8] generating a highly contaminated biomass with serious consequences for human health [9-13]. Lead (Pb) toxicity affects the central nervous system, cardiovascular, digestive and urogenital system, and causes different types of cancer [14-16].

The Pb absorption is affected by the concentration of other metals, pH and organic matter content [17] and bioaccumulation of chemical elements in plants depends on their concentrations in soil [10]. Bioaccumulation of toxic heavy metals pose a threat to human health, induce renal tumors, reduce cognitive, development, and increase blood pressure and cardiovascular diseases risk for adults [18, 19].

The transfer factor (TF), is the relationship between the concentration of metal in the aerial part of the plant and that of the soil [20, 21]. The TF quantifies the metal bioavailability and is an indicator of the extent of metal mobility [20, 22]. The TF is the key parameter of the heavy metal accumulation in plants, because it is the main pathway of human exposure to soil contamination by heavy metal accumulation [20].

Poly-metallic transformation of copper, zinc, silver, lead, indium, bismuth, gold, selenium, tellurium and antimony, emits toxic substances into the environment polluting the ecosystem [23].

In the central region of Peru, for more than 90 years, soils have been contaminated by metallurgical emissions of fine particulate

<sup>\*</sup>Jorge Castro-Bedriñana, Av. Mariscal Castilla 3909, El Tambo-Huancayo, +51 964408057 & jorgecastro@yahoo.com

material, rich in lead and other heavy metals [24], which have been deposited in the soil and they are available for plants [25, 26, 17]; in this case, Pb bioaccumulates in the pastures consumed by cattle, sheep and South American camelids.

Analysis of the soil surface layer (between 0 to 20 cm) will provide valuable information to study the dynamics of contamination of Pb from soil to plant [27].

A main activity of families living in Andean communities located near the metallurgical complex is the raising of sheep, alpacas and cows in large areas of natural pastures, and there is no information on the lead content of pastures consumed by these high Andean cattle.

This research contributes information on the soil-root-plant relationship, by determining the concentration of Pb in soil, root and natural and cultivated pastures and their transfer factors (Figure 1), contrasting the content of Pb in soil and grass of the study with levels of environmental quality safety [28, 29].

Results represent the most up-to-date cut in the content of Pb in the surface soil and pastures of a highly contaminated area of the central highlands of Peru. This information can be used to establish a better regulation of environmental and human health protection by Pb contamination.

Figure 1 shown the sequence of the pasture contamination by heavy metals. Self-created model

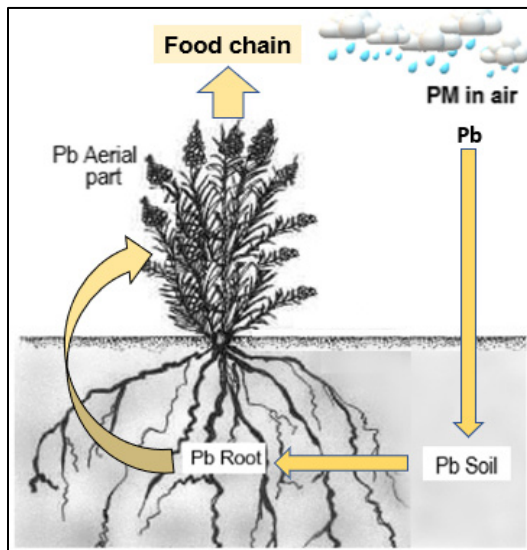


Figure 1: Sequence of pasture contamination by lead from metallurgical emissions. PM: Particulate Material (with heavy metal and other pollutants)

## 2. Materials and methods

### 2.1. Study area

Peasant community "Purísima Concepción de Paccha" (CCP-LO), of Yauli province, Junín-Peru, is situated between South Latitude  $11^{\circ} 31' 03''$  and West Longitude  $75^{\circ} 53' 58''$  (altitude 3,700) and located 10.2 km from metallurgical complex La Oroya (Figure 2), industry dedicated to poly-metallic transformation (copper, zinc, silver, lead, indium, bismuth, gold, selenium, tellurium and antimony), that emits fine particulate material (PM), loaded with heavy metals that pollute the ecosystem for more than nine

decades [23, 24]. PM rich in Pb and other heavy metals is deposited in the soil and water resources, and being easy transferred to the plants [25, 26, 17]. Figure 2 shown the geographical location o the CCP-LO.

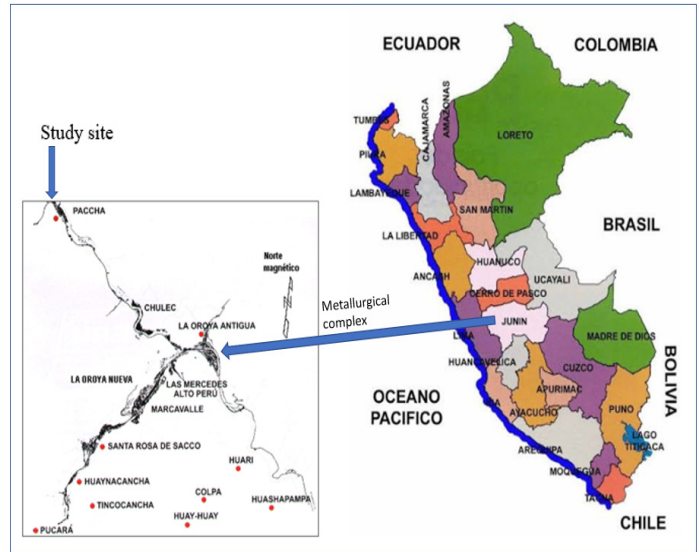


Figure 2. Geographical location of the peasant community of Paccha, study site

Sampling of soil, root and aerial part of natural and cultivated pastures was carried out in the rainy season (November to March 2018). These pastures are used to feed high Andean cattle (sheep>alpacas>cows). Natural grasses are mainly composed of *Festuca dolichophylla*, *Piptochaetium faetertonei*, *Bromus catharticus*, *Bromus lanatus* and *Calamagrostis heterophylla*, and small extensions of cultivated pastures associated with *Lolium perenne* and *Trifolium repens*. CCO-LO has approximately 6000 ha of communal land with natural pastures (NP) and six hectares of cultivated pastures (CP), distributed in different grazing sites to feed sheep, cows and alpacas. CP in study site was installed 15 years ago. The productive and nutritional quality of both pastures is poor.

Quantification of lead in samples soil, root and aerial part of the plants were carried out in the Baltic Control SAC Laboratory, accredited by the National Institute of Quality - INACAL, Peru.

### 2.2. Sample collection

The soil and grass samples collected for the study approximately correspond to 1 ha of natural pastures (NP) and 1 ha cultivated pastures (CP) (Figure 3).

In March 2018 (rainy season), a total of 60 samples were taken (20 parallel samples of soil, root and aerial part of natural and cultivated pastures, 10 samples for each pasture type) at twenty-five-meter zigzag intervals. Samples were taken from upper soil layer (0-20 cm) [30, 31,32] of 1 ha of NP and 1 ha of CP near the CCP-LO stable (Figure 3). Five random subsamples taken of approximate area of  $1m^2$  were mixed until 0.5 kg soil sample was completing in a polythene bag and then taken to the laboratory. Soil samples were air dried for 48 hours, and then sieved with 2 mm mesh to remove gravel, stone and other materials prior to analysis. Sample collection details are provided in [27, 33].

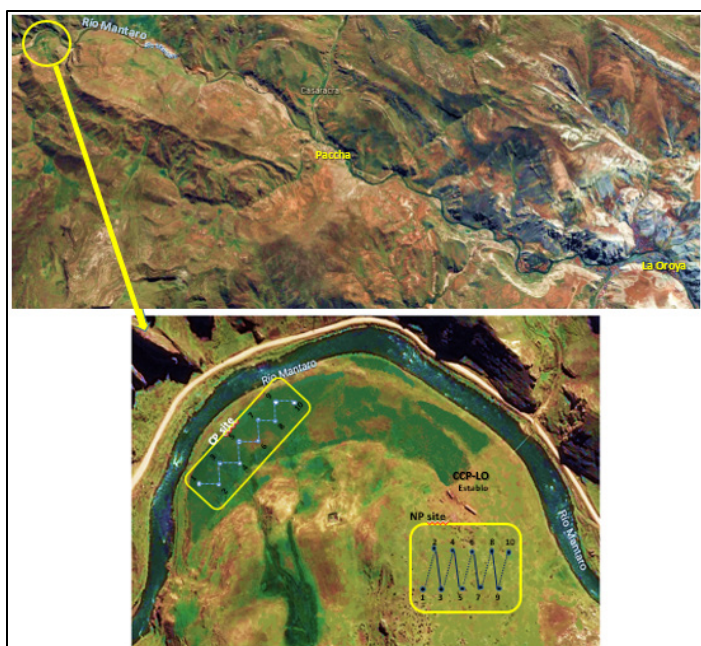


Figure 3. Soil and pasture sampling sites in CCP-LO. The image above is the map of the Paccha-Junin district, and shows the road from the city of La Oroya to Paccha; The bottom image is the sampling sketch in natural and cultivated pastures areas (NP n = 10; CP n = 10). La Oroya city is located 183.4 km from Lima (Capital of Peru) by the central highway. There is located the polymetallic metallurgical complex. Paccha District is located 10.2 km from La Oroya, and the "Comunidad Purísima Concepción de Paccha" (CCP-LO), where the cow stable is located, is approximately 40 minutes away by road. CCP-LO is characterized by its high altitude (3900-4500) and low temperatures (-3°C to 11°C). Community population: 315 families.

The forage samples were collected from the same place where soil samples were collected and on which the cows were grazing. The forage samples were divided into root and aerial part [33] and placed in paper bags to take to the laboratory.

### 2.3 Lead concentration quantification

For sample digestion according to USEPA method 3050B (SW-846) to extract the metals, 1 gram of the dried sieved soil was digested with repeated additions of concentrated nitric acid (HNO<sub>3</sub>) and hydrogen peroxide (H<sub>2</sub>O<sub>2</sub>). Hydrochloric acid (HCl) was added to the initial digestate and the sample is refluxed. The digestate was diluted to a final volume of 100 mL [34]. Lead concentration was determined by flame atomic absorption spectrometry (FLAA), following the AOAC-Official Method 975.03 protocol [35]. Analysis were in duplicate and the lead concentration units are expressed in mg / kg. To determine the concentration of Pb in the roots and aerial part of the pastures the same analysis procedure was followed.

Summary process:

1. Homogenize and eliminate foreign material
2. Sift the sample 2mm.
3. Dry the sample in an oven (30-35 °C / 4h)
4. Bag the subsamples.
5. Weigh 1 g of the sample and transfer to a 250 mL beaker.
6. Add 10 mL of HNO<sub>3</sub> (1: 1) and heat without boiling at 95 + -5 °C for 15 min.
7. Add 5 mL of HNO<sub>3</sub> (cc) until a complete reaction is achieved and concentrate up to 5 mL.

8. Add 2 mL of water and 3 mL HCl (minimum effervescence) and concentrate up to 5 mL
9. Filter and refine at a 100 mL vial. Apply the quality controls of the sample.
10. Calibration curve building and analysis the sample by flame atomic absorption spectroscopy (FLAA).
11. Report results in units of mg / kg.

Quality Control: Method blank (BK), Duplicate Sample (DM) and Control Pattern (PC) were performed in high and low range for every 15 samples. For the calibration curve, Pb Sigma-Aldrich 986 + -4 mg / kg was used as standard. In addition, the Pb detection limit was 0.2 mg/kg.

### 2.4 Statistical analysis

Information was processed in SPSS 23. Descriptive statistics were used and variance analyzes were conducted for lead contents in the soil, root and aerial part of the plant, with Tukey significance tests at a confidence level  $P < 0.05$ . To determine the difference in means between Pb in soil and grass with the maximum permissible limits, "t" tests were performed for a single sample. Maximum limits used for soil and grass were 70 and 30 mg / kg.

## 3. Results

### 3.1 Lead concentration in the soil, root and aerial part of pastures

The Pb concentrations in descending order were soil > root > grass ( $p < 0.01$ ). The data had normal distribution patterns. There were no statistical differences between natural pastures (NP) and cultivated pastures (CP) (Table 1, Figures 1, 2).

Table 1. Pb concentration in soil, root and aerial part of PN and PC in livestock area near the La Oroya Metallurgical Complex (mg / kg)..

Lead content	Average	Standard Deviation	Variance	Min.	Max.
PN soil	210.87a	40.37	1629.45	131.76	264.92
PC soil	224.75a	39.41	1553.38	171.12	284.13
PN root	184.37b	52.66	2773.48	102.92	251.49
PC root	169.13b	58.79	3456.45	102.73	263.61
Aerial part-PN	19.46c	3.12	9.75	14.55	23.81
Aerial part-PC	20.73c	2.51	6.32	16.65	23.88

Average values with different letters vary statistically ( $P < 0.05$ )

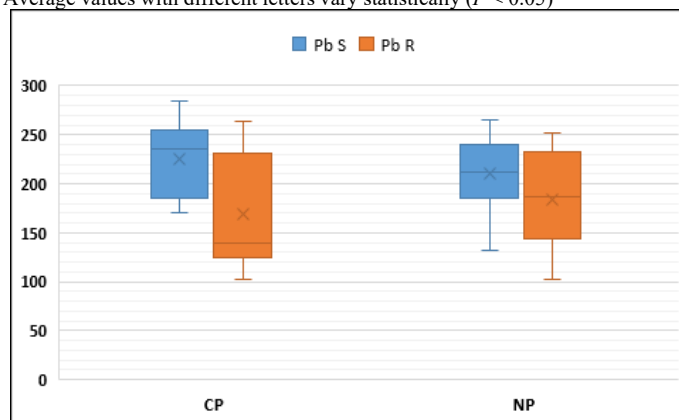


Figure 4. Pb content in the soil and root of cultivated and natural pastures (mg/kg)



Pb S: Soil Pb content, Pb R: Root Pb content, CP: Cultivated pastures, NP: Natural pasture

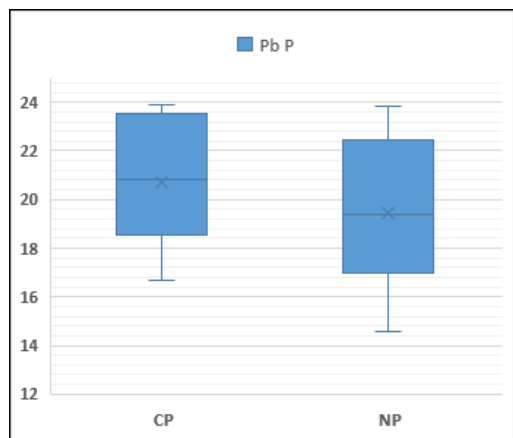


Figure 5. Pb content in aerial part of cultivated and natural pastures  
CP: Cultivated pastures, NP: Natural pasture

### 3.2 Transfer of Pb from soil to the root and aerial part of pastures

The transfer factors of soil Pb to the root of CP and NP were 0.75 and 0.87. The transfer factor of soil Pb to the aerial part of CP and NP was 0.092 for both.

In this study, the percentage of Pb transfer from the soil to the aerial part of the grasslands was 9.2% (Table 2, Figure 3), a percentage nine times higher than that reported in conditions of less pollution [9].

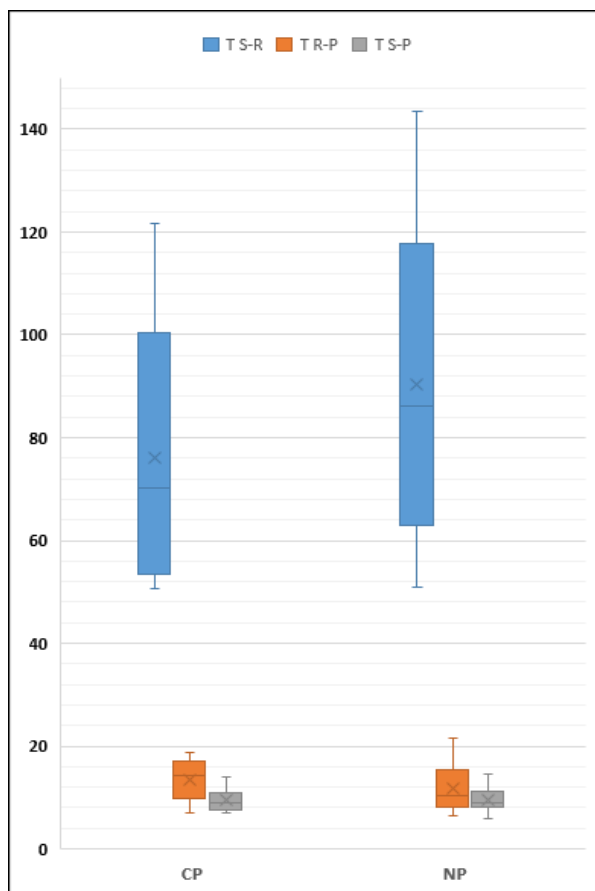


Figure 6. Pb transfer percentages in NP and CP sites

T S-R: Soil to root transference  
T R-P: Root to aerial parts transference  
T S-P: Soil to aerial part transference  
CP: Cultivated pastures, NP: Natural pasture

Table 2. Percentage of Pb transfer from soil to the root, and aerial part of NP and CP in livestock area near the La Oroya Metallurgical Complex (%)

Lead transfer	Average	Estándar Deviation	Variance	Min.	Max.
Soil-root, PN	90.29a	30.92	955.91	50.82	143.49
Soil-root, PC	76.01a	25.56	653.53	50.59	121.53
Root-aerial part, PN	11.68b	4.81	23.19	6.33	21.60
Root-aerial part, PC	13.43b	4.04	16.35	6.96	18.85
Soil-aerial part, PN	9.55c	2.43	5.92	5.93	14.60
Soil-aerial part, PC	9.51c	2.25	5.05	7.01	13.96

Average values with different letters vary statistically ( $P < 0.05$ ).

## 4. Discussion

La Oroya soils have received pollution since the metallurgical complex began operations in 1922, and has poured 0.39 Mt of Pb [36]. In 2008, in La Oroya and Paccha the average concentrations of PM<sub>2.5</sub> were 32.4 and 20.3  $\mu\text{g} / \text{m}^3$  [37], which exceed the ECA PM<sub>2.5</sub> = 15  $\mu\text{g} / \text{m}^3$  [38], and the average concentrations of PM<sub>10</sub> were 52.3 and 42.4  $\mu\text{g} / \text{m}^3$ , values similar to ECA PM<sub>10</sub> = 50  $\mu\text{g} / \text{m}^3$  [38]. At the end of the last century, in La Oroya-Yauli, average values of Pb in the air were reported exceeding the upper limit by 800% (1.5  $\mu\text{g} / \text{m}^3$ ). Between 2009 and 2014, reported Pb levels in air were up to three times more than upper limit [39,40].

Heavy metals contaminate water and soil, transfer and bioaccumulate in plants, and affect human and environmental health [25, 26].

Accumulated heavy metal contamination for decades in the study area would determine high concentrations of Pb in the soil, root and aerial part of NP and CP. The soils in the study area have more than 3 times of Pb than the maximum established in Peru (70 mg / kg) [28] and more than 3.5 times that established in Finland (60 mg / kg) [29]. It is reported that concentrations of Pb in the soil, between 10 and 30 mg / kg have no detrimental effects on plant growth [41].

Lead concentration in Paccha community soil is of high risk to human health, because it bioaccumulates in the crops produced. Excess Pb in soil affects its quality, microbial development and biodiversity [7] and in agri-food products it can cause a series of health problems [42-45].

Average concentration of Pb in NP and CP determined in this study (19.46 and 20.73 mg / kg), reflects accumulation of Pb over time, since the smelting began activities in 1922, as reported in other latitudes too [46]. High Pb content inhibits the absorption of all mineral elements in the plant [47], affects its performance [48], decreases food safety and quality, causing multiple adverse effects on human health [11,6,15,16].

In Caldas-Colombia, the Pb of soils adjacent to petrochemical activity is transferred and bioaccumulated in brachiaria crops, and the highest levels of Pb bioaccumulation have the following order: root> stem> leaves [25,26].

Average concentration of Pb in NP and CP in this study was 6.7 times higher than the critical value proposed by other researchers for vegetables 0.05-3.0 mg / kg [49]. Our results were similar than those observed in pastures areas near to La Oroya reported in a Missouri study [50]. The study soils have a high concentration of heavy metals compared to other parts of Peru and the world, which can lead to unwanted economic and social results.

Pb concentrations in NP and CP were similar and consistently higher than those observed in studies conducted in other latitudes [51,45]. This study shows that the bioaccumulation of Pb in the grass roots gives it control over its concentration in the aerial part of the grass. Of Pb concentration present in the soil, only 9.5% is transferred to the aerial pasture. Roots capture a large amount of Pb from the soil (> 83%), transferring 12% of Pb to the aerial part of the plant; However, concentration of Pb in the edible part of the pasture is a threat of toxicity to high Andean cattle, according to another research [52].

In areas near the refineries, Pb contents in 31 brachiaria species, is values between 9.8 and 16.0 mg / kg, being higher closer to the emission focus. In places around the exploration wells, Pb contents between 9.7 and 13.2 mg / kg are reported [25,26].

Average Pb in the pastures of the study area was lower than those recorded around sites containing lead slag in Nigeria, forage grasses had between 209-899 mg / kg, with an average of 425 ± 79.0 mg / kg [53].

Although the average Pb content in the aerial part of the pastures produced in the study area did not exceed the allowed limit of the European Union (30 mg / kg), it exceeds the normal range of 5-10 mg / kg recommended by other authors [54]. Considering as a limit value of Pb in pastures 10 mg / kg [54], the average of Pb in pastures of this study was 2 times higher, not being suitable for feeding cattle [55].

Regarding cultivated pastures, in *Trifolium alexandrinum*, *Brassica campestris* and *Avena sativa* associations, average concentrations of Pb was between 36.5 and 60.21 mg / kg [52], values higher than the European Union toxic level (30 mg / kg) [56], and those found in this study.

In New Zealand pastures, an average value of Pb is reported in grass (10.6 mg / kg) with a range of 4.4 to 26.8 mg / kg [27]; observing that the toxicity of Pb causes a decrease in the percentage of germination, growth, dry biomass of roots and shoots, alteration of mineral nutrition, reduction in cell division and inhibition of photosynthesis [43,57].

NP and CP increase the accumulated amount of Pb in the root to a higher Pb content in soil, as observed in another study [58]. Accumulation of Pb in the aerial part of the grass is also increased to a greater amount of Pb in soil and root. Comparing the results obtained in both types of pastures, the accumulated amounts of Pb in the roots and the aerial part were similar in NP and PC. In both types of pasture, the concentration of Pb in the roots was higher than that of the shoots, which suggests that the transport of lead from the roots to the shoots is restricted and the root maintains a high Pb content in its structure, and the cumulative amounts of lead in the aerial part of the plants were greater than those reported in other studies [58].

## 5. Conclusion

Pb concentration was significantly higher in the soil than in the root and aerial part of natural and cultivated pastures used in Andean livestock food -in areas close to metallurgical emissions.

Lead level in soil and grass exceeded the toxic levels suggested by national and international standards; So, the soils and pastures are intoxicated.

The information for the ecosystem studied is useful to take measures to reduce the adverse effects on human health by the consumption of food produced in these soils. This evidence should be used to establish action plans for removal and remediation.

## Acknowledgments

This study was funded by competitive funds from Canon, Sobrecanon y Regalías Mineras administered by the Universidad Nacional del Centro del Perú.

To the authorities of the Comunidad Campesina Purisima Concepción de Paccha-La Oroya, for the facilities in carrying out this study.

## Conflict of interest

All the authors declare that there is no conflict of interests regarding the publication of this manuscript.

## References

- [1] Osinergmin. La industria de la minería en el Perú: 20 años de contribución al crecimiento y desarrollo económico del país. Organismo Supervisor de la Inversión en Energía y Minería, 2017. [http://www.osinergmin.gob.pe/seccion/centro\\_documental/mineria/Documentos/Publicaciones/Osinergmin-Industria-Mineria-Peru-20años.pdf](http://www.osinergmin.gob.pe/seccion/centro_documental/mineria/Documentos/Publicaciones/Osinergmin-Industria-Mineria-Peru-20años.pdf).
- [2] Suvarapu LN, Baek SO. Determination of heavy metals in the ambient atmosphere: a review. *Toxicol. Ind. Health* 33, 79–96, 2017. <https://doi.org/10.1177/0748233716654827>.
- [3] Ogabiela EE, Udiba UU, Adesina OB, Hammuel C, Ade-Ajayi FA, Yebpella GG, Mmereole UJ, Abdullahi M. Assessment of metal levels in fresh milk from cows grazed around Challawa industrial Estate of Kano, Nigeria. *Journal of Basic and Applied Scientific Research*, 1(7): 533-538, 2011.
- [4] Castro J, Chirinos D, Tejada de Rivero D. Plomo en la sangre del cordón umbilical y su impacto sobre el peso, longitud, hemoglobina y APGAR en. *Revista de Toxicología*, 29(0212–7113):100-106, 2012.
- [5] Lovell A, Magee N, Nunez S, Mitt K. Biosorption and Chemical Precipitation of Lead Using Biomaterials, Molecular Sieves, and Chlorides, Carbonates, and Sulfates of Na & Ca. *Journal of Environmental Protection*, 4:1251–1257, 2013. <https://doi.org/10.4236/jep.2013.411145>.
- [6] President's Task Force, on Environmental, Health Risks and Safety, & Risks to Children. Key Federal Programs to Reduce Childhood Lead Exposures and Eliminate Associated Health Impacts, (November): 1–64, 2016. <https://portal.hud.gov/hudportal/documents/huddoc?id=FederalProgramUpdate.pdf>.
- [7] Rábago I. Capacidad de amortiguación de la contaminación por plomo y cadmio en suelos de la Comunidad de Madrid. Tesis Doctoral. Universidad Complutense de Madrid, 2010.
- [8] Nascimento SS, Silva EB, Alleoni LR, Graziotti PH, Fonseca FG, Nardis BO. Availability and accumulation of lead for forage grasses in contaminated soil. *Journal of Soil Science and Plant Nutrition*, 14 (4), 783-802, 2014.
- [9] Li Y, MCcrory DF, Powell JM, Saam H, Jackson-Smith D. A survey of selected heavy metal concentration in Wisconsin dairy feeds. *J. Dairy Sci.* 88, 2911, 2005
- [10] Grytsyuk N, Arapis G, Perepyatnikova L, Ivanova T, Vynograds'ka V. Heavy metals effects on forage crops yields and estimation of elements accumulation in plants as affected by soil. *Science of the Total Environment*, 354(2–3), 224–231, 2006. <https://doi.org/10.1016/j.scitotenv.2005.01.007>



- [11] Nava-Ruiz MA. Efectos neurotóxicos de metales pesados (cadmio, plomo, arsénico y talio). Arch Neurocién (Mex), 16(3), 140–147, 2011.
- [12] Castro J, Chirinos Peinado D, Ríos E. Lead content and placental weight and its association with gestational age, weight, length and hemoglobin in newborns of metallurgical region-Peru. Revista de Toxicología, 33(2), 2016.
- [13] Singh MK, Jha D, Jadoun J. Assessment of Physico-chemical Status of Groundwater Samples of Dholpur District, Rajasthan, India. International Journal of Chemistry, 4(4), 96–104, 2012. <https://doi.org/10.5539/ijc.v4n4p96>
- [14] Tchounwou P, Yedjou C, Patlolla A, DJS. Heavy Metals Toxicity and the Environment. NIH Public Access, (EXS. 2012; 101: 133–164, 2014. <https://doi.org/10.1007/978-3-7643-8338-1>.
- [15] Tepanosyan G, Maghakyan N, Sahakyan L, Saghatelian A. Heavy metals pollution levels and children health risk assessment of Yerevan kindergartens soils. Ecotoxicology and Environmental Safety, 142, 257–265, 2017. <https://doi.org/10.1016/j.ecoenv.2017.04.013>
- [16] Tepanosyan G, Sahakyan L, Belyaeva O, Maghakyan N, Saghatelian A. Human health risk assessment and riskiest heavy metal origin identification in urban soils of Yerevan, Armenia. Chemosphere, 184, 1230–1240, 2017. <https://doi.org/10.1016/j.chemosphere.2017.06.108>
- [17] Olayinka OO, Akande OO, Bamgbose K, Adetunji MT. Physicochemical Characteristics and Heavy Metal Levels in Soil Samples obtained from Selected Anthropogenic Sites in Abeokuta, Nigeria. J. Appl. Sci. Environ. Manage. Vol. 21 (5):883-891, 2017. DOI: <https://dx.doi.org/10.4314/jasem.v21i5.14>
- [18] Harmanescu M, Alda L, Bordean D, Gogoasa I, Gergen I. Heavy metals health risk assessment for population via consumption of vegetables grown in old mining area; a case study: Banat County, Romania. Chemistry Central Journal, 5(1), 64, 2011. <https://doi.org/10.1186/1752-153X-5-64>.
- [19] Rim-Rukeh A. Uptake of Heavy Metals by Okro (*Hibiscus Esculentus*) Grown on Abandoned Dump Sites in Effurun, Nigeria. Journal of Emerging Trends in Engineering and Applied Sciences (JETEAS) 3 (4): 640-644, 2012.
- [20] Papaioannou D, Kalavrouziotis IK, Koukoulakis PH, Papadopoulos F, Psoma P. Interrelationships of metal transfer factor under wastewater reuse and soil pollution. Journal of Environmental Management, 1–9, 2017. <https://doi.org/10.1016/j.jenvman.2017.04.008>.
- [21] Bu-Olayan AH, Thomas BV. Combined effects of particulates dispersion and elemental analysis in desert plants: a modeling tool to air pollution. International Journal of Environmental Science and Technology, 13(5), 1299–1310, 2016. doi:10.1007/s13762-016-0968-5.
- [22] Kachenco, A.G., Singh, B. Heavy metal contamination in vegetables grown in urban and metal smelter contaminated sites in Australia. Water Air Soil Pollut. 169, 101e123, 2006.
- [23] Alvarez-Berrios N, Campos-Cerqueira M, Hernández-Serna A, Delgado A, Román-Dañobeytia F. Impacts of small-scale gold mining on birds and anurans near the Tambopata Natural Reserve, Peru, assessed using passive acoustic monitoring. Tropical Conservation Science, 9(2), 832–851, 2016. <https://doi.org/10.1177/194008291600900216>.
- [24] Barrios-Napuri C. El desarrollo empresarial desde la perspectiva local. España: Red Académica Iberoamericana Local Global. Universidad de Málaga, 2008. <http://www.eumed.net/libros-gratis/2008b/403/index.htm>.
- [25] Peláez-Peláez MJ. Evaluación del estrés abiótico en *Brachiaria spp.* inducido por bioacumulación de cadmio y plomo, en una zona alejada al corredor petrolífero de Barrancabermeja (Colombia). Tesis Doctoral. Universidad Nacional de Colombia, 2016.
- [26] Peláez-Peláez MJ, Bustamante CJ, Gómez LE. Presencia de cadmio y plomo en suelos y su bioacumulación en tejidos vegetales en especies de *Brachiaria* en Magdalena medio colombiano. Revista.luna.azul. 43:82-101, 2016.
- [27] Martin AP, Turnbull RE, Rissmann CW, Rieger P. Heavy metal and metalloid concentrations in soils under pasture of southern New Zealand. Geoderma Regional 11,18–27, 2017. <https://doi.org/10.1016/j.geoder.2017.08.005>
- [28] MINAM. DS N°011-2017-MINAM. “Aprueban Estándares de Calidad Ambiental (ECA) para Suelo. Perú: El Peruano, 2017.
- [29] Ministry of the Environment, Finland. Government Decree on the Assessment of Soil Contamination and Remediation Needs 214/2007, March 1, 2007. Ministry of the Environment, Finland.
- [30] MINAM. Guía para muestreo de suelo, 72, 2014. <http://www.minam.gob.pe/calidadambiental/wp-content/uploads/sites/22/2013/10/GUIA-PARA-EL-MUESTREO-DE-SUELOS-final.pdf>
- [31] Li, F., Huang, J., Zeng, G. et al. Toxic metals in topsoil under different land uses from Xiandao District, middle China: distribution, relationship with soil characteristics, and health risk assessment. Environ Sci Pollut Res 22, 12261–12275, 2015. Doi:10.1007/s11356-015-4425-7
- [32] Li F, Zhang J, Huang J, Huang D, Yang J, Song Y, Zeng G. Heavy metals in road dust from Xiandao District, Changsha City, China: characteristics, health risk assessment, and integrated source identification. 2016. Environ Sci Pollut Res Int. 23(13):13100-13, 2016. Doi: 10.1007/s11356-016-6458-y
- [33] García-Gallegos E, Hernández-Acosta E. García-Nieto E, Acevedo-Sandoval O. Contenido y traslocación de plomo en avena (*Avena sativa* L.) y haba (*Vicia faba* L.) de un suelo contaminado. Revista Chapingo Serie Ciencias Forestales y del Ambiente 17(1):19-29, 2011. DOI: <https://doi.org/10.5154/r.chscfa.2010.02.002>.
- [34] EPA. Method 3050B: Acid digestion of sediments, sludges, and soils. Revision 2, 1996 <https://www.epa.gov/sites/production/files/2015-06/documents/epa-3050b.pdf>
- [35] Mertens D. AOAC Official Method 975.03. Metal in Plants and Pet Foods. Official Methods of Analysis, 18th edn. Editors: Horwitz W, and GW Latimer. Chapter 3, pp 3-4, AOAC-International Suite 500, 481. North Frederick Avenue, Gaithersburg, Maryland. USA, 2005.
- [36] Díaz W. Estrategia de gestión integrada de suelos contaminados en el Perú. Revista del Instituto de Investigación, FIGMMG-UNMSM 19(38):103-110, 2016.
- [37] Arotoma KS. Distribución de las fuentes del material particulado en la zona alta y media de la cuenca del Mantaro - ciudades de Huancayo, Jauja, Junín, Concepción, La Oroya, Paccha. Repositorio UAP,2014. <https://vdocuments.es/tesiscomposicionqaerosolesuap.html>.
- [38] MINAM. Decreto Supremo N° 003-2008-MINAM. Aprueban los estándares nacionales de calidad ambiental para aire. Lima 21 de agosto de 2008.
- [39] Doe Run Perú. Historia de la empresa. 2019. <http://www.doerun.com.pe/content/pagina.php?PID=124>. Tomado el 19 de abril 2019.
- [40] SPDA. La Oroya: registraron metales pesados en el aire cuando el complejo metalúrgico no operaba. SPDA Actualidad Ambiental. 2016. <http://www.actualidadambiental.pe/?p=35070>.
- [41] Mlay PS, Mgumia Y. Levels of lead and copper in plasma of dairy cows, pastures, soil and water from selected areas of Morogoro suburbs, Tanzania. Livestock Research for Rural Development. Volume 20, Article #60, 2010. <http://www.lrrd.org/lrrd20/4/mlay20060.htm>.
- [42] Ma W. Lead in mammals, environmental contaminants in biota. CRC Press, pp 595–607, 2011.
- [43] Sharma P, Dubey RS. Lead toxicity in plants. Braz J Plant Physiol 17:35–52, 2005.
- [44] Rodrigues SM, Pereira ME, Duarte AC, Römkens PF. Soil–plant–animal transfer models to improve soil protection guidelines: A case study from Portugal. Environment International, 39(1),27-37, 2012. <https://doi.org/10.1016/j.envint.2011.09.005>.
- [45] Reiser R, Simmler M, Portmann D, Clucas L, Schulin R, Robinson B. Cadmium concentrations in New Zealand pastures: relationships to soil and climate variables. J. Environ. Qual. 43 (3), 917–925, 2014.
- [46] Wuana RA, Okieimen FE. Heavy metals in contaminated soils: a review of sources, chemistry, risks and best available strategies for remediation. ISRN Ecology Volume 2011, Article ID 402647, 20 pages. <http://dx.doi.org/10.5402/2011/402647>
- [47] Yilmaz K, Akinci İE, Akinci S. Effect of lead accumulation on growth and mineral composition of eggplant seedlings (*Solanum melongena*). New Zealand Journal of Crop and Horticultural Science, 37(3), 189–199, 2009. <https://doi.org/10.1080/01140670909510264>.
- [48] Alloway B. Heavy Metals in Soils: Trace Metals and Metalloids in Soils and Their Bioavailability. Environmental Pollution, Springer Science+Business Media Dordrecht, 2013. <https://doi.org/10.1007/978-94-007-4470-7>.
- [49] Tokaliog'lu Ş, Kartal Ş, & Güneş A. Determination of Heavy Metals in Soil Extracts and Plant Tissues at Around of a Zinc Smelter. Int. J. Environ. Analyt. Chem. 80(3):201-217, 2001. Doi:10.1080/03067310108044370.
- [50] Proyecto El Mantaro Revive. 2012. Resultados de la evaluación de la calidad de suelo de la zona alta y media de cuenca del río Mantaro – Perú. Cáritas Huancayo. <https://es.slideshare.net/ElMantaroRevive/el-mantaro-revive-resultados-de-la-evaluacion-de-la-calidad-de-suelo-de-la-zona-alta-y-media-de-cuenca-del-ro-mantaro-per>.
- [51] Longhurst RD, Roberts AH, Waller JE. Concentrations of arsenic, cadmium, copper, lead, and zinc in New Zealand pastoral topsoils and herbage. New Zeal. J. Agr. Res. 47 (1), 23–32, 2004.
- [52] Iqbal Z, Ahmad K, Aisha N, Mustafa I, Ibrahim M, Fardous A, Gondal S, Hussain A, Arshad F, Rasul I, Yousaf M, Fawad A, Sher M, Hussain A, Ahmad H, Rashid U. Heavy Metals Concentration in Soil-Plant-Animal Continuum under Semi-Arid Conditions of Punjab, Pakistan. Pakistan J. Zool., vol. 47(2), pp. 377-382, 2015.

- [53] Ogundiran MB, Ogundele DT, Afolayao PG, Osibanjo O. Heavy MetaLs Levels in Forage Grasses, Leachate and Lactating Cows Reared around Lead Slag Dumpsites in Nigeria. *Int. J. Environ. Res.* 6(3):695-702, 2012.
- [54] Kabata-Pendias A, Pendias H. Trace Elements in Soils and Plants. 4th ed. CRC Press Inc. 548 Pages, 2010. ISBN 9781420093681. <https://doi.org/10.1201/b10158>
- [55] Shah FU, Ahmad N, Masood KR, Peralta-Videa JR, Ahmad FD. Heavy Metal Toxicity in Plants. *Plant Adaptation and Phytoremediation*, 71–97, 2010. doi:10.1007/978-90-481-9370-7\_4.
- [56] Oficial Journal of the European Union. Directiva 2005/87/CE de la Comisión por la que se modifica el anexo I de la Directiva 2002/32/CE del Parlamento Europeo y del Consejo, sobre sustancias indeseables en la alimentación animal, en lo referente al plomo, el flúor y el cadmio. 2005. <https://www.boe.es/doue/2005/318/L00019-00024.pdf>.
- [57] Ekmekci Y, Tanyolac D, Ayhan B. A crop tolerating oxidative stress induced by excess lead: maize. *Acta Physiol Plant* 31:319–330, 2009.
- [58] Win Mi Htwe, Yin Yin Kyawt, Sarayut Thaikua, Yuriko Imai, Susumu Mizumachi and Yasuhiro Kawamoto. Effects of lead contamination in soils on dry biomass, concentration and amounts of lead accumulated in three tropical pasture grasses. *Japanese Society of Grassland Science, Grassland Science*, 62, 167-173, 2016. <https://doi.org/10.1111/grs.1212>.

## Big Data Analytics Using Deep LSTM Networks: A Case Study for Weather Prediction

Shweta Mittal<sup>\*1</sup>, Om Prakash Sangwan<sup>2</sup>

<sup>1</sup>Research Scholar, Department of Computer Science and Engineering, Guru Jambheshwar University of Science & Technology, Hisar, Haryana, India, 125001

<sup>2</sup>Professor, Department of Computer Science and Engineering, Guru Jambheshwar University of Science & Technology, Hisar, Haryana, India, 125001

### ARTICLE INFO

Article history:

Received: 23 November, 2019

Accepted: 31 January, 2020

Online: 09 March, 2020

Keywords:

Big Data

Spark

Weather Prediction

LSTM

RNN

### ABSTRACT

Recurrent Neural Networks has been widely used by researchers in the domain of weather prediction. Weather Prediction is forecasting the atmosphere for the future. In this proposed paper, Deep LSTM networks has been implemented which is the variant of RNNs having additional memory block and gates making them capable of remembering long term dependencies. Fifteen years hourly meteorological data of Brazil weather stations for the period of 2000-2016 collected from Kaggle.com has been analyzed for 1 hour and 24-hour time lag using Keras libraries on Spark framework. Hidden layers of the network have been increased up to three to examine its impact on accuracy of the network and it was found that network with 2 hidden layers provides good accuracy in lesser learning runtime. From the experimental results, it is also concluded that Adam optimizer provides best results when compared with SGD and RMSProp optimizer.

### 1. Introduction

This paper is an extension of work based on Machine Learning Techniques for Big Data Analytics originally presented in 2019 9th International Conference on Cloud Computing, Data Science & Engineering (Confluence) [1]. Weather prediction is one of the vital applications of technology to forecast the atmosphere for the future and has its wide application in number of domains such as forecasting air flights delay, satellites launching, crop production, natural calamities etc. Weather prediction can be classified into 4 categories depending on the time of forecast : a) Very Short Term Prediction: forecast for few hours in advance b) Short Term: forecast for days in advance c) Medium Term: forecast for weeks in advance d) Long Term: for months-years in advance. In the early days, data collected from several weather stations were fed into some numerical models which made the use of statistics to predict the future. While with the growing popularity and tremendous applications of Machine Learning Techniques, availability of high speed processors, new improved tools and techniques, researchers are now experimenting with ML techniques in meteorological domain too.

Neural Networks is one of the most popular Machine Learning techniques but it lacked its popularity in the late 90's due to gradient descent problem and limited processing power of the computers leading to very high learning time. As the technology progressed further, various techniques like parallel processing, High Performance Computing clusters, GPUs etc. have been developed which when applied in NN results in tremendous improvement of their performance.

RNN are the recurrent neural networks with the feedback connection but they might get trapped in Vanishing Gradient Problem. LSTM (Long Short Term Memory neural networks, introduced by Hochreiter and Schmidhuber in 1997) are gated RNNs which overcomes the above-mentioned issue by creating the gradients that neither explode nor vanish with time. It is composed of 1 memory unit and 3 gates namely input, output and forget gate which uses sigmoid activation function to decide which information they need to input, output and forget. LSTM has self-loops with conditioned weights controlled by forget gate to generate paths where gradient can flow for greater time [2]. It has also an advantage of learning long term dependencies, thereby widely used in text sequencing domain. Architecture of LSTM

\* Shweta Mittal, Av.Email: shwetamittal019@gmail.com

networks has been described in Figure 1. LSTMs are trained using BPTT i.e. Back Propagation through Time, thus overcomes vanishing gradient problem but it might get stuck in local optima.

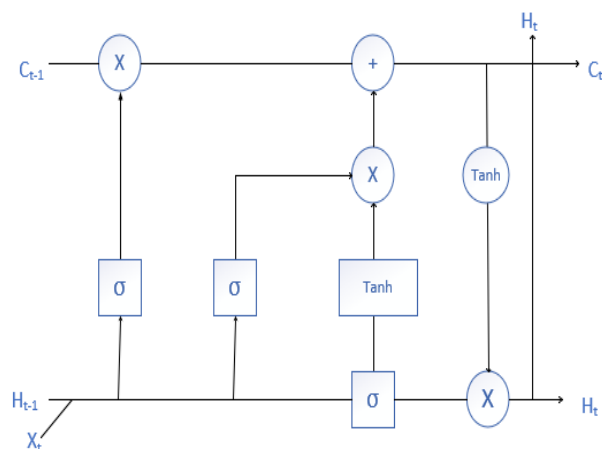


Figure 1: Architecture of LSTM: Image Source [3]

## 2. Literature Review

In this section, a detailed review has been conducted on work done by various researchers for application of NN in the field of weather prediction. A study on various Data Mining algorithms popularly used in the field of weather prediction has been conducted and several challenges that may occur while applying traditional data mining techniques were highlighted [4]. In [5], the authors analyzed 30 years of Hong Kong metrological data using 5 layered Deep NN with 4 layered Stacked Auto Encoders to learn raw data features with SVR for prediction. NMSE (Normalized Mean Square Error), R Square and DS (Directional Symmetry) metrics have been used for evaluation purpose. In [6], the reviewers analyzed weather data collected from [www.weatherunderground.com](http://www.weatherunderground.com) which was first normalized and then fed to 3 layered BPNN model to obtain non-linear relationships.

IGRA dataset collected across 60 stations was analyzed by authors to design data driven kernel and to provide an efficient inference procedure [7]. Best validation results were obtained using 2 stacked RBM with hidden neurons 50 and 150. In [8], the authors used CNN for the first time to predict monthly rainfall of Australia and the results proved that CNN performs better in comparison to prediction model used by Bureau of Meteorology and MLP for months with high annual average rainfall. Researchers also proposed CFPS-HGA (Climate features and neural network parameters selection-based hybrid genetic algorithm) for setting neural network parameters and the proposed algorithm performed better [9].

Meteorological data collected from BKMKG (for the period 1973-2009) and ENSO data from NOAA was analyzed by researchers using RNN, CRBM and Convolutional Networks [10]. In [11], the authors implemented NARX NN (Non Linear Auto regressive with exogenous variables), a type of recurrent NN for predicting multiple weather attributes and the results concluded that proposed algorithm performed better than CBR (Case Based

Reasoning). In [12], researchers proposed a new layer i.e. Dynamic Convolutional layer which used filter in addition to feature maps from the previous layer to predict the sequence of rain radar images using Caffe library and Stochastic Gradient Decent optimizer.

In [13], the researchers compared the performance of deep neural NN with shallow NN for short term wind prediction. NN parameters were reduced using PMI (Partial Mutual Information) based IVS algorithm and the results proved that 3 layered stacked auto encoders performed better. In [14], the authors proposed Deep Multilayer Perceptron using Cascade learning and implanted it on H1-B Visa applications record and cardiac dataset and the results proved that proposed model has less run time and greater accuracy.

In [15], the authors proposed 2 layers stacked LSTM model (each layer has independent LSTM model for every location) for weather data obtained from Weather Underground website from 2007 to 2014. In [16], the authors compared the performance of ARIMA model and LSTM (weather variables are combined) on weather data collected from Weather Underground for the period 2012 to 2016 and it was concluded that LSTM performs better than ARIMA.

In [17], the authors proposed deep LSTM model for wind prediction on the data from Manchester Wind Farm for 2010-2011 and the proposed algorithm performed better than BPNN and SVM. Best results were obtained from the model consisting of 3 hidden layers constituting 300, 500 and 200 neurons. In [18], 15 years of hourly meteorological data for 9 cities in Morocco was analyzed by authors using multi-stacked LSTM to forecast 24 and 72 hours weather data. Missing values were eliminated using forward filling and RMSProp optimizer was used.

## 3. Experimental Study

As per the survey done in Section 2, it can be concluded that LSTM is one of the most popular and successfully used technique in the domain of weather prediction. Thus, in this experimental study, multi-stacked LSTM model has been implemented on Spark platform to determine the best architecture for the task of weather prediction. For the analysis purpose, dataset of 2 GB from INMET (National Meteorological Institute - Brazil) has been used which consists of hourly weather data from 122 weather stations of various south-eastern states of Brazil i.e. Rio de Janeiro, Sao Paulo, Minas Gerais and Espirito Santo from 2000 to 2016 [19]. Brazil is the largest country in the South America and its temperature rarely fall below 20 degrees. In the proposed experiment, a computer with 1TB memory, 16 GB RAM and 1.8 GHz processor has been used. Dataset includes 31 features and around 9.7 million (9,779,168) rows. All the dataset is first loaded into the Spark dataframe and unnecessary columns i.e. wsnm, wsid, elvt, lat, lon, inne, city, prov, mdct, date, yr, mo, da, hr, tmax, tmin have been deleted from our schema (Only 15 attributes have been preserved as mentioned in Table 1).

Data pre-processing is the pre-requisite of any analytics process. All the null values have been replaced with zero and the

results are cited in Table 2. Several other ways to deal with null values are as follows: a) Replace nulls with zero in case of numerical attributes b) Replace with mean/median/mode values c) Use algorithms that support missing values d) Remove the rows having null values.

Table 1: Attributes for weather prediction

Attribute	Description
Prcp	Amount of precipitation in millimeters (last hour)
Stp	Air pressure for the hour in hPa to tenths (instant)
Smax	Maximum air pressure for the last hour in hPa to tenths
Smin	Minimum air pressure for the last hour in hPa to tenths
Gbrd	Solar radiation KJ/m2
Temp	Instant Air Temperature (Celsius degrees)
Dewp	Instant Dew Point (Celsius degrees)
Dmax	Maximum Dew Point (Celsius degrees)
Dmin	Minimum Dew Point Temperature (Celsius degrees)
Hmdy	Relative Humidity of Air (%)
Hmax	Maximum Relative Air Humidity (%)
Hmin	Minimum Relative Air Humidity (%)
Wdsp	Instant Wind Speed (meters per second)
Wdct	Wind direction in radius degrees (0-360)
Gust	Wind Gust Intensity (meters per second)

Input to the proposed LSTM network is prcp, stp, smax, smin, gbrd, dewp, dmax, dmin, hmdy, hmax, hmin, wdsp, wdct, gust, temp at (t-1)<sup>th</sup> hour and the output is temperature at (t)<sup>th</sup> hour and at (t+24)<sup>th</sup> hour. Architecture of the proposed network has been described in Figure 2. Input attributes are normalized between 0 and 1 via pyspark.ml.MinMaxScaler and training and validation data has been split in the ratio 80:20.

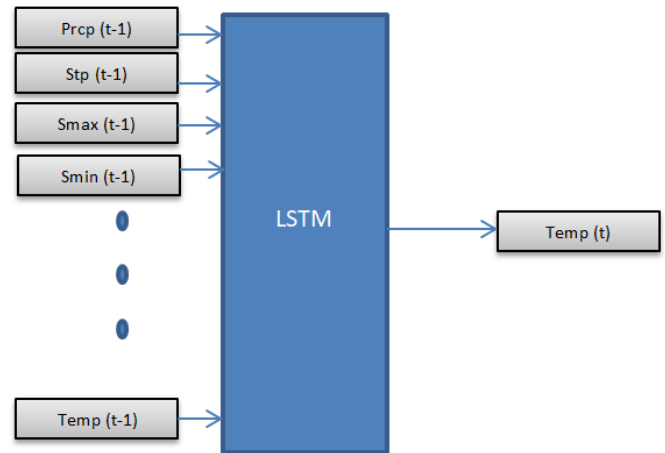


Figure 2: Architecture of LSTM network

Table 2: Number of nulls

Attributes	Number of null values
Prcp	8371184
Stp	0
Smax	0
Smin	0
Gbrd	4108820
Dewp	475
Dmax	310
Dmin	807
hmdy	0
Hmax	12
Hmin	44
Wdsp	925561
Wdct	0
Gust	316474
Temp	31

#### 4. Experimental Results

Let I, H and O be the number of neurons in input layer, hidden layer and output layer respectively. Models are trained using Keras module (with Tensorflow backend) which has dense library for implementing LSTM networks. Weights to be optimized in the LSTM networks are as follows:

$$\begin{aligned}
 W1 &= 4 * I * H; & U1 &= 4 * H * H; \\
 B1 &= 4 * H; & W2 &= H * O; \\
 B2 &= O & \dots & (1)
 \end{aligned}$$

For H=5 (5 units in LSTM with 1 hidden layer), I=15 (15 input attribute) and O=1 (1 output attribute), W1= 4\*5\*15=300, U1=4\*5\*5=100, B1=4\*5=20, W2= 5\*1=5, B2=1. Thus, there are total of 426 parameters which needs to be optimized.

Two separate networks have been implemented, one provides output temperature at t<sup>th</sup> hour and the other network provides output at (t+24)<sup>th</sup> hour. In the proposed study, the number of hidden neurons has been varied from 10 to 30 and the number of hidden layers has been increased up to 3. Results of both the case studies have been mentioned in Table 3. Performance of Adam (Adaptive Moment Estimation), SGD (Stochastic Gradient Decent) and RMSProp (Root Mean Square Prop) optimizers has also been compared for 2 hidden layers comprising 10 and 20 neurons respectively for 24 hours' time lag and results are described in Table 4. From the results, it can be concluded that Adam optimizer performs best whereas SGD performs worst. Thus, Adam optimizer has been used in all the implemented case studies. Mean Absolute Error (MAE) metrics has been used for the evaluation purpose. Run time of the network (in floating point number) has also been analyzed to determine the complexity of the network.



Table 3: MAE of LSTM networks with 1 hour and 24-hour time lag

S. No	Number of hidden layers	Number of hidden units	Iterations	1 hour time lag		24 hour time lag	
				MAE	Runtime	MAE	Runtime
1	1	10	100	0.015151	28041.47	0.041649	30256.38
2	1	20	100	0.015462	29292.39	0.041582	29889.34
3	1	30	100	0.015365	30854.15	0.042124	28289.06
4	2	10,10	100	0.015088	48892.43	0.040463	49878.65
5	2	20,20	100	0.015077	49898.42	0.040839	46737.57
6	2	30,30	100	0.015259	50805.43	0.040060	46829.74
7	2	10,20	100	0.015124	42302.25	0.040020	52487.23
8	3	10,10,10	100	0.015269	124915.8	0.040546	101543.68

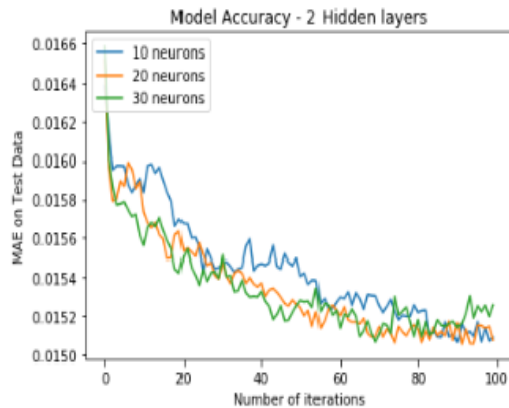


Figure 3: MAE of LSTM with 2 hidden layers for 1-hour time lag



Figure 6: MAE with 1 and 2 hidden layer, each having 30 neurons each for 24 hour time lag

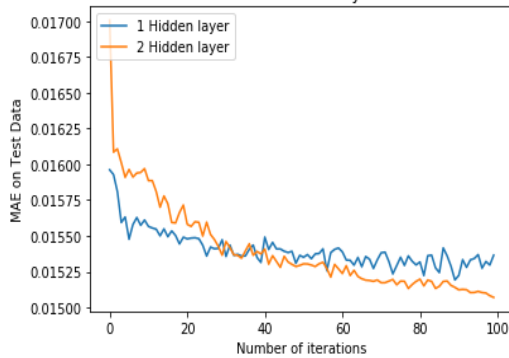


Figure 4: MAE with 1 and 2 hidden layers, each having 30 neurons each for 1 hour time lag



Figure 5: MAE of LSTM with 2 hidden layers for 24-hour time lag

Table 4: comparison of MAE for various optimizers for 24-hour time lag

Optimizers/Metric	MAE	Accuracy	Runtime
Adam	0.04002	6.64686E-06	52487.2306
Rmsprop	0.05972	5.62427E-06	51896.5460
SGD	0.04142	6.64686E-06	40895.8979

Figure 3 and Figure 5 illustrates the comparison of MAE with 2 hidden layers comprising 10, 20 and 30 neurons each for 1 hour time lag and 24 hour time lag respectively over 100 iterations. For 1 hour time lag, network with 2 hidden layers comprising 20 neurons each provides best results (with the lowest MAE value of 0.015077 as stated in Figure 3) whereas for 24 hour time lag,

network with 2 hidden layers comprising 10 and 20 neurons respectively provides best results with the MAE value of 0.040020.

Figure 4 shows the comparison for networks of 1 hidden layer having 30 neurons with the network of 2 hidden layers comprising 30 neurons each for 1 hour time lag and it can be inferred that network with 2 hidden layers has low MAE value as compared to network with 1 hidden layer. Similarly, Figure 6 shows comparison for networks of 1 hidden layer having 30 neurons with the network of 2 hidden layers comprising 30 neurons each for 24 hour time lag and it can be inferred that network with 2 hidden layers has low MAE i.e. 0.040060 value as compared to network with 1 hidden layer i.e. MAE value of 0.042124.

From the case studies implemented, it can also be observed that MAE for 1 hour time lag is comparatively low, thus gives more accurate results as compared to network with 24 hour time lag i.e. network with short term predictions provides higher accuracy as compared to network with medium term predictions.. More combinations of the hidden neurons and layers can be explored in the near future to obtain better results.

## 5. Conclusion and Future Work

In this paper, Deep LSTM network has been implemented on 15 years meteorological data. Number of hidden layers has been increased up to 3 and it can be concluded that increasing the number of hidden neurons in the layer does not necessarily increases the accuracy of the model as network might start learning the linear relationship between the attributes. Also, increase in the number of layers in the model increases the run time of network by marginal amount, thus increasing the complexity of the network.

There are number of combinations possible for choosing the adequate number of hidden neurons and hidden layers in the network which can provide the minimum MAE. Manually testing all such combinations will be a quite tedious task. Thus, process of selection of number of hidden layers and hidden neurons needs to be automated.

Also, the algorithm takes quite longer time to run on single CPU. Thus, it becomes hard to increase the number of hidden layers and neurons beyond a significant point. Parallel processing of neural network might help us in reducing the time complexity of the network. Time complexity can further be reduced by employing more number of processors to do a task or by using the high speed GPUs. In future, it would be interesting to study the reduction in time complexity by implementing the above algorithms on increased number of processors and on GPUs.

## Conflict of Interest

The authors declare no conflict of interest.

## References

[1] S. Mittal, O.P. Sangwan, "Big Data Analytics using Machine Learning Techniques" in 2019 9th International Conference on Cloud Computing, Data

Science & Engineering (Confluence), Noida, India. <http://dx.doi.org/10.1109/CONFLUENCE.2019.8776614>.

[2] I. Goodfellow, Y. Bengio, A. Courville, Deep Learning, MIT Press, 2016.

[3] [https://en.wikipedia.org/wiki/Long\\_short-term\\_memory](https://en.wikipedia.org/wiki/Long_short-term_memory).

[4] S. Mittal, O.P. Sangwan, "Big Data Analytics Using Data Mining Techniques: A Survey" in book: Advanced Informatics for Computing Research, 264-273, 2018 Second International Conference, ICAICR, Shimla, India. [http://dx.doi.org/10.1007/978-981-13-3140-4\\_24](http://dx.doi.org/10.1007/978-981-13-3140-4_24).

[5] J. Liu, Y. Hu, J. Jia You, P. Wai Chan, "Deep Neural Network Based Feature Representation for Weather Forecasting" in 2014 International Conference on Artificial Intelligence (ICAI), Las Vegas, Nevada, USA.

[6] Ch. J. Devi, B.S. Prasad Reddy, K. Vaghdhan Kumar, B. Musala Reddy, N. Raja Nayak, "ANN Approach for Weather Prediction using Back Propagation" International Journal of Engineering Trends and Technology, 3(1), 20-23, 2012.

[7] A. Grover, A. Kapoor, E. Horvitz, "A Deep Hybrid Model for Weather Forecasting" in 2015 21th ACM SIGKDD International Conference on Knowledge Discovery and Data Mining, KDD, 379-386, Sydney, NSW, Australia. <http://dx.doi.org/10.1145/2783258.2783275>.

[8] A. Hiader, B. Verma, "Monthly Rainfall Forecasting using One-Dimensional Deep Convolutional Neural Network," IEEE Access, 6, 69053 – 69063, 2018. <http://dx.doi.org/10.1109/ACCESS.2018.2880044>.

[9] A. Hiader, B. Verma, "A novel approach for optimizing climate features and network parameters in rainfall forecasting" Soft Computing, Springer, 22(24), 2018. <https://doi.org/10.1007/s00500-017-2756-7>.

[10] A. Galih Salman, B. Kanigoro, Y. Heryadi, "Weather forecasting using deep learning techniques" in 2015 International Conference on Advanced Computer Science and Information Systems (ICACSIS), Depok, Indonesia. <http://dx.doi.org/10.1109/ICACSIS.2015.7415154>.

[11] S. Biswas, N. Sinha, B. Purkayastha, L. Marbianing, "Weather prediction by recurrent neural network dynamics" Int. J. Intelligent Engineering Informatics, 2(2/3), 166-180, 2014. <http://dx.doi.org/10.1504/IJIEI.2014.066208>.

[12] B. Klein, L. Wolf, Y. Afek, "A Dynamic Convolutional Layer for Short Range Weather Prediction" in 2015 IEEE, Conference on Computer Vision and Pattern Recognition (CVPR), Boston, MA, USA. <http://dx.doi.org/10.1109/CVPR.2015.7299117>.

[13] M. Dalto, J. Matusko, M. Vasak, "Deep neural networks for ultra-short-term wind forecasting" in 2015 IEEE, International Conference on Industrial Technology (ICIT), Seville, Spain. <http://dx.doi.org/10.1109/ICIT.2015.7125335>.

[14] A. Gupta, H. Kumar Thakur, R. Shrivastava, P. Kumar, S. Nag, "Big Data Analysis Framework Using Apache Spark and Deep Learning" in 2017 IEEE, International Conference on Data Mining Workshops (ICDMW), New Orleans, LA, USA. <http://dx.doi.org/10.1109/ICDMW.2017.9>.

[15] Z. Karevan, J. Suykens, "Spatio-temporal Stacked LSTM for Temperature Prediction in Weather Forecasting" Cornell University, 2018.

[16] A. Galih Salman, Y. Heryadi, E. Abdurahman, W. Suparta, "Weather Forecasting Using Merged Long Short-Term Memory Model (LSTM) and Autoregressive Integrated Moving Average (ARIMA) Model" Journal of Computer Science, 14(7), 930-938, 2018. <https://doi.org/10.3844/jcssp.2018.930.938>

[17] Q. Xiaoyun, K. Xiaoning, Z. Chao, J. Shuai, M. Xiuda, "Short-Term Prediction of Wind Power Based on Deep Long Short-Term Memory" in 2016 IEEE, PES Asia-Pacific Power and Energy Engineering Conference (APPEEC), Xi'an, China. <http://dx.doi.org/10.1109/APPEEC.2016.7779672>.

[18] M. Akram Zaytar, C. El Amrani, "Sequence to Sequence Weather Forecasting with Long Short-Term Memory Recurrent Neural Networks" International Journal of Computer Applications, 143(11), 2016. <http://dx.doi.org/10.5120/ijca2016910497>.

[19] <https://www.kaggle.com/PROPPG-PPG/hourly-weather-surface-brazil-southeast-region>.

## The Acquiring Process of Entrepreneurship Competencies in Realist Airbrush Art

Bayu Rahmat Setiadi<sup>1,\*</sup>, Suparmin<sup>2</sup>, Slamet Priyanto<sup>2</sup>, Henny Pratiwi<sup>1</sup>, Sugiyono<sup>1</sup>

<sup>1</sup>Department of Mechanical Engineering Education, Universitas Negeri Yogyakarta, Yogyakarta, Indonesia

<sup>2</sup>Department of Mechanical Engineering Education, Universitas Sarjanawiyata Tamansiswa, Yogyakarta, Indonesia

### ARTICLE INFO

Article history:

Received: 14 October, 2019

Accepted: 05 February, 2020

Online: 09 March, 2020

Keywords:

Realist Airbrush

Art and Technologies

Acquiring Process

Vocational High School

### ABSTRACT

One of the creative industries with rapid growth is the airbrush industry. Airbrush art, especially realist, is identical to the field of automotive engineering in the combination of art and technology. The research is directed to prove how the difficult realist airbrush competency can be achieved by Vocational High School (VHS) students in a short time. Also, the research synchronises the increase in entrepreneurial understanding of VHS students in real business incubation in the realist airbrush industry. The final results show that entrepreneurial learning needs to add elements of art as a stage in the acquisition of real competencies.

## 1. Introduction

The creative industry is one of the creative economies that can stimulate the economy in Indonesia. Some of these creative sectors have great opportunities in solving the problem of unemployment in Indonesia [1]. Creative industries support almost half of Indonesia's foreign exchange [2]. Data shows that the number of entrepreneurs from the creative industries is 49% spread widely in some province in Indonesia where Yogyakarta Province as the centre [3].

Creative industries that grow in Indonesia have several sub-sectors include animation, architecture, design, photography, music, crafts, culinary, fashion, research and development, publishing, film, advertising, interactive games, performance art, visual arts, information technology, television, radio, and video. Some of these sectors, six sub-sectors with the highest growth, are television, film-animation-video, performing arts, crafts, and visual communication design [4]. One of the most desirable sub-sectors is craft and art [5]. Yogyakarta City is one of the contributors to the arts and crafts business in regional, national, and international export marketing [6].

The growth of the creative arts industry in Yogyakarta is a reflection of artists in Indonesia as inspiration for ideas and creativity. One of the trendy creative endeavours in this city is airbrush art. The famous airbrush in this city is Planet Airbrush Potlot. Potlot has been established since 2000 and has produced

hundreds of airbrush works on automotive, painting, wall, and other media. Potlot won various international events. According to an art perspective, the realist airbrush technique is very complicated and is in great demand by many people because of the high level of detail and animate the character of the artwork [7]. So, Yogyakarta could be said as a place for artists in exploring art [8].

The effort to open a realist airbrush, as exemplified in the previous paragraph, explains that there are good prospects for Vocational High Schools (VHS) to produce graduates as airbrush entrepreneurs [9]. The trend of shifting from VHS graduates to entrepreneurs is due to the limited number of jobs for VHS graduates to get a new job. However, leading graduates to create airbrush art is an option to reduce the unemployment level of VHS graduates.

Based on the previous description, the researcher wants to examine how VHS students who are doing internships in the realist airbrush industry can be skilled in simple airbrushing. Besides, observing the process of acquiring entrepreneurial competencies about the business is the key to this paper because the research is unique and can be an inspiration for business people to be interested in opening up new business fields.

## 2. Combining Art in Automotive for New Business Incubation

### 2.1. Collaboration between creative industry subsector in Indonesia

\* Bayu Rahmat Setiadi, Email: bayursetiadi@uny.ac.id

The creative industry in Indonesia has a variety of sub-sectors. The Creative Economy Agency or abbreviation of Bekraf Indonesia has released 16 strategic sub-sectors, including animation, architecture, design, photography, music, crafts, culinary, etc. Some of these sub-sectors were developed in several iconic big cities such as Yogyakarta (handicraft city), Pekalongan (city of Batik), Bandung (fashion city) [10]. The iconic cities became a centre for business development and creative industries as well as references from various regions [11].

The collaboration between various industry sub-sectors is a good strategy in order to produce quality products. The products currently available are a combination of multidisciplinary or better known as Science, Technology, Engineering, Arts, and Mathematics (STEAM) [12]. Science and technology need to work together with art to manufacture products that are more accepted by society. It indicates that the creative industries sub-sectors need to collaborate dynamically and flexibly so that the products in the creative industries become more diverse and quality.

### 2.2. Prospective realist airbrush as a promising business

Fine art has two types, namely, pure and applied art [13]. Pure art, or better known as first works, is an expression of the soul that is etched through dots, lines, paintings, and other forms of images. Applied art is a form of application of artists to the media that it has designed. Airbrush, as an art-based painting technique, is an applied art that is expressively determined by painting in the media [14].

Realist airbrushes have advantages in producing real artwork. The examples are such as in murals, posters, contemporary, and painting [15]. Not many people are experts in painting realists in certain media. A high level of difficulty in drawing and depth in inspiration determines the success of a realist. Also, the airbrush technique requires much experience so that the results are more realistic and easily understood by connoisseurs of art [16]. Various challenges in airbrush art make the techniques needed in the business of painting and airbrush. Therefore, a realistic airbrush with complicated media such as vehicles, motorcycles, cars, trucks, and buses is an excellent business opportunity.

### 2.3. VHS automotive students have potential in the realist airbrush industry entrepreneurship

The curriculum determines VHS graduates to work, go to college, and be entrepreneurs [17]. The current curriculum design

in Indonesia refers to the 2013 Curriculum. The contents of the curriculum with the priority of practicum indicate a change in mindset for VHS to increase psychomotor ability compared to cognitive and adaptive. For example, automotive skills in the curriculum spectrum in Indonesia limit the practice of basic painting. If this continues, the tendency of students to get late for the first job becomes a common problem in Indonesia. The entrepreneurship is like a medicine needed in solving the unemployment problem in Indonesia.

Policies in Indonesia encourage entrepreneurship in vocational education. Many studies have explored the opportunities for creative industry employment as a potential face of new entrepreneurs. Cheap, collaborative capital, a wide variety of products, and the dynamics of consumer change are ideal potentials in entrepreneurial learning. In the case of automotive engineering, the business of marketing and repair services are frequent, and consumers have regular customers who certainly reduce the interest of entrepreneurship for beginners.

## 3. Research Method

The study used a mixed-method with an explanatory cycle model. This method is in line with the process of acquiring competencies that have three observed research stages. The first step using phenomenology to reveal the process of achieving student competence in airbrush techniques. The next step is adopting experimentation in the form of pre-test and post-test to examine the first hypothesis. The last step is testing the second hypothesis with pre-test and post-test in order to validate the improvement of entrepreneurship skills in airbrush realism after the incubation process was carried out.

The population is 30 students at VHS Ma'arif-Salam, Magelang Regency, majoring in automotive engineering. Data collection techniques used were interviews and observations and questionnaires. Interviews were conducted to obtain in-depth information from the instructor. Meanwhile, the pre-test and post-test instruments will ask questions related to increasing understanding of both airbrush and entrepreneurship training — data analysis by reducing the critical information based on coding and besides, interpreting the findings through a crosscheck of interviews and observations to the instructor. Descriptive statistics were used to measure the understanding of both airbrush and entrepreneurship training.



Figure 1: The Art of Collaborating with Automotive



4. Results

The acquisition of entrepreneurial competence in the realist airbrush has two main scopes. They are achieving airbrush success and success in opening a business. The results of the two studies are mutually simultaneous to prepare VHS graduates to open the automotive business in the realist airbrush field. Based on observations, interviews, and data reduction, the flow chart as obtained for VHS students who were said to be amateur workers.

Figure 2 describes the process of obtaining entrepreneurial competence in airbrush skills. The process illustrates that the repetition of the process occurs as a stage of student learning. For example, students are often less thorough in sanding and caulking. The results of sandpaper and picking should be checked for smoothness because it has an impact on the final product. Therefore, the initial work raises many related cycles as capital to prepare an applicable and neat airbrush media. The improvement of airbrush realist skills is carried out continuously by conducting tests at the beginning and providing posttest after treatment.

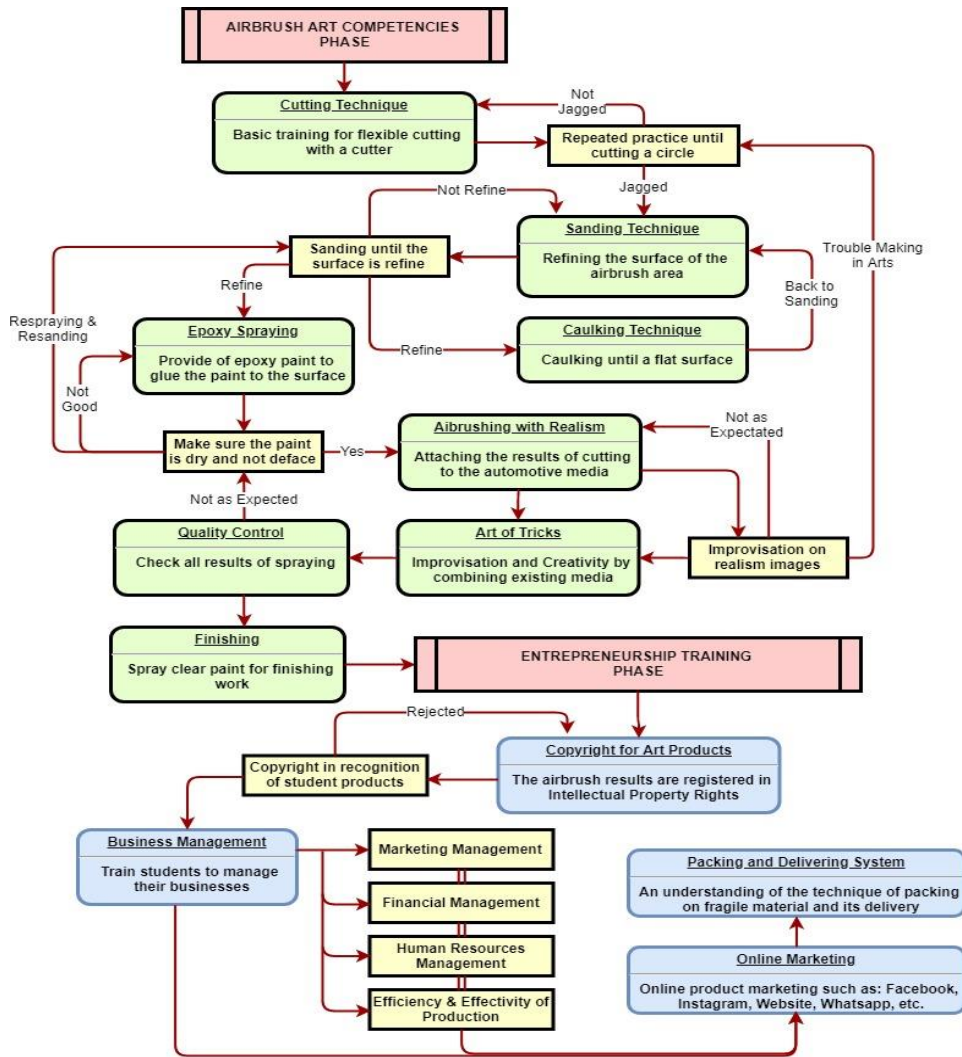


Figure 2: The Process of Forming Entrepreneurship Competence in the Automotive Realist Airbrush Business

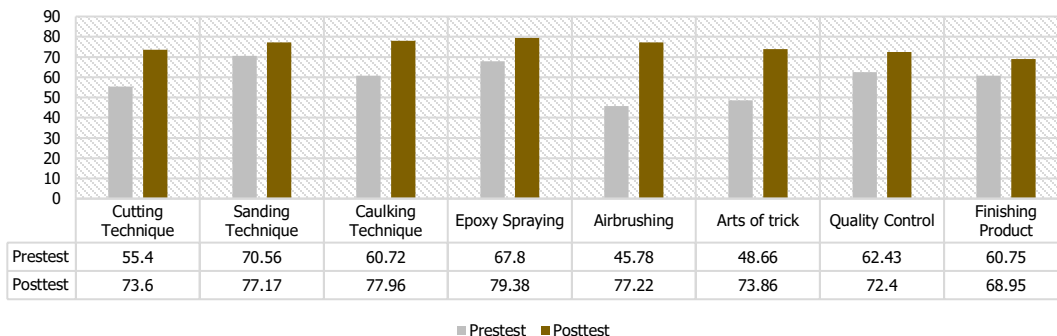


Figure 3: Realist Airbrush Skills in Pretest and Posttest



There is a significant influence on students' skills due to airbrush training (Fig. 3). More than one-fifth of the posttest outperformed the pretest score, indicating that students' interest in painting was very high. Substantially, the enthusiasm of students to continue on the entrepreneurial step becomes an opportunity for them to be confident in opening a realist airbrush business. Positive responses to the creative industries in this sector need to be encouraged comprehensively.

The challenge in airbrush training based on interviews are cutting techniques, airbrushing, and arts of tricks. All three techniques require a lot of practice and material. These obstacles can be overcome if they often practice continuously to form these skills. Behaviorally, a child's skills will work well if he does repetitive work according to the object being worked on the workplace. Meanwhile, constructivism point of view states that learning can build independence in the field of arts, creation, and innovation.

The entrepreneurial skills of VHS students are measured by doing pretest and posttest before the airbrush training is carried out, and after they get the entrepreneurial knowledge. In the posttest, the skill of students increased by 11.38% compared to pretest. The following is a graph of the increasing entrepreneurial development of VHS students. The improvement of realist airbrush skills examination is carried out continuously by conducting tests at the beginning through a pretest and giving a posttest after treatment.

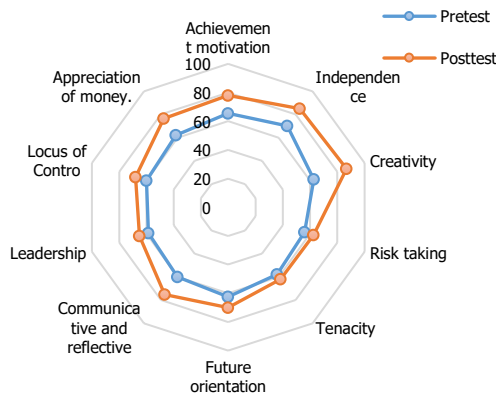


Figure 4. Distribution of VHS Student Entrepreneurship Experience Progress

The distribution of VHS student entrepreneurship experience progress diagram (Fig. 4) shows that there is an increase in all aspects of entrepreneurship criteria. The remarkable improvement is an increase in creativity, which is a quarter per cent of the value of the two tests. In the other side, there is a concern in the low level of tenacity. The short-term training and entrepreneurial experience have not significantly increased their tenacity level, but the entrepreneurship training after completing the product provides a significant increase in other criteria.

## 5. Discussions

Arts and automotive would be two beautiful fields of science if they integrated. Maeda proves that the existence of art in automotive design will increase the sale value of the vehicle [12]. A significant increase is very noticeable when automotive products begin to be marketed at certain specific events. The

research findings show the acceleration of students' ability in the mastery of art in the automotive field on airbrush realism. The primary abilities of students become the first reason in increasing their motivation and interest to explore airbrush science based on the needs of automotive work.

Entrepreneurship that is in line with skills is an excellent opportunity to pursue the field of expertise [18]. Students with airbrush skills have a big challenge to open the airbrush business later after they graduate. This entrepreneurial theory will undoubtedly oppose the assumption of Prosser & Quigley theory that working in the automotive field is required to work in the automotive industry [19]. This assumption began to shift since Dewey gave the freedom to determine the goals and lives of students following the needs and opportunities of students [20]. However, this finding is part of providing information to schools in Indonesia that VHS has great potential to direct graduates to become entrepreneurs.

## 6. Conclusion

There is a significant influence on students' skills due to airbrush training. More than 20% of the posttest outperformed the pretest score, indicating that students' interest in painting was very high. The distribution of VHS student entrepreneurship experience progress diagram also shows that there is an increase in all aspects of entrepreneurship criteria. The remarkable improvement is an increase in creativity which increase 25% after the training.

## Conflict of Interest

The authors declare no conflict of interest.

## Acknowledgment

Our thanks to the Directorate of Research and Community Service - Ministry of Research, Technology, and Higher Education of the Republic of Indonesia for funding research into the development of creative industries for VHS students. Researchers are grateful to all those who helped the research process.

## References

- [1] B. R. Setiadi and Suparmin, "Providing Space for Creative Industry Sub-Sectors to Meet the Labor Market for Vocational School Graduates," in *Advances in Social Science, Education and Humanities Research*, 2017, vol. 102, no. Ictvt, pp. 309–313.
- [2] M. E. Pangestu, *Ekonomi Kreatif Indonesia 2025*, no. 5. Jakarta: Departemen Perdagangan RI, 2015.
- [3] Bekraf, *Opus creative economy outlook 2019*. Jakarta: Badan Ekonomi Kreatif, 2019.
- [4] S. R. Maryunani and I. R. Mirzanti, "The Development of Entrepreneurship in Creative Industries with Reference to Bandung as a Creative City," *Procedia - Soc. Behav. Sci.*, vol. 169, no. August 2014, pp. 387–394, 2015.
- [5] ICCEI, "KADIN Dorong Ekonomi Kreatif Yogyakarta," Indonesian Chamber of Commerce and Industry, 2017.
- [6] DIY Tourism Office, "Statistik Kepariwisata 2015," Yogyakarta, Indonesia, 2015.
- [7] X. Wang, "Realist painting and its relationship to my creative practice Realist painting and its relationship to my creative practice," Edith Cowan University, 2010.
- [8] M. D. Marianto, "Surrealist Painting in Yogyakarta," University of Wollongong, 1995.
- [9] B. R. Setiadi, Suparmin, S. Priyanto, and P. Roniwijaya, "Tracking the potential of vocational high school students leading to eighteen strategic

- creative industry sub-sectors in Indonesia,” IOP Conf. Ser. Mater. Sci. Eng., vol. 535, no. 1, 2019.
- [10] F. Z. Fahmi, S. Koster, and J. van Dijk, “The location of creative industries in a developing country: The case of Indonesia,” *Cities*, vol. 59, pp. 66–79, 2016.
- [11] M. B. Alexandri, E. Maulina, A. Chan, and R. W. S. Sumadinata, “Creative Industries : Existence of Arts Traditional Industries in Indonesia,” *Acad. Strateg. Manag. J.*, vol. 18, no. 1, pp. 1–12, 2019.
- [12] J. Maeda, “STEM + Art = STEAM,” *STEAM*, vol. 1, no. 1, pp. 1–3, 2013.
- [13] C. P. Magill, “Pure and Applied Art: A Note on Johann Peter Hebel,” 1957, pp. 183–188.
- [14] J. Lu, C. Barnes, S. DiVerdi, and A. Finkelstein, “RealBrush: Painting with examples of physical media,” *ACM Trans. Graph.*, vol. 32, no. 4, 2013.
- [15] A. Oliver, “Critical realism in contemporary art,” University of Pittsburgh, 2014.
- [16] M. A. A. Soltan, “An Investigation into the History of the Airbrush and the Impact of the Conservation Treatment of Airbrushed Canvas Paintings Mohamed,” University of Northumbria, 2015.
- [17] H. Retnawati, S. Hadi, and A. C. Nugraha, “Vocational high school teachers’ difficulties in implementing the assessment in curriculum 2013 in Yogyakarta Province of Indonesia,” *Int. J. Instr.*, 2016.
- [18] B. R. Setiadi, Suparmin, and Samidjo, “Preparing engineering students for entrepreneurial creative industries,” *Glob. J. Eng. Educ.*, vol. 20, no. 2, pp. 127–131, 2018.
- [19] P. Sudira, “Indonesia vocational education praxis betwen,” in *Empowering Vocational Education and Training to Elevate National Economic Growth*, 2014, pp. 190–200.
- [20] J. Dewey, *Democracy and Education*. Hazleton: The Pennsylvania State University The, 2001.

## Dynamic Behavior of Multi-Story Concrete Buildings Based on Non-Linear Pushover & Time History Analyses

Sherif Gamal Abd-Elhamid<sup>1,\*</sup>, Reham Mohamed Galal Ebrahim El-Tahawy<sup>2</sup>, Mohamed Nour El-Din Fayed<sup>3</sup>

<sup>1</sup>Structural engineer at ENNPI, Structural engineering Department, Ain Shams University, 11311, Cairo, Egypt

<sup>2</sup>Associate Professor, Structural engineering Department, Ain Shams University, 11311, Cairo, Egypt

<sup>3</sup> Professor, Structural engineering Department, Ain Shams University, 11311, Cairo, Egypt

### ARTICLE INFO

Article history:

Received: 01 January, 2020

Accepted: 22 February, 2020

Online: 09 March, 2020

Keywords:

Reinforced concrete structures

Non-linear time history analysis

Pushover analysis Response reduction/modification factor

### ABSTRACT

In many countries and regions in the world, earthquakes are one of the most common natural disasters, which affect both human life and property. To avoid negative effects of earthquake, the nonlinear response of structures under dynamic loading should be accurately modeled to investigate their actual behavior under earthquake loading to ensure safe and sound design. To yield proper results, accurate representative structural models should be developed for the elements resisting lateral loading and representative ground motions pertaining to the site should be employed. Then relating such response to that of elastic behavior should be conducted to correlate response modification factors in design codes with actual response. The main objective of the research is to investigate the effect of basements existence and considering soil pressure on retaining walls on the seismic response modification factor for reinforced concrete structures, based on ABAQUS software analysis results using pushover analysis and time history analysis. For this purpose, experimental results of individually tested RC structures are used in order to verify modeling technique to be adopted.

## 1. Introduction

RC structures designed to withstand earthquakes must have enough strength and stiffness to control deflection and prevent any possible collapse. Recent seismic design codes include R factors in definition of lateral forces used for seismic design to reduce the design elastic spectral acceleration to account for its components yielding.

R factor reflects the structure capacity to behave in-elastically without collapsing. In fact, the response reduction / modification factor is a combined effect of over strength, redundancy and ductility. Response modification factors play an important role in the seismic design. No other parameter in the design base shear equation affects the design actions in a seismic framing system as does the value assigned to R-factor.

## 2. Literature Review

A summary of previously available analytical work was conducted for this study is presented as follows.

- In 2008, Asgarian and Shokrgozar [1] evaluated response reduction/modification factor(R), over-strength and the ductility of buckling-restrained braced frames. Seismic building codes considered a decrease in design loads; considering that, the RC structures have substantial over-strength and the capacity of energy dissipation. The ductility and over-strength were included in design through a reduction/modification factor(R). The basic fault in code actions was using linear methods not considering nonlinear behavior. Over strength in RC structures is connected to the fact that, maximum lateral strength of a RC structure usually beats its design strength. It was perceived that the response reduction/modification factor(R) decreases as the building height increases.
- In 2014, Apurba Mondal [2] focused on estimating the value of the response reduction/modification factor (R) for realistic reinforced concrete(RC) structures detailed and designed based on Indian standard (IS) for that they made models

\*Corresponding Author Name: Sherif Gamal AbdelHamid, [sherif\\_gamal9@yahoo.com](mailto:sherif_gamal9@yahoo.com)

[www.astesj.com](http://www.astesj.com)

<https://dx.doi.org/10.25046/aj050219>

consist of 3, 5, 9 & 13 stories reinforced concrete (RC) frames and analysis was carried out with non-linear static method using static push-over analysis. The results explained that the Indian standard (IS) recommendation for a higher value response reduction/modification factor (R) than actual value of response reduction/modification factor (R) is potentially dangerous.

- In 2014, Hakim [3] aimed to investigate building performance on resisting expected seismic loadings. Two 3D reinforced concrete (RC) frames were analyzed using the push-over analysis following (ATC-40). One was designed based on a design practice which takes in account only gravity load and other frame was designed based on Saudi Building Code (SBC-301) [4]. The results explained that the RC structure designed considering only gravity load was found not sufficient. While, the RC frame designed based on (SBC 301) satisfies Immediate Occupancy (IO) acceptance criteria following (ATC-40).
- In 2015, El Azizi [5] tested six RC walls under displacement controlled quasi-static cyclic lateral loading. The walls had three different configurations, rectangular, flanged and end confined. The study aimed at calculating and comparing the ductility capacities of the three configurations. Figure (1) shows the used wall configurations and reinforcement details. The results of the study show that the flanged and end confined walls had a significantly higher ductility capacity than their rectangular counterparts. El-Azizi suggested assigning different seismic force reduction factors for walls with different cross sectional configurations.

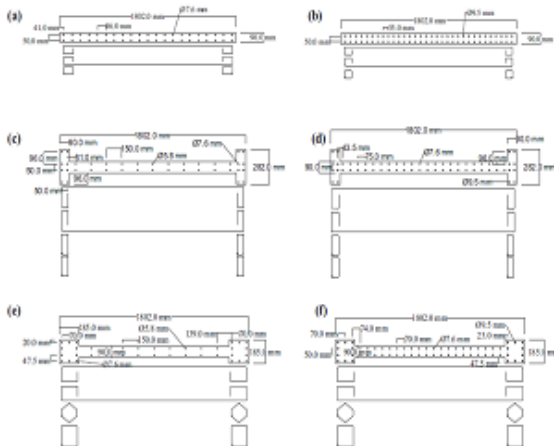


Figure 1: Wall Configurations and Reinforcement (El-Azizi et al., 2015)

- In 2016, Bholebhavi [6] modeled RC SMRF with medium rise that have irregularity in elevation, vertical irregularity and in Plan irregularities to evaluate the (R) factor for irregular RC structures using the non-linear static analysis. The results explained that as percentage of horizontal irregularities increases R-value decreases, as a percentage of sudden vertical irregularities increases, R-value was decreasing and a structure with gradual irregularities in elevation didn't show considerable deviation in R-value.

- In 2004, Sungjin [7] studied the different factors that have effect on ductility. Evaluation of distortion capacity of the RC columns was important in performance-based seismic design. The capacity of RC columns in deformation was being expressed in various ways, which are drift, curvature ductility or displacement ductility. The effect of axial load, reinforcement ratio, volumetric ratio, concrete strength and shear span to depth ratio of the confining reinforcement, on various ductility factors were discussed and evaluated.

### 3. Non-Linear Numerical Model for RC Structures

#### 3.1. Element Model

The ABAQUS program [8] is a powerful, intuitive, finite element program developed and maintained by Hibbit, Karlsson and Sorensen, Inc. (HKS) through their company established in 1978. The ABAQUS system consists of a pre-processor ABAQUS/Standard, ABAQUS/Explicit and a postprocessor ABAQUS/Viewer or ABAQUS/CAE. The program is completely modular allowing the user to acquire and load only the modules that are needed. The input data for the program include nodal points, type of element, loading condition, material properties, dimensioning of the geometry of the structure, the restraints of nodes, the required type of analysis and the termination criteria.

#### 3.2. Material model

In order to obtain accurate analysis, proper material models were needed. To be able to understand the mechanical behavior to final failure, it was important that this non-linear behavior could be simulated in the finite element analyses. The nonlinearities of the concrete in compression and the steel were accounted for with plasticity models. Three major effects cause the non-linear response of reinforced concrete namely:

- Crushing of concrete in compression.
- Cracking of concrete in tension.
- Yielding of reinforcement.

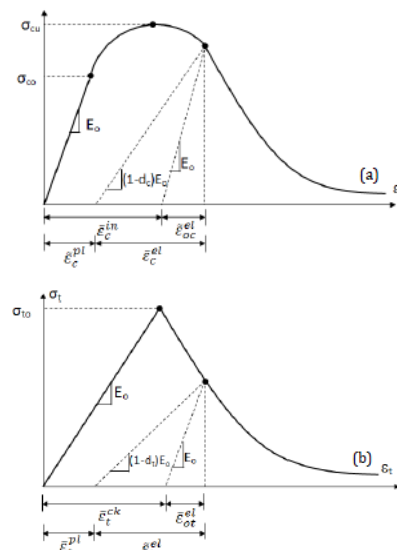


Figure 2: Behaviour of concrete under axial compressive (a) and tension (b) strength (ABAQUS User Manual, 2008 [9])

Nonlinearities also arise from the interaction of the constituents of reinforced concrete such as, bond - slip between reinforcing steel and surrounding concrete, aggregate interlock at a crack and dowel action of the reinforcing steel crossing a crack. The steel elements were provided with isotropic multi linear elasto-plastic material model.

The degradation of the elastic stiffness is characterized by two damage variables,  $d_t$  and  $d_c$ , which are assumed to be functions of the plastic strains, temperature, and field variables:

$$d_t = d_t(\varepsilon_t^{pl}, \theta, f_i) : 0 \leq d_t \leq 1$$

$$d_c = d_c(\varepsilon_c^{pl}, \theta, f_i) : 0 \leq d_c \leq 1$$

The damage variables can take values from zero, representing the undamaged material, to one, which represents total loss of strength. If  $E_0$  is the initial (undamaged) elastic stiffness of the material, the stress-strain relations under uni-axial tension and compression loading are, respectively:

$$\sigma_t = (1 - d_t)E_0(\varepsilon_t - \varepsilon_t^{pl})$$

$$\sigma_c = (1 - d_c)E_0(\varepsilon_c - \varepsilon_c^{pl})$$

#### 4. Response Reduction Factor

The response reduction/modification factor (R) simply represents the ratio of the maximum lateral force if the structure remains elastic ( $V_e$ ) to the lateral force ( $V_d$ ), it is designed to withstand [10]. R factor is an essential seismic design parameter that is typically used to describe the inelasticity level expected in lateral load resisting systems during earthquakes. And depends on the over-strength factor ( $\Omega$ ), the ductility factor ( $R_\mu$ ), the damping factor ( $R_\xi$ ), and the redundancy factor ( $R_R$ ) as indicated in equation (5) as suggested by ATC-19 [11].

$$R = \Omega \cdot R_\mu \cdot R_R \cdot R_\xi \quad (5)$$

The relationship between response reduction/modification factor (R), over-strength factor ( $\Omega$ ) and ductility factor ( $R_\mu$ ) is presented in Figure (3), assuming that  $R_\xi$  and  $R_R$  equal to (1.0).

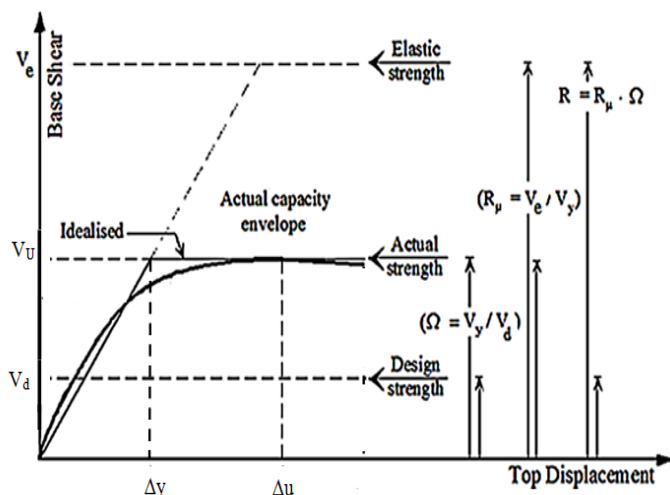


Figure 3: Relationship between response reduction/modification factor(R), over-strength factor ( $\Omega$ ) and ductility factor ( $R_\mu$ )

#### 4.1. Response Reduction Factor (R) in International Codes

##### i. ECP and ASCE Codes

The seismic force values used in design of RC buildings are conducted by dividing forces that would be associated with elastic response by a response modification factor. Table 1 illustrates the values recommended for the response modification factors in ECP code [12] and ASCE code [13].

Table 1: R factor in ECP &ASCE codes

code	R-values		
	Structural System	Type	R
Egyptian code	(RC) Moment resisting frame	Sufficient ductility	7
		Not Sufficient ductility	5
ASCE-7-10 code	(RC) Moment resisting frame	Special	8
		Ordinary	3
		Intermediate	5

##### ii. EUROPE (Eurocode 8)

The seismic design procedure in Euro-code is a single level design procedure that reduces the elastic spectral demands to the strength design level through use of a period-dependent response factor, known as “behavior factor q”. This behavior factor differs as a function of building stiffness, regularity, strength, structural system and ductility. As shown in Figure (4), if  $\frac{L_1+L_3}{L} > 0.2$ , then the structure is irregular. Hence behavior factor shall be reduced by 20%. Table 2 shows the basic values of the behavior factor  $q_0$ .

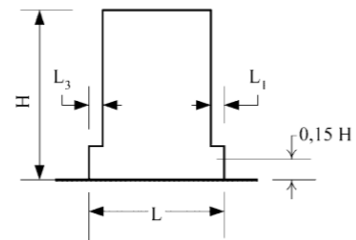


Figure (4): Criteria for regularity in Euro code [14]

Table 2: Basic value of the behavior factor,  $q_0$ , for systems regular in elevation

STRUCTURAL TYPE	DCM	DCH
Frame system, dual system, coupled wall system	$3,0\alpha_u/\alpha_1$	$4,5\alpha_u/\alpha_1$
Uncoupled wall system	3,0	$4,0\alpha_u/\alpha_1$
Torsionally flexible system	2,0	3,0
Inverted pendulum system	1,5	2,0

$\alpha_1$  and  $\alpha_u$  are defined as follows:

$\alpha_1$  is the value by which the horizontal seismic design action is multiplied in order to first reach the flexural resistance in any member in the structure, while all other design actions remain constant.

$\alpha_u$  is the value by which the horizontal seismic design action is multiplied, in order to form plastic hinges in a number of sections sufficient for the development of overall structural instability, while all other design actions remain constant. The factor  $\alpha_u$  may be obtained from a nonlinear static (pushover) global analysis.



, frames or frame-equivalent dual systems:

- One-storey buildings:  $\alpha_u/\alpha_1=1.1$ ,
- Multistory, one-bay frames:  $\alpha_u/\alpha_1=1.2$ ,
- Multistory, multi-bay frames or frame-equivalent dual structures:  $\alpha_u/\alpha_1=1.3$ .

**5. Model Verification**

In this respect, two experimental output data for reinforced concrete(RC) frames using pushover analysis and an additional experimental output data based on nonlinear time history analysis (three records for each) were compared with the output results from ABAQUS 6.14 software analytical models in order to check the reliability and validity of a nonlinear finite element model. As a measure for the evaluation, the error in the results were calculated as follows.

$$\% \text{ Error} = \left( \frac{\text{Analytical mean value} - \text{Experimental mean value}}{\text{Experimental mean value}} \right) \times 100\%$$

*5.1. Experimental Data*

Model-1:

S. Z. Korkmaz et al. 2010 [15] Tested one bay, two-story bare reinforced concrete (RC) specimen with no infill wall under a reversed cyclic loading. The goal of this test was to report on an experimental study about the Turkish EQ Code on proposed strengthening method. The specimens were subjected to lateral load that simulate the seismic action at the story level. Cycles were named as forward and backward cycles. Also, axial load was applied to top of columns. The test setup, instrumentation and loading system is presented in Figure (5). Dimensions and details of test specimens are presented in Figure (6). Figure (7) shows the ABAQUS analysis model conducted for this model. While Figure (8) shows plastic hinges formation & crushing in concrete.

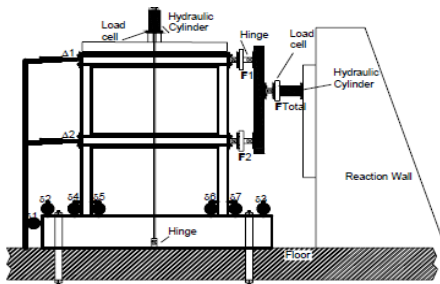


Figure 5: Test setup, loading system and instrumentation

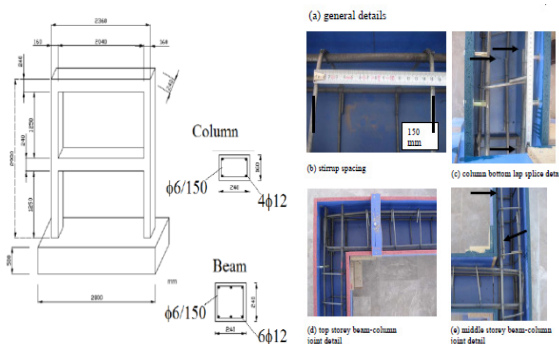


Figure 6: Dimensions and details of test specimens

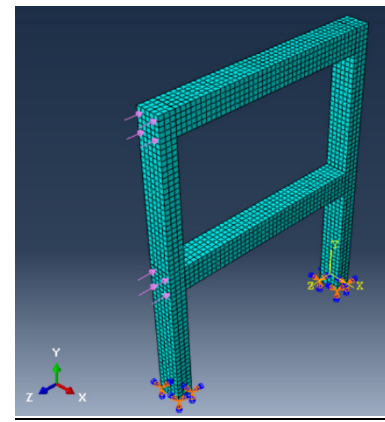


Figure 7: ABAQUS analysis model conducted for model 1

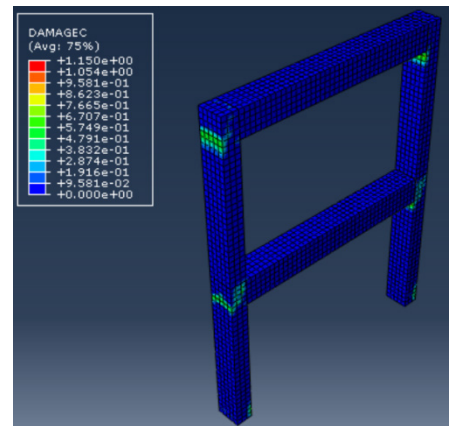


Figure 8: Plastic hinges formation & crushing in model-1

Model-2:

Ch. G. Karayannis et al. 2005 [16]. Tested single bay single story bare reinforced concrete (RC) frame specimen was constructed and tested under lateral loading. The test aims to study behavior of bare and masonry in-filled reinforced concrete (RC) frames under lateral cyclic loading, Reinforcement detailing of the reinforced concrete (RC) frame model is presented in Figure (9). Test setup is shown in Figure (10). Propagation of cracks was recorded for bare frame as presented in Figure (11). Figure (12) shows the ABAQUS analysis model conducted for this model. While Figure (13) shows plastic hinges formation & crushing in concrete.

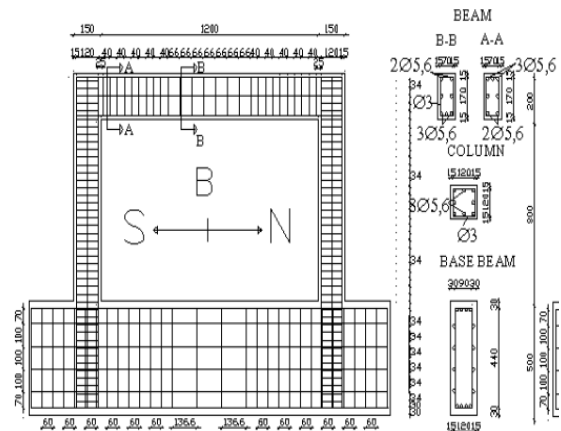


Figure 9: Reinforcement detailing of the reinforced concrete (RC) frame model (mm)

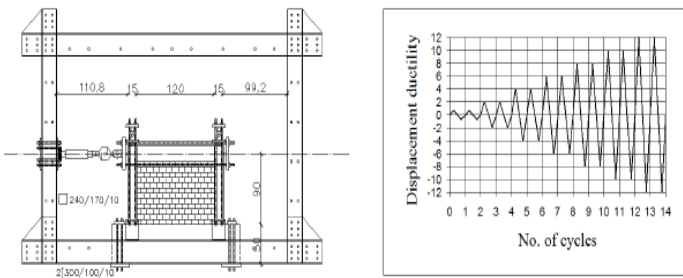


Figure 10: Test setup (cm) and loading program

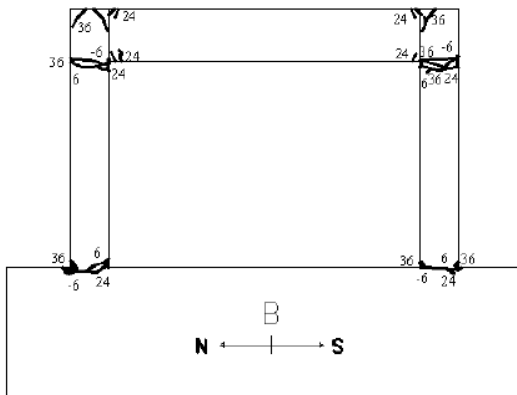


Figure 11: Propagation of cracks for bare frame

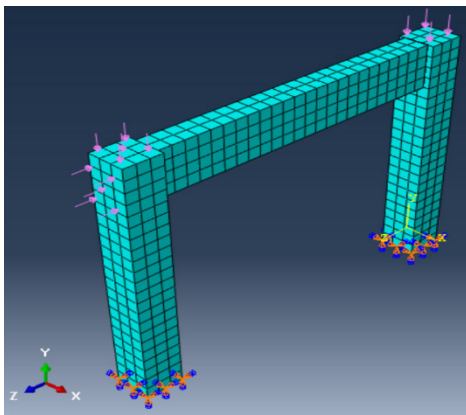


Figure 12: ABAQUS analysis model conducted for model-2

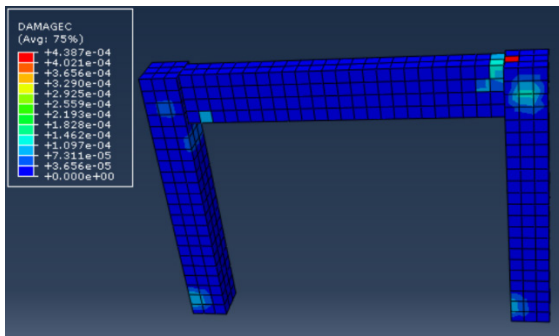


Figure 13: Plastic hinges formation & crushing in model 2

**Model-3:**

Behzad Fatabiet al.2012 [17]. Tested ten story height moment resisting building frame under shaking table using time history analysis with three records of earthquake to study dynamic [www.astesj.com](http://www.astesj.com)

response of structures. Benchmark earthquakes including the 1995 Kobe, the 1994 Northridge and the 1940 El Centro earthquakes are adopted. Figure (14) illustrate the shaking table tests on the fixed-base ten story model structures. Figure (15) shows the ABAQUS analysis model conducted for this model.

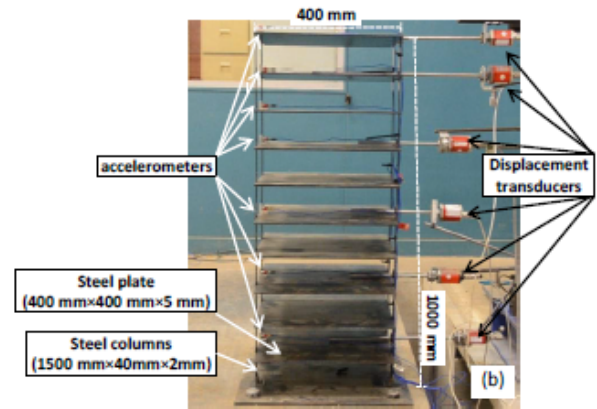


Figure 14: Ten story fixed-base model structure for shaking table tests

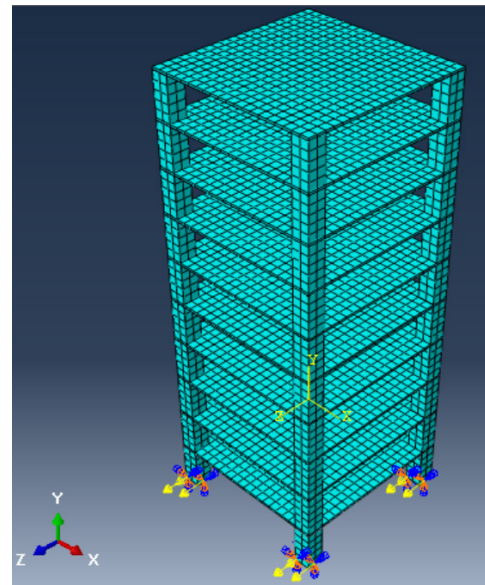


Figure 15: ABAQUS analysis model conducted for model-3

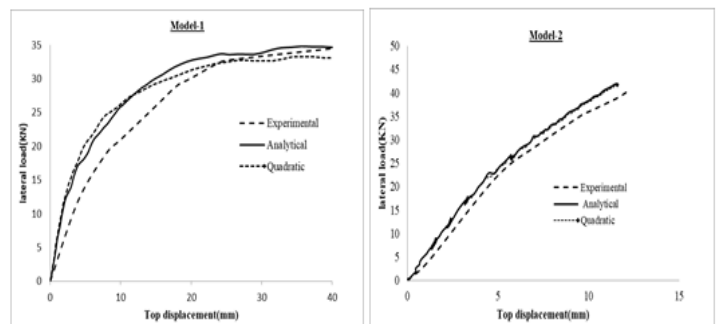


Figure 16: Modeling Results for reinforced concrete (RC) frames specimens

**5.2. Verification of Experimental Results**

A comparison between experimental and analytical load-displacement curves for all reinforced concrete frames is presented in Figures (16) & (17). The figure shows that the analytical load-

displacement curves are matching the experimental load-displacement curves. The quadratic curve also refers to the analytical results but using quadratic meshing instead of linear meshing, considering that using quadratic meshing in the analysis increases the accuracy of results. As shown in Figure (16), using quadratic meshing make the error smaller.

Table (3) shows the comparison between experimental and analytical values of ultimate flexural strength.

Table 3: Results for models-1 & 2 (Pushover analysis)

Model	Experimental (shear)	Analytical (shear)	% Error	Experimental (displacement)	Analytical (displacement)	% Error
	Q <sub>ult</sub> (KN)	Q <sub>ult</sub> (KN)		Δ <sub>ult</sub> (mm)	Δ <sub>ult</sub> (mm)	
1	34.51	34.77	0.75%	40	31.50	21.25
2	40.50	41.85	3.33%	12.21	11.50	5.82

While for model-3, time history results were verified as shown in Table (4) & Figure (17)

Table 4: Results for model-3 (Time history analysis)

Story No.	(NORTHRIDGE 1994)		(KOBE 1995)		(ELCENTRO 1940)	
	Experimental displacement	Analytical displacement	Experimental displacement	Analytical displacement	Experimental displacement	Analytical displacement
0	0	0	0	0	0	0
1	1	0.98	1	1.04	1	0.966
3	5	5.79	2.5	2.66	2.5	1.95
5	11	11.65	6	5.3	5	5.82
7	16	16.2	9	8.25	7.5	7.65
9	17.8	18	12.5	11.1	8.5	9.3
10	18	18.8	13	12.01	9	10.9

% Error (NORTHRIDGE 1994)		% Error (KOBE 1995)		% Error (ELCENTRO 1940)	
Story No.	Displacement	Story No.	Displacement	Story No.	Displacement
0	0	0	0	0	0
1	2.00	1	4.00	1	3.40
3	15.80	3	6.40	3	22.00
5	5.91	5	11.67	5	16.40
7	1.25	7	8.33	7	2.00
9	2.86	9	11.20	9	9.41
10	4.44	10	7.62	10	21.11

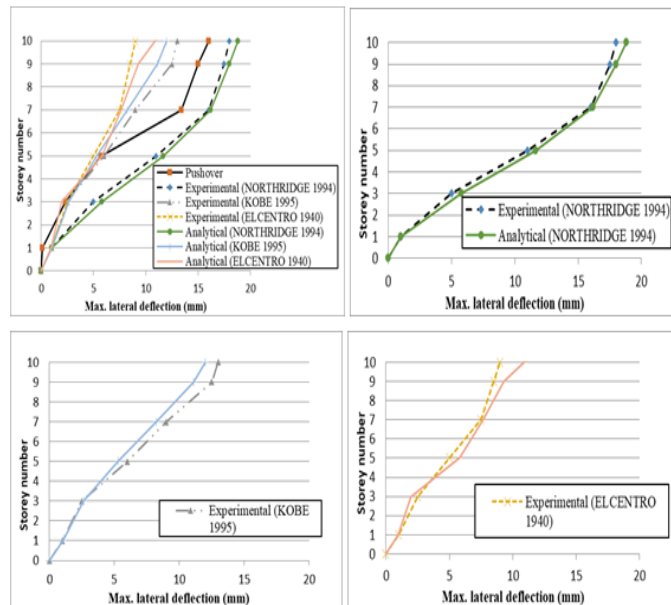


Figure 17: Results for Time history Analysis Records.

5.2.1. Observations from verification models:

Since the comparison between experimental and analytical results showed a negligible error, consequently the ABAQUS

analytical models could be considered to capture the real behavior of the RC concrete frames.

- It's observed that using quadratic meshing in ABAQUS increased the accuracy in results because:
  - The high order approximation for the finite element (keeping the same size) leads to a smaller error for the solution if all parameters (boundary conditions, geometry, materials) are sufficiently smooth. Thus the quadratic approximation is better than linear one.
  - Triangular shapes for FE of low order (linear) leads to the larger error (locking for bending)
  - Small size of FE leads to the smaller error (but it leads to many FE's).
- It's observed that full detailed reinforcement modeling for columns & beams in ABAQUS model increased accuracy of results.

6. Parametric Study

6.1. Modeling Data

Three case studies were analyzed to investigate the effect of basements on (R) factor. Figures (18), (19), (20) & (21) show the case studies geometry (plans, sections & details) used for modeling. The case studies configurations were selected to simulate a huge number of buildings that contain the same elements with a proper distribution in plan. In the first two cases, retaining walls were used to support the two stories in basement, as the RC building contains two stories in basement and five typical stories above ground with an upper roof, but in the first case the soil pressure on retaining walls was taken in account while modeling, while in the second case the soil pressure was neglected. In the third case, no retaining walls were used, so the RC building contains ground, first floors and five typical floors with an upper roof. Their structural system is combined between RC frames and cores. Figure (16) shows reinforcement details for columns, beams & cores.

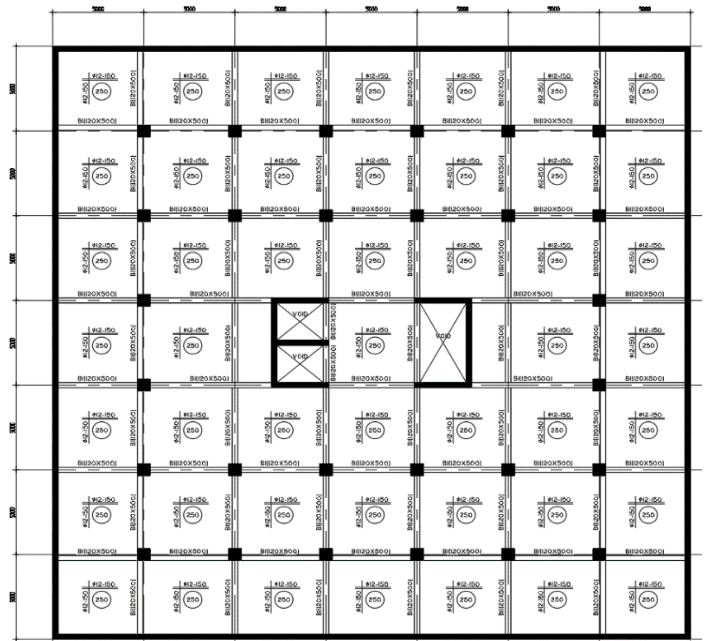


Figure 18: 1st & 2nd case study geometry (for two stories in basements)



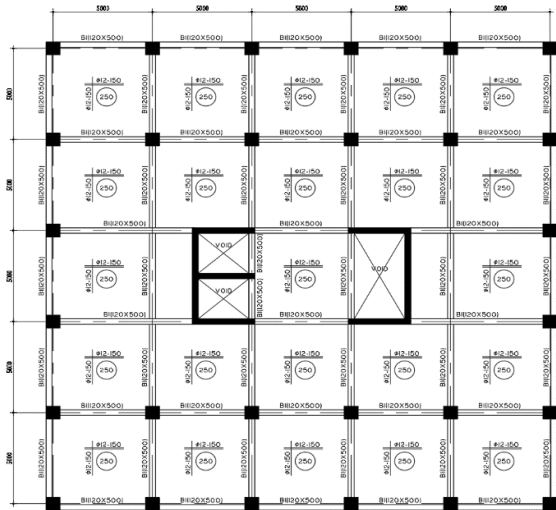


Figure 19: 1st & 2nd case study geometry (for five stories in super structure)

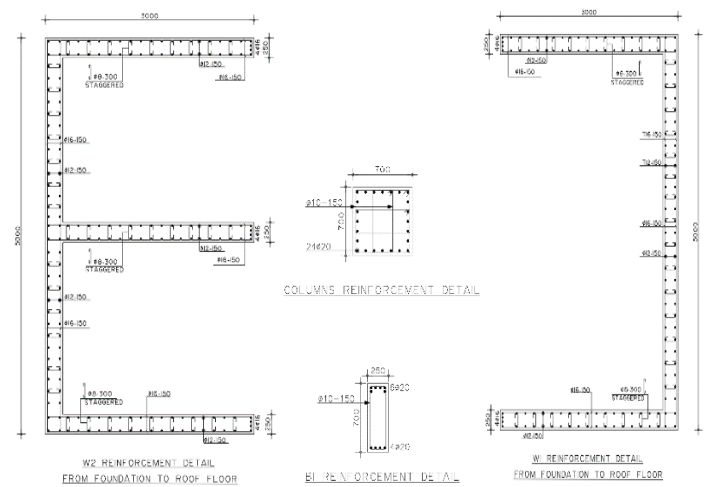


Figure 22: Case studies geometry (reinforcement details)

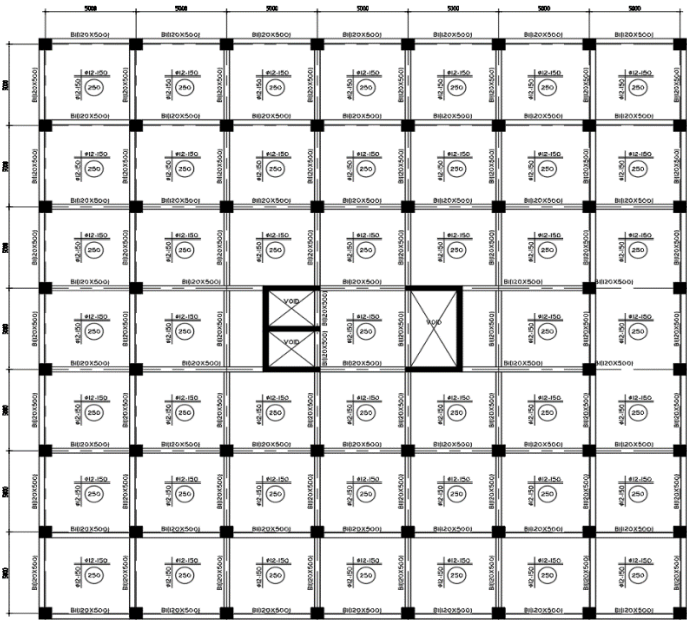


Figure 20: 3rd case study geometry (for ground & first floors)

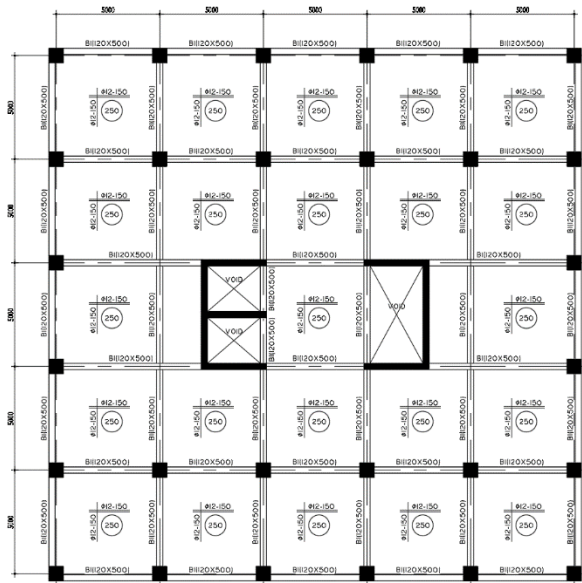


Figure 21: 3rd case study geometry (for five typical stories)

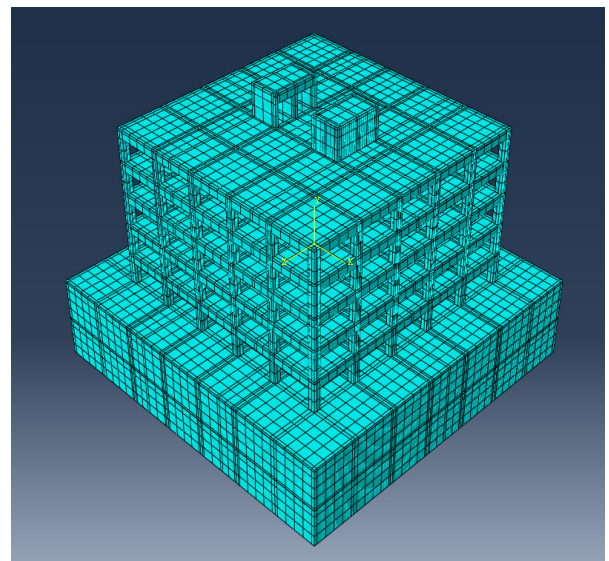
The following material properties were used in the parametric study:

- Concrete compressive strength (cube) ( $f_{cu}$ ) = 40 MPa
- Concrete young's modulus ( $E_c$ ) = 26587.215 MPa
- Specific weight for concrete = 25 kN/m<sup>3</sup>
- Steel yield strength ( $f_y$ ) = 400 MPa for vertical reinforcement and stirrups
- Steel young's modulus ( $E_s$ ) = 200 GPa
- Specific weight for steel = 78.5 kN/m<sup>3</sup>
- Specific weight for steel = 78.5 kN/m<sup>3</sup>

Vertical load was assigned to all levels, as follows:

- For basement stories & typical floors:  
Floor Cover = 2 kN/m<sup>2</sup>, Walls load = 2 kN/m<sup>2</sup> and Live Load = 2 kN/m<sup>2</sup>.
- For roof floor & upper roof floor:  
Floor Cover = 2.5 kN/m<sup>2</sup> and Live Load = 2 kN/m<sup>2</sup>.

Figure (23) shows the ABAQUS modeling for concrete solid meshed elements and steel wire elements, while Figure (24) shows the boundary conditions for the concrete footing had locked translational degrees of freedom in all directions.



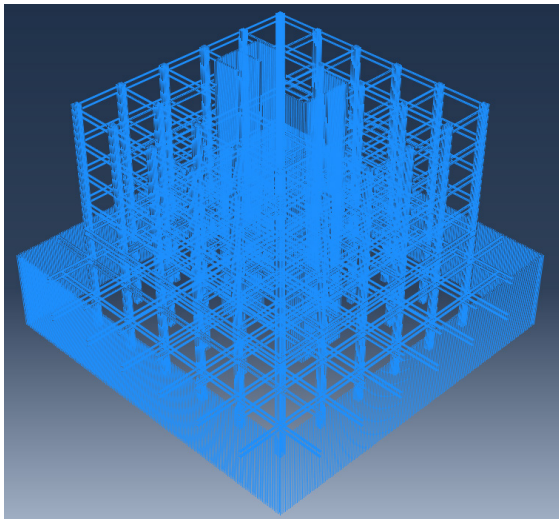


Figure 23:(a): 1st Case study ABAQUS model (concrete meshed elements & steel wire elements)

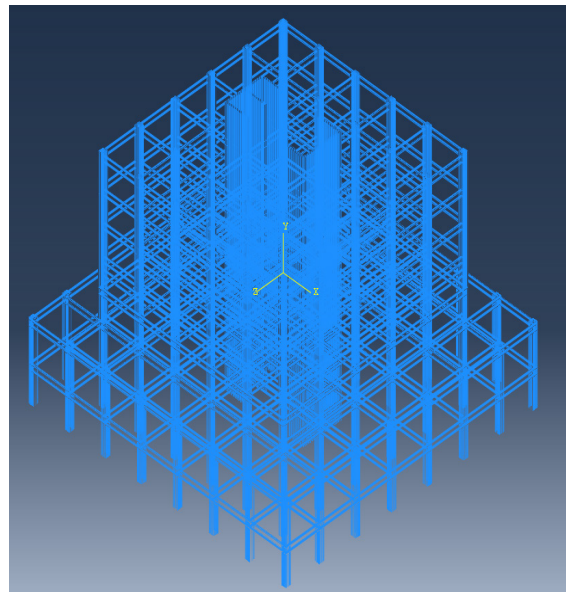
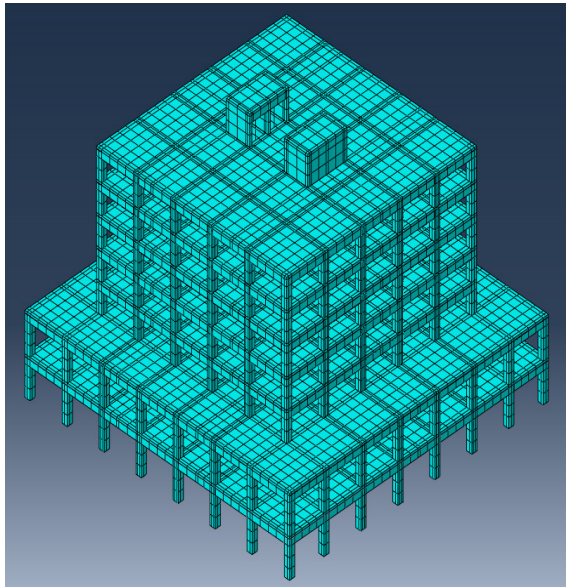


Figure 23.(b): 3rd Case study ABAQUS model (concrete meshed elements & steel wire elements)

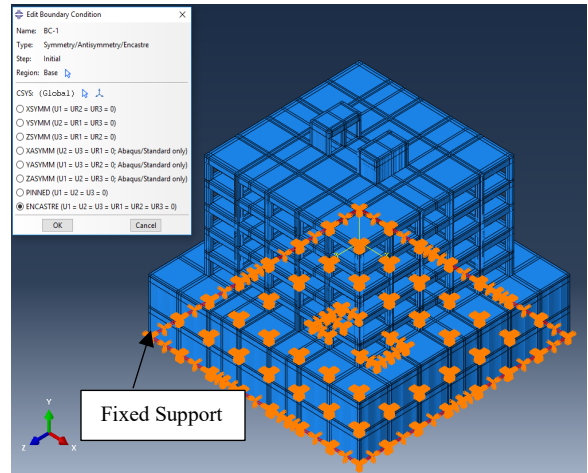


Figure 24.(a): 1st Case study ABAQUS model (boundary conditions)

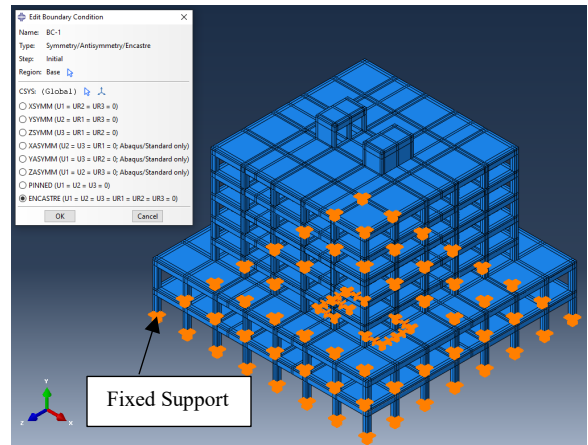


Figure 24.(b): 3rd Case study ABAQUS model (boundary conditions)

## 6.2. Methods of Analysis

Two methods of analysis are used in the parametric study in order to model RC buildings considered in this study. These methods are non-linear static pushover analysis and non-linear time history analysis.

### 6.2.1. Pushover model

The incremental load assigned in pushover analysis model developed for RC buildings was considered to increase from basement to the top level of the building until amplification factor for load = 1.0, as shown in Figure (25).

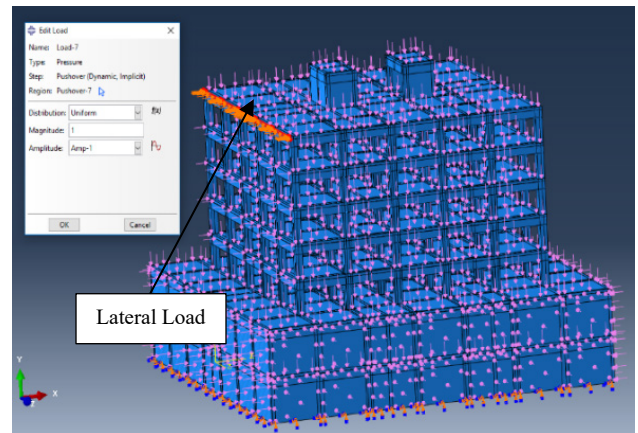


Figure 25.(a): 1st Case study ABAQUS models (loading)



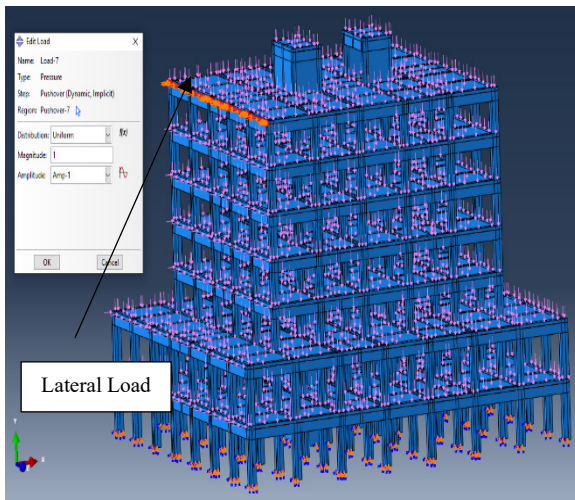


Figure 25.(b): 3rd Case study ABAQUS models loading

### 6.2.2. Time history models

A series of three earthquakes with low, medium, and high frequencies were selected for the nonlinear dynamic analyses to be assigned for the 1<sup>st</sup> case study and the 3<sup>rd</sup> case study. By reference the PEER database (PEER 2006) [18], time history of selected earthquakes along with peak ground acceleration (PGA) and year of occurrence of the earthquake are illustrated in Figure 26. The maximum value for base shear is considered as per ECP code recommendations; in case of studying three earthquakes.

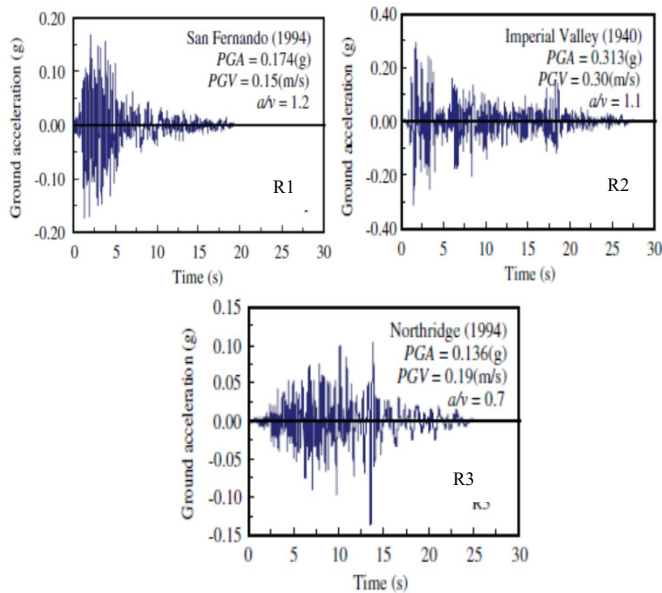


Figure 26: Time history of selected ground motions

### 6.3. Failure criteria

The analyses were continued until the earlier from two options as per ECP code requirements:

- Stress in reinforcement = 400MPa
- Strain in concrete = 0.002 at maximum compressive strength according to ECP code [19], as shown in Figure (27). Figure (28) shows deformation for the 1<sup>st</sup> case study, while figure (29) shows plastic hinges formation & crushing in concrete for the 3<sup>rd</sup> case study.

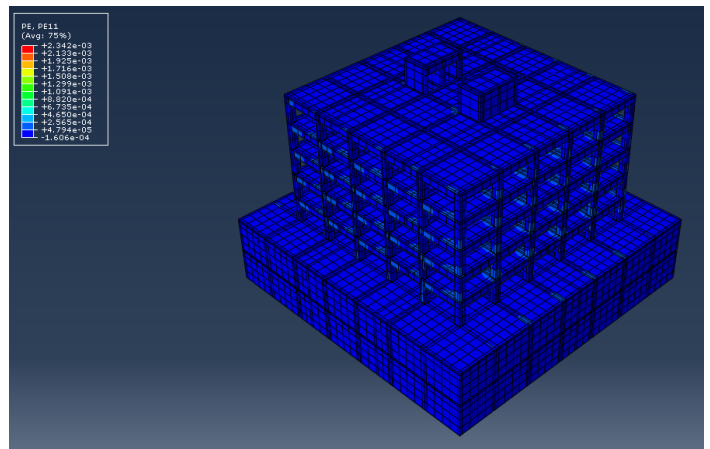


Figure 27: Strain for concrete

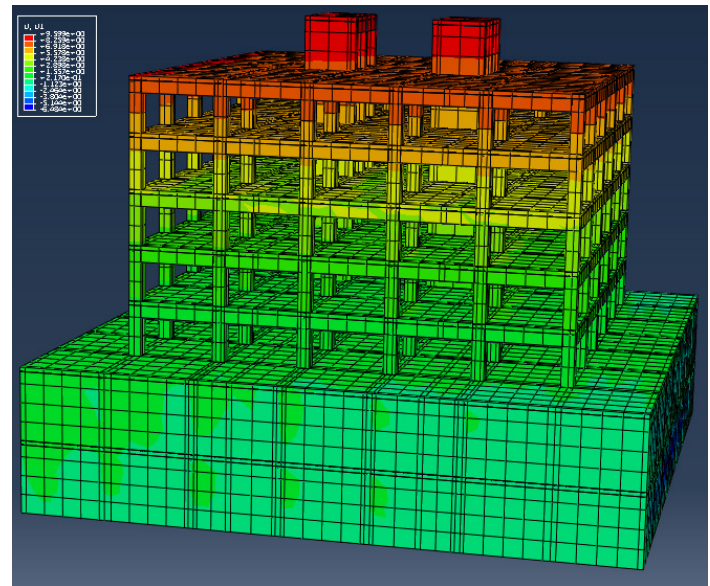


Figure 28: Deformed shape for the 1st case study

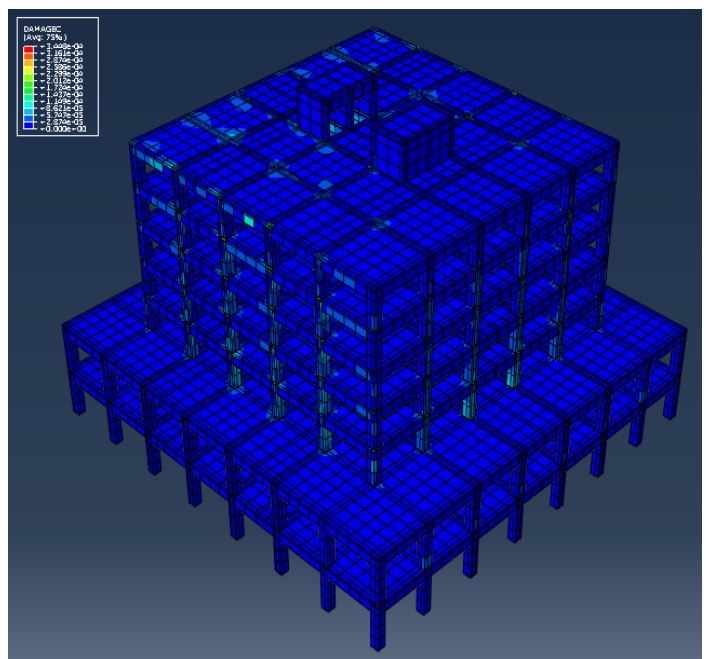


Figure 29: Plastic hinges formation & crushing in concrete for the 3rd case study

6.4. Observations from The Parametric Study

6.4.1. Pushover Results

The results for base shear, displacement & calculated response modification factor considering pushover analysis are listed in Table (5) and Figures (30), (31) & (32).

Table (5): Results for studied RC buildings based on pushover analysis

Case study	V <sub>u</sub> (kN)	V <sub>d</sub> <sup>d</sup> (kN)	T <sup>e</sup> (second)	T <sup>f</sup> (second)	R <sub>s</sub> <sup>g</sup>	Δ <sub>u</sub> <sup>h</sup> (mm)	Δ <sub>y</sub> <sup>i</sup> (mm)	μ <sup>j</sup>	R <sub>μ</sub> <sup>k</sup>	R
1 <sup>a</sup>	7191.07	4314.64	0.73	0.706	1.67	7.82	3.52	2.22	2.22	3.71
2 <sup>b</sup>	7202.17	4321.30	0.73	0.714	1.67	14.08	7.02	2.01	2.01	3.36
3 <sup>c</sup>	2231.73	1339.04	0.73	0.952	1.67	20.03	6.00	3.34	3.34	5.58

<sup>a</sup>The first case study where retaining walls were used and soil pressure was assigned to them.

<sup>b</sup>The second case study where retaining walls were used and soil pressure wasn't assigned to them.

<sup>c</sup>The third case study where retaining walls weren't used.

<sup>d</sup>V<sub>d</sub> Design base shear equal 60% of the ultimate load capacity as suggested by Uang (1991) [20].

<sup>e</sup>T Calculated max. time period as per ECP requirements, time period shall not exceed (1.2\*0.05 \*h<sup>0.75</sup>)

<sup>f</sup>T Fundamental period obtained from ETABS model for multi degree of freedom

<sup>g</sup>R<sub>s</sub> = V<sub>u</sub> / V<sub>d</sub>

<sup>h</sup>Δ<sub>u</sub> Max Top displacement at V<sub>u</sub>, calculated based on peak load, as recommended by Park, R., and Paulay, T,1988 [21].

<sup>i</sup>Δ<sub>y</sub> yield displacement, calculated based on equivalent elasto plastic yield as recommended by Park, R. & Paulay, T,1988 [21].

<sup>j</sup>μ =Ratio between the ultimate displacement and the yield displacement (Δ<sub>u</sub>/ Δ<sub>y</sub>).

<sup>k</sup>R<sub>μ</sub> Function of μ depends on time period, as per Newmark & Hall assumptions [22]:

T < 0.2 seconds R<sub>μ</sub>=1  
 0.2 < T < 0.5 seconds R<sub>μ</sub>=√(2μ - 1)  
 T > 0.5 seconds R<sub>μ</sub>=μ

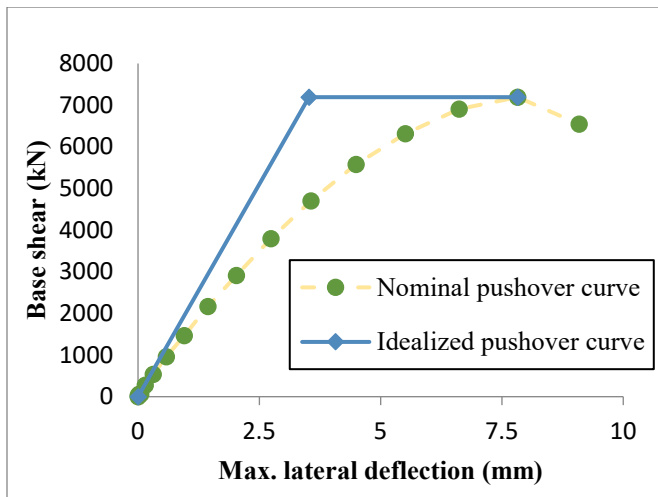


Figure 30: Base shear versus top displacement (nominal curve & idealized curve) for 1st case study

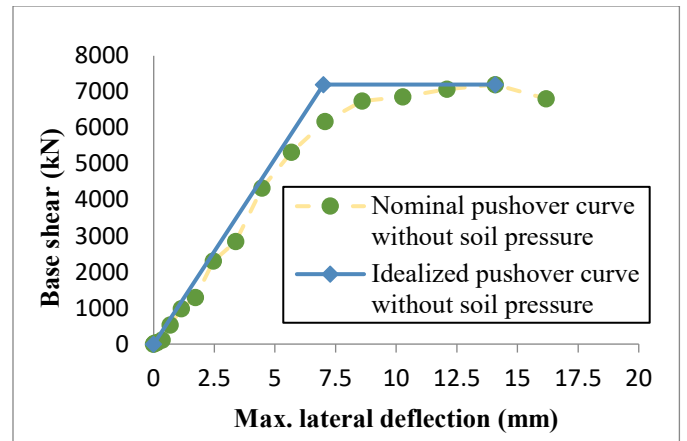


Figure 31: Base shear versus top displacement (nominal curve & idealized curve) for 1st case study without soil pressure

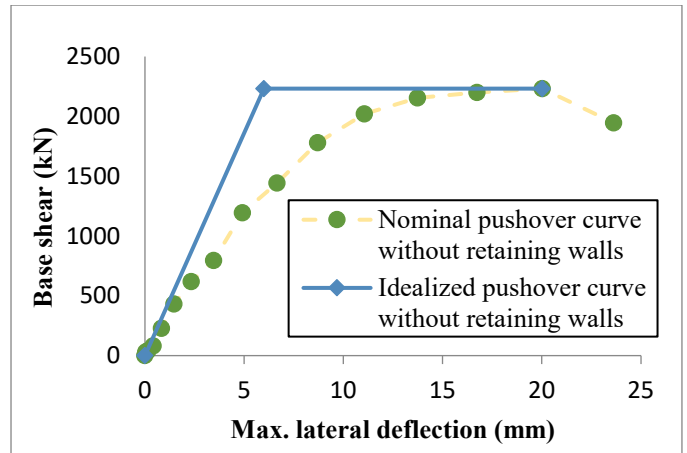


Figure 32: Base shear versus top displacement (nominal curve & idealized curve) for 2nd case study

6.4.2. Time history Results

The results for time history analysis models developed for the RC building (1<sup>st</sup> & 3<sup>rd</sup> case studies) are listed in Tables (6) & (7).

Table (6): Results for all reinforced concrete (RC) frames models based on time history analysis

Case study	Record	PGA	PGA (Max.)	(V <sub>d</sub> = 4314.64 kN)	
				V <sub>e</sub> (kN)	R = V <sub>e</sub> / V <sub>d</sub>
1 <sup>st</sup>	1- San Fernando (1994)	0.174g	1.55g	18578.7	4.31
	2- Northridge (1994)	0.136g	1.03g	17251.7	4.00
	3- Imperial Valley (1940)	0.313g	1.19g	16143.1	3.74
	Max.				4.31

Case study	Record	PGA	PGA (Max.)	(V <sub>d</sub> = 1339.04 kN)	
				V <sub>e</sub> (kN)	R = V <sub>e</sub> / V <sub>d</sub>
3 <sup>rd</sup>	1- San Fernando (1994)	0.174g	1.55g	9028.17	6.67
	2- Northridge (1994)	0.136g	1.03g	8431.26	6.30
	3- Imperial Valley (1940)	0.313g	1.19g	7943.55	5.93
	Max.				6.67

Table 7: Comparison between time history results and pushover results for the 1st &amp; 3rd case study

Case study	Time history	Pushover
	R	R
1 <sup>st</sup>	4.31	3.71
3 <sup>rd</sup>	6.67	5.58

## 7. Conclusions

A parametric study was conducted to illustrate how the response modification factor would be affected in case of existence of multi-story basements, number of stories underground and taking in account the pressure effect from soil besides the retaining walls. The first main objective was to determine the R-value. While the second main objective was to compare the calculated response modification factor (R) values for reinforced concrete (RC) shear walls with those specified in ECP and international codes.

Some interesting conclusions could be extracted from the parametric study regarding the building behavior, taking in account that the calculated R values could be related only to similar RC structures, as follows:

- The (R) factor values, calculated for the RC structures with two basement stories and supporting retaining walls doesn't match ECP code recommended values, because the stiffness increases due to existence of retaining walls, which isn't considered in ECP code.
- The (R) factor values calculated using pushover analysis & time history analyses for the RC structures without basement stories (3<sup>rd</sup> case study) are close to that recommended in ECP & ASCE codes.
- The (R) factor values, calculated from analytical models for the RC structures with basement stories (1<sup>st</sup> case study), match the recommended values in Euro code. As the Euro code specify unique values for (R) factor for RC structures that have irregularity in elevation (a reduction of 20% shall be used), which is not considered in ECP code.
- The (R) factor increases with a significant value when removing retaining walls, while it decreases when neglecting soil pressure on retaining walls, as the ductility factor increases and the time period increases.
- The time period calculated from analysis models increases when removing retaining walls, as the RC structure stiffness decreases when removing retaining walls.
- The (R) factor is very sensitive to the existence of the retaining wall, while it isn't as much as sensitive for considering soil pressure on retaining walls, due to changing in stiffness in case of existence of retaining walls.
- Pushover analysis gives results for (R) factor that are close to time history analysis results.
- From pushover analysis, Increasing number of stories from five, ten to fifteen leads to a larger displacement, also a larger ductility factor.
- From pushover analysis, Increasing number of stories from five, ten to fifteen leads to a bigger (R) factor.

## Conflict of Interest

The authors declare no conflict of interest.

## Notations

- DCM: Ductility Class Medium
- DCH: Ductility Class High
- $E_s$ : Steel Young's Modulus
- $E_c$ : Concrete Young's Modulus
- $F_{cu}$ : concrete Compressive Strength
- EQ: Earthquake
- $f_y$ : Steel Yield Stress
- FE: Finite Element
- R: Response Reduction/Modification Factor
- RC: Reinforced Concrete
- $R_\mu$ : Ductility Factor
- $V_u$ : Maximum Base Shear
- $\Delta y$ : Yield Displacement
- $\mu$ : Ductility Capacity
- $\Omega$ : Over-Strength Factor

## References

- [1] Asgarian and Shokrgozar et al. "BRBF response modification factor", Journal of Constructional Steel Research, 2008.
- [2] Apurba Mondal et al. (Performance-based evaluation of the response reduction factor for ductile RC frames), 2014. DOI: 10.1016/j.engstruct.2013.07.038
- [3] Hakim et al. "Seismic Assessment of an RC building using pushover analysis", Saudi Arabia, 2014. DOI:10.5281/zenodo.14043
- [4] (SBC-301) Saudi Building Code.
- [5] El Azizi et al., "Assessment of the seismic performance of reinforced masonry and reinforced concrete shear wall buildings", M.Sc. Thesis, Faculty of Engineering, Ain Shams University, Cairo, Egypt, 2015.
- [6] Bholebhavi Rahul D.1, Inamdar V.M., "An Evaluation of Seismic Response Reduction Factor for Irregular Structures Using Non-Linear Static Analysis" International Journal of Innovative Research in Science, Engineering and Technology, ISSN (Online): 2319-8753, ISSN (Print): 2347-6710, Issue 5, May 2016. DOI:10.15680/IJRSET.2016.0505136
- [7] Sungjin BAE, "What Do We Know About The Performance-Based Design Of Columns?" Issue August 2004.
- [8] ABAQUS software V6.14.
- [9] ABAQUS/Standard Analysis User's Manual, Version 6.14.
- [10] Bedeir, H., "Assessment of the seismic performance of reinforced masonry and reinforced concrete shear wall buildings", M.Sc. Thesis, Faculty of Engineering, Ain Shams University, Cairo, Egypt, 2016.
- [11] Applied Technology Council (ATC). (2008). "Quantification of building seismic performance factors." ATC-63, Project rep., 90% draft, Redwood City.
- [12] ECP (Egyptian Code of Practice for loading), 2012.
- [13] ASCE 7 (Minimum Design Loads for Buildings and Other Structures. American Society of Civil Engineers. USA), 2005. [https://doi.org/10.1061/\(ASCE\)0733-9445\(2005\)131:3\(507\)](https://doi.org/10.1061/(ASCE)0733-9445(2005)131:3(507))
- [14] Eurocode 8 Provisions (2004).
- [15] S. Z. Korkmaz, "Experimental study on the behavior of non-ductile infilled RC frames strengthened with external mesh reinforcement and plaster composite, Issue 18 November 2010. <https://doi.org/10.5194/nhess-10-2305-2010>
- [16] Ch. G. Karayannis et al. "Seismic behavior of infilled and pilotis RC frame structures with beam-column joint degradation effect", The Democritus University of Thrace, Greece, 2005. DOI: 10.1016/j.engstruct.2011.06.006
- [17] Behzad Fatabiet, , Effect of Dynamic soil-pile-structure interaction on seismic response of mid-rise moment resisting frames", Issue June 2012.
- [18] PEER database (PEER 2006).
- [19] ECP (Egyptian Code of Practice for design), 2017.
- [20] Uang, C., "Establishing R (or R<sub>w</sub>) and Cd factors for building seismic provisions", J. Struct. Eng., 117(1). 19-28, (1991). DOI: 10.1061/(ASCE)0733-9445(1991)117:1(19)
- [21] Park, R., and Paulay, T "Reinforced Concrete Structures", Wiley, New York, 1988. DOI: 10.1002/9780470172834.ch5
- [22] Newmark, N. M., and Hall, W. J., "Earthquake spectra and design", EERI Monograph Series, Earthquake Engineering Research Institute, Oakland, Calif, 1982. DOI: 10.1007/s11803-016-0341-1



# Transfer Learning and Fine Tuning in Breast Mammogram Abnormalities Classification on CBIS-DDSM Database

Lenin G. Falconi<sup>\*1</sup>, Maria Pérez<sup>1</sup>, Wilbert G. Aguilar<sup>1</sup>, Aura Conci<sup>2</sup>

<sup>1</sup>Escuela Politécnica Nacional, Facultad de Ingeniería de Sistemas, 170517, Ecuador

<sup>2</sup>Federal Fluminense University, VisualLab, Computer Institute, 24210-240, Brazil

## ARTICLE INFO

Article history:

Received: 15 January, 2020

Accepted: 18 February, 2020

Online: 11 March, 2020

Keywords:

Transfer Learning

Fine Tuning

Convolutional Neural Networks

Mammogram classification

## ABSTRACT

Breast cancer has an important incidence in women mortality worldwide. Currently, mammography is considered the gold standard for breast abnormalities screening examinations, since it aids in the early detection and diagnosis of the illness. However, both identification of mass lesions and its malignancy classification is a challenging problem for artificial intelligence. In this work, we extend our previous research in mammogram classification, where we studied NasNet and MobileNet in transfer learning to train a breast abnormality malignancy classifier, and include models like: VGG, Resnet, Xception and Resnext. However, training deep learning models tends to overfit. This problem is also carried out in this work. Our results show that Fine Tuning achieves the best classifier performance in VGG16 with AUC value of 0.844 in the CBIS-DDSM dataset.

## 1 Introduction

This work is an extension of our work originally presented in IWS-SIP 2019 [1] about mammogram abnormalities classification using *Transfer Learning* (TL) with Mobilenet [2] and Nasnet [3]. In this paper, we also address the classification problem of mammogram abnormalities using the CBIS-DDSM [4] dataset, but we extend the experimentation in transfer learning to other ImageNet pre-trained convolutional neural network (ConvNet) models like: Resnet, Resnext, Xception; to name a few. Finally, *Fine Tuning* (FT) is used in order to address the overfitting problem and improve previous results on the CBIS-DDSM dataset.

Despite the increase in understanding of breast cancer as a disease, it is still a major public health problem worldwide because of the incidence and mortality rates it presents [5]. According to the International Agency for Research on Cancer (IARC), this illness is the second most frequent form of cancer among women worldwide with 2,088,849 (11.6%) new cases and 626,679 (6.6%) of deaths [6]. The mammogram exam remains the gold standard for screening examination, mainly because it is the only screening test that has proven to reduce mortality [7]. However, mammography has some limitations like the variability of its sensitivity, which is inversely proportional to breast density, the false positive and negative rates, and the patient's exposure to radiation [7]. Other

screening tests available are: ultrasound, magnetic resonance (MRI), tomosynthesis, and infrared thermography [8]-[9]; in most cases, the aforementioned screening tests are used as adjunct tests.

The mammogram exam diagnostic relies on the radiologist's experience for detection. However, 10% of all woman screened for cancer are called back for additional testing and just as little as 0.5% of them are diagnosed with breast cancer [10]. This shows that it is important to design CAD systems that aid specialists, and train new ones, in breast lesions detection. A "classic" CAD system is comprised of 5 main stages: image pre-processing, image segmentation or region of interest (ROI) definition, feature extraction and selection, classification, and performance evaluation [9, 11]. However, this model can be said to be in change due to advances in the field of machine learning, specifically in *Deep Learning*; which allows to automatically learn representations of data with multiple levels of abstraction through deep convolutional neural networks [12]. For instance, in the field of computer vision, the classification of natural images has shown an incredible increase in performance since 2012, when the AlexNet ConvNet model to classify natural images in 1000 categories presented in [13] achieved a 15.3% top 5 test error rate. As a matter of fact, the stages of feature extraction and classification can be solved directly by a ConvNet [14]. This reduces the need for feature hand engineering, which was tradition-

\*Corresponding Author: Lenin G. Falconi, lenin.falconi@epn.edu.ec



ally used to create the feature vector, because a ConvNet is able to synthesize its own feature vector [15]. All of this confirms the point indicated in [11] that the development in both image techniques and computer science enhance the interpretation of medical images.

The success of ConvNets and deep learning in computer vision tasks such as image classification heavily relies on the number of examples used in training the model under the supervised learning paradigm [16]. Unfortunately, mammogram public datasets are not “deep enough”. In this context, transfer learning and fine tuning are deep learning techniques that can aid the development of accurate enough classifiers by transferring knowledge from another domain where large datasets are available. One of the main problems when dealing with small number of examples in training is overfitting. Transfer Learning and Fine Tuning aid in overcoming this disadvantage of working with ConvNets.

In this work, we aim to classify region of interest images from mass tumors of the CBIS-DDSM [4] dataset. We extend our previous experimentation presented in [1] by using different ConvNets models and also the Fine Tuning technique in order to increase the performance of the classifier of breast mammogram abnormalities in benign and malignant. Our research results indicate that Fine Tuning is able to train an accurate classifier and overcome overfitting. Also, we have included the ROC curve metric to measure the performance of the classifiers here studied.

The remainder of this paper is organized as follows: In Section 2, we perform a review of machine learning concepts related to the current research; specifically convolutional neural networks, transfer learning and fine tuning. Literature review of related works in the field is in Section 3. Our proposed experimental method, dataset, and model are presented in Section 4. Section 5 presents experimental data results. Finally, discussion and future works are presented in Section 6 and 7, respectively.

## 2 Deep Learning Background

### 2.1 Convolutional Neural Networks

Models based on the Convolutional Neural Networks (ConvNets) architecture have been able to achieve high accurate results in image classification and detection tasks in the ImageNet[17] dataset, under the supervised learning paradigm and back-propagation. That is the case of residual networks, proposed in [18], which achieved a 3.57% error rate in the ImageNet test set in 2015.

Traditional pattern recognition classifiers rely on a hand designed feature extractor that derives relevant information from the raw input data [16]. Thus, the feature extraction step aims to reduce the dimension of the data while characterizing the raw input data (image, sound, etc.) meaningfully so that a trainable classifier is able to categorize its feature vectors [16, 19]. However, the design of the feature extractor requires specialized knowledge about the data (hand-engineering) that, in some cases, could be unknown [19]. On the contrary, ConvNets eliminate the feature extraction process by absorbing it in their architecture [16]. As pointed out in [14], the structure of a ConvNet combines both: the feature extraction and classification steps in one single model that is trained on back-propagation; the feature extraction task is, therefore, learned from data in the first layers of the model, while the last full connecting

layers constitute the classifier task. The LeNet-5 ConvNet, proposed in [15] to solve the handwritten classification task, reduces the input image of  $32 \times 32$  into a 120 vector that is called *the feature vector*. Thus, the feature vector can be used with any type of trainable classifier to solve the classification task. In fact, this approach is used in [19], where LeNet-5 is used as a black box feature extractor for several Support Vector Machines (SVM) that are trained based on it. Something similar is performed by [14], where the authors build an AlexNet [13] like model, trained it on a large dataset, and then use the trained model as a feature extractor to train new classifiers; however, their approach is more similar to a transfer learning set-up, as it will be discussed in Section 2.2.

The deepness in the number of layers of the ConvNets has been increasing in order to obtain better results since year 2012. However, the number of layers cannot be increased indefinitely due to the vanishing and exploding gradient problems. In order to overcome this problem, the structure of the traditional ConvNet, comprised basically of convolutional and pooling layers, has been revisited. An example of those architecture designs are found in Residual Networks[18], MobileNet[2], Inception[20] and NasNet[3] ConvNets. Also the study of regularization functions has been of aid in avoiding the overfitting of the Networks in training [21, 22]. For a review of the state of the art in Convolutional Neural Networks the reader may review the works of: [12, 15, 23, 24].

Thus, ConvNets have some advantages compared with traditional artificial neural networks (ANN): reduction of training parameters by shared weights, local connections and object location invariance [12]. An ANN depends on all the connections between its layers; which increases the number of parameters to train, and makes the training of the model more expensive computationally. On the contrary, a ConvNet reduces the number of parameters trained because the convolution operation is of the local type. Yet, the main disadvantages of the ConvNet model are: the training time, which may be large since it is an hyper-parametrized model, and the susceptibility to overfitting. The most important aspect of ConvNets, as a deep learning method, consists in being a *Representation Learning* method that automatically discovers a representation of the data that is used for classification and detection tasks [12], as previously discussed. This is specially important because it implies that the need for carefully hand engineer feature extractors is not required. Remind that the feature extractor is embedded in the design of the ConvNet and, therefore, learned from data.

The success of a ConvNet relies in its architecture as well as on training the model with enough number of samples. Unfortunately, public mammogram datasets do not have as many examples as the number used per category in the ImageNet dataset. In order to overcome this difficulty, TL and FT are studied as a means to train deep ConvNets in order to classify mammogram abnormalities. In this Section we review the concept of TL and FT as it is used in this article.

### 2.2 Transfer Learning

A definition of the term is found in [25] and [26]. In their work, the purpose of TL is defined as to improve the performance of a learning algorithm in a target learning task  $\mathcal{T}^T$  (i.e. pathology classification) over a target domain  $\mathcal{D}^T$  (i.e. mammogram ROI images) by using

the knowledge of the learning algorithm trained in a source learning task  $\mathcal{T}^S$  (i.e. 1000 category classification) over a source domain  $\mathcal{D}^S$  (i.e. natural images) which is larger than the target domain where:

$$\mathcal{D}^S \neq \mathcal{D}^T \quad (1)$$

$$\mathcal{T}^S \neq \mathcal{T}^T \quad (2)$$

Depending on the relations defined by (1) and (2), different categories of TL are defined in literature. However, it is important to consider that computer vision tasks are particular and different from their corresponding data mining tasks. Thus, despite the fact that a mammogram image is very different from a natural image, the visual properties of objects in an image are general (i.e. edges, textures, shapes, etc.).

In a ConvNet, the knowledge is represented by the value of the weights trained by the back-propagation algorithm on each layer. Therefore, TL implies using the pre-trained ConvNet as a feature extractor or replacing the last original layer with a set of layers that are trained to obtain the target learning task desired. The latter is the approach that we have followed in our experiments. One of the main advantages in this technique is that training time is reduced by not re-training the whole ConvNet, but only the added layers or a trainable classifier in the case of using the pre-trained ConvNet as a feature extractor itself.

### 2.3 Fine Tuning

In this case, some of the last layers of the pre-trained ConvNet are re-trained with the new images  $I \in \mathcal{D}^T$ . Thus, the ConvNet is divided in two parts. Let us define  $\gamma$  as the layer from which the re-training of the ConvNet will occur. If the original ConvNet model has  $L$  layers, similarly to TL, we can replace the last original layer and add some layers in order to obtain the desired target learning task. Differently to TL, we also choose a  $r$  number of layers before the last one that are also to be trained. This means that the original weights from layer 0 to layer  $\gamma - 1$  are preserved or frozen. FT presents more computing resources and time training since the number of parameters to be trained is increased by the  $r$  layers that are added to the training queue.

### 2.4 Over and Underfitting

A machine learning algorithm may suffer of two problems when training: overfitting and underfitting. The former reduces the capacity of the model to predict new unseen data which means that the model has a high variance. The latter, means that the model is not complex enough to reflect the nature of the data and find a pattern [27]. ConvNet models are characterized by being overparameterized; which means that the parameters of the model exceed the size of the training data [28]. The overfitting problem is reflected when plotting the train vs validation accuracy curve of the model. The difference between the train and validation curve should be minimum. In order to overcome overfitting in ConvNets, Data Augmentation, Regularization, and Early Stopping are usually used. Data augmentation is a basic strategy that consists in increasing the size of the dataset by performing transformations to the original

images (i.e. rotation, zoom, reflection, etc). On the other hand, regularization techniques aim to penalize extreme parameter weights values (e.g.  $L_2$  regularization) [27] or controlling the co-adaptation between neurons (e.g. Dropout) [13]. Early Stopping is also considered a regularization technique which aims to interrupt training when the performance of the ConvNet degrades on the validation set. This prevents that the model learn a form of statistical noise [29].

As discussed earlier, TL and FT may also prevent overfitting since the ConvNet model is not whole retrained; in other words, TL and FT have less parameters to learn compared to training a model from randomly initialized weights. In the present work, Dropout [30] and Early Stopping have been used as regularization techniques altogether with data augmentation; these are changes introduced in this work that differ from our previous experiment.

## 3 Related Works

### 3.1 Search Process

In our previous work [1], we used the methodology by [31], in order to find relevant works for study. Table 1 shows the search string designed to retrieve information from: Springer Link, Science Direct (Elsevier), IEEE Xplore, Scopus, Web of Science, ACM digital library, and PubMed. A total of 174 studies (including our previous work) were gathered from each repository as shown in Table 2. From these studies, a total of 32 primary documents were retrieved according to a selection study process where documents should have experimental methodology with results regarding the use of transfer learning in mammogram breast cancer classification.

Table 1: Search String

“breast cancer” AND (“classification” OR “detection” OR “prediction”) AND (“ensemble learning” OR “transfer learning”) AND mammo*
---

Table 2: Search Results

Database	#Publications: 2014-2018
Scopus	38
IEEE	12
Science Direct	51
PubMed	10
ACM	25
Web of Science	23
Springer	15
<b>Total</b>	<b>174</b>

### 3.2 Literature review discussion

In our literature review, the most common ConvNet used for transfer learning is the model proposed in [13], named *AlexNet*, with a total

of 12 cases. The second most frequent model found is VGG16. These results are shown in Figure 1.

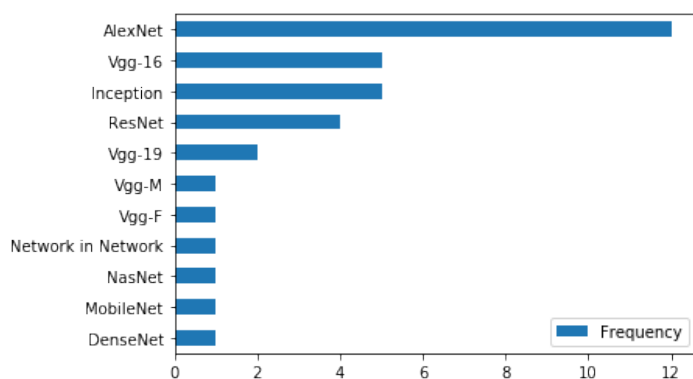


Figure 1: ConvNets used in Literature. This bar plot shows the frequency of the pre-trained ConvNets used in the primary documents retrieved for our literature review. The most used model corresponds to AlexNet (12 cases). At a second place are VGG16 and Inception (5 cases each). Next is ResNet (4 cases) and VGG19 (2 cases).

In mammogram mass abnormality classification and detection there are two main approaches found in literature: a) Processing the whole mammogram image and b) processing the region of interest. The former is found in [32, 33]. Their aim is to find an “*end to end design*”. Our approach belongs to the latter, where the ROI image is extracted. In fact processing a whole mammogram images in their original size seems to be a problem itself because mammogram images far exceed the traditional size used in many trained ConvNets in the ImageNet dataset. An interesting approach for an end to end design is proposed in [34]; In their work, the principles of the YOLO [35] architecture are used. However, the mammogram is also resized to  $448 \times 448$ .

As in the case of mammogram classification, Transfer Learning and Fine Tuning are used differently by different authors in literature. In the next subsection this differences are enlightened and discussed.

### 3.2.1 Transfer Learning as a Feature Extractor

In this case, the pre-trained ConvNet is used to extract a feature vector which is later used to train another kind of classifier algorithm like Support Vector Machines (SVM). This case is illustrated in [36]; the author extracts several feature vectors from different layers of the pre-trained AlexNet and trains Support Vector Machines (SVM) for each case. In the end, the author builds an ensemble of SVM. Other similar examples are found in [37, 38].

### 3.2.2 Transfer Learning as a new ConvNet Classifier

In this case, the last full connecting layer of the pre-trained ConvNet may be substituted with a set of additional layers, where the last full connecting layer has only one neuron and the logistic regression for binary classification, or just the number of random initialized neurons required in proportion to the new classification task. For instance, in the case of benign vs malignant classification of the mammogram abnormality this can be achieved with a single neuron

or two. Only the added layers are trained while the rest of the ConvNet’s weights remain frozen. This approach is tested in both our current and previous work [1]. In a similar fashion, VGG16[39], GoogLeNet[40] and AlexNet[13] are trained in TL in [41].

### 3.2.3 Transfer Learning as weight initialization

In this case the whole ConvNet is re-train but uses the values of the ImageNet pre-trained ConvNet model as initial values for the weights. The last full connecting layer with 1000 categories is substituted by one or two neurons to address the binary classification problem [42]-[43].

### 3.2.4 Fine Tuning

This is the most common technique found in literature. In this case, the model’s last full connecting layer is substituted with the number of neurons needed for the new classification or a set of new layers are added before the output layer. Differently to *transfer learning as a new ConvNet*, some of the last layers of the model are re-trained with the new data as indicated in Section 2.3. For example, VGG16[39], InceptionV3[20], and ResNet50 [18] are fine tuned in [44]; the author found that when the number of convolutional blocks exceeds 2, the accuracy of the fine tuned model drops. Also, a comparison of the classification performance between the training of VGG16 in FT and using it as a feature extractor is explored in [45].

### 3.2.5 Data Augmentation and Pre-processing

In literature there is some discussion about the impact of both data augmentation and pre-processing of the medical image. As stated by [46], the achievements in medical images visual tasks with deep learning do not only rely in the ConvNet model but also in the pre-processing of images. For instance, some of the pre-processing methods found in literature are: global contrast normalization (GCN), local contrast normalization, and Otsu’s threshold segmentation. However, there is some discussion about improving the image quality. In [37] is reported that global contrast normalization did not aid in improving the experimental results presented in the paper.

Since datasets are not so large, data augmentation is used by almost all researchers. Some of the most common techniques used are: rotations and cropping. However, the rotation operation yields to distortion of the original image. Because of this reason, right angle rotations are preferred to random rotation angles [37, 43, 44].

## 4 Proposed Approach

### 4.1 Transfer Learning and Fine Tuning Model

The problem to solve is to classify ROI patch mammogram images  $\mathcal{I}$  in two classes  $\mathcal{Y} = \{\textit{benign}, \textit{malignant}\}$ . In a supervised learning paradigm this means to find a prediction function  $\phi(\cdot)$  that maps an input space  $\mathcal{X}$  formed by ROI patch mammogram images ( $\mathcal{I} \in \mathcal{X}$ ) to the output space  $\mathcal{Y}$  as indicated in (3)

$$\mathcal{Y} = \phi(\mathcal{X}) \quad (3)$$

However, since TL and FT are to be used to improve the performance of  $\phi(\cdot)$ , 3 may be written as indicated in 4

$$\mathcal{Y}^T = \phi^T(\mathcal{X}^T) \quad (4)$$

Function  $\phi^T(\cdot)$  is to be trained by using pre-trained ConvNets on the ImageNet dataset, which is denominated as  $\mathcal{X}^S$ . Therefore, our approach satisfies the relations indicated in (1) and (2), since both images and the classification task are different between source and target.

Our approach in both TL and FT consists in replacing the last full connecting layer related to the original ImageNet classification task with a set of layers as indicated in Table 3. The global average pooling (GAvg) layer helps to flatten the original model layer previous to the 1000 full connecting SoftMax classification. The classification layer is comprised of 1 neuron and the Sigmoid function.

Table 3: TL and FT Output

Global Average Pooling 2D
Full Connecting
Dropout
Classification Layer

In TL, only the last layers indicated in Table 3 are to be trained. In FT, we define the  $\gamma$  value that indicates the layer from which the training of the weights is to be performed. It is important to remember that all weights before  $\gamma$  remain with their original value from the ImageNet.

## 4.2 Dataset

In the present study, as well as our previous work, we use the Curated Breast Imaging Subset of DDSM (CBIS-DDSM)[4] which is an updated and standardized version of the Digital Database for Screening Mammography (DDSM). The dataset includes a subset of the DDSM data selected and curated by a trained mammographer. For our experiments we extract the ROI images from the mammogram images. We have only considered mass problems, leaving micro calcifications for a future work. The dataset is originally organized in train and test sets. The number of images per abnormality class and set type is shown in Table 4.

Table 4: Mass Images in CBIS-DDSM

Dataset Set Type	Benign	Malignant
Train	681	637
Test	231	147

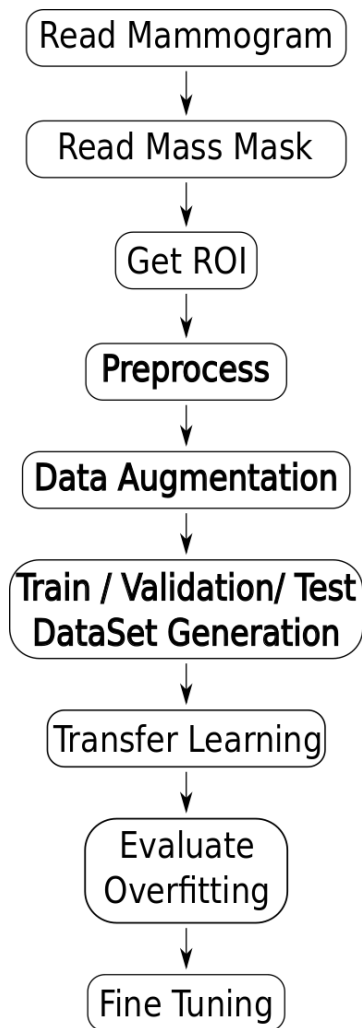


Figure 2: A diagram depicting the methodology followed in our research. First, mammogram and corresponding mass binary mask are read. The mask is used to extract the ROI from the mammogram image. Next, the ROI image is enhanced (pre-process). As a third step, data augmentation is used to increase the number of samples and create train, validation and test sets. Finally, transfer learning is performed and evaluated. The best non overfitting model is selected to be fine tuned

## 4.3 Methodology

The methodology followed in the current experiments is shown in Figure 2. First, the ROI images are extracted from the mammogram image by using the binary segmentation masks provided in the CBIS-DDSM dataset. After that, images are pre-processed to enhance contrast. Next, a single dataset is formed in order to use data augmentation and create three sets of data: train, validation and test. In this work, we do not use Otsu algorithm to segment the previously obtained ROI by creating an intermediate binary mask. This is because our previous work showed that training with the ROI image segmented with Otsu did not overcome the results obtained with the original background image. Finally, the models are trained in TL and FT, and their performance is evaluated. These steps are described in more detail below.

### 4.3.1 Image Pre-processing

In this section we present the steps performed in the pre-processing stage of our proposed method. The original mammogram image



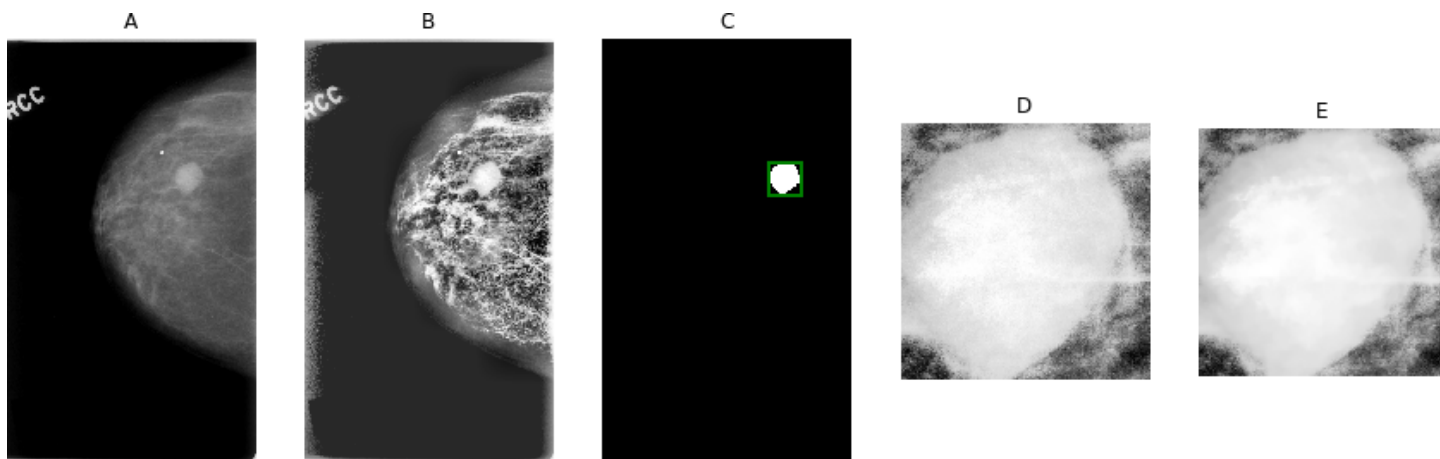


Figure 3: Image Preprocessing. A. The original CBIS-DDSM ROI mammogram image ( $4704 \times 2744$ ) normalized in UIN8 resolution ( $pixel\_value \in [0, 255]$ ). B. Mammogram image contrast is improved by using The CLAHE equalization algorithm. C. The binary mass mask provided in the dataset is used to find the ROI. D. The ROI is extracted from B step with a size corresponding to the Bounding Box ( $358 \times 346$ ) found in the binary mask. E. The ROI image in previous step is resized to  $328 \times 328$ , where we used a 8 pixel padding. Finally, the image is cropped around the center to obtain the final desired training dimensions for the ROI image of  $320 \times 320$  and Fast Non Local Means Denoising Algorithm is used to further filter ROI image scanning noise.

has a pixel value which ranges up to 65 535 (i.e. 16 bit resolution). In order to generate a dataset of PNG images saved in disk, we change the resolution of the images by normalizing them between 0 and 255, considering the minimum and maximum values of pixel in the original DICOM mammogram image. After that, and different to our previous work, we used the Contrast Limited Adaptive Histogram Equalization (CLAHE)[47] to improve image quality. By using the provided binary masks, we extract the ROI through the coordinates of a bounding box around the suspicious mass. A second normalization of the pixel value is carried out on the ROI considering the minimum and maximum pixel values in it. This originates ROI images with different width and height sizes. As in our previous work, aspect ratio is considered. In (5), the aspect ratio is defined; where  $r$  is the aspect ratio,  $w$  and  $h$  are the width and height of the image respectively.

$$r = w/h \quad (5)$$

Aspect ratio was considered previous to resizing the image in order to preserve the best quality possible from the original image in both, upsampling and downsampling procedures. For upsampling, cubic interpolation was used, whereas for downsampling, area interpolation gives best results. Also, images with an aspect ratio inferior to 0.4 and superior to 1.5 where removed from dataset.

$$\mathcal{I} = \{I|I \in \mathbb{R}^{w \times h}, 0.4 \leq r \leq 1.5\} \quad (6)$$

ROI images were resized to a final size of  $320 \times 320$ . This was achieved only with images whose aspect ratio was inside the limits presented in (6). Resizing the ROI images consisted in two parts: 1) we resized the ROI image to  $328 \times 328$ , 2) cropping around the center of the image. In other words, we have resized the original ROI image to a bigger size (with a padding of 8 pixels) and then cropped in the center of the image to obtain the desired size. Finally, the image is filtered with fast non local means denoising algorithm [48]. This is because CBIS-DDSM images are film mammography and appear to have some noise that has not been removed from the image. Figure 3 presents the steps carried out on image pre-processing for a

sample of the training set. Both, the full mammogram image and its corresponding binary mass mask are shown in sub-figures A and C respectively. Image C shows the identification of the bounding box. B presents the application of CLAHE on the mammogram image. Finally, E presents the processed ROI image after performing crop center on D which was extracted from B through the bounding box.

#### 4.3.2 Data Augmentation and Dataset Generation

In our previous work we did not use data augmentation and our models presented overfitting. In order to overcome this difficulty, we implemented the output structure indicated in Table 3 which uses dropout. As pointed out in Section 3.2.5, performing transformations over the images distorts them. Because of that, some researchers use right angles.

Table 5: Augmentation Operations

Operation	Probability	Parameters
Rotation	95%	Max Angle $15^\circ$
Shear	60%	Max value $25^\circ$
Histogram Equalization	60%	
Horizontal Flip	70%	
Bright	80%	min value: 0.6 max value: 1.2
Zoom	100%	min value: 1.0 max value: 1.2

In our case, we have used the Augmentor Library [49], which has been designed to permit rotations of the images limiting the degree of distortion. Additionally, the Augmentor library permits to apply other operations for data augmentation like zoom, bright, shear. The function uses a probability value to control the number of artificially created images. To augment the dataset, we first join both Train and Test sets. The dataset was increased to a total of 60 000 images, where 80% of the images are used for training, 10%

for validation and 10% for testing. The augmentation operations used are depicted in Table 5.

#### 4.3.3 Model Training

The generated augmented dataset is tested first in Transfer Learning. A total of 4096 neurons are used for the FC layer, a dropout value of 0.2, and a single neuron in the output layer (or classification layer, see Table 3) for binary classification. Early Stopping, with a patience of 50, was enabled in order to stop training when the performance degrades. A maximum number of 1 000 epochs is proposed. The learning rate for TL is  $1 \times 10^{-5}$ . The loss function is set to binary cross entropy and the optimization algorithm used is RMSProp [50]. Binary cross entropy was chosen because the classification layer of our model uses the Sigmoid activation function to discriminate between benign and malignant mass pathology by using one neuron. RMSProp, an adaptive gradient algorithm, is frequently used in computer vision tasks [51]. For instance, the results achieved in [52] indicate a better training result obtained by using RMSProp instead of Stochastic Gradient Descent (SGD). Also, as presented in [53], RMSProp outperforms other common optimization algorithms [51]. This has inspired the theoretical research in [51], where the authors establish the reasons of the success of RMSProp in deep learning and propose new algorithms for optimization. In our study, we consider that RMSProp is convenient for our image classification task because of the aforementioned reasons.

Transfer Learning was carried out in 20 models provided by the Keras API in Tensorflow v1.13.1 [54]. The models used are shown in Table 6.

Table 6: Pre trained ConvNets used

Vgg	Densenet	Inception	Nasnet
16, 19	121, 169, 201	v3, Resnet-v2	large, mobile
Mobilenet	Resnet	Xception	Resnext
v1, v2	50, 50v2, 101, 101v2, 152, 152v2	v1	50, 101

Each model performance is evaluated in the train-validation curve of accuracy. If the difference between train accuracy and test accuracy is over 10%, we consider that overfitting has occurred and the model is rejected. Once a suitable not overfitting model is found, FT is performed in order to further increase the performance of the selected classifier.

FT training parameters are: learning rate of  $2 \times 10^{-7}$ ; Dropout remains at 0.2. Respect to the FC neurons, only Global average pooling is performed. Binary cross entropy is set as the cost function and the optimization algorithm used is also RMSProp.

#### 4.3.4 Computing Resources

In order to train deep learning models it is necessary to use Graphical Processing Units (GPU). In our case we have used: Nvidia Tesla K80, with 12 GB of memory, Nvidia Tesla K40, with 12 GB of memory, and Nvidia GeForce RTX 2080, with 8 GB of memory.

Regarding software resources, our program used Tensorflow v13.1 [54] as the machine learning framework. For image data augmentation, as indicated before, the Augmentor library [49] was used.

## 5 Experimental Results

In this Section, we present our experimental results. As a difference wrt. to our previous work, we include additional metrics to evaluate the performance of the classification model such as the area under the ROC curve and the  $F_1$  Score. These metrics are described below. According to the methodology proposed in Figure 2, it is important to estimate the overfitting of the trained model  $\phi^T(\cdot)$ . In order to do so, let us define  $\beta$  as the overfitting ratio by comparing train ( $train\_acc$ ) and validation accuracy ( $valid\_acc$ ) as in

$$\beta = \frac{train\_acc}{valid\_acc} \quad (7)$$

If  $\beta \approx 1$ , we could say that  $train\_acc \approx valid\_acc$  and therefore that there is little overfitting. Values of  $\beta > 1$  will reflect that there is a considerable difference between train and validation accuracy, meaning that the model has overfitted.

### 5.1 Performance Metrics

The confusion matrix compares both the prediction of the trained classifier and the true labels provided in the test set. It consists of four main measures: true positives ( $TP$ ), true negatives ( $TN$ ), false positives ( $FP$ ), and false negatives ( $FN$ ). The total positive cases are  $P = TP + FN$ ; similarly, the total negative cases:  $N = TN + FP$ . From these measures, the true positive rate (8), false positive rate (9), and true negative rate (10) are derived.

$$TPR = \frac{TP}{P} \quad (8)$$

$$FPR = \frac{FP}{N} \quad (9)$$

$$TNR = \frac{TN}{N} \quad (10)$$

The elements over the diagonal belong to  $TP$  and  $TN$  and reflect all the correct classifications made by the model. The  $FP$  and  $FN$  correspond to wrongly classified cases. For instance,  $FN$  corresponds to a true malignant tumor that is classified as benign. From these measurements, metrics like: Accuracy (11),  $F_1$  Score (12), and the area under the ROC curve (13) are defined.

$$ACC = \frac{TP + TN}{TP + TN + FP + FN} \quad (11)$$

$$F_1 = \frac{2TP}{2TP + FP + FN} \quad (12)$$

$$AUC = \frac{1}{2} (1 + TPR - FPR) \quad (13)$$

## 5.2 Transfer Learning Experiment

The ImageNet pre-trained ConvNets presented in Table 6 are trained under TL to predict mammogram abnormalities classes in mammogram roi images.

Table 7: Transfer Learning Results

<i>Model</i>	<i>AUC</i>	<i>F<sub>1</sub>Score</i>	<i>ACC</i>
resnet-50-TL	0.861	0.858	0.861
mobilenet-TL	0.854	0.855	0.854
resnet-152-TL	0.853	0.847	0.853
resnet-101-TL	0.846	0.848	0.846
resnet-152v2-TL	0.844	0.845	0.844
resnet-50v2-TL	0.843	0.854	0.843
resnet-101v2-TL	0.832	0.833	0.832
densenet-201-TL	0.821	0.823	0.821
xception-TL	0.816	0.82	0.816
densenet-169-TL	0.812	0.816	0.812
resnext-101-TL	0.806	0.82	0.806
nasnet-l-TL	0.804	0.802	0.804
mobilenet-v2-TL	0.791	0.801	0.791
densenet-121-TL	0.79	0.79	0.789
inception-v3-TL	0.778	0.781	0.779
resnext-50-TL	0.777	0.764	0.777
inception-resnet-v2-TL	0.744	0.746	0.744
nasnet-m-TL	0.712	0.73	0.712
vgg16-TL	0.644	0.654	0.644
vgg19-TL	0.629	0.659	0.629

Table 8: Transfer Learning Overfitting Ratio  $\beta$ 

<i>Model</i>	<i>train_acc</i>	<i>test_acc</i>	$\beta$
vgg16-TL	0.65	0.64	1.01
vgg19-TL	0.64	0.63	1.02
resnet-50-TL	1.00	0.86	1.16
mobilenet-TL	1.00	0.85	1.17
resnet-152-TL	1.00	0.85	1.17
resnet-101-TL	1.00	0.85	1.18
resnet-152v2-TL	1.00	0.84	1.19
resnet-50v2-TL	1.00	0.84	1.19
resnet-101v2-TL	1.00	0.83	1.20
inception-resnet-v2-TL	0.90	0.74	1.21
densenet-201-TL	1.00	0.82	1.22
xception-TL	1.00	0.82	1.22
resnext-101-TL	0.99	0.81	1.22
densenet-169-TL	1.00	0.81	1.23
densenet-121-TL	0.98	0.79	1.24
nasnet-l-TL	1.00	0.80	1.24
mobilenet-v2-TL	1.00	0.79	1.26
resnext-50-TL	0.98	0.78	1.26
inception-v3-TL	0.99	0.78	1.27
nasnet-m-TL	0.91	0.71	1.28

As indicated in Section 4.3.3, 4096 output neurons and a dropout rate of 0.2 are used. The results achieved are shown in Table 7. The overfitting ratio stated in (7) is presented in Table 8. The results indicate that Resnet-50 has the best *AUC*, however its  $\beta$  shows that there is overfitting. On the contrary, both VGG16 and VGG19 do not present overfitting, but their classification performance is lower compared to Resnet-50. These results are reflected in Figure 4 and 5, where the plot train vs test accuracy is presented for Resnet-50 and VGG16, respectively.

## 5.3 Fine Tuning Experiment

According to the results indicated in Tables 7 and 8, we proceeded to train the VGG16 in Fine Tuning. Different deepness levels were tried in order to search for classification performance improvement. This is indicated through the  $\gamma$  value. VGG16 was trained from layers  $\gamma = 8$ ,  $\gamma = 10$ . In order to denominate the trained model, we propose to use the pre-trained ConvNet name followed by the layer from which fine tuning occurred and added the keyword FT to distinguish the model from those trained in TL mode. For instance, *VGG16-10-FT* means that VGG16 was fine tuned from layer 10. Similarly, we trained VGG19 at  $\gamma = 17$ . In all cases, only global average pooling followed by dropout and the classification layer were used; except for the case of *VGG16-8-FT*, where a full connecting layer of 4096 neurons was used.

The results obtained are shown in Table 9. We have complemented the experimental results with the Fine Tuning of models: Xception, Resnet101, Resnet152 and Resnet50. It is observable that the best results are achieved by VGG models. The best result achieved corresponds to the VGG16-8-FT. However, Table 10 suggest that the second best result (VGG16-10-FT) has less overfitting and therefore is preferred. In fact  $\beta$  value for VGG16-10-FT and VGG19-17-FT is similar, but the performance of the latter is poorer.

In Figure 6, the plot of train and validation accuracy vs the number of epochs for VGG16-10-FT is presented. Figure 7 shows the ROC curve obtained, whereas Figure 8 presents the confusion matrix for the test set generated.

Table 9: Fine Tuning Results

<i>Model</i>	<i>AUC</i>	<i>F<sub>1</sub>Score</i>	<i>ACC</i>
vgg16-8-FT	0.844	0.85	0.844
vgg16-10-FT	0.816	0.822	0.816
vgg19-17-FT	0.774	0.774	0.774
xception-127-FT	0.571	0.664	0.571
xception-122-FT	0.526	0.67	0.526
xception-130-FT	0.504	0.663	0.504
resnet-101-343-FT	0.5	0.667	0.5
resnet-101-340-FT	0.5	0.667	0.5
resnet-152-510-FT	0.5	0.667	0.5
resnet-50-173-FT	0.5	0.667	0.5
resnet-101-330-FT	0.5	0	0.5
resnet-152-513-FT	0.5	0	0.5
resnet-50-160-FT	0.5	0	0.5
resnet-50-170-FT	0.5	0	0.5

Table 10: Fine Tuning Overfitting Ratio  $\beta$

Model	train_acc	test_acc	$\beta$
vgg19-17-FT	0.82	0.77	1.07
vgg16-10-FT	0.87	0.82	1.07
vgg16-8-FT	0.92	0.84	1.09

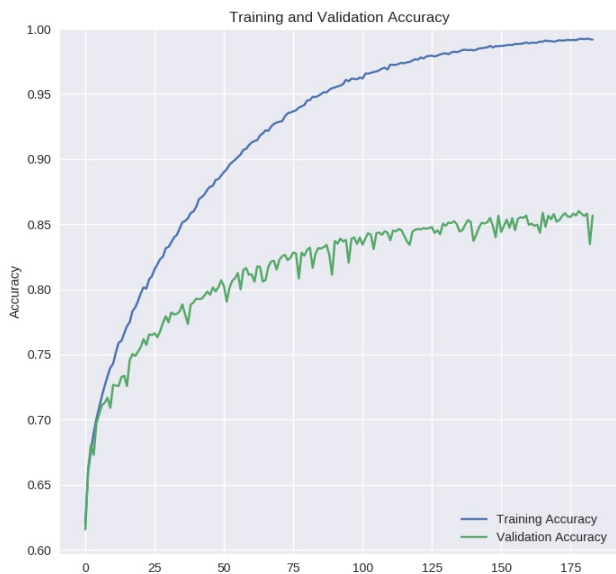


Figure 4: Comparison of the train and validation accuracy for **Resnet50-TL** when trained in transfer learning. As can be seen, despite that Resnet50 achieves an  $ACC = 0.86$  accuracy, the model presents overfitting due to the distance between both curves, described by the ratio  $\beta = 1.16$

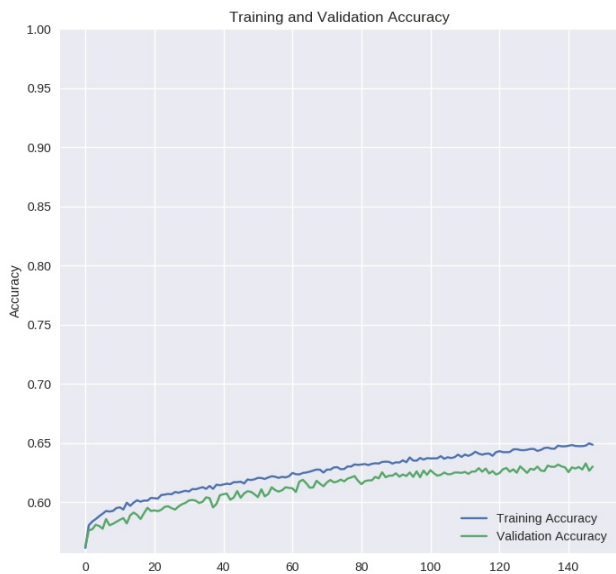


Figure 5: Comparison of the train and validation accuracy for **Vgg16-TL** when trained in transfer learning. VGG16 achieves a lower level of accuracy compared to Resnet50 ( $ACC = 0.64, \beta = 1.01$ ) but there is no overfitting, due to the little distance between train and validation curves.



Figure 6: Fine Tuning VGG16 achieves the best result for our dataset based on CBIS-DDSM ( $ACC = 0.87, \beta = 1.07$ ). Fine Tuning has overcome overfitting and managed to increase classification performance as comparing the train and validation curves for the accuracy metric show in this figure.

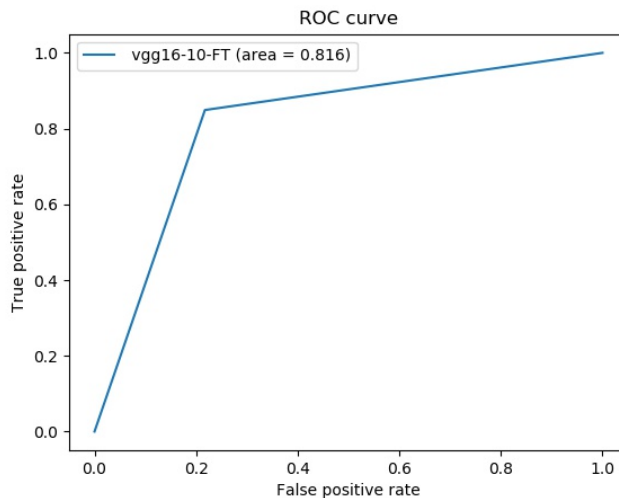


Figure 7: ROC Curve for the binary classification of ROI mammogram images test set. It depicts the performance of the Fine Tuned VGG16-10-FT model, which achieved  $AUC = 0.818$

Fine Tuning the VGG16 model from layer 10 ( $\gamma = 10$ ) helps to increase the performance of the classifier while controlling the overfitting ( $\beta = 1.07$ ), which means that train accuracy is 7% over the test accuracy.



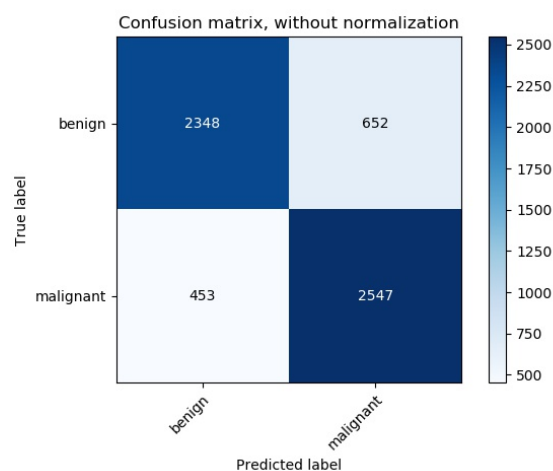


Figure 8: Confusion matrix of the VGG16-10-FT over the test set with 3000 images per category (malignant, benign). In this matrix, True Positive cases are 2547 (84.9%) and True Negatives are 2348 (78.2%). False Positive are 652 (21.7%) and False Negatives are 453 (15.1%). The VGG16 fine tuned model has been able to reduce false negative cases.

## 6 Conclusion

The present study compared the performance of TL and FT of different pre-trained ConvNet models on the ImageNet dataset such as: VGG, DenseNet, Inception, Resnet, Resnext and Xception. In our previous work, we have experimented with Nasnet and Mobilenet without data augmentation. This showed that the models had a trend to overfit. In order to overcome this problem and increase the performance of a Fine Tuned model, in this work we have used data augmentation as indicated in Section 4.3.2. Our experiments showed that increasing the dataset up to 30 000 images per category helped to achieve good results. Special care was taken to increase the dataset by using the Augmentor library [49] which permits to rotate images avoiding excessive distortion. Compared to our previous work, the image pre-processing has also been changed: instead of using histogram equalization, CLAHE was selected to enhance the contrast the images. Also, the image was resized to a bigger value in order to crop around the center. Finally, image filtering was applied to reduce the presence of noise in the image, as indicated in Section 4.3.1.

In order to estimate overfitting, we proposed a simple ratio relation described in (7). This permitted to conclude that models could achieve good results in classification metrics but overfit in the end. Considering this, we decided to increase the complexity of the model by using the fine tuning technique, where weights from layer 1 to  $\gamma - 1$  are frozen, and weights from layer  $\gamma$  until the end are trained with back-propagation. This allowed to increase the performance of both VGG16 and VGG19. Increasing the number of neurons in the FC layer of VGG16-8-FT improved the results but there is a slight overfitting.

The CBIS-DDSM dataset, despite the fact of having at most 1 696 examples for mass abnormality classification, their samples present some artifacts and noise, which is the reason why we used some pre-processing and filtering algorithms in order to improve the image. This is probably due to the fact that the original images

are of film type. Certainly, our experiments suggest that TL and FT of pre-trained ConvNets is able to classify film mammogram ROI images. However, the data augmentation increase of the original dataset is considerably. Therefore, public mammogram datasets of Full Digital Mammography, which has better quality than film, with enough sample data would aid to train better classifiers.

With respect to our previous work, we have also included new metrics to evaluate the performance of the classifier. This is important, since the accuracy metric is susceptible to be distorted when the dataset is skewed or unbalance. In other words, it tends to benefit the class with a majority of examples.

## 7 Future Works

The interest in improving CAD systems in mammography is clear since the disease is a public health problem with high rates of both incidence and mortality. In this and our previous work, we have used the CBIS-DDSM dataset mainly. In a future work, we aim to evaluate the performance of TL and FT in other datasets such as INbreast[55] and Mias[56].

Also, we will be addressing the problem of localization and detection of the mass in the mammogram image. This problem is also of interest and could be formulated from the classification problem here addressed. One of the important things to notice is the peculiarity of the size of the mammogram image compared to the size used in ImageNet trained ConvNets. Mammogram images are of considerable size and it could be of interest to design both the classifier and the object detection avoiding to excessively resize the original image.

**Conflict of Interest** The authors declare no conflict of interest.

**Acknowledgment** This research was carried out using the research computing facilities offered by Scientific Computing Laboratory of the Research Center on Mathematical Modeling: MODEMAT, Escuela Politécnica Nacional - Quito and those also provided by Corporación Ecuatoriana para el Desarrollo de la Investigación y la Academia (CEDIA). The authors also gratefully acknowledge the financial support provided by the Escuela Politécnica Nacional, for the development of the project PREDU 2016-013.

## References

- [1] L. G. Falconi, M. Pérez, and W. G. Aguilar. Transfer learning in breast mammogram abnormalities classification with mobilenet and nasnet. In *2019 International Conference on Systems, Signals and Image Processing (IWSSIP)*, pages 109–114, June 2019. doi: 10.1109/IWSSIP.2019.8787295.
- [2] Andrew G Howard, Menglong Zhu, Bo Chen, Dmitry Kalenichenko, Weijun Wang, Tobias Weyand, Marco Andreetto, and Hartwig Adam. Mobilenets: Efficient convolutional neural networks for mobile vision applications. *arXiv preprint arXiv:1704.04861*, 2017.
- [3] Barret Zoph, Vijay Vasudevan, Jonathon Shlens, and Quoc V Le. Learning transferable architectures for scalable image recognition. In *Proceedings of the IEEE conference on computer vision and pattern recognition*, pages 8697–8710, 2018.

- [4] Rebecca Sawyer Lee, Francisco Gimenez, Assaf Hoogi, Kanae Kawai Miyake, Mia Gorovoy, and Daniel L. Rubin. A curated mammography data set for use in computer-aided detection and diagnosis research. *Scientific Data*, 4:170177 EP –, Dec 2017. URL <https://doi.org/10.1038/sdata.2017.177>. Data Descriptor.
- [5] Kiven Eriq Lukong. Understanding breast cancer—the long and winding road. *BBA clinical*, 7:64–77, 2017.
- [6] World health organization. global health observatory. geneva: World health organization; 2018. [who.int/gho/database/en/](http://who.int/gho/database/en/). 2018.
- [7] Jennifer S Drukteinis, Blaise P Mooney, Chris I Flowers, and Robert A Gatenby. Beyond mammography: new frontiers in breast cancer screening. *The American journal of medicine*, 126(6):472–479, 2013.
- [8] D. Selvathi and A. Aarthypoomila. Performance analysis of various classifiers on deep learning network for breast cancer detection. volume 2018-Janua, pages 359–363. ISBN 9781509067305. doi: 10.1109/CSPC.2017.8305869.
- [9] Afsaneh Jalalian, Syamsiah Mashohor, Rozi Mahmud, Babak Karasfi, Abdul Rahman B Ramli, Communication Systems Engineering, Universiti Putra, Health Science, Universiti Putra, and Qazvin Branch. Review article : FOUNDATION AND METHODOLOGIES IN COMPUTER-AIDED. pages 113–137, 2017.
- [10] X. Zhang, Y. Zhang, E.Y. Y Han, N. Jacobs, Q. Han, X. Wang, and J. Liu. Whole mammogram image classification with convolutional neural networks. volume 2017-Janua, pages 700–704, 2017. ISBN 9781509030491. doi: 10.1109/BIBM.2017.8217738.
- [11] John Stoitsis, Ioannis Valavanis, Stavroula G Mouggiakakou, Spyretta Golemati, Alexandra Nikita, and Konstantina S Nikita. Computer aided diagnosis based on medical image processing and artificial intelligence methods. *Nuclear Instruments and Methods in Physics Research Section A: Accelerators, Spectrometers, Detectors and Associated Equipment*, 569(2):591–595, 2006.
- [12] Yann LeCun, Yoshua Bengio, and Geoffrey Hinton. Deep learning. *nature*, 521(7553):436, 2015.
- [13] Alex Krizhevsky, Ilya Sutskever, and Geoffrey E. Hinton. ImageNet classification with deep convolutional neural networks. *Communications of the ACM*, 60(6):84–90, jun 2017. ISSN 15577317. doi: 10.1145/3065386.
- [14] L. Hertel, E. Barth, T. Käster, and T. Martinetz. Deep convolutional neural networks as generic feature extractors. In *2015 International Joint Conference on Neural Networks (IJCNN)*, pages 1–4, July 2015. doi: 10.1109/IJCNN.2015.7280683.
- [15] Yann LeCun, Yoshua Bengio, et al. Convolutional networks for images, speech, and time series, the handbook of brain theory and neural networks, 1998.
- [16] Y Bengio. Convolutional Networks for Images, Speech, and Time-Series Unsupervised Learning of Speech Representations View project Parsing View project. Technical report, 1997. URL <https://www.researchgate.net/publication/2453996>.
- [17] Jia Deng, Wei Dong, Richard Socher, Li-Jia Li, Kai Li, and Li Fei-Fei. Imagenet: A large-scale hierarchical image database. In *2009 IEEE conference on computer vision and pattern recognition*, pages 248–255. Ieee, 2009. doi: 10.1109/cvprw.2009.5206848.
- [18] Kaiming He, Xiangyu Zhang, Shaoqing Ren, and Jian Sun. Deep Residual Learning for Image Recognition. Technical report. URL <http://image-net.org/challenges/LSVRC/2015/>.
- [19] Fabien Lauer, Ching Y. Suen, and Gérard Bloch. A trainable feature extractor for handwritten digit recognition. *Pattern Recognition*, 40(6):1816–1824, 2007. ISSN 0031-3203. doi: <https://doi.org/10.1016/j.patcog.2006.10.011>. URL <http://www.sciencedirect.com/science/article/pii/S0031320306004250>.
- [20] Christian Szegedy, Vincent Vanhoucke, Sergey Ioffe, and Jonathon Shlens. Rethinking the Inception Architecture for Computer Vision. Technical report. URL <https://arxiv.org/pdf/1512.00567.pdf>.
- [21] Evgeny A. Smirnov, Denis M. Timoshenko, and Serge N. Andrianov. Comparison of Regularization Methods for ImageNet Classification with Deep Convolutional Neural Networks. *AASRI Procedia*, 6:89–94, 2014. ISSN 22126716. doi: 10.1016/j.aasri.2014.05.013.
- [22] Nitish Srivastava, Geoffrey Hinton, Alex Krizhevsky, and Ruslan Salakhutdinov. Dropout: A Simple Way to Prevent Neural Networks from Overfitting. Technical report, 2014.
- [23] Waseem Rawat and Zenghui Wang. Deep Convolutional Neural Networks for Image Classification: A Comprehensive Review. *Neural Computation*, 29(9):2352–2449, sep 2017. ISSN 0899-7667. doi: 10.1162/neco\_a.00990. URL [http://www.mitpressjournals.org/doi/abs/10.1162/neco\\_a.00990](http://www.mitpressjournals.org/doi/abs/10.1162/neco_a.00990).
- [24] Neena Aloysius and M. Geetha. A review on deep convolutional neural networks. In *2017 International Conference on Communication and Signal Processing (ICCSP)*, pages 0588–0592. IEEE, apr 2017. ISBN 978-1-5090-3800-8. doi: 10.1109/ICCSP.2017.8286426. URL <http://ieeexplore.ieee.org/document/8286426/>.
- [25] Karl Weiss, Taghi M Khoshgoftaar, and DingDing Wang. A survey of transfer learning. *Journal of Big Data*, 3(1):9, 2016.
- [26] Sinno Jialin Pan and Qiang Yang. A survey on transfer learning. *IEEE Transactions on knowledge and data engineering*, 22(10):1345–1359, 2010.
- [27] Patrick Hill and Uma Kanagaratnam. *Python Machine Learning Sebastian Rashka*, volume 58. OUP, 2016.
- [28] Mingchen Li, Mahdi Soltanolkotabi, and Samet Oymak. Gradient descent with early stopping is provably robust to label noise for overparameterized neural networks. *CoRR*, abs/1903.11680, 2019. URL <http://arxiv.org/abs/1903.11680>.
- [29] Mingchen Li, Mahdi Soltanolkotabi, and Samet Oymak. Gradient descent with early stopping is provably robust to label noise for overparameterized neural networks. *CoRR*, abs/1903.11680, 2019. URL <http://arxiv.org/abs/1903.11680>.
- [30] Nitish Srivastava, Geoffrey Hinton, Alex Krizhevsky, Ilya Sutskever, and Ruslan Salakhutdinov. Dropout: a simple way to prevent neural networks from overfitting. *The journal of machine learning research*, 15(1):1929–1958, 2014. URL <http://jmlr.org/papers/v15/srivastava14a.html>.
- [31] Barbara Kitchenham and S Charters. Guidelines for performing Systematic Literature Reviews in Software Engineering. In *Engineering*, volume 2, page 1051. 2007. ISBN 1595933751. doi: 10.1145/1134285.1134500.
- [32] Gustavo Carneiro, Jacinto Nascimento, and Andrew P. Bradley. *Deep Learning Models for Classifying Mammogram Exams Containing Unregistered Multi-View Images and Segmentation Maps of Lesions*. Elsevier Inc., 1 edition, 2017. ISBN 9780128104095. doi: 10.1016/B978-0-12-810408-8.00019-5. URL <http://dx.doi.org/10.1016/B978-0-12-810408-8.00019-5>.
- [33] Stephen Morrell, Zbigniew Wojna, Can Son Khoo, Sebastien Ourselin, and Juan Eugenio Iglesias. Large-scale mammography CAD with deformable conv-nets. In *Lecture Notes in Computer Science (including subseries Lecture Notes in Artificial Intelligence and Lecture Notes in Bioinformatics)*, volume 11040 LNCS, pages 64–72, 2018. ISBN 9783030009458. doi: 10.1007/978-3-030-00946-5\_7. URL [http://link.springer.com/10.1007/978-3-030-00946-5\\_7](http://link.springer.com/10.1007/978-3-030-00946-5_7).
- [34] M.A. Al-masni, M.A. Al-antari, J.-M. Park, G. Gi, T.-S. T.-Y. Kim, P. Rivera, E. Valarezo, M.-T. Choi, S.-M. Han, and T.-S. T.-Y. Kim. Simultaneous detection and classification of breast masses in digital mammograms via a deep learning YOLO-based CAD system. *Computer Methods and Programs in Biomedicine*, 157:85–94, 2018. doi: 10.1016/j.cmpb.2018.01.017.
- [35] Joseph Redmon, Santosh Divvala, Ross Girshick, and Ali Farhadi. You only look once: Unified, real-time object detection. In *The IEEE Conference on Computer Vision and Pattern Recognition (CVPR)*, June 2016.
- [36] Benjamin Q Huynh, Hui Li, and Maryellen L Giger. Digital mammographic tumor classification using transfer learning from deep convolutional neural networks. *J. Med. Imag.*, 3(3):34501, 2016. doi: 10.1117/1.JMI.3.3.034501. URL [http://bhuyhnh.github.io/tl\\_jmi.pdf](http://bhuyhnh.github.io/tl_jmi.pdf).

- [37] Ana Perre, Luís A. Alexandre, and Luís C. Freire. Lesion classification in mammograms using convolutional neural networks and transfer learning. *Lecture Notes in Computational Vision and Biomechanics*, 27:360–368, jul 2018. ISSN 22129413. doi: 10.1007/978-3-319-68195-5\_40. URL <https://www.tandfonline.com/doi/full/10.1080/21681163.2018.1498392>.
- [38] Y. Hu, J. Li, and Z. Jiao. Mammographic mass detection based on saliency with deep features. In *ACM International Conference Proceeding Series*, volume 19-21-Aug, pages 292–297, 2016. ISBN 9781450348508. doi: 10.1145/3007669.3007714.
- [39] Karen Simonyan and Andrew Zisserman. VERY DEEP CONVOLUTIONAL NETWORKS FOR LARGE-SCALE IMAGE RECOGNITION. Technical report, 2015. URL <http://www.robots.ox.ac.uk/>.
- [40] Christian Szegedy, Wei Liu, Yangqing Jia, Pierre Sermanet, Scott Reed, Dragomir Anguelov, Dumitru Erhan, Vincent Vanhoucke, and Andrew Rabinovich. Going deeper with convolutions. In *The IEEE Conference on Computer Vision and Pattern Recognition (CVPR)*, June 2015.
- [41] Azam Hamidinekoo, Zobia Suhail, Erika Denton, and Reyer Zwiggelaar. Comparing the performance of various deep networks for binary classification of breast tumours. In *14th International Workshop on Breast Imaging (IWBI 2018)*, page 39, 2018. ISBN 9781510620070. doi: 10.1117/12.2318084.
- [42] Oliver Diaz, Robert Marti, Xavier Llado, and Richa Agarwal. Mass detection in mammograms using pre-trained deep learning models. In Elizabeth A. Krupinski, editor, *14th International Workshop on Breast Imaging (IWBI 2018)*, volume 10718, page 12. SPIE, jul 2018. ISBN 9781510620070. doi: 10.1117/12.2317681.
- [43] F. Jiang, H. Liu, S. Yu, and Y. Xie. Breast mass lesion classification in mammograms by transfer learning. In *ACM International Conference Proceeding Series*, pages 59–62, 2017. ISBN 9781450348270. doi: 10.1145/3035012.3035022.
- [44] Hiba Chougrad, Hamid Zouaki, and Omar Alheyane. Deep Convolutional Neural Networks for breast cancer screening. *Computer Methods and Programs in Biomedicine*, 157:19–30, apr 2018. ISSN 18727565. doi: 10.1016/j.cmpb.2018.01.011. URL <https://linkinghub.elsevier.com/retrieve/pii/S0169260717301451>.
- [45] Shuyue Guan and Murray Loew. Breast Cancer Detection Using Transfer Learning in Convolutional Neural Networks. In *2017 IEEE Applied Imagery Pattern Recognition Workshop (AIPR)*, pages 1–8. IEEE, oct 2017. ISBN 978-1-5386-1235-4. doi: 10.1109/AIPR.2017.8457948. URL <https://ieeexplore.ieee.org/document/8457948/>.
- [46] Geert Litjens, Thijs Kooi, Babak Ehteshami Bejnordi, Arnaud Arindra Adiyoso Setio, Francesco Ciompi, Mohsen Ghahfoorian, Jeroen A.W.M. van der Laak, Bram van Ginneken, and Clara I. Sánchez. A survey on deep learning in medical image analysis, dec 2017. ISSN 13618423. URL <https://linkinghub.elsevier.com/retrieve/pii/S1361841517301135>.
- [47] Karel Zuiderveld. Contrast limited adaptive histogram equalization. In *Graphics gems IV*, pages 474–485. Academic Press Professional, Inc., 1994.
- [48] Antoni Buades, Bartomeu Coll, and Jean-Michel Morel. Non-Local Means Denoising. *Image Processing On Line*, 1:208–212, 2011. doi: 10.5201/ipl.2011.bcm\_nlm.
- [49] Marcus D Bloice, Peter M Roth, and Andreas Holzinger. Biomedical image augmentation using Augmentor. *Bioinformatics*, 04 2019. ISSN 1367-4803. doi: 10.1093/bioinformatics/btz259. URL <https://doi.org/10.1093/bioinformatics/btz259>.
- [50] Geoffrey Hinton, Nitish Srivastava, and Kevin Swersky. Neural networks for machine learning lecture 6a overview of mini-batch gradient descent. *Cited on*, 14(8), 2012.
- [51] Mahesh Chandra Mukkamala and Matthias Hein. Variants of rmsprop and adapt with logarithmic regret bounds. In *Proceedings of the 34th International Conference on Machine Learning - Volume 70, ICML’17*, page 2545–2553. JMLR.org, 2017.
- [52] Andrej Karpathy and Li Fei-Fei. Deep visual-semantic alignments for generating image descriptions. In *The IEEE Conference on Computer Vision and Pattern Recognition (CVPR)*, June 2015.
- [53] Tom Schaul, Ioannis Antonoglou, and David Silver. Unit tests for stochastic optimization. *arXiv preprint arXiv:1312.6055*, 2013.
- [54] Martín Abadi, Ashish Agarwal, Paul Barham, Eugene Brevdo, Zhifeng Chen, Craig Citro, Greg S. Corrado, Andy Davis, Jeffrey Dean, Matthieu Devin, Sanjay Ghemawat, Ian Goodfellow, Andrew Harp, Geoffrey Irving, Michael Isard, Yangqing Jia, Rafal Jozefowicz, Lukasz Kaiser, Manjunath Kudlur, Josh Levenberg, Dan Mané, Rajat Monga, Sherry Moore, Derek Murray, Chris Olah, Mike Schuster, Jonathon Shlens, Benoit Steiner, Ilya Sutskever, Kunal Talwar, Paul Tucker, Vincent Vanhoucke, Vijay Vasudevan, Fernanda Viégas, Oriol Vinyals, Pete Warden, Martin Wattenberg, Martin Wicke, Yuan Yu, and Xiaoqiang Zheng. TensorFlow: Large-scale machine learning on heterogeneous systems, 2015. URL <http://tensorflow.org/>. Software available from tensorflow.org.
- [55] Inês C Moreira, Igor Amaral, Inês Domingues, António Cardoso, Maria Joao Cardoso, and Jaime S Cardoso. Inbreast: toward a full-field digital mammographic database. *Academic radiology*, 19(2):236–248, 2012.
- [56] P SUCKLING J. The mammographic image analysis society digital mammogram database. *Digital Mammo*, pages 375–386, 1994.

## Satisfaction of Old Graduates of Zootechnical Engineering for Improvement of Educational Quality at the UNCP

Jorge Castro-Bedriñana<sup>\*1</sup>, Doris Chirinos-Peinado<sup>1</sup>, Felipe Zenteno-Vigo<sup>1</sup>, Gianfranco Castro-Chirinos<sup>2</sup>

<sup>1</sup>Faculty of Zootechnics, Universidad Nacional del Centro del Perú, Huancayo, Perú

<sup>2</sup>Faculty of Psychology, Universidad Peruana de Ciencias Aplicadas, Perú

### ARTICLE INFO

*Article history:*

*Received: 26 December, 2019*

*Accepted: 22 February, 2020*

*Online: 09 March, 2020*

*Keywords:*

*Curriculum*

*Old graduate*

*Graduate satisfaction*

*Continuous improvement*

*Graduation profile*

*Competence approach*

*Professional performance*

*Curriculum update*

*Zootechnics program*

### ABSTRACT

*Concept of university higher education quality is linked to the relevance of an educational project that promotes institutional transformation to improve the comprehensive training of new professionals. In this context, the research objective is to determine the graduates satisfaction level, trained with curricula 1979, 1985 and 1995 who have more than 20 years of graduation from Zootechnical Faculty of the Universidad Nacional del Centro del Perú (UNCP), the main deficiencies perceived by graduates in curriculum development, areas of knowledge that should be reinforced and the reasons for dissatisfaction, and have more evidence for curriculum improvement. These plans respond to a traditional educational model, by objectives, without competence assessment system, repetitive learning, and insufficient laboratories implementation. A questionnaire was applied with questions to know the employment situation, continuing education, curricular relevance, areas to be reinforced and satisfaction level with training received in the study years. Sixty graduates in the research were considered, with systematic probabilistic sampling carried out in graduates meeting; This sampling is very efficient when there are a limited number of subjects that have the same qualities as the target population, that is, graduates of the UNCP Faculty of Zootechnics trained with 1979, 1985 and 1995 curricula. Data was analyzed in SPSS 23. Research provides information to improve the educational quality of UNCP zootechnical engineering academic program.*

### 1. Introduction

Universal access to higher education is a global commitment and is intended to minimize social inequality gaps [1], to contribute to scientific, technological and economic progress population [2]; for this, higher education institutions must be recognized for sustained quality assurance, self-regulation and relevant and efficient provision of their educational services [3]. In this context, to guarantee the satisfaction of the needs and expectations of students, graduates and interest groups, governments must monitor the quality of higher education through different strategies, which in Peru is carried out by the National System for the Evaluation, Accreditation and Certification of Educational Quality - Sineace, whose accreditation model for university programs sets 34 quality standards [4].

Demand for quality educational services not only comes from students satisfied with their training and educational services received, but from their parents or caregivers who cover educational expenses [5], and satisfaction of interest groups and employers; Therefore, the labor insertion of graduates and the achievement of educational objectives are monitored after 3 years of professional experience [6], to demonstrate the relevance of professional training with the needs of the environment and social demand [7].

A quality training process allows graduates to meet labor demand with high levels of satisfaction; therefore, the quality of higher education is reflected in the quality of its graduates [8], with full achievement of competencies defined in its profile [6].

The quality factors that evaluate comprehensive training are linked to the teaching-learning process, and consider 4 quality standards, with their indicators [6]:

<sup>\*</sup>Jorge Castro-Bedriñana, Av. Mariscal Castilla N° 3909, El Tambo-Huancayo. +51 964408057. [jorgecastro@yahoo.com](mailto:jorgecastro@yahoo.com)



- Curriculum: input profile and graduation profile with a focus on competencies, with general, basic and specialized areas, teaching strategies, relevance, evaluation and periodic updating.
- Teaching-learning process: articulate learning with research, development and innovation (RDi) and social responsibility with the participation of students and teachers; mobility agreements and exchange of experiences.
- Teacher management: adequate selection, evaluation, training and improvement, recognition and stimulation of teaching activity and intellectual production.
- Follow-up to students: adequate selection of new students, leveling programs to start and extracurricular activities that contribute to their training.

To assess achievement of competence and employability, representative information should be measured and collected to strengthen the teaching-learning process and update the curriculum, the graduation profile, improve teacher management and other related processes [6]. The satisfaction evaluation of graduates with different services offered by the university and its curriculum, in recent years have intensified in the search for the quality and excellence of higher education [9, 4].

It is necessary that university training programs analyze and reflect on their current situation and their environment, and redefine their purpose through dialogue with different interest groups, including graduates, to know their perceptions and expectations, in order to improve educational quality [10].

In major universities in the world, information about graduates is collected through surveys [11, 12, 13]. In Peru, all accredited university programs conduct follow-up surveys of their graduates, monitoring employability and fulfillment of educational objectives or career purposes [14].

Regarding careers linked to agriculture, the Inter-American Institute for Cooperation on Agriculture (IICA), as a result of Regional Meetings for the Modernization of Agricultural Sciences Faculties, more than two decades ago suggests improving the link with the environment [15], considering the scientific progress, technological, socio-economic and cultural changes, that today added to a context of climate change. Recent study by Sineace-Peru, called "Training offer and labor demand of technical and professional personnel in risk and disaster management and climate change", reveals that professional needs are directed to specialists who make climate change effects more bearable; Higher education institutions must shape their academic proposals in agricultural, environmental, biological and health careers [16].

Profiles of graduation from Zootechnical Faculties must guarantee the formation of transformative and integral human potential, which contributes to solve problems that delay the progress of family agri-food production and medium and large-scale production systems. Rural population requires appropriate production technologies to contribute to their food security [17], and on the other hand export agriculture should be intensified, as the country's fundamental economic livelihood, through the generation of modern technology for sustainable production and minimizing pollution environmental. This context demands radical changes in the curriculum to improve critical thinking, with soft skills, knowledgeable about their environment, with investigative

and innovation skills, committed to producers and accompany them in their development, with social responsibility.

In the Faculty of Zootechnics of UNCP, since its foundation in 1959, various curricula characterized by their linearity and minimum flexibility were applied [18]. In this context, the research objective was to determine the graduates satisfaction level, trained with curricula 1979, 1985 and 1995 who have more than 20 years of graduation from Zootechnical Faculty of the Universidad Nacional del Centro del Perú (UNCP), the main deficiencies perceived by graduates in curriculum development, areas of knowledge that should be reinforced and the reasons for dissatisfaction.

Research is structured as follows: Section 2 presents the methodology used in this study; descriptive and relational methodology, determining the correlation of evaluated variables. Section 3 shows the results obtained after conducting surveys. Section 4 presents the discussion of results and conclusions.

## **2. Material and method**

### *2.1. Type and level of research*

Cross-sectional, descriptive and relational study.

### *2.2. Sample framework for graduate satisfaction survey*

Survey was carried out to 60 graduates in professional activity for more than 20 years; 28.3% were formed with the 1979 curriculum, 40.0% with the 1985 curriculum and 31.7% with the 1995 curriculum. Sampling was systematic probabilistic, which is very efficient when there are a limited number of subjects with the same qualities as the target population [19], in this case, old graduates of the Faculty of Zootechnics - UNCP.

### *2.3. Collection of information and measuring instruments survey*

The information was collected by applying a semi-structured survey at a meeting of graduates, who studied with the curricula of 1979, 1985 and 1995.

The survey instrument considered general information on the date of graduation, the curriculum followed (1979, 1985 or 1995) and the highest academic degree. Specific information considered the perception about employability, work area, areas to reinforce the profile, qualification criteria of the study curriculum, curricular deficiencies, satisfaction level with the curricular consistency, and suggestions to reinforce the curriculum.

### *2.4. Statistical analysis*

Statistical analyzes were performed with SPSS 23, generating univariate descriptive results. Bivariate and multivariate correlations were also determined between the variables linked to the perception of graduates regarding their curricula followed during professional training.

## **3. Results**

Figures 1 to 4 show information on the number of respondents by curriculum, the highest academic degree obtained, employment level and professional work area.

More than 50% of graduates have obtained the professional title by thesis modality and only one had a Doctor degree (Figure

2). The majority work in public institutions, highlighting temporary jobs in areas other than zootechnics (Figure 3). Less than half work in activities related to animal production, animal health, livestock unit management, agricultural marketing, teaching and consulting in the agricultural area (Figure 4).

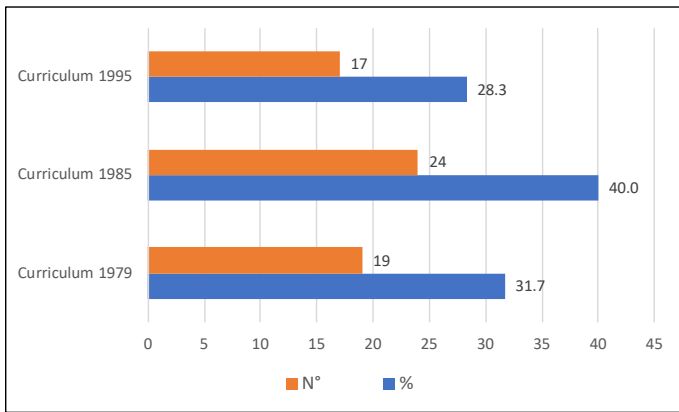


Figure 1. Graduates who participated in the survey

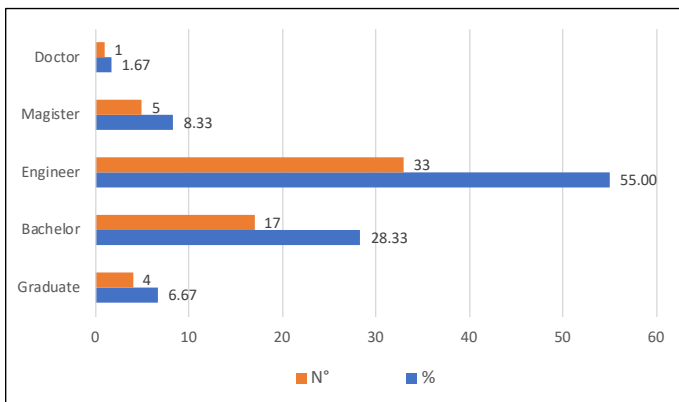


Figure 2. Highest grade of respondents

Figures 5 to 10 show the results of the areas of reinforcement suggested by the graduates, curriculum qualification and factors considered, suggestions for curriculum type, graduate achievements and the perception of curriculum relevance. Main five areas that graduates suggest strengthening in the curricula are strategic planning, social evaluation of investment projects, biotechnology and genetic engineering, livestock management, and budget and financing (Figure 5).

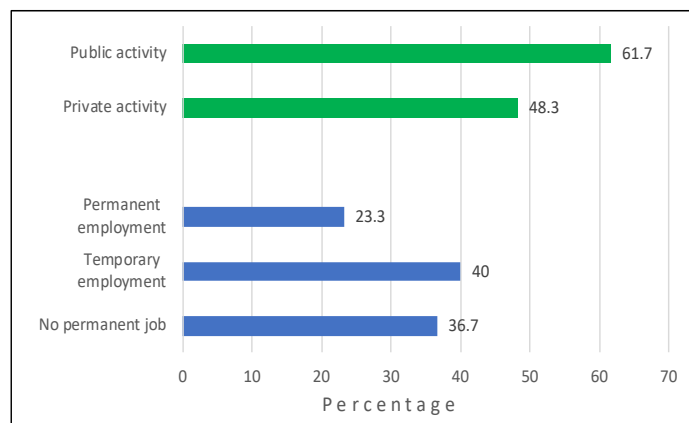


Figure 3. Employability of graduates

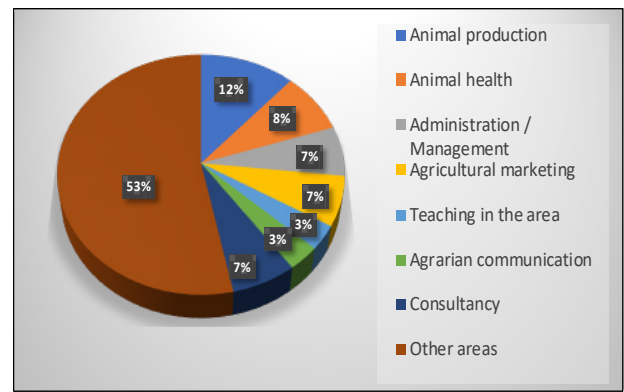


Figure 4. Graduates work area

Regarding the curriculum qualification, the majority consider "Regular" (Figure 6), and for improvement, additionally to consider areas to be reinforced, they suggest the development of modular or block curricular experiences; that is, by competencies (Figure 7). Additionally, for adequate curriculum development and guaranteeing the achievement of competencies, the program must establish strategies to improve the academic and research level of teachers (Figure 8). They consider having received an adequate theoretical basis and the practical aspects must be reinforced (Figure 9); For these reasons, the graduates of the study have perceived that the curriculum had little relevance (Figure 10).

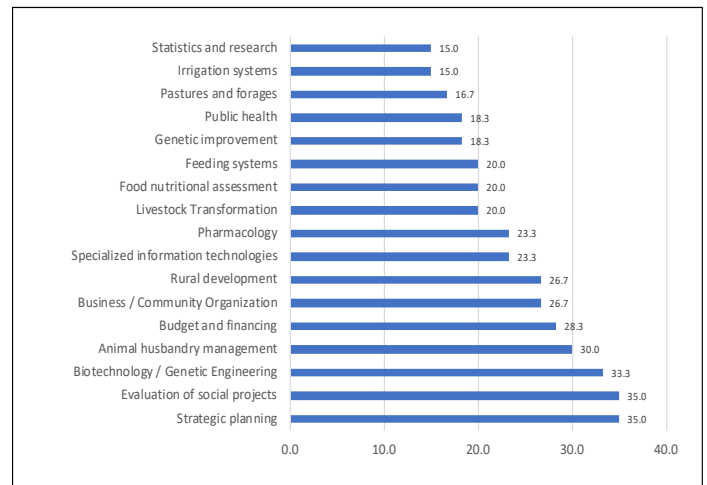


Figure 5. Areas to reinforce profile

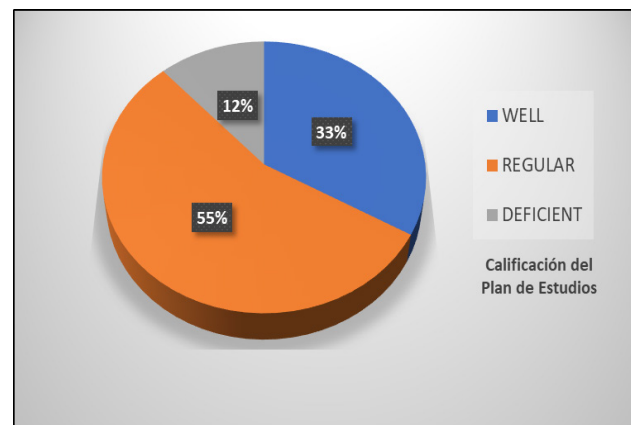


Figure 6. Qualification of the Curriculum by graduates

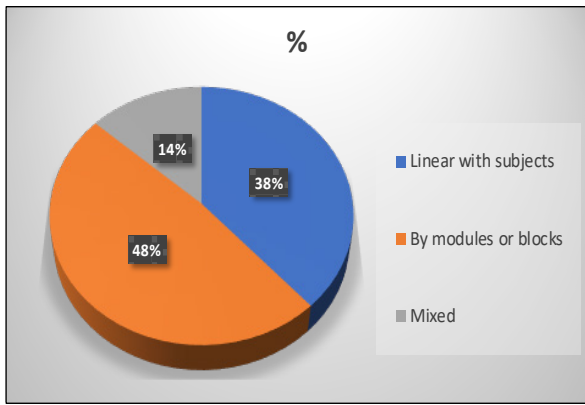


Figure 7. Suggestion of graduates to modify the Curriculum

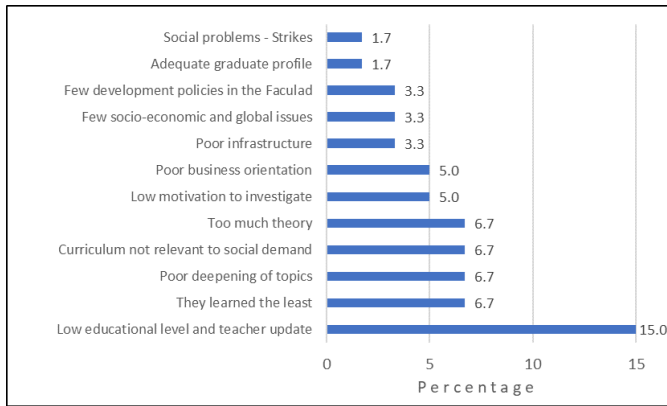


Figure 8. Factors considered to qualify the curriculum

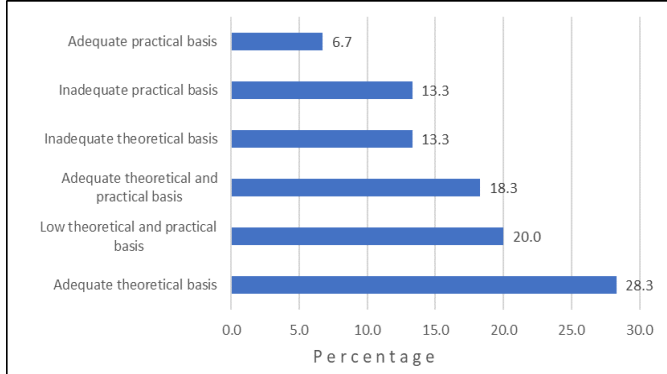


Figure 9. Achievements of graduates with a corresponding curriculum

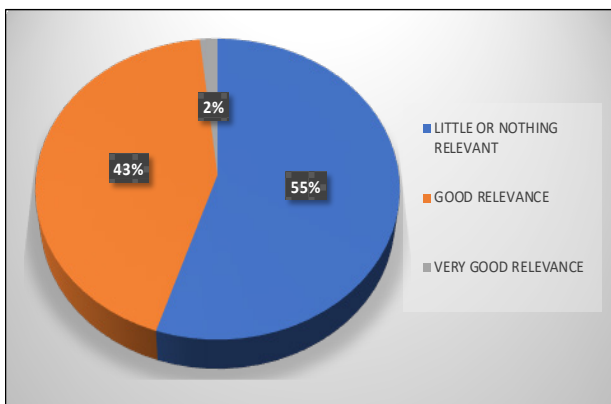


Figure 10. Relevance of the curriculum

The satisfaction level with professional training was 46.7% and not satisfied was 53.3%. Respect to specialized knowledge received, 23.3% was enough, 58.3% was not enough, and 18.3% was insufficient.

Figures 11 and 12 show the percentage of the main reasons for dissatisfaction in professional training and the perception of curricular deficiencies.

Among the main reasons for dissatisfaction with professional training they indicate having had non-innovative and outdated teachers, inappropriate graduation profile, and in the professional practice they do not apply everything they learned (Figure 11).

Graduates perceive that the main deficiencies in the curriculum are due to the superficial and outdated knowledge received during professional training, with priority cognitive curricular experiences.

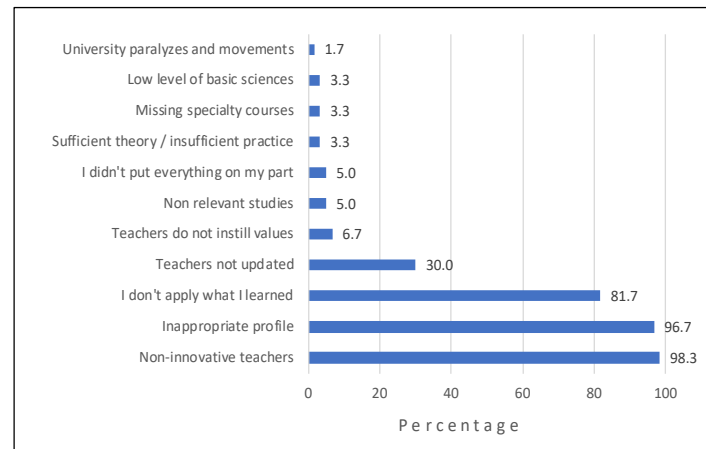


Figure 11. Main reasons for dissatisfaction in professional training

To determine the correlation that exists between some variables considered in the perception survey with curricula followed by graduates, it was considered: There is no correlation = 0; Moderate positive correlation = 0.3 to 0.5; Strong positive correlation > 0.5; Perfect positive correlation > 1.0.

Significant correlations were found between the variables linked to the perception of graduates regarding the curricula developed during professional training (Table 1).

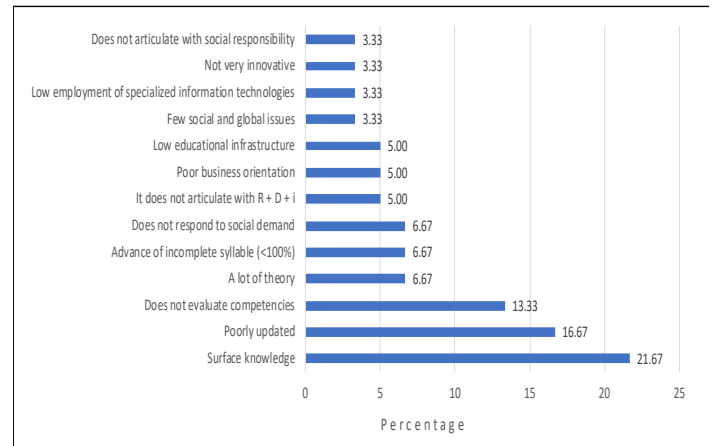


Figure 12. Perception of the curriculum deficiencies

Table 1. Spearman's correlation between some variables that showed statistical significance ( $P < 0.05$ )

Variable 1	Variable 2	r	P-value
Professional status of the graduate	Curriculum	0.434	0.001
Professional status of the graduate	Where you currently work	0.736	0.000
Professional status of the graduate	Main Work Area	0.725	0.000
Curriculum relevance	Expand work areas	0.333	0.009
Strengthen diagnostic knowledge	Strengthen knowledge in budget and financing	0.406	0.001
Strengthen diagnostic knowledge	Strengthen knowledge in business / community organization	0.435	0.001
Strengthen diagnostic knowledge	Strengthen knowledge in data analysis and interpretation	0.453	0.000
Strengthen diagnostic knowledge	Strengthen computer and informatic knowledge	0.319	0.013
Strengthen knowledge in budget and financing	Strengthen strategic planning knowledge	0.469	0.000
Strengthen knowledge in business / community organization	Strengthen knowledge in technology transfer	0.485	0.000
Strengthen knowledge in reproduction systems	Strengthen knowledge in feeding systems	0.515	0.000
Strengthen knowledge in reproduction systems	Strengthen knowledge in balanced ration formulation	0.523	0.000
Strengthen knowledge in food nutritional assessment	Strengthen knowledge in balanced ration formulation	0.528	0.000
Strengthen knowledge in food nutritional assessment	Strengthen knowledge in prevention and promotion of animal health	0.467	0.000
Strengthen knowledge in animal husbandry management	Strengthen knowledge in feeding systems	0.395	0.006
Strengthen knowledge in balanced ration formulation	Strengthen knowledge in technology transfer	0.571	0.000
Strengthen knowledge in balanced food processing	Strengthen knowledge in technology transfer	0.621	0.000
Strengthen knowledge in balanced food processing	Strengthen knowledge in animal husbandry management	0.492	0.000
Strengthen knowledge of cultivation and management of pastures and forages	Strengthen knowledge in technology transfer	0.395	0.002
Strengthen knowledge in education and agricultural communication	Strengthen knowledge in technology transfer	0.515	0.000
Strengthen knowledge in rural development	Strengthen knowledge in soil management	0.416	0.000
Strengthen knowledge in irrigation systems	Strengthen knowledge in silvopastoral management	0.522	0.000

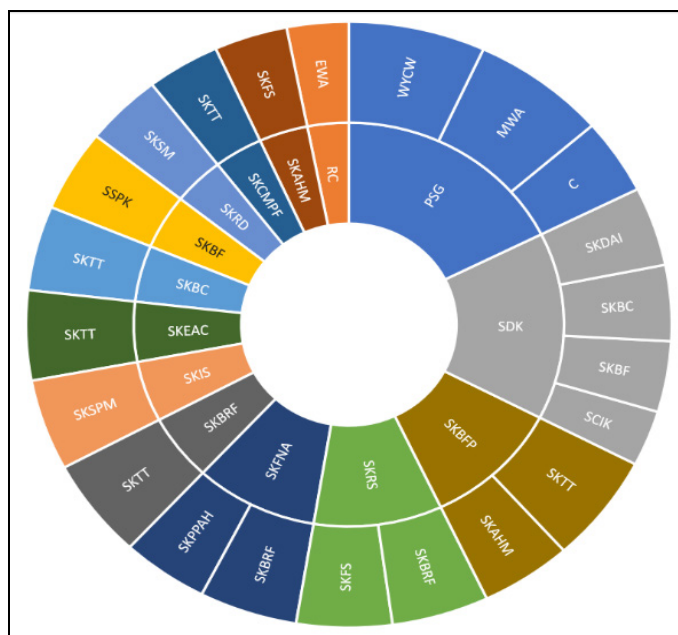


Figure 13. Solar projection of hierarchically coded correlations

C: Curriculum, EWA: Expand work areas, MWA: Main Work Area, PSG: Professional status of the graduate, RC: Curriculum relevance, SCIK: Strengthen computer and informatic knowledge, SDK: Strengthen diagnostic knowledge, SKAHM: Strengthen knowledge in animal husbandry management, SKBC: Strengthen knowledge in business / community organization, SKBF: Strengthen knowledge in budget and financing, SKBFP: Strengthen knowledge in balanced food processing, SKBRF: Strengthen knowledge in balanced ration formulation, SKCMPF: Strengthen knowledge of cultivation and management of pastures and forages, SKDAI: Strengthen knowledge in data analysis and interpretation, SKEAC: Strengthen knowledge in education and agricultural communication, SKFNA: Strengthen knowledge in food nutritional assessment, SKFS: Strengthen knowledge in feeding systems, SKIS: Strengthen knowledge in irrigation systems, SKPPAH: Strengthen knowledge in prevention and promotion of animal health, SKRD: Strengthen knowledge in rural development, SKRS: Strengthen knowledge in reproduction systems, SKSM: Strengthen knowledge in soil management, SKSPM: Strengthen knowledge in silvopastoral management, SKTT: Strengthen knowledge in technology transfer, SSPK: Strengthen strategic planning knowledge, WYCW: Where you currently work.

#### 4. Discussion

Research examines the satisfaction and experiences of graduates of the Zootechnical Faculty of UNCP with your professional training and the recommendations given to strengthen the curriculum and improve professional performance in the context of globalization, based on curricular experiences with 1979, 1985 and 1995 plans. This document contributes to knowledge in the field of quality assurance of higher education services [7].

In this study, the “Good” qualification of the curriculum is mainly based on the fact that graduates learned the minimum and regularly work in the profession. The “Regular” qualification responds to too much theory, and lack of practices, poor laboratory infrastructure, farms, classrooms, audiovisual equipment, agricultural equipment and tools, poor motivation to research and innovate, poor business orientation, superficiality in developed topics, low academic level teacher, poor teaching methodology, poor updating, incomplete syllable development, lack of socio-economic issues, lack of faculty development policies, low relevance of curriculum, and low engineering level that leads to problems of professional development.

Between Spearman's correlations that showed statistical significance ( $P < 0.05$ ), the professional situation of the graduate with the relevance of the curriculum, and with the place and area of work stands out [16]; observing greater economic benefits when better professional training was received (Table 1).

There is also a series of relationships between different subjects or issues, which demonstrate synergy and must be organized in the correct sequence, establishing an appropriate curriculum mapping with basic competencies as a requirement of specific competences [6].

The solar projection graph represents hierarchical data as concentric rings in a circle; the correlation values (r) have been coded as arcs within each ring. Each level of the hierarchy is represented by a ring or circle, the inner circle being the top of the hierarchy (Figure 13).



The “Poor” curricular qualification is directly related to the problems identified in the Zootechnics study program [20], indicating that the graduates are not formed in basis to require for the development for Peruvian agriculture; They have little insertion in the labor market, the quality of their training does not meet the requirements of employers. They have little capacity for entrepreneurship and commitment to the environment. These results force to carry out a curricular reform to move to teaching with a competency approach, in order to comply with standards of accreditation of university careers considered in the National System of Accreditation and Certification of Educational Quality of Peru [4, 6], redesigning the graduation profile that considers general and specific competences [21, 4, 6].

Regarding curricular relevance, the majority of respondents say that it does not respond to the needs of local and national reality, and should be modified in response to social demand and have a new professional with solid humanistic, scientific and technological training, with training capacity continuous, with comprehensive training and with social and environmental responsibility; processes in which authorities, teachers, students, graduates and properly identified interest groups must participate [4, 6].

Information of graduates is an important source of feedback for the study program and the university. The connection with the labor market contributes to the development of university social responsibility, and is a bridge between university and social context [22], determining the social role, positioning and relevance [23].

Monitoring graduates offers evidence for curriculum reform. The professional and personal performance of graduates allows identifying quality and efficiency indicators of higher education institutions [24].

The results of the study indicate that more than half of the graduates of the faculty of zootechnics UNCP, who studied with the curricula 1975, 195 and 1995 do not work in activities related to zootechnics (Figure 4), relevant aspect of the study, linked to the non-fulfillment of educational objectives of a public university [6]. Training professionals who do not work in your area means a loss to the State and society; and it is suggested to prioritize a comprehensive curriculum reform.

Information from graduates on educational quality, job placement and other characteristics facilitates the development of strengths and implementation of improvement plans for higher education institutions [25, 26]. Evaluation of satisfaction with academic and administrative services received in training is a right of graduates [27] and can be carried out through end of training surveys [28] and follow-up surveys after 3 or more years of professional practice [6]. In state institutions it is directly related to accountability to society, not only for the purpose of management transparency, but to demonstrate a quality educational service [29].

In this study, satisfaction of graduates is well below medical graduates of the Cienfuegos University of Cuba, where more than 80% of respondents expressed their satisfaction with the promotion and consolidation of personal qualities, as well as in the training received for the professional performance [30], however,

they showed dissatisfaction with regard to English language proficiency, new information and communication technologies, tutors and research advisors. A result similar to ours is dissatisfaction with the development of general or soft skills.

The improvement of university quality is not only caused by the increase in resources and infrastructure, but mainly by offering professionals trained and satisfied with the training received [31] and the information is needed to propose improvement plans. In this regard, the formative model by competences, seeks that the student relate theory to practice, which impacts on the achievement of professional competences [32].

Other studies on student satisfaction with curriculum content, teaching methods, infrastructure and facilities, teacher skills and student performance show that satisfaction levels are largely correlated with student academic performance, and with teacher skills [33] and with the teacher ability to interact with the students. The teacher's attitude excels in the student's interest [34].

Results show that graduates are satisfied with their training when they get a job in their professional area and in a suitable work place, with permanence of work. The ease of obtaining a job contributes to the appreciation of satisfaction and quality of the services received, and employers' satisfaction with the image and prestige of the higher institution that forms them [35, 36].

This study shows that the professional condition of the graduate is correlated with the relevance of the curriculum, place and work area (Table 1), aspects linked to the salary level [37, 38]. Engineers can earn more than social scientists, and these can earn more than teachers, but on average each will earn less if they are graduated from an institution of low selectivity and quality [39].

Graduates suggest strengthening knowledge in agricultural production systems, food security, public health and climate change, developing environmental awareness, synergistically integrating biotechnology and information technologies, having as transversal axes to RDi, and Social Responsibility, aspects which have to be prepared with the participation of interest groups [4, 6].

The general results of the study are similar to those of more than 20 years ago at the Universidad Nacional de Loja-Ecuador [40] who detected applicants and entrants without minimum knowledge for careers, with lacks of study and reading habits, without vocational guidance, with professional profiles without appropriate curricular research and not relevant, with archaic and traditional teaching systems, the master class and dictation subsisting, non-existence of a permanent system of curriculum evaluation, with memorized and fragmented learning, with evaluation based on exams, with insufficient implementation of laboratories and workshops, with outdated libraries, without research plans that allow the link between teaching, research and extension, with thesis without major scientific input and whose results were not disseminated. For these reasons they replaced the traditional educational model with a modular system that relates the university - society, integrating teaching, research and extension, around concrete problems of reality, implementing a modular academic system for transformation objects. The future of higher education was planned from the present, to face scenarios of high uncertainty and not easy to foresee [41], which implies new teaching-learning strategies, especially when university students

currently have an amazing management of virtual technology, which must be included in the curriculum, without detriment to interpersonal contact, revaluing the emotional and social intelligences of the person [42].

Our results aim to improve the generation of science and technology from the university through the application of a properly designed curriculum, since agricultural education is an essential factor in the success of agricultural development in different countries [43] and linked university programs the agricultural sector must guarantee the training of professionals of quality and excellence [44].

## 5. Conclusions

The study determined the main weaknesses of the 1979, 1985 and 1995 curricula based on semi-structured surveys applied to old graduates of the professional program of Zootechnics - UNCP who have more than 20 years of work experience.

Satisfaction level of graduates regarding their curricula, in general, ranges from Regular to Poor.

The research offers elements of judgment to readjust the curriculum and train a new zootechnic engineer, required for the sustained development of the country.

It is recommended that managers, teachers, students, graduates and interest groups of the professional program of Zootechnics take into account the results of this study for reflections of curriculum reform.

## Limitations

The conclusions of this study may have a limited generalized capacity for other zootechnical engineering programs, both in Peru and in other countries. The sample was intended to include all graduates of the Faculty of Zootechnics with the 1979, 1985 and 1995 curricula, but it was not possible for different places of current residences. The results should not be considered to characterize the relationship between the quality of the program and the job satisfaction of other universities due to the different environments. In this study, quality responds to the perceptions of graduates, which may vary based on relatively recent events in professional action and would have little to do with previous experiences in the academic career.

## Conflict of Interest

The authors declare no conflict of interest.

## Acknowledgment

To graduates who kindly gave their consent to participate in the survey, providing valuable contributions to be incorporated into the readjustment of the UNCP Zootechnics program curriculum.

## References

[1] European Commission/EACEA/Eurydice (2013). Education and training in Europe 2020: Responses from the EU Member States. Eurydice Report; Brussels: Eurydice. <https://op.europa.eu/en/publication-detail/-/publication/4cd55a97-854d-4fff-8ebd-3fd3f38ca58a/language-en>. <https://doi.org/10.2797/49490>.

[2] Ali, F., Zhou, Y., Hussain, K., Nair, P. K., & Ragavan, N. A. (2016). "Does higher education service quality effect student satisfaction, image and loyalty?: A study of international students in Malaysian public universities",

Quality Assurance in Education, Vol. 24 Issue: 1, pp.70-94, <https://doi.org/10.1108/QAE-02-2014-0008>.

[3] Nyagotti-Chacha, C. (2007). Public university, private funding: the challenges in East Africa. Higher Education in Postcolonial African Nations: Paradigm of Development, Decline, and Dilemmas.

[4] Sineace. (2016). Modelo de Acreditación para Programas de Estudios de Educación Superior Universitaria. Sistema Nacional de Evaluación, Acreditación y Certificación de la Calidad Educativa. Disponible en: <https://www.sineace.gob.pe/wp-content/uploads/2014/08/Anexo-1-nuevo-modelo-programas-Resolucion-175.pdf>

[5] Rajab, A., Panatik, S. A., Rahman, A, Rahman, H. A., Shaari, R. & Saat, M. (2011). Service quality in a research university: A postgraduate perspective. *Procedia - Social and Behavioral Sciences* 29 pp. 1830 – 1838. <https://doi.org/10.1016/j.sbspro.2011.11.431>.

[6] Sineace. (2018). Explicación de Estándares del Modelo de Acreditación para Programas de Estudios de Educación Superior Universitaria. Sistema Nacional de Evaluación, Acreditación y Certificación de la Calidad Educativa. <http://repositorio.sineace.gob.pe/repositorio/handle/sineace/5490>.

[7] Alhassan I, Sowley E, Nalarb R, Kassim A. (2019). Analysis of Graduate Satisfaction and Experience with Higher Education Services in a Ghanaian University. *European Journal of Educational Sciences, EJES* 2018 Vol.5 No.4 ISSN 1857- 6036. <http://dx.doi.org/10.19044/ejes.v5no4a2>.

[8] Belash, O., Popov, M., Ryzhov, N., Ryaskov, Y., Shaposhnikov, S. & Shestopalov, M. (2015). Research on university education quality assurance: Methodology and results of stakeholders' satisfaction monitoring. *Procedia - Social and Behavioral Sciences* 214:344-358. <https://doi.org/10.1016/j.sbspro.2015.11.658>

[9] Temizer, L. & Turkyilmaz, A. (2012). Implementation of Student Satisfaction index model in higher education institutions. *Procedia-Social and Behavioral Sciences* 46:3802-3806. <https://doi.org/10.1016/j.sbspro.2012.06.150>.

[10] Garzón CA. (2018). Modelo para el Seguimiento y Acompañamiento a Graduados (SAG), una visión holística de la gestión de la calidad de la educación superior. *Educación Vol. XXVII, N° 52:201-218*. <https://doi.org/10.18800/educacion.201801.011>

[11] Azah, M., Fatihah, S., & Abdul-Halim, I. (2012). Graduate students' perspectives on study environment based on exit. *Canadian Center of Science and Education*, 8(16). DOI: 10.5539/ass.v8n16p200

[12] Magid, M., Kamaruddin, N. & Azirawani, N. (2009). Quality assurance in higher education institutions: Exist survey among University Putra Malaysia graduating students. *International Education Studies*, pp. 25-32. DOI: 10.5539/ies.v2n1p25

[13] Othman, N. T. A., Misonon, R., Abdullah, S. R. S., Kofli, N. T., Kamarudin, S. K., & Mohamad, A. B. (2011). Assessment of programme outcomes through exit survey of chemical/biochemical engineering students. *Procedia Social and Behavioral Sciences*, pp. 39-48. <https://doi.org/10.1016/j.sbspro.2011.05.007>

[14] Sineace. (2019). Estas son las 78 carreras universitarias acreditadas por el Sineace en Lima. Disponible en: <https://www.sineace.gob.pe/estas-son-las-78-carreras-universitarias-acreditadas-por-el-sineace-en-lima/>

[15] Venezian E. y Chateaufneuf R. (1997). Implicaciones del MERCOSUR para la formación agronómica universitaria. Primera Jornada Regional de Modernización de Facultades de Agronomía. CECAP-IICA. San José de Costa Rica. ISSN: 0534-5391; no. A1/SC-97-09.

[16] Sineace, (2016b). Estudio de oferta formativa y demanda laboral de personal operativo, técnico y profesional asociado a la gestión de riesgos de desastres y del cambio climático. Sistema Nacional de Evaluación, Acreditación y Certificación de la Calidad Educativa. <http://bvpad.indeci.gob.pe/doc/pdf/esp/doc2656/doc2656-contenido.pdf>

[17] Chirinos. (2016). Seguridad alimentaria Nutricional en Poblaciones Vulnerables de la Región Central del Perú. Editorial JOSIMPRESORES SAC. Huancayo. ISBN. 978-612-00-2291-7. 270 pp.

[18] CFZ. (1995). *Plan Curricular de la Facultad de Zootecnia – 1995*. Consejo de Facultad de Zootecnia – Universidad Nacional del Centro del Perú. Huancayo. Perú

[19] Landa, M. & Ramírez, M. (2018). Design of a student satisfaction questionnaire for a professional level course under the inverted learning model. *Revista Páginas de Educación*. Vol. 11, Núm. 2.

[20] CFZ. (2002). *Plan Curricular de la Facultad de Zootecnia – 2002*. Consejo de Facultad de Zootecnia – Universidad Nacional del Centro del Perú. Huancayo. Perú.

[21] Ley Universitaria N° 30220 (2014). Presidencia del Consejo de Ministros. Presidencia del Perú. MINEDU. [http://www.minedu.gob.pe/reforma-universitaria/pdf/ley\\_universitaria.pdf](http://www.minedu.gob.pe/reforma-universitaria/pdf/ley_universitaria.pdf)

- [22] Ramírez, M. J, Reséndiz, M., y Reséndiz, M. E. (2017). Metodología de seguimiento de egresados para fortalecer la vinculación de la universidad con la sociedad. *Revista Global de Negocios*, 5(3), 99-111. <https://ssrn.com/abstract=2914540>.
- [23] Aldana de Becerra, G. M., Morales-González, F. A., Aldana-Reyes, J. E., Sabogal-Camargo, F. J., Ospina, A. R. (2008). Seguimiento a egresados. Su importancia para las instituciones de educación superior. *Teoría y praxis investigativa*, 3(2), 61-65. Recuperado de <https://dialnet.unirioja.es/servlet/articulo?codigo=3701001>.
- [24] Marulanda, J., Ortiz, E., Moratto, N., Arcila, A. (2010). Caracterización de egresados de la Universidad CES en las cohortes de 2003, 2005, 2007 y momento "0". *Revista CES Psicología* 3(1), 50-63. <http://revistas.ces.edu.co/index.php/psicologia/article/view/1156/745>.
- [25] Ivanaa, D. & Dragan, M. (2014). Challenges and implications in assessing graduates' satisfaction in an international study program. *Procedia Economics and Finance* 16 pp. 104 – 109. [https://doi.org/10.1016/S2212-5671\(14\)00780-1](https://doi.org/10.1016/S2212-5671(14)00780-1)
- [26] Uysal, F. (2015). Evaluation of the factors that determine quality in graduate education: Application of a satisfaction benchmarking approach. *Procedia - Social and Behavioral Sciences* 191 pp. 1034-1037. <https://doi.org/10.1016/j.sbspro.2015.04.386>
- [27] Hanapi, Z. & Nordin, M. S. (2014). Unemployment among Malaysia graduates: Graduates' attributes, lecturers' competency and quality of education. *Procedia - Social and Behavioral Sciences* 191 (2015) 1034 – 1037. <https://www.sciencedirect.com/science/article/pii/S1877042814012865>. <https://doi.org/10.1016/j.sbspro.2014.01.1269>
- [28] Cardona, M. M. & Bravo, J. J. (2012). Service quality perceptions in higher education institutions: The case of a Colombian university. *estud.gerenc.* 28 (2012) 23-29. [https://doi.org/10.1016/S0123-5923\(12\)70004-9](https://doi.org/10.1016/S0123-5923(12)70004-9).
- [29] Uceda, J., y Sánchez-Canales, M. (2018). Rendición de cuentas y cómo hacerla. Cátedra. Cátedra UNESCO. [http://catedraunesco.es/kathedra\\_folder/Uceda18-Rendicion\\_de\\_cuentas.pdf](http://catedraunesco.es/kathedra_folder/Uceda18-Rendicion_de_cuentas.pdf)
- [30] Rocha, M., Hernández, M., Ledo, M., Chávez, D. (2017). Satisfacción de egresados cubanos de la carrera de Medicina con la formación recibida. *Curso 2015-2016, Cienfuegos. Medisur* 15(4):509-515.
- [31] Paredes MG. (2014). Nivel de satisfacción de estudiantes y egresados de la Universidad Nacional de Asunción. *Revista Paraguaya de Educación*, 1(4):57-69. ISSN 2305-1787
- [32] Avendaño, C., Gutiérrez, K., Salgado, C., Alonso-Dos-Santos, M. (2016). Rendimiento Académico en Estudiantes de Ingeniería Comercial: Modelo por Competencias y Factores de Influencia. *Formación Universitaria* Vol. 9 N°3. doi: 10.4067/S0718-50062016000300002. <https://scielo.conicyt.cl/pdf/formuniv/v9n3/art02.pdf>
- [33] Fernández Rico, J. E., Fernández Fernández, S., Álvarez Suárez, A., y Martínez Cambor, P. (2007). Éxito Académico y Satisfacción de Estudiantes con la Enseñanza Universitaria, *Relieve*: 13(2).
- [34] Salinas, A., Morales, J., Martínez, P. (2008). Satisfacción del estudiante y calidad universitaria: un análisis explicatorio en la unidad académica multidisciplinaria agronomía y ciencias de la Universidad Autónoma de Tamaulipas, México. *Revista de Enseñanza Universitaria*, N.º31:39-55. <http://institucional.us.es/revistas/universitaria/31/4SalinasGuti.pdf>
- [35] Teixeira, S., Matos da Silva, J., Oom do Valle, P. (2014). A model of graduates' satisfaction and loyalty in tourism higher education: The role of employability. *Journal of Hospitality, Leisure, Sport & Tourism Education* 16(2015):30-42. doi:10.1016/j.jhlste.2014.07.002.
- [36] Espinoza, O., González, E., Loyola, J. (2018). Evaluación de la satisfacción de titulados de la carrera de psicología en Chile. *Innovación Educativa*. Vol. 18(76),171-192. <http://www.scielo.org.mx/pdf/ie/v18n76/1665-2673-ie-18-76-171.pdf>
- [37] de Vries, W., Vázquez-Cabrera, R., Ríos-Treto, D. (2013). Millonarios o malparados: ¿de qué depende el éxito de los egresados universitarios? *Revista Iberoamericana de Educación Superior*, vol. 4(9)3-20. <https://doi.org/10.22201/iissue.20072872e.2013.9.80>.
- [38] Humburg, M., van der Velden, R., Verhagen, A. (2013). The Employability of Higher Education Graduates: The Employers' Perspective. *European Commission. The Netherlands*. [https://www.researchgate.net/publication/265086055\\_The\\_Employability\\_of\\_Higher\\_Education\\_Graduates\\_The\\_Employer's\\_Perspective](https://www.researchgate.net/publication/265086055_The_Employability_of_Higher_Education_Graduates_The_Employer's_Perspective).
- [39] Eide, E., Hilmer, M., & Showalter, M. (2015). Is it where you go or what you study? the relative influence of college selectivity and college major on earnings. *Contemporary Economic Policy*, 34(1), 37-46. doi:10.1111/coep.12115.
- [40] Uquillas, S., Valarezo, C., Tituaña, L. (2019). El Sistema Académico Modular: Experiencias de la Universidad Nacional de Loja y Aprendizajes para la Innovación de la Universidad Ecuatoriana. Loja, Ecuador. <https://unl.edu.ec/sites/default/files/archivo/2019-12/EL%20SISTEMA%20ACADEMICO%20MODULAR.pdf>
- [41] Gutiérrez, Katuska (2007). El papel de la prospectiva en las instituciones universitarias desde una perspectiva conceptual. *Revista Informe de Investigaciones Educativas*, XXI, 79-91. <http://biblo.una.edu.ve/ojs/index.php/IIIE/article/view/547>.
- [42] Ruiz Ruiz, M. (2013). El futuro de la educación [superior]. Una reflexión entre la doxa y la episteme. *Educación*, 22(42), 7-27. Recuperado a partir de <http://revistas.pucp.edu.pe/index.php/educacion/article/view/5289>.
- [43] Mulder M., Kupper H. (2006). The Future of Agricultural Education: The Case of the Netherlands. *The Journal of Agricultural Education and Extension* 12(2). DOI: 10.1080 / 13892240600861658.
- [44] Tamboli, PM and Nene, YL. (2011). Revitalizing Higher Agricultural Education in India: Journey towards Excellence. *Asian Agri-History Foundation, Secunderabad 500009, India*. 316 pp.

## The Implementation of Smart Farming Application Based on the Microcontroller and Automatic Sprinkler Irrigation System of Agricultural Land

Ery Muchyar Hasiri<sup>1,\*</sup>, Asniati<sup>1</sup>, Mohamad Arif Suryawan<sup>1</sup>, Rasmuin<sup>2</sup>

<sup>1</sup>Department of Informatics Engineering, Faculty of Engineering, Universitas Dayanu Ikhsanuddin, South East Sulawesi 93711, Indonesia

<sup>2</sup>Department of Mathematics Education, Faculty of Teacher Training and Education, Universitas Dayanu Ikhsanuddin, South East Sulawesi 93711, Indonesia

### ARTICLE INFO

Article history:

Received: 01 January, 2020

Accepted: 25 February, 2020

Online: 09 March, 2020

Keywords:

Smart Farming Application

Microcontroller

Irrigation Technology

Agricultural Land

### ABSTRACT

This research to applying the application of e-smart farming to control the sprinkler irrigation on agricultural land. This study aims to be able to help farmers to solve the watering problems that are manually carried out into watering done automatically and controlled, besides that this research also obtained data about the level of moisture content from sensor soil moisture, air temperature from the temperature sensor, and rainfall data from Rain Sensor as well as setting the right time using automatically scheduled Real-Time Clock (RTC) for watering time. This system is a combination of hardware and software components. The hardware part consists of systems and software embedded in the form of android-based applications. Consists of three sections, namely the Sensor block, the farm station controller, and the home station controller at the farmer's house. The implementation of the smart farming application in this study obtained quite good results. The final results of this study indicate that the tools applied can assist farmers in implementing smart farming systems. The results can be seen in the success of several temperatures, soil humidity, and rain sensor tests. Moreover, there is no barrier between smart farming applications on the base station and the farm station using 2.4GHz Wireless ZigBee, and sending data in real-time from the sensor block on the farm station server using ESP8266. Besides, the sprinkler watering system also has no problems when watering agricultural land when receiving orders from the application

### 1. Introduction

Indonesia is an agrarian country, where agriculture is one of the main sectors of food production to be able to meet the demands of an increasingly growing human population. In agriculture, Irrigation is a necessary process that affects plants to be able to grow and produce. Traditional farmers always visit their farms regularly to check the level of soil moisture on their farms and based on the crop's need for water. Farmers need to wait a certain period before turning off the pump so that the water is allowed to flow in sufficient quantities in their fields. This Irrigation is a tool to save the problem of water that is not suitable for plantations and vegetation in dry places and during the dry season [1]. Moreover, the traditional irrigation method requires a lot of time and effort, especially when a farmer needs to irrigate several agricultural

fields that are distributed in different geographical areas. Traditionally farmers will be present in their fields carrying out the irrigation process.

The modern agricultural sector is a transition from conventional agricultural technology to modern agriculture, namely smart agriculture. Smart farming (SF) involves the incorporation of information and communication technologies into machinery, equipment, and sensors for use in agricultural production systems. New technologies such as the Internet of things and cloud computing are expected to advance this development, introducing more robots and artificial intelligence into farming [2]. Such technologies do not suffice on their own; instead, they must be judiciously combined to deliver meaningful information in near real-time [3]. The use of smart farming techniques can increase crop yields, while simultaneously

\*Corresponding Author: Ery Muchyar Hasiri, [erymuchyar82@gmail.com](mailto:erymuchyar82@gmail.com)



producing more output from the same amount of input [4]. Advances in communication technologies such as GSM and GPRS have enabled the remote control of irrigation systems [5]. However, with current technological developments, farmers can manage their agricultural land along with other jobs [6].

Smart agriculture can be a solution for the development of modern agriculture [7]. Innovative irrigation practices can enhance water efficiency, gaining an economic advantage while also reducing environmental burdens [8]. Smart irrigation systems are practical and efficient ways of Irrigation. It monitors weather, soil conditions, evaporation, and plant water use and automatically adjusts watering schedules [9]. Intelligent Irrigation is a self-controlled system that automatically controls the total irrigation system, where farmers do not need to be present in their fields. The system will send information to farmers about the data and conditions of their farmland. So that the intelligent system does not require more workers to embarrass the task of watering plants, and also the use of water will be more efficient [10].

Smart agriculture uses Information Technology (ICT) and specifically, the Internet of Things (IoT) and associated extensive analytic data to overcome these challenges through electronic crop tracking, as well as the environment, soil, fertilization, and planting conditions [11]. The intelligent farming system that is a system that can control; temperature sensor, soil moisture sensor, air humidity sensor and another sensor at the sensor node and The Wireless sensor network (WSN) consists of a large number of sensor nodes can collect data and are sent to the base station [12]. Smart agriculture relies on data transmission and data concentration from many sensors in remote receiving systems to allow the combination and analysis of various agricultural data that can be used as a basis for making decisions to control agricultural land [2].

Agricultural land irrigation can be used to automate the system by utilizing the development of microcontroller technology. With the microcontroller technology can be a monitor of condition soil moisture, an automatic system is needed to water the plants and observe soil moisture so that cultivation can be more comfortable than conventional agriculture [13]. The irrigation system using wireless sensor networks has installed these sensors, to collect the environment data and control the irrigation system via smartphone [14]. Predict plantation irrigation based on weather and soil measurement variables, but it is necessary to predict the irrigation needs of a field without any prior irrigation reports from the plantation [15]. The setup uses soil moisture sensors that measure the exact moisture level in the soil. This value enables the system to use an appropriate quantity of water, which avoids [16]. The use of mobile systems can quickly increase water content from online monitoring and control to realize irrigation automation [17]. This smartphone service is based on PDAs, GIS, GPS, and WS. It is not easy, flexible, mobile, practical, and smart to gather information and manage agriculture in decision making in agricultural production agriculture [18].

Automation of farm activities can transform agricultural domains from being manual and static to intelligent and dynamic, leading to higher production with lesser human supervision. Wireless Sensor Networks (WSNs), the Internet of things (IoT), and aerial mapping are nowadays being used very much in

agriculture. The developed multimedia platform can be controlled remotely by mobile phone [19]. Parameter controller via a remote device or internet service and its operation is carried out with a connecting sensor, wifi, a camera with a microcontroller [20]. Smart irrigation systems use IoT based on application controlled plant monitoring and monitoring systems via Smartphones [21].

The implementation of smart farming applications based on Automatic Sprinkler Irrigation systems can provide solutions for farmers where farmers are not required to work in the field. In this paper, we propose hardware and software prototype to be able to automate irrigation control from the smart farming application fully. We also use microcontroller Arduino and three main sensors, namely Soil Moisture Sensor, Temperature Sensor, and Rain Sensor, which use Wireless sensor network connections from Zigbee and Esp8266 Module. The soil moisture sensor is a comparator (LM393), which converts analog data to discrete with two soil probes consist of two thin copper wires of 5 cm each that can be immersed in the soil under test (Kumar Sahu & Behera, 2015). Temperature sensor DS18B20, the core functionality of the DS18B20 is its direct-to-digital temperature sensor. The resolution of the temperature sensor is user-configurable to 9, 10, 11, or 12 bits, corresponding to increments of 0.5 C, 0.25 C, 0.125 C, and 0.0625C, respectively [9]. To communicate Android with the main server, we use wireless ESP8266EX to host the application. ESP8266EX can boots directly from an external flash. ESP8266EX functions as a WIFI adapter. Wireless internet access can be added to a microcontroller-based design with simple connectivity (SPI/SDIO or I2C/UART interface) [22].

## 2. Application Design

This system is a combination of hardware and software components. The hardware part consists of systems and software embedded in the form of android-based applications. Consists of three sections, namely the Sensor block, the farm station controller, and the home station controller at the farmer’s house. Overall engineering design can be seen in figure 1.

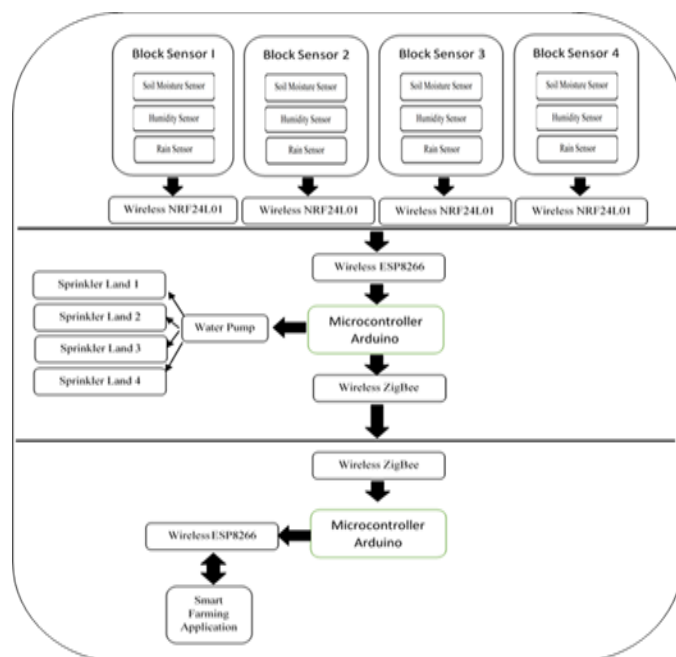


Figure 1. Overall Engineering Design

In testing the Real-Time Clock (RTC), the first watering time setting is done at 6:30 in the morning, and the second watering is at 4:30 pm and goes on every day. While on schedule management, fertilization is done scheduling once a week, which is done at 7:00 am every Thursday. In testing and measuring the moisture content using four soil moisture modification sensors connected to the ADC module and connected to Arduino Nano and NRF24L01 as senders of moisture content data to the Farm Station and forwarded to the smart Farming application on the smartphone, sensors are placed on four plots land. This humidity sensor is designed using two stainless steel rods of 5mm in diameter for two pieces for negative and positive voltage, with a length of each iron rod that is 15cm. At the base of the stainless steel, each cable is connected as a current stream to the ADC module. The input data from each stainless-steel bar is converted to a digital value in ADC, which becomes the data Value of ADC Sensor.

Convert the value from analog to Digital with the following method:  $ADC = (V_{in}/V_{ref}) * \text{Bit Maximum of Data}$ , which is the maximum number of bits of data that is 1023 starting at 0. To calculate the Input Voltage value ( $V_{in}$ ) on soil moisture sensors, where this input voltage is influenced by the amount of value detected by soil moisture sensors. Logarithms of calculations are as follows:

$V_{in} = \text{Value of Analog Sensor} \times (V_{ref}/\text{Number of Bit of Maximum Data})$ .

Then calculate the Difference value ( $n$ ) = Value of Bit Max Data (Dry) – Wet Standard Bit Value = 1023-350 = 673. So, to calculate the value of % Rh (Moisture Content Percentage) in Figures 4.b, namely by:

$Rh\% = [(Value of Bit Max Data - Analog Sensor Value)]/n \times 100\%$

Furthermore, calculating the sensitivity of soil moisture sensors in figure 4.d is by converting the Input Voltage value ( $V_{in}$ ) on the sensor from Volt to Millivolt with logarithms as follows:  $mV = Volt * 1000$ , So for sensitivity, i.e.,  $Sens = \%Rh / (mV)$ .

### 2.1. Scheme of Connection Between Home Station and Farm Station

Hardware in the form of electronic components, the first component placed in the Home Station as a home base of the farmer and the secondary component placed in the farm or field of the farmer as a Farm Station within 2 km. At Home Station, the components used consist of an Arduino Mega 2560 controller, ESP8266 wireless, Zigbee Pro 2.4 GHz. While at the Farm Station, the components consist of Arduino Mega 2560, Zigbee Pro 2.4 GHz Wireless Communication, NRF24L01 Wireless, Arduino Nano, Soil Moisture Sensor, DS18B20 Temperature Sensor, and Rain Sensor, Relay, Sollar Panel as a source of electricity use at the agriculture station. Laying sensor points on plots of land taken as wireless sensor network nodes of each area and interconnected wirelessly with ESP826 in the Controller Box at the Agricultural Station. Communication between stations uses Zigbee Pro 2.4 GHz wireless so that monitoring and control of farmlands/gardens can be done remotely while it is within reach of the communication signal. The system can work in real-time in transmitting data from each sensor node using NRF24L01 to Farm Station and then

forwarding the Home Station using Wireless Zigbee Pro 2.4 GHz. From the Home Station, the data is forwarded to the Smart Farming Application connected to ESP8266 wireless. The connection scheme between the Home Station and the Agriculture Station can be seen in Figure 2.



Figure 2. Scheme of Connection Between Home Station and Farm Station

### 2.2. The interface of e-smart Farming Application

In the application used in the control and monitoring of agricultural land by farmers using an Android-based platform with the application name smart farming, as shown in figure 2, Application Design Scheme of e-smart Farming. This e-smart farming application consists of several parts, namely: The First Form is to display the average graph in the form of temperature data with three conditions namely temperature  $<20^{\circ}C$  = Condition of Cold Temperature, temperature  $>21^{\circ}C$  up to  $<30^{\circ}C$  = Temperature of medium category (Warm) and temperature  $>31^{\circ}C$  categorized as hot temperature. The data of temperature displayed in the application are based on real-time input from the DS18B20 temperature sensor. On the first page there is also a moisture value/soil moisture content, which is divided into three conditions, namely soil moisture content  $<35\%$ , meaning that the soil experiences drought conditions, moisture content  $>35\%$  to  $69\%$  means that the soil is moist, while the soil moisture content  $>69\%$  are categorized as wetland. This soil water content data were obtained from sensor Soil Moisture data. Besides that, there is also a display of weather conditions in real-time from the Rain Sensor input, which displays rain or no rain conditions.

Sensor Soil Moisture and DS18B20 temperature sensors are each consisting of four sensors placed on four agricultural fields. The Second Form displays history in the form of a graph of average temperature and soil moisture in real-time. The Third Form is to display the scheduling of Watering, Leaf Fertilization, and Root fertilization, which in this method, watering is carried out automatically following the set schedule. The Fourth Form is to display the manual system on watering plants, which in the manual mode the watering plant is not following the set schedule in the settings menu but instead selects the on a button to activate manual watering, and the button off to disable watering manually. Besides, in this mode, there is a menu for manually mixing root/leaf fertilizers. Before the e-smart farming application can be used, what will be done is to connect an Android smartphone with esp8266 wireless on the home station. The Fifth Form is a page to set up a smartphone connection with Esp8266 wireless. The Sixth Form is the Settings page. On the settings page, there are three

menus, namely automatic watering settings, leaf fertilization settings, and root fertilization settings, which on this page sets the time so that the system works automatically based on the time set. The display of the Agriculture e-smart Application can be seen in Figure 3.

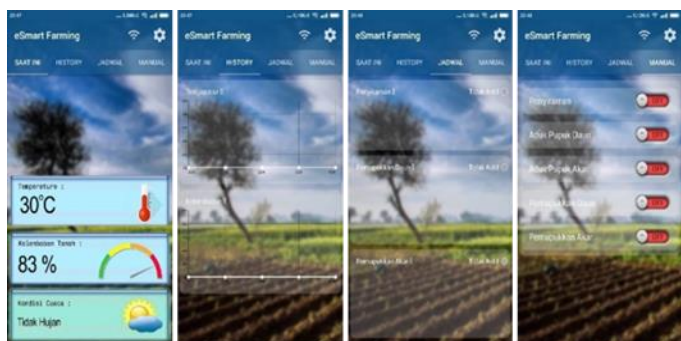


Figure 3. The interface of e-smart Farming Application

### 3. Result and Discussion

The results of the tests that have been carried out are by testing the Real-Time Clock (RTC), DS18B20 temperature sensor, Soil Moisture Sensor, and Rain Sensor. In checking the RTC, the first watering time setting is done at 6:30 am, and the second watering is at 4:30 pm and goes on every day. While on schedule management, fertilization is done scheduling once a week, which is done at 7:00 am every Thursday.

#### 3.1. Testing the Real-Time Clock (RTC) Temperature Sensor

The results of the tests that have been carried out are by testing the Real-Time Clock (RTC), DS18B20 temperature sensor, Soil Moisture Sensor, and Rain Sensor. In testing the DS18B20 temperature sensor, which is testing the input temperature sensor in the form of analog data then converted to digital values to display temperature per 24 hours can be seen in Figure 4.

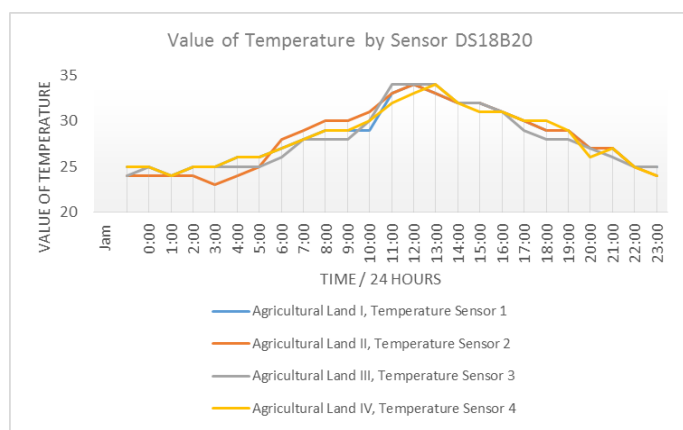


Figure 4. Value of temperature by sensor DS18B20

The output result of the DS18B20 sensor is quite precise to detect changes in temperature because the DS18B20 sensor can detect the smallest temperature changes  $5 / (212-1) = 0.0012$  Volt with a temperature range of  $-10^{\circ}\text{C}$  to  $+85^{\circ}\text{C}$ , with an accuracy value of  $\pm 0.5^{\circ}\text{C}$ . On temperature measurement in the research, area is the placement of four plots of land with each sensor placed on each of these fields, then the results obtained are on land 1 to the fourth land the lowest temperature is obtained at 23.00-04.00

with a temperature value  $< 26^{\circ}\text{C}$ , temperature is happening at 07.00-10.00 am and 05.00 -08.00 pm with temperature  $> 26^{\circ}\text{C}$ . While the temperature is classified as hot  $> 32^{\circ}\text{C}$  occurs at 00.00 - 03.00 pm. Conditions during the day with a temperature of  $> 32^{\circ}\text{C}$ , evaporation of soil water levels are also higher, causing soil moisture also to decrease, and water absorption in plants also decreases. With real-time temperature monitoring, it is intended that the condition of the plant does not experience dryness or lack of water when the temperature conditions increase  $> 32^{\circ}\text{C}$ . With the placement of temperature sensors on agricultural land, the system can work automatically in watering. Besides, the application also continues to receive information in the form of updating temperature data from changes in temperature detected by sensors in real-time on agricultural land.

#### 3.2. Testing of The Performance of Real-Time Clock (RTC) and Sensor Soil Moisture

Testing of the performance of RTC and Sensor Soil Moisture is carried out. Testing of RTC is carried out by monitoring in the form of timeliness of watering at the specified time, namely the first watering at 6:30 am and second watering at 4:30 pm, in the process of watering the system can work correctly and on time according to the specified schedule. While the measurement and testing of soil moisture sensors to the level of moisture content and soil moisture use sensor Soil Moisture. Stages of testing carried out by measuring the water content for 24 hours and determine the amount of water content absorbed by the soil. Measurements were made with two methods of time starting from the first watering time, which is from 6:30 am until 04:30 pm and continued on the second measurement starting from after the second watering, which is 04:30 pm until 06:30 am the next day.

The results of the measurement of soil water content obtained analog values that have been converted to 10-Bit ADC values on Arduino with Reference Voltage,  $V_{\text{ref}} = 5\text{Volt}$ . From the measurements and testing using soil moisture sensors on sensor 1 to sensor 4 in the first method, the initial measurement data at 06:00 am was obtained, in the form of the lowest average value of the ADC of 423, the moisture content of  $\text{Rh}\% = 89\%$ , with the input voltage ( $V_{\text{in}}$ ) received by the sensor which is 2.07 Volt and the sensor sensitivity value is 0.043 with the condition of the soil being wet after the first watering. Furthermore, the wet conditions only last  $\pm 3$  hours, namely 06:00 Am to 10:00 Am, with the ADC value which is increased to 571 with  $\text{Rh}$  dropped to 67% with the input voltage rising to  $V_{\text{in}} = 2,79$  Volt and the sensor sensitivity decreases namely 0.024 with the condition of the soil in humid conditions. The intensity of the sun's irradiation and soil absorption power also influence the decrease in the level of soil moisture due to evaporation and soil absorption power. The average percentage decrease in water content of about 4-5% per hour seen at the time conditions above 10:00 am to 5:00 Pm. The lowest level of water content is  $\text{ADC} = 758.5$  occur at 17:00:00 before the second watering time, with  $\text{Rh} = 39\%$ , the input voltage has increased, namely  $V_{\text{in}} = 3.74$  Volt and sensor sensitivity has decreased which is 0.011. At 05:00 pm, the condition of the soil is in a humid state or close to the dry value of 764-800.

The measurement carried out in the second method is to measure the level of water content when the second watering is



done at 06:00 Pm. In the second measurement, at the beginning of 06:00 Pm from the lowest average value of the ADC was obtained from the four soil moisture sensors, namely 434.8. With the percentage value of humidity (% Rh) = 87% and the input voltage (Vin), which is 2.12v and sensitivity of 0.041 with soil conditions in the Wet. The wetness level of the second watering is to last ± 7 hours from 6: 00 Pm to 02:00 Am. In these conditions, the average decrease is % Rh = 1-2%, this is influenced by the reduced intensity of evaporation by the sun at night and is only influenced by the level of soil absorption so that the decrease in water content at night is not the same as during the day. Changes in conditions from wet to damp occur at 02:00 Am. And up to the morning when the first watering average decreases % Rh = 1-2%. In the morning before the first watering, the soil conditions were still moist with ADC = 624, the percentage of water content (% Rh) = 59%, and the Input voltage (Vin) = 2.88V and sensor sensitivity = 0.019.

The results of measurements on the first and second watering on soil moisture sensors obtained data in the form of the lowest ADC values ranging from 423 to 434.8, with the percentage of water content (% Rh) ranging from 87-89%, and Input voltage (Vin) ranging 2,07-2,12Volt. Moreover, the sensitivity of soil moisture sensors ranges from 0.041-0.043. The lowest ADC value is the condition of the soil in the wet state, namely the percentage of Rh> 75% caused by the increased intensity of water from watering. For soil conditions in humid conditions, the ADC value ranges from 525 - 795, with the percentage of Rh = 33% -74%, and the voltage value at the sensor (Vin) ranges from 2.52 Volt-3.89 Volt. As well as the sensitivity of the sensor when the soil is moist, it ranges from 0.009-0.029. A comparison of measurement results from the tests carried out can be seen in Figure 5.

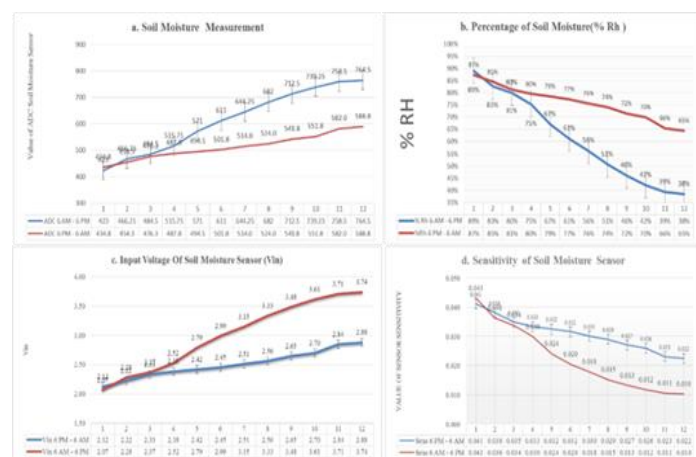


Figure 5. Soil Moisture Sensor Testing

### 3.3. Testing of Rain Sensors

For measurement and testing of rain sensors, it aims to measure the occurrence of rain or not. Which way the sensor works is that when there are raindrops and on the sensor panel, there will be an electrolysis process by rainwater to deliver electricity from the rain sensor module. In the measurement and testing of the rain sensor, it is done by observing analog values when the intensity of the raindrops, heavy rain, and no rain. Observation in figure 6 shows that the sensor ADC data when the conditions of heavy rain ranged from <250, and the conditions of raindrops> 250 and <500, and the

conditions for not raining were ADC> 500. the results of the Rain Sensor Measurement in the trial can be seen in Figure 6.

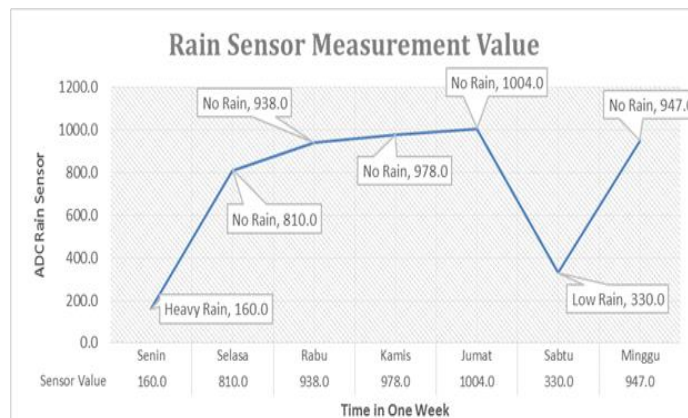


Figure 6. Measurement Chart of Rain Sensor

## 4. Summary

The implementation of the smart farming application in this study obtained quite good results. The final results of this study indicate that the tools applied can assist farmers in implementing smart farming systems. The results can be seen in the success of several temperatures, soil humidity, and rain sensor tests. Moreover, there is no barrier between smart farming applications on the base station and the farm station using 2.4 GHz Wireless ZigBee, and sending data in real-time from the sensor block on the farm station server using ESP8266. Besides, the sprinkler watering system also has no problems when watering agricultural land when receiving orders from the application.

Data obtained in the form of soil conditions and soil moisture are still in a standard condition that is very good for plant growth, due to regular and automatic watering twice a day, so that moisture and moisture content of the soil is maintained. In this study no dry or critical soil conditions were obtained, even though in the system and application the standard values of soil dryness were established with ADC values ranging from 800 to a maximum of 1023, percentage (Rh) = 33% - 0%, and input voltage (Vin) = 3.91Volt-5Volt and sensor sensitivity 0.008-0. If the condition of the sensor detects that the water content has been greatly reduced and the soil experiences drought, the system will give an alarm in the form of a warning to the smartphone farmers that the land is experiencing drought. So that the automation system on the Esmart Farming application can anticipate by doing automatic watering on agricultural land even though it is outside the morning or evening watering schedule. With applications and systems that can regularly work, scheduled and automatically, it is expected that plant growth in agricultural areas will also increase

## 5. Conclusion

The implementation of the smart farming application in this study obtained quite good results. The final results of this study indicate that the tools applied can assist farmers in implementing smart farming systems. The results can be seen in the success of several temperatures, soil humidity, and rain sensor tests. Moreover, there is no barrier between smart farming applications on the base station and the farm station using 2.4GHz Wireless



ZigBee, and sending data in real-time from the sensor block on the farm station server using ESP8266. Besides, the sprinkler watering system also has no problems when watering agricultural land when receiving orders from the application. If the condition of the sensor detects that the water content has been greatly reduced and the soil experiences drought, the system will give an alarm in the form of a warning to the smartphone farmers that the land is experiencing drought. So that the automation system on the Smart Farming application can anticipate by doing automatic watering on agricultural land even though it is outside the morning or evening watering schedule. With applications and systems that can regularly work, scheduled, and automatically, it is expected that plant growth in agricultural areas will also increase.

### Acknowledgment

The researcher would like to thank Dayanu Ikhsanuddin University, as well as all those who assisted with the research, which cannot be mentioned individually.

### References

- [1] O. P. Bodunde, U. C. Adie, O. M. Ikumapayi, J. O. Akinyoola, and A. A. Aderoba, "Architectural Design and Performance Evaluation of a Zigbee Technology-Based Adaptive Sprinkler Irrigation Robot," *Comput. Electron. Agric.*, vol. 160, no. March, pp. 168–178, 2019.
- [2] D. Pivoto, P. D. Waquil, E. Talamini, C. P. S. Finocchio, V. F. Dalla Corte, and G. de Vargas Mores, "Scientific development of smart farming technologies and their application in Brazil," *Inf. Process. Agric.*, vol. 5, no. 1, pp. 21–32, 2018.
- [3] M. J. O'Grady and G. M. P. O'Hare, "Modelling the smart farm," *Inf. Process. Agric.*, vol. 4, no. 3, pp. 179–187, 2017.
- [4] K. L. Krishna, O. Silver, W. F. Malende, and K. Anuradha, "Internet of Things Application for Implementation of Smart Agriculture System," *Proc. Int. Conf. IoT Soc.*, pp. 54–59, 2017.
- [5] U. Nagesh, S. G. Talekar, U. D. V., and P. S., "Application of MQTT Protocol for Real-Time Weather Monitoring and Precision Farming," *Int. Conf. Electr. Electron. Commun. Comput. Technol. Optim. Tech.*, 2017.
- [6] G. Shruthi, B. SelvaKumari, R. PushpaRani, and R. Preyadharan, "A-real time smart sprinkler irrigation control system," *Proc. - 2017 IEEE Int. Conf. Electr. Instrum. Commun. Eng. ICEICE, 2017*, vol. 2017-Decem, pp. 1–5, 2017.
- [7] A. Walter, R. Finger, R. Huber, and N. Buchmann, "Smart farming is key to developing sustainable agriculture," *Proc. Natl. Acad. Sci. U. S. A.*, vol. 114, no. 24, pp. 6148–6150, 2017.
- [8] L. Levidow, D. Zaccaria, R. Maia, E. Vivas, M. Todorovic, and A. Scardigno, "Improving water-efficient irrigation: Prospects and difficulties of innovative practices," *Agric. Water Manag.*, vol. 146, pp. 84–94, 2014.
- [9] P. Singh and S. Saikia, "Arduino-Based Smart Irrigation Using Water Flow Sensor, Soil Moisture Sensor, Temperature Sensor, and esp8266 Wifi Module," *IEEE Reg. 10 Humanit. Technol. Conf. 2016, R10-HTC 2016 - Proc.*, 2017.
- [10] C. K. Sahu and P. Bahera, "A Low Cost Smart Irrigation Control System," *IEE 2nd Int. Conf. Electron. Commun. Syst. ICECS*, no. Icecs, pp. 1146–1152, 2015.
- [11] P. P. Jayaraman, A. Yavari, D. Georgakopoulos, A. Morshes, and A. Zaslavsky, "Internet of Things Platform for Smart Farming: Experiences and Lessons Learnt," *Sensors*, vol. 16, no. 11, pp. 1–17, 2016.
- [12] C. M. Chidambaranathan, S. Handa, and M. Ramanamurthy, "Development of Smart Farming - a Detailed Study," *Int. J. Eng. Technol.*, vol. 7, no. 2, pp. 56–58, 2018.
- [13] L. Kamelia, M. Ramdhani, A. Faroqi, and R. V., "Implementation of Automation System for Humidity Monitoring and Irrigation System," *IOP Conf. Ser. Mater. Sci. Eng.*, 2017.
- [14] N. Kaewmard and S. Saiyod, "Sensor Data Collection and Irrigation Control on Vegetable Crop Using Smart Phone and Wireless Sensor Networks for Smart Farm," *ICWiSe 2014 - 2014 IEEE Conf. Wirel. Sensors*, pp. 106–112, 2014.
- [15] H. Navarro-Hellín, J. Martínez-del-Rincon, R. Domingo-Miguel, F. Sotavalles, and R. Torres-Sánchez, "A Decision Support System for Managing Irrigation in Agriculture," *Comput. Electron. Agric.*, vol. 124, pp. 121–131, 2016.
- [16] S. Rawal, "IoT based Smart Irrigation System," *Int. J. Comput. Appl.*, vol. 159, no. 8, pp. 7–11, 2017.
- [17] F. Zhang, "Research on Water-Saving Irrigation Automatic Control System Based on Internet of Things," *2011 Int. Conf. Electr. Inf. Control Eng. ICEICE 2011 - Proc.*, pp. 2541–2544, 2011.
- [18] L. Zheng et al., "Development of a smart mobile farming service system," *Math. Comput. Model.*, vol. 54, no. 3–4, pp. 1194–1203, 2011.
- [19] C. Cambra, S. Sendra, J. Lloret, and L. Garcia, "An IoT Service-Oriented System for Agriculture Monitoring," *IEEE Int. Conf. Commun.*, 2017.
- [20] S. R. Prathibha, A. Hongal, and M. P. Jyothi, "IoT Based Monitoring System in Smart Agriculture," *Proc. - 2017 Int. Conf. Recent Adv. Electron. Commun. Technol. ICRAECT, 2017*, pp. 81–84, 2017.
- [21] S. Vaishali, S. Suraj, G. Vignesh, S. Dhivya, and S. Udhayakumar, "Mobile Integrated Smart Irrigation Management and Monitoring System Using IOT," *Proc. 2017 IEEE Int. Conf. Commun. Signal Process. ICCSP 2017*, vol. 2018-Janua, pp. 2164–2167, 2018.
- [22] Espressif Systems IOT Team, "ESP8266EX Datasheet Version 4.3," *Espr. Syst. Datasheet*, 2015.

## An Algorithm to Improve Data Accuracy of PMs Concentration Measured with IoT Devices

Mihaela Balanescu<sup>1,\*</sup>, George Suci<sup>1</sup>, Marius-Alexandru Dobrea<sup>1</sup>, Cristina Balaceanu<sup>1</sup>, Radu-Ioan Ciobanu<sup>2</sup>, Ciprian Dobre<sup>2</sup>, Andrei-Cristian Birdici<sup>1</sup>, Andreea Badicu<sup>1</sup>, Iulia Oprea<sup>2</sup>, Adrian Pasat<sup>1</sup>

<sup>1</sup>Beia Consult International, Research & Development, 041385, Romania

<sup>2</sup>University Politehnica of Bucharest, Faculty of Automatic Control and Computers, 060042, Romania

### ARTICLE INFO

Article history:

Received: 15 January, 2020

Accepted: 25 February, 2020

Online: 09 March, 2020

Keywords:

Air Quality

IoT

Edge/cloud computing

PMs concentration

### ABSTRACT

Air pollution is responsible for increased morbidity and mortality due to respiratory problems mainly caused by long term exposure. Although the emissions of principal air pollutants are highly regulated, there is a lack of information about the real extent of personal exposure for an accurate health impact assessment. To tackle these challenges, local air pollution measurements and citizen involvement based on the small IoT devices became necessary. The Tel-MonAer platform is based on IoT devices and Edge/Cloud computing technologies and allows the (near) real-time monitoring of Particulate Matter air pollutants considering the complex chemistry and influence of various parameters (i.e. air humidity, wind speed, temperature). The aim of this paper is the assessment of the influence that air humidity has on the PM concentrations measured with IoT devices based on laser beam technologies. The results showed that in order to increase the accuracy of PM concentrations values a threshold value for relative humidity of 80% needs to be considered. When humidity values are below 80%, the PM concentration values are considered valid, while for values over the threshold, a specific correction algorithm needs to be applied. This paper presents the correction algorithm (based on the type of sensor and humidity) and the testing results (an increase of at least 2.5 times of the correlation coefficient between the corrected and reference values).

## 1. Introduction

This paper is an extension of the work originally presented in CSCS22: The 22<sup>nd</sup> International Conference on Control Systems and Computer Science, Bucharest, 2019 [1].

Worldwide, air pollution has extensive effects on the environment, human health and global economy, as research showed correlation between premature deaths and low air quality [2,3]. The extent of the consequences of air pollution levels are strongly related to the pollutant concentrations and the level of exposure. Until recently, the assessment of air quality has been strongly reliant on traditional monitoring networks, because of their accuracy, but they also have some disadvantages that should not be disregarded [4,5]. The main issues of these monitoring networks are high costs of acquisition, maintenance requirements, improper placement in areas with low pollution and the limited number of fixed stations, due to legal restrictions for location [6]. Therefore, the need for alternative air pollution measurements is

indisputable, in the context of spatial variability of air quality [7-9]. As a result of the variety of sensors on the market, the increased computing power and new communication protocols and the community-led sensing initiative, the topic of air pollution became a key research topic, at local and regional scale [10].

The research community expressed concerns particularly regarding the dangerous effects on human health of two key pollutants: nitrogen dioxide and particulate matter (PM). The latter is one of the most dangerous pollutants in terms of health effects, as it can cause a wide range of negative reactions, even at low concentrations [11]. Among them, the PM<sub>10</sub> (PM with diameter lower than 10  $\mu\text{m}$ ) and PM<sub>2.5</sub> (PM with diameter lower than 2.5  $\mu\text{m}$ ) are considered to have the greatest impact, as their effects are not only related to pollutant concentrations, but also to the frequency and the duration of exposure [12]. For individuals, there are also other factors that play important roles in the extent of air pollution effects, such as health status and age [13].

\*Mihaela Balanescu, mihaela.balanescu@beia.ro

The prime sources of particulate matter in the atmosphere are either natural, such as volcano eruptions and forest fires, or human-made, such as traffic, industry, agriculture, construction and other combustion processes. PM concentrations are particularly important to monitor due to the fact that they can be emitted not only from direct emission sources, but also from chemical reactions between different gases, such as NO<sub>x</sub> and SO<sub>2</sub> [14]. A comprehensive characterization of PM has to consider multiple factors: (1) mass; (2) elemental composition; (3) water-soluble ionic species; and (4) organic compounds. The traditional sampling systems based on gravimetric measurements of collected particles generate direct measurements of airborne particle mass. Moreover, during the sampling process, there is the possibility of losing the semi-volatile organic compounds and semi-volatile ammonium compounds (such as NH<sub>4</sub>NO<sub>3</sub>). The composition of the sample of PM is also decisive for the accuracy of the measurements, because the presence of ionic species (i.e. sulfate and nitrate compounds) increases the liquid water uptake of suspended particles and therefore, the particle dimension. Therefore, the chemical composition of the sample and the temperature heavily influence the correct assessment of PM concentrations in the atmosphere [15].

This paper presents an analysis of the variation of particulate matter (PM<sub>10</sub> and PM<sub>2.5</sub>) concentrations in relation to relative humidity. Chapter 2 compiles related work for data accuracy of PMs, Chapter 3 discusses the method that it is used, Chapter 4 presents the results, and lastly, Chapter 5 concludes the paper.

## 2. Related Work

The effects of different parameters on the data accuracy of PM concentrations were approached in several papers. The influence of wind and precipitation on different-sized particulate matter concentrations were investigated in paper [16], showing that the effects of atmospheric conditions differ, depending on the size of the particulate matter. The increase in wind speed can decrease the concentrations of fine PM, while decreasing the concentrations of coarse PMs. The authors also found a stronger negative impact of precipitation on PM<sub>10</sub> than on PM<sub>2.5</sub>.

In paper [17], authors analyze the way PM<sub>10</sub> concentrations are influenced by different meteorological parameters, such as pressure, relative humidity, temperature, wind speed, wind direction, CO, SO<sub>2</sub>, NO, NO<sub>2</sub>. A quantile regression model has been employed and the results showed that the influence of the independent variables was significant in at least one or more quantiles of the PM<sub>10</sub> concentrations. Among the analyzed parameters, relative humidity was proven to have a significant impact on quantiles 0.05 to 0.3 and an insignificant impact at higher quantiles.

The topic of the relationship between relative humidity and PM concentrations was approached in paper [18]. Authors found that PM concentrations in the atmosphere are closely correlated with the levels of relative humidity. It has been shown that high humidity conditions (between 70-100%) led to a reduction in PM<sub>2.5</sub> concentrations, while low-humidity conditions (below 70%), led to the increase in PM<sub>2.5</sub> concentrations. In case of PM<sub>10</sub> concentrations, humidity values below 45% had an accumulation effect, causing an increase in concentration, while an environment with humidity levels above 45% led to lower concentrations.

## 3. Methods

### 3.1. Tel-MonAer platform

The aim of the Tel-MonAer project was the development of a mobile, extensible and scalable system which integrates technologies such as the Internet of Things and Edge/Cloud Computing, for the purpose of monitoring and performing real time analysis of the risk factors of public health and the environment. The architecture of the IoT platform is presented in Figure 1.

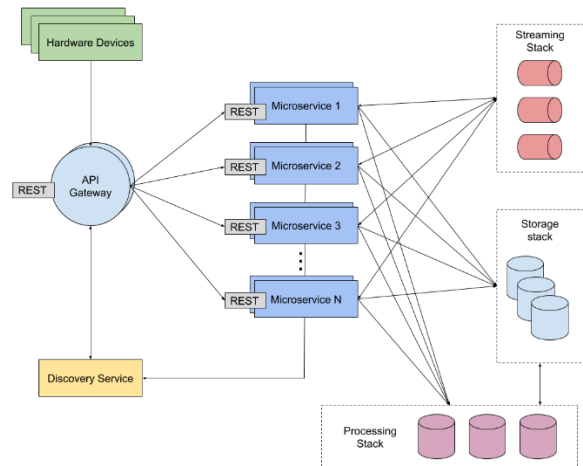


Figure 1: NETIoT architecture



(a).BEIA Consult, Romania.



(b).University Politehnica of Bucharest, Romania

Figure 2: Installed air-quality sensors that send the data the Tel-MonAer platform.

The platform registers every hardware device employed by the end-user, such as sensors or device gateways, with a unique ID. The data from the sensors is firstly received by the MQTT protocol, through a device gateway and then forwarded to a cloud gateway. The Tel-MonAer system is capable of simultaneously monitoring different air quality parameters such as SO<sub>2</sub>, NO<sub>x</sub>, CO, O<sub>3</sub>, PM<sub>10</sub>, PM<sub>2.5</sub>, as well as meteorological parameters (wind direction and speed, pressure, temperature, relative humidity).

The air quality data is currently being collected from IoT sensors in two locations: the premises of BEIA Consult International and University Politehnica Bucharest, as shown in Figure 2.

Tel-MonAer is designed to allow some specific features like availability and scalability. Moreover, the platform will permit further development. The architecture of the platform is based on microservices, because of the advantages of this model, such as independent, faster and more cost-effective development of each microservice and dedicated and specific databases for each component.

The high volumes of data stored by the Tel-MonAer platform demand a scalable and performant storage layer. For this purpose, Apache Cassandra database has been used because of its ability to scale almost linearly, to tackle failover situations and to automatically replicate data in more data centers.

The data is further processed by the platform, using two types of processing. Batch processing is used for analyzing the data received from multiple sensors and within a specific time frame and for performing predictions of possible evolutions. Real-time processing is used for event detection. We used Apache Spark, a general use engine for both real-time and batch processing, because of its advantages, such as in-memory processing, real-time stream processing and sophisticated analytics support.

### 3.2. Details of the method used

The parameters of the data set used to perform the analysis are: PM10 and PM2.5 concentration values, atmospheric pressure, atmospheric temperature and relative humidity. The measurements were performed in Bucharest using Libelium sensors. The parameters were measured between the 1<sup>st</sup> of November 2018 and the 28<sup>th</sup> of January 2019, with a frequency of 15 minutes.

The process of data acquisition follows several steps: accessing the gateway interface, connecting to the MySQL database interface to access the sensor data, logging into the phpMyAdmin interface, querying the database for hourly average values, downloading the data selected by the query function.

## 4. Experimental Results

The dataset resulted from the registered measurements contains 2133 values for every parameter. Firstly, a qualitative analysis of the data has been performed, in order to compare the measured values with standard data requirements. Secondly, a preliminary analysis has been carried out using statistical descriptive methods for the parameter, such as variation, mean value and standard deviation [1].

The variation of PM<sub>10</sub> and PM<sub>2.5</sub> concentrations function of relative humidity is presented in Figure 3 and Figure 4,

respectively. The results show an increase in PM concentrations for values of relative humidity greater than 90%. This is a strong indication of a measurement error, caused by the measurement method or by the complex chemistry of PMs.

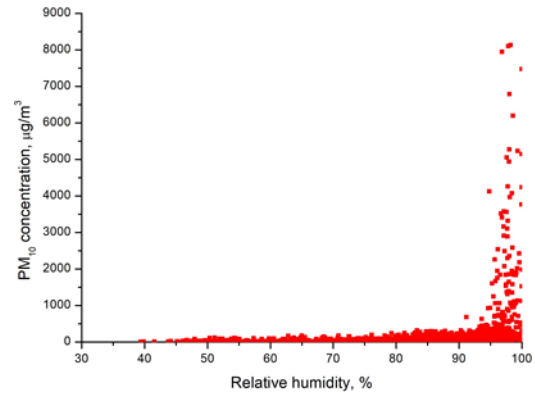


Figure 3: PM<sub>10</sub> concentration vs relative humidity for the entire data set

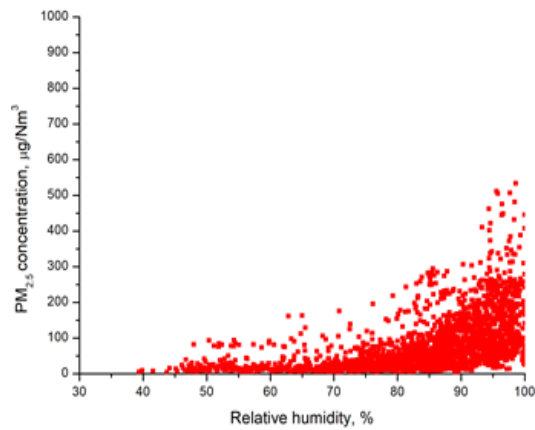


Figure 4: PM<sub>2.5</sub> concentration vs relative humidity for the entire data set

Considering the need to ensure the accuracy of measurements and the previous measurement results, it is necessary to determine a threshold value of relative humidity from which the measurements accuracy decrease. For this purpose, Pearson's correlation coefficients between relative humidity and PM concentrations were calculated for different data sub-sets. The results shown in Figure 5 indicate a stronger correlation for both types of PMs when relative humidity values are higher than 80%.

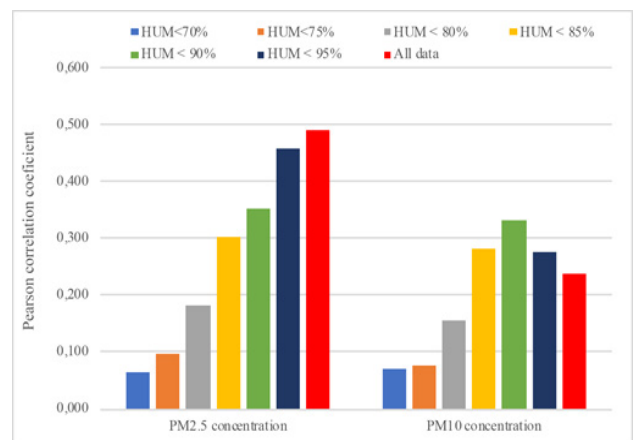


Figure 5: The absolute values of Pearson's correlation coefficients between PM<sub>2.5</sub> and humidity, respectively PM<sub>10</sub> and humidity, for selected data sub-sets.



In order to perform a comparative analysis, the absolute value of the correlation coefficients was used, and the threshold value of relative humidity was established at 80%. The dataset that resulted consists of 591 values and represents 27.7% of the total values registered.

The variation of measured PM<sub>10</sub> and PM<sub>2.5</sub> concentrations for the data sub-set corresponding to values of relative humidity lower than 80% are presented in Figure 6. For the same data sub-set, Figure 7 shows the PM<sub>10</sub> and PM<sub>2.5</sub> concentrations function of relative humidity.

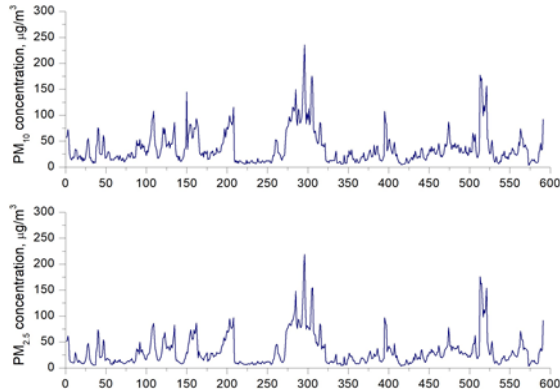


Figure 6: Variation of measured values for PM<sub>10</sub> and PM<sub>2.5</sub> concentration for the data sub-set (humidity < 80%).

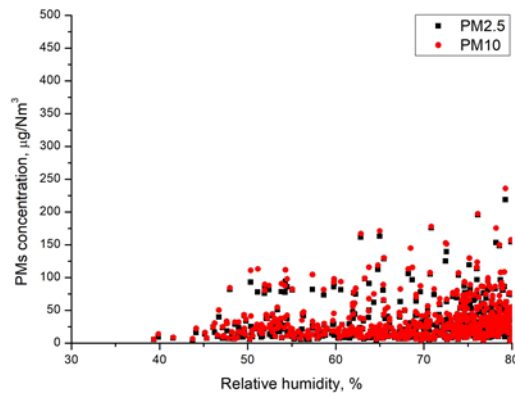


Figure 7: PM<sub>2.5</sub> and PM<sub>10</sub> concentration vs relative humidity for the data sub-set (humidity < 80%).

Table 1: Correction factors for humidity classes

Class name	Range of variation, (%)	Correction factor
K1	≤ 80	1
K2	80-85	1.5152
K3	85-90	2.3008
K4	90-95	3.3807
K5	95-98	6.6515
K6	> 98	14.4549

In order to make corrections that eliminate the influence of humidity on the values of PM concentrations, it is proposed a division by humidity classes for which the values of correction factors have been estimated. The correction factor values for

humidity classes were calculated as average values of the corresponding correction factors for the humidity values of each variation interval. The resulting values are presented in Table 1.

#### 4.1. Algorithm for correcting concentrations of PM<sub>2.5</sub> and PM<sub>10</sub>

Based on the information and data measured in the Tel-MonAer project, a correction algorithm (presented below) was developed for the concentration values of PM<sub>2.5</sub> and PM<sub>10</sub>.

##### Step 1. Determination of the correction factor for humidity

Each measured value of the relative humidity falls into the corresponding humidity class (according to Table 1) and then the correction factor corresponding to the class is identified)

##### Step 2. Correction for humidity of PM<sub>x</sub> concentration

For each value of the PM<sub>x</sub> concentration measured, the following formula is applied:

$$Conc PMx corr H = \frac{conc PMx measured}{FC} \quad (1)$$

Where:

PM<sub>x</sub> – x fraction of particulate matter (e.g. PM<sub>2.5</sub> and PM<sub>10</sub>);

Conc PM<sub>x</sub> corr H – the value of PM<sub>x</sub> concentration as a function of humidity;

Conc PM<sub>x</sub> measured – the value of the measured PM<sub>x</sub> concentration;

FC – the value of the correlation factor.

##### Step 3. Making the correction by reporting to the reference methods

For each value of the concentration corrected in Step 2, the formula applies:

$$Conc PMx corr = f(Conc PMx corr H) \quad (2)$$

Where the function is specific to each type of sensor, pollutant and mediation period.

##### Step 4. Calculation of the final concentration for the specified mediation interval.

The average value of the corrected concentrations for the specified mediation periods (hour, day) is calculated.

For the application and testing of the calculation algorithm, the concentration data of PM<sub>2.5</sub>, PM<sub>10</sub> and relative humidity acquired using a Libelium SCP station (with OPC-N3 sensor) was used. The station was installed outside the building of the CAMPUS Center, within the Politehnica University of Bucharest (Figure 8). The data set used corresponds to the period March 13-May 13, 2019.

The corrected values of the concentrations of PM<sub>2.5</sub> and PM<sub>10</sub> were calculated with the measurements made by the National Environmental Protection Agency, at the Morii Lake measuring point within the National Network for Air Quality Assessment (Figure 9).



Figure 8: Installation of the measuring equipment Libelium SCP at the CAMPUS center

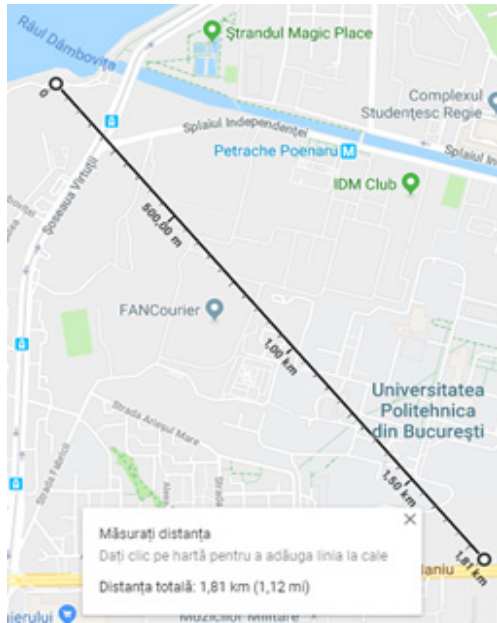


Figure 9: Distance between the Morii Lake monitoring point and the CAMPUS monitoring point

The correction algorithm was applied for  $PM_{2.5}$  and  $PM_{10}$  and the results were compared with the values of the measured concentrations at Morii Lake measurement point in the National Air Quality Assessment network.

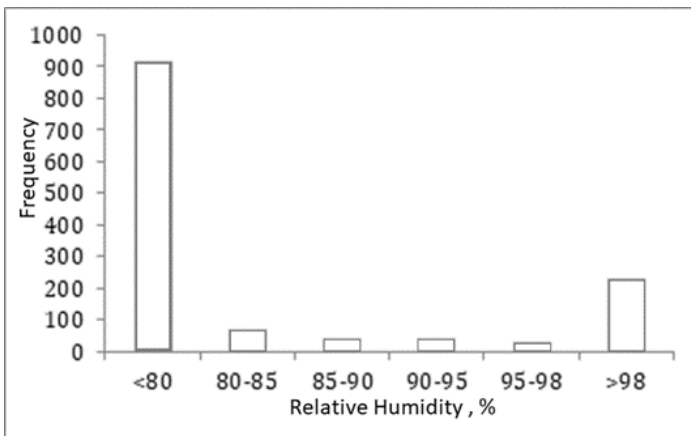


Figure 10: Histogram of relative humidity for the test period

#### 4.2. Application of the algorithm for $PM_{2.5}$

During the analyzed period (March 13 – May 13, 2019), there were recorded hourly values of relative humidity (Figure 10) below 80% in 915 hours (69% of the total) and values greater than

98% in 231 hours (17.42%). Thus, the correction algorithm for humidity will lead to the modification of the values for 31% of the recorded values.

The hourly concentrations measured (Figure 11) during the testing phase of the algorithm recorded values below  $7 \mu\text{g} / \text{Nm}^3$  in 32.43% of hours, values less than  $22 \mu\text{g} / \text{Nm}^3$  being measured in 80.24% of the total number of hours. Also 43 values over  $67 \mu\text{g} / \text{Nm}^3$  were recorded.

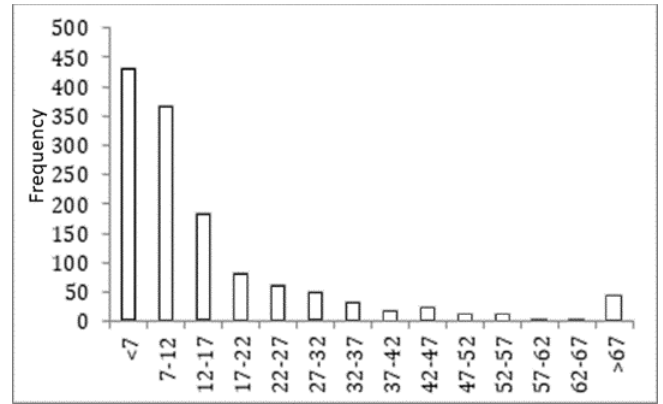


Figure 11: Histogram of the values of  $PM_{2.5}$  concentrations measured during the test period

By applying the algorithm, the very small values (below  $7 \mu\text{g} / \text{Nm}^3$ ) of the measured concentrations were increased and represent 1.52% of the total. Values lower than  $22 \mu\text{g} / \text{Nm}^3$  represent 83.45% of the total number of hours. The number of values greater than  $67 \mu\text{g} / \text{Nm}^3$  was reduced to one value (Figure 12).

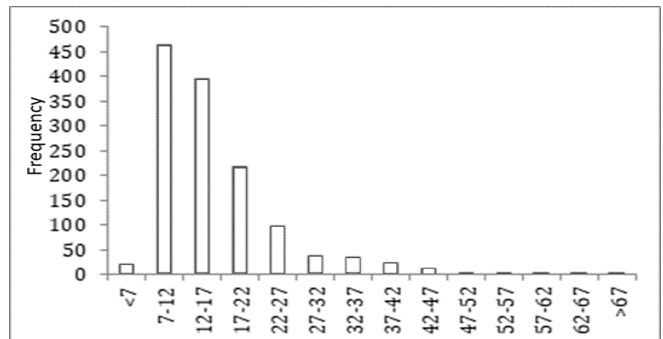


Figure 12: Histogram of  $PM_{2.5}$  concentration values corrected after applying the algorithm

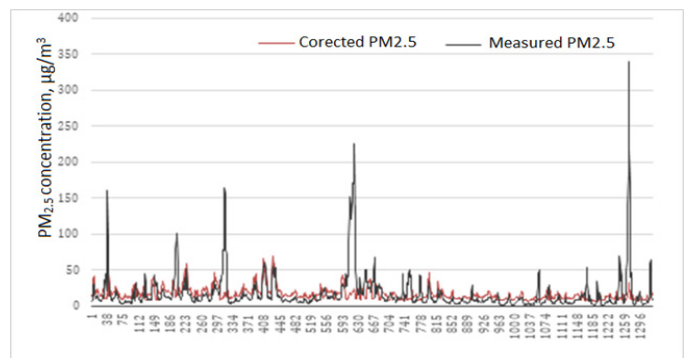


Figure 13: Measured and corrected concentration values of  $PM_{2.5}$  for the test period

Figure 13 shows the values of PM<sub>2.5</sub> concentrations measured and corrected for the test period. It is observed the elimination of the extreme values generated by the increase of humidity and the increase of the small values which represents the elimination of the underestimation of the measured values.

#### 4.3. Application of the algorithm for PM<sub>10</sub>

The hourly concentrations measured (Figure 14) during the testing phase of the algorithm recorded values below 12 µg / Nm<sup>3</sup> in 44.49% of the hours, values less than 44 µg / Nm<sup>3</sup> being measured in 92.23% of the total number of hours. Also, 33 values of over 92 µg / Nm<sup>3</sup> were recorded.

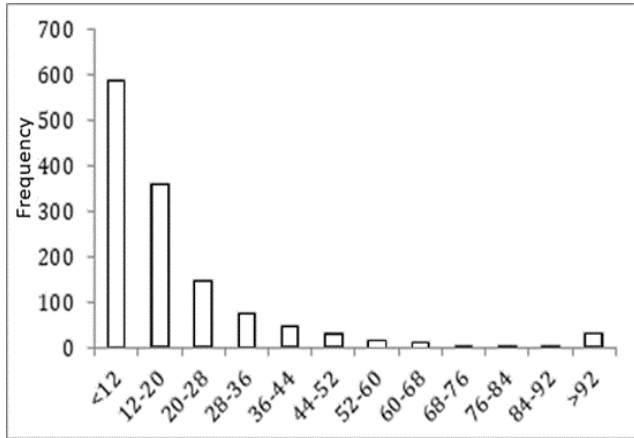


Figure 14: Histogram of PM<sub>10</sub> concentration values measured during the test period

By applying the algorithm, the very small values (below 12 µg / Nm<sup>3</sup>) of the measured concentrations were increased and represent 0.5% of the total. The number of concentrations greater than 92 µg / Nm<sup>3</sup> was reduced to a single value (Figure 15).

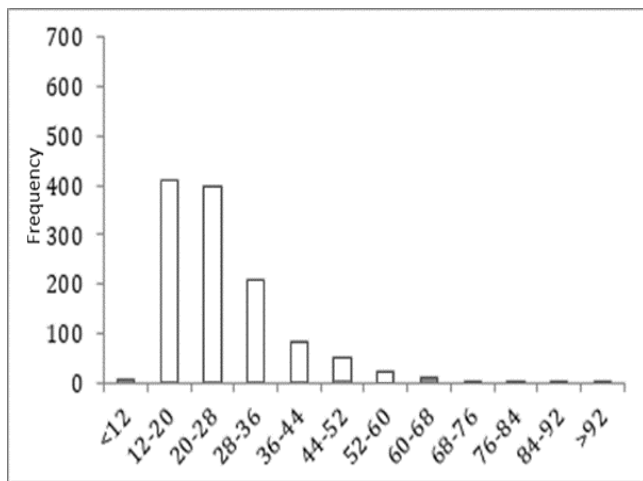


Figure 15: Histogram of PM<sub>10</sub> concentration values corrected after applying the algorithm

The following figure shows the values of PM<sub>10</sub> concentrations measured and corrected for the test period. It is observed the elimination of the extreme values generated by the increase of humidity and the increase of small values which represents the elimination of the underestimation of the measured values (Figure 16).

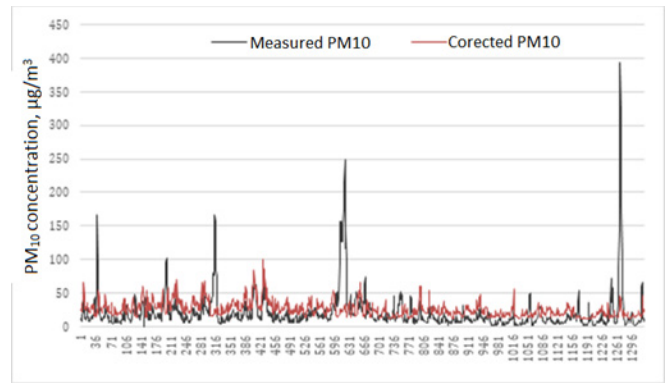


Figure 16: Values of concentrations measured and corrected by PM<sub>10</sub> for the test period

#### 4.4. Performance evaluation of the algorithm

The monitoring station at Morii Lake is urban-background type, the measured values being representative on an area with a radius of 1-5 km around the station. The CAMPUS Center where the Libelium sensors were located is within the representative area (1.8 km from the station). By placing it at a higher height, the effect of the pollution generated by car traffic was reduced, but it is also possible to reduce the measured values due to the height at which they were located.

The hourly PM<sub>2.5</sub> concentrations measured at the monitoring station at Morii Lake (Figure 17) were below the value of 22 µg / Nm<sup>3</sup> in 82.69% of the total number of hours.

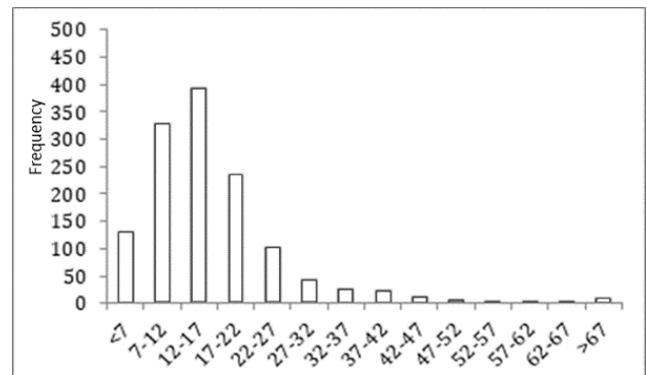


Figure 17: Histogram of the values of PM<sub>2.5</sub> concentrations measured at the Morii Lake point from the National Air Quality Network

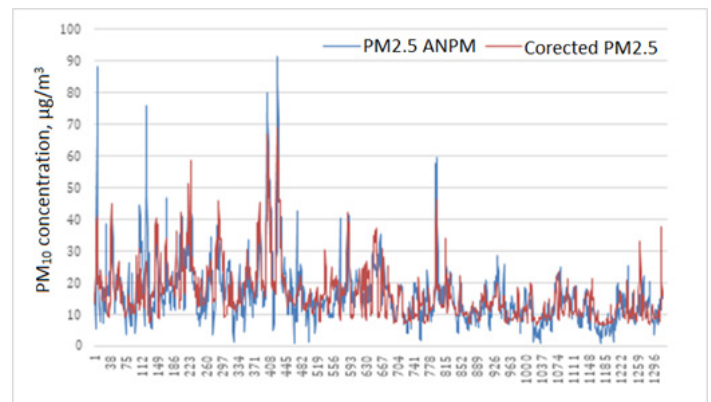


Figure 18: Values of corrected PM<sub>2.5</sub> concentrations and those measured by ANPM for the test period

The comparative graphical representation of the values of the corrected PM<sub>2.5</sub> concentrations and those measured by ANPM (Figure 18) during the testing period of the algorithm indicates close values and similar evolution trend.

The hourly PM<sub>10</sub> concentrations measured at the Morii Lake monitoring station (Figure 19) were below the value of 44 µg / Nm<sup>3</sup> in 94.94% of the total number of hours.

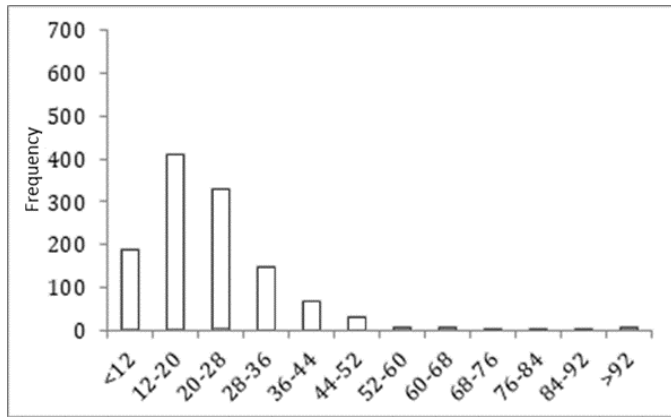


Figure 19: Histogram of the values of PM<sub>10</sub> concentrations measured at the Morii Lake point from the National Air Quality network

The comparative graphical representation of the values of the corrected PM<sub>10</sub> concentrations and those measured by ANPM (Figure 20) during the testing period of the algorithms indicates close values and similar evolution trend.

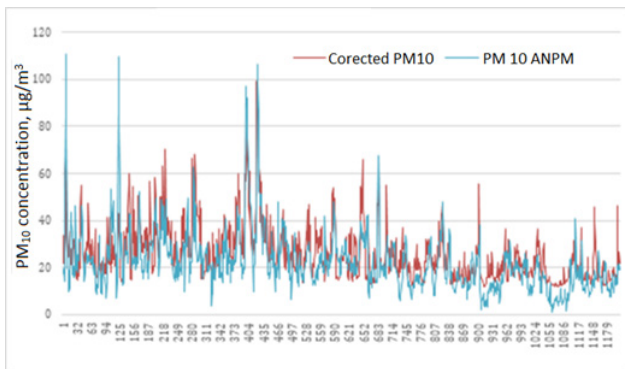


Figure 20: Values of corrected and officially measured concentrations of PM<sub>10</sub> for the test period

The efficiency of the correction algorithm was evaluated at this stage by the value of the Pearson correlation coefficients (Table 2).

Table 2: Pearson’s correlation coefficient values for the analyzed data sets

Concentration	Correlation coefficient	
	Measured values vs. ANPM values	Corrected values vs. ANPM values
PM <sub>2.5</sub>	0.268	0.688
PM <sub>10</sub>	0.216	0.663

This shows a 2.5-fold increase in the correlation coefficient for PM<sub>2.5</sub> concentrations, from a value of 0.268 (Libelium measured data vs. ANPM measured data).

For PM<sub>10</sub> concentrations, the value of the correlation coefficient increased 3-fold, from 0.216 (Libelium measured data vs ANPM measured data) to 0.663 (Libelium corrected data vs. ANPM measured data).

## 5. Conclusions and Future Work

The influence of relative humidity on the PMs concentration values is significant for the devices based on laser measurement technology. For this type of IoT devices we propose a threshold value for relative humidity of 80% under which to consider PMs measured concentration as valid. For the situation when relative humidity has values over 80%, a specific algorithm was developed. The algorithm corrects the PMs measured values considering the type of the sensors and the value of humidity.

The correction algorithm was tested on a data set containing PMs concentration values and other meteorological parameters for a period of two months. The results show an increase of at least 2.5 times of the correlation coefficient between the corrected values and those measured by the reference station of the National Air Quality Monitoring Network.

Future work will consider further testing of the algorithm and the development of a specific ML algorithm for air quality predictions.

## Conflict of Interest

The authors declare no conflict of interest.

## Acknowledgment

The work presented in this paper has been funded by Tel-MonAer project subsidiary contract no.1223/22.01.2019, from the NETIO project ID: P\_40270, MySmis Code: 105976 and by the WINS@HI project, PN-III-P3-3.5-EUK-2017-02-0038.

## References

- [1] CSCS19: The 22<sup>nd</sup> International Conference on Control Systems and Computer Science, 28-30 May 2019, Faculty of Automatic Control and Computers, University Politehnica of Bucharest, Romania. <https://cscs22.hpc.pub.ro/>
- [2] J. Ayres, “The mortality effects of long-term exposure to particulate air pollution in the United Kingdom,” Report by the Committee on the Medical Effects of Air Pollutants, 2010.
- [3] P. J. Landrigan, R. Fuller, N. J. Acosta, O. Adeyi, R. Arnold, A. B. Bald’e, R. Bertollini, S. Bose-O’Reilly, J. I. Boufford, P. N. Breyse et al., “The lancet commission on pollution and health,” *The Lancet*, vol. 391, no. 10119, pp. 462–512, 2018.
- [4] V. Hadjoannou, C. X. Mavromoustakis, G. Mastorakis, J. M. Batalla, I. Kopanakis, E. Perakakis, and S. Panagiotakis, “Security in smart grids and smart spaces for smooth IoT deployment in 5g,” in *Internet of Things (IoT) in 5G Mobile Technologies*. Springer International Publishing, 2016, pp. 371–397. [Online]. Available: [https://doi.org/10.1007%2F978-3-319-30913-2\\_16](https://doi.org/10.1007%2F978-3-319-30913-2_16)
- [5] M. Ianculescu, A. Alexandru, and E. Tudora, “Opportunities brought by big data in providing silver digital patients with ICT-based services that support independent living and lifelong learning,” in *2017 Ninth International Conference on Ubiquitous and Future Networks (ICUFN)*. IEEE, jul 2017. [Online]. Available: <https://doi.org/10.1109%2Ficufn.2017.7993817>
- [6] J. M. Batalla, K. Sienkiewicz, W. Latoszek, P. Krawiec, C. X. Mavromoustakis, and G. Mastorakis, “Validation of virtualization platforms for i-IoT purposes,” *The Journal of Supercomputing*, vol. 74, no. 9, pp. 4227–4241, aug 2016. [Online]. Available: <https://doi.org/10.1007%2Fs11227-016-1844-2>
- [7] J. S. Apte, K. P. Messier, S. Gani, M. Brauer, T. W. Kirchstetter, M. M. Lunden, J. D. Marshall, C. J. Portier, R. C. Vermeulen, and S. P. Hamburg, “High-resolution air pollution mapping with google street view cars:



- exploiting big data,” *Environmental science & technology*, vol. 51, no. 12, pp. 6999–7008, 2017.
- [8] D. Fecht, A. L. Hansell, D. Morley, D. Dajnak, D. Vienneau, S. Beevers, M. B. Toledano, F. J. Kelly, H. R. Anderson, and J. Gulliver, “Spatial and temporal associations of road traffic noise and air pollution in london: Implications for epidemiological studies,” *Environment international*, vol. 88, pp. 235–242, 2016.
- [9] H. Lin, T. Liu, J. Xiao, W. Zeng, L. Guo, X. Li, Y. Xu, Y. Zhang, J. J. Chang, M. G. Vaughn et al., “Hourly peak pm 2.5 concentration associated with increased cardiovascular mortality in guangzhou, china,” *Journal of Exposure Science and Environmental Epidemiology*, vol. 27, no. 3, p. 333, 2017.
- [10] T. Watkins, “Draft roadmap for next generation air monitoring,” Environmental Protection Agency, 2013.
- [11] K.-H. Kim, E. Kabir, and S. Kabir, “A review on the human health impact of airborne particulate matter,” *Environment international*, vol. 74, pp. 136–143, 2015.
- [12] A. Y. Watson, R. R. Bates, D. Kennedy et al., *Air pollution, the automobile, and public health*. National Academies, 1988.
- [13] S. Holgate, J. Grigg, R. Agius, J. R. Ashton, P. Cullinan, K. Exley, D. Fishwick, G. Fuller, N. Gokani, C. Griffiths et al., “Every breath we take: The lifelong impact of air pollution, report of a working party.” Royal College of Physicians, 2016.
- [14] F. Dominici, R. D. Peng, M. L. Bell, L. Pham, A. McDermott, S. L. Zeger, and J. M. Samet, “Fine particulate air pollution and hospital admission for cardiovascular and respiratory diseases,” *Jama*, vol. 295, no. 10, pp. 1127–1134, 2006.
- [15] J. G. Watson, J. C. Chow, H. Moosmüller, M. Green, and N. Frank, “Guidance for using continuous monitors in pm2.5 monitoring networks,” Nevada Univ. System, Desert Research Inst., Reno, NV (United States), Tech. Rep., 1998.
- [16] B. Zhang, L. Jiao, G. Xu, S. Zhao, X. Tang, Y. Zhou, and C. Gong, “Influences of wind and precipitation on different-sized particulate matter concentrations (pm 2.5, pm 10, pm 2.5–10),” *Meteorology and Atmospheric Physics*, vol. 130, no. 3, pp. 383–392, 2018.
- [17] K. Y. Ng and N. Awang, “Quantile regression for analysing pm10 concentrations in petaling jaya,” *Malaysian Journal of Fundamental and Applied Sciences*, vol. 13, no. 2, 2017.
- [18] C. Lou, H. Liu, Y. Li, Y. Peng, J. Wang, and L. Dai, “Relationships of relative humidity with pm 2.5 and pm 10 in the yangtze river delta, china,” *Environmental monitoring and assessment*, vol. 189, no. 11, p. 582, 2017.

## Hybrid Solar Thermal/Electricity Automated Oven

Ajah Onu Victor<sup>\*1</sup>, Emenike Ejiogu<sup>2</sup>

<sup>1</sup>Department of Electrical Engineering, University of Nigeria Nsukka, Nigeria

<sup>2</sup>African Centre of Excellence for Sustainable Power & Energy Development, University of Nigeria Nsukka, Nigeria

---

### ARTICLE INFO

Article history:

Received: 14 January, 2020

Accepted: 28 February, 2020

Online: 11 March, 2020

---

Keywords:

Sliding mode control

Solar thermal collector

Control law

---

### ABSTRACT

*This paper presents hybrid solar thermal/electricity automated oven. The work compares sliding mode control (SMC) to traditional PID control of the oven system using MATLAB/Simulink 2014b model. SMC control method shows faster rise and settling time. The control technique has been designed to automate change of temperature level of the oven by accepting multiple reference inputs. This has been implemented using microcontroller programmed in C++. Flat-plate solar thermal collector and paint curing oven have also been implemented for experimental test. The results obtain from the experiments are in conformity to the simulation results. The collector delivers 43.27% of the total energy required to operate the oven up to 120°C at 200W/m<sup>2</sup> solar insolation. Calculation of payback period for commercial viability on the cost of the collector installation indicates a year and four months for an average insolation of seven hours per day. These results demonstrate that the research work is effective and solves the problem of temperature control in curing modern organic paints and the challenge of power requirements in the operation of oven.*

---

## 1. Introduction

This paper is an extension of work originally presented in 2019 IEEE International Conference on Sustainable Energy Technologies and Systems (ICSETS) [1].

Precise temperature control of ovens is very essential to industries and firms that use them for productions. Paint curing for instance involves converting applied wet or powdered paint to dry and hard film. Paint may cure by solvent loss, chemical reaction, oxidation, melting and re-solidifying, or melting and crosslinking [2]. It may take few hours for liquid paints to dry but it takes days to months to cure properly. To reduce cure time, paint curing ovens are used to speed up the process under elevated temperature, and energy is usually required for reliable and stable curing of industrial coatings [2, 3].

The primary challenges of curing and drying ovens generally are temperature control and energy optimization. Various temperature control methods such as traditional PID control system, Adaptive and Fuzzy Algorithm, fuzzy-PID control system, etc. [4, 5, 6] have been proposed in other works. Also, there are

various methods energy can be made available to raise the temperature of oven and its content to required degree [7, 8]. The results obtained from the applications of these proposals show slow response time, delayed settling time, high overshoots and oscillations outside prescribed tolerance limits. Hence, they have not adequately met up with constraints in modern coatings and the complexity of curing ovens, especially when the different subsystems - heaters, air circulating fans, temperature sensors, etc. - have to work together to control temperature.

Moreover, as paint curing processes continue to improve, the tolerance limits have become much tighter from  $\pm 14^\circ\text{C}$  in liquid-based paints to  $\pm 5.6^\circ\text{C}$  in organic and powder paints [3, 9] which demands more robust control method that can track the set-point more accurately. On the other hand, Sliding Mode Control (SMC), a robust non-linear control method, has recently found wide applications to automatic control problems; largely due to its simple algorithm, order reduction, decoupling design procedure, disturbance rejection, insensitivity to parameter variations, simple implementation, high reliability and fast response [10, 11, 12].

The application of SMC to oven temperature control would provide the needed remedy since its comparison to the earlier mentioned control methods in other areas proved that SMC gives

---

<sup>\*</sup>Ajah Onu Victor, University of Nigeria Nsukka, Address, Contact No: +2348036878453 & Email: [ajahonuvictor@gmail.com](mailto:ajahonuvictor@gmail.com)

improved system performance [13, 14]. This work applies sliding mode control to paint curing oven temperature in order to overcome the inefficiencies of existing control methods. Sliding mode control (SMC), has many advantages and can track the desired temperature within limits. Solar thermal collector is incorporated to electric heating system for energy optimization.

## 2. Modeling and Simulation

### 2.1. Oven Modeling

Figure 1 is the block diagram model of energy flow in a convective oven system. The following assumptions were made in the modelling [15]:

- i. That all objects in the chamber are under thermal equilibrium condition.
- ii. The materials that compose the oven and the work-piece have constant physical properties and do not depend on temperature.
- iii. The heat capacity  $C = c_p \times m$  of insulators and supports of the oven are considered in the balance energy equation, where  $c_p$  and  $m$  are the specific heat and the mass of each component in the oven respectively.
- iv. The change of temperature  $T$  with respect to time,  $t$  has the following requirements:
  - a)  $\frac{dT}{dt}$  is maximum at  $t = 0$ , it is a non-increasing function of  $t$  and
  - b)  $\frac{dT}{dt} \rightarrow 0$  when  $t \rightarrow \infty$ .
- v. The energy of the chemical or phase transformation is neglect. It is assumed that no work enters or goes out from the oven
  - a) It is considered that the cavity and both air and body surfaces place in it are in thermal equilibrium.
  - b) The physical properties, as thermal conductivity and specific heat of oven components and work-piece materials, are constant.
  - c) The temperature change in the inner part of the oven satisfies the following restrictions:
    - i.  $\frac{dT}{dt} = \varepsilon \geq 0$ .
    - ii.  $\varepsilon$  is small in the heating process.
    - iii.  $\varepsilon(t)$  is maximum at  $t = 0$ , i.e., it is a decreasing function of  $t$ .
    - iv.  $\varepsilon(t) \rightarrow 0$  When  $t \rightarrow \infty$ .

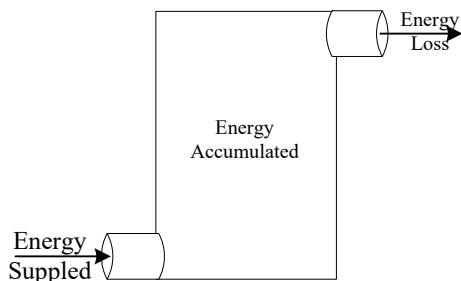


Figure 1: Convective oven energy flow model

The energy supplied  $E_s$ , to the convective oven is the sum of the accumulated energy  $E_u$ , and the energy loss  $E_L$ .

$$E_s = E_u + E_L \quad (1)$$

$$E_u = E_s - E_L = C_T \frac{dT}{dt} \quad (2)$$

The maximum heat energy loss

$$E_L = \frac{T - T_a}{R_T} \quad (3)$$

where,

$E_s, E_u$  and  $E_L$  are in Joules

$C_T =$  heat capacity  $= c_p \times m$  (of insulators, support,)

$c_p =$  specific heat capacity in (kJ/kgK)

$m =$  mass (in kg)

$T =$  temperature in the oven (in °K)

$T_a =$  temperature of the surrounding (in °K)

$R_T =$  total thermal resistance of the oven (in  $K \cdot \frac{m^2}{W}$ )

Putting (2) & (3) into (1) gives (4)

$$E_s - \frac{T - T_a}{R_T} = C_T \frac{dT}{dt} \quad (4)$$

Re-arranging (4) gives (5) which is the temperature evolution of the oven.

$$R_T C_T \frac{dT}{dt} + T = E_s R_T + T_a \quad (5)$$

The maximum oven temperature and time constant are expressed by (6) and (7) respectively.

$$E_s R_T + T_a = T_{max} \quad (6)$$

$$R_T C_T = \tau \quad (7)$$

Thus, (5) becomes (8).

$$\tau \frac{dT}{dt} + T = T_{max} \quad (8)$$

Since  $\tau$  &  $T_{max}$  are constants, (8) is a first order ordinary differential equation of the oven system and its solution is shown in equation (9).

$$T(t) = T_{max} \left( 1 - \exp \left[ \frac{-t}{\tau} \right] \right) + T_a \exp \left[ \frac{-t}{\tau} \right] \quad (9)$$

Putting (6) into (9) gives (10).

$$T(t) - T_a = E_s R_T \left( 1 - \exp \left[ \frac{-t}{\tau} \right] \right) \quad (10)$$

Equation (11) is the maximum temperature rise, hence the temperature rise of the system at any time instant is obtained by (12).

$$E_s R_T = \theta_{max} \quad (11)$$

$$\theta(t) = \theta_{max} \left( 1 - \exp \left[ \frac{-t}{\tau} \right] \right) \quad (12)$$

Taking the Laplace transform of equation (8) gives (13) which is the transfer function of the system.

$$\frac{T(s)}{E(s)} = \frac{R_T}{\tau s + 1} \quad (13)$$

### 2.2. Controller Design based on Sliding Mode Control

Equation (14) defines the sliding surface for nth order system [16, 17].

$$S = \left( \frac{d}{dx} + \lambda \right)^n \times e \quad (14)$$

Where,

$S$  = sliding surface

$\lambda$  = a positive integer

$n$  = the order of the system

$e$  = error

Re-arranging (5) gives (15), a first order equation.

$$\frac{dT}{dt} = \frac{1}{\tau} \{-T + E_s R_T + T_a\} \quad (15)$$

$T$  is the actual output, taking  $T_d$  as the reference input, the error,

$$e = T_d - T \quad (16)$$

Substituting for  $n$  and  $e$  into (14) gives (17).

$$S = \left( \frac{d}{dx} + \lambda \right)^{1-1} \times (T_d - T) \quad (17)$$

$$\therefore S = 1 \times (T_d - T = 0) \quad (18)$$

The equivalent control of SMC is obtained by taking the derivative of the sliding surface as shown in (19).

$$\dot{S} = \dot{T}_d - \dot{T} = 0 \quad (19)$$

$T_d$  is a constant  $\therefore \dot{T}_d = 0$

$$\dot{S} = -\dot{T} = 0 \quad (20)$$

Putting (15) into (20) gives (21)

$$\dot{S} = \frac{1}{\tau} \{T - R_T E_s - T_a\} = 0 \quad (21)$$

Making  $E_s$  the subject in (21) gives the equivalent control of the system (22).

$$E_{s-equ} = \frac{CT}{\tau} \{T - T_a\} \quad (22)$$

The switching control of SMC is given by (23).

$$E_{sw} = \begin{cases} Msign(S) & S > 0 \\ -Msign(S) & S < 0 \end{cases} \quad (23)$$

Where,

$S$  is the sliding surface and

$M$  is calculated based on Lipschitz function [18, 15].

SMC control law is given by (24).

$$U(t) = U_{equ} + U_{sw} \quad (24)$$

The control law in (25) is the summation of the  $E_{s-equ}$  and the switching control  $E_{sw}$  divided by the coefficient of  $E_s$  in (21)

$$E_s(t) = \frac{CT}{\tau} \{T - T_a\} + \frac{\tau}{R_T} (Msign(s)) \quad (25)$$

The stability of the system is verified using Lyapunov [18]

Taking the sliding surface  $S$ , as the Lyapunov function candidate  $\frac{1}{2}S^2$ ,

It will evaluate to common stability values:

$\frac{1}{2}S^2 > 0$  the system is unstable

$\frac{1}{2}S^2 = 0$  the system is stable

$\frac{1}{2}S^2 < 0$  the system is asymptotically stable

$$\frac{1}{2}S^2 = \dot{S}S \Rightarrow \frac{1}{\tau} (T - E_s R_T - T_a)(T_d - T)$$

$$\frac{1}{\tau} (T * T_d - T_d * E_s * R_T - T_d * T_a - T^2 + T * E_s * R_T + T * T_a)$$

Since the highest power of the function  $-T^2$  is negative,  $\frac{1}{2}S^2 < 0$ ; therefore, the system is stable.

### 2.3. Simulation using MatLab/Simulink

Simulation of the oven system carried out in MATLAB/Simulink, as shown in the Simulink model description in Figure 2. The figure shows the reference temperature  $T_d$  of 120°C as the desired set-point. The reference is compared to the actual oven temperature from the feedback loop to generate error signal. The error  $e$ , is used by the sliding mode controller to generate commands that regulates the quantity of heat energy that is delivered to the oven chamber.

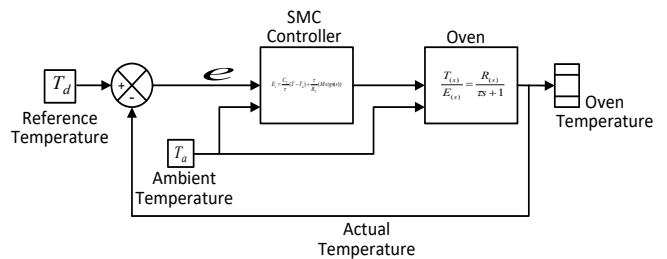


Figure 2: Simulink Model of SMC controlled Oven

The SMC controller is a Simulink model sub-system designed using (25). The ambient temperature,  $T_a$  is modelled in (26).

$$A_1 + A_2 \sin \varphi \quad (26)$$



Where,

$$A_1 = 25^{\circ}\text{C (Average room temperature)}$$

$$A_2 = 8^{\circ}\text{C (Chosen amplitude of variation)}$$

$$\varphi \leq 0 \leq 360 \text{ (In degrees)}$$

The oven block is a Simulink model sub-system too. It is created using (13) which is the transfer function describing the oven system behavior. The oven temperature block is a scope that logs the temperature evolution in the oven.

The simulation is repeated after the SMC controller sub-system has been replaced with Simulink PID block for comparison.

### 2.4. Simulation Results

The simulation results for the SMC controller is shown as a plot of temperature against time in Figure 3. From the graph the controller drives the system temperature to rise continually until the reference temperature of 120°C is reached. At steady-state the characteristic chattering effects of sliding mode controllers is seen as reviewed by a zoom-in of the plot. The highest and lowest peak of the chattering is ±0.3°C which are within the tolerance limits of most of the sensitive materials that are baked in oven such as some organic paints that require ±5.6°C.

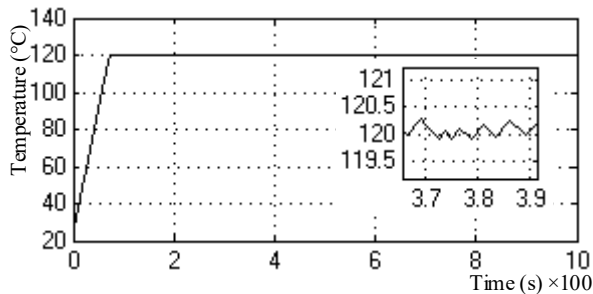


Figure 3: Plot of temperature vs time for SMC controlled oven

However, the simulation results after the SMC controller has been replaced by PID block shows high amplitude of oscillation at the steady-state region. The plot of temperature-time for the simulation is shown in figure 4.

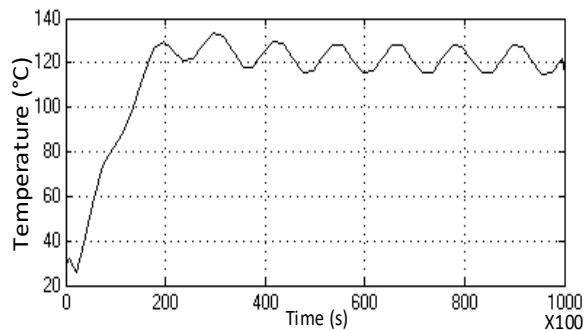


Figure 4: Plot of temperature vs time for PID controlled oven

The rise time for the PID controller is very long (11700s against <100s for the SMC).

Table 1 shows comparison of further analysis results generated from Matlab tools like stepinfo command.

Table 1: Comparison of SMC and PID controller for oven

Response	SMC Value	PID Value
Rise Time:	98.39 (s)	11700 (s)
Settling Time	124.14 (s)	64800 (s)
Settling Min	119.709°C	115.026
Settling Max	121.144°C	133.36°C
Overshoot:	0.9535%	11.13%
Undershoot:	0.2425%	4.145%
Peak vale:	121.144°C	133.36°C

Some important control factors have been compared as reviewed in Table 1.

- i. Rise time – this is the time taken for the system to rise from 10% of the steady-state value to 90% of the steady-state value (the steady-state value is 120°C). From the analysis the SMC controlled oven has 98.39 s rise time while the PID controlled oven has a rise time of 11700 s.
- ii. Settling time – this is the taken for the system to reach and remain within tolerance limits of steady-state value. The SMC controlled system has 124.14s and the PID controlled system has 64800 s to settle.
- iii. Settling max and min – are the highest and lowest temperature values in the oven after the system has reached steady-state.
- iv. Overshoot and undershoot – are the differences between the upper and lower limits of the system response and steady-state value expressed in percentage.
- v. Peak value – is the maximum temperature value attained inside the oven chamber.

The analysis results are evidence that the SMC controller performs better than PID controller for oven system. Hence, the system implementation is based on sliding mode control.

### 3. Implementations

#### 3.1. Software Designs

The simulation results of sliding mode control of oven temperature in MATLAB/Simulink 2014b indicates that the control method is an improvement on the existing control methods in for oven temperature control. Three key implementations that have been designed and built to verify SMC oven control on a practical oven system; these are convective paint curing oven, flat-plate air solar thermal collector and sliding mode controller unit.

Figure 5 and Figure 6 are the screen captures of the AutoCAD drawings of the oven and the collector respectively. The dimensions of the oven are a height of 1200mm, a length of 900mm and breadth of 600mm. It also has 1000mm length and 400mm breadth door framing; exhaust air channel of 100mm x 100mm x 1000mm and insulation layer thickness of 50mm.

Figure 5 shows control box that houses the controller, the keypad and display unit. Other things visible from the drawing are the power distribution box, the oven door lock and heater access door.

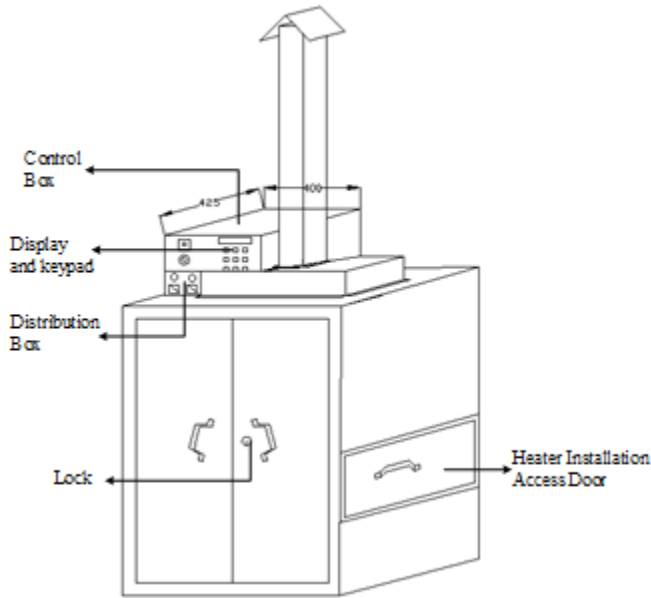


Figure 5: AutoCAD drawing of Convective paint curing oven

Figure 6 shows 2140mm x 2140mm flat-plate collector tilted at 16° angle for higher reception of radiation since extraction is by air forced. The drawing shows the glass cover, glass frame, extraction fan housing and inlet air channel.

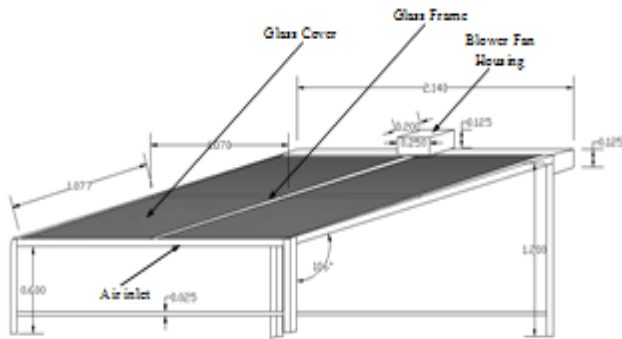


Figure 6: AutoCAD drawing of flat-plate air solar thermal collector

The design software is also used to generate the bill of materials (BOM), require for the implementation.

Figure 7 is screen capture of the control circuit diagram as designed in proteus software. It shows the microcontroller which is programmed using c++, a 16x2 LCD display, 3x4 matrix keypad electric heater control circuit and extraction fan controller for solar thermal collection.

### 3.2. Practical Implementation

The BOM generated from software is used to purchase the required materials need for the practical implementation. Figure 8(a) is a picture of the setup of the complete oven system with solar thermal collector and the control box. In the figure the chimney of the exhaust channel of can be seen on top of the oven and the control panel with the power distribution box mounted on the top left corner. The collector is place side by side with the oven and insulated host used to feed hot air extracted from the collector into the oven.

A zoom-in of the control box section is shown in Figure 8(b). It reviews the display, control box power switch, reset button, keypad and USB programmable port. The main power switches and fuse boxes are equally visible below the control box.

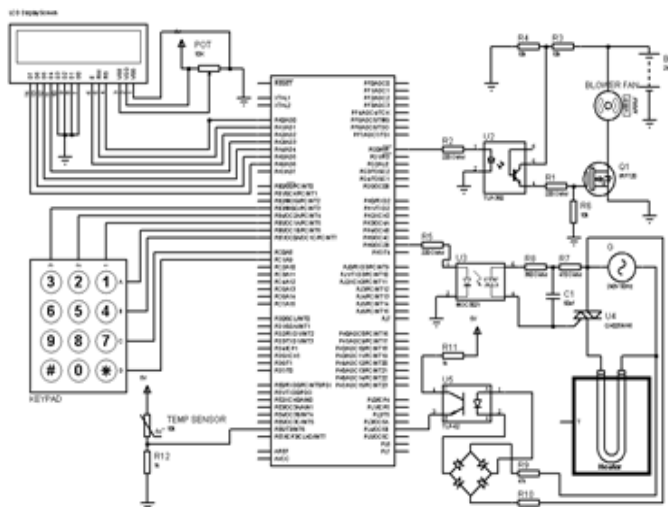


Figure 7: Proteus design of controller circuit diagram

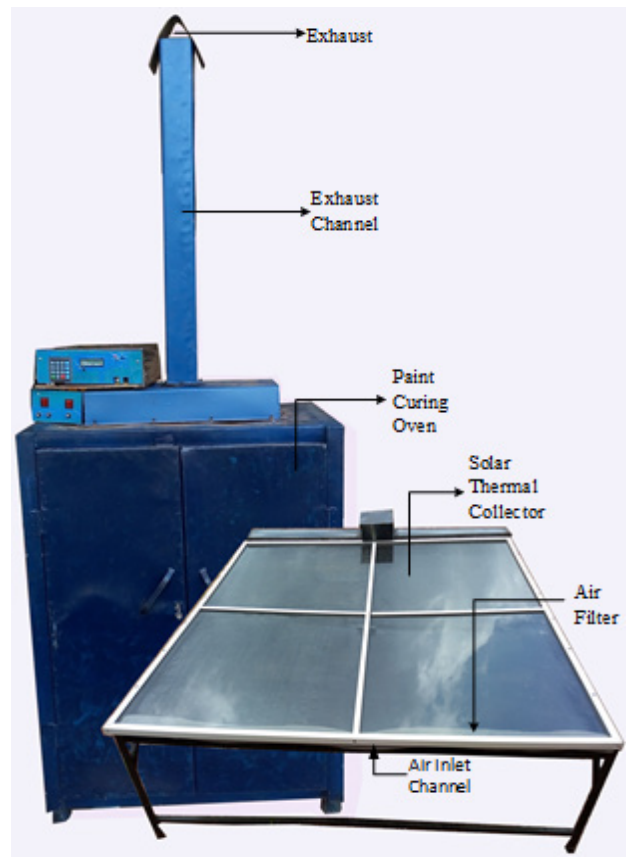


Figure 8(a): Picture of implemented system setup

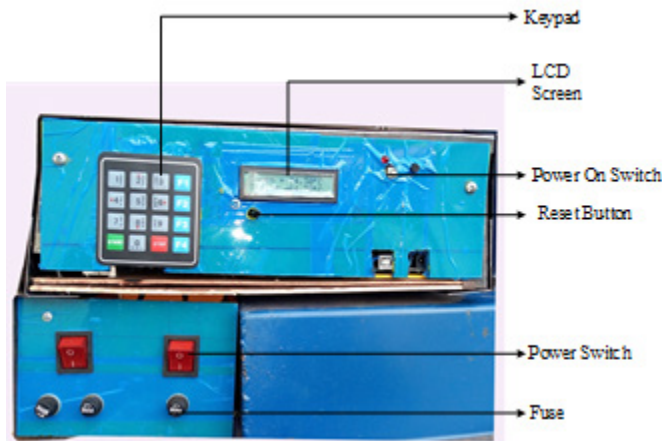


Figure 8(b): Picture of control box and power distribution box

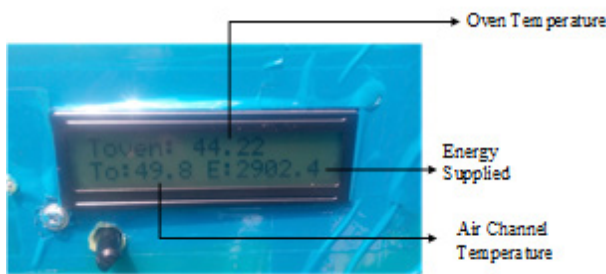


Figure 8(c): Picture of zoom-in display unit

Further zoom-in shown in Figure 8(c) is the real-time readings in the oven chamber as displayed by the LCD screen. They are the values obtained while the oven is powered by the solar collector alone. The value on top,  $T_{oven}$ , is the temperature on the oven at the instant of taking the snapshot, the value at the lower left,  $T_o$ , is the temperature of the hot air extracted from the collector and the value at the lower right of the screen,  $E$ , is the total energy delivered by the collector.

### 3.3. Program Flow of the Controller – Automated Oven

The control implementation allows for setting two temperature levels of temperature reference points which the oven will automatically migrate from one level to another. The flowchart algorithm in Figure 9(a) shows the program flow. It starts by initializing the variables,  $T_1$ ,  $T_2$ ,  $t_1$  and  $t_2$ .  $T_1$  is the first stage reference temperature for the cure (in Celsius) of paint that requires multiple temperature levels for proper cure.  $T_2$  is the second stage set-point;  $t_1$  is the time require for the paint to soak in the first temperature point;  $t_2$  is the soak time at the second temperature level. At the completion of initialization the processor reads the keypad and displays the numeric entry to the LCD screen. The processor evaluates the oven power control pin and toggle if need. This operation turns ON the air circulating fan in the oven at low speed. The processor reads the temperature sensors, which are negative temperature coefficient thermistors chosen because of their high sensitivities, fast responses, accuracies, and because they are suitable for temperature range of  $20^{\circ}\text{C}$  to  $120^{\circ}\text{C}$  of the paint cure oven built. The sensors data read are logged to external storage for analysis and simultaneously

used in the sliding mode control subroutine. The display is also updated in real-time. The SMC subroutine generates the command signals the processor uses regulate the speed of the extraction fan, circulating fan and the electric heater. The processor compares actual oven temperature to the first reference temperature,  $T_1$  of the oven; once the reference is reached a timer is set and the SMC maintains the actual temperature in the oven at that reference point until the set time is elapsed. At the expiration of the timer, the screen is displays “First Stage Completed” text and the SMC subroutine is updated with the second reference point which will enable the oven to automatically maintain a new temperature profile.

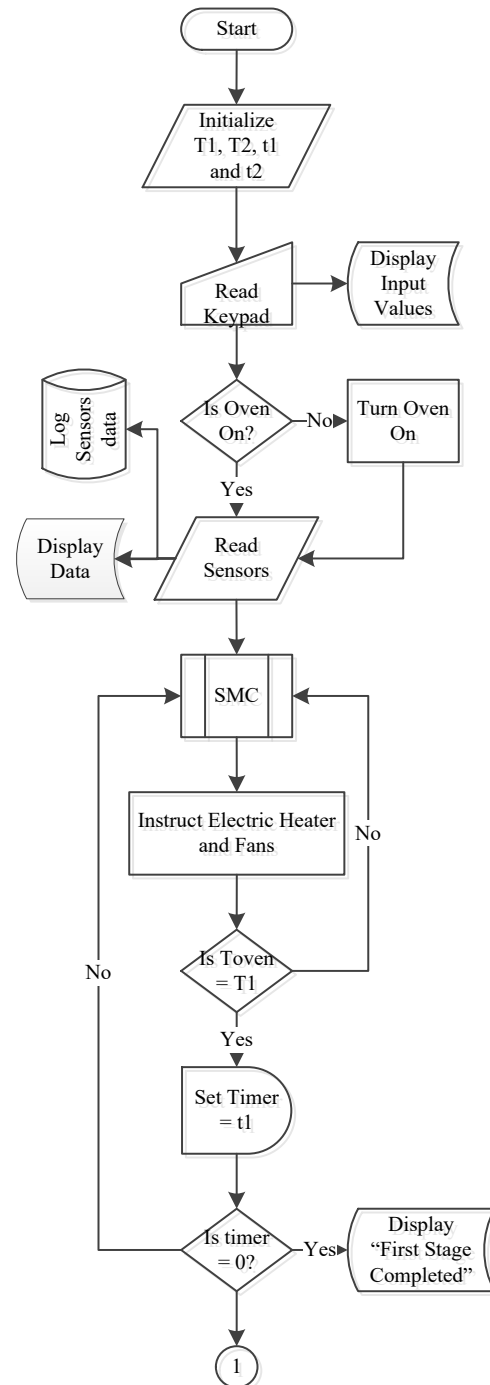


Figure 9(a): Flowchart of the controller – First stage

As the temperature reference is updated in the continued flowchart shown in Figure 9(b), the processor compares the temperature  $T_{out}$ , of hot extracted air from the collector to the new reference  $T_2$ . If  $T_{out}$  is greater than  $T_2$ , the electric heater is turned OFF so that the oven is solely powered by the collector; else the combined power sources continues as the SMC subroutine is called. The regulation of the electric heater, extraction and circulating fans by SMC generated signal begins to drive the oven temperature to the new reference point. Once again timer is set with the value of  $t_2$  and after the second stage soak time elapses "Paint Cured" is displayed on the LCD screen. The electric heater turned OFF and the oven shuts down.

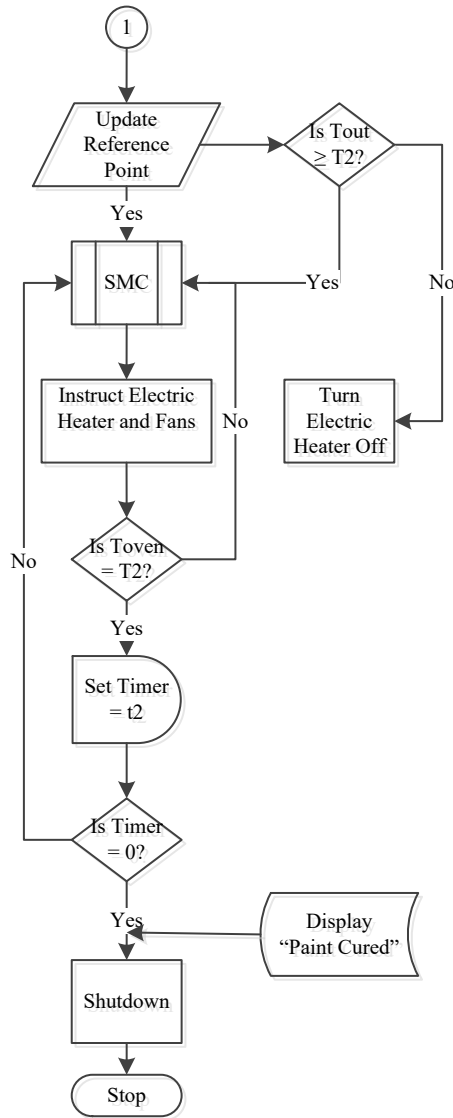


Figure 9(b): Flowchart of the controller – Second stage

Sliding mode control is a fast responds simple control method that switches between two discontinuous states in order to drive an output to track a reference input. Figure 10 is the flowchart algorithm of sliding mode control solar thermal/electricity powered oven. The control execution starts by reading three temperature variables; the reference temperature  $T_d$ , this changes for a multiple reference inputs ( $T_1$  or  $T_2$  as in the main flowchart).  $T_d$  is the desired temperature at any stage ( $T_1$  or  $T_2$ ). The second

variable is  $T_a$ , which is the temperature of the surroundings and the third variable is the actual temperature in the oven,  $T_{oven}$ .

$T_{oven}$  is continually acquired to track  $T_d$ . As the variables are updated the equivalent control  $E_{s-equ}$ , and the switching control  $E_{s-sw}$ , are computed. The equivalent control is the control mechanism that maintains  $T_{oven}$  to be steady once it reaches the sliding surface ( $T_d - T_{oven} = 0$ ). It is computed by taking the quotient of the total temperature rise in the oven chamber ( $T_{oven} - T_a$ ) and the total heat capacity of the oven  $\frac{1}{R_T}$ , (where  $\frac{1}{R_T} = \frac{C_T}{\tau}$  and  $\tau = C_T \times R_T$ ).

The switching control is the mechanism that drives the actual output  $T_{oven}$ , to the reference point  $T_d$  in order to reach the sliding surface. The operation is achieved by changing the state of the  $T_{oven}$  to be opposite in direction to any deviation from the sliding surface. That is taking the product of signum function of the error signal ( $sign(T_d - T_{oven})$ ), the heat capacity of the oven system  $C_T$  and a positive constant  $M$ , so chosen as to be greater than the maximum limit of the system disturbances.

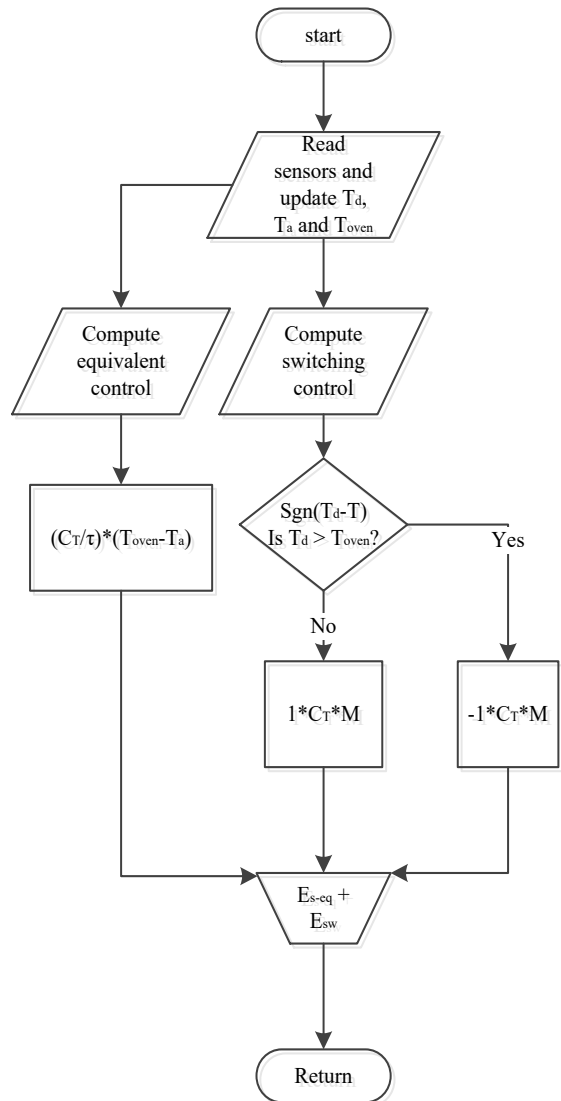


Figure 10: Sliding mode control flowchart



Table 2: Experimental test results

Quantity	Value
Rise Time	150.2369 (s)
Settling time	165.7523(s)
Settling Max.	60.8341 (°C)
Overshoot	1.7970 (%)
Undershoot	0 (%)
Peak	61.1800 (°C)
Peak Time	213.1673 (s)
Air Channel Temperature Max.	50.10 (°C)
Hydraulic Space Temperature Max.	69.7 (°C)
Collector Total Energy Supply	419,250.7 (W)

Signum function outputs +1 when the error signal is positive and -1 when the error signal is negative. The control signals from the equivalent control and the switching control are summed up in a Flowchart merger to get the control law of the sliding mode control. The control law generates the signal which is returned to the micro-controller and the process repeats until the paint is cured.

### 3.4. Experimental Test Results and Analysis

The system setup is for combined solar and electricity as sources of heat energy. The experiments are performed for single temperature reference and double temperature references. A plot obtained from the single temperature level test is shown in Figure 11. The plot shows the temperature evolution in thick blue line which is how the sliding mode controller drives the oven temperature to the reference temperature shown in black line.

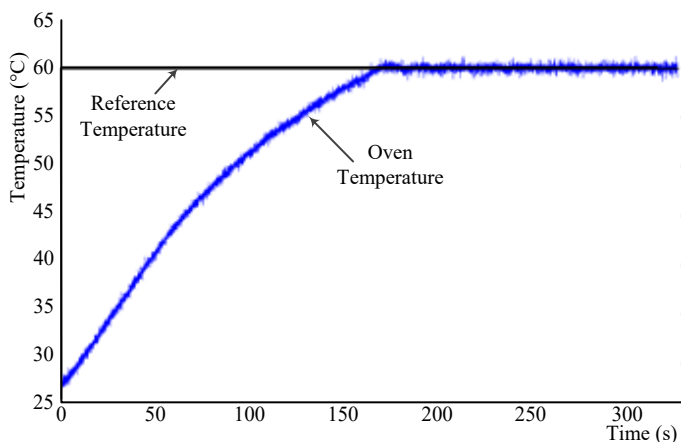


Figure 11: Oven temperature-time plot for a single reference point

Just as in the simulation results, the system has a rapid rise time in the experimental results; which demonstrates that the controller is an improvement over other convectional control methods. The controller also proves to be effective in tracking the reference temperature of 60°C with little or no deviation.

Table 2 is the statistical data collected from the analysis of oven temperature evolution logged in external drive while performing the experiment.

The table shows a rise time of 150.2369 s and settling time of 165.7523 s. It also shows settling maximum of about 60.8°C and an overshoot of about 1.8% with 0% undershoot. The maximum temperature recorded in the oven is 61.18°C which is the peak that occurred at 213.17 s.

The maximum temperature in the air channel that connects the solar collector to the oven is 50.10°C and the maximum temperature in the hydraulic space (gap between absorber plate and glass cover) of the collector is 69.7°C. The total energy supplied by the collector is 419,250.7 W.

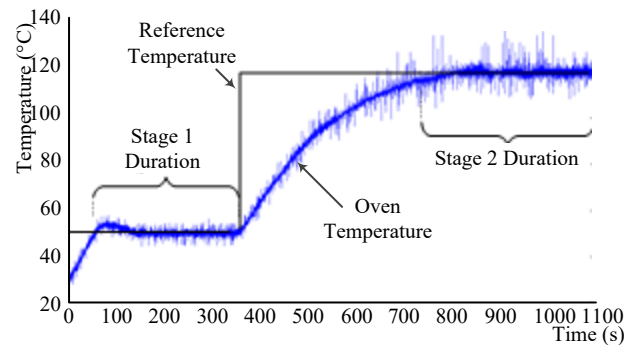


Figure 12: Oven temperature for double reference points

The second experimental demonstration test results are shown in the plot of Figure 12. The two reference points are 50°C and 120°C with each set to soak time of five minutes (300 s). The figure again shows that the controller effectively tracks multiple references at the various set time without much overshoot. However, noisy spikes begin to appear as the oven is in continuous use which become more pronounced as the temperature elevates. This is a design issue as a result of using thermistor with 150°C limit of maximum accurate range.

### 3.5. Payback Period and Energy Savings

Payback period is an estimate of the amount of time that is needed for cash inflow realized from a project to offset the initial cash outflow; it ignore the cost of maintenance [14-18] [19, 20, 21]. Powering of paint curing oven system with flat-plate air solar thermal collector to come with addition cost and the time required for the collector to generate energy that worth the cost.

In Table 2, the total energy the supplied to the oven by the collector is 419,259.7 W, for a period of 325 s. This is equivalent to 1,290 W/s

This implies that in one hour the collector can supply

$$1290 \times 60 \times 60 = 4,644 \text{ MJ} \quad (27)$$

Equation (27) shows that the collector generates 4.644 MJ of energy per hour. A kilowatt-hour of energy is 3.6 MJ and costs ₦47.8 in Nigeria that is equivalent of \$0.13 (or thirteen cent).

$$\Rightarrow \text{₦}47.80 \times \frac{4.644}{3.6} = \text{₦}61.66 \quad (28)$$

Equation (28) shows that the collector saves ₦61.66/hr

Assuming seven hours (7 hrs) of insolation per day over a period of one year (365 days) the equivalent cost of energy savings is ₦157,546.41 as shown in (29).

$$\text{₦}61.66 \times 7 \times 365 = \text{₦}157,546.41 \quad (29)$$

The cost of solar thermal collector in Figure 8(a) and its operation auxiliaries is ₦210,009.36; the payback period is thus:

$$\text{Payback period} = \frac{\text{total collector cost}}{\text{amount generated per year}} \quad (30)$$

$$\text{payback period} = \frac{210,009.36}{157,546.41} = 1.33 \text{ yrs} \quad (31)$$

The payback period is about sixteen months.

#### 4. Conclusion

This paper is an extension of work originally presented in 2019 IEEE International Conference on Sustainable Energy Technologies and Systems (ICSETS) [1]. It extends the control methodology approach and shows how the stability verification on the system model is done.

The work uses sliding mode control techniques and integration of solar thermal collector to solve oven temperature control and power optimization problem. Comparison of a model of an oven system designed and simulated in MATLAB/SIMULINK shows that sliding mode control method is an improvement over other control methods like PID control.

A convective paint curing oven has been built to verify the control method on paint curing process; Flat-plate air solar collector has also been built and incorporated into the oven system to reduce cost on utility bill. The developed control method was implemented for multi-stage temperature level using micro-controller and thyristor modules that switches electricity if the solar thermal collector is not supplying up to required temperature.

The system was setup and tested for verification and the experimental results show behavior similar to the simulation results. The results also show that the collector energy generation can payback the running and installation cost within sixteen months on an average insolation of 200W/m<sup>2</sup> in Nsukka. The collector provides 43.27% of the energy requirement by the oven when the oven operates at 120°C, which is considerably good.

#### Acknowledgment

This work is sponsored by Mirai Denchi Nigeria Limited

#### References

- [1] O. V. Ajah and E. C. Ejiogu, "Solar Thermal/Electricity Paint curing Oven," in *IEEE International Conference on Sustainable Energy Technologies and Systems (ICSETS)*, Bhubaneswar, India, Mar. 2019.
- [2] R. Talbert, "Curing," in *Paint Technology Handbook*, Boca Raton, USA, Press Taylor & Francis, 2008, pp. 161-167.
- [3] Despatch, "Industrial Oven Selection Guide," in *Thermal Processing Technology*, 8860 207th Street West Minneapolis, MN 55044 USA, Despatch, 2016.
- [4] N. Hambali, A. A. Rahim and A. A. Ishak, "Various PID Controller Tuning for Air Temperature Oven System," in *IEEE International Conference Proc. on Smart Instrumentation, Measurement and Applications (ICSIMA)*, Kuala Lumpur, 2014.
- [5] Y. Z. X. Gao and W. Guo, "Simulation and Research of Fuzzy Immune Adaptive PID Control in Coke Oven Temperature Control System," in *IEEE Proceedings of the 6th World Congress on Intelligent Control and Automation*, Dalian, China, 2006.
- [6] K. Ohishi, "Robust Temperature Control of Thermostatic Oven Based on Adaptive and Fuzzy Algorithm," in *IEEE Industrial Electronics Society IECON 15th Annual Conference*, 1989.
- [7] Z. Xuelei, W. Songling, C. Haiping and Z. Lanxin, "System Design and Economic Evaluation of Coke Oven Gas Utilization Projects," in *IEEE Conference*, 2010.
- [8] F. Pask, P. Lake, A. Yang and e. al., "Pask, F., Industrial oven improvement for energy reduction and enhanced process performance," in *Clean Techn Environ Policy*, 2017.
- [9] J. Kent, "http://www.pcimag.com," Apr., 2008. [Online]. Available: <https://www.pcimag.com/articles/95662-a-uniform-cure>. [Accessed 10 Feb., 2017].
- [10] E. C. Ejiogu, "High Performance Vector Control of the Induction Motor by Application of the Variable Structure System Theory," PhD Thesis, Shinshu University, Nagano-City, Japan, 1994.
- [11] V. I. Utkin, "Sliding Mode Control Design Principles and Applications to Electric Drives," *IEEE Trans. Industrial Electronics*, vol. 40, no. 1, p. 23 – 36, Feb, 1993.
- [12] K. D. Young, V. I. Utkin and Ü. Özgüner, "A Control Engineer's Guide to Sliding Mode Control," *IEEE Trans. Control Systems Technology*, vol. 7, no. 3, pp. 328-342, 1999.
- [13] B. Mohamed, M. Benyounes and Z. Souhila, "Comparison of Sliding Mode Control and Fuzzy Logic Applied to Wind Turbine Emulator," in *IEEE Conference 3rd International Symposium on Environmental Friendly Energie and Applications (EFEA)*, 2014.
- [14] M. Jzernik and K. Dal, "Experimental Comparison of Discrete Time Sliding Mode and Conventional, PI Current Controller for IM Drives," in *IEEE 12th International Power Electronics and Motion Control Conference*, 2006.
- [15] K. Eriksson, D. Estep and C. Johnson, *Applied Mathematics: Body and Soul Volume 1: Derivatives and Geometry in IR3*, Singapore: Springer, 2004.
- [16] V. Ajah and G. A. a. E. Ejiogu, "Sliding Mode Temperature Control for Hybrid Solar/Electricity Oven," *International Journal of Mechatronics, Electrical and Computer Technology (IJMEC)*, vol. 10, no. 37, pp. 4654 - 4664, July, 2020.
- [17] A. Victor, "Sliding Mode Temperature Control: Hybrid Solar Thermal/Electricity Paint Curing Oven," M.Eng Thesis, Electrical Engineering University of Nigeria, Nsukka, 2018.
- [18] N. Derbel, G. Jawhar and Z. Quanmin, *Applications of Sliding Mode Control*, Singapore: Springer, 2017.
- [19] S. Stelling, T. Y. R. Syah, R. Indrawati and D. Dewanto, "Role of Payback Period, ROI, and NPV for Investment in Clinical Health Business," *International Advanced Research Journal in Science, Engineering and Technology (IARJSET)*, vol. 5, no. 7, pp. 78 - 82, July, 2018.
- [20] A. F. AWOMEWE and O. Oludele Olawale, "THE IMPORTANCE OF THE PAYBACK METHOD IN," *Blekinge Institute of Technology, Blekinge*, 2018.
- [21] M. K. Al-Ani, "A Strategic Framework to Use Payback Period in Evaluating the Capital Budgeting in Energy and Oil and Gas Sectors in Oman," *International Journal of Economics and Financial Issues (IJEFI)*, vol. 5, no. 2, pp. 469 - 475, 2015.

# A Study on the Effects of Combining Different Features for the Recognition of Handwritten Bangla Characters

Halima Begum<sup>\*</sup>, Muhammed Mazharul Islam

Department of Electrical and Electronic Engineering, East West University, Dhaka 1212, Bangladesh

## ARTICLE INFO

Article history:

Received: 23 January, 2020

Accepted: 26 February, 2020

Online: 16 March, 2020

Keywords:

Handwritten Bangla character recognition

Artificial neural network

Shadow feature

Longest run feature

Chain code histogram feature

Gabor filter

Feature combinations

## ABSTRACT

This paper studies and compares the effectiveness of four different features and their combinations on the recognition accuracy of handwritten Bangla characters. The longest run, chain code histogram, shadow, and Gabor filter based features and their eleven (11) combinations were tested on a standard Bangla database of 15,000 basic handwritten characters to compare their recognition performances. From the experiments performed, it was observed that the combination of the longest run, chain code histogram, and the shadow features (having feature vector sizes of 20, 20, and 16 respectively) produce the highest recognition accuracy of 84.01%. Furthermore, inclusion of a feature with a large vector size compared to the other features in the combination generally dominates the recognition accuracy. In our case, inclusion of the Gabor filter-based features with a vector size of 1024 in the combination produced a recognition accuracy of 69.71%, which is worse than the accuracy obtained using the other three features. The analysis of the results indicates that the combinations of different feature vectors produce better accuracy as long as the sizes of each individual feature vector is comparable with each other in the combination.

## 1 Introduction

Handwritten character recognition has wide commercial applications, e.g., automatic letter sorting based on postal code, extracting information from bank checks and filled up forms, digitization of old handwritten books and documents etc. However, the similarity of shapes of different characters in a particular language, as well as the high variability in the handwritten scripts by different writers makes it quite a challenging task to correctly identify the characters in any language.

Bangla is ranked as the 6th most spoken language in the world and is spoken by nearly 230 million people. In Bangla, there are 50 basic character classes: 11 vowels and 39 consonants. There are also vowel modifiers, consonant modifiers, and other compound characters. Several characters in Bangla have identical shapes, which are only distinguished by the presence of a dot, a short straight line, a curved line, or by the number of loops, strokes etc. These characteristics have given Bangla its unique but complex nature. For recognition of handwritten characters, the obvious similarity of the characters of different classes can hurt the overall accuracy of a system.

Research on Bangla handwritten character recognition is comparatively new. Broadly speaking, two types of research trends are observed in handwritten character recognition. One is the extraction of features from the scanned character images and

then employing a classifier to identify the characters based on the extracted features. Another recent trend is to use convolutional neural network to perform the task of both feature extraction and classification. Success of the first type of methods largely depend on the careful selection of features, while the second type of methods heavily rely on the design of the network structure and the number as well the variability of sample data used to train the network.

Bhowmik et al. [1] used stroke based features on a database of 25,000 characters with recognition accuracy of 84.33%, while Rahman et al. [2] used a multi stage approach on a database comprised of 20 different samples of 49 categories each, with recognition accuracy of 88.38%. Bag et al. [3] used skeletal concavity/convexity of characters along two directions with a recognition accuracy of 60.6%. Basu et al. [4] used an artificial neural network with multi layer perceptron (MLP) on a database of 10,000 characters. Rahman et al. [5] used a convolutional neural network (CNN) to perform the task of both feature extraction and classification on their own dataset of 20000 samples with a recognition accuracy of 85.96%. Alom et al. [6] applied deep CNN for Bangla handwritten character recognition. Although a few of them used large datasets, but these were not publicly available. Therefore, it was not possible to compare the effectiveness of different features proposed by researchers.

Previously, we worked on the combination of three different

<sup>\*</sup>Halima Begum, East West University, A/2, Jahurul Islam Avenue, Jahurul Islam City, Aftabnagar, Dhaka 1212, Bangladesh, +88-09666775577-ext 186, & hab@ewubd.edu

features, namely Longest run features (LR), Chain code histogram features (CH) and features extracted using Gabor filter [7]. As a classifier, artificial neural network with back propagation algorithm was considered. We used a publicly available benchmark database [8] of basic Bangla characters and obtained an recognition accuracy of 76.47% considering the combination of the longest run and chain code histogram features [7].

In this paper, we used the same standard database to study and compare the effectiveness of different combinations of four types of features: shadow feature, chain code histogram feature, longest run feature and feature extracted using Gabor filters, in recognizing Bangla handwritten (isolated) basic characters. The purpose of this research is not only to identify the best combinations of features but also to identify the general condition of feature combinations to yield better recognition accuracy.

## 2 Brief Description of the Database and Preprocessing of the Character Image

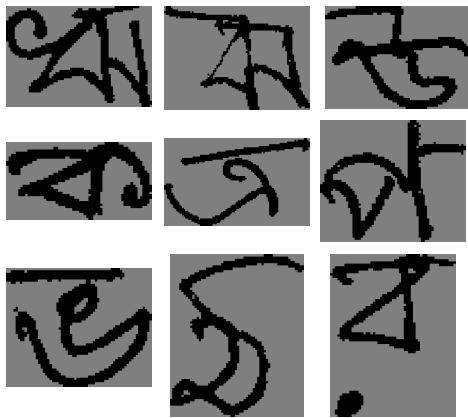


Figure 1: Randomly selected samples from the CMATER training database

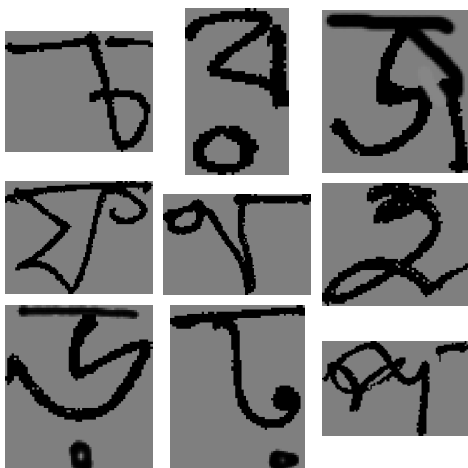


Figure 2: Randomly selected samples from the CMATER test database

In this paper, a benchmark database named ‘CMATERdb 3.1.2’ has been used [8]. The data was collected by the ‘Center for Microprocessor Application for Training Education and Research’ (CMATER), a research laboratory of Jadavpur University, India. The hand written isolated characters were collected from native

Bangla writers of different age, sex and educational groups in formatted data sheets designed by them. The collected data sheets were optically scanned in gray scale with a resolution of 300 dpi. In this way, a total of 15,000 characters of 50 character classes were collected (i.e. 300 character samples for each class). The character images vary from a size of 50 × 17 pixels to 589 × 667 pixels. The images were already divided into a training set and a test set. For any class of character, the number of images in the training set and the test set are 240 and 60 respectively. Fig. 1 shows a few randomly selected samples of Bangla characters from the training database, and Fig. 2 shows samples from the test database.

For recognizing handwritten characters, it is sufficient to work with binary images because the color of the characters do not contribute any additional information in classifying the characters. Binarizing the images also reduce the computational overhead. Furthermore, the size of the images must be uniform across the dataset for proper classification. Therefore, each image was size normalized to 128 × 128 pixels.

Fig. 3 and Fig. 4 show the samples of the preprocessed data. The foreground of the images (i.e. the character strokes) has a binary value of 1, while the background has a value of 0.

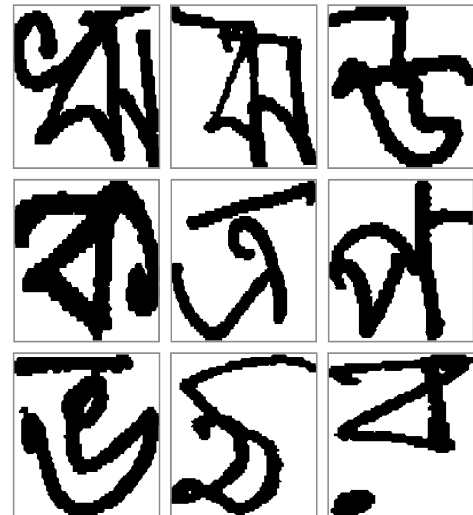


Figure 3: The preprocessed samples from the CMATER training database

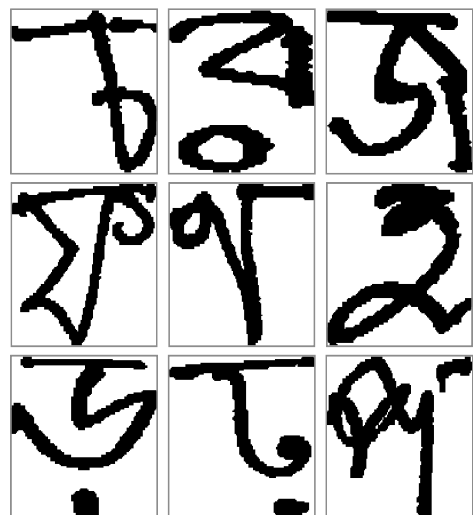


Figure 4: The preprocessed samples from the CMATER test database



### 3 Description of Features

In order to obtain a good recognition accuracy from a classifier, appropriate features need to be extracted from the character images. Researchers generally look to define features that are unique to the in-class characters but differ significantly between inter-class characters.

In this paper, four features, namely shadow feature, chain code histogram feature, longest run feature, and feature extracted using Gabor filters and their different combinations have been used.

#### 3.1 Shadow Feature

A shadow of a character is the projection of that character in a particular direction (typically on the image borders). The shadow feature computes the length of the shadow in each direction of projection. Projections along the vertical and horizontal directions were considered in this paper [9].

To extract the shadow feature from each of the character images, it was first divided into eight octants as shown in Fig. 5. For each octant, the length of the shadows (of the character segment falling into that octant) were computed on two perpendicular borders. The length of the shadow along a perpendicular border of an octant was divided by the total length of that border to obtain a normalized value and was considered as a feature.

Therefore, a total of 16 shadow features from each character image were obtained. Fig. 6 demonstrates the shadow feature extraction scheme for a sample character (of 16 by 16 pixels), where arrows show the direction of the projection of shadows.

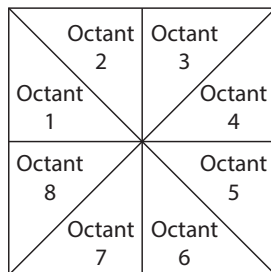


Figure 5: Octants for obtaining shadow features of image

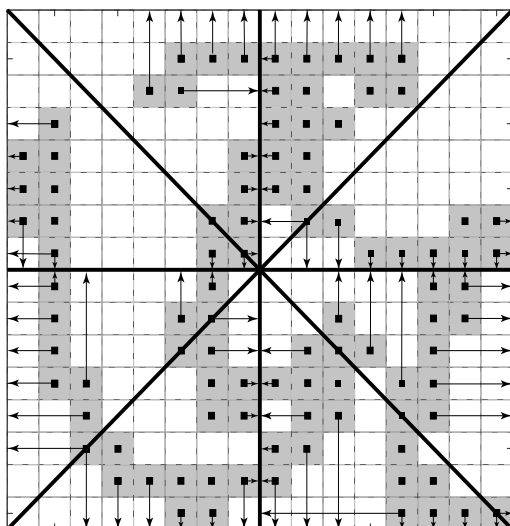


Figure 6: Horizontal and vertical shadow features of image for each octant

#### 3.2 Chain Code Histogram Feature

The chain code carries the information of the shape and the size of a character image. In this method, the directions of movement along the character's boundary are encoded using a numbering scheme and this allows for a compact representation and reduction of data [10, 11].

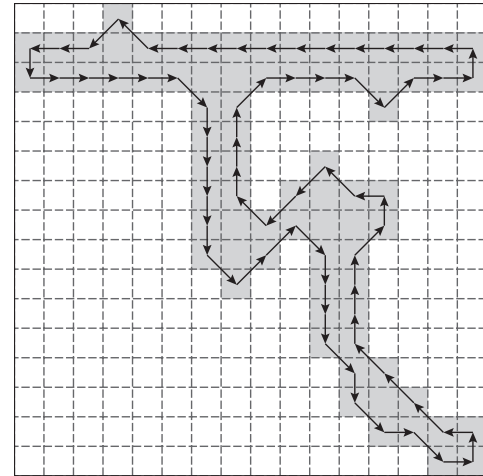


Figure 7: Illustration of the change of direction of boundary pixels for the whole character image

In this paper, to extract this feature, the boundary pixels of the character image (which must be 8-connected or 4-connected) were first detected using Moore's contour tracing algorithm [12] and then the changes in the direction of the boundary pixels were coded using a scheme proposed by Freeman [13]. Fig. 7 illustrates the change in the direction of the boundary pixels for a sample Bangla character. In the figure, the direction changes along the boundary are denoted with arrows. The change in the direction between two neighboring pixels is coded using Freeman's chain code. The numbering scheme for the code is illustrated in Fig. 8.

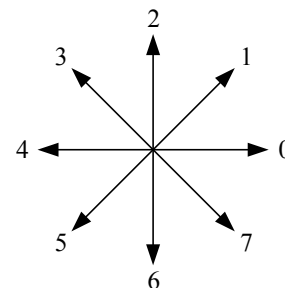


Figure 8: Illustration of the numbering scheme proposed by Freeman's Chain code considering 8 connectivity of pixels

For example, if the movement from one pixel to the next is along 0°, then the movement is coded as the number 0, if the direction of movement is 45°, then the movement is coded as the number 1 and so on.

Moreover, in the case of character images, the general practice is for the opposite directed movements to be coded with the same value, that is, 0° and 180° are both considered as code 0, 45° and 225° are both coded as 1, 90° and 270° are both coded 2, and 135° and 315° are both coded as 3 [9]. This modification reduces the chain code to four values.

Using the modified chain code, the frequency of occurrence of each directional code (histogram) for a character image was calcu-





Figure 12: Original sample image before applying Gabor filter

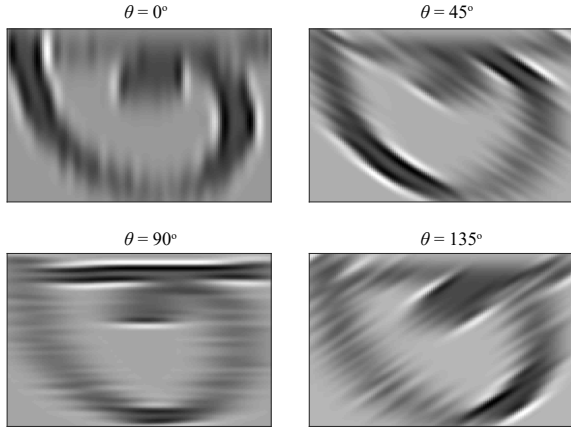


Figure 13: Filtered sample image with enhanced directional feature

As the four filtered images has size  $128 \times 128$  each, therefore, in this paper, these were down-sampled to get sub-sampled images of size  $32 \times 32$  each. The four filtered sub-sampled images were then averaged and used as a feature. This was done to reduce the high dimensionality of the feature vector. The feature vector size for each character image is thus  $32 \times 32 = 1024$ .

### 4 Artificial Neural Network

An artificial neural network (ANN) was used as the classifier to identify the characters. The ANN consists of nodes in different layers with inter connections [15], where the nodes are distributed in mainly three types of layers, i.e. (i) input layer, (ii) output layer, and (iii) one or more hidden layers. Mathematically, the output of a layer of the neural network can be defined as the weighted sum of  $n$  input signals,  $x_j = 1, 2, \dots, n$ , and the firing of the neurons are controlled by the activation function. The output is expressed as,

$$y = f \left( \sum_{j=1}^n w_j x_j + b \right) \tag{3}$$

where  $f(\cdot)$  is the sigmoid activation function,  $w_j$  is the weight associated with the  $j$ -th input and  $b$  is the bias.

We used a feed-forward neural network architecture (with a vanilla structure), where each layer is fully connected to the next as shown in Fig. 14. In the figure,  $w_{ij}^L$  is the weight of the connection between the  $i$ -th node in the layer  $(L - 1)$  to  $j$ -th node in the layer  $L$ .

To train the network,  $p$ -numbers of input-output pairs (called training pairs), defined as  $\{(\mathbf{x}^{(1)}, \mathbf{d}^{(1)}), (\mathbf{x}^{(2)}, \mathbf{d}^{(2)}), \dots, (\mathbf{x}^{(p)}, \mathbf{d}^{(p)})\}$  are used. Here, each input  $\mathbf{x}^{(r)} = [x_1^{(r)}, x_2^{(r)}, \dots, x_n^{(r)}]^T$  is a feature vector in  $n$ -dimensional space, and each corresponding output  $\mathbf{d}^{(r)} = [d_1^{(r)}, d_2^{(r)}, \dots, d_m^{(r)}]^T$  (where  $d_q^{(r)} \in [0, 1]$ ) is a vector in  $m$ -dimensional space.

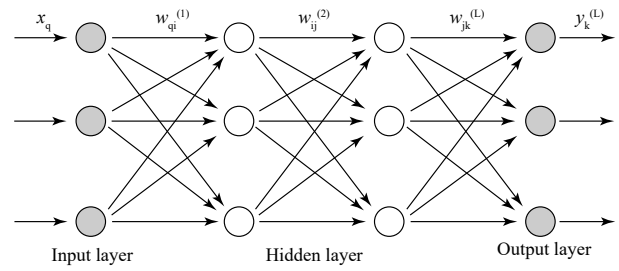


Figure 14: Artificial neural network

Note that,  $m$  is the number of classes. In the vectors  $\mathbf{d}^{(r)}$ , only the correct class element has a value of 1, and all other elements have values of 0. The cost function is defined between the predicted class ( $\mathbf{y}$ ) and the actual class ( $\mathbf{d}$ ) over the entire training range as,

$$E = \frac{1}{2} \sum_{k=1}^p \|\mathbf{y}^{(k)} - \mathbf{d}^{(k)}\|^2 \tag{4}$$

During the training phase, the back-propagation learning algorithm is used to optimize the weight values through the minimization of the squared error cost function [16].

### 5 Classification Results and Analysis

The extracted features from the training data set characters were used as the inputs of the ANN for varying number hidden layers (up to 500), and the recognition accuracy was checked on the test data set. Therefore, the features obtained from the training data actually train the network, and the recognition accuracy indicates how well the trained network is able to recognize the test data set.

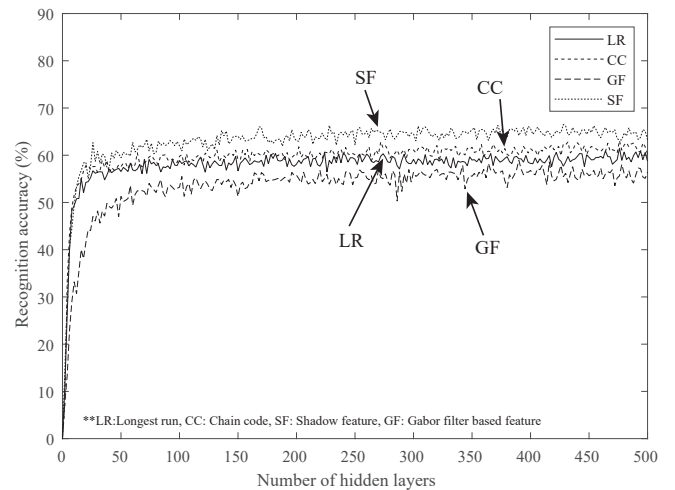


Figure 15: Recognition accuracy of test data for single feature sets

Figure 15 shows the recognition accuracy on the test data against different number of hidden layers, where only single features were used. The recognition performance based on the shadow feature seems to be better than the other three individual features. On the other hand, the recognition performance based on the features extracted using the Gabor filter produces the poorest results among the four.

Figure 16 shows the recognition accuracy on the test data against different number of hidden layers, where different combinations of features (taken two at a time) were used.

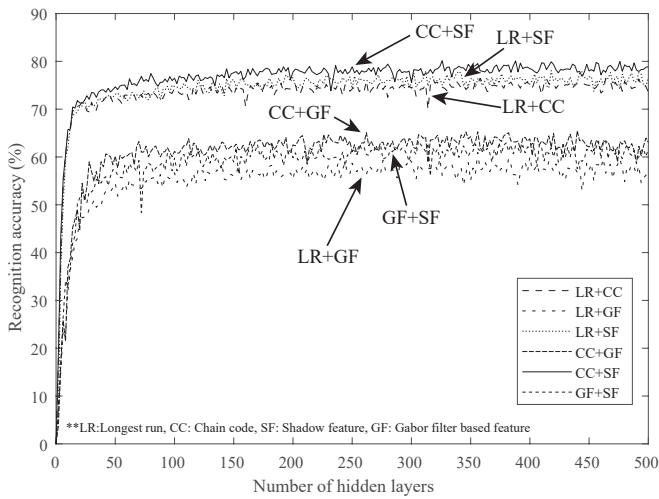


Figure 16: Recognition accuracy of test data for feature sets taken in pairs

Again, the recognition accuracy seems to be poor whenever any combination were used which involved features extracted using the Gabor filter. The combinations (excluding the Gabor filter based features) also produce better results than the those obtained using individual features.

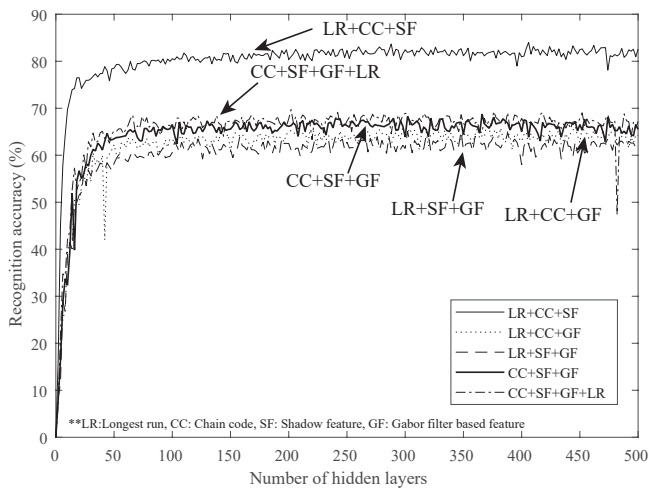


Figure 17: Recognition accuracy of test data for feature sets taken three or more at a time

Figure 17 shows the recognition accuracy on the test data against different number of hidden layers, where different combinations of features (taken more than two at a time) were used. Like the previous case, the recognition accuracy is better without the Gabor filter based features. The recognition accuracy for all the feature combinations (excluding the Gabor filter based features) produce the best results among the combinations.

Table 1 summarizes the maximum recognition accuracy of the neural network (on the test data) under different feature sets and their combinations. The optimal number of hidden layers of the network are also shown in the table.

For the individual feature sets, the highest recognition accuracy is 66.51% using the shadow features, while the recognition accuracy is the lowest (i.e. 59%) for the Gabor filter based feature. It is noted that the shadow feature produces a better result although the feature vector size is only 16, which is the lowest among all the individual feature sets used in this paper, while the

Gabor filter based feature performs poorly, although the size of this feature vector is the largest (i.e. 1024).

Table 1: Classification performance of different feature sets and their combinations

No.	Feature name	Number of features	Classification accuracy	Number of hidden layers
1	Longest run (LR)	20	61.52%	476
2	Chain code histogram (CC)	20	63.47%	476
3	Gabor filter (GF)	1024	59%	428
4	Shadow feature (SF)	16	66.51%	390
5	LR and CC combination	40	76.47%	358
6	LR and GF combination	1044	60.96%	356
7	LR and SF combination	36	78.07%	418
8	CC and GF combination	1044	65.49%	440
9	CC and SF combination	36	80.13%	326
10	GF and SF combination	1040	63.54%	464
11	<b>LR, CC, and SF combination</b>	<b>56</b>	<b>84.01%</b>	<b>406</b>
12	LR, CC, and GF combination	1064	66.68%	370
13	LR, SF, and GF combination	1060	65.11%	348
14	CC, SF, and GF combination	1060	68.77%	366
15	CC, SF, LR and GF combination	1080	69.71%	202

However, higher recognition accuracy was obtained when we used combinations of features on character images. There are six possible combinations of feature sets taken two at a time, four possible combinations of feature sets taken three at a time, and only one combination of all the four feature sets. Looking at the recognition accuracy when using the combinations, it can be seen that a combination of longest run, chain code histogram, and shadow feature produces the best results, i.e. 84.01%. The number of features of this combination was only 56.

It is seen that, any combination of features that contains the Gabor filter based feature produces a comparatively lower accuracy result. The reason for this is, the feature vector size of the Gabor filter based feature is more than 50 times larger than any of the other three individual features, i.e. while the feature vector size of the Gabor filter based feature is 1024, those of the longest run, chain code histogram, and shadow features are 20, 20 and 16 respectively. As a result, the Gabor filter based feature overshadows the other features in these combinations. Therefore, since the Gabor filter based feature itself does not produce a very good recognition accuracy (i.e. only 59%), the recognition accuracy produced by these combinations are weighed down by this dominating sized feature.

Combinations of the other three features (i.e. longest run, chain code histogram, and shadow feature) produce relatively better recognition accuracy, because, the size of the feature vectors of all the three feature sets are comparable. Moreover, for a particular class, some of the character images recognized by each feature sets are non-overlapping. That is, some characters which are *not* recognized using one feature set, are recognized when using another feature set.



Therefore, to get a better recognition accuracy, more than one feature sets are necessary, and the feature vectors of these sets should be comparable in size, otherwise, the results may be dominated by a particular feature set and the purpose of combining different feature sets may not be fulfilled.

## 6 Conclusion

In this paper, we have compared the effectiveness of four feature sets (shadow, longest run, chain code histogram and Gabor filter based feature) on Bangla handwritten isolated basic character recognition. Moreover, the effectiveness of 11 different combinations of these features were also studied. A benchmark database with 15,000 samples of Bangla basic characters was used for this comparative study.

We observed that, among the individual features, the shadow feature was more effective in Bangla handwritten character recognition compared to the other three features, although its feature vector size was only 16. On the other hand, among the combination of features, the combination of the shadow feature, the longest run feature and the chain code histogram feature yielded the best recognition accuracy, i.e. 84.01%, with a feature vector size of 56 only. In this combination, the size of the feature vectors from the shadow, longest run, and chain code histogram features were 16, 20, and 20 respectively, which are comparable. This implies that, in this combination, the three different features have equal contribution in recognizing the character classes. If the combination includes a feature with a larger vector size (compared to the size of other feature vectors in the combination), then it can strongly influence the recognition accuracy. In our case, when the Gabor filter-based feature (with a vector size of 1024) was added to the combination, it resulted in a comparatively poor performance than those obtained with the combinations of the other features. Therefore, we can surmise that, the combination of features performs better in recognizing character classes as long as the size of the feature vectors are comparable.

In this paper, although we have used hand-coded features, and a feed-forward neural network with backward propagation, but the recent trend is to use convolution neural networks (CNNs). In CNNs, the number of layers is many, and the structure of the network allows for the hidden layers to become sensitized to different features during training. We mainly avoided CNNs because of the small size of the available database, but in our future work, we would like to use CNNs to evaluate the recognition accuracy of handwritten characters and compare with the results obtained in this paper.

## References

- [1] T. K. Bhowmik, U. Bhattacharya, S. K. Parui, "Recognition of Bangla Handwritten Characters Using an MLP Classifier Based on Stroke Features" in 11th International Conference, ICONIP 2004, Calcutta, India, 2004. [https://doi.org/10.1007/978-3-540-30499-9\\_125](https://doi.org/10.1007/978-3-540-30499-9_125)
- [2] A. F. R. Rahman, R. Rahman, and M. C. Fairhurst, "Recognition of handwritten Bengali characters: a novel multistage approach" *Pattern Recognition*, **35**(5), 997-1006, 2002. [https://doi.org/10.1016/s0031-3203\(01\)00089-9](https://doi.org/10.1016/s0031-3203(01)00089-9)
- [3] S. Bag, P. Bhowmick, G. Harit, "Recognition of Bengali Handwritten Characters Using Skeletal Convexity and Dynamic Programming" in 2011 Second International Conference on Emerging Applications of Information Technology, Kolkata, India, 2011. <https://doi.org/10.1109/eait.2011.44>
- [4] S. Basu, N. Das, R. Sarkar, M. Kundu, M. Nasipuri, D. K. Basu, "A hierarchical approach to recognition of handwritten Bangla characters" *Pattern Recognition*, **42**(7), 1467-1484, 2009. <https://doi.org/10.1016/j.patcog.2009.01.008>
- [5] M. A. H. Akhand, M. M. Rahman, P. C. Shill, S. Islam, M. M. H. Rahman, "Bangla Handwritten Numeral Recognition using Convolutional Neural Network" in 2015 International Conference on Electrical Engineering and Information Communication Technology (ICEEICT), Dhaka, Bangladesh, 2015. <https://doi.org/10.1109/iceeict.2015.7307467>
- [6] M. Z. Alom, P. Sidike, M. Hasan, T. M. Taha, V. K. Asari, "Handwritten Bangla character recognition using the state-of-the-art deep convolutional neural networks" *Computational Intelligence and Neuroscience*, **2018**, 1-13, 2018. <https://doi.org/10.1155/2018/6747098>
- [7] H. Begum, A. Rafid, M. M. Islam, "Recognition of Bangla Handwritten Characters using Feature Combinations" in 2018 5th IEEE Uttar Pradesh Section International Conference on Electrical, Electronics and Computer Engineering (UPCON), Gorakhpur, India, 2018. <https://doi.org/10.1109/upcon.2018.8597076>
- [8] N. Das, K. Acharya, R. Sarkar, S. Basu, M. Kundu, M. Nasipuri, "A benchmark image database of isolated Bangla handwritten compound characters" *International Journal on Document Analysis and Recognition (IJDAR)*, **17**(4), 413-431, 2014. <https://doi.org/10.1007/s10032-014-0222-y>
- [9] D. R. Birajdar, M. M. Patil, "Recognition of off-line handwritten Devanagari characters using combinational feature extraction" *International Journal of Computer Applications*, **120**(3), 1-4, 2015. <https://doi.org/10.5120/21204-3883>
- [10] Y. Qian, W. Xichang, Z. Huaying, S. Zhen, L. Jiang, "Recognition Method for Handwritten Digits Based on Improved Chain Code Histogram Feature" in Proceedings of 3rd International Conference on Multimedia Technology (ICMT-13), Guangzhou, China, 2013. <http://doi.org/10.2991/icmt-13.2013.53>
- [11] R. C. Gonzalez, R. Woods, *Digital Image Processing*, Prentice Hall, 2008.
- [12] U. Pape, "Implementation and efficiency of Moore-algorithms for the shortest route problem" *Mathematical Programming* **7**(1), 212-222, 1974. <https://doi.org/10.1007/BF01585517>
- [13] H. Freeman, "On the encoding of arbitrary geometric configurations" *IRE Transactions on Electronic Computers*, **EC-10**(2), 260-268, 1961. <https://doi.org/10.1109/tec.1961.5219197>
- [14] D. Gabor, "Theory of communication. Part 1: The Analysis of Information" *Journal of the Institution of Electrical Engineers - Part III: Radio and Communication Engineering*, **93**(26), 429-441, 1946. <https://doi.org/10.1049/ji-3-2.1946.0074>
- [15] S. Haykin, *Neural Networks: A Comprehensive Foundation*, Prentice Hall PTR, 1994.
- [16] C. M. Bishop, *Pattern Recognition and Machine Learning*, Springer, 2006.

## Control of Electrostatic Suspension System Using Pulse Width Modulation

The Truyen Le\*

*Department of Mechanical Engineering of Ho Chi Minh City University of Food Industry, 140 Le Trong Tan Street, Ho Chi Minh City, 760310, Viet Nam*

### ARTICLE INFO

*Article history:*

*Received: 31 January, 2020*

*Accepted: 02 March, 2020*

*Online: 13 March, 2020*

*Keywords:*

*Electrostatic suspension system*

*Pulse width modulation*

*Silicon wafer*

### ABSTRACT

*Electrostatic suspension systems have great potential applications in contactless transportation objects since they allow many different materials to be suspended. The electrostatic suspension will be widely applied in practice if the system cost is inexpensive. This paper presents an electrostatic suspension system controlled by using pulse width modulation (PWM). The use of PWM in electrostatic suspension system will reduce the system cost since inexpensive switching power amplifiers could be applied instead of linear analogue power amplifiers, which are bulky and costly. The simulation and experimental results are performed and showed that PWM can be used effectively to control the position of the levitated object in the electrostatic suspension.*

### 1. Introduction

The electrostatic suspended actuation can be used in a special environment without problems caused by friction, abrasion or lubrication. The electrostatic suspension systems can levitate many different materials without any contact, therefore, they are useful in micro-bearings, contactless levitation and transportation of silicon wafers [1, 2], aluminum hard disks media [3] and glass panels [4]. The electrostatic suspension systems could be also used effectively for the process of handling materials. Generally, the material handling process requires containers containing the material processed. However, if the melting point of material treated is higher than that of the material of container, this handling process becomes difficulty. The contactless levitation performed by the electrostatic suspension system can help this handling process perfectly performs since it is devoid of using any container for handling materials.

Generally, electrostatic suspension systems require several kV voltages to create enough electrostatic force for the suspension process. So, the traditional electrostatic systems use the high analogue voltage amplifiers to amplify the low output voltage signals of the feedback controller. However, these devices are very cumbersome, especially they are expensive components [5-7]. Moreover, electrostatic suspension system requires many electrodes to suspend wide flexible objects result in an increase in the number of these devices. This leads to an increase in the cost

of the suspension system and it hinders the widespread application of electrostatic suspension in practice [8]. Therefore, it is necessary to develop the low-cost contactless electrostatic suspension systems to improve its applicability in practice.

Modulation technique is widely applied in many industrial fields, however, this method has not been successfully applied in the field of contactless suspension by electrostatic forces. The use of modulation techniques in this field is attractive because it allows employing the inexpensive switching power amplifiers instead of expensive analog high voltage amplifiers.

Many modulation techniques such as integral pulse frequency modulated [9], pulse width modulation [10], and pulse width pulse frequency modulation [11] are applied in industrial systems. Among them, PWM is widely used because it has many advantages such as robust against disturbances and easily implemented. It could be found application of PWM in motor controls [12], pneumatic and hydraulic actuators [13-14], shape memory alloy actuator [15, 16], 3-RPR parallel robot [17], pneumatic valves [18, 19], Electro-Mechanical Actuator [20], and in piezo air jet actuators [21]. This paper introduce a contactless suspension system by using modulation techniques. In this paper, the PWM is used to modulate an PID controller (Proportional-Integral-Derivative) in order to control the position of the suspended object. Experimental results prove that the contactless suspension by electrostatic forces could be implemented by using the PWM-modulated PID controller. The system provides an accurate position control with an inexpensive switching power amplifier.

\* The Truyen Le, Email: [truyenlt@cntp.edu.vn](mailto:truyenlt@cntp.edu.vn)

## 2. Experimental setup

The schematic of 1 d.o.f (degree of freedom) contactless suspension system by electrostatic force is introduced in Fig. 1. The external disturbance forces  $F_{ext}$  is small and it is ignored. Thus, the dynamic motion of the object could be presented by [22]:

$$m\ddot{z} = mg - F_e - F_d \quad (1)$$

where:

$m$ : the mass of the object,

$z$ : the gap between the object and the electrode,

$F_e$ : the electrostatic force,

$F_d$ : the damping force,

$mg$ : the gravitational force.

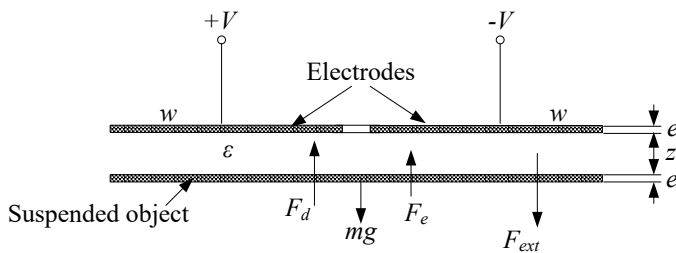


Figure 1: The schematic of 1 d.o.f contactless suspension system by electrostatic force

The electrostatic can be expressed as [22]:

$$F_e = \frac{1}{2} \epsilon A \left(\frac{V}{z}\right)^2 \quad (2)$$

in which,

$V$ : the supplied voltage,

$\epsilon$ : the permittivity of the air, its value is  $8.854 \times 10^{-12}$  F/m

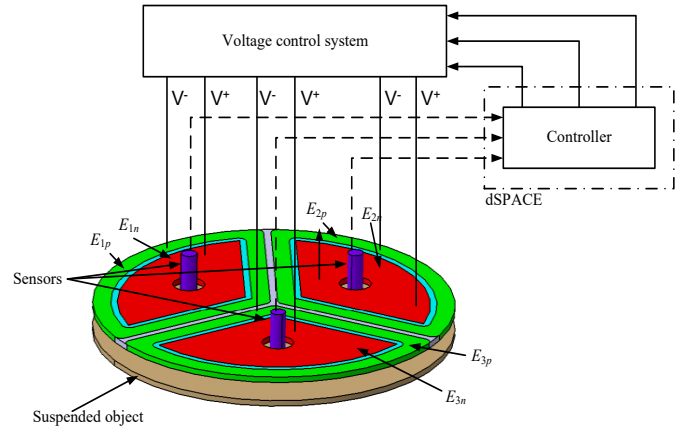
$A$ : the area of electrode.

Equation (2) reveals that the supplied voltage  $V$  must be controlled for the stabilization of the levitated object.

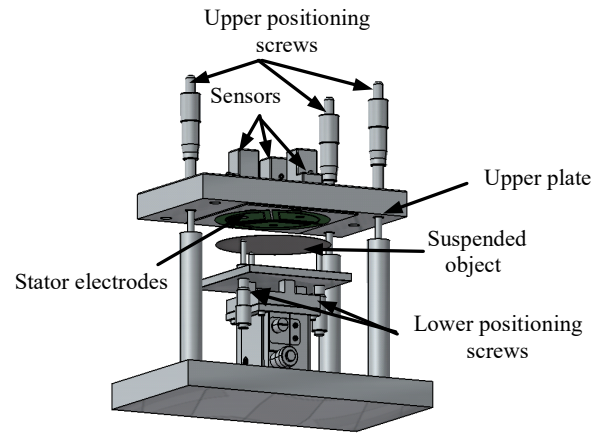
The schematic and experimental system used to perform the contactless suspension are presented in Fig. 2. The electrostatic suspension system using PWM consist of four major components: stator electrodes, position sensors, and circular shaped suspended object (4-inch silicon wafer). The process of contactless levitation of the object (4-inch silicon wafer) needs to be controlled in five degree of freedoms that are the horizontal plane, vertical movement, pitching, and rolling [23]. However, the displacements of the object in the horizontal plane are passively balanced without any active control due to the regenerative force created by the edge field that will pull the object back into position where object and electrode overlap.

The remaining three degrees of freedom that are rolling, pitching and vertical displacements must be balanced by the active control of the force acting on the object [22]. This could be performed by using three fan shape electrodes that are directly

positioned above the object. Each electrode is designed to include an external electrode  $E_{ip}$  and an internal electrode  $E_{in}$ , ( $i=1, 2, 3$ ). The positive voltage provides to the external electrode, and the negative voltage supply to the internal electrode. Three external electrodes are arranged in a circle with the same diameter of the object [8]. Three position sensors are placed in the center hole of each electrode #1, #2 and #3 to detect positions of suspended object, respectively. The electrode surface is covered with an insulating layer with a thickness of  $80 \mu\text{m}$  to prevent short circuits if the suspended object comes in contact with electrodes.



a) Schematic view of an experimental setup



b) Suspension system



Figure 2. Experimental apparatus [22]

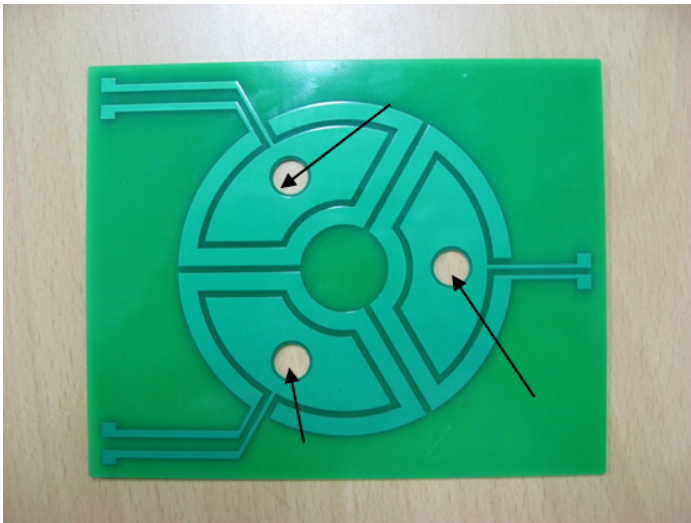
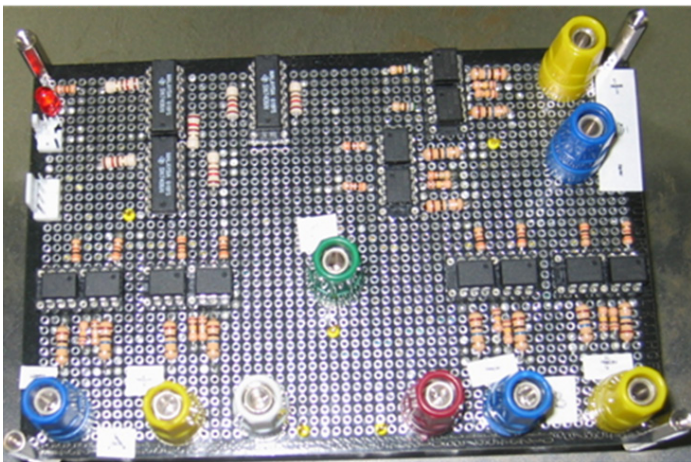


Figure 3. Stator electrodes

Contactless suspension of a suspended object is performed by using a controller implemented by using dSPACE data acquisition system. The design of controller is described in section 3. The position of the object is detected by the position sensors, and the position signal is fed to the controller. The voltage supplied to the electrode will occur in an on-off action according to the position sensor signals by the switching circuit. The switching power amplifier provides the charged voltage and discharged voltage to the external and internal electrode  $E_p$  and  $E_n$  parts of each electrode, respectively. The switching power circuit is designed by using power metal-oxide-semiconductor field-effect transistor (MOSFET). For controlling MOSFET, the drive chip IR2104 is employed. The switching power amplifier circuits are presented in Fig. 4.



### 3. PWM-PID controller designed for the electrostatic suspension system

The mechanisms implement of PWM in this paper is presented in Fig. 5. It includes of a triangular carrier wave with a constant frequency  $r(t)$  and a bang-bang trigger [13]. It notes that the amplitude of carrier wave is greater than the greatest amplitude of the control signal. The difference  $e(t)$  between the control signal and the carrier wave is fed to the bang-bang trigger. The value of

$e(t)$  will determine the bang-bang trigger outputs that are  $A_c$  or  $-A_c$ . Namely, the bang-bang trigger output is  $A_c$  corresponding to the on-state if the value of  $e(t)$  is positive and bigger than the bang-bang trigger threshold, otherwise, its output is  $-A_c$  corresponding to the off-state. The bang-bang trigger will change state twice in a cycle since the carrier wave is triangular. The pulse width is equal to the times during the value  $e(t)$  is bigger than the bang-bang trigger threshold. Thus, the frequency of the pulse generated is the same as the carrier wave and its amplitude is constant.

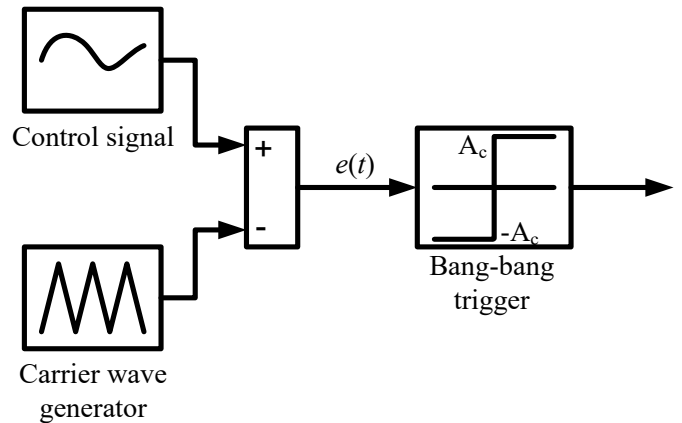


Figure 5. The mechanisms to implement PWM

Figure 6 describes in detail of mechanism to implement a modulated pulse with a triangular carrier wave  $r(t)$ , the bang-bang trigger threshold, in that case, is equal zero, where  $T_c$  and  $2A_r$  are called the period and amplitude of carrier wave  $r(t)$ , respectively.

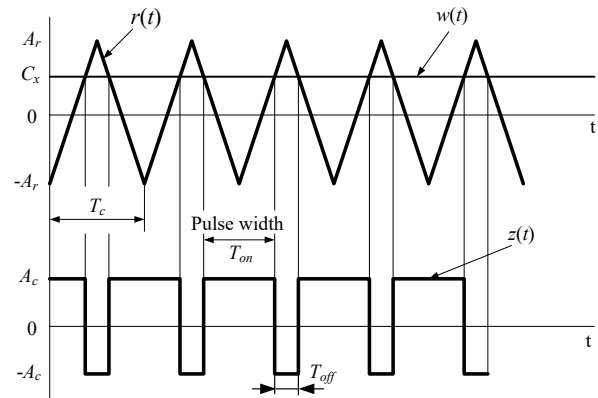


Figure 6. A mechanism implement of the modulated pulse

If the input values are constant then the mean time of output value is given by [13]:

$$\overline{z(t)} = \frac{A_c}{A_r} C_x = \frac{A_c}{A_r} \overline{w(t)} \quad (3)$$

where  $\overline{z(t)}$  is the mean time of  $z(t)$ , and  $\overline{w(t)}$  is the mean time of  $w(t)$  for the period of  $T_c$ .

Equation (3) reveals that the mean time of the PWM output is proportional to the  $\overline{w(t)}$  because the ratio  $A_c/A_r$  is a constant and it does not depend on time. In other words, the pulse width is directly proportional to the control signal amplitude.



$T_{on}$  is called the on-time or PW and it is the time required for the bang-bang trigger output moves from value  $A_c$  to  $-A_c$ . Otherwise, the time required for the bang-bang trigger output moves from  $-A_c$  to  $A_c$  called the off-time,  $T_{off}$ . The duty cycle (DC) of the PW modulated is equal the percentage of the on-time to the period and is presented by [13]:

$$DC = \frac{T_{on}}{T_{on}+T_{off}} \% \quad (4)$$

Equation (3) also reveals that the output  $\bar{z}(t)$  is approximately proportional to the  $\bar{w}(t)$ , therefore, if the input signal  $w(t)$  is a time varying then the frequency of input signal  $w(t)$  must be large enough to obtain the almost constant value of output  $\bar{z}(t)$  [20].

In this paper, the controller that combines PID (proportional-integral-derivative) and PWM are used to control the displacement of suspended object in the contactless electrostatic suspension system because this combination provides many advantages such as robust against disturbances and easily implemented. The idea is using PID controlling the PWM duty cycle. PID is well-known controller, and it is widely applied in many process control. This controller includes of three control terms that are proportional, integral and derivative term. The proportional term ( $K_p$ ) provides an control action proportional to the error signal. The integral term ( $K_I$ ) effects on the steady-state errors. The derivative term ( $K_D$ ) effects on the transient response [24].

The proper value of duty cycle is determined by PWM-PID controller as [16]:

$$DC = \frac{T_c DC\%}{100} \quad (5)$$

where  $DC\% = K_p e + K_D \dot{e} + K_I \int e dt$ ,  $e$  is the error between the current position of suspended object and reference position.

The suspension system with 3 d.o.f is illustrated in Fig. 7. The suspended object is levitated by three independent stator electrodes. Each pair of electrode ( $E_{1p}, E_{1n}$ ), ( $E_{2p}, E_{2n}$ ) and ( $E_{3p}, E_{3n}$ ) is supplied by control voltage accordingly to the corresponding sensor signals. The PWM converts the PID controller output into a pulse series between on-voltage ( $V_{ON}$ ) and off-voltage ( $V_{OFF}$ ) with a duty cycle value between 0 and 100% which is determined by Eq. (5). As a result, the electrostatic forces  $F_1, F_2$ , and  $F_3$  generated by three pair electrodes ( $E_{1p}, E_{1n}$ ), ( $E_{2p}, E_{2n}$ ) and ( $E_{3p}, E_{3n}$ ), respectively, are controlled.

#### 4. Simulations and Experimental results

The suspended object (4-inch silicon wafer) with a radius of 50 mm, the thickness of 0.71 mm, and a mass of 9.1 g is used. The suspended gap is 320  $\mu\text{m}$ , and the initial position of silicon wafer is set at 350  $\mu\text{m}$ . Based on Eq. (2), the bias voltage is calculated as  $V_0 = 480$  V.

Therefore, the on-voltage (charged voltage)  $V_{ON}$  should be bigger than the bias voltage, was set at  $V_{ON} = V_0 + 50\%V_0$ , i.e. 780 V, the off-voltage (discharged voltage)  $V_{OFF}$  was 0 V. The controller was implemented digitally in dSPACE system and three optical fiber position sensors used to measure the gap length

(Model PM-E, Nanotex Co.). Figure 8 presents the control block diagram for the suspension system.

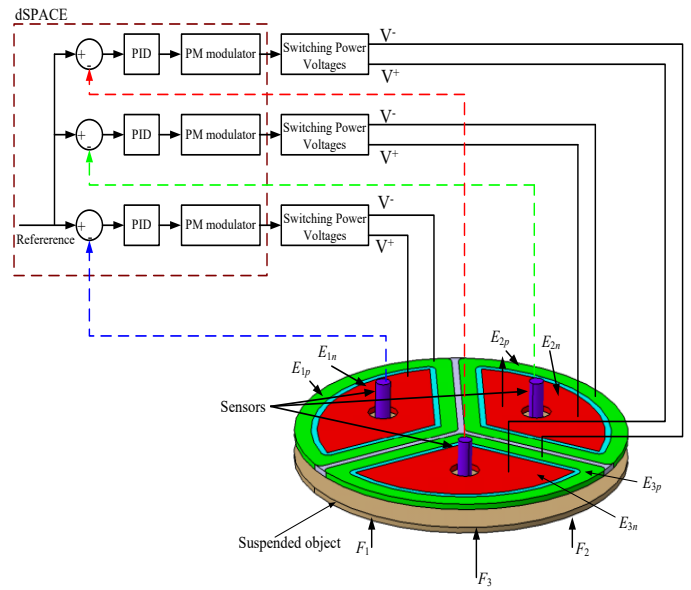


Figure 7. Control system of the 3 d.o.f electrostatic suspension system

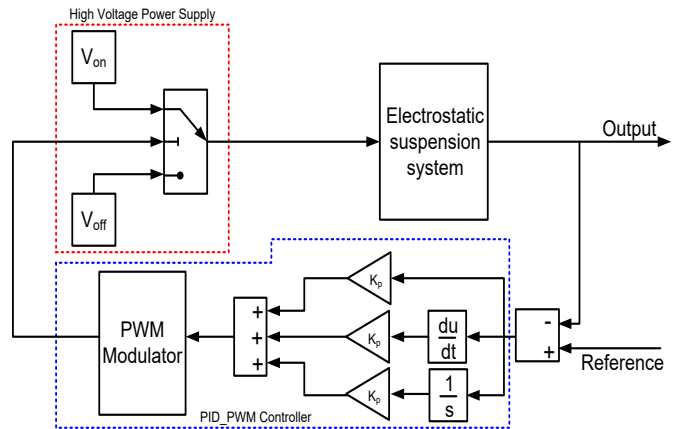


Figure 8. The PID-PWM control diagram for the suspension system

The gains of PID controller strongly influences on the performance of suspended object. Simulations are implemented to obtain the optimal values of the PID gains [24]. The simulation results in Fig. 9 reveal that steady state error reduced when PID gains are increased. The set of parameters of PID gains  $K_p = 10e30$ ,  $K_D = 2000$  and  $K_I = 12e23$  is chosen to apply in experiments.

Figure 10 shows a response plot performed experimentally. The object is suspended at a reference position with an amplitude of oscillation at the electrodes #1, #2 and #3 are around 0.9  $\mu\text{m}$ , 1  $\mu\text{m}$  and 1.2  $\mu\text{m}$ , respectively. It is observed in Fig. 10 that the oscillation is very small. Figure 11 shows the applied voltages to electrodes during the suspension process.

Several electrostatic systems successfully apply the on-off controller to control the position suspended object such as simple on-off controller [7], delay controller [25], variable structure controller [8].

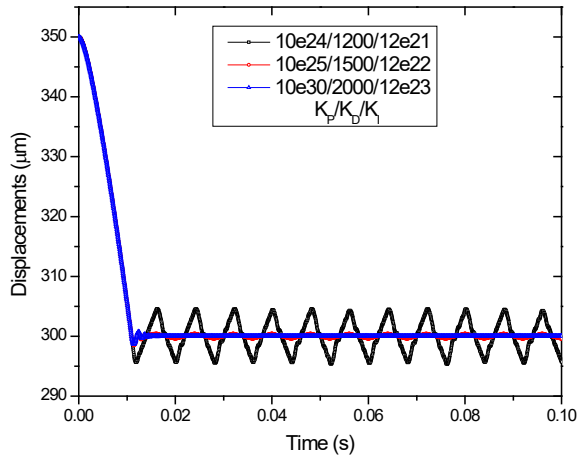
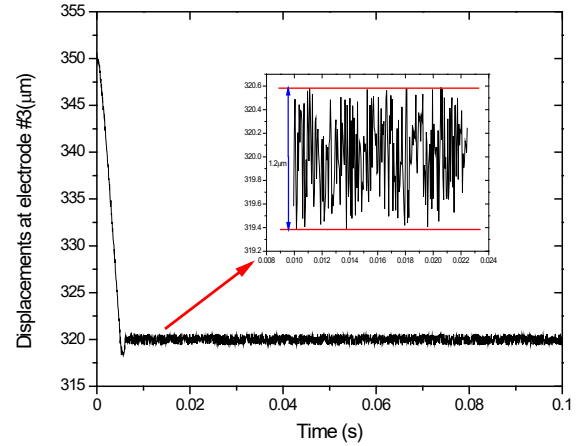
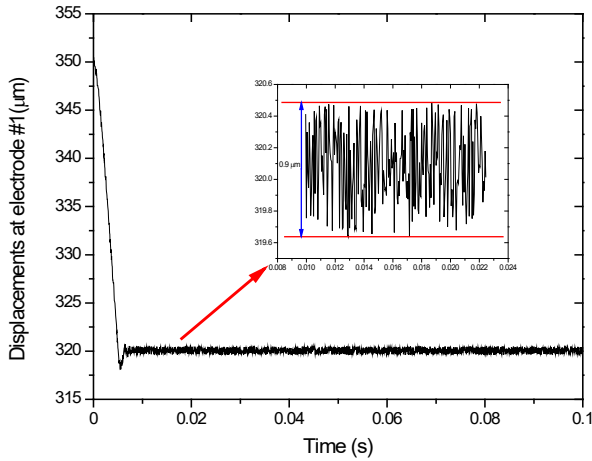


Figure 9. Simulation results of suspension

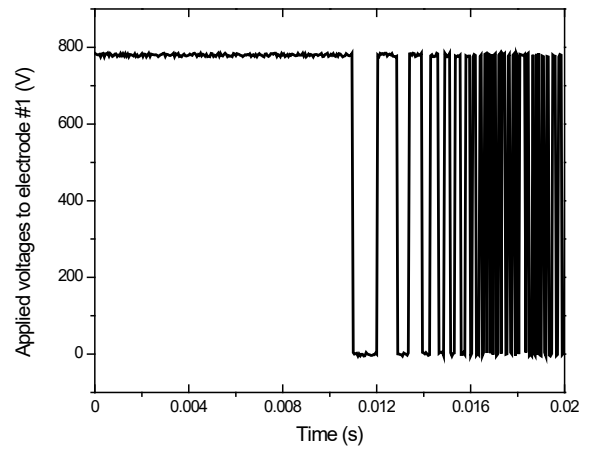


c) Displacements at electrode #3

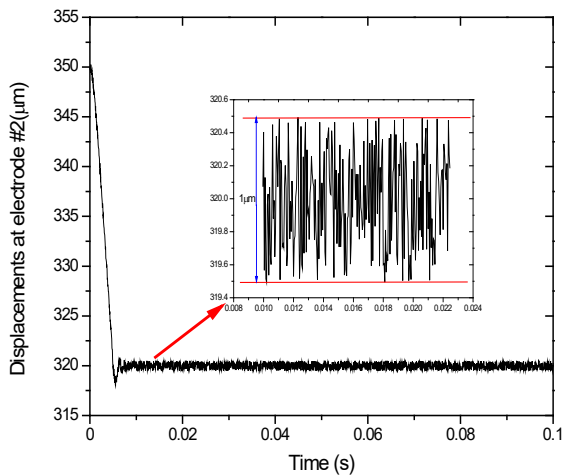
Figure 10. Displacements of the 4-inch silicon wafer during the suspension process



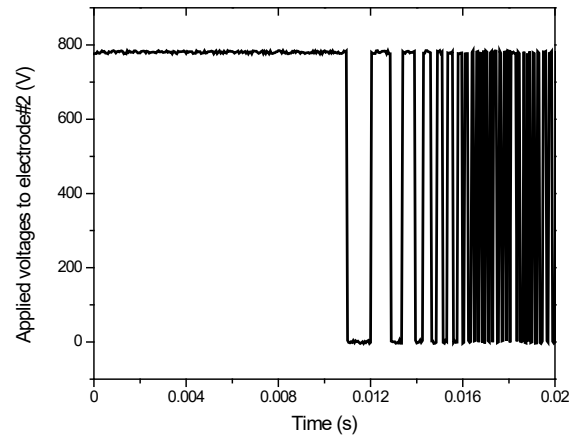
a) Displacements at electrode #1



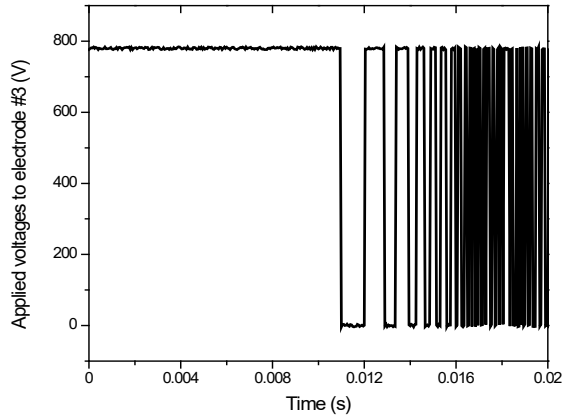
a) Applied voltage to electrode #1



b) Displacements at electrode #2



b) Applied voltage to electrode #2



c) Applied voltage to electrode #3

Figure 11. Applied voltages to electrodes during the suspension process.

Each of the above controllers has its advantages in each specific case. However, considering the parameters of the amplitude of oscillation, the PID-PWM controller has advantages compared to the remaining on-off controller. Comparison data of on-off controllers are presented in Table 1. The comparison shows that the electrostatic suspension system using PID- PWM controller provides a very good response with very small fluctuations of the suspended object.

Table 1: The amplitude of oscillation of several on-off controller

Type of controller	Amplitude of oscillation
Simple on-off	~ 6.5 μm
Delay controller	~ 4.5 μm
Variable structure controller	~ 2.3 μm
PID-PWM controller	~ 0.9 μm

**Conclusion**

This paper presents an electrostatic suspension system using PID-PWM controller. Simulation and experimental results reveal the effectiveness of this electrostatic suspension system. Application of pulse width modulation in electrostatic suspension system makes possible the use of inexpensive switching power amplifier instead of linear analogue power amplifier employed in previous systems, therefore, the system cost is reduced.

**Conflict of Interest**

The authors declare no conflict of interest.

**Acknowledgment**

The authors are very grateful for the support received from the University of Ulsan and Ho Chi Minh City University of Food Industry for this project.

**References**

[1] J. U. Jeon, J. Jin and T. Higuchi, “Electrostatic suspension of 8-inch Silicon wafer,” Proc. Inst. Electrosta. Japan, vol. 21, no. 2, pp. 62-68, 1997.  
 [2] J. Jin, T. C. Yih, T. Higuchi and J. U. Jeon, “Direct Electrostatic Levitation and Propulsion of Silicon Wafer,” IEEE Trans. Industry Applications, vol. 34,

no. 5, pp. 975-984, 1998. DOI: 10.1109/28.720437  
 [3] J. Jin, T. Higuchi, and M. Kanemoto, “Electrostatic levitator for Hard Disk Media,” IEEE Trans. Industrial Electronics, vol. 44, no. 5, pp. 467 - 473, 1995. DOI: 10.1109/41.466330  
 [4] J. U. Jeon and T. Higuchi, “Electrostatic suspension of Dielectrics,” IEEE Trans. Industry Electronics, vol. 45, no. 6, pp. 938-946, 1998. DOI: 10.1109/41.735338  
 [5] J. Jin and T. Higuchi, “Direct Electrostatic Levitation and Propulsion,” IEEE Trans. Industrial Electronics, vol. 44, no. 2, pp. 234-239, 1997. DOI: 10.1109/41.564162  
 [6] E. West, A. Yamanoto and T. Higuchi, “Transportation of Hard Disk Media Using Electrostatic Levitation and Tilt Control,” IEEE Int. Conf. Robotics (ICRA), Pasadena, USA, pp. 755-760, 2008. DOI: 10.1109/ROBOT.2008.4543296  
 [7] J. U. Jeon and S. Lee, “Electrostatic suspension system of silicon wafer using relay feedback control,” J. Korean society of Precision Engineering, vol. 22, no. 10, 56-64, 2005.  
 [8] T. Le, “A variable structure controller for a cost-effective electrostatic suspension system,” Transactions of the Institute of Measurement and Control, vol. 41, no. 2, 2019. https://doi.org/10.1177/0142331219826663  
 [9] R. N. Clark and G. F. Franklin, “Limit cycle oscillations in pulse modulated systems,” J. Spacecr. Rockets vol. 6, pp. 799–804, 1969. https://doi.org/10.2514/3.29704  
 [10] A. Kempski, R. Strzelcki, R. Smolenski and Z. Fedyczak Z, “Bearing current path and pulse rate in PWM-inverter-fed induction,” 2001 IEEE 32nd Annual Power Electronics Specialists Conf. (Vancouver, Canada) vol. 4 (Piscataway, NJ: IEEE) pp. 2025–2030, 2001. DOI: 10.1109/PESC.2001.954419  
 [11] T. C. Anthony, B. Wei and S. Carroll, “Pulse-modulated control synthesis for a flexible spacecraft,” J. Guid. Control Dyn. Vol. 13, no. 6, pp. 1014–22, 1990. https://doi.org/10.2514/3.20574  
 [12] L. Petrua and G. Mazenb, “ PWM Control of a DC Motor Used to Drive a Conveyor Belt,” Procedia Engineering, vol. 100, pp. 299 – 304, 2015. doi: 10.1016/j.proeng.2015.01.371  
 [13] M. Shih and M. Ma, “Position control of a pneumatic cylinder using fuzzy PWM control method,” Mechatronics, vol. 8, pp. 241–53, 1998. https://doi.org/10.1016/S0957-4158(98)00005-1  
 [14] M. M. Gade and K. K. Mangrulkar, “Modeling and PWM Control of Electro-Pneumatic Actuator for Missile Applications,” IFAC PapersOnLine vol. 51, no.1, pp. 237–242, 2018. https://doi.org/10.1016/j.ifacol.2018.05.057  
 [15] N. Ma and G. Song, “Control of shape memory alloy actuator using pulse width modulation,” Smart. Mater. Struct., vol. 12, pp. 712–719, 2003. https://doi.org/10.1088/0964-1726/12/5/007  
 [16] J. Ko, M. B. Jun, G. Gilardi, E. Haslam and E. J. Park, “ Fuzzy PWM-PID control of cocontracting antagonistic shape memory alloy muscle pairs in an artificial finger,” Mechatronics, vol. 21, pp. 1190–1202, 2011. https://doi.org/10.1016/j.mechatronics.2011.07.003  
 [17] S. A. Moezi, M. Rafeeyan, E. Zakeri and A. Zare, “Simulation and experimental control of a 3-RPR parallel robot using optimal fuzzy controller and fast on/off solenoid valves based on the PWM wave,” ISA Transactions, vol. 61, pp. 265-286, 2016.  
 [18] M. Pipan and N. Herakovic, “Closed-loop volume flow control algorithm for fast switching pneumatic valves with PWM signal,” Control Engineering Practice, vol. 70, pp. 114-120, 2018. https://doi.org/10.1016/j.conengprac.2017.10.008  
 [19] B. Zhang, Q. Zhong, Ji Ma, H. Hong, H. Bao, Y. Shi and H. Yang, “Self-correcting PWM control for dynamic performance preservation in high speed on/off valve,” Mechatronics 55 (2018) 141-150. https://doi.org/10.1016/j.mechatronics.2018.09.001  
 [20] Y. Peng, Y. J. Zhang, D. T. Liu and L. S. Liu, “ Degradation estimation using feature increment stepwise linear regression for PWM Inverter of Electro-Mechanical Actuator Microelectronics,” Reliability, vol. 88–90, pp. 514–518, 2018. https://doi.org/10.1016/j.microrel.2018.06.025  
 [21] Y. Zhao and B. Jones, “Pulse width modulated reinforced piezo air jet actuators,” Mechatronics, vol. 7, no. 1, pp. 11-25, 1997. https://doi.org/10.1016/S0957-4158(96)00040-2  
 [22] T. T. Le, J. U. Jeon1, S. J. Woo and T. Higuchi, “An electrostatic suspension system using piezoelectric actuators,” Smart Mater. Struct., vol. 21 (2012) 025012 (8pp).  
 [23] T. T. Le and J. U. Jeon, “Stability analysis of a time-optimally controlled electrostatic suspension system and suspension experiments in a vacuum,” Proc. IMechE Part C: J. Mechanical Engineering Science, vol. 225, pp. 88-100, 2010. https://doi.org/10.1243/09544062JMES1925

- [24] K. H. Ang and G. Chong, "PID Control System Analysis, Design, and Technology," IEEE Transactions on control systems technology, vol. 13, no. 4, pp. 556-576, 2005.  
DOI: 10.1109/TCST.2005.847331
- [25] T. T. Le and J. U. Jeon, "Time Delay Effects on Performance and Stability of a Low Cost Electrostatic Suspension System," International journal of precision engineering and manufacturing, vol. 11, no. 4, pp. 549-557, 2011.  
<https://doi.org/10.1007/s12541-010-0063-7>



## System of Sequential D-Optimal Identification for Dynamic Objects in Real-Time Scale

Fatuev Victor\*, Mishin Anton

Department of Computer Technology, Tula state university, 300012, Russia

### ARTICLE INFO

Article history:

Received: 14 January, 2020

Accepted: 06 March, 2020

Online: 13 March, 2020

Keywords:

D-optimal identification

real time scale

estimation of unknown

parameters

technical complex

synthesis of the testing signal

### ABSTRACT

The article is devoted to the formalization and development of the theory of sequential experimental design for optimal identification of dynamic objects. The algorithmic and technical support for a system of sequential D-optimal identification for a wide class of dynamic objects in real time is considered. This system is universal and can be used for optimal identification of real objects and continuous technological processes.

## 1. Introduction

This paper is an extension of work originally presented in 8th Mediterranean Conference on Embedded Computing (MECO) [1].

The construction of adequate models of the dynamic objects under study is an important step in solving any applied task. With a known or given structure of the dynamics model, the problem of experimental statistical parametric identification is usually solved. The quality of the resulting dynamic regression model (DRM) is determined by the probabilistic properties of the estimates for the unknown model parameters and its predictive properties.

If active influence at the input of the object is allowed, then the optimal parametric identification task can be formulated and solved, the purpose of which is to obtain an optimal dynamic regression model that satisfies the selected criterion.

The most universal optimality criteria used in the design of the experiment are the equivalent D- and G-optimality criteria, which simultaneously minimize the generalized variance of estimates for unknown model parameters and the maximum in terms of planning space variance of the output prediction according to the regression model [2-5].

When constructing dynamics models satisfying these criteria, it becomes necessary to formalize and solve additional problems:

- synthesis of optimal test signals [1, 4-11];

- technical implementation of optimal identification procedures in real time, which is especially important.

As a rule, DRMs have a nonlinearly parameterized structure. Therefore, their optimal identification is possible on the basis of the theory of sequential design of the experiment [2, 3], adapted to the problems of dynamics. Based on this theory, an original procedure of sequential D-optimal identification (DPPI) [1, 5-9] was developed, which allows us to study a wide class of linear and nonlinear dynamic objects described by input-output models and state spaces. Thus, the scientific novelty of this study lies in the development for the classical theory of experimental design and the development of methodology. Algorithmic and technical support of the original real-time control systems with optimal identifying studies of a wide class of dynamic objects.

## 2. Short description of DPPI

Let's Consider the class of dynamic objects described by regression models, represented in the form:

$$Y(n\Delta t) = \Phi(\vec{A}, \vec{U}) + e(n\Delta t),$$

where  $\vec{A}$  - is the vector of unknown parameters of the dynamic regression model;  $Y(n\Delta t)$  - discrete value of the output of the object.

As the factors of planning discrete values of input signal are accepted:

\*Fatuev Victor, Tula, Russia, +7(960) 597 74 46 vfatuev@inbox.ru

$$\vec{U}^T = (u((n-1)\Delta t), u((n-2)\Delta t), \dots, u((n-l)\Delta t))$$

DPPI is implemented in real time as follows.

At the time of starting the system, an arbitrary non-degenerate "seed" test signal is supplied to the input of the identifiable object through the actuator, the implementation of which determines the initial NLSM estimate of the vector of unknown model parameters and its covariance matrix. These data are used in planning the first stage of the procedure. When planning the next stage, the NLSM estimation and its covariance matrix are used, obtained from the results of all previous stages, including "seed" testing. The planning goal is to synthesize a part of the local D-optimal plan, which implies one or more planned exit measurements at the planned stage of the procedure. The choice of the number of planned measurements of the output is carried out on the basis of effectiveness criterion for the implementation of the procedure, taking into account the cost per unit of testing time, the cost of one measurement of the output, as well as the sensitivity function of the dispersion function of the DRM to estimates of unknown model parameters.

Each point of the plan corresponds to a piece of piecewise-constant testing signal, which must be implemented at the input of the object before the moment of the planned measurement of the output. The continuity of the test signal is ensured by "sewing" sections on  $\gamma_i$  clock cycles according to the algorithm:

$$u_i((n-l+j)\Delta t) = u_{i-1}((n-\gamma_i+j)\Delta t), i=1,2,3,\dots; j=0,1,\dots,(\gamma_i-1),$$

where  $i$  – is the number of the sector.

If it is more efficient to plan several exit measurements at the stages of DPPI, then the synthesis of part of the local D-optimal plan implemented at the  $(N+1)$  - th stage is carried out according to the algorithm:

$$\begin{aligned} \vec{U}_{N+1,i} &= \arg \max_{\vec{U} \in U_0} \nabla \Phi^T(\hat{A}_N, \vec{U}) \text{cov}(\hat{A}_{N,i-1}) \nabla \Phi(\hat{A}_N, \vec{U}) \\ \text{cov}(\hat{A}_{N,i}) &= \left( I - \frac{\text{cov}(\hat{A}_{N,i-1}) \nabla \Phi(\hat{A}_N, \vec{U}_{N+1,i}) \nabla \Phi^T(\hat{A}_N, \vec{U}_{N+1,i})}{\sigma_e^2 + \nabla \Phi^T(\hat{A}_N, \vec{U}_{N+1,i}) \text{cov}(\hat{A}_{N,i-1}) \nabla \Phi(\hat{A}_N, \vec{U}_{N+1,i})} \right) \times \\ &\times \text{cov}(\hat{A}_{N,i-1}) \end{aligned}$$

where  $\vec{U}_{N+1,i}$  - is  $i$ -th point of the part of the local D-optimum plan, defining  $(N+1)$ -th stage of DPPI;  $\text{cov}(\hat{A}_{N,i})$  - covariance matrix of vector  $\hat{A}_N$ , if to specify it due to the results of  $i$  planned measurements of the output on  $(N+1)$ -th stage.

The implementation of DPPI ends at the stage in the planning of which the difference between the locally optimal plan synthesized in parts and the D-optimal one will become insignificant:

$$\left\| \max_{\vec{U} \in U_0} \nabla \Phi^T(\hat{A}_N, \vec{U}) \text{cov}(\hat{A}_N) \nabla \Phi(\hat{A}_N, \vec{U}) - \frac{q}{N} \sigma_e^2 \right\| < \varepsilon,$$

where  $q$  – is the number of unknown parameters of model;  $\sigma_e^2$  - is dispersion of random output component;  $\varepsilon$  – a priori set small value.

Planning for the next stage begins from the moment the previous stage is completed. Therefore, it is relevant to minimize the planning time, which depends on the characteristics of the optimization and estimation algorithms used, as well as using the sequence of implementation for the plan points when constructing the test signal, taking into account the need for its level to remain constant over the planning interval.

A detailed algorithm for the implementation of DPPI is given in [1].

### 3. Description of the system architecture

A DPPI implementing system should consist of the following elements:

- Calculation Computer;
- programmable logic controller (PLC);
- sensors for measuring the output parameters of the identified object;
- actuators for realization of test signals.

The main functions implemented by the computer calculation computer [3-6,11]:

- planning of the DPPI stages;
- determination of discrete values for sections of minimum length testing signals and moments of planned output measurements.
- control of time instants for planned output measurements. At times when it is required to take data, the calculator issues a request for the programmable controller. It is supposed to use Ethernet as a communication port.

Functions implemented by the PLC:

- data collection from sensors of identifiable object output variables at planned time points;
- transfer of this data to the calculation computer for subsequent registration and processing. A diagram of the computing complex for solving problems of D-optimal sequential identification in real time is shown in [1]

The block diagram of a system of D-optimal sequential identification in real time is given in [1].

### 4. Calculation Computer

The software of the calculation computer implements 4 processes:

- the process of implementing the procedure of sequential D-optimal identification.
- the process of data requesting from the PLC;
- process of creating a control signal for actuator;
- scheduling process.

At each stage of the D-optimal identification procedure, the time moments of the change in the signal levels of the control action determining the piecewise-constant testing signal, and the

moments of requesting data from the output of the object are determined, which leads to the execution of processes 2 and 3.

The process of requesting data from the PLC occurs according to the following algorithm. At times when it is necessary to request data from the PLC, the software of calculation computer transfers the high execution priority to this process. A data request begins. After sending the request, the program will wait for a response of 100 ms. If no response is received, another request will be made. After 3 failed exchanges in a row, the program will end with an error. If the data was received, they will be written to shared memory [12] for process of sequential D-optimal identification. After completing this process, the software will block it until the next moment in time for requesting data from the PLC.

Exchange with the PLC will occur via Modbus TCP protocol. This is a modification of the MODBUS protocol for working in top/ip networks. Modbus is based on the Master-Slave architecture, where in this case the calculation computer will be the master, and the PLC will be the slave responding to requests.

The process of creating a control signal for actuators operates as follows. At times when it is necessary to change the testing signal, execution priority will be given to this process. A signal will be sent to the control device. After completing this process, the software will block it until the next moment in time of changing the level of the test signal.

During the operation of the software, it may turn out that the execution times of processes 2 and 3 may coincide, which may lead to the fact that one of these processes will not be completed in time. To eliminate this, process execution is spaced on different processor cores.

Fig. 1 shows how priorities are allocated and, accordingly, when the implementation of the corresponding process begins

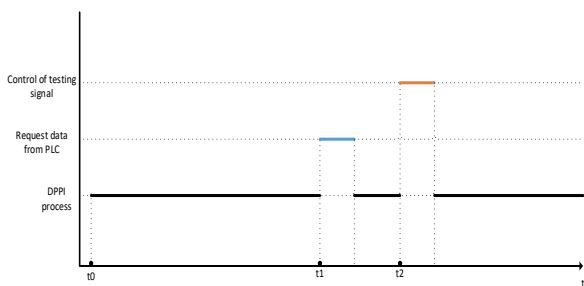


Figure 1: Prioritization of the processes of the calculation computer by time.

Fig. 1 shows that from time  $t_0$ , which is the conditional start of the software, the high priority is always given to the process of implementing the sequential D-optimal identification procedure. The time instants  $t_1$  and  $t_2$  correspond to the time instants calculated during the planning phase of the DPPI.

Due to the fact that processes must be launched at certain points in time, it is required to implement another process that will monitor the execution time of the rest - the scheduler. The reason for its creation is that the RTOSs do not have their own software timers, and standard functions can lead to time fluctuations [12,13]. That why, own software timer needed to create. By using this timer, the scheduler will issue commands to transfer control to the processes described above.

## 5. Programmable logic controller

PLC is a device that works in cycles and performs two main functions

- inputs polling;
- execution of a user program that records the data received at the inputs and further transfers this data via Ethernet to the computer at the scheduled times.

To ensure high system reliability, it is required that the PLC respond to requests from the computer with high speed. This is achieved by the fact that:

- PLC provides a high frequency of data acquisition from sensors (estimated value of 100 Hz);
- The PLC, having received a request from the calculator at the scheduled time, instantly sends the last received data to the calculator.

PLCs are equipped with both discrete and analog inputs, which allows you to take data from the corresponding sensors without the use of additional equipment, such as analog-discrete converters. Data received from the PLC to the computer will be written to the data log file.

Most PLCs, in terms of receiving information, work with the MODBUS protocol based on the Master-Slave architecture [14-16], where the master is the PLC itself, while the slaves are surveyed sensors. The master initiates exchanges by sending requests. Such exchanges can be both individual and broadcast for all slave devices. The slave device responds to a request addressed to it. Upon receipt of a broadcast request, a response by slaves is not generated.

PLC connection to the object under study depends on the sensor, with which you can measure the output parameter of interest to us. Most often, these sensors have RS-485 and RS-232 communication lines, which will require analog ports and Modbus RTU protocol. Sensors operating over the Ethernet communication line are increasingly appearing. Such devices will require an Ethernet router, and the PLC will operate using the Modbus TCP protocol. In both cases, to receive data from sensors, PLC send request with the command 0x03 - registers reading [16].

In addition, PLC can be used as actuator, thanks to the presence of discrete inputs and outputs. The control is implemented as follows: the Calculation Computer sends a discrete output write command to the PLC - 0x05; when recording a discrete output, 2 values 0 and FF are used; Having accepted the command, the PLC, depending on the setting, will create a control action. The control action can be of two types:

- By analogue output. In this case, the numerical value of the test signal will be sent to the device for changing the input parameter.  $u_1$  for 0 and  $u_2$  for FF;
- By discrete output. In this case, the PLC sends a pre-programmed value received from the calculation computer to the actuator of the object

The algorithms for data request by the calculation computer and the operation of the PLC are given in [1].

The features of the technical implementation of DPPI for the identification of the reaction process of methanol and oxygen for the production of formaldehyde are considered in [1].

The developed system is universal and can be used for optimal identification of continuous technological processes in various industries.

### Conflict of Interest

We declare there is no conflict of interest.

### Acknowledgment

TSU (Tula state university), Tula, Russian Federation.

### References

- [1] Fatuev V.A., Mishin A.A. Realization of Optimal Identification Tasks for Dynamic Systems in Real Time Scale. 2019 8th Mediterranean Conference on Embedded Computing (MECO), 2019, pp. 537-540. DOI: 10.1109/MECO.2019.8760138
- [2] Fedorov V.V. *Teoria optimalnogo experimenta* [Theory of optimal experiment], Moscow, Science, 1971, 312 p.
- [3] Krug G.K., Fatuev V.A. Synthesis of D-optimal testing signal for one class of dynamic objects. *Avtomatika i telemekhanika* [Automation and Remote Control], 1974, no. 8, pp. 73-77. (In Russia)
- [4] Krug G.K., Fatuev V.A. Synthesis of D-optimal testing signal for one class of dynamic objects. *Avtomatika i telemekhanika* [Automation and Remote Control], 1974, no. 8, pp. 73-77. (In Russia)
- [5] Fatuev V.A. *Optimalnaya identifikaciya i upravlenie dinamicheskimi sistemami. Ucheb. posobie* [Optimal identification and management of dynamic systems. Allowance]. Tula, 2019. 120 p.
- [6] Fatuev V.A., Khrapova A.G., Morozova A.N. Algorithmic ensuring realization of serial procedure D-optimal identification in real time. *Izvestiya TulGU. Tekhnicheskie nauki* [News of TSU. Technical science]. 2014, no. 11. part 2. pp. 612 – 620. (in Russia)
- [7] Fatuev V.A., Mishin A.A. Control of the experiment with optimum identification of dynamic systems in real time. 2018 7th Mediterranean Conference on Embedded Computing (MECO). 2018. pp.1-4. DOI: 10.1109/MECO.2018.8406057
- [8] Fatuev V.A., Mishin A.A. Algorithmic and technical ensuring for the implementation of the procedure for optimal identification of dynamic system in real time scale. *Izvestiya TulGU. Tekhnicheskie nauki* [News of TSU. Technical science]. 2018, no. 12. part. 2. pp. 315-323. (in Russia)
- [9] Bahvalov L.A. On a problem of input signal synthesis on the statistical identification of linear dynamic systems. *Tekhnicheskaya kibernetika* [Technical Cybernetics]. 1974, no. 3. pp. 191-196. (in Russia)
- [10] Boroduk V.P., Kirichenko A.V. Constructing the optimal input signal to identify multichannel dynamic objects. *Trudy MEI* [Works of MEI] 1975, no. 241. pp. 30 -36. (in Russia)
- [11] Oslender D.M., Ridgeley J.R., Ringenberg J.D. *Upravlayushie programmi dlya mekhanicheskikh sistem:obyektno-orientirovannoe proektirovanie sistem realnogo vremeni* [Control programs for mechanical systems: Object-oriented design of real-time systems], Moscow, 2004, 416 p.
- [12] Burdonov I.B., Kosachev A.S., Ponomarenko V.N. *Operacionnie sistemi realnogo vremeni* [Real-time operating systems], Moscow, 2006, 98 p.
- [13] Burdonov I.B., Kosachev A.S., Ponomarenko V.N. *Operacionnie sistemi realnogo vremeni* [Real-time operating systems], Moscow, 2006, 98 p.
- [14] Minaev I.G., Sharapov V.M., Samoilenko D.G. *Programmruemie logicheskie kontrolleri v avtomatizirovanih sistemah upravleniya* [Programmable logic controllers in automated control systems], Stavropol, 2010, 128 p.
- [15] Parr E. *Programmruemie kontrolleri: rukovodstvo dlya ingenera.* [Programmable Controllers: Engineer's Guide], Moscow, 2007, 516 p.
- [16] Modicon modbus protocol reference guide - North Andover, 1996 – URL: [http://modbus.org/docs/PI\\_MBUS\\_300.pdf](http://modbus.org/docs/PI_MBUS_300.pdf)



# Enhancing an SDN Architecture with DoS Attack Detection Mechanisms

Ranyelson Neres Carvalho, Lucas R. Costa\*, Jacir Luiz Bordim, Eduardo Adilo Pelinson Alchieri

Department of Computer Science - Institute of Exact Sciences - University of Brasília - 70910-900 - Brazil

## ARTICLE INFO

### Article history:

Received: 03 December, 2019

Accepted: 20 February, 2020

Online: 25 March, 2020

### Keywords:

Software Defined Network (SDN)

Denial of service (DoS)

Attack identification

OpenFlow

Entropy

Chi-square

## ABSTRACT

A Software Defined Network (SDN) architecture is characterized by decoupling the data plane and control plane. This feature enables the establishment of a programmable environment in which the control plane acts under the data plane, managing and configuring the network over a standard protocol, such as OpenFlow. Although there are numerous benefits to the SDN architecture, security is still a matter of concern, as the decoupling expands the attack surface on the network. Denial of service (DoS) attacks is one of the major challenges for the SDN architecture, mainly due to the vulnerabilities existing between the control and data planes. This paper proposes an enhancement to the SDN architecture enhanced with DoS attack detection mechanisms. Two techniques have been evaluated to identify of DoS attacks: entropy and chi-square. Both techniques use OpenFlow switches statistics so that it is possible to distinguish benign traffic from spurious traffic. Experimental results show that entropy and chi-square present similar results in terms of spurious flow detection accuracy. However, on average, chi-square requires about 14.89% fewer packets to detect the attack when compared to entropy.

## 1 Introduction

Software Defined Networks (SDN) is an upcoming network architecture that provides a more simplified and flexible way to manage a network. One of the main aspects of a SDN network is decoupling the data plane from the control plane. When this architecture is employed, the control plane is responsible for managing the entire network through operational decisions, coordinating and adding new functionalities. While the data plane is classified as the network infrastructure and its tasks are routing, dropping packets on the network, as well as transmitting information regarding packets to the control plane. The communication between the two planes (control and data plane) is carried out through a protocol. The most widely used protocol is OpenFlow, which is characterized as a generic method of communication between the controller (control plane) and switches (data plane) [1]. Despite the numerous benefits provided by an SDN architecture, network security is still a matter of concern [2]. Decoupling the two planes presents new challenges to network security, since in conventional networks, security mechanisms are often defined through a combination of configurations between both planes [3].

Denial of Service (DoS) attacks are one of the major challenges for a SDN network, mainly due to the vulnerabilities present in the communication between the two planes [4]. In this architecture, the main goals of a DoS attack are to exhaust the controller's process-

ing capacity or reduce the bandwidth of an application, which is usually accomplished by generating large volumes of traffic through multiple hosts with spoofed addresses [5].

DoS attack detection has been broadly researched in traditional networks, where most of the proposed works employ knowledge-based methods, as can be seen in [6, 7, 8]. However, the use of statistical methods or machine learning also proves to be effective for detecting a DoS attack. Such methods are commonly used in the literature to identify deviations in traffic behavior patterns, presenting high accuracy for this purpose. In [9], for example, the authors suggested a scheme based on machine learning to detect DoS attacks in conventional networks, where they propose a neural network designed to classify legitimate from spurious traffic.

In contrast to the aforementioned works, this article proposes a DoS attack detection mechanism in SDN. In addition, this paper proposes an enhancement to the SDN architecture with a mechanism that works alongside the controller to detect DoS attacks. Two techniques are evaluated to detect DoS attacks: **entropy** [10] and **chi-square** [11]. In the OpenFlow protocol, the controller can collect information about the switches to calculate statistics. These values are used to differentiate spurious traffic from legitimate traffic. The main contributions of this paper are a mechanism that allows the definition of an adaptive detection threshold that may reflect optimal network behavior and the use of different OpenFlow protocol header fields to characterize DoS traffic. Among its features, the

\*Corresponding Author: Lucas Rodrigues Costa, Campus Darcy Ribeiro. Asa Norte, Brasília, DF - 70910-900 - Brazil, lucasrc.rodri@gmail.com

proposed mechanism encompasses the following characteristics:

1. the implementation resides at the control plane SDN, allowing it to obtain data from the whole network with greater precision, instead of a specific switch as used in a conventional network;
2. development of a mechanism to detect DoS attacks using OpenFlow switches statistics, thus enabling the use of different OpenFlow protocol header fields to characterize DoS traffic.

Experimental evaluation of the proposed solutions indicates that the entropy-based mechanism is slightly more accurate in identifying spurious flow at the cost of requiring a larger number of packets to detect attack compared to the chi-square-based mechanism.

The remainder of this paper is structured as follows. Section 2 introduces the SDN concepts. Section 3 presents how SDN DoS attacks work and how chi-square-based and entropy-based attack detection mechanisms work. Section 4 presents the anomaly detection techniques (entropy and chi-square) and how they can be used to detect DoS attacks. In Section 5 presents a brief overview of the related works. Section 6 introduces the proposed detection method applied to an SDN. Finally, Section 7 presents the simulation results, followed by the conclusion in Section 8.

## 2 Software Defined Networks and OpenFlow

The OpenFlow protocol is known as one of the first standards for Software Defined Networks (SDN), it enables communication between data planes and switch. It also allows the management of the query table used by the hardware to specify the next step of each received packet. There is a logical division between the data and control layers (a.k.a. planes), which establishes a programmable environment [1]. The planes that make up the SDN architecture are depicted in Figure 1.

The application layer consists of SDN applications for high-level management of network resources and support of the control layer below. The north interface is used for establishing the communication between the application layer and the control layer [12]. The control layer is in charge of programming and managing the data plane. It is composed of controllers that use the data obtained by the data layer and establishes all the procedures and actions to be performed by the network infrastructure [13].

The infrastructure layer (data plane) is made up of forwarding devices (switches and routers). This layer is responsible for local information monitoring and statistical collection [1]. The south interface is responsible for the communication between data layer and controller [14]. The best-known interface is the OpenFlow protocol, which allows the controller to observe the flow table of the switches, in order to implement actions through a standardized interface.

The protocol architecture is composed of: (i) OpenFlow switches that form the data plane; (ii) the control plane, which includes one or more controllers; and (iii) a secure communication channel, which links the switches to the control layer. An OpenFlow

switch consists of a flow table and a secure communication channel. The flow table is formed by a set of input flows in which each input has an associated behavior, such as discarding, forwarding and sending the packet to the controller. This table is formed by actions, rules and counters. The rules are constituted from one or more header fields and correlated to a set of actions, which specify how the packets will be processed. The counters store statistics for switch flows, such as bytes received and transmitted, number of packets and the elapsed time since the flow was inserted into the switch. This feature allows the collection of statistics that can be used for specific purposes, such as detecting network anomalies, estimating the delay and so on. The collection of statistics can be achieved with a flow or a group of flows. The secure communication channel is the path used to transport information between the controller and the switch and vice versa [15].

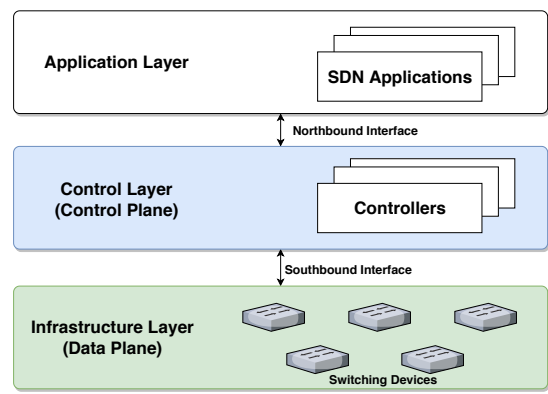


Figure 1: SDN architecture.

The packets processed by the OpenFlow switch are compared with the flow table and if a corresponding entry is found, the respective action will be taken. Otherwise, the packet will be forwarded to the control layer through the secure communication channel and the switch will wait for instructions from the controller. When receiving a packet, the controller performs the action that was previously established in its configuration for this type of flow. For example, remove or add new information from the flow table and apply the rule to the switches.

## 3 Denial of Service in SDN

A denial of service (DoS) attack on an SDN network can target both the data plane and the control plane [4]. These attacks are often known for generating excessive amounts of malicious traffic over a short period of time, in order to exhaust the resources of a victim or an infrastructure. DoS attacks are characterized by a high volume of traffic that floods the network, reducing or preventing a victim from being accessed [5]. In the data plane, this attack can deplete the flow table entries of the switches, through false streams generated by the attacker using the same source address [4]. In the control plane, the attack can cause a bottleneck in the communication channel between the controller and the switch [4]. In this situation, the attacker can exhaust the controller's processing efficiency by forwarding packets

with different headers that do not correspond to any flow already defined in the switch. This will force the switch to send control packets to the controller, since there is no rule to forward that malicious packet. DoS attacks can be even more complex when they are orchestrated in a distributed way and are known as Distributed Denial of Service (DDoS) attacks. These attacks can be even more detrimental to the network, while also increasing the complexity and the cost to defend the victim.

DoS attacks can be classified into two main groups: volumetric attacks and non-volumetric attacks (low volume or low rate) [16]. The latter covers attacks in which specific vulnerabilities of the communication protocol are exploited, causing the exhaustion of some of the victim's resources. The former, on the other hand, includes attacks where large volumes of traffic flood the victim. It aims to exhaust the victim's processing capacity or bandwidth preventing legitimate requests to reach the victim. Volumetric attacks can be further divided into direct and reflexive attacks. Direct attacks send traffic directly to the victim while reflection attacks use intermediate hosts (reflectors) to flood the victim. In this work, we restrict to SYN Flood-type attacks, characterized as a direct-volumetric attack.

The SYN Flood attack is based on sending a large number of TCP connection requests to the server, the SYN segments are sent with different source addresses, that are usually spoofed. For each SYN sent, the server must respond with a SYN-ACK segment, waiting for a confirmation message (ACK) to configure the connection. Since the source address of the SYN packet is usually false, the ACK response will never arrive because the SYN-ACK was sent to a nonexistent address. Causing TCP connections to remain in a semi-open state (SYN-RECV), where the memory resources are not released. With a large volume of false SYN segments sent, the server's TCP connection queue is flooded, causing the server to eventually crash. This, in turn results in a state in which the server cannot respond to any requests from TCP clients [17].

## 4 Anomaly Detection Techniques

Anomaly detection techniques help in identifying patterns outside the expected behavior. They can be performed through collection, filtering, and data processing.

Detection mechanisms play a key role in the DoS attack detection scenario. Beitollahi et al. [18] classifies the detection mechanisms based on the algorithm used for the detection. According to this classification, there are four groups: (i) statistical techniques; (ii) wavelets analysis; (iii) point of sequential change; and (iv) machine learning techniques. In statistical techniques, the profile of normal traffic flow is provided by the header information in the packet, which is then compared to the spurious traffic. Wavelet analysis techniques describe an input signal in terms of spectral components, which are representations of amplitudes or intensities. At the point of sequential change, filtered traffic is treated as a time series, i.e. a collection of observations made sequentially over time. Detection of a change in time is provided by evaluating all past data, where one must distinguish between two processes states: out of control or under control. Finally, machine learning techniques are capable of transforming data into intelligent actions, allowing decision-making to be performed automatically. This work focuses

on statistical techniques.

Statistical techniques analyze various properties of specific fields in packet headers during normal traffic conditions. Then, by using statistical properties, the system creates a reference model for normal traffic. When the statistical properties calculated for the traffic show differences from the reference model, it is possible to observe traffic conditions that could indicate an attack. This kind of technique uses two basic components for detection: an observation window and a detection threshold. The size of the observation window can be based on the length of time or the number of packets to be analyzed. The threshold is used to capture variations that go beyond predetermined limits. Some statistical methods, such as chi-square and entropy, can report such type of information [6] [19].

### 4.1 Chi-square (a.k.a. $\chi^2$ )

Chi-square is a measure that portrays the difference between two probability distributions. The basic principle of this method is to compare proportions, that is, the possible divergences between the frequencies observed and expected for a certain event [20]. The equation is defined as follows:

$$\chi^2 = \sum_{j=1}^m \left[ \frac{(o_j - p_j)^2}{p_j} \right], \quad (1)$$

where  $m$  is the total number of occurrences observed in a window  $w_i$ ,  $o_j$  is the observed frequency for each class and  $p_j$  is the expected frequency for that class. When the frequencies observed are very close to the expected value, the chi-square value is small. Otherwise, chi-square will assume high values.

### 4.2 Entropy

Shannon entropy [10] is a well-known and valuable concept in information theory. It measures the probability of an event occurring concerning the total number of events, through which it is possible to describe the degree of dispersion or concentration of a distribution. The equation is defined as follows:

$$H = - \sum_{j=1}^m p_j \log p_j, \quad (2)$$

where  $m$  is the number of different occurrences in an observation window  $w_i$  and  $p_j$  is the probability associated with each occurrence  $j$  in the window. In other words,  $p_j$  is the occurrence frequency of every single item divided by the total number of items. The result of this calculation varies between 0 and  $\log m$  [21]. Higher values indicates more disperse data in the distribution. Lower value indicates maximum concentration in the distribution. In other words, if the entropy is low then the randomness of the distribution is also low and vice versa.

## 5 Related Works

Research on the use of statistical methods to detect DoS attacks has grown over the years [20]. Statistical methods such as chi-square and entropy are great representatives of this class, as they present

excellent results for this purpose in traditional networks [22], [23], [7], [21].

One of the major problems with using such detection mechanisms in traditional networks is that each edge switch has only local network traffic, so it is not possible to have a global network scanning scenario. Therefore there is no mechanism that can provide a network overview. Such a limitation can make it difficult to detect an attack when it is distributed throughout the network. In addition, there is a relatively high cost of deploying the detection mechanism on each edge device that make up the network, which may become unfeasible depending on the infrastructure.

In the SDN context, there are some works that proposed the use of statistical analysis to evaluate possible changes in traffic from a DoS attack. In [24], the authors suggested a detection mechanism that uses data plane entropy from a programmable switch. The authors in [25] proposed the use of entropy in the control plane, taking advantage of the controller overview to detect traffic changes that may characterize the DoS attack. Although the mentioned works use entropy, they do not present the volume of packets necessary for the detection of the attack and other methods are not explored in the presented proposals.

This work proposes a solution for detecting DoS attacks in SDN that takes advantage of the controller's network traffic knowledge. That is, unlike traditional network approaches where each switch implements local strategies, we take advantage of the controller overview to detect anomalies. To be more specific, this paper implements and evaluates statistical DoS detection mechanisms, entropy and chi-square, which are incorporated at the controller. The details of the proposed solution are presented and evaluated in the subsequent sections.

## 6 Proposed solution to detect DoS attacks in SDN

In the SDN architecture, traffic flow monitoring and the execution of pre-established actions are performed by the control plane. The controller operates with the OpenFlow switches, exchanging information and statistical data via specific communication channels [3]. This data includes the number of bytes, the number of packets and the elapsed time that the flow was established on the switch. These can be forwarded to the controller in an organized way, through a timer, which requests the current set of data from the switch for a group of flows or a certain flow. All input streams are managed by flow tables in the switch. If a stream is not configured in its flow table, the switch sends an asynchronous message named *packet.in* to the controller. Otherwise, the stream follows the behavior determined by its flow table. This message is sent whenever there is no corresponding flow entry in the switch flow table. Thus, the controller will add a flow rule or eliminate flows from the flow table.

The use of spurious IP addresses is common in DoS attacks. In the course of an SYN Flood DoS attack, all spoofed source IP addresses target the victim's IP. In an SDN, there will be no entries in the flow tables for spoofed addresses, so the spurious flows will be forwarded to the controller via *packet.in*. If the packet rate is too high, such as in a DoS attack, the controller's resources will start to run out. In this situation, a high rate of spoofed addresses can

overload the controller. The consequence of this will be the flooding of the communication channel between the data and the control plane, making it impossible for legitimate streams to be routed to their destination. Considering that it is possible to identify a new stream in the network and that during a DoS attack, this stream will have non-standard characteristics of the normal traffic. Then it is possible to measure this divergence through techniques that detect anomalies like chi-square and entropy. These techniques can identify changes in traffic that can be characterized as a DoS attack.

To develop the DoS attack detection mechanism using statistical analysis techniques it is necessary to define four components: observed field, observation window, statistical method, and the detection threshold.

### 6.1 Observed field

The available packet header fields to be analyzed include source IP address, destination IP address, source port, destination port, packet size, and etc. It is possible to extract packet header information at runtime. Each strategy should define the field to be analyzed that allows characterizing spurious traffic from legitimate traffic during a denial of service attack.

### 6.2 Observation window

The observation window corresponds to the number of packets (window size  $L$ ) that will be analyzed by the mechanism. Within each observation window  $w_i$ , the frequency at which the field to be observed appears is computed in  $O(L^2)$  time. The probability of occurrence of the fields of interest is measured as follows:

$$p_j = \frac{o_j}{L}, \quad (3)$$

where  $o_j$ , ( $1 \leq j \leq L$ ) is defined as the frequency of the observed fields in  $w_i$ ,  $|w_i| = L$  is the number of packets in  $w_i$  and  $p_j$  is the probability of occurrence of the field observed in  $w_i$ .

### 6.3 Statistical method

The statistical method consists in applying one of the methods defined by the mechanism, chi-square (Equation 1) or entropy (Equation 2), defined as  $\delta$ , from the observed frequency ( $o_1 \dots o_j$ ) and the probability of occurrence of the field ( $p_1 \dots p_j$ ) in the window ( $w_i$ ). The calculated values are stored in a list containing the previously calculated values. These values will serve as the basis for setting the detection threshold.

### 6.4 Detection threshold

The detection threshold  $T_{w_i}$  defines the sensitivity of the proposed mechanism. The calculation of the threshold is given as:

$$T_{w_i} = \begin{cases} T_{w_i}, & i = 1 \\ T_{w_i}\alpha + (1 - \alpha)T_{w_{i-1}}, & i > 1 \end{cases} \quad (4)$$

where  $T_{w_i}$  represents the current value of the applied anomaly method calculated,  $T_{w_{i-1}}$  represents the estimated value in the previous window ( $w_{i-1}$ ) without attack and  $\alpha$  is the smoothing coefficient. The coefficient  $\alpha$  assumes values ( $0 \leq \alpha \leq 1$ ), then that the closer to 1, the greater the weight applied to recent information and the



closer to 0 the greater the weight applied to past information. In this way, the threshold can be adjusted according to the characteristics of the network to reduce the incidence of false alarms.

### 6.5 DoS Attack Detection Mechanism

Based on the components above, this work presents a new statistical DoS attack detection mechanism for an SDN architecture. Note that, unlike other works presented in the literature, the proposed strategy can adjust the DoS detection threshold limits at runtime. The proposal is presented in Algorithm 1.

---

#### Algorithm 1 DoS Attack Detection Mechanism

---

**Input:**  $T_{w_1}$ ,  $L$ ,  $\alpha$

```

1:  $i \leftarrow 2$ 
2:  $attack \leftarrow \text{"false"}$ 
3: while true do
4:    $w_i \leftarrow \{\}$ 
5:   while  $|w_i| \leq L$  do
6:      $f \leftarrow$  extract the observed field from  $packet\_in$ 
7:      $w_i \leftarrow w_i \cup \{f\}$ 
8:   end while
9:   Compute  $o_j$  and  $p_j \forall j \in w_i$ 
10:   $\delta \leftarrow StatisticalMethodResult(w_i)$ 
11:  if  $\delta > T_{w_i}$  then
12:     $T_{w_i} \leftarrow T_{w_i}\alpha + (1 - \alpha)T_{w_{i-1}}$ 
13:  end if
14:  if  $\delta > T_{w_i}$  then
15:     $attack \leftarrow \text{"true"}$ 
16:  else
17:     $attack \leftarrow \text{"false"}$ 
18:     $i \leftarrow i + 1$ 
19:  end if
20: end while

```

---

Initially, the controller receives as input the initial threshold value ( $T_{w_1}$ ), window size ( $L$ ) and smoothing coefficient ( $\alpha$ ). It is assumed that in the first window there is no attack and that the first threshold ( $T_{w_1}$ ) has already been calculated (lines 1 – 2). The controller starts a loop that always keeps analyzing all  $packet\_in$ 's (line 3). As packets enter the OpenFlow controller input queue, the controller start window as empty (line 4) and then extracts the field to be parsed by the proposed detection engine (lines 5 – 8). The parsed field corresponds to a predefined field from the available header fields in the packets. The observation window  $w_i$  is composed of these fields until they reach a predetermined size.

In this article, we employ sizes of 20, 60, and 100 packets parsed for the source IP address field, as we will see in Section 7. When the observation window is filled, that is, when  $|w_i| = L$ , the observed frequency ( $o_1 \dots o_j$ ) and the probability of occurrence ( $p_1 \dots p_j$ ), for all fields in the window ( $w_i$ ), as calculated in (line 9). With all observed frequency values and all calculated probabilities, it is possible to perform the statistical analysis defined for the detection mechanism (chi-square or entropy) in  $w_i$ , where  $\delta$  is defined (line

<sup>1</sup>The relationship between the  $\delta$  and  $T_{w_i}$  depends on the field to be analyzed. For example, if the field is the source IP, use  $\delta > T_{w_i}$ , if the field is the destination IP, use ( $\delta < T_{w_i}$ ).

10). If the variable denoting the attack is set to *false* (line 11), then the window threshold ( $T_{w_i}$ ) is updated. If the value of the statistical method is above the threshold ( $\delta > T_{w_i}$ )<sup>1</sup> the DoS attack is detected (lines 14 – 16), otherwise, it will be considered as legitimate traffic ( $attack = \text{"false"}$ ), increments  $i$  and the loop runs again.

### 6.6 Complexity Analysis

The time complexity of the proposed solution is analyzed as follows. To calculate the frequency of the observed field, it is necessary to analyze the entire observation window, of size  $m$ , for each element, so its time complexity is  $O(m^2)$ . To calculate chi-square or entropy it is necessary to calculate the number of distinct occurrences in the window. So in the worst case, we have window size  $m$ , thus  $O(m)$ . Thus, overall, the total time complexity of window detection analysis is  $O(m^2)$ .

## 7 Experiments

In order to evaluate the proposed architecture, we implemented the proposed detection model and analyzed its performance. The following sections present the experimental environment, the methodology, the metrics considered in our analysis and the results observed in the experiments.

### 7.1 Experimental Setup and Methodology

The experiments were performed using Mininet as an emulator of an SDN architecture [26]. In Mininet the switches and controllers operate under the OpenFlow protocol enabling the implementation of SDN applications. The controller used was POX, which enables rapid prototyping in the Python language to create features in the network [27]. The controller has been implemented to collect source IP addresses of new incoming packets. A function was developed for calculating packet statistics. The experiments were performed on the Ubuntu 16.04 LTS operating system, using a core i5 7400 3.0 GHz CPU with 4Gb of RAM.

The proposed detection mechanism is not influenced by the size of the network, but by the volume of packets that make up the observation window. To this end, using a network topology was considered in order to allow balancing the workload between the victim and the attacker. The topology consists of 4 OpenFlow switches, 9 hosts and 1 controller POX. The IPs range from 10.0.0.1 to 10.0.0.9, with host 10.0.0.3 being the victim server and host 10.0.0.7 the attacker. The range of spurious IPs are generated at random. The bandwidth of each link is 100 Mbps, as shown in Figure 2. The victim's host is located on the "Switch OpenFlow 2" network and the DoS attacker performs the attack from the "Switch OpenFlow 4" network.

The generation of legitimate packets is performed using the Scapy [28]. Scapy is a tool that allows creating TCP and UDP packets. The spoofed SYN packets are generated using the tool Hping [29]. This tool is used for security testing on networks operating as a packet generator for the TCP/IP protocol. Two types of

traffic were generated: normal traffic and spurious traffic. Normal traffic is used to obtain the statistical values used by the detection mechanisms of anomalies (chi-square and entropy) under normal conditions. With this, it is possible to define the detection threshold, based on Equation 4. Spurious traffic is injected to verify the behavior of the solution.

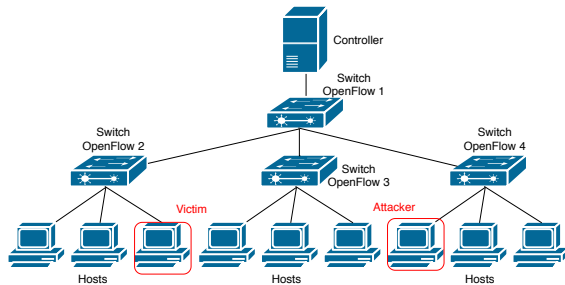


Figure 2: Network topology.

To analyze the proposed solution, SYN Flood attacks were simulated by calculating the entropy and chi-square values using source IP addresses with different observation window sizes and smoothing coefficients (threshold) to identify the attack traffic. In the experiments, 20,500 packets were considered. The observation windows had the following sizes: 20, 60 and 100 packets. The window is moved sequentially with the same number of packets from the previous window without overlap, as shown in Figure 3. The smoothing coefficients ( $\alpha$ ) evaluated were: 0.1, 0.5 and 0.9. The simulation time of each experiment was 200 s, and in the hundredth second the SYN Flood attack was started at a rate of 250 packets per second from a host belonging to the “Switch OpenFlow 2” network. The rate of legitimate packets is 5 packets per second. Five simulations of each method were performed to analyze the behavior of the solution.

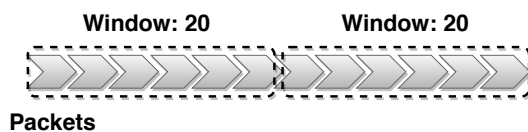


Figure 3: Moving windows

Figures 4 and 5 show the outputs of the chi-square and entropy values. Such values are obtained by Equations (1) and (2), respectively. The observed field was the source IP address, the observation windows have the size of 60 packets and the smoothing coefficient of 0.5 for the detection threshold.

The observation period shows 200 seconds of analysis, which at a rate of 250 packets per second generates about  $\approx 833$  windows of 60 packets. Before the onset of the attack, the chi-square and entropy measurements are in the range of 180 to 220 for the chi-square and 0.44 to 0.49 for the entropy for the normal traffic. During the attack, there is a considerable increase in these values in both techniques. The reason for this is that the source IP address is changed in each new packet, due to the attack characteristic, which causes the source

IP address quantities to increase substantially filling the entire observation window, causing an anomaly. In the case of the chi-square, a peak is observed at the beginning of the attack injection, but during and after the attack, the values return to a normal traffic situation. Entropy, in turn, best classifies the beginning and end of the attack, differentiating the attack period from a normal traffic situation. It is important to note that the chi-square is asymmetric, generating a peak only at the beginning of the attack, after the end of the attack there is a slight change between the observed values.

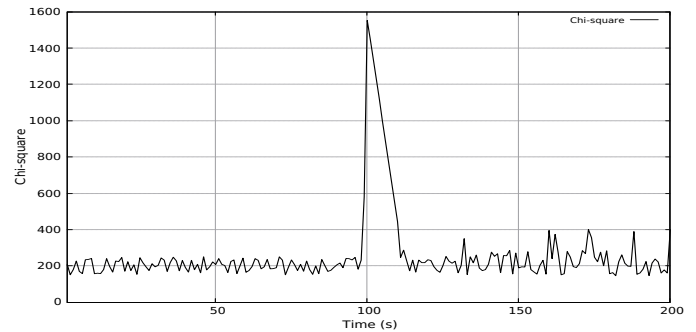


Figure 4: DoS attack identification using chi-square.

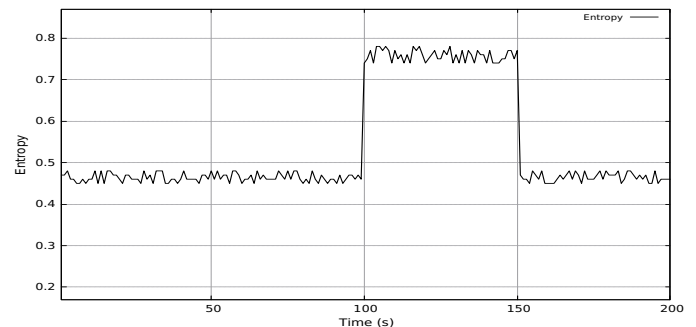


Figure 5: DoS attack identification using entropy.

It can be observed that both methods can identify anomalies in the network based on the deviation of the traffic distribution. The two methods were compared to identify which method has the highest detection rate and the lowest false alarm rate in the proposed SDN architecture model.

## 7.2 Metrics

The quality of the results was measured using a confusion matrix. Table 1 exemplifies the matrix model used. The matrix is composed of predicted values (results obtained) and actual values (expected results) of normal traffic and spurious traffic, based on the rates of false negative ( $FN$ ), false positive ( $FP$ ), true negative ( $TN$ ) and true positive ( $TP$ ).

Table 1: Confusion matrix.

Predicted	Actual	
	Attack	Normal
Attack	TP	FP
Normal	FN	TN

The *FN* rate is given by the number of packets classified as normal (negative) but that are confirmed as attack packets (positive). The *FP* rate is given by the number of packets classified as attack packets (positive) but they are confirmed as normal (negative) packets. On the other hand, *TN* rate indicates the number of packets correctly classified as legitimate (negative) and *TP* rate represents the number of packets correctly classified as attack packets (positive).

In this work, we use precision, recall and *F1*-score to evaluate the effectiveness of the proposed DoS detection mechanisms.

Precision represents the proportion of positive identifications that were correctly identified. This metric measures the quality of the results and is defined as follows:

$$\text{Precision} = \frac{TP}{TP + FP}. \tag{5}$$

Recall is the proportion of positives that have been identified correctly, measuring the completeness of the mechanism. This metric is defined as follows:

$$\text{Recall} = \frac{TP}{TP + FN}. \tag{6}$$

*F1*-score is defined as a harmonic mean between precision and recall, aiming to bring the balance between both, to indicate the overall performance of the technique. High *F1*-score values indicate that the detection technique presents more accuracy. this metric is defined as follows:

$$F1 = \frac{(2 * TP)}{(2 * TP + FP + FN)}. \tag{7}$$

### 7.3 Results

The confusion matrix for the entropy and the chi-square can be seen in Table 2 and 3, respectively. The data in the table was obtained based on the simulation results for each statistical method presented. The smoothing coefficient can be observed immediately to the left at the beginning of each method analyzed.

The smoothing coefficient plays an important role in the definition of detection thresholds since it is responsible for defining the detection sensitivity of the proposed method. Through it is possible to assign weights to the values and thus the threshold represents an exponential weighted moving average, whose latest values have more weight. A very low coefficient may leave the solution more sensitive to small variations in the values obtained, providing a higher detection, but this sensitivity may cause an increase in the *FP* rate. On the other hand, a very high coefficient provides greater freedom for the change in the values obtained and consequently a lower detection resulting and an increase in the rate of *FN*. It is therefore ideal to seek a balance for the smoothing coefficient in order to provide it with an appropriate threshold that reflects well the characteristics of the network and can reduce these rates while maintaining an acceptable level of accuracy.

The size of the window is related to the accuracy of attack detection. We can note that the larger the window, the greater the accuracy in detecting the attack, this is due to the large number of

packets that fill the window reflect in a greater representativity of the data to be observed, however this size can cause a greater consumption of resources by part of the controller and slower detection because the number of packets the solution needs to fill the window is larger. For a small window, we can observe a low precision in the results, because the observed values represent a small part of the total set to be analyzed, in contrast, we obtain a faster detection, providing a lower consumption of resources.

Considering the analyzed parameters of the smoothing coefficients and observation windows, the mechanisms had similar behaviors, although the entropy was 0.59% more accurate on average than the chi-square, due to the reduction of the *FP* and *FN* rate in both cases.

Figure 6 shows the result of the Precision. We can see that the mechanism can correctly identify spurious traffic in an acceptable way, avoiding false positives. Figure 7 shows the result of the Recall. The results show that the mechanism can effectively separate what is spurious traffic from legitimate traffic.

Figure 8 shows the result of the *F1* score. Although entropy provides higher accuracy when compared to chi-square results, it requires a larger packet volume to detect any change in traffic, which can increase detection time. For example, for the 60-packet window with a smoothing coefficient of 0.1 ( $\alpha = 0.1$ ), the entropy needed to analyze approximately 582 packets to detect the attack, the equivalent of  $\approx 10$  windows, while the chi-square needed only 478 packets, the equivalent of  $\approx 8$  windows, reducing the volume of packets evaluated by about 17%, as shown in Figure 9. This is because chi-square allows the comparison between two consecutive distributions, allowing to detect much changes faster. Unlike entropy, which represents the dispersion of several values in a given probability distribution. In summary, chi-square has reduced on average by 14.89% of the number of packets to be analyzed in the observation windows used.

It is important to note that the results presented do not take into account the attack rate, because the proposed solution focuses on analyzing the behavior of the observation windows and the sensitivity of the detection thresholds, finding the ideal balance between these components in order to meet the needs of the network operator.

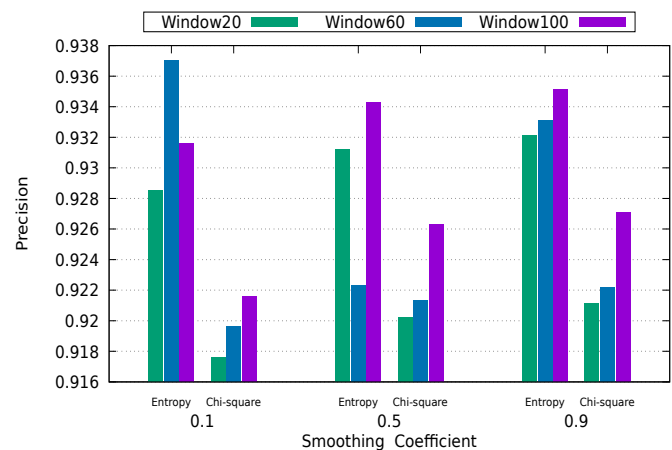


Figure 6: Precision results.

Table 2: Entropy confusion matrix.

$\alpha$	Window 20			Window 60			Window 100		
	Predicted	Actual		Predicted	Actual		Predicted	Actual	
		Attack	Normal		Attack	Normal		Attack	Normal
$\alpha = 0.1$	Attack	95.5%	8.9%	Attack	95.7%	8.6%	Attack	95.9%	8%
	Normal	4.5%	91.1%	Normal	4.3%	91.4%	Normal	4.1%	92%
$\alpha = 0.5$	Attack	95.1%	7.2%	Attack	95.5%	6.7%	Attack	95.6%	6.6%
	Normal	4.9%	92.8%	Normal	4.5%	93.3%	Normal	4.4%	93.4%
$\alpha = 0.9$	Attack	94.4%	6.6%	Attack	94.7%	6%	Attack	94.8%	5.9%
	Normal	5.6%	93.4%	Normal	5.3%	94%	Normal	5.2%	94.1%

Table 3: Chi-square confusion Matrix

$\alpha$	Window 20			Window 60			Window 100		
	Predicted	Actual		Predicted	Actual		Predicted	Actual	
		Attack	Normal		Attack	Normal		Attack	Normal
$\alpha = 0.1$	Attack	95%	9.7%	Attack	95.2%	9.6%	Attack	95.6%	9.3%
	Normal	5%	90.3%	Normal	4.8%	90.4%	Normal	4.4%	90.7%
$\alpha = 0.5$	Attack	94.7%	7.6%	Attack	95.1%	7.1%	Attack	95.3%	7%
	Normal	5.3%	92.4%	Normal	4.9%	92.9%	Normal	4.7%	93%
$\alpha = 0.9$	Attack	93.8%	6.9%	Attack	94%	6.5%	Attack	94.1%	6.3%
	Normal	6.2%	93.1%	Normal	6%	93.5%	Normal	5.9%	93.7%

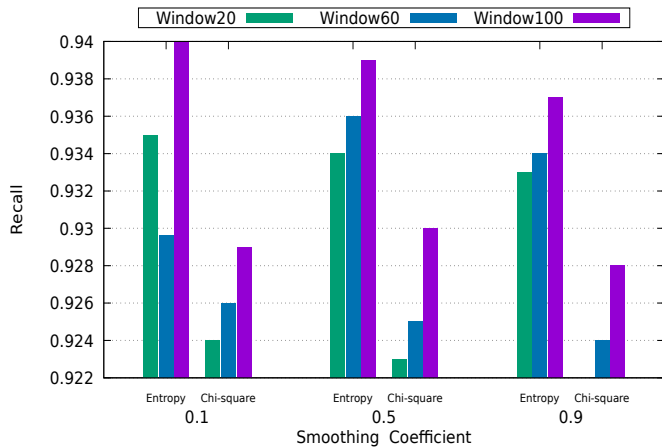


Figure 7: Recall results.

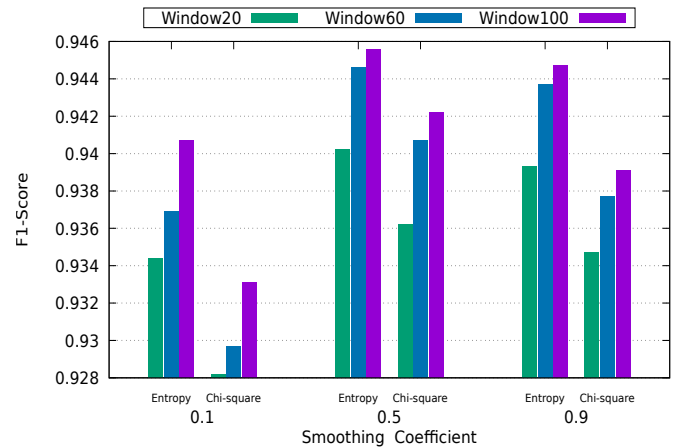


Figure 8: F1-Score results.



Finally, Figure 10 shows the result of time detection. The smoothing coefficient plays an important role in this regard as it allows manipulating the sensitivity of the mechanism which can result in faster or slower detection. For example, coefficient 0.1 provides more immediate alerts, unlike coefficient 0.9, at the cost of higher *FP* and *FN* rates. This is due to the weight of information given to the mechanism for calculating the detection threshold.

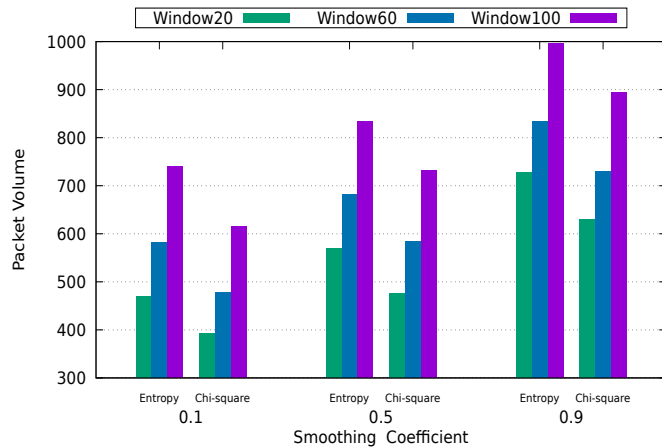


Figure 9: Packet volume.

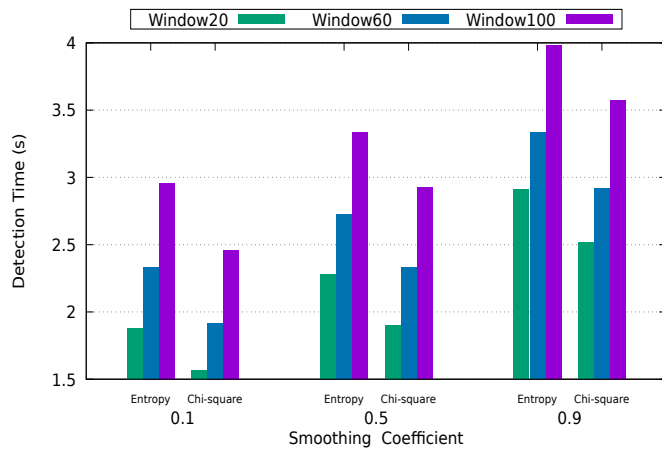


Figure 10: Detection Time.

## 8 Conclusion

This paper proposes a solution for the detection of DoS attacks based on the use of any mechanism for the detection of network anomalies. The mechanism works alongside the controller. Two techniques are evaluated for the detection of DoS attacks: entropy and chi-square. Both techniques were evaluated in terms of the rate of false positives and false negatives. From the experimental results, chi-square and entropy could detect the TCP-SYN Flood attack with an acceptable accuracy rate. The entropy was a little more accurate due to the reduction in the number of false positives and false negatives, around 0.59%, while the chi-square detects the anomaly with a smaller number of packets, on average 14.89% less entropy. One

of the main benefits of the proposed solution is its versatility. Any parameter in the solution can be changed to suit the characteristics of the network. The detection field (i.e, source IP, destination IP, source port and source port), detection threshold and window size can be configured to meet SDN requirements. As future work, we want to handle this information to establish mitigation strategies in SDN architectures under different scenarios and different attack rates.

**Conflict of Interest** The authors declare no conflict of interest.

**Acknowledgment** This work is partially supported by the MC-TIC/RNP/CTIC (Brazil) through the project P4Sec.

## References

- [1] D. Kreutz, F. Ramos, P. Verssimo, and C. Rothenberg, "Software-Defined Networking: A Comprehensive Survey," *IEEE*, 2014.
- [2] D. Kreutz, F. M. Ramos, and P. Verissimo, "Towards Secure and Dependable Software-defined Networks," in *Proceedings of the Second ACM SIGCOMM Workshop on Hot Topics in Software Defined Networking*, ser. HotSDN '13. New York, NY, USA: ACM, 2013, pp. 55–60. [Online]. Available: <http://doi.acm.org/10.1145/2491185.2491199>
- [3] A. Lara, A. Kolasani, and B. Ramamurthy, "Network innovation using open-flow: A survey," *IEEE communications surveys & tutorials*, vol. 16, no. 1, pp. 493–512, 2014.
- [4] D. M. F. M. e Otto Carlos Muniz Bandeira Duarte, "Authflow: authentication and access control mechanism for software defined networking," in *Ann. Telecommun.*, vol. 71, 12 2016, pp. 607 – 615.
- [5] F. Lau, S. H. Rubin, M. Smith, and L. Trajkovic, "Distributed denial of service attacks," vol. 3, 02 2000, pp. 2275 – 2280 vol.3.
- [6] S. Tritilanunt, S. Sivakorn, C. Juengjinchaoen, and A. Siripompisan, "Entropy-based input-output traffic mode detection scheme for DoS/DDoS attacks," in *2010 10th International Symposium on Communications and Information Technologies*, Oct 2010, pp. 804–809.
- [7] A. Bhandari and A. Sangal, "Destination Address Entropy based Detection and Traceback Approach against Distributed Denial of Service Attacks," *I. J. Computer Network and Information Security*, vol. 8, pp. 9–20, jul 2015.
- [8] K. Kurihara and K. Katagishi, "A Simple Detection Method for DoS Attacks Based on IP Packets Entropy Values," in *2014 Ninth Asia Joint Conference on Information Security*, Sep. 2014, pp. 44–51.
- [9] J. Li, Y. Liu, and L. Gu, "DDoS attack detection based on Neural Network," in *2010 2nd International Symposium on Aware Computing*, Nov 2010, pp. 196–199.
- [10] C. Shannon, "A mathematical theory of communication," vol. 27, pp. 379–423, 1948.
- [11] M. Broniatowski and S. Leorato, "An estimation method for the Neyman chi-square divergence with application to test of hypotheses," *Journal of Multivariate Analysis*, vol. 97, no. 6, pp. 1409 – 1436, 2006. [Online]. Available: <http://www.sciencedirect.com/science/article/pii/S0047259X06000194>
- [12] A. Taha, "Software-Defined Networking and its Security," 2014.
- [13] M. Casado, T. Koponen, R. Ramanathan, and S. Shenker, "Virtualizing the Network Forwarding Plane," *Workshop on Programmable Routers for Extensible Services of Tomorrow*, 2010.
- [14] N. McKeown, T. Anderson, H. Balakrishnan, G. Parulkar, L. Peterson, J. Rexford, S. Shenker, and J. Turner, "OpenFlow: Enabling Innovation in Campus Networks," *SIGCOMM Comput. Commun. Rev.*, vol. 38, no. 2, pp. 69–74, Mar. 2008.
- [15] O. N. Foundation, "Openflow switch specification 1.0," vol. 1, pp. 1–44, december 2009.
- [16] R. A. J. Gondim, "Mirror Saturation in Amplified Reflection DDoS," *JNIC-Jornadas Nacionais de Investigacin en Ciberseguridad*, 2019.
- [17] R. Bani-Hani and Z. Al-Ali, "Syn flooding attacks and countermeasures: A survey," 04 2013.

- [18] H. Beitollahi and G. Deconinck, "Analyzing well-known countermeasures against distributed denial of service attacks," *Computer Communications*, vol. 35, no. 11, pp. 1312 – 1332, 2012.
- [19] J. Tajer, A. Makke, O. Salem, and A. Mehaoua, "A comparison between divergence measures for network anomaly detection," in *7th International Conference on Network and Service Management*, 2011.
- [20] L. Feinstein, D. Schnackenberg, R. Balupari, and D. Kindred, "Statistical approaches to DDoS attack detection and response," in *Proceedings DARPA Information Survivability Conference and Exposition*, vol. 1, April 2003, pp. 303–314 vol.1.
- [21] S. Sharma, S. K. Sahu, and S. K. Jena, "On selection of attributes for entropy based detection of DDoS," in *International Conference on Advances in Computing, Communications and Informatics*, 2015.
- [22] F. Leu and C. Pai, "Detecting DoS and DDoS Attacks Using Chi-Square," in *2009 Fifth International Conference on Information Assurance and Security*, vol. 2, Aug 2009, pp. 255–258.
- [23] S. Oshima, A. Hirakawa, T. Nakashima, and T. Sueyoshi, "DoS/DDoS Detection Scheme Using Statistical Method Based on the Destination Port Number," in *2009 Fifth International Conference on Intelligent Information Hiding and Multimedia Signal Processing*, Sep. 2009, pp. 206–209.
- [24] A. C. Lapolli, J. A. Marques, and L. P. Gaspar, "Offloading Real-time DDoS Attack Detection to Programmable Data Planes," in *IFIP/IEEE International Symposium on Integrated Network Management*, 2019.
- [25] R. Carvalho, J. L. Bordim, and E. A. P. Alchieri, "Entropy-based DoS Attack identification in SDN," *21st Workshop on Advances in Parallel and Distributed Computational Models*, 2019.
- [26] M. Team, "Mininet - an instant virtual network on your laptop (or other pc)." [Online]. Available: <http://mininet.org/>
- [27] M. MC, "NOX." [Online]. Available: <https://github.com/noxrepo/pox>
- [28] Scapy, "Packet crafting for Python2 and Python3." [Online]. Available: <https://scapy.net/>
- [29] S. Sanfilippo, "Hping - Active Network Security." [Online]. Available: <http://www.hping.org/>

## A Psychovisual Optimization of Wavelet Foveation-Based Image Coding and Quality Assessment Based on Human Quality Criteria

Abderrahim Bajit<sup>\*1</sup>, Mohammed Nahid<sup>2</sup>, Ahmed Tamtaoui<sup>3</sup>, Mohammed Benbrahim<sup>1</sup>

<sup>1</sup>Ibn Toufaily University, GERST Electrical Engineering Department, National School of Applied Sciences, Kénitra, Morocco

<sup>2</sup>Mohammed V University, SC Department, INPT Institute, Rabat, Morocco

<sup>3</sup>Hassan II University, Electrical Engineering Department, Faculty of Sciences and Technologies, Mohammedia, Morocco

### ARTICLE INFO

Article history:

Received: 29 December, 2019

Accepted: 20 February, 2020

Online: 20 March, 2020

Keywords:

Discrete Wavelet Transform DWT

Psycho-visual Quality Criteria

Wavelet Foveation Filter FOV

Just Noticeable Difference JND

Contrast Threshold Elevation

Embedded Image Coder SPIHT

Objective Quality Metric FWVDP

Subjective Quality Metric

Mean Opinion Score MOS.

### ABSTRACT

In the present article, we introduce a foveation-based optimized embedded and its optimized version image coders thereafter called VOEFIC/MOEFIC and its related foveation wavelet visible difference predictor FWVDP coding quality metric. It advances a visually advanced foveal weighting mask that regulates the wavelet-based image spectrum before its encoding by the SPIHT encoder. It intends to arrive at a destined compression rate with a significant quality improvement for a disposed of binary budget, witnessing separation, and a foveal locale that locates the object in the zone of concern ROI. The coder embodies a couple of masking achieves build on the human psycho-visual quality criteria. Hence, the coder administers the foveal model to weigh the source wavelets samples, reshapes its spectrum content, adapts its shape, discards or somewhat shrinks the redundant excess and finally enhances the visual quality. The foveal weighting mask is computed indoors wavelet sub-bands as come after. First, it administers the foveal wavelet-based filter depending on the intention point so that it removes or at least reduces the imperceptible frequencies around the zone of concern. Next, it augments the picture contrast according to wavelet JND thresholds to manage brightening and nice the contrast above the distortion just notable. Once refined, the weighted wavelet spectrum will be embedded coded using the standard SPIHT to reach a desired binary bit budget. The manuscript also advances a foveation-based objective quality evaluator that embodies a psycho-visual quality criterion identified with the visual cortex framework. This investigator furnishes a foveal score FPS having the power of detecting probable errors and measuring objectively the compression quality. Keep in mind that the foveal coder VOEFIC and its visually upgraded variant MOEFIC, have similar complexity as their reference SPIHT. In contrast, their gathered data highlight the visual coding advancement and the boost ratio purchased in its quality gain.

### 1. Introduction

In multi-channel wavelet picture coding [1], psycho-visual investigations show that spatially, the goals, or examining thickness, has the most noteworthy incentive at the purpose of the fovea and descends quickly aside from that seeing point depending on the glancing angle. Therefore, when a spectator eyewitness glances at a zone in a natural picture, the locale encompassing the purpose of obsession is anticipated toward his fovea. At that point,

examined with the most noteworthy thickness and thusly saw with the most elevated differentiation affectability. Overall, the viewing thickness and contrast susceptibility diminishes significantly with expanding the glancing angle regarding the gazed point. The inspiration driving the foveal compression is that there exists significant high-recurrence data excess in the fringe districts.

In the vision, an image can capably be addressed by discarding or somewhat shrinking the redundant excess, considering the foveal point (s) and the watching space. The foveal masking plans to filter a constant resolution picture, with the end goal that when the spectator glances at his interested zone, he could not recognize

Abderrahim BAJIT, National School of Applied Sciences ENSA, Ibn Toufaily University, Kénitra Morocco, [abderrahim.bajit@gmail.com](mailto:abderrahim.bajit@gmail.com)

the unlikeness among the source picture and its foveal variant around the locale of intrigue. As illustrated in Figure .1, we administer the foveal mask to the BARBARA test picture and subjectively compare its quality to its original version. As a result, when we center our attention on a gazed zone, both pictures grant the likewise appearance. However, in peripheral regions, the disparities are significant. On the other hand, the foveal quality becomes acceptable, but its reference still distorted. In addition, the foveal coder is practiced adopting three vital parameters, the viewing distance ( $V=4$ ), the bit rate (0.15bpp), and the regarded zone (the face middle) which specify the region of intrigue ROI.

In the literature, various strategies inexact the ideal foveal channel. In [2], a pyramid architecture is prescribed to focus pictures. In [2-5], the foveal channel comprises of a set of low-pass bands with different cutoff frequencies. In [3], the configuration of the foveal mask relies upon the Laplacian pyramidal design. In [2-5], the foveal masking strategy implements a non-uniform arranging design [6-9] that lacks the integration of psycho-visual properties. Lately, incredible achievement has been furnished by a couple of wavelet picture coders that are based zones of concern (ROI), like the coders implemented in [4-9], their psychovisual variant accurate in [10-12] and the norm JPEG2000 cited in [14].

The previous solution doesn't fuse the Watson's psycho-visual compression approach that is founded on the quality criterions examinations of the wavelets filter 9/7 [13-14] to aggregate the clarity of its coefficients distortion limits [14-16], then to quantify them visually and finally to furnish an enhanced lossless squeezing. In the last plan, the merge of psychovisual aspect isn't appropriated, similar to luminance and contrast hiding or edge rise [17-20], whose specific characteristics is to spatially refine these picture features and also to reform every single conceal recurrence to the observer's visual cortex. Abusing this reality, we adjust the picture technical aspect (luminance acclimating and difference hiding), to fine-tune conceal frequencies as indicated by the JND limits [15] and to still quantize proficiently the picture spectrum among the zones of concern ROI.

Once a picture is coded, the gained quality needs to be evaluated. To attain this objective, one may find in the literature a series of "Image Fidelity Assessor" (IFA) [21-24]. Based on the "Visible Difference Predictor" VDP [25] and its wavelet-based variant WVDP [26-35], we suggest a psycho-visual assessor that integrates the "Human Visual System HVS" quality criterions [31-33]. Our foveal metric named thereafter FWVDP adapts the original wavelet coefficients, provides a foveal score FPS aiming to predict the probability of detecting the coder introduced errors.

This manuscript includes the following section: first, it advances the flow diagram of the foveal coder. After, it explains, in the second section, how to implement, the wavelet-based foveal masking. Then, it highlights in the third section, how to compute and implement the visual threshold elevation model integrating the wavelet-based edges (JND) entitled "Just Notable Differences". This way, it improves the content of the weighted wavelet spectrum and subsequently optimizes coding. Then it details, in the fourth section, how to evaluate the foveal coding quality based on the foveation wavelet-based visible distortion predictor model to conclude our visual encoder performances. Finally, it emotionally and neutrally discards, in the last section, the results gathered depending on the viewing distance, the bit rate, and the regarded zone which specify the region of intrigue ROI.



Figure. 1. Barbara original test image (left) and its foveated version (right) for a viewing distance  $V = 4$  and binary targeted bit rate  $\text{bpp} = 0.125$ .

## 2. Foveation Wavelet-Based Visual Image Coding Diagram

We advance in Figures 2 and 3, the flow process of the VOEFIC coder "Visually Optimized Embedded Foveation Image Coder" [12] and its upgraded variant MOEFIC the "Modified Optimization Embedded Foveation Image Coder". The two coders comprise five successive stages itemized as come after. In the initial trail, it transforms the source picture utilizing a discrete wavelet DWT that play out a cortical-like decay [1] exploiting a 9/7 biorthogonal filter [13-14] which, in view of its extraordinary mathematic criterions [15] guarantees an ideal reproduction as prescribed by the standard coder JPEG2000 [12-13].

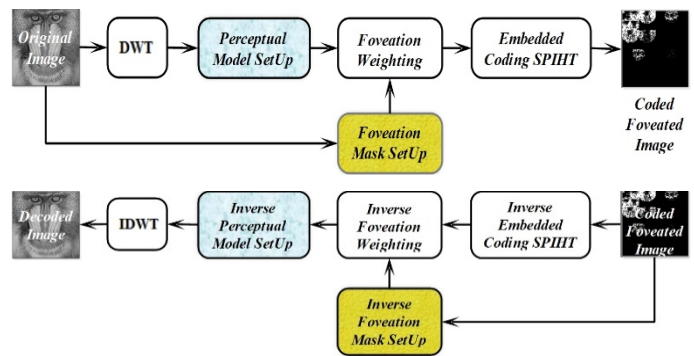


Figure 2: Foveation Wavelet-Based Visual Embedded Image Coding and Decoding flow diagrams based together on a Psycho-Visual Upgrading Tools.

In the following trail, related to the fixation point and its related observation distance we compute the wavelet-based foveal filter [2-5]. Its main aim is to eliminate or reduce invisible frequencies in the peripheral regions of the zone of concern ROI (section III). Then in the subsequent trail, according to the wavelet notable difference edges, we figure the contrast veiling known as limits height [14-16]. Its task starts first on computing the luminance concealing identified with the foveation wavelet coefficients. At that point, it uses the perceptual JND [15] edges required for contrast redress. This activity shadows undetectable differentiation parts and lifts above JNDs limits every single noticeable one concerning the degree of wavelet edges (Section IV).

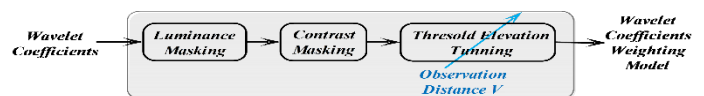


Figure 3: Visually Optimized Wavelet Weighting Process

The primary reason for our upgraded visually based masking layout and exclusively furnished to the MOEFIC coder (VOEFIC coder upgraded variant) [10-12] is its capacity of regulating none directly the picture spectral contents regarding the visioning



conditions. This parameter, as it develops from a lower to higher values, the spectral form plans to cover the significant frequencies. For low separations, the obtained channel spread significantly lower spectrum contents. Oppositely, for higher length, the mask removes, this time, substantially higher image spectral frequencies.

In the last advance, we administer a progressive coder to salable code with different compression rates our visually ballasted wavelet samples till arriving at destined goal identified with a disposed of binary budget. For this scope, we have opted for the use of the SPIHT progressive encoder, which is itself an advanced variant that appertains to the clan of "Embedded Zero Tree Wavelet EZW" Coder commenced early by Shapiro [36] and heightens alongside by A. Said and W. A. Pearlman [37-39].

### 3. Conceiving and Configuring a Wavelet Foveal Filter

In the guise of the observer framework, the HVS is profoundly space-variation in testing, encoding, preparing, and understanding, and in light of the fact that the spatial goals of the visual cortex is most noteworthy all over the gazed region, and diminishes quickly with the working up of the eccentricity, we register the foveation channel [2-5]. By misusing its preferences, it is conceivable to decrease or evacuate impressive high frequencies and unfortunate data from the fringe districts and still perceptually reproduce with a brilliant nature of the decoded picture. To reach this aim; we apply the upcoming process shown in Figure 5. First, we locate the fixation point and calculate the distortion for all pixels with respect to this point. Then, we convert these distortions to eccentricities  $e$  given cycle/degree. Next, we compute the cut-off frequency  $f_c$  (cycle/degree) beyond which, all higher frequencies become invisible (eq. 1) which limits the visible frequencies with no aliasing display in the human visual cortex. Moreover, based on the half display resolution  $f_d$  (eq. 2) (cycle/degree), we obtain the minimum frequency (cycle/degree) so known to us as the Nyquist frequency  $f_m$  (eq. 3) which determinates the visible spectrum.

$$f_c = \frac{e_2 \ln\left(\frac{1}{CT}\right)}{\alpha(e+e_2)} \quad (1), \quad f_d = \frac{r}{2} = \frac{\pi Nv}{360} \quad (2), \quad f_m(x) = \min(f_c, f_d) \quad (3)$$

Here  $f$  refers to the spatial recurrence (cycles/degree),  $e_2 = 2.3$ ,  $\alpha = 0.106$ ,  $CT_0 = 1/64$ ,  $e = \text{atan}\left(\frac{d(x)}{Nv}\right)$  eccentricity (degree),  $x$  point in image,  $d$  distortion,  $v$  distance,  $N$  image resolution.

The best filter parameters can be obtained in [2-5,31,35]. Finally, from the contrast threshold  $CT$  we reach the error sensitivity  $S_f$  that can be expressed as follow:

$$CT(f, e) = CT_0 \exp\left(\alpha f \frac{e+e_2}{e_2}\right)$$

$$S_f(v, f, x) = \begin{cases} \frac{CS(f, e(v, x))}{CS(f, 0)} = \exp(-0.0461 f \cdot e(v, x)) & \text{pour } f \leq f_m(x) \\ 0 & \text{pour } f > f_m(x) \end{cases}$$

The foveation channel alters the picture range contingent upon the survey perception separation. Its shape wipes out logically higher frequencies with expanding perception separation. Therefore, the onlooker is continuously unfit to recognize high frequencies when the distance increments [2-5] Figure 4.

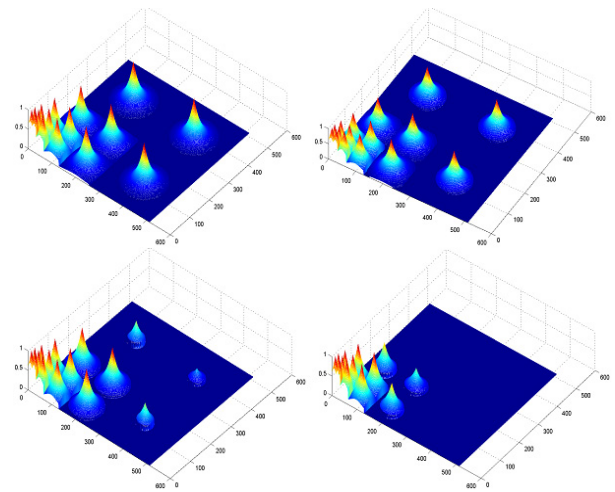
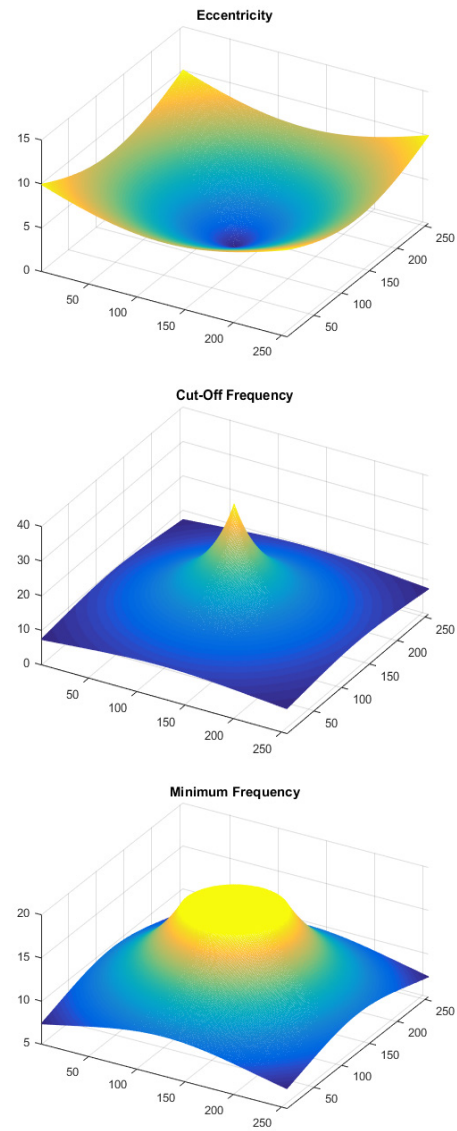


Figure 4. Foveation wavelet-based models designed according to the following survey distance  $V = 1, 3, 6$  and  $10$ . With increasing observation distances, the shadowed regions increase and the foveal filter sensitivity value decrease.



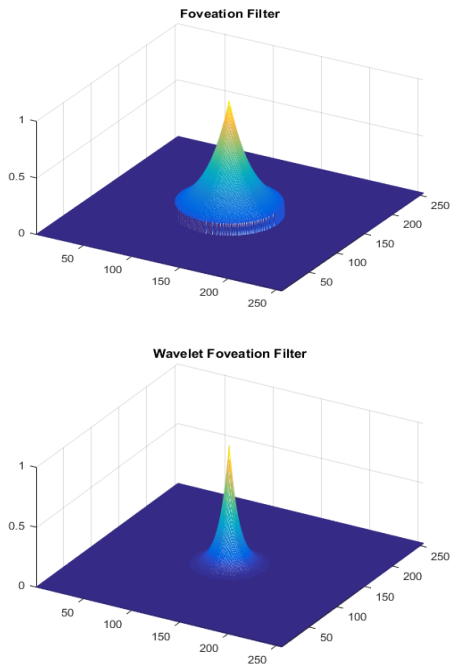


Figure. 5. Foveation Wavelet-Based Visual Weighting Filter process implementation stages computed for one wavelet sub-band. We plot successively its components as come after eccentricity angle, Cut-off frequency avoiding aliasing cortical display, Minimum visible frequency concerning the half media resolution (Nyquist-Frequency), Contrast Sensitivity Function, Foveation Wavelet filter.

#### 4. Contrast Adjust based on Elevation to JND Thresholds

The fundamental advance received in our coding strategy is its complexity covering the masking layout, which we only embrace right now. In fact, we administer this activity to the first wavelet range. Its origination depends on three psycho-visual criterions to visually develop and configure the weighting mask, progressively: first, it decides the perceptual edges JND experimented by Watson [14-16], at that point, it arranged the brightening [17-20] (otherwise called, luminance concealing), Contrast redress [17-20] known as edge height. Once figured, the model is applied to wavelet coefficients in the wake of guaranteeing a cortical-like decay [1], at that point contrasted with the genuine model handled by the renowned human visual cortical disintegration which we at long last confirm their ideal relationship.

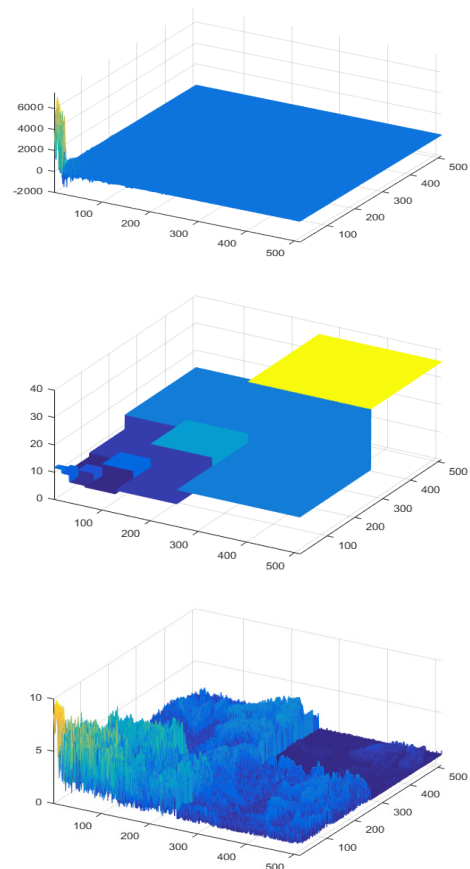
To arrive at this point, we initially register the JND limits [8-9] utilizing a base location identified with wavelet sub-groups. These edges were gathered from the psychophysical tests prepared by Watson. The accomplished edges values relate solely to the Daubechies linear phase wavelet channel [13-14]. Displaying edges in picture pressure relies upon the mean luminance over a chose district in the picture. To figure the differentiation affectability we consider its variety that we can refine utilizing luminance veiling redress mark. In this manuscript, we regulate this veiling with a constant set to 0.649, in light of force work, received appropriate in the JPEG2000 picture coder [13-14].

Likewise, differentiate amendment or complexity limit rise is a second factor that influences essentially the recognition edge. This rise remembers that the permeability of one picture design part changes altogether with the nearness of a picture masker compound [17-20]. Complexity veiling revises the variety of the

location edge of an example segment as an element of the hider content. The covering result alludes to us as a differentiation capacity of an objective limit contrast a hider. Right now, coefficients speak to the masker signal info picture to code outwardly, while the quantization twisting speaks to the objective sign [17-20]. In display 6, we process the wavelet foveation-based visually adapted masking layout. It explains progressively the visual covering impact on the image content. It displays first, the original wavelet coefficients, then plots the JND thresholds [15], next draws the contrast masking effect, then plots the foveation filter and finally its impact on the outwardly weighted variant.

To start with, the procedure breaks down the first picture to give wavelet coefficients - initial step-. At that point figures their relating perceptual edges JND - second step-. These limits depend upon both to Daubechies linear phase channel. It registers next, the foveal filter FOV to foveate the wavelet areas of intrigue ROI and reshape their range [2-10]-third step-. From that point forward, it adjusts the picture relating luminance [17-20] - fourth step-and raises the complexity as per perceptual limits [14-16]. At last, - in the fifth step-, it administers the planned channel to load the wavelet samples and scalable encodes them as indicated by SPIHT described coding reasoning [36-37].

We advance in Figure 6, the masking process conceived specially for the LENA test picture at a granted review separation  $V=4$ . This task explains how we restyle the picture wavelet spectrum regarding our visual loads and explains how the channel influences the wavelet dispersion across sub-bands. It impressively reshapes medium and low frequencies that comprise normally the fundamental image substance. Keep in mind that, we can regulate the shape conditionally to a changeable perception separation.



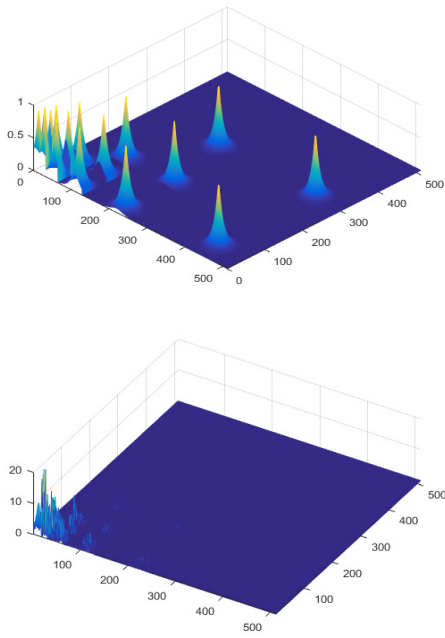


Figure 6. Visually Optimized Foveation-based Weighting Model exclusively conceived for the LENA test image, for her face as foveal region and for a survey distance  $V = 4$ . We cover successively its stages as come after the Wavelet-based Frequency Spectrum, the Limit of Visible Distortions JND, Contrast Elevation, Foveal Filter FOV, and the visually adapted foveal image frequency spectrum to be progressively coded by the standard coder SPIHT.

### 5. Foveation-based Unbiased Quality Investigator

To quantize the strategies of image coding quality, we contrast dependably the measures concurring with abstractly to the *opinion averaged notes* (MOS). The utilization of scientific models, like, the “average squared distortion” (MSE) and its streamlined variant the “Peak Signal to Noise Ratio” (PSNR) are straightforward and spatially processed. Notwithstanding, these measurements correspond ineffectively to the MOS averaged notes that rely upon favorable conditions ensuring the cortical quality criteria [33].

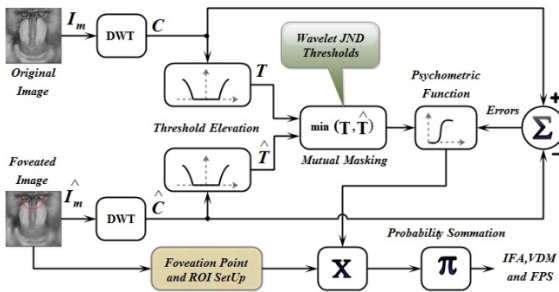


Figure 7: Foveation Wavelet-based Visible Difference Predictor.

As of late, we exercise a cortical-like measurements depending on the psychovisual properties to streamline the interaction factor with the opinion average notes MOS. It expects the merged blunders in a picture naturally unrecognizable to the human onlooker [21-24]. The VDP metric [25] unlike such metrics, enlivens on a cortical transform that intercepts a significant level of visual errors dependably on the picture components. In fact, Wavelet depending metrics get productive in picture coding, due to its closeness to the cortical decay. Regardless of its channels restriction, the wavelet-based investigator yields an exemplary quality gauge and add to advancing the picture squeezing plans.

Right now, we have built up another cortical-like picture quality measurement; labeled “Foveation Wavelet-based Visible Difference Predictor FWVDP” that appeared in Figure 7. It is a foveal form of its native variant WVDP [25-30]. It sums noticeable blunders exercising the “Minkowski Aggregation” to arrive at the obvious contrast guide and yields, obviously [25-30], the foveal mark FPS employing a “Psychometric Activity” [23]. The foveal metric regulates both the source and degraded picture utilizing the advanced arranging mask we conveyed in sections 3 and 4. Along these lines, it disposes of all imperceptible data and looks at just the significant ones. At that point, it moves these blunders to the “Minkowski Addition” [23] entity to arrive at the obvious distortions map and their foveal factor FPS utilizing the “Psychometric Activity”. Therefore, it supplies productively to psycho-visual coders planning to upgrade their exhibition. It communicates the capacity to see noticeable blunders inside wavelet channels. Its recognition likelihood recipe is as come after:

$$P(\lambda, \theta, i, j) = 1 - \exp\left(-\left|\frac{FOV(\lambda, \theta, i, j) \cdot D(\lambda, \theta, i, j)}{JND(\lambda, \theta, i, j)^\alpha}\right|^\beta\right)$$

Here, the term  $D(\lambda, \theta, i, j)$  means degradations at the area  $(\lambda, \theta, i, j)$ ,  $JND(\lambda, \theta, i, j)$  refers to the visual edge,  $\alpha$  and  $\beta$  are refining constants,  $P$  the error probability. Propelled from the Minkowski Summation, and exercised indoors image wavelet spectrum, the probability summation furnishes the aimed mark as come after:

$$FPS = \exp\left(-\frac{1}{MN} \sum_{i,j} |P(\lambda, \theta, i, j)|\right) : M, N \text{ denote the image size}$$

Keep in mind that with increasing values of the FPS mark approaching the unit the degraded image reaches its excellent quality. Oppositely, the degraded image attend its poor quality.

### 6. Gathered Results Analysis

In the vision, all coders are completely subject to their quality measurement which hypothetically and effectively corresponds well with its subjective reference issued from the opinion averaged note MOS. Right now, we experimented with foveal coder MOEFIC and its native variant VOEFIC engaging 8 bits gray scale pictures. We also surveyed their quality exercising the FWVDP foveal wavelet metric for the former and its streamlined variant FVDP for the later. For such reason, we study the MOEFIC and VOEFIC coding quality coding to their reference, separately with VOEFIC for the former and to SPIHT for the later. To arrive at this point, we conveyed three assessment manners that act objectively, subjectively and quantitatively, as a function of the bit binary budget spending and survey conditions.

The main methodology counts completely upon the scores FPS acquired from the coding quality assessment afforded by the coders SPIHT, and its visually revised variants VOEFIC, and MOEFIC experienced together on standard test grayscale pictures. As appeared in figures 8, 9, 10, 11 and 12, the outcomes are done for expanding squeezing rates changing from **256:1** conforming to 0.0039bpp till **2:1** corresponding to 0.5bpp and a viewing separation constant grabbing its value in the set: **{1,3,6,10}**. Accordingly, all methodologies support that exceptionally for low spending plan (below 0.0625bpp), numerous spatial blunders are noticeable in the SPIHT coder picture, while visual coders MOEFIC and VOEFIC display substantially more fascinating data with regards to the locales of concern. So also, at the intermediate squeezing rate (beneath 0.125bpp), the SPIHT coder despite everything giving obscured pictures, while the foveal variants coders show a huge quality over the entire picture. Then again, for a higher compression rate (above 0.25bpp), the foveal coders’ quality remains constantly better than its reference one. At long



last, when the compression rate arrives at a high piece pace, all the mentioning coders approach a uniform appearance and their afforded images become indistinguishable at the entire images.

The qualitative manner affords the average scores of the advanced coders and of their reference. As exhibited in Figures 8-9, we emotionally highlight the MOEFIC, VOEFIC, and SPIHT coder images. We inspect the approach on the “BARBARA” test picture for spending compression rate and fixed perception length V. This experience affirms the abstract quality documentation to the target esteems identified with its corresponding property score FPS. It affirms that, at a lower compression rate, the candidate coders MOEFIC and VOEFIC results keep up significant-quality over the entire picture. So also, for the intermediate spending plan, the witnessed images zones are pitifully unmistakable in the reference coder pictures. However, those areas are emphatically recognizable to the visual coders' images that emphasize significantly the whole picture contents. For higher compression rates and survey distances, the visual coders behave superbly well at the whole analyzed image, as well as the images offered by the SPIHT encoder become significant.

In the QUANTITATIVE methodology, we contrast the visual quality boost ratio against its reference SPIHT as come after:

$$100 * \frac{(FPS_{VOEFIC} - FPS_{SPIHT})}{FPS_{SPIHT}}$$

$$100 * \frac{(FPS_{MOEFIC} - FPS_{VOEFIC})}{FPS_{VOEFIC}}$$

We can finish up as filled in tables 1, 2 and 3, with expanding parallel spending compression rate and also perception conditions the quality addition develops continuously up. This establishes our coder/assessor upgrading aim in terms of additional enhancement.



Figure 8: The foveal coder visually optimized VOEFIC (left column) contrast its Reference SPIHT coder (right column) with accompanied FPS values granted by the Quality Metric FWVDP experienced for BARBARA test picture, for changeable binary budget and fixed survey distance. The former has its values in the set: a. 0.0156bpp, b. 0.0313bpp, c. 0.0625bpp, d. 0.125bpp, and e. 0.25bpp and the latter has its value set to V = 4.

**ISAECT20 INITIAL PRODUCT**

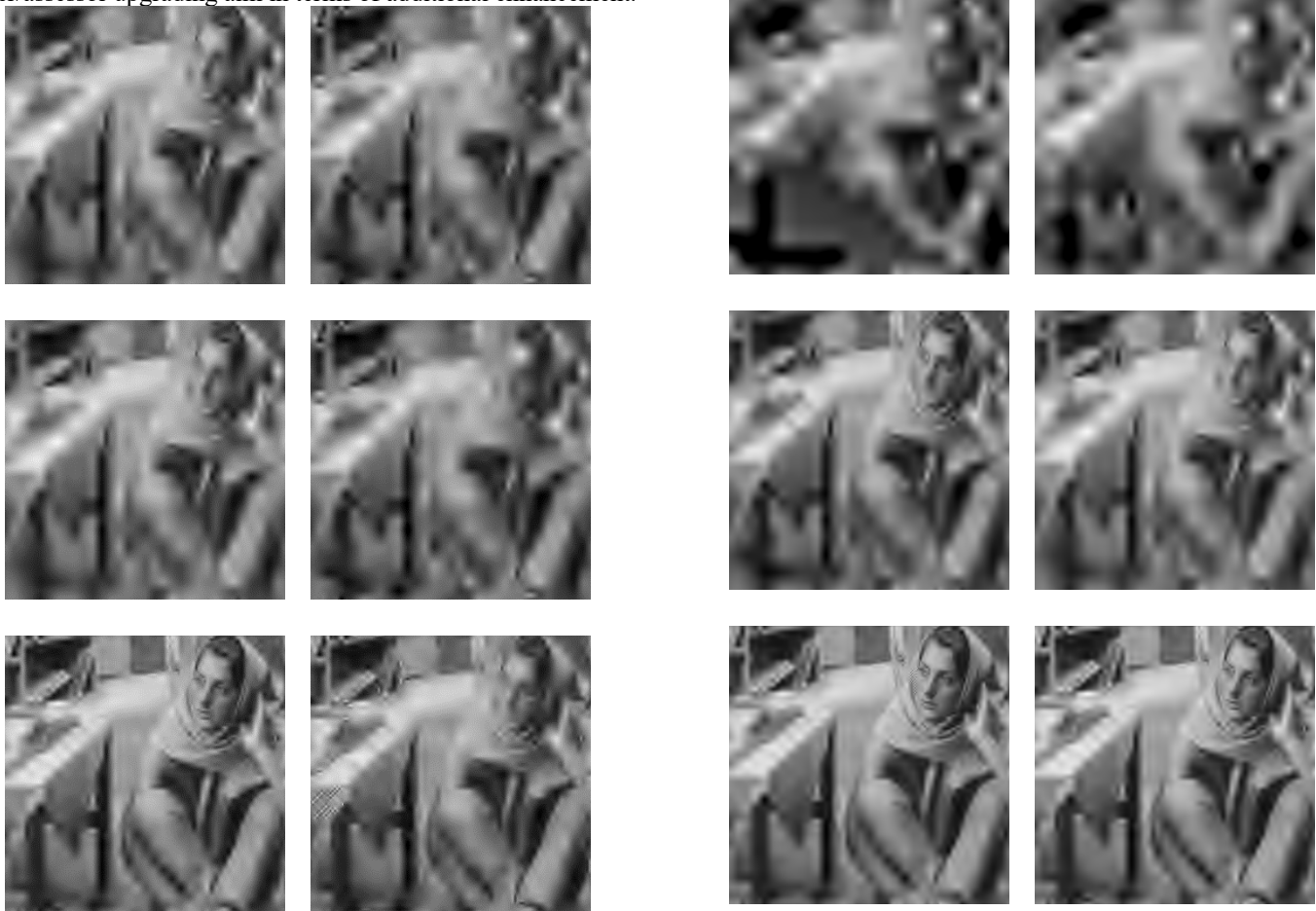
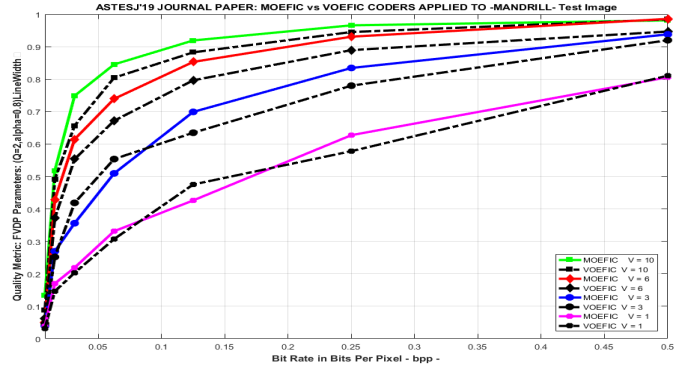
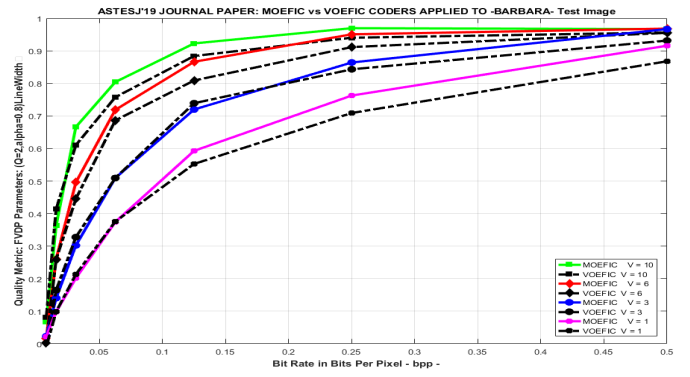






Figure 9: The foveal coder visually optimized **MOEFIC** (left column) contrast its legacy version **VOEFIC** coder (right column) with accompanied **FPS** values granted by the Quality Metric **FWVDP** experienced for **BARBARA** test picture, for changeable binary budget and fixed survey distance. The former has its values in the set: a. **0.0156bpp**, b. **0.0313bpp**, c. **0.0625bpp**, d. **0.125bpp**, and e. **0.25bpp** and the latter has its value set to **V = 4**.



**ASTESJ'20 LIMITED PRODUCT**

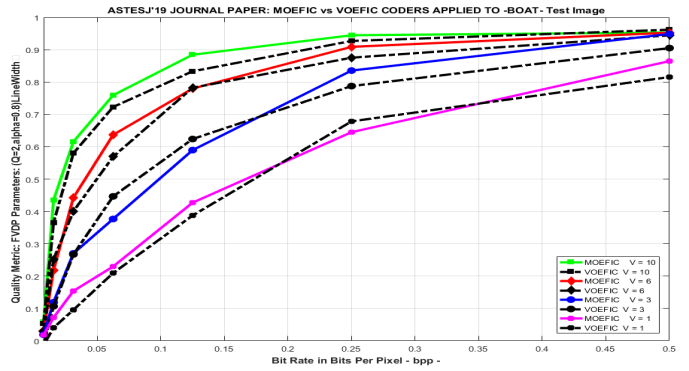
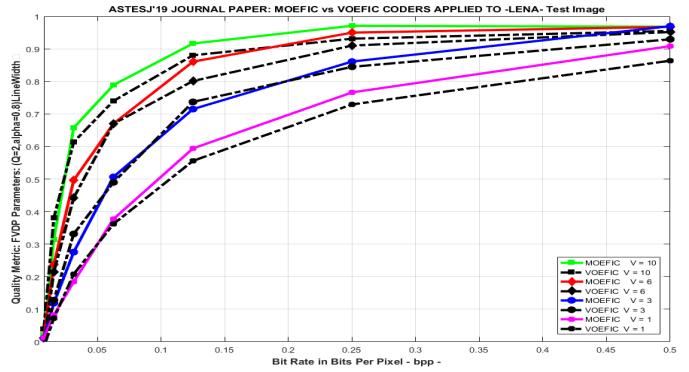
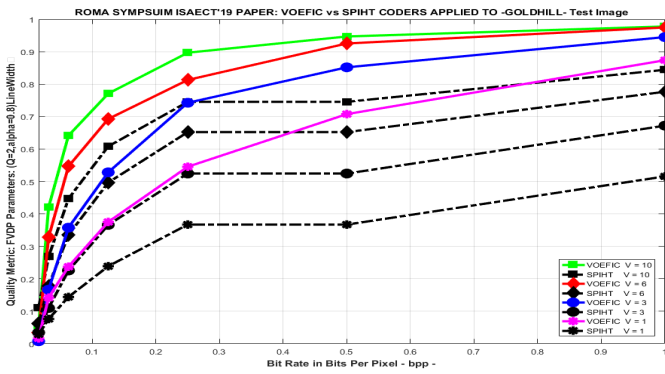
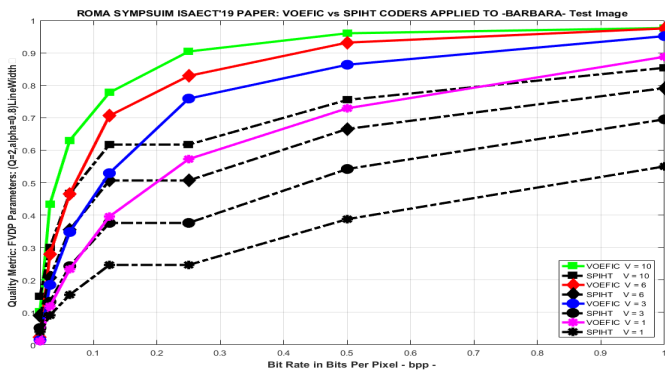


Table 1: VOFEIC vs SPIHT quality boost ratio based on the FVDP Quality Metric experienced for the test pictures: BOAT, MANDRILL, BARBARA, and LENA for changing survey distances and still binary budget.

Targeted Binary Budget	Quality boost ratio (%)			
	LENA	BARBARA	MANDRILL	BOAT
BPP = 0.0625	8.9022	4.4205	5.1243	6.9512
BPP = 0.25	26.3367	34.5819	22.4297	16.6942
BPP = 1	94.2398	74.7420	53.1172	58.8734

ISAECT20 INITIAL PRODUCT

Table 2: VOFEIC vs SPIHT quality benefits granted by FVDP Quality Metric experienced for the test pictures: BOAT, MANDRILL, BARBARA, and LENA for changeable binary compression rates and still survey separation.

Viewing Separation	Quality boost ratio (%)			
	LENA	BARBARA	MANDRILL	BOAT
V = 1	29.8790	50.2645	91.4849	64.2214
V = 3	22.6332	35.6187	64.7933	45.1057
V = 6	13.6161	22.5175	39.6148	38.8212
V = 10	16.5556	23.0739	26.2814	26.3661

ISAECT'20 INITIAL PRODUCT

Table 3: MOEFIC vs VOFEIC quality boost ratio based on the FWVDP metric experienced for the test pictures: BOAT, MANDRILL, BARBARA, and LENA for changeable binary compression rates and still survey separation.

Viewing Separation	Quality boost ratio (%)			
	LENA	BARBARA	MANDRILL	BOAT
V = 1	22.8005	47.6810	14.0676	11.6146
V = 3	28.3076	77.9034	3.2422	39.7098
V = 6	26.8725	66.7592	3.7920	3.3685
V = 10	5.1945	0.9735	14.0159	6.6470

ASTESJ'20 LIMITED PRODUCT

7. Biased and Unbiased Quality Correlation Factor

Right now, we will present the subjective quality assessor. This abstract methodology computes a quality scale named MOS (Mean Opinion Score) which midpoints the emotional estimates applied on pictures coded by our coders for various squeezing rates. First, the measures are gathered dependent on an investigation built up by a gathering of eyewitnesses of alternate class, age, and sex on an abstract scale differing from exceptionally poor to a particular quality. Then, a MOS factor calculation is established to approve the utilization of the MOEFIC and VOFEIC visual coders over the standard coder SPIHT and to validate our FWVDP foveal metric.

Table 4: Necessary conditions to experience Subjective Evaluation

Experienced Pictures	Standard Pictures
Environment	Environment of Normal Desk
Viewing Separation V	This choice belongs to the spectator
Perceiving Time	Limitless
Observers Number	Between 15 and 39
Score Range	Between 0 and 1

7.1. Requirements for an Abstract Quality Assessors

The instinctive aspect assessment is standardized according to CCIR suggestions [10, 31-33], initially intended for TV pictures. We plan to assess the identified differences among a candidate and reference pictures and embrace instinctive measures. We expect the utilization of Fränti conditions [40-41] required for this assessment experimentation, as suggested in the CCIR

recommendation detailed in [42-43] and summarized in Table. 4. Assuming that these conditions are regarded, we standardize the assessment range to evade extra blunders environment dependent.

7.2. MOS Quality Factor Experimentation

To satisfy the relationship among the unbiased measures (vector X) and the biased measures (vector Y), we administer the matching coefficient evolved as come after:

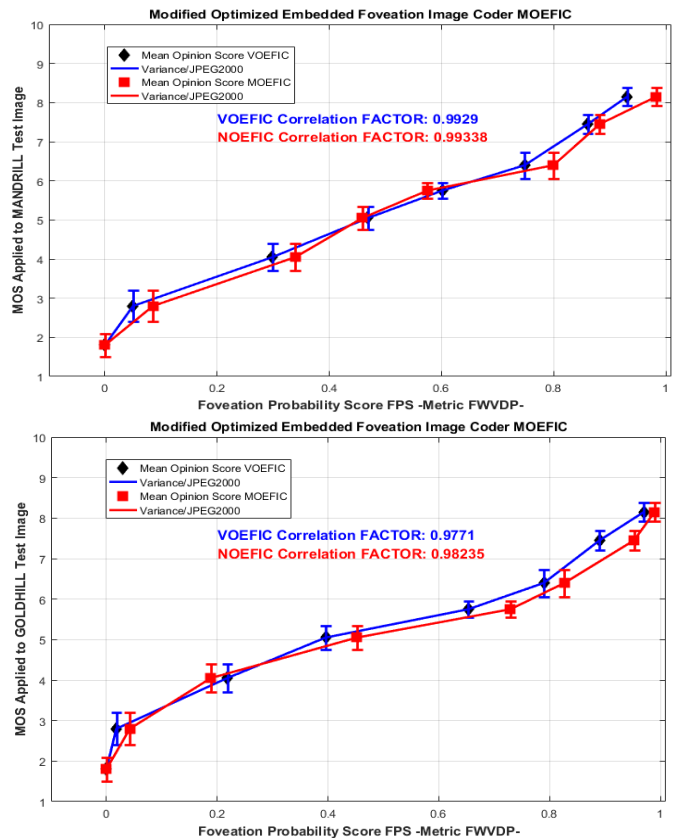
$$\rho(X, Y) = \frac{\sum_{i=1}^n (X_i - \bar{X})(Y_i - \bar{Y})}{\sqrt{\sum_{i=1}^n (X_i - \bar{X})^2} \sqrt{\sum_{i=1}^n (Y_i - \bar{Y})^2}}$$

Where  $X_i$  and  $Y_i$ , n, refer separately the array elements of X and Y. n refers to the total of elements.  $\bar{X}$  and  $\bar{Y}$  mean, individually, the mean of the arrays X and Y values, according to the accompanying equation:  $\bar{X} = \frac{1}{n} \sum_{i=1}^n X_i$

and decides the inconstancy note, as follow:  $Var(X) = \frac{1}{n} \sum_{i=1}^n (X_i - \bar{X})^2$

7.3. Results of subjective quality assessment

To explore the MOS figuring, refer to [10, 31-33], to fit the conditions to be respected before launching the subjective assessment. As shown in figure 13, the subjective score experienced by the MOS metric is compared to its objective scores FPS provided by the FWVDP assessor and deployed to highly textured test images and distorted at different bit rates by the JPEG2000 coder. This is to demonstrate a superior relationship between the objective and the subjective measures. This is highlighted in figure 13. This correlation is approved for the visual coders MOEFIC and VOFEIC (with a significant improvement for the former), however, it is disapproved for the SPIHT coder.



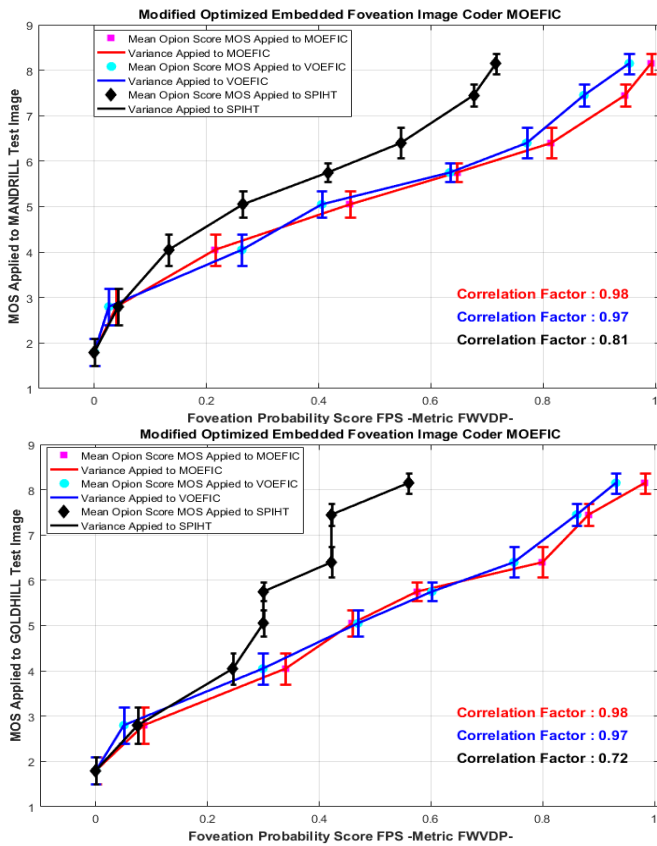


Figure 13: Opinion Averaged Notes using MOS vs FPS scores using FWVDP foveal metric experienced to “GOLDHILL” and “MANDRILL” images under MOEFIC/VOEFIC/SPIHT coders as indicated by the accompanying arrangement: resolution 512x512 degraded pictures, JPEG2000 reference coding, number of spectators=24, Degraded pictures versions=24, .Separation=4.

## 8. Conclusion

In this manuscript, we submitted a novel picture coder MOEFIC, that is labeled "Modified Optimization Embedded Foveation Image Coding". It takes its advantages from its adapted variant VOEFIC, that is baptized "Visually Optimized Embedded Foveation Image Coder" and largely explained in [10]. We have conceived these coders regarding their forerunner EVIC [11], MEVIC [12], POEZIC [38], as well as their foveal variant POEFIC that was elaborated in [39]. We additionally presented the quality evaluator FWVDP, that is entitled "Foveation Wavelet Visible Difference Predictor" [32-33]. The pair of the referenced frameworks manages precise cortical properties by the integration of the human psychophysical weighting models. They consolidate progressively the foveation channel (FOV), the wavelet visible distortions edges (JND), the contrast elevation above those JND limits dependent on luminance adaptation and contrast correction.

The ultimate model, when is applied to the wavelet-based picture spectrum, will reshape its range. Therefore, it will keep its significant data situated in the looked locale of intrigue and disposes of all subtle and repetitive ones. Thusly, we encoded and assessed the valuable data, which as indicated by the obsession point, using a paired spending squeezing rate and a perception separation. Consequently, we arrived at an increasingly upgraded picture quality contrasted with the reference form that has processed straightforwardly the initial wavelet-based picture spectrum. The foveal coder and its corresponding foveal assessor

register together psychovisual-like transform, which regardless of its recurrence sub-bands constraint upgrades the picture transformation, limits perceptually increasingly pertinent blunders, arrives at the purpose binary rate and advances the ocular aspect contrasted with that provided by the mentioning SPIHT [37]. It likewise directly refine the picture spectrum contingent upon the coding aspect and the survey conditions. Indeed, when the perception separation increases taken away lower level to the greatest values, the picture adapted spectrum shape will spread the significant wavelet channels that, naturally, are the zones of interest located in low and medium frequency bands.

Besides, we highlighted in this manuscript three evaluation approaches aiming to validate the suggested coders. We meant here, the objective validation based on foveal score FPS that is provided by the mentioned assessor (FWVDP). The subjective validation, which is based on averaged spectator's notes (MOS). The quantitative and qualitative approaches that are based on the boost ratio for the former and the interaction factor between the objectives scores and the subjective notes for the later. This validation process was administered to the visually advanced coder MOEFIC, to its adapted variant VOEFIC, and to their mentioning coder SPIHT. As highly discussed above, all gathered fruits from obtained results approve our perceptual coders in terms of quality improvement and binary budget optimization.

To finish our unobtrusive work, note that we assembled, talked about and contrasted the got outcomes and distinctive assessment techniques we implied unbiased, biased, qualitative and quantifiable ways to deal with endorse and approve our work.

## References

- [1] S. G. Mallat, "Multi-frequency channel decomposition of images and wavelet models", IEEE Trans. Acoust., Speech, Signal Processing, Vol. 37, 2091-2110, 2000.
- [2] P. Kortum and W. S. Geisler. "Implementation of a foveated image coding system for image bandwidth reduction." In Proc. SPIE: Human Vision and Electronic Imaging, Vol. 2657, 350-360, 1996.
- [3] W. S. Geisler and J. S. Perry. "A real-time foveated multiresolution system for low-bandwidth video communication", Proc. SPIE, Vol. 3299, 1998.
- [4] Zhou Wang, Alan Conrad Bovik "Embedded Foveation Image Coding, IEEE transactions on image processing, Vol. 10, Oct. 2001.
- [5] S. Lee, M. S. Pattichis, and A. C. Bovik., "Foveated video compression with optimal rate control", IEEE Trans. Image Processing, vol. 10, pp. 977-992, July 2001.
- [6] Andrew Floren, Alan C. Bovik, "Foveated Image and Video Processing and Search", Academic Press Library in Signal Processing, Volume 4, 2014, Pages 349-401, Chapter 14
- [7] J. C. Galan-Hernandez, V. Alarcon-Aquino, O. Starostenko, J. M. Ramirez-Cortes, Pilar Gomez-Gil, "Wavelet-based frame video coding algorithms using fovea and SPECK", Engineering Applications of Artificial Intelligence Volume 69 March 2018, Pages 127-136
- [8] Rafael Beserra Gomes, Bruno Motta de Carvalho, Luiz Marcos Garcia Gonçalves, «Visual attention guided features selection with foveated images», Neuro computing Volume 12023, November 2013, Pages 34-44
- [9] J. C. Galan-Hernandez, V. Alarcon-Aquino, O. Starostenko, J. M. Ramirez-Cortes, Pilar Gomez-Gil, «Wavelet-based frame video coding algorithms using fovea and SPECK», Engineering Applications of Artificial Intelligence Volume 69, March 2018, Pages 127-136
- [10] Bajit, A., Benbrahim, M., Tamtaoui, Rachid, E., "A Perceptually Optimized Wavelet Foveation Based Embedded Image Coder and Quality Assessor Based Both on Human Visual System Tools", 2019, ISACET'2019 -IEEE-International Symposium on Advanced Electrical and Communication Technologies, ROMA, 2020.
- [11] Bajit, A., Nahid, M., Tamtaoui, A, Lassoui, A, "A Perceptually Optimized Embedded Image Coder and Quality Assessor Based on Visual Tools" 2018, ISACET 2018 -IEEE-International Symposium on Advanced Electrical and Communication Technologies, 2018.
- [12] Bajit, A., Nahid, M., Tamtaoui, A, Lassoui, A, "A Perceptually Optimized Embedded Image Coder and Quality Assessor Based on Visual Tools", ASTESJ'19 –Special Issue- CFP for Special Issue on Advancement in

- Engineering and Computer Science, Volume 4, Issue 4, Page No 230-238, 2019.
- [13] Michael Unser, and Thierry Blu., "Mathematical Properties of JPEG2000 Wavelet Filters", IEEE Transaction on Image Processing, Vol. 12, n. 9, Sep. 2003.
- [14] Z. Liu, L. J. Karam and A. B. Watson., "JPEG2000 Encoding With Perceptual Distortion Control", IEEE Transactions on Image Processing, Vol. 15, N. 7, July 2006.
- [15] A.B Watson, G.Y.Yang, J.A.Solomon, and J.Villasonor. "Visibility Of Wavelet Quantization Noise", IEEE Trans. Image Processing, Vol. 6, n. 8, 1164-1175, 1997.
- [16] Y. Jia, W. Lin and A. A. Kassim., "Estimating Just-Noticeable Distortion for Video", IEEE Transactions on Circuits and Systems for Video Technology, Vol. 16, 820829. July 2006.
- [17] Watson and J. A. Solomon., "A model of visual contrast gain control and pattern masking", J. Compar. Neurol., Vol. 11, 1710-1719, 1994.
- [18] J. M. Foley., "Human luminance pattern-vision mechanisms: masking experiments require a new model", J. Compar. Neurol., Vol. 11, N. 6, 1710-1719, 1999.
- [19] S. Daly, W. Zeng, J. Li, S. Lei., "Visual masking in wavelet compression for JPEG 2000", in: Proceedings of IS&T/SPIE Conference on Image and Video Communications and Processing, San Jose, CA, Vol. 3974, 2000.
- [20] D. M. Chandler and S. S. Hemami., "Dynamic contrast-based quantization for lossy wavelet image compression", IEEE Trans. Image Process. 14(4), 397410, 2005.
- [21] Z. Wang, A. C. Bovik, H. R. Sheikh, and E. P. Simoncelli., "Image Quality Assessment: From Error Visibility to Structural Similarity", IEEE Transactions on Image Processing, Vol. 13, N.4, April 2004.
- [22] H.R. Sheikh, A. C. Bovik, and G. de Veciana., "A Visual Information Fidelity Measure for Image Quality Assessment", IEEE Trans on Image Processing, Vol.14, pp. 2117-2128, N.12, Dec. 2005.
- [23] J. G. Robson and N. Graham., "Probability summation and regional variation in contrast sensitivity across the visual field", Vis. Res., vol. 19, 409-418, 1981.
- [24] S. J. P. Westen, R. L. Lagendijk and J. Biemond., "Perceptual Image Quality based on a Multiple Channel HVS Model", Proceedings of ICASSP, 2351-2354, 1993.
- [25] S. Daly. "The visible differences predictor: An algorithm for the assessment of image fidelity, in Digital Images and Human Vision", Cambridge, MA: MIT Press, 179-206, 1993.
- [26] Andrew P. Bradley. "A Wavelet Visible Difference Predictor", IEEE Transactions on Image Processing, Vol. 8, No. 5, May 1999.
- [27] E. C. Larson and Damon M. Chandler. "Most apparent distortion: full-reference image quality assessment and the role of strategy," Journal of Electronic Imaging, 19(1), 011006. Jan Mar 2010.
- [28] Yim and A. C. Bovik, "Quality assessment of deblocked images," IEEE Trans on Image Processing, vol. 20, no. 1, pp. 88-98, 2011.
- [29] Zhou Wang, Qiang Li", Information Content Weighting for Perceptual Image Quality Assessment, IEEE TRANSACTIONS ON IMAGE PROCESSING, VOL. 20, NO. 5, MAY 2011.
- [30] M. Oszust., "Full-Reference Image Quality Assessment with Linear Combination of Genetically Selected Quality Measures", , in PLOS ONE journal, Jun 24, 2016
- [31] M. Nahid, A. Bajit, A. Tamataoui, El. Bouyakhf " Wavelet visible difference measurement based on human visual system criteria for image quality assessment", Journal of Theoretical and Applied Information Technology, Vol. 66 No.3 p:736-774 2014
- [32] M. Nahid, A. Bajit, A. Tamataoui, El. Bouyakhf " Wavelet Image Coding Measurement based on the Human Visual System Properties", Applied Mathematical Sciences, Vol. 4, no. 49, 2417 - 2429, 2010
- [33] Nahid, M., Bajit, A., Baghdad, "A., Perceptual quality metric applied to wavelet-based 2D region of interest image coding" SITA- 11th International Conference on Intelligent Systems, 2016.
- [34] Mario Vranješ, Snježana Rimac-Drlje, Krešimir Grgić, "Review of objective video quality metrics and performance comparison using different databases", Signal Processing: Image Communication, Volume 28, Issue 1 January 2013, Pages 1-19
- [35] Xikui Miao, Hairong Chu, Hui Liu, Yao Yang, Xiaolong Li, "Quality assessment of images with multiple distortions based on phase congruency and gradient magnitude", Signal Processing: Image Communication, Volume 79, November 2019, Pages 54-62
- [36] J. M. Shapiro. "Embedded image coding using Zero-Trees of wavelet coefficients", IEEE Trans. Signal Processing, Vol.41, 3445-3462, 1993.
- [37] A. Said and W. A. Pearlman., "A new fast and efficient image codec based on set partitioning in hierarchical trees", IEEE Trans. Circuits and Systems for video Technology, Vol. 6, 243-250, June 1996.
- [38] A. Bajit, A. Tamtaoui & al, "A Perceptually Optimized Foveation Based Wavelet Embedded ZeroTree Image Coding" Int. Journal of Computer, Elecl, Aut, Control and Information Eng Vol:1, No:8, 2007,
- [39] A. Bajit, A. Tamtaoui & al, "A Perceptually Optimized Wavelet Embedded ZeroTree Image Coder" International Journal of Computer and Information Engineering Vol:1, No:6, 2007
- [40] Pasi Fränti, "Blockwise distortion measure for statistical and structural errors in digital images", Signal Processing: Image Communication, Volume 13, Issue 2 August 1998 Pages 89-98 C.
- [41] Deng, Z. Li, W. Wang, S. Wang, L. Tang, A. C. Bovik "Cloud Detection in Satellite Images Based on Natural Scene Statistics and Gabor Features" IEEE Geoscience and Remote Sensing Letters, 2018.
- [42] L. Stenger Signal Processing: Image Communication, Volume 1, Issue 1 June 1989, Pages 29-43, "Digital coding of television signals—CCIR activities for standardization"
- [43] Erika Gularte, Daniel D. Carpintero, Juliana Jaen, "Upgrading CCIR's foF2 maps using available ionosondes and genetic algorithms" Advances in Space Research Volume 61, Issue 71 April 2018 Pages 1790-1802.



## **A Framework for Plans Permeable Breakwater Eco-Friendly Building Identification and Characteristics Materials Construction Study Case at Demak Village**

Denny Nugroho Sugianto<sup>1,2,\*</sup>, Sugeng Widada<sup>1</sup>, Anindya Wirastriya<sup>1,2</sup>, Aris Ismanto<sup>1,2</sup>, Retno Hartati<sup>4</sup>, Widianingsih<sup>4</sup>, Agus Indarjo<sup>4</sup>, Suripin<sup>5</sup>

<sup>1</sup>*Department of Oceanography, Diponegoro University, Semarang 50275, Indonesia.*

<sup>2</sup>*Center for Coastal Rehabilitation and Disaster Mitigation Studies, Semarang 50275, Indonesia.*

<sup>3</sup>*Doctorate Programme of Coastal Resources Management/Aquatic, Diponegoro University, Semarang 50275, Indonesia.*

<sup>4</sup>*Department of Marine Science, Diponegoro University, Semarang 50275, Indonesia.*

<sup>5</sup>*Department of Civil Engineering, Diponegoro University, Semarang 50275, Indonesia.*

---

### **ARTICLE INFO**

*Article history:*

*Received: 27 September, 2019*

*Accepted: 11 March, 2020*

*Online: 20 March, 2020*

---

*Keywords:*

*Submerged breakwater*

*ocean wave*

*Jepara*

*coastal protection*

*mitigation*

---

---

### **ABSTRACT**

*Demak is located on the north coast of Java, precisely in Central Java Province, Indonesia which has many problems related to erosion and shoreline degradation. This study attempts to analyze, identify, and select the materials to build eco-friendly permeable breakwater in Demak. The research was conducted during 2014, consist of several activities, i.e. identified the condition of breakwaters position, materials, and construction, did literature study of identification type breakwaters, study area, sediment, chemical reaction, then reverse design and modification for eco-friendly permeable breakwater. The result is a design of eco-friendly permeable breakwater which used a material of PVC pipe and Bamboo. PVC has excellent chemical resistance, also will increase sedimentation process and accelerate coastal changes towards the sea. Effectiveness level of breakwater made from combination of tire and PVC was 62%, and reveal to be more economical than other general-purpose plastics such as PE, PP, or PS.*

---

## **1. Introduction**

Demak is located on the north coast of Java, exactly in Central Java Province, Indonesia that interesting to observed [1][2]. This area has many problems related to erosion and shoreline degradation [3]. Coastal abrasion in the north coast of Java is mainly influenced by ocean dynamics, like wave action, long shore current, and sea level rise also land subsidence that caused erosion [4]. It would affect to shoreline line, and dangerous for community live in surrounding area.

Many attempts have been made to build breakwaters and plant mangrove to decrease abrasion. In 2014, Indonesian Ministry of Marine and Fisheries built breakwater using hybrid nature concept, this building can control hydrodynamics and deformation of wave energy. However, it was not effective to reduce wave energy, and sediment was not trapped inside perfectly [5][6]. Another problem was the evidence of wood

boring community which attack the bamboo pole used. Woodborers bore into wood not only for shelter but often also for nourishment [7]. This study attempts to analyse, identify, and plan the materials to build an eco-friendly permeable breakwater in Demak Coast.

## **2. Literature Study**

### *2.1. Study Area*

Indonesia is a maritime country which has 13,487 islands; 3'257'483 km<sup>2</sup> water area, and 95,181 km<sup>2</sup> coastline [8]. Demak is one of the coastal areas, direct facing Java Sea. This research was conducted in Timbulsloko Village, Demak. This aims of research was to identify the condition of breakwaters position, materials, and construction.

Java Sea Wave has a uniqueness that is generated by the wind that is bounded by the islands of Java, Sumatra, Kalimantan and the Sulawesi Islands [8]. Demak has many problems related to

---

\*Denny N. Sugianto, Email: [dennysugianto.oceanography@gmail.com](mailto:dennysugianto.oceanography@gmail.com)

erosion and shoreline changing [9]. The changing of coastal area is because the soil type of Demak is alluvial which is susceptible to coastal erosion process [2]. Provincial Development Planning Agency (Bappeda) reported that in 2007 Central Java Province faced coastal mangrove degradation, and the result of the study, in 2014 the ground cover vegetation of coastal mangrove was only 5.381,15 ha [10].

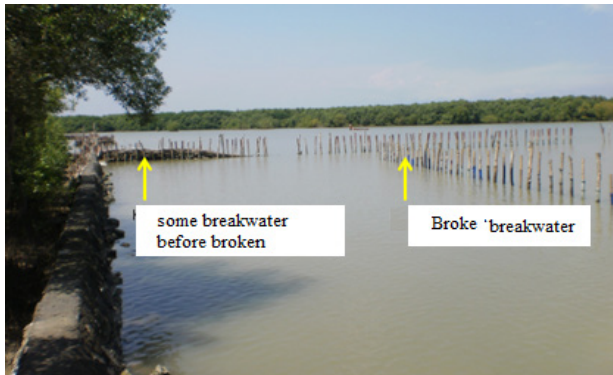


Figure 1: Submerged breakwater experiment layout.



Figure 2: Problem face by materials of breakwaters (source : research study in 2014).

## 2.2. Coastal Structure Type

Several types of coastal structure be important role to prevent coastal morpho-dynamics. Proper layouts of coastal structures can lead to less intense sand transport near the beach [11]. Some types of coastal buildings are revetment, groin, jetty and reduce wave energy [12]. These buildings have several roles and functions. Revetment buildings are built on shorelines were used to protect beaches directly from wave attacks. Groins are building jutting from the beach into the sea used to capture or restrain movement of sediment along the coast, so the sediment transport along the coast is reduced. Groynes are protective structures, but, on the contrary, they may induce local strong flow around the head zone [12]. Jetty is a perpendicular building of coastline that is placed on both sides of the river mouth [11]. Setting of jetty construction can impact the longshore transport [13]. The third group is the breakwater (breakwater), which consists of 2 types, they are offshore and on-shore breakwaters [14] [15]. Waves break on these nearshore bars can reduce the level of wave energy [16]. Breakwaters protect shorelines from beach erosion and lessen the impacts on water quality and landscape [17]. Offshore

breakwater widely used as coastal protection against erosion by destroying the wave energy before it reaches the shore while the breakwater connecting the beach used to protect the waters of the port from wave disturbances, so that the ships can be docked [11] [18].

## 2.3. Wave Breaker Structure

The main characteristic of a wave-permeable breakwater is that a wave can move through the breakwater without changing its profile, while wave diffraction is not dependent on whether the structure is permeable or not [19] [20] [21]. Wave energy can induce sediment transport and shoreline changes [22] and also implication of breakwater orientation can be designed or altered to sediment transport in a desired direction [23]. Those sometimes constructed as countermeasures against beach erosion where the availability of sediments for nourishment is limited [24]. The construction of breakwater influenced by wave energy and sediment transport patterns of the study area [25].

The effectiveness of structure type to reduce wave energy is influenced by the geometric shape and configuration of the breakwater placement, as well as the water depth, height and wave period. The length of the breakwater and its distance from the shoreline determines the shoreline and sediment changes collected behind the breakwater structure concerned. There are some type of wave breaking structures as presented in Tabel 1.

## 2.4. Phytoplankton, Benthic Organism and Boring Community

To get phytoplankton samples, researches used plankton net for phytoplankton with 100  $\mu\text{m}$  nets and 20 cm holes placed behind the boat and pulled with 10 m long nylon ropes for 10 minutes. The distance traveled is about 500 m and the volume of filtered seawater for each transport of plankton is 350  $\text{m}^3$ .

Then the sample is transported and taken to a laboratory where it is arranged in 5% buffered formalin. Researchers use a hemocytometer under a compound microscope to count and identify phytoplankton cells. The van veen grab sampler is used to collect samples of benthos, the assemblage of organisms inhabiting the seafloor. The benthos in the sediment samples recovered after sieving through 0.5 mm mesh sieve and preserved with 10% formalin mixed with rose-bengale was brought to the laboratory in polythene bags.

Sediment with benthos were transferred to a large, white-bottomed tray, and the animals were hand sorted in laboratory. After this preliminary examination, the whole sample was treated with 70% alcohol and kept for further analysis.

Phyto-plankton in Demak coast were found consisted of two classes, i.e. Bacillariophyceae and Dinophyceae. Nine teen phytoplankton species (80 %) from Bacillariophyceae class were Amphipora, sp., Amphora, sp., Bacteriastrum sp., Biddulphia sp., Chaetoceros sp., Corethron sp., Coscinodiscus sp., Eucampia sp., Fragilaria sp., Leptocylindrus, sp., Melosira, sp., Navicula sp., Nitzschia sp., Pelagothrix sp., Pleurosigma sp., Rhizosolenia sp., Skeletonema sp., Thallasiotrix sp., Triceratium sp and dominated by Pleurosigma sp. Dinophyceae phytoplankton found in the study area were Peridium sp., Ceratium sp., Dinophysis sp. and Diploneis sp.

Table 1: Some types of wave breaking structures and their disadvantages and advantages.

Types	Disadvantages	Advantages
1. Type of box-concrete (concrete cube)	<ul style="list-style-type: none"> <li>- Requires a lot of large stone (rock weight more than 300 kg per grain) in large quantities.</li> <li>- Needs a strong foundation for the sludge.</li> <li>- Cheaper cost</li> </ul>	<ul style="list-style-type: none"> <li>- From the technical point of view is very effective as wave energy damper.</li> <li>- Concrete cube have different gravity of about 2.4 times of the water weight or about 2.4 tons for 1 m<sup>3</sup> of concrete.</li> <li>- In terms of data execution, easy in structuring.</li> </ul>
2. Wooden Building Type	<ul style="list-style-type: none"> <li>- The poles are not tight enough to withstand the incoming waves.</li> </ul>	<ul style="list-style-type: none"> <li>- Can reduce the rate of coastal erosion and catch sediment in protected areas.</li> </ul>
3. Tires combined PVC	<ul style="list-style-type: none"> <li>- Will only be effective and work well for the following coastal conditions: (1) wave height, H &lt; 3.0 m and wave period T = 4-8 seconds; (2) current velocity V &lt; 0.5 m / s; (3) tidal range &lt; 1.1 m; (4) coastal slope (slope) 0,1% &lt; tan <math>\theta</math> &lt; 0,5%; (5) water depth &lt; 2 m; And a sediment diameter of 0.20 mm &lt; D50 &lt; 0.30 mm.</li> <li>- PVC and tires have weaknesses because the materials used more quickly brittle.</li> </ul>	<ul style="list-style-type: none"> <li>- Will encourage the sedimentation process and accelerate coastal changes towards the sea.</li> <li>- Level of breakwatereffectiveness of combined tire and PVC type is 62%.</li> <li>- More economical</li> </ul>
4. Concrete Buis Type	<ul style="list-style-type: none"> <li>- Less environmentally friendly</li> </ul>	<ul style="list-style-type: none"> <li>- Concrete material is stronger, durable and not easily damaged due to wind conditions and waves that occur.</li> <li>- Effectiveness level of Concrete Buis type is 85%.</li> </ul>
5. Bamboo Combined Tires Type	<ul style="list-style-type: none"> <li>-</li> </ul>	<ul style="list-style-type: none"> <li>- Ease of self-help by community and non-government organizations.</li> <li>- Low cost.</li> <li>- Ease in obtaining material.</li> </ul>
6. Brushwood dam / Permeable dam / Hybrid engineering type	<ul style="list-style-type: none"> <li>-</li> </ul>	<ul style="list-style-type: none"> <li>- Allows to capture maximum sediment and minimize abrasion strength.</li> <li>- Reduces wave energy and does not reflect waves.</li> <li>- Creating a calm water condition for mud sediment.</li> <li>- No need for cross section or grounding as in breakwater combined bamboo tire type.</li> </ul>

The analysis shows that benthic organisms found in all study area mostly polychaeta (95%) consist of 8-21 species and 5% of bivalve and crustacean. Polychaetes have an important role in the function of benthic communities, in terms of recycling and reworking benthic sediments, bioturbation sediments and in the burial of organic matter. Polychaetes are abundant in most marine and estuary environments, both in terms of numbers of individuals and species. [26]. Polychaetes, by their burrowing and feeding activity, may considerably enhance various sedimentary processes. This benthic community take a great advantage from sedimentation as the impact of breakwater construction.

The bamboo and wood materials used as material construction were found attacked by boring organism *Barnea cf. candida* (Figure 1) which is one of the most abundant and diversified of modern pholadid bivalves [27]. The colour of this boring bivalves

were white, periostracum yellowish or light brown with inner surfaces white. Their shell were thin and brittle, elongate-oval, shaped rather like a date; anterior and posterior margins rounded, gaping posteriorly. Sculpture of corrugated concentric ridges and radiating lines, developed as sharp tubercles where they intersect, most pronounced anteriorly. They are filter-feeders and bore into inorganic and organic substrates of variable hardness and, occasionally, into waterlogged and decayed wood [27]. The diverse and abundance of phytoplankton in the study area provide excellent food the the bivalves so that *Barnea cf. candida* were found very dense (15-21 indiv./10 cm<sup>2</sup>) and caused the wood broken. The bamboo was also heavily attached by oysters (*Crassostrea sp.*) so the bamboo become weak and broken. Pholads such as *Barnea sp.* are particularly aggressive in tropical waters and causing extensive damage to wood[28].

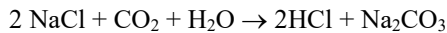


Marine borers are wood boring invertebrates and other hard objects in the sea and brackish waters (as their habitat and foraging). Its nature that drills wood will cause damage to the wood structure and reduce the strength of the wood, and crustacean borers including multiple species commonly known as gribbles Goodell 2000 [29] [28]. Both shipworms and gribbles attack the wood piles for shelter and, at least in the case of shipworms, wood can also be digested through the aid of microbial symbionts [30] to supplement filter feeding nutrition.

2.5. Phytoplankton, Benthic Organism and Boring Community

Chemical reaction happen in breakwater inside materials construction which is sank in water. In study area a water has characteristics of salt water (55% Cl, 4% Mg, 8% SO<sub>4</sub>, 31% Natrium, Ca, etc), this shows good for phytoplankton growth.

There were several breakwater type such as tires-bambo combination (Figure 3), Bamboo and Concrete Buis Type (Figure 5). Waste tyres contain a carbon (84,10%), oxygen (10,36%), sulfur (0,48%), silicon (0,07%), and Zn (5,04%). Carbon inside in waste tyres will produce more CO<sub>2</sub> and it will make acid condition in aquatic :



Salt + Carbon dioxide + Water → Acid + Metal Carbonates

In the location where the Concrete Buis Type was used as breakwater, it showed more effective as wave energy reducer. Concrete materials have 2.4 times of the water weight or about 2.4 tons for 1 m<sup>3</sup> of concrete. Concrete material is stronger, durable and not easily damaged by wind and waves [31][4]. However this type is less-environmental-friendly because produce heavy metals such as Pb, Ag, and Cr.



Figure 3: Breakwater of tires bambo combination type in study area.

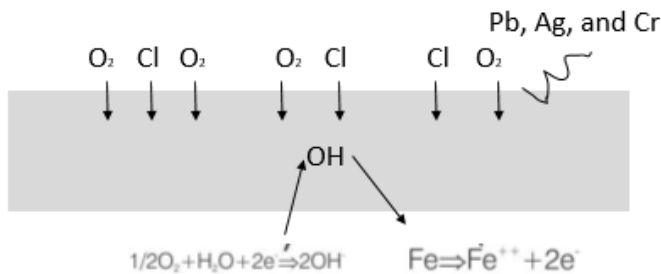


Figure 4 Chemical reaction inside concrete buis type.

10 elements were selected: barium, strontium, cadmium, chromium, cobalt, copper, manganese, nickel, vanadium, and

mercury for further investigation. Some of these metals, Cd, Cr, Ni and Hg, are known as poisons or are suspected carcinogens. Metal air emissions are the biggest concern because of the health risks resulting from this release. Several studies in cement have tried to study the fate and distribution of metals found in waste fuels. The amount of mercury transferred to the clinker or cement is difficult to determine because of the high volatility.



Figure 5: Breakwater of concrete buis type built on 2012.

2.6. Phytoplankton, Benthic Organism and Boring Community

Indonesia has two characteristics season depend on the rainfall. There are four condition regularly happened which were known as northwest-northeast monsoon, first transitional season, southeast-southwest monsoon and the second transitional season. The differences of wave length and wave height are influenced by seasonal variation. Characteristics of waves study is very important because it deal with the strength of wave.

Research report by Ismanto et al [9] stated that the sediment concentration distribution model results in Figure 3. Seen from tides scenario that the highest flood tide (Figure 6a) change the concentration of sediment dominant with a distance of 6 km from the source of pollutants where sediment concentration values ranging between 0,015 - 0,045 kg/m<sup>3</sup>. While the condition of the lowest tide ebb sediment concentrations scattered small enough dominance in which the value of sediment concentration ranges between 0,01 - 0,03 kg/m<sup>3</sup> with a distance of 3 km distribution (Figure 6b). This sediment transport patterns affected by the tidal patterns, where the pattern of sediment transport and the direction of ocean currents towards to near the shore in accordance with the conditions of simulated at high tide. According to Gyr and Hoyer [11] sediment transport patterns are not only influenced by the mass of water flow patterns but also depend on monsoon different wind conditions. The simulation shows that the distribution of sediment is quite small because of the small ocean currents velocity.

3. Result and Conclusion

This study found several factors affected the breakwater effectiveness in Demak coastline, so there is urgent need to select construction materials for breakwaters which are economic, high durability, and eco- friendly. Basically, ecosystem rehabilitation activities is an attempt to restore the degraded ecosystem. This integrated approach is called eco-friendly permeable breakwater, i.e. brushwood dam breakwater type. Based on the characteristics area, there are several materials which may be chosen to construct the breakwater as given in Table 1.



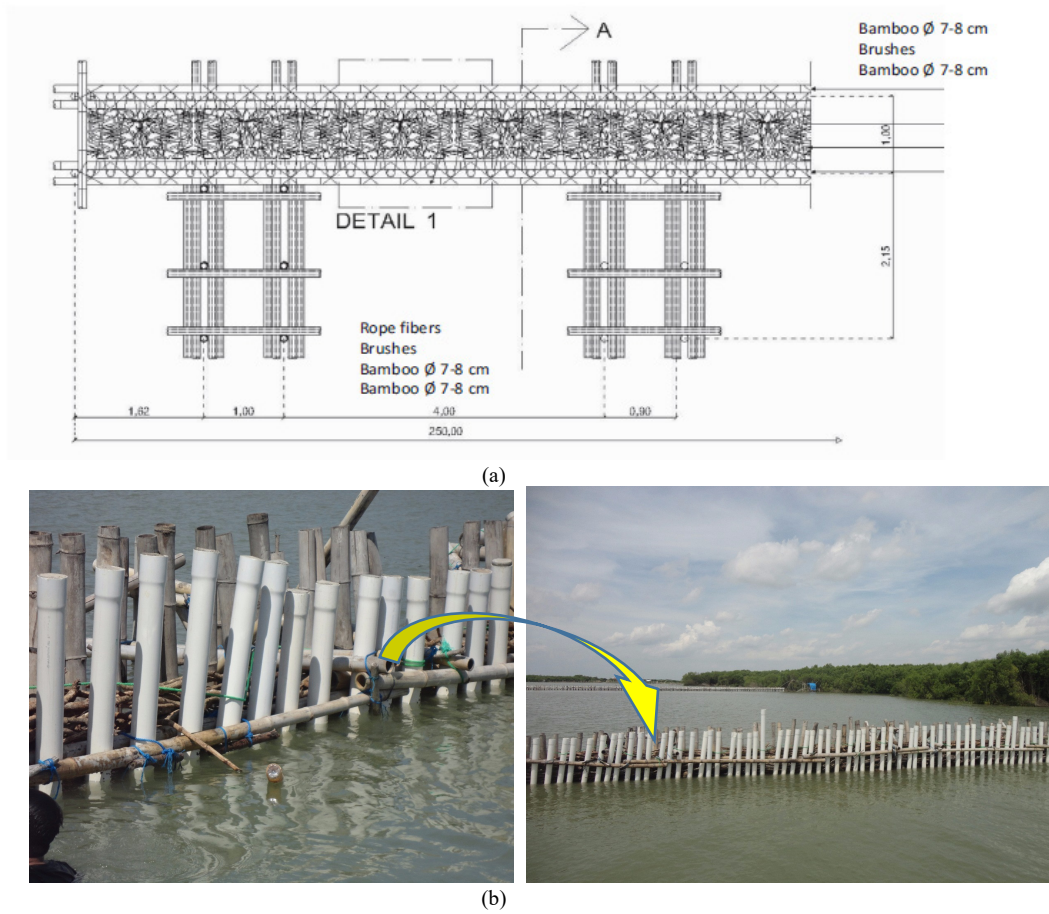


Figure 6: (a) Design of eco-friendly hybrid permeable breakwater

Table 2 : Economic analysis of construction materials.

Materials	Durability	Treatment	Cost (USD)/meter
PVC	4 - 5 years	Interfenced by human (almost no)	90 – 100
Bamboo	3 – 4 years	Attacked by boring community (slower)	80 - 90
Wood	8 month – 2 years	Attacked by boring community (faster, more quickly damage)	60 - 75
Pipe Concrete (Ø 90 cm)	7 – 10 years	Heavy weight, landslide by sediment, chemical reaction	250 - 350

The construction of this type of breakwater restore the habitats for mangroves replant which require surface sedimentation, the greater sedimentation rates the faster mangrove growth. The sedimentation rate is in the proportion with sediment concentration in the water column, in which could be increased by dredging agitation and restoration motion. Massive structures (pipe concrete) were too expensive. The bamboo and PVC combination type permeable breakwater would naturally provides a variety of ecosystem needs, such as coastal protection (adjustable according to sea level rise), fishery resources, as a nursery of marine biota, and improve water quality.

#### 4. Conclusion

Based on the analysis among factors caused breakwater damage's in study area of Timbul Sloko village of Demak regency

is chemical reaction, characteristics sediment, and crustacean borers. Eco-friendly permeable breakwater type aims to restore mud beaches for mangroves replant by restoring lost areas due to erosion and abrasion.

The best materials recomend for eco-friendly permeable breakwater are the bamboo and PVC combination. PVC has excellent chemical resistance, cause increase of sedimentation process and accelerate coastal changes towards the sea. Effectiveness level the bamboo and PVC combination breakwater type is 62%, and more economical than other general-purpose plastics such as PE, PP, or PS.

#### Conflict of Interest

The authors declare that there is no conflict of interest regarding

the publication of this paper.

## Funding Statement

The work was funded by Ministry of Research Technology and Higher Education (Ristek Dikti) Republic of Indonesia, with grant number 257-104/UN7.P4.3/PP/2019.

## Acknowledgment

We would like to thank to Oceanography Department Diponegoro University, Center for Coastal Rehabilitation and Disaster Mitigation Studies (CoRem-PKMBRP) - Center of Excellence Science and Technology (PUI), LPPM Diponegoro University and Ministry of Research Technology and Higher Education (Ristek Dikti) Republic of Indonesia for funding our research.

## References

- [1] M.A. Marfai, "The hazards of coastal erosion in Central Java, Indonesia: An overview," *Malaysia Journal of Society and Space*, vol. 7, no. 3, pp. 1 – 9, 2011.
- [2] Badan Pusat Statistik, "Kecamatan dalam angka di Demak," 2012.
- [3] S. Bagli and P. Soille, "Morphological automatic extraction of Pan-European coastline from Landsat ETM+images," *International Symposium on GIS and Computer Cartography for Coastal Zone Management*, October, Genova, 2012.
- [4] Suripin, D.N. Sugianto and M. Helmi, "Mangrove restoration with environment friendly permeable breakwater," *Asian Journal Biotech Environemental*, vol. 19, no. 1, 2016.
- [5] P. Hawati, D. N. Sugianto, S. Anggoro, et al., "Waves induce sediment transport at coastal region of Timbulsloko Demak," *IOP Conf. Series: Earth and Environmental Science*, vol. 55, Article ID 012048, 2017.
- [6] I. Alifdini, Y.O. Andrawina, D.N. Sugianto, et al., "Technology application of oscillating water column on the Sungai Suci Beach as solutions for make a renewable energy in Coastal Bengkulu, Indonesia," *3rd Asian Wave and Tidal Energy Conference (AWTEC) Proceeding*, vol. 2, Nanyang Technological University, Singapore, 2016.
- [7] I.M.S. Borges, A.A. Valente, P. Palma, et al., "Changes in the wood boring community in the Tagus Estuary: a case study," *Marine Biodiversity Records*, vol. 3, pp. 1-7, 2010.
- [8] D.N. Sugianto, M. Zainuri, A. Darari, et al., "Wave height forecasting using measurement wind speed distribution equation in Java Sea, Indonesia," *International Journal of Civil Engineering and Technology*, vol. 8, no. 5, pp. 604-619, 2017.
- [9] A. Ismanto, M. Zainuri, S. Hutabarat, et al., "Sediment transport model in Sayung District, Demak," *IOP Conf. Series: Earth and Environmental Science*, vol. 55, Article ID 012007, 2017.
- [10] J. Gu, Y. Ma, B. Wang, et al., "Influence of near-shore marine structures in a beach nourishment project on tidal currents in Haitan Bay, facing the Taiwan Strait," *Journal of Hydrodynamics*, vol. 28, no. 4, pp. 690-701, 2016.
- [11] B. Triatmodjo, "Teknik Pantai (Coastal Engineering)," Beta Offset, Yogyakarta, 1999.
- [12] A. Safarzadeh, A. H. Zaji and H. Bonakdari, "Comparative assessment of the hybrid genetic algorithm-artificial neural network and genetic programming methods for the prediction of longitudinal velocity field around a single straight groyne," *Applied Soft Computing*, vol. 60, pp. 213-228, 2017.
- [13] E. Garel, C. Sousa and O. Ferreira, "Sand bypass and updrift beach evolution after jetty construction at an ebb-tidal delta," *Estuarine, Coastal and Shelf Science*, vol. 167 (A), pp. 4-13, 2015.
- [14] J. Shen, H. Wu and Y. Zhang, "Subsidence estimation of breakwater built on loosely deposited sandy seabed foundation: Elastic model or elasto-plastic model," *International Journal of Naval Architecture and Ocean Engineering*, vol. 9, no. 4, pp. 418-428, 2017.
- [15] H.D. Soo, W.C. Cho, J. S. Yoon, et al., "Applicability of multiple submerged narrow-crested breakwaters for reduction of mean water level in rear side and flow control," *Journal of Coastal Research: Special Issue*, vol. 79, pp. 179-183, 2017.
- [16] B. Grasmeyer, "Process-based cross-shore modelling of barred beaches," *Nederlandse Geografische Studies*, vol. 302, pp. 19 – 251, 2002.
- [17] D.S. Hur, W.D. Lee and W.C. Cho, "Characteristics of wave run-up height on a sandy beach behind dual-submerged breakwaters," *Ocean Engineering*, vol. 45, pp. 38–55, 2012.
- [18] S. Baker, N. Sultan, A. Cornett, et al., "Physical modelling and design optimizations for a new port in Brazil. coastal structures and solutions to coastal disasters, 2015: resilient coastal communities," *Proceedings of the Coastal Structures and Solutions to Coastal Disasters Joint Conference*, pp. 838-847, 2015.
- [19] I. Aouiche, L. Daoudi, E.J. Anthony, et al., "Alongshore variations in morphology and incident wave energy on a human-impacted coast: Agadir, Morocco," *Journal of Coastal Research*, vol. 1, no. 75, pp. 1027-1031, 2016.
- [20] I. Alifdini, D.N. Sugianto, Y.O. Andrawina, et al., "Identification of wave energy potential with floating oscillating water column technology in Pulau Baai Beach, Bengkulu," *IOP Conf. Series: Earth and Environmental Science*, vol. 55, Article ID 012040, 2017.
- [21] D. Dykstra, X. Xing, and C. Devick, "Floating breakwater modeling and design for oyster point marina," *Coastal engineering practice*, "Proceedings of the 2011 Conference on Coastal Engineering Practice", pp. 903-916, 2011.
- [22] V. Noujas, K.V. Thomas, L. S. Nair, et al., "Management of shoreline morphological changes consequent to breakwater construction," *Indian Journal of Marine Sciences*, vol. 43, no. 1, pp. 54-61, 2014.
- [23] N.L. Jackson, M.D. Harley, C. Armadori, et al., "Beach morphologies induced by breakwaters with different orientations," *Geomorphology*, vol. 239, pp. 48–57, 2015.
- [24] Y. Kuriyama and M. Banno, "Shoreline change caused by the increase in wave transmission over a submerged breakwater due to sea level rise and land subsidence," *Coastal Engineering*, vol. 112, pp. 9-16, 2016.
- [25] L. Benedet, J.P.F. Dobrochinski, D.J.R. Walstra, et al., "A morphological modeling study to compare different methods of wave climate schematization and evaluate strategies to reduce erosion losses from a beach nourishment project," *Coastal Engineering*, vol. 112, pp. 69-86, 2016.
- [26] P. Hutchings, "Biodiversity and functioning of polychaetes in benthic sediments," *Biodiversity and Conservation*, vol. 7, pp. 1133-1145, 1998.
- [27] S. Monari, "Phylogeny and biogeography of pholadid bivalve *Barnea* (Anchomasa) with considerations on the phylogeny of Pholadoidea," *Acta Palaeontologica Polonica*, vol. 54, no. 2, pp. 315–335, 2009.
- [28] R. Lopez-Anido, A.P. Michael, B. Goodell, et al., "Assessment of Wood Pile Deterioration due to Marine Organisms," *J. of Waterway, Port, Coastal and Ocean Engineering*, vol. 130, no. 2, pp. 70-77, 2004.
- [29] B. Goodell, "Wood products: deterioration by insects and marine organisms," *Encyclopedia of materials science and technology*, Elsevier, New York, 2000.
- [30] E.A. Lawry and C.S. L. Arrowsmith, "Monitoring of geotextile offshore breakwaters to enhance mangrove re-vegetation," *Australian Coasts and Ports*, pp. 497-501, 2015.
- [31] A.F. Zakki, D.M. Bae, S. Susilo, et al., "Structure design and characteristic analysis of buckling strength on swedge frame pressure hull with finite element analysis," *ARPN Journal of Engineering and Applied Sciences*, vol. 12, no. 3, pp. 821-833, 2017.

## Implementing an AGV System to Transport Finished Goods to the Warehouse

Nuno Correia<sup>1</sup>, Leonor Teixeira<sup>2,\*</sup>, Ana Luísa Ramos<sup>3</sup>

<sup>1</sup>Department of Economics, Management, Industrial Engineering and Tourism, University of Aveiro, 3010-193 Aveiro, Portugal

<sup>2</sup>Institute of Electronics and Informatics Engineering of Aveiro / Research Unit on Governance, Competitiveness and Public Policies, Department of Economics, Management, Industrial Engineering and Tourism, University of Aveiro, 3010-193 Aveiro, Portugal

<sup>3</sup>Research Unit on Governance, Competitiveness and Public Policies, Department of Economics, Management, Industrial Engineering and Tourism, University of Aveiro, 3010-193 Aveiro, Portugal

### ARTICLE INFO

Article history:

Received: 01 January, 2020

Accepted: 22 February, 2020

Online: 20 March, 2020

Keywords:

Automated guided vehicle (AGV)

Automotive industry

Productivity

Waste

### ABSTRACT

*This work describes a case study carried out in an automotive company. The main objective was to increase the productivity of the last workstation of an assembly line by implementing an AGV System to transport finished goods to the warehouse. A comprehensive analysis of Value Added and Non-Value Added activities were performed to understand the current state of the workstation. By using the Spaghetti Diagram, the worker's movements were mapped and quantified. To eliminate motion and material transport and therefore increase productivity, an AGV system was implemented. To design this particular system, it was necessary to determine the required number of AGVs and their capacity, picking and delivery locations and the flow path. Activities such as transporting the containers and moving around to pick up the same containers were eliminated, thus contributing to a better ergonomics and an increase in safety. The Cycle Time was also reduced and therefore productivity was increased.*

## 1. Introduction

Due to the organizations' desire to grow and scale up their business, the global marketplace has become highly competitive. This leads organizations to enter on a crusade of continuous improvement to guarantee sustained customer satisfaction and to level up competitiveness with other organizations [1].

Customers thinking is changing. They have become more demanding for cutting-edge products and services at a lower price and that can be delivered to them in the shortest period possible [2]–[4].

To satisfy the customer on these demands, a new management philosophy emerged - Lean Manufacturing, whose primary goal is the maximization of value for the customer by eliminating production wastes [5]. Nowadays, companies focus on reducing waste and Non-Value Added activities. One of the examples is the internal movement of materials. By improving this aspect, it is possible to improve the distribution and manufacturing flows efficiency [6]. One way of improving the internal material

handling and reduce Non-Value Added activities is by implementing Automated Guided Vehicle (AGV) Systems. An AGV is a driverless transport system that is used to move all types of materials in an automated way. With these systems, it is possible to fully automate material flows between several departments. The design of an AGV system involves many concerns. The main ones are guided-path design, estimation of a number of vehicles required, vehicle scheduling, idle-vehicle positioning, battery management, and vehicle routing and deadlock resolution [7].

This paper describes the work that was carried out in an automotive company that produces car components and assembles gearboxes. Its main goal was to improve the productivity of the last assembly line workstation, through the reduction of wastes by implementing an AGV system. To accomplish this objective several aspects were studied. First, the Value Added (VA) and Non-Value Added (NVA) activities were mapped and the wastes in the workstation were highlighted and quantified. To implement the AGV system it was necessary to determine: (i) the required number of AGVs and their capacity, (ii) picking and delivery locations, (iii) flow paths and (iv) speeds in different sections.

\* Leonor Teixeira, Email: [lteixeira@ua.pt](mailto:lteixeira@ua.pt)



This paper is organized as follows: the current section makes a brief introduction to the project as well as to its objectives and methodology. The second section presents a literature review on Lean Manufacturing and Automated Guided Vehicle systems. In the third section, it is presented the case study and in the fourth and last section, it is described the main conclusions of the work.

## 2. Literature Review

### 2.1. Lean Manufacturing

It all started with the introduction of Toyota Production System (TPS) [8]. TPS target was to remove any kind of waste and inconsistency in the production system. Its foundations are Just-In-Time (JIT) and Jidoka [9]. JIT aims to produce only what is necessary and only when requested [10]. Jidoka is the ability to stop production the moment a defect is detected.

Lean manufacturing philosophy focuses on customer value maximization through the elimination of production wastes [11]. This philosophy has a set of tools for eliminating waste, optimizing workflow, reducing cost and improving quality [12]. Examples of these tools are one-piece flow, standardized work, inventory management, cellular manufacturing, poke yoke, workplace organization, synchronous manufacturing, kaizen and scrap reduction waste [13].

The lean concept applies to almost all industries [14]. Some industry examples are chemical, aerospace, electronics and services [15]–[17].

*Muda* is the Japanese word for waste. If an activity does not add value to a product is considered waste. By consuming time and resources, it makes the product more expensive [18]. In a manufacturing context, three types of operation are undertaken according to [19], namely, (i) Non-Value Adding (NVA); (ii) Necessary but Non-Value Adding (NNVA); (iii) Value-Adding (VA). NVA activities are pure waste and they should be eliminated. NNVA operations are wasteful but they are necessary for the process itself. VA operations are related to the conversion or processing of an item in any stage of the process, adding value to the product.

### 2.2. Eight Wastes

The seven wastes in an industrial environment that were identified by [8] are inventory, defects, motion, over-processing, overproduction, transportation and waiting periods. Overproduction is considered the most serious waste because it triggers the other six types of waste. This leads to additional transportation, excessive handling, an increase in stock levels, more waiting time and so on. Recently an additional waste was identified by [20], which is people's talent. For an efficient flow of goods or services, these wastes should be minimized.

### 2.3. Spaghetti Diagram

A *spaghetti* diagram is a visual tool that shows materials and people flow during a process, inside a factory, being these flows represented by lines. According to [21] it gives a full picture in the identification of the following problems:

- Cross-traffic – Paths that have intersection will cause congestion and delays;

- Backtracking – Material moving backward, in the opposite way of normal flow;
- Distance traveled – Distance traveled by materials and people in the plant;
- Procedure – understand if the sequence of operations is the most suitable one or the equipment placement is the right one.

The purpose of these diagrams is to find solutions on how to shorten the distances traveled by people and materials.

In a manufacturing environment, there are flows from different domains. The seven flows of lean manufacturing are the flow of raw material, the flow of work-in-progress, the flow of finished goods, the flow of machines, the flow of operators, the flow of engineering and the flow of information [22]. The mapping of the flows mentioned above allows us to understand how people and materials interact to add value to the product [23].

### 2.4. Automated Guided Vehicle (AGV)

AGVs are driverless vehicles that run on the plant floor which have the capacity of carrying loads. These are designed to perform their operations without direct human guidance and are used in a wide variety of industrial applications [24]. To achieve the benefit of integrated automation, they are interfaced with other automated systems [25]. AGV systems have been frequently used as material handling equipment in the manufacturing context [26] and it represents the most versatile means of moving materials automatically [25]. Firstly, AGVs provide automated loading, transportation, and unloading capabilities. Therefore, there are several applications where AGVs can be used, such as manufacturing plants, container terminals, material handling systems, warehouses and service industries [27]. They are being integrated in these systems because they provide a wide range of benefits in economic, environmental and social sustainability dimensions [28]–[30], including labor cost savings [31], increased productivity [32], enhanced safety [33], reduced emissions [34] and energy consumption [35].

AGVs are versatile enough to transport more than one load at the same time. A load refers to a number of items arranged in such a way (ordered or not) that they can be transported as a single object. A container or a pallet are some examples of a unit load [36]. By transporting multiple loads, the number of vehicles needed may reduce and throughput of a system may increase. Additional loads may be picked up while transporting a previously assigned load. The benefit of using multi-load vehicles includes a reduction in the number of vehicles' empty trip time and total distance traveled [7].

An AGV system must be built to satisfy a specific need and suited to different situations. When designing an AGV system, several factors should be considered, such as, the available budget, the quantities to be moved, the goods to be handled, the distance travel and the type of production system that the AGV will serve [25]. According to [37], the following tactical and operational issues have to be addressed in designing an AGV system:

- Flow path layout - Flow path can be unidirectional and bidirectional. A flow is unidirectional when vehicles travel in only one direction. When vehicles travel in both directions the



flow is bidirectional. However, in a bidirectional flow, vehicles cannot travel in opposite directions at the same time.

- Traffic management: prediction and avoidance of collisions and deadlocks number and location of pick-up and delivery points - For safety and collision-free travel, sensors are attached to AGVs. Another method is splitting the shop floor into control zones. By doing this, only one vehicle at the same time is allowed to travel through the control zone. Consequently, at any given time, a zone is occupied by only one vehicle while others are waiting for that zone to be free.

The choice of the location of pick-up and delivery points is important. It influences the operational performance. The goal is to reduce the distance traveled and waiting times of loads avoiding bottlenecks at pick-up and delivery points. This factor is even more important when large AGV systems are displayed.

- Vehicle requirements – The number of vehicles heavily influences the performance of AGV systems [37]. To ensure that the system runs smoothly without any problems, enough vehicles should be available. However, due to economic, congestion and space availability reasons, the number of vehicles should not be overestimated.
- Vehicle dispatching – Dispatching rules should be used when selecting vehicles for transportation, by selecting the most favorable one for a good performance.
- Vehicle routing and scheduling – if an AGV is allocated to one task a route and schedule should be planned. A route indicates the path which should be taken by the AGV when making a pick-up or delivery. The related schedule gives arrival and departure times of the AGV at each segment, pick-up and delivery point, and intersection during the route to ensure collision-free routing.
- The positioning of idle vehicles – the location of idle vehicles should be defined so the waiting times of loads for transport are low. By assuring this, AGVs will respond quickly when they are requested.
- Battery management - batteries are used as a fueling system. Like any other battery, it needs to be charged or changed at a given time. The charging or changing time should not be forgotten because it impacts system performance (vehicles required, throughput, congestion, and costs).
- Failure management – when few AGVs are used, the probability of congestion will be low, and its occurrence will be unnoticed on the system performance. When there are a lot of AGVs being used, failures' probability will be higher. These failures might cause congestion and deadlocks in the system.

### 3. Case Study

The company involved in this case study produces components for car motors and also gearboxes. More specifically, the project was at the gearbox assembly line. The main goal is to improve the productivity of the last assembly line workstation (workstation Y) by reducing NVA activities such as movements and transportation. With this in mind, an AGV system was implemented to transport empty containers from the warehouse and then full containers from the assembly line's last station to the warehouse.

#### 3.1. Workstation Y

It is at workstation Y where the final details are applied to the product. Once this is accomplished, the finished products are scanned and stored in a container in batches of eight or twelve (Operation 1). These are the sizes of the available containers. Then they are transported by an assembly line worker to the production leaving the area (Operation 2). Even though the containers have wheels, the weight of a full container ranges between 420kg to 600kg and the worker has to move them between 50 to 75 times during a shift. After this, the worker is responsible for putting an empty container in his workstation (Operation 3 and 4). This operation flow can be seen in Figure 1, as well as the Spaghetti Diagram reflecting the worker's movements.

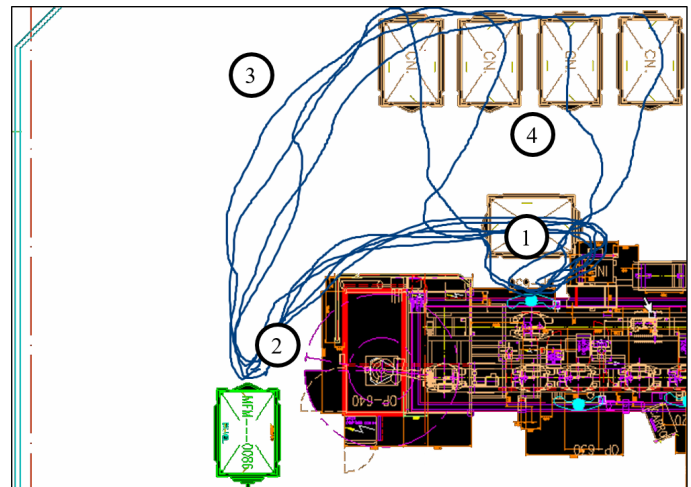


Figure 1: Workstation Y before AGV implementation with the corresponding Spaghetti Diagram.

Then a logistic operator comes, hitch all the available containers and transport them to the warehouse. There he unhitches the containers and put them into shelves with a fork lifter.

Each activity performed by the worker was defined as VA or an NVA activity, as proposed by [38]. Figure 2 depicts an analysis of VA and NVA of the production activity in the analysis. Most of the NVA is the result of excessive motion and containers transport by the assembly line worker. These activities must be reduced because they do not add value.

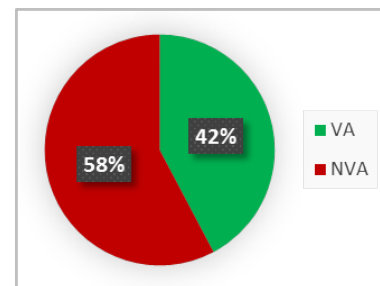


Figure 2: VA and NVA analysis before AGV implementation.

Looking at the ergonomics dimension this workstation is also critical because of the repeated movement of heavyweights executed by the worker. This can lead to health issues and the probability of occurring an accident is bigger. After identifying the wastes, they were quantified as shown in Table 1. Traveled



The number of round-trips required is related to the assembly line productivity and the AGV capacity. In Table 2, it is possible to see the calculations' results based on Figure's 3 calculation sheet. If the number of AGVs is too small, the assembly line may stop due to the lack of containers but if the number of AGVs is too big, it may overload the system and it will be a large investment without necessity.

The AGV capacity must not exceed three containers due to the factory layout. If the number of containers is higher than three, in some corners, there is a chance of clashing with each other and therefore product quality may be affected. In addition, it is even possible that they cross-areas reserved for people's movements, increasing the chance of an accident. According to Table 2, and considering arguments above, the optimal number of AGVs for this system is two.

Even though two AGVs are enough for this system, some prevention actions were made. For example, if a round trip takes more time than expected for some reason, the AGV may not arrive in time at the Workstation Y. Then the worker from this station does not have a container to store the gearbox and therefore the assembly line may stop. To prevent this situation, an extra container was placed near this workstation. If an AGV does not arrive in time, the worker can store the gearbox in this container and when the AGV arrives, he can replace the containers.

**4. Results**

To validate the model and confirm that the estimation of the number of AGVs was correct, some data were collected to compare the estimated values and the real values. After the AGV implementation, round trip and unloading time were measured. These are the real values and the same formula was used. The main purpose was to validate this method.

The data collected was slightly different from what was estimated. Despite these differences, the calculations with new data reveal that the number of AGVs required is still the same (Table 3). This confirms that the formula used is suitable for this kind of system.

Table 3: Data before and after the AGV implementation for a shift.

	Estimated Values	Real Values	Δ
Unloading AGV (minutes)	5	4.22	-0.78
Average Loaded travel Time (minutes)	4.63	5.08	+0.45
Average Unloaded travel Time (minutes)	4.07	4.99	+0.92
Number of AGVs	1.84	1.88	+0.04

After the AGV implementation, several improvements have been recorded. The main goal was to reduce the Non-Value activities such as motion and materials' transports from workstation Y to the warehouse.

The improvements depend on the type of container used at the moment. If the container size is 8, the worker has to move more containers, therefore, increasing the distance traveled. All the

container manipulations were eliminated. Now the worker of the workstation Y never leaves its station. He only focuses on finishing the product and put it in the container. Only body rotation is needed, as can be seen in the Spaghetti Diagram in Figure 4. Therefore, he no longer has to transport the heavy containers, improving this station from an ergonomics dimension and his well-being. Many efforts to do his job were eliminated. The results of the AGV implementation for a shift are summarized in Table 4.

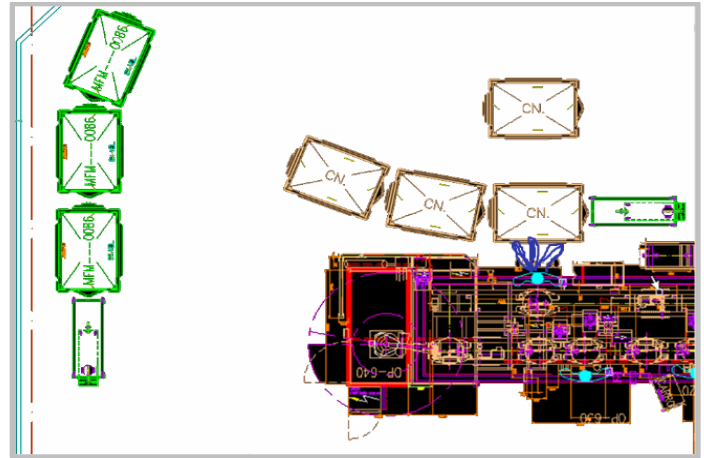


Figure 4: Workstation Y after AGV implementation with the corresponding Spaghetti Diagram.

All of the improvements contributed to Non-Value added activities reduction, something that Lean Manufacturing aims for. As mentioned above all the distance traveled transporting the containers by the worker was eliminated. Therefore, the percentage of Non-Value added activities declined. The remaining Non-Value added activities are validation and control activities that are essential for the process as shown in Figure 5.

Table 4: Data before and after the AGV implementation for a shift.

Wastes identified at Workstation Y	Container Size = 8		Container Size = 12	
	Before	After	Before	After
Containers manipulations	150	0	100	0
Loads transported (tonnes)	39	0	36	0
Distance traveled (kilometers)	2,6	0	1,75	0
Time spent moving (minutes)	50	0	50	0

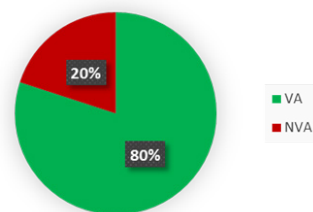


Figure 5: VA and NVA analysis after AGV implementation.

The time that was spent moving the containers as part of the cycle time. By eliminating this, the cycle time was improved and all the variability associated with the container transport. The cycle time is now 39.57 seconds. This represents an improvement of 13%. This workstation is now under the Takt time desired and therefore is able to produce the quantities desired in the available time.

It was also possible to eliminate a logistics worker and a convenient means of transport (logistic train) from the production area. This worker now is located at the unloading area and is responsible for placing the full containers on the shelves from the two assembly lines existing in the factory. Activities such as hitching and unhitching the containers do not exist anymore because they are attached to the AGV. The workplace is now more organized because there is no need for an excessive number of containers laying around.

## 5. Conclusions

The company wants to automate materials flows inside the factory to achieve a flexible system and to eliminate waste in operations that involve transporting material from one point to another. Its ultimate goal is to remove all the fork lifters and others mean of transport that requires humans, in the production area, increasing not only flexibility but also safety.

Number of AGVs required, the proper AGV speed, active and inactive AGV positioning, AGV capacity, load and unload locations, and tasks linked to electronic tags to give orders to the AGVs, had to be determined. All these features needed to be determined so that the assembly line never stopped.

With the implementation of the AGV system, it was possible to eliminate the transport of heavy loads by the operator and the excess of containers at the workstation, thus contributing to better ergonomics, an increase of safety and greater productivity. The worker has stopped manipulating containers between 100 and 150 times during a shift. In a full shift, this represents: (i) between 36 and 39 tons of material is not transported anymore by the worker, (ii) by not transporting this material, the worker stops walking between 1.75 and 2.6 kilometers and (iii) the time-traveling was reduced in 50 minutes. Being an automatic system and with security features incorporated, the probability of happening any accident between people and vehicles also was reduced and consequently safety improved. The risk of having damaged pieces during transport was also minimized. Having these systems means having the right product, at the right quantity, at the right time, and the right location, reducing stock at the assembly line. This led to a full synchronization between logistics and production regarding gearboxes.

In the short term, it may be an expensive system, but when integrated with other applications it may be worthwhile because then it is possible to have a fully flexible system that can be changed easily saving money and time.

For a future project and to integrate all processes between production and logistics, an AGV system at unloading finished product at the warehouse should be designed, using AGV Fork lifters. In the way, it would be possible a full integration from the beginning of production until the storage at the warehouse. Another topic that should be addressed is how to maintain the

RFID in good shape (like preventive maintenance), to minimize AGV stops, due to non-reading or incorrect reading from its RFID reader. In addition, a simulation study is being developed to analyze the operational performance of the entire system to improve it continuously. This study incorporates AGV failures to test some scenarios regarding the system's robustness.

## Conflict of Interest

The authors declare no conflict of interest.

## Acknowledgment

This work was financially supported by Institute of Electronics and Informatics Engineering of Aveiro funded by National Funds through FCT - Foundation for Science and Technology, in the context of the project UIDB/00127/2020; and by the research unit on Governance, Competitiveness and Public Policy (project POCI-01-0145-FEDER-008540), funded by FEDER funds through COMPETE 2020 and by national funds through FCT - Foundation for Science and Technology.

## References

- [1] J. Singh, V. Rastogi, R. Sharma, "Implementation of 5S practices: A review." *Uncertain Supply Chain Management* 2 (3): 155–162, 2014. <https://doi.org/10.5267/j.uscm.2014.5.002>
- [2] R. J. Tersine, J. G. Wacker, "Customer-aligned Inventory Strategies: Agility Maxims." *International Journal of Agile Management Systems* 2 (2): 114–120, 2000. <https://doi.org/10.1108/14654650010337122>
- [3] H.C.W. Lau, B. Jiang, F. T. S. Chan, R. W. L. Ip, "An Innovative Scheme for Product and Process Design." *Journal of Materials Processing Technology* 123 (1): 85–92, 2002. [https://doi.org/10.1016/S0924-0136\(02\)00068-7](https://doi.org/10.1016/S0924-0136(02)00068-7)
- [4] G. T. S. Ho, H. C. W. Lau, C. K. M. Lee, A. W. H. Ip, "An Intelligent Forward Quality Enhancement System to Achieve Product Customization." *Industrial Management and Data Systems* 105 (3): 384–406, 2005. <https://doi.org/10.1108/02635570510590174>
- [5] I. Belekoukias, J. Garza-Reyes, V. Kumar, "The Impact of Lean Methods and Tools on the Operational Performance of Manufacturing Organizations." *International Journal of Production Research* 52 (18): 5346–5366, 2014. <https://doi.org/10.1080/00207543.2014.903348>
- [6] J. Tompkins, J. White, Y. Bozer, J. Tanchoco, *Facilities planning*. 3rd ed. USA: Hamilton Printing Company, 2003.
- [7] T. Le-Anh, M.B.M. De Koster, 2006. "A review of design and control of automated guided vehicle systems." *European Journal of Operational Research* 171 (1): 1–23, 2006. <https://doi.org/10.1016/j.ejor.2005.01.036>
- [8] T. Ohno, *The Toyota Production System: Beyond Large-scale Production*. Portland, OR: Productivity Press, 1988.
- [9] J.K. Liker, *The Toyota Way: 14 Management Principles from the World's Greatest Manufacturer*. New York: McGraw-Hill, 2004.
- [10] S. Tiwari, R. Dubey, N. Tripathi, "The Journey of Lean." *Indian Journal of Commerce and Management Studies* 2 (2): 200–208, 2011. <https://doi.org/10.17010/pijom/2016/v9i9/101509>
- [11] J. Womack, D.T. Jones, *Lean Thinking: Banish Waste and Create Wealth in Your Corporation*. New York: Free Press, 2003.
- [12] H.D. Koning, J.P.S. Verver, J.V.D. Heuvel, S. Bisgaard, R.J.M.M. Does, "Lean six sigma in healthcare." *Journal for Healthcare Quality* 28 (2): 4–11, 2006. <https://doi.org/10.1111/j.1945-1474.2006.tb00596.x>
- [13] R.S. Russell, B.W. Taylor, *Operations Management*. 2nd ed. Upper Saddle River, NJ: Prentice-Hall, 1999.
- [14] V. Crute, Y. Ward, S. Brown, A. Graves, "Implementing Lean in Aerospace – Challenging the Assumptions and Understanding the Challenges." *Technovation* 23 (12): 917–928, 2003. [https://doi.org/10.1016/S0166-4972\(03\)00081-6](https://doi.org/10.1016/S0166-4972(03)00081-6)
- [15] D. Bowen, W. Youngdahl, "Lean Service: In Defense of a Production Line Approach." *International Journal of Service Industry Management* 9 (3): 207–225, 1998. <https://doi.org/10.1108/09564239810223510>
- [16] P. Atkinson, "Creating and Implementing Lean Strategies." *Management Services* 48 (2): 18–33, 2004.
- [17] F. Abdi, S. Shavarini, S. Hoseini, "Glean Lean: How to Use Lean Approach in Services Industries?" *Journal of Services Research* 6 (Special Issue): 191–206, 2006.



- [18] J.C. Chen, L. Ye, B. D. Shady, "From Value Stream Mapping toward a Lean/Sigma Continuous Improvement Process: An Industrial Case Study." *International Journal of Production Research* 48 (4): 1069–1086, 2010. <https://doi.org/10.1080/00207540802484911>
- [19] Y. Monden, *Toyota Production System: An Integrated Approach to Just-in-Time*. 2nd ed. Norcross, GA: Industrial Engineering and Management Press, 1993.
- [20] J. K. Liker, D. Meier, *The Toyota Way Fieldbook: A Practical Guide for Implementing Toyota's 4Ps*. New York, London: McGraw-Hill, 2006.
- [21] F. E. Meyers, J. R. Stewart, *Motion and Time Study for Lean Manufacturing*. 3rd ed. Upper Saddle River, NJ: Prentice-Hall, 2002.
- [22] J.R. Black, *The Toyota Way to Healthcare Excellence: Increase Efficiency and Improve Quality with Lean*. Chicago, IL: Health Administration Press, 2008.
- [23] K. J. Hayes, N. Reed, A. Fitzgerald, V. Watt, "Applying lean flows in pathology laboratory remodelling." *Journal of Health Organization and Management* 28 (2): 229-246, 2014. <https://doi.org/10.1108/JHOM-03-2013-0064>
- [24] R. Pandey, A. Singh, "Utilization of AGVs and Machines in FMS Environment." *Journal of Material Sciences & Engineering*. 5 (4): 263, 2016. <https://doi.org/10.4172/2169-0022.1000263>
- [25] O. R. Ilić, "Analysis of the number of automated guided vehicles required in flexible manufacturing systems." *The International Journal of Advanced Manufacturing Technology* 9 (6): 382–389, 1994. <https://doi.org/10.1007/BF01748483>
- [26] S.E. Kesen, Ö. F. Baykoç, "Simulation of automated guided vehicle (AGV) systems based on just-in-time (JIT) philosophy in a job-shop environment." *Simulation Modelling Practice and Theory*. 15 (3): 272–284, 2007. <https://doi.org/10.1016/j.simpat.2006.11.002>
- [27] H. Fazlollahtabar, M. Saidi-Mehrabad, J. Balakrishnan, "Mathematical optimization for earliness/tardiness minimization in a multiple automated guided vehicle manufacturing system via integrated heuristic algorithms." *Robotics and Autonomous Systems* 72: 131-138, 2015. <https://doi.org/10.1016/j.robot.2015.05.002>
- [28] R.C. Craig, S.R. Dale, "A framework of sustainable supply chain management: moving toward new theory." *International Journal of Physical Distribution & Logistics Management* 38 (5): 360-387, 2008. <https://doi.org/10.1108/09600030810882816>
- [29] M. Kannegiesser, H.-O Günther, N. Autenrieb, "The time-to-sustainability optimization strategy for sustainable supply network design." *Journal of Cleaner Production* 108: 1-13, 2015. <https://doi.org/10.1016/j.jclepro.2015.06.030>
- [30] H. Wu, K. Lv, L. Liang, H. Hu, "Measuring Performance of Sustainable Manufacturing with Recyclable Wastes: a Case from China's Iron and Steel Industry". *Omega*, 2016.
- [31] A. Gosavi, S.E. Grasman, "Simulation-based optimization for determining AGV capacity in a manufacturing system." In: *Proceedings of the Institute of Industrial Engineers Research Conference*, Miami, FL: 574-578, 2009.
- [32] A. Negahban, J.S. Smith, "Simulation for manufacturing system design and operation: literature review and analysis." *Journal of Manufacturing Systems* 33: 241-261, 2014. <https://doi.org/10.1016/j.jmsy.2013.12.007>
- [33] V.G. Duffy, F.F. Wu, P.P.W. Ng, "Development of an Internet virtual layout system for improving workplace safety." *Computers in Industry* 50: 207-230, 2003. [https://doi.org/10.1016/S0166-3615\(02\)00121-5](https://doi.org/10.1016/S0166-3615(02)00121-5)
- [34] H. Geerlings, R. Van Duin, "A new method for assessing CO2-emissions from container terminals: a promising approach applied in Rotterdam." *Journal of Cleaner Production* 19: 657-666, 2011. <https://doi.org/10.1016/j.jclepro.2010.10.012>
- [35] M. Acciaro, G. Wilmsmeier, "Energy efficiency in maritime logistics chains. Research in Transportation Business & Management 17: 1-7, 2015. <https://doi.org/10.1016/j.rtbm.2015.11.002>.
- [36] I. F. Vis, "Survey of research in the design and control of automated guided vehicles." *European Journal of Operation Research*. 170: 677-709, 2006. <https://doi.org/10.1016/j.ejor.2004.09.020>
- [37] J.R. Van der Meer, "Operational control of internal transport system." PhD thesis, Erasmus University, Rotterdam, 2000
- [38] B.H. Maskell, "Performance Measurement for World Class Manufacturing." Cambridge, MA: Productivity Press, 1991.
- [39] K.R. Fitzgerald, "How to estimate the number of AGVs you need." *Modern Materials Handling*: 79, 1985.

## Safety in Industry 4.0: The Multi-Purpose Applications of Augmented Reality in Digital Factories

Lorenzo Damiani\*, Roberto Revetria, Emanuele Morra

Genoa University, DIME (Department of Mechanical Engineering), 16145, Genoa, Italy

### ARTICLE INFO

Article history:

Received: 10 January, 2020

Accepted: 01 March, 2020

Online: 20 March, 2020

Keywords:

Augmented Reality

Health and Safety

Industry 4.0

Digital Twin

Emergency Management

### ABSTRACT

The digital factory is a concept signing a new era for industry, the so-called Industry 4.0, in which ordinary production systems like manufacturing plants, machineries and utilities are being equipped with diagnostic and sensitive instrumentation to be connected to digital shared networks. This data-sharing, through the big data management techniques, is a fully integrated base on which digital tools can be installed and exchange information. Data stored from physical world of machines can be redirected to simulation environments like Digital Twins and can be inspected, for several purposes like predictive analysis, by humans too. On top of these scopes, within the realization of an Internet of Things, there is safety, especially in industrial sites where injury risk for operators and workers is a key factor for production sustainability. This paper, starting from a tested case study in mechanical stressed monitoring, focuses on the application of upgraded augmented reality systems for safety practices, expanding the area of interest to electric and overheating risk mitigation in electrical equipment and to emergency management.

## 1. Introduction

This paper is an extension of a work originally presented 2019 Spring Simulation Conference (SpringSim), Tucson, Arizona, USA [1]; the extended paper, starting from the prevention of mechanical risk for shelving structures, underlines the evolution of augmented reality applications for safety, expanding its area of interest to overheating risk mitigation in electrical equipment and to emergency management. Opportunities for safety improvements are also given by the availability on the market of tools and devices to be connected to the AR main equipment, for example like thermo-camera or gas detection sensors to be mounted on smart glasses. In the current competitive scenario manufacturing companies are facing the challenge of digital transformation, as demonstrated by the arrival of Industry 4.0 [2]. This new paradigm is known as “the fourth industrial revolution” and it refers to new production patterns, including new technologies, productive factors and labor organizations, which are completely changing the production processes and the relationship between customer and company with relevant effects on the supply and value chains [3].

In the next chapters, the technology under study is described in terms of both hardware/software set-up kit and safety practical

applications in industrial sites. In particular, AR devices are related to the main following topics:

- Mechanical risk prevention for steel shelving breakdown due to overloaded storing situations;
- Overheating risk prevention for electrical equipment and devices in case of power overload or short circuit;
- Fire risk and emergency management due to overcrowding or critical emergency situation (big fires, explosion, pollution, evacuation in hospitals, airports, schools).

## 2. Application Development

### 2.1. Augmented Reality Equipment

Several augmented reality equipment and platforms are available on the market for professional purposes: an important assessment on the best SDK and devices to be used has been done by this research group, basing on a market research specific for AR Application in industrial working environment. Basing on the work of Mladenov et al. [4], a specific process for finding the most efficient support has led to the result that smart glasses are the best way to overlay AR objects on the real world or to get information from specific symbols placed on real objects of interest. One of the best features of smart glasses, suitable for safety for workers, is the opportunity to allow hands-free AR experiences. The diffusion of

\* Lorenzo Damiani, Email: [lorenzo.damiani@unige.it](mailto:lorenzo.damiani@unige.it)

these devices has increased the opportunity of developing new AR mobile apps compatible with these gadgets, in order to increase easiness in connection.

The wearable device selected for the development of the AR applications in object are F4 smart glasses, produced by Glass Up an Italian start-up company. These are equipped with a screen on the right lens. The optical system allows a field of view with an angle of 22°, the effect obtained is the same as a 70" screen positioned at a distance of 5 m. The 3D view is possible even if the glasses are not binocular. The glasses are equipped with a video-camera which allows video sharing in real time and the data can be visualized through the software "Dashboard". Therefore, the F4 glasses allow both remote assistance and "on the job training" through explicit videos or images. F4 glasses presented in Figure 1.



Figure 1: Glass-Up F4 VR glasses.

Because of AR technology recent diffusion, long term effects on workers' health have not already been isolated. From a recent study [5], AR technology might represent a benefit for health of users, due to operator's mental workload reduction. But in other studies [6], Head-Mounted Devices like smart glasses, are said to utilize a field of view that is smaller than human's, which could cause headaches, dizziness nausea after a prolonged period of use. Additionally, the HMD is associated with discomfort caused by the weight and a limitation of usage for users that need to use regular goggles. A parallel can be done with Virtual Reality technology, characterized by a longer experience. The key concern from the literature is VR-induced sickness, experienced by a large proportion of VR participants, even if it is not completely clear the exact reason for that disease [7]. A maximum consecutive utilization time period can be safely regarded within 1 hour, before relax. A further study on these aspects should be done.

The software can capture an image and re-send it to the user enriched with additional explicit data, text or drawings to improve the information acquisition, or can highlight in real time [8 – 10] elements in the field of view to focus the user's attention. Several different sensors are optionally available for the F4 glasses: an accelerometer, a compass, a gyroscope, a barometer, a hygrometer, a led torch, plug-in sensors and voice control, all with connections to Wi-Fi, LTE and Bluetooth. It is possible to install a 32X32 thermo-camera too or a gas detection sensor on the glasses support. Electric feeding and interaction with the user are ensured by a USB port.

In general, data can be collected by an electronic card, like the Arduino one, receiving electric signals from dedicated sensors. The card can be programmed trough a software based on C++ language and then data are sent to a platform to be analyzed and elaborated: a specific Wi-Fi module can be used and connected to Arduino card. Data received by the server from sensors on site can be compared to historical data, threshold or safety alarm values and then being sent back to operators equipped with AR visors to be visualized in real time through the glasses lens. Operator is enabled to receive only desired data in many ways: one of these is the QR codes detection, which are applied on surfaces or specific points in order to recognize for examples specific components or safety zones of interests. QR codes identity unique destinations for inquiring or inspection and enable the server to release only the desired data. This level of interconnection is a significant part of the digital factory concept, representing the Internet of Thing in which humans are in the center of information exchange. In Figure 2 below, the main logic concept is depicted.

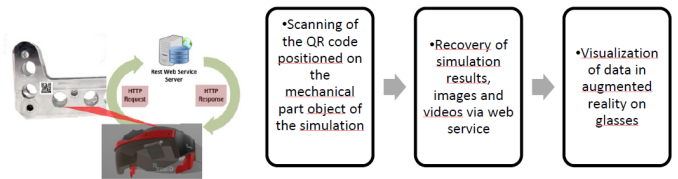


Figure 2: Logics of the application with QR code.

A specific case of application is described in chapter 3.1 regarding strain gauges connection. The same connection path can be used with other tools, for example for sending information to server with a thermo-camera. A similar application under study is described in chapter 3.2. In general, images processing techniques can be inherited by other specific application or case-study [11-15].

## 2.2. Software Development

For safety application using the Arduino system, it is possible and worthy to program the card in a dedicated environment, which is free of charge. The Arduino program is an IDE (Integrated Development Environment). The source code of the programs, called sketch, is a simple text file with .ino extension. The main elements are:

- 1) Text editor;
- 2) Message area;
- 3) Text console;
- 4) Tool bar;
- 5) Menu bar;
- 6) Status bar.

The basic sketch structure is subdivided in two parts:

- The first part, composed by the setup() function, used to configure the card;
- The second part, composed by the loop() function which contains the program executable in a loop.

Data transmission occurs thanks to the ESP8266 router connection, which occurs through AT commands allowing the chip to dialogue with the modem and send data to a server. The data is received by ThingSpeak, the IoT development platform, which analyzes the data coming from the two sensors. The ThingSpeak basic entity is the channel, each of the variables composing a channel are called fields, a maximum number of 8 fields are allowed per each channel.

### 2.3. Thermography Tools

In industrial environments, thermography is used to identify hot spots that lead to failures in mechanical and electrical systems. Early detection of anomalies allows you to avoid production stoppages and save money. In the mechanical field, thermographic control identifies overheating caused by friction between bearings, joints, transmissions and couplings. Thermographic applications in the mechanical field are characterized by high operating and investigation temperatures. The study of temperatures requires careful precautions by the operator. Since the thermographic operator must carry out shooting in an environment where high temperature sources are present, it is necessary to provide shielding systems to reduce as much as possible the reflection effects on the component to be analyzed. On the analysis of mechanical components, in addition to the analysis on bearings and transmission belts, there are frequent analysis of pipes temperature distribution, of boilers, of alternators and production systems of electricity, control-checks of tank levels.

In power transmissions it is necessary to check that there are no abnormal frictions caused by a malfunction. The mechanical faults typically detected are:

- Overheating of the engines;
- Rollers at suspect temperature;
- Overload of the pumps;
- Hot pads;
- Axial overheating of the pumps.

With these controls it is possible to detect the "weak ring" of the system, so that production activity can be guaranteed thanks to immediate interventions. The plants that are subjected to thermographic analysis have the advantage of a production continuity, this would not be possible if they were not monitored continuously, because the damage would be detectable only after the damage happens, forcing the plant to stop. Thermographic applications in the mechanical field are generally characterized by very high operating and investigation temperatures. The investigation of temperatures requires special precautions by the operator; mechanical applications are usually distinguished by an accumulation of temperature following friction phenomena in correspondence with the movement of certain components.

Thermal imaging cameras are commonly used to inspect electrical systems and components of all sizes and shapes. The most commonly detectable faults with thermal imaging cameras can be found in high voltage installations:

- Oxidation of high voltage circuit breakers;
- Overheating of the connections;

- Imperfect fixing of the connections;
- Insulator failure.

When checking electrical systems, it is very important to know the load, the maximum allowed temperatures of the components analyzed. It is necessary to know the external conditions of the component; if a standard survey is carried out externally, it is necessary to know the wind speed and other climatic factors that can affect the temperature of the element. For internal surveys it is necessary to know if there are room cooling systems or convective effects caused by the cooling system of the component itself. Before making measurements of the element to be analyzed, it is necessary to prepare high emissivity points so that the most precise temperature can be read in the case of analysis of conductive metals. In a situation in which the inspection takes place in closed cabinets that cannot be opened without risk for safety of the operator himself, it is recommended to prepare special windows with germanium monocrystalline lenses. In addition, the electrical are different between low voltage and high voltage devices. Thermal imaging cameras are used for low voltage installations such as electrical panels and engine control panels. These checks are carried out to avoid breakdowns or fires. Problems caused by load imbalances; corrosion phenomena can occur.

Examples of failures that are detectable with thermal imaging cameras in low voltage devices include:

- High resistance connections;
- Corrosion of connections;
- Damage to the internal fuse;
- Internal circuit breaker faults;
- Inefficient connections and internal damage.

Instead, for high voltage installation, heat is a relevant factor. When the electric current passes through an element that offers resistance, it generates heat. A high resistance corresponds to an increase in heat. Over time, the resistance of the electrical connections increases. This can be caused by corrosion which causes an increase in temperature which can bring to component failure, possible accidents, unnecessary consumption due to the energy used to generate heat. If not controlled, the heat can reach a level that melts the connections.

Examples of failures that are detectable with thermal imaging cameras in high voltage devices include:

- Oxidation of high voltage circuit breakers;
- Insulator failure;
- Imperfect fixing of the connections;
- Overheating of the connections.

The thermal imaging camera is a particular camera, which detects the intensity of the infrared radiation of a body, it is therefore not an instrument that sees or detects the temperature. Starting from the detected radiation, through an electronic processing of the machine, a digital radiometric type image is obtained in which it is possible to view the temperature of the object.



The essential components of a thermo-camera are (Figure 3):

- Lens;
- Sensor.

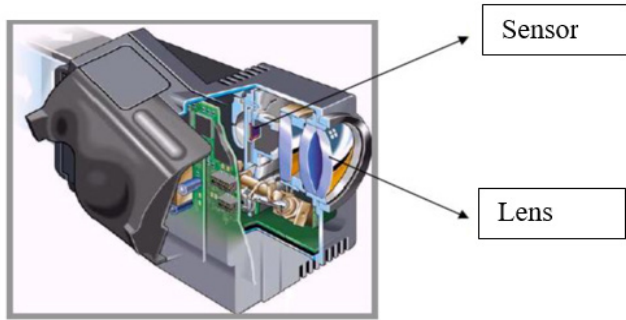


Figure 3: Glass-Up F4 VR glasses.

This image can be viewed as a digital photo or as a video depending on the use of the machine and the software that elaborates the electronics result. The thermal imaging camera is a device similar to a digital camera, which stores the image or frame by converting the infrared, invisible to the human eye, into a visible image represented in false colors. The thermal imaging camera must have adequate optics in relation to the fields of intervention to be analyzed. The optics are made up of germanium lenses, a material that prevents entry to the spectrum of visible radiation, while it is transparent to the passage of the infrared band (with a wavelength between 2 and 14 microns). The focus is electronically controlled by the processing unit or carried out manually by the operator by means of a ring on the lens. Thermal imaging cameras on the market today are divided into two types, cooled and uncooled. The highest accuracies are obtained with cooled thermal imaging cameras, which however present problems that do not exist in the other group and often have higher costs; these are the reasons why, especially in the construction field (where less precision is required for many parameters), uncooled thermal imaging cameras have a greater diffusion.

### 3. Safety Applications

#### 3.1. Mechanical risk for metallic shelving breakdown

This application is provided by strain gauges, which are measuring sensors glued to critical metallic components of the whole shelving structure: physical working behavior for this system is based on the direct proportionality between deformation and the consequent variation of electric resistance of the gauges. The resistance is electrically connected to a Wheatstone bridge which is able to provide a voltage signal, proportional to deformation, to the Arduino card [9].

In the former paper [1], from which the present extension is derived, a test with calibration is done on a piece of metallic structure and results are exposed.

The hardware components employed for directing data to storing system are listed below (figure 4):

- Strain gauges, to keep information about the deformation and the level of mechanical stress (see figure 2 for installation details);

- A Wheatstone bridge with electric resistors as a transducer for the resistance variation detection;
- HX711 amplifier, to make the signals compliant with Arduino card input voltage levels;
- Rapid prototyping card Arduino Mega2560;
- Wi-Fi module ESP8266 to send the data to the ThingSpeak server.

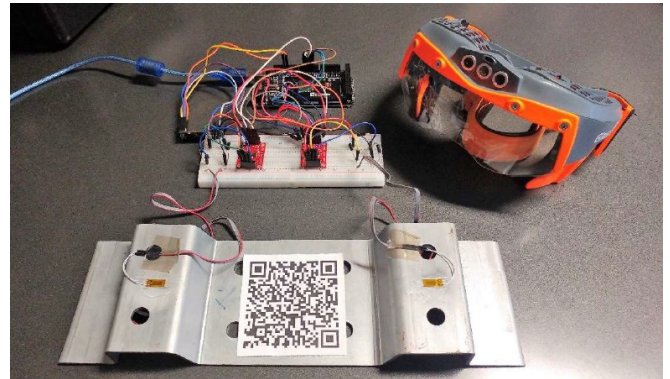


Figure 4: Set-up kit for strain gauges.

In addition to this configuration, a model of the metallic components under analysis has been realized in MATLAB Finite Element Analysis Toolbox (FEA) to simulate the stress state of the metal shelving. The FEA analysis is carried out online. Since the finite elements model of the shelf is very simple, the computational time required for the parameters calculation does not require more than 5 seconds per each run.

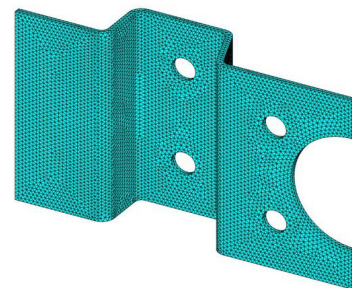


Figure 5: Mesh of the geometry.

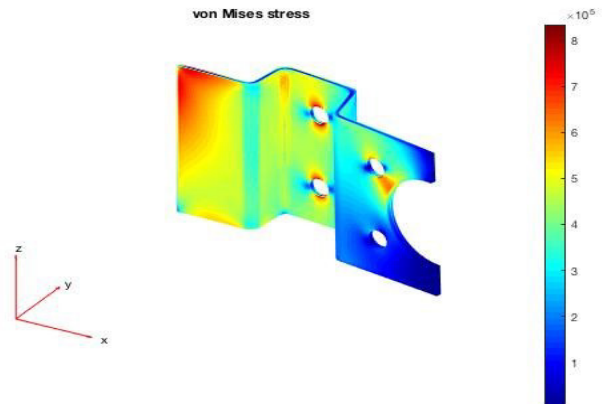


Figure 6: FEM simulation results.

### 3.2. Overheating risk for electrical equipment

The use of AR visor can be coupled with a very powerful tool for thermographic analysis of electrical equipment like switchgears, cables and busbars, circuit breakers, transformers. The use of a thermo-camera mounted on the smart glasses allows the operator to isolate specific components, identified by a QR code glued onto, simply watching at those and then to compare images got by the thermo-camera with historical images of the same components. Procedure to be established and tested for a case study is:

1. Operator looks at the electrical component of interest with smart glasses equipped with thermo-camera;
2. QR code of the component is detected and information is sent to the server;
3. An image is captured by the thermo-camera and sent to the server by the Wi-Fi glasses connection;
4. A comparison between the actual infrared image and an image of the ordinary status, or of a previous one derived with the QR code activation, can be done by an application programmed on the server,
5. Alarm signal or alert indication can be sent to glasses and received by the operator if the temperature parameters are in danger zone or next to fire ignition;
6. Overlaying of historical infrared images with the real equipment can be done with AR programming apps and sent to operators for direct comparison on site in real time.

### 3.3. Safety management in emergency situations

AR application for safety management of building can be achieved with QR code technique. QR codes reading by smart glasses can support rescue teams with quick information about, for example, particular areas in which fire prevention and overcrowding can create difficulties during the evacuation phase in a general emergency situation. Information can be regarded as the total amount of people counted by specific devices placed at the entrance doors, images captured by video-cameras placed in the rooms, known hazards beyond closed doors or fire alarm status derived from fire detection systems. Information can be obtained through an Internet of Thing interconnection of the devices used for monitoring [10].

## 4. Results

In Figure 7 stress monitoring activity on the metallic shelving is represented on a time base of 8 minutes for both the sensors installed. In the diagram, the Stress Yield Limit [%] (i.e. the ratio between the measured stress and the yield stress of the material) as a function of time is drawn. A comparison between loaded and unloaded structure is clearly visible after time 22:28 when stress goes flat.

The same situation can be calculated with a model programmed in MATLAB language, showing stress mechanical components and the size/location of the maximum stress points as parameters change. As stated above, the example test discussed in this paper is a simplification, since the stresses measured are only in the axial

direction and calibration has been effected by a traction machine. FEA allows an in-depth analysis of the stress status for a correct positioning of the sensors, and might ensure a precise description of the shelving stress status; starting from a local stress measurement there would be the possibility to create a visual representation of the stress status with a chromatic scale.

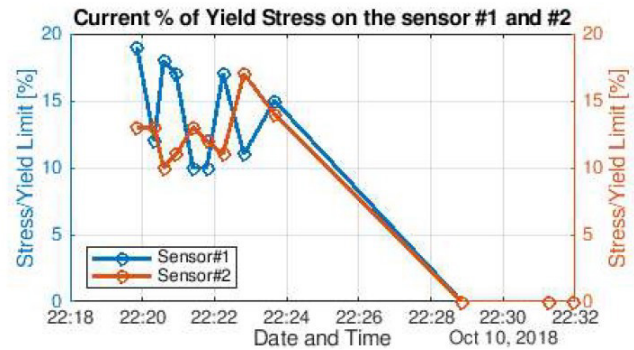


Figure 7: Stress monitoring on the shelving equipped with two strain gauges

First results obtained from the thermography application are encouraging because of the ease of use and the quick inspection from far away from the equipment. Finer adjustments on the images elaboration are under study.

## 5. Conclusions

Excellent results obtained with AR application applied to mechanical risk assessment for shelving structures underline the opportunity of extending this technology concept to other safety applications in industrial environments. Actually two main applications are under study and will be tested for safety improvements of workers and operators expecting the same results. This paper has presented in the previous chapters two experimental applications in which AR visors are the key factor for putting humans in the center of a digital revolution for safety best practices in industrial sites. Important benefits for AR application of smart glasses can be received with the implementation of the voice command feature, in order to further increase “hands-free” operations; system is actually under test. AR technology become a practical safety prevention tool that can be used in hazard management and reduction.

Advantages of this technology, confirmed with the new applications exposed are:

- Data intuitiveness;
- Easiness of use, updating and upgrading;
- High speed for data exchanging;
- Quick support for sudden decision making by safety operators;
- Multi-purpose hazard application with the same device and SDK.

Future developments of this work will provide the assessment of the platform in action, and the evaluation of the data collected during operation.

## **Conflict of Interest**

The authors declare no conflict of interest.

## **Acknowledgment**

Authors would like to acknowledge Genoa University.

## **References**

- [1] Revetria R., Tonelli F., Damiani L., Demartini M., Bisio F., Peruzzo N., A real-time mechanical structures monitoring system based on digital twin, IoT and augmented reality, SpringSim-MSM 2019, April 29-May 2, Tucson, AZ, USA. DOI: 10.22360/springsim.2019.msm.001.
- [2] Kolberg D., Zühlk D., 2015, Lean Automation enabled by Industry 4.0 Technologies, IFAC-PapersOnLine 48-3 (2015), pp. 1870–1875. Damiani, L., Giribone P., Mzoughi K., Revetria R., A Hybrid Simulation Model for Hospital Complex Plants Risk Evaluation, 2017, Engineering Letters, 25.2.
- [3] Demartini, M., Tonelli, F., Damiani, L., Revetria, R., Cassettari, L. Digitalization of manufacturing execution systems: The core technology for realizing future smart factories (2017) Proceedings of the Summer School Francesco Turco, 2017-September, pp. 326-333.
- [4] Mladenov B., Damiani L., Giribone P., Revetria R., A Short Review of the SDKs and Wearable Devices to be Used for AR Application for Industrial Working Environment. Proceedings of the World Congress on Engineering and Computer Science 2018 Vol I, WCECS 2018, October 23-25, 2018, San Francisco, USA, pp. 137-142.
- [5] De Souza Cardoso L.F., Martins Queiroz Mariano F.C., Zorzalac E.R., A survey of industrial augmented reality, Computers & Industrial Engineering, 139, January 2020, 106159.
- [6] Fiorentino, M., Uva, A. E., Gattullo, M., Debernardis, S., & Monno, G. (2014). Augmented reality on large screen for interactive maintenance instructions. Computers in Industry, 65, 270–278.
- [7] Nichols S., Patel H., Health and safety implications of virtual reality: a review of empirical evidence, Applied Ergonomics 33 (3), May 2002, pp. 251-271.
- [8] J. Wang, L. Zhang, L. Duan, R. Gao, A new paradigm of cloud-based predictive maintenance for intelligent manufacturing, March 2015, Journal of Intelligent Manufacturing, DOI: 10.1007/s10845-015-1066-0.
- [9] Hoffmann K., 1989, An introduction to measurements using strain gages, Hottinger Baldwin Messtechnik GmbH, Darmstadt.
- [10] Revetria, R., Catania, A., Cassettari, L., Guizzi, G., Romano, E., Murino, T., Improta, G., Fujita, H. Improving healthcare using cognitive computing based software: An application in emergency situation (2012) Lecture Notes in Computer Science (including subseries Lecture Notes in Artificial Intelligence and Lecture Notes in Bioinformatics), 7345 LNAI, pp. 477-490.
- [11] Cheikhrouhu E., Imed Jabri, M.N Lakhoua, Yosra Mlouhi, Tahar Battikh, Lotfi Maalej, Application of Image Processing Techniques for TV Broadcasting of Sporting Events, International Journal of Advanced Computer Science and Applications, Vol.6, N°6, 2015, pp. 138-148.
- [12] Wang H., Zhang X., Damiani L., Giribone P., Revetria R., Ronchetti G., Transportation Safety Improvements Through Video Analysis: An Application of Obstacles and Collision Detection Applied to Railways and Roads, Transactions on Engineering Technologies 2018, DOI: 10.1007/978-981-10-7488-2\_1.
- [13] Damiani, L., Demartini, M., Guizzi, G., Revetria, R., Tonelli, F., Augmented and virtual reality applications in industrial systems: A qualitative review towards the industry 4.0 era (2018) IFAC-PapersOnLine, 51 (11), pp. 624-630.
- [14] Damiani, L., Revetria, R., Volpe, A. Augmented reality and simulation over distributed platforms to support workers (2016) Proceedings - Winter Simulation Conference, 2016-February, art. no. 7408476, pp. 3214-3215.
- [15] Demartini, M., Tonelli, F. Quality management in the industry 4.0 era (2018) Proceedings of the Summer School Francesco Turco, 2018-September, pp. 8-14.

## Analyzing Job Tenure Factors in Private and Public Companies in Albania by Using Cox Proportional Hazards Model

Lule Basha\*, Eralda Gjika, Llukan Puka

Department of Applied Mathematics, Faculty of Natural Science, University of Tirana, Tirana, Albania

### ARTICLE INFO

Article history:

Received: 04 December, 2019

Accepted: 23 January, 2020

Online: 20 March, 2020

Keywords:

Job tenure

Survival analysis

Cox proportional hazards model

MIC method

### ABSTRACT

Job tenure is an important factor for both employees and employers. Sometimes, for employees, this time is a criterion in starting new job, and also for employers when they have to hire new employees. It measures the length of time that employees have been in their current job or with their current employer. Analyzing factors, which affect the job tenure, is important for companies, as well as for employee.

Job tenure is a duration concepts, so we have applied survival analysis to model the tenure for Albanian employees, in several different private and public companies.

First, Kaplan-Meier method is used to estimate the survival function for time. Then Cox proportional hazards model is used to assess the impact of the predictors in job termination. This study demonstrated the important role that the current age of the employee, the age at which he started the job, salary, gender, position, education, marital status and years of work in front of the current position may have on job tenure.

### 1. Introduction

The analysis of employment processes and estimation of factors that affect job tenure is frequently made by using survival analysis. Several authors have studied the effect that wages have on staying at work using microeconomic data [1,2]. Gregory-Smith and Thompson [3] have inspected the job tenure of CEOs in the United Kingdom and their exit using survival analysis. Jackowska and Wycinka [4] have made an assessment of the last period of employment for unemployed persons. Kohara, Sasaki, and Machikita [5] present that job tenure is an evidence of a job full of quality after unemployment. Grzenda and Buczyński [6] have assessed the employee turnover using competing risks models. Chaudhuri, Reilly, and Spencer [7] examine the effects of age and tenure on job satisfaction. Altunbaş, Thornton and Uymazc [8] analyze if there is a link between job tenure of an employee and misconduct by US banks. Worker aging has affected in the job tenure distribution. Also, a shift toward longer-duration jobs is because of the declining business [9, 10, 11].

Sometimes, for employees, job tenure is an important criterion in starting new job, and for employers when they have to hire new employees. When the time of staying in employment relationship with the same employer and the same job position is too long (more than 5 years), the worker has the advantages of being considered a loyal employee.

But on the other hand, employees may become less motivated [12, 13]. When the time of staying in employment relationship with the same employer and the same job position is very short (less than 2 years), the employees have the opportunity to gain more experience working in different job positions and with different people.

Survey reports by Wolfe [14] have shown that the average job tenure for employees is around 7 years. From the results, fifth of workers have been in the same company and in the same job position for more than ten years, while more than a third of them stay for 5-10 years.

Bureau of Labor Statistics [15], for year 2018, have shown that older employees have a median job tenure higher compared with the median time for younger ones. If an employee is 55 to 64 years old, the median job tenure is around ten years, while for an employee ages 25 to 34, this time is 2.8 years. Older employees have been in the same job for ten years or more, while younger employees are more likely to have short job tenure. In January 2018, 74 percent of employees from 16 to 19 years old have been in a current job for one year or less. Only 12 percent of employees ages 30 to 34 had job tenure for 10 years or more, where for employees between 60 to 64 years old, more than half of them had this job tenure.

In this study, we have examined of the characteristics of 887 employees, in several different private and public companies, in Albania. We will adopt Kaplan-Meier method [16], and the Cox

\*Lule Basha, University of Tirana, Tirana, Albania, [lule.hallaci@fshn.edu.al](mailto:lule.hallaci@fshn.edu.al)

[www.astesj.com](http://www.astesj.com)

<https://dx.doi.org/10.25046/aj050233>



proportional hazards model [17], in modeling the duration of job tenure. Our data are right censoring because some employees are still in the same company and in the same job position by the end of the sample.

In addition to the survival time, job tenure and indicator variable, we have taken into consideration also other variables that are thought of as important factors in the job tenure. The factors studied are the current age of the employee, the age at which he started the job, salary, gender, position, education, marital status and years of work in front of the current position. This study determine the factors which affect the job tenure using Cox proportional hazards model.

The analysis is done through R software, using *survival()* *coxphMIC()* and *ggplot2()* packages.

## 2. Materials and methods.

### 2.1. Cox proportional hazards (Cox PH) model

The Survival analysis models the timing of events by using statistical methods. Cox proportional hazards model is a regression model for the survival data, which analysis the relationship between covariates and survival [18]. This model has been proposed by Cox, 1972, [17] and the hazard function relates with covariates as follows

$$h(t | Z) = h_0(t) \exp\left(\sum_{j=1}^p \beta_j z_j\right) = h_0(t) \exp(\beta^T Z) \quad (1)$$

where  $Z = (Z_1, \dots, Z_p)^T$  is the vector of covariates for a particular individual,  $\beta = (\beta_1, \dots, \beta_p)^T$  is a parameter vector of regression coefficients and  $h_0(t)$  is the baseline hazard function. This function is the hazard function when all covariates are ignored and shows how the risk changes with time. Factors effect on the hazard function in a multiplicative way and the baseline hazard function stay an unspecified and nonnegative function of time, even with the addition of explanatory covariates.

In the Cox PH model, the ratio of hazard functions for different individuals does not depend on time. For two individuals with covariate values  $z_1 = (z_{11}, \dots, z_{p1})^T$  and  $z_2 = (z_{12}, \dots, z_{p2})^T$ , the hazard ratio [17] is:

$$\begin{aligned} HR &= \frac{h(t | z_1)}{h(t | z_2)} = \frac{h_0(t) \exp\left(\sum_{j=1}^p \beta_j z_{j1}\right)}{h_0(t) \exp\left(\sum_{j=1}^p \beta_j z_{j2}\right)} \\ &= \exp\left(\sum_{j=1}^p \beta_j (z_{j1} - z_{j2})\right) \end{aligned} \quad (2)$$

### 2.2. Maximum Partial Likelihood Estimate

In regression models, the most common method for parameter estimation is the maximum likelihood method. To use the likelihood function, we should know the distribution of the data. However, one of the main features of the Cox model is that the baseline hazard function is not identified parametrically. Therefore, the ordinary likelihood function cannot be used for the Cox PH

model. As an alternative, a method called *Maximum Partial Likelihood Method* has been proposed by Cox.

Sufficient conditions for the estimation of the *maximum partial likelihood function*, when there are missing at random variables data, have been provided by Chen, Ibrahim and Shao [19]. They also provide necessary conditions in the case of no missing data.

The partial likelihood function is:

$$L(\beta) = \prod_{i=1}^D \frac{\exp\left(\sum_{j=1}^p \beta_j z_{j(i)}\right)}{\sum_{l \in R_{(i)}} \exp\left(\sum_{j=1}^p \beta_j z_{jl}\right)} \quad (3)$$

where  $t_1, t_2, \dots, t_D$  are the observed survival times [19].

The log-partial likelihood function is:

$$\begin{aligned} l(\beta) &= \log L(\beta) = \log \prod_{i=1}^D \frac{\exp\left(\sum_{j=1}^p \beta_j z_{j(i)}\right)}{\sum_{l \in R_{(i)}} \exp\left(\sum_{j=1}^p \beta_j z_{jl}\right)} \\ &= \sum_{i=1}^D \left\{ \beta^T z_{(i)} - \log \left[ \sum_{l \in R_{(i)}} \exp(\beta^T z_l) \right] \right\} \end{aligned} \quad (4)$$

The set of individuals who are at risk at time  $t_i$  is  $R_{(i)}$ . Parameters estimation is obtained by using the Newton-Raphson iterated method, to solve the simultaneous equations:

$$\frac{\partial(l(\beta))}{\partial \beta} = 0 \quad (5)$$

### 2.3. Adequacy assessment of the proportional hazards model

The next step after selecting the model, is to evaluate the assumption of proportionality and the goodness of fit, thus we evaluate the fitted model. In order to verify the proportional hazard assumption, there are graphical methods, statistical tests, and time-dependent variables. There are different types of residuals for a proportional hazard model such as: Cox-Snell residuals [20], Schoenfeld residuals by Schoenfeld [21], deviance residuals [22] and dbeta residuals.

*Schoenfeld residuals* [21] are given by

$$R_{ji} = \delta_i \left[ z_{ij} - \frac{\sum_{l \in R_{(i)}} z_{jl} \exp(\hat{\beta}^T z_l)}{\sum_{l \in R_{(i)}} \exp(\hat{\beta}^T z_l)} \right] \quad (6)$$

where  $j=1, 2, \dots, p$  and  $i=1, 2, \dots, n$ .

This method was modified by Grambsch and Therneau [23]. These residuals are good estimators if we want to check for the time trend or for the lack of proportional hazards assumption, because they have the same properties as random walk. A non-zero slope shows that the proportional hazard model is not valid, because the conditions of proportionality are not met. Except graphical methods, Schoenfeld has proposed a global goodness-of-fit test.

2.4. Stratified proportional hazards model

The assumption of proportional hazards model may not always be met in practical situations. To accommodate the non-proportional hazards cases, Cox model can be modified using the concept of stratification for the covariate that does not satisfy the proportionality. This model has the form:

$$h_s(t | Z) = h_{0s}(t) \exp\left(\sum_{j=1}^p \beta_j z_j\right) = h_{0s}(t) \exp(\beta^T Z) \quad (7)$$

where  $s = 1, 2, \dots, k$  for  $k$  strata and  $h_{0s}(t)$  are  $s$  unknown baseline hazard functions [24].

By using stratification we get different baseline hazard functions for each stratum, but the coefficients of the variables taken into consideration are ordinary across strata. In a stratified Cox proportional hazards model, the assumptions of proportionality hold within each stratum, but it does not necessarily hold for the combined data. There are also special cases when the effect of the factor differs within strata [24].

2.5. Minimizing approximated Information Criteria

The vector of regression coefficients can be estimated by maximizing the partial log-likelihood [17]. To indicate the zero elements in  $\beta$  and the nonzero ones, we have to look for methods obtained from penalized partial likelihood function. Selection of important covariates in survival analysis is possible by using best subset selection (BSS) algorithm or the regularization one.

Su, Wijayasinghe, Fan, and Zhang [25] elaborated Minimizing Approximated Information Criteria (MIC) method to handle sparse estimation of Cox PH models. This model enjoys the advantages of best subset selection (BSS) algorithm and the regularization one.

3. Study population

In our analysis we have analyzed job tenure for 887 employees, in Albania. Job tenure is the time that employees have been in their current job or with their current employer. The analysis is based on samples taken from the database of employees, in several different private and public companies.

The study period is January 1991 - December 2018. The start time is the time when the employee begins the financial relationship with the employer. End time is the time of interruption of financial relations. The job tenure time is month.

A major problem encountered when analyzing survival data is that of censored data. In this study, censored data refers to those employees who were still working at the time when the data was last updated. In this study, with time, we refer to the job tenure in months and the survival function gives the probability that the employee will stay in a working relationship for a certain time.

On the other hand, the hazard function gives us the potential risk that the employee will terminate the relationship with the company after a certain time.

In addition to the survival time, time from the beginning of the relationship with the company, until the end of the term and the indicator variable, whether or not an employee is still working, we have taken into consideration also other variables that are thought of as important factors in the job tenure. The factors studied are the

current age of the employee, the age at which he/she started the job, salary, gender (male, female), position (engineer, supervisory, specialist, financier and other positions (driver, cleaner, babysitter, etc.)), education (middle school, high school and university), marital status (married, unmarried) and years of work in front of the current position.

4. Results

Among the 887 employees, 534 of them (60%) were still in work in December 2018, and 353 of them (40%) had interrupted the employment relationship with the company. The average job tenure for employees who are not in work, is around 4 years, 35% of the workers have been in the same job position, with the same employer, for more than 8 years.

If we consider the job tenure for employees still at work, together with the job tenure for the employees how are not at work, we see that 26 % of the workers have been in the same company and in the same job position, for more than 10 years and 30% of them for less than 2 years.

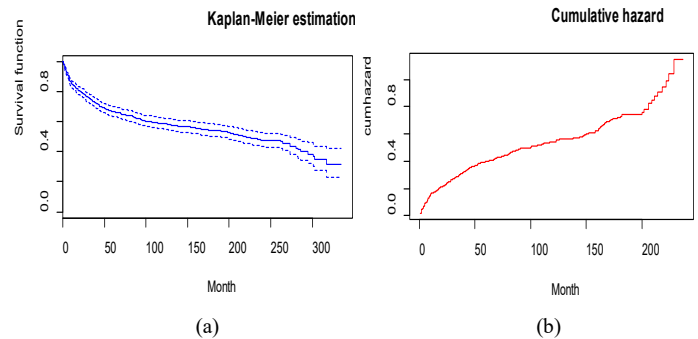
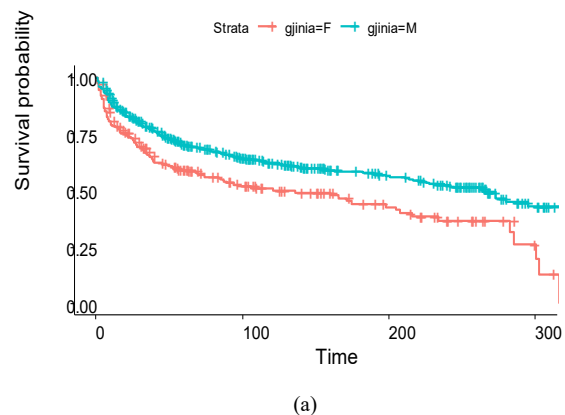


Figure 1: Estimated survival function (a) and cumulative hazard function (b), for job tenure.

Figure 1 shows that the probability of job tenure in the first year since the start of the work reaches 84.6%. The minimum period of time spent in a current job is one month and the maximum time is 317 months, approximately 26 years.

The first quartile of job tenure is 33 months; in other words, 25% of employees interrupt their relationship with the company within 33 months from their beginning. The possibility of extending the job tenure at least 217 months from the start is 50%.

Also, we have made a gender-related comparison to evaluate whether there is any difference in job tenure between them. From the studied data, we have that, 29% are women and 71% are male.



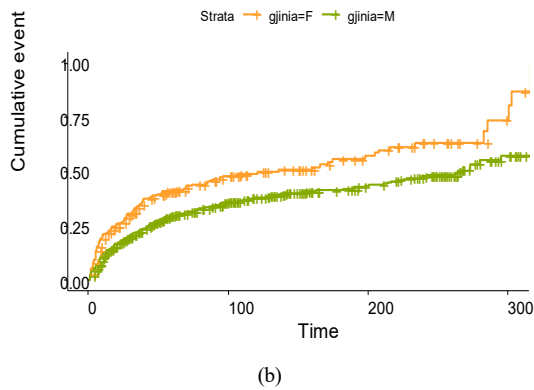


Figure 2: Kaplan-Meier estimation curves (a) and cumulative hazard (b) for male and female

Figure 2 shows that for men the estimated survival curve lies above the survival curve for women. This is as a result of the fact that job tenure for men is greater than that for women. Half of the men will interrupt employment relationships within 262 months, while women within 121 months. The probability of staying in relationship with the company in the first year is 87% for males and 78.5% for females. The first quartile of job tenure is 42 months, 25% of men will leave the company within 42 months, while women within 17 months.

To study whether the two Kaplan-Meier curves for gender are statistically equivalent, statistical tests (log-rank test, Gehan-Wilcoxon test and Peto-Peto test) have been used. From their results there is a statistically significant difference between Kaplan-Meier curves for women and that for men, with a critical value almost zero. The inhibiting effect young children have on the work lives of wives may help account for differences in job tenure by marital status. To assess whether there is a difference in job tenure between married and unmarried employees, we have used survival curves.

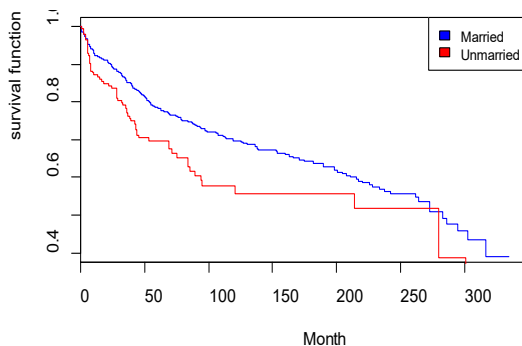


Figure 3: Kaplan-Meier estimation curves for married and unmarried employees

Figure 3 shows that the survival curve for married employees, measured by the Kaplan-Meier method, lays above the survival curve for the unmarried employees, which mean that the job tenure for married employees is greater than that of unmarried employees. At a time of 150 months of work, 75% of married employees are still at work, while only 50% of the unmarried will be in work at this time.

We have used the Cox proportional hazard model, in order to assess the *impact of the factors in job tenure*, as a semi-parametric model for the survival analysis. Initially, we have built dummy variables for actual age, age at the beginning of the job and the

salary. The variables are:  $ageA = 1$  if the employee is between 20-30 years old and  $= 0$  otherwise,  $ageB = 1$  if the employee is between 30-50 years old and  $= 0$  otherwise, if one employee is over 50 years old than  $ageA = 0$  and  $ageB = 0$ . The same is done with the age at the beginning of the job. For the salary:  $salA = 1$  if the employee has a salary up to 40,000 and  $= 0$  otherwise,  $salB = 1$  if the employee has a salary 40,000-70,000 and  $= 0$  otherwise, if one employee has a salary greater than 70,000,  $salA = 0$  and  $salB = 0$ .

Table 1: Cox proportional hazard analysis

Variable	coef	exp(coef)	Pr(> z )
Ywcp	-0.0043	0.9957	0.0000***
genderM	-0.3622	0.6961	0.020*
maritalstMarried	-0.13	0.8932	0.4959
educMiddle	1.1520	3.1650	0.0453
educUniversity	0.3051	1.357	0.5631
posEngineer	-0.0439	0.9570	0.8324
posSupervisory	-2.354	0.0950	0.0000***
posOther	-1.1450	0.3182	0.0000***
posSpecialist	-1.4420	0.2366	0.0000***
ageA	1.2740	3.5750	0.0005***
ageB	1.1020	3.0110	0.0000***
agebiA	-2.6150	0.0732	0.0000***
agebiB	-1.5440	0.2136	0.0000***
salA	-2.8370	0.0586	0.0083**
salB	-0.2013	0.8177	0.1869
Likelihood ratio test= 373.3 on 15 df, p=<2e-16			
Wald test = 234.7 on 15 df, p=<2e-16			

where: ywcp-years of work in front of the current position; genderM-gender (male); maritalstMarried- marital status (married); educMiddle-education (middle school); educUniversity- education (university); posEngineer-position (engineer); posSupervisory-position (supervisory); posSpecialist-position(specialist); posOther-other positions (driver, cleaner, babysitter, etc.); ageA-employee age 20-30; ageB-employee age 30-50; ageA- age at the beginning of the job 20-30; ageB- age at the beginning of the job 30-50; salA- salary up to 40,000; salB- salary 40,000-7000;

The variables are rated as significant using a 0.05 level. The results are obtained from *survival()* package, in R statistical software.

Table 2: Final Cox proportional hazard model

Variable	coef	exp(coef)	Pr(> z )
ywcp	-0.0040	0.9960	0.0000
genderM	-0.3622	0.6961	0.020
posEngineer	-0.6097	0.5435	0.0000
posSupervisory	-2.0140	0.1334	0.0000
posOther	-1.5470	0.2130	0.0000
posSpecialist	-1.5940	0.2030	0.0000
ageA	1.5800	4.8530	0.0000
ageB	1.1690	3.2180	0.0000
agebiA	-2.3820	0.0923	0.0000
agebiB	-1.3950	0.2478	0.0000
salA	-2.6340	0.0718	0.0095
salB	-0.4061	0.6662	0.0063
Concordance= 0.813 (se = 0.013 )			
Likelihood ratio test= 339.4 on 12 df, p=<2e-16			
Wald test = 220.4 on 12 df, p=<2e-16			
Score (logrank) test = 374.3 on 12 df, p=<2e-16			

The first column of the table shows the parameters estimation, with the partial likelihood method. The second column shows the hazard ratio. According to the Cox PH analysis, variables: *actual age*, *age at the beginning*, *salary*, *gender*, *time of work before the current job (ywcp)* and *position* in the company are significant variables with a *p-value* which is less than 0.05. The *marital status* variable and *education* are not targeted as important factor. We can observe this from *p-values* and also from *confidence intervals of hazard ratio* which contain the null value of one.

Based on the results of Table 1, we perform Cox PH multivariate model using the stepwise selection method with all the variables that have a *p-value* of less than or equal to 0.05. These results are presented in the following table, which also presents the final model.

The Cox proportional hazard model of our data, based on table 2, referred to the theoretical Cox model, equation 1, is given by:

$$\begin{aligned}
 h(t | z) = & h_0(t) \exp(-0.004ywcp - 0.36genderM \\
 & - 0.6posEngineer - 2posSupervisory - 1.5posOther \\
 & - 1.5posSpecialist + 1.5ageA + 1.1ageB - 2.3agebiA \\
 & - 1.3agebiB - 2.6salA - 0.4salB)
 \end{aligned}
 \tag{8}$$

From this model we can conclude that the greater the age at the moment of the beginning of the job, the higher the salary and the greater the number of years in work before this job, the possibility of dismissal is smaller. The position and the gender affect negatively in the interruption of the relationship between the employee and the company, while the age, affect positively in dismissal.

If we keep the other variables constant, the estimated risk of dismissal for an employee, with age less than 30 years is approximately equal to  $\exp(1.58)=4.853$  times higher than an employee with age greater than 50 years old. Employees between 30 years old to 50 years old at the time they start the job have 75% less risk of being dismissed than an employee over 50 years old at the moment he/she begin the job.

If we assumed that two employees are of the same gender, have one job position, belong to the same age category, the hazard ratio for an employee with salary between 40,000 to 70,000, compared to an employee with a salary fewer than 40,000, is 9.28. So, employees with a salary between 40,000 to 70,000 have 9.28 fewer risks to be dismissed, compared to employees with a salary fewer than 40,000.

Table 3: Model checking using Schoenfeld residuals.

	rho	chisq	p
Ywcp	0.0055	0.0110	0.9163
genderM	0.0588	1.1500	0.2845
posFinancier	-0.0696	1.4100	0.2346
posOther	0.0338	0.3540	0.5520
posSpecialist	-0.0032	0.0028	0.9579
posSupervisory	-0.1436	0.0000	0.9999
ageA	-0.0187	0.0846	0.7712
ageB	-0.0879	1.7000	0.1923
agebiA	-0.0233	0.1340	0.7147
agebiB	-0.0115	0.0332	0.8554
salA	0.0347	0.2980	0.5853
salB	-0.1975	13.700	0.0002
GLOBAL	NA	25.400	0.0129

For a male, the risk of being dismissed is reduced by 30% compared to a female. If the job position of an employee is an engineer, this reduces the risk of leaving with 45% compared to a financier. The likelihood-ratio tests, Wald test and the score test in this case, show that the underlying hypothesis, the assumption that all the coefficients are zero, is rejected.

The next step after selecting the model, is to evaluate the assumption of proportionality. We have used Schoenfeld residuals to evaluate if the variables taken into account in the model meet the requirements of the proportional hazard.

From Table 3 it is clear that the variable *salB* does not meet the PH conditions with a *p-value* less than 0.05. Also, the global test is not quite statistically significant.

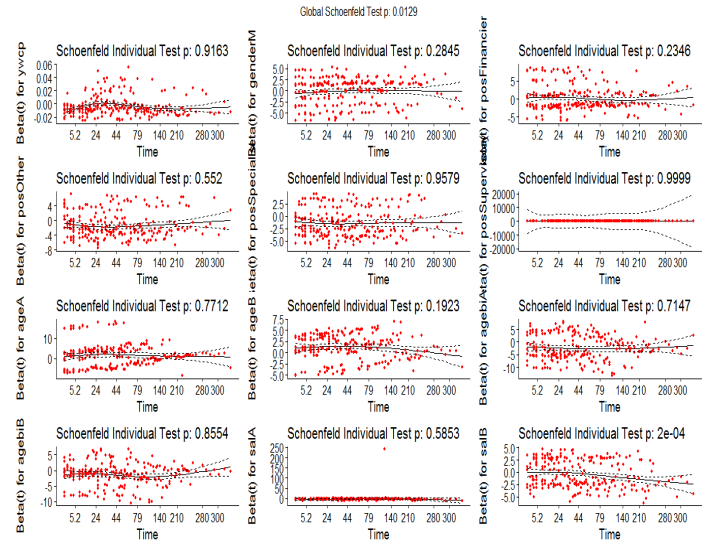


Figure 4: Schoenfeld residuals

Figure 4 shows the plot of Schoenfeld residuals for actual age, age at the beginning, salary, gender, time of work before the current job and position in the company versus survival time (job tenure). Slope of the fitted linear regression line for variable *salB* is different from zero, because the *p-value* is  $0.002 < 0.5$ . Salary violates the assumption of proportionality; thus we can conclude that this variable may depend on time.

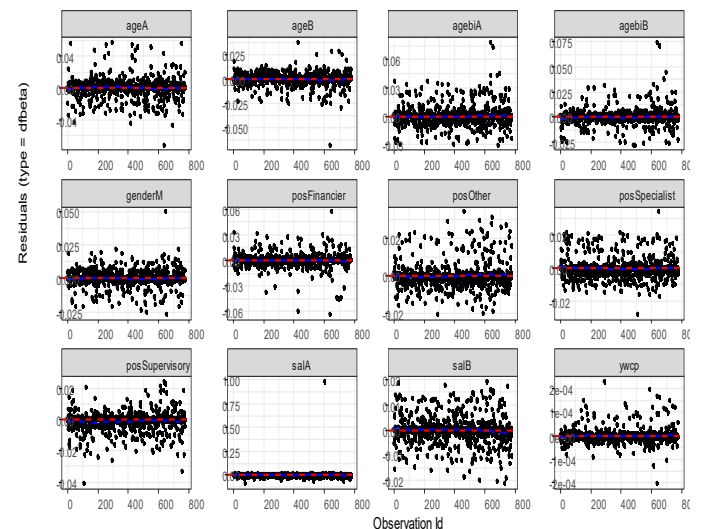


Figure 5: Graph of dfbeta indexes for the Cox model.



Slopes taken from the fitted linear regression lines for actual age, age at the beginning, gender, time of work before the current job and position are not significantly different from zero, since their p-values are greater than 0.05.

We have visualized the *dfbeta* values, for each covariate, to test outliers. These plots, given in figure 5, show the estimated differences in the regression coefficients and the magnitudes of the largest *dfbeta*.

For some variables the *dfbeta* indexes have a greater value then the others. But the above index plots show that none of the sample affects individually.

From the plots of Schoenfeld residuals we concluded that the variable *salary* does not meet the assumption of proportionality. One way to deal with this is by using the stratified Cox regression model. The results of the new model are given in Table 4.

Table 4: Results for the stratified Cox model

	coef	exp(coef)	Pr(> z )
ywcp	-0.0037	0.9963	0.0000
genderM	-0.4507	0.6371	0.0003
posEngineer	-0.6097	0.5435	0.0000
posSupervisory	-2.2815	0.1021	0.0000
posOther	-1.5090	0.2211	0.0000
posSpecialist	-1.5290	0.2167	0.0000
ageA	1.6050	4.9770	0.0000
ageB	1.2500	3.4920	0.0000
agebiA	-2.3500	0.0954	0.0000
agebiB	-1.4370	0.2376	0.0000

Table 4 shows that all the variables are statistically significant after stratification.

Also, Schoenfeld residuals given in Table 5 show that all variables meet the PH assumption.

Table 5. Testing the PH assumption by using Schoenfeld residuals, for the stratified model.

	rho	chisq	p
Ywcp	0.0269	0.2690	0.6042
genderM	0.1037	3.5700	0.0587
posEngineer	0.0865	2.1800	0.1394
posSupervisory	-0.0685	0.0000	0.9999
posOther	0.0999	2.8700	0.0900
posSpecialist	0.1117	3.3800	0.0658
ageA	-0.0030	0.0021	0.9635
ageB	-0.0385	0.3550	0.5515
agebiA	-0.0300	0.2180	0.6402
agebiB	-0.0322	0.2660	0.6063
GLOBAL		14.2000	0.2234

Also from Table 5 we can see that the global test is quite statistically significant.

Additionally, the MIC (minimizing approximated information criteria) method was used in the selection of variables. The results are given in Table 6 and are taken with the R package *coxphMIC* [26].

MIC started with maximum partial likelihood method given by the first column. From the last two columns of the table we get the

estimates for the coefficients, which show that the selected variables are the same as those selected by the Cox PH method.

Table 6: Variable selection with MIC method.

	beta0	p.value	beta.MIC	se.beta.MIC
Gender	0.1439	0.0058	0.1476	0.0527
Position	-0.5434	0.0000	-0.5432	0.0530
ageA	0.7430	0.0000	0.7487	0.0976
ageB	0.6205	0.0000	0.6236	0.0828
agebiA	-0.8385	0.0000	-0.8457	0.1294
agebiB	-0.5442	0.0000	-0.5489	0.1049
salA	0.4442	0.0000	0.4560	0.0478
salB	-0.0251	1.0000	0.0000	NA

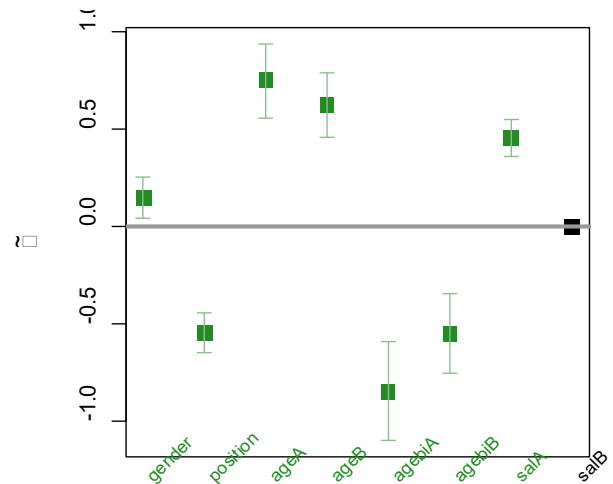


Figure 6: Error bar plot for MIC estimates of gamma and beta, together with the 95% confidence intervals. The selected variables are highlighted in green.

Figure 6 presents variables which are statistically significant with the MIC method. The selected variables are green in color, and are also associated with their confidence intervals. We can see that variable *salB* is not considered as significant covariates. The first plot is the error bar plot for estimators.

### 5. Conclusion

In this study, we have examined of the characteristics of 887 employees, in several different private and public companies, in Albania. We have used the Cox PH model in order to assess the impact of the factors in job tenure. According to the Cox PH analysis, variables: actual age, age at the beginning, salary, gender, time of work before the current job and position in the company are statistically significant, while the status variable and education are not targeted as important factor.

The findings of the present study showed that the average job tenure of an employee on a given company is approximately 187 months, different from the results taken by Wolfe [14].

Among employees, 26 % of them have been in the same company and in the same job position, for more than 10 years and 30% of them for less than 2 years. Job tenure for men is greater than that for women.

Young workers have the lowest levels of job tenure. Employees aged between 30 to 50 years at the time they start the job have 75% less risk of being dismissed than an employee over 50 years old at the moment he begin the job. Employees with a

salary between 40,000 to 70,000 have 9.28 fewer risks to be dismissed, compared to employees with a salary fewer than 40,000. Men have higher overall median levels of tenure than women, their risk of being dismissed is reduced by 30% compared to a female.

[26] R. Nabi, X. Su X. coxphMIC: An R package for sparse estimation of Cox proportional hazards models via approximated information criteria. Ar.Xiv:1606.07868v2. (2017)

## References

- [1] J. Kettunen. Effects of wages on job tenure. *Journal of income distribution*. Volume 9, Issue 2, Pages 155-169. (2000) [https://doi.org/10.1016/S0926-6437\(00\)00011-1](https://doi.org/10.1016/S0926-6437(00)00011-1)
- [2] L. Munasinghe, T. Reif, A. Henriques. Gender gap in wage returns to job tenure and experience. *Labour Economics*, Volume 15, Issue Pages 1296-1316. (2008) <https://doi.org/10.1016/j.labeco.2007.12.003>.
- [3] I. Gregory-Smith, S. Thompson, P.W. Wright. Fired or Retired? A Competing Risks Analysis of Chief Executive Turnover. (2009)
- [4] B. Jackowska, E. Wycinka. Analysis of the last employment period of the unemployed: the application of the Cox model. *Folia economica* 255. (2011)
- [5] M. Kohara, M. Sasaki, T. Machikita. Is longer unemployment rewarded with longer job tenure? *Journal of the Japanese and International Economies*. Volume 29, Pages 44-56. (2013) <https://doi.org/10.1016/j.jjie.2013.06.002>
- [6] W. Grzenda, M. Buczyński. Estimation of employee turnover with competing risks models. *Folia Oeconomica Stetinensia*. (2015) DOI: 10.1515/fofi-2015-0035.
- [7] K. Chaudhuri, K. Reilly, D. Spencer. Job satisfaction, age and tenure: A generalized dynamic random effects model. *Economics letters*. (2015) <https://doi.org/10.1016/j.econlet.2015.02.017>
- [8] Y. Altunbaş, J. Thornton, Y. Uymazc. CEO tenure and corporate misconduct: Evidence from US banks. *Finance Research Letters*, Volume 26, Pages 1-8. (2018) <https://doi.org/10.1016/j.frl.2017.11.003>
- [9] J.P. Hausknecht, C. Trevor. Collective turnover at the group, unit, and organizational levels: Evidence, issues, and implications. *Journal of Management*, 37 (1), pp. 352-388. (2011)
- [10] H. Hyatt, J. Spletzer. The shifting job tenure distribution. *Labour Economics*. (2016) <https://doi.org/10.1016/j.labeco.2016.05.008>
- [11] J. Son, Ch. Ok. Hangover follows extroverts: Extraversion as a moderator in the curvilinear relationship between newcomers' organizational tenure and job satisfaction. (2019) <https://doi.org/10.1016/j.jvb.2018.11.002>
- [12] T. Ng, D. Feldman. Does longer job tenure help or hinder job performance? *Journal of Vocational Behavior*. Volume 83, Issue 3. (2013) <https://doi.org/10.1016/j.jvb.2013.06.012>
- [13] C Chen, Y. Kao. Moderating effects of work engagement and job tenure on burnout—performance among flight attendants. *Journal of Air Transport Management*. Volume 25, Pages 61-63. (2012) <https://doi.org/10.1016/j.jairtraman.2012.08.009>
- [14] P. Wolfe. Trends in Job Tenure—and What Employers Should Do About Them. (2017) <http://blog.indeed.com/2017/06/29/trends-job-tenure/>
- [15] Bureau of Labor Statistics. “About the U.S. Bureau of Labor Statistics” Accessed Oct. 14, 2019.
- [16] E. Kaplan, P. Meier. Nonparametric estimation from incomplete observations. *Journal of the American Statistical Association*, vol. 53, pp. 457–481. (1958)
- [17] D.R. Cox. Regression models and life tables, *Journal of the Royal Statistical Society B*, 34, 187-202. (1972).
- [18] T. Therneau, P. Grambsch. *Modeling Survival Data: Extending the Cox Model*, New York: SpringerVerlag. (2000).
- [19] M. Chen, J. Ibrahim, Q. Shao. Maximum likelihood inference for the Cox regression model with applications to missing covariates. *Journal of Multivariate Analysis*. (2009). <https://doi.org/10.1016/j.jmva.2009.03.013>
- [20] D. R. Cox, E.J. Snell. A general definition of residuals (with discussion). *Journal of the Royal Statistical Society, Series B* 30:248-275. 5. (1968).
- [21] D. Schoenfeld D. Partial residuals for the proportional hazards regression model. *Biometrika* 69(1):239-241. (1982).
- [22] T.M. Therneau, P.M. Grambsch, T.R. Fleming. Martingale-Based Residuals and Survival Models. *Biometrika*, 77, 147—160. (1990).
- [23] P.M. Grambsch, T.M. Therneau. Proportional Hazards Tests in Diagnostics Based on Weighted Residuals. *Biometrika*, 81, 515—526. (1994).
- [24] L. Thompson, R. Chhikara, J. Conkin. Cox Proportional Hazards Models for Modeling the Time To Onset of Decompression Sickness in Hypobaric Environments. NASA/TP–2003–210791. (2003).
- [25] X. Su X, C. S. Wijayasinghe, J. Fan, Y. Zhang. Sparse estimation of cox proportional hazards models via approximated information criteria. *Biometrics*, 72:751–759 (2016).

## The Effectiveness of Personality-Based Gamification Model for Foreign Vocabulary Online Learning

Hasung Kang, Gede Putra Kusuma\*

*Computer Science Department, BINUS Graduate Program - Master of Computer Science, Bina Nusantara University, Jakarta, Indonesia, 11480*

---

### ARTICLE INFO

#### Article history:

Received: 29 November, 2019

Accepted: 28 February, 2020

Online: 20 March, 2020

---

#### Keywords:

Gamification

e-Learning

Personalized Learning

Foreign Language Learning

Big Five Personality

Hybrid Learning Model

---

### ABSTRACT

*Currently, there is a growing interest for applying gamification in e-learning due to innovations in technologies and pedagogies. However, motivation and engagement related problems can arise when the gamification elements are not personalized to match the individual's needs. Therefore, this research proposes a Hybrid Learning Model that combines both Gamification and Personality Traits to increase academic achievement and motivation for students who are studying foreign languages online. The methodology for the Hybrid Learning Model includes three different stages: pre-play stage where the students' personalities are gathered using the Big Five Personality questionnaire, gameplay stage where students' dominant personalities are examined to create gamified learning systems based on the Felder-Silverman Learning Style Model, and the post-play stage where the effectiveness of the Hybrid Learning Model is measured through a recall test to measure achievement and an ARCS motivation questionnaire to measure motivation using various statistical analysis. The Hybrid Learning Model is applied to a language learning web application named VocaManager and tested the Korean vocabulary skills of non-native students who were learning Korean at a local language center in Indonesia. Using SPSS software, the results showed that students who studied under the Hybrid Learning Model had a significant improvement in both their learning achievements and motivation. In addition, the research revealed a significant positive correlation between students' motivation and students' academic achievements.*

---

### 1. Introduction

E-learning is currently the largest domain (17.6%) of trending journal topics within the field of gamification [1]. Current models of gamification in e-learning focus on applying extrinsic game-like elements such as levels, challenges, point systems, and rankings to create a user experience that engages students to complete learning tasks [2]. Popular online language learning applications such as Duolingo has already provided 60 language courses in 23 different languages to its online users [3]. The application integrates gamification principles by implementing ranking systems for its users and providing in-app virtual currencies that can be spent on rewards. While these gamification elements may produce short-term motivation and engagement, studies from [4] have shown that gamification elements often offer only short-term engagement and a research by [5] have revealed that external rewards tend to eventually undermine students' internal motivation over time. The

research reveals that once the temporary external stimuli from the gamification elements disappear, users' motivation usually disappears along with it.

However, personalization in learning can be a way to increase students' motivation. Researcher [6] applied the Personalized Learning Environment (PLE) system that influenced high motivation scores for engineering undergraduates. The PLE system allowed the students to self-direct their learning process by choosing the course materials and the pace of learning. The students' motivation and satisfaction for learning increased because of their learning environment that supported their personal interests and skills. In an educational context, personalized learning encompasses a diverse range of personalization based on the learners' personal information. However, within e-learning, personalization of learning styles [7, 8] and personalities [9, 10] are common topics studied among researchers to help improve students' motivation and academic achievements.

---

\*Corresponding Author: Gede Putra Kusuma, [inegara@binus.edu](mailto:inegara@binus.edu)

The shortcoming of the current gamification model in e-Learning is the lack of personalization of the gamification elements that best fits with each student's individuality. Thus, the purpose of this paper to propose a Hybrid Learning Model that combines both personality and gamification elements to create appropriate learning systems that effectively increase students' motivation and academic achievement. This paper has the following order: 1. Related works on personality based gamification. 2. Background theory and methods. 3. Methodology used for the Hybrid Learning Model and research implementation. 4. Results and discussion of the experiment. 5. Conclusion of the paper along with future studies and improvements.

## 2. Related Works

In recent years, there have been various studies related to personality based gamification for e-learning. Researchers [11] conducted a study on the effectiveness of different e-learning gamification elements based on introvert/extrovert personalities for undergraduate students studying Object Oriented Design Methodology. Similarly, researcher [12] conducted a study on the perceived playfulness or the enjoyment of various gamification elements based on introverted and extroverted personalities for an e-learning system. In both of their studies, the results showed that each personality responded positively and negatively with certain gamification elements. In particular, extrovert learners have positive responses towards more gamification elements such as progress bars and leaderboards whereas introvert learners enjoy using fewer gamification elements.

A different study by [10] applied the Myers-Briggs Type Indicator (MBTI) to determine various learning styles for undergraduate students majoring in Computer Science. The research revealed that students' personalities can be a practical tool to guide appropriate content and structure of computer-based learning systems. Likewise, researchers [13] examined the relationship between personality traits using MBTI and learning styles using the Felder-Silverman Index of Learning Styles for millennial students learning online. The results showed that online learning allows the freedom to create one learning material while implementing various gamification elements that best fits with the students' personalities. In the study, Extrovert/Introvert personality is positively correlated with Active/Reflective learning style, Sensing/Intuitive personality is positively correlated with Sensing/Intuitive learning style, Thinking/Feeling personality is positively correlated with Verbal/Visual learning style, and Judging/Perceiving personality is positively correlated with Sequential/Global learning style.

Researchers [14] measured the drop-out rate and motivation based on the Big Five personality model for high school students learning Microsoft Excel online. The study revealed that for some personality types, the gamification elements helped in increasing motivation while for other personalities types, the gamification elements did not provide much benefit. By depicting the Kaplan-Meier graphs for gamified and non-gamified learning models for each personality types, highly conscientious learners prefer to have fewer gamification elements to motivate them, whereas highly extraverted learners are motivated by various gamification elements such as badges and points. In addition, highly neurotic learners are negatively affected by gamification elements. While

for both agreeableness and openness, the research did not reveal any significant effect due to a small number of these personality types.

Currently, many research related to personality based gamification for e-learning reveal a significant correlation between students' personalities and their interactions with various gamification elements. However, prior studies offer only a few guidance on the effectiveness of applying personality based gamification in real-life learning situations, particularly on how it affects students' academic achievements and motivation. Thus, this study aims to apply the personality based gamification using the Hybrid Learning Model for vocabulary learning online to test whether it significantly improves the students' academic achievements and motivation.

## 3. Theory and Methods

### 3.1. Gamification

Gamification in learning utilizes game elements and systems into a non-game related education context [15]. With improvements in technology, gamification is applied to various e-learning scenarios such as Massive Open Online Course and web applications. The main benefits of utilizing gamification in learning is to help increase students' motivation and engagement with the learning material [16]. Researcher [11] summarizes the eight main gamification elements that are commonly used in online education: Points are the currency that measures the success or achievement of learners, Levels represents the difficulty of the learning material along with learners' progression, Leaderboard displays the ranking of all participants' scores to create competition, Progress Bar maps the activities learners have to complete to progress through the course, Feedback is the system's response when learners interact with a learning activity to create engagement, Badges are rewards given upon completion of activities, Chat allows communication with other members to facilitate discussion, and Avatar allows customization of virtual identity such as photos, username, and password.

### 3.2. Big Five Personality Traits

Previous research by [17] confirms that students' personalities can be used to determine a specific learning styles. A well-established personality model is the Big Five Personality Traits proposed by Costa and McCrae [18]. It categorizes five different personality traits that are abbreviated as OCEAN (Openness, Conscientiousness, Extraversion, Agreeableness, Neuroticism). To determine an individual's personality, scores are measured for each of the five different personalities and a high score in one personality reveals stronger tendencies specific to that respective personality trait [19]. The explanation of each personalities are as follows:

- Openness is associated with intellectual curiosity. People with Openness personality are usually creative, curious, open-minded, and excited to try out new experiences.
- Conscientiousness relates with the adherence to social norms. People who are conscientious usually have a strong sense of work ethic, responsibility, organization, and performance.



- Extraversion deals with self-confidence. People who are extraverted usually are energetic, active, talkative, bold, and care little about what others think of them.
- Agreeableness is associated with sociability. People with Agreeableness personality are usually cooperative, kind-hearted, trusting, forgiving, and flexible.
- Neuroticism relates with a person's negative emotions. It measures the scale of negative human emotions such as anxiety, instability, insecurity, and social distress.

### 3.3. Felder-Silverman Learning Styles

Learning styles are defined as students' individual way of taking in information and processing their thoughts [20]. The Felder-Silverman Learning Style Model (FSLSM) provides four dimensions of learning styles to categorize students' preferred learning methods [21]. Understanding the different learning styles can help improve students' enjoyment and motivation in learning. The four dimensions of learning styles are as follows:

- Sensing-Intuitive dimension relates to preference on how one perceives or take in information. Sensing learners likes to focus on the concrete examples and strict information while doing practical real-world tasks. Conversely, Intuitive learners tend to think more conceptually and learn information better through theoretical and abstract frames.
- Visual-Verbal dimension relates to the preference on how the information is presented. Visual learners tend to remember things better when they see the related information in forms of visuals such as charts, pictures, and graphs. Verbal learners, on the other hand, tend to remember things that are spoken to them or they have seen in plain writing such as books and documents.
- Active-Reflective dimension relates to the preference on how information is processed. Active learners enjoy processing the information through hand-on interactions with the source material and they prefer large group learning and communication rather than individual learning. Reflective learners, however, prefer thinking and mediating about the learning material alone.
- Sequential-Global dimension relates to the preference on how information is organized and progress toward understanding information. A sequential learner prefers learning in processed step-by-step logical format that has clear objectives. Global learners, however, enjoy a more holistic learning where they can meaningfully piece together random bits of information into one big picture.

### 3.4. ARCS Motivation Model

An established theory in measuring motivation within the context of e-learning is the ARCS Motivation Model proposed by John Keller [22]. Motivation plays an important part in learning because it can be a predictor of academic achievement. A study by [23] reveals that college students with high self-motivation were less prone to dropping out of school compared to their unmotivated peers who had higher dropout rates. The ARCS model measures the following four aspects of motivation in learners:

- Attention refers to how attractive the learning material is to the learner. It relates to learning that incites curiosity and attention for the learner.
- Relevance refers to the relatability between the learning material and the student's personal experience. A relevant learning is one that has a benefit when applying to the student's real-life scenarios.
- Confidence refers to the student's perception on his or her ability to learn and understand the material. A confident learner does not experience anxiety during learning as they are sure that they can do the tasks well.
- Satisfaction refers to the positive feelings the student has towards the learning. A satisfied learner will enjoy the learning process and will likely to continue study the materials.

## 4. Methodology

### 4.1. The Hybrid Learning Model

Expanding on the previous related works, the proposed Hybrid Learning Model combines students' personalities and gamification elements to create specific learning outcomes for e-learning. In particular, this model applies the Big Five Personality Traits, Gamification elements, Felder-Silverman Learning Styles, and the ARCS Motivation to help increase students' academic achievement and motivation. As shown in Figure 1, the Hybrid Learning Model consists of three main stages: Pre-Play stage, Gameplay stage, and Post-play stage.

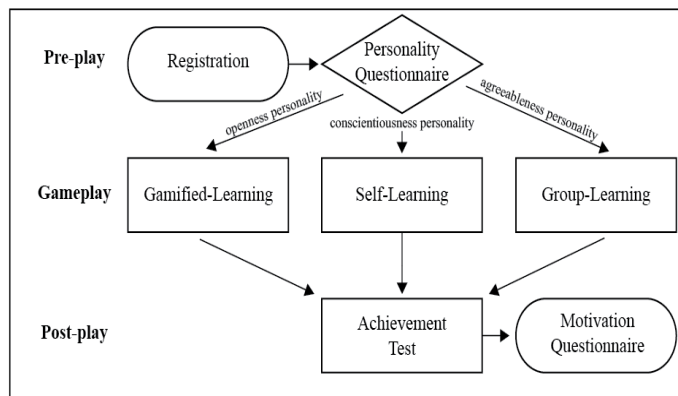


Figure 1: The proposed Hybrid Learning Model

For this research, the Hybrid Learning Model is applied to a web-based Korean vocabulary learning application named "VocaManager." The web application is created using the basic programming languages of HTML, PHP, CSS, JavaScript to create the website interface and MySQL for the database management system. The purpose of the application is to help students effectively learn new vocabulary words everyday by using their personalities to output a specific learning system that best fits the students. In addition, the application functions both on mobile devices and computers to help increase usability. The homepage of "VocaManager" for different devices is shown on Figure 2. As previously mentioned, the core features of the Hybrid Learning Model are the three different stages of pre-play, gameplay, and post-play.

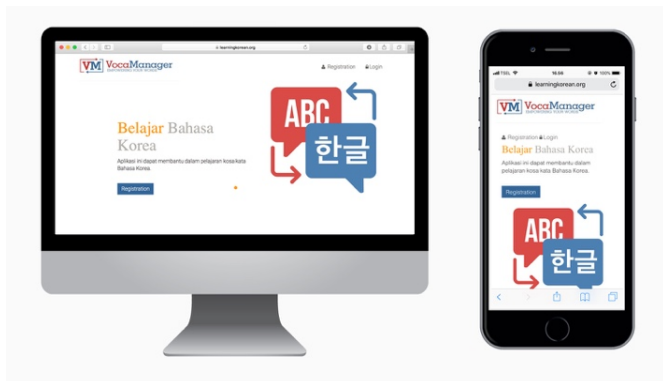


Figure 2: Adaptive display of VocaManager homepage

During the pre-play stage, students' personal information and their personalities are gathered and stored in the database to be used to predict learning styles. When the students first use the learning application, they must create an avatar and register their personal information (name, gender, email) along with their user id and password into the system's database as shown in Figure 3. The system then creates a unique identification number for each student to store their individual personality type along with their motivation and achievement scores.

After the students' initial login, they are redirected to take a personality questionnaire using The Big Five Inventory-2 Extra-Short Form (BFI-2-XS) developed by [24]. Due to the time constraints and to prevent the likelihood of learners to carelessly picking an answer to finish the questionnaire, the experiment used a succinct abridged questionnaire consists of 15 different questions using a 5-point Likert scale ranging from 5 for "strongly agree," down to 1 for "strongly disagree." The application of the pre-play stage is shown in Figure 3.

Once the system has calculated the scores of each of the five personality types, the students move on to the gameplay stage where they will study under specific learning models based on their highest personality trait score.

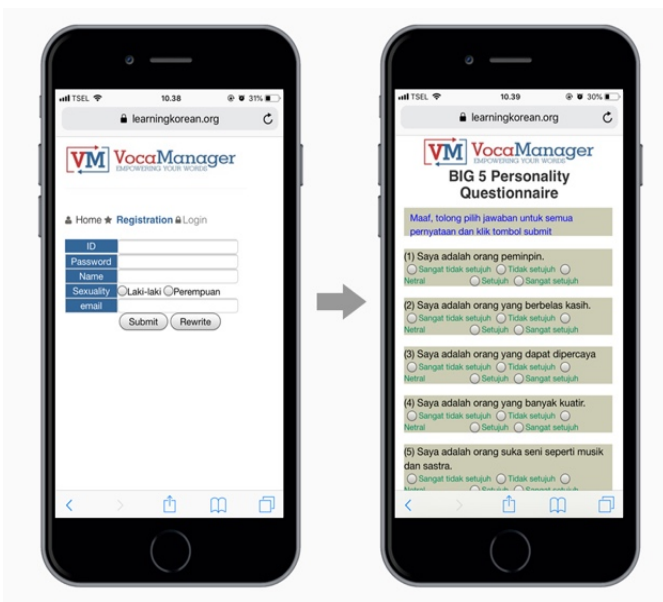


Figure 3: Pre-play: registration and personality questionnaire

As mentioned previously, different personality types react positively or negative to certain learning styles and gamification elements. A research by [25] examined the correlation between students' personality and students' preferred learning style. The research applied the Big Five Personality Traits to measure students' personality and the Felder-Silverman Learning Style Model to match their learning styles. The results highlighted that the students' personalities can be a predictor for their preferred learning styles. A different study by [26] revealed that certain gamification elements and learning activities have a positive impact on learners' motivation based on the Felder-Silverman Learning Style Model. By combining these various research, the proposed Hybrid Learning Model creates unique learning systems that best fit with the students' personalities, as shown in Table 1.

After determining the students' highest personality scores, the Hybrid Learning Model chooses the appropriate learning system with specific gamification elements. Because only three out of the five personalities (Openness, Conscientiousness, Agreeableness) are considered in this research, if a student scores the highest in either Extraversion or Neuroticism, then the system will choose next highest personality score. In the case of a tie for the highest score, the students take both learning systems and the average scores from both systems will be used for analysis.

Students with Openness personality tend to learn visually and actively. These students retain information better when they are aided with visual graphics. To accommodate this, these students require a gamified learning system with various gamification elements for them to actively learn and explore. The gamification elements that are used are challenge, points, leaderboards, competition, progress bar, and rewards. For the basic challenge, students learn new vocabulary words through randomized alphabet blocks in which students have to click on the respective blocks to form the meaning of the words as shown in Figure 4.

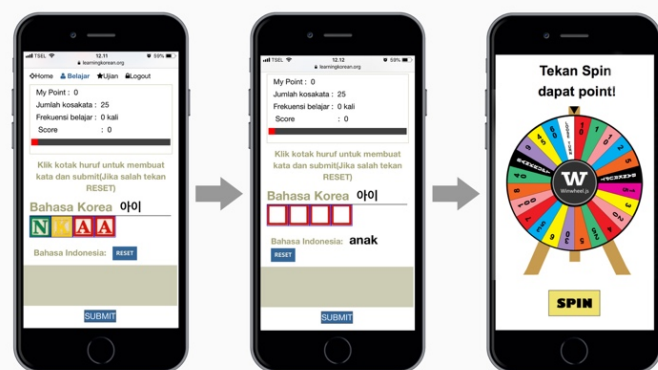


Figure 4: Openness visual learning system

This creates a visual and active learning experience different from the traditional learning method of just simply memorizing the word. This learning model also has an integrated point system. After completing a set of 25 different vocabulary words, students spin the wheel to have the chance to earn variety of points. There is no limit on the amount of times the students can study and spin to earn points. Students' individual points are then displayed on a real-time public leaderboard. At the end of the learning period of three days, the top three students with the highest points on the leaderboard are rewarded with gift cards.

Table 1: Gamified learning systems based on the research of Siddiquei [25] and Zaric [26]

Big Five Personality [18]	Core Learning Styles [25]	Preferred Gamification Elements [26]	Learning Systems [26]
Openness	Visual, Active	Badges, Leaderboards, Points, Levels, Feedback, Time Track, Progress Bar, Competition	Questions with visual elements/pictures
Conscientiousness	Sensing, Intuitive	Badges, Levels, Feedback, Stories, Progress Bar	Practical tasks with strict information
Agreeableness	Active, Sensing, Visual, Sequential	Badges, Leaderboards, Points, Levels, Feedback, Time Track, Progress Bar, Competition	Case studies with multiple steps
Extraversion	Positively correlated to all learning styles	All gamification elements	None; too broad to create a specific learning system
Neuroticism	Negatively correlated to all learning styles	None	None; learners don't enjoy gamification elements

Students who scored high in conscientiousness are sensing and intuitive learners. They learn information in a systematic and organized way and prefer concrete and practical procedures. As mentioned in a study by [14], highly conscientious learners do not particularly need gamification elements such as points, rewards, and leaderboards to motivate them. However, these students do enjoy the elements of feedback and progress bar within gamification. Thus, for these students, a self-learning system with subtle gamification elements such as logging, repetition, and hints have been applied. As shown in Figure 5, the basic learning task is to type in correct definition, but here students can keep track of their learning progress by seeing their frequency of study or how many times they have completed the lesson.

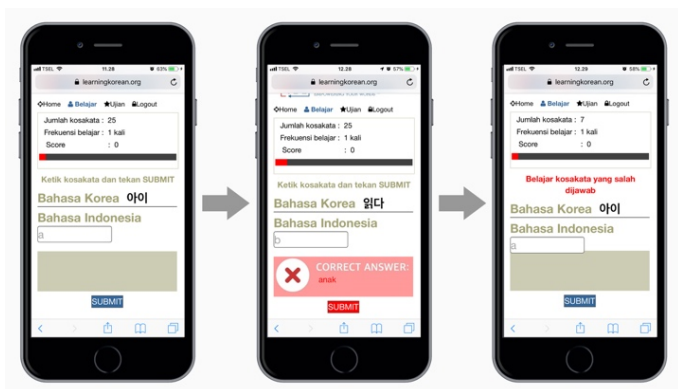
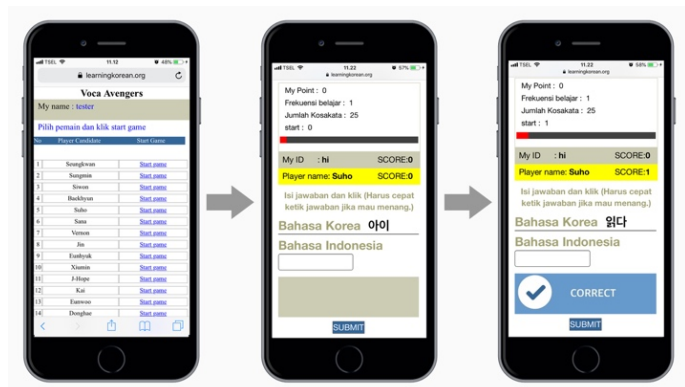


Figure 5: Conscientiousness practical learning system

Students with high agreeableness enjoy learning that are active, sensing, visual, and sequential. They tend to learn sequentially in small increment steps with the cooperation of other members to motivate one another. For this learning system, students study vocabulary words by participating in a group activity called “Voca Avengers”. The main gamification elements that are highlighted in this learning system is the avatar, time tracking, competition, and points. Prior to learning, students first create their unique avenger username and go through answering 25 different vocabulary definitions. Simultaneously, on the back end, the learning system records the students’ completion time for each word and stores them into the system database. Thus, students with agreeableness personality will learn by first choosing another student to study with. Here, whoever can type the correct definition faster will receive a score for that respective word as shown in Figure 6. The winner of the round is decided by who has the highest score after 25 vocabulary questions. Similar to the openness learning system, whoever win the match at the end can spin the wheel to earn points that can be later exchanged for gift cards. Furthermore, the completion time of the students are updated in the database after each round if the time completed is faster than the previous time. This is meant to motivate the students study the words faster each time they learn while improving the quality of each other’s



learning. Students can repeat this learning process as much as they desire.



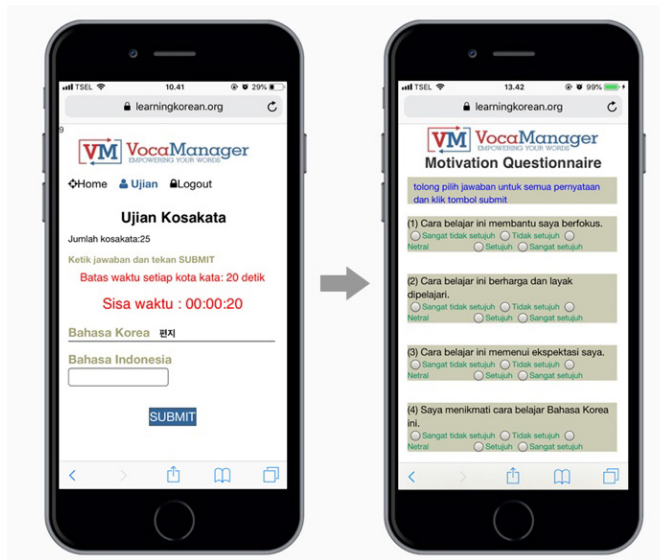
According to a research by [25], students with high extraversion have positive learning tendencies for all the learning styles which are Seeking-Intuitive, Visual-Verbal, Active-Reflective, and Sequential-Global. These students enjoy learning in variety of forms with various gamification elements. Therefore, for the purposes of this research which is to examine specific personality based gamification, the extraversion personality encompasses too broad of learning styles to a concrete learning system with specific gamification elements. Thus, it cannot be created to be objectively measured as it is a combination of all the different learning styles. Students who scored the highest in extraversion will learn based on their second highest personality score.

Contrarily, students with high neuroticism have negative correlation with all of the four learning styles. This coincides with a study by [14] stating that gamification elements have a negative effect on the motivation for highly neurotic learners as they considered the elements to be “silly” and “toylike.” These students have low motivation to learn in general as they tend to suffer from anxiety and moodiness. Therefore, it is difficult to determine a specific learning system due to their impulsive behaviors and their lack of interest for learning. Similar to the extraversion personality, for the purposes of this research, a specific learning system cannot be created and these students will learn based on their second highest personality score.

The last stage in the Hybrid Learning Model is the data collection stage. After completing the learning period in the gameplay stage for three days, the following day, students take a vocabulary proficiency test online. The proficiency is measured through a memory-recall test where students have to type in the definition of each vocabulary word within 20 seconds. The time limitation is implemented to help prevent students from looking up the definition elsewhere. The test consists of a total of 25 questions based on vocabulary words the students have learned during the gameplay stage. The test score results are then collected from all the different learning systems and are stored into the database for analysis.

After their proficiency test, students immediately take the ARCS Motivation. The questionnaire measures the scale of students’ attention, relevance, confidence, and satisfaction for the learning systems they have used. The questionnaire includes a total

of 12 questions (3 questions for each variable) based on a 5-point Likert scale from 5 being “strongly agree” to 1 being “strongly disagree.” The motivation questions are formed based on a similar study done by [27] to measure student’s academic motivation and have been adjusted to fit within the context for vocabulary learning. At the end of questionnaire, students can write their subjective feedback on their learning experience using the hybrid learning model. Figure 7 shows the system’s application for the post-play stage.



#### 4.2. Participants

The research was conducted to all Indonesian students taking the introductory Korean Language course at a Korean Language Center in Indonesia. Due to the limited number of Indonesian students studying Korean, 33 students participated in the experiment. The participants consisted of 31 females and 2 males and were between the ages of 18 and 27 years old interested in learning Korean. The majority of the participants were female due to the growing interest of Korean pop music and Korean dramas among young female adolescent in Indonesia. The learning objective for the experiment was to learn 100 different Korean vocabulary words from TOPIK (Test of Proficiency in Korean) to help prepare the students who wished to take the TOPIK exam.

#### 4.3. Research Implementation

The purpose of this research is to test whether the proposed Hybrid Learning Model as applied to vocabulary learning online is effective in increasing motivation and academic achievements. To confirm or deny this, two different learning models for studying 25 vocabulary words were presented to the students: the non-hybrid model and the hybrid model. As shown in Figure 8, the non-hybrid model is also a web learning application, but it does not include gamification elements such as leaderboards, points, and levels. Also, the students do not take the personality questionnaire prior to learning. The basic learning system for the non-hybrid model is that the students type in the definition and the system has a binary response of either “correct” and “incorrect” with the correct definition. It mimics the traditional method of learning vocabulary online. However, for the proposed hybrid model, students must



first take a personality questionnaire online and based on their personality scores, the application determines a learning system with specific gamification elements as discussed previously.



Figure 8: Non-hybrid learning system without gamification

The participants went through four learning intervals, learning 25 vocabulary words each interval, over a two-week period. In the first week, all the students had two learning intervals using the non-hybrid model. Each learning intervals lasted for three days, and on the fourth day students took the both the proficiency test and the motivation questionnaire. On the second week, the students had two learning intervals using the hybrid model. Similarly, after each learning intervals, students took the proficiency test and the motivation questionnaire. After two weeks of learning, the proficiency test and motivation scores from both models were analyzed and compared.

#### 4.4. Hypotheses

Current research finds a positive effect and correlation for personality based gamification. Thus, this research hypothesizes that students learning with the hybrid model would be more motivated to learn and produce higher academic achievements than students using the non-hybrid model. In addition, this research seeks to find if there is any correlation between students' motivation and achievements, and to check whether motivation can affect academic achievements and vice versa. The three main hypotheses are summarized as follows:

- H1: The Hybrid Learning Model will increase students' motivation.
- H2: The Hybrid Learning Model will increase students' academic achievements.
- H3: There is a correlation between students' motivation and achievements.

### 5. Results and Discussion

#### 5.1. Validity and Reliability Test

Prior to testing the main hypotheses, a validity and reliability test was conducted for both the Big Five Personality Questionnaire and the ARCS Motivation Questionnaire to examine whether the dataset can be analyzed scientifically. A concurrent validity was tested by comparing similar questionnaires from [24, 27] and finding the Pearson Product Moment Correlation Coefficient to assess the accuracy of the questionnaires. The Pearson Correlation

results for the Big Five Personality Questionnaire is shown in Table 2.

Table 2: Big Five Personality questionnaire validity test

Personality Question	Pearson Correlation	Sig. (p)
I am leader.	.667**	.000
I am forgiving.	.584**	.000
I can be trusted.	.648**	.000
I worry a lot.	.554**	.001
I like Arts.	.592**	.000
I am full of energy.	.659**	.000
I see the best in people.	.614**	.000
I am organized.	.653**	.000
I am emotional.	.523**	.002
I am creative.	.607**	.000
I am friendly.	.592**	.000
I respect others.	.392*	.024
I am resilient.	.591**	.000
I am often disappointed.	.330	.060
I am a deep thinker.	.566**	.001

\*. Correlation is significant at the 0.05 level (2-tailed).  
 \*\*. Correlation is significant at the 0.01 level (2-tailed).

Table 3: ARCS Motivation questionnaire validity test

ARCS Motivation Question	Non-Hybrid		Hybrid	
	Pearson Correlation	Sig. (p)	Pearson Correlation	Sig. (p)
The learning method helped me focus.	.781**	.000	.808**	.000
The learning method is valuable.	.783**	.000	.793**	.000
The learning meets my expectation.	.743**	.000	.805**	.000
I enjoyed the learning.	.886**	.000	.747**	.000
The learning method aroused my learning.	.805**	.000	.772**	.000
The learning method motivated me to learn more Korean.	.795**	.000	.824**	.000
I can apply the learning in daily life.	.869**	.000	.852**	.000
I want to continue to use the learning method to study Korean.	.757**	.000	.823**	.000
The learning method is interesting.	.811**	.000	.711**	.000
The learning method helps me prepare for the TOPIK test.	.749**	.000	.815**	.000
I can complete the learning method well.	.828**	.000	.748**	.000
I want to continue to use this learning method for other subjects.	.767**	.000	.662**	.000

\*\* Correlation is significant at the 0.01 level (2-tailed)

The results showed that all but the 14th question of “I am often disappointed” has a correlation value greater than .3, which is an industry standard for a question to be considered valid. The slight margin for the 14th question may have caused by the inherent negative nature of the question where participants may have been uncomfortable to answer it truthfully which skewed the overall correlation. However, since the 14th question measures a person’s neuroticism and this study does apply the neuroticism personality in the Hybrid Learning Model, it can be concluded that overall, the Big 5 Personality Questionnaire is considered valid.

Table 3 shows the validity test results for ARCS Motivation Questionnaires for both non-hybrid and hybrid models. In both cases, all the questions have correlation values that are greater than .3 and all questions are statistically significant with a p value = .000, making the overall motivation questionnaire valid.

To measure the questionnaires’ reliability or the internal consistency, the Cronbach’s Alpha was measured for the Big 5 Personality Questionnaire and the ARCS Motivation for Non-Hybrid and Hybrid models. According to [28], the Cronbach’s Alpha has been the standard value in scientific research reported for scale reliability. The Cronbach’s Alpha results are shown in Table 4, where N represents the number of questions that were asked in the questionnaire.

Table 4: Cronbach’s Alpha results for all questionnaires

Questionnaire	Cronbach’s Alpha	N
Big 5 Personality	.843	15
Non-Hybrid ARCS Motivation	.945	12
Hybrid ARCS Motivation	.941	12

For the questionnaire to be considered reliable, the alpha value should equal to or be greater than 0.7 [29]. The results showed that  $\alpha = .843$  for the Big 5 Personality Questionnaire,  $\alpha = .945$  for the non-hybrid model ARCS Motivation Questionnaire, and  $\alpha = .941$  for the hybrid model ARCS Motivation Questionnaire. Since all three of the questionnaires’ alpha values were greater than 0.7, the questionnaires were all reliable and consistent.

### 5.2. Descriptive Statistics

Descriptive statistics such as the mean and standard deviation for the achievement test scores were compared for both models as shown in Figure 9. The results showed that both the mean test and motivation scores were higher for students learning with the hybrid model. The mean test scores for the hybrid model was 93.61 out of 100 while the non-hybrid model produced an average score of 68.85. For the achievement test scores, the average score for the hybrid model were 25 points higher than the non-hybrid model. This implies that students with the hybrid model had greater academic success compared to the students with the non-hybrid model. Moreover, the standard deviation for the hybrid model, which was 8.56, was significantly lower than the non-hybrid model, which was 29.93. This shows that students learning with the hybrid model had less of a wide score gap between the highest score and the lowest score and that the students with the hybrid model produced consistently higher test scores compared to the students learning with the non-hybrid model.

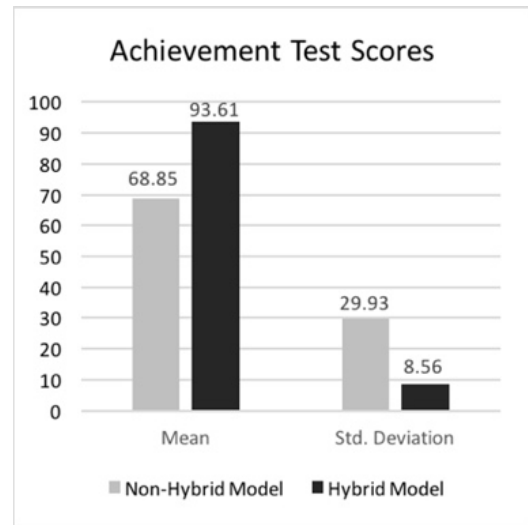


Figure 9: Achievement test scores descriptive statistics

The descriptive statistics for the motivation scores were compared in Figure 10. For the motivation scores, the hybrid model produced an average score of 4.19 while the non-hybrid produced an average score of 3.08. Similarly, the ARCS motivation scores for students learning with the hybrid model was higher by an average of 1 point compared to the non-hybrid model. Since the ARCS motivation scores are based on a 1-5 point Likert scale, a one point difference in motivation score is significant. This implies that students learning with the hybrid model had greater enjoyment and engagement with the learning systems. Furthermore, many students gave the subjective feedback that the hybrid model helped in their learning. However, the standard deviation for the ARCS motivation scores did not differentiate much between the two learning models, which was 0.46 for the hybrid model and 0.56 for the non-hybrid model. This may be caused by the smaller range of possible score outcomes from the 1-5 Likert scale. Regardless, students learning with the hybrid model had greater motivation and enjoyment in their learning compared to students who learned with the non-hybrid model.

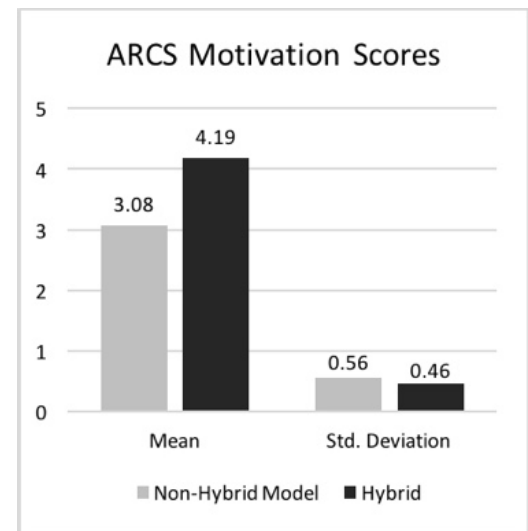


Figure 10: ARCS motivation scores descriptive statistics

Comparing the descriptive statistics for both learning models gives an overview that the hybrid model produced both greater

achievement test scores and ARCS motivation scores. However, to test scientifically whether a significant difference exists between the two models, a parametric or non-parametric statistics must be conducted depending on the distribution of the datasets.

### 5.3. Non-Parametric Statistics

Prior to testing for significance using parametric statistics, the dataset of the test scores and motivation scores must first be checked for normal distribution [30]. If the dataset is normally distributed, then parametric statistics can be used, but if it is not normally distributed, non-parametric statistics must be utilized to analyze the dataset. Using SPSS software, the Shapiro-Wilk [31] statistical measurement was used to test whether a data sample came from a normal distribution and the results are shown in Table 5.

Table 5: Normality test results using Shapiro-Wilk

Normality Test		Shapiro-Wilk Sig.
Non-Hybrid	Test Scores	.002
	Motivation Scores	.003
Hybrid	Test Scores	.000
	Motivation Scores	.158

A dataset is considered normally distributed when the significance value is greater than .05. However, the results showed the sig. values of .002, .003, .000, and .158. In fact, all except the hybrid model motivation scores have a significance value that is less than .05. Three out of the four datasets are not normally distributed. The slightly skewed distribution may have caused by a relatively small sample size of the participants. As a result, to test the three main hypotheses, non-parametric tests must be used when analyzing the test and motivation scores for both the non-hybrid and the hybrid model.

To test H1 and H2, the non-parametric Mann-Whitney U test was used to compare the two independent variables, which are the non-hybrid model scores and hybrid model scores. This test is a common alternative to the parametric t-test when the dataset is not normally distributed [32]. The Mann-Whitney U test compares the number of times the scores from the hybrid model ranked higher than the scores from the non-hybrid model. The results are shown in Table 6.

Table 6: Mann-Whitney U test results for significance

Mann-Whitney U	Learning Model	Mean Rank	Asymp. Sig (2-tailed)	N
Test Scores	Non-Hybrid	25.36	.000	33
	Hybrid	41.64		33
Motivation Scores	Non-Hybrid	23.14	.000	33
	Hybrid	43.86		33

The mean rank for the test scores were 41.64 for the hybrid model and 25.36 for the non-hybrid model. As for the motivation scores, the hybrid model had 43.86 mean rank while the non-hybrid model had 23.14 mean rank. The mean ranks for both the test scores and motivation scores in the hybrid learning model were on 18 ranks higher than the non-hybrid learning model. This implies that students who learned with the hybrid model overall had better scores in both their academic test scores and motivation scores when compared to the non-hybrid model. Moreover, since

the p value < .05 for both the test scores and the motivation scores, there was a significant difference test scores and motivation scores between the two models. These results support hypothesis H1 that the Hybrid Learning Model significantly increases students' academic achievement, and also affirms hypothesis H2 that the Hybrid Learning Model significantly increases students' motivation.

To test for hypothesis H3, a non-parametric Spearman's Rank Correlation Coefficient test was used to examine the linear relationship between the students test scores and motivation scores. This test is an alternative measurement to the parametric Pearson Product Moment Correlation in comparing the relationships between two variables [33]. The results are shown in Table 7.

Table 7: Spearman's Rank Coefficient Results

Learning Model	Spearman's rho correlation coefficient	Sig. (p)
Non-Hybrid	.693**	.000
Hybrid	.755**	.000

\*\* . Correlation is significant at the 0.01 level (2-tailed).

In both learning models, the p = .000 which implied a significant correlation between the achievement test scores and motivation scores. The results support hypothesis H3 that a correlation exists between students' motivation and academic achievement. Moreover, since the Spearman's coefficient was .693 for the non-hybrid model and .755 for the hybrid learning model, there exists a strong positive correlation between students' achievement test scores and motivation scores. This implies that as students' motivation increases so will their academic achievement, and vice versa. The result is consistent with other similar research done by [34] which found a correlation coefficient of .79 between students' learning motivation and achievement for students studying the Indonesian language.

## 6. Conclusion

Many studies have discussed the impact of personality traits on gamification elements when learning online, but few have implemented the effectiveness of personality based gamification in real-life scenarios. Thus, in this research, the Hybrid Learning Model that combines both gamification elements and personality traits was applied to a web learning application named VocaManager that was designed to teach foreign vocabulary words. Based on the experiment, the Hybrid Learning Model resulted in a significant increase in students' motivation and students' academic achievements when compared to the traditional method of learning online. Furthermore, there exists a strong positive correlation between students' motivation and students' achievements. The implication of this study reveals an important innovation for e-learning today. By matching the students' individual personalities with specific gamification elements, students can feel more motivated to learn, which in turn, increases their academic achievement. Justification can be made to choose VocaManager over existing online vocabulary learning systems because VocaManager provides the students with a specific learning environment that best fits their personalities and learning

styles. This method of learning has proved to be effective because the students showed an increase in their academic achievement and motivation when learning with the hybrid learning model. Moreover, VocaManager provides a unique learning experience that is different from existing learning systems which normally has one type of a learning system. Hence, the majority of the students who learned with VocaManager gave a subjective feedback that they would want to continue learn using VocaManager for their daily vocabulary learning.

The main limitations for this research was the small sample size due to the limited number of students studying at that time. For future research, the participants can be gathered from schools rather than local language centers to increase the number of students available for the experiment. Furthermore, due to the limited research material available, this study did not create specific learning systems for the students with Extraversion and Neuroticism personality. For future studies, however, a more comprehensive research can be done specifically for these two personalities, and finding methods to combine other personality models such as the Myers-Briggs Type Indicator to help create appropriate learning systems for the gaps within Extraversion and Neuroticism personalities. Lastly, for future studies, incorporating other areas of personalization such as gender, age, and demographics using data mining techniques can be further researched to create an even more curated learning systems for the students to improve their learning motivation and academic achievements.

As innovation within e-learning continues to develop and grow, this research paper provides several recommendation to the current e-Learning system. First, online learning should create uniquely different learning systems that are personalized to the individuality of the learners based on their personality, age, gender, and background. Secondly, online learning systems should integrate various academic field of studies into e-Learning such as Computer Science, Psychology, Game Studies, and Design to optimize the learning experience and environment for the learners. Thirdly, it is important for educators today to have a personal understanding of their students in order to create learning materials and environments that best supports the students to succeed. By applying these adjustments, this research paper reveals that not only do the learners increase their academic achievements, but also their motivation to learn the subject material significantly increases.

## References

- [1] J. Kasurinen and A. Knutas, "Publication trends in gamification: A systematic mapping study," *Computer Science Review*, 27, 33–44, 2018. doi:10.1016/j.cosrev.2017.10.003.
- [2] F. L. Khaleel, N. S. Ashaari, T. S. M. T. Wook, and A. Ismail, "Gamification Elements for Learning Applications," *International Journal on Advanced Science, Engineering and Information Technology*, 6(6), 868, 2016. doi:10.18517/ijaseit.6.6.1379.
- [3] D. Huynh, L. Zuo, and H. Iida, "Analyzing Gamification of 'Duolingo' with Focus on Its Course Structure," *Lecture Notes in Computer Science Games and Learning Alliance*, 268–277, 2016. doi:10.1007/978-3-319-50182-6\_24.
- [4] R. V. Roy and B. Zaman, "Need-supporting gamification in education: An assessment of motivational effects over time," *Computers & Education*, 127, 283–297, 2018. doi:10.1016/j.compedu.2018.08.018.
- [5] K. Kim and S. J. G. Ahn, "Rewards that undermine customer loyalty? A motivational approach to loyalty programs," *Psychology & Marketing*, 34(9), 842–852, 2017. doi:10.1002/mar.21026.
- [6] B. Balakrishnan, "Motivating engineering students learning via monitoring in personalized learning environment with tagging system," *Computer Applications in Engineering Education*, 26(3), 700–710, 2018. doi:10.1002/cae.21924.
- [7] S. V. Kolekar, R. M. Pai, and M. P. M.m., "Adaptive User Interface for Moodle based E-learning System using Learning Styles," *Procedia Computer Science*, 135, 606–615, 2018. doi:10.1016/j.procs.2018.08.226.
- [8] Ö. Özyurt and H. Özyurt, "Learning style based individualized adaptive e-learning environments: Content analysis of the articles published from 2005 to 2014," *Computers in Human Behavior*, 52, 349–358, 2015. doi:10.1016/j.chb.2015.06.020.
- [9] A. Tlili, F. Essalmi, M. Jemni, Kinshuk, and N.-S. Chen, "Role of personality in computer based learning," *Computers in Human Behavior*, 64, 805–813, 2016. doi:10.1016/j.chb.2016.07.043.
- [10] J. Kim, A. Lee, and H. Ryu, "Personality and its effects on learning performance: Design guidelines for an adaptive e-learning system based on a user model," *International Journal of Industrial Ergonomics*, 43(5), 450–461, 2013. doi:10.1016/j.ergon.2013.03.001.
- [11] M. Denden, A. Tlili, F. Essalmi, and M. Jemni, "Educational Gamification Based on Personality," 2017 IEEE/ACS 14th International Conference on Computer Systems and Applications (AICCSA), 2017. doi:10.1109/aiccsa.2017.87.
- [12] D. Codish and G. Ravid, "Personality Based Gamification – Educational Gamification for Extroverts and Introverts," CHAIS '14 - Conf. Study Innov. Learn. Technol. Learn. Technol. Era, 36–44, 2014.
- [13] A. Kamal and S. Radhakrishnan, "Individual learning preferences based on personality traits in an E-learning scenario," *Education and Information Technologies*, 24(1), 407–435, 2018. doi:10.1007/s10639-018-9777-4.
- [14] W. Ghaban and R. Hendley, "How Different Personalities Benefit From Gamification," *Interacting with Computers*, 31(2), 138–153, 2019. doi:10.1093/iwc/iwz009.
- [15] D. N. Karagiorgas and S. Niemann, "Gamification and Game-Based Learning," *Journal of Educational Technology Systems*, 45(4), 499–519, 2017. doi:10.1177/0047239516665105.
- [16] R. S. Alsawaier, "The effect of gamification on motivation and engagement," *International Journal of Information and Learning Technology*, 35(1), 56–79, 2018. doi:10.1108/ijilt-02-2017-0009.
- [17] P. Buckley and E. Doyle, "Individualising gamification: An investigation of the impact of learning styles and personality traits on the efficacy of gamification using a prediction market," *Computers & Education*, 106, 43–55, 2017. doi:10.1016/j.compedu.2016.11.009.
- [18] P. T. Costa and R. R. McCrae, "The Five-Factor Model and the NEO Inventories," *Oxford Handbooks Online*, 2009. doi:10.1093/oxfordhb/9780195366877.013.0016.
- [19] T. Aidt and C. Rauh, "The Big Five personality traits and partisanship in England," *Electoral Studies*, 54, 1–21, 2018. doi:10.1016/j.electstud.2018.04.017.
- [20] T. A. Litzinger, S. H. Lee, J. C. Wise, and R. M. Felder, "A Psychometric Study of the Index of Learning Styles," *Journal of Engineering Education*, 96(4), 309–319, 2007. doi:10.1002/j.2168-9830.2007.tb00941.x.
- [21] S. Graf, S. R. Viola, T. Leo, and Kinshuk, "In-Depth Analysis of the Felder-Silverman Learning Style Dimensions," *Journal of Research on Technology in Education*, 40(1), 79–93, 2007. doi:10.1080/15391523.2007.10782498.
- [22] J. M. Keller, "First principles of motivation to learn and e3-learning," *Distance Education*, 29(2), 175–185, 2008. doi:10.1080/01587910802154970.
- [23] E. E. Meens, A. W. Bakx, T. A. Klimstra, and J. J. Denissen, "The association of identity and motivation with students academic achievement in higher education," *Learning and Individual Differences*, 64, 54–70, 2018. doi:10.1016/j.lindif.2018.04.006.
- [24] C. J. Soto and O. P. John, "Short and extra-short forms of the Big Five Inventory–2: The BFI-2-S and BFI-2-XS," *Journal of Research in Personality*, 68, 69–81, 2017. doi:10.1016/j.jrp.2017.02.004.
- [25] N. L. Siddiquei and D. R. Khalid, "The relationship between Personality Traits, Learning Styles and Academic Performance of E-Learners," *Open Praxis*, 10(3), 249, 2018. doi:10.5944/openpraxis.10.3.870.
- [26] N. Zaric, S. Scepanović, T. Vujicic, J. Ljucovic, and D. Davcev, "The Model for Gamification of E-learning in Higher Education Based on Learning Styles," *ICT Innovations 2017 Communications in Computer and Information Science*, 265–273, 2017. doi:10.1007/978-3-319-67597-8\_25.
- [27] C.-H. Su and C.-H. Cheng, "A mobile gamification learning system for improving the learning motivation and achievements," *Journal of Computer Assisted Learning*, 31(3), 268–286, 2014. doi:10.1111/jcal.12088.
- [28] K. S. Taber, "The Use of Cronbach's Alpha When Developing and Reporting Research Instruments in Science Education," *Research in Science Education*, 48(6), 1273–1296, 2017. doi:10.1007/s11165-016-9602-2.
- [29] A. Christmann and S. V. Aelst, "Robust estimation of Cronbachs alpha," *Journal of Multivariate Analysis*, 97(7), 1660–1674, 2006. doi:10.1016/j.jmva.2005.05.012.



- [30] A. Ghasemi and S. Zahediasl, "Normality Tests for Statistical Analysis: A Guide for Non-Statisticians," *International Journal of Endocrinology and Metabolism*, 10(2), 486–489, 2012. doi:10.5812/ijem.3505.
- [31] S. S. Shapiro and M. B. Wilk, "An analysis of variance test for normality (complete samples)," *Biometrika*, 52(3-4), 591–611, 1965.
- [32] N. Nachar, "The Mann-Whitney U: A Test for Assessing Whether Two Independent Samples Come from the Same Distribution," *Tutorials in Quantitative Methods for Psychology*, 4(1), 13–20, 2008. doi:10.20982/tqmp.04.1.p013.
- [33] A. J. Bishara and J. B. Hittner, "Testing the significance of a correlation with nonnormal data: Comparison of Pearson, Spearman, transformation, and resampling approaches," *Psychological Methods*, 17(3), 399–417, 2012. doi:10.1037/a0028087.
- [34] A. Riswanto and S. Aryani, "Learning motivation and student achievement: description analysis and relationships both," *COUNS-EDU: The International Journal of Counseling and Education*, 2(1), 2017. doi:10.23916/002017026010.

## Optimization of Low Temperature Differential Stirling Engine Regenerator Design

Hind El Hassani<sup>\*1</sup>, Nour- Eddine Boutammachte<sup>2</sup>, Sanae El Hassani<sup>3</sup>

<sup>1</sup>ENSA Engineering School, Industrial Department, Sidi Mohamed Ben Abdellah University, 30050, Morocco

<sup>2</sup>ENSAM Engineering School, Energy Departement, Moulay Ismail University, 50000, Morocco

<sup>3</sup>ENSA Engineering School, Chouaib Doukkali University, 24000, Morocco

### ARTICLE INFO

Article history:

Received: 06 January, 2020

Accepted: 10 March, 2020

Online: 20 March, 2020

Keywords:

Stirling engine

Regenerator

Optimization

Pressure drop

Heat transfer coefficient

### ABSTRACT

Stirling engines working with relatively low temperature are attractive for the future, especially for applications like water pumping without concentration system and low temperature heat recovery. The present work is the continuation of a series of works on the optimization of this type of machines. The main objective of this paper is to investigate the performance of low temperature differential Stirling engine (LT-SE) regenerator by adopting a theoretical model based on heat transfer and frictional pressure drop correlations. Since the speed and the Reynolds number of this type of machines are low, the correlations concerning pressure drop were validated by comparing the calculated results with experimental measurements on a LT-SE prototype. Based on this model, several calculations were conducted in order to know how LT-SE designers can attain a desired value for regenerator effectiveness. In fact, the effect of six parameters on regenerator performances was investigated. Studied parameters are: engine speed, regenerator volume, regenerator porosity, wires diameter, working fluid type and regenerator fibers arrangement. The effect of these parameters was especially checked on pressure drop, heat transfer coefficient, regenerator and engine efficiencies. Results indicated many designing recommendations for LT-SE having the same power range of our prototype: a regenerator length around  $L_{reg} = 1.41 \times \text{displacer stroke}$ , a wire diameter around  $d_w = 0.15\text{mm}$ , a porosity around  $\beta = 0.75$ . Results indicated also that the most performant working fluid is Helium.

## 1. Introduction

The Stirling engine is one of the methods for converting heat into mechanical energy with a theoretically maximum efficiency [1,2]. This is due to the use of the regenerator, which is a heat exchanger acting as an energy economizer [3]; It is a porous matrix, with a great storage capacity of thermal energy and a great heat transfer surface [4]. Stirling engine regenerators are generally composed either from woven screens or random fibers [5].

During half of the Stirling motor cycle, heat is transferred from the working fluid to the matrix. During the other half, the heat is transferred in the opposite direction. Thus, for a whole cycle, the transferred heat between working fluid and the matrix is null.

The very first mathematical theories for regenerator's functioning description were published around 1920, more than

100 years after Stirling engines invention. Later, experimental and theoretical studies of regenerators were conducted in order to identify thermodynamic phenomena acting in this important component, and to predict Stirling engines behavior. Examples of these studies include those of Kays and London [6], who presented correlations between parameters based on experimental studies in order to find out the working fluid Darcy friction factor. Later, Sodré and Parise [7] conducted experimental tests in order to identify the pressure drop in an annulus duct filled of a woven matrix. Similarly, Tanaka et al. [8] have studied flow and heat transfer characteristics of the regenerator for a periodic flow. Many numerical studies were also conducted in order to analyze the flow through regenerator matrices based on 3D CFD Modeling [9]. The finite element method seems suitable for such analysis as indicated by Rühlich and Quack [10], Gedeon and Wood [11], Ibrahim et al. [12, 13], Tew et al. [14] and others. These studies have stressed the importance of flow simulation for understanding

<sup>\*</sup>Corresponding Author: Hind El Hassani, hind\_elhassani@yahoo.fr

characteristics of fluid friction. Combined experimental and numerical studies have quantified the pressure drop and heat transfer rate [15]. In addition, effort has been invested to study the design and structural parameters of mesh type regenerators of Stirling cryocoolers [16].

The present study contributes to the optimization of a category of solar low temperature differential Stirling engines (LT-SE). Prototypes were designed and constructed within a cooperation framework between Dresden University- Germany, and Moulay Ismail University- Morocco. These prototypes are designed to be simple and cheap for providing a solar pumping water system, and thus, contributing to human development [17].

Since this category of Stirling motors is to be developed and optimized, the authors studied earlier many parameters to find out there optimal values [18]. This paper aims to complete this development process by studying and optimizing one of the critical components of this type of engines: the regenerator.

In the literature, studies about regenerators are focused on high and moderate temperature differential Stirling engines. This paper aims to fill out the existing lack about regenerators of low temperature differential engines [19,15]. In this work a theoretical study of regenerators is held, taking into account the pressure drop inside it, heat transfer coefficient, regenerator and engine efficiencies. Since the speed and the Reynolds number of this type of machines are low, the correlations concerning pressure drop were validated by comparing the calculated results with experimental measurements on a LT-SE prototype.

After validation of the theoretical model, a parametrical study is conducted in order to find optimal values of a number of design and functioning parameters. The considered prototype is a beta type of LT-SE, called SUNWATER 3. Figure 1 and Table 1 present its main components and geometrical specifications.

Table 1: Technical specifications and calculation data of SUNWATER 3

Parameter	Value
Displacer diameter	1.35 m
Absorber diameter	1.51 m
Working piston diameter	0.29 m
Regenerator volume	0.063 m <sup>3</sup>
Fibers arrangement	Random
Hot temperature	70°C
Cold temperature	20 °C
Working fluid	Air
Cooling system	Water cooled
Section area of the regenerator housing	≈ 0.36 m <sup>2</sup>
Average pressure	≈ 1.1 bars

## 2. Theoretical analysis

In order to identify the effect of a number of regenerator parameters on its efficiency and on LT-SE efficiency, some correlations and equations were adopted, which are suitable for Stirling engines characteristics’.

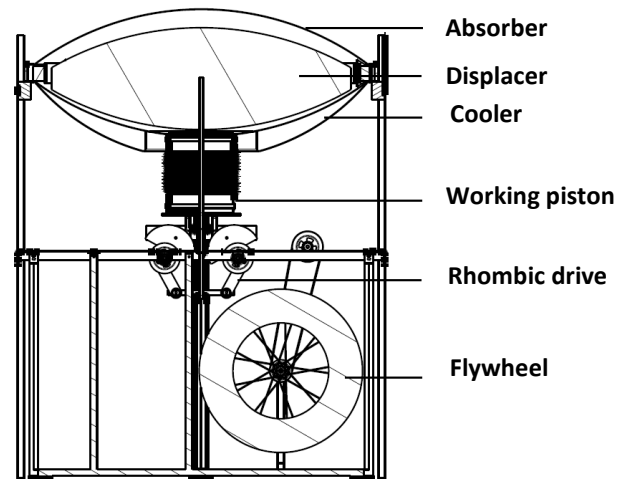


Figure 1: Illustration of SUNWATER 3

### 2.1 Correlations for Darcy friction factor and Nusselt number

Experimental studies of Gedeon and Wood [11] about regenerators have led to the correlations of Darcy friction factor and Nusselt number for two types of regenerators: felts and woven screens, given in equations (1 - 4):

- Felts fibers [11] :

$$f = \frac{192}{Re} + 4.53 Re^{-0.067} \quad (1)$$

$$Nu = (1 + 1.16 Pe^{0.66})\beta^{2.61} \quad (2)$$

- Woven screens [10]:

$$f = \frac{129}{Re} + 2.91 Re^{-0.103} \quad (3)$$

$$Nu = (1 + 0.99 Pe^{0.66})\beta^{1.79} \quad (4)$$

With:

- Re is the Reynolds number, defined as :

$$Re = \frac{d_h u_R \rho}{\mu}$$

- $\beta$  is porosity, calculated as following :

$$\beta = \frac{\text{Volume du vide}}{\text{Volume total}}$$

- $u_R$  is fluid velocity [20] :

$$u_R = \frac{Q_m}{\beta A \rho}$$

- $d_h$  is the hydraulic diameter, for porous matrices, defined in [21] as:

$$d_h = \frac{\beta d_w}{1 - \beta}$$

- Pe and Pr are respectively Peclet and Prandtl numbers, given as :

$$Pe = Re \cdot Pr$$

$$Pr = \frac{\mu C_p}{k}$$

### 2.2. Convective heat transfer coefficient and pressure drop:

The convective heat transfer coefficient is defined based on Nusselt number as follows:

$$h = \frac{k Nu}{d_h}$$

The pressure drop in the regenerator is defined by [20]:

$$\Delta P = f L_{reg} \rho u_R^2 / 2 d_h \quad (5)$$

### 2.3. Regenerator efficiency

Based on Tanaka et al. work [8], the regenerator efficiency can be expressed based on the number of transfer units as follows:

$$\varepsilon = \frac{NTU}{2 + NTU} \quad (6)$$

with:

$$NTU = \frac{\bar{h} A_{wg}}{C_p \bar{Q}_m} \quad \text{and} \quad A_{wg} = \frac{4(1 - \beta)V}{d_w}$$

$\bar{h}$  et  $\bar{Q}_m$  are average values of convective heat transfer coefficient and mass flow rate respectively.

### 2.4. Engine efficiency

In order to evaluate LT-SE efficiency taking into account regenerator characteristics, we adopt (7). Pressure drop in other heat exchangers (absorber and cooler) was not considered, as it is relatively low in comparison with the charge loss in the regenerator and does not affect the regenerator evaluation [8][22].

$$\eta = \frac{-(W_{ind} - W_r)}{-W_c + Q_{perte}} \quad (7)$$

$W_{ind}$  is the indicated work, which does not take into account any loss.  $W_r$  is the work lost in the regenerator by friction of the fluid against regenerator fibers.  $W_c$  is the work during the expansion. And  $Q_{perte}$  is the heat that hot source should give additionally, due to the regenerator imperfection.

$W_e$  suppose that during the passage of the fluid from the hot side to the cold side, the same heat amount ( $Q_{perte}$ ) should be evacuated additionally by the cold source, due to the regenerator imperfection. These energies are calculated as in (8).

$$Q_{perte} = m C_p (T_c - T_f)(1 - \varepsilon) \quad (8)$$

The indicated work is calculated based on the variation of the total volume and the instantaneous pressure. Two Schmidt hypothesis were adopted; the harmonic variation of engine volumes, and the uniform pressure inside the engine [23]. Our machine can be represented as in Figure 2.

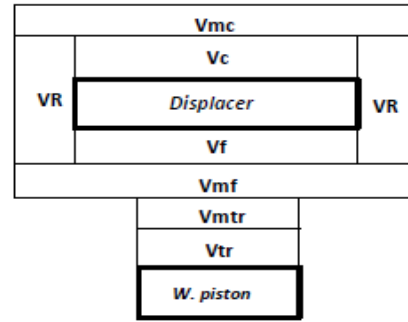


Figure 2: Schematic representation of a beta Stirling engine [23]

$V_{mc}$ ,  $V_{mf}$  and  $V_{mtr}$  are dead volumes in the hot side, cold side and in the working space respectively.  $V_R$  is the regenerator volume,  $V_{tr}$ ,  $V_C$  and  $V_f$  are the working space, hot and the cold instantaneous volumes respectively.

$dV_e$  and  $dV_c$  are respectively the variation of the total volume during the expansion and the compression.  $V_e$ ,  $V_c$ ,  $V_{tr}$  are defined in (9 - 12).

$$V_c = \frac{V_{sc}}{2} (1 + \cos(\theta + \alpha)) \quad (9)$$

$$V_f = \frac{V_{sc}}{2} (1 - \cos(\theta + \alpha)) \quad (10)$$

$$V_{tr} = \frac{V_{Str}}{2} (1 + \cos\theta) \quad (11)$$

Applying the ideal gas law, we can write:

$$p = mr \left( \frac{V_c}{T_c} + \frac{V_f}{T_f} + \frac{V_{Tr}}{T_f} + \frac{V_r}{T_r} + \frac{V_{mc}}{T_c} + \frac{V_{mf}}{T_f} + \frac{V_{mtr}}{T_f} \right)^{-1} \quad (12)$$

Using Schmidt theory for our beta type Stirling engine, we find the following expression of instantaneous pressure, according to engine flywheel rotation angle  $\theta$  [23]:

$$P = \frac{mr/k}{1 + \left(\frac{A}{R}\right) \cos(\theta - \beta)} \quad (13)$$

With:

$$k = \frac{V_{sc}}{2T_c} + \frac{V_{sc}}{2T_f} + \frac{V_{Str}}{2T_f} + \frac{2V_r}{T_f + T_c} + \frac{V_{mc}}{T_c} + \frac{V_{mf}}{T_f} + \frac{V_{mtr}}{T_f} \quad (14)$$



$$A = \frac{1}{2} \left[ \left( \frac{V_{Str}}{T_f} \right)^2 + \left( \frac{V_{Sc}}{T_c} - \frac{V_{Sc}}{T_f} \right)^2 - 2 \frac{V_{Str}}{T_f} \left( \frac{1}{T_f} - \frac{1}{T_c} \right) V_{Sc} \times \cos \alpha \right]^{\frac{1}{2}} \quad (15)$$

$$\tan \beta = \frac{\left( \frac{1}{T_f} - \frac{1}{T_c} \right) \sin \alpha}{\frac{V_{Str}}{T_f \times V_{Sc}} - \left( \frac{1}{T_f} - \frac{1}{T_c} \right) \cos \alpha} \quad (16)$$

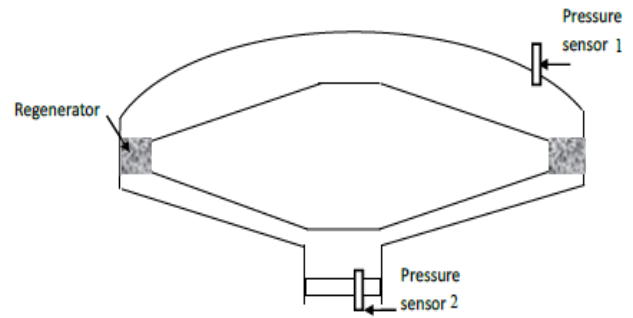


Figure 3: Experimental measurement of pressure drop [24]

$W_r$  is calculated based on the pressure drop  $\Delta P$  [20]:

$$W_r = - \oint \Delta P dVc = - \sum \Delta P dVc \quad (17)$$

$$\begin{aligned} W_{ind} &= - \int P dVc - \int P dVf \\ &= - \sum P dVc \\ &\quad - \sum P dVf \end{aligned} \quad (18)$$

$$W_e = - \int P dVc = - \sum P dVc \quad (19)$$

### 3. Validation set up and parametric study

The correlating expressions for pressure drop produced by wood [11] concern two types of regenerator material: woven screens and metal felts. These felts have a random fiber orientation but with the fibers lying predominantly transverse to the flow direction. In SUNWATER 3 prototype, we use random fiber regenerator due to its simplicity and cost. For this reason, an experimental study is carried out to verify the validity of these correlations for our case. Measurement of pressure drop was conducted for SUWATER 3 [24] in order to compare experimental results to theoretical calculations. Pressure sensors in hot and cold sides were installed (Figure 3).

After the experimental validation, effects of many regenerator parameters are studied for finding their optimal values. The parameters are: engine speed, regenerator volume, porosity, wire diameter, working fluid type, and fibers arrangement. The impact of the former parameters on pressure drop in the regenerator, heat transfer coefficient, the regenerator and the engine efficiencies was investigated using equations developed in the theoretical analysis.

Results were found using a calculation program on Microsoft EXCEL, which calculates for a thermodynamic cycle (a complete revolution of the engine flywheel), at a step of  $1^\circ$ , the engine internal chambers instantaneous volumes  $V_c$ ,  $V_f$  and  $V_{tr}$ , the mass flow rate, the instantaneous pressure, the hydraulic diameter, the fluid velocity, Reynolds number, pressure drop, heat transfer factor, etc.

The prototype SUNWATER 3 was taken as a calculation example. Table 2 indicates data for studied cases. Each studied case shows effect of the variation of selected parameter on engine performance.

## 4. Results and discussions

### 4.1. Experimental validation of pressure drop correlation

Figure 4 presents experimental results. It shows the variation of the difference between pressures given by sensors 1 and 2 in time. This pressure difference represents the pressure drop in the engine.

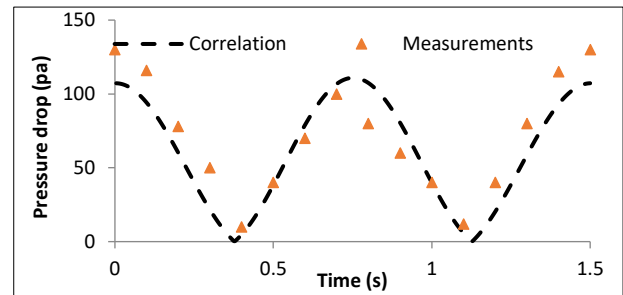


Figure 4: Pressure drop measurement and calculation during one cycle

The comparison between experimental and theoretical curves shows a good agreement, despite some small differences. These differences are due to the structure of our regenerator, and to the fact that sensors give pressure drop caused by regenerator and heat exchangers in hot and cold side, whereas the model gives the pressure drop caused by the regenerator only. Indeed, the pressure drop in the machine is mostly due to the regenerator. This result validates the calculation model adopted, especially for pressure drop correlation. Therefore, we can use the developed model to conduct a parametric study for optimization of LT-SE.

### 4.2. Effect of engine speed

In order to find the effect of engine speed on regenerator and engine efficiencies, we calculated the former values for many

engine's speeds (data are available in Table 2, case 1). Results are shown in Figure 5.

Figure 5: Variation of regenerator and engine efficiencies according to engine speed

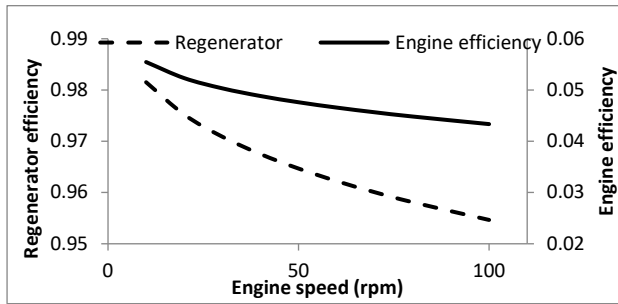


Table 2: The parameters range of parametric study

Case	Engine Speed (rpm)	Regenerator length (m)	Porosity $\beta$ (-)	Wire diameter $d_w$ (mm)	Fluid type	Fibers type
1	[10-100]	0.1	0.9	0.2	Air	random
2	40	[0,03-0,5]	0.9	0.2	Air	random
3	40	0.1	[0,6-1]	0.2	Air	random
4	40	0.1	0.75	[0,05-0,5]	Air	random
5	40	0.1	0.8	0.2	variable	random
6	40	0.1	0.8	0.2	Air /Helium	variable

Figure 5 shows that engine performances decrease as engine speed increases. This result is due to the increasing of pressure drop in regenerator with speed. High speed has also bad effect on heat transfer in regenerator, because of the low time contact between the gas and the matrix. Hence, it is advisable to run LT-SE at a low speed in order to improve its performance.

#### 4.3. Effect of regenerator volume

In order to identify the regenerator volume effect on LT-SE for a fixed cross section area, we varied the regenerator length (Table 2, case 2) and calculated pressure drop, convective heat transfer coefficient and regenerator and machine efficiencies. Results are shown in Figures 6 and 7.

Figure 6 indicates that heat transfer coefficient is not affected by the regenerator length, as hydraulic diameter and engine speed have not changed. However, pressure drop decreases with the increase of the regenerator length.

Figure 7 indicates that it exists an optimal regenerator length ( $L_{reg} = 0.12m$ ), for which the engine efficiency is maximum. After this value, the negative effect of pressure drop is more significant than the increasing of the contact surface between the gas and the regenerator. The optimal regenerator length for LT-SE is then about:

$$L_{reg} = 1.41 \times \text{diplacer stroke}$$

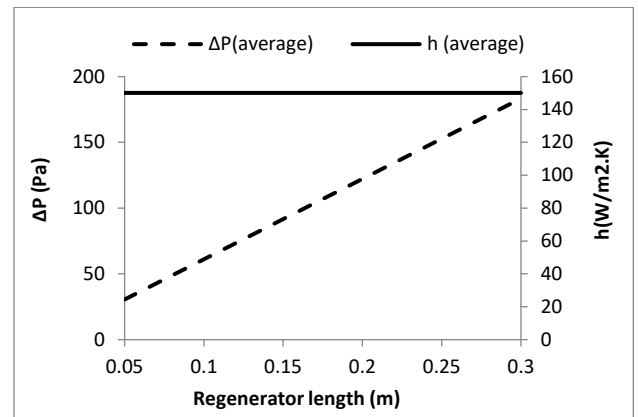


Figure 6: Effect of regenerator length on pressure drop and heat transfer coefficient

#### 4.4. Effect of porosity

Figure 8 presents the effect of porosity on pressure drop and heat transfer coefficient of the regenerator (Table 2, case 3). It indicates that pressure drop decreases with increase of regenerator porosity. Considering heat transfer coefficient, the value of porosity which maximizes it is  $\beta = 0.8$ .

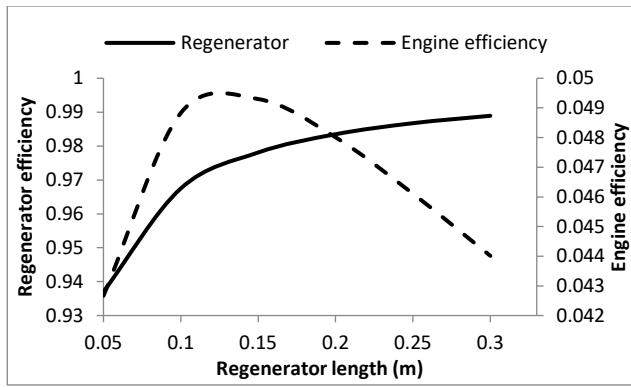


Figure 7: Effect of regenerator length on engine and regenerator efficiencies

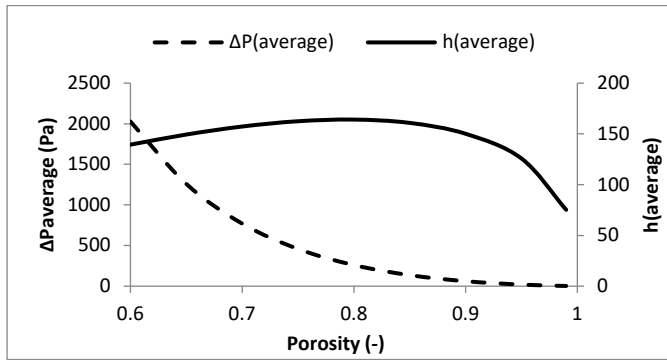


Figure 8: Variation of heat transfer coefficient and charge loss according to porosity

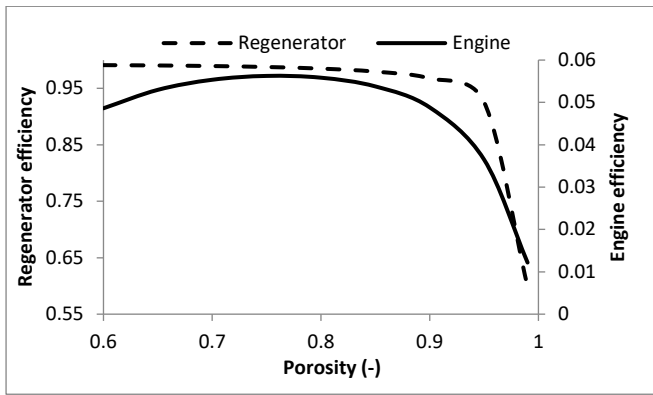


Figure 9: Variation of regenerator and engine efficiencies according to porosity

Figure 9 shows the effect of porosity on the regenerator and engine efficiencies. It indicates that these efficiencies follow the same trend as the heat transfer coefficient. Thus, it's recommended to adopt the optimal value  $\beta=0.8$ , giving the best performances.

#### 4.5. Effect of regenerator wire diameter

The effect of regenerator wire diameter (Table 2, case 4) is illustrated on Figure 10. An optimal value for wire diameter is found to be  $d_w=0.15mm$ , corresponding to hydraulic diameter  $d_h=0.45mm$ .

Work of Tanaka et al. [8] based on experimental tests indicates also an optimal wire diameter. They found, for regenerators longer than 70mm (which is the case for our adopted values), that

there is an optimal value for wire diameter. But it was not defined, due to smaller variation range of regenerator length.

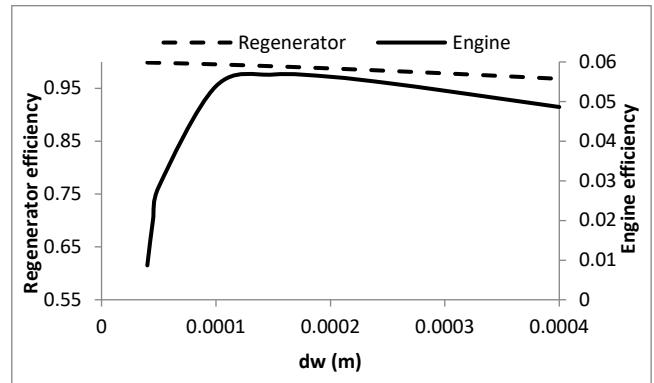


Figure 10: Variation of engine and regenerator efficiencies according to wire diameter dw

#### 4.6. Effect of working fluid

Effects of three working fluids: hydrogen, helium and air, on regenerator and engine efficiencies were investigated.

Figures 11 and 12 present the effect of working fluid type on the variation of heat transfer coefficient and pressure drop during a complete cycle. Calculation data are available in Table 2, case 5. These figures indicate that hydrogen is the most performant fluid among the studied fluids, giving the best heat transfer coefficient and causing the less pressure losses. These results are due to the fact that hydrogen is the lightest and less viscous fluid among the studied fluids (see Table 3).

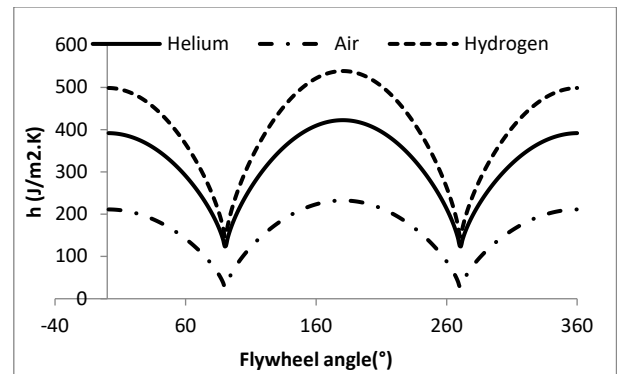


Figure 11: Cyclic variation of heat transfer coefficient for several working fluids

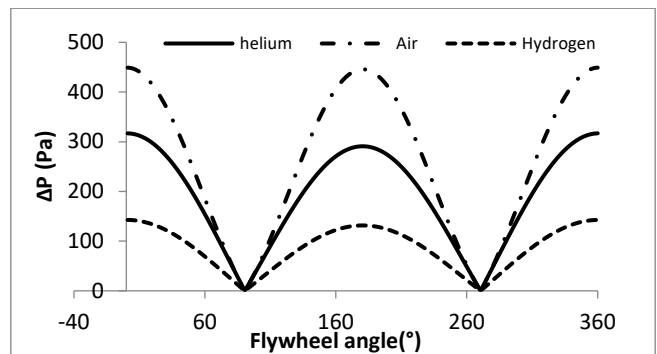


Figure 12: Cyclic pressure drop variation for several working fluids

Figure 13 indicates the regenerator and engine efficiencies for the studied working fluids. Helium and hydrogen give the best performance compared to air. We can also note that although hydrogen has the highest heat transfer coefficient and causes less pressure drop, helium gives the best engine performances. This is due to the fact that helium density is greater than that of hydrogen (see Table 3), which has the effect of increasing the mass of gas inside the machine, and causes consequently more energy absorption.

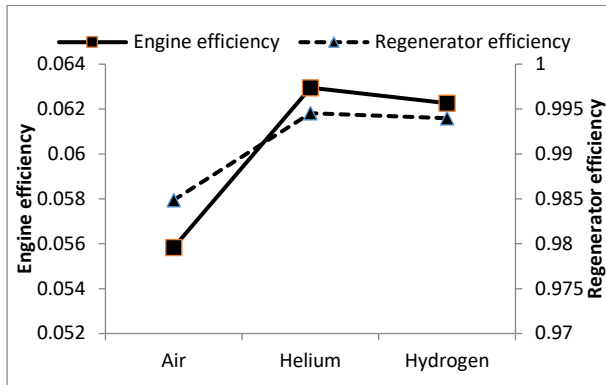


Figure 13: Engine and regenerator efficiency for many working fluids

Table 3: Fluids properties [25]

Fluid	Density at (20°C)	Viscosity at 20°C (Pa.s)	Specific Heat Cp at 20°C (J/Kg K)
H <sub>2</sub>	0.0827	8.7454E-06	14307
Helium	0.16422	0.000019586	5195
Air	1.204	0.00001825	1007

#### 4.7. Effect of regenerator type

Figure 14 shows the effect of the regenerator fibers arrangement on engine efficiency (Table 2, case 6). Studies were made for air and helium due to availability of air and high performance of helium.

This figure indicates a higher performance for woven screens regenerators in comparison with random fiber ones, especially for speeds greater than 50 rpm. However, the speed range of LT-SE is generally low, as confirmed by Kolin [26]. Then, while designing LT-SE, the use of random fibers is a justified choice due to the acceptable performance, availability and low price.

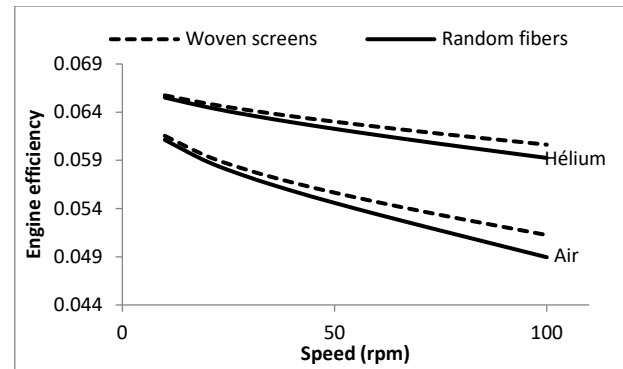


Figure 14: Engine efficiency for two regenerator types

## 5. Conclusion

In order to contribute to the development of LT-SE regenerators' design, a calculation model was developed, validated and used to analyze the effect of six regenerator parameters in order to find out their optimized values. Studied parameters are: engine speed, regenerator volume, regenerator porosity, regenerator wire diameter, working fluid type and regenerator fibers arrangement. Results indicated a number of optimization recommendations of LT-SE:

- Low speed is preferred in order to reduce the pressure drop and to enhance the heat exchange in regenerator;
- A regenerator length around  $L_{reg}$  should be adopted, where :

$$L_{reg} = 1.41 \times \text{displacer stroke}$$

- The optimal value for wire diameter is:  $d_w = 0.15 \text{ mm}$ , corresponding to a hydraulic diameter  $d_h = 0.45 \text{ mm}$ ;
- Porosity of the regenerator matrix should have a moderate value ( $\beta = 0.75$ );
- The most performant working fluid is helium. However, because of the recurring sealing problems on Stirling engine performance, the use of air is most adequate (available and for free);
- The use of woven screens regenerators is not necessary for engines running at low speed ( $< 50 \text{ rpm}$ ), random fibers give acceptable performance. At higher speed, woven screens regenerators are more suitable, giving better engine efficiency.

By following the guidelines presented in this paper, an appropriate configuration for LT-SE can be selected.

## Nomenclature

Parameter	Signification- Unit
$A$	Section area of the regenerator housing ( $m^2$ )
$A_{wg}$	Wetted area ( $m^2$ )
$C_p$	Specific heat of fluid at constant pressure ( $J/kg K$ )
$d_h$	Hydraulic diameter (m)
$d_w$	Wire diameter (m)
$f$	Darcy Friction factor (-)
$h$	Convective heat transfer coefficient ( $W/m^2 k$ )
$k$	Thermal conductivity ( $W/mK$ )



$L_{reg}$	Regenerator length (m)
$Nu$	Nusselt number (-)
$NTU$	Number of transfer units (-)
$Pe$	Peclet number (-)
$Pr$	Prandtl number (-)
$Q_m$	Mass flow rate (kg/s)
$Q_{perte}$	Heat lost due to regenerator imperfection (J)
$Re$	Reynolds number (-)
$r$	Specific gas constant (J/kg K)
$T_c, T_f$	Absorber a cooler temperatures respectively
$T_r$	Regenerator temperature
$u$	Fluid velocity (m/s)
$V_c$	Expansion volume
$V_f$	Compression volume
$V_{mc}$	Dead volumes in the absorber side
$V_{mf}$	Dead volume in the cooler side
$V_{mtr}$	Dead volume in the working space
$V_{sc}$	Maximal volume of hot space
$V_{str}$	Maximal volume of working space
$V_R$	Regenerator volume
$V_{tr}$	Working space instantenous volume
Greek symbols	
$\alpha$	Phase angle (°)
$\beta$	Porosity (-)
$\theta$	Flywheel angle (°)
$\rho$	Density (kg/m <sup>3</sup> )
$\varepsilon$	Regenerator efficiency (-)
$\mu$	Dynamic viscosity (kg/ms)
$\eta$	Engine efficiency (-)

### Conflict of interest

The authors declare no conflict of interest.

### References

[1] R.Stirling, Stirling air engine and the heat regenerator, Patent no, 4081, 1816.  
 [2] K.Wang,S.R. Sanders, S. Dubey, F.H. Choo, F. Duan, “ Stirling cycle engines for recovering low and moderate temperature heat: A review” Renew. Sustain. Energy Rev., 62, 89–108, 2016. <https://doi.org/10.1016/j.rser.2016.04.031>  
 [3] C. Toro, N. Lior, “Analysis and comparison of solar-heat driven Stirling, Brayton and Rankine cycles for space power generation” Energy, 120, 549–564, 2017. <https://doi.org/10.1016/j.energy.2016.11.104>  
 [4] S K. Andersen, H. Carlsen, P.G. Thomsen, “Numerical study on optimal Stirling engine regenerator matrix designs taking into account the effects of matrix temperature oscillations” Energy Convers. Manag., 47, 894–908, 2006. <https://doi.org/10.1016/j.enconman.2005.06.006>  
 [5] L. Sun, T.w. Simon, S. Mantell, M. Ibrahim, D. Gedeon, R. Tew, “Thermo-fluid experiments supporting microfabricated regenerator development for a

Stirling spacepower engine”, in 2009, 7th International energy conversion engineering conference, Denver, Colorado 2009. 10.2514/6.2009-4579  
 [6] W. Kays, A. London, Compact Heat Exchangers.,New York: McGraw-Hill, 1984.  
 [7] J.R. Sodré, J.A. R. Parise, “Friction Factor Determination for Flow Through Finite Wire-Mesh Woven-Screen Matrices” J. Fluids Eng., 119, 847–851, 1997. <https://doi.org/10.1115/1.2819507>  
 [8] M. Tanaka, I. Yamashita, F. Chisaka, “Flow and heat transfer characteristics of the Stirling engine regenerator in an oscillating Flow” JSME Int. J., 33, 283–9, 1990. <https://doi.org/10.1299/jsmeb1988.33.2.283>  
 [9] S. Alfarawi, R. Al Dadah, S. Mahmoud, “Potentiality of new miniature-channels Stirling regenerator”, Energy convers. Manag., 133-264, 2017. <https://doi.org/10.1016/j.enconman.2016.12.017>  
 [10] I. Rühlich, H. Quack , New regenerator design for cryocoolers, Technische Universiat, Dresden,1999.  
 [11] D. Gedeon, J. Wood, Oscillating-flow regenerator test rig: hardware and theory with derived correlations for screens and felts, NASA CR (N°198442), 1996.  
 [12] MB. Ibrahim, T. Simon, D. Gedeon, R. Tew , ”Improving performance of the Stirling converter: redesign of the regenerator with experiments”, Computation and modern fabrication techniques, Cleveland State University, 2001.  
 [13] MB. Ibrahim., Danila, D., Simon, T.W., Gedeon, D., Tew, R. , “Computational Modeling of a Segmented-Involute-Foil Regenerator for Stirling Engines” J. Thermophys. Heat Transf., 23, 786–800, 2009. <https://doi.org/10.2514/1.40330>  
 [14] R. Tew , R. Dyson, S.D. Wilson, R. Demko. , Stirling convertor CFD model development and regenerator R&D efforts, in December 2004, In 2004, AIP Conference Proceedings 746,NASA, 2004. DOI: 10.1063/1.1867183  
 [15] Anders S. Nielsen, Brayden T. York, Brendan D. MacDonald, “ Stirling engine regenerators: How to attain over 95% regenerator effectiveness with sub-regenerator and thermal mass ratios”, 253, Applied Energy, 2019. <https://doi.org/10.1016/j.apenergy.2019.113557>  
 [16] K.V. Srinivasan, A. Manimaran, M. Arulprakasajothi, M.Revanth, Vijay A. Arolkar, “Design and development of porous regenerator for Stirling cryocooler using additive manufacturing” Therm. Sci. Eng. Prog. , 11, 195-203, 2019. <https://doi.org/10.1016/j.tsep.2019.03.013>  
 [17] N. Boutammachte, J. Knorr, ”Field-test of a solar low delta-T Stirling engine” Sol. Energy, 86, 1849–1856, 2012. <https://doi.org/10.1016/j.solener.2012.03.001>  
 [18] H. El Hassani, N. Boutammachte, M. Hannaoui, “Study of some power influencing parameters of a solar low temperature Stirling engine”, European Journal of Sustainable Development, 3(2), 109-118. <http://dx.doi.org/10.14207/ejsd.2014.v3n2p109>, 2014.  
 [19] R. Gheith, F. Aloui , S. Ben Nasrallah, “Study of temperature distribution in a Stirling engine regenerator”, Energy Convers. Manag., 88, 962-972, 2014. <https://doi.org/10.1016/j.enconman.2014.09.043>  
 [20] K. Hirata, I. Iwamoto, K. Hamaguchi, “Performance evaluation for a 100 W Stirling engine” in 1997 8th International Stirling engine conference, University of Ancona, Italy, 19–28, 1997.  
 [21] S. Wilson, R. Dyson, R. Tew, R. Demko, Experimental and computational analysis of unidirectional flow through Stirling engine heater head”. Nasa center for aerospace information, 2006.  
 [22] D. Berchowitz, I. Urieli, Stirling Cycle Machine Analysis. Adam Hilger, 1984.  
 [23] H. El Hassani, N. Boutammachte, J.Knorr, M. Hannaoui, “Study of a low-temperature Stirling engine drivenby a rhombic drive mechanism”, Int. J. Energy Environ. Eng., 4, 40-50, 2013. <https://doi.org/10.1186/2251-6832-4-40>  
 [24] D. Chen, “Untersuchung zur Optimierung eines solaren Niedertemperatur-Stirlingmotors”, Ph.D Thesis, Technischen Universität Dresden, 2004.  
 [25] H. El Hassani, “ Etude théorique et expérimentale des paramètres régissant le fonctionnement des moteurs Stirling à basse température”, Ph. D Thesis, Moulay Ismail University, 2014.  
 [26] I. Kolin, Stirling Motor: History- theory- practice, Dubrovnik- Zagreb University Publications, 1991.

## Electronic Steering of the Vehicle Axle with Force Feedback

Tomas Pawlenka\*, Jaromir Skuta, Jiri Kulhanek

*Faculty of Mechanical Engineering, Department of Control Systems and Instrumentation, VSB – Technical University of Ostrava, 708 00, Czechia*

---

### ARTICLE INFO

*Article history:*

*Received: 14 January, 2020*

*Accepted: 29 February, 2020*

*Online: 20 March, 2020*

---

*Keywords:*

*steering wheel*

*force feedback*

*Steer-by-Wire*

*autonomous vehicles*

---

---

### ABSTRACT

*The technology of electronic steering with force feedback is related to electronic vehicle control. This technology is also known as "steer-by-wire" technology and is specific in that there is not any mechanical connection between the axle and the steering wheel. This technology is currently not very widespread. However, developments in the automotive industry are slowly moving towards this technology in the context of autonomous vehicles. This study includes a review of current technologies in this area and suggests a technical solution for Steer-by-Wire technology and its verification in the real vehicle model in the university environment.*

---

### 1. Introduction

The paper follows the work that was presented at the International Carpathian Control Conference (ICCC) [1]. This work dealt with the design of the electronic steering wheel and will be briefly described in this article as well. This article is further expanded by research about Steer-by-Wire technology and axle control using linear servos and a designed electronic control system. The main goal of this work is to make some progress in the area of Steer-by-Wire technology.

The technology of Steer-by-Wire is currently very widespread not only in the automotive industry. It is most often mentioned in connection with autonomous vehicles. It is a very special technology which must meet rules for safe and reliable operation. To ensure the safety of drivers and all road users, vehicles equipped with these systems must contain many electronics and sensors. However, the development of these technologies is still underway, and it will take some time to fully deploy to normal traffic.

In modern vehicles, systems that interfere with vehicle control are already implemented. However, we cannot call them autonomous. An example of such a system is a parking assistant, adaptive cruise control or a system that holds the vehicle in the traffic lane.

Electronic vehicle control technology can be solved in many ways. It depends only on our requirements. As a first requirement, we can consider the independent steering or steering of both wheels simultaneously. Yamaguchi and Murakami [2] described a standard Steer-by-Wire model with one steering motor, which controls both wheels together via rack and pinion. It is based on a classic electric power steering system without a mechanical connection with a steering wheel. An example of a driving assistant system is described by Liu et al. [3] and it is based on the same principle. As another requirement can be considered the physical principle of the selected actuators. Ye et al. [4] explain the model of the vehicle's electro-hydraulic system that controls the steering of all four wheels.

Other issues in this area can provide feedback to the driver according to the road surface or advanced methods of control. The solution may be to implement force, torque and yaw rate sensors or accelerometers as described in [5-7]. A very interesting solution is also described by Fahami et al. [8]. They propose an algorithm to create force feedback torque based on the current measurement of the DC motor.

For advanced methods of control, a bilateral control scheme to improve vehicle handling can be mentioned, which was proposed by Zheng et. al. [9].

The main content of this paper is about the proposal of an electronic steering system technical solution, which is based on a

---

\*Corresponding Author: Tomas Pawlenka, [tomas.pawlenka@vsb.cz](mailto:tomas.pawlenka@vsb.cz)

clear electric principle. This choice depends on a lower price than electrohydraulic systems. It utilizes independent steering of both front wheels with the use of power linear servos mounted on each wheel.

Figure 1 shows the block diagram of the chosen technology. It consists of a steering wheel unit, steering control system and two independent linear actuators. The steering wheel unit is designed for generating force feedback and setting the desired steering angle and the steering control system serves for controlling linear servos according to the desired steering angle set by a driver.

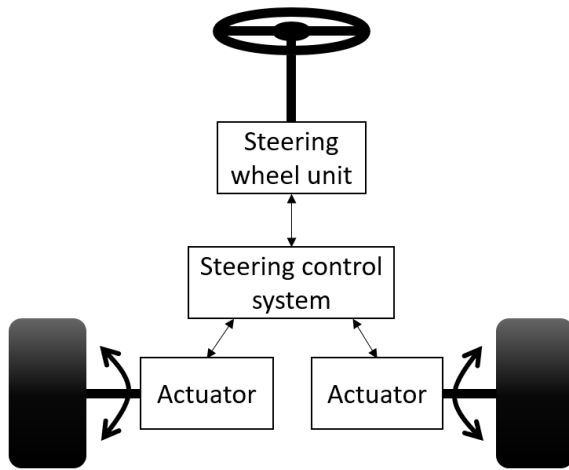


Figure 1 – Block structure of the proposed system

## 2. Design of steering wheel unit

In the beginning, the model of the steering wheel unit was designed. There are more options to create a steering wheel unit to control the steering and generate force feedback to the driver. In [2] the steering wheel rotation is proposed utilizing a motor and a belt drive. This method of torque transmission was also chosen in this work for easier implementation. The disadvantage of the gears is the play between the teeth, which in this case could cause steering insensitivity.

The main task of the proposed system is to provide the steering wheel position to the steering control system and generate force feedback to the driver. Force feedback is generated by a DC motor. The DC motor shaft is coupled to the steering wheel via a dual belt drive, which increases the final torque of the steering wheel.

The angle of the steering wheel is measured using the SEAT automotive position sensor. The advantage of this sensor is that it provides data over the CAN bus and it is also very reliable due to its robust design.

The Arduino UNO board was selected as the main control unit and it was interfaced with the CAN bus shield based on MCP2515 chip. The power of the DC motor is controlled by the dual H-bridge according to the PWM signal in the range of 0-5 V from the Arduino unit. Part of the design is also a current sensor. It measures the direction and value of the DC motor current. The

current direction is important to determine if the driver affects the steering wheel with any force.

Figure 2 shows the whole structure of the steering wheel unit with the possibility of setting parameters through a computer application. As can be seen from the picture, the structure is divided into three levels according to their main task.

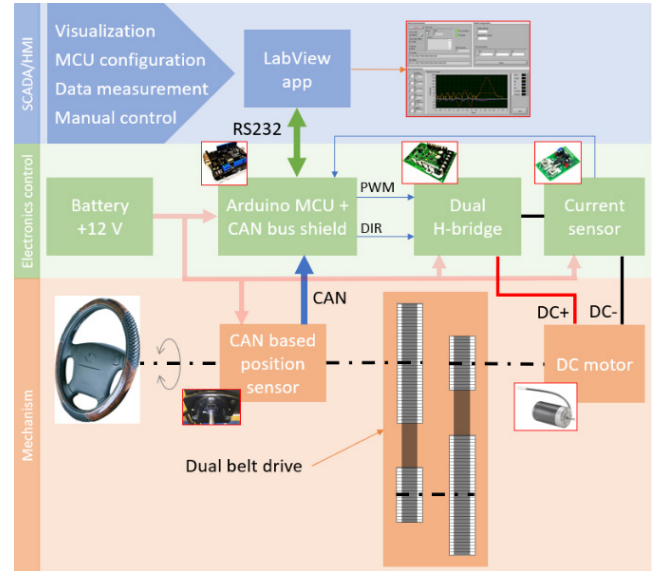


Figure 2 - Block diagram of the steering wheel unit

### 2.1. Construction design and assembly

As the feedback motor, the DOGA 162 was chosen. It is a motor that uses permanent magnets to generate a magnetic field. The principle is based on the mutual attraction of the positive and negative poles [10]. The initial torque of the chosen motor is about 1 Nm from the datasheet. Parameters like performance, size, weight, availability, and price played a major role in the choice of this DC motor.

As already mentioned, the power transfer of the feedback motor to the steering wheel shaft was designed by a dual belt drive. The belt drive was designed to meet the requirement for the resulting torque. First, the gear ratio was defined as the same for both gears as 4.5. HTD pulleys with the required number of teeth were then selected based on the gear ratio. The total gear ratio through both gears was calculated as 20.25. Then it was necessary to calculate the minimal axial distance between pulleys. The actual axial distance was then selected based on the standard lengths of the Continental HTD belts.

The equations and formulas for obtaining the belt length are described in [1].

The calculation of the resulting starting torque of the DC motor is also described in [1].

Finally, the initial torque from the total gear ratio has been calculated and it can be noted that its value meets the specified

requirement of 20 Nm. This value can be considered as enough for this application.

In Figure 3, the mechanical construction of the model is shown. The prototype frame is made of metal sheets and threaded rods. All shafts were mounted with the construction frame through ball bearings fixed in bearing holders. The position sensor was connected to the steering wheel shaft using a 3D printed connecting part.

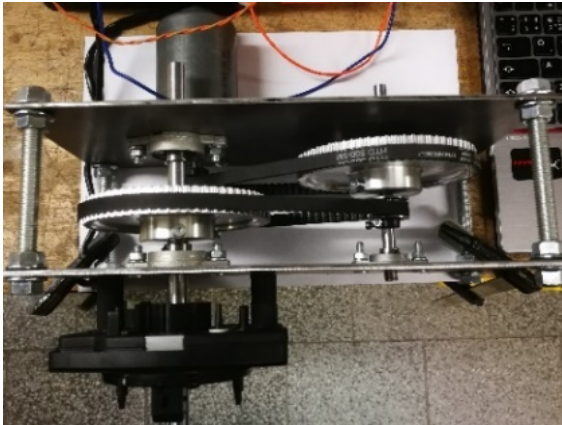


Figure 3 – Realized mechanism of the steering wheel unit

## 2.2. Electronics control system

The design of the electronic control system includes the selection of suitable components and their correct connection for safe operation.

Figure 4 describes a regulation loop showing which components represent the controller, the system and the measured feedback.

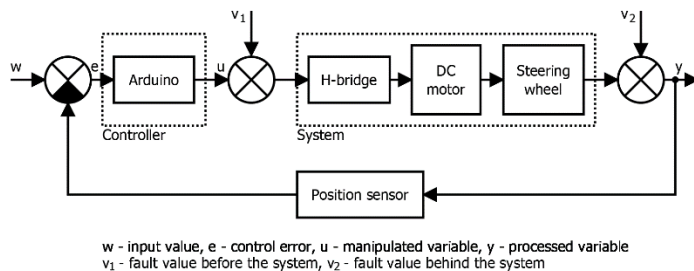


Figure 4 – The regulation loop of the electronic steering wheel unit

The controller is the evaluation board Arduino UNO. The manipulated variable is generated by the PWM signal in the 0-5 V range. The system consists of a dual H-bridge, DC motor, dual belt drive, and steering wheel. The dual H-bridge controls the power of the DC motor based on the manipulated variable. The steering wheel position reference value can be considered as an input. The actual controlled position can be considered as the output. The position feedback is measured by the already mentioned sensor based on CAN.

The CAN bus is a communication standard used for data transfer in the automotive industry. A twisted-pair copper line is usually used as the transmission medium [12].

The position sensor provides data about the current position and speed of rotation. The sensor resolution is 240 values per revolution. Measurement of its ranges was performed using the PCAN-USB interface from Peak System.

The Arduino unit was developed as an open-source platform. For programming, it is possible to use the development environment Arduino, which is free. The main function of this unit is to measure and control the position of the steering wheel. For this purpose, the PID control algorithm was implemented in the Arduino. Another function is cyclical data sending via a serial interface to a computer application. In addition to sending data, the unit can also receive data in the form of configuration commands from the application.

The mentioned application was developed in LabView from National Instruments. This environment uses a block structure for programming. The final design is shown in Figure 5.

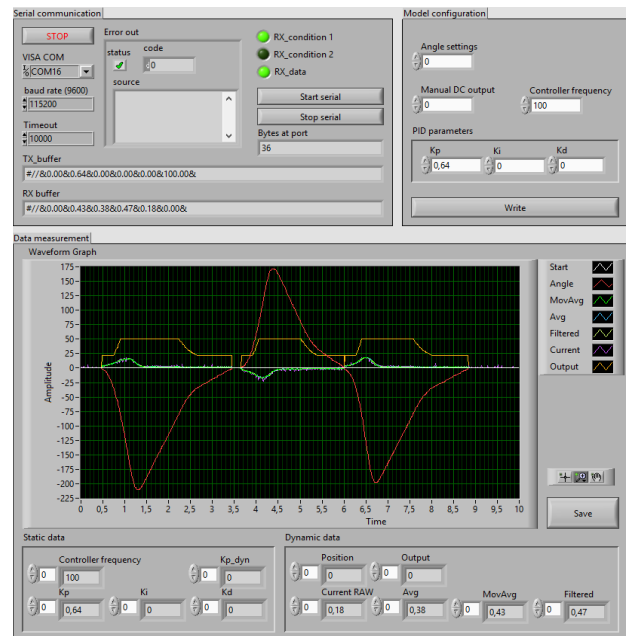


Figure 5 – Steering wheel unit application

The application was designed and divided into three sections. The first section consists of serial communication settings, error indicators and the display of received and sent buffers to or from the Arduino unit.

The second section is for model configuration and manual control. There is the possibility of manually adjusting the steering wheel angle as an offset position or DC motor power in the 0-255 PWM range to measure step response. This section also contains a form for setting PID controller parameters and controller frequency.

The last section includes tools for data measurement and visualization. Except for the graph, which shows the last values on the selected timeline, this section also contains numeric indicators of current values. Measured data can be saved to TDMS file using the save button.



### 2.3. System identification and controller design

An important part of the work is to determine the parameters of the proposed model. Deterministic methods based on measured step response were chosen for system identification. For step response measurement, the developed application was used. That was measured during the steering wheel rotation of 360 degrees. The step size was set to match the maximum motor power. According to the step response, it was found out that it is the integration system. It will not stabilize.

The inertia integration system can be described by the following form of the transfer function [13]:

$$G(s) = \frac{1}{T_I s} \cdot \frac{1}{(T_1 s + 1)^n} \quad (1)$$

Integral time and inertia were obtained using standard identification methods. The calculations revealed that it is a first-order system defined by the following form of the transfer function [13]:

$$G(s) = \frac{k_1}{s \cdot (T_1 s + 1)} \quad (2)$$

Subsequently, a step response was simulated using a calculated transfer function in Matlab Simulink. The accuracy of the simulated step response was verified by comparison with the measured step response. Figure 6 shows that the transfer function parameters have been calculated correctly.

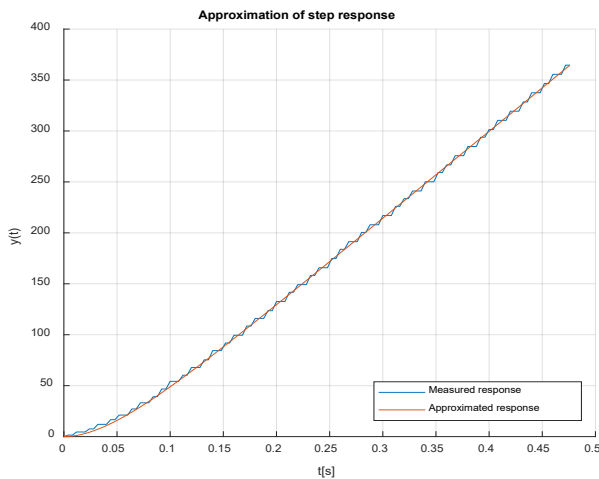


Figure 6 – Step response approximation

The controller parameters were then calculated for the derived transfer function. The Desired model method was used for this purpose. This method established a PD controller for the first-order integration system.

The following equation shows the transfer function of a conventional PD controller in the discrete form [14]:

$$G_R(z) = k_p \cdot \left( 1 + \frac{T_D}{T} \cdot \frac{z - 1}{z} \right) \quad (3)$$

Where:

- $k_p$  – proportional gain,
- $T_D$  – derivative time
- $T$  – controller sample time

The controller parameters were obtained for 0 % overshoot and 100 Hz sampling frequency. The calculation of the parameters is given by the following formulas [14]:

$$T_D^* = T_1 - \frac{T}{2} \quad (4)$$

$$k_p^* = \frac{1}{\alpha \cdot T \cdot k_1}$$

Where:

- $T_1$  – transfer function time constant,
- $k_1$  – transfer function coefficient,
- $T$  – sample rate
- $\alpha$  – table coefficient

Figure 7 shows the process of control with proposed parameters while turning the steering wheel. To facilitate steering wheel rotation, the manipulated variable was limited to 20% of DC motor power.

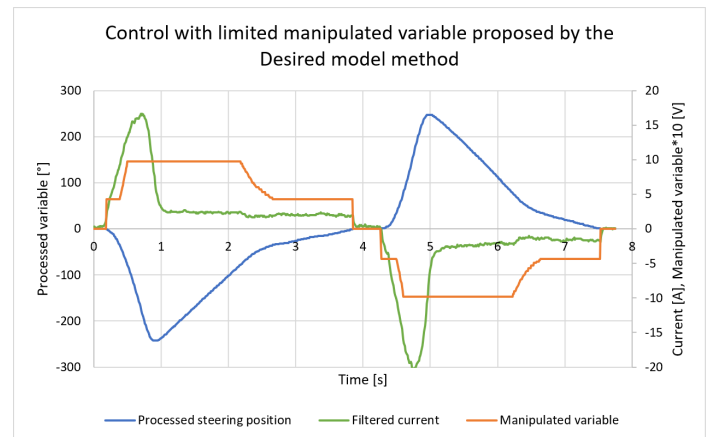


Figure 7 – Final process of control

The graph also contains the measurement of feedback motor load using the current sensor based on ACS758. Due to high noise, the signal was adjusted using an exponential filter.

The exponential filter is described by equation below [15]:

$$y_F(i) = K_F \cdot y_M(i) + (1 - K_F) \cdot y_F(i - 1) \quad (5)$$

$$y_F(1) = y_M(i), 0 < K_F \leq 1$$

Where:

- $y_F(i)$  – new filtered value,
- $K_F$  – filtration coefficient,
- $y_M(i)$  – measured value,
- $y_F(i-1)$  – previous filtered value

The value of the filtration coefficient was chosen as 0.03.

Figure 8 shows the different methods of current signal conditioning. There is a comparison of moving average and exponential filtration.

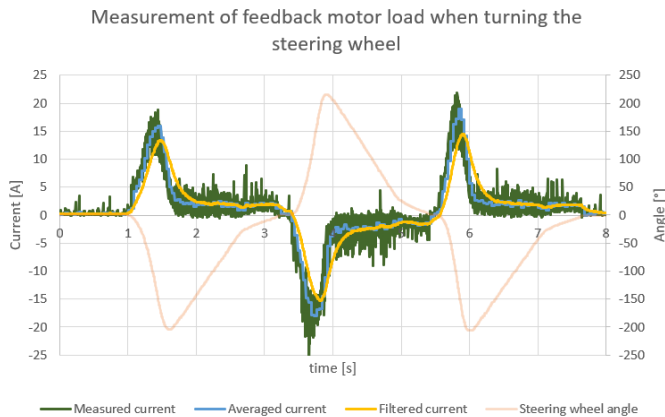


Figure 8 - Feedback motor load while turning the steering wheel

The solution for the future implementation of other systems such as parking assistance or vehicle stabilization can be designed advanced control with dynamic change of controller parameters depending on the required power of the motor.

In Figure 9, the prototype model of the electronic steering wheel is shown.

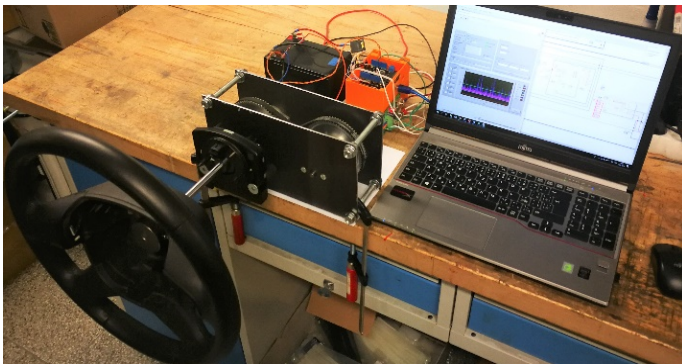


Figure 9 – Electronic steering wheel unit prototype model

### 3. Design of the steering control system

In the design of the steering control system, it was necessary to select appropriate components such as actuators or control unit. As the actuators, the super duty linear servos were selected for the wheel steering. These actuators were selected according to the calculated parameters described in [16]. This linear actuator can exert a force greater than 2 kN and includes a 10 kΩ potentiometer to provide information about the current position. For the control of linear drives, the cRIO from National Instruments together with Roboclaw motor driver was chosen.

The same procedure as for the steering wheel unit was performed to determine the PID controller parameters. This means that experimental identification was performed first. Then the controller parameters were derived for the determined transfer function [16].

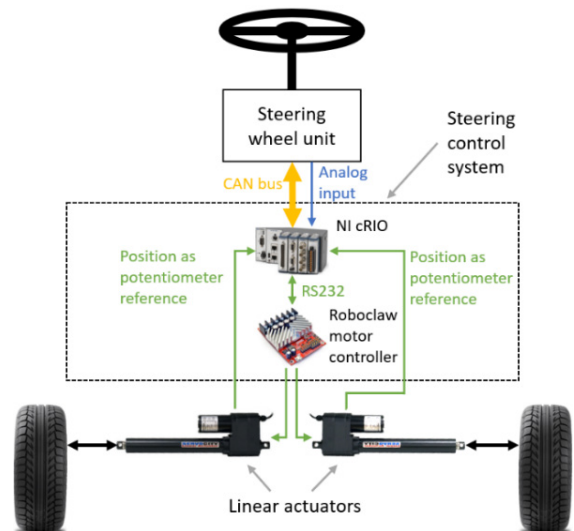


Figure 10 – Structure of the proposed electronic steering system, [16]

Figure 10 shows the whole structure of the proposed steering control system with selected components.

Figure 11 shows the linear actuators mounted on the axles of the test vehicle.



Figure 11 – Picture of testing vehicle with steer-by-wire technology

Finally, the program of the control system was created in LabView. The cRIO was not only used for testing, but also as a main unit of the steering control system. The control system also implements the condition of Ackermann steering geometry. The calculation of the Ackermann formula is described in [16].

Ackermann steering geometry is based on the different steering angles of the inner and outer wheels when the vehicle turns. The aim is that the turn radius of both wheels ideally has a

common midpoint. As a result, the tires are not so stressed when cornering the vehicle. The principle and more detailed information are described by Zhao et al. [17]. They deal with the design of the steering mechanism based on Ackermann.

#### 4. Results and future work

This chapter summarizes the results of this work. During this work, two systems were developed which communicate with each other. The first is the steering wheel unit, which is used to set the desired position of wheels and generate force feedback back to the driver. The maximum torque of the feedback DC motor was calculated as 20 Nm. The second system controls the linear actuators of both wheels.

Figure 12 shows the final relation between the steering angle of both wheels and the steering wheel position. The difference between wheels is given by Ackermann steering geometry of our car.

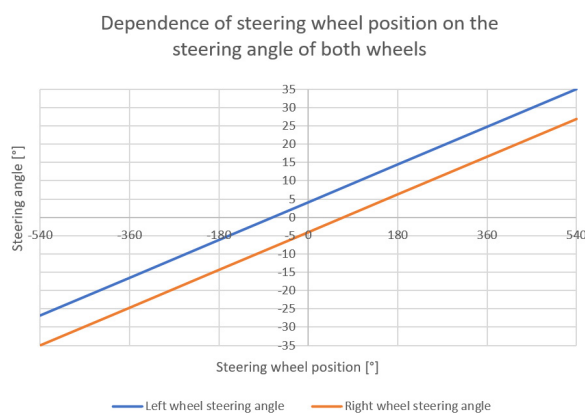


Figure 12 – Relationship between steering angle and steering wheel position

The goal of further development is to find a solution for road surface feedback and get it to the driver through the steering wheel. The solution can be force or torque sensors in combination with accelerometers or yaw rate sensors mounted on the wheels of the vehicle as described in [18, 19].

#### 5. Conclusion

The current automotive world is moving towards autonomy and the replacement of mechanical systems by electronic ones. Therefore, this work was focused on the design and implementation of electronic vehicle control without a mechanical connection between the axle and the steering wheel. In this work were developed and implemented two systems that can communicate with each other. The first system is the steering wheel unit and the second is the steering control system. The steering wheel unit represents a steering wheel coupled to a DC motor using a dual belt drive and the position is measured by CAN based sensor. The main role of this system is to transmit the requirement for the steering angle of the wheels in the form of an analog signal to the steering control system. The other role is to generate force feedback back to the driver by the steering wheel.

The steering control system is represented by the control unit, motor controller and two linear actuators for turning the wheels.

The result of this work is the possibility of independent control of both wheels according to the steering wheel position. The advantage of independent control is software geometry adjustment. The proposed system was tested on the real model of the electric car at the university.

#### Conflict of Interest

The authors declare no conflict of interest.

#### Acknowledgment

This work was supported by the European Regional Development Fund in the Research Centre of Advanced Mechatronic Systems project, CZ.02.1.01/0.0/0.0/16\_019/0000867 within the Operational Programme Research, Development and Education and the project SP2020/57 Research and Development of Advanced Methods in the Area of Machines and Process Control supported by the Ministry of Education, Youth and Sports.

#### References

- [1] T. Pawlenka and J. Škuta, "Electronic Steering With Force Feedback," 2019 20th International Carpathian Control Conference (ICCC), Krakow-Wieliczka, Poland, 2019, pp. 1-5. doi: 10.1109/CarpathianCC.2019.8765925
- [2] Y. Yamaguchi and T. Murakami, "Adaptive Control for Virtual Steering Characteristics on Electric Vehicle Using Steer-by-Wire System", IEEE Transactions on Industrial Electronics, vol. 56, no. 5, pp. 1585-1594, 2009. Available: 10.1109/tie.2008.2010171.
- [3] X. Liu et al., "Driving Assist System for Ultra-Compact EVs—Fundamental Consideration of Muscle Burden Owing to Differences in the Drivers' Physiques", Actuators, vol. 7, no. 3, p. 44, 2018. Available: 10.3390/act7030044.
- [4] M. Ye, Q. Wang and S. Jiao, "Robust H<sub>2</sub>/H<sub>∞</sub> Control for the Electrohydraulic Steering System of a Four-Wheel Vehicle", Mathematical Problems in Engineering, vol. 2014, pp. 1-12, 2014. Available: 10.1155/2014/208019.
- [5] G. Yin, N. Chen and P. Li, "Improving Handling Stability Performance of Four-Wheel Steering Vehicle via  $\mu$ -Synthesis Robust Control", IEEE Transactions on Vehicular Technology, vol. 56, no. 5, pp. 2432-2439, 2007. Available: 10.1109/tvt.2007.899941.
- [6] H. Yan, W. Zhang and D. Wang, "Wheel Force Sensor-Based Techniques for Wear Detection and Analysis of a Special Road", Sensors, vol. 18, no. 8, p. 2493, 2018. Available: 10.3390/s18082493.
- [7] J. Pytka et al., "Determining Wheel Forces and Moments on Aircraft Landing Gear with a Dynamometer Sensor", Sensors, vol. 20, no. 1, p. 227, 2019. Available: 10.3390/s20010227.
- [8] S. Fahami, H. Zamzuri and S. Mazlan, "Development of Estimation Force Feedback Torque Control Algorithm for Driver Steering Feel in Vehicle Steer by Wire System: Hardware in the Loop", International Journal of Vehicular Technology, vol. 2015, pp. 1-17, 2015. Available: 10.1155/2015/314597.
- [9] H. Zheng, J. Hu and Y. Liu, "A bilateral control scheme for vehicle steer-by-wire system with road feel and steering controller design", Transactions of the Institute of Measurement and Control, vol. 41, no. 3, pp. 593-604, 2017. Available: 10.1177/0142331217734502.
- [10] K. Kozeka, "A Motor Driven by Permanent Magnets Alone; A Clean and Abundant Source of Electromagnetic Energy from Iron and Other Ferromagnetic Materials", Natural Science, vol. 09, no. 09, pp. 319-329, 2017. Available: 10.4236/ns.2017.99031.
- [11] V. Bhandari, Design of machine elements. New Delhi: McGraw-Hill Education (India), 2017.
- [12] J. Škuta and J. Kulhánek, "Controll of car LED lights by CAN/LIN bus," Proceedings of the 2015 16th International Carpathian Control Conference (ICCC), Szilvasvarad, 2015, pp. 486-489. doi: 10.1109/CarpathianCC.2015.7145128.
- [13] P. Noskiewič, Modelování a identifikace systémů. Ostrava: Montanex, 1999.
- [14] M. Vítečková, Základy automatické regulace, Přeprac. 2. vyd. Ostrava: VŠB - Technická univerzita Ostrava, 2008.

- [15] H. Ravinder, "Forecasting With Exponential Smoothing Whats The Right Smoothing Constant?", *Review of Business Information Systems (RBIS)*, vol. 17, no. 3, pp. 117-126, 2013. Available: 10.19030/rbis.v17i3.8001.
- [16] Lawrance, "Steering by Wire for Sport Car", Diploma thesis, Ostrava, 2019.
- [17] J. Zhao, X. Liu, Z. Feng and J. Dai, "Design of an Ackermann-type steering mechanism", *Proceedings of the Institution of Mechanical Engineers, Part C: Journal of Mechanical Engineering Science*, vol. 227, no. 11, pp. 2549-2562, 2013. Available: 10.1177/0954406213475980.
- [18] J. Iqbal, K. Zuhaib, C. Han, A. Khan and M. Ali, "Adaptive Global Fast Sliding Mode Control for Steer-by-Wire System Road Vehicles", *Applied Sciences*, vol. 7, no. 7, p. 738, 2017. Available: 10.3390/app7070738.
- [19] J. Tian, J. Tong and S. Luo, "Differential Steering Control of Four-Wheel Independent-Drive Electric Vehicles", *Energies*, vol. 11, no. 11, p. 2892, 2018. Available: 10.3390/en11112892.



## **A Systematic Literature Review of Vessel Anomaly Behavior Detection Methods Based on Automatic Identification System (AIS) and another Sensor Fusion**

Nova Muhammad Ferlansyah\*, Suharjito

*Department of Computer Sciences, BINUS Graduate Program-Master of Computer Sciences, Bina Nusantara University, Jakarta, Indonesia, 11480*

---

### **ARTICLE INFO**

*Article history:*

*Received: 10 October, 2019*

*Accepted: 04 March, 2020*

*Online: 20 March, 2020*

---

*Keywords:*

*Automatic Identification System*

*Anomaly Detection*

*Vessel traffic Behavior*

---

### **ABSTRACT**

*The high flow of vessel traffic affects the difficulty of monitoring vessel in the middle of the sea because of limited human visibility, occurrence of vessel accidents at the sea and other illegal activities that illustrate abnormal vessel behavior such as oil bunkering, piracy, illegal fishing and other crimes that will continue and will certainly have an impact on losses in several aspects. the author collects studies using Automatic Identification System (AIS) data as a basis for analysis to see the behavior of vessels at the sea, in addition to that AIS data can also be combined with other sensor data to strengthen monitoring of vessel movements at the sea, this is very supportive in detecting the anomalous behavior of vessel that often occur outside the reach of human vision or the sea patrol on duty. This paper uses the Systematic Literature Review (SLR) method in identifying, evaluating, and interpreting various methods of studies related to vessel anomalous behavior at the sea the author highlights several methods that are always applied to studies that already exist in detecting vessels anomalous behavior, the study detected the movement of vessel with AIS data from the history of vessel locations and fusion with another sensor in seeing movements of abnormal vessel behavior through patterns that were formed. This paper refers to various studies and reviews some of them about the use of AIS track data history in vessel including combining with other data to detect anomalous behavior of vessel, the results of the analysis are used to find out activities that have the potential for illegal activities or other crimes that can be detrimental and can be used as decision making, the authors hope the results of this paper can be an option to be applied to the surveillance system of vessel around the territorial waters in order to guard against crime and other illegal behavior*

---

## **1. Introduction**

The development of information technology in the maritime sector for vessel behavior is monitoring, has been recently developed to facilitate monitoring of vessels in the sea waters. Automatic Identification System (AIS) is an important part of supporting the safety of vessels in the sea when sailing. For all transport vessels with a load of 300 Gross Tonnage (GT), passenger vessels (domestic and international lines), and other types of vessels with international lines required to use AIS, prevent collision accidents between vessels and seeing the pattern of vessel movements [24].

Comprehensive supervision needs can be done directly by using physical observation at the sea, but direct observation has

certain weaknesses when it's carried out, such as the availability of sea transportation fleets and crew by preparing high operational costs, this is very important to be the main concern in supervising and maintaining very wide waters and need new ways of monitoring vessels at the sea. In addition to physical observations and movement patterns, the vessel has an identity that can provide information about the condition and origin of the vessel, there needs to be rules regarding the use of the identity of the vessel as one of the supporting feasibility of vessels in sailing by standardization in the form of legality [15].

Many vessels which certainly enter the obligation to use the AIS device for safety at the sea, it is difficult to know the route of the tanker when it is far from the shore or the mainland, the extent of sea waters in Indonesia is a condition as a problem in

---

\* Nova Muhammad Ferlansyah, [ferlansyah@rocketmail.com](mailto:ferlansyah@rocketmail.com)

monitoring activities of vessels at the sea, a method is needed in monitoring the vessel so it can be monitored properly.

Generally the vessel sails by using a predetermined route, but in traffic conditions in the sea waters many choices of paths can be used, see the anomalies of vessel movements can be seen from the density of vessel traffic [14], from this method we can see the position of the vessel around the lane or outside of the lane. The potential for vessels to do anomalies is very large because the number of vessels passing in the sea waters is very much a concentration of areas that become centers of supervision activities, in this case, areas that often occur piracy, accidents or special areas that deserve attention, or in terms of another is the Area Of Interest (AOI).

## 2. Basic Concept

### 2.1. Automatic Identification System (AIS)

The factor of increasing sea accidents is that vessels are not identified through electronic navigation devices that can provide information on the location, vessel speed, direction of the vessel's direction, and vessel's identity. In 2004 AIS was implemented which was primarily aimed at avoiding collisions and accidents, besides being a supporter of information for coastal operators it was also used to monitor vessel traffic as a marine navigation for vessel supervision [2].

### 2.2. International Maritime Organization (IMO)

In 1996 the priority of human safety on the vessel became high because of accidents recorded 3559 events at that time, the legality of the vessel became one of the first steps in detecting and regulating various information on the condition of the vessel and vessel activity information by their functions and capabilities [16]. Also, IMO is very focused on vessel safety regulations at the sea, and IMO numbers are listed on electronic data variables Automatic Identification System (AIS) through the rules of International Telecommunications Union (ITU) with data sent via radio packages transmitted by encapsulation standards according to the National Marine Electronics Association (NMEA) 0183 [2].

### 2.3. Vessel Anomaly Behaviour

Traffic movements of vessels in the sea in the recent digital era are very much used for various activities that can be used as supporting data to make decisions, from various types of vessels that cross-sea waters, utilization of vessel movement data stored for a certain period when displayed, can shows the behavior patterns of vessels that vary from the various travel routes that have been passed. The pattern of normal vessel behavior is abnormal, or it can be called anomaly which has own pattern which can be used as an analysis material for vessel movement designations

## 3. Proposed Methodology

The Biolchini Systematic Literature Review (SLR) method involves identifying, evaluating, and interpreting all available and relevant research, through questions from the research topics and phenomena favored by researchers. Individual studies that contribute to systematic studies are called primary studies, while systematic studies are themselves forms of secondary studies.

Biolchini separated the guidelines for implementing SLR in 3 phases, namely: (i) planning; (ii) execution; (iii) analysis of the results.

During the literature review, there are 2 checking areas, namely in the planning protocol and execution protocol area. If the problems are found in each of the checking areas, the reviewer must return to the previous stage.

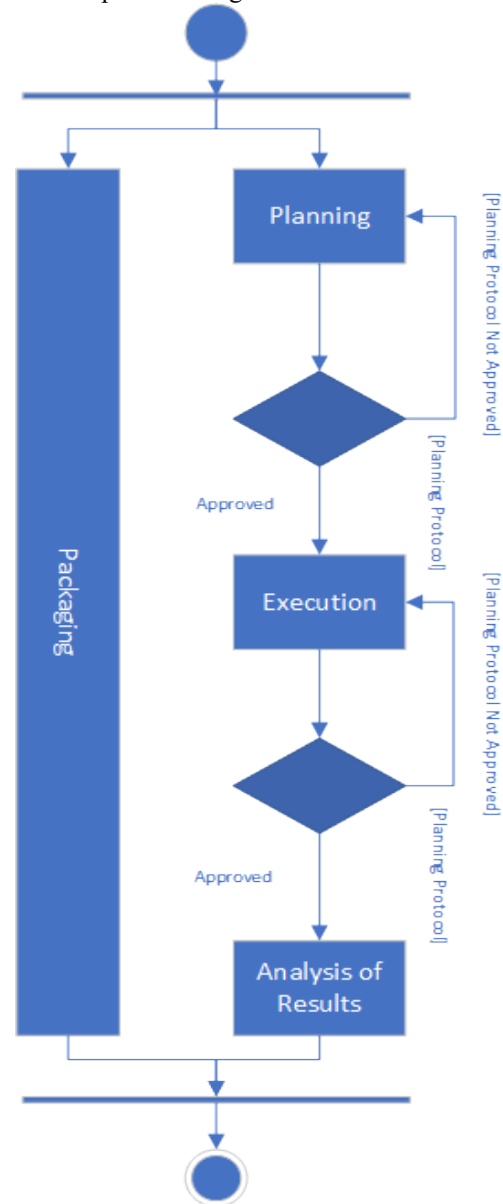


Figure 1: Process in carrying out SLRs [11]

### 3.1. Planning Review

The planning steps consist of [11]:

- (i) Formulating questions;
- (ii) Selection of data sources and search strategies;
- (iii) Selection of studies.

Each step will be described as follows:

#### 3.1.1 Formulate Question

The focus of this study is to find out how to detect the vessel anomalies by using AIS data. For this reason, many questions are

designed to obtain answers from the results of this literature review.

- Question 1 (Q1). In the publication forum, what are the discussions on how to detect vessel anomalies?
- Question 2 (Q2). What methods are often used to detect vessel anomalous behavior?
- Question 3 (Q3). Developmental trend method for detecting vessel anomalous behavior in the last 5 years?
- Question 4 (Q4). What is the contribution of each of the ways to detect vessel anomalous behavior?

### 3.1.2 Selection of Data Sources and Search Strategies

In this literature review the data sources that will be used are available papers on the website page:

- (1) Elsevier (<http://www.elsevier.com>);
- (2) The Journal of Navigation (<https://www.cambridge.org>);
- (3) IEEE (<https://ieeexplore.ieee.org>);
- (4) Reasearch Gate (<https://www.researchgate.net>).

The more data sources used, the greater the chance to find the appropriate literature.

The strategy in conducting searches is built through determining keywords and synonyms from the focus of the study. Keywords and synonyms can be connected to logical conector OR and AND, as follows:

(AIS OR "Automatic Identification System" OR "AIS vessel movement")AND("vessel anomaly behaviour" OR "vessel anomaly detection" OR "vessel anomaly tracking" OR "ais vessel" OR "vessel movement").

Search all databases: Elsevier, Cambridge, IEEE, Researchgate.

### 3.1.3 Paper Selection

The destination website search engine is likely to produce a large number of papers. Though not necessarily all the papers are relevant to the purpose of the study. Therefore, further, identification is needed to obtain papers that are primary studies. Identification can be done by applying inclusion and exclusion criteria. The application of inclusion and exclusion criteria will guarantee that the paper used is a paper that truly fits the context of the study.

Inclusion criteria:

1. Paper that explains concepts, benefits, techniques, methods, strategies and everything in detecting vessel behavior
2. Papers presented in English.

Exclusion Criteria:

1. Papers that only focus on the discussion of AIS.
2. Papers that only focus on the discussion of Anomaly Detection.

The procedure for selecting papers is done by speed reading techniques for all primary study candidates. Speed reading is reading the abstraction section of the available paper. Furthermore, based on the inclusion and exclusion criteria made, it can be determined whether the paper can be used as the primary study.

### 3.2 Execution

Based on the planned review that has been prepared, the next step is to execute the plan. The execution of the search string on the four pages of the website which is used as the source of the data produces 64 papers which are the primary study candidates as Table.

Table 1: Related or No Related Articles

No.	Database	Related	No. Related
1	IEEE	6	15
2	ScienceDirect	9	22
3	ACM Digital Library	3	9

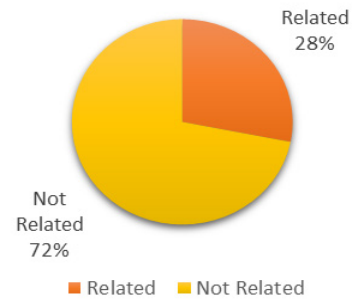


Figure 2: Based on related and unrelated primary journal studies

The total number of 64 publications found 72% related and 28% not related to Figure 2 related to the domain being searched, this result can answer question Q1 to map important data sources that can be used for further studies. Publications that are following the domain of 72% including journals and conferences.

The further inclusion criteria are applied and exclusion by reading the abstraction part of all primary study candidates. Application of criteria inclusion and exclusion produced as many as 18 journals that related

## 4. Results and Discussion

After knowing the results conducted through primary studies originating from the publication forum, there were 18 in accordance with the domains of 17 journals and 1 conference in figure 3. From the results of the primary study, we can see that few related domains discussing Vessel Anomaly Behavior Detection Methods Based on Automatic Identification System (Q1) in several source database forums.

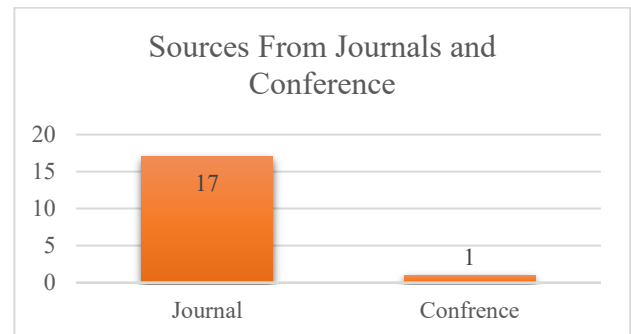


Figure 3: Based on related sources from journals and Conferences studies

Table 2 : Related Journals and Conferences

Journal Databases	Year of Publication				
	2013	2014	2015	2017	2018
Institute of Electrical and Electronics Engineers (IEEE)			J01. [7] J02 [9]	J01. [23] J02. [28]	J01 [22] J02 [1]
Science Direct		J01. [26] J02. [5]	J01. [4] J02 [12]	J01 [6]	J01. [21] J02. [33] J03. [32] J04. [29]
Association for Computing Machinery (ACM)	C01. [17]			J01. [18]	J01 [30]

4.1. Question 1 (Q1)

Conducting studies of various publications obtained from various sources to look for methods related to the anomalous of the vessel’s behavior, the selection of methods is carried out by using the biolchini method to include grouping sources that are related and not related.

From the other side, the use of human decisions is part of a process that cannot be avoided if a wise decision is needed, not only to determine correctly or wrongly, humans here as operators to take an important role in determining the final results of decisions taken based on events and information received through the system or direct observation. In the Figure 4, the Bayesian Network method functions to produce decisions from the conditions encountered [3]. The loss of AIS information in the search for the position of the vessel being monitored is a common thing, whether it occurs because of intentional or not, such as the vessel operator accidentally turns off the AIS device [3] where is installed in the vessel or the AIS device is not functioning properly can occur but this needs to be a serious concern because if the vessel is in the middle of the sea and far from the human view, the AIS information is very useful to see the position, and movement of the vessel.

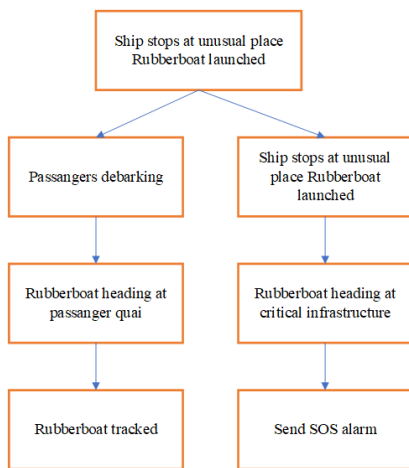


Figure 4: Possible scenario model of a Bayesian network [17]

Information contained in the AIS Data is in the form of location data (longitude and latitude), time stamp, speed over ground (SOG), course over ground (COG), heading, vessel ID (MMSI, IMO, Call Sign, Flag), and others [29]. One of the anomalous

activities on a vessel can be known through, not detected by the vessel with signal loss or not receiving AIS information from the vessel, it is necessary to detect the loss of vessel AIS information by combining other data to see from observations of synthetic aperture radar (SAR), if AIS information data is not detected. Figure 5 shows how to combine information through AIS and SAR data to detect the position of the vessel.

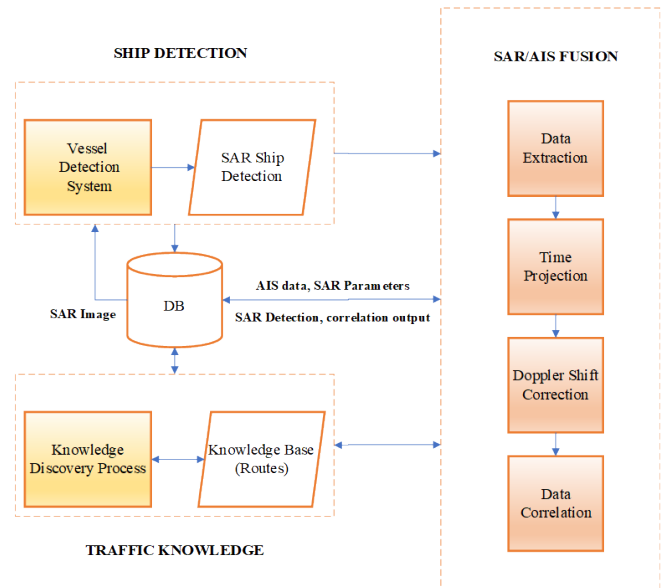


Figure 5: Combine data SAR and AIS [17]

Detecting anomalies can also be seen from the trajectory that is traversed using the history of stored data then compared to using normal trajectory data as a reference for determining whether the vessel is conducting anomalous movements or not, this is can answer question Q2 [23] [12] [26] [33],

4.2. Question 2 (Q2)

The method that describes the route to be used as a detection of vessel behavior through travel history and movement patterns of the vessel, according to P. Fu et al. vessel behavior analysis detects the movement of vessels out on the trajectory path [23] that is normally traversed. The data source used in the method of using the vessel trajectory is using AIS historical data.

Besides detecting anomalies can determined also through the estimated hours of arrival of the vessel, related to the delay of the



vessel which can cause concern about the activities of the vessel which, of course if it is in the middle of the sea [1], in 2019 the prediction method for vessel delay by detecting the prediction of vessel arrival time greatly helped to detect vessel anomalies from analysis through time (Q3).

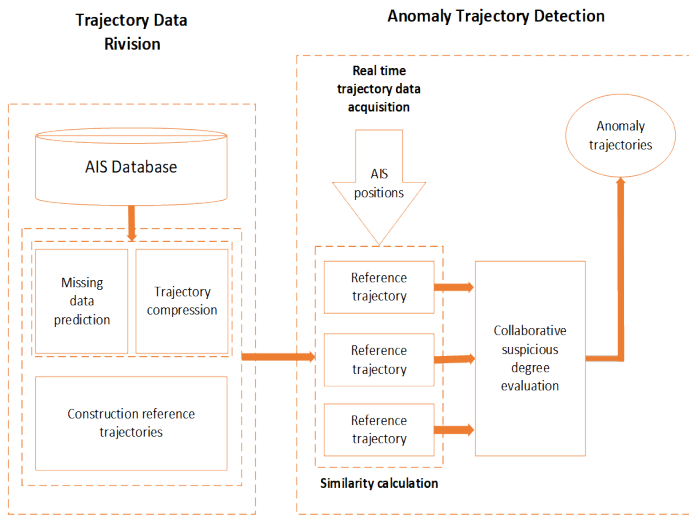


Figure 6: Framework movement trajectory path [23]

#### 4.3. Question 3 (Q3)

Trends use historical data of ship travel and movement based on time passed, a valid approach to finding areas where ships repeatedly show changes in direction [22], and a combination of some data other than the AIS sensor, one of which is to combine data, i.e. synthetic aperture radar (SAR) to detect the position of ships at the sea using radar sensors [7].

In addition to monitoring vessels, observing activities through monitoring anomalous activities can also be used in certain areas of the intensity of vessels carrying out activities in the area based on certain times and seasons [6]. Each method has the character and way of detecting vessel anomalies, most of which use historical data to see the movement patterns of vessels from crossed trajectories, use prediction of vessel arrival times, and analyze the consistency of AIS signals sent, this is very helpful in investigating incidents that have occurred and is likely to be used as information for deciding detecting vessel anomalous behavior, in conditions of oil smuggling, vessel hijacking and others (Q4).

#### 4.4. Question 4 (Q4)

The contribution made is to make it easier for the monitoring officer to know the activities of the ship through the movement or position of the ship at the sea. From the various methods reviewed in this paper, it is explained that monitoring by relying on limited human visibility will be very difficult if the ship in the middle of the sea is difficult to know the movement, the method that has been conveyed from several studies above explained related to utilizing AIS data and combining data using other sensor data to capture the activities of ships at the sea, of course will be very helpful in analyzing and making decisions of events that are caught to be able to provide recommendations if they occur anomaly in ship behavior, interested parties can use the above methods as a reference tool in detecting the behavior of ship anomalies at the sea.

## 5. Conclusions

Vessel anomalous behavior generally performs unusual activities when the vessel travels from point A to point B, of course, the factor of determining anomalies is very varied, referring for not detection of the AIS signal of the vessel, unusual vessel movements, estimated time arrival, the vessels are in the region outside the usual trajectory, changes or shifts in the direction of the vessel with addition significant speed, and other factors not following the actual shape or form such as anomalies to the identity of the vessel, or the vessel is not in other normal conditions. From the results of a survey conducted that the study of literature generally states that anomalies are carried out through activities or conditions not in a state of reasonableness, it can be used to determine what is happening in the field, based on methods carried out to detect vessel anomalous behavior, of course, observations the behavior of vessels with the behavior of land vehicles is very different in terms of location and term that can still be reached, compared to the unstable sea conditions and the vast expanse of sea.

From this literature study, the researcher concludes that from various methods used to detect anomalies, it is very helpful for surveillance operators to supervise ships without having to check vessels one by one with heavy traffic conditions, and the number of ships that are not small as initial detection, related to this role humans are still used as final decision-makers to compare with data and other information because there are no standard categorizations of anomalies on ships and are listed as general references, and high considerations because they involve the law. The anomaly detection method is also useful for the safety of the vessel at the sea protected from collisions between vessels and prevented illegal activity

## References

- [1] A. Alessandrini, F. Mazzarella, and M. Vespe, (2019) "Vessel Tracking Data," *IEEE Trans. Intell. Transp. Syst.*, vol. 20, no. 1, pp. 7–15
- [2] Bekkadal, F. (2009, October). Emerging maritime communications technologies. In *Intelligent Transport Systems Telecommunications*, 358–363.
- [3] Carthel, C. C. (2007). Multisensor tracking and fusion for maritime surveillance. In *Information Fusion*, 1–6.
- [4] D. Zissis, E. K. Xidias, and D. Lekkas, (2015) "A cloud based architecture capable of perceiving and predicting multiple vessel behaviour," *Appl. Soft Comput. J.*
- [5] E. Osekowska, H. Johnson, and B. Carlsson, (2014) "Grid size optimization for potential field based maritime anomaly detection," *Transp. Res. Procedia*, vol. 3, no. July, pp. 720–729.
- [6] E. Osekowska, H. Johnson, and B. Carlsson, (2017) "Maritime vessel traffic modeling in the context of concept drift," *Transp. Res. Procedia*, vol. 25, pp. 1457–1476.
- [7] F. Mazzarella, M. Vespe, and C. Santamaria, (2015) "SAR Vessel Detection and Self-Reporting Data Fusion Based on Traffic Knowledge," *IEEE Geosci. Remote Sens. Lett.*, vol. 12, no. 8, pp. 1685–1689.
- [8] Fawcett, T. (2006). An introduction to ROC analysis. *Pattern recognition letters*, 861–874
- [9] F. Papi et al., (2015) "Radiolocation and tracking of automatic identification system signals for maritime situational awareness," vol. 9, no. July 2014, pp. 568–580.
- [10] Garuba, D. S. (2010). Trans-border economic crimes, illegal oil bunkering and economic reforms in Nigeria. *Policy brief series*, 15
- [11] J. Biolchini, P.G. Mian, A.C.C. Natali, G.H. Travassos. (2005), *Systematic Review in Soft-ware Engineering, Technical Report RT-ES 679/05*, Federal University of Rio de Janeiro, Rio de Janeiro, RJ, Brazil.

- [12] J.-H. OH, K. KIM, and J.-S. JEONG, (2015) "A Study on the Risk Analysis based on the Trajectory of Fishing Vessels in the VTS Area\*," *UMK Procedia*, vol. 2, pp. 38–46.
- [13] Juba, B. M.-D. (2015, February). Principled Sampling for Anomaly Detection. In *NDSS*.
- [14] Kowalska, K. &. (2012). Maritime anomaly detection using Gaussian Process active learning. In *Information Fusion (FUSION)*, 1164-1171.
- [15] Laxhammar, R. F. (2009, July). Anomaly detection in sea traffic—a comparison of the gaussian mixture model and the kernel density estimator. In *Information Fusion*, 2009, 756-763.
- [16] Li, K. X. (2001). Maritime legislation: new areas for safety of life at sea. *Maritime Policy & Management*, 225-234.
- [17] L. Rothkrantz and K. Scholte, (2013) "A Surveillance System of a Military Harbour Using an Automatic Identification System," pp. 169–176.
- [18] L. Zhao, (2017) "A Correction Method for Time of Vessel Trajectories Based on AIS," pp. 83–88.
- [19] Mazzarella, F. V. (2017). A novel anomaly detection approach to identify intentional AIS on-off switching. *Expert Systems with Applications*, 110-123
- [20] Nanduri, A. &. (2016, April). Anomaly detection in aircraft data using Recurrent Neural Networks (RNN). In *Integrated Communications Navigation and Surveillance (ICNS)*, 5C2-1.
- [21] P. Chen, Y. Huang, J. Mou, and P. H. A. J. M. Van Gelder, (2018) "Vessel collision candidate detection method: A velocity obstacle approach," *Ocean Eng.*, vol. 170, no. October, pp. 186–198.
- [22] P. Coscia, P. Braca, S. Member, L. M. Millefiori, F. A. N. Palmieri, and P. Willett, (2018) "Multiple Ornstein-Uhlenbeck Processes for Maritime Traffic Graph Representation," vol. 9251, no. c, pp. 1–13.
- [23] P. Fu, H. Wang, K. Liu, X. Hu, and H. U. I. Zhang, (2017) "Finding Abnormal Vessel Trajectories Using Feature Learning," *IEEE Access*, vol. 5, pp. 7898–7909.
- [24] Sak, H. S. (2014). Long short-term memory recurrent neural network architectures for large scale acoustic modeling. In *Fifteenth annual conference of the international speech communication association*.
- [25] Silveira, P. A. (2013). Use of AIS data to characterise marine traffic patterns and vessel collision risk off the coast of Portugal. *The Journal of Navigation*, 879-898.
- [26] S. Mascaro, A. Nicholson, and K. Korb, (2014) "International Journal of Approximate Reasoning Anomaly detection in vessel tracks using Bayesian networks," vol. 55, pp. 84–98.
- [27] Vadaine, R. H. (2018). Multi-task Learning for Maritime Traffic Surveillance from AIS Data Streams.
- [28] V. F. Arguedas, G. Pallotta, and M. Vespe, (2018) "Maritime Traffic Networks: From Historical Positioning Data to Unsupervised Maritime Traffic Monitoring," *IEEE Trans. Intell. Transp. Syst.*, vol. 19, no. 3, pp. 722–732.
- [29] X. Wu and V. A. Zaloom, (2018) "Study of travel behavior of vessels in narrow waterways using AIS data – A case study in Sabine-Neches Waterways," vol. 147, no. October 2017, pp. 399–413.
- [30] Y. Jiang, B. Li, H. Zhang, Q. Luo, and P. Zhou, (2018) "A Novel Classification Scheme of Moving Targets at Sea Based on Ward's and K-means Clustering," pp. 1–5.
- [31] Yang, X. S. (2018). Position Detection and Direction Prediction for Arbitrary-Oriented Vessels via Multiscale Rotation Region Convolutional Neural Network. *arXiv preprint arXiv*, 1806.04828.
- [32] Y. Shu, W. Daamen, H. Ligteringen, M. Wang, and S. Hoogendoorn, (2018) "Calibration and validation for the vessel maneuvering prediction ( VMP ) model using AIS data of vessel encounters," *Ocean Eng.*, vol. 169, no. October, pp. 529–538.
- [33] Z. Chen, J. Xue, C. Wu, L. Qin, L. Liu, and X. Cheng, (2018) "Classification of vessel motion pattern in inland waterways based on Automatic Identification System," vol. 161, no. September 2017, pp. 69–76

## Scapy Scripting to Automate Testing of Networking Middleboxes

Dr. Minal Moharir<sup>1,\*</sup>, Karthik Bhat Adyathimar<sup>2</sup>, Dr. Shobha G<sup>3</sup>, Vishal Soni<sup>4</sup>

<sup>1</sup>Associate Professor, Computer Science and Engineering, RV College of Engineering, Bengaluru-560059, India

<sup>2</sup>Student, Computer Science and Engineering, RV College of Engineering, Bengaluru-560059, India

<sup>3</sup>Professors, Computer Science and Engineering, RV College of Engineering, Bengaluru-560059, India

<sup>4</sup>Senior Manager, Engineering at Citrix Systems Inc, Bengaluru-560042, India

### ARTICLE INFO

*Article history:*

*Received: 28 December, 2019*

*Accepted: 22 February, 2020*

*Online: 23 March, 2020*

*Keywords:*

*Automatic Identification System*

*Anomaly Detection*

*Vessel traffic Behavior*

### ABSTRACT

Middleboxes like load balancers are being used by all the corporations to manage and support their infrastructures. These devices see a large amount of bandwidth every day. This might include a range of protocols which might be varying from network layer to the application layer. This traffic can be corrupt or malicious thus causing these devices to fail or get exploited. Citrix NetScaler Application Delivery Controller (ADC) is one of such ADC which provides supple transportation services for conventional, containerized and microservice applications from the data centre or any cloud. NetScaler supports robust security, excellent L4-L7 load balancing, authentic Global server load balancing (GSLB), and enhanced uptime. Scapy is one of the most powerful and interactive packet manipulation software. Scapy is a powerful network manipulation module which is distributed as a python module. Python being a powerful scripting language helps in exploring this in various use cases. In this paper we discuss using Scapy with Python to script application layer protocols with controlled packet structure which helps in testing these middleboxes. We use these modules to explore Citrix Netscaler ADC which is widely being used. Our present work involves development of server-client Model for the following protocols namely FTP, HTTPS and TFTP. FTP protocol developed using scapy has support for both IPv4 and IPv6. All these scripts built using scapy are open sourced.

## 1. Introduction

Scapy is a software developed in Python. It supports low level packet manipulation. It can be used to build tools to support testing and exploitation of networking modules. Scapy can easily interpret packets of a different variety of protocols, push them on the wire, and capture them. It can send requests and responses. The various functions of Scapy tool is as shown in figure 1. Scapy can handle most traditional undertakings like filtering, tracerouting, examining, unit tests, assaults or system revelation without much of a stretch [1]. Scapy can supplant hping, arpspoof, arp-sk, arping, p0f and even a few sections of Nmap, tcpdump, and tshark.

Scapy likewise performs extremely well on a considerable measure of other explicit assignments that most different tools can't deal with, such as sending invalid packets, infusing your own 802.11 layers, joining procedures (VLAN hopping ARP

store harming, VOIP translating on WEP scrambled channel). The thought is straightforward. Scapy primarily completes couple of major functions such as sending packets and in turn accepting responses. We can build the packets with the required parameter let that be a TCP/UDP or even the lower layer details like window size, acknowledgement number. This has the huge favourable position over tools like Nmap or hping that only lets you deal with known packets. Scapy lets the user to listen to the packets on the network, filter the required ones and alter/forge/forward them [2].

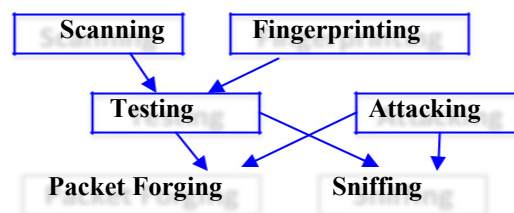


Figure 1: Scapy Functions

\* Dr. Minal Moharir, [minalmoharir@rvce.edu.in](mailto:minalmoharir@rvce.edu.in)

## 2. Methodology of Protocol Enhancement to Scapy

Scapy has a Python module which lets a developer script the required features and test them easily. It is currently supported with both Python2 and Python3. It can be simply imported and its function for packet manipulation can be used. This was made use of to develop different Server-Client modules of protocols FTP, TFTP and HTTPS. These were the major requirement for the testing of Citrix Netscaler ADC. The methodology followed for packet manipulation to Scapy is shown in figure 2[3].

To achieve easy prototyping initially a TCP module is built using Scapy scripting. This lets us write any application layer protocol over it. Scapy has easy to use function for listening on the network i.e packet sniffing with the packet filters. This lets us intervene with an ongoing TCP connection on the network. This TCP module had 2 parts, listener and responder. The listener is a background thread which listens to the packets on the network with the given filter and acknowledge them. This was achieved by maintaining Sequence and Acknowledge number on which atomic operations for read and update were performed. Once the TCP data is received, this was placed in a synchronized Queue which then can be accessed using the APIs. This was built so that any higher layer protocol built can make use of it directly without worrying for the lower level details of packet filters and packet parsing. This module opens sourced and is later used with FTP and HTTPS. TFTP is a UDP protocol and it is simpler to build hence no such module had to be scripted. The main objectives of this paper is, to explore Scapy Tool with its different features support. Further to enhance TFTP, FTP, HTTPS protocol support to scapy.

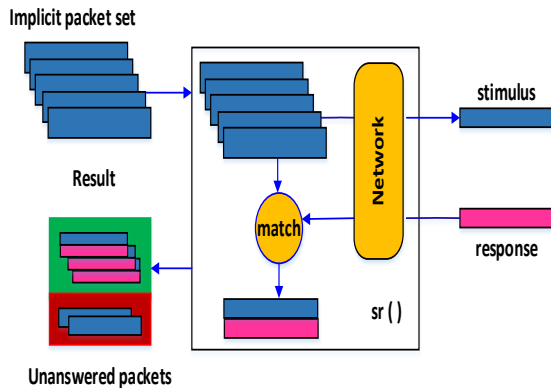


Figure 2: Packet Manipulation in Scapy

## 3. Protocol Enhancement to Scapy

### 3.1. FTP

FTP: File Transfer Protocol (FTP) is one of the most popular and preferred Internet protocols for sending and receiving huge files between computer systems over TCP/IP connections. FTP is a best example of client-server architecture. FTP is implemented on two communications channels between purchaser (client) and server. FTP comprised of two channels namely control and data channel. The overall architecture controlling is implemented by control channel. The file transmission is carried out using data channel. The clients send connection request to server before downloading any data from server side. FTP allows purchaser to upload, download, remove, and rename, flow and replica files on

a server. The working of FTP protocol is as shown in figure 3. Generally, a user officially gets activated on to the FTP server to manage their desired records or files. On the other hand servers make a few or all in their content to be had without login, also referred to as anonymous FTP [4].

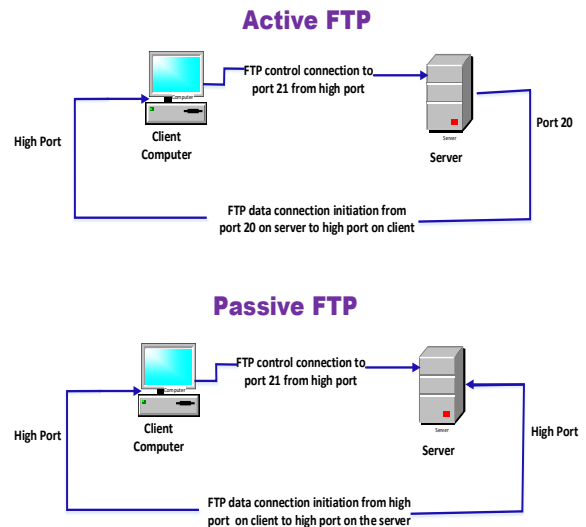


Figure 3: FTP working Principle

FTP sessions can be implemented in two modes namely passive and active mode. The active mode is implemented by initiating a client's a command channel request. In response the server initiates a data connection and starts sending data. On the other hand, in passive mode, the server uses the command channel to send the client the information it needs to open a data channel. As in passive mode the client initiates all connections, it works well across firewalls and Network Address Translation gateways. The code snippet used to implement FTP client is as shown in figure 4.

```

7 class FTPClient:
8
9     __passive_cmd = ['LIST', 'STOR', 'RETR']
10
11     def __init__(self, src, dst, sport, dport, verbose=False, logfile=None):
12
13         self.tcp_connection = TCP_IPv4(src, dst, sport, dport)
14
15         self.tcp_connection.handshake()
16
17         self.close = False
18
19         self.logfile = logfile
20
21         self.logger_thread = Thread(target=self.logger)
22         self.logger_thread.start()
23
24         self.passive_port = None
25         self.passive_mode = False
--

```

Figure 4: Code Snippet FTP client

Now a day's most of the file transfer applications are implemented using HTTP. Moreover, FTP is still widely used to transfer files "behind the scenes" for banking applications, the services which are used to build websites like Wix or SquareSpace and etc. It is also used in Web browsers, to download new applications [5]. The code snippet used to implement FTP server is as shown in figure 5.



TFTP service runs on well-known UDP port of 69. TFTP has to furnish its own session support as it used UDP an unreliable connectionless service. The file transferred using TFTP account for an independent exchange. The requesting client node sends either an RRQ (read request) or WRQ (write request) packet, along with the filename and the transfer mode to be used. As a response a server sends ACK (acknowledgement) packet to a received DATA packet if it is a WRQ message. Server responds with a DATA packet if it is an RRQ message (the client port is shown). On receiving each ACK message the sending host sends numbered DATA packets to the destination host. The last message contains a full-sized block of data. The numbered ACK packets is sent by the destination node for each received DATA packet [7]. The code snippet used to implement TFTP client is as shown in figure 7

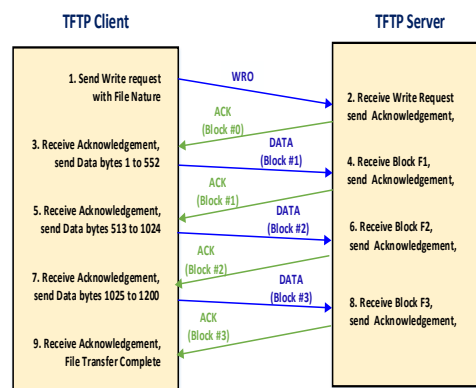


Figure 6: TFTP working Principle

TFTP service runs on well-known UDP port of 69. TFTP has to furnish its own session support as it used UDP an unreliable connectionless service. The file transferred using TFTP account for an independent exchange. The requesting client node sends either an RRQ (read request) or WRQ (write request) packet, along with the filename and the transfer mode to be used. As a response a server sends ACK (acknowledgement) packet to a received DATA packet if it is a WRQ message. Server responds with a DATA packet if it is an RRQ message (the client port is shown). On receiving each ACK message the sending host sends numbered DATA packets to the destination host. The last message contains a full-sized block of data. The numbered ACK packets is sent by the destination node for each received DATA packet [7]. The code snippet used to implement TFTP client is as shown in figure 7.

```

44
45 # initialize the fields
46 def __init__(self, src, dst, sport, dport, seqno, ackno):
47     """
48     Initializes the src, dst parameters.
49     """
50     self.src = src
51     self.dst = dst
52
53     self.sport = sport
54     self.dport = dport
55
56     self.tcp_conn = TCP_IPv4(src, dst, sport, dport, seqno, ackno)
57     print(src, dst, sport, dport)
58     self.tcp_conn.listener.connection_open = True
59
60

```

Figure 5 Code Snippet FTP Server

### 3.2. TFTP

The tiny and fastest file transfer can be implemented using Trivial File Transfer Protocol (TFTP). TFTP is companion of User Datagram transport Protocol (UDP) which is layered on the UDP. It can be used along with Internet Protocol both the version IPv4 or IPv6. TFTP is an elementary simple file transfer protocol. It was developed around 1980. TFTP provides functionality to copy files across a network (a very basic form of FTP). It is officially published in [RFC2347]. As it is so simple, it occupies very small amount of memory which makes it more convenient to use. Therefore, booting or loading the configuration of systems is implemented using TFTP. It includes thin client, wireless base stations without any storage and routers. TFTP does not support any security features such as authentication or encryption mechanisms. All the files in the TFTP directory can be directly accessible to the user. The working of TFTP protocol is as shown in figure 6. The absence of security feature makes TFTP dangerous over the open Internet which makes TFTP suitable only on private local area networks. It is an alternative to FTP when FTP is costlier or tougher to implement. The example of these services includes down-loading firmware, software and configuration data to network devices [6].

```

114 # Main client class
115 class TFTPClient:
116     # Initialize fields
117     def __init__(self, src, dst, sport, dport):
118         self.mode = "octet"
119         self.src = src
120         self.dst = dst
121         self.sport = sport
122         self.dport = dport
123         self.basic_pkt = IP(src=self.src, dst=self.dst)/UDP(sport=self.sport, dport=self.dport)
124         self.verbose = False
125
126     # Interactive shell
127     def interactive(self):
128         inp = ""
129         while "exit" not in inp:
130             sys.stdout.write(">>> ")
131             inp = raw_input().split(" ")
132             if len(inp) == 1:
133                 inp.append(None)
134             self.run_command(inp[0], inp[1])
135             print "Done"
136

```

Figure 7: Code Snippet TFTP client

This is just like simple Automatic Repeat Request (ARQ) protocol, extended to retransmission of packet when there is a packet is lost. The last DATA packet must contain less than a maximum-sized block of data. It shows that it is the last block of the transfer. In TFTP data transmission happens in lockstep [8]. It means only one packet (either a block of data or an 'acknowledgement') is ever in flight on the network at any point of time. This windowing limitation makes TFTP low throughput and high latency protocol over links. The code snippet used to implement TFTP server is as shown in figure 8.

```

11 # For a get request, TFTPReader class will listen and store the file
12 class TFTPReader:
13     # Initializing fields
14     def __init__(self, src, dst, sport, dport, filename):
15         self.src = src
16         self.dst = dst
17         self.dport = dport
18         self.sport = sport
19         self.basic_pkt = IP(src=self.src, dst=self.dst)/UDP(sport=self.sport)
20         self.block = 1
21         self.filename = filename
22         self.verbose = False
23         with open(self.filename, "w") as f:
24             f.write("")
25

```

Figure 8: Code Snippet TFTP Server

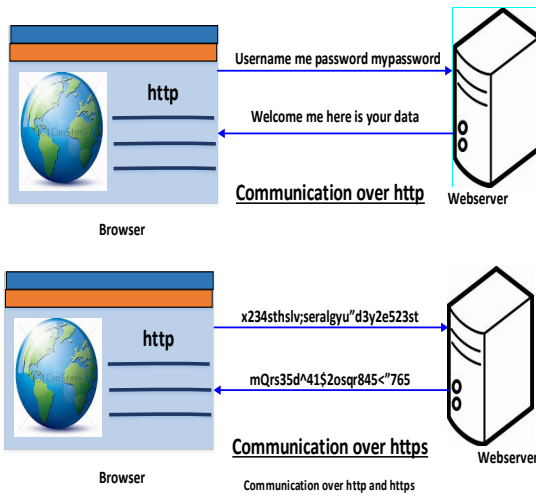


Figure 9: HTTPS working Principle

### 3.3. HTTPS

HTTPS is a Hyper Text Transfer Protocol Secure. The secure communication between two systems e.g. the browser and the web server is implemented using HTTPS [9]. The difference between communication over http and https is as shown in figure 9.

We can analyse from the above figure, the data transfer using http between the browser and the web server is in the hypertext format, on the other side https transfers data in the encoded format. Thus, https safeguards data from hackers for eavesdropping and changing it during the transmission between browser and webserver. Further, though the hackers able to hack the transmission, they will not be able to read it because the message is in encoded format. HTTPS uses the Secure Socket Layer (SSL) or Transport Layer Security (TLS) protocols to setup a secure link between the browser and the web server. TLS is the extended version of SSL [10].

Secure Socket Layer (SSL): SSL establishes an encrypted link between the two systems to implement data security for secure communication. The HTTPS code snippet is as shown in figure 10

```

10 def tis_client(ip, request, tis_version, ciphers, extensions):
11     resp = None
12     with TLSocket(client=True) as tis_socket:
13         try:
14             tis_socket.connect(ip)
15             print("Connected to server: %s" % (ip,))
16         except socket.timeout:
17             print("Failed to open connection to server: %s" % (ip,), file=sys.stderr)
18         else:
19             try:
20                 server_hello, server_kex = tis_socket.do_handshake(tis_version, ciphers, extensions)
21             except TLSProtocolError as tpe:
22                 print("Got TLS error: %s" % tpe, file=sys.stderr)
23             else:
24                 resp = tis_socket.do_round_trip(TLSPLAINTEXT(data=request))
25                 tis_socket.close()
26
27     if CONTEXT:
28         print(tis_socket.tis_ctx)
29     return resp
    
```

Figure 10 Code Snippet HTTPS

The communication can be in the form of browser to server, server to server or client to server. The main aim of SSL to ensure secure and private data transfer between the two systems. The https is essentially http over SSL. SSL sets up an encrypted link using an SSL certificate. This certificate is also known as a digital certificate.

## 4. Results

Scapy uses the Python interpreter as a command board. That means that you can directly use the Python language (assign variables, use loops, define functions, etc.) The paper is implemented by creating wrapper classes in Python to support different protocol using Scapy.

FTP module [11] has both server and client modules. This also has support for both IPv4 and IPv6. One of the features of the client module is to let the user specify the source IP and port for communication. This is not supported by any of the existing FTP clients. This helps in analyzing the working of the load balancer on how it performs when a large number of requests come in with different source IP/port. To achieve this, there is one more feature of selecting the number of concurrent connections to the server. Now this lets us test the middleboxes when the traffic floods in. This also supports different commands to be used on different concurrent connections with the help of command file as input. All these features are exposed as command line parameters. Also, all the features can be read with the help command (python client.py -h). Also further information is explained in detail in repo's readme.

The FTP protocol support is as shown in the following figures. The wrapper class was developed to support FTP with Scapy for IPV4 and IPV6 shown in figure 11 and figure 12 respectively.

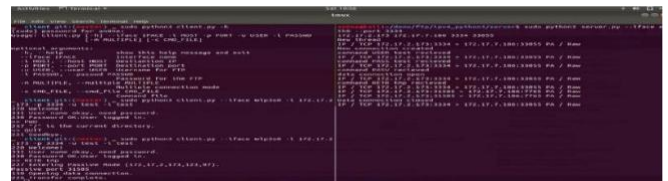


Figure 11: FTP IPV4 sessions

The file transfer with IP format with different read/write session is shown in screen shot for both IPV4 and IPV6.

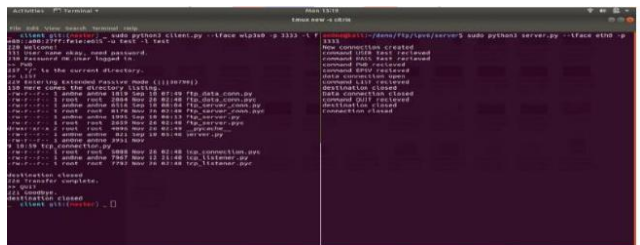


Figure 12 FTP IPV6 sessions

The implementation also supports multiple files transfer to single connection or single file transfer to multiple connections as shown in figure 13 and figure 14 respectively.

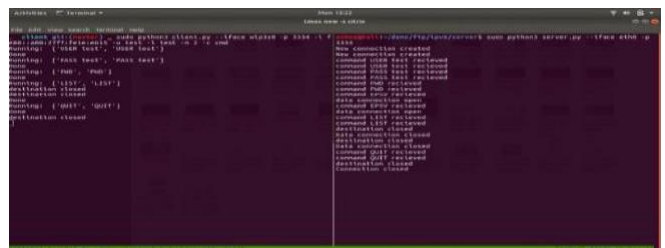


Figure 13 FTP IPV6 Multiple connections

The output shows different connection has received same file.

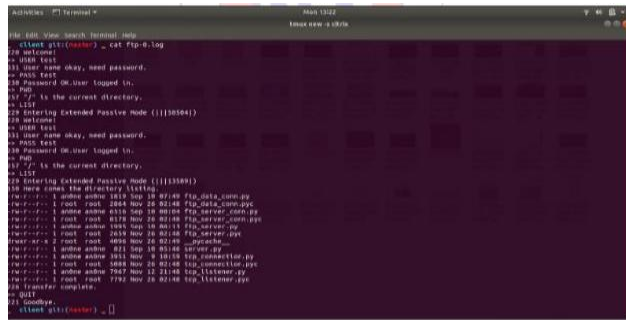


Figure 14 FTP IPV6 Multiple connections

Similarly HTTPS module was built to support various parameters to be used during SSL/TLS negotiation. This made use of one more Python module scapy-ssl\_tls. This has support for selecting the Ciphersuite, TLS version as well as TLS extensions. All the features are exposed as command line parameters and can be viewed using help (python client.py -h). The HTTP request to be sent can be given as an input file specifying all the HTTP parameters and the output will be written to the file specified in the command line. It also supports curl like command by specifying the URL in the command line.

The execution of the developed wrapper class to support HTTPS with Scapy is shown in figure 15.

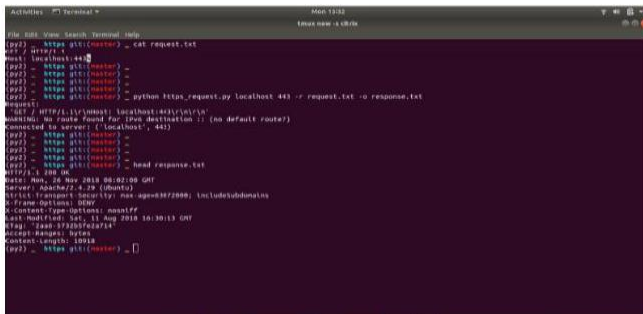


Figure 15 HTTPS client

TFTP module was also built using Scapy. TFTP is a simple request response protocol and has a simpler architecture. Similar to FTP various features like multiple concurrent requests, source IP/port options etc which are exposed as command line parameters. The connectionless small is transfer is generally implemented using trivial File Transfer (TFTP). The TFTP client server protocol support is as shown in figure 16 and 17 respectively

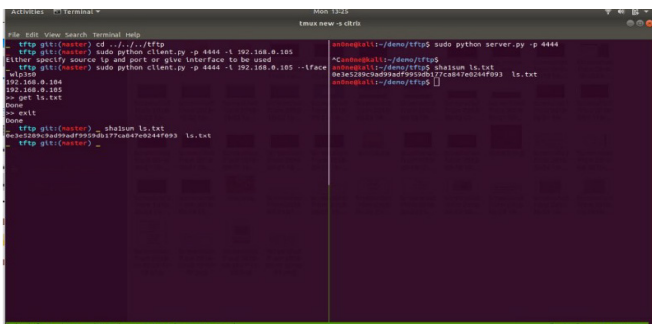


Figure 16 TFTP Client usage

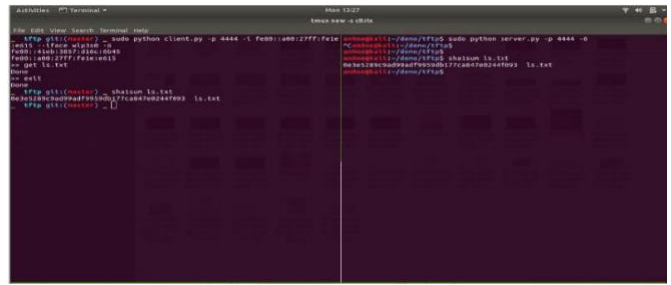


Figure 17 TFTP Server usage

## 5. Conclusion

There have been issues where when the load balancers see a new/broken packet structures it fails to parse and causing undefined behavior. This cannot be found out general test cases since a malicious user is capable of injecting malicious packets which are not handled by the design. These cases can be very frequent and the middleboxes needs to be robust. Here we have developed python modules for protocols like FTP, TFTP and HTTPS where the packets can be generated with varied parameters like controlled TCP source IP/port, number of parallel connections, encryption parameters etc. This lets us test the load balancer with various packet structure which might not be a part of everyday traffic but might be capable of crashing or compromising of the middleboxes. For this purpose, we develop the protocol support to the system such that it we can craft our own packets from the raw structure and manipulate as we need. Using Scapy we can add additional functionalities to the protocol and use it. With Scapy it is easy to play with packets and hence it is a very powerful tool.

The enhancement to this paper can implemented as addition of data link layer protocol support to the scapy, build interactive GUI for usage, Secure protocols such as SFTP, FTPS etc can be implemented.

## Conflict of Interest

The authors declare no conflict of interest.

## Acknowledgment

The authors would like to thank Team Citrix for their support and guidance while implementing this project work.

## References

- [1] RFC4346] Dierks, T. and C. Allen, "The TLS Protocol Version 1.0", RFC 2246, DOI 10.17487/RFC2246, January 1999, <https://www.rfc-editor.org/info/rfc2246> SSL/TLS packet structure, handshake protocol implementation, ciphers supported. Creating reliable and private connection
- [2] [RFC4346] Dierks, T. and E. Rescorla, "The Transport Layer Security (TLS) Protocol Version 1.1", RFC 4346, DOI 10.17487/RFC4346, April 2006, <https://www.rfc-editor.org/info/rfc4346>. Change in ciphers supported from previous versions. Difference and improvements in security parameters.
- [3] Rohith Raj S, Rohith R, Minal Moharir, Shobha G, SCAPY- A powerful interactive packet manipulation program, IEEE International Conference on Networking, Embedded and Wireless Systems (ICNEWS), 27-28 Dec. 2018
- [4] Khamar Ali Shaikh, A Karthik Bhat, Minai Moharir, A Survey on SSL Packet Structure, IEEE 2nd International Conference on Computational Systems and Information Technology for Sustainable Solution (CSITSS), 21-23 Dec. 2017. DOI: 10.1109/CSITSS.2017.8447634

- [5] A. Soumya Mahalakshmi et al., "A study of tools to develop a traffic generator for L4 – L7 layers", 2016 International Conference on Wireless Communications Signal Processing and Networking (WiSPNET), pp. 114-118, 2016 DOI: 10.1109/WiSPNET.2016.7566102
- [6] S Bansal, N Bansal, "Scapy – A Python Tool For Security Testing", J Comput Sci Syst Biol, vol. 8, pp. 140-159, 2015 System Application," Ph.D Thesis, Chongqing University, 2005.
- [7] <https://github.com/karthikbhata97/ScapyTCP>
- [8] <https://github.com/karthikbhata97/scapy-ftp>
- [9] [https://github.com/tintinweb/scapy-ssl\\_tls](https://github.com/tintinweb/scapy-ssl_tls)
- [10] <https://github.com/karthikbhata97/scapy>



## The Adventure of BipBop: An Android App Pathfinding Adventure Game

Gredion Prajena<sup>1\*</sup>, Jeklin Harefa<sup>1</sup>, Andry Chowanda<sup>2</sup>, Alexander<sup>1</sup>, Maskat<sup>1</sup>, Kamal Rahman<sup>1</sup>, Muhammad Naufal Fadhil<sup>1</sup>

<sup>1</sup> Computer Science Department, School of Computer Science, Bina Nusantara University, Jakarta, Indonesia 11480

<sup>2</sup> Game Application Technology Department, School of Computer Science, Bina Nusantara University, Jakarta, Indonesia 11480

### ARTICLE INFO

*Article history:*

*Received: 27 December, 2019*

*Accepted: 07 February, 2020*

*Online: 23 March, 2020*

*Keywords:*

*Adventure Puzzle, Culture Game,*

*Artificial Intelligence,*

*A\* algorithm,*

*Traditional House*

### ABSTRACT

*The purpose of this research is to build an android based pathfinding adventure game where user gets information about Indonesian culture, especially the traditional houses including the folk songs and the traditional weapons in certain areas. The method used is by questionnaires, interviews, observation, and literature study. This application also implements the A\* algorithm to solve the pathfinding problems. The result of this research is "The Adventure of BipBop" app that can make the user can feel the experience of playing that is not only entertaining but also as a medium to convey about the culture of Indonesia and help preserve the traditional house of Indonesia. Most of the respondents find out that the application can provide Indonesian culture well (91.7%). Furthermore, this application can realize about 84.5% of players to help preserve the traditional culture in Indonesia.*

### 1. Introduction

Nowadays, technology has been evolved tremendously in many aspects, especially in smartphones. With this evolving technology, the lifestyle especially in working and collaborating with someone else has become easier [1]. Almost every person has a smartphone, especially those who live in a city. Research in 2016 figure out the number of smartphones equivalent to one for every fifth person on earth [2]. Smartphone operating system still dominated by Android which has 75.27% market share worldwide in May 2019 [3]. With a smartphone, we can do many activities like communication, entertainment, finance, shopping, and play game. Among those activities, playing games remains one of the most engaging categories for smartphone users [4] and Gaming is the main entertainment feature on a smartphone [5]. The game does not only serve as entertainment but also allows the player to learn about many things [6] [7]. Pathfinding is a common feature for various applications including games. Pathfinding generally refers to find the shortest route between two endpoints [8]. Some pathfinding algorithms, like Depth-First Search (DFS), Breadth-First Search (BFS), Hill-Climbing Search, Dijkstra's, A Star (\*) algorithm was created for solving the pathfinding problem. Based on those popular pathfinding algorithms, the A\* algorithm considered as the most popular pathfinding algorithm in Artificial Intelligence Games and widely used in pathfinding and graph traversal [9]. Hence, this paper will use A\* for the enemy to chasing after player inside this game.

\*Gredion Prajena, Email: [gprajena@binus.edu](mailto:gprajena@binus.edu)

As the largest archipelago country in the world, Indonesia has a variety of cultures, ranging from the local, national, or even the foreign culture that existed before Indonesia's independence. The manifestations of the diversity of Indonesian cultures consist of traditional houses, traditional dances, traditional clothing, folk songs, traditional musical instruments, performing arts, and folklore [10]. However, currently, the world is facing the 4T revolution (Technology, Telecommunication, Transportation, Tourism) that has dominant globalizing force so that the boundaries between regions are increasingly blurred and lead to the creation of a global village as predicted by McLuhan (McLuhan is a popular communication scientist and critic because the concept is about the global village, medium is the message and its predictions about the World Wide Web 30 years before it was discovered). This condition raises problems in the weakening of cultural heritage [11]. One example of the fading of Indonesian culture is the traditional houses. This can be seen from the news about traditional houses in Indonesia. News from merdeka.com said, Lontiok tourism house located on Kuok Belimbing Island, Bangkinang Barat District, Kampar Regency, Riau. If it was once famous for its antique, it is now weathered because it is not maintained [12]. Besides, based on the information obtained from the news portal makassar.tribunnnews.com also wrote, the condition of the Wotu traditional house in Wotu Sub-District, East Luwu, South Sulawesi, was left abandoned by the government. Around the traditional house which has 72 concrete pillars already overgrown with wild plants, many roofs have been dislodged, new floors and walls have been installed 50 percent. The development

has stopped for 7 years ago [13]. Then, at the end of January 2018, there was news about the Toraja Traditional House in the Benteng Somba Opu area which suffered severe damage to the roof and floor because it was not maintained so it looked alarming [14].

To overcome the fading of Indonesian culture, it needs synergic participation from parents, society, education, and government as an effort to respect the regional culture by providing knowledge of local culture to children and implemented as part of daily life [15]. By utilizing sophisticated technology, and with the increase in the gaming industry on smartphones, a game about Indonesian culture that can restore the interest of many people to love Indonesian culture. There are several kinds of research that have been done to make an application about learning Indonesian culture through games based on android. Alexander et. al. developed "Indonesian National Culture", a puzzle that takes the theme of Indonesian Culture with helping the younger generation get to know and maintain various cultures in Indonesia. Besides that, this puzzle game also can be used as a learning media.

From the background and reference studies that have been explained, this paper wants to increase user awareness about Indonesian culture by building a game adventure puzzle with the Indonesian culture theme, especially in the traditional house. Specifically, the traditional houses that will be focused on this research, including Central Java, West Java, Irian Jaya, West Sumatera, and Bali. Users will have given task through the storyline to fix the broken traditional house by collecting material in the game. And, this game will have information about the traditional house and some information about the culture in the corresponding area. To make the app more challenging, this game will implement Artificial Intelligence pathfinding. This app named The Adventure of BipBop.

From the formulation of the problem, this paper contributes to providing knowledge and information about Indonesian culture through the game. Hence, can increase the level of awareness and interest of the community in helping to preserve traditional houses. This paper also gives the exploration and variety of adventure games based on Android with Pathfinding.

## 2. Recent Work

Artificial Intelligence and Level Design in-game task demand increasingly [16] because Artificial Intelligence and Level Design can make the game more fun and challenge. Pathfinding is one of the Artificial Intelligence that can be implemented in various applications especially in-game. In this game, Pathfinding Algorithm is used for moving the object from the starting point to endpoint in this research Pathfinding will move the enemy from the initial location to the player. For Level Design, the Adventure of BipBop will have several tasks that use traditional houses and use islands in Indonesia. The research said one of the important things to build successful serious games is engaging the learners [17]. With Pathfinding and Level Design, this game is expected can have good user engagement.

From the journal entitled "Android Based Indonesian Information Culture Education Game" by Kidi, et. al. explain about an educational game called "Merah Putih". In this game, the player will become an Indonesian citizen character who meets with a foreign citizen named Robert who invites the player to

accompany him around to the areas in Indonesia. Inside the game, players will select existing stages by selecting areas on the map in Indonesia. A map is divided into ten areas that can be entered by players. Each stage of the game will consist of three games where two games are varied and different sets for each stage, and there is a quiz at the end of the game to hone the player's ability to get to know the culture in Indonesia. There is also a new hidden bonus game that will open when the player gets the perfect score for a stage. When the player finishes running and plays a stage, then the player will get a reward in the form of objects where the object can be seen in the collection of players and players can see information about the objects that have been obtained and information about the province. Objects collected are usually common objects that come from areas in Indonesia. Besides the player will also get a star per the value obtained after the player finished playing a stage. Stars can be collected and later used to upgrade the game to assist players in completing the game [18].

In a journal entitled "Indonesian Culture Learning Application Based on Android" by [19] explained the game application called "Indonesian National Culture". This game is a puzzle that takes the theme of Indonesian culture. This game aims to help the younger generation get to know various cultures in Indonesia and maintain a historical culture native to Indonesia. Besides, the game has a function as a learning media obtained from several studies conducted (Setiawan, Handojo, & Hadi, 2017). This application is divided into several menus, namely Learn, Quiz, Game, Login, Gallery, Exit. Quiz menu is a game in the form of a quiz to test the knowledge of users related to the scope of culture discussed in the game application. The cultural elements in this game are traditional dance, traditional house, and historical place.

Those 2 research create 2D puzzle game applications regarding Indonesian Culture Learning Based on Android, and this paper will use a 3D puzzle game with a pathfinding algorithm, hence can engage the player and give different experiences in learning Indonesian Culture.

## 3. Proposed Method

This research will be divided into three stages. The first stage is requirement analysis and concept story design, where the initial study performed by surveying the respondents and analyze the result to design the game concept. The second stage is preparing all the asset including visual, audio, and build the app using Unity. And finally, the last stage is the evaluation of the proposed game.

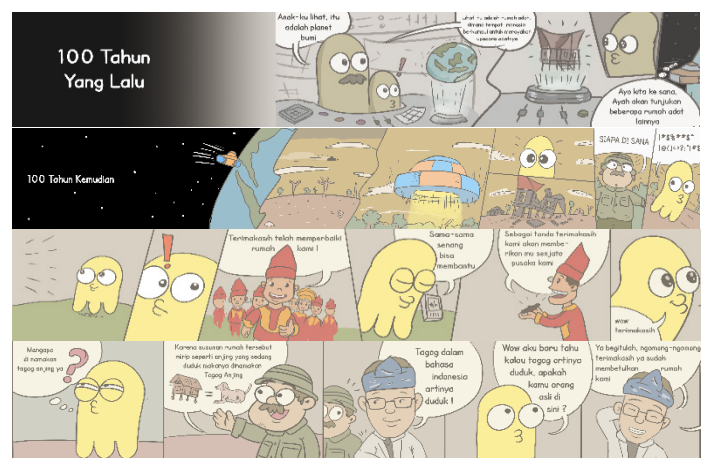


Figure 1. Story

In the first stage, the initial study was performed by surveying 255 respondents (52.2% are male) with most of them are the students in the higher education system. In the survey, most respondents (72.9%) are using Android for their mobile operating system. While for the game genre, 43.9% of them like to play adventure games and 52.6% of them interested in an adventure puzzle game with Indonesia’s traditional house themed.

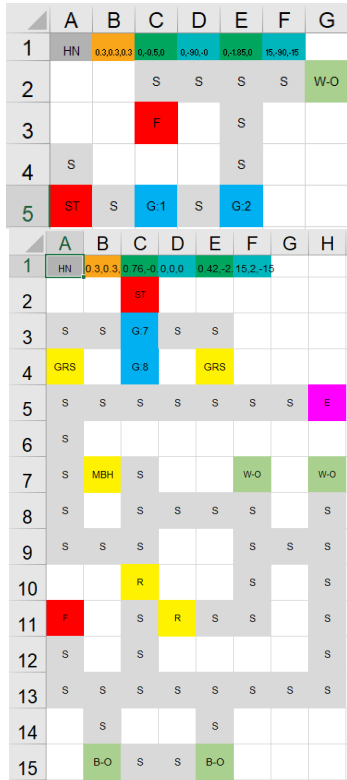


Figure 2. Map for Level 1 Stage 1 & Level 5 Stage 3

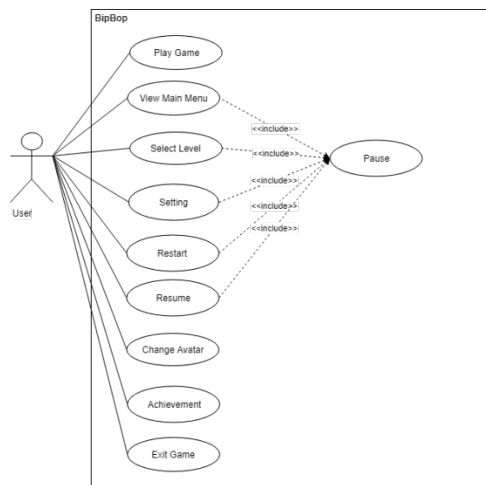


Figure 3. BipBop Use Case Diagram

The second stage is developing the asset, app, map, level design, features, and algorithm. This game will have ten features (see FIGURE 3). This game started with a story about a space creature called BipBop that come to earth and accidentally found the traditional house in Indonesia. Unconsciously, He interested in it, but He must leave earth to avoid known by a human (see FIGURE 1). After one hundred years passed by, He comes again to earth and discovers traditional houses have been broken. He

wants to help human to fix it by collecting the material needed. This game will use a combination of adventure and puzzle genre and use maps for playing area. This game will have 5 main levels, where for each level there will have 3 stages and each stage will have different maps. The game map needs to be well prepared or pre-processed before the A\* algorithm can work [9], the example map of each stage can be seen in Figure 2. TABLE 1 shows the description of each variable columns:

Table 1. Variable Map Description

Column	Description
A1 (HN)	prefab model from the traditional house
B1	size / scale of the traditional house model with format of $x,y,z$
C1	position of a traditional house with the format of $x,y,z$
D1	rotation of traditional house with the format of $x,y,z$
E1	position of the traditional house when it's damaged with the format of $x,y,z$
F1	rotation of traditional house when it's damaged with the format of $x,y,z$
S (grey color)	The passable road by both the player and the enemies
ST (red color)	the starting point of the player
F (red color)	the checkpoint where the player aims to complete the game
W-O / B-O (green color)	the position of the materials (W-O for wood; B-O for brick)
R (yellow color)	the position of the stone (obstacle)
MBH (yellow color)	the position of the moving box (horizontally)
GRS (yellow color)	the position of the grass (BipBop can hide behind the grass to avoid the enemies)
E (pink color)	the position of the enemy
G:x (blue color)	the position of trigger guide screen based on the number. Number 7: Be Careful, don't let you get close to the enemy Number 8: The grass will help you to hide from the enemy

For each stage, the player must collect all the items and go to checkpoint. Besides, there will be a different level of difficulty and the enemies who will always chase the player by using the A\* pathfinding algorithm (see FIGURE 4). A\* algorithm will be used to move the enemy from the initial location to the player location and prevent the enemy from obstacles. As we see in FIGURE 4, first the algorithm will check if the enemy needs to search player location. If the player location is found, the enemy will move to the player, if not the enemy will move randomly. Then the algorithm will detect nodes to find the closest path to the player. And after that, the algorithm will find the closest path from enemy

to player by avoiding the obstacles. The algorithm will run continuously chasing the player, even when the player moving.

```

IF enemy in front of traffic light THEN
  Stop pathfinding searching
  Stop enemy moving
ELSE
  Search player location with A*
ENDIF

IF player target located THEN
  Move enemy to player target location
ELSE
  Move enemy randomly
ENDIF

OPEN_SET
CLOSE_SET

first_node
target_node

Input first_node to OPEN_SET

LOOPING
node = node in OPEN_SET list that have lowest F_COST
Remove correspondent node from OPEN_SET
Insert correspondent node to CLOSE_SET

IF node is target_node THEN
  return
ENDIF

FOREACH around_node from node THEN
IF around_node is obstacle or exist in CLOSE_SET THEN
  skip to next around_node
ENDIF

IF newest G_COST value lower than around_node OR
around_node does not exist in OPEN_SET THEN
  SET G_COST around_node
  SET H_COST around_node
  SET F_COST around_node
  SET node to parent from around_node

IF around_node does not exist in OPEN_SET THEN
  Insert around_node to OPEN_SET
ENDIF
ENDIF
ENDFOREACH
ENDLOOPING
    
```

Figure 4. Pseudocode for Pathfinding Algorithm



Figure 5. Map of Indonesia

There are 34 traditional houses in Indonesia [20] and the proposed game will use 5. The first level is Rumah Gadang from West Sumatra, and the player must finish all stages to continue to the next level. After the player finishes all stages, then the proposed game will show the map of Indonesia with a pinned location (see FIGURE 5). The second level is Rumah Adat Tagog Anjing from West Java. The third level is Rumah Adat Joglo from Central Java. The fourth level is Rumah Adat Bali from Bali. The fifth level is Rumah Adat Honai from Papua. When finished all the stages, the player will get a new item from the villages and the proposed game will show a description of the item and house.

During playing the game, the player can pause or reset to the initial condition.

In the third stage, the proposed game was evaluated using a questionnaire. Based on the questionnaire distributed, the number of respondents is 60, and most of them are university students. The detailed results of the questionnaire are described in the next section.

#### 4. Result and Discussion

In this section the game has been developed, when the player opens the app it will show four menus (see FIGURE 6), achievement (trophy icon), change character color (paint roller icon), settings (gear icon), and Start (button “mulai”). The achievement will show items given to the player when finishing a certain level. The default color of BipBop character is yellow but the player can change the color by choosing icon paint or change character color, and the player will be provided various colors to choose. In settings, the player can configure to turn on/off the music and the sound effect, besides change the control position and reset the game data. When the player chooses button Start, it will bring the player to the game. For the initial set, the player will see the story of the space creature called BipBop that comes to earth and discover the traditional house. After that, the game starts with a game guide such as how to control the character, how to collect items, tips, and how to finish the stage. For the first level, the player will play in West Sumatra. The game area of the given map is the land above the sea, the player needs to move the character by using game control shown on the screen. If the character moves out of the land, the character will sink then the game will stop and show time spent. The player can repeat the game without limits and the game will update the best time for each stage. During the game, the player also can pause by pushing the top left corner button, the player can reset position to the initial, and exit to the menu. Each level in this game consists of 3 stages, and after the player finishes one level, the player will get items and can go to the next level (see FIGURE 6). The difficulties of the game will increase along with the level, various obstacles will appear in every level such as some boxes that will block the movement of the player, so the player needs to move the box first, the box can use as a foothold as well. Another obstacle is the enemy that can chase the BipBop character, if the enemy hits the BipBop then the player loses. The enemy will move to chase the player with A\* pathfinding algorithm, hence it will chase wherever the player moves. This game will store data to file-based database [21], the detail column of the data can be seen in TABLE 2.

Table 2. BipBop File Database

Variable Name	Variable Type	Description
CURRENT_STAGE	Integer	Determine the stage that will be used when starting the game
CURRENT_LEVEL	Integer	Determine the level to be used when starting the game



Variable Name	Variable Type	Description
LEVEL_STATE	Integer	Determine the game level status, the status is 0 (not yet completed level) and 1 (has completed level)
TIME_ELAPSED	Float	Save time spent when completing the stage
LAST_LEVEL	Integer	Save the last progress level of the player
LAST_STAGE	Integer	Save the last progress stage of the player
AFTER_FINISH	Integer	Defines the screen when you have finished the game
BEST_TIME_n	Float	Save the best time for each level (n)
LEVEL_STATE_n	Integer	Save the level status played by level (n), the status is 0 (not yet completed level) and 1 (has completed level)



Figure 6. BipBop (Main Menu, Game Guide, Playing Game, Level Finish, Traditional House, Item)

This study evaluated by two methods, self-assessment and user-assessment. In the self-assessment evaluation, this game measured by 9 general principles of User Interface for games [22] as well as Five Measurable Human Factor [23] those assessments also supported by the user’s questionnaire.

For evaluating user satisfaction, this study has conducted the survey using a questionnaire to sixty people chosen randomly. Respondents will get a link to the game app, try the game, and then fill the survey questions (see FIGURE 7). The result of the questionnaire more than half of the respondents agreed that this game is easy to operate (80%), yet have good gameplay (83.3%), game design (90%) and features (85%). They also affirm the instructions in the game are easy to understand (98.3%). And then, this game makes them realize that the Indonesian traditional houses are now becoming obsolete (80%) and this game also can become a medium to convey (88.3%) and learn Indonesian culture (91.7%). Finally, after they play this game, they interested to help preserve Indonesian traditional house (84.9%).



1. Do you think this game is easy to operate? a. Yes b. No	6. Do you think this game has provided information about Indonesian culture well? a. Yes b. No
2. Is the gameplay of this game good enough? a. Yes b. No	7. Do you think this game is appropriate as a medium to convey Indonesian culture especially in traditional houses? a. Yes b. No
3. Are the features provided good enough? a. Yes b. No	8. Can you learn about Indonesian culture through this game, especially about Indonesian traditional houses? a. Yes b. No
4. Are the instructions given easy to understand? a. Yes b. No	9. Do you realize that through this game, Indonesian traditional houses are now becoming obsolete? a. Yes b. No
5. Do you think the design of this game is good? a. Yes b. No	10. Are you interested in this application to help preserve Indonesian traditional houses? a. Yes b. No

Figure 7. Questionnaire Form

## 5. Conclusion and Future Work

This research gives information about Indonesian culture especially in the traditional house called BipBop. This adventure and puzzle game has several features that support the player to save and pause the game, customize the character, and save the best time for each level. This game also has a game guide to help the player understand how to play, various difficulties with items and the enemy. Based on the evaluation conducted, the BipBop game can give information about Indonesian culture (91.7%) and after trying this game, people realize that Indonesian traditional house is now becoming obsolete (80%). The BipBop game also can act as a medium to convey (88.3%) and learn (91.7%) Indonesian traditional house. Moreover, this game can make the user interested to help preserve Indonesian traditional house (84.9%). All these successes supported by the ease of operation the game (80%), good gameplay (83.3%), game design (90%) and features (85%). For future work, there are several improvements can be added to this game, such as adding multiplayer, more detail information about the culture and folk songs in a related area.

### Conflict of Interest

The authors declare no conflict of interest.

### Acknowledgment

This research is partially supported by BINUS University.

### References

- [1] E. Isabela, J. Drona, N. Fadhilah, D. F. Tanoto, J. Harefa, G. Prajena, A. Chowanda and A. , "NYAM: An Android Based Application for Food Finding Using GPS," in 3rd International Conference on Computer Science and Computational Intelligence 2018, Jakarta, 2018. <https://doi.org/10.1016/j.procs.2018.08.189>
- [2] B. Carton, J. Mongardini and Y. Li, "A New Smartphone for Every Fifth Person on Earth: Quantifying the New Tech Cycle," IMF Working Paper, 2018.[Online].Available: <https://www.imf.org/~media/Files/Publications/WP/2018/wp1822.ashx>
- [3] "Mobile Operating System Market Share Worldwide," 13 June 2019. [Online]. Available: <http://gs.statcounter.com/os-market-share/mobile/worldwide>.
- [4] "Smartphone Usage and Behaviour Report," Kantar IMRB & MMA, 2016. [Online].Available: [https://www.mmaglobal.com/files/documents/mma\\_kimrb\\_smartphone\\_report\\_overview.pdf](https://www.mmaglobal.com/files/documents/mma_kimrb_smartphone_report_overview.pdf)
- [5] L.-F. Olatz, M. Niko, K. Maria, G. Mark and K. D. J., "Mobile gaming and problematic smartphone use: A comparative study between Belgium and Finland," *Journal of Behavioral Addictions*, pp. Volume 7, Issue 1, 2017. <https://doi.org/10.1556/2006.6.2017.080>
- [6] M. Hartono, M. A. Candramata, K. N. Adhyatmoko and B. Yulianto, "Math Education Game for Primary School," 2016 International Conference on Information Management and Technology (ICIMTech), pp. 93-96, 2016. <https://doi.org/10.1109/ICIMTech.2016.7930309>
- [7] Y. L. Prasetyo, S. Rambito, A. Yudhistira, S. F. Aulia and A. Chowanda, "Teaching Social Critique to Adults with A Desktop Horror Myth Game," 3rd International Conference on Computer Science and Computational Intelligence 2018, pp. 624-631, 2018. <https://doi.org/10.1016/j.procs.2018.08.224>
- [8] X. Cui and H. Shi, "A\*-based Pathfinding in Modern Computer Games," *IJCSNS International Journal of Computer Science and Network Security*, VOL.11 No.1, January 2011, pp. 125-130, 2011.
- [9] N. H. Barnouti, S. S. M. Al-Dabbagh and M. A. S. Naser, "Pathfinding in Strategy Games and Maze Solving Using A\* Search Algorithm," *Journal of Computer and Communications*, vol. 4, pp. 15-25, 2016. <https://dx.doi.org/10.4236/jcc.2016.411002>
- [10] O. Indriani, M. Shaifuddin and M. , "UPAYA MENINGKATKAN KEMAMPUAN MENGIDENTIFIKASI KEANEKARAGAMAN BUDAYA INDONESIA MELALUI METODE TALKING STICK," *Jurnal Didaktika Dwija Indria (SOLO)*, (Vol 1, No 3 (2013): JULI, Jurnal Mahasiswa PGSD), 2013.
- [11] A. P. Wardhanie, "PERANAN MEDIA DIGITAL DALAM MEMPERTAHANKAN BUDAYA LOKAL INDONESIA DI ERA GLOBALISASI," *Prosiding Strengthening Local Communities Facing The Global Era*, pp. 348-354, 2017.
- [12] A. Sani, "Tak lagi antik, Rumah Lontioik kini lapuk dan tidak terawat," 10 May 2016. [Online]. Available: <https://www.merdeka.com/peristiwa/tak-lagi-antik-rumah-lontioik-kini-lapuk-dan-tidak-terawat.html>.
- [13] I. Ismar, "Terbengkalai, HAM-Luwu Timur Desak Bupati Selesaikan Rumah Adat Wotu," 3 March 2018. [Online]. Available: <https://makassar.tribunnews.com/2018/03/03/terbengkalai-ham-luwu-timur-desak-bupati-selesaikan-rumah-adat-wotu>.
- [14] Saldy, "Memprihatinkan, Begini Kondisi Rumah Adat di Benteng Somba Opu, Lihat Foto-fotonya," 23 January 2018. [Online]. Available: <https://makassar.tribunnews.com/2018/01/23/memprihatinkan-begini-kondisi-rumah-adat-di-benteng-somba-opu-lihat-foto-fotonya>.
- [15] Widiastuti, "ANALISIS SWOT KERAGAMAN BUDAYA INDONESIA," *Jurnal Ilmiah WIDYA*, vol. 1, no. 1, pp. 8-14, 2013.
- [16] A. S. Nery and A. C. Sena, "Efficient A\* Co-processor for Reconfigurable Gaming Devices," 17th Brazilian Symposium on Computer Games and Digital Entertainment, Volume 2018-November, 6 February 2019, Article number 8636904, pp. 97-106, 2019. <https://doi.org/10.1109/SBGAMES.2018.00021>
- [17] M. D. Kickmeier-Rust and A. Holzinger, "Teaming up with artificial intelligence: The human in the loop of serious game pathfinding algorithms," 7th International Conference on Games and Learning Alliance, Volume 11385 LNCS, 2019., pp. 354-363, 2019. [https://doi.org/10.1007/978-3-030-11548-7\\_33](https://doi.org/10.1007/978-3-030-11548-7_33)
- [18] N. Kidi, B. Kanigoro, A. G. Salman, Y. L. Prasetyo, I. Lokaadinugroho and A. A. Sukmandhani, "Android Based Indonesian Information Culture Education Game," 2nd International Conference on Computer Science and Computational Intelligence 2017, pp. 99-106, 2017. <https://doi.org/10.1016/j.procs.2017.10.015>
- [19] A. Setiawan, A. Handoyo and R. Hadi, "Indonesian Culture Learning Application based on Android," *International Journal of Electrical and Computer Engineering (IJECE)*. Vol. 7, No. 1, February 2017, pp. 526-535, 2017. <http://doi.org/10.11591/ijece.v7i1.pp526-535>
- [20] R. Rizky and T. Wibisono, *Mengenal Seni & Budaya Indonesia*, Jakarta: CIF (Penebar Swadaya Group), 2015.
- [21] K. Yusof and M. Man, "Efficiency of Flat File Database Approach in Data Storage and Data Extraction for Big Data," *Indonesian Journal of Electrical Engineering and Computer Science*, pp. 460-473, 2018. <http://doi.org/10.11591/ijeecs.v9.i2.pp460-473>
- [22] E. Adams, *Fundamentals of Game Design (3rd Edition)*, New Riders Publishing, 2014.
- [23] B. Shneiderman, C. Plaisant , M. Cohen, S. Jacobs, N. Elmqvist and N. Diakopoulos, *Designing the User Interface: Strategies for Effective Human-Computer Interaction (6th ed.)*, Pearson, 2016.

## Evolutionary Quantum Technology: The Future with Holographic Plasma Voxel

Yogi Udjaja\*

Computer Science Department, School of Computer Science, Bina Nusantara University, Jakarta, Indonesia 11480

### ARTICLE INFO

*Article history:*

*Received: 11 October, 2019*

*Accepted: 09 January, 2020*

*Online: 23 March, 2020*

*Keywords:*

*Evolution*

*Quantum Technology*

*Future*

*Holographic Plasma Voxel*

*Holography*

*Hologram Technology*

*User Experience*

### ABSTRACT

*This current situation will affect the future, technology models that are unthinkable or which impossible to happen pops up one by one. Like the hologram, this technology began to develop as a solution to increase user comfort in operating a system that is needed. This paper explains the development of hologram technology that is currently available and what the prediction of future technology models will be.*

### 1. Introduction

The future is unpredictable, but by understanding the advantages that shape this period—one of them is the development of human education which gives rise to creativity that affects human and computer interactions—based on this we can learn where to look for it and how to interpret what is found [1]. Many models have been found or developed from various researchers, such as algorithm optimization [2], skin cancer detection systems [3], learning applications for visually impaired children [4], making hydroponic tower systems for people want to plant with limited space [5], mathematics learning applications [6], recommendation system [7], website engine [8], strategic game experience [9-11], game for learning Japanese language [12,13], improvement performance teacher system [14,15], technology enhance learning system [16], cat disease detection system [17], determining teacher engagement [18], and much more.

The more days discoveries in the technology sector are increasing, it causes the order of life in the world such as lifestyle, education and all processes that occur change. One of the changes can be seen from the user experience, where there are many ways to present graphs in augmented reality and virtual reality.

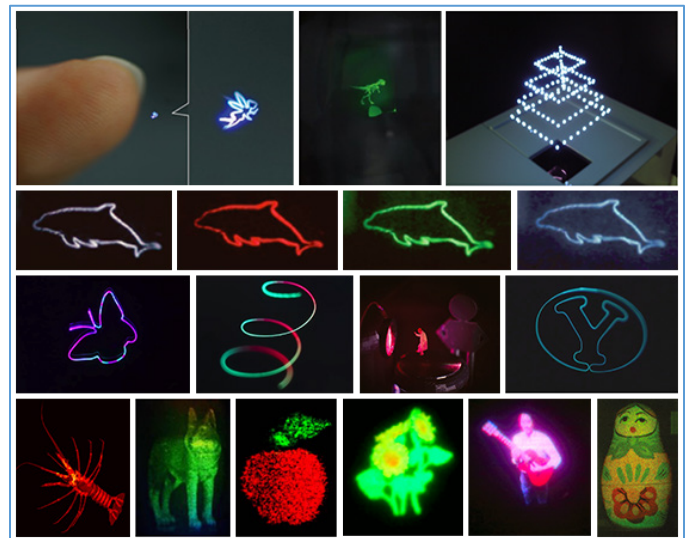


Figure 1: Holographic Projections

Presentation of the graph is currently still using a special device, experience still has discomfort in a physiological perspective [19]. Because of this, holographic display are developed, where the container used is air, as in figure 1 made by ref. [19-30]. The technique of making holograms is called holography, this technique has been widely used and developed by researchers, on

\*Yogi Udjaja, Jakarta, Indonesia 11480, +62 898 268 3399, udjaja.yogi@gmail.com, yogi.udjaja@binus.ac.id

[www.astesj.com](http://www.astesj.com)

<https://dx.doi.org/10.25046/aj050240>



the other hand the technology used is still not able to be used by the general public, because based on the size of the hardware and system it still requires a lot of development.

## 2. History of Holography

### 2.1. Holography

In 1947 the holography was discovered by Gabor [31], which produced random patterns of light intensity that varied spatially. Then in 1961 Leith and Upatnieks adopted the work of Gabor and applied it to laser beams free space and still produced the same model. It did not stop there, in 1966 found computer generated hologram (CGH) by Brown and Lohman, using numerical calculations to calculate wave phase information on the hologram interface can simplify the recording process through programming. This breakthrough opens up many new findings to create virtual objects that are seen in a real state but their forms do not exist in a static or dynamic state using spatial light modulators (SLM) [32].

Furthermore in 1982 Aspect et al. those from the University of Paris discovered subatomic particles in which electrons can connect to each other regardless of the distance that separates. This changed the world view of the principle held by Einstein, that no communication can travel faster than the speed of light, because when faster than the speed of light is the same as breaking the barrier of time [33].

The inventions continue to be developed, many physicists try to understand Aspect's findings, the results found a more radical explanation. Where according to one physicist from the University of London, Bhom explained that Aspect's findings do not have objective reality, apart from the solidity of the universe, subatomic particles can relate to each other apart from separate distances, where the separation produces an illusion called a hologram [33].

Currently holograms can be defined as three-dimensional images made based on interference patterns from coherent light waves (laser light) [34]. While the holography is a hologram making technique by recording and reconstructing the light wave fronts without amplifying and distributing the specified phase [35]. In making it, to form a hologram requires high-speed computing so that appropriate of the shapes and models are displayed as desired.

Based on previous research, a hologram is formed from the energy produced by a laser, the following are research has been done to make a hologram:

In Table 1 can be seen the research of Kimura et al. (2006) [20] and Saito et al. (2008) [21], produces 100 and 1000 Dot / Sec, but has not been able to produce a hologram. Then in the study of Ochiai et al. (2016) holograms can be produced using femtosecond lasers with energies of 30-100fs, 2mJ and 269fs, 50µJ with 1 color [22]. Then developed again by Hayasaki and Kumagai (2018), where the hologram has several colors produced

from femtosecond lasers with energy <100fs, 4.3µJ [19] (see figure 1).

Table 1: Research to Produce Holographic Projections

Researcher	Type of Laser	Energy of Laser	Dot/Sec
Kimura et al. (2006)	Nanosecond	Ns Normal	100
Saito et al. (2008)	Femtosecond	100fs	1000
Ochiai et al. (2016)	Femtosecond	30-100fs, 2mJ	1000
Ochiai et al. (2016)	Femtosecond	269fs, 50µJ	200000

### 2.2. Voxel

To display a hologram a volumetric approach is used with a predetermined diffraction pattern [36]. Literally a hologram is formed based on a dot produced from a laser beam that forms certain patterns (see figure 1). The element for the hologram is known as the volume pixel (voxel)—model 3D of pixels.

### 2.3. Computer Generated Hologram

Currently the technology for generating holograms has been widely circulated, such as: augmented reality (AR), virtual reality (VR) and mixed reality (MR) devices [37], but the technology can still cause vergence-accommodation disparity which can lead to inconvenience headache and nausea [36]. Then to avoid this, a holography technique called computer generated hologram (CGH) was developed using a laser beam.

The use of lasers is still a lot that can be developed, from the hardware and software side to security in use, because when playing with lasers can affect the health of the eyes and skin, if you do not use a protective eye and skin will be damaged.

In the Research Ochiai et al. (2016) suggest using anti-radiation glasses until this technology already has its own security, on the other hand it also documented several observations and studies when laser light exposed to the skin can also cause lesions, counted in 50ms - 6000ms starting from small wounds up to >2000ms will burn skin surface [21]. This discovery is the same as the computer was first discovered, where it is still large in size, requires a large amount of money, is functional which is limited and difficult to carry everywhere. In accordance with the principle of calm technology, as time goes by all technology is made so that people do not realize that they are interacting with the technology itself [38].

### 2.4. Spatial Light Modulator

Spatial light modulator (SLM) is a dynamic device that can modify light according to the position of the object [39]. According to Ref. [39], there are 2 types of SLM, namely:

- **Liquid Crystal on Silicon (LCoS)**  
As the name, this SLM uses birefringent liquid crystal molecules that are parallel because of the voltage applied to the electrode at the bottom.
- **Micro-Opto-Electro-Mechanical Systems (MOEMS)**  
MOEMS is a device that uses a micro-opto-mechanical element or like a mirror driven by electrical impulses.



What is often investigated by researchers in the holography field is LCoS, because LCoS can produce a holographic pattern with full wave changes. Each voxel can be arranged, so that luminous patterns can be displayed and direct energy in a certain order.

### 2.5. Deep Learning

Machine Learning is very useful for handling large-scale and high-dimensional data. There are several methods that support machine learning, one of the most prominent is the artificial neural network (ANN) [40]. ANN's extraordinary learning ability significantly outperforms conventional machine learning techniques. This has been proven in various disciplines.

As time goes by, because of the many human needs, then machine learning evolved into deep learning to solve existing problems. Deep learning is a representation learning method that has a level of representation starting from raw data into a complex composition of transformations and functions [41]. Where the architecture is a multilevel neural network, so that it can know more about something. As an example for the introduction of an object in an image, based on existing data deep learning is able to recognize shapes, know the name and position of objects in the image, and can predict events that will occur (Object detection, classification and prediction), besides that it can also be used to reconstruct and improve the quality of voxels so that images produced from CGH from low-quality resolution become high-quality resolutions [42-49].

### 3. Future Research and Experience System

Holographic Plasma Voxel (HPV) is a naming taken from a plasma laser that produces a volume of pixels (Voxel) in the real world so that it forms a pattern that is currently called a hologram. This hologram technology is very useful for progress in various fields such as computer aided design, medical imaging and navigation [50]. In addition, this future technology is predicted to be used in the future as befits a smartphone that we use today, as everyone can interact directly with real entities and many applications such as education, games and others can be felt in real terms. For example in figure 1 there are several animal shapes that are made into holograms, the hologram can be further developed into a virtual pet for the introduction of animals to children or to eliminate phobias of animals.

### 4. Discussion and Conclusion

The evolution of time has made different holographic models, from one set of modes to another, where each newly emerging generation inherits the existing pattern from the previous one [51]. Over the past 70 years research has been carried out to produce holograms by reflecting light repeatedly using parallel mirrors. This has a tremendous impact, because it can fulfill all physiological aspects and provide a natural experience without causing visual fatigue because it does not use special devices such as glasses or other devices [52]. Until now this technology still being developed, and the phenomenon predicted by Einstein and other researchers is still being investigated. Based on the current situation, the law of causality is always in the investigation, this

can be seen from the advantages and disadvantages of existing technology, all of which can be used as learning for the future.

### References

- [1] Grudin, J. (2018, April). From Tool to Partner: The Evolution of Human-Computer Interaction. In *Extended Abstracts of the 2018 CHI Conference on Human Factors in Computing Systems* (p. C15). ACM.
- [2] Girsang, A. S., Tanzil, F., & Udjaja, Y. (2016, November). Robust adaptive genetic K-Means algorithm using greedy selection for clustering. In *Knowledge, Information and Creativity Support Systems (KICSS), 2016 11th International Conference on* (pp. 1-5). IEEE.
- [3] Udjaja, Y. (2018). ANDROID APPLICATION FOR DETECTION OF SKIN CANCER USING EXPERT SYSTEM. *Social Economics and Ecology International Journal (SEEIJ)*, 2(1), 1-8.
- [4] YanFi, Udjaja, Y., & Sari, A. C. (2017). A Gamification Interactive Typing for Primary School Visually Impaired Children in Indonesia. *Procedia Computer Science*, 116, 638-644.
- [5] Yunanto, A., Aslamiah, A. H., Darmawan, D., Santoso, I., & Udjaja, Y. (2016). PENGEMBANGAN EKONOMI SOSIAL DALAM SEKTOR PERTANIAN DENGAN MENGGUNAKAN HYDROPONIC TOWER SYSTEM.
- [6] Udjaja, Y., Guizot, V. S., & Chandra, N. (2018). Gamification for Elementary Mathematics Learning in Indonesia. *International Journal of Electrical and Computer Engineering (IJECE)*, 8(6).
- [7] Gunawan, F. E., Maryanto, A., Udjaja, Y., Candra, S., & Soewito, B. (2016, November). Improvement of E-learning quality by means of a recommendation system. In *Knowledge, Information and Creativity Support Systems (KICSS), 2016 11th International Conference on* (pp. 1-4). IEEE.
- [8] Udjaja, Y. (2018). EKSPANPIXEL BLADSY STRANICA: Performance Efficiency Improvement of Making Front-End Website Using Computer Aided Software Engineering Tool. *Procedia Computer Science*, 135, 292-301.
- [9] Kristiadi, D. P., Udjaja, Y., Supangat, B., Prameswara, R. Y., Warnars, H. L. H. S., Heryadi, Y., & Kusakunniran, W. (2017, November). The effect of UI, UX and GX on video games. In *Cybernetics and Computational Intelligence (CyberneticsCom), 2017 IEEE International Conference on* (pp. 158-163). IEEE.
- [10] Sasmoko, Halim, S. A., Indrianti, Y., Udjaja, Y., Moniaga, J., & Makalew, B. A. (2019, March). The Repercussions of Game Multiplayer Online Battle Arena. In *2019 International Conference of Artificial Intelligence and Information Technology (ICAIIIT)* (pp. 443-447). IEEE.
- [11] Sasmoko, Harsono, J., Udjaja, Y., Indrianti, Y., & Moniaga, J. (2019, March). The Effect of Game Experience from Counter-Strike: Global Offensive. In *2019 International Conference of Artificial Intelligence and Information Technology (ICAIIIT)* (pp. 374-378). IEEE.
- [12] Udjaja, Y. (2018). Gamification Assisted Language Learning for Japanese Language Using Expert Point Cloud Recognizer. *International Journal of Computer Games Technology*, 2018.
- [13] Udjaja, Y., Renaldi, Steven, Tanuwijaya, K., & Wairooy, I. K. (2019). The Use of Role Playing Game for Japanese Language Learning. *Procedia Computer Science*, 157, 298-305.
- [14] Sasmoko, Indrianti, Y., Widhoyoko, S. A., Udjaja, Y., & Tanurwijaya, A. (2018, August). Teacher Engagement Interventions through ITEI Apps. In *2018 6th International Conference on Cyber and IT Service Management (CITSM)* (pp. 1-4). IEEE.
- [15] Sasmoko, Indrianti, Y., Widhoyoko, S. A., Udjaja, Y., & Rosyidi, U. (2018, August). Performance Change With or Without ITEI Apps. In *2018 6th International Conference on Cyber and IT Service Management (CITSM)* (pp. 1-4). IEEE.
- [16] Udjaja, Y., Indrianti, Y., Rashwan, O. A., & Widhoyoko, S. A. (2018, October). Designing Website E-Learning Based on Integration of Technology Enhance Learning and Human Computer Interaction. In *2018 2nd International Conference on Informatics and Computational Sciences (ICICoS)* (pp. 206-212). IEEE.
- [17] Aulia, A., Udjaja, Y., Wairooy, I. K., Hutama, A. P., Shabira, D. K., & Muhtadin, S. Android Application to Detect Cat Disease Using an Expert System.
- [18] Sasmoko, Moniaga, J., Indrianti, Y., Udjaja, Y., & Natasha, C. (2019, July). Designing Determining Teacher Engagement Based on The Indonesian Teacher Engagement Index Using Artificial Neural Network. In *2019 International Conference on Information and Communications Technology (ICOIACT)* (pp. 377-382). IEEE.

- [19] Hayasaki, Y., & Kumagai, K. (2018, June). Volumetric display with holographic femtosecond laser accesses. In *Digital Holography and Three-Dimensional Imaging* (pp. DTu5F-1). Optical Society of America.
- [20] Kimura, H., Uchiyama, T., & Yoshikawa, H. (2006, July). Laser produced 3D display in the air. In *ACM SIGGRAPH 2006 emerging technologies* (p. 20). ACM.
- [21] Saito, H., Kimura, H., Shimada, S., Naemura, T., Kayahara, J., Jarusirisawad, S., ... & Asano, A. (2008, February). Laser-plasma scanning 3D display for putting digital contents in free space. In *Stereoscopic Displays and Applications XIX* (Vol. 6803, p. 680309). International Society for Optics and Photonics.
- [22] Ochiai, Y., Kumagai, K., Hoshi, T., Rekimoto, J., Hasegawa, S., & Hayasaki, Y. (2016). Fairy lights in femtoseconds: aerial and volumetric graphics rendered by focused femtosecond laser combined with computational holographic fields. *ACM Transactions on Graphics (TOG)*, 35(2), 17.
- [23] Ochiai, Y. (2016, May). 8-4: Invited Paper: Pixels towards Pixies: Post-Multimedia interactions with Air-Based Media. In *SID Symposium Digest of Technical Papers* (Vol. 47, No. 1, pp. 79-82).
- [24] Yamada, S., Kakue, T., Shimobaba, T., & Ito, T. (2018). Interactive holographic display based on finger gestures. *Scientific reports*, 8(1), 2010.
- [25] Smalley, D. E., Nygaard, E., Squire, K., Van Wagoner, J., Rasmussen, J., Gneiting, S., ... & Costner, K. (2018). A photophoretic-trap volumetric display. *Nature*, 553(7689), 486.
- [26] Im, D., Cho, J., Hahn, J., Lee, B., & Kim, H. (2015). Accelerated synthesis algorithm of polygon computer-generated holograms. *Optics Express*, 23(3), 2863-2871.
- [27] Choo, H. G., Chlipala, M., & Kozacki, T. (2019). Visual perception of Fourier rainbow holographic display. *ETRI Journal*.
- [28] Huang, Z., Marks, D. L., & Smith, D. R. (2019). Out-of-plane computer-generated multicolor waveguide holography. *Optica*, 6(2), 119-124.
- [29] Bianco, V., Memmolo, P., Leo, M., Montresor, S., Distante, C., Paturzo, M., ... & Ferraro, P. (2018). Strategies for reducing speckle noise in digital holography. *Light: Science & Applications*, 7(1), 48.
- [30] Kim, J., Lim, Y., Hong, K., Kim, H., Kim, H. E., Nam, J., ... & Kim, Y. J. (2019). Electronic Tabletop Holographic Display: Design, Implementation, and Evaluation. *Applied Sciences*, 9(4), 705.
- [31] Shimobaba, T., & Ito, T. (2019). *Computer Holography: Acceleration Algorithms and Hardware Implementations*. CRC Press.
- [32] Huang, L., Zhang, S., & Zentgraf, T. (2018). Metasurface holography: from fundamentals to applications. *Nanophotonics*, 7(6), 1169-1190.
- [33] Talbot, M. (1991). *The holographic universe*.
- [34] Awad, A. H., & Kharbat, F. F. (2018, February). The first design of a smart hologram for teaching. In *Advances in Science and Engineering Technology International Conferences (ASET), 2018* (pp. 1-4). IEEE.
- [35] Cviljušac, V., Divjak, A., & Modrić, D. (2018). Computer Generated Holograms of 3D Points Cloud. *Tehnički vjesnik*, 25(4), 1020-1027.
- [36] Khan, J., Blackwell, C., Can, C., & Underwood, I. (2018, May). 16-1: Invited Paper: Holographic Volumetric 3D Displays. In *SID Symposium Digest of Technical Papers* (Vol. 49, No. 1, pp. 177-180).
- [37] El Saddik, A. (2018). Digital Twins: The Convergence of Multimedia Technologies. *IEEE MultiMedia*, 25(2), 87-92.
- [38] Poslad, S. (2011). *Ubiquitous computing: smart devices, environments and interactions*. John Wiley & Sons.
- [39] Collier, R. (2013). *Optical holography*. Elsevier.
- [40] Jo, Y., Cho, H., Lee, S. Y., Choi, G., Kim, G., Min, H. S., & Park, Y. (2019). Quantitative phase imaging and artificial intelligence: a review. *IEEE Journal of Selected Topics in Quantum Electronics*, 25(1), 1-14.
- [41] LeCun, Y., Bengio, Y., & Hinton, G. (2015). Deep learning. *nature*, 521(7553), 436.
- [42] Thanh, N., Xue, Y., Li, Y., Tian, L., & Nehmetallah, G. (2018). Deep learning approach to Fourier ptychographic microscopy. *Optics Express*.
- [43] Shimobaba, T., Endo, Y., Nishitsuji, T., Takahashi, T., Nagahama, Y., Hasegawa, S., ... & Ito, T. (2018). Computational ghost imaging using deep learning. *Optics Communications*, 413, 147-151.
- [44] Göröcs, Z., Tamamitsu, M., Bianco, V., Wolf, P., Roy, S., Shindo, K., ... & Ozcan, A. (2018). A deep learning-enabled portable imaging flow cytometer for cost-effective, high-throughput, and label-free analysis of natural water samples. *Light: Science & Applications*, 7(1), 66.
- [45] Liu, T., de Haan, K., Rivenson, Y., Wei, Z., Zeng, X., Zhang, Y., & Ozcan, A. (2019). Deep learning-based super-resolution in coherent imaging systems. *Scientific reports*, 9(1), 3926.
- [46] Sun, Y., Xia, Z., & Kamilov, U. S. (2018). Efficient and accurate inversion of multiple scattering with deep learning. *Optics express*, 26(11), 14678-14688.
- [47] Metzler, C., Schniter, P., & Veeraraghavan, A. (2018, July). prDeep: Robust phase retrieval with a flexible deep network. In *International Conference on Machine Learning* (pp. 3498-3507).
- [48] Shimobaba, T., Takahashi, T., Yamamoto, Y., Endo, Y., Shiraki, A., Nishitsuji, T., ... & Ito, T. (2019). Digital holographic particle volume reconstruction using a deep neural network. *Applied optics*, 58(8), 1900-1906.
- [49] Zhang, H., Fang, C., Xie, X., Yang, Y., Mei, W., Jin, D., & Fei, P. (2019). High-throughput, high-resolution deep learning microscopy based on registration-free generative adversarial network. *Biomedical Optics Express*, 10(3), 1044-1063.
- [50] St-Hilaire, P., Benton, S. A., Lucente, M. E., Jepsen, M. L., Kollin, J., Yoshikawa, H., & Underkoffler, J. S. (1990, May). Electronic display system for computational holography. In *Practical Holography IV* (Vol. 1212, pp. 174-183). International Society for Optics and Photonics.
- [51] Dvali, G. (2018). A Microscopic Model of Holography: Survival by the Burden of Memory. *arXiv preprint arXiv:1810.02336*.
- [52] Isomae, Y., Shibata, Y., Ishinabe, T., & Fujikake, H. (2017). Design of 1- $\mu\text{m}$ -pitch liquid crystal spatial light modulators having dielectric shield wall structure for holographic display with wide field of view. *Optical Review*, 24(2), 165-176.

## A Sustainable Multi-layered Open Data Processing Model for Agriculture: IoT Based Case Study Using Semantic Web for Hazelnut Fields

Şahin Aydın\*, Mehmet Nafiz Aydın

Kadir Has University, Department of Management Systems, 34083, Turkey

### ARTICLE INFO

Article history:

Received: 01 January, 2020

Accepted: 19 March, 2020

Online: 23 March, 2020

Keywords:

Open Data

Open Data Processing Model for Agriculture

Multi-layered Open Data

Processing Model

Semantic Web in Agriculture

IoT in Hazelnut farming

### ABSTRACT

In recent years, several projects which are supported by information and communications technologies (ICT) have been developed in the agricultural domain to promote more precise agricultural activities. These projects account for different kinds of key ICT terms such as internet of things (IoT), wireless sensors networks (WSN), cloud computing (CC). These projects are used for different agricultural products; and it is a well-known fact that they can be essential to perform precise agricultural activities for the relevant agricultural products. The implementation of these projects successfully depends on the extent to which various stakeholders provide support by leveraging relevant data, gathered from heterogenous data sources. Agriculture domain has a great number of stakeholders. These stakeholders need sophisticated data and appropriate intelligence to get benefits in order to perform precise agricultural activities. Authors agreed with scholars that "Open Data" idea, which means accessing data published on the web and available in a machine-readable format is an appropriate way to get benefits for precise agriculture by relevant stakeholders. In this paper, authors shall investigate the open data term in an agricultural context, create an open data processing model, and develop an IoT-based solution to gather environmental data from agricultural fields. Authors also show viability of the proposed model by developing an ICT-based solution. Considering the socioeconomic importance of hazelnut for Turkey, the stakeholders of hazelnut domain still have problems such as availability, meaningful, accuracy of the hazelnut related data. Therefore, authors shall focus on hazelnut within the scope of this paper.

### 1. Introduction

This paper is an extension of work originally presented in the 6th International Conference on Control Engineering & Information Technology (CEIT), in 2018 [1].

Agriculture increases employment that covers more than third of the world population via exportation and domestic income which makes it one of the leading sectors in the world. [2]. Turkey which is the leader country in terms of hazelnut production in the world, has an important role for contributing more information with respect to hazelnut production cycle from this aspect. As well as Turkey is the leader of hazelnut production, it is leading producer of dried apricots, raisins, and dried figs [3]. Since having such a convenient weather quality which only a few countries could have for hazelnut production, Turkey, has 75% of overall

production and 70-75% of the exportation. Furthermore, considering that there have been 4 million people correspond with almost 5% of the overall population of Turkey, who are concerned with hazelnut produced over an area of 550-600 thousand hectares, this makes hazelnut quite important in terms of socio-economic aspect [4]. In Turkey, statistics concerning agricultural products, including hazelnut are presented as only hypertext markup language (HTML) pages, spreadsheets, and comma-separated files (CSV) by Turkish Statistical Institute (TUIK). The context of hazelnut data presented by TUIK contains just a certain type of statistical information. However, the domain stakeholders such as farmers, experts, researchers, and analysts might generate more detailed and sophisticated data regarding hazelnut so that gaining knowledge from it must be straightforward and obvious. In order to achieve that, the data must include basic parameters used for the general management of the accession and environmental and field-specific parameters. This kind of data, freely available to use and

\*Şahin AYDIN, Email: aydinoglu.sahin@gmail.com

republish and in machine-readable format, might give a chance to stakeholders for removing the obstacles of implementation of sustainable hazelnut production. Examples of issues regarding hazelnut, which might be commonly encountered by domain stakeholders, might be indicated as follows: limited information or uncertainty about supply and demand side. In addition, there are several problems regarding hazelnut production such as aging hazelnut gardens, land element and position, soil texture, blights, fertilizing, treatment, less pollination, less pruning, agricultural pests, price fluctuation, increase of hazelnut production areas uncoordinatedly, and lack of persistent exportation policies [5]. Furthermore, there exist positive or negative correlations between environmental factors and hazelnut production. For instance, a sudden drop in the temperature negatively affects hazelnut production. It is not generally possible to access this type of data for such a particular agricultural product. However, it might be a solution to leverage the reference body of knowledge and analyze the reports of scientific experiments by accessing this data. The data obtained from scientific experiments are not usually allowed for using by any stakeholders out of the relevant communities [6]. However, considering the presence of barriers for accessing such kind of data, most of organizations belonging to government or private sector are in charge of removing them and making the data freely accessible. Nevertheless, aforementioned permission barriers should be removed for hazelnut stakeholders to meet requirement accessing, reusing, and publishing sophisticated data regarding hazelnut as well.

In this paper, we shall look in detail into processing open data gathered from different data sources and a designed model, considering very exclusive layers from stakeholders' perspectives.

This paper begins with an introduction section in which the research problem is explained. Second section is the research background section that mentions some key terms regarding the model's layers. Then, open data processing model is disclosed in the model, followed by the findings section. Lastly, a case study, which is developed as an exclusive system to demonstrate the model viability, was explained in the implementation section.

## 2. Research Background

In Turkey, hazelnut production is being dominantly performed in the zone of Black Sea which comprises of two different areas named as First Standard District (FSD) and Second Standard District (SSD) respectively. While SSD is composed of the west and the middle areas of Black Sea zone, FSD is located in the east of the Black Sea zone. Although there are similarities between two areas, it should be noted that considerably differences such as environmental characteristics and climate conditions are exist between them as well. The aforementioned dissimilarities might generate an obvious discrepancy in hazelnut production year by year. When one looks at the statistical data of last thirty years in agricultural production, one sees that on average 520.198 tons hazelnut were produced in Turkey, and such data demonstrates that the position of Turkey as a leader in hazelnut production in the world. Turkey exports significant amount of hazelnut every year. The statistical data regarding agricultural exportation in the year 2019 illustrate that Turkey exported at about 320 thousand tons of hazelnut and it received 2 billion 28 million dollars of revenue via this. It has been identified that there are not adequate researches and studies about how to utilize contemporary ICT for such valuable agricultural product. Therefore, a multi-layered model

based on open standards for demonstrating how to process agricultural data is proposed considering the hazelnut which is a dominant agricultural product produced in a wide range area in Turkey in this study. Multi-layered model enables us to distinguish the essential layers such as data sources, data processing, semantic annotation, data storage, services, applications and users functions physically and logically. In addition, it enables interoperability for each layer to accomplish performing sustainable agricultural activities. There are a number of important benefits of the multi-layered approach. For instance, the multi-layered approach is secure, and its management is easy. It is also scalable, flexible and provides more efficient development abilities. Adding new features to the developed system is easy as well. That is why, a multi-layered model is presented and detailed within this study.

Although extensive research has been carried out on agricultural ICT technologies, not many studies exist which adequately focus on hazelnut. Furthermore, there is not a model which meets the requirements of hazelnut agricultural activities as well. So, a multi-layered open data processing model which aims to conduct sustainable agricultural activities of hazelnut is proposed as a part of this study.

The model proposed is essentially based on two pillars: the very idea of "Open Data", and "Semantic Web" approach to data modeling. Authors shall first provide a basic understanding of these pillars so that conceptual foundation of the proposed model is established. Publishing the data in machine-readable format using favorable open standards and open formats by enabling stakeholders to access, read, reuse, and share it with no license limit or permission barriers might be described as "Open Data" [7]. Furthermore, ICT's role is to facilitate distribution of data to users from various stakeholders in the relevant domain. Eliminating heterogeneity of data sources in the agricultural domain might be possible by using the strength of semantic web technologies. It is necessary to publish data using open standards and in machine-readable format to meet requirements of providing processable data by software agents. Semantic Web (SW) aims transforming data into suitable format which might be processed by software agents and human via software tools [8]. As well as SW eases retrieving the data by human or software agents via making interrelations between the objects. The linked data, which might be usable in varied formats on the web and published under open license, must be in structured and machine-readable format [9]. Resource Description Framework (RDF) is used to display information on the web as guided and identified data. It usually serves data including, but not limited to, personal information, social networks, metadata about digital artifacts. Furthermore, it contributes as a way of combination over diverse sources of information. The structure of SPARQL which is being used for querying RDF data, is described semantically considering this specification [10].

Utilizing semantic web technologies is quite efficient way to present domain-specific data on the web. It might ensure removing difficulties in terms of presenting data in appropriate formats, which can be processed by both software agents and humans. RDF, which is widely used and known as common standard for sharing data semantically on the web, has strong characteristics to ease merging data obtained from heterogeneous sources. Merging data obtained from varied sources might be performed using ontologies. RDF, which plays a significant role in SW's world in terms of



presenting data, is main pillar in terms of generating ontology regarding varied domains [11]. RDF also enables improving schemas in time with no requirement for changing by data consumers [12].

### 3. Model and Findings

As mentioned in the previous sections, authors created a multi-layered open data processing model, and focused on the hazelnut agricultural product. Even though this model focuses on a sustainable agricultural production lifecycle of hazelnut in this study, it is convenient for all agricultural products as well. This model is created by considering data sources, data processing, semantic annotations, data storage, services, applications, and users. The proposed open data model which demonstrates how to process data obtained from heterogeneous agricultural data sources and designed as multi-layered includes varied layers such as types of data sources (IoT devices, statistical data from government, market data, farmers, and other data sources); storing and processing raw data; semantic annotation layer (agricultural

product ontology, other ontologies and data interchange engine); data storage layer (graph databases, relational databases, cloud databases, RDF and XML file-based storage options and database service); services layer (XML web services, REST web services, web APIs, mobile services, analysis services, reporting services and SPARQL query services); applications layer (unified web based data platform based on open formats, mobile applications and desktop applications); and lastly, end users layer. The overall model and its each layer, proposed in this study, are being demonstrated in Figure 1.

The data are generally gathered from heterogeneous sources such as farmers, sensors, government statistical data, and market data in the agriculture domain. There is no doubt that the most important one of these heterogeneous data sources is “farmers”. As a significant data source in terms of the model, farmers, play a vital role for performing agricultural production life cycle. Considering the hazelnut production cycle, there is much varied information regarding hazelnut might be collected by consulting of farmers.

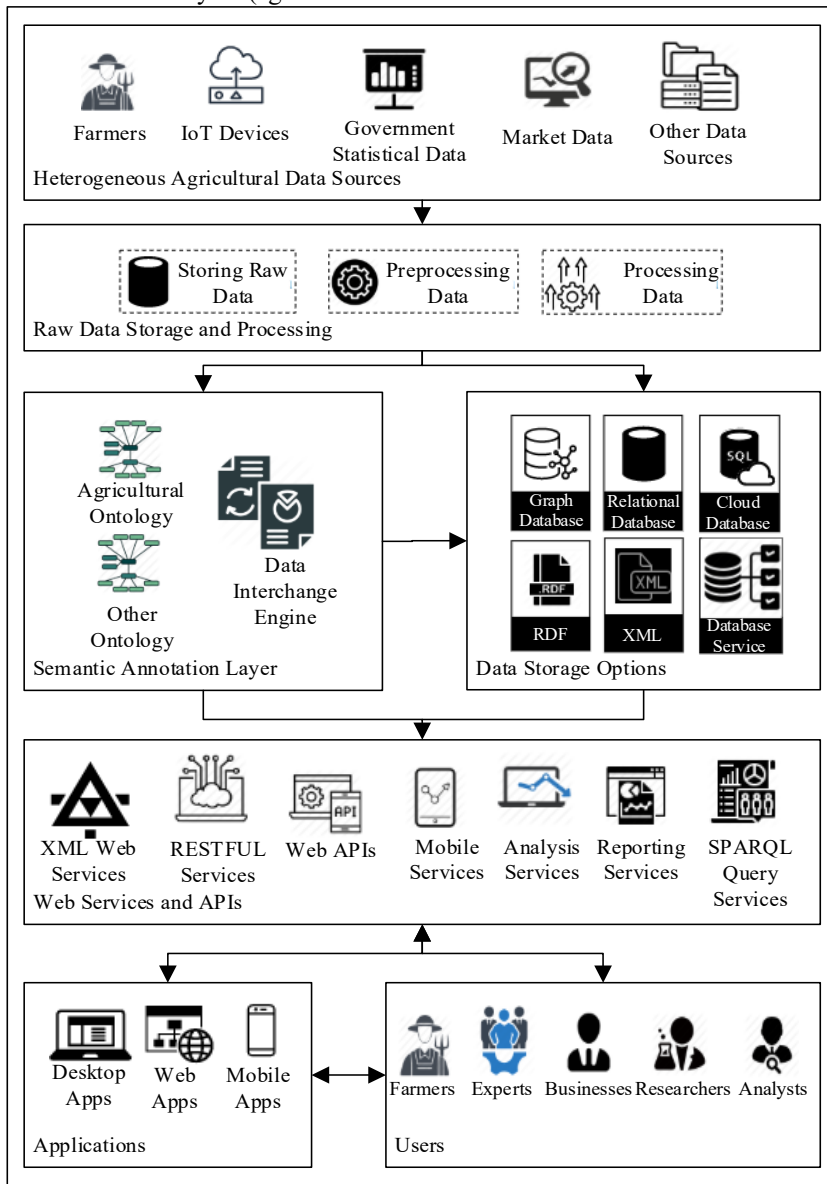


Figure 1: Overall Architecture of Open Data Model

For instance, age productivity and morbidity of trees, observation for soil fertility, the number of trees in orchards, location of orchards (southern slopes or northern slopes), pruning hazelnut trees, fertilization, agricultural spraying, cropping system, propagation method, irrigation method, overall vegetation surrounding the collecting site, stoniness, rockiness etc.

Today, IoT devices have been frequently used for varied domains such as smart cities, industries, education, health, and agriculture. These devices generally consist of a wide range of sensors which are used to collect specific data pertaining to environmental characteristics of site. Collecting and processing data with respect to these characteristics facilitates performing precise agricultural activities. Sensors might provide sensitive measurement values concerning slope, weather temperature, velocity of wind, rainfall, soil moisture, soil Ph, frost (date of most recent frost, minimum temperature, duration of temperature below 0°C), relative humidity (diurnal and seasonal range), light intensity, leaf anatomy, etc.

Agricultural production stats, which are a sort of official statistics data, are recorded by government agencies. The open data model takes into consideration the importance of statistical data concerning agricultural production so, it adopts them as an element of overall architecture. The statistical records regarding many varied domains in Turkey are compiled, evaluated, and published by TUIK [13]. The data with respect to agriculture domain are generally published by TUIK as spreadsheet, comma-separated values, and HTML files, which might be accessed through TUIK web platform.

Marketing operations in agriculture domain include several procedures such as production plan, burgeoning, reaping, classifying, packaging, shipping, managing storehouse, transforming agricultural products into food, delivery, promote, and sale, required for movement of a product from farmers to buyers [14]. It is a very crucial cycle for any agricultural product, so the proposed model contains it as a data source element. The experts, researchers, and analysts who are interested in relevant agricultural products might contribute to the system by loading some exclusive data. So, these kinds of data sources are defined as other data sources in the open data model.

According to NIST (National Institute of Standards and Technology), “cloud computing (CC) is a model for enabling ubiquitous, convenient, on-demand network access to a shared pool of configurable computing resources such as networks, servers, storage, applications, and services, that can be rapidly provisioned and released with minimal management effort or service provider interaction” [15]. Considering the strength and robust characteristics of CC, it has been recommended that data storages, services and applications of the proposed model should serve on the cloud. Raw Data Storage and Processing Layer (RDSandPL) comprises component of raw data storing (SRD), component of data preprocessing (PPD), and component of data processing (PD). Data obtained from heterogeneous agricultural data sources are stored into varied data storage options such as relational databases, graph databases, cloud databases, RDF files, and XML files via SRD. It is worth bearing in mind that any stakeholder might need to handle data obtained from heterogeneous sources in raw form. That's why, it is significant storing data in raw format using recommended data storage options according to open data model point of view.

Considering the data gathered from heterogeneous agricultural data sources might be incomplete, incorrect, or irrelevant, it is important to emphasize the requirement of a mechanism to detect and correct them. According to open data model, this mechanism is being corresponded with PPD component. Preprocessing the data ensures removing incompleteness and inconsistency with respect to the raw data and transforming such data into meaningful format to analyze effectively [16]. As well as, PPD decomposes raw data, it aims to apply exclusive techniques concerning preprocessing to such data. Applying preprocessing techniques such as data integration, data enhancements, data enrichment, data transformation, data reduction, data discretization and data cleansing boosts quality of the data [17]. Some of the traditional data preprocessing methods such as K-neighbors Classifier, Logistic Regression, Gaussian Naïve Bayes, Decision Tree, and Support Vector Machine might be used for sensor data, but it should be noted that the major purpose of development of these methods are not to apply them to sensor data [18]. This component is also responsible for semantic annotation of streaming data obtained from sensors, using existing or new ontologies. By this means, semantic annotation of streaming sensor data facilitates data integration processes between varied data sources and open data platforms. In addition, this component solves noisy and redundant problems of sensor data streams, solves missing value problems, detects anomalies related to data, and manages data heterogeneity using the strength of semantic web technologies [19].

The aim of carrying out the preprocessing techniques and methods to the sensor stream data is to build a robust technical infrastructure for data processing component of the proposed model. Data processing means that acquiring meaningful information from preprocessed raw data. Acquiring meaningful information enables users to make estimations for the future via implementing varied analyze techniques and allows creating analytical solutions. So, it is important to bear in mind that having such a component is essential in terms of open data model. The design principles proposed by Begoli and Horey, which allows using varied analytical techniques and substantially interested in maximizing the controllable factors, provide easily exploring and analyzing the data by researchers [20]. The practical analytical solutions are ensured corresponding with these design principles for stakeholders by component of data processing of open data model.

When implementation of relevant methods and techniques is completed by the components of RDSandPL, it is required transforming data into RDF datasets. The data interchange component of Semantic Annotation Layer (SAL) is in charge of transforming data into RDF datasets. The proposed model recommends using agricultural product ontologies to transform data into RDF datasets.

Ontologies distinctly specify conceptualization by means of constructing abstract and simplified view of a particular domain which requires to be represented [21]. Combining a number of objects and concepts, which are related to knowledge that is supposed to be expressed and making interrelations between them might be described as conceptualization [22]. The aim of generating ontologies is not merely to identify the conceptualization or point out the widespread savvy of a particular domain. In addition, they are utilized as conceptual models which provide common understanding to facilitate communicating

between varied types of software application systems and among people [23]. Nowadays, there exist several ontologies which are still being in use, concerning the agriculture domain. AGROVOC, one of the commonly known agricultural ontologies, was developed by Food and Agriculture Organization (FAO) of the United Nations in the early of the 1980s. Furthermore, it is the most popular and well-known agricultural thesaurus all over the world. AGROVOC, which is formed as linked dataset, is based on SKOS-XL (Simple Knowledge Organization System eXtension for Labels) concept scheme, and it comprised of more than thirty-five concepts which are defined in up to twenty-nine different languages. [24]. Institute for Learning & Research Technology created SKOS(Simple Knowledge Organization System) with the aim of providing linked and distributed knowledge organization systems such as controlled vocabularies, thesauri, taxonomies, and folksonomies [25]. SKOS-XL, as an extension version of SKOS, facilitates identifying lexical entities and making interrelationships among them, with the additional support [26]. The focus of this study is on the development of open data processing model. Therefore, authors intend to develop a comprehensive ontology using descriptors of hazelnut as future work [27]. Both RDF (Resource Description Framework) and OWL (Web Ontology Language) have vital role in the world of semantic web and are popular technologies which might be utilized to accomplish the aforementioned objective. RDF and OWL are the most known standards of semantic web technologies for describing data on the web. OWL is developed based on RDF and extends it including exclusive components such as axioms, classes, object properties, data properties, datatypes, individuals etc. [28]. OWL is the common, well-known, and standard language to create ontologies. Moreover, it has three sublanguages to meet different requirements such as OWL Full, OWL DL, and OWL Lite.

Data gathered from different data sources and processed by RDSandPL might be stored in graph databases, relational databases, cloud databases, XML files, and RDF files, which are recommended as data storage options in the open data model. The proposed open data model is noted the importance of converting raw data into RDF datasets. Therefore, transforming data gathered from varied sources into triple store which means subject, predicate, and object, has been built as a component of semantic annotation layer. Due to RDF datasets have robust features in terms of storage and indexing [29], they have been considered as a storage option in the proposed open data model. Relational databases component of data storage layer (DSL) is in charge of storing relational data. Graph databases component of DSL is in charge of storing data as graphs. Cloud databases might store data as both graphs and relational. Database services, which is a component of DSL, provide a secure connection, session management, user mapping, user authentication, and authorization between components of services layer (SL).

Another essential layer of proposed model is the services layer, which consists of seven different types of services: XML web services, REST web services, web APIs, mobile services, analysis services, reporting services, and SPARQL query services. According to W3Schools, “web services are defined as self-contained and self-describing application components that can be discovered using UDDI, be used by other applications, and they communicate using open protocols“ [30]. Web Services and APIs Layer (WSandAL), which is in charge of providing interoperability between mobile, desktop, and embedded software applications and databases, is a significant part of the proposed

model. While providing interoperability by WSandAL, the RESTful Services component of this layer plays an important role. Software agents, tools and applications, which are being developed using different or similar development technologies, utilize agricultural data by consuming RESTful Services. Another important feature of the proposed model is mobility. To meet this requirement, it strongly recommends developing mobile applications. It is, therefore, needed to generate mobile services to develop an efficient infrastructure for mobile devices. Mobile services, which provide connection to different kinds of mobile devices must take part in the proposed model. Stakeholders might be limited by lack of knowledge to apply data analysis methods to agricultural data. The proposed model recommends building analysis services to solve this problem.

Designing and publishing detailed reports are required to develop usable software systems which aims to process data. Reporting Services component of open data model aims to meet these requirements. It enables domain stakeholders create dynamic, well-designed and detailed reports. As mentioned in previous section of this study SPARQL is the language to query RDF datasets which are stored in files or graph databases. In the proposed open data model, creating queries using this particular language and compiling them are provided and facilitated by service component named SPARQL Query Service.

Applications Layer (AL) allows end users to access agricultural data obtained from heterogeneous data sources. AL consists of web, mobile and desktop applications which enable us to import, export, report, analyze, and query data.

There are a number of varied end users belonging to proposed open data model, called domain stakeholders such as farmers, researchers, businesses, analysts, and domain experts. Domain stakeholders are provided to utilize data which are gathered from heterogeneous agricultural data sources and might be consumed through the WSandAL and processed by applications layer. Considering the importance of accessing, reusing, and processing such data, it allows domain stakeholders of hazelnut agricultural product construct common knowledge with respect to performing agricultural activities in an efficient way. Every year, several exploratory investigations are performed to estimate total amount of hazelnut production by different institutions of Turkey. However, these current exploratory investigations to find out the hazelnut production of a further year are limited because of unforeseen circumstances with respect to hazelnut harvest. Unfortunately, some discrepancies are seen among the estimations which are carried out by different government agencies every year. Due to the hazelnut price per kilogram is being affected from these discrepancies negatively, rapid price fluctuations are being seen for hazelnut in Turkey. When one takes into consideration the problems for hazelnut market, each user in other words domain stakeholder, play a vital role in terms of the proposed open data model.

The proposed open data model reveals that how each of stakeholders might exploit the processed and published agricultural data for removing the obstacles and problems concerning any particular agricultural product. The proposed open data model by its data processing perspective might enable farmers who have a key role in agriculture domain plan their production cycle effectively. The domain experts and researchers might take preventive measures to prevent further spread of the agricultural

diseases by producing the meaningful information using the applications and services developed based on the proposed open data model. Varied kinds of statistical analysis with respect to market, investment, and employment might be undertaken by analysts utilizing the conferred data by proposed open data model. Statistical analysis presented by analysts might be used to support making effective decisions concerning market share of agricultural businesses for the future.

#### 4. Implementation

The proposed multi-layered open data processing model is introduced within the previous sections. In this part of the study, a prototype of the electronic system is developed by establishing a wireless sensor network (WSN), which consists of varied sensors and other electronic devices in order to test the viability of the proposed model. This implementation is only focused on streaming data from IoT devices to the databases through web services. Other aspects of the proposed model shall be elaborated in different studies in future studies. There are three sensor nodes named router 1, router 2, and router 3 in the developed system, respectively. These nodes transmit measured data to the coordinator. This system structure is an implementation of ordinary WSN. Figure 2 presents the architecture of the developed wireless sensor network.

Weather temperature, weather humidity, weather pressure, carbon monoxide, nitrogen, oxygen, and ultraviolet detection sensors have been plugged on router 1; digital light intensity, soil moisture, and precipitation detection sensors have been plugged on router 2; and accelerometer and gyroscope sensor have been plugged on router 3. Table 1 illustrates which sensor measures what type of measurements, and which sensor is plugged on which router. While some of these sensors measure different types of environmental events or changes at the same time, some of them measure only one event or change. Weather pressure, temperature, humidity changes have been detected by only one sensor named BME280. Likewise, rates of carbon monoxide, hydrocarbons and oxidizing gases such as NO<sub>2</sub> have been measured by only one sensor named MICS-4514. Arduino Uno microcontroller boards based on ATmega328P have been used to plug the sensors and

measure their values in the system. XBee is one of the most popular modules which allows devices connect to each other through wireless. So, XBee Pro S2C modules have been seen an appropriate embedded solution for established wireless sensor network to transmit data from routers to the coordinator. The coordinator consists of a Raspberry Pi 3 small single-board computer, an Arduino Uno, and an XBee Pro S2C module. Raspberry Pi has been included in WSN to run a universal windows application, which is in charge of reading, visualizing, and storing real-time data stream obtained from sensors. This application communicates with the coordinator device to read the data stream through serial port. The real-time data stream, which is visualized in favorable visualization objects by universal application, are stored in databases through web services. Figure 3 illustrates how sensor measurements are visualized by universal windows application on Raspberry Pi.

ZigBee is an international open standard and communication protocol, which depends on IEEE 802.15.4 and ensures low-power, low-cost, low-data-rate, and wireless mesh networking. [31]. Zigbee has three kinds of node types, such as coordinator, router, and end device. However, the developed WSN does not include any end device. Each of the XBee modules belonging to WSN were configured to API operating mode, which provides data transmission to multiple destinations with no requirement, using command mode. Receiving success and failure status of each transmitted RF packet is facilitated in this mode. In addition, the operation of identifying the source address of each received packet is readily provided by this mode. The routers transmit data, which is gathered via sensors, in an exclusive format named frame, represented as a ZigBee packet to the coordinator. The structure of the frame data; in other words, a ZigBee packet, which is used by the routers to transmit sensor data stream towards the coordinator, is demonstrated in Figure 4. The structure of frame data differs in compliance with the objectives of the API frame. The frame data structure of the established wireless sensor network, represented in Figure 4, consists of the fields, such as start delimiter, length, frame type, frame id, 64-bit destination address, options, RF data, and checksum.

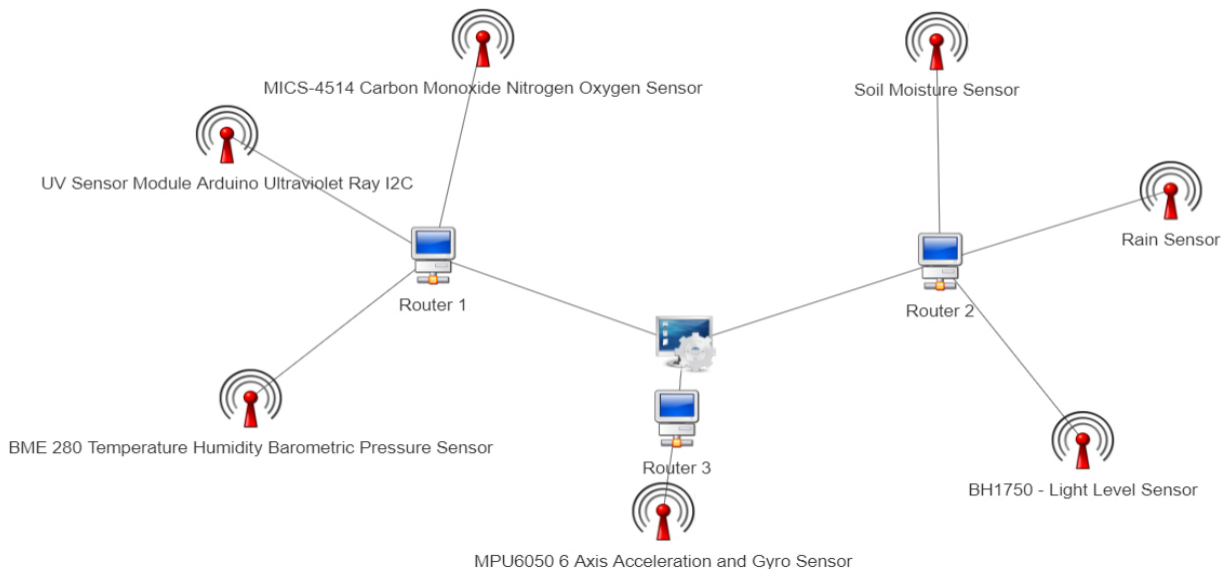
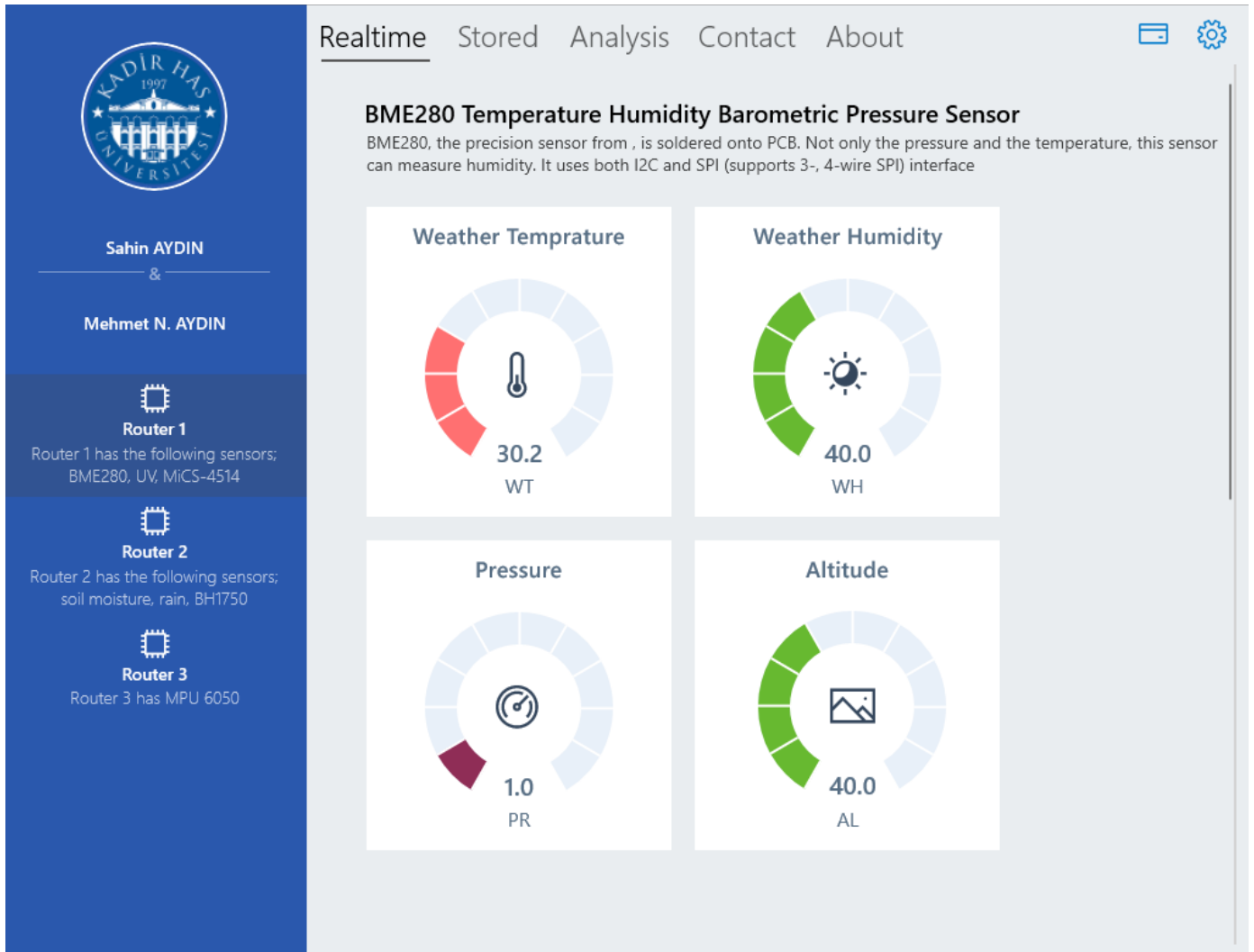


Figure 2: Developed WSN Architecture



Table 1: Sensors plugged on routers

Router Name	Sensor Name	Measurements
Router 1	BME280 Temperature Humidity Barometric Pressure Sensor	Temperature Humidity Pressure
	GUVA-S12SD UV Sensor Module Arduino Ultraviolet Ray I2C	UV radiation in sunlight
	MICS-4514 Sensor	CO concentration Hydrocarbons Oxidizing gases
Router 2	Soil Moisture Sensor	Soil Moisture
	BH1750 - Light Level Sensor	Light Intensity
	Rain Sensor	Rain detection and rainfall intensity measurement
Router 3	MPU6050 (Gyroscope + Accelerometer + Temperature) Sensor Module	Accelerometer Gyroscope Temperature



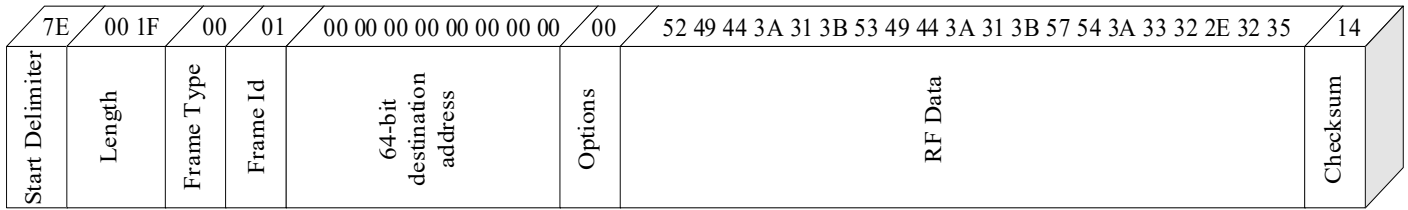


Figure 4: Frame Data Format

Weather Temperature Data (Last 25 Measurements)

SENSOR TYPE NAME	TYPE NAME	TYPE DEFINITION	VALUE	DATETIME
BME 280 Temperature Humidity Barometric Pressure Sensor	Weather Temperature	WT	32.434	2/2/2020
BME 280 Temperature Humidity Barometric Pressure Sensor	Weather Temperature	WT	32.404	2/2/2020
BME 280 Temperature Humidity Barometric Pressure Sensor	Weather Temperature	WT	32.446	2/2/2020 10:03:53 PM
BME 280 Temperature Humidity Barometric Pressure Sensor	Weather Temperature	WT	32.426	2/2/2020 10:03:45 PM
BME 280 Temperature Humidity Barometric Pressure Sensor	Weather Temperature	WT	32.419	2/2/2020 10:03:39 PM
BME 280 Temperature Humidity Barometric Pressure Sensor	Weather Temperature	WT	32.414	2/2/2020 10:03:32 PM

The sensor data are transmitted from the routers to the coordinator using key-value pair identifiers. For instance, the frame data, represented in Figure 4, refers to “RID:1;SID:1;WT:32.25”. The key-value pairs of this frame are RID:1, SID:1, and WT:32.25, respectively. Likewise, the values are 1, 1, and 32.25 as well. The keys, RID, SID, and WT stand for router id, sensor id, and temperature, respectively.

When the data are transmitted to the coordinator and transformed into a meaningful format by universal application, storage operations are performed by DPL. Data are stored in two different types of database management systems, such as Microsoft MS SQL Server and Neo4j graph database system, which are a component of data storage layer. Neo4j, which is a graph database management system, increases the system performance, provides flexibility and agility. Figure 6 presents the

data stored in Neo4j. RDF file-based data storage option is used to store and export sensor data for this case study. Table 3, Table 4, Table 5 represent RDF/XML, Notation 3, and N-Triples datasets, respectively. These datasets can be created using the sensor listing UI of the open data platform represented in Figure 5.

The data gathered from sensors and stored on databases must be published in a suitable format for applications running on different platforms. Therefore, REST web services were developed using Windows Communication Foundation (WCF), which is a framework for building service-oriented applications. Furthermore, web services for Windows platforms were developed in the same way. Table 2 illustrates the formatted data in JSON (JavaScript Object Notation) format. Developed web services are accessible to stakeholders.

Table 2: Example of JSON data

```
[{
  "Id": 2,
  "SensorDataAddedDatetime": "\Date(1580635128430+0300)\",
  "SensorDataType": 2,
  "SensorDataValue": "32.45",
  "SensorId": 1000
}]
```

Table 3: Example of RDF/XML dataset

```
<?xml version="1.0" encoding="utf-8"?>
<!DOCTYPE rdf:RDF [
  <!ENTITY rdf 'http://www.w3.org/1999/02/22-rdf-syntax-ns#'>
  <!ENTITY rdfs 'http://www.w3.org/2000/01/rdf-schema#'>
  <!ENTITY xsd 'http://www.w3.org/2001/XMLSchema#'>
  <!ENTITY sensorData 'http://www.opendatainagriculture.com/sensors#'>
]>
<rdf:RDF xml:base="http://www.opendatainagriculture.com/sensors" xmlns:rdfs="http://www.w3.org/2000/01/rdf-schema#"
xmlns:xsd="http://www.w3.org/2001/XMLSchema#" xmlns:sensorData="http://www.opendatainagriculture.com/sensors#"
xmlns:rdf="http://www.w3.org/1999/02/22-rdf-syntax-ns#">
  <rdf:Description rdf:about="http://www.opendatainagriculture.com/sensors/datatype#WeatherTemperature">
    <sensorData:DataTypeId>2</sensorData:DataTypeId>
    <sensorData:Datetime>2/2/2020 10:04:07 PM</sensorData:Datetime>
    <sensorData:SensorTypeId>1000</sensorData:SensorTypeId>
    <sensorData:SensorTypeName>BME 280 Temperature Humidity Barometric Pressure Sensor</sensorData:SensorTypeName>
    <sensorData:TypeDef>WT</sensorData:TypeDef>
    <sensorData:TypeName>Weather Temperature</sensorData:TypeName>
    <sensorData:Value>32.434</sensorData:Value>
  </rdf:Description>
</rdf:RDF>
```

Table 4: Example of Notation 3 dataset

```
@base <http://www.opendatainagriculture.com/sensors>.
@prefix rdf: <http://www.w3.org/1999/02/22-rdf-syntax-ns#>.
@prefix rdfs: <http://www.w3.org/2000/01/rdf-schema#>.
@prefix xsd: <http://www.w3.org/2001/XMLSchema#>.
@prefix sensorData: <http://www.opendatainagriculture.com/sensors#>.

<http://www.opendatainagriculture.com/sensors/datatype#WeatherTemperature> sensorData:DataTypeId "2";
    sensorData:Datetime "2/2/2020 10:04:07 PM";
    sensorData:SensorTypeId "1000";
    sensorData:SensorTypeName "BME 280 Temperature Humidity Barometric Pressure Sensor";
    sensorData:TypeDef "WT";
    sensorData:TypeName "Weather Temperature";
    sensorData:Value "32.434".
```

Table 5: Example of N-Triples dataset

```
<http://www.opendatainagriculture.com/sensors/datatype#WeatherTemperature>
<http://www.opendatainagriculture.com/sensors#DataTypeId> "2".
<http://www.opendatainagriculture.com/sensors/datatype#WeatherTemperature>
<http://www.opendatainagriculture.com/sensors#SensorTypeId> "1000".
<http://www.opendatainagriculture.com/sensors/datatype#WeatherTemperature>
<http://www.opendatainagriculture.com/sensors#SensorTypeName> "BME 280 Temperature Humidity Barometric Pressure
Sensor".
<http://www.opendatainagriculture.com/sensors/datatype#WeatherTemperature>
<http://www.opendatainagriculture.com/sensors#TypeName> "Weather Temperature".
<http://www.opendatainagriculture.com/sensors/datatype#WeatherTemperature>
<http://www.opendatainagriculture.com/sensors#TypeDef> "WT".
<http://www.opendatainagriculture.com/sensors/datatype#WeatherTemperature>
<http://www.opendatainagriculture.com/sensors#Value> "32.434".
<http://www.opendatainagriculture.com/sensors/datatype#WeatherTemperature>
<http://www.opendatainagriculture.com/sensors#Datetime> "2/2/2020 10:04:07 PM".
```

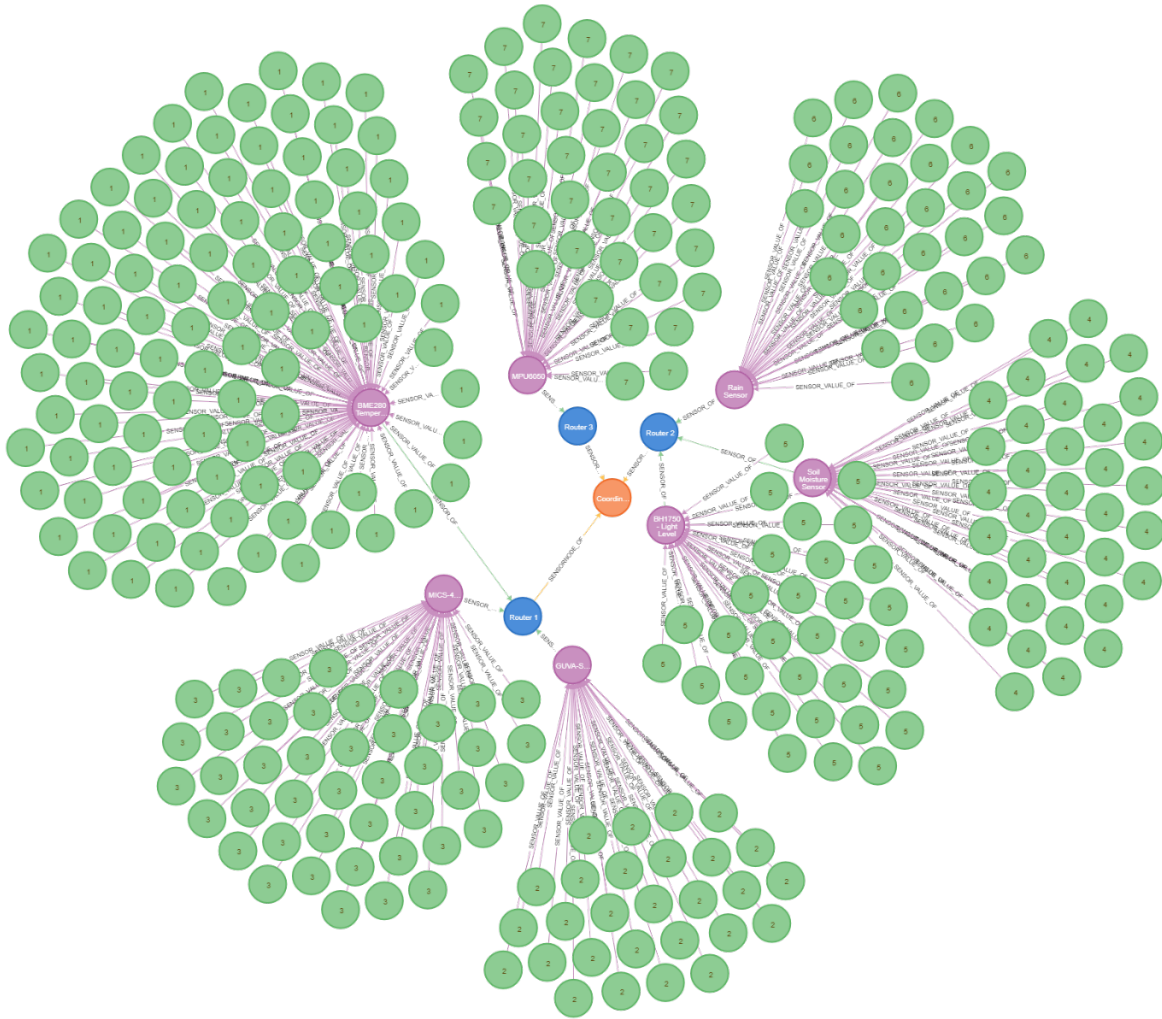


Figure 6: Storing sensor data in Neo4j Graph Database

**SPARQL Query**

You can write your SPARQL statements using this form.

DataAcquisitionForms.rdf
DataAcquisitionFormsProperties.rdf
Ontologies.rdf
SensorData.rdf

SELECT \* WHERE {{{ ?s ?p ?o }}}}

Execute

Figure 7: SPARQL query service

Created RDF datasets might be manipulated using SPARQL query language through SPARQL query service, which is represented in Figure 7. This service filters files in compliance with the “.RDF” extension and creates buttons for each of them. Stakeholders should click to load the relevant dataset on SPARQL query service engine. After the loading process is completed, it should be written to execute the query into the text area.

## 5. Conclusion and Future Work

In this paper, authors proposed a multi-layered open data processing system that consists of different layers and components. All layers and its components were explained; and an implementation regarding sensors was developed and summarized in the implementation section. Authors examined only one aspect



in this implementation. However, there are four other aspects in terms of heterogeneous data sources. These other aspects are worth discussing and examining in the future. Also, authors tried to justify the suitability of the data life cycle in terms of the proposed multi-layered model by implementing the wireless sensor network system. Authors feel that this study enhances academic understanding of creating a multi-layered open data processing model. However, the life cycle of other data from other data sources should be examined and justified for viability. In addition, authors mentioned creating hazelnut ontology, but did not its development and description. As a future work, an ontology for hazelnut shall be created and adapted to the model. In addition, authors are planning to develop an open data platform based on the proposed model. Stakeholders will be able to create data acquisition forms using agricultural trait dictionaries to gather structured data regarding the relevant agricultural product without requiring strong technical skills. The platform will allow obtaining environmental data from heterogenous sensors and will be able to map these sensor measurements with relevant classes of agricultural trait dictionaries. By this means, domain-specific data will be able to be published in varied open formats using the developed platform. A number of restrictions of this study and areas for future research should be mentioned; and the following ones might be given as examples: difficulty of gathering data from farmers (lack of knowledge of technology usage), defining the boundaries of gathering market data, determining the potential data sources, which is defined as “*Other Data Sources*” in heterogeneous data sources layer, and spreading the usage of applications mentioned in “*Applications Layer*”.

### Conflict of Interest

The authors declare no conflict of interest.

### Acknowledgment

This project is partly supported by Scientific Research Fund (2018-BAP-14) of Kadir Has University.

### End notes

Web-based Open Data Platform can be accessed using the following URL: <http://www.opendatainagriculture.com/>

### References

- [1]. Ş. Aydın, U. Ünal and M. N. Aydın, "Open Data in Agriculture: Sustainable Model Development for Hazelnut farms using semantics," 2018 6th International Conference on Control Engineering & Information Technology (CEIT), Istanbul, Turkey, 2018, pp. 1-6. doi: 10.1109/CEIT.2018.8751875
- [2]. Melissa J. Perry, Agricultural Health and Safety, Editor(s): Stella R. Quah, International Encyclopedia of Public Health (Second Edition), Academic Press, 2017, Pages 38-44, ISBN 9780128037089
- [3]. Agriculture and Food. [online] Available at: <http://www.invest.gov.tr/en-US/sectors/Pages/Agriculture.aspx> [Accessed 21.07.2018].
- [4]. Turkey's Hazelnut. [online] Available at: <http://www.ftg.org.tr/en/turkish-hazelnutturkeys-hazelnut.html> [Accessed 21.07.2018].
- [5]. Fındık Veriminde ve Üretiminde Temel Sorunlar. [online] Available at: <http://www.findikihracati.com/findik/findik-veriminde-ve-uretiminde-temel-sorunlar.html> [Accessed 21.07.2018].
- [6]. Peter Murray-Rust, Open Data in Science, Serials Review, 34:1, 52-64, 2008, <https://doi.org/10.1080/00987913.2008.10765152>.
- [7]. Carolan, L., Smithy, F., Protonotarios, V., Schaap, B., Broad, E., Hardinges, J., Gerry, W., 2015, How can we improve agriculture, food and nutrition with open data? , Open Data Institute.
- [8]. I. Szilagyı and P. Wira, "Ontologies and Semantic Web for the Internet of Things - a survey," IECON 2016 - 42nd Annual Conference of the IEEE

- Industrial Electronics Society, Florence, 2016, pp. 6949-6954. <https://doi.org/10.1109/IECON.2016.7793744>.
- [9]. Berners-Lee, T., 2006, Linked Data, <https://www.w3.org/DesignIssues/LinkedData.html> [Accessed 23.07.2018].
- [10]. SPARQL 1.1 Query Language. [online] Available at: <https://www.w3.org/TR/2013/REC-sparql11-query-20130321/> [Accessed 23.07.2018].
- [11]. Lata, Swaran & Sinha, Bhaskar & Kumar, Ela & Chandra, Somnath & Arora, Raghu, Semantic Web Query on e-Governance Data and Designing Ontology for Agriculture Domain. International Journal of Web & Semantic Technology. 4., 2013 <http://doi.org/10.5121/ijwest.2013.4307>.
- [12]. Resource Description Framework. [online] Available at: <https://www.w3.org/RDF/> [Accessed 23.07.2018]
- [13]. Available at: <http://www.turkstat.gov.tr/UstMenu.do?metod=gorevYetki> [Accessed 24.07.2018].
- [14]. Agricultural Marketing. [online] Available at: [https://en.wikipedia.org/wiki/Agricultural\\_marketing](https://en.wikipedia.org/wiki/Agricultural_marketing) [Accessed 24.07.2018]
- [15]. Mell, P., G., Tim, 2018, National Institute of Standards and Technology, Information Technology Laboratory – a nonregulatory federal agency within the U.S. Department of Commerce – <http://csrc.nist.gov/groups/SNS/cloud-computing>.
- [16]. Aisha Siddiqa, Ibrahim Abaker Targio Hashem, Ibrar Yaqoob, Mohsen Marjani, Shahabuddin Shamsirband, Abdullah Gani, Fariza Nasaruddin, A survey of big data management: Taxonomy and state-of-the-art, Journal of Network and Computer Applications, Volume 71, 2016, Pages 151-166, ISSN 1084-8045, <https://doi.org/10.1016/j.jnca.2016.04.008>.
- [17]. I. Taleb, R. Dssouli and M. A. Serhani, "Big Data Pre-processing: A Quality Framework," 2015 IEEE International Congress on Big Data, New York, NY, 2015, pp. 191-198. <https://doi.org/10.1109/BigDataCongress.2015.35>.
- [18]. Zhong Y, Fong S, Hu S, Wong R, Lin W. A Novel Sensor Data Pre-Processing Methodology for the Internet of Things Using Anomaly Detection and Transfer-By-Subspace-Similarity Transformation. Sensors (Basel). 2019;19(20):4536. Published 2019 Oct 18. <https://doi.org/10.3390/s19204536>.
- [19]. Jason J. Jung, Semantic preprocessing for mining sensor streams from heterogeneous environments, Expert Systems with Applications, Volume 38, Issue 5, 2011, Pages 6107-6111, ISSN 0957-4174 <https://doi.org/10.1016/j.eswa.2010.11.017>.
- [20]. E. Begoli and J. Horey, "Design Principles for Effective Knowledge Discovery from Big Data," 2012 Joint Working IEEE/IFIP Conference on Software Architecture and European Conference on Software Architecture, Helsinki, 2012, pp. 215-218, <https://doi.org/10.1109/WICSA-ECSA.2012.32>.
- [21]. Thomas R. Gruber, Toward principles for the design of ontologies used for knowledge sharing?, International Journal of Human-Computer Studies, Volume 43, Issues 5-6, 1995, Pages 907-928, ISSN 1071-5819, <https://doi.org/10.1006/ijhc.1995.1081>.
- [22]. N. F. Noy and C. D. Hafner, "The State of the Art in Ontology Design: A Survey and Comparative Review", AIMag, vol. 18, no. 3, p. 53, Sep. 1997, <https://doi.org/10.1609/aimag.v18i3.1306>.
- [23]. Cristani, Matteo & Cuel, Roberta, A Survey on Ontology Creation Methodologies. Int. J. Semantic Web Inf. Syst.. 1., 2005, 49-69. 10.4018/jswis.2005040103.
- [24]. LNCS About AGROVOC Page. [online] Available at: <http://aims.fao.org/standards/agrovoc/concept-scheme>, last [Accessed 2019/01/15].
- [25]. Dean Allemang, Jim Hendler, Chapter 10 - SKOS—managing vocabularies with RDFS-Plus, Editor(s): Dean Allemang, Jim Hendler, Semantic Web for the Working Ontologist (Second Edition), Morgan Kaufmann, 2011, Pages 207-219, ISBN 9780123859655, <https://doi.org/10.1016/B978-0-12-385965-5.10010-X>.
- [26]. LNCS SKOS Simple Knowledge Organization System eXtension for Labels (SKOS-XL). [online] Available at: <https://www.w3.org/TR/skos-reference/skos-xl.html>, [Accessed 2019/01/15].
- [27]. Koksall, A. I., Gunes, N., Descriptors for Hazelnut, Bioversity International and FAO, 2008.
- [28]. Pollock, J., T.: Semantic Web for Dummies. 1st edn. Wiley Publishing, Inc., Canada, 2009, ISBN: 978-0-470-39679-7.
- [29]. Luo Y., Picalausa F., Fletcher G.H.L., Hidders J., Vansummeren S., Storing and Indexing Massive RDF Datasets. In: De Virgilio R., Guerra F., Velegrakis Y. (eds) Semantic Search over the Web. Data-Centric Systems and Applications. Springer, Berlin, Heidelberg, 2012, [https://doi.org/10.1007/978-3-642-25008-8\\_2](https://doi.org/10.1007/978-3-642-25008-8_2).
- [30]. XML Web Services. [online] Available at: [https://www.w3schools.com/xml/xml\\_services.asp](https://www.w3schools.com/xml/xml_services.asp) [Accessed 25.07.2018].
- [31]. DIGI International Inc., XBee/XBee-PRO S2C Zigbee RF Module User Guide, 2018

## Methodology for Assessing Synchronization Conditions in Telecommunication Devices

Juliy Boiko<sup>\*1</sup>, Ilya Pyatin<sup>1</sup>, Oleksander Eromenko<sup>2</sup>, Oleg Barabash<sup>3</sup>

<sup>1</sup>*Khmelnytskyi National University, Department of Telecommunications and Radio Engineering, 29016, Ukraine*

<sup>2</sup>*Khmelnytskyi National University, Department of Physics and Electrical Engineering, 29016, Ukraine*

<sup>3</sup>*State University of Telecommunications, Department of Mathematics, 03110, Ukraine*

### ARTICLE INFO

*Article history:*

*Received: 11 January, 2020*

*Accepted: 10 March, 2020*

*Online: 23 March, 2020*

*Keywords:*

*Synchronization*

*Modulation*

*Dispersion of Error*

*Interpolation*

*Timing Error*

*Signal to Noise Ratio*

### ABSTRACT

*This paper represents analysis of principles providing maximally reliable delay estimation of signal synchronization devices in telecommunication. Clock synchronization schemes on the base of stochastic models, graph-analytic interpretation, analytical functional description and their parameters selection in case of real complex hindrance are analyzed. Dependences between dispersion of maximally reliable estimation of synchronization devices and signal to noise ratio (SNR) are represented. Analytical expressions and dependences are obtained for deviation of synchronization error with respect to SNR at the output of discriminator. Diagrams of state are formed for assessment of digital synchronization device in case of error state. Calculated error of numerical solution of the equation of a stationary grid method. We obtain the schedule of the distribution of the probability density synchronization errors for different values of the normalized time. The functions performed by the symbolic synchronization circle, features of the construction of the timing error detector (TED) are analyzed. The Gardner, Early-Late, Mueller & Muller TED, their error and the S-curve equation are investigated. The dependence of the relative timing error on the SNR is obtained. The article examines the effects of interpolation and decimation conditions in the forming filters of digital communication systems.*

## 1. Introduction

This paper is an extension of work originally presented in conference name "Quality Assessment of Synchronization Devices in Telecommunication" that is published in 2019 IEEE 39th International Conference on Electronics and Nanotechnology (ELNANO) [1].

The proposed paper (additionally) presents experimental results for evaluating the effect of interpolation conditions and decimation for energy gain of telecommunication facilities on phase shift keying modulation, as well as comparative analysis of error detectors of symbol synchronization of coherent communication network with QPSK modulation has done.

The main purpose of the presented results is to supplement and summarize information on the specifics and nature of synchronization conditions in the means of determining the factors

<sup>\*</sup>Corresponding Author : Juliy Boiko, Khmelnytskyi National University, 29016 Ukraine, [boiko\\_julius@ukr.net](mailto:boiko_julius@ukr.net)

that qualitatively influence the factors contributing to the noise immunity of modern information processing systems [2,3]. The coherent and quasicohherent methods for signal receiving require phase locked loop (PLL) frequency as obligate component which forms the reference signal from the received oscillation [4]–[6]. To receive discrete information a system needs clock, word and frame synchronization. The important task of synchronization, which is to form reference oscillation at the receiving side of wireless connection, in most of the cases, becomes complicated due to influence of noise, which distorts the received signal, and in some cases due to random character of the signal itself [2].

Such events entail fluctuational phase deviation, which is formed by reference oscillation synchronization system. The effectiveness of data transmission lowers consequently because of losses in transmission of data required for not only synchronization but also for the signal search time and transition onto monitoring mode for all synchronization systems of the receiver. This raises the question of improving synchronization system especially in

case of using in communication systems frequency, phase and quadrature methods of digital modulation [7]–[9].

Papers [4,5] represent linear and nonlinear analysis of clock synchronization devices. Probability of acquisition and probability of cycle slip are estimated. The main factors, which increase an error in increasing and decreasing reliability of system synchronization in time, are analyzed.

The represented research is conducted in progress of results published in [3]–[6]. We use various stochastic models with expanded technical interpretation of Markov’s modeling, cumulant method and method for statistic linearization. Besides, upgrading circuit structure of the manipulated signal receiver in order to optimize it by using solutions aimed at removing reverse effect, synthesis of the receiver structure with synchronization devices and defining character of signal to noise ratio influence on accuracy of synthesized clock synchronization devices are important.

The research outcome represents novelty, which consists in using stochastic model to describe synchronization error. Significance of the research consists in estimating clock transition distribution density. The criteria and algorithm is developed to provide optimal operation of synchronizer in condition of hindrance.

## 2. Stochastic Model of Synchronization System

### 2.1. Semigraphical Interpretation of Clock Synchronization Systems

In article [1], [7], a stochastic model of a synchronization system was proposed. Model of synchronization system is described by stochastic equations in accordance to the scheme Fig. 1. The following symbols are used:  $\xi=\xi(t)$  - input influence,  $\hat{\xi}=\hat{\xi}(t)$  - influence assessment,  $\gamma = \gamma(t) = (\xi(t) - \hat{\xi}(t))/T$  - normalized synchronization error,  $\rho(\gamma)$  - discriminatory characteristics,  $h(\gamma)$  - fluctuation characteristics,  $n(t)$  - Gaussian white noise,  $f(\varepsilon)$  - transient pulse function of the linear dynamic element, which describes the effect of processing output signal and adjustment of the clock generator frequency Fig.1.

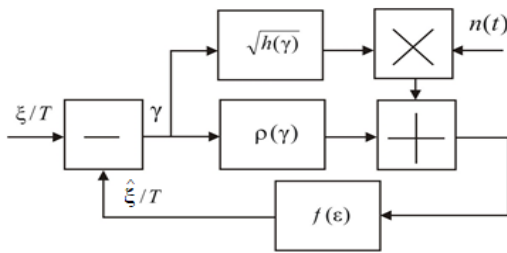


Figure 1: The research clock synchronization scheme

Assumption is made that: the influence is slow process, stable due to large amount of symbol intervals; assessment of the target influence is a slow process; normalizing random processes and fluctuation of discriminator’s output signal is the condition to be used; spectral density  $G(\omega, \gamma)$  is assumed stable in the tract transmission frequency band  $G(0, \gamma)$  and fluctuation component is represented as the white noise.

The synchronization system is described as automatic control system. The input influence is represented as  $r(t)=U(t)+n(t)$ . The

signal is represented analogously as the following:  $U(t) = U_0 \sum_i S_i h(t - iT - \xi)$ ,  $h(t)=1, 0 \leq t \leq T, h(t)=0, t \in (0, T)$ .

Thus, the pulses sequence is given  $U_0$  - having rectangular form  $h(t)$ , which represents binary character data stream  $S_i \in \{+1, -1\}$ ,  $n(t)$  - Gaussian white noise. The research is conducted in order to identify discriminatory and fluctuational characteristics. The synchronization error is specified by  $\gamma = (\xi - \hat{\xi})/T$ . The pulse sequences to identify synchronization error are represented in Fig. 2.

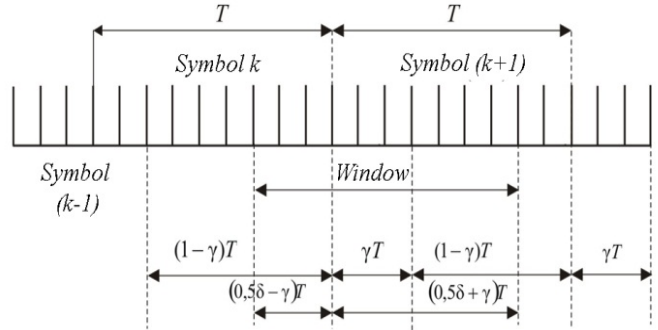


Figure 2: Pulse sequences in synchronization system

The dispersion of fluctuational error in synchronization system is to be defined using the equation of Markov’s random process, which density of probability distribution  $P=P(\gamma, t)$  is expressed by Fokker-Planck equation [10,11]:

$$\frac{d\gamma}{dt} + k\alpha(\gamma) = k\sqrt{h(\gamma)}n(t), \quad 0 \leq t, \quad (1)$$

$$\gamma(0) \sim P_0(\gamma).$$

where  $P_0(\gamma)$  - initial density distribution of synchronization error.

$$\frac{\partial P}{\partial t} = -\frac{\partial}{\partial \gamma}(A(\gamma)P) + \frac{1}{2} \frac{\partial^2}{\partial \gamma^2}(Z(\gamma)P), \quad P(\gamma, 0) = P_0(\gamma) \quad (2)$$

where  $U_0(\gamma)=-k\alpha(\gamma)$ ,  $Z(\gamma)=k^2S(0, \gamma)$ .

The solution of equation (2) at synchronization system stationary mode  $\frac{\partial P}{\partial t} = 0$  is found as:

$$P(\gamma) = c^{-1} \exp\left(-\int_0^\gamma \frac{2h_0^2\chi_0\alpha_n(U) + dh(U)/dU}{h(U)} dU\right), \quad |\gamma| \leq 1/2 \quad (3)$$

where  $\chi_0=4/U_0kT$  - parameter opposite to normalized noise band of the synchronization system linear model [12]-[15];

$c = 2 \int_0^{1/2} \exp\left(-\int_0^\gamma \frac{2h_0^2\chi_0\alpha_n(U) + dh(U)/dU}{h(U)} dU\right) d\gamma$  - normalizing constant.

Synchronization system accuracy is assessed by dispersion of normalized synchronization error:

$$\sigma_\gamma^2 = 2 \int_0^{1/2} \gamma^2 P(\gamma) d\gamma \quad (4)$$

The mathematical modeling will be performed and error dispersion influence will be assessed in dependence on signal to noise ratio for some values of  $\chi_0$  parameter. In particular Fig. 3 demonstrates assessment carried out for  $\delta_0 = \delta_{0opt}(h_0^2)$ .

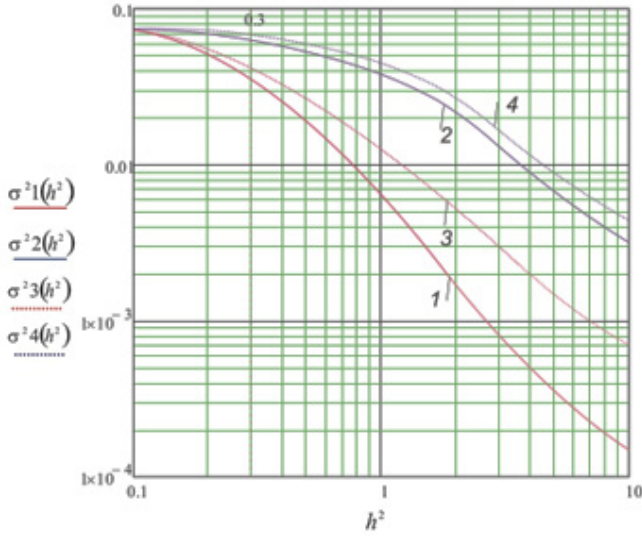


Figure 3: Graphs of dispersion error  $\sigma_\gamma^2$  dependence on signal to noise ratio  $h^2$ : 1-  $\chi_0=100, \delta_0 \rightarrow opt$ ; 2-  $\chi_0=25, \delta_0 \rightarrow opt$ ; 3-  $\chi_0=100, \delta_0=1$ ; 4-  $\chi_0=25, \delta_0=1$

The conducted research has indicated that in case of narrowing synchronization system band the dispersion of fluctuational error reduces. In Fig. 3 solid lines 1 and 2 demonstrate effect that the window width minimizes synchronization error dispersion for each value of signal to noise ratio, however lines 3 and 4 demonstrate constant width of the window.

Analysis of transition mode of synchronization system can be done with the use of numerical solving Fokker-Planck equation by grid method when distribution density of synchronization error changes. The equation (5) will be used with inserting normalized time  $t_H = 4\omega t$ , where  $\omega = k_1 k_2 U_0 T / 4$  - noise band of linear model of synchronization system. In this case the canonic form of stochastic Fokker-Planck equation for distribution density  $P = P(\gamma, t_H)$  can be written.

$$\frac{\partial P}{\partial t_H} = \frac{\partial}{\partial \gamma} (\alpha(\gamma)P) + \frac{1}{D_0} \frac{\partial^2}{\partial \gamma^2} (h(\gamma)P), \quad (5)$$

$$t_H \geq 0, \quad P(\gamma, t_H) = P(\gamma \pm 1, t_H), \quad P(\gamma, 0) = 1$$

In the research the distribution density of the initial condition will be assumed uniform,  $D_0 = 2h_0^2 / \omega T$  - equation parameter,  $\Delta F_{nor} = \omega T$  - normalized noise band.

Stationary solution of equation (5) is used for numerical solution (2) by grid method. The essence of this method is in inserting the grid having nodes  $x_k = x_0 + k\xi$ ,  $k=0, \pm 1, \pm 2, \dots, \pm N$ ,  $x_0=0$ ,  $\xi = 1/2N$ ,  $t_l = t_0 + \delta_l$ ,  $l=0, 1, 2, \dots$ ,  $\tau_0=0$ ,  $\xi, \delta$  - grid. The grid function is represented as  $\hat{h}_{k,l} = \hat{h}(\gamma, t_H)$  when  $\gamma = x_k$ ,  $t_H = t_l$  and differential

operators are replaced with difference ones. Initial conditions are:  $P_{k,0}=1$ ,  $k \in (0, \pm N)$ ,  $P_{-N,l} = P_{N,l}$ ,  $P_{N+1,l} = P_{-N+1,l}$ ,  $P_{-N-1,l} = P_{N-1,l}$ . References testify that solution is possible to find at the new layer on conditions mentioned above [16]. The stability condition of the difference scheme is worthy to mention:  $\delta/\xi^2 < D_0/2$ .

The equation (5) rewritten with recurrent formulas becomes:

$$P_{k,l+1} = P_{k,l} + \frac{\delta}{2\xi} (\alpha_{k+1} P_{k+1,l} - \alpha_{k-1} P_{k-1,l}) + \frac{\delta}{D_0 \xi^2} (h_{k+1} P_{k+1,l} - 2h_k P_{k,l} + h_{k-1} P_{k-1,l}) \quad (6)$$

$$l=0, 1, 2, \dots \quad \omega(\varphi, \tau) = 1/2\pi \cdot (\text{ch}\tau - \text{ch}\tau \cdot \cos\varphi)$$

The error should be assessed by comparing grid functions of two types – the accurate and the numerical solutions; and by finding  $\Delta = (\omega_n(\varphi, \tau) - \omega_a(\varphi, \tau)) / \omega_a(\varphi, \tau) \cdot 100\%$  along the layers in nodes of selected grid.

This approach will be used to assess error of clock synchronization. Fig. 4 shows transient process, Fig. 5 – dependences of numerical solution (6), and Fig. 6 represents graphs, which describe process of setting on stationary mode at error probability  $p_0 = 10^{-3}$ , in case of minimum shift keying (GMSK) digital modulation [1].

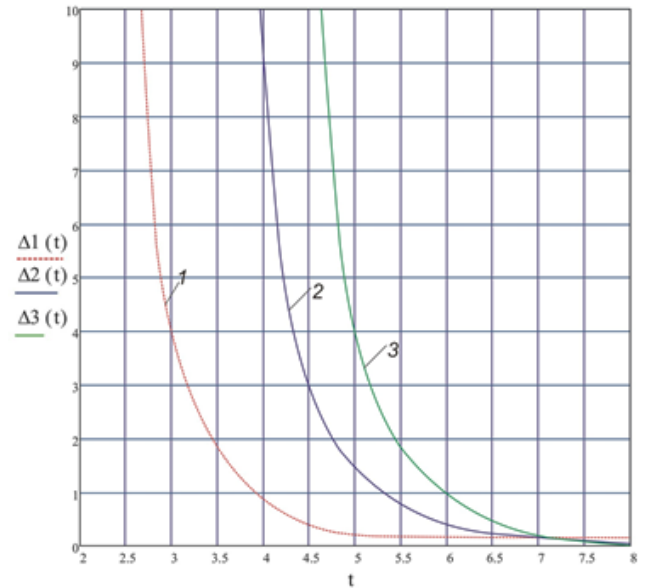


Figure 4: Graphs of transient processes  $t_H$  (condition:  $p_0=10^{-3}$ ): 1-  $\omega t = 5 \cdot 10^{-2}$ ; 2-  $\omega t = 1 \cdot 10^{-2}$ ; 3-  $\omega t = 1 \cdot 10^{-3}$

Modeling parameters are:  $\Delta F_{nor} = 5 \cdot 10^{-2}$ ;  $\xi = 0.01$ ,  $\delta = 0.001$ .

The research has identified less than one percent error in numerical search of solution using grid method Fig. 5.

The research results in form of graphs which describe transient process for the value of SNR that corresponds to error probability  $p_0 = 10^{-3}$  (Fig. 6) and assessed dependences of transient process duration in a system in case of deviation of current dispersion  $\sigma_{current}^2$  of synchronization error on its value in stationary mode  $\sigma_{stationary}^2$ , testify that in case of narrowing band in synchronization



system, what means reducing monitoring error, the transient process time gets increased (Fig. 4).

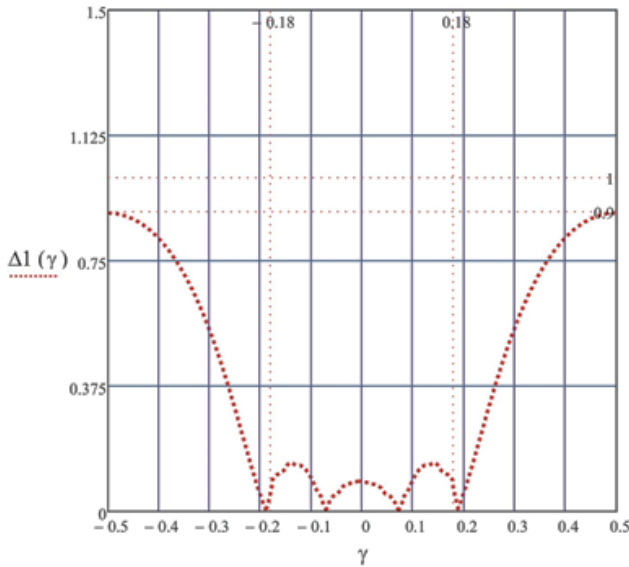


Figure 5: Numerical stationary solutions by grid method:  $\Delta l$  - given in percent's

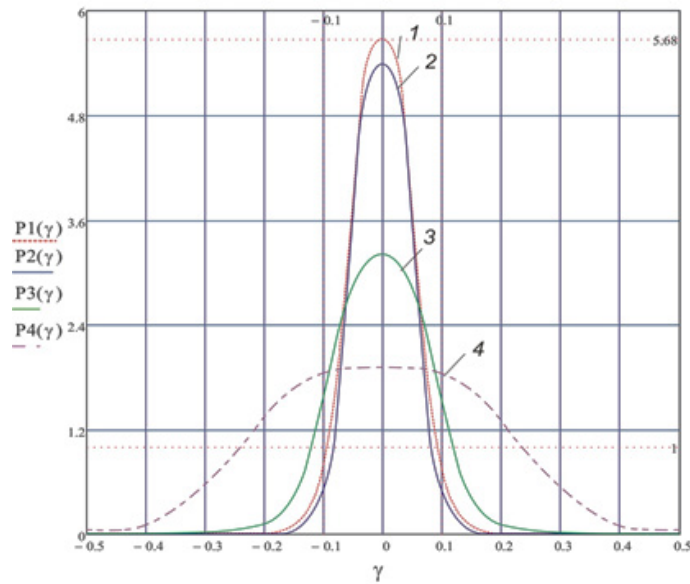


Figure 6: Graphs of density of probability distribution at different values of normalized time  $t_H$  (condition:  $p_0=10^{-3}$ ,  $\omega t=5 \cdot 10^{-2}$ ): 1 - stationary state; 2 -  $t_H=2$ ; 3 -  $t_H=1$ ; 4 -  $t_H=0.5$

Besides, in case when the band of synchronization system changes then getting on stationary mode goes with larger number of symbols.

### 3. Investigation Inaccuracy of Symbol Timing Error Detector

In the modern digital communication system, the sampling rate plays an important role. High-speed signal processing can be implemented by usage of digital converters with increasing or decreasing sampling rate [17].

An important part of the digital interface used for radio frequency communication systems is the frequency converter

(FC). The FC main function is to convert one or more data channels from the main band format into a radio signal consisting of modulated carriers belonging to a set of one or more mentioned radio frequencies. This is achieved in two stages: increasing the sampling rate by interpolation, providing spectrum generation and suppressing interpolation images by filtration and shifting the spectrum of the signal to the desired carrier frequencies using a multiplier and a heterodyne [18,19].

#### 3.1. Symbol Timing Recovery Circuit

The symbol timing recovery circuit has the block diagram shown in Fig. 7. Time synchronization is performed using a PLL consisting of three main units: TED, contour filter and interpolation control [20, 21].

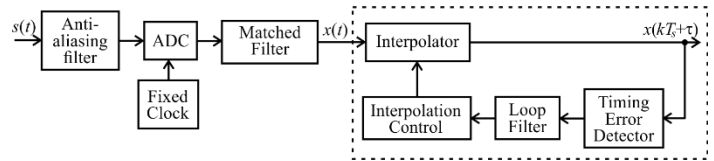


Figure 7: Structural diagram of the symbolic synchronization circle

The figure  $x(t)$  shows signal sampling after the matched filter;  $x(kT_s + \tau)$  is a symbolic signal adjusted for the offset of the clock signal between the transmitter and receiver.

The purpose of characters synchronization is to create  $N$  samples at the output of the matched filter for each character interval so that one of the samples is aligned with the maximum opening of the eye-diagram [7]. A sample rate of the received signal  $u(t)$  is received at a fixed rate  $1/T$ , which is asynchronous with the rate of symbols transmission. The ADC generates samples of the input signal at a rate of  $N$  samples per symbol. The  $N$ -th count of this signal can be represented by the expression:

$$r(nT) = G_a \sum_m a(m) p(nT - mT_s - \tau) + w(nT)$$

The time delay  $\tau$  is estimated by samplings  $x(nT)$  which are asynchronous samplings at the output of the matched filter. Samples are not aligned in characters. The role of symbol synchronization over time is to "move" samples to the right moments. Another name for "moving" samplings over time is interpolation [20]. Because the time synchronizer must adapt to an unknown time delay, the interpolator must be adaptive. With proper operation, the interpolator generates agreed output filter signals that are aligned across characters and optimal sampling points.

The main disadvantage of the scheme shown in Fig. 7, is an interpolation jitter that occurs when  $T_s \neq NT$ . In this case the result of the interpolation is displayed in average for each  $N$  sample. But on condition of  $T_s \neq NT$ , the fractional timing error accumulates and as a result it reaches the value of the character length. At a time when this is happening the interpolator outputs  $N-1$  of the samples or  $N+1$  after the previous interpolated samples to compensate for the difference depending on the sign of the fractional timing error. This interpolation jitter is particularly problematic if the data bits need to be retransmitted synchronously to some other destination.

In general, the TED generates an error signal once for each character based on the current synchronization estimate and using

the matched filter input  $r(nT)$  and the matched filter output  $x(nT)$ . In other words, the discrete-time error signal is updated with a frequency of characters.

It can be supposed that there is an ideal interpolator that calculates the interpolation polynomial  $x(kT_s + \hat{\tau})$  using the estimation  $\hat{\tau}$  of the time delay and the output signals of the matched filter. The interpolation polynomial can be represented by the expression:

$$x(kT_s + \hat{\tau}) = K \sum_m a(m)r_p((k-m)T_s - \tau_e) + v(kT_s + \hat{\tau}) \quad (8)$$

where  $\tau_e = \tau - \hat{\tau}$  is a timing error and  $K = G_d/T$ . The TED generates a signal that is a function of the timing error  $\tau_e$ . The TED output signal  $e(kT_s)$  is a function of the interpolated output signals of the matched filter and the data symbols (or their estimates). The TED characteristics are described by the  $S$ -curve  $g(\tau_e)$ .

Symbolic synchronization relies on a change of data sign when determining a synchronization error signal. For a QPSK modulation communication system the error signal oriented to symbol-synchronization system solution is determined by the expression:

$$e(k) = \text{sign}\{a_0(k)\} \dot{x}(kT_s) + \text{sign}\{a_1(k)\} \dot{y}(kT_s) \quad (9)$$

where  $\dot{x}(kT_s)$  and  $\dot{y}(kT_s)$  - are derivatives in time outputs of respectively common-mode and quadrature matched filters.

### 3.2. Error Signal Characteristics

The derivative of the correlation function of the matched filter is shown in Fig. 8.

This error signal is derived from an estimate of the maximum likelihood of synchronization bias. The operation of a derivative obtaining can be replaced by the structure of management of early-late counts for both common-mode and quadrature components.

Character synchronization according to Gardner is a non-data feedback method. The timing error detector requires at least two samples per symbol, one of which is the point where a decision can be made.

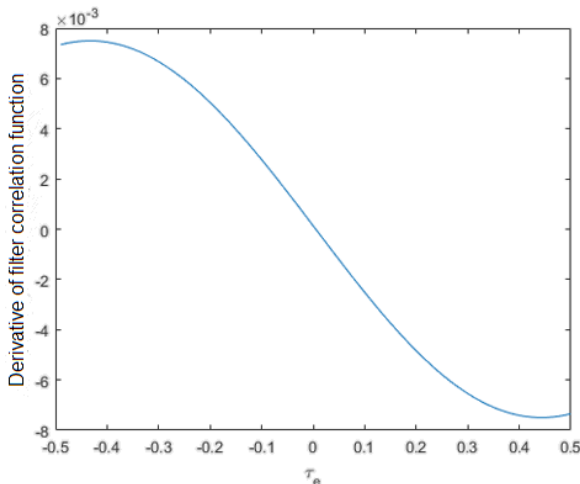


Figure 8: Derivative of autocorrelation function of spectral raised-cosine pulse type filter

The Gardner timing error detector is based on the detection of zero crossing on eye diagrams and is designed to work with BPSK and QPSK [7].

For a Gardner detector at arbitrary fixed  $\hat{\tau}$ , the synchronization error  $e(k)$  is independent of any rotation of the carrier phase [17]. The Gardner TED has an error signal defined by the expression:

$$e(k) = x((k-1/2)T_s + \hat{\tau}) [x((k-1)T_s + \hat{\tau}) - x(kT_s + \hat{\tau})] \quad (10)$$

$S$ -curve for GTED turns out by transformation  $e(k)$  through  $\tau_e$  and calculating the desired value:

$$g(\tau_e) = K^2 E_{avg} \sum_m r_p((m-1/2)T_s - \tau_e) [r_p((m-1)T_s - \tau_e) - r_p(mT_s - \tau_e)]$$

The Early-Late detector restores the phase of input character synchronization using a non-data feedback method.

The optimum moment of sampling signals coincides with the moment of maximum average eye-diagram opening. The maximum eye opening diagram occurs at a time when the average slope of the eye-diagram is zero. The nonzero slope at  $t = \tau$  are the points on the trajectory corresponding to the absence of the data sign change. Symbolic synchronization relies on data sign changes to get the correct synchronization error signal. The TED Early-Late works with 2 samples per symbol. The data-dependent detector synchronization error signal looks like:

$$e(k) = a(k) [x((k+1/2)T_s + \hat{\tau}) - x((k-1/2)T_s + \hat{\tau})]$$

where  $T_s$  - is usually chosen as a value that is conveniently represented by the sampling rate.

The  $S$ -curve for TED Early-Late is obtained by calculating the expected value of the error signal:

$$g(\tau_e) = KE_{avg} [r_p(T_s/2 - \tau_e) - r_p(-T_s/2 - \tau_e)] \quad (12)$$

Shedule of  $S$ -curve is shown in Fig. 9.

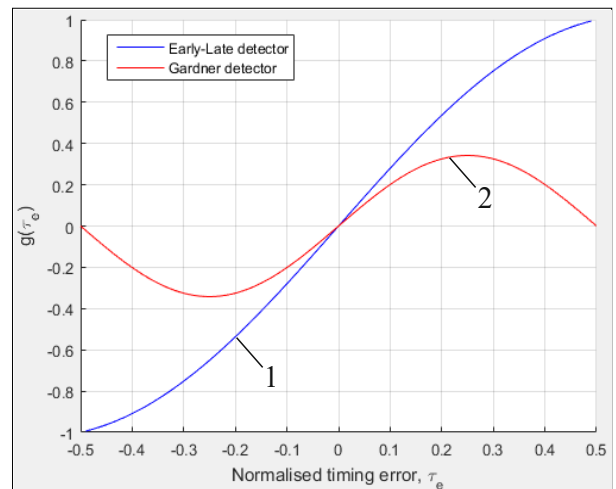


Figure 9:  $S$ -curve of detectors of timing error (1 – is a Early-Late detector; 2 – is a Gardner detector)

The Mueller & Muller detector implements a decision-oriented method of data-driven feedback that requires a preliminary restoration of the carrier phase [22]. The Mueller & Muller timing error detector operates on matched filter output signals generated at 1 sample per character. The symbol synchronization error signal is determined by the expression:

$$e(k) = a(k-1)x(kT_s + \hat{\tau}) + a(k)x((k-1)T_s + \hat{\tau}) \quad (13)$$

where  $\hat{\tau}$  - is the estimation of clock delay;  $x(kT_s + \hat{\tau})$  - is the interpolation polynom;  $a(k)$  - is the  $k$ -th received signal symbol;  $T_s$  - is the duration of the character;  $\tau$  - is the unknown time delay.

The  $S$ -curve is obtained by calculating the expected value  $e(k)$  for  $x(kT_s - \tau_e)$  and  $x((k-1)T_s - \tau_e)$ . The  $S$ -curve for the detector of data-dependent synchronization error is determined by the expression:

$$g(\tau_e) = KE_{avg} [r_p(T_s - \tau_e) - r_p(-T_s - \tau_e)] \quad (14)$$

The  $S$ -curve is the slope estimation of  $r_p(\tau_e)$  using the values  $r_p(t)$  of time symbol before and after  $-\tau_e$ . Since  $r_p(t)$  is an autocorrelation function, it is symmetric about  $\tau_e=0$ . As a result, the  $S$ -curve is zero at  $\tau_e=0$ .

The dependence schedule of the relative synchronization error on the SNR for the TED of Early-Late, Gardner and Mueller & Muller is shown in Fig. 10.

So, the relative synchronization error increases when the SNR is less than 10 dB. Early-Late TED has the most uniform dependence.

When demodulating digital signals, it is desirable that the sampling rate of the signal can be multiple of its keying rate (each character must have the same number of counting's). However, the sampling rate of the input signal from the ADC is generally fixed but the manipulation speed may change. The solution to this problem is the signal resampling.

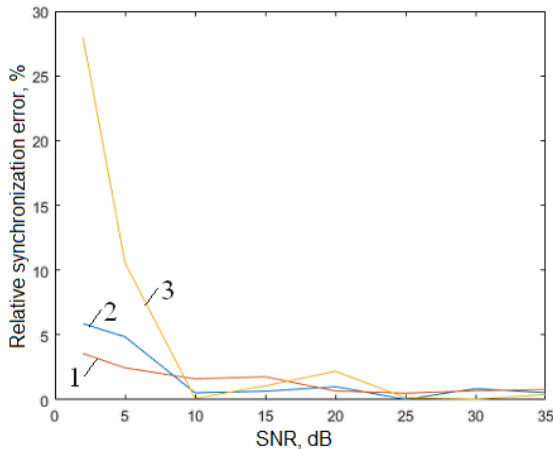


Figure 10: Dependency of relative synchronization error on the SNR for TED (1 - is the Early-Late detector; 2 - is the Gardner detector; 3 - is the Mueller & Muller detector)

#### 4. Conditions of Interpolation and Decimation Signals

The phase modulation techniques should be used to study the effect of conditions of interpolation and decimation signals on telecommunication facilities power.

The estimation should be carried out by determining the energy gain in case of change of the coefficients of interpolation and decimation of the agreed forming filters. Recommendations should be given as to the conditions for changing the coefficients and using the symbolic synchronization system to stabilize the modes of the digital communication system when using interpolation and decimation in the forming filters.

Background information for estimating the effect of interpolation and decimation signals on the power of telecommunications facilities with phase manipulation will be presented by noise immunity graphs (BER dependence on  $E_b/N_0$ ) and evaluation of signal processing quality by constellation diagrams (signal constellations: Scatter Plot) [7]. It is necessary to evaluate the dependencies of the bit error rate (BER) on the SNR ( $E_b/N_0$ ) for the different graphs of error synchronization detector and interpolation (decimation) coefficients in the forming filters.

Fig. 11, Fig.12 and Fig.13 show the results of the study of the bit error rate (BER) on the SNR ( $E_b/N_0$ ) at the coefficients of interpolation and decimation ( $k_i-d$ ) of matched forming filters equal to 10 and 50 for different types of modulation. Simulink models of digital systems with different types of modulation and different coefficients of interpolation and decimation ( $k_i-d$ ) of forming filters for QPSK modulation are investigated.

To achieve  $BER=10^{-4}$  when using QPSK modulation and increasing the interpolation coefficient - decimation of forming filters from 2 to 50, it is necessary to increase the ratio ( $E_b/N_0$ ) by 14 dB. The most energy-efficient is BPSK modulation. In this case, increasing the coefficients of interpolation and decimation from 10 to 50 requires an increase in the ratio ( $E_b/N_0$ ) by 7 dB for  $BER=10^{-5}$ .

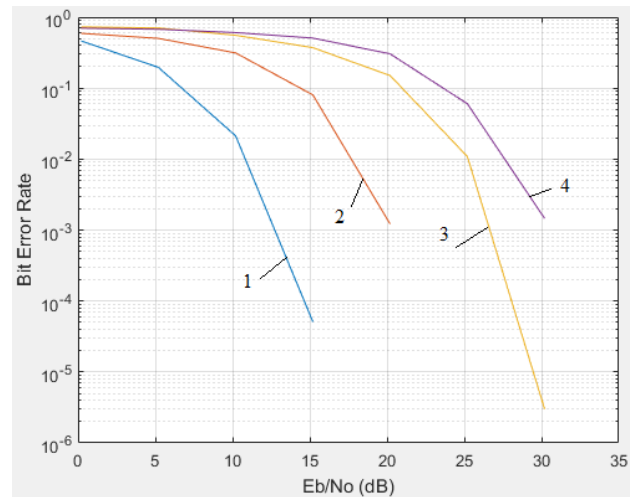


Figure 11: Noise immunity curves of communication system for QPSK modulation with interpolation and decimation coefficients ( $k_i-d$ ) of forming filters (1 -  $k_i-d=2$ ; 2 -  $k_i-d=10$ ; 3 -  $k_i-d=50$ ; 4 -  $k_i-d=100$ )

The timing error detector produces an error signal  $e$ , which is related to the difference between the unknown time offset  $\tau$  and the offset estimate in time space  $\hat{\tau}$ . The PLL adjusts the estimate  $\hat{\tau}$  so that it is close to the time offset  $\tau$  and reduces the error signal to zero. The logarithmic likelihood ratio  $L$  is differentiated with  $\tau$  to get the error signal and the equation  $dL/d\tau_e$  which is solved by PLL.

The Gardner detector and the Mueller-Muller detector are the most commonly used as a synchronization error detector.

The dependence of the bit error rate (BER) on the SNR ( $E_b/N_0$ ) for different timing error detector circuits and the interpolation and decimation coefficients 2 and 50 in the forming filters for QPSK modulation are shown in Fig.14 and Fig. 15.

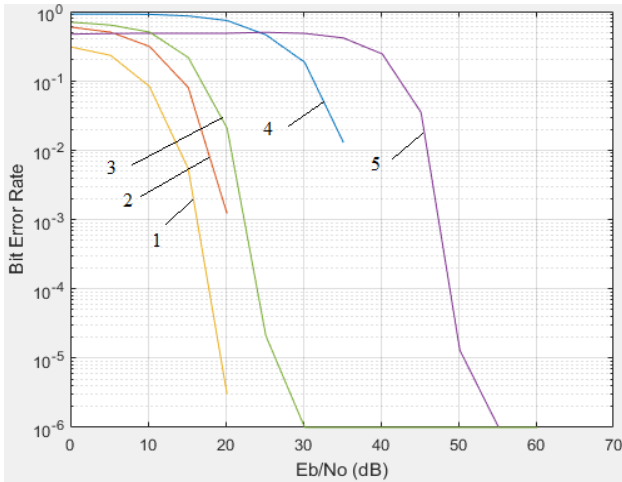


Figure 12: Noise immunity curves (Bit error rate (BER) on the SNR ( $E_b/N_0$ ) at  $k_r-d=10$  for modulation (1 – BPSK; 2 – QPSK; 3 – DQPSK; 4 – QAM-16; 5 - DBPSK)

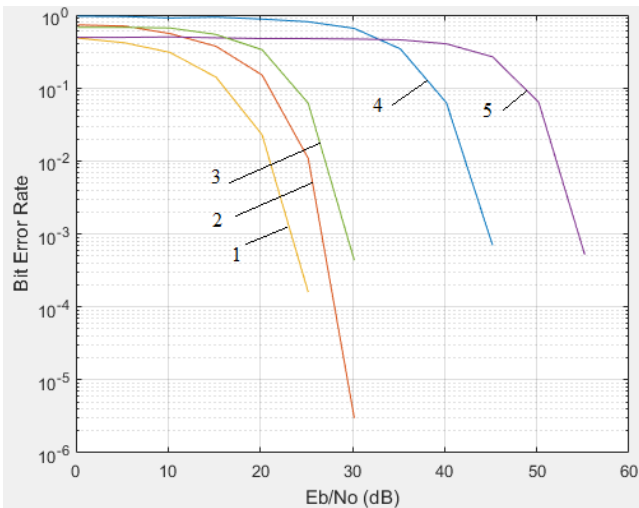


Figure 13: Noise immunity curves (Bit Error Rate (BER) on the SNR ( $E_b/N_0$ ) at  $k_r-d=10$  for different types of modulation (1 – BPSK; 2 – QPSK; 3 – DQPSK; 4 – QAM-16; 5 - DBPSK)

The Gardner detector has feedback that is unrelated to data and it is independent of carrier frequency recovery [23]. It is suitable for both basic bandwidth and modulated carrier systems. In the presence of noise, the effect of the resynchronizing method improves as the excess bandwidth increases (the recession rate for a spectral raised-cosine pulse type filter).

The Mueller-Muller detector has decision-making feedback that requires a prior restoration of the carrier phase. This method has no noise of its own when the input signal has Nyquist pulses (in the output of a spectral raised-cosine pulse type filter).

Fig. 16 a, b (Scatter Plot1, Scatter Plot2) presents a constellation diagram showing the signal constellation before and

after the symbolic synchronization circle and showing the effect of the synchronization error on the transmitted constellation [7], [24].

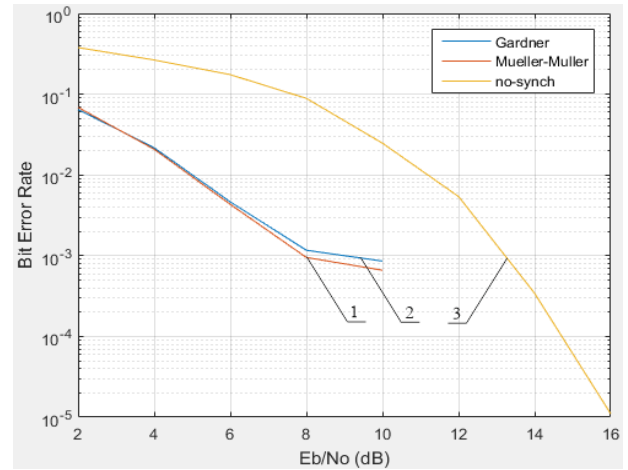


Figure 14: Noise immunity curves of communication system with QPSK modulation and  $k_r-d=2$  (1 – is a Mueller & Muller detector; 2 – is a Gardner detector; 3 – is the absence of symbol synchronization)

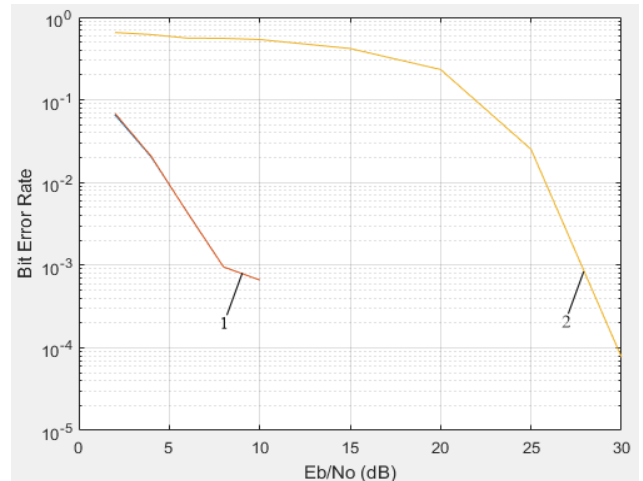


Figure 15: Noise immunity curves of communication system with QPSK modulation and  $k_r-d=50$  (1 – is a Gardner detector; 2 – is the absence of symbol synchronization)

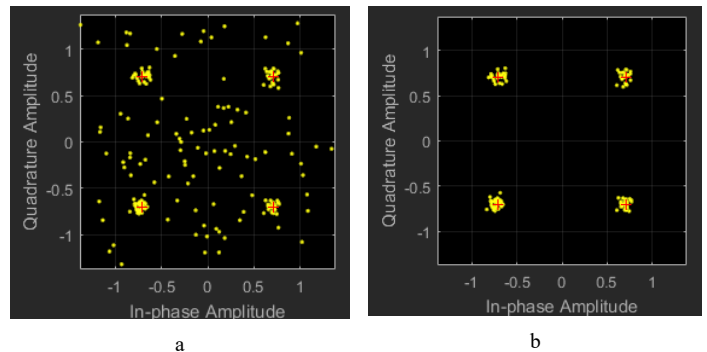


Figure 16: Constellation diagrams (a - Scatter Plot1; b - Scatter Plot2)

In the presence of noise, the output of the Mueller-Muller method improves as the excess pulse width ratio decreases and it is good for narrowband communication systems. The symbol synchronizer unit corrects the asymmetry of the clock pulses and restores the frame synchronization of the QPSK system, which has



a variable synchronization error [25,26]. For a signal to noise ratio of 20 dB, the resulting bit error rate is less than  $10^{-3}$ , indicating that the signal is being restored.

### 5. Conclusions

Paper represents obtained analytical and graphical research that bonds influence of SNR and accuracy of clock synchronization device on condition of their equal noise bands defined that at the level of  $\sigma^2_{\gamma}=10^{-3}$ . The benefit proposed methodology for of clock synchronization device makes almost 2.7 dB.

Studies of Mueller & Muller, Gardner, Early-Late timing error detectors have been performed. As the SNR decreases, there is an increase of the synchronization error. The Mueller & Muller detector has a 20% greater synchronization error than the Gardner and Early-Late detectors with a 2 dB SNR. The Early-Late detector has a larger S-curve, the most uniform dependence of the relative synchronization error on the SNR, which decreases from 4% to 1% with increasing SNR from 2 dB to 35 dB.

To achieve BER =  $10^{-4}$  when using QPSK modulation and increasing the interpolation-decimation coefficient of forming filters from 2 to 50, it is necessary to increase the ratio ( $E_b/N_0$ ) for 14 dB. The most energy-efficient is BPSK modulation. In this case, increasing the coefficients of interpolation and decimation from 10 to 50 requires an increase in the ratio ( $E_b/N_0$ ) by 7 dB for BER =  $10^{-5}$ .

To achieve the bit error rate BER =  $10^{-3}$  when using symbolic synchronization, it is possible to reduce the SNR of synchronization for the interpolation and decimation coefficient of the forming filters equal to 2. When the interpolation and decimation coefficient of forming filters increases up to 50, the SNR at the receiver input reduces to 20 dB. Thus, the introduction of a symbolic synchronization system helps to stabilize the operation of the digital communication system when using interpolation and decimation in forming filters.

### References

[1] J. Boiko, O. Eromenko, I. Kovtun, S. Petrushchuk, "Quality Assessment of Synchronization Devices in Telecommunication," in 2019 IEEE 39th International Conference on Electronics and Nanotechnology (ELNANO), Kyiv, Ukraine, 2019. <https://doi.org/10.1109/elnano.2019.8783438>.

[2] A. I. Semenko, N. I. Bokla, M. Y. Kushnir, G. V. Kosovan, "Features of creating based on chaos pseudo-random sequences," in 2018 14th International Conference on Advanced Trends in Radioelectronics, Telecommunications and Computer Engineering (TCSET), Slavske, Ukraine, 2018. <https://doi.org/10.1109/tcset.2018.8336383>.

[3] W. Wei, Z. Hongen, C. Suzhi, "Error Analysis and Correction of Time-Frequency Synchronization Based on Packet Switching," in 2017 International Conference on Dependable Systems and Their Applications (DSA), Beijing, China, 2017. <https://doi.org/10.1109/dsa.2017.40>.

[4] D.R. Stephens, Phase-Locked Loops for Wireless Communications, Springer, 2002.

[5] F. Brandonisio, M.P. Kennedy, Noise-Shaping All-Digital Phase-Locked Loops, Springer, 2014.

[6] S. Huang, S. Liu, M. Liu, J. Hu, Z. Zhu, "Low-Noise Fractional-N PLL With a High-Precision Phase Control in the Phase Synchronization of Multichips," IEEE Microwave and Wireless Components Letters, 28(8), 702-704, 2018. <https://doi.org/10.1109/lmwc.2018.2842680>.

[7] J. Boiko, V. Tolubko, O. Barabash, O. Eromenko, Y. Havrylko, "Signal processing with frequency and phase shift keying modulation in telecommunications," *Telkommika (Telecommunication Computing Electronics and Control)*, 17(4), 2025-2038, 2019. <http://dx.doi.org/10.12928/telkommika.v17i4.12168>.

[8] A. Rai, V. N. Kumar, "Wideband acquisition technique for QPSK demodulator," in 2016 IEEE International Conference on Recent Trends in Electronics, Information & Communication Technology (RTEICT), Bangalore, India, 2016. <https://doi.org/10.1109/rteict.2016.7807869>.

[9] L. Zhang, Z. He, "A modified timing synchronization algorithm for QPSK in digital receiver," in 2011 2nd International Conference on Artificial Intelligence, Management Science and Electronic Commerce (AIMSEC), Dengleng, China, 2011. <https://doi.org/10.1109/aimsec.2011.6011207>.

[10] P. Bondalapati, W. Namgoong, "Timing Jitter Distribution and Power Spectral Density of a Second-Order Bang-Bang Digital PLL With Transport Delay Using Fokker-Planck Equations," *IEEE Trans. on Very Large Scale Integration (VLSI) Syst.*, 27(2), 398-406, 2019. <https://doi.org/10.1109/tvlsi.2018.2878665>.

[11] W. Zhang, "An Analytical Solution of the Fokker-Planck Equation in the Phase-Locked Loop Transient Analysis," *IEEE Trans. on Communications*, 35(7), 773-775, 1987. <https://doi.org/10.1109/tcom.1987.1096849>.

[12] G. Hui, B. Chenghao, Z. Hongjun, L. Fanghui, L. Lei, "Synchronization Error Estimation of High-speed AD Sampling Based on Digital Phase Discrimination," in 2018 Cross Strait Quad-Regional Radio Science and Wireless Technology Conference (CSQRWC), Xuzhou, China, 2018. <https://doi.org/10.1109/csqrwc.2018.8455461>.

[13] H. Li, Z. Wang, H. Wang, "Research and implementation of high speed parallel carrier synchronization algorithm," in 2017 IEEE 9th International Conference on Communication Software and Networks (ICCSN), Guangzhou, China, 2017. <https://doi.org/10.1109/iccsn.2017.8230073>.

[14] F. Shaikh, B. Joseph, "Simulation of synchronous reference frame PLL for grid synchronization using Simulink," in 2017 International Conference on Advances in Computing, Communication and Control (ICAC3), Mumbai, India, 2017. <https://doi.org/10.1109/icac3.2017.8318790>.

[15] I. Park, I. Jang, W. Jung, S. Kim, "Noise immunity modeling and analysis of delay-locked loop," in 2015 IEEE 19th Workshop on Signal and Power Integrity (SPI), Berlin, Germany, 2015. <https://doi.org/10.1109/sapiw.2015.7237401>.

[16] C. Zhang, X. Zhao, X. Wang, X. Chai, Zhang Z, X. Guo, "A Grid Synchronization PLL Method Based on Mixed Second- and Third-Order Generalized Integrator for DC Offset Elimination and Frequency Adaptability," *IEEE Journal of Emerging and Selected Topics in Power Electronics*, 6(3), 1517-1526, 2018. <https://doi.org/10.1109/jestpe.2018.2810499>.

[17] Q. Chen, M. Li, "Modified Gardner algorithm for bit synchronization in high-order QAM system," in 2013 International Conference on Computational Problem-Solving (ICCP), Jiuzhai, China, 2013. <https://doi.org/10.1109/iccps.2013.6893575>.

[18] T. Chang, K. Lee, G. Chen, S. Chiu, J. Yang, "Super resolution using trilateral filter regression interpolation," in 2017 IEEE 2nd International Conference on Signal and Image Processing (ICSIP), Singapore, Singapore, 2017. <https://doi.org/10.1109/siprocess.2017.8124511>.

[19] J. Boiko, I. Kovtun, S. Petrushchuk, "Productivity of telecommunication systems with modified signal-code constructions," in 2017 4th International Scientific-Practical Conference Problems of Infocommunications. Science and Technology (PIC S&T), Kharkov, Ukraine, 2017. <https://doi.org/10.1109/infocommst.2017.8246374>.

[20] W. Chen, M. Huang, X. Lou, "Sparse FIR Filter Design Based on Interpolation Technique," in 2018 IEEE 23rd International Conference on Digital Signal Processing (DSP), Shanghai, China, 2018. <https://doi.org/10.1109/icdsp.2018.8631685>.

[21] S.K. Mitra, A. Mahalonobis, T. Saramaki, "A generalized structural subband decomposition of FIR filters and its application in efficient FIR filter design and implementation," *IEEE Trans. on Circuits and Systems II: Analog and Digital Signal Processing*, 40(6), 363-374, 1993. <https://doi.org/10.1109/82.277881>.

[22] K. M. Whelan, F. Balado, N. J. Hurley, G. C. M. Silvestre, "A Two-Dimensional Extension of the Mueller and Müller Timing Error Detector," *IEEE Signal Processing Letters*, 14(7), 457-460, 2007. <https://doi.org/10.1109/lsp.2006.891321>.

[23] P. Harati, A. Dyskin, I. Kalfass, "Analog Carrier Recovery for Broadband Wireless Communication Links," in 2018 48th European Microwave Conference (EuMC), Madrid, Spain, 2018. <https://doi.org/10.1109/eumc.2018.85>.

[24] C. C. Cheng, S. Hikmet, S. Sezginer, Yu T. Su, "Enhanced Spatial Modulation With Multiple Signal Constellations," *IEEE Trans. on Communications*, 63(6), 2237-2248, 2015. <https://doi.org/10.1109/tcomm.2015.2422306>.

[25] A. Wadhwa, U. Madhoo, "Near-Coherent QPSK Performance With Coarse Phase Quantization: A Feedback-Based Architecture for Joint Phase/Frequency Synchronization and Demodulation," *IEEE Trans. on Signal Processing*, 64(17), 4432-4443, 2016. <https://doi.org/10.1109/tsp.2016.2568169>.

[26] I.R. Parhomey, J.M. Boiko, O.I. Eromenko, "Features of digital signal processing in the information control systems of multipositional radar," *Journal of Achievements in Materials and Manufacturing Engineering*, 2(77), 75-84, 2016. <https://doi.org/10.5604/17348412.1230101>.

# Extending Movable Surfaces with Touch Interaction Using the VirtualTablet: An Extended View

Adrian H. Hoppe<sup>\*1</sup>, Felix Marek<sup>1</sup>, Florian van de Camp<sup>2</sup>, Rainer Stiefelhagen<sup>1</sup>

<sup>1</sup>Karlsruhe Institute of Technology (KIT), Institute for Anthropomatics and Robotics (IAR), cv:hci Lab, 76131 Karlsruhe, Germany

<sup>2</sup>Fraunhofer IOSB, Interactive Analysis and Diagnosis (IAD), 76131 Karlsruhe, Germany

## ARTICLE INFO

Article history:

Received: 07 January, 2020

Accepted: 04 February, 2020

Online: 30, March, 2020

Keywords:

VirtualTablet

Virtual environment

Virtual reality

Touch interaction

Haptic feedback

## ABSTRACT

*Immersive output and natural input are two core aspects of a virtual reality experience. Current systems are frequently operated by a controller or gesture-based approach. However, these techniques are either very accurate but require an effort to learn, or very natural but miss haptic feedback for optimal precision. We transfer ubiquitous touch interaction with haptic feedback into a virtual environment. To validate the performance of our implementation, we performed a user study with 28 participants. As the results show, the movable and cheap real world object supplies an accurate touch detection that is equal to a laserpointer-based interaction with a controller. Moreover, the virtual tablet can extend the functionality of a real world tablet. Additional information can be displayed in mid-air around the touchable area and the tablet can be turned over to interact with both sides. Therefore, touch interaction in virtual environments allows easy to learn and precise system interaction and can even augment the established touch metaphor with new paradigms.*

## 1 Introduction

Virtual Reality (VR) has established itself at a consumer level. Many different VR systems immerse the user in an interactive environment. However, the different systems all have their distinct input devices. For newer users, we witnessed, it is quite difficult to just *pull the trigger* or *press the grip button*, since users do not see their own hands, but only the floating input device. More natural interfaces are needed. Gesture interaction via a camera that is mounted on the Head Mounted Display (HMD) lets the user grab virtual objects and manipulate the Virtual Environment (VE) effortlessly. But, haptic sensations are missing.

We therefore present VirtualTablet - A touchable object that is made of very cheap materials and can have any size or shape. This paper is an extension of work originally presented in the IEEE Conference on Virtual Reality and 3D User Interfaces (VR) [1]. It presents further detail regarding related work, implementation and design as well as evaluation and results. This paper makes two technical contributions: First, VirtualTablet supplies touch interaction on a movable surface captured by a movable camera. Second, different

interaction techniques are presented that increase the functionality of the tablet to more than the capability of a real-world tablet.

## 2 Related Work

Haptic feedback increases performance and usability [2]–[4]. Different systems can be used to realize haptic feedback for a user. With active haptics, users wear a device that exerts pressure or a force on the user's hand. Scheggi et al. [5] use small tactile interfaces at the fingertips. The interfaces press down on the fingers if an object is touched. The VRGluV<sup>1</sup> is an exoskeleton that allows to constrain the movement of the fingers, thereby providing haptic feedback. With passive haptics the user touches real objects to receive feedback. The real objects can be tracked, for example with markers, and then displayed in the VE. Simeone et al. [6] track different real objects, e.g. a cup or an umbrella, as well as the head and hands of the user. They showed that the virtually displayed object does not need to match the real object perfectly. Some variation of material properties or shape allow the use of a broader range of virtual objects even if the set of real world objects is limited.

<sup>\*</sup>Adrian H. Hoppe, Fraunhoferstr. 1, 76131 Karlsruhe, Germany, +49 721 6091 307 & adrian.hoppe@kit.edu

<sup>1</sup>see <https://vrgluV.com/>

If users start navigating in the VE, a mismatch between the location of the real and virtual objects may occur. To overcome this, movable haptic proxies or redirection techniques can be used. Araujo et al. [7] use a robotic arm to move a haptic surface to block the user's hand when it gets close to a virtual object. The head of the robotic arm can be rotated and exchanged, hereby providing a wide range of haptic surfaces. i.e. different textures, a pressure sensor, a interactive surface, physical controls or even a heat emitter. Kohli [8] implemented a touch interaction using an IMPULSE system that tracks the finger via a LED. Utilizing space warping, it is possible to alter the movement of the user's hand in the real world, without the user noticing. By steering the hand towards a real world object, haptic feedback can be given by a virtual object at another position. Azmandian et al. [9] track cubes and a wearable glove with markers on a table surface. The users hand and forearm, as well as some virtual cubes are displayed in the VE. By redirecting the hand of the user while reaching for the virtual objects, they provide haptic sensations for several virtual cubes with a single real world cube. Cheng et al. [10] apply the same principle. Using eye tracking and an OptiTrack system they predict what virtual object will be touched. The movement of the virtual hand is then modified so that a user corrects their real world movement. This allows Cheng et al. to only use a hemispherical surface as a touch proxy. Most of these techniques require a rather static scene and a non navigating user and are thereby not suitable for full body VR experiences.

The presented systems above all give a haptic feeling to the user, but have limited input capabilities. To overcome this, Medeiros et al. [11] use a tracked tablet in a CAVE environment. Depending on the orientation of the tablet, the respective view into the virtual world is rendered on the touch screen. A user can select and manipulate objects by clicking on them in the rendered view or using a set of control buttons. The tablet is tracked by an external tracking system using markers. Xiao et al. [12] use the internal sensors of a Microsoft HoloLens to allow touch interaction on static surfaces. The system is much more flexible as all of the above systems, since it does not require the user to put on gloves or to set up an external tracking system. Using the depth sensors and a segmentation algorithm the hands of the user are recognized and the fingertips extracted. A RANSAC algorithm detects surfaces in the room. Combining these allows for touch interaction with haptic feedback on a real world surface. There is no need to visualize the hands or the surface for the user, since the HoloLens is an augmented reality (AR) HMD and the user sees the real objects. However, only static surfaces are used.

### 3 Implementation

The VirtualTablet system is implemented on a HTC Vive Pro VR HMD<sup>2</sup>. The Vive features a  $1440 \times 1600$  pixels display per eye with a 90 Hz refresh rate. The field of view of the Vive is  $110^\circ$ . Using the Lighthouse tracking system and an IMU the pose of the HMD is detected in a room area of  $5 \times 5 m^2$ . Moreover, the Vive has a stereo camera on the front of the HMD<sup>3</sup>. Each camera has a resolution of

<sup>2</sup>see <https://www.vive.com/de/product/vive-pro/>

<sup>3</sup>see <https://developer.vive.com/resources/knowledgebase/intro-vive-srworks-sdk/> and <https://www.stereolabs.com/blog/vive-pro-ar-zed-mini/>

$640 \times 480$  pixels with a refresh rate of 60 Hz and a field of view of  $96^\circ$  horizontal and  $80^\circ$  vertical. The camera can be accessed with the SRWorks toolkit with a latency of about 100 ms with SRWorks to 200 ms with the ZED Mini. SRWorks supplies depth information with an accuracy of  $\pm 3$  cm at 1 m and  $\pm 10$  cm at 2 m distance from the camera. The minimal distance is 30 cm.

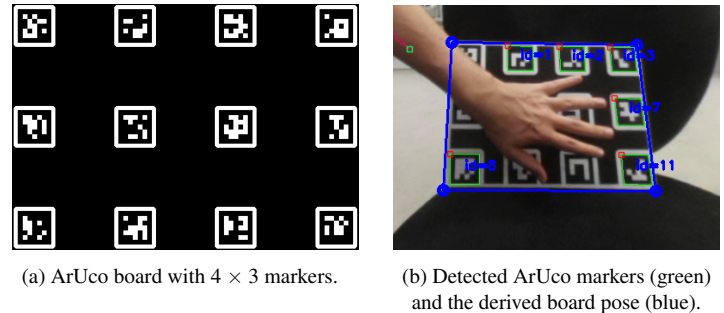


Figure 1: Setup and Detection of the ArUco board.

To detect the movable objects, ArUco markers [13] are used. They provide a position and rotation in respect to the camera, given their real world size. The VirtualTablet consists of a simple rigid base, for example a piece of acrylic glass or cardboard, pasted up with ArUco markers. Because the hand of the user will overlap with some markers while interacting, the markers are spread out over the board (see Figure 1). ArUco markers can be uniquely identified, therefore allowing the use of more than one VirtualTablet at the same time.

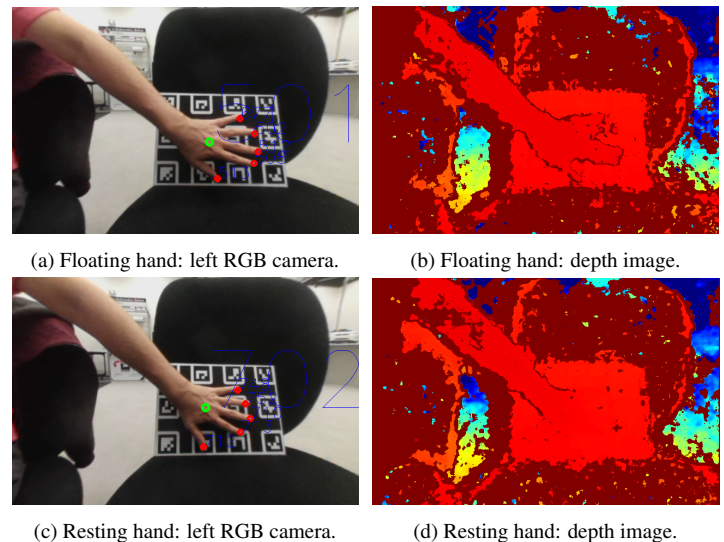


Figure 2: Front camera images of a hand hovering above the board and touching the board. Dark red color in the depth image mark invalid depth information.

To detect the fingertips, a segmentation algorithm is used, since the hand of the user cannot be reconstructed from the given depth information (see Figure 2). First, the hand is extracted from the RGB image by first masking out the board. An interacting hand will be inside this area. Since the ArUco board only consists of black and white colors, we subtract these colors from the image which results in a binary representation of the segmented hand. Pixels



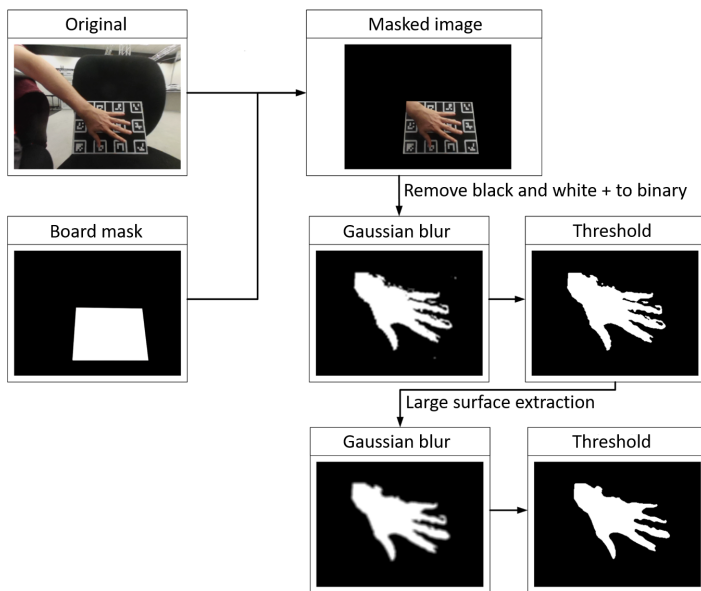


Figure 3: Hand segmentation process.

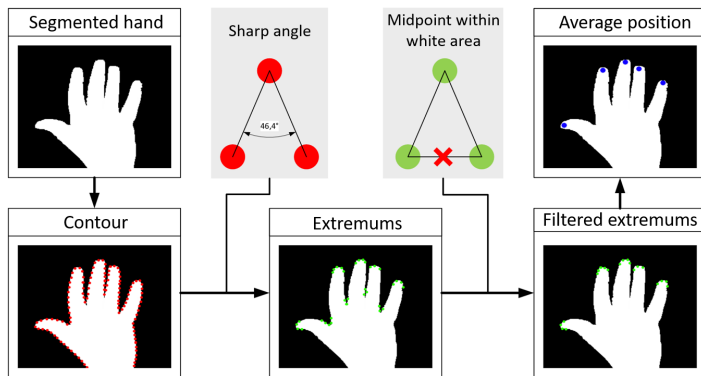


Figure 4: Fingertip detection process.

with a black or white color are removed in the HSV color space at a threshold with a low saturation (white) or a low brightness (black), i.e.  $S \leq 80$  or  $V \leq 40$  (scale from 0 to 255). As Figure 3 shows, the binary image is then enhanced by a blur filter, the application of a threshold and the extraction of larger surfaces<sup>4</sup>. There are other ways to extract the hand by using skin color, so this approach can be easily exchanged if the background skin colors or lighting conditions change. Second, the fingertips are detected by calculating the extreme values of the contour of the hand [14]. This is done by calculating the angle between three points on the contour that are for our camera setup 18 pixels apart from each other (see Figure 4). To track the fingertips from one frame to another a distance-based tracking algorithm similar to [12] is used. Combined with the depth information from the stereo camera the 2D tracked location of the user's fingers can be projected into the 3D space relative to the HMD. To have a more robust depth value an average of  $11 \times 11$  pixels is calculated around the 2D fingertip location. Since the pose of the surface and the fingertips are known, a touch can be detected. If the finger is closer than 0.5 cm to the surface, a click is triggered.

<sup>4</sup>see <https://medium.com/@muehler.v/simple-hand-gesture-recognition-using-opencv-and-javascript-eb3d6ced28a0>

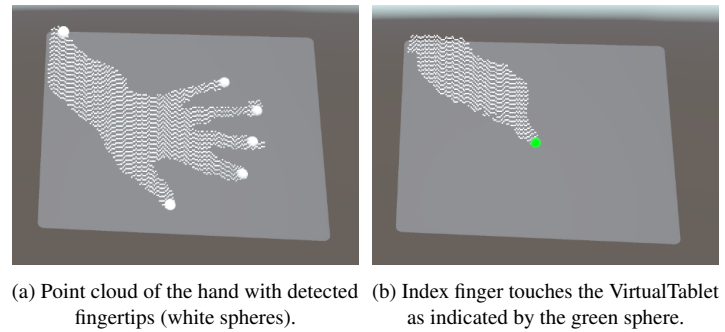
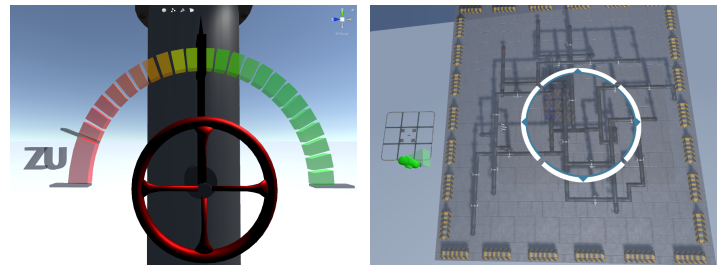


Figure 5: Visualization of the VirtualTablet and the user's hand.

To visualize the VirtualTablet and the user's hands in VR, the engine Unity3D<sup>5</sup> is used. At the location of the real tablet, a virtual tablet with the same size and shape is rendered (see Figure 5). To give the user a visual feedback of the location of her or his hand, a 3D point cloud is rendered. White spheres at the fingertips highlight currently tracked fingers. The sphere turns green if a touch is detected.

The VirtualTablet can be used as normal tablet which is familiar to many users. However, VR allows to enhance and extend the interaction with the tablet. The following subsections describe different techniques that are enabled by VirtualTablet.

### 3.1 Moving the VirtualTablet



(a) A virtual valve wheel that can be turned by holding the VirtualTablet at the wheel's location and rotating it. (b) The map of the VE can be moved by tilting the VirtualTablet. A green symbol represents the current location of the player. The user can teleport to a location by touching it.

Figure 6: Examples for a rotating tablet interaction.

Even without the touch recognition the VirtualTablet allows different forms of interaction. The position and rotation of the tablet can be used as an input to e.g. open a menu or change a value if held inside a trigger volume. If a user holds the tablet into a virtual object, an action can be triggered. By rotating the tablet at the location of a wheel, the wheel can be turned (see Figure 6a). We implemented a navigation mechanism that allows the user to move a map around by tilting the tablet (see Figure 6b). If the user touches a location she or he is teleported there.

Since the VirtualTablet has ArUco markers on both sides, it can recognize touch on both surfaces. This can be used to give the

<sup>5</sup>see <https://unity3d.com/>



user a more natural way to navigate through menus. If the user flips the tablet around, a different user interface is displayed. In our application it is used to switch between an information interface and a map display for navigation.

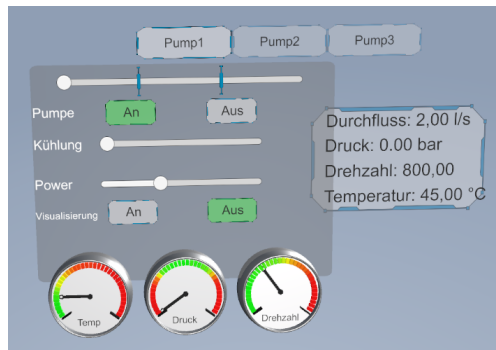


Figure 7: A menu that extends non-interactable information over the edges of the physical tablet.

### 3.2 Extending the VirtualTablet

VR allows to display information at any given location. In reality, displays are much more constrained and information cannot (yet) be displayed in mid-air. The VirtualTablet allows to extend the displayed content over the edges of the physical tablet (see Figure 7). All interactable elements, like buttons and sliders, are displayed on the touchable surface. Other informations are arranged around the tablet.

### 3.3 Duplicating the VirtualTablet



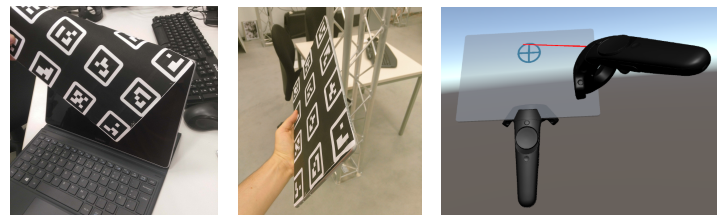
(a) Mobile acrylic glass.

(b) Mounted cardboard.

Figure 8: Different interaction surfaces.

Physical tablets are expensive, rely on a power supply and only come in distinct shapes and sizes. With our approach multiple

interactable surfaces can be created fast and cheap. As seen in Figure 8 we created a small mobile tablet and a larger mounted interaction surface. The different surfaces can be used in parallel.



(a) Attaching the ArUco board to the capacitive touchscreen tablet.

(b) Holding the capacitive touchscreen tablet.

(c) Laserpointer and interaction surface attached to the HTC Vive controllers.

Figure 9: Setup of the input techniques for comparison with the VirtualTablet.

## 4 Evaluation

To evaluate the proposed system and interaction methods, a user study was performed. We designed an application that allows a user to control different machines and valves in a factory using the VirtualTablet. The task of the user was to react to a breach in the pipe system. While solving the issues, the user interacted repeatedly with the extended interaction methods described above.

### 4.1 Independent Variables

To compare the detection performance of the VirtualTablet, other input methods were implemented. A capacitive touchscreen tablet was equipped with a ArUco board (see Figure 9a and 9b). The capacitive tablet uses the same hand visualization as the VirtualTablet, but the touch detection from the display as a ground truth. The size of the tablet is about 1 cm smaller in width and 0.5 cm smaller in height than the acrylic glass VirtualTablet. The default interaction tools for the HTC Vive are the provided controllers. The pose of the controllers is tracked with sub-millimeter accuracy [15]. Applications often use a laser pointer to interact with a handheld menu (see Figure 9c). This virtual pointer technique is effective and efficient [16]. Furthermore, a normal capacitive tablet in a non-VR scenario was used to evaluate the ground truth precision of touch interaction for the given tasks.

The user study was performed in a within-subjects design. The independent variables are the the four described techniques VirtualTablet, CapacitiveTablet and Controller (all in VR) as well as the NonVRTablet. To compensate for the effects of learning and fatigue the conditions were counterbalanced.

### 4.2 Procedure

First, the users tested the extended interaction methods in the factory application. Second, the users were asked to perform several click and draw interactions with the tablet as in [12]. Users were presented with 6 targets which appeared four times each per technique. Each target had a size of  $5 \times 5$  cm, independent of the condition. As a result each user performed  $6 \times 4 \times 4 = 96$  clicks in total. The order of the click targets was random, but pre-calculated for each

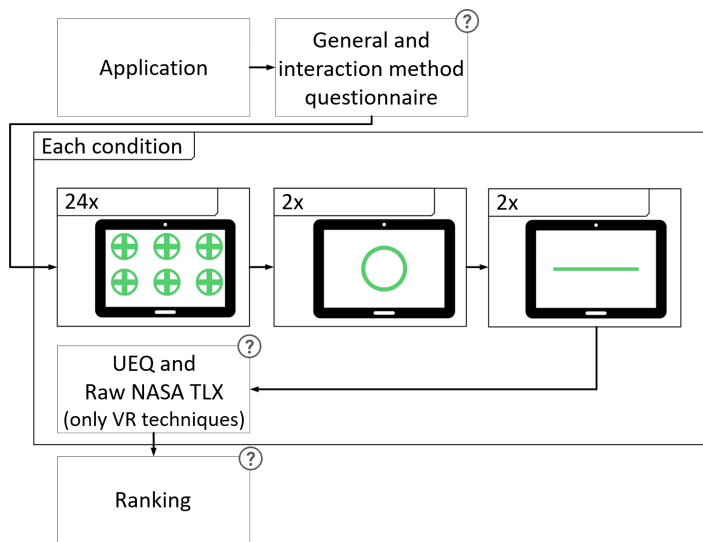


Figure 10: Procedure of the user study. Question mark indicates questionnaire.

technique so each user had the same sequence. For the shape tracing task, users were asked to trace a given figure (circle and line) as closely as possible and finishing their drawing by clicking a button. Each shape was drawn twice. The full procedure is listed in Figure 10.

### 4.3 Participants

28 people (4 female) participated in the user study with an age distribution of 2 under 20 years, 13 from 21-30 years, 8 from 31-40 years and 5 larger than 40 years. All of which had prior experience with touch input. On a scale of 1 (none) to 7 (very much), users had  $\bar{O} 3.2 \pm 1.9$  experience with VR, 15 users had used a tracked controller before.

## 5 Analysis

### 5.1 Selection

The precision of the target selection was measured by recording the position of the touch and calculating the distance to the center of the target. We removed 49 outlier points (1.8%) with a distance of more than three standard deviations from the target point (as in [12], [17]). Also, the time taken was measured.

### 5.2 Tracing

For the shape tracing tasks, we measured how much of the target area was filled. Furthermore, the percentage of pixels painted inside the image was calculated. This value is an indication how accurately a user could draw inside the target area. Moreover, we calculated the average distance of the touch point to the target shape with the width of the brush and the shape removed. Also the duration of drawing was measured.

### 5.3 Performance and User Experience

To assess the qualitative performance and experience of the different hardware setups, we used Raw NASA TLX [18] and the shortened version of UEQ, the UEQ-S [19] as a usability measurement. These questionnaires were only collected for the VR techniques since the NonVRTablet is only used as a ground truth for precision. At last, users were asked to rank the three VR techniques on a 7-point Likert scale regarding wearing comfort, quality of input and an overall ranking.

### 5.4 Statistical analysis

We present the results as average value ( $\bar{O}$ ) with standard deviation ( $\pm$ ). We used the *rTOST* [20] as a equivalence test and the *Mann-Whitney-Test* [21] as a significance test. Both tests do not assume a normal distribution of the sample set. To calculate the power of the effects, *Cohen's d* [22] is used.

## 6 Results

### 6.1 Selection accuracy

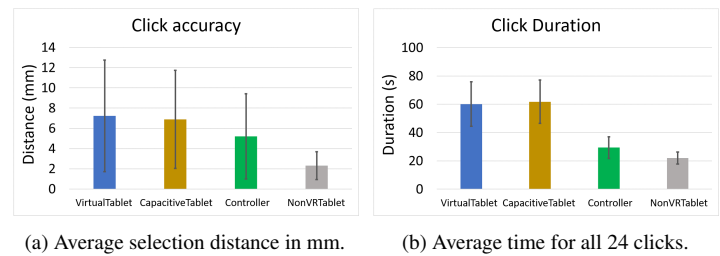


Figure 11: Accuracy and duration of selections.

Table 1: Average selection distance in mm. The 6 targets are coded as T/B = top or bottom row and L/C/R = left, center or right column.

	Total	TL	TC	TR	BL	BC	BR
<b>VirtualTablet</b>							
$\bar{O}$	6,877	6,528	5,401	7,155	8,005	7,272	6,910
$\pm$	4,869	4,701	3,603	4,827	5,287	5,287	4,985
<b>CapacitiveTablet</b>							
$\bar{O}$	6,488	6,553	6,491	7,218	6,752	5,877	6,023
$\pm$	4,077	3,765	4,198	3,853	4,790	4,093	3,581
<b>Controller</b>							
$\bar{O}$	4,827	5,028	5,039	5,221	4,905	4,162	4,614
$\pm$	3,291	3,445	2,929	3,619	3,345	2,783	3,501
<b>NonVRTablet</b>							
$\bar{O}$	2,246	2,527	2,118	2,301	2,562	2,159	1,820
$\pm$	1,231	1,300	1,160	1,287	1,308	1,033	1,148

The results of the selection tasks are listed in Figure 11a and Table 1. The three VR input methods VirtualTablet, CapacitiveTablet

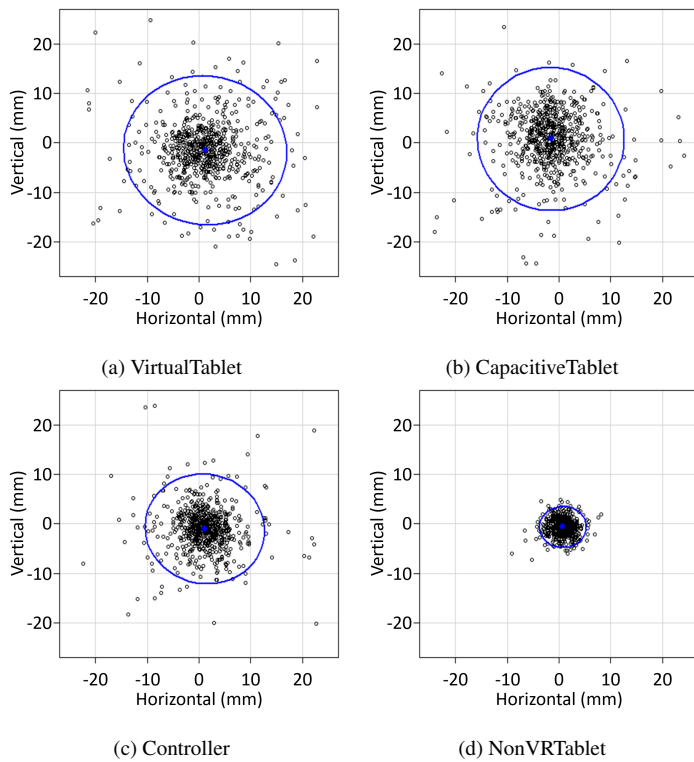


Figure 12: 95% confidence ellipses.

Table 2: rTOST equivalence test between pairs of VirtualTablet (VT), CapacitiveTablet (CT) and Controller (C)

	VT - C	VT - CT	CT - C
<b>Epsilon</b>	2,315	2,315	2,315
<b>Avg. diff.</b>	1,652	-0,001	-1,658
<b>df</b>	687,239	759,937	778,250
<b>Cohen's d</b>	0,412	0,065	0,370
<b>p value</b>	0,003	0,000	0,001

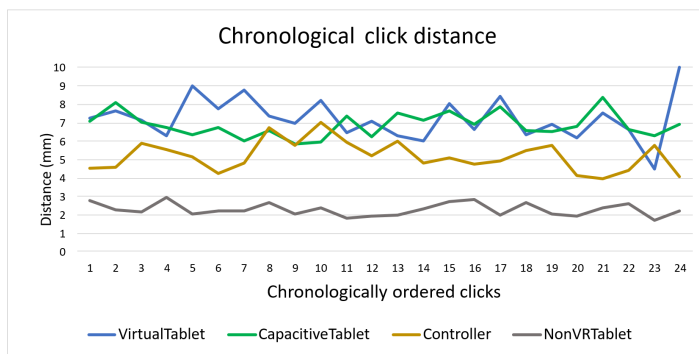


Figure 13: Average distance of clicks chronologically ordered.

and Controller have a selection accuracy of about 5 to 7 mm. The 95% confidence ellipses in Figure 12 show visually, what the rTOST test (see Table 2) confirms. All three VR input methods are equivalent. The epsilon of 2.315 is the average distance of the ground truth tablet interaction, meaning this value represents the accuracy of the users in a best case scenario. Analysis of the accuracy of the

Table 3: Average duration for 24 selections.

	VirtualTablet	CapacitiveTablet	Controller	NonVRTablet
$\emptyset$	60,120	61,770	29,350	22,060
$\pm$	15,690	15,270	7,695	4,243

6 targets as seen in Figure 1 reveals, that the VirtualTablet detection has a higher accuracy of about 1 mm at the top row. The other techniques do not show such a large difference. Also, no learning effect can be detected in the collected data. Figure 13 shows the average distances to the center in a temporal order. The difference from the center stays approximately the same over the period of the selection task. The total amount of time needed to perform the selection task with each input technique is shown in Figure 11b and Table 3. Users took about twice as much time with the VirtualTablet and CapacitiveTablet in regards to the Controller interaction and almost three time as much in comparison to the NonVRTablet.

### 6.2 Tracing accuracy

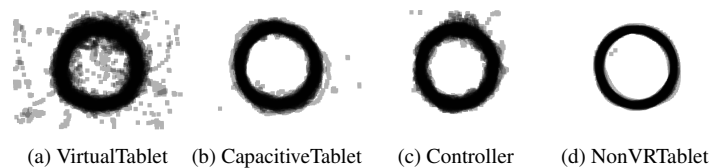


Figure 14: Stacked drawings of all circle traces.

Table 4: Shape tracing accuracy for the circle.

	VirtualTablet	CapacitiveTablet	Controller	NonVRTablet
<b>% of drawing inside target area</b>				
$\emptyset$	35,131	47,709	45,059	63,884
$\pm$	8,884	11,847	11,239	8,949
<b>% of target area filled</b>				
$\emptyset$	56,840	66,057	63,671	77,615
$\pm$	14,452	16,490	17,694	13,091
<b>Average distance to target shape (mm)</b>				
$\emptyset$	4,274	2,960	2,892	1,873
$\pm$	2,106	1,851	1,003	0,590
<b>Drawing duration (s)</b>				
$\emptyset$	15,688	8,128	6,455	5,277
$\pm$	8,540	2,877	3,542	2,378

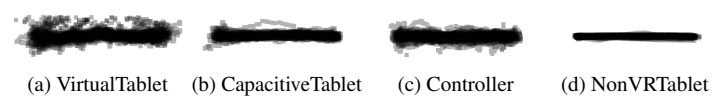


Figure 15: Stacked drawings of all line traces.

Table 5: Shape tracing accuracy for the line segment.

	VirtualTablet	CapacitiveTablet	Controller	NonVRTablet
<b>% of drawing inside target area</b>				
Ø	39,058	56,813	49,715	82,004
±	9,464	14,805	18,014	11,840
<b>% of target area filled</b>				
Ø	61,949	67,469	64,202	78,607
±	13,468	17,716	23,724	11,706
<b>Average distance to target shape (mm)</b>				
Ø	4,340	2,757	3,430	2,400
±	1,383	1,387	1,640	0,848
<b>Drawing duration (s)</b>				
Ø	6,885	3,909	3,148	2,521
±	4,075	1,424	2,179	1,172

The results for the shape tracing task are shown in Table 4 and 5 for the circle target and line target respectively. Drawing with the NonVRTablet achieves the highest tracing accuracy regarding percentage of drawing inside the target area and target area filled. The CapacitiveTablet is on average slightly better than the Controller and VirtualTablet condition. The standard deviation is smallest for the VirtualTablet and the NonVRTablet. The average distance towards the circle target area is very similar to this, with the NonVRTablet performing best with 1.9 mm accuracy and VirtualTablet performing worst with a distance of 4.3 mm. For the line segment, the average distance of the CapacitiveTablet is very close to the NonVRTablet with 2.8 mm to 2.4 mm. The detected touches of the VirtualTablet have the highest average distance (4.3 mm), but are not so far away from the Controller tracing (3.4 mm). Figures 14 and 15 show the shape traces of all users on top of each other. The touch detection of the VirtualTablet leads to a lot of smaller errors outside of the target area. The ground truth touch of the CapacitiveTablet is a lot more stable. The Controller drawings appear shaky. The NonVRTablet matches the target area the most.

Regarding shape tracing duration, the Controller is on average faster, but more inaccurate than the CapacitiveTablet. The NonVRTablet is the quickest and the VirtualTablet takes the most time.

### 6.3 Performance and User Experience

The results of the evaluation show that the arrangement of the extended menus with information displayed outside the interactable area was clear (see Table 6). It was also very useful to have more than one input surface. Teleportation with the tilting map has a medium difficulty. During the user study users often needed help to initially understand what they needed to do. Yet, once learned, participants quickly got better. Turning the valves with the orientation of the tablet and using the displayed buttons and sliders also has a medium difficulty. The pose of the tablet and touch input is recognized medium-well. The participants are happy with the interaction distance, which is due to the camera sensor at least 30 cm in front of the HMD. Input delay was quite high (mostly due to the

Table 6: 7 point Likert scale questionnaire for different aspects of the extended interaction techniques of the VirtualTablet.

Questions	Value 1	Value 7	Ø	±
Information outside the input area was...	unclear	clear	5,143	1,597
Using more than one input surface are was...	practical	impractical	2,429	1,116
Teleportation with the tilting map was...	easy	difficult	4,107	1,718
Using the tablet orientation as input was...	easy	difficult	3,607	1,800
Using the buttons and sliders was...	easy	difficult	3,643	1,315
Reaction of touch input was was...	expected	unexpected	3,786	1,319
Recognition of tablet pose was...	expected	unexpected	2,571	1,400
Minimum distance for input was...	too far away	just right	5,071	1,534
Input delay was...	annoying	undisturbing	3,786	1,839
Haptic surface for input was...	helpful	unnecessary	1,500	1,086

cameras), which is a little bit annoying for the users. However, the haptic surface for hand gesture input is clearly rated as helpful.

Figure 16 shows the results of the UEQ-S ratings. The pragmatic quality is very good for the Controller, positive for the CapacitiveTablet and neutral for the VirtualTablet (positive evaluation from a value of 0.8 and more). the hedonic quality is rated positive for all techniques, with the VirtualTablet and Controller rated best. The overall result shows that the Controller technique works very well. However, both touch surface interactions receive a positive rating. Compared to the supplied benchmark ratings from the UEQ Data Analysis Tool [23] the VirtualTablet is ranked as bad for the pragmatic quality, above average for the hedonic quality and below average overall.

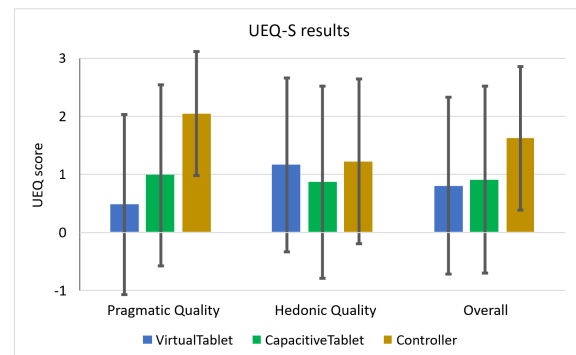


Figure 16: Results of UEQ-S.

The CapacitiveTablet is below average for all three categories. The Controllers are ranked as excellent for the pragmatic quality and overall. Their hedonic quality is above average. The difference between the Controller technique and the two touch techniques is significant for the pragmatic quality ( $p \leq 0.001$ ) and overall



( $p \leq 0.002$  and  $p \leq 0.012$  for the difference towards the VirtualTablet and CapacitiveTablet respectively).

The results of the Raw NASA TLX as seen in Figure 17 show that the Controller ranks best in all categories. The VirtualTablet ranks worst in almost all categories, except for the physical demand.

Users rank the wearing comfort of the VirtualTablet and the Controllers as good, the CapacitiveTablet as below medium (see Figure 18). The quality of input is ranked best for the Controllers, good for the CapacitiveTablet and below medium for the VirtualTablet. Overall, the participants rank the Controller as good and the tablet techniques as medium.

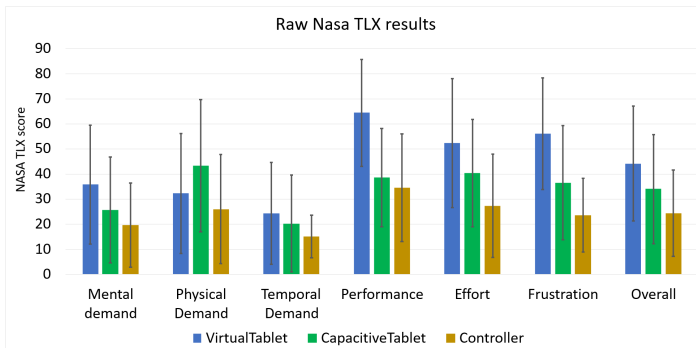


Figure 17: Results of Raw NASA TLX.

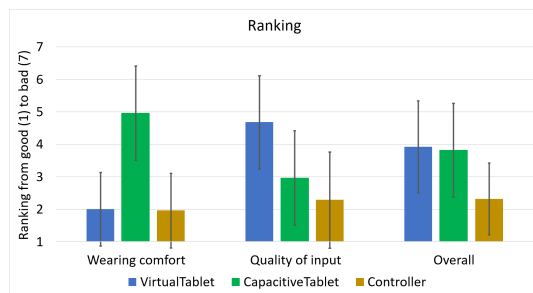


Figure 18: Rankings of the techniques.

## 7 Discussion

The rTOST test shows that both the VirtualTablet and the Controller interaction perform equally in a selection task. The precision of the VirtualTablet is about 6.9 mm, which is over half as small as the average size of a fingertip with 1620 mm in diameter [24]. The precision is good enough to interact with objects of suggested minimum target sizes, e.g. 9.6 mm [25] or 7-10 mm<sup>6</sup>. Because of the larger temporal delay, the tablet interaction is slower. This yields to longer interaction times and also affects the precision of the task execution, since the visualized hand and tablet locations did not match current location of their real world counterpart. The interaction with a controller is different compared to touch interaction. A user often only twists the wrist to point the laser towards another target. This is quicker than moving the whole hand, but it also induces more jitter as the larger standard deviations show. The shape tracing task

shows that the touch detection of VirtualTablet is not robust enough. Due to the large amount of noise and invalid data in the calculated depth information, the touch detection is not able to always detect a continuous touch and sometimes detects false positives. The touch detection also fails, if a user obscures the fingertip with her or his own hand. This explains the larger time difference and usability issues of the VirtualTablet compared to the CapacitiveTablet and Controller techniques, which recognize the touch through sensors.

VR does not allow the user to see her or his own hand. A good visualization of the user's hand is therefore necessary to achieve good results. The used point cloud and fingertip spheres depend on the segmentation of the hand. The blur during head movements and the automatic brightness adjustments dampen the quality of the image. However, the point cloud representation by itself seems to be not so easy to understand spatially. The impact of the hand visualization in the shape tracing task is lower than in the selection task for the CapacitiveTablet, because the user receives direct feedback from her or his touch point on the capacitive display and can compensate for any hand visualization delay or errors. Thus, the CapacitiveTablet performs better than the VirtualTablet.

The haptic surface for the interaction was rated as very helpful during the application task. This was also indicated through comments by the participants. The acrylic glass material is very lightweight (120 g) compared to the touchscreen tablet with battery (754 g) which leads to a lower physical demand and a higher wearing comfort (Vive controllers 2 × 203 g). The impact of the weight will be even larger at longer sessions of usage.

The comparable MRTouch system [12] shows slightly better selection precision ( $\emptyset 5.4 \pm 3.2$  mm) when compared to the VirtualTablet. However, the VirtualTablet interaction uses movable touch surfaces, which induce additional precision errors. Furthermore, because MRTouch is an AR augmented reality (system, there is no need for a hand or surface visualization. But, the visualization in VR is crucial and has a larger impact on the precision and usability of the input technique. Tracing accuracy of VirtualTablet and MRTouch are comparable with an average distance of  $\emptyset 4.0 \pm 3.4$  mm for MRTouch. Although the AR HMD of MRTouch uses a time of flight depth sensor and infrared cameras, the touch detection works with a threshold distance of 10 mm (ours 5 mm) which could lead to a touch recognition before the user reached the surface. The very accurately tracked Controllers show a similar target selection result as VirtualTablet and MRTouch. This shows that touch input in VR and AR is very accurate, even with the present issues regarding inaccurate tracking.

Our ground truth baseline (NonVRTablet with  $\emptyset 2.3 \pm 1.4$  mm avg. distance to target) shows that there is room for improving the accuracy of the presented technique. Yet, the extended functionality, e.g. extending the user interface over the edges of the physical surface, turning the tablet around for a menu switch or changing the pose of the tablet to control a device, has a benefit that a real-world touch tablet cannot offer.

## 8 Conclusion and Future Work

We presented VirtualTablet, a movable surface that allows familiar touch interaction to control the VE. VirtualTablet is intuitive to

<sup>6</sup>see <https://support.google.com/accessibility/android/answer/7101858>

control, cheap, lightweight and can be shaped into any form and size. It can be used as an extension to currently supported input hardware, like controllers, since it does not require any additional hardware setup (except the board itself) and does not alter the VR HMD in any way. The haptic surface is helpful and the implementation allows an accurate selection of targets which is comparable to a laserpointer-based interaction using controllers.

The hardware used in this study has high latency and large noise levels. This yields to issues with continuous touch detection and dampens the overall accuracy of the system. For future work we would like to use a different camera and/or depth sensor to resolve these challenges. Also, other sensors like a capacitive touch foil on the tablet could be used to eliminate the problems of occlusion. We proposed several new interaction techniques that extend the usefulness of touch interaction in VR environments. With better tracking, further exploration of the design space of touch in VR will be possible. Another aspect that we need to improve is the hand visualization so that users get a better understanding of their finger positions. Mesh- or skeleton-like representations could be used for this purpose.

**Conflict of Interest** The authors declare no conflict of interest.

**Acknowledgment** We want to thank all of the participants of the user study for taking the time to provide us with very helpful feedback and insights.

## References

- [1] A. H. Hoppe, F. Marek, F. van de Camp, and R. Stiefelwagen, "Virtualtablet: Extending movable surfaces with touch interaction", in *2019 IEEE Conference on Virtual Reality and 3D User Interfaces (VR)*, Mar. 2019, pp. 980–981. DOI: 10.1109/VR.2019.8797993.
- [2] D. Markov-Vetter, E. Moll, and O. Staadt, "Evaluation of 3d selection tasks in parabolic flight conditions: Pointing task in augmented reality user interfaces", in *Proceedings of the 11th ACM SIGGRAPH International Conference on Virtual-Reality Continuum and Its Applications in Industry*, ser. VRCAI 12, Singapore, Singapore: Association for Computing Machinery, 2012, 287294, ISBN: 9781450318259. DOI: 10.1145/2407516.2407583.
- [3] E. Koskinen, T. Kaaresoja, and P. Laitinen, "Feel-good touch: Finding the most pleasant tactile feedback for a mobile touch screen button", in *Proceedings of the 10th International Conference on Multimodal Interfaces*, ser. ICMI 08, Chania, Crete, Greece: Association for Computing Machinery, 2008, 297304, ISBN: 9781605581989. DOI: 10.1145/1452392.1452453.
- [4] C. S. Tzafestas, K. Birbas, Y. Koumpouros, and D. Christopoulos, "Pilot evaluation study of a virtual paracentesis simulator for skill training and assessment: The beneficial effect of haptic display", *Presence*, vol. 17, no. 2, pp. 212–229, Apr. 2008, ISSN: 1054-7460. DOI: 10.1162/pres.17.2.212.
- [5] S. Scheggi, L. Meli, C. Pacchierotti, and D. Prattichizzo, "Touch the virtual reality: Using the leap motion controller for hand tracking and wearable tactile devices for immersive haptic rendering", in *ACM SIGGRAPH 2015 Posters*, ser. SIGGRAPH 15, Los Angeles, California: Association for Computing Machinery, 2015, ISBN: 9781450336321. DOI: 10.1145/2787626.2792651.
- [6] A. L. Simeone, E. Velloso, and H. Gellersen, "Substitutional reality: Using the physical environment to design virtual reality experiences", in *Proceedings of the 33rd Annual ACM Conference on Human Factors in Computing Systems*, ser. CHI 15, Seoul, Republic of Korea: Association for Computing Machinery, 2015, 33073316, ISBN: 9781450331456. DOI: 10.1145/2702123.2702389.
- [7] B. Araujo, R. Jota, V. Perumal, J. X. Yao, K. Singh, and D. Wigdor, "Snake charmer: Physically enabling virtual objects", in *Proceedings of the TEI 16: Tenth International Conference on Tangible, Embedded, and Embodied Interaction*, ser. TEI 16, Eindhoven, Netherlands: Association for Computing Machinery, 2016, 218226, ISBN: 9781450335829. DOI: 10.1145/2839462.2839484.
- [8] L. Kohli, "Redirected touching: Warping space to remap passive haptics", in *2010 IEEE Symposium on 3D User Interfaces (3DUI)*, Mar. 2010, pp. 129–130. DOI: 10.1109/3DUI.2010.5444703.
- [9] M. Azmandian, M. Hancock, H. Benko, E. Ofek, and A. D. Wilson, "Haptic retargeting: Dynamic repurposing of passive haptics for enhanced virtual reality experiences", in *Proceedings of the 2016 CHI Conference on Human Factors in Computing Systems*, ser. CHI 16, San Jose, California, USA: Association for Computing Machinery, 2016, 19681979, ISBN: 9781450333627. DOI: 10.1145/2858036.2858226.
- [10] L.-P. Cheng, E. Ofek, C. Holz, H. Benko, and A. D. Wilson, "Sparse haptic proxy: Touch feedback in virtual environments using a general passive prop", in *Proceedings of the 2017 CHI Conference on Human Factors in Computing Systems*, ser. CHI 17, Denver, Colorado, USA: Association for Computing Machinery, 2017, 37183728, ISBN: 9781450346559. DOI: 10.1145/3025453.3025753.
- [11] D. Medeiros, L. Teixeira, F. Carvalho, I. Santos, and A. Raposo, "A tablet-based 3d interaction tool for virtual engineering environments", in *Proceedings of the 12th ACM SIGGRAPH International Conference on Virtual-Reality Continuum and Its Applications in Industry*, ser. VRCAI 13, Hong Kong, Hong Kong: Association for Computing Machinery, 2013, 211218, ISBN: 9781450325905. DOI: 10.1145/2534329.2534349.
- [12] R. Xiao, J. Schwarz, N. Throm, A. D. Wilson, and H. Benko, "Mrtouch: Adding touch input to head-mounted mixed reality", *IEEE Transactions on Visualization and Computer Graphics*, vol. 24, no. 4, pp. 1653–1660, Apr. 2018, ISSN: 2160-9306. DOI: 10.1109/TVCG.2018.2794222.
- [13] S. Garrido-Jurado, R. Muoz-Salinas, F. Madrid-Cuevas, and M. Marn-Jimenez, "Automatic generation and detection of highly reliable fiducial markers under occlusion", *Pattern Recognition*, vol. 47, no. 6, pp. 2280–2292, 2014, ISSN: 0031-3203. DOI: 10.1016/j.patcog.2014.01.005.
- [14] N. S. Chethana, Divyaprabha, and M. Z. Kurian, "Design and implementation of static hand gesture recognition system for device control", in *Emerging Research in Computing, Information, Communication and Applications*, N. R. Shetty, N. H. Prasad, and N. Nalini, Eds., Singapore: Springer Singapore, 2016, pp. 589–596, ISBN: 978-981-10-0287-8.
- [15] D. C. Niehorster, L. Li, and M. Lappe, "The accuracy and precision of position and orientation tracking in the htc vive virtual reality system for scientific research", *i-Perception*, vol. 8, no. 3, 2017. DOI: 10.1177/2041669517708205.
- [16] I. Poupyrev, T. Ichikawa, S. Weghorst, and M. Billingham, "Egocentric object manipulation in virtual environments: Empirical evaluation of interaction techniques", *Computer Graphics Forum*, vol. 17, no. 3, pp. 41–52, 1998. DOI: 10.1111/1467-8659.00252.
- [17] C. Harrison, H. Benko, and A. D. Wilson, "Omni-touch: Wearable multitouch interaction everywhere", in *Proceedings of the 24th Annual ACM Symposium on User Interface Software and Technology*, ser. UIST 11, Santa Barbara, California, USA: Association for Computing Machinery, 2011, 441450, ISBN: 9781450307161. DOI: 10.1145/2047196.2047255.
- [18] S. G. Hart, "Nasa-task load index (nasa-tlx); 20 years later", *Proceedings of the Human Factors and Ergonomics Society Annual Meeting*, vol. 50, no. 9, pp. 904–908, 2006. DOI: 10.1177/154193120605000909.
- [19] M. Schrepp, A. Hinderks, and J. Thomaschewski, "Design and evaluation of a short version of the user experience questionnaire (ueq-s)", *International Journal of Interactive Multimedia and Artificial Intelligence*, vol. 4, p. 103, Jan. 2017. DOI: 10.9781/ijimai.2017.09.001.
- [20] K. K. YUEN, "The two-sample trimmed t for unequal population variances", *Biometrika*, vol. 61, no. 1, pp. 165–170, Apr. 1974, ISSN: 0006-3444. DOI: 10.1093/biomet/61.1.165.
- [21] H. B. Mann and D. R. Whitney, "On a test of whether one of two random variables is stochastically larger than the other", *The Annals of Mathematical Statistics*, vol. 18, no. 1, pp. 50–60, 1947, ISSN: 00034851. DOI: 10.1214/aoms/1177730491.

- [22] J. Cohen, *Statistical power analysis for the behavioral sciences*. (2nd ed.) 1988.
- [23] A. Hinderks, M. Schrepp, and J. Thomaschewski, "A benchmark for the short version of the user experience questionnaire", Sep. 2018. DOI: 10.5220/0007188303730377.
- [24] K. Dandekar, B. I. Raju, and M. A. Srinivasan, "3-D Finite-Element Models of Human and Monkey Fingertips to Investigate the Mechanics of Tactile Sense", *Journal of Biomechanical Engineering*, vol. 125, no. 5, pp. 682–691, Oct. 2003, ISSN: 0148-0731. DOI: 10.1115/1.1613673.
- [25] P. Parhi, A. K. Karlson, and B. B. Bederson, "Target size study for one-handed thumb use on small touchscreen devices", in *Proceedings of the 8th Conference on Human-Computer Interaction with Mobile Devices and Services*, ser. MobileHCI 06, Helsinki, Finland: Association for Computing Machinery, 2006, 203210, ISBN: 1595933905. DOI: 10.1145/1152215.1152260.

## Mutual Reduction in the Coupling of the MIMO Antenna Network Applied to the Broadband Transmission

Chafai Abdelhamid<sup>1</sup>, Hedi Sakli<sup>\*1,2</sup>

<sup>1</sup>MACS Research Laboratory LR16ES22, National Engineering School of Gabes, Gabes University, 6029 Gabes, Tunisia.

<sup>2</sup>EITA Consulting, 5 Rue du Chant des oiseaux, 78360 Montesson, France.

### ARTICLE INFO

Article history:

Received: 13 December, 2020

Accepted: 18 March, 2020

Online: 26 March, 2020

Keywords:

UWB antenna

MIMO antenna

SRRs metamaterial

### ABSTRACT

In this article, a new form of UWB (ultra-wide-band) antenna operating to the desired specifications, obtained from a base antenna to which some modifications are made. The proximity of the antennas causes a mutual coupling phenomenon thus generating an apparent modification of their characteristics. It is therefore crucial to have the minimum level of insulation with a small possible separation distance between the antennas to ensure efficient operation of our multiple input and multiple output (MIMO) system. The separation spacing between the antennas is close to  $0.15\lambda_0$  ( $\lambda_0$  is the wavelength in free space), where the coupling can be very weak. To overcome this weakness, two efficient methods are applied to minimize mutual coupling in a four-element MIMO antenna, such as the use of the neutralization line and the use of split ring resonator metamaterial (SRR). The objective of our paper is, on the one hand the design of UWB antenna, and on the other hand to minimize the coupling between four UWB-MIMO antennas using the two methods of isolation mentioned above. A coupling minimization of more than 15 dB is obtained using the neutralization line and more than 20 dB with the use of metamaterial while maintaining the operating band and radiation specifications of the MIMO antennas.

### 1. Introduction

In recent years and today, the MIMO antenna has demonstrated its ability to improve the efficiency and capacity of the satellite communication system [1]. Despite the advantages of the MIMO antenna in modern technology, mutual coupling is a delicate challenge, given the small distance between the elements [2,3]. The effects of the interaction between all components of the MIMO antenna array have the effect of reducing the operation of the system by increasing the correlation coefficient and the channel loss. This reduces the antenna gain and distortion of the antenna pattern. Radiation [3-5], and consequently reduces the efficiency of the MIMO antenna. The influence of the near fields performed by the neighboring antenna with the presence of the surface waves has a great influence on the radiating elements in the emission-reception system and more precisely on the coupling between antennas [1,6]. In cases where the antennas are placed on dielectric substrates with low permittivity [3], the fields of the antennas are very close, a very strong coupling these produce. The problems related to antenna linkages have increased since the end

of the 20th century. Many research studies have been conducted and are continuing to improve the characteristic radiation efficiency of antennas. Metamaterial are a promising research topic in various fields, in particular electromagnetism [7], whether for circuit applications (filters, phase shifters, etc.) or for radiation applications (antennas, diffraction, stealth). These are elaborate materials, consisting of periodic elements of small size (relative to the wavelength) and providing, in specific frequency bands, particular properties different from those of natural materials [8,9]. Potential benefits of these structures include, for example, miniaturization of antennas, expansion of their bandwidth or reduction of inter-element coupling within a network. To take into account the constraints inherent in the need for discretion and to respond to the current trend of low thickness solutions, we favored a planar technology for the design of this new antennal solution. The delicate compromise between bandwidth, dimensions and electrical performance leads us to propose a new radiating print. In this article, we propose a very wide bandwidth rectangular patch antenna on a FR4 substrat, with insertion of the notches at the ground plane and shape modifications for the radiating element. Compared with conventional microstrip antennas, the

\*Corresponding Author : Hedi Sakli, hedi.s@eitaconsulting.fr



bandwidth is around 15 GHz for a reflection coefficient of -10 dB. A physical structure is proposed to minimize the mutual coupling between the elements constituting the MIMO system with four patches very close to each other. Two isolation techniques are studied and compared in this article. Starting with the use of an isolation technique called DGS (Defected Ground Structure) is to introduce changes to the structure of the ground plane to change the current distribution. In MIMO systems, the effect of the notch filter is applied in order to reduce the mutual coupling between the radiating antennas. The application of the DGS method is to introduce slits on the ground plane [10-12] The DGS solution is very easy to implement since its operation depends on the resonance frequency rather than the types of antennas, so a combination of this technique with the technique called "neutralization technique" (NL) used to decouple the two UWB antennas. MIMO placed side by side and involves inserting a line between the elements in a well-defined position or short-circuit when the antenna are positioned very closely on a small mass plane. Noting that the electromagnetic coupling presented between two patches nearby is mainly of the capacitive type [12,13]. Indeed, by introducing an inductance between the two patches, a rejection filter behavior allows decoupling [14,15]. A decoupling of the order of 14 dB is obtained in the operating band [3.2 - 17.7] GHz. The second solution is to use a structure based on metal rings (Split Ring Resonators or SRR) with a permeability of negative value. Four SRRs in series are located along the distance between two adjacent antennas and two opposite antennas forming the symbol (+) based on the upper layer of the FR4 substrate to separate the antennas from each other to ensure good isolation. Mutual coupling between the elements of the MIMO antenna systems can be greatly reduced, with isolation greater than 10 dB over the majority of the antennas operating band.

In this paper, the design of UWB antenna is presented. The coupling between four UWB-MIMO antennas using the two methods of isolation (NL and metamaterial) is minimized. The gain of isolation between antennas more than 15 dB using the neutralization line and more than 20 dB with the use of metamaterial are obtained while maintaining the operating band and radiation specifications of the MIMO antennas.

**2. Antenna characterization**

We start at the beginning of our design with a square-shaped printed antenna powered by microstrip line. The choice of the power line is based on the fact that this line must have a characteristic impedance of 50 ohms, adapted over a very wide frequency band. The geometry of this antenna consists of a rectangular patch printed on the top face of a FR4 type substrate. The ground plane is a partial plane printed on the bottom surface of the substrate. The reflection coefficient modulus of the initial antenna is greater than -10 dB for frequencies in the band [3 - 11] GHz. But in the band [11 - 16.7] GHz the modulus of reflection is less than -10 dB (see figure 1 curve a). This antenna is therefore not well suited over the entire frequency band studied (X, Ku and Ka bands). According to the influence of the modifications made on the base antenna, and in order to improve its characteristics and mainly its adaptation as well as obtaining an ultra-wide band operation The design is made by introducing some modifications on the structure of the base antenna, in particular on the shape of

the radiating element and by adding slots on the patch and on the ground plane; we present in this part our complete antenna with all the modifications made. Figure 2 presents the geometric shape as well as the dimensions of our antenna presented. The different characteristics of the antenna will be presented and commented. Figure 1 presents the geometry as well as the dimensions of the proposed antenna printed on a substrate FR4 of relative permittivity  $\epsilon_r = 4.4$ , loss tangent  $\tan \delta = 0.02$  and thickness equal to 1.6 mm. The parameters associated with the structure of the antenna studied are shown in Table 1.

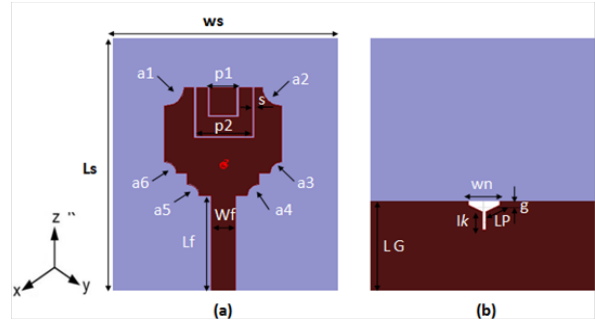


Figure 1: Structure of the patch antenna studied: (a) In front view (b) bottom view.

Table 1: Geometric parameters of the studied antenna.

Parameters	Values (mm)	Parameters	Values (mm)
$W_S$	25.52	$L_S$	31
$W_{Pa}$	14.52	$L_{Pa}$	14.52
$W_F$	2.85	$L_F$	13.52
$L_G$	12.62	$H_{Su}$	1.6
$a_1$	1.45	$g$	0.36
$a_2$	1.5	$l_l$	7.5
$a_3$	1.1	$L_p$	1.62
$a_4$	1.1	$wn$	3.1
$a_5$	1.1	$L_k$	0.75
$a_6$	1.1	$L_p$	2.35
$p_1$	10		
$p_2$	4		

This antenna has a reflection coefficient of -10 dB over the entire frequency band [3.1 - 16.8] GHz (Figure 2 curve b).

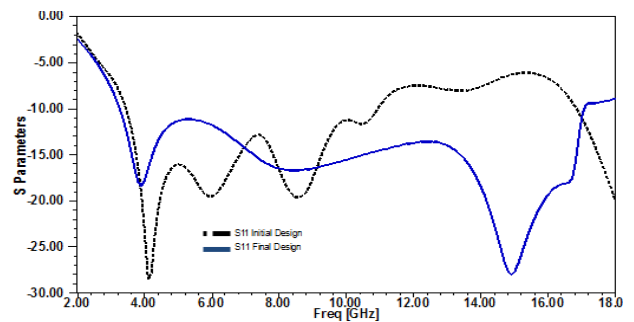


Figure 2: Reflexion coefficient S11 of the UWB antenna: (a) Initial design, (b) Final design.

The influence of modification is clearly visible in the improvement of the adaptation.

**3. NL Decoupling structure design**

At the beginning a research was done to show the effect of the neutralization line on the general radiating element and more

precisely on the insulation between the elements that constituted our system. The basic idea of this method was to compensate for the complex electromagnetic coupling existing between the neighboring antennas by opposite coupling reaction. As the coupling between the antennas is capacitive, the line mainly makes it possible to provide a reaction or an inductive effect to oppose the capacitive effect of the coupling between antennas [16]. This technique has been used to guarantee improved isolation of several multi-antenna systems [17]. Moreover, the neutralization line supports strong currents so that the direction of current is directed towards the antenna itself to radiate and not towards the power port of the second antenna. In addition, it is possible to cancel the coupling of all the paths [16]. Then this method is the one selected to improve the isolation of the four patch antennas of our multi-antenna system. The insertion of the line is done in the area where the amplitude of the currents is the highest, which corresponds to the zones of low impedances. A simple four-element structure has been used. The width and length of the microstrip antenna are the same. The separation distance between the four elements is  $0.15\lambda_0$ . The MIMO antenna structure is based on a FR4 type substrate  $60 \times 48$  mm in size with a permittivity ( $\epsilon_r$ ) of 4.4 mm and a thickness of 1.6 mm. The proposed antenna scheme is shown in figure 3. NL was placed between items like shown in Figure 4.

the parameters S11, S22, S33 and S44, which are in coincidence. The scattering parameters simulated are shown in figure 5. By comparing the two simulation results without and with NL, it is noted that the parameters of the Sii reflection coefficients (S11, S22, S33 and S44 are the same because of the symmetry of the structure) are not strongly modified, the MIMO antenna covered a very wide bandwidth of -10 dB.

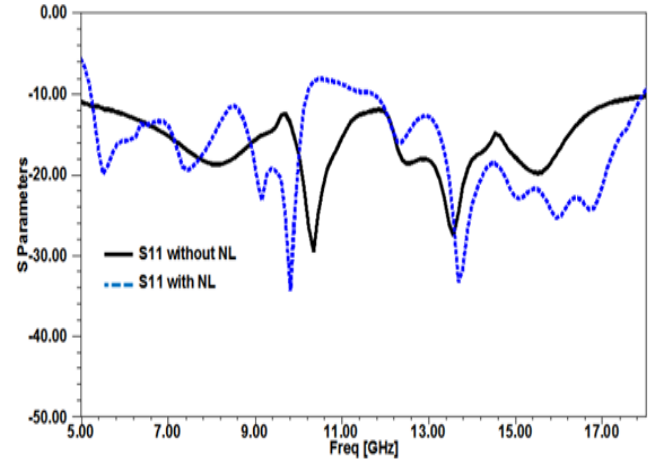


Figure 5: Reflexion coefficient S11 of the UWB antenna without and with NL

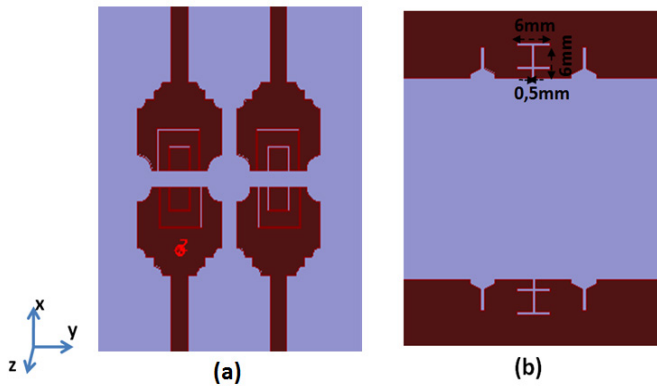


Figure 3: MIMO studied with four elements without NL.

### 3.2. Isolation Parameters Analysis

The transmission parameters  $S_{ij}$  from antenna  $j$  to antenna  $i$  ( $S_{21}$ ,  $S_{31}$  and  $S_{41}$ ) reveal and show that the adjacent antennas are strongly coupled with a decoupling method that is easy to design and execute compared to that presented in several articles. The parameter level is decreased for our current MIMO system. According to the results obtained by simulation, it has been found that the influence of an NL makes it possible to find an acceptable decoupling level for a network of four antennas. This helps us to create a model similar to the one created by simulation. Compared to the MIMO-UWB antenna without NL application, our studied MIMO antenna not only preserves the overall performance for each element, but also further minimizes the coupling of 21 dB at 15 GHz and 15 dB at 8 GHz and presents an isolation more than 15 dB, (see figures 6, 7 and 8).

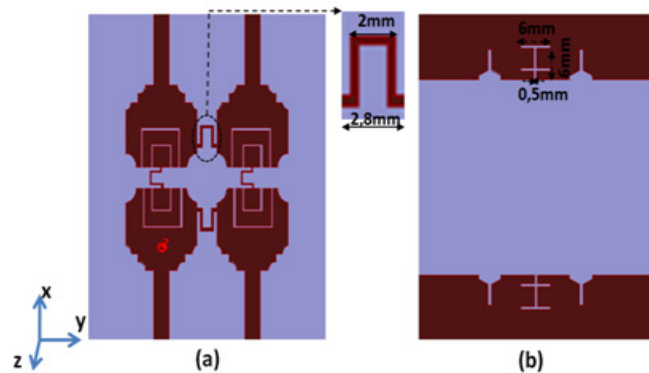


Figure 4: MIMO studied with four elements: with NL

### 3.1. Reflexion coefficient (Sii) Analysis

Several simulations have been carried out to find the optimal position of the neutralization line to maintain the bandwidth in adaptation. The simulation result has shown a small assignment on

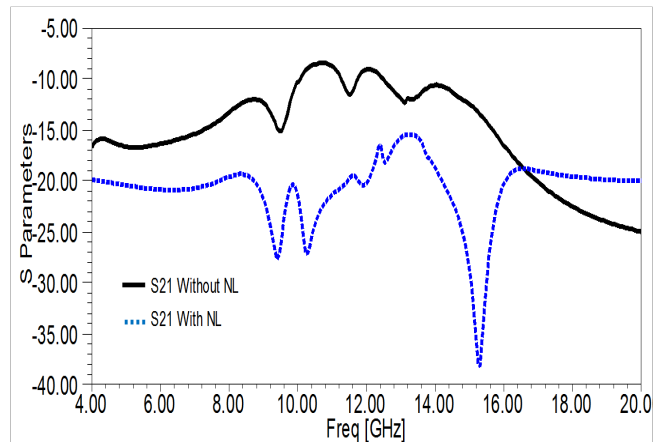


Figure 6: Parameters S21 simulated of MIMO antennas (adjacent) without and with NL

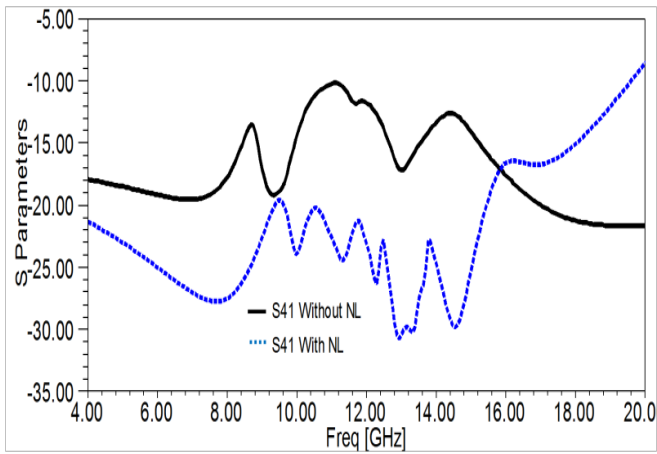


Figure 7: Parameters S41 simulated of MIMO antennas (opposite) without and with NL

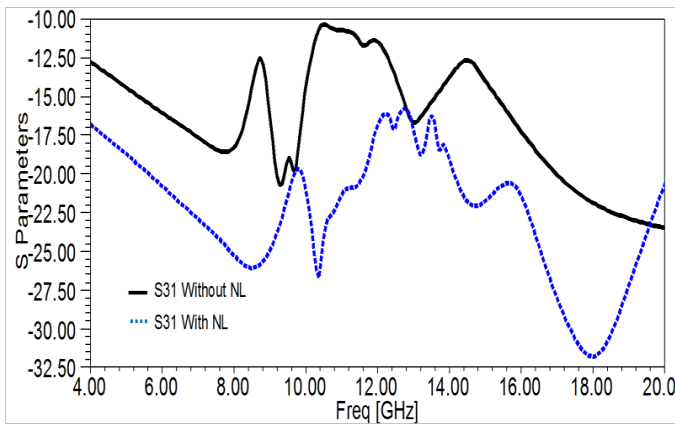


Figure 8: Parameters S31 simulated of MIMO antennas (symmetrical) without and with NL

#### 4. Structure and decoupling of metamaterials

Research has been carried out to ensure and obtain an electromagnetic mulberry allows to isolate the flux and the interference to the radiation of proximity of adjacent antennas. Subsequently, a proposed method based on the application of the metamaterial was presented which makes it possible to minimize the coupling levels [17]. So at the beginning a design of a SRR presented to ensure the operation around the band of frequencies mentioned initially and are suitable the impact on the resonance of the components of the MIMO antenna. The applied SRR unit cell has been dimensioned for band operation. The substrate used for the simulation is the FR4 which has a relative permittivity of 4.4, tangential losses of the order of 0.002 and a thickness of 1.6 mm. The external side of the square is equal to 2.4 mm. The width of the track in copper is 0.3 mm. The width of the cut of the rings is 0.34 mm (figure 9).

With the aim of guaranteeing isolation over our entire frequency band, we are doing a study on the size of the SRR aperture in order to see the influence of this variation on the resonance frequency of SRR. According to the simulation results mentioned in the figure 10 and figure 11, we notice well that we have a relationship of proportionality between the increasing of the opening for the two rings of our SRR and the resonant frequency that evolves with the opening.

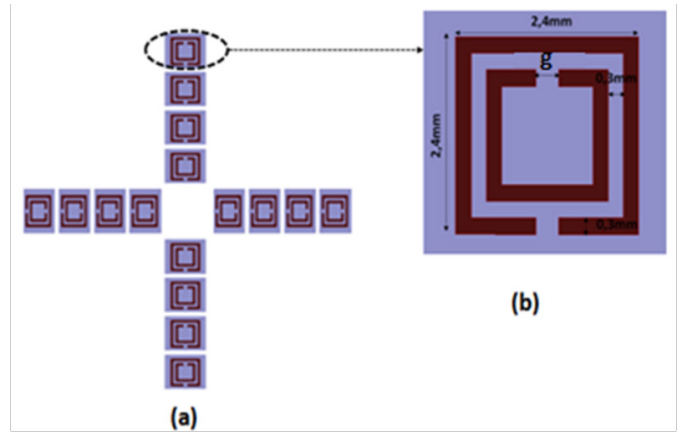


Figure 9: Geometric of studded split ring resonators: (a) 4x4 unit cells in front view and (b) Unit cell

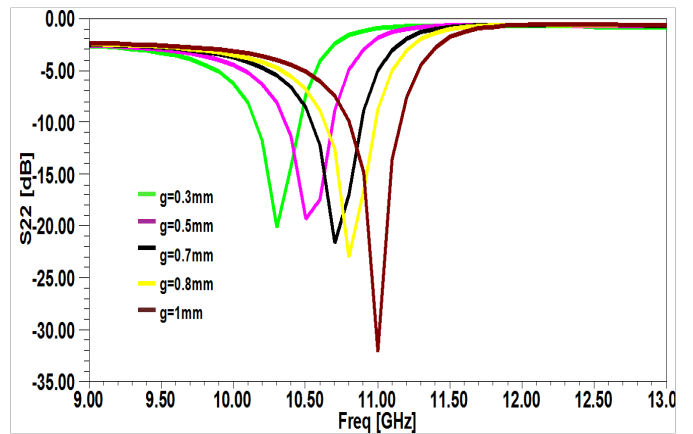


Figure 10: Parameter of S22 for several aperture values in the SRR

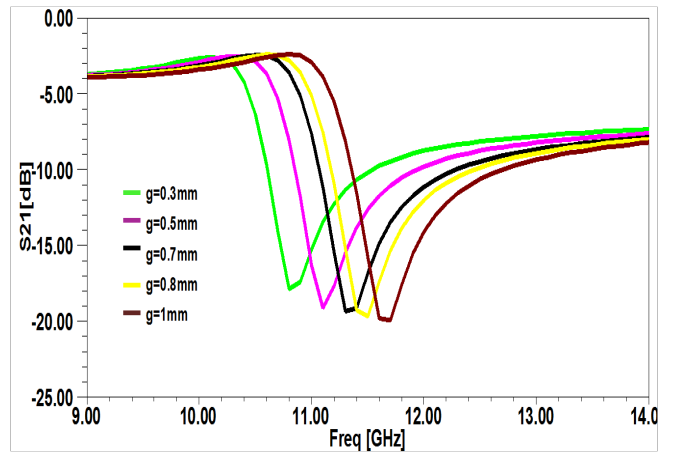


Figure 11: S21 parameters for several aperture values in the SRR

The structures are placed between the antennas at an optimized separation distance at  $0.15\lambda_0$  and are composed of 4 groups of SRRs over the substrate. Each group has four integrated SRR units between the antennas for good isolation between the antenna elements. This configuration is illustrated in Figure 12. In this part, we are going to study the influence of an SRR cell network between the two adjacent antennas. We have looked for presenting an electromagnetic blackberry in order to isolate radiation fluxes and interferences from the proximity of adjacent antennas. So a proposed solution based on the use of the

metamaterial has been presented which allows stopping or minimizing the propagation of surface waves, thus reducing the mutual coupling in a MIMO antenna.

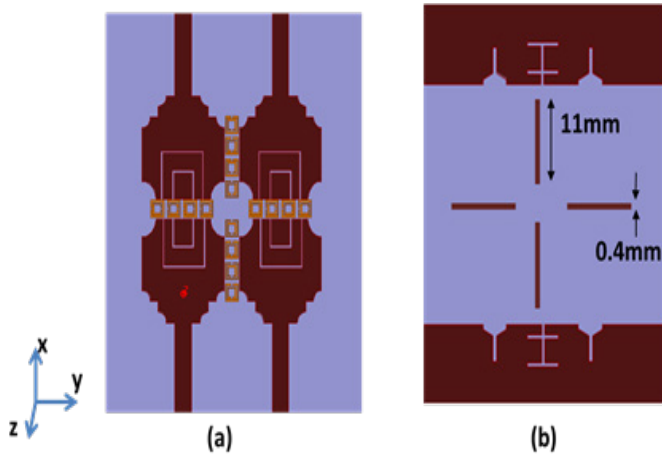


Figure 12: UWB MIMO antenna associated with SRR cells in front view and bottom view.

#### 4.1. Reflexion coefficient ( $S_{11}$ ) Analysis

We note that the simulated structure has a stability of the  $S_{11}$  reflection coefficients of four MIMO antennas with SRRs over the entire desired band. Figure 13 indicates the parameters  $S_{11}$  of the proposed antenna. The influence of the material is clearly visible in the improvement of the adaptation of the antenna. We can conclude that the structure with the application of the SRR contributed to the increase of the MIMO antenna performance in terms of reflection coefficient and consequently allowed us to obtain a better ULB structure.

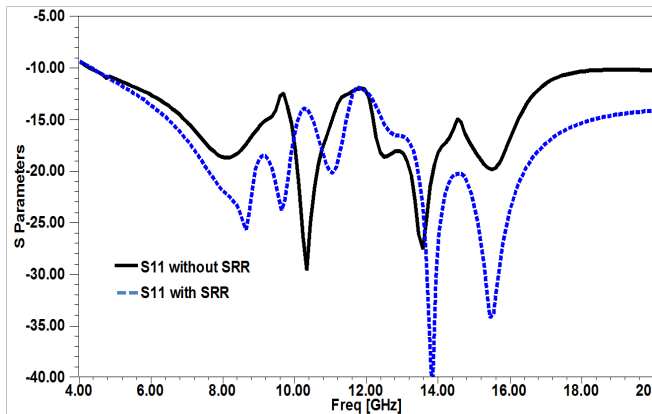


Figure 13: Reflexion coefficient  $S_{11}$  of the UWB antenna with SRR.

#### 4.2. Isolation Parameters ( $S_{i1}$ ) Analysis

Inter-element electromagnetic coupling presents a difficulty between the components during start-up. Here, a chain of separation between the elements is an assembly of two periodic networks consisting of metallic line and a resonator network makes it possible to have a negative permeability whereas the line network is characterized by a negative permittivity. The assembly of these two networks contributes to having a negative permittivity and permeability at the same time. The SRR chain at

the highest point of the substrate was used to ensure isolation improvement. As previously reported, the mutual coupling is more important in the case where the radiating elements are very close. For this reason, we are interested in this approach to the analysis of the mutual coupling between each two adjacent, opposite and symmetrical antennas. In fact, as shown in figures 14, 15 and 16, the initial mutual coupling measured in terms of transmission coefficient at the frequency of 10.7 GHz was -7.2 dB, -10.1 dB and -11.6 dB between antenna 1 and 2, 1 and 3, 1 and 4 respectively. After the use of SRR, the isolation becomes more improved to obtain the value of -24.3 dB, -22.2 dB and -27.6 dB between antenna 1 and 2, 1 and 3, 1 and 4 respectively. Thus, the condition of having a mutual coupling lower than -17 dB imposed to maintain the performance of a MIMO system.

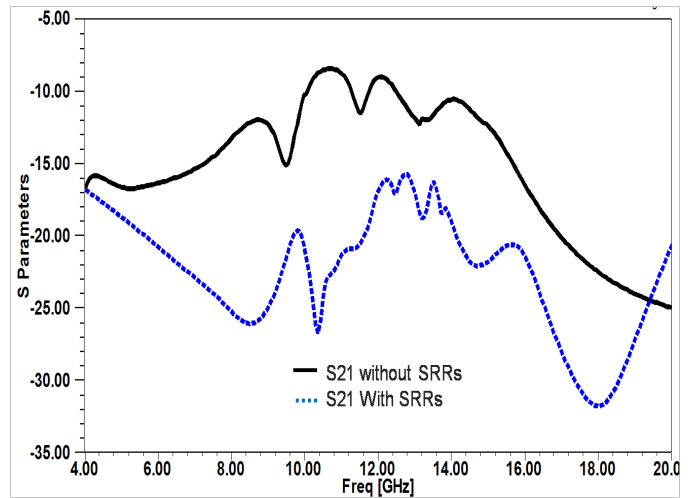


Figure 14: Parameters  $S_{21}$  simulated of MIMO antennas (adjacent) without and with metamaterial.

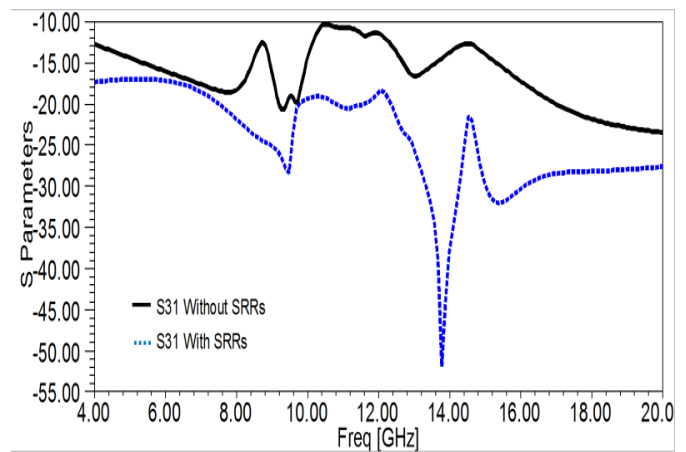


Figure 15: Parameters  $S_{31}$  simulated of MIMO antennas (symmetrical) without and with metamaterial.

The observation on the figures 14, 15 and 16 showing the transmission coefficients indicates better quality with reduced power losses across the desired band. An isolation protection gain of more than 10 dB over the entire band is achieved. This is explained by the isolation performance between the antennas with this predicted structure. This separation between the antennas ensuring the efficiency of the transmission system constituting our space links.



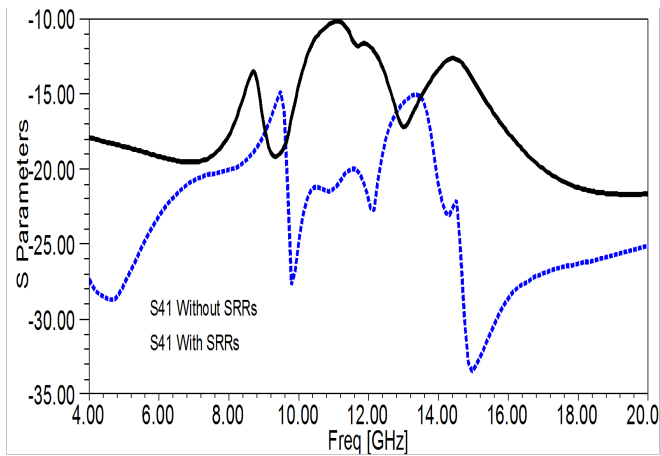


Figure. 16: Parameters S41 simulated of MIMO antennas (opposite) without and with metamaterial.

## 5. Conclusion

In this article, we presented a new structure of a MIMO antenna array that belongs to the UWB ultra-wideband UWB antennas categories. We presented several approaches to improve the performance of MIMO systems. The simulation relating to a MIMO antenna has been completely described, have shown great efficiency for the improvement of the isolation of a system consisting of four UWB antennas originally presented. The results of electromagnetic simulation have shown the gain provided by these techniques for increasing the isolation between antennas in the band of interest. A solution that seems to be relevant is obtained using the neutralization line technique. For this solution, the insulation in the UWB band is greater than 18 dB. Another solution made it possible to highlight the role of the split-ring resonator, in the design of UWB microband antennas with the insertion of periodic SRR structures. We were able to increase the isolation without losing the UWB characteristics. These results show that the proposed structures contribute to meeting the requirements of modern communication systems dedicated to 5G.

## References

- [1] M. A. Vázquez, *et al.*, "Precoding in multibeam satellite communications: Present and future challenges," *IEEE Wireless Commun.*, vol. 23, no. 6, pp. 88–95, Dec. 2016.
- [2] B. H. G. Gao, L. He, S. Wang, and C. Yang, "Investigation of A Reconfigurable Dual Notched UWB Antenna by Conceptual Circuit Model and Time-Domain Characteristics," *Microwave and Optical Technology Letters*, vol. 59, pp. 1326–1332, 2017.
- [3] A. Iqbal, O. A. Saraereh, A. W. and S. Bashir, "Mutual Coupling Reduction Using F-Shaped Stubs in UWB-MIMO Antenna", *IEEE Access* vol. 6, pp. 2755–2759, 2018.
- [4] I. Szini, A. Tatomirescu, and G. F. Pedersen, "On Small Terminal MIMO Antennas, Harmonizing Characteristic Modes with Ground Plane Geometry," *IEEE Antenna Propag. Trans. On*, vol. 63, no. 4, pp. 1487 - 1497, 2015.
- [5] B. H. G. Gao, L. He, S. Wang, and C. Yang, "Investigation of A Reconfigurable Dual Notched UWB Antenna by Conceptual Circuit Model and Time-Domain Characteristics," *Microwave and Optical Technology Letters*, vol. 59, pp. 1326–1332, 2017.
- [6] L. Malviya, R. K. Panigrahi and M. V. Kartikeyan., "A 2x2 Dual-Band MIMO Antenna with Polarization Diversity for Wireless Applications," *Progress In Electromagnetics Research C*, vol. 61, pp. 91-103, 2016.
- [7] A. Dadgarpour, M. S. Sorkherizi and A. A. Kishk, "Wideband, Low loss Magneto Electronic Dipole Antenna for 5G Wireless Network with Gain Enhancement Using Meta Lens and Gap Waveguide Technology Feeding," *IEEE Transactions on Antennas and Propagation*, vol. 64, no. 12, pp. 5094 - 5101, 2016.

- [8] M. S. Sharawi, S.K. Podilchak, M. T. Hussain and Y. M. M. Antar, "Dielectric Resonator Based MIMO Antenna System Enabling Millimeter-Wave Mobile Devices," *IET Microwaves, Antennas & Propagation*, vol. 11, no. 2, pp. 287 – 293, Jan. 2017.
- [9] G. K. S. Pandey, H. S. Bharti, P. K. Meshram, M. Kumar, "Design and Analysis of  $\Psi$ -Shaped UWB Antenna with Dual Band Notched Characteristics," *Wireless Personal Communications*, vol. 89, pp. 79-92, 2016.
- [10] R. B. Rani and S. K. Pandey, "A CPW-Fed Circular Patch Antenna Inspired by Reduced Ground Plane and CSRR Slot for Uwb Applications with Notch Band," *Microwave and Optical Technology Letters*, vol. 59, issue 4, pp. 745-749, 2017.
- [11] G. K. Pandey, H. S. Singh, P. K. Bharti and M. K. Meshram, "Design and Analysis of Multiband Notched Pitcher-Shaped UWB Antenna" *International Journal of RF and Microwave Computer-Aided Engineering*, vol. 25, pp. 795–806, 2015.
- [12] A. P. Singh, R. Khanna, and H. Singh, "UWB Antenna With Dual Notched Band For WIMAX and WLAN Applications," *Microwave and Optical Technology Letters* vol. 59, pp. 792–797, 2017.
- [13] T. Jiang, T. Jiao, and Y. Li, "Array mutual coupling reduction using L-loading e-shaped electromagnetic band gap structures," *International Journal of Antennas and Propagation*, vol. 2016, Article ID 6731014.
- [14] S. Zhang and G. Pedersen, "Mutual coupling reduction for UWB MIMO antennas with a wideband neutralization line," *IEEE Antennas and Wireless Propagation Letters*, vol. 15, pp. 166-169, 2016.
- [15] C. Abdelhamid, M. Daghari, H. Sakli and C. Hamrouni, "A New UWB-MIMO Multi-Antennas With High Isolation For Satellite Communications," *15th International Wireless Communications & Mobile Computing Conference (IWCMC)*, Maroc, pp. 152-155, 24-28 Jun 2019. (978-1-5386-7747-6/19/\$31.00 ©2019 IEEE).
- [16] T. Jiang, T. Jiao, Y. Li, and W. Yu, "A low mutual coupling MIMO antenna using periodic multilayered electromagnetic band gap structures," *Applied Computational Electromagnetics Society Journal*, vol. 33, no. 3, pp. 305-311, 2018.
- [17] K. Wei, J. Li, L. Wang, Z. Xing, and R. Xu, "Mutual coupling reduction by novel fractal defected ground structure band gap filter," *IEEE Transactions on Antennas and Propagation*, vol. 64, pp. 4328-4335, 2016.

# Antenna Radiation Performance Enhancement Using Metamaterial Filter for Vehicle to Vehicle Communications Applications

Marwa Daghari<sup>\*1</sup>, Hedi Sakli<sup>1,2</sup>

<sup>1</sup>MACS Research Laboratory, National Engineering School of Gabes, Gabes University, 6029, Tunisia.

<sup>2</sup>EITA Consulting 5 Rue du Chant des oiseaux, 78360 Montesson, France

## ARTICLE INFO

Article history:

Received: 28 November, 2019

Accepted: 12 February, 2020

Online: 30 March, 2020

Keywords:

Metamaterial

Frequency Selective Surface (FSS)

Antenna

V2V communications

## ABSTRACT

*In this work, an integrated metamaterial filter design in close proximity with monopole antenna is proposed for vehicular communication applications. A cylindrical screen formed by an array of metamaterial cells is designed to be reflective at 5.9 GHz in order to enhance antenna performance in intelligent vehicle transport systems. The unit cell proposed design based on Frequency Selective Surface (FSS) is made of a square loop element glued to a thin substrate to ensure a band-stop filtering behavior. This geometry is symmetrical providing the advantage of polarization independency and exhibiting angular stability up to 45° for both Transverse Electric (TE) and Transverse Magnetic (TM) modes. More importantly, antenna gain and directivity enhancement are illustrated when the cylindrical FSS layer is added at a small distance from the monopole radiator. Antenna bandwidth reduction is also detected due to the presence of the added FSS layer which is suitable for Vehicle to Vehicle (V2V) communications.*

## 1 Introduction

Nowadays, road traffic is becoming much heavier than before, so that intelligent communication between moving vehicles is even more important to improve road safety and optimize the flow of traffic [1] - [2]. Vehicular communication is an emerging wireless technology in which the major objective is to enable vehicles to interact with each other and share information about certain road issues. The V2V communication system is based on the IEEE 802.11p protocol where a Dedicated Short Range Communication system (DSRC) frequency of 5.8755.925 GHz is used for information exchanges between vehicles [3] - [4].

Wireless Access in Vehicular Environments (WAVE) has been achieved by antennas installed on the vehicle roofs and the performance of communication systems depends mainly on the configuration of the antennas. Generally, for wireless devices, a simple environment is required to ensure their proper operation. However that is not the case in an electromagnetic vehicular environment. Rather it is considered a complex environment due to the existence of a multitude of signals, systems, and very high electromagnetic interferences [5] - [6]. Electromagnetic Compatibility (EMC) becomes a solution to protect circuits and radio-receiving apparatus from disturbing effects. It depends on the ability of the equipment or systems to function satisfactorily in their electromagnetic environ-

ment without introducing intolerable electromagnetic disturbance to anything in that environment [7]. Shielding control technique consisting on filtering is a solution to ensure this EMC. In this case EMI signals will be stopped outside the operating band.

Commonly, Radio Frequency (RF) filters are added after the antenna in the circuit and then connected to it with a transmission line. But a RF filter with a bulky size is the major limiting factor that increases losses and circuit size. However, an integrating filter and antenna in a single component showed enhancement in the system performances by reducing losses, complexity and size [8]. Added filters are built with Frequency Selective Surfaces (FSS) [9] to realize remarkable shielding and preserve antenna radiation characteristics simultaneously. FSS is a periodic metamaterial structure assembly of one or two dimensions, either metallic patches on a substrate or as apertures in a thin conducting sheet, with a filtering behavior [10].

In literature, little research integrates the antenna with FSS based on metamaterials to reduce electromagnetic interferences and improve antenna radiation performances. In [11], a way based on FSS is proposed to reduce Radar Cross Section (RCS) of microstrip array antenna. Planar FSS cells with absorptive property over low band 1.9-7.5 GHz and a transmissive performance at 11.05 GHz is used to reduce the out-of-band RCS and simultaneously preserve the antenna array radiation performance. In [12] - [13], conical

\*Corresponding Author: Marwa Daghari, Email:marwadaghari@gmail.com

FSS radome located in close proximity of a monopole antenna is proposed and it shows a narrow pass-band response which is very useful for out of band RCS control. Ayan Chatterjee in [14], proposed a conformal cylindrical FSS for radiation diversity of monopole dielectric resonator antenna. This FSS reflective at 5 GHz is placed close to the antenna and improved the bandwidth from 26.8 % to 53.67 % in 4-6 GHz. Later, in [15], different curvatures of a conformal FSS to achieve beamwidth control in a dual band monopole antenna were demonstrated. Unit FSS design exhibit a miniaturization of  $0.07 \lambda_0$ . The design of a corner reflector based on this FSS cell achieves different beamwidth of 58 degrees and  $190^\circ$  with 8.30 and 6.8 dBi at 3.5 GHz and 5.8 GHz respectively.

In this paper we propose a 3-D cylindrical filter-antenna for wireless vehicular communication. This filter is designed to be reflective at 5.9 GHz frequency dedicated for wireless communication in a vehicular environment. It is made with an array of FSS cells blinded on cylindrical form and integrated with a monopole antenna at a close distance in order to enhance the radiation performance in gain, directivity and bandwidth. Simulation results show a good filtering response independently of incident wave angle and polarization. Also, an improvement in directivity, gain and S-parameters of antenna is observed. Moreover, bandwidth reduction is shown which is suitable for vehicular communication applications in an Internet of Things (Vehicles) environment.

The rest of the paper is structured as follows: Section II describes the proposed FSS unit cell design and simulations. Then, the design and characteristics of the antenna with the cylindrical filter at 5.9 GHz are detailed in section III. Simulation works, are also discussed in this section. Conclusions are finely summarized in the last section.

## 2 Proposed metamaterial filter

Frequency selective surface FSS are usually constructed from a periodic assembly of one or two dimensional resonant structures. These structures can be metallic patches of arbitrary geometries or their complementary geometry may have aperture elements similar to patches within a metallic screen [16]. In the neighborhood of the element resonances, these surfaces exhibit total transmission or reflection response depending on the FSS cell design. So, they may be categorize as having a low-pass, band-pass, band-stop and high-pass filter behavior [17]. The performance of FSS mainly depends on geometry, element size and spacing, dielectric thickness, electrical characteristics, the incident angle of the excitation wave and polarization. Later a new class of FSS called miniaturized FSS is investigated. In this class of FSS, instead of using a resonant structure, the constituting element consists of a lumped inductor and capacitor properly arranged in a compact form which is respectively coupled to the magnetic and electric fields of an incident wave. So, an L-C circuit filter is formed and the overall dimensions of the unit cell can drastically be reduced [10]. Figure 1 shows a capacitor formed between two adjacent metallic strips with a separation distance of  $s$ , where  $s \ll \lambda$ . If a vertically polarized TEM wave acts on this structure, positive and negative charges accumulate on the lower and upper strips respectively. This creates a capacitor whose capacity is proportional to the length of the ribbon  $L$ , and inversely

proportional to the separation distance  $s$  [10]. For a thin metal wire with a width of  $W$ , it acts locally as an inductance for a TEM wave whose magnetic field is perpendicular to the wire. By cascading the capacitive and inductive surfaces compactly, a parallel L-C circuit is formed and performs as a first-order resonator of  $f = \frac{1}{(2.\pi.\sqrt{LC})}$ . The manufacture of this type of circuit can be easily obtained by printing a capacitor and an inductor on both sides of the dielectric substrate.

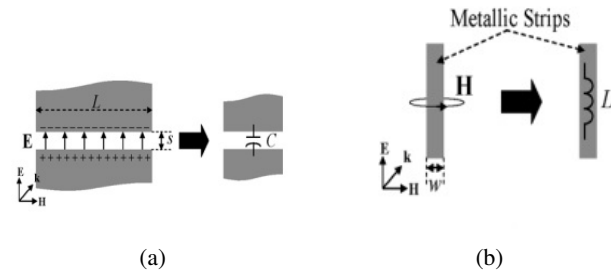


Figure 1: (a) Capacitance  $C$  is formed between the adjacent edges of two coplanar microstrips, (b) Inductance  $L$  associated with a metallic strip.

The first step in the design of a desired FSS cell using the proposed architecture above is to design the constituting resonators. The resonant frequency of the resonator can be determined by evaluating the effective inductance and capacitance of the unit cell. A first order approximation for the value of the capacitance is provided in [10].

$$C = \epsilon_0 \cdot \epsilon_{eff} \cdot \frac{2.D}{\pi} \cdot \log\left(\frac{1}{\sin\left(\frac{\pi.s}{2.D}\right)}\right) \quad (1)$$

The capacitance value is determined by the cell length  $D$ , the gap width between the two adjacent strip  $s$ , and the effective dielectric constant of the supporting substrate. The inductance value, however, is only determined by the length and width of the metallic strip  $W$  and  $D$  [10].

$$L = \mu_0 \cdot \frac{2.D}{2.\pi} \cdot \log\left(\frac{1}{\sin\left(\frac{\pi.W}{2.D}\right)}\right) \quad (2)$$

In the design of this miniature FSS it is important to choose the constituent unit, the substrate and the existence or not of FSS multilayers. All these parameters control the FSS frequency response such as bandwidth, operating frequency, sensitivity to polarization and incidence angle.

In this paper we propose an FSS unit cell with a stop-band filtering response at the resonance frequency of 5.9 GHz. It basically consists of a rectangular loop on the top side of RT5880 substrate with a relative permittivity of 2.2, dielectric loss tangent of 0.0009 and thickness of 0.127 mm. The unit cell has a dimension  $D$  and it is called periodicity. It has a size of  $\frac{\lambda_0}{7}$  compared to the wavelength at the operating frequency of 5.9 GHz. Parameter  $a$  represents the loop width and  $s$  is the gap between them. The whole cell geometry varies the symmetry propriety to the directions of polarization for horizontal and vertical polarized waves. This topology is illustrated in Figure 2 and Figure 3.

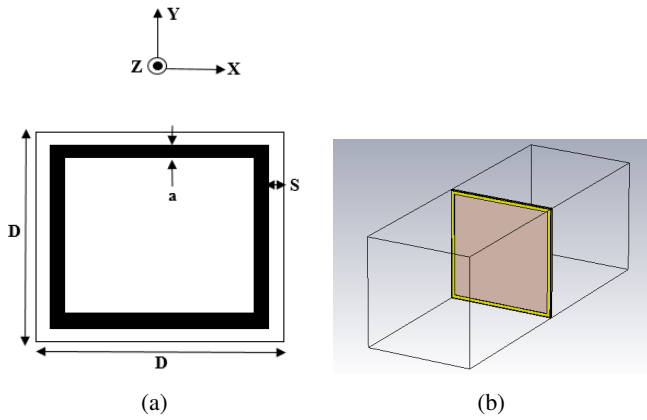


Figure 2: (a) FSS cell topology. (b) FSS cell on 3D.

### 2.1 Parametric study and simulations results

To synthesize the miniaturized FSS element, we initially assign its structural parameters according to the equations (1) and (2) in the CST studio as follows:  $D = 7 \text{ mm}$ ,  $a = 0.2 \text{ mm}$  and  $s = 0.05 \text{ mm}$ . A parametric study is done for periodicity value  $D$ , Loop width  $a$  and also for Gap between loops  $s$  in order to select the best configuration which gives more performances at 5.9 GHz resonant frequency. Transverse Electric (TE) mode is adopted in the parametric simulations. Based on results of reflection and transmission coefficients shown in Figure 4, it may be noted that, the FSS cell behaves as a pass-band filter. Furthermore, the variation of parameters  $D$ ,  $a$  and  $s$  have significant effects on the resonant frequency. In fact, for transmittive performances with the increase of periodicity  $D$ , loop width  $a$  and the gap  $s$ , the resonance frequency is shifted from 5.9 GHz towards high frequency band. For reflective performance it can be seen that, the reflection zero value gets close to 0 dB with the increase of all parameters values. Clearly, the transmittive and reflective performances are dependent on the geometric parameters of the FSS cell.

In Table.1, the optimized geometric parameters values of the proposed FSS cell are given.

Table 1: Optimized geometric parameter of FSS cell at 5.9 GHz.

Parameters	Value (mm)
Periodicity: $D$	7.1
Loop width: $a$	0.1
Gap: $s$	0.1

As a recommendation in telecommunication systems, it is important that the FSS must be isotropic with respect to different polarizations and also insensitive to the incident angles of the electric field. In this case it is necessary that the transmission and reflection characteristics remain invariant when the polarization and the angle of incidence of the incoming wave change. To put in evidence these characteristics, and using the values of the optimized geometric parameters of the FSS cell, the transmission and reflection coefficients are evaluated for both TE and TM polarization modes and they are shown in Figure 4. Simulation results indicate that the FSS cell has a stop-band filter response with a reflective -10 dB bandwidth of 8.66

GHz at 5.9 GHz. An isotropic cell behavior is also observed because of identical values of transmission and reflection coefficients in the TE and TM modes. Thus, the proposed metamaterial cell structure enables the polarization independent operation.

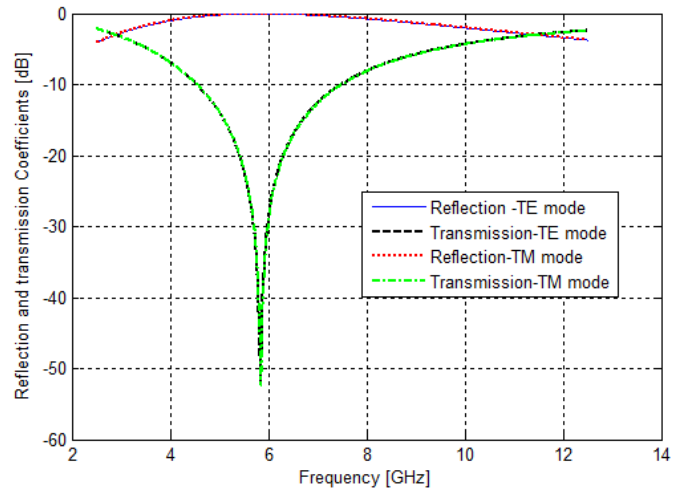


Figure 3: Transmission and reflection coefficients simulations for TE and TM modes at normal incidence.

The comportment of the cell under oblique incidence in TE and TM mode respectively, is calculated and depicted in Figures 5 and 6. From these results, we can see how the reflection zero changes when the incident angle increases over 45°. In addition, it is observed that the FSS response is opposite for TE and TM modes according to the change of incidence angles. In fact, the amplitude levels of the reflection coefficient is failing with the increase of the incidence angle value in TM mode but it is more rapid in TE mode. This is because the surface impedance is proportional to the angle of incidence in TM mode whereas in TE mode it is the opposite [10]. It is to be noted that the proposed structure is isotropic and it has a stable performance for different incidence angles and polarizations.

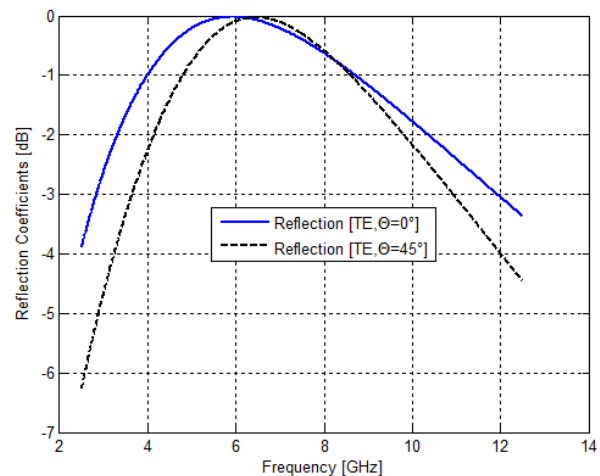
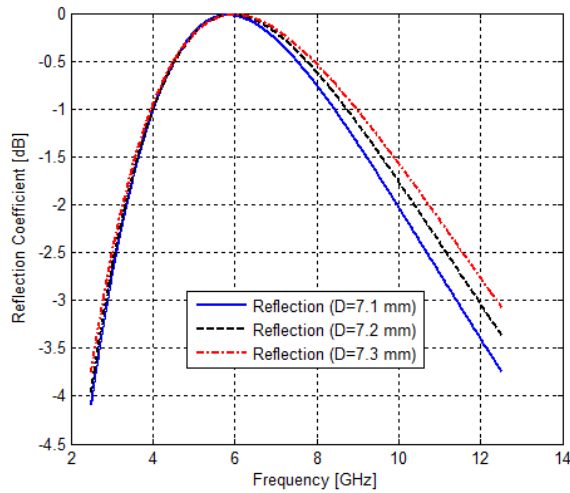
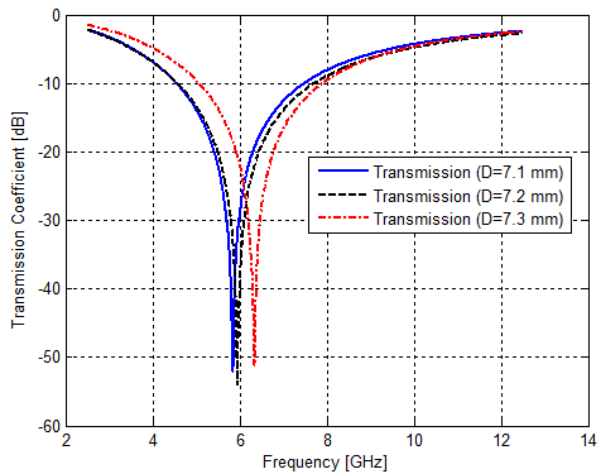


Figure 4: Reflection characteristics for TE mode at different angle of incidence.

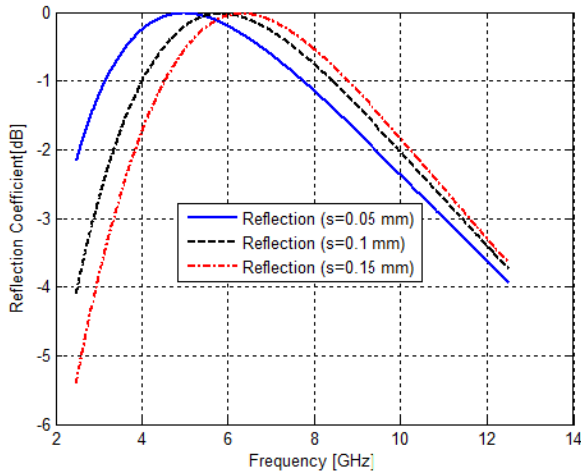




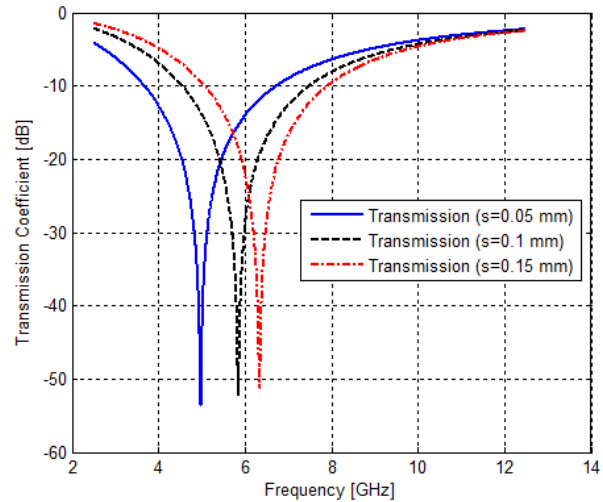
(a) Variation of reflection coefficient with the periodicity  $D$  as a parameter.



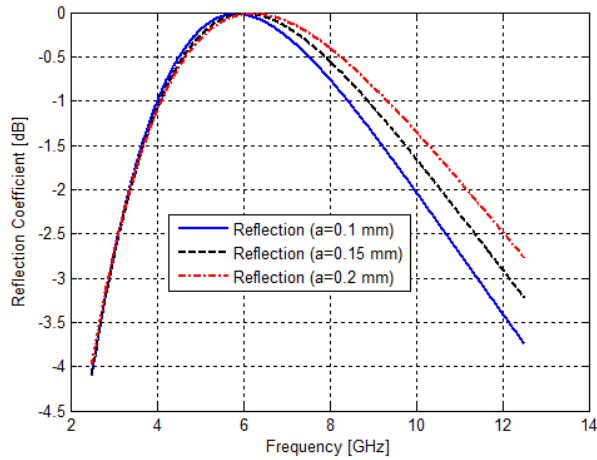
(b) Variation of transmission coefficient with the periodicity  $D$  as a parameter.



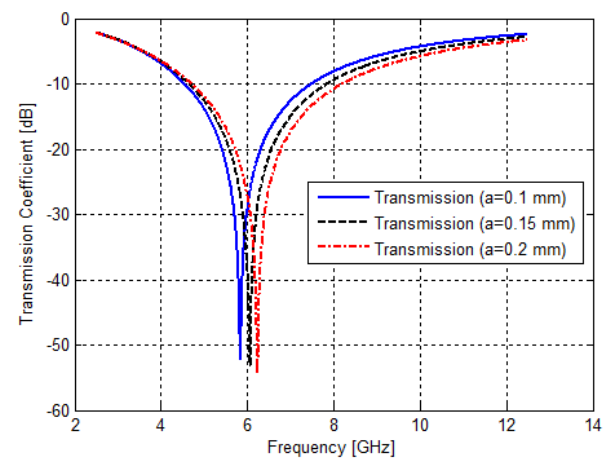
(c) Variation of reflection coefficient with the gap  $s$  as a parameter.



(d) Variation of transmission coefficient with the gap  $s$  as a parameter.



(e) Variation of reflection coefficient with the loop width  $a$  as a parameter.



(f) Variation of transmission coefficient with the loop width  $a$  as a parameter.

Figure 5: Simulated transmission and reflection coefficient value of proposed FSS unit cell.

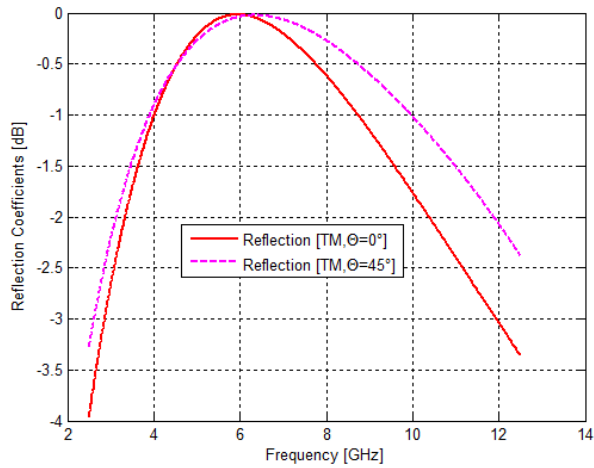


Figure 6: Reflection characteristics for TM mode at different angle of incidence.

### 3 Integrated design of antenna and meta-material filter

As is well known, the monopole antenna is widely used in V2V communications because of its omnidirectional radiation characteristics [18]. So, it has been chosen as the reference antenna. It is designed to operate at 5.9 GHz with a PEC circular reflecting ground plane. Large ground plane with Radius of 48 mm ( a distance of  $\lambda$  ) is taken to accommodate after, the integrated curved FSS. The length of the PEC wire  $L$  is 11.75 mm acting as a quarter-wave monopole and his radius ( $R_m$ ) is taken 0.45 mm. This monopole is fed by a 50  $\Omega$ . The proposed antenna design is shown in Figure 7.

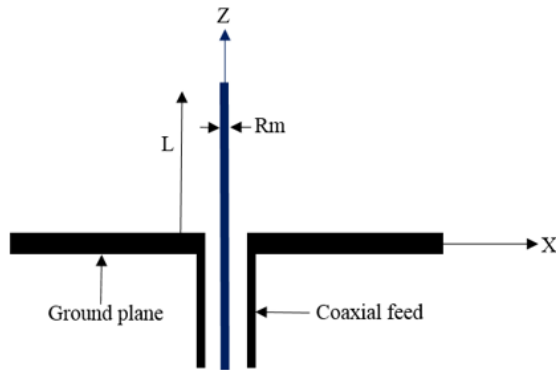


Figure 7: Cross-section view of the monopole antenna.

In order to verify the effect of the proposed FSS on bandstop filtering, an array of  $9 \times 42$  unit cells as studied above is designed and then mapped on a cylindrical curved surface. The radius of the cylinder is chosen to keep the radial distance ( $R_c$ ) between the antenna and the reflector around  $\lambda$  (near to 48 mm) with respect to the 5.9 GHz center frequency. This conformal FSS is then placed above the antenna ground plane. The monopole is laid on the center axis of the cylindrical FSS radome to keep axi-symmetry of the whole structure. The filter-antenna design is shown in Figures 8 and 9.

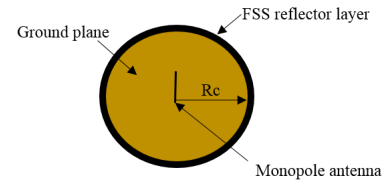


Figure 8: Top view of monopole with conformal FSS reflector.

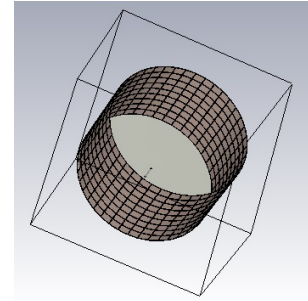


Figure 9: 3-D view of monopole with conformal FSS reflector.

Simulations of the composite design with and without cylindrical FSS are performed with CST-microwave studio in order to study the performance of the FSS filter when it is added to the antenna. The simulated reflection coefficient ( $S_{11}$ ) of the antenna with and without the conformal reflector are shown in Figure 10. It can be see from this figure, that the input reflection coefficient value changes significantly and was improved from -16.11 dB to -26.85 dB at 5.9 GHz. Furthermore, -10 dB bandwidth of the antenna decreases from 1.35 GHz to 239 MHz around the 5.9 GHz center frequency. So, it is much narrower which is very suitable for V2V communication in Dedicated Short Range Communication system (DSRC) frequency.

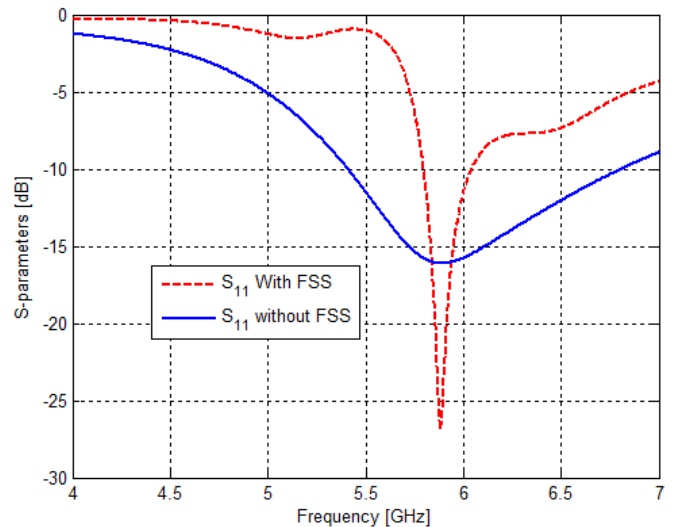


Figure 10: Simulated input reflection coefficient  $S_{11}$  of the antenna with and without curved FSS.

Radiation patterns with  $\phi=90$  at 5.9 GHz of the monopole antenna and the corresponding FSS filter are shown in Figures 11 and 12. From these patterns, omnidirectional radiation characteristics

of the monopole antenna are kept. It is also clearly observed that with FSS, the antenna radiates more directivity. In fact, directivity was improved from 4 dBi to 5.54 dBi with the integration of the conformal FSS reflector. In addition, antenna gain increases from 4 dBi to reach 5.55 dBi with the FSS layer at 5.9 GHz. Total radiation efficiency of 95% of the antenna is also noted in the presence of the proposed cylindrical conformal FSS reflector layer. These results can be explained by the presence of constructive interferences of the phase component of radiated and reflected waves in the direction opposite to the FSS [19].

So, based on the above simulated results, one can deduce that the radiation characteristics of antenna were improved. The conformal FSS cylindrical layer can act as a RF filter which is directly added on to the antenna. It can be used in reducing interferences and shielding antenna especially in electromagnetic vehicular environment.

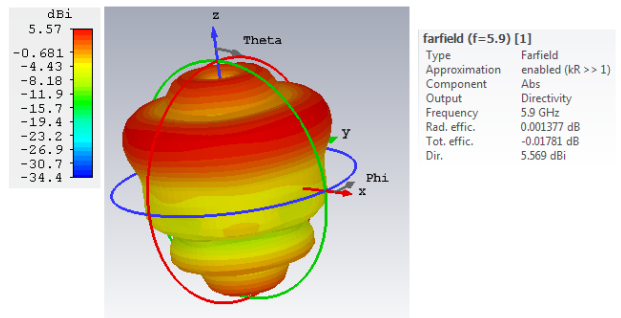


Figure 13: 3-D radiation pattern of monopole antenna with FSS reflector layer.

## 4 Conclusions

Due to the unreliable characteristics of the wireless medium, performance guarantees concerning the quality of the communication cannot be easily given. EMI in electromagnetic vehicular environments can distort the function of wireless devices. Therefore, the use of filter added on the antenna may be very beneficial to reduce the EMI effect. In this paper, a cylindrical conformal filter-antenna for V2V application is proposed. This design based on the cylindrical resonant FSS screen and placed at a small distance from the monopole element, enhances the radiation performance at 5.9 GHz. It provides an improvement in directivity by 1.55 dBi, in gain by 1.5 dB and also demonstrates also a narrow bandwidth which is mainly recommended for V2V communications. These results were successfully demonstrated by numerical simulations and in a future work by experimental prototypes. Moreover, due to its design simplicity and having only one layer, this filter should bear a low fabrication cost.

## References

- [1] Yang, Q., Wang, H., "Towards trustworthy vehicular social network," *IEEE Communication Magazine*, Vol. 53, No. 8, 42-47, 2015.
- [2] Aisopoulos, P., Kantartzis, N., Zygiridis, T., Kosmanis, T., *system "emi characterization on automotive electronics."*, 2010.
- [3] Groupe, L. W., and al., "IEEE standard for wireless access in vehicular environments (wave)-multi-channel operation," *IEEE Std*, 1609-4, 2016.
- [4] Khairnar, V., D., Kotecha, K., "Performance of vehicle-to-vehicle communication using IEEE 802.11p in vehicular ad-hoc network environment," *arXiv preprint arXiv: 1304-3357*, 2013.
- [5] Rakhshan, A., "The effect of interference in vehicular communications on safety factors," *arXiv preprint arXiv:1706.05758*, 2017.
- [6] Schmidt-Eisenlohr, F., "Interference in vehicle-to-vehicle communication networks", feb. 9, 2010.
- [7] Rybak, T., Steffka, M., "Automotive electromagnetic compatibility (EMC)," *Springer Science and Business Media*, 2004.
- [8] Chuang, C., T., Chung, S. J., "New printed filtering antenna with selectivity enhancement," in *2009 European Microwave Conference (EuMC). IEEE*, 747-750, 2009.
- [9] Bayatpur, F., Sarabandi, K., "Multipole spatial filters using metamaterial based miniaturized element frequency selective surfaces," *IEEE Transactions on Microwave Theory and Techniques*, Vol. 56, No. 12, 2742-2747, 2008.
- [10] Sarabandi, K., Behdad, N., "A frequency selective surface with miniaturized elements," *IEEE Transactions on Antennas and Propagation*, Vol. 55, No. 5, 1239-1245, 2007.

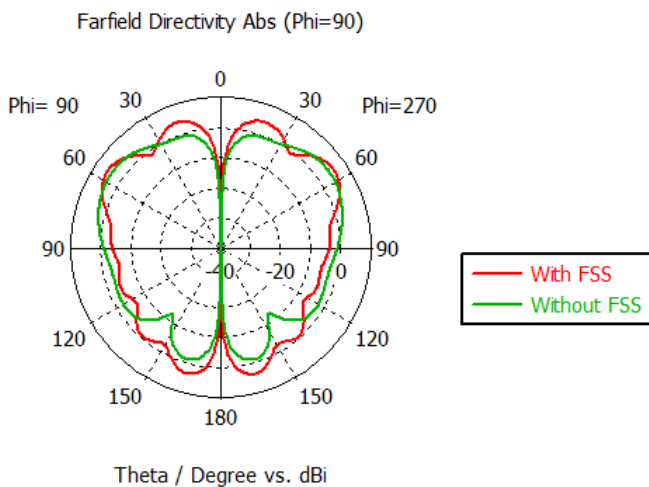


Figure 11: 2-D view of radiation pattern (directivity) of monopole antenna with/without FSS layer.

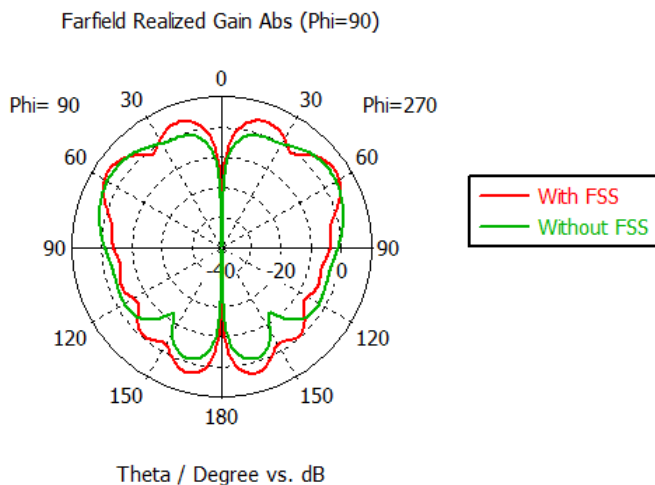


Figure 12: 2-D view of radiation pattern (gain) of monopole antenna with/without FSS layer.

- [11] Xue, J., Jiang, W., Gong, S., "Wideband rcs reduction of microstrip array antenna based on absorptive frequency selective surface and microstrip resonators," *International Journal of Antennas and Propagation*, Vol. 2017, 2017.
- [12] Lin, B., Du, S., Zhang, H., e, X., "Design and simulation of frequency selective radome together with a monopole antenna," *Applied Computational Electromagnetics Society Journal*, Vol. 25, No. 7, 620-625, 2010.
- [13] Zhou, H., Qu, S., Li, B., Wang, J. Ma, H., Xu, Z., Peng, W., Bai, P., "Filter-antenna consisting of conical fss radome and monopole antenna," *IEEE Transactions on Antennas and Propagation*, Vol. 60, No. 6, 3040-3045, 2012.
- [14] Chatterjee, S. K., Parui, A., "Frequency dependent directive radiation of monopole dielectric resonator antenna using a conformal frequency selective surface," *IEEE Transactions on Antennas and Propagation*, vol. 65, no. 5, 2233-2239, 2017.
- [15] Mondal, K., "Bandwidth and gain enhancement of microstrip antenna by frequency selective surface for wlan, wimax applications," *Saadhana*, Vol. 44, No. 11, 233, 2019.
- [16] Bayatpur, F., Sarabandi, K., "Single layer high order miniaturized element frequency selective surfaces," *IEEE Transactions on Microwave Theory and Techniques*, Vol. 56, No. 4, 774-781, 2008.
- [17] Munk, B. A., "Frequency selective surfaces: theory and design", *John Wiley and Sons*, 2005.
- [18] Mishra, V., Abegaonkar, M. P., Kurra, L., Koul, S. K., "A configuration of fss and monopole patch antenna for bidirectional gain enhancement applications," in *2018 IEEE Indian Conference on Antennas and Propagation (InCAP)*, IEEE, 1-4, 2018.
- [19] Li, J., Zeng, Q., Liu, R., Denidni, T. A., "A gain enhancement and flexible control of beam numbers antenna based on frequency selective surfaces," *IEEE Access*, Vol. 6, 6082-6091, 2018.



## Shear Strength of Unreinforced Masonry Walls Retrofitted with CFRP

Sanaa El Malyh<sup>\*1</sup>, Azzeddine Bouyahyaoui<sup>1</sup>, Toufik Cherradi<sup>1</sup>, Ancuta Rotaru<sup>2</sup>, Petru Mihai<sup>3</sup>

<sup>1</sup>Department of Civil Engineering, Mohammadia School of Engineer, Mohammed V University of Rabat, Morocco.

<sup>2</sup>Department of Transportation Infrastructure and Foundations, Gheorge Asachi Technical University of Iasi, Faculty of Civil Engineering and Building Services, Romania.

<sup>3</sup>Department of Concrete Structures, Building Materials, Technology and Management, Gheorge Asachi Technical University of Iasi, Faculty of Civil Engineering and Building Services, Romania.

### ARTICLE INFO

Article history:

Received: 14 February, 2020

Accepted: 19 March, 2020

Online: 27 March, 2020

Keywords:

Stiffness

Strengthening

Composite materials

Carbon fiber reinforced polymer

Unreinforced masonry wall

### ABSTRACT

This paper investigates the in plane behavior of unreinforced masonry (URM) walls externally strengthening on both sides by different configurations of unidirectional carbon fiber reinforced polymer (CFRP) wraps. In order to evaluate the effectiveness of using the strengthening systems to improve the in plane behavior of masonry walls, the experimental program was conducted by testing four specimens. Initially, URM wall without retrofitting system; considered as a reference; was tested. The other specimens were retrofitted on both sides by different configurations of unidirectional CFRP wraps. Walls were tested following diagonal tensile (shear) test method. Then the effect of position, spacing, and reinforcement ratio on ductility, stiffness, shear behavior and failure modes of URM wall were evaluated. Experimental results confirmed the effectiveness of using CFRP in improving energy dissipation, strength, stiffness and ductility of URM wall. Furthermore, the strengthening system affected in a direct way the shear capacity and the deformability of URM walls.

## 1. Introduction

URM walls are widely used in many structures around the world due to many factors, like cost-effective, time of construction and durability; they are constructed by using different materials (bricks, stones, mortar, etc.). The interaction between their different elements influence in a direct way their behavior, which is characterized, in the most cases by diagonal shear failures, sliding shear deformations and compression failures [1]. The seismic assessment of existing buildings in Basel indicates that during a moderate earthquake about 45% to 80% of existing URM buildings will experience damages grade 4, equivalent to heavy damage or grade 5 which correspond to destruction [2].

URM walls still have many limitations; they are sensitive to shear and tensile forces produced by seismic loads. Besides, after earthquakes, several damages were occurred in buildings; but the most important ones were located in URM walls [3]. The fact that URM walls are more vulnerable to damage during earthquakes,

push many researchers to investigate the influence of vertical compression due to different loads, in plane and out of plane lateral loading on unreinforced masonry walls [4]. The infill panel damage depends on various parameters, for [5], it is related to the lack of connection between crossing walls, improper location and dimensions of openings. On the other hand, for [6], it depends on many factors, but in most cases, it is related to the use of inappropriate materials, inadequate masonry units, incorrect cross section of the wall, irregular wall openings and improper roofing. However, the probability of out of plane failure enhances because of the inappropriate connections between crossing walls, openings placement and the absence of connecting units between external and internal leaves of the wall sections [7]. The masonry piers subjected to in plane-loading shows different types of failure mechanisms [8], the first type is rocking failure, which appears when the horizontal load increase, it is characterized by bed joints cracks in tension, shear that appears by the compressed masonry and finally by the overturning of the wall and simultaneous crushing of the compressed corners. The second type is shear cracking, appeared when the inclined diagonal cracks performed

\* Sanaa EL MALYH, Email: selmalyh@gmail.com

at peak resistance. For the last failure mechanism, it performed when walls under reversed seismic loading show important sliding planes, which developed in bed joints with tensile horizontal cracks. The shear compression behavior of unreinforced masonry walls was studied also by [9]; the results show that the comportment of brick masonry walls under seismic loading is influenced by their height/width ration and by the vertical stress. Under seismic loading, URM walls show a strong degradation in stiffness and strength, which produced many damages in buildings. In literature the behavior of URM walls, and especially when it was considered as compression elements had been widely studied, furthermore, the necessity of using FRP as strengthening systems to reinforce URM walls with FRP was investigated by many researchers [10]-[15], also, their effectiveness in reinforcing masonry structures was highlighted by [16]-[18]. Sheets of unidirectional carbon fiber or glass fiber placed on two sides of the walls, which were subjected to diagonal compression to determine the shear strength and shear elastic modulus of retrofitted masonry walls; results indicate an increase of 55% of strength [19]. For [20], the application of fiber reinforced polymer grids to new or existing buildings is very easy and cheap, it permits to enhance strength and energy dissipation. Other researchers [21] tested URM clay units walls retrofitted by FRP composites rods and laminates under diagonal loading to deduce their shear performance. Rods were placed on masonry bed joints. The pseudo-ductility and the shear capacity increases up to 200%. One-side strengthened walls did not indicate an important increase in pseudo-ductility. However, for two-sides symmetrical strengthening, wall results show an increase in the ultimate load and the pseudo-ductility.

The shear collapse mechanisms of one face retrofitted panels reinforced with different configuration FRP laminates subjected to diagonal compression was not remarkably modified. However, the two-side retrofitted panels show less brittle failure and an increase in the ultimate capacity [22]. Additional researchers [23] tested panels retrofitted on one side by cementitious matrix grid composite (CMG) system, results indicate that at the ultimate stage, the cracks did not pursue the line of action of the splitting load but they follow the line of minimum resistance. The failure of some panels appeared in bed and head joint of mortar, for the shear-capacity, it was characterized by the feeble connection between mortar and units-Tuff stones, but the failures of other panels were characterized by debonding along the mortar joints forming a stepped appearance. Comparing the efficiency of different configurations of reinforcing systems applied on URM, the full surface coverage and inclined plates retrofitting systems are the most effective configurations [24].

The principal alternative of FRP is an innovative composite materials system, and particular type of textile-reinforced mortar (TRM) it's a Fabric Reinforced Cementitious Matrix (FRCM) material, which contain fibers embedded into an inorganic matrix, that characterized by better homogeneity with masonry because of its small content of polymeric resin. There is different type of FRCM that depends in which type of textiles they were produced (steel, glass, basalt, carbon, aramid. etc.) and depends on the textile characteristics (unidirectional or bi-directional). FRCM system had been studied by many researchers [25] and [26], which studied experimentally FRCM material that constituted from dry fiber grid in inorganic matrix with short fibers in tensile and bond.

In addition, [27] performed a shear test on historic walls strengthened by means of jacketing with GFRP (Glass Fiber Reinforced Plastics) mesh, implanted in an inorganic matrix; results had shown an important amelioration in lateral load-carrying capacity of up to 1060% while compared to the control panels, in addition, the shear parameters were identified by [28, 29-30]. The behavior of half-scale single leaf unreinforced masonry walls retrofitted by composite (URM-WRC) was tested under dynamic in-plane loading to analyze the behavior of URM walls with and without composite material [31]. [32] Had used a recent retrofitting technique in URM walls, which was tested under diagonal compressive force, results show that FRP systems enhance the shear strength of the walls.

Recently, NSM FRP attracted an important amount of researchers, because it affords important advantages. Usually, it used to retrofit reinforced concrete structures. The NSM procedure starts with surface preparation, groove sawing and application of the adhesive. This technique has a high adherence with retrofitted surface, and more protected by the material that cover the NSM material from different type of damages. The NSM FRP system is better than externally bonded FRP [33]. For [34], the bond behavior of FRP-concrete depends on the strength of the concrete and the adhesive, cross-section of retrofit system (FRP), spacing between FRP reinforcement and concrete edge, also by spacing between FRP, bond length and characteristics of different types of materials. In regards to NSM method, the most effectiveness retrofitting systems to work with is thin rectangular strip because it has many advantages, like decreasing of debonding, and increasing confinement around the thin rectangular strip [35].

## **2. Experimental Program**

### *2.1. Materials Characterization*

Clay brick units were tested under uni-axial compressive machine in accordance with ASTM C67 [36]; the average compressive strength is 11.28N/mm<sup>2</sup>, and for the maximum strain is 0.074 and the modulus of elasticity is 148.30N/mm<sup>2</sup>.

For the first types of mortar used in the construction of the walls, six cubes of mortar of each type were tested under uni-axial compressive test following ASTM C109/C109M [37]. For the mortar type M5 the average compressive strength is 3.31N/mm<sup>2</sup> corresponding to strain of 0.0015 and modulus of elasticity of 2203.52N/mm<sup>2</sup>. For the mortar used on the surface of the wall the average compressive strength is 13.85 N/mm<sup>2</sup>, the maximum strain is 0.00038 and modulus of elasticity is 36579.18 N/mm<sup>2</sup>. Following EN 1015-11 [38], nine normalized mortar specimens were tested to determine the flexural and compressive strength of mortar applied to wall sides and to bed and head joints of walls, models were tested under three-point bending, then the obtained pieces of flexural test were tested in compression. The compressive strength of the first type of mortar is equal to 4.47N/mm<sup>2</sup> and for the second type is 27.84N/mm. More details about the properties of different materials are presented in the table 1.

Sikadur 330, constituted from thixotropic epoxy based impregnating resin and adhesive, mixed in a ratio of 4:1, were used for impregnation of six CFRP coupons with dimensions of

Table 1: Details about different materials

Material types	Dimensions (mm)	Type of test	Standard used	Compressive strength(N/mm <sup>2</sup> )
Mortar ( Apply on bed and head of joints)	40*40*160	Flexural and compression strength	EN 1015-11	4.47
	50*50*50	Compression strength	ASTM C109/C109M	3.31
Mortar (Apply on wall surface)	40*40*160	Flexural and compression strength	EN 1015-11	27.84
	50*50*50	Compression strength	ASTM C109/C109M	13.85
Clay bricks	240*115*63	Compression strength	ASTM C-67-05	11.28
Masonry prism (3 units of brick linked by mortar)	240*200*63	Compressive test	ASTM C1314 [39]	10.83
Masonry prism (2 units of brick linked by mortar)	240*130*63	Bond strength of mortar-masonry	ASTM C952[40]	17.43

15x250mm. First, the dry specimens were put on a thin layer of epoxy resin, which were applied on plastic fixed on regular surface, and another thin layer of epoxy applied on coupons, then second plastic used to cover the specimens. The air removed by using a grooved roller, then extra epoxy resin removed by covering specimens with a flat surface of wood. Characteristics of epoxy given by the manufacturer: for flexural E-Modulus, Tensile Strength and Tensile Modulus of Elasticity values are respectively 3800N/mm<sup>2</sup>, 30N/mm<sup>2</sup> and 4500N/mm<sup>2</sup>.

Tabs with dimensions of 15\*56mm were fixed to all the extremities of coupons by adhesive Sikadur-30, which based on a mixture of epoxy resin and special filler in a ratio of 3:1. All the specimens were cured for seven days before being tested on a tensile machine following ASTM D3039/D3039M [41]. The table 2 presents the mechanical characteristics of CFRP used.

Table 2: Characteristics of fibers

Material type	Fibers density	Thickness (mm)	Elongation at rupture
CFRP (ISO10618) [42]	1.82 g/cm <sup>3</sup>	0.129	1.7 %
	Tensile strength (N/mm <sup>2</sup> )	Tensile modulus of elasticity (N/mm <sup>2</sup> )	
	>4000	230000	
Laminate (EN 2561) [43]	0.129	Nominal thickness (mm)	Tensile strength (N/mm <sup>2</sup> )
		Average Characteristics	
		3500	3200
		Modulus of Elasticity in Tension (KN/mm <sup>2</sup> )	
		225	220

2.2. Preparation of Different Specimens

The experimental study passed through several stages; first, URM walls with dimension of 1200\*1200\*115mm were constructed by qualified masons using clay brick masonry units with dimension of 240\*115\*63mm, linked by a 10mm joint layer of mortar, then URM walls were cured for 28 days. The procedure of strengthening masonry walls started with surface coatings, which consist of preparing walls by cleaning the both sides of walls and especially the joints from dust with a high pressure of air. Before the application of strengthening materials, walls sides were wetted, and then a thin layer of primer and mortar of a nominal thickness of 12mm were applied to walls surfaces. The

main role of primer and mortar is to provide a leveled surface of URM walls; 28 days after, different configurations of CFRP wraps were applied to wall surface after applying the first epoxy resin layer, then a second layer was used to fix CFRP wrap. Then all the strengthened walls were cured for seven days before being tested (figure 1).



Figure 1: Different steps of retrofitting URM wall by the CFRP wraps



2.3. Description of Different Configurations and Test Instrumentation

Details of the aforementioned walls strengthened by diverse configurations of CFRP (figure 2) are illustrated in table 3.

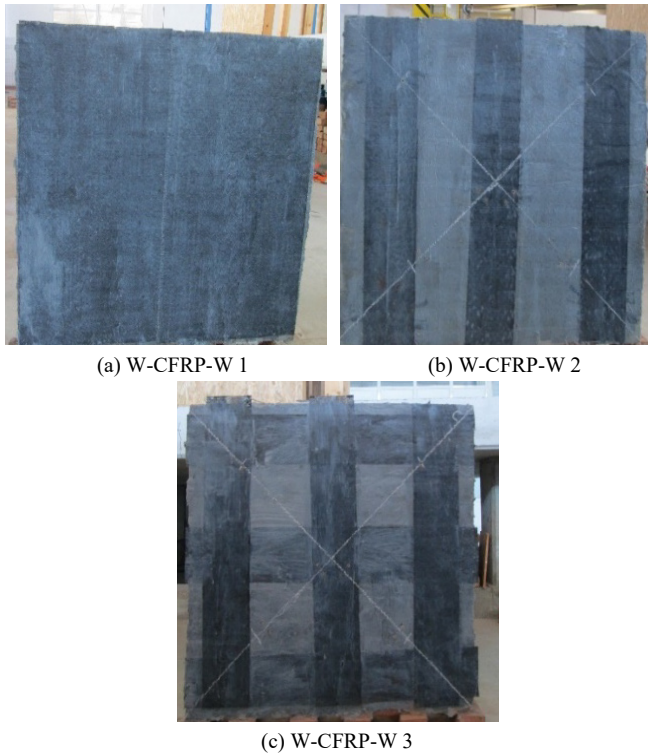


Figure 2: Specimens retrofitted with different configurations

Table 3: Retrofit details applied on each side

Designation	Ratio (%)	Configuration	Dimensions of CFRP (mm)
URM-W-R	-	-	-
W-CFRP-W1	100	Full face	1200*1200
W-CFRP-W2	50	3 Vertical	200*1200
W-CFRP-W3	75	3Verticals & 3 horizontals	6*(200*1200)

\* URM-W-CFRP-W-X-: URM: unreinforced masonry, W: wall, CFRP-W: carbon fiber reinforced polymer, W: wrap, X: number of wall.

After the preparation of all specimens, the next step is the determination of diagonal tensile strength of walls reinforced by CFRP. Initially, special attention was given to the specimen transportation from the construction zone to the testing machine by taking into consideration all the security measures in order to keep the same properties and avoiding any deterioration of walls. In accordance with ASTM E519-02[44], the wall was fixed between two steel shoes, which were placed on top and lower corners of the wall to permit the transmission of machine load. Then, four 500mm LVDT's were installed on each side of the wall, to record shortening in the vertical diagonal (compression) and lengthening in the horizontal diagonal directions (traction). Before starting test of each wall, all LVDTs were calibrated. The load applied at the upper point of the wall on the vertical diagonal in the gravity direction through hydraulic jack. The fourth walls

were tested by applying load continuously. Measurement of in-plane displacement of different specimens were recorded automatically through LVDTs by using special data acquisition system. The figure 3 presents the test machine and the emplacement of different equipment.

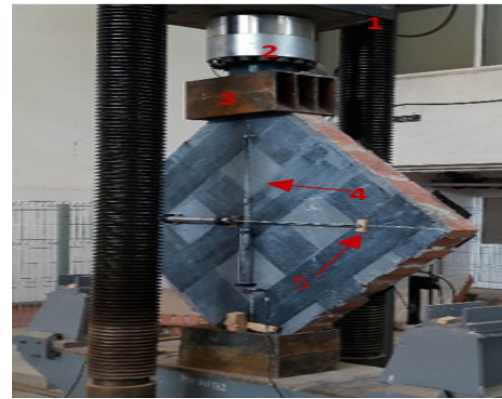


Figure 3: Setup of the diagonal tensile test: (1) Steel frame; (2) Loading plate; (3) Steel shoe; (4) Vertical LVDT; (5) Horizontal LVDT

3. Experimental Results

Four walls were tested to failure, one was considered as reference and others were retrofitted on both sides by three different configurations. For the first wall, the unidirectional CFRP wrap covered the both wall surfaces with an overlay in vertical direction of 250mm in the middle of the wall. Then, three vertical CFRP wraps with a width of 200mm and length of 1200mm were used to reinforce the second specimen. For the last wall, it was reinforced by vertical and horizontal CFRP wraps of the same dimension 200\*1200mm. Failure modes and Shear stress-strain curves are described in the next part.

3.1. Test Observations



(a) URM side I (b) URM side II

Figure 4: Failure mode of unreinforced masonry wall



For the first configuration (W-CFRP-W 1), the wall surfaces were entirely retrofitted by CFRP. It was characterized by a symmetrical behavior on its both sides. While increasing compressive loading, diagonal cracks were observed in masonry substrate and shear tensile is transferred via the interface between masonry and CFRP wrap, as a result a partial delamination of CFRP occurred in two opposite directions perpendicular to the vertical diagonal that occur the failure of tested. The CFRP shows their effectiveness in holding the masonry wall that react in this case as one element, consequently an important resistance of the tested wall to in-plane strength was observed. In addition, load-bearing capacity of both sides increased (figure 5).



Figure 5: Failure mode of W- CFRP-W 1

For the second configuration (W-CFRP-W 2), both sides of wall were reinforced by three vertical unidirectional CFRP wraps with a width of 200mm. While increasing diagonal compression loading, the strength of wall increase too, then cracks on both sides of the wall started in masonry between each two vertical CFRP wrap, at the upper and lower corners parallel to the direction of the applied load. The cracks propagation continue in a diagonal direction until they reach the middle vertical reinforcement, which started to delaminate partially from the upper line of reinforcement until it will measure for Side I, 40 cm and for side II, 30cm. Despite the fact that bricks have many cracks, but the reinforced wall, remains stable. Furthermore, no collapse produced while transporting tested wall. Delaminating were located and observed at the end of cracked masonry that transferred tensile load via interface masonry-CFRP wrap (figure 6).

For the third configuration (W-CFRP-W 3), failure mode in the strengthened wall started by subsequent diagonal cracks in masonry and in CFRP wrap, parallel to compression load direction, which was followed by the delamination and rupture of

CFRP wrap in two extremities of the wall. Moreover, a diagonal slippage of some layers situated on the top corner of the wall, which contain just one and a half brick forming a stepped appearance and causing the failure of the walls (figure 7).

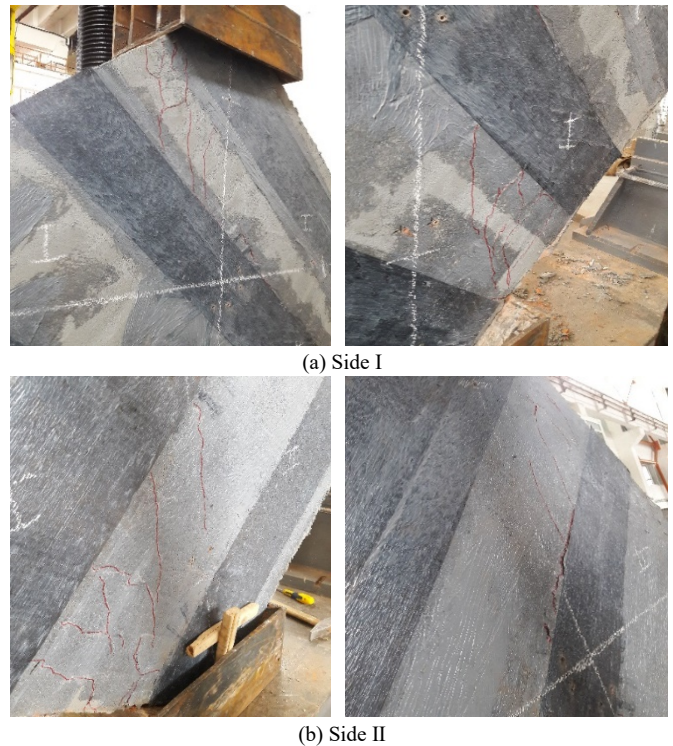


Figure 6: Diagonal shear cracking and delamination of CFRP wraps



Figure 7: Diagonal shear cracking along the diagonal and delamination of CFRP wraps of the strengthened wall

### 3.2. Shear Stress-Strain Curves

According to ASTM E519-02 [44], the shear stress and strain for the tested specimens are calculated by the following formulas:

$$S_s = \frac{0.707P}{A_n}$$

Where,  $S_s$  is the shear stress, MPa;  $P$  is the applied load, N;  $A_n$  is the crossed area of the specimen,  $\text{mm}^2$  which calculated by the following formulas:

$$A_n = \left(\frac{W+h}{2}\right) * t * n$$

Where  $W$  and  $h$  correspond to the width and the height of the specimen in mm;  $t$  presents the total thickness of specimen, mm; and  $n$  is the percent of the gross area of the unit that is solid, expressed as a decimal.

The shear strain is calculated as follows:

$$\gamma = \frac{\Delta V + \Delta H}{g}$$

Where  $\Delta V$  is the vertical strengthening, mm; and  $\Delta H$  is the horizontal strengthening, mm; and  $g$  is the vertical gage length, mm.

The modulus of rigidity  $G$  or modulus of elasticity in shear is calculated by:

$$G = \frac{S_s}{\gamma}, \text{ MPa.}$$

The figure 8 illustrates the shear stress-strain curves, which were deduced following ASTM E519-02 [44].

The results of the diagonal compression tests on the fourth walls (Shear stress, shear stress, modulus of rigidity, initial and peak loads and their corresponding displacement) are illustrated in table 4.

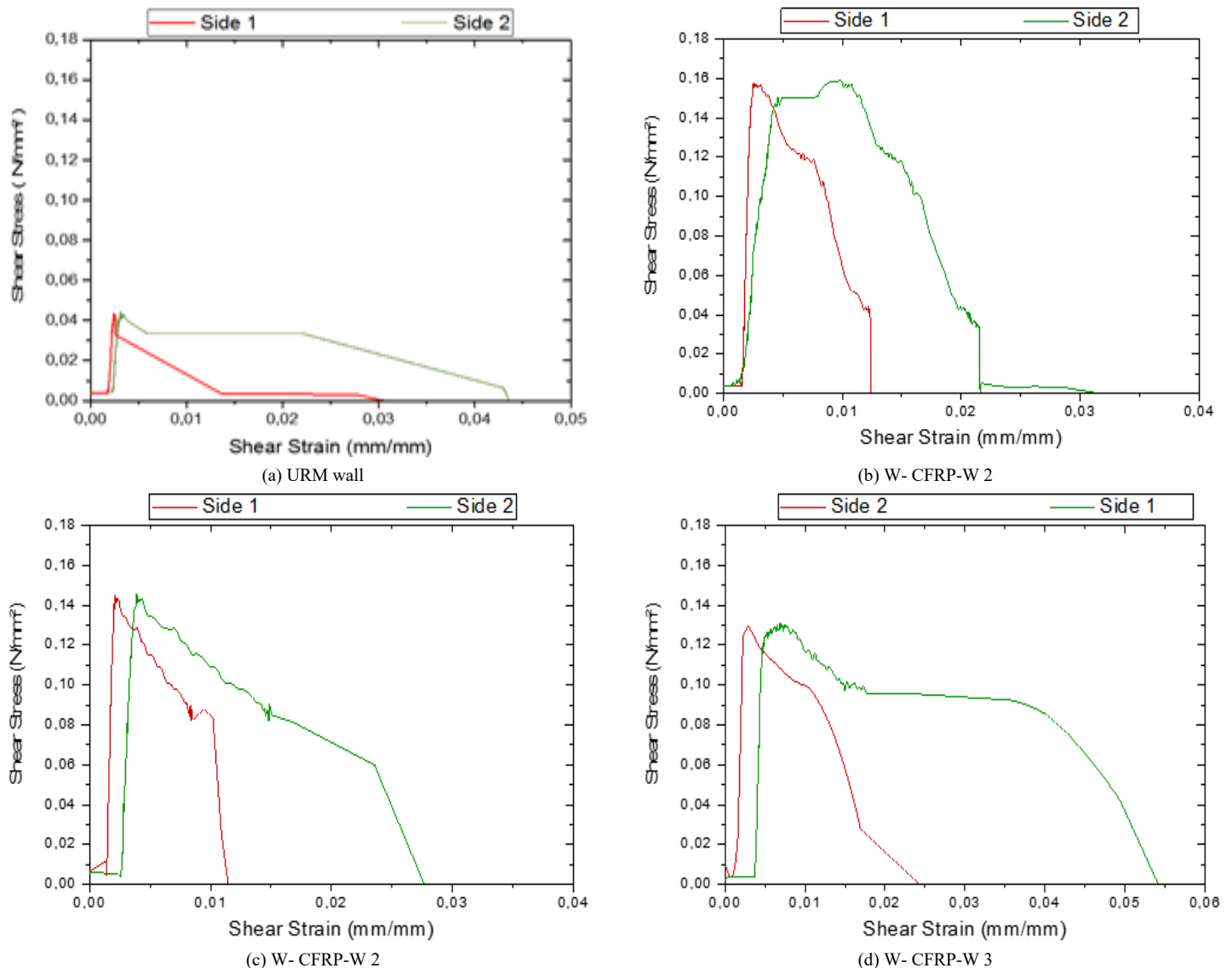


Figure 8: Shear Stress-Strain Curves of the tested specimens

Table 4: Results of diagonal compression tests

Configuration type	Side N <sup>o</sup>	Load (KN)	$\Delta V$ (mm)	$\Delta H$ (mm)	Shear stress (N/mm <sup>2</sup> )	Shear strain (mm/mm)	Modulus of Rigidity (MPa)
Initial Cracks							
URM	1	7.9	0.62	0.65	0.04	0.0026	15.38
	2		1.24	0.52		0.0035	11.43
W- CFRP-W 1	1	30.8	1.20	0.18	0.16	0.0028	57.14
	2		4.83	0.37		0.01	16.00
W- CFRP-W 2	1	27.9	0.97	0.08	0.14	0.0021	66.67
	2		1.8	0.14		0.0039	35.90
W-CFRP-W 3	1	24.7	1.02	0.7	0.13	0.0034	38.24
	2		1.46	3.02		0.009	14.44
Failure points							
URM	1	9.3	0.62	0.65	0.05	0.0026	18.46
	2		1.24	0.52		0.0035	13.71
W- CFRP-W 1	1	32.3	1.2	0.18	0.17	0.0028	60.71
	2		4.83	0.37		0.01	17.00
W- CFRP-W 2	1	29.4	1.03	0.15	0.15	0.0023	65.22
	2		1.90	1		0.0058	25.86
W-CFRP-W 3	1	26.2	1.02	0.7	0.13	0.0034	38.24
	2		1.46	3.02		0.009	14.44

#### 4. Discussion

The wall surfaces were covered by different configurations of unidirectional CFRP wrap. The figure 8 presents the Shear Stress-Strain curves of retrofitted panels, which characterized by serial increase and decrease in the carrying load due to successive cracks propagated in masonry and transmitted to the strengthening system (unidirectional CFRP wraps). The curves shown that in the first step the behavior of all strengthened specimens depends on the beginning on the mechanical properties of masonry wall then the CFRP wrap start to react. All the tested walls were tested in compression following ASTM E519-02 [44] to determine the shear strength.

The experiment started by testing unreinforced masonry wall. The maximum compression load carried by the specimens was 9.3KN, which correspond to the following vertical and horizontal displacements, for the first side 0.62mm and 0.65mm and for the second side 1.24mm and 0.52mm. When the specimen reaches its load bearing capacity its behavior was characterized by brittle failure started from the top corner of the wall fixed on steel shoes, then the cracks propagated in bed and head joints and diagonal shear cracks were observed which cause a total detachment of an important part of URM wall.

For the second wall, both sides were entirely reinforced by unidirectional CFRP wrap, the peak compressive diagonal load supported by this specimen was 32.3KN, which associated to the following vertical and horizontal displacement, for the first side, 1.2mm and 0.18mm for the second side 4.83mm and 0.37mm. In this case, the reinforced wall had an important strength in compression and in tension; furthermore the behavior of this specimen was characterized by a high ductility and an increase in energy dissipation. Then when the wall reached its maximum load bearing capacity, its strength decrease and cracks initiated from the top and propagated until reaching the bottom of the wall along

the loading direction, then the unidirectional CFRP wrap partially delaminate in opposite directions consequently the compressive strength decreased.

The third tested Wall, was reinforced on each side by three vertical symmetrical layers of unidirectional CFRP wrap, its failure occurred by successive diagonal cracks parallel to load direction and across the bed and head joints. The cracks appeared between the two parallel layers on the top corner of the wall, and then it propagated until reaching the bottom of the wall and appeared between the other parallel layers. Some cracks appeared in the layer situated in the middle of the wall, which start to delaminate from its mid-height. The specimen reaches 29.4KN corresponding to the vertical and horizontal displacement, for side one 1.03mm and 0.15mm and for the second side 1.9mm and 1mm, which present an increase of more than 3 times in peak load capacity when it's compared to the URM wall.

The last specimen is characterized by less load bearing capacity, equal to 26.2KN corresponding to the vertical and horizontal displacement, for the first side 1.02mm and 0.7mm and for the second side, 1.46mm and 3.02mm. In this case, the failure mechanism, diagonal shear cracking initiated along the mortar joints and bricks on the direction of the applied load followed by the delamination of unidirectional CFRP wrap, and then a detachment of the top corner of wall accompanied by a high decrease in strength were observed.

#### 5. Conclusions

This study presented the experimental results of three masonry walls retrofitted by using different configurations of the CFRP wrap under diagonal compression were investigated to evaluate the influence of the strengthening system on energy dissipation, stiffness and strength. Based on the experimental results the following conclusions can be drawn:



- The first results of URM wall tested under compression loading were characterized by brittle behavior due to the feeble strength of mortar joints when it is compared to the bricks, which occur a shear slip failure accompanied in some case by some cracks in the masonry substrate.
- All retrofitted walls showed a high ductility and an increase in energy dissipation in the beginning, furthermore similar behavior before failure initiated by progressive cracks in masonry, which behave as one element due to the presence of CFRP wrap, that had different reactions to compression loading. Such as a de-bonding, rupture, and delamination from a different point of masonry wall, finished in all the cases by failure. Different failure modes were remarked in the test such as shear cracking, brittle failure, compression strut, delamination, shear sliding.
- The experimental results shows that the retrofitted walls exhibited a high resistance to shear failure. The load bearing capacity of the strengthened walls increased from 26.2KN to 32.3KN when it compared to URM wall, which equal to 9.3KN.
- For the configuration type 1 and type 2, while increasing loading, diagonal shear cracks started along the mortar joints, then the failure resulted immediately after rupture and delamination of the strengthening system. They had a high shear strength, stiffness and ductility; moreover, even after their failure the walls remain stable.
- The results of configuration type 2 with reinforcement ratio of 50% had significant ductility and deformability, despite the small ratio used of CFRP wrap, the diagonal tension characteristics were improved, which prove that the strength of strengthened wall depends not only on reinforcement ratio but also on the position and direction of the strengthening system.
- The configuration type three, strengthened by 75% of strengthening system had less energy absorption capacity and a feeble strength against the compression loading when it compared to the other configurations. In addition, it was characterized by a brittle behavior caused by serial cracks followed by the failure of a part of the wall. This configuration presents less safety, which make its amelioration necessary.
- For the strain-stress curves show in the beginning of the test a linear behavior of the specimens followed by the nonlinear behavior when the specimen reaches their maximum carrying capacity. Consequently, the failure of the retrofitted specimens had occurred when the masonry substrate attained its peak load bearing capacity, then the CFRP wrap start to keep the masonry as one unit and absorb the tensile compression through energy transmitted by masonry via the interface mortar and resin.
- Retrofitting materials with their tensile strength capacity augment deformations ability of URM wall by holding them. This study showed the efficiency of the strengthening system in enhancing security of structures during an earthquake by improving the compression strength, energy dissipation, stiffness and ductility of URM wall. The compressive strength of the strengthened walls had experimentally observed to be 181.72% to 247.31% higher than URM wall.

- Additional experimental investigations will present the next phase of research.

### Conflict of Interest

The authors declare no conflict of interest with any individual or organization.

### Acknowledgments

The authors acknowledge the support and the assistance afforded by SIKA Iasi.

### References

- [1] S. El Malyh, A. Bouyahyaou, T. Cherradi, "Review on influence of infilled on the seismic behavior of frame structures" *Journal of Engineering and Applied Sciences.*, 14(2), 356-372, 2019. DOI: 10.36478/jeasci.2019.356.372.
- [2] K. Lang, "Seismic vulnerability of existing buildings" PhD thesis, Institute of Structural Engineering Swiss Federal Institute of Technology, Zurich, Switzerland, 188, 2002.
- [3] D. F. D'Ayala, S. Paganoni, "Assessment and analysis of damage in L'Aquila historic city centre after 6th April 2009" *Bulletin of Earthquake Engineering.*, 9(1), 81-104, 2011. <https://doi.org/10.1007/s10518-010-9224-4>
- [4] H. Kaplan, H. Bilgin, S. Yilmaz, H. Binici, A. Öztas, "Structural damages of L'Aquila (Italy) earthquake" *Natural Hazards and Earth System Sciences.*, 10(3), 499-507, 2010. <https://doi.org/10.5194/nhess-10-499-2010>
- [5] M. Inel, H. B. Ozmen, E. Akyol, "Observations on the building damages after 19 May 2011 Simav (Turkey) earthquake" *Bulletin of Earthquake Engineering.*, 11(1), 255-283, 2013. DOI: 10.1007/s10518-012-9414-3
- [6] Y. S. Tama, A. Solak, N. Cetinkaya, G. Sen, S. Yilmaz, H. Kaplan, "Damages to unreinforced masonry buildings by the Van earthquakes of 23 October and 9 November 2011" *Natural Hazards and Earth System Sciences.*, 13(2), 329-337, 2013. <https://doi.org/10.5194/nhess-13-329-2013>
- [7] N. Cetinkaya, I. Turkmen, "Damages of Masonry School Buildings on 2010 Karakocan-Elazig Earthquake" *International Balkans Conference on Challenges of Civil Engineering.*, 2011. <http://dspace.epoka.edu.al/handle/1/524>
- [8] G. Magenes, G. M. Calvi, "In-plane seismic response of brick masonry walls" *Earthquake engineering & structural dynamics.*, 26(11), 1091-1112, 1997. [https://doi.org/10.1002/\(SICI\)1096-9845\(199711\)26:11<1091::AID-EQE693>3.0.CO;2-6](https://doi.org/10.1002/(SICI)1096-9845(199711)26:11<1091::AID-EQE693>3.0.CO;2-6)
- [9] A. Anthoine, G. Magonette, G. Magenes, "Shear-compression testing and analysis of brick masonry walls" in *Proceedings of the 10th European Conference on Earthquake Engineering.*, 1657-1662, 1995.
- [10] A. Bilotta, F. Ceroni, G.P. Lignola, A. Prota, "Use of DIC technique for investigating the behaviour of FRCM materials for strengthening masonry elements" *Composites Part B: Engineering.*, 129, 251-270, 2017. <https://doi.org/10.1016/j.compositesb.2017.05.075>
- [11] J. Guerreiro, J. Proença, J. G. Ferreira, A. Gago, "Experimental characterization of in-plane behaviour of old masonry walls strengthened through the addition of CFRP reinforced render" *Composites Part B Engineering.*, 148, 14-26, 2018. <https://doi.org/10.1016/j.compositesb.2018.04.045>
- [12] N. Ismail, J. Ingham, "Polymer textiles as a retrofit material for masonry walls" *Proceedings of the Institution of Civil Engineers, Journals of Structures & Buildings.*, 167(1), 15-25, 2014. DOI:10.1680/stbu.11.00084
- [13] A. Jafari, A.V. Oskouei, M. Bazli, R. Ghahri, "Effect of the FRP sheet's arrays and NSM FRP bars on in-plane behavior of URM walls" *Journal of Building Engineering.*, 20, 679-695, 2018. <https://doi.org/10.1016/j.job.2018.09.018>
- [14] G. Mantegazza, A. Gatti, A. Barbieri, "Retrofitting concrete and masonry building: FRCM a new emerging technology" *XII Konferencja Naukowo-Techniczna Problemy Remontowe W Budownictwie Ogólnymi Obiektach Zabytkowych REMO.*, 6-8, 2006.
- [15] G. Marcari, G. Manfredi, A. Prota, M. Pecce, "In-plane shear performance of masonry panels strengthened with FRP" *Composites Part B : Engineering V.*, 38(7-8), 887-901, 2007. doi:10.1016/j.compositesb.2006.11.004 888



- [16] A.Z. Fam, S.H. Rizkalla, G. Tadros, "Behavior of CFRP for prestressing and shear reinforcements of concrete highway bridges" *ACI Structural Journal*, 94 (1), 77-86, 1997.
- [17] E. Grande, M. Imbimbo, E. Sacco, "Bond behaviour of CFRP laminates glued on clay bricks: experimental and numerical study" *Composites Part B: Engineering*, 42 (2), 330-340, 2011. DOI: 10.1016/j.compositesb.2010.09.020.
- [18] T.C. Triantafillou, "Strengthening of masonry structures using epoxy-bonded FRP laminates" *Journal of composites for construction* 2., 2 (2), 96-104, 1998. [https://doi.org/10.1061/\(ASCE\)1090-0268\(1998\)2:2\(96\)](https://doi.org/10.1061/(ASCE)1090-0268(1998)2:2(96))
- [19] A. Borri, M. Corradi, A. Vignoli, "Seismic upgrading of masonry structures with FRP" in 7th International Conference on Inspection Appraisal Repairs and Maintenance of Buildings and Structures, Nottingham, United Kingdom., 43-54, 2001.
- [20] R.A. Sofronie, "Seismic strengthening of masonry in buildings and cultural heritage" in 6th National Congress on Seismology and Seismic Engineering., 81-100, 2004.
- [21] S. Grandò, M. R. Valluzzi, J. G. Tumialan, A. Nanni, "Strengthening of URM clay walls with FRP systems" in *Fibre-Reinforced Polymer Reinforcement for Concrete Structures World Scientific*, 2, 1229-1238, 2003.
- [22] M.R. Valluzzi, D. Tinazzi, C. Modena, "Shear behavior of masonry panels strengthened by FRP laminates" *Construction and Building materials*, 16(7), 409-416, 2002. DOI:10.1016/S0950-0618(02)00043-0
- [23] A. Prota, G. Marcari, G. Fabbrocino, G. Manfredi, C. Aldea, "Experimental in-plane behavior of tuff masonry strengthened with cementitious matrix-grid composites", *Journal of Composites for Construction*, 10 (3), 223-233, 2006. DOI:10.1061/(ASCE)1090-0268(2006)10:3(223)
- [24] M. ElGawady, P. Lestuzzi, M. Badoux, "A review of retrofitting of unreinforced masonry walls using composites" in *Proc. 4th International Conf. on Advanced Composite Materials in Bridges and Structures*. CSCE., 2004.
- [25] A. Nanni, "A new tool for concrete and masonry repair" *American Concrete Institute (ACI)*, 34(4), 43-49, 2012. <http://worldcat.org/oclc/4163061>
- [26] F.G. Carozzi, A. Bellini, T. D'Antino, G. de Felice, F. Focacci, L. Hojdis, L. Laghi, E. Lanoye, F. Micelli, M. Panizza, "Experimental investigation of tensile and bond properties of Carbon-FRCM composites for strengthening masonry elements" *Composites Part B: Engineering*, 128, 100-119, 2017. DOI:10.1016/j.compositesb.2017.06.018
- [27] M. Corradi, A. Borri, G. Castori, R. Sisti, "Shear strengthening of wall panels through jacketing with cement mortar reinforced by GFRP grids" *Composites Part B: Engineering*, 64, 33-42, 2014. DOI:10.1016/j.compositesb.2014.03.022
- [28] D. Arboleda, G. Loreto, A. De Luca, A. Nanni, "Material characterization of fiber reinforced cementitious matrix (FRCM) composite laminates" in *Proceedings of 10th International Symposium on Ferrocement and Thin Reinforced Cement Composite*, Havana, Cuba, October., 12-17, 2012.
- [29] C. Calderini, S. Cattari, S. Lagomarsino, "The use of the diagonal compression test to identify the shear mechanical parameters of masonry" *Construction and building materials*, 24 (5), 677-685, 2010. DOI:10.1016/j.conbuildmat.2009.11.001
- [30] T. C. Rilem, "LUM B6 Diagonal tensile strength tests of small wall specimens, 1991" *RILEM Recommendations for the testing and use of constructions materials*, 488-489, 1994. doi: 10.1617/2351580117.152
- [31] M. A. ElGawady, P. Lestuzzi, M. Badoux, "A seismic retrofitting of unreinforced masonry walls using FRP" *Composites Part B: Engineering*, 37(2-3), 148-162, 2005. <https://doi.org/10.1016/j.compositesb.2005.06.003>
- [32] H. Mahmood, J. M. Ingham, "Diagonal compression testing of FRP-retrofitted unreinforced clay brick masonry wall" *Journal of Composites for Construction*, 15 (5), 810-820, 2011. DOI:10.1061/(ASCE)CC.1943-5614.0000209
- [33] D. J. Oehlers, R. Rashid, R. Seracino, "IC debonding resistance of groups of FRP NSM strips in reinforced concrete beams" *Construction and Building Materials*, 22 (7), 1574 -1582, 2008. DOI:10.1016/j.conbuildmat.2007.03.021
- [34] R. Seracino, N. M. Jones, M. S. Ali, M.W. Page, D. J. Oehlers, "Bond strength of near-surface mounted FRP strip-to-concrete joints" *Journal of Composites for Construction*, 11(4), 401-409, 2007. [https://doi.org/10.1061/\(ASCE\)1090-0268\(2007\)11:4\(401\)](https://doi.org/10.1061/(ASCE)1090-0268(2007)11:4(401))
- [35] L. De Lorenzis, J. G. Teng, "Near-surface mounted FRP reinforcement: An emerging technique for strengthening structures" *Composites Part B: Engineering*, 38 (2), 119-143, 2007. DOI:10.1016/j.compositesb.2006.08.003
- [36] ASTM C-67, *Standard Test Methods for Sampling and Testing Brick and Structural Clay Tile*. ASTM International, American Society for Testing and Materials, West Conshohocken, PA, 2005.
- [37] ASTM C109/C109M, *Standard Test Method for Compressive Strength of Hydraulic Cement Mortars (Using 2-in. or [50 mm] Cube Specimens)*. ASTM International, American Society for Testing and Materials. West Conshohocken, PA, 2016.
- [38] EN 1015-11, *Methods of Test for Mortar for Masonry – Part 11: Determination of Flexural and Compressive Strength of Hardened Mortar*. European Committee for Standardization, Brussels, 1993.
- [39] ASTM C-1314-02a, *Standard Test Method for Compressive Strength of Masonry Prisms*, ASTM International, American Society for Testing and Materials. West Conshohocken, PA, 2002.
- [40] ASTM C952, *Standard Test Method for Bond strength of Mortar to masonry Units*. ASTM International, American Society for Testing and Materials, West Conshohocken, PA, 2002.
- [41] ASTM D 3039/D 3039M, *Standard Test Method for Tensile Properties of Polymer Matrix Composite Materials*. ASTM International, American Society for Testing and Materials, West Conshohocken, PA, 2000.
- [42] ISO 10618, *Carbon fiber- Determination of tensile properties of resin-impregnated yarn*, 2004.
- [43] EN 2561, *Carbon fiber reinforced plastics. Unidirectional laminates. Tensile test parallel to the fiber directions*, 1995.
- [44] ASTM E 519-02, *Standard test method for diagonal tension (Shear) in masonry assemblages*. ASTM International, West Conshohocken, PA, 2002.

## **In-Plane Shear Behavior of Unreinforced Masonry Walls Strengthened with Fiber Reinforced Polymer Composites**

Sanaa El Malyh<sup>\*1</sup>, Azzeddine Bouyahyaoui<sup>1</sup>, Toufik Cherradi<sup>1</sup>, Ancuta Rotaru<sup>2</sup>, Petru Mihai<sup>3</sup>

<sup>1</sup>*Department of Civil Engineering, Mohammadia School of Engineer, Mohammed V University of Rabat, Morocco.*

<sup>2</sup>*Department of Transportation Infrastructure and Foundations, Gheorge Asachi Technical University of Iasi, Faculty of Civil Engineering and Building Services, Romania.*

<sup>3</sup>*Department of Concrete Structures, Building Materials, Technology and Management, Gheorge Asachi Technical University of Iasi, Faculty of Civil Engineering and Building Services, Romania.*

---

### ARTICLE INFO

*Article history:*

*Received: 21 February, 2020*

*Accepted: 19 March, 2020*

*Online: 27 March, 2020*

---

*Keywords:*

*Composite materials*

*In plane*

*Masonry Wall*

*Strengthening*

*Fiber Reinforced Polymer*

*CFRP*

*Energy dissipation*

---

### ABSTRACT

*Unreinforced masonry (URM) wall is one of the oldest types of walls used around the world. During earthquakes, URM walls present a real danger to life safety due to their behavior characterized by a brittle failure caused by their feeble shear resistance to in-plane loads, which make their strengthening necessary. Numerous studies had been used fiber reinforced polymer (FRP) as strengthening systems to upgrade the seismic behavior of masonry walls. In this study, the effectiveness of using carbon fiber reinforced polymer (CFRP) to increase the energy dissipation and the load carrying capacity of URM walls subjected to in-plane loading is experimentally investigated. Tests were carried on five walls subjected to diagonal compression loadings, one wall was considered as a reference and the other were retrofitted by different configurations of unidirectional CFRP wraps. Despite the advantages associated with the use of such systems, it remains expensive to use, therefore in this study, different ratio and configurations of CFRP wraps were used to reinforce masonry walls to enhance their resistance with less costs. The parameters under investigation are the dimensions, the number and the orientation of CFRP layers. It was concluded that the CFRP enhance the shear resistance and the deformability of URM walls. Results show The CFRP wraps had a significant influence on the URM wall behavior. Important amelioration of deformations and ultimate shear strength were observed when the specimen reaches its peak load, it was determined that the use of CFRP wrap even in smaller ratios increased ductility, the load-bearing capacity and the in-plane shear strength capacity of the masonry walls. The compressive strength of the strengthened walls had experimentally observed to be 147.31% to 319.35% higher than URM wall. The CFRP wraps presents an important solution for the improvement of the in-plane behavior of masonry walls.*

---

## **1. Introduction**

After moderate or severe earthquakes, several damages occurred in structures and the most important ones were located in URM walls, which have shown less resistance to in-plane loadings. The fact that masonry walls were not covered in the design stage and in analyzes had led to important damages. Moreover, the seismic codes do not take into consideration the

nonlinear response of these elements. Their failure due to either wind or earthquake is susceptible to be brittle and unexpected.

The evaluation of the buildings in Basel revealed that 45 to 80% of the existing URM buildings would experience damage grade 4 or 5, which correspond to very heavy damage and destruction [1], [2]. The fact that URM Walls are vulnerable to earthquakes makes their strengthening necessary. Recently different techniques had been developed to improve the seismic

---

\* Sanaa EL MALYH, Email: selmalyh@gmail.com

performance of existing or new URM structures, like the reinforcement by using fiber-reinforced polymer (FRP), which has an important displacement, elastic deformations, and effective in nonlinear domain. In addition, FRP is a cheap material, assure structure safety, can provide a high level of strength, and easy to deploy because most of them are characterized by a small weight and easy to apply to structures.

In literature, diverse strengthening systems were used by researchers the common ones are glass FRP, aramid FRP and carbon FRP, which were experimentally investigated to test their efficiency to upgrade the resistance of the walls by applying seismic loading either on the out plane or on in-plane directions.

Even if the FRPs have many advantages, but it has many limitations such as it cannot be applied to humid surfaces, no vapor permeability due to the presence of resin, however, they replace resin by a cementations matrix as an alternative of external retrofitting technique [3]-[5]. In addition, it could influence the architecture, and presents additional charges [6].

Experimental results of clay brick walls externally strengthened with glass FRP and aramid FRP laminates subjected to out-of-plane loads showed a significant increase in the flexural capacity [7]. Several researches have shown that the strength of masonry panels externally strengthened with FRP and subjected to diagonal compression loadings enhanced up to 15 and 70% [8].

The in-plane shear of URM walls retrofitted with composite materials were inspected within experimental or numerical studies. Results demonstrated that the use of retrofitting systems increases significantly the in-plane shear capacity of URM walls [9]-[11]. Even if the retrofit systems have an important effect on the ultimate strength of the wall; however, the FRP did not reach its ultimate strength at failure [12]-[17]. Stratford et al. [18] Investigated masonry walls reinforced by GFRP sheets, no remarkable amelioration in ductility was remarked, however the shear capacity increased by 65%. Reinforcement with FRP can be partial by using strips or total by applying the reinforcement to the entire surface of the walls [19].

Different configurations of reinforcement with CFRP plates using the NSM technique (horizontal reinforcement on one side, horizontal reinforcement on two sides and horizontal-vertical reinforcement on two sides of the wall) were used by [20] to repair the damaged masonry walls. Results show that the walls with the horizontal and the vertical reinforcement had the highest energy dissipation, resistance and deformation capacity. For Gharib et al.

[21], the ductility and strength of the wall increased when using the vertical reinforcement bars. In addition, in the case of reinforcement by two horizontal layers, the resistance did not increase when it compared to walls reinforced with a single layer. Increasing the number of shear reinforcement layers is more effective when the fibers have angles of 0-90 °.

## 2. Objectives of Research

The main objective of this paper is to determine adequate retrofitting systems with the highest efficiency, which may enhance the stability of structures with less amount of FRP, to minimize costs with less intervention to maintain the same aspect of the original architecture of different type of structures. In this study, diverse configurations of strengthening system applied to four URM walls were tested under compression loading. Analyses of the experimental results are performed and a comparison between the five specimens was carried out to analyze the effect of CFRP wrap ratios on the energy dissipation, strength, stiffness and other mechanical characteristics of URM walls.

## 3. Experimental Program

An experimental program was pursued to investigate the in-plane behavior of the standardized specimens following ASTM E-519 [22], which provides a standard test method for testing masonry walls under diagonal compression loads to determine diagonal tension strength. The test consists of testing panels of 1200\*1200mm fixed at the ends of their diagonal by two steel shoes, the diagonal compression forces were applied via the steel shoe located at the top corner.

All the masonry walls had the same dimension, and they were strengthened by different configurations of unidirectional CFRP wrap. The variables considered in this study were the ratio, number of layers and their dispositions. The principal aim of these tests is to investigate the influence of the orientation and the ratios of the reinforcement on the behavior of masonry walls.

### 3.1. Materials Characterization

The specimens were constructed by using clay bricks with dimension of 240\*115\*63mm, two types of mortar were applied one for linking bricks and the other was used on the wall faces. The unidirectional CFRP wrap used to reinforce URM walls via the interface of resin. The mechanical characteristics of aforementioned materials are illustrated in the table 1, table 2 and table 3.

Table 1: Characteristics of fibers according to ISO 10618 [23]

Type of material	Fibers density	Thickness of CFRP wrap	Tensile strength (N/mm <sup>2</sup> )	Tensile modulus of elasticity (N/mm <sup>2</sup> )	Elongation at rupture
CFRP	1.82 g/cm <sup>3</sup>	0.129 mm	>4000	230000	1.7 %

Table 2: Characteristics of fibers according to EN 2561 [24]

Type of material	Tensile strength (N/mm <sup>2</sup> )		Modulus of Elasticity in Tension (KN/mm <sup>2</sup> )		Nominal thickness (mm)
Laminate	Average	characteristics	Average	Characteristics	0.129
	3500	3200	225	220	

Table 3: Details about different materials

Material types	Dimensions (mm)	Type of test	Standard used	Compressive strength (N/mm <sup>2</sup> )
Mortar ( Apply on bed and head of joints)	40*40*160	Flexural and compression strength	EN 1015–11 [25]	4.47
	50*50*50	Compression strength	ASTM C109/C109M [26]	3.31
Mortar (Apply on wall surface)	40*40*160	Flexural and Compression strength	EN 1015–11[25]	27.84
	50*50*50	Compression strength	ASTM C109/C109M [26]	13.85
Clay bricks	240*115*63	Compression strength	ASTM C-67-05 [27]	11.28
Masonry prism (3 bricks) of brick linked by mortar)	240*200*63	Compressive test	ASTM C1314 [28]	10.83
Masonry prism (2 units of brick linked by mortar)	240*130*63	Bond strength of mortar-masonry	ASTM C952 [29]	17.43

### 3.2. Specimens Preparations

The preparation of the specimens passed through several stages; initially walls with dimension of 1200\*1200\*115mm were constructed by using clay brick units with dimension of 240\*115\*63 mm connected by 10mm mortar joints. The URM walls were cured for 28 days. The process of the application of CFRP wrap started with cleaning the both sides of the specimens from dust with a high pressure of air, and each face was wet.

The next step consists of applying a thin layer of primer followed by a layer of mortar, which were also cured for 28 days. Then to fix CFRP wrap two layers of epoxy-resin are applied one is used directly on the wall faces and the other is used after positioning different configurations of CFRP wrap. All the specimens were retrofitted on both faces. After seven days, the walls were tested under diagonal compression loading.

The abbreviations used for the specimens are URM-WR, W- 1D-CFRP, W- 3D-CFRP, W-2DX- CFRP and W- 2DX-2V-CFRP. The details about the configuration types used in this experiment are listed in table 4.

Table 4: Description of different configurations

Designation	Retrofit details applied per side		
	Ratio (%)	Configuration	Width (mm)
URM-W-R	-	-	-
W-1D-CFRP	41	One diagonal	350
W-3D-CFRP	53	Three parallel diagonals	(300) & 2(200)
W-2DX-CFRP	74	Diagonal (X)	2(350)
W-2DX-2V-CFRP	90	Two verticals & diagonal (X)	2(350) & 2(200)

### 3.3. Test Instrumentation

Five samples of masonry walls subjected to in-plane loadings are tested to failure, one is considered as a reference and the others

are reinforced by different configurations of CFRP wrap. The compressive loads were applied using hydraulic jacks and transmitted via steel shoe located on the top corner of the standardized tested walls. The shortening and lengthening were measured and recorded by two horizontal and vertical linear variable displacement transducers (LVDTs), which were installed on both faces of each wall. All the specimens were tested under similar rate loading until they reach the initial peak loading, but after that different incremental loading were applied.

## 4. Experimental Results

Different specimens under diagonal compression loading were tested to failure following ASTM E 519-02 [22]. Deformations of each case were presented by shear stress-strain curves. The test results indicated that each retrofitting system had special behavior related to many factors such as the position and the orientation of CFRP wrap that influence on the ability of the specimen to resist to diagonal compression loading. In all cases, retrofitting system enhanced the shear strength, the energy dissipation and the deformations of masonry panels before failure.

### 4.1 Test Observation

The tested specimens show different behaviors, which depend on the configuration used to retrofit URM walls. While increasing the in-plane loading, the masonry walls cracked and the shear stress-strain curves show a serial variation in load carrying capacity characterized by several increases and decreases in the peak load, due to the retrofitting systems, which absorb the deformations and enhance the shear strength of masonry substrates.

Under diagonal compression loadings, cracks propagated diagonally in the URM wall, from the top corner, parallel to loading direction, and across the wall width. While increasing compressive stress, the diagonal tension and the shear stress increased too, then diagonal shear cracks in bed and head joints followed by few cracks in the bricks were observed. However, when the specimen reached its maximum load bearing capacity of 9,3KN, a brittle failure is produced by a shear sliding along the mortar joints occurred a detachment of a significant part of wall figure 1.



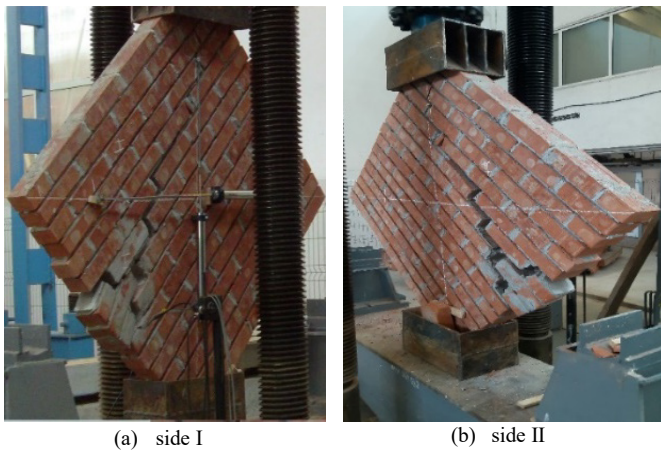


Figure 1: Failure mode of unreinforced masonry wall

The failure of the second specimen (W-1D-CFRP) started gradually by continuous diagonal shear cracking that propagates along the brick surface and across the mortar, accompanied by delamination in several points on the diagonal CFRP wrap and finished by the detachment of a considerable part of the wall and the shear slippage of a layer of masonry substrate at one edge. The stability of the wall reduced even after stopping the test, the specimen collapse and presented a potential danger figure 2.



(a) Shear cracking (Side I)



(b) Shear cracking (Side II)

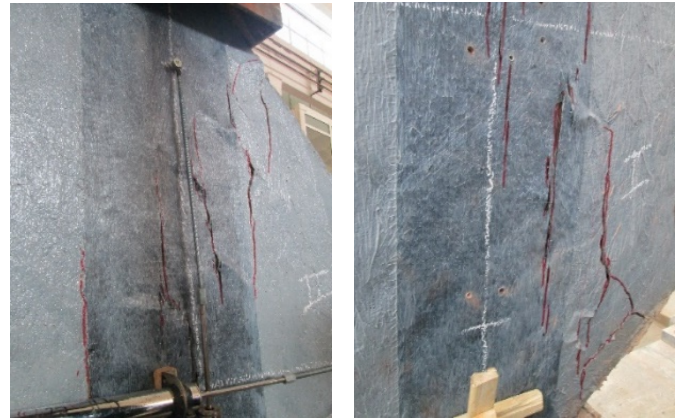
Figure 2: Failure mode of W-1D-CFRP

However, the use of CFRP wrap enhanced the strength and the stiffness of the wall. The peak load reached, in this case, is 23KN, which presents an increase by a factor of 2.5 when it compared to URM. When the third case (W- 3D-CFRP) reached the ultimate

load bearing capacity, which is equal to 37.8 KN, cracks initiated simultaneously from opposite directions parallel to the vertical compression loading, although due to the interface between masonry wall and CFRP wrap, the shear force transmitted to the diagonal CFRP wrap, which was cracked too. The behavior, in this case, is similar to equivalent diagonal strut, which was performed by the appearance of cracks between the two opposite loading shoes corners. An increase in shear strength, deformation, energy dissipation and carrying capacity of masonry wall were observed. Besides, the failure of the specimen is occurred in a high compression load started by successive cracks in masonry followed by delamination in the strengthening system. Consequently, a sudden descent in strength provided figure 3.



(a) Delamination and shear cracking (Side I)



(b) Delamination and shear cracking (Side II)

Figure 3: Failure mode of W- 3D-CFRP

For the fourth specimen (W-2DX-CFRP), no cracks observed during the test, indeed they were produced directly after wall reached its maximum load bearing capacity 27.4KN, accompanied by the delamination of CFRP wrap located at several points on the vertical diagonal direction. The failure of the surfaces of some bricks in the bottom and in the top corners of walls was observed figure 4.

The last specimen (W-2DX-2V-CFRP) reached the highest compression strength, and the maximum load bearing capacity of 39KN without failure. Indeed delamination of CFRP wrap occurred in the center of the wall and propagated along the diagonals in two directions, although no damages were remarked in the vertical layers. In addition, diagonal cracks developed along the diagonal loading direction. The specimen had similar behavior on its both sides figure 5.



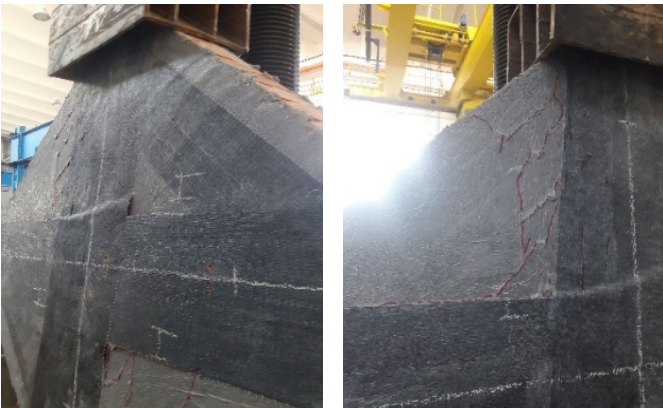


(a) Delamination and shear cracking (Side I)



(b) Delamination and shear cracking (Side II)

Figure 4: Failure mode of W- 2DX-CFRP



(a) Delamination and shear cracking (Side I)



(b) Delamination and shear cracking (Side II)

Figure 5: Failure mode of W- CFRP-W 1

#### 4.2. Shear Stress-Strain Curves

According to ASTM E519-02 [22], the shear stress and strain for the tested specimens are calculated by the following formulas:

$$S_s = \frac{0.707P}{A_n}$$

Where,  $S_s$  is the shear stress, MPa; P is the applied load, N;  $A_n$  is the crossed area of the specimen,  $\text{mm}^2$  which calculated by the following formulas:

$$A_n = \left(\frac{W+h}{2}\right) * t * n$$

Where W and h correspond to the width and the height of the specimen in mm; t presents the total thickness of specimen, mm; and n is the percent of the gross area of the unit that is solid, expressed as a decimal.

The shear strain is calculated as follows:

$$\gamma = \frac{\Delta V + \Delta H}{g}$$

Where  $\Delta V$  is the vertical strengthening, mm; and  $\Delta H$  is the horizontal strengthening, mm; and g is the vertical gage length, mm.

The modulus of rigidity G or modulus of elasticity in shear is calculated by:

$$G = \frac{S_s}{\gamma}, \text{ MPa.}$$

A general overview of the experimental results, including displacements, the ultimate load and their corresponding strain and stress values were presented in the table 5.

The figure 6 and figure 7 present the shear stress-strain curves of the tested walls characterized by a serial increase and decrease due to the successive cracks propagated in masonry and transmitted to CFRP wrap.

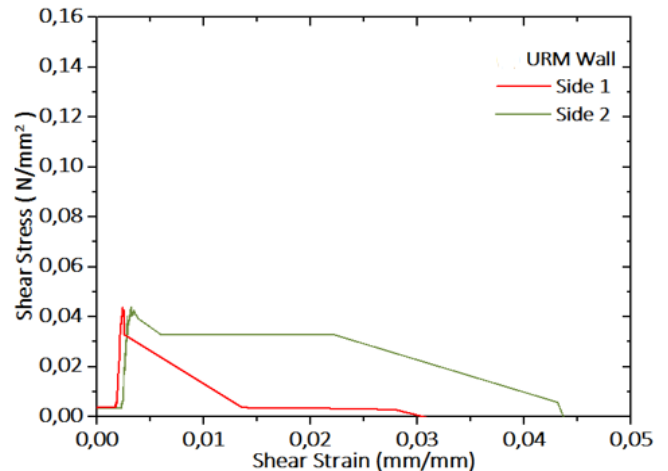


Figure 6: Shear Stress-Strain curves of the reference URM wall

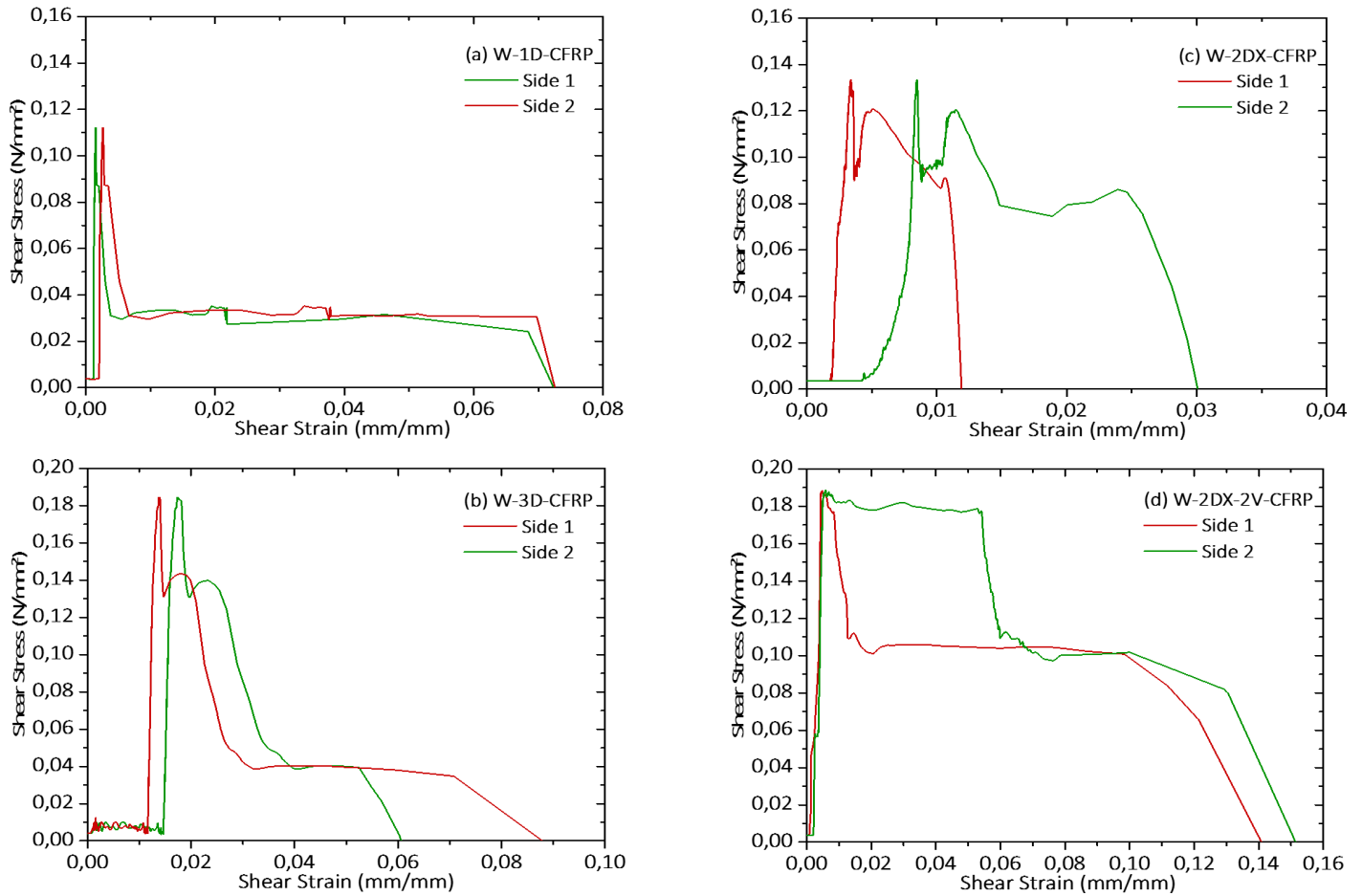


Figure 7: Shear Stress-Strain curves of the retrofitted walls

Table 5: Results of diagonal compression

Configuration type	Side N°	Load (KN)	$\Delta V$ (mm)	$\Delta H$ (mm)	Shear stress (N/mm <sup>2</sup> )	Shear strain (mm/mm)	Modulus of Rigidity (MPa)
Initial cracks							
URM	1	7.9	0.62	0.65	0.04	0.0026	15.38
	2		1.24	0.52		0.0035	11.43
W- 1D-CFRP	1	21.5	0.273	0.51	0.11	0.0016	70.39
	2		0.467	0.887		0.0027	40.70
W- 3D-CFRP	1	36.3	1.59	7.19	0.186	0.0176	10.58
	2		1.219	5.751		0.0139	13.32
W-2DX-CFRP	1	26	1.141	0.571	0.133	0.0034	38.9
	2		0.884	3.359		0.0085	15.69
W-2DX-2V-CFRP	1	37.5	2.05	0.493	0.19	0.0051	37.80
	2		2.263	0.989		0.0065	29.56
Failure points							
URM	1	9.3	0.62	0.65	0.05	0.0026	18.46
	2		1.24	0.52		0.0035	13.71
W- 1D-CFRP	1	23	0.273	0.51	0.12	0.0016	75.25
	2		0.467	0.887		0.0027	43.51
W- 3D-CFRP	1	37.8	1.592	7.188	0.194	0.0176	11.03
	2		1.219	5.751		0.0139	13.89
W-2DX-CFRP	1	27.4	1.141	0.571	0.1404	0.0034	41
	2		0.884	3.359		0.0085	16.54
W-2DX-2V-CFRP	1	39	2.05	0.493	0.1998	0.0051	39.30
	2		2.263	0.989		0.0065	30.72

## 5. Discussion

The seismic performance of URM walls relies on the capacity of CFRP wrap to maintain the stability and avoid failure. Retrofitted walls exhibited a high resistance to shear failure, characterized by the appearance of cracks either in the steel shoes corners or in the loading direction.

The use of the reinforcement system improved the integrity, the strength and the peak loading capacity of URM walls from 9.3KN to 39KN. All the specimens had a linear behavior in the beginning until they reached the maximum force, then serial cracks and delamination occurred at several points providing an important decrease in stiffness until the shear strength reached its maximum.

In all cases, the CFRP wrap reduced walls damages and enhanced safety. Indeed, each configuration influenced in a different way the behavior of URM wall. The failure of W-1D-CFRP is characterized by a brittle behavior and a shear failure caused by serial cracks followed by the detachment of a large part of the specimen.

The W-2DX-2V-CFRP configuration had the highest shear strength even after the specimen failure the wall remains stable, nevertheless, it presents an expensive solution in comparison to W-3D-CFRP, which had a significant shear strength and require a less ratio of CFRP wrap.

The use of CFRP wrap is recommended to minimize wall damages and increase the shear resistance of URM structures. The combination of vertical and horizontal configuration provides the highest shear resistance. Consequently, CFRP wrap presents an effective solution to upgrade the integrity and the seismic response of URM.

## 6. Conclusions

Five standardized walls were built using clay brick units, one was considered as reference and others were retrofitted by different configurations of CFRP wraps. The diagonal tensile strength of the specimens was evaluated through diagonal compression tests. This experimental research led to the following results:

- The reference wall showed a fragile behavior with a less shear strength values.
- The failure of the retrofitted panels started in all cases by progressive cracks in masonry, which behaved as one element due to the presence of CFRP wrap, their reactions to in-plane loading depends on the retrofitting configuration, which was observed such as a de-bonding, rupture, and delamination of CFRP wrap in diverse point of masonry wall.
- Due to the epoxy used in the interfaces, a partial delamination was observed in some cases and all the specimens had high strength, even after they reach their maximum strength, the tested specimen remains stable without collapsing.
- The retrofitting system restrains the URM wall from shear failure and shear sliding; it enhanced their strength up to 319%.

- All the used configurations, improved considerably the load bearing capacity of the specimens from 2.5 to 4.2 times.
- Despite the small ratio of reinforcement used in some cases like the specimen W-3D-CFRP; it achieves a high load bearing capacity of 37.8 KN when it's compared to the specimens W-DX-CFRP and W-2DX-2V-CFRP, with CFRP wrap ratios of 74% and 90%, which reached the following load bearing capacities of 27.4KN and 39KN.
- The configuration W-2DX-2V-CFRP attained the highest shear strength to in-plane loading. However, results show that the best cost improvement ratio is in configuration W-3D-CFRP, which has increased the strength of the wall by 306% by deploying only a ratio of 53% of CFRP wrap.
- An interesting relation is remarked between the disposition of CFRP wrap, the shear strength and the stiffness of the walls.
- The FRPs retrofitting systems are effective in increasing the in-plane strength and the deformability of URM walls.
- The compressive strength of the strengthened walls had experimentally observed to be 147.31% to 319.35% higher than URM wall.

## Conflict of Interest

The authors declare no conflict of interest with any individual or organization.

## Acknowledgments

The authors acknowledge the support and the assistance afforded by SIKA Iasi.

## References

- [1] K. Lang, "Seismic vulnerability of existing buildings. PhD dissertation, Institute of Structural Engineering". Department of Civil, Environmental and Geomatics Engineering., Swiss Federal Institute of Technology, Zurich, Switzerland, 2002.
- [2] S. El Malyh, A. Bouyahyaouo, T. Cherradi, "Review on influence of infilled on the seismic behavior of frame structures". *Journal of Engineering and Applied Sciences*, 14(2), 356-372, 2019. DOI: 10.36478/jeasci.2019.356.372.
- [3] ICC Evaluation Service, "Acceptance criteria for masonry and concrete strengthening using fiber reinforced cementitious matrix (FRCM) composite systems" Tech. Rep. AC434, ICC Evaluation Service, Whittier, Calif, USA, 2013.
- [4] S. Babaeidarabad, F. De Caso, A. Nanni, "URM walls strengthened with fabric-reinforced cementitious matrix composite subjected to diagonal compression". *Journal of composites for Construction*, 18(2), 2013. DOI: 10.1061/(ASCE)CC.1943-5614.0000441
- [5] A. Prota, G. Marcari, G. Fabbrocino, G. Manfredi, C. Aldea, "Experimental in-plane behavior of tuff masonry strengthened with cementitious matrix-grid composites." *Journal of composites for Construction*, 10(3), 223-223, 2006. DOI:10.1061/(ASCE)1090-0268(2006)10:3(223)
- [6] M. ElGawady, P. Lestuzzi, M. Badoux, "A review of conventional seismic retrofitting techniques for URM". In: proceedings of 13th international brick and block masonry conference. Amsterdam, July 4-7, 2004.
- [7] J. G. Tumialan, N. Galati, A. and Nanni, "Fiber-reinforced polymer strengthening of unreinforced masonry walls subject to out-of-plane loads." *ACI Structural Journal*, 100(3), 312-329, 2003.
- [8] H. Santa María, G. Duarte, A. Garib, "Experimental investigation of masonry panels externally strengthened with CFRP laminates and fabric subjected to in-plane shear load". 13th WorldConference on Earthquake Engineering Vancouver, B.C., Canada, August 1-6, 2004.
- [9] M. Bruneau, "State-of-the-art report on seismic performance of unreinforced masonry buildings". *Journal of Structural Engineering*, 120 (1), 230-251, 1994.



- [10] R. Capozucca, "Experimental analysis of historic masonry walls reinforced by CFRP under in-plane cyclic loading". *Composite Structures*, 94(1), 277-289, 2011. DOI: 10.1016/j.compstruct.2011.06.007.
- [11] A. P. Russell, "Characterization and seismic assessment of unreinforced masonry buildings," Ph.D. thesis, University of Auckland, New Zealand, 2010.
- [12] Y. Zhuge, "FRP Retrofitted URM walls under in-plane shear: review and assessment of available models". *Journal of Composites for Construction*, 14(6), 743-753, 2010.
- [13] M. R. Ehsani, H. Saadatmanesh, A. Al-Saidy, "Shear behavior of URM retrofitted with FRP overlays". *Journal of Composites for Construction*, 1(1), 1997. [https://doi.org/10.1061/\(ASCE\)1090-0268\(1997\)1:1\(17\)](https://doi.org/10.1061/(ASCE)1090-0268(1997)1:1(17))
- [14] V. Bosiljkov, A. W. Page, V. Bokan-Bosiljkov, R. Zarnic, "Performance based studies of in-plane loaded unreinforced masonry walls". *Masonry International*, 16 (2), 39-50, 2003.
- [15] A. Benedetti, E. Steli, "Analytical models for shear-displacement curves of unreinforced and FRP reinforced masonry panels". *Construction and Building Materials*, 22(3), 175-185, 2008. DOI: 10.1016/j.conbuildmat.2006.09.005.
- [16] A. H. Salmanpour, N. Mojsilovic, J. Schwartz, "Deformation capacity of unreinforced masonry walls subjected to in plane loading: A state-of-the-art review". *International Journal of Advanced Structural Engineering*, 22, 2013. <https://doi.org/10.1186/2008-6695-5-22>
- [17] G. Magenes, G. M. Calvi, "In-plane seismic response of brick masonry walls". *Earthquake Engineering and Structural Dynamics*, 26(11), 1091-1112, 1997. [https://doi.org/10.1002/\(SICI\)1096-9845\(199711\)26:11<1091::AID-EQE693>3.0.CO;2-6](https://doi.org/10.1002/(SICI)1096-9845(199711)26:11<1091::AID-EQE693>3.0.CO;2-6)
- [18] T. Stratford, G. Pascale, O. Manfroni, B. Bonfiglioli, "Shear strengthening masonry panels with sheet glass-fiber reinforced polymer". *Journal of Composites for Construction*, 8(5), 434-443, 2004. [https://doi.org/10.1061/\(ASCE\)1090-0268\(2004\)8:5\(434\)](https://doi.org/10.1061/(ASCE)1090-0268(2004)8:5(434))
- [19] A. Mosallam, S. Banerjee, "Enhancement in in-plane shear capacity of unreinforced masonry (URM) walls strengthened with fiber reinforced polymer composites Composites". 42(6), 1657-1670, 2011. DOI: 10.1016/j.compositesb.2011.03.015
- [20] K. M. C. Konthesingha, M. J. Masia, R. B. Petersen, N. Mojsilovic, G. Simundic, A. W. Page, "Static cyclic in-plane shear response of damaged masonry walls retrofitted with NSM FRP strips – An experimental evaluation". *Journal of Engineering Structures*, 50, 126-136, 2013. <https://doi.org/10.1016/j.engstruct.2012.10.026>
- [21] T. Gharib, A. Gabor, E. Ferrier, "Analyse expérimentale du comportement au cisaillement des murs en maçonnerie de pierre renforcés par matériaux composites TRC & NSM FRP". 33èmes Rencontres de l'AUGC, ISABTP/UPPA, May 2015.
- [22] ASTM E 519-02, Standard test method for diagonal tension (Shear) in masonry assemblages. ASTM International, West Conshohocken, PA, 2002.
- [23] ISO 10618, Carbon fiber- Determination of tensile properties of resin-impregnated yarn, 2004.
- [24] EN 2561, Carbon fiber reinforced plastics. Unidirectional laminates. Tensile test parallel to the fiber directions, 1995.
- [25] EN 1015-11, Methods of Test for Mortar for Masonry – Part 11: Determination of Flexural and Compressive Strength of Hardened Mortar. European Committee for Standardization, Brussels, 1993.
- [26] ASTM C109/C109M, Standard Test Method for Compressive Strength of Hydraulic Cement Mortars (Using 2-in. or [50 mm] Cube Specimens). ASTM International, American Society for Testing and Materials. West Conshohocken, PA, 2016.
- [27] ASTM C-67, Standard Test Methods for Sampling and Testing Brick and Structural Clay Tile. ASTM International, American Society for Testing and Materials, West Conshohocken, PA, 2005.
- [28] ASTM C-1314-02a, Standard Test Method for Compressive Strength of Masonry Prisms, ASTM International, American Society for Testing and Materials. West Conshohocken, PA, 2002.
- [29] ASTM C952, Standard Test Method for Bond strength of Mortar to masonry Units. ASTM International, American Society for Testing and Materials, West Conshohocken, PA, 2002.

## Territorial Sales Redesign Using Geotechnical Tools

Diana Sánchez-Partida<sup>\*1</sup>, Moises Ernesto Sánchez-Castro<sup>1</sup>, José-Luis Martínez-Flores<sup>1</sup>, Patricia Cano-Olivos<sup>1</sup>, Martin Straka<sup>2</sup>

<sup>1</sup>Department of Logistics and Supply Chain Management, UPAEP University, 17 Sur 901, Barrio de Santiago, CP 72410 Puebla, Puebla, México

<sup>2</sup>Faculty of Mining, Ecology, Process Control and Geotechnologies, Technical university of Kosice, Letná 9, 042 00 Košice, Slovak Republic.

### ARTICLE INFO

*Article history:*

*Received: 16 January, 2020*

*Accepted: 06 March, 2020*

*Online: 27 March, 2020*

*Keywords:*

*Territorial Design*

*Geographical Information System (GIS)*

*Location-Allocation Problem*

*P-Median Problem*

*Constraint of impedance*

### ABSTRACT

*In recent years there has been technological growth in the field of facility location, considering it as a significant factor to achieve greater competition among companies. The present work gives a methodological solution for a territorial redesign in a Mexican automotive parts distribution company with the support of Geotechnological tools like Geographic Information Systems (GIS) and Global Positioning System (GPS). The objective of this research is the improvement of customer service and, at the same time, a reduction in logistics costs. In this research, were evaluated and proposed two scenarios. The first the re-allocation of the current customers to the nearest distribution center, obtaining a decrease of the distance of 5.08%; and a second scenario where the opening of four peripheral warehouses reduces up to 24.6% of the total kilometers traveled. Currently, the company is evaluating which scenario is the most convenient for the company based on its resources and expansion plans. The value of this work is to be taking into account real-world results and manage a large amount of data as well as consider the constraint of impedance.*

## 1. Introduction and Literature Review

There could be many causes and variables for which a company does not obtain or maximize their profits. Some could be market competition, a lot, or little demand for products. However, for this research, we will focus on transportation costs that the company invests in distributing the products because the charge that generates to deliver the product to the final customer, is the expenses influence to the final price of the product, consequently in the business competitiveness.

For helping to reduce transportation costs, many companies choose to open more Distribution Centers (CEDIS). Ghiani et al. [1] define a Distribution Center as "the place mainly used in the large-scale distribution for the storage of products from different manufacturers, for distribution to the points of sale (and possibly another application belonging to the firm), located in a specific geographical area." Moreover, their location must be analyzed to use as a strategy of cost reduction.

Because of opening, a CEDI is more expensive than opening a peripheral warehouse, and many companies take this option.

Ghiani et al. [1] define a peripheral warehouse as "it is a warehouse served by a central warehouse and used for distribution of products to customers. Its objective is to ensure a better quality of customer service. Moreover, its operation cost is reduced because this warehouse only has an operational workforce.

There are many ways to select a correct place for the facility, but the competition and the technological innovation to this day make critical the use of different tools such as the use of Geographic Information Systems (GIS). Lo & Yeung [2] define GIS as "Computer-based systems specifically designed and implemented for two subtle but interrelated purposes, managing geospatial data, and using that data to solve spatial problems." Church & Murray [3] also define a GIS as "A system of hardware, software, and procedures designed for decision making throughout the acquisition, administration, analysis, and output of spatially referenced information."

For this study, we did an extensive search to know the applications of logistics, supply chain management, and GIS, finding a variety of applications implemented. One of the most common uses of GIS has been to support location sciences along

<sup>\*</sup>Diana Sánchez-Partida, Email: [diana.sanchez@upaep.mx](mailto:diana.sanchez@upaep.mx)

[www.astesj.com](http://www.astesj.com)

<https://dx.doi.org/10.25046/aj050248>

with access to necessary spatial information, including the extraction of coordinates from location points and the attribute associated with a geographical location [4, 5].

Another case is in [6] where used GIS and Global Positioning System (GPS) to track assets within the supply chain, he cites the example of Walmart that avoid increasing the inventory costs or shortages of inventory using these technologies to curb these deficiencies giving them continuous monitoring your goods. Li et al. [7] demonstrated that genetic algorithms (GA) could be used with GIS to effectively solve spatial decision problems to locate optimal places to establish facilities using data such as population and transportation, apply GIS and solve it with GA where multiple objectives are incorporated to have as exit the best locations.

The application of GIS in recent years has been extended, whether in the public or private sector. It is due to this advance that logistics and supply chain management have found in this technology like such a promising future. [8] make use of the GIS procedures together with Multicriteria Analysis (MCA) to improve the logistics for an electricity plant whose source is biomass, applied a set of criteria for the use of sustainable land. The research considers several scenarios evaluating a growing number of biomass plants and located the best location.

Another similar case is [9], where used a model with a multicriteria technique called MAIRCA that is used to classify and select suitable locations for this case, the site of an ammunition deposit. [10, 11] make use of GIS and optimization models to improve biomass availability and minimize costs and calculate delivery costs in the cotton industry. [12] propose a tool for monitoring resources by integrating a model of information construction (BIM) and GIS within a single system where the path of the chain's status is enabled, supply, and provides warning signs to ensure the delivery of materials. [13] present some other case studies where GIS and BIM are integrated, citing each platform or software used in each study.

A case of the management of the green supply chain (GSCM) is presented [14], in which it develops and implements a GIS tool on the internet to encourage the furniture industry to make a waste collection process of wood for easier recycling. The application helped identify the closest producer of a specific wood waste material in a particular geographical area so that the buyer can obtain the shortest route to collect wood waste with the minimum cost of collection.

[15] combine GIS, simulation and optimization methods for the location of biofuel facilities and design of a supply chain to minimize the cost that it causes, here the GIS were used as precursors to select locations of facilities of biofuel utilizing a series of decision factors such as candidate facilities, crop area potential, and transportation materials. This work served to identify the locations and offered support for decision-makers to determine the optimal costs, energy consumption, and emissions for the candidates.

Approaching the use of GIS applied, [16] makes use of the models of Location-Allocation, where evaluates the possibilities of these applied to the field of service geography, and it is a case study related to the spatial analysis of primary care centers in the city of

Lujan, Argentina. In [17], where is analyzed data from car travel time collected through smartphones (GPS) by Google and where it applies the GIS tools and Python programming language. Establishing an initial framework as well as to extract, analyze and visualize data, as results achieve the calculation of the fluctuation during the day, the estimation of travel time variability, and an estimate of the origin-destination (OD) matrix applied to a regional analysis in the city of Kaunas City.

For last, [18] developed a desktop tool where he makes use of the Google Maps Application Programming Interface (API), where he dynamically updated the transport network and obtained a reliable estimate of the travel time matrix. The results obtained by comparing them with those obtained by running this data with the ArcGIS Network Analysis module. Thus demonstrating its advantages, one of the main criticisms compared to the ArcGIS method is that it requires prior preparation of the network and that the data is not updated continuously, unlike the Google Maps API. Also, having peak hour data, all of the above applied to a case study to estimate the travel time in the hospital accessibility assessment.

Following the last study, one of the main criticisms is the updating of spatial data. [19] evaluate the Open Street Map (OSM) data according to several quality criteria in the case developed in QGIS using existing functions and adding new sequences for the spatial data management. It allowed the researchers to evaluate the integrity of the spatial data using fundamental indicators. The study also proposed a heuristic approach to test the navigability of OSM data; the scripts developed to provide an intuitive method to evaluate OSM data based on quality indicators can be easily used to assess the suitability of data use from any region.

Another way to reduce transportation costs by [20] is to organize the sales territories for a company with 11 sales managers to be assigned to 111 sales coverage units in Mexico. The assignment problem is modeled as a mathematical program with two objective functions. One objective minimizes the maximum distance traveled by the manager, and the other objective minimizes the variation of the sales growth goals concerning the national average. A weights method is selected to solve the bi-objective non-linear mixed-integer program. Some instances are solved using commercial software with long computational times. Also, a heuristic and a metaheuristic based on simulated annealing were developed.

A well-designed territory enhances customer coverage, increases sales, fosters excellent performance and rewards systems, and lower travel costs. [21] consider a real-life case study to design the sales territory for a business sales plan. The business plan consists of assigning the optimal quantity of sellers to a territory, including the scheduling and routing plans for each seller. The problem is formulated as a combination of assignment, scheduling, and routing optimization models. The solution approach considers a meta-heuristic using a stochastic iterative projection method for large systems. Several real-life instances of different sizes were tested with stochastic data to represent rise/fall in the customers' demand as well as the appearance/loss of customers.

For this study, we created two scenarios and used geotechnical tools to evaluate the geographical distribution of current

customers, current CEDIS, and the opening of peripheral warehouses due to the company is thinking of expanding its operations. That is why two scenarios were developed to reduce the delivery distance to customers by improving the service level and thereby minimizing the logistics costs. The first proposal is the re-allocation of customers to the nearest CEDI. Moreover, the second proposal is the opening of a new peripheral warehouse that helps to improve the indicators above further and expand its operations.

## 2. Problem Description

Currently, the company has 11 distribution centers (CEDIS), including the headquarters in Puebla city, spread throughout the Mexican Republic which has around 710 employees, 38,000 square meters for storage in the warehouses, accounts with more than 150 national delivery routes and daily deliveries to more than 350 cities. The company was founded in 1984 when they acquired the group of retail stores called "Refacciones Puebla" (1953), to later be acquired gradually by a North American company and one of the largest business conglomerates in the world that currently operates in the United States, Canada, Mexico, and New Zealand.

The company has been undergone many changes. It started as a family business in the city of Puebla and later was expanded throughout the country. The geographical distribution of the CEDIS currently follows an ambiguous customer allocation criterion and, because they have been opened gradually and empirically, detailed location studies have not been carried out. They have opened CEDIS, where there was a higher concentration of population and vehicular fleet, thinking that this is a good market. Nevertheless, a problem of the company is that the location of the CEDIS does not serve its closest customers, causing longer delivery times, long routes, higher distribution costs, and therefore lowering the level of customer service.

Therefore, we have seen the need to give a new proposal that integrates new variables, for example, so far have not taken other criteria such as distance CEDIS to customers and equity in each one of the centers. As a result, there are no clear criteria as to what is the area of influence of each distribution center; there is no clear

delimitation of the sales territories, for example, there are cases where several sales agents from other regions can coexist in the same area generating a self-internal competition.

## 3. Methodology

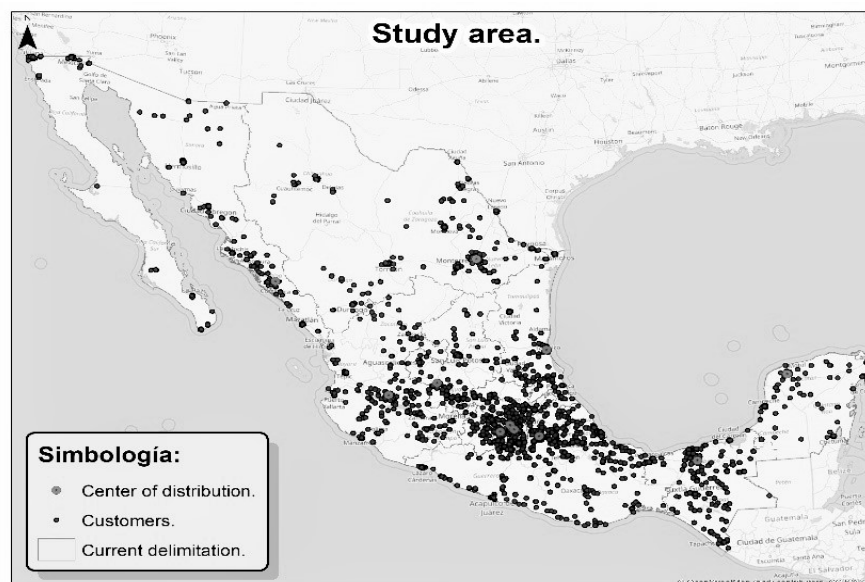
### 3.1. Data Collection

Burkholder [22] defines spatial data as "those numerical values which it represents, the location, size, and shape of objects found in the physical world." In our case, the spatial data corresponding to the location of the company's customers. We obtained the spatial data with the support of the field sales force of the company, approximately 140 people from the 11 CEDIS that received training.

The training consisted of the use of Geotechnological tools such as the use of the Global Positioning System (GPS) to obtain data such as Latitude, Longitude, and Business Name of the active customers of the company. The information collected in the field were validated; the points were attached to reality with the support of GIS functions to give quality to this information. For the realization of this project, several spatial data sources were used, such as internal and external data.

Internal spatial data: As mentioned at the beginning, we obtained the spatial information of the customers formed by 8911 records of customer locations, collected from July 2016 to August 2017. Moreover, we took the current geolocation of each CEDI.

External spatial data: As a source of external data, the OpenStreetMap base cartography (dataset) was used (OSMF, 2017) accessed on 10th May 2018 retrieved from (<https://www.openstreetmap.org>) which was a project founded in 2004 and today had positioned itself as the most famous example of Voluntary Geographical Information (VGI) on the internet [23]. The OSM project is made up of a massive global community of collaborators worldwide that contribute to keeping information on roads, trails, shops, and many more places around the world updated. We selected this cartography because it is continuously updated and useful free under an open license.



Study area. Source: self-made.



According to [24] have increased the number of developers, industries, researchers, and other users who are making use of OSM in their applications. OSM has been compared favorably with other spatial data sources regarding spatial quality, as well as citing several examples of navigation and routing applications that make direct use of OSM data.

For this work, the cartographic base of OSM was extracted to generate the road network corresponding to the update of December 2017. Then, delimit the area of influence of each distribution center with data from Municipalities of the National Institute of Statistics and Geography (INEGI, 2017) retrieved from (<http://www.inegi.org.mx>) accessed on 10th June 2018; corresponding to a total of 2464 municipalities that are spatially represented by polygons. All the data has been given in shapefile format (.shp) because it is considered a standard form in the GIS environment. Figure 1 shows the area of study. Currently, the company has 11 CEDIS and 8911 active customers established throughout the Mexican Republic delimited by polygons that represent the service area of each distribution center.

For this study, we developed two scenarios solved with GIS and geospatial tools based on Location-Allocation methods. In the first scenario, we evaluated how the current allocation of customers for each distribution center is compared with a reassignment of customers with the current configuration of CEDIS; that is, customers will be assigned to their nearest distribution center.

In the second scenario, we evaluated the current allocation of customers in the same way, but we proposed the opening of four peripheral warehouses following the business plan of the company. The purpose of the opening peripheral warehouses is because the company looks for improving the service level at the same time that creates new customers. A multiple regression analysis was performed to establish which municipality has better as commercial potential and where the company does not have any CEDI.

For this regression analysis, only was considered five variables because they were the most representative at the municipality level. The variables considered are the total population, automotive vehicles registered, spare parts sales business, municipal Gross Domestic Product (GDP), and personnel employed in the industrial sector. Multiple regression was run for a total of 2464 Municipalities. Then, we took the four municipalities with the most significant potential and where the company does not have a CEDI; these are Ciudad Juarez, Tijuana, Querétaro, and San Luis Potosí. Furthermore, it was generated a midpoint within the municipality to simulate the location of the peripheral warehouses. It is applied only for this study, while in the future, to have higher precision is suggested local research of facilities. The decision will be taken according to the needs of the company. Later, to identify and analyze the coverage and distances of current CEDIS to their customers, we apply a Location-Allocation model available in ArcGIS and its extension Network Analyst tools 27 [25].

The Location-Allocation model within the GIS environment has six different types of models based on various assumptions: (1)

Minimize Impedance, (2) Maximize Coverage, (3) Maximize capacitated coverage, (4) Minimize Facilities, (5) Maximize Attendance, (6) Maximize Market Share y (7) Target Market Share [26]. For this study, the first model was applied due to the nature of the problem.

### 3.2. Minimize Impedance Problem

Minimize Impedance Problem attempts to find locations for a set of facilities that can minimize the sum of all weighted costs among all demands to reach the nearest facility. This type of problem is also known as P-Median that was developed by [27, 28]. In other words, the objective of the problem is to determine the appropriate locations for a specific number of facilities such that the total sum of the impedance weight can be minimized. That means that the demand is assigned to an installation multiplied by the impedance of the installation. The model has a set of constraints.

The first set of constraints is that any demand outside all impedance limits of the facilities will be considered unassigned. The second set of constraints is that for service installation has all the demands that fall within the impedance limit assigned to that installation. Finally, the last set of constraints is that the demands located within the impedance limit of more than one installation will be assigned to the nearest facility.

The problem of minimizing impedance has many applications in both the public and private sectors, including the location of retail stores, libraries, schools, hospitals, and others. Having as well as the main objective for the private sector to minimize costs and maximize efficiency, this model will reduce the total transportation costs; its use is the most appropriate for the private sector. Therefore, for the scenarios, it was decided to use this model to minimize the total distance.

### 3.3. Model Formulation of P-Median

This section shows the formulation of the P-Median problem [29]:

$$\text{minimize} \quad \sum_{i \in I} \sum_{j \in J} c_{ij} x_{ij} \quad (1)$$

$$\text{Subject to} \quad \sum_{j \in J} x_{ij} = 1 \quad \forall i \in I \quad (2)$$

$$\sum_{j \in J} y_j = p \quad (3)$$

$$x_{ij} - y_j \leq 0 \quad \forall i \in I; j \in J \quad (4)$$

$$x_{ij}, y_j \in \{0,1\} \quad \forall j \in J \quad (5)$$

$$x_{ij} \geq 0 \quad \forall i \in I; j \in J \quad (6)$$

$p$  The number of facilities to locate

$x_{ij}$  The fraction of customer demand  $j$ ,

which is supplied from the installation  $i$ .

$$y_i = \begin{cases} 1 & \text{If a facility is located in the candidate site } i \\ 0 & \text{otherwise} \end{cases}$$

The objective function (1) minimizes the weighted total cost. Constraint (2) means that all the demand on the demand site  $j$  must be satisfied. Constraint (3) precisely requires  $p$  facilities to be located. Constraint (4) indicates that the demand nodes can only be assigned to open facilities. Constraint (5) stipulates that the location variables must be integer and binary. Finally, the constraint (6) specifies that variable assignments be nonnegative. Bear in mind that this model does not consider the constraint of impedance, it is contained in the GIS environment.

### 3.4. Methodology Summary

The first step is to design a network based on the updated OSM cartography. Once we had our network, to generate the scenario one, the Location-Allocation model was run in ArcGIS, taking the current customer's locations and the facilities as the current CEDIS in order to have the customers assigned to the nearest CEDI minimizing the distances traveled. Scenario two was starting from the same network. The model was again run with the 11 CEDIS plus the four peripheral ones, with a total of 15 facilities and with the same demand from current customers. Here the customers were grouped by primary areas or municipalities and were located to the territories. In Figure 2, is presented a Territorial Redesign methodology.

## 4. Results

As a result of the first model, which consisted of the reallocation of current customers to the nearest distribution center. We observed that there was a decrease in the total kilometers traveled between the current allocation of customers from the re-allocation result. The reduction was from 1,537,814 km to 1,459,744 km, which represents an improvement of 5.08% of the distance total traveled. Only to measure it is 7.6 times the geodesic distance from Mexico City to Moscow, that is, the shortest between two points on a curved surface, as can be seen in Table 1.

In Figure 3, it can be seen that the CEDIS of Culiacán, México Norte, Mexico Sur, León, Toluca, and Villahermosa would increase their mileage, but Puebla decreases, approximately, half of the kilometers due to the re-allocation customers to other CEDIS.

Figure 4 graphically represents the proposed re-allocation for scenario one, representing a different color on the map, which would be the service area of each current distribution center.

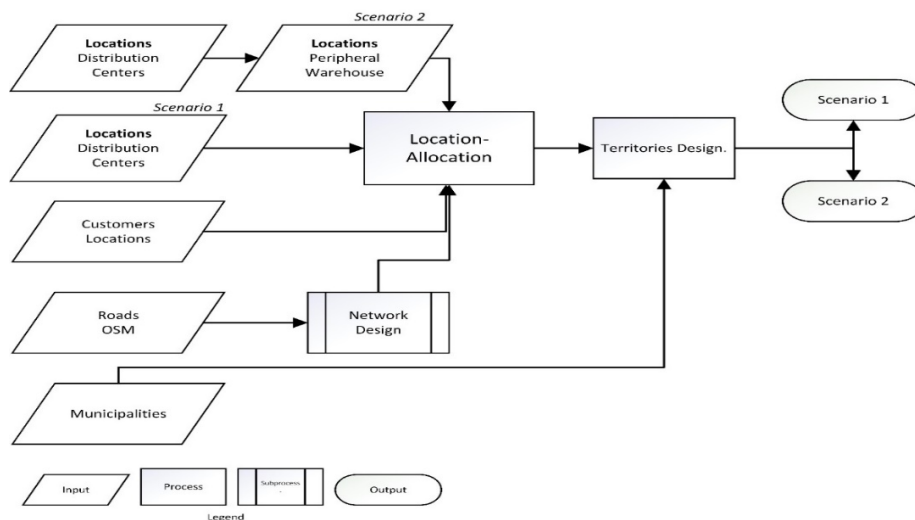


Figure 2: Proposed methodology. Source: self-made.

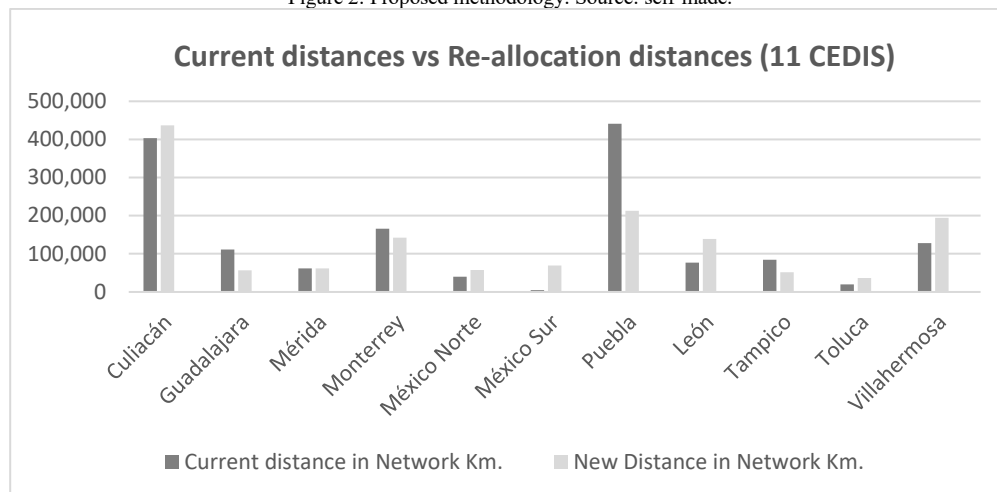


Figure 3. Current distances vs. New distances for the customers' Re-allocation (11 CEDIS). Source: self-made.

Table 1: Comparative between the current allocation and re-allocation of customers. Source: self-made.

Scenario 1						
Current Allocation			Re-allocation			
id	Distribution center	Current distance in Network Km	Current customers	New distance in Network Km	Re-allocated customers	%
1	Culiacán	403,064	908	436,617	969	-8.32
2	Guadalajara	111,725	887	57,120	707	48.87
3	Mérida	61,684	451	61,684	450	0
4	Monterrey	165,845	940	142,056	919	14.34
5	México Norte	39,788	1,086	57,911	1110	-45.55
6	México Sur	5,042	348	69,263	717	-1273.65
7	Puebla	441,305	2,083	212,585	1445	51.83
8	León	76,691	488	138,966	709	-81.2
9	Tampico	84,619	484	52,116	406	38.41
10	Toluca	19,882	469	36,662	539	-84.4
11	Villahermosa	128,170	767	194,763	940	-51.96
<b>Totals</b>		<b>1,537,814</b>	<b>8,911</b>	<b>1,459,744</b>	<b>8911</b>	<b>5.08</b>

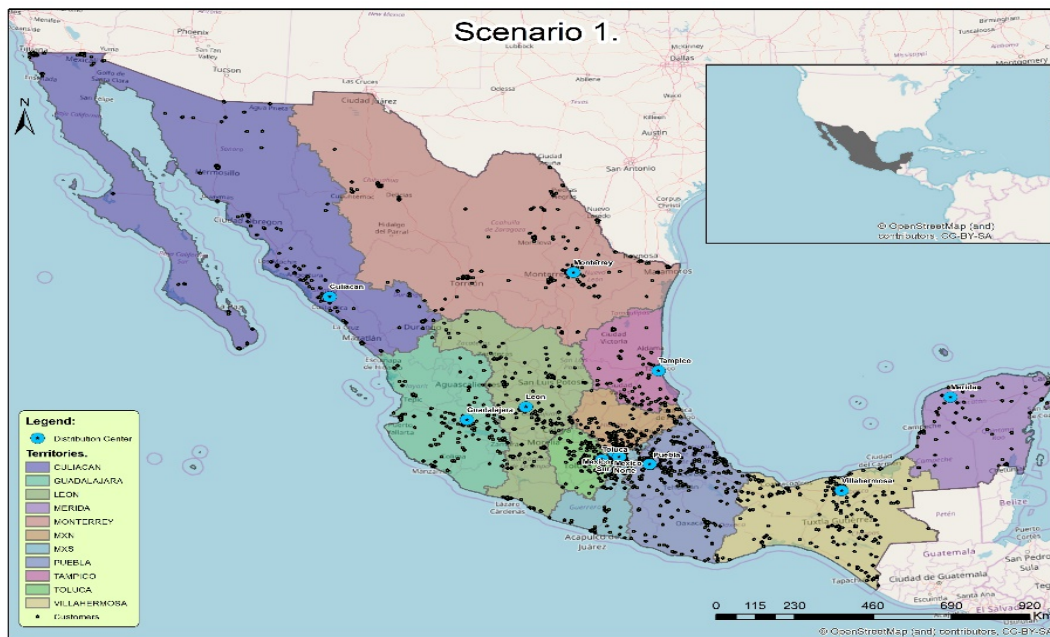


Figure 4. Territorial redesign for scenario one. Source: self-made.

For scenario two, the data was run to obtain a configuration where each current customer was re-allocated to the nearest distribution center according to the network—taking into account four peripheral warehouses that serve as auxiliary to the 11 principal CEDIS. After having solved this configuration, we obtain a reduction of 24.6% of the total trips. With this configuration, we would go from 1, 537, 814 km to 1, 159, 510 km, and there would

be a reduction of 378, 304 km; it is imperative to emphasize that it is a summation of the CEDIS to each one of the customers at the national level.

With the results of this allocation, we verified that there is a significant reduction in kilometers of the CEDIS of Culiacán, Puebla, and Monterrey, which would be absorbed by Tijuana, México Sur, and Ciudad Juárez as shown in Table 2.

Table 2: Comparative results of Scenario 2. Source: self-made.

Scenario 2							
id	Current Distribution			Re-allocation			%
	Distribution Center	Warehouse type	Current distance in Network Km	Current customers	New distances in Network Km	Re-allocated customers	
1	Culiacán	Distribution center	403,064	908	92,085	736	77.1537523
2	Tijuana	Peripheral warehouse	0	0	79,082	148	-100
3	Guadalajara	Distribution center	111,725	887	54,962	698	50.8059969
4	Mérida	Distribution center	61,684	451	62,006	451	-0.5220154
5	San Luis Potosí	Peripheral warehouse	0	0	67,329	391	-100
6	Monterrey	Distribution center	165,845	940	89,886	836	45.8011999
7	Mexico Norte	Distribution center	39,788	1,086	51,710	1,098	-29.963808
8	Ciudad Juárez	Peripheral warehouse	0	0	35,070	79	-100
9	México Sur	Distribution center	5,042	348	69,282	648	-1274.0976
10	Querétaro	Peripheral warehouse	0	0	22,375	220	-100
11	Puebla	Distribution center	441,305	2,083	213,227	1,441	51.6826231
12	León	Distribution center	76,691	488	45,836	278	40.2328826
13	Tampico	Distribution center	84,619	484	47,247	389	44.165022
14	Toluca	Distribution center	19,882	469	33,721	552	-69.605673
15	Villahermosa	Distribution center	128,170	767	195,691	946	-52.680815
Totals		15	1,537,814	8,911	1,159,510	8,911	24.6001142

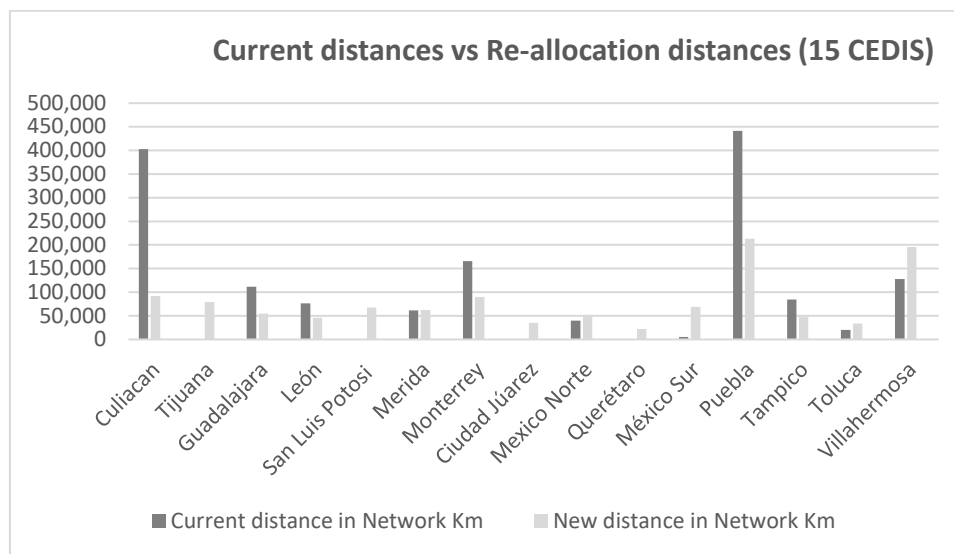


Figure 5: Current distances vs. New distances for the customers’ Re-allocation (15 CEDIS). Source: self-made.

Figure 5, we can see the reductions of kilometers for Culiacan, Puebla, and Monterrey CEDIS because other CEDIS and the new proposed as peripheral warehouses like Tijuana, San Luis Potosí, Ciudad Juárez, and Querétaro now serve these customers.

As a result of the Scenario two, we can see in Figure 6, and the four other territories have been created for each new center of the peripheral distribution, as mentioned, they will be administered by another distribution center to cover the demand of the customers assigned to these territories.



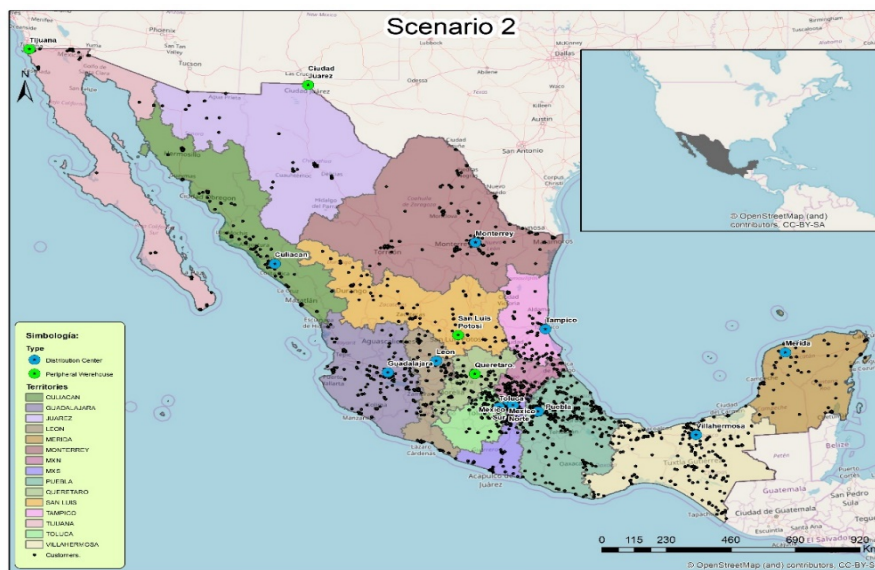


Figure 6. Territorial redesign of scenario 2. Source: self-made.

## Discussion and Conclusion

Comparing the two scenarios, we can discuss that for Scenario one; there is a decrease of 5.08 % concerning the total distance. In the same way, the company will obtain a reduction in the costs of transport and raise the service level. For Scenario 2, where the 11 current CEDIS and four peripherals warehouses are considered. Likewise, there is a reduction in mileage of 24.6%. This configuration would have higher coverage to customers and lower transportation costs, but this would depend on the number of the peripheral warehouses opened. This scenario must be made an economic evaluation due to the investment that entails the opening of new facilities. The value of this work is to be taking into account real-world results and manage a large amount of data as well as consider the constraint of impedance. The continuation of this study will be compared to the operating cost of the peripheral warehouse and the variations of income for each CEDI.

In conclusion, establishing four peripheral warehouses, the routes that were considered foreign and thus more expensive because the route has a long time to arrive with the customers, now are considered as local routes. With this proposal, the local routes guarantee the delivery in a maximum 3 hours instead of 24 to 36 hours. Moreover, the proposal generates the plus of being able to attract more customers in the new territories and always improving the service level to the customers.

## Conflict of Interest

The authors declare no conflict of interest.

## Acknowledgment

The corresponding author wants to acknowledge financial support from Consejo Nacional de Ciencia y Tecnología (CONACyT) with the number of scholarships (391444) and the Popular Autonomous University of the State of Puebla (UPAEP University).

## References

- [1] G. Ghiani, G. Laporte, R. Musmanno, *Introduction to Logistics Systems Management*, Wiley, 2013.
- [2] C. Lo, A. Yeung, *Concepts and Techniques in Geographic Information Systems*, Pearson Prentice Hall, 2007.
- [3] R. Church, A. Murray, *Business Site Selection, Location Analysis, and GIS*, Wiley, 2009.
- [4] R. Church, "Location modelling and GIS." In: P. Longley, M. Goodchild, D. Maguire, D. Rhind, *Geographical information systems*, 293-303, Wiley, 1999.
- [5] R. Church, "Geographic information systems and location science" *Comput Oper Res*, 29, 541–562, 2002.
- [6] B. Alhenaki, "Using GIS/GPS to Optimize Supply Chain Management and Logistics at Walmart" *International Journal of Scientific & Engineering Research*, 7, 745-748, 2016.
- [7] X. Li, A. Gar-On, "Integration of genetic algorithms and GIS for optimal location search" *International Journal of Geographical Information Science*, 19, 581-601, 2005.
- [8] M. Delivand, A. Cammerino, P. Garofalo, M. Monteleone, "Optimal locations of bioenergy facilities, biomass spatial availability, logistics costs, and GHG (greenhouse gas) emissions: a case study on electricity productions in South Italy" *Journal of Cleaner Production*, 99, 129-139, 2015.
- [9] L. Gigovic, D. Pamucar, Z. Bajic, M. Milicevic, "The Combination of Expert Judgment and GIS-MAIRCA Analysis for the Selection of Sites for Ammunition Depots" *Sustainability*, 8, 1-30, 2016.
- [10] F. Zhang, J. Wang, S. Liu, S. Zhang, J. Sutherland, "Integrating GIS with an optimization method for a biofuel feedstock supply chain, *Biomass and Bioenergy*, 98, 194-205, 2017.
- [11] K. Sahoo, G. Hawkins, X. Yao, "GIS-based biomass assessment and supply logistics system for a sustainable biorefinery: A case study with cotton stalks in the Southeastern US" *Applied Energy*, 182, 260-273, 2016.
- [12] J. Irizarry, E. Karan, F. Jalaei, "Integrating BIM and GIS to improve the visual monitoring of construction supply chain management" *Automation in Construction*, 31, 241–254, 2013.
- [13] Z. Ma, Y. Ren, "Integrated Application of BIM and GIS: An Overview" *Procedia Engineering*, 196, 1072 – 1079, 2017.
- [14] A. Susanty, D. Sari, W. Budiawan, Sriyanto, H. Kurniawan, "Improving green supply chain management in the furniture industry through Internet-based Geographical Information System for connecting the producer of wood waste with the buyer" *Procedia Computer Science*, 83, 734–741, 2016.
- [15] F. Zhang, D. Johnson, M. Johnson, D. Watkins, R. Froese, J. Wang, "Decision support system is integrating GIS with simulation and optimization for a biofuel supply chain" *Renewable Energy*, 85, 740-748, 2016.
- [16] G. Buzai, "Location-allocation models applied to urban public services Spatial analysis of Primary Health Care Centers in the city of Luján, Argentina" *Hungarian Geographical Bulletin*, 62, 387-408, 2013.
- [17] V. Dumbliauskas, V. Grigonis, A. Barauskas, "Application of Google-based data for travel time analysis: Kaunas City case study" *Promet-Traffic & Transportation*, 29, 613-621, 2017.

- [18] F. Wang, Y. Xu, "Estimating O-D Travel Time Matrix by Google Maps API: Implementation, Advantages, and Implications" *Annals of GIS*, 17(4), 199-209, 2011.
- [19] S. Sehra, J. Singh, R. Singh, "Assessing OpenStreetMap Data Using Intrinsic Quality Indicators: An Extension to the QGIS Processing Toolbox" *Future Internet*, 9, 1-22, 2017.
- [20] E. Olivares-Benitez, P.N. Ibarra, S. Nucamendi-Guillén, O.G. Rojas, "Multi-Objective Territory Design for Sales Managers of a Direct Sales Company." In *Optimizing Current Strategies and Applications in Industrial Engineering*, 160-178, IGI Global, 2019.
- [21] L. Hervert-Escobar, V. Alexandrov, "Territorial design optimization for business sales plan" *Journal of Computational and Applied Mathematics*, 340, 501-507, 2018, <https://doi.org/10.1016/j.cam.2018.02.010>
- [22] E. Burkholder, "Spatial Data, Coordinate Systems, and the Science of Measurement" *Journal of Surveying Engineering*, 127, 143-156, 2001.
- [23] J. Arsanjani, A. Zipf, P. Mooney, M. Helbich, "An introduction to OpenStreetMap in Geographic Information Science: Experiences, research, and applications." In: A. Jokar, A. Zipf, P. Mooney, M. Helbich, Eds. *OpenStreetMap in GIScience, Lecture Notes in Geoinformation and Cartography*, 1-18, Springer International Publishing Switzerland, 2015.
- [24] P. Mooney, M. Minghini, "A Review of OpenStreetMap Data. In: Foody G. See L. Fritz S. Mooney P. Olteanu-Raimond A. Fonte C. and Antoniou V" Eds. *Mapping and the Citizen Sensor*, 37-59, London: Ubiquity Press, 2017.
- [25] ESRI 2011. *ArcGIS Desktop: Release 10*. Redlands, CA: Environmental Systems Research Institute.
- [26] ESRI 2018. *Location-allocation analysis-Help | ArcGIS Desktop, Desktop.arcgis.com*, Retrieved from [http://desktop.arcgis.com/en/arcmap/latest/extensions/networkanalyst/locationallocation.htm#ESRI\\_SECTION1\\_F8182D9F421E4EA4AEE11E7B360E1340](http://desktop.arcgis.com/en/arcmap/latest/extensions/networkanalyst/locationallocation.htm#ESRI_SECTION1_F8182D9F421E4EA4AEE11E7B360E1340) (accessed on 10th May 2018).
- [27] S. Hakimi, "Optimum location of switching centers and the absolute centers and medians of a graph" *Oper Res*, 12, 450-459, 1964.
- [28] S. Hakimi, "Optimum distribution of switching centers in a communication network and some related graph-theoretic problems" *Oper Res*, 13, 462-475, 1965.
- [29] G. Laporte, S. Nickel, F. Saldanha da Gama, *Location Science*, Springer, 2015.

# Wilson-Hilferty-type Approximation for Poisson Random Variable

Paolo Giammatteo<sup>\*1</sup>, Tania Di Mascio<sup>2</sup>

<sup>1</sup>Università degli Studi dell'Aquila, Center of Excellence DEWS, 67100 L'Aquila, Italy

<sup>2</sup>Università degli Studi dell'Aquila, Department of Information Engineering, Computer Science and Mathematics DISIM - Center of Excellence DEWS, 67100 L'Aquila, Italy

## ARTICLE INFO

Article history:

Received: 20 November, 2019

Accepted: 05 February, 2020

Online: 04 April, 2020

Keywords:

Poisson random number generator

Poisson distribution

Non-linear transformation

## ABSTRACT

The possibility to apply non-linear transformation of the Wilson-Hilferty type to the Poisson random variable is investigated using an analytic approach, in order to improve the convergence towards the large-parameter Gaussian limit. Considering the already existing non-linear transformation for the Gamma distribution, the original Wilson-Hilferty and a higher-order transformations are showed and approximations for the Gamma function are illustrated. From this, an approximate algorithm which exploits standard Gaussian random numbers is established, in order to generate Poisson random numbers of any parameter  $m$ . The algorithm performance is also assessed. The convenience of this approximate approach it resides in the fact that simulations often could be computationally demanding so that optimized algorithms have to be adopted for the efficient extraction of Poisson random numbers with variable parameter  $m$ .

## 1 Introduction

The Poisson  $k \in \mathbb{N}$  (discrete) and standard Gamma  $x \in \mathbb{R}^+$  (continuous) random variables are characterized by the asymmetric probability distributions:

$$p_k(m) = \frac{m^k \exp(-m)}{k!}, \quad f(x, \alpha) dx = \frac{x^{\alpha-1} \exp(-x)}{\Gamma(\alpha)} dx \quad (1)$$

which depend on a single dimensionless parameter  $m \in \mathbb{R}^+$  or  $\alpha \in \mathbb{R}^+$ . The parameter coincides with both average and variance of the random variables while the skewness asymmetry parameter, equal to  $m^{-\frac{1}{2}}$  for the Poisson and  $2\alpha^{-\frac{1}{2}}$  for the Gamma distributions, tends to zero in the limit of large parameter values. Correspondingly both random variables weakly approach to a Gaussian limit for  $m \rightarrow \infty$  or  $\alpha \rightarrow \infty$ . These distributions are useful for the description of several phenomena involving Poisson and other random processes relevant to fundamental and applied research fields. The distributions share the same functional form with the roles of variable and parameter exchanged and therefore are also a representative example of conjugate a priori in the Bayesian formalism [1].

The availability and evolution of computing hardware [2]-[3] and the development of computational methods requiring the repeated generation of random numbers according to these distributions has stimulated the development of accurate and fast algorithms.

Most of these algorithms are based on different implementations of the rejection method, random variable transformations or their combination [4]. Exact algorithms for the generation of random numbers for the Poisson, Gamma, Beta and Binomial distributions were early introduced by Ahrens and Dieter [5], while specific improved algorithms for the Gamma [6, 7] and Poisson [8]-[13] random numbers have been extensively discussed. Versatile fast algorithms for repeated extractions of random numbers from the same discrete distribution (also Poisson with parameter  $m$ ) were developed by Marsaglia and co-workers [14]. They are based on the random access to suitable pre-calculated tables that contain the integers to be generated in such a way that they are drawn with the desired probability.

Approximate methods often provide useful alternatives especially when a wide range of large parameter values are encountered. The large-parameter Gaussian limit for the Poisson and Gamma distributions suggests the possibility to generate approximate random numbers with linear transformations of the type:

$$k \approx m + \sqrt{m} z, \quad x \approx \alpha + \sqrt{\alpha} z \quad (2)$$

from a standard Gaussian random number  $z$  generated using well established approaches. It can be expected that more complex non-linear transformations may provide more efficient strategies to exploit the Gaussian random number  $z$ . In the historical paper

<sup>\*</sup>Paolo Giammatteo, DEWS Via Vetoio 1 67100 Coppito (AQ) Italy, paolo.giammatteo@univaq.it

by Wilson and Hilferty (WH) [15] non-linear transformations of the form  $x = (a + bz)^p$  were investigated to provide approximate confidence intervals for the  $\chi^2$  random variable (a Gamma with semi-integer parameters) from the Gaussian confidence intervals. A useful transformation was obtained using  $p = 3$ .

The possibility to use the WH transformation to approximate the Poisson cumulative distribution was recently emphasized in a paper of Lesch and Jeske [16] exploiting a relationship between the Gamma and Poisson random variables through the cumulative distribution function. In this paper, considering  $P_k(m)$  as the Poissonian cumulative distribution function, and  $\Phi(x)$  the Gaussian cumulative distribution function, the following approximation is stated:

$$P_k(m) \simeq 1 - \Phi((c - \mu)/\sigma) \tag{3}$$

where  $c = (m/(1+k))^{1/3}$ ,  $\mu = 1 - 1/(9(1+k))$  and  $\sigma = 1/(3\sqrt{1+k})$ . Since the Eq. (3) is not explicable with a formula which expresses the Poisson as dependent variable of a Gaussian variable, an explicit non-linear transformation is still missing according to our knowledge.

In this paper we are interested in finding a non-linear transformation for the Poisson random variable exploiting the Gaussian random variable, in the spirit of the WH approach used for the Gamma random variable [15, 7]. Our interest in the generation of Poisson random numbers was motivated by the effort to develop a Kinetic Monte Carlo computer simulation of the classical nucleation process [17] and was required for an approximate treatment of the high transition rate region. The method has been recently applied to compute the homogeneous crystalline nucleation rate in undercooled liquid Ni [18] for comparison with experimental data. In the parameter range  $m \leq 50$ , an efficient exact approach was adopted combining the method of Marsaglia [14], tabulated for integer parameter values, with a  $O(m)$  algorithm correction for the decimal part of  $m$ . While, for larger  $m$ , the following non-linear transformation from a standard Gaussian random number  $z$ , was adopted:

$$k = \left[ \left[ \max \left( \frac{2}{3} m^{1/6} z + m^{2/3}, 0 \right) \right]^2 + \frac{1}{3} \right]. \tag{4}$$

Eq. (4), that has apparently never been suggested before, was introduced in a previous paper without derivation [17]. In this paper an analytic justification for the above expression is illustrated. It will be shown that this approximation can be obtained with an approach analogous to WH transformation for the Gamma random variable. The aim is to find the optimal transformation in a given class of functions for which the Taylor expansion about the maximum of the logarithm of the transformed probability density, is closer to a parabolic shape. It is believed that this transformation can be useful in many applications requiring an efficient generation of Poisson random numbers with parameters  $m \gtrsim 10$  (variable in a wide range) and represents a good trade off between computing time and accuracy.

The paper is organized as follows. In Sec. 2 the WH transformation and a higher order formula for the Gamma distribution are presented. Furthermore, approximations to the Gamma function are discussed in the same section, exploiting the two transformation. The non-linear transformation method is extended to the Poisson

distribution in Sec. 3 and the previous transformation (4) established. The approximation errors on the cumulative and probability distributions are investigated in Sec. 4. Conclusions are drawn in Sec. 5.

## 2 Considerations on WH-type Approximations for the Gamma Random Variable and Gamma Function

The original WH paper [15] is focused on the Gamma random variable whose probability density is  $f(x, \alpha)$  in Eq. (1), related to the Erlang ( $\alpha \in \mathbb{Z}^+$ ), and  $\chi^2$  ( $2\alpha \in \mathbb{Z}^+$ ) distributions. The spirit of the original approach is to look for a non-linear transformation of the type:

$$x = y(z)^p = [a + bz + \psi(z)]^p \tag{5}$$

where  $x$  is the Gamma random variable,  $z$  is the transformed random variable, and  $a, b$  and  $p$  are suitable constants to be determined in such a way that  $z$  is closely approximated by a standard Gaussian random variable. The original WH approach considers  $\psi(z) = 0$ , but it is possible to extend the class of transformations including an analytic correction  $\psi(z)$  with  $\psi(0) = 0, \psi'(0) = 0, \psi''(0) = 0$ . Throughout this paper the Lagrange's primes notation will be used and the successive derivatives of  $f(x)$  are indicated as  $f'(x), f''(x), f'''(x), f^{(4)}(x), f^{(5)}(x)$

The differentials  $dx$  and  $dz$  of the original and transformed random variables, according to Eq. (1), are related by:

$$dx = p y(z)^{p-1} y'(z) dz = p [a + bz + \psi(z)]^{p-1} [b + \psi'(z)] dz. \tag{6}$$

If we transform the Gamma density function (1) according to transformation (5), the resulting transformed probability density is:

$$f(x, \alpha) dx = g(z, \alpha) dz = \frac{P}{\Gamma(\alpha)} \exp[\phi(z)] dz \tag{7}$$

where  $g(z, \alpha)$  is the new Gamma density function expressed through the  $z$  variable and obtained replacing equations (5) and (6) in  $f(x, \alpha)$  of Eq. (1). Therefore,  $\phi(z)$  is defined as:

$$\phi(z) = (\alpha p - 1) \ln [y(z)] - y(z)^p + \ln [y'(z)]. \tag{8}$$

Since we are interested in obtaining a Gaussian approximation through the transformation in Eq. (2), the function  $\phi(z)$  at the exponent in Eq. (7), could be approximated by a parabolic function named  $\tilde{\phi}(z)$ :

$$\phi(z) \simeq u + vz^2 = \phi(0) - \frac{1}{2}z^2 = \tilde{\phi}(z) \tag{9}$$

with  $u = \phi(0)$  and  $v = -1/2$ . So, the minimal analytic requirements that  $\phi(z)$  must satisfy in  $z = 0$  are:

$$\phi'(0) = 0, \quad \phi''(0) = -1, \quad \phi'''(0) = 0. \tag{10}$$

in order to recall a parabolic shape and therefore a Gaussian density function for  $g(z, \alpha)$  in the neighborhood of the peak  $z = 0$ .



In the simplest case, corresponding to the original WH transformation [15], where  $\psi(z) = 0$ , it is demonstrated that Eq. (5) is:

$$x = [a(\alpha) + b(\alpha)z]^3 = \left[ \left( \alpha - \frac{1}{3} \right)^{\frac{1}{3}} + \frac{1}{3} \left( \alpha - \frac{1}{3} \right)^{-\frac{1}{6}} z \right]^3 \quad (11)$$

where:

$$a = a(\alpha) = \left( \alpha - \frac{1}{3} \right)^{\frac{1}{3}}, \quad (12)$$

$$b = \frac{1}{3} a^{-\frac{1}{2}} = b(\alpha) = \frac{1}{3} \left( \alpha - \frac{1}{3} \right)^{-\frac{1}{6}}. \quad (13)$$

Always in the WH demonstration [15], the parameter  $p$  results  $p = 3$ . This choice is endorsed by the fact that  $p = 3$  implies that  $\phi'''(0) = 0$  for a wide class of  $\psi(z)$  functions where  $\psi^{(4)}(z) = 0$ , which is obviously true for  $\psi(z) = 0$ .

It is possible, however, to find transformations which improve the parabolic approximation for  $\phi(z)$  imposing the additional condition  $\phi^{(4)}(0) = 0$  to the others showed in Eq. (10). A good choice is to adopt a cubic  $\psi(z)$  term of the type:

$$\begin{aligned} \psi'''(0) &= 6c b^3, \\ \psi(z) = c b^3 z^3 &\Rightarrow \psi^{(4)}(0) = 0, \\ \psi^{(5)}(0) &= 0. \end{aligned} \quad (14)$$

Imposing the conditions in Eq. (10) and  $\phi^{(4)}(0) = 0$ , the complete higher order transformation is given by:

$$x = [a(\alpha) + b_4(\alpha)z + c b_4(\alpha)^3 z^3]^3 \quad (15)$$

with  $p = 3$ ,  $a(\alpha)$  equal to Eq. (12) and:

$$b = b_4(\alpha) = \frac{1}{3} \left( \alpha - \frac{1}{3} \right)^{-\frac{1}{6}} \left( \frac{5}{3} - \frac{2}{3} \sqrt{\frac{6\alpha - 3}{6\alpha - 2}} \right)^{-\frac{1}{2}} \quad (16)$$

$$c = -a \left[ 1 - \sqrt{1 - \frac{1}{6a^3}} \right]. \quad (17)$$

Furthermore, the previous Gaussian approximation to the transformed Gamma distribution (7) can be used to compute approximately the integral corresponding to the  $\Gamma(\alpha)$  function in the spirit of the saddle point integration approach:

$$\begin{aligned} \Gamma(\alpha) &= \int_0^\infty x^{\alpha-1} \exp(-x) dx \\ &\approx 3 \int_{-\infty}^\infty \exp \left[ \phi(0) - \frac{z^2}{2} \right] dz \\ &= 3 \exp[\phi(0)] \sqrt{2\pi}. \end{aligned} \quad (18)$$

With respect to the usual Stirling approximation, the two non-linear transformations (11) and (15) produce integrand functions of  $z$  better approximated by a standard Gaussian. Recalling that:

$$\begin{aligned} \phi(0) &= (3\alpha - 1) \log(a) - a^3 + \log(b), \\ \exp[\phi(0)] &= a^{(3\alpha-1)} b \exp(-a^3) \end{aligned} \quad (19)$$

the following approximations  $\Gamma_{WH}(\alpha)$  and  $\Gamma_4(\alpha)$  to the  $\Gamma(\alpha)$  function are obtained:

$$\Gamma_{WH}(\alpha) = \sqrt{2\pi} \left( \alpha - \frac{1}{3} \right)^{(\alpha-\frac{1}{2})} e^{-(\alpha-\frac{1}{3})} \quad (20)$$

$$\Gamma_4(\alpha) = \sqrt{2\pi} \left( \alpha - \frac{1}{3} \right)^{(\alpha-\frac{1}{2})} e^{-(\alpha-\frac{1}{3})} \left( \frac{5}{3} - \frac{2}{3} \sqrt{\frac{6\alpha - 3}{6\alpha - 2}} \right)^{-\frac{1}{2}}. \quad (21)$$

The modulus of the relative error  $\epsilon(\alpha) = \left| 1 - \frac{\Gamma_a(\alpha)}{\Gamma(\alpha)} \right|$  of the two previous above approximations  $\Gamma_a(\alpha)$ , is reported in Fig. 1 and compared to the Stirling formula and the Stirling series (with two terms):

$$\Gamma_{St}(\alpha) = \sqrt{2\pi(\alpha-1)} \left( \frac{\alpha-1}{e} \right)^{\alpha-1} \quad (22)$$

$$\Gamma_{S2}(\alpha) = \sqrt{2\pi(\alpha-1)} \left( \frac{\alpha-1}{e} \right)^\alpha \left( 1 + \frac{1}{12(\alpha-1)} + \dots \right). \quad (23)$$

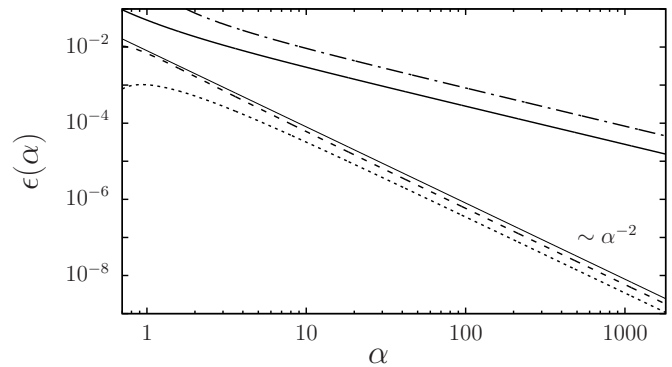


Figure 1: Relative error  $\epsilon(\alpha)$  of various approximations to the  $\Gamma(\alpha)$  function. The curves refer to: the Stirling approximation  $\Gamma_{St}(\alpha)$  (dot-dashed line), the WH approximation  $\Gamma_{WH}(\alpha)$  (solid line), the higher-order WH approximation  $\Gamma_4(\alpha)$  (dashed line), the first two terms of the Stirling series expansion  $\Gamma_{S2}$  (dotted line). The thin straight line is a guideline for the eye corresponding to an  $\alpha^{-2}$  behaviour.

It is possible to notice that the approximations obtained by the WH approach (20) and (21) are better than the Stirling formula (22). In particular, the higher-order WH approximation (21) is characterized by a relative error decreasing as  $\alpha^{-2}$ , similarly to the approximation obtained including the first two terms of the Stirling series (23).

### 3 The WH-type Approximation for the Poisson Distribution

The possibility to obtain an approximation to the Poisson cumulative distribution function, using a relationship between the Poisson and Gamma random variables (exploiting the application of the WH transformation to the latter) was emphasized [16]. In this approach the transformation  $z(k)$  for the Poisson distribution, cannot however

be easily inverted to obtain an explicit  $k(z)$  relationship, analogous to the  $x(z)$  transformations for the Gamma distribution.

In this section an approach similar to the one mentioned in Sec. 2, and therefore referred to as a WH-type transformation, is applied to the Poisson distribution. Two additional complications arise: the first is that for a discrete random variable it is necessary to approximate the distribution with a continuous probability density, the second is the requirement to expand  $k! = \Gamma(k+1)$  at the denominator introducing an additional approximation. For these reasons there is no scope in pushing the expansion order while the accuracy of the final transformation will have to be numerically assessed. An advantage of the discrete nature of the approximated random variable is that the transformation will eventually inject finite  $z$  intervals into a single  $k$  value and the possible effects of the transformation singularity will be masked.

The simplest continuous approximation to the Poisson distribution (the approximate normalization is not relevant for the following arguments) is given by:

$$p_k(m) = \frac{m^k \exp(-m)}{k!} \quad \rightarrow \quad f(k, m) \approx \frac{m^k \exp(-m)}{\Gamma(k+1)}. \quad (24)$$

The class of transformation  $k(z)$  considered in the present work is of the type:

$$k(z) = [a(m) + b(m)z]^q + c. \quad (25)$$

The opportunity to include an additional constant term  $c$ , with respect to (5) with  $\psi(z) = 0$ , is suggested by a flexibility requirement for the successive conversion into integer numbers. The general form of (25) and the resulting optimal functional dependencies  $a(m)$ ,  $b(m)$  and exponent  $q$ , are expected to be compatible with relatively fast numerical computations.

The probability density of the transformed random variable is obtained as usual:

$$f(k, m) dk = \frac{m^{k(z)} \exp(-m)}{\Gamma(k(z)+1)} q b(m) [a(m) + b(m)z]^{q-1} dz \quad (26)$$

$$= \exp[\varphi(z)] dz$$

where:

$$\varphi(z) = k(z) \ln(m) - m - \ln[\Gamma(k(z)+1)] + \left(1 - \frac{1}{q}\right) \ln[k(z) - c] + \ln[b(m)] + \ln(q). \quad (27)$$

Similarly to the Gamma case treated in Sec. 2, the aim is to find the optimal parameters in such a way that the function  $\varphi(z)$  (27) at the exponent of the transformed probability density is close to a parabolic function in the neighbourhood of  $z = 0$ .

In order to calculate the derivatives of  $\varphi(z)$  respect to  $z$ , an explicit approximate functional expression for the logarithm of the

Gamma function is required and, according to Eq. (20), it is possible to write:

$$\ln[\Gamma(k(z)+1)] \approx \frac{1}{2} \ln(2\pi) + \left[k(z) + \frac{1}{2}\right] \ln\left[k(z) + \frac{2}{3}\right] - \left[k(z) + \frac{2}{3}\right]. \quad (28)$$

An approximate expression for  $\varphi(z)$  (27) is obtained exploiting Eq. (28), retaining the leading terms in  $k \ln(k)$ ,  $k$ ,  $\ln(k)$  and neglecting constants or lower order terms as:

$$\varphi(z) \approx -k(z) \ln[k(z)] + k(z) + k(z) \ln(m) - \frac{1}{2} \ln[k(z)] + \left(1 - \frac{1}{q}\right) \ln[k(z)] + O(1). \quad (29)$$

Correspondingly the first three approximated derivatives are:

$$\varphi'(z) \approx \left\{ \ln(m) - \ln[k(z)] + \left(\frac{1}{2} - \frac{1}{q}\right) \frac{1}{k(z)} \right\} \cdot q b(m) [k(z) - c]^{(1-\frac{1}{q})} \quad (30)$$

$$\varphi''(z) \approx \left\{ (\ln(m) - \ln[k(z)]) \left(1 - \frac{1}{q}\right) - 1 \right\} \cdot q^2 b^2(m) k(z)^{(1-\frac{2}{q})} \quad (31)$$

$$\varphi'''(z) \approx \left\{ \left(\frac{1}{q} - 1\right) + \left[ (\ln(m) - \ln[k(z)]) \left(1 - \frac{1}{q}\right) - 1 \right] \left(1 - \frac{2}{q}\right) \right\} \cdot q^3 b(m)^3 k(z)^{(1-\frac{3}{q})} \quad (32)$$

where further terms of order  $O(1)$  have been neglected in the second and third derivatives and the condition  $k(z) \gg c$  accounted for. The analytic conditions to be imposed to equations (30), (31) and (32) are that these first three derivatives of  $\varphi(z)$  in  $z = 0$  should satisfy:

$$\varphi'(0) = 0, \quad \varphi''(0) = -1, \quad \varphi'''(0) = 0. \quad (33)$$

The condition on the first derivative requires that the term in curly brackets in Eq. (30) vanishes:

$$0 = \ln(m) - \ln(a^q + c) + \left(\frac{1}{2} - \frac{1}{q}\right) \frac{1}{a^q + c} \approx \ln(m) - \ln(a^q) - \frac{1}{a^q} \left[ c - \left(\frac{1}{2} - \frac{1}{q}\right) \right]. \quad (34)$$

In this expression the identity  $k(0) = a^q + c$  was used and, considering that  $c \ll k \approx a^q$ , the logarithm was expanded to the first order as  $\ln(a^q + c) \approx \ln(a^q) + \frac{c}{a^q}$  and the denominator in the last term approximated as  $a^q + c \approx a^q$ . In order to satisfy Eq. (34) it is possible to choose:

$$a(m) = m^{\frac{1}{q}}, \quad c = \frac{1}{2} - \frac{1}{q}. \quad (35)$$

By evaluating (31) in  $z = 0$ , considering that to the  $O(1)$  order  $\ln(m) - \ln[k(0)] \approx 0$  and the term in curly brackets is  $\approx -1$ , imposing the condition  $\varphi''(0) = -1$ , it is found that:

$$b(m) = q^{-1} k(0)^{\left(\frac{1}{q} - \frac{1}{2}\right)} \approx q^{-1} a^{\frac{(2-q)}{2}}. \quad (36)$$

Finally, retaining only  $O(1)$  terms in the curly brackets of Eq. (32), the condition  $\varphi'''(0) = 0$  yields:

$$\frac{1}{q} - 1 + \frac{2}{q} - 1 = 0 \Rightarrow q = \frac{3}{2}. \quad (37)$$

The solution for  $q$  from (37) inserted into (35) and (36) defines all optimal transformation parameters as:

$$q = \frac{3}{2}, \quad a(m) = m^{\frac{2}{3}}, \quad b(m) = \frac{2}{3} m^{\frac{1}{6}}, \quad c = -\frac{1}{6}. \quad (38)$$

The proposed  $k(z)$  transformation thus takes the form:

$$k(z) = \left[ m^{\frac{2}{3}} + \frac{2}{3} m^{\frac{1}{6}} z \right]^{\frac{3}{2}} - \frac{1}{6}. \quad (39)$$

The performance and meaning of transformation (39) is illustrated in Fig. 2 for a typical Poisson distribution with a relatively low parameter value ( $m = 10$ ). The small (\*) symbols are exact numerical results, reported at the ordinate integer values  $k$  and  $k + 1$  and abscissa  $z$  such that the cumulative distributions of the Poisson random variable (up to  $k$  included) and of the standard Gaussian (up to  $z$ ) coincide, that is:

$$\exp(-m) \sum_{\ell=0}^k \frac{m^\ell}{\ell!} = \frac{1}{\sqrt{2\pi}} \int_{-\infty}^z \exp\left(-\frac{y^2}{2}\right) dy. \quad (40)$$

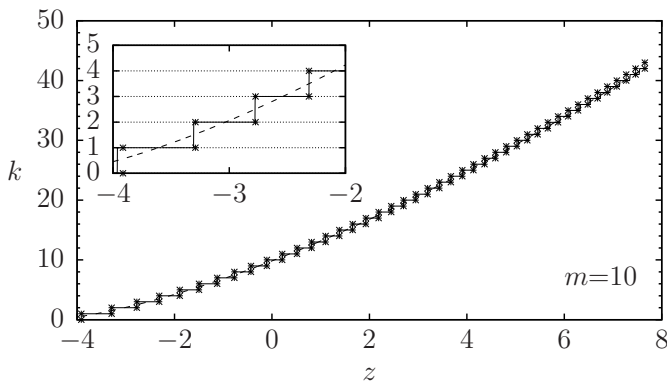


Figure 2: Relationship between the standard Gaussian  $z$  and Poisson  $k$  (parameter  $m = 10$ ) random variables. Couples  $(z, k)$ ,  $(z, k + 1)$  (\*) symbols where a matching between the corresponding cumulative distributions occurs, according to Eq. (40). Proposed non linear transformation (dashed curve) Eq. (39). Stepwise discretized transformation Eq. (41). The small  $k$  range is magnified in the inset.

The dashed curve is the approximate transformation (39) that clearly interpolates the numerical result for the exact discrete random variable. In order to use the continuous transformation to generate correctly integer values, a continuity correction has to be applied. This can be performed by adding a constant shift  $+\frac{1}{2}$  to

<sup>1</sup>This operator corresponds to the C floor function and is indicated as  $\lfloor \dots \rfloor$

the transformation and taking the largest integral value that is not greater than the resulting real number<sup>1</sup>. The discretized version of the transformation is therefore:

$$k = \left\lfloor \left( m^{\frac{2}{3}} + \frac{2}{3} m^{\frac{1}{6}} z \right)^{\frac{3}{2}} + \frac{1}{3} \right\rfloor. \quad (41)$$

This expression corresponds to the stepwise curve reported in Fig. 2 that closely reproduces the exact numerical steps (symbols \*) especially in the  $|z| < 3$  high probability region. The remote possibility that a large negative  $z$  results in a negative  $k$  is overcome by the max operator in the final transformation, anticipated in Eq. (4), that injects these cases in the  $k = 0$  random number.

## 4 Accuracy Assessment

Several statistical indicators can be considered to investigate the errors of the proposed approximation (4) in comparison with the linear transformation (2) or the one proposed in the paper of Chang [19] and of Lesch [16]. As described by Lesch [16], useful statistical indicators quantify the maximum deviations on both the probability and the cumulative distributions and can be defined respectively as the maximum absolute difference between the exact Poisson probability  $p_k$  and the approximate probability  $f_k$ ,

$$M_p = \max_k |p_k - f_k| \quad (42)$$

and, the maximum absolute difference between the exact Poisson  $P_k$  and the approximate  $F_k$  cumulative distributions:

$$M_c = \max_k |P_k - F_k|. \quad (43)$$

The dependence of these two indicators as a function of  $m$  is illustrated in Fig. 3 in double logarithmic plots, which quantifies the precision of the approximations.

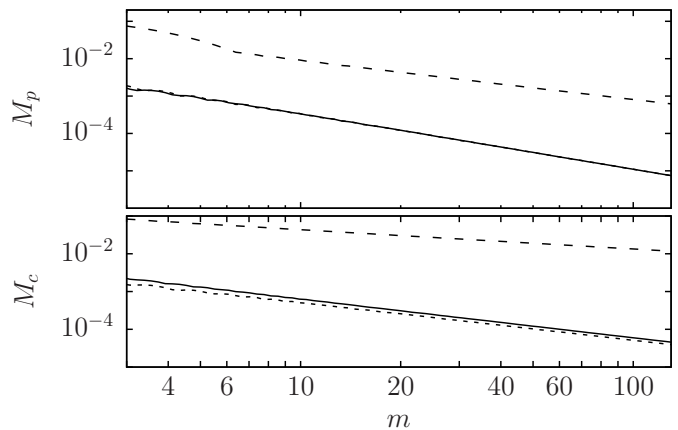


Figure 3: Double logarithmic plot of the dependence of the two statistical indicators  $M_p$  (42) and  $M_c$  (43) as a function of the Poisson parameter  $m$ . The performance of the proposed non-linear transformation (solid lines) is compared with the linear transformation (dashed lines) and the transformation proposed by Lesch [16] (dotted lines). This latter curve overlaps with the solid line in the  $M_p$  case.

The behaviour of the two indicators are showed in each sub-plot for the linear (Eq. 2 with dashed line), the non-linear (Eq. 4 with solid line) and the Lesch transformations ([16] with dotted line). It is possible to notice that, for the non-linear transformation, the two indicators decrease with increasing  $m$  roughly as  $m^{-1.5}$  in both the case. So, the performance of the proposed approximation (4) is substantially equivalent to the one proposed by Lesch [16] with the advantage of the availability of an explicit  $k(z)$  expression for the random number generation.

The  $\chi^2$  test is also performed and showed in Fig. 4 as a function of the sample number  $N$ . As in Fig. 3, the indicator is reported for three different number of degree of freedom  $nc$  (7, 57, 89), which correspond respectively to different values of the Poisson parameter  $m$  (1, 60.24, 144.89). The  $\chi^2$  value is reported for the linear (Eq. 2 with dashed line), the non-linear (Eq. 4 with solid line) and the Lesch transformations ([16] with dotted line). The horizontal line represents the  $\chi^2$  level of significance considered at 5%. Under the line, the hypothesis test is considered verified and the random numbers obtained through the transformation (4) are considered distributed as a Poisson function. This means that the approximation is good. Furthermore, its goodness improves with the increasing of the degree of freedom  $nc$ , and so with the increasing of the Poisson parameter  $m$ .

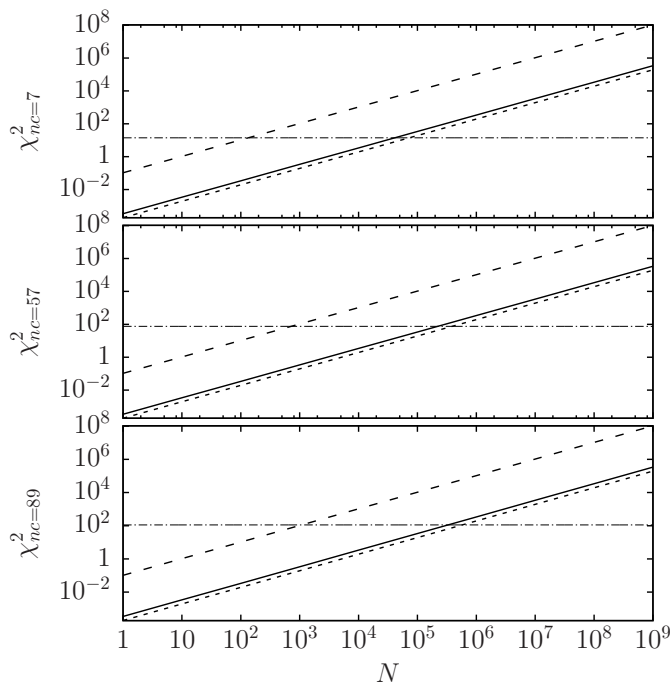


Figure 4: The dependence of the statistical indicator  $\chi^2$  as a function of the sample dimension  $N$ . The performance of the proposed non-linear transformation (solid lines) is compared with the linear transformation (dashed lines) and the transformation proposed by Lesch [16] (dotted lines). The plot are showed for three different case of degree of freedom  $nc$ , which correspond to different value of the Poisson parameter  $m$ . In particular for  $nc = 7$   $m = 1$ ,  $nc = 57$   $m = 60.64$  and  $nc = 89$   $m = 144.89$ . The horizontal line represents the level of significance of 5% taken from the  $\chi^2$  table under which the hypothesis of the  $\chi^2$  test is verified.

It is evident the better performance of the proposed non-linear transformation (solid line) respect to the linear one, furthermore, its goodness increases with the increasing of the degree of freedom.

As in the case of the previous statistical indicators, the proposed approximation (4) is substantially equivalent to the one proposed by Lesch [16].

## 5 Conclusions

In this paper WH type non-linear transformation between a standard Gaussian random variable  $z$  and Poisson  $k$  random variable was investigated. The historical WH transformation, was revisited and its corresponding approximations to the Gamma function were investigated. The WH approach was extended to the Poisson random variable and a relatively simple transformation was established. The accuracy of the transformation was assessed as a function of the Poisson parameter  $m$ .

This result provide an analytic justification for the proposed transformation (4) to generate approximate Poisson random numbers for arbitrary parameter  $m$  introduced in the previous paper [17]. The proposed transformation has a relatively simple functional structure and can be implemented using fast library routines for the evaluation of square roots `sqrt`, while the slower `pow` function is not required. The execution of (4), including the generation of the Gaussian random number, requires about 53 ns on a 3.7 GHz 64-bit processor and the reliability of the generated random numbers is fully acceptable for  $m \geq 10$  for most applications. The improved reliability of the generated random number with respect to the simpler linear transformation  $m + \sqrt{m}z$  fully justifies the required additional 4 ns of computing time.

While a large number of exact methods for the generation of Poisson random number with different characteristics are described in the literature [8], [11]-[14], the present method is expected to provide a useful approximate alternative for several possible applications. Marsaglia's method [14], for example, is useful for repeated extractions from the same distribution (parameter  $m$ ), since different arrays are required if  $m$  changes. Our method for sure is slower and less precise (since it is an approximation) than the Marsaglia's method, anyway it is a valid alternative for the cases where  $m$  varies over time, giving a good trade-off between precision computing speed. A possible application filed of the proposed algorithm is the filed of embedded systems and Wireless Sensor Networks (WSN)[20, 21], where the aspect just mentioned has its importance.

The method actually provides an explicit expression for the random number generation, implementing the ideas of the usage of the WH non-linear transformation recently emphasized in the educational literature [16]. Furthermore, this paper intend to be an hint for a more precise mathematical work in which to provide analytical bounds and how the proposed transformation is related to the central limit theorem. Finally, last observation, this method could be the basis for a new rejection method, increasing its random number generation accuracy.

**Conflict of Interest** The authors declare no conflict of interest.

## References

- [1] G. D'Agostini. Bayesian inference in processing experimental data: principles and basic applications. *Reports on Progress in Physics*, 66:1383–1419, 2003.



- <https://doi.org/10.1088/0034-4885/66/9/201>.
- [2] M. Faccio, F. Federici, G. Marini, V. Muttillio, L. Pomante, and G. Valente. Design and validation of multi-core embedded systems under time-to-prototype and high performance constraints. In *2016 IEEE 2nd International Forum on Research and Technologies for Society and Industry Leveraging a better tomorrow (RTSI)*, 2016. <https://doi.org/10.1109/RTSI.2016.7740546>.
- [3] V. Muttillio, G. Valente, F. Federici, L. Pomante, M. Faccio, C. Tieri, and S. Ferri. A design methodology for soft-core platforms on fpga with smp linux, openmp support, and distributed hardware profiling system. *EURASIP Journal on Embedded Systems*, 2016(1):15, Sep 2016. <https://doi.org/10.1186/s13639-016-0051-9>.
- [4] L. Devroye. *Non-Uniform Random Variate Generation*. Springer, 1986. <https://doi.org/10.1007/978-1-4613-8643-8>.
- [5] J. H. Ahrens and U. Dieter. Computer methods for sampling from gamma, beta, poisson and binomial distributions. *Computing*, 12:223–246, Sep. 1974. <https://doi.org/10.1007/BF02293108>.
- [6] G. Marsaglia. The squeeze method for generating gamma variates. *Computers and Mathematics with Applications*, 3:321–325, 1977. [https://doi.org/10.1016/0898-1221\(77\)90089-X](https://doi.org/10.1016/0898-1221(77)90089-X).
- [7] G Marsaglia and W. W. Tsang. A simple method for generating gamma variables. *ACM Transactions on Mathematical Software*, 26(3):363–372, Sep. 2000. <https://doi.org/10.1145/358407.358414>.
- [8] G. S. Fishman. Sampling from the poisson distribution on a computer. *Computing*, 17:147–156, Jun. 1976. <https://doi.org/10.1007/BF02276759>.
- [9] A. C. Atkinson. The computer generation of poisson random variables. *Journal of the Royal Statistical Society. Series C (Applied Statistics)*, 28:29–35, 1979. <https://doi.org/10.2307/2346807>.
- [10] A. C. Atkinson. Recent developments in the computer generation of poisson random variables. *Journal of the Royal Statistical Society. Series C (Applied Statistics)*, 28:260–263, 1979. <https://doi.org/10.1007/BF02243478>.
- [11] L. Devroye. The computer generation of poisson random variables. *Computing*, 26:197–207, 1981. <https://doi.org/10.1007/BF02243478>.
- [12] C. D. Kemp and A. W. Kemp. Poisson random variate generation. *Journal of the Royal Statistical Society. Series C (Applied Statistics)*, 40:143–158, 1991. <https://doi.org/10.2307/2347913>.
- [13] W. Hormann. The transformed rejection method for generating poisson random variables. *Insurance: Mathematics and Economics*, 12:39–45, Feb. 1993. [https://doi.org/10.1016/0167-6687\(93\)90997-4](https://doi.org/10.1016/0167-6687(93)90997-4).
- [14] G. Marsaglia, W. W. Tsang, and J. Wang. Fast generation of discrete random variables. *J. of Statistical Software*, 11:1–11, July 2004. <https://doi.org/10.18637/jss.v011.i03>.
- [15] E. B. Wilson and M. M. Hilferty. The distribution of chi-square. *Proceedings of the National Academy of Sciences of the USA*, 17:684–688, 1931. <https://doi.org/10.1073/pnas.17.12.684>.
- [16] S. M. Lesch and D. R. Jeske. Some suggestions for teaching about normal approximations to poisson and binomial distribution functions. *Journal of the American Statistical Association*, 63:274–277, Aug. 2009. <https://doi.org/10.1198/tast.2009.08147>.
- [17] A. Filippini and P. Giammatteo. Kinetic monte carlo simulation of the classical nucleation process. *J. Chem. Phys.*, 145:211913, 2016. <https://doi.org/10.1063/1.4962757>.
- [18] A. Filippini, A. Di Cicco, S. De Panfilis, P. Giammatteo, and F. Iesari. Crystalline nucleation in undercooled liquid nickel. *Acta Materialia*, 124:261–267, 2017. <https://doi.org/10.1016/j.actamat.2016.10.076>.
- [19] C. H. Chang, J. J. Lin, N. Pal, and M. C. Chiang. A note on improved approximation of the binomial distribution by the skew-normal distribution. *The American Statistician*, 62(2):pp. 167–170, May 2008. <https://doi.org/10.1198/000313008X305359>.
- [20] S. Marchesani, L. Pomante, M. Pugliese, and F. Santucci. Definition and development of a topology-based cryptographic scheme for wireless sensor networks. In Marco Zuniga and Gianluca Dini, editors, *Sensor Systems and Software*, pages 47–64, Cham, 2013. Springer International Publishing. [https://doi.org/10.1007/978-3-319-04166-7\\_4](https://doi.org/10.1007/978-3-319-04166-7_4).
- [21] L. Pomante, M. Pugliese, S. Marchesani, and F. Santucci. Winsome: A middleware platform for the provision of secure monitoring services over wireless sensor networks. 2013. <https://doi.org/10.1109/IWCMC.2013.6583643>.

# A Critical Analysis of Usability and Learning Methods on an Augmented Reality Application for Zoology Education

Diego Iquiria-Becerra<sup>\*</sup>, Michael Flores-Conislla, Juan Deyby Carlos-Chullo, Briseida Sotelo-Castro, Claudia Payalich-Quispe, Carlo Corrales-Delgado

*Universidad Nacional de San Agustín de Arequipa, Perú*

---

## ARTICLE INFO

*Article history:*

*Received: 16 January, 2020*

*Accepted: 11 March, 2020*

*Online: 07 April, 2020*

---

*Keywords:*

*Augmented reality*

*Education*

*Zoology*

*Usability*

---



---

## ABSTRACT

*In recent years, research has been conducted focused on the use of technologies in the classroom, but one of the main problems is to demonstrate that the use of this technology favors learning compared to traditional methods. One of these technologies is augmented reality that allows seeing virtual objects superimposed in the real world, but to achieve its correct use it is necessary to evaluate the usability that is the ease with which an interface is used. In this work we develop and analyze from two perspectives an educational application for zoology that uses augmented reality, a first perspective is usability, where an analysis has been carried out on how the correct design of an augmented reality application should be focusing on heuristic evaluations, the second perspective is at the educational level where we analyze it at the classroom level where we measure the different learning methods (Traditional Learning, Self Learning, and Guided Learning) and which one should be used.*

---

## 1 Introduction

This paper is an extension of work originally presented in XIII Latin American Conference on Learning Technologies (LACLO) [1]. The emergence of new technologies creates a need to adopt new strategies in the classroom, which complement the learning process to improve the way of teaching.

This research focuses on conducting a case study from the perspective of usability and learning methods of an application of augmented educational reality for the teaching of zoology. Usability is understood as the degree to which users interact with an application that must be effective, efficient and easy to learn [2].

The learning methods have been based on game-based learning where three different methodologies were used (Traditional, Self and Guided) [3].

In the design of the application, we have taken as a basis the traditional method of teaching zoology where cards with descriptions of animals are used, which have been transformed into markers, these markers are recognized by a mobile device that generates a model of the animal and its habitat in 3D. Finally, the case study was carried out in an educational institution where students were divided into groups to which an evaluation was made before and after using the application.

### 1.1 Augmented Reality

Augmented reality (AR) is a variation of virtual environments (VE) or virtual reality (VR). The Figure 1 shows a vision of the continuity between virtuality and reality defined by Milgram in 1995 [4], where VE technologies completely immerse the user in a synthetic environment (right of the Figure 1), not being aware of the real world that surrounds it. In contrast, AR allows the user to see virtual objects superimposed in the real world. Therefore, AR complements reality instead of completely replacing it [5].

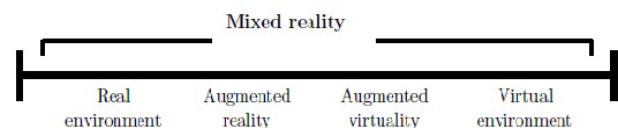


Figure 1: Milgram's reality-virtuality continuum [6]

Azuma defines AR as a technology that meets three characteristics [7]:

1. Combines real and virtual.
2. Interactive in real time.

<sup>\*</sup>Diego Alonso Iquiria Becerra, Arequipa, Per, diquiria@unsa.edu.pe

3. Registered in 3-D.

## 1.2 Usability

Usability is an attribute that evaluates the ease with which a user interface is used; It can also refer to methods to improve ease of use during the design process [2].

The 5 main components of usability are defined by the following questions:

1. Learning: How easy is it for users to perform basic tasks the first time they encounter the design?
2. Efficiency: Once users have learned the design, how quickly can they perform tasks?
3. Easy to remember: When users return to the design after a period of not using it, how easily can they restore their competition?
4. Errors: How many errors do users make, how serious are these errors and how easy can they recover from errors?
5. Satisfaction: How nice is it to use the design?

. An important point is utility, which refers to the functionality of the design: Does it do what users need? [2].

ISO 9241 is a standard focused on quality, providing requirements and recommendations relating to the attributes of the hardware, software, and environment that contribute to the usability and ergonomic principles that guide them [8].

Specifically, ISO 9241-11 tells us that the objective of the design and evaluation of systems, products, and services for usability is to allow users to reach goals effectively, efficiently and with satisfaction, taking into account the context of use. Thus, it defines usability as "The extent to which a system, product or service can be used by specific users to achieve specific objectives with effectiveness, efficiency, and satisfaction in a specific context of use" [8] [9].

Usually, to measure usability according to ISO 9241-11, it is done by user tests, the advantage of these is that resources can be quite modest. The number of users varies, but a small sample of 5 to 8 users can identify 80-85% of usability problems in a controlled environment.

The goal of usability evaluation is to see the degree to which a system is easy and pleasant to use, to determine the scope of its usability, using robust, reliable and objective metrics [10]. The evaluation of traditional systems is based on predefined usability methods. These can be classified as Inspection methods, test methods and user reports [10]- [12].

## 1.3 Learning Methods

### 1.3.1 Traditional Learning

In the traditional teaching method participants are required to attend the classes in the fix hour and place regularly and receive training face to face, mainly in the form of verbal and textual ones. What is more remarkable is that this method of teaching is provided in the same way for all learners [13].

Therefore, this method generates space-time limitations since it is only performed at predetermined times and is limited to only being carried out in classrooms [14].

### 1.3.2 Self Learning

According to Acosta, self learning is a form of active learning in which students, guided by a facilitator, autonomously increase their skills in a specific area [15].

Operational units of students or autonomous work teams are established, which choose a situation or reality to investigate by team, then establish their baseline of competencies, then choose their learning objectives, finally design a simulation scenario, experience it and reflect. Likewise, self-learning can be understood as the process in which the student is involved in the construction of their learning, thus promoting autonomous work [16].

### 1.3.3 Guided Learning

Guided learning lies midway between direct instruction and free learning, presenting a learning goal, and scaffolding the environment while allowing students to maintain a large degree of control over their learning [17].

Guided learning approaches are effective because they create learning situations that encourage students to become active and engaged partners in the learning process [17].

## 1.4 Zoology Education

Children from birth have a scientific interest in exploring and knowing the objects and beings of their environment, for this reason, the teaching of science and technology encourages their curiosity, discovery and the pleasure to learn, as well as providing sensitivity and respect for the environment and living things, specifically in the area of zoology which focuses on animal studies.

In the first years of age, children develop their ability to understand nature in their environment, where the student questions, reflects and thinks about the beings that inhabit it, for this reason, the Ministry of Education of Peru (MINEDU) proposes the use of learning paths to guide the correct teaching of students [18].

So that the student can progress in the learning pathways of the zoology area, it is expected that they will be able to explain the beings of nature-based on evidence from various sources of information and that they will be able to describe in their own words the characteristics or qualities of living beings in their environment based on previous knowledge.

According to MINEDU, the learning paths for zoology teaching are the competences, capacities, and indicators which focus on [18]:

- Competence: It is intended that the student explain the physical world based on their scientific knowledge and that their scientists understand and apply knowledge, arguing them scientifically.
- Capacity: The student must be able to recognize animals according to their characteristics and must be able to relate an animal according to its environment.

- Indicators: The student must describe the characteristics of the animals, must mention their similarities between their descendants and parent and must relate them according to their environment.

Once the learning path is completed; students will be able to: learn the characteristics and needs of living beings, understand that living beings are born from another living being, grow and develop, similarities between parents and descendants and the names of Animals and the place they inhabit.

Another central point in the learning paths is the map of progress that are instruments that allow identifying the progress of the students, to have greater clarity regarding the expectations that are expected of them regarding each established competence [18].

At a more specific level, the progress maps contain a clear and agreed definition of the learning goals that must be achieved by all students at the end of a learning cycle, in this way we can determine that the progress maps provide us with all the information necessary of the students according to each competition [19].

Finally, the materials used in the classes are [18]:

- Metal board and magnetized animal parts.
- Cards with descriptions of the animals.
- Paper, markers and duct tape.
- Science and Environment Book provided by MINEDU.

## 2 Related Works

In recent years, interest in the use of augmented reality for teaching in children has increased. Different previous investigations have built applications through programs such as Unity (Multi-platform video game engine) used in conjunction with augmented reality libraries such as Vuforia. A study [20] shows a mobile application of augmented reality to reinforce student learning and experience, among the activities of the application was the 3D visualization of the Earth by focusing the view on the encyclopedia and being able to visualize an animal model in 3D using as markers bills from different countries. All this allowed increasing the curiosity of the student by stimulating his memory since he related the virtual 3D models with the physical elements.

In another study, they developed educational software in Unity for teaching physics where a methodology for the evaluation of didactic usability was proposed [21].

Another study [22] is about how to create educational software using augmented reality combined with Bloom's Taxonomy, whose main purpose was to stimulate spatial reasoning by improving the children's learning process. In another investigation [23], an application has been created which takes a specific image of an anatomy atlas and converts it into a three-dimensional and dynamic model, which allows improving the interactivity of the student in the learning process, in that system they are stored in a database the different scanned photos of the anatomy atlas and then are consulted by the application, they made the three-dimensional models in Unity3D and Maya, one of the most important points of that research is that it encourages students' self-learning.

Teaching an alphabet can be complicated at times, but augmented reality also works for these cases, as in this study [24], where an attractive and interesting learning process of the Hijaiyah alphabet is developed through a mobile application using augmented reality technology. The purpose of this application is to encourage children's interest in learning the Hijaiyah alphabet. This application uses smartphones and markers. It was built using Unity and the Vuforia library, as well as Blender for modeling 3D objects. To use the application, the smartphone camera tracks the marker and once it is identified, the marker will have projected the objects of the Hijaiyah alphabet in three-dimensional form. Finally, the user can learn and understand the form and pronunciation of the Hijaiyah alphabet by touching the virtual button on the marker.

Augmented reality can also be used in the area of chemistry as in the application called PeriodikAR [25], which is an application developed for the Android platform through the use of the Vuforia library. The tracking technique used is without a marker. This application runs dynamically to provide certain information about the elements in an animated video. The information includes the name of each element, atomic number, boiling point, melting point, density, atomic mass, standard atomic weight, oxidation state, symbol, phase, element category, electron configuration, and electron orbital display. In this case, the dynamic term means that all the markers and animated videos of the application can be added or subtracted without modifying the source code of the application. It is because all the markers and the storage of animated videos are placed in a different place from the application storage. This application aims to increase interest in studying chemical elements. Finally, another work [26] focuses on an Android application that teaches playing musical instruments. This application was made using technologies such as augmented reality Vuforia, 3D modeling with Blender and Unity 3D.

## 3 Zoology Augmented Reality Application

### 3.1 Application Overview

The application was developed for mobile devices that have a camera, which recognizes the markers found on the cards; the markers contain images of the animals in their environment. The target audience is kindergarten students, who can interact with the virtual animals that appear in their habitat.

The objective of the application is to provide new technological tools to the classroom, specifically the cards with virtual reality markers, which will allow students to interact and recognize the animals according to their characteristics and their environment. Additionally, activities in the application focused on self-learning were added, where the student recognizes the animals based on their shadow, these activities contain a system of scores and notifications; in order to generate continuous feedback between the student and the application.

### 3.2 Hardware and Software

For the development of the application, we have used Android mobile devices version 7.0 or higher, which had a gyroscope. Also, a computer with the following features was used: Intel Core I7



processor, 8 GB of RAM, 1 TB of storage memory and an Nvidia GeForce GTX 980M graphics card.

The programs that were used were: Unity 3D and Vuforia for the main development of the application, Inkscape for graphic design and Audacity for audio editing.

### 3.3 Activities

The application will teach about the animals of the following groups: mammals, birds, reptiles, fish and amphibians as shown in Figure 2, the application will have five levels that represent the learning sessions of each day: Monday, Tuesday, Wednesday, Thursday and Friday, as seen in Figure 3, we will describe the activities of each level below:

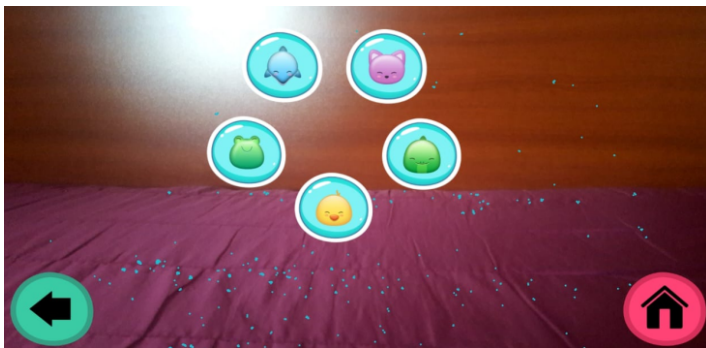


Figure 2: Groups of animals: mammals, birds, reptiles, fish and amphibians (Source: Own Elaboration)

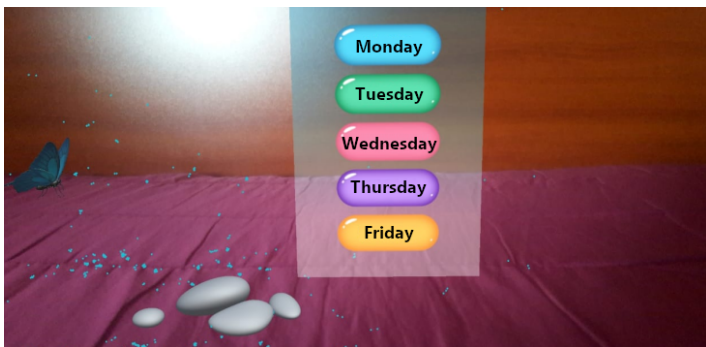


Figure 3: Application levels: Monday, Tuesday, Wednesday, Thursday and Friday (Source: Own Elaboration)

#### 3.3.1 Monday

It is the first level of the lessons, in which students learn the names and descriptions of each of the animals. They can also observe the models of each of the animals.

#### 3.3.2 Tuesday

In this level, the animations of each animal are presented, which are interactive through the use of touch.

#### 3.3.3 Wednesday

At this level, 3d animal models are presented in a 3d environment that represents their habitat as seen in Figure 4.



Figure 4: 3d animal models in their habitat (Source: Own Elaboration)

#### 3.3.4 Thursday

This level shows the 3d animal models that were seen in the previous levels but on a real scale, as seen in Figure 5.

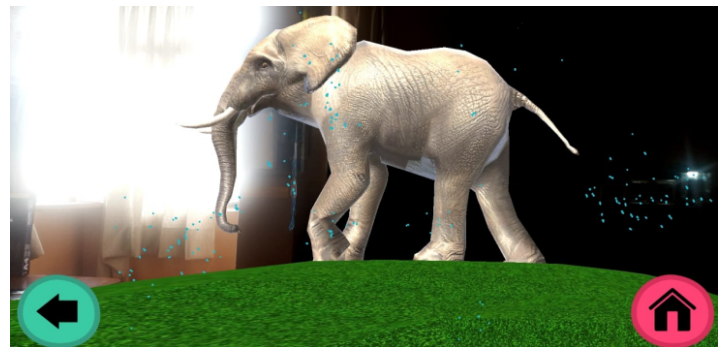


Figure 5: Real-size animal 3d model with animations (Source: Own Elaboration)

#### 3.3.5 Friday

Final level, the student link the animals to their habitat, which are selected randomly. The student must drag the animal with its corresponding habitat, see Figure 6.



Figure 6: Activity to relate animals with their habitats (Source: Own Elaboration)

## 4 Methodology

### 4.1 Usability Evaluation

To perform the evaluation, we made use of user tests that contain a combination of task completion rates, errors, task times and task level satisfaction. Two ways of testing were considered:

- Formative: Provides immediate feedback to improve learning
- Summative: Evaluate what has been learned.

The experiences to evaluate and improve user interaction with the application was formative, and the problems were quantified in terms of frequency and severity, we monitored the users who had problems, we measured the time it took to complete a task and we determined whether they completed the tasks correctly. The method used to evaluate the results is described below.

#### 1. Task Time: The time a user spends in an activity, specifically:

- Completion task time: Time for users to complete the task correctly.
- Failure task time : Time for users to complete the task incorrectly.
- Total task time: Total duration of time users spend on a task.

#### 2. Errors: The capture of touch events in the activities of the application, considering actions such as:

- ACTION DOWN: This event is manifested when the screen is pressed and we don't move the pointer anywhere.
- ACTION MOVE: This event is manifested when after pressing the screen we proceed to move the pointer, in other words, when we do these 2 events will appear, the ACTION DOWN and then when moving the pointer the ACTION MOVE event will appear.
- ACTION UP: This event is manifested when we lift the finger or pointer of the screen, for this event to occur, the ACTION DOWN event must have occurred before.
- ACTION OUTSIDE: This event is manifested when the event occurs outside the normal limits of an user interface element.

#### 3. Effectiveness: Measured by the rate of completed tasks and the rate of errors in tasks, the following will be analyzed: Completed tasks, Objectives achieved, Errors in a task, Tasks with errors and Intensity of task error.

#### 4. Efficiency: It is measured by the time it takes to complete a task, it will be analyzed: Task time, Time efficiency, Profitability, Production time ratio, and Unnecessary actions.

#### 5. Satisfaction: The perception of the ease of use of a system is measured, if they can be completed immediately after a task (post-task questionnaires), at the end of a usability session (post-test questionnaires), or outside of A usability test is analyzed.

### 4.2 Evaluation Learning Methods

#### 4.2.1 Participants

A total of 45 5-year-old children participated in the study, they were kindergarten students of a national school; There were a greater number of men (62.2 %) than women, the students belonged to two classrooms.

#### 4.2.2 Method

The students were divided into three groups chosen at random, they were given the first test to measure their knowledge about zoology, this test focused on presenting a group of thirteen animal cards, of which the students had to recognize the name and habitat of different animals.

Subsequently, each group was assigned a different teaching method, a first group used the traditional learning where the teacher used cards with descriptions of the animals to teach them about zoology, the second group were given mobile devices and a set of markers that contained figures of animals with which students should self-learning about animals, finally, the third group used mobile devices and markers but their learning was led by a teacher who guided and explained about the different animals.

After the end of the learning session, a second evaluation was carried out on the students in which the acquired knowledge was measured.

## 5 Results

### 5.1 Usability Results

To evaluate the results, three aspects of usability were considered: Effectiveness, efficiency, and satisfaction. We capture the events of user interaction with the application in Friday activity.

The measurement by task completion rate and task error rate are shown in Figure 7.

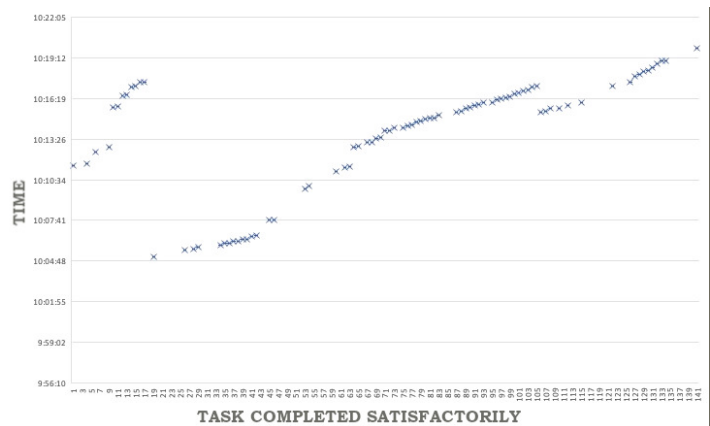


Figure 7: Tasks completed satisfactorily (Source: Own Elaboration)

To analyze the results, the tasks completed in the sample of 141 tasks were observed as a collection of points in time, the position of each point on the vertical axis (y) is the time at which the value

was collected. Tasks that do not have a point associated were not completed successfully.

To recognize effectiveness as a characteristic of the usability evaluation of the application, the total percentage of tasks completed with or without cognitive errors related to animals was considered. Figure 8 shows that 91% represents the total of complete tasks with or without cognitive errors, while 9% represents tasks that did not reach the objective. Comparing the result with the percentage of tasks completed, 31% represents tasks completed with cognitive errors.

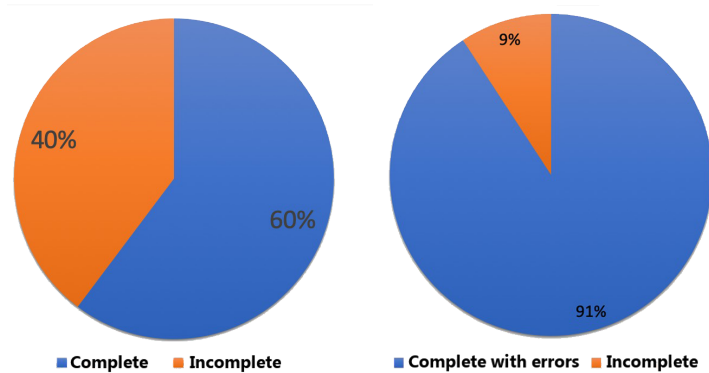


Figure 8: Percentage of completed tasks and complete tasks with errors (Source: Own Elaboration)

To recognize the efficiency, we considered the task time in the accomplishment of the task and an average time of 5 seconds was considered. Of the sample size of 141 tasks, only the time of 128 tasks that were completed was considered. In Figure 9, the time of accomplishment of each task is observed; The average time ranges from 0 seconds to 5 seconds, considering the highest peak with 23 seconds and the lowest peak 0 seconds.

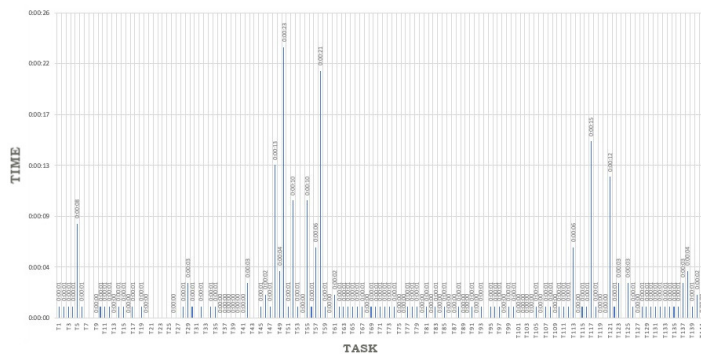


Figure 9: Task Time (Source: Own Elaboration)

In Figure 10, it is observed that the tasks completed within the average time of 5 seconds represent 91%, being a total of 116 tasks. While the remaining 9% represents a total of 12 tasks that obtained a task completion time greater than 5 seconds. According to the evaluation of this characteristic of Usability, the high percentage of tasks completed within the average time assigned is observed, therefore, it can be affirmed that the application in Friday activity complies with this aspect of usability by 91%.

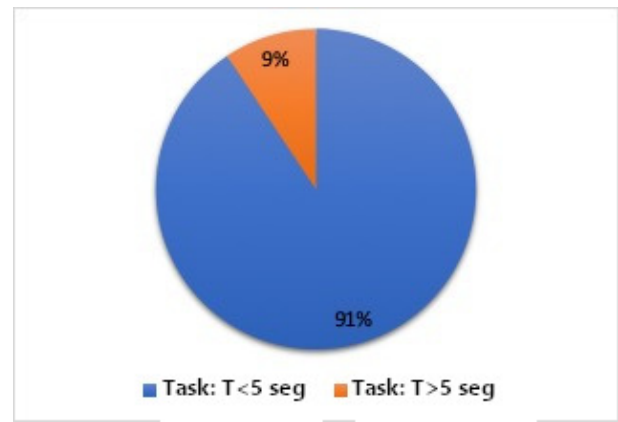


Figure 10: Percentage of the execution time of a task (Source: Own Elaboration)

To know satisfaction, we measured with the SUS (System Usability Scale) questionnaire, an instrument of Likert scale of 10 items. The evaluation was carried out immediately after the interaction, which allowed the evaluators to record their initial feelings and responses with greater certainty.

According to the results presented in Figure 11, the SUS score obtained is 69. Since the theoretical maximum is 100, we can deduce good but not excellent usability of the system.

SUS QUESTIONNAIRE											
RATING FROM 1 TO 5:											
1: TOTAL DISAGREE											
5: TOTAL AGREE											
QUESTIONS	E1	E2	E3	T1	T2	PSY	A1	A2	A3	A4	Pts
1 I think I would use this application frequently	5	5	5	5	4	4	4	4	4	5	4.5
2 I find this application unnecessarily complex	1	1	1	1	1	1	1	1	1	1	1
3 I think the application was easy to use	4	4	4	4	5	5	5	5	5	4	4.5
4 I think I need help from a person with technical knowledge to use this application.	3	3	3	3	4	4	4	4	4	3	3.5
5 The functions of this application are well integrated	4	4	4	4	4	4	4	4	4	4	4
6 I think the application is very inconsistent	2	2	2	2	1	1	1	1	1	2	1.5
7 Most people would learn to use this application very quickly.	5	5	5	5	5	5	5	5	5	5	5
8 I find that the application is very difficult to use	1	1	1	1	2	2	2	2	2	1	1.5
9 I feel confident using this application.	5	5	5	5	4	4	4	4	4	5	4.5
10 I needed to learn many things before being able to use this application.	2	2	2	2	2	2	2	2	2	2	2

E= Engineer      T= Teacher      PSY= Psychologist      A= Education Assistant

Figure 11: SUS questions of the application (Source: Own Elaboration)

## 5.2 Results Learning Methods

To analyze the results obtained from the pre-test and the post-test we decided to apply the regression and correlation of data, which were applied to both the names of the animals and the habitat of the animals of the following thirteen animals: cow, shark, frog, penguin, polar bear, lion, giraffe, gorilla, seal, elephant, crocodile, sea horse, and owl.

In the Figure 12, the data was processed with the STATA (Software for Statistics and Data Science) tool where a regression equation was used that explains the students' learning about the names of the animals which turned out to be in inverse function of the self-learning method, that is that by applying the method of



self-learning, the learning of animal names is reduced but there is a direct relationship between guided learning and traditional learning.

A regression equation was used for the analysis of animal name learning, this equation is a function of self-learning plus guided learning towards traditional learning.

. regress ANIMAL NAME SELF LEARNING GUIDED LEARNING TRADITIONAL LEARNING				
Source	SS	df	MS	Number of obs = 45
Model	6.94039066	3	2.31346355	F(3, 41) = 41.17
Residual	2.30405378	41	.056196434	Prob > F = 0.0000
				R-squared = 0.7508
				Adj R-squared = 0.7325
				Root MSE = .23706
Total	9.24444444	44	.21010101	

ANIMAL NAME	Coef.	Std. Err.	t	P> t	[95% Conf. Interval]	
SELF LEARNING	-.0088418	.0183371	-0.48	0.632	-.0458744	.0281908
GUIDED LEARNING	.1384828	.0125899	11.00	0.000	.1130569	.1639087
TRADITIONAL LEARNING	.0203049	.0201334	1.01	0.319	-.0203553	.0609652
_cons	-.5299198	.1554088	-3.41	0.001	-.8437742	-.2160653

Figure 12: Regression of animal name learning between different learning methods (Source: Own Elaboration)

$$\begin{aligned}
 \text{LEARNING ANIMAL NAME}^{(\wedge)} &= \\
 &- 0.0088418 \text{ Self learning} \\
 &+ 0.1384828 \text{ Guided learning} \\
 &+ 0.0203049 \text{ Traditional learning} + u
 \end{aligned}$$

The negative self-learning coefficient indicates that it has an inverse relationship with the learning of animal names, that is, when the learning of animals is achieved, self-learning has little influence. On the other hand, guided learning and traditional learning have a positive sign in their coefficients, which indicates that they influence the learning process.

For this reason the model is significant in its entirety, since its p-value of F is 0.0000 which is lower than the significance level of 5%.

The independent variables (Self learning; Guided learning; Traditional learning) explain the variable learning of animal names by 75.08%.

With which we determine the following:

- The self learning variable is not significant for the model since the p-value of its coefficient is 0.632 which is less than 5%.
- The guided learning variable is significant for the model since the p-value of its coefficient is 0.000 which is less than 5%.
- The traditional learning variable is not significant for the model since the p-value of its coefficient is 0.319 which is greater than 5%

In the same way, we perform another analysis with the data corresponding to the names of the animals where it is stated that the variable that has the greatest correlation with the learning of the name of the animals as seen in the Figure 13 is the guided learning

with 86.21 % and the variable that has a negative correlation of -5.99% is the traditional learning.

. corr ANIMAL NAME SELF LEARNING GUIDED LEARNING TRADITIONAL LEARNING (obs=45)				
	NAME	SELF	GUIDED	TRADITIONAL
ANIMAL NAME	1.0000			
SELF LEARNING	-0.0599	1.0000		
GUIDED LEARNING	0.8621	-0.0263	1.0000	
TRADITIONAL LEARNING	0.1079	0.0031	0.0342	1.0000

Figure 13: Correlation of animal name learning between different learning methods (Source: Own Elaboration)

On the other hand, we perform another regression equation was used for the analysis of animal habitat learning, this equation is a function of self-learning plus guided learning towards traditional learning. 14.

. regress ANIMAL HABITAT SELF LEARNING GUIDED LEARNING TRADITIONAL LEARNING				
Source	SS	df	MS	Number of obs = 45
Model	8.27600752	3	2.75866917	F(3, 41) = 49.14
Residual	2.30177026	41	.056140738	Prob > F = 0.0000
				R-squared = 0.7824
				Adj R-squared = 0.7665
				Root MSE = .23694
Total	10.5777778	44	.24040404	

ANIMAL HABITAT	Coef.	Std. Err.	t	P> t	[95% Conf. Interval]	
SELF LEARNING	.0153236	.0201697	0.76	0.452	-.0254098	.0560571
GUIDED LEARNING	.1841973	.015174	12.14	0.000	.1535529	.2148417
TRADITIONAL LEARNING	-.0155931	.0183617	-0.85	0.401	-.0526744	.0214902
_cons	-.7618375	.1579508	-4.82	0.000	-1.080826	-.4428494

Figure 14: Regression of animal habitat learning between different learning methods (Source: Own Elaboration)

$$\begin{aligned}
 \text{LEARNING ANIMAL HABITAT}^{(\wedge)} &= \\
 &0.0153236 \text{ Self learning} \\
 &+ 0.1841973 \text{ Guided learning} \\
 &- 0.0155931 \text{ Traditional learning} + u
 \end{aligned}
 \tag{1}$$

The negative traditional learning coefficient indicates that it has an inverse relationship with the learning of animal habitat, that is, when the learning of animals habitat is achieved, traditional learning has little influence. On the other hand, guided learning and self learning have a positive sign in their coefficients, which indicates that they influence the learning process.

The model is significant in its entirety since its p-value of F is 0.0000 which is below the significance level of 5%. The independent variables (Self learning; Guided learning; Traditional learning) explain the variable learning of the location of the animals by 78.24%.

With which we determine the following:

- The self learning variable is not significant for the model since the p-value of its coefficient is 0.452 which is less than 5%.



- The guided learning variable is significant for the model since the p-value of its coefficient is 0.000 which is less than 5%.
- The traditional learning variable is not significant for the model since the p-value of its coefficient is 0.401 which is greater than 5%

Additionally, we perform another analysis with the data corresponding to the habitat of the animals as seen in Figure 15, where it is stated that the variable that has the greatest correlation with the learning of the location of the animals is the guided learning with an 88,07% and the variables that have a negative correlation of -1.62% and -0.74% are those of self and traditional learning respectively.

```

. corr ANIMAL HABITAT SELF LEARNING GUIDED LEARNING TRADITIONAL LEARNING
(obs=45)
    
```

	HABITAT	SELF	GUIDED	TRADITIONAL
ANIMAL HÁBITAT	1.0000			
SELF LEARNING	-0.0162	1.0000		
GUIDED LEARNING	0.8807	-0.0792	1.0000	
TRADITIONAL LEARNING	-0.0074	0.0229	0.0600	1.0000

Figure 15: Correlation of animal habitat learning between different learning methods (Source: Own Elaboration)

Finally, we made a comparison between the pre-test and post-test of the different learning methods as seen in Figure 16, in which the guided learning was the one that obtained the highest percentage of improvement, they get to improve the understanding of animals and the habitat in 48.6% followed by self learning with a 30.5% improvement and finally traditional learning that obtained only 21%.

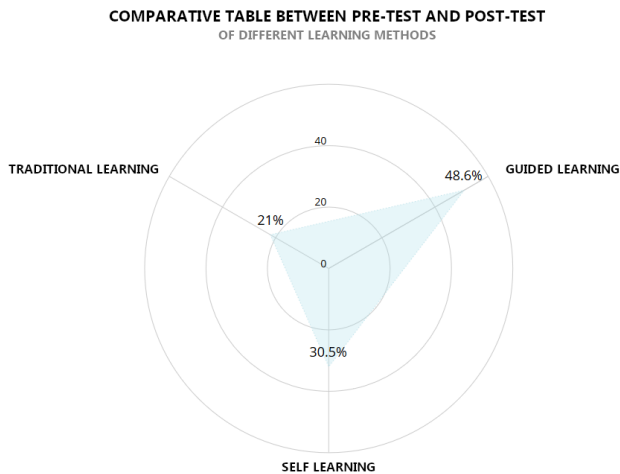


Figure 16: Comparative table between pre-test and post-test of different learning methods (Source: Own Elaboration)

## 6 Conclusions and Future Works

### 6.1 Conclusions

According to the usability characteristics established by ISO 9241-11 presented in this research, it provides a practical way to

evaluate the usability of AR applications. Thus, the proposal is expected to become part of the AR application development process, which will allow users to perform tasks that achieve the objectives of effectiveness, efficiency, and satisfaction.

During the evaluation carried out in the development of the applications, several design problems were found including the use of AR techniques in the application. When the end-users of the application are children, it is advisable not to use markers for the recognition of 3D elements, it was difficult to keep their attention on pointing to the marker and at the same time seeing the recognition image. Due to these first tests, the application uses navigation and selection techniques. Therefore, it is concluded that to choose the interaction techniques depends on the requirements of the application. The same set of techniques will not work well in all situations.

An important observation was that children seemed to understand how to use the augmented reality application as soon as they began to interact with technology.

In the process of development and evaluation of the application, it is essential to involve teachers in the development of activities directly related to the needs of students, especially if the application is aimed at children 5 years old; since it allows researchers to have a better overview and better understand the problems that could occur.

We can conclude that the applications of AR that follow the principles of usability help in the motivation and learning of children.

When analyzing the results obtained in the tests we determine that for the recognition of animal names a guided learning method turns out to be better than a self-learning.

Which was because the application failed to explain the name correctly, since it was not repeated and when it was heard at the same time that the sound generated by the animal caused a distraction in the students and did not take the corresponding attention unlike of guided learning, where the teacher indicated the animal they should look for and explained information about the animal that is complemented by the visualization of the 3D model.

As for the habitat, the guided learning method turned out to be the best, because with traditional learning the student could not identify visually the environment where the animal lived, since the habitat was described orally, on the other hand in the car if the student could recognize the environment, but since there were no dialogues that would indicate information about the environment, the student had to rely on his previous knowledge to identify the correct name of the environment, finally when comparing the post-test and the pre-test we identified that the guided learning method obtained a higher score reaching 48.3% of positive responses.

With which we have been able to conclude that the use of augmented reality does show improvements in traditional education, but the best method to carry out education through this technology is that the teacher guides the student on what to do and can maintain at all times the control of the actions that each student will take.

### 6.2 Futures Work

Articles focused on the use of augmented reality in the classroom will continue, while many will focus on short-term research, it

is also necessary to consider long-term research and the use of other technologies, so we suggest the following topics that could be investigated:

- Add specific ergonomic tests regarding the user experience. It is also recommended to consider ergonomics usability issues in terms of interaction with mobile devices.
- Perform more extensive tests using the evaluation proposal presented to evaluate new virtual contents and the use of other types of 3D interactivity techniques or sensors.
- Perform new educational activities that focus on Machine Learning to improve the free education process and serve as a complement to targeted education.
- Find new technologies of augmented reality that not only focus on markers such as ARCore for the creation of new educational activities focused on the topic of zoology.
- The creation of other augmented reality applications that explain natural phenomena that occur in the student environment is proposed.

**Acknowledgment** Thanks to the Universidad Nacional de San Agustín de Arequipa for support in the research.

## References

- [1] D. A. I. Becerra, B. D. S. Castro, M. M. F. Conislla, and C. Corrales-Delgado, "Augmented reality applied in the design of learning activities in zoology," in *2018 XIII Latin American Conference on Learning Technologies (LACLO)*, IEEE, 2018, pp. 121–126.
- [2] J. Nielsen, "The usability engineering life cycle," *Computer*, vol. 25, no. 3, pp. 12–22, 1992.
- [3] E. Danniels and A. Pyle, "Definir el aprendizaje basado en el juego," *Aprendizaje basado en el juego. Actualizado en febrero de*, 2018.
- [4] P. Milgram, H. Takemura, A. Utsumi, and F. Kishino, "Augmented reality: A class of displays on the reality-virtuality continuum," in *Telemanipulator and telepresence technologies*, vol. 2351. International Society for Optics and Photonics, 1995, pp. 282–292.
- [5] S. E. Schaeffer, "Usability evaluation for augmented reality," 2014.
- [6] P. Milgram and F. Kishino, "A taxonomy of mixed reality visual displays," *IEICE TRANSACTIONS on Information and Systems*, vol. 77, no. 12, pp. 1321–1329, 1994.
- [7] R. T. Azuma, "A survey of augmented reality," *Presence: Teleoperators & Virtual Environments*, vol. 6, no. 4, pp. 355–385, 1997.
- [8] M. Kurosu, "Nigel bevan and concepts of usability, ux, and satisfaction," *Journal of Usability Studies*, vol. 14, no. 3, 2019.
- [9] M. Georgsson, N. Staggers, E. Årsand, and A. Kushniruk, "Employing a user-centered cognitive walkthrough to evaluate a mhealth diabetes self-management application: A case study and beginning method validation," *Journal of biomedical informatics*, vol. 91, p. 103110, 2019.
- [10] G. Cockton, "Usability evaluation," 2012.
- [11] H. Martínez and P. Bandyopadhyay, "Analysis of four usability evaluation methods applied to augmented reality applications," *Helsinki, Finland: Helsinki Institute for Information Technology (HIIT)*, 2014.
- [12] O. Sharhorodska and D. Iquira, "Interaction of low cost mobile virtual reality environments—using metaphor in an astronomy laboratory," in *International Conference on Human-Computer Interaction*. Springer, 2019, pp. 293–300.
- [13] M. Gharibpoor, S. Sargazi, and M. Aref, "Efficiency evaluation of e-learning compared to traditional education in human resource development (case study: Small and medium enterprises in shiraz)," in *7th International Conference on e-Commerce in Developing Countries: with focus on e-Security*. IEEE, 2013, pp. 1–8.
- [14] J. E. Thiele, "Learning patterns of online students," *Journal of Nursing Education*, vol. 42, no. 8, pp. 364–366, 2003.
- [15] C. L. Costa, A. M. Nicolás, J. A. G. Méndez, M. d. G. A. Martínez, and J. L. D. Agea, "Enseñando con metodología de autoaprendizaje en entornos simulados (maes©). un estudio cualitativo entre profesores y alumnos de grado en enfermería," *Educación Médica*, vol. 20, pp. 52–58, 2019.
- [16] C. J. Z. Rodríguez, P. García-Martínez, C. Ferreira, I. Fernández, and J. J. Miret, "Sistemas interactivos eficientes para la tutorización y el autoaprendizaje de óptica basados en la resolución gráfica de problemas," *Optica pura y aplicada*, vol. 46, no. 2, pp. 197–203, 2013.
- [17] D. S. Weisberg, K. Hirsh-Pasek, and R. M. Golinkoff, "Guided play: Where curricular goals meet a playful pedagogy," *Mind, Brain, and Education*, vol. 7, no. 2, pp. 104–112, 2013.
- [18] MINEDU. (2016) Programa curricular educacin inicial. [Online]. Available: <http://www.minedu.gob.pe/curriculo/pdf/programa-curricular-educacion-inicial.pdf>
- [19] M. J. Ramos Haro, G. García Figueroa, E. Y. Quinteros Hajar, M. J. Niño Correa, M. Ventura Panduro, W. Palomino Noa, J. M. Camavilca Vega, J. A. Pezo de la Cuba, L. Velasco Taipe, C. Yupán Cárdenas et al., "Rutas del aprendizaje¿ qué y cómo aprenden nuestros niños y niñas?: II ciclo. área curricular ciencia y ambiente, 3, 4 y 5 años de edad. versión 2015," 2015.
- [20] "An educational augmented reality app to facilitate learning experience." *2017 International Conference on Computer and Applications (ICCA), Computer and Applications (ICCA), 2017 International Conference on*, p. 279, 2017.
- [21] D. Alonso Iquira Becerra, J. Herrera Quispe, R. Guillermo Apaza Aceituno, G. Mary Poma Vargas, F. Gabriela Fernandez Zamora, J. Luis Huilca Mango, G. Paulina Ancasí Figueroa, A. Alexis Perez Vizcarra, and J. Willian Torres Chana, "Evaluation of a gamified 3d virtual reality system to enhance the understanding of movement in physics," 01 2017, pp. 395–401.
- [22] "Playful and interactive environment-based augmented reality to stimulate learning of children." *2016 18th Mediterranean Electrotechnical Conference (MELECON), Electrotechnical Conference (MELECON), 2016 18th Mediterranean*, p. 1, 2016.
- [23] J. A. Juanes, D. Hernández, P. Ruisoto, E. García, G. Villarrubia, and A. Prats, "Augmented reality techniques, using mobile devices, for learning human anatomy," in *Proceedings of the Second International Conference on Technological Ecosystems for Enhancing Multiculturality*, ser. TEEM '14. New York, NY, USA: ACM, 2014, pp. 7–11.
- [24] R. F. Rahmat, F. Akbar, M. F. Syahputra, M. A. Budiman, and A. Hizriadi, "An interactive augmented reality implementation of hijaiyah alphabet for children education," in *Journal of Physics: Conference Series*, vol. 978, 2018.
- [25] A. A. K. Oka Sudana, A. Setiawan, and I. P. A. E. Pratama, "Augmented reality for chemical elements: Periodikar," *Journal of Theoretical and Applied Information Technology*, vol. 90, no. 1, pp. 88–92, 2016, cited By :2.
- [26] M. K. Zhaparov and U. Assanov, "Augmented reality based on kazakh instrument "dombyra"," in *8th IEEE International Conference on Application of Information and Communication Technologies, AICT 2014 - Conference Proceedings*, 2014.

# Hybrid Autogyro: Model and Longitudinal Control for Wind Gust Energy Conversion Using Autorotation

Jonathan Flores Santiago<sup>\*1</sup>, Sergio Salazar Cruz<sup>1</sup>, Rogelio Lozano Leal<sup>1,2</sup>

<sup>1</sup>UMI-LAFMIA 3175 CNRS, CINVESTAV, 07360, Mexico.

<sup>2</sup>Sorbonne Universités, UTC-CNRS, UMR 7253 Heudiasyc, Compiègne, France.

## ARTICLE INFO

Article history:

Received: 14 January, 2020

Accepted: 11 March, 2020

Online: 07 April, 2020

Keywords:

Autorotation

Longitudinal Control

Hybrid autogyro

## ABSTRACT

In the new technologies for producing electricity from wind gusts, a new class of wind power converter has been proposed. The hybrid autogyro uses the principle of autorotation to generate lift. This paper proposes to take advantage of this rotation to also generate energy. There are systems that use flying wings or airplanes to reach winds that blow in layers of the atmosphere that are inaccessible to traditional wind turbines. Wind gusts are disturbances that significantly affect the behavior of this kind of aircraft. However wind gust is the source of energy and this wind speed increases with the aircraft's altitude. This paper reviews the mathematical model of the hybrid autogyro aircraft and proposes a control algorithm to ensure that the vehicle remains horizontal in forward flight, in this way is possible to maximize the generated energy, this concept is tested in numerical simulations.

Symbol	Description
$a_0, a_1, b_1$	Coning, forward, and side flapping angles.
$F$	Force vector $[X \ Y \ Z]^T$ .
$g$	acceleration due to gravity.
$H$	Angular momentum vector.
$I_{xx}, I_{yy}, I_{zz}$	Inertia matrix components.
$K_p, K_i, K_d$	Gain of control terms.
$L, M, N$	Torques around $x, y$ and $z$ axes.
$m$	Autogyro mass.
${}^pN, {}^pE, {}^pD$	Inertial frame positions (north, east, and down).
$P, Q, R$	Body rotation rates about $x, y,$ and $z$ directions.
$\mathbb{R}$	Rotational matrix, body to inertial frame.
$TAF$	Total aerodynamic force.
$U, V, W$	Linear velocities in $x, y,$ and $z$ axes.
$v$	Velocity vector $[U \ V \ W]^T$ .
$X, Y, Z$	Forces in $x, y,$ and $z$ directions.
$\delta$	Deflection angle of elevator.
$\tau$	Torque vector $[L \ M \ N]^T$ .
$v$	Noise.
$\phi, \theta, \psi$	Euler angles (roll, pitch, yaw).
$\omega$	Body rotation rate vector $[P \ Q \ R]^T$ .
$\Omega_{3,4}$	Matrices of rotation rates.
$(\cdot)_A$	Aerodynamic.
$(\cdot)_a$	Air relative.
$(\cdot)_d$	Desired angle.
$(\cdot)_w$	Air relative velocities.

$(\cdot)^i$	Inertial frame.
$(\cdot)_e$	Error.
$(\cdot)_{fus}$	Fuselage.
$(\cdot)_{ht}$	Horizontal tail.
$(\cdot)_{pid}$	Proportional, integral and derivative terms.
$(\cdot)_r$	Rotor.
$(\cdot)_{vt}$	Vertical tail.

## 1 Introduction

The arrival of the 21st century brought a great advance in technology. Unmanned Aerial Vehicles (UAV's) are now the object of interest by sectors of society that find more and more applications, for example to explorer areas which are difficult to access or imply high risk for humans [1]. UAV's present great advances in design and control, due to the versatility of the applications [2, 3]. On the other hand, well-known techniques that use natural resources such as solar radiation, wind gusts or the water flow of rivers, could be improved by using UAV's for inspection and maintenance work [4, 5]. Furthermore, wind generators, solar panels, hydroelectric dams among others, have high-impact environmental and economic costs. In addition, there are cases in which geographical and environmental areas have very specific characteristics [6].

In recent years, air vehicles have presented advances in design and control thanks to a large number of applications and scopes.

\*Jonathan Flores Santiago, Gustavo A. Madero, Mexico City 07360, Contact +525523711324, Email: jonathan.flores@cinvestav.mx

One of the advances is to generate energy using wind gusts. In [7] the authors present a study of the technologies used to generate energy. The techniques used for wind gusts can be arranged in three main groups of generation [8]:

- On board.
- Ground generation.
- On board and ground generation.

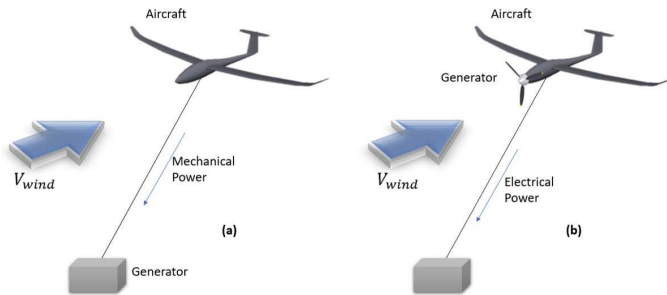


Figure 1: (a) Ground generation. (b) Generation on board.

On board case has the purpose of converting the wind gust to energy using electric generators like the *Makani* Company [9]. Ground generation case, the traction generated by the gust of wind on the aircraft which is attached to some mechanism on the ground. In [10]-[13] are presented different techniques to transform that traction force into energy. This technology is developed to obtain benefits from wind gusts once the aircraft is on the air. However take-off and landing of the aircraft are high risk maneuvers and are performed manually.

The first model of the autogyro was developed by Glauert and Wheatley in the early 30's [14, 15], who introduced the concept of *blade element impulse*, a phenomenon responsible for the state of autorotation. Developed by the Spanish engineer Juan de la Cierva in 1923, the autogyro can be described as the antecedent of the modern helicopter. The principle of self-rotation consists of a free rotation wing for the elevation generated by the induced wind. This aircraft is powered by engine (equivalent in classic airplane). Thanks to self-rotation, landing and take-off are possible on a much shorter runway, even under specific wind conditions, short take-offs or *jump start* is possible. There is a great variety of aircrafts applied to the generation of energy and there are different techniques of flight for obtaining energy.

This paper proposes an autogyro with fuselage and a control surfaces as an airplane to generate pitching moment. The main difference is that it uses a free rotating wing which changes the angle of the lateral inclination to generate the roll moment of the aircraft, similar to the classic helicopter. The implementation of a fixed wing for the autogyro fuselage is presented in [16]-[19], the improvement in performance is shown by the authors.

The paper is organized as follows: Section 2 presents the autorotation in vertical flight and forward flight. Section 3 describes the mathematical model of the autogyro and its dynamics. Section 4 describes the longitudinal control law. Section 5 is devoted to the energy conversion. Final remarks are given in the conclusions in section 6.

## 2 Autorotation

### 2.1 Autorotation in vertical flight

Sometimes an auto start system (engine that drives the rotor) is used for the take-off at a very short distance, producing an almost vertical take-off. Similarly, the landing is done almost vertically and in slow-soft landing. The autogyro as others aircrafts obtains the lift from the wind upwards that crosses the disc formed by the rotation of its main rotor inverse to the helicopters. This wind gust generates aerodynamic forces along each propeller which allow the autorotation [20, 21].

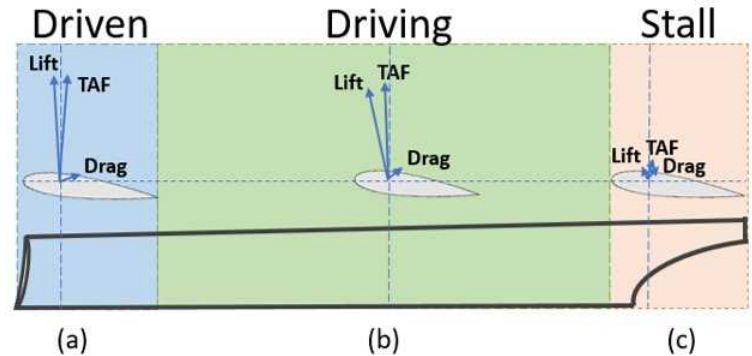


Figure 2: (a) Driven: A bearing force is generated orthogonal to the wind incidence, the total aerodynamic force is soft-opposite to the rotation. (b) Driving: A greater lift force is produced, the region farthest from the center hub is the one with the highest speed, the total aerodynamic force is positive to the rotation. (c) Stall: Mechanically it is where the axis of rotation and hub of the helices is located.

The Lift force, Drag force and the Total Aerodynamic Force or TAF are the forces with which it is possible to generalize its operation and that vary along the regions of each blade [22].

### 2.2 Autorotation in Forward flight

Landing and take-off are important stages in flight. The forward displacement generates aerodynamic forces that must be considered. The autorotation, takes advantage of the wind incidence. The autogyro must remain in forward flight to generate lift in the same way as an airplane.

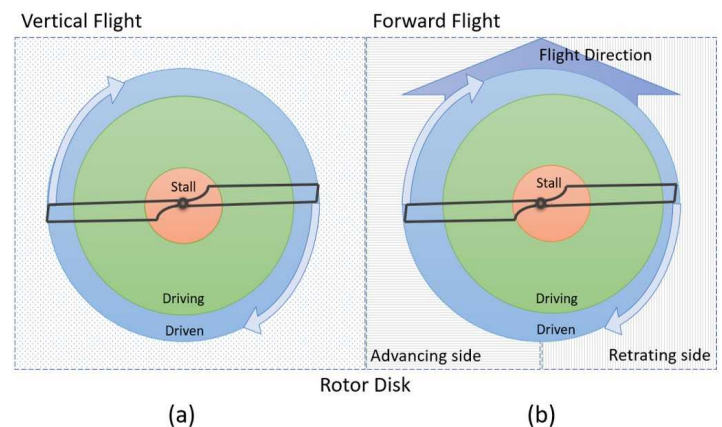


Figure 3: From a top view its possible to separate the rotation disk in left and right hemispheres, therefore the rotation is clockwise.



Figure 3 shows the aerodynamic forces due to the relative wind generated by the forward flight of the autogyro. The forward blade corresponds to the right hemisphere and the retreating blade corresponds left hemisphere. This relative movement of the forward blade presents an increase in its total aerodynamic force which is larger than the one produced by the retracting blade. This difference induces an angular momentum that could cause an overturn [23, 24]. A semi-cyclic plate is able to control the orientation by tilting the rotor disc using the roll moment [25].

### 3 Mathematical model

#### 3.1 Equations of motion

The six-degree of freedom rigid body dynamics equations will be developed in this section. The fundamental relations between forces and linear momentum rates and torques and angular momentum rates are

$$\begin{aligned} F &= m\dot{v}^i \\ \tau &= \dot{H}^i \end{aligned} \quad (1)$$

where  $H$  is the angular momentum vector with the derivatives taken with respect to the inertial frame  $*^i$  [26]. The force and torque vectors  $F = [X \ Y \ Z]^T$  and  $\tau = [L \ M \ N]^T$  are

$$\begin{aligned} F &= m(\dot{v} + \omega \times v) \\ \tau &= \dot{H} + \omega \times H \end{aligned} \quad (2)$$

where the derivatives are taken with respect to the airframe

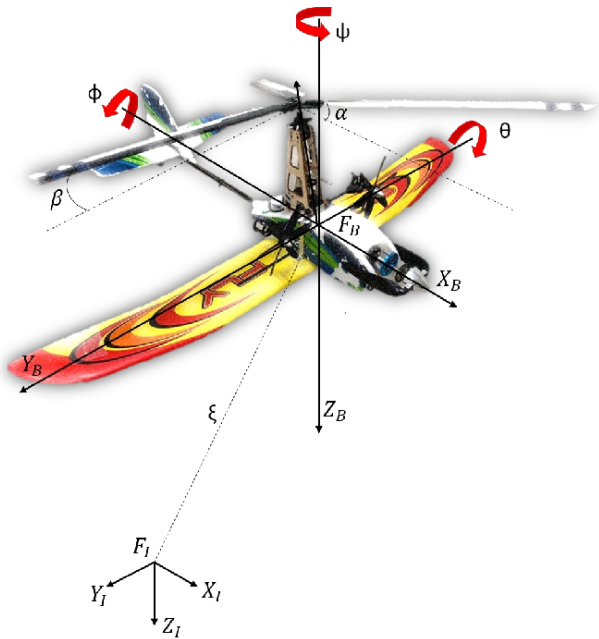


Figure 4: Autogyro Diagram

and  $v = [U \ V \ W]^T$  is the relative velocities vector and  $\omega = [P \ Q \ R]^T$  is the rotation rates vector. Then, using the matrix cross product, the angular momentum is

$$\omega \times v = \Omega_3 v = \begin{bmatrix} 0 & -R & Q \\ R & 0 & -P \\ -Q & P & 0 \end{bmatrix} \begin{bmatrix} U \\ V \\ W \end{bmatrix} \quad (3)$$

The force and moment equations can be rewritten as

$$\begin{aligned} \frac{1}{m} F &= \dot{v} + \Omega_3 v \\ \tau &= I\dot{\omega} + \Omega_3 I\omega \end{aligned}$$

where the individual state derivatives represents the forces and moments vectors, where it is established that in a hybrid autogyro the autorotating propeller is considered as a passive element, therefore the remaining dynamics may well be represented as that of a fixed-wing aircraft according to [27].

$$\begin{bmatrix} \dot{U} \\ \dot{V} \\ \dot{W} \end{bmatrix} = \frac{1}{m} \left( \begin{bmatrix} X_A \\ Y_A \\ Z_A \end{bmatrix} + \begin{bmatrix} X_r \\ Y_r \\ Z_r \end{bmatrix} + C^T \begin{bmatrix} 0 \\ 0 \\ mg \end{bmatrix} \right) + \begin{bmatrix} RV - QW \\ PW - RU \\ QU - PV \end{bmatrix} \quad (4)$$

$$\begin{bmatrix} \dot{P} \\ \dot{Q} \\ \dot{R} \end{bmatrix} = \begin{bmatrix} I_{xx} & 0 & 0 \\ 0 & I_{yy} & 0 \\ 0 & 0 & I_{zz} \end{bmatrix}^{-1} \left( \begin{bmatrix} L_A \\ M_A \\ N_A \end{bmatrix} + \begin{bmatrix} L_r \\ M_r \\ N_r \end{bmatrix} + \begin{bmatrix} QR(I_{yy} - I_{zz}) \\ RP(I_{zz} - I_{xx}) \\ PQ(I_{xx} - I_{yy}) \end{bmatrix} \right) \quad (5)$$

The weight vector  $g = [0 \ 0 \ mg]^T$  must be included with the direction cosine matrix or rotational matrix  $\mathbb{R}$ , which rotates vectors from the body to the inertial frame. Euler angles describe the rotation with respect to the inertial frame.  $\mathbb{R}$  matrix transform vectors from the body to the inertial frame and is defined as

$$\begin{aligned} \mathbb{R} &= \begin{bmatrix} c_\phi c_\theta & c_\psi s_\theta s_\phi - s_\psi c_\phi & c_\psi s_\theta c_\phi + s_\psi s_\phi \\ s_\phi c_\theta & s_\psi s_\theta s_\phi + c_\psi c_\phi & s_\psi s_\theta c_\phi - c_\psi s_\phi \\ -s_\theta & c_\theta s_\phi & c_\theta c_\phi \end{bmatrix} \\ &= \begin{bmatrix} C_{xx} & C_{xy} & C_{xz} \\ C_{yx} & C_{yy} & C_{yz} \\ C_{zx} & C_{zy} & C_{zz} \end{bmatrix} \end{aligned} \quad (6)$$

where  $c_\phi$  corresponds to  $\cos \phi$ ,  $s_\phi$  corresponds to  $\sin \phi$  and the same for  $c_{\theta,\psi}$  and  $s_{\theta,\psi}$  [28]. The relation between Euler angles and the body angular velocities is the following

$$\begin{bmatrix} P \\ Q \\ R \end{bmatrix} = \begin{bmatrix} \dot{\phi} - \dot{\psi} \sin \theta \\ \dot{\theta} \cos \phi + \dot{\psi} \cos \theta \sin \phi \\ -\dot{\theta} \sin \phi + \dot{\psi} \cos \theta \cos \phi \end{bmatrix} \quad (7)$$

The Euler angles derivatives are

$$\begin{bmatrix} \dot{\phi} \\ \dot{\theta} \\ \dot{\psi} \end{bmatrix} = \begin{bmatrix} P + (Q \sin \phi + R \cos \phi) \tan \theta \\ Q \cos \phi - R \sin \phi \\ (Q \sin \phi + R \cos \phi) \sec \theta \end{bmatrix} \quad (8)$$

Finally, the equations for the position are defined in the local coordinate frame as

$$\begin{bmatrix} {}_p \dot{N} \\ {}_p \dot{E} \\ {}_p \dot{D} \end{bmatrix} = \mathbb{R} \begin{bmatrix} U \\ V \\ W \end{bmatrix} \quad (9)$$

where  ${}_p N$ ,  ${}_p E$ ,  ${}_p D$  represent the inertial frame positions (north, east, and down).

### 3.2 Wind model

The wind is introduced in the local frame, the body velocities  $[U \ V \ W]$  are converted to local velocities through the direction cosine matrix  $\mathbb{R}$ . The wind velocities can be subtracted and the result converted back to the body frame to obtain the air relative velocity

$$\begin{bmatrix} U_a \\ V_a \\ W_a \end{bmatrix} = \mathbb{R}^T \left( \mathbb{R} \begin{bmatrix} U \\ V \\ W \end{bmatrix} - \begin{bmatrix} U_w \\ V_w \\ W_w \end{bmatrix} \right) \quad (10)$$

where  $(\cdot)_a$  and  $(\cdot)_w$  represent air relative and air relative velocities respectively. For simulation proposes, the wind is generated by the equation

$$v_w = (1 + v_{wind})v_{w_i}G_w \quad (11)$$

where  $v_w$  is the constant wind intensity. A zero mean Gaussian noise *turbulence* term  $v_{wind}$  with standard deviation  $\sigma_{wind}$  is added to 1 to perturb  $v_{w_i}$ , this signal is then shaped by  $G_w$  to smooth the turbulence, where  $G_w$  is a first order low pass filter.

### 3.3 Forces and Moments

#### 3.3.1 Rotor Forces and Moments

The forces and moments produced by the rotor considering the distance of the rotor hub from the vehicle center of gravity and if the flapping angles are assumed small, the equations can be simplified with sine and cosine approximations.

$$\begin{bmatrix} X_r \\ Y_r \\ Z_r \end{bmatrix} = \begin{bmatrix} -T_{a_1} \\ T_{b_1} \\ -T \end{bmatrix} \quad (12)$$

$$\begin{bmatrix} L_r \\ M_r \\ N_r \end{bmatrix} = \begin{bmatrix} -T_{b_1}z_r \\ T_{x_r} - T_{a_1}z_r \\ 0 \end{bmatrix}$$

#### 3.3.2 Aerodynamic Forces and Moments

The total aerodynamic forces and moments in the equations of motion are:

$$\begin{bmatrix} X_A \\ Y_A \\ Z_A \end{bmatrix} = \begin{bmatrix} X_{fus} \\ Y_{fus} + Y_{vt} \\ Z_{fus} + Z_{ht} \end{bmatrix} \quad (13)$$

$$\begin{bmatrix} L_A \\ M_A \\ N_A \end{bmatrix} = \begin{bmatrix} -Y_{fus}z_{fus} - Y_{vt}z_{vt} \\ X_{fus}z_{fus} - Z_{ht}x_{ht} \\ Y_{vt}x_{vt} \end{bmatrix}$$

The approach to estimate these forces and moments is to assume that, similar to a helicopter, the lift force is generated by a rotating wing. However, an important aerodynamic difference is that the wind flow is upward through the rotor. Another difference is the absence of the moment produced by the helicopter motor. It is possible to find a more complete study in [29] where similar details to other aircrafts are considered.

## 4 Control Structure

Separate lateral and longitudinal controllers are constructed in decoupled modes and the two can be integrated with minimal risk of interference.

### 4.1 Longitudinal Control Design

The longitudinal dynamics is governed by a PID controller as an internal loop for attitude control. The controller includes the input pitch angle. The corresponding output is the deflection angles of the elevator  $\delta_e$ . The longitudinal control law is as follows:

$$\delta_e = \left[ (\theta_d - \theta) K_{p\theta} - p \right] K_{pq} + K_{iq} \int \left[ (\theta_d - \theta) K_{p\theta} - p \right] dt \quad (14)$$

$$+ K_{dp} \frac{d \left[ (\theta_d - \theta) K_{p\theta} - p \right]}{dt}$$

the desired angle is represented by  $\theta_d$ . The Classical PID control strategy is used to control the attitude of the aircraft [26, 16] due to the fact that the attitude of the hybrid autogyro and the energy generation are independent processes. The PID Tuner app in Matlab was used for automatically tuning the gains of a controller to achieve a balance between performance and robustness.

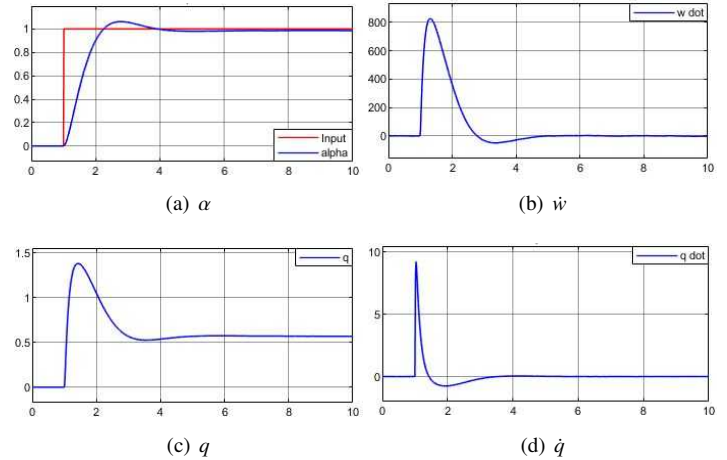


Figure 5: Step response. The response of the vehicle to the change of reference.

The inner loop PID controller for the longitudinal control corresponds to the pitch attitude control. The altitude control compares the pitch angle and desired pitch angle and uses it for pitch stabilization to reach the desired altitude (Figure 5). Then it commands the angle of the elevator to control the hybrid autogyro pitch and correct the angle of attack. The longitudinal control of the autogyro commands the flight up and down. In the presence of wind it is necessary to consider the angle of attack of the autogyro which must be regulated to keep the lift at acceptable level. Furthermore, the rotor can be tilted laterally to make the autogyro turn [30]. To reduce the lifting force loss during the turning and maintain the altitude, this paper adopts the pitching elevator feedforward control method of the propeller (roll moment).

The response of the Hybrid Autogyro to a change of direction presents an effective control before the variation in the reference that may come from the change of direction in the altitude. Figure 6 presents the response of the angle of attack due to a disturbance or a change in altitude, the autogyro reaches its horizontal reference.

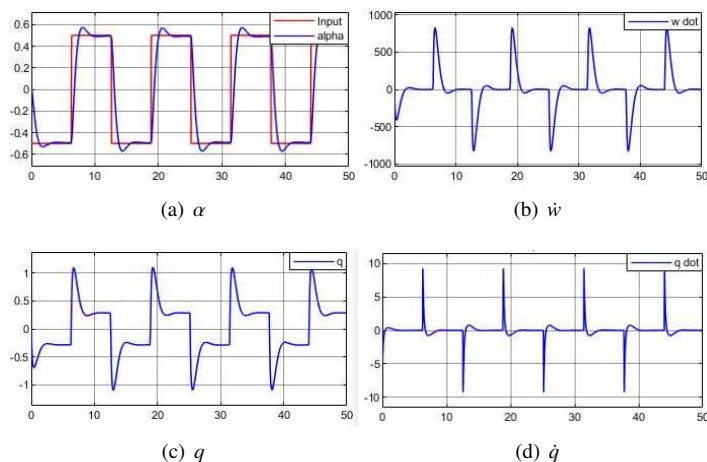


Figure 6: Square wave signal response.

## 5 Energy conversion

According to [31] the wind velocity variation can be observed in terms of the altitude. As shown in Figure 7, a terrain with obstacles like buildings or high trees produces a reduction in the wind velocity. In higher levels above ground we can find higher wind velocities but in fact also greater amount of opposite wind gust, which are considered as strong disturbances. The wind velocity variation versus the height above ground exhibits a parabolic shape depending on the ground roughness.

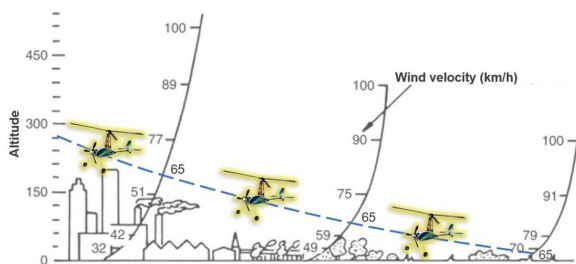


Figure 7: Altitude vs Wind speed for equilibrium flight 65km/h.(image taken from [31]).

If the speed of the autogyro (induced by the motor) is equal to the minimum wind speed required for the lift, then the autogyro performs a stationary or suspended flight without displacement. Actually, finding this balance in wind speed represents an ideal for energy conversion. The autogyro can remain in flight without using energy in the engine, which represents the highest energy consumption during the flight. Other avionics components (servomotors, sensors, autopilot, etc.), only used for the attitude control, represent a lower energy consumption, which means an increase in flight time [32]. The higher wind speed could represent

a negative displacement to the advance of the autogyro, in other words, it would be necessary to anchor the autogyro as a kite.

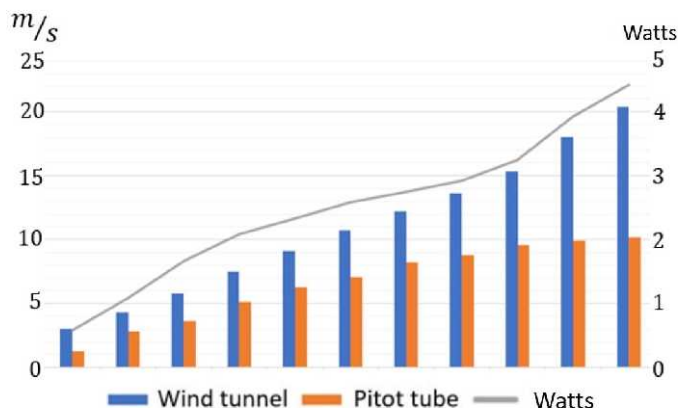


Figure 8: Wind speed vs energy in flight.

When the wind speed is above 65 km/h, the use of the main motor for producing lift may not be necessary. However the longitudinal control is crucial to improve the performance in the generation of energy (Figure 8).

$$V_{wind} \approx 65km/h \rightarrow 5Wh. \quad (15)$$

## 6 Conclusions

The hybrid autogyro uses the principle of autorotation to generate lift and in this paper has proposed to take advantage of this rotation for energy generation by placing generators on the frame. However, the wind speed should be considerably higher to flight an autogyro than the wind required for fixed-wing vehicles. Therefore, the autorotation serves simultaneously to generate lift and to generate energy. It has been observed that it is important to consider the mathematical model and control algorithm of the autogyro to obtain a good behavior of the aircraft. Consequently and because wind gusts are also non-constant disturbances, the implementation of a control strategy that improves performance in altitude control is important for power generation. Nonetheless the wind is the source for power generation at high altitude.

A wide range of topics for the UAV's that pursue the generation of energy, such as aerodynamics, avionics, control and energy is presented in this paper. Currently these areas are continually being developed promoting clean and renewable energy through specific UAV's projects.

### Conflict of Interest

The authors declare no conflict of interest.

### Acknowledgment

This project was funded by UMI-LAFMIA 3175 CNRS, CINVESTAV and UTC, CNRS, UMR 7253 Heudiasyc. Finally to the National Council of Science and Technology (CONACYT) for the support.

## References

- [1] Rao, B., Gopi, A. G., & Maione, R. (2016). The societal impact of commercial drones. *Technology in Society*, 45, 83-90.
- [2] Luppici, R., & So, A. (2016). A technoethical review of commercial drone use in the context of governance, ethics, and privacy. *Technology in Society*, 46, 109-119.
- [3] Finn, R. L., & Wright, D. (2016). Privacy, data protection and ethics for civil drone practice: A survey of industry, regulators and civil society organisations. *Computer Law & Security Review*, 32(4), 577-586.
- [4] Rakha, T., & Gorodetsky, A. (2018). Review of Unmanned Aerial System (UAS) applications in the built environment: Towards automated building inspection procedures using drones. *Automation in Construction*, 93, 252-264.
- [5] Jo, J., Jadidi, Z., & Stantic, B. (2017, October). A Drone-Based Building Inspection System Using Software-Agents. In *International Symposium on Intelligent and Distributed Computing* (pp. 115-121). Springer, Cham.
- [6] Del Río, P. (2010). Analysing the interactions between renewable energy promotion and energy efficiency support schemes: The impact of different instruments and design elements. *Energy Policy*, 38(9), 4978-4989.
- [7] Cherubini A, Papini A, Vertechy R, Fontana M. (2015). Airborne Wind Energy Systems: A review of the technologies. *Renewable and Sustainable Energy Reviews*, 51, 1461-1476.
- [8] Breukelman, P., Kruijff, M., Fujii, H. A., Maruyama, Y. (2014). A new wind-power generation method employed with high altitude wind. In *International Conference and Exhibition, Grand Renewable Energy*, Tokyo July.
- [9] <https://makanipower.com>
- [10] Ahmed M, Hably A, Bacha S. (2013). Kite generator system modeling and grid integration. *IEEE Transactions on Sustainable Energy*, 4(4), 968-976.
- [11] White FM, Wolf DF (1968). A theory of three-dimensional parachute dynamic stability. *Journal of aircraft*, 5(1), 86-92.
- [12] Argatov I, Rautakorpi P, Silvennoinen R. (2009). Estimation of the mechanical energy output of the kite wind generator. *Renewable Energy*, 34(6), 1525-1532.
- [13] Canale M, Fagiano L, Milanese M. (2009). KiteGen: A revolution in wind energy generation. *Energy*, 34(3), 355-361.
- [14] Wheatley JB. (1935). An Aerodynamic analysis of the autogyro rotor with a comparison between calculated and experimental results.
- [15] Glauert H. (1926). A general theory of the autogyro (Vol. 1111). HM Stationery Office.
- [16] Song, Z., Cai, Z., Li, K., Zhao, J., Liu, N. (2017, June). Model and Attitude Control of a Miniature Hybrid Autogyro. In *Chinese Intelligent Automation Conference* (pp. 751-760). Springer, Singapore.
- [17] Liu, N., Cai, Z., Ma, Y., Wang, Y. (2017). Control and Flight Testing of a Miniature Compound Autogyro. In *AIAA Atmospheric Flight Mechanics Conference* (p. 3891).
- [18] Hou, J., Cai, Z., Zhao, J., Wang, Y., Liu, N., Song, Z. (2017, December). Fuzzy and PSO-based PID controller for a hybrid autogyro attitude control. In *Control Conference (ASCC), 2017 11th Asian* (pp. 2160-2165). IEEE.
- [19] Mackertich S, Das T. (2016, July). A quantitative energy and systems analysis framework for airborne wind energy conversion using autorotation. In *American Control Conference (ACC), 2016* (pp. 4996-5001). IEEE.
- [20] Duda, H., Pruter, I. (2012). Flight performance of lightweight gyroplanes. In *28th International Congress of the Aeronautical Sciences*, Brisbane, Australia.
- [21] Handbook, F. A. A. (2000). 8083-21. Rotorcraft Flying Handbook.
- [22] Lin, Q., Cai, Z., Wang, Y. (2014, August). Design, model and attitude control of a model-scaled gyroplane. In *Guidance, Navigation and Control Conference (CGNCC), 2014 IEEE Chinese* (pp. 1282-1287). IEEE.
- [23] Wheatley, J. B. (1934). The aerodynamic analysis of the gyroplane rotating-wing system.
- [24] Lopez, C. A., Wells, V. L. (2004). Dynamics and stability of an autorotating rotor/wing unmanned aircraft. *Journal of guidance, control and dynamics*, 27(2), 258-270.
- [25] Houston, S. S. (1998). Identification of autogyro longitudinal stability and control characteristics. *Journal of Guidance, Control, and Dynamics*, 21(3), 391-399.
- [26] Deyst, J. J., & George, S. (2005). Simulation and control design of a gliding autogyro for precision airdrop (Doctoral dissertation, Massachusetts Institute of Technology).
- [27] Arnold, U. Investigation of gyroplane flight mechanics (in German). Master Theses, Institute of Flight Systems, Braunschweig, 1988.
- [28] Lozano, R. (Ed.). (2013). Unmanned aerial vehicles: Embedded control. John Wiley and Sons.
- [29] D. H. Lorenz Meier and M. Pollefeys, "px4: A node-based multithreaded open source robotics framework for deeply embedded platforms," *International Conference on Robotics and Automation (ICRA)*, 2015.
- [30] Breukelman, P., Kruijff, M., Fujii, H. A., Maruyama, Y. (2014). A new wind-power generation method employed with high altitude wind. In *International Conference and Exhibition, Grand Renewable Energy*, Tokyo July.
- [31] Hartmann, D. L. (2015). *Global physical climatology* (Vol. 103). Newnes.
- [32] Flores, J., Salazar, S., & Lozano, R. (2019, June). Hybrid autogyro: Airborne wind gust energy conversion using autorotation. In *2019 International Conference on Unmanned Aircraft Systems (ICUAS)* (pp. 1255-1260). IEEE.



## Using Metaheuristics-Based Methods to Provide Sustainable Market Solutions, Suitable to Consumer Needs

Ricardo Simões Santos<sup>\*1</sup>, António João Pina da Costa Feliciano Abreu<sup>2</sup>, Joaquim José Rodrigues Monteiro<sup>3</sup>

<sup>1</sup>GOVCOPP Universidade de Aveiro, ISEL, Polytechnic Institute of Lisbon, 1959-007, Portugal

<sup>2</sup>CTS-UNINOVA Universidade Nova de Lisboa, ISEL, Polytechnic Institute of Lisbon, 1959-007, Portugal

<sup>3</sup>INESC-ID Lisboa, ISEL, Polytechnic Institute of Lisbon, Portugal, 1959-007, Portugal

### ARTICLE INFO

Article history:

Received: 01 January, 2020

Accepted: 19 March, 2020

Online: 04 April, 2020

Keywords:

Sustainability

Energy efficiency

Household Appliances

Multi-criteria

Multi-objective Optimization

Evolutionary Algorithms

Simplex

### ABSTRACT

Nowadays the buildings sector is one of the key sectors to achieve sustainability, with the correspondent consumers, in particular, the household consumers, having the need to perform sustainable choices every day, regarding the appliances to be acquired from the market. This is not only due to government's growing concerns about sustainability but also with the consumers on having sustainable solutions, given the different economic, social (including their comfort) and environmental needs. However, the existence of several electrical appliances on market, with all their different issues, brands and models, together with the several tradeoffs referred before, difficult the consumer's choices, on having sustainable solutions in the market. Therefore, this work, presents an approach, by using Multi-Attribute Value Theory (MAVT), integrated with metaheuristics, which uses Evolutionary Algorithms (EA) to provide suitable and sustainable market solutions to a consumer, according to its own needs. Based on the achieved solutions and considering the relative importance, given to each consumer, and regarding each dimension of sustainability, it's possible to achieve several savings, namely electrical and water consumption, CO<sub>2</sub> emissions, among others. A case study shall be shown, to demonstrate the applicability of the proposed approach.

## 1. Introduction

This paper is an extension of work [1] originally presented in 2019 International Young Engineers Forum (YEF-ECE), held in Nova University, Costa da Caparica, Lisbon, Portugal.

Sustainable measures are relevant to reach environmental and economic sustainability, particularly regarding the reduction of energy production dependency from fossil fuels, where buildings account for about 30–43 % of the final energy consumed [2-3].

Based on [4], and from the percentage referred above, the household's sector represents approximately 18 % of the final electric energy consumed in the world, which represents an important sector to be improved in terms of energy efficiency, and through the adoption of sustainable appliances.

According to [5-7], there were some improvements regarding energy efficiency, and related to electrical appliances, by

establishing reglementary labeling measures, to provide relevant information to the consumer.

Some of these issues include energy consumption, machine's noise, refrigerator capacity, water consumption, among others [7].

According to [7], such measures, have been arisen, not only in the European countries but as well as in other world regions, such as Africa, America and Asia.

Although the importance of such measures to reach sustainability, there are too much options available in the market, which makes it difficult to know what's the best solution to choose, in order to attend the consumer's needs [6-7].

The difficulty raises, when each appliance has its own set of features, which can be different according to the appliance's brand and model to acquire [4-5].

Considering the diversity of options from the market, and related to each energy service (e.g. lighting, air conditioners, refrigerators, etc.), the number of possible combinations could exponentially rise.

\* Ricardo Santos, Email: ricardosimoessantos84@gmail.com

The use of optimization algorithms, to assist the consumer on its decisions, allows the achievement of efficient and even sustainable solutions, regarding the household appliances to acquire.

However, and due the high combinatorial nature of the problem referred before, the use of traditional optimization techniques, could present some disadvantages, regarding the efficiency on reaching a feasible solution, as well as with the number of potential and feasible solutions available to the consumer [8]. This could happen, since that some optimization techniques, based on gradient methods, could be stuck into to a local maxima or minima, limiting therefore, the exploitation of the entire feasible region [8-9].

An alternative way to surpass such disadvantages, could pass by using Evolutionary Algorithms (EA), given the widely use, reflected on the number of works from the literature, on solving optimization problems in less time than other traditional optimization methods (e.g. [8-12]).

Other approaches have been used by the authors, in order to develop an integrated approach that allows to achieve sustainable solutions.

In [1][13-14] the authors have started to use a single objective approach to achieve efficient solutions from the market of household appliances.

The successful contribution to the main goal of their research, have led them to adapt the first approach into a Multiobjective one, given the several dimensions of sustainability (referred before) to attend, and considering each household appliance, related to each energy service to be acquired, namely; Economic, Social and Environment.

In order to consider other kind of consumer's issues, such as its social preferences (e.g. reliability, design, performance, among others) we've applied multiple-attribute value theory (MAVT). This theory allows to model the consumer's choices, as well as other preferences regarding the environment (e.g. CO<sub>2</sub> savings, water savings, noise, among others) and the economic dimension (e.g. initial investment, noise, water consumption, among others) [15].

All the dimensions referred above have some constraints, suitable to each case (e.g. number of building occupants, area of the room to be climatized, the type of division, among others), such as the ones related with human comfort (e.g. minimum illuminance to achieve visual comfort, noise, minimum air conditioner to achieve heating comfort), with economy (e.g. budget, water consumption), and environmental (e.g. water savings, CO<sub>2</sub> savings, among others). To maximize each dimension, modelled according to MAVT, it was used optimization techniques to get sustainable solutions from the market to the consumer, by acting on three dimensions (or objective functions) referred before.

According to [16], Evolutionary Algorithms (EA), have been applied with success, to solve many optimization problems within less time, when compared with other methods. However, such methods, uses too many control parameters, which makes them, quite sensitive to the input values, therefore, the need to adjust them [16-17], by performing some robustness and sensitive tests.

The aim of this research, is to propose an approach, where MAVT is integrated with Non-Dominated Sorting Genetic Algorithm II (NSGAI) [18], based on genetic algorithms (GAs), in order to provide the consumer with sustainable solutions from the market, that not only attends it needs, but as well the tree

dimensions referred before; Economic, Social and Environmental. To pursue this goal, we've tested, validated and presented in [1], a first approach, which has consisted in one objective function regarding the economic dimension, where it was tried different problem formulations, to study their influence in terms of results.

Based on the works presented on [1] we've selected the objective function with the best results and tested the entire model's robustness, regarding the influence of GAs parameters. Some results are presented with this preliminary approach.

The 2<sup>nd</sup> approach presented here, will integrate the developments achieved with the 1<sup>st</sup> one, into a Multiobjective model by using NSGAI optimization method, where not only economic dimension will be included, but also the environmental one as well. For this purpose, new attributes will be added to the model, regarding the environmental dimension, whose diversity and the correspondent units involved, will be integrated into a unique model by recurring to MAVT.

Finally, it will be obtained a combined solution that attends the economic and environmental dimensions, in order to pursue the main goal referred before. A case study will be presented here, to illustrate the applicability of the method, by presenting an example of a set of a feasible and sustainable solutions, suitable to the consumer needs.

## 2. Literature review

Several methods such as scenario's analysis (e.g. [19]), are frequently used to simulate a constrained set of solutions.

However, some methods are essentially economical, by allowing the consumers to obtain highest values of energy savings, given the same value of investment (e.g. [17]). Other methods, existed on literature, allows to deal with different issues (e.g. savings with Greenhouse Gas (GHG) emissions, benefit-cost analysis, initial investment costs, among others). Such methods are mainly related to retrofitting measures (e.g. [20]), where some of them are even combined with technologies too (e.g. [21]).

However, there is some limits with these approaches, since they don't consider other relevant factors, such as the environment, the labelling system and legal and social issues as well, to find suitable solutions, to fulfill the requirements of the occupants of the building. These methods also don't consider the attributes, regarding each electrical appliance, which varies according to the number of building's occupants.

Recently, some works are based on multi-criteria decision-making (MCDM) methods, in order to help a consumer to solve his problems regarding the measures of retrofitting with their own building's, by accounting not only energy efficiency factors, but also assuring the comfort of the building's occupants (e.g. [15]).

Regarding other works from the literature, there is other MCDM models, based on MAVT approaches, allowing therefore, the integration of optimization with multicriteria methods, which allows the achievement of feasible solutions, selected based on a set of attributes, organized according to a set of criteria (e.g. [15]).

However, these methods don't account the different attributes, related to each electrical appliance existed on market and adjusted to the individual needs of the occupants.

The use of Metaheuristics to achieve from the energy problems' solving, a set of feasible solutions (e.g.[8]), by using particle swarm optimization, e.g. [11], by using genetic algorithms, among others existed on literature), have been increased in the last years. However, none of these approaches, have been considered

into a combined method, that allows the consumer, to pick from the market, a set of sustainable appliances, based on its preferences.

### 3. Objectives

In order to fulfill the gap referred on literature review, the main objective of this research work is to present an approach to assist an household consumer, who wants to buy sustainable appliances, existed on market, for its home, that not only allows to fulfill its needs, but also allows to accomplish a set of requirements regarding sustainability, based on the three dimensions of sustainability referred before, namely, the Consumer's economic well-being, social well-being and Consumer's environment well-being.

Additionally, it will be presented two approach, which allows to obtain several and alternative solutions from the market, facing therefore, some contingencies that eventually may occur, namely the situations of "out of stock" for instance, given an electrical appliance initially recommended by this method.

The approach developed here, also considers economic, social and environment constraints, regarding each energy service considered in this work.

### 4. Research Method

#### 4.1. Problem description and case study

The problem presented in this work has considered a consumer, who is intended to acquire a set of household appliances, available on market.

The pre-criteria, considered by the algorithm to pre-select a set of appliances existed on market (Table 1), were instantiated according to the number of occupants, existed in the building. In this case study, it was considered a family (which includes the decision-agent) of 4 occupants.

Table 1: Criteria used

Criteria used	Appliance	Quantity
<ul style="list-style-type: none"> <li>Air conditioners (types) considered:</li> <li>Zone to be heated/ cooled by the air conditioner</li> <li>Capacity (minimum)</li> </ul>	Air Conditioner	<ul style="list-style-type: none"> <li>Mono split</li> <li>Multisplit,</li> <li>Portable</li> <li>Living room</li> <li>9923,7 BTU</li> </ul>
<ul style="list-style-type: none"> <li>Capacity, based on the number of household's occupants</li> </ul>	Washing Machine	<ul style="list-style-type: none"> <li>5 kg</li> </ul>
<ul style="list-style-type: none"> <li>Load capacity.</li> </ul>	Dishwasher	<ul style="list-style-type: none"> <li>10 Cutleries</li> </ul>
<ul style="list-style-type: none"> <li>Useful volume, available for cooking based on the number of occupants</li> </ul>	Oven	<ul style="list-style-type: none"> <li>44,2 cm x 61,8 cm</li> </ul>
<ul style="list-style-type: none"> <li>Type of dryer machines</li> <li>Load capacity</li> </ul>	Dryer machine	<ul style="list-style-type: none"> <li>By condensation ;</li> <li>6 kg</li> </ul>
<ul style="list-style-type: none"> <li>Technology</li> </ul>	Lighting	<ul style="list-style-type: none"> <li>Halogen</li> <li>CFL</li> <li>Fluorescent</li> </ul>
<ul style="list-style-type: none"> <li>Capacity of the fridge</li> <li>Type of fridge, based on the number of occupants</li> </ul>	Refrigerator	<ul style="list-style-type: none"> <li>120 liters</li> <li>Refrigerator</li> <li>Combined type.</li> </ul>

However, the values regarding each attribute, can be modified, based on the number of occupants, existed in the building.

Thus, the appliances, was pre-selected from the market, by using the criteria presented on Table 1, in order to reduce the decision space, considering therefore, only the suitable solutions to the consumer needs. This was done, in order to increase EA's efficiency, regarding both approaches, by achieving optimal solutions with less time.

#### 4.2. 1<sup>st</sup> Approach – Single objective model

The 1<sup>st</sup> approach, proposed in this work, can be seen on Figure1, where each consumer's option ( $x_{ij}$ ), regards to an existent solution from the market, which can be defined as a choice  $i$ , belonged to a certain type of appliance (energy service)  $j$ , to be acquired by the consumer. Considering the trade-offs referred before, together with the diversity of features, related to each solution, the consumer will deal with a problem of combinatorial nature, whose number of combinations are dependent on the number of options to be considered, regarding each dimension. The 20 million combinations (approximately) considered in this work, can be reduced, by considering that the consumer cannot perform any choices ( $x_{ij}$ ), given its limited budget.

Furthermore, and based on Table 1, all the equipment's, were pre-selected according to the number of occupants, in order to meet the consumer requirements (e.g. washing machine capacity, capacity of the fridge, etc.). Issues, such as air conditioner minimum capacity, minimum illuminance among others, was also considered here and compiled in a set of criteria (Figure1).

Additionally, it was also considered the influence of the consumer usage profile, regarding each potential solution/option  $x_{ij}$ , based on the assumptions presented on Table 2, for the case study considered.

Such assumptions have included the number of hours that each household appliance will perform for each day, which was then extrapolated for a monthly and yearly basis.

Table 2: Assumptions, according to consumer usage profile

Emission factor [gCO <sub>2</sub> /kWh]	674,6	Discount Factor [%]	7,0	
Life cycle (usage phase) considered [years]:	11	Annual Factor	7,1	
Electrical Energy tariff [€/kWh]	0,171			
Electrical appliance	Profile of Usage (h)			
	Day	Week	Month	Year
Air Conditioning	3	14	60	719
Dryer Machine	1,2	8,4	32	361
(Electric) Oven	7	7	31	360
Refrigerator	11	76	333	3960
Lighting	3,1	21	94	1080
Dish Washer Machine	1,1	7,7	32	360
Washer Machine	1,5	10,5	31	358

These parameters have some influence on consumption, regarding each household appliance. Therefore, their savings, was achieved through the comparison of each efficient solution with the correspondent standard one. The consumer can also define its

own profile of usage, according to its needs, or by using the profile, considered in this work, by default.

Regarding each individual efficient solution  $(x_{ij})$ , it was determined the correspondent savings,  $S_{cons,i,j}(x_{ij})$  and  $S_{inv,i,j}(x_{ij})$ , respectively for the consumption and investment and regarding each option  $i$ , belonging to an appliance type  $j$ . Both savings, were obtained, based on the comparison between the efficient values of consumption and investment, and the correspondent standard solution (i.e. less efficient), regarding to an appliance/energy service type  $j$ . The value, resulted from this difference, was then discounted, according to the life cycle period (usage phase) considered, by applying a discount factor (Table 2).

Based on the approach, shown on Figure1, the decision variables are:

$$x_{ij} : j(\text{appliance type}) = \{1..7\} \wedge i(\text{options}) = \{1..n_i\} \quad (1)$$

With the objective to maximize  $V_R(x_{ij})$ , i.e.:

$$\max V_R(x_{ij}) : V_R \in \square \wedge x_{ij} \in \{0,1\} \quad (2)$$

Based on work of [22], the value of  $V_R$ , can be achieved by:

$$V_R^{(n)} = \sum_{i=1}^{20} \left( \frac{P_{cons,i,j}(x_{ij})}{P_{inv,i,j}(x_{ij})} \right) \cdot \frac{I_{inv,ef_{ij}}(x_{ij})}{I_{stdj}} \cdot x_{i1} + \sum_{i=1}^{11} \left( \frac{P_{cons,i,2}(x_{i2})}{P_{inv,i,2}(x_{i2})} \right) \cdot \frac{I_{inv,ef_{ij}}(x_{i2})}{I_{total}} \cdot x_{i2} + \sum_{j=3}^7 \sum_{i=1}^{10} \left( \frac{P_{cons,i,j}(x_{ij})}{P_{inv,i,j}(x_{ij})} \right) \cdot \frac{I_{inv,ef_{ij}}(x_{ij})}{I_{stdj}} \cdot x_{ij} \quad (3)$$

Given that only one option  $i$ , can be chosen, regarding each appliance, the correspondent constraints are:

$$R_1(x_{i1}) : \sum_{i=1}^{20} x_{i1} = 1 \wedge x_{i1} \in \square, \forall i = \{1..20\} \wedge x_{i1} = \{0,1\} \quad (4)$$

$$R_2(x_{i2}) : \sum_{i=1}^{11} x_{i2} = 1 \wedge x_{i2} \in \square, \forall i = \{1..11\} \wedge x_{i2} = \{0,1\} \quad (5)$$

$$R_k(x_{ij}) : \sum_{i=1}^{10} x_{ij} = 1 \wedge k = \{3..7\} \wedge x_{ij} = \{0,1\}, \forall i = \{1..10\}, j = \{3..7\} \quad (6)$$

The budget constraint, can be modeled by using the total investment (budget) and according to the following expression:

$$R_8(x_{ij}) : I_{total}(x_{ij}) = \sum_{i=1}^{20} x_{i1} * I_{ef_{i1}} + \sum_{i=1}^{11} x_{i2} * I_{ef_{i2}} + \sum_{j=3}^7 \sum_{i=1}^{10} x_{ij} * I_{ef_{ij}} \quad I_{total} \in \square \quad (7)$$

On Figure2, it's presented the EA's individual framework.

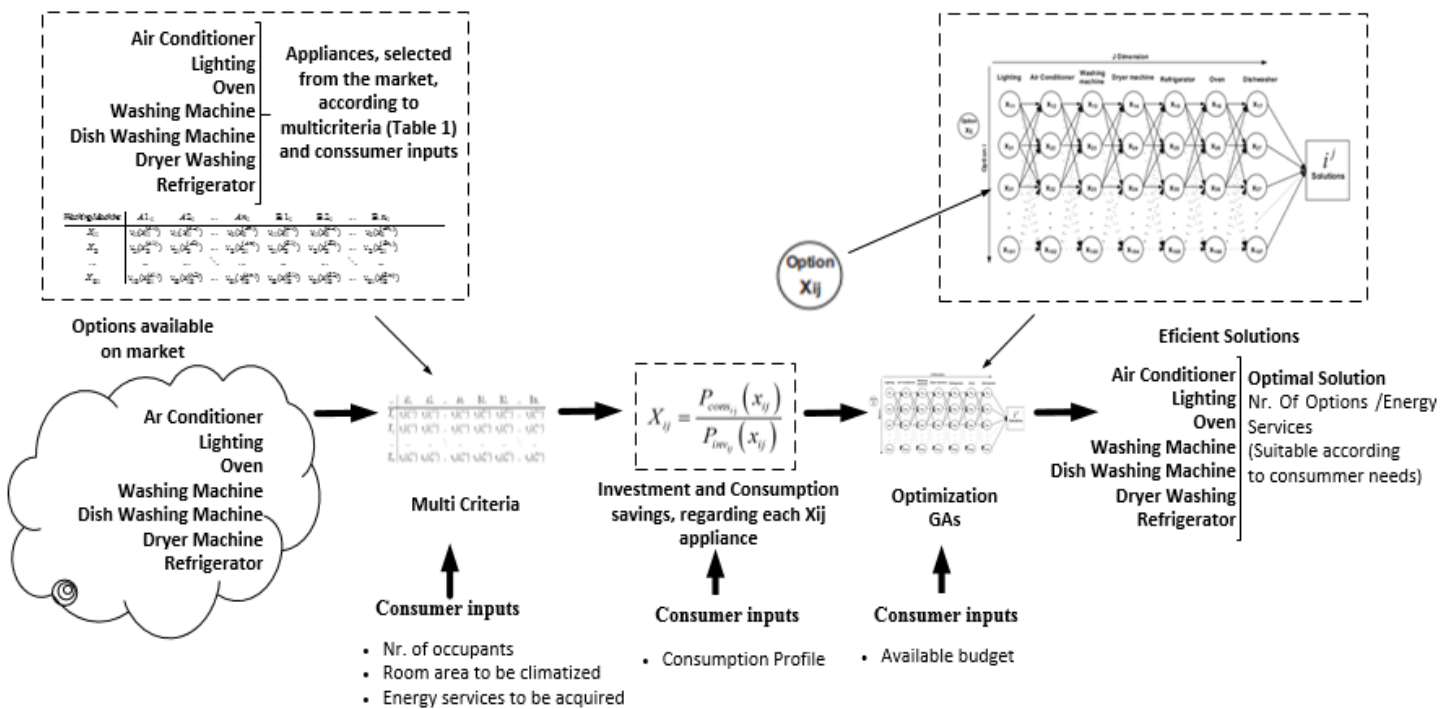


Figure 1(a): 1<sup>st</sup> Approach – Single objective approach

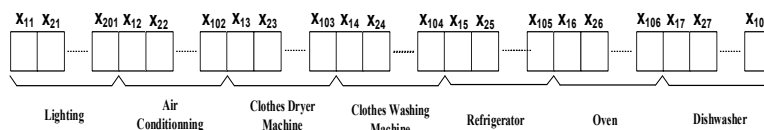


Figure 1(b): EA's individual framework (single objective approach)



Table 3. Definition of the problem dimensions, according to each energy service considered and criteria used

Energy Service	Dimension	Ref.	Dimension	Ref.	Dimension	Ref.
	A-Economics		B-Social		C-Environment	
Ilu—lighting	Energy Efficiency Classification	Ilu.A1	Durability (h)	Ilu.B1	CO <sub>2</sub> e Emissions (Life Cycle—Usage Phase) [kg]	Ilu.C1
	Energy Cons. Savings (Life Cycle—Usage phase) [€]	Ilu.A5	Color Rendering Index (CRI) [%]	Ilu.B5	CO <sub>2</sub> e Emissions (Life Cycle—Production Phase) [kg]	Ilu.C3
AC—Air Conditioner	Energy Efficiency Classification (Heating)	AC.A1	Noise (Indoor) [dB]	AC.B1	CO <sub>2</sub> e Emissions (Life Cycle—Production Phase) [kg]	AC.C1
	Energy Efficiency labelling (Cooling)	AC.A6	Customer Service (warrant)	AC.B9	CO <sub>2</sub> e Emissions (Life Cycle—Usage Phase) [kg]	AC.C3
---	---	---	---	---	---	---
FE.—Oven (Electric)	Energy Efficiency Classification	FE.A.1	CO <sub>2</sub> e Emissions (Life Cycle—End Use Phase) [kg]	FE.B1	CO <sub>2</sub> e Emissions (Life Cycle—Usage Phase) [kg]	FE.C.1
	Investment cost [€]	FE.A.5	CO <sub>2</sub> e Emissions (Life Cycle—End Use Phase) [kg]	FE.B.5	CO <sub>2</sub> e Emissions (Life Cycle—End Use Phase) [kg]	FE.C.3
MLL—Dishwasher	Energy Efficiency Classification	MLL.A.1	Water Consumption (Life Cycle—Usage phase) [l]	MLL.B.1	CO <sub>2</sub> e Emissions (Life Cycle—Usage phase) [l]	MLL.C.1
	Water Cons. Savings (Life Cycle—Usage phase) [€]	MLL.A.6	Customer Service (warrant)	MLL.B.6	Water Consumption (Life Cycle—Usage phase) [l]	MLL.C.4

### 4.3. 2<sup>nd</sup> Approach – Multiobjective model involving 2 dimensions

The 2<sup>nd</sup> Approach, was pretended to study the interaction between 2 of the three existed dimensions, regarding sustainability, namely Economics vs Social Wellbeing and Economics vs Environment Wellbeing. To do this, it was included the formulation presented and studied before, regarding economic wellbeing, and the two other dimensions, by recurring to Multiattribute Value Theory (MAVT). This was preformed, in order to convert the objective function (3) (Economic Wellbeing) into a correspondent one, without units involved, to be added further into the other dimensions (Social and/or Environmental). After, the tests performed with multiobjective approach (2 dimensions), we have combined the three objective functions, regarding the three dimensions referred before, into one objective function, to achieve sustainable results, regarding the three dimensions. The assumptions presented before, were the same as well as the case study to apply the approach.

The criteria adopted here, are also the same, although there is the possibility of being changed, based on the number of occupants, existed in the building.

As it referred before, such pre-selection allows to reduction of the decision space, by considering only the available solutions,

adjusted to the needs of the consumer. Such pre-selection, contributes also to rise the efficiency of NSGAI, by getting optimal solutions within less time. To pursue this, the proposed approach, has been developed by starting to consider at first 2 and then, the 3 dimensions of the problem. Both cases, are based on the approach described on Figure 2.

Each potential solution ( $x_{ij}$ ), is regarded from an option  $i$ , which is correspondent to the energy service  $j$  to be bought by the consumer from the market. Like the first approach, the consumer’s consumption profile (Table 2), was considered, in order to preform Life Cycle Cost Assessment (LCCA) to achieve for each appliance, the corresponding savings, in terms of water consumption ( $S_{H2O.Cons,i,j}(x_{ij})$ ), energy consumption ( $S_{E.Cons,i,j}(x_{ij})$ ) and initial investment ( $S_{inv,i,j}(x_{ij})$ ). All these savings, have been obtained from the comparison between the more efficient solution and the less efficient one (“standard” solution).

By considering several factors, regarding each appliance, as well as the consumer’s social, environmental and economic

concerns, a set of criteria was established based on the consumer preferences,

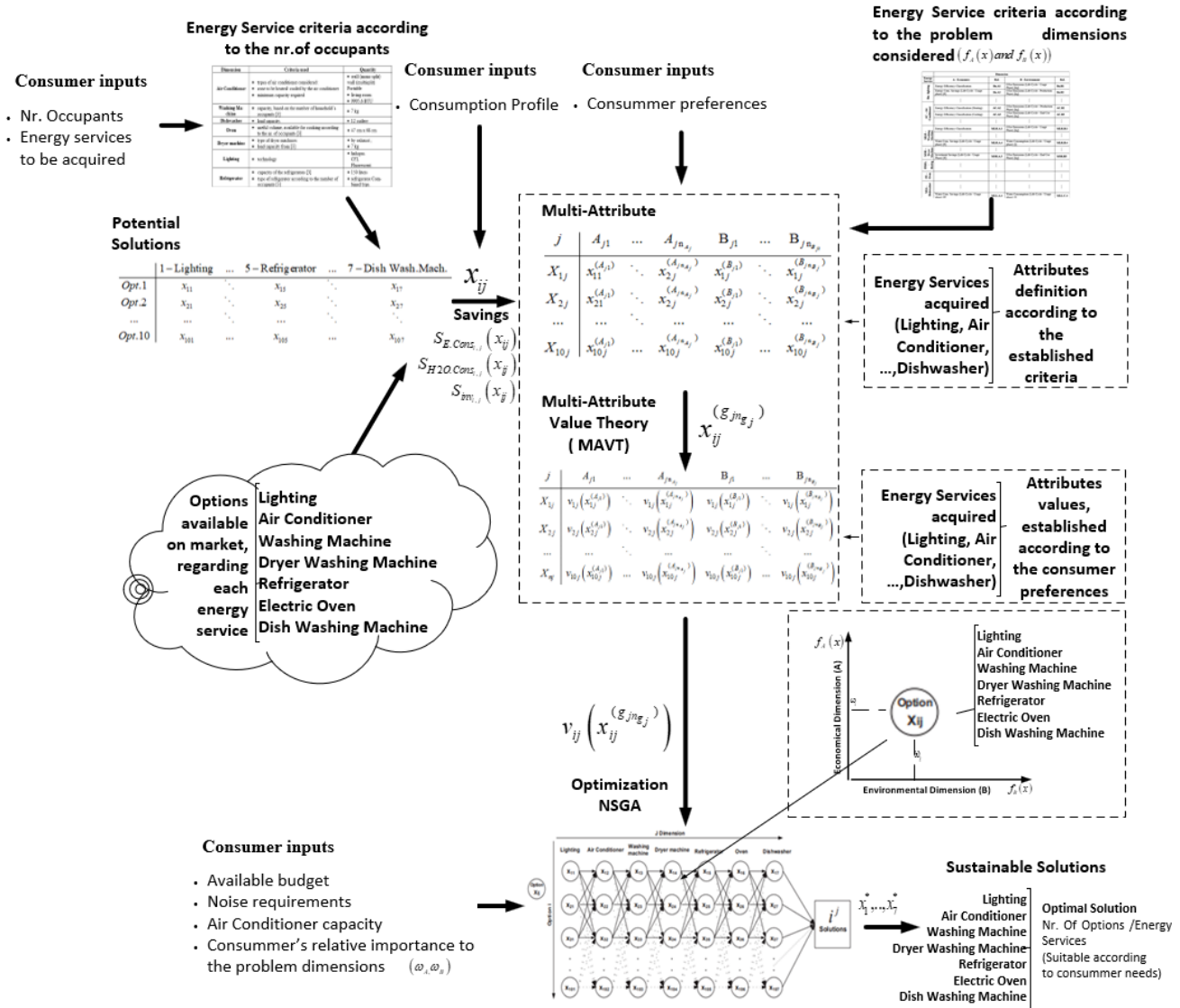


Figure 2: 2<sup>nd</sup> Proposed approach – Multiobjective approach with MAVT

A.C.	$A_{21}$	$A_{22}$	...	$A_{2n_{A_2}}$	$B_{21}$	$B_{22}$	...	$B_{2n_{B_2}}$	$C_{21}$	$C_{22}$	...	$C_{2n_{C_2}}$
$X_{12}$	$x_{12}^{(A_{21})}$	$x_{12}^{(A_{22})}$	...	$x_{12}^{(A_{2n_{A_2}})}$	$x_{12}^{(B_{21})}$	$x_{12}^{(B_{22})}$	...	$x_{12}^{(B_{2n_{B_2}})}$	$x_{12}^{(C_{21})}$	$x_{12}^{(C_{22})}$	...	$x_{12}^{(C_{2n_{C_2}})}$
$X_{22}$	$x_{22}^{(A_{21})}$	$x_{22}^{(A_{22})}$	...	$x_{22}^{(A_{2n_{A_2}})}$	$x_{22}^{(B_{21})}$	$x_{22}^{(B_{22})}$	...	$x_{22}^{(B_{2n_{B_2}})}$	$x_{22}^{(C_{21})}$	$x_{22}^{(C_{22})}$	...	$x_{22}^{(C_{2n_{C_2}})}$
...	...	...	...	...	...	...	...	...	...	...	...	...
$X_{102}$	$x_{102}^{(A_{21})}$	$x_{102}^{(A_{22})}$	...	$x_{102}^{(A_{2n_{A_2}})}$	$x_{102}^{(B_{21})}$	$x_{102}^{(B_{22})}$	...	$x_{102}^{(B_{2n_{B_2}})}$	$x_{102}^{(C_{21})}$	$x_{102}^{(C_{22})}$	...	$x_{102}^{(C_{2n_{C_2}})}$

a)

A.C.	$A_{21}$	$A_{22}$	...	$A_{2n_{A_2}}$	$B_{21}$	$B_{22}$	...	$B_{2n_{B_2}}$	$C_{21}$	$C_{22}$	...	$C_{2n_{C_2}}$
$X_{12}$	$v_{12}(x_{12}^{(A_{21})})$	$v_{12}(x_{12}^{(A_{22})})$	...	$v_{12}(x_{12}^{(A_{2n_{A_2}})})$	$v_{12}(x_{12}^{(B_{21})})$	$v_{12}(x_{12}^{(B_{22})})$	...	$v_{12}(x_{12}^{(B_{2n_{B_2}})})$	$v_{12}(x_{12}^{(C_{21})})$	$v_{12}(x_{12}^{(C_{22})})$	...	$v_{12}(x_{12}^{(C_{2n_{C_2}})})$
$X_{22}$	$v_{22}(x_{22}^{(A_{21})})$	$v_{22}(x_{22}^{(A_{22})})$	...	$v_{22}(x_{22}^{(A_{2n_{A_2}})})$	$v_{22}(x_{22}^{(B_{21})})$	$v_{22}(x_{22}^{(B_{22})})$	...	$v_{22}(x_{22}^{(B_{2n_{B_2}})})$	$v_{22}(x_{22}^{(C_{21})})$	$v_{22}(x_{22}^{(C_{22})})$	...	$v_{22}(x_{22}^{(C_{2n_{C_2}})})$
...	...	...	...	...	...	...	...	...	...	...	...	...
$X_{102}$	$v_{102}(x_{102}^{(A_{21})})$	$v_{102}(x_{102}^{(A_{22})})$	...	$v_{102}(x_{102}^{(A_{2n_{A_2}})})$	$v_{102}(x_{102}^{(B_{21})})$	$v_{102}(x_{102}^{(B_{22})})$	...	$v_{102}(x_{102}^{(B_{2n_{B_2}})})$	$v_{102}(x_{102}^{(C_{21})})$	$v_{102}(x_{102}^{(C_{22})})$	...	$v_{102}(x_{102}^{(C_{2n_{C_2}})})$

b)

Figure 3: Example of evaluation table regarding the Air Conditioning appliance's type: (a)  $x_j^{(gjt)}$ ; (b)  $v_{ij}(x_j^{(gjt)})$ .

regarding each energy service, for the three problem dimensions, i.e., A-Economics, B-Social and C- Environment. Some of these attributes, are described on Table 3. Then, and based on such attributes, MAVT was used to assist the consumer, by evaluating a set of alternative solutions, obtaining therefore, a set of evaluation tables, each one regarding to an energy service. On Figure 3, it's described an example, regarding a table, correspondent to the energy service "Air Conditioning".

Through the value attributes, obtained by using MAVT, it was used the additive model to aggregate all the evaluation tables. Such model has resulted into 3 different objective functions, regarding each one, to a sustainability's dimension of the problem. The three objective functions considered above, were further optimized, by recurring to an optimization algorithm, based on NSGAI.

As it referred on previous sections, the problem presented here, is from the type of combinatorial nature, whose number of combinations, is related to the dimension of the sample. In this work, it was considered 10 alternatives per energy service. However, the combinations' number was reduced, since that, the consumer cannot make any choices, given its budget. Other constraints were also accounted in this work, namely the appliances noise maximal requirements and the air conditioner capacity. Thus, and after being applying MAVT, the problem stated in this work, can be modeled as follows:

$$\begin{aligned} \max \quad & V_D(x), \quad c / D = A, B, C \\ \text{s.t } x \in X \quad & c / V_D(x) = [V_A(x), V_B(x), V_C(x)]^T \end{aligned} \quad (8)$$

Where  $x$ , is the vector of decision, i.e.:

$$x \in X : x \in \{x_{ij}^{(A_j)}, x_{ij}^{(B_j)}, x_{ij}^{(C_j)}\} \wedge t, i, j \in \square \quad (9)$$

with,

$$\begin{aligned} i &= \{1, 2, \dots, 10\} \wedge j = \{1, 2, 3, \dots, 7\} \wedge \\ \wedge t &= \left\{ \left\{ 1, \dots, n_{A_j} \right\} \cup \left\{ 1, \dots, n_{B_j} \right\} \cup \left\{ 1, \dots, n_{C_j} \right\} \right\} \wedge n_{A_j}, n_{B_j}, n_{C_j} \in \square \end{aligned} \quad (10)$$

The  $V_A(x)$ ,  $V_B(x)$  and  $V_C(x)$ , defines the objective functions, considering each problem dimension, i.e.:

$$V_g(x) = \sum_{j=1}^{n_j} \sum_{t=1}^{n_{g_j}} v_j(x_j^{(g_j)}) \quad w / g = \{A, B, C\} \wedge v_j(x_j^{(g_j)}) \wedge n_j, n_{g_j}, t, j \in \square \quad (11)$$

Therefore, the objective functions are:

$$\text{Economic Well-being} : \max V_A(x) = \sum_{j=1}^{n_j} \sum_{t=1}^{n_{A_j}} v_j(x_j^{(A_j)}) \quad (12)$$

$$\text{Social Well-being} : \max V_B(x) = \sum_{j=1}^{n_j} \sum_{t=1}^{n_{B_j}} v_j(x_j^{(B_j)}) \quad (13)$$

$$\text{Environment Well-being} : \max V_C(x) = \sum_{j=1}^{n_j} \sum_{t=1}^{n_{C_j}} v_j(x_j^{(C_j)}) \quad (14)$$

The 1<sup>st</sup> objective function, were based on previous work [9]. The following approaches (with 2 and 3 objectives), uses the additive model based on MAVT, to obtain an unique objective function, based on the 2 and 3 objective functions (according to the approach used) pondered by the consumer's concern ( $\omega_g$ ), i.e.:

$$\begin{aligned} V(V_A(x), V_B(x)) &= \omega_A \cdot V_A(x) + \omega_B \cdot V_B(x) + \omega_C \cdot V_C(x) = \\ &= \sum_{j=1}^{n_j} \left( \omega_A \sum_{t=1}^{n_{A_j}} v_j(x_j^{(A_j)}) + \omega_B \sum_{t=1}^{n_{B_j}} v_j(x_j^{(B_j)}) + \omega_C \sum_{t=1}^{n_{C_j}} v_j(x_j^{(C_j)}) \right) \end{aligned} \quad (15)$$

The constraints, regarding economic and environment well-being/dimensions, are:

Available Budget ( $\eta_{avail.}$ ):

$$r_1 : \sum_{j=1}^{n_{dim}} I_j(x_j) \leq \eta_{avail.} \Leftrightarrow \sum_{j=1}^{n_{dim}} x_j^{(A_j)} \leq \eta_{avail.} \quad (16)$$

With

$$A_{jt} = \{A_{14}, A_{26}, A_{35}, A_{44}, A_{54}, A_{64}, A_{75}\} \wedge n_{dim}, t, j \in \square \quad (17)$$

Environment-Noise:

$$r_j : Noise_j \leq Max.Noise_j \Leftrightarrow x_j^{(B_j)} \leq Max.Noise_j \quad (18)$$

With:

$$B_{jt} = \{B_{24}, B_{35}, B_{44}, B_{54}, B_{64}, B_{75}\} \wedge n_{dim}, t, j \in \square \quad (19)$$

The NSGAI individual framework, presented on Figure 4, regards the approach for the 2 and 3 dimensions of sustainability presented next. For the approach with 2 dimensions, the structure is the same, although considering only 2 dimensions each. Instead of binary codification, regarding the 1<sup>st</sup> approach (one objective), NSGAI's codification have used real one. The model, developed here, will be deployed, by using the case study referred before, on previous section.

## 5. Results & Discussion

### 5.1. 1<sup>st</sup> Approach – Single objective model

Based on what was referred before, the 1<sup>st</sup> approach, has consisted into an EA's single objective approach, whose codification used, was binary, to ensure the existence of a unique individual solution at a time, and regarding appliance's type.

The approach presented here, was implemented by using MATLAB software, given its efficiency when dealing with data, which are organized into matrices. Our previous work ([1]) has allowed us to improve our EA's behavior by testing different objective functions, as well as different parameters values. To assess the quality of EA's solutions, it was used Simplex, which was implemented by using General Algebraic Modeling System (GAMS) software.

The best formulation, achieved at the time from ([1]), was the one presented on previous section. The results, presented next, were achieved, by using the following parameters:



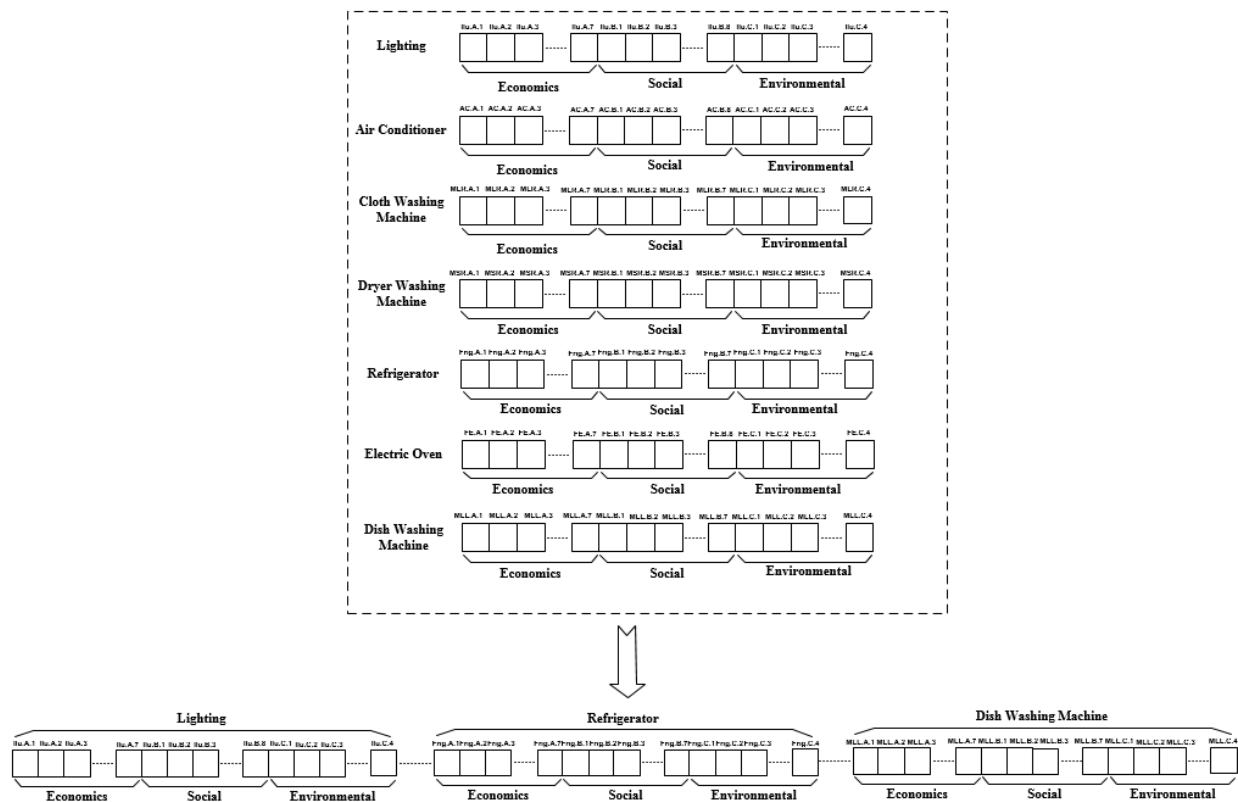


Figure 4: Individual framework (regarding the 2 and 3 objective approaches)

- Population size: 130
- Selection technique: roulette method
- Crossover technique: double point
- Crossover ratio: 0,55
- Mutation technique: bit string
- Mutation ratio: 0,02
- Convergence ratio: 0,002
- Maximum number of iterations/generations: without limits

On previous work ([1]), it was assessed the best fitness function (and objective function), based on the average values of the correspondent  $V_r^{(n)}$  objective, by performing 12 runs/budget.

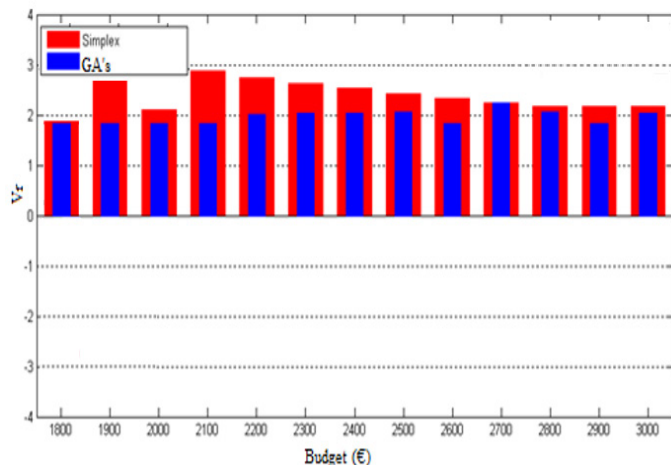


Figure 5: Average values of  $V_r$ , considering each value of budget constraint scenario

The EA's behavior, regarding the exploitation of feasible region, was also exploited, by using budget scenario constraint (eq. (7)). Although SIMPLEX, provides the best values, GAs, can also provide good solutions, considering the proximity of both values, By considering the present objective function, EA was also more efficient (on average) than other fitness functions assessed and studied on [1][14]. On Fig.5, it's presented also the average values of  $V_r$  (objective/fitness function), regarding the present formulation and considering both methods; GAs and SIMPLEX.

Although SIMPLEX, provides the best values, GAs, can also provide good solutions, considering the proximity of both values, regarding each budget constraint scenario.

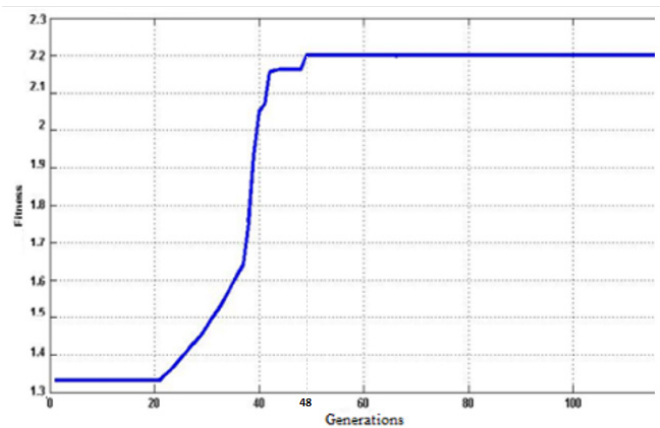


Figure 6: Example of fitness evolution from the best individual/generation (budget scenario of 1900 €)

The performance of GAs is shown on Figure 6, considering a 1900 € budget constraint scenario. On average, the steady state was achieved with 51 generations and considering 12 runs/budget constraint scenario.

On Table 4, it's described a feasible solution achieved with the approach described in this study, regarding a budget scenario constraint of 2700 Euros.

It is also shown the CO<sub>2</sub> avoided emissions (i.e. savings), regarding this solution, by comparing it with the less efficient.

Furthermore, the consumer has the information about what brand and model, regarding each appliance type to be acquired, as well as other information, such as the life cycle of each equipment and the savings in terms of electrical energy consumption, by comparing an efficient appliance with a less efficient one.

Table 4. Solution achieved by using EA's approach

Dimension	Stand. Solution Total Invest.	Effic. sol. Total Invest. (€)	Invest. Saving (€)	Consum. Saving (€)	CO <sub>2</sub> Savings (kg)	Life cycle	Brand	Model
Lighting	15,89	10,55	5,34	58,44	28,50	8000h	Philips	GENIE ESAVER 11W/827
Air Conditioning	368,0	299,0	69,00	1315,60	1315,57	10 yrs	Electro	TC N12KRH PORT
Refrigerator	250,0	529,0	-279,0	704,11	8,50	10 yrs	Indesit	TAN13FFS
Dishwasher Machine	310,0	349,0	-39,00	3,20	6,20	10 yrs	Fagor	1LF-011S
Washing Machine	262,0	294,0	-32,00	6,85	94,80	10 yrs	Zanussi	FLN1009
Oven	170,0	199,0	-29,00	1,30	2,60	10 yrs	Candy	FST100X
Clothes dryer	349,0	419,0	-70,00	11,32	1,800	10 yrs	Indesit	1SL79C
<b>Total:</b>	<b>1724,9</b>	<b>2099,6</b>	<b>-374,7</b>	<b>2100,80</b>	<b>1458,0</b>	-	-	-

Given the stochasticity of the GAs, as a metaheuristic method, it was made a statistical study to evaluate the consistency of the model, which was developed on previous works [1][13].

5.2. 2<sup>nd</sup> Approach – Multiobjective model

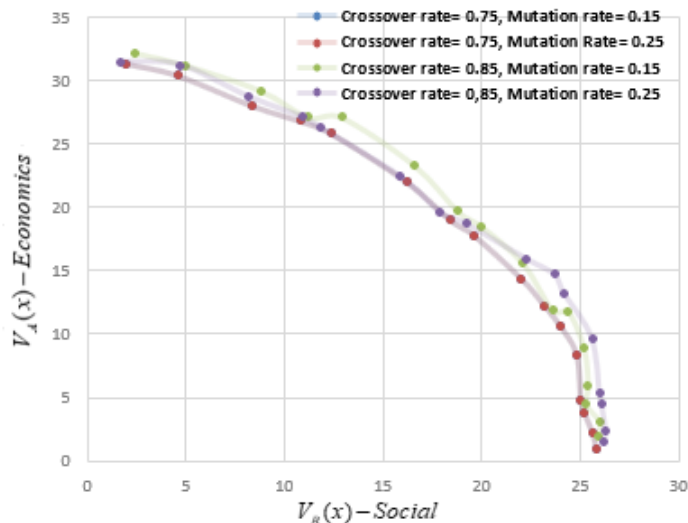
In order to achieve sustainable solutions, and based on Section 4.3, a Multiobjective method, based on NSGAI (Non-Sorting Genetic Algorithm II) ([18]), was coded on Matlab, by accounting the NSGAI's parameters, regarding each NSGAI's phase, namely; selection (roulette), crossover (double point) and mutation (normal random). The other parameters (crossover, mutation rate and initial population) were established after several simulations. Parameters such as the crossover rate, the mutation rate and the population size (120 individuals), were also experimented. With regards to the stopping criteria, it was chosen a parameter value of 80, as being the maximum number of iterations/generations allowed. It was considered several arrangements of crossover and mutation rates of NSGA-II, to obtain a suitable arrangement ( Table 5).

Table 5. Values, regarding the arrangements of crossover and mutation rates

Experiment	Crossover Rate	Mutation Rate
1	0.75	0.15
2	0.75	0.25
3	0.85	0.15
4	0.85	0.25

Therefore, it was used the following NSGAI's parameters: population size of 120 individuals, a maximum number of 80 iterations, a mutation rate of 0,15 and a crossover rate of 0,75.

In the Figure 7, it's shown the pareto frontier, for different arrangements of crossover and mutation rates.



After the tuning with NSGAI's parameters, the Pareto frontier in Figure 9, was therefore achieved, with each one of the 16 nodes, representing an optimal solution of the problem. In other words, each node represents a set of individual solutions (appliances from the market), related each one, to an energy service.

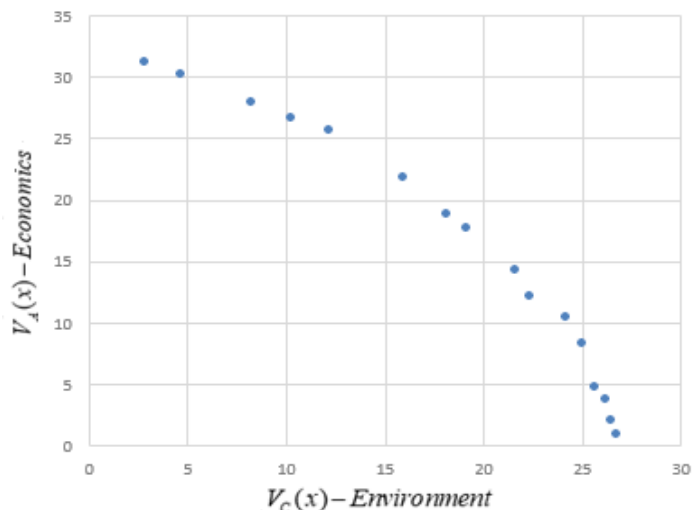


Figure 8. Pareto frontier (last generation) Economical vs Environmental

( $\omega_A = 0,73$ ,  $\omega_B = 0,00$ ,  $\omega_C = 0,27$ )

Such calculations were performed, by considering a scenario where the consumer only considers the Economic and Environment concerns, i.e.,  $\omega_A = 0,73$ ,  $\omega_B = 0,00$  and  $\omega_C = 0,27$  (Figure 10).

The trade-off, existed between the two dimensions, can also be noted through Figure 8, since the reduction on economic well-being, leads to an increase of the environment well-being.

Table 6, shows the results from one of the nodes achieved here, by assuming a budget constraint value of 2250 €.

Table 6. Solution achieved: Economical vs Environmental ( $\omega_A = 0,73$ ,  $\omega_B = 0,00$ ,  $\omega_C = 0,27$ )

Dimension	Stand. Solution Total Invest. (€)	Effic. sol. Total Invest (€)	Invest. Saving (€)	Consum. Saving (€)	CO <sub>2</sub> Savings (kg)	H <sub>2</sub> O Savings (l)	Brand	Model
Lighting	15.89	09.53	5.34	59.40	28.90	-	GE	EFL23W
Air Conditioning	368.00	299.00	69.00	1320.60	1322.60	-	Whirlpool	PACW9HP
Refrigerator	250.00	529.00	-279.00	708.10	8.70	-	BECKEN	Bc2016 1x
Dishwasher Machine	310.00	349.00	-39.00	3.20	7.80	429.07	Bosch	SMS25A100E
Washing Machine	262.00	294.00	-32.00	6.90	94.80	351.02	INDESIT	EWE71252 W
Oven	170.00	199.00	-29.00	1.70	2.33	-	Zanussi	ZZB21601XV
Clothes dryer	349.00	419.00	-70.00	12.30	1.82	-	Electrolux	EDP2074PDW
<b>Total:</b>	<b>1727.89</b>	<b>2098.53</b>	<b>-374.66</b>	<b>2112.20</b>	<b>1466.95</b>	<b>780.09</b>	-	-

Through the values, presented above, we can see that if the consumer, choses the optimal solutions provided by NSGAII, he can save 1737,54 € approximately, having also CO<sub>2</sub> and water savings. Both values are per year, for a life cycle of 10 years.

The same, were performed, by considering a scenario where the consumer only considers the Economic and Social concerns, i.e.,  $\omega_A = 0,73$ ,  $\omega_B = 0,27$  and  $\omega_C = 0,00$  (Figure 9).

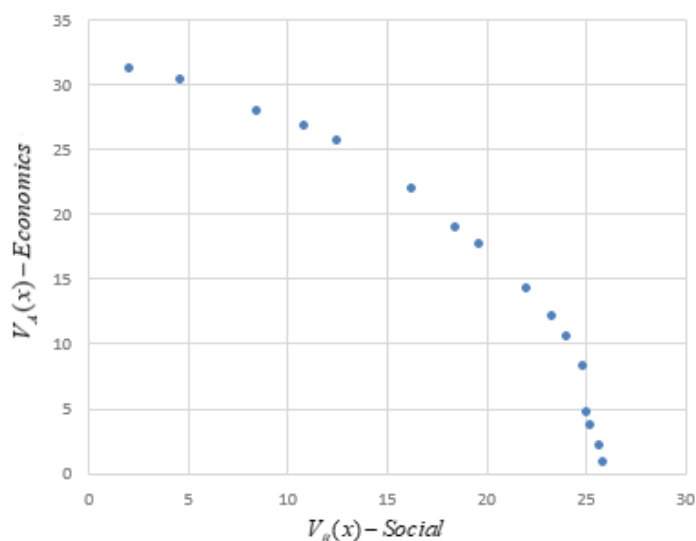


Figure 9. Pareto frontier regarding the last generation; Economical vs Social ( $\omega_A = 0,73$ ,  $\omega_B = 0,27$ ,  $\omega_C = 0,00$ )

Through the last iteration/generation, it was obtained sixteen feasible solutions, achieving therefore, an example of a Pareto frontier. One of the nodes achieved with this scenario, is shown on Table 7, by considering a budget of 2250 € and a life cycle of 10 years.

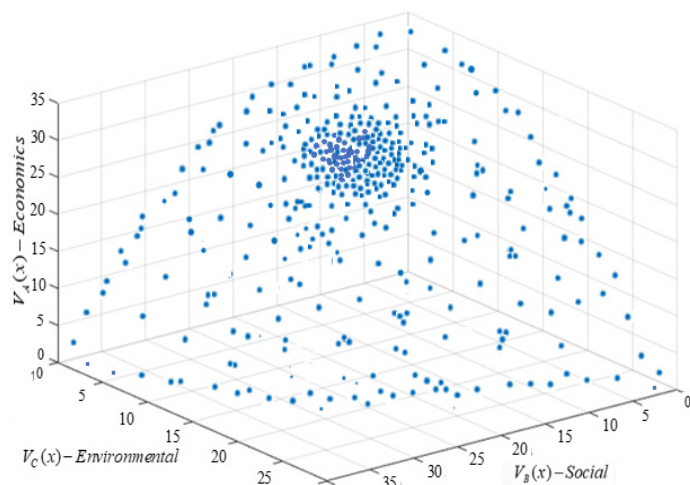
Table 7. Solution achieved: Economical vs Social ( $\omega_A = 0,73$ ,  $\omega_B = 0,27$ ,  $\omega_C = 0,00$ )

Dimension	Stand. Solution Total Invest. (€)	Effic. sol. Total Invest (€)	Invest. Saving (€)	Consum. Saving (€)	CO <sub>2</sub> Savings (kg)	H <sub>2</sub> O Savings (l)	Brand	Model
Lighting	15.89	69.65	5.34	59.40	27.60	-	OSRAM	3316242
Air Conditioning	352.00	279.00	69.00	1319.50	1322.60	-	SAMSUNG	AQV09PSBN
Refrigerator	250.00	529.00	-279.00	708.10	9.72	-	Candy	CFET 6182W
Dishwasher Machine	320.10	351.99	-38.10	2.20	6.90	423.02	BALAY	3V5303IP
Washing Machine	262.00	294.00	-32.00	6.90	95.10	317.04	Siemens	WI12A222E5
Oven	171.00	701.00	-28.30	2.82	2.33	-	Electrolux	EZC2430AOX
Clothes dryer	368.00	449.00	-68.00	10.20	1.82	-	BOSCH	WTE84107EE
<b>Total:</b>	<b>1738.99</b>	<b>2673.64</b>	<b>371.06</b>	<b>2109.12</b>	<b>1458.90</b>	<b>740.06</b>	-	-

According to the values on Table 7, the consumer can save up to 1738.06 €, through the selection of the appliances mentioned above. Additionally, there also savings with CO<sub>2</sub> and water as well, with both values being expressed as savings/years and based on the life cycle considered here.

Based on both trade-offs, presented above, it was considered a scenario with the three dimensions and their correspondent consumer's relative importance, i.e., Economical vs Social vs Environmental ( $\omega_A = 0,66$ ,  $\omega_B = 0,23$  and  $\omega_C = 0,11$ ).

In order to pursue the main goal, referred before, it was performed a scenario where the consumer considers the 3 dimensions of sustainability, i.e., Economic, Social and Environment concerns, i.e.;  $\omega_A = 0,66$ ,  $\omega_B = 0,23$  and  $\omega_C = 0,11$  (Figure 10).



Through Figure 10, it can be seen that the crowding distance, between the final solutions obtained, regarding the obtained Pareto surface, is higher in the region where the Economic dimension is more dominant. Such dominance order is followed by the Social, and at last, the Environmental dimension. Such dominance order, is somehow expected, given the relative importance's values (weight) considered in this case, and regarding each dimension considered, i.e.;  $\omega_A = 0,66$ ,  $\omega_B = 0,23$  and  $\omega_C = 0,11$ .

One of the nodes, represented on that surface, are shown on Table 8, considering a budget of 2250 €, for 10 years of life cycle.

Table 8. Example of a solution obtained from this approach. Economical vs Social vs Environmental ( $\omega_A = 0,66$ ,  $\omega_B = 0,23$ ,  $\omega_C = 0,11$ )

Dimension	Stand. Solution Total Invest. (€)	Effic. sol. Total Invest (€)	Invest. Saving (€)	Consum. Saving (€)	CO <sub>2</sub> Savings (kg)	H <sub>2</sub> O Savings (l)	Brand	Model
Lighting	16.88	49.04	5.35	62.20	28.90	-	Phillips	LEDspotMV
Air Conditioning	352.00	279.00	69.00	1319.50	1315.70	-	SAMSUNG	AQV09P5BN
Refrigerator	234.00	399.00	-265.00	709.30	9.72	-	BECKEN	Bc2016 1x
Dishwasher Machine	310.00	349.00	-39.00	3.20	6.90	423.00	Bosch	SMS25AI00E
Washing Machine	272.20	249.90	-33.00	5.60	95.10	322.10	INDESIT	EWE71252 W
Oven	171.00	701.00	-28.30	2.82	2.20	-	Electrolux	EZC2430AOX
Clothes dryer	368.00	449.00	-68.00	10.20	1.70	-	BOSCH	WTE84107EE
Total:	1724.80	2475.94	-262.65	2112.30	1460.22	745.10	-	-

According to Table 8, the consumer, can save up to 1849,65 €, avoiding approximately 1460,22 kg of CO<sub>2</sub> and saving 745,10 liters of water, with both values expressed as savings/years, and based on 10 years as the life cycle considered in this study.

Through the performance of such scenarios, we can see some coherence with the application of  $\omega_A$ ,  $\omega_B$  and  $\omega_C$ .

An example is the water savings achieved, where it is more noticed when the correspondent Environment weight ( $\omega_C$ ), is increased.

## 6. Conclusions & Further Work

This paper follows a research line, where the main goal is to present a method to provide sustainable electrical household appliances from the market to a household consumer. On previous work, and at a first stage, it was formulated a single objective problem, although considering only the environmental impacts (CO<sub>2</sub> savings) and the economic savings, each one, related to the initial investment and energy consumption. Both indicators, were calculated, by performing the correspondent lifecycle cost assessment (LCCA) of each household appliance, and during the correspondent usage phase.

It was also used Genetic Algorithms (GAs) to achieve several and different feasible solutions, whose quality were tested through the comparison with the results achieved from simplex method.

Then, the approach was formulated by considering a multiobjective problem, although by exploring 2 dimensions at a time, and by recurring to MAVT and NSGA II methods

This approach has used a set of established criteria, in order to perform a pre-selection of candidate solutions existed on market, and suitable to the consumer needs. The purpose was to redefine the decision space, composed by a set of candidate solutions, and based on each type of household appliance considered to be acquired by the consumer.

Furthermore, it was adopted additional criteria, to be further integrated with MAVT, in order to achieve a model with the consumer preferences and based on the 3 problem dimensions presented.

The objective was to improve the consumer well-being, regarding each sustainability's dimension referred above, and based on their importance, given by the consumer.

When achieving the MAVT model, it was also included the ecological impact in terms of water and CO<sub>2</sub> savings, as well as economic issues, such as energy consumption and initial investment savings, based on the lifecycle cost assessment (LCCA) of each household appliance. Social issues were also included, by integrating the consumer's preferences in terms of design, reliability and other issues, including even the visual and thermal comfort. Then NSGAII was applied, by achieving sustainable solutions from the market, that maximizes the tree dimensions referred before.

The approach presented here, also allows a consumer, to achieve a set of savings regarding issues such as; CO<sub>2</sub> emissions, energy and water consumption.

As further work, this approach could be applied into other energy services/household appliances, for instance, with a relevant impact in terms of sustainable development (e.g. information technology's equipment's such as computers, printers, among others).

## References

- [1] R. Santos, J. C. O. Matias and A. Abreu, "An approach to provide efficient choices to a household consumer," 2019 International Young Engineers Forum (YEF-ECE), Costa da Caparica, Portugal, 2019, pp. 46-51. doi: 10.1109/YEF-ECE.2019.8740824
- [2] IEA: Energy Efficiency 2017 – Market Reports Series, OECD/IEA (2017)
- [3] Gul, M., Patidar. S. (2015). Understanding the energy consumption and occupancy of a multi-purpose academic building, In Energy and Buildings, Volume 87, Pages 155-165, ISSN 0378-7788
- [4] ADENE: Manual da Etiqueta Energética, ADENE, Lisboa ISBN: 978-972-8646-36-3 (2017)
- [5] Wong, I., L., Krüger, E., Comparing energy efficiency labelling systems in the EU and Brazil: Implications, challenges, barriers and opportunities, In Energy Policy, vol.109, pp. 310-323, Springer, Heidelberg (2017)
- [6] Fell, M.: Energy services: A conceptual review, Energy Research & Social Science, vol.27, pp.129--140, Springer (2017)
- [7] Hoxha, E., Jusselme, T. (2017), On the necessity of improving the environmental impacts of furniture and appliances in net-zero energy buildings, In Science of The Total Environment, Volumes 596–597, Pages 405-416, ISSN 0048-9697
- [8] Ting, T.O.; Rao, M.V.; Loo, K.C. (2006) A novel approach for unit commitment problem via an effective hybrid particle swarm optimization. IEEE Trans. Power Syst., 21, 411–418.
- [9] Ferreira, F.A.; Lemos, F.A.B. (2010) Unbalanced electrical distribution network reconfiguration using simulated annealing. In Proceedings of the 2010 IEEE/PES Transmission and Distribution Conference and Exposition: Latin America (T&D-LA), Sao Paulo, Brazil, 8–10; pp. 732–737.
- [10] Agrawal, P.; Rao, S. (2014), Energy-aware scheduling of distributed systems. IEEE Trans. Autom. Sci. Eng. , 11, 1163–1175.



- [11] Ko, M.J.; Kim, Y.S.; Chung, M.H.; Jeon, H.C.(2015), Multi-objective design for a hybrid energy system using genetic algorithm. *Energies*, 8, 2924–2949.
- [12] Randall, M., Rawlins, T., Lewis, A., Kipouros, T., Performance Comparison of Evolutionary Algorithms for Airfoil Design, In *Procedia Computer Science*, vol. 51, pp. 2267-2276, Springer Heidelberg (2015)
- [13] R.S. Santos, J.C.O. Matias, A. Abreu, F. Reis, Evolutionary algorithms on reducing energy consumption in buildings: An approach to provide smart and efficiency choices, considering the rebound effect, *Computers & Industrial Engineering*, Volume, 126,2018,Pages 729-755,ISSN 0360 8352, <https://doi.org/10.1016/j.cie.2018.09.050>
- [14] Santos, R., Abreu, A., Matias, J.C.O.,Energy Efficiency in buildings by using evolutionary algorithms: An approach to provide efficiency choices to the consumer, considering the rebound effect, IFIP International Federation for Information Processing 2018, 2018-03-29, book-chapter Part of ISBN: 978-3-319-78574-5
- [15] Pombo, O., Allacker, K., Rivela, B., Neila, J., (2016) Sustainability assessment of energy saving measures: a multi-criteria approach for residential buildings retrofittingda case study of the Spanish housing stock, *Energy Build.* 116 pp.384e394.
- [16] Aghay Kaboli , S. Hr., Selvaraj, J., Rahim, N.A.,(2017) Rain-fall optimization algorithm: A population based algorithm for solving constrained optimization problems, *Journal of Computational Science*, Volume 19, Pages 31-42, ISSN 1877-7503, <https://doi.org/10.1016/j.jocs.2016.12.010>.
- [17] Cortés, P., Muñuzuri, J., Berrocal-de-O, M., Domínguez, I., (2018) Genetic algorithms to optimize the operating costs of electricity and heating networks in buildings considering distributed energy generation and storage, *Computers & Operations Research*, Volume 96, Pages 157-172, ISSN 0305-0548, <https://doi.org/10.1016/j.cor.2018.01.020>.
- [18] K. Deb, A. Pratap, S. Agarwal and T. Meyarivan, "A fast and elitist multiobjective genetic algorithm: NSGA-II," in *IEEE Transactions on Evolutionary Computation*, vol. 6, no. 2, pp. 182-197, April 2002. doi: 10.1109/4235.996017
- [19] Chuah, J. W., Raghunathan, A., Jha, N. K. (2013), ROBESim: A retrofitoriented building energy simulator based on EnergyPlus, *Energy Build.*, vol. 66, pp. 88–103.
- [20] Asadi, E., Silva, M. G., Antunes, C. H., Dias, L. (2012), Multi-objective optimization for building retrofit strategies: A model and an application, *Energy Build.*, vol. 44, pp. 81–87
- [21] Mauro, G.M., Hamdy, M., Vanoli, G.P., Bianco, N., Hensen, J.L.M. (2015) A new methodology for investigating the cost-optimality of energy retrofitting a building category, *Energy Build.* 107 pp. 456 e 478.

## A Comparative Analysis of ARIMA and Feed-Forward Neural Network Prognostic Model for Bull Services

Jude B. Rola<sup>\*1</sup>, Cherry Lyn C. Sta. Romana<sup>2</sup>, Larmie S. Feliscuzo<sup>2</sup>, Ivy Fe M. Lopez<sup>3</sup>, Cherry N. Rola<sup>4</sup>

<sup>1</sup>Visayas State University, Department of Computer Science and Technology, Baybay City, 6521-a, Philippines

<sup>2</sup>Cebu Institute of Technology-University, Cebu City, 6000, Philippines

<sup>3</sup>Philippine Carabao Center-Visayas State University, 6521-a, Philippines

<sup>4</sup>Visayas State University, Department of Liberal Arts and Behavioral Sciences, Baybay City, 6521-a, Philippines

### ARTICLE INFO

Article history:

Received: 13 January, 2020

Accepted: 16 March, 2020

Online: 04 April, 2020

Keywords:

Time series forecasting

ARIMA

Artificial neural network

### ABSTRACT

Bull service is the natural copulation by a purebred male carabao with a female counterpart. This is part of the bull loan agenda of the Philippine Carabao Center-Visayas State University (PCC-VSU), one of the 12 regional centers of PCC. For the past years, PCC-VSU used averaging of bull services count of previous years and sometimes did a little tweaking of the formulas in setting annual targets. Some targets fell short in the actual accomplishment that may have led to achieving lesser animal products. There is a need for resource optimization. Resource optimization through Auto-Regressive Integrated Moving Average (ARIMA) and Artificial Neural Network (ANN) forecasting can be used in the setting of goals of future number of copulations. This study deals with the comparative assessment of ARIMA and ANN in 4-step and 12-step ahead time series forecasting of bull services. This endeavor dealt with quarterly data from 2002 to 2017. In ARIMA, the for 4-step ahead (1-year) forecasting had the data from 2002 to 2016 for training while data from 2017 was employed for testing. ARIMA 12-step ahead (3-year) forecasting had data from 2002 to 2014 for training and 2015 to 2017 for testing. The ANN 4-step ahead prediction made use of data from 2002 to 2015 for training, 2016 for validation and 2017 for testing. ANN 12-step forecasting had data from 2002 to 2011 for training, 2012 to 2014 for validation and 2015 to 2017 for testing. R studio, a tool for statistical computing was employed in the analysis. Based on the performance measures Root Mean Square Error, Mean Absolute Percent Error and Mean Absolute Error the ANN outshines the ARIMA in both 4-step and 12-step ahead forecasting. The ANN forecasting can surely help in optimizing the center's resources. The forecasting of bull services using multivariate series is recommended.

### 1. Introduction

Bull service is the natural breeding by a purebred male carabao/water buffalo with a female mate. Dealing with the comparison of forecasting methods that predict bull services, this paper is an extension of the work originally presented in the 2019 International Conference on Multimedia Analysis and Pattern Recognition (MAPR) [1]. Bull service is among the services offered by the Philippine Carabao Center-Visayas State University

(PCC-VSU) under the bull loan program which promotes water buffalo or carabao propagation and genomic enhancement.

PCC-VSU is among the 12 regional centers of PCC spread across the Philippine archipelago. The center is a government agency founded in 1992 through the Republic Act 7307. Other services it offers are artificial insemination (AI), buffalo semen distribution, and farmers and technicians' training [2]. PCC-VSU is mandated to deliver these services in region 8 comprising 6

\* Jude B. Rola, Philippines, 63-53-563-7068/ jude.rola@vsu.edu.ph

provinces namely: Biliran, Leyte, Southern Leyte, Northern Samar, Samar, and Eastern Samar.

In the past, PCC-VSU used mean computation of bull services count of recent previous years and sometimes did little adjustment of formulas in setting annual targets. Some targets would fall short in the actual accomplishment and some would go over. Achieving more than the actual is an advantage but achieving low because of the low target does not optimize the animal and human resources. Forecasting bull services can help the center in the target setting and in optimizing its resources. It may help in aiming high to accomplish more. More bull services conducted means more animal products are produced – higher income especially for small-scale animal raisers. The focal purpose of this inquiry is to explore and compare the 4-step (1 year) and 12-step ahead (3 years) time series forecasting performance of Auto-Regressive Integrated Moving Average (ARIMA) and multi-layer artificial neural network (ANN) on bull services to improve the target setting competence of the center. In [1], only a single-layer ANN was used while in this research endeavor a multi-layer ANN was employed. This analysis utilized quarterly bull services data from 2002 to 2017. R studio was utilized in the analysis. The performance of ARIMA and ANN models were tested using the following measures: Root Mean Square Error (RMSE), Mean Absolute Percent Error (MAPE), and Mean Absolute Error (MAE).

In 2015, [3] combined ARIMA with Deep Belief Net (DBN) in predicting the residual of prediction results. Experimental results showed an effective forecast. Relatively, [4] produced a model to forecast the crude matters required for plastic products based in revenue data. The short-term prediction had relatively fine accuracy.

On the other hand, [5] established a neural network model with 4 input stratum neurons, 8 hidden stratum neurons and 1 output stratum neuron that effectively forecast information security incidents. [6] established an ANN model for forecasting and optimization of solar energy potential. Another model was produced in the study of [7] for wind speed forecasting. A recurrent neural network model was designed and implemented also by [8] for repairable system failure analysis. Another by [9] produced an ANN model that successfully predicted the rainfall one-step ahead. None of these tackled bull services prognostic modeling using a multi-layer ANN. A thorough web search was performed and none has been found as well hence, the purpose of the study.

## 2. Method

### 2.1. Box-Jenkins Method or Autoregressive Integrated Moving Average (ARIMA)

Autoregressive-Moving Average (ARMA) model incorporates a broad collection of non-stationary time series. It is then simplified producing an ARIMA. With the past data, the differencing technique is utilized to enhance stationarity into the modelling. The modelling decomposes the data into an autoregressive (AR) process, integrated (I) process, and a moving average (MA) of prognostic oversight.

The purpose of the AR procedure is to take a recollection of historical events, the I procedure is responsible for easing data stationarity, hence helps in easier prediction. Forecasting is more accurate with longer past data as it learns eventually. To achieve a transformation of a non-stationary procedure into a stationary one, a random walk is employed. A procedure  $\{y_t\}$  is articulated to observe an Integrated ARMA model, conveyed by ARIMA (p, d, q), if  $dy_t = (1-B)^d \varepsilon_t$  is ARMA (p, q). The prognostic model can be written as

$$\varphi(B)(1 - B)^d Y_t = \theta(B)\varepsilon_t \tag{1}$$

where

$$\varphi(B) = 1 - \varphi_1 B - \varphi_2 B^2 - \dots - \varphi_p B^p$$

$$\theta(B) = 1 - \theta_1 B - \theta_2 B^2 - \dots - \theta_q B^q$$

$\varepsilon_t \sim WN(0, \sigma^2)$ , WN signifying White Noise. B indicates the backshift operator ( $By_t = y_{t-1}$ ). The  $d$  is a non-negative integer that is known as the integration parameter. The ARIMA (p, d, q) model becomes an ARMA (p, q) model when  $d=0$ .

The 3 stages of ARIMA are identification, estimation and testing, and forecasting application. The constraints of the provisional chosen model at the identification part are approximated at the estimation stage while the model’s adequacy is evaluated at the estimation and testing stage. When the model is unsatisfactory, the process is repeated until a sufficient model is selected [10]. Figure 1 depicts the ARIMA or Box-Jenkins modeling phases created by [11].

The Box-Jenkins Method or ARIMA is employed to forecast the trend of bull services for the next 4-quarters and 12-quarters. Its forecasts are then compared to the ANN’s. The method that gives better prediction may help in determining the possible number of bulls and manpower that possibly maybe involve in carrying out bull services.

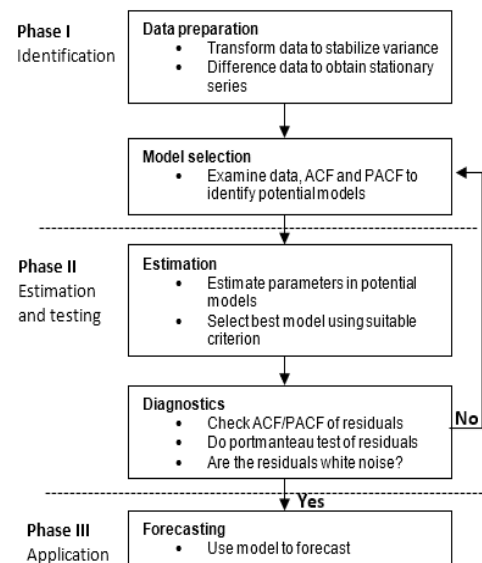


Figure 1: Box-Jenkins or ARIMA modeling approach.

2.2. Artificial Neural Network (ANN)

As great function estimators, the ANNs, commonly used in forecasting, pattern recognition, and control engineering replicate the human intellect. The Multi-Layer Perceptron (MLP) is an ANN of a feed-forward construct that is a compound layer network usually with 3 tiers namely: the input, the hidden, and the output layers. The MLP diagram, adapted from [3] is shown in Figure 2.

Each layer of the network has neurons or units. The neurons at the input layer obtain inputs from external entity and reproduce these inputs to the neurons of the hidden stratum. As the input signal components with the weights go beyond the biases, the neurons on the hidden layer can fire. A similar thing could happen among hidden and output layers. The neurons at the hidden and output layer generate function utilized logistic sigmoid depicted in (2) [3].

$$f(x) = \frac{1}{1 + \exp(-x/\epsilon)} \quad \epsilon : \text{Gradient} \quad (2)$$

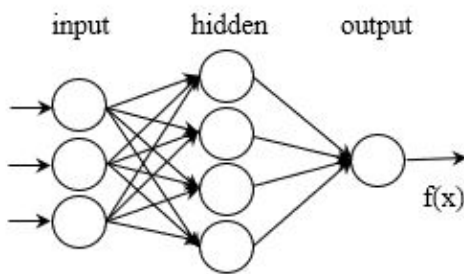


Figure 2: The structure of a multilayer perceptron.

2.3. Performance Evolution and Error Estimations

Some of the evaluation functions utilized in determining the success of the ARIMA method are Akaike information criterion (AIC), Bayesian information criterion (BIC), adjusted coefficient of determination ( $R^2$ ), mean absolute percent error (MAPE), root mean square error (RMSE), and mean absolute error (MAE) [11, 12]. AIC and BIC select models with more accuracy and of low error in out-of-sample forecasting. The errors of these techniques are computed by the coefficient of determination and MAPE [12, 13, 14]. The MAPE is calculated by getting the difference between predicted and actual value. The outcome of subtraction is divided by the actual value, multiplied by 100, and then divided by the number of samples [15]. RMSE presents the concentration of data near the line of best fit. Aside from forecasting, it is widely utilized in regression and climatology analyses [16]. It is employed to measure the projection error values of potential models for a specific dataset [17]. MAE, on the other hand, entails adding the magnitudes of the errors and dividing it by n [18].

3. Experimental Results

3.1. Data and Modeling Tool

Figure 3 shows the time series chart of bull services covering 2002 to 2017. In ARIMA modeling, the for 4-step ahead (1-year) forecasting had the data from 2002 to 2016 (60 samples) for training while data from 2017 was employed for testing. ARIMA 12-step ahead (3-year) forecasting had data from 2002 to 2014 (52 samples) for training and 2015 to 2017 for testing.

On the other hand, ANN 4-step ahead prediction made use of data from 2002 to 2015 (56 samples) for training, 2016 for validation and 2017 for testing. ANN 12-step forecasting had data from 2002 to 2011 (40 samples) for training, 2012 to 2014 for validation and 2015 to 2017 for testing. R studio was the statistical computing tool utilized for both ARIMA and ANN modeling.

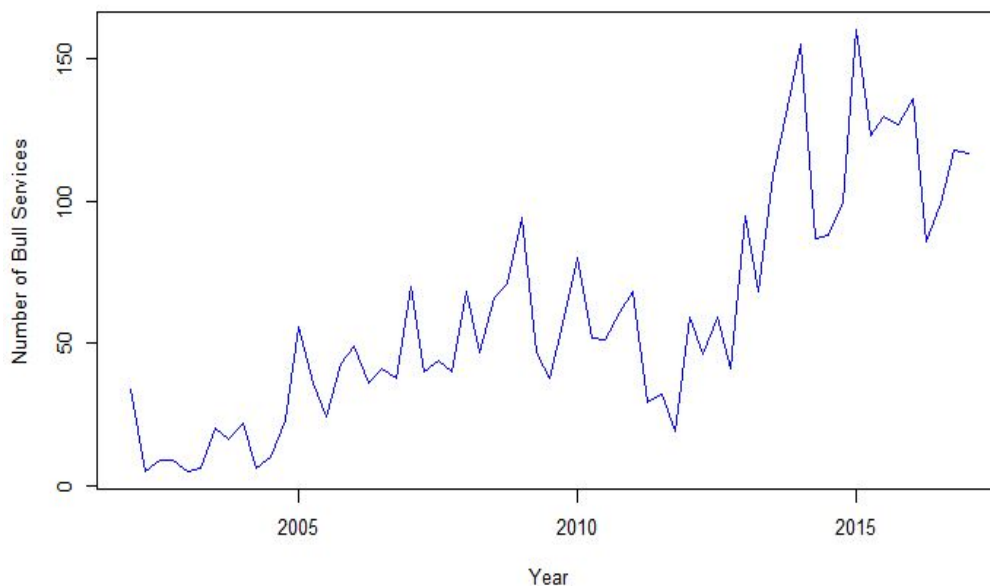


Figure 3: Time series plot of bull services (2002-2017).



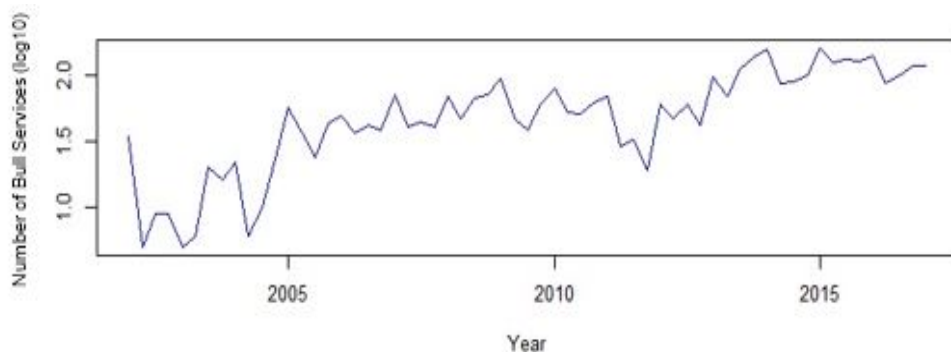


Figure 4: Logarithmic- transformation of bull services data series.

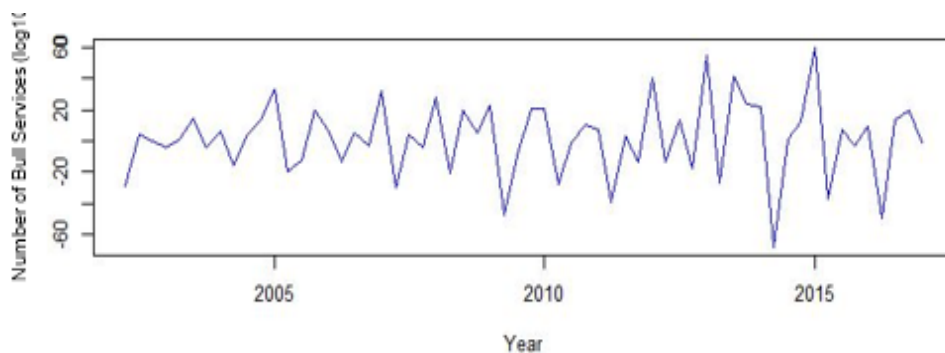


Figure 5: Differenced Bull Services Data

### 3.2. Preprocessing Data

The time series plot of bull services from 2002 to 2017 is shown in Figure 3. There is a growing activity inclination from the beginning to the initial quarter of 2009. During the sophomore quarter of the same year to the last quarter of 2012, a fall in the number of services can be observed. It starts to rise again in the initial quarter of the following data point. The primary quarter of 2014 is considered as its peak; however, 2014 falls again. Furthermore, the initial periods of 2005 to 2012 depicts the greatest number of bull services.

Generally, just like the other regional centers, along the years PCC-VSU may have met some challenges in the implementation of the bull services that were evident in the years 2010 to 2015 due to few significant fluctuations of data. The factors that may have affected it were the social and economic aspect of the bull loan beneficiary, willingness in adapting the process of acquiring bulls, PCC and LGU staff monitoring difficulties, political intervention in choosing recipients, and bull handlers' expertise deficiency. These factors were manifested in the study of [19].

There was a logarithmic conversion or transformation of data as shown in Figure 4 since there was no stationarity in the methods which predict series ( $Y_t$ ) of raw data. The process makes data stationary on variance. The log transformation equation is depicted in (3). The transformed data were used in both ARIMA and neural network forecasting.

$$Y_t^{new} = \log_{10} Y_t \quad (3)$$

The data were then subjected to one-time differencing to transform its mean to stationary (on logged) (Figure 5).

### 3.3. ARIMA Model

For both the 4-step ahead (1-year) and 12-step ahead (3 years) bull services forecasting, the best model is ARIMA (1,1,1) (2,0,0) [4] based on AIC, BIC, and AIC<sub>c</sub>. Table 1 and Table 2 presents the AIC<sub>c</sub> values.

### 3.4. Feed-forward Neural Network Model

The suitable ANNs for both 4-step ahead and 12-step ahead bull services forecasts were chosen from various examined networks in the training stage; but, only sample results of different input parameters are presented on this paper (Table 3 and Table 4) employing the following number of epochs: 100, 500 and 1000. The learning rate used was 0.001. For shorter-term forecasting, the finest outcome was produced by the model which comprises 20 input neurons (window width), 12 hidden neurons and 4 output neurons trained for 1000 epochs (Table 3).

For longer-term forecasting, the best outcome was from the network which consists of 4 input neurons (window width), 4 hidden neurons and 12 output neurons trained for 100 epochs (Table 4). There was no overfitting that occurred in ANN modeling as the same network structures in both 4-step and 12-step ahead forecasting gave the most accurate prediction in the validation and testing stage.

Table 1: Statistical results of different ARIMA parameters for PCC-VSU bull services (4-step ahead forecast).

ARIMA	AIC <sub>c</sub>
(0, 1, 0)	-5.43
(0, 1, 1)	-14.21
(0, 1, 1) (1, 0, 0) [4]	-15.76
(1, 1, 1) (1, 0, 0) [4]	-18.20
(1, 1, 0) (1, 0, 0) [4]	-13.43
(1, 1, 2) (1, 0, 0) [4]	-16.08
(0, 1, 0) (1, 0, 0) [4]	-14.10
(2, 1, 2) (1, 0, 0) [4]	-15.14
(1, 1, 1)	-12.54
<b>(1, 1, 1) (2, 0, 0) [4]</b>	<b>-19.87</b>
(0, 1, 1) (2, 0, 0) [4]	-17.25
(2, 1, 1) (2, 0, 0) [4]	-17.43
(1, 1, 0) (2, 0, 0) [4]	-15.98
(1, 1, 2) (2, 0, 0) [4]	-17.43
(0, 1, 0) (2, 0, 0) [4]	-16.60
(2, 1, 2) (2, 0, 0) [4]	-14.89

Table 2: Statistical results of different ARIMA parameters for PCC-VSU bull services (12-step ahead forecast).

ARIMA	AIC <sub>c</sub>
(0, 1, 0)	4.60
(0, 1, 1)	-1.98
(0, 1, 1) (1, 0, 0) [4]	-2.35
(1, 1, 1) (1, 0, 0) [4]	-3.59
(1, 1, 0) (1, 0, 0) [4]	-0.39
(1, 1, 2) (1, 0, 0) [4]	-1.24
(0, 1, 0) (1, 0, 0) [4]	-1.15
(1, 1, 1)	-0.17
<b>(1, 1, 1) (2, 0, 0) [4]</b>	<b>-3.70</b>
(0, 1, 1) (2, 0, 0) [4]	-2.33
(2, 1, 1) (2, 0, 0) [4]	-1.13
(1, 1, 0) (2, 0, 0) [4]	-1.12
(1, 1, 2) (2, 0, 0) [4]	-1.13
(0, 1, 0) (2, 0, 0) [4]	-1.91

Table 3: Statistical performance of ANN model for bull services (4-step ahead forecast; learning rate =0.001).

Network Structure	RMSE	MAPE (%)	MAE	RMSE	MAPE (%)	MAE	RMSE	MAPE (%)	MAE
	100 epochs			500 epochs			1000 epochs		
20-3-4	0.14	6.91	0.13	0.04	1.83	0.04	0.07	2.66	0.05
20-4-4	0.14	6.87	0.13	0.15	6.22	0.12	0.15	6.00	0.12
20-5-4	0.17	8.21	0.16	0.15	7.49	0.15	0.14	5.87	0.12
20-6-4	0.13	6.33	0.12	0.16	8.00	0.16	0.15	7.28	0.14
20-7-4	0.14	6.91	0.13	0.15	6.67	0.13	0.16	7.28	0.14
20-8-4	0.15	6.76	0.13	0.14	7.16	0.14	0.14	6.10	0.12
20-9-4	0.15	7.20	0.14	0.13	6.07	0.12	0.15	7.32	0.14
20-10-4	0.16	7.51	0.15	0.18	8.45	0.17	0.14	6.70	0.13
20-11-4	0.15	6.54	0.13	0.17	7.78	0.15	0.16	6.93	0.14
<b>20-12-4</b>	0.16	7.63	0.15	0.13	6.48	0.13	<b>0.02</b>	<b>0.55</b>	<b>0.01</b>

Table 4: Statistical performance of ANN model for bull services (12-step ahead forecast; learning rate =0.001).

Network Structure	RMSE	MAPE	MAE	RMSE	MAPE	MAE	RMSE	MAPE	MAE
	100 epochs			500 epochs			1000 epochs		
4-3-12	0.11	4.01	0.08	0.08	3.30	0.07	0.09	3.86	0.08
<b>4-4-12</b>	<b>0.07</b>	<b>2.77</b>	<b>0.06</b>	0.10	3.88	0.08	0.09	3.70	0.08
4-5-12	0.14	4.44	0.09	0.15	6.14	0.13	0.19	7.46	0.15
4-6-12	0.13	5.29	0.11	0.15	5.62	0.12	0.12	4.70	0.10
4-7-12	0.12	4.78	0.10	0.08	3.05	0.06	0.13	5.64	0.12
4-8-12	0.13	4.77	0.10	0.20	7.84	0.16	0.18	6.88	0.14
4-9-12	0.18	7.65	0.16	0.09	2.99	0.06	0.22	8.57	0.18
4-10-12	0.16	6.09	0.12	0.19	6.81	0.14	0.25	9.79	0.20
4-11-12	0.18	6.64	0.14	0.50	20.67	0.43	0.24	9.20	0.19
4-12-12	0.34	6.39	0.25	0.25	10.11	0.21	0.21	7.35	0.15

3.5. Comparison of ARIMA and ANN Model

The comparative analysis utilized the testing datasets. In terms of performance error measures RMSE, MAPE, and MAE, the ANN model outperforms the ARIMA in both 4-quarter or 1-year bull natural mating forecasting (Table 5) although ARIMA is known as good in short-term forecasting in many cases [20]. The ARIMA model RMSE, MAPE, and MAE errors are 0.13, 6.45% and 0.12, respectively while ANN scored 0.02, 0.55% and 0.01. This clearly shows ANN to be better because its error values are smaller than the ARIMA. Figure 6 depicts a graph of ARIMA 4-step ahead forecasts while Figure 7 shows the ANN forecast (y-axis is on logged). The blue line exhibits the forecasted data and the red one represents the actual. Subscribing to the values above, forecasted data by ANN is closer to the target data than the ARIMA's (Figure 6 and 7).

For 12-step ahead or 3-year forecasting, ANN is still better than its counterpart. Table 6 shows the empirical outcome of ARIMA's RMSE, MAPE, and MAE scores of 0.08, 3.31% and 0.07 while ANN scores 0.07, 2.77% and 0.06. Figure 8 portrays a graph of the ARIMA 12-step ahead forecast whereas Figure 9 (y-axis is on logged) exhibits the ANN's. Still subscribed to the values above, forecasted data by ANN is closer to the target data than the ARIMA's (Figure 8 and Figure 9) since ANN got smaller error values than ARIMA.

RMSE is utilized since this study analyzes different models of the same dataset [17]. Conferring to [21], both models generated good models since the models scored lower than 10% of MAPE. MAE is employed as a common performance measure for time series forecasting [17]. Generally, the results subscribe to the study of [22] and [23] that ANN is better than ARIMA in forecasting.

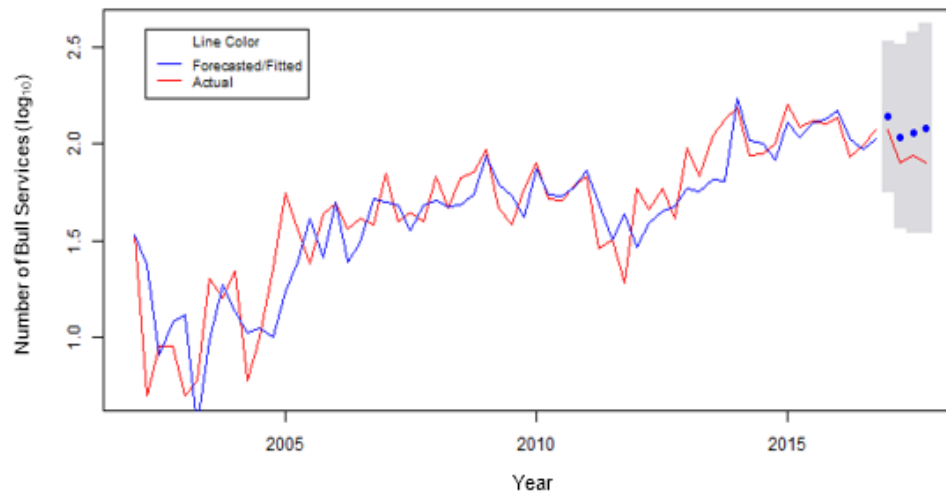


Figure 6: ARIMA 4-step ahead forecast.

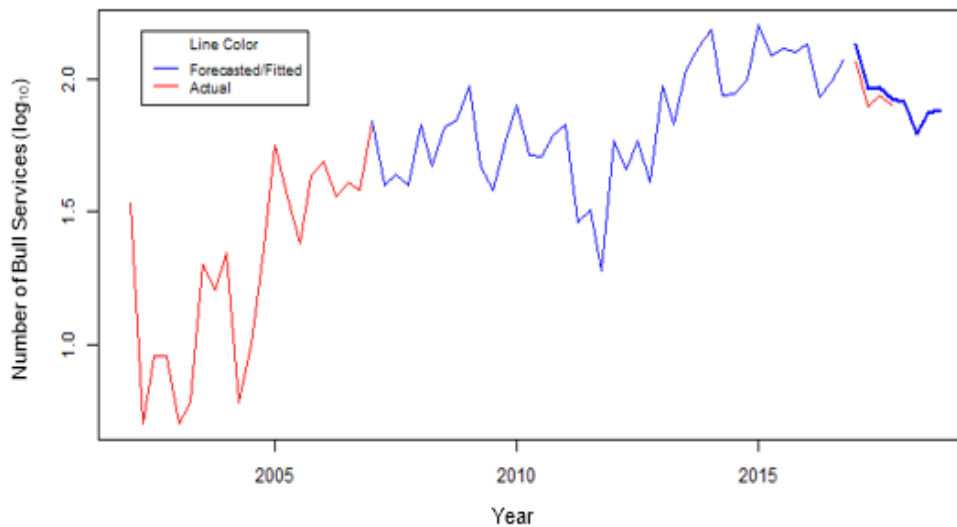


Figure 7: ANN 4-step ahead forecast.

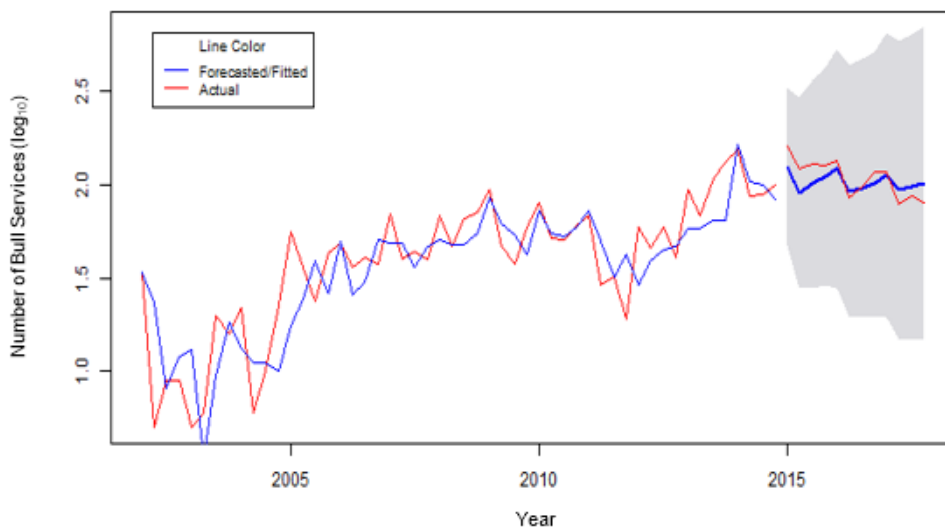


Figure 8: ARIMA 12-step ahead forecast

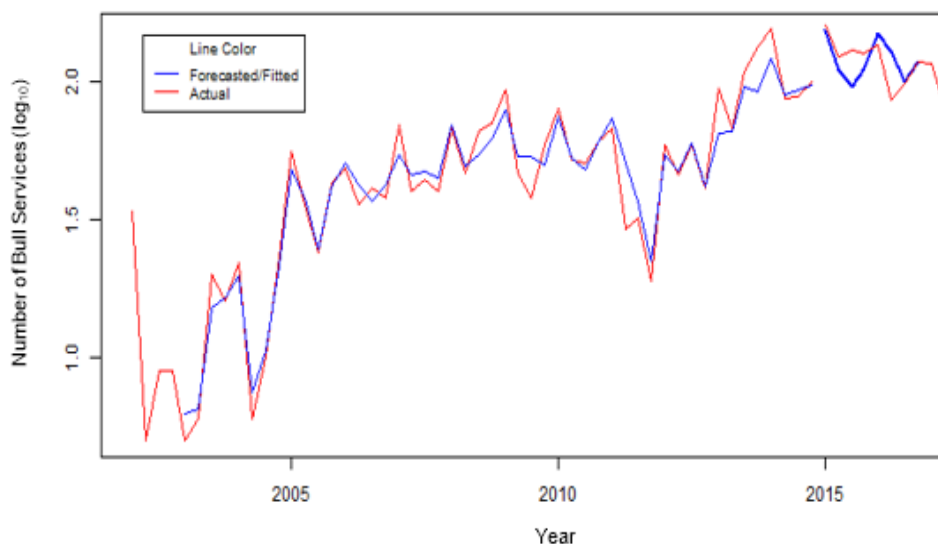


Figure 9: ANN 12-step ahead forecast.

Table 5: ARIMA and ANN model error (4-step ahead forecast).

Method	RMSE	MAPE (%)	MAE
ARIMA	0.13	6.45	0.12
Neural Network	0.02	0.55	0.01

Table 6: ARIMA and ANN model error (12-step ahead forecast).

Method	RMSE	MAPE (%)	MAE
ARIMA	0.08	3.31	0.07
Neural Network	0.07	2.77	0.06

#### 4. Conclusion and Future Work

As a pioneering study in forecasting bull services, the experimental outcomes attained with data on the execution of ARIMA and ANN models in time sequence forecasting have been exhibited. The performance of the ARIMA and ANN predictive models established in this study was assessed. Though both models are showing good forecasting capability based on RMSE, MAPE, and MAE values, the ANN surpasses the traditional ARIMA in both 4-step and 12-step ahead bull natural mating forecasts. The ANN with a single hidden layer indeed can satisfactorily estimate any continuous function that agrees with theoretical corroborations. The ANN forecasting can surely help in optimizing the PCC-VSU's resources. A prognostic modeling of bull services using multivariate series is recommended.

#### Conflict of Interest

The authors declare that there is no conflict of interest in laying this paper to publication.



## Acknowledgment

The authors' profound gratitude to the following individuals/institutions: Roopam Upadhyay, Jiashen Liu, Visayas State University, Department of Computer Science and Technology-VSU, Philippine Carabao Center-VSU, Prof. Winston M. Tabada, Dr. Norberto E. Milla, and the College of Computer Studies of the Cebu Institute of Technology-University.

## References

- [1] J. B. Rola, C. L. C. Sta. Romana, L. S. Feliscuzo and I. F. M. Lopez, "ARIMA prognostic application to bull services for resource usage optimization," in *2019 International Conference on Multimedia Analysis and Pattern Recognition (MAPR)*, Ho Chi Minh, 2019, <https://doi.org/10.1109/MAPR.2019.8743539>.
- [2] PCC, "Philippine Carabao Center annual report 2018," PCC, Muñoz, 2018.
- [3] T. Hirata, T. Kuremoto, M. Obayashi, S. Mabu and K. Kobayashi, "Time series prediction using DBN and ARIMA," in *International Conference on Computer Application Technologies*, Matsue, Japan, 2016, <https://doi.org/10.1109/CCATS.2015.15>.
- [4] B. Siregar and Fahmi, "Forecasting of raw material needed for plastic products based in income data using ARIMA method," in *5th International Conference on Electrical, Electronics and Information Engineering (ICEEIE)*, Malang, Indonesia, 2017, <https://doi.org/10.1109/ICEEIE.2017.8328777>.
- [5] A. S. Katasev, L. Y. Emaletdinova and D. V. Kataseva, "Neural Network model for information security incident forecasting," in *International Conference on Industrial Engineering, Applications and Manufacturing (ICIEAM)*, Moscow, Russia, 2018, <https://doi.org/10.1109/ICIEAM.2018.8728734>.
- [6] S. Leholo, P. Owolawi and K. Akindeji, "Solar energy potential forecasting and optimization using Artificial Neural Network: South Africa Case Study," in *Amity International Conference on Artificial Intelligence (AICAI)*, Dubai, United Arab Emirates, 2019, <https://doi.org/10.1109/AICAI.2019.8701372>.
- [7] J. C. Palomares-Salas, J. G. de la Rosa, J. G. Ramiro, J. Melgar, A. Aguera and A. Moreno, "ARIMA vs. Neural Networks for wind speed forecasting," in *International Conference on Computational Intelligence for Measurement Systems and Applications (CIMS A)*, Hongkong, 2009, <https://doi.org/10.1109/CIMS A.2009.5069932>.
- [8] S. L. Ho, M. Xie and T. N. Goh, "A comparative study of Neural Network and Box-Jenkins ARIMA modeling in time series prediction," *Comput. Ind. Eng.*, vol. 42, pp. 371-375, 2002.
- [9] M. K. Aiden and K. C. Tripathi, "A Neural Network model for time series forecasting of U.P. East Rainfall," in *International Conference on Advances in Computing, Communication Control and Networking (ICACCCN2018)*, Greater Noida (UP), India, India, 2018, <https://doi.org/10.1109/ICACCCN.2018.8748734>.
- [10] M. Kumar and M. Anand, "An application of time series ARIMA forecasting model for predicting sugarcane production In India," *St. Bus. Econ.*, vol. 9, no. 1, pp. 81 - 94, April 2014.
- [11] S. Makridakis, S. C. Wheelwright and R. J. Hyndman, *Forecasting: methods and applications*, New York, USA: John Wiley, 2008.
- [12] S. A. DeLurgio, *Forecasting principles and applications*, Boston, MA, USA: Irwin McGraw-Hill, 1998.
- [13] R. A. Yaffee and M. McGee, *Introduction to time series analysis and forecasting: with applications of SAS and SPSS*, 1st edition, San Diego, London, Boston, New York, Sydney, Tokyo, Toronto: Academic Press, Inc., 2000.
- [14] SAS Institute Inc., *SAS/ETS®13.2 User's guide*, Cary, NC, USA.: SAS Institute Inc., 2014.
- [15] M. Akpınar and N. Yumusak, "Year ahead demand forecast of city natural gas using seasonal time series methods," *Energies*, vol. 9, no. 9, p. 727, 2016.
- [16] A. Barnston, "Statistics how to," *Weather Forecast.*, vol. 34, no. 6, 1992, [https://doi.org/10.1175/1520-0434\(1992\)007<0699:CATCRA>2.0.CO;2](https://doi.org/10.1175/1520-0434(1992)007<0699:CATCRA>2.0.CO;2).
- [17] R. J. Hyndman and A. B. Koehler, "Another look at measures of forecast accuracy," *Int. J. Forecasting*, vol. 22, no. 4, p. 679-688, 2006, <https://doi.org/10.1016/j.ijforecast.2006.03.001>.
- [18] C. J. Willmott and K. Matsuura, "Advantages of the mean absolute error (MAE) over the root mean square error (RMSE) in assessing average model performance," *Clim. Res.*, vol. 30, pp. 79-82, 2005, <https://doi.org/10.3354/cr030079>.
- [19] G. C. E. Bumanlag, M. P. Tolentino, E. D. Manlapig and E. P. Palacpac, "A case study on the implementation of the bull loan program in selected PCC regional centers," in *2nd International Conference on Agriculture, Environment and Biological Sciences (ICAEB S-15) August 16-17, 2015*, Bali, Indonesia, 2015.
- [20] X. Li and Z. Zhang, "A time series forecasting based on ARIMA for Minqin value of output related to water resources," in *2012 International Symposium on Geomatics for Integrated Water Resource Management*, Lanzhou, 2012, <https://doi.org/10.1109/GIWRM.2012.6349588>.
- [21] C. D. Lewis, "Industrial and business forecasting methods," *Butterworths*, vol. 2, pp. 194-196, 1982.
- [22] A. A. Adebisi, A. O. Adewumi and C. K. Ayo, "Comparison of ARIMA and Artificial Neural Networks models," *J. Appl. Math.*, vol. 2014, 2014.
- [23] N. Kohzadi, M. S. Boyd, B. Kermanshahi and I. Kaastra, "A comparison of artificial neural network and time series models for forecasting commodity prices," *Neurocomputing*, vol. 10, pp. 169-181, 1996.

## A Comprehensive Study of Privacy Preserving Techniques in Cloud Computing Environment

Bayan O Al-Amri, Mohammed A. AlZain, Jihad Al-Amri, Mohammed Baz, Mehedi Masud\*

College of Computers and Information Technology, Taif University, Saudi Arabia

### ARTICLE INFO

*Article history:*

*Received: 06 December, 2019*

*Accepted: 04 March, 2020*

*Online: 04 April, 2020*

*Keywords:*

*Cloud computing, Multi-clouds, cloud storage, Privacy-preserving, Data privacy, multi-key, deep learning*

### ABSTRACT

*The huge growth in cloud storage utilization over the past years has made a big demand for an advanced technique and strong tools to make services even more practical and secure. Data privacy in cloud computing has become one of the biggest concerns for both individuals and organizations which adds more pressure on cloud service providers to gain more trust. This paper surveys various privacy-preserving techniques in cloud computing fields, and addresses the highlights and tools used in each technique with an explanation of what and why these tools were used. This work aims to focus on the most innovative and strongest techniques that researchers has figured and tested so far.*

## 1. Introduction

Cloud computing as defined by NIST [1] “a model for enabling convenient, on-demand network access to a shared pool of configurable computing resources (e.g., networks, servers, storage, applications, and services) that can be rapidly provisioned and released with minimal management effort or service provider interaction”.

Over the years, cloud services have expanded more and more to catch the interests and demands of the users with less cost features of its services [2]- [5]. Users like normal individuals, or big expanding companies, or even governments, are all interested in the modern magic of safeguarding knowledge and information (AKA data). Though, perfection is nearly a wish in real life as well as in digital world, it seems that there are still a lot of work to do to reach the 100% of safety[5]-[7]. But aside from wishes, work and knowledge should be invested to prevent the most damage possible for the sake of integrity and privacy – preserving of data stored in clouds all over the network [8]-[10].

In cloud environment, data must be kept secure and save. If harm is done on the service provided to users regarding any kind of application serving a demand. Such as quick accessing from any place in the world, data storing, security measures against attacks, and many more of other privileges brought to users of cloud services [2] [11] [12] . There exist a lot of third-party cloud computing service and support providers of data, administration

for processes, and much more of various needed services in the field. Their services yet are not just profitable, but offers even more of abilities in farm out data to cloud platform [13] [14] Cloud computing systems permit users to execute calculations on a massive quantity of data without building a whole groundwork from scratch [15] [16]. Yet, sending user’s data to the cloud server in the form of a plaintext may endanger it to complete disclosure, which is a huge fail in privacy preserving condition [16]. Therefore, in aim to protect those data there should be some procedures and techniques to accomplish this goal. One of them is the mechanism of hiding data [17]-[19] by using specific calculations and algorithms.

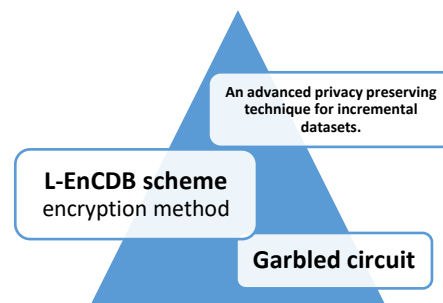


Figure 1: privacy preserving techniques.

## 2. Major Privacy Preserving Techniques

In this section the paper discusses three current privacy preservation techniques, which are most intriguing.

\* Mehedi Masud, College of Computers and Information Technology, Taif University, Saudi ArabiaAddress, mmasud@tu.edu.sa

2.1. L-EnCDB Scheme

L-EnCDB is a novel lightweight encryption mechanism for databases[20]. This encryption method is using a format preserving encryption (FPE) scheme proposed with the L-EnCDB [20]. Secret and confidential data are generally encrypted before publishing to clouds for security necessities that results in a huge demand in practical operational databases. This is considered as a challenging mission; therefore, the authors proposed this technique claimed to success the challenges by addressing the following results:

- The technique supports practical SQL-based queries[20].
- Maintaining database structure [20].

After a detailed examination it turns out that this proposed technique is proven to be fairly practical and secure within the current security model [20]. The traditional methods of applying security to data used to be by encrypting data with techniques such as public key encryption, and symmetric key encryption [18] [21] [17, 22] [23], yet they change data types which makes it difficult to use them in database applications for several operations in SQL such as queries [20]. But still, all these data are categorized as private assets, along with information extracted through queries, so they cannot be unprotected if traditional encryption techniques do not meet the desired measures. This gives data owners a mission to both secure data and send them in an changeable form [20].

This is why L-EnCDB scheme was suggested. It proposes a trivial encrypted database method signified by L-EnCDB, this method promises to achieve the necessities discussed beforehand, which are securing data without changing their format in a database to perform practically all kinds of operations needed in database applications [20]. L-EnCDB can be successfully executed by using (FPE) technique and character string scheme, this way a data format can be preserved while in cipher text form [20]. In the proposed L-EnCDB scheme, a trivial FPE scheme is proposed to support its trivial context for privacy preserving data in a database [20].

Note that the use of FPE enhancing security in databases in an obvious manner, its mission is to create a cipher text that is not changeable from plain text, thus the researchers developed a new FPE method, it basically has three algorithms, which they are, setup, encryption, decryption [20].

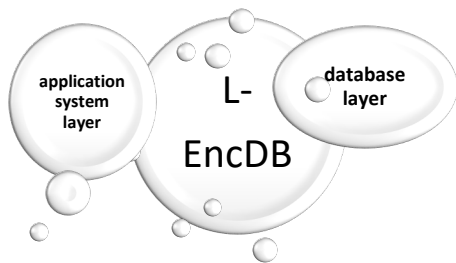


Figure 2: L-EncDB layers [20]

2.1.1 L-EncDB layers

There are two layers in this system, the first layer is the application system layer where several encryption methods (FPE, FQE, OPE) are used in several SQL queries, and the interface

installed in the database will perform SQL analysis, encrypt, and create cipher texts, while the second layer is a database layer which is responsible for permitting developers to only perform SQL related functions, and also offer data services [20].

Security concepts:

SQL analysis interface is installed at the application layer or user’s side of the system. In this system there expected to be a way to secure the key used in this encryption method, two kinds of adversaries might be colluded with the system’s security:

- Those who target the database, with an attack to encrypted data and a database structure.
- Adversaries who target both the database and system’s applications.

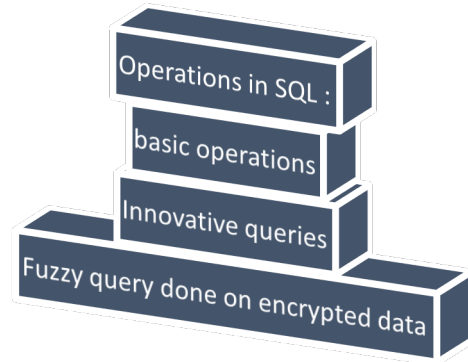


Figure 3: The three SQL operations on cloud[20].

Adversaries can gain entrée to interfaces or manipulate SQL applications in many ways, either by targeting the whole arrangement of the database, or by changing, building sentences in both ways of encryption and decryption. L-EnCDB is believed to be more practical supporting fuzzy queries in SQL, and it offers a lighter and easier way to perform operations over data and sharing data securely to cloud providers. In conclusion, L-EnCDB is suggested as an innovative technique that assures security and privacy preserving measures for data on cloud databases, capable of applying security over SQL application and various operations related to SQL in general, furthermore, with the ability of keeping data type and construction after applying encryption operations on them.

Along with the above advantages, it guarantees privacy preserving for queried data from the database, which means securing valuable data when linking the database to the cloud. This technique has been experimented and resulted that it is effectively secure when demonstrated over a huge database to achieve a stronger enhanced privacy preserving operations, as the founders of this advanced technique has viewed their scheme to prove a privacy preserving queries done on encrypted NoSQL database, thus for the sake of making the technique extra efficient it will be going under more examinations in the future for evaluations over cipher text, and will provide more effort to enhance privacy preserving querying from database along with a stronger publishing method supported by their method .

## 2.2 A Privacy Preserving Technique for Incremental Datasets:

Cloud Computing (CC) is known of being the service that offers data storage in a huge and powerful base between interconnected data servers and parties[5] [24], in which users of the service can share their data for storage or operations[25]. For the time being, there has been many cases of attacks on this simple service usage of sharing and storing. Therefore, the protection of data became a needed condition in the field of CC privacy. To fulfill this approach, there has been a lot of techniques proposed to protect data, some of them involve encryption techniques[18], such as FHE, but it does not serve well in case of incremental data sets due to its large cypher text. There exist other techniques which their concept is basically about anonymizing data sets to produce a secure and privacy preserving solution for shared data on clouds. But still, it's not achieving the paramount protection over the growth of datasets on CC, the spreading of enormous data capacity athwart several storage points bounds the privacy preservation. In this new anonymization technique, it is suggested to achieve a stronger security for huge data usage over several and increased datasets on cloud computing. The ability of privacy preservation and enhanced privacy necessities is verified over evaluation.

Many encryption techniques have been advanced and put under operating situations to maintain the security and preserve privacy for important data, yet they weren't useful enough due to some weaknesses and high cost.

Preserving privacy has other techniques which are the anonymization techniques such as generalization, anonymized data k anonymity, the anatomization, L-diversity. The incremental anonymization technique is basically about dividing anonymized data into several small blocks then be stored in the cloud, the anonymization is based on the level of K. The novel anonymized data will be initialized to allow the addition of more data to the cloud. Though, the new advanced anonymization technique is not built upon anonymization algorithms only, but along with storage and other operations, it preserves privacy of cloud data. Privacy necessities are maintained by an inception in the K-anonymity model.

### Two major targets are reached:

- 1- An enhanced privacy preserving in cloud computing is brought successfully by the new anonymization technique, even though the utility of data storage in clouds is increased
- 2- In the case of performance overhead increased, data's privacy will be preserved without using another anonymization algorithm. Operation's time and data storage will be preserved tool.

### How it works?

D\* is the anonymized dataset of D

Anonymization level: K

B: blocks of data.

Both D and D\* are installed in the cloud.

B is added to the cloud as:

$$B = \{b_1, b_2, \dots, b_n\}$$

Then it will be added to D several times.

After that, the following  $(D + b_i)^*$  is generated, the target is to avoid performing a complete anonymization to  $D + b_1 + b_2 + \dots + b_n$  every time new blocks of  $b_i$

Is added. Why? Because the operation is complicated resulting this procedure to be impractical and costly.

How to anonymize data without repetition?

When the new data (b) are generalized upon K-old( $b^*$ ), then added to previously added data D\*. We check K-anonymous status and see if it is violated and the anonymized datasets are over-generalized, then comparing and testing K-new to K-old:

- If K-old is minor than K-new? Socialization is made on sets with largest.
- K-old = K-new? Data is exported.
- Uneven generalization cases: carried out upon K-old.

Aauthors in their work [13] represented an algorithmic code of the advanced anonymization technique. Noting that implementation time is depending on blocks numbers, while manifestation randomness is resulting from data variation. In summary, the new incremental anonymization technique should reach the operational goal efficiently plus overpowering performance overhead. Accordingly, the advantages of performing the new incremental anonymization technique is shown in decreasing the severe escalation in time and cost compared to the current anonymization techniques. Typically, clouds capacity of data is huge. It is revealed that the new anonymization technique can broadly enhance the privacy preservation on incremental datasets compared to recent techniques. This advanced incremental anonymization technique is proven to be unaffected by the deviationK, and also proven to successfully preserve privacy and confidentiality demands

## 2.3 Garbled circuit

In the environment in which users trust their private data to third party servers AKA Clouds, there became a noticeable growth in using this type of data storage.

The need to preserve privacy has increased a lot recently, and it's not only urgent for companies and governments for big data, also to keep individual's information in their mobile devices away from disclosure as well, its keeping all data of all kinds and amounts protected. A portable device user shares data to a garbled circuit to perform calculations, these calculations are executed by the others server giving back the outcome of garbled calculations, this is showing the technique's way of procedures and measures to secure data and preserve privacy, this will guarantee the privacy



even if the calculating server did not gain data from all servers in the circuit. This technique includes the innovative use of the secured PRG of Blum et al. which allows the user to practically gain back the outputs of the computation along with assuring that it's been done accurately by the evaluator. Both the server and the user's processes will be analyzed by the system, to provide a privacy-preserving mechanism to user's device. Then the time of proceeding and constructing the above operations will be dignified to estimate the garbled circuit for multiple servers, proving the practicability of the secure cloud computing for mobile systems[26].

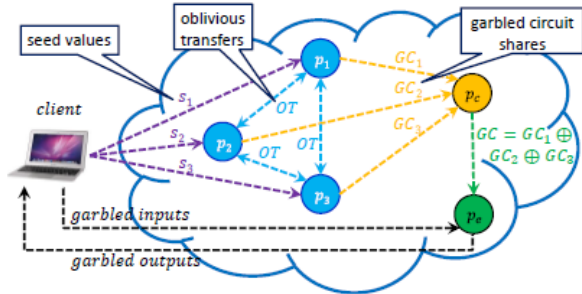


Figure4: secure cloud computing model with a mobile client using  $(2+2)=5$  servers  $\{ P1,P2,P3,Pc,Pe\}$  [26]

To explain the figure above, here are the details and steps as shown in figure 5:

1. Client sends seed values  $s_1, s_2, s_3$  to  $p_1, p_2, p_3$  respectively.
2.  $p_1, p_2, p_3$  interact with one another to construct their shares of the garbled circuit,  $GC$ .
3.  $p_1, p_2, p_3$  send their shares  $GC_1, GC_2, GC_3$ , respectively, to  $p_c$ .
4.  $p_c$  computes  $GC = GC_1 \oplus GC_2 \oplus GC_3$ , and sends it to  $p_e$ .
5. Client generates garbled inputs, and sends them to  $p_e$ .
6.  $p_e$  evaluates  $GC$ , and sends the garbled outputs to the client.

Figure 5: Explanation and Steps for GC [26]

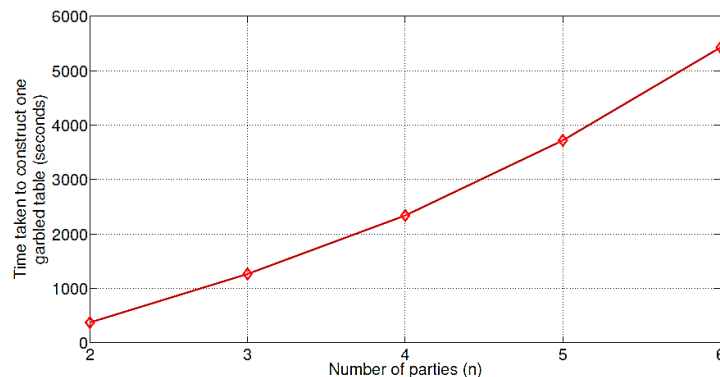


Figure 6: Consumed Time for Building the GC[26].

**Approach highlights:**

- In the proposed preserving of privacy solution of this approach, researchers compared their scheme with Gentry's FHE scheme, noting that it only uses one server, but in comparison with their solution they prove it is more useful and secure explaining that with every garbled significance with a size of  $(nk+1)$  bits, for every input and output chain, the user simply interactions  $O(nk)$  bits with the server  $P_e$ .
- The consumed time in the process of building and checking the Garbled Circuit:

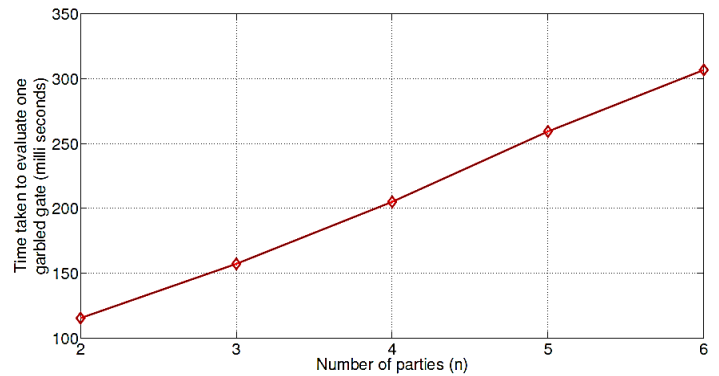


Figure 7: Consumed Time for Checking GC[26]

Fig. 6 displays the time consumed to build a single garbled compilation as a function of n. note that GC can be built in a corresponding way at every gate, and in this way, it can shrink the consumed time for building circuits. Fig. 7 displays the stage of checking a single garbled gate as a function of n. it's been shown that calculation is ominously faster than building, in case it's been done offline.

GCs can feely complete the requested operations when they already have been pre-operated and checked for a quicker response time for users.

Because of the unfeasibility of FHE schemes, due to the large cipher text, there has been an alternative solution using Yao's garbled circuits, for secure computations, it's been used with the multiparty computations with some other computations. In this scheme of multiparty computations, private inputs are held by several parties to attain the outputs of operations. However, in this advanced GC scheme, which is considered as a secure cloud computing system, users can only attain operation outputs from holding the preserved inputs in garbled method. Nevertheless, this upgraded GC scheme has been proven to match the necessities of preserved cloud servers by engaging several public cloud servers to operate the tasks of building and checking garbled circuits.

- By using this advanced GC, the user will be able to validate if in instance some unauthorized party has actually checked the GC, all that is effectively processed without engaging FHE encryption.
- Mobile user is the only one who has the authorization to deliver inputs to the secure computing model and attains outputs of the operations in garbled method.

- User’s privacy of data inputs and outputs of the operations will be preserved despite the possibility of an evolving occurred between the checking server and a cloud exploiting in the process of constructing the GC.

This technique suggested an innovatively secure and confirmable cloud computing using several servers, the technique associates the protocol of et al. Goldreich (the secure multi-party computation protocol). And Beaver et al.’s GC design, along with the PRG method of Blum et al. Mobile user’s privacy of data inputs and outputs of the operations will be preserved despite the possibility of an evolving occurred between the checking server and a cloud exploiting in the process of constructing the GC. A false checker will be discovered by not delivering values without the operations demanded, the system will perform an analysis for both sides, server and user of this system.

2.4 Information-Centric Approach:

Authors in [27] proposed a system using information-centric approach which makes cloud data self-intelligent. In this approach usage policy is used to encrypt and package cloud data. The data access mechanism consults its policy, create a virtualization environment, and assesses the trustworthiness of the data environment (using Trusted Computing). The architecture is shown in the Figure 8. The system is suitable in a corporate setting, in which database containing sensitive information need to be protected against external administrators, service providers, and local administrators. The system allows via machine readable rights expressions depth control over information that is allotted to a particular user.

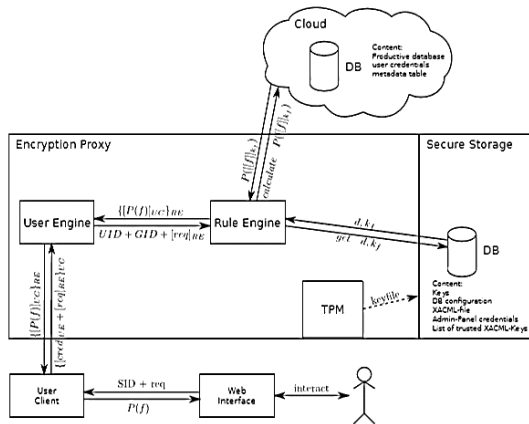


Figure 8: Information-centric approach [27]

2.5 Secure data-exchange in a cloud-based collaborative health care environment:

The authors in [28] presents a secure Cloud-based big data framework for collaborative healthcare service providers to efficiently store and manage large-scale health data. Each cloud data source exchange data using pair-wise communication for user queries by creating an on-the-fly data-exchange session. It provides a platform for sharing or exchanging health data residing

in multiple clouds for the purpose of data analysis, decision making, and improving patients’ treatment. The framework does not need a central third-party security mechanism (e.g., Public Key Infrastructure). Concerning pair-wise, on-the-fly data exchange, the authors presents a two-phase security protocol that uses pairing-based cryptography. Each cloud computes a secret session key dynamically by computing a pairing in an elliptic curve.

2.6 Privacy preserving data storage technique in cloud computing:

Authors in [29] proposed data fragmentation for privacy preserving data storage and retrieval. The mechanism protects the data unavailable when an unauthorized person compromised to one of this data splits in multi-cloud architecture. A decomposition technique introduced in this paper proves that privacy preserving information storage in multi-cloud is achieved. Based on the experiments, redundant storage of information is extremely efficient for data availability.

3. Results

In summary, all the techniques discussed above, here are some points and remarks regarding every method and some noticeable highlights, addressed in the following table:

Table 1: Privacy-Preserving Techniques in Cloud Computing

Field of remarks Tech Name	Type of Privacy Preserving	Cloud field	Tools
EnCDB scheme	Encryption	This technique is applied over data on cloud database	L-EncDB & FPE
An advanced privacy preserving technique for incremental datasets.	Data anonymization encryption method	Preserving incremental data on cloud	Anonymization algorithm
Garbled circuit	PRG encryption over Garbled circuits.	While outsourcing data between multiple cloud servers	PRG method & a secure multiparty computation protocol

In Table 1 we addressed the three privacy preserving techniques in terms of main differences, tools and types of preserving techniques practiced in each one of them, as in the EnCDB scheme, encryptions using a format preserving encryption (FPE) scheme proposed with it is the method of privacy preserving here while it is an anonymization encryption method in the second technique using an advanced anonymization algorithm, the garbled circuit uses a PRG encryption method over the circuits.

The purposes and fields to apply each method differs in terms of the timing and practicability of performing them whether it is while outsourcing data between multiple cloud servers in the

Garbled circuit technique or where it is applied over data on cloud database in the EnCDB scheme, or it is for the sake of preserving incremental data on cloud in the second technique we addressed in this paper.

#### 4. Conclusion

This paper describes the importance of data security and why we need privacy preserving techniques in cloud computing. The paper discusses different surveyed privacy preserving techniques proposed by researchers. Summary of the three important techniques are discussed. The cloud computing field is improving and offering several solutions to serve this goal privacy preserving. We believe that this paper will help whom ever has the need to improve further techniques in the privacy preserving field, to enhance a better yet stronger approaches.

#### References:

- [1] (NIST), <http://www.nist.gov/itl/cloud/>.
- [2] AlZain, M.A., et al. Cloud computing security: from single to multi-clouds. in 2012 45th Hawaii International Conference on System Sciences. 2012: IEEE.
- [3] AlZain, M.A., B. Soh, and E. Pardede. Mcdb: using multi-clouds to ensure security in cloud computing. in 2011 IEEE Ninth International Conference on Dependable, Autonomic and Secure Computing. 2011: IEEE.
- [4] AlZain, M.A., B. Soh, and E. Pardede, A new model to ensure security in cloud computing services. Journal of Service Science Research, 2012. 4(1): p. 49-70.
- [5] AlZain, M.A., B. Soh, and E. Pardede, A survey on data security issues in cloud computing: From single to multi-clouds. Journal of Software, 2013. 8(5): p. 1068-1078.
- [6] AlZain, M.A., B. Soh, and E. Pardede. A byzantine fault tolerance model for a multi-cloud computing. in 2013 IEEE 16Th International Conference On Computational Science And Engineering. 2013: IEEE.
- [7] AlZain, M.A., B. Soh, and E. Pardede. A new approach using redundancy technique to improve security in cloud computing. in Proceedings Title: 2012 International Conference on Cyber Security, Cyber Warfare and Digital Forensic (CyberSec). 2012: IEEE.
- [8] AlZain, M.A., Data security, data management and performance evaluation in a multi-cloud computing model. 2014.
- [9] AlZain, M.A., et al., Byzantine Fault-Tolerant Architecture in Cloud Data Management. International Journal of Knowledge Society Research (IJKSR), 2016. 7(3): p. 86-98.
- [10] Samra, H.E., B. Soh, and M.A. Alzain. A Conceptual Model for an Intelligent Simulation-Based Learning Management System Using a Data Mining Agent in Clinical Skills Education. in 2016 4th International Conference on Enterprise Systems (ES). 2016: IEEE.
- [11] AlZain, M.A., et al., Managing Multi-Cloud Data Dependability Faults, in Knowledge-Intensive Economies and Opportunities for Social, Organizational, and Technological Growth. 2019, IGI Global. p. 207-221.
- [12] Subashini, S. and V. Kavitha, A survey on security issues in service delivery models of cloud computing. Journal of network and computer applications. 34(1): p. 1-11.
- [13] Aldeen, Y.A.A.S., M. Salleh, and Y. Aljeroudi, An innovative privacy preserving technique for incremental datasets on cloud computing. Journal of biomedical informatics. 62: p. 107-116.
- [14] Fox, A., et al., Above the clouds: A berkeley view of cloud computing. Dept. Electrical Eng. and Comput. Sciences, University of California, Berkeley, Rep. UCB/EECS, 2009. 28(13): p. 2009.
- [15] JoSEP, A.D., et al., A view of cloud computing. Communications of the ACM. 53(4).
- [16] Liu, Z., et al. Secure storage and fuzzy query over encrypted databases. in International Conference on Network and System Security: Springer.
- [17] AlZain, M.A., Utilization of Double Random Phase Encoding for Securing Color Images. International Journal of Computer Applications, 2018. 975: p. 8887.
- [18] Faragallah, O.S., et al., Investigation of Chaotic Image Encryption in Spatial and FrFT Domains for Cybersecurity Applications. IEEE Access, 2020.
- [19] Faragallah, O.S., et al., Secure color image cryptosystem based on chaotic logistic in the FrFT domain. Multimedia Tools and Applications, 2019: p. 1-25.
- [20] Li, J., et al., L-EncDB: A lightweight framework for privacy-preserving data queries in cloud computing. Knowledge-Based Systems. 79: p. 18-26.
- [21] Sodhi, G.K., et al., Preserving Authenticity and Integrity of Distributed Networks through Novel Message Authentication Code. Indonesian Journal of Electrical Engineering and Computer Science, 2018. 12(3): p. 1297-1304.
- [22] Faragallah, O.S., et al., Block-based optical color image encryption based on double random phase encoding. IEEE Access, 2018. 7: p. 4184-4194.
- [23] AlZain, M.A., Efficient Image Cipher using 2D Logistic Mapping and Singular Value Decomposition. INTERNATIONAL JOURNAL OF ADVANCED COMPUTER SCIENCE AND APPLICATIONS, 2018. 9(11): p. 196-200.
- [24] Alraddady, S., et al., Deployment of Fog Computing During Hajj Season: A Proposed Framework. Procedia Computer Science, 2019. 161: p. 1072-1079.
- [25] Alzain, M.A. and E. Pardede. Using multi shares for ensuring privacy in database-as-a-service. in 2011 44th Hawaii International Conference on System Sciences. 2011: IEEE.
- [26] Premnath, S.N. and Z.J. Haas, A practical, secure, and verifiable cloud computing for mobile systems. Procedia Computer Science. 34: p. 474-483.
- [27] Greveler, U., B. Justus, and D. Lochr. A privacy preserving system for cloud computing. in 2011 IEEE 11th International Conference on Computer and Information Technology. 2011: IEEE.
- [28] Masud, M. and M.S. Hossain, Secure data-exchange protocol in a cloud-based collaborative health care environment. Multimedia Tools and Applications. 77(9): p. 11121-11135.
- [29] Kartheeban, K. and A.D. Murugan. Privacy preserving data storage technique in cloud computing. in 2017 IEEE International Conference on Intelligent Techniques in Control, Optimization and Signal Processing (INCOS): IEEE.

## Optimal Flow Analysis of a Unified Energy System with Effects of P2G

Haseeb Yar Hiraj\*, Wenping Qin, Muhammad Abbas, Muhammad Zeeshan Adil

Taiyuan University of Technology, Electrical & Power Engineering, College of Electrical Engineering, 030000, China

---

### ARTICLE INFO

*Article history:*

*Received: 02 January, 2020*

*Accepted: 19 March, 2020*

*Online: 04 April, 2020*

---

*Keywords:*

P2G

Integrated Energy System

Newton Raphson method

Bi-directional Energy Conversion

---

---

### ABSTRACT

*The reformation of energy hubs has significantly augmented the apprehensions about the levels of dependency between different energy sources which often can also be discussed as independent systems conventionally. This research brings focus on the formulation and analysis of an integrated system with bi-directional energy conversions and its effects on the stability of the system for the benefit of overall secure and cost-effective operations. A general unification approach is adopted for the integration of two energy systems to execute optimal flow analysis in the form of one system based on Newton-Raphson scheme. PV solar energy is added into the system via electrical power system (EPS) to analyze the effects of renewable energy on electric network. A case study is presented to analyze the operational status of EPS and natural gas system (NGS) and effects of different factors on each system. The applicability of the proposed method is established by analysis of 20-Node Belgian gas network combined with IEEE-39 test system. The proposed method verifies not only that integrated systems with P2G capabilities and bi directional conversion increases the rate of smooth and reliable operations significantly but also discusses the limitations still present.*

---

### 1. Introduction

In recent years, with the widely use of natural gas fired generators and the encouraging functionality of Power to Gas (P2G) technology, the dependency between electrical systems and gas Networks is getting more adaptive worldwide [1-4]. In light of these developments, it is Indispensable to model the electrical and gas networks as a unified energy system. [5, 6].

The influence and implementation of renewable energy resources, such as wind and solar energy, have rapidly increased during the last few years in response to the scarcity of fossil fuels, global warming and climate change. Considering current environmental challenges and shortage of energy, it has become more of a global consensus to switch towards renewable energy [7, 8]. Literature and design of the future 100% renewable energy are well discussed in [9, 10]. Renewable energy resources play an imperative and effective role in the accomplishment of sustainable and environmentally friendly power generation. However, the unpredictable nature and uncertainty of it causes imbalance in supply and demand. To address this issue, gas fired generators (GPG) with faster response ability can be employed. On the other hand, large scale energy storage technologies should be

implemented to accumulate the excessive renewable energy [11]. A P2G which converts electricity into hydrogen and synthetic natural gas (CH<sub>4</sub>) presents a promising solution to energy storage [1]. To solve problems like excessive energy accumulation and reduction of carbon dioxide (CO<sub>2</sub>) can be achieved by the development of an integrated energy network with P2G capabilities. Achieving such system also lies in economic benefits, such as integrated operations of coupled networks that yield an overall optimal outcome. [12-15]. Security and optimal reliability have always been an obstacle in achieving such a deeply interdependent system. Natural gas networks and electrical energy supplying systems are entirely dependent on each other for inputs which causes disruption in one system if there is any uncertainty in the proportional system and it affects the overall performance of the unified system.

Previously, extensive studies have been led in electrical systems and natural gas exclusively, but an integrated system analysis is still inadequate [16]. The state-of-the art reviews on integrated energy system are well documented and presented in [17, 18]. Many important, game changing technical constraints are often ignored or overlooked to ease the complexity when modeling a unified system, even though the technical model is responsible for secure, efficient and productive operations. [18]. Different tactics have been projected over time to create a unified gas and

---

\*Haseeb Yar Hiraj, Email: [haseebyar@gmail.com](mailto:haseebyar@gmail.com)



electricity network. A multi time period combined gas and electricity network optimization model is discussed in [19], and it considers the changeable nature of gas flows and grid auxiliaries. Another model discussed in [20] suggests a multi stage model for co-planning and optimal co-expansion for a unified system. The consistency of the system is mainly prone to the threats like operations under abnormal conditions, such as surges and shutdowns [21]. Different possible impacts and advantages of P2G in a unified system are discussed in detail in Qadrdan et al. [22].

In order to further extend the research and analysis of a unified system with an optimal power flow, a comprehensive model is required. Thus, this research puts emphasis on design and implementation of a unified energy system with P2G capabilities to convert energy in to different forms and store efficiently. Nodal balance is the most effective method to obtain non-linear equations for the power and gas flows. On the basis of equations achieved for a unified system, a case study has been conducted to demonstrate the feasibility of the proposed approach on the IEEE-39 test system connected with Belgium-20 node gas network by the means of integrated formulation and connection between two systems using gas-compressors, P2G and gas-fired power plants. The effects of renewable PV energy and power output are investigated the effects of pressure in a gas network are studied to relate its significance on the overall system. The notable outcomes this research provides are:

- A coherent integrated system of electrical energy with gas network, which includes gas compressors, the power-to-gas and gas-fired power plants.
- Mathematical simulations are performed in MATLAB to validate the precision and viability of the proposed technique.
- The effects of injecting renewable energy in to the system has been tested with the help of a case study.
- The properties of P2G on electrical infrastructure and natural gas system are discussed.
- The limitations of the proposed technique are discussed.

The remaining part of the paper is structured as follows. Modelling of power system and gas network is presented in section 2. Section 3 offers a detailed unification of gas and electrical system into one interdependent network. Section 4 illustrate the case study of such system and discusses the numerical simulations and results. Section 5 discusses the results and conclusions drawn from this piece of research.

## 2. Modelling

### 2.1. Power System Formulation

Power stream analysis are of boundless significance in design and operation of power systems. In a power system, power flow calculations are mainly performed to collect voltage magnitude and associated angles for each bus [23]. Bus voltage V and nodal admittance matrix Y are expressed in polar coordinates in following form.

$$V_i = |V_i| \angle \theta_i = |V_i| (\cos \theta_i + j \sin \theta_i) \quad (1)$$

$$Y_{ij} = |Y_{ij}| \angle \theta_{ij} = |Y_{ij}| (\cos \theta_{ij} + j \sin \theta_{ij}) = G_{ij} + jB_{ij} \quad (2)$$

The real power of the system and reactive power at different busses can be calculated as follows

$$P_i = |V_i| \sum_{j=1}^N |V_j| (G_{ij} \cos \theta_{ij} + B_{ij} \sin \theta_{ij}) \quad (3)$$

$$Q_i = |V_i| \sum_{j=1}^N |V_j| (G_{ij} \sin \theta_{ij} + B_{ij} \cos \theta_{ij}) \quad (4)$$

Here, in equation (3) & (4)  $\theta_{ij} = \theta_i - \theta_j$ . It establishes the polar form of the power flow equations. By using these equations, calculations can be performed for net active power  $P_i$  and reactive power  $Q_i$  entering the bus  $i$ . Let  $P_{g,i}$  and  $P_{d,i}$  denotes the power generated and power consumed at a specific node. The nodal power balance equations can be defined as

$$\Delta P_i = P_{g,i} - P_{d,i} - |V_i| \sum_{j=1}^N |V_j| (G_{ij} \cos \theta_{ij} + B_{ij} \sin \theta_{ij}) \quad (5)$$

$$\Delta Q_i = Q_{g,i} - Q_{d,i} - |V_i| \sum_{j=1}^N |V_j| (G_{ij} \sin \theta_{ij} + B_{ij} \cos \theta_{ij}) \quad (6)$$

### 2.2. Gas Flow Formulation

Gas flow equations, compression power calculations and nodal mass balance methodology is an ideal way to achieve a steady state model of natural gas system. On the basis of the principle of isothermal flow properties, it is observed that long distance pipelines can achieve constant values of temperature [24]. Therefore, the temperature nonconformity and elevation changes in gas pipelines are ignored in this research. This work concentrates on the steady state isothermal flow of the gas in pipelines and the nodal balance equations produced are stated below

#### i. Pipe Flow Equation

$$G_{gas,km} = C \left( \frac{T_b}{p_b} \right) D_{km}^{2.5} \left( \frac{p_k^2 - p_m^2}{L_{km} \gamma G T_{a,km} Z_{af,km}} \right)^{0.5} E_{p,km} \quad (7)$$

The friction factor  $f_{km}$  is given in SI units as

$$f_{km} = \frac{0.009407}{\sqrt[3]{D_{km}}} \quad (8)$$

Pipe diameter is the only factor included to determine the value of friction factor. The eq. 8 which shows the physical characteristics of a pipeline with fixed gas composition can be simplified by a single constant  $C_{km}$  [25].

$$C_{km} = C \left( \frac{T_b}{p_b} \right) D_{km}^{2.5} \left( \frac{1}{L_{km} \gamma G T_{a,km} Z_{af,km}} \right)^{0.5} E_{p,km} \quad (9)$$

So, a more compressed form of Eq. (8) for the gas flow from node k to m can be written as

$$\Pi_k - \Pi_m = R_{km} G_{gas,km}^2 \quad (10)$$

Where  $\Pi_k = p_{p_k}^2$ ,  $\Pi_m = p_m^2$  and  $R_{km} = \frac{1}{C_{km}}$  which denotes the hydraulic resistance coefficient of the channel.

ii. *Compression Power Calculation*

The compression ratio (CR) has a relationship with break horsepower and gas flow rate in the compressor. In other words, compression ratio (CR) is of absolute value of discharge pressure to the absolute value of suction pressure [26].

$$CR = \frac{P_m}{P_k} = \left(\frac{\Pi_m}{\Pi_k}\right)^{0.5} \quad (11)$$

$$BHP_{km} = K_{GC} Z_a G_{GC,km} \left[ \frac{T_s}{E_c \eta_c} \right] \left[ \frac{C_k}{C_k - 1} \right] \left[ \left( \frac{P_m}{P_k} \right)^{\frac{C_k - 1}{C_k}} - 1 \right] \quad (12)$$

$$BHP_{km} = K_{GC} Z_a G_{GC,km} \left[ \frac{T_s}{E_c \eta_c} \right] \left[ \frac{C_k}{C_k - 1} \right] \left[ \left( \frac{\Pi_m}{\Pi_k} \right)^{\frac{C_k - 1}{2C_k}} - 1 \right] \quad (13)$$

In eq. (12), (13)  $K_{GC}$  is a constant and its value depends on the unit of  $G_{GC,km}$ . Generally, for MM scfd, the value of  $K_{GC}$  is 0.0854; it is worth mentioning that 1 MMscfd of gas flow at 15 degrees Celsius equals 1177m<sup>3</sup>/h in flow rate. So, the value of  $K_{GC}$  is  $7.26 \times 10^{-5}$  if the unit of  $G_{GC,km}$  is given as 1177m<sup>3</sup>/h.

iii. *Nodal Gas Balance Equation*

The nodal gas balance equation indicates the sum of the inflows and outflows at the node should must be zero.

$$G_{s,k} - G_{d,k} - \sum_{mek} G_{gas,km} = 0 \quad (14)$$

Assuming a natural gas distribution network with N nodes and M branches, a reference node is pre-set with given nodal pressure. The unknown variables include (N-1) nodal pressure and M pipeline flow are unknown variables in the system.

2.3. *Integrated Natural Gas and Power System*

In any integrated system, GPG and P2G are essential in energy conversion process.

i. *Gas Fired Power Generation*

Power plant efficiency is specified in terms of heat rate (HR). The ratio of heat given up by natural gas in relation to its lower calorific value (LHV), to the total power available at GPG is known as HR [27]. The SI unit of heat rate is MJ/MWh. So, a lower heat value rate and higher efficiency is stated in [28] as

$$\eta_{GPG} = \frac{3600}{HR} \quad (15)$$

The mathematical relationship of power generation and natural gas network based on the heat rate curve can be presented as

$$HR = \alpha + \beta P_{g,GPG} + \gamma P_{g,GPG}^2 \quad (16)$$

The coefficients  $\alpha, \beta, \gamma$  define the efficiency in the energy

conversion process. On the account of these mathematical equations, the gas consumption  $G_{d,GPG}$  (m<sup>3</sup>/h) can be calculated about roughly from

$$G_{d,GPG} = \frac{HR \cdot P_{g,GPG}}{LHV} \quad (17)$$

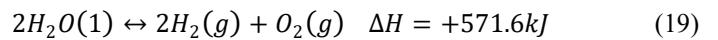
The amount of gas flow required to meet energy demands can be calculated using the power plant efficiency.

$$G_{d,GPG} = \left( \frac{3600}{\eta_{GPG} LHV} \right) P_{g,GPG} \quad (18)$$

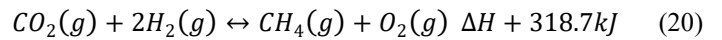
In above equation, the value of LHV is from 35.40 to 39.12 MJ/m<sup>3</sup> [29].

ii. *Power to Gas*

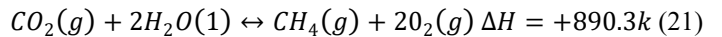
Hydrogen gas is produced as a result of power to gas conversion and it can be used as a fuel to gas networks. Hydrogen gas as an input to the gas network comes with its drawbacks such as adverse effects on pipelines, burners, boilers or even gas engines. This leads to many restrictions imposed on injecting hydrogen as a fuel to gas networks [22]. Methane gas ( $CH_4$ ) has always been the most ideal choice to be used as a fuel. P2G process consists of two steps: electrolysis and methanation. In first step, water is split into hydrogen and oxygen. The chemical reaction is given in [30] as



Sabatier reaction is the process for synthesis of hydrogen and carbon dioxide in to methane gas and this process is called methanation.



The production of methane makes the process of compression, metering and injecting to natural gas network makes it more reliable. Combining both reactions (19) and (20), the overall reaction of P2G is stated as



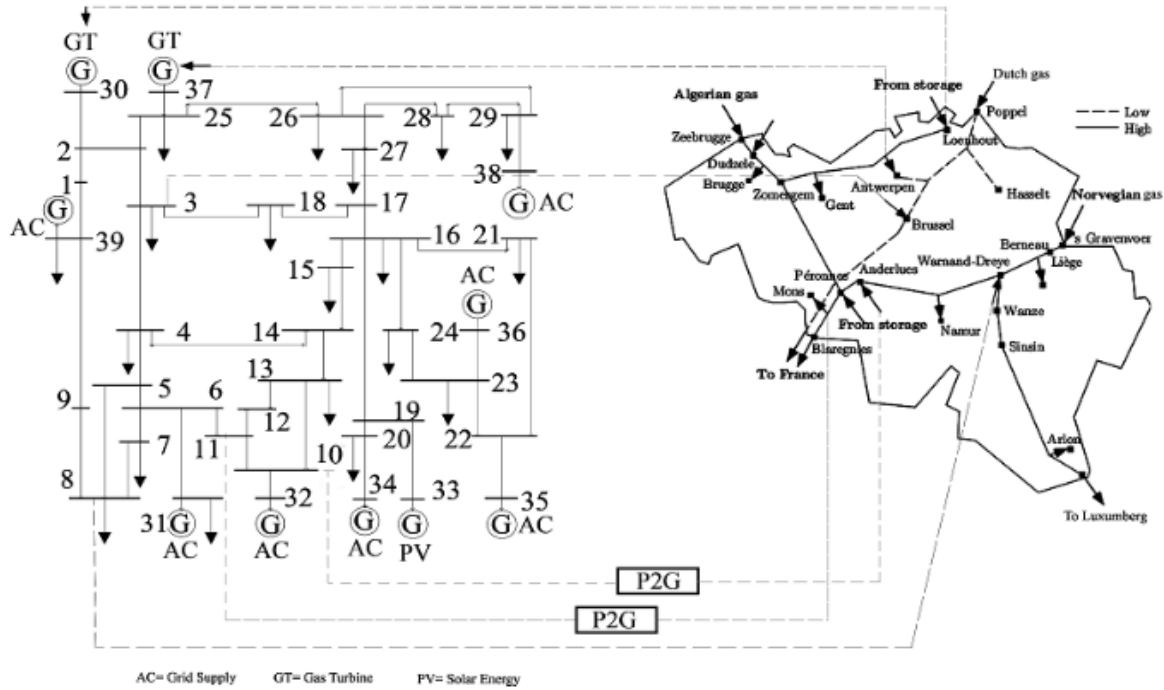
3. **Unification of Systems**

Proposed flow models of both systems can be gathered to form a unified energy system, so that its steady state energy distribution can be analyzed in terms of its input and output. Nonlinear equations representing power flow and gas flow systems obtained by nodal balance are stated as

$$P_i = |V_i| \left| \sum_{j=1}^N |V_j| \right| (G_{ij} \cos \theta_{ij} + B_{ij} \sin \theta_{ij})$$

$$Q_i = |V_i| \left| \sum_{j=1}^N |V_j| \right| (G_{ij} \sin \theta_{ij} + B_{ij} \cos \theta_{ij})$$

$$\Delta G_k = G_{s,k} - G_{d,k} - \sum_{mek} G_{gas,km} \quad (23)$$



BHP is measured in ft.lbs/sec and it can be converted to power unit (MW). One horsepower equals to 745.7 watts. Thus, the new form of power consumed by compressor is

$$P_{GC,km} = 745.7 \times 10^{-6} \times BHP_{km} \quad (24)$$

$$P_{GC,km} = K'_{GC} Z_a G_{gas,km} \left[ \frac{T_s}{E_c \eta_c} \right] \left[ \frac{C_k}{C_{k-1}} \right] \left[ \left( \frac{\Pi_m}{\Pi_k} \right)^{\frac{C_k-1}{2C_k}} - 1 \right] \quad (25)$$

So,

$$\Delta P_{GC} = P_{GC} - K'_{GC} Z_a G_{gas,km} \left[ \frac{T_s}{E_c \eta_c} \right] \left[ \frac{C_k}{C_{k-1}} \right] \left[ \left( \frac{\Pi_m}{\Pi_k} \right)^{\frac{C_k-1}{2C_k}} - 1 \right] \quad (26)$$

Newton Raphson method is widely used for solving nonlinear equations. Take a point X close to the possible exact solution, then the linearization of all nonlinear equations at X can be presented using Taylor expansion as stated in [31].

$$F(X) = -J \times \Delta X \quad (27)$$

Here, in this equation, X represents all the unknown variables and F(X) represents all the mismatches, then

$$F(X) = [\Delta P \ \Delta Q \ \Delta \Pi \ \Delta G \ \Delta P_{GC}]^T \quad (28)$$

Partial derivatives for Jacobean matrix are stated as

$$J = \begin{bmatrix} \frac{\partial \Delta P}{\partial \theta} & \frac{\partial \Delta P}{\partial |V|} & \frac{\partial \Delta P}{\partial P_{GPG}} & \frac{\partial \Delta P}{\partial P_{P2G}} & \frac{\partial \Delta P}{\partial P_{GC}} & 0 & 0 \\ \frac{\partial \Delta Q}{\partial \theta} & \frac{\partial \Delta Q}{\partial |V|} & 0 & 0 & 0 & 0 & 0 \\ 0 & 0 & 0 & 0 & 0 & \frac{\partial \Delta \Pi}{\partial \Pi} & \frac{\partial \Delta \Pi}{\partial G_{gas}} \\ 0 & 0 & \frac{\partial \Delta G}{\partial P_{GPG}} & \frac{\partial \Delta G}{\partial P_{P2G}} & \frac{\partial \Delta G}{\partial P_{GC}} & \frac{\partial \Delta G}{\partial \Pi} & \frac{\partial \Delta G}{\partial G_{gas}} \\ 0 & 0 & 0 & 0 & \frac{\partial \Delta P_{GC}}{\partial P_{GC}} & \frac{\partial \Delta P_{GC}}{\partial \Pi} & \frac{\partial \Delta P_{GC}}{\partial G_{gas}} \end{bmatrix}$$

#### 4. Case Study

We established a case study to demonstrate the proposed unified modelling and solution. An IEEE-39 test system is combined with Belgium 20-node gas network as shown in fig. 1. The electricity infrastructure is consisted of total 39 busses and 46 branches, built on ten generators with seven of them connected with AC big grid, two gas fired generators and one generator producing energy from PV solar. A total of twenty-one loads are attached to the electrical network including two nodes specified for P2G conversions. The node 30 and 37 represents the gas fired generators, node 33 is a PV solar based renewable energy, and node 10 and 11 are with the pressurizers installed while the node 3 and 8 converts electrical energy in to gas by the means of P2G. The 20-node gas network is composed of nineteen pipelines and twenty nodes. The nodal pressure is specified as 1MPa on the reference node. The nodal parameters are given in table 1. Flow

rate and pipeline capacity for each pipeline are presented in Table 2.

Table 1: Nodal Parameters of NGS

No.	Name	Gas Supply (m3/h)	Gas demand (m <sup>3</sup> /h)	Gas pressure (Kpa)
1	Zeebugge	17.24682076	0	63.65693325
2	Dudzele	11.55	0	63.59142946
3	Brugge	0	5.88	63.29836967
4	Zomergem	0	0	59.91755089
5	Loenhout	7.2	0	60.6756345
6	Antwerpe	0	6.05	57.58851446
7	brussel	0	7.88	57.58851446
8	haseelt	26	0	66.2
9	Berneau	0	0	65.568138
10	Liege	0	9.55	62.97687116
11	Warnand	0	0	61.54785195
12	Namur	0	1.71	58.91868179
13	Anderlues	1.8	0	56.82349342
14	Peronnes	1.44	0	56.48709817
15	Mons	0	10.27	53.6465546
16	Blaregnies	0	23.42	50
17	Wanze	0	0	61.19625306
18	sinsin	0	0	58.30205055
19	Arlon	0	0.33	45.77828544
20	Petange	0	1.16	45.24689417

Table 2: Branch Parameters of NGS

N	From bus	To bus	Pipeline Capacity (C)	Flow rate
1	1	2	6.02338	250.16
2	2	3	4.91796	204.26
3	3	4	1.18128	49.06
4	5	6	0.31663	13.15
5	6	7	0.38556	16.01
6	7	4	0.47633	19.78
7	4	14	0.81219	33.73
8	8	9	3.02268	125.53
9	9	10	1.51121	62.77
10	10	11	1.35167	56.14
11	11	12	0.92943	38.6
12	12	13	0.95238	39.56
13	13	14	2.69374	111.88
14	14	15	1.90476	79.11
15	15	16	1.20467	50.03
16	11	17	0.22681	9.42
17	17	18	0.08012	3.33
18	18	19	0.04127	1.71
19	19	20	0.16679	6.93

i. Effects of Renewable Energy

In order to investigate the impact of power supplied by PV Solar and fluctuation of power demand on the integrated system, a stochastic data of PV solar energy is injected in to the electric network at node 33. The PV solar data is obtained from 20KW solar power panel installed at Taiyuan University of technology. Its parameters and rated values are given in table 3. The analysis

shows that energy produced from the PV solar has a great and direct impact on power demand. Not only that the renewable energy produced can be useful for the peak rectification purposes but it can also be stored as gas if surplus.

Table 3. Rated Parameters of the Solar Module

Installed rated capacity	20 KW
Total sets	13
Face direction	25 Degrees south
Max Power (Per string)	270 W
Rated voltage	38.10 V
Rated current	9.45 Amps
Invertor	Sun 2000-33KTL
Inverted Max I/P Dc	33800 W
Max I/P voltage	1000 V
Total O/P	30000 W
Max active power	3300 W
Rated O/P Voltage	380 V
Max O/P current	48 Amps
Max Harmonic distortion	3 %

The MATLAB simulations shown in Figure 2-3 describes the trends of PV solar output and power demand for the month of June 2018. It is observed that demand tends to be decreasing during the night hours and can be easily compensated with the input available by primary source of energy but as the demand increases during the day time and at noon it can be met by adding additional renewable energy into the system. The output of PV solar is always irregular and alternating by nature. There is no output during the night hours but even during the daylight the output varies constantly due to different factors like weather conditions, humidity and availability of sunlight. This property also shows the reverse trend ability of PV output to the electricity demand because of the fluctuation in production. Thus, a backup capacity such as GPG is required to provide peak regulation, while a large-scale storage technology such as P2G is increasingly needed to store the surplus solar power to accommodate the growing supplies of intermittent renewable energy. This technique therefore, imposes a strong emphasis on the presence of P2G in a unified energy system. Renewable energy like solar and wind depends upon various factors which cannot be controlled and are natural, but by injecting the renewable energy into a primary network or stored in for of P2G if surplus, can provide with many potential benefits such as meeting peak demand and increasing overall efficiency. Thus, the prosed technique can be further studied to make a unified system more sophisticated.

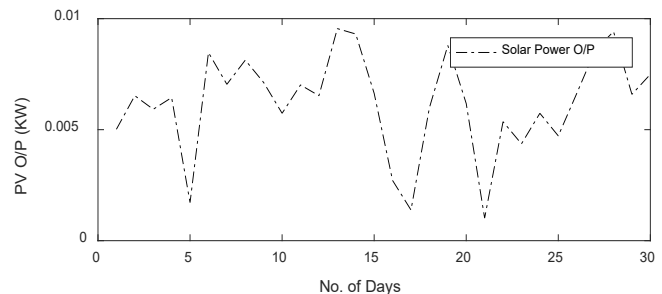


Figure 2: Daily average Output Power of the Solar Module for the Month of June 2018



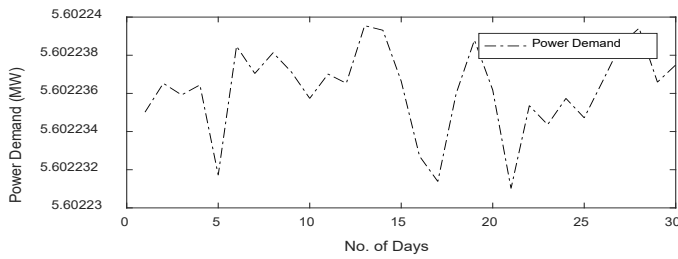


Figure 3: Fluctuations in Power demand

ii. *Effects of Integrated System and P2G on Gas Network*

Previously a large amount of literature has been entirely focused on how P2G helps in mitigating power losses and energy losses in an integrated system with respect to its electrical network such as mitigation effects of P2G in an integration system in terms of its total energy loss, power consumed by gas compressors and fluctuations in renewable energy. However, this study tries to demonstrate the effects of P2G on the gas network. Table 1 stated the Gas supply and Gas Demand along with Gas pressure at each node of the NGS. Whereas the branch parameters are listed in Table 2. Pipeline capacity and flow rate for each node are calculated using these parameters in MATLAB to simulate the effect of P2G on a unified system. Figure 4 shows that gas flow rate is independent of the pipeline capacity. The nodes receiving energy from electrical system via P2G has a rising flow rate. Whereas, nodes transferring gas into the electrical system has comparatively lowest flow rates. These barriers are mostly because of the elevation throughout the pipeline and temperature variations. These issues can be addressed by adding multiple pressurizers and compressors along to the pipeline to maintain a constant pressure regardless of the flow rate of the gas pipeline. In figure 5 it can be seen that by adding pressurizers, the pressure in the gas network can be maintained. Adding pressurizer or compressors can reduce the pressure drop even if the flow rate fluctuates.

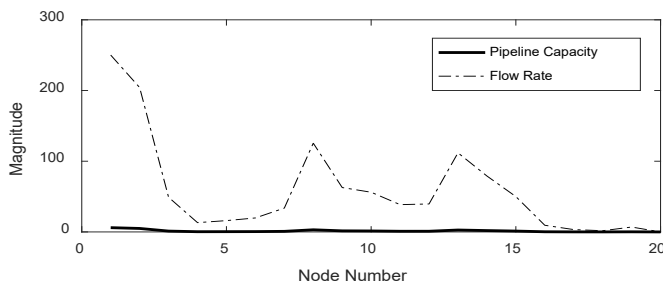


Figure 4: Pipeline capacity and its effect on flow rate

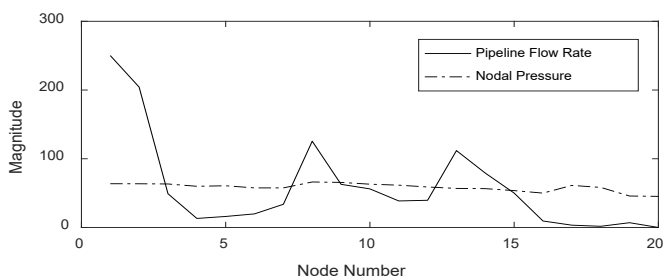


Figure 5: Pressure variation at each node

Just like the voltage stability in an electrical system is a vital factor in reliability of the system, the nodal gas pressure is an important factor for secure operation of gas networks. Figure 5 compares the pressure at each node with respect to the flow rate of the respective node. By using the proposed approach of adding pressurizers at nodes with weak flow rates, the pressure of the pipelines can be maintained within a specified range. From the results of this study, this is clear that, the proposed methodology helps in maintaining the pressure in the gas network for smooth operations.

5. Conclusion

This paper proposed an integrated system of energy flow between electric and gas network with a bi-directional energy conversion. The model studied and implemented to analyse the effects shows that renewable energy is of high importance and with the help of P2G it can be stored in the form of gas for future use. The conventional modelling of this infrastructure has been expanded to consider the unification of two systems and injecting renewable energy in form of solar. The set of non-linear equations representing the harmonized natural gas and electrical system have been obtained based on nodal flows respectively and later solved with the help of Jacobian matrix. Numerical example has been presented to demonstrate the prowess of the proposed method with strong emphasis on the integration of two systems. The system can be studied for future research purposes as to circumvent the problems like environmental temperature and elevation of pipelines and to coup with intermittent nature of renewable energy.

Nomenclature

Indices:

s, d, g supply, demand, generation  
 GPG, P2G, GC gas-fired power generation, power to gas, gas compressor

Parameters:

$C$  Constant 77.54 for gas flow formulation in English units  
 $CR$  Compression ratio  
 $C_{GPG}$  proportional relationship of energy conversion from gas to power in GPG  $m^3/MWh$   
 $C_{P2G}$  Conversion of electrical energy in to gas using P2G  $m^3/MWh$   
 $C_{km}$  Overall transmission coefficient for an individual pipeline,  $(m^3/h)/kPa$   
 $C_k$  Specific heat ratio for the natural gas  
 $D_{km}, L_{km}$  Inside diameter of pipeline in meters, pipeline length in Kms  
 $E_{p,km}$  Pipeline efficiency, dynamic value no larger than 1.0  
 $E_c$  Compression parasitic efficiency, 0.99 for centrifugal units  
 $f_{km}$  Friction factor  
 $G_{ij}, B_{ij}, Y$  electrical inductance, electrical susceptance, line admittance matrix

$G_{gas,km}, G_{s,k}, G_{d,k}$	gas flow, gas supply, gas demand at node $k$ , $m^3/h$
$HR$	The heat rate, MJ/MW h
$J$	Jacobian matrix
$K_{GC}$	Constant of compressor
$LHV$	Lower heating value MJ/ $m^3$
$p_B$	gas pressure at base condition, kPa
$P_{g,i}, P_{d,i}$	Active power generated of bus $i$ , active power demand of bus $i$ , MW
$Q_{g,i}, Q_{d,i}$	Reactive power generated of bus $i$ , reactive power demand of bus $i$ , MVar
$R_{km}$	Hydraulic resistance coefficient of the pipeline, kPa/( $m^3/h^2$ )
$T_s$	Suction temperature of compressor,
$T_b$	Gas temperature at base condition, K (273+ °C)
$T_{a,km}$	Average absolute temperature of pipeline, K (273 + °C)
$V, Y$	Bus voltage, nodal admittance matrix
$Z_{km}$	Resistance coefficient of pipeline, $KPa^2/(MW)^2$
$Z_a$	Average compressibility factor
$\gamma_G$	Natural gas specific gravity
$\eta_c, \eta_{GPG}, \eta_{P2G}$	Compression efficiency, energy efficiency of GPG, energy efficiency of P2G
<b>Variables</b>	
$BHP_{km}$	Brake horsepower consumed by gas compressor, horsepower
$G_{d,GPG}$	Gas consumption in GPG
$G_{s,P2G}$	Gas generation in P2G, $m^3/h$
$G_{d,p2G}$	Gas consumed by P2G system, by gas compressor
$P_{GC,km}$	Power generated by GPG, MW
$p_m, p_k$	The nodal pressure at both end of pipeline, $m^3/h$
$\Pi_k, \Pi_m$	$\Pi_k = p_k^2, \Pi_m = p_m^2$
$ V_i , \theta$	Magnitude of voltage, angle of voltage

**References**

[1] G. Guandalini, S. Campanari, and M. C. Romano, "Power-to-gas plants and gas turbines for improved wind energy dispatchability: Energy and economic assessment," *Appl. Energy*, vol. 147, pp. 117-130, Jun. 2015.

[2] S. Clegg and P. Mancarella, "Integrated modeling and assessment of the operational impact of power-to-gas (P2G) on electrical and gas transmission networks," *IEEE Trans. Sustain. Energy*, 2015, vol. 6, no. 4, pp. 1234-1244, Oct. 2015.

[3] P. J. Hibbard and T. Schatzki, "The interdependence of electricity and natural gas: current factors and future prospects," *Electr. J.*, vol. 25, no. 4, pp. 6-17, May 2012.

[4] M. Qadrdan, J. Wu, N. Jenkins, and J. Ekanayake, "Operating strategies for a GB integrated gas and electricity network considering the uncertainty in wind power forecasts," *IEEE Trans. Sustain. Energy*, vol. 5, no. 1, pp. 128-138, Jan. 2014.

[5] Z. Wei, S. Chen, G. Sun, D. Wang, Y. Sun, and H. Zang, "Probabilistic available transfer capability calculation considering static security constraints and uncertainties of electricity-gas integrated energy systems," *Appl. Energy*, vol. 167, pp. 305-316, Apr. 2016.

[6] Z. Wei, S. Chen, G. Sun, D. Wang, Y. Sun, and H. Zang, "Probabilistic available transfer capability calculation considering static security constraints and uncertainties of electricity-gas integrated energy systems," *Appl. Energy*, vol. 167, pp. 305-316, Apr. 2016.

[7] Yu XH, Xue YS. Smart grids: A cyber-physical systems perspective. *Proc IEEE* 2016; 104(5):1058-70.

[8] Ahlgren LW. The dual-fuel strategy: An energy transition plan. *Proc IEEE* 2012; 100(11):3001-52.

[9] Mathiesen BV, Lund H, Connolly D, Wenzel H, Østergaard PA, Möller B, et al. Smart energy systems for coherent 100% renewable energy and transport solutions. *Appl Energy* 2015; 145: 139-54.

[10] Connolly D, Lund H, Mathiesen BV, Leahy M. The first step towards a 100% renewable energy-system for Ireland. *Appl Energy* 2011; 88:502-7.

[11] Chen, S., Wei, Z., Sun, G., Cheung, K. W., & Sun, Y. (2016). Multi-linear probabilistic energy flow analysis of integrated electrical and natural-gas systems. *IEEE Transactions on Power Systems*, 32(3), 1970-1979.

[12] C. Unsuhay-Vila, J. W. Marangon-Lima, A. C. Zambroni de Souza, I. J. Perez-Arriaga, and P. P. Balestrassi, "A model to long-term, multi-tiarea, multistage, and integrated expansion planning of electricity and natural gas systems," *IEEE Trans. Power Syst.*, vol. 25, no. 2, pp. 1154-1168, May 2010.

[13] C. Correa-Posada and P. Sanchez-Martin, "Security-constrained optimal power and natural-gas flow," *IEEE Trans. Power Syst.*, vol. 29, no. 4, pp. 1780-1787, Jul. 2014.

[14] X. Xu, H. Jia, D. Wang, D. C. Yu, and H-D. Chiang, "Hierarchical energy management system for multi-source multi-product microgrids," *Renew. Energy*, vol. 78, pp. 621630, Jun. 2015.

[15] J. Qiu, Z. Dong, J. Zhao, K. Meng, F. Luo, and Y. Chen, "Expansion co-planning for shale gas integration in a combined energy market," *J. Mod. Power Syst. Clean Energy*, vol. 3, no. 3, pp. 302-311, Mar. 2015.

[16] Erdener BC, Pambour KA, Lavin RB, Dengiz B. An integrated simulation model for analyzing electricity and gas systems. *Int J Electr Power Energy Syst* 2014; 61:410-20.

[17] Mancarella P. MES (multi-energy systems): an overview of concepts and evaluation models. *Energy* 2014; 65:1-17.

[18] Ouyang M. Review on modeling and simulation of interdependent critical infrastructure systems. *Reliab Eng Syst Saf* 2014; 121:43-60.

[19] Chaudry M, Jenkins N, Strbac G. Multi-time period combined gas and electricity network optimization. *Electr Power Syst Res* 2008; 78:1265-79.

[20] Qiu J, Dong ZY, Zhao JH, Xu Y, Zheng Y, Li C, et al. Multi-stage flexible expansion co-planning under uncertainties in a combined electricity and gas market. *IEEE Trans Power Syst* 2015; 30:2119-29.

[21] Hernandez-Fajardo I, Dueñas-Osorio L. Probabilistic study of cascading failures in complex interdependent lifeline systems. *Reliab Eng Syst Saf* 2013; 111: 260-72.

[22] Qadrdan M, Abeysekera M, Chaudry M, Wu J, Jenkins N. Role of power-to-gas in an integrated gas and electricity system in Great Britain. *Int J Hydrog Energy* 2015; 40:5763-75.

[23] Grainger J, William Stevenson J. *Power system analysis*. New York: McGraw-Hill; 1994.

[24] Bagajewicz M, Valtinson G. Computation of natural gas pipeline hydraulics. *Ind Eng Chem Res* 2014; 53:10707-20.

[25] Martinez-Mares A, Fuerte-Esquivel CR. A unified gas and power flow analysis in natural gas and electricity coupled networks. *IEEE Trans Power Syst* 2012; 27:2156-66.

[26] Mokhatab S, Poe WA, Speight JG. *Handbook of natural gas transmission and processing*. Burlington (MA, USA): Gulf Publishing Company; 2006.

[27] Sheldrake AL. *Handbook of electrical engineering: for practitioners in the oil, gas and petrochemical industry*. 1st ed. Chichester (West Sussex, England); Hoboken (NJ, USA): Wiley; 2002.

[28] Beér JM. High efficiency electric power generation: the environmental role. *Prog Energy Combust Sci* 2007; 33:107-34.

[29] Shahidehpour M, Fu Y, Wiedman T. Impact of natural gas infrastructure on electric power systems. *Proc IEEE* 2005; 93:1042-56.

[30] Grond L, Schulze P, Holstein J. *Systems analyses power to gas: a technology review*. Groningen; 2013.

[31] Bergen AR, Vittal V. *Power systems analysis*. 2nd ed. Upper Saddle River (NJ): Prentice Hall; 2000.

## Author Identification for Marathi Language

C. Namrata Mahender\*, Ramesh Ram Naik, Maheshkumar Bhujangrao Landge

Department of CS and IT, Dr.B.A.M.University, Aurangabad-431004 (MS), India

---

### ARTICLE INFO

Article history:

Received: 22 July, 2019

Accepted: 09 December, 2019

Online: 04 April, 2020

---

Keywords:

Plagiarism detection

Author identification

Marathi language.

---

### ABSTRACT

This is era of new technology; most of information is collected from internet, web sites. Some people uses data from research papers, thesis, and website as it is and publish as their own research without giving proper acknowledgement. This term is known as plagiarism. There are two types of plagiarism detection methods, i) Extrinsic plagiarism detection ii) Intrinsic plagiarism detection. Through extrinsic plagiarism utilizing reference corpus plagiarism is observed, while in intrinsic plagiarism identification, using author's writing style, plagiarism can be identified. If the anonymous text is written by unknown author. By using authorship analysis we can find original author of text. Authorship analysis is having three types i) Author identification ii) Author characterization and iii) Similarity detection. This paper mainly focuses on author identification for Marathi language. To calculate projection in two different files, we used feature vectors of main author file and summary file of other authors. The result of average projection shows, there is similarity in main author file and summary file of different authors, it also shows summary file of each author is having impact of main author file.

## 1. Introduction

Plagiarism includes copying material, every word from phrase or as a paraphrase, from any book to websites, course notes, oral or visual displays, lab reports, pc assignments, or artistic works. Plagiarism includes reproducing any individual else's work, whether or not it be posted article, chapter of a book, a paper from a buddy or some file, or whatever. In addition, plagiarism involves the exercise of employing another person to alter or revise the work that a student submits as his or her own, whoever that other man or woman may be. Authorship identification is the ability to identify unidentified authors based on their previous work and statements. The main method in authorship identification is to look at and identify features by an author using stylometric features. We can find the writing style of author by identifying textual features that they used while writing document [1].

### 1.1. Authorship Analysis

Authorship analysis is a method of analyzing the features of the writing part in order to draw conclusions from its authorship [1]. Authorship analysis having three types: i) Authorship

Identification, ii) Authorship characterization, iii) Similarity detection.

*A. Authorship identification:* It defines the likelihood of a part of the writing being produced by a specific author by examining the author's other writings.

*B. Authorship characterization:* Authorship characterization reviews the characteristics of an author and produces the author profile based on his or her writing.

*C. Similarity detection:* Similarity detection examines several pieces of writing and judges whether they have been published by a single author without actually identifying the author [1].

## 2. Literature Survey

The PAN workshop brought together experts and researchers around the exciting and future-oriented topics of plagiarism detection, authorship identification, and the detection of social software misuse. It started in 2009. But relevant to Plagiarism the track started in 2011. The table1 shows that PAN Features used, and technique applied from the year 2011 to 2018.

---

\*C. Namrata Mahender, Department of CS and IT, Dr.B.A.M.University, Aurangabad-431004 (MS), INDIA, [nam.mah@gmail.com](mailto:nam.mah@gmail.com)

Table 1: PAN Features and technique used from the year 2011 to 2018.

Reference Number	Features	Technique used
[2]	Bag of words features are used	In this paper author used Approach over known authors documents, using support vector machines. author treat each paragraph as a separate document and apply the n-cut clustering algorithm
[3]	1. Lexical features 2. Character level 3. various length-related features 4. syntax related features	In this paper author was used Support vector machine classifier for classification.
[4]	Language-dependent Content and Stylometric Features	Author used SVM and random forests as classifiers and regressors.
[5]	Word ngrams, Character ngrams, POS ,tag ngrams, Word lengths, Sentence lengths ,Sentence length ngrams ,Word richness ,Punctuation ngrams ,Text shape ngrams.	Author explored three different regressor algorithms: trees, random forests, and support vector machines.
[6]	n-gram	PPM (Prediction by Partial Matching) compression algorithm based on an n-gram statistical model.
[7]	phrase-level and lexical-syntactic features 1. Word prefixes 2. Word suffixes 3. Stopwords 4. Punctuation marks 5. N-grams(one gram to Fivegram features calculated) 6. Skip-grams (one gram to Fivegram features calculated) 7. Vowel combination 8. Vowel permutation	A similarity vector using the LSA algorithm for each word in the test documents Different distance/similarity measures were tested, including the Jaccard similarity for the vocabulary feature vector, the cosine similarity for the Frequency vector of all the combined Lexical syntactic features and Chebyshev Distance, Euclidean distance and cosine similarity for the LSA vectors.
[8]	1. Character 2. Words 3. Lemma and Part of Speech	Our method is based on the analysis of the average similarity (ASUnk) of an unknown authorship text with the closeness to each of the samples of an author, comparing it to the Average Group Similarity (AGS) between samples of an author.
[9]	Bag of words using character n-grams	Author used Ensemble Particle Swarm Model Selection (EPSMS) for the selection of classification models for each data set. For classification we used the neural network classifier implemented in the CLOP toolbox
[10]	stylometric features 1. Basic features 2. Lexical features 3. Character features 4. Syntactic features 5. Coherence features	Author follows the unmasking approach.
[11]	1. length of the sentences, 2. variety of vocabulary, 3. Words, n-characters grams, n-4. Words gram, punctuation marks.	Author compares all documents inside a corpus using the cosine similarity, euclidean distance or the correlation coefficient. For the task of Author Verification, we used the Classification and Regression Trees (CART) algorithm which constructs binary trees using the features and thresholds that



		yield the largest information gain at each node
[12]	profiles of character 3-grams for representing information about the Different categories of authors.	Baseline (accuracy) obtained in cross-genre classification by age and gender using Naive Bayes, tf-idf word representation.
[13]	word bag, stop word bag, punctuation bag, part of speech (POS) bag	KNN Algorithm is used
[14]	1. counting text elements 2. constructing syntactic n-grams	Integrated syntactic graph is used.
[15]	1.Char Sequences 2.Word Uni-grams 3. POS-tags Features	PCA Linear SVC
[16]	phoneme-based features, character-based features, token-based features, syntax-based features, semantic-based features	k-NN classifier
[17]	signatures, chat slang, context, emotionality, semantic similarity, Jaccard similarity and BOW	NB classifier
[18]	Stylistic Features 1.Stylometry based approaches 2.Content based approaches 3.Topic based approaches	Navies Bayes, Support Vector Machine, Random Forest, J48 and Logistics. These algorithms was used.
[19]	lexical, syntactic and graph-based features	Support Vector Machines (SVM).
[20]	character n-grams	Vector Space Model, Similarity Overlap Metric
[21]	Basic Statistics, Token Statistics, Grammar Statistics, Stop-Word Terms, Pronoun Terms, Slang Terms, Intro-Outro Terms, Bigram Terms, Unigram Terms, and Terms.	Supervised vote/veto meta-classifier approach
[22]	Stylometric features or word n-grams.	k-NN classifier
[23]	n-grams	Distance measure technique used.
[24]	n-Grams	Support Vector Machine classifier
[25]	n-grams	Local n-gram Technique is used.
[26]	Bag of words, Bigram, Trigram, Comma Dots, Numbers, Capitals, Words per paragraph, Sentences per paragraph, Square brackets.	Support Vector Regression and Neuronal Networks models
[27]	n-grams of POS tag sequences	vector space model
[28]	stylistic and statistical features	SVM, Bayes, KNN
[29]	stylometric features ranging from characters to syntactic and semantic units	SVM
[30]	n-grams	SVM
[31]	First words of sentences or lines, nouns, verbs, punctuation.	principal component analysis
[32]	stylometric properties, grammatical characteristics and pure statistical features	SVM classifier
[33]	Linguistic Features	SVM
[34]	n-grams	LSA
[35]	Unigram-Tf-idf, Unigram Character, Character4-gram	GenIM method
[36]	Stylistic Total number of words Average number of words per sentence	SVM, K-means clustering Algorithm implemented in CLUTO

	Binary feature indicating use of quotations Binary feature indicating use of signature Percentage of all caps words Percentage of non-alphanumeric characters Percentage of sentence initial words with first letter capitalized Percentage of digits Number of new lines in the text Average number of punctuations (!?,:;) per sentence Percentage of contractions (won't, can't) Percentage of two or more consecutive non-alphanumeric characters. Lexical Bag of words (freq. of unigrams) Perplexity Perplexity values from character 3-grams Syntactic Part-of-Speech (POS) tags Dependency relations Chunks (unigram freq.)	
[37]	Elimination of stopwords, punctuation symbols and xml tags	Rocchio, Naïve Bayes and Greedy

### 3. Text Corpus

Similar to other language work, work in the Marathi language is also appreciable. But the work is not accessible as an online resource, so far it's offline. Actually, there is no generic Marathi text corpus accessible. For the development of text corpus, we have considered 10 paragraphs for taking summary from 50 users in their own writing. We have used 500 summary files from 50 users as a database for author identification.

रात्रीचे जेवण लवकर घ्यावे.त्यामुळे त्याचे पचनही चांगले होते आणि स्थूलपणा कमी होण्यास मदत होते.प्रत्येकाने ही तत्त्वे नेटाने,नित्यनेमाने पाळली तर स्थूलपणा कमी होण्यास मदत होईल आणि चरबीचे थर निघून जातील.तसेच शरीर हलके होईल.त्यामुळे मन प्रसन्न,आनंदी राहील.स्थूलपणा हा बदललेल्या जीवनशैलीचा दुष्परिणाम आहे.घरी बनवलेले रुचकर,सात्त्विक जेवण ज्यात वरण,भात,चपाती वा भाकरी,भाजी,कोशिंबीर,दही,उसळ या सर्वांचा समावेश असेल,तर स्थूलपणाला सहज रामराम ठोकणे शक्य आहे.

Figure 1: Sample file from database

अन्न हे पूर्णब्रह्म आहे अन्न हे रुचकर करण्यासाठी त्यात आपले मनशांती असणे गरजेचे आहे जेव्हा आपण जेवणात अन्न ग्रहण करतो तेव्हा आपण व्यवस्थित चावणे हे गरजेचे असते.जेवणात वरण,भात,चपाती,वा भाकरी, उसळ,कोशिंबीर असणे हे स्थूलपणाला रामराम ठोकणे आहे पण हे अन्न आपण नित्यनेमाने करणे आवश्यक आहे.

Figure 2: Sample Summary written by Author

### 4. Proposed System

We would like to propose a system for Author Identification in Marathi Language. The system workflow is given below:

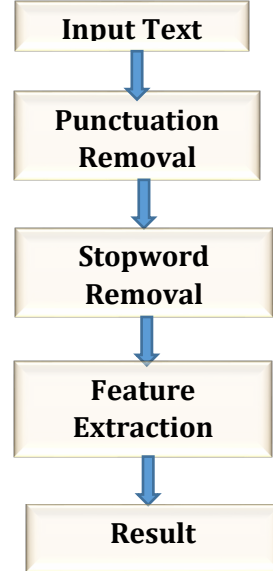


Figure3: Proposed System for Author Identification for Marathi Language

#### 4.1. Input Text

First the system reads two files. Main file and summary of written by Authors file. The file format is .txt

#### 4.2. Punctuation removal

This step removes the punctuations present in the file, e.g. punctuations = "!()-[]{};:'\",<>./?@#\$\$%^&\* \_~"

4.3. Stopword Removal

Stop words are simply a set of words widely used in any language. Here are the Stopwords:

Table 2. List of Stopwords

या	त्यांनी	हा	पण
व	सुरु	ही	जेव्हा
यांनी	करून	करण्यात	त्या
हे	जर	याच्या	त्याच्या
तर	असून	ता	मात्र
ते	आले	तेव्हा	परंतु
असे	त्यामुळे	हा	पण

Table 3: Features of Original Sample files

main files	avg sen len by char	avg sen len by word	hapax legema	hapax dislegama	avg word freq class	avg sen len
OG_File1	1198	57	423.41	0.11	1.79	7
OG_File2	1441	74	441.88	0.19	1.55	9
OG_File3	1612	79	443.08	0.1	1.77	9
OG_File4	2797	128	492.72	0.07	1.84	7
OG_File5	2896	154	508.75	0.09	1.95	7
OG_File6	2757	141	499.04	0.06	1.89	7
OG_File7	2841	141	503.69	0.04	1.82	7
OG_File8	991	63	417.43	0.12	1.69	13
OG_File9	740	30	358.35	0	1	4
OG_File10	1173	44	417.43	0.1	1.76	11

5. Feature Extraction

Feature extraction can be defined as the process of extracting a set of new features from the set of features generated in the selection stage feature. Feature extraction is a basic and fundamental step to pattern Recognition and machine learning problem. There is no text corpus available for Marathi language.

We concentrated on two major features: Lexical features and Vocabulary richness features. These include features like Average sentence length by word, Average sentence length by character, AvgWordFrequencyClass, Avg sentence length, Hapax legomenon, Hapax dislegemena.

We have extracted the following features:

5.1. Lexical features

1. Average length of sentence by word
2. Average length of sentence by character
3. AvgWordFrequencyClass

4. Avg sentence length

5.2. Vocabulary richness features

1. Hapax legomenon
2. Hapax dislegemena

Hapax Legomena and Hapax DisLegemena

Hapax Legomena is a term that appears only once in a sense, either in the written record of the whole language, a single text. Hapax legomenon it is a Greek phrase which means something that told onetime only.

Similarly, Hapax DisLegemena is the word that is used twice. Following table3 shows that features of original sample files from database.

Table 4: Features of Author1 files

Files	Avg_SentLengthByChar	Avg_SentLengthByWord	hapaxLegemena	hapaxDisLegemena	Avg Word Frequency Class	Avg sentence length
File1	758.0	44.0	391.20	0.054	1.7	15
File2	1049.0	68.0	426.26	0.24	1.53	34
File3	943.0	57.0	409.43	0.183	1.65	14
File4	1149.0	67.0	423.41	0.084	1.75	17
File5	1243.0	75.0	436.94	0.072	1.78	15
File6	1465.0	90.0	453.25	0.22	1.52	45
File7	754.0	44.0	395.12	0.04	1.92	15
File8	572.0	41.0	376.12	0.131	1.76	14
File9	538.0	25.0	349.65	0.064	1.87	8
File10	645.0	28.0	361.09	0.00	1.0	14

Table 5: Features of Author2 files

Files	Avg_SentLengthByChar	Avg_SentLengthByWord	hapaxLegemena	hapaxDisLegemena	Avg Word Frequency Class	Avg sentence length
File1	877.0	49.0	397.02	0.1041	1.81	12
File2	1076	59.0	411.08	0.113	1.75	10
File3	1296.0	71.0	429.04	0.089	1.83	18
File4	1366.0	72.0	434.38	0.069	1.87	15
File5	1103	84.0	438.35	0.059	1.82	14
File6	678	82.0	538.0	0.079	1.79	16
File7	899	65.0	458.0	0.085	1.84	15
File8	523.0	30.0	349.65	0.033	1.84	8
File9	442.0	19.0	317.80	0.0	1.0	5
File10	869.0	37.0	380.66	0.04	1.84	9

Table 6: Features of Author3 file

Files ↓	Avg_SentLenghtByCh	Avg_SentLenghtByWord	hapaxLegemena	hapaxDisLegemena	AvgWordFrequencyClass	Avg sentence length
File1	777.0	47.0	395.12	0.1063	1.80	23
File2	880	67.0	412.11	0.13	1.82	20
File3	1390.0	86.0	449.98	0.154	1.87	29
File4	1230	82.0	468.25	0.123	1.85	22
File5	1178	86	434.0	0.14	1.78	24
File6	879	81.0	398.0	0.13	1.87	22
File7	758	58.0	369.0	0.15	1.83	20
File8	627.0	41.0	376.12	0.176	1.62	14
File9	598.0	34.0	361.09	0.23	1.62	11
File10	686.0	36.0	371.35	0.051	1.90	36

Table 7: Features of Author4 file

Files ↓	Avg_SentLenghtByCh	Avg_SentLenghtByWord	hapaxLegemena	hapaxDisLegemena	AvgWordFrequencyClass	Avg sentence length
File1	758.0	47.0	389.18	0.050	1.71	23
File2	796	49.0	387.10	0.02	1.74	22
File3	947.0	51.0	397.02	0.02	1.88	25
File4	864.0	53.0	434.0	0.03	1.85	23
File5	1164	52.0	489	0.086	1.83	20
File6	1516.0	84.0	0.051	445.43	1.82	10
File7	1526.0	94.0	456.43	0.1392	1.67	19
File8	496.0	29.0	343.39	0.074	1.77	14
File9	565.0	27.0	343.39	0.0	1.0	13
File10	1071.0	53.0	404.30	0.058	1.82	18

Table 8: Features of Author5 file

Files ↓	Avg_SentLenghtByCh	Avg_SentLenghtByWord	hapaxLegemena	hapaxDisLegemena	AvgWordFrequencyClass	Avg sentence length
File1	794.0	45.0	391.20	0.090	1.78	11
File2	1056.0	64.0	418.96	0.157	1.72	16
File3	1020.0	56.0	398.21	0.18	1.85	14
File4	2093.0	104.0	468.21	0.061	1.83	9
File5	1524.0	102.0	485.11	0.071	1.84	10
File6	1754.0	107.0	480.12	0.078	1.86	12
File7	1825.0	111.0	475.35	0.11	1.74	16
File8	715.0	46.0	387.12	0.12	1.72	23
File9	631.0	31.0	358.35	0.0	1.0	10
File10	812.0	31.0	378.41	0.07	1.86	10



6. Result

$$\text{projection} = \frac{\overline{AS} \cdot \overline{OS}}{|\overline{AS} \cdot \overline{OS}|} \tag{1}$$

$\overline{AS}$  Feature vector of summary file written by author  
 $\overline{OS}$ -> Feature vector of main author file from database

Table 9: Projections of main author file on summary file written by author

Projection of File1			Projection of File2			Projection of File3		
Feature vector of original file	Feature Vector of Author file	Projection	Feature vector of original file	Feature Vector of Author file	Projection	Feature vector of original file	Feature Vector of Author file	Projection
O1 S1	A1 S1	1259.96	O2 S2	A1 S2	1502.67	O3 S3	A1 S3	1656.90
O1 S1	A2 S1	1267.24	O2 S2	A2 S2	1505.64	O3 S3	A2 S3	1671.39
O1 S1	A3 S1	1260.77	O2 S2	A3 S2	1493.81	O3 S3	A3 S3	1671.71
O1 S1	A4 S1	1260.08	O2 S2	A4 S2	1490.71	O3 S3	A4 S3	1659.55
O1 S1	A5 S1	1263.03	O2 S2	A5 S2	1504.15	O3 S3	A5 S3	1664.60
Projection of File4			Projection of File5			Projection of File6		
Feature vector of original file	Feature Vector of Author file	Projection	Feature vector of original file	Feature Vector of Author file	Projection	Feature vector of original file	Feature Vector of Author file	Projection
O4 S4	A1 S4	2797.49	O5 S5	A1 S5	2904.78	O6 S6	A1 S6	2783.81
O4 S4	A2 S4	2817.58	O5 S5	A2 S5	2882.72	O6 S6	A2 S6	2471.87
O4 S4	A3 S4	2791.57	O5 S5	A3 S5	2896.68	O6 S6	A3 S6	2719.10
O4 S4	A4 S4	2722.88	O5 S5	A4 S5	2870.66	O6 S6	A4 S6	2789.41
O4 S4	A5 S4	2839.97	O5 S5	A5 S5	2917.76	O6 S6	A5 S6	2794.38
Projection of File7			Projection of File8			Projection of File9		
Feature vector of original file	Feature Vector of Author file	Projection	Feature vector of original file	Feature Vector of Author file	Projection	Feature vector of original file	Feature Vector of Author file	Projection
O7 S7	A1 S7	2753.51	O8 S8	A1 S8	1059.29	O9 S9	A1 S9	816.28
O7 S7	A2 S7	2763.22	O8 S8	A2 S8	1057.72	O9 S9	A2 S9	810.570
O7 S7	A3 S7	2777.38	O8 S8	A3 S8	1066.46	O9 S9	A3 S9	819.15
O7 S7	A4 S7	2869.40	O8 S8	A4 S8	1054.22	O9 S9	A4 S9	818.94
O7 S7	A5 S7	2879.50	O8 S8	A5 S8	1072.00	O9 S9	A5 S9	820.94
Projection of File10								
Feature vector of original file	Feature Vector of Author file	Projection						
O10 S10	A1 S10	1228.20						
O10 S10	A2 S10	1242.74						
O10 S10	A3 S10	1230.19						
O10 S10	A5 S10	1240.36						

Table 10: Average projection of main author on dependent author

Name of Projection Files	Average projection of each file
File1	1262.22
File2	1499.401
File3	1664.835
File4	2793.904
File5	2894.525
File6	2711.718
File7	2808.606
File8	1061.944
File9	817.1817
File10	1237.416

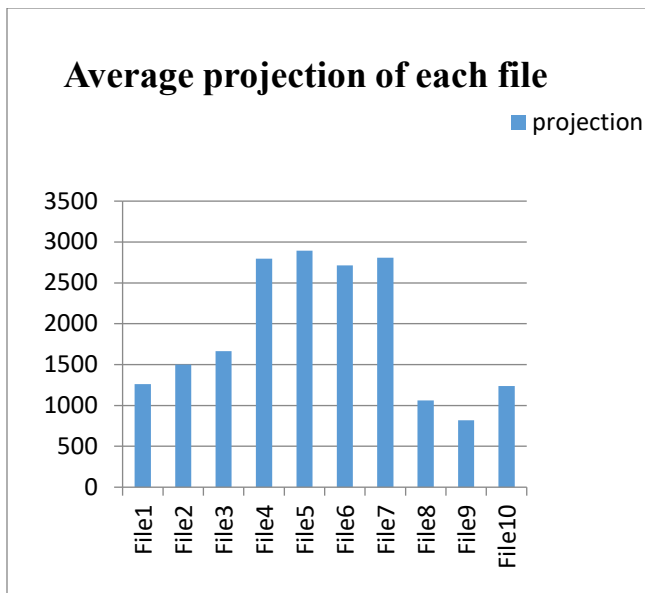


Figure 4: Average projection of each file

Above figure 4 shows average projection of 10 files. We have calculated feature vector of main author file and feature vector of summary file written by author, we calculated projection these two vectors for 10 different sample summary files of five authors. It shows there is similarity in main author file and summary file of each author. Summary file of author is having impact of main author file. Above graph shows file number 4,5,6,7 are having more projection of main author file.

## 7. Conclusion

Authorship identification is the ability to identify unidentified authors based on their previous work and statements. We have created database of 500 summary files from 50 users for author identification. After doing literature survey on features used for author identification, we selected some features like Lexical features and vocabulary richness features. By using feature vector of main author file and summary file of authors, we calculated projection of 10 files. The result of average projection shows, there is similarity in main author file and summary file of different authors. The figure4 shows summary file of each author

is having impact of main author file, Summary file number 4,5,6,7 are having more projection of main author file. Currently, most of Marathi native speakers are contributing their research for various topics in Marathi language, but some of researchers are using information from various sources like research papers, books, thesis without giving acknowledgement. There is need to restrict these type of conditions. There is no Author identification tool available for Marathi language. This tool will be helpful to perform quality research in Marathi language.

## Acknowledgment

Authors would like to acknowledge and thanks to CSRI DST Major Project sanctioned No.SR/CSRI/71/2015(G), Computational and Psycholinguistic Research Lab Facility supporting to this work and Department of Computer Science and Information Technology, Dr. Babasaheb Ambedkar Marathwada University, Aurangabad, Maharashtra, India.

## References

- [1] Zheng, R., Li, J., Chen, H., & Huang, Z. "A framework for authorship identification of online messages: Writing-style features and classification techniques", *Journal of the American society for information science and technology*, 57(3), 378-393. 2006, DOI: 10.1002/asi.20316.
- [2] Akiva, Navot. "Authorship and Plagiarism Detection Using Binary BOW Features" CLEF (Online Working Notes/Labs/Workshop) 2012.
- [3] Argamon, S., & Juola, P. "Overview of the international authorship identification competition at PAN-2011". In CLEF (Notebook Papers/Labs/Workshop). 2011.
- [4] Bartoli, A., De Lorenzo, A., Laderchi, A., Medvet, E., & Tarlao, F. "An author profiling approach based on language-dependent content and stylistometric features". In Conference and Labs of the Evaluation forum (Vol. 1391). CEUR. 2015.
- [5] Bartoli, A., Dagri, A., De Lorenzo, A., Medvet, E., & Tarlao, F. "An author verification approach based on differential features". In Conference and Labs of the Evaluation forum (Vol. 1391). CEUR. 2015.
- [6] Bobicev, V. "Authorship detection with PPM". In Proceedings of CLEF. 2013.
- [7] Alhijawi, B., Hriez, S., & Awajan, A. "Text-based Authorship Identification-A survey". In 2018 Fifth International Symposium on Innovation in Information and Communication Technology (ISIICT) (pp. 1-7). IEEE.2018. DOI: 10.1109/ISIICT.2018.8613287
- [8] Castro, D., Adame, Y., Pelaez, M., & Muñoz, R. "Authorship verification, combining linguistic features and different similarity functions", CLEF (Working Notes). 2015.
- [9] Escalante, H. J. "EPSMS and the Document Occurrence Representation for Authorship Identification", Notebook for PAN at CLEF 2011.
- [10] Feng, V. W., & Hirst, G. "Authorship verification with entity coherence and other rich linguistic features", In Proceedings of CLEF (Vol. 13) 2013.
- [11] Fréry, J., LARGERON, C., & Juganaru-Mathieu, M. "Ujm at clef in author identification", Proceedings CLEF-2014, Working Notes, 1042-1048. 2014.
- [12] Ucelay, M. J. G., Villegas, M. P., Funez, D. G., Cagnina, L. C., Errecalde, M. L., Ramirez-de-la-Rosa, G., & Villatoro-Tello, E. "Profile-based Approach for Age and Gender Identification", In CLEF (Working Notes) (pp. 864-873). 2016.
- [13] MR Ghaeini. "Intrinsic Author Identification Using Modified Weighted KNN" -Notebook for PAN at CLEF 2013.
- [14] Gómez-Adorno, H., Sidorov, G., Pinto, D., & Markov, I. "A graph based authorship identification approach". Working notes papers of the CLEF, 2015.
- [15] HaCohen-Kerner, Y., Miller, D., Yigal, Y., & Shayovitz, E. "Cross-domain Authorship Attribution: Author Identification using char sequences, word unigrams, and POS-tags features", Working Notes of CLEF. 2018.
- [16] Halvani, O., Steinebach, M., & Zimmermann, R. "Authorship verification via k-nearest neighbor estimation". Notebook PAN at CLEF. 2013.
- [17] Hernández, D. I., Guzmán-Cabrera, R., & Reyes, "A. Semantic-based Features for Author Profiling Identification" First insights Notebook for PAN at CLEF 2013.

- [18] Pervaz, I., Ameer, I., Sittar, A., & Nawab, R. M. A. "Identification of Author Personality Traits using Stylistic Features", Notebook for PAN at CLEF 2015.
- [19] Vilariño, D., Pinto, D., Gómez, H., León, S., & Castillo, E. "Lexical-syntactic and graph-based features for authorship verification". In Proceedings of CLEF, 2013.
- [20] Jayapal, A., & Goswami, B. "Vector space model and Overlap metric for Author Identification", Notebook for PAN at CLEF 2013.
- [21] Kern, R., Klampfl, S., & Zechner, M. "Vote/Veto Classification, Ensemble Clustering and Sequence Classification for Author Identification", Notebook for PAN at CLEF 2012.
- [22] Kern, R. "Grammar Checker Features for Author Identification and Author Profiling" In CLEF 2013 Evaluation Labs and Workshop-Working Notes Papers.2013.
- [23] Kocher, M., & Savoy, J. "Author Identification" Working Notes Papers of the CLEF.2015.
- [24] Kourtis, Ioannis, and Efstathios Stamatatos "Author identification using semi-supervised learning", CLEF 2011: Proceedings of the 2011 Conference on Multilingual and Multimodal Information Access Evaluation (Lab and Workshop Notebook Papers), Amsterdam, the Netherlands. 2011.
- [25] Layton, Robert, Paul Watters, and Richard Dazeley" , Local n-grams for Autho Identification". Notebook for PAN at CLEF 2013.
- [26] Ledesma, P., Fuentes, G., Jasso, G., Toledo, A., & Meza, I. "Distance learning for author verification" In Proceedings of the conference pacific association for computational linguistics, PACLING (Vol. 3, pp. 255-264). 2003.
- [27] López-Anguila, Rocío, Arturo Montejo-Ráez, and Manuel Carlos Díaz-Galiano "Complexity Measures and POS n-grams for Author Identification in Several Languages", SINAI at PAN@ CLEF 2018.
- [28] Mechti, S., Jaoua, M., Faiz, R., & Belguith, L. H. "On the Empirical Evaluation of Author Identification Hybrid Method".2015.
- [29] Mikros, G. K., & Perifanos, K. "Authorship identification in large email collections: Experiments using features that belong to different linguistic levels". Notebook for PAN at CLEF, 2011.
- [30] Moreau, E., Jayapal, A., & Vogel, C. "Author Verification: Exploring a Large set of Parameters using a Genetic Algorithm", Notebook for PAN at CLEF In Working Notes for CLEF 2014 Conference (Vol. 1180, p. 12). CEUR Workshop Proceedings. 2014.
- [31] Foltýnek, T., Meuschke, N., & Gipp, B. "Academic plagiarism detection: a systematic literature review", ACM Computing Surveys (CSUR), 52(6), 112. 2019.
- [32] Pimas, O., Kröll, M., & Kern, R. "Know-Center at PAN 2015 author identification", Working Notes Papers of the CLEF. 2015.
- [33] Ruseti, S., & Rebedea, T. "Authorship Identification Using a Reduced Set of Linguistic Features" Notebook for PAN at CLEF 2012.
- [34] Satyam, A., Dawn, A. K., & Saha, S. K. "A Statistical Analysis Approach to Author Identification Using Latent Semantic Analysis", Notebook for PAN at CLEF. 2014.
- [35] Seidman, S. "Authorship verification using the impostors method", In CLEF 2013 Evaluation Labs and Workshop-Online Working Notes. 2013.
- [36] Solorio, T., Pillay, S., & Montes-y-Gómez, M. "Authorship Identification with Modality Specific Meta Features", PAN, 1, 11. 2011.
- [37] Vilariño, Darnes, et al. "Baseline Approaches for the Authorship Identification Task".

## Pyrolysis of Beech Wood in A Continuous Drop Tube Reactor in Comparison to A Batch Reactor

Chetna Mohabeer<sup>1,\*</sup>, Nourelhouda Boukaous<sup>2</sup>, Antoinette Maarawi<sup>1</sup>, Lokmane Abdelouahed<sup>1</sup>, Abdeslam-Hassen Meniai<sup>2</sup>, Mustapha Chikhi<sup>2</sup>, Bechara Taouk<sup>1</sup>

<sup>1</sup>Normandie Univ, INSA Rouen Normandie, UNIROUEN, Laboratoire de Sécurité des Procédés Chimiques, LSPC EA-4704, 76000 Rouen, France

<sup>2</sup>Faculté de Génie des Procédés, Université de Constantine 3, 25000 Constantine, Algeria

### ARTICLE INFO

#### Article history:

Received: 07 January, 2020

Accepted: 19 March, 2020

Online: 04 April, 2020

#### Keywords:

Pyrolysis

Beech wood

Drop tube reactor

Batch spoon-fed reactor

### ABSTRACT

The goal of this research work is first to investigate the comparison between a batch and a continuous pyrolysis reactor (at 500, 550 and 600 °C) and the eventual differences and similarities that are obtained by analysing the obtained liquid and gas compositions. All the products formed were examined: liquids by GC-MS/FID and Karl Fischer titration, gases by GC-FID/TCD and solids by thermogravimetric analysis (TGA). It was observed that even though not the same pyrolytic reactor was used, the parameters rendering the maximum yield of bio-oil were the same in both cases: 500 °C under 500 mL/min N<sub>2</sub> (~58 wt. %). Furthermore, it was observed that while changing the temperature affected significantly the product distribution, varying the gas residence time did not cause much change to the product distribution. This was due to the fact that pyrolysis was occurring within the same intermediate regime ( $\tau$ : ~9 min), and that the limiting factor of the reaction was thus the biomass particle residence time (20.6 s), not that of the gas. Finally, the observations obtained for product distributions and evolution for both the batch and the continuous setups were compared, and discrepancies between results from the two setups were found. This led to the conclusion that comparisons between reactors of different scales need to be undertaken with caution as the results might not be directly comparable.

## 1. Introduction

This paper is an extension of work originally presented in the 10<sup>th</sup> International Renewable Energy Congress (IREC) [1]. Depletion of fossil-based fuels has become an important environmental issue. A more sustainable alternative to the use these fuels would be the use of a “green” bio-fuel and a promising route to achieve this goal would be to convert biomass into a product known as “bio-oil” through the pyrolysis process [2]. Lam et al. [3] conducted an exhaustive review that showed that most biomass pyrolysis studies at laboratory scale are performed on batch, or semi-batch, reactors due to the ease which they provide. However, among the different studies led on continuous biomass pyrolysis in literature, another commonly-used technology is the drop tube reactor (DTR), named also the entrained flow reactor or the free fall reactor [3, 4]. This study undertakes a comparison of these two experimental setups.

A number of studies was led on pyrolysis in batch reactors and a pertinent one was that of Bajus [5]. They studied beech wood pyrolysis at temperatures between 350 and 450 °C in a batch reactor and found that the products formed on average were 25.1 wt. % non-condensable gas, 44.3 wt. % liquid and 30.6 wt. % char. The non-condensable gas products comprised mainly of carbon monoxide and carbon dioxide while the liquids contained mostly acetic acid, formic acid, furfural, lactic acid and levoglucosan. Another study led by Demirbas [6] examined the effect of varying reaction temperature (350-525 °C) on the pyrolytic products of hazelnut shell, olive husk, beech and spruce wood samples. The experiments were performed in a fixed-bed tubular reactor. They observed that a significant oil fraction contained phenols and that the water content oscillated around 15-30 wt. % of the total oil mass. They also found that the bio-oil recovered at 500 °C included elevated concentrations of acetic acid, 1-hydroxy-2-butanone, 1-hydroxy-2-propanone, methanol, 2,6-dimethoxyphenol, 4-methyl-2,6-dimethoxyphenol and 2-cyclopenten-1-one.

\*Chetna Mohabeer, 685 Avenue de l'Université, 76800 Saint-Etienne-Du-Rouvray, France, +33232956667, chikirsha.mohabeer@insa-rouen.fr



Concerning studies led on drop-tube reactors, Guizani et al. [7] conducted experiments using a free-fall reactor by varying operational conditions for biomass pyrolysis: temperature (450-600 °C), biomass particle size (370-640  $\mu\text{m}$ ) and gas residence time (12.6-20.6 s). They firstly observed that more elevated temperatures, along with more elevated particle sizes, caused a decrease in bio-oil yield. Among the various operating conditions, it was seen that temperature of the reactor and the particle size impacted greatly the product distribution without influencing notably properties of the bio-oil, namely, acidity. Sun et al. [8] conducted another interesting study on this subject where flash pyrolysis of rice husk and sawdust was performed in a free fall reactor within a temperature range of 700 to 1000 °C. Results from their study have demonstrated that temperature affected the reaction significantly; when temperature increased, gas yield increased as well while liquid and solid yields lessened. The authors also noted that at less elevated temperatures, the improvement in gas production could be owing to a boost in the formation of CO and CH<sub>4</sub> whereas, at higher temperatures, it concerned increased CO<sub>2</sub> and H<sub>2</sub> production.

Based on the values obtained for residence time for this study, it can be inferred that the pyrolysis regime used was an intermediate one. Now, as stated in literature [9–13], results obtained from fast and intermediate regimes are similar to each other. The latter regime was also the one obtained from the pyrolysis experiments in the batch, spoon-fed reactor ( $\tau$ : ~9 min based on heated length of reactor). As the same pyrolysis regime reigned in both setups, the results are comparable in terms of operating conditions (like biomass used, reaction temperature and gas residence gas).

This research work presents liquid and gas results obtained for pyrolysis reactions conducted in a batch, spoon-fed reactor (SFR) and a continuous DTR, respectively. This research is a follow-up to our previous studies [13–15] and many of the comparisons makes use of the results derived from these studies. The aim is firstly to establish a comparison between the two reactors and then, study the subsequent similarities and differences obtained from the products of the two setups. To further corroborate these observations, the results were also compared to those obtained from a micro pyrolyser [16]. To the best of our knowledge, such a comparison has rarely been undertaken before, despite the importance of knowing and understanding the variation in results obtained when upscaling a process (changing reactor technology and scale of the process). Ultimately, this study can help attest whether comparing results obtained from different reactor technologies is reliable or not, and why.

## 2. Experimental Section

### 2.1. Materials used

The biomass used for this study, beech wood having an average particle size of 400  $\mu\text{m}$ , was supplied by ETS Lignex Company. The elemental and proximate analyses for the biomass can be found in the supplementary materials (Tables A.1 and A.2). The C, H and N contents (elemental analysis) of the samples were measured by the use of a CHN elemental analyser (Flash 2000, Thermofisher Scientific). The proximate analysis was obtained via thermogravimetric analysis (TGA), using a STD Q600 equipment, according to the protocol described by Garcia et al. [17].

[www.astesj.com](http://www.astesj.com)

## 2.2. Experimental and analytical setup

### 2.2.1 Experimental setup

Previous studies conducted by our research group detail the reactor layout, experimental protocol and analytical procedures undertaken for experimental runs in the spoon-fed reactor [13–15]. Now, the experimental runs in continuous mode were performed in a drop tube reactor, as is illustrated by Figure 1. Biomass was fed through the top of the DTR by a screw conveyor (GLD 77.0, Tremie 5L from Gericke). A 2 m heated length of the pyrolysis reactor was used. A char collector to gather solid residues of biomass pyrolysis was placed at the bottom of the DTR. This collector was kept at 300 °C through the use a heating shell to ensure that the condensable pyrolysis vapours entering it stayed in vapour form. However, sometimes, some fine solid particles got swept away by the gas/vapour flow and escaped the char collector. Two cyclones (efficiency: 85 % each) were positioned at the vapour exit of the DTR so as to capture these particles away from the gas flow. It should be noted that the whole system was kept at 300 °C in order to prevent condensation of vapours.

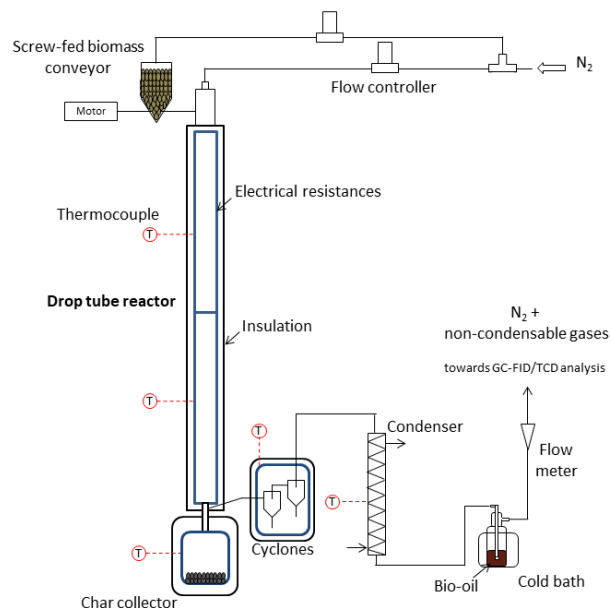


Figure 1: DTR layout

The pyrolysis experiments were performed by altering the temperature of the DTR (500, 550 and 600 °C) and the nitrogen flow rate (0.5, 1 and 2 L/min) in order to vary the gas residence time ( $\tau$ ). The list of experiments has been presented in Table 1. It should be noted that the gas residence time has been calculated based only on the nitrogen flow rate. The experimental protocol followed was: first, the reactor was set to the temperature desired and the nitrogen flow rate was controlled at the exit to make sure that there were no leaks. Then, the system was allowed to stabilise for about two hours. Afterwards, a biomass feed rate of 2 g/min was introduced in the reactor and the reaction was left to occur for 60 minutes. After the experiment, the heat was cut and the experimental system left to cool. The collection of char was done at temperatures below 150 °C so as to prevent it from burning at the contact of air. The collection of bio-oil was done by using a solvent: acetone with 99.98% purity, with, as internal standard, a known added amount of nonane.

Table 1: List of pyrolysis experiments and corresponding gas residence times

Nitrogen flow rate (L/min)*	Gas residence time, $\tau$ (min)	DTR temperature ( $^{\circ}\text{C}$ )
0.5	9.27	500
		550
		600
1	4.63	500
		550
		600
2	2.32	500
		550
		600

\*Measured at room temperature and pressure

### 2.2.2 Analytical setup for pyrolytic products

#### Gas Chromatography (GC) Analyses

The liquid and gaseous products formed were then recovered and analysed using the protocol described by our previous work [13]. The bio-oil collected was analysed using a gas chromatograph-mass spectrometer instrument GC-MS (Varian 3900-Saturn 2100T) with a VF-1701ms (Agilent) (60 m  $\times$  0.25 mm  $\times$  0.25  $\mu\text{m}$  film thickness) column. The same temperature programme as Charon et al. [18] was used. The identification of the liquid components was done using Varian WS (WorskStation) and NIST 2002 software. A GC-FID (flame ionisation detector) Scion 456-GC Bruker instrument was used to quantify the compounds once the identity of the peaks was obtained and confirmed. The same column as for the GC-MS was used. The temperature programme used was the same as for the GC-MS, only, the final temperature used was 240  $^{\circ}\text{C}$  instead of 280  $^{\circ}\text{C}$ . The obtained compounds were finally classified into chemical “families”, each having the same main functional group.

The non-condensable gases (NCG) were mostly composed of CO, CO<sub>2</sub>, CH<sub>4</sub> and H<sub>2</sub>. C<sub>2</sub>H<sub>2</sub>, C<sub>2</sub>H<sub>4</sub> and C<sub>2</sub>H<sub>6</sub> (represented as ‘C<sub>2</sub>’) and C<sub>3</sub>H<sub>4</sub>, C<sub>3</sub>H<sub>6</sub> and C<sub>3</sub>H<sub>8</sub> (represented as ‘C<sub>3</sub>’) were also present in less significant proportions. The gases were analysed with a gas chromatograph instrument (Clarus 580, Perkin Elmer), equipped with an FID and a thermal conductivity detector (TCD). A Shincarbon St 100 120 column, a methaniser and a hydrogen generator completed the build of the equipment.

### 2.3 Karl Fischer (KF) titration

A Metrohm 870 KF TitrinoPlus apparatus was used to perform volumetric KF titrations. An aqualine sodium tartrate solution along with Hydranal Composite 5 were used as titrating agents and Hydranal Methanol Rapid was used as working medium. The pyrolysis oil samples were weighed on an analytical precision balance. After weighing, the sample was placed into the titration vessel of the KF apparatus. The titration started when the sample was completely dissolved. Each sample was measured in triplicate, which allowed the calculation of a 99 % confidence interval.

### 2.4 Thermogravimetric analysis (TGA)

Weight loss as a function of temperature was recorded using a thermobalance (TA Instrument Explorer Q600) from 20  $^{\circ}\text{C}$  to 800  $^{\circ}\text{C}$ . In a typical experiment, 5-10 mg of sample were placed in

[www.astesj.com](http://www.astesj.com)

an alumina crucible and heated under a N<sub>2</sub> flow (50 mL/min). A heating rate of 15  $^{\circ}\text{C}/\text{min}$  was used.

## 3 Results and discussion

### 3.1 Results from drop tube reactor (DTR)

The major chemical compounds identified and the different families they were grouped into have been summarised in Table 2.

Table 2: Major chemical compounds identified and their different chemical families

Chemical family	Major molecules identified
Alcohols	1,2-Propanediol, 3-methoxy-, 2-Furanmethanol, 6-Hepten-1-ol, 5-methyl-, 2,4-Hexadien-1-ol, Resorcinol, 3-Heptanol, 3,6-dimethyl-, Thymol, 1,2-Benzenediol
Aldehydes	2-Heptenal, (E)-, 2-Pental, (E)-, 3-Furaldehyde, 2-Furancarboxaldehyde, 5-methyl-, Benzaldehyde, 2-hydroxy-
Alkanes	Hexane, 3,3,4,4-tetramethyl-, Nonane, Decane
Aromatics	Benzene, o-Xylene, Benzene, 1,3-dimethyl-, 1H-Indene, 3-methyl-, Naphthalene, 1,2-dihydro-, Azulene, Naphthalene, 2,6-dimethyl-
Amides	N-Methoxy-N-methylacetamide, Benzenacetic amide
Carboxylic acids	Acetic acid, Acetohydroxamic acid, Propanoic acid, Benzoylformic acid
Esters	Acetic acid, 1-methylethyl ester, 1,1-Ethandiol, diacetate, Phenol, 4-(2-propenyl)-, acetate
Furans	Furan, 2,3,5-trimethyl-, Furan, 2-ethyl-, Vinylfuran, Benzofuran, 2-methyl-
Guaiacols	Phenol, 2-methoxy-, Phenol, 2,6-dimethoxy-, Phenol, 4-ethyl-2-methoxy-
Ketones	1-Hexen-3-one, 2-Hexanone, 3,4-dimethyl-, 2-Cyclohexen-1-one, 2-Cyclopenten-1-one, 1H-Inden-1-one, 2,3-dihydro-
Phenols	Phenol, Phenol, 2-methyl-, Phenol, 2,4,6-trimethyl-, Phenol, 4-ethyl-, 1-Naphthalenol
Carbohydrates	Levoglucozan, 3,4-O-Isopropylidene-d-galactose

### 3.2 Defining optimal conditions for pyrolysis reaction in the DTR

The mass balance values obtained for the various experimental runs are presented in Figure 2. It is worth mentioning that mass balances of above 85 % were found experimentally for each run. This discrepancy can be explained by the fact that there still remained a fraction of the liquid produced on the walls of the DTR installation that was lost even if every attempt was made to collect all of it. Therefore, the mass balances were completed to 100 % with respect to the liquid fraction.

It can firstly be observed from the previous figure that the lowest temperature (500  $^{\circ}\text{C}$ ) tested gave rise to the largest amount

of char produced (between 13 and 18 wt. %) and the smallest amount of non-condensable gases formed (between 28 to 30 wt. %). In contrast to the latter observations, 600 °C, the highest temperature utilised corresponded to the lowest amount of char (around 9 to 10 wt. %) and the highest amount of non-condensable gases (49-55 wt. %). Now, so as to detail these findings, the degree of conversion of the biomass at different temperatures, that is, the fraction of biomass that was converted to its pyrolytic products at each pyrolytic temperature, was analysed through TGA under a nitrogen flow rate of 0.5 L/min and the results obtained have been illustrated in Figure 3. The figure also depicts the evolution of the percentage of each pyrolytic product at different reactor temperatures.

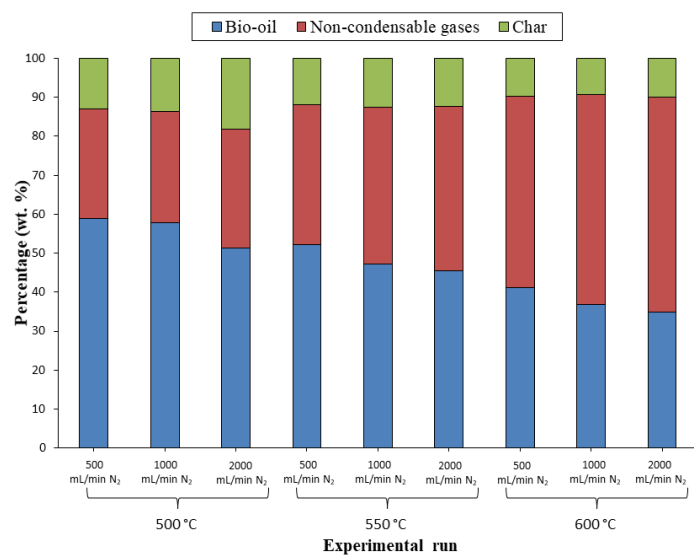


Figure 2: Mass balances of pyrolysis experiments

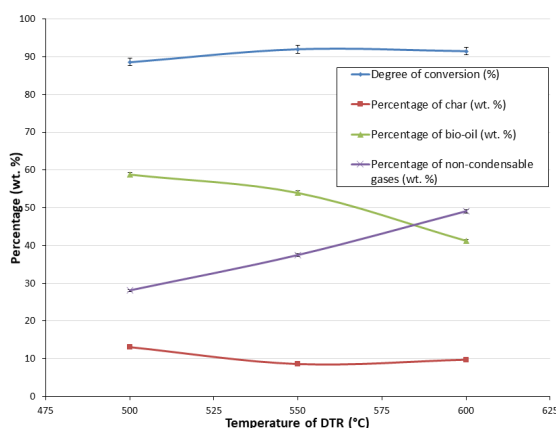


Figure 3: Degree of biomass conversion (TGA) at different DTR temperatures at  $\tau = 9.27$  min

It can be seen from the previous figure that the tendency of the degree of conversion and that of the char percentage were opposing ones, as were the evolution of bio-oil and gas percentages. It can therefore be claimed that the gas production bears a direct correlation to the reactor temperature, and that the liquid formation a negative one, that is, at higher temperatures, an improvement in gas formation and a diminishment in liquid

production will be witnessed. This observation can be explained by the fact that cracking reactions are favoured at higher temperatures [19], and so, at those temperatures, larger liquid molecules decompose into smaller, gaseous ones. The same observations were obtained from the SFR, as mentioned in previous works [13, 14].

It was also observed that the experiment performed at 500 °C under 0.5 L/min N<sub>2</sub> produced the most elevated bio-oil output (58.8 wt. %). These conditions corresponded to the same ones obtained in the SFR [14].

### 3.3 Influence of gas residence time on pyrolysis liquid and gas products

#### 3.3.1 Liquid product composition

As previously mentioned, in order to elicit a variation in the gas residence time in the DTR, carrier gas (N<sub>2</sub>) flow rate was changed from 0.5 to 2 L/min. Table 1 shows the resulting residence times. Then, the liquid product compositions for the pyrolysis of beech wood obtained at different reactor temperatures were analysed. Figure 4 illustrates the composition obtained at 500 °C in the DTR. The ones obtained for other reactor temperatures have been tabulated in Table 3.

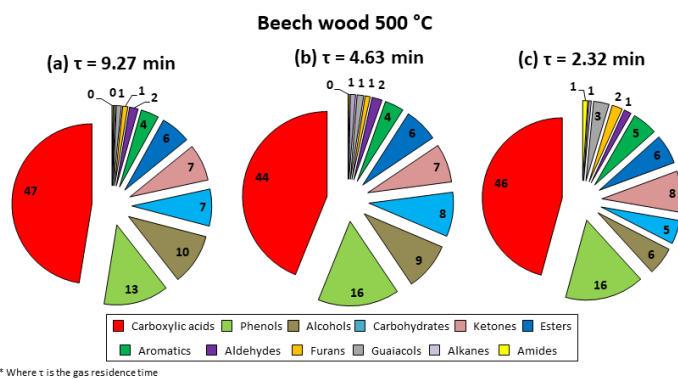


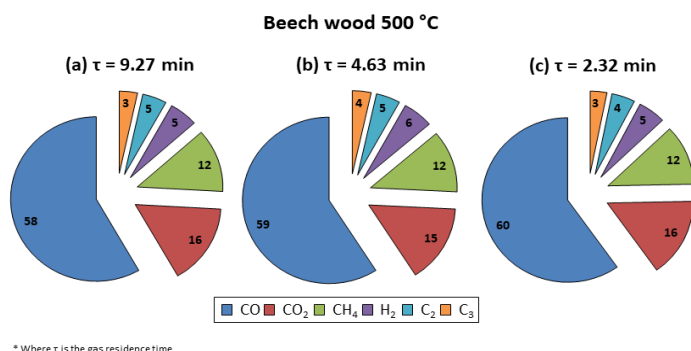
Figure 4: Liquid product compositions obtained for pyrolysis of beech wood at 500 °C in DTR

As it can be seen in Figure 4, although gas residence times have more than halved (9.27 min to 4.63 min to 2.32 min), product compositions were not much influenced. Further calculations were conducted to try to understand the happenings throughout the reaction. These calculations have been compiled in the supplementary materials. From these calculations, it was found that the biomass particle residence time in the reactor was 2.20 s, which was much lower than the gas residence times used (see Table 2). This observation led to the understanding that the parameter that controlled the formation of products and the dynamics of the reaction, that is, the limiting parameter, was in fact the biomass particle residence time, not the gas residence time. Thus, even if the carrier gas flow were increased, hence diminishing gas residence time, the liquid product distribution would undergo no appreciable change as long as the pyrolysis reaction took place in a regime wherein the biomass particle residence time was less than the gas residence time. The same observation was also made by Guizani et al. [7], Jahirul et al. [20] and Ellens [21]. Now, it could be stipulated that raising the N<sub>2</sub> flow rate to higher values would help to overcome this obstacle.

However, for this specific setup, technical restrictions did not allow the flow rate used to be any higher than 2 L/min.

### 3.4 Gas product composition

NCG were also examined while the N<sub>2</sub> flow rate was altered. Figure 5 illustrates the different NCG compositions obtained at 0.5, 1 and 2 L/min N<sub>2</sub> at 500 °C, while the compositions at other temperatures have been listed in the supplementary materials (Table A.3).



\* Where τ is the gas residence time

Figure 5: Gas product compositions obtained for pyrolysis of beech wood at 500 °C in DTR

As can be observed from Figure 5, the pattern for the gas composition resembled that for the liquid composition: the gas composition was not majorly influenced by elevating the carrier gas flow rate. Following this, the same inference can be made: even if the gas residence time changes, the gas product distribution is not majorly affected if the pyrolysis regime is not altered.

### 3.5 Comparison of results from the SFR and the DTR

#### 3.5.1 Liquid product composition

To enhance the visual representation of the various chemical families, pie charts were constructed for the different temperatures and nitrogen flow rates used. An example is Figure 6 (composition of beech wood bio-oil obtained at 500 °C under 0.5 L/min N<sub>2</sub> in DTR compared to that obtained in SFR under same conditions). A similar analysis was performed for each bio-oil produced (at 500, 550 and 600 °C under N<sub>2</sub> flow rates of 0.5, 1 and 2 L/min) and the results have been presented in Table 3.

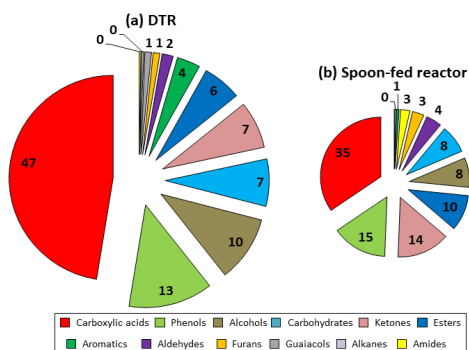


Figure 6: Composition of beech wood bio-oils obtained at 500 °C and τ = 9.27 min in DTR and spoon-fed reactor (τ = 9 min) (mol. %)

It can be observed from Figure 6 that carboxylic acids, phenols and alcohols were the most important chemical families present in the oils. These findings concord to a certain extent with the results

found when the SFR was used; the only dissimilarity was that the oils obtained from the SFR contained a higher quantity of ketones and esters. This difference may be explained by the variation in the collected oil components: concerning the DTR, using a more important amount of biomass led to a more significant production of bio-oil, which demanded the use of a smaller amount of solvent so as to be collected. This enabled the detection of compounds which had been present only in negligible fractions in the oil obtained from the SFR, which had been more dilute (338 detected compounds vs. 255 in spoon-fed reactor). The observed variation may also be due to the change in reaction technology used. However, these results vary slightly from those that Guizani et al. [7] obtained. They investigated the fast pyrolysis of biomass in an entrained flow reactor by changing reactor temperature, size of particles and vapour residence time. The major oil components observed by them were aldehydes, ketones and carboxylic acids. This difference might stem from the fact that even though beech wood was used as raw material for their study, they used a gas residence time of 20.6 s for a mean biomass particle size of 640 μm, which both differ from the conditions used in this study. Nevertheless, their maximum oil yield, 62.4 wt. %, was found to be formed at 500 °C, which this time, coincided with the findings presented in this study.

Now, it is interesting to study increasing reactor temperature influences the major families present in oil (the trend has been illustrated in Figure 7). The influence on all the other chemical families has been depicted in the supplementary materials, Figures A.1 (a)-(l).

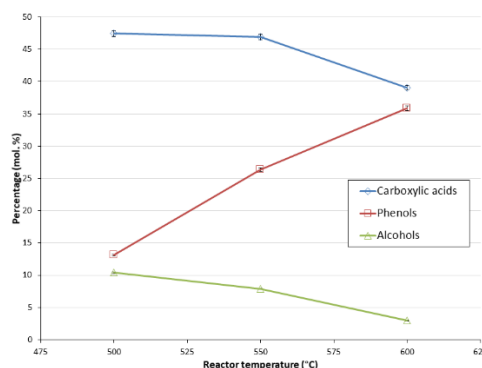


Figure 7: Evolution of major bio-oil components with increasing DTR reactor temperature (τ = 9.27 min)

Figure 7 shows clearly that both carboxylic acid and alcohol percentages decreased when temperature increased, while the opposite trend was portrayed by phenols. These findings do not completely match the results from the spoon-fed reactor, where an increasing trend with temperature was noted for the carboxylic acids.

The diminishment in the percentage of carboxylic acids corresponded with a sharp increase in the percentage of phenol. As mentioned in our previous work [13], carboxylic acids and phenols tend to be negatively correlated; this means that, when one experiences an increase, the other undergoes a reduction. This observation has been well-depicted in Figure 7. Now, a certain difference from results obtained from the SFR has been observed.



Table 3: Chemical family percentages (mol. %) in bio-oil samples obtained from DTR

Experimental conditions	Chemical families present (mol. %)											
	Carboxylic acids	Alkanes	Aromatics	Alcohols	Aldehydes	Amides	Ketones	Esters	Furans	Guaiacols	Phenols	Carbohydrates
500 °C 0.5 L/min N <sub>2</sub>	47.44	0.36	3.64	10.38	1.74	0.25	7.45	6.10	1.04	1.02	13.12	7.45
500 °C 1 L/min N <sub>2</sub>	43.88	1.00	3.65	9.18	1.94	0.26	7.38	6.48	0.97	1.26	15.55	8.46
500 °C 2 L/min N <sub>2</sub>	45.75	0.53	5.09	5.67	1.49	1.01	8.35	5.99	2.13	3.15	16.03	4.81
550 °C 0.5 L/min N <sub>2</sub>	46.91	0.55	2.95	4.04	1.75	0.90	5.94	5.00	1.02	1.05	26.33	3.57
550 °C 1 L/min N <sub>2</sub>	46.34	0.29	2.60	7.92	1.40	0.72	7.24	3.28	1.00	1.04	24.88	3.29
550 °C 2 L/min N <sub>2</sub>	47.90	1.59	3.63	5.76	1.66	0.15	6.56	3.88	0.98	1.07	23.74	3.08
600 °C 0.5 L/min N <sub>2</sub>	39.04	0.33	4.90	2.97	1.76	2.08	4.75	5.21	0.71	0.98	35.90	1.38
600 °C 1 L/min N <sub>2</sub>	38.35	0.21	2.80	3.60	1.31	1.98	4.78	8.59	1.26	1.21	34.71	1.21
600 °C 2 L/min N <sub>2</sub>	39.75	0.34	3.50	3.37	1.69	2.53	5.66	4.37	0.82	1.18	35.09	1.69

This variance can be explained firstly by the fact that a higher number of molecules was detected for the DTR and secondly, by the operational conditions of the two reactors used, which varied significantly. This finding illustrates that changing a reaction scale from lab to pilot may ensue in differences in the results obtained, and the same may be observed when reaction technology is changed from batch or semi-continuous to continuous. The latter statement is further corroborated by Table 4, where results obtained from different pyrolysis technologies used have been presented to better grasp the similarities and differences.

Table 4: Comparison of different pyrolysis technologies

	$\mu$ -pyrolyser	SFR	DTR
Amount of raw material	~mg	~g	~100 g
No. of molecules identified	92	255	338
Liquid fraction	Major compounds	40-46 % acetic acid No levoglucosan	35 % acetic acid 8 % levoglucosan
	Trend of acetic acid with reactor temperature	$\square$	$\square$
Gas fraction	No gas analysis performed as only traces were detected	Detection of: 45 % CO 40 % CO <sub>2</sub> 11 % CH <sub>4</sub> 3 % H <sub>2</sub>	Detection of: 58 % CO 16 % CO <sub>2</sub> 12 % CH <sub>4</sub> 5 % H <sub>2</sub>
References	[16]	[13, 14]	This study

### 3.6 Gas product composition

NCG went through the same analysis that liquid products did. Figure 8 represents the gas product distributions obtained for samples at 500 °C under 0.5 L/min N<sub>2</sub> in the DTR and the SFR. Results compiled from diagrams showing NCG compositions when reaction conditions are varied have been listed in Table A.3, found in the supplementary materials.

Firstly, it was observed that CO was the majorly present species (58 vol. %). This result concurs with that of Guizani et al. [7] (58.4 vol. %), and the variance from what was found with the SFR was not very large (45 vol. % for CO, the major gas component). However, it was witnessed that the gaseous product distribution changed slightly with DTR use: a more important fraction of each NCG component was detected. This may be owing to the fact that, as it was with the liquids, a higher amount of biomass was supplied to the DTR than to the SFR and this led to the production of more concentrated NCG, enabling easier detection of smaller gas molecules that were henceforth less dilute

in the carrier gas. Furthermore, Figure 9 was obtained by analysing the trend of each NCG component at 0.5 L/min N<sub>2</sub> with increasing reactor temperature. The graphs obtained with the use of other flow rates have been presented in the supplementary materials, Figures A.2 and A.3.

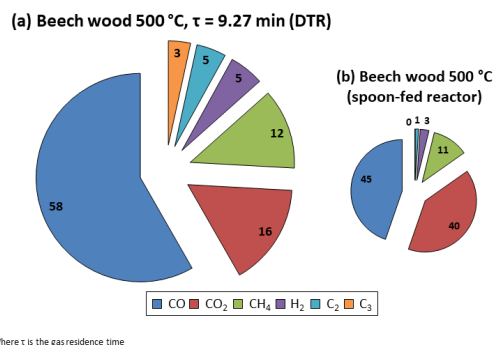


Figure 8: Composition of beech wood NCG obtained at 500 °C in DTR and spoon-fed reactor (vol. %)

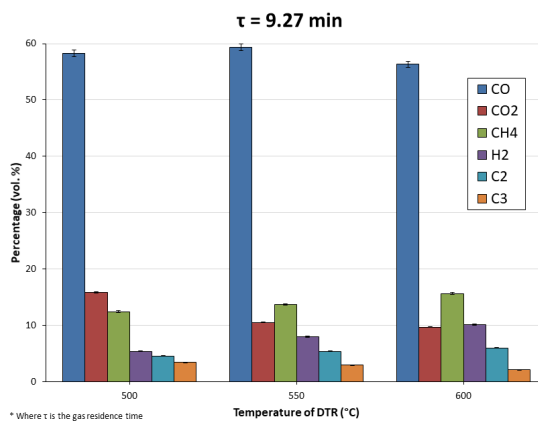


Figure 9: Evolution of NCG components (vol. %) with DTR temperature at  $\tau = 9.27$  min

The NCG composition evolved quite feebly at different DTR temperatures: a spike of CO was noted at 550 °C while increasing pyrolysis temperature caused a CO<sub>2</sub> percentage decrease. All other gaseous compounds, excluding C<sub>3</sub>, went through a raise in percentage with increasing reactor temperature. The general increase in CO and decrease in CO<sub>2</sub> trend observed with the SFR when reaction temperature was increased, somewhat shifted when the DTR was used. In this case, it was seen that whilst a decrease in the percentage of CO<sub>2</sub> was indeed witnessed, CO percentage remained almost stable (as CO was the major component). Still, if quantitative values are taken into consideration, a raise in the volume of CO can be observed, substantiating the theory that mounting the temperature of the reactor indeed privileged cracking reactions and thereby, formation of gas molecules, as per what was mentioned previously.

### 3.7 Water content of liquid products

KF titration method was utilised to estimate water content for each experiment. The detailed results can be found in Figure 10. It can be observed that a reduction in the water content was caused by a raise in the temperature of DTR (maximum water content: 48 wt. % at 600 °C under 1 L/min N<sub>2</sub>). This coincided with a

reduction in some chemical families such as alcohols, carbohydrates and carboxylic acids as well. Similar findings were made by Lehto et al. [22]. It can be therefore be claimed that elevating the temperature of the reactor promoted the dehydration of the previously-mentioned chemical families.

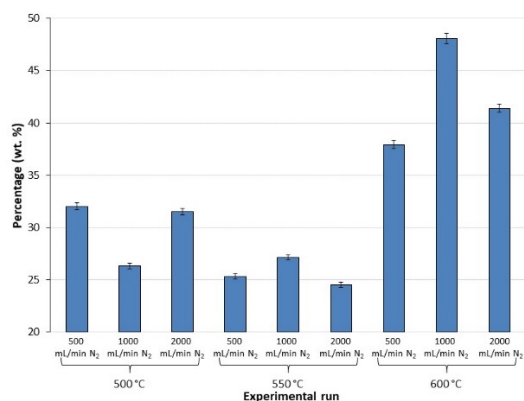


Figure 10: Water content (wt. %) of bio-oils obtained from each experimental run

### 3.8 Oxygen content of liquid products

The elevated oxygen fraction of pyrolytic oils, which renders them highly functionalised [23], remains a crucial challenge to their mainstream use. This high functionality is what causes the bio-oils to be relatively highly viscous, acidic and unstable and to possess low calorific values. Therefore, acquiring an indication of the oxygen fraction formed directly from the compounds found in the bio-oil (oxygen fraction derived from humidity not included) is key to be able to understand the behaviour of the oil and therefore, find a way to improve its properties. The theoretical calculation of the oxygen content was conducted from the weight of the oxygen atoms present in the compound. Figure 11 illustrates the evolution of the bio-oils' oxygen content (mol. %) obtained at DTR different temperatures under various N<sub>2</sub> flow rates.

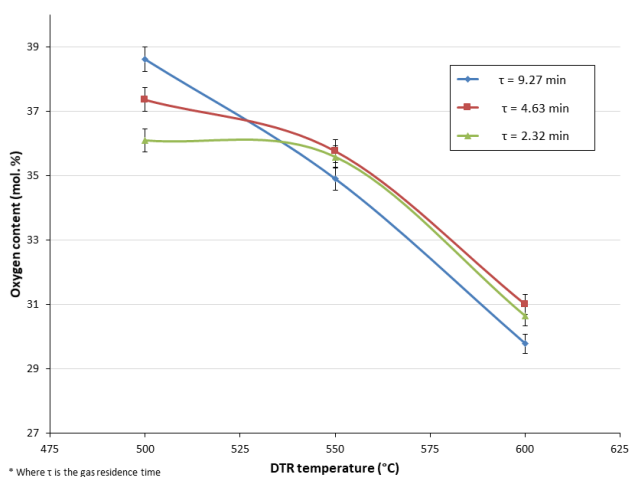


Figure 11: Oxygen content (mol. %) of bio-oils obtained from all experimental runs

It can be observed that increasing the temperature of the DTR caused the oxygen content to lessen. This finding corroborates the fact that cracking reactions and the elimination of certain oxygen-

containing chemical groups are favoured by more elevated reaction temperatures. Thus, the formation of smaller, gaseous molecules was privileged. Hence, at more elevated temperatures, a less significant amount of liquid was collected and some of the oxygen atoms escaped in the gas fraction. Nonetheless, the global bio-oil oxygen content remained quite high (29-40 mol. %) in contrast to that of the bio-oils obtained from the spoon-fed reactor (average of 33 mol. %) and also, that of fossil-derived fuels (~1 %) [24].

## 4 Conclusion

The results pertaining to liquid and gas products obtained for a continuous pyrolysis reaction in a DTR were presented in this study. The goal of this research work was first to investigate a comparison a batch and a continuous pyrolysis reactor and the subsequent existing differences and similarities by examining the obtained liquid and gas compositions. The temperature of the DTR and the gas residence time were primarily changed to study the effect on the pyrolytic products. Even though not the same pyrolytic reactor was used, it was observed that the parameters rendering the maximum yield of bio-oil were the same in both cases: 500 °C under 500 mL/min N<sub>2</sub> (~58 wt. %). It was also observed that while changing the temperature affected significantly the product distribution (it was seen that the use of higher temperatures gave rise to higher amounts of gas products and a more acidic oil), changing the gas residence time did not cause much change to the product distribution. This was due to the fact that pyrolysis was occurring within the same intermediate regime ( $\tau$ : ~9 min), and that the reaction limiting factor was the residence time of the biomass particle (20.6 s), not that of the gas. Finally, many inconsistent findings were observed between the spoon-fed and the continuous setups. This means that when comparisons are undertaken for results obtained from setups of different scales, it should be with caution as the results might not be directly comparable. This fact highlights the need for deeper research so as to understand the differences in the results obtained from differently-scaled reactors.

## Conflict of Interest

The authors declare no conflict of interest.

## Acknowledgment

This project has been funded with the support from the European Union with the European Regional Development Fund (ERDF) and the Regional Council of Normandie.

## References

- [1] N. Boukaous, L. Abdelouahed, M. Chikhi, A.-H. Meniai, and B. Taouk, 'Combustion behaviour of several Mediterranean biomass sources and their blends biomass/char', in *2019 10th International Renewable Energy Congress (IREC)*, 2019, pp. 1–6, doi: 10.1109/IREC.2019.8754608.
- [2] G. Gentile, A. Cuoci, A. Frassoldati, T. Faravelli, and E. Ranzi, 'A comprehensive cfd model for the biomass pyrolysis', *Chemical Engineering Transactions*, pp. 445–450, 2015, doi: 10.3303/CET1543075.
- [3] S. S. Lam, R. K. Liew, A. Jusoh, C. T. Chong, F. N. Ani, and H. A. Chase, 'Progress in waste oil to sustainable energy, with emphasis on pyrolysis

- techniques', *Renewable and Sustainable Energy Reviews*, vol. 53, pp. 741–753, Jan. 2016, doi: 10.1016/j.rser.2015.09.005.
- [4] L. Lu, Y. Jin, M. R. Nakamura, M. J. Castaldi, and K. Yoshikawa, 'An Investigation on Cocombustion Behaviors of Hydrothermally Treated Municipal Solid Waste with Coal Using a Drop-Tube Reactor', *Journal of Combustion*, 2012. [Online]. Available: <https://www.hindawi.com/journals/jc/2012/282851/>. [Accessed: 20-Sep-2018].
- [5] M. Bajus, 'Pyrolysis of woody material', *Petroleum & Coal*, vol. 52, no. 3, pp. 207–214, 2010.
- [6] A. Demirbas, 'The influence of temperature on the yields of compounds existing in bio-oils obtained from biomass samples via pyrolysis', *Fuel Processing Technology*, vol. 88, no. 6, pp. 591–597, Jun. 2007, doi: 10.1016/j.fuproc.2007.01.010.
- [7] C. Guizani, S. Valin, J. Billaud, M. Peyrot, and S. Salvador, 'Biomass fast pyrolysis in a drop tube reactor for bio oil production: Experiments and modeling', *Fuel*, vol. 207, pp. 71–84, Nov. 2017, doi: 10.1016/j.fuel.2017.06.068.
- [8] S. Sun, H. Tian, Y. Zhao, R. Sun, and H. Zhou, 'Experimental and numerical study of biomass flash pyrolysis in an entrained flow reactor', *Bioresource Technology*, vol. 101, no. 10, pp. 3678–3684, May 2010, doi: 10.1016/j.biortech.2009.12.092.
- [9] A. Hornung, 'Intermediate Pyrolysis as an Alternative to Fast Pyrolysis', *BioEnergy IV: Innovations in Biomass Conversion for Heat, Power, Fuels and Chemicals*, Jun. 2013.
- [10] A. S. N. Mahmood, J. G. Brammer, A. Hornung, A. Steele, and S. Poulston, 'The intermediate pyrolysis and catalytic steam reforming of Brewers spent grain', *Journal of Analytical and Applied Pyrolysis*, vol. 103, pp. 328–342, Sep. 2013, doi: 10.1016/j.jaap.2012.09.009.
- [11] I. D. V. Torri et al., 'Bio-oil production of softwood and hardwood forest industry residues through fast and intermediate pyrolysis and its chromatographic characterization', *Bioresour. Technol.*, vol. 200, pp. 680–690, Jan. 2016, doi: 10.1016/j.biortech.2015.10.086.
- [12] K. Kebelemann, A. Hornung, U. Karsten, and G. Griffiths, 'Intermediate pyrolysis and product identification by TGA and Py-GC/MS of green microalgae and their extracted protein and lipid components', *Biomass and Bioenergy*, vol. 49, pp. 38–48, Feb. 2013, doi: 10.1016/j.biombioe.2012.12.006.
- [13] C. Mohabeer, L. Abdelouahed, S. Marcotte, and B. Taouk, 'Comparative analysis of pyrolytic liquid products of beech wood, flax shives and woody biomass components', *Journal of Analytical and Applied Pyrolysis*, vol. 127, pp. 269–277, Sep. 2017, doi: 10.1016/j.jaap.2017.07.025.
- [14] C. Mohabeer et al., 'Production of liquid bio-fuel from catalytic de-oxygenation: Pyrolysis of beech wood and flax shives', *Journal of Fuel Chemistry and Technology*, vol. 47, no. 02, pp. 153–166, Feb. 2019.
- [15] C. Mohabeer, L. Reyes, L. Abdelouahed, S. Marcotte, and B. Taouk, 'Investigating catalytic de-oxygenation of cellulose, xylan and lignin bio-oils using HZSM-5 and Fe-HZSM-5', *Journal of Analytical and Applied Pyrolysis*, vol. 137, pp. 118–127, Jan. 2019, doi: 10.1016/j.jaap.2018.11.016.
- [16] J. D. Murillo, E. A. Ware, and J. J. Biernacki, 'Characterization of milling effects on the physical and chemical nature of herbaceous biomass with comparison of fast pyrolysis product distributions using Py-GC/MS', *Journal of Analytical and Applied Pyrolysis*, vol. 108, pp. 234–247, Jul. 2014, doi: 10.1016/j.jaap.2014.04.010.
- [17] L. Garcia, M. L. Salvador, J. Arauzo, and R. Bilbao, 'Influence of catalyst weight/biomass flow rate ratio on gas production in the catalytic pyrolysis of pine sawdust at low temperatures', *Ind. Eng. Chem. Res.*, vol. 37, pp. 3812–3819, 1998.
- [18] N. Charon et al., 'Multi-technique characterization of fast pyrolysis oils', *Journal of Analytical and Applied Pyrolysis*, vol. 116, pp. 18–26, Nov. 2015, doi: 10.1016/j.jaap.2015.10.012.
- [19] Y. Fan, Y. Cai, X. Li, N. Yu, and H. Yin, 'Catalytic upgrading of pyrolytic vapors from the vacuum pyrolysis of rape straw over nanocrystalline HZSM-5 zeolite in a two-stage fixed-bed reactor', *Journal of Analytical and Applied Pyrolysis*, vol. 108, pp. 185–195, Jul. 2014, doi: 10.1016/j.jaap.2014.05.001.
- [20] M. I. Jahiril, M. G. Rasul, A. A. Chowdhury, and N. Ashwath, 'Biofuels Production through Biomass Pyrolysis —A Technological Review', *Energies*, vol. 5, no. 12, pp. 4952–5001, Nov. 2012, doi: 10.3390/en5124952.
- [21] C. Ellens, 'Design, optimization and evaluation of a free-fall biomass fast pyrolysis reactor and its products', *Graduate Theses and Dissertations*, Jan. 2009.
- [22] J. Lehto, A. Oasmaa, and Y. Solantausta, 'Fuel oil quality and combustion of fast pyrolysis bio-oils'. 2013.
- [23] J. D. Adjaye and N. N. Bakhshi, 'Production of hydrocarbons by catalytic upgrading of a fast pyrolysis bio-oil. Part I: Conversion over various catalysts', *Fuel Processing Technology*, vol. 45, no. 3, pp. 161–183, Dec. 1995, doi: 10.1016/0378-3820(95)00034-5.
- [24] S. Xiu and A. Shahbazi, 'Bio-oil production and upgrading research: A review', *Renewable and Sustainable Energy Reviews*, vol. 16, no. 7, pp. 4406–4414, Sep. 2012, doi: 10.1016/j.rser.2012.04.028.
- [25] Engineering ToolBox, 'The Engineering Toolbox', 2001. [Online]. Available: <https://www.engineeringtoolbox.com/>. [Accessed: 04-Oct-2018].



**Supplementary Materials**

Table A.1 illustrates the elemental analysis of the raw material used as feed for this study, while Table A.2 presents the proximate analysis of beech wood based on thermogravimetric measurements.

Table A.1: Elemental analysis of biomass used

Biomass/Biomass Component used	Elemental analysis (wt. %)			
	Carbon	Hydrogen	Nitrogen	Oxygen
Beech wood (BW)	47.38	6.11	<0.01	46.51

Table A.2: Proximate analysis of different raw materials based on TGA experiments (wt. %)

	Humidity	Volatile matter	Fixed carbon	Ash
Beech wood (BW)	7.44	74.19	17.52	0.85

*Hydrodynamic calculations for pyrolysis reaction occurring in DTR*

- Determining terminal velocity,  $u_t$ , of biomass particles

Using Stoke's law,  $u_t = \sqrt{\frac{4 \cdot g \cdot d (\rho_{N_2} - \rho_{biomass})}{3 \rho_{N_2} \cdot C_D}}$ , for  $0.1 < Re < 1000$

Where  $\rho_{N_2} = 0.5956 \text{ kg/m}^3$  and  $\rho_{biomass} = 840 \text{ kg/m}^3$

d: biomass particle diameter = 0.0004 m

g: gravity = 9.812 m/s<sup>2</sup> [25]

Re: Reynold's number =  $\frac{\rho_{N_2} \cdot D \cdot u_t}{\mu}$ ,

where  $\mu$ : dynamic viscosity of carrier gas =  $3.49 \times 10^{-5} \text{ kg/m.s}$  [25]

$C_D$ : drag coefficient =  $\left(\frac{24}{Re}\right) (1 + 0.14Re^{0.7})$

To determine the terminal velocity of the biomass particle, an iterative calculation is required. The Reynold's number,  $Re_0$  is first calculated for an initial value of  $u_{t,0} = 3 \text{ m/s}$  [21], followed by the drag coefficient  $C_{D,0}$  and finally, once again, the terminal velocity,  $u_{t,1}$ . This process repeats itself; the values of  $Re_1$  (using  $u_{t,1}$ ),  $C_{D,1}$  and then,  $u_{t,2}$  and so on are obtained n times until  $(u_{t,n}^2 - u_{t,n-1}^2)^2 = 0$ .

The values thus found were:  $Re = 15.41$ ;  $C_D = 3.04$ ;  $u_t = 1.08 \text{ m/s}$

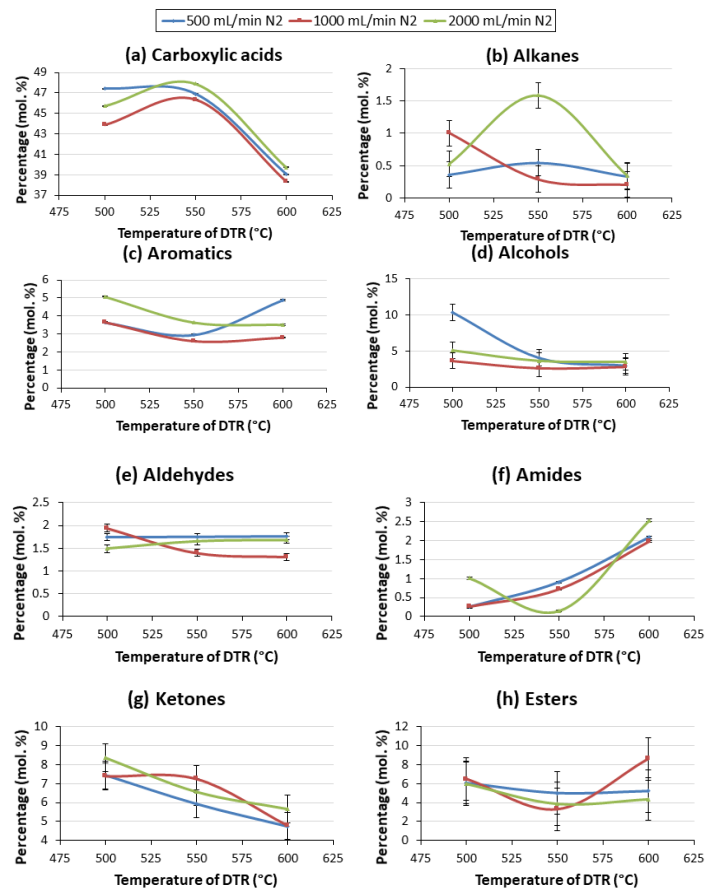
$\therefore t_{particle}$ : residence time of biomass particle =  $\left(\frac{L_r}{u_t}\right) = 2.20 \text{ s}$ , where  $L_r$  is the length of the reactor.

The following Table A.3 details the different NCG compositions obtained for the various experimental runs performed.

Table A.3: NCG compositions (vol. %) obtained for all experimental runs

Experiment performed	vol. %					
	CO	CO <sub>2</sub>	CH <sub>4</sub>	H <sub>2</sub>	C <sub>2</sub>	C <sub>3</sub>
500 °C, 0.5 L/min N <sub>2</sub>	58.27	15.86	12.46	5.39	4.60	3.43
500 °C, 1 L/min N <sub>2</sub>	59.06	15.16	12.08	5.69	4.51	3.50
500 °C, 2 L/min N <sub>2</sub>	59.80	15.53	11.86	5.23	4.42	3.15
550 °C, 0.5 L/min N <sub>2</sub>	59.38	10.54	13.68	7.98	5.41	3.00
550 °C, 1 L/min N <sub>2</sub>	60.08	10.47	13.27	7.84	5.30	3.04
550 °C, 2 L/min N <sub>2</sub>	60.46	10.44	12.69	7.95	5.19	3.28
600 °C, 0.5 L/min N <sub>2</sub>	56.32	9.70	15.64	10.14	6.00	2.19
600 °C, 1 L/min N <sub>2</sub>	56.60	9.59	15.11	10.41	5.93	2.36
600 °C, 2 L/min N <sub>2</sub>	56.44	9.56	14.56	11.17	5.79	2.48

Figures A.1 (a)-(l) illustrate the evolution of the different chemical families present in the bio-oil samples obtained under different nitrogen flow rates with increasing DTR temperature.



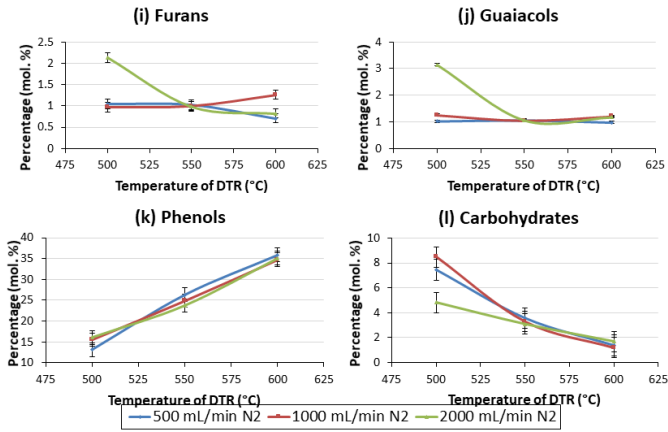


Figure A.1 (a)-(l): Evolution of chemical families (mol. %) in bio-oil samples obtained under different nitrogen flow rates with DTR temperature

Figures A.2 and A.3 depict the evolutions of the non-condensable gas compositions obtained with increasing DTR temperature under different gas flow rates, except that obtained with 500 mL/min N<sub>2</sub>, as it was presented in the main text.

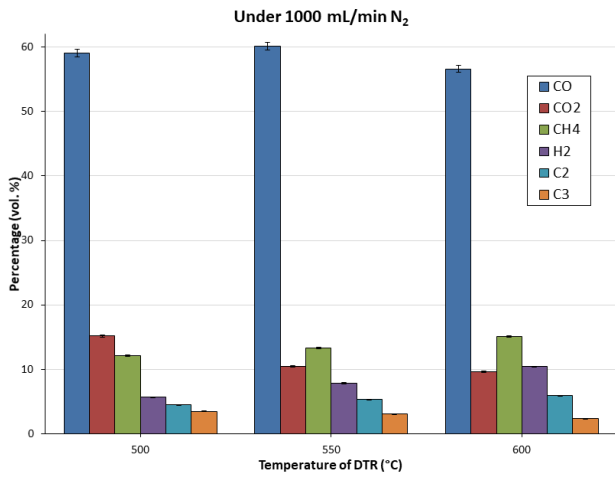


Figure A.2: Evolution of NCG components (vol. %) with DTR temperature at  $\tau = 4.63$  min

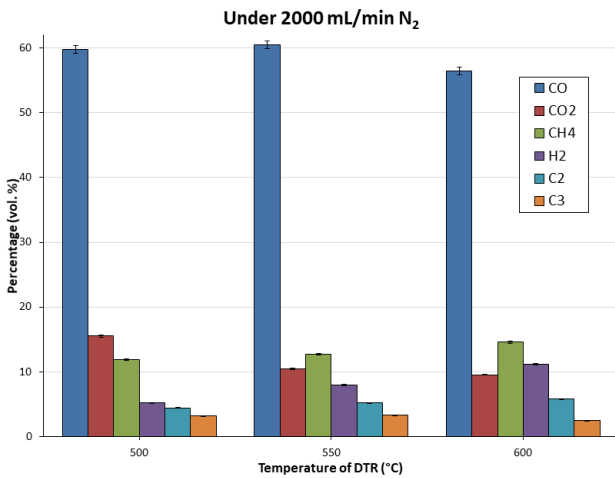


Figure A.3: Evolution of NCG components (vol. %) with DTR temperature at  $\tau = 2.32$  min

## **Promoting Continuous Professional Development Among Academics from A Vocational College by Using A Practical Workshop Based on Arduino Technology**

Arthur James Swart\*, Pierre Eduard Hertzog

*Central University of Technology, Faculty of Engineering, Built Environment and Information Technology, Bloemfontein, South Africa*

---

### ARTICLE INFO

*Article history:*

*Received: 17 November, 2019*

*Accepted: 27 March, 2020*

*Online: 04 April, 2020*

---

*Keywords:*

*practice*

*e-learning*

*pre-post test*

---

### ABSTRACT

*The internet of things has resulted in the design and development of many electronic sensors that need to be integrated with various technologies. Engineering academics need ongoing training relating to this integration as they need to subsequently teach their students. This relates to continuous professional development. The purpose of this article is to illustrate how engineering academics from a vocational college have been able to engage with the theory and practice of sensor integration with Arduino technology, thereby strengthening or reconstructing their conceptual knowledge of these electronic components. A case study is used where experts in electrical engineering designed and facilitated an academic development workshop (2 days in duration) to address a need for continuous professional development. Eighteen academics from a local vocational college attended this workshop where the first goal was to determine their conceptual knowledge of 10 electronic components using an electronic responsive system (pre-test). The second goal was to facilitate a "hands-on" laboratory session where academics had to physically integrate various sensors with an Arduino microcontroller. A post-test online questionnaire was then used to determine their conceptual knowledge again, in order to ascertain the impact of the workshop. Results indicate that their conceptual knowledge was reconstructed with regard to the purpose and use of capacitors, Zener diodes, transformers, ultrasonic sensors, reed switches and passive infrared receivers. A problematic question arose relating to photocells in the first workshop that was held in 2017, which was resolved by the facilitators prior to offering a second workshop in 2018. Positive feedback was received from the participants regarding the relevance and presentation of the workshops. The novelty of this work relates to the design of a practical workshop where all participants are engaged to either strengthen, or reconstruct, their conceptual knowledge regarding electronic components that may be integrated with Arduino technology.*

---

### **1. Introduction**

This article is an extension of work originally presented at the 12<sup>th</sup> International Conference on Sensing Technologies, held in Limerick Ireland from 3-6 December 2018. The original paper considered the importance of academic development workshops and focussed on the results of one such workshop that was offered to academics from a vocational college in 2017 [1]. The current article adds to the discussion by highlighting the importance of continuous professional development (as suggested by the reviewers), by detailing the four practical assignments that were

designed for the workshop and by including the results of a second workshop that was offered in 2018. The results of this second workshop are especially important, as a question relating to one of the sensor components caused some confusion among the participants in the first workshop offered in 2017. The revised question attained the goal of strengthening the conceptual knowledge of the participants.

Students or academics need to be engaged on a personal level, where their conceptual knowledge is either strengthened or reconstructed in order to enhance their intellectual capacity, thereby enriching their lives. Reconstructing knowledge refers to identifying gaps or errors in one's thinking, which first needs to be

---

\* Arthur James Swart, 685 Email : [drjamesswart@gmail.com](mailto:drjamesswart@gmail.com)

deconstructed before it can be reconstructed again in the correct way. One way of achieving this is by fusing theory and practice, which is mandatory in engineering education [2, 3]. Students must be allowed to experiment actively in a laboratory, where theory and practice are linked to real-world problems. Academics must be allowed to put into practice their acquired theoretical knowledge (new or old) in an academic development workshop that could lead them to enhancing their teaching practice.

Academic development workshops are successful tools of change in teaching practice and post-workshop evaluations operate as indicators of impact [4]. An academic's teaching practice must be investigated on a regular basis to determine areas of self-improvement. This forms part of the Scholarship of Teaching and Learning [5] and also of continuous professional development [6]. TVET (technical and vocational education and training) college academics should also engage with this, as they seek to prepare their students to meet the needs of industry, and especially as engineering technicians. Their conceptual knowledge of their field should be strengthened, or reconstructed, on a regular basis, so as to build capacity within the college regarding new technologies. Such expertise is required within any discipline, including electrical engineering, where the study and application of electronic components (including sensors) and microcontrollers is constantly evolving.

Many microcontrollers require a software program to execute commands [7] that can be achieved by significant "hands-on" practice [8]. The internet of things has been defined as a massive network where a diversity of electronic components are used to collect all kinds of data, including sound, light, heat, electricity, mechanics, chemistry, biology, and position [9]. Training academics to effectively integrate many of these electronic components with a specific microcontroller may enable them to teach their students more effectively, and thereby helping academics fulfil their teaching responsibilities. It may further help students to be better equipped to meet the needs of Industry.

The purpose of this research is to illustrate how engineering academics from a vocational college have been able to engage with the theory and practice of sensor integration with Arduino technology, thereby strengthening or reconstructing their conceptual knowledge of these electronic components. The link between academic development workshops and continuous professional development is firstly explained, along with the structure of the practical workshop. The research methodology, results and conclusions then follow.

## 2. Academic Development Workshops Linked to Continuous Professional Development

Research suggests that relevant academic development workshops are critical to enhance the quality of education, as they enable participants to acquire new and innovative teaching and learning practices [10]. Education should never be static. This requires academics to constantly reflect on their teaching practices, seeking innovative ways to improve it. Academic development workshops provide opportunities for such improvement by promoting a culture of reflective practice [11]. These workshops are vital within a dynamic higher education landscape. However, to be effective, they need to be facilitated by experts within a relevant field of study [12]. They should also aim to fuse theory

and practice, which may be achieved through a practical workshop. Goals of such workshops must include the transfer of theoretical and technological knowledge, the acquisition of practical hands-on skills [13] and the reinforcement of conceptual knowledge through practice [1].

A practical workshop regarding the production of Educational videos was held at the University of Huddersfield. This was a 'hands-on' workshop where the participants worked in pairs developing a script and a visual storyboard for their educational videos. Participants learnt about the range of videos and multimedia that can be used in the educational environment and how this could *benefit learners* [14].

A practical workshop on engineering ethics was held at the University of Nottingham in Malaysia. A post-workshop survey revealed that the participants knowledge on engineering ethics had not significantly improved, but it had *motivated* them to act more ethically [15].

A further important goal of practical workshops should be to address Continuing Professional Development (CPD). CPD has been defined as the maintenance and enhancement of knowledge expertise and competence of professionals throughout their careers according to a plan that is formulated to meet the needs of an individual [16]. In a PhD study that explored the impact of short CPD courses on the professional development of teachers, it was found that only one CPD course (duration of one day) focusing on subject-specific information had valuable impacts on the teacher's practice [17].

Demonstration of CPD is increasingly required for re-certification of professionals in the workplace [18]. The certification of professional engineers in SA is done by the Engineering Council of South Africa (ECSA). ECSA has an online CPD recording system that consists of 3 main categories, namely development activities, work-based activities and individual activities. Development activities include attending conferences, workshops and colloquiums. Work-based activities include engineering work and mentoring candidate engineering practitioners. Individual activities include supervision of postgraduate students, evaluation of dissertations, publishing research articles and membership of a recognized voluntary association, such as the IEEE. A minimum of 25 credits must be obtained over a five-year cycle to remain registered as a professional Engineer or Technologist. Only ECSA recognised voluntary associations and tertiary institutions with accredited engineering programs may validate CPD developmental activities [19].

## 3. Structuring Practical Workshops

Practical workshops should be bottom-up approaches. They should provide equal engagement by all participants [20]. This can be achieved by using an electronic responsive system (ERS) where individual participant engagement is maintained. Attending a workshop does not guarantee meaningful engagement, as the participant may not actively engage in the discussions due to shyness or distractions. Encouraging active engagement is required to achieve the following primary outcomes of any developmental workshop:

- Agency; individuals need to act voluntarily and independently, making their own decisions [21].



- Ownership; individuals need to actively participate in decision taking [22].
- Active learning; individuals need to be personally involved [23] by pressing knobs, sketching images, etc.
- Satisfaction of learning; individuals learn from their own misconceptions, as their ideas are shared and scrutinized by others in a “secretive” way [24].

In this research, training is defined as strengthening, or reconstructing, the conceptual knowledge of TVET academics regarding the integration of electronic components with Arduino technology. An academic development workshop, or practical workshop, is used to achieve this aim.

#### 4. The Practical Workshop Used in This Research

The practical workshop reported on in this article featured two stages. In stage one, the conceptual knowledge of the participants was reviewed with regard to 10 electronic components (including 5 sensors). In stage two, the software programming skills of the participants were enhanced through repeated practice and interaction with an Arduino microcontroller. The practical workshop was designed by experts in electrical engineering who have published extensively on this topic. Their most recent contributions considered the effective use of Arduino in engineering education [25], the use of Arduino in energy monitoring [26] and the use of Arduino in evaluating the performance of pico-solar systems [27].

The first stage of the workshop required participants to engage with two Microsoft PowerPoint presentations. The main presentation covered the workshop program, learning outcomes and requirements for CPD. Content relating to the purpose and application of 10 electronic components and sensors were also included. A second presentation was designed using Turning Point Software that enables interactivity between the facilitator and participants. This presentation contained a number of multiple-choice questions that were answered in real-time by the participants, in an effort to determine their conceptual knowledge of the selected components and sensors.

This interactive presentation necessitates the use of a transmitter (resembling a calculator) and receiver (USB device connected to a PC). Voluntary responses of each participant (*agency* involved) is transmitted (*active learning* as keys need to be pressed) wirelessly to the receiver. Once all responses have been received, then the results are visually displayed on the next slide for all to see and analyse (this contributes to *ownership* as each contributes to the discussion). Discussions on the real-time results then follow to help the participants to either strengthen their conceptual knowledge of the components and sensors, or to deconstruct and then reconstruct it again (*satisfaction of learning* occurs as perceptions are shared and compared). These results also enable the facilitator to identify gaps or misconceptions in the thinking of the participants, thereby spending more time clarifying the purpose and application of specific components. The results of this interactive presentation were saved for future analysis.

In the second stage of the practical workshop, the facilitators discussed the basic fundamental theory of the hardware and

software associated with the Arduino microprocessor. This included:

- Identifying the key differences between the UNO and MEGA microprocessors;
- Listing the available inputs, outputs and basic connections on the UNO microprocessor;
- Structuring a basic C program in the Arduino integrated development environment (IDE); and
- Reviewing various codes for integrating components and sensors onto the UNO microprocessor.

Four practical assignments were designed for the participants to complete, with each one requiring a specific software program that had to be uploaded to an UNO microprocessor. Four steps had to be followed for each assignment

- Compile a basic software program on the computer;
- Wire the component or sensor to the microprocessor using a breadboard;
- Upload the program using a USB cable; and
- Troubleshoot any errors.

The first assignment required the participants to connect a Liquid Crystal Display (LCD) to the UNO microprocessor where the name of the participant had to be visually shown on the display. The second assignment required the participants to integrate a light dependent resistor (LDR), or photocell, with the UNO microprocessor, where the previously used LCD would now display the resistance value of the LDR. The third assignment required the participants to integrate with the Arduino microprocessor to measure distance and then display it on the LCD. This assignment is described next in detail with regard to the four steps that participants needed to follow. In this way, each assignment built on the first one, as the LCD was subsequently used in all the remaining assignments. This is a form of scaffolding, where support was initially given by the facilitators to the participants regarding the integration of the LCD in the first assignment. However, this support relating to the LCD was withdrawn from subsequent assignments and replaced with support for other components and sensors.

The **first step** requires a *software program code*. An example of this code is displayed in Figure 1. In line 1, the LCD library is included and in line 2 the connection pins for the LCD module is defined. The LCD is also defined as a two row LCD with 16 characters per row. The trigger pin of the ultrasonic sensor is also declared as an output and the eco pin as an input. In line 13 of the main loop, the ultrasonic function is called. The measured distance is calculated by this function and placed in the “distance” variable. The cursor position of the LCD is set to row 0 and character 0 where after “Ultrasonic” is written to the LCD. The cursor is then moved to character 0 of the second line and “distance:” is written to the position. The measured distance is then displayed on the LCD, with mm as the unit.

```

1 #include <LiquidCrystal.h>
2 LiquidCrystal lcd(12,11,5,4,3,2);
3 int trigPin = 9;
4 int echoPin = 10;
5 long distance;
6 long duration;
7 void setup() {
8   lcd.begin(16, 2);
9   pinMode(trigPin, OUTPUT);
10  pinMode(echoPin, INPUT);
11 }
12 void loop() {
13   ultrasonic();
14   lcd.setCursor(0,0);
15   lcd.clear();
16   lcd.print("Ultrasonic");
17   lcd.setCursor(0,1);
18   lcd.print("distance : ");
19   lcd.print(distance);
20   lcd.print("cm");
21   delay(200);
22 }
23 void ultrasonic() {
24   digitalWrite(trigPin, LOW);
25   delayMicroseconds(2);
26   digitalWrite(trigPin, HIGH);
27   delayMicroseconds(10);
28   digitalWrite(trigPin, LOW);
29   duration = pulseIn(echoPin, HIGH);
30   distance = duration*0.034/2;
31 }

```

Figure 1: Arduino code for assignment 3

Figure 2 shows the schematic diagram for assignment 3. The participants use the information in this circuit diagram to physically integrate the required sensors with the Arduino microcontroller with the aid of a breadboard. The Arduino UNO, the LCD and the ultrasonic sensor can be observed in Figure 3 that represents the **second step** in the assignment, being the *wiring of the sensor* to the microcontroller. This wiring diagram provides a real-life image of each component, thereby helping the participant to select the correct component from the electronic kit that was provided to them in the laboratory. This diagram is drawn by the participants using a free electronic CAD software, named Fritzing that can be downloaded from the internet. This wiring diagram further assists the participants with fault-finding, as connection mistakes are common. This links to the **fourth step** of the assignment, namely *troubleshooting*, that is also required during the third step of the other three assignments.

**Step three** requires the participants to *upload the program* to the Arduino microprocessor via the IDE. The participants first need to resolve any errors, as indicated by the IDE (the line in the code that contains the error is highlighted). Common errors that novice programmers make may include format and punctuation in the commands. The commands are also case sensitive, and many errors stem from upper- and lower-case letters. Before uploading, the participants also need to set the output in the IDE to Arduino UNO if the UNO board is used, as there are many boards in the Arduino family. The output port in the IDE also needs to be set to the port that the Arduino UNO is connected to. Many upload errors stem from either wrong board or port selections before uploading the code. The upload process usually takes only a few seconds and, if successful, the program will immediately start executing on the Arduino microprocessor.

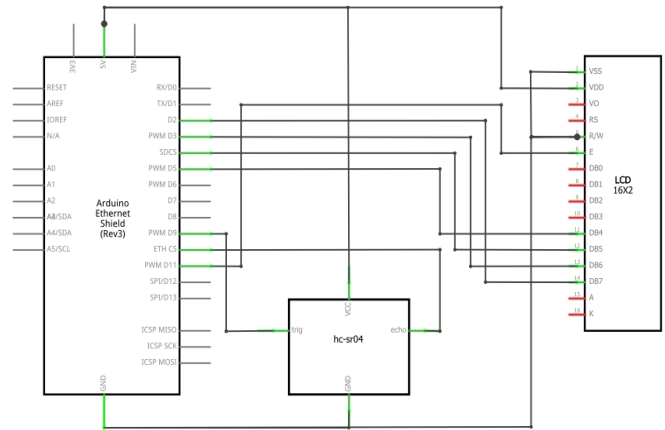


Figure 2: Schematic for assignment 3

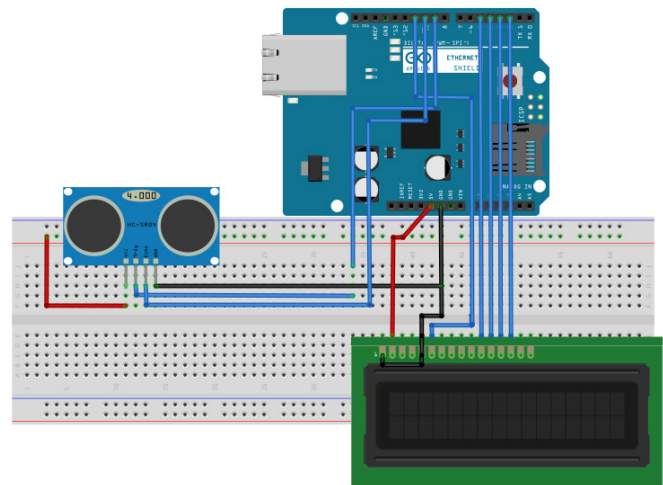


Figure 3: Breadboard for assignment 3

The learning outcome of the fourth assignment required a passive infrared sensor (PIR) and buzzer to be integrated with an UNO microprocessor, where the LCD would indicate an alarm condition. Participants had to again repeat the aforementioned steps for this assignment.

## 5. Research Methodology

A case study is used for this research where the results cannot be generalized. However, a case study can provide practical insights about industry-specific problems that are being addressed and therefore enable learning and changes in practice to occur [28]. In this research, insights into the conceptual knowledge of TVET academics are presented that can impact their workplace practice as they teach and train students in electrical engineering. This knowledge of the participants was either strengthened, or needed to be reconstructed, with regard to 10 electronic components and sensors. The findings of this case study further seek to establish if the designed workshop attained its aim of promoting CPD and if any changes needed to be made to enhance future workshops.

The practical workshop was first presented in 2017 that was attended by 10 TVET academics. The number of participants was limited to 10 to enable more personal attention to be given by the facilitators. This is especially required during the programming

and troubleshooting stages. A second workshop was presented in 2018 that was attended by 8 TVET academics.

A pre-post test, with no control group, was used to determine the impact of the practical workshop on the conceptual knowledge of the participants. A similar approach has been documented for nursing education [29]. Similar multiple-choice questions were posed for both tests that provided the participants with a predefined list of electronic components and sensors to choose from. Each question was phrased to cover a specific purpose relating to each component. The pre-test was administered during the first stage of the workshop using an ERS. The post-test was administered at the end of the second stage of the workshop using Google Forms. Grades from these tests were analysed quantitatively and are presented in the form of a radar chart. This helps to visually identify which electronic component the participants know well, and which ones require more discussion so that their conceptual knowledge may be reconstructed.

Feedback from the participants was also obtained in the post-test with regard to the facilitators and the workshop. Eight closed-ended questions were asked using a 5-point Likert scale. The profile of the academics was initially obtained during the first stage of the workshop using the ERS. This also helped to train the participants in using the ERS correctly. The end goal of the profile is to better contextualise the results.

## 6. Results and Discussions

Figure 4 shows the profile of the workshop participants for 2017, while Figure 5 shows the profile for 2018. More than 90% of the participants were older than 30 years, validating them as academics with life experience. The noted disciplines of the academics validate the relevance of this Arduino based practical workshop, as the majority of the participants (60% + 50% from 2017 and 2018 respectively) were from electrical engineering. It is true that Arduino technology is used by individuals from a wide range of fields, including electrical engineering [25, 30]. The third part of the profile presents the home languages of the participants (right hand side of Figure 4 and Figure 5). Four languages are shown that is not uncommon for SA where 11 official languages are spoken [31]. A dominant language in 2017 was Afrikaans, while in 2018 it was Sesotho. Figure 6 illustrates the perceptions of the participants regarding the workshop facilitators.

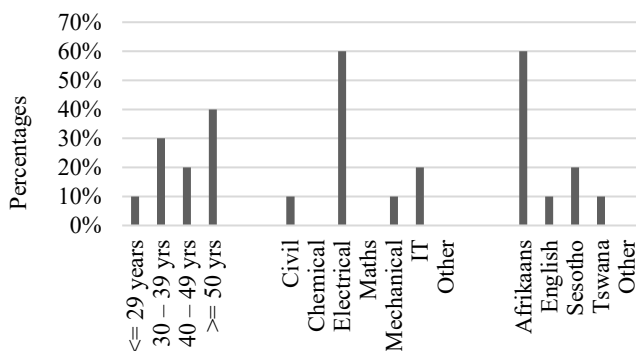


Figure 4: 2017 participant profile

The majority of the participants (67%) rated their time management skills as very good, while 89% rated their presentation skills in the same way. 89% of the participants agreed

that the subject knowledge of the facilitators was very good. Finally, 94% of the participants rated the academic professionalism of the facilitators as very good. Literature suggests that good time management in education is vital [32] as are good presentation skills [33]. It is equally important that a facilitator personally possesses the relevant subject knowledge [12] and academic professionalism (this may include shared values, unselfish concern for others, relevant expertise, logical thinking, use of evidence, conceptual and theoretical rigour and the unbiased pursuit of truth [34]).

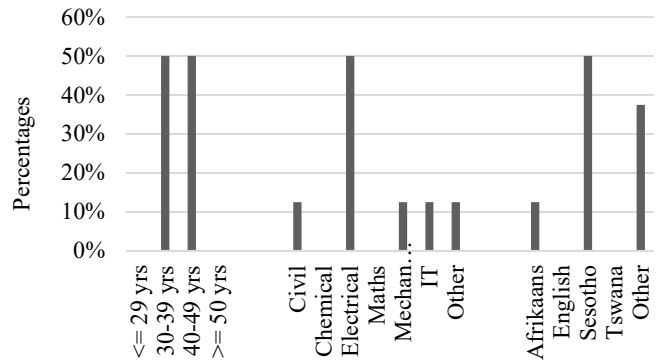


Figure 5: 2018 participant profile

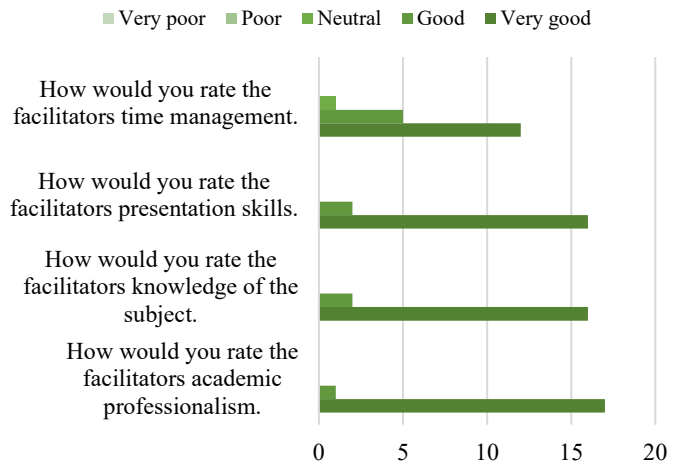


Figure 6: Participant perceptions regarding the facilitators

Figure 7 indicates the perceptions of the participants with regard to the workshop itself. The majority of the participants (94%) agreed that the workshop venue was appropriate. Appropriate facilities enhance not only the learning process, but also contributes to student satisfaction [35]. Time management is of great importance to academics in TVET colleges who need to cover specific course content in a limited amount of time [36]. Wasting time is therefore not an option. Many of the participants expressed the view that the practical workshop was not a waste of time (83% disagreed with the given statement). The majority (61%) further agreed that the workshop was relevant to their work responsibilities. This correlates well with the disciplines shown in Figure 4 and Figure 5, where 10 out of the 18 participants (56%) came from electrical engineering. However, it further correlates with literature showing the relevance of Arduino in different disciplines [25, 30]. A good indication that the workshop was valuable relates to the fact that 89% of the participants strongly

agreed that they would recommend it to their colleagues. Table 1 shows the conceptual knowledge questions that were used in the pre-post test.

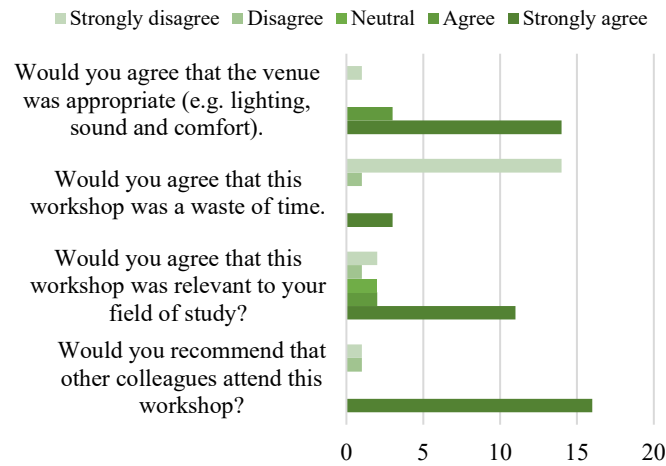


Figure 7: Participant perceptions regarding the workshop

Table 1: Questions used in the pre- and post-test

Number	Questions	Possible choices
Q5	Allow an AC signal to pass, while blocking a DC signal	Capacitor
Q6	Reduce the number of electrons flowing in a circuit	Resistor
Q7	Provide voltage regulation	Zener Diode
Q8	Block direct current in only one direction	Diode
Q9	Isolate two different circuits	Transformer
Q11	Measure the amount of water in a JOJO tank	Ultrasonic sensor
Q12	Determine if the door to your home is open	Reed Switch
Q13	Used as a smoke detector	Photocell
Q14	Switch on a light when a person enters a room	PIR receiver
Q15	Determine if a car's boot is open (no magnets available)	Tilt sensor

The first five questions (Q5 – Q9) focused on basic electronic components, such as the capacitor, resistor, Zener diode, diode and transformer. The next five questions (Q11 – Q15) focussed on sensor based electronic components, including the ultrasonic sensor, reed switch, photocell, PIR and tilt sensor. Participants were expected to engage with the majority of these components during their practical “hands-on” work in the laboratory. Knowledge of these components would be required before they can be correctly applied and connected to an Arduino microprocessor. The pre-test sought to establish the conceptual knowledge of the participants regarding these electronic components, which was then deconstructed (if their initial perceptions were wrong) and then re-constructed during the rest of

the practical workshop. The post-test sought to establish whether the participant conceptual knowledge had been strengthened (if their initial perceptions were right) or had been re-constructed.

The pre-test was done at the start of the workshop using an ERS. Immediate feedback of all the participant responses was presented and analysed in order to strengthen or reconstruct relevant conceptual knowledge. The post-test was done at the end of the workshop using Google Forms, as the academics were in a computer-based laboratory with Internet access. The scores for the pre-test (dotted line) and post-test (solid line) for 2017 and 2018 are shown in Figure 8 and Figure 9 respectively.



Figure 8: Participant responses to the conceptual knowledge questions for 2017

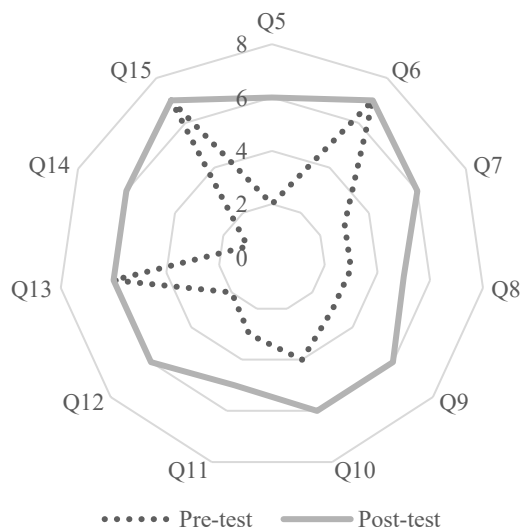


Figure 9: Participant responses to the conceptual knowledge questions for 2018

Questions 5, 7 and 9 indicate that the workshop impacted positively on the conceptual knowledge of the participants regarding the capacitor (Q5), the Zener diode (Q7) and the transformer (Q9). Only a few participants could correctly select the transformer in the pre-test as a component which may be used to



isolate two different circuits. However, the majority of the participants selected the correct answer in the post-test. This suggests that the academics' conceptual knowledge was reconstructed. No improvement was noticed regarding resistors (Q6) in both workshops (2017 and 2018). Participants also did not struggle in identifying the purpose of a diode (Q8) in 2017, although this did prove a little challenging in 2018 (3 out of 8 correctly identified the purpose with the pre-test). This may indicate that resistors and diodes are well known, and well used, by these participants.

Question 10 (Q10) was added in the second workshop to incorporate an inductor, as it was missing from the first workshop. Participants struggled to identify its purpose in the pre-test (4 out of 8) while seven participants correctly identified its purpose in the post-test for 2018.

Questions 11 through 15 relate to other electronic sensors that are commonly integrated with Arduino technology (see Table 1). Improvements in conceptual knowledge are evident for Q11 (Ultrasonic sensor), Q12 (Reed Switch) and Q14 (PIR). This reconstruction of knowledge can surely benefit these academics in terms of improving their own teaching practice. Participants strengthened their conceptual knowledge regarding the tilt sensor (Q15), as they correctly identified its purpose in the pre-test and in the post-test.

Pre-test results for the photocell in 2017 (Q13 in Figure 8) revealed that 8 out of the 10 academics would use it as a light sensor. The question was phrased as follows "Please select the component that you would use for a day/night sensor". Obviously, the participants could associate the term "photo" with "light", and thereby selected the photocell as the desired component. However, the post-test revealed that only 3 academics would use it as a smoke detector, which is a decrease of 50% from the pre-test with regard to the conceptual knowledge of the participants. The question in the post-test considered a different application for the photocell and was phrased as follows "Please select the component that you would use as a smoke detector". The majority of the participants could not deduce that the presence of smoke would interrupt the reception of light by the photocell, thereby affecting its resistance and triggering an alarm condition. This indicated that more time needed to be allocated to the discussion of the photocell in future workshops and that the facilitators needed to revisit this question in the post-test.

This was done prior to the second workshop that was offered in 2018. The question was revised to state: "Please select the component that you would use to switch a light on when it becomes dark". Phrasing the two questions differently, but using the same application, by using synonyms for the key words' day (being light) and night (being dark) resonated more with the participants. Results in Fig. 9 show NO decrease in the participant's conceptual knowledge for this component (Q13), but an actual strengthening of it. The correct response to the purpose of the photocell, or LDR, was observed for both tests in 2018. Using different applications (day/night sensor versus a smoke sensor) for the same component (photocell) proved a little problematic for the majority of the participants. This can further be addressed in the first stage of future workshops by discussing with

the participants a greater variety of applications for each of the electronic components.

## **7. Conclusions**

The purpose of this article was to illustrate how engineering academics from a TVET college were able to engage with the theory and practice of sensor integration with Arduino technology, thereby strengthening or reconstructing their conceptual knowledge of these electronic components. A practical workshop, or academic development workshop, was designed and facilitated by experts in electrical engineering. The 2-day workshop consisted of two stages that were presented to 18 academics from a TVET college in SA during 2017 and in 2018. The first stage sought to obtain the conceptual knowledge of TVET academics relating to 10 electronic components and sensors using a pre-test. The second stage related to four practical assignments that the participants needed to complete in a laboratory, followed by an online post-test that was again used to determine their conceptual knowledge. This was done to determine the value, and impact, of the practical workshop.

Conceptual knowledge regarding capacitors, Zener diodes, transformers, ultrasonic sensors, reed switches and PIR had to be deconstructed, and then reconstructed again during the workshop for many of the participants. However, their conceptual knowledge regarding photocells deteriorated in 2017, requiring the facilitators to review their discussion on it. This was done before the second workshop was offered in 2018. The results of the revised question showed no decrease in the participant's conceptual knowledge for this component in 2018, but an actual strengthening of it. A key recommendation in this regard is to retain the same application for each electronic component between the pre-test and post-test. However, synonyms or different phrases could be used between the two questions. Another option is to enhance the discussion after the pre-test, but before the post-test, by providing participants with a greater variety of applications for each of the electronic components.

Conceptual knowledge regarding resistors, diodes and tilt sensors were strengthened, as the results between the pre- and post-test remained similar. TVET academics further indicated that the practical workshop was relevant to their work and that they would encourage fellow colleagues to attend future workshops.

A limitation of this study is related to the small sample size, where only 18 TVET college academics attended the workshops. However, the research methodology chosen was a case study that aims to explore and describe a setting where the researcher can gain a more in-depth understanding of what he/she is seeking. In this research, the facilitators were seeking to determine if the practical workshop (the setting) that they designed would be able to help TVET college academics to strengthen, or reconstruct, their conceptual knowledge of electronic components that may be integrated with the Arduino technology. This was achieved as only one question had to be rephrased in the pre and post-test. Subsequent offerings of this practical workshop should therefore not present any major challenges with regard to determining conceptual knowledge, as it has been validated on two occasions.

It is recommended that more such academic development workshops be offered as practical workshops by field experts to

enable fellow academics to either strengthen, or reconstruct, their conceptual knowledge of relevant technologies. This would also greatly contribute to meeting the requirements of CPD, as required by professional engineering bodies around the world.

### Conflict of Interest

The authors declare no conflict of interest.

### Acknowledgment

The authors wish to acknowledge the financial support of the Manufacturing, Engineering and Related Services SETA (merSETA) in South Africa.

### References

- [1] Swart, A. J. and Hertzog, P. E., "Engaging academics from an engineering training college with Arduino sensors using an academic development workshop," presented at the ICST 2018, 12th International Conference for Sensing Technology, Limerick, Ireland, 2018.
- [2] Grinter, L. E., "Responsibility in engineering education," *The Journal of Higher Education*, **25**(5), 258-261, 1954.
- [3] Swart, A. J., "Does it matter which comes first in a curriculum for engineering students – theory or practice?," *IJEEE, International Journal of Electrical Engineering Education*, **47**(2), 189-199, 2010. DOI:10.7227/IJEEE.47.2.8.
- [4] McCulloch, A. and Loeser, C., "Does research degree supervisor training work? The impact of a professional development induction workshop on supervision practice," *Higher Education Research & Development*, **35**(5), 968-982, 2016.
- [5] Swart, A. J., Luwes, N., Olwagen, L., Greyling, C., and Korff, C., "Scholarship of teaching and learning – "What the hell" are we getting ourselves into?," *EJEE, European Journal of Engineering Education*, **42**(6), 653-667, 2016. DOI:10.1080/03043797.2016.1214689.
- [6] Mardapi, D. and Herawan, T., "Community-Based Teacher Training: Transformation of Sustainable Teacher Empowerment Strategy in Indonesia," *Journal of Teacher Education for Sustainability*, **21**(1), 48-66, 2019. DOI:10.2478/jtes-2019-0004.
- [7] Umelo, N., Amadi, A., Obodoze, F., and Onyibe, C., "A Multi-purpose Hardware Efficient Temperature Regulator with LCD Display," *International Journal of Computer Engineering and Information Technology*, **9**(10), 254-257, 2017.
- [8] Yükksekaya, M. and Haberal, O. E., "An Efficient Microcontroller Course With An Affordable And Easy To Use Development Setup," presented at the EPESS, The Eurasia Proceedings of Educational & Social Sciences, 2015.
- [9] Fan, Y. B. and Liu, H., "Study on Application Model of Internet of Things for Green Manufacturing," *Applied Mechanics and Materials*, **484**(1), 187-190, 2014. DOI:10.4028/www.scientific.net/amm.484-485.187.
- [10] Vorster, J. and Quinn, L., "Privileging knowledge, creating knowers: An analysis of a formal programme for university lecturers," *Re-Imagining Academic Staff Development: Spaces for Disruption*, edited by L. Quinn, 71-88, 2012.
- [11] Ndebele, C., "Deconstructing the narratives of educational developers on the enabling and constraining conditions in their growth, development and roles as educational staff development facilitators at a South African University," *International Journal of Educational Sciences*, **6**, 103-115, 2014. DOI:10.1080/09751122.2014.11890123.
- [12] Makondo, L. and Makondo, O., "The Interplay between South African Higher Education Context and Academic Development," *Anthropologist*, **17**(2), 301-309, 2014. DOI:10.1080/09720073.2014.11891438.
- [13] Swart, A. J., "Distance Learning Engineering Students Languish Under Project-Based Learning, But Thrive in Case Studies and Practical Workshops," *IEEE Transactions on Education*, **59**(2), 98-104, 2016. DOI:10.1109/TE.2015.2453349.
- [14] Gibbs, G. R., "Workshop: Producing educational videos: design and workflow issues," presented at the Inspire Conference, HEA Social Sciences Conference, The Studio, Manchester, 2015.
- [15] Ooi, P. C. and Tan, M. T., "Effectiveness of workshop to improve engineering students' awareness on engineering ethics," *Procedia-Social Behavioral Sciences*, **174**(2015), 2343-2348, 2015. DOI:10.1016/j.sbspro.2015.01.898.
- [16] Manley, K., Martin, A., Jackson, C., and Wright, T., "A realist synthesis of effective continuing professional development (CPD): A case study of healthcare practitioners' CPD," *Nurse education today*, **69**, 134-141, 2018. DOI:10.1016/j.nedt.2018.07.010.
- [17] Cole, M. J., "An Exploration of the Long-Term Impacts of Short CPD Workshops," PhD, Northumbria University, 2018.
- [18] Mack, H. G., Golnik, K. C., Murray, N., and Filipe, H. P., "Models for implementing continuing professional development programs in low-resource countries," *MedEdPublish*, **6**, 1-18, 2017. DOI:10.15694/mep.2017.000018.
- [19] Cruywagen, H., "Continuing professional development for the quantity surveying profession in South Africa: commentary," *Acta Structilia: Journal for the Physical Development Sciences*, **14**(2), 91-103, 2007. DOI:hdl.handle.net/10520/EJC110013.
- [20] Kasimba, R., "Training and Development Programs in Educational Institutions: A Human Factor Approach," *Journal of Gleanings from Academic Outliers*, **3**(1), 64-86, 2014.
- [21] Altbach, P., "Higher education and the WTO: Globalization run amok," *International Higher Education*, **23**, 2-4, 2015.
- [22] Shapiro, J. P. and Stefkovich, J. A., *Ethical leadership and decision making in education: Applying theoretical perspectives to complex dilemmas*. New York: Routledge, 2016.
- [23] Spooner, E., *Interactive Student Centered Learning: A Cooperative Approach to Learning*. Lanham: Rowman & Littlefield, 2015.
- [24] Ryan, M. and Ryan, M., "Theorising a model for teaching and assessing reflective learning in higher education," *Higher Education Research & Development*, **32**(2), 244-257, 2013. DOI:10.1080/07294360.2012.661704.
- [25] Hertzog, P. E. and Swart, A. J., "Arduino - Enabling engineering students to obtain academic success in a design-based module!," presented at the EDUCON 2016, IEEE Global Engineering Education Conference, Abu Dhabi, UAE, Dusit Thani Hotel, 2016.
- [26] Swart, A. J. and Hertzog, P. E., "LED's as viable power loads for experimental purposes relating to PV modules in pico-solar systems," presented at the ICETAS 2017, AMA International University Bahrain, Bahrain, 2017.
- [27] Swart, A. J. and Hertzog, P. E., "Evaluating the Performance of Small-Scale PV Modules in a Semi-Arid Area to Identify any Anomalies," *IJST, Indian Journal of Science and Technology*, **12**(28), 1-9, 2019. DOI:10.17485/ijst/2019/v12i28/147001.
- [28] Love, P. E., Zhou, J., and Matthews, J., "Project controls for electrical, instrumentation and control systems: Enabling role of digital system information modelling," *Automation in Construction*, **103**, 202-212, 2019. DOI:10.1016/j.autcon.2019.03.010.
- [29] Neafsey, P. J., "Computer-assisted instruction for home study: a new venture for continuing education programs in nursing," *The Journal of Continuing Education in Nursing*, **28**(4), 164-172, 1997. DOI:10.3928/0022-0124-19970701-06.
- [30] Schlingloff, B.-H., "Towards a curriculum for model-based engineering of embedded systems," in *Tagungsband des Dagstuhl-Workshops*, H. Giese, et al., Eds., ed Munchen: fortiss GmbH, 2014, pp. 83-90.
- [31] Robertson, S.-A. and Graven, M., "Exploring South African mathematics teachers' experiences of learner migration," *Intercultural Education*, **26**(4), 278-295, 2015. DOI:10.1080/14675986.2015.1071754.
- [32] Kirillov, A. V., Tanatova, D. K., Vinichenko, M. V., and Makushkin, S. A., "Theory and practice of time-management in education," *Asian Social Science*, **11**(19), 193-204, 2015. DOI:10.5539/ass.v11n19p193.
- [33] Hori, T. and Alley, M., "W-10 Rethinking Oral Presentations for Engineers in a Global Society," presented at the JSEE, Japanese Society for Engineering Education Annual Conference, Tokyo City University, Setagaya Campus, 2017.
- [34] Kolsaker, A., "Academic professionalism in the managerialist era: A study of English universities," *Studies in Higher Education*, **33**(5), 513-525, 2008. DOI:10.1080/03075070802372885.
- [35] Hanssen, T.-E. S. and Solvoll, G., "The importance of university facilities for student satisfaction at a Norwegian University," *Facilities*, **33**(13), 744-759, 2015. DOI:10.1108/F-11-2014-0081.
- [36] Buthelezi, Z. and Training, "Lecturer experiences of TVET College challenges in the post-apartheid era: a case of unintended consequences of educational reform in South Africa," *Journal of Vocational Education*, **70**(3), 364-383, 2018. DOI:10.1080/13636820.2018.1437062.

## The Usability Evaluation of Academic Progress Information System (SIsKA-NG)

Gede Indrawan\*, I Made Agus Oka Gunawan, Sariyasa

Computer Science Department, Universitas Pendidikan Ganesha, 81116, Indonesia

---

### ARTICLE INFO

#### Article history:

Received: 27 January, 2020

Accepted: 22 February, 2020

Online: 04 April, 2020

---

#### Keywords:

Performance Measurement

Retrospective Think Aloud

User Experience Questionnaire

---

### ABSTRACT

*Limited functionalities of the Academic Progress Information System (SIsKA) has direct consequences on the quality of thesis management service at the authors' magister study program of the authors' university. This research focused on the significant improvement from the previous User Experience Questionnaire (UEQ) result of SIsKA. That significant improvement was based on the recommendations from the previous Heuristic Evaluation (HE) and two additional usability evaluation methods. All of those improvements have been applied to the new Academic Progress Information System that was called SIsKA Next Generation (SIsKA-NG). Overall, there are three usability evaluation methods were used in this research, namely the Performance Measurement (PM), the Retrospective Think Aloud (RTA), and the UEQ. The PM through the effectiveness analysis and the efficiency analysis each provided 11 and 16 recommendations, while The RTA provided 39 recommendations. The UEQ provided the assessment on SIsKA-NG with level excellent on aspect of attractiveness, efficiency, dependability, stimulation, and novelty; and with level good on aspect of perspicuity. It was considered as a significant improvement of the UEQ result of SIsKA-NG compared to the previous UEQ result of SIsKA because of the better assessment on four aspects with level excellent on SIsKA-NG, namely attractiveness, efficiency, dependability, and novelty. Same assessments are on two aspects, namely perspicuity and stimulation. SIsKA-NG still need to be improved based on the aspect of perspicuity, additional recommendations from the conducted Focus Group Discussion, and procedural White Box testing for code evaluation.*

### 1. Introduction

This paper conformed to the scope of the journal in Computer software and applications (A6) of Engineering & Technology topic. It addressed a particular complex system related to the thesis management information system. This paper is an extension of the work originally presented as a best paper in The 3rd Third International Conference on Informatics and Computing (ICIC) [1]. This paper focused on the significant improvement from the previous User Experience Questionnaire (UEQ) result of SIsKA. That significant improvement was based on the recommendations from the previous Heuristic Evaluation (HE) [1] and two additional usability evaluation methods conducted in this research, namely the Performance Measurement (PM) and the Retrospective Think Aloud (RTA). All of those improvements have been applied to the new Academic Progress Information System that was called SIsKA Next Generation (SIsKA-NG).

SIsKA itself is Indonesian abbreviation of "Sistem Informasi Kemajuan Akademik".

SIsKA that has been used at the authors' magister study program (refer to "the authors' study program" on the next discussion) of the authors' university has been able at certain level to manage the academic progress of the postgraduate student (refer to "the student" on the next discussion) related to their thesis research [1][2]. The future works of that previous research are on improving the UEQ result and following up the user interface improvement recommendations based on the HE using expert respondents.

This research focused on that future works and following up the recommendations from two additional usability evaluation methods, namely the PM and the RTA. The usability evaluation by involving the user respondents has an advantage on information about how the users use the system as well as problems faced directly by them [3]. There are three categories of usability

---

\* Gede Indrawan, 685 Email : [gindrawan@undiksha.ac.id](mailto:gindrawan@undiksha.ac.id)



evaluation methods, namely inspection, testing, and inquiry [4]. This research used both of testing and inquiry for observing the users and their response to get the improvement recommendations.

This paper is organized into several sections, i.e.: Section 1 (Introduction) describes the problem background related to the improvement of SIsKA based on its previous UEQ result [1]; Section 2 (Literature Survey) describes the related works in area of usability testing methods; Section 3 (Research Method) contains the research stages for all of SIsKA improvements applied to SIsKA-NG; Section 4 (SIsKA-NG) provides several aspects related to its initial design and implementation; Section 5 (Result and Discussion) covers SIsKA-NG usability evaluation; and finally, Section 6 (Conclusion and Future Work) consists of some important concluded points.

**2. Literature Survey**

There are many usability testing methods that have been developed and tested to provide recommendations for improving a system. In one study, Ita et al. [1] successfully utilized the HE to produce recommendations based on expert aspects in the interface field. The PM is another usability testing method, where in one research, Widyanti et al. [5], used it in evaluating the interface of online transportation. The PM was used to obtain quantitative data to analyze the level of effectiveness and efficiency when the users carry out certain tasks [4][5][6]. Widyanti et al. combined the PM with the RTA, where the RTA is a Think Aloud method that can be combined with other usability methods [7][8]. Elling et al. [8] combined with eye movements method in analyzing the behavior of system users. Those research [5][8] provided a list of recommendations for the improvement of the system being evaluated.

In addition to usability testing, the level of satisfaction of user experience also needs to be calculated by determining the aspects to be evaluated [1]. The inquiry method is one method that can be used to evaluate user experience [4]. The UEQ, as one type of Questionnaire, usually takes 3-5 minutes to read and complete the questionnaire [9]. The UEQ has the questionnaire items that can make the respondents do not think too long to fill out the questionnaire [10]. The purpose of the UEQ is to compare the level of user experience between two products, test the user experience of a product, and determine area of improvement [11]. The UEQ has the advantage of measuring aspects of user experience of the product very quickly [12].

In our research, we combined the PM method with the RTA method by involving system users. We also calculated the satisfaction value of user experience using UEQ to get aspects of user experience that must be improved. This research is not limited to obtain system improvement recommendations as in the previous studies [1][5][8], but also carried out the implementation phase at the authors' postgraduate program server. So that the recommendations for improvements that are obtained directly can be tested by the users and of course will get other recommendations, closely related to the system implementation environment.

**3. Research Method**

Figure 1 shows the research method in the form of a flow chart. The initial stage of this research was to design and to implement

SIsKA-NG that follows up the previous HE recommendations [1] related to the user interface improvement of SIsKA web page (refer to "page" on the next discussion), as shown by Table 1. Note that Table 1 has been updated by additional expert recommendations since the previous publication [1].

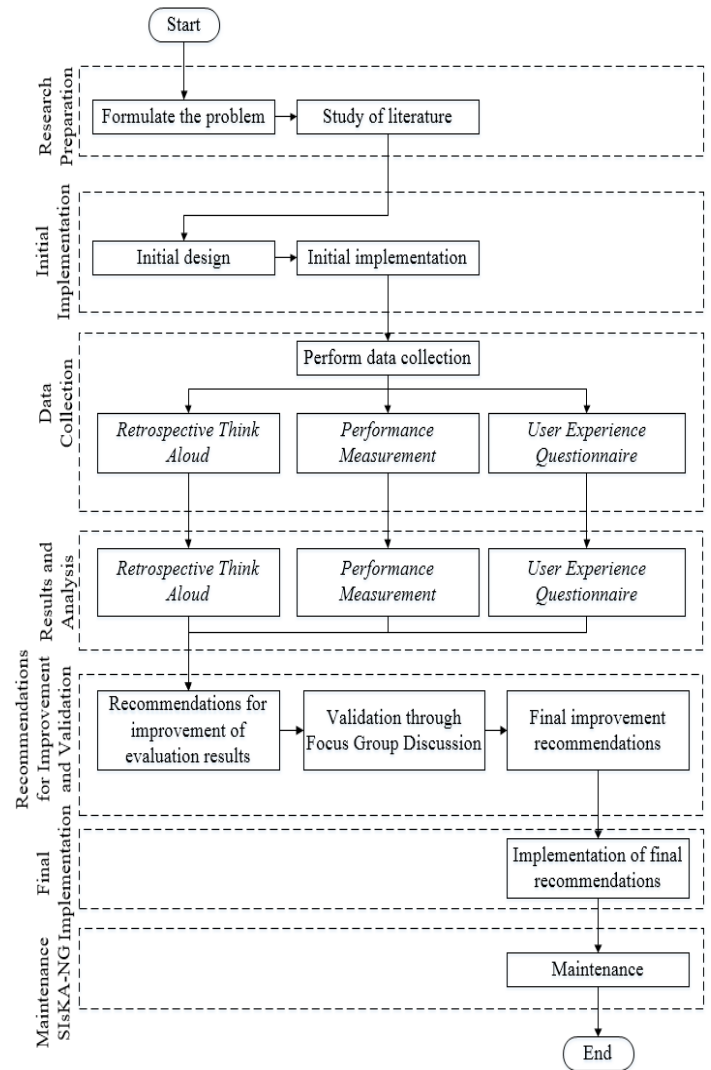


Figure 1: Research Method

The usability evaluation with the PM and the RTA was conducted afterwards, and their improvement recommendations were then validated by SIsKA-NG manager, namely the authors' study program manager and the authors' postgraduate program Information Technology (IT) manager. The process was continued to implement the recommendations on SIsKA-NG at the authors' postgraduate program server. The maintenance was conducted after establishing the implementation.

The UEQ used 20 respondents [11][13] who carried out certain tasks according to the pages being evaluated [14]. Evaluation on the administrator pages used 25 tasks, the lecturer pages used 14 tasks, and the student pages used 21 tasks. Each respondent run each task 2 times to get a difference in the level of effectiveness and efficiency. The final stage of data collection was filling in the questionnaire (Figure 2) combined with the additional questions to clarify the answers of the respondents [15].



Table 1: The Updated Previous Recommendations of SIsKA

No	Violated principle(s)	Recommendation(s)
1	Visibility of system status (feedback). When the confirmation to delete the data appears, the "Delete" button is blue, while the "Back" button is red.	<ol style="list-style-type: none"> <li>1. Use standard color of buttons, such as red for "Delete" button and blue for "Back", so the users do not misunderstand and make a mistake.</li> <li>2. There should be a response that distinguishes visually when the object is given an action (selected, pressed, etc.).</li> <li>3. Naming the menu and the page in accordance with its content.</li> <li>4. Color must be clear on the button or functional system.</li> </ol>
2	Use Control and Freedom. The users are forced to change the password if the password is the same with the username.	<ol style="list-style-type: none"> <li>1. Instead of forcing the users to change the password, they should be given a warning. The users have the freedom to decide either to change or to leave their password.</li> <li>2. There should be a feature to manage personal account data of each user, including sensitive information such as password.</li> </ol>
3	Flexibility and Efficient of Use. Search feature does not exist yet, there is only a search in the table, which is not appropriate.	The search feature should be placed at the upper right corner of the page according to the standard system interface in general.
4	Recognition rather than Recall. There is no error warning message when the users make a mistake.	<ol style="list-style-type: none"> <li>1. The system do not prevent the users from making a mistake. For an example, in making examination schedule. If the users have to add schedule first, the button to manage the participants should be disabled so that they are prevented to press the button.</li> <li>2. The added schedule feature is done one by one, so that the users do not make a mistake, such as pressing the manage button of the participant first and then creating the examination schedule data.</li> </ol>
5	Consistency and Standards. The "Add" menu is inconsistent.	<ol style="list-style-type: none"> <li>1. The menu should be consistent, should add "Add" menu in lectures data page.</li> <li>2. Consistency on the use of grammar in naming menus provided by the system.</li> <li>3. Consistency on color selection on the system.</li> </ol>
6	Aesthetic and Minimalist Design. There is no clear instructions/description on any given page, so the users can only guess the content/intent of the page.	Each page is given a clear and informative description so that the users do not guess the intent of the page. For an example, the student home page still empty. It should be filled with the informative information, such as the registration flow of the proposal to the thesis examination; or the information related to the history of the stage passed by the student (see next Figure 4).
7	Error Prevention. The system do not prevent the users from making a mistake.	<ol style="list-style-type: none"> <li>1. The system needs to prevent the users from making a mistake, such as providing a message to make sure whether they actually logout or not.</li> <li>2. Provision of automatic data entry feature or the system provides clear data format, such as date, time, and telephone number.</li> <li>3. Provision of warning feature about data or action that can cause error.</li> </ol>
8	Help and Documentation. There is no help menu.	<ol style="list-style-type: none"> <li>1. Creating a help menu to make it easier for the users to use the system, including: 1) News; 2) System Guidance; and 3) Frequently Asked Question (FAQ).</li> <li>2. Creating a site map to make it easier for the users to navigate the system.</li> </ol>
9	Match between system and real world	The use of grammar that can be understood directly by the users in accordance with their expectations.

		1	2	3	4	5	6	7		
The product should look enjoyable	annoying	○	○	○	○	○	○	○	enjoyable	1
The product should be understandable	not understandable	○	○	○	○	○	○	○	understandable	2
The product should be creative	creative	○	○	○	○	○	○	○	dull	3
The product should be easy to learn	easy to learn	○	○	○	○	○	○	○	difficult to learn	4
Using the product should be valuable	valuable	○	○	○	○	○	○	○	inferior	5
Using the product should be exciting	boring	○	○	○	○	○	○	○	exciting	6
Using the product should be interesting	not interesting	○	○	○	○	○	○	○	interesting	7
The interaction with the product should be predictable	unpredictable	○	○	○	○	○	○	○	predictable	8
I should perform my tasks with the product fast	fast	○	○	○	○	○	○	○	slow	9
The product should be inventive	inventive	○	○	○	○	○	○	○	conventional	10
The interaction with the product should be supportive	obstructive	○	○	○	○	○	○	○	supportive	11
The product should look good	good	○	○	○	○	○	○	○	bad	12
The product should be easy	complicated	○	○	○	○	○	○	○	easy	13
The product should look pleasing	unlikable	○	○	○	○	○	○	○	pleasing	14
The product should be leading edge	usual	○	○	○	○	○	○	○	leading edge	15
The product should look pleasant	unpleasant	○	○	○	○	○	○	○	pleasant	16
The interaction with the product should be secure	secure	○	○	○	○	○	○	○	not secure	17
Using the product should be motivating	motivating	○	○	○	○	○	○	○	demotivating	18
The interaction with the product should be meet my	meets expectations	○	○	○	○	○	○	○	does not meet expectations	19
I should perform my tasks with the product efficient	inefficient	○	○	○	○	○	○	○	efficient	20
The product should be clear	clear	○	○	○	○	○	○	○	confusing	21
I should perform my tasks with the product practical	impractical	○	○	○	○	○	○	○	practical	22
I should perform my tasks with the product organized	organized	○	○	○	○	○	○	○	cluttered	23
The product should look attractive	attractive	○	○	○	○	○	○	○	unattractive	24
The product should look	friendly	○	○	○	○	○	○	○	unfriendly	25
The product should be innovative	conservative	○	○	○	○	○	○	○	innovative	26

Figure 2: Twenty-Six Statement Items of UEQ

4. SIsKA-NG

Based on Table 1, the initial design of SIsKA-NG with its main functionalities is elaborated by using a use case diagram [16], as shown by Figure 3. The use case diagram shows the main functionalities related to the management of research, involving three stages of examination (proposal, pre-thesis, and thesis), and three kinds of user (administrator, lecturer, and student). Part of those examination stages was shown by Figure 4. Related to kinds of user, the administrator manage any data related to the student research, including research data, examination prerequisites, and examination schedule. The students can submit their research data and examination prerequisites, and later view examination schedule, as well as list of existing researchs. The lecturers have access to see the examination schedule related to their role as a supervisor or an examiner. All those described functionalities can be done by the users if they have logged in to SIsKA-NG.

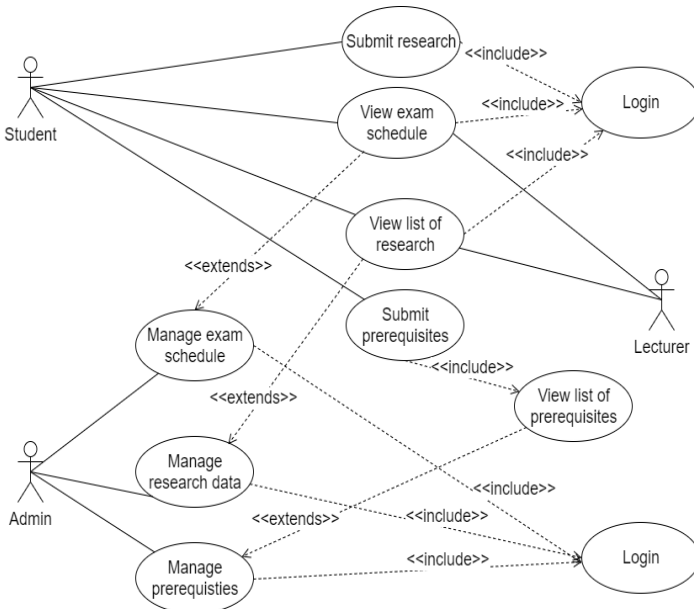


Figure 3 Use Case Diagram of SIsKA-NG

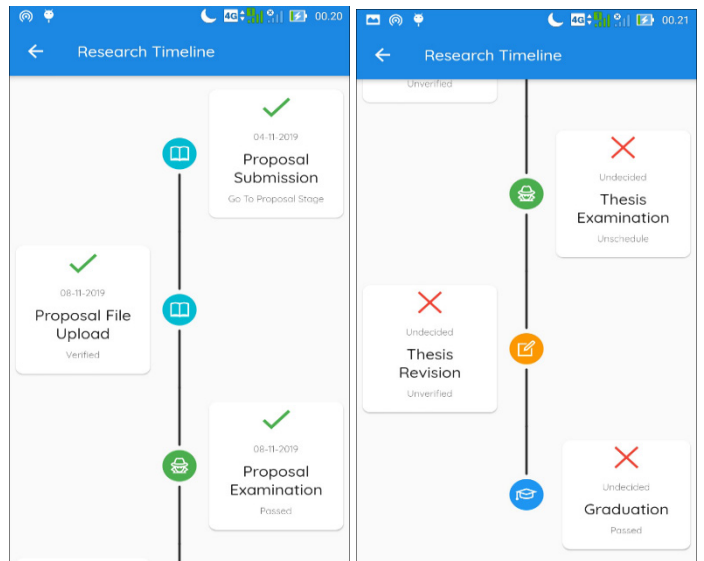


Figure 4 Part of the Student's Examination Stages of SIsKA-NG on its mobile application: Proposal (Left); Thesis (Right)

Figure 5 shows an the Entity Relationship Diagram (ERD) of SIsKA-NG with the entities and their relationships that are described by using the Crow's Foot model [17] from the previous recommendations [1], as shown by Table 1. There are 17 entities related to each other. These entities in the ERD is used for SIsKA-NG new database implementation.

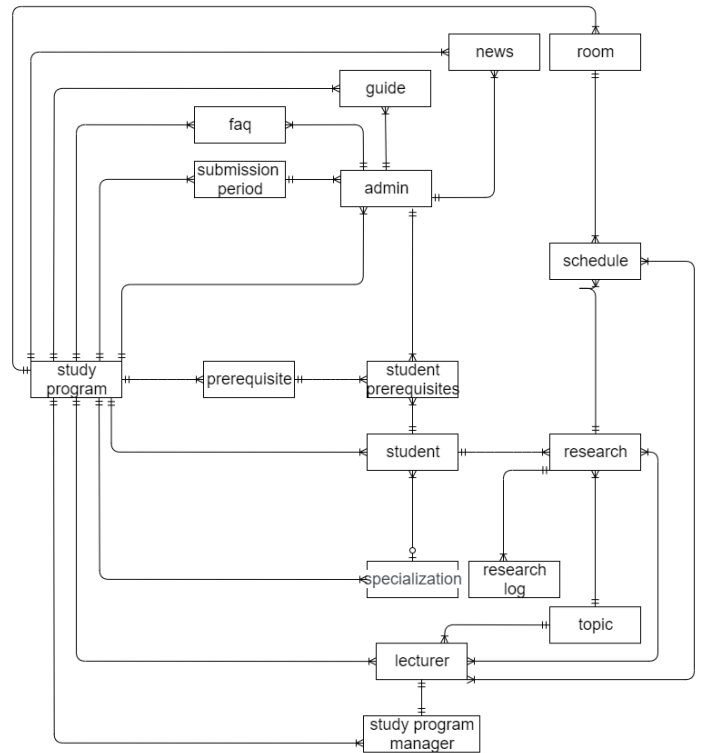


Figure 5 ERD of of SIsKA-NG

The ERD also shows relationship type of one-to-one and one-to-many. For example, one-to-one relationship connects the lecturer and the study program manager since only one lecturer can be a study program manager, meanwhile one-to-many relationship

connects the specialization and the student since one specialization can be assigned to many students.

In addition to the functionality requirement design using use case diagram and ERD, an analysis was also carried out for non-functionality requirement related to the implementation. Table 2 shows the non-functionality requirement that are tailored to the authors' postgraduate program server specification. Based on Table 2, a web framework CodeIgniter was used to improve the novelty aspect of SIsKA-NG technology. That framework supports PHP 5.6 and one of the latest web technologies [18][19].

Table 2 Non-Functionality Requirement of SIsKA-NG

No	Requirement	Specification
1	Web Server	Apache: 2.4.x
2	DBMS	MySQL: 5.x
3	PHP	PHP: 5.6

The result of the initial implementation based on the previous recommendations (Table 1) produced SIsKA-NG with an improved interface. As an example, Figure 6 shows the administrator starting page.

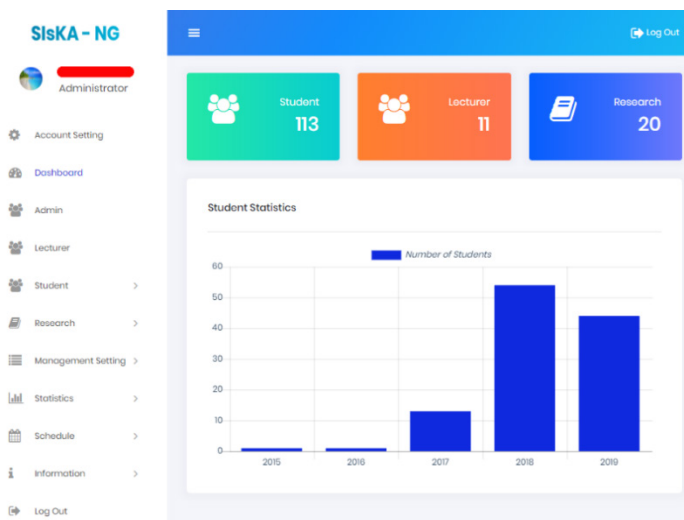


Figure 6: SIsKA-NG initial implementation of the Administrator Starting Page

## 5. Result and Discussion

### 5.1. The Performance Measurement

The PM was conducted through the effectiveness analysis and the efficiency analysis. The effectiveness of SIsKA-NG was obtained by counting the number of failures that occur when the respondent completes the task. The effectiveness analysis was conducted by reviewing the video of the work done by the respondent to see the factors that cause the respondent failed to complete the task. All factors that cause failure were then summarized so get a final list of causes of failure and recommendations for the improvement.

Table 3 shows the result of SIsKA-NG effectiveness analysis. On the administrator pages, there are four factors that cause failure, namely: 1) Unclear menus that need to be regrouped and renamed; 2) Less effective position of the student prerequisites sub menu; 3) Less effective position of the action button; and 4) Less effective

display button. On the lecturer page, there are four factors that cause failure, namely: 1) Less effective position of the action button; 2) Less clear icon of the action button; 3) Less clear filter feature of each research stage and the examination schedule; and 4) The clarity of the grammar on the page. On the student page, there are four factors that cause failure, namely: 1) Less effective position of the action button; 2) Less clear icon of the action button; 3) The examination schedule that does not directly displays the detail schedule; and 4) The clarity of the grammar on the page. Table 4 shows the list of the recommendations based on the effectiveness analysis.

Table 3: The Result of SIsKA-NG Effectiveness Analysis

Pages	1 <sup>st</sup> Test		2 <sup>nd</sup> Test	
	Errors	Percentage	Errors	Percentage
Administrator	23	4,60%	5	1%
Lecturer	20	7,14%	8	2,86
Student	14	3,33%	9	2,14%

The efficiency of SIsKA-NG was obtained by comparing the time spent by the respondent on the first and the second trial. This efficiency calculation used a statistical comparison of the Mann Whitney U-test. Comparison of work time data from two experimental groups requires two hypotheses for each task, namely:

- H0 : There is no time difference in the completion of task [task number] between the first trial and the second trial.
- H1 : There is time difference in the completion of task [task number] between the first trial and the second trial.

Final computation of the efficiency data processing was done by comparing the *p*-value generated from the Mann Whitney U-test [6] of each task with a value of  $\alpha$  equal to 0.05. If the *p*-value is greater than 0.05, the decision taken do not reject H0. Analysis of the factors causing the efficiency is also done if H1 is true. Analysis of the factors causing this level of efficiency is done by reviewing the video of the work done by the respondent to see the factors causing the difference in task completion time. All factors are then summarized to obtain a final list of causes of the time difference in efficiency and its recommendations for the improvement.

Based on the results of *p*-value comparison of each task with value  $\alpha$ , then statistically there are 4 tasks that do not have a significant difference and 21 other tasks that have a significant difference from the completion time of each task on the administrator page. On the lecturer page, there are 10 tasks that do not have a significant difference and 4 other tasks that have a significant difference from the completion time of each task. On the student page, there are 10 tasks that do not have a significant difference and 11 other tasks that have a significant difference from the completion time of each task.

Tasks that show a significant difference in processing time are then analyzed in terms of causal factors by re-observing the video of respondent's work. It was found that on the administrator page, many respondents have difficulty in finding the action buttons and menus grouping that are unclear, so that in the first trial more time was needed to search for menus or functions for task completion.

On the lecturer and the student pages, significant time differences in some assignments were also found caused by inconsistent and unclear buttons positions, besides unclear grammar. Table 5 shows the list of the recommendations based on the efficiency analysis.

Table 4: The Recommendations based on the Effectiveness Analysis

No	Pages	The Recommendations
1	Administrator	<ol style="list-style-type: none"> <li>1. Be clear on the group and the name of the menus related to their function.</li> <li>2. The student prerequisites sub menu should be moved to the main menu.</li> <li>3. The action button should be moved to the left position of the page.</li> <li>4. The display button should be removed so the users only need to input the filter data.</li> </ol>
2	Lecturer	<ol style="list-style-type: none"> <li>1. The action button should be moved to the left position of the page.</li> <li>2. The icon of the action button should be easy to understand.</li> <li>3. Be clear on filter feature at each research stage and exam schedule.</li> <li>4. Be clear on the grammar on the page.</li> </ol>
3	Student	<ol style="list-style-type: none"> <li>1. The action button should be moved to the left position of the page.</li> <li>2. The icon of the action button should be easy to understand.</li> <li>3. The examination schedule should directly displays the detail schedule.</li> <li>4. Be clear on the grammar on the page.</li> </ol>

Table 5: The Recommendations based on the Efficiency Analysis

No	Pages	The Recommendations
1	Administrator	<ol style="list-style-type: none"> <li>1. Be clear on the group and the name of the menus related to their function.</li> <li>2. The action button should be moved to the left position of the page.</li> <li>3. The save button should be moved to the bottom position of the page.</li> <li>4. The display button should be removed so the users only need to input the filter data.</li> <li>5. The entire examination schedule should be displayed and could be filtered afterwards.</li> <li>6. Active Menu Tab should be colored for the visual clarity to the users.</li> <li>7. Help text should be added for the usage clarity to the users.</li> </ol>
2	Lecturer	<ol style="list-style-type: none"> <li>1. The save button should be moved to the bottom position of the page.</li> <li>2. Filter feature should be added to the stages in all research submenus.</li> <li>3. The display button should be removed so the users only need to input the filter data.</li> </ol>

3	Student	<ol style="list-style-type: none"> <li>1. Be clear on the group and the name of the menus related to their function.</li> <li>2. The action button should be moved to the left position of the page.</li> <li>3. The save button should be moved to the bottom position of the page.</li> <li>4. Summary of the previous research stage is automatically displayed when the users add research data.</li> <li>5. The examination schedule should directly displays the detail schedule.</li> <li>6. Active Menu Tab should be colored for the visual clarity to the users.</li> </ol>
---	---------	---

### 5.2. The Retrospective Think Aloud

Table 6, Table 7, and Table 8 show the summary of difficulties, problems, suggestions, and/or criticisms on SIsKA-NG page of the administrator, the lecturer, and the student, respectively. Related to the position mentioned further, it referred to the position at SIsKA-NG page.

Table 6: Summary of the RTA on the Administrator Pages of SIsKA-NG

No	Respondent Code	Summary
1	R01, R04, R05, R06, R08, R10, R12, R14, R15, R16, R17, R19, R20	Features/aspects on the main menu and perspicuity: <ol style="list-style-type: none"> <li>1. Menus seem unclear and should be grouped based on their similar function.</li> <li>2. Menus should stay visible so that when the users are at the bottom position, there is no need to scroll up to find them.</li> <li>3. Information of each form's field should be added to avoid user confusion.</li> <li>4. Alternating background color of row should be used for the visual clarity of data row.</li> <li>5. Tabs at the revision section of each research stage seem unclear and should be filled with distinguishing colors.</li> <li>6. Error notifications will stay visible, with the users having the freedom to close them.</li> </ol>
2	R01, R02, R03, R05, R06, R07, R08, R09, R11, R13, R14, R15, R17, R18, R19, R20	Features/aspects of the system button: <ol style="list-style-type: none"> <li>1. The save button should be moved to the bottom position of the page.</li> <li>2. The system functional button should be moved to the left position of the page.</li> <li>3. The display button should be removed for automatic data display.</li> </ol>
3	R01, R02	Features/aspects on the information menu: <ol style="list-style-type: none"> <li>1. Content should be enriched.</li> <li>2. The FAQs should be categorized specifically for the lecturer and the student.</li> </ol>
4	R08, R09	Features/aspects on the account setting:



No	Respondent Code	Summary
		<ol style="list-style-type: none"> <li>Account feature should be placed at the upper-right position for the easy access.</li> <li>Logged-in user display should be clickable to access the account management page.</li> </ol>
5	R05	Feature/aspect on the student prerequisites: its menu should be grouped according to each research stage.
6	R08	Feature/aspect on the file upload: there should be a preview when uploading image data.
7	R11	Feature/aspect on the system bug: data sorting fixation on the submission page.

Table 7: Summary of the RTA on the Lecturer Page of SIsKA-NG

No	Respondent Code	Summary
1	R01, R04, R05, R06, R07, R12, R13, R17, R18, R20	Features/aspects on the data filter: <ol style="list-style-type: none"> <li>Filter feature should be added to all menus at the research stages.</li> <li>Filter feature should be added according to the examination role.</li> </ol>
2	R02, R05, R06, R08, R09, R10, R12, R14, R15, R17, R18, R19, R20	Features/aspects of the system button: <ol style="list-style-type: none"> <li>The icon of the button should be easy to understand.</li> <li>The action button should be moved to the left position of the page.</li> <li>The display button should be removed on the schedule page.</li> </ol>
3	R03	Feature/aspect on the information menu: content should be enriched.
4	R03, R08	Feature/aspect on the account setting: account feature should be placed at the upper-right position for the easy access.
5	R11, R14, R16	Feature/aspect on the main menu: There should be a separation between menu groups for the visual clarity to the users.

Table 8: Summary of the RTA on the Student Page of SIsKA-NG

No	Respondent Code	Summary
1	R01, R03, R05, R06, R07, R08, R10, R11, R12, R14, R15, R16, R17, R19	Features/aspects on the main menu and perspicuity: <ol style="list-style-type: none"> <li>Menus seem unclear and should be grouped based on their similar function.</li> <li>Menus should stay visible so that when the users are at the bottom position, there is no need to scroll up to find them.</li> <li>Information of each form's field should be added to avoid user confusion.</li> <li>Unnecessary fields should be removed to avoid user confusion.</li> </ol>

No	Respondent Code	Summary
		<ol style="list-style-type: none"> <li>5. Tabs at the revision section of each research stage seem unclear and should be filled with distinguishing color.</li> <li>6. Error notifications will stay visible, with the users having the freedom to close them.</li> <li>7. Each stage in the timeline should be given a distinguishing color for the visual clarity of the stages that have been passed (see Figure 4).</li> </ol>
2	R01, R02, R03, R04, R05, R06, R07, R08, R09, R11, R13, R14, R15, R18, R19, R20	Features/aspects of the system button: <ol style="list-style-type: none"> <li>The save button should be moved to the bottom position of the add or edit page.</li> <li>The action button should be moved to the left position of the start page of each menu.</li> </ol>
3	R02	Feature/aspect on the information menu: content should be enriched.
4	R08, R09	Features/aspects on the account setting: <ol style="list-style-type: none"> <li>Account feature should be placed at the upper-right position for the easy access.</li> <li>Logged-in user display should be clickable to access the account management page.</li> </ol>
5	R10, R13, R18	Features/aspects on the research stage: summary from the previous stage is automatically seen when adding research data of the recent stage.
6	R07, R17	Features/aspects on the student prerequisites: <ol style="list-style-type: none"> <li>The student only need to upload prerequisite files according to the prerequisite requirement.</li> <li>Its menu should be grouped according to each research stage.</li> </ol>
7	R04, R11, R12, R18, R20	Feature/aspect on the examination schedule: detail schedule for the logged-in student should be displayed directly.

### 5.3. The User Experience Questionnaire

After following up the PM and the RTA recommendations, SIsKA-NG was used for the UEQ. The questionnaire was filled out by 20 respondents using SIsKA-NG. The UEQ value of 26 statement items (see Figure 2) obtained from each respondent was processed by using the provided UEQ Data Analysis Tool [9][13]. At the data analysis stage, testing was carried out by comparing the value of each aspect with the product data set available in the UEQ Analysis Data Tool. Benchmark test can describe the relative quality of SisKA-NG compared to the other products. Benchmark test result are divided into five categories, namely *Excellent*, *Good*, *Above Average*, *Below Average*, and *Bad*. Data obtained from the UEQ was the result of SIsKA-NG user experience measured

through six aspects, namely *attractiveness*, *perspicuity*, *efficiency*, *dependability*, *stimulation*, and *novelty* [11].

Figure 7 shows the result where Good category was obtained for *perspicuity* aspect. This category means that 25% of the products in the dataset are better than SISKA-NG while 50% of the others are worse. Excellent category was obtained for aspect of *attractiveness*, *efficiency*, *dependability*, and *stimulation*. Those results are in the range of 10% best results. Excellent category was also obtained for novelty aspect but 10% of the products in the dataset are better than SISKA-NG while 75% of the others are worse.

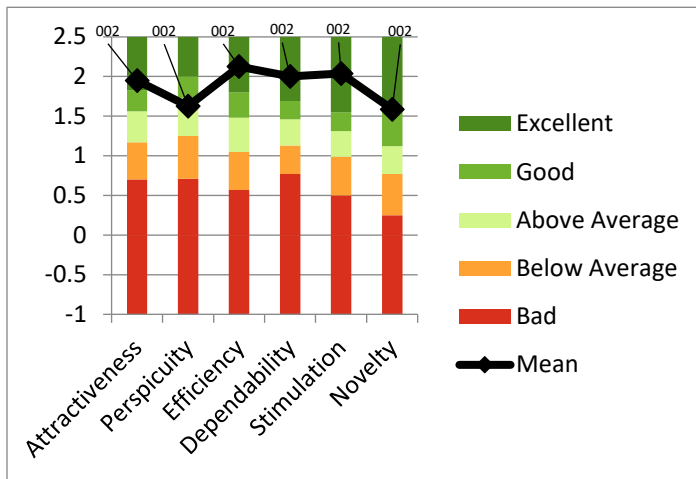


Figure 7: SISKA-NG Benchmark Graph

Previous SISKA with its six aspects each was assessed with the UEQ by score 1.59; 1.75; 1.64; 1.40; 1.56; and 1.10 [1]. The UEQ result of SISKA-NG, as shown by Figure 7, was considered as a significant improvement compared to the previous UEQ result of SISKA because of the better assessment on four aspects with level excellent, namely *attractiveness*, *efficiency*, *dependability*, and *novelty*. Same assessments are on two aspects, namely *perspicuity* (at level good even though SISKA has higher score) and *stimulation*.

#### 5.4. The Focus Group Discussion

Table 9 shows the additional recommendations that come from the Focus Group Discussion (FGD).

Table 9: The additional recommendations based on the FGD

No	The Recommendations
1	Addition of CSV file import feature for user data.
2	Printing of the examination schedule should be more attractive and based on existing design.
3	Addition of verification feature by the research supervisor.
4	Integration of the student prerequisites with the research submission.

The FGD discussed the result of the improvement recommendations obtained from the PM and the RTA evaluation. That FGD was conducted with the SISKA-NG administrator,

namely the authors' study program administrator and the authors' postgraduate program IT administrator. Those additional recommendations at Table 9 were considered as a reference for the further implementation.

#### 5.5. The Implementation

Figure 8 shows an example of the new interface of SISKA-NG, as one of the results of the final implementation based on the recommendations related to the menus grouping and the menus naming. That new interface is the result of the page improvement at Figure 6, which is the administrator starting page. Based on point 1 of the effectiveness recommendations of the administrator pages (Table 4), point 1 of the efficiency recommendations of the administrator pages (Table 5), and the RTA result, an improvement was made by grouping and by naming the menus related to their function.

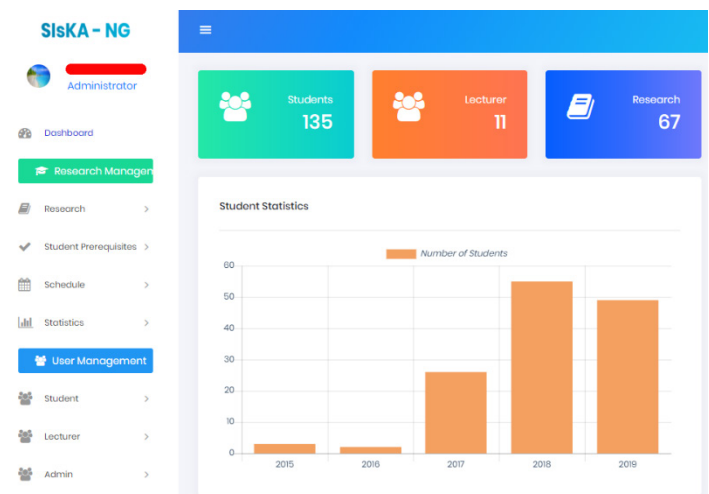


Figure 8 SISKA-NG final implementation of the Administrator Starting Page

#### 5.6. The Maintenance

SISKA-NG, which has been hosted at the authors' postgraduate program server, has been successfully used for the real case of student research data management. However, there are several things to be noted during the use, including:

- The framework code used was unstable at the authors' postgraduate program server in the code of Asynchronous JavaScript And XML (AJAX) [20][21] for displaying the initial table (Figure 9). This error occurred because some Internet Service Providers (ISPs) injected the advertising code that cause the AJAX code did not run perfectly. Based on in-depth testing, to avoid insertion of those advertisements SISKA-NG need to use the Hypertext Transfer Protocol Secure (HTTPS) Internet communication protocol.
- The authors' postgraduate program server need to be configured since the development Operating System (OS) was not the same as the production OS, neither do some software libraries needed (Figure 10).
- The file size that can be uploaded need to be adjusted because of recent 4MB limitation.

- Email notifications did not run at the server side, so additional email setting is required at the authors' postgraduate program server.
- The time to run a feature of SIsKA-NG need to be optimized by evaluating the structure of SIsKA-NG code.

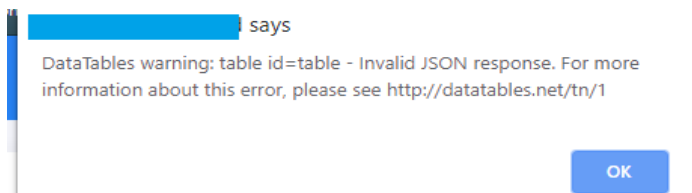


Figure 9: AJAX Error of SIsKA-NG

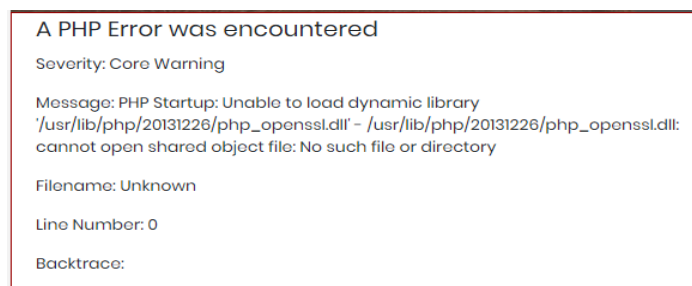


Figure 10: Software Library Error of SIsKA-NG

## 6. Conclusion and Future Work

This research has conducted significant improvement on the Academic Progress Information System that was called SIsKA-NG based on the usability evaluation. It gave better UEQ result of SIsKA-NG compared to the previous UEQ result of SIsKA since there are better excellent level assessment on four aspects of SIsKA-NG, namely *attractiveness*, *efficiency*, *dependability*, and *novelty*. Same assessments are on two aspects, namely *perspicuity* and *stimulation*. SIsKA-NG still need to be improved based on the aspect of *perspicuity*, additional recommendations from the conducted FGD, and procedural White Box testing for code evaluation.

### Conflict of Interest

The authors declare that there is no conflict of interest regarding the publication of this article.

### Acknowledgment

The authors would like to thank to Indonesian Ministry of Education and Culture that supported this work through research grant.

### References

[1] A. I. I. Paramitha, G. R. Dantes and G. Indrawan, "The Evaluation of Web Based Academic Progress Information System Using Heuristic Evaluation and User Experience Questionnaire (UEQ)," in *Third International Conference on Informatics and Computing (ICIC)*, 2018. <https://doi.org/10.1109/IAC.2018.8780430>.

[2] G. Indrawan, G. T. Heriawan, A. A. I. I. Paramitha, G. Wiryawan, G. B. Subawa, M. T. Sastradi, and K. A. Suchayana, "SIsKA: Mobile Based Academic Progress Information System," in *International Conference on Innovative Research Across Disciplines (ICIRAD)*, 2017.

<https://doi.org/10.2991/icirad-17.2017.24>.

[3] J. M. C. Bastien, "Usability testing: a review of some methodological and technical aspects of the method" *Int. J. Med. Inform.*, **79**(4), e18–e23, 2010. <https://doi.org/10.1016/j.ijmedinf.2008.12.004>

[4] S. Gupta, "A Comparative study of Usability Evaluation Methods" *Int. J. Comput. Trends Technol.*, **22**(3), 103–106, 2015. <https://doi.org/10.14445/22312803/IJCTT-V22P121>

[5] A. Widyanti and S. A. Q. Ainizzamani, "Usability evaluation of online transportation' user interface" in *International Conference on Information Technology Systems and Innovation (ICITSI)*, 2017. <https://doi.org/10.1109/ICITSI.2017.8331762>

[6] F. Z. Ghazizadeh and S. Vafadar, "A quantitative evaluation of usability in mobile applications: An empirical study" in *International Symposium on Computer Science and Software Engineering Conference (CSSE)*, 2017. <https://doi.org/10.1109/CSICSSSE.2017.8320120>

[7] S. Elling, L. Lentz, and M. de Jong, "Retrospective think-aloud method: Using eye movements as an extra cue for participants' verbalizations" in *Proceedings of the 2011 annual conference on Human factors in computing systems*, 2011. <https://doi.org/10.1145/1978942.1979116>

[8] M. W. M. Jaspers, "A comparison of usability methods for testing interactive health technologies: Methodological aspects and empirical evidence" *Int. J. Med. Inform.*, **78**(5), 340–353, 2009. <https://doi.org/10.1016/j.ijmedinf.2008.10.002>

[9] H. Santoso, M. Schrepp, R. Y. Kartono Isal, A. Yudha Utomo, and B. Priyogi, "Measuring the User Experience" *J. Educ. Online*, **13**(1), 58–79, 2016. <https://doi.org/10.9743/JEO.2016.1.5>

[10] B. Laugwitz, T. Held, and M. Schrepp, "Construction and Evaluation of a User Experience Questionnaire" in *Holzinger A. (eds) HCI and Usability for Education and Work. USAB 2008. Lecture Notes in Computer Science, vol 5298. Springer, Berlin, Heidelberg, 2008.* [https://doi.org/10.1007/978-3-540-89350-9\\_6](https://doi.org/10.1007/978-3-540-89350-9_6)

[11] M. Schrepp, A. Hinderks, and J. Thomaschewski, "Construction of a Benchmark for the User Experience Questionnaire (UEQ)" *Int. J. Interact. Multimed. Artif. Intell.*, **4**(4), 40–44, 2017. <https://doi.org/10.9781/ijimai.2017.445>

[12] D. S. S. Sahid, P. I. Santosa, R. Ferdiana, and E. N. Lukito, "Evaluation and measurement of Learning Management System based on user experience" in *The 6th International Annual Engineering Seminar (InAES)*, 2016. <https://doi.org/10.1109/INAES.2016.7821910>

[13] M. Schrepp, A. Hinderks, and J. Thomaschewski, "Applying the User Experience Questionnaire (UEQ) in Different Evaluation Scenarios" in *In: Marcus A. (eds) Design, User Experience, and Usability. Theories, Methods, and Tools for Designing the User Experience. DUXU 2014. Lecture Notes in Computer Science, vol 8517. Springer, Cham, 2014.* [https://doi.org/10.1007/978-3-319-07668-3\\_37](https://doi.org/10.1007/978-3-319-07668-3_37)

[14] J. Nielsen, T. Clemmensen, and C. Yssing, "Getting access to what goes on in people's heads?" in *Proceedings of the second Nordic conference on Human-computer interaction*, 2002. <https://doi.org/10.1145/572020.572033>

[15] A. Hinderks, M. Schrepp, F. J. Dominguez Mayo, M. J. Escalona, and J. Thomaschewski, "Developing a UX KPI based on the user experience questionnaire" *Comput. Stand. Interfaces*, **65**, 38–44, 2019. <https://doi.org/10.1016/j.csi.2019.01.007>

[16] M. Seidl, M. Scholz, C. Huemer, and G. Kappel, "The Use Case Diagram" in *UML @ Classroom. Undergraduate Topics in Computer Science. Springer, Cham, 2015.* [https://doi.org/10.1007/978-3-319-12742-2\\_3](https://doi.org/10.1007/978-3-319-12742-2_3)

[17] S. Hitchman, "The Details of Conceptual Modelling Notations are Important - A Comparison of Relationship Normative Language" *Commun. Assoc. Inf. Syst.*, **9**(1), 2002. <https://doi.org/10.17705/ICAIS.00910>

[18] X. Li, S. Karnan, and J. A. Chishti, "An empirical study of three PHP frameworks" in *2017 4th International Conference on Systems and Informatics (ICSAI)*, 2017. <https://doi.org/10.1109/ICSAI.2017.8248546>

[19] L. Lancor and S. Katha, "Analyzing PHP frameworks for use in a project-based software engineering course" in *Proceeding of the 44th ACM technical symposium on Computer science education*, 2013. <https://doi.org/10.1145/2445196.2445350>

[20] A. Mesbah, A. Van Deursen, and S. Lenselink, "Crawling AJAX-based web applications through dynamic analysis of user interface state changes" *ACM Trans. Web*, 2012. <https://doi.org/10.1145/2109205.2109208>

[21] M. Ying and J. Miller, "Refactoring legacy AJAX applications to improve the efficiency of the data exchange component" *J. Syst. Softw.*, **86**(1), 72–88, 2013. <https://doi.org/10.1016/j.jss.2012.07.019>

## Comparison Analysis Between Mobile Banking and Mobile Payment as Determinant Factors of Customer Privacy

Yakob Utama Chandra<sup>\*1</sup>, Bahtiar Saleh Abbas<sup>2</sup>, Agung Trisetyarso<sup>2</sup>, Wayan Suparta<sup>3</sup>, Chul-Ho Kang<sup>4</sup>

<sup>1</sup>Information Systems Department, School of Information Systems, Bina Nusantara University, Jakarta 11480, Indonesia

<sup>3</sup>Computer Science Department, Bina Nusantara University, Jakarta, 11480, Indonesia

<sup>3</sup>Department of Informatics, Faculty of Design and Technology Pembangunan Jaya University, South Tangerang, Indonesia

<sup>4</sup>Department of Electronics and Communication Engineering, Kwangwoon University, Seoul, South Korea

### ARTICLE INFO

*Article history:*

*Received: 15 December, 2019*

*Accepted: 25 February, 2020*

*Online: 04 April, 2020*

*Keywords:*

*Perceived Privacy*

*Privacy Concern*

*Trust*

*Mobile Banking*

*Mobile Payment*

### ABSTRACT

*Mobile banking and mobile payment are currently always used by customers for financial payments. With customer payments, it is usually easier to make payments with mobile payment, because it is more practical and direct than mobile banking. However, is the privacy of both platforms understood by the customer? Research questions to be answered: 1) What are the factors that influence privacy issues in mobile banking? 2) What are the factors that influence privacy issues with mobile payments? 3) What are the factors that influence confidence in mobile banking? 4) What are the factors that influence confidence in mobile payments? 5) Does the privacy factor influence the perceived privacy? 6) Does the confidence factor influence the perceived privacy? There are two research models and 12 (twelve) hypotheses for each model. Privacy risk, subjective norm, information management factors positive influence on privacy interest, and trust. Care about privacy and trust have a positive influence on mobile payment.*

## 1. Introduction

Smartphones can now have a variety of applications, ranging from standard applications on a smartphone itself, such as telephone, message, internet browser, to applications that customers download to meet customer needs. Most customers currently use mobile payment and mobile banking applications as applications that must be on smartphones in addition to social media applications [1][2].

Customer privacy is an essential factor in an application on a smartphone that aims to give customers confidence in the application company by maintaining privacy on every element of the customer. The customer feels safe about using the application if the application company on the smartphone can give customer privacy rights. The most important in terms of privacy in a smartphone application is the flow of information to the customer. The customer's concern about the ownership of data, and the

customer does not want data on smartphones to be in circulation without the customer's knowledge [3].

The privacy of customers can depend on the factors of institutions and the environment in the application itself. The more closely related to customer personal information, the higher the privacy issue for the safety and comfort of customer information. Underlying the existence of customer privacy is anticipating the prevention of problems that are more related to management practices. When customers want to care more about privacy, customer information can be better monitored. Therefore, the role of maintaining privacy is not only the regulation of the application but also the awareness of the privacy of the customer. In the privacy of customers themselves, there are two (two) concerns that affect the privacy of customers, namely internal drivers and external drivers. Internal drivers are something that influences customers because of privacy considerations from within the customer, and external drivers are something that

\* Yakob Utama Chandra, Email : yakob@binus.ac.id



influences customers because of privacy considerations from outside the customer and usually looks at the environment that exists in the customer [3], [4].

Applications that are of concern in this study are mobile banking and mobile payment applications from financial institutions. Mobile banking is a bank product that gives customers easy access to customers' savings at the bank so that mobile banking customers can easily do non-financial and financial transactions because they have access to customers' savings. While mobile payments, customers do not have savings at the financial institution, but the customer deposits money at the financial institution to facilitate transactions. Mobile payments are generally used to make payments for convenience in non-bank transactions [5]–[7].

With both platforms, namely mobile banking and mobile payment, the research questions in this study are 1) What are the factors that influence the privacy issues in mobile banking? 2) What are the factors that influence privacy issues with mobile payments? 3) What are the factors that influence confidence in mobile banking? 4) What are the factors that influence confidence in mobile payments? 5) Does the privacy factor influence the perceived privacy? 6) Does the confidence factor influence the perceived privacy?

To answer the research question above, this study will use a model, and there are two models, one for the mobile banking and mobile payment, with 12 (twelve) hypotheses for this research for each model:

- H1: Privacy Risk (PR) positive influence on the Privacy Concern (PC)
- H2: Propensity to Value Privacy (PVP) positive influence on the Privacy Concern (PC)
- H3: Subjective Norm (SN) positive influence on the Privacy Concern (PC)
- H4: Privacy Awareness (PA) positive influence on the Privacy Concern (PC)
- H5: Information Quality (IQ) positive influence on the Privacy Concern (PC)
- H6: Privacy Risk (PR) positive influence on the Trust (TR)
- H7: Propensity to Value Privacy (PVP) positive influence on the Trust (TR)
- H8: Subjective Norm (SN) positive influence on the Trust (TR)
- H9: Privacy Awareness (PA) positive influence on the Trust (TR)
- H10: Information Quality (IQ) positive influence on the Trust (TR)
- H11: Privacy Concern (PC) positive influence on the Perceived Privacy (PP)
- H12: Trust (TR) positive influence on the Perceived Privacy (PP)

This research used a quantitative approach by distributing questionnaires to 210 respondents.

## 2. Literature Review

### 2.1. Mobile Banking

Mobile banking or sometimes referred to as online banking is an application built by banks aimed at offering alternative channels to customers so that customers have access rights to use savings that are owned by customers. Customers can, therefore, be more satisfied with the use of the existing service facilities at the bank. For banks, operating costs will also be reduced by the existence of a mobile banking application, as banks do not have to provide the people needed to provide services to customers, but are represented by a mobile banking application [8][9].

### 2.2. Mobile Payment

Mobile payment, or better known as e-wallet or e-payment, is a breakthrough in non-bank financial institutions that strive to offer facilities or services to the public to make payments quickly. Customers only have to enter the balance of this mobile payment and then make a payment using a smartphone via QR Code or EDC available at the payment service, and the customer can quickly enter the customer pin to complete the payment. Mobile payment is generally more practical compared to mobile banking because, with mobile payments, it is not necessary to open a savings account, only by registering on the application and filling in money balances, it can be used directly for the execution of payments [9][10][11].

### 2.3. Perceived Privacy

Perceived privacy is something that the customer can accept for the privacy of current personal information when the customer registers with mobile banking and mobile payment. Perceived privacy means accepting all kinds of negative possibilities that result from the use of the application [12][13]. This perceived privacy is the goal to be pursued in this study, whereby privacy considerations and trust influence perceived privacy. Because the customer can accept any existing privacy, this influences the way the customer receives a real privacy issue and along with the trust that the customer understands. The customer can then prepare if there is a risk that arises because of the information collected about the application used by the customer [14].

### 2.4. Privacy Concern

Customers must understand that every application has a privacy setting, especially in applications that request data or smartphone settings from the customer. With the client's privacy issue, the client can feel comfortable and safe when using the application because the application has settings that can be made by the client and the client can adapt to the needs of the client in terms of different types of privacy that exist in the customer's smartphone application. Moreover, in highly sensitive applications such as mobile banking and mobile payment, it contains sensitive data that relates explicitly to customer money. The privacy problem is, therefore, something that the customer must take into account [15][16].

### 2.5. Trust

An essential factor in this research is trust, where trust is a condition that the customer believes that the application on the

smartphone can function correctly according to what the application developer has promised and ensures that all transactions can go smoothly. Besides, trust also in the sense that the client understands the business well how the business processes in the business can be carried out and by the promises made when the client reads or sees before the client installs the application on the client's smartphone and ensuring registration by providing data about the application is installed by the customer and is a sign that the customer uses the application well from start to finish [17][10].

### 2.6. Privacy Risk

Customers must be able to understand that every application installed on a smartphone sometimes requires customer information data to be entered into the application, and the customer must realize that the customer may lose information input or the data may be used by people who are not interested in the use of the application. Customers should realize that the risk to privacy can arise at any time because the data in each application can be taken by someone else or unknown to someone who has taken over the data [18][19].

### 2.7. The propensity to Value Privacy

Customers must respect the privacy created by the application developer to understand how privacy settings are made in the application. Customers are more likely to use the application without looking at the privacy settings in the application so that the customer cannot complain if something happens to the customer. Therefore, customers must understand and respect how privacy is created in applications by application developers [20].

### 2.8. Subjective Norm

Currently, more customers to see the terms of other customers and the behavior of other customers when using the same application for a specific purpose. In this way, the subjective norm can see how customers want to adapt to others who use the same application in psychological terms. It can be seen that customer factors follow what other people do and then psychologically apply to themselves [21].

### 2.9. Privacy Awareness

Customer awareness of privacy is certainly a concern and need when using applications, especially in applications where there are financial transactions. This is because privacy awareness forms the basis for the safety and ease of transactions such as mobile banking or mobile payment. Because customers with privacy awareness can make the necessary privacy settings when they start transactions in the previous phase to ensure that application developers always maintain privacy. The customer experience at the time of the transaction thus becomes positive and the absence of a negative thing that will happen to the customer, especially on the customer's psychological factors [22].

### 2.10. Information Control

Every customer has the right to control the information submitted in the online application. With the Information Control factor, the customer can easily set what is a priority for sharing or not. Because the client does not know that the entered data is being taken somewhere by the application developer so that the client can use the information check to adapt to the privacy policy that is available from a government or country in the client's area

and also find out how the information is useful for the customer himself. Openness to information is very vulnerable to the privacy of customers. Therefore, the information check of the application can be beneficial when you perform specific online transactions [21][22].

## 3. Research Methodology

In this study, researchers wanted to discover which factors influence privacy interests and trust in perceived privacy. The privacy interest and trust factors in this study are five factors, namely privacy risk (PR), the propensity to value privacy (PVP), subjective norm (SN), privacy awareness (PA), and information control (IC). With figure 2 above, this model is tested simultaneously on respondents who both use mobile banking and mobile payment. Researchers conducted the same respondents to find out how privacy is felt when using mobile banking and mobile payment in terms of privacy when using the application. With this model, the aim of this study can be achieved by looking at how consumers feel about the perceived privacy of mobile banking and mobile payment.

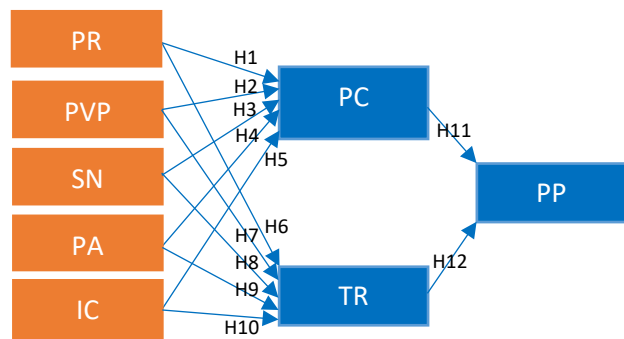


Figure 1. Research Model

### 3.1. Research Instrument

In this research in quantitative research, 31 statements are the same for mobile banking and mobile payment. So there are 62 statements in total. Respondents must complete all these statements in order to be able to measure the perceived privacy of respondents with a Likert scale. On this comparable scale, there are six choices of feelings felt by consumers, starting with number 1 the feeling of disagreeing with the statement until number 6 is a feeling that they strongly agree with the statement. Thirty-one statements to know perceived privacy, there are eight factors with details as follows: privacy risk (4 statements), propensity to value privacy (3 statements), subjective norm (3 statements), privacy awareness (3 statements), information control (4 statements), privacy concern (5 statements), trust (6 statements), and perceived privacy (3 statements). In addition to 31 statements for mobile banking and 31 statements for mobile payments, the questionnaire also asked about the identity of the respondents, namely the age of the respondents and the occupation of the respondents.

### 3.2. Data Collection Procedure

By using the sampling of the snowball technique, the data collection procedure is distributed online with Google Forms. The researcher used snowball sampling because the researcher did not know the exact population when questionnaires were distributed that started in September 2019 for 1 (one) a full month. With the use of Google Forms, the researcher has set the form if the

respondent who opens the online questionnaire is not a user of both applications on mobile banking and mobile payment, then the respondent is not counted as a respondent or invalid so that 31 answer statements in mobile banking and mobile payment. This is because there is a choice on Google Forms whether respondents use mobile banking and mobile payment? If both are not used, the respondent answers "no" and is then asked to end the form. So, it is beneficial for researchers to find out which are valid in this study. From the results obtained in this study, 210 respondents actively used mobile banking and mobile payment. Respondents' ages and occupations are shown in Table I.

Table 1. Number of Respondents

Description	Total Answer	%
N Total	210	100%
<i>Ages of Respondent</i>		
17 – 23 years old	167	80%
24 – 30 years old	8	4%
31 – 37 years old	11	5%
38 – 44 years old	13	6%
45 – 51 years old	9	4%
More than 51 years old	2	1%
<i>Occupation of the Respondent</i>		
Entrepreneur	2	1%
Employee	23	11%
Professional	16	8%
Higher Education Students	163	78%
High School Students	1	1%
Housewife	4	1%

#### 4. Result and Discussion

Correct respondent data are respondents who use mobile banking and mobile payment, a total of 210 respondents. Of the 210 respondents, 80% (167 respondents) were 17-30 years old. The remaining 20% were older than 30 years and older. Because the respondents in this study were 17-30 years old, the profession of respondents was at most students in higher education as much as 78% (163 respondents) With the identity of these respondents it can be concluded that the observed privacy will be assessed earlier in this study, especially more at the age of 17-30 and older professions as students in higher education, the results of this research are more focused on identity.

After knowing the identity of the respondent, we will look at how the test model designed in Chapter 3 is used to calculate the results of the questionnaire in this study, a statistical calculation tool to make the calculation more accurate. Researchers using the partial least squares of Smart Equations (PLS-SEM) [23]. This application is used to find the outer load for each indicator, the

composite reliability for each indicator, and the extracted average variance (AVE) for each indicator. The results of the calculation of each indicator are shown in Table II for the use of mobile banking and Table III for the use of mobile payment.

Table 2: Outer Loading, Validity, and Reliability of Mobile Banking Privacy

Latent Variables	Indicators	Loading	CA	CR	AVE
Privacy Risk (PR)	PR1	0.805	0.874	0.914	0.727
	PR2	0.883			
	PR3	0.860			
	PR4	0.860			
The propensity to Value Privacy (PVP)	PVP1	0.783	0.716	0.831	0.622
	PVP2	0.786			
	PVP3	0.796			
Subjective Norm (SN)	SN1	0.842	0.790	0.878	0.705
	SN2	0.878			
	SN3	0.798			
Privacy Awareness (PA)	PA1	0.880	0.737	0.852	0.658
	PA2	0.783			
	PA3	0.765			
Information Control (IC)	IC1	0.825	0.797	0.867	0.623
	IC2	0.846			
	IC3	0.845			
	IC4	0.716			
Privacy Concern (PC)	PC1	0.777	0.919	0.940	0.758
	PC2	0.866			
	PC3	0.916			
	PC4	0.883			
	PC5	0.904			
Trust (TR)	TR1	0.836	0.925	0.941	0.728
	TR2	0.874			
	TR3	0.760			
	TR4	0.892			
	TR5	0.890			
	TR6	0.860			
Perceived Privacy (PP)	PP1	0.913	0.900	0.938	0.834
	PP2	0.904			
	PP3	0.922			

In Table 2 above, based on 210 respondents who use mobile banking about outer loading is valid because it is more than 0.7.

Also, with the composite reliability valid because the composite reliability value is higher than 0.6. Furthermore, the AVE (Average Variance Extracted) also valid because the value is higher than 0.5, so it can be concluded that all statements from using mobile banking are all valid.

Table 3: Outer Loading, Validity, and Reliability of Mobile payment Privacy

Latent Variables	Indicators	Loading	CA	CR	AVE
Privacy Risk (PR)	PR1	0.773	0.871	0.912	0.722
	PR2	0.875			
	PR3	0.854			
	PR4	0.891			
The propensity to Value Privacy (PVP)	PVP1	0.751	0.721	0.829	0.618
	PVP2	0.768			
	PVP3	0.836			
Subjective Norm (SN)	SN1	0.806	0.779	0.872	0.694
	SN2	0.879			
	SN3	0.812			
Privacy Awareness (PA)	PA1	0.882	0.728	0.847	0.650
	PA2	0.790			
	PA3	0.742			
Information Control (IC)	IC1	0.761	0.795	0.868	0.624
	IC2	0.869			
	IC3	0.852			
	IC4	0.762			
Privacy Concern (PC)	PC1	0.826	0.925	0.944	0.770
	PC2	0.867			
	PC3	0.893			
	PC4	0.924			
	PC5	0.876			
Trust (TR)	TR1	0.830	0.927	0.943	0.733
	TR2	0.879			
	TR3	0.804			
	TR4	0.873			
	TR5	0.898			
	TR6	0.848			
Perceived Privacy (PP)	PP1	0.933	0.914	0.946	0.854
	PP2	0.896			
	PP3	0.943			

After calculating statistics on mobile banking users, on Table III above shows the result of 210 respondents of mobile payment on the same respondents. In Table III in the outer loading, all statements are valid because the outer loading is more than 0.7. The composite reliability is also valid because the composite reliability value is higher than 0.6. And in the AVE (Average Variance Extracted), are all higher than 0.5, so it can be concluded that all statements about respondents who use mobile payment is all valid.

The SmartPLS application, there is a process called bootstrapping to test internal and external models. This application increases the total number of 210 respondents to 1000 samples for this research, and the alpha error is 5%. The level of proximity for general information can be achieved with the use of bootstrapping.

The bootstrapping for testing the values for hypothesis or path correlation with values of original samples, T statistics, and P values. According to the T-Table, the valid or acceptable T-Statistics is above 1.96. While P Values should below 0.05. The results of the hypothesis for mobile banking can be seen in Table IV and Figure 3. Then, the result of the hypothesis for mobile payment can be seen in Table V and Figure 4.

Table 4: Result of Mobile Banking Hypothesis

Hypothesis	Paths	Original Sample	T-Statistic	P Values	Result
H1	PR → PC	0.424	5.386	0.000	Significant
H2	PVP → PC	0.193	1.912	0.056	Not Significant
H3	SN → PC	0.150	2.015	0.044	Significant
H4	PA → PC	-0.015	0.166	0.868	Not Significant
H5	IC → PC	0.048	0.575	0.565	Not Significant
H6	PR → TR	-0.011	0.187	0.852	Not Significant
H7	PVP → TR	-0.043	0.494	0.621	Not Significant
H8	SN → TR	0.333	3.918	0.000	Significant
H9	PA → TR	0.177	1.957	0.051	Not Significant
H10	IC → TR	0.337	3.542	0.000	Significant
H11	PC → PP	-0.051	1.438	0.151	Not Significant
H12	TR → PP	0.855	33.679	0.000	Significant

The results of Table IV about mobile banking users indicate that there is 5 (five) path correlation that significant in using mobile banking. They are privacy risk (PR) to privacy concern (PC), subjective norm (SN) to privacy concern (PC), subjective norm (SN) to trust (TR), information control (IC) to trust (TR), and trust (TR) to perceived privacy (PP).



The results of Table V about mobile payment users indicate that there are 6 (six) path correlations that significant in using mobile banking. They are privacy risk (PR) to privacy concern (PC), subjective norm (SN) to privacy concern (PC), subjective norm (SN) to trust (TR), information control (IC) to trust (TR), privacy concern (PC) to perceived privacy (PP), and trust (TR) to perceived privacy (PP).

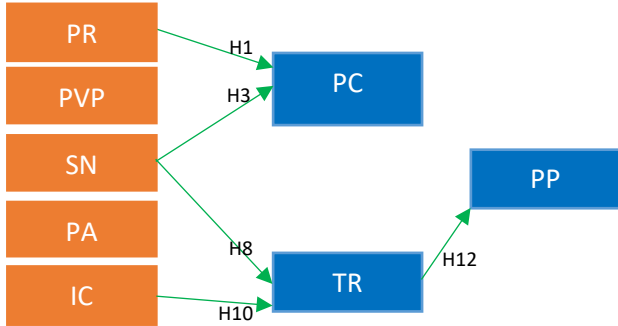


Figure 2. Result of mobile banking hypotheses

Table 5: Result of Mobile payment Hypothesis

Hypothesis	Paths	Original Sample	T-Statistic	P Values	Result
H1	PR → PC	0.405	4.876	0.000	Significant
H2	PVP → PC	0.221	1.828	0.068	Not Significant
H3	SN → PC	0.216	2.707	0.007	Significant
H4	PA → PC	-0.005	0.055	0.956	Not Significant
H5	IC → PC	-0.052	0.625	0.532	Not Significant
H6	PR → TR	0.024	0.336	0.737	Not Significant
H7	PVP → TR	-0.121	1.404	0.161	Not Significant
H8	SN → TR	0.268	3.058	0.002	Significant
H9	PA → TR	0.078	0.911	0.363	Not Significant
H10	IC → TR	0.523	6.483	0.000	Significant
H11	PC → PP	-0.085	2.177	0.030	Significant
H12	TR → PP	0.865	32.629	0.000	Significant

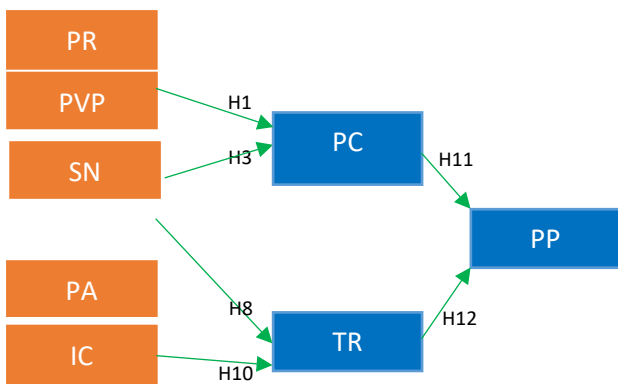


Figure 3. Result of mobile payment hypotheses

5. Conclusions

There is an exciting uniqueness in this study. The results obtained show that in the hypothesis, there are almost similarities that are statistically calculated for the same respondents as the use

of mobile banking and mobile payment. In general, the same essential factors between mobile banking and mobile payment are privacy risk and subjective norm regarding privacy, subjective norms, and information control for trusts. This shows the similarity between mobile banking and mobile payment.

However, the difference that occurs is in mobile banking; privacy considerations do not have a significant effect on perceived privacy, while mobile payments for privacy and trust have a significant effect on perceived privacy. So the unique feature of this study is that privacy is significantly more critical for consumers to feel the perceived privacy.

In short, mobile banking is a product issued by a bank with a good reputation and building new electronic channels to facilitate consumers' use of bank access. Consumers will, therefore, have more confidence in the use of mobile banking issued by banks trusted by consumers. The bank also has an explicit agreement for consumers to use every product and service available in mobile banking. Such as the general terms and conditions that consumers must agree on when using mobile banking. This makes consumers feel comfortable with financial transactions with mobile banking.

That is why trust is perceived as valuable by consumer trust. The confidence that consumers have in the use of mobile banking also comes from important factors, namely the subjective standard and information control. The subjective norm is to follow what is driven or created by the social environment of consumers so that consumers also see from the perspective of others. An information check is a consumer who can easily use mobile banking with a check on the privacy of information about a consumer. Regarding privacy issues that are not significant to the perceived privacy. Concerning privacy issues, consumers who use mobile banking come from significant privacy risk and subjective standards. This is because consumers are still concerned about their privacy when using mobile banking, particularly concerning monitoring the risk of privacy and also subjective standards based on an understanding of the social environment of mobile banking for consumers.

With mobile payment, the same applies to mobile banking because of privacy and trust. Where privacy considerations are also significantly influenced by privacy risk and subjective norm. This is because consumers understand the privacy risks to be understood, and consumers also know that there are restrictions on the use of mobile payments so that consumers do not overthink about the risks that arise, so that consumers have understood the privacy risk. Moreover, on the subjective norm, consumers have been influenced by the social environment on the use of mobile payment and see from environmental factors that everything can go according to procedures agreed between the consumer and the manager of the mobile payment.

With mobile payment, however, privacy concerns significantly affect perceived privacy, which is what distinguishes between mobile payment and mobile banking. What has been explained above is that privacy issues in mobile banking do not affect perceived privacy. For the trust, the same thing with mobile banking is that there are subjective standards and information control factors that significantly affect trust. Moreover, the trust

factor has a significant effect on the perceived privacy. Viewed from the same two fields in financial technology, consumers will feel the same in terms of confidence in mobile payment. Because of the subjective norm that consumers feel in the social environment and also information management, that gives consumers more freedom to control the receipt and provision of information on the mobile payment platform.

### Conflict of Interest

The authors declare no conflict of interest.

### References

- [1] S. Rathore, "Adoption of digital wallet by consumers," *BVIMSR's J. Manag. Res.*, vol. 8, pp. 69–75, 2016.
- [2] T. T. T. Pham and J. C. Ho, "The effects of product-related, personal-related factors and attractiveness of alternatives on consumer adoption of NFC-based mobile payments," *Technol. Soc.*, vol. 43, pp. 159–172, 2015.
- [3] V. Kumar and W. Reinartz, "Customer Privacy Concerns and Privacy Protective Responses," pp. 285–309, 2018.
- [4] P. Su, L. Wang, and J. Yan, "How users' Internet experience affects the adoption of mobile payment: a mediation model," *Technol. Anal. Strategy. Manag.*, vol. 30, no. 2, pp. 186–197, 2018.
- [5] A. C. Teo, G. W. H. Tan, K. B. Ooi, T. S. Hew, and K. T. Yew, "The effects of convenience and speed in m-payment," *Ind. Manag. Data Syst.*, vol. 115, no. 2, pp. 311–331, 2015.
- [6] A. Upadhayaya, "Electronic Commerce and Mobile payment," vol. I, no. March, pp. 37–41, 2012.
- [7] K. B. Ooi and G. W. H. Tan, "Mobile technology acceptance model: An investigation using mobile users to explore smartphone credit card," *Expert Syst. Appl.*, vol. 59, pp. 33–46, 2016.
- [8] M. A. Shareef, A. Baabdullah, S. Dutta, V. Kumar, and Y. K. Dwivedi, "Consumer adoption of mobile banking services: An empirical examination of factors according to adoption stages," *J. Retail. Consum. Serv.*, vol. 43, no. December 2017, pp. 54–67, 2018.
- [9] Y. U. Chandra, "Bank vs Telecommunication Mobile payment : System Analysis , Purchase , and Payment Method of GO- Mobile CIMB Niaga and T-Cash Telkomsel." no. November, pp. 165–170, 2017.
- [10] Y. U. Chandra, D. M. Kristin, J. Suhartono, F. S. Sutarto, and M. Sung, "Analysis of Determinant Factors of User Acceptance of Mobile Payment System in Indonesia (A Case Study of Go-Pay Mobile Payment)," *Proc. 2018 Int. Conf. Inf. Manag. Technol. ICIMTech 2018*, no. September, pp. 454–459, 2018.
- [11] M. Karsen, Y. U. Chandra, and H. Juwitasary, "Technological factors of mobile payment: A systematic literature review," *Procedia Comput. Sci.*, vol. 157, pp. 489–498, 2019.
- [12] Y. Chang, S. F. Wong, C. F. Libaque-Saenz, and H. Lee, "The role of privacy policy on consumers' perceived privacy," *Gov. Inf. Q.*, vol. 35, no. 3, pp. 445–459, 2018.
- [13] Y. Yang, Y. Liu, H. Li, and B. Yu, "Understanding perceived risks in mobile payment acceptance," *Ind. Manag. Data Syst.*, vol. 115, no. 2, pp. 253–269, 2015.
- [14] A. Rauzzino and J. C. Correa, "Diferencias por sexo de los «Millenials» sobre la privacidad percibida en Snapchat," *Suma Psicol.*, vol. 24, no. 2, pp. 129–134, 2017.
- [15] K. Degirmenci, "Mobile users' information privacy concerns and the role of app permission requests," *Int. J. Inf. Manage.*, vol. 50, no. April 2019, pp. 261–272, 2020.
- [16] A. R. Jung, "The influence of perceived ad relevance on social media advertising: An empirical examination of a mediating role of privacy concern," *Comput. Human Behav.*, vol. 70, pp. 303–309, 2017.
- [17] N. E. Frye and M. M. Dornisch, "When is trust not enough? the role of perceived privacy of communication tools in comfort with self-disclosure," *Comput. Human Behav.*, vol. 26, no. 5, pp. 1120–1127, 2010.
- [18] J. Henriksen-Bulmer, S. Faily, and S. Jeary, "Privacy risk assessment in context: A meta-model based on contextual integrity," *Comput. Secur.*, vol. 82, pp. 270–283, 2019.
- [19] G. de Kerviler, N. T. M. Demoulin, and P. Zidda, "Adoption of in-store mobile payment: Are perceived risk and convenience the only drivers?," *J. Retail. Consum. Serv.*, vol. 31, pp. 334–344, 2016.
- [20] H. Jia and H. Xu, "Measuring individuals' concerns over collective privacy on social networking sites," *Cyberpsychology*, vol. 10, no. 1, 2016.
- [21] F. Xu, K. Michael, and X. Chen, "Factors affecting privacy disclosure on social network sites: An integrated model," *Electron. Commer. Res.*, vol. 13, no. 2, pp. 151–168, 2013.
- [22] I. D. Anic, V. Škare, and I. Kursan Milaković, "The determinants and effects of online privacy concerns in the context of e-commerce," *Electron. Commer. Res. Appl.*, vol. 36, no. June, 2019.
- [23] C. M. Ringle, S. Wende, and J.-M. Becker, "SmartPLS 3." SmartPLS GmbH, 2015.

## Object Classifications by Image Super-Resolution Preprocessing for Convolutional Neural Networks

Bokyoon Na<sup>\*</sup>,<sup>1</sup>, Geoffrey C Fox<sup>2</sup>

<sup>1</sup>Dept. of Computer Engineering, Korea Polytechnic University, 429-793, Korea

<sup>2</sup>School of Informatics, Computing, and Engineering, Indiana University, 47408, USA

### ARTICLE INFO

Article history:

Received: 25 January, 2020

Accepted: 12 March, 2020

Online: 04 April, 2020

Keywords:

Object classification

Super-resolution

Convolutional neural networks

Machine learning

### ABSTRACT

Blurred small objects produced by cropping, warping, or intrinsically so, are challenging to detect and classify. Therefore, much recent research is focused on feature extraction built on Faster R-CNN and follow-up systems. In particular, RPN, SPP, FPN, SSD, and DSSD are the layered feature extraction methods for multiple object detections and small objects. However, super-resolution methods, as explored here, can improve these image analyses working on before or after convolutional neural networks. Our methods are focused on building better image qualities into the original image components so that these feature extraction methods become more effective when applied later. Our super-resolution preprocessing resulted in better deep learning in the number of classified objects, especially for small objects when tested on the VOC2007, MSO, and COCO2017 datasets.

### 1. Introduction

This paper extends the work presented at the 2018 IEEE International Conference on Big Data [1]

Since Krizhevsky et al. [2] introduced specifically designed CNN (Convolutional Neural Network) architectures, there have been various methods for increasing the object classification rate. [3]-[8] have shown performance to be increased compared to the shallow learning in neural networks. These days CNNs have around a 90 percent object classification rate for unblurred or slightly blurred images. Moreover, algorithms in [9], [10] introduced much faster detection times, an increased number of classes, and object segmentations in addition to the Softmax and linear regression algorithms.

Recently, to reduce misdetections and detection failures on CNNs, research has been conducted, such as on generative adversarial networks (GAN) [11]-[13], GAN with reinforcement learning [14], and Capsule networks [15]. GAN solved many of the problems from adversarial noises. Sara Sabour et al. in [15] have attained considerably better results than CNNs on MultiMNIST with smaller sized training data sets. However, Capsule networks, which are groups of neurons learning to detect a particular object within a region of the image [15] do not perform as well as CNNs on larger images even though Capsule networks improve CNNs' weaknesses caused by pose information (such as

precise object position, rotation, size, and so on). Also, Capsule networks require much more computing resources than CNNs.

Even though these studies demonstrate that there have been many improvements in CNNs, there are still detection failures caused by blurred images or low-resolution images. For example, in [16], 100 images were randomly chosen, and these images were preprocessed at a resolution, which was three times lower than the original images in order to generate cropped or warped images, which are called regions of interest (ROI). Following this, they were interpolated using bilinear or bicubic interpolation and then were tested in [4]. These interpolation methods may cause aliasing effects on the images and make larger regions of interest. Therefore, a new method might be needed to generate less aliased and higher-resolution ROIs from original images in CNNs.

Since CNNs were introduced, the most common image size has been approximately 256x256 pixels. Examples in the Spatial Pyramid Pooling network, Faster R-CNN, and ConvNet are tested for the adequateness of the image size. Also, in [17]-[20], it was shown that a recurrent neural network model is able to extract features from an image by selecting a sequence of regions and processing each region at high resolution. Therefore, object detections from ROIs are very common in CNNs.

In [2], Krizhevsky et al. described ImageNet, which has 15 million labeled images with 22,000 categories and variable resolution image sizes and adopted down-scaled rectangular

<sup>\*</sup>Bokyoon Na, Email : bkna@kpu.ac.kr

images from ImageNet dataset. They reported results on 10,184 categories and 8.9 million images. [3], [6] classified 21 object classes from ImageNet, PASCAL VOC 2007 [16]. However, most research is conducted with VOC2007 20+1 classes even though there are datasets with more than several hundred categories. Recently [9] trained and tested using 80 object classes in the fastest object detection speed. In future research, more than 200,000 object categories should be considered to distinguish objects such as human beings.

There are a number of practical applications for processing low-quality images. These include surveillance cameras, black-box systems in vehicles, and cameras in mobile phones. However, it may be difficult to increase the quality of images in surveillance camera systems because of the limited capacity for storage, insufficient night vision, and dark image sensors. In particular, current night visioning algorithms do not have procedures for good image quality. In the case of black-box systems in vehicles, vibrations and low electric power consumption may cause poor image compression, inability to zoom quickly, or lack of focus. Finally, in mobile phone cameras, the limits of the zoom algorithm can cause images to be blurry or target objects to be small.

In this paper, we will present our research on improving rates of object classification through preprocessing before classification neural networks.

## 2. Related Research

Compared to the previous CNN algorithms, [3], [21] have shown more new algorithms for feature extracting or new initial parameters. Paper [3] also improved CNN using “region proposals” technique and sliding window. Their new methods increase the speed of object detection, which allows the images to be processed in almost real-time. Using region proposals, the Fast YOLO model in [9] processed 155 frames per second.

In [6], Keiming He et al. had used variable size image datasets and were able to get the best results for training and testing of images after achieving when the shorter side of the input image was maximum 392 pixels. Also, their results indicated that scale is an important factor in recognition processing. Thus, they suggested that the spatial pyramid pooling model and they found that the detection of objects had better performance among several scaled datasets. The main reason for this was because the objects which were detected often occupied significant regions of the whole image. But cropped or warped images caused to get lower accuracy rates than when using the same model on the undistorted full images.

Upon reading this related research, we were motivated to achieve better object recognition performance in (1) regions of interest and (2) high-resolution regions of interest which are cropped areas from input images. High-resolution image cropping is a solution which can come from super-resolution methods.



Figure 1: Cropping and warping. This image is from [6]

In [22], super-resolution is said to construct high-resolution images by adding of new pixels which have high frequency components to the neighbor pixels, instead of adding simply computed new pixels. The frequency components are from multiple observed low-resolution images or from a single low-resolution image.

There are four categories in super-resolution algorithms such as prediction, edge-based, statistical, and example-based methods. Among them, the space-coding based method, which is a kind of example-based method, is popular nowadays.

Let  $X$  denote the high-resolution image desired and  $Y_k$  be the  $k$ th low-resolution observation. Assume the image system captures iteratively  $k$  low-resolution images of  $X$ , where the low-resolution iterations are related with the high-resolution image  $X$  by

$$Y_k = D_k H_k F_k X + V_k, k = 1, 2, \dots, k, \quad (1)$$

where  $F_k$  represents the geometric warp (motion information) on the  $X$ ,  $H_k$  is the linear space-variant blurring effects,  $D_k$  is the down-sampling decimation operator, and  $V_k$  is the additive zero-mean Gaussian noise. Equation (1) can be represented in matrices

$$\begin{bmatrix} Y_1 \\ Y_2 \\ \vdots \\ Y_k \end{bmatrix} = \begin{bmatrix} D_1 H_1 F_1 \\ D_2 H_2 F_2 \\ \vdots \\ D_k H_k F_k \end{bmatrix} \mathbf{X} + \underline{V} \quad (2)$$

or equivalently,  $Y = \mathbf{W}\mathbf{X} + \theta$ .

The obtained model (2) is a classic restoration, and the Expectation-Maximization (EM) estimator or the MAP can be applied in order to restore the image  $X$ . Similarly to the above image observation model, statistical approaches in [23] relate the super-resolution restoration steps in iteration toward optimal restoration. Therefore, the super-resolution reconstruction is cast into a full Bayesian framework, and by sum rule and Bayes’ theorem. Finally, if we can estimate  $\mathbf{W}$ , then  $X$  can be obtained as a popular maximum a posteriori (MAP), or  $X$  can even be reduced to the simplest maximum likelihood (ML) estimator, which can be treated by an Expectation-Maximization (EM) algorithm in machine learning.

In [24], two kinds of super-resolution algorithms are introduced. Compared with the multiple-image super-resolution algorithm, the single image super-resolution algorithm uses a training step for the relationship between a set of high-resolution images and their low-resolution equivalents. This relationship is then used to predict the missing high-resolution components of the input images. There are three steps in this process: the registration (motion estimation), the restoration, and the interpolation to construct a high-resolution image from a low-resolution image or multiple low-resolution images [25].

In addition to the EM algorithm for single image super-resolution, [26]-[25] present methods that employ a mixture of experts (MoE) to jointly learn the features by separating global and local models (space partitioning and local regressing). These are solved by an expectation and maximization (EM) for joint learning of space partitioning and local regressing. Generative Adversarial Networks (GAN) method in [29] is proposed using generative networks and discriminative networks to restore most



likely original images with reducing of the mean squared reconstruction error.

In this paper, we will apply a single image super-resolution method to get better detection rates from a single image dataset.

### 3. Image Resolution Improvements

There are two approaches to improving input image quality. The first is to apply the super-resolution directly to the input images then have the CNN take the super-resolution image as the input image. The second is to apply the super-resolution only to bounding boxes. The second method may reduce the necessary computing power.

Shaoqing Ren et al. [4] implemented the interpolation algorithm for two purposes. One was to fix the input image size from variable input images, and the other was for the selective search algorithm to extract feature maps from input images. Detector extends networks for windowed detection by a list of crops or selective search (or EdgeBoxes) feature maps and then interpolates them to fix the size into one of the bounding boxes. Thus, this method may have more effects on bounding boxes for small objects, as shown in Figure 2. In [6], this method was described in detail in Section 4. In future research, we will implement CNN with extended images which are preprocessed using the super-resolution method instead of interpolation. In this paper, we propose using super-resolution as pre-processing before CNN to increase the image size to approximately 492x324 pixels.

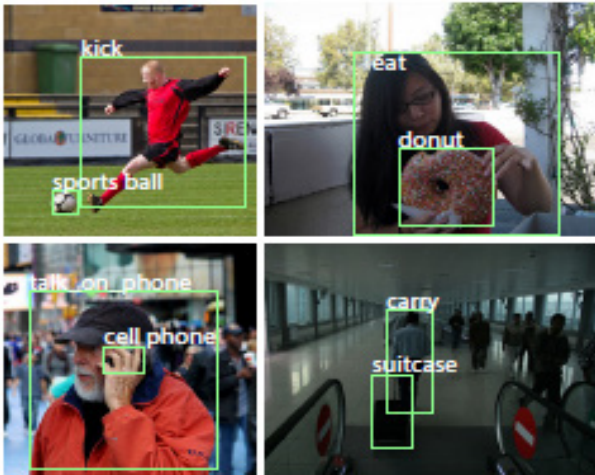


Figure 2: Images with either full-size objects or small-sized objects. These examples are from [30]

Thus, we will first describe a single image super-resolution method to enhance the quality of the image in preprocessing before forwarding image data to the input layer of CNN. Then, it is followed by the CNN algorithm to classify preprocessed images.

#### 3.1. Super-resolution as Pre-processing

In image analysis, there have been distinct improvements related to convolution neural networks. However, we will focus on preprocessing image samples by super-resolution methods. For example, if a cropped 166x110 pixel image is extracted from a larger image of 640x480 pixels, the cropped image is usually too small to feed into the input layer of CNN models to get good results

in object recognition. Thus, we will import a super-resolution method before the input layer of CNN or for bounding boxes.

We propose a Mixture of Experts (MoE) model to solve problems in anchor-based local learning, which are optimizing the partition of feature space and reducing the number of anchor points. The MoE model will be solved by Expectation-Maximization (EM) algorithm. The objective of a MoE model is to partition a large complex set of data into smaller subsets via the gating function. This preprocessing is built with the lazy neighbor embedding, anchor-based local learning approach, sparse coding, and deep convolution neural networks, respectively.

Component regressors,  $W_i$ , and an anchor point,  $v_j$  have the following relationship as an expert which means that each of the model component classifiers or regressors is highly trained:

$$\min_{\{v_1, v_2, \dots, v_k; w_1, w_2, \dots, w_k\}} \sum_{j=1}^N \sum_{i=1}^K c_{ji} \|h_j - W_i l_j\|^2, \quad (3)$$

where  $l_j$  is a low resolution path,  $h_j$  is the corresponding high resolution patch,  $v_j$  is the nearest anchor point for  $l_j$  and  $c_{ji}$  is a continuous scalar value which represents the degree of membership of  $l_j$ .

However, we propose a mixture of experts, which is one of the conditional combined mixture models in [31][32], in order to partition an image data into smaller subsets (as gating networks to determine which components are dominant in the region) and to determine the best (as experts to make predictions in their own regions).

In general, this a mixture of experts model can be trained efficiently by maximum likelihood using the EM algorithm in the M step. For every iteration, the posterior probabilities are calculated and reweighted for patches, and then we get LR/HR patch pairs  $(l_j, h_j)$  through the expectation of the log-likelihood as an E-step. During M-step, anchor points and regressors are updated, which is a softmax regression problem. After training, which is saving the trained anchor points and the projection matrices, a super-resolution image from the given input low-resolution image can be constructed by collecting all the patches from regressed low-resolution patches and averaging the overlapped pixels.

In order to compare the performance of our proposed method with that of interpolation methods, in addition to images produced by the super-resolution method, bilinear and bicubic interpolated images will also be generated.

#### 3.2. Object classification

As the object classification model, we decided to implement the CNN mostly based on the Faster R-CNN [4] because these networks support variable image sizes as the input data of CNN and sliding widow proposal scanning for the convolution network. Most importantly, the detection speed to predict an object is almost as fast as real-time. In YOLO or SSD, a group of an object can be detected, and the Faster R-CNN is enough to meet our goal. As mentioned earlier, Faster R-CNN uses the region proposal approach to detect an object from variable input image sizes. But the size ratio of the region proposal to the whole image is critical

to detect the object. As shown in Figure 2, sometimes objects from small bounding boxes are ignored because the object may be deformed or aliased during cropping or warping. With a better quality image, CNN will make better quality cropped or warped bounding boxes. This means we can distinguish our proposed method from other interpolated data.

As the pre-processing, the super-resolution is implemented on MATLAB on Linux and Intel® Xeon. Our proposed neural networks are implemented in two ways. For one example, CNN is implemented only on Intel® Xeon CPU 2.30GHz, and as another example, CNN is implemented based on Intel® Xeon CPU 2.30GHz and eight GPUs in four NVIDIA Tesla K80 GPU boards. Since our purpose is not to find how fast objects are detected but rather how many objects are detected, we do not discuss these different platforms anymore.

Our proposed CNN has built to predict region proposals in terms of region proposal networks (RPN), which are implemented by deep convolution networks (a kind of fully convolutional network [6]) [2][8]. This RPNs can predict region proposals with wide ranges of input image sizes and aspect ratios in contrast to conventional neural networks. The RPN also runs on pyramids of regression references (or pyramid of anchors), not on pyramids of images. It has benefits on running speeds.

The detection modules are organized as below: Multiple convolution layers convolve an input image and output feature maps. Then feature maps are given to the RPN. The RPN, in terms of a sliding window with a Multi-boxing method, generates a set of rectangular object proposals as a deep, fully convolutional network. A wide range of input image scales is fixed into given anchor sizes. After the RPN, conventional CNN predicts objects using the classification layer and bounds a box around the detected object using the regression layer.

In addition, for the storage usage of CAFFE, we make constraints on reading input images from the given image dataset. In our deep CNN model allowing multiple scaled image sizes, the maximum number of region proposals is  $w$  (the width of the image) multiplied by  $h$  (the height of the image) multiplied by  $k$  (the number of anchors of a region proposal). This means that the region proposal network requires a considerable amount of memory space. Therefore, we limited the feeding of the number of input images in hidden layers to less than or equal to 20 simultaneous images. Other than CAFFE, we used a version of the Keras model, which uses Tensorflow and GPUs. This other implementation had similar results. Therefore, we will not discuss it in this paper.

For the training of our CNN model, we use model parameters given in [4], which are actually initialized by pre-training model parameters of ImageNet. We test 9000 images from datasets with PASCAL VOC 2007 and also tests with Microsoft's COCO dataset. As we said before, we consider more only on the number of detected objects but not the improving or computational speeds. Therefore, we are pretty sure that our model training procedure is adequately fitted to our purpose.

For each region proposal from an input image, an object is randomly counted on, and we randomly sample 256 anchors in an image as a mini-batch size. Instead of considering the super-  
[www.astesj.com](http://www.astesj.com)

resolution method on selected region proposals instead of interpolation methods, any input images with variable sizes or shapes can be supported with better cropped or warped regions. But we do not consider this right now. We will leave this for future research. Instead, we processed with low-resolution images as the input dataset, processing super-resolution on these images, then detecting objects.

#### 4. Performance Evaluations

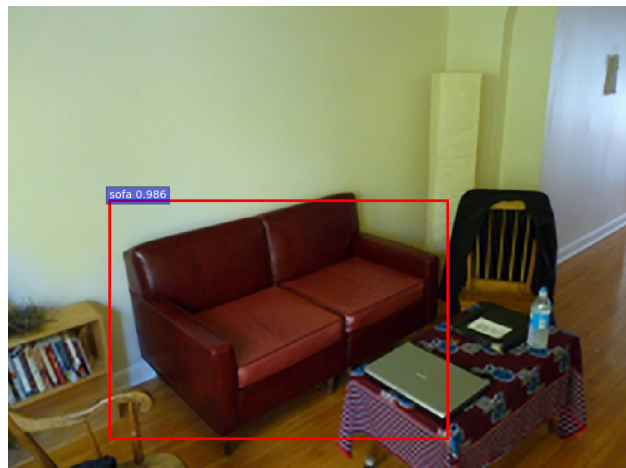
To detect objects from images in CNNs, there are two kinds of popular file formats as input datasets. Those formats are JPG and Bitmap. However, we have considered several more image file formats as well as JPG and Bitmap formats to get better image quality for preprocessing and to get better detection objects during testing images. While datasets such as PASCAL VOC2007 or COCO are generated images with the JPG file format, in super-resolution processing, the JPG format did not seem to offer results as good as the Bitmap format. Such effects on preprocessing, we decided to use Bitmap format, and then we worked to convert the images from JPG format into BMP format before a preprocessing procedure. Also, we scaled down the image size, reducing each width and height by a factor of three to generate images of lower quality, instead of directly collecting cropped or warped images. Then, the image was further processed with bilinear and bicubic interpolations, as well as the super-resolution method. Thus, we built three different image datasets as preprocessing in our proposed method.

In our model, we implemented the preprocessing procedure based on [26]. Rather than training with nearly 50 images as in most of the published single image super-resolution models, we trained our model based on their initial parameters and with 100 PASCAL VOC2007 images and COCO images. We did not find any considerable overfitting with this number of training images. We generated images as the preprocessing of our method with randomly selected images from PASCAL VOC2007 [16][33], images from [34], and additionally with the COCO dataset images. Newly built images after our preprocessing are similar categories and the number of objects in an image. Therefore, we tested the object classification with 520 images randomly extracted from VOC2007 and 1224 images from COCOs MSO [35].

As shown in Figure 3, we knew that the dataset was annotated with a different number of objects compared to our intuition, and our proposed model found it. For example, the first image of Figure 3 was annotated with no number of any designated object, but our proposed model caught an object or several objects, as shown in the image. The second image of Figure 3 shows that a sofa was detected even though the image was annotated with no object. Because of these differences, we decided to use roughly the given annotations from the given dataset. A larger number of people than the labeled number was detected in the third image of Figure 3. This meant that we needed to manually count the number of objects in each image in the dataset to get the precision-recall measures.

##### 4.1. Comparison of Output Pictures

Even though some of the images from the PASCAL VOC 2007 were detected as the image had no objects in the designated



person detections with  $p(\text{person} | \text{box}) \geq 0.8$

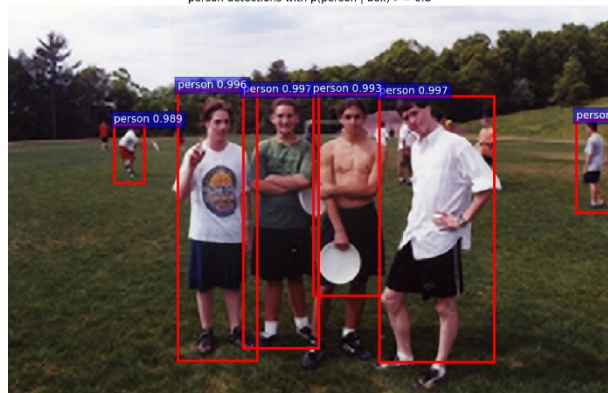


Figure 3: Some Images labeled with no objects on annotated dataset but detected objects by our method.

categories, multiple objects in the categories are detected from almost all of the images, as shown in the results given in Table 10. There were three different preprocessing models, namely bilinear interpolation, bicubic interpolation, and our super-resolution method. After the preprocessing of input images, our model for object detection was set with a learning rate of 0.001 to train and detection scores with 0.8 or higher compared with ground truths (IoU) at the testing stage. Our model has 21 categories that are randomly selected and which are independent of each other.

As shown in Figure 4, Figure 5, and Figure 6, green color bars (the first column) show the number of detected objects in each

category as given by bilinear interpolation, blue color bars (the second column) show the number as given by bicubic interpolation, and red color bars (the third column) show the results for our proposed approach. Both the number of objects detected as y-coordinate and the detection rate as x-coordinate are shown.

As shown in Table 1, our model detects more objects than the other two models, but the average detection scores are not very different. This demonstrates that our model generates improved input images of which objects had lower scores than 0.8 compared with ground truth images in the other two models, which are then fed into the CNN which is able to increase the number of detections of categories. Here we mean the detection score is the probability that the detected object belongs to the class. Therefore, objects with near- or over-threshold scores (80% or above) are included even though they did not get the scores over the threshold value in the bilinear or bicubic interpolation models. Figure 4 shows the number of detected objects from the PASCAL VOC 2007 dataset and the comparison between them.

In Table 1, Table 2, In Figure 7, our proposed model detects a chair which is quite a small object compared with the image size, while the other two models did not detect this ‘chair’ object. It is looked like that a small change by preprocessing before CNN can make a big difference. Even though the other chair, which is bigger than the chair, is detected in all three models, our proposed model has a little higher score. Thus, we can conclude our model can help to improve image qualities in image analyses. In particular, with video surveillance camera systems, our model may help to detect more objects. Therefore, we are interested in surveillance camera systems as a future research topic.

#tp means the number of correctly predicted objects (true positive), and the mean column shows the classification average probabilities predicted.

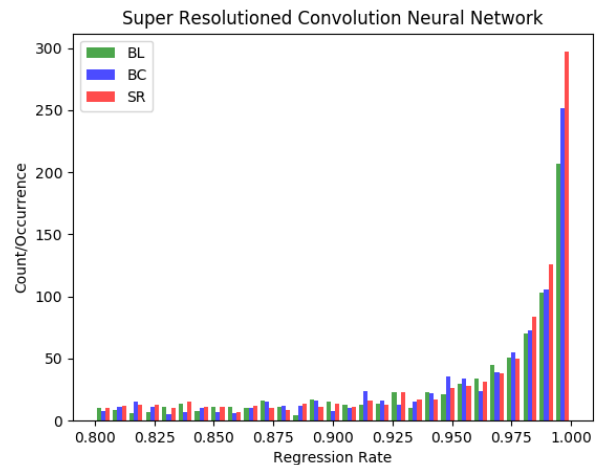


Figure 4: Histogram for object detection models: images from VOC 2007 dataset.

With the dataset of Microsoft MSO as another image dataset for testing object classification, we present results in Figure 5 and Table 2. As with the VOC2007 dataset, our proposed model detects more objects than the two other models. This indicates that the image quality of low scored objects improved, leading to



better detection. In other words, in our model, the image quality of low-scored objects improved, leading to detection scores (which is the probability that the object is the class) above 80%.

The main change in the COCO 2017 test dataset [36] is that instead of an 83K/41K train/validation split, the split is now 118K/5K for train/validation. Also, for testing, in 2017, the test set only had two splits (dev / challenge), instead of the four splits (dev / standard / reserve / challenge) used in previous years. For training of this dataset, we followed similar procedures as we did in PASCAL VOC 2007. For this dataset, we present the results in Figure 6 and In Figure 7, our proposed model detects a chair which is quite a small object compared with the image size, while the other two models did not detect this ‘chair’ object. It is looked like that a small change by preprocessing before CNN can make a big difference. Even though the other chair, which is bigger than the chair, is detected in all three models, our proposed model has a little higher score. Thus, we can conclude our model can help to improve image qualities in image analyses. In particular, with video surveillance camera systems, our model may help to detect more objects. Therefore, we are interested in surveillance camera systems as a future research topic.

. The total number of detected objects using our model was much bigger than the bilinear or bicubic models. However, the mean probabilities of detected objects were similar or a little bit lower. This indicates that many objects which were not detected with bilinear or bicubic interpolation methods were detected with our method.

Table 1: The number of detected objects on each category and the prediction scores on three different preprocessing and CNN with the PASCAL VOC2007 dataset.

Classes	Bilinear		Bicubic		Our Method	
	#tp	mean	#tp	mean	#tp	mean
aeroplane	25	0.9569	29	0.9472	27	0.9787
bicycle	16	0.9602	17	0.9697	18	0.9520
bird	18	0.9204	25	0.9178	30	0.9500
boat	16	0.9330	18	0.9260	20	0.9276
bottle	19	0.9222	17	0.9208	15	0.9331
bus	26	0.9626	25	0.9639	26	0.9588
car	93	0.9662	100	0.9671	104	0.9710
cat	11	0.9427	10	0.9665	11	0.9739
chair	25	0.9273	34	0.9368	45	0.9320
cow	11	0.9149	12	0.9216	16	0.9385
dining table	7	0.9317	7	0.9420	12	0.9193
dog	37	0.9559	36	0.9657	35	0.9565
horse	30	0.9560	34	0.9574	37	0.9694
motorbike	13	0.9467	13	0.9630	16	0.9581
person	405	0.9546	432	0.9575	466	0.9590
potted plant	10	0.9467	12	0.9194	18	0.8767
sheep	15	0.9275	13	0.9380	14	0.9227
sofa	7	0.9191	8	0.9175	8	0.9475
train	7	0.9193	4	0.9276	4	0.9572
tvmonitor	25	0.9653	25	0.9729	26	0.9479
Total	816	0.9415	871	0.9450	<b>948</b>	<b>0.9465</b>
misclassified	25		21		<b>39</b>	

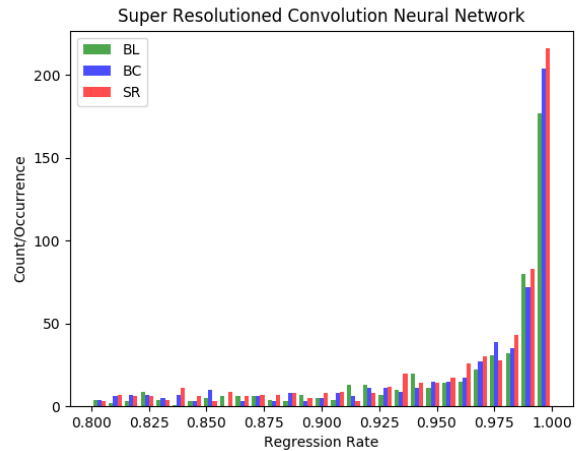


Figure 5: Histogram for object detection models: images from the MSO dataset.

#### 4.2. Big vs. Small ROI Pictures and Their Detection Rates

As mentioned above, if an object is sufficiently large relative to the size of the image which contains the object in a region proposal, objects from interpolated images with bilinear or bicubic methods are identified satisfactorily and sometimes may have better performance means that there is a higher probability that the object is identified as being in the specified class. However, the model we have proposed obtains much better results when the objects are from small bounding boxes, or if there is a small ratio of object size to the size of the image which contains the object (it means small anchor boxes in region proposals).

Table 2: The number of detected objects on each category and the prediction scores on three different preprocessing and CNN with the MSO dataset.

Classes	Bilinear		Bicubic		Our Method	
	#tp	mean	#tp	mean	#tp	mean
aeroplane	5	0.9650	6	0.9300	9	0.9263
bicycle	1	0.9992	2	0.9112	1	0.9978
bird	50	0.9512	59	0.9521	75	0.9627
boat	1	0.8301	1	0.9771	1	0.9713
bottle	23	0.9074	24	0.9062	21	0.9117
bus	3	0.9954	3	0.9954	3	0.9871
car	16	0.9641	19	0.9558	18	0.9499
cat	11	0.9639	10	0.9829	11	0.9540
chair	19	0.9299	20	0.9270	22	0.9393
cow	5	0.9452	6	0.9488	7	0.9584
dining table	3	0.9410	4	0.8927	4	0.9072
dog	42	0.9559	47	0.9636	50	0.9478
horse	11	0.9728	11	0.9726	15	0.9362
motorbike	4	0.9487	4	0.9529	4	0.9588
person	302	0.9715	318	0.9718	340	0.9719
potted plant	4	0.9023	5	0.8756	9	0.9035
sheep	1	0.8780	1	0.9353	4	0.9064
sofa	3	0.9204	3	0.9099	6	0.9261
train	6	0.9746	7	0.9529	8	0.9522
tvmonitor	6	0.9720	6	0.9804	10	0.9248
Total	516	0.9444	556	0.9447	<b>618</b>	<b>0.9447</b>
misclassified	86		82		<b>92</b>	



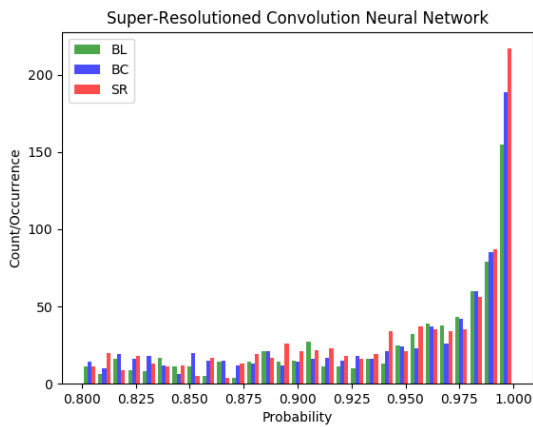


Figure 6: Histogram for object detection models: images from COCO 2017 dataset.



Figure 7: Examples of small object scales through three models

In Figure 7, our proposed model detects a chair which is quite a small object compared with the image size, while the other two models did not detect this ‘chair’ object. It is looked like that a small change by preprocessing before CNN can make a big difference. Even though the other chair, which is bigger than the chair, is detected in all three models, our proposed model has a little higher score. Thus, we can conclude our model can help to improve image qualities in image analyses. In particular, with video surveillance camera systems, our model may help to detect more objects. Therefore, we are interested in surveillance camera systems as a future research topic.

### 5. Conclusion

Our proposed model appears particularly powerful in three scenarios; firstly, where there are relatively small objects in large pictures; secondly, where there is warping in the region proposals approach; and finally, with object detection from cropped images. Commonly, there are many noisy video images from surveillance camera systems, especially with night vision systems. Our method will remove a significant amount of aliased or mosaicked areas in these images, and so help to detect more objects. We compared our scheme with other approaches on three datasets showing an increased object in each case.

In future work, we will implement the super-resolution method confined to the bounding box areas. This will reduce the needed computational resources and allow us to use this method in real-time processing [37] and achieve better object recognition in this application. We will demonstrate this capability using modern streaming software environments [38].

Table 3: The number of detected objects on each category and the prediction scores on three different preprocessing and CNN with the COCO 2017 dataset.

Classes	Bilinear		Bicubic		Our Method	
	#tp	mean	#tp	mean	#tp	mean
aeroplane	9	0.9652	10	0.9502	11	0.9684
bicycle	1	0.8821	2	0.9012	3	0.9250
bird	5	0.9471	10	0.9066	17	0.9277
boat	5	0.9002	5	0.8908	7	0.8896
bottle	20	0.9116	25	0.9100	19	0.9160
bus	15	0.9725	16	0.9590	15	0.9456
car	24	0.9503	29	0.9251	28	0.9388
cat	6	0.9274	7	0.9235	10	0.9075
chair	26	0.9193	28	0.9169	36	0.9174
cow	12	0.9190	14	0.9287	14	0.9384
dining table	10	0.8989	9	0.9049	9	0.9063
dog	12	0.9184	12	0.9183	12	0.9047
horse	7	0.9219	8	0.9293	6	0.9402
motorbike	11	0.9604	14	0.9550	18	0.9368
person	411	0.9547	460	0.9521	498	0.9534
potted plant	16	0.8806	11	0.8824	15	0.9002
sheep	2	0.9585	2	0.9880	2	0.9977
sofa	3	0.9398	3	0.9015	2	0.8760
train	9	0.9358	10	0.9269	9	0.9427
tvmonitor	26	0.9461	24	0.9457	25	0.9544
Total	734	0.9305	805	0.9258	<b>869</b>	<b>0.9293</b>
misclassified	104		106		<b>113</b>	

### Acknowledgment

This work was supported by the 2017 sabbatical year research grant of the Korea Polytechnic University.

Geoffrey Fox was partially supported by NSF CIF21 DIBBS 1443054 and NSF CINES 1835598. We thank the Futuresystems group for the computational resources.

## References

- [1] Bokyoon Na, Geoffrey Fox, "Object Detection by a Super-Resolution Method and a Convolutional Neural Networks", IEEE International Conference on Big Data (Big Data) (2018)
- [2] Alex Krizhevsky, Ilya Sutskever, Geoffrey E. Hinton. "ImageNet Classification with Deep Convolution Neural Networks". In *Advances in Neural Information Processing Systems (NIPS)*, (1097-1105). (2012).
- [3] Girshick Ross. "Fast R-CNN". arXiv: 1504.08083v2 [cs.CV] 27 Sep 2015.
- [4] Shaoqing Ren, Kaiming He, Ross Girshick, and Jian Sun. "Faster R-CNN: Towards Real-time Object Detection with Region Proposal Networks". arXiv:1506.01497v3[cs.CV] 6 Jan 2016.
- [5] David Berthelot Schumm, Luke Metz Thomas. "BEGAN: Boundary Equilibrium Generative Adversarial Networks". arXiv: 1703.10717v2 [cs.LG]. (2017).
- [6] Keiming He, Xiangyu Zhang, Shaoqing Ren, and Jian Sun. "Spatial Pyramid Pooling in Deep Convolutional Networks for Visual Recognition". arXiv:1406.4729v4. (2015).
- [7] Ross Girshick, Jeff Donahua, Trevor Darrell, Jitendra Malik, "Region-Based Convolution Networks for Accurate Object Detection and Segmentation", *IEEE Transactions on Pattern Analysis and Machine Intelligence Vol. 38, NO.1*, 2016.
- [8] Karen Simonyan, Zisserman Andrew. "Very Deep Convolutional Networks for Large-Scale Image Recognition". ICLR. (2015).
- [9] Joseph Redmon, Santosh Divvala, Ross Girshick, Ali Farhadi, "You Only Look Once: Unified, Real-time Object Detection", The IEEE Conference on Computer Vision and Pattern Recognition (CVPR), 2016, pp. 779-788
- [10] Kaiming He, Georgia Gkioxari, Piotr Dollár, Ross Girshick, "Mask R-CNN", The IEEE International Conference on Computer Vision (ICCV), 2017, pp. 2961-2969
- [11] Ghosh Nachum and Debiprasad Ofir. <https://www.quora.com/What-are-Generative-Adversarial-Networks-GANs>.
- [12] Tim Salimans Goodfellow, Wojciech Zaremba, Vicki Cheung Ian. "Improved Techniques for Training GANs". arXiv:1606.03498v1. (2016).
- [13] Takeru Miyato M Dai, Ian Goodfellow Andrew. "Adversarial Training Methods for Semi-Supervised Text Classification". ICLR. (2017).
- [14] Ian J. Goodfellow Pouget-Abadie, Mehdi Mirza, Bing Xu, David Warde-Farley, Sherjil Ozair, Aaron Courville, Yoshua BengioJean. "Generative Adversarial Nets". arXiv:1406.2661v1. (2014).
- [15] Sara Sabour, Nicholas Frosst, Geoffrey E. Hinton, "Dynamic Routing Between Capsules", *Advances in Neural Information Processing Systems 30 (NIPS 2017)*
- [16] M. Everingham Van Gool, C. K. I. Williams, J. Winn, and A. ZissermanL. "The PASCAL Visual Object Classes Challenge 2007 (VOC2007) Results". (2007).
- [17] Achanta R., Estrada F., Wils P., Süsstrunk S. "Salient Region Detection and Segmentation". In: Gasteratos A., Vincze M., Tsotsos J.K. (eds) *Computer Vision Systems. ICVS 2008. Lecture Notes in Computer Science*, vol 5008. Springer, Berlin, Heidelberg. (2008)
- [18] Volodymyr Mnih, Nicolas Heess, Alex Graves, and Koray Kavukcuoglu. "Recurrent Models of Visual Attention". arXiv:1406.6247v1[cs.LG] 24 Jun 2014.
- [19] Jimmy Lei Ba, Volodymyr Mnih, and Koray Kavukcuoglu. "Multiple Object Recognition with Visual Attention". arXiv:1412.7755v2[cs.LG] 23 Apr 2015.
- [20] Karol Gregor Danihelka, Alex Graves, Danilo Jimenez Rezende, Daan Wierstra Ivo. "DRAW: A Recurrent Neural Network For Image Generation". arXiv:1502.04623v2[cs.CV] 20 May 2015.
- [21] J.R.R. Uijlingsvan de Sande, T. Gevers, and A.W.M. Smeulders K.E.A. "Selective Search for Object Recognition". IJCV. (2012).
- [22] Michael Elad, Arie Feuer, "Restoration of a Single Superresolution Image from Several Blurred, Noisy, and Undersampled Measured Images", *IEEE Transactions on Image Processing*, Vol. 6, No. 12, December 1997
- [23] Jianchao Yang, John Wright, Thomas S. Huang, and Yi Ma, "Image Super-Resolution Via Sparse Representation", *IEEE TRANSACTIONS ON IMAGE PROCESSING*, VOL. 19, NO. 11, pp2861, NOVEMBER 2010
- [24] Nasrollahi Kamal, Guerrero Escalera Sergio, Rasti Pejman, Anbarjafari Gholamerza, Baro Xavier, J. Escalante Hugo, Moeslund B. Thomas. "Deep Learning based Super-Resolution for Improved Action Recognition". In *International Conference on Image Processing Theory, Tools and Applications (IPTA)* IEEE Signal Processing Society. (2015).
- [25] Brian C. Tom, Aggelos K. Katsaggelos, Nikolas P. Galatsanos. "Reconstruction of a high resolution image from registration and restoration of low resolution images". In *Proceedings of IEEE International Conference on Image Processing*, pages 553-557, 1994
- [26] Kai Zhang Wang, Wangmeng Zuo, Hongzhi Zhang, Lei ZhangBaoquan. "Joint Learning of Multiple Regressors for Single Image Super Resolution". *IEEE Signal Processing Letters*. Vol. 23 No. 1. (2016).
- [27] Zhaowen Wang Liu, Jianchao Yang, Wei Han, Thomas Huang Ding. "Deep Networks for Image Super Resolution with Sparse Prior". ICCV. (2015).
- [28] Chao Dong Change Loy, Kaiming He, Xiaoou Tang Chen. "Image Super Resolution Using Deep Convolution Networks". arXiv:1501.00092v3.v (2015).
- [29] Christian Ledig Theis, Ferenc Huszar, Jose Caballero, Andrew Cunningham, Alejandro Acosta, Andrew Aitken, Alykhan Tejani, Johannes Totz, Zehan Wang, Wenzhe ShiLucas. "Photo-Realistic Single Image Super Resolution Using a Generative Adversarial Network". arXiv:1609.04802v5[cs.CV]. (2017).
- [30] Georgia Gkioxari, Ross Girshick, Piotr Dollár, Kaiming He, "Detecting and Recognizing Human-Object Interactions", *The IEEE Conference on Computer Vision and Pattern Recognition (CVPR)*, 2018, pp. 8359-8367
- [31] Bishop Christopher. "Pattern Recognition and Machine Learning". Springer. (2006).
- [32] Zhang Zhang, Baoquan Wang, Wangmeng Zuo, Hongzhi ZhangKai. "Joint Learning of Multiple Regressors for Single Image Super-Resolution". *IEEE Signal processing letters*, Vol. 23, No.1. (2016).
- [33] Olga Russakovsky Deng, Hao Su, Jonathan Krause, Sanjeev Satheesh, Sean Ma, Zhiheng Huang, Andrej Karpathy, Aditya Khosla, Michael Bernstein, Alexander C. Berg and Li Fei-Fei Jia. "ImageNet Large Scale Visual Recognition Challenge". arXiv:1409.0575. (2014).
- [34] Olga Russakovsky Deng, Hao Su, Jonathan Krause, Sanjeev Satheesh, Sean Ma, Zhiheng Huang, Andrej Karpathy, Aditya Khosla, Michael Bernstein, Alexander C. Berg and Li Fei-Fei Jia, "ImageNet Large Scale Visual Recognition Challenge 2017". (2017).
- [35] Zhang Ma, Shuga Sameki, Mehrnoosh Sclaroff, Stan Betke, Margrit Lin, Zhe Shen, Xiaohui Price, Brian Much, Radom Jianming. "Salient Object Subitizing". *IEEE Conference on Computer Vision and Pattern Recognition (CVPR)*. (2015).
- [36] Tsung-Yi Lin, Michael Maire, Serge Belongie, Lubomir Bourdev, Ross Girshick, James Hays, Pietro Perona, Deva Ramanan, C. Lawrence Zitnick, Piotr Dollár. "Microsoft COCO: Common Objects in Context", arXiv:1405.0312 [cs.CV]
- [37] Xinyuan Huang, Geoffrey C. Fox, Sergey Serebryakov, Ankur Mohan, Pawel Morkisz, Debojyoti Dutta, "Benchmarking Deep Learning for Time Series: Challenges and Directions", *Stream-ML workshop at IEEE Big Data Conference, Los Angeles CA December 10, 2019*
- [38] Vibhatha Abeykoon, Supun Kamburugamuve, Kannan Govindrarajan, Pulasthi Wickramasinghe, Chathura Widanage, Niranda Perera, Ahmet Uyar, Gurhan Gunduz, Selahattin Akkas, Gregor Von Laszewski, and Geoffrey Fox, "Streaming Machine Learning Algorithms with Big Data Systems", *Stream-ML workshop at IEEE Big Data Conference, Los Angeles CA December 10, 2019*

# Interaction Model and Respect of Rules to Enhance Collaborative Brainstorming Results

Thierry Gidel<sup>\*1</sup>, Andrea Tucker<sup>2</sup>, Shigeru Fujita<sup>3</sup>, Claude Moulin<sup>4</sup>, Kenji Sugawara<sup>3</sup>, Takuo Suganuma<sup>5</sup>, Yuki Kaeri<sup>6</sup>, Norio Shiratori<sup>7</sup>

<sup>1</sup>Sorbonne Universités, Université de Technologie de Compiègne, COSTECH EA 2223, 60200, France

<sup>2</sup>Interuniversity Center for Research in Education, Université de Lille, CIREL EA 4354, France

<sup>3</sup>Faculty of Information and Computer Science, Chiba Institute of Technology, Narashino-shi, Chiba-ken, Japan

<sup>4</sup>Sorbonne Universités, Université de Technologie de Compiègne, JR Unit CNRS 7253, Heudiasyc, 60200, France

<sup>5</sup>Cyberscience Center, Tohoku University, Sendai, Miyagi, Japan

<sup>6</sup>Faculty of Media Studies, Department of Media Studies, Mejiro University, 4-31-1 Nakaochiai, Shinjuku-ku, Tokyo, Japan

<sup>7</sup>Research and Development Initiative, Chuo University, 1-13-27 Kasuga, Bunkyo-ku, Tokyo 112-8551, Japan

---

## ARTICLE INFO

### Article history:

Received: 14 January, 2020

Accepted: 21 March, 2020

Online: 09 April, 2020

---

### Keywords:

Creative problem solving

Interaction model

Multi-agent system

Multi-touch device

Methodological rules

---

## ABSTRACT

*This paper presents a collaborative interaction model (CIAO) and several behaviour rules that could enhance brainstorming results. The model is composed of five elements which may be used during brainstorming sessions, consisting of activities performed by participants which are characteristic of different modes of interaction. Some sequences of these interactions may be considered more or less adequate than others. In particular, in order to get better results during brainstorming activities participants must respect certain rules when they write their ideas and when they consider notes written by somebody else. We argue that a multi-agent system can recognize different interaction modes and verify the respect of these rules by analyzing videos and notes produced by the participants in real time. Such a system must be trained as a machine learning system before being used during actual meetings. This system can simplify the role of the meeting facilitator. It can send a summary of the meeting situation, such as the proportion of each mode of interaction and identify behaviors that may need to be addressed. We present how feedback could be sent individually or addressed to the entire team. We will begin by presenting the interaction model, then propose an automatic recognition of these modes from video recordings and log analysis. We also address the necessity of rules and the structure of a multi-agent system which is able to verify whether or not the participants are respecting them. Finally, we propose how experiments could show the level of acceptance of such a system by users. The goal of this prospective research is to define a non-intrusive system that can be used during brainstorming sessions, based on an interaction model to enhance the quality of meeting results.*

---

## 1 Introduction

This paper is an extension of work originally presented in the 23rd IEEE International Conference on Computer Supported Cooperative Work in Design [1]. Several research projects have proposed various architectures for supporting activities, in particular creative problem solving, in the context of collaboration between teams situated in different locations. Their front-ends typically involve rich user

interfaces and some of them use large multi-touch surfaces[2]-[4]. The user interface of such tools should be synchronized between sites to ensure a continuity of experience. Their back-end is mainly based on a managing multi-agent system situated in the cloud that supports the functions of the applications (such as storing data and synchronization). To facilitate the collaboration, provide a sense of presence, and ensure awareness of other team members' actions and oral conversations, the sites must have specific equipment (cameras

---

\*Corresponding Author, +33 3 44 23 52 10 & thierry.gidel@utc.fr



and microphones).

Figure 1 shows two people working during brainstorming activities around a large multi-touch table in France, at the Université de Technologie de Compiègne (UTC) while communicating with a remote team situated in Japan, at the Chiba Institute of Technology (CIT). In this image, we can see that people use virtual keyboards on the table for creating digital notes. At the same time, they can see the other team (on the right section of the board), from several angles. The team in France can also observe the similar multi-touch device used by the other team (left part of the board).

The initial stage of a project meeting is often brainstorming, which requires a facilitator to manage member contributions.

From a technological point of view, these types of collaboration environments reach a high level of quality that should allow people to obtain good results during their collaboration. However, it appears that is not always true due to some practical, methodological and behavioural reasons:

**Practical reasons:** people do not know how to use these systems and, for example, cannot find the right way to activate a menu, a virtual keyboard, etc. in order to perform a task. Beyond the software, the hardware may also be slow or not as responsive as the user might expect.

**Methodological reasons:** collaboration is a complex process with multiple steps, which are not necessarily completed in a specific order. Participants do not necessarily know which is the best step to choose, when to move to the next step or repeat previous one in order to make their collaborative activity successful.

**Behavioural reasons:** people do not necessarily know how to conduct themselves when they are in a group meeting. It is the role of the meeting facilitator to help, to encourage or to set limits to, for instance, ensure equal participation. Everybody should be able to participate and use competencies at their best. This can be particularly complex in multi-cultural teams with potential language barriers. Moreover, it is not always easy to find a meeting facilitator with enough expertise to manage collaborative sessions and produce interesting results.

Our long term objective is to bring an AI based support to facilitators dynamically in order to make the meeting management easier especially when several distant teams need to collaborate. We claim that such a support could be useful to tackle methodological and behavioural issues. The first step was to define an interaction model between users, presented in Section 3. The second step will be the real-time AI based analysis of all the digital footprints left by meeting participants. This will allow us to get as many indications as possible on what is happening during the meeting. Digital footprints must be understood globally: audio/video recording of sessions with several cameras and several points of view, event logs of people performing activities on the large multi-touch devices. Then, the digital footprint data needs to be analysed and we need to define how the results of this analysis are communicated to the meeting facilitator and participants.

In the following sections we present some behaviour rules concerning brainstorming session, the collaborative interaction model (CIAO), and the architecture of a framework able to deliver advice to a meeting facilitator. The last section describes how the facilitator could communicate tips and hints to meeting participants.

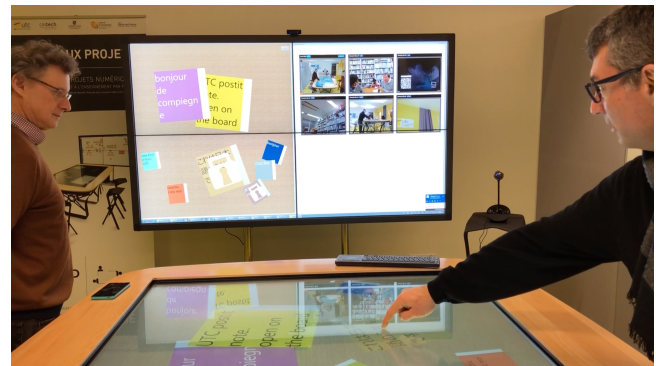


Figure 1: Environment with large multi-touch tabletop

## 2 Creative Problem Solving

### 2.1 Brainstorming

Creative problem solving is a key activity of teamwork that leads to novel ideas with great value [5]. Multi-touch and multi-user systems are expected to support this type of collaborative work by allowing cognitive stimulation through shared space [6, 7], common views, joint attention, awareness [8, 9] and social interactions[10].

Group brainstorming is one of the most popular creative problem solving methods [11] but it is often misused and the role of the group facilitator is often underestimated[12].

This seems especially critical when it comes to multi-disciplinary, multi-cultural distributed teams[13]. That is why we propose in this article to develop a complete system that could capitalize on the positive impact of multi-touch, multi-user devices based on cognitive simulation and social comparison processes[14, 15], simultaneous written and oral interactions [16, 17], AI and multi-agent based systems that would facilitate the team-work during creative problem solving and, more specifically, brainstorming sessions.

### 2.2 Rules

In order to encourage better results during brainstorming activities participants must follow some rules. Osborn[18] outlined four guidelines for brainstorming: (1) criticism is excluded, (2) free-wheeling and wild ideas are encouraged, (3) the greater the number of ideas, the greater the likelihood of useful ideas, (4) combination and building on others' ideas is welcome.

### 2.3 Barriers and propositions for effective implementation

Based on an extensive literature review, the main barriers to effective brainstorming are summarized by Isaksen [12] as (1) judgments during generation, (2) members giving up on the group and (3) an inadequate structure of interaction. In section 3 we first propose a model of interaction between users during general meetings and then we show how to analyze people's behaviour according to this model. Currently, analysis is done manually, looking at video recordings. A first objective of our research is to enable the automatic analysis of



videos, based on deep learning techniques. A second objective is to define acceptable and unacceptable structures of interaction during meetings.

To avoid judgment, which leads to inhibition due to fear of critical evaluation, voice and video analysis will track those attitudes and generate appropriate responses, either directed to one person (in a semi-private way), to a sub group (a local team on a specific site) or to the full team (simultaneously on all remote sites).

In order to avoid cognitive inertia or uniformity, wild ideas could be inserted within the group production by a computer support system in such a way as to be unable to identify the idea's origin.

One of the reasons for members giving up on the group is social loafing or freeriding. To avoid this, the setting will allow participants to view, through peripheral vision, others' production of ideas. This use of a matching of effort effect is supposed to work if there is a good group dynamic. To initiate this dynamic, the system could set challenges to stimulate the global team or the local sub-teams in terms of numbers of ideas generated, by displaying and announcing when each sub-group has produced ten more ideas. This could be associated with encouragement to extend their effort, which is known to lead to increased participation[19]. This kind of tool would require an experienced facilitator to avoid potentially harmful competition between sub-groups, or even encourage a team vs. computer competition.

System architecture and front-end software are designed to avoid inadequate interaction with devices. However, the way to favour adequate interaction between people, is still a meeting management issue. We propose a first step towards an automatic recognition of adequate and inadequate sequences of interaction between people during meetings thanks to video analysis.

The fact that all participants can write their ideas simultaneously will help to avoid production blocking [20] and limited airtime issues that are a common problem in oral brainstorming, where one person talks at a time. Simultaneous processing could even be encouraged by the challenges proposed previously. As it is true that we often think of more ideas than we could write down, a particular attention should be granted to text entry interaction: keyboard, auto-completion, word suggestion, spelling and grammar check, etc. to speed up the writing process.

We propose to develop a system that handles those major problems by helping the facilitator in his/her managing role, not aiming to replace this role. It must be seen as a critical added value. Nevertheless, the group facilitator has no ubiquitous power and he/she can only be in one location. Therefore, the system should help complete repetitive tasks and act as a relay in each sub-group. The system's contribution would include reinforcing the guidelines (follow the rules) and encouraging the participants. The system could also have a more direct interaction with the facilitator, as a timekeeper, suggesting the right time to shift from the production to the sorting phase, for instance, to maintain the group energy and productivity. That is the objective we would like to pursue.

## 2.4 *Brainstorming process and rules*

Brainstorming is a phase where people try to express ideas about the topic of a new project. Everyone is free to propose new ideas

and there should be no limitations.

Generally people write ideas on post-it notes. In previous papers [2, 3] we showed that virtual post-it notes organized on large multi-touch devices present advantages over paper notes. That defines the context of our research: brainstorming activities using large multi-touch devices (tables and boards) during meetings recorded with video cameras. To respect privacy, videos are used for real time analysis as explained in the next sections. The research seeks to facilitate brainstorming by making these rules explicit.

As people are not always aware of the brainstorming rules, an automatic system supporting the respect of these social and process rules must be well integrated and as symbiotic as possible. Because it is difficult for the facilitator or group leader of a remote brainstorming session to ensure that the rules are followed in all sites, having a system supporting the animation role would be of great help. We define two types of rules: social/behavioural rules and process/note content rules.

## 2.5 *Rules regarding behavior*

During brainstorming activities, people are free to propose ideas. Nobody should feel constrained because it leads to a hesitation to express ideas. Ideas are to be analyzed in a later step, which will weed out those ideas that do not correspond to the topics developed in the project. That means that everybody must respect any proposal and not be critical of any idea during the brainstorming phase. There are at least three ways to criticize: by voice (e.g. someone saying "this is not compatible with our project"), by gesture (e.g. somebody raises an arm or turns the head or makes disapproving facial expressions) and deleting someone else's idea before discussion.

## 2.6 *Rules regarding note content*

Only the author of a note is really aware of its meaning. However, somebody else reading a note must make sense of it. So, the way to write a note must not be ambiguous. Some syntactic rules, even if they are not extensive, may avoid some misunderstandings. Notes must not contain only a few words, but complete sentences. It is a good way to ensure that people have really expressed their ideas in a way that is comprehensible for other team members. Following this rule may also help people to fully develop an idea before proposing it.

## 2.7 *Other phases of project management*

Brainstorming is usually only one step of the project or problem solving process. Ideas produced during brainstorming activities need to be organized, filtered, and sometimes repeated if the group feels that there are not enough ideas to move the project forward. For that reason, the system analyzing the respect of syntactic rules may be used for other, more semantic tasks. It should be possible for this system to recognize similar ideas, new ideas and bring attention to them. New ideas are ideas where the content has not be reused in other notes.

### 3 Collaborative Interaction Model

#### 3.1 Analysis Model

Behaviors that can be observed during globally collaborative work include cooperation, individual work, presentation of that work etc. As such, we propose five modes of interaction which break globally collaborative work into its finer details: individual work, communication, coordination, cooperation and collaboration[21]. We define each of these modes as:

- **Individual Work:** moments when individuals retreat from the group in order to reflect and construct their ideas [22], as well as work performed on tasks with which they were entrusted by the group.
- **Communication:** this mode of interaction allows individuals to introduce new information into the group, creating the point of departure for a shared vision [22]. Communication can take the form of providing information orally, presentations or adding written notes into shared spaces.
- **Coordination:** denotes the organization of activities (events, behaviors and actions) that structure and organize tasks in order to facilitate cooperative work [23].
- **Cooperation:** is produced following individual work, often preceded by the division of tasks amongst group members [24]. It appears as the results are put back together. This pooling of individual work necessitates negotiation to synchronize each actors representations.
- **Collaboration:** designates the co-elaboration, co-evolution, or co-construction of tasks and ideas by participants in order to reach a common goal [23, 22]. The most fundamental difference between collaboration and cooperation relates to how the production is constructed: together (in the case of collaboration), to the point that it is difficult to determine who contributed what; separately (in the case of cooperation).

These modes of interactions are mobilized, in a non-linear manner, by participants during work sessions and over the course of long-term projects. The project environment, methods and tools used, intervention or instructions given by the moderator, influence the behavior of participants and as such, the emergence of these modes of interaction.

We go on to present the targeted production of the different modes as well as some elements regarding the complexity of the interactions that make them up.

#### 3.2 Targeted Production

Targeted production leave traces either on tools or meeting video recordings. In this section we present the elements we can detect in the video.

- **Individual Work:** individual work is shown through reflection, aiming at the construction of ideas and meaning with the goal

of eventually re-introducing the elements they judge as useful for the group. Producing written notes can be observed on video recordings and also on logs produced by the tools, because notes are written using virtual keyboards on multi-touch devices. Parsing these logs, we can also analyze the content of notes and detect those which do not respect predetermined guidelines or are interesting because the idea they contain has not yet been produced/shared with the group.

- **Communication:** Each member of the group is likely to have different results and ideas based on their individual work and experiences. Those ideas need to be introduced to allow new information into the group's discussions. This can be observed on recordings through speech, especially immediately following individual work or through actions on the device, such as sending a note from one surface to another (moving the idea from an individual work space to a collective one).
- **Coordination:** In collective sessions, coordination discussions allow for the definition of tasks and identification of responsibilities. This can be observed through the content of the conversation, related to organization and planning or through the type of tool being used, such as a GANTT. It is also typical to see a change in coordination following the intervention of a coach, as they often challenge the work that is being done.
- **Cooperation:** The division of tasks necessitates a pooling of work that is completed individually (or in sub-groups). This combining requires the establishment of consensus after having considered the information, opinions and arguments of each member. This can be detected based in the content of the discussion in audio recordings. Typically few notes are produced during this phase, but we see the modification of existing digital objects, instead.
- **Collaboration:** The group works together to co-produce a shared vision of concepts, of solutions, strategies, which is materialized through writing, models, reports or presentations. This, again, can be detected based on the content of the discussion in audio recordings.

The concept of globally collaborative work is introduced in [21] which examines some aspects of physical-digital workspaces, focusing on multi-user, multi-touch technologies and shows how different workspaces impact collaboration.

#### 3.3 Manual Video Annotation

At the UTC, students have courses about project management. We installed a class environment in which there are five cubicles, each one containing a large multi-touch table and a large multi-touch board. We used software developed by the Ubikey start-up<sup>1</sup>. During these management courses, students work on several case studies, performing activities mediated by these new tools and experimental working methods. For research purposes, the Ubikey software allows each action on these devices to produce a digital event that

<sup>1</sup>Ubikey proposes a collaborative visual management tool consisting of two large multitouch surfaces (a table and a board) as well as a suite of applications which makes their use simple by supporting many kind of activities, including brainstorming.

could be tracked in near real-time on a log file. Each session produce hundreds of events registered in the log.

Each cubicle in the class environments also contain a system of four cameras able to record students' activities, behaviour and discussions. With the agreement of the students, we have recorded more than fifty hours of videos that we have manually analyzed. Figure 2 shows the view from the different cameras in one cubicle. For privacy reasons, we show the devices before the students enter the room.



Figure 2: Views from cameras for video recording

For analyzing the videos, we divided each recording into thirty seconds sequences and annotated them with one or more tags corresponding to the interaction modes described previously. This was a huge but very interesting work that consolidated our model. Figure 3 shows an excerpt of an annotation video file. For each sequence, we indicated which interaction mode appeared. The number simply represents the associated mode of interaction (8 for collaboration, 7 for cooperation, etc..) This system allowed us to avoid coding errors and graph the sequences more easily, demonstrating when and how these modes of interaction overlapped.

A	B	C	D	E	F
Time	Collaboration	Cooperation	Coordination	Communication	Individual Work
00:00:00					
00:00:30					4
00:01:00					4
00:01:30					
00:02:00					
00:02:30					
00:03:00					4
00:03:30				5	4
00:04:00			6	5	4
00:04:30				5	4
00:05:00		8		6	4
00:05:30				5	4
00:06:00					4
00:06:30					4
00:07:00		8		5	4
00:07:30		8			4
00:08:00				6	5
00:08:30			7		5
00:09:00					4
00:09:30			7		5
00:10:00			7		4
00:10:30			7		4

Figure 3: Excerpt of an Excel sheet containing video annotation

### 3.4 Automatic Video Annotation

We claim that an AI based automatic video annotation, together with a log event analysis could automate the video annotation process. Machine learning or inductive learning is based on software that learns from previous experiences and builds a model for predicting intelligent results for newly fed inputs (see figure 4). Such a computer program improves performances as more and more examples are available. In our case, we benefit of a large video corpus manually annotated. We think we can feed enough data to this machinery software for it to learn patterns, with the final output being the annotations according to the five annotation criteria defined in section 3.

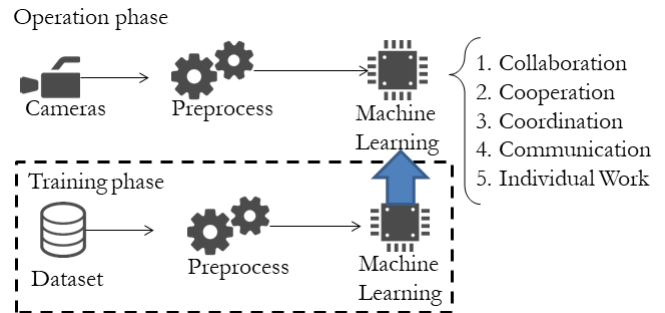


Figure 4: Video analysis, general training and prediction pipeline

Our first experiments were focused on using the already annotated video recordings to build and train a deep-learning action recognition model capable of directly recognizing each of these modes of interaction. We used the videos which were already manually annotated as training data. As of today, seven meetings have been manually annotated. Of those seven meetings, two also have the digital footprint logs associated with the devices used, and two more have been captured using four different points of view. We decided to discard the two videos taken from the ceiling viewpoint as they were too different from the rest of the dataset. This left a training dataset of around 8 GB and 12 hours. As the annotations were taken on 30 seconds intervals, we further cut the each video into the corresponding 30 seconds segments witch left us with 1473 annotated videos of 30 seconds. We finally doubled this number adding left-right flipped copies of each for a final training dataset of 2946 data points.

We based our work on the Inflated Inception model<sup>2</sup> described in [25] and used the TensorFlow framework<sup>3</sup>. This network has already been successfully used by their authors in [26] with weights trained on the Kinetics dataset [27] to improve the SOTA predictions on another action dataset performed by Google and described in [28] through transfer learning. In order to accommodate the weights, each video was first cropped to a frame size of 224 x 224 px and then had their RGB values normalized in [-1,1]. Our trials were run on a Tensorflow docker container with access to 64 Gb of RAM, Intel(R) Xeon(R) CPU E3-1230 v6 @ 3.50GHz and an Nvidia 2080 Ti with 11GB.

However, our first experiments met with some difficulties. Video sequences we annotated have a duration of thirty seconds, whereas

<sup>2</sup>See the following repository for the Keras implementation of this model we used: <https://github.com/dlpcb/keras-kinetics-i3d>

<sup>3</sup>TensorFlow initially developed by Google researchers is now an open source tool available in several programming languages. See <https://www.tensorflow.org/>

current action recognition datasets and models focus on shorter video sequences. Moreover, those datasets, and the models built upon them, focus on the recognition of atomic actions which are on a different semantic level versus the annotations we are trying to obtain. This implies the need for an intermediate semantic step in our models' architecture and the partial if not total retraining of said models. Finally, another difficulty we met was the relative limitations of our computing capabilities : the original network was trained on 500,000 iterations using 16 V100 GPUs each with at least 16GB of memory. This considerably slowed our trials with added memory and performance management, the original I3D in itself occupying 10 GB of video memory when accounting for the space needed for the input data. This is by no means a blocking factor, but hardware capabilities should not be ignored in future experimentations.

Moreover, the reason why humans choose a category when annotating is often not only based on video element recognition like a hand gesture or an interaction with an object but may also be based on vocal interactions and on their activity on the multi-touch surfaces. This led us to surmise the need of a multi modal approach combining video, audio and digital footprints. We especially believe our model will benefit from the event logs devices and thus, we plan to focus future experiments on leveraging this wealth of data to augment the video approach.

## 4 A Support Mechanism for Remote Brainstorming Analysis

In this section we study the questions presented above from a technological point of view and discuss the characteristics that an automatic (coaching) system must master to support brainstorming and the different tasks necessary to detect when a rule is not followed. We explain how this can be done by a multi-agent system. Each agent can detect a default and then produce an alert when something wrong appears. However some regulation is necessary in order to propose efficient feedback to participants. Also, when rules are correctly followed and the team is producing good results, we detail how this could be encouraged.

### 4.1 Architecture

We are able to make use of existing system architectures, which have been designed to support team activities (managing support system). Figure 5 shows a simplified architecture of a management system (left) and the added coaching system we plan to develop (right). Notes and video streams are sent by the local devices to the cloud managing system, where they are treated by its agents and dispatched to the other sites.

We will design another multi-agent system (coaching support system) which can be installed on the same cloud server that receives the streams from the different sites thanks to the managing support system agents; it will produce feedback that can be dispatched to the sites by the managing system agents. The new system can receive the streams because it can request them from the managing agents. It will be necessary to develop a new interface to provide feedback to each site, but, from a technical point of view, the work required

to design and implement it is negligible. A multi-agent system is suitable for developing a heterogeneous distributed system. Our multi-agent system is in compliance with the FIPA architecture and uses the FIPA-ACL communication protocol. Agents can make decisions according to a rule-based inference system. Rule descriptions are declarative and rules are associated with a dynamic priority level. Agents run procedures associated with the rules that are chosen. No machine learning method is implemented here.

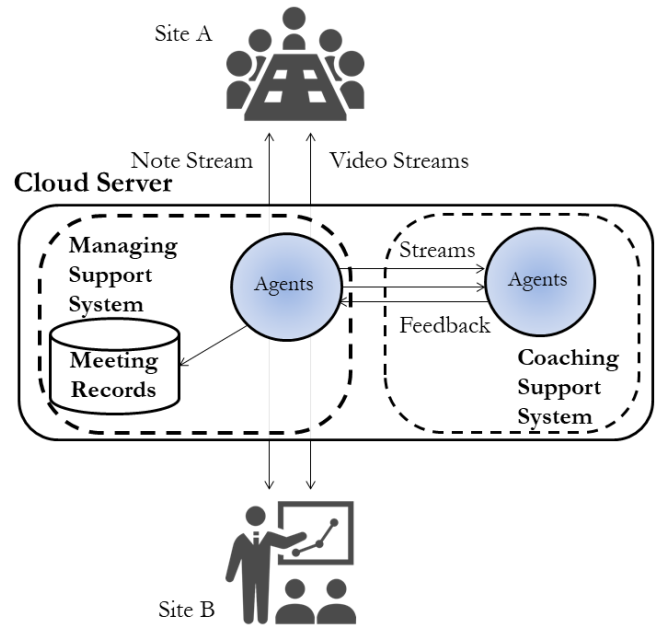


Figure 5: Multi-agent systems managing collaboration between remote teams

We believe that the coaching system must consist of two layers: a detection layer and a regulation layer. In the first layer, the agents detect the activities done by each person (production of an idea, criticism, facial expression...) and produces alerts after each detection. Other agents track the number of ideas produced during a session and produces alerts based on a comparison between sub-group metrics (i.e. returning to the notion of competition), standard production metrics (i.e. the systems default settings for what good production looks like), and on group goals and/or the specificity of the group according to the facilitator.

In the second layer, regulation agents analyze the different alerts (positive and negative) coming from the detection layer agents. According to pre-defined rules, these agents decide what feedback should be given, when and to whom (see figure 6).

### 4.2 Identification of participants

It is necessary to identify all the participants in a meeting. An identifier is sufficient, personal data should not be required. The system must give feedback either to one participant, to a sub-group at one specific site or to all the participants at all sites. It is when a message has to be sent to one individual or to identify the source of a particular idea that the identifier is necessary.

When using a large multi-touch surface, people use virtual keyboards to enter content into post-it notes. It is easy to add a unique



symbol on this keyboard and then a camera can associate a participant to a keyboard for identification. If necessary, facial recognition maybe used to add identifiers to participants. An piece of individual feedback, dedicated to a single participant, could be achieved thanks to an individual written notification, like a pop-up attached to the virtual keyboard he/she is using, making it discreet.

### 4.3 Behavioural Rules

According to the examples we proposed in the previous section, there are three ways to express disapprobation of an idea: by voice, by gesture or by deleting a note. Because of this, we believe that the installation must include different types of devices: i) cameras for video streams transfer, ii) microphones for better capturing individual voices and iii) multi-touch screens where the activity is performed. Several video streams are transferred to agents belonging to the detection layer. Agents use their own algorithm to analyze either gestures, voice or faces. Representations of notes are also transferred to detection layer agents.

### 4.4 Syntactic Rules

A note contains a text which expresses an idea about the brainstorming subject. The rule concerning an idea specifies that the text must be a complete and expressive phrase. This avoids any misunderstanding and ambiguity. The analysis of a note is described in section 4.6.

In the detection layer an agent is associated with each participant (i.e. with each identifier). It receives structures representing notes containing their content, the participants' identifiers and other meta-data (timestamp, etc.). The natural language processing support of each agent is able to detect acceptable notes and refuse others.

The system uses different kinds of rules. Rules will be checked through experimentation and inconsistencies, then adjusted manually.

manage syntactic alerts. All the alerts produced during the activities are compiled in shared memory (see figure 7). Globally, the regulation agents have different tasks: they determine the given situation of the meeting: is it the beginning, middle or end of the session?; they count the number of positive alerts (rules followed, production rate) and negative alerts (rules not followed); they check the production rate of each participant (a participant is considered inactive when the number of notes is low); they propose feedback.

A feedback agent is in charge of ordering and producing definitive feedback to participants. Feedback agreement from participants (a record of whether or not the feedback is acceptable or helpful) are also stored in the shared memory (however their exploitation will be performed in a future research).

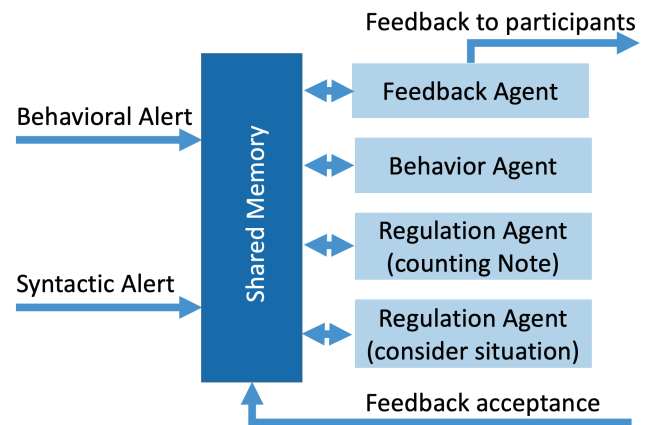


Figure 7: Regulation layer

### 4.6 Design of Text Processing System

This subsection describes the life cycle of a note within the agent layers (see figure 8). The note counting mechanism counts each participant's note. The number of notes may launch feedback that is designed to reinforce his/her enthusiasm.

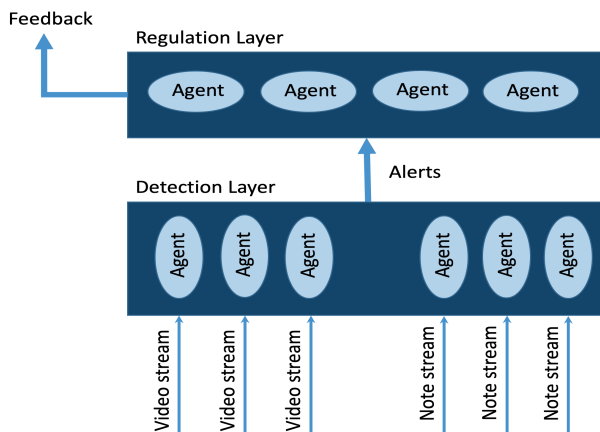


Figure 6: Multi-agents system layers

### 4.5 Regulation System

The regulation agents consist of two main categories: behaviour agents that manage behavioural alerts and regulation agents that

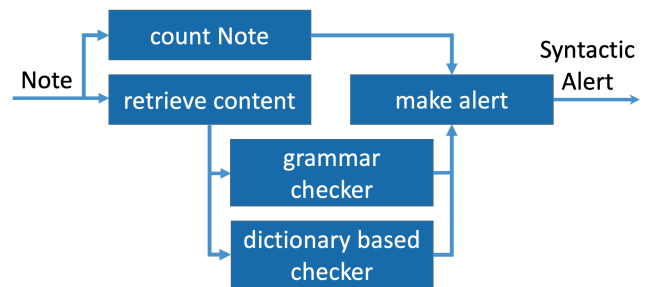


Figure 8: Text checker on note

The text of a note is checked by a dictionary and grammar checker. The dictionary based checker verifies if words are contained in predefined dictionaries and associates a value to each word. The grammar checker verifies syntactically the text of each note using a tool such as the LanguageTools. An alert is launched if this global evaluation is not high enough.

#### 4.7 Design of Image and Voice Processing System

In this subsection we detail the main components of a checking mechanism for a video stream (see Figure 9): The facial recognition mechanism identifies a participant; the gesture recognition mechanism categorizes a participant's actions; the emotion recognition mechanism associates a participant's face to a class of emotions; finally the tone of voice recognition mechanism associates a participant with a class of emotions. The voice recognition mechanism achieves a speech to text transformation.

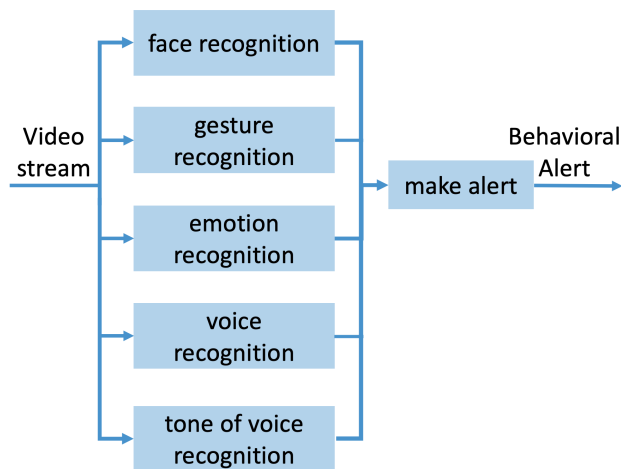


Figure 9: Video checker

These recognition systems require large data sets to learn to categorize faces, emotions and gestures. Alerts produced by this mechanism will have a relative score which indicates the level of reliability of the identification.

Different tools can be used for these mechanisms. Open source projects OpenCV[29] with YOLO[30] are suitable for identifying a participant. The OpenPose tool[31, 32] can detect human body, hands, facial and foot key-points on single images; the Microsoft Emotion engine[33] recognizes emotion categories from Kinect sensors.

Of course, non-verbal communication depends largely on participants' language, nation, region, age or personal experience and its analysis requires a good deal of testing.

### 5 Feedback For Rule Respect

In this section we detail the way an automatic system could give feedback in real time to the participants of a brainstorming meeting about the respect of rules. The feedback is based on the different types of rules we identified in previous sections.

The main questions are when, how, to whom to deliver the feedback and if hints are necessary. Another question is how to avoid interfering with the meeting by being as discreet as possible, while also being sensitive to participants' emotions to help create a safe psychological space.

Both individual and generic messages have to be integrated in the coaching system. Individual notifications are dedicated to a specific person, for instance because he/she does not follow one

rule consistently. This means that the system is able to refer to and recognize all the participants of a meeting. This could be achieved through an individual written notification, like a pop-up attached to a keyboard (see section 4.2).

Common notifications can be sent to a group of people, for instance, a local team (i.e. a distant team would not receive it). If the regulation layer of the coaching system considers that the same rule is not followed by several people in the same place, a local verbal or written message could be sent to the local team. A verbal message could be heard by the other team, so if we want to avoid this possibility, it is better to choose to send a message written on the large multi-touch surface.

Social interactions are important in brainstorming activities. The notifications should not divert participants from their work. Therefore, the number of notifications should be adjusted to the situation and should take into account the group dynamic and notification content.

The balance between feedback to motivate or correct behaviors should be taken into account. This means positive comments such as "good job, you are producing lots of ideas, keep it up!" are as important as constructive feedback such as "be careful, you should not criticize other people's ideas".

Finally, specificity of the team should be taken into account in the way the feedback is delivered. For instance, cultural bias could lead to different ways of producing and interpreting feedback.

## 6 Evaluation Scenario

In this section we explain how we will test the coaching system. It is necessary to evaluate the efficiency of the system at both a technical and acceptance level.

The first step is to test the quality of the coaching system at the detection layer with the production of alerts. Different scenarios creating notes automatically will be played and statistics about the number of alerts delivered by the system analyzed. Video with specific gestures and faces will be created and proposed to the agents. When the rate of recognition is satisfactory we can begin the second step of our evaluation, i.e. the test of the regulation layer.

Based on pre-recorded videos and notes from a session, we determine what feedback individuals and the team should receive. It is a test relying on subjective judgments made by researchers, but based on the rules outlined previously. Researchers will manually balance individual and global feedback delivery for timeliness and content. When a satisfactory rate of feedback is delivered by the coaching system we can begin the third step of the evaluation, i.e. experiments with real scenarios and real participants playing foreseen sequences.

The last step of the experiment will focus on the way people accept to respect constraints during brainstorming activities and receive feedback during their work. Prior to the experiment, participants will receive instructions about the rules to be followed during the session in order to make the conditions explicit. We will conduct experiments in two ways: i) brainstorming activities managed only by a human in charge of the facilitation to ensure the respect of the rules, ii) brainstorming activities where an automatic system gives feedback together with a human facilitator.

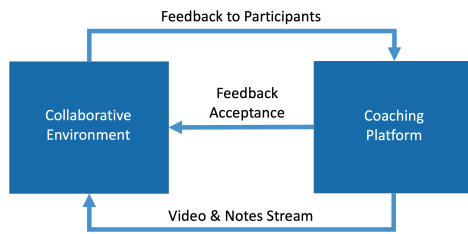


Figure 10: Exchanges between systems

The results of the last experiment will be evaluated by observers who monitor how people react when they receive feedback. We postulate that the user interface may allow participants to react when they are notified, with a very quick action such as pressing a button on the notification itself. In this way, we can consider a loop where the coaching system registers the level of feedback acceptance by the participants (see figure 10).

Our objective is not to cancel out the role of the facilitator because integrating a coaching system into pre-existing support system architecture can be difficult, but also because the role of the facilitator is fundamental. The coaching system is only an assistant which allows the facilitators to devote time to their main tasks, such as managing the group dynamic.

## 7 Research limitations

This position paper defines our research goals, details our propositions on how to achieve this goal and describes our three step research protocol for evaluation. As presented, we are already facing difficult technical challenges that we need to overcome in order to carry out this research, such as automatic video annotation issues. We also foresee some tricky problem to be solved with regards to fine tuning the rules implemented in the regulation system. Finally, once the technical issues are solved, acceptance of this type of system by both the participants and the coach needs to be thoroughly evaluated.

## 8 Conclusion

In this paper, we have presented how brainstorming results could be enhanced if meeting participants observed several simple practical, methodological and behavioural rules. We have proposed a model of interactions between people during collaborative meetings. We have described how an AI based analysis system could both summarize the state of a meeting according to this model and give advice to a meeting facilitator and the participants.

We hypothesise that a technological support system could help meeting facilitators with their group management tasks if it is able to analyze whether or not behavioural and methodological rules are followed and if it produces efficient and adapted feedback.

We proposed an architecture for such a system and explained the way we can conduct the necessary experiments for testing its implementation and the way people receive and agree with the feedback.

In the context several teams situated in different locations, this model and associated architecture could help supporting activities

and in particular creative problem solving. It therefore could be integrated into existing computer supported collaboration tools along with video-conferencing systems. In a future work, we would like to implement new technical functionalities such as an automatic learning system based on analysis of previously recorded sessions. Additionally, we would like to study the retroactive feedback acceptance by participants on the system itself. For instance, an agent would be able to understand and adjust its behavior in order to achieve the highest impact on the targeted participant. This means that the agent would need to learn from participant feedback acceptance and choose the appropriate way to give feedback to each participant.

## References

- [1] T. Gidel, S. Fujita, C. Moulin, K. Sugawara, T. Sukanuma, Y. Kaeri, and N. Shiraori. Enforcing methodological rules during collaborative brainstorming to enhance results. In *2019 IEEE 23rd International Conference on Computer Supported Cooperative Work in Design (CSCWD)*, pages 356–361, 2019.
- [2] Y. Kaeri, K. Sugawara, C. Moulin, and T. Gidel. Agent-based design of iot applications for remote brainstorming support. *2018 IEEE 22nd International Conference on Computer Supported Cooperative Work in Design (CSCWD)*, pages 820–825, 2018.
- [3] Y. Kaeri, C. Moulin, K. Sugawara, and Y. Manabe. Agent-based system architecture supporting remote collaboration via an internet of multimedia things approach. *IEEE Access*, 6:17067–17079, 2018.
- [4] Y. Kaeri, K. Sugawara, C. Moulin, and T. Gidel. Agent-based management of support systems for distributed brainstorming. *Advanced Engineering Informatics*, 44:101050, 2020.
- [5] *The International Handbook of Creativity*. Cambridge University Press, 2006.
- [6] P. Marshall, R. Morris, Y. Rogers, S. Kreitmayer, and M. Davies. Rethinking ‘multi-user’: An in-the-wild study of how groups approach a walk-up-and-use tabletop interface. In *Proceedings of the SIGCHI Conference on Human Factors in Computing Systems, CHI ’11*, pages 3033–3042, New York, NY, USA, 2011. ACM.
- [7] Y. Rogers, Y. kyung Lim, W. R. H. PhD, and P. Marshall. Equal opportunities: Do shareable interfaces promote more group participation than single user displays? *Human Computer Interaction*, 24(1-2):79–116, 2009.
- [8] R. Fleck, Y. Rogers, N. Yuill, P. Marshall, A. Carr, J. Rick, and V. Bonnett. Actions speak loudly with words: unpacking collaboration around the table. In *Proceedings of the ACM international conference on interactive tabletops and surfaces*, pages 189–196. ACM, 2009.
- [9] S. Conversy, H. Gaspard-Boulin, S. Chatty, S. Valès, C. Dupré, and C. Ollagnon. Supporting air traffic control collaboration with a tabletop system. In *Proceedings of the ACM 2011 Conference on Computer Supported Cooperative Work, CSCW ’11*, pages 425–434, New York, NY, USA, 2011. ACM.
- [10] O. Shaer, M. Strait, C. Valdes, T. Feng, M. Lintz, and H. Wang. Enhancing genomic learning through tabletop interaction. In *Proceedings of the SIGCHI Conference on Human Factors in Computing Systems, CHI ’11*, pages 2817–2826, New York, NY, USA, 2011. ACM.
- [11] K. L. Dugosh and P. B. Paulus. Cognitive and social comparison processes in brainstorming. *Journal of Experimental Social Psychology*, 41(3):313 – 320, 2005.
- [12] S. G. Isaksen and J. P. Gaulin. A reexamination of brainstorming research: Implications for research and practice. *Gifted Child Quarterly*, 49(4):315–329, 2005.
- [13] N. Michinov and C. Primois. Improving productivity and creativity in online groups through social comparison process: New evidence for asynchronous electronic brainstorming. *Computers in Human Behavior*, 21(1):11 – 28, 2005.
- [14] B. A. Nijstad, W. Stroebe, and H. F. Lodewijckx. Cognitive stimulation and interference in groups: Exposure effects in an idea generation task. *Journal of Experimental Social Psychology*, 38(6):535 – 544, 2002.
- [15] K. Dugosh, P. Paulus, E. Roland, and H.-C. Yang. Cognitive stimulation in brainstorming. *Journal of Personality and Social Psychology*, 79(5):722–735, 2000.

- [16] B. A. Nijstad, W. Stroebe, and H. F. Lodewijkx. Production blocking and idea generation: Does blocking interfere with cognitive processes? *Journal of Experimental Social Psychology*, 39(6):531 – 548, 2003.
- [17] M. Diehl and W. Stroebe. Productivity loss in brainstorming groups: Toward the solution of a riddle. *Journal of Personality and Social Psychology*, pages 497–509, 1987.
- [18] A. F. Osborn. *Applied imagination; principles and procedures of creative thinking*. Scribner, 1953.
- [19] D. Johnson and R. Johnson. *Learning together and alone: cooperation, competition, and individualization*. Prentice-Hall, 1975.
- [20] C. M. Hymes and G. M. Olson. Unblocking brainstorming through the use of a simple group editor. In *Proceedings of the 1992 ACM Conference on Computer-Supported Cooperative Work, CSCW 92*, page 99106, New York, NY, USA, 1992. Association for Computing Machinery.
- [21] A. Tucker, T. Gidel, and C. Fluckiger. Designing physical-digital workspaces to support globally collaborative work. In *Proceedings of the Design Society: International Conference on Engineering Design*, pages 109–118. Cambridge University Press, 2019.
- [22] S. D. Teasley and J. Roschelle. Constructing a joint problem space: The computer as a tool for sharing knowledge. In S. P. L. . S. J. Derry, editor, *Computers as Cognitive Tools*, pages 229–258. Hillsdale, NJ: Lawrence Erlbaum Associates, 1993.
- [23] M. J. Baker. Collaboration in collaborative learning. *Interaction Studies*, 16(3):451–473, 2015.
- [24] K. A. Bruffee. Sharing our toys: Cooperative learning versus collaborative learning. *Change: The Magazine of Higher Learning*, 27(1):12–18, 1995.
- [25] J. Carreira and A. Zisserman. Quo Vadis, Action Recognition? A New Model and the Kinetics Dataset. *arXiv:1705.07750 [cs]*, Feb. 2018.
- [26] R. Girdhar, J. Carreira, C. Doersch, and A. Zisserman. A Better Baseline for AVA. *arXiv:1807.10066 [cs]*, July 2018.
- [27] W. Kay, J. Carreira, K. Simonyan, B. Zhang, C. Hillier, S. Vijayanarasimhan, F. Viola, T. Green, T. Back, P. Natsev, M. Suleyman, and A. Zisserman. The Kinetics Human Action Video Dataset. *arXiv:1705.06950 [cs]*, May 2017.
- [28] C. Gu, C. Sun, D. A. Ross, C. Vondrick, C. Pantofaru, Y. Li, S. Vijayanarasimhan, G. Toderici, S. Ricco, R. Sukthankar, C. Schmid, and J. Malik. AVA: A Video Dataset of Spatio-temporally Localized Atomic Visual Actions. *arXiv:1705.08421 [cs]*, May 2017.
- [29] G. Bradski. The OpenCV Library. *Dr. Dobb's Journal of Software Tools*, 2000.
- [30] J. Redmon, S. Divvala, R. Girshick, and A. Farhadi. You only look once: Unified, real-time object detection. In *2016 IEEE Conference on Computer Vision and Pattern Recognition (CVPR)*, pages 779–788, June 2016.
- [31] Z. Cao, T. Simon, S.-E. Wei, and Y. Sheikh. Realtime multi-person 2d pose estimation using part affinity fields. In *CVPR*, 2017.
- [32] T. Simon, H. Joo, I. Matthews, and Y. Sheikh. Hand keypoint detection in single images using multiview bootstrapping. In *CVPR*, 2017.
- [33] Ms emotion engine. <https://azure.microsoft.com/en-gb/services/cognitive-services/emotion/>.



## Design of Interactive Aids for Children's Teeth Cleaning Habits

Cheng Chuko, Fang-Lin Chao\*, Hsin-Yu Tsai

*Department of Industrial Design, Chaoyang University of Technology, Taichung, 436, Taiwan, R.O.C.*

### ARTICLE INFO

*Article history:*

*Received: 09 February, 2020*

*Accepted: 25 March, 2020*

*Online: 04 April, 2020*

*Keywords:*

*Product design*

*Arduino*

*Teeth cleaning*

*Interactive aids*

### ABSTRACT

*Dental plaque is considered a possible causative agent of major dental diseases. People must develop oral care skills at an early age with family support. This study aims to assist parents and to reduce children's fear while cleaning their teeth. An interactive game challenges children's brushing ability. Arduino modules and software platform were utilized to build a functional prototype. The status of the palm movements identified using a sensing module within brusher. When the cumulative number of swipes exceeds a specified target, the LED moves to the next position. Children became more attentive and adjusted to their corresponding tooth positions according to changes in the hippo's dental light. The average brushing time increased to 226 seconds, with the assistance of the partner. An interactive novelty toothbrush with Bluetooth module was built and evaluated. The contribution of the work is observing children's needs and guide them to brush their teeth from an intimate perspective.*

## 1. Introduction

The most common dental problem of concern in children is dental caries. Dental plaque is considered a possible causative agent of major dental diseases. Oral health affects chewing, nutrition, speaking, socializing. As a result, people must develop oral care skills at an early age. The implementation of oral disease prevention includes education and the integration of family support. This design study aims to assist parents and to reduce children's fear while cleaning their teeth.

### 1.1. Oral Health Education

Advocacy and family coordination are vital for implementing oral health education. Children are often unfamiliar with initial skills. A survey of Taiwan's 3-6 year-olds showed that the average permanent dental caries experience index (DMFT) of school children was 3.31. This index indicates the need for promoting children's oral health programs. Taiwanese children prefer sugary drinks, which have a high correlation with severe dental caries. The frequency of sugary drinks for children in Taiwan is 4-6 times a week. Therefore, it is necessary to implement oral health education and implement correct dental cleaning habits from early childhood.

Good oral hygiene is dependent upon the effectiveness and the ease with which the procedure is carried out. The most common preventive dental program is the modified Bass approach [1] (Figure 1). Domestic academics and American public health

scholars also recommend the Bass method for its high efficiency and "horizontal short-distance movements." Its main points are:

- (1) Place the toothbrush at a 45-degree angle on the gum line.
- (2) Brush using a gentle circular motion: downward for the upper teeth and upward for the lower teeth, and brush 2-3 teeth at a time.
- (3) Use the same procedure for the lower teeth, except rotating in an upward direction toward the medial teeth.

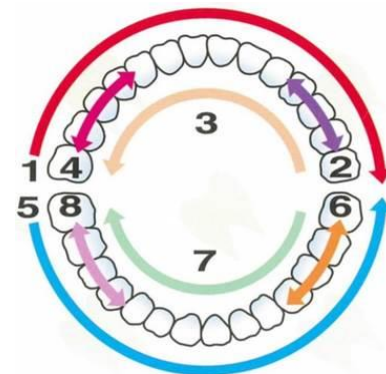


Figure 1. Brushing sequence of the Bass method.

A reduction of interdental plaque and gingival inflammation requires a suitable brushing technique. Poyato-Ferrera et al. [2] found that the modified Bass method is superior for supragingival

\* Fang-Lin Chao, Email: flin@cyut.edu.tw

plaque removal. Studies also show that the modified Bass technique was useful for children [3,4]. The Scrub and Bass methods (with flossing) are effective in eliminating or reducing plaque and gingivitis in 11-year-old children using a junior toothbrush.

### 1.2. Analysis of Existing Products

Extant products seek to attract young children with appealing anthropomorphic images. It is difficult for purely informational products that lack substantial interaction to keep young children engaged for a long time (Figure 2). These textbooks are like a toy and cannot be interacted with in person; so it is not easy to raise the expectation of continuous exploration.



Figure 2. Interactive dental cleaning products (a) gamebook, (b) music-induced voice cleaning.

Philips Sonicare marketed by Oral Healthcare (Figure 3) is a companion product for teeth cleaning that is currently on the market. Power toothbrushes remove plaque more effectively by brush head motion. For example, Sonicare claims to remove plaque as a result of dynamic fluid activity [5]. Studies show that the use of a Sonicare Airfloss results in less removal of tooth enamel when compared to the use of a standard toothbrush [6]. A reduction in plaque in the posterior and hard-to-reach areas indicated the benefit of the design [7].



Figure 3. Sonicare children's toothbrush.

Sonicare features include timed tooth cleaning, an app music reminder to change the part of the mouth being brushed every 30 seconds, and a link with an interactive game app. Its advantage is flexible content; however, the user must be familiar with smartphone operation. Another study [8] identified several other oral health-focused apps in the Apple App Store and Google Play. Apps identified using the following search phrases: oral health, dental health, teeth health, tooth health, dental care, and oral care. However, the quality of the reviewed apps was generally poor [9]. Apps need theoretically grounded content and adherence to ethical design principles for persuasive health technologies. The Oral-B and Sonicare apps can connect with a phone via Bluetooth. However, those apps performed poorly on standard usability heuristics [10].

## 2. Survey and Analysis

First, we surveyed the toothbrushing habits of children to find suitable entry points for product design. Items included current brushing status, the attitudes of children and parents toward tooth brushing, and methods of parental assistance in building dental cleaning habits.

### 2.1. Method

A total of 204 families with schoolchildren in the age range of 3-6 years old were selected in a randomized controlled family survey. The inclusion criteria used to select the samples for the study were as follows: (i) healthy children between the age group; (ii) schoolchildren who live with their parents. The survey distributed through both paper and website.

### 2.2. Results and Discussion

According to the survey data, more than half of the families were double-income families, and only 40% of the carers were full-time caregivers. At present, more than 90% of the parents demonstrated an awareness of oral care. However, more than 70% of children needed to be accompanied by their parents when brushing their teeth. More than 70% of families reported purchasing education material or products for oral health care. 3.5 % families reported their child had tooth decay, and less than 20% of children demonstrated knowledge of preventative oral care.

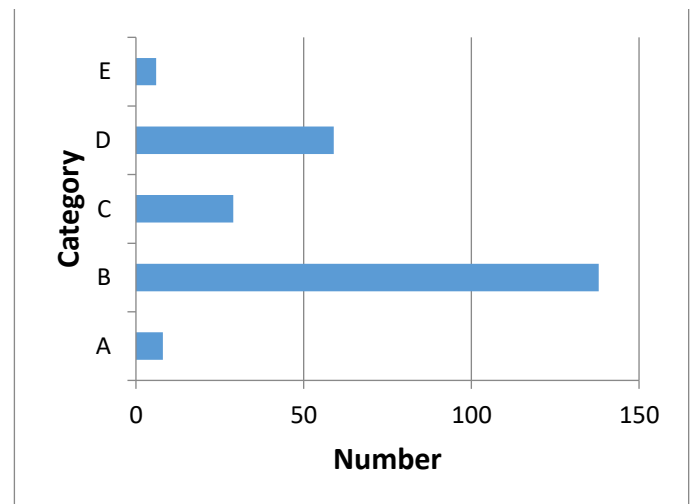


Figure 4. Children's brushing habits.

The Figure 4 shows the level of brushing reported by the families, as follows:

- A: Child has not yet begun to brush their teeth.
- B: The parent brushes child's teeth.
- C: The child is self-motivated to brush teeth.
- D: Parent motivates a child to brush teeth.
- E: The child brushes teeth with parental assistance.

Items B, D, and E involved parental participation, so the children could not take the initiative to complete these tasks themselves. Therefore, an educational product that plays the role of a parent could hypothetically reduce the burden on parents. If the product is impressive, the design could improve children's motivation to brush their teeth and improve the effectiveness of tooth cleaning.

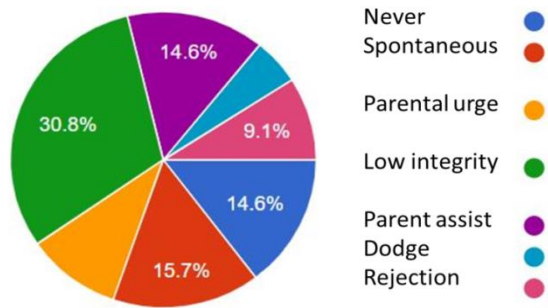


Figure 5. Children's behavior and attitude towards teeth cleaning

As shown in Figure 5, less than 20% of children can brush their teeth independently, and the rejection rate is quite high, at 15%. Low quality meant that although the child brushed their teeth, they did not do so carefully, so they remained at risk for tooth decay. The survey results revealed the Bass method needs more promotion to families.

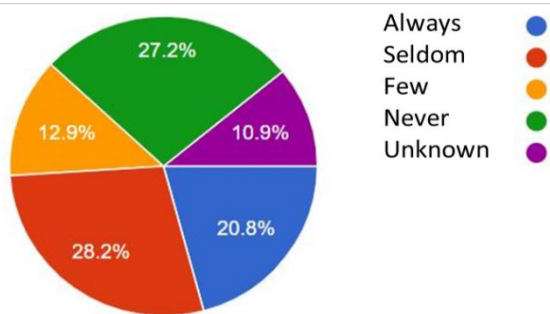


Figure 6. How often do children brush their teeth with the Bass method?

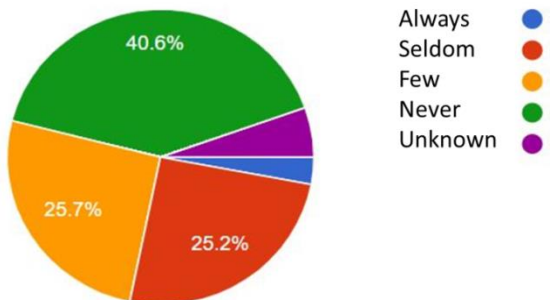


Figure 7. Completeness of Golden Teeth 333 code

As shown in Figure 6, parents report that only 21% of children can brush their teeth with the Bass method. Most children or parents are not familiar with the main points of the Bass method. The data also shows that there is a need to increase through auxiliary tools.

The "333 Code" refers a better way to brushing teeth: at least three times a day, brushing one's teeth within 3 minutes after a meal and brushing one's teeth for more than 3 minutes each time. Only less than 10% of people reported performing it correctly.

The Association of Dental Surgeons points out that the rate of tooth decay in children is high, with an average of five cases of tooth decay per child. The Department of Health appeals to all age groups, from infants, adolescents, and the elderly for independent health management.

The market survey found that most parents had an awareness of establishing healthy habits (Figure 7): 79.2% reported wanting to comply as much as possible, but also reported difficulties with implementation. Researchers hoped that assisted design could develop independent healthcare habits in children from an early age.

### 3. Design Approaches

Through the questionnaire survey, we understand that the current situation of children's learning is significantly different from our expectations. Through various design concepts, we proposed to increase children's attempts with interactivity, attract them to try and reduce the burden on parents. Through the sharing mechanism, excellent performance can be linked with parents' rewards to form a positive learning cycle.

#### 3.1. Problem Definition

The target user age for this study was 3- to 6-year-old children. The goal was to remove children's fear of cleaning teeth and implement tooth cleaning habits without parental assistance. It is easier to develop a habit if the process is enjoyable. A suitable game design challenges children depending on their age and ability. Suitable game types for children include distinguishing color, number, and order, recognition, and memory. At the age of five, children have basic concepts of mathematics, association, and space. Simple vocabulary games can reduce the fear of tooth brushing in children and assist parents in encouraging children's oral health.

A bionic "dentist partner" draws children's gazes and reduces the rejection of oral cleaning appliances. Interaction and encouragement between parents and children allow children to develop habits. A visually appealing form supplemented by smart monitoring functions facilitates observation of cleaning status. A "dentist partner" game uses an LED screen to ensure that children are excited to complete the cleaning process using the Bass method.

It is not easy to cultivate oral cleaning habits at an early stage, and some children are repulsed by stimulation. Toy toothbrushes and electric toothbrushes often appeal to children with cute shapes, but parents' supervision is required to urge children to clean their teeth properly. Adding childlike connotations and introducing stories makes cleaning teeth more fun for children.

#### 3.2. Arduino and Control Circuit

Arduino is a typical software tool for building a variety of devices with available peripherals, tools, and techniques. The



Arduino ecosystem includes LED, Servo motors and stepper motors, wireless connectivity, and the Internet of Things. The technical forum provides more prominently featured in the advanced projects. We utilized a 4-digit 7-segment display [12] with a common cathode and a digit display that turns on when the digit pin state is LOW. The lights are lit one by one in the order of the brush. The user needs to stay in this position until the light index changes. The status of the palm movements identified using IMU inertial sensor to read the accumulated number of brush. When the cumulative number of swipes exceeds a specified target, the light moved to the next position to lead children's interaction (Figure 8).

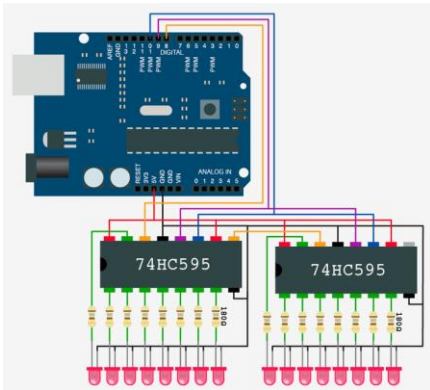


Figure 8. Hardware circuit. The device is comprised of an Arduino Nano microcontroller, MPR 121 Multiplexer, MPU 6050 IMU, and a Bluetooth [11]

### 3.3. Product Design

The initial concept of oral healthcare aid inspired by a whack-a-mole game. Instead of striking a mole, the idea of the game was transformed into brushing specific teeth. The device design based on an anthropomorphic hippopotamus with an open mouth and exposed teeth. A capsule machine inside the device rewarded children with a surprise gift following tooth brushing (Figure 9). Children were trained in good tooth brushing habits through daily cleaning, with additional help from a parent app.



Figure 9. Final concept sketch

The model built by vacuum forming with a polyurethane mold. The buckled structure utilized to take into account the size of the body and the internal configuration (Figure 10). The appearance of the model set to a medium-sized doll, which intended to stimulate children's alertness and curiosity.

The chassis contained the dental cleaning indicator and timing function and could transmit the cleaning record, time spent

brushing, and conditions to a parent's mobile phone. The hippo-shaped teeth had indicator lights to indicate a brushing location. An Arduino program controlled the LED. Each tooth lit up sequentially according to Bass method and sensed whether there was brushing at the corresponding position. The toothbrush handle equipped with an electronic induction device, a Bluetooth module, and a battery, and the indicator light indicates the position of the brush; the inertial sensor [13] on the toothbrush handle detects whether the toothbrush is shaking to confirm that the child is brushing correctly. The counter and timer of the system can accumulate the number and time to identify the brushing situation.



Figure 10. Assembly drawing of main accessories and appearance.

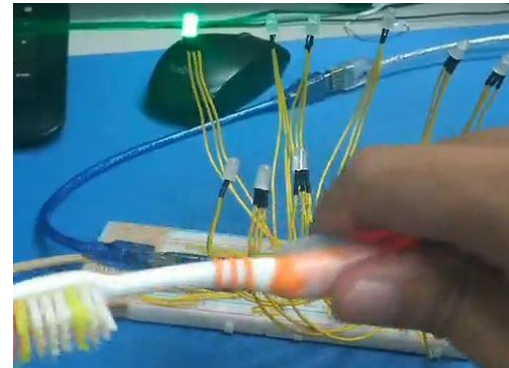


Figure 11. Sensors and LED indication configuration and the brush with an inertial sensor that wirelessly connected with the main circuit board.

Specifications of internal parts were as follows: Arduino Nano, HC-06 Bluetooth module, 74594 SIPO shift register, R.T.C. clock, 5mm LED\*10, and Servo motor (Figure 11). The tooth faces indicated with different colors: green for the external surface, blue for occlusal surface, and red for the internal surface.

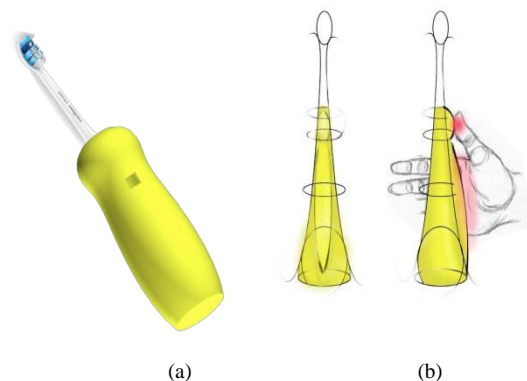


Figure 12. The rendering of toothbrush and (a) actual installation appearance, and (b) grip shape of a possible design.





Figure 13. Operation flow and parent APP interface screen diagram.

The module comprised of a 3-watt speaker and a 3.7V lithium batteries. A brush circuit board contained the Power Module (ADIO-5VCH + ADIO-USB-0506 Boost Module), Arduino IMU inertial sensor, and MPU-6050. An indicator interface placed inside each tooth, which lit up to indicate cleaning progress. The current installation appearance, and future possible grip shape are display in Figure 12.

### 3.4. User Interface. Design

The product placed in homes or classrooms. The intended users were children who had just begun to clean their teeth. Parents or teachers could use the game machine to demonstrate brushing to children.

Children have their feelings and tastes; designers of new technologies need to remind that children are an entirely different user. Researchers suggested "children had more direct involvement with technology developers" for technology development and invited children to test before it released [14]. The interactive experience is the basis for the toy design. Lacking researches on children's interactive experience causes mismatching of children's needs [15]. Popular toys are a dominant entertainment medium. Traditional toys have the function of supporting children's growth [16]. The user interface of a child-friendly product is one of the elements of a successful design.

The Figure 13 shows the operation process and parent's APP interface. This app can record the score and progressing of cleaning events, gift sticker reward, and parent responses. A monthly calendar is helpful to view children's oral cleaning status and progress. Designers are required to avoid using symbolic images that confuse children. The contrast formed by different color blocks is natural to arouse the user's visual interest. Deleting extra pages simplifies the process and only shows what is needed to convey important messages—the interface mainly based on natural and pleasant feelings, and brighter colors matched with cute fonts.



Figure 14. Product usage test: after the sensor has been swiped for a set number of times, the indicators will jump in the sequence. The reward gift is placed in the mouth of the villain on the lower right.

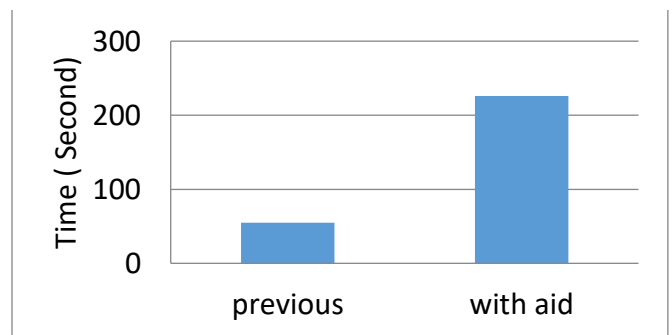


Figure 15. Product usage test: the average brushing time

### 3.5. User's Test

The product usage test carried on in both family house and kindergarten classrooms (Figure 14). The researcher invited five children to complete the brushing steps according to the light of assisting partners and record children's responses and the total time of brushing. From the experiment, we observed that children

became more attentive and adjusted to their corresponding tooth positions according to changes in the hippo's dental light. Figure 15 is the average brushing time result; the autonomous brushing is often completed quickly (55 seconds) with the disadvantage of less fulfilling the requirements. But the average time for brushing increased to 226 seconds with the assistance of the hippo partner. The teacher's required value is 180 seconds (3 min.) [2], and the average acting time is higher. During the boot test, the child must wait for the light to change position (time delay), so it will take more time to follow at the beginning. The classroom setting also takes advantage of the children's inclination to increase enthusiasm within a peer-collective situation [3].

Children were happy to follow the LED display of the hippo and complete the steps of brushing their teeth through interaction. When parents need to accompany them, the child will also be stressed; parents' time is limited and it is not easy to maintain good mood. Through the records left by the interaction with the companion, parents can reward and respond to the child after watching it. This approach reduces tension and wasted time on both sides.

However, the mechanism of this model encountered some configuration problems. The brush's rod is insufficiently supported, so when the child brushes his teeth, the head is biased; water may flow along the toothbrush rod into the circuit area in the handle. The added electronic induction circuit does increase the issue of safety and must be waterproof and damp-proof before entering the application. At present, the size of the product is large, and the toothbrush grip also weighs a significant amount. The component and device size can reduce in the future with the help of electrical and mechanical engineers in the cross-domain design.

#### 4. Conclusions

Throughout the investigation, the researchers identified the current educational need for dental care. An interactive novelty toothbrush with Bluetooth module was built and evaluated. Building cross-domain design teams allowed conceptual revision and determination in the early stages of design. Through cooperation with electrical engineers and circuit implementation of Arduino, design elements were combined. The children connected with parents through the app interface. This design can reduce the burden of parental supervision and contribute to the positive cycle of child interaction. At present, the cost of firmware hardware is high, so it is more suitable for teaching aids. In the future, the miniaturization of electronic parts will make the product more suitable for children.

#### Conflict of Interest

The authors declare no conflict of interest.

#### Acknowledgment

The authors acknowledge the electrical engineers in cross-domain design and programming.

#### References

- [1] <https://www.buysplat.com/pages/bass-brushing-technique>
- [2] M. Poyato-Ferrera, J. J. Segura-Egea, and P. Bullón-Fernández. "Comparison of modified Bass technique with normal toothbrushing practices for efficacy in supragingival plaque removal" *International Journal of Dental Hygiene*, 1(2), 110-114, 2003. <https://doi.org/10.1034/j.1601-5037.2003.00018.x>
- [3] E. Robinson, "A comparative evaluation of the Scrub and Bass Methods of toothbrushing with flossing as an adjunct (in fifth and sixth graders)." *American Journal of Public Health*, 66(11), 1078-1081, 1976. <https://ajph.aphapublications.org/doi/pdf/10.2105/AJPH.66.11.1078>
- [4] S.P. Patil, P.B. Patil, and M.V. Kashetty. "Effectiveness of different tooth brushing techniques on the removal of dental plaque in 6–8-year-old children of Gulbarga." *Journal of International Society of Preventive & Community Dentistry*, 4(2), 113, 2014. <https://doi.org/10.4103/2231-0762.138305>
- [5] P.R. Warren, M.A. Cugini, B.V. Chater, and J. Strate, "A review of the clinical efficacy of the Oral-B oscillating/rotating power toothbrush and the Philips Sonicare toothbrush in normal subject populations" *International Dental Journal*, 54(6), 429-437, 2004. <https://doi.org/10.1111/j.1875-595X.2004.tb00300.x>
- [6] T. J. Holley, J. A. Ross, and T. L. Hottel, "Efficacy of Philips Sonicare AirFloss compared to manual brushing and flossing: an in vitro study" *The Journal of the Tennessee Dental Association* 94(1), 34-36, 2014. <https://europepmc.org/article/med/25241500>
- [7] G.I. McCracken, P.M. Preshaw, L. Heasman, "Efficacy of plaque removal of the Sonicare Elite versus the Sonicare Advance from hard-to-reach sites" *Journal of Clinical Periodontology*. Nov;31(11):1007-1011, 2004. DOI: 10.1111/j.1600-051x.2004.00604.x.
- [8] B. Tiffany, P. Blasi, S.L. Catz, and J.B. McClure, "Mobile apps for oral health promotion: Content review and heuristic usability analysis" *JMIR mHealth and uHealth*, 6(9), p.e11432., 2018.
- [9] N. Nayak, S. Nayak, M. Vikneshan, S. Acharya, and D. Sathiyabalan, "Smartphone apps: A state-of-the-art approach for oral health education" *Journal of Oral Research*, 8(5), 386-393, 2020. <https://doi.org/10.17126/10.17126/joralres>.
- [10] F. Zotti, D. Dalessandri, S. Salgarello, M. Piacino, S. Bonetti, L. Visconti, C. Paganelli, "Usefulness of an App in improving oral hygiene compliance in adolescent orthodontic patients" *The Angle Orthodontist*, (1), 101-107, 2016. <https://doi.org/10.2319/010915-19.1>
- [11] J. Blum, *Exploring Arduino: Tools and techniques for engineering wizardry*, John Wiley & Sons, 2019.
- [12] N. Cameron, *4-Digit 7-Segment Display*, Arduino Applied. Apress, Berkeley, CA, 119-136, 2019.
- [13] A. Verma, G. Culbertson, and K. Ramani, "Chiron: interpreting signals from capacitive patterns and inertial sensors for intuitive shape modeling" *CHI'14 Extended Abstracts on Human Factors in Computing Systems*, 1831-1836, 2014. <https://doi.org/10.1145/2559206.2581161>
- [14] A. Druin, "The role of children in the design of new technology." *Behaviour and information technology*, 21(1), 1-25, 2002.
- [15] X. Lv & R. Peng, "User experience research of toy design" In *IEEE 11th International Conference on Computer-Aided Industrial Design and Conceptual Design, CAID and CD'2010*, 2, 943--946. DOI: 10.1109/CAIDCD.2010.5681811
- [16] A.A. Naufal, and A. Suzianti, "Design thinking approach for product innovation design of educational toys" In *Proceedings of the 2019 5th International Conference on E-business and Mobile Commerce*, 69-74, 2019. <https://doi.org/10.1145/3332324.3332337>

## Alternative Braking Method for Small Scaled-Wind Turbines Connected DC Green House with Analogical Experiment on Blade Destruction

Anupa Koswatta<sup>1</sup>, Faramarz Alsharif<sup>2</sup>, Yasushi Shiroma<sup>1</sup>, Mahdi Khosravy<sup>3</sup>, Shiro Tamaki<sup>1\*</sup>, Junji Tamura<sup>2</sup>

<sup>1</sup> Graduate school of Engineering, University of the Ryukyus, 903-0213, Japan.

<sup>2</sup> School of Earth, Energy and Environmental Engineering, Kitami Institute of Technology, 090-8501, Japan.

<sup>3</sup>Media Integrated Communication Laboratory, Osaka University, 565-0871, Japan

### ARTICLE INFO

Article history:

Received: 01 February, 2020

Accepted: 25 February, 2020

Online: 04 April, 2020

Keywords:

Small-Scaled Wind Turbine

Wind turbine brake

Eddy current brake

Over-rotation

Strong wind

### ABSTRACT

To supply a stable and efficient electricity, small-scaled wind turbine's brake system plays an immense role in various wind speeds. Small-wind power generation systems are difficult to operate in strong wind region since the turbine could be over-rotated and damaged if the brake system is not robust enough to maintain a stable angular velocity. Most of the small-scaled wind turbines use friction brakes to control the turbine speed for a stable electricity output. Since the friction brake are run out of time and needs frequent maintenance and eventually replacement, we introduce an eddy current based wind turbine brake system which is contactless with the rotor as an alternative to the friction brake system. The advantage of the proposed brake system is that the energy loss due to the friction will be reduced and will be more durable than the friction brake. The flow of this study is at first we did the analogical experiment of blade destruction to set to the maximum allowed angular velocity. Later, in order to verify the performance and stability requirement the mathematical implementation of eddy current brake system have done in DC-Green house for various wind penetration. Eventually the feasibility of eddy current brake system is confirmed in simulation results.

### 1. Introduction

The Wind energy provide a vast energy contribution to the modern world energy requirements. Recently its development made a huge impact to the world energy needs. Wind energy has a long history for more than 130 years [1]. In the early age of the wind industry, windmills were used to pump water for farms. Nowadays larger scale wind turbines can produce up to 10MW and Small wind turbines can produce less than 100 kilowatts. However, management of the wind energy sources has been always challenging as it has a considerable effect on different aspects of the power system such as the power quality [2], power harmonics and inter-harmonics [3], power line communications [4], etc. In this regard, research topics regarding how to obtain a maximum power output for high speed wind input without destroying the small-scaled wind turbine system can be considered as one of the important research areas of the wind energy. Because in high speed wind conditions the turbines output could be overloaded and could destroy the small-scaled wind turbine due to

low inertia momentum. Therefore, in such wind condition, the wind operation must be stopped to avoid being damage to the small scaled wind turbine.

In this research, our work is about how to operate the wind turbine in such storm condition and how to generate the electricity without damaging the turbine. In the simulation results we have shown that it is possible to use eddy current magnetic brake system on the proposed method for the stall control. Wind turbine brake system plays an important role when there is storm condition. Most of the modern wind turbines use the friction brakes to control the rotation of the rotor of the wind turbine [5]. The brake pads are the important part to slower or stop the rotation of the rotor in strong wind situation. Therefore, these brake pads should be made for long term use. But still the modern wind turbine brakes can be used for few years, after that either it should be repaired or replaced by a new brake pad. Therefore, our aim is to introduce this magnetic brake system to replace the current friction brake system. The main specialty of this magnetic brake is there is no mechanical contact with the rotor for controlling the speed of the turbine. Therefore,

\*Shiro Tamaki, Email: shiro@ie.u-ryukyuu.ac.jp

[www.astesj.com](http://www.astesj.com)

<https://dx.doi.org/10.25046/aj050264>



this eddy current brake system is an alternative method to the conventional friction-based brake system [6]. Also, magnetic brake system required less maintenance than the conventional brake system [7].

In this paper, at first, we explain about small-scaled wind turbine blade which is destroyed due to experimental tension test that equivalent to centrifugal force due to over rotation of the blade. Afterwards the application of the magnetic brake and the eddy current brake were introduced. Later the mathematical modeling of the system and simulation results were explained.

## 2. Analogical experiment of blade destruction

Wind turbine blades are often destroyed by strong winds. The reason is due to the centrifugal force on the blades triggers into over-rotation by strong winds. In order to realize a tensile force equivalent to the centrifugal force until the blade destroys, the blade was subject to a tensile test. Figure 1 shows the test status of the broken wind turbine blade. In otherwords, this analogical experiment is done in order to obtain the safety margin of the blade. This experiment stands for loading force (i.e. equivalent to centrifugal force) to the blade until it breaks out. Through this experiment we can calculate the force that may cause destruction of the blade. Once the destructive force is obtained then we can recalculate the maximum allowed angular velocity. The material of the blade is made by FRP (Fiber Reinforced Plastic). Figure 2 shows the experimental results of tension test of the blade. In this figure the horizontal axis stands for the displacement of the blade against the axis of the blade. Then vertical axis shows the tension force to the blade. Figure 2 was obtained using Microsoft Excel software. In this experiment, when the tensioned force reach to approximately 27 kN, at that point the blade is destroyed. So, in order to avoid such destruction, we have to concern safety margin. As it is obvious in Figure 2, tensioned force is linear with respect to displacement up to 6 mm. However, after 6mm the characteristics of the blade becomes non-linear against to force. Concerning safety margin and non-linearity of curve, we set the maximum allowed force to 4.5kN.



Figure 1. Broken wind turbine blade

Equation (1) shows the relation between tensioned force that is equivalent to centrifugal force and angular velocity as well the parameter and value are shown in table 1 below this equation.  $F_{max}$  stands for allowable maximum force, m is the weight and r is the length of blade.

$$F_{max} = m r \omega_{max}^2 \quad (1)$$

Table 1: Specification of the blade

Parameter	Value	Unit
$F_{max}$	4.5	kN
m	4.5	kg
r	1	m
$\omega_{max}$ (without margin)	31.622	rad/s

According to equation (1) and table 1, the allowable maximum angular velocity  $\omega_{max}$  is 31.622 rad/s (point A in the Figure 2), which is 4.5kN. We did not set the maximum angular velocity to the obtained value since safety margin is taken. Therefore, we put a secondary safety margin value as 29 rad/s (point B in the Figure 2) and primary safety margin value as 25 rad/s (point C). By doing so, we can obtain low penetration value 3.8kN for 29rad/s and 1kN for 25rad/s which is less than 4.5kN. From point A to point D can be considered as the blade destruction area. After point D the blade was broken. Hence, we set the  $\omega_{max}$  as follows,

$$\omega_{max} = 25 \text{ rad/s.}$$

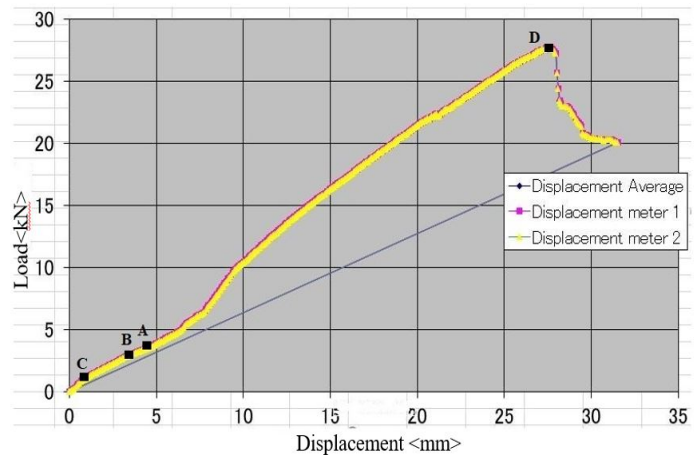


Figure 2. Blade destruction chart

## 3. Mechanism of eddy current brake

### 3.1. Eddy current theory

Some specific theories are related to the eddy current theory, such as the Faraday law of induction, the Lenz law and Fleming's right hand rule. Eddy current theory-based instruments are currently applied on many areas modern day. Some examples include bomb detectors and Electric meter for residence, among others.

Faraday law of induction states that a magnetic field can produce a current in a closed circuit when the magnetic flux linking to the circuit is changing [8]. Equation (2) introduces the mathematical expression of the Faraday law of induction,



$$\varepsilon = - \frac{d\Phi}{dt} \quad (2)$$

where,  $\varepsilon$  and  $\Phi$  stands for electromotive force and magnetic flux, respectively.

Assuming this magnetic flux induced on a copper plate and its resistor is  $R_c$  and  $I$  is the induced eddy current on a copper plate. We can obtain the mathematical expression as (3), According to ohm's law,

$$-\varepsilon = R_c I_{\text{eddy}} \quad (3)$$

From (2) and (3) we can obtain the eddy current as the following equation indicates.

$$I_{\text{eddy}} = - \frac{1}{R_c} \varepsilon \quad (4)$$

Therefore, it can be stated that induced eddy current can be calculated using (4).

### 3.2. Lenz law

Lenz law states that the direction of an induced electromagnetic force (e.m.f) is always such that it tends to set up a current opposing the motion or the change of flux responsible for inducing that e.m.f [9]. Eddy currents are the loops of currents which are induced due to the moving of a non-ferromagnetic conductor and a magnetic field according to the Faraday's law of induction as the equation above highlights. The path of the eddy current induced in the non-ferromagnetic material shaped in the form of a loop and it build up a magnetic field opposite to that of magnet [10]. The blue lines in the Figure 3 display the eddy currents induced on the conductor plate. The magnitude of the eddy current induced in the conductor is proportional to the size of the magnetic field. Also, the rotating copper plate which is attached to the rotor will exert a drag force from the permanent magnet. This drag force will operate as the brake force to control the angular velocity of the small scaled wind turbine. The reason for using the copper plate is that it's a non-ferromagnetic material. For ferromagnetic materials the eddy current will not be induced. Each time when the copper plate rotates the magnetic flux on the copper plate is changing. As a result of magnetic flux change the braking force will create due to the interaction of the eddy current on the plate and the magnetic field. Therefore, the magnet exerts a drag force on the copper plate. As a result of this, the rotation of the angular velocity of the copper plate decreases.

Nowadays electromagnetic brake systems are used widely such as in industrial applications, gym appliances, rollercoasters, recreation equipment's and maglev trains among others. This magnetic brake system is considered as a very efficient brake system because of its non-contact braking operation [11]. The advantage of this braking system is that, when the force become stronger, the magnetic force creates a stronger force against the system, relatively. Figure 3 shows how eddy current brake works. Only one section of the magnets was shown to describe the illustration more precisely. However, in the brake system incorporated multiple magnets to produce a strong braking force on the braking plate.

Figure 4 displays the braking plate with induced eddy current. B1 and B2 are the induced magnetic field on the copper plate from the magnet.

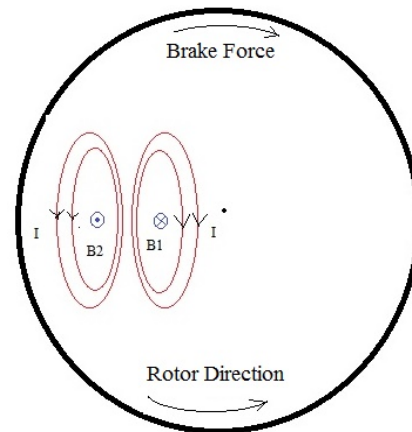
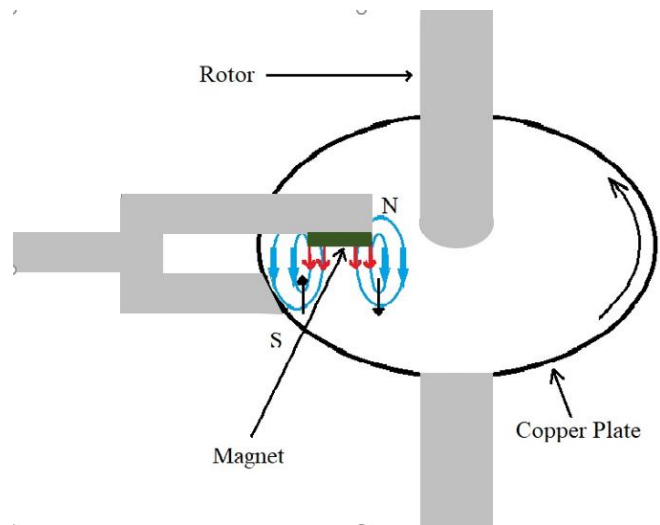


Figure 4. Braking plate

Mathematical expression for B is in (5). Here B denotes magnetic flux density and magnetic intensity denotes by H.  $\mu$  represent the permeability of the atmosphere.

$$B = \mu H \quad (5)$$

The brake force is created as a result of the induced eddy current according to the Fleming's left-hand rule. While the rotor rotates counterclockwise the braking force will occur in clockwise direction.

## 4. Conventional method and proposed method and its application

Nowadays the conventional wind turbines use different types of control methods to get an efficient, stable and long-term durability power. Pitch control [12,13], yaw control, friction [14-16] control is popular control method are being used. In the friction control method, the brake pads are being used to control the angular velocity of the rotor. However, such brakes cannot be used long-term, since they need to be repaired or replaced if the brake pads were broken. Our proposed brake system, on the other hand, utilizes a magnetic eddy current brake system which controls the angular velocity in a non-contact manner with the rotor. In spite of the friction brake system that has the contact with the rotor, our

proposed method is contactless. Hence, it is adequate for long-term usage, rather than the time span offered by the conventional one.

The arrangement of magnets is displayed in Figure 5 in which the braking torque occurs in the opposite direction of the disk rotation.

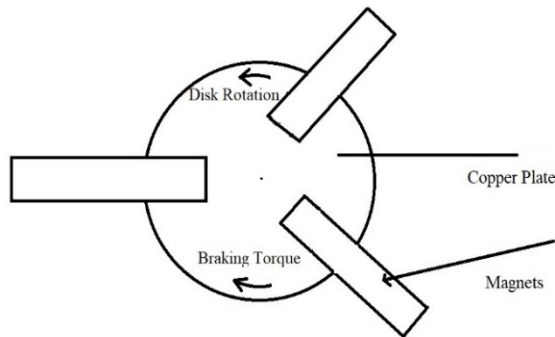


Figure 5. Cross section of the brake

When the small-scaled wind turbine angular velocity increases the copper plate angular velocity will increase simultaneously because the plate is attached to the rotor. When copper plate velocity increases the drag force on the plate from the induced eddy current also will be increased. Therefore, the angular velocity of the turbine will be controlled.

#### 4.1. The structure of proposed brake system

In order to implement the eddy current contact less brake system, we have designed the following system shown in Figure 6. The principle is based on the eddy current occurrence that requires non-ferromagnetic low resistor material is implemented by the copper plate and magnetic flux is set in the arm as it is shown in Figure 5. The principle of brake system is that when the angular velocity exceeds 25rad/s, the two magnets will be turned in between the copper plates in parallel using the arm that controlled by servo motor. As a result of this matter, due to rotation of plate and changing magnetic flux the emf is induced and eddy current will flow. Consequently, angular velocity of rotor will decrease due to

the induced magnetic brake force. Hence, the excessive angular velocity will be restricted to the referenced value. Here, microcontroller has the controller role in the brake system. It measured the angular velocity and control the movement of arm by servo motor. By assumption of following prototype system, we construct the flow diagram of the system in next section.

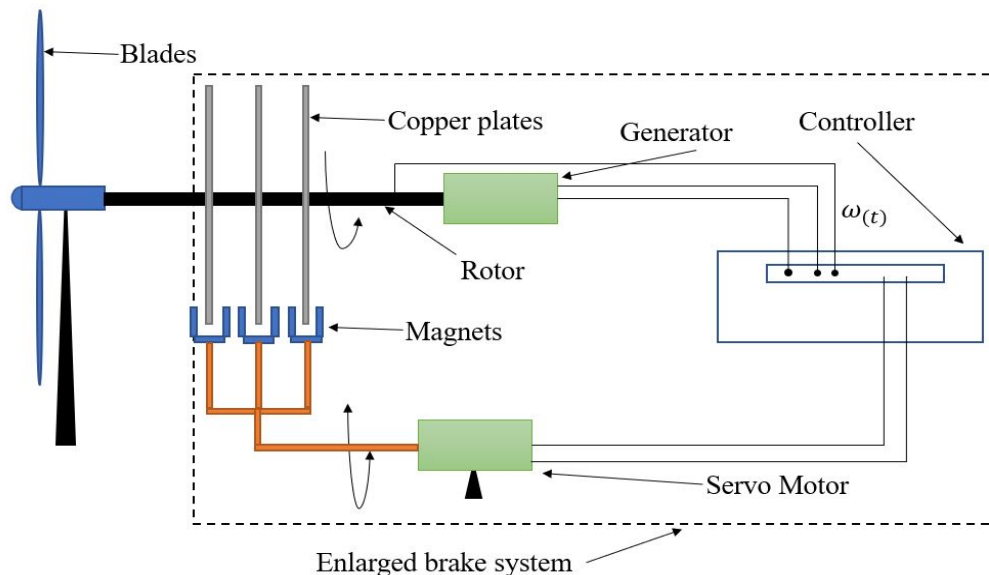
#### 4.2. Flow diagram of the system

After the small-scaled wind turbine received the input wind, the flow will divide into mechanical power ( $P_{mech}$ ) and power captured from wind ( $P_{\omega}$ ). Then the subtraction of power captured from wind and mechanical power can obtain electrical power ( $P_e$ ). Afterward  $P_e$  will go through 3  $\phi$  power generator ( $P_g$ ). Then the power received from the AC generator will distribute to AC/DC converter which includes rectifier and low-pass filter. At this stage the alternate current will convert to the direct current and it will charge the batteries for the purpose of supplying electricity to the DC green-house system. The load is variable. This process is displayed in the Figure 7.

When the measurement system receives the angular velocity  $\omega(t)$  of the small-scaled wind turbine the measurement system will send the measured angular velocity  $\omega_m$  to the system controller. Afterwards the system controller will obtain the  $\omega_{error}$  by calculating the difference between the reference value of angular velocity  $\omega_{ref}$  and  $\omega_m$ . Then, the system controller will turn on the servo motor to rotate the magnet closer to the braking plates. At this point, the magnetic brake force  $f_m$  will reduce the rotation of the brake plate as a result of the induced eddy current on the copper plate. This process was illustrated in Figure 8. In the next section mathematical modeling of entire system is described in detail.

#### 4.3. Mathematical modeling

In this section the entire dynamics model of system is introduced. The system consists of small-scaled wind turbine, mechanical shaft, 3 $\phi$  generator, DC converter and the DC bus in order. The DC bus is providing power to the loads at the end. The pattern of loads is shown in later section.



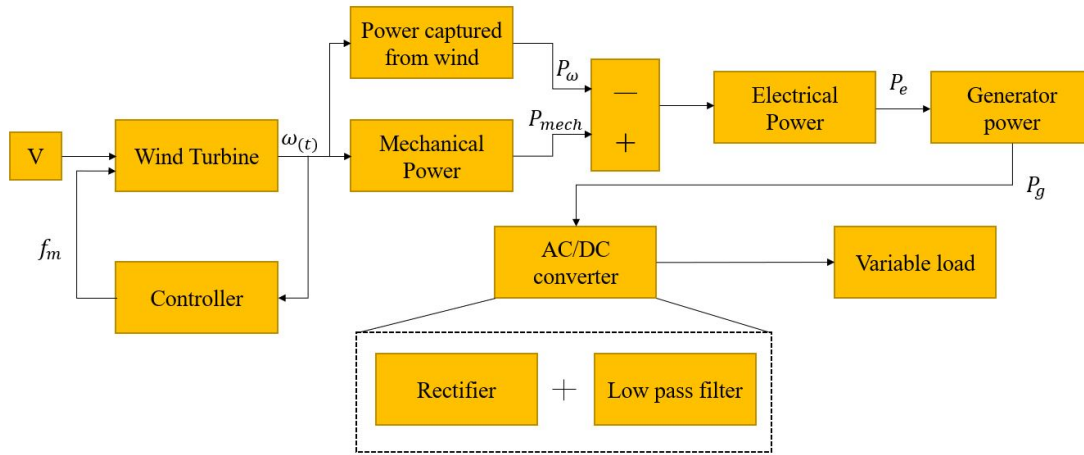


Figure 7. Flow diagram of the entire system

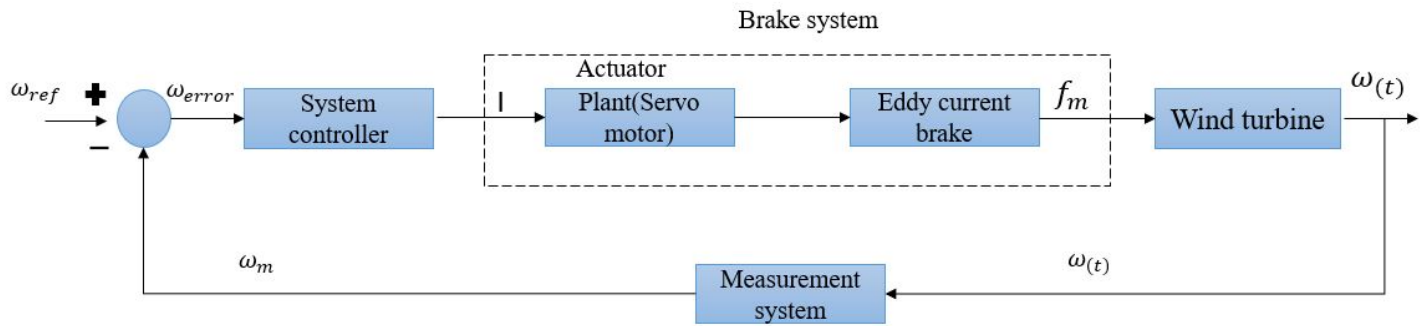


Table 2: Parameters

Symbol	Name
$J_\omega$	Inertia moment of the blade
$\omega$	Angular Velocity
$\rho$	Density of atmosphere
$A$	Area swept by blade
$R$	Length of blade
$V_{(t)}$	Speed of wind
$f_r$	Axis friction factor
$\mu$	Permeability
$q_m$	Magnitude of the magnetic field of the magnet
$q_c$	Magnitude of the magnetic field of the copper plate
$d$	Distance between copper plate and magnet
$a_{adj}$	Decision functional adjustment
$\omega_{ref}$	Reference value of angular velocity
$\omega_m$	Measured angular velocity
$I$	Eddy Current
$C_p$	Power coefficient
$C_t$	Torque coefficient
$\eta_g$	Generator power coefficient
$\eta_{DC}$	Rectifier efficiency of DC converter

At first, we introduce the dynamics of the conventional model of small-scale wind turbine and afterwards the dynamics of the proposed method will be shown. The table 2 shows the parameters [www.astesj.com](http://www.astesj.com)

identification of the whole system. Additionally, the power efficiency of 3  $\phi$  generator and DC converter is considered as they are connected to the turbine shaft directly without coupling any gear.

The conventional dynamics of equation (6) represents the dynamics of the conventional small-scaled wind turbine system

$$J_\omega \frac{d\omega(t)}{dt} = \frac{1}{2} C_T \rho A R V_{(t)}^2 - f_r \omega(t) \quad (6)$$

In order to show the stability of the system we apply the Laplace transform and made two assumptions to linearize the system

Assumption 1;  $V_{(t)}$  is a constant value,

Assumption 2;  $\omega_{(0)} = 0$ .

Since velocity is constant the Laplace transform of the input term can be considered as  $U_{(s)}$ .

Here,  $s$  is the Laplace operator

The Laplace transform of angular velocity and its derivative can be obtain by following transformation rules

$$\mathcal{L}[\omega(t)] = \Omega_{(s)}$$

$$\mathcal{L}\left[\frac{d\omega(t)}{dt}\right] = s\Omega_{(s)} - \omega_{(0)} = s\Omega_{(s)}$$

Therefore, the Laplace transform of equation (6) is (7)

$$J_\omega s\Omega_{(s)} = U_{(s)} - f_r \Omega_{(s)} \quad (7)$$

Through equation (7) we obtain the transfer function of conventional method shown in (8).

$$\Omega_{(s)} = \frac{1}{J_{\omega}s + f_r} U_{(s)} \quad (8)$$

For (8) the bode plot is shown in Figure 9 to describe that how angular velocity responds to wind velocity that may contains various frequency components.

The parameter of transfer function is set to as following:

$$f_r = 0.2; J_{\omega} = 12;$$

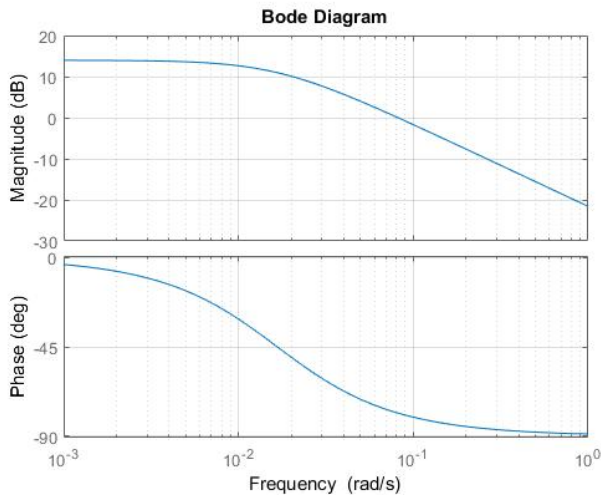


Figure 9. Bode diagram of transfer function of (8)

As it can be seen in Figure 9, the gain for low frequency components the output of transfer function will include up to 15 dB. This means that if there is a constant wind velocity (rated velocity) penetrates the turbine, the angular velocity increases rapidly. However, the natural wind velocity spectrum varies from low to high frequencies. As it is clear, in high frequency domain the gain is decreasing drastically. Therefore, the analysis of wind velocity spectrum [17] becomes significant that how affect the turbine rotation behavior. However, in this study we are not go through this.

Next for the stability analysis, from the transfer function we can obtain the pole of conventional method that the denominator of equation (8) is set to be 0. Hence, we have as following:

$$J_{\omega}s + f_r = 0$$

Eventually the pole of system (8) is

$$s = -\frac{f_r}{J_{\omega}} < 0$$

The system is stable, since the pole is negative. So, we can conclude that the small-scaled wind turbine system has a stable behavior. The proposed method is shown by applying with combination of the eddy current and decision function.

The equation below expresses the proposed torque equation.

$$T_B = \frac{1}{2} C_T \rho A R V_{(t)}^2 - T_{axis} - f_m f_{(\omega(t))} \quad (9)$$

The torque equation is shown in Figure 10.

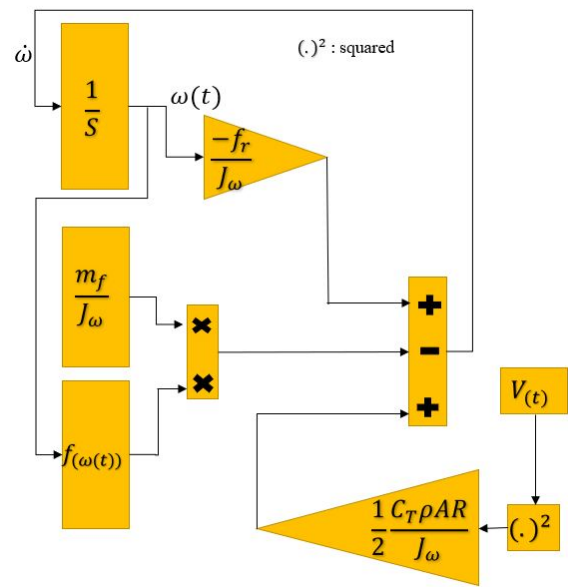


Figure 10. Flow of the torque equation

As it is clear in the above equation, conventional method of break system to restrict the angular velocity has done by  $T_{axis}$  which the technique was to varying the friction by brake pad. However, in this study since the  $-f_m f_{(\omega(t))}$  term is proposed as contactless break method, the  $T_{axis}$  is considered as the friction of shaft coupled to the generator which can be assumed to be a constant value. Therefore, for the sake of contactless purpose the magnets are utilized in order to magnetize the copper plate and as results the eddy current will flow. The torque earned from term  $f_m$  is single set permanent magnetic brake torque on the rotor which is

$$f_m = \mu \frac{2q_m q_c}{4\pi d^2} \quad (10)$$

Where,  $d$  is the distance from copper to each magnet and  $q_m$  and  $q_c$  stands for magnitude of the magnetic field.

For the sake of stronger torque creation from magnetization, in this study we set 3 sets of permanent magnetic brake in parallel as described in Figure 5, the above equation becomes as follows

$$f_m = \mu \frac{6q_m q_c}{4\pi d^2} \quad (11)$$

Furthermore, equation (12) represents the decision function [18-19].

$$f_{(\omega(t))} = \frac{1}{\pi} \tan^{-1} \left( \alpha_{adj} (\omega_{(t)} - \omega_{ref}) \right) + 1/2 \quad (12)$$

The decision function acts as a switch to brake system to decide at what moment the  $\omega_{(t)}$  exceeds  $\omega_{ref}$ . Therefore, whenever, angular velocity exceeds the reference value it will be activated. However, the performance of decision function depends on the coefficient  $\alpha_{adj}$  which is analyzed in the later section.

Next,  $T_B$  is the torque of the blade which can be written as below equation.

$$T_B = J_{\omega} \frac{d\omega(t)}{dt} \quad (13)$$

Where,  $J_{\omega}$  is the inertia moment of the blade.



Finally,  $T_{axis}$  represents the axis friction torque as described as follows

$$T_{axis} = f_r \omega(t) \tag{14}$$

Where,  $f_r$  is axis friction factor.

It is notable that in conventional brake system this term was controlled to regulate and restrict the angular velocity [20]. However, we are not going through it in this paper.

The application of this study is to install 3  $\phi$  generator and rectifies its output to provide a DC power supply to the loads. Load considered to be DC-Green house that will describe the details in later section. The schematic of rectification and smoothing of its output, in other words the conventional DC converter consists of 6 diodes, capacitor and resistor which these two elements are used as the low-pass filter to smoothen the rectified output waves. Figure 11 represents a schematic of the generator which considered to be 3  $\phi$  power supply, full wave rectifier and low pass filter and a battery parallel with loads.

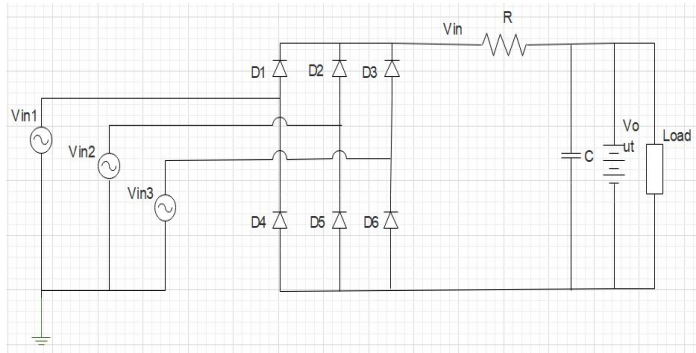


Figure 11 Three phase voltage circuit diagram with rectifier and low pass filter.

Equation (15) shows the low pass filter dynamics.

$$V_{in} - V_{out} = RC \frac{dV_{out}}{dt} \tag{15}$$

From (15) we can obtain the transfer function of low pass filter shown in following equation (16),

$$G_{LFP} = \frac{1}{1+sRC} \tag{16}$$

Where,  $s$  is Laplace operator.

As it can be seen it is significant to choose the  $R$  and  $C$  value to obtain a stable output to the loads. However, in this study, we are not going to the detail of designing the low-pass filter.

Now let us consider the power dynamics in order to obtain the anticipated generated electrical power from generator. According to the following equation the subtraction of  $P_{mech}$  by  $P_e$  is equivalent to  $J_{\omega} \omega \frac{d\omega(t)}{dt}$ . In other words, mathematical expression is as follows

$$J_{\omega} \omega \frac{d\omega(t)}{dt} = P_{mech} - P_e \tag{17}$$

Since  $P_{mech}$  is obtained by wind turbine characteristic formula,  $P_e$  can be anticipated by simple manipulation of above equation.

$$P_e = P_{mech} - J_{\omega} \omega \frac{d\omega(t)}{dt} \tag{18}$$

As mentioned previously, in this study since the efficiency is considered we define an output power efficiency of a 3 $\phi$  AC generator and its rectification since the load is DC bus.

The output power of the 3 $\phi$  AC generator displayed in (19).

$$P_G = \eta_g P_e \tag{19}$$

Here,  $\eta_g$  is the power coefficient of the generator and  $P_e$  is the electrical power received to the generator.

Further, equation (20) shows the converted DC power.

$$P_{DC} = \eta_{DC} P_G \tag{20}$$

where,  $\eta_{DC}$  represents the efficiency of rectifier of DC converter.

As considering the power stability analysis, it is significant that the produced power from wind turbine has adequate capacity of power in order to provide power to the loads. Therefore, the final stage of power conversion that is  $P_{DC}$ , this should satisfy the power to the loads constantly and globally in time domain which includes the transient and steady response.

Suppose that we have a function such as following (21)

$$\Gamma(P_{DC}, P_L) = \frac{P_{DC} - P_L}{P_{DC}} \tag{21}$$

which  $\Gamma(\dots)$  stands for remnant function. The remnant function is composed of remnant power normalized by final stage power output that is DC converter output. Here, if and only if  $\Gamma$  is Semi Positive-definite function then the power supply is globally stable. The Below equation is used to verify the power supply stability.

$$\Gamma(P_{DC}, P_L) \geq 0 \tag{22}$$

Once the above equation is satisfied, then the required capacity is adequate for entire system. Besides, for above equation, in any situation  $\sup_{vt} \Gamma(P_{DC}, P_L) \leq 1$  is satisfied so that the load's installation percentage can be determined. The satisfactory analysis and evaluation is done in later section as simulation.

#### 4.4. Extension of the proposed method

From now on we will explain the extension of the proposed method which is about adding  $C_p$  and  $C_t$  as variables into the system. In equation (23)  $\lambda$  stands for tip speed ratio which is equal to the linear velocity of the wind turbine blade divided by the wind velocity.  $\omega$  is the angular velocity of the blade and  $R$  is the radius of the blade [21].

$$\lambda = \frac{\omega R}{V} \tag{23}$$

Equation (24) represents the power coefficient of the wind turbine. Here,  $\beta$  is the blade pitch angle. We assume the blade pitch angle value is 0 for this study.

$$C_p = 0.5176 \left( \frac{116}{\lambda_i} - 0.4\beta - 5 \right) e^{-\frac{21}{\lambda_i} + 0.0068\lambda} \tag{24}$$

Where  $\frac{1}{\lambda_i} = \frac{1}{\lambda + 0.08\beta} - \frac{0.035}{\beta^3 + 1}$ .

In this research pitch angle is assumed to be 0 constantly. Therefore,

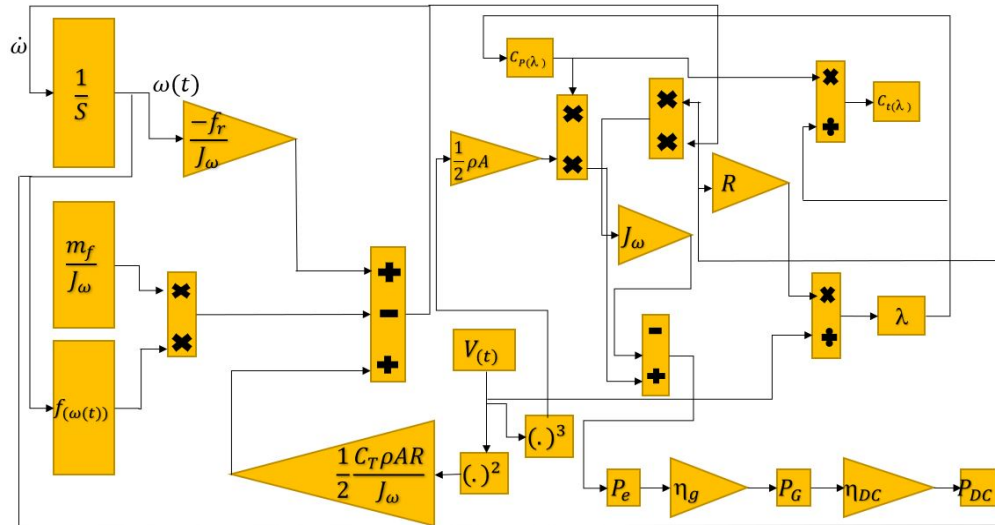


Figure 12. Expanded block diagram including  $C_p$  and  $C_t$

$$\lambda_i = \frac{\lambda}{1 - 0.035\lambda}$$

Equation (25) displays the torque coefficient

$$C_t = \frac{C_p}{\lambda} \tag{25}$$

The extended flow diagram of the [22] article is displayed in Figure 12. Note that  $(.)^2$  and  $(.)^3$  represent the mathematical operation as squared and cubed of input, respectively.

#### 4.5. Analysis of decision function behavior

The decision function has an important role to do as regulation of angular velocity while it is operating. When angular velocity is greater than the reference value the decision function value will be greater than 0.5. Then the eddy current brake system will activate to reduce the angular velocity of the rotor.

For behavior analysis of decision function, let's give an artificial set of angular velocity that is  $\omega = 2 \times t$  which  $t$  stands for time as shown in Figure 13. We used MATLAB/Simulink software to plot the following figures shows in this section.

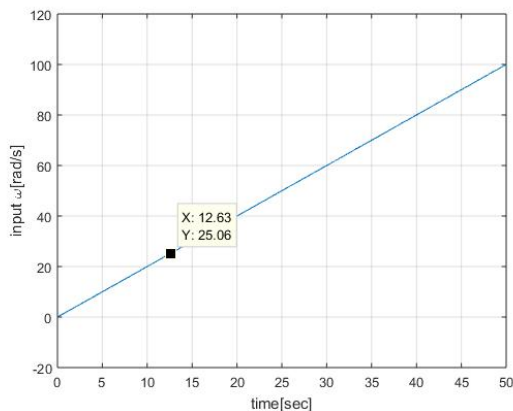


Figure 13. Input wind

For performance analysis of decision function  $a_{adj}$  is a critical coefficient. Therefore, we applied different  $a_{adj}$  values such as 0.1, [www.astesj.com](http://www.astesj.com)

0.5, 1, 10, 200 to observe the output behavior of decision function. The triggered angular velocity value is set to be 25 rad/s. For these different  $a_{adj}$  values, the behavior of the decision function with respect to time is shown in Figure 14. For high values of  $a_{adj}$  such as 200 the decision function value is almost 1 at approximately 12 seconds which also can be seen in Figure 13 that at 12 sec angular velocity reaches 25 rad/s. According to Figure 15, when the  $a_{adj}$  is 0.1 the decision function's output has lower value comparing to the other  $a_{adj}$  values that are greater than unity. The decision function has a lower value in the beginning means that the brake system has already started to work when the angular velocity is below 25rad/s as shown in Figure 15. When the decision function output value is at 0.5 the brake system is triggered. When the  $a_{adj}$  increases the decision function value is converging to 1 for brake mode. That means the system must use a higher  $a_{adj}$  value in order to get an efficient brake control system. According to Figure 15 the highest  $a_{adj}$  value is 200. As it is clear in Figure 15, the area of non-braking mode except  $a_{adj} = 200$  line (ideal mode) is shown in the gray color mesh and other area is for the braking mode.

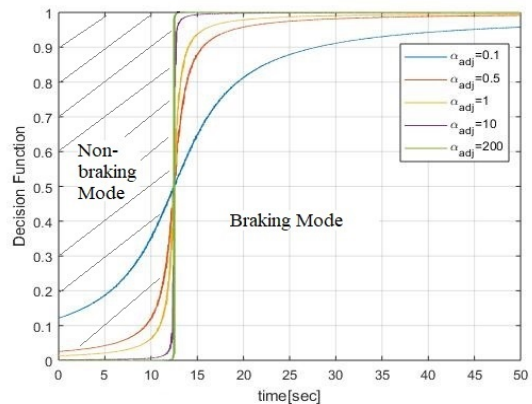


Figure 14. Performance of decision function against time

However, in reality it is hard to realize a system with  $a_{adj} = 200$  due to microcontroller process time and may not have enough capability to calculate speedily. Therefore, some internal delay

may occur in the system and stability and performance analysis should be done for system including time delay element [23-25]. However, in this study, since we focus on behavior of brake system performance, instead of analyzing the delay system we set the  $\alpha_{adj}$  to an acceptable value. Hence, we applied the  $\alpha_{adj}$  as 10 to which has adequate transient response according to Figure 14 and at the same time is considered to be a reasonable value for implementation in actual case.

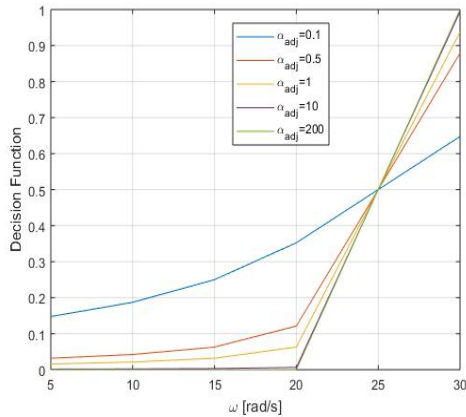


Figure 15. Decision function against angular velocity

### 5. Simulation and Results

In this section, first, we built the mathematical model of the control system then we simulated it in the MATLAB/Simulink based environment. At first we simulate the angular velocity response for different mean velocities from 10 to 30 m/s. Next we set two patterns of input wind velocity and observe the angular velocity behavior. One set is a regular rising and declining wind velocity (pattern No.1) and the other one is a random one (pattern No.2) which are shown in results. Additionally, for each pattern, in order to observe the decision function performance, we have shown the offsets between the  $\omega_{ref}$  and  $\omega_{steady}$  with respect to  $\alpha_{adj} = 6$  to 200. The offset stands for the subtraction of reference angular velocity by steady response which concerns system performances. Eventually, for both patterns, to observe the power provision stability evaluation function  $\Gamma(P_{DC}, P_L)$  is shown with regard to time response.

#### 5.1. Simulation conditions

In this simulation, power coefficient and torque coefficients are considered as variables. Previously in [1] power coefficient and torque coefficient were constants. Simulation time for this research is 1000s. Sampling time is 0.1s. The load as shown in Figure 16 is applied to entire simulation. The input load behavior changes depending on various conditions in DC-green house such as weather, temperature, light condition. In the greenhouse the power consumption is varying through day and night time. Specially in night time the power consumption would be higher since many devices are in operation. Such as the LED lights which exposes light to products, microcontrollers and sensors. Therefore, we created the load that applies in real case to verify the proposed system that while restriction of angular velocity weather it is possible to provide an adequate power to the loads or not. However, for the sake of simplicity for analysis as it is expressed duration time is set to 1000 s.

Table 3 displays the parameters values with the SI units

Table 3: Values of the Parameters

Symbol	Value	Unit
$J_\omega$	12	$kg.m^2$
$\omega$	Variable	$rads^{-1}$
$\rho$	1.225	$kg.m^3$
$A$	3.14	$m^2$
$R$	1.5	m
$V(t)$	Variable	$ms^{-1}$
$f_r$	0.2	$kg.m^2s^{-1}$
$\mu$	$4\pi 10^{-7}$	$T.m.A^{-1}$
$q_m$	$62.5 \cdot 10^9$	A.m
$q_c$	$0.1 \cdot 10^{-4}$	A.m
$d$	0.05	m
$\alpha_{adj}$	10	
$\omega_{ref}$	25	$rads^{-1}$
$\eta_g$	0.9	
$\eta_{DC}$	0.9	

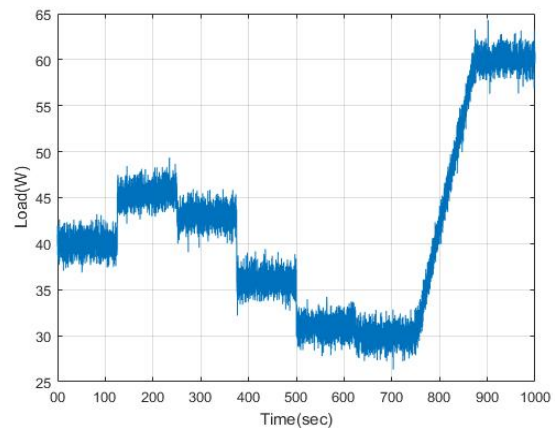


Figure 16. Pattern of the load

#### 5.2. Results

From now on, Figure 17 to Figure 21 displays the angular velocity behavior for different input average velocities of 10, 15, 20, 25 and 30 m/s in order with controller decision function coefficient is set to  $\alpha_{adj} = 10$  and the stall angular velocity or the referenced one is considered to be 25 rad/s as it has been chosen in section 2.

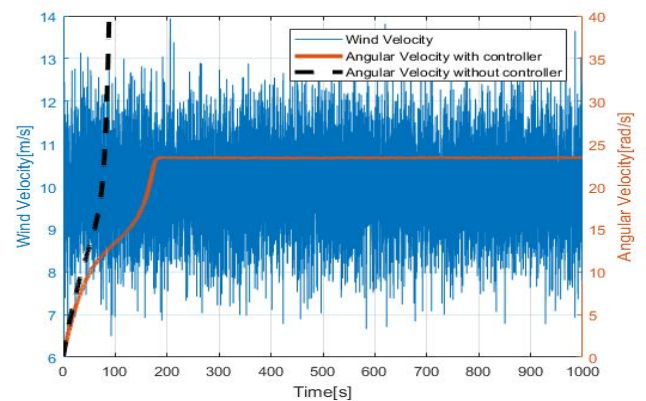


Figure 17. Stall control chart for average wind 10m/s



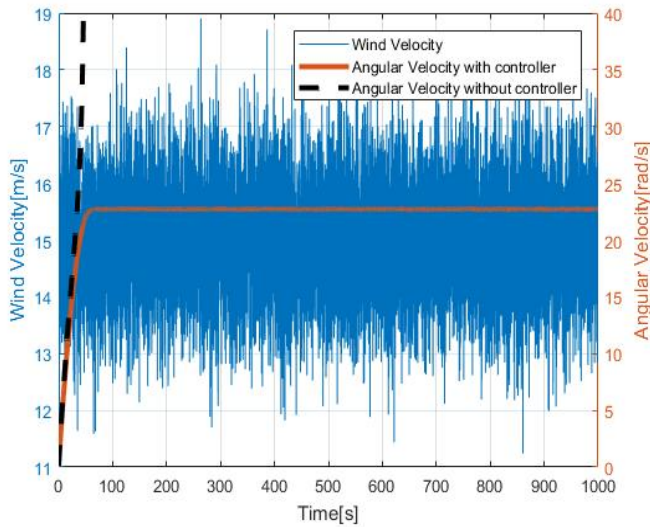


Figure 18. Stall control chart for average wind 15m/s

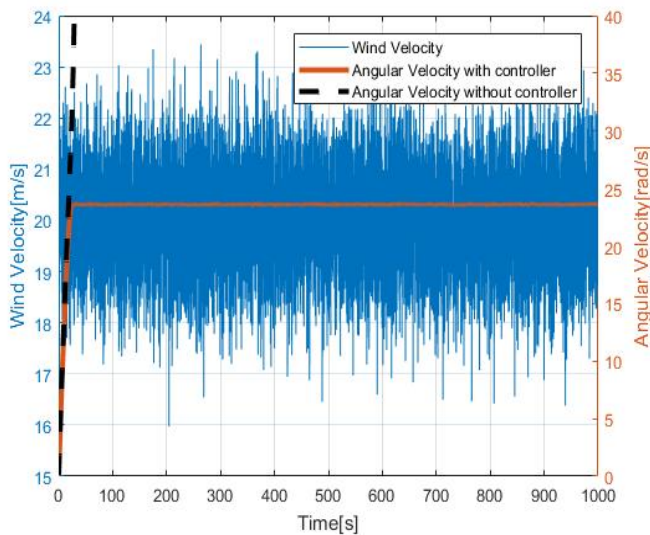


Figure 19. Stall control chart for average wind 20m/s

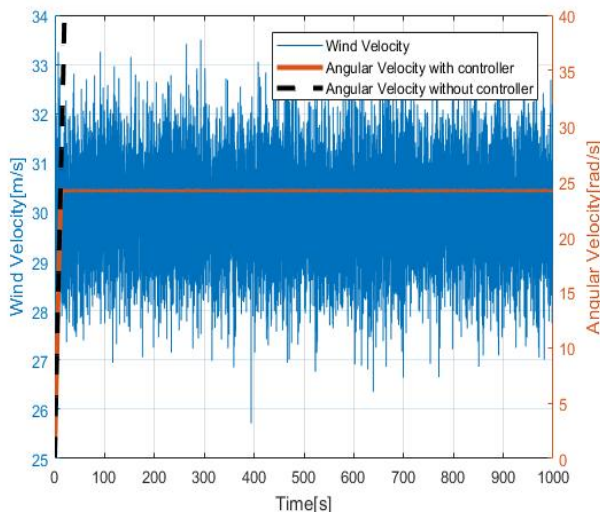


Figure 20. Stall control chart for average wind 25m/s

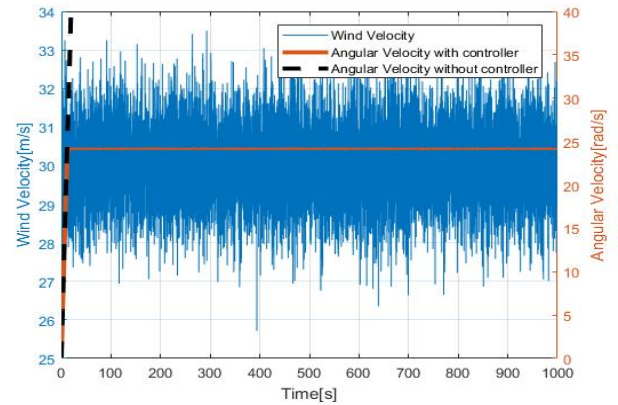


Figure 21. Stall control chart for average wind 30 m/s

By analyzing the Figure 17 to Figure 21 it is obvious that the magnetic brake system restricts the angular velocity up to 25 rad/s for average wind velocities of 10m/s to 30m/s. However, without controlling it will diverge and system becomes unstable. Moreover, the transient response of decision function seems to be adequate. Therefore, we can conclude that  $\alpha_{adj} = 10$  has a stable behavior and acceptable performance. Following Figure 22 summarize the angular velocity behavior when the input wind velocity changes from 10m/s to 30m/s.

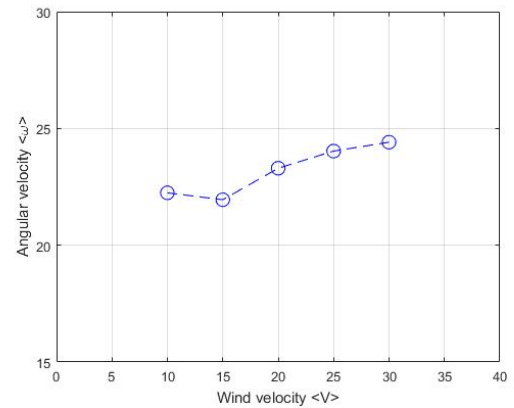


Figure 22. Wind velocity from 10m/s to 30m/s against angular velocity

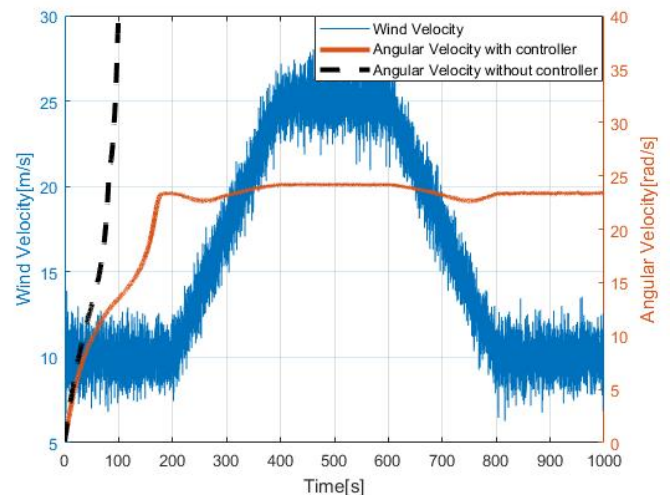


Figure 23. Angular velocity behavior for wind velocity pattern No. 1



Figure 23 and 24 explain how the brake system works with and without the proposed control. Angular velocity without the brake control is displayed using the broken line which is diverging on the Y-axis for both wind patterns. The maximum average wind velocity in this simulation is 25m/s and the minimum value is 5m/s. Patterns of input velocity have been created artificially.

As it is shown in above figure, the behavior of angular velocity with proposed controller against the input wind velocity pattern No.1 has a stable attitude with respect to time. As well, it is visible that the angular velocity is controlled up to 25rad/s even during high wind penetration conditions which is during 400 to 600 sec.

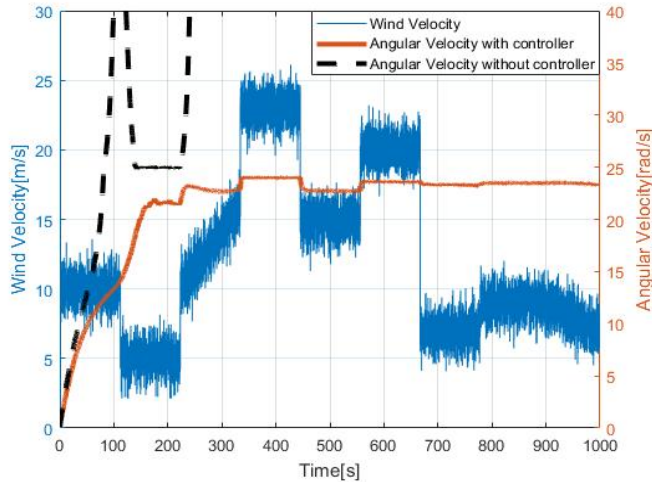


Figure 24. Angular velocity behavior for wind velocity pattern No. 2

In Figure 24, it is clear that even though angular velocity with proposed controller fluctuates but it has stable response and have been suppressed up to 25 rad/s and cease the excessive rotation. The arise of fluctuation of angular velocity is due to the wind pattern that have been penetrated to the wind turbine. Therefore, the angular velocity behavior should be enhanced for such sudden changes of wind velocity. However, for now it satisfies the requirement. Therefore, mechanical point of view, we can conclude that the angular velocity can be sustained to a desired or referenced value by proposed method.

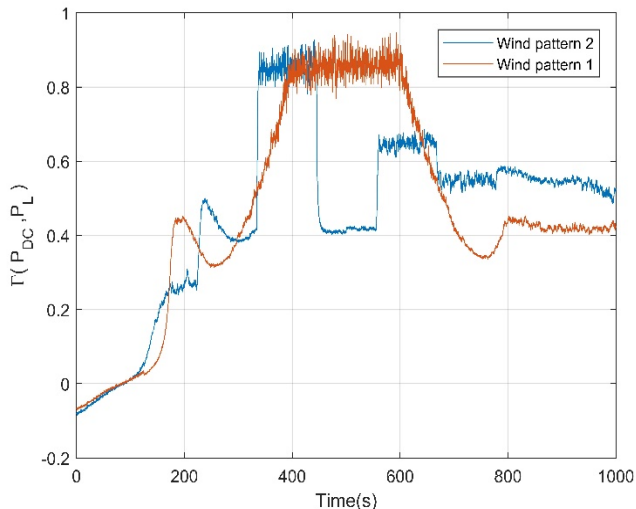


Figure 25. Time response of evaluation function for wind pattern 1 and 2

Next the power provision is evaluated by evaluation function which has been defined previously. Following Figure 25 is shown the evaluation function for the wind velocity pattern No. 1 and 2, respectively.

As it is obvious, except the transient duration, equation (21) is satisfied. Hence, the proposed controller can also provide an adequate power supply to loads and restricts the angular velocity. Also, the power output contains the remnant quantity of power particularly during high wind penetration that means it can be stored to power bank or charges the peripheral batteries.

Finally, in order to ensure the decision function performance that is part of controller the offsets of referenced angular velocity and steady value of angular velocity with controller has been plotted with respect to  $\alpha_{adj}$  in Figure 26.

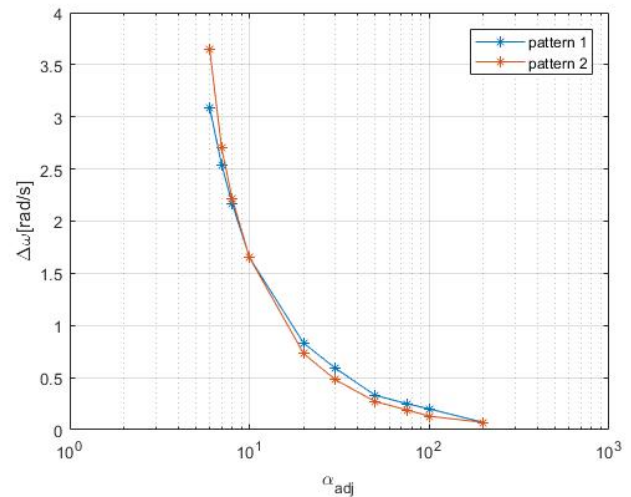


Figure 26. Offset for average wind velocity 20m/s

As it is clear in above figure, if the  $\alpha_{adj} < 10$ , then the corresponding offset increase. On the other side, if  $\alpha_{adj} > 10$ , then the corresponding offset would decrease. This means for higher value of factor, performance of the system improves since the offset decreases. However, as have been discussing, it is fairly hard to set  $\alpha_{adj}$  to high value due to microcontroller processor capability for realization. Therefore,  $\alpha_{adj}$  can be set to 10 according to the above since it is not too high value and at the same time it has sufficient performances.

## 6. Conclusion

In this paper, we have simulated an eddy current magnetic brake system for the small-scaled wind turbines. In strong wind condition, several types of control methods utilized to get the desired electricity output for small-scaled wind turbines. But still the modern wind turbines unable to get a stable generated electricity output when there is a storm condition. In storm condition, most of the wind turbines stop their operation to protect the turbine and it's all components. As we have seen from the simulation results it is possible to conclude that using the eddy current brake system, we can limit the angular velocity below 25rad/s when there is storm condition and satisfies the power provision to the loads, simultaneously. Since there is no mechanical connection with the rotor and the brake system, we

believe it may be able to use for much longer time than the conventional friction brake system. Thus, for future works, we will apply the Lyapunov function for the stability analysis. Moreover, in this paper the trigger of angular velocity is set based on physical destructive value. However, maximum power point should also be considered for enhancing the efficiency. Therefore, we will use the maximum Power Point Tracking Method (MPPT) to get a maximum power output from objected wind turbine. Additionally, pitch controlling method is a very useful method to control the wind turbine operation. Since we haven't applied this method to the proposed system in this paper, we will apply pitch control method as future work for this system. Finally, the integration of pitch angle control and proposed eddy current brake system will be implemented.

### Conflict of Interest

The authors declare no conflict of interest.

### Reference

- [1] J.F. Manwell, J.G. McGowan, A.L. Rogers, *Wind Energy Explained*, John Wiley and Sons, 2009.
- [2] E. Santos, M. Khosravy, M.A. Lima, A.S. Cerqueira, C.A. Duque, "ESPRIT associated with filter bank for power-line harmonics, sub-harmonics and inter-harmonics parameters estimation". *INT. J. ELEC. POWER*, **118**, p.105731, 2020. <https://doi.org/10.1016/j.ijepes.2019.105731>
- [3] E. Santos, M. Khosravy, M.A. Lima, A.S. Cerqueira, C.A. Duque, and A. Yona, "High accuracy power quality evaluation under a colored noisy condition by filter bank ESPRIT" *Electronics*, **8**(11), p.1259, 2019. <https://doi.org/10.3390/electronics8111259>
- [4] A.A. Picorone, T.R. de Oliveira, R. Sampaio-Neto, M. Khosravy, M.V. Ribeiro, "Channel characterization of low voltage electric power distribution networks for PLC applications based on measurement campaign", *INT. J. ELEC. POWER.*, **116**, p.105554, 2020. <https://doi.org/10.1016/j.ijepes.2019.105554>
- [5] Y.B. Lee, G.C. Lee, J.D. Yang, J.W. Park, D.C. Baek, "Failure analysis of a hydraulic power system in the wind turbine" *ENG. FAIL. ANAL.* **107**, 104218, 2020. <https://doi.org/10.1016/j.engfailanal.2019.104218>
- [6] R. Yazdanpanah, M. Mirsalim, "Hybrid electromagnetic brakes: design and performance evaluation" *IEEE T. ENERGY CONVER.*, **30**(1), 60-69, 2015. <https://doi.org/10.1109/TEC.2014.2333777>
- [7] H. Sodano, J.S. Bae, "Eddy current damping in structures" *The Shock and Vibration Digest.*, **36**(6), 469-478, 2004. <https://doi.org/10.1177/0583102404048517>
- [8] J. D. Kraus, K. R. Carver, *Electromagnetics*, 2nd ed. McGraw Hill, 1973.
- [9] John Bird, *Electrical circuit theory and technology*. Third edition, Newnes, 2007
- [10] M. O. Gulbahce, D.A. Kocabas, I. Habir, "Finite element analysis of a small power eddy current brake" *Proceedings of 15th International Conference MECHATRONIKA*, Prague, Czech Republic, 2013.
- [11] K.J. Lee, K. Park, "Optimal robust control of a contactless brake system using an eddy current" *Mechatronics*, **9**(6), 615-631, 1999. [https://doi.org/10.1016/S0957-4158\(99\)00008-2](https://doi.org/10.1016/S0957-4158(99)00008-2)
- [12] F. Asharif, S. Tamaki, T. Nagado, T. Nagata M.R. Asharif, "Analysis of non-linear adaptive friction and pitch angle control of small-scaled wind turbine system," *Future Generation Information Technology FGIT 2011, Control and Automation CA*, Springer-Verlag, Lecture Note: Communication in Computer and Information Science, 26-35, December 2011. [https://doi.org/10.1007/978-3-642-26010-0\\_4](https://doi.org/10.1007/978-3-642-26010-0_4)
- [13] F. Alsharif, J. Tamura, S. Tamaki, K. Anupa, M. Futami, "Dynamics modification of passive pitch control for small-scaled wind turbine" *Grand Renewable Energy 2018*, Yokohama, Japan, June 2018. [https://doi.org/10.24752/gre.1.0\\_147](https://doi.org/10.24752/gre.1.0_147)
- [14] F. Asharif, S. Tamaki, H. Tepei, T. Nagado, T. Nagata, "Feasibility confirmation of angular velocity stall control for small-scaled wind turbine system by phase plane method" *IEEK Transactions on Smart Processing and Computing*, **2**(4), 240-247, 2013.
- [15] F. Asharif, S. Tamaki, T. Nagado, M. R. Alsharif, "Comparison and evaluation of restrain control in wind turbine with various shock absorber considering the time-delay" *International Journal of Control and Automation*, Vol. **5**(3), 111-131, September 2012.
- [16] F. Asharif, M. Futami, S. Tamaki, T. Nagado, K. Asato, "Stability and performance analysis of passive and active stall control of small-scaled wind turbine system by phase plane method" *Proceedings of IEEE, International Conference on Intelligent Information and BioMedical Sciences (ICIIBMS 2015)*, 27-33, OIST, Okinawa, Japan, November 2015. <https://doi.org/10.1109/ICIIBMS.2015.7439483>
- [17] E. Branlard, A. T. Pedersen, J. Mann, N. Angelou, A. Fischer, T. Mikkelsen, M. Harris, C. Slinger, B. F. Montes, "Retrieving wind statistics from average spectrum of continuous-wave lidar" *Atmos. Meas. Tech.*, **6**, 1673-1683, 2013. <https://doi.org/10.5194/amt-6-1673-2013>
- [18] F. Asharif, S. Tamaki, T. Hirata, T. Nagado, T. Nagata, "Design of electromagnetic and centrifugal force pitch angle stall controller on application to small-scaled wind turbine system" *International Symposium on Stochastic Systems Theory and Its Applications*, 2013. <https://doi.org/10.5687/sss.2014.231>
- [19] F. Asharif, M. Futami, S. Tamaki, T. Nagado, K. Asato, "Stability and performances analysis of electromagnetic stall control system by phase plane method" *47th ISCIE International Symposium on Stochastic Systems Theory and Its Applications*, Hawaii, USA, December 2015. <https://doi.org/10.5687/sss.2016.345>
- [20] F. Asharif, S. Tamaki, T. Nagado, T. Nagata, M. R. Asharif, "Design of adaptive friction control of small-scaled wind turbine system considering the distant observation" *International Conference of Control and Automation*, LNCS Springer, 213-221, November 2012. [https://doi.org/10.1007/978-3-642-35264-5\\_30](https://doi.org/10.1007/978-3-642-35264-5_30)
- [21] N. Karakasis, A. Mesemanolis, C. Mademlis, "Wind turbine simulator for laboratory testing of a wind energy conversion drive train" *8th Mediterranean Conference on Power Generation, Transmission, Distribution and Energy Conversion (MEDPOWER)*, 2012. <https://doi.org/10.1049/cp.2012.2033>
- [22] K. Anupa, F. Asharif, S. Yasushi, K. Ken, S. Tamaki, J. Tamura, "Contactless magnetic braking control unit for small-scaled wind turbines for dc green house" *The 34th International Technical Conference on Circuits/Systems, Computers and Communications*, Jeju Shinhwa World, Republic of Korea, 2019. <https://doi.org/10.1109/ITC-CSCC.2019.8793443>
- [23] F. Asharif, S. Tamaki, T. Nagado, T. Nagata M. R. Asharif, "Application of internal model controller for wind turbine system considering time-delay element" *8th International Conference on Informatics in Control, Automation and Robotics*, 199-202, Noordwijkerhout, Netherlands, July 28-31, 2011.
- [24] F. Asharif, S. Tamaki, T. Nagado, T. Nagata, "Analysis of hybrid robust controller considering disturbance, noise and time-delay" *18th Iranian Conference on Electrical Engineering Isfahan*, Iran, *Proceeding of IEEE Conference 978-1-4244-6760-0/10*, 11-13, May 2010. <https://doi.org/10.1109/IRANIANCEE.2010.5506990>
- [25] F. Asharif, S. Tamaki, T. Nagado, T. Nagata, M. Rashid, M. R. Asharif, "Feedback control of linear-quadratic-integration including time-delay system" *The 24th International Conference on Circuit-Systems, Computers and Communication*, ITC-CSCC'09, 1054-1057, Jeju, Korea, July 5-8, 2009.

## On the Ensemble of Recurrent Neural Network for Air Pollution Forecasting: Issues and Challenges

Ola Surakhi\*, Sami Serhan, Imad Salah

The University of Jordan, Computer Science Department, King Abdulla II Faculty for Information Technology, 11942, Jordan

---

### ARTICLE INFO

Article history:

Received: 28 February, 2020

Accepted: 27 March, 2020

Online: 04 April, 2020

Keywords:

Ensemble Methods

Recurrent Neural Network

Time-series Forecasting

---

### ABSTRACT

Time-series is a sequence of observations that are taken sequentially over time. Modelling a system that generates a future value from past observations is considered as time-series forecasting system. Recurrent neural network is a machine learning method that is widely used in the prediction of future values. Due to variant improvements on recurrent neural networks, choosing of the best model for better prediction generation is dependent on problem domain and model design characteristics. Ensemble forecasting is more accurate than single model due to the combination of more than one model for forecasting. Designing an ensemble model of recurrent neural network for time-series forecasting applications would enhance prediction accuracy and improve performance. This paper highlights some of the challenges that are faced by the design of the ensemble model of different recurrent neural network versions, and surveys some of the most relevant works in order to give a direction of how to conduct ensemble learning research in the future. Based on the reviewed literature, we propose a framework for time-series forecasting based on the using of ensemble technique.

## 1. Introduction

Atmospheric aerosol concentrations have attracted increasing worldwide attention during the past years due to its effect on human health and the environment [1]. According to The World Health Organization (WHO), it is estimated that around 7 million people die every year due to air pollution [2]. Therefore, having real time information about air pollutants concentration could help in controlling air pollution and preventing health issues that are related to its effect [3].

Recently, many researchers have put forward efforts to improve the approach to air pollution prediction. The methods of predicting air pollution concentration, in general, fall into two categories: deterministic and statistical. Deterministic models simulate the spatiotemporal distributions of air pollutants at different scales and directions by using statistical methods [4, 5, 6]. Deterministic models use physics and chemical reactions in the atmosphere to model emission and transformation of air pollutants. These models are considered theoretical models that are based on sophisticated priori knowledge, inconsistent and limited data [7, 8].

Statistical models use statistics-based models to predict air pollutants concentrations. Regression, Time Series, and

Autoregressive Integrated Moving Average (ARIMA) are the most common statistical approaches that are used in the environment science prediction [9, 10, 11]. Due to a non-linear relationship between air pollutant concentration and metrological parameters, advanced statistical approaches based on machine learning algorithms are needed such as ensemble learning algorithms [12] and recurrent neural network (RNN) [13].

RNN is a type of artificial neural network that has a cycle within the network graph which maintains the internal state. RNN is able to predict in sequence prediction problems that involve a time component. This makes it suitable to be applied in applications that utilize a sequence of observations over time, such as Biomedicine, Meteorology, Genomics and more. Within the environmental engineering field, RNN has been used to predict air pollution. Due to its influence of more than one metrological parameter (such as temperature, pressure, humidity, etc), the air pollution prediction is considered as a multivariant time-series prediction problem.

Long Short-Term Memory Unit (LSTM), is a state-of-the-art model of RNN that is recently used to predict air quality [14, 15]. Many variants of RNN have been developed with different characteristics. They include GRU (gated recurrent unit), Vanilla LSTM and more.

---

\* Ola Surakhi, Email: [ola.surakhi@gmail.com](mailto:ola.surakhi@gmail.com)

[www.astesj.com](http://www.astesj.com)

<https://dx.doi.org/10.25046/aj050265>

Several attempts have been made to better predict accuracy of time-series forecasting problems using RNN models. In order to obtain advantages of several recurrent neural network models, a combination of different models can be applied. The ensemble of multi-models is a suitable solution [16]. Combining a different number of recurrent neural network models can enhance forecasting performance and increase accuracy. Conversely, ensemble methods may lead to an increase in the cost of computation time that is needed to train multi-models based on the number of models utilized. This paper will highlight some of the challenges that are faced in the application of different recurrent neural networks for forecasting applications, especially air pollution forecasting in terms of performance and accuracy. The contributions of this paper are summarized as follow:

1. Summarize the state-of-the-art recurrent neural network models that have been applied in the application of forecasting air pollution.
2. Study of challenges of designing a recurrent neural network model.
3. Recommend some of the issues that will have to be tackled before designing recurrent neural network.
4. Present the advantages of using ensemble method to enhance forecasting performance.
5. Analyze and compare the performance of different ensemble recurrent neural network for time-series forecasting applications.
6. Propose a framework for time-series forecasting based on the using of ensemble technique.

The reminder of this paper is organized as follow: Section 2 will give a brief description of the air pollution concept along with the methods that are used for its prediction. Section 3 will provide details of recurrent neural networks, some of its variations and the challenges of its design. Section 4 will present the ensemble model concepts design. Section 5 will propose the framework for time-series forecasting. Section 6 will offer the conclusion.

## 2. Air Pollution

In urban cities, air pollution is one of the most significant environmental concerns that has a great impact on health and the ecosystem. Air pollution effects air quality and is one of the causes for various diseases such as heart disease, chronic obstructive pulmonary disease, acute and chronic respiratory conditions and cancers [2]. Air pollutants can be formed due to a chemical reaction with other pollutants and atmospheric physics. The prediction of air pollutants can enhance the scientific understanding of air pollution and provide valuable information concerning the contribution of each pollutant toward the cause of air pollution [17-21]. This information will provide public authorities the time to manage pollution so as not to exceed acceptable levels.

According to World Health Organization (WHO), 7 million people die every year due to air pollution. PM<sub>2.5</sub> (particulate matter less than 2.5 micrometers in diameter) is the air pollutant that is the most likely cause of the majority of death and disease. Ozone is another pollutant that is the cause of some of the major

respiratory diseases. Oxides of Nitrogen (NO<sub>x</sub>), a major contributor to ozone, is also linked to significant health risks [2].

Due to its harmful effect on human health, some major cities, such as Los Angeles and New York, have identified air pollution as one of the main health dangers [22], and so, air pollution technology has become an important topic for the creation of smart environment and for the delivery of clean air for citizens.

Many researches have been conducted over past years to propose and develop a predictive model for the concentration of air pollutants. The accuracy of these models differs based on the methods that have been employed. However, it is still a challenge to develop an accurate predictive model for the concentration of air pollution due to the existence of many factors that influence its performance [23].

The methods of predicting air pollution can be classified into two categories [24]: deterministic and statistical methods. Deterministic methods simulate the physical and chemical transformation, emission and desorption of pollutants in terms of metrological variables in the atmospheric physics. Statistical methods apply statistic-based models to predict future air pollution from historical data. These methods involve a time-series analysis. It includes linear regression [25], the autoregressive moving average (ARMA) method [26], the support vector regression (SVR) method [27], the artificial neural network (ANN) method [28], and hybrid methods [29] to understand the relationship between the concentration of air pollutants and metrological variables.

Artificial neural network is a machine learning technique that provides convincing performance in the field of time-series forecasting and prediction. ANN can incorporate complex non-linear relationships between the concentration of air pollutants and metrological variables. Various ANN structures have been developed to predict air pollution over different study areas, such as neuro-fuzzy neural network (NFNN) [30], Bayesian neural network [31] and Recurrent neural network (RNN) [32, 33]. RNN has been applied in many studies involving time-series prediction, such as traffic flow prediction [34] and wind power prediction [35]. In the area of air pollution, RNN is suitable to capture the dynamic nature of the atmospheric environment [24]. It can learn from a sequence of inputs to model the time-series of air pollution.

## 3. Recurrent Neural Network

Recurrent Neural Network is a type of machine learning algorithm that was developed in 1980 [36]. It is the neural network model that is most likely used for time-series forecasting problems. RNN are designed with memory to remember things from past occurrences that can be useful for prediction of the future events. Its structure has a recurrent edge between hidden nodes. So, RNN not only uses input data but also uses the output of the previous steps to make current predictions.

Figure 1 shows a simplified structure of RNN with one input layer and one output layer. The input can be considered as a sequence of vectors through time  $t$  such as  $\{x_t, x_{t+1}, x_{t+2}, \dots\}$  where  $x_t = (x_0, x_1, x_2, \dots, x_N)$ . the input units are fully connected with hidden units, where the connections are defined by weights value. The hidden layer contains units that are connected to each



other with recurrent connection through time to define memory of the system.

The hidden units are connected with output units. As the inputs are sequential through time, the feedback loop forms the cyclical structure that allow a sequential input to loop in the layer. This means that the output of step  $t-1$  is fed back to the network to influence output of step  $t$  [36].

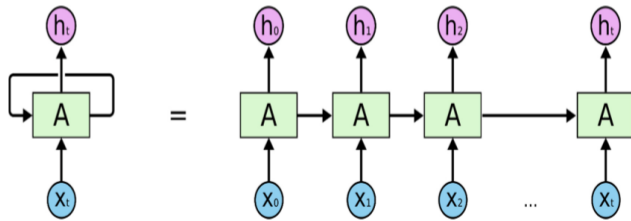


Figure 1: Recurrent Neural Network [36]

RNN can deal with sequential input and produce sequential output. The input is considered internally dependent where RNN can capture this dependency with time relation. Some application areas of RNN with sequential data include handwriting recognition [37], video captioning [38] and music composition [39].

To learn input-output relationship, RNN uses a nonlinear activation function at each unit. Nonlinear activation function is more powerful than linear activation function. It is differentiable and can deal with nonlinear boundaries.

RNN uses Backpropagation algorithm during learning process to update and adjust network weights [40]. As the updating follows the modifications during feedback process, it is commonly referred to as the backpropagation through time (BPTT). The BPTT works backward through the network layer by layer from the network output, updating the weights of each layer according to the layer's calculated portion of the total output error. The weights are changing with proportion to the derivative of error with respect to the weights value, this includes that nonlinear activation function is differentiable. The changing of weights represents distance between current output and desired target.

Computing error derivative through time is done at each iteration to make a single update and capture dependencies between parameters in order to optimize results. Updating weights back into every timestep takes time and slows learning.

Two main issues may occur during weights update, exploding gradient and vanishing gradient. The exploding gradient happens when the algorithm assigns a high importance to the weights. On long sequence data, RNN gradients may explode as weights become larger with increasing of gradients during training. While vanishing gradients happens when the partial derivation of error is very small, multiplying its value with learning rate to update weights will not be a big change compared with previous iteration. This cause network to iteratively learn with no much changes as memory will hardly learn correlation between input and output and thus will ignore long term dependencies.

Several solutions have been proposed in the literature to overcome vanishing and exploding gradient. The most popular are Long short-term memory (LSTM) and Gated recurrent unit (GRU) which are explained next in this section.

Long short-term memory (LSTM) [41] is a variant of RNN that is used to solve the problem of short-term memory. LSTM uses gate mechanism that control the flow of data. The gate decides whether the coming input data is important to be kept in the memory or not. RNN keeps all the data during the learning process, even if the update is very small and not important (vanishing problem). The gates in LSTM store important data even if it is long for a prolonged period of time. This makes LSTM capable of learning long-term dependencies as a default. Repeating modules structure in LSTM is different than RNN. Each module has four interacting layers with a unique method of communications, as shown in Figure 2.

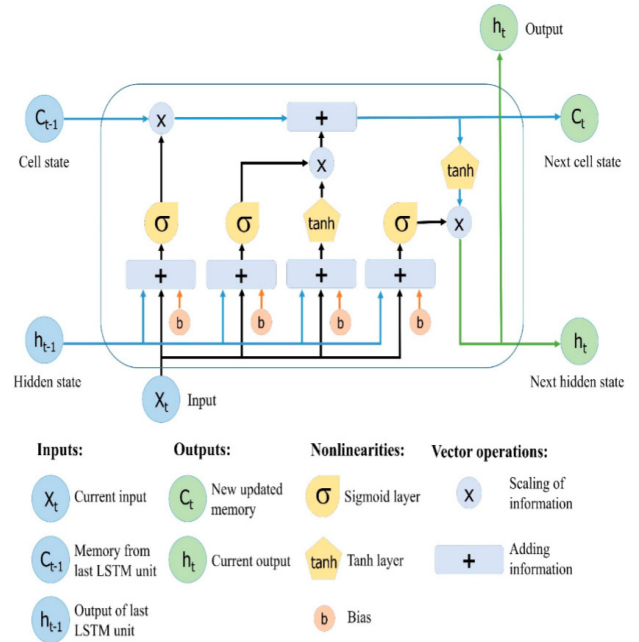


Figure 2: LSTM structure [42]

The LSTM structure consists of memory block called cells. The cell state and hidden states are transferred to the next cell. The cell state is the data flow that allows data to be transferred unchanged to the next cell. Cell state is the long-term memory. The gates are similar to layers that perform some matrix operations to add or remove data from the cell state. Gates control the memorizing process to avoid long term dependency problem. The input gate and forget gate manage cell state.

Gated recurrent unit (GRU) is another variant of RNN [43]. GRU have faster learning process than LSTM and with fewer gates and shorter memory. GRU has two gates, update gate and reset gate, with no output gate in contrast to LSTM. Update gate controls information flow from the previous activation and the addition of new information. Reset gate is inserted into the candidate activation. GRU outperforms LSTM for music and speech applications [44].

The inputs to RNN, LSTM and GRU are one-dimensional vectors. Bidirectional LSTM process sequential input with opposite direction with two hidden states that accept past data and future data [45]. Bidirectional LSTM is suitable with the application where current information is influenced by previous and future inputs such as speech [46].

Choosing the appropriate algorithm among RNN versions is dependent on the problem domain and requirements. The main factor here is to improve the learning process by obtaining a satisfiable accuracy that has a low error rate and reasonable speed up. The model performance of all RNN versions is dependent on the optimization of the network hyperparameters. The hyperparameters define the neural network architecture and determine the behaviour of the algorithm for the given dataset. They include: activation function, number of hidden layers, number of neurons in each layer, sequence length, learning rate, weights initialization, number of epochs, batch size, dropout rate and feature extraction.

Finding the optimal selection for each parameter for the optimization of network performance is a challenge. The most widely applied method for the selection of hyperparameters of a given algorithm on a given dataset are grid search and random search. In grid search, all possible combinations of parameters are tested. This method is time consuming and dependent on several hyperparameters that are essential for it to be optimal. As more parameters are included, the complexity increases. However, random search chooses a random point from the parameters space, and unlike grid search which considers all possible combinations, random search is much faster with less complexity.

Selecting hyperparameters is a data driven method that requires fitting the model and validating it on the existing data, which make the process expensive [47, 48].

Table 1 summarizes the neural network hyperparameters that influence network performance, along with a list of some methods that are used to set each one up.

Choosing the value of each hyperparameter depends on the problem and its domain. Machine learning problems can be classified into two categories: classification and regression; similar for the activation function. Some of the activation function are used for classification problems, such as softmax, and some are used for regression problems, such as ReLu. The distribution of the dataset aids in determining the activation function that effect the behavior of the training.

Table 1: neural network hyperparameters

Hyperparameter	Description	Methods
Activation function	Mathematical function used to generate output value	Sigmoid, ReLu, softmax, tanh
Optimization algorithm	The mathematical method used to update network weights to make accurate prediction and minimize loss function value	Gradient decent, AdaGrad, Adam, RMSProp
Loss function	The difference between model prediction values and actual, which is needed to predict	Mean square error, mean absolute error, cross entropy
Number of hidden layers	Number of hidden layers in the network that add a	Experimental

	hierarchy learning capacity	
Number of neurons	Number of neurons at each layer that affects the learning capacity of the network	Experimental
Learning rate	Steps forward to move weights in the direction opposite to gradient	Experimental
Weights initialization	Initial weight values	Normal distribution, uniform distribution, identity matrix, random orthogonal matrix
Number of epochs	Number of iterations	Experimental
Batch size	Number of input samples, how often to update weights of the network	Experimental
Dropout rate	Number of connections to be dropped during training	Randomly
Feature extraction	Set of features used to train predictive model	Filter method, wrapper method, embedded method

Neural networks are trained using stochastic gradient descent, which maps inputs to outputs from training data. This requires the choosing of a suitable loss function for the given problem. The model, with a given set of weights, makes prediction and, error is calculated; the optimization algorithm then updates the weights so that the following evaluation will reduce the error.

Depending on the properties of the problem and the goals of designed model, an optimization algorithm and loss function can be selected that guarantee a satisfiable result.

The number of hidden layers, number of neurons in each layer, batch size and number of epochs can influence the performance of training in terms of speedup and increase complexity. For problems where speed is not important, fixing parameters to increase accuracy by selecting large values, as needed, may not be a big issue. Determining the optimal number is a large task, and it can be done by repeating the same experiment and calculating statistics summary, which can then be compared with each configuration.

The learning rate communicates to the optimizer of the learning algorithm as to how far to move the weights in response to the estimation error after weight updating. If it is small, the training is more reliable, but more time will be needed. If it is high, then training may not converge or may even diverge. Learning rate is one of the most important parameters that need to be tune correctly

before training the neural network, and its value has a great influence on the training results and network performance. Learning rate value ranges between 0.0 and 1.0.

The weight of the neural network should be initialized to a small random value. By doing this, the hidden layer will acquire a chance to generate different signals. If the weights are initialized with the same value, then the hidden layer will generate same signal. The initialization should be asymmetric (different) so that the model can find different solutions to the problem. Choosing the method that is best able to initialize the weight of the network in a way that would enhance its performance is a challenge and considered as an entire field of study.

Dropout is a technique proposed by Srivastava, et al. in 2014 to select randomly neurons to be dropped during training [49]. After each epoch, selected dropout neurons do not contribute to the activation on the forward pass, and their weights are not updated in the backward pass.

Neuron dropping during the training signifies that other neurons weights are tuned to specific features of the dataset, and this provide some specialization to training data. Selecting dropout neurons randomly gives the network a better generalization, since the un-dropped neurons will need to handle the representation to make prediction of the missing neurons, which will be led to a reduction in the overfitting of the training data and enhance performance.

Feature extraction means to select those features from the dataset that are more related to the problem and effect the training results. Irrelevant, unneeded and redundant features can be eliminated from the data before training the model. Thus, those features cannot influence the accuracy of the model. Small number of features reduces the complexity of the model, and vice versa.

Selecting the optimal value for each network hyperparameters in a way that it will enhance the performance of the model is mainly dependent on the problem domain and its dataset. The greater the parameters of hyperparameters that need to be tuned, the greater the time needed to tune them. It is preferred to select the minimum number of subsets for the hyperparameters that will influence the performance of the related problem.

### 3.1. Recurrent Neural Network for Forecasting Air Pollution

There are many studies that applied the recurrent neural network for forecasting application. In this section, we will introduce some of these works that have specifically focused on the prediction of air pollution. along with a summary of the tuned hyperparameters for each, the main contributions of each one, the conducted results and pitfalls of each work are summarized in Table 2.

Lim, et al. used recurrent neural network to design a model that predicts various types of air quality over three different area in Daegu Metropolitan City, Korea. The author examined the model over different time steps and found that the error is small when the length of input data is about 30 or lower [50]. Authors [51] developed a forecasting model by combining convolution neural network (CNN) and Long Short-Term Memory to predict particulate matters (PM2.5). Li, at al., proposed a novel long short-term memory neural network extended (LSTME) model that inherently considers spatiotemporal correlations for air pollutant concentration prediction [24]. TAO, et al., proposed a model that combines RNN and CNN for air pollution forecasting [52]. Sun, et al., proposed a spatial temporal PM2.5 concentration prediction framework using GRU, which is an extension of RNN [53]. Athira, et al., proposed a deep learning architecture that consists of input layer, a recurrent structure with three neural networks: RNN, LSTM and GRU, and a prediction layer to predict PM10 [54]. Xayasouk, et al., combined RNN with GRU to predict PM10 and PM2.5 in Seoul, South Korea. The proposed model can forecast the concentration of the future 20 days based on previous history data [55].

Brian, et al., used RNN with LSTM to predict an 8-hour average surface ozone concentration based on hourly air monitoring station measurements [56]. Rao, et al., proposed an RNN-LSTM framework for quantification and prediction of air quality [57]. Zhao, et al., applied RNN to forecast daily Air Quality Classification (AQC) in three different cities in the United States, including Los Angeles (LA), Houston (HOU) and Atlanta (ALT) [58]. Karimian, et al., implemented three machine learning approaches: Multiple Additive Regression Trees (MART), a Deep Feedforward Neural Network (DFNN) and a new hybrid model based on long short-term memory (LSTM) to forecast PM2.5 concentration over different time length. LSTM achieved best results [59]. Septiawan and Endah proposed the implementation of Backpropagation Through Time (BPTT) algorithm on three models of RNN: Elman RNN, Jordan RNN, and a hybrid network architecture to predict air pollutant concentration [60].

#### 3.1.1 Discussion about Related Works

From the above-mentioned related works, several recommended points can be concluded:

1. Each region has its specific features that are distinct from one another. The air quality research is recommended to be carried out region wise.
2. The data pre-processing is an important step that eliminate noise and reduce outliers. Different techniques that handle missing data generate different accuracy.

Tables 2: Comparison between recent works on applying RNN for air pollution forecasting

Related Works	Hyperparameters used	Application Area	Main contributions	Experimental results	Pitfalls
Lim et al. [50]	Sequence input, epochs, batch size, dropout, optimizer	Daegu Metropolitan City, Korea	a. The authors used RNN to predict various kinds of air quality of Daegu	a. As input data is 30 or lower, accuracy increased. b. Nadam and RMSprop	a. Small number of iterations are used b. Metrological parameters that influence air pollution prediction are not

			<p>metropolitan city.</p> <p>b. Various experiments were conducted with different variables: input length, different activation functions, number of neurons on hidden layer</p>	<p>activation function outperform Adam and Adagrad.</p> <p>c. The accuracy increased as number of neurons increased in hidden layer.</p>	<p>considered in the experiment</p> <p>c. Proposed work was not compared with previous works in the literature</p>
Huang and Kuo [51]	SELU activation function	Beijing, China	<p>a. A combination of CNN and RNN are proposed to predict PM<sub>2.5</sub></p> <p>b. Comparing proposed model with several machine learning methods</p>	Proposed work achieved higher accuracy comparing with traditional methods	<p>a. Only two metrological parameters are considered in the proposed work</p> <p>b. Selected epoch is used to avoid overfitting, more effective methods can be used</p> <p>c. Proposed model was not tested with different hyperparameters</p>
Li et al. [24]	two LSTM layers and one fully connected layer	Beijing, China	<p>a. Proposed a model of LSTM that consider spatiotemporal correlations for air pollution prediction</p> <p>b. Comparing proposed model with another statistical-based model</p> <p>c. Apply a random search method with k-fold cross validation to find optimal selection of hyperparameters network architecture</p>	Better prediction performance with higher prediction precision achieved by proposed model	Using large time lag, the prediction performance of proposed model decreases with high value of RMSE.
Tao et al. [52]	CNN contains two layer, RNN two layers with 80-neurons	Beijing, China	<p>a. Propose a framework that combines 1D convnets (convolutional neural networks) and bidirectional GRU (gated recurrent unit) neural networks for PM<sub>2.5</sub> concentrations</p>	<p>a. For a certain number of neurons in hidden layer of GRU, overfitting problem may occur after that</p> <p>b. Autocorrelation coefficient indicates that earlier events have a weaker</p>	Comparison is made by shallow machine learning methods and some deep learning algorithms. It would be more efficient to compare proposed model with some model that used CNN to extract features such as one proposed in [50]



			b. Comparing proposed work with seven machine learning methods	effect on current status c. Deep learning method outperform shallow machine learning methods in prediction performance d. Proposed model shows higher precision	
Sun et al. [53]	Not mentioned	Shenyag, China	Propose a spatial-temporal GRU-based prediction model to predict PM <sub>2.5</sub> hourly concentration	Proposed work outperforms other machine learning methods that are used in the paper for experimental comparison	a. No network configuration with different parameters was used in the proposed work b. Proposed work focused on effect of convolutional variables, while time interval is important as air pollution change over time
Athira et al. [54]	Learning rate, batch size, epochs, RMSprop optimizer	China	Use different RNN models with different learning rate to forecast air pollution from AirNet data	Three models performed well in prediction, where GRU outperform other models	a. Deep learning models were used before to predict air pollution. b. Results of proposed work were not compared with previous works
Xayasouk et al. [55]	Sequence input, optimizer Adam	Seoul, Korea	Propose a prediction model that combines RNN with GRU to predict PM <sub>10</sub> and PM <sub>2.5</sub> in the next 7, 10, 15 and 20 days	Proposed model can predict the concentration of particular matter value for the next future	Proposed model was not evaluated in terms of performance of other deep learning models
Brian et al. [56]	Learning rate, activation function, uniform distribution for weight initialization, dropout, feature selection, epochs	Kuwait	a. Propose a framework with LSTM to predict 8-hours average surface ozone concentrations b. Use Decision Tress to extract features	a. Feature extraction b. Sensitivity analysis of parameters led to tune network efficiently c. RNN shows better prediction results comparing with FFNN and ARIMA	RNN was used previously in past studies to forecast air pollutants
Rao et al. [57]	Adam optimizer	Visakhapatnam, India	Propose a model using RNN and LSTM to predict hourly of various air pollutants by considering temporal sequential data of pollutants	Proposed approach archives better performance than Support Vector Machine (SVM) in terms of evaluation metrics.	Network tuning parameters is not mentioned in the proposed work, where difference between then in term of accuracy is not tested neither mentioned

Zhao et al. [58]	Data length	The united states	Use RNN to propose a prediction model to predict air quality classifications in three different cities in the U.S.	RNN outperform two machine learning techniques: SVM and Random Forest	Data length comparison was done in a daily basis, for real-time forecasting, the hourly basis data may give more accurate comparison. The results of RNN and other methods are close to each other for one day time length.
Karimian et al. [59]	Data length	Tehran, Iran	Evaluate three methods for PM <sub>2.5</sub> forecasting by implementing models based on Multiple additive regression trees (MART) and deep neural network (DFNN and LSTM) concepts.	a. LSTM for 48-h predictions outperformed the other two models with higher accuracy b. advanced machine learning models, MART, produced better PM <sub>2.5</sub> estimates than the DFNN model	Number of metrological data was used with no consideration of its importance on increasing/decreasing accuracy of model
Septiawan and Endah [60]	the number of hidden neurons, learning rate, minimum error, and maximum epoch on the accuracy of BPTT	London, England	a. Apply BPTT algorithm with Elman RNN, Jordan RNN, and hybrid network architecture to predict the time series data of air pollutant concentration in determining air quality b. Use autoregressive (AR) process to determine the number of input neurons	Jordan RNN gives smallest value of Mean Absolute Percentage Error (MAPE)	The effects of other features such as metrological data is not mentioned

3. The input variables play an important role on improving the prediction accuracy of the model. For the air pollution domain, the metrological data inputs have a great influence on the variability of air pollutants. The increasing number of input data does not guarantee enhancement of the accuracy of the prediction model, in [52]. It is highly recommended those inputs that are highly correlated with the predicted value (air pollutants concentrations) be included.

4. Recurrent neural networks are suitable to capture non-linear mapping from the sequence of inputs and spatiotemporal evolution of air pollutants. It is highly recommended that they are applied to the domain of air pollutants concentration prediction.

5. The performance of selected algorithm is dependent on the selected hyperparameters.

6. Batch normalization is a technique that is used to automatically standardize inputs to a layer in the deep learning architecture in

order to accelerate the training process and improve performance as listed in [51].

7. Regularization is a technique that is used to reduce weights of the network in order to prevent overfitting and to improve generalization of the model as done in [51]. Generalization means satisfactory performance of the new input data, and not only for the data for which the model was trained.

8. Input variables with different units and different distributions increase the difficulty of training and thereby generate a large weight value. When working with deep learning neural network, such as RNN, data pre-processing is a recommended step before training. The data is either normalized or standardized to make input variables with small values and within the same range (usually between 0 and 1).

9. For time series problems, the amount of input data inputted to the model is a critical parameter that influence the prediction

accuracy. As input data is shorter, more recent information is reflected [50].

10. Since air pollution is a dynamic parameter that changes over time, the time length is an important factor to be considered as it effects the performance of the predictive model. Air pollution may change within the hour, the day or even more, and so the prediction results will also be changed based on the time length. It is recommended to describe behaviour of air pollutants

concentration over time to fine tune the optimal time length before training.

#### 4. Ensemble Learning

Neural networks algorithms are a nonlinear method that uses stochastic training algorithms to learn. This means that learning algorithm can capture nonlinear relationship in the data even if it is complex, but this is dependent on the initial conditions of the training, the initial random weights and the initial parameters tuning. This means that different algorithms will produce different set of weights, which in turn will produce different predictions. This is referred to the neural network as a high variance technique. Conversely, there are hundreds of machine learning algorithms to be selected from for any predictive problem, and choosing the best one that will give the optimal results in terms of accuracy and performance is a challenge. A successful approach to helping in the selection of the best algorithm that will improve the prediction performance and reduce variance is to train multiple models and then combine the prediction of these models. This is called ensemble learning technique.

The ensemble technique is a machine learning method that combines different base models to produce one optimal predictive model [61, 62]. For the ensemble to produce a better result, each individual model should produce an accurate result with different error on the input data [63]. Ensemble can result in better prediction than single model prediction.

Ensemble involves training different multiple networks with the same data, each model is used to make a prediction, which are then combined in a way to generate a final prediction. Some advantages of using ensemble method can be include the following:

1. Improve prediction accuracy
2. Reduce the impact of the following problems which rise when working with single model:
  - a. High variance: when the amount of data is small comparing to the search space
  - b. Computational variance: when the learning method faces a difficulty to find the best solution within search space
  - c. High bias: when the searching space does not contain the solution of corresponding problem

##### 4.1. How to Ensemble Neural Network Methods?

The oldest ensemble neural network approach is called “committee of networks”. It is a collection of networks where each network is trained with the same problem dataset, and each network then produces its actual output. The average of these output predictions is evaluated to produce a final prediction. The

number of models used in ensemble is usually small, three, five or ten trained models to maintain the performance of the technique. Since training multiple models will increase computation and complexity, so ensemble is often kept small. The general idea of ensemble method is shown in Figure 4.

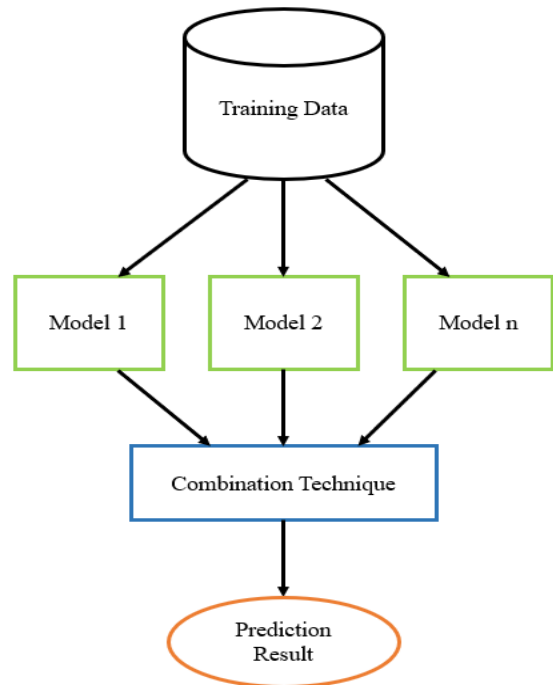


Figure 3: General idea of ensemble method

As shown in Figure 3, the major elements of ensemble method are:

1. Training Data: dataset of the problem
2. Ensemble Models: the set of neural network methods used in ensemble
3. Combination Technique: the way to produce final prediction from output of ensemble models

Varying any one of these elements will influence the performance of the ensemble model. It is a challenge to find the best selection to have a final optimal model. The details of each element are explained below.

#### Training Data

Varying the training data for each model of the ensemble can be done in different ways. The popular one is k-fold cross validation. In the k-fold cross validation, the dataset is divided into k-samples, where each sample is different than the other. A k-models are used for ensemble, where each model uses one sample from a k-samples set.

Bootstrap aggregation, or shortly bagging, is another approach. Here, the dataset is resampled by replacement, and a new dataset is fed into the training model. The composition of each dataset is different, thereby generating different errors from the models. Another approach involves a random selection of data from the dataset.

Training the ensemble models with different samples from the dataset will examine the performance of the model for the different data. It is preferable to have a low correlation in the prediction results of each ensemble members. The predictions of each model are then combined which greater stability and better performance prediction.

### Ensemble Models

The performance of any learning algorithm depends on the initial conditions, that is, the selection of hyperparameters to tune algorithm in a way to produce an optimal result. The model can give many results depending on the selection, some that are good, and others that are not. Training more than one algorithm will result in a set of sub-optimal solutions that when averaging them may give an improved estimate.

Each model will produce an error. The model selection should be in a way that results in a low correlation of errors made by each model. To achieve this, it is recommended to tune each model with different capacity and conditions (different number of neurons and layers and different learning rate, etc.).

### Combination Techniques

There are three ways of combining model prediction into the ensemble prediction which are:

1. **Bagging:** Choose different subsamples from the dataset to build multiple models for each sample. The final output is the average of each prediction for all of the sub-models. There are different bagging models such as:

- a. **Bagged Decision Tree:** Performs well with algorithms that have high variance.
- b. **Random Forest:** An extension of Bagged Decision Tree where samples are taken by replacement.
- c. **Extra Trees:** A modification of Bagged Decision Tree where random trees are constructed from samples of the training dataset.

2. **Boosting:** Build multiple models where each learn to fix the prediction error of the model before it in the chain. The common boosting ensemble models are:

- a. **AdaBoost:** Works by weighing instances in the dataset, so the algorithm can pay less or more attention to their weight while building subsequent models.
- b. **Stochastic Gradient Boosting:** A random subsample of the training data is selected at each iteration and used to fit the base learner.

3. **Voting:** Build multiple models with some statistics (such as mean) to combine prediction.

A summary of ensemble machine learning algorithms used to enhance performance of models on forecasting problems is shown in Figure 4.

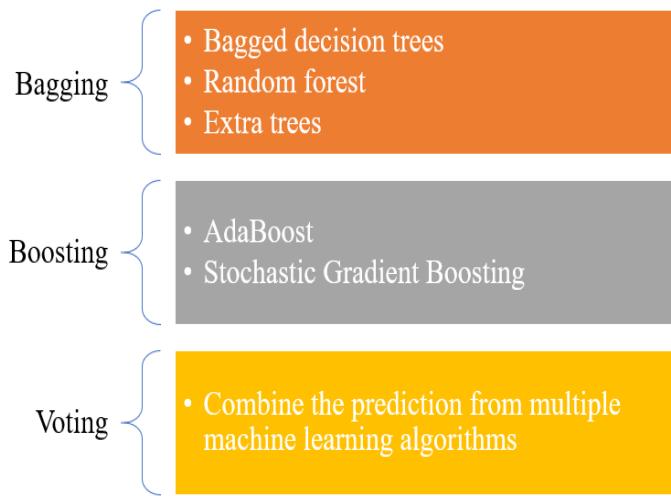


Figure 4: Ensemble Machine Learning Algorithms

### 4.2. Ensemble Learning Applications

Ensemble learning methods have been applied in different forecasting applications and decision making in various applications [64, 65]. It has been shown in that efficiency of ensemble models is greater than single model in terms of accuracy [66, 67]. A summary of some of those applications are introduced below.

Siwek and Osowski used wavelet transformation and ensemble of neural networks to improve accuracy of prediction of PM10 [66]. The authors applied four neural networks: Multilayer perceptron, Support vector machine for regression, Elman network and radial basis function network. All of them are different and independent.

A randomly selected data samples from the entire dataset is fed to each model, and the final output of each model is fed into another neural network. The results of the proposed model show an improvement in the performance in terms of accuracy.

In the biomedical field, Peimankar and Puthusserypady proposed an ensemble model using recurrent neural networks to detect P-wave in electrocardiogram. The authors used four deep recurrent neural networks. The four networks are trained on the data to extract features, where their output is combined for the final detection of P-waves. The results show a high classification accuracy [67]. Tan, Et al., proposed an ensemble of recurrent neural networks for predicting enhancers, a DNA fragment [68]. In wind forecasting application, Cheng. et al., proposed an ensemble method for probabilistic wind forecasting. The authors used recurrent neural network with different architecture (LSTM, GRU and Dropout layer) for ensemble models, and adaptive neuro fuzzy inference system which were used for combination of final prediction [69]. An adaptive boosting (AdaBoost) combined with Extreme Learning Machine (ELM) for multi-step wind speed forecasting proposed in [70].



Table 3: Analysis of ensemble methods in time-series forecasting applications

Related works	Ensemble method	Combination method	Number of base models	Application domain	Results
Siwek and Osowski [66]	Neural network ensemble	Non-linear mixing	10	Air pollution prediction	Mean Absolute Error (MAE), The Mean Absolute Percentage Error (MAPE), The Root Mean Square Error (RMSE), Correlation Coefficient (R) and Index of Agreement (IA)
Peimankar and Puthusserypady [67]	LSTM ensemble	Dempster-Shafer theory (DST)	4	P-waves detection in ECG recordings	Achieved 98.48% accuracy and 97.22% sensitivity
Tan, Et al. [68]	Bagging	Voting	8	Enhancer classification	achieved sensitivity of 75.5%, specificity of 76%, accuracy of 75.5%, and Matthews Correlation Coefficient (MCC) of 0.51
Cheng. et al. [69]	Hybrid ensemble of wavelet threshold denoising (WTD), RNN and Adaptive Neuro Fuzzy Inference System (ANFIS)	ANFIS	6	Wind speed prediction	(RMSE), (MAE) and normalized mean absolute percentage error (NMAPE)
Peng, et al. [70]	A combination of the improved AdaBoost.RT algorithm with the Extreme Learning Machine (ELM)	Additive of models	5	Wind speed forecasting	RSME, MAE and MASE
Borovkova and Tsiamas [71]	Stacking	Average	12	Intraday stock predictions	AUC
Qi, et al. [72]	Bagging	Voting	8	Chinese Stock Market	accuracy is 58.5%, precision is 58.33%, recall is 73.5%, F1 value is 64.5%, and AUC value is 57.67%
Choi and Lee [73]	LSTM ensemble	Adaptive Weighting	10	Time-series forecasting	(MAE) and (MSE)[

In the stock market prediction, many studies have been proposed based on ensemble methods. Borovkova and Tsiamas proposed an ensemble using LSTM for intraday stock predictions [71]. Qi, et al., used eight LSTM neural network with Bagging method to establish ensemble model for the prediction of Chinese Stock Market [72]. A general time-series forecasting model was proposed in [73] using LSTM ensemble model. The authors used multiple LSTM models where final prediction outputs are combined in a dynamically adjusted way. Table 3 summarize the analysis of previous works.

4.3. Discussion of related works

Ensemble learning is the method that combines multiple models to enhance prediction accuracy over one model performance. Analysing the challenges of using ensemble method in the time-series applications includes advantages and disadvantages of combination technique used. Table 4 summarize advantages and disadvantages of each ensemble combination method discussed in this paper [74, 75].

Table 4: Advantages and disadvantages of ensemble method

Method	Advantages	Disadvantages
--------	------------	---------------

Bagging	<ul style="list-style-type: none"> <li>- Used for classification and regression problems</li> <li>- Performs well in the presence of noise</li> <li>- Each model works separately</li> </ul>	<ul style="list-style-type: none"> <li>- Need to perform multiple pass on the dataset</li> <li>- Dataset size should be known in advance</li> </ul>
Boosting	<ul style="list-style-type: none"> <li>- Improve power of weak model</li> <li>- Fast and simple</li> <li>- Can identify noise</li> </ul>	<ul style="list-style-type: none"> <li>- Need to perform multiple pass on the dataset</li> <li>- AdaBoost is sensitive to outliers</li> <li>- Accuracy is influenced by sufficiency of data</li> </ul>
Voting	<ul style="list-style-type: none"> <li>- Accuracy increases as number of member increases</li> </ul>	<ul style="list-style-type: none"> <li>- High computational time</li> </ul>

When designing a predictive model for time-series application based on ensemble method, the size affect performance of model. As the number of base models increases, the accuracy improves but will lead to increasing in the computational time and storage space [76]. Determining the optimal number of base models is a research challenge. Some related works proposed the use of pruning ensemble which reduce complexity and enhance performance [77, 78, 79].

In order to increase performance of ensemble model, it is recommended to use different samples for different base models with different features for each model, and to tune each model with different selection of hyperparameters to increase diversity [80].

**5. Ensemble Recurrent Neural Network Method**

Based on the analysis of previous studies that have been designed as an ensemble model, the framework for ensemble of recurrent neural network for time-series applications can be divided into two main phases: Data Preparation Phase and Ensemble Model Design Phase. The details of each phase are:

1. Data Preparation: Getting the data ready for machine learning algorithm. It is not useful to use real values of data for learning. The data should be consistent, within the same range, and not contain any noise. This includes the following steps:

a. Data Decomposition: Time-series data can be divided into systematic and non-systematic. The systematic data comprises of components from time-series data that are consistent and recurrent. Non-systematic data are components that are not consistent and considered as noise. The systematic components can be defined as follow:

1. Level: The average value of the series data.

2. Trend: Increasing or decreasing of data.
3. Seasonality: Repetitive patterns in the data.

Time-series data can be viewed as a level of components depending on the degree of consistency of the dataset. Splitting the data to components can be useful for better understanding of the problem during time forecasting.

b. Cleaning: Cleaning data from missing and noise values.

c. Normalization: Useful to normalize data to be within the same range, usually between -1 and 1. Two popular choices can be used: minmax scaler and standard scaler.

d. Data Transformation: There are different ways to transform data for processing, which depends on the problem domain. For time-series problem, the data should be re-framed as a supervised machine learning problem. This means that output from previous time step is transformed into an input for the next time step.

e. Data Split: Dividing data into two subsets, training and testing. Usually data is split into 80% training and 20% testing.

4. Features Engineering: This phase includes a processing of data to select most important features that influence the prediction results. In most machine learning applications, feature importance is an essential step which can be performed in numerous ways. For time-forecasting prediction problem, most of the previous works applied mathematical correlation to find a relationship between input and output variables [51, 24, 52, 53, 56]. When there are many features to be entered into the network for training, then finding the correlation between the target output value and these features will reduce complexity of training and enhance performance. The model can then be used with proper input features that can effect on the prediction.

Pearson correlation is the most popular method used to find correlation between two variables.

5. Ensemble Models Selection: This phase contains two main steps:

a. Determining the recurrent neural network models (LSTM, GRU, Bidirectional, etc) which will be used on ensemble design.

b. Hyperparameters Tuning by designing selected algorithms by setting different hyperparameters selection. This means that each algorithm will generate a different error where the correlation between the error values for all algorithms will be low enough to achieve generalization of the model.

6. Combining Models Prediction: The results from each model of ensemble algorithms will be combined using one of the combination ensemble techniques, as described previously, to generate the final prediction of the model.

The overall framework proposed in this paper is presented in Figure 5.

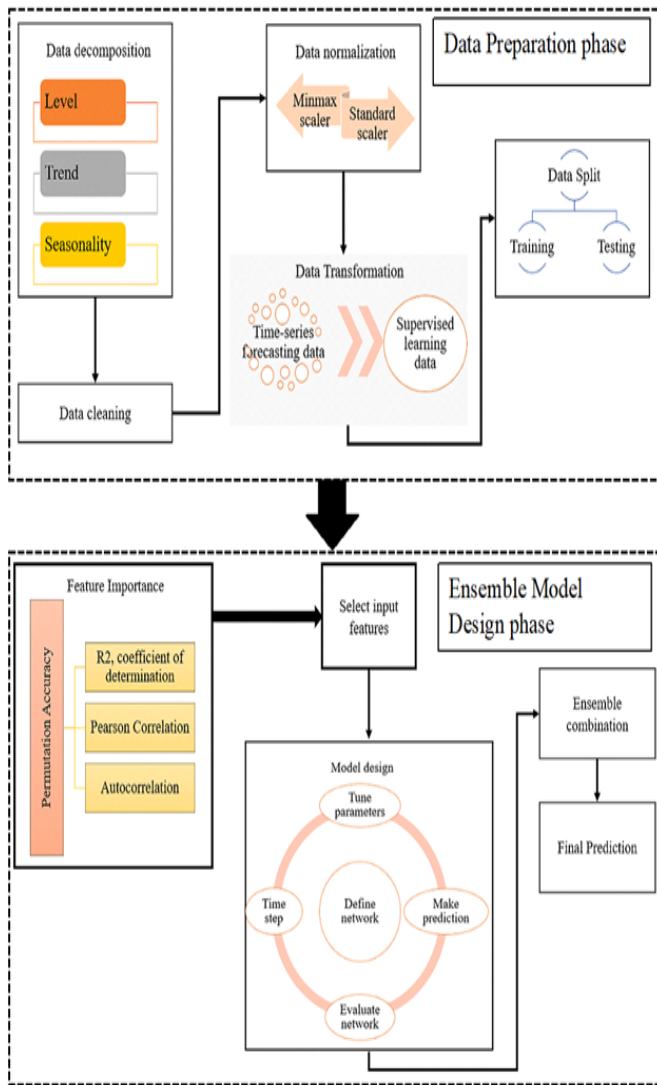


Figure 5: ensemble of recurrent neural network framework

## 6. Conclusions

This paper reviewed several studies that have been applied on recurrent neural network for time-series forecasting applications. The reviewed works give an idea of how to conduct a research for air pollution forecasting using optimization techniques of recurrent neural network and ensemble method. The proposed idea can be formulated on the framework which is divided into two main phases: Data preparation phase and Ensemble model design phase. The Data preparation phase is responsible on cleaning, normalizing and transforming data to a supervised form.

The output of this phase will generate a more consistent data with no noise, duplication and unrelated information. Having consistent training data will affect on the performance by increasing prediction accuracy. Ensemble model design phase includes the choosing of best recurrent neural network design after tuning each model with different parameters, ensemble method type and combination technique. It is recommended to use different subset of samples, different features for each model and tune each model with different parameters to achieve diversity.

The proposed model can be applied in most time-series forecasting applications. This paper focuses on the air pollution forecasting where ensemble method of recurrent neural networks could be suitable for pollution estimation.

## Conflict of Interest

The authors declare no conflict of interest.

## References

- [1] Lelieveld, J., Evans, J. S., Fnais, M., Giannadaki, D. & Pozzer, A. (2015). "The contribution of outdoor air pollution sources to premature mortality on a global scale". *Nature*
- [2] WHO Global Ambient Air Quality Database. <https://www.who.int/airpollution/data/en/>. Accessed:393 2019-08-17
- [3] Zheng, Y., Liu, F., Hsieh, H. (2013). "U-Air: when urban air quality inference meets big data". In: *Proceedings of the 19th ACM SIGKDD. International Conference on Knowledge Discovery and Data Mining*
- [4] Baklanov, A., Mestayer, P.G., Clappier, A., Zilitinkevich, S., Joffre, S., Mahura, A., Nielsen, N.W. (2008). "Towards improving the simulation of meteorological fields in urban areas through updated/advanced surface fluxes description". *Atmospheric Chemistry and Physics*
- [5] Kim, Y., Fu, J.S., Miller, T.L. (2010). "Improving ozone modeling in complex terrain at a fine grid resolution: Part I: examination of analysis nudging and all PBL schemes associated with LSMs in meteorological model". *Atmospheric Environment*
- [6] Jeong, J.I., Park, R.J., Woo, J., Han, Y., Yi, S. (2011). "Source contributions to carbonaceous aerosol concentrations in Korea". *Atmospheric Environment*
- [7] Vautard, R., Builtjes, P., Thunis, P., Cuvelier, C., Bedogni, M., Bessagnet, B., Honore, C., Moussiopoulos, N., Pirovano, G., Schaap, M. (2007). "Evaluation and intercomparison of Ozone and PM10 simulations by several chemistry transport models over four European cities within the CityDelta project". *Atmospheric Environment*
- [8] Stern, R., Builtjes, P., Schaap, M., Timmermans, R., Vautard, R., Hodzic, A., Memmesheimer, M., Feldmann, H., Renner, E., Wolke, R. (2008). "A model intercomparison study focussing on episodes with elevated PM10 concentrations". *Atmospheric Environment*
- [9] Lee, M.; Brauer, M.; Wong, P.; Tang, R.; Tsui, T. H.; Choi, C.; Chang, W.; Lai, P. C.; Tian, L.; Thach, T. Q.; Allen, R.; Barret, B. (2017). "Land use regression modeling of air pollution in high-density high-rise cities: A case study in Hong Kong". *Science of The Total Environment*
- [10] Nhung, N. T.; Amini, H.; Schindler, C.; Joss, M. K.; Dien, T. M.; ProbstHensch, N.; Perez, L.; Künzli, N. (2017). "Short-term association between ambient air pollution and pneumonia in children: A systematic review and meta-analysis of time-series and casecrossover studies". *Environmental Pollution*
- [11] Zafra, C.; Ángel, Y.; Torres, E. (2017). "ARIMA analysis of the effect of land surface coverage on PM10 concentrations in a high-altitude megacity". *Atmospheric Pollution Research*
- [12] Cannon, A. J.; Lord, E. R. (2008). "Forecasting summertime surface level ozone concentrations in the Lower Fraser Valley of British Columbia: An ensemble neural network approach". *Journal of the Air & Waste Management Association*
- [13] Zhao, X.; Zhang, R.; Wu, J. L.; Chang, P.C. (2018). "A deep recurrent neural network for air quality classification". *Journal of Information Hiding and Multimedia Signal Processing*
- [14] A. G. Salman, Y. Heryadi, E. Abdurahman, and W. Suparta, (2018). "Single layer & multi-layer long short-term memory (LSTM) model with intermediate variables for weather forecasting," *Procedia Comput. Sci.*
- [15] Y. Tsai, Y. Zeng, and Y. Chang, (2018). "Air pollution forecasting using RNN with LSTM," in *Proc. IEEE 16th Int. Conf. Dependable, Autonomic Secure Comput., 16th Int. Conf. Pervasive Intell. Comput., 4th Int. Conf. Big Data Intell. Comput. Cyber Sci. Technol. Congr. (DASC/PiCom/DataCom/CyberSciTech)*, Athens, Greece
- [16] Jae Young Choi and Bumshik Lee, (2018). "Combining LSTM Network Ensemble via Adaptive Weighting for Improved Time Series Forecasting", *Mathematical Problems in Engineering*

- [17] Yu, S.; Mathur, R.; Schere, K.; Kang, D.; Pleim, J.; Otte, T. (2007). "A detailed evaluation of the Eta-CMAQ forecast model performance for O<sub>3</sub>, its related precursors, and meteorological parameters during the 2004 ICARTT study". *J. Geophys. Res.*
- [18] Wang, Y.J.; Zhang, K.M. (2009). "Modeling near-road air quality using a computational fluid dynamics model", *CFD-VIT-RIT. Environ. Sci. Technol.*
- [19] Tong, Z.; Zhang, K.M. (2015). "The near-source impacts of diesel backup generators in urban environments". *Atmos. Environ.*
- [20] Tong, Z.; Baldauf, R.W.; Isakov, V.; Deshmukh, P.; Zhang, M.K. (2016). "Roadside vegetation barrier designs to mitigate near-road air pollution impacts". *Sci. Total Environ.*
- [21] Keddem, S.; Barg, F.K.; Glanz, K.; Jackson, T.; Green, S.; George, M. (2015). "Mapping the urban asthma experience: Using qualitative GIS to understand contextual factors affecting asthma control". *Soc. Sci. Med*
- [22] Chen, L.-J.; Ho, Y.-H.; Lee, H.-C.; Wu, H.-C.; Liu, H.-M.; Hsieh, H.-H.; Huang, Y.-T.; Lung, S.-C.C. (2017). "An Open Framework for Participatory PM<sub>2.5</sub> Monitoring in Smart Cities". *IEEE Access*
- [23] Jiangshe Zhang and Weifu Ding, (2017). "Prediction of Air Pollutants Concentration Based on an Extreme Learning Machine: The Case of Hong Kong", *Environmental Research and Public Health*
- [24] Xiang Li, Ling Peng, Xiaojing Yao, Shaolong Cui, Yuan Hu, Chengzeng You, Tianhe Chi, (2017). "Long short-term memory neural network for air pollutant concentration predictions: Method development and evaluation", *Environmental Pollution*
- [25] Li, C., Hsu, N.C., Tsay, S. (2011). "A study on the potential applications of satellite data in air quality monitoring and forecasting". *Atmos. Environ*
- [26] Box, G.E.P., Jenkins, G.M. (1976). "Time series analysis: forecasting and control". *J. Operational Res. Soc*
- [27] Nieto, P.G., Combarro, E.F., Del Coz Díaz, J.J., Montes, E. (2013). "A SVM-based regression model to study the air quality at local scale in Oviedo urban area (Northern Spain): a case study". *Appl. Math. Comput*
- [28] Hooyberghs, J., Mensink, C., Dumont, G., Fierens, F., Brasseur, O. (2005). "A neural network forecast for daily average PM<sub>10</sub> concentrations in Belgium". *Atmos. Environ*
- [29] Diaz-Robles, L.A., Ortega, J.C., Fu, J.S., Reed, G.D., Chow, J.C., Watson, J.G., MoncadaHerrera, J.A. (2008). "A hybrid ARIMA and artificial neural networks model to forecast particulate matter in urban areas: the case of Temuco, Chile". *Atmos. Environ*
- [30] Mishra, D., Goyal, P. (2016). "Neuro-fuzzy approach to forecast NO<sub>2</sub> pollutants addressed to air quality dispersion model over Delhi, India". *Aerosol Air Qual. Res*
- [31] Martha A. Zaidan I, Lubna Dada, Mansour A. Alghamdi, Hisham Al-Jeelani, Heikki Lihavainen, Antti Hyvärinen and Tareq Hussein, (2019). "Mutual Information Input Selector and Probabilistic Machine Learning Utilisation for Air Pollution Proxies", *Applied Sciences*
- [32] A. G. Salman, Y. Heryadi, E. Abdurahman, and W. Suparta, (2018). "Single layer & multi-layer long short-term memory (LSTM) model with intermediate variables for weather forecasting," *Procedia Comput. Sci.*, vol. 135, pp. 89–98
- [33] Y. Tsai, Y. Zeng, and Y. Chang, (2018). "Air pollution forecasting using RNN with LSTM," in *Proc. IEEE 16th Int. Conf. Dependable, Autonomic Secure Comput., 16th Int. Conf. Pervasive Intell. Comput., 4th Int. Conf. Big Data Intell. Comput. Cyber Sci. Technol. Congr. (DASC/PiCom/DataCom/CyberSciTech)*, Athens, Greece, pp. 1074–1079.
- [34] Yuelei Xiao and Yang Yin, (2019). "Hybrid LSTM Neural Network for Short-Term Traffic Flow Prediction", *information*
- [35] E. C. Eze, C.R Chatwin, (2019). "Enhanced Recurrent Neural Network for Short-term Wind Farm Power Output Prediction", *Journal of Applied Science*
- [35] Olah, C. (2018). "Understanding LSTM Networks". Available online: <http://colah.github.io/posts/2015-08-Understanding-LSTMs>
- [35] Graves, A.; Schmidhuber, J.; Koller, D.; Schuurmans, D.; Bengio, Y.; Bottou, L. (2009). "Offline Handwriting Recognition with Multidimensional Recurrent Neural Networks". In *Advances in Neural Information Processing Systems 21*; Curran Associates, Inc.: Dutchess County, NY, USA, pp.545–552.
- [36] Yang, Y.; Zhou, J.; Ai, J.; Bin, Y.; Hanjalic, A.; Shen, H.T.; Ji, Y. (2018). "Video Captioning by Adversarial LSTM". *IEEE Trans. Image Process.* 27, 5600–5611
- [37] Eck, D.; Schmidhuber, J. (2002). "Learning the Long-Term Structure of the Blues". In *Proceedings of the Artificial Neural Networks—ICANN 2002*, Madrid, Spain
- [38] Bengio, Y.; Simard, P.; Frasconi, P. (1994). "Learning long-term dependencies with gradient descent is difficult". *IEEE Trans. Neural Netw.* 5, 157–166
- [39] Hochreiter, S.; Schmidhuber, J. (1997). "Long short-term memory". *Neural Comput.* 9, 1735–1780.
- [40] Yan, S. "Understanding LSTM and Its Diagrams". Available online: <https://medium.com/mlreview/understanding-lstm-and-its-diagrams-37e2f46f1714>
- [41] Cho, K.; Van Merriënboer, B.; Gulcehre, C.; Bahdanau, D.; Bougares, F.; Schwenk, H.; Bengio, Y. (2014). "Learning Phrase Representations using RNN Encoder–Decoder for Statistical Machine Translation". In *Proceedings of the 2014 Conference on Empirical Methods in Natural Language Processing (EMNLP)*, Doha, Qatar
- [42] Chung, J.; Gulcehre, C.; Cho, K.; Bengio, Y. (2014). "Empirical evaluation of gated recurrent neural networks on sequence modelling". In *Proceedings of the NIPS 2014 Workshop on Deep Learning*, Montreal, QC, Canada
- [43] Raza H. A. et al., (2019) "Analysis the effect of 500kv High-Voltage Power Transmission Line on the Output Efficiency of Solar-Panels," in *2019 International Conference on Electrical, Communication, and Computer Engineering (ICECCE)*, pp. 1–6.
- [44] Graves, A.; Jaitly, N.; Mohamed, A. (2013). "Hybrid speech recognition with Deep Bidirectional LSTM". In *Proceedings of the 2013 IEEE Workshop on Automatic Speech Recognition and Understanding*, Olomouc, Czech Republic
- [45] Saleh Albelwi and Ausif Mahmood. (2017). "A framework for designing the architectures of deep convolutional neural networks". *Entropy*
- [46] Sean C Smithson, Guang Yang, Warren J Gross, and Brett H Meyer. (2016). "Neural networks designing neural networks: multi-objective hyperparameter optimization". In *Computer-Aided Design (ICCAD), 2016 IEEE/ACM International Conference on*, pages 1–8. *IEEE*
- [47] Nitish Srivastava, Geoffrey Hinton, Alex Krizhevsky, Ilya Sutskever, Ruslan Salakhutdinov, (2014). "Dropout: A Simple Way to Prevent Neural Networks from Overfitting", *Journal of Machine Learning Research* 15
- [48] Y. Lim, I. Aliyu and C. Lim, (2019). "Air Pollution Matter Prediction Using Recurrent Neural Networks with Sequential Data", *Conference paper*, DOI: 10.1145/3325773.3325788
- [49] Chiou-Jye Huang and Ping-Huan Kuo, (2018). "A Deep CNN-LSTM Model for Particulate Matter (PM<sub>2.5</sub>) Forecasting in Smart Cities", *sensors*
- [50] QING TAO, FANG LIU, YONG LI, AND DENIS SIDOROV, (2019). "Air Pollution Forecasting Using a Deep Learning Model Based on 1D Convnets and Bidirectional GRU", *IEEE Access*
- [51] Xiaotong Sun, Wei Xu, Hongxun Jiang, (2019). "Spatial-temporal Prediction of Air Quality based on Recurrent Neural Networks", *Proceedings of the 52nd Hawaii International Conference on System Sciences*
- [52] Athira V, Geetha P, Vinayakumar R, Soman K P, (2018). "DeepAirNet: Applying Recurrent Networks for Air Quality Prediction", *International Conference on Computational Intelligence and Data Science*
- [53] Thanongsak Xayasouk, Guang Yang, HwaMin Lee, (2019). "Fine Dust Predicting using Recurrent Neural Network with GRU". *International Journal of Innovative Technology and Exploring Engineering (IJITEE)*
- [54] Brian S. Freeman, Graham Taylor, Bahram Gharabaghi & Jesse Thé, (2018). "Forecasting air quality time series using deep learning", *Journal of the Air & Waste Management Association*
- [55] K Srinivasa Rao, Dr. G. Lavanya Devi, N. Ramesh, (2019). "Air Quality Prediction in Visakhapatnam with LSTM based Recurrent Neural Networks", *IJ. Intelligent Systems and Applications*
- [56] Xiaosong Zhao, Rui Zhang, Jheng-Long Wu and Pei-Chann Chang, (2018). "A Deep Recurrent Neural Network for Air Quality Classification", *Journal of Information Hiding and Multimedia Signal Processing*
- [57] Hamed Karimian, Qi Li2, Chunlin Wu, Yanlin Qi, Yuqin Mo, Gong Chen, Xianfeng Zhang and Sonali Sachdeva, (2019). "Evaluation of Different Machine Learning Approaches to Forecasting PM<sub>2.5</sub> Mass Concentrations", *Aerosol and Air Quality Research*
- [58] Widya Mas Septiawan and Sukmawati Nur Endah, (2018). "Suitable Recurrent Neural Network for Air Quality Prediction With Backpropagation



Through Time”, 2nd International Conference on Informatics and Computational Sciences

- [59] Zhou and Jiang, NeC4.5: (2004). “Neural Ensemble Based C4.5”. IEEE Transactions on Knowledge and Data Engineering, vol. 16, no. 6, pp. 770-773
- [60] Ahmed A. et al., (2019) “Modeling and Simulation of Office Desk Illumination Using ZEMAX,” in 2019 International Conference on Electrical, Communication, and Computer Engineering (ICECCE), pp. 1–6.
- [61] Kok Keng Tan, Nguyen Quoc Khanh Le , Hui-Yuan Yeh, and Matthew Chin Heng Chua, (2019). “Ensemble of Deep Recurrent Neural Networks for Identifying Enhancers via Dinucleotide Physicochemical Properties”, Cells
- [62] A.Peimankar,S.J.Weddell,T.Jalal,andA.C.Laphorn, “Evolutionary multi-objective fault diagnosis of power transformers,” Swarm and Evolutionary Computation, 2017. vol. 36, pp. 62–75.
- [63] R. Polikar, (2006). “Ensemble based systems in decision making,” IEEE Circuits and systems magazine, vol.6, no.3, pp. 21–45
- [64] A.Peimankar, S.J. Weddell, T.Jalal, and A .C. Laphorn, (2018). “Multi-objective ensemble forecasting with an application to power transformers,” Applied Soft Computing, vol. 68, pp. 233–248
- [65] S. Hochreiter and J. Schmidhuber, (1997). “Long short-term memory,” Neural Computation, vol. 9, no. 8, pp. 1735– 1780
- [66] K. Siwek and S.Osowski, (2012). “Improving the accuracy of prediction pf PM10 pollution by the wavelet transformation and an ensemble of neural predictors”, Engineering Applications of Artificial Intelligence
- [67] Abdolrahman Peimankar and Sadasivan Puthusserypady, (2019). “AN ENSEMBLE OF DEEP RECURRENT NEURAL NETWORKS FOR P-WAVED ETECTION IN ELECTROCARDIOGRAM”, ICASSP
- [68] Kok Keng Tan, Nguyen Quoc Khanh Le, Hui-Yuan Yeh and Matthew Chin Heng Chua, (2019). “Ensemble of Deep Recurrent Neural Networks for Identifying Enhancers via Dinucleotide Physicochemical Properties”, Cells
- [69] Lilin Cheng, Haixiang Zang , Tao Ding , Rong Sun , (2018). Miaomiao Wang, Zhinong Wei and Guoqiang Sun, “Ensemble Recurrent Neural Network Based Probabilistic Wind Speed Forecasting Approach”, Energies
- [70] Peng, T.; Zhou, J.Z.; Zhang, C.; Zheng, Y. (2017). “Multi-step ahead wind speed forecasting using a hybrid model based on two-stage decomposition technique and AdaBoost-extreme learning machine”. Energy Convers. Manag
- [71] Svetlana Borovkova and Ioannis Tsiamas, (2019). “An ensemble of LSTM neural networks for high-frequency stock market classification”, Wiley
- [72] Xie Qi, Cheng Gengguo, Xu Xu and Zhao Zixuan, (2018). “Research Based on Stock Predicting Model of Neural Networks Ensemble Learning”, MATEC Web of Conferences 232, 02029
- [73] Jae Young Choi and Bumshik Lee, (2018). “Combining LSTM Network Ensemble via Adaptive Weighting for Improved Time Series Forecasting”, Mathematical Problems in Engineering
- [74] de Souza, E. N., & Matwin, S. (2013). “Improvements to Boosting with Data Streams Advances in Artificial Intelligence” (pp. 248-255): Springer
- [75] Oza, N. (2001). Online Ensemble Learning. (PhD), University of California, Berkeley
- [76] Antonino A. Feitosa Neto, Anne M. P. Canuto and Teresa B Ludermir, (2013). “Using Good and Bad Diversity Measures in the design of Ensemble Systems: A Genetic Algorithm Approach”, IEEE Congress on Evolutionary Computation, pp. 789 – 796. IEEE
- [77] Lacoste, A., Laroche, H., Laviolette, F., & Marchand, M. (2014). “Sequential Model-Based Ensemble Optimization” arXiv preprint arXiv:1402.0796
- [78] R. E. Banfield, L. O. Hall, K. W. Bowyer and W. P. Kegelmeyer. (2002). “Ensemble Diversity Measures and Their Application to Thinning”, Information Fusion, vol. 6, no. 1, pp. 49-62, Elsevier B.V
- [79] Sylvester, J., Chawla, N. (2006). “Evolutionary Ensemble Creation and Thinning”, In: IJCNN 06 International Joint Conference on Neural Networks, pp. 51485155, IEEE.
- [80] Wang, S., & Yao, X. (2013). “Relationships Between Diversity of Classification Ensembles and Single-Class Performance Measures”, Knowledge and Data Engineering, IEEE Transactions on, vol. 25, No. 1, pp. 206219. IEEE.

# A Simple Modelling Tool for Fast Combined Simulation of Interconnections, Inter-Symbol Interference and Equalization in High-Speed Serial Interfaces for Chip-to-Chip Communications

Davide Menin<sup>\*1</sup>, Thomas Bernardi<sup>1</sup>, Alessio Cortiula<sup>1</sup>, Martino Dazzi<sup>1,2</sup>, Alessio De Pr<sup>1</sup>, Mattia Marcon<sup>1</sup>, Marco Scapol<sup>1</sup>, Andrea Bandiziol<sup>3</sup>, Francesco Brandonisio<sup>3</sup>, Andrea Cristofoli<sup>3</sup>, Werner Grollitsch<sup>3</sup>, Roberto Nonis<sup>3</sup>, Pierpaolo Palestri<sup>1</sup>

<sup>1</sup>University of Udine, Polytechnic Department of Engineering and Architecture, Via delle Scienze 206 33100 Udine, Italy

<sup>2</sup>Now with IBM Zurich, Switzerland

<sup>3</sup>Infineon Technologies Austria, 9500 Villach, Austria

---

## ARTICLE INFO

### Article history:

Received: 14 January, 2020

Accepted: 20 February, 2020

Online: 10 April, 2020

---

### Keywords:

Chip-to-chip communications

Modelling

Equalization

---

---

## ABSTRACT

We describe an efficient system-level simulator that, starting from the architecture of a well-specified transmissive medium (a channel modelled as single-ended or coupled differential microstrips plus cables) and including the system-level characteristics of transmitter and receiver (voltage swing, impedance, etc.), computes the eye diagram and the bit-error rate that is obtained in high-speed serial interfaces. Various equalization techniques are included, such as feed-forward equalization at the transmitter, continuous-time linear equalization and decision-feedback equalization at the receiver. The impact of clock and data jitter on the overall system performance can easily be taken into account and fully-adaptive equalization can be simulated without increasing the computational burden or the model's complexity.

---

## 1 Introduction

This paper extends the work presented at the 42<sup>nd</sup> International Conference on Information and Communication Technology, Electronics and Microelectronics (MIPRO 2019) [1] and describes a simple and efficient tool for fast system-level simulation of high-speed serial interfaces, a topic that has received much attention in the past two decades due to its relevance in modern electronic systems: As the miniaturization of CMOS integrated circuits (IC) keeps following the path described by Moore's law [2], the amount of components integrated onto single devices, the number of functionalities available on single ICs and their speed increases significantly every few years. Over the last decades, evidence has arisen that the major bottleneck in performance shifted from computational capabilities and the associated power consumption towards communication between different ICs [3]. In fact, many applications such as modern microprocessors, servers, micro-controllers, FPGAs, even portable devices and, recently, automotive systems require High-Speed I/O (HSIO) modules capable of handling data rates up to 128 Gb/s with energies per bit as low as 1 pJ [4–9]. Moreover, as in many appli-

cations chip area and pin availability pose strict design constraints, the aforementioned devices cannot support parallel I/O that would reduce the data rate of individual channels, implying that such communications need to be implemented as high-speed serial interfaces (HSSI). In the present paper, the terms HSIO and HSSI will be used interchangeably to denote high-speed serial communication devices.

At multi-Gb/s data rates, performances are highly affected by impedance discontinuities in the interconnections due to PCB characteristics, presence of vias and package features; non-perfect impedance matching due to fabrication imperfections or poor compatibility for different devices; and by the dispersive nature of the transmissive medium at high frequencies [4, 10]. All these phenomena concur in causing Inter-Symbol Interference (ISI), which manifests itself as a smoothing and widening of the pulses sent along the channel so that they are superimposed to other symbols transmitted in the neighbouring unit intervals (UIs), thus increasing the Bit-Error Rate (BER) at the receiver, dramatically impairing the quality of the transmission [4, 10, 11].

In order to cope with this, HSIOs are required to implement complex equalization strategies, both at the transmitter or at the receiver,

---

\*Davide Menin, Via delle Scienze 206, 33100 Udine (Italy), menin.davide@spes.uniud.it

and in the analog, mixed-signal or digital domains [10, 12–15]. Such techniques include Feed-Forward Equalization (FFE) at the transmitter, Continuous-Time Linear Equalization (CTLE) and Decision-Feedback Equalization at the receiver [10]. FFE uses an FIR filter that applies a pre-distortion to the transmitted pulses in order to preemptively compensate for the channel distortion; CTLE comprises a peaking amplifier mainly employed to compensate for the high frequency attenuation of the channel and possibly provide additional gain control at low frequency; in DFE the history of recent received bits is stored into a shift register and used to correct the received analog signal in order to cancel ISI at the input of the slicer, either through FIR or IIR filters.

One of the main challenges in the design and implementation of such equalization techniques is the fact that HSIOs are supposed to operate on a variety of channels whose features are unknown at design time. Thus, the optimal parameters of the equalizers cannot be precisely known and set a priori during the design phase, unless the resulting suboptimal performance can be tolerated, when it does not completely impede communication. Even in such rare cases where the transmissive medium is well known, the design itself is intrinsically dependent on process, voltage and temperature (PVT) variations and technology corners, all of which need to be counteracted by the equalizers. Therefore, calibration and adaptation strategies are required in order to find the optimal equalization parameters for the actual channel [13, 15–17]. Full adaptation automatically performs such a task, and is usually implemented in the form of Sign-Sign Least-Mean Squares (SS-LMS) algorithms due to the short time required to adjust the equalization parameters and the simplicity of their realization [11, 12, 15, 16, 18–21].

Moreover, HSIOs are also equipped with algorithms for clock and data recovery (CDR), and even performance monitoring, hence making up very complex electronic systems [12, 22]. Such a complexity cannot be conveniently handled through transistor-level descriptions because of the extremely long simulation times that they require. Therefore, various system-level models have been proposed in the last decades to aid the design of HSSIs, mainly using statistical techniques [19, 23–26]. Such tools are very important for the initial system-level assessment in the design of chip-to-chip HSIOs for selecting design specifications such as the number of equalization taps, the amount of high-frequency content that needs to be equalized, evaluating the Signal-to-Noise Ratio (SNR) and the overall jitter that can be tolerated without degrading the BER.

The design and analysis of HSIOs comprising a variety of complex equalization techniques require efficient system-level models capable of producing fast and accurate predictions of the system behaviour. Extending the work presented in [1] and relating it with contributions from [19, 27], this paper shows how fast system-level simulations of high-speed serial interfaces can be performed with a simple modular model. The paper proceeds as follows: Section 2, starting from the architecture of a generic HSSI, describes the numerical model, how it evaluates performance accounting for jitter and how fully-adaptive equalization is computed; Section 3 shows some sample simulation results and comparisons with post-layout transistor-level simulations, demonstrating the capabilities of the proposed approach; finally, conclusions are drawn in Section 4.

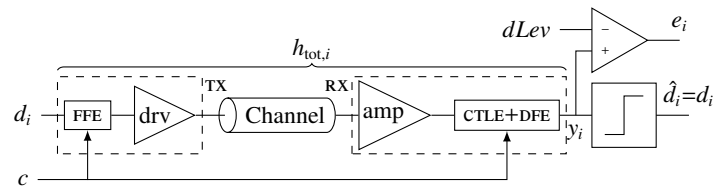


Figure 1: Scheme of a generic high-speed serial interface with equalization:  $h_{tot,i}$  is the overall pulse response of the TX (FFE+driver) + channel + RX (amplifier+CTLE+DFE) system;  $c$  is a generic equalization parameter (e.g. a filter tap), which may be either statically set or automatically adapted [19].

## 2 Model Description

### 2.1 Architecture of the Transceiver

In order to accurately model the system performance of a generic HSIO device, the general model depicted in Figure 1 and extensively described in [19] is considered: Denoting by the subscript  $i$  the sampling instant  $t_b = iT_B$  (where  $T_B$  corresponds to a bit period, i.e. one Unit Interval UI), the data sequence  $d_i$  is sent by the differential transmitter TX at a bitrate  $f_b = 1/T_B$ , optionally implementing FFE; the channel, whose sampled pulse response is  $h_{ch,i}$ , can be modelled either as two independent single-ended lines or as a coupled differential line; the receiver RX contains an amplifier, a CTLE and a DFE, and produces the analog voltage  $y_i$ ; the slicer makes decisions on such a voltage ( $\hat{d}_i = \text{sign}(y_i)$ , i.e.  $\hat{d}_i = 1$  if  $y_i > 0$  V and  $-1$  otherwise) and its sampling point can be modified with respect to the one determined by the CDR in order to perform optimal sampling [12, 19]; moreover, when performing full adaptation, the analog voltage  $y_i$  is compared with a reference voltage  $dLev$  [15] to determine the error  $e_i$  (i.e. the distance of the actual sample to  $dLev$ , usually defined as the desired voltage level corresponding to a '1' bit), and use this information to perform adaptation. Assuming that the BER is small (either because the channel has low loss or because it is well equalized), the reconstructed data  $\hat{d}_i$  is equal to the transmitted data  $d_i$ .

### 2.2 Numerical Model of the Transceiver

The numerical model implemented in Matlab exploits a fast approach for the modelling of ISI and equalization in HSIOs, the flowchart of which is here summarised in Figure 2 and detailed in the following paragraphs.

#### 2.2.1 Transmitter

The idealised transmitted waveform is modelled as the trapezoidal pulse  $v_{\text{pulse}}(t)$ , shown in Figure 3a and characterised by its duration, amplitude and by the slope of its edges (rise and fall times  $t_{\text{rise}} = t_{\text{fall}}$ ); such a waveform is easily Fourier-transformed, giving  $V_{\text{pulse}}(f)$ , to which FFE is applied by summing weighted delayed versions of the transformed pulse itself:

$$V_{\text{TX}}(f) = V_{\text{pulse}}(f) \sum_{n=0}^{N_{\text{FFE}}-1} w_n e^{-i\omega n T_b}, \quad (1)$$

where  $w_n$  are the weights of the  $N_{\text{FFE}}$  FFE taps, subject to the constraint  $\sum_{n=0}^{N_{\text{FFE}}-1} |w_n| = 1$  due to the fact that the power available in the

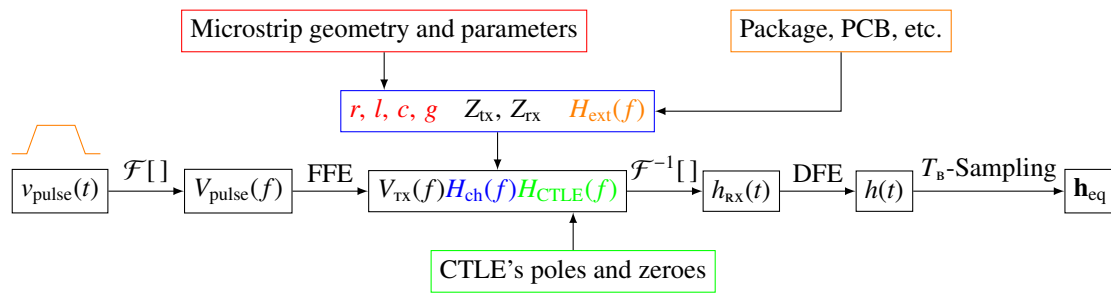


Figure 2: Diagram of the procedure implemented to obtain the received pulse response [1].  $\mathcal{F}$  and  $\mathcal{F}^{-1}$  stand for the Fourier and the inverse Fourier transforms, respectively.

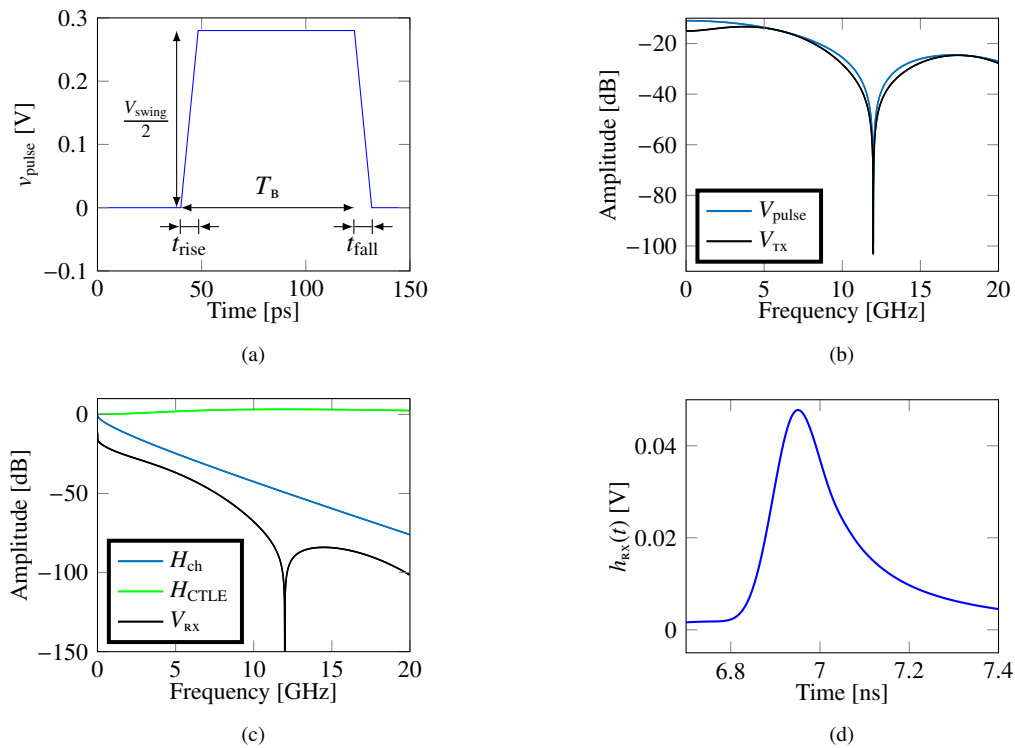


Figure 3: Example based on a PCIe 4.0 channel attenuating 20 dB at 6GHz, showing the waveforms elaborated by the fast modelling tool according to the flow of Figure 2 [1, 19]. (a) shows the transmitted trapezoidal pulse  $v_{pulse}(t)$ ; (b) reports the corresponding Fourier transform prior to ( $V_{pulse}(f)$ ) and after application of FFE ( $V_{tx}(f)$ ); (c) shows  $H_{ch}(f)$ ,  $H_{CTLE}(f)$ , and the result of their multiplication with  $V_{tx}(f)$ ; (d) shows the subsequent inverse Fourier transform prior to DFE  $h_{rx}(t)$ , the application principle of which is shown in Figure 5.

driver is limited. The effect of such an operation is shown in the frequency domain in Figure 3b.

The proposed approach considers a transmitter’s impedance which is kept constant and does not change at high or low outputs, as is the case in Input-Output Buffer Information Specification (IBIS) models [28, 29]. Moreover, the pulse shape used in the proposed method (trapezoidal shape with  $t_{rise} = t_{fall}$ ) is chosen in order to exploit the channel’s linearity and hence use the channel’s pulse response in the various computations instead of its step response [26]; in other words, a sequence of pulses  $v_{pulse}(t)$  having the same amplitude results in a constant voltage level, which is not the case with other pulse shapes, see [30].

### 2.2.2 Communication Channel

The transmissive medium is generally modelled as a differential line, made up either of two independent microstrips (to simulate

lines placed at some distance from each other as to minimise interactions) or a single coupled microstrip excited with an odd mode (to realistically reproduce differential signalling). This is then used to reproduce the salient features of any other type of transmission line, such as the target attenuation at a certain frequency or its characteristics impedance.

The microstrip features are computed from the line’s geometry and material parameters following the approach defined in [31–36] for single-ended lossy microstrips, or extended to the coupled case according to [37, 38], and then used to extract its per-unit-length parameters  $r(f)$ ,  $l(f)$ ,  $c(f)$ ,  $g(f)$  considering dielectric losses and skin effect, all of which are among the main contributors to ISI [4].

Such a result can then be combined with  $H_{ext}(f)$ , a transfer function representing the socket or package and incorporating notch filters, which can be used to take into account discontinuities, vias, etc. in order to provide a complete description of realistic channels.



$H_{\text{ext}}(f)$  can be calculated with a model of the package, e.g. in terms of parasitic resistance, inductance and capacitance, which allows a straightforward evaluation of its transfer function in terms of poles and zeroes, while the contributions due to impedance discontinuities or vias can be taken into account by fitting the features of actual measurements of the transmission line's  $S$  parameters to the transfer function of notch filters in the form

$$H_{\text{notch}}(f) = \frac{1 + 2\xi(if)/f_0 + (if)^2/f_0^2}{1 + 2(1 - \xi)(if)/f_0 + (if)^2/f_0^2}, \quad (2)$$

where  $\xi$  is the filter's damping factor and  $f_0$  is its notch frequency.

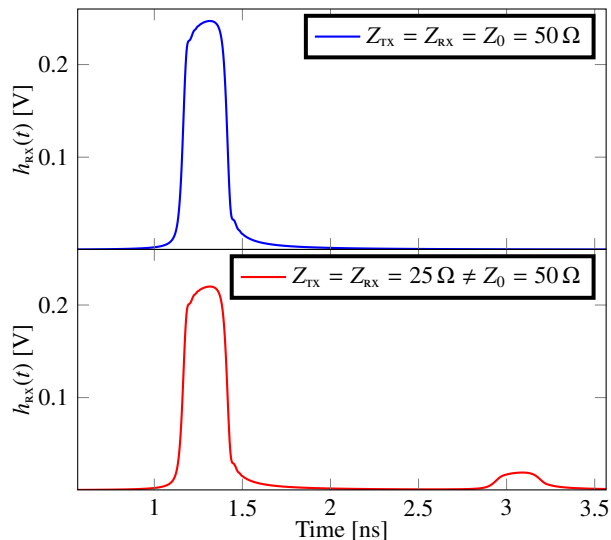


Figure 4: Effect of mismatch on the received pulse response: On top,  $Z_{\text{TX}} = Z_{\text{RX}} = Z_0 = 50 \Omega$ ; below,  $Z_{\text{TX}} = Z_{\text{RX}} = 25 \Omega$ ,  $Z_0 = 50 \Omega$ , showing reflections due to such a mismatch. Transmission at 4 Gb/s over a low-loss channel (approximately  $-3$  dB at Nyquist frequency).

Using as additional parameters the driver's and the receiver's termination impedances ( $Z_{\text{TX}}$  and  $Z_{\text{RX}}$ , respectively), the transmission line transfer function is computed from the telegrapher's equations as

$$H_{\text{ch}}(f) = \frac{e^{-\gamma L}(1 + \Gamma_{\text{RX}})(1 - \Gamma_{\text{TX}})}{1 - \Gamma_{\text{TX}}\Gamma_{\text{RX}}e^{-2\gamma L}} H_{\text{ext}}(f), \quad (3)$$

where  $\gamma = \sqrt{(r + i\omega l)(g + i\omega c)}$  is the propagation coefficient,  $L$  is the line length and  $\Gamma_{\text{TX/RX}} = \frac{Z_{\text{TX/RX}} - Z_0(f)}{Z_{\text{TX/RX}} + Z_0(f)}$  are the reflection coefficients corresponding to the transmitter and the receiver. Note that, due to the inclusion of  $Z_{\text{TX/RX}}$ , (3) takes into account possible non-perfect matching among driver, transmission line and receiver, which is shown as an example in Figure 4: The mismatch produces a reflection that contributes to ISI.

### 2.2.3 Receiver

The CTLE is modelled as a rational function  $H_{\text{CTLE}}(f)$  characterised by the CTLE's poles and zeroes; optionally, an extraction of the CTLE's transfer function from simulations of the transistor-level HSIO can be used to reproduce more accurately a realistic implementation (and the frequency response of other analog blocks in the receiver can be similarly taken into account). The received

signal associated to the transmitted trapezoidal pulse has spectrum  $V_{\text{RX}}(f) \triangleq V_{\text{TX}}(f)H_{\text{ch}}(f)H_{\text{CTLE}}(f)$ ; an example of this is shown in Figure 3c with some of its sub-components.

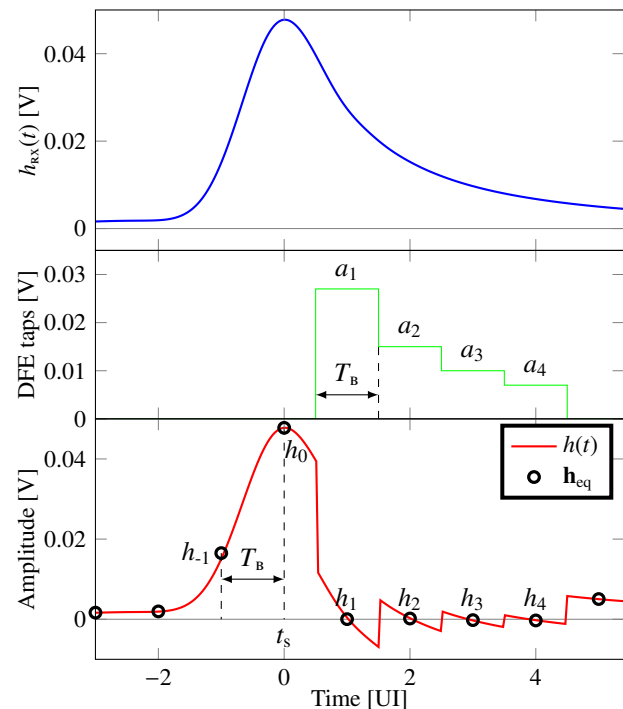


Figure 5: Procedure used by the model to apply the DFE correction to the received analog pulse response  $h_{\text{RX}}(t)$  to obtain  $h(t)$  and eventually its sampled version  $\mathbf{h}_{\text{eq}}$ . The DFE taps are rectangular pulses 1 UI wide and centred on the sampling point determined by the CDR.

The received pulse response  $h(t)$  at the slicer's input is then obtained through inverse Fourier transform of  $V_{\text{RX}}(f)$  using the procedure in [39], yielding  $h_{\text{RX}}(t)$  (an example of  $h_{\text{RX}}(t)$  is shown in Figure 3d). Application of the DFE correction is performed as shown in Figure 5, i.e. by subtracting from  $h_{\text{RX}}(t)$  rectangular pulses with amplitude equal to the tap weights  $a_i$  and centred on the sampling point determined by the CDR.

The procedure above implicitly assumes that the CDR has reached its steady state and is locked. Its impact on the behaviour of the HSSI is twofold: It determines the sampling point for data, error and edge samples (which is related to the position of the "rectangles" associated to the DFE, as mentioned above), while the jitter at its output is responsible for a reduction of BER (as will be explained in Section 2.4). For what the sampling point is concerned, we can simply assume that the data samples correspond to the maximum of the pulse response  $h(t)$ ; alternatively, an Alexander CDR [40] can be emulated by determining the time instants corresponding to  $h_{\text{RX},-0.5}$  and  $h_{\text{RX},0.5}$  (which are the positions of the edge samples of the CDR in a real implementation [27]) and then assume that the data sample is exactly in between. On top of it, an algorithm for optimal sampling point may be used to determine a shift from the output of the CDR, which results in an improved sampling position [12, 19]. Any of the above can be selected and all of them aim at sampling as close to the centre of the eye as possible in order to reduce the probability of error.

Sampling by the bit period  $T_b$  is eventually performed in order to

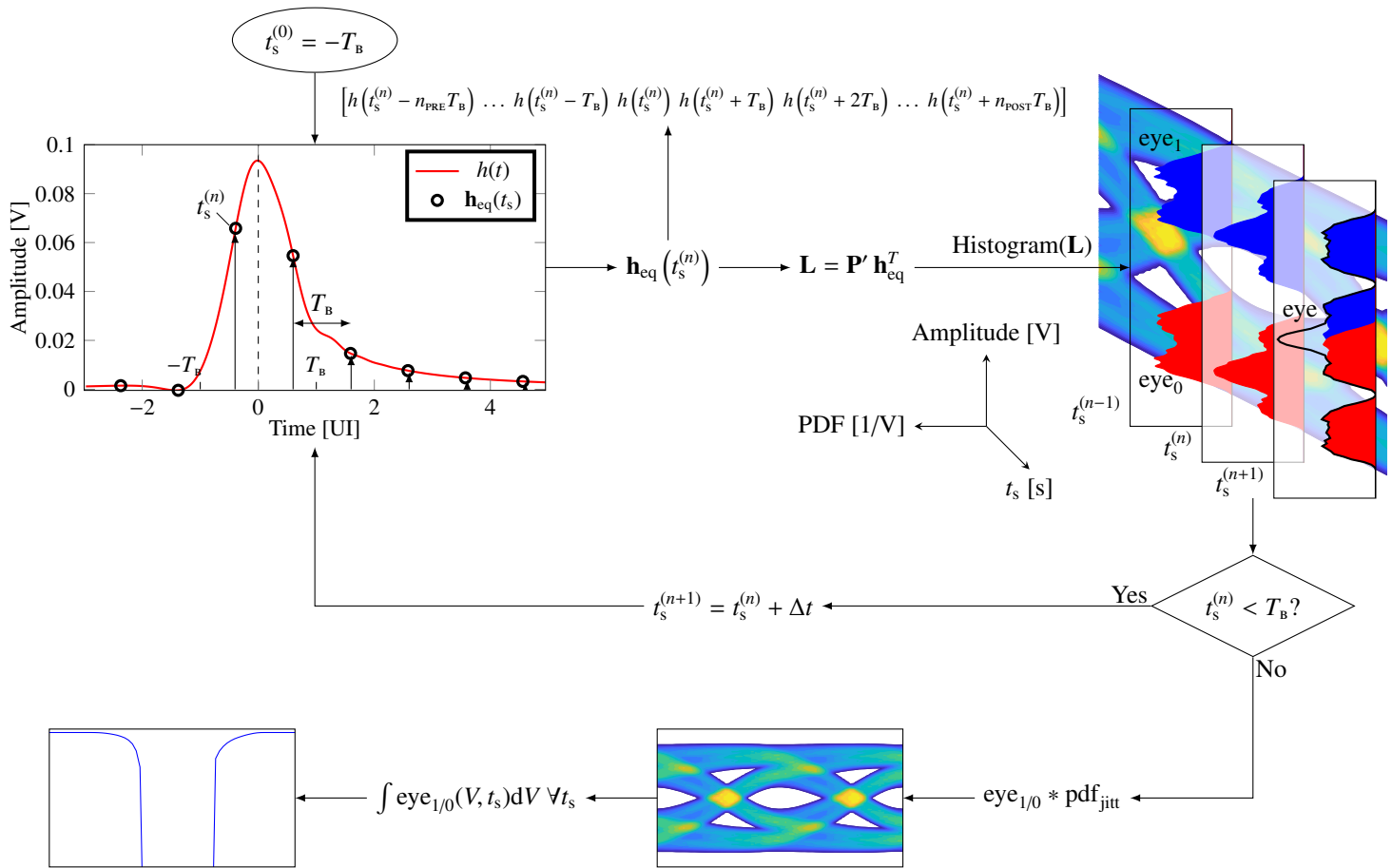


Figure 6: Diagram of the procedure used to evaluate the HSSI performance in terms of eye diagram and bathtub plot, as explained in Section 2.3. All plots and diagrams are obtained by transmitting at 12 Gb/s over a channel losing 14.3 dB at Nyquist frequency, with the FFE applying a de-emphasis of  $-2.5$  dB; no DFE is applied for the sake of demonstrating the working principle of the proposed method. From an initial sampling point  $t_s^{(0)} = -T_B$ , at each iteration  $n_{PRE} + n_{POST} + 1$   $T_B$ -spaced samples of  $h(t)$  are taken to form  $\mathbf{h}_{eq}(t_s^{(n)})$ ; at each sampling point, histograms of  $\mathbf{L}$  are computed to determine the corresponding PDFs, represented in the drawing at the top right as cross sections of the eye diagram; the procedure is repeated until  $t_s$  reaches  $T_B$  and then the eye diagram and bathtub plot are computed taking into account jitter at the receiver.

obtain the analog voltages (vector  $\mathbf{h}_{eq} = [h_{-n_{PRE}} \dots h_{-1} h_0 h_1 \dots h_{n_{POST}}]$ ) that would be sensed at the input of the slicer at sampling time.

### 2.3 Evaluating the HSSI Performance

Performances of the transceiver are determined mainly by computing the eye diagram, constructed by folding the received signal over a time length of 1 UI, which allows to observe all the transitions that take place during operation of the serial link and their density; and by calculating the bathtub plot, which shows the cumulative distribution function of the received errors over the same time span of the eye diagram, indicating the sampling positions that result in an increased BER [4]. Both such metrics require probabilistic calculations in order to maintain computation times low [19, 23].

From the sampled pulse response  $\mathbf{h}_{eq}$  one can compute all possible values of the voltage  $y_i$  at the samplers, due to all the possible sequences of bits that can be sent, as

$$\mathbf{L} = \mathbf{P} \mathbf{h}_{eq}^T, \quad (4)$$

where  $\mathbf{L}$  is a column vector containing such voltage levels and  $\mathbf{P}$  is a permutation matrix which contains all the possible bit sequences of a certain length that can be transmitted. In fact,  $\mathbf{P}$  is structured as a

truth table: It features a number of columns equal to  $n_{PRE} + 1 + n_{POST}$ , where  $n_{PRE}$  and  $n_{POST}$  are the number of pre- and post-cursors, respectively, which can be chosen according to their relevance in the pulse response; while the number of rows is  $2^{n_{PRE} + 1 + n_{POST}}$ , i.e. the number of all possible sequences composed of  $n_{PRE} + 1 + n_{POST}$  bits. In other words,  $\mathbf{L}$  considers all the possible ways in which the samples of the pulse response can combine due to ISI, hence simulating observation of the received analog voltage  $y_i$  over a sufficiently long time span. Moreover,  $\mathbf{L}$  implicitly depends on the choice of the sampling instant  $t_s$  through the sampled pulse response  $\mathbf{h}_{eq}$ .

$$\mathbf{P}' = \begin{pmatrix} -1 & 1 & -1 & -1 \\ -1 & 1 & -1 & 1 \\ -1 & 1 & 1 & -1 \\ -1 & 1 & 1 & 1 \\ 1 & 1 & -1 & -1 \\ 1 & 1 & -1 & 1 \\ 1 & 1 & 1 & -1 \\ 1 & 1 & 1 & 1 \end{pmatrix}. \quad (5)$$

By assuming that the eye is vertically symmetric (the transceiver behaviour when transmitting a '1' bit is the same as though a '0' was sent, just with a sign reversal), only the cases in which  $\hat{d} = 1$

are useful for the purpose of computing the HSIO performance. By coding the '1' and '0' bits as 1 and -1 values, respectively, and keeping only the non-redundant rows, e.g. for one pre- and two post-cursors such a reduced matrix (denoted by  $\tilde{\mathbf{L}}$ ) reads

Equation (4) provides an easy way to compute the eye diagram and the bathtub plot. The eye diagram can be computed by sampling  $h(t)$  at various  $t = t_s \in [-T_b/2, T_b/2]$ , where  $T_b$  is the bit period (1 UI), and creating histograms  $\text{eye}_1(V, t_s)$  of the corresponding  $\mathbf{L}(t_s)$ ; due to the fact that the eye for the '0' bit is just the flipped version of the one for the '1' bit (as follows from the assumption of symmetry), they can be combined to obtain the overall eye diagram

$$\text{eye}(V, t_s) = \frac{\text{eye}_1(V, t_s) + \text{eye}_1(-V, t_s)}{2}. \quad (6)$$

The bathtub plot, i.e. the BER corresponding to a voltage threshold equal to 0 V as a function of the sampling instant  $t_s$ , is then given by the probability that a '1' bit is misinterpreted for a '0' (that is the same as the probability that a '0' bit is misinterpreted for a '1', due to the above assumption of symmetry):

$$\text{BER}(t_s) = \int_{-\infty}^0 \text{eye}_1(V, t_s) dV. \quad (7)$$

The overall procedure for computing the eye diagram and the bathtub plot is shown in Figure 6, summarising the flow described in this Section and in the following.

### 2.4 Including the Effect of Jitter

The effect of jitter on the receiver can be optionally taken into account by simply convolving the single  $\text{eye}_{1/0}$  of (6) and the probability density function of sampling time  $t_s$  corresponding to the jitter component of interest  $\text{pdf}_x(t_s)$  [41]. As an example, considering an oscillator in the receiver affected by random jitter, the period jitter of which has variance  $\sigma_{\text{PJ}}$  (in other words, a clock with phase noise going as  $1/f^2$ , which means that the jitter values in different periods are uncorrelated) and a CDR having a bandwidth  $BW_{\text{CDR}}$ , the squared variance of the absolute jitter present in the recovered clock can be easily shown to be given by

$$\sigma_{\text{RJ}}^2 = \frac{\sigma_{\text{PJ}}^2}{4\pi T_b BW_{\text{CDR}}}. \quad (8)$$

The simple example shown in Figure 7 assumes a jitter characterised by a Gaussian distribution described as

$$\text{pdf}_G(t_s) = \frac{1}{\sqrt{2\pi}\sigma_{\text{RJ}}} e^{-\frac{1}{2}\left(\frac{t_s}{\sigma_{\text{RJ}}}\right)^2}, \quad (9)$$

where  $\sigma_{\text{RJ}}$  is the variance of the random jitter affecting the recovered clock as per (8), which in general may include other sources than random jitter of the clock alone.

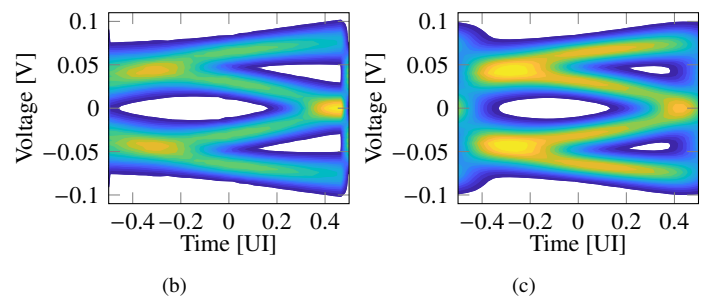
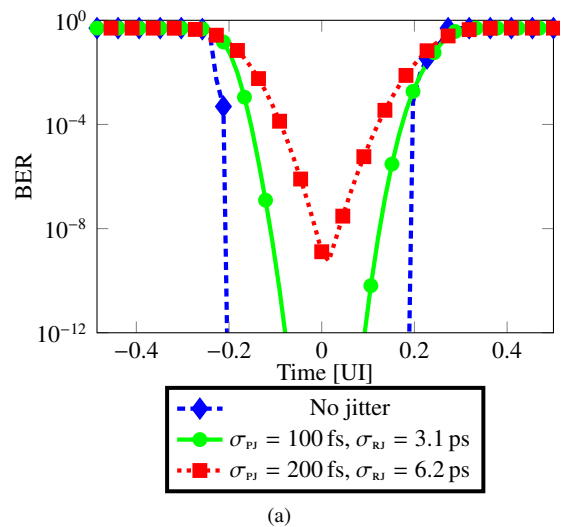


Figure 7: PCIe 4.0 channel attenuating 20 dB at 6 GHz; approximately 4 dB of FFE de-emphasis, first 4 post-cursors cancelled by the DFE. The random jitter applied at the receiver's recovered clock is calculated according to (8) assuming a CDR bandwidth  $BW_{\text{CDR}} = 1$  MHz. (a) BER bathtub plots; eye diagrams with (b) no random jitter and (c)  $\sigma_{\text{RJ}} = 6.2$  ps random jitter on the recovered clock.

### 2.5 Including Fully-Adaptive Equalization

As briefly mentioned in the Introduction, the problem concerning the optimal settings of the equalizers' parameters is not trivial, and often one must resort to full adaptation in order to automatically find optimal equalization parameters. The implementation of fully-adaptive techniques based on an SS-LMS algorithm in the simulation approach described in this paper is relatively straightforward and was thoroughly described in [19]: Briefly, it involves computing quantities in the form

$$c^{(k+1)} = c^{(k)} + \mu_c \text{sign}(\hat{d}_i) \text{sign}(e_j), \quad (10)$$

where  $\mu_c$  is the step size,  $\hat{d}$  is the data sample received at time  $i$ ,  $e_j$  is the error at time  $j = i + k$  between the analog voltage  $y_j$  at the samplers and the desired voltage  $dLev$  corresponding to a '1' bit and  $c^{(k)}$  is the  $k$ -th iteration on a generic parameter that can be adapted (the taps amplitude of FFE or DFE, the positions of poles and zeroes in a CTLE modelled e.g. as  $H_{\text{CTLE}}(s) = c_0 + c_1 s$ , the sampling phase as well as  $dLev$  itself). Note that  $\text{sign}(\hat{d}_i) \text{sign}(e_j)$  corresponds to correlating the error made at a certain time with the bit received at possibly another time in the past or in the future, where obviously the latter can be considered only when data and errors are parallelized before computation of the fully-adaptive algorithm [8, 17, 27, 42–44]. Such correlations provide information

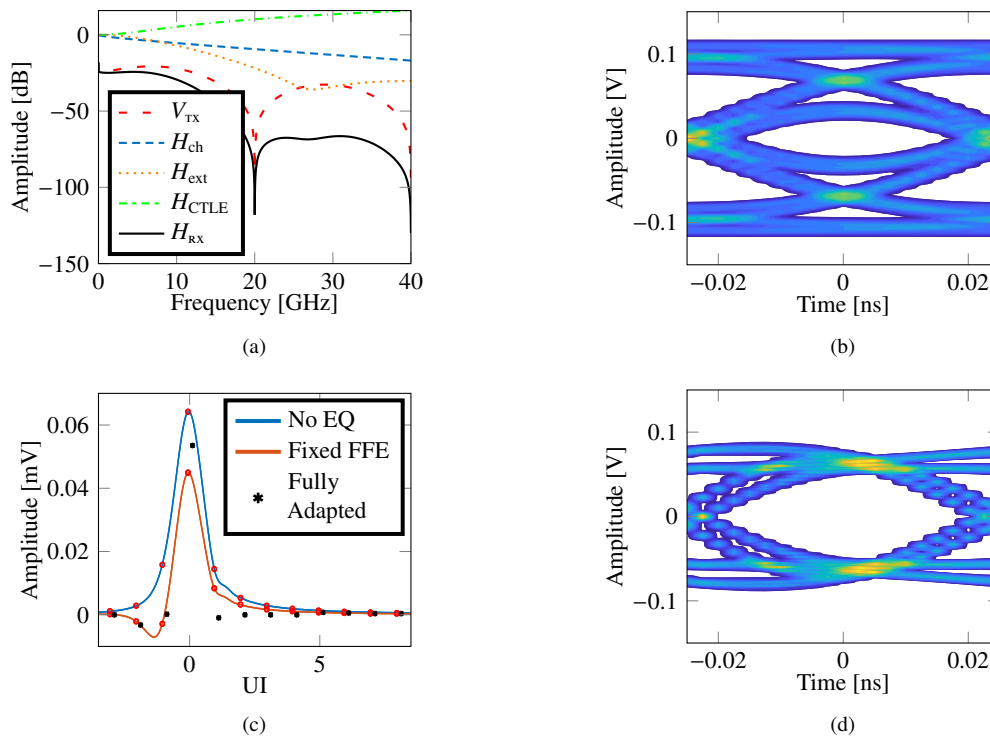


Figure 8: Simulation of a channel with 12 dB attenuation at 10 GHz and fixed 2-tap FFE. All the relevant Fourier transforms of signals and transfer functions of the transceiver are plotted in (a); the eye diagram prior to equalization is shown in (b); (c) shows the pulse response prior to equalization (solid blue line), after the fixed FFE (solid orange line) and after application of the fully-adaptive loop (Figure 10) and subsequent sampling (black asterisks); (d) shows the resulting equalised eye diagram.

on whether to increase or decrease the corresponding parameter  $c$  and bring it to convergence, and are usually collected and averaged over time [12, 27]. Such a correlation can be easily evaluated from  $\mathbf{h}_{eq}$  by multiplication with a matrix similar to  $\mathbf{P}'$  of (5) (further mathematical details are given in [19]).

By applying equalization to the pulse response of the transceiver plus channel, as mentioned in Section 2.2, iteration of (4) and Equation 10 provides the evolution over time of the adaptation procedure until the equalization parameters converge in the neighbourhood of the optimum [19].

### 3 Results

As an example of the power and versatility of the proposed approach, we consider here the fully-adaptive equalization of an HSIO transmitting at 20 Gb/s with rise/fall times equal to 20 % of the UI and  $\pm 0.25$  V differential voltage swing on a channel attenuating 12 dB at 10 GHz. A fixed 2-tap FFE with a pre-emphasis of approximately 6 dB ( $w_{-1} = -0.25$ ,  $w_0 = 0.75$ ) was applied at transmit side to reduce the first pre-cursor. The package was described by an LC  $\pi$ -network with  $L = 2$  nH and  $C = 100$  fF, while an impedance discontinuity was modelled by adding a notch filter with  $\xi = 0.1$  centred at  $f_0 = 27$  GHz; both features were included through the function  $H_{ext}(f)$  mentioned in Section 2.2.2. Figure 10 shows the resulting simultaneous adaptation of  $dLev$ , CTLE's zeroes, DFE taps and sampling phase as a function of the number of iterations performed by the fully-adaptive algorithm described above. As expected,  $dLev$  converges to the average value corresponding to

the '1' bit (i.e. the peak value of  $h(t)$ :  $h_0$ ) and, as it approaches such a value, the other equalization parameters start to adapt and eventually converge: The DFE taps reach the values of the corresponding post-cursors ( $h_1$ ,  $h_2$  and  $h_3$ ), while the phase is shifted w.r.t. the position determined by the CDR to a value that zeroes the first pre-cursor. Frequency representations of all relevant signals and transfer functions of the transceiver are plotted in Figure 8a, the unequalised eye diagram is depicted in Figure 8b, the channel pulse response is shown in Figure 8c prior to equalization, after the fixed FFE and after full adaptation, a situation to which corresponds the eye diagram of Figure 8d.

In order to validate the proposed numerical model, a comparison was carried out in [27] between the eye diagram obtained with the model itself and that obtained through post-layout transistor-level simulations. An HSSI for automotive applications implemented in 28 nm planar CMOS technology was simulated at 12 Gb/s at transistor level with full adaptation enabled; the numerical model was then used as a comparison in terms of performance and behaviour of the SS-LMS adaptive algorithm when the HSIO was used to communicate over a realistic, high-loss channel ( $-33$  dB at 6 GHz) representing a transmission line as will likely be defined by the MIPI A-PHY standard. The results of Figure 9 show a good degree of accuracy in reproducing the transistor-level simulations when relevant features of the post-layout transistor-level implementation (chiefly, the transfer functions of the CTLE and of the Variable-Gain Amplifiers in the receiver) were extracted and used in the tool, as explained in Section 2.2.3.

As a means of comparison, in order to observe convergence of



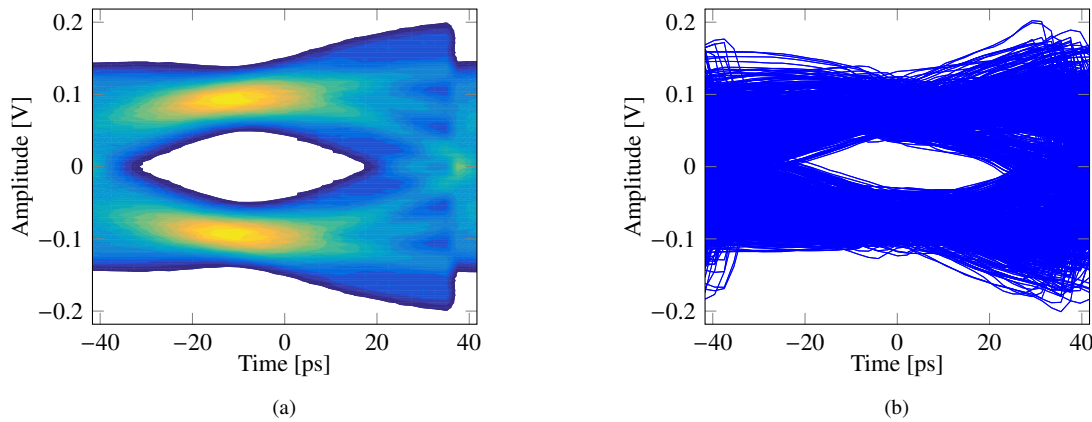


Figure 9: Eye diagrams after convergence of the SS-LMS equalization loops on a MIPI A-PHY channel [27] as obtained through (a) post-processing of the pulse response with the proposed method and (b) transistor-level simulations.

the fully-adaptive algorithm and be able to compute an eye diagram containing enough UIs, transistor-level simulations run at a speed of about 6 h per  $\mu\text{s}$  of simulation for at least  $1 \mu\text{s}$ , whereas the proposed method takes about 5 s to provide the results.

The above is meant to be just a rough comparison, mainly because the various models do not necessarily implement all the components of an HSIO (e.g. the transistor-level simulation does not consider the digital part of the system), but it still provides some figures to consider when dealing with such kind of simulations.

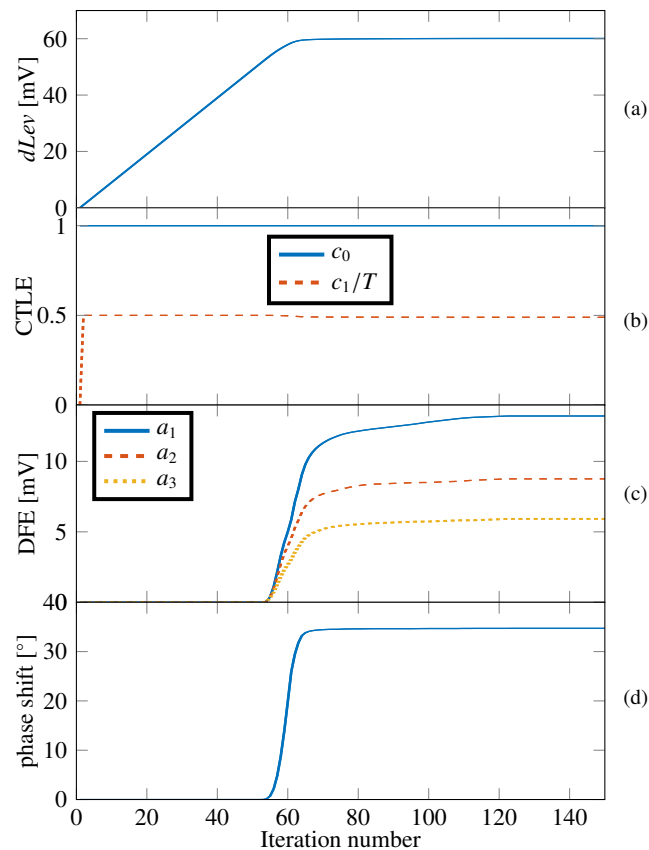


Figure 10: Simulation of a channel with 12 dB attenuation at 10 GHz and fixed 2-tap FFE; the trapezoidal pulse was sent at 20 Gb/s bitrate, it has 20 % rise/fall time and  $\pm 0.25 \text{ V}$  swing differential voltage. From top to bottom, (a)  $dLev$  drives adaptation of (b) first-order CTLE, (c) 3-tap DFE and (d) optimal sampling point.

## 4 Conclusions

We have presented a fast tool exploiting a simple modelling approach to evaluate the performance of high-speed serial interfaces for chip-to-chip communications. An efficient probabilistic algorithm was developed to evaluate the eye diagram with low computational effort. Sharing the same motivations of other similar models developed in the past in the literature, such an approach represents a powerful alternative to time-domain simulations, since complex systems working with BER as low as  $10^{-15}$  require simulating very large amounts of bit periods, which may be very time consuming. The effect of the most common equalization strategies, of CDR techniques, of jitter and of full adaptation of the equalizers can be easily included in the model, so that the proposed simulation approach can be used for the system-level assessment of high-speed interfaces that need to comply with various standards. As examples of the capabilities of the proposed approach, we reported results from two interfaces: One transmitting at 20 Gb/s over a relatively low-loss channel ( $-12 \text{ dB}$  at Nyquist frequency) and another operating at 12 Gb/s over a high-loss MIPI A-PHY line ( $-33 \text{ dB}$  at Nyquist frequency). Both cases show that the combination of various equalization techniques is required to obtain suitable BERs, and that the proposed approach provides results that are comparable with much longer, time-domain post-layout transistor-level simulations, thus demonstrating the power of our model to evaluate the performance of realistic high-speed serial interfaces.

**Conflict of Interest** The authors declare no conflict of interest.

Preliminary tests employing behavioural models for the HSSI indicate a simulation speed of about 7.3 s per  $\mu\text{s}$  of simulation (not

**Acknowledgement** The authors would like to thank prof. Luca Selmi (University of Modena and Reggio Emilia) for support.

## References

- [1] A. Cortiula, M. Dazzi, M. Marcon, D. Menin, A. Bandiziol, A. Cristofoli, W. Grollitsch, R. Nonis, and P. Palestri, "A simple and fast tool for the modelling of inter-symbol interference and equalization in high-speed chip-to-chip interfaces," in *The 42nd Int. Conf. on Information and Communication Technol., Electronics and Microelectronics (MIPRO)*, Opatija, Croatia, May 2019, pp. 116–120. doi: 10.23919/MIPRO.2019.8756752.
- [2] G. Moore, "Cramming more components onto integrated circuits," *Electronics*, vol. 38, no. 8, pp. 114–117, Apr. 1965.
- [3] H. Tamura, "Looking to the Future: Projected Requirements for Wireline Communications Technology," *IEEE Solid-State Circuits Mag.*, vol. 7, no. 4, pp. 53–62, 2015. doi: 10.1109/MSSC.2015.2477017
- [4] T. C. Carusone, "Introduction to Digital I/O: Constraining I/O Power Consumption in High-Performance Systems," *IEEE Solid-State Circuits Mag.*, vol. 7, no. 4, pp. 14–22, Fall 2015. doi: 10.1109/MSSC.2015.2476016
- [5] Y. Chen, P.-I. Mak, L. Zhang, and Y. Wang, "A 0.002-mm<sup>2</sup> 6.4-mW 10-Gb/s Full-Rate Direct DFE Receiver With 59.6-Channel Loss at Nyquist Frequency," *IEEE Trans. Microw. Theory Techn.*, vol. 62, no. 12, pp. 31073117, Dec. 2014. doi: 10.1109/TMTT.2014.2360697.
- [6] N. J. Endo, "Wireless Communication In and Around the Car: Status and Outlook. ES3: High-Speed Communications on 4 Wheels: What's in Your next Car?" in *2013 IEEE Int. Solid-State Circuits Conf. Dig. of Tech. Papers*, Feb. 2013, pp. 515–515. doi: 10.1109/ISSCC.2013.6487598.
- [7] J. Kim et al., "A 112 Gb/s PAM-4 56 Gb/s NRZ Reconfigurable Transmitter With Three-Tap FFE in 10-nm FinFET," *IEEE J. Solid-State Circuits*, vol. 54, no. 1, pp. 29–42, 2019. doi: 10.1109/JSSC.2018.2874040
- [8] J. Lee, K. Park, K. Lee, and D.-K. Jeong, "A 2.44-pJ/b 1.62–10-Gb/s Receiver for Next Generation Video Interface Equalizing 23-dB Loss With Adaptive 2-Tap Data DFE and 1-Tap Edge DFE," *IEEE Trans. Circuits Syst. II*, vol. 65, no. 10, pp. 1295–1299, Oct. 2018. doi: 10.1109/TCSII.2018.2846677
- [9] Z. Toprak-Deniz, J. E. Proesel, J. F. Bulzacchelli, H. A. Ainspan, T. O. Dickson, M. P. Beakes, and M. Meghelli, "A 128-Gb/s 1.3-pJ/b PAM-4 Transmitter With Reconfigurable 3-Tap FFE in 14-nm CMOS," *IEEE Journal of Solid-State Circuits*, vol. 55, no. 1, pp. 19–26, Jan. 2020. doi: 10.1109/JSSC.2019.2939081
- [10] J. F. Bulzacchelli, "Equalization for Electrical Links: Current Design Techniques and Future Directions," *IEEE Solid-State Circuits Mag.*, vol. 7, no. 4, pp. 23–31, Fall 2015. doi: 10.1109/MSSC.2015.2475996
- [11] J. W. M. Bergmans, *Digital Baseband Transmission and Recording*. Springer, 1996, ch. Adaptive Reception, pp. 373–450.
- [12] V. Balan, O. Oluwole, G. Kodani, C. Zhong, R. Dadi, A. Amin, A. Ragab, and M.-J. E. Lee, "A 15–22 Gbps Serial Link in 28 nm CMOS With Direct DFE," *IEEE J. Solid-State Circuits*, vol. 49, no. 12, pp. 3104–3115, 2014. doi: 10.1109/JSSC.2014.2349992
- [13] H. Higashi et al., "A 5-6.4-Gb/s 12-channel transceiver with pre-emphasis and equalization," *IEEE J. Solid-State Circuits*, vol. 40, no. 4, pp. 978–985, Apr. 2005. doi: 10.1109/JSSC.2005.845562
- [14] S. Palermo, S. Hoyos, S. Cai, S. Kiran, and Y. Zhu, "Analog-to-Digital Converter-Based Serial Links: An Overview," *IEEE Solid-State Circuits Mag.*, vol. 10, no. 3, pp. 35–47, Aug. 2018. doi: 10.1109/MSSC.2018.2844603
- [15] V. Stojanović et al., "Autonomous dual-mode (PAM2/4) serial link transceiver with adaptive equalization and data recovery," *IEEE J. Solid-State Circuits*, vol. 40, no. 4, pp. 1012–1026, Apr. 2005. doi: 10.1109/JSSC.2004.842863
- [16] H.-J. Chi, J.-S. Lee, S.-H. Jeon, S.-J. Bae, Y.-S. Sohn, J.-Y. Sim, and H.-J. Park, "A Single-Loop SS-LMS Algorithm With Single-Ended Integrating DFE Receiver for Multi-Drop DRAM Interface," *IEEE J. Solid-State Circuits*, vol. 46, no. 9, pp. 2053–2063, Sep. 2011. doi: 10.1109/JSSC.2011.2136590
- [17] J. Savoj et al., "Wideband flexible-reach techniques for a 0.5–16.3 Gb/s fully-adaptive transceiver in 20nm CMOS," in *Proc. of the IEEE 2014 Custom Integrated Circuits Conf.* IEEE, Sep. 2014, pp. 1–4. doi: 10.1109/CICC.2014.6945980.
- [18] S. Dasgupta, C.R. Johnson, and A.M. Baksho, "Sign-sign LMS convergence with independent stochastic inputs," *IEEE Trans. Inf. Theory*, vol. 36, no. 1, pp. 197–201, Jan. 1990. doi: 10.1109/18.50391
- [19] D. Menin, A. De Pr, A. Bandiziol, W. Grollitsch, R. Nonis, and P. Palestri, "A Simple Simulation Approach for the Estimation of Convergence and Performance of Fully-Adaptive Equalization in High-Speed Serial Interfaces," *IEEE Trans. Compon. Packag. Manuf. Technol.*, vol. 9, no. 10, pp. 2079–2086, Oct. 2019. doi: 10.1109/TCPMT.2019.2911177
- [20] S. U. H. Qureshi, "Adaptive equalization," *Proc. IEEE*, vol. 73, no. 9, pp. 1349–1387, Sept 1985. doi: 10.1109/PROC.1985.13298
- [21] B. Widrow, J. M. McCool, M. G. Larimore, and C. R. Johnson, "Stationary and nonstationary learning characteristics of the LMS adaptive filter," *Proc. IEEE*, vol. 64, no. 8, pp. 1151–1162, 1976. doi: 10.1109/PROC.1976.10286
- [22] B. Casper, "Clocking Wireline Systems: An Overview of Wireline Design Techniques," *IEEE Solid-State Circuits Magazine*, vol. 7, no. 4, pp. 32–41, 2015. doi: 10.1109/MSSC.2015.2476015
- [23] A. Sanders and J. D'Ambrosia, "Designcon 2004 channel compliance testing utilizing novel statistical eye methodology," 2004.
- [24] G. Balamurugan, B. Casper, J. Jaussi, M. Mansuri, F. O'Mahony, and J. Kennedy, "Modeling and Analysis of High-Speed I/O Links," *IEEE Trans. Adv. Packag.*, vol. 32, no. 2, pp. 237–247, May 2009. doi: 10.1109/TADVP.2008.2011366
- [25] D. Oh, J. Ren, and S. Chang, "Hybrid Statistical Link Simulation Technique," *IEEE Trans. Compon. Packag. Manuf. Technol.*, vol. 1, no. 5, pp. 772–783, May 2011. doi: 10.1109/TCPMT.2011.2118209
- [26] J. Ren and K. S. Oh, "Multiple Edge Responses for Fast and Accurate System Simulations," *IEEE Trans. Adv. Packag.*, vol. 31, no. 4, pp. 741–748, Nov. 2008. doi: 10.1109/TADVP.2008.2002201
- [27] D. Menin, A. Bandiziol, W. Grollitsch, R. Nonis, and P. Palestri, "Design and Simulation of a 12 Gb/s Transceiver with 8-Tap FFE, Offset-Compensated Samplers and Fully-Adaptive 1-Tap Speculative/3-Tap DFE and Sampling Phase for MIPI A-PHY Applications," *IEEE Trans. Circuits Syst. II*, 2019. doi: 10.1109/TCSII.2019.2926152. [Online]. Available: <https://ieeexplore.ieee.org/document/8752403/>
- [28] G. Signorini, C. Siviero, M. Telescu, and I. S. Stievano, "Present and future of I/O-buffer behavioral macromodels," *IEEE Electromagn. Compat.*, vol. 5, no. 3, pp. 79–85, 2016. doi: 10.1109/MEMC.0.7764256
- [29] J. N. Tripathi, V. K. Sharma, and H. Shrimali, "A Review on Power Supply Induced Jitter," *IEEE Trans. Compon. Packag. Manuf. Technol.*, vol. 9, no. 3, pp. 511–524, Mar. 2019. doi: 10.1109/TCPMT.2018.2872608
- [30] A. Cristofoli, P. Palestri, N. D. Dalt, and L. Selmi, "Efficient Statistical Simulation of Intersymbol Interference and Jitter in High-Speed Serial Interfaces," *IEEE Trans. Compon. Packag. Manuf. Technol.*, vol. 4, no. 3, pp. 480–489, Mar. 2014. doi: 10.1109/TCPMT.2013.2282530
- [31] M. Dazzi, P. Palestri, D. Rossi, A. Bandiziol, I. Loi, D. Bellasi, and L. Benini, "Sub-mW multi-Gbps chip-to-chip communication Links for Ultra-Low Power IoT end-nodes," in *2018 IEEE Int. Symp. on Circuits and Syst. (ISCAS)*, May 2018. doi: 10.1109/ISCAS.2018.8351893 pp. 1–5.
- [32] E. Denlinger, "Losses of Microstrip Lines," *IEEE Trans. Microw. Theory Techn.*, vol. 28, no. 6, pp. 513–522, Jun. 1980. doi: 10.1109/TMTT.1980.1130112
- [33] W. Getsinger, "Microstrip Dispersion Model," *IEEE Trans. Microw. Theory Techn.*, vol. 21, no. 1, pp. 34–39, Jan. 1973. doi: 10.1109/TMTT.1973.1127911
- [34] E. Hammerstad and O. Jensen, "Accurate Models for Microstrip Computer-Aided Design," in *MTT-S Int. Microwave Symp. Dig.*, vol. 80. MTT006, 1980. doi: 10.1109/MWSYM.1980.1124303 pp. 407–409.
- [35] M. Kirschning and R. Jansen, "Accurate model for effective dielectric constant of microstrip with validity up to millimetre-wave frequencies," *Electron. Lett.*, vol. 18, no. 6, p. 272, 1982. doi: 10.1049/el:19820186
- [36] H. Wheeler, "Transmission-Line Properties of a Strip on a Dielectric Sheet on a Plane," *IEEE Trans. Microw. Theory Techn.*, vol. 25, no. 8, pp. 631–647, Aug. 1977. doi: 10.1109/TMTT.1977.1129179
- [37] M. Kirschning and R. Jansen, "Arguments and an accurate model for the power-current formulation of microstrip characteristic impedance," *Archiv der elektrischen Übertragung: AEÜ*, vol. 37, pp. 108–112, mar 1983.
- [38] M. Kirschning and R. Jansen, "Accurate Wide-Range Design Equations for the Frequency-Dependent Characteristic of Parallel Coupled Microstrip Lines," *IEEE Trans. Microw. Theory Techn.*, vol. 32, no. 1, pp. 83–90, Jan. 1984. doi: 10.1109/TMTT.1984.1132616
- [39] T. Brazil, "Causal-convolution – a new method for the transient analysis of linear systems at microwave frequencies," *IEEE Trans. Microw. Theory Techn.*, vol. 43, no. 2, pp. 315–323, Feb. 1995. doi: 10.1109/22.348090

- [40] Alexander, J.D.H., "Clock recovery from random binary signals," *Electron. Lett.*, vol. 11, no. 22, pp. 541–542, Oct. 1975. doi: 10.1049/el:19750415
- [41] V. Stojanović and M. Horowitz, "Modeling and analysis of high-speed links," in *Proc. of the IEEE 2003 Custom Integrated Circuits Conf., 2003.* IEEE, 2003, pp. 589–594. doi: 10.1109/CICC.2003.1249467.
- [42] G. R. Gangasani et al., "A 32 Gb/s Backplane Transceiver With On-Chip AC-Coupling and Low Latency CDR in 32 nm SOI CMOS Technology," *IEEE J. Solid-State Circuits*, vol. 49, no. 11, pp. 2474–2489, Nov. 2014. doi: 10.1109/JSSC.2014.2340574
- [43] J. Han, Y. Lu, N. Sutardja, K. Jung, and E. Alon, "A 60Gb/s 173mW receiver frontend in 65nm CMOS technology," in *2015 Symp. on VLSI Circuits (VLSI Circuits)*, June 2015, pp. C230–C231. doi: 10.1109/VLSIC.2015.7231268.
- [44] T. Shibasaki et al., "A 56Gb/s NRZ-electrical 247mW/lane serial-link transceiver in 28nm CMOS," in *2016 IEEE Int. Solid-State Circuits Conf. (ISSCC).* IEEE, Jan. 2016, pp. 64–65. doi: 10.1109/ISSCC.2016.7417908.

# Understanding Human Perception of Vibrotactile Feedback in Walking and Running Tasks

Emel Demircan<sup>\*1</sup>, Elliot Recinos<sup>2</sup>, I-Hung Khoo<sup>3</sup>, Sharon Teng<sup>4</sup>, Will Wu<sup>5</sup>

<sup>1</sup>Mechanical and Aerospace Engineering, Biomedical Engineering, California State University Long Beach, 90803, U.S.A.

<sup>2</sup>Mechanical and Aerospace Engineering, California State University Long Beach, 90803, U.S.A.

<sup>3</sup>Electrical Engineering, Biomedical Engineering, California State University Long Beach, 90803, U.S.A.

<sup>4</sup>Department of Physical Therapy, California State University Long Beach, 90803, U.S.A.

<sup>5</sup>Department of Kinesiology, California State University Long Beach, 90803, U.S.A.

## ARTICLE INFO

Article history:

Received: 19 January, 2020

Accepted: 27 March, 2020

Online: 10 April, 2020

Keywords:

Haptic Feedback

Locomotion

Motion Training

## ABSTRACT

Vibrotactile feedback is increasingly becoming an essential feedback component in several non-medical and medical areas. One area that vibrotactile feedback has not been explored as an intervention tool is in sports science. In addition, vibrotactile feedback lacks scientific evidence as a feedback mechanism within the sports world. A portable vibrotactile feedback system was developed to understand how a human perceives vibrotactile feedback while performing walking and running tasks. The system incorporates a model-based simulation framework to check human motion and visualize key performance metrics. We performed a pilot study on twenty-six subjects to understand the accuracy of human perception of vibrotactile feedback using the system we developed. Here, we investigated the type, number, and location of haptic feedbacks that would yield better subject perceived accuracy during walking and running. Findings suggested that staggered vibrotactile feedback would lead to higher accuracy than continuous vibrotactile feedback especially when more than two motors were used. For the subjects perception accuracy for all motor combinations, we observed an average that was 9.3% higher for walking compared to running. For one motor, the perception accuracy decreased by only 3.38% while running compared to walking. The decrease was much more significant for higher combinations of motors. The decrease in the perception accuracy of the motor locations was significantly less for both staggered ( $p < 0.001$ ) and one motor ( $p < 0.001$ ) vibration modes.

## 1 Introduction

This paper is an extension of work originally presented in IEEE International Conference on Ubiquitous Robots (URAI 2019) [1]. A key in quantifying and improving locomotion is identification of useful, tractable metrics and providing useful feedback. The most fundamental metric for our study, and arguably of most interest to many affected populations, is an estimate of injury risk. Despite the health benefits, a high number of lower extremity injuries can be linked to running [2, 3]. Estimates suggest that 10-20% of Americans run regularly, with 40-50% of these injured annually [4], although causation is more complex, with a survey of results across 17 published studies, involving a range specific population

characteristics (age, experience, gender, etc.) showing annual injury rates can vary from 19% to 79% [5]. Among running injuries, 50% of injuries occur at the knee joint and the most common diagnosis is patellofemoral pain (PFP) [3, 5]. PFP can lead to severe pain and disability and is a precursor of knee osteoarthritis [6]. Real-time feedback is an effective method for motion and gait retraining. Augmented feedback has been shown to be a useful part in the process of learning a motor task and has been shown to enhance effects of walking and running gait programs [7, 8]. Different feedback modalities such as visual, audio, or vibrotactile feedback have been shown to effectively modify knee and impact loading [9]-[13]. Vibrotactile feedback is increasingly becoming an essential feedback component in several non-medical and medical areas [14]. Among

\*Corresponding Author: Emel Demircan, 1250 Bellflower Blvd, ECS-645, California State University Long Beach, CA, 90840, emel.demircan@csulb.edu



vibrotactile feedback, coin vibration motors are chosen for being non-invasive, safe, low cost, small size, and its ability to be effective when placed at almost anywhere on the body [15]-[18]. Vibrotactile feedback can also be a means of delivering cues to a user learning new motor skills [19] or for patients undergoing rehabilitation therapy [20]. Models that are data-driven have been implemented to train gaits involving a combination of different kinematic modifications [21]. One study compared how combining haptic feedback with visual feedback had a greater effect in the learning performance for lower extremity tasks than the feedbacks alone [22]. A different study pointed out that wearable feedbacks in the form of haptic and auditory are commonly used in clinical applications for human gait [23]. Knee and trunk motion are the gait parameters most associated with retraining using wearable feedback [23]. Both visual-auditory feedback and visual-tactile feedback provide advantages in reducing reaction times and improving performance [24]. It has been observed that combining visual feedback with tactile feedback works best when performing multiple tasks that have high cognitive workload conditions [24]. In a study that evaluated assistive navigation systems for the blind, auditory feedback resulted in a 22 times higher cognitive load than haptic feedback [25]. Previous studies have observed that vision feedback provides a high degree of precision [12]. Vibration provides simple and intuitive feedback, particularly when vision is otherwise occupied [21]. In addition, vibration conveys Cartesian space directional cues well. Another benefit of haptic feedback systems is that they can provide feedback to multiple body segments and thus allow modifications of multiple gait parameters [21]. Motor tasks can be guided by using immediate feedback on complex tasks to provide proprioceptive information [14]. Several studies have shown how effective feedback can be in gait retraining and learning a task that can also slow down the progression of joint diseases [9]-[11]. Research still does not provide insight on how feedback needs to be provided and combined in the system to yield better results. It is important to maintain latency as low as possible since it is highly dependent on the motor task and type of vibrotactile stimuli.

To enhance motor learning, visual feedback can be provided in the process of gait retraining. This type of feedback facilitates external focus which has been shown to be beneficial for motor learning due to its ability of promoting automaticity in movement control [26]. Depending on the timing that the feedback is delivered, it can be divided into concurrent (online, real-time) and terminal (at the end) [27]. Concurrent feedback has been reported to enhance learning of complex motor tasks [28] and is especially helpful in early phase of learning [27]. Knowledge of Performance and Knowledge of Results are the two categories of Terminal feedback. While knowledge of performance provides feedback regarding the execution of the task (i.e. joint kinematics and kinetics of gait), knowledge of results pertains information related to the response outcome rather than about the movement (i.e. VO<sub>2</sub> consumption during gait) [29]. Terminal feedback has been found to promote motor learning and facilitates motor retention [27]. Despite studies that focus on multi-modal feedback mechanisms on human kinematics, there is a lack of understanding on how feedback interfaces can be used with cyber-physical systems to improve response and engagement. Several studies demonstrate that there is not enough evidence yet to support implementation of tactile feedback to enhance

performance [7, 16, 30].

In addition to augmented feedback systems, there has been much research in developing smart wear with integrated sensors, with applications in different areas. Some recent examples that involve soft suits which can be used in daily activities include the following: (i) A sensing suit using elastic tights and hyper-elastic strain sensors was developed for lower limb biomechanics measurements [31]; (ii) A knee pad and ankle wearable system that contains soft stretchable sensors was developed to track and analyze the joint position of lower limbs [32]; (iii) An IMU integrated shirt, with conductive yarn for circuit patterning and flexible printed circuit boards for interconnections, was designed for posture monitoring [33]; (iv) Leggings with stretch sensors were designed to detect knee valgus [34], commonly observed in athletes at risk of knee injuries; (v) A soft exo-suit, which consists of: a waist belt, leg strap, calf wrap, insole, load cells, gyroscopes, and Bowden cables, was developed to help improve walking in post-stroke patients [35]; (vi) The commercial product by Athos includes a compression shirt and shorts with integrated IMU and EMG sensors, and provides visual information on muscle efforts using a smartphone app ([www.liveathos.com](http://www.liveathos.com)); (vii) a portable gait asymmetry rehabilitation system that delivers vibrotactile cues based on gait phase measurement to improve gait symmetry for individuals with stroke [20, 36].

It remains unclear how haptic mode (e.g., simultaneous or staggered) or number of motors affects individuals perception of haptic feedback during locomotion. In this study, we present a portable haptic feedback system that uses actuators [37]-[39] to provide the wearer with real-time haptic feedback during locomotion. We designed the system with the wearers comfort during locomotion in mind by making it portable and lightweight. Using this system, we conducted a pilot study to examine subject perceived haptic feedback during different types of haptic mode and numbers of motors during walking and running. Coin-based vibrotactile actuators were chosen and mounted on custom 3D printed cases to avoid impeding the human body's natural motion. We had 3 main questions in mind when we designed the experiments: (i) How many vibration motors can a subject perceive at once?; (ii) Where on the subjects body should the haptic feedback be provided?; (iii) How effective are the subjects when interpreting higher orders of haptic feedback occurring simultaneously?

Our study is an extension of work originally presented in IEEE International Conference on Ubiquitous Robots (URAI 2019) [1]. Here, we provide a more comprehensive understanding of human interpretation of vibrotactile feedback during walking and running, including the effect of feedback locations. For future work, we plan to train subjects on how interpret haptic cues to increase their performance using this framework and suit by altering key kinematic variables during locomotion.

## 2 Vibrotactile Feedback

For the preliminary experiment, we developed a vibrotactile feedback system that consists of the following three subsystems: (1) the hardware, that is comprised of 10 vibrotactile motors (10 x 2.7 mm Coin Mobile Phone Vibration Motor) and 1 Bluetooth-enabled Arduino-Nano microcontroller, (2) an in-house made GUI that sends

Bluetooth commands to the vibrotactile systems microcontroller, and (3) a custom button panel that is placed on a treadmill to record the subjects haptic response (Figure 1).

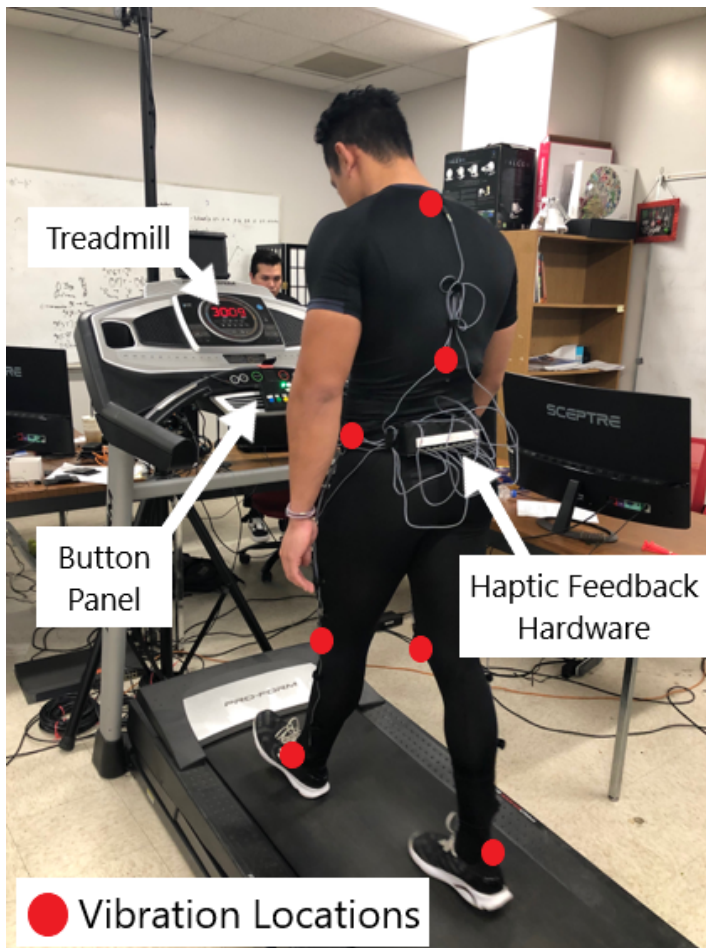


Figure 1: Subject wearing the wireless sensing and feedback system.

Our frameworks GUI is a Windows Presentation Foundation (WPF) application, that uses the 32feet.NET library to discover and connect to the vibrotactile feedback systems Bluetooth module, and a wired serial communication protocol to connect to the custom button panel. When connected to the haptic suit system, the experimenter can use the GUI to manually actuate the 200Hz (slightly below the peak sensitivity of fast-acting mechanoreceptors [40]) haptic suit motors and motor combinations by clicking on the appropriate radio buttons. Figure 2 shows how the motor actuation type (continuous or staggered) and duration of actuation can be manually changed by the experimenter using the GUI. Note that the GUI also provides visual feedback to the experimenter on what motors are being actuated by coloring in the circles that correspond to activated motors on the GUIs body model. When the Start Auto button is pressed, the GUI performs an automatic procedure in which motor actuation commands are executed. Specifically, the sequence and order of actuation modes are based on the selected Subject Number while the time gap between each actuation is randomly chosen at run time to be the subject-specific sequence.

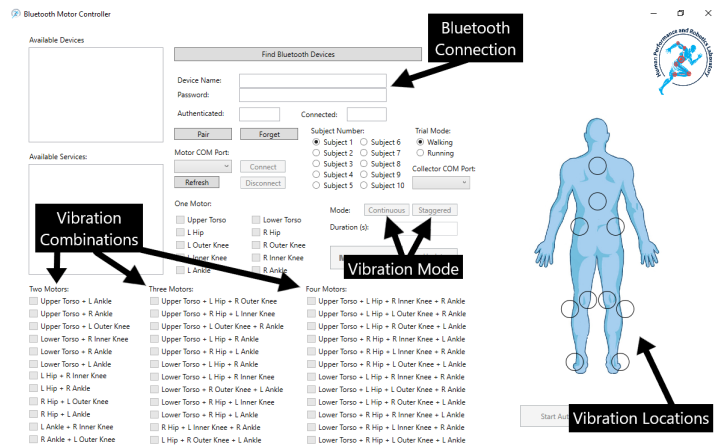


Figure 2: GUI for the vibrotactile feedback experiment.

While the automatic procedure is running, a separate thread is instantiated and used to collect the subject response data outputted by the custom button panel. The GUI automatically logs: the haptic command events, the subjects response input, and the timestamps at which these events occur, during the automatic procedure of the main process thread. When the automatic procedure finishes, the haptic events and subject response events are combined with the timestamps and then analyzed based on each events unique keywords. The subject response events are grouped with their respective actuator commands (by determining the closest actuator command event to the response event) and, with the use of specific event keywords, compared with their respective actuator commands to quantify the accuracy of the subjects response. For example, the subjects response will be reported as false (zero) if the subjects response is TORSO when the haptic feedback command was activated as LOWER TORSO + L KNEE (Continuous) since the subject failed to perceive the correct feedback. The software then calculates statistical results with the use of the ClosedXML library and saves both statistical and experimental data as an Excel file.

### 3 Simulation Framework

The simulation framework was developed to read existing OpenSim models and build them with the Unity game engine environment. OpenSims musculoskeletal properties and definitions are implemented by the framework. This allows the framework to acquire unique behaviors that are only found in OpenSims software. A few unique behaviors include muscle path joints that move during motion, conditional muscle path joints, and application of cubic spline for joint connectivity. The framework takes advantage of Unitys editor window to allow the user, while in edit mode, to upload and adjust dynamic OpenSim models. The simulation framework is capable of symbolic calculus and matrix operations due to implementations of the ALGIB numerical analysis and data-processing library [41], C++ Mathematical Expression Toolkit Library (ExprTK) [42], MITs Math.NET Symbolics [43]. At runtime of the framework, the user can symbolically solve both kinematic and muscular Jacobians of an OpenSim multi-body model using the Math.NET Symbolics library. This allows the user to generate the

symbolic expression that can be used by the ExprTk library. Due to the high computation expense of symbolic interpretations, dynamic compilation functionality was implemented. Dynamic compilation allows the framework to compile and save symbolic expressions to be used in future runtimes. The simulation framework has the capability to solve complex and dynamic computations during motion tracking due to the implementation of dynamic compilation with Math.Net Symbolics closed-form symbolic computation. The framework can perform these computations at a framerate of 100 FPS or higher depending on the computer specifications. The framework generates generalized coordinates by implementing algorithms to decompose motion of a body [44]-[46] and can act as an interface for generic motion tracking.

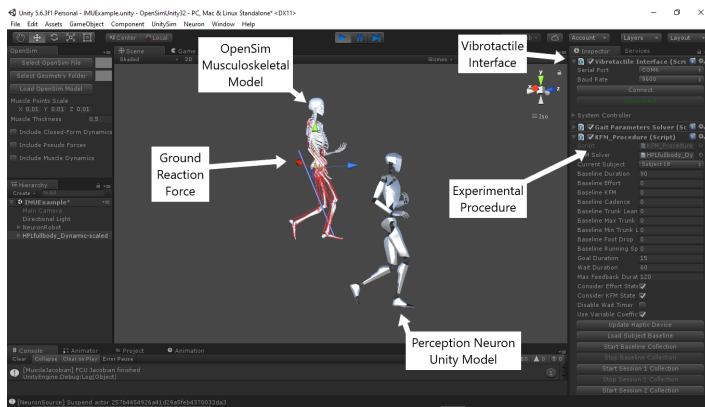


Figure 3: Simulation Framework.

To evaluate the motion tracking interfaces performance, a Perception Neuron full-body IMU suit was integrated into the framework. As expected, Noitom already provides the software (Axis Neuron) and the rigged humanoid model required to use the IMU motion capture system within Unity. As designed, the only task that must be completed to use the IMU motion capture system with our framework is to connect the individual limbs of the humanoid model to the appropriate JointTracker elements. The ground reaction forces are estimated by our framework using the motion data from IMU and the subject-specific mass matrix. The simulation framework provides haptic feedback commands to an Arduino nano microcontroller that is Bluetooth enabled. The simulation framework connects to the microcontroller through a haptic feedback interface script that connects to the Bluetooth communication port at 9600 baud rate (Figure 3). Once connected, the simulation runs an experimental procedure script that tracks different kinematic metrics and sends vibration commands in the form of strings to the microcontroller.

Effective indicators of joint loading that can be used in injury prevention and sports performance are joint moments. Progression of patellofemoral joint (PFJ) osteoarthritis can be related to flexion moment impulse and peak knee flexion [47]. High PFJ reaction force and stress has been associated to increased knee flexion moment that suggests requirements for greater quadriceps force [48, 49]. Our framework estimates the 3-dimensional joint moments in real-time using the inverse dynamics algorithm. Both the kinematic and kinetic values estimated by our framework were validated against the data reported in the literature [47]. The novel

simulation framework and the motion/force data will be used in our future study to estimate joint contact forces and other performance metrics (i.e. metabolic cost) during locomotion.

## 4 Experiments

This section presents the experimental evaluation, including experimental setup, subjects and data collection, and statistical analysis.

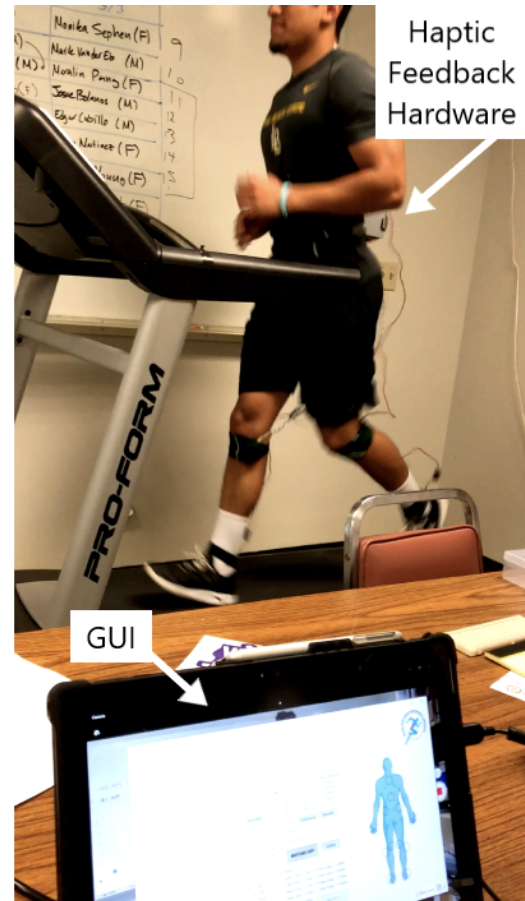


Figure 4: Experimental Setup and System GUI.

### 4.1 Subjects

Eighteen subjects (10 males, 8 females, age:  $22.5 \pm 3.0$  years, BMI:  $22.6 \pm 3.6 \text{ kg/m}^2$ ) participated in the study. All subjects reported no pain or symptoms while walking or running, nor history of surgery or sensory deficit. To have scientifically correct subject-specific scaling for the modeling purposes in our future work, we did not include children or the elderly. Inclusion criteria for subject recruitment are the following: (1) between ages of 18 and 40 years old; (2) familiar with running on a treadmill; and (3) run at least 8 miles/week for 4 weeks prior to participation. Exclusion criteria for subject recruitment are the following: (1) History of lower extremity or low back surgery that may affect running kinematics, muscle activation, or kinetics; (2) low back or lower extremity discomfort or pain during the data collection or within 3 months prior of the experiment; and (3) any mental or physical condition that prevents

the subject from performing the exercises or tasks safely. Medical clearance and written informed consent forms approved by the California State University, Long Beach Human Subjects Review Board (IRB : 1300259-2) were obtained from the participants.

#### 4.2 Experimental Setup

We used the same experimental setup detailed in our previous work [1]. The experiment consisted of 4 trials that got divided into walking and running. Subjects were tasked to perform two walking and two running trials on a treadmill at self-selected comfortable speed (walking:  $1.1 \pm 0.2$  m/s, running:  $2.2 \pm 0.2$  m/s). Each trial lasted between 12 to 14 minutes. During each trial, subjects experienced vibrations by motors placed over 10 locations of his/her body bony landmarks: upper and lower back, bilateral posterior superior iliac spines, bilateral medial and lateral femoral epicondyles, and bilateral lateral malleoli.

Two types of vibrations were implemented, continuous and staggered. During continuous vibration, the combinations of motors vibrated at the same time. During staggered vibrations, the motors vibrated in a sequential manner for the combination of motors. A 0.5 second delay was programmed between each motor during the vibration sequence. The vibration commands included up to a combination of four motors in a pre-determined random order. Subjects were tasked to verbally report the number and location of the vibration motors they perceived during the experiment. The subject was also tasked to report the vibration locations using the button panel on the treadmill. Subjects were informed if the trial was continuous or staggered with verbal instructions and an LED light on the button panel.

#### 4.3 Data Collection

Feedback perception accuracy (FPA), which is defined as the percent accuracy of detecting correct number and location of vibration motors, was calculated for each combination. The average reaction time for each subject was collected during each trial. Subjects comfort level of wearing the system during locomotion was immediately reported after each experiment using a ten-point bipolar Likert-type scale.

#### 4.4 Statistical Analysis

Two-way repeated measures ANOVA was used to evaluate effects of number of motors (i.e., 2, 3, and 4) and vibration modes (i.e., continuous and staggered) on FPA during walking and running. The FPA (%) between the first and second trial for walking and running and for the different vibration modes (staggered or continuous) was compared using paired-sample t-tests. Separate t-tests were performed independently for male (M) and female (F) subjects. An alpha of 0.05 was set for the statistical significance level.

## 5 Results

Overall, FPAs were greater than 50% in all motor and activity conditions in staggered mode. On the other hand, FPAs reached above

50% only during two motor condition in continuous mode. Results of ANOVAs showed significant number-of-motor, vibration-mode, and interaction effects ( $p < 0.001$ ) for both walking and running. FPAs reduced as the number of motors increased. Compared to continuous mode, staggered mode yields higher FPAs, especially when the number of motors increased. When examining staggered or continuous mode alone, FPAs were significantly higher during walking than running ( $p = 0.04$  and  $0.01$ , respectively) with a mean difference of 8%.

Table 1: Table P-Values, averages, and standard deviations for walking and running trials

Task	p-Value	Trial 1 (%)	SD (%)	Trial 2 (%)	SD (%)
Walking	0.584	60.63	11.50	61.99	14.09
Running	0.384	54.40	12.64	56.10	12.07

Table 1 shows the respective FPA p-values, averages, and standard deviations for trial 1 and trial 2 during walking and running. The FPA means for walking and running, respectively, showed an increase of 2.23% and 3.12% that suggests effective learning for both types of locomotion.

Table 2: Table P-Values, averages, and standard deviations for males and females

Task	p-Value	Male (%)	SD (%)	Female (%)	SD (%)
Walking	0.052	66.09	10.74	55.33	10.74
Running	0.136	58.96	9.39	50.61	13.18

Table 2 shows the respective FPA p-values, averages, and standard deviations for males and females during walking and running. A decrease of 12.60% in the standard deviation from walking to running was observed among the male population. An increase of 22.70% in the standard deviation from walking to running was observed among the female population.

Table 3: Table P-Values, averages, and standard deviations for vibration modes

Task	p-Value	S (%)	SD (%)	C (%)	SD (%)
Walking	0.0001	50.72	9.14	74.84	17.24
Running	0.0001	44.14	8.23	69.05	18.54

Table 3 shows the respective FPA p-values, averages, and standard deviations for continuous (C) vibrations and staggered (S) vibrations during walking and running. A decrease of 9.95% in the standard deviation from walking to running was observed within the continuous vibration mode. An increase of 7.49% in the standard deviation from walking to running was observed within the staggered vibration mode. Figure 6 shows the FPA averages for 1, 2, 3, and 4 motors. Most notably, 1 motor yielded an FPA of 92.78 for walking.

The overall FPA decreased when the subjects were asked to verbally identify the location of the vibrotactile devices they felt. The average decrease for detecting one motor location was 2.98% during



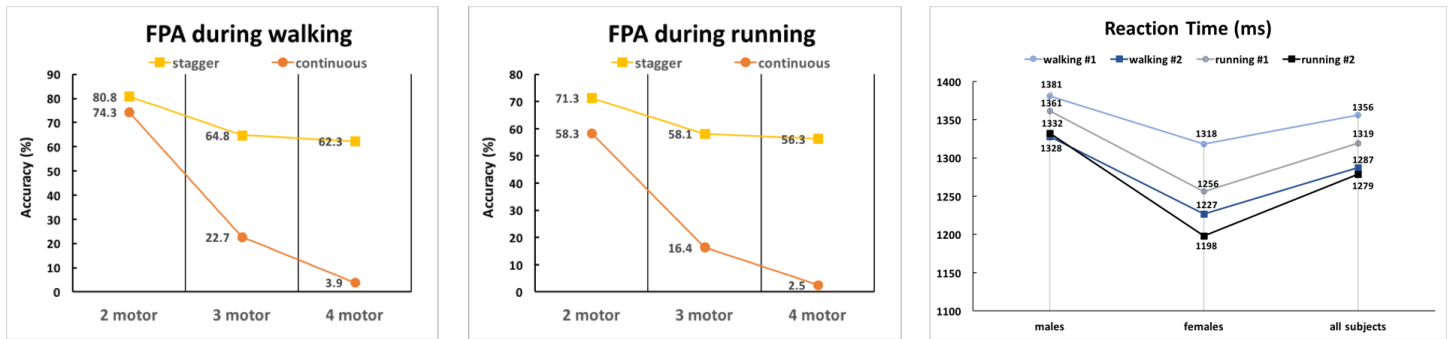


Figure 5: FPA during walking (left), FPA during running (middle), and reaction time (right).

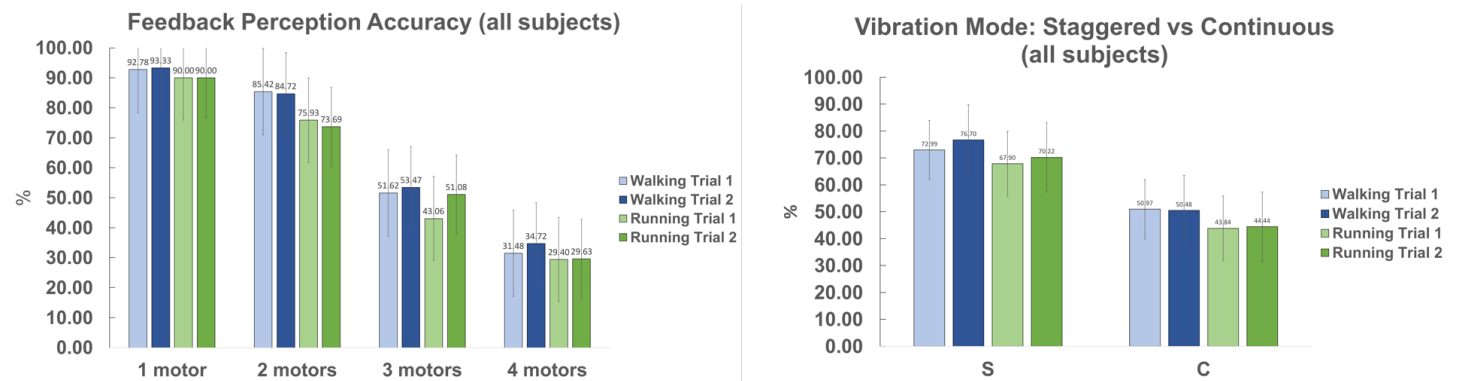


Figure 6: FPA for subjects (left); Vibration modes: staggered vs. continuous (right).

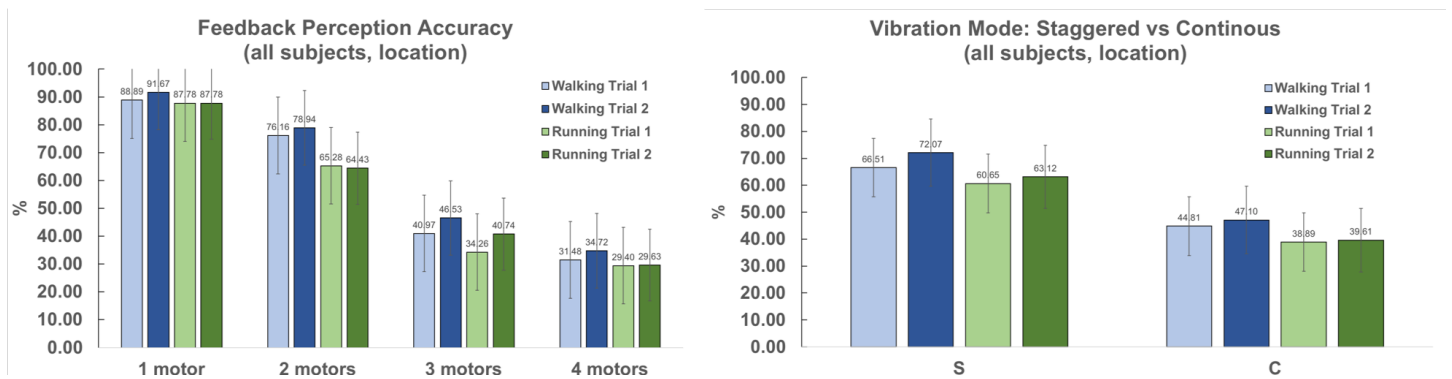


Figure 7: FPA of the feedback locations on subjects (left); Vibration modes: staggered vs. continuous (right).

walking and 2.46% during running (see Figure 7 (left)). For staggered vibration mode, there was an average of 7.45% and 10.39% decrease in FPA of the correct location of vibrotactile motors during walking and running, respectively. For continuous vibration mode, the decrease was more significant: 9.39% and 11.08% decrease in FPA of the correct location of vibrotactile motors during walking and running, respectively (see Figure 7 (right)).

The results from Figure 5 (left and middle) suggest that staggered vibrations are easier to perceive by humans. This can be observed by comparing the loss in FPA as the number of simultaneous stimuli increases. Figure 5 (left and middle) show a greater loss (slope) for continuous vibrations as the number of motors is increased compared to staggered, which has less of a negative slope. This may suggest that cognitive load is less when trying to identify vibrations that are staggered throughout body locations compared to simultaneous continuous vibrations. This shows promise when trying to maintain low cognitive load for motor and gait training. Figure 6 (right) and Figure 7 (right) both reinforce that staggered is much more suitable when you want a person to perceive total number of stimulation and accurately distinguish among different locations. Another possible reason that staggered is a more suitable form of haptic feedback for motor and gait training is because it has been observed that continuous vibration on the same location may lead to numbness of that section of the skin [50]. Meanwhile, staggered vibrations provide the user with rest periods that may reduce the numbness associated to constant stimulation. As mentioned in the experiment section, subjects reported an average comfort level score of 8.4 using the bipolar Likert-type with a ten-point scale. Subjects average reaction times can be observed in Figure 5 (right).

## 6 Discussion

For this paper, we explored human perception of vibrotactile feedback using a portable system that provides vibrations during walking and running tasks. Findings from our previous study gave insight of how vibrotactile feedback is perceived by humans during locomotion. This study showed that staggered vibrotactile feedback would yield greater subject perceived accuracy during locomotion especially when more than two motors were used. This study provides valuable insights into the feasibility of vibration mode and number of motors during locomotion. Information obtained from this study can be used to improve the haptic feedback systems design and experimental protocol.

This study's results set a foundation to develop multi-modal feedback systems to improve performance during walking and running. We plan to incorporate the simulation framework into the multi-modal system to provide different feedback modalities for coordinated motions. Previous studies have observed that vision feedback provides a high degree of precision [12]. Vibration provides simple and intuitive feedback, particularly when vision is otherwise occupied [21]. In addition, vibration conveys Cartesian space directional cues well. By integrating visual, audio, and haptic feedback, we will combine their advantages to provide rich and intuitive feedback to improve human performance and decrease the risk of injuries during locomotion.

**Conflict of Interest** The authors declare no conflict of interest.

**Acknowledgment** The design of the study and collection, analysis, and interpretation of data were funded by California State University Long Beach Faculty Seed Grants.

## References

- [1] Demircan, E., Recinos, E., Abella, J.R., Khoo, I., Teng, S., Wu, W.: Perception accuracy of vibrotactile feedback during locomotion. In: 16th International Conference on Ubiquitous Robots, UR 2019, Jeju, South Korea, June 24-27, 2019, pp. 673–677 (2019). doi:10.1109/URAI.2019.8768771
- [2] Koplán, J.P., Rothenberg, R., Jones, E.: The natural history of exercise: a 10-yr follow-up of a cohort of runners. *Medicine & Science in Sports & Exercise* **27**(8), 1180–1184 (1995)
- [3] Taunton, J.E., Ryan, M.B., Clement, D.B., McKenzie, D.C., Lloyd-Smith, D.R., Zumbo, B.D.: A retrospective case-control analysis of 2002 running injuries. *British journal of sports medicine* **36**(2), 95–101 (2002)
- [4] Fields, J.C., W.K.M., J.J.C. Karl B.1; Sykes: Prevention of running injuries. *Current Sports Medicine Reports* **9**, 176–182 (2010)
- [5] van Gent, R.N., Siem, D., van Middelkoop, M., van Os, A.G., Bierma-Zeinstra, S.M.A., Koes, B.W., Taunton, J.E.: Incidence and determinants of lower extremity running injuries in long distance runners: a systematic review. *British journal of sports medicine* **41**(8), 469–480 (2007)
- [6] Thomas, M.J., Wood, L., Selfe, J., Peat, G.: Anterior knee pain in younger adults as a precursor to subsequent patellofemoral osteoarthritis: a systematic review. *BMC Musculoskeletal Disorders* **11**(1), 201 (2010)
- [7] Shull, P.B., Damian, D.D.: Haptic wearables as sensory replacement, sensory augmentation and trainer review. *J Neuroeng Rehabil* **12**(1) (2015)
- [8] Agresta, C., Brown, A.: Gait Retraining for Injured and Healthy Runners Using Augmented Feedback: A Systematic Literature Review. *Journal of Orthopaedic and Sports Physical Therapy* **45**(8), 576–584 (2015)
- [9] Barrios, J.A., Crossley, K.M., Davis, I.S.: Gait retraining to reduce the knee adduction moment through real-time visual feedback of dynamic knee alignment. *J Biomech Eng.* **43**(11), 2208–2213 (2012). doi:10.1016/j.jbiomech.2010.03.040
- [10] Riskowski, J.L., Mikesky, A.E., Bahamonde, R.E., Burr, D.B.: Design and validation of a knee brace with feedback to reduce the rate of loading. *J Biomech Eng.* **131**(8) (2009). doi:10.1115/1.3148858
- [11] Dowling, A.V., Fisher, D.S., Andriacchi, T.P.: Gait modification via verbal instruction and an active feedback system to reduce peak knee adduction moment. *J Biomech Eng.* **132**(7) (2009). doi:10.1115/1.4001584
- [12] Wheeler, J.W., Shull, P.B., Besier, T.F.: Real-time knee adduction moment feedback for gait retraining through visual and tactile displays. *J Biomech Eng.* **133**(4) (2011). doi:10.1115/1.4003621
- [13] Crowell, H.P., Milner, C.E., Hamill, J., Davis, I.S.: Reducing Impact Loading During Running with the Use of Real-Time Visual Feedback. *J of Orth and Sports Phy Ther* **40**(4), 206–213 (2010)
- [14] VanBreda, E., Verwulgen, S., Saeys, W., Wuyts, K., Peeters, T.: Vibrotactile Feedback as a Tool to Improve Motor Learning and Sports Performance: A Systematic Review. *BMJ Open Sport and Exercise Medicine* **3**, 21–53 (2017)
- [15] Bark, K., Hyman, E., Tan, F., Cha, E., Jax, S.A., Buxbaum, L.J., Kuchenbecker, K.J.: Effects of Vibrotactile Feedback on Human Learning of Arm Motions (V), 1–42 (2015). doi:10.1109/TNSRE.2014.2327229.Effects
- [16] Alahakone, A.U., Senanayake, S., Arosha, M.: Vibrotactile feedback systems: current trends in rehabilitation, sports and information display. In: *Advanced Intelligent Mechatronics* (2009). ASME International Conference
- [17] Bannwart, M., Pyk, P., Kiper, D., Eng, K., Gassert, R., Kim, Y.: 2013 International Conference on Virtual Rehabilitation : Philadelphia, Pennsylvania, USA, 26-29 August 2013.
- [18] Weber, P., Ruekert, E., Calandra, R., Peters, J., Beckerle, P.: IEEE RO-MAN 2016 : the 25th IEEE International Symposium on Robot and Human Interactive Communication : 25th Anniversary : August 26 to August 31, 2016, Teachers College, Columbia University, New York, U.S.A.
- [19] Van Der Linden, J., Schoonderwaldt, E., Bird, J., Johnson, R.: MusicJacket - Combining motion capture and vibrotactile feedback to teach violin bowing. *IEEE Transactions on Instrumentation and Measurement* **60**(1), 104–113 (2011). doi:10.1109/TIM.2010.2065770

- [20] Afzal, M.R., Lee, H., Yoon, J., Oh, M.K., Lee, C.H.: Development of an augmented feedback system for training of gait improvement using vibrotactile cues. 2017 14th International Conference on Ubiquitous Robots and Ambient Intelligence, URAI 2017, 818–823 (2017). doi:10.1109/URAI.2017.7992833
- [21] Shull, P.B., Lurie, K.L., Cutkosky, M.R., Besier, T.F.: Training multi-parameter gaits to reduce the knee adduction moment with data-driven models and haptic feedback. *J Biomech Eng.* **44**(8), 1605–1609 (2011). doi:10.1016/j.jbiomech.2011.03.016
- [22] Koritnik, T., Koenig, A., Bajd, T., Riener, R., MuniH, M.: Comparison of visual and haptic feedback during training of lower extremities. *Gait and Posture* **32**(4), 540–546 (2010). doi:10.1016/j.gaitpost.2010.07.017
- [23] Shull, P.B., Jirattigalachote, W., Hunt, M.A., Cutkosky, M.R., Delp, S.L.: Quantified self and human movement: A review on the clinical impact of wearable sensing and feedback for gait analysis and intervention. *Gait and Posture* **40**(1), 11–19 (2014). doi:10.1016/j.gaitpost.2014.03.189
- [24] Burke, J.L., Prewett, M.S., Gray, A.A., Yang, L., Stilson, F.R.B., Coovert, M.D., Elliot, L.R., Redden, E.: Comparing the effects of visual-auditory and visual-tactile feedback on user performance: a meta-analysis. In: Proc. of the 8th International Conference on Multimodal Interfaces, Canada, pp. 108–117 (2006)
- [25] Martinez, M., Constantinescu, A., Schauerte, B., Koester, D., Steifelhagen, R.: Cognitive evaluation of haptic and audio feedback in short range navigation tasks. In: Proc. of the International Conference on Computers for Handicapped Persons, ICCHP, pp. 128–135 (2014)
- [26] Shea, C.H., Wulf, G.: Enhancing motor learning through external-focus instructions and feedback. *Human movement science* **18**, 553–571 (1999)
- [27] Sigrist, R., Rauter, G., Riener, R., Wolf, P.: Augmented visual, auditory, haptic, and multimodal feedback in motor learning: A review. *Psychonomic Bulletin & Review* **20**(1), 21–53 (2012)
- [28] Wulf, G., Shea, C.H.: Principles derived from the study of simple skills do not generalize to complex skill learning. *Psychonomic Bulletin & Review* **9**(2), 185–211 (2002)
- [29] Salmoni, A.W., Schmidt, R.A., Walter, C.B.: Knowledge of results and motor learning: a review and critical reappraisal. *Psychological bulletin* **95**(3), 355–386 (1984)
- [30] Choi, S., Kuchenbecker, K.J.: Vibrotactile display: Perception, technology, and applications. In: Proceedings of the IEEE, pp. 2093–2104 (2013). IEEE
- [31] Mengüç, Y., Park, Y.-L., Martinez-Villalpando, E., Aubin, P., Zisook, M., Stirling, L., Wood, R.J., Walsh, C.J.: Soft wearable motion sensing suit for lower limb biomechanics measurements. In: Robotics and Automation (ICRA), 2013 IEEE International Conference On, pp. 5309–5316 (2013). IEEE
- [32] Totaro, M., Poliero, T., Mondini, A., Lucarotti, C., Cairolì, G., Ortiz, J., Beccai, L.: Soft smart garments for lower limb joint position analysis. *Sensors* **17**(10), 2314 (2017)
- [33] Kang, S.-W., Choi, H., Park, H.-I., Choi, B.-G., Im, H., Shin, D., Jung, Y.-G., Lee, J.-Y., Park, H.-W., Park, S., *et al.*: The development of an imu integrated clothes for postural monitoring using conductive yarn and interconnecting technology. *Sensors* **17**(11), 2560 (2017)
- [34] Pettys-Baker, R., Compton, C., Utset-Ward, S., Tompkins, M., Holschuh, B., Dunne, L.E.: Design and development of valgus-sensing leggings. In: 2017 Design of Medical Devices Conference, pp. 001–0501700105017 (2017). American Society of Mechanical Engineers
- [35] Awad, L.N., Bae, J., Odonnell, K., De Rossi, S.M., Hendron, K., Sloot, L.H., Kudzia, P., Allen, S., Holt, K.G., Ellis, T.D., *et al.*: A soft robotic exosuit improves walking in patients after stroke. *Science translational medicine* **9**(400), 9084 (2017)
- [36] Afzal, M.R., Lee, H.-s., Oh, M.-k., Lee, J.-h., Yoon, J.: Effects of Vibrotactile Feedback on Human Learning of Arm Motions. *BioMed Research International* **2015**, 1–4 (2014)
- [37] Rogers, J.A.: A clear advance in soft actuators. *Science* **341**, 968–969 (2013)
- [38] Majidi, C.: Soft robotics: A perspective - current trends and prospects for the future. *Soft Robot* **1**, 5–11 (2014)
- [39] Yeo, W.-H., Kim, Y.-S., Lee, J., Ameen, A., Shi, L., Li, M.: Multifunctional epidermal electronics printed directly onto the skin. *Adv Mater* **25**, 2773–2778 (2013)
- [40] Verrillo, R.T.: Age related changes in the sensitivity to vibration. *Journal of gerontology* **35**(2), 185–193 (1980)
- [41] C++/C# Numerical Analysis Library
- [42] C++ Mathematical Expression Library (ExprTk)
- [43] Math.NET Symbolics
- [44] Mladenova, C., Mladenov, I.: Vector decomposition of finite rotations. *Reports on Mathematical Physics* (2011)
- [45] Brezov, D., Mladenova, C., Mladenov, I.: Vector decomposition of rotations. *Geometry and Symmetry in Physics* (2012)
- [46] Dobrowolski, P.: Swing-twist decomposition in clifford algebra. *CoRR* (2015)
- [47] Teng, H.-L., MacLeod, T.D., Link, T.M., Majumdar, S., Souza, R.B.: Higher knee flexion moment during the second half of the stance phase of gait is associated with the progression of osteoarthritis of the patellofemoral joint on magnetic resonance imaging. *Journal of Orthopaedic and Sports Physical Therapy* **45**(9), 656–664 (2015)
- [48] Ho, K., Blanchette, M., CM., P.: The influence of heel height on patellofemoral joint kinetics during walking. *Current Sports Medicine Reports* **35**, 271–275 (2012)
- [49] Teng, H.-L., C.M., P.: Sagittal plane trunk posture influences patellofemoral joint stress during running. *J Orthop Sports Phys Ther.* **44**(10), 785–792 (2014)
- [50] Guo, W., Ni, W., Chen, I.M., Ding, Z.Q., Yeo, S.H.: Intuitive vibro-tactile feedback for human body movement guidance. 2009 IEEE International Conference on Robotics and Biomimetics, ROBIO 2009, 135–140 (2009). doi:10.1109/ROBIO.2009.5420612

## The Capacity Factor of Renewable Energy Power Plants During Electric Power Peak Times in Jeju Island

Zulmandakh Otgongerel, Gaemyoung Lee\*, Ankhzaya Baatarbileg

*Department of Electrical Engineering Jeju National University, Jeju, 63243, South Korea*

### ARTICLE INFO

*Article history:*

*Received: 29 January, 2020*

*Accepted: 27 March, 2020*

*Online: 08 April, 2020*

*Keywords:*

*Renewable energy*

*Solar power plant*

*Wind power plant*

*Capacity Factor*

*Peak period*

### ABSTRACT

*Jeju Island is the largest island of South Korea and has an independent electric supply system. The island has a special energy plan that realizes itself a carbon-free region by 2030. Wind and solar energy resources are considered as an important means. The introduction of weather-variable renewable energy generation sources into the electric power system makes it unstable. The main content of this study was to investigate the capacity factor of large scale renewable energy (solar, wind) power plants operated in Jeju Island during the electric power peak time. We can see their utilization rate or contribution rate during the power peak time by the value of their capacity factors. The largest 18 solar power plants (SPP) and 8 wind power plants (WPP) on the island were chosen and the 4, 12, 25, 50 and 100% electric power peak times were set for this study. There are two electric power peak seasons, summer and winter, in Jeju Island when the electric power demand arrives at peak. Generation of renewable energy plants depends on weather and the climates of the 5 regions of Jeju Island are a little different from one another. So, we investigated the difference between the average capacity factors of the 5 region's renewable plants. WPPs showed a high contribution to the power grid only during winter peak time and SPPs did high contribution to the power grid only during summer peak time, while WPPs showed low contribution to the power grid during summer peak time and SPPs did low contribution to power grid during winter peak time. WPPs and SPPs have inter-compensation relation in the aspect to contribute to the power grid.*

### 1. Introduction

Population increase and industrialization have resulted in rapid increases in energy consumption and greenhouse gas (GHG) emissions. Therefore, many countries have been focusing on the wider application of renewable energy. South Korea also announced the "Renewable Energy 3020 Plan" in 2017 [1]. The global utilization of renewable energy increases annually and renewable plants are one of the largest factors in the world energy system. The capacity of the renewable power plants installed in 2018 was 181 GW and the annual electric energy generated by renewable sources grew by an average of 3.8 percent from 1990 until 2018, which is higher than the average increase rate of 2.9 percent of total electricity generation [2]. In addition, renewable power capacity totaled 2,378 GW (including hydropower) and 1,246 GW (not including hydropower). By the end of 2018, 230 countries proposed 100% renewables in at least one sector, and 169 countries adopted renewable energy targets. [3]. The international

energy agency reported that wind power systems are the second fastest growing source of renewable electric energy after solar power systems. Furthermore, between 1990 and 2018, growth of electric energy generated by wind power plants from 3.8 TWh to 745.2 TWh showed an average annual increase rate of 20.7% [4]. Between 2005 and 2017, the world photovoltaic electricity production increased from 4TWh to 444TWh [5]. In 85 countries, states and provinces with renewable portfolio standards have the targets to produce more than 50% of their electric energy using renewable energy plants [6]. These documents showed that solar and wind resources are the lead renewable energies worldwide and this power plant technology has developed rapidly over the last few years.

Jeju's regional government announced the "Carbon Free Island by 2030 Plan (CFI2030 Plan)" in 2012 [7], which is to realize itself a carbon-free region by 2030. The capacity of renewable (solar and wind) electric power plants were expected to reach 4.15GW by 2030, which consists of on-shore wind power plants 0.45 GW, off-

\*Gaemyoung Lee, Jeju National University, myounglk@jejunu.ac.kr

[www.astesj.com](http://www.astesj.com)

<https://dx.doi.org/10.25046/aj050268>



shore wind power plants 1.9 GW and photovoltaic power plants 1.8 GW.

Also, about 377,000 electric vehicles will run on the island by 2030 [8]. In the case of the Jeju Island, WPPs and SPPs were estimated about 260.6MW and 160.8MW in 2018 [9]. In the aspect of supply and consumption of electric energy, demand and supply must be always equal to each other. Namely, the electric power of the supply side must be always equal to one of the demand side. Also, the supply side always has more than electric power capacity than the demand side needs and then has sufficient electric generation plants to supply timely the demand side with electric energy. The problem is that renewable electric power plants such as WPPs and SPPs can't always control the amount of generation according to the request of the demand side because their generation depends on the weather. Unlike the existing other power generation resources, renewable power generation sources cannot be rated. If extra generation facilities that cover the stop of the renewable electric power plants were reserved, the problem will be solved, but it needs big cost. Therefore, the estimation of the average contribution of renewable electric power plants during the electric power peak time when most generation facilities will be operated is very important.

There are a few case studies on how to approximate the supply capacity of renewable power resources [10, 11]. Some studies used the capacity factor as a measure of how much energy is generated by power plants compared to their maximum output. Ref [12] explained and compared the peak-period capacity factor method and effective load-carrying capability method, and Ref [13] analyzed the capacity value of locations in the south-western United States. Similarly, ref [14] estimated the capacity factor of SPPs in Korea.

The electric energy supply side must have sufficient electric power during even electric power peak times in summer and winter seasons. It is very important in designing a stable energy mix for a region to know the past statistical contribution of renewable power plants (SPPs and WPPs) during the peak times in the peak seasons because the renewable power plants cannot be always operated when the demand increases. This study is going to examine the contribution of SPPs and WPPs to the power grid by evaluating their capacity factors during the electric power peak times in Jeju Island.

## 2. Methodology

### 2.1. Regional grouping of renewable power plants

Jeju Island is the largest island in South Korea and locates in North-East Asia. The island has four distinct seasons. Winter is cool and dry while summer is hot, sometimes rainy and humid [15]. In the case of renewable energy plants, unlike conventional thermoelectric power plants, their power capacity possible to supply is determined by climate or weather. To suggest the regional generation characteristics of renewable power plants, grouping them needs according to the climates of the regions at which they are installed. In this study, 8 wind power plants and 18 solar power plants were selected and grouped into the three and the four regions respectively. Furthermore, we chose the WPPs and SPPs with the power capacity of more than 0.5MW and 15MW respectively for this study.

The Korea Meteorological Administration divided Jeju Island into the 5 regions according to weather; western, eastern, southern, northern and mountain regions.

Figure 1 shows the regional grouping of solar power plants (SPPs). The mountain region is not selected because it has a few SPPs. In this paper, we selected the SPPs that have generation data for more than two years.

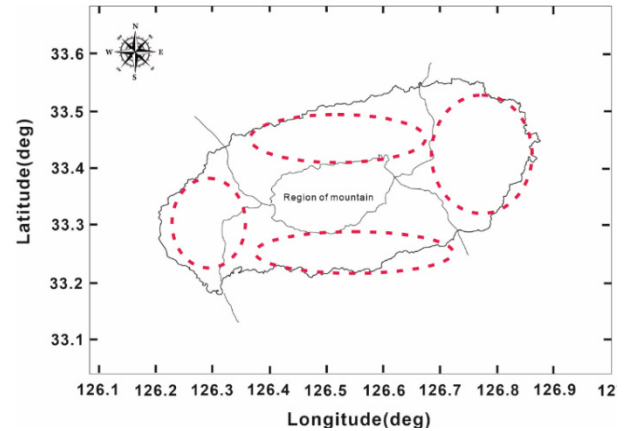


Figure 1: Regional grouping of solar power plants

Figure 2 shows the regional grouping of wind power plants. Wind farms were usually constructed in the west and east parts because both regions have a strong windy climate. Let call the 3 regions western, eastern and southern regions respectively.

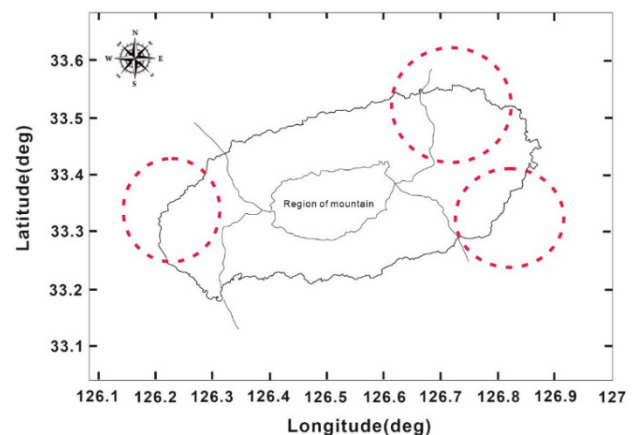


Figure 2: Regional grouping of wind power plants

### 2.2. Data sources

The data on the hourly average electric power demand of Jeju Island for three years (2015-2017) was used to define its electric power peak time and was obtained from the Korean Power Exchange Company (KPX). The data on the hourly electric energy generated by wind and solar powers over three years (2015-2017) are also obtained from KPX.

### 2.3. Choosing the electric power peak seasons

Figure 3 shows the average electric power demand of Jeju Island for three years (2015-2017). The electric power peak occurred in July and August in the summer season and December and January in the winter season.

Winter electric power peak season was chosen from December to January and the summer electric power peak season was done from June to August in this study.

2.4. Defining the electric power peak times

The electric power peak time can be selected from the data on the electric demand during the electric power peak day within the specific period, or can be done from the data on the average electric demand during the specific electric power peak season. We choose the latter because, usually, the renewable power plants always operate in the case that weather matches. In this study, the data on the average electric demand during the winter and the summer electric power peak seasons was used in determining the electric power peak time.

This study suggested an electric power peak time system with the five types of electric power peak times: the 4, 12, 25, 50 and 100% electric power peak times. They mean to have the 1, 3, 6, 12 and 24 hours intervals, respectively, in the order of the volume of electric power demand. Let's call them as the % electric power peak times. The electric power demand curve in Figure 4 shows the July-August average power demand for the 3 years (2015-2017) in the respective time interval. In Figure 5 does the December-January's one. We selected the % electric power peak times during the summer and the winter electric power peak seasons from Figure 4 and 5.

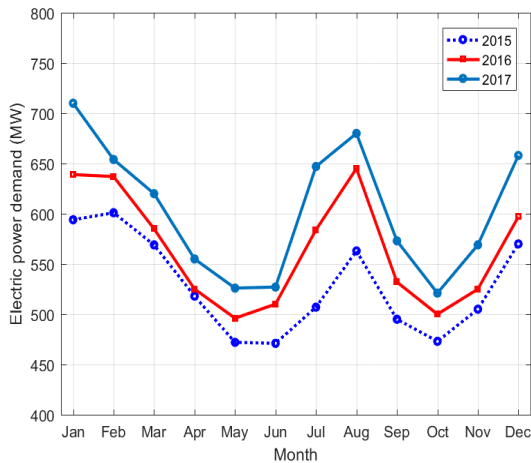


Figure 3: Monthly average electric power demand on the island (2015-2017)

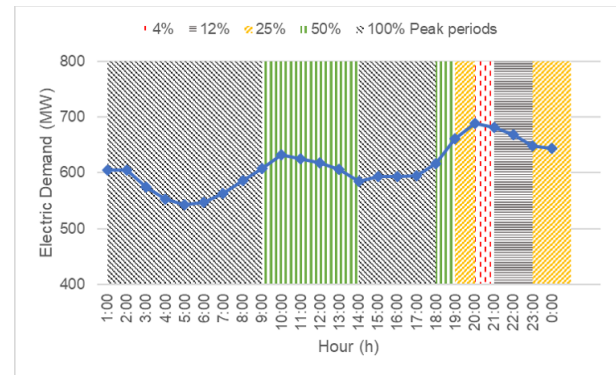


Figure 5: Classification of the % peak periods in winter (Dec-Jan)

2.5. Calculation of the capacity factor

The utilization rate of an electric power plant can be estimated as the parameter, capacity factor. The capacity factor of an electric power plant, *CF* is obtained following equation:

$$CF = \frac{GE(Wh)}{T(day) \times 24(hour/day) \times C(W)} \times 100(\%) \quad (1)$$

where *T* is the period that the plant has been operated, *C* is its electric power capacity and *GE* is the electric energy generated during the time interval *T* by it. The capacity factor of the *N* electric power plants, *CF(N)* is obtained by the equation:

$$CF(N) = \sum_{i=1}^N \frac{GE_i(Wh)}{T_i(day) \times 24(hour/day) \times C_i(W)} \times 100(\%) \quad (2)$$

where *T<sub>i</sub>* is the period that the *i* plant has been operated, *C<sub>i</sub>* is the electric power capacity of the *i* plant and *GE<sub>i</sub>* is the electric energy generated during the time interval *T<sub>i</sub>* by the *i* plant. The capacity factor of multiple plants is calculated as the weighted average value and is not as simple an arithmetic average.

3. Results & Discussion

3.1. Capacity factors of wind power plants and solar power plants during 2015-2017 in Jeju Island.

Yearly-average capacity factors of WPPs and SPPs in the respective hour interval are shown in Figure 6 and Figure 7, respectively. The capacity factor of an electric power plant means the utilization rate of the plant. The operation of wind or solar power plants depends on weather.

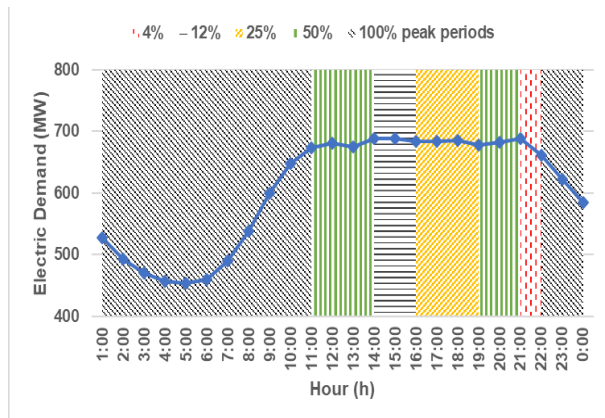


Figure 4: Classification of the % power peak periods in summer (Jul-Aug)

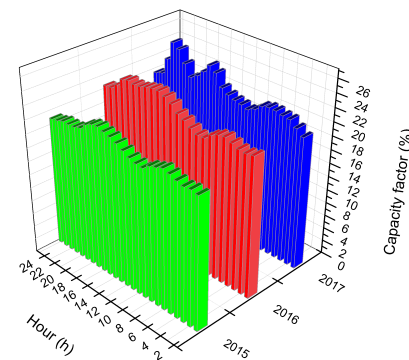


Figure 6: Average CF of WPP on the island (2015-2017)

Figure 6 shows some regular trend of generation time of WPPs, namely generation amount increasing in the morning and in the evening. This trend attributes to an island climate that regular wind flows from sea to land in the morning and from land to sea in the evening. Figure 6 shows the capacity factor range from 19% to 25%.

Figure 7 shows a daily trend of SPPs, the capacity factors of SPPs ranging from 0% to 50%. Generation occurs only daytime and reaches the peak at noon because 100% of SPPs in Jeju Island is the fixed type which does not track moving sun.

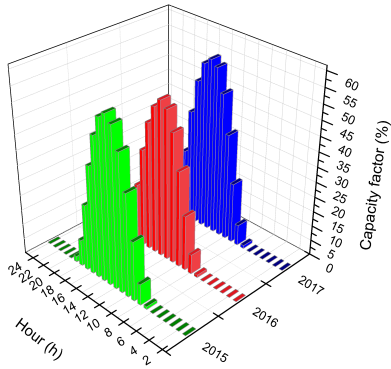


Figure 7: Average CF of SPP in the island (2015-2017).

Table 1 shows the yearly average capacity factors of regional WPPs and SPPs. The western region is shown to have better competitiveness for solar power plant business.

Table 1: Average CF of renewables on an island (2015-2017).

Region	North	East	South	West
Wind power plant	-	23.2%	22.2%	21.0%
Solar power plant	12.6%	12.8%	13.5%	17.1%

### 3.2. Capacity factor of the wind power plants during the electric power peak times

Figure 8 and Figure 9 show the capacity factors of the 3 regional wind power plants during summer and winter electric power peak times, respectively. The capacity factors are ranged from 9% to 15% during all summer % peak times in all regions in Figure 8, while those are ranged from 32% to 38% during all winter % peak times in all regions in Figure 9. The average annual capacity factor of WPPs over 3 years (2015-2017) in Jeju was calculated as 22.1%. Therefore, we can say WPPs in Jeju make a larger contribution to the electric power supply system in winter than in summer.

Generation of WPPs in summer is much below the annual average. Let's compare the difference of the 3 regional capacity factors of WPPs. In the summer peak time within 50% peak time, WPPs in the southern region makes a larger contribution to the electric power supply system than WPPs in the eastern and the western regions by about 1-3% in capacity factor. In the winter peak time within 50% peak time, WPPs in the western region make a larger contribution to the electric power supply system than

WPPs in the eastern and the southern ones by about 1-3% in capacity factor. But, we can think that, in the winter peak time, there is no difference in the capacity factors of the 3 regions' WPPs because they have more than 30% capacity factor.

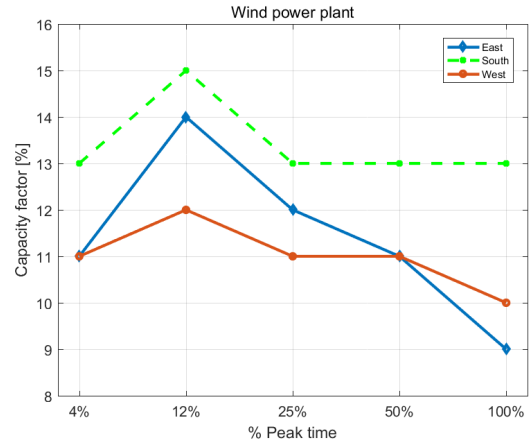


Figure 8: Capacity factor of the wind power plants during the summer electric power peak season (July-Aug)

Next, let's discuss whether WPPs generate more electric energy at peak time than at the nonpeak time. Figure 8 and Figure 9 show that the values of capacity factors at 4, 12 and 25% peak times are larger than those at 100% peak time. Generation by wind and solar cannot increase when we want or demand for electric energy increases. Also, it is necessary and important that WPPs and SPPs generate statistically more electric energy during peak time than during nonpeak time though their generation depends on the weather. WPPs in any region of Jeju Island, luckily, generated statistically more electric energy during electric power peak time than during electric power nonpeak time.

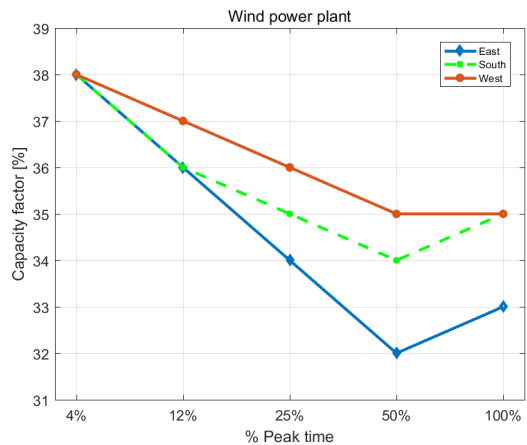


Figure 9: Capacity factor of wind power plants during winter electric power peak season (Dec-Jan)

### 3.3. Capacity factor of the solar power plants during the electric power peak times

Figure 10 and Figure 11 show the capacity factors of the 4 regional solar power plants during summer and winter electric power peak times, respectively. The capacity factors are ranged from 0% to 32% during all summer % peak times in all regions in Figure 10, while those are ranged from 0% to 12% during all winter % peak times in all regions in Figure 11.

The average annual capacity factor of SPPs over 3 years (2015-2017) in Jeju was calculated as 14.0%. Therefore, we can see that SPPs in Jeju Island contribute greatly to the electric power supply system during summer peak time except during 4% peak time with 1 hour duration, while they do not contribute to it and have the capacity factor below the annual average in winter peak time. Figure 11 shows the contribution of SPPs in all regions to an electric power supply system is zero within 25% peak time duration during the winter peak time.

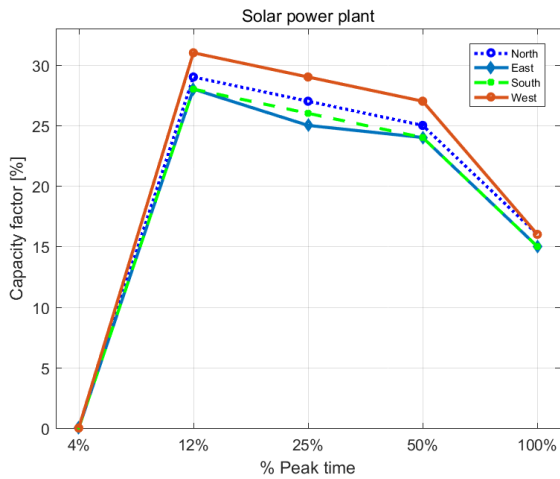


Figure 10: Capacity factor of the solar power plants during the summer electric power peak season (July-Aug)

In the case of SPPs, the regional difference of contribution to the electric power supply system is not shown during the summer and winter electric power peak times, but it is distinguished that the capacity factor of SPPs in the northern region is half of it in other regions during the winter peak time.

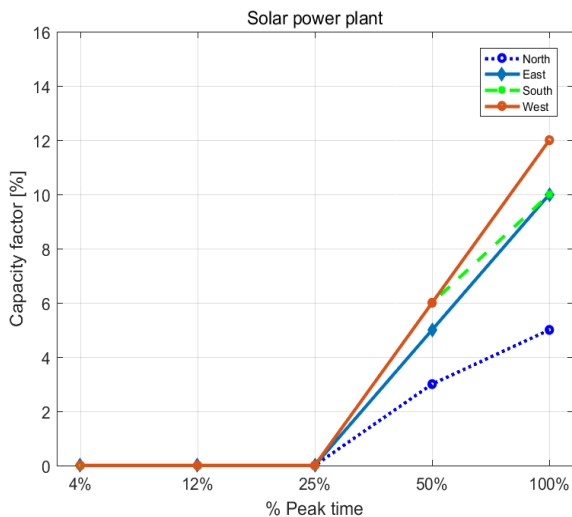


Figure 11: Capacity factor of solar power plants during winter electric power peak season (Dec-Jan)

### 3.4. Total discussion

In Jeju Island, there are two seasonal electric power peak times. They are the summer and winter peak times. Summer peak time attributes to cooling load and winter peak time to the heating load. We can see, from the electric demand patterns of Figure 4

and Figure 5, that, in the case of the summer peak time, considering the peak duration until 50% peak time needs and, in the case of the winter peak time, considering the peak duration until 25% peak time does.

WPPs showed a high contribution to the power grid only during the winter peak time and SPPs did high contribution to the power grid only during the summer peak time, while WPPs showed low contribution to the power grid during the summer peak time and SPPs did low contribution to power grid during the winter peak time. WPPs and SPPs have inter-compensation relation in the aspect to contribute to the power grid. We think this inter-compensation relation may usually take place in other regions of the world. It is lucky in aspect to penetrate WPPs and SPPs on large scale. Nevertheless, it will be a big problem, in the future that SPPs will have been penetrated on large scale, SPPs can't make any contribution to the power grid during the 4% peak time in summer in Jeju Island because the peak time is at evening.

It is one of the most important research themes in the renewable field to evaluate how much the specific renewable plants contribute to the power grid during the electric power peak time. This paper is to have examined the contribution of WPPs and SPPs to the power grid during the winter and summer power peak times in Jeju Island to be a carbon-free region by 2030. We were able to understand easily the contribution of renewable plants through introducing the concept of the % peak time in this paper.

### 4. Conclusion

The supply side must have sufficient electric power during even power peak times in summer and winter seasons. It is very important in designing a stable energy mix for a region to know the past statistical contribution of renewable power plants (SPPs and WPPs) during the peak times because the renewable power plants cannot be always operated when the demand increases. This study examined the contribution of SPPs and WPPs to the power grid by evaluating their capacity factors during the electric power peak times in Jeju Island.

The large scale solar and wind power plants in Jeju Island were grouped into four and three regions, respectively, depending on climates of their location. The % peak time was defined and is divided into the 4%, 12%, 25%, 50% to 100% peak times.

WPPs showed a high contribution to the power grid only during winter peak time and SPPs did high contribution to the power grid only during summer peak time, while WPPs showed low contribution to the power grid during summer peak time and SPPs did low contribution to power grid during winter peak time. WPPs and SPPs have inter-compensation relation in the aspect to contribute to the power grid. We were able to understand easily the contribution of renewable plants through introducing the concept of the % peak time in this paper.

### References

This research was supported by the 2019 scientific promotion program funded by Jeju National University



## References

- [1] IEA, Key World Energy Statistics 2018.
- [2] IRENA (2019), Renewable Energy Statistics 2019, The International Renewable Energy Agency, Abu Dhabi.
- [3] Report citation Renewables 2019 Global Status Report REN21, 2019
- [4] Renewables information: overview (2019 edition), International Energy Agency.
- [5] A.Gusmao M.Grossbock, Sandi Aramco "Capacity value of photovoltaic and wind power plants in an isolated Mini-grid in the Kingdom of Saudi Arabia" conference paper.
- [6] Korea wind and energy industry association (2018) <http://www.kweia.or.kr/> (accessed 30 August 2018).
- [7] Sang-Hyun Kang, "Analyzing the Capacity of an ESS for Mitigating the Fluctuations in the Dongbok-Bukchon Wind Farm" Jeju National University, the Degree of the master, 2017
- [8] Seyed Hossein Madani, Ramteen Sioshansi, Paul Denholm" Comparison of Capacity Value Methods for Photovoltaics in the Western United States" Technical Report NREL/TP-6A20-54704, July 2012.
- [9] Shuai Lu, Nader Samaan, Ruisheng Diao, Pevel Etingov "Capacity Value of PV and Wind Generation in the NV Energy System" Pacific Northwest national laboratory, September 2012.
- [10] Navid Haghdahi, Anna Bruce, Iain MacGill, and Robert Passey "Impact of distributed Photovoltaic Systems on Zone Substation Peak Demand" IEEE Transactions on sustainable energy, Vol9, No 2, April.2018.
- [11] Seyed Hossein Madaeni, Student Member, IEEE Ramteen Sioshansi, Member, IEEE, and Paul Denholm, Member, IEEE "Estimating the Capacity Value of Concentrating Solar Power Plants: A Case Study of the Southwestern United States" conference paper.
- [12] Suchitra Subramaniyan, Mobi Mathew, Dr. Jami Hossain "Renewable Energy Capacity Value Estimation using Peak Period Method in Rajasthan" 2018 3<sup>rd</sup> International Conference for Convergence in Technology, India, Apr 06-08,2018.
- [13] Mehdi Shahriari, Seth Blumsack "The capacity value of optimal wind and solar portfolios" Energy 148 (2018) 992-1005.
- [14] Cai Jilin, Xu Qingshan, Wang Xudong, Jiang Ling "Estimation for the Capacity Value of PV and Wind Plants Considering Output Correlation" Published by Elsevier Ltd, 1876-6102, 2017.
- [15] Chunhyun Paik, Yong Joo Chung, Young-Jin Kim "CF-based Approximation Approach for Calculating Capacity Credit of Solar Power in Korea" Journal of the Korean Solar Energy Society Vol37, No5, pp.13-26, October 2017

## **Approach to Combine an Ontology-Based on Payment System with Neural Network for Transaction Fraud Detection**

Ahmed EL Orche\*, Mohamed Bahaj

<sup>1</sup>*Faculty of Sciences and Technologies, Hassan 1st University, Settat, Morocco*

---

### ARTICLE INFO

*Article history:*

*Received: 17 November, 2019*

*Accepted: 18 March, 2020*

*Online: 08 April, 2020*

---

*Keywords:*

*Ontology*

*Machine learning*

*Neural network*

*Payment system*

*Fraud*

---

---

### ABSTRACT

*Fraud, as regards means of payment, means the behavior of any legal or natural one that makes an abnormal or irregular use of a way of payment, elements of it or information contained therein, to improperly obtain an honest, service or enrichment, and or causing financial damage to the one that has distributed the means of payment to a user or a 3rd party; Contests in bad faith a legitimate payment order of which she is that the initiator. during this paper we are getting to propose an approach to managing the risks, it consists to mix a machine learning with an ontology-based on a payment system to succeed in this objective. Machine learning may be a field of study that improves their performance in solving tasks without being explicitly programmed by each. An ontology is that the structured set of terms and ideas that represent the meaning of an information field, whether by the metadata of a namespace, or the elements of a domain of knowledge.*

---

### **1. Introduction**

Artificial Intelligence (AI) has come to the fore, with many companies using them to develop their solutions and/or services. If AI is a global concept, Machine Learning (ML) is a technology that allows machines to access data so that they can learn, predict, and categorize information. ML is a branch of artificial intelligence, which is mainly based on the automatic construction of statistical models based on the widest possible body of learning.

Deep Learning is a sub-branch of this discipline, which uses as model neural networks, very complex with many layers. This approach, which has been made popular by the availability of low-cost computing power.

With AI and ML, companies can enrich and leverage this information. Finally, via pre-established models, they will be able to test the results obtained and reiterate them throughout the life cycle.

The adoption of ML has been accelerated by increased data processing power, the development of Big Data and advances in statistical modeling.

It relies on complex statistical methods and high computing power. At the heart of this concept, however, is a very simple idea.

By identifying relationships, the most influential cause-and-effect of the past, a machine can learn to make accurate predictions for the future. The ML is based on powerful computers that are guided by human intelligence to sift through billions of data and identify cause-and-effect relationships. Then all this information is introduced in a variety of algorithms to come up with predictions. With time, computers improve in identifying these cause-and-effect relationships, they exploit the knowledge they have acquired and use it to refine the algorithms. It is "learning" that takes place and with a much faster processing speed than that of the human brain.

The fraud tracked and resolved by ML?

Fraud detection is a big challenge. However, Fraudulent transactions are few and represent a very small part of the activity within an organization. Nevertheless, a small percentage of the business can quickly turn into significant financial losses without the right tools and systems in place to deal with. Cybercriminals are smart. The traditional fraud schemes are no longer effective, they have made them evolve. The good news is that with Machine Learning advances, systems can learn, adapt and discover new ways to prevent fraud.

On the other hand, many strengths make ML such a powerful and effective tool in the fight against fraud:

---

\* Ahmed EL Orche, Email: [ahmed.elorche@gmail.com](mailto:ahmed.elorche@gmail.com)

- Facilitate real-time decision-making: Rule-based systems, to determine the types of orders to accept or reject, require a lot of time and manual interaction. The ML can help evaluate a large number of transactions in real-time.
- Improving Accuracy: Cybercriminals have become more sophisticated and more skilled at hiding fraud. ML can often be more effective than humans in detecting subtle or unintuitive patterns to identify fraudulent transactions. It can also help avoid "false positives", good orders that are mistakenly identified as fraudulent.
- React quickly to change: Fraudsters constantly changing tactics. ML continually analyzes and processes new data, and then updates its models autonomously to reflect the latest trends.
- Reduce Costs: Technological innovations have reduced the costs associated with ML solutions and the computer systems that can make them work. As ML improves accuracy, it also reduces costly false positives and minimizes the time and cost of manual revisions.

In general, fraud management solutions rely on two types of ML models to combat payment fraud. On one side are static models that learn to identify fraud at a given moment by sifting through millions of past transactions. Static models are effective in identifying historical patterns of fraud and tend to work well after they are implemented. The problem is that there is no way to update or to adjust these models as new patterns of fraudulent activity emerge. On the other side are ML models based on self-learning that continually integrate data from new transactions to adapt and recognize evolving fraud patterns.

Self-learning models are very effective in identifying the latest fraud techniques. However, the "black box" nature of these models makes it almost impossible for a human to follow, control or adjust what the machine learns, which means that the model can suddenly cause enormous problems if he makes bad choices and starts blocking reliable customers.

All ML solutions are not based solely on static models or self-learning models. There is a middle ground that can compensate for ML weaknesses by combining an automated system with a rules-based approach. The rules serve as a guideline for companies to better control fraud decisions in real-time.

An ontology is an explicit specification of a conceptualization and a conceptualization is an abstract and simplified worldview that one wants to represent for a given goal (Gruber, 1993). The explicit representation of information occupies a place important in software development.

In the case of classical software development, we are interested in data structures centered on algorithms that enable ease of understanding and maintenance as well as efficiency in terms of memory and execution time. What interests the developer of the ontology is rather a representation centered on a conceptualization answering the aims of the ontology. This conceptualization is based on the real world because it consists of a simplified vision of it.

The representation of knowledge by ontology has several advantages that make this technology interesting. The attributes that are retained here are its simplicity, its flexibility, the possibility of applying reasoning and the possibility of questioning it at various levels of abstraction.

Describing data in an ontology is an important phase in the approach proposed in this paper, [1] presents a method to migrate a relational database to an ontology by taking into account the semantics of the data, this method is based on two levels ontology model (TBOX) and individuals (ABOX), it is the same method as we adopted. While the [1] presents this method, the aim of the [2] is the synchronization between the RDB and the ontology.

The history of AI shows that knowledge is important for intelligent systems. In many cases, better knowledge could also be more important in solving a task than better algorithms. To possess truly intelligent systems, knowledge must be captured, processed, reused and communicated. The ontologies support of these tasks.

The term "ontology" can be defined as an explicit specification of conceptualization. The ontologies capture the structure of the domain, which is to say the conceptualization. This includes the domain model with possible restrictions. The conceptualization describes the knowledge of the domain, not the particular situation of the domain. In other words, the conceptualization does not change or changes very rarely. The ontology is then the specification of this conceptualization - the conceptualization is specified using a particular modeling language and particular terms. A formal specification is necessary to be able to process ontologies and operate on ontologies automatically.

An ontology describes an area, while a knowledge base (based on an ontology) describes a particular situation. Each knowledge-based system or agent has its knowledge base. Only what can be expressed using an ontology can be stored and used in the knowledge base. When an agent wants to communicate with another agent, he uses the constructions of certain ontologies. To understand communication, ontologies must be shared between agents.

This paper is only an extension of a work already started in papers [2]-[5], and the added value is how we combine an ontology-based on a payment system with a machine learning to detect and prevent frauds on a payment system.

In [3] and [4], an approach has been proposed and described for detecting and preventing suspicious transactions on a payment system using an ontology. the approach shares and adopts rules to prevent cases of fraud on an ontology-based on a payment system. In [2] and [5], we described the way to migrate a relational database to an ontology, this approach allows to explain well the first steps of our work, because most of the payment systems in the world use this type of databases, algorithms, and rules are well described in papers to migrate schema and data. The other papers in the references are all discussing how to fight or prevent fraud in any system via machine learning and/or how to design and present an ontology. Each paper enriches the current paper with the following. For large multi-stakeholder systems such as the electronic payment systems that we are trying to study, [6] proposes to what degree the ontology must be heavy to meet the

needs of the different players in this system. the paper presents a set of important requirements in this paper and will be pre-requisites in the design in the current ontology. in addition to that, we will also take into consideration the modeling of the graphic means used in [7], guide and help the experts in the field to determine the "best" adaptation to existing rules to capture all fraudulent transactions and, respectively, omit all legitimate transactions as presented in [8], how semantic technologies could make investigations of cybercrime more efficient in [9]. this paper also builds on the strength of BIM on semantic web technology to establish an ontology of risk knowledge [10]. in another way, our approach takes into consideration the study which presents an approach lies in the use of the technique-driven by the ontology which not only minimizes the data the cost of modeling but also makes the expert system extensible and reusable for different applications [11]. and finally, it takes into consideration the possibility of arriving at a formal integrative ontology and sufficiently general generic primitives to describe the semantics of the concepts of specialized knowledge domains is far from being acquired [12].

## 2. Payment systems

The Internet allows us to shop, pay bills, make transfers and buy everything without having to move. With the growth of purchases made on the web, the concern about the security of electronic payments is still present. Online trading platforms ensure secure payment methods to gain the trust of customers. To check if online payments are secure, you first need to understand things like how purchases and electronic payments work.

### 2.1. Payment systems architecture

A payment system is an infrastructure of the financial market dedicated to the transfer of funds by clearing and/or settlement based on a or several means of payment. It is made up of elements below:

- A formal multilateral agreement between an operator which can be a central bank, or a structure interbank and financial institutions called "participants";
- Operating rules and procedures standardized.
- A technical infrastructure agreed between operator and participants.
- A risk management system both at the level of the operator than of the participants.
- One or more means of payment. Way to payment is an instrument for transferring funds, whatever the medium or process used. As an illustration, cash, check, transfer, bill of exchange, promissory note as well that direct debit is means of payment.

Electronic payment systems involve the six participants as Figure 1 shows.

- Cardholder designates the holder of a bank card, of which he is the bearer. It is the bank that issues it, on the one hand to its name and with its logo, and on the other hand to the name of the holder.

- The payment card is a small plastic rectangle, measuring 85.60 × 53.98 mm, offered by financial institutions. It is equipped with a magnetic card and a chip, which allows electronic reading from a distance.

Synonymous with a credit card, the payment card is both in the name of the issuing bank and in the name of its holder. It allows the latter to make withdrawals from ATMs, to pay for purchases from a large number of merchants, as well as on virtual terminals on the Internet. The amount is then debited from his bank account.

- An acceptor is a commercial or service establishment that accepts, for its account or that of its network, the payment of goods or services via an electronic money instrument.
- An acquirer is an entity or entities that hold deposit accounts for the acceptor (merchant) card and to whom the card acceptor transmits transaction data. The acquirer is responsible for collecting information on transactions and settlement with the acceptor.
- The payment system network is an institution that transmits information and funds through a payment system network. It may operate as an agent or a principal.

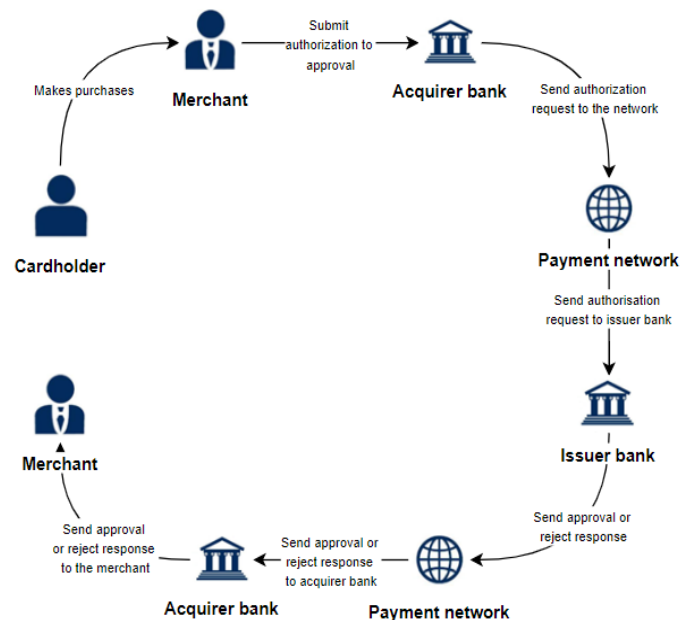


Figure 1: Payments system process

### 2.2. Electronic payment: principle and operation

Electronic payment replaces traditional payment in internet transactions. Today, with businesses opening up to e-commerce and Internet users increasingly connected, electronic payment is used by a majority of consumers in countries around the world. The advantage of online transactions is accessibility and speed. There is no need to move or queuing in department stores.

### 2.3. Electronic payment methods

To make an online payment, it should have a powered account. Several online payment methods have been developed in recent



years. The smart card can pay for purchases in the store using the TPE, but also to make payments online. With digitalization, the wallet or electronic wallet facilitates transactions. No need to enter each time the figures of a card so that a payment is validated.

Today, with the opening on electronic payments, several directives are available that help ensure that transactions are secure:

- **SSL:** All sites on which you are trading, must use SSL to ensure the security of sensitive information and data on their site. SSL is represented by the small padlock in the URL bar and the web address that starts with HTTPS.
- **PCI compliance:** it protects against fraud. The data is encrypted and is not visible. PCI DSS (Data Security Standards in the Payment Card Industry) is a standard that tells merchants who use the web the requirements they must meet. These are designed to provide data protection, detect vulnerabilities, control access, monitoring, and information security policy. PCI compliance also considers the creation of tokens in a future release.
- **Tokenization:** This is a way to encrypt payment data. When a person enters the details of his credit card, they will be stored in the form of a token. In other words, the token will replace this information.
- **3D Secure:** this is to consider a password that will be sent to the owner of the card for example before validating the payment. In this case, every time a transaction is made with this card, the password is required.

In the same logic of these means of payment, we are confronted with a dynamic and changing market, with many new means of payment that proliferate, and we see the importance and growth of the use of payment methods more and more secure.

### 3. Payment system fraud

#### 3.1. How an online transaction works

To understand the risks of fraud, one must first understand who is involved in an online transaction. There are you, your client, the payment gateway provider and the payment corporate or company (Visa, MasterCard, American Express, etc.).

When a customer pays for their order it is not PayPal for example that transfers the money, but the customer's credit company that funds. The advance will be made in the measures where the card number is valid and the holder of it has enough credit for the transaction.

#### 3.2. Risks and consequences

In the financial world, an online transaction is considered as no card transaction. This is the most difficult type of transaction to protect, mainly because it is not possible to verify the identity of the cardholder. As a merchant, it is not necessary to be alarmed, but it is necessary to be aware that the current legal provisions favor the customer. Unfortunately, it has no guarantee that it will receive the money or any real remedy in the event of fraud. Even if the credit company authorizes the transaction if this card is

declared stolen, the credit company will reimburse the legitimate cardholder and it will lose the money.

Unfortunately, payment gateway providers cannot offer recourse when the credit company reimburses its customers for fraud. However, it is possible to configure gateways so that warn the customer when a transaction seems fraudulent. People who shop online are not recognized for their patience. it should make a compromise between a platform with a quick and easy payment process, which could have vulnerabilities and a safer but more complex platform that could discourage some customers.

#### 3.3. Fraud at the instant payment time, between tracking and profiling, the parade is called "artificial intelligence"

The issue of fraud takes on a new dimension with instant payment.

Artificial intelligence, which has been used to secure and prevent payment fraud, is even more justified for instant payment. One of its great strengths is to have flexible algorithms, which can lead to both millisecond controls on a mass of data, to adapt to changing behaviors, and profile the fraudsters. A human is unable to integrate these data in the time of his reasoning. Today, only an algorithm is adapted to block and advise the human in his decision making.

Although artificial intelligence demonstrates its ability to diagnose, anticipate and stop some of the fraud, it will remain complementary to the traditional parades implemented. The first step is to secure the hardware or acquisition channel, to block the entrance. As a priority, secure the smartphone, which is currently experiencing massive cyber-attacks, by downloading ad hoc software, listening parade and remote phone handshake. The second step, the enrollment to the service then the registration of the immediate beneficiaries, by strong authentication using application, token or biometric device based on artificial intelligence. In the third step, after entering the payment data, the payer confirms his payment by strong authentication. Fourth step, the bank or the payment service provider gives its agreement after the traditional controls of the type primo-use, ceilings, lists of beneficiaries, destination country, by integrating finer indicators generated by tools of scoring.

The success of building the Fraud Risk Management Building on the instant payment will go through a mixed.

### 4. Combining ontology and neural networks in the payment system.

An ontology-based on an electronic payment system is defined as a set of knowledge describing this domain, Once the ontology has been developed, it must also be managed. For example, building an ontology-based on another shared top ontology and using a modular design usually means use and easier maintenance. In this chapter, we focus on a part of the ontology related to the payment transactions to study and manage fraud cases.

This is the aim of which we will combine machine learning with this part of the ontology.

Figure 2 describes the approach using an ontology-based on the payment system and machine learning. creating and maintaining

an ontology-based on this system is not easy. and there are several ways to proceed. to adopt an approach to:

- Migrate all databases and data into ontologies according to a well-defined structure in an automatic way.
- Create ontology silently but this approach requires investigation of more resources for migration, synchronization, and maintenance.
- Follow a semi-automatic approach, by creating an ontology-based in a first step on the databases then add an extension to add more semantics and for describing non-existing cases in the database, functional and decisional cases Etc. the data migration must be automatic for the data of the database and by user intervention for external data.

Using machine learning to detect or prevent cases of fraud in this approach is done by an ontology data analysis by machine learning, extraction is generally done by the language Sparql with a data preparation in the form of machine learning.

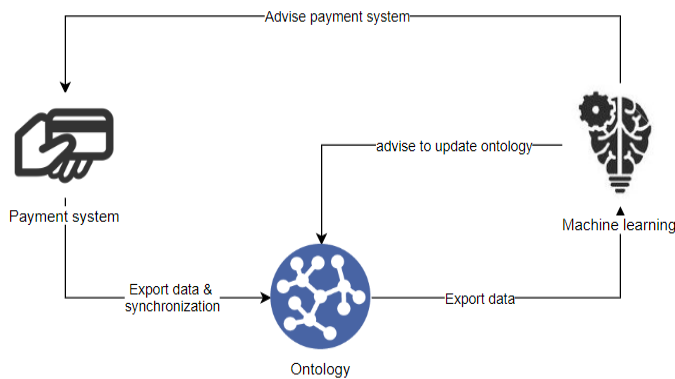


Figure 2: Combining ontology with Machine learning

In [2] and [5], we proposed an approach to migrate a relational database towards an ontology in 2 levels. the first level focuses on extracting the RDB schema, then creating an ontology model that is made up of a set of classes with data type properties and link to each other by object properties. This model constitutes the TBOX part of the ontology. The second level aims at extracting the data from the RDB and using it for assertions of the different elements of the model obtained at the first level. All of these assertions constitute the ABOX part of the ontology.

#### 4.1. Neural network for fraud detection

The detection of payment fraud has two very particular characteristics. The first is the very limited time in which the decision of acceptance or rejection must be made. The second is the huge amount of credit card transactions that need to be processed at some point. For example, millions of card transactions take place every day.

The Operating Principle of Neural Network Based Fraud Detection relies entirely on the operating principle of the human brain. The technology of neural networks has made a computer capable of thinking. While the human brain learns from past experiences and uses its knowledge or experience to decide in

everyday life, the same technique is applied with payment fraud detection technology.

When a consumer uses their credit card, there is a fixed pattern of credit card usage, created by the way the consumer uses their credit card. The use of the data neuron network for last years makes it possible to better understand the model of the use of a credit card by a consumer. The neural network contains information on the different categories of cardholders, such as cardholder occupation, income, occupation can fall into one category, while in another category, related information, this information includes the number of major purchases, the frequencies of major purchases, the place where these types of purchases take place, etc.

Within a specified time. Despite the pattern of card use, neural networks are also trained within the varied card frauds previously encountered by a bank. supported the card usage model, the neural network uses a prediction algorithm on this model data to classify the fact that a selected transaction is fraudulent or genuine. When the card is used by an unauthorized user, the neural network-based fraud detection system verifies the pattern employed by the fraudster and matches the rationale of the primary cardholder on whom the neural network has formed, if the pattern matches the neural network. declare the transaction ok.

The neural network layer during a card when a transaction arrives for authorization, it's characterized by a stream of authorization data fields that contain information identifying the cardholder and thus the characteristics of the transaction. Other data fields are often saved during a feed of the authorization system.

In most cases, banks don't archive logs of their authorization files. Only transactions sent by the merchant for payment are archived by the cardboard processing system of the bank. Thus, a gaggle of transaction data has been composed of an extract of the data stored within the Bank's settlement file.

Fraud detection model doesn't suggest that the transaction should exactly match the model, but the neural network to determine how far there is a difference if the transaction is on the brink of the model, the transaction is ok otherwise if there's a huge difference then the prospect of being an illegal transaction increases and thus the neural network declares the transaction by default. The neural network is supposed to provide a real value output between 0 and 1. There are cases where the transaction made by a legal user is different and it is also possible that the illegal person uses a card that corresponds to the model used for the formation of the neural network. Transaction OK probably fraudulent Age, income, occupation, cardholder Number of great purchases on the cardboard Frequency of major purchases Location where the transaction was made Detection of card fraud via a neural network.

#### 4.2. Neural network

A neural network is the association of elementary objects, in a complex graph. The main networks are distinguished by the organization of the graph, that is to say, their architecture, their level of complexity, by the type of neurons and finally the objective: supervised learning or not, optimization, dynamic systems, etc.

In summary, a biological neuron is a cell that is characterized by:

- Synapses, connection points with other neurons, fibers nervous or muscular.
- Dendrites or neuron inputs.
- Axons, or exits the neuron to other neurons or muscle fibers.
- The kernel activates the outputs according to input stimulations.

By analogy, the formal neuron is a model that is characterized by a state internal  $s \in S$ , input signals  $x_1, \dots, x_p$  and an activation function:

$$s = h(x_0, \dots, x_p) = g(\alpha_0 + \sum_{j=1}^n \alpha_j x_j) = g(\alpha_0 + \alpha'x) \quad (1)$$

The activation function performs a transformation of an affine combination input signals,  $\alpha_0$ , constant term, being called through the neuron.

This affine combination is determined by a vector of weight  $[\alpha_0, \dots, \alpha_p]$  associated with each neuron and whose values are estimated in the learning phase. They constitute the memory or distributed knowledge of the network.

The different types of neurons are distinguished by the nature of their activation function. The main types are:

- Linear  $g$  is the identity function,
- Seuil:  $g(x) = 1_{[0,+\infty[}(x)$
- Sigmoide:  $g(x) = 1/(1 + e^x)$
- Rectified linear unit:  $g(x) = \max(0, x)$
- Softmax: for each  $k \in \{1 \dots K\}$ ,  $g(x)_j = \frac{e^{x_j}}{\sum_{k=1}^K e^{x_k}}$
- Radiale:  $g(x) = \sqrt{1/2\pi}e^{-x^2/2}$
- Stochastic:  $g(x) = 1$  with probability  $\frac{1}{1 + e^{-x/H}}$ , 0 if not (H intervenes as the temperature in a simulated annealing algorithm).

Linear, sigmoidal, Rectified linear unit, softmax models are well adapted to learning algorithms involving (see below) a backpropagation gradient because their activation function is differentiable; these are the most used. The threshold model is probably more in line with the biological reality but poses learning problems. Finally, the stochastic model is used for global optimization problems of disturbed functions or again for analogies with particle systems (Boltzman machine).

#### 4.3. Multilayer Perceptron

The multilayer perceptron (PMC) is a network composed of successive layers. A layer is a set of neurons that have no connection between them. An input layer reads incoming signals, a neuron by input  $x_j$ , an output layer responds to the system. According to the authors, the input layer that does not introduce

any changes is not counted. One or more hidden layers participate in the transfer.

In a perceptron, a neuron of a hidden layer is input connected to each of the neurons of the previous layer and output to each neuron of the next layer.

For the sake of consistency, the same notations have been kept through the different chapters. Thus, the inputs of a network are still denoted  $X_1, \dots, X_p$  as the explanatory variables of a model, while the weights of the inputs are parameters  $\alpha, \beta$  to be estimated during the learning procedure and the output, is the variable  $Y$  to explain or target the model.

A multilayer perceptron thus realizes a transformation of the input variables:  $Y = f(x_1, \dots, x_p; \alpha)$  where  $\alpha$  is the vector containing each of the parameters  $\alpha_{jk}$  of the  $j$ th input of the  $k$ th neuron of the  $l$  layer; the input layer ( $l = 0$ ) is not parameterized, it only distributes the inputs on all the neurons of the next layer

A so-called universal approximation theorem shows that this elementary structure with a single hidden layer is sufficient to take into account the classic problems of modeling or statistical learning. Indeed, any regular function can be approached uniformly with arbitrary precision and in a finite domain of the space of its variables, by a network of neurons comprising a layer of finite number hidden neurons all having the same function of activation and a linear output neuron. Attention, this result, which seems contradictory to the structures of deep learning, is theoretical, it masks difficulties of learning and stability for complex problems in a very big dimension.

In the usual way and regression (quantitative  $Y$ ), the last layer consists of a single neuron equipped with the identity activation function whereas the other neurons (hidden layer) are equipped with the sigmoid function.

In binary classification, the output neuron is also equipped with the sigmoid function, whereas in the case of discrimination with  $m$  classes, the output neuron integrates a softmax activation function with values in  $\mathbb{R}^m$  and sum unit. These  $m$  values are comparable to the probabilities of belonging to a class. Thus, in regression with a perceptron at a hidden layer of  $q$  neurons and an output neuron, this function is written:

$$y = f(x; \alpha, \beta) = \beta_0 + \beta'_z \quad (2)$$

where  $z_k = g(\alpha_{k0} + \alpha'_k x)$ ;  $k = 1, \dots, q$

Suppose that we have a learning base of size  $n$  of observations  $(x_1, \dots, x_p, y_i)$  explanatory variables  $X_1, \dots, X_p$  and the variable to predict  $Y$ . Consider the simplest case of regression with a network consisting of a linear output neuron and a  $q$ -layer neuron whose parameters are optimized by least squares. This is generalized to any differentiable loss function and therefore to  $m$  class discrimination. The learning is the estimation of the parameters  $\alpha_j = 0, p$ ;  $k = 1, q$  and  $\beta_k = 0, q$  by minimization of the quadratic loss function or that of a classification entropy function:

$$Q(\alpha, \beta) = \sum_{i=1}^n Q_i = \sum_{i=1}^n [y_i - f(x; \alpha, \beta)]^2 \quad (3)$$

In elementary networks, a simple option to avoid over-learning is to introduce a penalization or regulation term, as in ridge

regression, into the criterion to be optimized. This then becomes  $Q(\theta) + \gamma||\theta||^2$ . The higher the value of the  $\gamma$  (decay) parameter, the lower the weight of the neuron inputs can take chaotic values, thus helping to reduce the risk of over-learning.

The user must therefore determine:

1. The input variables and the output variable; to submit to them as for all statistical methods, possible transformations, normalizations.
2. The architecture of the network: the number of hidden layers that correspond to an ability to deal with problems of non-linearity, the number of neurons per hidden layer. These two choices directly affect the number of parameters (weight) to be estimated and therefore the complexity of the model. They participate in the search for a good compromise bias/variance that is to say the balance between quality of learning and quality of forecasting.
3. Three other parameters are also involved in this compromise: the maximum number of iterations, the maximum error tolerated and a possible term of a regulation ridge (decay).
4. The learning rate and a possible strategy of the evolution of it.
5. The size of the sets or batches of observations considered at each iteration.

In practice, all these parameters cannot be adjusted simultaneously by the user. This one is confronted with choices mainly concerning the control of the over-learning: to limit the number of neurons or the duration of learning or to increase the coefficient of penalization of the standard of the parameters. This requires determining an error estimation mode: sample validation or test, cross-validation or bootstrap.

#### 4.4. Combining the ontology with a neural network

Figure 3 describes an example of the ontology proposed in this paper, and that will be used as a data source for machine learning.

The ontology as proposed in [2] is defined as follow:

$$O = \{C, DO, DT, I\} = \{TBOX, ABOX\} \quad (4)$$

Where:

**TBOX** :  $\{C, dataType, \{objectProperty\}\}$

$C = (className, classeParent),$

$dataType$

$= (dataTPDomain, dataTPName, dataTPRange),$

$ObjectProperty$

$= (objectPDomain, objectPName, objectPRange)\}$

And:

**ABOX** :  $\{I /$

$I = (IName, IType, dataTypeList, objectPropertyList) /$

$dataTypeList = \{(dTPName, dTPtype, dTPvalue)\},$

$objectPropertyList = \{(objectPropertyName, ITarget)\}\}$

Weka is open source software issued under the GNU General Public License. It is a collection of machine learning algorithms for data mining tasks. It contains tools for data preparation, classification, regression, clustering, association rules mining, and visualization. all experiences done for this paper are implemented through it.

Attribute-Relation File Format (ARFF) are files developed by a machine learning project from the Computer Science Department of Waikato University for use with the Weka machine learning tool. it is an ASCII text file describing a list of instances sharing a set of attributes.

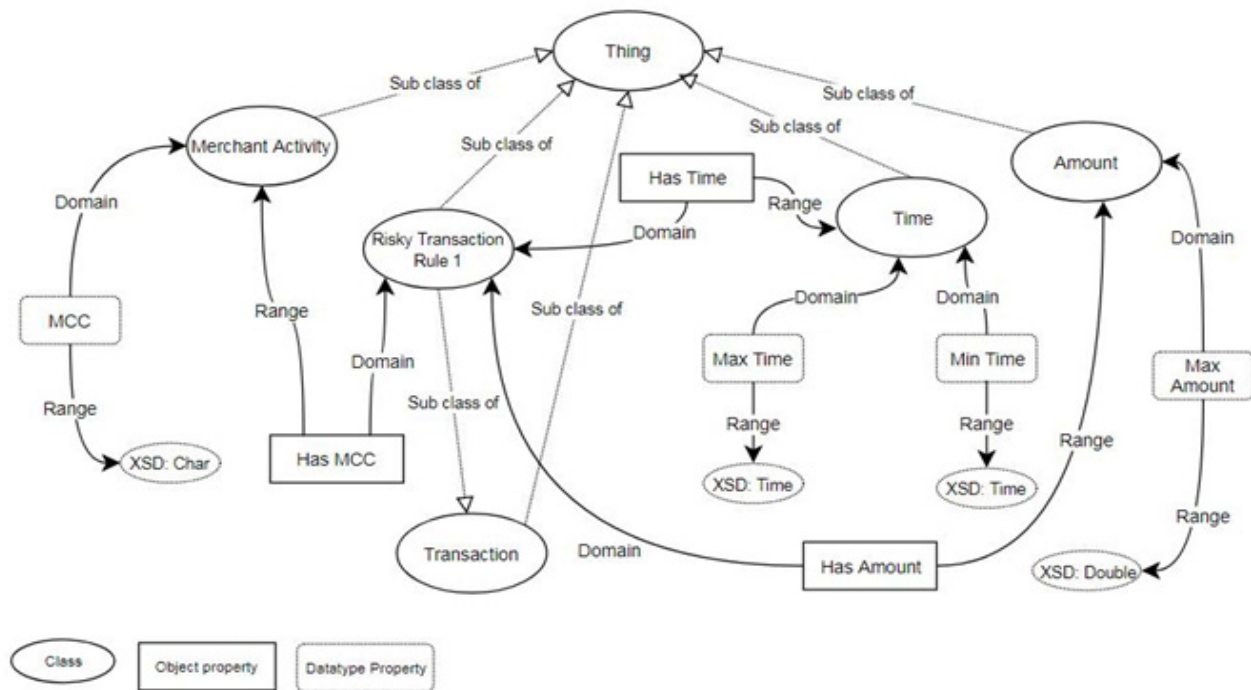


Figure 3: Part of ontology-based on a payment system



ARFF files contain two sections. The first is the Header information, the second is the Data information.

**ARFF Header Section**

The Header of the ARFF file contains the relation name and a list of the attributes with their types. The relation name is defined as the first line.

The format is:

```
@relation <relation-name>
```

where <relation-name> is a string and must be quoted if the name includes spaces.

The declarations of the attributes are presented in the form of an ordered sequence of attribute instructions. The attribute in the dataset has its declaration which uniquely defines the name of that attribute and its data type. The order of the attributes indicates the position of the column in the data section of the file.

The format is:

```
@attribute <attribute-name> <datatype>
```

where the <attribute-name> must start with an alphabetic character. If spaces are to be included in the name, then the entire name must be quoted.

The <datatype> can be any of the four types (version 3.2.1) supported by Weka:

- String.
- Numeric.
- <Nominal-specification>.
- Date [<date-format>].

where <nominal-specification> and <date-format> are defined below. The keywords numeric, string and date are case insensitive.

The ontology-based on a payment system is very large, but in our case, we are only interested in the part of the transactions to try to take and detect the cases of fraud, that's why we will migrate via Sparql to an ARFF file the data we need and that are related to the

transaction. The extraction of data is done via the requests Sparql in the form of triples (subject, predicate, object).

Then the format of the attribute will in the case of Nominal-specification as:

```
@attribute <attribute-name> <'Predicate;Subject;Object'>
```

Example:

```
@relation AEO_PAYMENT_SYS
@attribute transaction_ref real
@attribute card_number real
@attribute bank_network {'BNKNWK;100001;10','BNKNWK;100001;11','BN, ...
@attribute bank_bin {'BNKBIN;100001;200001','BNKBIN;100001;200002', ...
@attribute bank_country {'BNKCRY;100001;301','BNKCRY;100001;302!', ...
...
@attribute class {'H','M','L'}
```

**ARFF data Section**

The ARFF Data section of the file contains the data declaration line and the actual instance lines.

**The data Declaration**

The data declaration is a single line denoting the start of the data segment in the file. The format is: @data

**The instance**

Each instance is represented on a single line, with carriage returns denoting the end of the instance.

Attribute values for each instance are delimited by commas. They must appear in the order that they were declared in the header section.

@data

```
'23000000155623173083012','1400007623528765','BNKNWK;100005;11','BNKBIN;100005;200009',...L
'23000000155623138374641','1400007626995405','BNKNWK;100005;10','BNKBIN;100005;200004',...M
'23000000155623161382386','1400007606073039','BNKNWK;100003;11','BNKBIN;100003;200005',...L
'23000000155623195794287','1400007637878184','BNKNWK;100003;10','BNKBIN;100003;200004',...H
```

Figure 4 below shows an example or ARFF file that generated from ontology and will be executed into the weka tool:

```
@relation AEO_PAYMENT_SYS
@attribute transaction_ref real
@attribute card_number real
@attribute bank_network {'BNKNWK;100001;10','BNKNWK;100001;11','BNKNWK;100002;10','BNKNWK;100002;11','BNKNWK;100003;10','BNKNWK;100003;11','BNKNWK;100004;10','BNKNWK;100004;11','BNKNWK;100004;12','BNKNWK;100004;13','BNKNWK;100004;14','BNKNWK;100004;15','BNKNWK;100004;16','BNKNWK;100004;17','BNKNWK;100004;18','BNKNWK;100004;19','BNKNWK;100004;20','BNKNWK;100004;21','BNKNWK;100004;22','BNKNWK;100004;23','BNKNWK;100004;24','BNKNWK;100004;25','BNKNWK;100004;26','BNKNWK;100004;27','BNKNWK;100004;28','BNKNWK;100004;29','BNKNWK;100004;30','BNKNWK;100004;31','BNKNWK;100004;32','BNKNWK;100004;33','BNKNWK;100004;34','BNKNWK;100004;35','BNKNWK;100004;36','BNKNWK;100004;37','BNKNWK;100004;38','BNKNWK;100004;39','BNKNWK;100004;40','BNKNWK;100004;41','BNKNWK;100004;42','BNKNWK;100004;43','BNKNWK;100004;44','BNKNWK;100004;45','BNKNWK;100004;46','BNKNWK;100004;47','BNKNWK;100004;48','BNKNWK;100004;49','BNKNWK;100004;50','BNKNWK;100004;51','BNKNWK;100004;52','BNKNWK;100004;53','BNKNWK;100004;54','BNKNWK;100004;55','BNKNWK;100004;56','BNKNWK;100004;57','BNKNWK;100004;58','BNKNWK;100004;59','BNKNWK;100004;60','BNKNWK;100004;61','BNKNWK;100004;62','BNKNWK;100004;63','BNKNWK;100004;64','BNKNWK;100004;65','BNKNWK;100004;66','BNKNWK;100004;67','BNKNWK;100004;68','BNKNWK;100004;69','BNKNWK;100004;70','BNKNWK;100004;71','BNKNWK;100004;72','BNKNWK;100004;73','BNKNWK;100004;74','BNKNWK;100004;75','BNKNWK;100004;76','BNKNWK;100004;77','BNKNWK;100004;78','BNKNWK;100004;79','BNKNWK;100004;80','BNKNWK;100004;81','BNKNWK;100004;82','BNKNWK;100004;83','BNKNWK;100004;84','BNKNWK;100004;85','BNKNWK;100004;86','BNKNWK;100004;87','BNKNWK;100004;88','BNKNWK;100004;89','BNKNWK;100004;90','BNKNWK;100004;91','BNKNWK;100004;92','BNKNWK;100004;93','BNKNWK;100004;94','BNKNWK;100004;95','BNKNWK;100004;96','BNKNWK;100004;97','BNKNWK;100004;98','BNKNWK;100004;99','BNKNWK;100004;100','BNKNWK;100004;101','BNKNWK;100004;102','BNKNWK;100004;103','BNKNWK;100004;104','BNKNWK;100004;105','BNKNWK;100004;106','BNKNWK;100004;107','BNKNWK;100004;108','BNKNWK;100004;109','BNKNWK;100004;110','BNKNWK;100004;111','BNKNWK;100004;112','BNKNWK;100004;113','BNKNWK;100004;114','BNKNWK;100004;115','BNKNWK;100004;116','BNKNWK;100004;117','BNKNWK;100004;118','BNKNWK;100004;119','BNKNWK;100004;120','BNKNWK;100004;121','BNKNWK;100004;122','BNKNWK;100004;123','BNKNWK;100004;124','BNKNWK;100004;125','BNKNWK;100004;126','BNKNWK;100004;127','BNKNWK;100004;128','BNKNWK;100004;129','BNKNWK;100004;130','BNKNWK;100004;131','BNKNWK;100004;132','BNKNWK;100004;133','BNKNWK;100004;134','BNKNWK;100004;135','BNKNWK;100004;136','BNKNWK;100004;137','BNKNWK;100004;138','BNKNWK;100004;139','BNKNWK;100004;140','BNKNWK;100004;141','BNKNWK;100004;142','BNKNWK;100004;143','BNKNWK;100004;144','BNKNWK;100004;145','BNKNWK;100004;146','BNKNWK;100004;147','BNKNWK;100004;148','BNKNWK;100004;149','BNKNWK;100004;150','BNKNWK;100004;151','BNKNWK;100004;152','BNKNWK;100004;153','BNKNWK;100004;154','BNKNWK;100004;155','BNKNWK;100004;156','BNKNWK;100004;157','BNKNWK;100004;158','BNKNWK;100004;159','BNKNWK;100004;160','BNKNWK;100004;161','BNKNWK;100004;162','BNKNWK;100004;163','BNKNWK;100004;164','BNKNWK;100004;165','BNKNWK;100004;166','BNKNWK;100004;167','BNKNWK;100004;168','BNKNWK;100004;169','BNKNWK;100004;170','BNKNWK;100004;171','BNKNWK;100004;172','BNKNWK;100004;173','BNKNWK;100004;174','BNKNWK;100004;175','BNKNWK;100004;176','BNKNWK;100004;177','BNKNWK;100004;178','BNKNWK;100004;179','BNKNWK;100004;180','BNKNWK;100004;181','BNKNWK;100004;182','BNKNWK;100004;183','BNKNWK;100004;184','BNKNWK;100004;185','BNKNWK;100004;186','BNKNWK;100004;187','BNKNWK;100004;188','BNKNWK;100004;189','BNKNWK;100004;190','BNKNWK;100004;191','BNKNWK;100004;192','BNKNWK;100004;193','BNKNWK;100004;194','BNKNWK;100004;195','BNKNWK;100004;196','BNKNWK;100004;197','BNKNWK;100004;198','BNKNWK;100004;199','BNKNWK;100004;200','BNKNWK;100004;201','BNKNWK;100004;202','BNKNWK;100004;203','BNKNWK;100004;204','BNKNWK;100004;205','BNKNWK;100004;206','BNKNWK;100004;207','BNKNWK;100004;208','BNKNWK;100004;209','BNKNWK;100004;210','BNKNWK;100004;211','BNKNWK;100004;212','BNKNWK;100004;213','BNKNWK;100004;214','BNKNWK;100004;215','BNKNWK;100004;216','BNKNWK;100004;217','BNKNWK;100004;218','BNKNWK;100004;219','BNKNWK;100004;220','BNKNWK;100004;221','BNKNWK;100004;222','BNKNWK;100004;223','BNKNWK;100004;224','BNKNWK;100004;225','BNKNWK;100004;226','BNKNWK;100004;227','BNKNWK;100004;228','BNKNWK;100004;229','BNKNWK;100004;230','BNKNWK;100004;231','BNKNWK;100004;232','BNKNWK;100004;233','BNKNWK;100004;234','BNKNWK;100004;235','BNKNWK;100004;236','BNKNWK;100004;237','BNKNWK;100004;238','BNKNWK;100004;239','BNKNWK;100004;240','BNKNWK;100004;241','BNKNWK;100004;242','BNKNWK;100004;243','BNKNWK;100004;244','BNKNWK;100004;245','BNKNWK;100004;246','BNKNWK;100004;247','BNKNWK;100004;248','BNKNWK;100004;249','BNKNWK;100004;250','BNKNWK;100004;251','BNKNWK;100004;252','BNKNWK;100004;253','BNKNWK;100004;254','BNKNWK;100004;255','BNKNWK;100004;256','BNKNWK;100004;257','BNKNWK;100004;258','BNKNWK;100004;259','BNKNWK;100004;260','BNKNWK;100004;261','BNKNWK;100004;262','BNKNWK;100004;263','BNKNWK;100004;264','BNKNWK;100004;265','BNKNWK;100004;266','BNKNWK;100004;267','BNKNWK;100004;268','BNKNWK;100004;269','BNKNWK;100004;270','BNKNWK;100004;271','BNKNWK;100004;272','BNKNWK;100004;273','BNKNWK;100004;274','BNKNWK;100004;275','BNKNWK;100004;276','BNKNWK;100004;277','BNKNWK;100004;278','BNKNWK;100004;279','BNKNWK;100004;280','BNKNWK;100004;281','BNKNWK;100004;282','BNKNWK;100004;283','BNKNWK;100004;284','BNKNWK;100004;285','BNKNWK;100004;286','BNKNWK;100004;287','BNKNWK;100004;288','BNKNWK;100004;289','BNKNWK;100004;290','BNKNWK;100004;291','BNKNWK;100004;292','BNKNWK;100004;293','BNKNWK;100004;294','BNKNWK;100004;295','BNKNWK;100004;296','BNKNWK;100004;297','BNKNWK;100004;298','BNKNWK;100004;299','BNKNWK;100004;300','BNKNWK;100004;301','BNKNWK;100004;302','BNKNWK;100004;303','BNKNWK;100004;304','BNKNWK;100004;305','BNKNWK;100004;306','BNKNWK;100004;307','BNKNWK;100004;308','BNKNWK;100004;309','BNKNWK;100004;310','BNKNWK;100004;311','BNKNWK;100004;312','BNKNWK;100004;313','BNKNWK;100004;314','BNKNWK;100004;315','BNKNWK;100004;316','BNKNWK;100004;317','BNKNWK;100004;318','BNKNWK;100004;319','BNKNWK;100004;320','BNKNWK;100004;321','BNKNWK;100004;322','BNKNWK;100004;323','BNKNWK;100004;324','BNKNWK;100004;325','BNKNWK;100004;326','BNKNWK;100004;327','BNKNWK;100004;328','BNKNWK;100004;329','BNKNWK;100004;330','BNKNWK;100004;331','BNKNWK;100004;332','BNKNWK;100004;333','BNKNWK;100004;334','BNKNWK;100004;335','BNKNWK;100004;336','BNKNWK;100004;337','BNKNWK;100004;338','BNKNWK;100004;339','BNKNWK;100004;340','BNKNWK;100004;341','BNKNWK;100004;342','BNKNWK;100004;343','BNKNWK;100004;344','BNKNWK;100004;345','BNKNWK;100004;346','BNKNWK;100004;347','BNKNWK;100004;348','BNKNWK;100004;349','BNKNWK;100004;350','BNKNWK;100004;351','BNKNWK;100004;352','BNKNWK;100004;353','BNKNWK;100004;354','BNKNWK;100004;355','BNKNWK;100004;356','BNKNWK;100004;357','BNKNWK;100004;358','BNKNWK;100004;359','BNKNWK;100004;360','BNKNWK;100004;361','BNKNWK;100004;362','BNKNWK;100004;363','BNKNWK;100004;364','BNKNWK;100004;365','BNKNWK;100004;366','BNKNWK;100004;367','BNKNWK;100004;368','BNKNWK;100004;369','BNKNWK;100004;370','BNKNWK;100004;371','BNKNWK;100004;372','BNKNWK;100004;373','BNKNWK;100004;374','BNKNWK;100004;375','BNKNWK;100004;376','BNKNWK;100004;377','BNKNWK;100004;378','BNKNWK;100004;379','BNKNWK;100004;380','BNKNWK;100004;381','BNKNWK;100004;382','BNKNWK;100004;383','BNKNWK;100004;384','BNKNWK;100004;385','BNKNWK;100004;386','BNKNWK;100004;387','BNKNWK;100004;388','BNKNWK;100004;389','BNKNWK;100004;390','BNKNWK;100004;391','BNKNWK;100004;392','BNKNWK;100004;393','BNKNWK;100004;394','BNKNWK;100004;395','BNKNWK;100004;396','BNKNWK;100004;397','BNKNWK;100004;398','BNKNWK;100004;399','BNKNWK;100004;400','BNKNWK;100004;401','BNKNWK;100004;402','BNKNWK;100004;403','BNKNWK;100004;404','BNKNWK;100004;405','BNKNWK;100004;406','BNKNWK;100004;407','BNKNWK;100004;408','BNKNWK;100004;409','BNKNWK;100004;410','BNKNWK;100004;411','BNKNWK;100004;412','BNKNWK;100004;413','BNKNWK;100004;414','BNKNWK;100004;415','BNKNWK;100004;416','BNKNWK;100004;417','BNKNWK;100004;418','BNKNWK;100004;419','BNKNWK;100004;420','BNKNWK;100004;421','BNKNWK;100004;422','BNKNWK;100004;423','BNKNWK;100004;424','BNKNWK;100004;425','BNKNWK;100004;426','BNKNWK;100004;427','BNKNWK;100004;428','BNKNWK;100004;429','BNKNWK;100004;430','BNKNWK;100004;431','BNKNWK;100004;432','BNKNWK;100004;433','BNKNWK;100004;434','BNKNWK;100004;435','BNKNWK;100004;436','BNKNWK;100004;437','BNKNWK;100004;438','BNKNWK;100004;439','BNKNWK;100004;440','BNKNWK;100004;441','BNKNWK;100004;442','BNKNWK;100004;443','BNKNWK;100004;444','BNKNWK;100004;445','BNKNWK;100004;446','BNKNWK;100004;447','BNKNWK;100004;448','BNKNWK;100004;449','BNKNWK;100004;450','BNKNWK;100004;451','BNKNWK;100004;452','BNKNWK;100004;453','BNKNWK;100004;454','BNKNWK;100004;455','BNKNWK;100004;456','BNKNWK;100004;457','BNKNWK;100004;458','BNKNWK;100004;459','BNKNWK;100004;460','BNKNWK;100004;461','BNKNWK;100004;462','BNKNWK;100004;463','BNKNWK;100004;464','BNKNWK;100004;465','BNKNWK;100004;466','BNKNWK;100004;467','BNKNWK;100004;468','BNKNWK;100004;469','BNKNWK;100004;470','BNKNWK;100004;471','BNKNWK;100004;472','BNKNWK;100004;473','BNKNWK;100004;474','BNKNWK;100004;475','BNKNWK;100004;476','BNKNWK;100004;477','BNKNWK;100004;478','BNKNWK;100004;479','BNKNWK;100004;480','BNKNWK;100004;481','BNKNWK;100004;482','BNKNWK;100004;483','BNKNWK;100004;484','BNKNWK;100004;485','BNKNWK;100004;486','BNKNWK;100004;487','BNKNWK;100004;488','BNKNWK;100004;489','BNKNWK;100004;490','BNKNWK;100004;491','BNKNWK;100004;492','BNKNWK;100004;493','BNKNWK;100004;494','BNKNWK;100004;495','BNKNWK;100004;496','BNKNWK;100004;497','BNKNWK;100004;498','BNKNWK;100004;499','BNKNWK;100004;500','BNKNWK;100004;501','BNKNWK;100004;502','BNKNWK;100004;503','BNKNWK;100004;504','BNKNWK;100004;505','BNKNWK;100004;506','BNKNWK;100004;507','BNKNWK;100004;508','BNKNWK;100004;509','BNKNWK;100004;510','BNKNWK;100004;511','BNKNWK;100004;512','BNKNWK;100004;513','BNKNWK;100004;514','BNKNWK;100004;515','BNKNWK;100004;516','BNKNWK;100004;517','BNKNWK;100004;518','BNKNWK;100004;519','BNKNWK;100004;520','BNKNWK;100004;521','BNKNWK;100004;522','BNKNWK;100004;523','BNKNWK;100004;524','BNKNWK;100004;525','BNKNWK;100004;526','BNKNWK;100004;527','BNKNWK;100004;528','BNKNWK;100004;529','BNKNWK;100004;530','BNKNWK;100004;531','BNKNWK;100004;532','BNKNWK;100004;533','BNKNWK;100004;534','BNKNWK;100004;535','BNKNWK;100004;536','BNKNWK;100004;537','BNKNWK;100004;538','BNKNWK;100004;539','BNKNWK;100004;540','BNKNWK;100004;541','BNKNWK;100004;542','BNKNWK;100004;543','BNKNWK;100004;544','BNKNWK;100004;545','BNKNWK;100004;546','BNKNWK;100004;547','BNKNWK;100004;548','BNKNWK;100004;549','BNKNWK;100004;550','BNKNWK;100004;551','BNKNWK;100004;552','BNKNWK;100004;553','BNKNWK;100004;554','BNKNWK;100004;555','BNKNWK;100004;556','BNKNWK;100004;557','BNKNWK;100004;558','BNKNWK;100004;559','BNKNWK;100004;560','BNKNWK;100004;561','BNKNWK;100004;562','BNKNWK;100004;563','BNKNWK;100004;564','BNKNWK;100004;565','BNKNWK;100004;566','BNKNWK;100004;567','BNKNWK;100004;568','BNKNWK;100004;569','BNKNWK;100004;570','BNKNWK;100004;571','BNKNWK;100004;572','BNKNWK;100004;573','BNKNWK;100004;574','BNKNWK;100004;575','BNKNWK;100004;576','BNKNWK;100004;577','BNKNWK;100004;578','BNKNWK;100004;579','BNKNWK;100004;580','BNKNWK;100004;581','BNKNWK;100004;582','BNKNWK;100004;583','BNKNWK;100004;584','BNKNWK;100004;585','BNKNWK;100004;586','BNKNWK;100004;587','BNKNWK;100004;588','BNKNWK;100004;589','BNKNWK;100004;590','BNKNWK;100004;591','BNKNWK;100004;592','BNKNWK;100004;593','BNKNWK;100004;594','BNKNWK;100004;595','BNKNWK;100004;596','BNKNWK;100004;597','BNKNWK;100004;598','BNKNWK;100004;599','BNKNWK;100004;600','BNKNWK;100004;601','BNKNWK;100004;602','BNKNWK;100004;603','BNKNWK;100004;604','BNKNWK;100004;605','BNKNWK;100004;606','BNKNWK;100004;607','BNKNWK;100004;608','BNKNWK;100004;609','BNKNWK;100004;610','BNKNWK;100004;611','BNKNWK;100004;612','BNKNWK;100004;613','BNKNWK;100004;614','BNKNWK;100004;615','BNKNWK;100004;616','BNKNWK;100004;617','BNKNWK;100004;618','BNKNWK;100004;619','BNKNWK;100004;620','BNKNWK;100004;621','BNKNWK;100004;622','BNKNWK;100004;623','BNKNWK;100004;624','BNKNWK;100004;625','BNKNWK;100004;626','BNKNWK;100004;627','BNKNWK;100004;628','BNKNWK;100004;629','BNKNWK;100004;630','BNKNWK;100004;631','BNKNWK;100004;632','BNKNWK;100004;633','BNKNWK;100004;634','BNKNWK;100004;635','BNKNWK;100004;636','BNKNWK;100004;637','BNKNWK;100004;638','BNKNWK;100004;639','BNKNWK;100004;640','BNKNWK;100004;641','BNKNWK;100004;642','BNKNWK;100004;643','BNKNWK;100004;644','BNKNWK;100004;645','BNKNWK;100004;646','BNKNWK;100004;647','BNKNWK;100004;648','BNKNWK;100004;649','BNKNWK;100004;650','BNKNWK;100004;651','BNKNWK;100004;652','BNKNWK;100004;653','BNKNWK;100004;654','BNKNWK;100004;655','BNKNWK;100004;656','BNKNWK;100004;657','BNKNWK;100004;658','BNKNWK;100004;659','BNKNWK;100004;660','BNKNWK;100004;661','BNKNWK;100004;662','BNKNWK;100004;663','BNKNWK;100004;664','BNKNWK;100004;665','BNKNWK;100004;666','BNKNWK;100004;667','BNKNWK;100004;668','BNKNWK;100004;669','BNKNWK;100004;670','BNKNWK;100004;671','BNKNWK;100004;672','BNKNWK;100004;673','BNKNWK;100004;674','BNKNWK;100004;675','BNKNWK;100004;676','BNKNWK;100004;677','BNKNWK;100004;678','BNKNWK;100004;679','BNKNWK;100004;680','BNKNWK;100004;681','BNKNWK;100004;682','BNKNWK;100004;683','BNKNWK;100004;684','BNKNWK;100004;685','BNKNWK;100004;686','BNKNWK;100004;687','BNKNWK;10000
```

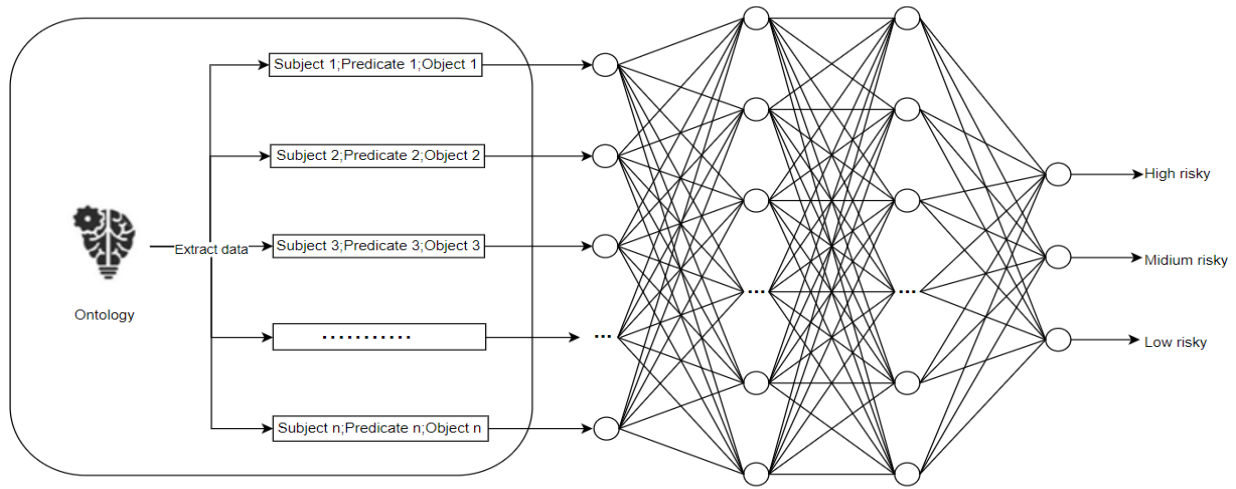


Figure 5: Combining ontology and neural network process

Figure 5 shows the extraction of data from ontology, creation an ARFF file, then combining this data with a neural network for classification according to the class levels defined by users.

4.5. Comparison and statistics:

The statistics below show the results of a comparison study to live the performance of the neural networks and ontology to detect cases of fraud. within the initiative, we applied the neural network directly on data downloaded from the payment system, within the second step, we created an ontology-based on these data, then we applied the same neural network on this ontology. Table 1 shows the statistics and percentages obtained. as a conclusion, it's seen that the mixture of neural networks and ontology allows having an improvement of precision on the detection of fraud.

Table 1: Statistics for Detection fraud

Class	Neural network on normal data		Neural network on Ontology data	
H(High)	27	0,27%	35	0,35%
M(Medium)	88	0,88%	100	1%
L(Low)	9885	98,85	9865	98,65%

The results are shown in figures 6 and 7 visualize a classification with a multilayer perceptron where we distingue if the transaction is high, medium or low risk done by neural network on ontology data.

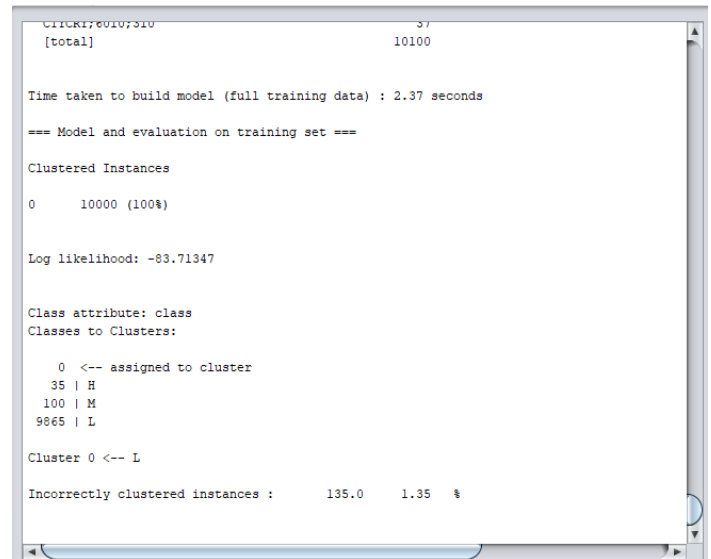


Figure 7: Results visualizing

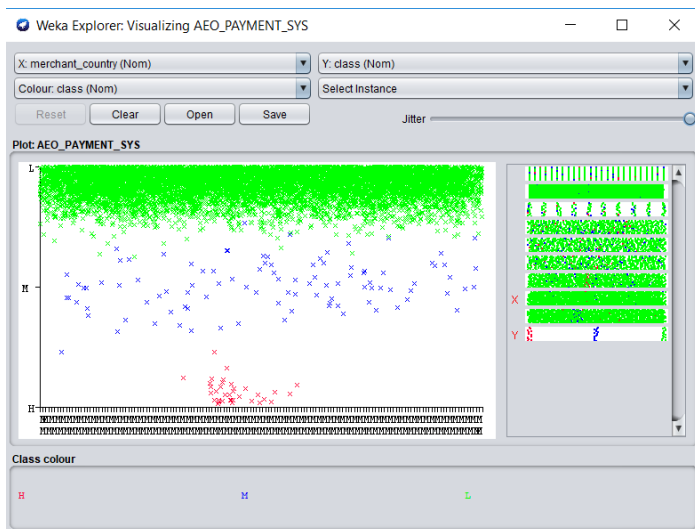


Figure 6: Results visualizing

5. Conclusions

The growth of payment card fraud and the evolution of artificial intelligence is the purpose of this paper. Our overall goal is to identify anomalies in a payment system to detect the largest number of fraudulent activities with a reasonable number of false positives.

There are several approaches and techniques used to detect the frauds in the payment system, which transactions are normal or fraudulent. The main advantage of the proposed approach is to combine semantics concepts with machine learning to achieve the goal of the paper.

In this paper, we have proposed the use of an ontology with machine learning for the detection of payment system frauds. The performance of this approach is evaluated on an ontology with the neural network method. The experimental phase proves that the

use of structured data in an ontology is very effective in detecting anomalies. In future work, we will focus on including SVM, Decision Tree, and KNN in terms of precision, AUC on building and implement a new architecture capable of detecting fraudulent transactions, then make a comparison and deduce the best method to combine with the ontology.

## References

- [1] Jamal Bakkas, Mohamed Bahaj, Abderrahim Marzouk ; "Direct Migration Method of RDB to Ontology while Keeping Semantics"; International Journal of Computer Applications (0975 – 8887) Volume 65– No.3, March 2013.
- [2] Ahmed EL ORCHE, Mohamed BAHAJ; "Using framework to synchronize ontology with relational database"; Journal of Theoretical and Applied Information Technology 31st May 2016. Vol.87. No.3; ISSN: 1992-8645; E-ISSN: 1817-3195
- [3] Ahmed EL ORCHE and Mohamed BAHAJ; "Approach to use ontology based on electronic payment system and machine learning to prevent Fraud"; The 2nd International Conference on Networking, Information Systems & Security, March 27-29, 2019, Rabat, Morocco.
- [4] Ahmed EL ORCHE, Mohamed BAHAJ; "Ontology-based on electronic payment fraud prevention"; Proceeding of 5th International Congress on Information Science and Technology; ISBN: 978-1-5386-4385-3; IEEE Catalog Number: CFP1867R-ART; October 21-27, 2018; P.143
- [5] Ahmed EL ORCHE, Mohamed BAHAJ; "A Method for Updating RDB of Ontology while keeping the Synchronization between the OWL and RDB"; ARPN Journal of Systems a and Software; ISSN 2222-9833; VOL. 4, NO. 4, July 2014.
- [6] Kingston, J., Schafer, B., & Vandenburghe, W.; "Ontology Modelling in the Legal Domain - Realism Without Revisionism"; Proceedings of the KI2003 Workshop on Reference Ontologies and Application Ontologies, Hamburg, Germany, September 16, 2003.
- [7] Ali Ahmadian Ramaki, Reza Asgari, and Reza Ebrahimi Atani; "Credit card fraud detection based on ontology graph", International Journal of Security, Privacy and Trust Management ( IJSPTM), Vol. 1, No 5, October 2012.
- [8] Tova Milo, Slava Novgorodov, Wang-Chiew Tan; "Interactive Rule Refinement for Fraud Detection"; Proceedings of the VLDB Endowment, v.9 n.13, p.1465-1468, September 2016.
- [9] Rodrigo Carvalho, Michael Goldsmith, Sadie Creese; "Applying Semantic Technologies to Fight Online Banking Fraud"; European Intelligence and Security Informatics Conference; 2015.
- [10] L.Y. Ding, B.T. Zhong, S.Wu, H.B. Luo; "Construction risk knowledge management in BIM using ontology and semantic web technology"; Safety Science 87 (2016) 202–213.
- [11] Quratulain Rajput, Nida Sadaf Khan, Asma Larik, Sajjad Haider; "Ontology-Based Expert-System for Suspicious Transactions Detection"; Computer and Information Science; Vol. 7, No. 1; 2014 ISSN 1913-8989 E-ISSN 1913-8997.
- [12] Gunnar Declerck, Audrey Baneyx, Xavier Aimé, Jean Charlet; "A quoi servent les ontologies fondationnelles ?"; 23èmes Journées francophones d'Ingénierie des Connaissances (IC 2012), Jun 2012, Paris, France. pp. 67-82, 2012.

## Minimizing the Cleaning Cost in Flash Based Storage Sub-Systems by Proliferating the Valid Data Copying Process

Hisyamuddin Kasim, Amir Rizaan Abdul Rahiman\*, Nor Asilah Wati Abdul Hamid, Thinagaran Perumal

*Department of Computer Science, Universiti Putra Malaysia*

### ARTICLE INFO

*Article history:*

*Received: 27 November, 2019*

*Accepted: 22 February, 2020*

*Online: 08 April, 2020*

*Keywords:*

*Sector*

*Flash memory*

*Garbage collection*

*Storage*

### ABSTRACT

*Flash memory reliability and the performance have been confirmed as an improvement in the storage subsystem technological advancement, especially in supporting an embedded system solution. Conversely, the main constraint of the storage device is the erase-before-write characteristic in handling both write and re-write I/O operations. More attention must be taken into consideration to handle both I/O operations. To overwhelm this constraint, a time-consuming garbage collection scheme has been introduced. This paper presents an optimized cleaning scheme that significantly reduces the required cleaning collection cost without interfering the memory I/O operations. The candidate sector to be erased is being determined by a score factor together with an erasure count before selecting the actual victim sector to be cleaned. The experimental results show the proposed approach assists in reducing the garbage collection cost since the number of sectors used in handling the I/O operations is being minimized. Even the sector becomes the candidates, but the score factor will be the tiebreaker to determine whether the sector needs to be cleaned or not. On the contrary, the proposed scheme increases the number of copy operations due to new sector requirement while the degree of the wear-levelling emulate the standing sector cleaning scheme.*

### 1. Introduction

Recently, flash memory has become the predominant semiconductor storage device that offers some outstanding features such as zero noise, solid-state reliability, low power consumption, small and lightweight natures, and great shock-resistant [1 – 4]. Its primary application is a storage device used for storing and transferring data in various electronic appliances such as smartphones, digital cameras, a global positioning system (GPS) device, just to name a few.

On the contrary, the flash memory has two operating characteristics namely, i) out-place-updating policy, and ii) high cleaning cost requirement. Those characteristics bring some technical challenges in designing and implementing an efficient storage sub-system, especially in an embedded system. Rewrite an existing data at the recent location in the device results in I/O operational overheads. Thus, the out-place-updating policy has been employed where the updated data is being stored into a new location while the initial copy of the data is set as garbage [5 – 6]. Conversely, the frequent data rewrite increases the amount of garbage which resulting in lesser device-free spaces. The garbage needs to be cleaned to guarantee the continuous data storing

process. Moreover, the device could wear out and leads to its end lifetime as compared to the classical hard drive. The cleaning in the flash memory is being implemented on a sector unit rather than page unit where it may contain valid data that is used by particular applications. Thus, the entire valid data in the sector need to be transferred or copied into the available free pages in the available sectors. The cleaning process and the sector utilization level, the ratio between the number of valid data and the total pages per sector have been considered the stimulus of flash memory I/O access performance, energy consumption and device persistence. Several studies those focusing on recognizing the accurate victim sector selection to be erased have been proposed in the literature. The objectives of the studies are to minimize the cleaning cost and lengthen the storage device lifespan [7 – 13]. The cleaning cost refers to the required I/O accessing time in executing the cleaning operation.

This paper proposes a sector cleaning scheme, called candidate selection garbage collection (CSGC). Unlike the existing schemes, the candidate or the victim sector in the CSGC scheme is being determined according to the score factor together with the erasure count before the selection of the actual sector to be cleaned. The scoring factor helps in selecting the actual victim sectors which result in the least cleaning cost. According to the simulation results

\* Amir Rizaan Abdul Rahiman, Email: [amir\\_r@upm.edu.my](mailto:amir_r@upm.edu.my)

[www.astesj.com](http://www.astesj.com)

<https://dx.doi.org/10.25046/aj050270>



performed, the CSGC scheme offers lower erasure operation among the existing sector cleaning and emulate the similar degree of wear-levelling with the existing cleaning scheme. Conversely, the scheme requires higher copy operation as compared to the previous schemes since it repopulated the valid data more rapidly after the cleaning process had been initiated. The remainder of this paper is organized as follows. Section 2 discusses the related works on a garbage collection scheme. Section 3 discusses and explain the proposed CSGC scheme. The experimental setup and the performance evaluation are being discussed in Section 4 while Section 5 presents the conclusions of this study.

## 2. Backgrounds and Related Works

In general, there are two types of flash memory in the current market, i) NOR-flash and ii) NAND-flash [14]. The characteristics comparisons between both flash memory types are being tabulated in Table 1. In this study, we limit our discussion on the NOR-flash and will refer to it as the flash memory in this paper.

### 2.1. Flash Memory Characteristics

Flash memory is a tiny and lightweight semiconductor storage device and known as a block-and-page-based storage device. The page is a basic accessing unit and a group of pages form a sector unit or block. Both read and write I/O accesses are executed in the page unit while the erase is being executed in the sector unit. Each page has two dissimilar sized areas, data and a spare area. The data area is a location where the actual data being stored while the spare area keeps assisting information about the data area.

Table 1: NAND-flash and NOR-flash Characteristics [15]

Operations	NAND-flash	NOR-flash
Read unit	Page (512 + 16 bytes)	Byte/word
Access time	7 μs (initial access) 50 ns (serial access)	90 ns (random access)
Write unit	Page (512 + 16 bytes)	Byte/word
Write time	200 μs	8 μs/byte 16 μs/Word (4 ms/528 bytes)
Erase unit	Block (8k + 256 bytes)	Sector (8k/64k bytes)
Erase time	2 ms	1 s

As tabularized in Table 1, the NAND-flash has slower read operation but offer faster write operation. Therefore, it is being used as a substitution for the classic storage sub-system (e.g., magnetic hard disk) and known for its enormous capacity. On the other hand, the NOR-flash memory offers fast read operation which is being carried out in a byte unit. However, it has slower written I/O operation. Moreover, the NOR-flash is known for its XIP capability where it runs the BIOS directly from the memory device. Therefore, the NOR-flash memory is being used as an alternative to the main memory of a personal computer or embedded microcontroller system. Rather than copying a program into a RAM, the XIP capability can execute a program directly from the storage. Thus, reduce the total memory usage as an extension of a portion of memory.

In flash memory, updating the existing data is done via the out-place-policy. Therefore, the page unit falls into three states (*free*, *valid*, and *invalid*). The free page is a page unit without any

data and is ready for storing new and updated data while the valid page is a page containing the latest version or actual data. The invalid page is a page containing garbage or dead data. Moreover, each memory sector has a limited number of erasure cycles. Therefore, excessive sector erasures can cause the block to be permanently spoilt or damage. To overcome this limitation, a wear-leveling policy that wears down all memory sectors as evenly as possible is essential in flash memory.

### 2.2. Sector Cleaning in Flash Memory

Figure 1 below shows the cleaning process in the flash memory is carried out in three underlying phases. First, the victim sector/s is being determined based on the cleaning thresholds. Second, the entire valid data reside in the sector are being recognized and being copied into available free pages located in a spare sector. Third, upon completion of the copying, the victim sector is being erased. Moreover, if all pages in the victim sector are invalid, the sector can automatically be erased without requiring the copying process cost since the cleaning requires only the constant erasure cost.

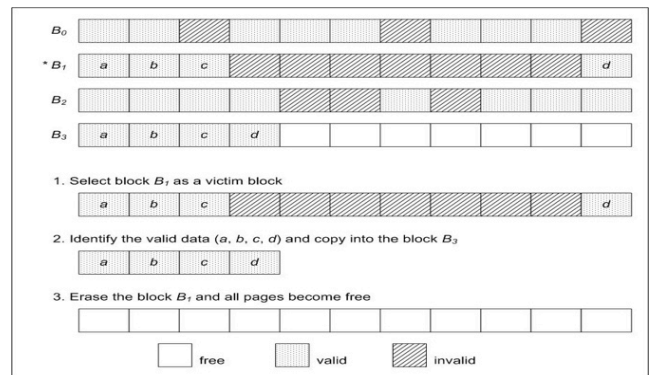


Figure 1: Three Phases in The Semi-automatic Cleaning Process in Flash Memory

### 2.3. Cleaning Algorithms in Flash Memory

There are various studies are focusing on defining the victim sector and re-organizing valid data when the garbage collection is initiated in the flash memory. Most studies are focusing on the NAND-flash type. The two objectives of the studies are minimizing the cleaning cost and guaranteeing the memory sectors are evenly worn. In the NOR-flash environment, the sector cleaning process is handled by freeing up both valid and invalid pages for the next iteration of live pages or bytes to be written in the erased victim sector. The life expectancy of the device is being determined according to the status of sector usage. For example, to utilize the sector life cycle, the proportional of sector erasure count and the re-use level are being taken into consideration. Moreover, the dense and the energy usages of the NOR-flash are less as compared to the NAND-flash. Thus, in NOR-flash, the cleaning process becomes a challengeable task since the cleaning operation is quite slow as compared to other I/O operations. Following are the cleaning schemes those focusing on the NOR-flash type.

The flash resident file system (FLAREFS) scheme dynamically proposed sector cleaning scheme with a wear-leveling policy that keeps a region of sectors clean and available for storing the updated data [16]. To determine the victim sector, the scheme will keep tracking the status of every physical busy page in a meta-table. A such number of sectors is required for the

meta-table that makes the scheme consumes extra storage space. Moreover, the scheme requires extra space for handling the valid data copying process when the cleaning process is being initiated. When the cleaning is being initiated, the established greedy technique (sector with the highest amount of garbage) is being used to select the victim sector.

In the least first garbage collection (LFGC) scheme [17], all the dirty sectors (another name for a victim block) are being clustered according to the candidate region and resident region. Unlike the FLAREFS, the LFGC scheme uses hot and cold classification technique in reorganizing the valid data found in the victim sector. The well-defined cold-detection scheme has been used to classified hot and cold valid data. Those sectors belong to the candidate region are being selected to be erased when the cleaning is being initiated. On the contrary, if the candidate region does not have any sector, the least erase count sector in the device will be the victim sector.

Niv and Phillipe have proposed the two garbage collection schemes called Lazy Gecko and Logarithmic Gecko [18]. Both schemes require metadata to perform the sector cleaning with the minimum cleaning cost. In the Lazy Gecko, the RAM-resident bitmap called Page Validity Bitmap (PVB) is being used to store the up-to-date status of the pages to allow the victim sector selection and valid page identification. However, the scheme works efficiently when the PVB is ample to store the copying process information. Note that, the size of the metadata is very important for caching the frequently accessed I/O in the embedded system. Thus, to minimize the metadata size, the Logarithmic Gecko has been proposed to overcome the highly RAM consumption in the Lazy Gecko solution. The scheme similar to Lazy Gecko, but the information in the PVB is being stored in the flash-resident reverse map.

From the above studies, we have observed that the sector cleaning schemes that combine the victim block selection with the valid data reorganizing procedures assists in achieving the sector cleaning process objectives. Most of the schemes use the greedy approach in determining the victim block to be erased. Using the similar approach, this paper presents the score factor consideration together with the sector erasure count to verify the suitable victim sector that requires the minimum cleaning cost. The victim sector will be select as the candidate for the cleaning before the cleaning can be executed. Moreover, these two screening parameters will give the exact victim sector. Therefore, it has given us the motivation to propose an optimized sector cleaning scheme that guarantees the I/O performance in the flash memory.

### 3. Candidate Selection Garbage Collection (CSGC)

Table 2 lists the data structures used in the phases to determine the appropriate candidate sector. As illustrated in Figure 2, the cleaning process in the CSGC scheme will go through three (3) consecutive phases without exception in regulating the candidate sector selection. In the figure, the sector refers to the available block in the flash memory device.

First, when the cleaning process has been initiated, the scheme will check if all the sectors in the device are either free or not. This stage becomes a preliminary task to verify whether the cleaning process can be executed or not. Then, move to the second stage. In

this stage, the availability for executing the copying process is being determined according to the *free\_pages* variable. This stage is required to proceed with the candidate selection for the copying process when the candidate block was selected. Note that, the valid data/pages reside in the candidate sector must be copied into the available free sector in the memory. The busy pages within the sector will not be selected if the file where the pages reside is in the current execution state. The reason is, copying and migrating these pages require longer waiting time for the sector to be ready for the cleaning process.

Table 2: Data Structure in The CSGC Candidate Sector Selection

Variables	Description
<i>fs-</i>	The sectors in the flash memory are in free state
<i>p_free</i>	All pages in the sector are empty
<i>free_pages</i>	The available free pages in the sector
<i>pages_per_sector</i>	Total pages in each block of the memory
<i>p_busy</i>	The valid pages in the sector

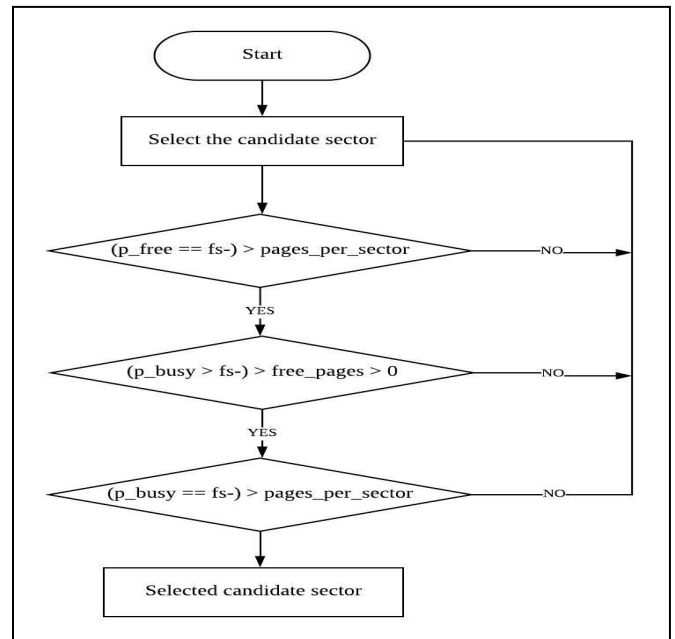


Figure 2: Candidate Sector Selection Process in The CSGC Scheme

Furthermore, if the sector has no free pages but has the non-busy pages, then the copying process become the main priority. At this stage, if the sector has the only free pages but in a different sector, this sector will not be chosen as the candidate sector. After completing the third stage, then the candidate sector is being decided. Only the sector that has the largest amount of non-busy pages will select for the cleaning process. This selection also can fully utilize sector usage lifecycle. Unlike the previous cleaning schemes, the CSGC scheme uses a scoring system to select the candidate sector for the erasure. The scoring *sec\_ers\_diff* parameter is being calculated according to the difference value between the maximum sector erasure count (denoted by *max\_ers*) and the sector header erase (denoted by *header\_ers*) count as shown below:

$$sec\_ers\_diff = max\_ers - header\_ers \quad (1)$$

Parameter *sec\_ers\_diff* in (1) defines the score factor for every sector in the device. The sector with the highest score factor will be selected as the candidate sector. However, if the sector has the same highest score, it will choose based on the sector index number. For example, both sector 1 and sector 2 have the same score value, then sector 1 will be chosen as the candidate. Then, the candidate sector cleaning cost (*cost*) is being calculated according to the following equation:

$$cost = (sec\_ers\_diff \times 100) + (free\_pages \times 100) + (invalid\_pages \times 100) + (p\_busy \times 100) \quad (2)$$

To ensure the efficiency of the victim sector selection, the calculation is being measured for every I/O accessing iterations. As shown in Figure 3, each sector will have the erase count, and the score factor. To maintain the consistency of the erased sector to prolong its lifespan, the erasure count of each sector will keep updates and monitoring. The only thing separating each sector is based on highest score factor and the sector starting digit.

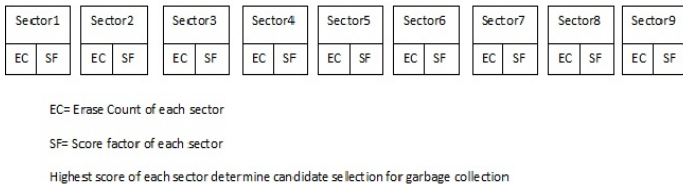


Figure 3: The Score Factor Counting in The Sector

#### 4. Simulation and Experiment Results

##### 4.1. Simulation Model and Parameter

The CSGC scheme is evaluated through proper computer simulation. The evaluation performance of the scheme is being compared with the existing sector cleaning schemes in terms of the total block erasure count and the copying process involved. In addition, the degree of wear-levelling is being discovered for the proposed scheme. The simulation model was programmed using the STM32F1 architecture that targeted for the embedded system simulation. Table 3 shows the actual technical specifications of the memory device in the STM32F1 architecture. In the simulation, the threshold level of the available free space in the device is being set to 15% for initiating the cleaning process. Table 4 shows the actual device specification being executed on the Linux Kernel 4.1 environment during the simulation.

Table 3: STM32F1 Simulation Parameters

Sector Header size	Page size	Page Header size
<i>niffs_sector_hdr</i>	<i>niffs_page_hdr:data</i>	<i>niffs_page_hdr:data</i>
<i>ers_cnt</i>	<i>id : flag</i>   .... <i>\obj_id</i> <i>\spix</i>	<i>id : flag</i>   .... <i>\obj_id</i> <i>\spix</i>

Table 4: The Evaluation Parameter Framework

Parameters	Value
Number of sectors in device	2 <sup>16</sup>
Sector size	8 Kbytes
Page per sector	512
Page size	16 bytes
Working buffer size	16 bytes

Figure 4 shows how the wireless sensor data is being collected for the I/O accessing pattern that is used in the simulation as the simulation data benchmarking.

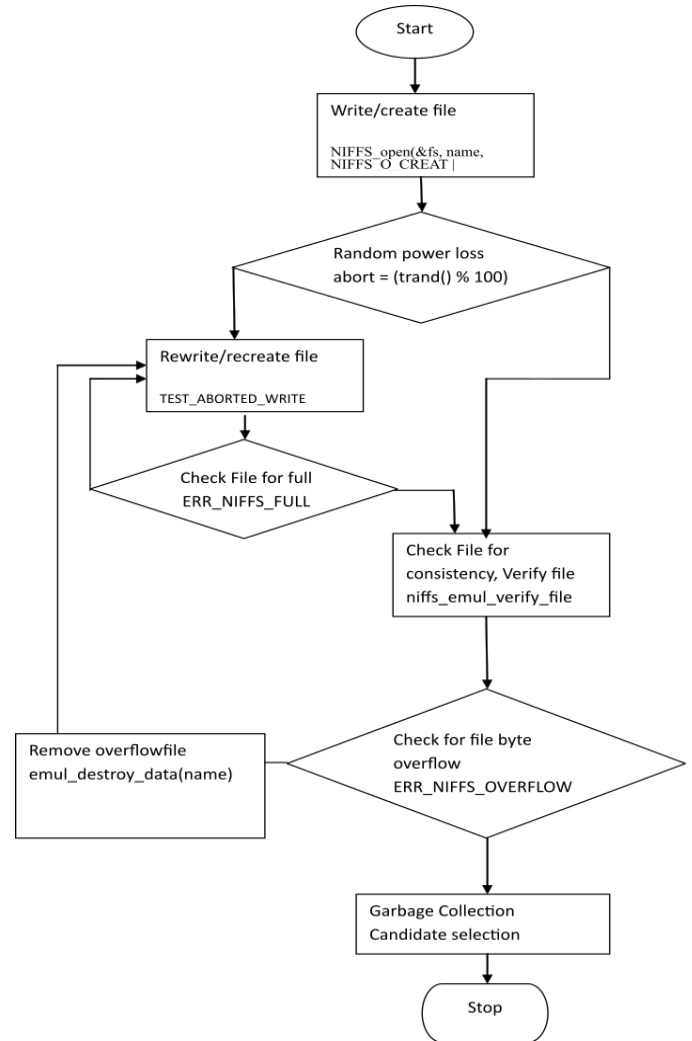


Figure 4: The Random Data Establishment in Simulation

##### 4.2. Results and Discussions

The three performance matrices, i) number of erase operation, ii) number of copying the valid data and iii) degree of wear-levelling are being discovered in the simulation when the cleaning process is being initiated. The matrices are based on the storing and updating the random I/O accessing pattern captured from the designated testing framework. The following figures illustrate the evaluation results for the matrices.

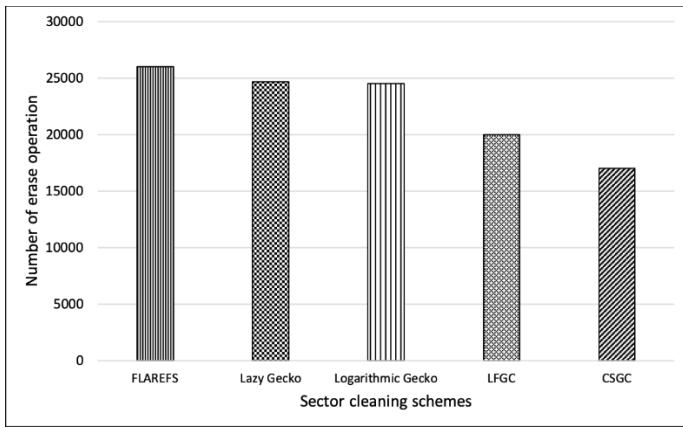


Figure 5: The Sector Erasure Count

As compared to existing garbage collection schemes, the CSGC scheme requires the lowest sector erasure counts. The lowest block erasure count is aligning with the minimum cleaning process cost since the number of involved sectors during the garbage collection process is being reduced. This is due to the candidate sector in the scheme will be evaluated again according to the score factor to confirm whether the sector can be erased or not.

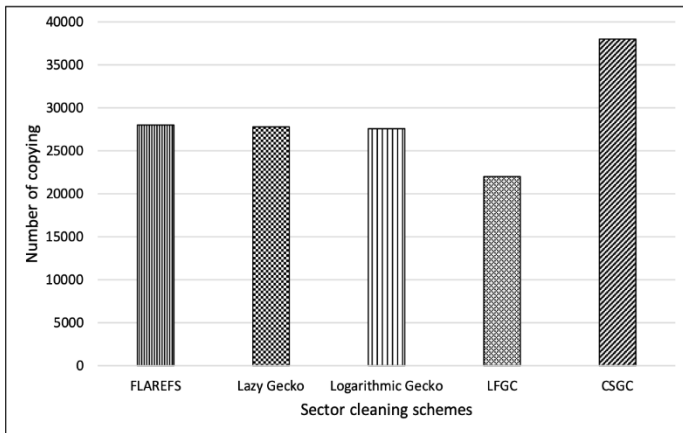


Figure 6: The Valid Data Copying Amount

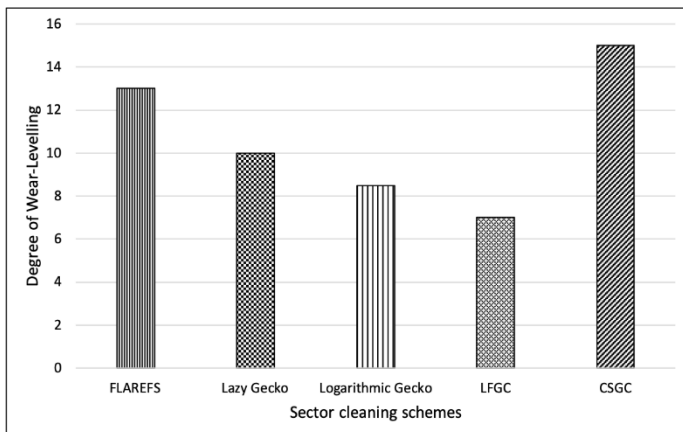


Figure 7: Degree of Wear-Leveling

On the contrary, as shown in Figure 6, the CSGC requires the most copying process. The scoring factor has increased the CSGC scheme to employ the new sector during the valid data copying

process. As compared to the existing schemes, the gap difference is a considerable disparity. Note that, in the CSGC scheme, during the candidate sector selection, the existing valid data in the sector might be transferred into a new sector according to the state of the candidate sector. In the simulation, we have counted this copying process and that is the main reasons why the gap difference is quite large as compared to the existing schemes. Moreover, the degree of wear-leveling exceeding the existing sector cleaning schemes.

## 5. Conclusion and Future Work

The garbage collection scheme is a mandatory process in flash memory due to the necessarily erase-before-write characteristic. Several studies have been carried out to optimize the time-consuming erasure process due to the characteristic. Unlike the existing sector cleaning scheme, the CSGC scheme emphasizes on selecting the candidate sector for the valid data copying prior in selecting the actual victim block to be cleaned. The candidate sector is not necessarily the victim block to be erased. With the sector scoring factor and the erasure count, the actual victim sector with low cleaning cost can be determined appropriately. Moreover, the consistency of the erased sector is a pledge. Even though the number of the cleaning process is reduced significantly, the proposed CSGC scheme requires more copying processes when the garbage collection process is being initiated. Also, the degree of wear-leveling increase significantly. This is due to the busy pages are being copied earlier when the candidate sector has been selected. The scoring factor determines this approach earlier before the sector is being confirmed to be erased. For further study, an efficient calibration measurement will be used in reducing the process of a valid copy of the data once the sector candidate is determined. In the present study, the selection of candidates is based on the score factor derived from the difference between the maximum sector erasure count and the sector header erasure count.

## Conflict of Interest

The authors declare no conflict of interest.

## Acknowledgment

The work is supported by the Geran Putra (GP) GP/2018/9596300 and we would also like to thank Universiti Putra Malaysia for providing technical assistance.

## References

- [1] R. Agarwal, M. Marrow, "A Closed-form Expression for Write Amplification in NAND Flash" in 2010 IEEE Globecom Workshops, Miami, FL, 2010. <https://doi.org/10.1109/GLOCOMW.2010.5700261>
- [2] Y. Zhang, H. Zhang, C. Wang, "Reliability-aware low energy scheduling in real time systems with shared resources" Journal Micro. and Microst., 52(C), 312 – 324, 2017. <https://doi.org/10.1016/j.micpro.2017.06.020>
- [3] Y. Zhou, F. Wu, P. Huang, X. He, C. Xie, J. Zhou, "An Efficient Page-level FTL to Optimize Address Translation in Flash Memory" in Proc. ACM the 10<sup>th</sup> European Conference on Computer Systems, Bordeaux, France, 2015. <https://doi.org/10.1145/2741948.2741949>
- [4] F. Chen, B. Hou, R. Lee, "Internal parallelism of flash memory-based solid-state drives" ACM Trans. on Storage, 12(3), 1 – 39, 2016. <https://doi.org/10.1145/2818376>
- [5] S. K. Panigrahi, C. Maity, A. Gupta, "A simple wear leveling algorithm for NOR type solid storage device" CSI Trans. on ICT, 2(1), 65 – 76. 2014. <https://link.springer.com/article/10.1007/s40012-014-0047-3>
- [6] S. y. Park, E. Seo, J.y. Shin, S. Maeng, J. Lee, "Exploiting internal parallelism of flash-based SSDs" IEEE Comp. Arch. Letters, 9(1), 9 –12. 2010. <https://doi.org/10.1109/L-CA.2010.3>



- [7] P. Olivier, J. Boukhobza, E. Senn, "Micro-benchmarking Flash Memory File-system Wear Leveling and Garbage Collection: A Focus on Initial State impact" in Proc. 15<sup>th</sup> International Conference on In Computational Science and Engineering (CSE), Nicosia, Cyprus, 2012. <https://doi.org/10.1109/ICCSE.2012.67>
- [8] M.C. Yang, Y.M. Chang, C.W. Tsao, P.C. Huang, Y.H. Chang, T.W. Kuo, "Garbage Collection and Wear Leveling for Flash Memory: Past and Future" in Proc. International Conference on Smart Computing (SMARTCOMP), Hong Kong, China, 2014. <https://doi.org/10.1109/SMARTCOMP.2014.7043841>
- [9] O. Kwon, K. Koh, J. Lee, H. Bahn, "FeGC: An efficient garbage collection scheme for flash memory based storage systems. *Journal of Syst. and Soft.*, 84(9), 1507 – 1523, 2011. <https://doi.org/10.1016/j.jss.2011.02.042>
- [10] S. Mittal, J.S. Vetter, "A survey of software techniques for using non-volatile memories for storage and main memory system" *IEEE Trans. on Parallel and Dist. Sys.* 27(5), 1537 – 1550, 2016. <https://doi.org/10.1109/TPDS.2015.2442980>
- [11] J. Y. Paik, R. Jin, T.S. Chung, "Data recovery aware garbage collection mechanism in flash-based storage devices" *IEICE Trans. on Info. and Sys.*, E101.D(9), 2404 – 2408, 2018. <https://doi.org/10.1587/transinf.2017EDL8255>
- [12] C. C. Chung, D. Sheng, N.M. Hsueh, "A high-performance wear-leveling algorithm for flash memory system" *IEICE Electronics Express*, 9(24), 1874 – 1880, 2012. <https://doi.org/10.1109/APCCAS.2012.6419105>
- [13] Y.P Hu, N. Xiao, X.F. Liu, "An elastic error correction code technique for NAND flash-based consumer electronic devices" *IEEE Transactions on Consumer Electronics*, vol. 59, no. 1, pp. 1-8, 2013.
- [14] M. Lin, S. Chen, "Efficient and intelligent garbage collection policy for NAND flash-based consumer electronics" *IEEE Trans. on Cons. Electronics*, 59(3), 538 – 543, 2013. <https://doi.org/10.1109/TCE.2013.6626235>
- [15] A. R. Rahiman, P. Sumari, "Minimizing the Garbage Collection Time in Flash Memory Using Efficient Data Allocation Scheme" in Proc. 2009 IEEE Region 10 Conference (TENCON2009), Singapore, 2009. <https://doi.org/10.1109/TENCON.2009.5396010>
- [16] S. Fazackerley, R. Lawrence, "A Flash Resident File System for Embedded Sensor Networks" in Proc. IEEE 24<sup>th</sup> Canadian Conference on Electrical and Computer Engineering (CCECE), Niagara Falls, ON, Canada, 2011. <https://doi.org/10.1109/CCECE.2011.6030693>
- [17] G. Xu, Y. Liu, X. Zhang, M. Lin, "Garbage collection policy to improve durability for flash memory" *IEEE Trans. on Cons. Elect.*, 58(4), 1232 – 1236, 2012. <https://doi.org/10.1109/TCE.2012.6414990>
- [18] N. Dayan, P. Bonnet, "Garbage collection techniques for flash-resident page-mapping FTLs". *arXiv preprint arXiv:1504.01666*

# Securing Hybrid SDN-based Geographic Routing Protocol using a Distributed Trust Model

Lylia Alouache<sup>\*1</sup>, Mohamed Maachaoui<sup>2</sup>, Rachid Chelouah<sup>1</sup>

<sup>1</sup>ETIS CNRS ENSEA UMR 8051. Computer science, CY Cergy Paris University, 95000, France

<sup>2</sup>Quartz Laboratory. Computer science, CY Cergy Paris University, 95000, France

## ARTICLE INFO

Article history:

Received: 15 January, 2020

Accepted: 10 March, 2020

Online: 12 April, 2020

Keywords:

IoV

Routing protocols

SDN

QoS

Security

Availability

Reliability

Integrity

Trust

## ABSTRACT

In this paper, the vulnerabilities and the security attacks against vehicular networks, SDN architecture and some security solutions for SDVN are studied. Secondly, a complete and improved version of the secure HSDN-GRA routing protocol based on a distributed trust model is proposed where public keys of the vehicles are managed in a distributed way. Besides, in this approach, a weight is assigned to every vehicle, which is calculated from its freeloading and its trust values per those of the neighbors. The trust value is deduced from the historical interactions stored in a log of communication errors. To measure the trust value, three unreliable behaviors occurred in a time interval are considered. The vehicle with the role of cluster head hosts a list of each vehicles misbehaviors forming a log of communication errors. A vehicle will be chosen as the next relay according to its weight. As a positive result of this complete proposed approach, the following security requirements are achieved: the vehicle's authentication and the data integrity are guaranteed by a signature mechanism, whereas an encrypted function is used to ensure the confidentiality of the exchanged data. The goal is to protect the routing process against malicious and unstable nodes. Finally, the implementation details and simulation analysis are given, and a comparative study between the secure and the insecure HSDN-GRA is presented in the presence of a percentage of malicious nodes in the network. The perspective of managing non-collaborative vehicles is briefly introduced as future work.

## 1 Introduction

The Vehicular Adhoc Networks (VANET) suffers from many lacks such as delays of communication because of the multi hop scenarios, frequent links failures because of the nodes mobility, and also a low security due to the several attacks and intrusions against the wireless and the heterogeneous network.

In our previous works [1][2], the SDN paradigm has been identified as a suitable approach for dealing with: the dynamic and large scale environment, the robustness of communication, the heterogeneity of the network concerning applications and the communication technologies, the routing strategies and also the security issues [3].

However, finding the best way to implement the controller to suit to vehicular networks constraints is unresolved, especially because of the SDVN vulnerabilities. The security and the routing features are controlled by the SDN Controller. Whereas, the data plane applies according to the controller rules, since it is devoid of intelligence.

As a result, the location choice of the controller is critical, as robust and secure communications depends on the robustness, the reliability and the availability of this controller.

This paper represents an extended version of our previous work [1] entitled "Securing Southbound Interface of HSDN-GRA Vehicular Routing Protocol using a Distributed Trust" that is published in 2019 Fourth International Conference on Fog and Mobile Edge Computing (FMEC). We described an IoV communication use case based on the SDN architecture, to root IoV's data in a secure and robust manner from a source to a destination. The proposition was a preliminary approach without simulation analysis.

In this extended paper, we firstly discuss the security vulnerabilities of vehicular networks, SDN paradigm and SDVN networks. Secondly, we propose to secure the HSDN-GRA routing protocol by using an encrypted function and trust model [1]. In this trust model, each new vehicle broadcast its public key to its neighbors,

\*CY Cergy Paris University, Avenue du Parc 95000 Cergy Grance, +33769265726 & lae@eisti.eu

all the keys are managed in a distributed way. Besides, the described approach aims to assign a weight  $\omega$  to each vehicle.  $\omega$  is deduced from the free load value as well as the trust value of each vehicle per those of their neighbors.

To deduce the trust value of a vehicle, this approach uses the error log of HSDN-GRA protocol [4], as the historical misbehaviors of a vehicle gives its trust rate. three types of unreliable behaviors that a vehicle had in a period of time are considered. The list of each vehicle's misbehavior is stored in an error log and embedded on a specific cluster head vehicle. A vehicle can be the next relay according to its weight value.

the advantage of the proposed solution is the improvement of security in the communication process, indeed, vehicle authentication and data integrity are obtained using a signature mechanism, while the confidentiality of the data exchanged is provided by an encryption function. the main purpose of secure HSDN-GRA is to protect the routing process from malicious and unstable vehicles.

The present paper is organized as follows: Section 2 studies the security attacks against vehicular networks and SDN architecture and some security solutions for SDVN. Section 3 describes our Secure HSDN-GRA approach. The implementation details and simulation analysis is presented in Section 4. Finally, Section 5 concludes the main contributions and summarizes the perspective of an incentive scheme in order to manage the non-collaborative vehicles.

## 2 Background and Related Work

In the survey [2] realized by Alouache et al., the SDN architecture is described as an alternative to secure the network and to ensure the data integrity. In fact, a global overview of the system is achievable thank to the SDN controller. It collects information about the entire network traffic instead of exchanging a large amounts of information. As a result, it provides a better and reliable security mechanism than those applied to the traditional network [5].

### 2.1 Security Attacks in Vehicular Networks

Vehicular networks suffer from several attacks which compromise the main security requirements. [6].

In Table 1 non exhaustive list of these attacks are given.

### 2.2 Security Attacks in SDN Architecture

The SDN paradigm also has its own vulnerabilities, they are principally related to the characteristics, the location and the crucial role of the controller, as well as the control data flow exchanged between the control plane and the data plane [7].

Table 2 exposes a non exhaustive list of attacks related to the SDN paradigm.

## 2.3 Security Solutions for SDVN

Despite the vulnerabilities exposed in Table 1 and those mentioned in Table 2, and since SDN exceeds the limits of traditional mechanisms, it can be beneficial for IoV security deficiencies.

Table 1: Vehicular Network Attacks vs Security Requirements

Attacks in Vehicular Networks	Authentication	Availability	Confidentiality	Integrity	Non-repudiation
Denial of Service (DoS)		x			
Distributed DoS		x			
Jamming		x		x	
Malware attack		x	x	x	
GPS Spoofing	x	x			
Hijacking of session	x				
Position faking	x				
Illusion attack	x	x			
Bogus information attack	x	x			
GPS Spoofing	x	x			
Snooping			x		
Identity reveling			x		
Location tracking			x		
Brute force	x		x		
Eavesdropping			x		
Sink Hole attack		x	x	x	
Black Hole attack		x		x	
Masquerade attack	x			x	
Message tempering				x	x
Message suppression				x	x
Message reply	x				x
Repudiation		x			x

In fact, the SDN controller labels and isolates suspect flows and their sources, consequently, the data plane will not process the

packets coming from these flows.

Besides, the IoV network is heterogeneous and uses a set of communication technologies such: WAVE, DSRC, LTE, etc. having their own security policies, therefore, due to the SDN controller and its given global overview, these security policies can be deployed without conflict, which reinforces the security of the whole IoV system.

In addition, the centralization and the abstraction provided by the controller give the administrators the possibility to update any security policy based on observed unreliable behaviors. Table 3 describes how SDN can be a solution for security issues.

Table 2: SDN Attacks vs Security Requirements

SDN attacks in SDN Architecture	Authentication	Availability	Confidentiality	Integrity	Non-repudiation
DoS on the Data plane		x			
Distributed DoS on the Control plane		x			
Controller identity spoofing	x	x	x	x	x
Flow based forwarding attack				x	x
Flow table alteration			x	x	

Table 3: Security in IoV with SDN Architecture

Action	details
Intrusion detection	The SDN controller manages the nodes authentication and detects malicious intrusions.
Attacks identification	The SDN controller monitors the exchanged flows emanating from all the nodes to detect any setting alteration.
Self recovery mechanism	The SDN controller hosts rules to automatic recovery against any attack.

Recently, some research papers deal with both routing and security issues in vehicular networks by adopting the SDN paradigm.

The Improvised Trust based Ad-hoc On-demand Distance Vector routing (I-TAODV) is proposed by Vasudes et al. in [8], it aims to secure routing in a multi hop scenario.

Based on a metric called trust value, the authors propose an algorithm to identify the trusted vehicles, and another one to identify the malicious ones.

This protocol is built on the SDN paradigm, where the control plane

monitors forwarding, reversing, trust of forwarding Vehicle, trust of reverse vehicle, path trust and network performances.

Zhang et al. elaborate The Software-Defined Trust based Ad hoc On-demand Distance Vector routing (SD-TAODV) in [9]. The process of route discovery, route maintenance, the reverse and forwarding paths are chosen by the control plane.

They also use a trust management mechanism which is represented by a bi-objective function, it tries to optimize two objectives: the node trust and the path trust calculated respectively by Trust Node Calculation Process and Path Trust Calculation Process They are used to enhance the Route Discovery Process of TAODV.

### 3 Securing the HSDN-GRA

The HSDN-GRA protocol presented in the research [4] exploits a log of communication errors where three types of vehicle’s misbehavior are stored: link failures, random reception of Beacon messages, and non-acknowledgement of previous messages.

To estimate the trust value, the vehicle communication history is observed and tracked from the log of communication error. In this extended paper, we use the trust value of each vehicle with comparison to the trust values of all its neighbors.

The trust is described as the expectation and the belief that a vehicle has about other vehicles concerning future behaviors.

Its estimation is based on 1) experiences and evidences collected in the past either directly or indirectly, and 2) the knowledge about the vehicles nature, and/or on recommendations from trusted entities [10]-[12].

This trust value in addition to the free load value of each vehicle are aggregated to assign a weight  $\omega$  to each vehicle. This weight will be used to elect the best relay at each step of the routing process.

The routing rules are commonly governed by two types of controllers in HSDN-GRA: the semi-centralized controller represented by the cluster head, and the distributed controllers represented by the cluster members.

Figure 1 shows an IoV communication scenario using the HSDN-GRA routing protocol based on a semi-centralized SDN architecture.

A vehicle tries to access to an Internet service is requested by a vehicle, but the request fails because the closest infrastructure is down. So it switches to the vehicles on the road for routing its request.

The network is divided on clusters and Cluster heads are elected. Each Cluster Head contains a part of the control plane (the error log). The second part is distributed on the rest of the cluster members.

until reaching the destination, the request transits through vehicles with a hop by hop approach. Each vehicle selects its next relay with respect to the controller policy i.e.: The one who has the best relative trust value and the best relative free load value.



Hypothesis:

- In this extended paper, we opt for the highway scenario, this choice is guided by the stability of vehicle's speed.
- At first, the free load and the trust values of vehicles are equal and optimal.
- Malicious-Vehicles  $\ll$  Reliable – Vehicles.

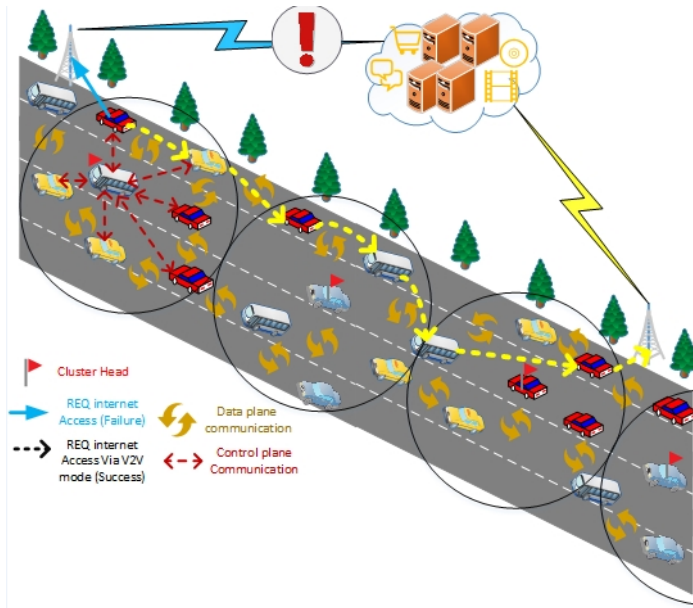


Figure 1: A Use Case of IoV Communication with a Hybrid SDN Architecture

The following subsections describe the securing HSDN-GRA steps.

### 3.1 Public key Distribution

- all the vehicles exchange a define Beacon to form a a one hop neighboring.
- Each vehicle sends its Public Key  $Pkey$  to the one hop neighbors, and receives back their  $Pkey$ .
- At this initialization step, because of the absence of cluster head, only the distributed controllers embedded on each vehicle are operational.
- Each vehicle has a weight  $\omega$ , it exploits the load capacity  $l_i$  deduced from the received Beacons, and the trust value  $Trust_i$  calculated from the log of communication errors according to Formula 1. The weight  $\omega$  of each vehicle is calculated from Formula 2 by all the neighbors, and the true value will be confirmed by the majority.
- The election of the Cluster Head is realized by a distributed consensus after the initialization period of time  $T$  has passed, the one with the largest weight  $\omega$  will be the Cluster Head.

$$Trust = \left( \frac{1}{Popularity} \right) \quad (1)$$

$$\omega(v)_i = \left( \frac{l_i}{\sum_{j=1}^m l_j} + \frac{Trust_i}{\sum_{j=1}^m Trust_j} \right) \quad (2)$$

where  $m$  is the number of neighbors.

-To monitor the communication errors of each neighbor, in the beginning, before electing cluster heads, logs are distributed within all the vehicles. The trust rate is estimated by exploiting all the distributed logs. So, initially each vehicle:

- Monitors its neighbors and has it own log
- Calculates the weight  $\omega$  of each neighbor
- Then, each vehicle broadcasts in a map the  $Pkey_i$  of each neighbor and their associated weight  $\omega$  values:

$$NeighborPkeyMap = \{Pkey_i, \omega_i\}, \text{ With } i \in \{1, m\}$$

The algorithm 1 describes how the public key distribution as well as the weight of each vehicle is managed.

#### Algorithm 1: Public Key Distribution (PKD)

```

1 Let  $Pkey_i$  be a the public key of vehicle  $V_i$ ;
2 Let  $NeighborsPkeyMap < Pkey, \omega >$  be a the map in which
  a vehicle  $V$  store the public key and the weight of its
  neighbors;
input : Vehicle  $V$ 
output :  $NeighborsPkeyMap$ 
3 Initialization:  $NeighborsPkeyMap = \emptyset$ ;  $\omega_{V_i} = null$ ;
   $Pkey_i = null$ ;
4 for each vehicle  $V_i$  do
5   |  $Broadcast(Beacon_{V_i})$ ;
6   |  $Broadcast(Pkey_{V_i})$ ;
7 end
8 for each vehicle  $V$  do
9   |  $Receive(Beacon_{V_i})$ ;
10  |  $Receive(Pkey_{V_i})$ ;
11  |  $Trust_i = \left( \frac{1}{Popularity_i} \right)$ ;
12  |  $\omega(V)_i = \left( \frac{l_i}{\sum_{j=1}^m l_j} + \frac{Trust_i}{\sum_{j=1}^m Trust_j} \right)$ ;
13  |  $Insert(< Pkey_{V_i}, \omega(V_i) >, NeighborsPkeyMap)$ ;
14 end
15  $Broadcast(NeighborsPkeyMap)$ ;

```

### 3.2 Cluster Head Election

-Using all the received  $NeighborsPkeyMap_i$ , a vehicle  $V$  confirms the reliable weight value  $\omega_i$  of each neighbor  $V_i$  and the association  $(V_i/Pkey_i)$ . i.e, a coherent contain of the  $NeighborsPkeyMap$  is deduced by the majority who give the same values.

-On each vehicle a consensus occur to chose as Cluster Head the vehicle with the largest weight  $\omega$ .

-The variable "IsCh" will be *True* in the Beacon for the Cluster Head, while the rest of vehicles will keep the value *False*.

-The elected Cluster Head, representing the Semi-Centralized SDN controller, will now hosts the log of communication errors related

to it cluster.

The algorithm 2 details the Cluster Head election.

**Algorithm 2: Secure Cluster Head Election (SCEA)**

```

1 Let  $NeighborsPkeyMap_i < Pkey, \omega >$  be a the maps
  received by V from each neighbor;
  input : Vehicle V
  output : ClusterHead
2 Initialization:  $Max\omega = \omega; PkeyMax = Pkey;$ 
  ClusterHead = null;
3 for each vehicle V do
4   Receive( $NeighborsPkeyMap_i$ );
5   FixTrueValueof( $NeighborsPkeyMap$ ) By the Majority;
6   if ( $NeighborsPkeyMap.\omega_i > Max\omega$ ) then
7      $Max\omega = NeighborsPkeyMap.\omega_i;$ 
8      $PkeyMax = NeighborsPkeyMap.Pkey_i;$ 
9   else
10    if ( $NeighborsPkeyMap.\omega_i == Max\omega$ ) and
11      ( $NeighborsPkeyMap.Pkey_i < PkeyMax$ ) then
12         $Max\omega = NeighborsPkeyMap.\omega_i;$ 
13         $PkeyMax = NeighborsPkeyMap.Pkey_i;$ 
14    end
15    ClusterHead =  $V_{Max\omega};$ 
16    if (ClusterHead = V) then
17       $Beacon_V.isCH = True;$ 
18      Send(NewBeacon);
19      Receive(ErrorLog) from previous Cluster Head
20      or from the neighbors at initialization;
21      Filter(ErrorLog);
22    else
23      Reset( $NeighborsPkeyMap_i$ );
24    end
  end
  
```

**3.3 Secure Control Plane of HSDN-GRA**

In this section, the Secure HSDN-GRA is detailed. Once the first election of the Cluster Head occurred, the vehicles signs all their Beacons. The objective is to guarantee the authentication. Figure 2 expose the Beacon message structure.

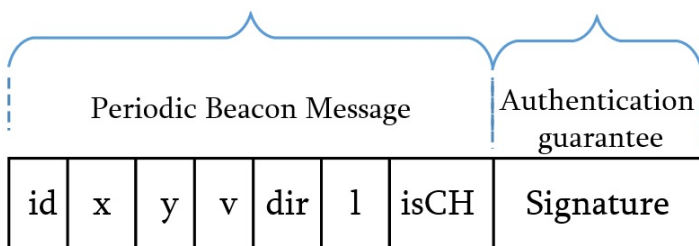


Figure 2: Beacon Message structure in Secure HSDN-GRA

The structure of the messages exchanged via the southbound interface are represented in Figure 3.

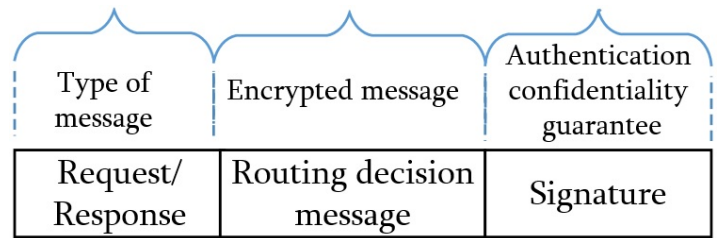


Figure 3: Structure of Southbound Messages in Secure HSDN-GRA

As the confidentiality of the control decisions, especially about the next hops, need to be preserve, we also propose to secure the southbound interface used in HSDN-GRA routing protocol.

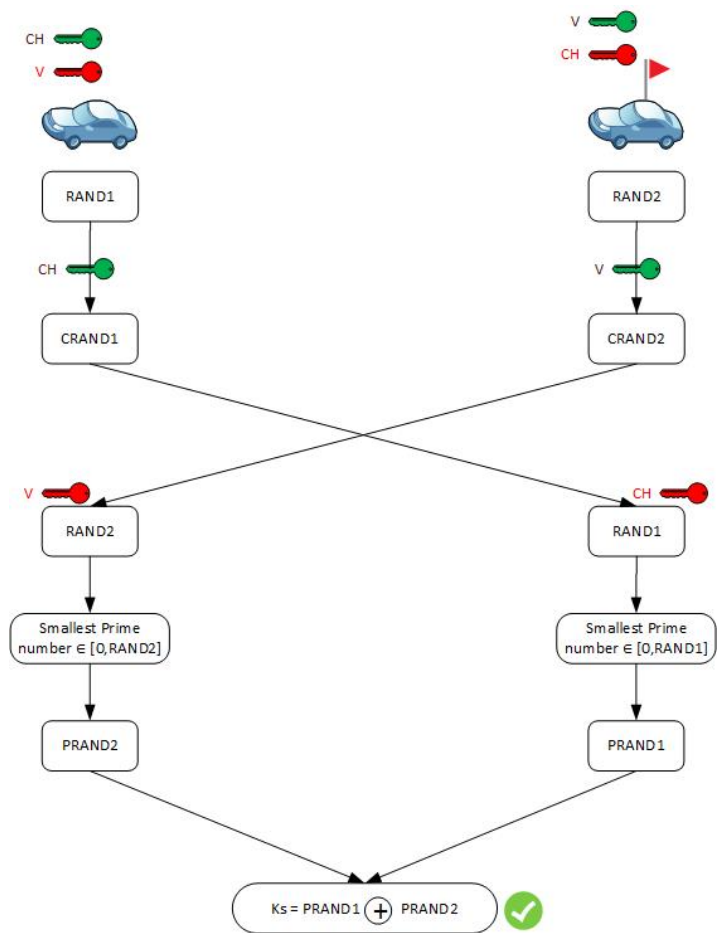


Figure 4: Secret Key creation between the Cluster Head and a vehicle V

To encrypt the data flow of the southbound interface, we are inspired from the symmetric encryption algorithm AES [13]. A secret key  $K_s$  is exchanged between each vehicle and its Cluster Head. The public keys  $Pkey$  already shared are exploited to deduce  $K_s$ .

A vehicle V and its Cluster Head exchange two random numbers  $RAND1$  and  $RAND2$  encrypted respectively with  $Pkey_{CH}$  and  $Pkey_V$ .

Then, the Cluster Head decrypt with its private key  $RAND1$

and choose the smallest prime number  $PRAND1$  in the interval  $[0,RAND1]$ . The vehicle  $V$  decrypt also with its private key  $RAND2$  and choose the smallest prime number  $PRAND2$  in the interval  $[0,RAND2]$ .

Finally, the secret key  $K_s$  is given using the formula 3. The symbol  $\oplus$  representing the Exclusive Or logical operation.

$$K_s = (PRAND1 \oplus PRAND2) \tag{3}$$

Figure 4 illustrate how the secret key  $K_s$  is formed by the Cluster Head and a vehicle  $V$  in order to encrypt the southbound interface communications.

Figure 5 illustrate communications inside a cluster of Secure HSDN-GRA.

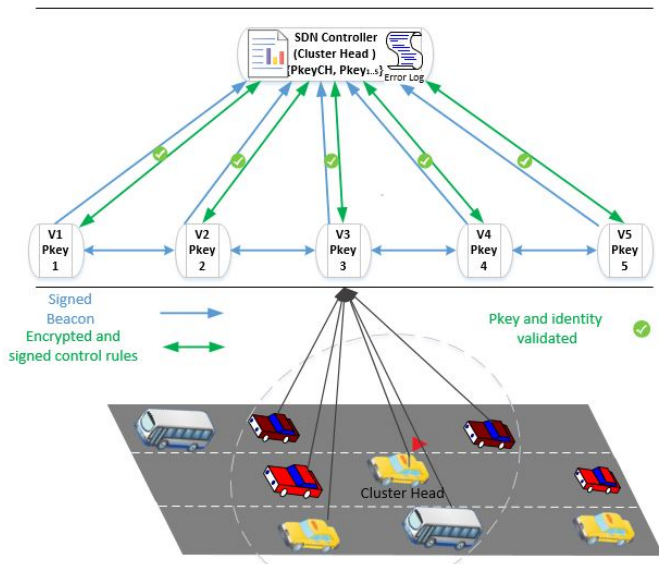


Figure 5: Communication inside a Cluster of Secure HSDN-GRA

### 3.4 Secure Incoming Vehicles in a Cluster

Three steps are required to integrate a new vehicle in a cluster:

- The new vehicle  $V_n$  broadcast its Beacon and its  $Pkey$  to announce its self.
- All the neighbors inside the Cluster reply to  $V_n$  with the identifier and the  $Pkey$  of the Cluster Head, while sending the triplet  $(V_n, Pkey_n, \omega_n)$  to the Cluster Head.
- The Cluster Head analyzes all the received triplets  $(V_n, Pkey_n, \omega_n)$  in order to confirm the identity of  $V_n$ . It deduces the percentage of veracity of this triplet, from the number of vehicles who affirm it. After that, a Challenge-Response mechanism [14] is exploited associate definitively  $V_n$  to  $Pkey_n$ .

These steps are respectively illustrated by Figure 6, Figure 7 and Figure 8.

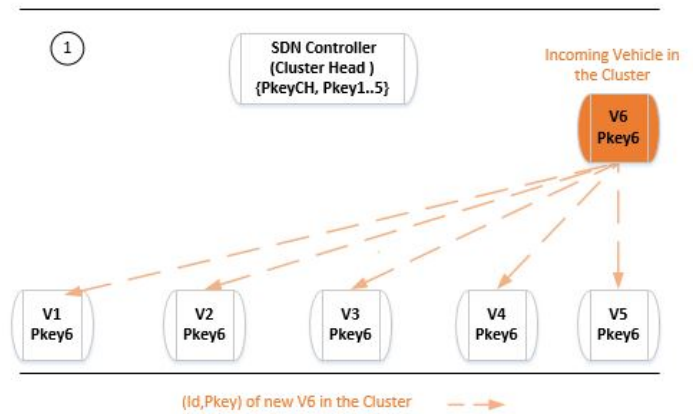


Figure 6: Incoming Vehicle in the Cluster: Phase 1

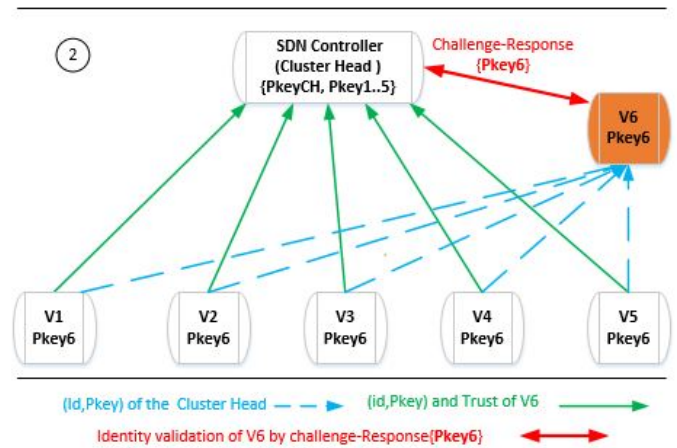


Figure 7: Incoming Vehicle in the Cluster: Phase 2

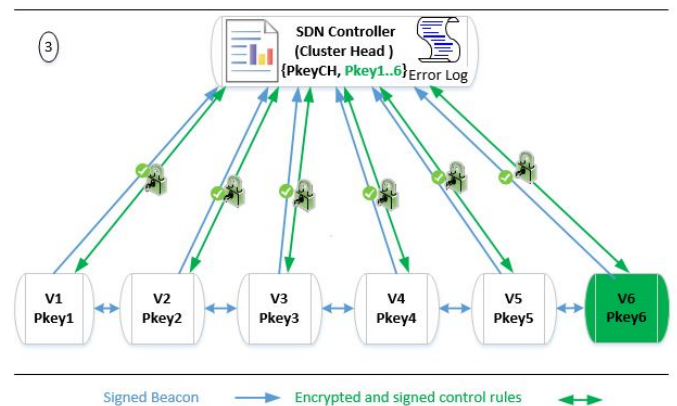


Figure 8: Incoming Vehicle in the Cluster: Phase 3

### 3.5 Secure Outgoing vehicle from a Cluster

This section shows the behaviour of secure HSDN-GRA in case of outgoing vehicle. Two cases are identified:

The first case deals with a cluster member which formulates a Request-To-Leave message the steps are:

- The Cluster member sends a Request-to-Leave message to the Cluster Head
- A Challenge-Response mechanism [14] is launched to confirm that the request is formulated by the pretending cluster member.
- After the authentication, an ACK message is sent by the Cluster Head to the leaving vehicle as an acknowledgement of its request. Meanwhile, the Cluster Head also broadcasts a  $Revoke(V, Pkey)$  message inside the cluster in order to delete the keys of the outgoing vehicle.
- ACK messages confirming the revocation of this vehicle are sent to the Cluster Head by all the cluster members.

- ACK messages confirming the revocation of this vehicle are sent by all the Cluster members.

The two cases are combined in the algorithm 3.

Figure 9 shows a Cluster member outgoing scenario.

It encompasses the two cases. The black circle details the Request-to-Leave scenario, while the rest explains the revocation procedure.

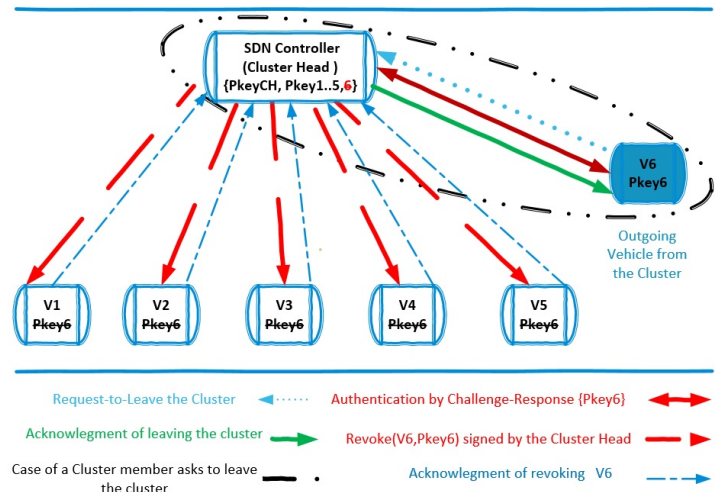


Figure 9: Outgoing Cluster Member Management

**Algorithm 3: Secure Outgoing Vehicle From a Cluster (SOC)**

```

1 Let  $\tau$  be the Beacon interval and  $ToF$  be the maximum delay
  of receiving Beacons;
input : Vehicle  $V$ 
output : Cluster
2 Initialization:  $ToF = 5\tau$ ;
3 for each Cluster do
4   if ( $V$  wants to leave a Cluster) then
5     Send(Request – To – Leave) to the Cluster Head;
6     if (Challenge – Response(ClusterHead,  $V$ ) is
7       verified by the Cluster Head) then
8       Send(ACK) by the Cluster Head to  $V$ ;
9       Broadcast(Revoke( $V, Pkey$ )) to the cluster
10      members;
11    end
12  else
13    if ( $Receive(Beacon_V) \notin [\tau, 5\tau]$ ) then
14      Broadcast(Revoke( $V, Pkey$ )) to the cluster
15      members;
16    else
17      Reset( $ToF$ );
18    end
19  end

```

The second case concerns the revocation of the vehicles that don't respect the periodicity of Beacons, as they are considered as unreliable.

In this paper, at every time-out  $\tau$ , vehicles are supposed to send and receive back Beacons. Besides, a Timer-of-Freshness  $ToF$ , initialized to  $5\tau$ , is assigned to each Cluster member sending a Beacon. The Cluster Head launches and decrements  $ToF$  when it receives a new Beacon message from a Cluster member.

If the Cluster Head receives t Beacon in the time interval  $[\tau, 5\tau]$ , the  $ToF$  value is refreshed and reset to its initial value. Otherwise, the Cluster member is considered as unreliable and need to be excluded from the cluster according to the following steps:

- If the  $ToF$  has passed, the Cluster Head broadcasts a  $Revoke(V, Pkey)$  message within its cluster.

## 4 Simulation Analysis

In this simulation, we simulate a scenario of the Secure HSDN-GRA routing packets in IoV.

We develop a simulation with traffic condition similar to the situation in Figure 1.

Table 4: NS2 Simulation Parameters

Parameters	Specification
Simulation time	300s
Simulation area	1000m X 1000m
Number of nodes	[20-300]
Speed	[50-140] km/h
Propagation model	Two Ray Ground
Medium capacity	6 Mbps
Transmission range	310 m
Transport layer	UDP



## 4.1 NS2 Implementation

The simulation is done under a Ubuntu 10.04 Linux machine where we have installed the new version of network simulator NS2.34[15] and VanetMobiSim[16].

The simulation parameters are summarized in Table 4.

Some simulation functions in C++ are summarized in listing 1 (cf. Appendix 5).

## 4.2 Experimental Results

The goal of this evaluation consist of the study of attack resilience and routing performances of the secure HSDN-GRA protocol against the insecure HSDN-GRA protocol.

Percentage rate of data delivery and average end to end delay are chosen as indicators of routing performances.

The comparative study is done for different combinations of metrics like: the presence of malicious nodes, the clusters density and the vehicles speed.

the routing decisions of HSDN-GRA protocol are guided by the one-hop neighbors, besides, the secure HSDN-GRA protocol aims to detect and avoid malicious nodes. So, the routing performances will be positively affected by the improvement of routing behavior in presence of malicious nodes

### 4.2.1 Effect of Malicious Nodes

In this section, we observe in Figure 10 that the Secure HSDN-GRA presents better packet delivery ratio than the baseline HSDN-GRA once an increased number of malicious nodes are introduced in the simulation.

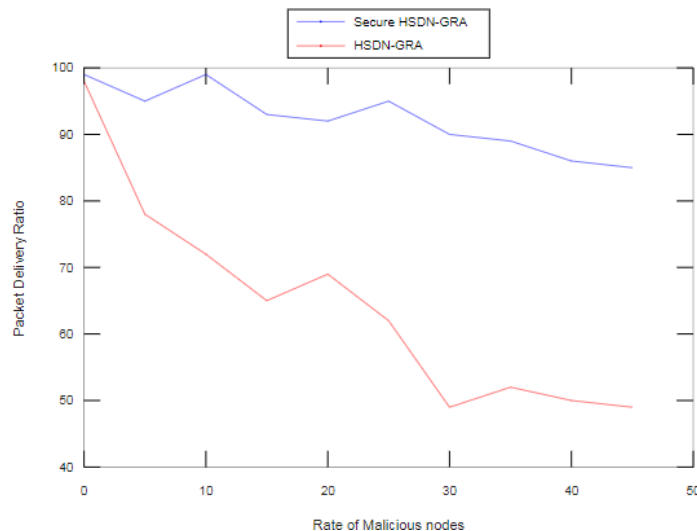


Figure 10: Packet Delivery Ratio vs. Number of Malicious Nodes

Indeed, the Secure HSDN-GRA elects as a relay the neighbor with the best trust value as well as the maximum free load with comparison to the whole neighbors, furthermore, the exchanged packets are signed and encrypted with a secret key  $K_s$  which makes the alteration and the destruction of packets more difficult.

Besides, the Secure HSDN-GRA also outperforms the baseline HSDN-GRA of delay in the presence of an increased number of malicious nodes in the simulation as shown in Figure 11.

In fact, the Secure HSDN-GRA takes into account the trust value of each relay with comparison to the whole neighbors as well as the corresponding average free load before choose it. It makes the HSDN-GRA more resilient.

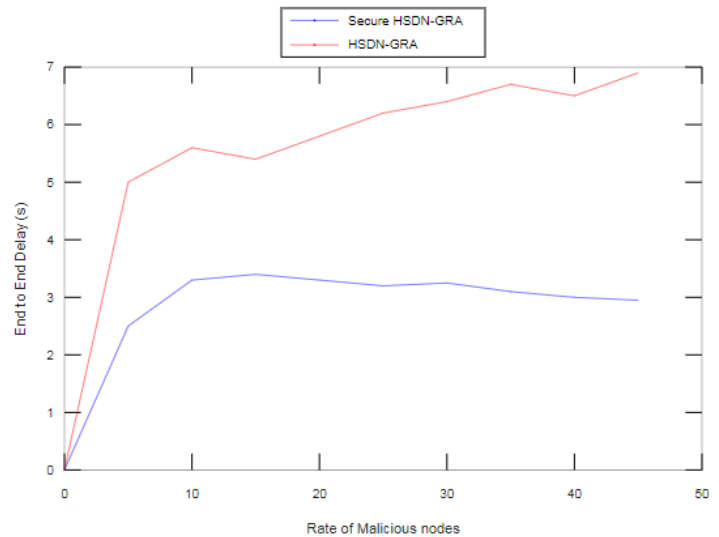


Figure 11: Average End to End Delay vs. Number of Malicious Nodes

### 4.2.2 Effect of Cluster nodes Density

Figure 12 and Figure 13 show respectively the impact of clusters density on the behaviour of both Secure HSDN-GRA and baseline HSDN-GRA in term of packet delivery ratio and delay especially in the presence of 20% of malicious nodes.

Firstly, for both Secure HSDN-GRA and baseline HSDN-GRA the increase density inside clusters offer better packet delivery ratio because more relays can be exploited. However, the packet delivery ratio is more satisfying when the relays are chosen according to the trust analysis estimated by the network.

Then, we observe in Figure 12 that Secure HSDN-GRA deliver an average of 30.28% of packets more that baseline HSDN-GRA in the presence of 20% of malicious nodes.

Besides, we can deduce that the authentication and the encrypted communications decrease the number of packets alteration, packet lost and malicious intrusion.

Secondly, we can observe that Secure HSDN-GRA reduce the delay comparing to baseline HSDN-GRA because the relays are chosen according to their trust values in order to guarantee the local acknowledgement of each packet sent and reduce the error recovery, consequently the delay is reduced.

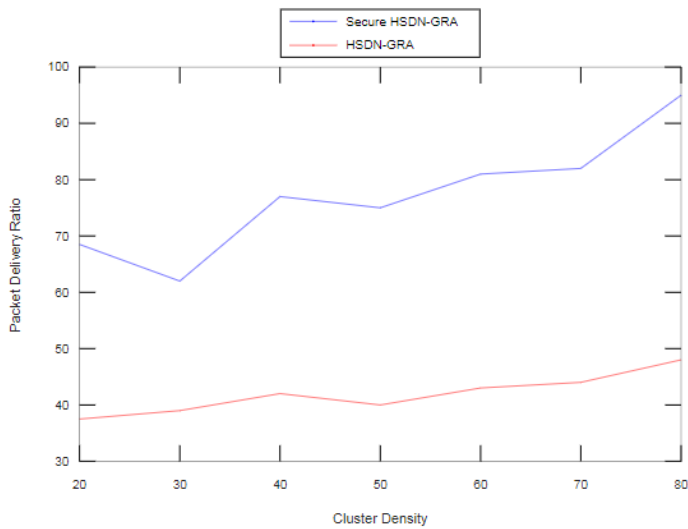


Figure 12: Packet Delivery Ratio vs. Clusters Density with 20% of malicious nodes

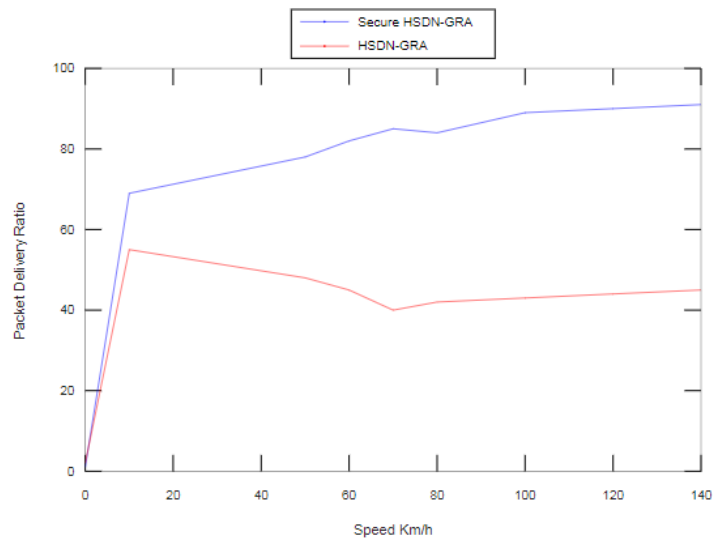


Figure 14: Packet Delivery Ratio vs. Speed with 20% of malicious nodes

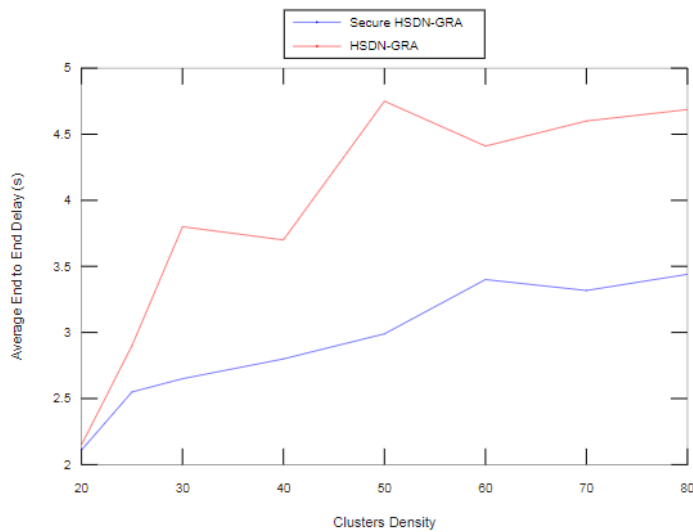


Figure 13: Average End to End Delay vs. Clusters Density with 20% of malicious nodes

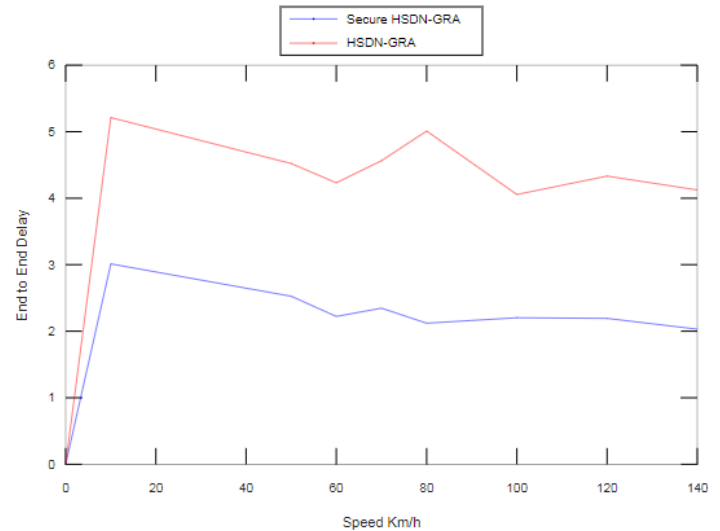


Figure 15: Average End to End Delay vs. Speed with 20% of malicious nodes

#### 4.2.3 Effect of Vehicles Speed

Figure 14 and Figure 15 show the impact of vehicles speed against the Secure HSDN-GRA and baseline HSDN-GRA in the presence of 20% of malicious nodes.

The results in Figure 14 show that the secure HSDN-GRA outperform the baseline HSDN-GRA in term of packet delivery ratio, besides, we can observe that the increase speed stabilizes the packet delivery ratio for the both protocols.

For the delay performances, we can observe in Figure 15 that Secure HSDN-GRA reduces the delay when the speed, furthermore, it surpasses the baseline HSDN-GRA, it is due to the stability of the clusters on the highways and the packets destination are reached faster, since the relays are chosen according to the direction of the destination.

## 5 Conclusion

The result of applying the SDN architecture on vehicular network consist of making the routing strategies optimal, especially for with load balancing, security policies and also for the network heterogeneity management.

Indeed, it aims to select the most suitable channels and frequencies for data transmission at a specific time according to the context and the requirements.

Besides, it implements various security policies and exploits them adaptively according to the requirements. Finally, the nodes are balanced thanks to the global view given by the control plane.

In this paper, a secure HSDN-GRA for more robustness is exposed, a trust model is built between nodes, and the communications

between the nodes as well as those of the southbound interface are secured with an encryption function. Even if we have a performing and securing routing protocol, in a totally distributed system it is difficult to guarantee the cooperation of all the entities without any rewards in turn, the selfish nodes constitute an obstacle of communication in a totally distributed network, so as a future perspective, a solution based on blockchain paradigm will be integrated in secure HSDN-GRA in order to tackle selfish nodes and stimulate their cooperation.

**Acknowledgment** This project was supported by Initiative d'Excellence Paris//Seine.

## References

- [1] Lylia Alouache et al. "Securing Southbound Interface of HSDN-GRA Vehicular Routing Protocol using a Distributed Trust". In: *Fourth International Conference on Fog and Mobile Edge Computing, FMEC 2019, Rome, Italy, June 10-13, 2019*. 2019, pp. 90–97.
- [2] Lylia Alouache et al. "Survey on IoV routing protocols: Security and network architecture". In: *International Journal of Communication Systems* 32.2 (2019), pp. 38–49.
- [3] Antonio Di Maio et al. "Enabling SDN in VANETs: What is the Impact on Security?" In: *Sensors* 16.12 (2016).
- [4] L Alouache et al. "Toward a hybrid SDN architecture for V2V communication in IoV environment". In: *2018 Fifth International Conference on Software Defined Systems (SDS)*. Barcelona, Spain, 2018, pp. 93–99.
- [5] P. Baskett et al. "SDNAN: Software-Defined Networking in Ad-Hoc Networks of Smartphones". In: *2013 IEEE 10th Consumer Communications and Networking Conference (CCNC)*. Las Vegas, NV, USA, 2013, pp. 861–862.
- [6] M. Azees, P. Vijayakumar, and L. Jegatha Deborah. "Comprehensive survey on security services in vehicular ad-hoc networks". In: *IET Intelligent Transport Systems* 10.6 (2016), pp. 379–388.
- [7] M. Liyanage et al. "Opportunities and Challenges of Software-Defined Mobile Networks in Network Security". In: *IEEE Security Privacy* 14.4 (2016), pp. 34–44.
- [8] H. Vasudev and D. Das. "A trust based secure communication for software defined VANETs". In: *2018 International Conference on Information Networking (ICOIN)*. 2018, pp. 316–321.
- [9] D Zhang et al. "Software-defined Vehicular Ad Hoc Networks with Trust Management". In: *the 6th ACM Symposium on Development and Analysis of Intelligent Vehicular Networks and Applications*. DIVANet '16. Malta, Malta: ACM, 2016, pp. 41–49. ISBN: 978-1-4503-4506-4.
- [10] Seyed Soleymani et al. "Trust Management in Vehicular Ad-Hoc Network: a Systematic Review". In: 2015 (2015).
- [11] N. Bimeyer et al. "Assessment of node trustworthiness in VANETs using data plausibility checks with particle filters". In: *2012 IEEE Vehicular Networking Conference (VNC)*. 2012, pp. 78–85.
- [12] Junhai Luo, Xue Liu, and Mingyu Fan. "A Trust model based on fuzzy recommendation for Mobile Ad-hoc Networks". In: *Computer Networks* 53.14 (2009), pp. 2396–2407. ISSN: 1389-1286.
- [13] Jim Schaad. *Use of the Advanced Encryption Standard (AES) Encryption Algorithm in Cryptographic Message Syntax (CMS)*. RFC 3565. 2003. URL: <https://rfc-editor.org/rfc/rfc3565.txt>.
- [14] Margaret Rouse. *Challenge - Response Authentication Definition: What does Challenge - Response Authentication mean?* <https://searchsecurity.techtarget.com/definition/challenge-response-system>. Accessed: 2018-05-30.
- [15] Teerawat Issariyakul and Ekram Hossain. *Introduction to Network Simulator NS2*. 1st ed. Springer Publishing Company, Incorporated, 2008. ISBN: 0387717595, 9780387717593.
- [16] Jrme Hrri et al. "Vehicular mobility simulation with Vanet-MobiSim". In: *SIMULATION* 87.4 (2011), pp. 275–300.

## Appendix

Table 5 presents the abbreviations used throughout the paper.

Table 5: Abbreviations used in the paper

ACK	Acknowledgment
AES	Advanced Encryption Standard
DoS	Denial-of-Service
DSCR	Dedicated Short-Range Communication
FMEC	International Conference on Fog and Mobile Edge Computing
GPS	Global Positioning System
HSDN-GRA	Hybrid SDN-based Geographic Routing Protocol with Multi-agent Approach
IoV	Internet of Vehicle
I-TAODV	Improvised Trust based Ad-hoc On-demand Distance Vector routing
LTE	Long Term Evolution
SDN	Software-Defined Networking
SD-TAODV	Software-Defined Trust based Ad hoc On-demand Distance Vector routing
SDVN	Software-Defined Vehicular Networking
TAODV	Trust based secure routing in AODV routing protocol
ToF	Timer-of-Refresh
UDP	User Datagram Protocol
V2V	Vehicle-to-Vehicle
VANET	Vehicular Ad Hoc Network
WAVE	Wireless Access in Vehicular Environments

Listing 1: Some NS2 Simulation Functions

```
static inline double jitter (double max, int be-random-)
```

```
static class ANGLEclusterHeaderClass : public PacketHeaderClass
static class ANGLEclusterClass
ANGLEclusterClass() :
TclClass("Agent/ANGLEcluster"):
public TclClass ("PacketHeader/ANGLEcluster", sizeof(hdr-all-
anglecluster))
void ANGLEclusterHelloTimer::expire(Event *e)
UpdPosTimer::expire(Event *e)
StateTimer::expire(Event *e)
PERTimer::expire(Event *e)
EndElecTimer::expire(Event *e)
ANGLEclusterAgent::ANGLEclusterAgent() : Agent(PT-ANGLECLUSTER)
int ANGLEclusterAgent::command(int argc, const char*const* argv
)
void ANGLEclusterAgent::SendHello()
void ANGLEclusterAgent::SendBeacon(u_int8_t type)
void ANGLEclusterAgent::SendMSG()
void ANGLEclusterAgent::SendRoutingMSG(nsaddr_t s, nsaddr_t d, int
i)
void ANGLEclusterAgent::sendACK(nsaddr_t node, float seqnumber)
void ANGLEclusterAgent::sendPkey()
void ANGLEclusterAgent::sendRequestToLeave(nsaddr_t node)
void ANGLEclusterAgent::sendRevoke(nsaddr_t node)
void ANGLEclusterAgent::receive(Packet* p, Handler*)
void ANGLEclusterAgent::RecvHello(Packet *p)
void ANGLEclusterAgent::RecvBeacon(Packet *p)
void ANGLEclusterAgent::RecvCHBeacon(Packet *p)
void ANGLEclusterAgent::RecvRoutingMsg(Packet *p)
void ANGLEclusterAgent::ReceiveACK(Packet *p)
void ANGLEclusterAgent::ReceiveRevoke(Packet *p)
void ANGLEclusterAgent::timeout()
tosend ANGLEclusterAgent::caluclWeight()
int ANGLEclusterAgent::search(nsaddr_t inode)
void ANGLEclusterAgent::getSpeed()
void ANGLEclusterAgent::getmovspeed(double * sp)
void ANGLEclusterAgent::getLoc()
void ANGLEclusterAgent::GetLocation()
void ANGLEclusterAgent::updcord()
void ANGLEclusterAgent::signalPre()
void ANGLEclusterAgent::signalRouting()
void ANGLEclusterAgent::showState()
void ANGLEclusterAgent::PurgeTable(u_int8_t num)
void ANGLEclusterAgent::secretKey()
void ANGLEclusterAgent::signature(Packet* p, Handler*)
void ANGLEclusterAgent::crypt(Packet* p, Handler*)
int ANGLEclusterAgent::numofNeighbors()
int ANGLEclusterAgent::existmember()
void ANGLEclusterAgent::Popularity(nsaddr_t node, int cas)
double ANGLEclusterAgent::Frequency(nsaddr_t node, int cas)
int ANGLEclusterAgent::getPopularity(nsaddr_t node)
double ANGLEclusterAgent::getFrequency(nsaddr_t node)
nsaddr_t ANGLEclusterAgent::unReliableNode()
float ANGLEclusterAgent::getTrust(nsaddr_t node)
void ANGLEclusterAgent::updatePositions()
void ANGLEclusterAgent::endelection()
void ANGLEclusterAgent::VehicleState()
void ANGLEclusterAgent::RecvPresMSG(Packet *p)
void ANGLEclusterAgent::BestNode(nsaddr_t node, double pd)
nsaddr_t ANGLEclusterAgent::NextRelay()
void ANGLEclusterAgent::Revoke(nsaddr_t node)
```



## An ISO 25010 Based Quality Model for ERP Systems

Emmanuel Peters<sup>1,\*</sup>, George Kwamina Aggrey<sup>2</sup>

<sup>1</sup>Computer Science and Information Technology, Accra Institute of Technology, P.O.Box AN 19782, Accra-North, Ghana

<sup>2</sup>Computer Science and Information Technology, University of Cape Coast, P.O. Box PMB, Cape Coast, Ghana

---

### ARTICLE INFO

Article history:

Received: 01 November, 2019

Accepted: 07 January, 2020

Online: 10 April, 2020

---

Keywords:

ERP systems

Software Quality Model

ERP systems Quality Model

ISO 25010 Model

---

---

### ABSTRACT

Higher Education Institutions (HEIs) have begun rapidly adopting, selecting and implementing ERP systems due to the call by various governments to streamline their processes and practices. While ERPs are expanding at much faster rate, there is pressure on most HEIs to ensure quality. For quality model, ISO/IEC 25010 is an international standard for software and systems quality evaluation. With the introduction of three specific new sub-factors, this paper presents a new model based on the ISO/IEC 25010 for the evaluation of quality enterprise resource planning (ERP) systems. This new model can be used to select and adopt ERP systems in higher education institutions. It can also serve as a guide in implementing ERP systems in higher education institutions. The new model comprises eight factors which include functional suitability, reliability, usability, performance efficiency, compatibility, security, maintainability and portability. These eight quality factors are further divided into thirty-four (34) sub-factors. Thus, the outcome of this study is a model developed for quality evaluation of ERP systems in HEIs.

---

## 1. Introduction

ERP systems are designed to allow smooth and easy flow of information across functional areas of an institution or organization. They are made to address problems of information disjointments or “Islands of information” in organizations. Enterprise resource planning (ERP) systems have been introduced into higher educational institutions to integrate and computerize most of the business operations which include recruitment, admission, financial aid, student records, and most academic and administrative services [1]. According to [2], ERP systems have several advantages in HEIs: (1) improved information access for planning and managing institutional resources; (2) faculty, students and employees get improved services; (3) reduced business risks and (4) income and expenditure improved efficiently. By implementing such systems, HEIs are expected to improve quality and productivity of their operations. Due to these advantages, many higher education institutions have spent time, money and effort in the implementation of ERP systems [3].

The market of ERP systems is expected to reach \$41.69 billion in sales by 2020 [4]. However, studies have shown that there are challenges in the selection and implementation of ERP systems especially among higher education institutions. Studies about educational institution’s information systems have all been about

e-book systems [5] and e-learning websites [6], thereby ignoring the ERP systems. Several software and systems quality models [5], [7, 8] have been developed to evaluate the quality of ERP systems in HEIs, but none of these has adapted the ISO 25010 as their base model. It is therefore, necessary to adapt this international standard (ISO 25010) which has been in existence since 2011, for quality evaluation of ERP systems in HEIs.

The study seeks to refine and extend the quality model of ISO 25010. Since ISO 25010 extends and refines the ISO 9126, there is the need to extend and refine the existing quality models of ERP systems in HEIs. Based on the ISO 25010, this paper presents a new model for quality ERP systems evaluation in HEIs since models are not static.

## 2. Literature Review

Several quality models in the literature were developed for software and systems evaluations. Thus, ERP systems selection and adoption in higher education would require a careful adaptation. This section gives the highlights on two popular software and systems quality models in the literature, their advantages and disadvantages. Based on these two models, we then propose an appropriate software quality model for ERP systems in HEIs. These two popular software and systems quality models are ISO 9126 and ISO 25010 quality models.

---

\*Emmanuel Peters, Email: [peterse30@gmail.com](mailto:peterse30@gmail.com)

### 2.1. ISO 9126 Model

ISO 9126 is an international standard for software quality evaluation. It was originally presented in 1991 and fully adapted in 1992. The ISO 9126 quality model addresses three aspects of software quality which are; the internal quality, the external quality and the quality in use [9]. ISO 9126 model therefore, evaluates the quality of software product based on the external, internal and quality in use attributes. The quality attributes are presented as a hierarchical structure of factors and sub-factors. The highest level comprises of six factors that are further decomposed into twenty one (21) sub-factors on the lowest level. ISO 9126 a derivation of McCall's model expresses 21 sub-attributes that every quality software product must exhibit. According to [9] the ISO 9126 model comprises of the following four part standards:

- ISO/IEC 9126-1 (ISO/IEC, 2001a): This standard defines an updated quality model.
- ISO/IEC 9126-2 (ISO/IEC, 2003a): This standard defines a set of external metrics.
- ISO/IEC 9126-3 (ISO/IEC, 2003b): This standard defines a set of internal metrics.
- ISO/IEC 9126-4 (ISO/IEC, 2001b): This standard defines a set of quality in use metrics.

### 2.2. ISO 25010 Model

ISO 25010 is an international standard for software and systems quality evaluation. This standard has gone through three important updates in 2007, 2011 and 2017 [10]. This standard is also known as the SQuaRE (Systems and software Quality Requirements and Evaluation) model. It describes software product quality and quality in use as well. According to [10] ISO 25010 was developed from an update of ISO 9126 model. According to them, the previous model (ISO 9126) has six (6) factors and twenty-one (21) sub-factors. By simple comparison of the two models, "security" and "compatibility" were the only two factors introduced together with their sub-factors into the ISO 25010. The quality attributes in this model are presented starting from top factors down to the sub-factors. The top level composes eight factors that are further decomposed into thirty one (31) sub-factors on the down level. ISO 25010 a derivation of ISO 9126 model describes thirty-one (31) attributes that every quality software product must exhibit.

Many researchers [11 - 13] have adapted the ISO 25010 standard to propose new quality models in their studies. As an international standard, the ISO 25010 model has also been adapted in this study to develop new ERP systems quality model.

## 3. New ERP System Quality Model

Even though there are specific software quality models developed for specific software products evaluations, majority of software quality models are general and common for all types of software products. For instance, ISO 25010 has factors which are general for evaluating quality of every type of system and software products. Moreover, many systems and software products have their own factors or features which must be considered during evaluation. Therefore, for an evaluation of software and systems

products, the existing software quality models should be carefully selected, modified or extended. This means the quality factors and sub-factors of a quality model should be adjusted to fit or match the new system being evaluated and not the vice versa. Thus, this study adapts the ISO 25010 to assess quality of ERP systems in HEIs.

Although, there are several researches on quality of software products based on ISO 9126 model in education environments [5, 6] studies on adapting ISO 25010 model to evaluate ERP systems in HEIs are very rare. Thus, the novelty about this study is the proposed quality model based on ISO 25010 for ERP systems quality evaluations in HEIs. Even though ISO 9126 has been used severally in developing other models to evaluate ERP systems, this new ISO 25010 model has also been developed to improve, replace and extend it. Since systems and software products are becoming increasingly complex and sophisticated nowadays, new quality models are also needed to evaluate them. Therefore, quality models based on the ISO 25010 are needed to evaluate ERP systems in HEIs.

Many researchers [11 - 13] have adapted the ISO 25010 in their studies. The generality of ISO 25010 quality model makes it easy to be adapted into developing many specific software quality models such as the ERP systems quality model. In adapting models like ISO 25010, researchers would mostly eliminate some quality attributes or factors, add new attributes or redefine the existing attributes of the model. This study adds and redefines the sub-factors of the ISO 25010 in order to suite a quality model for ERP systems evaluations in HEIs. The new ERP system quality model describes eight (8) factors including functional suitability, reliability, usability, performance efficiency, compatibility, security, maintainability and portability which are further decomposed into thirty four (34) sub-factors. Three new sub-factors have been introduced into the ISO 25010 model in this study. Supportability and searchability have been added as sub-factors under usability and archivability has also been added as a sub-factor under security. The section that follows describes the three new sub-factors, existing factors and sub-factors of the ISO 25010 model adapted for this study.

### 3.1. Definition and Justification of the three new sub-factors

**Supportability:** This feature can be defined as the ability of the system or software to provide certain basic needs to its users. It is the extent to which a software or system can assist its users in completing basic tasks. In higher education institutions (HEIs), most of the users of the ERP systems are not ICT trained experts therefore; they will need certain supports from the system in order to complete most of their tasks. They would need certain instructional programs and hints to be able to accomplish these basic tasks. ERP systems are huge systems which must include all these instructional programs and hints to enable its users to use them comfortably. Therefore, supportability is added as a sub-factor under usability factor.

**Searchability:** This feature of a system or software defines the capability of a software or a system to quickly find or obtain information from its database. It is the degree at which software or system can quickly find or obtain its information. Again, ERP systems are huge information systems that can store large information about organizations and institutions. Information

about students, teaching and non-teaching staffs and administrative processes can be stored by these systems. For that matter, ERP systems must include features or tools that will assist its users in finding information quickly. For this reason, searchability is also added as a sub-factor under usability factor.

**Archivability:** Archivability feature or factor of a system can be defined as the set of tools or techniques of a system used in preserving or reserving information for future reference. In other words, it is the extent to which a system can preserve its information for future references. For instance, in higher education institutions, it is mandatory to preserve outgoing students' records for future references. It is important therefore, to employ ERP systems that can preserve and reserve students' records for future references. Based on this reason, archivability is added as a sub-factor under security factor.

### *3.2. Functional Suitability*

This quality factor describes the extent to which a software product or system provides functions that satisfy the stated and implied needs of stakeholders when used under specified conditions [14]. This quality factor has been divided into three lower-factors including functional completeness, functional correctness and functional appropriateness [12, 14]. Since ERP systems in HEIs come with various functional applications, there must be a quality factor such as functional suitability to help evaluate these functions. Hence, functional suitability has been adapted in the new ERP system quality model.

### *3.3. Reliability*

Reliability factor expresses the capability of a system or software product to maintain its level of performance or specified functions under specified conditions for a specified time period. Four lower-factors are associated to reliability factor namely maturity, availability, fault tolerance and recoverability [13, 14]. This quality factor has been adapted in our new ERP system quality model to assess the reliability of various functions and services that ERP systems provide in HEIs under certain stated conditions.

### *3.4. Usability*

According to [14] usability factor describes the extent to which software or system product can be used to achieve specified goals with effectiveness, efficiency and satisfaction in a specified context of use. The usability factor has set of lower-factors which include appropriateness recognizability, learnability, operability, user error protection, user interface aesthetics and accessibility [13]. In this study, supportability and searchability were added as lower-factors under usability to help evaluate the operations of ERP systems in HEIs. Since usability is an important quality factor to every software or systems that include ERP systems, it has been adapted in our new ERP system quality model.

### *3.5. Performance Efficiency*

The performance efficiency factor describes the ability of software product or system in managing the given amount of resources to provide and maximize performance [14]. This quality factor has also been decomposed into three lower-factors including

time behaviour, resource utilization and capacity [12]. Performance efficiency has been adapted into the new ERP system quality model to assess the resource allocation and use of the ERP systems when providing required services and functions in HEIs.

### *3.6. Compatibility*

Compatibility factor is the capability of the software products or system to interact with other software products or systems without any glitches. That is the ERP system performs its required functions while sharing the same hardware or software environments with other systems. Compatibility factor has two lower-factors namely co-existence and interoperability [13, 14]. Again, adapting this quality factor in the new ERP system quality model will assist the evaluation of information exchange and sharing of common environment by the ERP system with other software products and systems.

### *3.7. Security*

According to [14] security factor is about how the software products or systems protect its information and data (information resources) from unauthorized persons or from other software products or systems. The security factor comes with set of lower-factors which include confidentiality, integrity, non-repudiation, accountability and authenticity [12, 14]. In this study, archivability has been added as a lower-factor under security to evaluate the operations of ERP systems in HEIs. Since security is an important quality factor to every software or systems that include ERP systems, it has been adapted into our new ERP system quality model.

### *3.8. Maintainability*

The ability of software products or systems to be modified, corrected, or adapted to current changes in the environment describes its maintainability feature. Five lower-factors including modularity, reusability, analyzability, modifiability and testability were associated to maintainability [11]. Applying this quality factor to the new ERP system quality model will suggest that the ERP systems in HEIs should permit modifications or corrections without much difficulty.

### *3.9. Portability*

The ability of software products or systems to be transferred from one hardware, software or other operational or usage environment to another operational platform defines its portability feature [14]. Three lower-factors including adaptability, installability and replaceability describe portability feature [12]. This quality factor has been adapted into the new ERP system quality model to evaluate ERP systems operations in different hardware and software platforms and across different environments.

In the light of all the analysis done in this study, Table 1 and Figure 1 present the new quality model based on the ISO 25010 standard. This new quality model includes the eight (8) main factors and thirty-four (34) sub-factors. The proposed model shows how these quality factors and sub-factors have been adapted to evaluate the quality of ERP systems in HEIs.

Table 1: ERP System quality model in HEIs

<b>Factor</b>	<b>Sub-Factor</b>	<b>Explanation</b>
<b>Functional Suitability</b>	Functional completeness	Does ERP system cover all specified tasks and user objectives?
	Functional correctness	Can ERP system provide correct results with the needed degree of precision?
	Functional appropriateness	Does ERP system’s function facilitate the accomplishment of specified tasks and objectives?
<b>Reliability</b>	Maturity	Does ERP system meet the needs of its users under normal operations?
	Availability	Can the ERP system be operational and accessible at a time needed for use?
	Fault tolerance	Can the ERP system operate as planned despite the malfunction hardware or software existence?
	Recoverability	During a disaster, can ERP system recover and re-establish the system to its desired state?
<b>Usability</b>	Appropriateness recognizability	Can ERP system be easily recognized by users as an appropriate product or system to solve their needs?
	Learnability	Can ERP system be learnt more easily?
	Operability	Can ERP system be easily operated and controlled?
	User error protection	Does the ERP system protect users against making errors?
	User interface aesthetics	Does the ERP system user interface look pleasant and satisfactory?
	Accessibility	Can the ERP system be accessed by specified users under specified conditions?
	Supportability	Can the ERP system provide basic operational instructions and hints to its users when in operation?
	Searchability	Can information be easily searched, found or located with the ERP system?
<b>Performance Efficiency</b>	Time behaviour,	Can ERP system response and process events faster?
	Resource utilization	Can ERP system utilize information resources efficiently?
	Capacity	Do ERP system parameters meet their system requirements?
<b>Compatibility</b>	Co-existence	Can the ERP system perform its required operations efficiently while sharing its environment and information resources with other products or systems?
	Interoperability	Can ERP system interact with other systems or software products?
<b>Security</b>	Confidentiality	Can ERP system ensure that information resources are accessible only to those authorized to have access?
	Integrity	Does ERP system prevent unauthorized access to information resources or modification of data?
	Non-repudiation	Can the ERP system prove an action or an event believed to have taken place?
	Accountability	Can the ERP system uniquely trace or account for an action or event of an entity?
	Authenticity	Can the ERP system be used to identify its users and resources?
	Archivability	Does the ERP system preserve and protect its past records for future references?
<b>Maintainability</b>	Modularity	Is the ERP system composed of discrete components or modules for easy usage?
	Reusability	Can the modules in ERP system be used to operate other modules in the same ERP system?



	Analyzability	How fast does the ERP system diagnose or troubleshoot problems?
	Modifiability	Can the ERP system be changed or updated without introducing bugs or degrading the existing standards?
	Testability	Does ERP system provide test criteria for testing certain actions or changes in the system?
<b>Portability</b>	Adaptability	Can ERP system be moved or transferred easily to other environment or platform without any glitches?
	Installability	How quickly and easily can ERP system be configured?
	Replaceability	Can ERP system be substituted easily with similar system in the same environment?

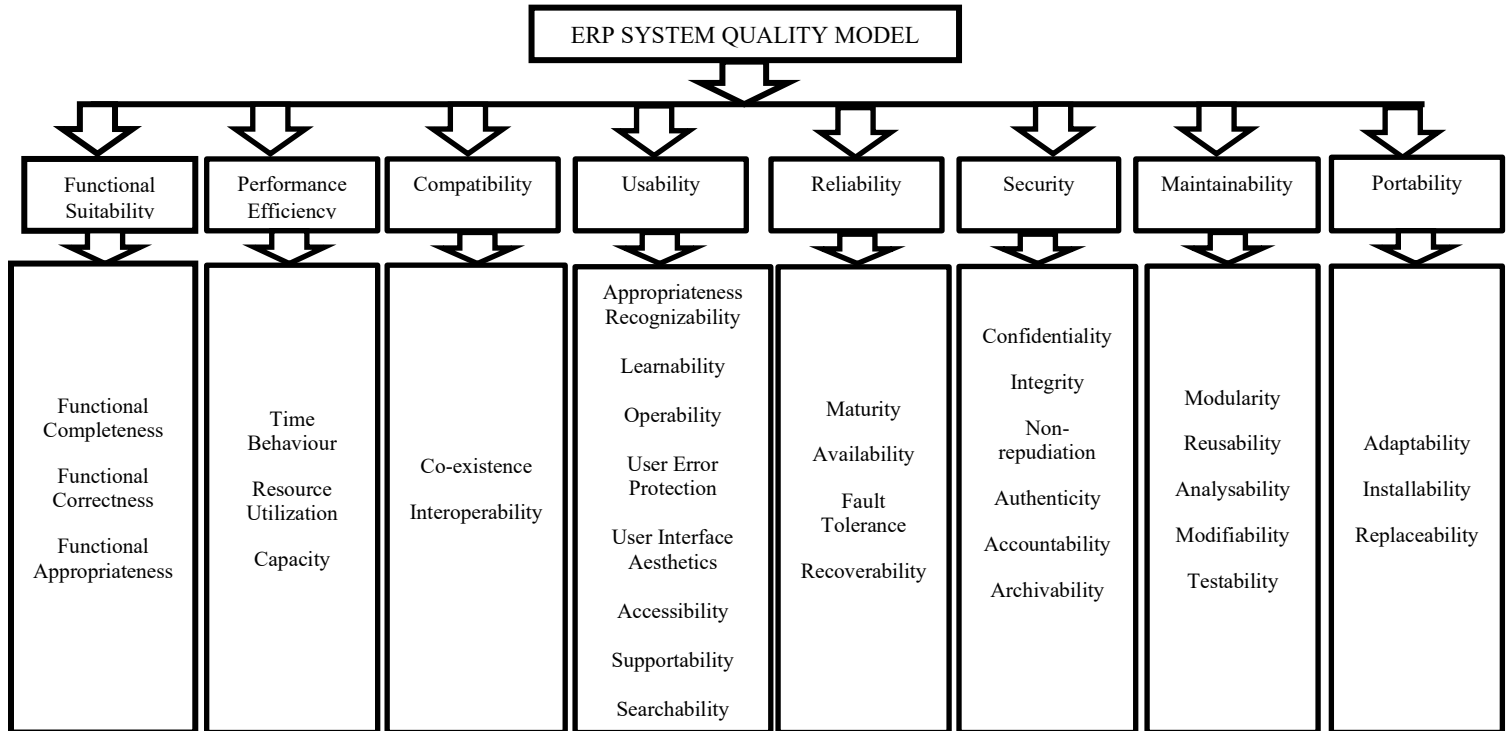


Figure 1: ERP System Quality Model

#### 4. Conclusion

A new quality model for evaluating the quality of ERP systems in higher education institutions has been proposed. The model's quality factors and sub-factors were based on the ISO 25010 standard. To our knowledge, this model is first of its kind proposed for the evaluation of ERP systems in HEIs. The study brings to forth three important contributions which include the comparison of two popular software quality models, identification of quality factors of ERP systems and the ISO 25010 standard as a base for the new quality ERP systems model in HEIs. Further studies to establish the relationships between the quality factors and sub-factors of this model in HEIs will be presented in the next paper. The results of the further study will enable us to understand the interrelation and the influence that these sub-factors would have on the quality factors of this model.

#### Conflict of Interest

The writers of this document declare no conflict of interest.

#### Acknowledgment

The writers of this piece of work want to acknowledge the grace and mercy of God for His enablement, continual guidance and assistance towards the completion of this document. We are also grateful to all those who one way or the other contributed to the success of this research study.

#### References

- [1] Ghuman, K.; Chaudhary, S. (2012) "Incorporation of ERP in Educational Institutions: An Empirical Study", International Conference on Technology and Business Management, pp. 318-324
- [2] Rabaa'i, A.; Bandara, W.; Gable, G. (2009a) "ERP systems in the higher education sector: a descriptive study", Proceedings of the 20th Australasian Conference on Information Systems, pp. 456-470
- [3] Swartz, D. and Orgill, K. (2001). "Higher Education ERP: Lessons Learned", EDUCAUSE Quarterly, (2), pp. 20-27.
- [4] Allied Market Research, 2015
- [5] Fahmy, S., Haslinda, N., Roslina, W. and Fariha, Z. (2012). "Evaluating the Quality of Software in e-Book Using the ISO 9126 Model". International Journal of Control and Automation Vol. 5, No. 2.

- [6] Padayachee, I., Kotze P. and Van der Merwe, A. (2010). "ISO 9126 External Systems Quality Factors, Sub-Factors and Domain Specific Criteria for Evaluating E-Learning Systems", In Proceedings of SACLA Conference.
- [7] Alrawashdeh, T.A., Muhairat, M., & Althunibat, A., (2013) "Evaluating the Quality of Software in ERP Systems Using the ISO 9126 Model", International Journal of Ambient Systems and Applications (IJASA) Vol.1, No.1, March 2013.
- [8] Djouab, R. and Bari, M. (2016) "An ISO 9126 Based Quality Model for the e-Learning Systems", International Journal of Information and Education Technology, Vol. 6, No. 5, May 2016
- [9] ISO/IEC TR 9126-4 (2004) "Software Engineering- Product Quality - Part 4: Quality in Use Metrics". International Organization for Standardization, Geneva, Switzerland.
- [10] Peters, E., & Aggrey, G. K. (2019a, March). "Evaluating the Effectiveness of ERP Systems in HEIs: A Proposed Analytic Framework". In 2019 International Conference on Computing, Computational Modelling and Applications (ICCMA) (pp. 40-45). IEEE.
- [11] França, J.M.S., Soares, S. M. (2015). "SOAQM: Quality Model for SOA Applications based on ISO 25010", Proceedings of the 17th International Conference on Enterprise Information Systems (ICEIS-2015), pages 60-70
- [12] Haoues, M., Sellami, A., Ben-Abdallah, H. and Cheikhi, L. (2017). "A guideline for software architecture selection based on ISO 25010 quality related factors", Int J Syst Assur Eng Manag (November 2017) 8(Suppl. 2):S886–S909
- [13] Iqbal, H. and Babar, M. (2016). "An Approach for Analyzing ISO / IEC 25010 Product Quality Requirements based on Fuzzy Logic and Likert Scale for Decision Support Systems", International Journal of Advanced Computer Science and Applications, Vol. 7, No. 12
- [14] ISO/IEC (2011). ISO/IEC 25010 – "Systems and Software Engineering - Systems and Software Quality Requirements and Evaluation (SQuARE)" - System and Software Quality Models. Technical report.

## Combination of Salient Object Detection and Image Matching for Object Instance Recognition

Evan Kristia Wigati, Gede Putra Kusuma\*, Yesun Utomo

Computer Science Department, BINUS Graduate Program - Master of Computer Science, Bina Nusantara University, Jakarta, Indonesia, 11480

### ARTICLE INFO

Article history:

Received: 06 January, 2020

Accepted: 11 March, 2020

Online: 10 April, 2020

Keywords:

Object Instance Recognition

Foreground Detection

Salient Object Detection

Feature Matching

Geometric Verification

### ABSTRACT

Object Instance Recognition aims to classify objects specifically and usually use a single reference image. It is possible to be used in many applications such as visual search, information retrieval and augmented reality. However, various things affect the appearance of the objects, which makes the recognition process harder, especially if a single reference image is used. In this paper, we proposed a combination method between Salient Object Detection and Object Instance Recognition using Image Matching and Geometric Verification. Salient Object Detection is used during initial processing (feature extraction), while Geometric Verification is performed using Best Score Increasing Subsequence (BSIS). Experimental results showed that the  $F_\beta$  score and Mean Absolute Error (MAE) of saliency map on Stanford Mobile Visual Search Dataset (SMVS) are quite satisfactory. While the results of the combination method show 1.92% performance improvement than the previous method which is BSIS without Salient Object Detection.

### 1. Introduction

Computer vision deals with the extraction of valuable information from the contents of digital images, real-world objects, or videos. One of many problems that exists in computer vision is object recognition. The study of object recognition has been done over decades since the 1960s [1], which makes it an old task and sometimes described as a challenging task. There are two approaches in Object Recognition: Object Classification and Object Instance Recognition / Fine-Grained Recognition. Object Classification means classifying objects in general categories/class *i.e.* human, animal, and vehicle. While Object Instance Recognition means recognizing objects in specific categories/class *i.e.* book covers, DVD covers, soda cans, and canned food [2] with one or small reference images per class. Fine-Grained Recognition also means recognizing objects in specific categories/class, but with small visual differences, which needs large number of reference images per class.

This paper focuses on proposing a method for Object Instance Recognition that combines Salient Object Detection and Image Matching with Geometric Verification.

Most previous works in Object Instance Recognition are feature-based. Such works include Triplets of feature descriptors

proposed by Zitnick *et al.* [2]. Kusuma *et al.* proposed Object Recognition using Weighted Longest Increasing Subsequence [3]. Xie *et al.* proposed Dense Feature extraction using SIFT and pose base verification [4], Best Increasing Subsequence (BIS) and image matching for Object Instance Recognition is proposed by Kusuma and Harjono [5] and the development of BIS which is Best Score Increasing Subsequence (BSIS) using SURF for feature extraction and image matching is proposed by Kusuma *et al.* [6]. Meanwhile, there are also deep learning methods for Object Instance Recognition, such as Held *et al.* proposed feed-forward neural network for a single image [7].

The most approach in Object Instance Recognition uses feature-based approach because of single image reference, and it is becoming unpopular nowadays because of deep learning. However, the performance of deep learning deteriorates when there is only a single reference image per class. This capability is still needed for certain applications such as visual search and augmented reality. Therefore, this research tries to develop better feature-based approach with the hope of improving its accuracy.

There are few reasons why feature-based is used rather than deep learning approaches in this research. One of them is because there is only one reference image per class which means deep learning approach is not suitable to use. In this research, Geometric Verification is used as a method to verify the similarity

\*Corresponding Author: Gede Putra Kusuma, [inegara@binus.edu](mailto:inegara@binus.edu)

score between the reference and testing images and to increase the accuracy. Geometric Verification needs spatial locations of features, and it is produced by a feature-based approach, not by deep learning. Even though deep learning extracts local features, but the location information of the features is not preserved.

Commonly, feature-based approach extract features from the raw image, but it could waste time and unimportant features can be extracted too. Instead of extracting features from the raw image, it is beneficial to extract features only from salient image areas. There is a method called Salient Object Detection which detects noticeable or important objects in an image. It works by narrowing down which image region to be extracted, so it can be more focused and accurate only on the noticeable object in the image. Therefore, Salient Object Detection is used for masking the feature extraction.

There are many types of Salient Object Detection methods from hand-crafted to deep learning approach. Such as Salient

object using shape prior extraction which proposed by *Jiang et al.* [8], Graph-based manifold ranking from *Yang et al.* [9], Contrast-based filtering from *Perazzi et al.* [10], Histogram-based contrast from *Cheng et al.* [11], and Window composition from *Feng et al.* [12]. But, based on our literature study, hand-crafted approaches are a bit outdated both in accuracy and processing times. Hence, recently many researchers use deep learning approach that performs well and overcomes the hand-crafted method. For example, Multi-Context Deep Learning using CNN as proposed by *Zhao et al.* [13]. While *Li and Yu* [14] proposed the Deep Contrast Network method which used CNN for extracting features efficiently and produce accurate results than other methods. *Liu and Han* [15] proposed a deep hierarchical saliency network. *Li et al.* [16] proposed a Multiscale Refinement Network (MSRNet). *Wang et al.* [17] used RFCN for saliency detection and *Qin et al.* [18] performs CNN combined with the Residual Refinement Module (RRM).

Table 1: Summary related works in Object Instance Recognition

Category	Methods	Datasets	Performance Measure (evaluation)	Results
Conventional method (Feature-based)	Image Matching, Grouping features in triplet, Geometric Hashing [2]	118 objects divided into 2: 1. Non-occluded single object 2. occluded multiple objects	ROC Curve	<b>Detection Rate:</b> 1. Single object: 78.8% 2. Multiple objects: 81.1%
	Image Matching and Geometric Verification using Weighted Longest Increasing Subsequence (WLIS) [3]	1. Stanford Mobile Visual Search (SMVS) 7 Categories 2. Their dataset 2 Categories 3. Images from internet: 1300 images.	1. E value = $(CRR * CJR) / (1 + IRR)$	<b>Average E:</b> 1. SURF+ WLIS: > 20% better than SURF matching > 4% better than SURF+RANSAC
	Dense Feature extraction, RANSAC Pose Estimation and Multimodal Blending [4]	1. Willow 2. Challenge	1. Precision 2. Recall 3. F score	<b>Willow &amp; Challenge (sequentially):</b> Precision: 0.9828, 1.000 Recall: 0.8778, 0.9977 F score: 0.9273, 0.9988
	Best Increasing Subsequence (BIS) [5]	1. Stanford Mobile Visual Search (SMVS) 7 categories. 2. Non-related images from internet	1. E measure = $(CRR * CJR) / (1 + IRR)$	<b>Average E measure:</b> SURF+BIS: 82.34% SURF+WLIS: 77.43% SURF+RANSAC Homography: 73.51% SURF Only: 53.49%
	Best Score Increasing Subsequence (BSIS) [6]	1. Stanford Mobile Visual Search (SMVS) 7 categories. 2. Non-related images taken from internet.	1. E measure = $(CRR * CJR) / (1 + IRR)$	<b>Average E measure:</b> SURF+BSIS: 86.86% SURF+BIS: 82,34% SURF+WLIS: 77,43% SURF+RANSAC Homography: 73,51%
Deep Learning	CNN model with CaffeNet architecture [7]	1. RGB-D 2. BigBird	Accuracy	<b>Testing Accuracy:</b> 1. Single view object during training: - Textured object: 73.8% - Untextured object: 60.0% - Overall: 63.9% 2. Object with occlusion and real background: 44.1%



This paper delivers a combination method for Object Instance Recognition that consists of Salient Object Detection, Image Matching, and Geometric Verification. The goal of this paper is to propose a new method for Object Instance Recognition that produce reliable results for the case of one reference image available per class.

## 2. Related Works

### 2.1. Related Works of Object Instance Recognition

Object Instance Recognition is a more refined method of object recognition that provides information about the attribute of an object such as the object’s name. There is another method which is quite like Object Instance Recognition called Fine-Grained Recognition. The difference from Object Instance Recognition is that Fine-Grained Recognition uses many training or reference images and usually employs a deep learning approach. Meanwhile, Object Instance Recognition is defined as a method that commonly uses a single reference image per class. Nowadays, Object Instance Recognition method that uses one reference image becomes unpopular. Only a few researches that explained about Object Instance Recognition, can be seen in Table 1. That is because deep learning becomes more well-known and Fine-Grained Recognition become a new challenge in recent years.

From Table 1, it can be seen that performance measurement varies because Object Instance Recognition is an old method. However, researchers tried to show their contribution to the development of Object Instance Recognition. The same table showed that feature-based approach is more reliable than deep learning when one reference image per class is used. Deep Learning performs well when many reference images in each class are available.

### 2.2. Related Works of Salient Object Detection

Salient Object Detection aims to highlight, predict and distinguish between an object of interest and its background object [19]. It works by predicting the object of interest in an image. There are many previous works in Salient Object Detection that researchers have done as seen in Table 2.

From Table 2, both Conventional and deep learning approaches are still used for Salient Object Detection. However, according to our observation, since 2015 deep learning is becoming more popular and promising to perform Salient Object Detection. It can achieve higher F-score and MAE compared to conventional methods. For example, *Qin et al.* [18] proposed CNN combined with residual refinement to produce an accurate saliency map. It can be seen from the result, the proposed method gets high F-score and MAE in six datasets such as SOD, ECSSD, DUT-OMRON, PASCAL-S, HKU-IS and DUTS-TE, also overcome other methods. Hence, deep learning becomes the best approach for Salient Object Detection nowadays.

## 3. Combination of Salient Object Detection and Image Matching

Figure 1 shows the flowchart of the combination method between Salient Object Detection [18] and Image Matching with Geometric Verification based on [6]. The process mainly divided

into 5 steps: Salient Object Detection (step 1), Feature Extraction, Feature matching and pre-filtering features (steps 3-5b). Calculating the pair score (step 6), Geometric Verification (step 7-8) and Acceptance/Rejection of the results (step 9-10). Feature extraction for the testing image is slightly different because it uses a saliency map to extract features.

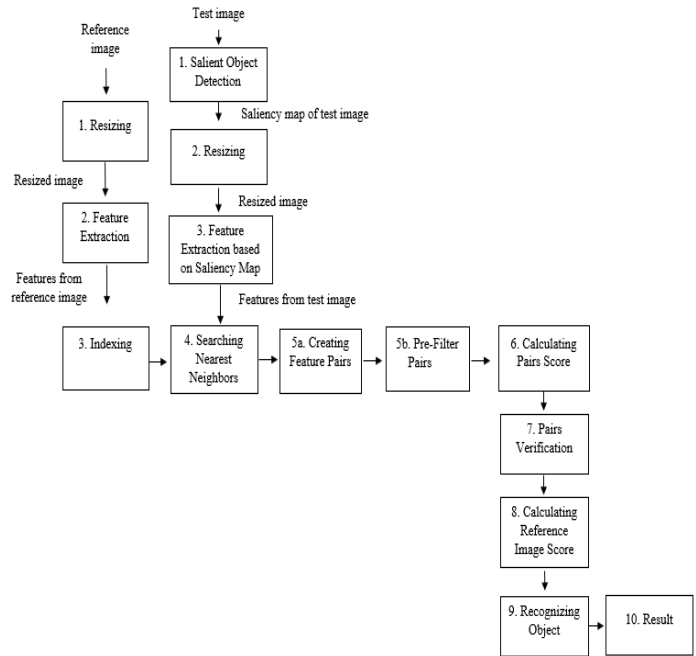


Figure 1: Flowchart of the combination method

The method begins by resizing reference and testing images, while the saliency map is resized along with testing images. The feature extraction is performed directly for the reference image, which means without using a saliency map, while the testing image is used a saliency map to extract features. All feature extraction is done using the Speeded Up Robust Feature (SURF) [22]. Then, all extracted features will be indexed to ease pair candidates searching. Later, all matched pair candidates which pass the threshold will be given similarity score and then passed to Geometric Verification to verify its pairs. Geometric Verification will determine the correct pairs based on the highest similarity score between reference and testing images. To accept/reject testing images, a threshold will be used. Only when the testing image’ score is higher than the threshold, it will be accepted. In this research, Salient Object Detection is used only for the pre-processing method and image matching with Geometric Verification for the main process.

### 3.1. Salient Object Detection

This research uses a Convolutional Neural Network (CNN) model for Salient Object Detection [18]. The method is called Boundary-Aware Salient Object Detection (BASNet) which is a predict-refine model. The method was chosen as the Salient Object Detection technique because it is relatively new, appearing in 2019 and provides good results. The architecture of BASNet based on [18] can be seen in Figure 2.

Table 2: Summary related works in Salient Object Detection

Author	Methods	Datasets	Performance Measure	Results
Conventional Methods	Energy minimization and combination between bottom-up saliency information and object-level shape prior [8]	2 datasets used: 1. Achanta et al. [20] 2. MSRA-B	1. F alpha 2. Boundary Box Displacement Error (BDE)	<b>F alpha:</b> The proposed method consistently achieves the highest F alpha on both datasets. <b>BDE:</b> The proposed method gets the lowest BDE (above 20 but less than 25)
	Manifold ranking [9]	3. datasets used: 1. MSRA 2. MSRA-1000 3. DUT-OMRON	1. F measure	<b>F measure:</b> 1. In MSRA and MSRA-1000: the method performs well to achieve the highest precision and recall. 2. DUT-OMRON: the method still performs poorly.
	Saliency filters using N-D Gaussian filtering, SLIC algorithm, K-means [10]	1. Natural images from [21]	1. F measure 2. Mean Absolute Error (MAE)	<b>F measure:</b> Approximately above 0.8 but less than 0.9 (only shown in the chart) <b>MAE:</b> In range 0.3-0.4 ( only shown in chart)
	SaliencyCut using histogram and spatial information region-based contrast [11]	3 datasets used: 1. Achanta et al. [20] 2. MSRA10K 3. THUR15K	1. F measure 2. True Positive Ratio (TPR)	<b>F measure:</b> Achanta dataset: above 0.9, MSRA10K: in range 0.8-0.9 (only shown in chart). <b>TPR:</b> Top 50 retrieval results: 78.2% and Top 100: 78.4%.
	Segment-based window composition algorithm [12]	2 datasets used: 1. PASCAL VOC 07 2. MSRA	1. Average precision. 2. F measure:	<b>F measure:</b> 1. MSRA: 0.82
Deep Learning	SLIC and CNN with global and coarse context [13]	5 datasets used: 1. ASD 2. SED1 3. SED2 4. ECSSD 5. PASCAL-S	1. F measure	<b>F measure:</b> 1. ASD: 0.9548 2. SED1: 0.9295 3. SED2: 0.8903 4. ECSSD: 0.7322 5. PASCAL-S: 0.7930
	Deep Contrast Learning based on CNN model using pixel level-segment pooling stream and CRF model [14]	5 datasets used: 1. MSRA-B 2. HKU-IS 3. DUT-OMRON 4. PASCAL-S 5. SOD	1. F measure 2. MAE	<b>F measure:</b> 1. MSRA-B: 0.916 2. HKU-IS: 0.904 3. DUT-OMRON: 0.757 4. PASCAL-S: 0.822 5. SOD: 0.832 <b>MAE:</b> 1. MSRA-B: 0.047 2. HKU-IS: 0.049 3. DUTOMRON: 0.080 4. PASCAL-S: 0.108 5. SOD: 0.126
	Global-View CNN + Hierarchical Recurrent CNN [15]	4 datasets used: 1. ECSSD 2. MSRA10K, 3. DUT-OMRON 4. PASCAL-S	1. F measure	<b>F measure (only shown in chart):</b> Above 0.8 and close to 0.9: 1. ECSSD, MSRA10K Above 0.7 and less than 0.8: 1. DUT-OMRON, PASCAL-S
	Fully Convolutional Multiscale Refinement Network (MSRNet) [16]	6 datasets used: 1. MSRA-B 2. PASCAL-S 3. DUT-OMRON 4. HKU-IS 5. ECSSD 6. SOD	1. F-measure 2. Mean Absolute Error (MAE)	- MSRA-B: 0.930, 0.042 ( <b>F measure, MAE</b> ) PASCAL-S: 0.852, 0.081 DUT-OMRON: 0.785, 0.069 HKU-IS: 0.916, 0.039 ECSSD: 0.913, 0.054 SOD: 0.847, 0.112 -New dataset for salient object instances (1000 images)
	Recurrent Fully Convolutional Networks (RFCN) [17]	4 datasets used: 1. SED1 2. ECSSD 3. PASCAL-S 4. HKU-IS	1. F measure 2. Mean Absolute Error (MAE)	<b>F measure:</b> 1. SED1: 0.8811 2. ECSSD: 0.8713 3. PASCAL-S: 0.7784 4. HKU-IS: 0.8564 <b>MAE:</b> 1. SED1: 0.0750 2. ECSSD: 0.0668 3. PASCAL-S: 0.1049 4. HKU-IS: 0.0547
	CNN, Predict Module (Encoder – Decoder) and Residual Refinement Module [18]	6 datasets used: 1. SOD 2. ECSSD 3. DUT-OMRON 4. PASCAL-S 5. HKU-IS 6. DUTS-TE	1. F measure, 2. Relax F measure 3. Mean Absolute Error (MAE)	<b>F measure, Relax F measure and MAE sequentially:</b> 1. SOD: 0.851, 0.603, 0.114 2. ECSSD: 0.942, 0.826, 0.037 3. DUT-OMRON: 0.805, 0.694, 0.056 4. PASCAL-S: 0.854, 0.660, 0.076 5. HKU-IS: 0.928, 0.807, 0.032 6. DUTS-TE: 0.860, 0.758, 0.047

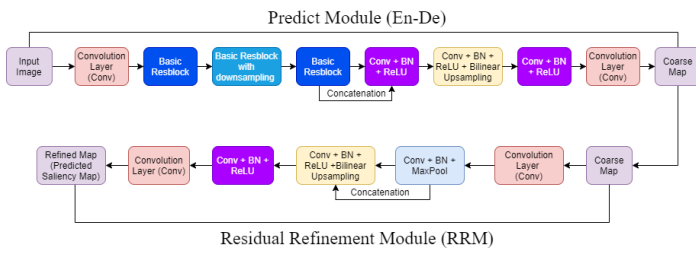


Figure 2: BASNet Architecture based on [18]

The method is divided into 2 stages, predict module and Residual Refinement Module (RRM). The model uses ResNet-34 as a backbone. Predict module is designed as an encoder-decoder model, which able to capture low and high-level details at the same time. Where RRM is designed to refine the saliency map of the predicting module by learning the residuals between saliency map and ground truth. To reduce overfitting, the last layer of each decoder stage is supervised by ground truth image which inspired by Holistically Nested Edge.

Predict module consists of Encoder-Decoder parts. The encoder part has a convolution layer and six stages of basic resblock for each part. Encoder part is based on ResNet-34, but some modifications are made to the input layer, which does not have a

Illustration of the RRM model can be seen in Figure 3. The RRM module consists of 4 stages of encoder-decoder, where each stage only has one convolution layer. Each layer has 64 filters size 3x3, batch normalization and, ReLU function. By using non-overlapping max pooling for down-sampling and bilinear interpolation for up-sampling, final saliency maps are obtained.

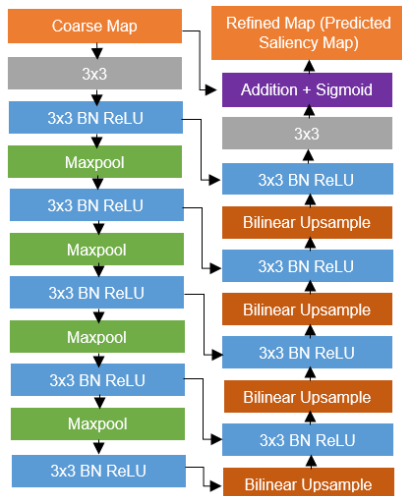


Figure 3: Residual Refinement Module on BASNet [18]

### 3.2. Image Matching and Geometric Verification using Best Score Increasing Subsequence (BSIS)

Image Matching and Geometric Verification using BSIS [6] is performed after features from testing and reference images are extracted. Features extraction will be done using Speeded Up Robust Features (SURF) [22]. It was chosen because it is relatively fast compared to other feature extraction methods. Since SURF returns features in vector forms, it is indexed using KD-Tree [23]. Indexed features from testing and reference images then enter the nearest neighbor steps, by using Euclidean distance

pooling operation after the input layer and has 64 convolution filters with size 3x3 stride 1, which makes the feature map have the same resolution as the input image. The original ResNet-34 has the quarter resolution in the feature map.

To capture global information from the encoder part, a bridge is made which consists of three convolution layers with 512 dilated (dilation = 2) 3x3 filters. The decoder part almost similar to the encoder in which each stage consists of three convolution layers, Batch Normalization (BN), and ReLU activation function. Decoder part works by concatenating feature maps of up-sampled output from the previous stage and next stage in the encoder, to achieve side-output saliency maps. The output of bridge and decoder stage is fed to 3x3 convolution layer to perform bilinear up sampling and sigmoid function. The process produces seven saliencies which has the same size with the input image's size, where the highest accuracy of coarse maps is taken to the refinement module.

The residual refinement module (RRM) is designed as a residual block that refines the predicted coarse saliency maps. Refined saliency maps are obtained from saliency coarse map added with saliency residual map as shown in Equation (1).

$$S_{refined} = S_{coarse} + S_{residual} \quad (1)$$

to find N (N=100) closest pair features. Pair features are then subjected to filtering by keeping only those with dissimilarity scores lower than the pre-filter threshold as defined in Equation (2).

$$Pre - Filter Threshold = m - K * \sigma \quad (2)$$

where  $m$  is the mean of Gaussian distribution and  $K$  is a constant value. In this case,  $K = 3$  with the purpose that features that are not quite potential still can be evaluated in pair verification step. Pair candidates with scores less than or equal to the threshold will be taken to the next step. Pair candidates that pass the pre-threshold will be given a pair score using Equation (3).

$$P_w = \left( \frac{distance(P_{QF}, P_{TF}) - m}{\sigma} \right)^2 \quad (3)$$

$P_w$  is pair weight/score.  $P_{QF}$  is a point feature of testing/query image  $\in$  set of testing/query features.  $P_{TF}$  is a point feature of a training/reference image  $\in$  set of training/reference features.  $m$  is the mean of Gaussian distribution which calculated using median and  $\sigma$  is a standard deviation. After assigning a score, the verification of each pair is doing using the BSIS method. This method determines the target object based on the highest similarity score and it is proven that the method is invariant to affine transformation. Figure 4 shows illustrated Geometric Verification on BSIS. The reference and testing image in Figure 4 are used only to show how BSIS works, both images are not from the SMVS dataset.

All pair scores in Figure 4 are only illustrative which are calculated using Equation (3). Number 1-6 (under bicycle image) represents test features and 0-6 represent train features along with its feature name and features that are paired. For example, feature C is paired to two different train features (R, T) which results in two feature pairs; P5, P6.

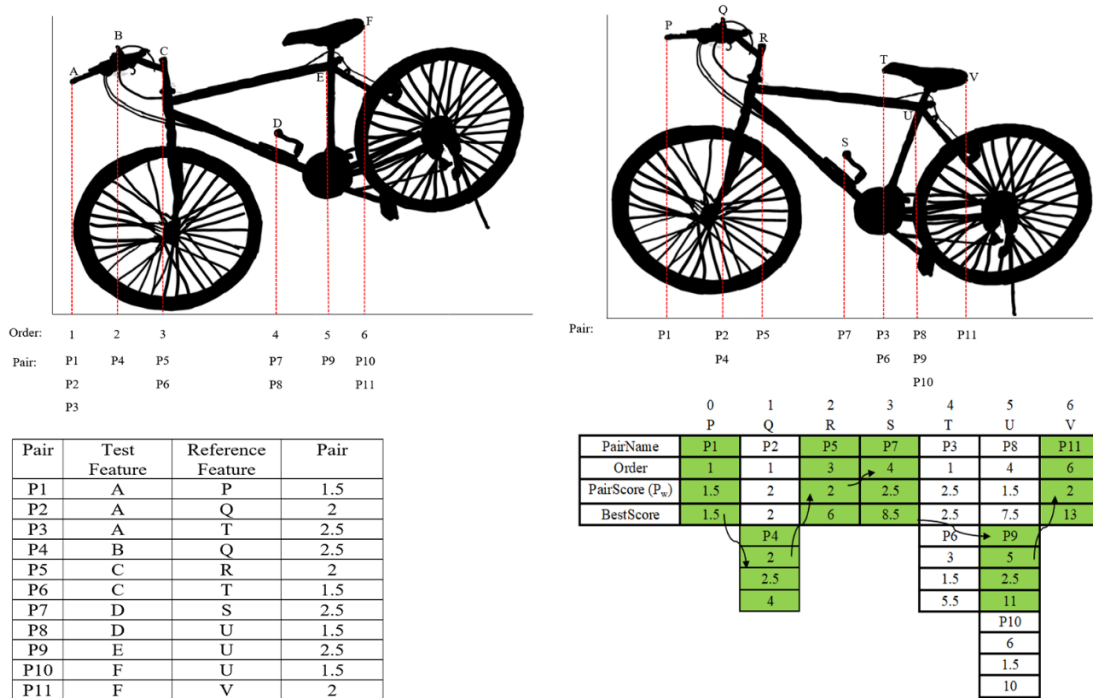


Figure 4: Illustrated Geometric Verification using Best Score Increasing Subsequence. Right: Reference Image, Left: Testing Image

The best score is obtained based on the highest total similarity score and the correct sequence. The correct sequence must meet the following requirements: pair candidates must not in the same column and higher-order numbers must be chosen than the current pair candidates, not the other way around. The correct sequence according to Figure 4 is P1, P4, P5, P7, P9, P11 with total similarity score = 13. This correct sequence is obtained by performing repetition and rotation of the image, either by X-axis or Y-axis.

Acceptance or rejection of an image is based on the similarity score. If the score is higher than the threshold as shown in Equation (4), the image is accepted or matched with the reference image or otherwise.

$$Acceptance\ Threshold = m + (L * \sigma) \quad (4)$$

Where  $m$  defines mean of Gaussian Distribution and  $\sigma$  defines the standard deviation from the top 60 best results for the query or test images. While  $L$  is a parameter value of the Gaussian Threshold for each category of SMVS dataset.  $L$  value is determined for each category based on experimental results; therefore,  $L$  value may be different for each category.

## 4. Experimental Results

### 4.1. Datasets

This research used two datasets: SMVS (Stanford Mobile Visual Search) dataset [24] and 1300 negative images taken from the internet. Salient Object Detection is evaluated using the SMVS dataset, while Object Instance Recognition is evaluated using the SMVS dataset and 1300 negative images. SMVS dataset used has 7 out of 8 categories. Only 7 categories of SMVS dataset were used so the results could be compared with previous methods that also use 7 categories, especially BSIS which is the benchmark in this research. The categories are *Book Covers*, *Business Cards*, *CD Covers*, *DVD Covers*, *Museum Paintings*, *Print*, and *Video*

*Frames*. Each category has 91-101 classes and each class has 5 images (1 image for reference and 4 images for testing). Negative images are images that are not included in the training/reference images. The purpose to use negative images is to evaluate our method whether it could correctly recognize images that are not included in the training/reference images. Details of the SMVS dataset can be seen in Table 3.

Table 3: Details of SMVS Dataset

Category	Class	Training image	Testing Image
Book Covers	101	101	404
Business Cards	100	100	400
CD Covers	100	100	400
DVD Covers	100	100	400
Museum Paintings	91	91	364
Print	100	100	400
Video Frames	100	100	400

### 4.2. Implementation and Experimental Setup

The Salient Object Detection method used comes from [18], Fine-tuning were performed to their pre-trained model. Using the SMVS dataset, the model is tuned so it fits the 7 categories. We took 1 image per class in 7 categories, total 692 images are used for training images. During the training, based on BASNet each image is resized to 256 x 256 and randomly cropped to 224 x 224 and for testing, each input image is first resized to 256 x 256 then resized back to the original size of the input image.

For Object Instance Recognition, BSIS was modified so that it can be used in this research [6]. Both reference and testing images are resized into 640 x 640 for feature extraction. The methods were implemented on Pytorch 1.0.0 and A four-core PC with AMD Ryzen 1500x 3.5GHz (with 8GB RAM) and a GTX 1050TI GPU for Salient Object Detection and Visual Studio 2019 (C# language) for Best Score Increasing Subsequence (BSIS).



### 4.3. Evaluation Metrics

This section will explain about evaluation techniques used in this research which combines two methods: Salient Object Detection and Object Instance Recognition.

Salient Object Detection is evaluated using two methods:  $F_\beta$  measure and Mean Absolute Error (MAE).  $F_\beta$  measure is a standard way to evaluate predicted saliency map.  $F_\beta$  measure is obtained from precision and recall which is calculated by comparing the saliency map to the ground truth mask.  $F_\beta$  measure is calculated using Equation (5).

$$F_\beta = \frac{(1 + \beta^2) \times \text{Precision} \times \text{Recall}}{\beta^2 \times \text{Precision} + \text{Recall}} \quad (5)$$

$\beta$  is set to = 0.3 to weight the precision more than the recall [25]. The maximum  $F_\beta$  ( $\max F_\beta$ ) of each category SMVS is reported in this paper.

Like  $F_\beta$  measure, Mean Absolute Error (MAE) also a standard way to evaluate saliency maps. MAE denotes the average absolute difference per pixel between the saliency map and ground truth. The formula of MAE can be seen in Equation (6).

$$MAE = \frac{1}{H \times W} \sum_{x=1}^H \sum_{y=1}^W |S(x,y) - G(x,y)| \quad (6)$$

where H denotes height, W denotes the width of the image. S (x, y) represents the x-y coordinate of the saliency map and G (x, y) represents the x-y coordinate of the ground truth mask.

Meanwhile, Object Instance Recognition is evaluated using E measure Firstly, E measure is introduced by [3] which aims to calculate the result between positive and negative images. In E measure, three main values are used to calculate the value of E:

- **Correct Recognition Rate (CRR)** is a number of the correct and accepted images divided by total positive images.
- **Incorrect Recognition Rate (IRR)** is a number of positive images that incorrectly recognized divided by total positive test images.
- **Correct Rejection Rate (CJR)** is a number of negative images that are rejected divided by total negative test images.

Therefore, E measure can be calculated using Equation (7).

$$E = \frac{CRR \times CJR}{(1 + IRR)} \quad (7)$$

## 4.4. Results

### 4.4.1. Salient Object Detection

This section shows the result of  $\max F_\beta$  and MAE Salient Object Detection in the SMVS dataset. The results are based on 50 test images are taken from each category in the SMVS dataset. There are no criteria when selecting 50 images, the images are taken randomly, and each test image only represents one class. There are 350 test images for seven categories of SMVS dataset. Since the SMVS dataset did not provide the ground truth image, we need to make the ground truth mask of the test images.

[www.astesj.com](http://www.astesj.com)

Table 4:  $\max F_\beta$  and MAE score of seven categories SMVS dataset for 50 images

Category	$\max F_\beta$	MAE
Book Covers	0.928	0.083
Business Cards	<b>0.993</b>	<b>0.012</b>
CD Covers	0.937	0.070
DVD Covers	0.977	<b>0.017</b>
Museum Paintings	<b>0.985</b>	<b>0.020</b>
Print	<b>0.979</b>	0.031
Video Frames	0.935	0.084

Table 4 shows the score of  $\max F_\beta$  (higher is better) and MAE (lower is better). The **bolded** number indicates the top three performances. The highest  $\max F_\beta$  and the lowest MAE are possessed by *Business Cards*. This may be influenced by several factors, such as business card object's is easy to spot in the image because there are no other objects that attract attention in the background of the same image and business cards does not have many form variations (which may be quite similar to train image). While *CD Covers*, *Video Frames*, and *Book Covers* respectively become the three lowest categories. Although the MAE of *Book Covers* is better than *Video Frames*, the difference is only 0.001. Therefore, *Book Covers* and *Video Frames* can be categorized equivalent in terms of MAE. Reasons for these three categories could be due to the wide variety of test images, there are other interesting objects in the background of the same image, and during the training process may be few numbers of training images/iterations could affect the result. However, the results can be categorized as a good result. Figure 5 shows the Example of the input image, ground truth image, and results from the saliency map in the SMVS dataset.

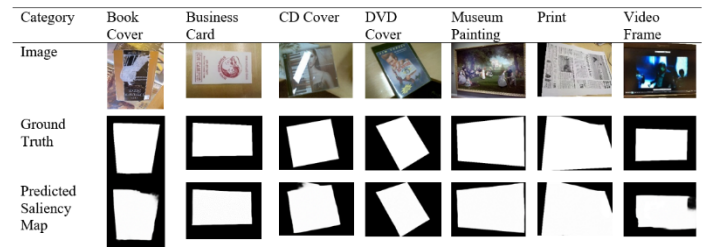


Figure 5: Example of Image, Ground Truth (GT) and Saliency Map of SMVS Dataset

### 4.4.2. Object Instance Recognition using BSIS

This section presents the result of the proposed method. Compared to other existing methods, our proposed methods can overcome others. The results are shown by the E score in Table 5.

In Table 5, results for WLIS, BIS, and BSIS are taken from the paper [6]. Our results can be seen in the fourth column "BSIS with Salient Object Detection". **Bold** indicates E scores higher than others. Overall, our work overcomes WLIS and BIS in every category of the SMVS dataset. While in BSIS, our result still cannot surpass E score BSIS in the *Print* category. Although most of the high score is owned by BSIS with Salient Object Detection, the average E score does not significantly increase with only 1.92% higher from 86.86% to 88.78%.

Table 5: E score of BSIS, BSIS with Salient Object Detection and other existing methods

Category	Methods			
	WLIS[3]	BIS[5]	BSIS[6]	BSIS with Salient Object Detection
Book Covers	87.52%	95.22%	96.98%	<b>97.70%</b>
Business Cards	62.83%	64.34%	70.69%	<b>79.35%</b>
CD Covers	83.49%	87.00%	91.15%	<b>93.30%</b>
DVD Covers	88.70%	94.76%	97.19%	<b>97.88%</b>
Museum Paintings	74.47%	86.69%	86.93%	<b>89.48%</b>
Print	48.60%	52.25%	<b>66.60%</b>	63.99%
Video Frames	96.43%	96.10%	98.52%	<b>99.75%</b>
<b>Average</b>	77.43%	82.34%	86.86%	<b>88.78%</b>

## 5. Conclusion

In this paper, we proposed a combination method for Object Instance Recognition. The method is a combination of Salient Object Detection and Image Matching with Geometric Verification using BSIS. Based on the experimental result, the fine-tuned model Salient Object Detection performs well on the SMVS dataset. Maybe, better improvement for *F-measure* and *MAE* can be achieved by adding more training images and increase the iteration number. While in Object Instance Recognition, the proposed method that is combination of Salient Object Detection and Image Matching can be concluded improve the E score but not significant, the increase is only 1.92% higher than the previous method BSIS without Salient Object Detection.

From this research, it can be concluded that the proposed combination method can improve the E score in SMVS dataset, but not significant. Many factors could influence the results such as, using Salient Object Detection in the SMVS dataset is not too beneficial because the object is clear and the background images are clean, i.e. there are no background objects that are interfering with the foreground object.

## References

- [1] A. Andreopoulos and J. K. Tsotsos, "50 Years of object recognition: Directions forward," *Comput. Vis. Image Underst.*, vol. 117, no. 8, pp. 827–891, 2013.
- [2] C. L. Zitnick, J. Sun, R. Szeliski, and S. Winder, "Object Instance Recognition Using Triplets of Feature Symbols," *Technology*, pp. 1–15, 2007.
- [3] G. P. Kusuma, A. Szabo, L. Yiqun, and J. A. Lee, "Appearance-Based Object Recognition Using Weighted Longest Increasing Subsequence," in *International Conference on Pattern Recognition*, 2012.
- [4] Z. Xie, A. Singh, J. Uang, K. S. Narayan, and P. Abbeel, "Multimodal Blending for High-Accuracy Instance Recognition," *2013 IEEE/RSJ Int. Conf. Intell. Robot. Syst.*, 2013.
- [5] K. D. Harjono and G. P. Kusuma, "Object Instance Recognition Using Best Increasing Subsequence," *2016 11th Int. Conf. Knowledge, Inf. Creat. Support Syst.*, 2016.
- [6] G. P. Kusuma, K. D. Harjono, and M. T. D. Putra, "Geometric Verification

Method of Best Score Increasing Subsequence for Object Instance Recognition," *2019 6th Int. Conf. Inf. Technol. Comput. Electr. Eng.*, pp. 1–5, 2019.

- [7] D. Held, S. Thrun, and S. Savarese, "Deep Learning for Single-View Instance Recognition," no. March, 2015.
- [8] H. Jiang, J. Wang, Z. Yuan, T. Liu, and N. Zheng, "Automatic salient object segmentation based on context and shape prior," *Proceedings Br. Mach. Vis. Conf. 2011*, pp. 110.1-110.12, 2011.
- [9] C. Yang, L. Zhang, H. Lu, X. Ruan, and M. H. Yang, "Saliency detection via graph-based manifold ranking," *Proc. IEEE Comput. Soc. Conf. Comput. Vis. Pattern Recognit.*, pp. 3166–3173, 2013.
- [10] F. Perazzi, P. Krahenbuhl, Y. Pritch, and A. Hornung, "Saliency Filters: Contrast Based Filtering for Salient Region Detection," *IEEE Conf. Comput. Vis. Pattern Recognit.*, 2012.
- [11] M.-M. Cheng, N. J. Mitra, X. Huang, P. H. S. Torr, and S.-M. Hu, "Global Contrast Based Salient Region Detection," *{IEEE} Trans. Pattern Anal. Mach. Intell.*, vol. 37, no. 3, pp. 569–582, 2015.
- [12] J. Feng, Y. Wei, L. Tao, C. Zhang, and J. Sun, "Salient Object Detection by Composition," in *International Conference on Computer Vision*, 2011.
- [13] R. Zhao, W. Ouyang, H. Li, and X. Wang, "Saliency Detection by Multi-Context Deep Learning," *IEEE Conf. Comput. Vis. Pattern Recognit.*, pp. 1265–1274, 2015.
- [14] G. Li and Y. Yu, "Deep Contrast Learning for Salient Object Detection," *IEEE Conf. Comput. Vis. Pattern Recognit.*, pp. 478–487, 2016.
- [15] N. Liu and J. Han, "DHSNet: Deep Hierarchical Saliency Network for Salient Object Detection," *IEEE Conf. Comput. Vis. Pattern Recognit.*, pp. 678–686, 2016.
- [16] G. Li, Y. Xie, L. Lin, and Y. Yu, "Instance-Level Salient Object Segmentation," in *IEEE Conference on Computer Vision and Pattern Recognition (CVPR)*, 2017, pp. 247–256.
- [17] L. Wang, L. Wang, H. Lu, P. Zhang, and X. Ruan, "Salient Object Detection with Recurrent Fully Convolutional Networks," *IEEE Trans. Pattern Anal. Mach. Intell.*, 2018.
- [18] X. Qin, Z. Zhang, C. Huang, C. Gao, M. Dehghan, and M. Jagersand, "BASNet: Boundary-Aware Salient Object Detection," in *Conference on Computer Vision and Pattern Recognition (CVPR)*, 2019, pp. 7479–7489.
- [19] J. Zhang, F. Malmberg, and S. Sclaroff, *Visual Saliency: From Pixel-Level to Object-Level Analysis*, 1st ed. Springer International Publishing, 2019.
- [20] R. Achanta, S. Hemamiz, F. Estraday, and S. Sússtrunky, "Frequency-tuned salient region detection," *2009 IEEE Comput. Soc. Conf. Comput. Vis. Pattern Recognit. Work. CVPR Work. 2009*, vol. 2009 IEEE, no. Ic, pp. 1597–1604, 2009.
- [21] D. Martin, C. Fowlkes, D. Tal, and J. Malik, "A Database of Human Segmented Natural Images and its Application to Evaluating Segmentation Algorithms and Measuring Ecological Statistics," in *Proceedings Eighth IEEE International Conference on Computer Vision. ICCV 2001*, 2001.
- [22] H. Bay, T. Tuytelaars, and L. Van Gool, "SURF: Speeded-Up Robust Features," in *European Conference on Computer Vision*, 2006, pp. 404–417.
- [23] J. L. Bentley, "Multidimensional Binary Search Trees Used for Associative Searching," *Commun. ACM*, vol. 18, no. 9, 1975.
- [24] V. R. Chandrasekhar et al., "The stanford mobile visual search data set," *Proc. Second Annu. ACM Conf. Multimed. Syst. - MMSys '11*, p. 117, 2011.
- [25] R. Achanta, S. Hemamiz, F. Estraday, and S. Sússtrunky, "Frequency-tuned salient region detection," *2009 IEEE Comput. Soc. Conf. Comput. Vis. Pattern Recognit. Work. CVPR Work. 2009*, no. Ic, pp. 1597–1604, 2009.

## Statistical Aspects of the Environment of Albanian Students Who Were Admitted to Higher Public Education Institutions in the Year 2014

Feruze Shakaj<sup>1,\*</sup>, Markela Muça<sup>2</sup>, Klodiana Bani<sup>2</sup>

<sup>1</sup>Ministry of Education and Sports (MES), Street "Durrësit" Nr.23, 1001 Tiranë, Albania

<sup>2</sup>University of Tirana, Faculty of Natural Sciences, Department of Applied Mathematics, "Zogu I" Boulevard, Nr. 25/I, 1060, Tiranë, Albania

### ARTICLE INFO

Article history:

Received: 20 February, 2020

Accepted: 10 March, 2020

Online: 10 April, 2020

Keywords:

Study Programs

Administrative Units

national graduation

group's hierarchy analysis

ward's methods, distance

### ABSTRACT

The research presents a statistical analysis that characterizes the environment of the admitted students to Higher Public Education Institutions, by providing an overview of student's distribution to the courses of studies offered by universities in Albania, such as, economy, medicine, technical etc., and grouping them according to the relative density of 38 (thirty eight) administrative units /districts. The aim of the research focuses on the trends that these units present in the main areas of study mentioned above. We want to see if there is a connection between them and the courses of studies. So, in other words to see the trends according to district. The clustering was performed using the Ward's method of Cluster Analysis (CA Hierarchy Methodology). This research seeks to develop a very careful description in order to detect typical features and furthermore to understand the situation. The assessment combines a total analysis to a relative comparative analysis of study programs offered by universities. Also, it analyzes different indicators.

The analysis is based on a choice obtained from the NG 2014 (National Graduation) of Ministry of Education and Sports (MES). The software used is SPSS Statistic 25.

### 1. Introduction

Cluster Analysis (hereinafter referred to as the CA) is an analytical technique that is used to classify or group data in a finite number and small groups based on two or more variables. There are several algorithms for CA and each of them is aimed to measure the distance between the observed individuals and observation groups. The objects, part of the established groups, can be instances or variables. The data pool can be numerical or categorical. The categorical data can be obtained from quantitative or qualitative data. [1]

CA is supported by a number of software packages like SAS, SPSS, BMDP, which are often available in academic and other computing environments. (A brief description and sources for these and other packages are provided by Romesburg [2])

Another issue in CA is the interpretation of groups. In fact, interpretation of groups that result from arithmetic procedure is not very clear. An important role in the identification of groups,

plays the distance between objects. Usually, a graphical representation helps in distinguishing before applying any method. We must be careful in case when there are no real groups for the data sets, but the method contains a partition. This is because we don't know the number of clusters that will emerge in our sample. [3]

CA is divided into Hierarchical and non - Hierarchical. Our study focuses on the implementation of hierarchical methodology in which clusters are given in hierarchically through a dendrogram at different levels of division [4]

Algorithms for Cluster Hierarchical Analysis are two types:

1. Agglomerative (collective)
2. Divisive (distribute)

These algorithms are completely the opposites of each other.

CA's Agglomerative Algorithm functions by grouping data one by one based on the nearest distance from all data distances [5]

\*Corresponding Author: Feruze Shakaj, shakajferuze@gmail.com

[6]. All agglomerative hierarchical grouping procedures start with a matrix of differences between objects. At the beginning of the agglomeration process, each object is considered as a separate cluster. For an N pool of initial objects, the first group will result in N- 1 clusters, the second in N -2, and so on until a single cluster will collect and contain all the objects [6], [7].

There are several methods to achieve this result where some of the most important ones are mentioned below:

1. Single Distance – nearest or single linkage,
2. Complete Distance – farthest or complete linkage,
3. Average – average distance or average linkage,
4. Centroid distance,
5. Ward's method – minimized square amount of Euclidian distances (SSEs.)

## 2. Literature review

The main motive behind writing this article is that educational development is essential to the improvement of socio-economic development of a country. The article discusses the choices of the students admitted to HEI. On the other hand, this aspect is not discussed as detached from the secondary education, but as attached to it, because the secondary education is the initial point which forms the students' inclinations towards higher education.

It is a well-known fact that HEI have an essential impact on the social development. So, the main role of HEI is to teach students to be able to develop research skills and to offer services to the community. By doing this role the HEI help students to secure a job in the future. Our main objective is that the HEI should cooperate with education institutions of secondary education, in order to foster and orient students towards their true inclinations.

In the field of economic development, the Higher Education contributes towards the increase of productivity and competition, mainly through the growth of human capital. Another role of HEI is that they through their cooperation with government and non-government institutions related to employment, can know better the labour market needs, in order to orient their curricula towards these needs. Our article aims to analyse the environment of the students admitted to universities, in order to offer some suggestions to improve the quality of Higher Education. These suggestions are related to Higher Education capabilities to attract students and the possibilities of offering employment for a great number of graduates, contributing in creating a Knowledge-based Society.

In this study are analysed all the Albanian students, who won a place in Public HEI, in the year 2014, based on districts. The main aim of this article is to examine if group analysis of the students based on districts could produce any results that can be used for the objectives mentioned above. The study is performed through hierarchical cluster analysis group, categorizing the districts based on nine main education fields, and the respective winners for each field. The main objective of this study is to produce

quantitative data of the winners in Higher Public Education, academic year 2014-2015, based on districts. The article aims to look into details of the winners based on districts, in the fields determined by us before, in order to compare different districts according to the fields, or to highlight the similarities between the districts.

A very important role that the HEI play is that, they contribute to the development of competition between countries, by creating scientific centres, or their branches, where is needed. This study helps the HEI, to direct their offer, in a clear and well-oriented way towards the students that come from the districts, where the inclinations of high school seniors are exactly those that serve the universities to increase the quality of the education. Universities can use this study to develop career strategies that helps not only them, but also the education institutions of the pre-university education. Thereby, the universities and industries become strong partners to the new concepts development that go toward a higher competition.

The curriculum in Albanian universities is an example of this, which lately has started to rely in the improvement of competition in Higher Education, creating knowledge centres in different scientific fields, which will cooperate closely with a great number of different industries. Taking into great consideration the problems of competition in Higher Education, in the context of the increase of students' number, some authors [7] [8]. emphasize the crucial role of skills and knowledge management in the socio-economic development of a country. This explains an increase in demand of higher-order thinking and the need of graduated students, who develop competencies that offer advantages in the labour market and different industries.

On the other hand, Bucharest Message to the 2009 World Conference on Higher Education – Experiences and Recommendations from the Europe [8] attracts our attention to the fact that:

*“Population decline and changes in age distribution are affecting higher education systems in most countries in the UNESCO Europe Region, with a consequence that higher education institutions see the need to compete for students both nationally and internationally, with the risk that international migration be required in order to overcome shortages of skilled labour”.*

*“In this context, new competencies for new demands of the labour market must be anticipated and increased opportunities for higher education and lifelong learning need to be created for he modern tendencies to the development of higher education emphasize the fact of the increase of the number of students admitted to universities, in other words the massification of higher education. Instead of addressing directly the issue of massification, [9]. well-known authors in this field, what happens is that this is included in the discussions of higher education as an external factor that impact the teaching, observations and related services.*



Another challenge of our education system, in particular higher education is to offer optimal conditions in all aspects, in a way that elite students, (approximately 3000-4000 a year), who for many years have chosen to study abroad, can have all the appropriate conditions to study in Albania. The phenomena of elite migration is linked directly to the socio-economic development of a country, because by the movement of highly skilled elites, our country not just losing our renowned intellectuals, but also losing our specialized labour force, or that is called the brain drain of a country.

A considerable number of authors, especially in the last decade considered the higher education from the perspective of economic policies and employment [10], [11], [12], [13] giving attention to the aspect of linkage between growth of human capital and economic development. The discussed studies so far are trying to give a thorough point of view of higher education, not only based on economic perspectives, but also emphasizing benefit analysis of individuals, who have completed higher education. Thus, analysis show that graduates have better chances of employment and are less exposed towards the risk of longer unemployment. Besides that, the importance of these findings, is very debatable for transition countries, which are faced with a very high rate of unemployment. Despite the fact, that the observations of this article discussed above, are very general in their nature, this study analysis the trends of Albanian higher education, in a way that it is exactly the higher education in our country that should be competitive, and why not aiming to be competitive to European countries as well.

### 3. Methodology

In this study we will use Ward's Method of Hierarchal Cluster Analysis (CA) which is an important method in grouping data [14]Ward's is also known as the minimum variance method because it merges at each stage the cluster pair whose union minimizes the increase in the error of all square numbers within the group based on the Euclidean distance. Between the centroid it tends to produce homogeneous clusters and a homogeneous hierarchy and its definition as a gravity cluster provides a useful way to represent a cluster [15].

This method is similar to the Linkage method that starts with N Clusters, which contain an object but uses the sum of SSE squares to determine the two next batches at each step of the algorithm. Square Sample Error (SSE) is defined as:

$$SSE = \sum_{i=1}^K \sum_{j=1}^{n_i} (y_{ij} - \bar{y}_i)^2 \quad (1)$$

Where  $y_{ij}$  is I object in the group (Cluster) i and  $n_i$ - is the object number in group (Cluster) i. [16] Ward's method shows that the distance between Cluster A and B is equal to the square sum when we join them

$$\Delta(A, B) = \sum_{i \in A \cup B} \|\bar{x}_i - \bar{m}_{A \cup B}\|^2 - \sum_{i \in A} \|\bar{x}_i - \bar{m}_A\|^2 - \sum_{i \in B} \|\bar{x}_i - \bar{m}_B\|^2$$

$$= \frac{n_A n_B}{n_A + n_B} \|\bar{m}_A - \bar{m}_B\|^2 \quad (2)$$

Where  $\bar{m}_j$  is the center of cluster j and  $n_j$  is the number of points in it.  $\Delta$  is the marginal cost of cluster's A and B combination. Through the hierarchical method, the sum of squares begins with zero because each point is in the cluster itself and it grows as we merge clusters (Distances between Clustering, Hierarchal Clustering 2009),

### 4. Information on the database

In this study we have considered the group of all winners in the Higher Public Education Institutions of the academic year 2014-2015. This group is pulled out from the National Graduation database of National Agency of Exams in the Ministry of Education and Sports. The used database is composed from n=18390 rows where each of them belongs to a winner. The initial table contains this data and it is organized in fields such as: Name, Father's Name, Surname, and study program, acceptance code of study, university, faculty, state, and district. We emphasized that the focus here are all the Albanian Higher Education Institutions. In addition, all study programs belonging to the same field of study have been named equally in all universities that offer this field of study. Example, study programs such as General Nursing, Imaging, General Medicine, Dentistry, Pharmacy etc., belongs to the group named "medical". Using Microsoft Office Access Database from the initial table, after making the necessary modifications, we have built an absolute density contingency table that shows for each city and for each district the number of winners in each of the fields of study we want to review. Likewise, we took care not to have missing values in the data by replacing all the latter with "zero" value. In this way we avoid problems during the grouping process. By using SPSS functions, the absolute densities are all turned to relative densities and they are used to group via Ward's method of Cluster Hierarchical Analysis. We have used relative densities as we noticed that the classification through district groups was clearer and the results were more readable.

Table 1: Number of groups and members for each

Cluster	Number of districts	Members
1	5	Berat, Kamëz, Korçë, Lushnje, Pogradec
2	27	Bulqizë, Delvinë, Devoll, Dibër, Gjirokastrë, Gramsh, Has, Kavajë, Kolonjë, Krujë, Kuçovë, Kukës, Kurbin, Lezhë, Librazhd, Malësi e Madhe, Mallakastër, Mat, Mirditë, Peqin, Përmet, Pukë, Sarandë, Skrapar, Tepelenë, Tiranë Qark, Tropojë
3	5	Durrës, Elbasan, Fier, Shkodër, Vlorë
4	1	Tiranë

5. Experiment results

As we have mentioned above, we have used Ward’s method of Cluster Analysis (CA Hierarchy Methodology). By using this method, data is categorized in four groups, having an intersection as in Figure 1. The Table presents a summary of the number of groups and districts that are categorized in each one of them. We highlight the fact that the grouping is based on the districts (this analysis is done based on administrative divisions before the territorial reform, where Albania was divided into 38 districts). In order to build graphics for each group, we have used absolute density, which we will present interpreting each one of them.

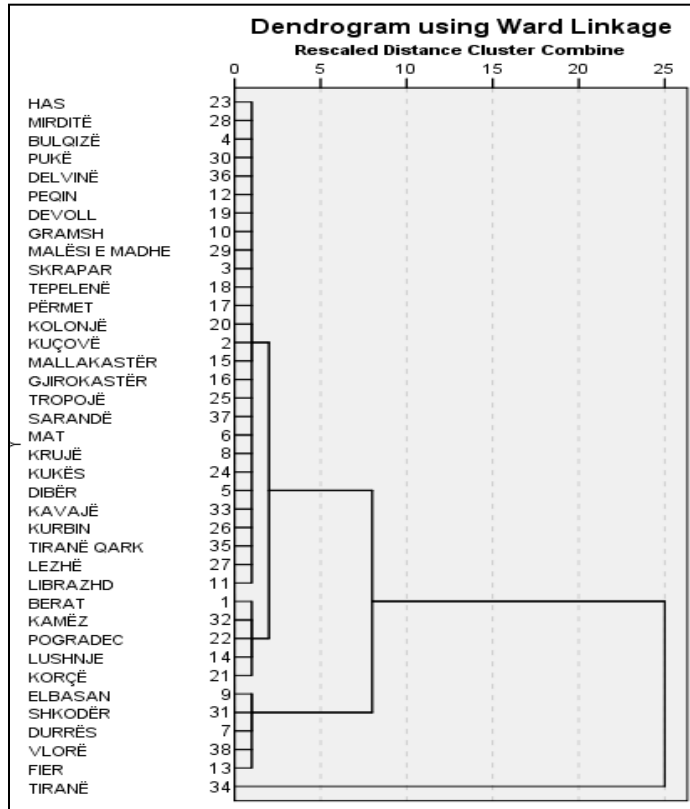


Figure 1: Dendrogram tree data

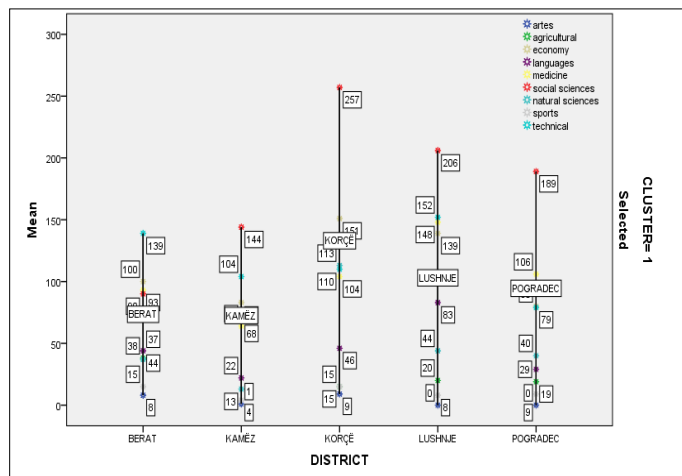


Figure 2: Group 1

Figure 2 notes that in the first group there are districts of: Berat, Kamëz, Korçë, Lushnje and Pogradec. The most interesting fact in this group is that starting from the numbers in small square boxes, (which show the number of winners in each field of study), and referring to the graphic’s legend, we note that the districts of this group have the largest number of winners in the field of Social Sciences.

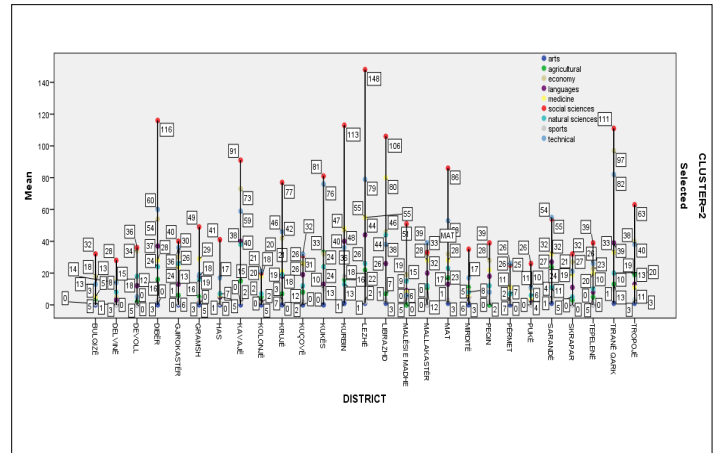


Figure 3: Group 2

Figure 3, notes that in the second group there are all districts, which have approximate number of students and there are mainly not of very large districts of the country. It is worth emphasizing the fact that, if we refer to the legend, the number of winners in the study field of Technical Sciences is almost equal in all districts. Also, we can note that in this group, all districts have the largest number of winners in the field of Social Science. It is very interesting to emphasize the fact noted by the graphic that even form the smaller districts, there are high school seniors students, who are winners in the Fine Arts Study Programs, highlighting the fact that these courses of study have a very limited number of student quotas, varying form 1 to 50 admissions for a study program

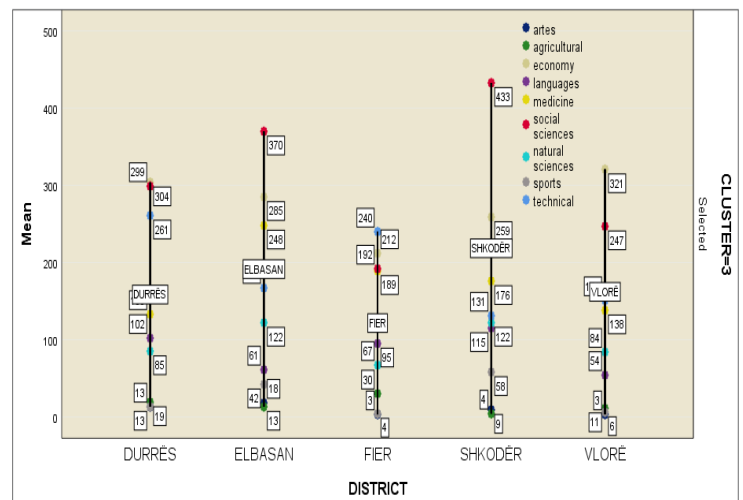


Figure 4: Group 3

Figure 4, notes that in the third group, districts of: Durrës, Elbasan, Fier, Shkodër, Vlorë, are grouped together. Also, the graphic shows that, these districts have approximately the same number of students, who are winners in Public HEI. In in this group, it is worth noting the fact that these districts have the same number of winners in the field of Foreign Languages. Meanwhile, in this group, it is clear that we have a considerable number of winners in the field of Social Sciences.

Figure 5, notes that in the third group, the district of Tirana is on its own, which makes sense because this district has the largest number of students who apply to universities. It is very important to emphasize the fact that in the district of Tirana, we see a visible trend of students, who apply to Economic, Technical and Sport Sciences, taking into consideration the fact that in the country level, there are not many students, who apply to these courses of study.

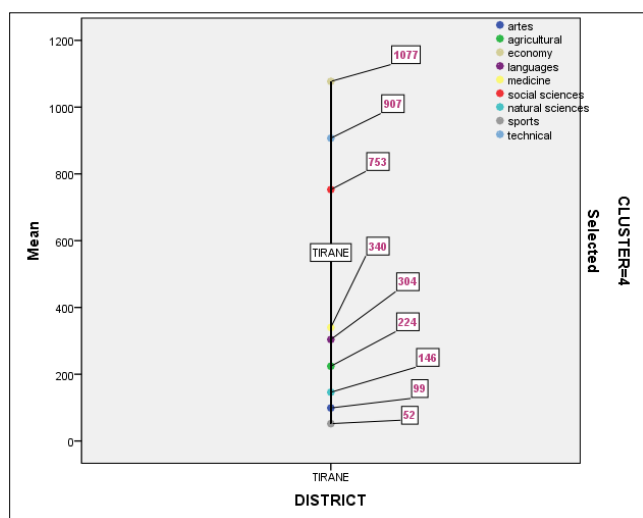


Figure 5: Group 4

## 6. Conclusions

The statistical analyses of the distributions shows that, admitted students in the field of Social Sciences, mainly come from the districts of Berat, Kamëz, Korçë, Lushnje and Pogradec. Almost, all of smaller districts of the country have approximately the same number of students admitted in the field of Technical Engineering. The largest number of students, admitted in the field of Natural Sciences, come from the districts of: Elbasani, Durrësi, Fieri, Shkodra and Vlora. The students are distributed evenly among all districts. Tirana District students are mainly inclined towards Economic, and Sport Sciences, whereas they are less inclined towards Natural Sciences.

## References

- [1] Muça M., Baani K., Shakaj F., "Combining the hierarchal and non-hierarchal methods for acluster analysis: a case study for classification of students accordin to their results.," in *SPNA*, Tirana, 2014.
- [2] R. H.C, Romesburg, 1984.

- [3] Muça M., Bani K., Shakaj F., "Combining the hierarchal and non-hierarchal methods for a cluster analysis: a case study for classiffication of students according to their results.," in *SPNA*, Tirana, 2014.
- [4] Aggarwal C. C., Reddy, C. K, "Data clustering Algorithms Application," 2015.
- [5] Fung, B. C. M., Wang, K., & Ester, M., " Hierarchical Document Clustering.," 2006.
- [6] Singh, W., Hjorleifsson, E., & Stefansson, G., " Robustness of three hierarchical agglomerative clustering techniques for ecological data.," 2010.
- [7] E. Egron-Polak, "100 voices. A decade of inspiration and achievements in higher education (p. 43). Bucharest: UNESCO-CEPES," 2009.
- [8] UNESCO, " Bucharest message to the 2009 world conference on higher education – Experiences and recommendations from the Europe region. UNESCO Forum on Higher Education in the Europe Region.," Bucharest, Romania., 2009.
- [9] Mora, J. G., & Vila, L. E, " The economics of higher education. In R. Begg (Ed.), the dialogue between higher education research and practice (pp. 121–13). Dordrecht: Kluwer Academic Publishers.," 2003.
- [10] Del Rey, E., & Racionero, M., " Financing schemes for higher education. European Journal of Political Economy, 26, 104–113.," 2010.
- [11] A. (. Schwarzenberger, "Public/private funding of higher education: A social balance. Hannover: HIS: Forum Hochschule.," 2008.
- [12] Strehl, F., Reisinger, S., & Kalatschan, M., "Funding systems and their effects on higher education systems, Paris: OECD Publishing. OECD Education Working Papers 6.," 2007.
- [13] J. Ward, "Hierarchical Grouping to Optimize an Objective Function," *Journal of the American Statistical Association.*," 1963.
- [14] Murtagh, F. Legendre, P., "Ward's Hierarchical Agglomerative Clustering Method: Which Algorithms Implement Ward's Criterion?. *J Classif* 31, 274–295.," 2014.
- [15] M. Lorr, "Cluster analysis for social scientists.," 1983.
- [16] Ferreira, L., Hitchcock, D.B., "A COMPARISON OF HIERARCHICAL METHODS FOR CLUSTERING FUNCTIONAL DATA."

## Analysis of Two-Dimensional Electron Gas Formation in InGaAs-Based HEMTs

Itsuki Takagi, Takuma Kato, Hirohisa Taguchi\*

Department of Electrical and Electronic Engineering, School of Engineering, Chukyo University, Nagoya, 4668666, Japan

### ARTICLE INFO

Article history:

Received: 06 March, 2020

Accepted: 31 March, 2020

Online: 10 April, 2020

Keywords:

2 DEG

InGaAs HEMTs

Potential shape

### ABSTRACT

*In this study, a theoretical simulation was performed using the Schrodinger-Poisson method to elucidate the formation factors for two-dimensional electron gas in InGaAs-based HEMTs. No visible change was observed in the carrier density and the potential shape. The inflection point of the energy level and the agreement of the energy level in each dimension were confirmed for the change in the number of carriers in the channel layer. It was found that the number of electrons at this coincidence point almost coincided with the number of electrons in the IV characteristics measured by the previous research for each gate voltage. The change in carrier state suggested that a 2DEG was formed. In addition, by considering the transport of carriers on the crystal lattice plane as a cause of the inflection point of the energy level, it was suggested that it might be caused due to the occurrence of the degeneracy process at a certain moment. From these results, it was experimentally and theoretically shown that the formation of 2DEG was caused by the carrier degeneration and the state change.*

### 1. Introduction

The InGaAs crystal is a ternary compound semiconductor known for forming the channel layer of a high electron mobility transistor (HEMT) [1]-[3]. Generally, the HEMT structure is constructed by using a heterojunction with a heterogeneous semiconductor crystal. For this reason, band discontinuity occurs at the crystal surface bonding interface. Furthermore, in the electrostatic potential caused by the space charge under thermal equilibrium, band bending occurs [4], [5]. Thus, an electron transport layer called a two-dimensional electron gas (2DEG) is formed in the channel layer [5]. As an advantage of the 2DEG formation, transmitted electrons are hardly scattered by impurities, and excellent high-speed transmission with low noise is obtained [6, 7]. Research on the characteristics such as the high-speed transmission and low noise in HEMTs has been performed on InGaAs crystals as well as on HEMTs that combine other materials [8]-[10].

However, there are few reports on the principle of 2DEG formation. Due to the formation principle of 2DEG, the quantum size effect (quantum confinement effect) has been reported [11], [12]. This is a phenomenon that occurs when the carriers are confined in a widened region spanning the de Broglie wave. It is often used as an explanation for a low-dimensional structure for the 2DEG interpretation in a quantum dot. This phenomenon

forms the basis for creating the channel layer of a few nanometers in HEMT fabrication [13], [14].

However, we have experimentally observed the moment of 2DEG formation in InGaAs-based HEMTs as a previous study [15]. Figure 1 shows a part of the experimental result of the previous research. In this experiment, the IV characteristics were measured by setting the drain voltage applied to the device to a very small value from -0.5 mV to 4.8 mV. In addition, a decrease in the drain current was found for InGaAs-based HEMTs when irradiated with light at a wavelength of 1480 nm. From figure 1, it is evident that the drain current sharply spikes at a certain voltage value. In addition, the timing at which the current value rises was shifted due to its dependence on the light intensity. When the HEMT operation was viewed, high-speed operation was found at the moment of the rise of the current value, and a rapid improvement in electron transport speed was obtained. It was considered that 2DEG was formed or expressed at this moment.

From the above, it is assumed that a 2DEG is formed from at a certain moment. The explanation of the quantum size effect alone is not sufficient for the principle of 2DEG formation.

Therefore, the purpose of this study was to elucidate the formation factor of 2DEG in InGaAs-based HEMTs. A theoretical simulation was performed on an InGaAs-based HEMT; physical

\*Corresponding Author; Hirohisa Taguchi, E-mail [htaguchi@sist.chukyo-u.ac.jp](mailto:htaguchi@sist.chukyo-u.ac.jp)



parameters of the device were compared with the experimental data shown in figure 1, and the factors involved in the formation of 2DEG were discussed.

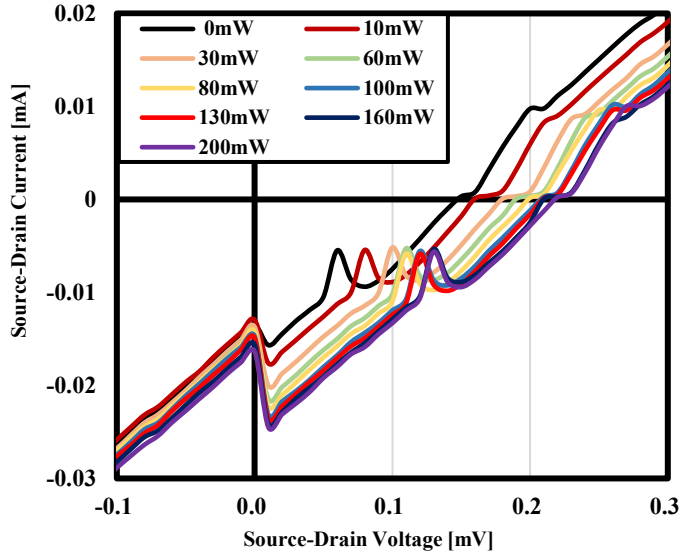


Figure 1: A part of the experimental results of the previous research.

## 2. Experiment Methods

### 2.1 Device Structure Model

A cross-sectional view of the device structure used in this experiment is shown in Figure 2. Theoretical calculations near the channel layer were performed from the barrier layer to the buffer layer in the simulations performed in this study. Table 1 summarizes the parameters for each layer.

### 2.2 The Schrödinger -Poisson Method

In this analysis, Wolfram Mathematica 12 was used as the theoretical calculation software. The Schrodinger-Poisson method using local density approximation in density functional theory was employed as the solver [16]. This solver calculates the parameters such as the energy level, wave function, potential function, and the carrier density function of the electron-hole system in the HEMT structure. The direction perpendicular to each layer plane was defined as the x-axis, and a one-dimensional calculation was performed. The used mathematical formulas are described below. A time-independent Schrodinger equation was introduced to describe the quantum mechanical effects that occur in the HEMT structures [17].

$$\left[ -\frac{\hbar^2}{2} \frac{d^2}{dx^2} \left( \frac{1}{m^*(x)} \right) + V(x) \right] \psi_m(x) = E_m \psi_m(x) \quad (1)$$

Where  $\psi$  is the wave function,  $E$  is the energy eigenvalue,  $V$  is the potential energy,  $\hbar$  is the Dirac constant, and  $m^*$  is the effective mass of electrons and holes of the target material. The solution to the Schrodinger equation gives the wave function associated with the energy. The wave function represents a spatial probability distribution indicating the presence of electrons and holes at a specific energy level. In this calculation, the carrier function defines the potential energy function. Therefore, the time dependence of the potential was not considered. Subsequently, the

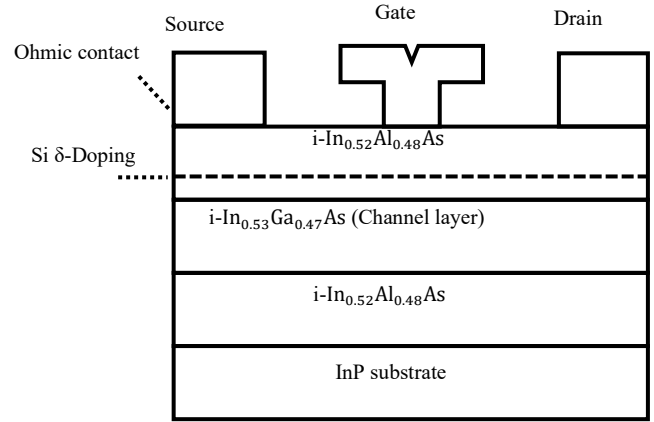


Figure 2: The cross-sectional view of the device structure used in this experiment.

carrier density was calculated. The carrier density of a semiconductor in an equilibrium state within the parabolic band approximation can be calculated from the following equation [18].

$$n_s = \int g(E) f(E) dE \quad (2)$$

$$p_s = \int g(E) [1 - f(E)] dE \quad (3)$$

Here,  $g(E)$  is a density of states function, and  $f(E)$  is a Fermi-Dirac distribution function.

$$f(E) = \frac{1}{1 + e^{\frac{E - E_F}{k_B T}}} \quad (4)$$

The density of states function gives the number of states per unit volume and unit energy in the  $\mathbf{k}$ -space. In this analysis, the electron and hole states in the same HEMT structure were compared in three and two dimensions.

$$g_{3D}(E) = \frac{(2m^*)^{\frac{3}{2}}}{2\pi^2 \hbar^3} \sqrt{E - E_F} \quad (5)$$

$$g_{2D}(E) = \frac{m^*}{\pi \hbar^2} \sum_N \theta(E - E_N) \quad (6)$$

When calculating the carrier distribution at the target potential, the carrier distribution in the channel layer region was not uniform with the triangular wave potential in the HEMT. The band edge of the triangular potential was strongly bent at the junction interface. Therefore, a band structure was mounted on the potential of the Schrodinger equation. This forms a constraint within the domain of the wave function [19]. In this case, the square of the wave function was a probability distribution function and it represents the probability of a particle having a specific energy level  $E_n$  in the region.

From these, the carrier density is;

Table 1: Summarizes the parameters for each layer.

$$n(x) = \left[ \int g(E) f(E) dE \right] |\psi(x)|^2 \quad (7)$$

$$p(x) = \left[ \int g(E)[1 - f(E)] dE \right] |\psi(x)|^2 \quad (8)$$

This time, in order to calculate the carrier density for a specific energy level, after performing indefinite integration, the energy eigen value of the object was substituted into the energy dependence function (state density and distribution function). Subsequently, the potential function  $V(x)$  of the HEMT structure was introduced. In this analysis, the potential function in the HEMT structure was defined by the following equation.

$$V(x) = -q\phi(x) + \Delta E_c(x) + V_{xc}(x) \quad (9)$$

The first term of  $V(x)$  is introduced by the Poisson equation. In this equation, the electrostatic potential is related to the space charge distribution in the system [20].

$$\frac{d}{dx} \left( \epsilon_0 \epsilon_r(x) \frac{d}{dx} \right) \phi(x) = -\rho(x) \quad (10)$$

$$\rho(x) = q[p(x) - n(x) + N_D^+(x) - N_A^-(x)] \quad (11)$$

Here,  $\epsilon_r(x)$  represents the relative permittivity of each material,  $\epsilon_0$  represents the permittivity in a vacuum, and  $\rho(x)$  represents the charge distribution of the semiconductor. In addition,  $n(x)$  and  $p(x)$  is the carrier density of electrons and holes, and  $N_D^+(x)$  and  $N_A^-(x)$  is the ionization dopant density by acceptors and donors.

Solving the Poisson equation defines the electrostatic potential  $-q\phi(x)$ . In addition, the band discontinuity  $\Delta E_c(x)$ , and the exchange correlation potential  $V_{xc}(x)$  are defined. The exchange correlation potential  $V_{xc}(x)$  is an interpolation formula developed by Hedin and Lundqvist and plays a role to change the Schrodinger equation for one particle system into an equation for another particle. This time, the Stern and Das Sarma format was adopted [21,22].

$$V_{xc}(x) = - \left[ 1 + 0.03683 r_s \ln \left( 1 + \frac{21}{r_s} \right) \right] \left( \frac{2}{\pi \alpha r_s} \right) R_y^* \quad (12)$$

$$R_y^* \text{ (Rydberg Constant)} = \frac{q^2}{8\pi\epsilon_0\epsilon_r(x)\beta} \quad (13)$$

$$\alpha = \left( \frac{4}{9\pi} \right)^{\frac{1}{3}}, \quad \beta = \frac{16\pi^3\epsilon_0\epsilon_r(x)\hbar^2}{m^*(x)q^2} \quad (14)$$

$$r_s = \frac{r_0}{\beta} = \left( \frac{4\pi\beta^3 C(x)}{3} \right)^{-\frac{1}{3}} \quad (15)$$

$$r_0 \text{ (Wigner-Seitz radius)} = \left( \frac{3}{4\pi C(x)} \right)^{\frac{1}{3}} \quad (16)$$

$$\therefore C(x) = n(x) \text{ or } p(x) \text{ (Electron or Hole density)} \quad (17)$$

### 2.3 Calculation Method

In the simulation method, initially, a Poisson equation is calculated as a trial function. At this time, the calculation is

performed under the condition that the electron and hole densities are set to 0. Thus, the well-type potential in the band offset state in the thermal non-equilibrium state was determined. The Schrodinger equation was calculated for the obtained electrostatic potential. Thereafter, the carrier density and the carrier concentration were calculated using the obtained energy eigen value and wave function. At this time, three-dimensional and two-dimensional systems were used for the density of states function. An exchange-correlation potential was defined from the obtained carrier density.

Table 1: Targeted Layers and Materials

Target Layers	Materials	Layer Width [nm]	Doping Density [cm <sup>-3</sup> ]	Effect of Gate Voltage [%]
Barrier	InAlAs	100	0	100 (Schottky barrier)
Doping	InAlAs (Si doped)	0.2	1.5×10 <sup>20</sup>	50
Spacer	InAlAs	20	0	50
Channel	InGaAs	15	0	25
Buffer	InAlAs	100	0	0

The calculation was repeated using these parameters. In this analysis, the change in potential shape due to the gate voltage was incorporated into the program, and the dependence at each gate voltage was compared. The potential function is as follows;

$$V'(x) = V(x) - qV_g(x) \quad (18)$$

The effect of the gate voltage on each layer was dependent on the distance from the surface of the Schottky junction (see Table 1). For the purpose of reproducing a gradually increasing electronic state, the carrier density was defined by superposition of the carrier densities obtained in each calculation. This was done to reproduce the situation of the previous study [15] in the simulation. As a result, the equations were not self-consistent and did not converge. Therefore, the convergence condition was derived from the IV characteristics obtained in previous studies as the convergence criterion for the calculation [15]. The electron concentration was calculated using the theoretical formula of the drain current in the linear region of the IV characteristic. After that, experiments and theory were compared for each obtained parameter.

### 3. Results

#### 3.1 The shape of Potential ( $V_g = 0$ )

The potential shape of the electron-hole system is shown in figure 3. As a result of the simulation, a potential shape known as the HEMT structure was obtained. For the energy eigen values, the ground level and the second level (excitation level) were

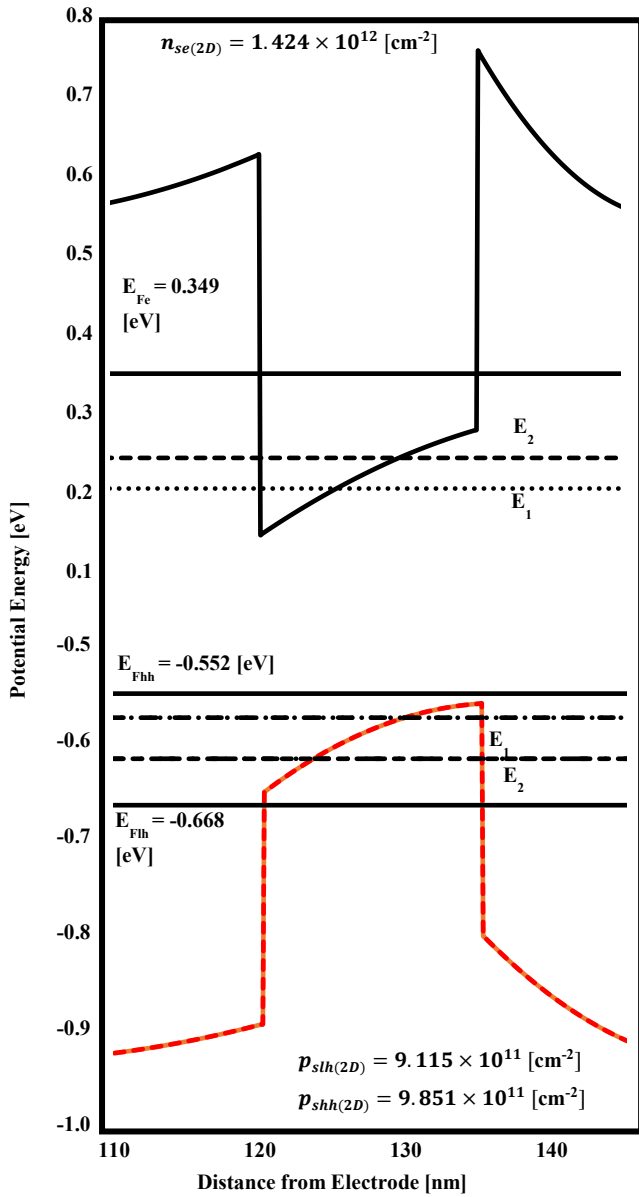


Figure 3: The potential shape in the electron-hole system ( $V_g=0$ ).  $E_1$  and  $E_2$  are energy levels,  $n_{se}$  is the electron density,  $E_{Fc}$  is the electron Fermi level,  $E_{Fhh}$  is the heavy hole Fermi level,  $E_{Flh}$  is the light hole Fermi level,  $p_{slh}$  is the light hole sheet density, and  $p_{shh}$  is the heavy hole sheet density, respectively.

obtained as solutions for the triangular wave potential. The subsequent energy levels were found to be around 0.545 eV. This was the result of level formation in the InAlAs layer by Si doping. In the hole system, two types of heavy holes and light holes were separately simulated. No significant change was observed in the potential shape; a paired potential was formed for the electron system.

### 3.2 The Carrier density ( $V_g = 0$ )

The results of the carrier density distribution are shown in figure 4. In this simulation, calculations were performed by defining the density of states function as two-dimensional and three-dimensional. From figure 4, no difference in the carrier distribution was found between the two-dimensional and three-dimensional orders in the electronic system. The hole density in the two-dimensional hole system does not vary significantly. The

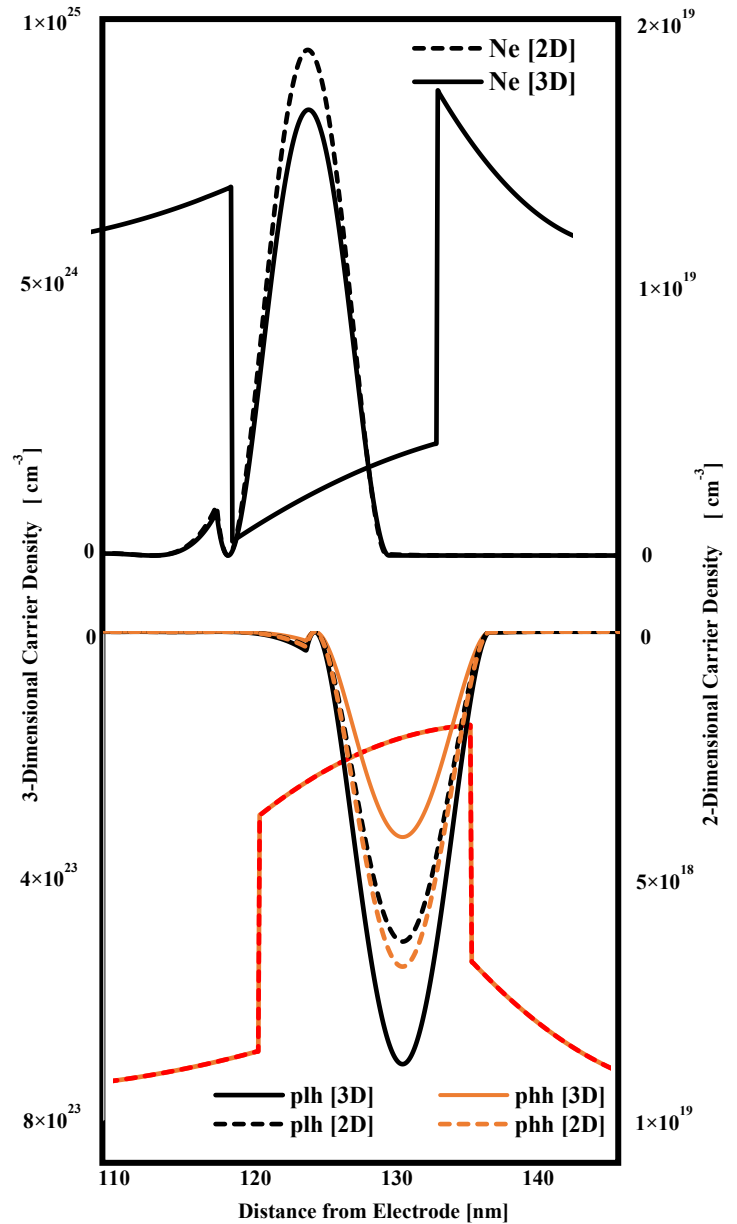


Figure 4: The carrier density distribution ( $V_g = 0$ ). The p\_lh means light hole density and p\_hh means heavy hole density. 2D means a 2-dimensional state, and 3D means a 3-dimensional state.

light holes had about three times as many hole carriers as the heavy holes in the hole density of the three-dimensional system. This was considered to be due to the difference between the light and heavy hole effective mass values.

### 3.3 The Energy Level ( $V_g = 0$ )

The result of the dependence of the energy eigenvalue on the number of electrons was shown in figure 5. The three-dimensional energy eigen value was not affected by the quantum size effect. Therefore, the three-dimensional energy eigen values are not discretized. Figure 5 plots a total of the three energy eigen values, one energy eigenvalue in a three-dimensional system, a ground level, and an excitation level in a two-dimensional system. From figure 5, it was found that the energy eigenvalue of the three-dimensional system rapidly changed with the increase in the

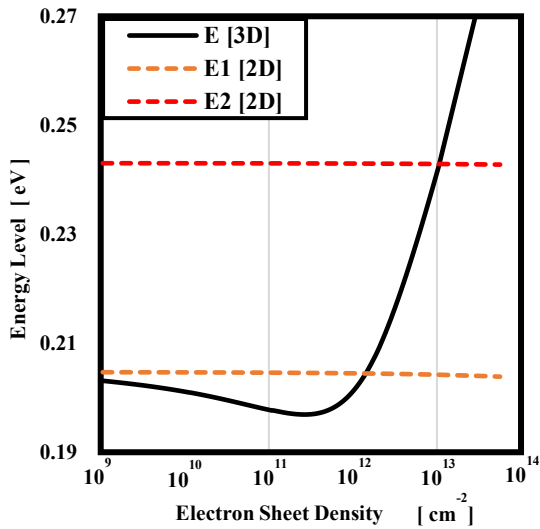


Figure 5: The dependence of the energy eigenvalue on the number of electrons.

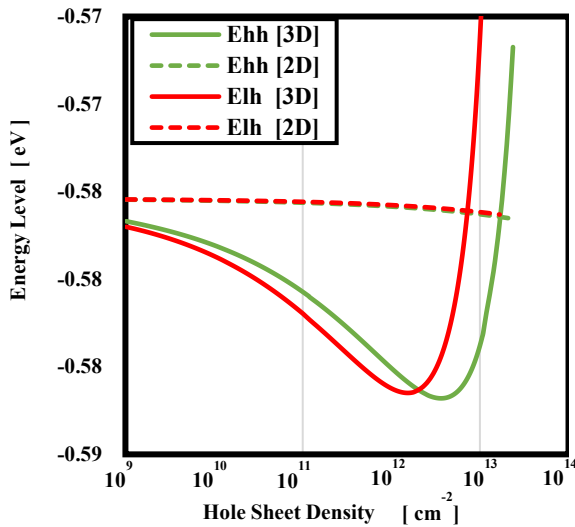


Figure 6: The dependence of the energy eigenvalue on the hole concentration.

number of electrons in the channel layer. In addition, it was found that there was an inflection point in the three-dimensional system where the energy changed from a decreasing trend to an increasing trend. Furthermore, it was observed that the energy eigenvalue of the three-dimensional system coincides with the ground level of the discrete two-dimensional system at a certain number of electrons. When comparing the number of electrons at this time with the result calculated from the IV characteristics.

$$\text{IV Characteristics} \square 1.429 \times 10^{12} \text{ [cm}^{-2}\text{]}$$

$$\text{Theoretical Value} \square 1.424 \times 10^{12} \text{ [cm}^{-2}\text{]}$$

It was found that the number of electrons almost coincided with the number of electrons at the moment when the peak was generated (at the moment when the shape of the IV characteristic changed abruptly). Subsequently, the dependence of the energy eigenvalue on the hole concentration is shown in figure 6. The energy eigenvalues in the two-dimensional system were the same for both the light and heavy holes (Elh and Ehh). However, in the

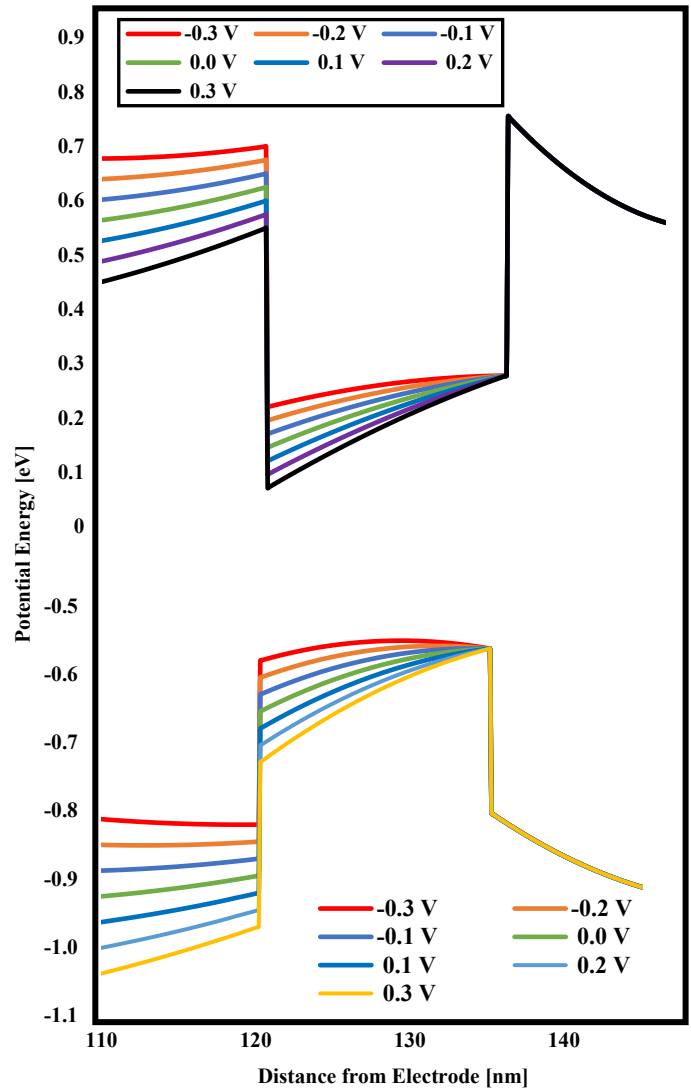


Figure 7: The potential shapes at each gate voltage.

eigenvalues of the energy in the three-dimensional system, the existence of an inflection point was confirmed at a certain moment with the increase in the number of holes, as in the electron system. In addition, the timing at which this inflection point occurs differs between a light hole and a heavy hole. It was found that the timing deviation occurred first in the light holes and then in the heavy holes. In this simulation, the initial settings of the trial function and the quasi-Fermi level in the heterostructure were set in such a way that the hole concentrations of light and heavy holes were the same. Therefore, it was considered that the difference in the effective mass and the like, affects the hole system.

### 3.4 The Gate-Voltage dependence of each parameter

#### 3.4.1 The shape of Potential

The potential shapes at each gate voltage are shown in figure 7. In the electron system, it was found that when a negative gate voltage was applied, the potential shape gradually changed to a well-shaped potential such as the band offset. It was also found that when a positive gate voltage was applied, the potential shape formed was a triangular wave potential deeper towards the



electrode. The table 2 summarizes the energy eigenvalues in a two-dimensional system for each potential. As it can be seen from the table 2, it was found that the energy eigenvalues such as the ground level, also changed according to the value of the applied gate voltage. On the other hand, in the hole system, little change in shape was observed for light holes and heavy holes, resulting in a pair with the electron system. The figure 7 plots the potential shape of heavy holes.

Table 2: Summarizes the energy eigenvalues in a two-dimensional system for each potential.

Gate Voltage [V]	Ground State [eV]	Second Level (Excited State) [eV]
0.3	0.14622	0.22147
0.2	0.16584	0.22299
0.1	0.18519	0.23293
0	0.20445	0.24296
-0.1	0.22356	0.25313
-0.2	0.24230	0.26366
-0.3	0.26005	0.27519

### 3.4.2 The Carrier density

Subsequently, the results of the carrier distribution for each gate voltage are summarized in figure 8. In the electronic system, it was confirmed that as a negative gate voltage was applied, the electron distribution shifted toward the substrate. On the other hand, when the gate voltage was positive, the distribution did not fluctuate so much. In the case of the hole system, when the gate voltage was negative, it was found that the voltage slightly shifted to the electrode side. When the gate voltage was positive, almost no change in the hole distribution was observed as in the case of the electron system. Figure 8 plots a two-dimensional system since no change in distribution was observed in two and three dimensions.

### 3.4.3 The Energy Levels

The dependence of the energy eigenvalue with the number of electrons on the gate voltage is shown in figure 9. The existence of an inflection point at a certain number of electrons for the energy eigenvalues of the three-dimensional system was confirmed under all gate voltage conditions. The table 3 shows the electron concentration at the time of occurrence of the inflection point in the electron energy eigenvalue function at each gate voltage. As shown in table 3, under all conditions, the electron number, at the moment when the peak occurs in the IV characteristic almost coincides with the electron areal density at the point indicating the inflection point in the energy eigenvalue function. Figure 10 shows the result of the energy eigenvalue with respect to the gate voltage in the hole system. The inflection point of the energy eigenvalue in the three-dimensional system was observed under each gate voltage condition. The table 4 summarizes the hole concentrations at the time of occurrence of the inflection point in the energy eigenvalue function of heavy holes and light holes at each gate voltage.

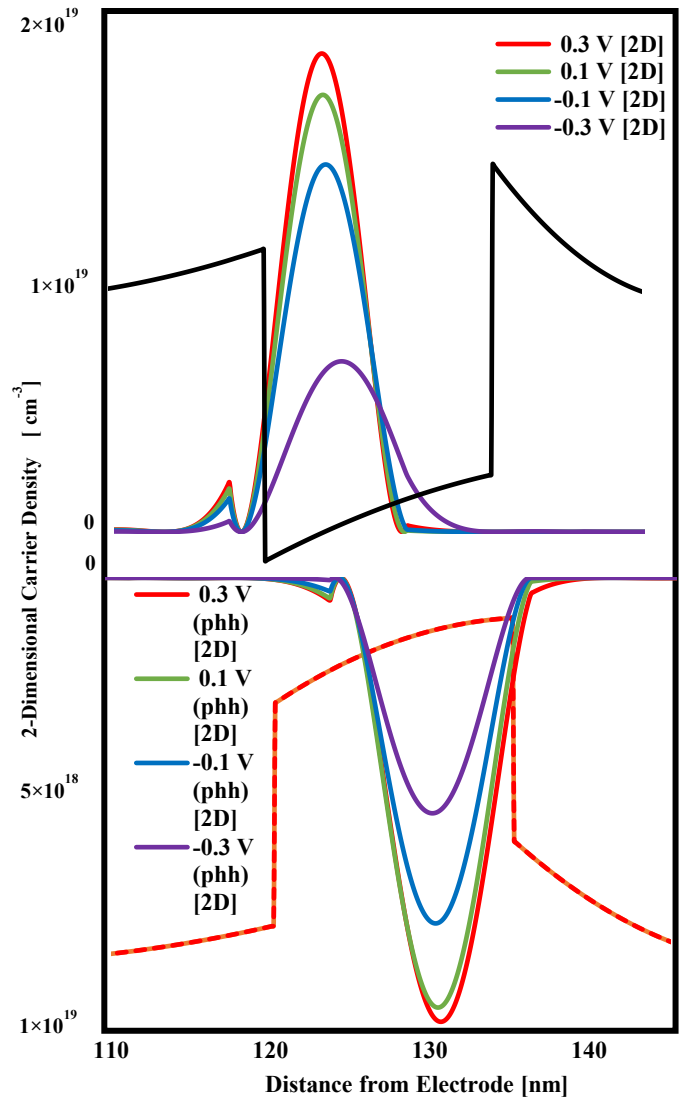


Figure 8: The carrier distribution for each gate voltage

Table 3: The electron concentration at the time of occurrence of the inflection point in the electron energy eigenvalue function at each gate voltage.

Gate Voltage [V]	Simulated Result (Inflection Point) [cm <sup>-2</sup> ]	Electron sheet Density (IV Characteristic) [cm <sup>-2</sup> ]
0.3	1.576 × 10 <sup>12</sup>	1.580 × 10 <sup>12</sup>
0.2	1.541 × 10 <sup>12</sup>	1.552 × 10 <sup>12</sup>
0.1	1.458 × 10 <sup>12</sup>	1.475 × 10 <sup>12</sup>
0	1.424 × 10 <sup>12</sup>	1.429 × 10 <sup>12</sup>
-0.1	1.260 × 10 <sup>12</sup>	1.271 × 10 <sup>12</sup>
-0.2	1.047 × 10 <sup>12</sup>	1.089 × 10 <sup>12</sup>
-0.3	7.271 × 10 <sup>11</sup>	7.142 × 10 <sup>11</sup>

Table 4: Summarizes the hole concentrations at the time of occurrence of the inflection point in the energy eigenvalue function of heavy holes and light holes at each gate voltage.

Gate Voltage [V]	Light Hole (Inflection Point) [cm <sup>-2</sup> ]	Heavy Hole (Inflection Point) [cm <sup>-2</sup> ]	Electron sheet Density (Before Rising current) [cm <sup>-2</sup> ]	Electron sheet Density (Rising current at Peak) [cm <sup>-2</sup> ]
0.3	2.036 × 10 <sup>12</sup>	4.103 × 10 <sup>12</sup>	1.580 × 10 <sup>12</sup>	2.485 × 10 <sup>12</sup>
0.2	1.749 × 10 <sup>12</sup>	3.916 × 10 <sup>12</sup>	1.552 × 10 <sup>12</sup>	2.481 × 10 <sup>12</sup>
0.1	1.577 × 10 <sup>12</sup>	3.725 × 10 <sup>12</sup>	1.475 × 10 <sup>12</sup>	2.421 × 10 <sup>12</sup>
0	1.534 × 10 <sup>12</sup>	3.590 × 10 <sup>12</sup>	1.429 × 10 <sup>12</sup>	2.275 × 10 <sup>12</sup>
-0.1	1.331 × 10 <sup>12</sup>	3.387 × 10 <sup>12</sup>	1.271 × 10 <sup>12</sup>	1.981 × 10 <sup>12</sup>
-0.2	1.140 × 10 <sup>12</sup>	3.168 × 10 <sup>12</sup>	1.089 × 10 <sup>12</sup>	1.811 × 10 <sup>12</sup>
-0.3	7.410 × 10 <sup>11</sup>	2.906 × 10 <sup>12</sup>	7.142 × 10 <sup>11</sup>	1.531 × 10 <sup>12</sup>

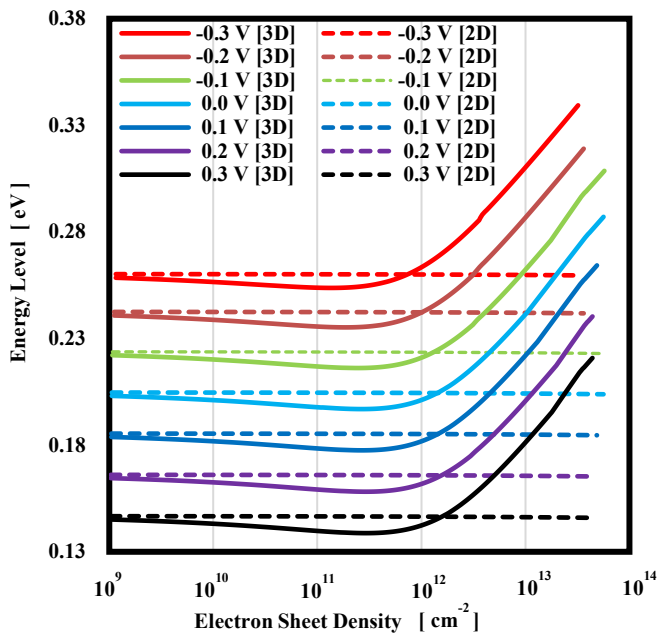


Figure 9: The dependence of the energy eigenvalue with the number of electrons on the gate voltage.

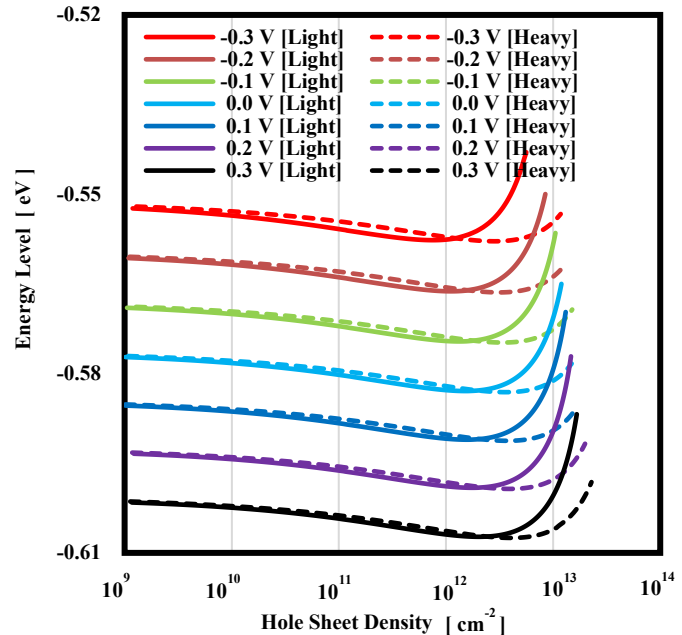


Figure 10: The energy eigenvalue with respect to the gate voltage in the hole system.

## 4. Discussions

### 4.1 The shape of Potential

From the simulation results, it was confirmed that the shape of the potential changes with respect to the gate voltage. These results suggest that the change in the Fermi level is related to the factors that cause the shape of the potential with respect to the gate voltage condition [23].

In the HEMT structure, the Fermi level of the metal electrode matches the Fermi level of the barrier layer material due to the Schottky junction between the metal electrode and the barrier layer material. Thereby, the difference between the work function and the electric affinity was formed as a Schottky barrier, and a hetero junction was established.

The gate electrode also has a Schottky junction with the barrier layer. The Fermi level of the metal electrode changes due to the minority carriers generated when a gate voltage was applied. As a result, it was considered that a potential shape change had occurred. The heterostructure was formed by a thermal

equilibrium state. This means that the Fermi levels for each material and the metal electrode were the same, and the potential shape must have continuity [24]. The application of the gate voltage causes a change in the Fermi level on the metal electrode side and changes the Schottky barrier. In the process of changing to the non-equilibrium state, the potential in the barrier layer changes to satisfy the equilibrium state to maintain continuity. The potential shapes of the doping layer and the spacer layer, which were continuous layers, were changed accordingly.

In this simulation, the Fermi level in the device was defined using pseudo Fermi level. Therefore, it was impossible to discuss the change of Fermi level in detail. However, it is true that each energy eigen value changes with the change of the potential shape. It means that when the energy states in the device are changed, it should also cause change in the Fermi level.

### 4.2 The changes of Energy level

#### 1) In the electron system

The energy eigen value of the electron system changed from showing a decreasing tendency to an increasing tendency at a

certain number of electrons. The above result suggests that in the process of forming 2DEG, the inflection point of this energy eigenvalue changes the electronic state from three-dimensional to two-dimensional.

Electrons in the channel layer try to select an energy state at a given energy level as a solution [25]. In the system simulated this time, it is an exchange correlation potential function treated as another particle system instead of one particle system. The interpretation of the obtained energy level is the minimum energy state that the electron can take. In this case, electrons have to occupy the ground level, having a low energy and most stable; it will be arranged on the reciprocal lattice point corresponding to the ground level around the energy. As a result, the electron-electron spacing becomes uniform, and the interaction between the electrons decreases. Then, it was considered that the energy value of the electrons tends to decrease. On the other hand, when the number of electrons supplied to the channel layer gradually increases, the number of electrons that can be arranged at the reciprocal lattice point around the ground level exceeds at a certain moment; the electron level starts to degenerate. As a result, the electron-electron spacing becomes non-uniform, thus the interaction between electrons is considered to increase. The results of this simulation suggest that the peak value of the number of electrons observed in the IV characteristics was due to the formation of 2DEG in the channel layer.

## *II) In the hole system*

It is considered that the inflection point occurs in the hole system due to the occurrence of the same phenomenon as in the electron system as described above. In this case, in the hole system, the number of holes generated in light holes and heavy holes was completely different. In the hole system, as in the electron system, the change to a two-dimensional system due to the degeneracy process is manifested by the presence of a two-dimensional hole gas (2DHG) [26], [27]. As a result of this simulation, the inflection point of the energy eigenvalue of light holes is generated during the onset of the IV characteristic (figure 1). From the results of the IV characteristics, a decrease in the drain current due to light irradiation at the forward bias can be confirmed. The current value temporarily increases due to light irradiation. However, the amount of current decrease after the IV characteristic peak value has decreased significantly as the light irradiation intensity increases. After reaching the IV characteristic peak value, the recombination ratio of electrons and holes increases. Therefore, it is suggested that the formation of 2DEG and the formation of 2DHG in the hole system promoted the recombination rate.

## **5. Conclusions**

In this study, a theoretical simulation by the Schrodinger-Poisson method was performed to elucidate the formation factors of two-dimensional electron gas in InGaAs-based HEMTs. No significant change was observed in the carrier density and the potential shape. For the change in the number of carriers in the channel layer, the inflection point of the energy level and the agreement of the energy level in each dimension were found. It was found that the number of electrons at this coincidence point almost coincided with the number of electrons in the IV characteristics measured by the previous research for each gate voltage. The change in carrier state suggested that a 2DEG was formed. In addition, considering the transport of carriers on the

crystal lattice plane as a cause of the inflection point of the energy level, it was suggested that it might be caused by the occurrence of the degeneracy process at a certain moment. From these results, it was experimentally and theoretically shown that the formation of 2DEG was caused by carrier degeneration and state change.

## **Conflict of Interest**

The authors declare no conflict of interest.

## **Acknowledgment**

The authors are grateful to the Chukyo University Research Found for financial assistance with this research.

## **References**

- [1] Fathimulla, A., Abrahams, J., Loughran, T., Hier, H., 1988. High-performance InAlAs/InGaAs HEMTs and MESFETs. *IEEE Electron Device Lett.* 9 (7), 328 – 330. DOI: 10.1109/55.733
- [2] Behet, M., Van der Zanden, K., Borghs, G., 1998. Metamorphic InGaAs/InAlAs quantum well structures grown on GaAs substrates for high electron mobility transistor applications. *Appl. Phys. Lett.* 73, 2760. <https://doi.org/10.1063/1.122582>
- [3] Malmkvist, M., Wang, S., Grahn, J. V., 2008. Epitaxial Optimization of 130-nm Gate-Length InGaAs/InAlAs/InP HEMTs for High-Frequency Applications. *IEEE T. Electron Dev.* 55 (1), 268 – 275, 2008. DOI: 10.1109/TED.2007.910613
- [4] Newson, D.J., Merrett, R.P., Ridley, B.K., 1991. Control of gate leakage in InAlAs/InGaAs HEMTs. *Electron. Lett.* 27 (17), 1592 – 1593. DOI: 10.1049/el:19910996
- [5] Rathi, S., Jogi, J., Gupta, M., Gupta, R.S., 2009. Modeling of hetero-interface potential and threshold voltage for tied and separate nanoscale InAlAs-InGaAs symmetric double-gate HEMT. *Microelectron. Reliab.* 49 (12), 1508-1514. [doi.org/10.1016/j.microrel.2009.07.044](https://doi.org/10.1016/j.microrel.2009.07.044)
- [6] Thome, F., Massler, H., Wagner, S., Leuther, A., Kallfass, I., Schlechtweg, M., Ambacher, O. Comparison of two W-band low-noise amplifier MMICs with ultra-low power consumption based on 50nm InGaAs mHEMT technology. 2013 IEEE MTT-S International Microwave Symposium Digest (MTT). SEATTLE, WA, USA. DOI: 10.1109/MWSYM.2013.6697362
- [7] Schlee, J., Rodilla, H., Wadefalk N., Nilsson P.Å., Grahn J., 2014. Cryogenic noise performance of InGaAs/InAlAs HEMTs grown on InP and GaAs substrate. *Solid State Electron.* 91, 74-77. [doi.org/10.1016/j.sse.2013.10.004](https://doi.org/10.1016/j.sse.2013.10.004)
- [8] Duh, K.H.G., Chao, P.C., Ho, P., Tessmer, A., Liu, S.M.J., Kao, M.Y., Smith, P.M. Ballingall, J.M. W-band InGaAs HEMT low noise amplifiers, 1990. IEEE International Digest on Microwave Symposium. Dallas Convention Center, Dallas, Texas, USA, IEEE, DOI: 10.1109/MWSYM.1990.99650
- [9] Xu H., Sanabria C., Chini A., Keller S., Mishra U.K., York, R.A., 2004. A C-band high-dynamic range GaN HEMT low-noise amplifier. *IEEE Microw. Wirel. Co.* 14 (6), 262-264. DOI: 10.1109/LMWC.2004.828020
- [10] Yan, T., Zhang, T., Li, P., Zhang, S., 2018. Study of microwave damage effect on HEMT low noise amplifier under different drain voltage bias. *Microelectron. Reliab.* 82, 228-234. [doi.org/10.1016/j.microrel.2017.10.028](https://doi.org/10.1016/j.microrel.2017.10.028)
- [11] Zhou, J.R., Ferry, D.K., 1993. Modeling of quantum effects in ultrasmall HEMT devices. *IEEE T. Electron Dev.* 40(2), 421 – 427. DOI: 10.1109/16.182523
- [12] Krokidis, G., Xanthakis, J.P., Uzunoglu, N.K., 2008. A fully 2-dimensional, quantum mechanical calculation of short-channel and drain induced barrier lowering effects in HEMTs. *Solid State Electron.* 52 (5), 625-631. [doi.org/10.1016/j.sse.2007.10.021](https://doi.org/10.1016/j.sse.2007.10.021)
- [13] Taguchi, H., Kawaguchi, M., Hayakawa, M., Nakamura, Y., Iida, T., Takanashi, Y., 2006. Frequency Dependence of Drain Conductance due to Hole Accumulation in InAlAs/InGaAs High Electron Mobility Transistors. *Japan J. Appl. Phys.* 45 (1), 4960-4967. [doi.org/10.1143/JJAP.45.4960](https://doi.org/10.1143/JJAP.45.4960)
- [14] Takanashi Y. "Frequency Dependence of Drain Conductance due to Hole Accumulation in InAlAs/InGaAs High Electron Mobility Transistors", *Japanese Journal of Applied Physics*, Vol. 45, Part 1, pp. 4960-4967, 2006, [doi.org/10.1143/JJAP.45.4960](https://doi.org/10.1143/JJAP.45.4960)

- [15] Taguchi H., Murakami H., Oura M., Iida T., Takanashi T., Analysis of Deviation of Threshold Voltage from Hole Accumulation Model at High Excitation, 2006, *Jpn. J Appl. Phys.* 45, 8549-8556. doi.org/10.1143/JJAP.45.8549.
- [16] Takagi I., Tanabe H., Taguchi H., Analysis of the low-electron-density state of a channel layer in InGaAs High electron mobility transistors, Proceedings of International Symposium on Engineering and Applied Science, Legian Bali, Kuta, Indonesia, 238-249, 2019.
- [17] Lyumkis E., Mickevicius R., Penzin O., Polsky B., Sayed E. K., Wettstein A., Fichtner W., Simulations of quantum transport in HEMT using density gradient model, 24th Annual Technical Digest Gallium Arsenide Integrated Circuit (GaAs IC) Symposium, Monterey, California, USA, IEEE. doi: 10.1109/GAAS.2002.1049067.
- [18] Lin L. D., Ping Y. Z., 2006. Self-consistent analysis of double- $\delta$ -doped InAlAs/InGaAs/InP HEMTs. *Chin. Phys.* 15, 2735-2741, doi.org/10.1088/1009-1963/15/11/046.
- [19] Neophytou N., Rakshit T., Lundstrom S. M., 2009. Performance analysis of 60-nm Gate-Length III-V InGaAs HEMTs: simulations versus experiments, *IEEE Transact Electron Devices*, 56, 7, 1377-1387. doi: 10.1109/TED.2009.2021437.
- [20] Verma N., Gupta M., Gupta R.S., Jogi J., 2013. Quantum modeling of nanoscale symmetric double-gate InAlAs/InGaAs/InP HEMT, *JOURNAL OF SEMICONDUCTOR TECHNOLOGY AND SCIENCE*, 13, 4, 342-354. doi.org/10.5573/JSTS.2013.13.4.342
- [21] Said T., Kelsall R. Pilgrim N., 2006. Simulation of electron transport in InGaAs/AlGaAs HEMTs using an electrothermal Monte Carlo Method, *IEEE Transact. Electron Devices*. 53, 8, 1768-1774, 2006. doi: 10.1109/TED.2006.877698
- [22] Roy M., Gurman S. J., 2001. An investigation of the use of the Hedin-Lundqvist exchange and correlation potential in EXAFS data analysis. *J. Synchrotron Rad.* 8, 1095-1102. doi.org/10.1107/S0909049501006434.
- [23] Nayak C., Simon H. S., Stern A., Freedman M., Sarma D.S., 2008. Non-Abelian anyons and topological quantum computation. *Rev. Mod. Phys.* 80, 1083-1090. doi.org/10.1103/RevModPhys.80.1083
- [24] Taguchi H., Sato T., Oura M., Iida T., Takanashi Y., 2008. Dependence of carrier lifetime of InAlAs/InGaAs high-electron-mobility transistors on gate-to-source voltage. *Jpn. J Appl. Phys.* 47, 4S, 2858-2862. doi.org/10.1143/JJAP.47.2858.
- [25] Krantz J. R., Mayer C. D., Bloss L. W., 1990. The influence of Fermi-level pinning at the GaAs substrate on HEMT threshold voltage. *Solid-State Electron.* 33, 9, 1189-1195. doi.org/10.1016/0038-1101(90)90098-Y.
- [26] Yoshida H., Mozume T., Nishimura T., Wada O., 1998. Intersubband transitions in InGaAs/AlAs coupled double quantum well structures for multi-wavelength all-optical switching. *Electron. Lett.* 34, 9, 913-915. doi: 10.1049/el:19980605.
- [27] Shina S.H., Park Y.H., Koob H.C., Songa Y.H., Song J.D., 2017. GaSb/InGaAs 2-dimensional hole gas grown on InP substrate for III-V CMOS applications, *Curr. Appl. Phys.* 17, 7, 1005-1008. doi.org/10.1016/j.cap.2017.03.018.



# HDR Image Tone Mapping Approach Using Multiresolution and Piecewise Linear Perceptual Quantization

Quoc Thai Pham, Ba Chien Thai \*

The University of Danang, University of Science and Technology, 54 Nguyen Luong Bang Street, Danang city, Vietnam

## ARTICLE INFO

Article history:

Received: 07 January, 2020

Accepted: 03 April, 2020

Online: 16 April, 2020

Keywords:

High Dynamic Range

Low Dynamic Range

Tone Mapping Operators

Multiresolution

Contrast Enhancement

Human Visual System

Tone Mapped Quality Index

## ABSTRACT

This paper discusses a new Tone Mapping (TM) approach converting a High Dynamic Range (HDR) image into a Low Dynamic Range (LDR) image able at the same time to extract the relevant details and enhance the contrast of LDR images to ensure a good LDR image visual quality. This approach uses an advantage of multiresolution and piecewise linear perceptual quantization. While multiresolution part at each resolution level extracts much more detail information from HDR image to become a LDR coarse image, perceptual quantizer part adjusts the LDR coarse by the pixel's distribution using a piecewise linear function so that the final LDR image can be visualized near human visual system. Simulation results provide good results, both in terms of visual quality and TMQI metric, compared to existing competitive TM approaches.

## 1 Introduction

High Dynamic Range (HDR) image Tone Mapping (TM) is an interesting subject. The objective is to find a trade-off between the relevant information such as details, contrast, brightness... to be preserved or discarded in the image ensuring a good visual quality of the displayed image on Low Dynamic Range (LDR) devices that would be appreciated by observers.

Three e-books in [1], [2] and [3] fairly describe a state of the art on HDR image TM approaches. This paper just quickly reviews the developed TM strategies that caught our attention because of their performance. In [4], the TM approach uses an edge-preserving bilateral filter to decompose the HDR image into two layers: a base layer encoding large-scale variations and a detail one. Contrast is then reduced only in the first layer while the details are kept unchanged. This TM reduces the HDR contrast while preserving the image details. In [5], an adaptive logarithmic mapping method of luminance values works with the adjustment of the logarithmic basis depending on the radiance of the pixels. A subband architecture related on an oversampled Haar pyramid representation in [6], is presented. The re-scaling of subband coefficients according to a gain control function reduces the high frequency magnitudes and

boosting low ones. A TM optimization approach with adjusting a histogram between linear mapping and the equalized histogram mapping in [7] is developed. Then revisited histogram equalization approaches are discussed in [8]. The modification of this approach is made with both histogram equalization and human sensitivity to the light function.

A second generation of wavelets based on the edge content of the image avoiding having pixels from both sides of an edge in [9] is proposed. A separable non-linear multiresolution approach based on essentially non-oscillatory interpolation strategy has been investigated in [10]. This work relates to the singularities such as edge points in their mathematical models preserving then the structural information of the HDR images. The results provided in [9], [10] and [11] show that the decomposition of the HDR image on different resolution levels would seem to be a good strategy.

The proposed HDR image TM approach has two main goals namely the preservation of the details that relates to multiresolution and the adjustment of the contrast that relates to perceptual linear adjustment in accordance with the LDR display devices. It is composed of four stages in Figure 1. The first one judiciously decomposes the HDR image into different subbands (section 2.1). The second one concerns the weighting strategy of the subband

\*Corresponding Author Name: Ba Chien Thai. Address: The University of Danang, University of Science and Technology, 54 Nguyen Luong Bang Street, Danang city, Vietnam. Contact No: (+84)867992782 & Email: tbchien@dut.udn.vn

coefficients (section 2.2). The third one reconstructs the coarse LDR image (section 2.3). Finally the fourth one adjusts the contrast according to a perceptual linear quantizer (section 2.4). Section 3 discusses the simulation results. Section 4 concludes the paper.

## 2 Proposed HDR image tone mapping approach

This section concerns four stages of the proposed HDR image TM mapping approach such as decomposition, weighting, reconstruction and contrast adjustment stages.

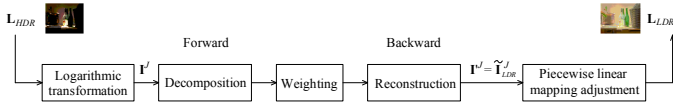


Figure 1: Diagram block of the proposed HDR image TM algorithm.

Let introduce some notations. Assume that size  $N^J \times M^J$  is the original HDR image at the finest resolution level  $J$ . Define the index  $j$  which refers to the resolution level with  $j = 0, \dots, J - 1$ . Denote  $l_{HDR}$  the HDR image luminance. In the rest of this paper, the HDR image luminance is considered in the logarithm domain since it is well adapted to the human visual system. It is denoted  $I^j$  and defined as follows  $I^j = \{I^j(x_n, y_m) = \log_{10}(l_{HDR}(x_n, y_m))\}$  where  $1 \leq n \leq N^j$  and  $1 \leq m \leq M^j$ . Hence  $I^j(x_n, y_m)$  is the HDR logarithm luminance value of the pixel located at position  $(x_n, y_m)$  on the image.

### 2.1 First stage: HDR image multiscale decomposition

The decomposition of the HDR image consists to go from the finest resolution level  $J$  to the coarsest resolution level 1. At a given resolution level  $j$  (with  $1 \leq j \leq J$ ), the algorithm deals with the approximation coefficients denoted  $I^j(x_n, y_k)$  (with  $1 \leq n \leq N^j$  and  $1 \leq k \leq M^j$ ) computed at resolution level  $j$ . The approximation resolution level  $I^j(x_n, y_m)$  is divided into 4 blocks  $I^j := (I^{j-1}, d_{HL}^{j-1}, d_{LH}^{j-1}, d_{HH}^{j-1})$  (with  $LL$  is Low Low,  $LH$  Low High,  $HL$  High Low and  $HH$  High High) which saves into a non-redundant way. The decomposition is thus iterated on  $I^{j-1}$  until  $j = 1$ . The original HDR image  $I^J$  is then represented by  $3J + 1$  subbands or resolution levels  $I^J := (I^0, d_{HL}^0, d_{LH}^0, d_{HH}^0, \dots, d_{HL}^{J-1}, d_{LH}^{J-1}, d_{HH}^{J-1})$ .

### 2.2 Second stage: Weighting strategy of the subband coefficients

In order to reduce the dynamic range of the HDR image, the TM approach proposes to weight the approximation and detail coefficients in an appropriate way before performing the adaptive lifting scheme backward process described in section 2.3.

Denote  $N_l$  the number of resolution levels equal to  $J$ ;  $E_a$  the entropy of the approximation coefficients at the coarsest resolution level ( $j = 1$ ); and  $E_d^j$  the entropy of the detail coefficients at resolution level  $j$  (such as  $d_{HL}^j, d_{LH}^j$  and  $d_{HH}^j$ ) getting therefore  $N_l + 1$

entropies ( $E_a, E_d^0, E_d^1, \dots, E_d^{j-1}, \dots, E_d^{N_l-1}$ ). From these entropies, positive weights smaller than one are deduced as follows:

$$\begin{cases} \alpha_a = \frac{\sum_{i=1}^{N_l} E_d^i}{E_a + \sum_{i=1}^{N_l} E_d^i} \text{ for } j = 1 \\ \alpha_d^j = \frac{E_a + \sum_{i=1, i \neq j}^{N_l} E_d^i}{E_a + \sum_{i=1}^{N_l} E_d^i} \text{ for } j = 1, \dots, N_l \end{cases} \quad (1)$$

$\alpha_a$  (respectively  $\alpha_d^j$ ) is the weight associated to the approximation (respectively detail) coefficients at resolution level  $j = 1$  (respectively  $j$ ).

The coefficients of the four coarsest resolution levels are first modified according to:

$$\begin{aligned} I^0 &= \alpha_a \times I^0, & d_{HL}^0 &= \alpha_d^0 \times d_{HL}^0, \\ d_{LH}^0 &= \alpha_d^0 \times d_{LH}^0, & d_{HH}^0 &= \alpha_d^0 \times d_{HH}^0. \end{aligned} \quad (2)$$

The approximation subband, denoted  $I^1$ , is then reconstructed (see section 2.3) and the number of levels is reduced to  $N_l - 1$ . The  $N_l$  entropies (associated to  $3N_l - 2$  subbands) are calculated again to update the weights  $\alpha_a, \alpha_d^j$  (equation (1) with  $N_l = N_l - 1$ ). After that, these weights are applied on the coefficients  $I^1, d_{HL}^1, d_{LH}^1, d_{HH}^1$  to build  $I^2$  as explained above. This process is iterated until  $N_l = 1$  to reconstruct the coarse tone mapped HDR image denoted  $\tilde{I}_{LDR}^J$ , called coarse LDR image.

### 2.3 Third stage: Reconstruction of the coarse LDR image

The reconstruction is worked inversely to the decomposition stage. Assume at the resolution levels  $j-1$ , the next step consists to recover the approximation coefficients  $I^j$  of size  $N^j \times M^j$  using 4 weighted blocks  $I^{j-1}, d_{LH}^{j-1}, d_{HL}^{j-1}$  and  $d_{HH}^{j-1}$ . The reconstruction is iterated to finally build the image  $I^J$  later called coarse LDR image which is denoted  $\tilde{I}_{LDR}^J$ .

### 2.4 Fourth stage: Piecewise linear perceptual quantizer

To enhance the contrast, this stage proposes to adjust locally the distribution of the coarse LDR image logarithm luminance  $\tilde{I}_{LDR}^J$  according to the HVS using a piecewise linear function. The  $\tilde{I}_{LDR}^J$  values are first sorted and statistically classified into equal  $B$  bins defined by cutting points denoted  $c_{uLDR}^i$ . A non-uniform histogram equalization is also performed with  $c_{nuLDR}^i$  cutting points with  $1 \leq i \leq B$ . The lower bound (cutting point) of each bin is then adjusted as follows:

$$\tilde{I}_{LDR}^J(1) = \beta(c_{nuLDR}^i - c_{uLDR}^i) + c_{uLDR}^i, \quad (3)$$

where  $\beta$  is a positive parameter smaller than 1.

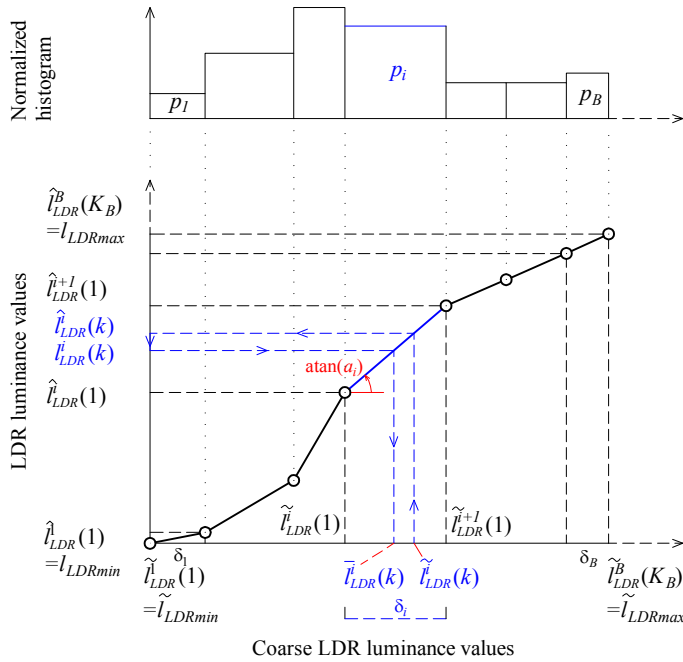


Figure 2: Piecewise linear modelization ("s-shaped" curve).

Therefore the  $\tilde{l}_{LDR}^j$  values are classified into non-uniform  $B$  bins as follows:

$$\tilde{l}_{LDR}^j = \{\tilde{l}_{LDR}^j(k) \text{ for } k = 1, \dots, N^j \times M^j\} \quad (4)$$

$$\begin{cases} [\tilde{l}_{LDR}^j(1), \dots, \tilde{l}_{LDR}^j(K_1)] & \text{for bin 1,} \\ [\tilde{l}_{LDR}^j(1), \dots, \tilde{l}_{LDR}^j(K_2)] & \text{for bin 2,} \\ \dots & \\ [\tilde{l}_{LDR}^j(1), \dots, \tilde{l}_{LDR}^j(K_i)] & \text{for bin } i, \\ \dots & \\ [\tilde{l}_{LDR}^j(1), \dots, \tilde{l}_{LDR}^j(K_B)] & \text{for bin } B. \end{cases}$$

where  $K_i$  is the number of values in the  $i$ -th bin (with  $1 \leq i \leq B$ ;  $K_i > 0$ ) and satisfying the following relation  $\sum_{i=1}^B K_i = N^j \times M^j$ .

The "s-shaped" TM perceptual curve, as discussed in [12] and [13], is modelled by a piecewise linear curve on each bin (see Figure 2). Consider the  $i$ -th bin, defined by  $[\tilde{l}_{LDR}^j(1), \dots, \tilde{l}_{LDR}^j(K_i)]$ , the coarse LDR values are then modeled as follows:

$$\hat{l}_{LDR}^j(k) = a^i \tilde{l}_{LDR}^j(k) + b^i \text{ with } k \in [1, K_i], \quad (5)$$

The parameter  $a^i$  is unknown and deduced so that the norm- $M$  space error between the HDR value and its quantized version (denoted  $\tilde{l}_{LDR}^j(k)$ ) is minimized in the  $i$ -th bin:

$$\arg \min_{a^i} \|\tilde{l}_{LDR}^j(k) - \hat{l}_{LDR}^j(k)\|_M^M, \quad \text{with } M \geq 1. \quad (6)$$

This equation is rewritten as follows:

$$\arg \min_{a^i} \sum_{k=1}^{K_i} \left| \frac{\tilde{l}_{LDR}^j(k) - \hat{l}_{LDR}^j(k)}{a^i} \right|^M \cdot p_i, \quad (7)$$

where  $p_i = \frac{K_i}{\sum_{i=1}^B K_i}$ .

Extending equation (7) to all bins involves the computation of a global norm- $M$  space error  $\Psi$  deduced as follows:

$$\Psi = \sum_{i=1}^B \sum_{k=1}^{K_i} \left| \frac{\tilde{l}_{LDR}^j(k) - \hat{l}_{LDR}^j(k)}{a^i} \right|^M \cdot p_i. \quad (8)$$

The expected value  $\sum_{k=1}^{K_i} |\tilde{l}_{LDR}^j(k) - \hat{l}_{LDR}^j(k)|^M = \xi$ . Equation (8) is then simplified and becomes:

$$\Psi = \sum_{i=1}^B \frac{p_i}{(a^i)^M} \cdot \xi, \quad \text{with } a^i > 0. \quad (9)$$

Denote  $l_{LDRmin}$  (respectively  $l_{LDRmax}$ ) the minimum (respectively maximum) LDR luminance value. Introduce  $\delta^i$  as the interval between HDR luminance in two consecutive bins:

$$\delta^i = \tilde{l}_{HDR}^{i+1}(1) - \tilde{l}_{HDR}^i(1). \quad (10)$$

A constraint results in:

$$\sum_{i=1}^B a^i \cdot \delta^i = l_{LDRmax} - l_{LDRmin}. \quad (11)$$

Therefore the optimization problem is written as follows:

$$\arg \min_{a^i} \sum_{i=1}^B \frac{p_i}{(a^i)^M} \cdot \xi, \quad \text{s.t.} \quad \sum_{i=1}^B a^i \cdot \delta^i = l_{LDRmax} - l_{LDRmin}. \quad (12)$$

Solving analytically using the Lagrangian function, the slope  $a^i$  is deduced:

$$a^i = \frac{(l_{LDRmax} - l_{LDRmin}) \cdot (p_i)^{1/(M+1)}}{\sum_{i=1}^B \delta^i \cdot (p_i)^{1/(M+1)}}. \quad (13)$$

Therefore the unknown parameter  $b^i$  is calculated as follows:  $b^i = \tilde{l}_{LDR}^i(1) - a^i \times \tilde{l}_{HDR}^i(1)$  and LDR mapped values are deduced according to equation (5).

### 3 Simulation results

This section provides the performance of the proposed tone mapped HDR image. Simulations have been conducted under Matlab environment using the HDR Toolbox ([1]) with 300 test HDR images. The tone mapped image quality is measured with the TMQI (Tone-Mapped image Quality Index) metric [14]. For lack of space, we only present the results obtained with 8 HDR images ("Anturium", "Small Bottle", "Small Office", "Oxford Church", "Memorial", "Light", "Ward Flowers" and "Street Lamp") with different dynamic range (or contrast ratio) from 8.7 f-stops to 18.4 f-stops.

The proposed approach is compared to: (i) Li TMO [6] with Haar multiscale; (ii) Duan [7] using  $\beta = 0.5$ ; (iii) Fattal [9] using RBW method with parameters  $\alpha = 0.8$ ,  $\beta = 0.3$ ,  $\gamma = 0.8$ ; (iv) SEP ENO-CA [10] with parameters  $\alpha_1 = 0.3$ ,  $\alpha_2 = 0.7$ ; (ii) NONSEP ENO-CA [11]; (v) TMOs in HDR Toolbox: Durand [4], Drago [5], Reinhard [15], Ward [16], Tumblin [17], Schlick [18] with the default parameters as given in the HDR Toolbox. The different parameters are chosen so as to give the best results in terms of TMQI metric in all methods.

Table 1 provides the TMQI metrics. The proposed TM approach namely "Proposed\_LJ" is deployed with Biorthogonal 2.2 wavelet (bior2.2) properties,  $B = 256$ ,  $M = 2$ ,  $\beta = 0.25$ ,  $l_{LDRmax} = 255$ ,  $l_{LDRmin} = 0$  and  $J = 1, \dots, 5$ . Our approach is competitive to those



developed in the literature. More the number of resolution levels increase, more the performance increase.

Figure 3 compares the visual quality of the "Oxford Church" tone mapped image using "Duan" method and our approach. The stained glass window at the church background presents a better contrast and details with our approach although the TQMI are identical. Figure 4 compares the "Memorial" tone mapped image using "Duan" and "Fattal" methods and our approach. The details on tills (see Figure 4) and rosette (see Figure 5) are better rendered by our approach.

Figure 6 compares the visual quality of the "Ward Flowers" tone mapped image using "Fattal" and our approach. Some details, on flowers and rocks, are lost on "Fattal" tone mapped image compared to our approach. Moreover, our tone mapped image is of better contrast. A similar result is provided by Figure 7 where the HDR "Street Lamp" image has been mapped using "SEP\_ENO" method and our method. The brightness of our tone mapped is better.

Figure 8 compares the visual quality of the "small office" tone mapped image using "Duan", "Fattal", "Li" and our approach. Compared to other tone mapped images, "Li" tone mapped image doesn't seem to be natural. Indeed its normalized histogram given in Figure 9 shows that the pixel grey levels are limited to 60. Some of the details from outside the office (via the window) are lost on "Fattal" tone mapped image (brightness) contrary to our approach and

"Duan" method. Indeed the brightness on "Fattal" tone mapped image is confirmed by the pic corresponding to a grey level equal to 255 on its normalized histogram (see Figure 9). However "Duan" tone mapped image is a little darker (armchair, office wall) than our tone mapped image. This analysis is well supported by the normalized histograms of our approach and Duan method. The comparison of the histograms proves that our strategy stretches the too-dark areas and suppresses the too-bright areas.

The performance of our approach is confirmed on more than 300 test HDR images where the details and contrast are better represented than other competitive methods.

## 4 Conclusion

This paper proposed a new HDR image TM approach while preserving as much information of the HDR image as possible. This is essentially related to : (i) the weighting operation depending on the information of each subband; (ii) the adjustment of the coarse LDR image luminance distribution according to the perceptual piecewise linear function. Simulation results confirm the relevance of the proposed approach both in terms of the TMQI metric and the visual quality of the displayed image. These are results related to the advantage of using multiresolution and piecewise linear perceptual quantization.



Figure 3: "Oxford Church" HDR test image (15.5 f-stops) - Up image: proposed (5 levels, TMQI=0.986); Down image: "Duan" (TMQI=0.987).





Figure 4: "Memorial" HDR test image (18.4 f-stops) - Left image: proposed (5 levels, TMQI=0.952); Middle image: "Duan" (TMQI=0.936); Right image: "Fattal" (TMQI=0.928).

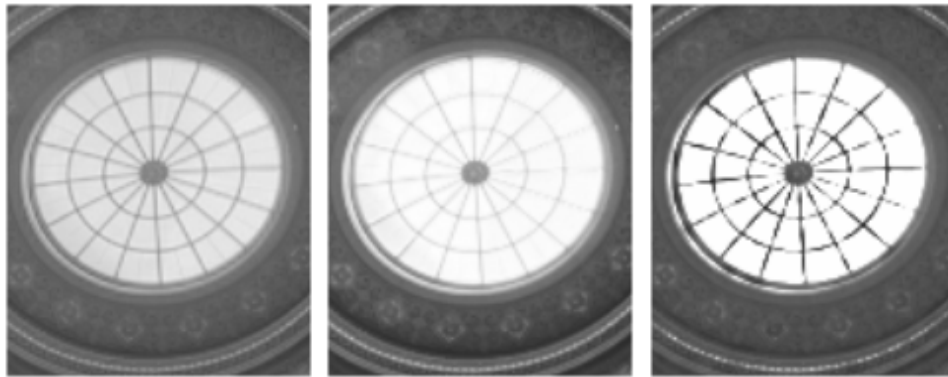


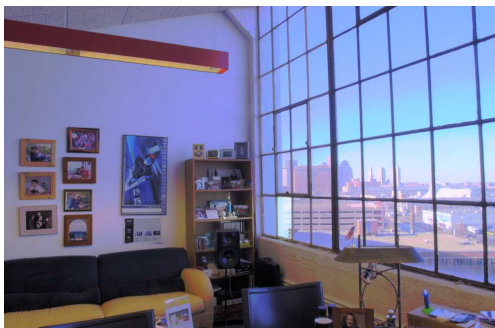
Figure 5: LDR luminance "Rosette" zoom - Left image: proposed (5 levels, TMQI=0.952); Middle image: "Duan" (TMQI=0.936); Right image: "Fattal" (TMQI=0.928).



Figure 6: "Ward Flowers" HDR test image (14.0 f-stops) - Up image: proposed (5 levels, TMQI=0.931); Down image: "Fattal" (TMQI=0.876).



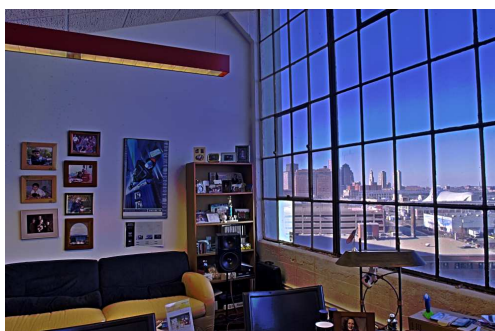
Figure 7: "Street Lamp" HDR test image (13.8 f-stops) - Up image: proposed (5 levels, TMQI=0.912); Down image: "SEP\_ENO" (TMQI=0.856).



(a) Proposed (0.949)



(b) Fattal (0.944)



(c) Li (0.855)



(d) Duan (0.956)

Figure 8: "Small Office" HDR tone mapped images.



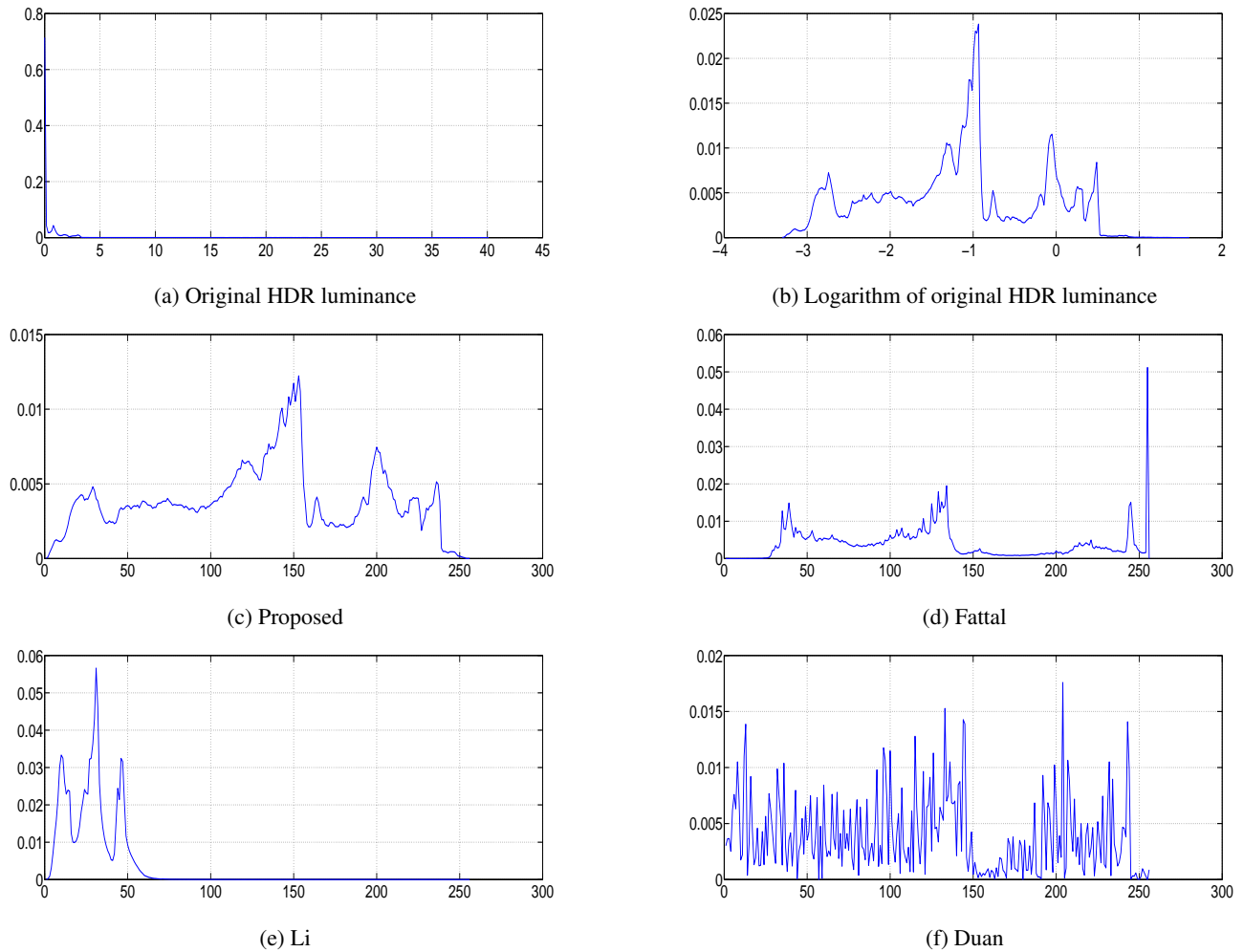


Figure 9: Normalized histograms of original "Small Office" HDR luminance and its tone mapped images.

Table 1: Tone Mapped Image Quality Index (TMQI)

TMOs/HDRi	Anturium	Small Bottle	Small Office	Oxford Church	Memorial	Light
DR (f-stops)	8.7	16.1	16.3	15.5	18.4	17.5
Durand [4]	0.812	0.893	0.826	0.930	0.815	0.801
Drago [5]	0.875	0.802	0.801	0.815	0.801	0.801
Li [6]	0.965	<b>0.955</b>	0.855	0.878	0.835	0.889
Duan [7]	<b>0.965</b>	0.917	<b>0.956</b>	<b>0.987</b>	<b>0.936</b>	0.970
Fattal [9]	0.890	0.929	0.944	0.890	0.928	<b>0.972</b>
SEP_ENO [10]	0.897	0.935	0.944	0.896	0.933	0.971
NONSEP [11]	0.939	0.874	0.936	0.821	0.833	0.933
Reinhard [15]	0.779	0.808	0.827	0.790	0.792	0.795
Ward [16]	0.807	0.784	0.776	0.818	0.796	0.790
Tumblin [17]	0.716	0.714	0.736	0.676	0.760	0.751
Schlick [18]	0.771	0.836	0.927	0.971	0.788	0.781
Proposed_L1	0.947	0.864	0.935	0.955	0.919	0.955
Proposed_L2	0.966	0.883	0.939	0.971	0.930	0.964
Proposed_L3	0.979	0.905	0.946	0.982	0.942	0.967
Proposed_L4	0.981	0.922	0.947	0.985	0.950	0.970
Proposed_L5	<b>0.983</b>	<b>0.934</b>	<b>0.949</b>	<b>0.986</b>	<b>0.952</b>	<b>0.970</b>

## Acknowledgment

This research is funded by Funds for Science and Technology Development of the University of Danang under project number B2019-DN02-51.

## References

- [1] Banterle, F., Artusi, A., Debattista, K., and Chalmers, A., "Advanced High Dynamic Range Imaging: Theory and Practice", AK Peters (now CRC Press), ISBN: 978-156881-719-4 (2011).
- [2] Dufaux, F., Le Callet, P., Mantiuk, R., Mrak, M., "High Dynamic Range Video 1st Edition : From Acquisition, to Display and Applications", ISBN: 9780081004128 (April 2016)
- [3] Reinhard, E., Heidrich, Wolfgang., Debevec, Paul., Pattanaik, S., Ward, G., and Myszkowski, K., "High Dynamic Range Imaging 2nd Edition: Acquisition, Display, and Image-Based Lighting", ISBN: 9780123749147 (May 2010).
- [4] Durand, F., and Dorsey, J., "Fast Bilateral Filtering for The Display of High-dynamic-range Images", ACM Transactions on Graphics (TOG) - Proceedings of ACM SIGGRAPH 21, pp. 257-266 (2002).

- [5] Drago, F., Myszkowski, K., Annen, T., and Chiba, N., "Adaptive Logarithmic Mapping for Displaying High Contrast Scenes", *Computer Graphics Forum* 22, pp. 419-426 (2003).
- [6] Li, Y., Sharan, L., and Adelson, E.H., "Compressing and Companding High Dynamic Range Images with Subband Architectures", *ACM Trans. Graph.* 24, pp. 836-844 (July 2005).
- [7] Duan, J., Bressan, M., Dance, C., and Qiu, G., "Tone-mapping High Dynamic Range Images by Novel Histogram Adjustment", *Pattern Recognition*, vol. 43, pp. 1847-1862 (2010).
- [8] Husseis, A., Mokraoui, A., and Matei, B., "Revisited Histogram Equalization as HDR Images Tone Mapping Operators", 17th IEEE International Symposium on Signal Processing and Information Technology, ISSPIT (December 2017).
- [9] Fattal, R., "Edge-Avoiding Wavelets and their Applications", *ACM Trans. Graph* (2009).
- [10] Thai, B.C., Mokraoui, A., and Matei, B., "Performance Evaluation of High Dynamic Range Image Tone Mapping Operators Based on Separable Non-linear Multiresolution Families", 24th European Signal Processing Conference, pp. 1891-1895 (August 2016).
- [11] Thai, B.C., Mokraoui, A., and Matei, B., "Image Tone Mapping Approach Using Essentially Non-Oscillatory Bi-quadratic Interpolations Combined with a Weighting Coefficients Strategy", 17th IEEE International Symposium on Signal Processing and Information Technology, ISSPIT (December 2017).
- [12] Dowling, J. E., "The Retina: An Approachable Part of the Brain", Cambridge, Belknap Press (1987).
- [13] Geisler, W. S., "Effects of Bleaching and Backgrounds on the Flash Response of the Cone System", *Journal of Physiology*, 312:413-434 (1981).
- [14] Yeganeh, H. and Wang, Z., "Objective Quality Assessment of Tone-mapped Images", *IEEE Trans. on Image Processing*, vol. 22, pp. 657-667 (February 2013).
- [15] Reinhard, E., and Devlin, K., "Dynamic Range Reduction Inspired by Photoreceptor Physiology", *IEEE Transactions on Visualization and Computer Graphics* 11, pp. 13-24 (2005).
- [16] Ward, G., Rushmeier, H., and Piatko, C., "A Visibility Matching Tone Reproduction Operator for High Dynamic Range Scenes", *IEEE Transactions on Visualization and Computer Graphics* 3, pp. 291-306 (1997).
- [17] Tumblin, J., and Rushmeier, H., "Tone Reproduction for Realistic Images", *IEEE Comput. Graph. Appl*, pp. 42-48 (1993).
- [18] Schlick, C., "Quantization Techniques for Visualization of High Dynamic Range Pictures", In *Proceeding of the Fifth Eurographics Workshop on Rendering*, pp. 7-18 (1994).



## Determinants of Students' Actual use of the Learning Management System (LMS): An Empirical Analysis of a Research Model

Charles Buabeng-Andoh<sup>\*1</sup>, Charles Baah<sup>2</sup>

<sup>1</sup>University of Education, Winneba, Department of ICT Education, Winneba, Ghana

<sup>2</sup>Pentecost University College, Department of IT, Ghana

### ARTICLE INFO

Article history:

Received: 02 January, 2020

Accepted: 27 March, 2020

Online: 14 April, 2020

Keywords:

Learning Management System  
Unified Theory of Acceptance and Use  
Structural Equation Model

### ABSTRACT

*This study built and tested a research model to determine the determinants that impact students' actual use of the learning management system. A survey questionnaire was used to gather data from 148 university students who used LMS in their course of study. The structural equation model was used to analyze quantitative data. The study revealed that (1) performance expectancy, effort expectancy and institutional support positively impacted students' actual use of LMS, (2) social influence and infrastructure support did not positively impact students' actual use, (3) gender had a significantly moderated effect on the correlation between institutional support and actual usage of technology. This study added to existing studies on the use of UTAUT in explaining students' actual use of technology in developing nations. Implications for practice, drawbacks and future directions are discussed.*

## 1. Introduction

Information technology has caused a series of changes in higher institutions by transforming the previous idea of learning [1]. The LMS is among the evolving technological tools that supports e-learning. LMS is a web-based system that facilitates web-based interaction between teachers and students [2], offers educators and trainers kits to develop and present study materials, check student involvement and assess learner performance, provides students with the means of networking with peers via chat, group conversation and video conferencing [3]. The most common LMS used in schools include Modular Object-Oriented Dynamic Learning Environment (MOODLE), Blackboard, WebCT and Desire2Learn [4]-[5]. Several higher learning institutions have spent millions of dollars in ICT facilities to aid the quality of the instruction process [6]-[7]. However, this capital spending will be useless if students do not accept the system [8]. A meta-analysis of LMS acceptance and use in sub-Saharan Africa (SSA) from 2007-2017 by [9], revealed a lack of research on LMS use in SSA. [9] proposed that further study should be conducted on the determinants of LMS use and acceptance in SSA by adopting the Unified Theory of Acceptance and Use of

Technology (UTAUT) model [9]. Additionally, [9] suggested that a more rigorous numerical analysis such as the structural equation model (SEM) be used to determine the factors that influence LMS usage. Therefore, it is critical to examine the determinants of LMS use and acceptance in SSA, particularly in Ghana.

This present study was conducted at Pentecost University College (PUC). The University College is found in Accra, Ghana, and has 2,500 students and 100 lecturers. In 2012, the University College implemented MOODLE LMS to supplement its standard face-to-face teaching. The MOODLE offers instructors with attributes such as course and user-management tools, discussion forums, quizzes and announcements to support their coaching experience. It also offers support in the management of the e-learning process by storing learners' information organized, making course materials accessible to learners, tracking learners' progress and generating reports, supporting collaboration with learners and providing testing and evaluation tools. It also allows learners to submit assignments. The MOODLE is used to support the teaching and learning process in any subject area. The system supports contents such as text, image, audio, and video to facilitate teaching and learning. Instructors register with the system to use it. After registration, the system validates the instructor's email address, approves it and activates it. Though

<sup>\*</sup>Corresponding Author; Charles Buabeng-Andoh, E-mail [cbandoh@hotmail.com](mailto:cbandoh@hotmail.com)

MOODLE LMS was introduced to deliver online courses to students in the institution, most of the lecturers and students have not adopted the system. Hence, for the successful use of the LMS, it is important to understand the determinants that impact the real usage of the LMS. Studies have revealed that the real implementation of LMS has not been fully studied in SSA nations [9], and even, the scanty studies on LMS have focused on technical issues ignoring inquiries on the determinants that impact users' real application of LMS [10]. These identified gaps have motivated the researchers to research into the determinants that affect the learners' actual application of LMS.

The objectives of this work are in two folds: (1) to explore the determinants that are significant for the use of e-learning system, in precise, the LMS in a Ghanaian university and (2) to build a research model integrating the factors that are directly essential for e-learning usage as well as to determine its efficacy in explaining students' actual use of LMS.

This manuscript is structured as follows: Initially, the theoretical model is described. Second, the new research model is discussed. Third, hypotheses are developed. Fourth, the research method (population, data collection, measures, and data analysis) is described. Fifth, the results of the study are explained. Sixth, the conclusion is drawn. Finally, drawbacks and future studies are discussed.

## 2. Theoretical Framework

### 2.1. The UTAUT

The UTAUT model, [11], is prevalent in studies relating to online learning. As shown in figure 1, the UTAUT model consists of four key constructs that influence the users' use of the technology. These constructs are performance expectancy (PE), effort expectancy (EE), social influence (SI) and facilitating conditions (FC). Additionally, the model consists of four moderating constructs. These are gender, age, experience and voluntariness of use [11]. Regarding the rate of application, UTAUT lags behind Technology Accepted Model (TAM) indicating that for the past decade, UTAUT is yet unpopular in reports in SSA [9]. Furthermore, a current study conducted on the use of technology, revealed that findings from studies using UTAUT might differ in diverse cultural settings [12], hence, it is essential to investigate UTAUT in diverse cultural backgrounds to augment the current literature on UTAUT. Therefore, this study used the UTAUT model to explain the determinants of students' actual use of LMS in universities in SSA.

## 3. The New Research Model

The main variables of the new research model were PE, EE, SI, IC and IS. The moderating variables were gender and age. In the new research model, the FC construct was broken into (1) IC and (2) IS. This is to determine the exact variable of facilitating condition construct which impacts students' actual use of LMS. In the new model, 'actual use' was used as an endogenous variable because of students' real application of LMS. Voluntariness and experience of use variables were excluded as explained by [13]. The introduction of IC, IS and actual use variables differentiate the

new research model from the original UTAUT (see Fig 1). Therefore, IC, IS, PE, EE and SI explain the level of the actual use of students' LMS. The research model for this study is shown in Figure 2 below.

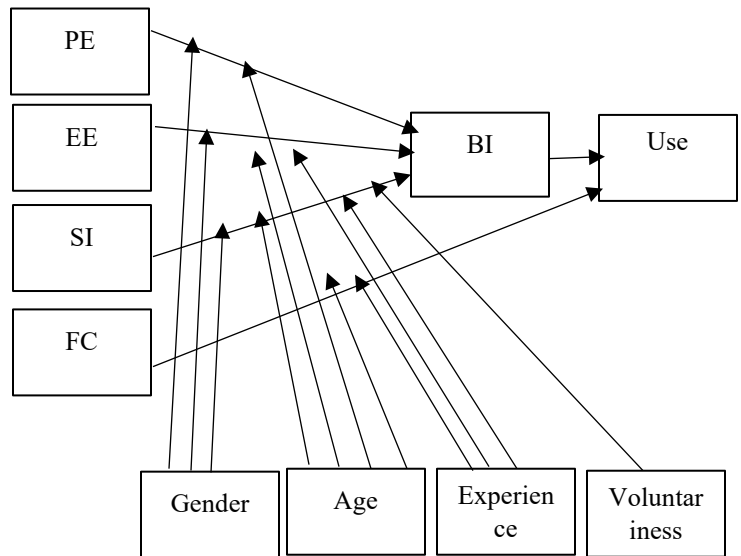


Figure 1: UTAUT model [11]

Note: BI stands for behavioral intention

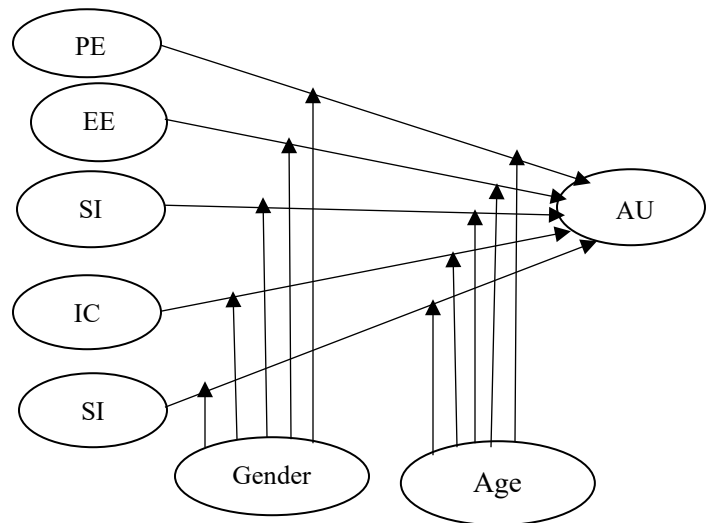


Figure 2: New study model

- PE is the belief that the performance of the user will increase with LMS use. [11].
- EE: is the trust that LMS will be easy to use [11].
- SI is a trust held by important people in the society that LMS in question should be used [11].
- IC is the belief that the technological facilities that support students to use the LMS exist.
- IS is the belief that the technological assistance the institutions offer exist.

- Actual use (AU): students' real application of the LMS.
- Gender: The gender of the student.
- Age: The age of the student.

#### 4. Hypothesis Development

##### 4.1. Performance Expectancy

PE is the belief that the performance of the user will increase with LMS usage [11]. According to [13] PE significantly related to technology usage. Similarly, [14] found that PE substantially related to the usage of a web-based tutoring system. Another study by [15] revealed that PE positively related to technology use. In related studies, it is shown that PE significantly impacts behavioral intention more strongly for men [11], [16]-[18]. Similarly, [11], [17], [19] have found that the older person drifts to use technology minimizes. Considering these pieces of evidence, the following hypotheses were deduced:

H1a: PE would have a significant effect on the AU of LMS.

H1b: The PE significant effect on AU of LMS would be higher when the student is male.

H1c: The PE significant effect on AU of LMS would be higher when the student is younger.

##### 4.2. Effort Expectancy

EE is the trust that the system will be easy to use [11]. According to [20], EE significantly influences the use of technology. Also, [21] revealed that EE significantly related to technology usage. In a related study, [13] found out that EE had a significant effect on students' use of LMS. In another study, [11], [17] have posited that age and gender play a moderating role in EE and users' behavioral intention. Based on the literature above, the under-listed hypotheses were developed:

H2a: EE would have a significant effect on the AU of LMS.

H2b: The EE significant effect on AU of LMS would be higher when the student is female.

H2c: The EE significant effect on AU of LMS would be higher when the student is young.

##### 4.3. Social Influence

SI is the extent one deems it important to use technology because a colleague or superior has asked him to use the technology [11]. Researchers, including [22] postulates that LMS usage ought not only to address the high-tech issues but also to consider the social environments where the technology is used. Also, [22] found that there is scant knowledge about the social issues regarding technology application in developing nations. In a similar work, [23] stated that SI positively influenced

technology use. Moreover, a study by [24] on learners' LMS implementation revealed that SI significantly impacted AU. In a comparable work, [25] confirmed that a significant correlation exists between SI and LMS usage intention. Furthermore, [8], [17] have reported that females are more inclined to be influenced by their colleagues to use technology than males. Additionally, [16] found that age moderates significantly on the association that exist between SI and behavioral intention to use technology.

From the evidence outlined above, the hypotheses below were deduced:

H3a: SI would have a significant effect on the AU of LMS.

H3b: The SI significant effect on AU of LMS would be higher when the student is female.

H3c: The SI significant effect on AU of LMS would be higher when the student is older.

##### 4.4. Facilitating Condition (FC)

FC is the level at which one believes that institutional and technical support are present to implement the system [11]. Training, support, institutional policy, ICT infrastructure, and leadership are the key elements considered to affect FC [26]. Many scholars have studied the impact of FC on LMS usage. [27] for instance, found out that technical support and lack of suitable equipment, and other resource availability issues significantly impacted LMS usage. [28] on the other hand, postulated that making computers and computer networks available to students will not necessarily influence usage but also administrative and institutional support should be in place to facilitate the system use. Numerous academicians also have stated the importance of support and training as core FC in e-learning use [29]-[30]. Besides, [9] has confirmed that FC significantly impacts students' usage of e-learning resources. [16] has also concluded in his study that age and gender significantly moderate FC and users' intention to use technology. In this study, FC was divided into IC and IS. From the above evidence, the following hypotheses were formulated:

H4a: IC would have a significant effect on the AU of LMS.

H4b: The IC significant effect on AU of LMS would be higher when the student is young.

H4c: The IC significant effect on AU of LMS would be higher when the student is female.

H5a: IS would have a significant effect on AU of LMS

H5b: The IS significant effect on AU of LMS would be higher when the student is female.

H5c: The IS significant effect on AU of LMS would be higher when the student is young.

#### 5. Method

In the present study, a case study approach was adopted based on the recommendation that it is a suitable strategy for studying

technological intervention in education [31]. Moreover, [32] states that case studies enable researchers to learn more from a particular situation.

5.1. Population and Data Collection Procedure

A total of 160 students took part in this study. The students were enrolled in undergraduate programs. A simple random sampling procedure was applied to choose the respondents from all the school year levels (Year 1 to Year 4) who were studying Business and Science courses. Before administering the questionnaires to the participants, they were told that their involvement was optional, and their anonymity was guaranteed. Additionally, the respondents were informed of the purpose of the study before administering the online questionnaire to them. The online questionnaires were completed after the respondents had taken a semester course. To enhance the rate of response, students were regularly reminded to complete the online questionnaires. Overall, 148 questionnaires were received. Of the 148 partakers, 69% were males and 31% were females, 23% were in the age range of 17 and 22 whereas 77% were more than 23 years, 40% of students were in Year 3 while 26% were in Year 2 (see Table 1). According to [33], a sample size between 100 and 150 cases is ideal for the Partial least square structural equation model (PLS-SEM). Consequently, a sample size of 148 students in this study was suitable for analysis using PLS-SEM.

5.2. Measures

The variables used in this study were taken from the earlier research works. The observed variables for EE, PE, SI, IS and IC were adapted from [11]. The PE construct contained four items; the EE composed of four variables; the SI had two variables. IC and IS, each comprised of five variables. A 5-point Likert scale was adopted and started from 1 representing “strongly disagree” to 5 representing “strongly agree”. On average, each partaker used at least 30 minutes to complete the questionnaire.

5.3. Data Analysis

PLS-SEM was used to analyze the quantitative data gathered from the respondents. PLS-SEM has been used in a broad array of disciplines such as Information Systems [34]. However, literature is lacking in the application of PLS-SEM in studies relating to LMS usage, particularly, in SSA [9]. Hence the use of PLS-SEM for the data analysis. The two-step approach of [35] was used for the PLS-SEM analysis. The first step measures the measurement model which comprises convergent and discriminant validities. The second step calculates the structural model.

6. Results

6.1. Measurement Model Assessment

6.1.1 Convergent Validity

The convergent validity was calculated on three stages: item reliability, composite reliability (CR) and average variance

extracted (AVE) [36]. The item reliability is measured by the factor loading of an item of the construct in the model. [33] posits that a factor loading of a construct is judged reliable if its value is equal to or higher than 0.5. Table 2 shows that the factor loadings of each construct’s items ranged between .56 and .93 confirming [33]’s assertion. Again, [33] postulates that, for a construct to be reliable, both its CA ( $\alpha$ ), as well as CR, should be greater than 0.7. From Table 2, CA as well as the CR of all the constructs exceeded 0.7, confirming the assertion of [33]. A further test of convergent validity, the AVE was conducted. Table 2 revealed that the AVEs of the constructs surpass 0.5 inferring that the convergent validity is acceptable [36].

Table 1: Demographics of the Respondents

Item	Type	Count	Proportion
Gender	Male	102	69%
	Female	46	31%
Total		148	100%
Age	17-22 (Young)	34	23%
	>=23 (Old)	114	77%
Total		148	100%
School year	First Year	34	23%
	Second Year	26	18%
	Third Year	59	40%
	Fourth Year	29	20%
Total		148	100%

Table 2: Convergent Validity

	AU	EE	IC	IS	PE	SI	CA	CR	AVE
AU1	<b>.90</b>	.47	.21	.35	.44	.22	.87	.92	.79
AU2	<b>.86</b>	.34	.18	.35	.38	.23			
AU3	<b>.91</b>	.47	.19	.33	.39	.20			
EE1	.35	<b>.76</b>	.41	.29	.46	.32	.79	.86	.62
EE2	.31	<b>.70</b>	.31	.15	.45	.30			
EE3	.41	<b>.83</b>	.34	.35	.55	.30			
EE4	.43	<b>.84</b>	.41	.34	.48	.35			
IC1	.16	.43	<b>.77</b>	.45	.29	.37	.72	.84	.64
IC2	.14	.35	<b>.78</b>	.32	.28	.31			
IC3	.21	.35	<b>.84</b>	.39	.28	.28			
IS1	.19	.21	.32	<b>.56</b>	.21	.33	.75	.83	.50



IS2	.30	.31	.37	<b>.78</b>	.20	.24			
IS3	.31	.30	.36	<b>.71</b>	.22	.33			
IS4	.24	.19	.31	<b>.72</b>	.16	.34			
IS5	.30	.27	.35	<b>.76</b>	.17	.34			
PE1	.39	.54	.28	.20	<b>.78</b>	.31	.78	.86	.60
PE2	.26	.41	.25	.12	<b>.66</b>	.18			
PE3	.41	.50	.33	.25	<b>.87</b>	.50			
PE4	.31	.47	.22	.24	<b>.77</b>	.46			
SI1	.24	.39	.39	.43	.46	<b>.93</b>	.79	.90	.82
SI2	.19	.34	.31	.36	.41	<b>.88</b>			

6.1.2 Discriminant Validity

Discriminant validity is measured by the following criteria: (1) Each construct’s loadings should exceed the cross-loadings of all the constructs [37]-[38], (2) the square roots of AVE of each construct should surpass the biggest squared correlations between any other construct [36]. Table 3 depicts the square roots of AVE (in bold) of each construct.

Table 3: Discriminant Validity

	AU	EE	IC	IS	PE	SI
AU	<b>0.89</b>					
EE	0.48	<b>0.78</b>				
IC	0.22	0.47	<b>0.80</b>			
IS	0.39	0.37	0.48	<b>0.71</b>		
PE	0.45	0.62	0.35	0.27	<b>0.77</b>	
SI	0.24	0.4	0.39	0.44	0.48	<b>0.91</b>

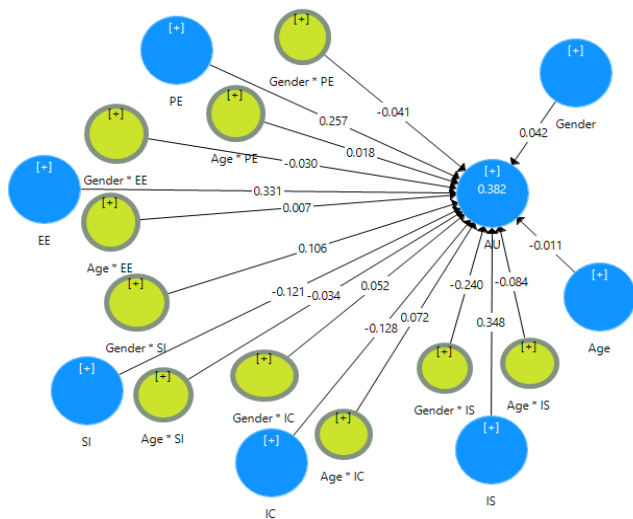


Figure 3: Structural model results

6.2. Structural Model Assessment

The bootstrap method of resampling of 5,000 iterations was performed to test the coefficients of the individual paths of the structural model. According to [39] the structural model's

explanation relies on the coefficient of determination, R<sup>2</sup>, to explain endogenous variable. The results of the structural model are given in Figure 3.

Table 4: Path Coefficients

Hypotheses	Path	Path coefficient	t-statistics	p-values	Result
H1a	PE -> AU	0.26	2.66	<b>0.01</b>	Confirmed
H1b	Gender * PE -> AU	-0.04	0.37	0.71	Unconfirmed
H1c	Age * PE -> AU	0.02	0.18	0.86	Unconfirmed
H2a	EE -> AU	0.33	3.32	<b>0.00</b>	Confirmed
H2b	Gender * EE -> AU	-0.03	0.32	0.75	Unconfirmed
H2c	Age * EE -> AU	0.01	0.07	0.95	Unconfirmed
H3a	SI -> AU	-0.12	1.31	0.19	Unconfirmed
H3b	Gender * SI -> AU	0.11	0.96	0.34	Unconfirmed
H3c	Age * SI -> AU	-0.03	0.39	0.69	Unconfirmed
H4a	IC -> AU	-0.13	1.39	0.16	Unconfirmed
H4b	Gender * IC -> AU	0.05	0.53	0.60	Unconfirmed
H4c	Age * IC -> AU	0.07	0.85	0.40	Unconfirmed
H5a	IS -> AU	0.35	3.40	<b>0.00</b>	Confirmed
H5b	Gender * IS -> AU	-0.24	2.36	<b>0.02</b>	Confirmed
H5c	Age * IS -> AU	-0.08	0.74	0.46	Unconfirmed

6.3. Hypotheses Testing

From Table 4, PE had a significant effect on actual use of LMS ( $\beta = 0.26, p = 0.01$ ), hence supporting H1a. Also, the effect of effort expectancy on students’ actual use of LMS was significant ( $\beta = 0.33, p = 0.00$ ), supporting H2a. Furthermore, IS had significant impact on actual use of LMS ( $\beta = 0.35, p = 0.00$ ), supporting H5a. However, SI ( $\beta = -0.12, p = 0.19$ ) and IC ( $\beta = -0.13, p = 0.16$ ) did not have a significant effect on the actual use of LMS, hence dH3a and H4a were not supported. Regarding the moderating effects of age and gender, gender moderated significantly on the correlation between institutional support and actual use of LMS ( $\beta = -0.24, p = 0.02$ ). Moreover, Figure 4 shows that, as institutional support increases the actual use also increases

for both males and female, but the increment is higher in females than in males, confirming H5b. However, the hypotheses H1b, H1c, H2b, H2c, H3b, H3c, H4b, H4c, and H5c were all not supported.

The actual use of LMS was significantly explained by PE, EE, SI, IC and IS, and the moderating effects of gender and age at  $R^2 = 0.38$ , showing the five independent variables and the two moderating variables explained 38% of the change in AU. Moreover, in this work, the value for the standardized root mean square residual (SRMR) was 0.069, suggesting a good model fit. This value confirms [40] assertion that SRMR value less than 0.1 gives an acceptable fit model. The result of the structural model is shown in Figure 3.

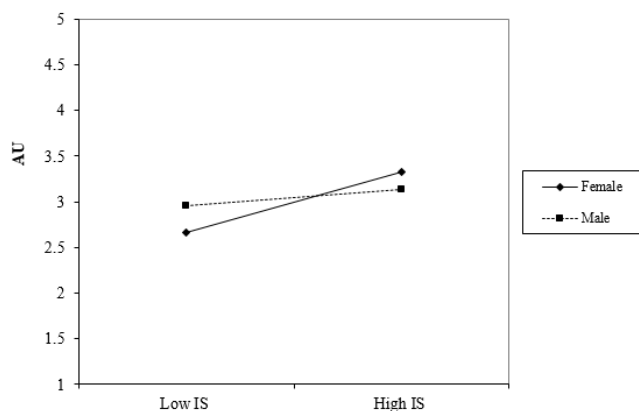


Figure 4: Moderating effect of gender on the correlation between Institutional Support (IS) and Actual Use (AU)

## 7. Discussions

This study intended to examine the determinants of students' actual use of the learning management system (LMS). [41] stated that knowing the determinants of an e-learning system is key to acquiring better discoveries and answers [42] also stressed that students and teachers should be encouraged to use the e-learning system. The research model accounted for 38% of the change in students' actual implementation of LMS, confirming that the new model is suitable in explaining learners' implementation of LMS.

The association between PE and actual usage of LMS was shown to be significant, implying that the greater the PE of a system, the greater the actual usage. Therefore, administrators should consider the benefits the students will gain from a system when planning to acquire one. This result was in agreement with previous studies [13], [14].

Furthermore, there was a significant correlation between EE and actual, implying that students will be willing to use the LMS if it is flexible, but will refuse to use the system if it is not flexible to use. This finding is in agreement with [11]. Additionally, this study revealed that SI did not significantly relate to actual use. This result is in disagreement with previous studies [23], [24]. This finding could be explained that the students are technology savvy and know the benefits of technology hence they do not need peers or any other entity to influence their use. Also, it was found that the IC did not impact the actual use of LMS. This means that

IC singly was not sufficient to stimulate learners' use of the system.

Finally, it was revealed that IS significantly related to students' actual use of LMS. This result is in agreement with prior works such as [27] [28]. Moreover, it was reported that as the institutional support increases so as actual usage increases for both males and females, but the increment is more significant in females than in males. This is in agreement with [16] who found out that gender moderated significantly on the correlation between facilitating condition and intention to use technology. According to [29], training and support are significant elements of individuals' use of technology.

## 8. Conclusion

The present study contributes to knowledge by providing first-hand data that the research model elucidates the determinants of learners' technology use. The research model elucidates 38% of the changes in learners' technology use. This finding has provided empirical data for studying several determinants that impact on students' actual application of technology. From a research point of view, this study primarily attempted to validate the findings from previous studies by empirically determining learners' actual implementation of LMS using UTAUT in unindustrialized nations. Future studies should examine other determinants such as technology self-confidence, individual innovativeness, and attitude that influence the usage of technology [43]. Although these may further explain the actual implementation of technology, it cannot assure us that the coefficient of determination of a new framework would be improved. To conclude, this study found that the new model was suitable for explaining the determinants of learners' actual application of technology.

## 9. Implication for Practice

PE and EE were found to be strongly related to the actual use. Irrespective of the usefulness of technology, users would be unwilling to use the technology if they find it to be cumbersome and difficult to use. Hence, management should consider the user-friendliness and flexibility of technology, as well as, its usefulness when adopting one. Additionally, educating academicians and learners would promote the use of technology in the instructional process. Furthermore, management in educational institutions should pay more attention to the provision of institutional support for learners and instructors. This would encourage lecturers and learners to use the online learning system to boost their self-confidence as well. [44] concluded that institutional support has a positive effect on the use of the e-learning learning system.

## 10. Drawbacks and Future Studies

The drawbacks of this study are: (1) Since this study involved one university, it is difficult to generalize the finding to other institutions, considering variations in the use of technology in different institutions. Therefore, future research should be done in other universities. (2) Thirty-eight percent (38%) of the change of

the dependent variable was elucidated by the exogenous variables. Other variables should be considered in future studies to unearth the outstanding 62%. (3) In this study, a cross-sectional strategy was adopted to gather data. In future studies, the longitudinal method ought to be employed to collect data from the partakers. (4) the use of other moderating factors is recommended for future studies. Finally, instead of using a questionnaire to collect data, future studies should use interviews to collect data from the partakers.

## References

- [1] A. Hassanzadeh, F. Kanaani, S. Elahi, "A model for measuring e-learning systems success in universities" *Expert Syst. Appl.* 39 (12), 10959–10966, 2012.
- [2] K. A. Al-Busaidi, K. and H. Al-Shihi. "Instructors' Acceptance of Learning Management Systems: A Theoretical Framework," *Communications of the IBIMA*, vol. 2010, 2010.
- [3] C.S. Nair, R. Patil, "A Study on the Impact of Learning Management Systems on Students of a University College in Sultanate of Oman", *Int. J. Comput. Sci.* 9(2), 379–385, 2012.
- [4] R. Ahmad, R. Edwards, R. Tomkinson, "The use of WebCT in distance learning course in university of manchester", *The Turkish Online J. Dist. Educ.* 7(2), 101-108, 2006.
- [5] C. Hong, Walker, D. A, "A confirmatory factor analysis of the Technology Acceptance", *General Linear Model J.I.*, 41(2), 22-29, 2015.
- [6] A.N. Islam, "Investigating e-learning system usage outcomes in the university context", *Comput. Educ.*, 69, 387–399, 2013.
- [7] M.. Waheed, K. Kaur, N. Ain, N. Hussain., "Perceived learning outcomes from moodle: an empirical study of intrinsic and extrinsic motivating factors", *Inf. Dev.* 32(4), 1001-1013, 2015.
- [8] N.D. Oye, N.A. Iahad, N. Ab.Rahim, "The history of UTAUT model and its impact on ICT acceptance and usage by academicians", *Educ. Inf. Tech.* 19(1), 251-270, 2014.
- [9] B. Bervell and I. N. Umar, "A decade of LMS acceptance and adoption research in Sub-Sahara African higher education: A systematic review of models, methodologies, milestones and main challenges", *Eurasia J. Math. Sci. Tech. Educ.* 13(11), 7269–7286, 2017.
- [10] T. Teo., N. Ruangrit, J. Khlaisang, T. Thammetarand, K.S. Jumngong, "Exploring e-learning acceptance among university students in Thailand: A National Survey", *J. Educ. Comput. Res.* 50(4), 489-506, 2014
- [11] V. Venkatesh, M.G. Morris, G.B. Davis, F.D. Davis, "User acceptance of information technology: Toward a unified view", *MIS Quart.* 27(3), 425–478, 2003.
- [12] W.R. King, J. He, "A meta-analysis of the technology acceptance model", *Inf. Manage.* 43(6), 740–755, 2006
- [13] N.D. Evans, and J. le Roux, "Modelling the acceptance and use of electronic learning at the University of Zululand", *S. Afric. J. Librar. Inf. Sci.* 81(2), 26-38, 2015.
- [14] P.C. Nanchang, "Student Acceptance of Web-based Learning System.Proceeding of the 2009 International Symposium on Web information Systems and application (WISA 2009)", China, 2009.
- [15] B. Sumak, G. Polancic, M. Hericko, "An empirical study of virtual learning environment adoption using UTAUT in 2010 Second Int. Conf. on Mobile, Hybrid, and On-line Learning ELML. Saint Maarten, 2010.
- [16] K. Ghalandari, "The effect of performance expectancy, effort expectancy, social influence and facilitating conditions on acceptance of e-banking services in Iran: The moderating role of age and gender", *Mid-East J. Scient. Res.*, 12(6), 801-807, 2012
- [17] O. A. Aliyu, C. Arasanmi, S. Ekundayo, "Do demographic characteristics moderate the acceptance and use of the Moodle learning system among business students?", *Int. J. Edu. Dev. Comm. Tech.*, 15(5), 165-178, 2019.
- [18] Wang, Y.-S., Shih, Y.-W., "Why do people use information kiosks? Validation of the Unified Theory of Acceptance and Use of Technology", *Govern. Inf. Quart.* 26(1), 158-165, 2009, doi:https://doi.org/10.1016/j.giq.2008.07.001
- [19] K. Magsamen-Conrad, S. Upadhyaya, C.Y. Joa, J. Dowd, (2015), "Bridging the divide: Using UTAUT to predict multigenerational tablet adoption practices", *Comput. Hum. Behav.* 50, 186-196, 2015.
- [20] N. Ain, K. Kaur, M. Waheed, "The influence of learning value on learning management system use: An extension of UTAUT2", *Inf. Dev.* 32(5), 1306-1321, 2016.
- [21] A. Raman, Y. Don, "Preservice teachers' acceptance of learning management software: An application of the UTAUT2 Model", *Int. Educ. Stud.* 6(7), 157–164, 2013.
- [22] T. Ali, H. Kate and L. Xiaohui, "Factors Affecting Students Acceptance of E-learning Environments in Developing Countries: A structural Equation Modeling Approach" *Int J. Inf. Educ. Tech.* 3(1), 54-59, 2013.
- [23] Y.L. Wu, Y.H. Tao, P.C. Yang, "The use of unified theory of acceptance and use of technology to confer the behavioral model of 3G mobile telecommunication users", *J. Stat. Manage. Syst.* 11(5), 919-949, 2008
- [24] A. Raman, Y. Don, R. Khalid, M. Rizuan, "Usage of Learning Management System (Moodle) among Postgraduate Students: UTAUT Model", *Asian Soc. Sci.*, 10(14), 186-192, 2014
- [25] A. Fidani and F. Idrizi. "Investigating students' acceptance of a learning management system in university education: A structural equation modeling approach" in 2012 ICT Innovation Web Proceedings, Macedonia, 2012.
- [26] V. Venkatesh, Bala, H, "Technology acceptance model 3 and a research agenda on interventions", *Decis. Sci.* 39(2), 273-315, 2008.
- [27] M. S. H. Khan, "Barriers to the introduction of ICT into education in developing countries: The example of Bangladesh", *Int. J. Inst.* 5(2), 61-80, 2012.
- [28] J. Brinkerhoff, "Effects of a long duration, professional development academy on technology skills, computer self-efficacy, and technology integration and beliefs", *J. Res. Tech. Educ.* 39(1), 22 – 43, 2006.
- [29] D. Jenkins, C. Mimbs, T. Kitchel, "Computer Literacy, Access, and Use of Technology in the Family and Consumer Sciences Classroom", *J. Fam. Consum. Sci. Educ.*, 27(1), 1–13, 2009.
- [30] R. Chen, "Investigating models for preservice teachers' use of technology to support student-centered learning", *Comput. Educ.*, 55(1), 32–42, 2010.
- [31] B.M. Sharan, *Qualitative Research: A Guide to Design and Implementation*, San Francisco: Wiley, 2009.
- [32] B. Flyvbjerg. "Five Misunderstandings About Case-Study Research", *Qual. Inqui.*, 12(2), 219-245, 2006.
- [33] J.F. Hair, G.T.M. Hult, C. Ringle, M. Sarstedt, *A Primer on Partial Least Squares Structural Equation Modeling (PLS-SEM)*, Thousand Oaks: Sage Publications, 2016.
- [34] A. Suh, C. Wagner, L. Liu, "Enhancing User Engagement through Gamification", *J. Comput. Inf. Syst.* 58(3), 204-213, 2018.
- [35] A. Ahmed et al., "Modeling and Simulation of Office Desk Illumination Using ZEMAX," in 2019 International Conference on Electrical, Communication, and Computer Engineering (ICECCE), 2019, pp. 1–6.
- [36] C. Fornell, D.F. Larcker, "Evaluating structural equation models with unobservable variables and measurement error", *J. Mark. Res.* 18(1), 39-50, 1981
- [37] W.W. Chin, "The partial least squares approach to structural equation modeling. In G.A. Macoulides (Ed.), *Methodology for business and management. Modern methods for business research*", Lawrence Erlbaum Associates Publishers, 1998.
- [38] J. Henseler, C.M. Ringle, Sinkovics, R.R, "The use of partial least squares path modeling in international marketing. In R.R. Sinkovics and P.N. Ghauri, Eds., *New Challenges to International Marketing*", Emerald Group Publishing Limited, 2009.
- [39] K.S. Ofori, H. Boateng, A.F. Okoe, I. Gvozdanovic, "Examining customers' continuance intentions towards internet banking usage", *Mark. Intell. Plann.* 35(6), 756-773, 2017
- [40] C. Sengul, E. Ilker (2015) "Comparison of model fit indices used in structural equation modeling under multivariate normality", *J. Mod. Appl. Stat. Meth.* 14(1), 2015.
- [41] R. Boateng, A.S. Mbrokroh, L. Boateng, P.K. Senyo, "Determinants of e-learning adoption among students of developing countries", *The Int. J. Inf. and Learn Technol.* 33(4), 248-262, 2016
- [42] D.D. Prior, J. Mazanov, D. Meacheam, G. Heaslip, J. Hanson, "Attitude, Digital literacy and self-efficacy: Flow-on effects for online learning behavior", *The Internet Higher Educ.*, 2016.
- [43] V. Venkatesh, J.Y. Thong, F.K. Chan, P.J.H., S.A. Brow, "Extending the two-stage information systems continuance model: Incorporating UTAUT predictors and the role of context", *Inf. Syst. J.* 21, 527–555, 2011.
- [44] Z. Yildirim, C.M. Reigeluth, S. Kwon, Y. Kageto, Z. Shao, "A comparison of learning management system in a school district: Searching for the ideal personalized integrated educational system (PIES)", *Interactive Learn, Environ.* 22(6), 721-736, 2014

## Commercialization Process of Disruptive Innovations in Corporate Ventures and Spinoff Companies: A Comparison

Javier Nieto Cubero<sup>\*1</sup>, Saheed Adebayo Gbadegeshin<sup>2</sup>, Carolina Consolación Segura<sup>3</sup>

<sup>1</sup>EINA University Center of Design and Arts, Autonomous University of Barcelona, Design Processes Research Group, 08017, Spain

<sup>2</sup>Turku School of Economics, University of Turku, Department of Management and Entrepreneurship, 20014, Finland & DeGesh Institute of Technology and Entrepreneurship; 20002, Nigeria

<sup>3</sup>ETSETB, Polytechnic University of Catalonia, Department of Management, 08034, Spain

### ARTICLE INFO

*Article history:*

*Received: 11 January, 2020*

*Accepted: 22 March, 2020*

*Online: 14 April, 2020*

*Keywords:*

*Commercialization*

*Transition Management*

*Disruptive Innovations*

*Ambidexterity*

*Corporate Venturing*

*Spin-off*

### ABSTRACT

*One of the most critical challenges that large companies, small enterprises and research institutes face, when commercializing their innovations, is the transfer process at the moment of scaling up. These organizations often transfer their innovation to either existing business units or create a new business entirely. The process of transferring innovations to an existing unit is known as corporate venture, while creating a new business is called spinoff. Both processes have been studied separately, but not yet together and from different business sectors and countries. In order to understand both processes, this article compares the commercialization of disruptive innovations from these sectors: electronics, information technology, telecommunications, engineering, healthcare, biotechnology or research equipment. The article used multiple case study methodology from commercialization projects carried out in large, small and medium-sized companies and research institutes based in Spain, Germany, UK and Finland. The findings showed that certain activities needed to be done at pre-transition /commercialization, transition/commercialization, and post-transition/commercialization phases to reach a successful transition. Furthermore, the study provides similarities between the corporate venture and spinoff approaches that include team formation, network development and getting the commitment from the company and stakeholders. Additionally, the article outlines divergences between the approaches which consist of innovation readiness, knowledge management or the activities of the post-transition phase. The article also provides insight for innovation scholars, commercialization practitioners, and business enterprises. Therefore, the article contributes to the commercialization of disruptive innovations.*

### 1. Introduction

In today's fast-paced technologically based environments, to keep long-term competitiveness, companies need to introduce disruptive and incremental innovations to markets [1,2]. The disruptive innovations need to be commercialized as it is argued by the scholars [3]. Unfortunately, the commercialization of these innovations has not been thoroughly studied [4], despite its importance within the innovation process [5]. Disruptive innovations are challenging to commercialize by both established enterprises and new businesses (specifically spinoffs). One of the

most critical challenges that mature corporations face at the commercialization phase is the transition of an innovation project to their business units for scaling up the project. Similarly, spinoff companies meet obstacles related to organizational factors when commercializing their disruptive innovation [6].

Thus, the corporate venture could be described as the exploration and exploitation of new technologies or products. It is detached from the corporate parent to avoid organizational inelasticity. Additionally, the term "corporate venture" could refer to "spin-in" according to [7]-[9]. Moreover, the commercialization of innovations by establishing a new enterprise is known as spinoff. Spinoff is defined as the creation of a new company to

<sup>\*</sup>J. Nieto Cubero, P. Santa Eulalia 25, 08017 Barcelona, +34 653560568, jnietoc@eina.cat

[www.astesj.com](http://www.astesj.com)

<https://dx.doi.org/10.25046/aj050278>



commercialize the business potential of a technology or innovation.

Currently, literature has explained the corporate venture process from many different perspectives, such as the corporate parent [10] or the corporate venture [11]. However, it is noted in the literature that there is a limited discussion on the venture transition at the moment of scaling up the innovation. Specifically, there is a limited scholarly discussion on how to design the transition process. Similarly, there is not yet a model that discusses activities needed for the successful transition of the corporate venture into the established company businesses [12] to reach the full commercialization of the innovation.

The existing literature also has explained the spinoff process from the parent organization and the academic entrepreneur's perspective. Nevertheless, few studies have focused on the commercialization process of the spinoff and how the innovation is transformed into a marketable product or service via the spinoff. Therefore, there is a need for in-depth knowledge of the commercialization process of spinoff [6].

Furthermore, ambidextrous literature has not yet provided a better explanation for the transferring of disruptive innovations in corporate entrepreneurship environments, by spin-in (corporate venture) or spinoff. Lastly, the current literature does not either provide a comparison among corporate ventures and spinoffs in their process of commercialization.

Therefore, the purpose of this article is to provide a better understanding of the commercialization process of disruptive innovations in the context of corporate venture and spinoff. It aims to provide critical factors and activities to perform in order to reach a successful scaling up innovation in these environments. To achieve these goals, it employed a qualitative research method.

The article also provides a comparison of the process of commercialization between corporate ventures and spinoffs in order to learn about the challenges they face in the commercialization process. The article offers both theoretical and practical knowledge to discourse on the commercialization process.

The rest of the article is organized as follows; Section 2 presents the theoretical background about the commercialization process in the corporate venture and spinoff, section 3 details the employed research method, section 4 presents the results obtained from the empirical studies, and section 5 presents discussion and conclusions. The last section presents contributions and limitations of the article as well as provides avenues to future research.

## **2. Theoretical Background**

Disruptive innovations are new technologies, techniques or knowledge that generate market and technological breakthroughs on macro and micro levels. These innovations embody new technology that causes a new market environment or generates different customer behaviors. These innovations are affected by S-curve(s): market, technology, or both, during their introduction to the marketplace [13,14]. More specifically, disruptive innovations are radical, and they distort existing ecosystems [15]. Thus, the disruptive innovation changes the relations among firms and

customers, modifies marketplace, overtakes current products and reconfigures the innovator's resources [16,17].

The corporate venture is often used to improve competitive positioning and transform corporations, their markets, and industries. It can also be used as opportunities to exploit value-creating innovations. The corporate ventures are startup-like structures that are idea-wise rooted in an established company. They are commonly used in exploration processes of disruptive innovations.

Thus, the corporate venture is, at this moment, described as the exploration and exploitation of new technologies or products, detached from the company's exploitation activities in an "incubation" cell structure that avoids organizational inelasticity and provokes resources and organizational renewal [18]-[20]. The corporate is notably essential when the innovation is still in an early phase, characterized by high uncertainties. Typically, the venture should be transferred to an existing business unit from the corporate parent creating profits within the firm. Meanwhile, the relationships between new corporate ventures and existing business units generate conflicts [21,22]. If this conflict is escalated, the incorporation of corporate venture into an existing corporate unit could be harmful to the development of the innovation and could also find hostility in the receiving team [23].

Notably, the corporate venture is different from intrapreneurship, which is described as infusing the mindset of entrepreneurs in the company's team and thus generating an innovative atmosphere within the company, as enunciated by [24]. Similarly, the corporate venture is different from the spinoff. While the corporate venture is a structurally separated unit with resources to manage innovation projects from idea to commercialization, the spinoff is an entirely new business created to develop and exploit the potential of the innovation.

The spinoff is defined as the generation of a new business to reach profits of new technology or innovation. This new business formation is attained by transferring innovation and other resources (e.g., intellectual property and human) from the originating organization. The originating organization consists of companies, universities or tertiary institutions and research institutes [25]. The spinoff also refers to a new firm that is established to commercialize business opportunities for a new technology that is developed by the research organizations [26]. Additionally, it could be a new company founded fundamentally to exploit an intellectual property that is developed by a university [27]. The spinoff is otherwise known as an academic spinoff, research-based spinoff or new technology-based firm.

### *2.1. Corporate Venture (CV)*

This article focuses on the transition phase of disruptive innovations, and particularly on the transference of innovations to a receiving business unit of the corporate parent.

Usually, a split exists among innovation teams and existing business units, as stated by [13]. Supported by research from [19], these scholars point out that there is not a defined process or methodology to guarantee the delivery of the innovation projects from research and development (R&D) at an acceptable level to the business unit before reaching the scaling-up phase. It has been

studied in literature through different perspectives, and it is described in the following paragraphs.

*Uncertainties perspective:* the scholars [28,13] outlined four kinds of uncertainties: technical, market-concerned, organizational and resources-based. Due to these uncertainties, disruptive innovations are usually substituted by incremental innovations [29]. Technical uncertainty includes the scientific knowledge base, technical feasibility and manufacturing process. The market-concerned uncertainty comprises the understanding of the new customer value, in relation to the existing competition [13]. The organizational uncertainty involves the organizational and managerial difficulties at integrating a disruptive innovation while pursuing exploitation activities. This uncertainty is mainly caused by unsupportive top management [10] or by the misfit among the corporate business unit and the innovation team [16]. The last uncertainty is resource-based. It addresses all the issues of acquisition of the resources to get successful exploitation of the disruptive innovation [30,31].

*Technology readiness:* the research from [32] offers an assessment tool to convert a technology invention into a profitable business, and the study of [33] provides a global view about the Technology Readiness Levels (TRL's). Nonetheless, these scholars only approach the phenomenon under a technology uncertainty perspective.

*Ambidexterity perspective:* the ambidexterity literature [20] introduces the construct of separated units for exploration and commercialization, coordinated at the top management level. This structural detachment guarantees that the exploration activities are preserved from the bureaucracies, managerial routines, and the culture of exploitation [34]. The works from [35,36,20] have enunciated that the detachment among exploration and exploitation activities foster the benefits of both [37]. Similarly, the work of [36] argues that ambidextrous organizations require methodologies to activate, organize and incorporate separated exploration and exploitation units in organizations.

Separation is mainly required to emphasize on disruptive exploration. Nevertheless, the detachment of these units from the corporate parent is a necessary yet insufficient condition for ambidexterity [38].

Notwithstanding the acknowledged obstacles for venture transition, the extant literature on the process of transference to an existing business is relatively scarce [39]. Research on integration mechanisms is still needed, and as [36] underlined, is required more research about how "transition should be done."

*Championship perspective:* many different scholars enunciate the relevance of having the support of a champion not only in the innovation team but also at senior management level [40,41]. Several studies also have studied the role of senior management in fostering integration and enhance synergies between exploration and exploitation units [12,35]. Moreover, the likelihood of transition success is also raised if a champion appears in the receiving unit [12, 13] or if it has the support of an informal network [31]. Clear and transparent communication is critical to recognize the right supporters within the corporate parent [29]. [11] also stresses the relevance of exchanges within corporations

not only at a management level but also between business units and other stakeholders of the firm.

Regarding CV, the disruptive innovation cell's managers are needed to smooth the integration of the project into the business unit by demonstrating the feasibility of the innovation, making concepts and benefits tangible and finding latent needs from customers.

### 2.1.1. Corporate ventures transition phases

The work from [12] distinguishes three stages in the transition from a separated venture to a one that is integrated into the established corporate structure: the pre-transition, the transition, and the post-transition phase. The pre-transition phase is described as a stage to develop connecting and learning activities between the CV and the parent business. During the transition phase, the hand-over moment takes place, and the venture is transferred to the corporate organization, while the post-transition phase is defined as the stage when the venture is incorporated in the established organization.

### 2.1.2. Specific activities in transition phases in corporate ventures

A summary of the existing literature on activities to perform in the commercialization process and activities to be performed within each phase of transition is displayed in Table 1.

### 2.2. Spinoff (CSO)

There are two approaches to the spinoff. The first approach is a planned spin-off. The planned spin-off is predetermined and is based on the plan of a parent organization. The parent organization often states that a new venture would stem from the commercialization activities of their project. The second approach is a spontaneously occurring spinoff. It happens when a new business venture is created unexpectedly. Generally, this spin-off does not get total support from the parent organization [42]. Commercializing innovation through a spinoff has been studied through different approaches. They are described in the following paragraphs.

*Strategic perspective:* From the strategic viewpoint, the scholars state that commercializing an innovation requires different strategies, orientations, and decisions. According to [43], there are three strategies: early adoption, adoption network configuration, and mainstream adoption. These authors explained that early adoption strategy is the method when a commercializing team adopts to create awareness, stimulate and motivate people to have a positive attitude towards the new product. Similarly, the authors stated that the adoption of a network configuration is the ability of the team to enable early buyers to be strong supporters of the product. Likewise, the authors mentioned that the mainstream strategy is the decision and effort of the team to transfer a configured network to the primary market. Still, from the strategic perspective, commercializing an innovation also requires different decisions to be made. [44] found that world-leading companies, well-known for their innovation commercialization, made critical decisions by placing commercialization as one of their highest priorities, establishing measurable objectives for proper management, and developing sufficient and essential competencies.

Table 1. Corporate venture activities in commercialization phases

Transition Phase	Category	Specific Activities	Scholars
Pre-Transition	Innovation project preparation for scale-up	Transition readiness assessment	O'Connor, Hendricks and Rice (2002), Rice, Leifer and O'Connor (2002) and van Burg et al. (2012). Rice, Leifer and O'Connor (2002) and van Burg et al. (2012). Kanter et al. (1991) Rice, Leifer and O'Connor (2002).
		Transition team	
		Transition plan	
	Conditions for validation	Achievement of first sales and running of pilot projects	Nieto (2018).
	Early-relations with the potential receiving business units	Training and personal exchange	van Burg et al. (2012).
		Cross-functional interfaces	Jansen et al. (2009).
		Liaison channeling and network building	Gassman et al. (2012).
		Horizontal interactions between teams	Raisch and Tushman (2016).
Transition	Transition time	Transference after achieving first sales	van Burg et al. (2012).
		Laying the groundwork for a significant market	Rice, Leifer and O'Connor (2002).
	Knowledge management	Transfer of the R&D team to the receiving business unit	Nieto (2018).
Post-transition	Specification of suitable KPI's in the business unit	Post transition autonomy. Performance metrics	van Burg et al. (2012).

*Marketing perspective:* The scholars, from the marketing viewpoint, seem to focus on the marketization of the disruptive innovation through innovation, according to [2]. The high technologies make use of disruptive innovations. Thus, marketing scholars state that innovation would be successful if the final consumers can accept them. Examples of prominent scholars in this group are [45,46]. To reinforce the credibility of this viewpoint, [47] argued that innovation would be successfully commercialized if it could be market oriented. This scholar stated that commercialization must start with the market and end with it. In a similar view, [48] added that the commercialization should

focus on the substitute products/services as well as on the functionality of commercializing products concerning its price. However, marketization is cumbersome, tedious and full of risks. According to [49], six challenges are awaiting the commercializers of disruptive innovation. The scholar stated that they market-concerned uncertainty, technological uncertainty, the inconsistency of new products in a complex multi-component system, difficulty in developing networks, the problem of ecosystem complexities and competition, and inherent risks of choice-making (especially with multiple and interdependent product-market options).

*Skills perspective:* From the skills perspective, the scholars emphasize how the commercialization should be accomplished. Examples of scholars in this perspective are [50,51]. [51] emphasized that innovation can reach the market successfully if the commercialization team can: (1) acquire and possess sufficient technological knowledge, (2) develop the innovation into a product which can be mass-produced, (3) establish commercialization process and relate it to growth strategy, (4) adhere to their process as a learning path, and coordinate and maintain a good network. Furthermore, [52] stressed that, though focused on the strategy, marketing skills are crucial for their successful commercialization. To assist practitioners, these scholars proposed market and user research tools, which include customer ethnography, emphatic designs, lead-user processes, investigating users, and the targeting of new markets.

Considering all these perspectives, the question of "what one has to do in commercializing disruptive innovation successfully in terms of activities" is fragmented depending on the perspective approach.

2.2.1. Spinoff commercialization phases

When commercializing disruptive innovations through a spinoff, three phases are recognized, as acknowledged by [53]-[56]. These phases are pre-commercialization, commercialization and post-commercialization. The pre-commercialization is the stage where any activity aiming at transforming new technology into products and services is done. The commercialization phase contains all the transformation efforts. The post-commercialization includes any attempt to make new products or services sustain market share at a profit for its commercializing team and companies.

2.2.2. Specific activities in commercialization phases in spinoffs

Based on the above grouping, the previous works describe the activities to perform in each phase and they are summarized in the following Table 2.

2.3. Relationship between CV's and CSO's in the commercialization stage.

The work from [57] discussed the role and relevance of internal corporate venturing and spinoffs as means to corporate renewal and to improve competitive positioning.

Meanwhile, similarities and differences between different corporate entrepreneurship structures have been researched by scholars, for instance between Startups and CV's, as enunciated by

Table 2. Spin-off activities in commercialization phases

Commercialization Phase	Specific Activities	Scholars
Pre-commercialization	Basic and applied science /discovery technology/ initiation /	Maine and Garnsey (2007), AbdRahima et al. (2015), Amadi-Echendu and John, (2008), and Pietzsch et al. (2009).
	Formulation/identification of technological opportunity/ Application idea initial technical and economic viability	Maine and Garnsey (2007), AbdRahima et al. (2015), Amadi-Echendu and John (2008).
	Reviewing the technology / Application	Eldred and McGrath (1997) and Amadi-Echendu and John (2008).
On-commercialization	Having a development team and organizing a senior review team / formalizing commercialization project	Eldred and McGrath (1997) and Rogers et al. (2004).
	Formalizing commercialization project	Rogers et al. (2004).
	Scanning and creation of potential alliances/identification of specific need of target market/ conducting of preliminary material investigation /	Maine and Garnsey (2007) and Chen and Panda (2005).
	Designing, building and testing of prototypes/designing and prototyping/design and development / Developing prototypes and integrating the prototype into existing products/incubation	Rogers et al. (2004), Maine and Garnsey (2007), Pietzsch et al. (2009) and Chen and Panda (2005).
	Development of technological product/service	AbdRahima et al. (2015) and Amadi-Echendu and John (2008).
	Customer testing and experimentation	Maine and Garnsey (2007).
	Verification of relating policies/ evaluation of make/buy decision/development of the pilot plant,	Rogers et al. (2004) and Maine and Garnsey (2007).
	Deciding on channels of distribution	Rogers et al. (2004).
	Final validation / final customer testing	Pietzsch et al. (2009) and Maine and Garnsey (2007).
	Developing a structured commercialization method / developing structured processes	Eldred and McGrath (1997) and Chen and Panda (2005).
Post-commercialization	Product launching and post-launching assessment/market, and acceleration	Pietzsch et al. (2009), Amadi-Echendu and John (2008).

[58], USO's (university spinoffs) and CV's, as stressed by [59], USO's and CSO's, as outlined by [60,61], or between IV's (independent ventures) and CV's [62]. Similarly, under the perspective of the leaders of the innovation units, commonalities and divergencies between corporate entrepreneurs and spinoff entrepreneurs have been discussed by [63].

The previous works show that the commercialization process of the corporate venture consists of pre-, transition, and post-transition. The phases are similar to the spinoff, which include pre-commercialization, commercialization and post-commercialization. The previous literature also states the different activities to be done at each phase. However, there is missing knowledge of the commercialization process of disruptive innovation via the corporate venture and spinoff. Thus, this article seeks to provide to the following research questions:

- What are the key activities that facilitate managing the transition and commercialization of disruptive innovations in corporate ventures and spinoffs?
- What are the differences and similarities in the process of commercialization between a corporate venture and a spinoff?
- Do corporate ventures face the same problems that spinoffs are confronted with?

### 3. Research design

#### 3.1. Methodology approach

In order to answer the research questions, a multiple case study approach has been selected. Case study research involves the examination of a phenomenon in its natural environment. The case study method is specifically appropriate to research new field areas, with a focus on "how" or "why" questions, related to a contemporary set of events. The study of multiple cases is usually considered as a more robust method, as it provides the observation and analysis of a situation in different settings. The multi-case method enables an understanding of the phenomenon beyond each project context and increases generalizability [64]. There were two sets of empirical data in this research. The first set was gathered for corporate ventures and the second for spinoffs.

##### 3.1.1. Corporate venture case selection and data collection

Potential disruptive innovation projects were evaluated according to criteria provided by the definitions of [65], who uses disruptive to describe innovations that could occur in a macro-level as well as micro-level contributions.

Based on the above criteria and according to [66], who state that theoretical sampling is a means to reach a high gain of insight, twelve corporate venture transition processes were selected. Nine of those samples found an internal existing business unit of the corporate parent to be integrated in. One of them found an external firm, and two projects employed a dual destination model to an internal business unit as well as to an external company. Eight of the samples have been successful in the transition process, and the other four were failure cases. The cases are presented in Table 3.

The companies have been named (Telco Co, FMCG Co, Appliances Co, Financial Co, Engineering Co). We also define the



name of the chosen projects as Tel1, Tel2, Tel3, Tel4, Tel5, Tel6, Fast1, App1, App2, Fin1, Eng 1, and Eng2. The real names of companies and projects are not displayed due to the confidentiality research agreements.

For the sample, data were collected through interviews with innovation unit managers and corporate innovation managers to achieve different perspectives on the success of the project, conflicts, key issues and evolution of the project transition, reaching a variety of insights. The research carried out 26 double interviews. Each interview took 1 to 1,30 hrs. Long. The interviews were performed in two rounds. The first round, to understand the overall context of the project and company and the second round to obtain a deeper understanding of each project’s details. During the conduction of the interviews, nevertheless, the interview guideline was regularly updated and enriched to be adapted to the insights obtained after the previously analyzed project. The documentation was complemented with secondary data about each project obtained from the corporate company.

**3.1.2. Spinoff case selection and data collection**

According to the criteria mentioned above, twenty spin-off companies were selected. They were chosen according to the type of disruptive innovations. Also, these companies were founded by serial entrepreneurs and business advisors. The details of the projects are also presented in Table 4. The spin-off projects were denoted by COY 1 to COY 20, respectively. The cases are presented in Table 4. Data were obtained through interviews. The study participants were contacted via email and telephone calls. After booking a date and venue, they were sent interview questions with themes. After a few weeks, the interviews were conducted. Each interview took more than 1 hour. All interview processes

were following the qualitative research guideline provided by [67]-[71].

**3.2. Data analysis**

Qualitative analysis needs a different approach than the quantitative analysis because of the nature of the collected data, mostly textual and descriptive. The research is focused on the process of transition and commercialization, and more specifically, on the tasks developed to overcome the challenges found during the process. The information obtained from interviews was transcribed and later analyzed by using open coding [72] to recognize patterns in transition activities and critical problems influencing the transference and commercialization of the innovation projects. The following step was the axial coding, identifying relationships between categories, organizing them hierarchically with interconnections and sub-categories. The last step was selective coding to produce a theory and recognize core categories. NVivo11 software was used for helping in the analysis and codification of qualitative data obtained at interviews. It is a software that supports data management, in the process of exploration and coding that is not linear, but iterative.

Similar patterns responding to the formulated research questions were codified, defining the main tasks to perform in order to overcome commercialization problems and barriers in corporate ventures and spinoffs. The theory that emerged from the interviews was compared with the existing literature leading to specific conclusions displayed in the following sections. Discovered similarities increase the validity of the findings and link old and new theory. Emerging differences show opportunities for new concepts and avenues for future research.

Table 3. Summary of corporate venture cases and interviewed profiles

Parent Company	Industry	Corporate Venture	Interviewed Profiles
TELCO CO	Telecommunications	Corporate organization	Product innovation director Design Research Lead
		Tel1 project	Head of product/project Head of Innovation Portfolio Innovation Business Development Manager
		Tel 2 project	Corporate Venture Leader Head of Innovation Portfolio
		Tel 3 project	Senior Technical Expert Head of Innovation Portfolio
		Tel 4 project	Service innovation Lead Head of Innovation Portfolio
		Tel 5 project	Head of commercial innovation Head of Innovation Portfolio Innovation Business Development Manager
		Tel 6 project	Corporate Venture Leader Head of Innovation Portfolio
FMCG CO	Laundry & Home Care	Fast 1 project	Innovation Manager - IoT Corporate Venture Leader
APPLIANCES CO	Home appliances	App 1 project	Innovation Transference Director Corporate Venture Leader
		App 2 project	Innovation Transference Director Corporate Venture Leader
FINANCIAL CO	Financial	Fin 1 project	Service Design Lead Product Innovation Director
ENGINEERING CO	Engineering	Eng 1 project	Division Manager
		Eng 2 project	Division Manager

Table 4. Summary of spinoff cases and interviewed profiles

Companies	Industry	Interviewed profiles
Coy 1	Electronics	CEO Chief Engineer
Coy 2	Environment Tech	CEO Chief Engineer
Coy 3	Healthcare Equipment	CEO Head of Venture Capital IPR Manager
Coy 4	Research Equipment	CEO Business developer Head of Venture Capital
Coy 5	Research Equipment	CEO
Coy 6	Electronics	CEO Chief Engineer
Coy 7	Research Instrument	CEO Business developer
Coy 8	Information Technology	Head of Venture Capital IPR Manager
Coy 9	Research Instrument	Principal lecturer
Coy 10	Optics	Head of Venture Capital
Coy 11	Biotechnology	Head of Venture Capital
Coy 12	Biotechnology	Head of Venture Capital
Coy 13	Electronics	Head of Venture Capital IPR Manager
Coy 14	Chemical Production	CEO
Coy 15	Information Technology	Head of Venture Capital IPR Manager
Coy 16	Electronics	Head of Venture Capital IPR Manager
Coy 17	Research Instrument	Head of Venture Capital IPR Manager
Coy 18	Information Technology	CEO Head of Venture Capital IPR Manager
Coy 19	Information Technology	Head of Venture Capital IPR Manager
Coy 20	Paper Production	Head of Venture Capital IPR Manager

#### 4. Empirical results

The first result of the empirical study is related to the key activities performed within the different phases of commercialization. These results are explained separately for Corporate Ventures and Spin-offs in the following subsections:

##### 4.1. Corporate ventures

Analyzing the readiness of the innovation projects, in all cases from the empirical setting, apart from having a clear value

proposition for customers and stakeholders, it was also necessary the achievement of first sales to obtain the interest of potential existing corporate units. This fact was enhanced when the innovation team had conducted real pilot programs.

The critical problem to overcome, as discovered across all cases, is the misfit between the R&D project and the established corporate unit. The structure of the business unit was not prepared for the disruptive project that they received. The misfit has been discussed previously by scholars such as [13]. Also, exploitation units could lack crucial knowledge and resources to develop the innovation project. Collaboration from the business members and identifying an owner in the business unit who support and promote the project becomes one of the main challenges in full commercialization.

Another critical barrier for the survival of the transferred venture was the sales expectations the receiving business unit had on the innovation project and the lack of specific and flexible performance metrics to control the development of the venture, as previously discussed by [12].

The interviews and the data collected from the sample, allow us to identify different team activities which are crucial within the different phases of the transference of the projects to the exploitation business units, as well as the critical organizational factors influencing commercialization, providing generalization to the previous work of [73]. They are described as follows.

##### 4.1.1. Pre-transition phase

###### a) Achievement of first sales and running of pilot projects.

Identifying leading customers willing to pay for the innovation is crucial in the maturity of the project. Another relevant key factor is obtaining real user traction, enhancing the interest of the corporate units, as enunciated by [73].

Moreover, the likelihood of conducting real pilot programs, and if possible, promoted by the customer enables the possibility of testing the hypotheses related to the projects linked to the particularities of the target market.

###### b) Early-relation with the potential receiving business unit.

Generating a relationship with the potential business unit and exchanging information concerning the R&D project seems to be crucial. The interaction between teams enables a better alignment with the corporate road map and enhances the involvement of the receiving team, as enunciated by [12,29,36,39].

It becomes relevant to recognize potential marketers in the first stages of the R&D process. These interactions could occur at managerial levels but also between the components of the teams.

This kind of relationship allows us to explain the value and potential of the innovation to gain the receiving team's trust. Communication should be transparent, transmitting the full knowledge obtained during the development phase, regarding the product, information about users and markets, including how the product has evolved and why.

Fostering communication between teams and the potential stakeholders for the innovation commercialization allows us to recognize possible future frictions, obtaining essential information to foresee how to overcome these barriers.

Finally, these cross-communications allow us to get more significant credibility for the innovation and future projects. It serves to identify key figures to obtain support from the base of the business unit, and from the management level, reaching a smoother integration.

c) *Search for champions and project support network.*

It has been observed in all the projects in the sample that senior management has played a supporting role, facilitating contacts and establishing bridges to look for potential marketers for the innovations. Identifying and involving a champion at the management level in the receiving team has been crucial to the success of the project. The role of informal networks has also been fundamental.

This championship perspective has been approached from the senior management perspective by [36,41]. [12,13] also pointed out the relevance of identifying an owner champion in the receiving business unit.

4.1.2. *Transition phase*

a) *Definition of the transition time.*

The different innovation unit managers underlined several tasks to get done to define the moment of transition:

- Once the R&D project has reached the first sales with a customer, it is convenient to build customer loyalty and obtain new sales with similar clients to confirm the potential of the innovation through establishing a broader and more stable customer base.
- Another crucial indicator is to have a refined and tested business and operating model ready to scale, a reliable team, and a sales road map.
- Apart from having the product ready, it is also necessary to get ready a technology platform and the complementary services to run the innovation.

These activities have not been discussed in previous literature.

b) *Transfer of the R&D team to the receiving business unit*

In the projects of the sample in which part of the innovation team was transferred to transmit all the knowledge acquired during the research and development phases, a positive effect was observed in the transition. This specific activity has not been discussed previously by scholars.

4.1.3. *Post-transition phase*

a) *Performance metrics.*

Business units that incorporate innovations from corporate ventures must also exploit more incremental or mature projects. For this reason, specific KPI's must be established to apply to both the business unit teams and the disruptive innovation projects they will exploit. This concept has been previously enunciated by [12].

4.1.4. *Other auxiliary tasks to carry out*

Besides the similar activities identified in the projects, other patterns also appeared, described here as follows:

- Several unit managers highlighted the importance of identifying and incorporating different profiles from the

business units to compose the needed team in the scaling up of the innovation. The search for these profiles aims not only to obtain the primary resources for growth but also to transform these future team members into potential champions of the innovation.

- Locating middle management champions at intermediate levels between the innovation team and the potential business unit was positive, acting as interfaces and transmitters of the benefits of the innovation.
- Another of the strategies recommended by different units and corporate innovation managers was to promote cross-movements of teams, incorporating temporary members from the innovation team into business units, enabling these profiles to approach the project from a business perspective, to detect possible future frictions.

These insights are new to literature.

4.2. *Spinoff*

It was noted during the interviews that technology entrepreneurs and business advisors acknowledged that certain activities have to be done before the actual commercialization and after it, defining pre-, on- and post-commercialization phases. Each phase has key activities; some of them previously not outlined in the scholarly works. The following section explains each of these critical activities according to the phases of commercialization.

4.2.1. *Pre-Commercialization Phase*

a) *Identification of innovation application.*

The study participants were able to identify an industrial process or sector where the innovation could be applied. They noted that the application should aim to solve a technical problem or social specific problem because its identification always enables commercializers to identify target markets for their innovations. This critical activity is also discussed by scholars such as [74]-[76].

b) *Professional protection of Intellectual Property.*

It is learned that IP protection happened after high-tech identified a business potential. The participants highlighted the importance of IP protection. They did not focus on ordinary protection, but rather professional protection. [54] emphasized the need for it.

c) *Establishing of the technology - business team.*

Previous works like [77,78] have stated that team formation plays an essential role in technology-based companies. The study participants plainly stated that a team should consist of someone who has a profound knowledge of the technology to be commercialized and someone who knows how to sell.

d) *Defining a clear target market.*

Scholars such as [45]-[47] have discussed this activity and concluded that marketization is a crucial pillar in commercialization. In the same perspective, the study participants shared that they succeeded in the commercialization because they were able to find a clear target market from the beginning of the commercialization challenge.

*e) Gathering sufficient market information.*

The study participants tried to gather sufficient market information. Participants stated that conducting market research ab initio is an essential step for commercialization success. They advised that commercializers should try to employ online and offline means to get market-related information on their target market. They added that the use of interpersonal networks to collect target market information played a significant role. This finding is in line with the recommendations of [48,53,57].

*f) Staying with the parent company.*

Participants shared that they preferred to stay with their research institutions while developing their technologies (during their early businesses). Interviewees said that it provides an opportunity to bring existing networks and resources into play during pre-commercialization. [53] acknowledged this activity in their previous study.

*g) Identification of different business models.*

Scholars like [79]-[81] explained that business model development is essential. This empirical study found it to be one of the tools that helped to make a business successful. Interviewees pointed out that every commercializer should know and develop several business models in which the best options can be selected in the future.

*4.2.2. On - Commercialization Phase*

*a) Product simplification.*

Participants stressed that product simplification is a key factor in the on-commercialization phase, suggesting that a new product should be able to work with existing systems or use existing infrastructure. This activity has a relationship with the recommendations of [43,48,49,77,78].

*b) Subcontracting / outsourcing.*

It was observed that the study participants preferred to work on their core technology and software aspects of the product while hardware and other parts were outsourced. They said that such a strategy enabled them to reach the market at the right time and to scale-up their production at a later stage of their company growth. This activity was also echoed by [43,53].

*c) Having direct contact with end-users.*

The participants understood that the real information for validating and improving the product solution came from end-users. Therefore, this key activity is often done during commercialization, as it is stated by [43,53,56,77,78].

*d) Testing and defining flexible business models.*

It is learned that the participants focused on testing while developing new business models.

*e) International awareness.*

The participants tried to attend international business events when developing their business models in order to improve awareness and develop networks. This activity has not yet been discussed by the previous scholars on the commercialization of innovations.

*f) Reference sales.*

The entrepreneur participants affirmed that one of their tasks during the commercialization stage is to make initial sales. They explained that this kind of sales is a pathway to sustainability. They shared that having references helps them to provide feedback for further development as well as create credibility for other clients and fundraising. This activity was discussed by [73] in the context of corporate ventures.

*g) Starting early internationalization.*

Study participants emphasized early internationalization during commercialization in order to develop a potential sales network.

*4.2.3. Post-Commercialization Phase*

*a) Getting feedback from initial buyers*

The study participants stressed that getting feedback is crucial for successful commercialization as a manner to satisfy customers as well as to offer more services, which in turn led to more revenue for the company. This activity is also outlined by [51,56].

*b) Managing the supply chain*

As it can be noted from the pre- and on-commercialization stages, the study participants advised commercializers to subcontract or outsource the manufacturing process. This activity is related to the work of [55], where the commercialization process from the supply chain point of view is explained.

## **5. Discussion and conclusions**

The case studies inform us about the different activities that corporate ventures and spin-offs carry out in order to confront the main challenges they encounter at pre-commercialization, on-commercialization and post-commercialization stages. The comparative analysis between the specific activities undertaken during the phases of commercialization allows us to define the main similarities and differences among the two structures upon scaling up the innovation project.

*5.1. Pre-transition/commercialization phase.*

Based on the analysis of collected data, the *commitment of organizational leaders and stakeholders* to commercialize the innovation appeared to be one of the most critical factors in both corporate ventures and spinoff cases. According to [6,77] for an innovation to be commercialized successfully, the organizational leaders and stakeholders must be committed to the process. The cases of this paper revealed that upper management support motivated the commitment of teams and project managers in commercialization teams. In the case of corporate ventures, early relations with the potential receiving business unit were crucial to search owners for the innovation project, as well as to get the involvement and support from all the layers in the commercialization unit. This network building could be obtained through bidirectional personnel exchange, education and training, cross-functional interfaces or horizontal interactions between teams. Endorsing the work of [8], the empirical results suggest that these activities contribute to balance the misfit (commitment, resources and objectives) among the R&D project and the existing



business unit, a key factor influencing the successful commercialization process.

*Team formation* at the moment of scaling up the innovation plays an essential role in technology-based companies, corroborating the work of [77]. The specific competencies and skills required for successful commercialization encourage corporate ventures and spin-offs to define and to form the right team to face this challenge with the appropriate resources of personnel. It was noted that a commercialization team consists of people from R&D and business people, or even teams with dual technical and business development competencies. Furthermore, the project managers of these cases have the attributes of an intrapreneur, which is a closely related arrangement to the champion approach in corporate ventures. These managers can integrate technological knowledge, business expertise and user perspective. The same feature is evident among the serial entrepreneurs of the spin-off companies.

*Team skills* and work methodologies seem to be similar in both cases. The disruptive innovation team integrates cross profiles beyond technological qualifications. Customer research, communication and sales skills are the most valued competencies.

*Collaboration or industrial networks* also appeared to be another relevant factor for the transition of disruptive innovations from the parent organization to a spin-in unit or spin-off company. The cases of this paper showed that the availability of partners in and out company is a must to facilitate commercialization. It was learned that such collaboration motivated the spin-in unit to be active and it encouraged spinoff entrepreneurs to exert more effort.

*Innovation project readiness.* Besides these similarities, some divergences emerged from the cases studied. The innovation project seems to be more developed in the case of corporate ventures than in the case of spinoffs. Whereas in corporate ventures, the focus is on validating, demonstrating and creating credibility on the potential receiving business unit, spinoff tries to ascertain the real value or business potential of the innovation project by way of clarifying the target market. Spinoffs do so by gathering enough market information or developing several business models in which the best options can be selected in the future. Based on the collected data, in the corporate venture cases, the realization of first sales is a necessary, yet insufficient, condition for transference. It is required also to conduct pilot programs to demonstrate real traction and to maximize learning from real market situations.

This difference could be motivated by a more goal-minded orientation on the part of the project leader and team components of the corporate venture, even if they work separately from the exploitative units of the parent company.

*IP property.* The analysis of the cases also reveals that corporate ventures are more financially supported and intellectual property protected thanks to their synergies with the corporate parent, while spin-offs must make an extra effort in IP protection and in search of funding and external partners.

### 5.2. Transition/Commercialization phase

*Knowledge transference.* In corporate venture cases, it is common that no one from the innovation team continues on the

receiving business unit that will exploit the innovation project. Is for this reason that the study outlines the critical importance of making the right transmission of the complete knowledge acquired and of balancing out the shortcomings in terms of responsibilities within the receiving team, as well as their different motivations and goals, which confirms the previous work from [73], focused on telco industry. The information collected during the project development stage should always be transmitted to the exploitation team for a better understanding of the real needs of the users, the customer's feedbacks, the stakeholder's key information and the integration of all this knowledge into the innovation commercialization. The transference of members of the R&D team helps to manage this knowledge.

*Innovation project readiness.* It can be noticed that some of the activities that spinoffs perform at the commercialization phase, such as product simplification, prototyping and testing with end-users or testing business models, are a "must" type of tasks that corporate ventures have to accomplish just before the transition time. For example, the innovation should have renewed the trust not only from users but also from clients, as well as have jumped to parallel market niches. The innovation project should also have a tested and refined business and operating model, a "go to market" strategy and the associated services developed to implement the innovation.

*Resources.* The limited resources that spin-offs have in comparison with corporate ventures make the former focus on their core business activities using subcontracting, while the latter devote their primary efforts to finding the right resources of personnel to exploit the disruptive innovation project.

*Awareness and networks.* Some of the activities that spin-offs perform at this phase are oriented to maximize awareness and to grow the sales network by the participation in business events, early internalization, creation of potential alliances and the definition and search for the right distribution channels. The synergies with the parent company in the case of corporate ventures help significantly when it comes to facing these challenges.

### 5.3. Post-transition/commercialization phase

It is during this phase when the approach from the two structures seems to be completely different, according to the analysis of the data collected from corporate ventures and spin-offs.

The following Table 5 summarizes the comparison between activities carried out by corporate ventures and spin-offs and the main challenges to overcome during the different phases of commercialization.

The insights gained from the spinoff cases reveal that even at this phase of post-commercialization, the process of refinement of the product is crucial, requiring the feedback from initial buyers.

Even if continuous refinement is also present in the mindset of corporate ventures, the activities performed by spinoffs during this phase are usually carried out by corporate ventures at the pre-transition phase so that they can offer an optimized product to the receiving business unit.

Table 5. Comparison between corporate venture and spin-off activities and challenges during the different phases of commercialization.

SPINOFF			CORPORATE VENTURE		
PHASE	CHALLENGES TO OVERCOME	ACTIVITIES	ACTIVITIES	CHALLENGES TO OVERCOME	PHASE
PRE-COMMERCIALIZATION	GETTING COMMITMENT FROM STAKEHOLDERS	Identification of technological opportunity  Application. Technical and economic viability	Early relations with potential business units  Personal exchange and training  Cross-functional interfaces	COMMITMENT FROM BU. SEARCH FOR CHAMPIONS	PRE-TRANSITION
	ASCERTAINING INNOVATION VALUE AND BUSINESS POTENTIAL	Targetting markets  Formulate different business models Gathering enough market information	Achieving first sales and running pilot programs	VALIDATION AND DEMONSTRATE REAL TRACTION	
			Reduce all remaining uncertainties	INNOVATION PROJECT READINESS	
	TEAM LACK OF RESOURCES AND SKILLS	Formation of the commercialization team	Definition and formation of the right team	TEAM LACK OF RESOURCES AND SKILLS	
	PROTECTION OF INNOVATION	IP protection			
ON-COMMERCIALIZATION	CONDITIONS FOR COMMERCIALIZATION	Reference sales  Product simplification. Ready or existing  Technology platform  Testing business models Prototype and testing with end-users. Final validation	Renew sales and open new niches  Clear operating model and technology platform technology platform. Complementary services Ready business model	CONDITIONS FOR TRANSITION TIMING	TRANSITION
	LACK OF RESOURCES	Subcontracting	Search for the right personal resources	RESOURCES LEVERAGING	
	AWARENESS AND SALES NETWORK	Participation in business events  Internationalization Creation of potential alliances Searching for distribution channels	Synergies with corporate parent	AWARENESS AND SALES NETWORK	
			Team transference for knowledge transferences	KNOWLEDGE MANAGEMENT	
POST-COMMERCIALIZ.	PROMOTING SPINOFF	Product launching and post launching. Market assessment			POST-TRANSITION
	REFINING INNOVATION PROJECT	Getting back from initial buyers			
	OPTIMIZATION VALUE CHAIN	Managing supply chain			
			Defining specific performance metrics	BALANCE EXPLORATION & EXPLOITATION PROJECTS	
		Searching for partial autonomy	KEEPING CV MINDSET		

The size and lack of resources that spinoffs have, push these kinds of organizations to focus part of their specific activities on this phase, in order to define and develop the supply chain, the commercialization, and the launching process that will help to scale up the innovation.

The study shows that in the cases of innovation projects from corporate ventures transferred to a business unit, they focus on keeping some autonomy of criteria and mindset (coming from the R&D team) in order to optimize the scaling up of the innovation in the corporate parent. Also, participants asked to define specific performance metrics that could be applied to the commercialization team in order to be able to balance explorative and exploitative projects.

## 6. Contributions and limitations

The main contribution of this article is that it provides the key commercialization activities for the corporate venture and spinoff. It outlines that team formation, network development, and early relations with potential commercializers and stakeholders are the important commercialization activities that the disruptive innovations require regardless the commercialization approach. Additionally, the article outlines that there are divergences between the corporate venture and the spinoff approach. These divergences include innovation readiness, knowledge management or the approach to the post-transition phase.

Another contribution of the article is the comparison of both corporate ventures and spinoff. Even though there are many literary works on both approaches, there is no scholarly work yet that compares them. This comparison shows that both approaches have various phases and each of the phases has several activities. It also provides an in-depth understanding of both approaches on the commercialization of disruptive innovation, stressing the common challenges corporate venture and spinoff face, as follows: ascertaining and validating the business potential of the innovation, getting the commitment from the corporate parent and stakeholders, overcoming the lack of resources and obtaining awareness and credibility from market and stakeholders.

Additionally, the article contributes to the practice by enhancing understanding of the commercialization process of disruptive innovation via the corporate ventures and spinoffs approaches. It outlines some key barriers that the practitioner might face during the process, as the misfit between the R&D project and the established corporate unit, the lack of specific and flexible performance metrics to control the evolution of the project or how to define the right conditions for the commercialization of the innovation

However, the article has some limitations, defining at the same time fields for future research. Firstly, the case study method applied in the article inherited the problem of generalization, as it is usually the case. This makes the findings of this article to be limited with regards to generalization. Although the findings are generic, which means they can be generalized, yet it is recommended that the findings' generalization is determined by the nature of the concerned technology, its industry and its target market.

Furthermore, this empirical research of the article does not incorporate the perspective of the managers of the business units that receive the innovation. Obtaining the vision from these profiles will enrich the data gathered regarding the research questions.

Further, the collected data were gathered from different countries. The corporate venture data were collected in Spain, Germany, and the UK, whereas spinoff data were collected in Finland. These countries have similarities and differences, and the latter might affect the findings of the article. Therefore, future studies could examine corporate venture and spin-off activities in the same country and the same industry.

Lastly, the findings of the article need to be confirmed through further research, something that creates room for future studies. For instance, it would be good to have a quantitative study where the identified activities are tested or a study of how the key activities impact the commercialization of technology-based companies' high-tech.

### **Conflict of Interest**

The authors declare no conflict of interest.

### **Acknowledgment**

The corresponding author would like to thank the Design Processes Research Group from EINA University Center of Design and Arts (Autonomous University of Barcelona) for their support.

### **References**

- [1] C. Lettl, "User involvement competence for radical innovation", *J. Eng. Technol. Manage.*, 24(1-2), 53-75, 2007. <https://doi.org/10.1016/j.jengtecman.2007.01.004>
- [2] J. Nieto Cubero and C. Consolación Segura, "The Role Teams and Organizational Factors Play in Disruptive Innovations in Ambidextrous Organizations" in the 2019 ICE/ITMC International Conference on Engineering, Technology and Innovation, Valbonne Sophia-Antipolis, France, 2019, 1-14. <https://doi.org/10.1109/ICE.2019.8792627>
- [3] S.A.Gbadegeshin, "The Commercialization Process of High Technologies: Case Studies from ICT, Cleantech and Life Sciences Industries" Ph.D. Thesis, University of Turku, Finland, 2019.
- [4] X.M.Song and M.M.Montoya-Weiss, "Critical development activities for really new versus incremental products", *J. Prod. Innovat. Manag.*, 15(2), 124-135, 1998. <https://doi.org/10.1111/1540-5885.1520124>
- [5] C.M. McDermott and G.C. O'Connor, "Managing radical innovation: an overview of emergent strategy issues", *J. Prod. Innovat. Manag.*, 19, 424-438, 2001. <https://doi.org/10.1111/1540-5885.1960424>
- [6] S.A. Gbadegeshin, S.A., "Commercialization process of high technologies: case study of finnish university spin-off", *Acad. Entrep. J.*, 23(2), 122, 2017.
- [7] S.A. Gbadegeshin, "Stating best commercialization method: An unanswered question from scholars and practitioners", *Int. J. Eco. Eng. Manag.*, 11(5), 1088-1094, 2017.
- [8] M.A. Kirchberger, and L. Pohl, "Technology commercialization: a literature review of success factors and antecedents across different contexts", *J. Technol. Transfer*, 41(5), 1077-1112, 2016. <https://doi.org/10.1007/s10961-016-9486-3>
- [9] K. Hindle and J. Yencken, "Public research commercialization, entrepreneurship and new technology-based firms: an integrated model", *Technovation*, 24(10), 793-803, 2004. [https://doi.org/10.1016/S0166-4972\(03\)00023-3](https://doi.org/10.1016/S0166-4972(03)00023-3)
- [10] R.A.Burgelman and L.R. Sayles, "Inside corporate innovation: strategy, structure and managerial skills", *Management*, 18(2), 179-185, 1986. <https://doi.org/10.3917/mana.182.0179>
- [11] S.A. Hill and J. Birkinshaw, "Strategy-organization configurations in corporate venture units: Impact on performance and survival", *J. Bus. Venturing*, 23(4), 423-444, 2008. <https://doi.org/10.1016/j.jbusvent.2007.04.001>
- [12] E. van Burg, S. de Jager, I.M.M.J. Reymen and M.Cloudt, "Design principles for corporate venture transition processes in established technology firms", *R&D Manage.*, 42(5), 455-472, 2012. <https://doi.org/10.1111/j.1467-9310.2012.00695.x>
- [13] M.P. Rice, R. Leifer, and G.C. O'Connor, "Commercializing discontinuous innovations: bridging the gap from discontinuous innovation project to operations", *IEEE T. Eng. Manage.*, 49(4), 330-340, 2002. doi: 10.1109/TEM.2002.806721
- [14] R. Garcia and R. Calantone, "A critical look at technological innovation typology and innovativeness terminology: a literature review", *J. Prod. Innovat. Manag.*, 19(2), 110-132, 2002. <https://doi.org/10.1111/1540-5885.1920110>
- [15] V. Govindarajan and P.K. Kopalle, "The usefulness of measuring disruptiveness of innovations ex-post in making ex-ante predictions", *J. Prod. Innovat. Manag.*, 23, 12-18, 2006. <https://doi.org/10.1111/j.1540-5885.2005.00176.x>
- [16] D. Dougherty, "Understanding new markets for new products", *Strateg. Manage. J.*, 11, 59-78, 1990. <https://doi.org/10.1108/00251749810223592>
- [17] R.A. Burgelman, "A process model of internal corporate venturing in the diversified major firm", *Admin. Sci. Quart.*, 28(2), 223-244, 1983. <https://doi.org/10.2307/2392619>
- [18] S. Ford, E. Garnsey and D. Probert, "Evolving corporate entrepreneurship strategy: technology incubation at Philips", *R&D Manage.*, 40(1), 81-90, 2010. <https://doi.org/10.1111/j.1467-9310.2009.00580.x>
- [19] G.C. O'Connor, and R. de Martino, "Organizing for radical innovation: An exploratory study of the structural aspects of RI management systems of large established firms", *J. Prod. Innovat. Manag.*, 23, 475-497, 2006. <https://doi.org/10.1111/j.1540-5885.2006.00219.x>
- [20] M.L. Tushman and C.A. O'Reilly, "Ambidextrous organizations: managing evolutionary and revolutionary change", *Calif. Manage. Rev.*, 38(4), 8-30, 1996. <https://doi.org/10.2307/41165852>
- [21] D.A. Levinthal and J.G. March, "The myopia of learning", *Strateg. Manage. J.*, 14, 95-112, 1993. <https://doi.org/10.1002/smj.4250141009>
- [22] H. Chesbrough, and C.L. Tucci, "Corporate Venture Capital in the Context of Corporate Innovation". EPFL Working Paper, Lausanne, 2005.



- [23] R.G. McGrath, "Exploratory learning, innovative capacity, and managerial oversight", *Acad. Manag. J.*, 44(1), 118-131, 2001. <https://doi.org/10.5465/3069340>
- [24] N. Thornberry, "Corporate entrepreneurship: Antidote or oxymoron?", *Eur. Manag. J.*, 19(5), 526-533, 2001. [https://doi.org/10.1016/S0263-2373\(01\)00066-4](https://doi.org/10.1016/S0263-2373(01)00066-4)
- [25] E. G. Carayannis, E.M. Rogers, K. Kurihara and M.M. Allbritton, "High-technology spin-offs from government, R&D laboratories and research universities", *Technovation*, 18(1), 1-11, 1998. [https://doi.org/10.1016/S0166-4972\(97\)00101-6](https://doi.org/10.1016/S0166-4972(97)00101-6)
- [26] F. Pimay, B. Surlemont and F. Nlemvo, "Toward a typology of university spin-offs", *Small Bus. Eco.*, 21(4), 355-369, 2003. <https://doi.org/10.1023/A:1026167105153>
- [27] S. Shane, *Academic Entrepreneurship: University Spin-offs and Wealth Creation.*, UK, Edward Elgar Publishing Ltd, 2004.
- [28] G.S. Lynn and A.E. Akgün, "Innovation strategies under uncertainty: A contingency approach for new product development", *Eng. Manag. J.*, 10(3), 11-18, 1998. <https://doi.org/10.1080/10429247.1998.11414991>
- [29] O. Gassmann, B. Widenmayer and M. Zeschky, "Implementing radical innovation in the business: the role of transition modes in large firms", *R&D Manage.*, 42(2), 120-13, 2012. <https://doi.org/10.1111/j.1467-9310.2011.00670.x>
- [30] R. Chandy and G. Tellis, "The incumbent's curse? incumbency, size, and radical product innovation", *J. Marketing*, 64(3), 2000. <https://doi.org/10.1509/jmkg.64.3.1.18033>
- [31] G.C. O'Connor, R. Hendricks and M.P. Rice, "Assessing transition readiness for radical innovation", *Res. Tech. Manage.*, 45(6), 50-56, 2002. <https://doi.org/10.1080/08956308.2002.11671533>
- [32] D. Clausing and M. Holmes, "Technology readiness", *Res. Tech. Manag.*, 53(4), 52-59, 2010. <https://doi.org/10.1080/08956308.2010.11657640>
- [33] J.C. Mankins, "Technology readiness and risk assessments: A new approach", *Acta Astronaut.*, 65(9), 1208-1215, 2009. <https://doi.org/10.1016/j.actaastro.2009.03.059>
- [34] C.A. O'Reilly and M.L. Tushman "The ambidextrous organization", *Harvard Bus. Rev.*, 82(4), 74-81, 2004.
- [35] G.C. Gilbert, "Change in the presence of residual fit: Can competing frames coexist?", *Organ. Sci.*, 17(1), 150-167, 2006. <https://doi.org/10.1287/orsc.1050.0160>
- [36] J.J.P. Jansen, M.P. Tempelaar, F.A.J. van den Bosch and H.W. Volberda, "Structural differentiation and ambidexterity: The mediating role of integration mechanisms", *Organ. Sci.*, 20(4), 797-811, 2009. <https://doi.org/10.1287/orsc.1080.0415>
- [37] C. Andriopoulos and M.W. Lewis, "Exploitation-exploration tensions and organizational ambidexterity: Managing paradoxes of innovation", *Organ. Sci.*, Special Issue on Ambidextrous Organizations, 20(4), 696-717, 2009. <https://doi.org/10.1287/orsc.1080.0406>
- [38] O.P. Kauppila, "Creating ambidexterity by integrating and balancing structurally separate inter-organizational partnerships", *Strateg. Organ.*, 8(4), 283-312, 2010. <https://doi.org/10.1177%2F1476127010387409>
- [39] S. Raisch and M.L. Tushman, "Growing new corporate businesses: From initiation to graduation", *Organ. Sci.*, 27(5), 1237-57, 2016. <https://doi.org/10.1287/orsc.2016.1081>
- [40] D.A. Garvin and L.C. Levesque, "Meeting the challenge of corporate entrepreneurship", *Harvard Bus. Rev.*, 84(10), 102-112, 2006.
- [41] M.L. Tushman and D. Lavie, "Exploration and exploitation within and across organizations", *Acad. Manag. Ann.*, 4(1), 109-155, 2010. <https://doi.org/10.5465/19416521003691287>
- [42] M. Steffensen, E.M. Rogers and K. Speakman, "Spin-offs from research centers at a research university", *J. Bus. Venturing*, 15(1), 93-111, 1998. [https://doi.org/10.1016/S0883-9026\(98\)00006-8](https://doi.org/10.1016/S0883-9026(98)00006-8)
- [43] F. Frattini, A. De Massis, V. Chiesa, L. Cassia and G. Campopiano, "Bringing to market technological innovation: What distinguishes success from failure", *Int. J. Eng. Bus. Manag.*, 4(15), 1 -11, 2012. <https://doi.org/10.1111/j.1540-5885.2006.00220.x>
- [44] T. M. Nevens, G. L. Summe, and B. Uttal, "Commercializing technology: What the best companies do", *Harvard Bus. Rev.*, 64(8), 154-163, 1990. <https://doi.org/10.1108/eb054310>
- [45] J.S. Gans and S. Stern, "The product market and the market for "ideas": commercialization strategies for technology entrepreneurs", *Res. Policy*, 32(2), 333-350, 2003. <https://dx.doi.org/10.2139/ssrn.317219>
- [46] J. Pellikka and P. Malinen, "Developing Commercialisation of Innovation in High Technology Industries – Regional Perspective", in 2011 56th International Council for Small Business (ICSB), Stockholm, Sweden, June 15-18, 2011.
- [47] P. Valiauga, "Commercialization of High-tech Radical Innovations: Case Studies of X-ray Imaging Technologies." in 2013 paper presented at the Aalto University School of Science, Finland, May 16, 2013. [http://noppa.aalto.fi/noppa/kurssi/tu-22.1500/luennot/TU-22\\_1500\\_povilas](http://noppa.aalto.fi/noppa/kurssi/tu-22.1500/luennot/TU-22_1500_povilas)
- [48] S.P. Nichols, "Module 1: An Introduction to Commercialization of Science and Technology. Converting Technology to Wealth Workshop". Austin, TX: IC2 Institute, The University of Texas at Austin. <http://ut.gtrade.or.kr/inc/download.asp?key=5288>
- [49] A. Dhebar, "Bringing new high-technology products to market: Six perils awaiting marketers", *Bus. Horiz.*, 59, 713-722, 2016. <https://doi.org/10.1016/j.bushor.2016.08.006>
- [50] A.D. Chandler, "Commercializing high-technology industries", *Bus. Hist. Rev.*, 79(3), 595-604, 2005. <https://doi.org/10.1017/S0007680500081460>
- [51] A.C. Fletcher and P.E. Bourne, "Ten simple rules to commercialize scientific research", *PLoS Comput. Biol.*, 8(9), e1002712, 2012. <https://doi.org/10.1371/journal.pcbi.1002712>
- [52] S. F. Slater and J. J. Mohr, "Successful development and commercialization of technological innovation: insights based on strategy type", *J. Prod. Innovat. Manag.*, 23(1), 26-33, 2006. <https://doi.org/10.1111/j.1540-5885.2005.00178.x>
- [53] E. Maine and E. Garnsey, "The commercialization environment of advanced materials ventures", *Int. J. Technol. Manage.*, 39(1/2), 49 -71, 2012. <https://doi.org/10.1504/IJTM.2007.013440>
- [54] J. E. Amadi-Echendu and R. T. Rasetlola, "Technology Commercialization Factors, Frameworks and Models" in 2011 IEEE/ITMC Conference, 144-148, 2011.
- [55] D. S. Rogers, D. M. Lambert, and A. M. Knemeyer, "The Product Development and Commercialisation Process", *Int. J. Logist. Manag.*, 15(1), 43 - 56, 2004. <https://doi.org/10.1108/09574090410700220>
- [56] J. B. Pietzsch, L. A. Shluzas, M. E. Paté-Cornell, P. G. Yock and J. H. Linehan, "Stage-gate process for the development of medical devices", *J. Med. Devices*, 3(021004), 1-15, 2009. <https://doi.org/10.1016/j.technovation.2017.03.003>
- [57] T. Elfving and N. Foss, "Corporate Renewal Through Internal Venturing and Spin-offs: Perspectives from Organizational Economics", No 97-7, IVS/CBS Working Papers, 97-7, 1997.
- [58] B. L. Golish, M.E. Besterfield-Sacre and L. J. Shuman, "Comparing Academic and Corporate Technology Development Processes", *J. Prod. Innovat. Manag.*, 25(1), 47-62, 2008. <https://doi.org/10.1111/j.1540-5885.2007.00282.x>
- [59] P.P. Georgallis and R. Durand, "Achieving High Growth in Policy Dependent Industries: Differences between Startups and Corporate-Backed Ventures", *Long Range Plann.*, 50(4), 487-500, 2017. <https://doi.org/10.1016/j.lrp.2016.06.005>
- [60] K. Wennberg, J. Wiklund and M. Wright, "The Effectiveness of University Knowledge Spillovers: Performance Differences between University Spinoffs and Corporate Spinoffs", *Res. Policy*, 40(8), 1128-1143, 2011. <https://doi.org/10.1016/j.respol.2011.05.014>
- [61] S.A. Zahra, E. Van de Velde and B. Larraneta, "Knowledge Conversion Capability and the Growth of Corporate and University Spinoffs", *Ind. Corp. Change*, 16(4), 569-608, 2007. <https://doi.org/10.1093/icc/dtm018>
- [62] R. C. Shrader and M. Simon, "Corporate Versus Independent new Ventures: Resource, Strategy, and Performance Differences", *J. Bus. Venturing*, 12(1), 47-66, 1997. [https://doi.org/10.1016/S0883-9026\(96\)00053-5](https://doi.org/10.1016/S0883-9026(96)00053-5)
- [63] T. Bager, H. Ottosson and T. Schott, "Intrapreneurs, Entrepreneurs and Spin-off Entrepreneurs: Similarities and differences", *Int. Small. Bus. J.*, 10(3), 2010. <https://doi.org/10.1504/IJESB.2010.033572>
- [64] R.K. Yin, *Case Study Research*, Thousand Oaks, CA: Sage Publications, 1994.
- [65] E. Danneels, "Disruptive technology reconsidered: a critique and research agenda", *J. Prod. Innovat. Manag.*, 21(4), 246-258, 2004. <https://doi.org/10.1111/j.0737-6782.2004.00076.x>
- [66] K.M. Eisenhardt, "Building theories from case study research", *Acad. Manag. Rev.*, 14(4), 532-550, 1989. <https://doi.org/10.2307/258557>
- [67] D. E. Gray, *Doing Research in the Real World*, Chapter 2: Theoretical Perspectives and Research Methodologies, USA: Sage Publications, 2013.
- [68] J. W. Creswell, *Research Design: Qualitative, Quantitative and Mixed Methods Approaches*. 3rd Ed., United Kingdom, London: Sage Publication, 2009.
- [69] P. Eriksson and A. Kovalainen, *Qualitative Methods in Business Research*, 1st Ed., United Kingdom, London: Sage Publications, 2008.
- [70] S. Rajasekar, P. Philominathan and V. Chinnathambi, *V.Rese. Method.*, 2016. <http://arxiv.org/pdf/physics/0601009.pdf>
- [71] N. Denzin and Y. Lincoln, *Handbook of Qualitative Research*, United Kingdom, London: Sage Publications, 2000.
- [72] J.M. Corbin and A. Strauss, *Basics of Qualitative Research*, 3rd Ed., Thousands Oaks: Sage Publications, 2008.



- [73] J. Nieto, "Managing Integration of Disruptive Innovations in Ambidextrous Organizations", in 2018 ISPIM Innovation Conference, Stockholm, Innovation, the Name of the Game, Stockholm: LUT Scientific and Expertise Publications, 2018.
- [74] N. Abd Rahima, Z. B. Mohamed, and A. Amrin, "Commercialization of emerging technology: The role of academic entrepreneur", *Soc. Behav. Sci.*, 169, 53 – 60, 2005. <https://doi.org/10.1016/j.sbspro.2015.01.285>
- [75] E. W. Eldred and M. E. McGrath, "Commercializing new technology", *Res. Tech. Manag.*, 40(1), 41-47, 1997. <https://doi.org/10.1080/08956308.1997.11671102>
- [76] J. E. Amadi-Echendu and A. John, "On the Commercialization of Trailing Knowledge and IP", in 2008 PICMET'08 Conference, Cape Town. Paper ID: 08R0018, 2008.
- [77] A. Al Natsheh, S.A. Gbadegeshin, A. Rimpiläinen and T. Mainela, "Technology-based entrepreneurship: measurement technology perspective", *Int. J. Res. Bus.*, 2(9), 26 – 42, 2013.
- [78] J. Che and R. Panda, "Review: Commercialisation of Piezoelectric Single Crystals for Medical Imaging Applications", in 2005 IEEE Ultrasonics Symposium, 235-240, 2005.
- [79] H. Chesbrough, "Business model innovation: opportunities and barriers", *Long Range Plann.*, 43(2), 354-363, 2010. <https://doi.org/10.1016/j.lrp.2009.07.010>
- [80] D.J. Teece, "Business models, business strategy and innovation", *Long Range Plann.*, 43(2), 172-194, 2010. <https://doi.org/10.1016/j.lrp.2009.07.003>
- [81] C. Zott, R. Amit and L. Massa, "The business model: recent developments and future research", *J. Manage.*, 37(4), 1019-1042, 2011. <https://doi.org/10.1177/0149206311406265>

## **Activerest: Design of A Graphical Interface for the Remote use of Continuous and Holistic Care Providers**

Nuno Martins<sup>1,\*</sup>, Jéssica Campos<sup>2</sup>, Ricardo Simoes<sup>2</sup>

<sup>1</sup>*Polytechnic Institute of Cavado and Ave / ID +, Barcelos, Portugal*

<sup>2</sup>*Polytechnic Institute of Cavado and Ave, Barcelos, Portugal*

---

### ARTICLE INFO

*Article history:*

*Received: 14 January, 2020*

*Accepted: 11 March, 2020*

*Online: 14 April, 2020*

---

*Keywords:*

*Pressure ulcers*

*Mobile application*

*Digital technologies*

*Healthcare mobile solution*

*Android*

---

### ABSTRACT

*One of the most prevalent physical limitations of both aging and accidents is immobility. Being bedridden requires great care to avoid the formation of pressure ulcers. Thus, the 'ActiveRest' project aimed to develop a textile mattress guard that will contribute to the prevention of pressure ulcers. This textile mattress guard integrates a monitoring system, based on a network of sensors (pressure, temperature, humidity), coupled with an intelligent non-invasive actuation system. The major innovation is that the actuation system only acts around high pressure loci, effectively relieving pressure in those critical areas. This system can operate autonomously and continuously adjusts its response to the data obtained by the real-time pressure sensor network. In addition, the system encompasses a mobile application that communicates in real-time with the mattress guard, and that enables caregivers to monitor the condition of a patient (and even receive an alert whenever their direct action is required). In the scope of ActiveRest, this paper describes the work pertaining to the digital technology component of the system, namely the graphic design and the development of the App necessary to convey the data to the caregiver. In this case, the main focus was the design of a graphic user interface, simple and customized towards distinct target audiences, which will facilitate the caregiver's work and interaction with the pressure ulcer prevention system.*

---

### 1. Introduction

In recent decades there has been a growth in average life expectancy in developed countries, according to a study published in The Lancet magazine, in 2020 for the first time in history there will be more people aged 65 years or more than aged 5 years or less [1].

In Portugal, in 1970 a person aged 65 could live on average more 13.5 years. In 2017, this number has risen to 19.5 years [2]. However, in 2013, the years considered healthy after 65 years of age had an average of 9.2 years.

Despite the increase in average life expectancy, aging still causes several types of limitations to the human body, it begins at 25 years and after the age of 60 accelerates its process which causes more physical and cognitive difficulties to the individual. In addition to aging, emerging diseases are also a factor that increases these limitations [3].

Immobility is one of the examples of physical limitations caused by aging and more prone diseases among the elderly. In

addition to numerous complications, one of the factors aggravated by it is the emergence of pressure ulcers (PU) which, according to the European Pressure Ulcer Advisory Panel (EPUAP), are defined as "a localized lesion of the underlying skin or tissue, usually over a bony prominence as a result of pressure or a combination of bone and torsional forces." [4]. In most cases, the emergence occurs when the patient is bedridden and has little or no mobility, which requires him or her to be accompanied by a health professional or family member to move to prevent PU.

Faced with this problem and given the seriousness of the emergence of a pressure ulcer for the patient and caregiver, as well as the economic burden on the national health services (NHS), there is a need to implement preventive measures, as well as timely therapeutic means to face the risk of pressure ulcers development.

So, the ActiveRest project, to which this paper is part, proposes a solution that can act on time to prevent this type of skin injury, while providing immediate relief from pressure on the user. This solution is composed of two components that complement each other, although they can act independently. One of these components is a textile guard that incorporates a sensing system composed of pressure, temperature and humidity sensors, three

---

\*Corresponding Author: Nuno Martins, [nunomartins.com@gmail.com](mailto:nunomartins.com@gmail.com)

risk factors for the development of PUs, together with an autonomous localized pressure relief system, which is based on an actuation mechanism. noninvasive, light and compact. The other component, which represents one of the innovative features of the proposed solution and which makes it stand out from the existing solutions in the market, constituting the central focus of this work, is the design of a digital graphic interface through which the user can interact with the product. safeguard, namely, access and manage the data derived from its performance.

Thus, this work aims to develop a Mobile Application (app), which will communicate with the guard via wireless, and which will enable the caregiver to check the patient's condition at any time. In this case, it is intended to implement two versions of the app that are suitable for patient monitoring in more technical or familiar environments (hospital / institutional or home environment). Thus, a home version was designed for use by family members and caregivers in the home environment. And another version designed for the institutional / hospital environment for use by doctors, nurses and other professionals/caregivers who have direct contact with patients, this version may be used in institutions such as nursing homes, retirement homes, rehabilitation centers / continuous care/palliative care, as well as in hospitals and other units that receive this category of patients.

Figure 1 presents an infographic perspective of the underlying approach taken by the ActiveRest project.



Figure 1: ACTIVEREST Project

The solution presented in this project, in addition to designing an application that is capable of displaying data from communication with the bedridden, also has a set of other features that complement the patient's treatment and give the application another level of protection. So, based on what has been said, the research carried out and presented in this article aimed to improve the development of a mobile application in order to design a more versatile and efficient solution that enables better results of the mobile application in the use of textile protection by the digital component.

## 2. Digital Transformation of Health in Portugal

Digital transformation is increasingly present in health and, in this sense, “several systems have been developed, implemented and updated to improve the quality of the information in healthcare provision and management, increase efficiency and technologically upgrade existing systems. , allowing for an improvement in public services provided to citizens [...]” [5].

In Portugal, the eHealth Summit event has been held in recent years where the main advances in the Health area are debated. Besides, several implementations of the concept have been observed in the country, an example is the Paperless Receipt (PR) which, according to the NHS, consists of the following: “With PR, the user may provide his doctor with an email and mobile number to receive prescribing information. At the time of consultation, he will be able to receive the treatment guide in paper form, or choose to receive it via email, and also access and consult it in the Citizen Area” [6]. In August 2018, the PR represented 97.02% compared to the traditional ones [7]. This figure reflects the effectiveness of the implementation of the system which, besides reducing costs and contributing to environmental preservation, has greater safety and control of the prescription of the medicine.

Henrique Martins, President of the Ministry of Health's Shared Services (HSS), states that “[...] we cannot continue to program and create digital solutions, assuming that people are sitting in front of a fixed terminal. People move. Healthy people do not go to the NHS much, nor do they want or seek health care... It is health that has to go after them and preferably in their pockets and everywhere. Therefore, all mobile digital transformation requires a paradigm shift in programming, creation, and the relationship of digital tools.” [8, p. 9]. In Portugal was created MySNS Carteira, an app that allows the user to consult his health information present in the National Register of User (NRU), through his own mobile phone. In May 2018 this was the most popular app in Portugal in the Health & Fitness category of the GooglePlay and AppleStore stores [9, 10].

MySNS Carteira is an example of mHealth - Mobile Health that “refers to the practice of medical and public health supported by mobile devices such as mobile phones, tablets, personal digital assistants (PDA) and wireless infrastructure. [...] mHealth covers all applications of telecommunications and multimedia technologies for providing health information.” [11].

In the Portuguese context, mobile applications are the most used medium in mHealth, with surveillance, monitoring and information exchange being the most used features in the development of these apps [12].

Through several initiatives, such as those mentioned above, Portugal distinguishes itself at the forefront of Digital Health Transformation with prominence among the member countries of the European Union [5]. Despite this achievement, SPMS President Henrique Martins has listed eight essential conditions for the country to continue with this advance: (1) Social and political motivation and support; (2) eSkills of health professionals and digital literacy of citizens; (3) Technical skills of technical staff in the State and in companies; (4) Strengthening the action of digital transformation agents; (5) Robust infrastructure, fast networks, and appropriate hardware; (6) Digital pillars and experience; (7) Mobile-to-start principle; (8) All2All thinking; CyberSecurity as a Service; TeleHealth as a principle rather than as a supplement [8].

Under these conditions, it is possible to observe that both health professionals and other citizens are fundamental elements for TDS in Portugal to continue to happen gradually. Through the support, receptivity, and use of technological systems, it will be possible to create a means of collaboration for this advance. And for these technologies to be successful before the public, the intervention of professionals specialized in technological and digital areas, such as programmers and designers, is required.

### **3. Mobile Health Applications**

Since its inception, the use of mobile applications has spread. The massification of mobile devices coupled with the expansion of easy access to the internet, justify the growing increase in their use. Other factors that contributed to this growth are the ability to be developed for various types of needs, and the mobility characteristic of mobile devices. The number of app store downloads is growing rapidly every year. In 2017 the number of downloads was 178.1 billion, the forecast is that this number will increase to 258.2 billion in 2022 [13].

Wireless technologies combined with mHealth enable healthcare to be increasingly connected. In the digital health market, mHealth has been the fastest growing technology since 2015 [14]. The diversity of mHealths present in online stores is extensive, being one of the fastest-growing categories. According to a statistical analysis by Statista, the Health & Fitness group is AppStore's eighth most popular group.

Through the use of wearable equipment (electronic devices that capture and send information and can be used as clothing accessories, such as a bracelet or watch) apps are developed for various uses and mainly for monitoring, storage and data exchange. FitBit is a company that manufactures a wearable technology-based wristband that collects fitness data from the wearer and uploads it to their smartphone storage. According to one study, the use of the bracelet proves to be effective in weight loss [15]. In addition, other research indicates that data collection by the device is accurate and reliable [16]. In 2016, the same company was in the top 50 on the list of the 500 fastest growing companies worldwide [17]. Just like the FitBit bracelet, there are many other solutions in this context, which have a good reception by the public.

Mobile applications have changed the global health scenario in both work and personal care. There is a wide variety of applications focused on this area, and the trend is its gradual increase, especially with the introduction of new devices that, together with smartphones, allow the development of increasingly accurate and new mHealths. functionalities. On the other hand, because it involves a delicate subject such as health, it is necessary that these applications have supervision by a regulatory body, especially those that indicate diagnosis, since the apps are not 100% safe, always requiring the review of a professional. Cybersecurity is also an important issue, namely in protecting the user's personal data.

Based on the objectives of the ActiveRest project, a mobile application was developed which, through data collection and exchange with the textile guard, enables better patient monitoring and, consequently, the prevention of pressure ulcers. Although there are already apps on the market that focus on the same theme of this research, they do not meet the needs of the equipment in question, for two main reasons: first because it is a device that has been developed since its inception, featuring certain particularities

and functionalities that set it apart from other equipment; and second for distancing itself from apps with unattractive aesthetics to the user, being one of the main goals the development of an app with an appealing aesthetics for different segments of the app users.

### **4. Research Contribution**

Pressure ulcers are classified by the NHS in the National Network of Integrated Continued Care group (RNCCI) which "has as its main objectives the provision of continuous and integrated health care and social support to people who, regardless of age, are in a situation of dependence and loss of autonomy" [18, p. 109]. Detailed information on health statistics and the burden of pressure ulcers on the economy has been provided by OCDE [19].

The DGS indicates that about 95% of pressure ulcers are preventable, as long as their degree of risk is identified in advance, so one of the factors that help prevent this problem is proper patient monitoring. One of the many problems that arise from the emergence of pressure ulcers is the increased length of stay of the patient causing the NHS greater financial burden.

The development of a mobile application that allows the caregiver to check the patient's condition at any time could improve the prevention of pressure ulcers in order to optimize patient monitoring through the guarding sensing system which will send data about your performance for the app. With the ease of mobility of mobile devices, healthcare professionals, through the use of guard and mobile applications, will have greater control over the risk of developing pressure ulcers in patients using this type of equipment.

Through the use of the app, the workload of professionals responsible for providing the necessary care to these patients tends to decrease, since the system works autonomously, alerting the caregiver whenever there is a need for repositioning, as well as which or which body regions are under pressure. The decrease in the appearance of pressure ulcers, in addition to bringing more quality of life to the patient and their caregiver, will also present to the NHS a decrease in the expenses resulting from this health problem.

### **5. State of Art**

For this analysis, we used mobile applications and device interfaces that integrate objects that act physically in the prevention/treatment of ulcers, such as mattresses with pressure sensors. The examples below correspond to existing applications/interface models that are designed to assist patients and their caregivers in the prevention and treatment of pressure ulcers, and also serve as an informative tool for this type of skin wound.

Applications and software analyzed: A) VA Pressure Ulcer Resource mobile application, B) XSENSOR - FORESITE PT software, C) uControl app and D) Lifelens.

The VA Pressure Ulcer Resource application developed for pressure ulcer and injury prevention is intended for US war veterans and their caregivers. Features such as history; sticky notes; notes; pressure and time monitoring graphs; alerts for the user to move around; a shortcut to get urgent care, as well as knowing where the nearest hospital is. These features allow the user to act proactively, through history and reminders, preventing the appearance of pressure ulcers. Alerts allow mobile users or



caregivers to act at certain times, helping the patient to move so that there are no very long periods of body immobility [20].

The XSENSOR – FORESITE PT created ForeSite PT, which is a body pressure monitoring system using a mattress cover and a touch screen monitor with software that analyzes and stores data. Real-time display of a body map of the pressure being exerted allows the user to act on body movement only when necessary. Graphs with the duration of the current position and the occurrence of repositioning allow the system to be used by different users, a common occurrence in hospitals. The timer indicates the time intervals to be reset and is positioned prominently on the interface because it is a key feature of the system, allowing the user greater control over patient movements [21].

Unitron is a multinational company with high experience in hearing solutions. As a member of the Sonova Group, Unitron develops high-performance hearing solutions that enable natural listening to sounds and speech. In addition to hearing aids, Unitron offers its users three applications: Remote Plus, uControl and Start Here. These applications allow the user to get the most out of the device by adjusting the volume and balance of the hearing aids. Constant assessment of user satisfaction is also allowed, as is communication between users. This application is developed for the senior public and differs from the vast majority found in this market by presenting an attractive and intuitive design, managing through graphic minimalism to effectively transmit messages to the UI [22].

Pressure Ulcer Prevention is a mobile application developed by the University of Southern California School of Medicine for patients with pressure ulcers to use as a follow-up, information and research about the disease, thus allowing the sharing of information with doctors or caregivers for better identification of causes and subsequent prevention. The application allows the user to photograph and annotate some parts of his body - specifically the areas most sensitive to the appearance of pressure ulcers - for monitoring. With this data, the app creates graphs showing the history of the monitored part. It also allows the user to create alerts to remind them to reposition themselves to avoid constant pressure on a certain area of the body. It has a didactic component where it tells the patient recommendations to reduce the risk of ulcers. And just like the previous mobile app, it even includes a shortcut for the user to make emergency calls [23].

Vista Medical is a company that develops technologies in the field of sensors and pressure mapping. This brand has developed the BodiTrack system that consists of a kind of sensor blanket and a USB cable for the integration of devices such as tablets and computers to access the product software.

This software allows the user to view the history of pressure exerted at a given time; visualization of areas with higher pressure; indicates the risk factor of each body part according to sensing; allows you to time the repositioning time; indicates the maximum pressure exerted during a selected period; ability to create alarms and real-time pressure mapping [24].

Lifelens is a Windows Phone 7 application that diagnoses malaria with 94% accuracy, which contrasts with 40% of conventional methods [25]. This app significantly reduces the costs of testing and traveling teams for testing, as it only requires the user to photograph blood already combined with special malaria dye, then a specific algorithm indicates if the patient is infected. Results can be sent via the Internet, along with GPS

coordinates, thus enabling faster interventions in disease outbreaks.

According to this analysis, it was possible to identify some functions that were the basis for the ActiveRest app project, namely: the real-time visualization of the pressure exerted by the body. This feature quickly and effectively provides you with information relevant to pressure ulcer prevention along with history, reminders, notes, pressure and time monitoring graphs.

The most relevant features for the study of the creation of the ActiveRest app were: the real-time visualization of the pressure exerted by the body to the local and general software. pressure ulcer prevention; pressure and repositioning history for better analysis of patient behavior; pressure and time monitoring reminders, diaries, and graphs for optimizing information catalysis.

An important detail found in the analyzed applications (table 1) was the presence of an emergency button that allows the user to quickly contact another person. However, it was observed that despite having an interesting concept, shortcuts in applications are confusing and with various actions to make the contact, causing the functionality to lose its main purpose. In ActiveRest we analyzed a more effective way to make this contact, allowing the user to perform the task with the fewest possible actions.

In the analysis of solutions for the prevention and treatment of pressure ulcers, it can be observed that the interfaces need a specific development, as well as the attention regarding UX because it is a product to be used by two audiences of different age groups. One of the challenges of this project was the development of interfaces that meet the needs of both segments.

Table 1: Comparative table of applications and software functionalities.

FUNCTIONALITY	APP - SOFTWARE				
	VA PRESSURE ULCER RESOURCE	PRESSURE ULCER PREVENTION	XSENSOR FORESITE PT	VISTA MEDICAL BODITRACK	UNITRON
Body Pressure Map					
Body Humidity Map					
Historic					
Sticky notes					
Daily					
Monitoring					
Data Graph					
Move Alert					
Emergency button					
UP's Information					
Stopwatch					

PRESENT
ABSENT

## 6. Mobile Application Development

Extensive analytical work on the literature on the types of mobile applications and graphic software interfaces in the area of pressure ulcer prevention devices / systems has culminated in an app proposal and its specifications have been defined. In this way, it was possible to define the necessary steps for the development of the app, among which the characterization of the people; the information architecture; wireframes and wireflows; the visual identity; prototyping; and the mobile application to the current development of textile protection.

### 6.1. Personas

Persona 1 - Bruno, 30, male nurse responsible for providing care and monitoring bedridden patients. He works in a large hospital and looks after a sector with 25 bedridden patients, some of whom have pressure sores and the remaining developmental risks. It uses the ActiveRest app along with the textile guard to monitor patients more effectively, enabling them to make better and more accurate patient surveillance and, when necessary, to take appropriate preventive measures early. It also uses the app to record and manage patient information, including repositioning history, humidity, pressure, temperature, and view notes and reminders.

Persona 2 - Joana, 42, journalist, responsible for accompanying her bedridden mother at home. Joana works at home but sometimes needs to be absent. Use the app and guard to know when to reposition her mother as well as to receive alerts when an abnormal or hazardous situation is detected, including critical pressure spikes and/or excessive temperature and humidity levels.

Persona 3 - Maria, 67, retired, has reduced mobility, so she spends many hours in bed. In addition to lack of mobility and sensitivity, which requires help to move and change her position, she also has memory problems, having some difficulty remembering to take the medicines. That said, Maria uses the app as a resource in her care, taking advantage of the app's alarmistic ability to reposition herself, as well as medication reminders, among other features that help her in her daily life and that provide her with preventive measures against her condition. She also uses the diary feature and reminder setting to create notes that may be important to present to the attending physician. She also makes use of the emergency call function as she has an imminent risk of myocardial infarction.

### 6.2. UX UI for audiences of different age

A aplicação móvel será utilizada por públicos de diferentes idades, sendo a idade inicial os 25 anos. O público jovem/adulto geralmente possui melhor literacia digital em comparação ao público idoso (65+). Por este motivo, foi necessária uma investigação a respeito do desenvolvimento de interfaces digitais para públicos com diferentes níveis de literacia digital.

The worldwide increase in the number of older people in an increasingly digital society requires that digital technology solutions were increasingly adapted to this public. The aging of the human body, even if currently possible, is one of the main obstacles in the use of digital media, due to the gradual loss of motor and mental abilities. However, the lack of use of appropriate solutions for this class of users in the development of digital interfaces is also one of the major factors for the frustration and withdrawal of the use of these technologies.

Data indicate that the usability of websites decreases 0.8% per year between the ages of 25 to 60 years, the reason is the increased time to complete each task on the page, and difficulties in interacting with the interface. This percentage tends to increase after age 60, a 75-year-old is 74% slower to use websites than a conventional 35-year-old. This is due to the consequences of human aging that contribute to it, among them it is possible to mention: the decrease of cognitive resources; of visual ability; the ability to memorize; of perception; and motor skills [3].

Nielsen says that designing only for the young audience may result in the elderly giving up the interface. In contrast, when designing for the elderly the chances of the interface being used by both audiences are significantly higher because the basis of the research will be for the development of an easily accessible interface for people with reduced mental and motor skills, so the interface can answer also to the young public that usually has these capacities in better condition. However, good practices for aesthetic design must be present in the project, as it is an important the attractive component for young audiences. Thus, the adaptability of the mobile application is an important resource to be used for both audiences to achieve greater success in using the app.

According to an analysis of several studies, it was possible to find different recommendations to be followed so that the interaction of senior users with digital interfaces is of the least possible frustration. These recommendations are based on human behaviour in a digital environment as they age, and the issues of decreased vision, motor coordination, and reduced memory capacity are the main factors for their development.

These recommendations, although based on the development of interfaces for the elderly, are largely similar to those indicated in the design for the adult audience. About the 10 Interface Design Usability Heuristics developed by Nielsen, the author states that: "The 10 Principles of Interface Design Usability are called heuristics because they are general rules rather than specific usability guidelines" [4].

With this research, it was possible to compile the analysed studies on the recommendations for interface design for seniors and then created a table where it is possible to briefly find these guidelines (Table 2). This table aims to facilitate and speed up the design of interfaces for seniors, so that following the suggestions in it is likely that the final product has a better solution for the user.

These recommendations have been used in the implementation of both versions of the app, so that both classes of users can use both versions of the app without causing them frustration or major handling difficulties.

### 6.3. Information Architecture

Information Architecture (AI) is a term created by designer Richard Saul Wurman. In his book "Information Architects" he states that the information architect is the "individual who organizes patterns inherent in data, transforming the complex into something clear" and who "creates the structure or map of certain information to enable others to create their path toward knowledge." It further states that "AI is the emerging profession of the 21st century, whose scope is shaped by current needs, focused on clarity, human understanding and the science of information organization." [26]

Table 2: Recommendations for the design of digital interfaces for the elder

NAVIGATION	TEXT	COLOR	GRAPHISM
Home page customization option;	Font size should not be less than 14pt;	Color contrast: 4.5: 1 or 3: 1, depending on font size;	Visual noise reduction;
Allow the user to enlarge the screen;	Use non-serif and non-condensed typography whenever possible;	Option to change the colors of the application, and the other version of the theme should have colors with more contrast;	The application icon must be easily recognizable;
Always inform the user of the current page;	80 characters per line in text;		Try to use familiar and user-recognizable symbols;
Minimum possible actions to perform tasks;	Avoid the use of justified text;	Actions when identified by colors should also, whenever possible, make use of text or symbols;	Buttons with clear language and distinct from the other features of the app and avoid having too small dimensions, with the recommended minimum size 9mm high or wide;
Avoid drastic changes to the application interface when updates occur;	Use few font styles as well as different types;	Avoid using colors such as blue and green on the same screen, as the elderly have difficulty distinguishing them in screens;	
Whenever there is an error-prone and irreversible action, ask the user for task verification and confirmation;	Create option to increase or decrease mobile application font size;		
The most important features should be visible on the first page avoiding the need for many interactions to find them;	Make use of clear and simple language that does not force the user to make too much memorial effort to identify an action;	In the background of texts avoid high contrast and opt for a pastel color so that there is no interference in reading due to the screen light;	
Make navigation as predictable as possible, as well as consistent with using the same features across all app pages;	Avoid the use of unnecessary words, where possible use a word to describe a function, always simply and clearly;		
Whenever possible, insert top and bottom navigation bars should be uniform throughout the app navigation and should have frequently used page access buttons such as Home;	Make clear the hierarchy of information, clearly and clearly exposing the titles, and the information, according to its degree of importance, should be highlighted or evidenced;		

In the case of a mobile application, the information architecture brings together the concepts that will be present in the project and logically segments the information that will give rise to the features to be inserted in the app. This step makes the development of functions more objective and understandable. It is possible to observe in Figure 2, the information architecture for the app that is intended to be developed within the ActiveRest project, through a demo with the main specifications of the app, taking into account the different scenarios of use of the guard.

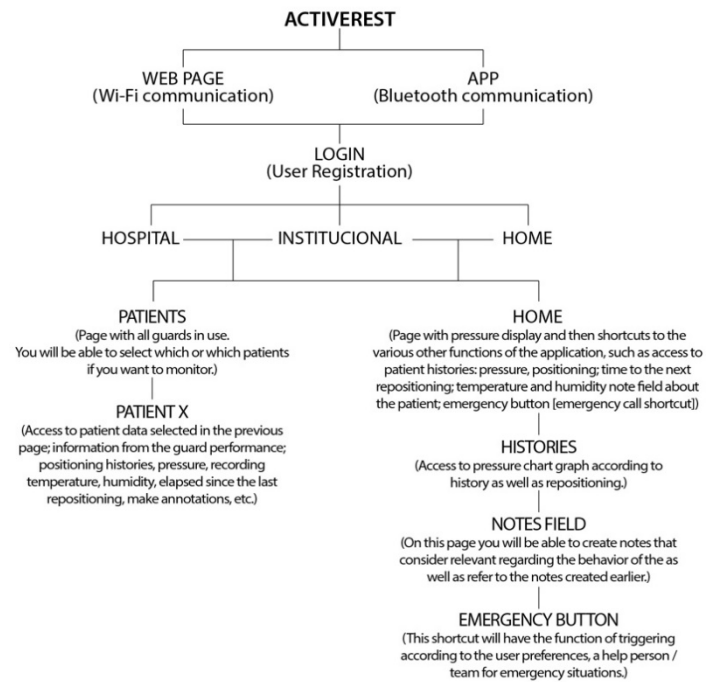


Figure 2: Information Architecture.

#### 6.4. Wireframe and Wireflow

The term wireframe derives from the term waterfall which is defined as a model where the structure process is schematic and sequential, being drawn from top to bottom. This model was described by Winston W. Royce in 1970. With the development of digital editing software, such as Adobe Photoshop, more flexible [27]. According to Brown "Wireframes are" crude "illustrations that show, to a greater or lesser extent, the content of each screen. They are called wireframes because they are usually rendered with simple lines, not very elaborate designs. They illustrate, among other things, what kind of information will be most important on each screen" [28].

From the developed wireframes, it was possible to create the wireflow, that is, the flowchart that will act through the drawn screens. This step made it possible to identify the effectiveness of fluidity in navigating the related functions.

#### 6.5. Visual identity and design guidelines

Regarding this project, the visual identity was developed to act in the mobile application and derived from the logo previously developed for it, and the main components derived from the logo used for the deployment of identity in the app were the colors and minimalist language.

According to the Interaction Design Foundation, design guidelines can be defined as: "sets of recommendations for good design practice. They are intended to provide clear instructions for designers and developers on how to adopt specific principles such as intuition, learning ability, efficiency, and consistency. Rather than dictating conventions, design guidelines provide helpful advice on how to achieve a design principle that can be platform-specific or cross-platform." (Interaction Design Foundation, 2017). This definition can be understood as a set of good practices to be adopted in the development of design projects. It is not mandatory to use them, but only advisable, to improve the harmony of language for the use [29].



In the user interface field, Google and Apple are the largest guidelines developers, this is because they have the two largest mobile operating systems, respectively, Android and iOS. According to IDC consultant, the two best-selling smartphone brands in Portugal in 2017 were Huawei and Samsung, both using the Android operating system. Nevertheless, a study by Marktest in November 2017 indicated that the sites audited by the Android group had a 30.8% access percentage, representing leadership over other systems [30]. Thus, the most used operating system in Portugal is Android, which is why the app was developed according to the guidelines established by Google for the design of mobile applications.

Google created Material Design, defining it as "a visual language that synthesizes the classic principles of good design with technological and scientific innovation." Thus, this concept can be understood as a set of guidelines that can be used for software development, directed mainly to the Android operating system. On the material.io website, the company offers several packages designed, based on scientific studies, in the concept of guidelines for the user interface. Also defined by UI Kits, this type of content is not required but has a high impact on mobile application development.

In summary, some of the advantages of using these UI Kits are that they are developed based on studies that seek the most satisfactory user possible interface and time optimization. First, on the part of the designer who can use this time in other components of the app design, and secondly on the part of the user, who can create a higher rate of application receptivity, as many components are known by him.

It is also possible to observe in these UI Kits the presence of several recommendations for elderly interface design as well as Nielsen's heuristics. Some examples as simple and straightforward language; visual noise reduction; use of non-serif typography; minimalist design; consistency and predictability in navigation; use of standards among others are inserted in the development of this material. Thus, the use of Google's UI Kit for ActiveRest application development was then defined as it had the interface developed for the Android operating system and these guidelines already fit the recommendations for designing applications for seniors as well as the use of parameters to be used for the adult audience. The images below demonstrate the design of some application screens using Google's UIKit.

### 6.6. ActiveRest App

After analyzing all the research carried out within all the necessary components for the development of a mobile application that responds to the adult and elderly public in the same digital environment, the application was designed. For its development, the recommendations for interface design for the elderly as well as Nielsen's heuristics were used:

- **Color and Icons:** The predominant color (#00AAAD) used is the same as the project logo. For better contrast, black and gray were used, as well as the use of white spaces to prevent visual noise, choosing the minimalist language. The settings can be changed the app theme to a higher contrast mode as well as change the font size. In Figure 3 can be seen the color option used and the option to change the font size. The icons are meant to be easily recognizable, thin lines were avoided, not to disturb the user's perception.



Figure 3: App Colors | Option to change font size | App icons.

- **Home and Repositioning Time:** on the homepage are the shortcuts to the most important functionalities of the application (see Figure 4), as well as the emphasis of the body pressure map and repositioning time that is present in most of the pages of the app for better control of the user.

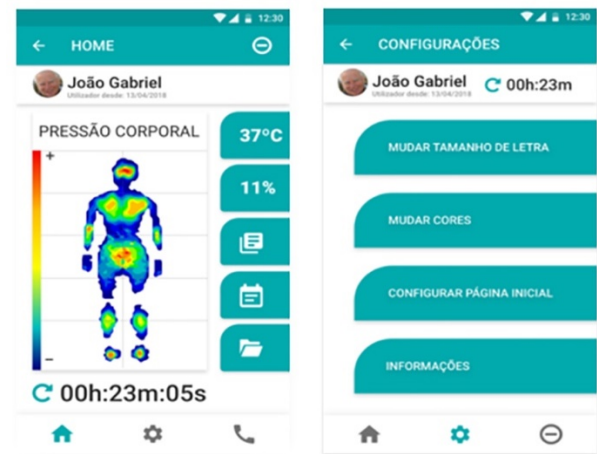


Figure 4: HOME-Domestic | SETTINGS-Hospital / Institutional screen (in the upper right corner is the timer).

- **Emergency Button:** was developed so that the user performs the minimum of actions to complete the task. We used windows to confirm the fulfilment of emergency requests to avoid unnecessary requests. These windows are positioned closer to the bottom of the interface so that the user can finalize the task with the least possible actions (see Figure 5).



Figure 5: EMERGENCY BUTTON screen and Home confirmation popUp.



- HOME version and HOSPITAL / INSTITUTIONAL version: The two versions of the app are similar in several respects, differing only in the following, the login mode that in the home version is done through the user and password credentials, and in the hospital / institutional version is done through the access PIN, the latter being the most common mode in hospital software; Emergency Button functionality is present only in the home version because it is not useful in a hospital / institutional setting.

### 6.7. Prototype

The prototypes can be tested in the following links:

- DOMESTIC: <https://marvelapp.com/ed2cbie>
- HOSPITAL (Institutional): <https://marvelapp.com/4id38ji>

## 7. Wireless Communication System

The Bluetooth Low Energy (BLE) communication protocol was selected to enable a simple and standard way to establish between the mattress guard and the developed mobile App. For each mattress guard, there will be a local electronic system (comprised of a printed circuit board with a processor, storage unit, and a BLE module), which will manage the power supply of the different electric components and obtain a signal input from them (namely, the sensors and actuators embedded on the mattress guard).

Control of the sensors and actuators is achieved through a microcontroller, which also stores the sensor information in the local storage unit. When the App establishes a connection with the mattress guard, by pairing the mobile device with the BLE module in the local mattress guard controller, data will start being transferred by Bluetooth and become available to the user. Conversely, whenever high pressure loci are detected above the defined threshold, the device will enable one or several of the actuators (according to a protocol developed within the ActiveRest project) in order to eliminate that pressure peak.

Figure 6 shows a schematic of the communication model between the mattress guard and its control and management electronic system, as well as the digital unit to where the data are sent by Bluetooth, becoming accessible to the user.

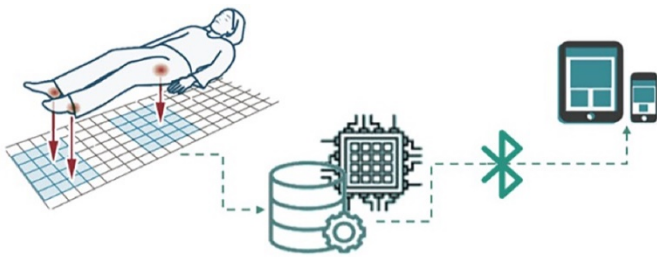


Figure 6: Scheme of the data communication model.

## 8. Android App Implementation

In order to validate the graphic model of the developed App, a prototype version was created, integrating the core features that can be tested by users and that are vital to the underlying purpose. These include the wireless communication between App and the mattress guard, and are essentially dependent on the hardware that acquires the signal and stores it for further processing. This App was developed using Android Studio version 3.1. It was compiled and further tested using a mobile phone running Android 7.0, and

featuring current standard hardware, including the required Bluetooth communications module.

The App initializes with the project logo. After the start-up screen, the user is presented with the first interactive screen, that displays data received from the mattress guard. This main screen intends to provide almost all relevant information the user requires for the purpose of monitoring the bedridden patient, and includes a graphical representation of the pressure mapping. In order to communicate with the mattress guard, the App employs the low energy Bluetooth protocol, using a pre-defined MAC address (configurable by the user), thus receiving data from the external on a regular time interval. The pressure data is processed into a color scale, which highlights specific pressure loci. The employed color scale goes from white (which stands for locations with pressure below a minimum setting, and which are not relevant), passing through a blue gradient (relatively low, but relevant pressure, usually implying the presence of a body), up to the highest pressure values, in red gradient (implying the pressure in that location has exceeded the threshold pressure for potential formation of ulcers). For every sensor present in the mattress guard, the value provided to the App is mapped onto this color scale and rendered in the two-dimensional grid that represents the physical device (see Figure 7.a). It was possible to use a simple and regular two-dimensional grid because all the sensors are spaced equally in the developed mattress guard, but this could be easily adjusted to any other physical configuration of the sensors.

Whenever the local pressure value exceeds the user-defined threshold (for which the project conducted a literature review and collected information from medical staff), it will induce an alarm, which can then trigger both (or either) a communication to a caregiver by text messaging, and a local notification / pop-up (with an audible trigger). Also, in order to allow analysis of the history of previous high pressure loci alerts, whenever the value exceeds the threshold it is stored in a list, which can then be accessed through a specific App page. This second App page, with the history of critical values, is shown in Figure 7.b. Note that in this view only the highlighted pressure loci are usually represented, but the user can quickly adjust the mapping threshold, for example to see how the overall pressure map evolved between alarm intervals. The pressure information is stored in a simple text file which later can be extracted from the device and transmitted to a caregiver or a physician.



Figure 7: Android App screenshots: (a) the main page where the data from the pressure mapping, and the temperature and humidity values are shown, as well as the repositioning timer, and (b) the page with the history of critical pressures that exceed the established threshold.

Last, the developed App includes a timer that send a notification to the caregiver after the specified interval. This is very useful for the regular repositioning of the patient which is a routine activity that needs to be performed on bedridden patients. The mattress guard does not intent to replace the standard repositioning protocols, but to complement them by identifying whenever a more urgent action is required, and thus, the timer was a feature request by all the professionals that were inquired during the early specification stage.

### 9. Usability tests

The usability test is one of the most important phases of the project, it is through it that the user will contact the product and will bring the designer answers regarding the usability and effectiveness of the developed interface. Loranger states that the main benefit is identifying design efficiency as well as the actual needs of users [31].

Nielsen states that five participants are the ideal number for taking a test and that, for best results, they should be short-lived and made up of simple tasks [32]. Usability testing can be developed early in the project, except when the product is for senior audiences. In this case, the prototype to be tested must be of high fidelity, because, due to the aging of cognitive abilities, this audience has a lower degree of abstraction and imaginary component [26, 27].

Loranger highlights nine important criteria to consider when preparing a usability test [33, 34]. They are: (1) Define the purpose of the test; (2) Define the format and scenario of the test (lab or field / moderate or unmoderated / face-to-face or remote); (3) Number of users; (4) Ensure that participants are suitable for the intended test; (5) Create tasks corresponding to the purpose of the study; (6) Perform a test run; (7) Collect metrics; (8) Create a script for the test; (9) Conduct the team test consisting of a moderator (who conducts the test) and an observer (who observes and takes notes).

During the test, it is essential to pay attention to the mode of communication with the participant so that the influence on the final action is as small as possible. Nielsen states that the Thinking Aloud method is the most important tool in a usability testusabilidade [35], asking the participant to say what he is thinking while performing the task is an important resource for assessing how the user interprets the interface. Interventions are discouraged when the participant is performing a task, questions should be unbiased to avoid naming interface elements and where possible answer the participant's questions with other questions and these should be exempt leading him to the conclusion by himself [24],[28]-[31].

After the completion of the test it will be through the analysis of the collected data that the success rates of each tested functionality will be found and, if necessary, redesigned to better fulfill the interface objective.

In the present project the usability tests were performed only with the interface developed to work in an institutional / hospital environment, were directed to three groups of participants, the first group was of eight nurses, the second two doctors, and the third five direct action assistants. It was decided to test the prototype in high fidelity in order to facilitate the participants' interaction with the product. A guide was developed for the documentation of the test, which contained a detailed description of each task to be requested for the participant, as well as areas for annotation of the

responses and their behavior. An app qualitative assessment questionnaire was also created for each test participant to complete at the end.

For data analysis, the profession and age range of each user was taken into account. The results indicated that the 31-40 age group had a higher success rate in using the interface. In terms of profession, nurses and physicians were the ones that represented the highest success rate. It is noteworthy that according to the questionnaire performed at the end of each test, these two classes were those that showed the greatest interest in mobile application adherence. It was identified that the questionnaire will not be the most appropriate tool to be used in usability tests, due to the fact that it presents different results from those collected in the monitoring guide, that is, the user's opinion did not always coincide with their own rate. of success in accomplishing each task. Results are shown in Figures 8 and 9.

With an 85% success rate, it was concluded that the HOSPITAL/ INSTITUTIONAL interface achieves the proposed objective. However, for better use of the app it is best to have the two features with a lower success rate (change timer and exit the application) be changed as these are key functions in using the app.

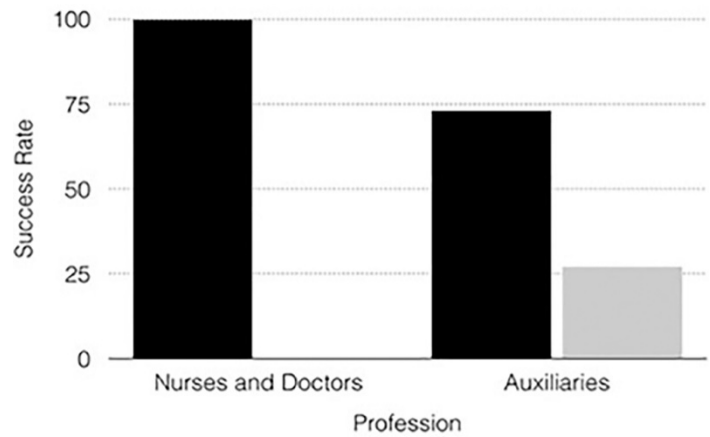


Figure 8: Profession Success Rate Chart; black: success rate; grey: failure rate. The graph comes from usability tests.

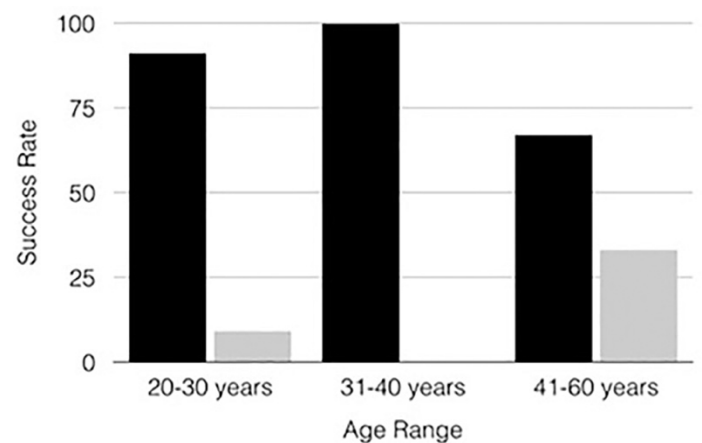


Figure 9: Age Success Rate Chart; black: success rate; grey failure rate. The graph comes from usability tests.

### 10. Conclusion

Pressure ulcers is a serious problem that significantly affects a patient's quality of life. This problem occurs mostly in the elderly,

with a high loss of physical health. Whether for economic or welfare issues, solutions focused on health care for the elderly are important preventive measures for the well-being of a society in which the average life expectancy of people tends to increase.

ActiveRest emerges as a solution focused on the prevention of UPs, through a textile shelter and a mobile support application. This project aims to offer patients (and their caregivers) a relevant contribution to their quality of life.

The present work had as main objective the development of the digital interface to work together with the 'ActiveRest' textile mattress guard. For the study it was necessary to examine the current panorama of digital technological investment in health with emphasis on the Portuguese market. In this way, it was possible to identify the current reality of health institutions as well as the existing solutions in the market to respond to this problem. The analysis of the behavior of the target public (adult and senior) was fundamental to understand what the real functionalities that these users need. It was also essential to analyze the solutions already on the market, these were selected according to similar functionalities that would be present in the ActiveRest project.

The application resulting from the investigation of this project, adapted with two versions to be used in a hospital environment and another in a home environment, even with the objective of working together with textile protection, is able to independently present support for prevention pressure ulcers. For example, the application's timer functionality provides the user with better control and optimization of time and, if there is a possible failure in blocking the application, it will continue to work. Features like Diary, Help Button and Reminders also do not require the backup feature. For a better use of the application, it will always be necessary to use textile protection, however, these components demonstrate that the mobile application remains operational and functional, even without using it.

## 11. Acknowledgements

Sandra Ventura (Texteis Penedo), Graça Bonifácio (CITEVE), José Casquilho (ComfortKeepers), Joana Fonseca (CENTI), Joana Almeida (CENTI), Miguel Ribeiro (CENTI), Pedro Pereira (CENTI), and Ricardo Carvalho (CENTI), for their contributions to the ActiveRest project. This research was supported by FEDER funds through the COMPETE 2020 Programme under project ActiveRest (project 18011 of the 33/SI/2015 call).

## References

[1] R. Suzman, J. R. Beard, T. Boerma, and S. Chatterji, 'Health in an ageing world - What do we know?', *The Lancet*, vol. 385, no. 9967. Lancet Publishing Group, pp. 484-486, 07-Feb-2015.

[2] E. instituto nacional de PORTDATA, 'Esperança de vida aos 65 anos: total e por sexo (base: triênio a partir de 2001)', *PORTDATA*, 2014. .

[3] J. Nielsen, 'Middle-Aged Users' Declining Web Performance', 2008.

[4] National Pressure Ulcer Advisory Panel et al., *Prevenção e Tratamento de Úlceras por Pressão: Guia de Consulta Rápida*, vol. 2, no. 1. 2014.

[5] H. Martins, 'Transformação digital e inovação na saúde em debate no "Portugal eHealth Summit"', *PÚBLICO*, 19-Mar-2018.

[6] Serviço Nacional de Saúde, 'Receita Sem Papel - SPMS', 2018. [Online]. Available: <http://spms.min-saude.pt/product/receita-sem-papel/>. [Accessed: 09-Sep-2018].

[7] SNS, 'Receita Sem Papel - Monitorização'. [Online]. Available:

<https://www.sns.gov.pt/monitorizacao-do-sns/receita-sem-papel/>. [Accessed: 09-Sep-2018].

[8] H. Martins, 'SNS digital e as condições da transformação digital na saúde', 2018.

[9] A Enfermagem e as Leis, 'MySNS Carteira: Aplicação móvel do SNS lidera na categoria de saúde e fitness | A Enfermagem e as Leis', 2018. [Online]. Available: <http://www.aenfermagemasleis.pt/2018/05/09/mysns-carteira-aplicacao-movel-do-sns-lidera-na-categoria-de-saude-e-fitness/>. [Accessed: 09-Sep-2018].

[10] G. Lins, 'MySNS Carteira (SPMS) | Guga Lins UX/UI Designer'. [Online]. Available: <https://www.gugalins.com/mysns-carteira/>. [Accessed: 10-Dec-2019].

[11] Innovatedmedtec, 'mhealth - what is mhealth?', 2018. [Online]. Available: <https://innovatedmedtec.com/digital-health/mhealth>. [Accessed: 09-Sep-2018].

[12] C. Duque, J. Mamede, and L. Morgado, 'Iniciativas de mHealth em Portugal mHealth initiatives in Portugal', 2017.

[13] Statista, 'Annual number of mobile app downloads worldwide 2022 | Statistic', 2018.

[14] Statista, 'Global digital health CAGR by major segment 2015-2020 | Statistic', 2018. [Online]. Available: <https://www.statista.com/statistics/387875/forecast-cagr-of-worldwide-digital-health-market-by-segment/>. [Accessed: 13-Sep-2018].

[15] J. M. Jakicic et al., 'Effect of Wearable Technology Combined With a Lifestyle Intervention on Long-term Weight Loss', *JAMA*, vol. 316, no. 11, p. 1161, Sep. 2016.

[16] K. M. Diaz et al., 'Fitbit®: An accurate and reliable device for wireless physical activity tracking.', *Int. J. Cardiol.*, vol. 185, pp. 138-40, Apr. 2015.

[17] Deloitte, '2016 Technology Fast 500™ Ranking Recognizing growth', 2016.

[18] Ministério da Saúde, 'Relatório anual acesso a cuidados de saúde nos estabelecimentos do sns e entidades convencionadas', 2018.

[19] OECD, *Health at a Glance 2017*. OECD, 2017.

[20] U.S. Department of Veterans Affairs, 'Resource App', no. March, 2017.

[21] XSENSOR, 'XSENSOR Technology - Accurate Pressure Imaging Sensors'. [Online]. Available: <https://xsensor.com/>. [Accessed: 10-Dec-2019].

[22] uControl, 'uControl'. [Online]. Available: [https://www.unitron.com/content/unitron/pt\\_PT/professional/hearing-solutions/accessories/hearing-instrument-accessories/ucontrol.html](https://www.unitron.com/content/unitron/pt_PT/professional/hearing-solutions/accessories/hearing-instrument-accessories/ucontrol.html). [Accessed: 10-Dec-2019].

[23] Pressure Ulcer Prevention (PUP) |, 'Pressure Ulcer Prevention (PUP) |'. [Online]. Available: <https://medicinegov.org/pressure-ulcer-prevention-pup/>. [Accessed: 10-Dec-2019].

[24] BodiTrak, 'BodiTrak - Wireless Bed Pressure Mapping System'. [Online]. Available: <https://www.boditrak.com/products/medical/bed-system.php>. [Accessed: 10-Dec-2019].

[25] Internetmedicine, 'The Lifelens Project: Smartphone App Diagnoses Malaria from Drop of Blood | InternetMedicine.com', 2014. [Online]. Available: <http://internetmedicine.com/2014/04/26/malaria1/>. [Accessed: 13-Sep-2018].

[26] J. Nielsen, '10 Usability Heuristics for User Interface Design', *Nielsen Norman Group*, 1995. [Online]. Available: <https://www.nngroup.com/articles/ten-usability-heuristics>. [Accessed: 12-Dec-2019].

[27] R. S. Wurman, P. Bradford, and G. P. Corp, *Information Architects*. Graphis, 1997.

[28] Timetoast, 'History of wireframing Timeline', *History of wireframing*

- Timeline, 2018. [Online]. Available: <https://www.timetoast.com/timelines/23833>. [Accessed: 28-Aug-2018].
- [29] G. L. Strunck, *Como criar identidades visuais para marcas de sucesso.*, 4<sup>a</sup>. Rio de Janeiro, 2007.
- [30] Interaction Design Foundation, 'What are Design Guidelines? | Interaction Design Foundation', 2017. [Online]. Available: <https://www.interaction-design.org/literature/topics/design-guidelines>. [Accessed: 06-Sep-2018].
- [31] H. Loranger, 'Usability Test, Even When You Know the Answer', 2018. [Online]. Available: <https://www.nngroup.com/articles/test-when-you-know-answer/?lm=why-you-only-need-to-test-with-5-users&pt=article>. [Accessed: 01-Dec-2019].
- [32] J. Nielsen, 'Why You Only Need to Test with 5 Users', *Nielsen Norman Gr.*, 2000.
- [33] A. Dickinson, J. Arnott, S. Prior, and A. Dickinson, 'Methods for human-computer interaction research with older people', *Behav. Inf. Technol. is*, vol. 26, no. 4, pp. 343–352.
- [34] H. Loranger, 'Checklist for Planning Usability Studies', 2016. [Online]. Available: <https://www.nngroup.com/articles/usability-test-checklist/?lm=users-real-data&pt=article>. [Accessed: 01-Dec-2019].
- [35] J. Nielsen, 'Thinking Aloud: The #1 Usability Tool', 2012. [Online]. Available: <https://www.nngroup.com/articles/thinking-aloud-the-1-usability-tool/>. [Accessed: 01-Dec-2019].



## Evaluation of Vapor Jet Refrigeration Cycle Driven by Solar Thermal Energy for Air Conditioning Applications: Case Study

Ishaq Sider, Khaled Sider\*

*Mechanical Engineering Department, Palestine Polytechnic University, Palestine*

---

### ARTICLE INFO

*Article history:*

*Received: 03 March, 2020*

*Accepted: 31 March, 2020*

*Online: 14 April, 2020*

---

*Keywords:*

*Air Conditioning*

*EES Software*

*Evacuated Tube*

*Solar Collector*

*Solar Thermal Energy*

*TRNSYS Software*

*Vapor Jet Refrigeration*

*Cycle*

---

### ABSTRACT

*The need for air conditioning in rural areas where there is no source of electricity, leads to look for alternative solutions. Usage of Solar thermal system drive vapor jet refrigeration cycle (VJRC) instead of the traditional air conditioning systems, contributes in the reduction of the Global Warming and Ozone Depletion. The main objective of this paper is to test the visibility of using VJRC driven by solar thermal energy in rural areas to cover the cooling load demand of a typical movable house unit (TMH). After the mathematical modeling of the VJRC, the characteristic curves and tables were obtained by using engineering equation solver (EES) software assuming a constant evaporator temperature and various generator and condenser temperatures. TRNBuild subsystem in TRNSYS software was used to emulate TMH cooling load demand using weather data for two selected locations (Hebron and Jericho cities). TRNSYS software was used to investigate the validity of the proposed system in summer (May to September) for the two suggested locations. Three main parameters were studied in the proposed system, location, evacuated tube solar collector (ETC) area and hot storage tank volume. The results of the overall simulation of the proposed system indicated that the system efficiency in Hebron city was much higher than Jericho city due to climate and design conditions. In addition, it is found that there were many options for the system size can be selected to provide a percentage of the human comfort.*

### 1. Introduction

The growing demand for human comfort has directed to a speedy increase in the use of the cooling system and, as a result, the demand for electricity especially in rural areas. Where the overall consumption from buildings, due to air conditioning systems, reach up to 40% in developed countries [1]. Palestine weather is considered an eligible candidate for the deployment of Renewable energy resources because Palestine allocated at the high sunny area where the annual average solar incident radiation is 5.4 kWh/m<sup>2</sup>/day. Deployment of a thermal refrigerator using solar energy, would provide a reasonable solution for such rural areas with advantage of decrease of energy consumption. Between the numerous technologies for the thermal refrigeration techniques, VJRC driven by solar thermal energy appear the most hopeful alternative to the vapor compression refrigeration cycle [2]. VJRC is simple to construct, robust, low operating maintenance and has no mechanical moving segments making it a highly unailing system which is capable of running low temperature heat from

solar energy or other substitute like waste heat, which can create a cheaper operation of the cooling system.

Constant pressure mixing ejector is more popular and efficient than constant area mixing ejector [3]. VJRC uses water, as a refrigerant which makes the system completely safe. Such systems were tested with high success in refrigeration in the early years of the last century. When using water as refrigerant, temperature attained is not enough for refrigeration applications but it is more efficient and satisfactory for air-conditioning, cooling, or chilling applications [4]. Water usage in VJRC has many advantages compared with other refrigerants, water is available and inexpensive, has a high latent heat, and has no environmental impacts such as ozone depletion and global warming.

Le Blanc and Parson the VJRC was first ones to develop the VJRC in early 1900. The deployment of VJRC was widespread in early 1930's for air-conditioning systems in large buildings [5]. The 1-D model of constant-pressure mixing ejector was initially developed in 1950 by Keenan et al [6]. In this model, the pressure of secondary and primary fluid is equivalent at the outlet of the

---

\*Corresponding Author: Khaled Sider, ksider@ppu.edu

nozzle. Where the two fluids mixing begins with constant pressure to reaches the inlet of the throat section. These concepts are still considered an effective for constant pressure mixing ejector. Several theoretical studies was carried out on operation conditions of the cycle such as the generator, condenser and evaporate temperature. Al-Khalidy [7], Rani [8] and Tashtoush et al [3] noted that the performance of the system decreased by increasing condenser temperature and decreasing evaporator and generator temperatures .Eames et al [9], Chunnanond et al [10] and Ruangtrakoon et al [11] experimented on a fixed geometry ejectors refrigerator Noticed that when the generator temperature increased the performance of the system decreased. Experimental results by Xiaoli Ma [12] using the water as refrigerant, Selvaraju [13] using R134a noted that the performance of the system increased up to maximum value at a certain generator temperature and then the performance goes to decreasing, and also [13] studied more than one ejector geometry and dimensions, and he noted that every ejector has an optimum and maximum performance at a certain value of generator temperature. Sun [14] study carried out on the variable geometry ejectors, it was noted that, with the variable geometry ejector. There are no limitations of the performance value of the system, when the generator temperature increased the performance increased without optimum generator temperature Thus, variable geometry ejectors are better than the of fixed geometry ejectors, which variable geometry ejector have a wide range of operation conditions to make it more flexible and reliable more the fixed geometry ejectors and more performance value. Variable geometry ejector can be achieved by using high industrial technology or by using more than one ejector in parallel in the same cycle, and only one ejector are used according to the performance of the system in the instant conditions .All the theoretical and experimental studies [7-14] concluded that the performance of the cycle increased when the evaporator temperature increased and the condenser temperature decreased.

Alexis and Karayiannis [15] studied the overall performance of the VJRC operated by solar energy and R134a as working fluid in the city of Athens along a period of 5 months from the beginning May until the end of September. It was found that the performance of the proposed system varied from 0.035 to 0.199 based on the operation conditions in which the generator temperature, condenser temperature and evaporator temperature varied. The temperatures were chosen between (82–92°C), (32–40°C) and (-10–0°C) respectively. Where the overall system performance varied from 0.014 to 0.101 with the same operation conditions in July. Kursad Ersoy et al [16] worked on a simulation study with R123 as working fluid, ETC as collector in Turkey climates. The performance of the VJRC and the evacuated tube collector were hourly varied by solar radiation and weather temperature. The maximum performance of the system occurred in the noon time. Tashtoush et al [17] simulation study using R134a as working fluid and 7 kW cooling load at Jordan climate noted that increasing the hot storage tank size could improve the amount of solar collector useful energy gain. Many researchers used TRNSYS software for studying solar thermal cooling systems and refrigeration systems. Pridasawas and Lundqvist [18] tested the effect of the operation conditions and solar collector types on the VJRC performance they used iso-butane as a refrigerant. Tashtoush et al [17] simulate the solar collector angle and area ,he was study the performance of VJRC for the climatic conditions of Jordan with R134a as a

refrigerant. Both of the aforementioned research were simulated in TRNSYS software. In addition, Ahmed et al [19], and Asim et al [20] used TRNSYS to simulate the absorption cooling system under climate of Egypt and Pakistan respectively.

This research aims to to use the TRNSYS software to simulate the VJRC under two different locations in Palestine; one in Hebron city which has a moderate weather and the second in Jericho city which has a very hot weather in summer. In addition, to estimate the possibility of compensate the cooling load demand of the TMH. Three main parameters were studied in the overall system, location, solar collector area and the storage tank volume.

## 2. Methodology

### 2.1. Location and Climate Description

Hebron city is located south of west bank at latitude 31.32°N and longitude 35.06°E. Hebron has relatively medium mean temperatures. The meteorological station is 1005 meters above sea level and the mean temperature is estimated 17.36 °C in 2015 according the Palestinian Meteorology (PAL MET) Agency [21]. Jericho city is located east of west bank at latitude 31.51°N and longitude 35.27°E. It is located in a relatively high mean temperature regions with summer temperatures rise up to 45 °C. The meteorological station is 260 meters below sea level and the mean temperature is estimated 24.77 °C for 2015 [21]

Figure. 1 shows the distribution of the ambient temperatures in the two cities, where the maximum ambient temperature in Hebron and Jericho cities reached to 38.7 °C and 45 °C respectively. Figure. 2 shows the distribution of the global horizontal solar radiation for the two cities, where the maximum hourly global horizontal solar radiation in Hebron city is 1157 W/m<sup>2</sup>, and the maximum hourly global horizontal solar radiation in Jericho city is 1180 W/m<sup>2</sup>.

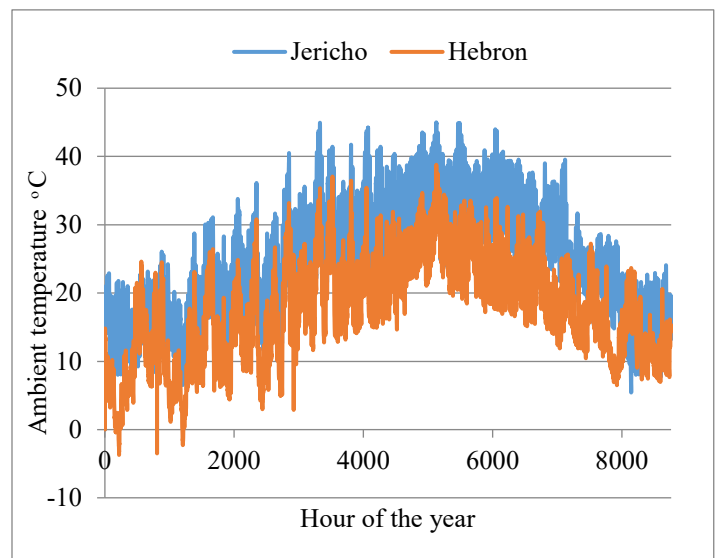


Figure.1. Annual distribution of ambient temperatures for Hebron and Jericho cities.

### 2.2. System Description

The proposed test system consists of three subsystems; VJRC subsystem, building cooling load subsystem and solar thermal

subsystem. Figure. 3 shows the Schematic diagram of the overall proposed system. The solar energy that collected by solar collector was converted into heat in the solar thermal subsystem and then used by the generator to operate the power cycle in the VJRC subsystem. The refrigeration load that produced by the VJRC subsystem was used to compensate the cooling load demand in the TMH unit to achieve the human comfort.

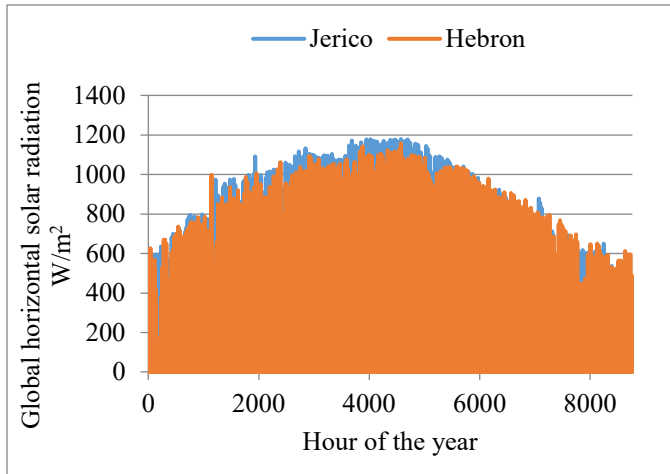


Figure. 2. Annual distribution of global horizontal solar radiation for Hebron and Jericho cities  $W/m^2$

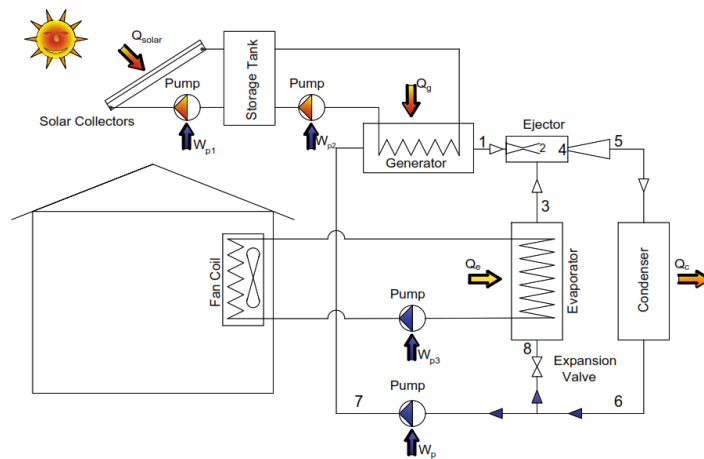


Figure.3. Schematic diagram of the proposed system.

### 2.2.1. VJRC description

Based on Figure. 3, it can be noticed that the VJRC subsystem consists of two cycles, the power cycle that consists from ejector, generator, condenser and circulation pump, and the refrigeration cycle that consists from ejector, evaporator, expansion valve and condenser. In the power cycle the primary fluid is vaporized by adding heat to the generator at high pressure, this fluid then passes through a supersonic ejector. In the ejector, the fluid velocity increased more than Mach number through the supersonic nozzle, and the pressure decreased to the evaporator pressure. The reduction in the pressure that occurs in the nozzle entrains the secondary fluid vapor from the evaporator. The two fluids then mix completely in the mixing chamber of the ejector and then enter the diffuser section where the mixed fluid velocity back decreases below Mach number and the pressure increased to reach the

condenser pressure. The mixed fluid then flows to the condenser where it is reject heat to the ambient and condensed into liquid.

A portion of the liquid that leaving the condenser goes to a circulation pump where it will be pumped to the generator to complete the power cycle, the other part enters and expands in the expansion valve and enters to the evaporator in the refrigeration cycle as a mixture. In the evaporator, the refrigerant evaporates producing a refrigeration load, and the resulting vapor is then sucked by the primary fluid into the ejector to complete the refrigeration cycle.

### 2.2.2. Building description

The reference TMH that has been selected in this study was produced by Alamour Company for industrial and trading in Bedy-Jeneen. It is rectangular shape  $8m \times 3m$ , and ceiling height is 2.6 m. It consists of two bedrooms, Kitchen and bathroom. Number of occupants are 3 persons. The sketch of TMH in Figure. 4 shows the architecture design, orientation and the zones dimensions.

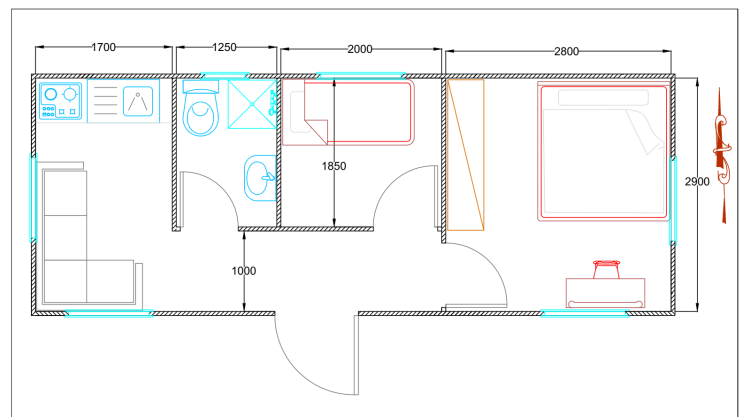


Figure.4. Architecture design of the TMH

### 2.2.3. Solar thermal subsystem

The ETC is the major component of the solar thermal subsystem, which collects the incident solar radiation from the sun, converts it into a heat, then transfers this heat to a heat transfer fluid (HTF), the energy which was collected then is carried by a circulated HTF to be used in a thermal energy storage tank.

### 2.2.4. Simulation

The current simulation study consists from three subsystems as mentioned. The VJRC was simulated by EES Software by with water as working fluid. The mathematical model and equations that used in this study are similar to the system used by Sun [14] for one-dimensional model of constant-pressure mixing ejector, which based on the steady flow energy equation, momentum and continuity equations [14]. In this subsystem the Mathematical model was carried out at various design conditions (generator, and condenser temperature), characteristic curves and tables for the VJRC were found where the generator temperature changed from  $80^{\circ}C$  to  $150^{\circ}C$  and the condenser temperature changed from  $25^{\circ}C$  to  $50^{\circ}C$  according to the weather and climate variations. The evaporator temperature was selected  $10^{\circ}C$  as fixed value. Characteristic tables for the cycle were created as an excel sheet

table to be used as input file in the TRNSYS software, where the generator and condenser temperature were varied with step of 1 °C and 0.5 °C respectively.

The building cooling load subsystem was hourly simulated using the TRNBuild subsystem in TRNSYS software. the cooling load demand of the TMH was simulated according to the weather data for the two locations. As the TRNBuild view, the cooling load into the building arises from both radiative heat flow to the windows and walls and convective heat flow to the air node. Where the convection heat transfer comes from infiltration, ventilation, gains due to the convective air flow from zones, internal surface gains and internal heat gains from people, equipment, illumination, radiators, etc. while the radiation heat transfer comes from, long wave radiation exchange between walls and all other walls, internal gains received by walls and windows, and solar radiation through zone windows and walls. [22]

The building prototype demonstrates the cooling load over the study period. The prototype is created in TRNBuild, Then the generated TRNBuild model is executed to TRNSYS simulation Studio as an input files by type 56 (multi-zone building). Noted that all the physical properties of the envelop constructions were taken according the Palestinian code for efficient buildings [23].

The overall solar thermal cooling system was hourly simulated by using the TRNSYS simulation studio that consist from VJRC subsystem as TRNSYS / Excel Coupling file (type 62) and the cooling load of the house by using Multi-zone building file(type 56), the overall simulation consider the solar energy collected by ETC at fixed optimum tilt angle 15 deg -based on the maximum amount of the total incident solar radiation for the study period[24], constant HTF flow at 0.02kg/s [25] and used hot energy storage tank to store the excess thermal energy for peak times or in the times where the sun radiation is absence. This energy delivered to the generator in the VJRC and used to operate the cycle and produce cooling effect in the evaporator. The cooling energy then delivered to a cooling coil to cover the cooling load demand of the house. Figure. 5 illustrated the overall TRNSYS simulation where the black solid lines represent the flow of system information, while the blue dotted lines show the flow of weather data Information, flow of control information and the flow of the output information from the simulation. In addition, Table 1 Shows the inputs and outputs descriptions of its elements [26].

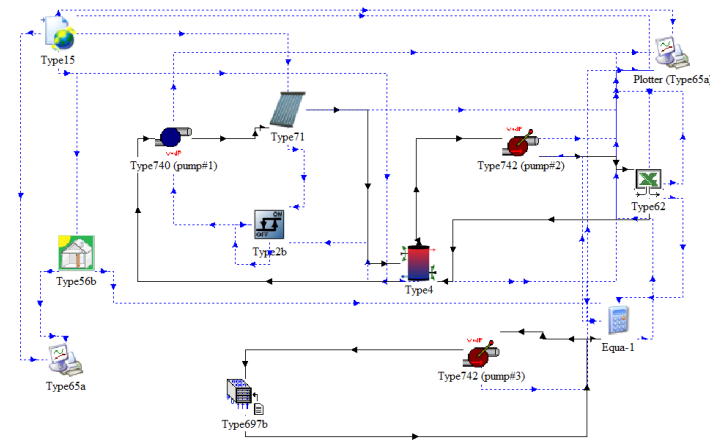


Figure.5. Simulation Studio window components for overall system

Table.1. Components of simulation Studio window and descriptions

Components	Descriptions
Whether data (type15-3)	This component supports of reading the weather data from an external weather data file. Type: Energy plus Weather (EPW) format with hourly intervals [21] Location: Hebron and Jericho cities/Palestine
Multi-zone building (type 56)	Models the thermal behavior of a building Desired inside temperature: 22 °C Area:24m <sup>2</sup> Height :2.6 m U-value of walls, roof, door and floor: 0.587 W/m <sup>2</sup> °C (50 mm sandwich panel) U-value of window: 2.877 W/m <sup>2</sup> °C (3-6-3 double glass aluminum frame window) Number of occupants: 3 persons Ventilation and infiltration :0.8 times per hour Heat gain from electrical equipment is 140 W Heat gain from lighting 10W/m <sup>2</sup> Maximum cooling load demand: 5.35 kW Seasonal cooling energy demands: 5749 kWh/season
Plotter (type 65a)	Plotter is used to display the simulation data and results
Solar Collector; Evacuated Tube (type71)	Models a single-phase evacuated tube solar collector. $\eta_0 = 80\%$ [23] $a_1 = 1.5 [W/(K \cdot m^2)]$ $a_2 = 0.005 [W/(K^2 \cdot m^2)]$ HTF: THERMINOL 66, operating temperature from 0 °C to 345 °C at atmospheric pressure and the average specific heat of 1.9 kJ/kg.K at 120 °C. Flow rate:0.02kg/s/m <sup>2</sup> Tilt angle 15° Azimuth: south. Area: variable (10,20,30,40,50,60 )m <sup>2</sup>
Storage Tank (Type4)	Models of a hot storage tank. HTF: THERMINOL 66 Maximum temperature:160°C U-value: 0.5 W/m <sup>2</sup> °C Volume: variable (0.5, 1, 1.5, 2) m <sup>3</sup>
Variable speed pump (Type742)	Models a variable speed pump HTF: THERMINOL 66
Single speed pump (Type740)	Models a single speed pump Flow rate:0.02kg/s/m <sup>2</sup> collector area HTF: THERMINOL 66
TRNSYS / Excel Coupling (Type62)	External model implements a link with Excel.
ON/OFF Differential Controller (Type2)	Controller with value of 0 or 1. Maximum storage tank set point temperature: 160°C
Cooling Coil (Type697)	Models an air cooled cooling coil. HTF: Water

### 3. Results and Discussion

The characteristic curves for the VJRC obtained from EES are shown in Figure. 6. The Figure. shows that the COP of the cycle increases as the generator temperature increased. The reason for this is that the pressure ratio of the power cycle increase and more secondary flow will be entrained from the evaporator. In addition, it can be seen that the COP decreased remarkably as the condenser temperature increased. This due to low secondary flow will be entrained as condenser temperature increases under high-pressure ratio in the refrigeration cycle. in some cases, the COP equal zero when the generator temperature is low and condenser temperature very high, in this case the ejector system is failure and there is no secondary fluid entrained and flow.

Hourly cooling load demand were simulated using TRNBuild in the two locations and integrated during the study period, Where the maximum cooling load demand during the study period for



Hebron and Jericho cities were: 5.35 kW and 7.02 kW respectively; and the total seasonal cooling energy demands were: 5749 kWh/year and 14864 kWh/year respectively, as shown in Figure. 7 .It can be noticed that Hebron city has less cooling load demand than Jericho. This is due to the lower ambient temperatures of Hebron city.

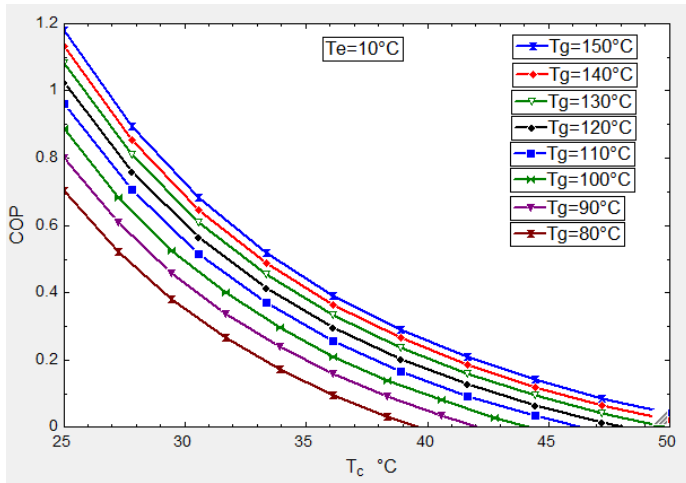


Figure.6. Characteristic curves for VJRC at 10°C evaporator temperature

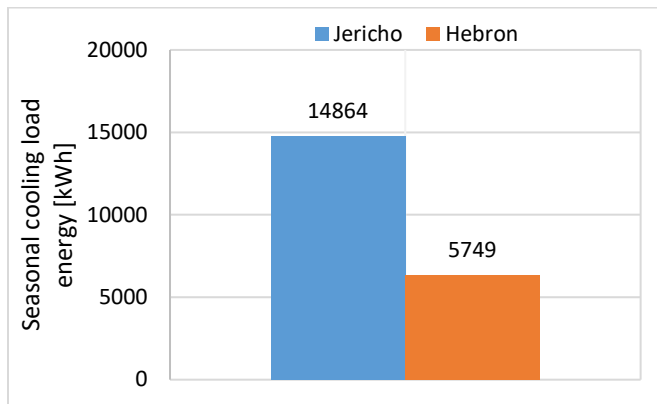


Figure.7. Total seasonal cooling energy demand for Hebron and Jericho cities

As rule of thumb the collector areas were chosen 10 m<sup>2</sup> to 60 m<sup>2</sup> with 5 m<sup>2</sup> step and the storage tank volume from 0.5 m<sup>3</sup> to 2 m<sup>3</sup> with 0.5 m<sup>3</sup> step for Hebron city. While for Jericho city, the collector areas were chosen from 10 m<sup>2</sup> to 150 m<sup>2</sup> with 10 m<sup>2</sup> step and the storage tank from 0.5 m<sup>3</sup> to 2 m<sup>3</sup> with 0.5 m<sup>3</sup> step. Figure. 8 shows the seasonal evaporator cooling energy as a percentage from the cooling energy demand at different collector area 10m<sup>2</sup> to 60m<sup>2</sup> and storage tank volume from 0.5m<sup>3</sup> to 2m<sup>3</sup> for Hebron city.

It can be noticed from Figure. 8 that the effect of the collector area has a proportional logarithmical effect on the evaporator cooling energy, where the evaporator cooling energy increased at high rate when the collector area was low and increased slowly after that. Therefore, the storage tank volume has a high impact on the system capacity and evaporator cooling load and energy. Figure. 8 also shows the effect of the storage tank volume on the evaporator cooling energy for Hebron city during the study period. It can be noticed that the relation between storage tank volume and the evaporator cooling energy availability is proportional at high

collector areas and inversely proportional at low collector area. It is because the temperature of the storage tank is a function of the tank volume, and it was affected strongly on the cycle COP as shown in characteristic curves.

Finally, from Figure. 8 it is clear that the seasonal evaporator cooling energy changed from 42% at 10m<sup>2</sup> collector area and 2m<sup>3</sup> storage tank volume to 98.9% at 60m<sup>2</sup> collector area and 2m<sup>3</sup> storage tank volume. The optimal values of the collector area and the storage tank volume can be selected according to the suitable evaporator cooling energy availability during the study period, also depends on the philosophy of the designer, economics issues and the related standards. From the chart there are more than one case can be selected for the system according to the evaporator cooling energy availability, for example 30 m<sup>2</sup> collector area & 1.5m<sup>3</sup> storage tank volume were selected where the cooling energy available represent is 95.4%, or 35 m<sup>2</sup> collector area & 1m<sup>3</sup> storage tank where the cooling energy available represent is 95.1% ,

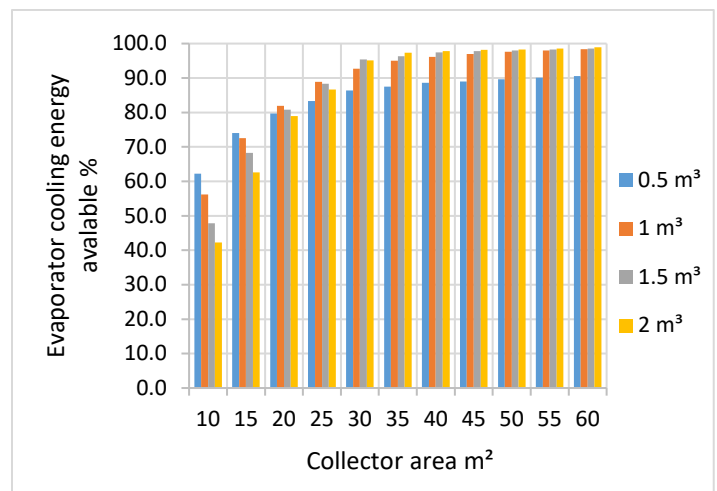


Figure. 8 Percentage of seasonal evaporator cooling energy from the cooling energy demand for Hebron city at different collector area and storage tank volume

For Jericho, the overall system parameters shows in Figure. 9 where the collector area varies from 10m<sup>2</sup> to 150m<sup>2</sup> and storage tank volume from 0.5m<sup>3</sup> to 2m<sup>3</sup>

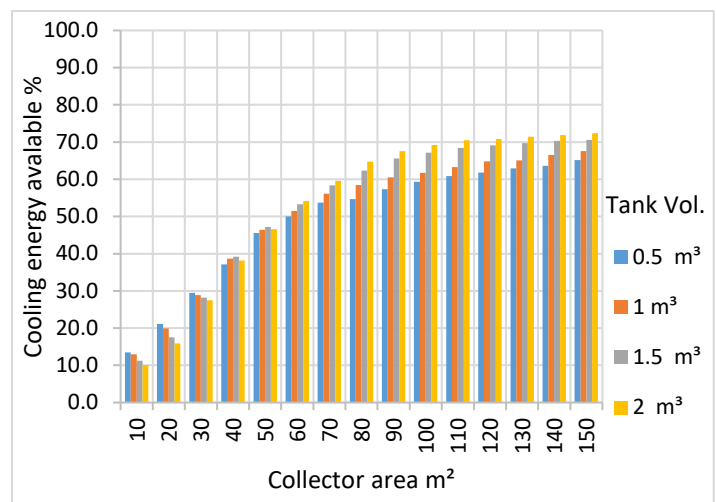


Figure.9. Percentage of seasonal evaporator cooling energy from the cooling energy demand for Jericho city at different collector area and storage tank volume

From Figure. 9 it is shown that the maximum seasonal evaporator cooling energy is reached to only 72.4 % at 150m<sup>2</sup> collector area and 2m<sup>3</sup> storage tank volume, where this value is very low. In Jericho the performance of the system was very low because the condenser temperature in the VJRC is high, also the cooling energy demand is high because the ambient temperature is high. This causes a very high extreme conditions that cannot be satisfied by the system at these conditions.

The overall efficiency is defined as the amount of cooled energy produces to the solar energy incident on the solar collectors. Figure 10 shows the system seasonal efficiency for both tested cities. It is noticeable that the overall seasonal efficiency in Hebron was higher than Jericho city in most cases. Also, the efficiency is inversely proportional to the area of the solar collectors as shown in aforementioned Figure.

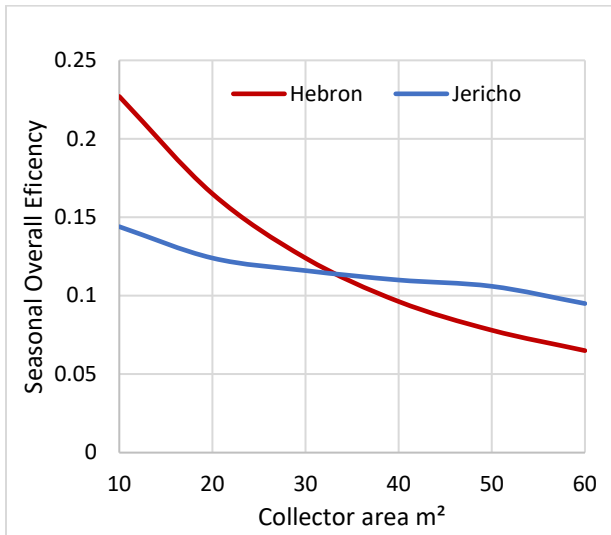


Figure.10. seasonal overall efficiency for Hebron and Jericho cities at different collector area at 1 m<sup>3</sup> storage tank volume.

#### 4. Conclusions

The study showed that solar thermal energy can operate the VJRC's to achieve human comfort as well as reducing the environmental impacts such as global warming and ozone depletion is worth considering spatially in rural areas with moderate ambient temperature. Results showed that the performance of the VJRC depends strongly on the operating conditions, where the cycle COP increases when the generator temperature increases. In addition, the COP decreases with the increasing condensing temperatures. By that, the generator temperature must be high and the condensing temperature should remain low to maintain a good performance for the cycle.

Results showed that the higher surface area of the solar collectors, the value of the cooling energy produced increases logarithmically. For example, in Hebron city the maximum evaporator cooling energy reached 62.1%, 95.4% and 98.9% of the required cooling demand at a surface area of the solar collectors 10, 30 and 60 m<sup>2</sup> respectively. While, the maximum evaporator cooling energy reached 14%, 58.8% and 72.4% of the required cooling demand at the surface area of the collector 10, 70 and 150 m<sup>2</sup>. Moreover, increase in the volume of the storage tank has a negative impact if the surface area of the solar collectors is low and a positive one if

the surface area of the solar collectors is large. For example, in Hebron city the value of the evaporator cooling energy was 62.1% to 42% of the required cooling demand at collector surface area 10 m<sup>2</sup> when the storage tank volume increased from 0.5 to 2 m<sup>3</sup>, while at solar collectors' area of 35 m<sup>2</sup> the evaporator cooling energy increased from 87.2% to 95.1%. The overall seasonal efficiency for the system in Hebron was higher than Jericho city in most of different circumstances which was tested.

Finally Using VJRC driven by solar thermal energy in Hebron city is thermally efficient in contrast to Jericho city where the proposed system showed a lack of cooling energy produced because a high condenser temperature. Where, applying this system in Hebron city can be done by the selection of more than one system size according to percentage of the human comfort needed.

#### 5. References

- [1] Pérez-Lombard, L., Ortiz, J. and Pout, C., 2008. A review on buildings energy consumption information. *Energy and buildings*, 40(3), pp.394-398.
- [2] Besagni, G., Mereu, R. and Inzoli, F., 2016. Ejector refrigeration: a comprehensive review. *Renewable and Sustainable Energy Reviews*, 53, pp.373-407.
- [3] Tashtoush, B., Alshare, A. and Al-Rifai, S., 2015. Performance study of ejector cooling cycle at critical mode under superheated primary flow. *Energy Conversion and Management*, 94, pp.300-310.
- [4] Dincer, I., 2017. *Refrigeration systems and applications*. John Wiley & Sons.
- [5] Meyer, A.J., Harms, T.M. and Dobson, R.T., 2009. Steam jet ejector cooling powered by waste or solar heat. *Renewable Energy*, 34(1), pp.297-306.
- [6] Keenan, J.H., 1950. An investigation of ejector design by analysis and experiment. *Journal of Applied Mechanics*, 17, p.299.
- [7] Al-Khalidy, N.A.H., 1997. Performance of solar refrigerant ejector refrigerating machine (No. CONF-9702141-). American Society of Heating, Refrigerating and Air-Conditioning Engineers, Inc., Atlanta, GA (United States).
- [8] Rani, S. and Sachdeva, G., 2015. Theoretical Performance Analysis of Vapour Jet Ejector for R 134a. *International Journal of Engineering, Management & Sciences*, 2, pp.300-310.
- [9] Eames, I.W., Aphornratana, S. and Haider, H., 1995. A theoretical and experimental study of a small-scale steam jet refrigerator. *International journal of refrigeration*, 18(6), pp.378-386.
- [10] Chunnanond, K. and Aphornratana, S., 2004. An experimental investigation of a steam ejector refrigerator: the analysis of the pressure profile along the ejector. *Applied Thermal Engineering*, 24(2-3), pp.311-322.
- [11] Ruangtrakoon, N., Aphornratana, S. and Sriveerakul, T., 2011. Experimental studies of a steam jet refrigeration cycle: effect of the primary nozzle geometries to system performance. *Experimental Thermal and Fluid Science*, 35(4), pp.676-683.
- [12] Ma, X., Zhang, W., Omer, S.A. and Riffat, S.B., 2010. Experimental investigation of a novel steam ejector refrigerator suitable for solar energy applications. *Applied Thermal Engineering*, 30(11-12), pp.1320-1325.
- [13] Selvaraju, A. and Mani, A., 2004. Analysis of an ejector with environment friendly refrigerants. *Applied Thermal Engineering*, 24(5-6), pp.827-838.
- [14] Sun, D.W., 1996. Variable geometry ejectors and their applications in ejector refrigeration systems. *Energy*, 21(10), pp.919-929.
- [15] Alexis, G.K. and Karayiannis, E.K., 2005. A solar ejector cooling system using refrigerant R134a in the Athens area. *Renewable Energy*, 30(9), pp.1457-1469.
- [16] Raza H. A. et al., "Analysis the effect of 500kv High-Voltage Power Transmission Line on the Output Efficiency of Solar-Panels," in 2019 International Conference on Electrical, Communication, and Computer Engineering (ICECCE), 2019, pp. 1-6.
- [17] Tashtoush, B., Alshare, A. and Al-Rifai, S., 2015. Hourly dynamic simulation of solar ejector cooling system using TRNSYS for Jordanian climate. *Energy conversion and management*, 100, pp.840-850.
- [18] Pridasawas, W. and Lundqvist, P., 2007. A year-round dynamic simulation of a solar-driven ejector refrigeration system with iso-butane as a refrigerant. *International Journal of Refrigeration*, 30(5), pp.840-850.
- [19] AHMED, M.H., MONTAGNINO, F., AMIN, A. and HASSAN, R., Modelling of Solar Absorption Cooling System under Egypt Climate Using TRNSYS. *Environment and Financial Science*, ISBN: 978-1-61804-361-0.
- [20] Asim, M., Dewsbury, J. and Kanan, S., 2016. TRNSYS simulation of a solar cooling system for the hot climate of Pakistan. *Energy Procedia*, 91, pp.702-706.

- [21] Palestinian Meteorology (PAL MET) in Palestine. <http://www.pmd.ps>.
- [22] Klein, S.A., Beckman, W.A., Mitchell, J.W., Duffie, J.A., Duffie, N.A., Freeman, T.L., Mitchell, J.C., Braun, J.E., Evans, B.L. and Kummer, J.P., 2004. Trnsys 16—Volume 6 Multizone Building Modeling with Type 56 and Trnbuild. Solar Energy Laboratory, University of Wisconsin: Madison, WI, USA.
- [23] Palestinian authority, Ministry of local government.2004. Energy Efficient Building Code. .
- [24] Masters, G.M., 2013. Renewable and efficient electric power systems. John Wiley & Sons.
- [25] Viessmann co., Technical Guide-Solar thermal systems 2009. <https://www.viessmann.com>.
- [26] Klein, S.A., Beckman, W.A., Mitchell, J.W., Duffie, J.A., Duffie, N.A., Freeman, T.L., Mitchell, J.C., Braun, J.E., Evans, B.L. and Kummer, J.P., 2005. Trnsys 16—Volume 3 Standard Component Library Overview. Solar Energy Laboratory, University of Wisconsin: Madison, WI, USA, p.92.

## On the Use of Triple Graph Grammars for Model Composition

Hatime Bencharqui<sup>\*1</sup>, Younes Moubachir<sup>2</sup>, Adil Anwar<sup>1</sup>

<sup>1</sup>Mohammed V University in Rabat. EMI, Siweb Team, Morocco

<sup>2</sup>Mohammed V University in Rabat. EMI, QSM Research Team, Morocco

### ARTICLE INFO

Article history:

Received: 30 October, 2019

Accepted: 18 March, 2020

Online: 14 April, 2020

Keywords:

Model-driven development;

Model composition;

Formal approach;

Triple graph grammars

AGG

### ABSTRACT

*In the software engineering research, several works focus on advantages of multi-modeling, which facilitate modeling a system by separating of concerns. The Model Driven Engineering approach relies on model to design software artefacts during the software development lifecycle. Handling such models involves describing some model management operators like 'composition'. That is an operation which consist to fuse a set of models into one (or more) incorporated model relating the application context. The present work, introduces a formal approach for UML-compliant model composition focused on three-actions: matching, checking and merging. Each composition action is represented by one or many graph transformations rules. The composition operator's syntax is specified with triple graph grammars (TGGs) formalism.*

## 1 Introduction

In Model Driven Engineering (MDE), model composition is critical process, especially in modeling complex system with multi-modeling approach [1]-[4]. The primary goal is to distinguish issues related to the software system as model-views in accordance with certain particular concerns [5]: components, sub-systems, abstraction views, interactions. The goal is to facilitate analyzing and designing activities tasks during software development process. Nevertheless, this would make difficult the to integrate the different sub-models throughout subsequent phases.

To deal with this difficult operation, it's very important to adopt appropriate approach, methods and techniques to maintain its consistency. The Model-Driven Engineering (MDE) approach is widely used that convert a process of integration to be operated automatically. In the model driven engineering approach these integration operations are assimilated to model transformations [6], [7]. However, this lacks formal foundations, and hence properties (e.g. commutative, associative) cannot be proven [8]. Such properties are useful to guarantee, that there is no influence of composition order in the operation of composition. we use the formal basis of graph grammars so that give a powerful background in the scope of model composition [9]. Some activities

related to MDE process can also be applied in Graph theory [9]-[13]. In addition, using graph transformations theory to formalize model makes it possible to use benefits and richness of current tools like AGG [14], Fujaba [15] and Great [10].

To tackle the model composition issue, we propose a new method that uses graph transformation with Triple Graph Grammars (TGGs). TGGs is defined as a formalism to handle models that use transformation rules. we explain a composition operator that we had developed in our previous work [16] in response to different contextual purposes.

The use of TGGs provides several benefits concerning model composition: excellent comprehension, simplicity to express declarative composition rules and an effective approach with formal software tools. Crucial analysis can also be used to automatically identify all interactions and contradictions between the graph production rules. In addition, a formalism depicting the composition operation is presented.

The formalism is founded on two models' relationships [8]. specifically, Models are subsequently considered to be graph-based artifacts, so we represent the relationships among models with two different equivalence categories. We will explore how composition operation can be accomplished by using relations between graphs.

\*Corresponding Author: Hatime Bencharqui, [bencharqui@gmail.com](mailto:bencharqui@gmail.com)



Our work is built up as bellows. In section 2, a case study is presented to illustrate the different concepts of our composition approach. Section 3 exposes a formalism based on graph theory, in order to define the concepts of models and their relationships. In section 4, elucidates the suggested method by implementing triple graph grammars and explores some experimental information. the section 5 is devoted to related works. Section 6 sums up our contributions and outlines some upcoming work.

## 2 Motivating Example

### 2.1 Case study

This section is devoted to a short overview of the modeling approach, after that, a case study is presented illustrating our composition method, that functions as a driving example to illustrate the compositional approach.

The purpose is to fuse two UML models developed separately by two distinct designers. We present the merging scenario using a Library Management System (LMS). To simplify the presentation, our example will focus only on the following actors and activities:

- Librarian save the loans and save the return of loans. To manage these, the librarian must know the identity of the borrower;
- Head Librarian manage books and members (add, delete, change);

Those actors have multiple concerns, so this will affect the way in which the system can be designed. The goal of the requirements analysis step is to identify functional requirements of the system. In this step, a use case diagram is used. (Figure 1).

Other models are used throughout the development process: class diagrams, state machines, etc. In this work, we will concentrate our studies on structural models.

In order to put into practice, the notion of point of view, Figure 2 and Figure 3 present class diagrams which are centered on each actor. Figure 2 illustrates an extract of the design model corresponding to the head librarian. We follow the same process to produce a design model (UML class diagram) for librarians and Library members.

### 2.2 Composition process

Our proposed method consists basically of three activities. First, we define between design models, some kind of relation of connection, the second activity consist of analyzing those established connections, and the last step consist of merging these models according to those correspondences. Composition process maintainability becomes easier due to the fact that the matching activity operation is sustainable than the merging one, which can be affected mainly by strategy modifications. Our proposed composition scheme will follow three different phases Figure 4: matchings step, checking step and merging step.

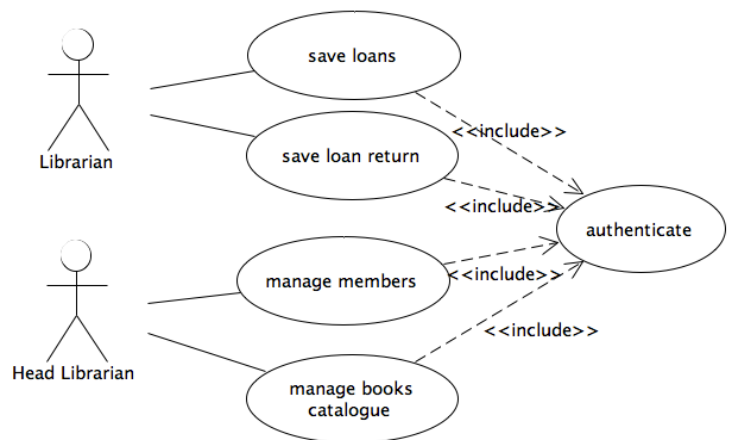


Figure 1: LMS snippet use case diagram.

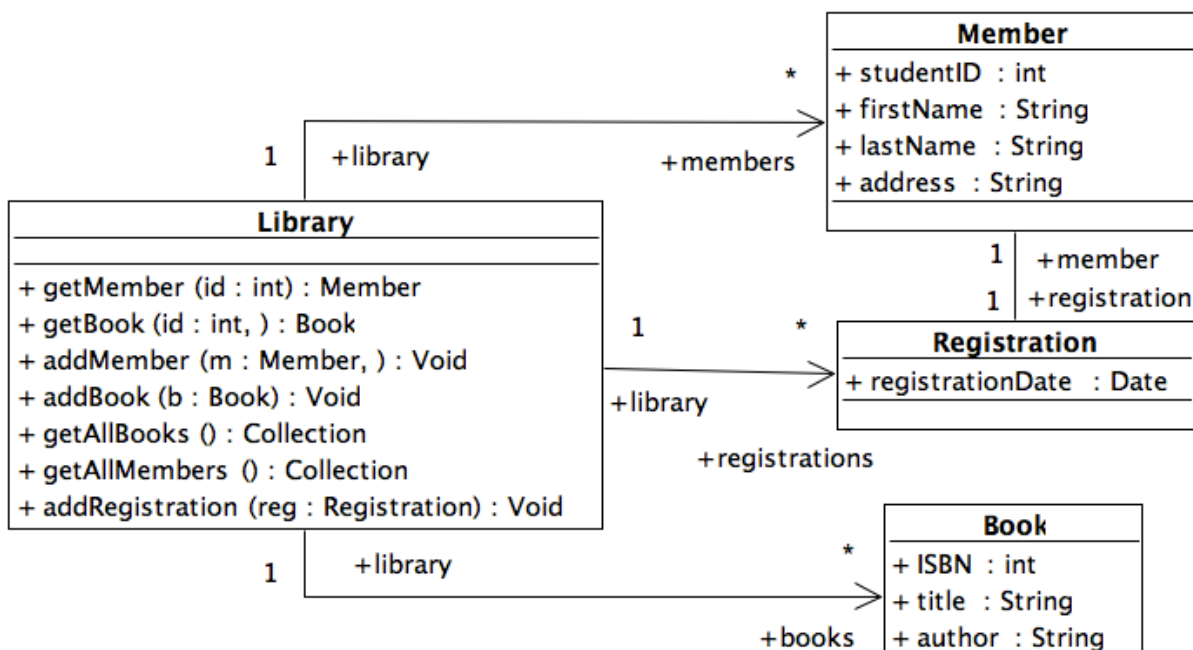


Figure 2: LMS snippet use case diagram.

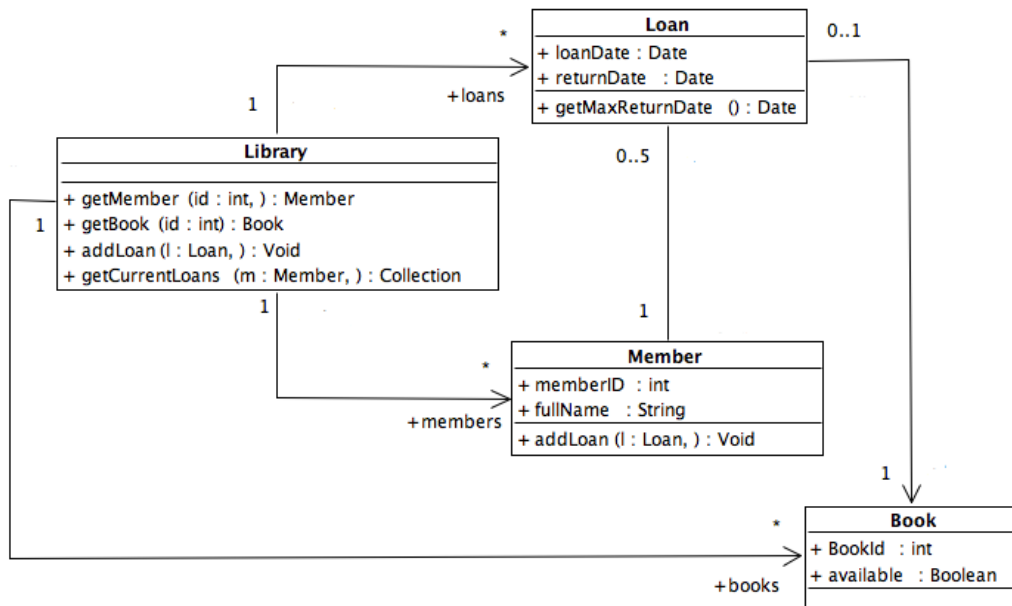


Figure 3: Snippet of Librarian actor design model

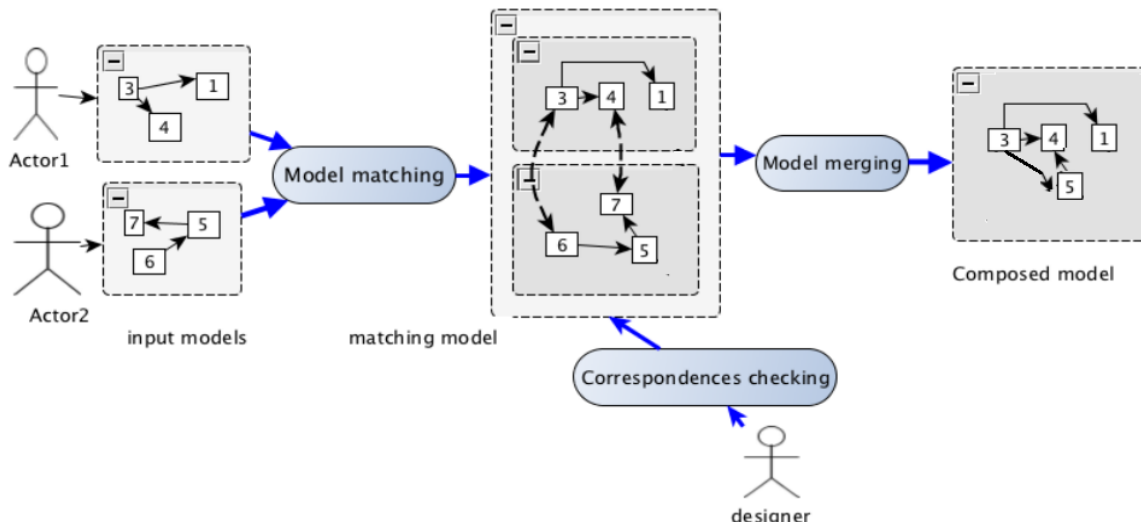


Figure 4: Merging process of the design models.

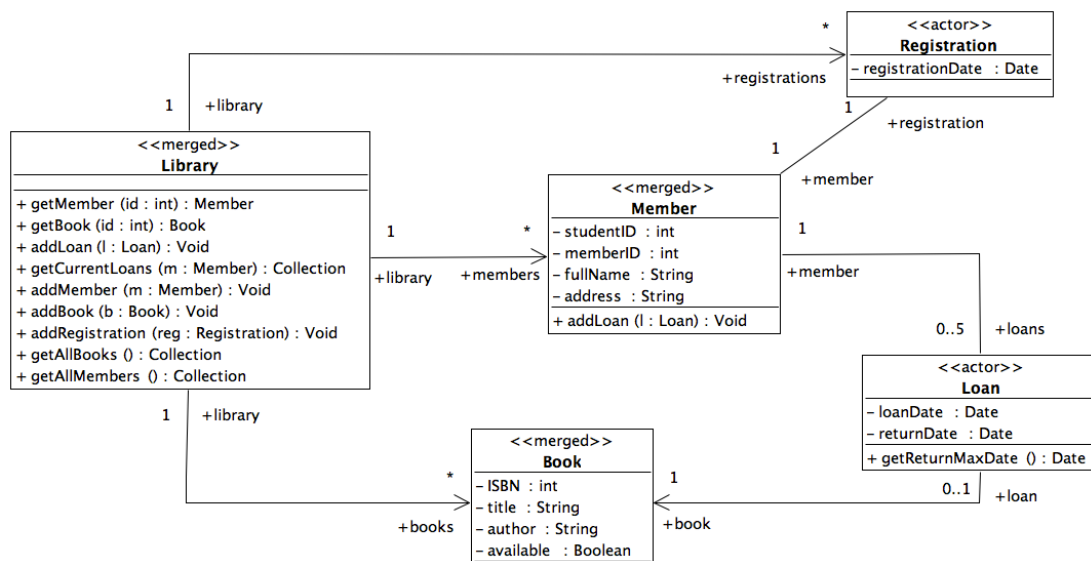


Figure 5: Class Diagram snippet of the LMS.

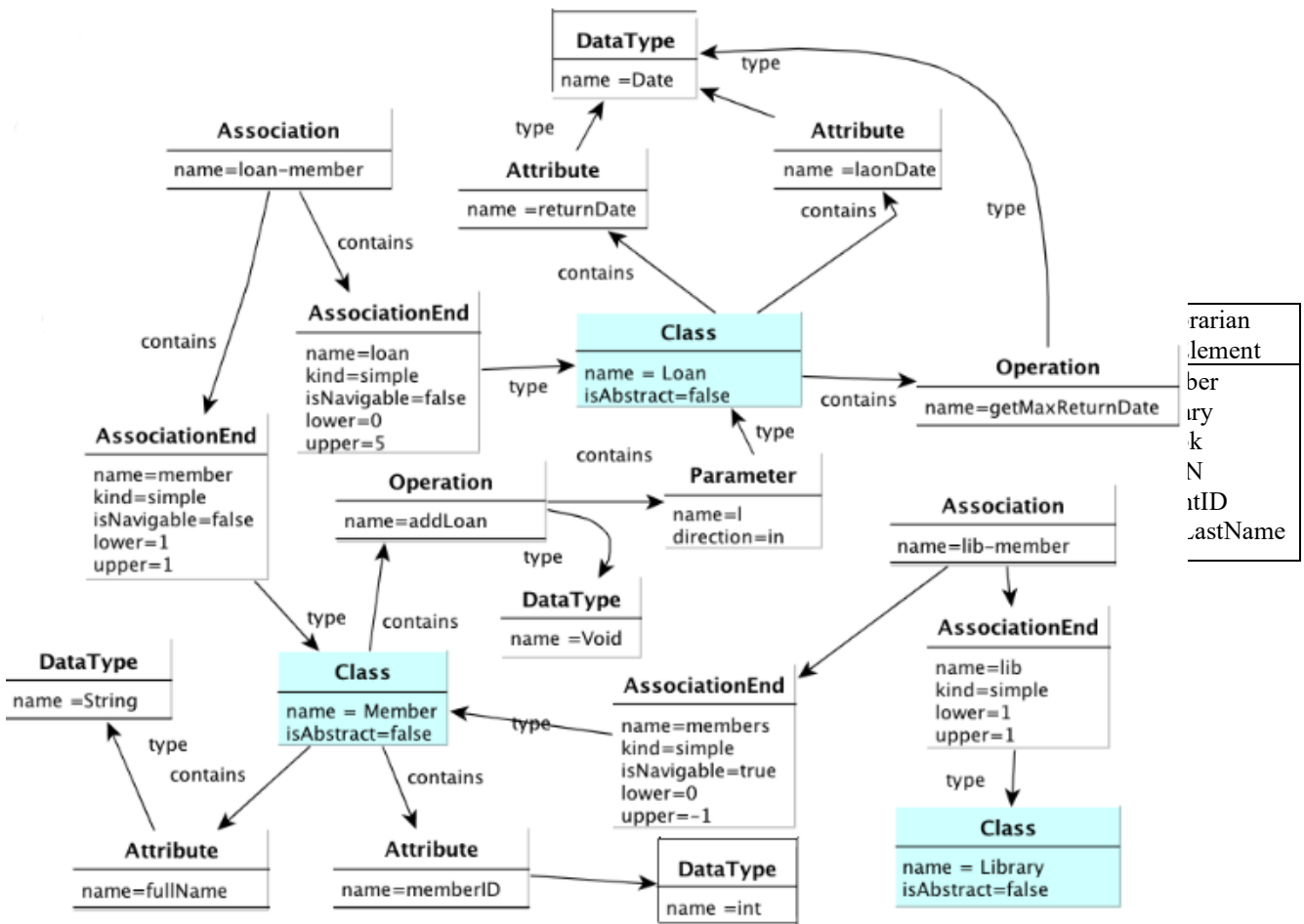


Figure 6:A graph depicting a UML class diagram as shown in figure 3.

2.2.1 Matching step

Model Matching approaches can be decomposed into three categories according to the way the corresponding model elements are matched. (i) matching based on static identity, in this case we employs single and unique identifiers (ii) matching based on signature (iii) matching based on similarity, within this technique, we compute the similarity value of an element feature, as an example, for UML class diagram, the similarity between two classes could be calculated by checking the similarities in their attributes or operations. The use of one technique instead of another depends on several factors such as the goal of the matching process and also the assumptions made about the application context, the nature of the models and their intention of use. For example, the static-based strategy won't be interesting for model merging purposes, since we don't look for elements which have the same value of the xml-id attribute but instead elements expressing the same principles, and designed to be similarly constructed. Additionally, Certain approaches focuses on similarity in graphs, for example, similarity flooding [17], To explore their matching degree, the authors use an algorithm to measure the resemblance of the adjacent nodes of elements. In addition, more the elements' neighbors are different, more the similarity between those two elements decreases. It was regarded as the basis for further matching and merging set of rules like Ontology matching [18], and BPM merging [19].

First of all, we identify in this step corresponding elements on the input models. This is can be achieved by creating correspondence links that relates these elements. This operation is called the model comparison, since the computation of some type of relationships is only automated at this point (Equality, Similarity, Aggregation, Generalization). Equality relationship specifies equality as equivalent to two or more model elements, so the same concept is represented by tow designers in two different models. It might exist another type of Similarity that indicates that two or even more elements are semantically similar but not identical.

It is very important to express a specific correspondence relationship to differentiate operations which come with the same signature [20] (name, returned type, a set of parameters) with two different behaviors. In order to illustrate the result of the step, consider design's models (Figure 2 and Figure 3) of the LMS example. These models can overlap in several ways: the classes Library, Book and Member of the Head Librarian model are likely to be the same as that in Librarian model. The BookId attribute defined on the Book class of the Librarian model is likely to be the same as the ISBN attribute of the head Librarian model. Similarly, the studentId and memberId attributes of the Member classes in models Figure 2 and Figure 3 respectively are likely to be the same as well. Assuming that all of these likely correspondences hold, the

following is the set of correspondences relationships between the Head Librarian and Librarian classes models (Table 1).

2.2.2 Correspondences checking step

It's commonly known that the related design models may present some consistencies because they have been constructed in a decentralized way; syntactic synonymy and certain differences within models are very probable. Applying some resolution strategies depend on how these cases are handled. For example, one can allow the matching of only a set of consistent models; others call for repair heuristics to correct inconsistencies before or during the matching operation. In our approach, we choose to repair conflicts after the matching step we tend to resolve conflicts, since checking the persisted elements wouldn't be difficult than resolving conflict at the first input models.

Testing and validation of correspondence relation could be done at this step. Potential inconsistencies can be identified between input models. For example, the same concept represented in two or even more classes appear with different names. For example, the attributes *memberId* and *studentId* have been identified as similar in the earlier step. Here the designer intervenes in order to delete this correspondence because those concepts are semantically deferent. Certain kinds of correspondence relationships can be defined manually, such as generalization, aggregation dependency., In the LMS example, the Member's name is represented in the Head Librarian and the Librarian viewpoint models respectively by (firstName, lastName) and (fullName). Here, the designer intervenes in order to manually draw the aggregation correspondence between those elements.

2.2.3 Merging Step

At this point, we have applied two techniques to merge models: merging technique and translating technique. We apply the merge technique on elements that are interconnected by the relations of equality. This is a default merging scenario, which is applied to relating elements among several models. Elements that have no corresponding one in the opposite model are by default translated into the merged model following the translation rules. In the case of 1 to many relationships, two merging strategies can be carried out, either representing the one element by the many or vice versa. In our example, we carried the second one (many-by-one).

The result of the composition process applied to the LMS example of Figure 2 and Figure 3 class diagrams is illustrated in Figure 5. We applied two stereotypes (merged and actor) to the merged model classes, those two stereotypes will help us to trace back the classes originated from one input model and which ones existed in both. For example, In the merged model, the library and member classes appear with the merged stereotype. Otherwise, the merge process labels classes with the stereotype actor (e.g., Registration class) that exist only in one source model. It is important to note that a tag attribute called actorName is added in order to trace the actors from which the class is originated.

3 Graph Transformation Theory

In the section above, we explain model composition operator is formalized over graph-based models, using graph transformation rules, also, how these are structured to create an

overall operator referred as compose, then we introduce some properties of it as well as their demonstrations.

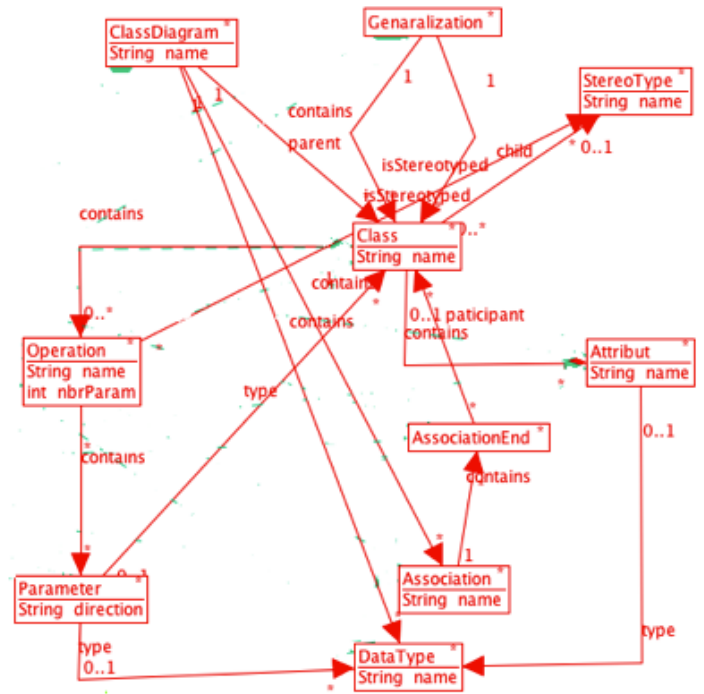


Figure 7: Type graph representing a simplified UML class diagrams metamodel with AGG tool .

As reported by various studies, MOF-compliant models are basically graphing [21]. The whole formalization is based on the representation of the models as attributed graphs. The main idea is to use the graph transformation theory to specify the composition operator using a set of visual and formal graph transformation rules. Using this formalism for model composition offers many benefits, like : Simplicity for declaratively expressing composition rules, good understanding, and also suitable technique with formal analysis tools. In particular, critical pair analysis that can be used to automatically detect dependencies and conflicts between graph production rules.

In the following, we assume that UML models (class diagrams) are formally defined as oriented, labelled, typed graphs. These graphs are conforming and satisfy the constraints defined by another graph called type graph.

3.1 Basic definitions

We present in the following some basic definitions that are necessary to define our composition operator.

Definition 1. (graph-based model)

We assume that UML class diagrams are oriented labelled typed graphs. Then, each model is represented as a graph  $Gr = (V_e; E_d; S_r; T_r; L_b; \Gamma_{Gr})$  such that  $V_e$  and  $E_d$  represent respectively vertices and edges of graph ( $E_d \subset V_e * V_e$ ), function source  $S_r: E_d \rightarrow V_e$  and function target  $T_r: E_d \rightarrow V_e$  that relates edge to a vertex, and a multilabeling function  $L_b$ . The multilabeling function  $L_b$  associates attributes to each element of the graph whether it is vertex or edge.



A graph morphism  $\Gamma_{Gr}: Gr \rightarrow TGr$  which associates a type to every element in  $Gr$ . Vertices and node types are defined in the graph  $\Gamma_{Gr}$  called the type graph; this represents the UML language meta-model graph representations.

Figure 6 gives an example of an oriented labelled typed graph. For instance, the Association-End node representing the member Association-End has a labeled output edge and targets the member's class node. This means that the aggregation Association named loan-member has as extremity the Class Member (Figure 3).

Corradini et al [22] proposed a powerful typing mechanism for graphs. This mechanism formalizes the conformance relationship between the models and the metamodel for the design language. Therefore, it is important to verify that it is conforms with a so-called TypeGraph. In the MDE method, the same principle is applied, where models conform to its meta-model [23]. The formal definition of type graphs is given below.

**Definition 2. (Type Graph)**

Let  $\Sigma V_e$  and  $\Delta E_d$  be a set of vertices types and edges types, respectively. Let  $Gr = (V_e, E_d, S_r, T_r; L_b; \Gamma_{Gr})$  be a graph. A type graph  $TGr$  is a labeled graph over  $\Sigma V_e$  and  $\Delta E_d$ .  $Gr$  is typed over  $TG$  if there exists a graph morphism  $\Gamma G$  from  $G$  into  $TG$  ( $\Gamma G: Gr \rightarrow TGr$ ).  $\Gamma Gr$  associates graph elements of  $Gr$  to nodes of  $TGr$ . This implies that nodes and edges of  $Gr$  are constrained by nodes from  $TGr$ .  $\Gamma_G: V_e * E_d \rightarrow \Sigma V_e \cup \Delta E_d$

The type graph required to represent graphic model is illustrated in Figure 7. It should be generic enough to fit for a subset of any UML class-diagram. This type graph expresses a restriction on the graph-based models that are allowed: it specifies which types of edges may occur between certain types of nodes. the well formedness of graph-model is constrained by existence of a graph-morphism to its typegraph.

**Definition 3. (Graph morphism)**

Given two graph-based models  $Gr1 = (V_{e1}, E_{d1}, S_{r1}, T_{r1}, L_{b1}, \Gamma_{Gr1})$  and  $Gr2 = (V_{e2}, E_{d2}, S_{r2}, T_{r2}, L_{b2}, \Gamma_{Gr2})$  a graph morphism  $h$  from  $Gr1$  to  $Gr2$  is a pair of functions  $h = (hnode, hedge)$ , with  $hnode: V1 \rightarrow V2$  and  $hedge: E_{d1} \rightarrow E_{d2}$  Such that :  $\forall e1 \in E_{d1}$   $hnode(S_{r1}(e1)) = S_{r2}(hedge(e1))$  and  $hnode(T_{r1}(e1)) = T_{r2}(hedge(e1))$

Graph morphisms are viewed as a set of mappings between models, our aim is to prove that those mappings preserve the models structure, in other words, if an edge belonging to the first model is mapped to an edge belonging to the second, then, there exist a mapping of its source and target vertices too [24].

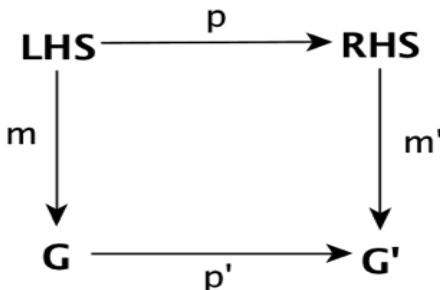


Figure 8: Graph transformation principle.

3.2 Graph transformation

**Definition 4. (Graph production (rule))**

Let LHS, RHS be two oriented, labelled and typed graphs. A graph production rule is a graph morphism  $p_r: LHS \rightarrow RHS$

In case of a given graph  $G_r$ , we apply a graph production rules  $p_r$  to perform transformation. This is made on three steps:

- (i) To find a correspondence in graph  $Gr$  on the left side of LHS.
- (ii) To remove element of the concrete graph that is linked to LHS but not RHS.
- (iii) To glue the context graph previously created with vertices and edges of RHS that possesses no equivalent in LHS. The formal definition of graph production rule, which respect the single pushout approach with injective graph morphisms, has been proposed in [25].

**Definition 5. (Graph transformation)**

Following the definition given in [25] A graph transformation  $G_r \Rightarrow_t G_r'$  is defined as a pair  $t = (p,m)$  composing of a graph production  $p_r: LHS \rightarrow RHS$  and an injective graph morphism  $m: LHS \rightarrow G_r$ . the use of category-theoretical construct, we may automate computing the morphisms  $m': RHS' \rightarrow G_r'$  and  $p_r': G_r \rightarrow G_r'$  that make the diagram  $(p_r;m)$  commute. The Graph  $G_r'$  is the outcome of the transformation applied by  $t$  to  $G_r$ . The Figure 8 illustrates the principles of this definition.

**4 Specifying Model Composition as Graph Transformations**

We introduce our approach in this section, that applies triple graph grammars [11] and also the use of this approach on model composition.

Triple graph grammars offer a declarative and visual formalism for description of model transformation. The TGG formalism is appropriate with the QVTMOF norm [26] for dealing with the problem of model transformation. Furthermore, A variety of models-driven development process activities such as model-refactoring [9], model-synchronization[12], model-integration [13], etc can also be achieved using it.

4.1 Meta9modeling

The main reason behind the use of metamodels is the specification of composition rules in the formalism of TGGs, and also metamodels that are conform with the MOF. In the example presented in Figure 9, metamodels (source and target) are specified by UM/MOF. A third metamodel is used as composition metamodel. It is a model that permits the definition of all the links types for the graphical specifications of composition rules.

In Model-driven engineering area, a model is conform to its metamodel, the same principle may apply to the theory of graphs, which means that a given graph is conform to its type graph [11]. A type graph specifies both nodes type, edges type and constraints between them.

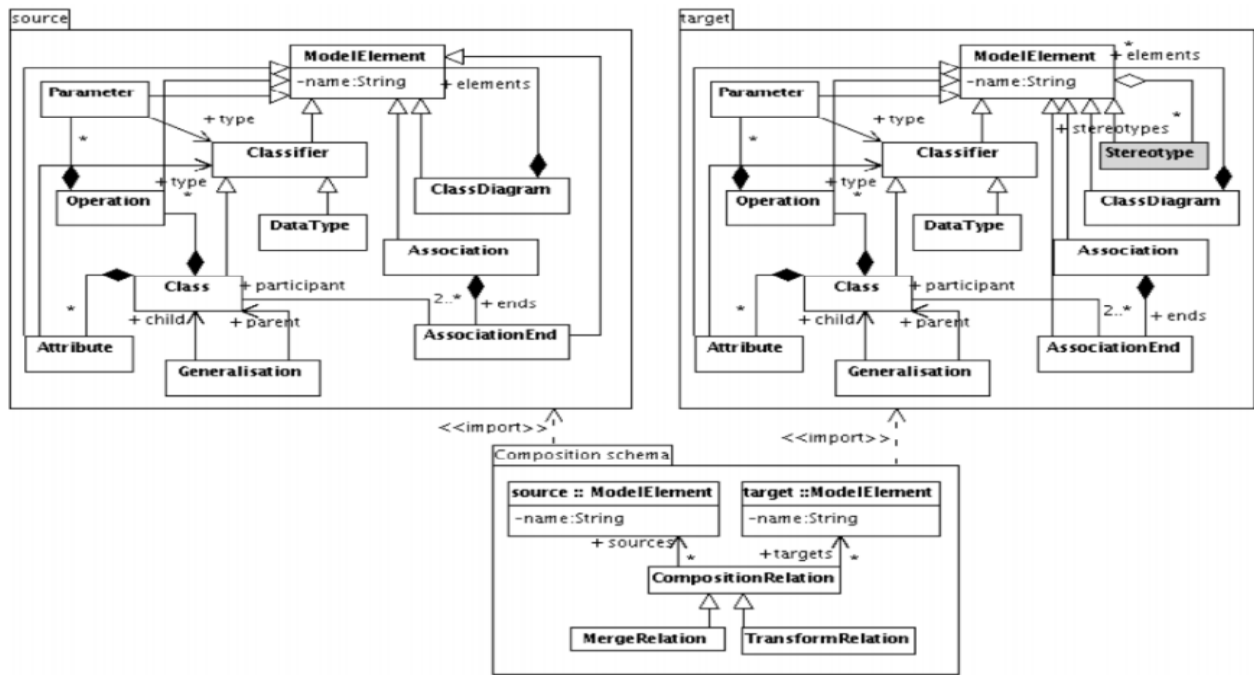


Figure 12:Composition metamodel.

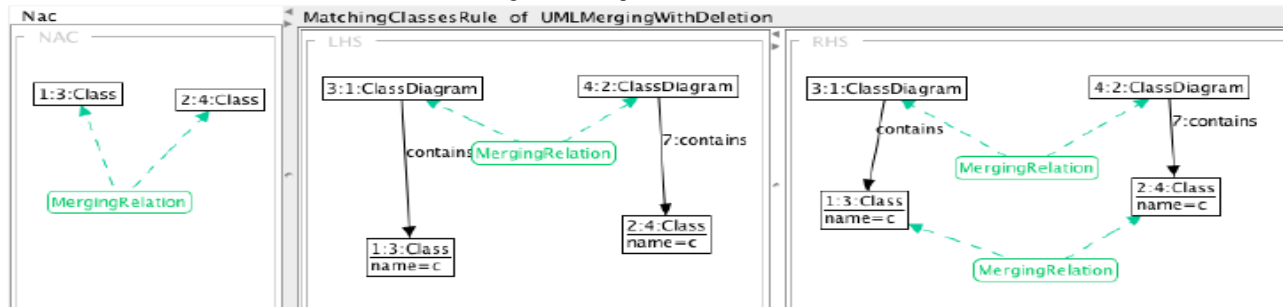


Figure 9: A example of a TGGs matching rule.

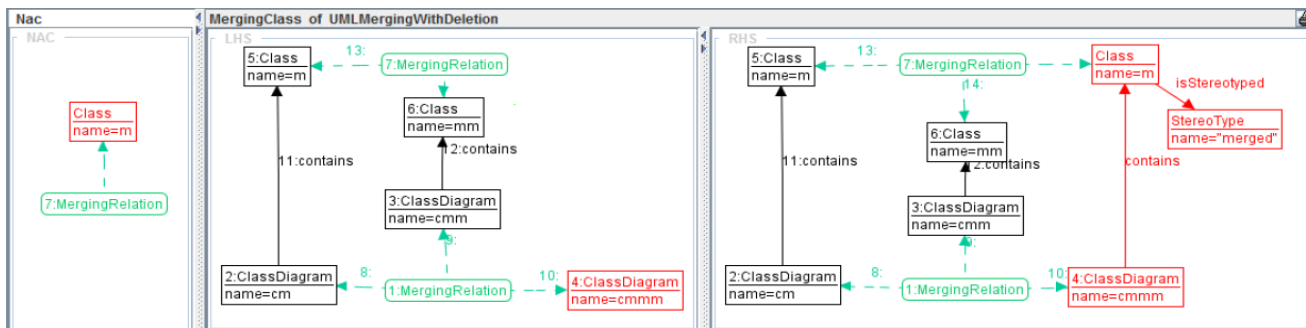


Figure 10: A example of a TGGs merging rule.

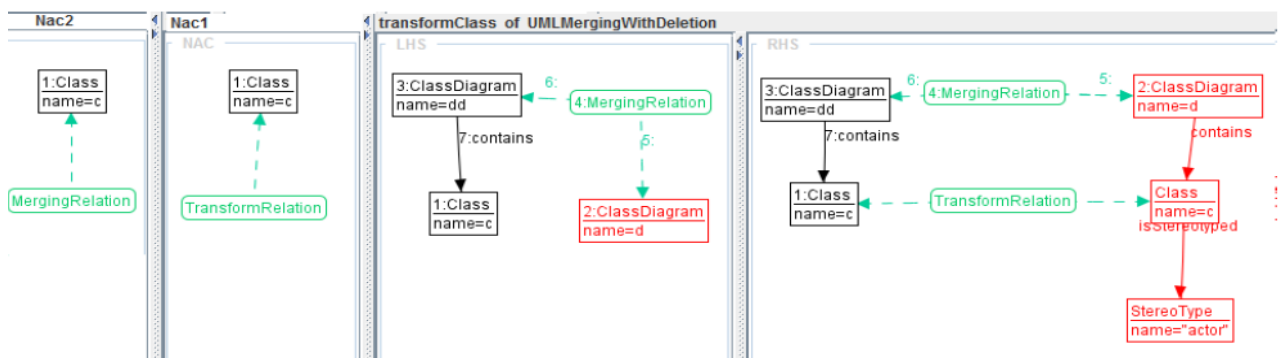


Figure 11:A example of a TGGs translation rule.

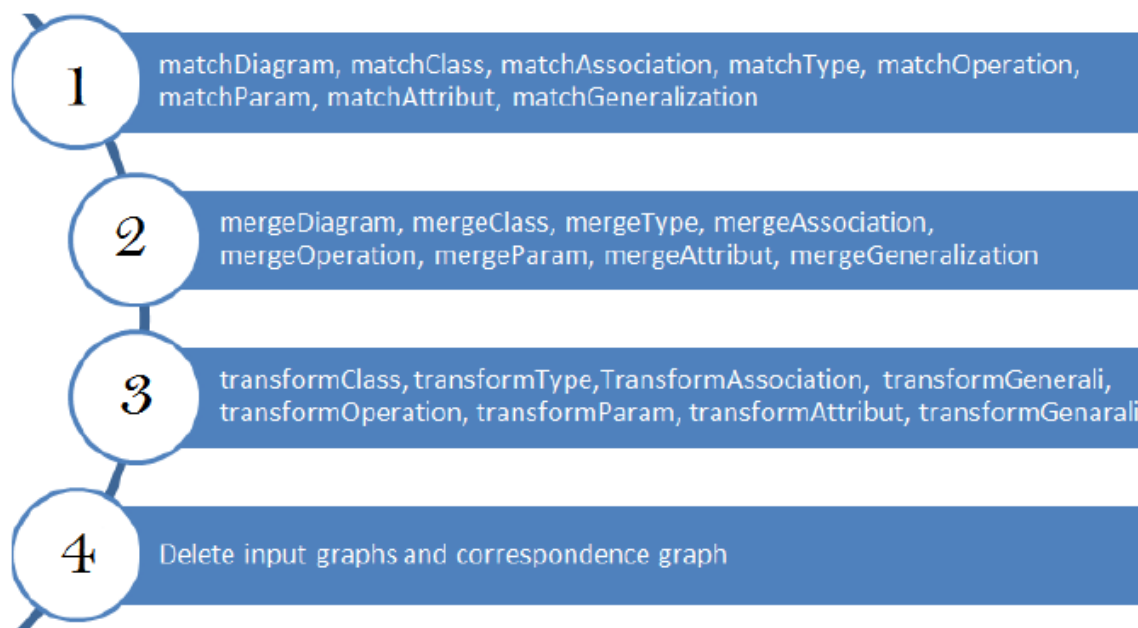


Figure 13:Transformation Rule layers.

The AGG defines metamodels as graph types. Typed attributed graphs are defined via node type inheritance, Nevertheless, node inheritance may not be allowed by the transformation rules and application requirements. this is the reason behind why we adopted a classical representation without node type inheritance. (Figure 9) illustrates packages via a subgraph. each type graph is shown in subgraphs. Related to the composition process, we may need to preserve and create a matching links between input model elements from the matching step. This will take us to use links for merging. by doing so, we create all of the matching links types needed to specialize the MergeRelation links type declaration. when link type is specialized, will determine a mapping link for every element type from source metamodels which would be used in the merging step producing elements in the merged model

#### 4.2 specifying Composition Rules using TGGs

With TGGs formalism, the graph-rewriting rules will show the way in which the elements of a pair of graphs are linked by a third-graph, so-called correspondence graph. Especially, Every TGG's rule consists of a rewriting pair of graphs and a third rewriting graph rules; those are used for checking and creating correspondence links between nodes of the two regarded graphs [13].

We recall that TGGs rules are considered as a set of declarative transformation rules of bidirectional graph transformations. In this section, we explain how, from these declaratives' specifications, we derive some transformation rules for model composition purposes. These rules are into three categories: matching, merging and translation rules.

The matching rules are first executed over input models. In this particular step, the transformation is in-place, only correspondence relations are set up. The TGGs rules compute a valid correspondence between two existing graphs [27]. Each rule execution looks for a pattern corresponding to the rule's LHS and not violating the NACs, if so, the RHS is produced and a correspondence pattern is arranged.

Figure 10 illustrates an example of a matching rule that creates a correspondence link between two equivalent classes. They are said equivalent if they hold the same name and belonging to two different models. Note that, a negative application condition is not shown, which eliminate many applications and creation correspondences links of this rule. As we have explained in the composition process section, some matching links could be created manually by the designer, so that they relate concept that are similar but differently modeled. Among the most important advantages of our method consist of separating the matching and merging operations. the main purpose of the merging transformation is treating the involved models and matching links as a single graph. The equivalent parts in the merged model are created by computing various matching links through merging rules. An example of a TGG rule that create a new class is given in Figure 11. In this rule, the newer class is linked to a merged model. The target production of the rule also specifies the generation of the merged stereotype according to our merging strategy.

Two classes that have the same label and but each of which belonging of a class diagram already merged (LHS). A merged class that has the same label as well as a merged stereotype is created, this will link the merged class to the merged class diagram. The default NACs guarantee the rules only apply once. AGG includes an editor for defining variables and attributes conditions. For instance, we used this feature to certify that the names of the two classes are identical in the Class Merging rule.

We have defined a set of transformation rules named "Translation rules". Those rules apply a simple default behavior which consists of creating, a deep duplicate of the source model in the target model. We show in Figure 12 a translation rule illustration applied to a single class. It generates a Class and a stereotype element by initializing their corresponding attributes with the provided values. We remember as explained before, that the merged model must be earlier produced by the corresponding merge rule to which the new produced class will be attached to.

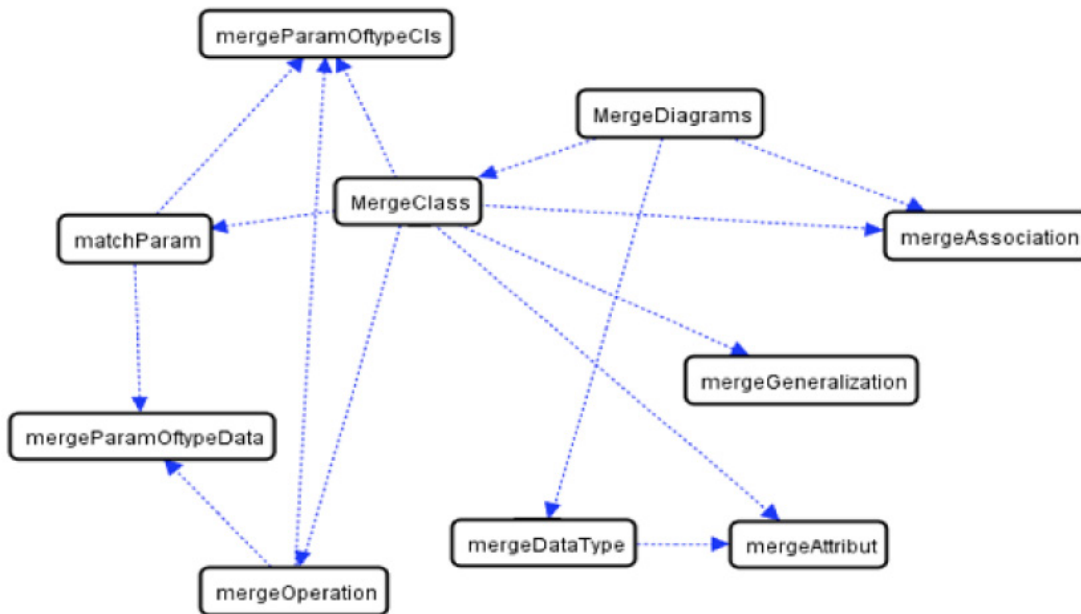


Figure 14: Sequential dependencies of merging rules.

### 5 Tool support

In order to validate the mentioned concepts, we carried out performed some practical experiments with AGG tool [14]. AGG tool is considered as one of the most known graph-based transformation tools implementing an algebraic approach for graph transformation. We have chosen this tool because it provides several advanced features of TGGs to specify complex transformations scenarios. As an example of advanced features, we can for example specify context constraints by using the specific attribute constraints. Also, we can specify a set of fillers with the concepts of Positive, Negative, and General Applications Conditions (PACs, NACs, and GACs). Within the GACs, one can apply combinations of former operators like AND, OR, FORALL over patterns. We can also perform some validations of graph transformation rules by applying advanced features by using consistency checking and critical pair analysis concepts. This is very useful to detect parallel conflicts and sequential dependencies [28]. Others features are applied to control flow of transformation rules, with rule sequences, layers and priority order [29].

#### 5.1 Specifying rule layers

in this logic So we can consider the fact of as to having the same logical order as in the composition process, we may used rule layers to identify specify the transformations ow and decrease the complexity of the trans- formation application conditions. ThusSo, the matching rules appear first, the trans- formation rules come after the application of merging rules, and, obviously, the deletion rules come after the transformation process. Figure 13. shows composition rules sorted by rule layers.

#### 5.2 Consistency checking with AGG

A consistency checking can be performed over the output model throughout consistency conditions (CC). A consistency condition describes graphically the graph properties as e.g. existence of a certain element or the independent of a certain rule. Also, a consistency condition is composed of a premise P and a

conclusion C. Formally; a consistency condition is a total injective morphism

$c: P \rightarrow C$ . This condition is said satisfied by a given graph G, if for all total injective morphisms  $p: P \rightarrow G$  there is a total injective morphisms  $q: C \rightarrow G$  such that  $q \circ c = p$ .

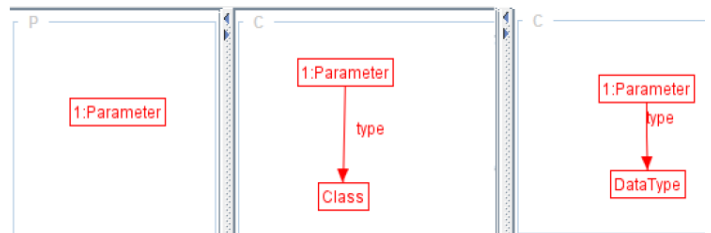


Figure 15: Dangling Parameter Type reference constraint.

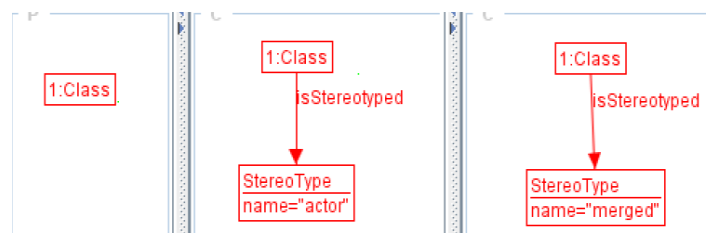


Figure 16: Check Class stereotypes constraint

In other words, for all the matches of the premise P in G, the conclusion C has to be fulfilled. We note that if we have multiple constraints then, G has to fulfill all these constraints. For instance, Figure 14 shows a consistency condition that specifies how to check that every parameter has necessarily a type. It is composed of one premise and two disjunctive conclusions (the satisfaction of one conclusion is enough). First, the premise is represented by a node of type parameter. Then, the associated conclusions assert that each node parameter has to be coupled (through- out the edge type) with either a node of type class or a node of type DataType.

Another example of a cc is depicted in Figure 15 which describes a consistency condition which specifies how to check



that every class has essentially a stereotype with an attribute named actor or merged. The premise of the CC is the node Class, and the conclusion is a class connected to Stereotype with an attribute name actor or merged. When checking those CC over our output model and a window appears having the message the graph fulfills this atomic.

The transformation configuration of the AGG tool gives one the ability to stop after the execution of each layer and check manually the satisfiability of the constraints of interest. This, evaluates the correctness of the graph resulting so far, and prevents errors to be propagated.

As our transformation is composed of two major and separate steps (matching and merging), it is more convenient to assess the matching phase before starting the composition phase. Afterwards, comes the final checking phase to validate and ensure the correction of the output graph. Thereafter, a brief description of the constraints to be checked after each step:

### 5.2.1 *Marching step*

After this transformation step finishes, we check either the transformation behaved as expected or not by running the appropriate constraints over the graph resulted as yet. These constraints play on the one hand the role of a syntactic checker. And on the other hand, they say if the set of transformation rules reaches all the graphs nodes. For instance, checking if all the classes are reached can be translated by the following constraint. For each node Class this class should either be merged to another class or simply transcribed as it is. In other words, each node Class has to be linked to a node MergeRelation or TransformRelation. The same constraints can be extended to all the of the source type graph (Attribute, Association, Parameter).

### 5.2.2 *Merging step*

After that the merging step reaches its end another validation process take place. Using the appropriate model constraints, we check if the transformation consults and transforms every matching relation (MergeRelation or TransformRelation). For example, every Class matching relation of type MergeRelation have to be linked to a Class with the stereotypes name merged. We expand it for every matching relation linked to any node type.

### 5.2.3 *Final checking*

Despite the fact that the previous checking steps help vanishing ambiguities, however, it is not satisfactory to tell that the results are correct. In some way, the constraints defined in this phase aid validating the syntactic properties of the output graph.

## 5.3 *Sequential Dependencies between rules*

This implementation activity is an important step to validate the syntactic correction of our composition process. During the definition of these constraints, we confronted a couple of difficulties, namely, the definition of complex constraints or negative ones. Other difficulties, adhere to those aged [9].

In fact, the graph of sequential dependencies between the transformation rules is computed by AGG, in order to retrieve the cross-dependency which in between (i.e is executing a rule depends on another execution). This graph is also intended to detect execution

cycles. We talk about execution cycles when a sequence of rules gives a way to a rule previously triggered to be executed for the same matching. This prevents the transformation to turn in empty. We computed this graph for the merging step of our composition process. While analyzing the graph in Figure 16, we conclude that the rules mergeClass, mergeData, and mergeAssociation depend on the rule mergeDiagram, so this rule should be triggered first. Also, we come out with the conclusion that no cyclic executions are present in this transformation layer.

## 6 **Related Works and Discussion**

In the MDE approach, model composition is now one of the relevant activities in MDE approach. According to [30], On the one side, matching requires consistency, efficiency and simplified approach. On the other side, the merging step requires; conflict identification and resolution and consistency preservation. In the section that follows, we used graph grammar to transform these requirements to model composition in an ad-hoc manner.

**Merging strategy:** This technique could be divided into in-place techniques and out-targeted techniques. The first one consists of merging the input models into one global model named the host model along with their correspondence model. This strategy has many advantages such as simplicity, so a new model is not necessary to define the global view. Nevertheless, the input models are no longer available and to return and get them back is not guaranteed. The second strategy maintains the inputs unchanged and completely computes their union into a novel target model.

**Conflicts management:** Conflict can occur when the input models overlap. Many solutions require merging only consistent models, this operation requires a preliminary step to conflict resolution. Matching process automation: this activity could be performed automatically, semi-automatically or manually. In certain situations, the designer must make the final drawings of models matching when dealing with inconsistencies or when describing other relationships that are not evident (e.g. generalization or aggregation).

**Change propagation:** Models are updated and revised regularly. Therefore, some model views require the transformation at the beginning stage of design. Therefore, it is important to preserve traceability between input models in order to avoid the merged model being computed in case of any change in the source models.

In [13], The authors proposed an approach based on multigraph grammar principle to generalize TGG formalism and which besides presents a method to deal with data integration in heterogeneous distributed environment. On the one side, the integration mechanism relies on declarative rules to define communication relations between models. On the other side, they derive from those rules a set of operational rules which ensure accuracy among models and are responsible for the propagation of attribute changes from one element to the linked one. As with TGGs we can define constraints that are fairly simple, we propose the use of Layered graph grammars in our approach that permits to minimize the difficulty of constraints properties. The propagation mechanism as well as the integration, updates and changes were addressed using graph transformation rules. In [31], an EMF-based model management framework is suggested, including a collection of generic modules. The framework is founded on three notions:

equivalent relations, inconsistency resolution and refreshment of the construct those steps are equivalent to our steps mentioned in our approach. To locate reused elements between two models, the Merge operator employs the equivalence relations specified in a metamodel. This method suppose consistency in the input models and consider only a simple relationship like a simple Association. this would facilitate automatization of matching operation.

Several approaches use matching step as primary step in model composition. UMLDiff [32] It introduces an automated structural-differentiating algorithm. UML-aware. Based on the name and structural similarity of two models, it generates all modifications in the form of a tree structure. the use of heuristics makes it possible to establish such correspondence between elements by comparing both structural and lexical similarity between them.

A related work called GenericDiff [33], takes into a count all feature information of models, pair-up feasibility predicates, and random walk tendency functions. This method compares two nodes to the recognizing of the Maximum Common Sub-graph (MCS) of two Typed Attributed Graphs by the use of an iterative process that propagates the distance value from nodes pair to node pair based on graph structure and probability distributions. The major weakness of this method is to specify the appropriate threshold.

Finally, EMF Compare framework [34] is developed with a high level of extensibility to deliver good performance and efficiency. Some techniques such as instances, statistics and heuristics are used to achieve the matching phase. the authors use some metrics to weight this formula such as element's name, their content, their types and the relations they have with other elements. In return a value ranging from zero to one, which will be balanced with additional factor's scores the similarity between the source and target elements.

## 7 Conclusion

To sum up, our work was a mere investigation conducted to test the practicality of our approach using a graph transformation by means of AGG which appears to be the appropriate one to achieve and satisfy the following representation and visualization requirements: it is an investigation that goes along with the objective of our work, it is mainly about formalizing the model composition activity to produce an integrated view of all the individual views. We are totally concluded that tools like AGG accomplish the requirements presented earlier. To this end, we are going to examine a list of languages and tools specialized on graph transformation such as Tiger EMF [35] in order to choose the more appropriate to our method. we have formalized graphically the process by means of graph transformations. Composition rules are specified graphically using TGGs formalism. A set of attributed graphs allows both source and target model formal representation as well as correspondence model. The matching process is really aimed at adding a set of links to features of the source model. The correspondence graph is used to facilitate the automatization of the merging step and enable the correspondence graph to be incrementally refined. It also helps the traceability of the composition phase to be enhanced. The scope of this research could be broadened to various lines. our method was specified and proved in case of UML models context. however, it is entirely generic because majority of specification concerns graphs features. Therefore, it can be simply applied to any graph-based model

composition. it is an important to automate the detection of possible concordances or conflicts between models towards implementing the proposed methodology to the big projects. So, we can use matching heuristics to compute similarities between elements of graph-based models.

## References

- [1] France R, Ray I, Georg G, Ghosh S. An aspect-oriented approach to design modeling. IEE Proceedings - Software, Special Issue on Early Aspects: Aspect-Oriented Requirements Engineering and Architecture Design 151,2004, 173-185.
- [2] Sabetzadeh M, Easterbrook S. An Algebraic Framework for Merging Incomplete and Inconsistent Views. 13th IEEE International Requirements Engineering Conference, (RE2005) pages 306-318, Washington, DC, USA, September 2005. IEEE Computer Society.
- [3] Finkelstein A, Kramer J, Goedicke M. Viewpoint Oriented Software Development. IC-SSEA. Toulouse, France, 1990, pages 337-351.
- [4] Clarke S. Extending Standard UML with Model Composition Semantics. Science of Computer Programming, 44 (2002). 71-100.
- [5] Chechik M. A relationship-based approach to model management. In Model-Based Methodologies for Pervasive and Embedded Software, 2009. MOMPES09. ICSE Workshop on, pages 11. IEEE.
- [6] [Kolovos D, Paige R, and Polack F. Merging models with the epsilon merging language (eml). Model Driven Engineering Languages and Systems, 2006. pages 215-229.
- [7] Anwar A, Ebersold S, Coulette B, Nassar M, and Kriouile A. A rule-driven approach for composing viewpoint-oriented models. Journal of Object Technology, 2010, 9(2):89-114.
- [8] Anwar A, Dkaki T, Ebersold S, Coulette B, and Nassar M. A formal approach to model composition applied to vuml. In the 16th IEEE International Conference on Engineering of Complex Computer Systems (ICECCS) 2011, on, pages 188-197. IEEE Computer Society.
- [9] Mens T, Van Eetvelde N, Demeyer S and Janssens D. Formalizing refactoring with graph transformations. Journal of Software Maintenance and Evolution: Research and Practice, 2005, 17(4):247-276.
- [10] Agrawal A, Karsai G, Neema S, Shi F and Vizhanyo A. The design of a language for model transformations. Software and Systems Modeling, 2006, 5(3):261-288.
- [11] Schrr A. Specification of graph translators with triple graph grammars. In Proceedings of the 20th International Workshop on Graph-Theoretic Concepts in Computer Science, 1994, pages 151-163. Springer-Verlag.
- [12] Giese H and Wagner R. Incremental model synchronization with triple graph grammars. Model Driven Engineering Languages and Systems, pages 543-557, 2006.
- [13] Knigs A and Schrr A. MDI: A rule-based multi-document and tool integration approach. Software and Systems Modeling, 5(4): 349-368, 2006.
- [14] Ahmed A. et al., "Modeling and Simulation of Office Desk Illumination Using ZEMAX," in 2019 International Conference on Electrical, Communication, and Computer Engineering (ICECCE), 2019, pp. 1-6.
- [15] Niere J and Zundorf A. Using Fujaba for the development of production control systems. Applications of Graph Transformations with Industrial Relevance, pages 301-304, 2000.
- [16] A. Anwar, A. Benallam, M. Nassar et B. Coulette. A Graphical Specification of Model Composition With Triple Graph Grammars. Lecture Notes in Computer Science (LNCS), volume 7706, p. 1 - 18. Springer, Heidelberg, 2013.
- [17] Melnik S, Garcia-Molina H, and Rahm E. Similarity flooding: A versatile graph matching algorithm and its application to schema matching. In Data Engineering, 2002. Proceedings. 18th International Conference on, pages 1171-128. IEEE, 2002.
- [18] Jean-Mary Y.R, Shironoshita E.P, and Kabuka M.R. Ontology matching with semantic verification. Web Semantics: Science, Services and Agents on the World Wide Web, 7(3):235-251, 2009.
- [19] La Rosa M, Dumas M, Uba R, and Dijkman R.M. Business process model merging: an approach to business process consolidation. ACM Transactions on Software Engineering and Methodology (TOSEM), 2012.
- [20] France F, Fleurey F, Reddy R, Baudry B, and Ghosh S. Providing support for model composition in metamodels. In Enterprise Distributed Object Computing Conference, 2007. EDOC 2007. 11th IEEE International, pages 253-253. IEEE, 2007.
- [21] Mens T. On the Use of Graph Transformations for Model Refactoring. GTTSE 2006: 219-257.

- [22] Corradini A, Montanari U, Rossi. Graph processes. *Fundamental Informaticae*, 26(34):241265, 1996.
- [23] Bezivin J. Model driven engineering: Principles, scope, deployment and applicability. In *Proceedings of 2005 Summer School on Generative and Transformation Techniques in Software Engineering*, 2005.
- [24] Marchand J, Combemale B, Baudry B, A Categorical Model of Model Merging and Weaving. In *4th International Workshop on Modelling in Software Engineering (MiSE 2012)*, in conjunction with ICSE 2012, IEEE, 2012.
- [25] Ehrig H and Lwe M. Parallel and distributed derivations in the single-pushout approach. *Theoretical Computer Science*, 109:123143, 1993.
- [26] OMG 2002. *OMG/MOF Meta Object Facility (MOF) 1.4. Final Adopted Specification Document*. formal/02-04-03.
- [27] Greenyer J and Kindler E. Reconciling tggs with qvt. *Model Driven Engineering Languages and Systems, LNCS* pages 1630, Springer-Verlag 2007.
- [28] Bottoni P, Taentzer G, and Schurr A. Efficient parsing of visual languages based on critical pair analysis and contextual layered graph transformation. In *Visual Languages, 2000. Proceedings. 2000 IEEE International Symposium on*, pages 59-60. IEEE, 2000.
- [29] Ehrig H, Ehrig K, De Lara J, Taentzer G, Varro D, and Varro -Gyapay S. Termination criteria for model transformation. *Fundamental Approaches to Software Engineering*, pages 4963, 2005.
- [30] Fortsch S and Westfechtel B. Differencing and merging of software diagrams. *State of the Art and Challenges*, 2007.
- [31] Boronat A, Cars J.A, Ramos I, and Letelier P. Formal model merging applied to class diagram integration. *Electronic Notes in Theoretical Computer Science*, 166:526, 2007.
- [32] Xing Z and Stroulia E. Umldiff: an algorithm for object-oriented design differencing. In *Proceedings of the 20th IEEE/ACM international Conference on Automated software engineering*, pages 5465. ACM, 2005
- [33] Xing Z. Model comparison with genericdiff. In *Proceedings of the IEEE/ACM international conference on Automated software engineering*, pages 135138. ACM, 2010.
- [34] Brun C and Pierantonio A. Model differences in the eclipse modelling framework. *UPGRADE, The European Journal for the Informatics Professional*, 2008
- [35] TFS Group, Technische Universitt Berlin. EMF Tiger (2009). <http://tfs.cs.tuberlin.de/emftrans>

## A Resolution-Reconfigurable Asynchronous SAR ADC with Segmented and Non-Binary Weighted Capacitance DACs

Chih-Hsuan Lin\*, Kuei-Ann Wen

Department of Electronic Engineering, University of National Chiao Tung (NCTU), Hsinchu 300, Taiwan

### ARTICLE INFO

Article history:

Received: 07 January, 2020

Accepted: 03 April, 2020

Online: 17 April, 2020

Keywords:

resolution-reconfigurable  
asynchronous SAR ADC  
segmented and non-binary  
weighted

### ABSTRACT

With the addition of thing of internet applications to 5G smartphones, mobile standby time and ultra-low-power sensing systems have become increasingly important. Nowadays, such sensing systems typically reduce power consumption to microwatts. This paper presents segmented and non-binary weighted capacitance DACs, low power, high resolution, an asynchronous clock, a spark-detect, vcm-based switching and direct switching, and reconfigurable 9- to 12-bit DACs to meet different sensing system applications. Multi-voltage is used to achieve microwatt-level power consumption. The analog/digit voltage is 1.5V/0.9V, respectively and can adjust the 4-mode resolutions (9/10/11/12 bits). The performance of the SNDR achieves 50.78, 58.53, 62.42, and 66.51db, respectively and consumes 2.69uW and results in a figure of merit (FoM) of 30.4fJ/conversion step for 12-bit mode.

### 1. Introduction

This paper refers to the previous paper titled “A Resolution-reconfigurable SAR ADC with Partially Thermometer Coded DACs.” [1] The Internet of Things uses multi-sensors recently. Using CMOS MEMS process to integrate different electronic systems are more and more frequent. The electronic system can reduce power consumption and maintain high-efficiency operations, which have always been important issues. The 3-axis CMOS MEMS accelerometer are capacitive sensors and capacitive sensitivities often less than 1fF/g. The circuit of the readout need to own a variable conversion gain of the capacitance to voltage to meet different needs. The circuit of the readout include a gain amplifier, correlated double sampling (CDS) and chopper, and a programmable gain amplifier (PGA). The readout circuit adopts time division multiplexing to reduce power consumption, and the output voltage of the three-axis accelerometer is given to the asynchronous SAR ADC with segmented and non-binary weighted capacitance DACs. This paper chooses a low power, high resolution, internally generated asynchronous clock, using a thermometer code to segment capacitors of the higher bits and improve the linearity for 3 MSB (the most significant bit), non-binary weighted DAC capacitance array for lower bits to avoid incomplete settle issues caused error and increase error correction capabilities, a spark-detect

schematic to avoid meta-stability issues, vcm-based switching and direct switching methodology to reduce the switching average energy and delay time, and uses negative voltage switch to adjust the resolution (12/11/10/9 bits), increase linearity and reduce leakage for reconfigurable resolutions. However, the average switching energy of the segment capacitance DAC array architecture is the same with Merged capacitor switching (MCS) and less than either the monotonic capacitor array or a conventional capacitor array architecture. [2]

### 2. Successive approximation register analog-to-digital converter architecture

#### 2.1. The analysis of the The architecture of the vcm-based switching architecture

Figure 1 shows the architecture of the vcm-based switching. The following is the operation process of the vcm-based switching architecture. The capacitance DAC array on the top plate and positive side of the bootstrapped switch to the input signal  $V_{ip}$  switches. The common-mode voltage  $V_{cm}$  (common-mode voltage) switch to the bottom plate capacitor. In the next phase, the input signal ( $V_{ip}$ ) float, and the comparator can collect the node voltages ( $v_{xp}$  &  $v_{xn}$ ) and make decision directly and does no switch any capacitor. The  $S_{10p}$  (MSB) is high when the input voltage  $V_{xp}$  is greater than  $V_{xn}$ . The maximum capacitor on bottom plate and the positive side switch from  $V_{cm}$  to  $V_{ref}$ , and

\*Corresponding Author: Chih-Hsuan Lin, [shsuanhsuan.ee01g@g2.nctu.edu.tw](mailto:shsuanhsuan.ee01g@g2.nctu.edu.tw)



the maximum capacitance on the bottom plate and negative side switch from Vcm to GND. The SAR ADC will duplicate this procedure until the least significant bit (LSB) make decision. Figure 2 shows the vcm-based switching functional flow diagram.

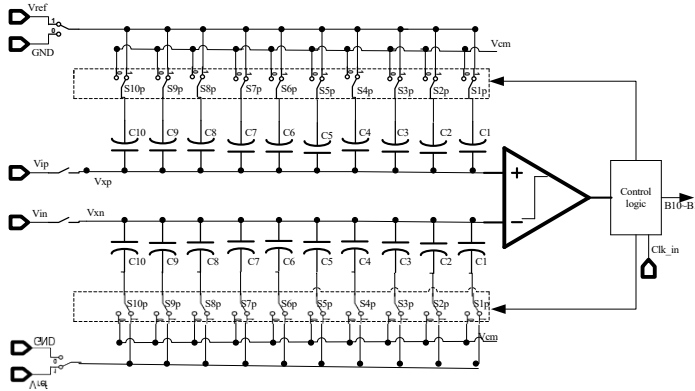


Figure 1. The architecture of the vcm-based switching

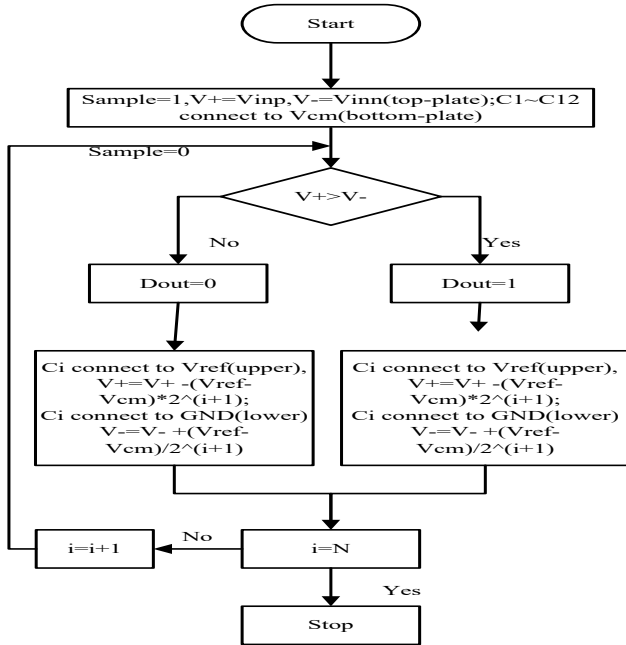


Figure 2. Vcm-based switching functional flow diagram

This paper proposes a new architecture use segmented capacitance DAC array for higher bits (3 bits) and non-binary weighted capacitance DAC array for lower bits (11 bits). In addition, using the architecture of differential to eliminate the effect of substrate noise and power noise to meet 12-bit accuracy. The ratio of all the capacitance DAC array is (256:256:256:256:256:256:112:64:32:20:10:8:4:2:2:1:1).

The higher bits (3 bits) divides the capacitor into 7 capacitors, each  $2^8 fF$ . The segmented capacitance DAC array use a thermometer code to segment and reduce the mismatch caused by the capacitor. Then the lower bits (11 bits) uses the non-binary weighted methodology. When the ADC which used binary weighting capacitance DAC array is in conversion state, external or internal interference maybe causes error decision and degrades the ADC's performance. This paper of the SAR ADC uses a non-binary weighted methodology and has 2 more cycle operations

than binary weighted methodology. It can continue to correct ADC digit representation by using excess 2 cycle operations. Figure 3 shows vcm-based switching architecture with both segmented and non-binary weighted capacitance DAC array.

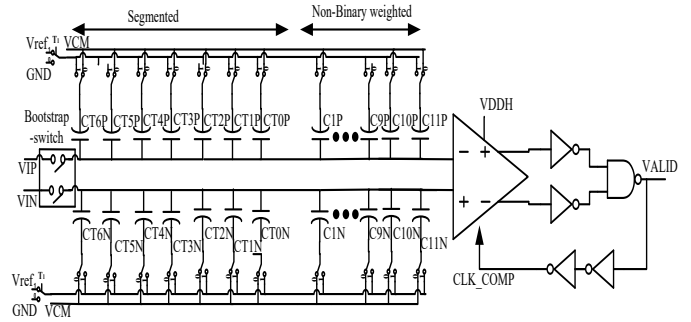


Figure 3. Vcm-based switching architecture with both segmented and non-binary weighted capacitance DAC array

Moreover, the formula of the average switching energy of the vcm-based switching architecture for this paper is “(1)” and  $341 CV_{ref}^2$ , which is smaller than the conventional switching method and the monotonic switching method. On the other hand, the number of switches is  $4(n+2)$  and the number of unit capacitors is  $2^{n-1}$  which is also smaller than the conventional switching method. [3,4]

$$E_{vcm-based,avg} = \sum_{i=1}^{n-1} 2^{n-3-2i} \cdot (2^i - 1) \cdot CV_{ref}^2 \quad (1)$$

### 2.2. Analysis of linearity

To make the lower bits of the SAR ADC has no quantization error, every split capacitor keeps "radix of 2" form. The non-binary weighted of the lower bits is (112:64:32:20:10:8:4:2:2:1:1) and 112C is  $2^6 Cu + 2^5 Cu + 2^4 Cu$ , 20C is  $2^4 Cu + 2^2 Cu$ , 10C is  $2^3 Cu + 2^1 Cu$ , 2C is  $2^1 Cu$ . The higher bits are implemented with 7 identical capacitor size which is  $2^8 Cu$ . The advantage of the DAC with thermometer coded is that it can make the higher bits have better linearity and DNL. The analysis of linearity is as follows.

The non-binary weighted capacitor array, each weighted capacitance can be expressed as [1][5]

$$C_i = 2^{i-1} C_u + 2^{i-1} \sigma_u = 2^{i-1} C_u + \delta_i \quad (2)$$

where  $i$  is an integer representing bit position,  $\delta$  is the error term,  $C_u$  is unit capacitor,  $D_n$  is the digital output,  $n$  is the number of bits,  $y$  is the digital output.

then, subtracting both the no error term of the nominal value  $\Delta V_{x,nominal}$  and the error term of the  $\Delta V_{x,binary}$ . The error term is expressed as follows

$$V_{error} = \Delta V_{x,binary} - \Delta V_{x,nominal} = \frac{2D_{n+2}\delta_{n+1} + 2D_{n+1}\delta_n + 2D_n\delta_{n-1} + 2D_{n-1}\delta_{n-2} + 2D_2\delta_1}{2^{n-1}C_u} V_{ref} \quad (3)$$

differential nonlinearity (DNL) is the difference of two adjacent code as shown in below:

$$DNL(y) = \frac{V_{error}(y) - V_{error}(y-1)}{LSB} \quad (4)$$

the maximum error is generated from 10...0 to 011...1, variance of the maximum DNL error can be expressed as

$$DNL_{\max(\text{non-binary})} = \frac{\sqrt{E[V_{\text{error}}^2(100 \dots 0) - V_{\text{error}}^2(011 \dots 1)]}}{\text{LSB}} = \sqrt{2^{n-1}} \frac{\sigma_u}{C_u} \quad (5)$$

integral nonlinearity (INL) is the difference between the ideal code and the actual code as shown below:

$$INL(y) = \frac{V_{\text{error}}(y)}{\text{LSB}} \quad (6)$$

the maximum error occurs during the code in '100...0', so the maximum INL is shown a

$$INL_{\max(\text{non-binary})} = \frac{\sqrt{E[V_{\text{error}}^2(100\dots 0)]}}{\text{LSB}} = \sqrt{2^{n-2}} \frac{\sigma_u}{C_u} \quad (7)$$

the maximum error of the segmented DAC's higher bits is generated from 10...0 to 011...1, variance of the maximum DNL error can be expressed as

$$DNL_{\max(\text{segmented})} = \frac{\sqrt{E[V_{\text{error}}^2(100 \dots 0) - V_{\text{error}}^2(011 \dots 1)]}}{\text{LSB}} = \sqrt{2^{n-4}} \frac{\sigma_u}{C_u} \quad (8)$$

The variation of the variance of the maximum DNL error of the binary weighted DAC and the variance of the maximum DNL error of the segmented DAC as follows:

$$\frac{DNL_{\max(\text{non-binary})}}{DNL_{\max(\text{segmented})}} \approx \frac{\sqrt{2^{n-1}} \frac{\sigma_u}{C_u}}{\sqrt{2^{n-4}} \frac{\sigma_u}{C_u}} = \sqrt{2^3} \quad (9)$$

### 3. ADC Architecture Design

#### 3.1. System architecture

Figure 4 shows the system architecture of the SAR ADC with segmented and non-binary weighted capacitance DACs. It is divided into analog part and digit part. The analog part includes bootstrap switch, comparator, the negative voltage switch, and negative voltage level shifter, the negative voltage switch power generator. The digit part includes the vcm-based switching and bit register control logic, an asynchronous clock, error correction schematic, and voltage level shifter. The digit part use VDDL (0.9V) and analog part use VDDH (1.5V) to save power and negative voltage NEG\_H2(-1.5V). The segmented capacitor DAC array has 3 bits and non-binary weighted capacitor DAC array has 11 bits. The capacitor DAC array include capacitor array and switch. Moreover, the resolution scale (RS) control uses RS\_I[1] and RS\_I[0] to generate RS0~2 and control the negative switch on positive side and negative side of DAC capacitance array, includes mux and a negative voltage switch. Both the power and ground of the negative switch on DAC capacitance array's positive side are VDDH and VIP+NEG\_H2 and the negative side are VDDH and VIN+NEG\_H2. The VIP and VIN are input signal. In addition, the voltage level shifter uses the contention mitigated

level shift (CMLS) architecture [6] and the unit capacitance uses 9fF.

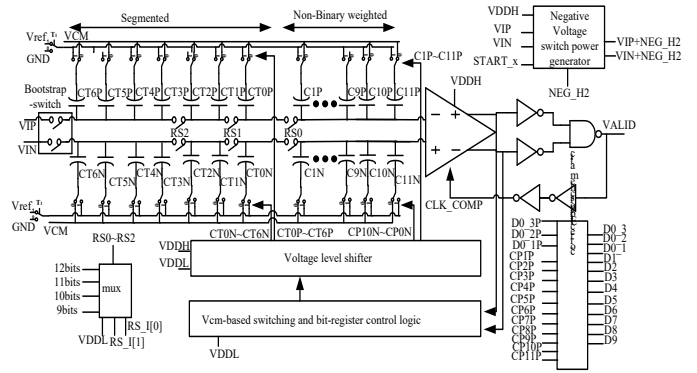


Figure 4. The system architecture of the SAR ADC with segmented and non-binary weighted capacitance DACs

#### 3.2. Sample and hold

Figure 5 shows the bootstrap switch, which performs the function of the sample-and-hold. Then the input signal (VI) achieves near the full range and can suppress the signal distortion to greater than 12 bits. [7] The operation of the bootstrap switch is shown in Figure 6. When CLKS is high, the voltage of the node VG fix at the voltage VDDH + VI to make the on-resistance of M10 keeps a small constant value, which can improve the linearity, reduce the significant distortion. When CLKS is low, the VG is low and M7&M10 turns off. From the simulation, the sample rate of 50Ks/s and get 8192 sample points in the Nyquist input frequency. Then taking fast Fourier transformations (FFT) for the bootstrap switch connect to the output load capacitor 18pf. The signal to noise and distortion ratio (SNDR) of sample-hold is 87.2db and an effective number of bits (ENOB) is 14.29.

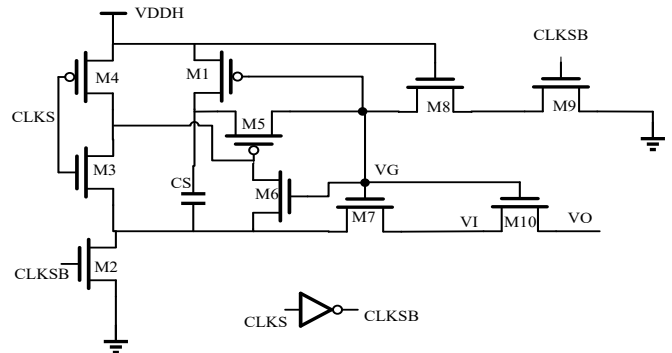


Figure 5. The bootstrap switch

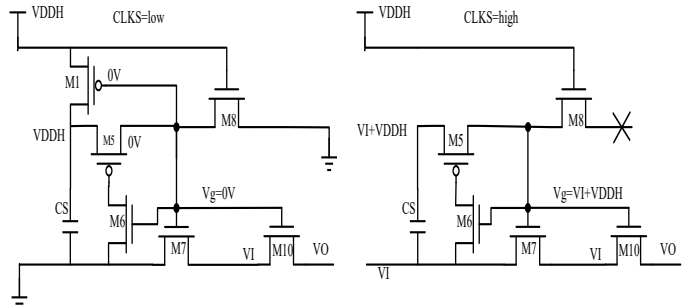


Figure 6. The operation of the bootstrap switch

3.3 Segmented control logic/RS control logic/negative voltage switch/negative power generator

Figure 7 shows the proposed segmented capacitance DAC array, non-binary weighted capacitance DAC array, and resolution scalable (RS). The vcm-based switching control logic for segmented capacitance DAC array use 3- to 7-bit binary-to-thermometer logic to divided into 7 equals  $2^{n-1}-T$  capacitances, and the T is 3. Moreover, the RS control logic uses 2- to 3-bit binary-to-thermometer decoder to generate RS0~RS2 and control the negative voltage switches on top plate of DAC capacitance array for higher bits. The 3- to 7-bit binary to thermometer code conversion logic expression is as follows.

$$T_6 = D_1 \cdot D_2 \cdot D_3 \quad T_5 = D_1 \cdot D_2 \quad T_4 = D_1 \cdot (D_2 + D_3)$$

$$T_3 = D_1 \quad T_2 = D_1 + (D_2 \cdot D_3) \quad T_1 = D_1 + D_2 \quad T_0 = D_1 + D_2 + D_3$$

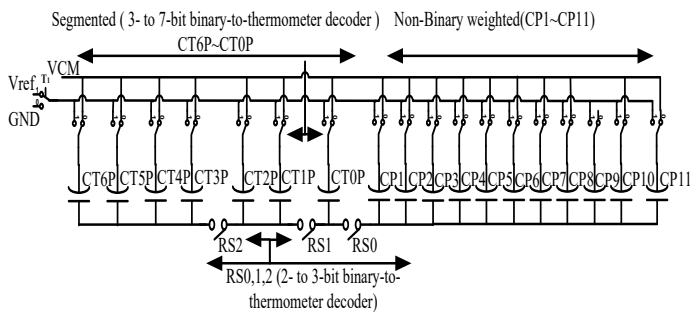


Figure 7. The segmented and non-binary capacitance DAC array on positive side

The negative voltage switch with both high linearity and low leakage is SW (M16&M17). Figures 8 and Figures 9 show the negative voltage switch schematic and operation. When SW turn off, CTRL is VI +NEG\_H2, and CTRLB is VDDH. When SW is on, CTRL is VDDH, and CTRLB is VI + NEG\_H2. This uses VDDH (1.5V) and VO2 (VI + NEG\_H2) as the control switching power supply generated from the negative power generator and VI comes from VIP and VIN. Thus, the negative voltage switch has high linearity and low leakage characteristics. Because VO2 (VI + NEG H2) can maintain, the junction voltage of SW (M16&M17) remains less than 1.8V, and SW (M16&M17) are 1.8V components. Therefore, SW can contribute less parasitic capacitance to the capacitance DAC array.

Moreover, Figure 10 shows the negative power generator of the negative voltage switch. When VDDH is ready, the START\_x is pulled from low to high, and both START\_x signal and CLK11 generate the START signal through “and gate” and negative voltage level shifter. When START is low, the M11 is off to make the NEG\_H2 voltage store in capacitor CB2, and the voltage of VO is VDDH. When START is high, the M11 is turn-on to make sure the VI signal is formed from the capacitance DAC array, and VO is VI + NEG\_H2. The voltage of VO generates VO2 through the unit gain buffer and generates the power supply of the negative switch. The control signal (RS\_I) of the negative switch generates both CTRL and CTRLB through the VDDH and VO2 to control SW (M16&M17). All components are 3.3v devices except SW (M16&M17). Then the negative voltage NEG\_H2(-1.5V) can be generated by the charge pump circuit method. Figure 13 shows the timing of the negative power generator.

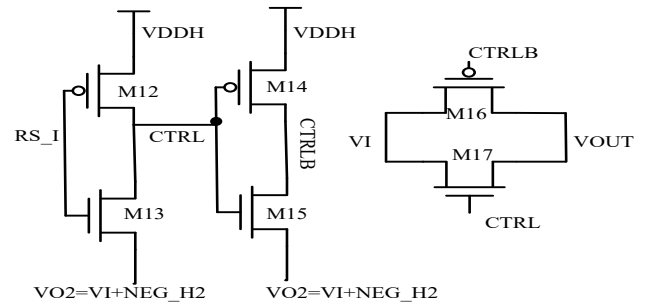


Figure 8. The negative voltage switch schematic with both high linearity and low leakage

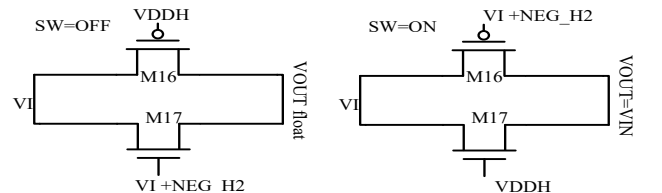


Figure 9. The negative voltage switch schematic with high linearity and low leakage operation.

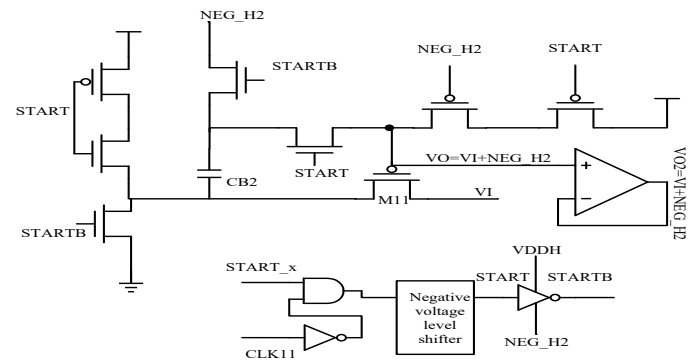


Figure 10. The negative power generator for the negative voltage switch

The negative voltage level shifter uses the CMLS architecture. It has smaller power consumption and delay than the conventional level shifter. As Figure 11 shows, all the schematics of the negative voltage level shifter are 3.3v devices. Both the VDDH and NEG\_H2 are 1.5V/-1.5V, respectively.

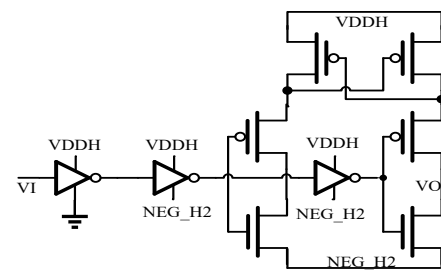


Figure 11. Schematic of the negative voltage level shifter [6]

3.4 Asynchronous clock/multi-phase clock/phase generator/vcm-based switching and bit register control logic/spark-detect/error correction

The previous paper describing the SAR ADC uses the synchronous clock cycle to complete the conversion state as follows. After sampling, the SAR ADC enters the conversion step of the N cycle. At the rising edge of each clock cycle, the comparator compares the voltage of both the capacitor DAC

array's positive ( $v_{xp}$ ) and negative sides ( $v_{xn}$ ). At the falling edge of each clock cycle, the comparator resets the voltage and enters the initial state. This action continues until the N clock cycle. From the comparator comparison to the comparator reset, each clock cycle is designed to be the same time. Because the comparison time of the comparator is related to the input voltage difference, when the input voltage difference is less than 1LSB, the comparator will require a longer comparison time. When the comparison time exceeds the clock cycle which is designed to be the same time, this will cause poor DAC settle time and degrade ADC performance. In addition, for N-bits SAR ADC, it takes N + 1 clock cycle to complete the conversion time, and an additional clock generator is required. To solve these problems, this paper uses an internally generated asynchronous clock to control the signal. The sampling rate is the clock rate, so the extra clock generator can be omitted. The asynchronous clock can adjust the length of each clock cycle in different environment due to internal circuit's delay and comparator. When the input voltage difference is larger than 1LSB, the comparator will have a shorter comparison time, and the clock cycle is shorter. In contrast, the input voltage difference is less than 1LSB, and the clock cycle is longer. This allows more time to poor DAC settle time and save time from fast DAC settle time.

The asynchronous clock generation process is as follows: The voltages of  $v_{xp}$  and  $v_{xn}$  pass the comparator to generate  $VO\_P1$  and  $VO\_N1$ . The differential signals ( $VO\_P1$  and  $VO\_N1$ ) can form VALID signal via inverter, "nand gate". Then the VALID signal merges  $CLKS$  and  $CLK11$  generates  $CLKC$  via "nor gate". Moreover,  $CLKC$  passes the delay line to increase the duty cycle of the asynchronous clock and form  $CLK\_COMP$ . The  $CLK\_COMP$  signal is the feedback control generated by internal circuit and the comparator. As Figure 12 shows, the generated clock cycle can be used to compare and reset its own state, and it can also be used to trigger vcm-based switching and bit register control logic.

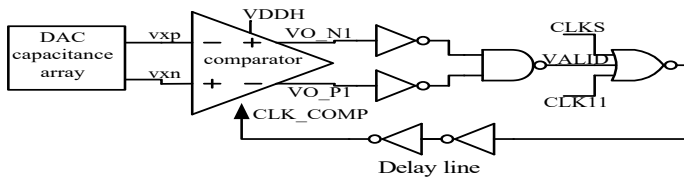


Figure 12. Asynchronous clock of this paper of the SAR ADC

When the sampling signal ( $CLKS$ ) and the asynchronous clock signal ( $CLKC$ ) is ready, the asynchronous clock signal ( $CLKC$ ) controls vcm-based switching and bit register control logic generates the multi-phase clock,  $CLK0\_3$ ,  $CLK0\_2$ ,  $CLK0\_1$ , and  $CLK1\sim CLK11$ . Then the  $CLK11$  signal will reset the node voltage of all the blocks of successive approximation register analog-to-digital converter to avoid wasting power. Figure 13 shows the timing diagram of the successive approximation register analog-to-digital converter. The multi-phase clock is represented as  $CLK_i$  and  $\sim CLK_i$  is  $CLK_i$  plus inverter. The number of  $i$  represent different multi-phase clock which are  $0\_3\sim 0\_1$  and  $1\sim 11$ .

The bit register control logic of the previous paper uses a synchronous clock signal to trigger D-flip-flop to generate the multi-phase clock and then uses D-flip-flop to switch the

capacitance DAC array's switch. [8] The bit register control logic of this paper is both the voltage of  $v_{xp}$  and  $v_{xn}$  of the capacitance DAC arrays that pass the comparator and inverter gate to generate  $OCMP\_P$  and  $OCMP\_N$  and are controlled by the asynchronous clock ( $CLKC$ ). The  $OCMP\_P$  and  $OCMP\_N$  signals go directly to the latch of the bit register control logic, as Figure 14 shows. This latch is dynamic logic and controlled by  $CLKS$ ,  $\sim CLK_i-1$ , and  $PHASEBi$ , as Figure 15 shows. The  $PHASEBi$  signal is used to control the latch and turn off and save power after the work is completed. Then it generates the corresponding digital outputs ( $LOLi$  and  $LORi$ ) and enters the vcm-switching control logic to switch the specified capacitor of the capacitance DAC array. In addition, the phase generator is controlled and generates  $PHASEBi$  by  $CLKS$ ,  $CLK_i$ , and  $CLK_i-1$ , as Figure 16 shows. Because the latch is dynamic logic, the delay time of the bit register is smaller than that of the previous version.

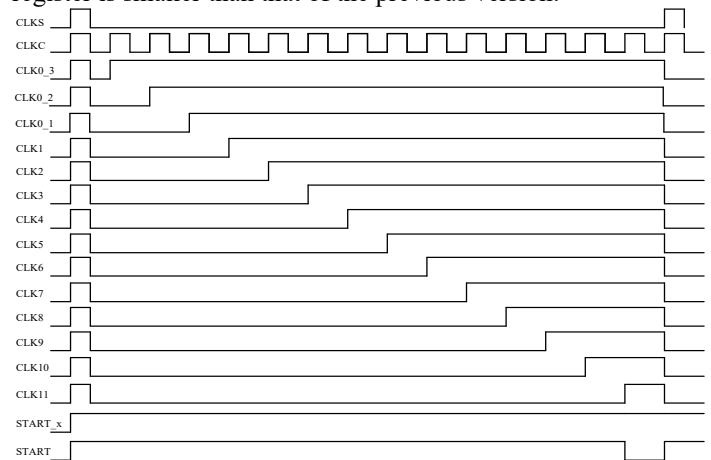


Figure 13. The timing diagram of the successive approximation register analog-to-digital converter

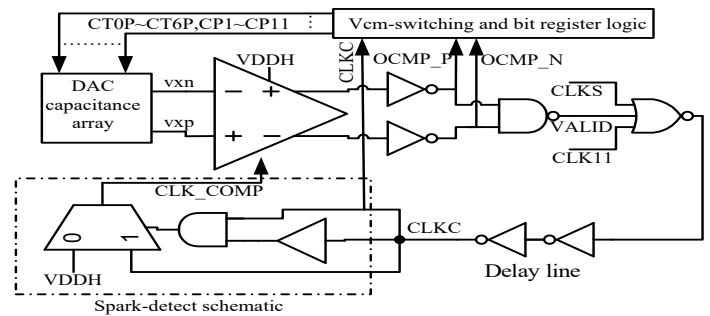


Figure 14. Vcm-based switching and bit register control logic and spark-code detect schematic

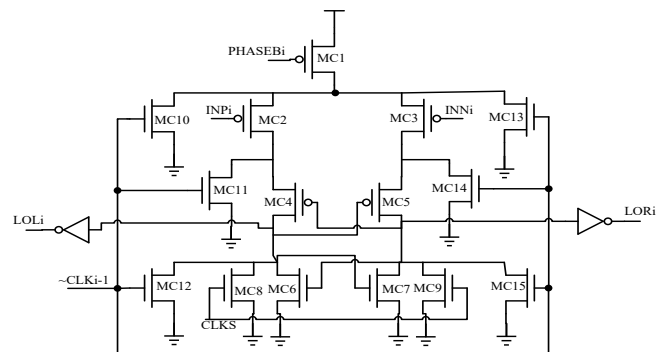


Figure 15. Latch





In addition, the comparator has a meta-stability issue. When the input voltage difference is less than 1LSB and close to zero, the comparator will take a longer comparison time. If the comparison time is larger than the sample rate and not determined, the ADC output digit code will generate a large error (sparkle codes). This issue is caused by the occasional inability of the comparator. To solve this issue, the spark\_detect schematic is designed. The CLKC form CLK\_COMP through buffer and mux. When the input voltage difference is less than 1LSB and close to zero, the comparator will take a longer comparison time. When the comparison time exceeds 4us and the comparator is not determined, the spark\_detect is low and CLK\_COMP is high, which will make the comparator reset to the initial state and then continue to the next comparison until the N+2 cycles are completed. The entire process loses 1~2 cycles, but there are still other cycles that can perform the comparison cycle to reduce the residual voltage that is the different voltages of both vxp and vxn and reduce the spark-code probability. Figure 14 shows the spark\_detect schematic.

### 3.5 Scalable voltage design

This paper uses multi-voltage to reduce power consumption and can be divided into two parts, include an analog part and a digital part. The level shifter is the bridge between the analog block and the digit block. Scaling down the supply voltage is a way to lower energy. The supply voltages of the analog block and digit block are 1.5V and 0.9V, respectively. The formula of the energy-per-conversion is “(10)”. The  $C_L(n+2)$  is the effective load capacitance, and  $V_{DD,digit}$  is the supply voltage of the digital part. The comparator energy-per-conversion, which are  $E_{COMP,reg}$  and  $E_{COMP,reset}$  in a cycle of comparison and reset, can be derived as “(11)”. [9,10] The n-bit SAR ADC needs n+2 comparison and reset cycles per conversion, the  $C_{load}$  is the comparator’s capacitive load,  $V_{eff}$  is the overdrive voltage of the transistor, and the  $V_{DD,analog}$  is the analog part’s power supply. The  $V_{cm}$ -based average switching energy is shown in Formula “(12)”, and the average switching energy is proportional to the transistor overdrive voltage squared and the capacitor dimension.

$$E_{DIG,CLK} = C_L(n + 2) \cdot V_{DD,digital}^2 \quad (10)$$

$$E_{COMP,reset} + E_{COMP,reg} = (n + 2)C_{load}V_{DD,analog}^2 + 2 \ln 2 \cdot (n + 2)^2 \cdot C_{load}V_{eff}V_{DD,analog} \quad (11)$$

$$E_{vcm-based,avg} = \sum_{i=1}^{n-1} 2^{n-3-2i} \cdot (2^i - 1) \cdot CV_{ref}^2 \quad (12)$$

### 3.6 Comparator

The comparator consists of two stages, as Figure 20 shows. The preamp of the first stage has a fixed current source (M5) and the second stage of the voltage amplifier and a latch make the output reach near full range. The offset voltage of the two differential end (VIP&VIN) of the comparator is classified to static offset and has no influence with the accuracy, but it will reduce the input range and the signal-to-noise ratio. Using a Monte Carlo simulation and add offset in the input differential pair (M1&M2), the SNR decreases slightly, and the effect of ENOB is little influenced.

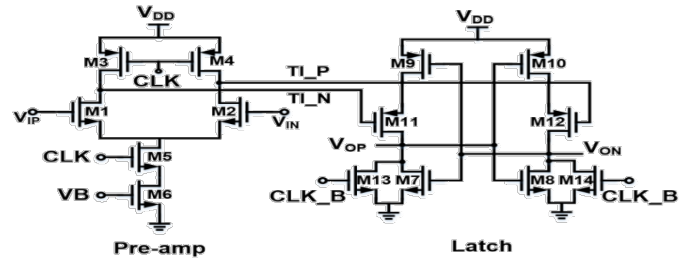


Figure 20. comparator [11]

This paper includes segmented and non-binary weighted capacitance DAC array, bootstrap switch, segmented control logic, RS control logic, negative voltage switch, asynchronous clock, vcm-based switching and bit register control logic, spark-detect, error correction, scalable voltage, comparator. The measurement results are described as follows. The input frequency is at the Nyquist rate and the maximum sampling rate is 50 KS/s. Then the output waveform gets 65536 points for the Fast Fourier Transform (FFT) analysis. The supply voltage of analog part is at 1.5V and the supply voltage of digital part is at 0.9V. The clock duty cycle is 22% and the clock period is 20us. The reconfigurable SAR ADC has 4 modes (12/11/10/9 bits), and the corresponding effective number of bits (ENOB) is 10.76/10.22/9.43/8.14 bits in the Nyquist input frequency ( $f_{in}$ ) and  $f_{in}$  is 25/25/25/25 KS/s, respectively. The power of the SAR ADC of this paper is 2.69uW for 12-bit mode and does not include the negative power generator. Table I shows the comparison of the SAR ADC results. Moreover, the input sine waveform with frequency 9.17968Khz, the sampling rate is 50Khz, and the number of sampling points is 65536. Then the sine waveform obtained is differential linearity(DNL) +0.82LSB/-0.25LSB and integral linearity(INL) +0.9LSB/-0.62LSB, as figure 21 shows. The measurement data was reported by Taiwan Semiconductor Research Institute (TSRI).

Table I: Comparison of the SAR ADC results

	[11]	[12]	The previous of the synchronous clock	This paper of the asynchronous clock
Resolution	10 bits	12 bits	12 bits	12 bits
Technology(um)	0.13	0.18	0.18	0.18
Supply voltage (V)(Analog/Digital)	1.0/0.4	1.8/	1.8/0.9	1.5/0.9
Area (mm2)	0.19	2.38	0.35	0.35
Sampling Rate (KS/s)	1	200	50	50
SNDR (dB)	56.54	69.6	68.6	66.51
Power (uW)	0.05	41.5	9.7	2.69
FoM (fJ/conversion)	94.5	84.6	88.4	30.4

From the measurement results, the ENOB of the SAR ADC has lost 0.4 to 0.7 bits for different resolutions. From comparison both the measurement result and simulation result of the INL and DNL, there are 0.2 to 0.4 LSB difference for 12-bit mode. The reason is that the ground part of the power supplier is disturbed by external noise. The solution is to use the linear regulator with ultra-low-noise to generate an independent power supply to the SAR ADC of this paper.

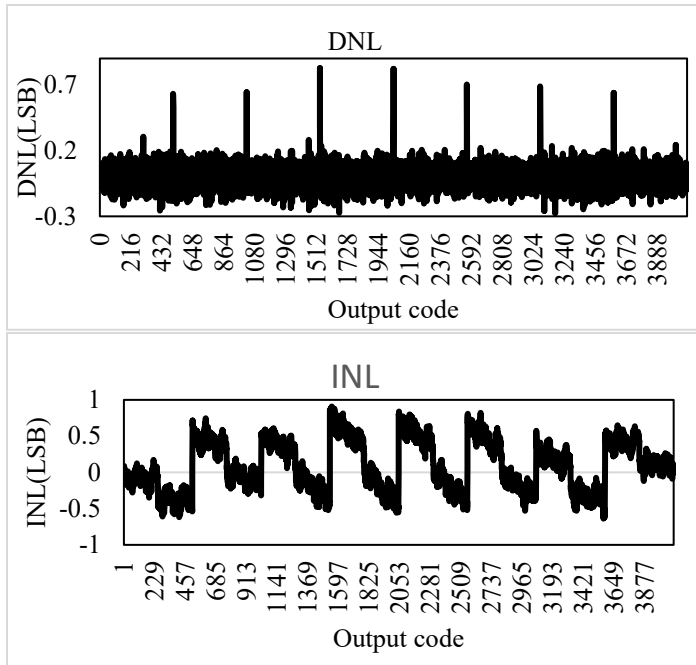


Figure 21. The DNL and INL of the SAR ADC of this paper

The layout of the DAC capacitor array is placed by a common-centroid method and add the dummy capacitors are around the DAC capacitor array to decrease the influence of process variation. The overall layout area is 810um x 430 um. Figure 22 shows the layout plan of the SAR ADC ,including the segmented DAC capacitor array for higher bits, non-binary weighted DAC capacitor array for lower bits, negative voltage switch, comparator, sample-and-hold (S/H), and switch and bit register control logic, error correction.

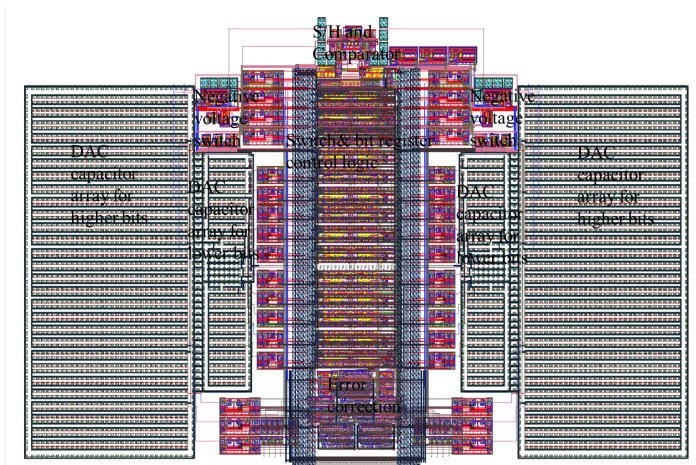


Figure 22. A resolution-reconfigurable asynchronous SAR ADC with segmented and non-binary weighted DACs layout plan

**Acknowledgment**

The authors appreciate the United Microelectronics Corporation (UMC) and Taiwan Semiconductor Research Institute (TSRI), for supporting the CMOS chip manufacturing.

**References**

- [1] H.-M. Lin, C.-H. Lin, and K.-A. Wen, "A resolution-reconfigurable and power scalable SAR ADC with partially thermometer coded DAC," *Advances in Science, Technology and Engineering Systems Journal*, vol. 3, January 2018.
- [2] V. Hariprasath, J. Guerber, S. H. Lee, and U. K. Moon, "Merged capacitor switching based SAR ADC with highest switching energy-efficiency," *Electron Lett.*, vol. 46, no. 9, pp. 620-621, 2010.
- [3] Yuan-Fu Lyu, "A low power 10-Bit 500-KS/s delta-modulated successive approximation register analog-to-digital converter for implantable medical devices," M.S. thesis, Institute of Electronics, National Chiao Tung University, Hsin Chu, 2012.
- [4] C. C. Liu, S. J. Chang, G. Y. Huang, and Y. Z. Lin, "A 10-bit 50-MS/s SAR ADC with a monotonic capacitor switching procedure," *IEEE J-Solid St Circ.*, vol. 45, no. 4, pp. 731-740, 2010.
- [5] S. Haenzsche and R. Schüffny, "Analysis of a charge redistribution SAR ADC with partially thermometer coded DAC," in *2013 European Conference on Circuit Theory and Design*, 2013, pp. 1-4.
- [6] C. Q. Tran, H. Kawaguchi, and T. Sakurai, "Low-power high-speed level shifter design for block-level dynamic voltage scaling environment," in *2005 International Conference on Integrated Circuit Design and Technology*, 2005. ICICDT 2005., 2005, pp. 229-232.
- [7] S. Wang and C. Dehollain, "Design of a rail-to-rail 460 kS/s 10-bit SAR ADC for capacitive sensor interface," in *2013 IEEE 20th International Conference on Electronics, Circuits, and Systems*, 2013, pp. 453-456.
- [8] H.-M. Lin and K.-A. Wen, "A low power reconfigurable SAR ADC for CMOS MEMS sensor," in *SoC Design Conference*, 2017, pp. 7-8.
- [9] M. Yip and A. P. Chandrakasan, "A resolution-reconfigurable 5-to-10-bit 0.4-to-1 V power scalable SAR ADC for sensor applications," *IEEE J-Solid St Circ.*, vol. 48, no. 6, pp. 1453-1464, 2013.
- [10] Z. Dai, C. Svensson, and A. Alvandpour, "Power consumption bounds for SAR ADCs," in *2011 20th European Conference on Circuit Theory and Design*, 2011, pp. 556-559.
- [11] D. Zhang, A. Bhide, and A. Alvandpour, "A 53-nW 9.1-ENOB 1-kS/s SAR ADC in 0.13- $\mu$ m CMOS for medical implant devices," *IEEE J-Solid St Circ.*, vol. 47, no. 7, pp. 1585-1593, 2012.
- [12] Y. H. Juan, H. Y. Huang, S. C. Lai, W. H. Juang, S. Y. Lee, and C. H. Luo, "A Distortion Cancellation Technique With the Recursive DFT Method for Successive Approximation Analog-to-Digital Converters," *IEEE Transactions on Circuits and Systems II: Express Briefs*, vol. 63, no. 2, pp. 146-150, 2016.

## Analysis of Vulnerabilities, Risks and Threats in the Process of Quota Allocation for the State University of Ecuador

Segundo Moisés Toapanta Toapanta<sup>1,\*</sup>, Andrés Aurelio García Henríquez<sup>1</sup>, Luis Enrique Mafla Gallegos<sup>2</sup>

<sup>1</sup>Department of Computer Science, Universidad Politécnica Salesiana (UPS), Guayaquil, 010102, Ecuador

<sup>2</sup>Faculty of Systems Engineering, Escuela Politécnica Nacional (EPN), Quito, 17-01-2759, Ecuador

### ARTICLE INFO

Article history:

Received: 15 January, 2020

Accepted: 02 April, 2020

Online: 17 April, 2020

Keywords:

Allocation of quotas Vulnerability  
Risks

Quotas

College entrance

Security Information

### ABSTRACT

Different models and standards of information security were analyzed, to adopt a model that mitigates vulnerabilities, risks and threats in the quota allocation process for the State University in Ecuador. The main objective is defining a prototype for the management of processes and information security in this type of organization. It was used the deductive and exploratory research method to analyze the information in the references. In this work, the characteristics of the attacks were analyzed. It turned out a model performs the detection and defense of attacks based on the differences in data and time between them and the browsing behavior of normal users. It was concluded that the prototypes presented as results are an alternative to improve the security of the processes and the flow of information and that these can be used as a reference in this type of organization.

## 1. Introduction

Universities State of Ecuador, for the admissions process students have implemented “Ser Bachiller”, which platform since the beginning of its implementation in 2018 has presented security problems that jeopardized the integrity of the system hurting students’ rights in their application. Higher education in Ecuador has undergone changes since the last decade, in the current Constitution the right to this is guaranteed, observing the principle of equal opportunities and permanency through the Organic Law on Higher Education (LOES), implemented in 2010, as it stated in the art. 71 on access and management of higher education institutions (IES) on art collecting tariffs.<sup>73</sup> Higher education platform of the State, has disadvantages in the application process for admission to universities, since there is the possibility of being manipulated by external agents, which makes seeing the process trustworthy, So that applicants can be affected in their desire to pursue a college career [1].

The aim of this study is to analyze vulnerabilities, threats and risks in the process of allocation of quotas for State Universities Ecuador and a quantitative methodology is applied, descriptive cross-sectional study under.

Although the computer platform uses reference frameworks to streamline and operationalize the admissions process, however, applied technology does not offer the best assurance to ensure non-interference of irregular actions that violate the integrity and confidentiality of the system.

Results affectation seen from the interface authentication of users “Ser Bachiller” system, problems in the security system for identifying risks, inconvenience for authentication and loss of access control on the intake system of education higher.

According to OWASP list errors most dangerous security-related software affect Web applications [2].

What are the benchmarks or standards that can be applied to prevent vulnerabilities, threats and risks in the process of allocation of quotas for state universities in Ecuador?

There are frameworks for optimization and good management of technological resources, technical criteria that are applied through effective systems. A typical system with service-oriented architecture (SOA) is front-end web applications, web services intermediary databases and background; They work in a harmonized way [3].

It is concluded that it is important to implement and apply the methodology OWASP Top Ten, so that the “Ser Bachiller” system cannot be hacked to attack any cyber as add-on armor and

\*Corresponding Author: Segundo Moisés Toapanta Toapanta, Email: [stoapanta@ups.edu.ec](mailto:stoapanta@ups.edu.ec)



protection to COBIT and COSO methodologies implemented in the allocation process quota system.

## 2. Materials and Methods

### 2.1 Prevention measures

The first vector in which can be implemented security layers is the network infrastructure as services is the entry route offered. Any measures to keep in mind is that, for example, in the case of online services within a corporate network, due to the fact that we can easily configure security layers as a check list (ACL), which controls network access based on IP applicants or firewall. The ISP is providing this router, but not always, the ISP not always allows us to configure these security measures, taking into account that in this case we should have an additional internal router in our network firewall how we allow to apply these security measures,

- Configuration: it is essential to review in detail the configuration of routers and firewalls to stop all IP that are not valid. Currently, the router is given adequate control of connections through logging options. Contingency plan: in any business, it is essential to have a protocol of action against any attacks from DOS. Thus, to produce the attack, security experts have a plan to follow, significantly minimizing the damage.
- IS / IPS: to explain IDS / IPS can detect any misuse valid as possible attack vectors protocols.
- Traffic: It is recommended to limit the tax on traffic coming from a single host in order to warn of a DoS attack that aims to saturate the server.
- DOS protection: These are services that will oversee the redirection of heavy traffic, thereby avoiding many requests affect the operation of the web.
- IP Block list: Blacklists allow identification of critical IP addresses and packet discard. This security measure can be done manually or automatically through block lists of the firewall.
- Filters: You can set limits on the amount of data processed simultaneously to filter, therefore, all kinds of abnormal packets. At this point, it is important to note that often, proxy servers allow many clients to connect from the same IP address of the server, which can generate the lock for no apparent reason.
- SYN cookies: if this security measure is used, information about SYN packets are no longer stored on the server but is sent as an encrypted cookie to the client. This way, a SYN flood attack compromises the ability of the equipment, but not the memory of the system.
- Load balancing: an effective measure against overload is the load distribution in the different systems. The use of load balancers can extend services to multiple physical machines. Thus, to some extent, controls the denial of service attacks.
- The need for complementary security technologies: in addition to using firewall systems and intrusion prevention, companies must have security solutions that certify successful mitigation of attacks known and unknown, including tools for analyzing network behavior, which systems can detect real-time signature. The intrusion

prevention systems against application vulnerabilities known. Active defense mechanism application levels. Active counter strategies emergency, alerting capabilities.

- Prepare for counterattacks, with a proactive and offensive defense system simultaneously: the design of a solid plan to integrate real-time technicians to ensure that tools, alerts, correlation and mitigation are properly managed. Make sure the team is ready to provide immediate assistance and active mitigation; or Figureht defensive actions as soon as the system is under attack. Active defense is equivalent to a backlash if it conforms to the last vestiges of DoS attacks and the incident is adjusted.
- Encryption: If engineering data security protects the network and other physical assets, such as servers, computers and databases, encryption protects the actual data and files stored on them or that travel between them over the Internet. Encryption strategies are crucial for any company that uses the cloud and are a great way to protect hard drives, data and files that are in transit via email, browsers or on their way to the cloud. If data is intercepted, encryption makes it difficult for hackers to do something with them. This is because encrypted data is unreadable to unauthorized users without the encryption key.
- Detection and response to a security breach: If suspicious actions occur in the network, for example, someone or something tries to enter, intrusion detection is activated. Systems network intrusion detection (NIDS) continuously monitor traffic network and passively to detect behaviors that appear illegal or abnormal mark for review. NIDS not only block this type of traffic, but also gather information about it and alert network administrators. However, despite all this, security violations continue to occur. That is why it is important to have a plan to respond to a data breach. They are prepared to act as an effective system. That system can update as often as necessary, for example,
- Strict access controls: a major concern is the loss of control of data for companies if the data is outside your firewall. This control extends to the belief that some employees of the cloud provider have general access to your sensitive data. A cloud provider is properly managed will have several features sharing responsibilities for the entire cloud solution without a single person who has full access to all components of the solution. In other words, no person has access level necessary to put the security or confidentiality of customer data at risk.
- Mitigation: once a threat has been detected, it must be mitigated. In the case of denial of service mitigation, it is to implement a series of measures that reduce the damage and, if possible, restore the compromised system services normally. These usually consist of increasing the pool of resources available for eliminating bottlenecks, increasing restriction of authentication systems through puzzles and lures, or update access lists and encryption policies.

### 2.2 Materials

The means and methods used in this research are based on the review of reference articles and general information sequence still steps to get the results. As users should check the configuration of our routers and firewalls for invalid or false IP detect that come from potential attackers. Overall, our internet

service provider (ISP) ensures that the router is updated with this configuration. On the other hand, state universities must protect both your network and your entire infrastructure to prevent attacks affect performance and safety of their customers.

We used information about items that have studied the situation in several universities in the world, for determining admission tests applied and what types of vulnerabilities have processes for allocating quotas in these institutions and likewise consider the situation of universities the public of Ecuador, with the application of the system of income, using tools to ensure the safety of students, to obtain a quota allowing him to study the career of their choice.

It is important for the Government of Jakarta, the measures in the field of education, because it affects the academic achievement of certain universities as a whole [4]. In Kazakhstan, this information technology and communication (ICT) improve and secure the quality of life in different areas including medicine, educational process and safety [5]. China's admission to the University is not only an examination system, it has also become a phenomenon of the social system [6]. Instead, Brazil is considered the entrance exam at several universities [7]. Also, at the Polytechnic University Timisoara (UPT) in Romania, the entrance exam for technical profile covers up to twelve math questions chosen at random from the exercise book [8]. All of them are considered, of utmost importance, to have a clear and fair entry process.

2.2.1 Vulnerability scan

Hackers are used to analyze networks actively or passively for holes and vulnerabilities. Analysts' data security professionals and vulnerability assessment are key elements in identifying potential holes and close them. Software safety analysis is used to exploit any vulnerability of a computer, network or communications infrastructure, prioritize and address each of them with safety plans that protect data, detect and react.

2.2.2 Frequency of vulnerabilities

- Very high frequency:** One or more times a day
- High frequency:** 1 time per week
- Average frequency:** 1 time a month
- Low frequency:** 1 time every two months
- Very low frequency:** 1 time every six months.

2.2.3 Testing Intrusion

The vulnerability analysis (identifying potential threats) may also include knowingly investigating a network or system to detect failures or intrusion testing. It is an excellent way to identify vulnerabilities in advance and devise a plan to solve them. If there are flaws in operating systems, problems with the default values, the code of some applications or other similar problems, an administrator expert network penetration testing can help you locate these problems and apply patches to make it less likely to have an attack.

Penetration testing involves performing manual or automated processes that disrupt servers, applications, networks and even end-user devices to see if it is possible intrusion occurred and where this division. From this, you can generate a report for

auditors as proof of compliance. A complete intrusion test can save you time and money on costly warn of attacks on weak areas not known.

Table 1: Comparison - Methodologies Security Applications

Frequency	Time
Very high frequency	1
High frequency	2
Half frequency	3
Low frequency	4
Very low frequency	5

In Table 1. The frequency that can be generated for each process threats an organization defined.

Downtime of the system can be another annoying side effect of unbridled attacks, so regular intrusion tests are an excellent way to avoid problems before they arise. Manufacturing division chewing establishes a framework for data leakage prevention to protect sensitive data and prevent unauthorized disclosure to third parties. DLP storage based tools apply to supervisors or even block any user activities and confidential data transmissions.

2.3 Methods

A quantitative, descriptive methodology under a cross-sectional applied also under a criterion Deductive information related articles were analyzed for:

- Identifying information related to the process for allocating quotas.
- Identify vulnerabilities or risks of universities in computer admissions process.
- Evaluate reference models leading to neutralize the risks and threats to the security of the admissions process.

In order to apply for a place at a public university in the country it is required to apply to the test designed by the SENESCYT, but in cities across the country have filed complaints, which can be reviewed in several newspapers of the city, also in the news and common citizenship, which, since its inception, has expressed dissatisfaction with the process.

It is important to review the steps for allocating quotas and the different problems presented in it.

2.3.1 Allocation of quotas

The institution responsible for the allocation of quotas is the Ministry of Higher Education, Science, Technology and Innovation (SENESCYT), who works for the benefit of students who want to aspire to a place in a public university, through the surrender of an examination It applied digitally, but has also been criticized by the public for various reasons, whether nonconformity by the mechanism adopted for a quota or for failing to assigning the desired career, on the other hand, some problems are attributed the platform used.

Computing services is the economic backbone of many different types of information systems [9].

For the system of income produces the best results in the

allocation of quotas is necessary to identify, first, information assets, then the possible threats also may recognize the vulnerabilities of the system, hence analyze the impact on the allocation quota, which can lead to finally manage systems that minimize or prevent damage to the system applied in universities. It is worth noting that in the midst of all this, the rate by which organizations and government are adopting the use of the web as they increase the useful resources [10].

Moreover, to combat increasing security risks, many software engineers recognize and analyze the abuse or misuse of the system to provide greater security to the beginning of the development of the system [11]. Firewalls analyze all incoming traffic, detect attacks using rules for policy expressions and blocks attacks detected [12].

In addition, in order to establish protection mechanisms on the platform, you should review the different articulated proposed by the Ecuadorian government, which are beneficial to students, so they can choose a career according to their profile, while their rights are violated citizens.

### 2.3.2 External computer threats

Because internal or external agents can threaten a digital platform, it is important to have a technical team that can identify, assess and eliminate or reduce their impact.

Regarding external threats, according PwC's Global Economic Crime Survey 2016 reports that there are organizations that had suffered losses from cybercrime for more than \$ 5 million, and these nearly a third reported losses in excess of \$ 100 million. In addition, Juniper Research reports that cybercrime increased the cost of data breaches to \$ 2.1 trillion worldwide by 2019; four times the estimated cost of violations in 2015 [13]. This alarmed security analysts, for which, before investing resources and efforts to defend itself, require first acknowledge the attacks received.

### 2.3.3 Internal computer threats

Internal threats affect the image of the institution as well as processes carried out, hurting users who use it. Institutions sometimes detected easily solved problems they have, like removing a magnetized article, which can affect the information, but also major issues such as the intrusion of unauthorized persons. At the organizational level are emerging efforts to improve security systems where filtering of information, analysis, penetration testing, development of best practices and defensive coding using a frame includes fully automated [14].

### 2.3.4 Vulnerabilities in the system

For the security of a system is considered to have access, some require web access to upload real-time information, the gateway is a channel to be careless, becomes vulnerable. For efficient mitigation of web-based attacks, the system must understand the context of the content of the information is processed and the

ability to filter content based on their effect on the target application [15].

Moreover, vulnerabilities become increasingly common in the computing environment, where in addition to the system, you should care for other peripherals that can give people access remote ill-intentioned, hurting the theft of information. Machine learning approaches for protecting texts have been applied to research in cybersecurity in the last decade [16].

### 2.3.5 Impact on quota allocations

Within the management of quotas for students who aspire to go to college, is a minority group that can

Enter, with the largest group, through preferential treatment in quotas.

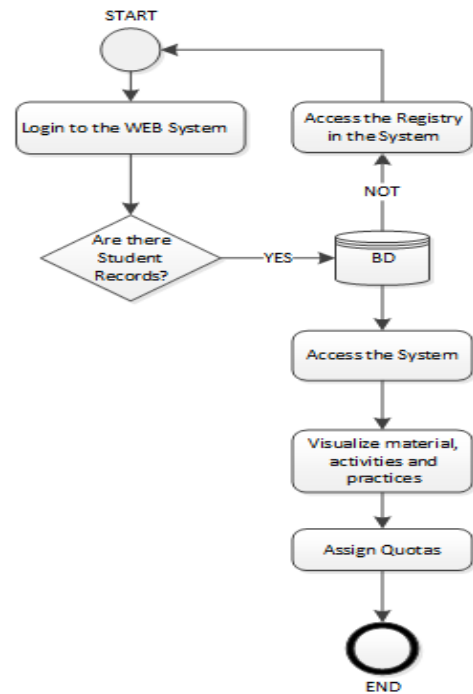


Figure.1: Description of the quota allocation process

In Figure 1 shows how the process of allocating quotas in state universities in Ecuador, do not maintain sufficient controls to ensure we get a quota for aspiration of university courses.

### 2.4 Security Tools

After establishing the threats and vulnerabilities, it is important to present alternatives to such security systems that may be compatible with other programs and can be more effective in their results. The threat to cyber security has increased exponentially [17].

### 2.5 Cobit (Control Objectives for Information and related technologies):

Is a framework designed to help implement strategies in technology, with the aim of unifying the processes presenting a comprehensive approach to business, ranked IT processes, criteria and information technology resources.

The components of the development and implementation of

the COBIT that allow streamline processes stand as follows:

2.5.1 Information criteria

This component is intended to adapt the control criteria, allowing requirements apply quality assurance processes quota allocation under the following aspects:

2.5.2 Effectiveness

It is related to the results of the selection process.

2.5.3 Efficiency

It is related to the ability to expedite the process of allocating quotas.

2.5.4 The integrity

It is to protect the information recorded by students in quota allocations, preventing it from being manipulated.

2.5.5 Disponibility

It refers to the application alternatives if the student was unable to complete the process within the platform.

2.5.6 Compliance

It is to follow the instructions recommended by the university to make quota allocations processes successfully. Also considering the introduction of IT processes, where this component is to establish strategies offering a better approach to the processes applied technology, classified in the following domains:

2.5.7 Plan and organize

Establishes strategies to attract students by offering them a good academic service.

2.5.8 Acquire and Implement

It allows for solutions in the classroom processes in view there is disagreement on the means of payment, so it is forced to enable electronic channels to perform them.

2.5.9 Monitor and evaluate

Evaluates the processes of quota allocations for their quality and performance.

2.5.10 Technological resources

This component aims at investing technology resources to the needs of the institution named below:

2.5.11 The applications

It provides applications for managing users based procedures

manuals.

2.5.12 Information

Stores the data in quota allocations for your application.

2.5.13 Infrastructure

It is related to the application of physical and logical components that enable the proper functioning of the applications.

2.5.14 People

Are those responsible for managing resources and monitoring systems implemented to mitigate the risks and threats that could arise [18].

2.5.15 The main features of the COBIT 5.0 include

- Identifies the most common risks within the organization.
- Implements technological resources best suited to form a robust technology architecture.
- Develops strategies for automating software.

2.5.16 Advantage

- Is a targeted approach to the needs of the business
- It comprises using the technology to improve its processes.
- Improves the functionality of integrated systems, using the availability of both technological and human resources.

2.5.17 Disadvantages

- It applies to all types of organizations involving information technology.
- It requires large investment of technological resources for standards compliance.
- It requires technical knowledge and commitment of all staff of the organization.

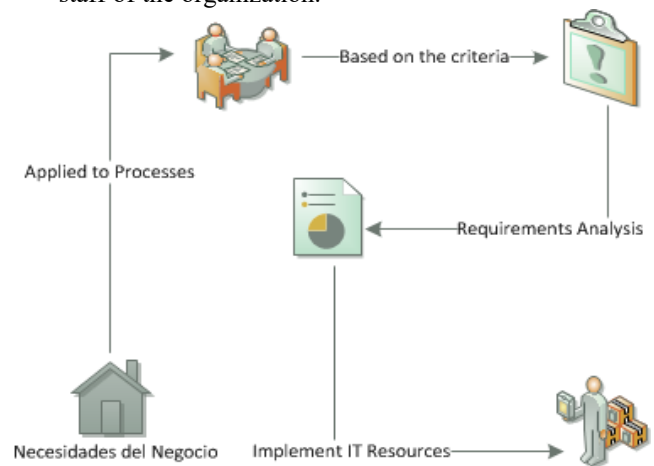


Figure.2: Overview of the COBIT 4.1

In Figure 2 the application of the COBIT 4.1 and the process, which a company, which also can be used for the allocation of quotas in a college is observed.



## 2.6 COSO ERM

This framework was created with the aim of identifying risks by obtaining data collected through the events presented, providing alternatives to mitigate risks in the business. Recently in research on corporate governance, internal control issues and Complex Enterprise Risk Management (ERM) have been the most debated in academic circles [19].

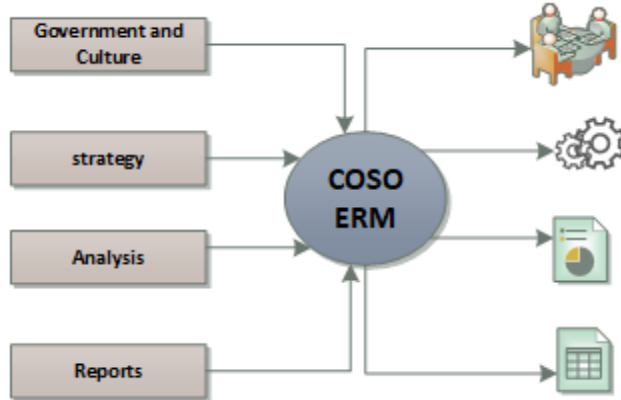


Figure.3: Description of the COSO ERM

In Figure 3, the complementary process is observed following this type of resource applied to a platform to solve problems presented.

The framework for the assessment and risk control comprises eight elements, which are described below:

### 2.6.1 Control environment

It refers when processes are vulnerable and can significantly affect the assets of the institution.

### 2.6.2 Setting objectives

It is to establish strategies to identify risks to address them adequately staffed.

### 2.6.3 Even ID

Locates vulnerable events in which it is exposed top-level platform and appropriate to mitigate the risks.

### 2.6.4 Risks evaluation

Classifies risk events by drawing heat maps to measure their impact on us platform quota allocations.

### 2.6.5 Risk Response

It is to obtain possible solutions once the threats that may affect the institution identified.

### 2.6.6 Information and communication

Is to communicate to all members within an organization,

measures to address risks to take.

### 2.6.7 Supervision and control

Monitors and monitor the activities assigned to those responsible for each vulnerable area in the institution.

This framework of risk management and internal control includes the following benefits:

- Sets strategies by identifying risk events.
- It allows staff to raise awareness about what steps to take response to risk events.
- Reduce the number of events and damaging consequences for the organization.
- Assesses the risks identified by developing heat maps to classify, reducing negative impacts.

### 2.6.8 Advantage and disadvantages

The advantage is that it understands the risks to which it is exposed to the organization. It establishes controls in their processes by identifying risks to the fulfillment of its objectives. Offers action plans, which involves the entire organization to achieve its strategic objectives.

The disadvantages are that it requires large investment of technological resources for standards compliance. It requires technical knowledge and commitment of all staff of the organization.

## 2.7 OWASP Top Ten (Project Open Web Application Security)

WASC addition, there are plans open up web applications (OWASP) makes visible security software [20]. This security system applications, was designed to raise awareness among organizations about the risks and threats that are exposed through the consequences this brings, with the aim of identifying the most critical risks, providing techniques and tools to counter increased risk events, as many methodologies applied are based on streamlining processes and identify risks without knowing how to counter them. Measures taken to protect network systems and data against attacks or intrusions: it is, by definition, a risk issue [21].

This project shows the most common problems presented in web applications, according to their criticality, taking into account any risks associated with exposure of sensitive data, which will be applied on the platform Bachelor Being under the following aspects:

### 2.7.1 Broken Authentication

It is used passwords with alphanumeric validations to prevent improper authentication session, in which they may be exposed when they expire passwords or credentials remembering, exposing sensitive information from intruders.

### 2.7.2 Loss of Access Control

It occurs when the parameters role assignment does not have validations on options granted, due to lack of functional testing by developers.

2.7.3 Registration and Monitoring Deficient

It refers to the lack of oversight that should have systems since submitted an incident does not have the capacity for immediate response.

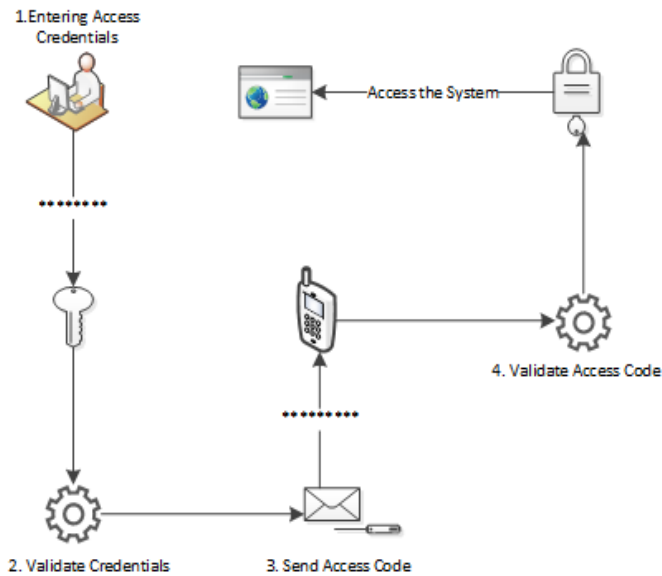


Figure.4: Hazard Identification Description OWASP TOP TEN

In Figure 4, the following process is observed OWASP TOP TEN to minimize security problems.

Functionality OWASP TOP TEN system:

- Assesses the results by the findings on the platform of higher education.
- Executes scan tests source code, allowing detecting potential vulnerabilities to which the web application is exposed.
- Establishes security controls to measure the impact can cause a cyber-attack.
- Validates the inputs and outputs of the application to rule no authentication Access to the user.
- It requires the implementation of tools to validate the quality of the code to prevent data leakage.
- To find solutions, but also new risks, which in the detection can be useful to identify technological resources.

2.7.4 Advantage

Applies in the cycle of software development considering Web security requirements. Explores possible threats through the most common risks presented. Implement mitigation strategies classified by types of threats.

2.7.5 Disadvantages

It requires specialized computer security analysts for troubleshooting. You need to know the business processes to be applied. No implementation is favorable when the software is developed.

3. Results

3.1 Comparative Methodology OWASP TOP TEN.

Shows that the methodology OWASP TOP TEN meet the acceptance criteria, as to the level of security it offers, by identifying and preventing threats that can occur on web platforms, providing responsiveness to counter events present.

Table 2: Comparison - Methodologies Security Applications

Evaluation criteria	COBIT	COSO ERM	OWASP Top Ten
Ensure access to application from secure locations.	DO NOT	DO NOT	YES
Ensure compliance with security policies and procedures.	YES	YES	YES
Determine the impact of events identified risks.	DO NOT	YES	YES
Implement technological resources to ensure the infrastructure.	YES	YES	YES
Monitor the behavior of services.	YES	YES	YES

Table 2 shows the comparison between COBIT, COSO ERM, OWASP TOP TEN observed.

Ecuador remains a country that is developing at the level of ICT [22]., It is for this inexperience, which is considered most work systems and cyber security risk [23].

Thus, the Ministry of Telecommunications and Information Society, "confirms that security problems persist Information [1].

In this paper the characteristics of the attacks are analyzed, active defense model is proposed and describe the corresponding model. This model makes detection and defense of attacks based on differences in the data and the time between them and the browsing behavior of ordinary users. Propose algorithms to detect attacks incoming, outgoing and forwarded. In addition, cooperatively they detect attacks by delivering its own detection statistics. To mitigate the potential risks to the integrity of an organization, it is necessary to define security policies in the strategic, tactical and operational level and to define the ICT department-level strategic management.

3.2 Monitoring attacks

The system is the victim of a denial-of-service attack. The network monitoring is done through tools, protocols, and control analysis records through applications. Finally, once you have identified the symptoms and vulnerabilities detected on the network, security measures are applied. The indicators were tested in trials are the alteration and packet loss. Since these are the parameters that directly, affect the quality of the service. Finally, the most notable indicator is the downtime that allowed the exact time who allowed us to know the exact time in which the service is no longer available.

3.3 ISO 27001

The standards give the organization the basis for developing a security management framework, which allows you to protect your important information assets, minimizing risks and optimizing investments and efforts required for protection. ISO

17799 presents a number of areas to manage, by applying controls or protection mechanisms, ranging from security systems, to aspects of physical security, human resources and general aspects of the organization.

A model offering a new cooperation between enterprises, can build dynamically. They are using a temporary network of independent organizations connected through information and communication technologies. Community projects can be directed by sharing resources, skills and practical skills and should implement security policies to protect resources from harmful attacks, preventing consequences such as loss of business. A security policy defined global information can be constructed as an extension of the local security policy of different organizations, avoiding start from scratch.

This solution offers the opportunity to focus only on security issues, respecting those who define govern trade within an organization. The question is, as an implant, a system of this type, which must be reliable, simple and must ensure the separation of the different fields.

Security services such as authentication, permission, confidentiality, integrity and traceability must be guaranteed within the infrastructure. ISO 27001 is an evaluation chart of the operating system information security. This prototype is based on ISO / IEC 27001; to mitigate the risks of information security, the variables that will be used are:

- Number = N
- Process = P
- Threat = X
- Frequency = Y
- Impact = Z
- Risk value = VR

Table 3: Risk Matrix

N	P	X	Y	Z	VR
one	Management strategies	The application of standards irregularly	3	4	12
		Difficulty in violation of the processes	3	4	2
		Acts of non-application process	7	8	9
two	IT security	Failure to follow the activities of political organizations	3	2	3
		Failure of processes	7	4	3
		Loss of resources (time, established agreements)	9	3	2

The number of processes in each organization will vary depending on their strategic objectives.

In Table 3 it can be determined that all the processes that are equal to or less than six obtained in risk value (RV) have no problems and all those that are greater than or equal to seven in the value of irrigation (RV) have to formulate strategies at the administrative level, technological, to define security policies that reduce the level of risk.

### 3.4 Equations

To mitigate the potential risks to the integrity of an organization, it is necessary to define security policies in the strategic, tactical and operational level and to define the ICT department-level strategic management.

The following formula applies in Table 3

$$N \rightarrow (P \subset X) \Rightarrow (Y * Z) = VR \quad (1)$$

In the formula 1 wherein determining the process number (N), process (P), threats (X) Frequency applied (Y) multiplied by the impact (Z) and the result obtained is the resistance value (VR). For the TVR is the sum of all risk values

$$TVR = \bar{X} = \frac{\sum x}{n} \quad (2)$$

Apply the formula two are:

$$TVR = (12 + 2 + 9 + 3 + 3 + 2) / 6$$

$$TVR = 31/6 = 5.16 \quad (3)$$

For the percentage of total risk values was:

$$PTTR = ((TVR / TTR) / 10) * 100\% \quad (4)$$

Apply the formula 4 which we are:

$$PTTR = (5.16 / 10) * 100\% = 51.6\% \quad (5)$$

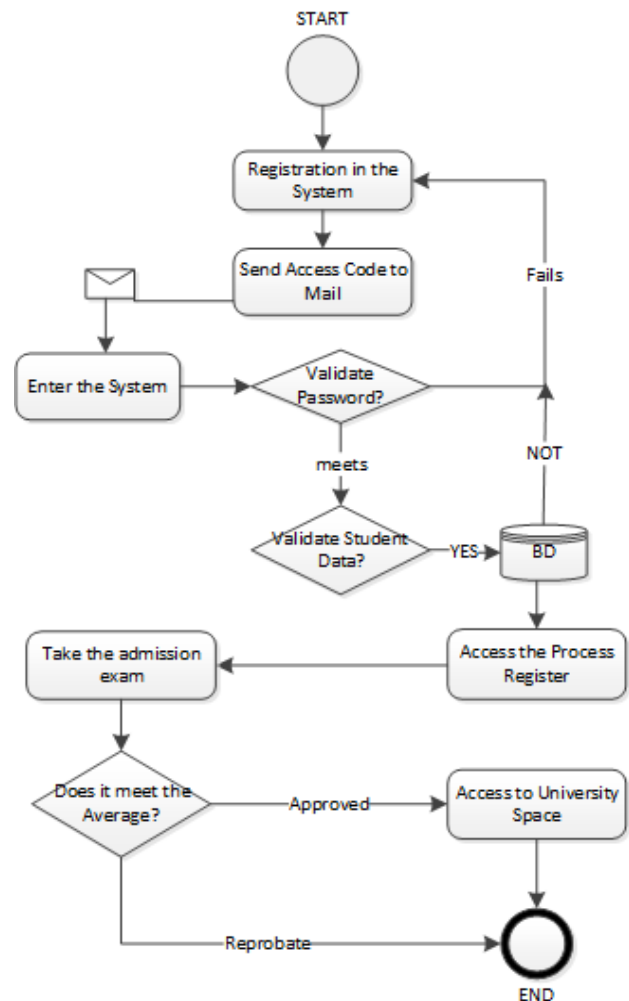


Figure 5: Diagram of the methodology OWASP Top Ten

### 3.5 Flowchart of the methodology OWASP Top Ten

Figure 5 provides the application of the methodology OWASP Top Ten, applying validations authentication must meet the quota allocation system to confront threats that may be exposed.

#### 4. Discussion

Achievements in this research are generic so they can follow the methodology and adapt to any specific organization considering your requirements. This research does not solve the security problems of telecommunications companies; only offered an alternative that mitigates risk levels in information security.

The results are directly related to other research in this regard; for each process security model that is carried over the Internet, you should be evaluated and should set up new processes and should be integrated models deemed appropriate. We believe that the use of our risk matrix we can find safety deficiencies for which state are in addition to this, we can learn a rating of overall risk that state universities may have.

The comparison between security processes applying each of the computing methodologies provides important knowledge about COBIT, COSO ERM, OWASP TOP TEN.

Methodologies do not provide complete assurance that the platform of Higher Education is not to be violated, because there are multiple threats on the web, which should be studied, such as lack of precision, failure to prevent surprises and lack of effectiveness.

To increase security in the identification process to minimize vulnerabilities, it is also the Transport Layer Security (TLS) tool is applied under a cryptographic protocol that ensures Internet communications to prevent attacks.

The methodology OWASP Top Ten is showing greater compatibility, it presents the necessary and reliable conditions to reduce the amount of potential threats.

#### 5. Conclusions and Future Work

In the future, it will analyze how it affects the security problems in the student population of the country.

After conducting research, we can conclude the following:

- The matrix-defined risk is an alternative to improve process safety and the flow of information and can be used as reference in these organizations.
- The different points presented in this research enable companies to create a clear picture of the different threats that are daily affected by day in order to take precautionary measures constants ratings director to its staff and consider the physical different topics day of its facilities to be much more organized models of their processes.

#### 6. Acknowledgment

The authors thank the Salesian Polytechnic University of Ecuador, a research group Guayaquil Headquarters "Computing, security and information technology for a Globalized World" (CSITGW) created in accordance with resolution 142-06-2017-07 -19 and the Ministry of Education. Superior Science, Technology and Innovation (Senescyt).

#### 7. References

- [1] S. Moisés Toapanta Toapanta and L. Enrique Mafla Gallegos, "An Approach

to Optimize the Management of Information Security in Public Organizations of Ecuador," *Fault Detect. Diagnosis Progn.*, no. November, 2020, doi: 10.5772/intechopen.88931.

- [2] F. Spoto et al., "Static identification of injection attacks in Java," *ACM Trans. Program. Lang. Syst.*, vol. 41, no. 3, 2019, doi: 10.1145/3332371.
- [3] S. Jan, A. Panichella, A. Arcuri, and L. Briand, "Automatic Generation of Tests to Exploit XML Injection Vulnerabilities in Web Applications," *IEEE Trans. Softw. Eng.*, vol. 45, no. 4, pp. 335–362, 2019, doi: 10.1109/TSE.2017.2778711.
- [4] E. Khudzaeva, F. Mintarsih, A. T. Muharam, and C. Wirawan, "Application of Clustering Method in Data Mining for Determining SNMP Quota Invitation UIN Syarif Hidayatullah Jakarta," *2018 6th Int. Conf. Cyber IT Serv. Manag. CITSM 2018*, no. Citsm, pp. 1–4, 2019, doi: 10.1109/CITSM.2018.8674329.
- [5] A. Zhamanov, Z. Sakhiyeva, R. Suliyev, and Z. Kaldykulova, "IoT smart campus review and implementation of IoT applications into education process of university," *2017 13th Int. Conf. Electron. Comput. Comput. ICECCO 2017*, vol. 2018-Janua, pp. 1–4, 2018, doi: 10.1109/ICECCO.2017.8333334.
- [6] Y. X. Li, Y. N. Miao, and S. Y. Lue, "A comprehensive analysis method of application in college entrance examination," *Proc. - 2017 Int. Conf. Netw. Inf. Syst. Comput. ICNISC 2017*, vol. 131, no. 1, pp. 131–134, 2017, doi: 10.1109/ICNISC.2017.00036.
- [7] I. C. Silveira and D. D. Maua, "University Entrance Exam as a Guiding Test for Artificial Intelligence," *Proc. - 2017 Brazilian Conf. Intell. Syst. BRACIS 2017*, vol. 2018-Janua, pp. 1–6, 2018, doi: 10.1109/BRACIS.2017.44.
- [8] A. Robu, I. Szeidert, I. Filip, C. Vasar, and R. Robu, "Online platform for university admission," *2018 9th Int. Conf. Information, Intell. Syst. Appl. IISA 2018*, 2019, doi: 10.1109/IISA.2018.8633616.
- [9] H. C. Huang, Z. K. Zhang, H. W. Cheng, and S. W. Shieh, "Web Application Security: Threats, Countermeasures, and Pitfalls," *Computer (Long. Beach. Calif.)*, vol. 50, no. 6, pp. 81–85, 2017, doi: 10.1109/MC.2017.183.
- [10] O. M. Awoloye, B. Ojuloge, and M. O. Ilori, "Web application vulnerability assessment and policy direction towards a secure smart government," *Gov. Inf. Q.*, vol. 31, no. S1, pp. S118–S125, 2014, doi: 10.1016/j.giq.2014.01.012.
- [11] K. Qian, R. M. Parizi, and D. Lo, "OWASP Risk Analysis Driven Security Requirements Specification for Secure Android Mobile Software Development," *DSC 2018 - 2018 IEEE Conf. Dependable Secur. Comput.*, pp. 1–2, 2019, doi: 10.1109/DESEC.2018.8625114.
- [12] R. Ranchal, B. Bhargava, P. Angin, and L. Ben Othmane, "EPICS: A Framework for Enforcing Security Policies in Composite Web Services," *IEEE Trans. Serv. Comput.*, vol. 12, no. 3, pp. 415–428, 2019, doi: 10.1109/TSC.2018.2797277.
- [13] N. S. Ali, "Investigation framework of web applications vulnerabilities, attacks and protection techniques in structured query language injection attacks," *Int. J. Wirel. Mob. Comput.*, vol. 14, no. 2, p. 103, 2018, doi: 10.1504/ijwmc.2018.10012241.
- [14] S. Braun, N. Dwenger, D. Kübler, and A. Westkamp, "Implementing quotas in university admissions: An experimental analysis," *Games Econ. Behav.*, vol. 85, no. 1, pp. 232–251, 2014, doi: 10.1016/j.geb.2014.02.004.
- [15] V. Mavroeidis and S. Bromander, "Cyber threat intelligence model: An evaluation of taxonomies, sharing standards, and ontologies within cyber threat intelligence," *Proc. - 2017 Eur. Intell. Secur. Informatics Conf. EISIC 2017*, vol. 2017-Janua, pp. 91–98, 2017, doi: 10.1109/EISIC.2017.20.
- [16] M. O. K. Qhw, "& \ EHU % XGJHW 2SWLPL ] DWLQR 7KURXJK 6HFXULW \ ( YHQW," pp. 1026–1031, 2017.
- [17] G. Husari, X. Niu, B. Chu, and E. Al-Shaer, "Using entropy and mutual information to extract threat actions from cyber threat intelligence," *2018 IEEE Int. Conf. Intell. Secur. Informatics, ISI 2018*, pp. 1–6, 2018, doi: 10.1109/ISI.2018.8587343.
- [18] J. S. Suroso and B. Rahadi, "Development of IT risk management framework using COBIT 4.1, implementation in it governance for support business strategy," *ACM Int. Conf. Proceeding Ser.*, vol. Part F1306, pp. 92–96, 2017, doi: 10.1145/3124116.3124134.
- [19] M. Rubino and F. Vitolla, "Corporate governance and the information system: How a framework for IT governance supports ERM," *Corp. Gov.*, vol. 14, no. 3, pp. 320–338, 2014, doi: 10.1108/CG-06-2013-0067.
- [20] E. Semastin et al., "Preventive measures for cross site request forgery attacks on Web-based Applications," *Int. J. Eng. Technol.*, vol. 7, no. 4, pp. 130–134, 2018, doi: 10.14419/ijet.v7i4.15.21434.
- [21] A. Razzaq, Z. Anwar, H. F. Ahmad, K. Latif, and F. Munir, "Ontology for attack detection: An intelligent approach to web application security," *Comput. Secur.*, vol. 45, no. 3, pp. 124–146, 2014, doi: 10.1016/j.cose.2014.05.005.



- [22] S. M. T. Toapanta, I. N. C. Ochoa, R. A. N. Sanchez, and L. E. G. Mafla, "Impact on administrative processes by cyberattacks in a public organization of Ecuador," *Proc. 3rd World Conf. Smart Trends Syst. Secur. Sustain. WorldS4 2019*, no. July, pp. 270–274, 2019, doi: 10.1109/WorldS4.2019.8903967.
- [23] N. M. Scala, A. C. Reilly, P. L. Goethals, and M. Cukier, "Risk and the Five Hard Problems of Cybersecurity," *Risk Anal.*, 2019, doi: 10.1111/risa.13309.

## Classification of Timber Load on Trucks

Jan Sikora\*, David Fojtik

Department of Control System and Instrumentation, VSB – Technical University of Ostrava, 708 00, Czech Republic

### ARTICLE INFO

Article history:

Received: 15 January, 2020

Accepted: 24 March, 2020

Online: 20 April, 2020

Keywords:

Truck

Wood

Neural network

Classification

Image

### ABSTRACT

All trucks heading into the paper mill MONDI, Slovakia, have to pass an automatic security check. It controls if storage of its wood load meets all standards of safety. Each truck is scanned by a group of 2D scanners. After that the inspection of timber load is done by a software with use of the data gained by these scanners. The security software is universal for all kinds of storage of timber loads. This article is dedicated to deal with a problem of classification a kind of wood storage on a semi-trailer. The classification is solved by training a convolutional neural network on datasets with recorded trucks of both kinds to learn patterns distinguishing them. The image classification is done with use of images recorded by a set of cameras. By determining a type of storage, it is possible to execute the safety check for a specific type of wood load with better result than the universal check.

## 1. Introduction

Deep learning as a promising field has been quickly involving during last years. Artificial neural networks, which are cornerstone of this field, have proven to achieve overwhelming results in many disciplines. Computer vision is one of such area, where deep learning techniques are being used for solving variety of tasks. Me and my colleagues were working on a particular computer vision task in the past. Back then, we solved the problem by analytic method with use of standard computer vision functions. Recently we decided to solve the same task by using deep learning techniques and compare the results. These objectives will be described in this paper, which is an extension of work originally presented in proceedings of the International Carpathian Control Conference 2019 [1].

Computer vision belongs to technologies in which deep learning techniques are widely used nowadays. Some of applications are for example image recognition, image processing [2], object detection [3], solving style transfer problem [4]. We cannot omit image classification problem [5], which is the issue of this paper.

Our classification problem is binary, i.e., the developed software must assign one of only two classes to the provided input data. In this particular case we are classifying kind of timber load stored on trucks. The classification should lead to a improve safety check of trucks heading into paper mill MONDI SPC, a.s. in Ruzomberok.

Similar problems of image classification have been solved in the past by applying supervised machine learning algorithms, which is the case of the article focused on classifying agricultural landscapes algorithms [6]. Next article solves the problem of cloud detection, that is binary classification problem, with use of large-scale gaussian processes classifier [7]. Next study shows a classification of heat emitting object with use of Convolutional Neural Network [8]. Network of such kind is also used in this work.

## 2. Recording Trucks

Before entering the paper mill MONDI SPC, each truck loaded with wood logs has to pass a safety check. For this purpose, a unique gate equipped with a set of 2D lidar scanners and a group of cameras has been developed and installed. Functionality and design of this gate are described in detail in the older article [9].



Figure 1: The scanning gate (left) with detail on a camera (right).

\*Corresponding Author: Jan Sikora, Email: [jan.sikora@vsb.cz](mailto:jan.sikora@vsb.cz)

Software executing the safety inspection of trucks use point cloud that represent a surface of each truck. These point clouds are obtained by the set of scanners while trucks are passing through the gate. The algorithm for safety check is universal for all kinds of timber load. We have an idea that can lead to improve success rate of the inspection, if we use a specific algorithm for relevant kind of timber storage.

But for that, we need to classify kind of wood storage of each truck, before running one of specifics inspection algorithm. This classification is the main goal of both original and this article. For this purpose, we can use the installed cameras, which serves now only for recording and storing an evidence of incorrectly loaded trucks.



Figure 2: Pictures of a truck from all three cameras.

### 3. Classification with use of Computer Vision Technology

The original article describes how we solved this classification problem with use of analytic functions belonging to the computer vision technology. These functions are described in detail in the book [10]. A final classification result of individual truck was determined by mean results of two classification methods.

#### 3.1. Top View Classification

First method works with images taken by a camera mounted on the top of the scanning gate. At the beginning of the recognition algorithm, the important area of taken image (highlighted by the blue quadrangular on the left part of Figure 3) is converted by perspective transformation into simulation of top view. Then the image is converted into grayscale one, on which the Canny algorithm for finding edges is applied.



Figure 3: Important area of image (left) and final image with founded lines [1].

Then lines are detected by use of Hough algorithm (see right part of Figure 3). Direction of those lines shows a type of wood storage.

#### 3.2. Side View Classification

This method uses images taken by cameras mounted on both sides of the scanning gate. Principle of this method is to find cross-sections of wood logs in truck's images. When they appear in significant percentage of image's area, then a truck is classified as transversely loaded one.

At first, via perspective transformation, an important part of an image is converted into a side view simulation. The perspective transformation is done due to easier wood logs' cross-sections detection when they transform from shape of ellipses to more or less circular shape.



Figure 4: Important area of image (left) and its perspective transformation into simulation of side view [1].

Then threshold is applied to find cross-sections of wood logs. Pure wood (cross-sections of wood logs) occur in variations of yellow color, from light to dark yellow. Whereas, tree bark (cylindrical surface of wood logs) occur in shades of brown or gray color. This feature is used in image processing to detect cross-sections of wood logs. Pixels belonging to cross-sections of wood logs are detected by applying threshold that define if pixels are within the range of yellow colors in HSV color spectrum (see Figure 5).

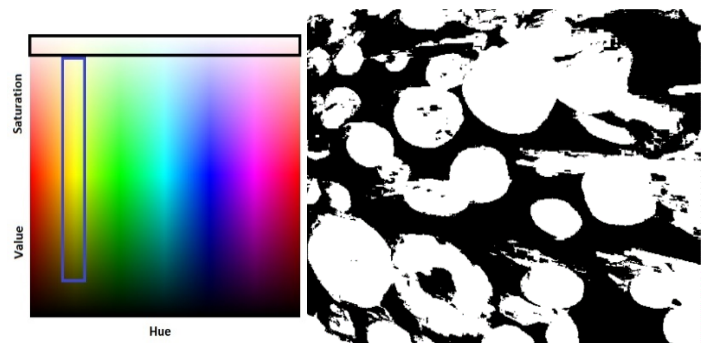


Figure 5: HSV color spectrum with marked ranges of yellow color (left) and threshold of both color ranges merged together on side view image (right)





The architecture of used neural network is based on VGG-19 model [13]. After using this model architecture to our classification dataset, we have done some experiments with the model configuration and slightly change its architecture. Final model is sequential, rather deep and consist of five convolutional layers. Every convolutional layer use ReLU (Rectified Linear Unit) as an activation function [14], and their kernels have a shape of 3 x 3. The number of filters increases with the depth of the model. First convolutional layer has only 32 filters, second one is made up from 64 filters, third and fourth layer have the same amount of 128 filters, and the last convolutional layer consists of 256 filters. After each of these convolutional layers, a max pooling operation, with pooling size of 2 x 2, is executed.

Then the model is flattened, and dropout function with rate of 0.5 is activated. In the end of the model are three densely connected layers. The number of units per layer is decreasing with depth from 1024 via 512 to 1. First two of these densely connected layers use ReLU activation function, whereas the last layer rely on Sigmoid activation function.

The neural network was trained for 120 epochs. The training has been done with RMSprop optimizer with 0.0001 learning rate. Choosing the hyper-parameters of the network have been done based on papers [15, 16]. Accuracy of the network was verifying on the validation dataset during training. As we can see from Figure 8, the validation accuracy stopped to follow the growing tendency of the training accuracy around 100<sup>th</sup> epoch. After that point the network started to memorize input data rather than finding a better classification pattern.

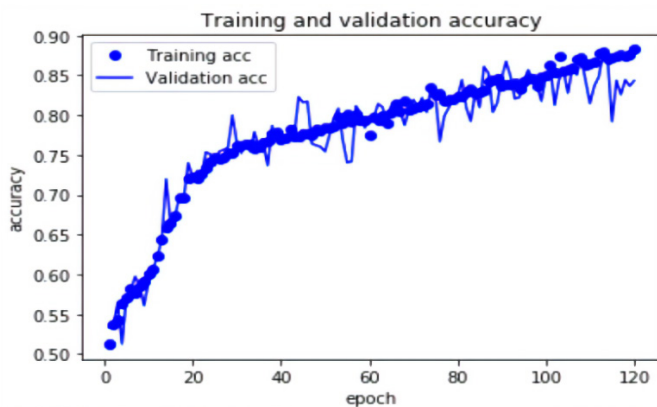


Figure 9: Training the network.

After initial training, a new neural network was trained with only a hundred epochs to avoid overfitting [17]. To combat overfitting, we used the techniques described in [18, 19], which help us to choose the best elements of model dealing with that problem, and set their parameters. These techniques were proven, via comprehensive experiments, to increase the model's classification success rate on new data. This final network was later examined on the testing dataset. The final classification accuracy achieved a result of 84.926 %, which is a great outcome received from our limited training dataset. With use of larger training dataset, we could achieve even greater success rate.

Although we tried to solve this task by training many different neural networks architectures with convolutional layers, the one described in this chapter has the best result.

The classification accuracy of the original paper with analytic approach has only slightly better result, that reached to 85,086 %. While maintaining almost identical classification accuracy, the new method is few times faster and need less computing energy.

## 5. Conclusion

The classification accuracy achieved by the trained convolutional neural network is 84.92%. This number is accuracy of an individual truck's image. When we classify a truck according to a mean result of all its images, we can reach up to 97.88% success rate.

This classification problem has already been solved in the original paper by analytic methods with use of computer vision technology. Back then we achieved similar result of 98% success rate.

Classification approach of this paper uses artificial neural network, and as such, it is more reliable in bad weather and light conditions. For example, snowing, raining, cloudy weather, or darkness at night, can lead to huge unreliability of analytic approach of the original paper, since it depends on finding yellow colour of wood log cross-sections. On the other hand, actual solution can be reliable even in those bad conditions, when the images of the training dataset include images with these situations.

Even though actual solution has not brought much better result, it is far faster and more energy efficient solution than the original one. The big future potential is by combining these two methods. The determining if a truck is longitudinally or transversely loaded will reach almost a hundred percent certainty by that. Then, we can upgrade the actual software for truck's safety inspection to work for a specific kind of timber load, and by that the safety check will be more precise.

## Conflict of Interest

The authors declare no conflict of interest.

## Acknowledgment

This work was supported by the European Regional Development Fund in the Research Centre of Advanced Mechatronic Systems project, CZ.02.1.01/0.0/0.0/16\_019/0000867 within the Operational Programme Research, Development and Education and the project SP2020/57 Research and Development of Advanced Methods in the Area of Machines and Process Control supported by the Ministry of Education, Youth and Sports.

## References

- [1] J. Sikora, D. Fojtík, J. Czebe and M. Mihola, "Storage kind recognition of truck's timber load", 2019 20th International Carpathian Control Conference (ICCC), Krakow-Wieliczka, Poland, 2019, pp. 1-4. <https://doi.org/10.1109/CarpathianCC.2019.8766049>

- [2] M. Jurek and R. Wagnerová, "Frequency Filtering of Source Images for LASER Engravers", 2019 20th International Carpathian Control Conference (ICCC), Krakow-Wieliczka, Poland, 2019, pp. 1-5. <https://doi.org/10.1109/CarpathianCC.2019.8766050>
- [3] S. Kanimozhi, G. Gayathri and T. Mala, "Multiple Real-time object identification using Single shot Multi-Box detection", 2019 International Conference on Computational Intelligence in Data Science (ICCIDS), Chennai, India, 2019, pp. 1-5. <https://doi.org/10.1109/ICCIDS.2019.8862041>
- [4] L. Gatys, A. Ecker and M. Bethge, "Image Style Transfer Using Convolutional Neural Network", 2016 IEEE Conference on Computer Vision and Pattern Recognition (CVPR), Las Vegas, USA, 2016, pp. 2414-2423. <https://doi.org/10.1109/CVPR.2016.265>
- [5] H. R. Roth et al., "Anatomy-specific classification of medical images using deep convolutional nets", 2015 IEEE 12th International Symposium on Biomedical Imaging (ISBI), New York, NY, 2015, pp. 101-104. <https://doi.org/10.1109/ISBI.2015.7163826>
- [6] D. C. Duro, S. E. Franklin, M. G. Dubé, "A comparison of pixel-based and object-based image analysis with selected machine learning algorithms for the classification of agricultural landscapes using SPOT-5 HRG imagery", 2012, Remote Sensing of Environment, vol. 118, pp. 259-272. <https://doi.org/10.1016/j.rse.2011.11.020>
- [7] P. M. Álvarez, A. P. Suay, R. Molina and G. C. Valls, "Remote Sensing Image Classification With Large-Scale Gaussian Processes", 2018, IEEE Transactions on Geoscience and Remote Sensing, vol. 56, pp. 1103-1114. <https://doi.org/10.1109/TGRS.2017.2758922>
- [8] A. D. Algarni, "Efficient Object Detection and Classification of Heat Emitting Objects from Infrared Images Based on Deep Learning", 2020, Multimedia Tools and Applications, pp. 1-24. <https://doi.org/10.1007/s11042-020-08616-z>
- [9] F. David, P. Petr, M. Miroslav and M. Milan, "Scanning of trucks to produce 3D models for analysis of timber loads", 2016 17th International Carpathian Control Conference (ICCC), Tatranska Lomnica, Slovakia, 2016, pp. 194-199. <https://doi.org/10.1109/CarpathianCC.2016.7501092>
- [10] G. R. Bradski, Learning OpenCV, Sebastopol: O'Reilly, 2008.
- [11] W. Rawat, Z. Wang, "Deep Convolutional Neural Networks for Image Classification: A Comprehensive Review", Neural Computation, **29**(9), 2352-2449, 2017. [https://doi.org/10.1162/neco\\_a\\_00990](https://doi.org/10.1162/neco_a_00990)
- [12] F. Chollet, Deep learning with Python, Manning Publications Co., 2018.
- [13] A. Koedwiady, S. M. Bedawi, C. Ou and F. Karry, "End-to-End Deep Learning for Driver Distraction Recognition", 2017, Image Analysis and Recognition, ICIAR 2017, Lecture Notes in Computer Science, vol. 10317, Springer, Cham. [https://doi.org/10.1007/978-3-319-59876-5\\_2](https://doi.org/10.1007/978-3-319-59876-5_2)
- [14] A. F. Agarap, "Deep Learning using Rectified Linear Units (ReLU)", arxiv 2018, ArXiv: 1803.08375
- [15] L. N. Smith, "A disciplined approach to neural network hyper-parameters: Part 1 -- learning rate, batch size, momentum, and weight decay", 2018, ArXiv: 1803.09820
- [16] H. Wu, Q. Liu and X. Liu, "A Review on Deep Learning Approaches to Image Classification and Object Segmentation", 2019, CMC-Computers, Materials & Continua, **60**(2), 575-597. <https://doi.org/10.32604/cmc.2019.03595>
- [17] H. Zhang, L. Zhang and Y. Jiang, "Overfitting and Underfitting Analysis for Deep Learning Based End-to-end Communication Systems", 2019 11th International Conference on Wireless Communications and Signal Processing (WCSP), Xi'an, China, 2019, pp. 1-6. <https://doi.org/10.1109/WCSP.2019.8927876>
- [18] A. F. Kamara, E. Chen, Q. Liu and Z. Pan, "Combining contextual neural networks for time series classification", 2020, Neurocomputing, vol. 384, pp. 57-66. <https://doi.org/10.1016/j.neucom.2019.10.113>
- [19] L. Pan, C. Li, S. Pouyanfar, R. Chen and Y. Zhou, "A Novel Combinational Convolutional Neural Network for Automatic Food-Ingredient Classification", 2020, Computers, Materials & Continua, vol. 62, pp. 731-746. <https://doi.org/10.32604/cmc.2020.06508>

## ROS Based Multimode Control of Wheeled Robot

Rajesh Kannan Megalingam\*, Santosh Tantravahi, Hemanth Sai Surya Kumar Tammana, Nagasai Thokala, Hari Sudarshan Rahul Puram, Naveen Samudrala

Department of Electronics and Communication Engineering, Amrita Vishwa Vidyapeetham, Amritapuri, India

### ARTICLE INFO

Article history:

Received: 15 January, 2020

Accepted: 25 March, 2020

Online: 20 April, 2020

Keywords:

Mobile robot

Python

Virtual network computing

Joystick

IoT

Android app

ROS

Multi-mode control

Speech

IP Address

Socket

Server - Client Protocols

### ABSTRACT

This research work mainly presents the design and development of a small-scaled wheeled robot, which can be controlled using multiple controlling interfaces using some new technological trends. Raspberry Pi 3 as the main controller, Python as the programming language integrated with the Robot Operating System (ROS) and Virtual Network Computing (VNC) for screen sharing are utilized in order to control the robot. Laptop Keys, Graphical User Interface (GUI) on PC, Virtual Network Computing on smart phones, Joystick connected to Laptop using python integrated with Robot Operating System, Voice commanding through an android app integrated with python and ROS and Internet of Things using a customized webpage with Node MCU as the controller are the dominant control interfaces. A Local Area Network is established in order to communicate with the micro-controllers wirelessly. The robot can be controlled with multiple interfaces by using its corresponding commands. The robot is made to survive in five different paths, controlled by all the six methods and the time for each response obtained was appraised and illustrated properly.

## 1. Introduction

Mobile robots are becoming increasingly popular across various sectors. They are used to assist with work processes and even accomplish tasks that are impossible, unreachable or dangerous for humans. Study of these robots had become an emerging field in the research world. Autonomous mobile robots (which can navigate themselves through an environment), guided robots (which travel through a pre-defined navigation route) and finally controllable robots (which travel according to the command received from a device). There are several types of mobile robots, which are controlled by different methods, depending on the need and operational conditions in the application environment. These robots are made resistant to harsh environments and are also available in several sizes too. Mobile robots had also introduced new trends in research.

The mobile robot, along with its control interfaces, is a simple device, made up of readily available materials. Raspberry Pi 3, which supports wireless communications, was selected as the single-board computer. PYTHON IDLE had been used as programming software to build keyboard and GUI control methods. The programs used for implementing the control methods were written in Python and were ROS integrated to implement joystick and voice control methods. This project also uses a Virtual Network Computing (VNC) viewer for smart phone purposes.

Six different methods were used to move the robot in desired direction: laptop PC, smart phone, GUI, joystick, voice command, IoT. The experimental results of three of these methods were already presented in [1] and in this research work, we added three more methods as extension of it. In [2] the voice command of eight languages is used for security system where as the app designed in this research work can take input command of many languages and can control the bot accordingly similar to that of [3]. Mobile control had been achieved using the VNC viewer by reducing its screen encoding time using the technique in [4]. IoT

\*Dr. Rajesh Kannan Megalingam  
Director, Humanitarian Technology (HuT) Labs, Amrita Vishwa Vidyapeetham,  
Kollam, Kerala, India, PIN: 690525.  
Email address: [raieshkannan@ieee.org](mailto:raieshkannan@ieee.org). Contact No: +91 9496120900

control method is similar to [5] but instead of an WIFI module and raspberry pi, we used NodeMcu which can both receive WIFI signal and control the robot. GUI and the laptop keys control were implemented by using raspberry pi as both microprocessor and microcontroller, where additionally Arduino in [6], and DSP in [7] were used for controlling the robot. This research work identifies the best method out of six selected modes of control. The best is determined based on the time difference between the time input is given and the robot finishes execution. This is to determine the speed efficiency of the robot, which is a major constraint in most of the situations. These tests conducted can be used to determine the speed with which these commands are transmitted and the processing speed of the controller board.

## 2. Motive

In recent times mobile robots have become more commonplace in various commercial and industrial applications. These robots are useful in reaching the places that are beyond human reach. Their uses are wide ranging. Primary motive behind the implementation of these mobile robots is to improve speed and efficiency. These robots when equipped with several types of sensors can improve functionality over wide range of applications. The robot can either move in an environment guided by the sensory inputs or be made to follow a specified trajectory. Usually, a terminal (computer user interface used to give input) is essential for controlling the bot. In situations where time is major constraint such as rescue robots, we need to send more commands to control the robot, our aim is to identify the best method for controlling such robots. Experimental results for three methods of control i.e. using Laptop, GUI, Mobile were tabulated before and are now extended by adding three more methods i.e. Joystick, Voice, IOT.

## 3. Related works

Condry and Nelson [8] presented a model that integrates control system gateways with smart IoT devices, using real-time challenge-response authentication for assured control operations. Agrawal et al. [9] offered a training method and algorithm, using a force-feedback joystick, with an “assist-as-needed” model for training vehicle drivers. [10] proposed a software structure, ASSOCIATES-ROS, for development of unresponsive, collaborative, multi-robot systems with copious software resources Shahzad [11] enlarged the Pymote structure to simulate packet-level performance. The extensions included radio propagation, energy consumption, and mobility. [12] discussed a new form of augmentative and alternative communication (AAC) device, for people with severe speech impairment. [13] proposed a method, to integrate the standard and throat microphone signals, for robust voice identification in clamorous environments. Kim’s team [14] proffered a novel approach to an auditory prototype, for robust speech identification in clamorous environments. [15] presented a book and straight forward hand gesture identification method, used in the mending of people who have flexibility issues,

specifically stroke patients and victims with spinal cord injury (SCI).

The authors of [16] explained the simulation of mobile robot using three stage torque control. Author delineated [17] implementation and assessed viability and execution of an embedded application of the Convolutional Neural Network (CNN) algorithm on the Raspberry Pi 3 computer. The CNN-embedded algorithm classifies and quantifies dissimilarities among the frames. The convolutional neural network (CNN) algorithm which they used to detect faults in SHM works by taking an input image, assign importance to various aspects/objects in the image and be able to differentiate one from other and counts these variations as faults, which may not be true always. This algorithm may give a count more than the actual number of faults. [18] describes the execution and working principles of transportable, flimsy user-interfaces to approach implanted distant home-systems and home-networks. Authors in [19] proposed RemoteUI, which performs more efficiently compared to VNC in terms of bandwidth.

Mobile robot with single control interface is presented in [20]. Stabilization and tracking of a robot using a predictive controller with a time varying system is proposed in [21]. Isolated control interface, push-button control based movable robots in an untold domain using wireless sensor technology is presented in the research work [22]. [23] concentrates on avoiding singularity issues rather than the control interface, in an over-stimulated, artificial poly directional, wheeled movable robot [24] used the robot operating system platform for planning motion of poly directional wheeled movable robot instead of the control interface. Authors of [25] explained a novel method to control an orthotic arm using the EOG signals and also proposed a method by which a second person could control it. A low cost auto-navigated wheelchair is designed by authors of [26] using fixed path navigation with a Raspberry Pi, Arduino and rotation encoders. It works on the principle of Distance estimation.

## 4. Architecture of the system

The system architecture, as shown in Figure 1, is comprised of three major components: the command block, controller block, and the mobility block. The command block is constituted of six interface units: keyboard, smart phone, GUI, joystick, voice command, IoT. Keyboard is the first control interface. The VNC viewer installed on the smartphone is used as the second control method. The third robot mobility control method is the GUI, installed on any PC; next is a joystick connected to a computer or laptop. Voice commands, sent through a mobile app and the sixth method is through IoT (Internet of Things) using a Node MCU (Single board Microcontroller) with the commands coming from a smart phone. The Wi-Fi communication interface is used for transmitting commands and controlling the robot. Single-board computer i.e. Raspberry Pi 3, a Node MCU interfaced with Wi-Fi and motor drivers make the controller block. The mobility block is comprised of motor drivers, the wheels and the motors. Python is the language used to send commands from microcontroller to



motor driver and in some of the methods, we used python programs integrated with ROS, to send commands.

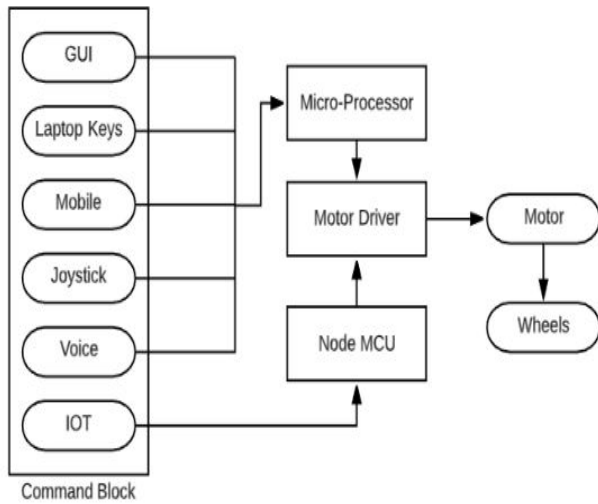


Figure 1: Robot Architecture

#### 4.1 Command Block

Graphical User Interface (GUI) allows the control of robot through simple graphics. The GUI was developed using Python language, five different graphical buttons were created which helps in controlling the robot: up, down, left, right and stop. The robot's front and back motion is controlled by the up and down buttons. The left turn, right turn and stop abilities of the robot is controlled with the help of left, right and stop button respectively.

VNC Viewer app is one of the means to control a wheeled bot, by a smart mobile phone through Wi-Fi communications. VNC viewer is used to control another computer by displaying its visual desktop on host computer connected over a network. Ensure that you have been given permission to remotely connect to the host computer. Once authentication is achieved, the VNC Viewer shows desktop of host computer in a new window. This is similar to the sharing desktop sharing of PC and controlling robot. VNC adapts itself automatically and dynamically to varying conditions, including differing screen contents and network bandwidths. VNC is also platform independent i.e. a Windows system can control a Linux system.

The keyboard of a laptop is used to send commands to the robot and control it to move in the desired direction. We used I, J, K, L and S keys in laptop to control the robot in various directions. Keys i, k, j, l and s are used to move the robot in forward, back, left, right directions and to stop the bot respectively.

A joystick is a input device which provides better control over the robot. It is easier to use by a human operator and steer a bot. Joystick often has one or more pushbuttons, called switches, whose positions can be monitored by the computer. The working of a joystick is based on the principle of conversion of physical movement into a digital signal, which when accepted by the device being controlled, produces the same results on the screen when connected to a computer.

#### 4.2 Mobility Block

The mobility block is constituted of motor drivers, wheels and DC motors. Because of speed efficiency DC motors were better than stepper motors and also DC motors were low weight, small size, and minimum cost. Speed of a DC motor can be controlled by controlled by varying the supply voltage of the controller. In the context of this paper's main objective, the robot should be as compact and lightweight as possible.

#### 4.3 Controller Block

The controller block's main components are a Raspberry Pi 3 computer and Node MCU. One of the six interfaces were used to send the commands. The controller block receives signal through WIFI, decodes these commands and generates control signal to the required modules to control the bot. The direction in which the robot moves is also being decided by the controller block depending on the received command.

### 5. Modelling the robot

The modeling of the robotic movements was carried out through three cases. The cases include - normal plane ground, robot going up an inclined plane and last, the robot going down the inclined plane. This kind of functional modeling offers an insight into the working of the robot in different terrains.

For all the equations presented here the following symbols are used and the meaning are as follows

N-Normal Force, Unit: Newton

m-Mass of robot, Unit: Kg

g-Acceleration due to gravity, Unit:m/s<sup>2</sup>

f<sub>s</sub>-Static force of friction,Unit:Newton

μ<sub>s</sub> -Coefficient of static friction

i<sub>d</sub> -Current drawn, Unit: Ampere

τ -Torque, Unit: Newton meter

K<sub>T</sub> -Torque constant for a DC motor, Unit: Newton meter/Amp

r-Radius of wheel

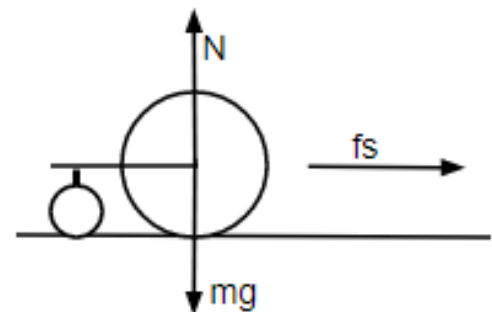


Figure 2: Robot on a flat surface

Considering the case of inclination angle zero i.e. plane ground, as shown in Figure 2,

$$N=mg \quad (1)$$

The force required to overcome friction is

$$F=\mu_s*N \quad (2)$$

$$F=m*g*\mu_s \quad (3)$$

The torque for the wheels comes from the DC motors

$$\tau=r*F \quad (4)$$

$$\tau=r*m*g*\mu_s \quad (5)$$

For a dc motor with constant input voltage

$$\tau=K_T*i_d \quad (6)$$

$$K_T*i_d =m*g*\mu_s \quad (7)$$

$$i_d=m*g*\mu_s/K_T \quad (8)$$

Here,  $i_d$  is the minimum current requirement for the bot.

Similarly, considering the cases of inclination, where the angle of inclination is  $\theta$ , as shown in Figure 3.

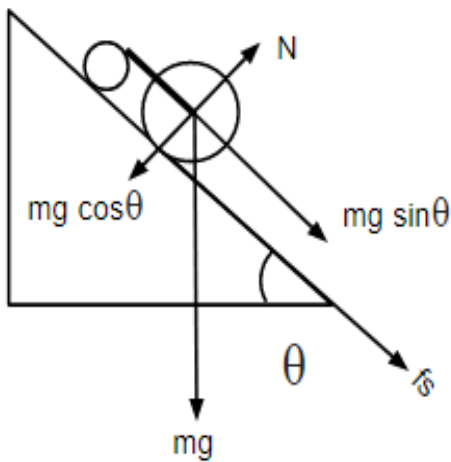


Figure 3: Robot moving up an inclined plane

$$N=m*g*cos\theta \quad (9)$$

Assuming the frictional force, between the inclined plane and the tires of the robot, is  $f_s$ ,

The force required to overcome friction is

$$F= (\mu_s*N) +(m*g*sin\theta) \quad (10)$$

$$F= (m*g*\mu_s*cos\theta) + (m*g*sin\theta) \quad (11)$$

$$F=r*m*g(cos\theta*\mu_s+ sin\theta) \quad (12)$$

The torque for the wheels comes from the motors connected.

$$\tau=r*F \quad (13)$$

$$\tau=r*m*g(cos\theta*\mu_s+ sin\theta) \quad (14)$$

For a dc motor with constant input voltage

$$\tau=K_T*i_d \quad (15)$$

$$K_T*i_d =r*m*g(cos\theta*\mu_s+ sin\theta) \quad (16)$$

$$i_d=r*m*g(cos\theta*\mu_s+ sin\theta) /K_T \quad (17)$$

Here,  $i_d$  is the minimum current'

Similar to the above case, considering the inclined plane with an inclination angle  $\theta$  and the robot moving down the plane as shown in Figure 4.

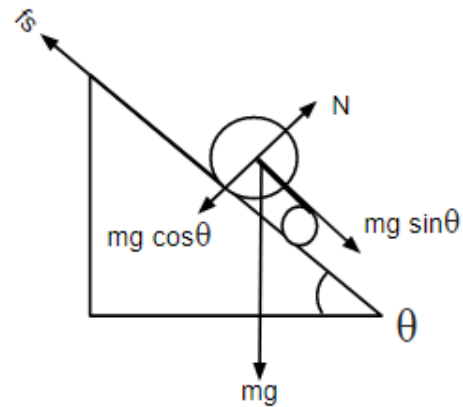


Figure 4: Robot moving down an inclined plane

Force required to overcome friction is

$$F= (\mu_s*N) -(m*g*sin\theta) \quad (18)$$

$$F= (m*g*\mu_s*cos\theta) -(m*g*sin\theta) \quad (19)$$

$$F=r*m*g(cos\theta*\mu_s- sin\theta) \quad (20)$$

The torque for the wheels comes from the motors connected.

$$\tau=r*F \quad (21)$$

$$\tau=r*m*g(cos\theta*\mu_s- sin\theta) \quad (22)$$

For a DC motor with constant input voltage

$$\tau=K_T*i_d \quad (23)$$

$$K_T*i_d =r*m*g(cos\theta*\mu_s- sin\theta) \quad (24)$$

$$i_d=r*m*g(cos\theta*\mu_s- sin\theta) /K_T \quad (25)$$

Here,  $i_d$  is the minimum current requirement.

## 6. Design and Implementation

Figure 5 shows about the mobile wheeled robot as implemented and tested by us in our lab. The hardware implementation comprises chassis of the robot, Raspberry Pi, circuitry for the control, motor drivers, motors, wheels, Node

MCU and powering unit for controllers. The control methods include GUI, smartphone, keyboard, Joystick, Voice command and IoT commands.

### 6.1 Robot Chassis

The chassis of the robot is a cardboard made using a laser-cut of dimensions 0.2032 meter by 0.127 meter providing provision for integrating the motors, castor wheel, circuit, Raspberry Pi and a power unit. Two DC motors can be attached to the body. The load that is being carried by the robot, affects its speed. The robot circuitry and the chassis are shown in Figure 5.

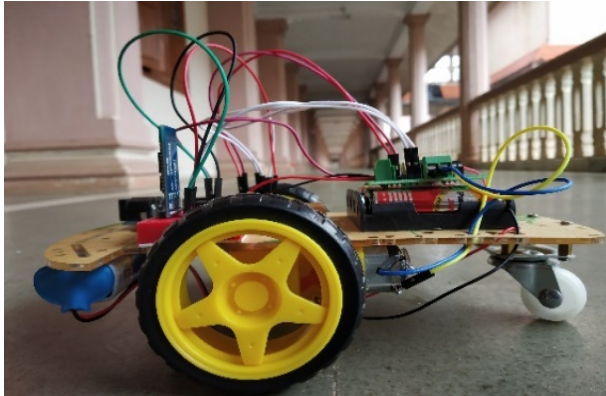


Figure 5: Mobile robot with its chassis and control circuitry

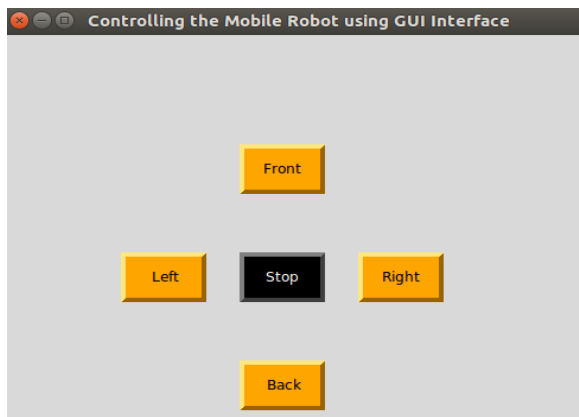


Figure 6: Python-based GUI on a laptop

### 6.2 Single Board Computer:

#### Raspberry Pi 3

Raspberry Pi 3, which is a single-board computer (SBC), is used as a micro-controller, with a 64-bit Quad core processor, GPU, ROM and Input/ Output pins on the System-on-Chip (SoC). It has 1.2 GHz single-core CPU, HDMI port, USB 2.0 port, GPIO pins and 1 GB RAM as its major parts. It is compatible with many Operating (OS) but “Raspbian” is the most commonly used OS.

#### Node MCU

NodeMCU is an open-source IoT platform.<sup>1</sup> It includes firmware that runs on the ESP8266 Wi-Fi SoC from Espressif Systems, and hardware which is based on the ESP-12 module. The board mainly consists of a built-in Wi-Fi-module, GPIO (General

Purpose Input / Output pins) as its major components. To program the board, we use Arduino-IDE installed with ESP8266 library which acts as a programming tool for it. The NodeMCU used is shown in Figure 9.

#### Motor Driver:

Motor driver acts as an interface between Microcontroller and the motors. Motor driver is used to control speed and direction of motor rotation through the PWM signal that is coming from the microcontroller. The L293D is designed to provide bidirectional drive currents up to 600-] mA, at voltages over the range from 4.5 V to 36 V.

### 6.3 Control Methods

A keyboard with standard functionality either the PC or laptop keys is implemented to control the robot as one of the methods as shown in Figure 8. Mobile phones which supports Android platform installed with VNC can be used as an optional method for driving the robot. Developed in Python, the GUI for control of the bot is shown in Figure 6. The GUI developed is very easy to use and can be controlled remotely in any direction. Robot can be remotely operated through mobile phone using the VNC viewer mobile app, as shown in Figure 7. This can be done using a local area network (LAN) in which the VNC will be running in a server PC and we can control the robot remotely by using a mobile phone by the process of screen sharing. This process will be carried out until both the PC and the mobile phones are connected to the same network. By this way the robot will be controlled using the same GUI but using the mobile phone as the controller.

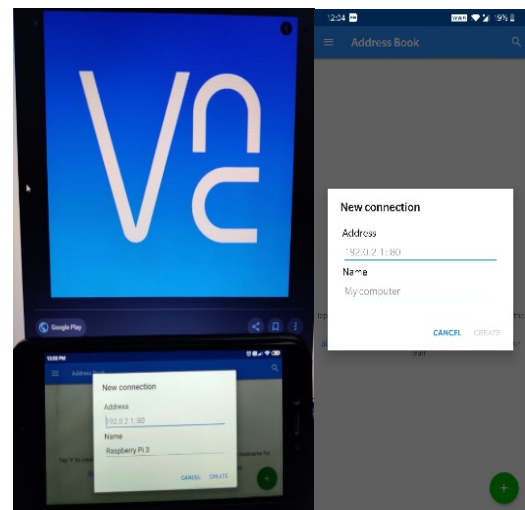


Figure 7: Mobile control using VNC

Raspberry Pi 3 is the major controller to drive the robot in stipulated environment. The motor driver acts as the mediator for supplying the power supply to the motors when a command arrives at the controller. Based on the commands given from any of the above-mentioned methods, the SBC intimates the motor driver and it regulates the speed according to the given command and passes to the wheels via motors.



Figure 8: Keyboard based Control

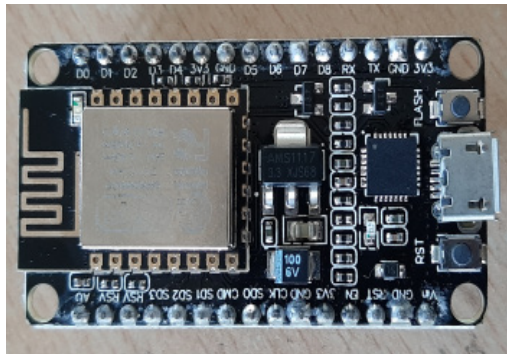


Figure 9: Node MCU

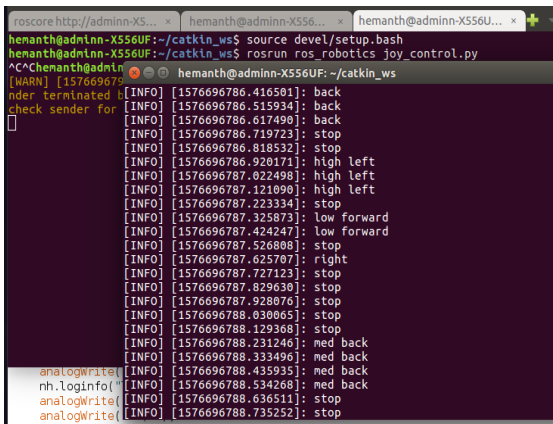


Figure 10: The commands received from the joystick

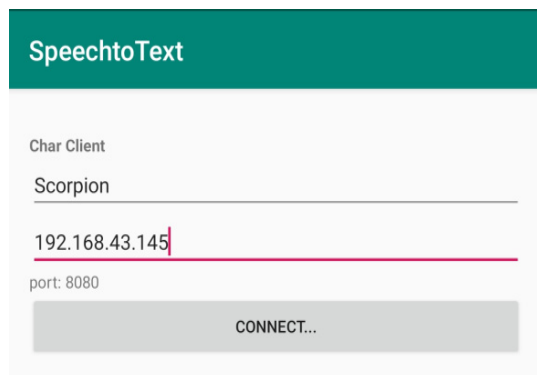


Figure 11: Speech App Interface for establishing a connection.

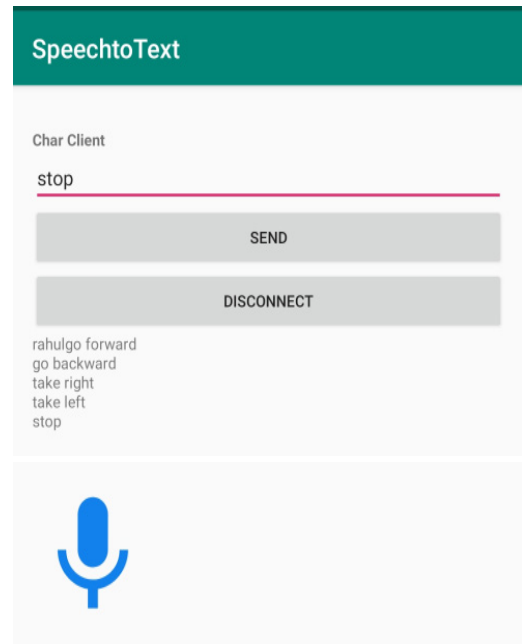


Figure 12: Sending voice commands using the app.

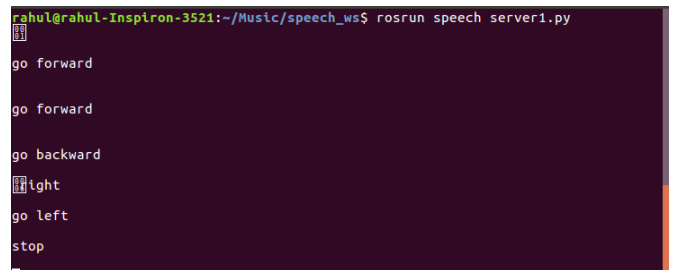


Figure 13: The data received from the VNC App.

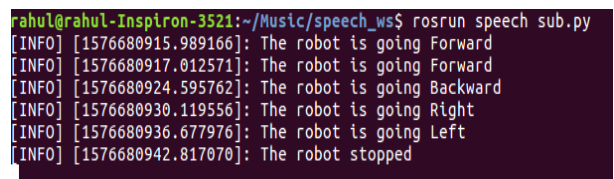


Figure 14: The received data from input device is being published to a Python file (where control is transferred to DC motors).

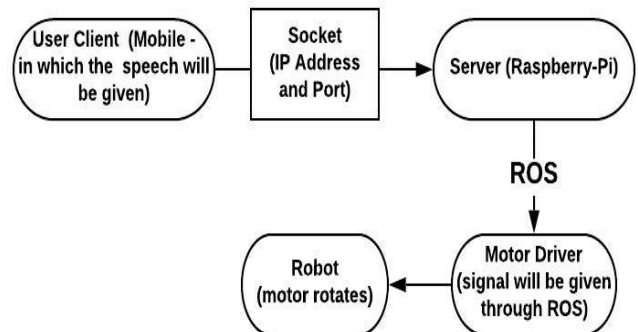


Figure 15: Flow chart of how data is being published to the Robot



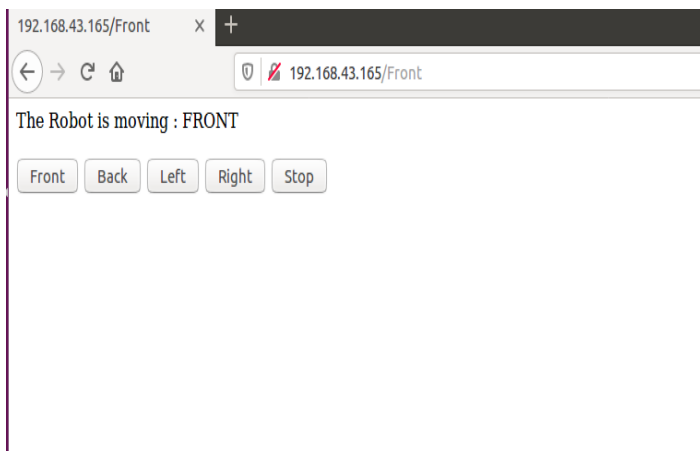


Figure 16: Web page created using html to control the robot.

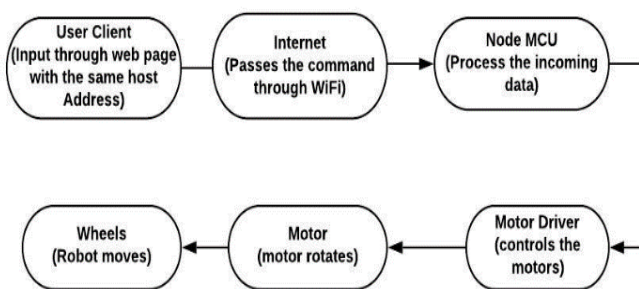


Figure 17: Flowchart for IoT control of mobile robot

The joystick used comprises of two 2 axis control sticks and 14 buttons. ROS integrated python file is used to transmit the commands given by the operator. The publisher node(program) establishes a connection between the user input data and the microprocessor. All these joystick commands from user are stored in a topic; these commands are then subscribed from the topic by the microprocessor (Raspberry-Pi 3). Based on the given input, Raspberry-pi 3 processes the data as shown in Figure 10, and send a signal to the motor driver, which facilitates the motor’s rotation in the desired direction.

Using this joystick, the bot is made to move in different directions: forward, backward, left, right, in different modes of speed - low, medium, high. The results obtained by operating the bot along several paths, in high-speed mode were noted and are tabulated.

There are different types of teleoperated robots, among which the major one is voice operated. There are several nodes which will act as publishers and subscribers to a topic. In this scenario, an app was created for controlling the robot as the input as the speech. The app interface is shown in Figure 11. This app basically works on socket programming. The socket programming is nothing but a server-client protocol. Here we are giving input from the app (using mobile) and it acts as a client. The hosted micro-controller (Raspberry -Pi) will be acting as a

server. In this, the server and client should be connected to the same IP Address and Port. Port is a channel through which the data is publishing from a client to a server. The IP Address and the Port together are called a Socket. On the server-side, the data is integrated with the Robot Operating System (ROS). Through socket, the connection establishes between the server and the client. The input voice-command is fed from the app, as shown in Figure 12. The data being sent from the client is conveyed to the Raspberry-Pi 3 computer, as shown in Figure 13. From the SBC the data is delivered to a Python file, via a topic. As shown in Figure 14, the file acts as a subscriber node(program), in this case. From there subscriber gives commands to the motor driver, which actuates, the robot to move. Transmission of data, from a mobile app to the Raspberry-Pi 3 is explained using a flow diagram in Figure 15.

We implemented next method of control using concepts of IoT. Considering the scenario of IoT, Node MCU was used as the microcontroller for driving the robot. Node MCU was selected the microcontroller, since it has a built-in Wi-Fi module to control the robot, remotely. In actually controlling the mobile robot using a web page. The webpage is being built through html and integrated with Arduino - IDE. The web page will have some set of commands to drive the robot as shown in Figure 16. The Node MCU needs to be connected to a Wi-Fi network; from any web browser, the control of robot is accessible by typing the link IP Address. Then the web page created can be seen. The web page shows buttons which can control the robot just by clicking on any one of them. The web page will be acting as a client and the Node MCU will be acting as a server. Through -client-server protocol, the connection is established between the web page and the robot. when the button is clicked, user data gets published to the Node MCU; from there the robot’s actions are based on the specific input command. All these steps are shown, as a flowchart in Figure 17, the bot was made to move in different directions along different paths, by this method.

## 7. Experiments and Results

An even rectangular plane surface is selected for the experiment. The surface is with dimensions 2.04 meters in length and 1.2 meters in breadth. The test area closely resembles realistic situations, as opposed to non-realistic one and it is chosen in a closed room. All these test analyses (control of the robot in different paths) were carried out on the same plane and the path followed by the bot was delineated by a tape. For the better analysis of the robot we have created five different paths for the robot to transverse: rectangular path, straight-then turn right, straight-then turn left, navigate a U-turn and a straight path. In the above-mentioned paths, we conducted 5 trials, using each of the six modes: Keyboard, GUI, Smartphone, joystick, Voice command, IoT. 30 trials in total were conducted for each of these different paths. The recordings during these trials, were tabulated, to determine which is the fastest using the six modes.

Table 1: Time taken by bot to cover Straight Line Path in all the methods

Trial No.	GUI (sec)	Mobile (sec)	Laptop keys (sec)	Joystick (sec)	Voice (sec)	IOT (sec)
1	5.1	5.1	5.0	5.2	6.1	5.2
2	5.3	5.2	5.2	5.4	6.2	5.2
3	5.3	5.1	5.0	5.5	6.1	5.2
4	5.4	5.2	5.3	5.3	6.2	5.3
5	5.1	5.4	5.5	5.4	6.4	5.5
Mean(sec)	5.3	5.2	5.1	5.3	6.2	5.2
Mean(rps)	1.9	2.0	2.0	1.9	1.7	2.0

Table 1 shows the transverse times for the robot using the straight-line path of 2 m in each of the six control modes. The analysis was recorded with the speed in revolutions per second (rps) being almost constant, but there is a negligible difference due to the latency of commands passed from the control end. Considering the results in which we have the lowest time taken method (using Laptop keys) and highest time taken method (using Voice), the analyzed difference between the timings is 1.07 (6.2 - 5.13). For this the number of commands required for controlling is one in all the above methods.

Table 2: Time taken by robot to cover Straight-right Path in all the methods

Trial No.	GUI (sec)	Mobile (sec)	Laptop keys (sec)	Joystick (sec)	Voice (sec)	IOT (sec)
1	8.4	8.2	8.2	8.4	9.2	8.5
2	8.6	8.5	8.5	8.6	9.5	8.5
3	8.7	8.2	8.6	8.7	9.2	9.0
4	9.0	8.5	8.2	9.1	9.5	8.5
5	8.8	8.4	8.2	8.9	9.4	8.9
Mean(sec)	8.7	8.3	8.2	8.7	9.3	8.9

Recordings that were noted in Table 2 shows the straight-right trajectory duration of robot with the help of six control methods. The distance travelled is 2.04 m in a straight line (forward) and 1.2 m in the right direction. Considering the results of lowest time taken method (Laptop keys) and highest time taken method (Voice) with the help of recordings, the difference between the timings is 1.12 (9.36 - 8.24). For this the number of commands used for controlling is three in all the above methods.

Table 3: Time taken by the robot to cover Straight-Left Path in all the methods

Trial No.	GUI (sec)	Mobile (sec)	Laptop keys (sec)	Joystick (sec)	Voice (sec)	IOT (sec)
1	9.4	8.6	9.0	9.4	10.2	9.5
2	9.5	8.7	8.9	9.5	10.4	9.3
3	9.5	8.2	9.1	9.5	10.3	9.4
4	9.0	8.7	9.2	9.0	10.2	9.5
5	9.5	8.5	9.0	9.5	10.1	9.4
Mean(sec)	9.3	8.5	9.0	9.3	10.2	9.4

In the scenario of the straight-left trajectory, the linear distance is 2 m and 1.2 m in a left direction and respective timings are recorded and they are shown in Table 3. In this scenario, the smartphone mode is the best in comparison to the other control modes by analysis. Considering the results of lowest time taken method (Mobile) and highest time taken method (Voice), the difference between the timings is 1.74 (10.24 - 8.5). Totally the number of commands used for controlling is three in all the methods.

Table 4: Time taken by the robot to cover 'U' turn Path in all the methods

Trail no	GUI (sec)	Mobile (sec)	Laptop keys (sec)	Joystick (sec)	Voice (sec)	IOT (sec)
1	13.4	14.8	13.3	13.2	15.8	13.2
2	13.3	14.9	13.3	13.4	15.9	13.3
3	13.0	14.9	13.3	13.3	15.9	13.4
4	13.4	14.4	13.4	13.1	15.4	13.4
5	13.3	14.6	13.4	13.2	15.6	14.0
Mean(sec)	13.2	14.7	13.3	13.3	15.7	13.4

Table 5: time taken by the robot to cover Rectangular Path in all the methods

Trial No.	GUI (sec)	Mobile (sec)	Laptop keys (sec)	Joystick (sec)	Voice (sec)	IOT (sec)
1	17.2	17.6	16.4	17.2	18.6	18.1
2	17.6	17.5	16.2	17.6	18.5	17.2
3	17.2	17.3	16.5	17.2	18.3	17.5
4	17.4	17.7	16.4	17.4	18.7	17.4
5	17.6	17.6	16.3	17.6	18.6	17.3
Mean(sec)	17.4	17.5	16.3	17.4	18.5	17.6

Table 4 gives the duration of the U-turn path covered by the robot. By the analysis, GUI mode provides the best timings compared to the other methods. The distance covered is 2 m linear up and down and breadth is 1.02 m. Considering the recordings, results of lowest time taken method (GUI) and highest time taken method (Voice), the difference between the timings is 2.76 (15.72 - 13.26). For this the number of commands used for controlling is five in all the above methods.

In the case of rectangular path, recordings of duration are shown in Table 5, With the analysis keyboard control shows better results in comparison to the other control modes. The results of lowest time taken method (Laptop keys) and highest time taken method (Voice) form the table V and the difference between the timings is 2.18 (18.54 - 16.36). For this the total number of commands used for controlling is seven in all the above methods.

### 8. Conclusion

From the results obtained from the experiments, we can observe that chosen 6 methods were equally efficient for simple paths. But, with the increase in complexity of the trajectory, the amount of control commands to be sent from user end also rises, which in turn increases the difference between time taken by the robot in different methods. So as this path complexity increases

Laptop keys and Joystick control methods turned out to be efficient methods to control the robot in less time compared to other methods. Limitation of our study is that all the experiments are carried out using a network of 2.4GHz band, where as an 5GHz band network can be used for fast communication and less time period for the paths. In future this research work can be extended by implementing with a greater number of methods with higher band for large scale robotic applications where time is a major constraint.

### Conflict of Interest

We, the authors of this paper hereby declare that we have no conflict of interest over the content presented in this paper.

### Acknowledgment

We sincerely thank Electronics and Communication Engineering department and Humanitarian Technology (HuT) labs of Amrita Viswa Vidhyapeetham, Amritapuri Campus for the persistent help and support in conducting this research.

### References

- [1] R. K. Megalingam, S. Tantravahi, H. S. S. Kumar, N. Thokala and H. S. Rahul, "Multimode Control of Wheeled Bot Using Python and Virtual Network Computing," *2018 4th International Conference on Computing Communication and Automation (ICCCA)*, Greater Noida, India, 2018, pp. 1-5. doi: 10.1109/CCAA.2018.8777597
- [2] Luis Fernando D Haro, Ricardo Cordoba, Jose Ignacio Rojo Rivero, Jorge Diez de la Fuente, Diego Avendano Peces, Jose Maria Bermudo Mera, "Low-Cost Speaker and Language Recognition Systems Running on a Raspberry Pi", *IEEE Latin America Transactions* Volume: 12 , Issue: 4 , June 2014
- [3] Kateryna Zinchenko, Chien-Yu Wu, Kai-Tai Song, "A Study on Speech Recognition Control for a Surgical Robot", *IEEE Transactions on Industrial Informatics*, Volume: 13, Issue: 2, April 2017
- [4] Ha-Young Ko, Jae-Hyeok Lee, Jong-Ok Kim, "Implementation and evaluation of fast mobile VNC systems", *IEEE Transactions on Consumer Electronics*, Volume: 58, Issue: 4, November 2012
- [5] G. O. E. Abdalla and T. Veeramanikandasamy, "Implementation of spy robot for a surveillance system using Internet protocol of Raspberry Pi," *2017 2nd IEEE International Conference on Recent Trends in Electronics, Information & Communication Technology (RTEICT)*, Bangalore, 2017, pp. 86-89. doi: 10.1109/RTEICT.2017.8256563
- [6] K. Krinkin, E. Stotskaya and Y. Stotskiy, "Design and implementation Raspberry Pi-based omni-wheel mobile robot," *2015 Artificial Intelligence and Natural Language and Information Extraction, Social Media and Web Search FRUCT Conference (AINL-ISMW-FRUCT)*, St. Petersburg, 2015, pp. 39-45. doi: 10.1109/AINL-ISMW-FRUCT.2015.7382967
- [7] J. D. Lee, Y. H. Wu, Y. J. Zhao, L. Y. Chen and H. I. Chen, "Development of mobile robot with vision inspection system and three-axis robot," *2018 3rd International Conference on Control and Robotics Engineering (ICCRE)*, Nagoya, 2018, pp. 6-10. doi: 10.1109/ICCRE.2018.8376424
- [8] Michael W. Condry, Catherine Blackadar Nelson, "Using Smart Edge IoT Devices for Safer, Rapid Response With Industry IoT Control Operations", *Proceedings of the IEEE* (Volume: 104, Issue: 5, May 2016
- [9] Sunil K. Agrawal, Xi Chen, Christina Ragonesi, James C. Galloway, "Training Toddlers Seated on Mobile Robots to Steer Using Force-Feedback Joystick", *IEEE Transactions on Haptics*, Volume: 5, Issue: 4, Fourth Quarter 2012
- [10] Zhongyuan Guo, Wenjing YANG, Minglong LI, Xiaodong YI, Zhongxuan CAI, Yanzhen WANG, "ALLIANCE-ROS: A Software Framework on ROS for Fault-Tolerant and Cooperative Mobile Robots", *Chinese Journal of Electronics*, Volume: 27, Issue: 3, 5 2018
- [11] Farrukh Shahzad, "Pymote 2.0: Development of an Interactive Python Framework for Wireless Network Simulations", *IEEE Internet of Things Journal*, Volume: 3, Issue: 6, Dec. 2016
- [12] Mark S. Hawley, Mark S. Hawley, Phil D. Green, Pam Enderby, Rebecca Palmer, Siddharth Sehgal, Peter O'Neill, "A Voice-Input Voice-Output Communication Aid for People With Severe Speech Impairment", *IEEE Transactions on Neural Systems and Rehabilitation Engineering*, Volume: 21, Issue: 1, Jan. 2013
- [13] M. Graciarena, H. Franco, K. Sonmez, H. Bratt, "Combining standard and throat microphones for robust speech recognition", *IEEE Signal Processing Letters*, Volume: 10, Issue: 3, March 2003
- [14] Doh-Suk Kim, Soo-Young Lee, R.M. Kil, "Auditory processing of speech signals for robust speech recognition in real-world noisy environments", *IEEE Transactions on Speech and Audio Processing*, Volume: 7, Issue: 1, Jan 1999
- [15] Rajesh Kannan Megalingam, Venkat Rangan, Sujin Krishnan, Athul Balan Edichery Alinkeezhil, "IR Sensor-Based Gesture Control Wheelchair for Stroke and SCI Patients", *IEEE Sensors Journal*, Volume: 16, Issue: 17, Sept.1, 2016
- [16] V. Gupta, N. Bendapudi, I. N. Kar and S. K. Saha, "Three-stage computed-torque controller for trajectory tracking in non-holonomic wheeled mobile robot," *2018 IEEE 15th International Workshop on Advanced Motion Control (AMC)*, Tokyo, 2018, pp. 144-149. doi: 10.1109/AMC.2019.8371077
- [17] A. Monteiro, M. de Oliveira, R. de Oliveira, T. da Silva, "Embedded application of convolutional neural networks on Raspberry Pi for SHM", *Electronics Letters*, Volume: 54, Issue: 11, 5 31 2018, 07 June 2018.
- [18] P.M. Corcoran, F. Papal, A. Zoldi, "User interface technologies for home appliances and networks", *IEEE Transactions on Consumer Electronics*, Volume: 44, Issue: 3, Aug 1998
- [19] Daniel Thommes, Ansgar Gerlicher, Qi Wang, Christos Grecos, "RemoteUI: A high-performance remote user interface system for mobile consumer electronic devices", *IEEE Transactions on Consumer Electronics*, Volume: 58, Issue: 3, August 2012
- [20] L. Labakhua, I. Martins and M. Igor, "Control of a mobile robot with Swedish wheels," *2017 IEEE International Conference on Power, Control, Signals and Instrumentation Engineering (ICPCSI)*, Chennai, 2017, pp. 267-272. doi: 10.1109/ICPCSI.2017.8392225
- [21] M. M. Ma, S. Li and X. J. Liu, "Tracking control and stabilization of wheeled mobile robots by nonlinear model predictive control," *Proceedings of the 31st Chinese Control Conference*, Hefei, 2012, pp. 4056-4061.
- [22] G. Mester, "Wireless sensor-based control of mobile robots' motion," *2009 7th International Symposium on Intelligent Systems and Informatics*, Subotica, 2009, pp. 81-84. doi: 10.1109/SISY.2009.5291190
- [23] C. P. Connette, C. Parlitz, M. Hagele and A. Verl, "Singularity avoidance for over-actuated, pseudo-omnidirectional, wheeled mobile robots," *2009 IEEE International Conference on Robotics and Automation*, Kobe, 2009, pp. 4124-4130. doi: 10.1109/ROBOT.2009.5152450
- [24] J. Yin, G. Yang, F. Zhao and H. Qiu, "Motion planning implemented in ROS for Omni-directional Wheeled Mobile Robot," *2015 IEEE International Conference on Information and Automation*, Lijiang, 2015, pp. 2695-2700. doi: 10.1109/ICInfA.2015.7279741
- [25] Rajesh Kannan Megalingam ; Vineetha Nandakumar ; A Athira ; G S Gopika ; Anjali Krishna "Orthotic arm control using EOG signals and GUI" *2016 International Conference on Robotics and Automation for Humanitarian Applications (RAHA)* Year: 2016 DOI: 10.1109/RAHA.2016.7931871
- [26] Rajesh Kannan Megalingam; Jeeba M. Varghese ; "Study and analysis of embedded system based indoor navigation on multiple platforms" *2016 International Conference on Communication and Signal Processing (ICCSP)* Year: 2016 DOI: 10.1109/ICCSP.2016.7754343

## Neural Network-based Efficient Measurement Method on Upside Down Orientation of a Digital Document

Yeji Shin, Youngone Cho, Hyun Wook Kang, Jin-Gu Kang, Jin-Woo Jung\*

Department of Computer Science and Engineering, Dongguk University, 04260, Seoul, Korea

### ARTICLE INFO

Article history:

Received: 15 January, 2020

Accepted: 24 March, 2020

Online: 20 April, 2020

Keywords:

Upside Down Detection

Optical Character Recognition,

Artificial Neural Network

Convolutional Neural Network

### ABSTRACT

As many digital documents are required in various environments, paper documents are digitized by scanner, fax, digital camera and specific software. In the case of a scanned document, we need to check whether the document is right sided or upside down because the orientation of the scanned document is determined by the orientation in which the paper document is placed. It is time-consuming for a person to check all the documents whether they are upside down. We propose an algorithm that can automatically determine upside down documents. The proposed artificial neural network-based method shows a high accuracy and efficiency in time for general documents. In addition, OCR-based method and CNN-based method were used to compare with the performance of the proposed method.

### 1. Introduction

Recently the use of digital documents has increased in various environments, such as the automation of business processes and factory system. The documents are digitized by scanner, fax, digital camera and specific software. The document may be scanned upside down because a person could put the paper in that way to the scanner without noticing it. If the scanned papers are in large quantity, there's no way to find out all the papers upside down other than doing it manually. In that case, we have to consume expensive time and cost for the checking process. Therefore, there are several studies to automatically determine the orientation of a digitized document without human checking when there is a large amount of non-digitized documents to be scanned.

The document orientation can be categorized into three categories [1]: landscape, portrait, and upside-down orientation. A few previous studies [1]-[5] have successfully developed some algorithms for determining document orientations from any angle. However, these studies have some limitation such that they cannot recognize the document orientation in special case of upside down [2, 3] or take high computational burden even though they can recognize the upside down [1, 4, 5]. The determination between landscape and portrait is usually done based on the skewed angle [2, 4]. Such studies based on the skewed angle may not determine between upside down and right sided when the orientation of the text inside the document is over 180 degrees. Thus, a different

approach is required to detect the orientation of documents that belong to these cases.

Some previous studies [4]-[9] shows efficient detection method for document orientation with English alphabet characters based on the ascender-descender (typography) ratio of text. Since the ascenders are usually more frequent than descenders, these methods rely on counting the numbers of ascenders and descenders in the text to make a decision on its orientation. Specifically, they extracted characters using OCR (Optical Character Recognition) engine and parsed the 'bbox value of the hOCR file with *Beautifulsoup*' [10]. And, they defined coordinate value information for each word obtained through the *bbox* tag of hOCR.

In OCR-based algorithm, Tesseract OCR [11] and *Beautifulsoup* [10] are usually used to determine whether the document is upside down or right sided through the coordinate value information of each word in hOCR.

In this paper, more efficient method is proposed to handle many documents immediately. For the small amounts of information for time efficiency and high recognition accuracy, structural information of the document and artificial neural network (ANN) [12] are used to determine between upside down and right sided without recognizing or analyzing characters.

Also, performance is verified by comparing between the proposed (ANN-based) method and the previous OCR-based method.

\*Corresponding Author: Jin-Woo Jung, Address, [jwjung@dongguk.edu](mailto:jwjung@dongguk.edu)



## 2. OCR (Optical Character Recognition)-based measurement method

Let us assume there are n-lines in an image and each line consists of k-words. The W of each word is defined as the summation of minimum and maximum coordinate values (min\_x, min\_y, max\_x, max\_y) for each word obtained through the bbox tag of hOCR. L<sub>j</sub> is defined as the summation of W<sub>i</sub> for every words in each line.

$$W_i = \min_x + \min_y + \max_x + \max_y \text{ for each word } i \dots\dots\dots (1)$$

$$L_j = W_1 + W_2 + \dots + W_k \text{ for each line } j \dots\dots\dots (2)$$

The document is determined as right sided if the value of L<sub>j</sub> increases, but upside down if it decreases. The following is the pseudo code for this the algorithm (Figure 1).

```

Input:
O ← Set of Wi of all words line by line
Output:
(true: right sided / false: Upside down) ← state

Initialization:
state ← false
increase ← 0
decrease ← 0

Begin
for i in len(lines) do
    sum ← O[i][1] + O[i][2] + O[i][3] + O[i][4]
    line_sum[i] ← sum

for i in len(line_sum) do
    if line_sum[i] <= line_sum[i+1] then
        increase ← increase + 1
    else
        decrease ← decrease + 1
    end if

if increase >= decrease then
    state ← true
end if

End
    
```

Figure 1. The pseudo code of OCR-based measurement algorithm

## 3. Artificial neural network (ANN)-based measurement method

### 3.1. Basic Idea

Many documents are written from left to right and top to bottom direction although titles, pictures, charts and so on may make exceptions. When the document can be separated as areas as shown in Figure 2, the ratio of the upper half non-background area to the lower half non-background area (defined as Top-to-bottom ratio), and the ratio of the left half non-background area to the right half

non-background area (defined as Left-to-right ratio) may be able to distinguish whether the document is upside down or right sided. Actually, the Top-to-bottom ratio and the Left-to-right ratio of three different types of documents are calculated as shown in Table 1. And for these documents (not for all documents), when Top-to-bottom ratio is greater than 1 or the Left-to-right ratio is greater than 1, we can see that the orientation is right sided.

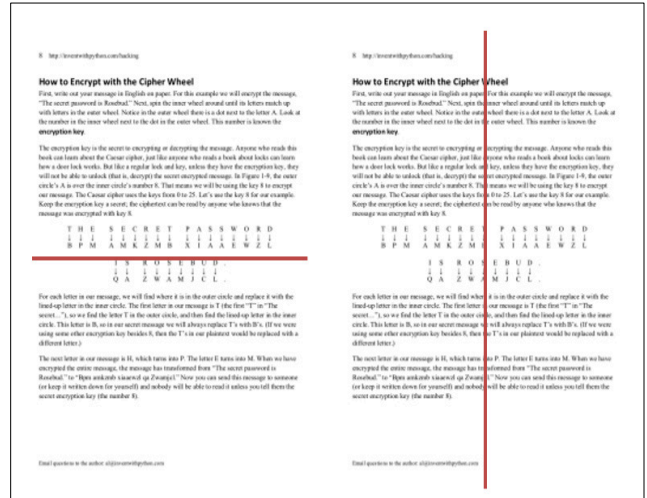


Figure 2. Sketch of basic idea

Table 1. Top-to-bottom ratios and Left-to-right ratios of three document samples

Document	State	Top-to-bottom ratio	Left-to-right ratio
Doc. 1	right sided	9.282392	7.849178
	upside down	0.107731	0.127402
Doc. 2	right sided	3.941437	1.16777
	upside down	0.253715	0.856333
Doc. 3	right sided	1.253945	1.446367
	upside down	0.797483	0.691387

However, experiments with 50 more documents with 10 different types have shown that if Top-to-bottom ratio and the Left-to-right ratio are less than 2, the distribution was scattered and not linearly separable as shown in Figure 3. So we have designed an algorithm based on ANN that can effectively and efficiently distinguish the upside down documents as shown in Section 3.2.

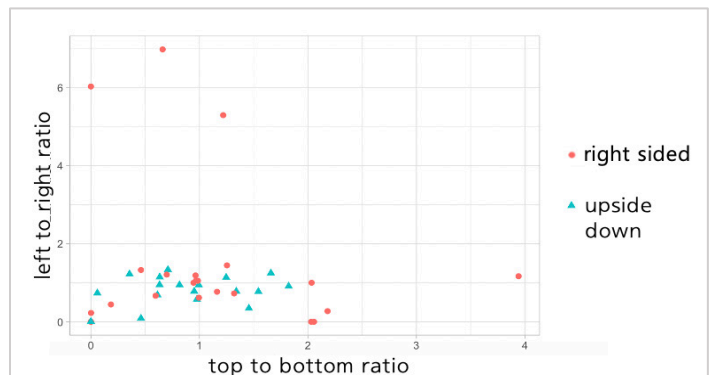


Figure 3. Feature plot for upside down and right sided state

3.2. Proposed algorithm

Artificial neural network (ANN)-based measurement method, it calculates the ratio of the upper half non-background area and the lower half non-background area. Similarly, it also calculates the ratio of the left half non-background area and the right half non-background area. These are used as feature values for training ANN to classify the upside down or not. And the recognition process of ANN gives the status of upside down automatically.

3.2.1 Feature extraction

We assumed that the characters are black and the algorithm for feature extraction is as follows:

Step1. Read the RGB color values of pixels from a scanned BMP image file for the given digital document.

Step2. Transform to the grayscale image and do thresholding with the threshold value, 33.

Step3. Calculate the number of black pixels at the upper half non-background area and the number of black pixels at the lower half non-background area. Subsequently, divide the number of black pixels in the top part by the number of black pixels in the bottom part like the below Eq. (3)

$$\text{Top-to-bottom ratio} = \frac{\text{Number of black pixels at the top}}{\text{Number of black pixels at the bottom}} \dots\dots\dots (3)$$

Step4. Calculate the number of black pixels on the left half non-background area to the number of black pixels on the right half non-background area. Thereafter, the number of black pixels on the left is divided by the number of black pixels on the right like this Eq. (4)

$$\text{Left-to-right ratio} = \frac{\text{Number of black pixels on the left}}{\text{Number of black pixels on the Right}} \dots\dots\dots (4)$$

Step5. Extract the input feature data for artificial neural network with the form of vector ('Top-to-bottom ratio', 'Left-to-right ratio', {'right sided' / 'upside down'})<sup>T</sup>.

3.2.2 Artificial neural network (ANN)

We have got the datasets of Top-to-bottom ratios and Left-to-right ratios from the section 3.2.1. To find appropriate structure of ANN, we tried 9 different structures by varying the number of hidden layers with 1, 2, 3 layers and the number of hidden nodes with 1, 3, 5 nodes as shown in table 2. By the results in Table 2, we decided the structure of ANN. The number of hidden layers is 1 and the number of hidden nodes are 5, whose structure shows the lowest error rate.

Table 2. Error rates of various ANN structures

#of hidden layers \ # of hidden nodes	1 layer	2 layers	3 layers
1 node	8.00	5.91	5.73
3 nodes	6.22	5.41	5.58
5 nodes	4.73	4.99	4.73

The artificial neural network system consisting of one hidden layer with five nodes calculates as in Figure 4.

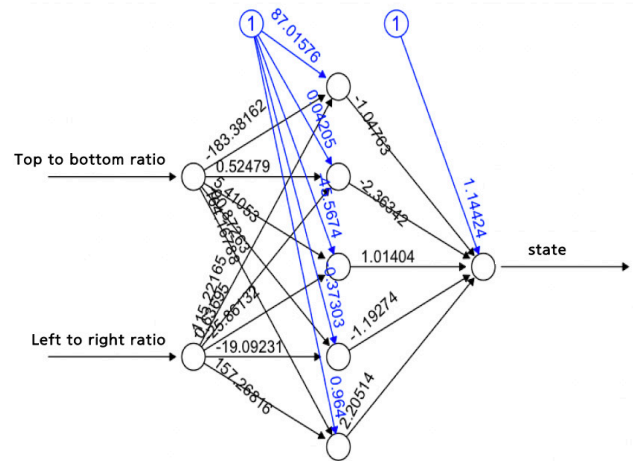


Figure 4. Proposed ANN Structure

Figure 5 shows the *min\_thresh* value of *neuralnet* function in R neuralnet library [13] according to the number of iterations to show the convergence of learning error. During the initial period up to 7,000 iterations, the *min\_thresh* value decreases rapidly but the value becomes almost constant from 30,000 iterations.

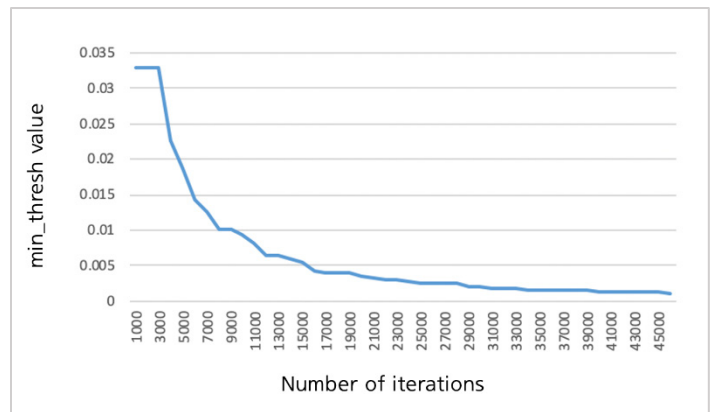


Figure 5. Error plot of ANN

The final decision can be derived by applying the input feature data to the trained artificial neural network. The trained ANN will decide whether the given document is right sided or upside down. The following Figure 6 explains the pseudo code of the trained ANN-based measurement method.

4. Convolutional neural network (CNN)-based measurement method

To extract the pattern information of pixels that are laid out in the document, we have used convolutional neural network (CNN) because it has shown a high performance in understanding images [14, 15]. The used CNN model in this paper has four hidden layers with different number of nodes for each corresponding layer as shown in Table 3 which showed superior results compared to other models. Activation function and 2D max\_pooling is applied followed by the first hidden layer. Then the output nodes of first hidden layer are fed into the second hidden layer. After applying

activation function and 2D max\_pooling, the output is flattened and an activation function is applied for linear operation. Then in the third hidden layer, drop\_out is done to avoid overfitting and to get rid of 30 % of the total number of nodes for generalization. After that, the last hidden layer with 1026 nodes are fed forward to the output layer.

**Input :**

TB ← Top-to-bottom Ratio

LR ← Left-to-right Ratio

**Output :**

(true: right sided / false: Upside down) ← Result

**Begin**

```

a ← sigmoid(87.01576 - 183.38162*TB - 115.22165*LR)
b ← sigmoid(0.04204546 + 0.52479163*TB + 0.63695455*LR)
c ← sigmoid(-45.567399 + 5.410532*TB - 25.861325*LR)
d ← sigmoid(-0.3730291 - 90.8726276*TB - 19.0923138*LR)
e ← sigmoid(0.9640014 + 164.1678818*TB + 157.2681645*LR)
    
```

```

state ← (1.144237 - 1.047632*a - 2.363419*b
        + 1.014042*c - 1.192740*d + 2.205141*e)
    
```

```

if state > 1.4 then
    Result ← true
else
    Result ← false
end if
    
```

**End**

Figure 6. The pseudo code of the trained ANN-based measurement Algorithm

Table 3. Used CNN structure

Layer Type	Output Shape	# of Params
conv2d_1 (Conv2D)	(None, 60, 60, 32)	832
activation_1 (Activation)	(None, 60, 60, 32)	0
max_pooling2d_1 (MaxPooling2)	(None, 30, 30, 32)	0
conv2d_2 (Conv2D)	(None, 30, 30, 64)	51264
activation_2 (Activation)	(None, 30, 30, 64)	0
max_pooling2d_2 (MaxPooling2)	(None, 15, 15, 64)	0
flatten_1 (Flatten)	(None, 14400)	0
activation_3 (Activation)	(None, 14400)	0
dense_1 (Dense)	(None, 512)	7373312
dropout_1 (Dropout)	(None, 512)	0
activation_4 (Activation)	(None, 512)	0
dense_2 (Dense)	(None, 2)	1026
activation_5 (Activation)	(None, 2)	0

For CNN training process, *adam* is used for the optimizer which is known to give better results compared to SGD (stochastic gradient descent) optimizer [16]. The error rates are measured with categorical cross entropy and the results are shown as in Figure 7. As for Figure 7, the error rate decreases as the training progresses along with the number of epochs.

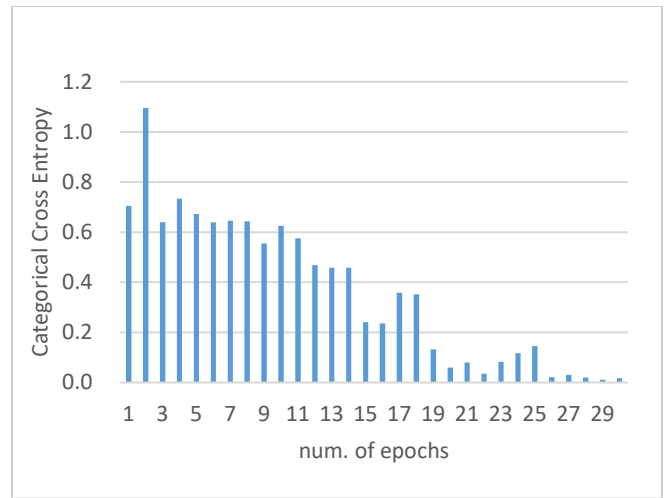


Figure 7. Categorical Cross Entropy per number of epochs in the trained CNN

**5. Experimental Results and Analysis**

*5.1. Experimental Setup*




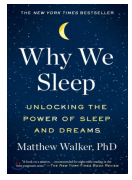
There are many types of documents and we have categorized into 4 groups such as general document, picture-oriented document, free style document and miscellaneous. The general document is a formal document composed of almost all characters. Almost all previous researches [1]-[8] were done with this kind of documents. The picture-oriented document such as the fairy tale book contains not only characters but also some pictures in many pages. The free style document and miscellaneous have no formats or styles. Table 4 shows 4 categories and 10 types of documents in each category.

Table 4. 4 categories and 10 types of documents

Category	No.	Document Type
General document	1	Culture book
	2	Technical book
	3	Paper
Picture-oriented document	4	Document consisting of more than half of pictures
	5	Fairy tale book
Free style document	6	Magazine
	7	Leaflet
Miscellaneous	8	Comic book
	9	Tabular document
	10	Book cover

The general document and picture-oriented document have a basic format and a certain number of characters. Others are free in their character size, deployment of characters and the number of words in a document. Table 5 shows some examples of 10 types of documents.

Table 5. Examples of each document type

		
1 Culture book	2 Technical book	3 Paper
		
4 Picture book	5 Fairy tale book	6 Magazine
		
7 Leaflet	8 Comic book	9 Tabular doc.
		
10 Book cover		

A total of 50 documents were used as training data. It is composed of 5 documents for each document type. 25 of the training data were right sided and the others were upside down. The documents are written in Korean or English. For the test, 100 documents were used as 10 images for each type of document. And 50 of the test data were right sided and the others were upside down.

We have implemented both OCR-based algorithm (See Figure 1) and ANN-based algorithm (See Figure 6) for whole documents. We have analyzed them with each category data and compared the ANN-based result with OCR-based result in each category. In addition, we have also implemented CNN-based algorithm (See Table 3) for the comparison with the ANN-based algorithm. To deal with various image size especially for the CNN-based algorithm, all input document images are converted to 64 \* 64 pixels. And the three-dimensional RGB array of the input image is converted into one dimensional array using gamma compression [17] giving weights according to the relative luminance of each pixel value. In addition, the time measured for the CNN-based algorithm is the elapsed time of the program including the time required for reading images but the training time.

### 5.2. Experimental Results

Experimental results of the general document are shown in Table 6 and the results of the picture-oriented document are in Table 7.

Table 6. Result of Category 1(General document)

Document type	OCR-based method		ANN-based method		CNN-based method	
	Accuracy	Average Time (s)	Accuracy	Average Time (s)	Accuracy	Average Time (s)
1	90%	2.580	90%	0.118	80%	1.049
2	80%	3.889	90%	0.071	90%	0.349
3	100%	4.700	90%	0.046	80%	0.368
All	90%	3.723	90%	0.078	83%	0.589

Table 7. Result of Category 2(Picture-oriented document)

Document type	OCR-based method		ANN-based method		CNN-based method	
	Accuracy	Average Time (s)	Accuracy	Average Time (s)	Accuracy	Average Time (s)
4	90%	1.773	70%	0.050	50%	0.992
5	70%	2.140	80%	0.190	70%	1.883
All	80%	1.957	75%	0.120	60%	1.438

Table 8. Result of Category 3(Free style document)

Document type	OCR-based method		ANN-based method		CNN-based method	
	Accuracy	Average Time (s)	Accuracy	Average Time (s)	Accuracy	Average Time (s)
6	100%	3.480	40%	0.042	70%	0.430
7	70%	1.724	40%	0.033	90%	0.391
All	85%	2.602	40%	0.038	80%	0.411

Table 9. Result of Category 4(Miscellaneous document)

Document type	OCR-based method		ANN-based method		CNN-based method	
	Accuracy	Average Time (s)	Accuracy	Average Time (s)	Accuracy	Average Time (s)
8	90%	0.784	40%	0.030	40%	1.063
9	90%	2.209	50%	0.030	60%	0.758
10	100%	0.794	60%	0.026	50%	0.562
All	93.3%	1.247	50%	0.029	50%	0.794

### 5.3. Discussion

In general documents (category 1 in Table 6) such as cultural books, technical books, and papers, both OCR-based algorithm and ANN-based algorithm have similar high accuracy in Table 6. But ANN-based algorithm shows tremendous time reduction. The ANN-based algorithm we proposed will have a high efficiency for checking a large number of documents automatically.



In picture-oriented documents (category 2 in Table 7) such as picture books and fairy tale books, OCR-based algorithm is a little better than ANN-based algorithm in accuracy (See Table 7). But the result is also seen that the time in ANN-based algorithm is shortened. This may be occurred by the reason that the result depends on our small number of experimental documents and it could be improved if we apply our algorithm with much more data. The thresholding method we used to be based on the fixed value. If the thresholding value can be adaptively changed as the given input image, then the performance could be enhanced.

In free style documents and miscellaneous documents (category 3 and 4 in Table 4) such as magazines, leaflets, comic books, tabular documents and book covers, OCR-based algorithm is better than ANN-based algorithm in accuracy (See Table 8 and 9). This may be occurred by the reason that there is a no formal document structure in the document type 6, 7, 8, 9. And, in case of book cover, there are more non-black characters than black characters. If the system can recognize all colors of characters exactly in high speed, then the performance could be enhanced.

The performance of ANN-based algorithm was also compared with that of CNN-based algorithm. Basically, the performance of CNN-based algorithm has less accuracy than ANN-based algorithm (See Table 6 and 7). This is based on the reason that the number of training data is limited to 50 documents for the comparison with other algorithms, and the image was resized into 64\*64 pixels by the complex structure of the CNN-based algorithm and as a result, the character was very distorted and became small. In the case of category 3 (See Table 8), CNN-based algorithm has better accuracy than ANN-based algorithm. It may be from the reason that many of the documents in category 3 include more non-black characters than black characters.

## 6. Conclusion

As a result, OCR-based algorithm shows high accuracy by the power of character recognition, but it takes more time because all words should be recognized in advance. CNN-based algorithm shows very limited power especially for the document type 2 and 7 due to the limited number of training data and resized image.

In contrast, ANN-based algorithm calculates two feature values derived from the document structure and can determine the orientation of the document immediately. ANN-based algorithm can greatly reduce the time using small information and can obtain high accuracy using the power of artificial neural network.

Additionally, we have conducted the experiments on the relatively free form of documents such as leaflets and magazines (category 3), comic books, tabular documents, and book covers (category 4). ANN-based algorithm determines the document structure immediately but the accuracy was significantly lower for these special cases.

## Conflict of Interest

The authors declare no conflict of interest.

## Acknowledgment

This research was partially supported by the MIST (Ministry of Science and ICT), Korea, under the national program for

excellence in SW supervised by the IITP (Institute for Information & Communications Technology Promotion) (2016-0-00017), partially supported by the KIAT(Korea Institute for Advancement of Technology) grant funded by the Korea Government(MOTIE : Ministry of Trade Industry and Energy) (No. N0001884, HRD program for Embedded Software R&D) and partially supported by the KIAT(Korea Institute for Advancement of Technology) grant funded by the Korea Government (MSS : Ministry of SMEs and Startups). (No. S2755615, HRD program for Enterprise linkages R&D).

## References

- [1] S. Lu, C. L. Tan, "Automatic document orientation detection and categorization through document vectorization" in Proceedings of the 14<sup>th</sup> ACM international conference on Multimedia, Santa Barbara, CA, USA, 2006. <http://doi.org/10.1145/1180639.1180673>
- [2] F. Hones, J. Lichter, "Layout extraction of mixed mode documents" Mach. Vision Appl., 7, 237-246, 1994.
- [3] M. Ali, "An object/segment oriented skew-correction technique for document images" in Proceedings of the 4<sup>th</sup> International Conference on Document Analysis Recognition, Ulm, Germany, 1997. <https://ieeexplore.ieee.org/document/620591/>
- [4] A. Hrishikesh, "A generic method for determining up/down orientation of text in roman and non-roman scripts" Pattern Recognition, 38(11), 2114-2131, 2005. <https://doi.org/10.1016/j.patcog.2004.12.011>
- [5] S. J. Lu, J. Wang, C. L. Tan, "Fast and accurate detection of document skew and orientation" in Proceedings of the International Conference on Document Analysis and Recognition, Vol.2, 684-688, 2007. <https://doi.org/10.1109/ICDAR.2007.4377002>
- [6] R. S. Caprari, "Algorithm for text page up/down orientation determination" Pattern Recognition Letters, 21, 311-317, 2000. [https://doi.org/10.1016/S0167-8655\(99\)00161-0](https://doi.org/10.1016/S0167-8655(99)00161-0)
- [7] B. T. Avila, R. D. Lins, "A fast orientation and skew detection algorithm for monochromatic document images" in Proceedings of the ACM symposium on Document engineering, 118-126, 2005. <https://doi.org/10.1145/1096601.1096631>
- [8] J. V. Beusekom, F. Shafait, T. M. Breuel, "Resolution independent skew and orientation detection for document images" in Proceedings of the SPIE Electronic Imaging: Document Recognition and Retrieval, Vol.7247, 72470K-72470K, 2009. <https://doi.org/10.1117/12.807735>
- [9] M. Kim, S. Yim, Y. Lee, M. Kim, J.-W. Jung, "A study on automated checking for upside down printed materials based on Optical Character Recognition" in Proceedings of the 2018 International Conference on Fuzzy Theory and Its Applications (iFUZZY), 2018. <https://doi.org/10.1109/iFUZZY.2018.8751690>
- [10] L. Richardson, Beautiful Soup Documentation, Crummy. <https://www.crummy.com/software/BeautifulSoup/bs3/documentation.html>
- [11] R. Smith, "An overview of the Tesseract OCR engine" in Proceedings of the IEEE 9<sup>th</sup> International Conference on Document Analysis and Recognition (ICDAR 2007), Vol. 2, 2007. <https://doi.org/10.1109/ICDAR.2007.4376991>
- [12] M. T. Hagan, H. B. Demuth, M. Beale, Neural Network Design, Boston Pws, 1996.
- [13] R Documentation. <https://www.rdocumentation.org/packages/neuralnet/versions/1.44.2/topics/neuralnet>
- [14] M. F. Aydogdu, M. F. Demirci, "Age Classification Using an Optimized CNN Architecture" in Proceedings of the International Conference on Compute and Data Analysis, Lakeland, FL, USA, 2017. <https://doi.org/10.1145/3093241.3093277>
- [15] M. A. Shibli, P. Marques, E. Spiridon, "Artificial Intelligent Drone-Based Encrypted Machine Learning of Image Extraction Using Pretrained Convolutional Neural Network (CNN)" in Proceedings of the 2018 International Conference on Artificial Intelligence and Virtual Reality, Nagoya, Japan, 2018. <https://doi.org/10.1145/3293663.3297155>
- [16] D. P. Kingma, J. Ba, "Adam: A Method for Stochastic Optimization" in Proceedings of the 3<sup>rd</sup> International Conference for Learning Representations, San Diego, 2015.
- [17] ITU-R, Studio encoding parameters of digital television for standard 4:3 and wide-screen 16:9 aspect ratios. [https://www.itu.int/dms\\_pubrec/itu-r/rec/bt/R-REC-BT.601-7-201103-I!!PDF-E.pdf](https://www.itu.int/dms_pubrec/itu-r/rec/bt/R-REC-BT.601-7-201103-I!!PDF-E.pdf)

## Evaluation of Mini-Hydro Power for Off Grid Electrification in Rural/Isolated Areas in Africa

Ogbuefi Uche Chinweoke<sup>1</sup>, Ene Princewill Chigozie<sup>\*2</sup>, Kenneth Chijioke Chike<sup>3</sup>

<sup>1</sup>Africa Centre of Excellence (ACE-SPED), University of Nigeria Nsukka, Enugu State, Nigeria

<sup>2</sup>Department of Electrical and Electronic Engineering, Enugu State University of Science and Technology (ESUT), Enugu State, Nigeria

<sup>3</sup>Department of Electrical Engineering, University of Nigeria, Nsukka, Enugu State, Nigeria

### ARTICLE INFO

Article history:

Received: 13 December, 2019

Accepted: 04 April, 2020

Online: 20 April, 2020

Keywords:

Mini-Hydro Power

Rural/Isolated dwellers

Output power

Small Hydro Power

Renewable energy resources

### ABSTRACT

Rural electrification and sustainable energy services to the less privileged is a major challenge faced in Nigeria. Off-grid power generation via small hydropower plant would mitigate this challenge. This Paper discusses the awareness and assessment of small hydro power for off-grid electrification in rural/isolated areas in Nigeria. In this research, the method of onsite data collection and evaluation was used. Data was measured and collected at water fall of 21 meters high. The velocity of the water and flow rate were measured and calculated respectively. From the onsite analysis carried out for a one-year period, the result shows output power generated in each month. The analytical observation revealed that the output power generated in the rainy season was higher than that of dry season. The data were compiled and plotted using Excel spreadsheet. The output power generated from the rainy season in Nigeria is higher than that of dry season. August has the highest output power (110.728867 kW), while December has the least output power (101.125352 kW). From the output power gotten we can term it a micro hydropower plant. With this each of the monthly generated power can serve 5 villages in rural/isolated areas with average connection of 200houses, assuming 100W compact power supply to each house hold. Nigeria as a developing country will gain a lot from Small Hydro Power (SHP) and it has minimal environmental hazard.

## 1. Introduction

Access to electrical energy is an essential enabler for economic and social economic development of any nation [1]. International Energy Agency (IEA) indicated that 95% of population without access to electricity are located either in sub-Saharan African or developing Asia and 84% are in rural areas making these locations stagnant and backward from developed world [2]. Taking a closer look at Small Hydro Power (SHP) system is one of the renewable energy technologies for generating electricity and mechanical power. The current technology of harnessing SHP uses potential energy in water as a result of presence of head in the river to drive the water turbine. SHP can be classified into pico, micro, mini and small systems, most first world counties rate is classes as follows; pico as a system that generate less than 10kW, micro has capacity of more than 10kW but less than 100kW, mini system has an installed capacity within the range of 100kW but less than 1MW and small systems between the range of 1MW but less than 10MW [3]. SHP is a

very robust issue than Photovoltaic system. SHP installed systems are placed to support diverse electrical needs ranging from institutional, community and even serving rural communities. SHP possess different benefits such it is environmentally friendly, it can fast track the provision of adequate, reliable, affordable and sustainable power to rural areas for socioeconomic growth. [4]. The levelized cost of Electricity (LCOE) of hydro \$0.057. Although the initial cost of setting up a hydro station is huge the running cost is very low [5]. Small hydro power (SHP) generation system is among a viable renewable energy technology and its suitable for rural electrification in Nigeria because majority of these isolated environments have rivers, streams and run-off waters which have potential to generate hydroelectric energy [6]. Development of energy from small, mini and micro hydropower projects are being encouraged worldwide because of its relative advantage as compared to other means of energy sources. The Hydropower is 29% as compared to petroleum which is 60%, natural gas is 9%, and coal is 2%. Figure 1 shows a pictorial view of them. They are safe and clean

\*Corresponding Author: Ene Princewill Chigozie, [eneh.princewill@esut.edu.ng](mailto:eneh.princewill@esut.edu.ng)

renewable source of energy also not expensive in terms of running cost [7].

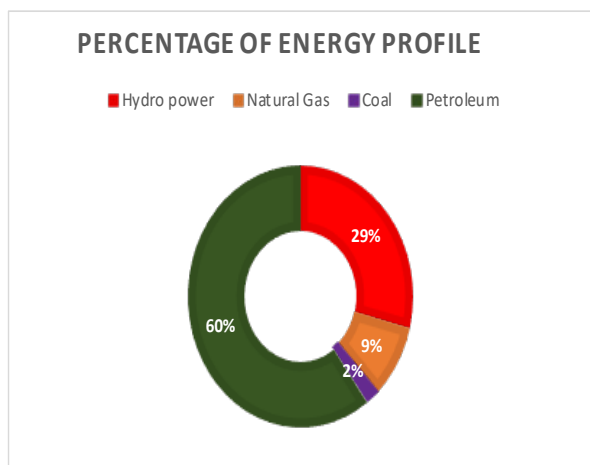


Figure 1: Profile for energy (in percentage)

Nigeria as a country is faced with an epileptic electrical energy supply. The country has numerous natural resources for generation of electrical energy to all its citizen such as the conventional fossil fuels of crude oil, tar sands, natural gas, coal as well as numerous renewable resources but still suffer from dwindling/unreliable energy supply with high tariffs rate paid by consumers of electricity, numerous grid collapse year in year out [8]. The world economic forum report 2020 revealed that high pollutant emission and its effect on climate is a major issue in the world [8, 9]. In order to tackle this backdrop the paper wishes to look at the possible solution to electrification problem in a selected community through small hydro power (SHP).

## 2. Energy Statistical Survey

### 2.1. Enugu Precipitation Rate

The zone has a tropical climate. In Enugu, the average annual temperature is 26.3°C in a year, the average rainfall is 1730mm (9). Table 1 shows the historical weather data for Enugu while Figure 2 shows a bar chart representation.

Table 1. Historical weather data for Enugu

Month	Average Temp. ( °C)	Precipitation rate(mm)
January	26.8	13
February	27.7	20
March	28.4	76
April	27.9	137
May	26.8	224
June	25.3	241
July	24.8	246
August	24	220
September	25.3	298
October	25.8	216
November	26.8	30
December	26.4	9

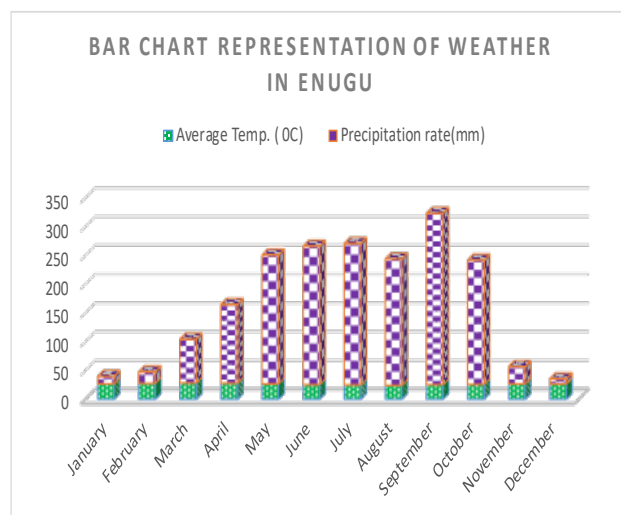


Figure 2. Bar chart representation

There exists a difference of 289mm of precipitation between the driest and wettest months with temperature variation of 4.4°C throughout the year [9].

### 2.2. Hydroelectric Power Distribution

As the world attempts to stall climate change by cutting emissions and dependence on fossil fuels, energy from renewable sources has become an integral part of global strategies. Table 2 shows different countries and hydroelectricity power generation. But hydroelectric power, despite being an important energy source in many nations around the world, is often overlooked. Figure 3 shows 2012 data taken from the US Energy Information Administration (EIA), which provides independent national and international energy statistics [10]

Table 2: Independent national and international energy statistics

Country	Billion kwh
China	856.35
Brazil	411.19
Canada	376.71
United States	276.24
Russia	164.42
Norway	140.47
India	124.57
Venezuela	81.19
Sweden	78.14
Japan	74.73

[10]

### 2.3. Economics of SHP

The major advantage of hydroelectricity is elimination of fuel cost. The cost of operating a hydroelectric plant is nearly immune to increases in the cost of fossil fuels such as oil, natural gas or coal, and no imports are needed, hence it is rarely affected by global economic and political changes. It is also worthy of note that hydroelectric plants also tend to have longer economic

lives than fossil-fuel-fired plants. Operating/labor costs are also usually low, as plants are automated and have few personnel on site during normal operation.

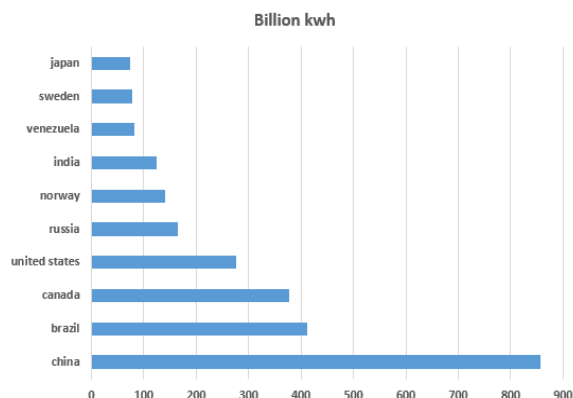


Figure 3: Energy statistic

It is also a fact that small hydro units in the range of 1MW to 30MW are often available from multiple manufacturers and that using standard “water to wire” packages, a single contractor can provide all the generator, ancillary switchgears, selecting from several standard designs to fit the site conditions [11].

#### 2.4. Small Hydropower Overview potential in Nigeria

Recent studies show that hydropower potential sites are distributed in 12 states and in the river basin. However, SHP potential sites exist in virtually all parts of Nigeria [3]. There are over 278 unexploited sites with total potentials of 734.3 MW. About eight small hydropower stations with aggregate capacity of 37.0MW has been installed in Nigeria by private companies and the government as shown in Table 3. Some around Jos Plateau, where there is 2MW station at Kwall fall on N’Gell river (river Kaduna) and 8MW station at Kurra fall, which was developed by a private company (NESCO) more than 75 years ago [3].

Table 3: Small hydropower stations installed in Nigeria by private companies and government [3]

S/n	River	State	Installed Capacity(MW)
1	Bagel(I) (II)	Plateau	1.0 , 2.0
2	Kurra	Plateau	8.0
3	Lere(I) (II)	Plateau	4.0, 4.0
4	Bakalor (I)	Sokoto	3.0
5	*Tiga	Kano	6.0
6	*Oyan	Ogun	9.9

There is varying information on the potential of small hydropower in Nigeria. According to UNIDO regional Centre on small Hydropower, the gross small hydropower potential (for plants up to 10MW) is 720 MW, the technical feasible potential is 605 MW and the economically feasible potential is 498.4MW. A study from 2006 identified 278 yet underdeveloped sites for small hydropower production with a total of 734.2MW (with a capacity of up to 30MW). Table 4 summarize the identified small hydro power potentials in Nigeria [3].

Table 4: Some feasible small hydro power in Nigeria [3]

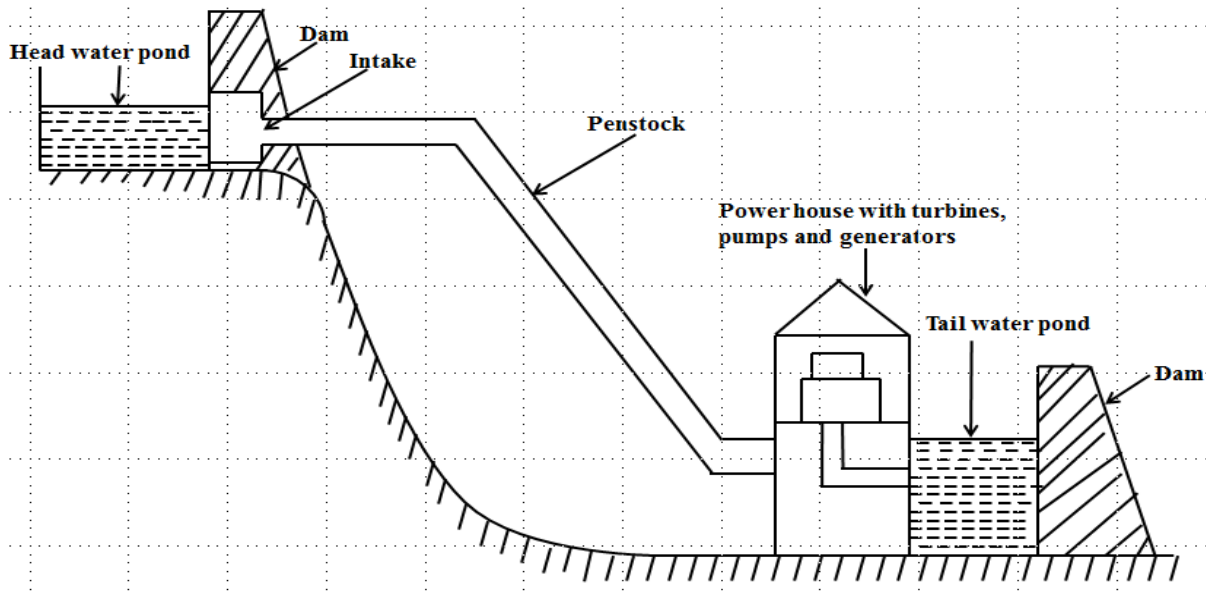
S/N	State	River basin	Places	Total (MW)
1	Sokoto	Sokoto-Rima	22	30.6
2	Katsina	Sokoto-Rima	11	8
3	Niger	Niger	30	117.6
4	Kaduna	Niger	19	59.2
5	Kwara	Niger	12	38.8
6	Kano	Hadejia-jamaare	28	46.2
7	Borno	Chad	28	20.8
8	Bauchi	Upper Benue	20	46.6
9	Gongol	Upper Benue	38	162.7
10	Plateau	Lower Benue	32	110.4
11	Benue	Lower Benue	19	69.2
12	Rivers	Cross River	18	258.1
Total			277	734.2

Nigeria as of today generates less than 4GMW of electricity but has the capability of increasing her generation through small hydropower (SHP) considering unharnessed potentials in the country as discussed in [11]. In other to increase the percentage contribution of hydroelectricity to the total energy mix and to extend electricity to rural and remote areas, we need to consider the economic, social and environmental benefits. Interpreted in [12], most of countries have access to large amounts of water through rivers and canal. With this hydro energy sources, electricity can be generated without polluting the environment. Electricity demand is on the everyday increase; it is therefore paramount to estimate the future potential of hydro power in Nigeria. Construe in [13], hydropower that is large and small, remains by far the most important of the “renewable energy” for electrical power production worldwide providing 19% of the planets electricity. Small-scale hydro is in mostly “run-of-river”, with no dam or water storage, and is one of the most cost-effective and environmentally benign energy technologies to be considered for rural electrification in less developed countries [14]. For development of such small hydro-power plants, simple and generally applicable procedures and methods for the design are lacking. The interest in small hydro-power resources is increasing but few published guidelines for project design. [14] outlined the merits of hydropower over fossil fuels, operating and maintenance costs are in favor of SHP development in Nigeria, being the lowest when compared with the situation in European countries. Challenges in locating a good site for the project which is essential to the success of the scheme with respect to sufficient flow rate and good head of water narrated in [3]. It should be known that flow rate is very essential for hydropower generation since the head at a proposed site is practically constant while the available flow is highly variable depending on the season (rainy or dry). The sole aim of this project is to check the potential energy that can be generated from SHP in Eziagu Water fall in Enugu State, Nigeria.

### 3. Proposed Scheme

In order to harness energy from the waterfall, certain design and





Parameters must be put in place to obtain a good result. A schematic diagram of small hydro power plant is depicted in Figure 4.

Figure 4 shows the Components of the SHP technology which include: head water pond, dam, intake, head race, penstock, and water turbine and generator: considering a modular design for low water flow and short descent, the under listed materials are to be used: *Generator*: For this design, a low speed and large diameter generator will be employed. *Turbine*: Kaplan turbine head ranging from 0 – 70m was employed. *Penstock*: Polyethylene (PE) or welded steel pipe of diameter of 1500mm was employed. *Generator speed governor*: Since Kaplan turbine is an axial-flow rotor with variable-pitch blade for variable load operation, speed governor is necessary for speed regulation of the generator to meet the load variation. Civil work for dam construction and power house is also a major phase of the SHP design that cannot be overlooked.

### 3.1. Ezeagu waterfall

Ezeagu is situated in south eastern part of Nigeria. The area possess much waterfalls, springs, streams, lakes and rivers within this Areas, but not all of them are suitable to set up a micro-hydro power station [15]. Ezeagu is located an hour thirty minutes’ drive from state capital Enugu. The waterfall rushes down the cliff with a thunderous sound that can be heard from a distance [15].

## 4. Materials and Method

One important hurdle to overcome for the successful analysis to be conducted is data collection. The data was collected from the site over a period of one year covering the two major seasons in Nigeria. The Ezeagu water fall has a measured head of water of 21m. Making use of a reference distance of 21m, the parameters were calculated as in

designed parameters. Figure 5 shows a pictorial view of the reference distance been measured whereas Figure 6 shows the site of the water fall. The average time for the month of June is calculated to be 3.047 seconds while the average time for the month of July was calculated to be 2.99seconds. Using this two parameters, Velocity was calculated. For June, Velocity was  $6.89 \text{ ms}^{-1}$ , and that of July  $7.02 \text{ ms}^{-1}$ .



Figure 5. Measurement of distance with measuring tape



Figure 6. Flowing water from the fall at Ezeagu

4.1. Design Parameters

To get the actual power that will be harvested from the assessment of this small hydro power, the following parameters are used; power output equations, overall efficiency, area, acceleration rate. They are defined and calculated as follows:

The Output Power equation for Hydro Power Plant is:

$$P_{out} = P_{gross} \times \eta \tag{1}$$

But  $\eta$  is the overall efficiency of the Hydro Power Scheme

$$P_{gross} = gHQ \tag{2}$$

Putting equation (2) into equation (1), we have:

$$P_{out} = gHQ \eta \tag{3}$$

$$\text{But } \eta = \eta_T \eta_G \tag{4}$$

Where:

$\eta_T$  is the efficiency of the turbine;  $\eta_G$  is the generator efficiency. Putting (4) into (3), we obtain:

$$P_{out} = gHQ \eta_T \eta_G \tag{5}$$

Where:  $g$  = Acceleration of free flow in  $m/s^2$ ;

$H$  = Gross Head in meters,  $Q$  = Design flow in  $m^3/s$ ,

$\eta_T$  = Efficiency of the turbine,  $\eta_G$  = Efficiency of the generator,  $P_{out}$  = Output Power in KW, and

$P_{gross}$  = Gross Power in KW.

Alternatively, flow rate,  $Q$ , can be calculated using the equations below:

$$A = \pi r^2 h \tag{6}$$

$$Q = \pi r^2 h \times V \tag{7}$$

$$V = \frac{\text{Distance } (D)}{\text{Time } (t)} \tag{8}$$

Where:  $A$  is the area of the penstock,  $h$  is the height of penstock,  $t$  is time in Seconds,

$V$  is the velocity of the following river in  $ms^{-1}$ .

$d$  is the diameter of the penstock in meter, whereas  $g$  and  $H$  remain as defined above.

$$d = 2.69 \left( \frac{n^2 Q^2 L}{H} \right)^{0.1875} \tag{9}$$

Where:  $L$  is the length of the penstock in meters and  $n$  is the manning coefficient.

$$L = \frac{gHt_g}{V} \tag{10}$$

$t_g$  is water acceleration constant in the pipe in seconds

$V$  is velocity in  $ms^{-1}$ .

The output power equation for turbine is:

$$P_{maxoutput} = gHQ \eta_{maxturbine} \tag{11}$$

Since the design is for low head, we make the following assumptions:

Height of penstock ( $h$ ) = 30m, Penstock diameter = 2000mm = 2m, Generator efficiency = 0.9, Turbine efficiency = 0.9, acceleration of free flow =  $9.81 m/s^2$ , radius of Penstock,  $r$  = 1m

Table 5: Time interval for first half of the year

January			February			March		
Interval	Time (Secs.)	Status (Stopwatch)	Interval	Time (Secs.)	Status (Stopwatch)	Interval	Time (Secs.)	Status (Stopwatch)
First Interval	3.23	Measured	First Interval	3.21	Measured	First Interval	3.18	Measured
Second Interval	3	Measured	Second Interval	3.12	Measured	Second Interval	3.1	Measured
Third Interval	3.25	Measured	Third Interval	3.25	Measured	Third Interval	3.11	Measured
<b>Average</b>	<b>3.16</b>			<b>3.19333</b>			<b>3.13</b>	

April			May			June		
Interval	Time (Secs.)	Status (Stopwatch)	Interval	Time (Secs.)	Status (Stopwatch)	Interval	Time (Secs.)	Status (Stopwatch)
First Interval	3.08	Measured	First Interval	3.12	Measured	First Interval	3.09	Measured
Second Interval	3.15	Measured	Second Interval	3.12	Measured	Second Interval	3.05	Measured
Third Interval	3.09	Measured	Third Interval	3.1	Measured	Third Interval	3	Measured
<b>Average</b>	<b>3.10666</b>			<b>3.11333</b>			<b>3.04666</b>	

Table 6: Time interval for second half of the year

July			August			September		
Interval	Time (Secs.)	Status (Stopwatch)	Interval	Time (Secs.)	Status (Stopwatch)	Interval	Time (Secs.)	Status (Stopwatch)
First Interval	3	Measured	First Interval	2.98	Measured	First Interval	3.03	Measured
Second Interval	3	Measured	Second Interval	2.99	Measured	Second Interval	3	Measured
Third Interval	2.97	Measured	Third Interval	2.97	Measured	Third Interval	3	Measured
<b>Average</b>	<b>2.99</b>			<b>2.98</b>			<b>3.01</b>	

October			November			December		
Interval	Time (Secs.)	Status (Stopwatch )	Interval	Time (Secs.)	Status (Stopwatch)	Interval	Time (Secs.)	Status (Stopwatch)
First Interval	2.98	Measured	First Interval	3.1	Measured	First Interval	3.24	Measured
Second Interval	3	Measured	Second Interval	3	Measured	Second Interval	3.26	Measured
Third Interval	2.97	Measured	Third Interval	3.24	Measured	Third Interval	3.29	Measured
<b>Average</b>	<b>2.98333</b> <b>3</b>			<b>3.11333</b> <b>3</b>			<b>3.26333</b> <b>3</b>	

Table 7: Calculated results.

Month	Average Time (s)	Velocity (m/s)	$A = \pi r^2 * h$ (m <sup>2</sup> )	$Q = AV$ (m <sup>3</sup> /s)	Power (W)	Power(kW)
<b>January</b>	3.16	6.6455696	94.26	626.4114	104421.5	<b>104.4215263</b>
<b>February</b>	3.193	6.5768869	94.26	619.9374	103342.3	<b>103.342319</b>
<b>March</b>	3.13	6.7092652	94.26	632.4153	105422.4	<b>105.422372</b>
<b>April</b>	3.107	6.7589314	94.26	637.0969	106202.8	<b>106.202775</b>
<b>May</b>	3.113	6.7459043	94.26	635.8689	105998.1	<b>105.99808</b>
<b>June</b>	3.047	6.8920249	94.26	649.6423	108294.1	<b>108.294067</b>
<b>July</b>	2.99	7.0234114	94.26	662.0268	110358.5	<b>110.358536</b>
<b>August</b>	2.98	7.0469799	94.26	664.2483	110728.9	<b>110.728867</b>
<b>September</b>	3.01	6.9767442	94.26	657.6279	109625.3	<b>109.625257</b>
<b>October</b>	2.983	7.0398927	94.26	663.5803	110617.5	<b>110.617507</b>
<b>November</b>	3.113	6.7459043	94.26	635.8689	105998.1	<b>105.99808</b>
<b>December</b>	3.263	6.4357953	94.26	606.6381	101125.4	<b>101.125352</b>

## 5. Results and Discussion

The investigation of velocity of the river, the flow rate, and the time in second to cover the reference distance was experimentally obtained and the results recorded. The velocity of the river was measured each month, with a distance of 21 meters as reference distance. During the experiment, the investigation was done three times which we denoted as: first interval, second interval and third interval; and their respective time in seconds were gotten using a stopwatch. The results recorded for the first half of the year and the second half of the year are shown in Tables 5 and 6. Results were obtained for a period of one year constituting the two seasons of Nigeria (Rainy and dry Season).

From Tables 5 and 6, it can be seen that it takes lesser time for the empty plastic water can to cover the reference distance of 21meters during the rainy season. The month with the least time to cover the reference distance is August with an average time interval of 2.98 seconds. While December with an average time interval of 3.26 seconds, as the highest time it took to cover the reference distance. It should be noted from the table that the time it took the plastic can to cover the reference distance was less in rainy season as compared to the dry season.

Table 7 shows the calculated results. Average time interval of each month was used for the calculation. To demonstrate how Table 7 was obtained, the output power for the month of August would be analyzed. The Average time of the month of August was gotten from

$$\text{Average Time} = \frac{2.98+2.99+2.97}{3} = 2.98 \text{ seconds.}$$

To get the velocity of the water fall, equation 8 was used. Substituting into equation 8, we have

$$\text{Velocity as } 7.0469799 \text{ m/s}$$

Substituting into equation 6 also gives the area as 94.26 m<sup>2</sup>. The flow rate, Q, was gotten from equation 7 as: 664.2483 m<sup>3</sup>/s. Substitution into equation 5 yields the output power as: 110728.9 W. or 110.728867 KW.

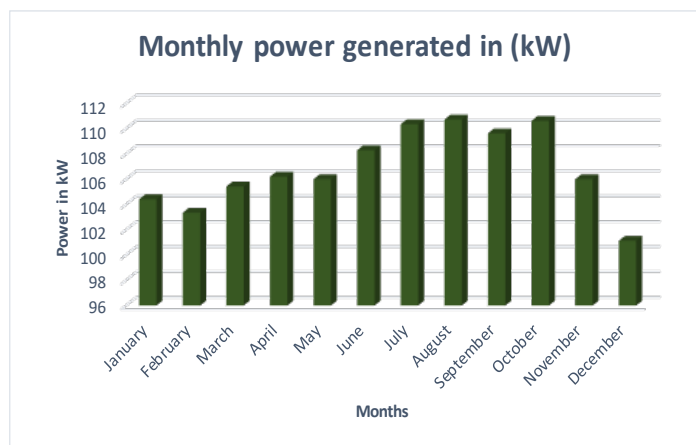


Figure 7: Monthly output Power.

The rest of the month was gotten in similar manner and Table 7 was completed with their respective results, while Figure 7 was gotten from the monthly output power.

Table 7 shows the velocity of the water fall, the flow and calculated output power of each month. It is obvious from Table 7 and Figure 7 that August has the highest value of velocity (7.0469799m/s), flowrate (664.2483 m<sup>3</sup>/s) and output power (110.728867 kW); while December has the lowest value of these quantities - 6.4357953m/s for the velocity, 606.638m<sup>3</sup>/s and 101.125352 kW for power output. It is worthy to note that the difference between the output power generated in rainy and dry season is not much. This is because, the water fall has almost equal rate of flow for all the months. Each of the monthly generated power can serve 5 villages in rural areas with average connection of 200houses, assuming 100W compact power supply to each house hold.

From the results in Table 7, the output power generated from the rainy season's month in Nigeria which is between months of June to October have the highest generated power with August having the highest output power of 110.728867 kW. December with an output power of 101.125352 kW has the least output power in dry season. From the output power gotten for each month we can term it a micro hydropower plant.

## 6. Conclusion

Result from the examined site shows that the site falls in the range of mini hydropower generation. As a way out to solve the epileptic nature of electrical supply mini hydropower could be used where site has a potential ability of generating power to the community thereby relieving the grid network from stress. There is a lot to gain from SHP because of little or no environmental hazard produced which is in line with recommendation of the World Economic Forum, Davos 2020 and also eradicating poverty in the rural communities

## References

- [1] Darfur Solar Electrification Project, project report, Khartoum, Feb. 2016 (Available online:7\_darfur\_solar\_electrification\_project\_final\_for\_signature\_0.pdf. Accessed on 24 July 2018).
- [2] UNDP Discussion Paper, "An integrated approach to tackle the challenge of rural development by bringing access to renewable energy for income generation and social development", Aug 2014. (Available online: 140901\_Integrated%20Rurl%20Electrification\_FINAL.pdf. Accessed on 20 July 2018).
- [3] S. Kaunda, Z. Kimambo, K. Nielsen "Potential of Small-Scale Hydropower for Electricity Generation in Sub-Saharan Africa", International Scholarly Research Network, vol. 2012, Article ID 132606, pp. 1-16.
- [4] W. S. Ebhota, P. Y. Tabakov, "The Place of Small hydropower electrification Scheme in Socioeconomic Stimulation of Nigeria", International Journal of Low-Carbon Technologies, vol. 13, 2018, pp. 311-319.
- [5] "How can developers use Levelised Cost of electricity to compare technologies?", United States Department of Energy (DOE) Energy Information Administration (EIA), 2017.
- [6] O. O. Fagbohun, "Studies on small hydro-power potentials of itapaji dam in Ekiti State, Nigeria", International journal of Engineering science invention, vol. 5 issue 1, 2016, pp. 28-36
- [7] J. A. Otun, J. I. Onemano, A. W. Alayande, "Assessment of the hydropower potential of kangimi reservoir in Kaduna State Nigeria", Nigeria Journal of Technology, vol. 31, No. 3, 2012, pp. 300 -307
- [8] Woes of power in Nigeria by FisayoAkinduro <http://thehopenewspapers.com/2016/03/woes-power-nigeria/>, accessed on 19<sup>th</sup> July 2017
- [9] "Climate: Enugu", content://com.sec.android.app.sbrowser/readi/0720083850.mhtml, accessed on 19th July,2018



- [10] S. Mishra, S. K. Signal, D.K. Khatod, "Optimal installation of small hydropower plant-A review", *Renewable Sustainable Energy Reviews*, vol. 15, 2011, pp 3862-3869.
- [11] H. S. Sachdev, A. K. Akella, N. Kumar, "Analysis and evaluation of small hydropower plants: A bibliographical survey" *Renewable Sustainable Energy Reviews* vol. 51, 2015, pp 1013-1022
- [12] C. P. Jawahar, P. A. Michael, "A review on turbines for micro hydro power plant", *Renewable Sustainable Energy Reviews*, vol.72, 2017, pp 882-887.
- [13] E. I. Igweonu, R. B. Joshua, "Small hydropower (SHP) development in Nigeria: issues, challenges and prospects" *Global Journal of Pure and Applied Science*, vol 18, No. 1&2, 2012, 53-58
- [14] S. O. Ohunakin, J. S. Ojolo, "Small Hydropower (SHP) Development in Nigeria: An assessment", *Renewable Sustainable Energy Reviews*, vol. 15, 2011 Doi:10.1016/j.rser.2011.01.003
- [15] "Ezeagu tourist complex Enugu State", <https://www.nigeriagallery.com/Nigeria/State-Nigeria/Enugu/Ezeagu-Tourist-complex.html>, accessed on 20<sup>th</sup>, July2018.

## Seismic Performance of Infilled Reinforced Concrete Buildings

Miloud Mouzzoun\*, Abdelkader Cherrabi

Department of civil engineering, Hassania School of Public Works, Morocco

### ARTICLE INFO

Article history:

Received: 10 January, 2020

Accepted: 31 March, 2020

Online: 20 April, 2020

Keywords:

Seismic  
Building  
Strut  
Reinforced  
SAP2000  
Concrete

### ABSTRACT

In the Moroccan seismic code, infill walls are considered as secondary elements and their lateral strength and stiffness are neglected in the design when considering horizontal seismic loads. In this article we propose to investigate the effect of infill on the seismic performance of the buildings. A 6-stories reinforced concrete frame building is investigated. The concept of equivalent strut is used for infill panel. Diagonal strut carries only compression forces. Strut properties are calculated according to the FEMA306. Software analysis SAP2000 is used to conduct numerical simulations. Numerical results show that there is a change in the internal forces, in the fundamental period of vibration and in the lateral story drift when masonry infill is included in the design. Seismic behavior of infill frame is different from that predicted by bare frame.

## 1. Introduction

Earthquakes occurred recently in the world, Northridge1994, Kobe 1995, Izmit1999 and Alhoceima2004, have shown that presence of masonry infill walls interact with the surrounding frames and change the seismic response of framed reinforced concrete buildings [1,2]. Behavior of masonry wall infilled frames have been investigated by many researchers, Polyakov1960 [3], Holmes1963 [4], Stafford1969 [5], Paulay and Priestly1992[6], Mehrabi1994[7], Negro1997[8], G. Al-Chaar2002 [9], P.G.Asteris2003 [10]. Most of these studies are focused on the behavior of single-frame single-bay infilled by unreinforced masonry under monotonic or cyclic lateral loading. The results of these studies indicate that masonry infill walls change the dynamic behavior of the building in terms of stiffness, strength, natural frequency and overall structural behavior. In Moroccan seismic code RPS2000 [11], infill walls are considered as secondary elements, their lateral stiffness and strength are neglected when considering loading due to horizontal components of ground motion earthquake. The aim of this paper is to investigate the influence of infill panels on the seismic performance. Lateral strength and stiffness of infill walls is considered by the concept of equivalent diagonal strut. Diagonal strut carries only compression forces. Pushover analysis is used to assess the seismic performance of building. Software analysis Sap2000 [12] is used to perform numerical simulations.

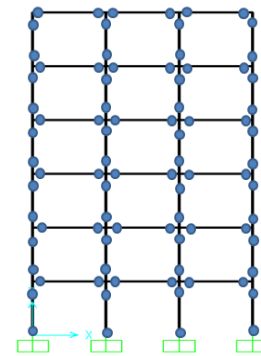


Figure 1: Bare frame with plastic hinges

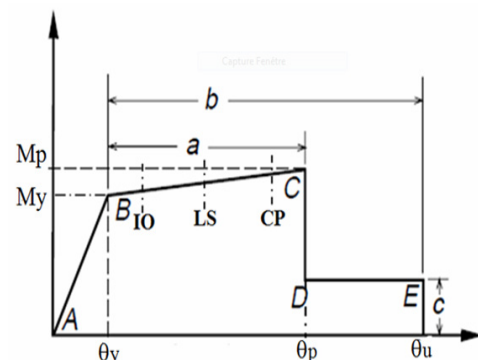


Figure 2: Moment –rotation relation of plastic hinge

\*Corresponding Author: Miloud Mouzzoun, mouzzoun.mouloud@gmail.com

## 2. Materials and methods

### 2.1. Modeling of concrete members

Frame members are idealized as elastic elements with a plastic hinge at each end. All material nonlinearities are concentrated in the plastic hinges. The properties of plastic hinges are defined as per FEMA 356 [13].

### 2.2. Modeling of infill wall

Lateral strength of infill wall is introduced in the analysis by modeling the infill wall by two diagonal struts. Diagonal strut carries only compression force. Properties of equivalent strut are calculated according to FEMA306 [14].

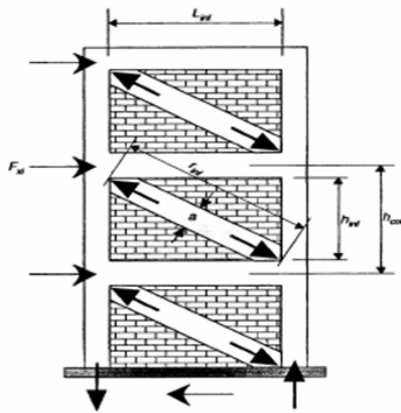


Figure 3: Diagonal strut for infill wall

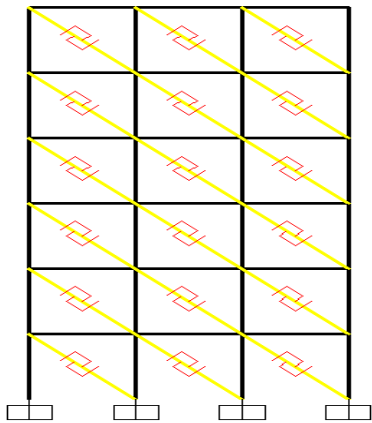


Figure 4: Link element idealization for compression strut

### 2.3. Parameters of diagonal strut

The width  $w$  of the equivalent strut is estimated according to Fema306. Nonlinearity is introduced in each diagonal strut by providing axial compression hinge.

$$w = 0.175d(\lambda H_c)^{-0.4} \quad (1)$$

$$\lambda = \sqrt[4]{\frac{E_m t \sin 2\theta}{4E_c I_c H_m}} \quad (2)$$

$$\theta = \tan^{-1} \frac{H_m}{L_m} \quad (3)$$

Where  $d$  is the strut diagonal length,  $E_m$  is the masonry modulus,  $E_c$  is the concrete modulus,  $H_c$  is the column height,  $H_m$  and  $L_m$  are the height and the width of infill wall respectively.  $I_c$  is the moment of inertia of column,  $t$  is the infill thickness,  $\theta$  is the angle of inclination of diagonal strut.

## 3. Numerical investigations

### 3.1. Building description

To study the influence of infill panel on the seismic behavior of the building, a six stories reinforced concrete building is considered. The total plan dimensions are 9m x 9m. Total height of the building is 18m. The height of each storey is 3m. The columns are 30cmx30cm, 35cmx35cm and 45cmx45cm, the beams are 25cmx30cm for all floors, and the slab thickness is 13cm for all floors. The superimposed loads are 2.5KN/m<sup>2</sup> and the live loads are 1.5KN/m<sup>2</sup>. Two models are considered, first model M1 is bare frame. The second model M2 is infill frame in which the lateral strength of infill is introduced by the concept of equivalent diagonal strut. The building is designed according to the RPS2000 and BAEL [15].

### 3.2. Properties of the diagonal strut

The frame properties are:

$$\begin{cases} \text{column} & 30.30 \\ \text{beam} & 25.30 \\ E_c & = 32164 \text{Mpa} \\ I & = 6.7510^{-0.4} \text{m}^4 \end{cases} \quad (4)$$

The infill wall properties are:

$$\begin{cases} H_m & = 2.7 \text{m} \\ L_m & = 2.70 \text{m} \\ t_m & = 15 \text{cm} \\ E_m & = 1100 \text{Mpa} \\ \theta & = \tan^{-1} \frac{H_m}{L_m} = 45^\circ \end{cases} \quad (5)$$

The parameter  $\lambda$  is given by:

$$\lambda = \left[ \frac{E_m t_m \sin 2\theta}{4E_c I_c H_m} \right]^{\frac{1}{4}} = 0.92 \quad (6)$$

The diagonal strut length  $d$  is given by:

$$d = \sqrt{H_m^2 + L_m^2} = 3.81 \text{m} \quad (7)$$

The width  $w$  of equivalent strut is given by:

$$W = 0.175d(\lambda H_c)^{-0.4} = 44\text{cm} \quad (8)$$

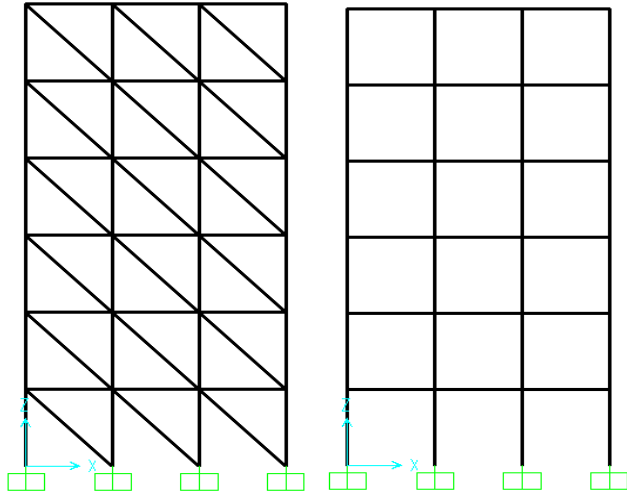


Figure 5: bare frame and infill frame models

Table 1: Mechanical properties and parameters of the study

Storey	disp (cm)	disp (cm)	Ratio (BF-IF)/BF
	Bare frame (BF)	Infill frame (IF)	
6° storey	5,02	2,14	57%
5° storey	4,48	1,94	56%
4° storey	3,54	1,61	54%
3° storey	2,52	1,21	52%
2° storey	1,36	0,72	47%
1° storey	0,47	0,28	40%

Table 2: Reinforcement of beams

Storey	Drift (%)	Drift (%)	RPS2000
	Bare frame	Infill frame	Drift limit (%)
6° storey	0,18	0,06	0,5
5° storey	0,31	0,11	0,5
4° storey	0,34	0,13	0,5
3° storey	0,38	0,16	0,5
2° storey	0,29	0,14	0,5
1° storey	0,15	0,09	0,5

Table 3: Reinforcement of columns

Column	Section	Long- reinf	Stirrups
1° Storey	45x45	12φ16	φ6 E=15cm
2° Storey	45x45	12φ16	φ6 E=15cm
3° Storey	35x35	12φ16	φ6 E=15cm
4° Storey	35x35	8φ16	φ6 E=15cm
5° Storey	30x30	8φ16	φ6 E=15cm
6° Storey	30x30	8φ16	φ6 E=15cm

## 4. Results and discussion

### 4.1. Lateral storey displacements

Maximum displacement at different stories is presented in the table 4 and 5. Figures, from 6 to 11 show the base shear versus storey drift. It can be seen that displacements decrease when lateral strength of masonry infill is considered in the model. There is a major reduction in the lateral storey displacements and storey drifts.

Table 4: Lateral storey displacements

Parameter	Value	Unit
Concrete grade	25	Mpa
Steel grade	500	Mpa
Seismic Zone	3	***
Site Factor	1.2	***
Behavior Factor	2	***
Importance Factor	1	***
Infill thickness	15	cm
Masonry strength	2	Mpa
Slab thickness	13	cm
Concrete modulus	32164	Mpa
Masonry modulus	1100	Mpa
Steel Modulus	200000	Mpa

Table 5: Storey drift of bare and infill frames

Beam	Section	Top- reinf	Bottom- reinf
1° Storey	25x30	4φ16+4φ12	4φ16+4φ12
2° Storey	25x30	4φ16+4φ12	4φ16+4φ12
3° Storey	25x30	4φ16+4φ12	4φ16+4φ12
4° Storey	25x30	4φ16+4φ12	4φ16+4φ12
5° Storey	25x30	4φ16+4φ12	4φ16+4φ12
6° Storey	25x30	4φ16+4φ12	4φ16+4φ12

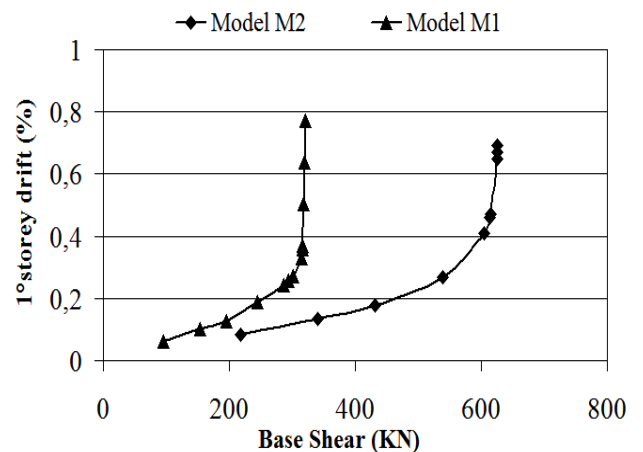


Figure 6: Base shear versus storey drift. 1° storey



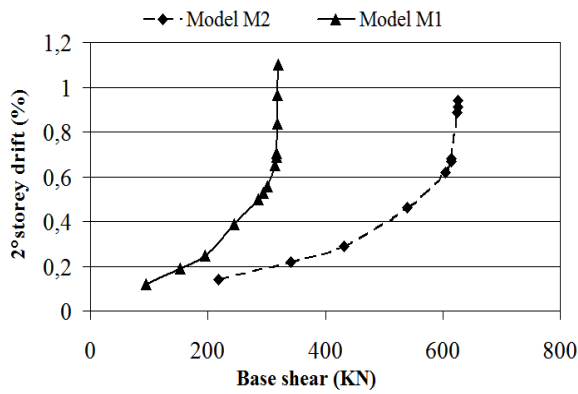


Figure 7: Base shear versus storey drift.2° storey

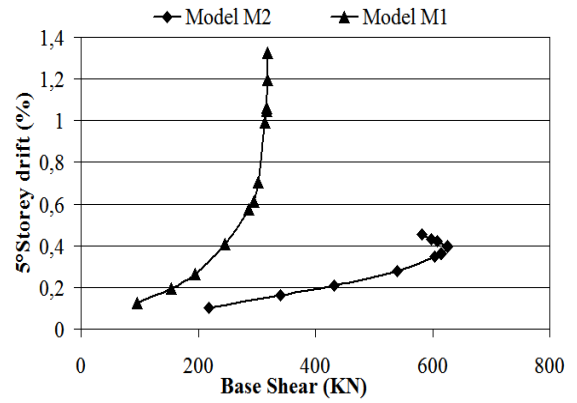


Figure 11: Base shear versus storey drift.6° storey

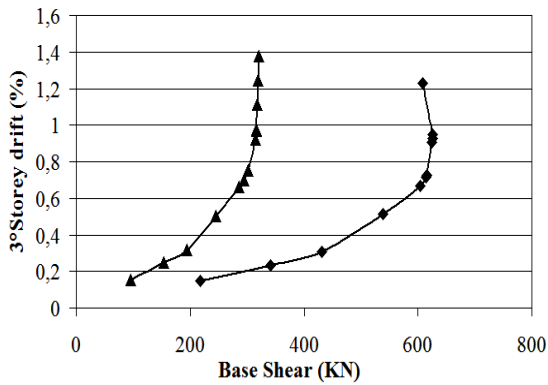


Figure 8: Base shear versus storey drift.3° storey

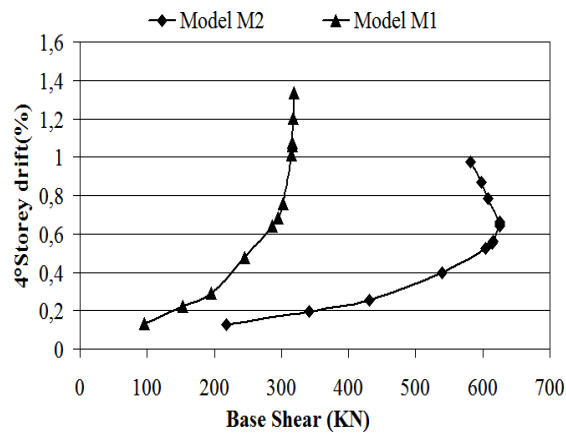


Figure 9: Base shear versus storey drift.4° storey

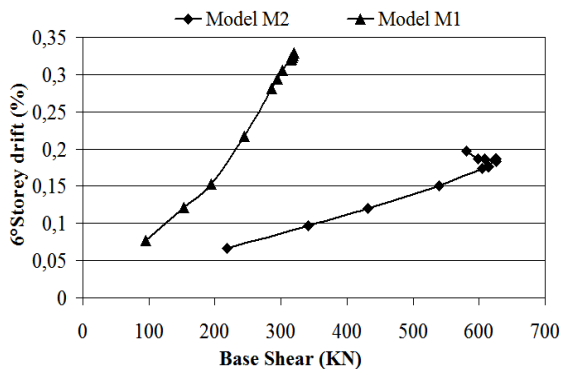


Figure 10: Base shear versus storey drift.5° storey

#### 4.2. Natural periods of vibration

Table 6 shows vibration periods of bare frame and infill frame. It is found that introduction of masonry infill wall increases the lateral rigidity of bare frame; consequently fundamental period of vibration will be decreased. Bare frame idealization, under estimates the seismic design base shear.

Table 6: Natural periods of vibration

Mode number	Infill frame	Bare frame
6° storey	0,251	0,419
5° storey	0,083	0,136
4° storey	0,049	0,078
3° storey	0,036	0,054
2° storey	0,029	0,042
1° storey	0,027	0,036

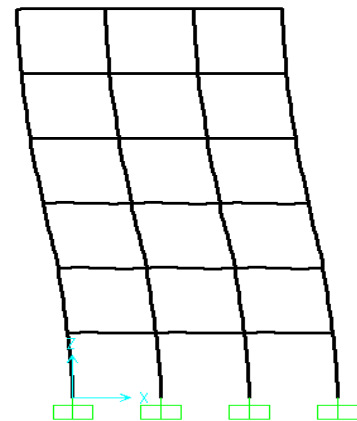


Figure 12: First mode of vibration (frequency=2.38Hz)

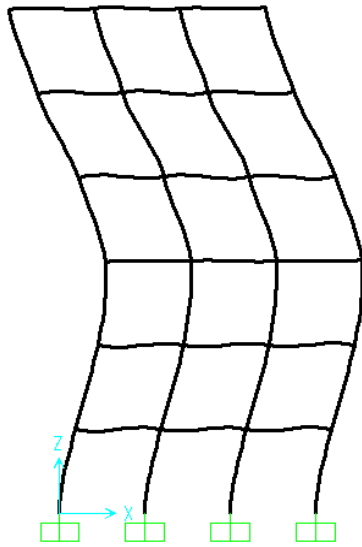


Figure 13: Second mode of vibration (frequency=7.35Hz)

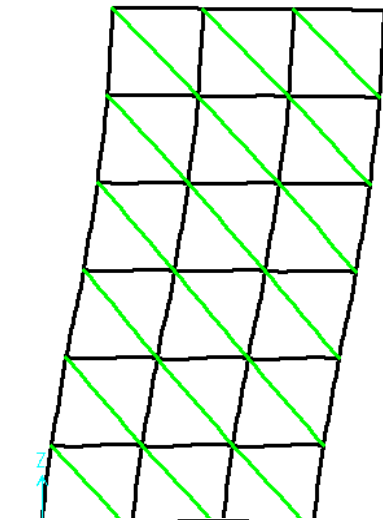


Figure 14: First mode of vibration (frequency=4Hz)

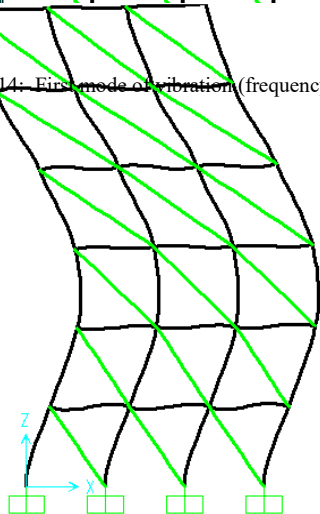


Figure 15: Second mode of vibration (frequency=12Hz)

### 4.3. Lateral strength and stiffness

Figure 16 shows capacity curves of bare and infill frames. It is found that lateral strength of infill frame is higher as compared to that of bare frame. The increasing in lateral stiffness reaches 2.5 times that of bare frame. Maximum strength of infill frame reaches 1.9 times that of bare frame. These numerical results obtained from this study agree with the experimental studies conducted by M.N Fardis et al [16], A.Hashemi et al [17] and A.Madan et al [18]. Experimental results indicate that, inclusion of masonry infill increases both lateral stiffness and strength of bare frame.

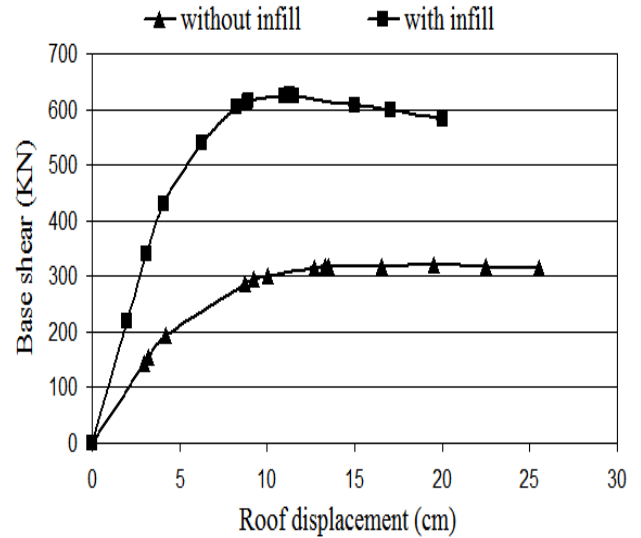
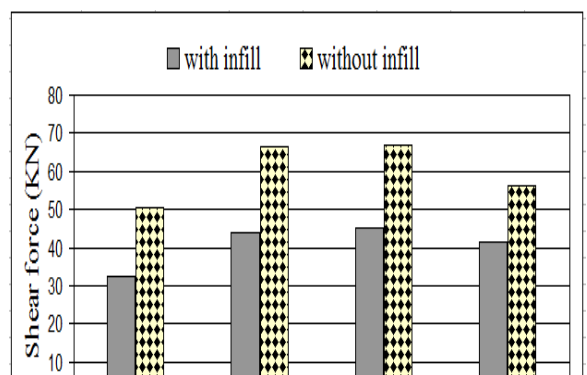
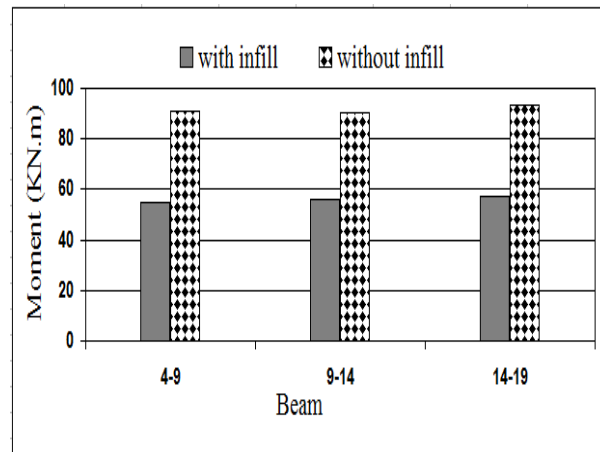


Figure 16: Pushover curves for bare and infill frame

### 4.4. Internal forces in the frame members

Figures 17, 18, 19 and 20 show the results of shear forces and bending moments obtained when lateral strength of infill is included or when it is ignored. It can be seen that there is an important change in the shear forces and bending moments in the frame members.



- Introduction of infill wall in the analysis reduces significantly seismic demands. The maximum reduction reaches 50% for lateral storey displacement and 66% for inter-storey drift.

Figure 20: Change in the bending moments. Beams

- Inclusion of infill wall enhances lateral capacity of building. Initial stiffness reaches 2.5 times that of frame without infill, while maximum strength of infill frame reaches 1.9 times that of bare frame.
- Numerical investigations show also that there is a change in the internal forces in the frame members when lateral strength of infill walls was included. Bending moments of bare frame reached 1.60 times that of infill frame, while shear forces of bare frame reached 1.50 times that of infill frame. The infill frame resists lateral loads as a trussed frame then, flexural effects will decrease significantly.

Finally, the results of this study as presented in previous tables and figures, suggest that masonry infill walls change the response of the building when subjected to horizontal seismic forces. Seismic response of infill frame is too much different from that predicted by bare frame.

### Conflict of Interest

The authors declare no conflict of interest.

### References

- [1] M.Mouzzoun and A.Cherrabi, "Seismic Behavior of reinforced concrete frame buildings with masonry infill" International Journal of GEOMATE, 17(63) 203–209, 2019.
- [2] M.Mouzzoun, "Seismic behaviour of reinforced concrete frame buildings with masonry infill" PhD thesis, Mohammadia School of engineers, Morocco, 2015.
- [3] S.V. Polyakov, "On the interaction between masonry filler walls and enclosing frame when loading in the plane of the wall" Earthquake Engineering Research Institute, San Francisco, 36-42, 1960.
- [4] M. Holmes, "Combined Loading on Infilled frames" Proceedings of the Institution of the Civil Engineers, 25, 31.1963.
- [5] S. Stafford and C. Carter, "A method for analysis for infilled frames" Proceedings of Institution of Civil Engineers, No. 7218, 31-48, 1969.
- [6] T.Paulay and M.N.Pristley, "Seismic design of reinforced concrete and masonry buildings" John Wiley, 1992.
- [7] A.B. Mehrabi, P.B.Shing, M.P.Schuller and J.L.Noland, "Experimental Evaluation of Masonry-Infilled RC Frames" ASCE Journal of Structural Engineering, 122(3), 228-237, 1996.
- [8] P. Negro and A. Colombo, "Irregularities induced by non structural masonry panels in framed buildings" Engineering Structures. 19(7), 576–585.1997.
- [9] G. Al-Chaar, Evaluating strength and stiffness of unreinforced masonry structures. US Army Corps of Engineers. Construction Engineering Research Laboratories, 2002.
- [10] P.G. Asteris. "Lateral stiffness of brick masonry infilled plane frames" Journal of Structural Engineering, 129(8), 1071–1079, 2003.
- [11] RPS2000, Moroccan seismic code, Ministry of housing, 2000.
- [12] CSI, Analysis Reference Manual for SAP2000, ETABS and SAFE, Computers and Structures, Inc. Berkeley, California, USA, 2005.
- [13] FEMA356, Federal Emergency Management Agency, NEHRP recommended Provisions for Seismic Regulations for New Buildings and Other Structures, 2000.
- [14] FEMA306, Evaluation of Earthquake Damaged Concrete and Masonry Wall Buildings, Basic Procedures Manual, Federal Emergency Management Agency, 1999.
- [15] BAEL, Analysis and design of reinforced concrete buildings according to limit states method. European Committee for Standardization, 1991.
- [16] M.N.Fardis, Experimental and numerical investigations on the seismic response of RC infilled frames and recommendations for code provisions, Report 6 of HCM-ECOEST Project, LNEC, Lisbon, 1997.
- [17] A.Hashemi, K.M.Mosalam, K.M, "Shake-Table Experiment on Reinforced Concrete Structure Containing Masonry Infill Wall" Journal of Earthquake Engineering and Structural Dynamics. 14(35), 1827-1852, 2006.

Figure 17: Change in the shear forces. Columns

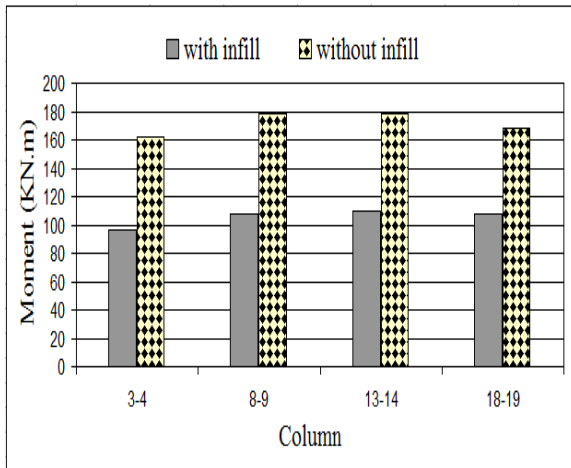


Figure 18: Change in the bending moments. Columns

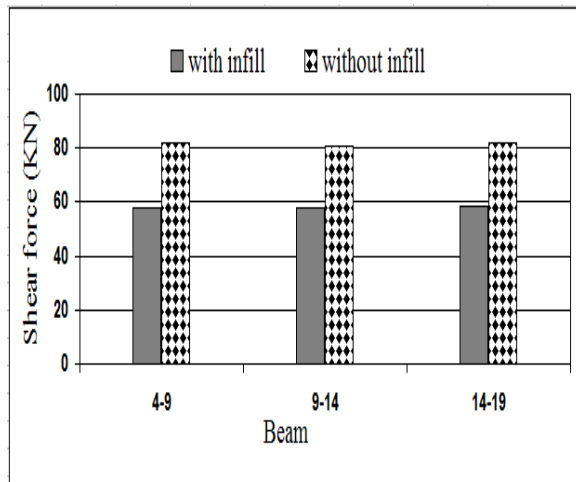


Figure 19: Change in the shear forces. Beams

## 5. Conclusion

In this study, the influence of infill walls on the seismic response of reinforced concrete buildings was investigated. The principal conclusions can be summarized as follows:

- Numerical simulations show that inclusion of masonry infill reduces significantly fundamental period. The maximum reduction reaches 40%. According to the response spectrum, when period decreases spectral acceleration increases, consequently the base shear design will be increased.

- [18] A. Madan, A.M. Reinhorn, J.B. Mander and R.E. Valles, "Modeling of masonry infill panels for structural analysis" ASCE Journal of Structural Engineering, 123(10), 1292-1297, 1997.



## Comparison of the RC-Triggered MOSFET-Based ESD Clamp Circuits for an Ultra-low Power Sensor System

Chih-Hsuan Lin\*, Kuei-Ann Wen

Department of Electronic Engineering, University of National Chiao Tung (NCTU), Hsinchu 300, Taiwan

### ARTICLE INFO

Article history:

Received: 17 February, 2020

Accepted: 11 April, 2020

Online: 20 April, 2020

Keywords:

ultra-low power

ESD

accelerometer

### ABSTRACT

*This paper uses the RC-triggered MOSFET-based electrostatic discharge (ESD) power clamp to conduct ESD from ESD events and not affect the ultra-low power sensor system. Then using the stacked device include stacked MOSFET or stacked BJT to reduce the leakage current which increases with temperature. Moreover, we compare gate-driven method and two-level-driven with both gate-driven and substrate-driven methods to determine the most efficient method in terms of layout area, leakage current, Human Body Model (HBM)/Machine Model (MM), and turn-on time. The proposed design of the power ESD clamp (IO15c/IO15e/IO15c\_resize) has an HBM ESD protection level with a Positive higher than 8KV, 5.5KV, 8KV, and an MM ESD protection level with a Positive higher than 600V, 300V, 1000V. The power ESD clamp (IO15c/IO15e) consumes nearly 3.5pW/16.45nW and 2.8pW/16.89nW at temperatures of 25°C and 125°C, respectively, when AVDD3 is 1.0V.*

## 1. Introduction

With internet of things applications being used in handheld devices, mobile phone standby time is becoming a key focus of consumers' attention. It has become increasingly important to study ultra-low power sensing systems in order to increase standby time. Nowadays, such systems generally reduce power consumption to less than the microwatt level. However, the current of traditional electrostatic discharge (ESD) power clamp leakage currents at high temperatures is greater than 1uA for a 180nm complementary metal-oxide-semiconductor (CMOS) process. This leakage current affects the stability of the ultra-low power sensor system. This paper uses the RC-triggered metal-oxide-semiconductor field-effect transistor (MOSFET)-based ESD power clamp to conduct ESD from ESD events and not affect the ultra-low power sensor system. Then, a stacked device, including a stacked MOSFET or stacked BJT, is used to reduce the leakage current that increases with temperature. However, the disadvantage of using a stacked device is that its size will be proportional to the number of stacked layers. This is because the stacked device must keep a certain ON-resistance as the BIGFET of the ESD power clamp (IO1) to keep the rate of heat flow and maintain the ESD level. Moreover, this paper compares two

methods to determine which method is the most efficient in terms of layout area, leakage, Human Body Model (HBM)/Machine Model (MM), and turn-on time. The methods are the gate-driven method and two-level-driven method with both the gate-driven and substrate-driven methods.

In addition, some microelectromechanical systems (MEMS) with small gap spacing operate using electrostatic forces. This may cause damage to their structures due to surface roughness, variations in structure geometries, variable gap spacing, and flexible moving components [1]. Further analysis of the problem determines that ESD is an effective charge injection source, which is considered to be a major reliability issue in MEMS [2]. In some studies, an analytical method of charge injection is performed, including using ESD in MEMS [3], [4]. This paper presents whole-chip ESD protection with an ultra-low power ESD clamp circuit to be applied to a 3D accelerometer.

In this paper, the proposed ESD power clamp can be fabricated using the Uniform Mechanical Code (UMC) 0.18mm standard CMOS-MEMS process. This paper is organized as follows: Section 1. introduces the ESD power clamp; Section 2. describes the ESD power clamp architecture considerations; Section 3. compares the RC-triggered MOSFET-based ESD clamp circuits and design; and Section 4. describes the measurement results and discussion.

\*Corresponding Author: Chih-Hsuan Lin, shsuanhsuan.ee01g@g2.nctu.edu.tw

[www.astesj.com](http://www.astesj.com)

<https://dx.doi.org/10.25046/aj050289>

## 2. Architecture considerations

Figure. 1 shows a schematic view of a sensor and the architecture of a whole-chip ESD protection circuit. The functions are detailed as follows: 1) When the input pin (VM) is zapped, the ESD current is led away by A\_PATH from the VM node through Q2, Q1 to VSUB; 2) When the input pin (VM) is zapped, the ESD current is led away by B\_PATH from the VM node through Q2, Q1, D1, D2, Q5 to VDN; 3) When the input pin (AVDD) is zapped, the ESD current is led away by C\_PATH from the AVDD node through Q1 to VSUB; 4) When the input pin (VDN) is zapped, the ESD current is led away by D\_PATH from the VDN node through Q5, D4, D3, Q1 to AVDD; 5) When the input pin (VUP) is zapped, the ESD current is led away by E\_PATH from the VUP node through Q1 to VSUB. 6) The zone with the black dotted line portrays the sensor model, and the accelerometer sensor is modeled by C1, C2, C3, C4, and C5 [5], [6]. When different ESD events occur, the electrostatic current will be led away through different paths, including A\_PATH, B\_PATH, C\_PATH, D\_PATH, E\_PATH, and ESD power clamp (Q1). The electrostatic current does not affect the performance of the sensor system and all of the junctions of the device are forward-biased for different paths. The forward-biased junction of the device generates less the rate of heat flow than the reverse-biased junction of the device and can improve ESD protection capability.

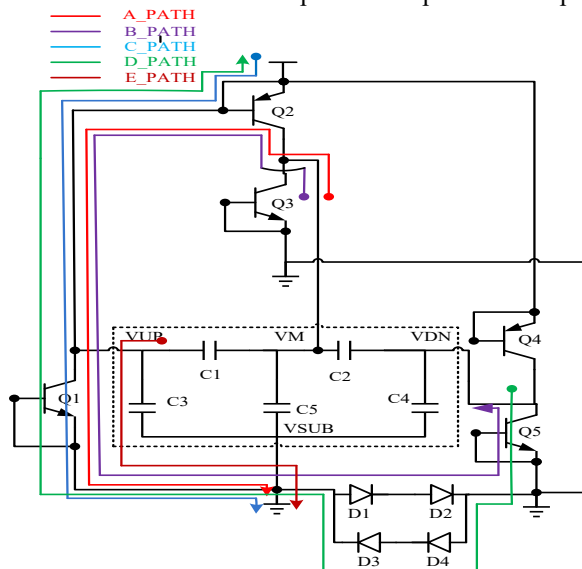


Figure. 1. Sensor and ESD protection circuit

## 3. Comparison the RC-triggered MOSFET-based ESD clamp circuits and designs

### 3.1. The RC-triggered MOSFET-based power clamp [7]

From the sensor and ESD protection circuit shown in Figure. 1, the ESD power clamp (Q1) is a large dimension of a 3.3V device to keep a certain ON-resistance and the rate of heat flow. The ESD power clamp (Q1) acts as the voltage gate in a low setting and will be divided into several 3.3V devices in parallel due to process reliability. The disadvantage of the ESD power clamp (Q1) is that it has a non-uniform conduction issue. When an ESD event occurs, the ESD power clamp (Q1) will be turned on, but the ESD power clamp (Q1) cannot simultaneously perform uniform conduction and degrade ESD protection capabilities. To solve the non-uniform conduction issue, an ESD power pad (IO1) is often

used. The ESD power pad (IO1) is an RC-filter and inverter that forms a RC-transient detector to detect an ESD event, as shown in the blue box in Figure. 2. When an ESD event occurs, the device (M2) is turned on and the detection point (O1) is pulled to a high setting. Then, the BIGFET is turned on and the electrostatic current travelling through the BIGFET is lead away. When the ESD event disappears, the device (M2) returns to a normal state, the detection point (O1) is pulled to a low setting, and the BIGFET stops conducting. Moreover, the ESD protection circuit uses a 3.3V device and a UMC ESD standard process, including a thinner gate oxide, shorter channel length, shallower drain/source junction, silicide block (SAB), Local Oxidation of Silicon/shallow trench isolation, lightly-doped drain/ESD-implantation structure, and layout rule. The layout rule includes SAB width, SAB to poly gate edge spacing, an n-type metal-oxide-semiconductor (NMOS) layout with inner N-well ring, channel width, channel length, drain contact to poly gate, source contact to poly gate, spacing from drain diffusion to guarding diffusion, etc. The overall power consumption of the ultra-low power sensor system is, however, at the microwatt level. When the ESD event disappears, the BIGFET is turned off and the BIGFET's leakage current will increase as the temperature rises. It will affect the overall performance of the ultra-low power sensor system. To solve this issue, the RC-triggered MOSFET-based power clamp (IO15) is used. [7]

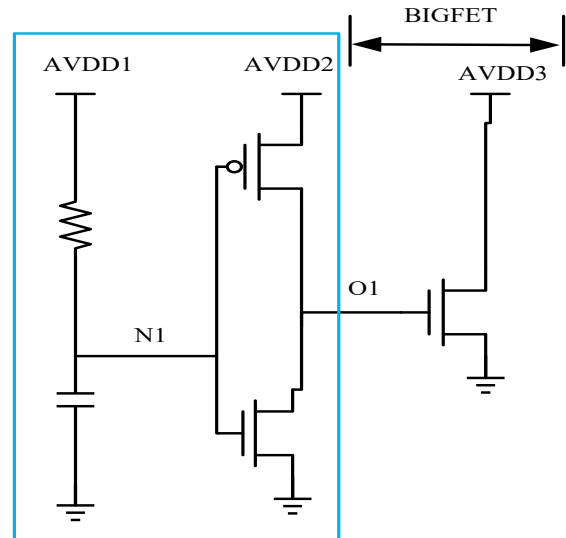


Figure. 2. ESD power clamp (IO1)

The IO15 description is as follows: The RC-transient detector, which is the RC-filter and inverter is the same as the ESD power clamp (IO1), and the ESD power clamp (IO15) uses a delay-line to divide into two paths, as shown by the red line in Figure. 3. The delay-line with parasitic capacitor (CL) increases the fully-on time of a stacked device (MN6\_1 and MN6\_2), which is separated from the BIGFET of the ESD power clamp (IO1) for the ESD event. Then, the ESD power clamp (IO15) uses the output of the delay-line to control the gate voltage of the stacked device. Moreover, it uses the stacked device to reduce the leakage current, and uses the RC-transient detector to control the delay-cell of small dimension size to lower the detection point (O1) time, as shown in Figure. 3. The capacitor uses a metal-oxide-metal capacitor to reduce the leakage current. The device sizes of the ESD power clamp (IO15) are chosen as Table 1.

Table 1. The device sizes of the ESD power clamp (IO15)

Name	W/L	Name	W/L		
MP1	6um/0.4um	MN1	1.5um/0.4um	R	50.33K
MP2 1	6um/0.4um	MN2 1	3.0um/0.4um	C	2.5P
MP3 1	6um/0.4um	MN3 1	3.0um/0.4um		
MP4 1	21um/0.4um	MN4 1	8.0um/0.4um		
MP5 1	21um/0.4um	MN5 1	8.0um/0.4um		
MP6 1N	864um/0.38um	MP6 2N	864um/0.38um		

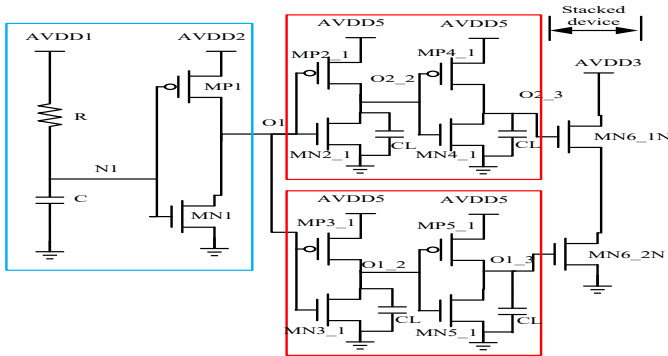


Figure 3. ESD power pad circuit (IO15)

3.2. Comparison of the RC-triggered MOSFET-based power clamp with the gate-driven method and two-level-driven with both the gate-driven and substrate-driven methods

Because the stacked device must keep a certain ON-resistance and the rate of heat flow as the BIGFET of the ESD power clamp (IO1) and maintain the ability ESD, the size of the stacked device will be proportional to the number of stacked layers. Then gate-driven method and two-level-driven with both gate-driven and substrate-driven methods are compared, respectively, to determine which method is the most efficient in terms of layout area, leakage, HBM/MM, and turn-on time. The gate-driven method, two-level-driven with both gate-driven and substrate-driven methods describe as follows.

The ESD power clamp (IO15c) uses RC-transient detector detect and delay-line as the IO15 and controls the gate voltage of the stacked MOSFET. The ESD power clamp (IO15c) uses the gate-driven method and the cross section of a stacked MOSFET, as shown in Figure. 4. When an ESD event occurs, the RC-transient detector pulls O1 to a high setting, then, through the delay-line, divides into two paths and controls the stacked MOSFET. The path from the top side controls the gate voltage (G1) of MNO1\_1~MNO1\_28 and the path from the bottom side controls the gate voltage (G2) of MNO2\_1~MNO2\_28. The electrostatic current will be divided into 28 paths, and heat will be generated from AVDD3 to GND, via the stacked MOSFET (MNO1\_1 and MNO2\_1)~(MNO1\_28 and MNO2\_28). The heat can be evenly distributed to different junctions to avoid thermal runaway. When the ESD event disappears, the stacked MOSFET is turned off and the leakage current is lower than the ESD power clamp (IO1).

By using the gate-driven method, the positive gate voltage will form strong versions of NMOS channels and will cause

electrostatic currents to flow through junctions, which are very shallow in depth. This will degrade ESD capability. The substrate-driven method can be used to avoid this issue [8] by having lower ON-resistance characteristics and evenly dissipating heat to a deeper junction to increase ESD capability. The cross section of the parasitic NPN junction is shown in Figure. 5. Moreover, the stacked MOSFET is divided into two levels. The first level uses a gate-driven method and the second level uses a substrate-driven method. The ESD power clamp (IO15e) uses the RC-transient detector and delay-line as IO15 to control the gate voltage of the first-level stacked MOSFET, and the substrate voltage of the second-level stacked BJT is controlled by the intermediate voltage of the first-level stacked MOSFET. The ESD power clamp (IO15e) uses the two-level-driven with both the gate-driven and substrate-driven methods and the cross section of the second-level stacked BJT, as shown in Figure. 6. When an ESD event occurs, the RC-transient detector pulls O1 to a high setting, then, through the delay-line, divides into two paths and controls the gate voltage of the first-level stacked MOSFET. The path from the top side controls the gate voltage (G1S) of MNR1\_1~MNR1\_14 and the path from the bottom side controls the gate voltage (G2S) of MNR2\_1~MNR2\_14. Then the electrostatic current flows through the first-level stacked MOSFET, which are (MNR1\_1 and MNR2\_1)~(MNR1\_14 and MNR2\_14), to generate the common intermediate voltage, which it uses to control the substrate voltage (G1R) of QS1\_1~QS1\_14 and QS2\_1~QS2\_14. Thus, the electrostatic current will be divided into 14 paths, and heat will be generated from AVDD3 to GND, via the first-level stacked MOSFET. Then, the electrostatic current will be divided into the remaining 14 paths, and heat will be generated from AVDD3 to GND, via the stacked BJT—(QS1\_1 and QS2\_1)~(QS1\_12 and QS2\_14)—to GND. The heat can be evenly distributed to different junctions, which are deeper than a gate-driven device to avoid thermal runaway. When an ESD event disappears, the stacked BJT and stacked MOSFET are turned off and the leakage current is lower than the ESD power clamp (IO1).

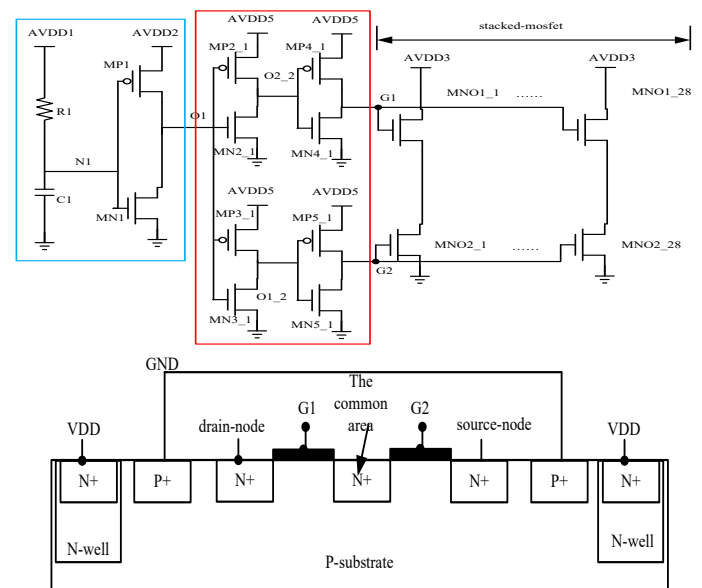


Figure 4. ESD power clamp (IO15c) and the cross section of the stacked MOSFET

This paper compares IO15c and IO15e by using the same layout area (95um\*144um), different component sizes and different methods. Because IO15e uses the substrate-driven method, it has one more mask (triple-well layer) than IO15c. IO15c's stacked MOSFET belongs to the same substrate and the drain node can be shared, so the layout area can be reduced so the size of the stacked MOSFET is 27um/0.44um. IO15e's first-level stacked MOSFET belongs to the same substrate and the drain node cannot be shared, whereas its second-level stacked BJT belongs to the same substrate and the drain node can be shared. Therefore, the layout area cannot be reduced and the size of the first-level stacked MOSFET is 13.5um/0.44um and the second-level stacked BJT is 27um/0.44um.

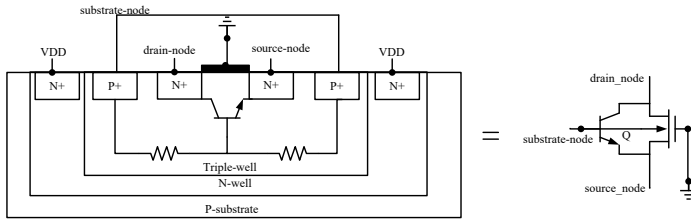


Figure. 5 Parasitic NPN junction

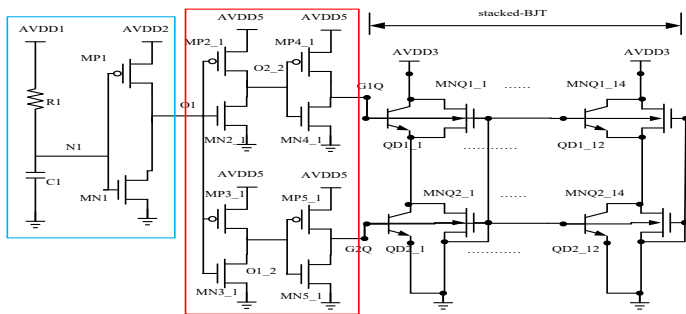


Figure. 6. ESD power clamp (IO15e) and the cross section of the stacked BJT

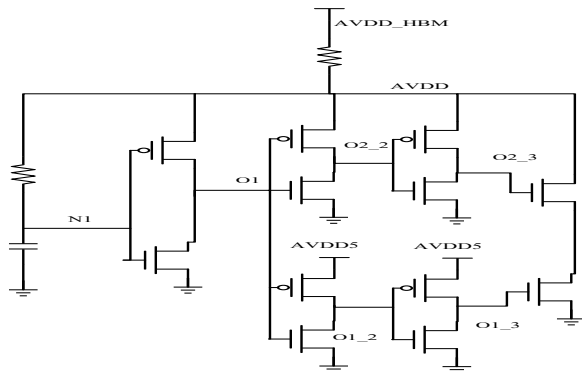


Figure. 7. ESD power clamp (IO15\_HBM)

By using transient simulation, it was confirmed that the voltage of each node is lower than the junction breakdown voltage of the 3.3V device, when AVDD\_HBM ranges from 0V to 3KV. The detection voltage of IO15 including nodes O1 and N1 which determines the turn-on time. Figure. 7 shows the ESD power clamp (IO15\_HBM) and series resistance (1500 ohms) for carrying out HBM simulation. Because the ESD power clamp (IO1) uses the RC-transient detector to drive large dimensions (BIGFET), and the ESD power clamp (IO15) uses the RC-transient detector to drive small dimensions of the delay-line, the turn-on time of IO15's detection point N1 is faster than the ESD power clamp (IO1) [5]. From the simulation results, AVDD is 12V, which is lower than the junction breakdown voltage, and the turn-on time of detection point N1 is 150ns for the ESD power clamp (IO15). The diagram of AVDD, N1, and O1 versus time is shown in Figure. 8. Moreover, when the ESD event disappears, all the IO1 and IO15 devices are turned off. Based on the simulation results, the total leakage current of both the ESD power pad (IO1) and the ESD power pad (IO15), with a typical process corner and a temperature of 25°C, are 464.4pA and 197.05pA, respectively. The ESD power clamp (IO15) has a lower rate of current leakage than the ESD power pad (IO1), and the stacked structure of the leakage current is smaller than that of the BIGFET.

In addition, in order to meet the specification of the sensor system, the size of the stacked MOSFETs ESD clamp (IO15c) is resized three times to achieve a larger-than-HBM ESD level of 4.5KV. The final measurement result of stabilized voltage, to reduce the leakage current that increases with temperature, is 1.0V. The original ESD clamp (IO15c) was changed to the ESD clamp (IO15c\_resize).

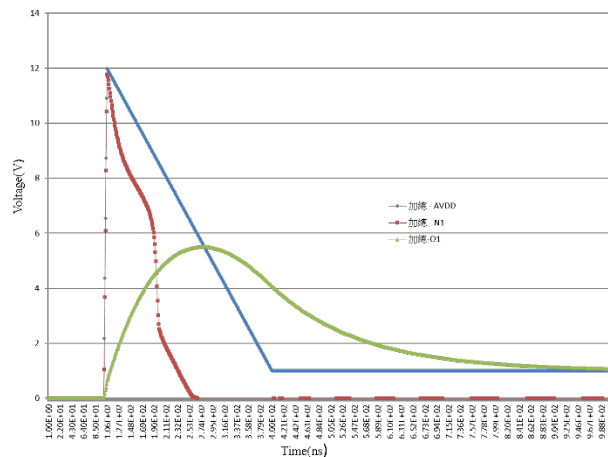


Figure. 8. IO15\_HBM simulation results

#### 4. Measurement results and discussion

Both IO15c and IO15e have the same layout area (95um\*144um), and compares with different methods include the gate-driven method and two-level-driven with both the gate-driven substrate-driven methods, respectively.

The ESD power clamp (IO15c/IO15e/IO15\_resize) is fabricated by the UMC 0.18um 1P6M CMOS-MEMS process; all devices use a 3.3V device. Figure. 9 shows VDD-VSS with a Positive mode and verifies the ESD level from VDD to VSS.



Table 2 shows the ESD power clamp (IO15c/IO15e/IO15\_resize) ESD test including HBM/MM for VDD to VSS with a Positive mode, the leakage current temperature of 25°C/125°C, the layout area, and the turn-on time when the VDD pin is zapped by a pulse [5], [6]. In addition, Figure. 10(a), 10(b) shows the turn-on time versus voltage, current of the ESD power clamp (IO15c\_resize)—the turn-on time is about 160ns when the VDD pin is zapped by a pulse and the ESD current is led away. For the electrical measurements of the (IO15c\_resize), the I-V characteristics and leakage currents versus AVDD are shown in Figure. 11(a). The (IO15\_resize) leakage current versus AVDD when VDD ranges from 0.5V to 1.5V and the temperature is 25°C is shown in Figure. 11(b).

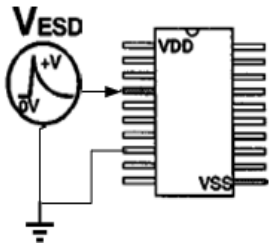


Figure. 9. VDD-VSS with Positive mode

Table 2. The ESD power clamp (IO15c/IO15e/IO15\_resize) ESD test

	IO15c	IO15e	IO15c_resize
turn-on time	160ns	160ns	160ns
leakage current at temperature of 25 °C /125 °C when AVDD3 is 1.0V	3.5pA/ 16.45nA	2.8pA/ 16.89pA	
leakage current at temperature of 25 °C /125 °C when AVDD3 is 1.8V	4.75pA/ 16.98nA	3.81pA/ 17.41nA	
HBM with Positive	8KV	5.5KV	8KV
MM with Positive	600V	300V	1000V
layout area(um*um)	95*144	95*144	95*387

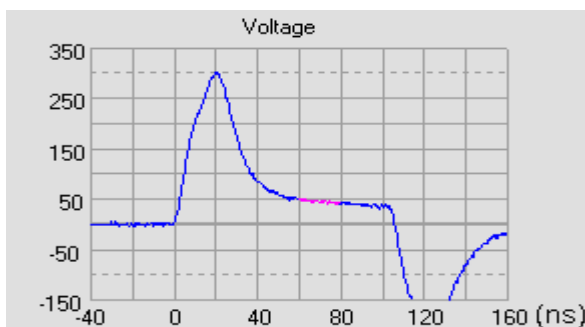


Figure.10. (a) The IO15c\_resize turn-on time versus voltage when the VDD pin is zapped by a pulse

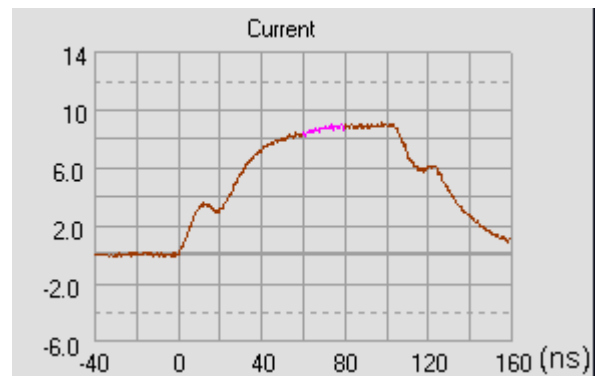


Figure.10. (b) The IO15c\_resize turn-on time versus current when the VDD pin is zapped by a pulse.

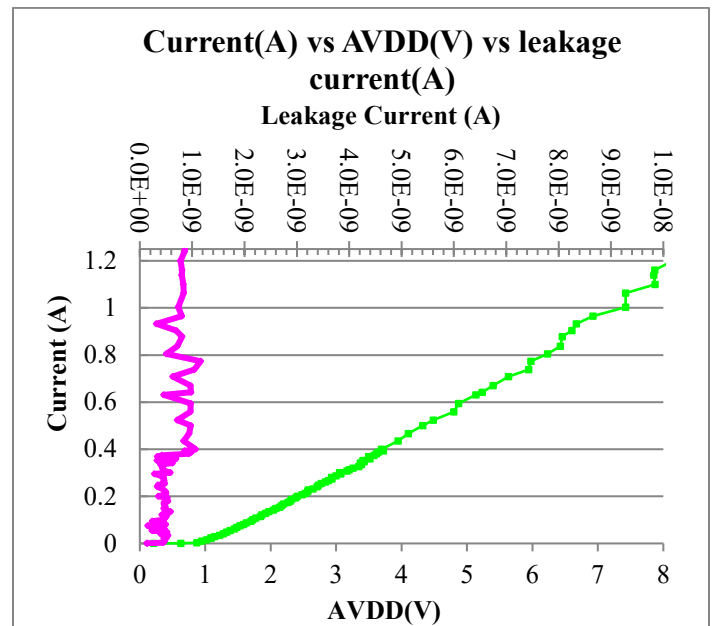


Figure. 11. (a) I-V characteristics of leakage current versus AVDD (IO15c\_resize)

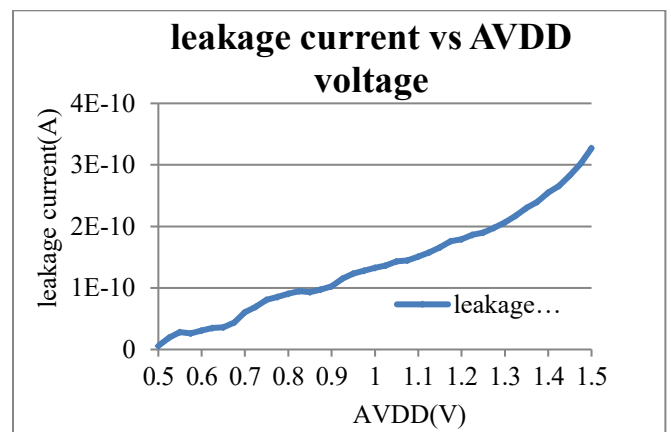


Figure. 11. (b) leakage current versus AVDD (IO15c\_resize)

According to the measurement results, the ESD power clamp (IO15c/IO15e/IO15\_resize) has a lower rate of current leakage and power consumption. It is expected to have less impact on and be suitable for ultra-low power sensor system applications. The proposed design has an HBM ESD level with a Positive higher

than 8KV, 5.5KV, 8KV, and the MM level protection with a Positive higher than 1000V, 300V, 600V MM ESD level. The proposed design for IO15c consumes 3.5pA/16.45nA at temperatures of 25°C/125°C when AVDD3 is 1.0V, and consumes 4.75pA/16.98nA at temperatures of 25°C/125°C when AVDD3 is 1.8V. The proposed design for IO15e consumes 2.8pA/16.89nA at temperatures of 25°C/125°C when AVDD3 is 1.0V, and consumes 3.81pA/17.41nA at temperatures of 25°C/125°C when AVDD3 is 1.8V. In addition, the proposed design includes an IO15c\_resize, which consumes 132.8pA at a temperature of 25°C when AVDD3 is 1.0V. The leakage current of the IO15c\_resize is larger than originally expected. The reason is that it is connected to the overall ESD protection circuit and affected by other ESD protection circuits. The layout area is 13680/13680/41040um<sup>2</sup>. Figure. 10 shows a dye photo of the ESD power clamp (IO15c/IO15e). Table 3 shows the ESD power clamp (IO12[9]/IO15c/IO15e/IO15\_resize) ESD test including HBM/MM for VDD to VSS with a Positive mode, leakage current, layout area, and turn-on time when the VDD pin is zapped by a pulse. The measurement data was reported by Integrated Service Technology Incorporated and Agilent 3458A.

From the analysis of the measurement results, IO15c/IO15c\_resize can be achieved higher than an HBM/MM ESD level of 4.5KV/400V by using the gate-driven method. IO15c can even shrink to 70~80% to achieve optimization. IO15e cannot reach an HBM/MM ESD level of 4.5KV/400V because the first-level gate-driven of the IO15e is effective, but the second-level substrate-driven of the IO15e does not have a full effect. Moreover, the common area is too small and the distance between the drain junction and the source junction is too close, so that a complete effective parasitic NPN junction or a complete stacked BJT cannot be formed. The solution to this issue is that a stacked BJT cannot share a drain junction, instead the parasitic NPN junction uses its own triple-well to isolate itself to achieve the stacked-BJT. However, the layout area will be larger than that of the IO15c, and an additional layer of triple-well is required, which is not cost-effective.

Table 3. The ESD power clamp (IO12/IO15c/IO15e/IO15c\_resize) ESD test

	IO12 [9]	IO15c	IO15e	IO15c resize
turn-on time		160ns	160ns	160ns
leakage current at temperature of 25 °C /125 °C when AVDD3 is 1.0V		3.5pA/ 16.45nA	2.8pA/ 16.89pA	
leakage current at temperature of 25 °C /125 °C when AVDD3 is 1.8V	24pA/ 66nA	4.75pA/ 16.98nA	3.81pA/ 17.41nA	
HBM with Positive	4.5KV	8KV	5.5KV	8KV
MM with Positive	400V	600V	300V	1000V
layout area(um <sup>2</sup> )	44800	13680	13680	41040

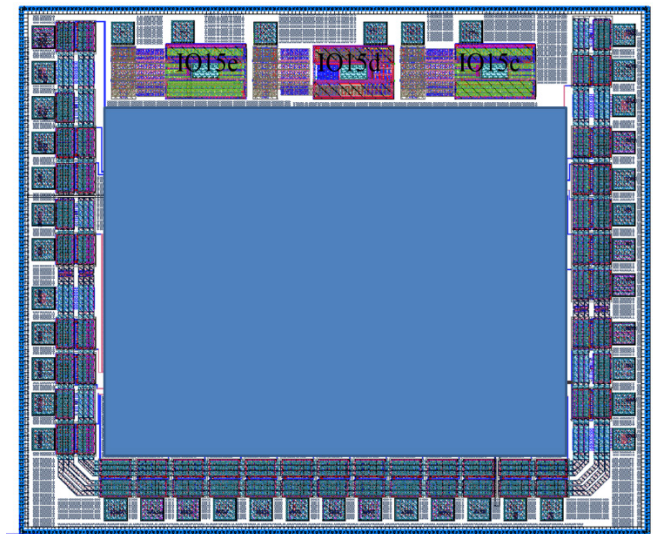


Figure. 12. Dye photo of whole-chip ESD protection and IO15c/e

### Acknowledgments

The authors appreciate the UMC and Taiwan Semiconductor Research Institute (TSRI), Taiwan, for supporting the CMOS chip manufacturing.

### References

- [1] J. Walraven, J. M. Soden, E. Cole, D. M. Tanner, and R. E. Anderson, "Human body model, machine model, and charge device model ESD testing of surface micromachined microelectromechanical systems (MEMS)," in 2001 EOS/ESD, pp. 236-246.
- [2] J. A. Walraven, J. M. Soden, D. M. Tanner, P. Tangyunyong, E. I. Cole Jr., R. E. Anderson, and L. W. Irwin, "Electrostatic discharge/electrical overstress susceptibility in MEMS: A new failure mode," in Micromachining and Microfabrication, 2000, pp. 30-39.
- [3] H. R. Shea, A. Gasparyan, H. B. Chan, S. Arney, R. E. Frahm, D. Lopez, S. Jin, and R. P. McConnell, "Effects of electrical leakage currents on MEMS reliability and performance," IEEE Trans. Device Mater. Rel., vol. 4, no. 2, pp. 198-207, 2004.
- [4] W. D. Greason, "Analysis of charge injection processes including ESD in MEMS," J. Electrostat., vol. 66, no. 11-12, pp. 602-608, 2008.
- [5] M. D. Ker, "Whole-chip ESD protection design with efficient VDD-to-VSS ESD clamp circuits for submicron CMOS VLSI," IEEE Trans. Electron Devices, vol. 46, no. 1, pp. 173-183, Jan. 1999.
- [6] M. D. Ker, T. Y. Chen, C. Y. Wu, and H. H. Chang, "ESD protection design on analog pin with very low input capacitance for high-frequency or current-mode applications," IEEE J. Solid-State Circuits, vol. 35, no. 8, pp. 1194-1199, Aug. 2000.
- [7] J. Li, R. Gauthier, S. Mitra, C. Putnam, K. Chatty, R. Halbach, and C. Seguin, "Design and characterization of a multi-RC-triggered MOSFET-based power clamp for on-chip ESD protection," in 2006 Electrical Overstress/Electrostatic Discharge Symposium, pp. 179-185.
- [8] M.-D. Ker, T.-Y. Chen, and C.-Y. Wu, "Substrate-triggered ESD clamp devices for use in power-rail ESD clamp circuits," Solid-State Electronics, vol. 46, no. 5, pp. 721-734, 2002.
- [9] Y. P. Chen, Y. Lee, J. Y. Sim, M. Alioto, D. Blaauw, and D. Sylvester, "45pW ESD clamp circuit for ultra-low power applications," in Proc. IEEE 2013 Custom Integrated Circuits Conf.

## **Towards Enterprise Technical Architecture for the Implementation of the South African NHI**

Farirai Chitsa, Tiko Iyamu\*

*Cape Peninsula University of Technology, Department of Information Technology, District Six, South Africa*

---

### **ARTICLE INFO**

*Article history:*

*Received: 12 February, 2020*

*Accepted: 07 March, 2020*

*Online: 20 April, 2020*

---

*Keywords:*

*Enterprise architecture*

*Technical architecture*

*Universal health coverage*

*National health insurance*

*IT project implementation*

---

---

### **ABSTRACT**

*This paper provides an insight about the significance of the enterprise technical architecture (ETA) in enabling and supporting the implementation of the South African National Health Insurance (NHI). Design: Existing documentations from both academic and government domains were gathered, and analyzed using the hermeneutics technique, from the perspective of interpretivist approach. Based on the analysis, the paper reveals the cruciality of the ETA in the implementation of the Universal health coverage (NHC) in the South African environment. The paper is intended to be of use for the core stakeholders of the NHI, which include governments' administrations, IT specialists, health practitioners, as well as academics.*

---

### **1. Introduction**

The national health insurance (NHI) is a universal health program, new in South Africa. At the time of this study in 2019, the program was being piloted. Owing to the newness of the program, stakeholders constituting a complex mixed bag, sensitivity nature of patients' datasets, and the complexity of information systems and technologies (IS/IT) solutions, the implementation will be inevitably challenging, which can potentially derail the entire program. From IS/IT perspectives, the challenges can be associated with factors such as lack of appropriate design and governance, which manifest into stagnation, disintegration of technology infrastructures, manipulation of information, and processes. Thus, an enterprise technical architecture (ETA) is required in addressing the fundamental challenges in enabling and supporting the implementation of the NHI.

The Universal Health Coverage (UHC) is a program that is aimed at increasing coverage and access to healthcare [1]. Both developed and developing countries such as Canada, Brazil, Taiwan, United states of America (USA), United Kingdom (UK) has adopted the program under different names, but with similar goals and objectives, in recent years [1]. It is National Health System (NHS) in the UK, Universal Health-care System (UHS) in Canada, and Obamacare in the USA [2]. The quality of life, as well as the healthcare of the Taiwanese, is said to have improved, leading to a better life expectancy as a result of the UHC in the

country [3]. The National Health Insurance (NHI) is the South African version of the UHC [4]. The department of health (DoH) is the custodian of the program.

The aim of the NHI is to ensure that all South Africans have access to good quality health care, disregarding their socio-economic status [4]. The anticipated benefits of NHI include elimination of out of pocket payments, removal of discrimination in terms of salary bracket, provision of universal health care to all with preference based on the illness and not affordability among others [5]. Cheng explains how the Taiwanese are benefiting from the country's NHI system, as they enjoy ease of access to health services including specialists, choice of health care provider and short waiting times [6]. The NHI is more about ensuring extended coverage and increased access to health services regardless of socio-economic status [7]. It is therefore intended to address challenges within the South African health sector, which has become severe due to the lack of equitable access to healthcare [4].

The UHC has yielded huge benefits to many countries such as the UK and Taiwanese [3]. The benefits hasn't been without challenges in some countries, from information technology (IT) perspective. In the USA, the Obamacare was hacked the same day it went on live [2]. The Canadian universal health-care system (UHC) is challenged with ease of access from different locations [8]. Cases and challenges from other countries are enough for the promoters and implementers of the South African NHI to be more prepared. Thus, there should be emphasis on the IS/IT solutions that enable and support the program. One of the approaches is to

---

\*Corresponding Author: Tiko Iyamu, Email: [connectvilla@yahoo.com](mailto:connectvilla@yahoo.com)

deploy the enterprise technical architecture (ETA) for the implementation of the NHI.

The assessment of the ongoing pilot of the NHI, it was reported that at the end of 2018, 20-million people were registered, but poor connectivity, hardware problems and lack of IT staff hinder some clinics from accessing the internet [9]. It has been proven that poorly designed systems affect the implementation of IT systems in healthcare [10]. Many of the IS/IT solutions' challenges manifest from lack of governance [11]. The ETA bridge the gap between enabler and the enabled, pragmatics assessment and of technology solutions in addressing needs, semiotics of IS/IT solutions' deployment [12]. The technical architecture stabilizes the deployment and use of IS/IT solutions in an environment [13]. Without architectural guidance, IS/IT solutions encounter challenges, and ultimately fail to enable and support goals and objectives towards fulfilment. It is based on this concern and gap that this study examines, and presents a discussion which can lead to the development and deployment of enterprise technical architecture (ETA) for the implementation of the South African NHI.

In order to give clearance, this paper is structured into six main sections, starting with the introduction, which is followed by reveal of related studies and the methodological approach that was applied in the study. Fourth section presents a discussion towards which an ETA can be built for the implementation of the NHI. Finally, a conclusion is drawn.

## **2. Related studies**

The use of IS/IT in the health sector improves the efficiency and effectiveness of the healthcare system [14], hence there is a need to invest more in the enabling solutions, to reduce some of the challenges [15]. This includes electronic storing as well as remote monitoring and accessing of patients' records [16].

The IS/IT solutions are increasingly used to play significant role in the delivering of healthcare services [17]. It was on this basis of signification that Phichitchaisopa and Naenna emphasized on the selection of ICT artefacts for enabling healthcare processes and activities [18]. This is to mitigate against the numerous challenges that constantly confront the health processes and activities, such as legislators, policy, governance, and systems design, integration and implementation [10]. The challenges can be worst in the South African environment in that it is a 'green field' for the UHC. Currently, public health facilities in South Africa are struggling in terms of the quality of service that they provide to the community [19]. There are poor ICT infrastructures in most parts of South Africa, which ultimately have impact on the adoption of health systems in the country [20]. This can be attributed to the state of IS/IT solutions that enable its functions. This makes case for more financial investment on IT solutions in enabling and supporting health care systems so as to improve service delivery through reponse time, and ease of access to patients' records [18]. Passchier therefore suggests the need for IT investment for the implementation of the NHI in the country [21].

The amount of investment on IS/IT does not necessarily determine the success or quality of the solutions. Successful implementation of IS/IT solutions is influenced by various factors, which the NHI is currently lacking. Child argue that successful

implementation of IT systems require interaction between the users, technologies, and organisational processes [19]. According to Cheng, the introduction of new technologies as well as velocity and variety of diseases can influence or strain IT systems including the budget [6]. In addition, connectivity, complexity of systems, reliability of software and hardware, human resources among others can also influence the implementation of ICT enabled systems such as the NHI [22]. These are factors and challenges that the South African NHI needs to focus on from the IS/IT perspective. Unfortunately, this aspect has been silent in the policy and strategic documents that gazetted between 2013 and to-date including some assessment reports [23, 9].

There has been so much emphases towards funding and other non-technical issues, and less attention on the enabler. In order to achieve the goals of UHC, the NHI system needs to be well financed [24]. This can be serious mistake. Like every other system, the NHI requires IS/IT solutions such as to software, hardware, network for its enablement [25]. However, the solutions include integration, security and governance, to ensure efficiency in operationalising and fulfilling the goals and objectives of the program.

As much as the use of ICT in health care systems has been increasing and of beneficial, it however, comes with challenges mainly regarding the concerns of security and privacy of sensitive data [26]. The challenges of implementation of IS/IT solution for healthcare service delivery can be attributed to many factors, such as cultural, economic, geographical and political settings of the environment [27, 1]. The Brazilian's unified health system is still facing challenges due to geographical factors which affect the equitable distribution of health care services in terms of resources and technologies [28]. Lack of standards can also affect the successful implementation of ICT solutions [29]. The Norwegian health sector experienced uncertainty of ICT infrastructure and solutions that was acquired without an architecture which led them to implementing one [30].

The NHI implementation requires combination, co-existence, and integration of various IS/IT solutions, such as software, hardware platforms, network protocols, and databases towards achieving its goals [8]. Interoperability is of paramount importance as medical data and information would be shared among different entities [31]. This is not without architectural deployment. Also, despite the interest and awareness to automate health information systems for NHI, which include transitioning from manual to electronic processes and interoperability of IS/IT solutions, the deployment of ETA is still silent. One of the definitions of the domain: ETA is a logically consistent set of principles, standards and models that are derived from vision, strategy in order to guide the engineering of IS/IT solutions within context [12].

## **3. Methodological approach**

This is an exploratory case study of the implementation of the South African NHI. Yazan defines this type of study as an inquiry of a phenomena, to gain a better understanding of a bigger class of units [32]. The conceptual and explanatory nature of the study makes the case approach suitable for the study [33].

The data was gathered from two sources, documentation relating to NHI by using the document analysis technique; and



transcript of focus group. These sources were considered most suitable for the following reasons: (1) the documents were passed into bill by the legislative arm of the government, making them authentic and legal, and (2) the focus group had a balanced representation from the public, government, and health practitioners.

The document analysis is often used to extract rich content. Sherif describes the technique as a detailed examination of data that can be collected from sources such as peer-reviewed articles, official reports, and policies documents with a specific goal of understanding the documents within context [34]. The technique helps to extract specific insights and key information for the purposes of the phenomenon being studied [35]. As shown in Table 1, different documents were collected for this study.

Table 1: Documentations

Title	Description	Source
National Health Insurance for South Africa Towards universal health coverage	1-80 pages: Government Gazette, 30 June 2017. No. 40955.	Department of health, Republic of South Africa. <a href="http://www.gpwonline.co.za">Www.gpwonline.co.za</a>
National Health Insurance for South Africa Towards universal health coverage	1-98 pages: Government Gazette, 11 December 2015. Ref No. 39506.	Department of health, Republic of South Africa. <a href="http://www.gpwonline.co.za">Www.gpwonline.co.za</a>
Status of NHI Pilot districts 12-month progress report	1-44 pages: Assessment of the NHI pilots. 25 May 2015.	Department of health, Republic of South Africa
National Health Insurance in South Africa	1-59 pages: Policy document for the NHI	Department of health, Republic of South Africa. <a href="http://www.gpwonline.co.za">Www.gpwonline.co.za</a>
National Health Insurance: pilot projects reveal deep problems	Assessment of pilot projects in 11 health districts countrywide between 2012 and 2017	Katherine Child, 28 July 2019.

The focus group method was employed it helps participants to recall their past experiences through interaction with other stakeholders [36]. A radio program was used as a source in the collection of data from the focus. The program was hosted by the South African Frequency Modulation (SAFM) on the <http://www.safm.co.za/sabc/home/safm/multimedia>. The SAFM is a national radio station. The station, arguably has the highest number of audience, listeners in the country. The participants included the host-presenter, two guests (each represented the government and health practitioners), and members of the community. The interview was conducted in the form of discussion. It was facilitated by the host-presenter between the guests and the callers (community members). It was an hour

program. The transcript of the podcast forms part of the data that was used in this study.

The data was analyzed by identifying, examining and interpreting subsets from technical and non-technical perspectives [37]. This was done through the hermeneutics approach, which helps to gain meaning and understanding of the text about the phenomenon being studied [38].

#### 4. Result and discussion

From the analysis of the NHI current state towards implementation, three factors: too much attention on political issues; imbalance between enabler and the enabled; and ETA insolation were found to be most prevalence. The factors as discuss below can potentially derail the implementation of the NHI, hence the deployment of ETA is crucially significant.

##### 4.1. Too much attention on political issues

It is critical to understand the factors that influence the deployment of the ETA is an environment. Many architecture projects are not successful because of the different challenges that they encounter in the process [39]. Some of the challenges are attributable to the gap that exists between the architects and other stakeholders, which manifest from attention being given to non-technical issues [40].

The implementation of the NHI has been overly politicized by the stakeholders, the political parties and some sections of the country. The policy and strategic documents that were gazetted between 2013 and to-date focus more on issues that manifest from political discourse. This includes how the NHI program will be funded; source of funding; and why should everyone be grouped or compelled to enroll in the program (DoH, 2017, 2015, 2013). As a result, there has been less attention on the enabling and supporting strategies towards successful implementation and practice of the NHI. Barrilleaux and Rainey explain how partisan politics outweigh universal healthcare program (Obamacare) at the expense of citizens [2]. This is a fundamental challenge which the South African government should take cognizance of, in the implementation of NHI.

##### 4.2. Imbalance between enabler and the enabled

The discussion about the NHI has come a long way, about ten years. It got intensified in the last two years, more in 2019 as the program got approval by the Parliament (legislative authority) and gazetted by cabinet. The approval paved way for actual implementation and realization of the goal and objectives of the program. This require a balance between the enabled (NHI program) and enabler (IS/IT solutions). However, over the years discourse including strategic and policy documents has been more of one sided, in favor of the enabled rather than the enabler. Taken the USA account and experience into consideration [2], this can be detrimental for the implementation of NHI.

The imbalance affects capability of the enabler, which require vast and detailed planning and assessment IS/IT solutions and infrastructures. These include health systems, hardware platforms, software, databases, and network protocols. To ensure workability and successful enabling and support of the NHI, standard, policy, and principle must be adhered, through which appropriate IS/IT

solutions and infrastructures are selected, for compatibility, integration, scalability and flexibility purposes. This is a report that the on-going pilot is experiencing challenges in some clinics, owing to lack of internet access caused by hardware and software failure as well as IT staff know-how [9]. The enterprise architecture (EA) which provides governance, standards, policies, and principles has hardly receive attention in the strategic documents [23]. A study highlights and explain how architecture can be used to manage complexities of systems [41].

4.3. Enterprise technical architecture in isolation

The government realizes the importance of health enterprise architecture [42]. What is missing is categorization of the domains, which is critical in the development of the EA. The pilot is already on-going without architecture, yet there are no signs of ETA development. The IS/IT solutions has dependency on each other, which makes their architectures, from platforms to integration critical. The ETA facilitates the integration, collaboration, standardization, deduplication, and reengineering of IS/IT solutions. Silo deployment of a domain or domains leads to lack of leverage and alignment between the enabled and the enabler [43]. As a result, many organizations are either unable to implement their ETA plans or only able to partially implement them [40].

The EA consists of domains which include business, information, application, and technical [44]. Although each of the domains has distinct objectives and deliverables, they are interconnected [45]. To avoid defragmentation, no domain is developed or deployed in isolation. Also, the domains are deployed in a chronological order, starting from the business to the technical architecture [46, 47]. This is to ensure holistic coverage, from business (health) goals and objectives, information exchanges and flows, to processing (eHealth) of activities and events [48]. This enacts integration and interoperability of systems towards successful implementation of the NHI systems

5. Enterprise technical architecture

In a more generic terms, an architecture is the art of designing a structure in order to manage the size and complexity [49]. An Architecture brings about pre and well planned procedures that are useful when implementing systems' complexities, which include integration, relationships of components [50] This study focuses on the enterprise technical architecture (ETA) domain of the enterprise architecture (EA) [47]. The technical architecture can be defined a set of standard guidelines that can be used to compel the choices of technology investment [51]. The architecture can be applied to guide any system because of its premise to provide a more solid foundation, enhanced support, and improved management approach [52].

The ETA has been employed to guide, support, manage, and govern IS/IT solutions in many walks of life, including the health sector [13]. From health system's viewpoint, an architecture is important in a system's life in that it is used to guide data collection and management of applications [53]. The need for systems in healthcare to support interoperability as well as data sharing makes it difficult to implement or develop systems without an architecture [50]. In the context of healthcare, Hayes argues that money can be saved if an architecture could be used to guide processes including the selection and deployment of IS/IT solutions [54].

The increasing interest in the ETA is primarily to ensure, and to prevent prohibitive circumstances, such as loss of datasets due to lack of security, lack of connectivity, increased procurement and maintenance costs of IS/IT solutions, unreliability, non-compatibility as well as uncertainty of software and hardware [25]. This enacts the ETA as a process and not a project that has a clear start and finish [55]. As shown in Figure 1, the ETA is defined as a four phase approach, which are objective, development, implementation, and strategic [12]. The deployment of the ETA can on iteration basis address the integration and interoperability problems in health care systems [31].

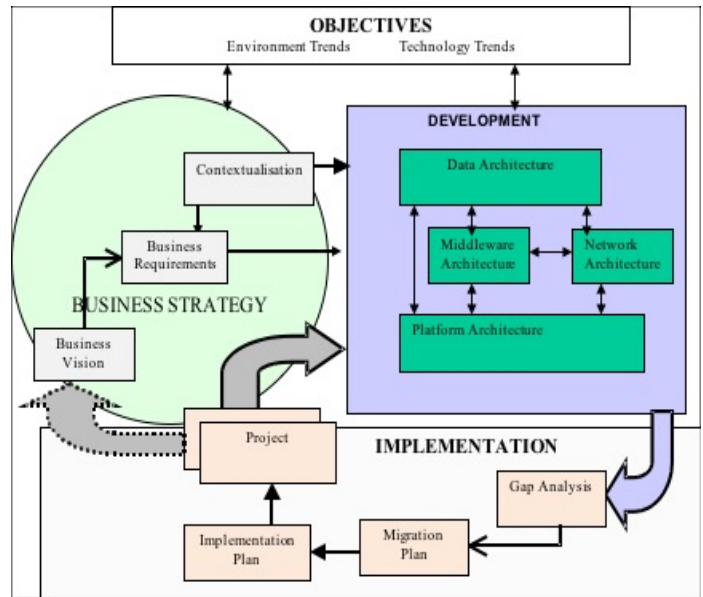


Figure 1: Technical Architecture Deployment [12]

Figure 1 is discussed, with focus on the cruciality of the ETA in the implementation of the NHI. It can be used to the four logical phases: Objectives, Business Strategy, Development, and Implementation are core in the deployment of technical architecture.

Phase 1: The ETA provides a baseline of the current and future states of an environment, which require managing change and gaining an accurate view of influencing factors [12]. No environment is stagnant, change is constant, which require the iterative approach of the ETA enabling the activities to the changing and transformative circumstances [56]. According to Gong and Janssen, the objectives shift and are refocused to align with societal or environmental needs [55]. The ETA facilitates assessment of the impact of technology change on the environment.

Phase 2: Phase 1 is the determinant factor for this phase [12]. This shows the ultimate dynamic and constantly changing nature of environment, which means that innovation is inevitable, and principles might become outdated. In this phase, technology challenges are addressed [55]. This allows the ETA to enable digitalization of health processes and activities toward quicker response in the delivering of services [56].

Phase 3: The development of the ETA is in four stages: requirements; classification of domains; documentation; and governance principles [12]. There are challenges in each of the

stages. To mitigate against the challenges, Banaeianjahromi, N., & Smolander suggest that it is crucial to understand the influencing factors during development [39]. In the context, there is a need to examine the relationship between architects and other stakeholders [40]. The development helps clarify the deployment and use of IS/IT solutions, which include processes, technical platforms, such as servers and databases, and of their mutual dependencies [57]. The development of the ETA provide insights into processes, available IS/IT solutions, and integrations methods [43].

Phase 4: As shown in Figure 1, the implementation phase consists of four stages: Gap analysis; Migration planning; Implementation planning; and Project [12]. Although architects are responsible for the implementation of the architectures, they depend on executives, on decision relating to non-technical issues, which often pose challenges to architecture solutions [40]. This can be attributed to lack of implementation strategy. Each component of the implementation should have assessment model. Otherwise, the development will continue to remain taxonomies [39].

## 6. Conclusion

In conclusion, the ETA should guide the implementation of the NHI. This should allow continuous examining and detecting of the factors that influence the implementation and practice of the program. These factors include technology infrastructures, information exchanges, and healthcare changing requirements (such as process, governance, and legislature).

The study discusses ETA towards its development for the implementation of the NHI in South Africa. The successful implementation of the NHI through the deployment of an ETA would be of interest and benefit to the stakeholders such as the policy-makers (government), health practitioners (doctors, nurses, and pharmacists) and the IT specialists, the enablers of the systems. Most importantly, development of an architecture will increase the society's confidence in the NHI program in that the ETA provides guidelines, which allow continuous examining and detecting of the factors that influence the implementation and practice of the program. The contributions of the study come from theoretical viewpoint. The theoretical contribution is the study's addition to existing literature from the perspectives of health informatics and ICT for development.

This study is limited, therefore it recommends that further studies should examine the factors that can influence the implementation of the NHI in South Africa, to understand the technology infrastructures, information exchange, and business (healthcare) requirements for the implementation of the NHI in South Africa. Through such studies an enterprise technical architecture can be developed, to guide the implementation of the NHI in the country.

## Conflict of Interest

The authors declare no conflict of interest.

## Acknowledgment

The authors would like to acknowledge and thank the Department of IT, CPUT for its support in carrying out this study. Input from the research forum at the IT department is also appreciated.

## References

- [1] M.R. Reich, J. Harris, N. Ikegami, A. Maeda, C. Cashin, E.C. Araujo, K. Takemi, T.G. Evans, "Moving towards universal health coverage: Lessons from 11 country studies" *The Lancet*, 387(10020), 811–816, 2016. [https://doi.org/10.1016/S0140-6736\(15\)60002-2](https://doi.org/10.1016/S0140-6736(15)60002-2)
- [2] C. Barrilleaux, C. Rainey, "The Politics of Need. State Politics & Policy" *Quarterly*, 14(4), 437–460, 2014. <https://doi.org/10.1177/1532440014561644>
- [3] J.Y. Lai, J. Wang, "Switching attitudes of Taiwanese middle-aged and elderly patients toward cloud healthcare services: An exploratory study" *Technological Forecasting and Social Change*, 92, 155–167, 2015. <https://doi.org/10.1016/j.techfore.2014.06.004>
- [4] N. Siegfried, T. Wilkinson, K. Hofman, K. Hofman, "Where from and where to for health technology assessment in South Africa? A legal and policy landscape analysis" *South African Health Review*, 41–48, 2017.
- [5] R. Marten, D. McIntyre, C. Travassos, S. Shishkin, W. Longde, S. Reddy, J. Vega, "An assessment of progress towards universal health coverage in Brazil, Russia, India, China, and South Africa (BRICS)" *The Lancet*, 384(9960), 2164–2171, 2014. [https://doi.org/10.1016/S0140-6736\(14\)60075-1](https://doi.org/10.1016/S0140-6736(14)60075-1)
- [6] T. Cheng, "Reflections On The 20th Anniversary Of Taiwan's Single-Payer National Health Insurance System" *Health Affairs*, 34(3), 502–510, 2015. <https://doi.org/10.1377/hlthaff.2014.1332>
- [7] W. Cape, "Pursuing Universal Healthcare Coverage through the implementation of NHI", 2015.
- [8] D. Martin, A.P. Miller, A. Quesnel-Vallée, N.R. Caron, B. Vissandjée, G.P. Marchildon, "Canada's universal health-care system: achieving its potential" *The Lancet*, 391(10131), 1718–1735, 2018. [https://doi.org/10.1016/S0140-6736\(18\)30181-8](https://doi.org/10.1016/S0140-6736(18)30181-8)
- [9] K. Child, "National Health Insurance: pilot projects reveal deep problems", 2019.
- [10] M. Jeffries, D. Phipps, R. L. Howard, A. Avery, S. Rodgers, D. Ashcroft, "Understanding the implementation and adoption of an information technology intervention to support medicine optimization in primary care: qualitative study using strong structuration theory" *BMJ open*, 7(5), e014810, 2017. <http://dx.doi.org/10.1136/bmjopen-2016-014810>
- [11] C. Johnston, L. Gillam, "Legal and Ethical Issues Arising from the Use of Emerging Technologies in Paediatric Healthcare" *QUT Law Review*, 18(2), 93–110, 2019.
- [12] T. Iyamu, "A Framework for Developing and Implementing the Enterprise Technical Architecture. *Journal of Computer Science and Information Systems*, 9(1), 189–206, 2012. <https://doi.org/10.2298/CSIS1011030401>
- [13] A. Zimmermann, R. Schmidt, K. Sandkuhl, M. Wißotzki, D. Jugel, M. Möhring, "Digital enterprise architecture-transformation for the internet of things" in 2015 IEEE 19th International Enterprise Distributed Object Computing Conference Workshops and Demonstrations, EDOCW: 130–138. DOI: 10.1109/EDOCW.2015.16
- [14] S. Devaraj, T.T. Ow, R. Kohli, "Examining the impact of information technology and patient flow on healthcare performance: A Theory of Swift and Even Flow ( TSEF ) perspective" *Journal of Operations Management*, 31(4), 181–192, 2013. <https://doi.org/10.1016/j.jom.2013.03.001>
- [15] W. Raghupathi, V. Raghupathi, "Big data analytics in healthcare: promise and potential, 2(1), 1–10, 2014. DOI: <https://doi.org/10.1186/2047-2501-2-3>
- [16] B.A.L. Kellermann, S.S. Jones, "What It Will Take To Achieve The As-Yet-Unfulfilled Promises" *Journal of Health Information Technology*, 32(1), 63–68, 2005. <https://doi.org/10.1377/hlthaff.2012.0693>
- [17] E.A. Booger, T. Arts, L.J. Engelen, T.H. Belt Van De, "What Is eHealth": Time for An Update? *JMIR Research Protocols*, 4(1) 2–5, 2015. DOI: 10.2196/resprot.4065
- [18] N. Pichitchaisopa, T. Naenna, "Original article: Factors Affecting the Adoption of Healthcare", 413–436, 2013.
- [19] L. Mhlaba, A. Parry, D. Blaauw, "Is National Health Insurance a viable option for South Africa? Experiences from other countries. *AfricaGrowth Agenda*, 2016(10), 8–12, 2016.
- [20] N. Leon, H. Schneider, E. Daviaud, "Applying a framework for assessing the health system challenges to scaling up mHealth in South Africa" *BMC Medical Informatics and Decision Making*, 12(1), 1–12, 2012. DOI: <https://doi.org/10.1186/1472-6947-12-123>
- [21] R. Passchier, "Exploring the barriers to implementing National Health Insurance in South Africa: The people's perspective" *South African Medical Journal*, 107(10), 836, 2017. DOI: 10.7196/SAMJ.2017.v107i10.12726
- [22] J. Ross, F. Stevenson, R. Lau, E. Murray, "Factors that influence the implementation of e-health: a systematic review of systematic reviews" *Implementation Science*, 11(1), 1–12, 2016. DOI: <https://doi.org/10.1186/s13012-016-0510-7>
- [23] Department of Health "policy documents for 2013 and 2015" 2017.
- [24] L. Liaropoulos, I. Goranitis, "Health care financing and the sustainability of health systems" *International Journal for Equity in Health*, 14(1), 5–8, 2015. DOI: <https://doi.org/10.1186/s12939-015-0208-5>



- [25] M. Aubakirov, E. Nikulchev, "Development of System Architecture for E-Government Cloud Platforms" *International Journal of Advanced Computer Science and Applications*, 7(2), 253–258, 2016. DOI: 10.14569/IJACSA.2016.070235
- [26] Q. Jiang, M.K. Khan, X. Lu, J. Ma, D. He, "A privacy preserving three-factor authentication protocol for e-Health clouds" *The Journal of Supercomputing*, 72(10), 3826–3849, 2016. DOI: <https://doi.org/10.1007/s11227-015-1610-x>
- [27] I. Odeyemi, J. Nixon, "Assessing equity in health care through the national health insurance schemes of Nigeria and Ghana: a review-based comparative analysis" *International Journal for Equity in Health*, 12(1), 1-18, 2013. DOI: <https://doi.org/10.1186/1475-9276-12-9>
- [28] L. Santos, A. Oliveira, J. Trindade, I. Barreto, P. Palmeira, Y. Comes, F. Santos, W. Santos, J. Oliveira, V. Pessoa, H. Shimizu, "Implementation research: towards universal health coverage with more doctors in Brazil" *Bulletin of the World Health Organization*, 95(2), 103-112, 2017. doi: 10.2471/BLT.16.178236
- [29] O. Hanseth, B. Bygstad, "Flexible generification: ICT standardization strategies and service innovation in health care" *European Journal of Information Systems*, 24(6), 645–663, 2015. <https://doi.org/10.1057/ejis.2015.1>
- [30] D.H. Olsen, "Enterprise Architecture management challenges in the Norwegian health sector" *Procedia Computer Science*, 121, 637–645, 2017. <https://doi.org/10.1016/j.procs.2017.11.084>
- [31] M. Sajid, K. Ahsan, "Role of Enterprise Architecture in Healthcare Organizations and Knowledge-Based Medical Diagnosis System" *Journal of Information Systems and Technology Management*, 13(2), 181–192, 2016. <https://doi.org/10.4301/S1807-17752016000200002>
- [32] B. Yazan, "The Qualitative Report Three Approaches to Case Study Methods in Education: Yin, Merriam, and Stake" *The Qualitative Report*, 20(2), 134–152, 2015.
- [33] H. Ridder, "The theory contribution of case study research designs" *Business Research*, 10(2), 281-305, 2017. DOI: <https://doi.org/10.1007/s40685-017-0045-z>
- [34] V. Sherif, "Evaluating preexisting qualitative research data for secondary analysis" *Forum Qualitative Sozialforschung/Forum:Qualitative Social Research*, 19(2), 2018.
- [35] M.P. Johnston, "Secondary Data Analysis: A method of which the time has come" *Qualitative and Quantitative Methods in Libraries (QQML)*, 3, 619–626, 2014. DOI: <http://dx.doi.org/10.17169/fqs-19.2.2821>
- [36] G. Guest, E. Namey, K. McKenna, "How Many Focus Groups Are Enough? Building an Evidence Base for Nonprobability Sample Sizes" *Field Methods*, 29(1), 3-22, 2016. <https://doi.org/10.1177/1525822X16639015>
- [37] A. Maxwell, T. Warner, F. Fang, "Implementation of machine-learning classification in remote sensing: an applied review" *International Journal of Remote Sensing*, 39(9), 2784-2817, 2018. doi.org/10.1080/01431161.2018.1433343
- [38] A.S. Lee, "Electronic Mail as a Medium for Rich Communication: An Empirical using Hermeneutic Interpretation", 18(2), 143–157, 1994.
- [39] N. Banaeianjahromi, K. Smolander, "Lack of communication and collaboration in enterprise architecture development" *Information Systems Frontiers*, 21(4), 877-908, 2019. DOI: <https://doi.org/10.1007/s10796-017-9779-6>
- [40] M. Dale, H. Scheepers, "Enterprise architecture implementation as interpersonal connection: Building support and commitment" *Information Systems Journal*, 30(1), 150-184, 2020.
- [41] O.A. Adenuga, R.M. Kekwaletswe, A. Coleman, "eHealth integration and interoperability issues: towards a solution through enterprise architecture" *Health Information Science and Systems*, 3(1), 1–8, 2015. DOI: <https://doi.org/10.1186/s13755-015-0009-7>
- [42] A. Gray, Y. Vawda, "Health policy and legislation" *South African health review*, 2016(1), 3-15, 2016.
- [43] R. Foorhuis, M. Van Steenberghe, S. Brinkkemper, W.A. Bruls, "A theory building study of enterprise architecture practices and benefits" *Information Systems Frontiers*, 18(3), 541-564, 2016. DOI: <https://doi.org/10.1007/s10796-014-9542-1>
- [44] D.D. Dang, S. Pekkola, "Systematic Literature Review on Enterprise Architecture in the Public Sector" *Electronic Journal of e-Government*, 15(2), 130-154, 2017.
- [45] T. Iyamu, *Enterprise Architecture: from concept to Practise* (2nd Ed.). Australia: Heidelberg Press, 2015.
- [46] K. Sandkuhl, U. Seigerroth, J. Kaidalova, "Towards Integration Methods of Product-IT into Enterprise Architectures" In 2017 IEEE 21st International conference on Enterprise Distributed Object Computing Workshop (EDOCW), Quebec City, Canada, 2017: DOI: 10.1109/EDOCW.2017.13
- [47] I. Shaanika, T. Iyamu, "Deployment of enterprise architecture in the Namibian Government: The use of activity theory to examine the influencing factors" *Electronic Journal of Information Systems in Developing Countries*, 71(1), 1–21, 2015. <https://doi.org/10.1002/j.1681-4835.2015.tb00515.x>
- [48] J. Whelan, G. Meaden, *Business Architecture: A Practical Guide*, Gower publishing, Ltd., 2016.
- [49] C. Fischer, R. Winter, S. Aier, "What is an enterprise architecture principle? Towards a consolidated definition" *Studies in Computational Intelligence*, 317(Ieee 2000), 193–205, 2010.
- [50] K. Hjort-Madsen, "Enterprise architecture implementation and management: A case study on interoperability" in 2006 Hawaii International Conference on System Sciences, Kauai, HI, USA 2006 DOI: 10.1109/HICSS.2006.154
- [51] R. Giachetti, "Design of enterprise systems: Theory, architecture, and methods. CRC Press, Taylor & Francis Group, 2016.
- [52] Z. Chen, X. Zhang, K. He, "Research on the Technical Architecture for Building CPS and Its Application on a Mobile Phone Factory" in 2017 Enterprise Systems 5th International Conference on Enterprise Systems: Industrial Digitalization by, ES 2017: 76–84. DOI: 10.1109/ES.2017.20
- [53] Y. Zhang, M. Qiu, C.W. Tsai, M.M. Hassan, A. Alamri, "Health-CPS: Healthcare cyber-physical system assisted by cloud and big data" *IEEE Systems Journal*, 11(1), 88–95, 2017. DOI: 10.1109/JSYST.2015.2460747
- [54] G. Hayes, "The NHS Information Technology (IT) and social care review 2009: A synopsis" *Informatics in Primary Care*, 18(2), 81–88, 2010. DOI: <http://dx.doi.org/10.14236/jhi.v18i2.757>
- [55] Y. Gong, M. Janssen, "The value of and myths about enterprise architecture" *International Journal of Information Management*, 46, 1-9, 2019. <https://doi.org/10.1016/j.ijinfomgt.2018.11.006>
- [56] J. Wichmann, M. Wißotzki, "An Exploration of Enterprise Architecture Research in Hospitals" In 2019 International Conference on Business Information Systems, Seville, Spain. [https://doi.org/10.1007/978-3-030-36691-9\\_8](https://doi.org/10.1007/978-3-030-36691-9_8)
- [57] E. Niemi, S. Pekkola, "The Benefits of Enterprise Architecture in Organizational Transformation" *Business & Information Systems Engineering*, 1-13, 2019. DOI: <https://doi.org/10.1007/s12599-019-00605-3>



## Face Recognition on Low Resolution Face Image With TBE-CNN Architecture

Suharjito\*, Atria Dika Puspita

Computer Science Department, Binus Graduate Program, Bina Nusantara University, 11480, Indonesia

---

### ARTICLE INFO

*Article history:*

*Received: 10 February, 2020*

*Accepted: 04 March, 2020*

*Online: 20 April, 2020*

---

*Keywords:*

*Low Resolution*

*Face Recognition*

*Trunk-Branch Ensemble CNN*

---

### ABSTRACT

*Face recognition in low resolution images has challenges in active research because face recognition is usually implemented in high resolution images (HR). In general, research leads to a combination of pre-processing and training models. Therefore, this study aims to classify low-resolution face images using a combination of pre-processing and deep learning. In addition, this study also aims to compare evaluation results based on differences in epoch values. In this research will use the Trunk Branch Ensemble - Convolutional Neural Network (TBE-CNN) as one of Convolutional Neural Network (CNN) architecture combined with the pre-processing method which is super resolution to get better accuracy compared to the state-of-art. Then the model is trained with different epoch values, that is 40 and 100, to comparing the best classification. This study was evaluated by YTD Dataset. Based on the test results, this proposed method has achieved better results compared to the previous method, which gives an increase of 1%. After that, training results from different epoch values used produce different accuracy at the training model but have no effect on validation and testing model. The training using epoch = 100 has an accuracy increase of 3% compared to training using epoch = 40 and the loss ratio obtained at the training is decreased by 20% compared to training at epoch = 40. Furthermore, optimization parameters used and reducing computing time when training models and validation will be future research.*

---

### 1. Introduction

Face recognition is a biometric that is used to recognize human faces. According to [1], face recognition is known as an image system that is used to try to get the identity behind the video being played and protected faces that have been labeled. The face has several components, such as the eyes, nose and mouth. From face components, it can produce millions of face variations throughout the world. The one that make a differences of each person's face are face shape, eyes, nose, mouth, and others. Based on the percentage of biometric usage described by [2], face recognition becomes the most usage on the system in Machine-Readable Travel Document MRTD with the graphic shown in Figure 1.

Face Recognition (FR) has become a very active research field due to the increasing demands of security, commercial applications and law enforcement applications [3]. For the examples of face recognition for security are finding someone's identity based on a face photo, authenticating to login into a smartphone, and others. In addition, face recognition can also apply to surveillance cameras.

Surveillance cameras are tools that help monitoring people in a room or area. Generally, face recognition is done on videos produced by surveillance cameras. But now, surveillance cameras have a low resolution, so the produced video also have low quality. This can be cause of face recognition accuracy tends to be low.

One of the face recognition methods that dealing with low-resolution problems and well-known today is deep learning. Deep learning is a new technology in machine learning that developed because along with the development of the GPU and the presence of big data has revives this technology. On the other hand, deep learning is a more accurate machine learning because they study the features of the data representation itself, so it minimize the require for programmer-based feature techniques [4].

One of the deep learning algorithms that can be used to face recognition is Convolutional Neural Network (CNN). CNN is a type of neural network that is used for image classification. The image here can be RGB or grayscale. CNN architecture is divided into 2, namely learning features and classification. There are 2

---

\*Corresponding Author: Suharjito, Email: [suharjito@binus.edu](mailto:suharjito@binus.edu)

stages of learning on CNN, namely feed-forward and backpropagation.

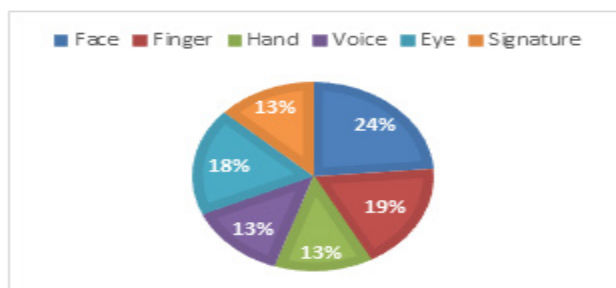


Figure 1: Comparison of the Most Widely Biometrics Used in MRTD Systems

In [5] the authors describe the four CNN architectures that are currently developed and be the subject of their research. The four architectures are Cross Correlation Mechanism CNN (CCM-CNN), TBE-CNN, HaarNet, and Canonical Face Representation CNN (CFR-CNN). From the accuracy obtained in the study proves that the TBE-CNN architecture and HaarNet have high accuracy for face recognition at low resolution. Previously, [6] conducted research using HaarNet on face recognition and compared it with Point-to-Set Correlation Learning (PSCL) architecture, Euclidean-to-Riemannian Metric (LERM) Learning, and TBE-CNN. And the results obtained for still-to-video prove that TBE-CNN is one of the best architectures for face recognition on low-resolution face images for still-to-video cases.

Trunk-Branch Architecture CNN (TBE-CNN) is one of the CNN architectures used to extract complementary features and patches around face landmarks through trunk and branches network. In the previous study, [7] has proposed two branch deep CNN method, which is a novel couple mapping using Deep Convolutional Neural Network (DCNN) and in this case using VGGFace pretrained model which is serves to mapping low and high-resolution face images into general space with non-linear transformations. And the proposed method has accuracy which is equal to 80.8% on the face size of 6 x 6 in the FERET dataset. After that, [3] proposed Deep Couple RestNet, which is a method whose architecture consists of 1 trunk using RestNet as the model and 2 branch networks (branch) using couple mapping to bring the distance between low and high resolution face images becoming certain resolutions and similar features will be placed in the new feature space. They also replaced the model in the trunk network with VGGFace and Light CNN for comparison and the results obtained were 93.6% for Coupled-ResNet, 83.7% for Coupled-VGGFace, and 80% for Coupled-Light CNN on the Labeled Face in The Wild (LFW) dataset for the size 8 x 8.

Adding pre-processing for face recognition at low resolutions is also widely used in research. According to [8] there are several pre-processing methods for solving low resolution face recognition problems such as Super Resolution (SR), feature-based representations likes local or global features, and structure-based representations likes coupled mappings, estimated resolution, and sparse representation. In the study, [3] used couple mapping on both branches to connect features on low and high-resolution face images into the same space. Likewise, [7] uses couple mapping on both branches and super resolution to construct low resolution face

images to high resolution. This method will be better if combined with deep learning.

The results of this learning can be used by the police or other authorities to find the target person if there is a face matches from the supervisor's surveillance camera. In this paper propose the development of the TBE-CNN architecture for face recognition at low resolution face images by combining methods in pre-processing and deep learning to perform face classifications on low-resolution face images. General research framework of this research defined as Figure 2.



Figure 2: General Research Framework

## 2. Related Work

On the pre-processing, [9] proposed a histogram alignment and image fusion approach. Generally, there's two way for image fusion, one is fusion in spatial domain and other is fusion in frequency domain. This research using curvelet coefficient for representation face feature because it proven excellently performance in representing facial features.

Two years later, [10] proposed Resolution-Invariant Deep Network (RIDN) to study the resolution of invariant features. To make the comparison achievable, they raised the LR image resolution through interpolation methods such as Bicubic. They used cosine distance metric to get recognition results that can be an evaluation material of the proposed method. RIDN looks for uniform features that feasible to extract invariant feature resolutions then equations between samples computed using common distance metrics such as Euclidean and cosine through feature space. RIDN applies a deep convolutional network to study the resolution of invariant features. The size used is 60 x 55 for high resolution images and 30 x 24 for low resolution face images.

Then, [11] uses a Discriminant Correlation Analysis (DCA) that can resolve the mismatch length of vector features and the relationship between the corresponding features in an improved low and high-resolution face image. Before analyzing the features, researchers looked for 2 linear transformation matrices using Canonical Correlation Analysis (CCA). CCA is a method that processes valuable multi-data, which has been widely used to analyze the same relationship between two sets of variables. And the images used for observation are low resolution (32 x 32, 16 x 16, and 8 x 8) and high resolution (128 x 128) images.

Finally, [12] proposes Discriminative Multi-Dimensional Scaling (DMS) which is a functions to link high resolution face images and low resolution face images and Local-consistency-preserving DMS (LDMS) are functions to connect high resolution images with high resolution images too. The problem in this study is to find the appropriate distance for low resolution face images and high-resolution images. In this study they used couple mapping method to find 2 mappings or projecting of low-resolution face images and high-resolution face images into the same subspace. DMS is also used to find hidden subspaces that roughly their distance in spaces  $\text{dist}(h_i, h_j)$ .  $h_i$  denoted as HR images that correspond to  $l_j$ . Gallery uses high-resolution images with test images that are larger than 32 x 32 and smaller than 16 x 16.

Table 1: Summary of State of Art

Publication	Problem	Methods
[9]	Face recognition at low resolution for observation image sizes 32 x 32, 16 x 16, and 8 x 8.	Face recognition at low resolution for observation image sizes 32 x 32, 16 x 16, and 8 x 8.
[10]	Face recognition at low resolution to look for features in the same observation image with the gallery.	Resolution-Invariant Deep Network (RIDN).
[11]	Low-resolution face recognition taken from surveillance cameras for image size problems tested with those in the gallery is different from low resolution for observation images size 32 x 32, 16 x 16, 8 x 8 and high resolution with observation picture size 128 x 128.	Use Canonical Correlation Analysis (CCA) and propose Discriminant Correlation Analysis (DCA).
[12]	Low resolution face recognition to adjust the matrix in low and high-resolution face images with observational image sizes less than 32 x 32 and more than 16 x 16.	Discriminative Multidimensional Scaling (DMS) and Local-consistency-preserved Discriminative Multidimensional Scaling (LDMS).
[3]	Face recognition at low resolutions with observational image sizes up to 8 x 8.	Deep Coupled ResNet, consist of one trunk network using ResNet and two branches using Coupled Mapping.
[7]	Face recognition at low resolutions with observational image sizes up to 6 x 6 sizes.	Two Branch with FECNN and SRFECNN (Combination of Super Resolution with FECNN).
[13]	Face recognition on video from surveillance cameras in the real world. The training dataset is taken from Face Detection on the surveillance camera.	CNN + Fine Tuning.
[14]	Face recognition in videos that have an unlimited variety of poses for still-to-video, video-to-still, and video-to-video cases.	Trunk Branch Ensemble – Convolutional Neural Network (TBE-CNN).

One of research that uses deep learning, [3] proposes Deep Couple RestNet. The architecture consists of 1 trunk and 2 branch networks. This network consists of convolutional layers, pooling, and 2 fully connected layers. The fully connected layer uses softmax and center-loss for interclass separation (classification). But to make a comparison, the authors replaced the model with VGGFace and LightCNN in the body tissue. The body network uses RestNet as its model while the branch network uses a couple mapping to close the distance between the low and high-resolution face images to a certain resolution and similar features will be placed in the new feature space.

Then [7] proposed the SRFECNN method which also offers high-resolution images because there is a super resolution CNN embedded in the architecture. The proposed method requires very little space, so it only requires a little memory. The proposed method is a novel couple mapping using a DCNN network (i.e. VGGNet) consisting of two DCNN branches for low and high-resolution face image maps into a common space with non-linear transformation.

The branch that handles high resolution images consists of 16 layers and the branch that handles low resolution face images consists of 5 super resolution layers connected to 14 layers (13 convolution layers and 1 fully-connected layer) and the third layer of fully connected layers will be used for so that the total classification for branches that deal with low-resolution face images is 19 layers. At the top branch which handles high resolution, 2 fully connected VGGnet layers removed so that the total layer at the top branch is 14 layers (13 convolution layers and 1 fully connected layer) of the total VGGnet layers.

This upper branch is called Feature Extraction Convolutional Neural Network (FECNN). Input image on the upper branch is 224

x 224 and other images than have other size will be done bicubic interpolation to an image size of 224 x 224. Bicubic interpolation used to resize the image as expected and softening the features of the image surface. The output are feature vectors with the number of elements is 4,096.

In lower branch that handles low resolution, the proposed method have 2 subnets. The first subnet called SRnet, using DCNN and the second subnet called FECNN, which is the same architecture as the upper branch. The output from SRnet will be the input for FECNN, which is an image with size 224 x 224. Input from the lower branch is a low-resolution face image that has been interpolated to size 224 x 224. The amount of weight used on SRFECNN is less than VGGnet, which is 141M.

The proposed method also uses Gradient Based Optimization to minimize the distance between low and high-resolution face images that are mapped into the same space by updating the DCNN weight via backpropagation on errors.

In addition, [13] used fine tuning in deep learning for face recognition. Fine tuning is a proposed method for constructing labelled datasets. Fine tuning is done on the face recognition model.

There are 3 stages in doing fine tuning. The first stage is to produce a rough dataset, such as collecting datasets obtained from surveillance cameras on lighting, poses, or expressions that vary by doing face detection and tracking. Then the second stage is refined dataset by labelling the dataset in each class using graph clustering from the VGG face model. Then the third stage, each class is purified by comparing its threshold values to eliminate duplication of datasets that are in each class. And the last step is to filter out classes, images that less than 100 classes will be eliminated.

Fine tuning is applied to VGG face models. The weight of VGG face model pre-training is done fine tuning by continuing back-propagation in the dataset. Only the fully connected layer that has been fine-tuned in the new dataset, so that makes the model fit the target.

At this time, [14] has proposed the architecture of the TBE-CNN. The architecture proposed also uses Mean Distance Regularization – Triplet Loss (MDR-TL) as a triplet loss function. This architecture consists of one body network and two branch networks. The body network used to study global features in face images while the branch network is used to study local features in face images. This architecture is evaluated by of still-to-video, video-to-still, and video-to-video case. All the previous work summarized on the Table 1.

### 3. Review Method

#### 3.1. Low Resolution

According to [8], low resolution images is one of the issues on face recognition because ideally face recognition is trained and carried out with high-resolution images. The examples of low-resolution images are small image sizes, low image quality, lighting, unlimited poses (unconstrained), blurred images, or can be a combination of all of them. According to [15], they also said that low-resolution images taken from down-sampling did not present good low-resolution images and had a decreased performance in terms of face recognition. Low resolution face images occur due to several factors such as inaccuracies (misalignment), decreased resolution and various types of poses (noise affection), lacks in effective features, different resolutions when the learning process and image classification process (dimensional mismatch).

Generally, to solve low-resolution images is convert the low-resolution images to high-resolution images, then conduct training and classification of images with high-resolution images.

Low resolution images better used to classify images globally than using high-resolution images. There are 2 concepts to find out the best image resolution for face recognition, the one is determining the best image resolution and determining the minimum resolution (resolution threshold value) used. The low-resolution image has smaller size than 32 x 24 with an eye-to-eye distance of about 10 pixels taken from a surveillance camera that has 320 x 240 QVGA resolution without a cooperative subject and generally contains noise and blur.

#### 3.2. Super Resolution

Super resolution or hallucination method is a technique to increase the resolution of low-sized images to high resolution. One method of super resolution is vision-oriented super resolution and recognition-oriented super resolution. Vision-oriented super resolution is a conventional super resolution technique that aims to obtain good visual reconstruction, but it's not usually designed for the recognition purpose. Whereas recognition-oriented super resolution is a technique that aims to enhance visual images to suit the recognition purpose because along with reduced image resolution, general super resolution techniques (vision-oriented super resolution) become more vulnerable to unlimited pose variations.

#### 3.3. Inception

Inception module is a module that acts as a multiple convolutional filter, where convolution is applied many times to the same input so it provide deeper convolution. Inception modules are generally illustrated by Figure 3. But the disadvantage of this inception is the large computational costs compared to simple convolution techniques.

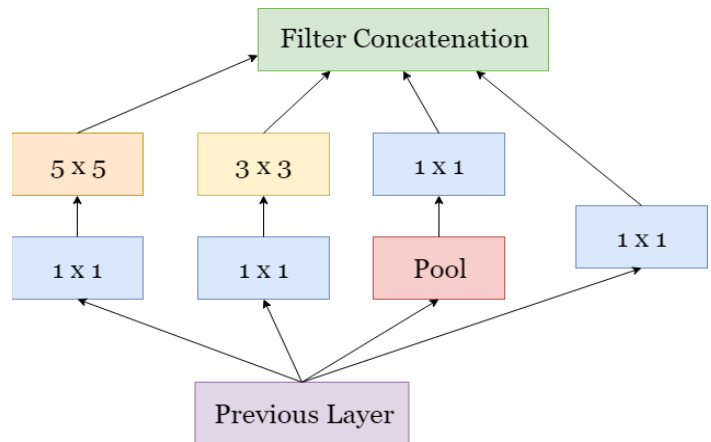


Figure 3: Common Inception Modules

#### 3.4. Trunk-Branch Ensemble – Convolutional Neural Network Architecture (CNN)

CNN is a special type of neural network for data processing which has a topology known as a grid. The CNN name indicates a network that uses mathematical operations called convolution. According to experiments from [16] shows an increases in the number of parameters in the convolutional network layer without increasing the height of the convolution layer making the increase proven ineffective. After doing convolution, pooling is carried out to summarize the output of adjacent groups of neurons in the same kernel map. There is 2 type of pooling, one is max pooling and other is average pooling [17]. In this proposed model will using max pooling. Then fully connected will applied for classification. This layer has fixed dimensions and discards spatial coordinates. And this layer can be seen as a convolution with a kernel that covers the entire input region [18].

TBE-CNN is an one of CNN architecture for extracting complementary features and patches around facial landmarks through trunk and branch networks [5]. Trunk networks contain several layers to absorb global information and branch networks contain several layers to absorb local information thereby reducing computation and effective convergence. Trunk network are trained to study facial representations for holistic facial images, and each branch network is trained to study facial representations for patch images cutted from one facial component [13]. On [14], they combine GoogLeNet [19] architecture with TBE-CNN.

On TBE-CNN, [14] divides the layer to extract features into 3 parts, namely the low, middle, and high level layers. Low and middle level layers used to represent features that store local information, so that network entities and branch networks can exchange local information in the lower and middle layers. While the high-level layer serves features representation that store global information.



3.5. SGD Optimizer

Stochastic Gradient Descent (SGD) is an extension of gradient descent where it's a modification of "batch" gradient descent and parameter updates are made after calculating a stochastic approximation of the gradient [20]. Gradient Descent calculate the gradient of cost function as much as number of training data. Many deep learning has powered by this algorithm. [21] explain that SGD have low memory usage, strong generalization ability, and incremental result. But SGD have sensitivity to learning rate hyperparameter. Based on research [22], they proven that SGD behaviour is also independent of the number of hidden units, as soon as this is large enough. Standard SGD notation are defined as follow:

$$x_{t+1} = Y(x_t - \eta g_t) = \operatorname{argmin}_{x \in X} \|x - (x_t - \eta g_t)\|_2^2 \quad (1)$$

Where its optimized function from  $\mathbb{R}^d \rightarrow \mathbb{R}, X = \mathbb{R}^d, x_t \in \mathbb{R}^d, \eta$  is a learning rate, and  $g_t$  is a gradient at each step of  $t$ . SGD reduce computational from Gradient Descent by multiply learning rate and cost gradient of 1 example at each training data without sum all gradient of cost function for each training data.

3.6. Softmax

The softmax loss function is a function used to represent the probability distribution of discrete variables with  $n$  possible values. The term "softmax" is a port-manteau of "soft" and "argmax" [23]. It is a typically good at optimizing the inter-class difference (i.e., separating different classes), but not good at reducing the intra-class variation (i.e., making features of the same class compact) [24]. The softmax function is most often used as the output of classifications. The softmax can be used within the model itself, if the model wants to choose one of  $n$  different options for several internal variables. The softmax function is define by equations (6) [25].

$$\operatorname{softmax}(x)_i = \frac{\exp(x_i)}{\sum_{i=1}^n \exp(x_i)} \quad (2)$$

Where,  $x_i$  is a vector input. Vector input might be negative value, or the sum is greater or less than one. So, after applying softmax function, the value will be range (0,1).

3.7. Ensemble Learning

Based on the understanding of [26], ensemble learning is a machine learning paradigm where several base learners or classifiers are trained to solve a problem, or one base learner is

trained several times to get the best accuracy or loss. Base learning is a model that will be combined in ensemble learning and the combination can be a neural network, deep learning, and others model, or it can be the same models. The concept of ensemble learning is generally illustrated in Figure 4.

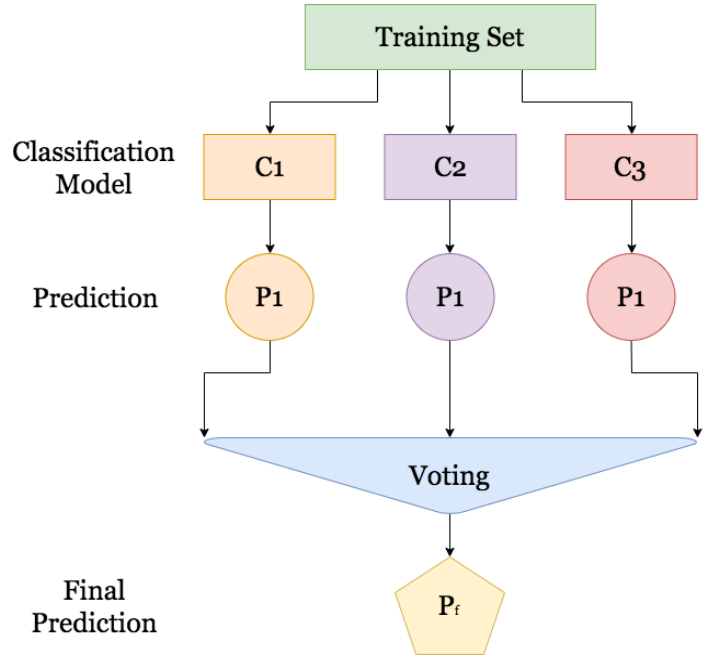


Figure 4: Common Ensemble Modules

The purpose of this combination is to produce better generalization performance compared to individual base learners. There are several methods in ensemble learning, the majority voting principle and the plurality voting principle [27]. Majority voting and plurality voting are ensemble learning methods where the way is to choose class labels or choose the highest accuracy (if the comparison uses accuracy) which is predicted from the whole base learner. The difference is the majority voting identically to binary classification while plurality voting is suitable for multiclass labels. Ensemble learning is denoted by equation (3) [27]:

$$\hat{y} = \operatorname{model}\{C_1(x), \dots, C_m(x)\} \quad (3)$$

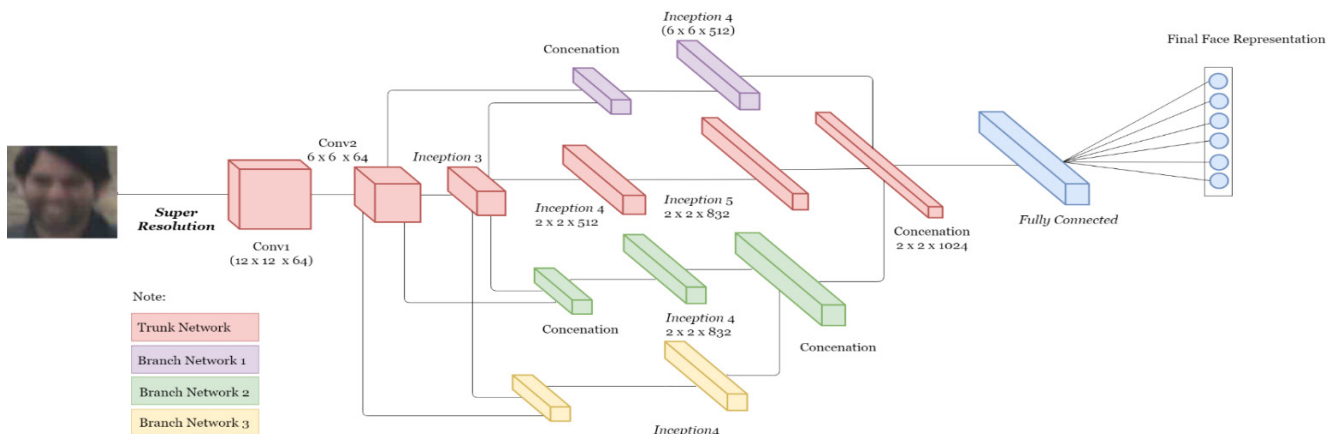


Figure 5: Common Ensemble Modules

Where the mode is the highest voting, C is the base learner or classifier and  $\hat{y}$  is the output that comes from the base learner or classifier that has the highest voting.

#### 4. Result and Discussion

##### 4.1. Dataset

In this study, the datasets used are YouTube Faces Database (YTD). The dataset used divided into training, validation, and testing with a portion of 70% for training, 20% for validation, and 10% for testing. Validation is done to avoid overfitting.

YouTube Faces Database (YTD) [28] is a dataset on face videos designed to study unlimited face recognition problems in video. This dataset contains 3,425 videos on 1,595 different subjects. All videos are downloaded from Youtube. The shortest clip duration is 48 frames, the longest clip is 6.070 frames, and the average length on the video clip is 181.3 frames. Total frame on this dataset is 621,126 image. In designing video datasets and benchmarks, [28] follow the example in the LFW image collection. YTD only contains video and provides still face image from a video that has been aligned on the same subject, whereas LFW only contains facial images that also on the same subject. The goal is to produce a collection of videos along with labels that indicate the identity of the people seen in each video. This dataset has enough blur, illumination, and lighting as the same as LFW dataset so YTD dataset able to verify algorithm performance for low resolution face recognition problem.

##### 4.2. Pre-Processing

Pre-processing will be carried out on the TBE-CNN architecture development to be built. The pre-processing technique that will be used is super resolution. Super resolution is used to increase image resolution from low resolution face images to high resolution images so that the pixels in the image increase and the entire image used is clearly visible. The super resolution technique will be using bicubic interpolation function when resizing the image (face alignment). Bicubic interpolation is one of the super resolution techniques that can make the images surface smoother so that the face image can be used to make recognition.

##### 4.3. Proposed Network Architecture

In the training phase, the face recognition model that will be used for TBE-CNN architecture development combined with pre-processing and model as shown in Figure 5. And this training will be using face training datasets and validation will be using face validation dataset. The dataset has been labeled before by their directories. The architecture consists of one trunk network and three branch networks. The trunk network will study global features. Whereas the branch networks will study the local features in image input. In the proposed architecture consist of a number of inceptions and use the Inception-v3 proposed by [29].

The branch two and three will be merging first before it will be merge to trunk and branch one. The parameter used described in Table 2 and the detail of model described in Table 3.

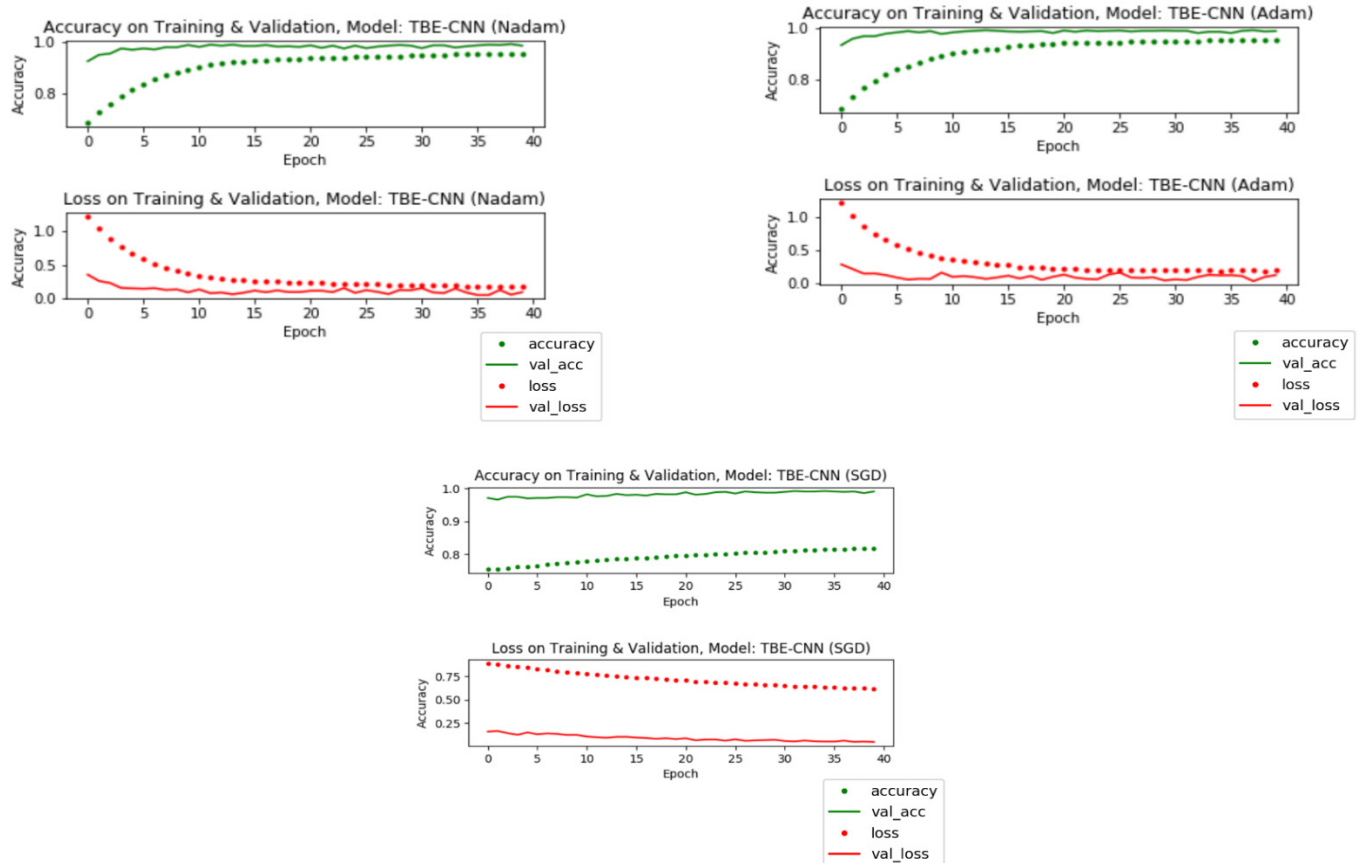


Figure 6: Training and Validation on TBE-CNN With Epoch 40

Table 2: Proposed Hyperparameter

Dataset	Parameter	Value
YTD	Learning Rate	1.0e-4
	Batch Size	32
	Optimizer	Adam, Nadam, and SGD
	Loss	categorical_crossentropy
	Validation Step	800 / batch size
	Activation	Softmax

In the fully connected layer, it will use the softmax function as its activation function and the results of this fully connected layer will be evaluated by confusion matrix that has been applied by [30]. The training using the same epoch and combine with SGD as optimizer with momentum value is 0.9 (based on empirical study) and learning rate is 1.0e-4. For generate training, validation, and testing dataset, it using data augmented that rescaled to 1/255, zoom range is 0.2, shear range is 0.2, and horizontal flip is false.

The previous architecture consists of two branch and combine with couple mappings to project LR image from HR images. But for this architecture, it will add one branch network on the bottom and combine with Super Resolution as pre-processing method to increase images resolution.

In this study, there are 2 epoch values used in the model, i.e. 40 and 100. In training and validation at epoch = 40, it requires 3 times training with the same number of epochs to get optimal accuracy.

And during the training process, the input trained using the GPU. For epoch = 100, the model is not trained in an ensemble and it run only once, so that this model training is called 3 Branch - Trunk Branch-CNN. For the model that was trained using epoch = 40, the model trained in an ensemble way, which is the model was trained 3 times with different optimizer, which is SGD, Adam, and Nadam. Both of these trainings using epoch = 100 and epoch = 40, started with random weight (initial weight).

4.4. Experiment Result and Discussion

By using the proposed model, the accuracy obtained is greater than that of state-of-art. However, based on the graph in Figure 5 shows that training and validation process with 3 different optimizers (ensemble learning).

Based on the training and validation using Adam optimizer shows that the accuracy at the last epoch in training was 98% while at the time of validation it was 99%. And for the loss in the last epoch in training by 20% while in validation by 18%. This is means that the difference in accuracy during training and validation is 1% and the difference in loss during training and validation is 2%.

Then in training and validation using Nadam optimizer shows that the accuracy in the last epoch in training was 97% while at the time of validation it was 99%. And for losses in the last epoch in training by 10% while in validation by 8%. This is means that the difference in accuracy during training and validation is 2% and the difference in loss during training and validation is 2%.

Table 3: Proposed Model Parameter

	Type (Name)	Kernel Size / Stride	Output Size
Low Level	convolution (Conv1)	7 x 7 / 2	12 x 12 x 64
	max pool	2 x 2 / 2	6 x 6 x 64
	convolution (Conv2)	3 x 3 / 1	3 x 3 x 192
Middle Level	inception (3a)		3 x 3 x 256
	inception (3b)		3 x 3 x 480
	max pool	2 x 2 / 2	3 x 3 x 480
High Level	inception (4a)		3 x 3 x 512
	inception (4b)		3 x 3 x 512
	inception (4c)		3 x 3 x 512
	inception (4d)		3 x 3 x 528
	inception (4e)		3 x 3 x 832
	max pool	2 x 2 / 2	3 x 6 x 832
	inception (5a)		3 x 3 x 832
	inception (5b)		3 x 3 x 1024
	concentration 1		3 x 3 x 1024
	concentration 2		3 x 3 x 1024
Fully Connected	flatten		1 x 36864
	dense	64 (dimension output)	1 x 64
	activation		1 x 64
	dropout	0.5	1 x 64
	dense	1591 (dimension output)	1 x 1591
	activation		1 x 1591

Whereas in training and validation using SGD optimizer shows that the accuracy in the last epoch in training was 82% while at the time of validation it was 99%. And for losses in the last epoch in training by 60% while in validation by 5%. This means that the difference in accuracy during training and validation is 17% and the difference in loss during training and validation is 55%.

From the results of these experiments, it can be concluded that training using Adam's optimizer provides the best results compared to the other 2 optimizers, both in terms of accuracy and loss that can be obtained. And SGD optimizer gives the lowest results compared to 2 other optimizers.

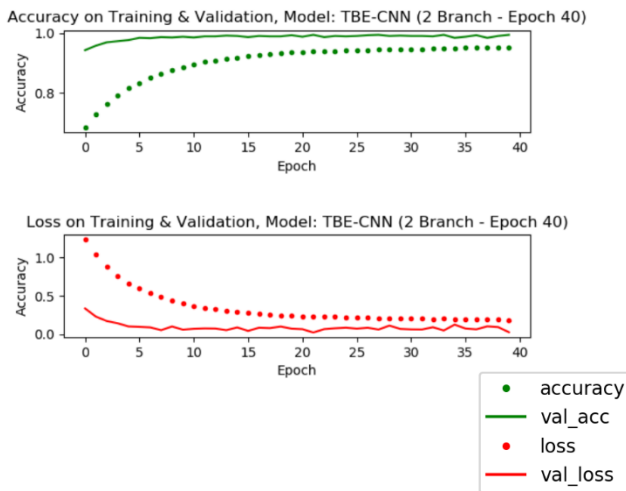


Figure 7: Training and Validation on TBE-CNN with 2 Branch

From the highest accuracy based on training using the ensemble approach, the accuracy will be compared with the model using 2 branches. In Figure 7 shows that the accuracy at the last epoch in training was 95% while at the time of validation it was 99%. And for the loss in the last epoch in training by 25% while in validation by 3%. This means that the difference in accuracy during training and validation is 4% and the difference in loss during training and validation is 22%.

Table 4: Comparison Accuracy

Method	Accuracy (%)
TBE-CNN (2 Branch)	99%
3 Branch-Trunk Branch Ensemble-CNN (Epoch 40 - Optimizer Adam)	100%
3 Branch-Trunk Branch Ensemble-CNN (Epoch 40 - Optimizer Nadam)	100%
3 Branch-Trunk Branch Ensemble-CNN (Epoch 40 - Optimizer SGD)	99%
3 Branch-Trunk Branch-CNN (Epoch 100)	99%

Because SGD provides the lowest accuracy, the next research is continued by changing the epoch value to 100 and using SGD as an optimizer model, the rest use the same parameters as the parameters used at epoch = 40. The change in epoch value is intended to compare training results, validation, and testing obtained when using different epochs. At epoch = 100, the weight used originates from initialization or does not use the weight of the training results and validation at epoch = 40. Based on the graph

in Figure 7 shows that the accuracy at the last epoch in training using epoch = 100 was 85% while at the time of validation it was 99%. And for the loss in the last epoch in training by 40% while in validation by 5%. This means that the difference in accuracy during training and validation is 14% and the difference in loss during training and validation is 35%.

When compared with the results of accuracy in training and validation using epoch = 40, the comparison of accuracy in training can be increased by 3%, while the accuracy ratio for validation is 0% (none). Then, for the comparison of accuracy obtained during training that is decreased by 20% and the loss ratio at the time of validation is 0% (none). On the testing phase, the model is tested using a confusion matrix. From the ensemble learning test results on Table 4 proved that the optimizer Adam and Nadam provide the best accuracy compared to other optimizers. In addition, epoch comparisons show on Table 5 do not provide significant accuracy differences during validation and testing, but on the Figure 6 and Figure 8 shows that epoch comparison provides increased accuracy and loss in training.

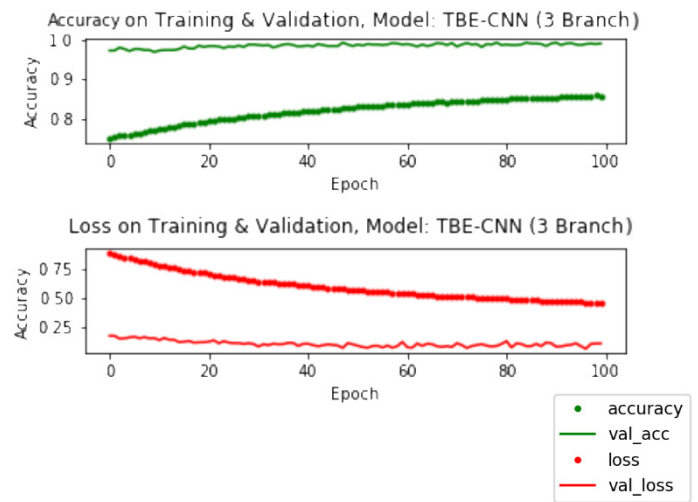


Figure 8: Training and Validation on TBE-CNN with 2 Branch

On the comparison to state-of-art, the accuracy obtained from the experimental results will be compared with [14]. The architecture also used a YTD dataset with an input size of 24 x 24. From the accuracy comparison in Table 4 it can be concluded that the 3 Branch - Trunk Branch Ensemble-CNN model is able to improve the accuracy of the previous method and the improvement is 1%.

### 5. Conclusion

In this paper proposed a method Trunk branch Ensemble-CNN and Trunk Branch-CNN with super resolution as pre-processing. The architecture consists of inception-v3 by GoogLeNet. The proposed architecture compared to previous architecture and evaluated by YTD dataset. And the results show that Adam and Nadam optimizer give the best accuracy on testing in ensemble learning and the proposed method provides better accuracy compared to state-of-art. Then, different epoch can affect the training performance results but not give significant improvement for validation and testing result. Furthermore, the optimization of parameter used and reduce computational time when model training and validation will be future work.



## Conflict of Interest

We declare that we have no affiliations with or involvement in any organization or entity with any financial interest (such as honoraria; educational grants; participation in speakers' bureaus; membership, employment, consultancies, stock ownership, or other equity interest, and expert testimony or patent-licensing arrangements), or non-financial interest (such as personal or professional relationships, affiliations, knowledge or beliefs) in the subject matter or materials discussed in this manuscript.

## References

- [1] K. Bhavani et al., Real time Face Detection and Recognition in Video Surveillance, *Int. Res. J. Eng. Technol.*, vol. 4, pp. 1562–1565 (2017)
- [2] T. Huang, Z. Xiong, and Z. Zhang, *Face recognition applications*. Springer, London (2011)
- [3] Z. Lu, X. Jiang, and A. Kot, Deep Coupled ResNet for Low-Resolution Face Recognition, *IEEE Signal Process. Lett.*, vol. 25, pp. 526–530 (2018)
- [4] J. S. Patil, Deep Learning in Low Resolution Image Recognition, *Vishwakarma J. Eng. Res.*, vol. 1, pp. 101–107 (2017)
- [5] S. Bashbaghi, E. Granger, R. Sabourin, and M. Parchami, Deep Learning Architectures for Face Recognition in Video Surveillance, *arXiv Prepr. arXiv1802.09990*, pp. 1–21 (2018)
- [6] M. Parchami, S. Bashbaghi, and E. Granger, Video-based face recognition using ensemble of haar-like deep convolutional neural networks, *2017 Int. Jt. Conf. Neural Networks*, pp. 4625–4632 (2017)
- [7] E. Zangeneh, M. Rahmati, and Y. Mohsenzadeh, Low Resolution Face Recognition Using a Two-Branch Deep Convolutional Neural Network Architecture, *Comput. Vis. Pattern Recognit.*, vol. 4, pp. 1562–1565 (2017)
- [8] Z. Wang, Z. Miao, Q. M. Jonathan Wu, Y. Wan, and Z. Tang, Low-resolution face recognition: A review, *Vis. Comput.*, vol. 30, pp. 359–386 (2014)
- [9] X. Xu, W. Liu, and L. Li, Low Resolution Face Recognition in Surveillance Systems, *J. Comput. Commun. Technol.*, vol. 2, pp. 70–77 (2014)
- [10] D. Zeng, H. Chen, and Q. Zhao, Towards resolution invariant face recognition in uncontrolled scenarios, *2016 International Conference on Biometrics (2016)*
- [11] M. Haghighat and M. Abdel-Mottaleb, Lower Resolution Face Recognition in Surveillance Systems Using Discriminant Correlation Analysis, *2017 12th IEEE Int. Conf. Autom. Face Gesture Recognit.*, pp. 912–917 (2017)
- [12] F. Yang, W. Yang, R. Gao, and Q. Liao, Discriminative Multidimensional Scaling for Low-Resolution Face Recognition, *IEEE Signal Process. Lett.*, vol. 25, pp. 388–392 (2018)
- [13] Y. Wang, T. Bao, C. Ding, and M. Zhu, Face Recognition in Real-world Surveillance Videos with Deep Learning Method, *2017 2nd Int. Conf. Image, Vis. Comput.*, pp. 239–243 (2017)
- [14] C. Ding and D. Tao, Trunk-Branch Ensemble Convolutional Neural Networks for Video-Based Face Recognition, *IEEE Trans. Pattern Anal. Mach. Intell.*, vol. 40, pp. 1002–1014 (2018)
- [15] P. Li, L. Prieto, D. Mery, and P. Flynn, Face Recognition in Low Quality Images: A Survey, *Comput. Vis. Pattern Recognit.*, pp. 1–15 (2018)
- [16] I. J. Goodfellow, Y. Bulatov, J. Ibarz, S. Amoud, and V. Shet, Multi-digit Number Recognition from Street View Imagery using Deep Convolutional Neural Networks, *Comput. Vis. Pattern Recognit.*, pp. 1–13 (2013)
- [17] K. He, X. Zhang, S. Ren, and J. Sun, Deep Residual Learning for Image Recognition, *2016 IEEE Conf. Comput. Vis. Pattern Recognit.*, pp. 770–778 (2016)
- [18] J. Long, E. Shelhamer, and T. Darrell, Fully convolutional networks for semantic segmentation, *Proc. IEEE Comput. Soc. Conf. Comput. Vis. Pattern Recognit.*, vol. 07, pp. 3431–3440 (2015)
- [19] C. Szegedy et al., Going deeper with convolutions, *Proc. IEEE Comput. Soc. Conf. Comput. Vis. Pattern Recognit.*, vol. 07, pp. 1–9 (2015)
- [20] S. Balaban, Deep learning and face recognition: the state of the art, *Biometric Surveill. Technol. Hum. Act. Identif. XII*, vol. 9457, pp. 94570B (2015)
- [21] J. Perla, Notes on AdaGrad Regret of AdaGrad, *arXiv*, pp. 1–5 (2014)
- [22] S. Mei, A. Montanari, and P.-M. Nguyen, A mean field view of the landscape of two-layer neural networks, *Proc. Natl. Acad. Sci.*, vol. 115, pp. E7665–E7671 (2018)
- [23] B. Gao and L. Pavel, On the Properties of the Softmax Function with Application in Game Theory and Reinforcement Learning, pp. 1–10 (2017)
- [24] F. Wang, J. Cheng, W. Liu, and H. Liu, Additive Margin Softmax for Face Verification, *IEEE Signal Process. Lett.*, vol. 25, pp. 926–930 (2018)
- [25] I. Goodfellow, Y. Bengio, and A. Courville, *Deep learning (Vol. 1)*. MIT press, Cambridge (2016)
- [26] Z. Zhou, *Ensemble Learning*, pp. 1–5
- [27] S. Raschka, *Python Machine Learning*. PACKT, Birmingham (2015)
- [28] L. Wolf, T. Hassner, and I. Maoz, Face recognition in unconstrained videos with matched background similarity, *Proc. IEEE Comput. Soc. Conf. Comput. Vis. Pattern Recognit.*, pp. 529–534 (2011)
- [29] C. Szegedy, V. Vanhoucke, S. Ioffe, J. Shlens, and Z. Wojna, Rethinking the Inception Architecture for Computer Vision, *Comput. Vis. Pattern Recognit. (2015)*
- [30] S. Turgut, M. Dagtekin, and T. Ensari, Microarray breast cancer data classification using machine learning methods, *2018 Electr. Electron (2018)*

## Review on Smart Electronic Nose Coupled with Artificial Intelligence for Air Quality Monitoring

Rabeb Faleh <sup>\*1,2</sup>, Souhir Bedoui<sup>2</sup>, Abdennaceur Kachouri<sup>2</sup>

<sup>1</sup>Computer and Engineering Networks Department, College of Computer and Information Sciences, Jouf University, Sakaka, Saudi Arabia

<sup>2</sup>Laboratory of Electronics and Information Technologies, Department of Electrical Engineering School of Engineering of Sfax, Sfax University, Sfax, Tunisia

### ARTICLE INFO

Article history:

Received: 13 February, 2020

Accepted: 10 April, 2020

Online: 20 April, 2020

Keywords:

E-nose

Artificial intelligence algorithms

Gas sensors

Pollution detection

Ensemble classifier

### ABSTRACT

*With the advent of the Internet of Things Technologies (IOT), smart homes, and smart city applications, E-Nose was created. Almost of gas sensors consisting the electronic nose system suffer from cross sensitivity and lack of selectivity. Coupling smart gas sensors with artificial intelligence algorithms can thus empower conventional gas sensing technologies and increase accuracy in gas detection. This study describes the overall types of smart gas sensors used in air quality control, signal pre-processing and extraction features. Also it presents pattern recognition methods used in E-nose applications including linear methods such as Linear Discriminant Analysis LDA, K-Nearest Neighbors KNN and Non-linear such as algorithms Support vector Machine SVM and Artificial Neural Network ANN and their impact on improving accuracy rate for gas detection. Finally, this paper summarizes by providing directions for about how to leverage the benefits of combining these classifiers which is known as Data fusion approach and ensemble classifiers.*

### 1. Introduction

Nowadays, with the advent of the Internet of Things (IOT), Society is interconnected with smart cities and the smart industry due to smart sensor growth. Among these sensors, smart gas sensors have been growth in many applications: food quality testing [1], environmental safety monitoring [2], Disease diagnosing [3], detecting the fresh vegetables freezing time [4]. Also, smart gas sensors cooperate with smart home and building application such as gas leakage [5].

One of the most issues in our life which is hazardous to our health is air pollution. Many works based on this field and created new instruments for monitoring the air quality [6], [7]. Due to its low cost, small size, robustness, the electronic nose approach is considered the most promising method among gas detection methods in several fields.

Electronic nose (E-nose) is mimicking the human olfactory system [8]. The e-nose system consists of two important elements: the hardware component that is an array of gas sensors coupled with the software component that is pattern recognition methods. They

are one of the most relevant artificial intelligence systems. The gas sensor array is made from different materials including thin metal oxide films, nanowires, and nanotubes. For each gas each sensor gives a different response. The collection of signals emitted by sensors that are exposed to the sample is called "cross selectivity" of the sensors, allowing a "fingerprint" to be formed and also called signature. All of the signatures constitute a database. Instead, these signatures demand that data processing methods be used to group gases into different groups. The gas identification process can be divided into four successive stages: Signal preprocessing, dimensionality reduction, classification, and validation. The preprocessing stage is often used to specify a certain number of parameters which are descriptive sensor response array [9]. Though pre-processing is based on the underlying sensor technology. At this point there are three general steps: simple manipulation, compression and normalization [10]. Principal Component Analysis is used for dimensionality reduction. This method is widely used in gas identification system and olfaction machine [11].

On the other hand, enhancing smart electronic nose performance is heavily dependent on the pattern recognition scheme in use. Artificial intelligence and machine learning algorithms are used to achieve successful discrimination, and pollutant gas detection.

\*Corresponding Author: Rabeb Faleh, Dept . of Computer and Engineering Networks , College of Computer and Information Sciences, Jouf University, Sakaka, Saudi Arabia, [rfhmidi@ju.edu.sa](mailto:rfhmidi@ju.edu.sa)

Some machine learning models have recently been explored in E-Nose applications. They can be divided into two categories. The first one is linear such as k-nearest neighbor (KNN) [12], linear discriminant analysis (LDA) [13]. The second one is nonlinear classification models such as the multilayer perceptron (MP) [14], radial basis function neural network (RBFNN) [15] and decision tree (DT) [16]. Support vector machine (SVM) is a promising classifier that has been widely applied in gas identification due to its kernel functions which solve non-linear problems [17].

In addition to individual classifiers, classifier ensemble has attracted considerable attention for E-nose pattern recognition [18]. Classifiers combination takes advantages of used individual classifiers to improve gas identification accuracy.

This review provides a summary of recent classification algorithms used in gas detection coupled with E-nose approach and the pertinent researches published in recent years in this field. The remainder of this paper is organized as follows: Section 2 presents a literature review on smart technologies for air quality monitoring and artificial intelligence algorithms. Section 3 exhibits related works about gas sensors and data preprocessing. Section 4 presents finding and discussion. Section 5 is a conclusion to summarize smart electronic nose investigation.

## 2. Literature review

Smart Cities applications are an important field of interest. Such technologies will be categorized into different categories by Smart Energy, Smart Lighting, Smart Transportation, Smart Parking, Smart Driving, Smart Buildings and Towns, Smart Grid, Smart Health and Smart Environment.

The notion of dedicated and non-dedicated sensors in smart city was introduced by authors in [19]. The first sort of compound sensors dedicated to a particular mission, including ambient sensors. Non-dedicated sensors are called embedded smartphone sensors such as accelerometer, gyroscope, GPS, microphone, and camera. The last form can be used for various applications. Derek Doran et al. described how people can be in use as human sensors to provide specific sources of information for smart cities. Authors developed a methodology to show how human sensors can support smartphones and other mobile devices through the provision of data streams [20].

For example, the authors in [21] identified an approach to energy sensing for Smart Buildings and Houses. The attitude consisted of voltage noise signatures or voltage signatures to categorize the operation of various devices and to note the similarity or difference between the harmonics 'spectral envelope and existing templates.

In this paper we will concentrate on Smart Environment sensing technologies more precisely pollution sensing technologies.

Regarding the harmful effects of polluting air, environmental control remains a significant challenge. This control involves expensive and fairly complex techniques. Hence the idea of designing an electronic nose is also called an artificial nose. Among smart sensing technologies, electronic nose (e-nose) can greatly enhance human quality of life. E-nose is an instrument capable of detecting odors and of distinguishing them. It consists of odor-sensitive sensors, a signal conditioning system and applications for data processing [22].

As shown in Figure 1, Gardner et al [23] identified an electronic nose as four main components. Next, a diffusion device that transfers air inside the instrument to be checked from the outside, then a chamber that contains the sensors, a signal processing device and a simple software for identification and classification.

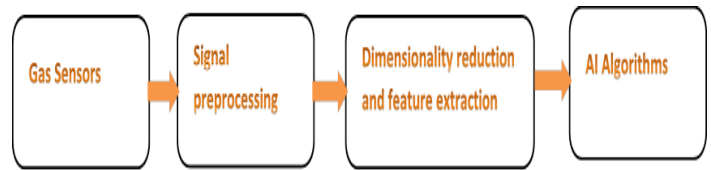


Figure1. Smart electronic nose system structure diagram

As seen in the figure1, Sensor array is the key component in electronic nose. Choice of materials is very important. The most used type is metal oxide MOX gas sensors [24]-[28] for different reasons. In fact MOX sensors have a very high sensitivity to various gases [29].

### 2.1. Feature extraction and dimensionality reduction

The most adopted data analysis method for reduction dimensionality is principal component analysis (PCA) which is a linear and unsupervised method [30]. PCA is a statistical tool allowing simple visualization of all related information. The PCA pathway includes as follows five phases [31]:

We typically have a data matrix of n observations on p correlated variables

- Compute data mean

$$\bar{x} = \frac{1}{n} \sum_i X_i \quad (1)$$

- Compute the standard deviation for each variable

$$s^2 = \frac{1}{n-1} \sum_{i=1}^n (X_i - \bar{x})^2 \quad (2)$$

- Compute covariance matrix

$$\hat{\Sigma} = \frac{1}{n} \sum_i (X_i - \hat{\mu})(X_i - \hat{\mu})^T \quad (3)$$

- Compute reduced centered matrix

$$X_i^* = \frac{X_i - \bar{x}}{s} \quad (4)$$

- Compute eigenvectors and eigenvalues

$$\hat{\Sigma} V = \Lambda V, \quad (5)$$

where  $\Lambda$  is the vector of eigenvalues of the covariance matrix.

Order eigenvalues in descending order  $\lambda_1 > \dots > \lambda_P$

We note PC1, PC2..., PCk... PCq the main component principal such that each has a linear combination of the original X1... Xp

$$PC_k = u_{1k}X_1 + u_{2k}X_2 + \dots + u_{pk}X_p \quad (6)$$

The  $u_{jk}$  coefficients are calculated in such a way that all  $PC_k$  is 2-2 uncorrelated variance and a maximum decreasing significance.

Main component characteristics are defined as follows: The first factor extracted in a main factor analysis typically accounts for a large amount of total variance in the observed variables. The second component will reflect a certain amount of variance in the data set which was not taken into account by the first component. It is going to be uncorrelated to the first part too. Components 1 and 2 are designed to have a zero association. The two axes obtained after running PCA, called main components, correspond to the highest individual values and contain most of the information. The main components contain the greatest variance of data, and are orthogonal.

Therefore, the percentage of the data variance expressed by each main component is determined using the corresponding own value.

The new set of data obtained with the linear orthogonal transformation was drawn in two or three dimensions, with the most important data set. Thus, PCA avoids consistency of the data and reduces the high dimensionality to smaller dimensions. However this method can't discriminate between gases classes. For this reason, we remedy this problem by using different AI algorithms.

## 2.2. AI algorithms and pattern recognition

After extracting from the sensor signal the most significant parameters, the data generated by a sensor array is grouped into a set of semi-, which are the output of the sensor array and a set of dependent variables. This data will be used by pattern recognition methods to identify detected gases [32]. Initially, electronic nose algorithms consist of three stages: drift calibration algorithms, preprocessing and extraction characteristics of signal, and methods for data analysis and classification with artificial intelligence algorithms [33].

Artificial intelligence algorithms can be divided into linear /non-linear algorithms considering that classification methods are supervised. The unsupervised methods are used for feature extraction and selection.

The methodology for the supervised multivariate analysis involves the labeling of the observations; a priori all the easily determined results are known. It is composed of two separate processes [34]:

- Training stage: This process is often carried out in the lab. It consists of building the prediction model with known X data, independent of the sensor response and the corresponding measured Y data.
- Evaluation test: In this step only the variables Y are computed. The X variables are calculated using the model

that was constructed during the learning process. They test the exactness and efficiency of the model.

### 2.2.1. Linear classification methods

Linear classification methods include linear discriminant analysis LDA, k-Nearest Neighbors (KNN) and Support vector machine (SVM) can train and identify high dimensional samples in gas recognition.

Like Principal Component Analysis (PCA), Linear Discriminant Analysis LDA is a dimension reduction factorial tool for exploring explanatory variables. It is used to view individual classes in an optimized graphic form. It is based upon Fisher's work in 1936.

Unlike PCA, LDA is a supervised dimension reduction process, which is based on each individual's quest for membership in a class specified a priori. The variables that classify individuals are a fortiori quantitative variables, while a qualitative variable defines the classes. LDA is in fact proposing two approaches: the first is concise. The second is predictive; it consists of deciding the class of allocation of n new individuals as defined by the same explaining variables.

Basic steps involved in the LDA algorithm:

- Calculate the within class scatter matrix

$$S_w = \sum_{i=1}^c S_i \text{ avec } S_i = \sum_i (X_i - \hat{\mu}_i) (X_i - \hat{\mu}_i)^T \quad (7)$$

Where  $\hat{\mu}_i$  is the mean of each class; and c is the number of classes.

- Calculate the between class scatter matrix

$$S_B = \sum_{i=1}^n n_i (\hat{\mu}_i - \hat{\mu}) (\hat{\mu}_i - \hat{\mu})^T, \quad (8)$$

where  $n_i$  is the number of observations for each class, is the mean of each class and  $\hat{\mu}$  is the mean of all the classes.

- Solve the eigenvalue problem

$$S_B V = \Lambda S_W V \quad (9)$$

The purpose of LDA is to maximize the following objective.

$$J(W) = \frac{W^T S_B W}{W^T S_W W} \quad (10)$$

- Implementing a K-Nearest Neighbors (KNN) classification model is simple, since it does not implement any learning function. The only metrics involved are the number K of the closer elements and the distance between the elements which we desire to classify [35]. It is necessary to choose distance so that the device works properly. The simplest distances allow for the achievement of satisfactory results. Euclidean distance, or Manhattan distance, is widely used to measure training sample similarity  $X = \{X_1, X_2, X_3... X_n\}$  to forecast data  $x = \{x_1, x_2, x_3... x_n\}$ .



- Support vector machine (SVM) is intended primarily for binary forecasting, i.e. two-class discrimination. Multi-class models were therefore built to understand more complex cases involving more than two classes. It is based on "kernel methods," which allow optimum separation of the data.
- SVM algorithms are very powerful for the identification of classes SVM determines the optimal hyperplan split between the groups to optimize the margin. There are two cases presented: linearly separable and nonlinear. Basic steps in the SVM algorithm; For the linearly separable case, the hyper plan has Equation (1).

$$f(x) = wx + b = 0 \tag{11}$$

The distance from a point to the plan is:

$$d(x) = \frac{|wx+b|}{\|w\|} \tag{12}$$

Maximize the distance means minimize  $\|w\|$ .

To reduce  $\|w\|$ , the Lagrange dual issue coefficients should be solved as follows:

$$w = \sum_i \alpha_i x_i y_i \tag{13}$$

$$w^T x + b = \sum_i \alpha_i x_i y_i x^T + b \tag{14}$$

Kernel functions will be added for the case which is not linearly separable. Example of such kernels,

Polynomial kernel (For MATLAB, "d" the order of the polynomial = 3 by default)

$$k(x_i, x) = (x_i x + 1)^d \tag{15}$$

RBF kernel ( $\delta = 1$  by default using MATLAB)

$$k(x_i, x) = \exp(-\delta \|x - x_i\|^2) \tag{16}$$

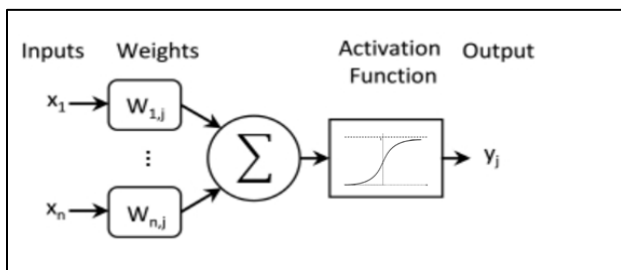


Figure 2. Principle of calculating formal neuron

Many researchers have created the Artificial Neural Network (ANN) because of its benefits of enhanced Big Data. It imitates the human brain, and solves several practical problems in different fields [36]. ANN performs its tasks as follows: As shown in Figure 2, each neuron receives and adds the signal from the previous layer that has a weight relation, compares weighted sum to threshold values and generates outputs by activation function such as

sigmoid function, radial basis [37]. There are two simple separate single layer and multilayer versions. All essential layers are interconnected in the first one. Within the second model, which is the multilayer structure, is divided into a layer of input, hidden layer, and layer of output. The number of hidden layers affects precision in classification and prediction [38].

For quantitative discrimination, MLP was used in many researches. V. Krivetskiy et al. [39] demonstrated in their research the identification of individual gasses by a single sensor, combined with methods for pattern recognition. Supervised learning algorithms were used to solve the classification problem: random forest, vector support machines (SVM), multilayer perceptron (MLP), (with one or two hidden layers). Only MLP had been used to solve the quantification problem. As an ANN disadvantage this requires a long period of training. To solve this problem, an algorithm named ELM has been proposed [40]. This is an algorithm of fast learning to feed the neural networks (SLFNs) into a single hidden layer. Instead of iterative tuning the output weights are generated randomly by the hidden node parameters. ELM's run time is therefore fast and demonstrates dominance over other classifiers [41]. The classification efficiency is clearly influenced by the parameters of the algorithm. Meanwhile, ELM's randomly generated input weights and hidden layer biases can make the algorithm unstable. Chao Peng et al[42] proposed an ELM-based Kernel Extreme Learning Machine (KELM) in combination with kernel functions for VOC detection to solve this problem. It was compared against SVM, KNN, and LDA. The results show that the KELM achieves the highest precision performance of about 95%.

Supervised methods are dedicated to quantitative classification such as the Linear Discriminant Analysis (LDA), Support Vector Machine (SVM) and the K-Nearest Neighbor method (KNN). It remains to be noted that artificial neural networks (ANN) are the most complex methods in terms of execution time and ease of implementation. ANN has been especially effective in predicting and classifying complex gas mixtures. In [43], researchers use ANN to model fuel-gas methanol output. A comparison of the main algorithms used for gas detection has been given in table 1.

Table 1: Sample Table

parameters	Classification algorithm			
	LDA	KNN	SVM	ANN
Interpretation simplicity	+	++	++	-
Ease of impelmentation	+	++	++	-
Execution Time	+	++	+	--
Classification quality	++	+	++	++

Very poor (--); poor (-); good (+); strongly good (++)

### 3. Related works

The main component for an electronic nose is a gas sensor array. A sensor for MOX gas is composed of many layers. First of

all, a silicone substrate is mounted on which is the dielectric membrane. The silicon oxide layer [44] or silicon oxide and silicon nitride bilayer will make up this membrane [45, 46]. Its function is to thermally insulate between the substrate and the sensitive layer [47]. Then the micro hotplate enables the detection of gaseous substances to exceed high temperatures. [48]. A Silicon Oxide passivation layer is deposited to separate the micro hotplate from the sensitive layer. The function of Sensitive layer is to react with the gaseous material. Tin oxide (SnO<sub>2</sub>), tungsten oxide (WO<sub>3</sub>) and zinc oxide (ZnO) are the most common and widely used metal oxides [49, 50].

Tungsten oxide (WO<sub>3</sub>) is very suitable for gas controlling applications [51, 52]. Take this latter material, for example, which is especially sensitive to ozone [53], A large number of researchers developed and tested a WO<sub>3</sub> gas sensor to detect various gases, such as NO<sub>2</sub>, where it was shown that the optimum working temperature for detecting this gas was approximately 225 °C [54] and H<sub>2</sub> where the best annealing temperature was just about 500 °C [55].

In [56], Joy Dutta et al proposed an Air Quality Monitoring System AQMD for tracking urban air pollution. They used two MQ135 and MQ7 air quality sensors, connected to an Arduino board that interacted with the Bluetooth module HC-05. Data were then moved to smartphones. Collected information from various users of smartphones then shaped the city's air quality index map for the outdoor and indoor environments.

Authors at [57] studied over a 20-day period the relationship between human activity and environment. Data from environmental monitoring stations and mobile networks is compiled to assess the air quality and weather. Consequently, authors demonstrated that stronger environmental analysis was achieved by incorporating information from various sources into sensing.

Persaud et al [58]'s application is to use a system that consists of polymer gas and quartz microbalance sensors to monitor the air quality in real time. This smart gas pump has been demonstrated for years to achieve and to detect complex mixtures of volatile substances.

The number of smart city electronic nose network applications is growing ever more. In 1995[59] Hodgins evacuated the first electronic nose research with the purpose of separating ethanol, dimethyl sulfide and diacetyl from water mixtures using CP sensors.

Authors in [24] studied an electronic nose response based on SnO<sub>2</sub> thin dioxide sensors to identify the presence of various gases such as CO, CH<sub>4</sub>, ISBU and EtOH with different concentrations ranging from 100ppm to 1000ppm. Results showed that the system can detect and recognize gasses with an error of less than 15%.

The ability of the electronic nose to identify and distinguish concentrations as low as 20 ppm for NO<sub>2</sub> and 5 ppm for CO was demonstrated in [25]. The main objective was to perform the indoor air quality control IAQ. Authors proposed an electronic nose based on an integrated gas sensor array and highly efficient

pattern recognition techniques for the quantification of carbon monoxide and nitrogen dioxide in mixtures of relative humidity and volatile organic compounds. The unit was composed of a metal oxide resistive sensor array, due to its low power consumption at high temperature and high sensitivity. Authors used a flimsy logic system. The goal was to extract the notable information from the response of the sensor array. The machine was able to distinguish and classify the presence of each pollutant in the test area, as well as their mixture.

Features selection is the key step in the classification scheme, which selects a subset from the original functions. In this context, Principal component analysis method was severely applied in the area of pollution monitoring.

For example, the overall objective of [60] was to apply a main component analysis (PCA) to air pollution data in order to provide a comprehensive definition of components that can be interpreted in terms of various air pollution sources and to investigate whether cause-specific daily mortality can be attributed to specific air pollution sources.

In [61] Wu and Kuo used data on air quality collected from eight automated air quality monitoring stations in central Taiwan and examined the connection between air quality variables and statistical analysis in an attempt to accurately represent the difference in air quality observed by each monitoring station and to create a suitable air quality classification system for the whole of Taiwan. The authors in[62] suggested a framework for defining and allocating sources of air pollution in an urban site in France. Using the key component analysis, the identification of the source profiles was achieved. In [63], PCA was used to compare air pollutions profiles of cities. PCA was applied in a study by [64].

However this method can't discriminate between gases classes. For this reason, we remedy this problem by using different AI algorithms.

For the pattern recognition stage, Hui et al [65], used LDA to detect and identify four different industrial gases, which achieved high classification rate and satisfactory predictive ability.

Researchers at [66] have used fishery LDA to classify mutton duck adulteration. For qualitative and quantitative analysis this approach was used. Mahdi Ghasemi et al.[67] suggested LDA as one of the discriminating methods for distinguishing and classifying various varieties of both grown and wild black caraway and cumin. The results show that LDA displays the highest precision performance near 100%.

In [68], wavelet energy has been extracted from the responses of e-nose and e-tongue for the classification of different grades of Indian black tea. Results confirm that classification rate using KNN have improved reaches 99.75%.

Researchers at [69] built on the Zynq platform a quick prototyping of the KNN-based gas identification system. For  $k = 1$  and  $k = 2$  the best results were obtained with a classification accuracy of

97.91 percent and 98.95 percent respectively. For example, a good  $k$  can be chosen via various heuristic techniques, such as cross-validation [70]. The value of  $k$  should be chosen on the basis of which classification error is minimised.

In comparison, KNN's biggest drawback is that after the training stage it is considered a slow learner. It does need an extensive test level, though. In order to address this problem, Mehmet Aci et al [71] proposed a hybrid classification system of  $k$  closest neighbour, Bayesian methods and genetic algorithm to solve these drawbacks by removing data that makes learning difficult.

Researchers in [72] have implemented hybrid KNN (HBKNN) classification approaches, which perform classification in high-dimensional space on the datasets with noisy attributes.

According to some researchers, they are outperforming many of the common methods of gas classification [73, 74]. Kyu-Won Jang et al [75] implemented a pairing plot scheme to classify gas form with SVM more effectively to detect CH<sub>4</sub> and CO. Apart from the classification task, the difficulty of machine learning methods is to estimate gas concentration or unknown gas concentration. In this context, researchers [76] applied Least-Squares Support-Vector-Machine-based (LS-SVM-based) nonlinear regression to determine the gas concentration of each constituent in a mixture.

SVM presents a considerable attention in gas classification in real time [77, 78]. R Faleh et al [52] showed in their research that successful classifications have been reached in the discrimination of three kinds of oxidizing and reducing gas using support vector machine.

In their research, Helli et al [26] used an electronic nose consisting of six Tagushi Gas Sensors for metal oxide (TGS-800, -813, -822, -825, -832, -2105) to track two gas forms: a reducing gas H<sub>2</sub>S and an oxidizing gas NO<sub>2</sub>. By applying Discriminant Factorial Analysis (DFA), they researched the capability of the sensor networks to detect the presence of these two gases in mixture or alone. This approach was applied to a complex reference atmosphere containing CO<sub>2</sub> and some humidity levels. DFA has proved to be a strong discriminator between different groups (H<sub>2</sub>S, NO<sub>2</sub> and H<sub>2</sub>S / NO<sub>2</sub> mixtures) and even between different concentrations for a single group.

The main research goal in [27] was to build an electronic nose containing five gas sensors (TGS 822, TGS 2442, TGS 813, TGS 4160, TGS 2600), a temperature sensor, a humidity sensor, and wind speed measurements to monitor carbon monoxide, carbon dioxide (CO, CO<sub>2</sub>) gasses for three different regions of Alexandria-Egypt along the Corniche River and two different rivers. The sensor array had been attached to a 16F628A microcontroller. After that, data clustering was implemented to investigate the relation between measurements from different sensors. Variance analysis (ANOVA) has been used to track critical variables which are to be inserted into the regression equation. Results showed that the electronic nose was able to prove

that the Corniche Street was the least polluted place while the most polluted was Abukir Street.

In research [79] Loutfi et al combined mapping of gas distribution with the definition of odors. The system is fitted with two electronic noses gathered into a handheld robot. The classification performance of ethanol and acetone in indoor experiments ranged from 88 to 100 per cent was very high.

In [80], authors analyzed the performance of the three electronic nose systems based solely on semi-conducting gas sensors (TGS880, TGS2600, and TGS1331), amperometric gas sensors (H<sub>2</sub>S-B4, CO-B4, 7SH CiTiceL) and both types of outdoor air quality sensors. They then compared the predictive potential of the e-noses gas concentration of four environmental gases, namely nitrogen dioxide, sulphur dioxide, ozone and carbon monoxide, with reference data from the air control system's stationary station. They concluded that the best results for prediction are obtained by integrating both types of sensors.

#### 4. Findings and discussion

In the above subsections, we have provided a detailed overview of individual classifiers such as SVM, KNN, ANN and ELM. Each of these algorithms has their problems. However, by combining certain processes, we can maximize the full benefits.

The data fusion or mixture of data is implemented to a wide variety of fields. To take an example: the human body, the human brain permanently merges knowledge from an object in order to determine its property.

In general, data fusion methods can be classified into three levels; low abstraction level, intermediate level and high level.

In order to determine the accuracy of agricultural and industrial olive oil samples, Natale et al. [81] have introduced two electronic nose systems based on specific sensor technologies (quartz resonators and metal oxide chemoreceptors). Researchers indicated that data fusion for the two abstraction levels: high (fusion of the key components) and low (fusion of sensor data) indicates that cooperation was formed from commercial samples between the two matrixes of animal product detection outcomes.

Pardo et al. [82] simultaneously used MOX sensors to measure more than one sensor property (i.e., conductivity and surface potential) with other types of sensor gases. This included the use of various types of sensors (so-called hybrid matrix) to reduce the linearity of the response and, therefore, achieve better discrimination.

A hybrid electronic nose (6 voltammetric and 15 potentiometric sensors) was used by Gutierrez et al. [83] to differentiate beer forms using data fusion and pattern recognition methods (PCA and LDA). They indicated that in comparison with the simple E-tongue, the performance of hybrid E-language systems using the latest approach of data fusion from different sensor types is more accurate.

Ensemble classifier is considered a mixture of a high level; an overall decision is made by merging the decisions of the classifiers used. This combination of classifiers can improve classification. Fusion requires modification of a learning ensemble to promote better classification accuracy. In other words, it is desirable to design and build a classification system using various combination classifiers to boost the overall classification accuracy.

Lijun Dang et al [84] have proposed a new fusion approach that carries out an efficient weighted base classifier process called an enhanced support vector machine ensemble (ISVMEN). Results show that the average accuracy of classification was increased from less than 86 % to 92.58% percent relative to that of base classifiers.

A novel hybrid approach to solving the problem of cross-selectivity of gases in electronic nose (E-nose) using the combination classifiers of support vector machine (SVM) and k-nearest neighbor (KNN) methods was proposed in research by R.Faleh et al [85]. The new coordinates calculated by PCA were used as inputs for classification by the SVM method. Finally, the classification achieved by the KNN method was carried out to calculate only the support vectors (SVs), not all the data. The proposed fusion approach has been shown to lead to the highest classification rate relative to the accuracy of the individual classifiers: KNN, SVM-linear, SVM-RBF, and SVM-polynomial.

The combination of SVM, PNN and LDA was shown a high accuracy rate compared to classification results obtained with individual classifiers [86]. Experimental findings show that the optimized Adaboost. M2 model, which solves a multi-class identification problem for Chinese herbal medicine, combined with SVM, PNN and LDA, achieves the best 91.75 %accuracy, compared to 87.62 % of the best single classifier SVM.

The above discussion shows that using multiple classifiers together lead to get maximum benefits in various applications.

## 5. Conclusion

Health and environmental effects whose origin is liability to air pollution requires monitoring and controlling air quality parameters. In this way we present this review summarizing various sensing technologies for air quality supervising. This paper was devoted primarily for Electronic nose technology. Metal oxide Gas sensor was then presented with different layers consisting a gas sensor. Signal processing for feature extraction based on PCA was then introduced. In addition, gas pattern recognition technology based on machine learning were detailed and compared. Finally, ensemble classifier notion was discussed as a solution to improve classification accuracy.

## References

[1] Apetrei,C; VirginiaBounegru,V,” Electronic Noses and Traceability of Foods”, Reference Module in Food Science, 2020  
 [2] Chen ,K; Gao W; Emaminejad S, et al. “Printed carbon nanotube electronics and sensor systems”. *Adv Mater*, 2016,Vol.28, 4397, doi:10.1002/adma.201504958

[3] Wilson, A. “Application of electronic-nose technologies and VOC-biomarkers for the noninvasive early diagnosis of gastrointestinal diseases”. *Sensors* 2018, 18, 2613,doi: 10.3390/s18082613  
 [4] Liu, L.; Li, X.; Li, Z.; Shi, Y. “Application of Electronic Nose in Detection of Fresh Vegetables Freezing Time Considering Odor Identification Technology”. *Chem. Eng. Trans.* 2018, 68, pp.265–270  
 [5] Zampolli ,S; Elmi ,I; Ahmed, F et al. An electronic nose based on solid state sensor arrays for low-cost indoor air quality monitoring applications. *Sens Actuators B*, 2004, 101, 39,doi: 10.1016/j.snb.2004.02.024  
 [6] Pangestu,E; Wonohardjoa, Gede Putra Kusumaa,” Air Pollution Mapping using Mobile Sensor Based on Internet of Things”, *Procedia Computer Science* ,2019,Vol.157,pp.638–645,doi: 10.1016/j.procs.2019.08.224  
 [7] Harrou, F.; Dairi, A.; Sun, Y.; Kadri, F. “Detecting Abnormal Ozone Measurements With a Deep Learning-Based Strategy”. *IEEE Sens. J.* 2018, 18, 7222–7232, doi:10.1109/JSEN.2018.2852001  
 [8] J.W. Gardner and P.N. Bartlett “A brief history of the electronic noses” *Sensors and Actuators B* 18-19 (1994) 211-220,doi: 10.1016/0925-4005(94)87085-3  
 [9] Pardo, M.; Sberveglier, G. “Comparing the performance of different features in sensor arrays”, *Sensors and Actuators B* (2007) pp 437–443,doi: 10.1016/j.snb.2006.09.041  
 [10] R.O.Duda,P.E.Hart and D.G.Stork,Pattern Classification,John Wiley&Sons,INc,New York,2000  
 [11] D. Grandjean et al. EXAFS and XANES,” study of a pure and Pd doped novel Sn/SnO xnanomaterial”,*J. Phys. Chem. B*, (2004), pp. 8876-8887,doi: 10.1021/jp0370627  
 [12] Ali, A.A.S.; Akbar, M.A.; Amira, A.; Bensaali, F.; Benammar, M.; Hassan, M.; Bermak, A. Fast Prototyping of KNN Based Gas Discrimination System on the Zynq SoC. *Qatar Found. Annu. Res. Conf. Proc.*, 2016, ICTOP1832, 10.5339/qfarc.2016.ICTOP1832  
 [13] Xiong, Y.; Xiao, X.; Yang, X.; Yan, D.; Zhang, C.; Zou, H.; Lin, H.; Peng, L.; Xiao, X.; Yan, Y.”Quality control of Lonicera japonica stored for different months by electronic nose”. *J. Pharm. Biomed.* 2014, 91, 68–72, 10.1016/j.jpba.2013.12.016  
 [14] Fayçal Benrekia , Mokhtar Attari and Mounir Bouhedda, “Gas Sensors Characterization and Multilayer Perceptron (MLP) Hardware Implementation for Gas Identification Using a Field Programmable Gate Array (FPGA)”, *Sensors* 2013, 13, 2967-2985; doi:10.3390/s130302967  
 [15] Saraoglu, H.M.; Selvi, A.O.; Ebeoglu, M.A.”Electronic nose system based on quartz crystal microbalance sensor for blood glucose and HbA1c levels from exhaled breath odor”. *IEEE Sens. J.* 2013, 13, 4229–4235,doi: 10.1109/JSEN.2013.2265233  
 [16] Jung Hwan Cho, Pradeep U. Kurup,” Decision tree approach for classification and dimensionality reduction of electronic nose data”, *Sensors and Actuators B: Chemical* Volume 160, Issue 1, 15 December 2011, Pages 542-548,doi: 10.1016/j.snb.2011.08.027  
 [17] Acevedo F., Maldonado S., Dominguez E., Narvaez A., Lopez F. Probabilistic support vector machines for multi-class alcohol identification. *Sens. Actuators B Chem.* 2007;122:227–235. doi: 10.1016/j.snb.2006.05.033  
 [18] Dietterich, T.G. (2000), “Ensemble methods in machine learning”, 1st International Workshop On Multiple Classifier Systems, Springer, Cagliari, pp. 1-15.  
 [19] HadiHabibzadeh, Zhou Qin, TolgaSoyata and BurakKantarci, Large Scale Distributed Dedicated- and Non-Dedicated Smart City Sensing Systems, doi: 10.1109/JSEN.2017.2725638, *IEEE Sensors Journal*  
 [20] Derek Doran, SwapnaGokhale and Aldo Dagnino, Human Sensing for Smart Cities, 2013 IEEE/ACM International Conference on Advances in Social Networks Analysis and Mining, ASONAM'13, August 25-29, 2013, Niagara, Ontario, CAN Copyright 2013 ACM 978-1-4503-2240-9 /13/08 .  
 [21] Froehlich, J.; Larson, E.; Gupta, S.; Cohn, G.; Reynolds, M.; Patel, S. Disaggregated End-Use Energy Sensing for the Smart Grid. *IEEE Pervasive Comput.*2011, 10, 28–39.  
 [22] S. Bedoui et al. Electronic Nose System and Principal Component Analysis Technique for Gases IdentificationAdvances in Systems, Signals and Devices, Volume 6, 2018, pp. 167-180. <https://doi.org/10.1515/9783110448375-011>  
 [23] Gardner, J.W.; Bartlett, P.N. A brief-history of electronic noses. *Sens. Actuators B Chem.* 1994, 18, 211–220.  
 [24] Negri, R.M.; Reich, S. Identification of pollutant gases and its concentrations with a multisensory array. *Sens. Actuators B Chem.* 2001, 75, 172–178. doi:10.1016/S0925-4005(01)00543-3  
 [25] S. Zampolli et al. An electronic nose based on solid state sensor arrays for low-cost indoor air quality monitoring applications/ *Sensors and Actuators B* 101 (2004) 39–46. doi:10.1016/j.snb.2004.02.024



- [26] Helli, O.; Siadat, M.; Lumbreras, M. Qualitative and quantitative identification of H<sub>2</sub>S/NO<sub>2</sub> gaseous components in different reference atmospheres using a metal oxide sensor array. *Sens. Actuators B Chem.* 2004, 103, 403–408. doi:10.1016/j.snb.2004.04.069
- [27] IMAN MORSI, Electronic Noses for Monitoring Environmental Pollution and Building Regression Model, 978-1-4244-1766-7/08/\$25.00 ©2008 IEEE
- [28] Ozmen Edward J. Wolfrum\*, Robert M. Meglen, Darren Peterson, Justin Sluiter, “Metal oxide sensor arrays for the detection, differentiation, and quantification of volatile organic compounds at sub-parts-per-million concentration levels”, *Sensors and Actuators B* 115 (2006) ,pp.322–329, 10.1016/j.snb.2005.09.026
- [29] Wang, C., Yin, L., Zhang, L., Xiang D. and Gao. R., “Metal Oxide Gas Sensors: Sensitivity and Influencing Factors”, *Sensors*, Vol: 10, No: 3, pp. 2088-2106, 2010,doi: 10.3390/s100302088
- [30] Ozmen A, Dogan E. “Design of a portable e-nose instrument for gas classifications”. *IEEE Trans Instrum Meas*, 2009, 58, 3609, 10.1109/TIM.2009.2018695
- [31] J.W. Gardner and P.N. Barlett “A brief history of the electronic noses” *Sensors and Actuators B* 18-19 (1994) 211-220
- [32] Simon M. Scott, David James, and Zulfiqar Ali, “Data analysis for electronic nose systems,” *Phil. Microchim Acta* 156, 183–207 (2007)
- [33] Zhesi Chen et al , “Smart gas sensor arrays powered by artificial intelligence”, *Journal of Semiconductors*, 2019, 40, 111601,doi: 10.1088/1674-4926/40/11/111601
- [34] FALEH Rabeb, BEDOUI Souhir, KACHOURI Abdennaceur, SAMET Mounir “An electronic nose for detection pollutant odorant and olfaction classification using neural network”, 14th international conference on Sciences and Techniques of Automatic control & computer engineering -pp 174-178, , 2013M. Young, *The Technical Writer’s Handbook*. Mill Valley, CA: University Science, 1989.
- [35] R.O.Duda,P.E.Hart and D.G.Stork, *Pattern Classification*, John Wiley&Sons,INc,New York,2000
- [36] Casey, J.G.; Collier-Oxandale, A.; Hannigan, M. Performance of artificial neural networks and linear models to quantify 4 trace gas species in an oil and gas production region with low-cost sensors. *Sens. Actuators Chem.* 2019, Vol.283,pp. 504–514,doi: 10.1016/j.snb.2018.12.049
- [37] Shaobin Feng et al, “Review on Smart Gas Sensing Technology”, *Sensors* 2019, 19, 3760,pp. 10.3390/s19173760
- [38] Casey, J.G.; Collier-Oxandale, A.; Hannigan, M. Performance of artificial neural networks and linear models to quantify 4 trace gas species in an oil and gas production region with low-cost sensors. *Sens. Actuators Chem.* 2019, 283, 504–514,doi: 10.1016/j.snb.2018.12.049
- [39] V. Krivetskiy et al, “Selective detection of individual gases and CO/H<sub>2</sub> mixture at low concentrations in air by single semiconductor metal oxide sensors working in dynamic temperature mode”, *Sensors and Actuators B: Chemical*, Vol. 254, 2018, pp. 502-513, 10.1016/j.snb.2017.07.100
- [40] Huang, G.B.; Zhu, Q.Y.; Siew, C.K. Extreme learning machine: Theory and applications. *Neurocomputing* 2006, 70, 489–501,doi: 10.1016/j.neucom.2005.12.126
- [41] Qiu, S.; Gao, L.; Wang, J. Classification and regression of ELM, LVQ and SVM for E-nose data of strawberry juice. *J. Food Eng.* 2015, Vol.144,pp.77–85,doi: 10.1016/j.jfoodeng.2014.07.015
- [42] Chao Peng et al, “Enhancing Electronic Nose Performance Based on a Novel QPSO-KELM Model”, *Sensors* 2016, 16, 520,doi: 10.3390/s16040520
- [43] Ye, J. Artificial neural network modeling of methanol production from syngas. *Pet. Sci. Technol.* 2019, 37, 629–632
- [44] Saxena, G., and Paily, R., “Performance improvement of square microhotplate with insulation layer and heater geometry”, *Microsystem Technologies*. Vol: 21, No: 11, pp. 2331-2338, 2015.
- [45] C. Rossi, P. Temple-Boyer, D. Estève, *Sens. Actuators A Phys.* 64, 241–245 (1998). [https://doi.org/10.1016/S0924-4247\(97\)01627-0](https://doi.org/10.1016/S0924-4247(97)01627-0)
- [46] D.S. Lee, Y.H. Choi, M.Y. Jun, in *Sensors*, 2012 IEEE (2012). doi:10.1109/icsens.2012.6411404
- [47] S. Bedoui, S. Gomri, H. Charfeddine Samet, A. Kachouri, in *International Multi Conference on Systems, Signals & Devices (SSD)* (2016). <https://doi.org/10.1109/SSD.2016.7473712>
- [48] H. Kumar, K.K. Sing, N. Sood, A. Kumar. And R.K. Mittal, “Design and Simulation of a Micro Hotplate for MEMS Based Integrated Gas Sensing System,” 978-1-4799-2179- 9/14/\$31.00 ©2014 IEEE.
- [49] M. Ahuja, R. Talwar, B. Prasad, *Rev. ICRTEDC* 1(2), 67–70 (2014)
- [50] S.D. Kim, B.J. Kim, J.H. Yoon, J.S. Kim, *J. Korean Phys. Soc.* (2007). doi:10.3938/jkps.51.2069
- [51] D. S. Lee, S. D. Han, J. S. Huh, and D. D. Lee, *Sens. Actuat. B Chem.*, 60, 57 (1999). Doi:10.1016/S0925- 4005(99)00244-0]
- [52] Rabeb Faleh ; Mehdi Othman ; Sami Gomri ; Khalifa Aguir ; Abdennaceur Kachouri, “A Transient Signal Extraction Method of WO<sub>3</sub> Gas Sensors Array to Identify Pollutant Gases”, *IEEE Sensors Journal*, Volume: 16, Issue: 9 , May1, 2016 ,doi: 10.1109/JSEN.2016.2521578
- [53] M. Bendahan, R. Boulmani, J. L. Seguin, and K. Aguir, *Sensor Actuat B-Chem.*, 100, 320 (2004). Doi:10.1016/j.snb.2004.01.023]
- [54] F. George, M.C. Leon, A. Ayo, B. Russell, *Sensors* (2010). doi:10.3390/s1006 05469
- [55] C. Wongchoosuk, A. Wisitsoraat, D. Phokharatkul, A. Tuantranont, T. Kerdraroen, *Sensors* (2010). Doi:10.3390/s1008 07705
- [56] Joy Dutta, Chandreyee Chowdhury, Sarbani Roy, Asif Iqbal Mridha, FirojGazi, Towards Smart City: Sensing Air Quality in City based on Opportunistic Crowd-sensing. *ICDCN '17*, January 04-07, 2017, Hyderabad, India © 2017 ACM .ISBN 978-1-4503-4839-3/17/01...\$15.00 doi:10.1145/3007748.3018286
- [57] Sagl, G.; Blaschke, T.; Beinat, E.; Resch, B. Ubiquitous Geo-Sensing for Context-Aware Analysis: Exploring Relationships between Environmental and Human Dynamics. *Sensors* 2012, 12, 9800–9822,doi: 10.3390/s120709800
- [58] K. C. Persaud, A. M. Pisanelli, S. Szyszko, M. Reichl, G. Horner, W. Rakow, H. J. Keding, and H. Wessels, “A Smart Gas Sensor for Monitoring Environmental Changes in Closed Systems: Results from the MIR Space Station,” *Sensors and Actuators B: Chemical*, vol. 55, 1999,doi: 10.1016/S0925-4005(99)00168-9
- [59] Hodgins, D. The development of an electronic nose for industrial and environmental applications. *Sens. Actuators B Chem.* 1995, 27, 255–258,doi: 10.1016/0925-4005(94)01597-B
- [60] CM Quant, PH Fischer, E Buringh, CB Ameling, DJM Houthuijs, FR Cassee “Application of principal component analysis to time series of daily air pollution and mortality” *RIVM report 650010035 /2003*
- [61] Edward Ming-Yang Wu and Shu-Lung Kuo “A Study on the Use of a Statistical Analysis Model to Monitor Air Pollution Status in an Air Quality Total Quantity Control District” *atmosphere* ISSN 2073-4433, 2013
- [62] zregorJasinski et al, Evaluation of the Electronic Nose Used for Monitoring Environmental Pollution, 2018 XV International Scientific Conference on Optoelectronic and Electronic Sensors (COE), 978-1-5386-4107-1/18/\$31.00 ©2018 IEEE
- [63] Marie Chavent, Herv\_e Guegan, Vanessa Kuentz, Brigitte Patouille, Jérôme Saracco “PCA and PMF based methodology for air pollution sources identification and apportionment” *Environmetrics*, Wiley-Blackwell, 20, pp.928-942. 2009
- [64] D.Voukantsis1 , K. Karatzas1, J. Kukkonen, T. Räsänen, A. Karppinen, M. Kolehmainen “Inter-comparison of air quality data using principal component analysis, and forecasting of PM10 and PM2.5 concentrations using artificial neural networks, in Thessaloniki and Helsinki” *Published in Science of The Total Environment*, 2011, 409(7), 1266- 76.
- [65] Hui Li et al, “Classification and Identification of Industrial Gases Based on Electronic Nose Technology”, *Sensors* 2019, 19, 5033; doi:10.3390/s19225033
- [66] ang, Qe t al, “Adulterant identification in mutton by electronic nose and gas chromatography-mass spectrometer”. *Food Control* 2019, 98, 431–438.
- [67] Mahdi Ghasemi-Varnamkhasti et al, “Differentiation of cumin seeds using a metal-oxide based gas sensor array in tandem with chemometric tools”, *Talanta*, doi:10.1016/j.talanta.2017.08.024
- [68] Mahuya Bhattacharyya Banerjee et al, « Black Tea Classification Employing Feature Fusion of E-Nose and E-Tongue Responses”, *journal of food engineering JFOE* 9409,2019, doi:10.1016/j.jfoodeng.2018.09.022
- [69] Ali, A.A.S.; Akbar, M.A.; Amira, A.; Bensali, F.; Benammar, M.; Hassan, M.; Bermak, A. Fast Prototyping of KNN Based Gas Discrimination System on the Zynq SoC. *Qatar Found. Annu. Res. Conf. Proc.* 2016
- [70] Gutierrez-Osuna, R.; Nagle, H.T. A method for evaluating data-preprocessing techniques for odour classification with an array of gas sensors. *IEEE Trans. Syst. Man Cybern. Part (Cybernetics)* 1999, 29, 626–632
- [71] Mehmet Aci, Cigdem \_Inan, Mutlu Avci, “A hybrid classification method of k nearest neighbor, Bayesian methods and genetic algorithm, *Expert Systems with Applications*, (2010) Vol. 37,pp. 5061–5067, 10.1016/j.eswa.2009.12.004
- [72] Yu, Z.; Chen, H.; Liu, J.; You, J.; Leung, H.; Han, G. Hybrid k-nearest neighbor classifier. *IEEE Trans. Cybern.* 2016, Vol.46, pp.1263–1275,doi: 10.1109/TCYB.2015.2443857
- [73] Wang, K.; Ye, W.; Zhao, X.; Pan, X. A support vector machine-based genetic algorithm method for gas classification. In *Proceedings of the 2nd International Conference on Frontiers of Sensors Technologies (ICFST)*, Shenzhen, China, 14–16 April 2017; pp. 363–366

- [74] Laref, R.; Losson, E.; Sava, A.; Siadat, M. Support Vector Machine Regression for Calibration Transfer between Electronic Noses Dedicated to Air Pollution Monitoring. *Sensors* 2018, Vol.18, 3716,doi: 10.3390/s18113716
- [75] Kyu-Won Jang, Jong-Hyeok Choi, Ji-Hoon Jeon and Hyun-Seok Kim, "Combustible Gas Classification Modeling using Support Vector Machine and Pairing Plot Scheme", *Sensors* 2019, Vol.19, 5018,doi: 10.3390/s19225018
- [76] Łukasz Lentka et al., "Determination of gas mixture components using fluctuation enhanced sensing and the LS-SVM regression algorithm", *Metrol. Meas. Syst.*, Vol. XXII (2015), No. 3, pp. 341–350,doi: 10.3390/s19225018
- [77] Bhaskar Navaneeth, M. Suchetha, " PSO optimized 1-D CNN-SVM architecture for real-time detection and classification applications", *Computers in Biology and Medicine*, Volume 108, May 2019, Pages 85-92
- [78] Yu Song a, Shaodong Xie, Yuanhang Zhang, Limin Zeng, Lynn G. Salmon, Mei Zheng "Source apportionment of PM2.5 in Beijing using principal component analysis/absolute principal component scores and UNMIX" *Science of the Total Environment* 372 (2006) 278–286
- [79] Loutfi, A.; Coradeschi, S.; Lilienthal, A.J.; Gonzalez, J. Gas distribution mapping of multiple odour sources using a mobile robot. *Robotica* 2009, Vol.27, pp.311–319. doi: 10.1017/S0263574708004694
- [80] Yeong Gwang Oh et al., " Adaptive SVM-based real-time quality assessment for primer-sealer dispensing process of sunroof assembly line", *Reliability Engineering & System Safety*, Volume 184, April 2019, Pages 202-212
- [81] Natale, D., et al., Comparison and integration of arrays of quartz resonators and metaloxide semiconductor chemoresistors. *Sens. Actuators B* 78, pp 303-309, 2001,doi: 10.1016/S0925-4005(01)00830-9
- [82] Pardo, M., Kwong, L.G., Sberveglieri, G., Brubaker, K., Schneider, J.F., Penrose, W.R., et al., 2005. Data analysis for a hybrid sensor array. *Sens. Actuators B* 106, pp136-143,doi: 10.1016/j.snb.2004.05.045
- [83] Gutierrez-Capitan, M., Santiago, J., Vila-Planas, J., Llobera, A., Boso, S., Gago, P., Martinez, M., Jimenez-Jorquera, C., 2013. Classification and characterization of different white grape juices by using a hybrid electronic tongue. *J. Agric. Food Chem.* 61 (39), pp 9325-9332,doi: 10.1021/jf402960q
- [84] Lijun Dang et al., " A novel classifier ensemble for recognition of multiple indoor air contaminants by an electronic nose", *Sensors and Actuators A* 207 (2014) ,67–74,doi: 10.1016/j.sna.2013.12.029
- [85] Rabeb Faleh, Sami Gomri, Mehdi Othman, Khalifa Aguir and Abdennaceur Kachouri, " Enhancing WO3 gas sensor selectivity using a set of pollutant detection classifiers", *Sensor Review Journal*, 2018, Vol. 38 No. 1, pp. 65-73,doi: 10.1108/SR-12-2016-0273
- [86] Xiyang Sun et al., " An optimized multi-classifiers ensemble learning for identification of ginsengs based on electronic nose", *Sensors and Actuators A: Physical* Volume 266, 15 October 2017, Pages 135-144,doi: 10.1016/j.sna.2017.08.052

## **A Comprehensive Survey on Image Modality Based Computerized Dry Eye Disease Detection Techniques**

Aditi Haresh Vyas\*, Mayuri A. Mehta

*Department of Computer Engineering, Sarvajani College of Engineering and Technology, Surat, 395001, Gujarat, India*

---

### **ARTICLE INFO**

*Article history:*

*Received: 08 February, 2020*

*Accepted: 25 March, 2020*

*Online: 20 April, 2020*

---

*Keywords:*

*Dry Eye*

*Disease detection*

*Tear film breakup*

*Lipid layer pattern*

*Image Processing*

*Deep learning*

---

### **ABSTRACT**

*Dry Eye Disease (DED) is one of the commonly occurring chronic disease today, affecting the vision of eye. It causes severe discomfort in eye, visual disturbance and blurred vision impacting the quality of life of patients. Due to recent advancements in Artificial Intelligence (AI) and rapid progress of analytics techniques, several image modality based computerized DED detection techniques are available in literature. These techniques transform image data into real and actionable insights and thus, provide new understanding and ways for better and quicker treatment. In addition, they assist ophthalmologist to diagnose dry eye disease precisely as well as to reduce the cost of healthcare. In this paper, we present a review on computerized DED detection techniques covering all available techniques. In addition, we present a parametric evaluation of these techniques based on our identified set of parameters. Though surveys on clinical DED detection techniques are available, this is the first attempt in literature to log down all computerized DED detection techniques at one place. Our survey will assist researchers and ophthalmologists to understand various technological advancements in the field of DED detection. As a little amount of work has been done in the field of automatizing dry eye disease detection, the field provides plenty of research opportunities to develop an automated efficient DED detection technique.*

---

### **1. Introduction**

Eye is a sensory organ of human body and is responsible for vision. Humans receive information of their surroundings through eyes. A transparent structure situated in front of the eye is referred as cornea [1-3]. In order to keep eyes healthy, cornea should be kept moist. A tear film located on the cornea helps to fulfill this need [2-4]. Tear film is a three layered structure having lipid layer on the outer surface, aqueous layer in middle and mucous layer in the inner portion of the cornea. It has several functions such as providing nourishment to the cornea, lubricating corneal surface and maintaining moisture of the eye. Certain factors such as prolonged use of electronic gadgets, old age, environmental conditions, medication, smoking habits and use of contact lens can disturb the tear film balance and can lead to evaporation of moisture from tear film causing dry eye disease [5-8].

Dry eye disease is a common and widespread eye disease in the world today. It is a growing health problem that affects significant percentage of population in the world [2-3, 7]. It occurs due to instability in tear film, reduction in tear production or

abnormality in tear producing glands. Symptoms of dry eye disease include blurred vision, burning sensation, sore and itchy eye, foreign body sensation and photophobia [3, 5-6]. If DED is left untreated, it can cause infection, corneal ulcer or blindness [9-11]. Clinical diagnosis of dry eye is a difficult task because it occurs due to different factors. A clinician sometimes requires multiple tests or repetitive tests for proper diagnosis. Some of the clinical tests used for diagnosis of dry eye are dry eye questionnaire such as Ocular Surface Disease Index (OSDI) [12] and Mc Monnies [13], tear film breakup time test, schirmer test and meibomian secretion scoring [4-6, 9, 11-14].

The major drawbacks of clinical are as follows: 1) Each clinical test takes long time to diagnose dry eye as it is performed manually. 2) Diagnosis by clinical test is subjective in nature 3) Accurate severity level of dry eye disease is not identified due to subjectivity in diagnosis and 4) Medication may be prescribed for incorrect period on the basis of inaccurate severity level. It was observed by research community that the computerization of clinical tests will help ophthalmologist and optometrist to bring objectivity and to increase accuracy of the diagnosis. Moreover, computerization makes diagnosis faster which in turn saves time

---

\*Aditi H. Vyas, Email: [aditi.vyas.9@gmail.com](mailto:aditi.vyas.9@gmail.com)

of ophthalmologist and gives him more time for counselling of patients. Several DED detection techniques have been proposed in literature.

In this paper, we summarize them along with corresponding clinical tests. Based on our study, we classify the techniques into following three major categories subject to the approach used to identify the dry eye disease: 1) Techniques based on tear film stability [15-25], 2) Techniques based on blink rate detection [26] and 3) Techniques based on amount of tear produced [27]. DED detection techniques based on tear film stability further differ from each other with respect to imaging modality. Hence, based on imaging modality used, we further classify them into three subcategories: techniques using fluorescein tear film video [15-22], techniques using lipid layer interference patterns [23-24] and techniques using thermal infrared images [25]. From our rigorous study on DED detection techniques, we have identified several parameters to evaluate them. We then present a comprehensive and comparative evaluation of these techniques based on identified parameters. To the best of our knowledge, this is the first attempt to note down all image modality based computerized DED detection techniques at one place. The objective of this survey is to discuss the some clinical tests and their corresponding computerized DED detection techniques as well as to emphasize the potential of DED detection techniques in the domain of healthcare. It has been observed that a little amount of work has been done in the field of automatizing dry eye disease detection and hence, it provides an ample amount of research opportunities in this field. The researchers may come up with an efficient new DED detection technique corresponding to any of the commonly adopted clinical tests.

The rest of this paper is organised as follows: Section II introduces the key concepts related to dry eye disease to understand its background. In addition, various clinical tests for which computerized techniques have been proposed are discussed in this section. Section III describes the proposed taxonomy of computerized DED detection techniques along with their detailed discussion. Section IV presents comparative analysis of DED detection techniques. In particular, the parametric evaluation of DED detection techniques based on identified parameters and summary of these techniques are presented in this section. Finally, conclusions and future work are specified in section V.

## 2. Dry Eye Disease and its Clinical Diagnosis

As shown in Figure 1, human eye is divided into two major parts: anterior segment and posterior segment [1]. Anterior segment mainly consists of iris, cornea, lens, pupil, anterior chamber and ciliary muscle. Posterior segment consists of sclera, retina, choroid, fovea, optic nerve and retinal blood vessels. Many diseases manifests themselves in eye such as corneal ulcer, diabetic retinopathy, age related macular degeneration, glaucoma, cataract, dry eye and so on. Amongst these diseases, dry eye is the most commonly occurring disease caused due to instable tear film on cornea.

Dry eye also known as keratoconjunctivitis sicca is defined as a multi-factorial disease characterized by unstable tear film causing a variety of symptoms and/or visual impairment, potentially accompanied by ocular surface damage [2-3]. It is

classified into two major categories: aqueous deficient dry eye and evaporative dry eye. Aqueous deficient dry eye refers to low production of tears. Evaporative dry eye refers to excess evaporation of tears from the eye. Both the categories show similar symptoms and may co-exist.

As diagnosis of dry eye disease is a difficult task, ophthalmologist sometimes requires performing different diagnosis tests to diagnose dry eye. Ophthalmologist starts diagnostic procedure by asking patient the history and symptoms related to dry eye disease. Predefined symptom questionnaires such as OSDI, Mc Monnies and Dry Eye Questionnaire are available to know the history and symptoms [12-13]. The questionnaire provides a score that serves as a basis to identify DED. A low score indicates normal eye and a high score indicates possibility of dry eye. However, ophthalmologist cannot completely rely upon questionnaire and hence, questionnaire procedure is often followed by different clinical tests.

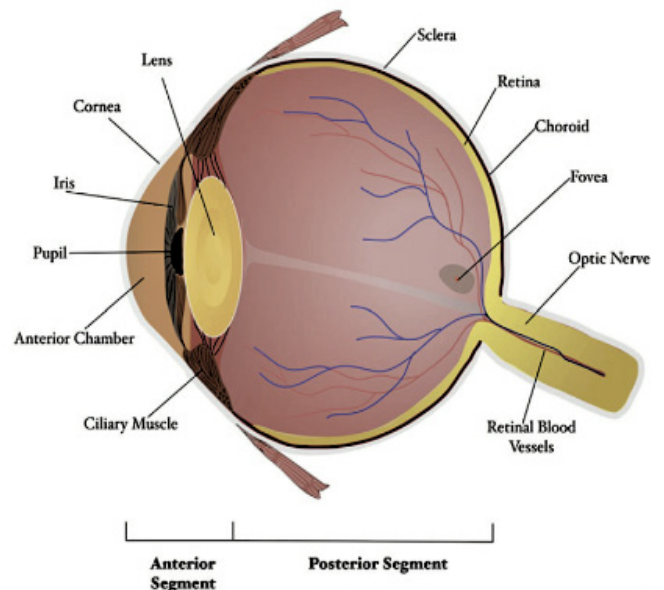


Figure 1: Anatomy of an Eye [1]

The clinical test is carried out to confirm the presence of dry eye disease. As shown in Figure 2, clinical tests are mainly categorized into three categories [2-4]: tests based on quantity of tears produced, tests based on quality of tear film and other laboratory tests. Each of these categories comprises of different clinical tests. Schirmer test, tear meniscus assessment test and phenol red thread test are the tests carried out measuring the quantity of tears. Lipid layer pattern assessment, tear breakup time test, osmolarity of tear film and non-invasive breakup test are the tests carried out considering the quality of tear film.

The remaining tests such as meibomian gland functioning test, confocal microscopy, impression cytology and bio microscopic examinations are the other tests conducted in clinics. Though several clinical tests are available, techniques have been proposed in literature only for four of them and hence, only those four clinical tests have been computerized so far. Before we discuss DED detection techniques, below we briefly describe those four clinical tests for better understanding of their corresponding DED techniques.



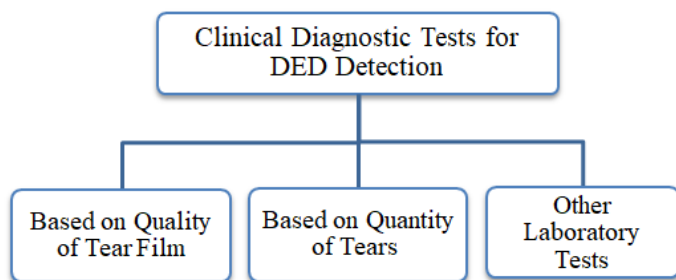


Figure 2: Clinical diagnostic tests for DED

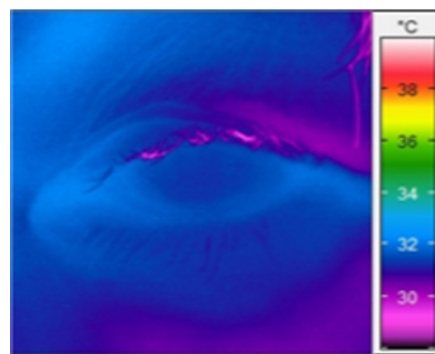


Figure 4: Thermal infrared image [25]

### 2.1. Tear film BreakUp Time (TBUT) Test

TBUT test measures the stability of the tear film. In TBUT test [2-5, 9], sodium fluorescein drops are instilled in the eye and are spread over the entire area of eye by directing the patient to blink few times. Subsequently, the ophthalmologist observes the tear film using slit lamp and measures the time (in seconds) at which the dark spot/s first appears in the tear film.

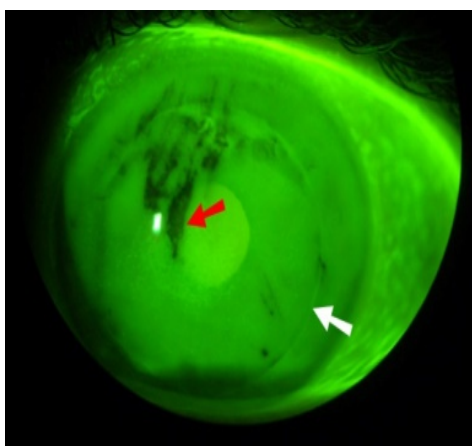


Figure 3: Tear film frame [22]

The appearance of the dark spot/s shows the instability of the tear film and thus, dry eye disease is detected. The time less than 5 seconds indicates dry eye, the time between 6 to 10 seconds indicates moderate dry eye and the time greater than 10 seconds indicates normal eye. Currently TBUT test is carried out manually by ophthalmologist or optometrist. The key shortcomings of manual TBUT test are it is time consuming and diagnosis done by it is subjective in nature as it depends on the observer. Figure 3 shows the breakup in tear film.

### 2.2. Infrared Thermography Images

In this test [3, 9], DED is detected based on the temperature of tear film. The infrared thermal camera is used to capture the eye image from which the temperature of tear film is measured. This temperature is also known as Ocular Surface Temperature (OST). OST varies when tear film is unstable. The variations in OST are captured by infrared radiations and are analyzed with the help of colour coded image. The sample colour coded image is shown in Figure 4. The variation appearing in OST is one of the ways to detect tear film instability and thereby to detect DED. A normal healthy eye does not show any variation in temperature. The major issues related to this clinical test are it takes higher time in diagnosis of DED and is expensive as well.

### 2.3. Lipid Layer Interference Pattern

Lipid layer is the first layer of the tear film. When light is projected over cornea, a pattern is formed over lipid layer [3, 8-9]. This pattern is captured using instrument called Tearscope Plus [23-24].

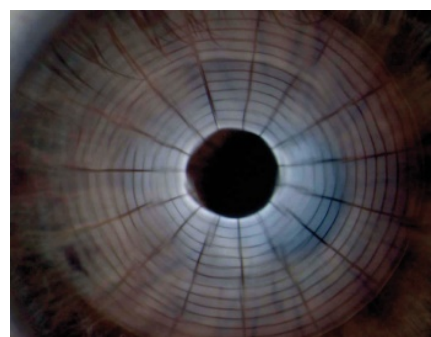


Figure 5: Lipid layer inference pattern [23]

As shown in Figure 5, it looks like a grid on lipid layer. The shape of pattern is classified into one of the following five categories: open meshwork, closed meshwork, wave, amorphous or colour fringe. These categories differ from each other with respect to colour and uniformity of lipid layer. The evaluation of lipid layer for non-uniformity and colour change assists in detection of DED.

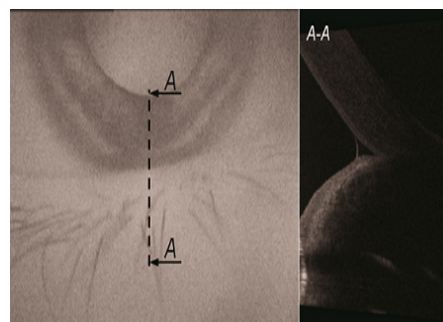


Figure 6: B-Scan of optical coherence tomography image [27]

### 2.4. Tear Meniscus Assessment

Tear meniscus [2, 6, 9, 27], also known as tear lake, is the collection of tears at the corners of eye. The measurement of its height, width and curves provide useful information for diagnosis of DED. Meniscus is measured manually using slit lamp or tearscope plus device by observing the quantity of tears in Tear

Lake. If tear quantity is less than approximate 0.2 mm, eye is considered as dry eye. Tear meniscus can also be measured from Optical Coherence Tomography (OCT) image. The sample optical coherence tomography image is shown in Figure 6.

### 3. Computerized DED Detection Techniques

Several DED detection techniques have been proposed over the years and are available in literature. As shown in Figure 7, we categorize them into three categories: techniques based on tear film stability, techniques based on blink rate detection and techniques based on amount of tears produced. These techniques aim to automatically identify the dry eye related area that indicates the presence or absence of DED.

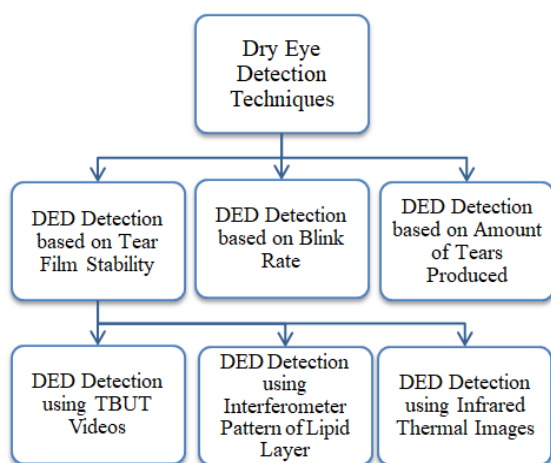


Figure 7: Classification of techniques for DED detection

The major steps involved in all these techniques are as follows: acquisition of eye image or eye video, pre-processing, feature extraction and classification.

#### 3.1. DED Detection Techniques based on Tear Film Stability

Tear film resides on the outer layer of eye. It maintains the moisture of eye. It becomes instable due to evaporation of moisture from eye and gets ruptured. As shown in Figure 7, the techniques that diagnose DED based on tear film instability are further classified into three sub-categories: techniques based on breakup measurement, techniques that use interferometer pattern of lipid layer and techniques that use infrared thermal image to detect DED. We now discuss the various techniques that fall under these sub-categories.

##### 3.1.1. Techniques based on Breakup Measurement

###### I. Automatic Detection of DED

The first automated DED detection technique was proposed in 2007 [15-16]. Input to this technique is an eye video that is captured using Eyescan device. We summarize the functioning of this technique in Figure 8. In this technique, input video is first divided into several frames. Then measurement areas are identified, where measurement area is the collection of frame/s that is/are captured when eye is completely open.

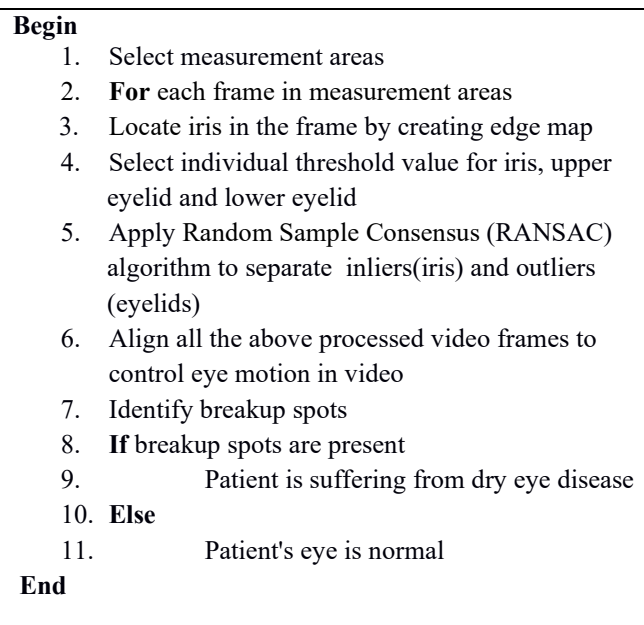


Figure 8: Major steps of automatic DED detection technique

In other words, it includes the frames that do not contain blink. Subsequently, iris is located in each frame of measurement area by creating edge map. This edge map is created using canny edge detection method. To eliminate illumination, to overcome blurring problem and to fit a circular mask, individual threshold values for iris, upper eyelid and lower eyelid are selected. All these video frames are then aligned to control the eye motion in video. Finally, breakup spots are identified by computing intensity value in each frame to know the presence of DED. If evolution curve of intensity values is created, it specifies the presence of dry eye disease.

#### II. Automation of Tear Film Breakup Test

In [17, 18], authors have proposed a technique for automatic detection of breakup spots. Input to this technique is an eye video. The major steps involved in this technique are depicted in Figure 9. During the first step, the measurement areas are detected from the input video. The key benefit of this technique is that unlike [15, 16], the measurement areas are detected automatically. They are detected based on symmetric difference in mean values of gray level of consecutive frames. High difference in mean values specifies the blink between two consecutive frames.

After locating the measurement areas, the Region of Interest (ROI) is located in each frame. The region of interest is iris on which the following three sub-steps are applied: identification of eye size, ROI alignment and ROI adjustment. Eye size is estimated using canny edge detection process and computing the size of circular mask. Next, eye movements in video are aligned by image registration process. Subsequently, iris is adjusted by cropping the background, eyelid and eyelashes portions that do not contain useful information.

The final step of this technique identifies the breakup spots using manually defined threshold value. For each frame in measurement areas, the histogram is created to calculate the threshold value of that frame. The largest value of gray level is

considered as black and is used as threshold value. If the threshold value of frame is higher than the manually chosen threshold value, the breakup spots are present. If evolution curve of breakup spots is created, patient is suffering from dry eye disease.

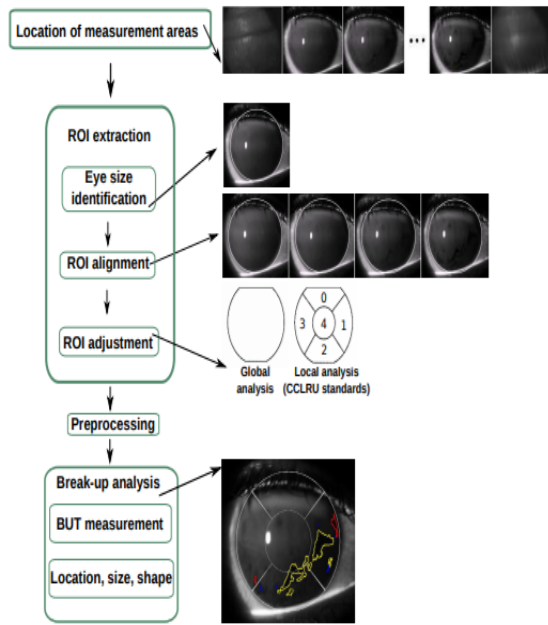
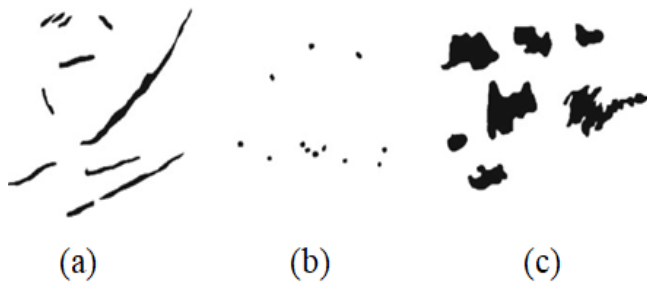


Figure 9: Flow of automation and analysis of TBUT [21]

The main drawback of this technique is that for every video in dataset, threshold value has to be selected manually due to difference in illumination condition and variation in quantity of fluorescein drops.

### III. Automation and Analysis of Tear Film Breakup Test

In [19-21], authors have extended the previous technique. The authors observed that the previous technique only examines the breakup spots. However, size, shape and location of these breakup spots can assist ophthalmologist in further assessment of tear film. Particularly, they assist ophthalmologist to indicate tear film contamination as well as to detect breakup accurately. Hence, they modified the previous technique via adding one more step location, size and shape as the last step as shown in Figure 9.



The initial steps of this technique are similar to previous technique [17-18]. After identification of breakup spots, rupture pattern is located in the last frame of video. Then two morphological operations, namely opening and closing, are

applied to the last frame to smoothen it. Next, the features such as moment, area, roundness, axis ratio, convexity and solidity are calculated. They are then fed to decision tree classifier which gives output as one of the three classes: streak, dot or pool as shown in Figure 10. Irrespective of the output pattern, the output represents the presence of DED.

### IV. Convolutional Neural Network based Screening of DED

In [22], authors have proposed a technique based on Deep Convolutional Neural Network (DCNN) to detect tear film breakup time. Input to this technique is an eye video. The technique consists of two major phases: training phase and testing phase. During training phase, each video frame is segmented into small-size images of 96x96 pixels. Input to DCNN is 96x96 pixels images. DCNN is trained on segmented images to predict one of the five classes: eyelash, tear film breakup area, tear film non-breakup area, sclera and eyelid. In testing phase, the input video is fragmented into frames for each second. The last frame (i.e. frame number 6) is given as the input to trained DCNN for identification of tear film breakup spot. Then probability map of breakup is created. Based on probability map, each of the frame numbers 1 to 5 is tested for appearance of breakup spot. If the breakup spot is present in the frame, dry eye disease is detected. The key limitation of this technique is that it limits dry eye detection up to 5 seconds (5 frames) and hence, is not able to identify further severity level of dry eye disease.

#### 3.1.2. Techniques based on Interference Pattern for Lipid Layer

Two techniques have been proposed under this category. They are a Computer Aided System to Support Dry Eye Diagnosis based on tear film maps (CASDES) [23] and iDEAS [24]. Input to both these techniques is image captured using tearscope plus device. The image captured using tearscope device is typically categorized into one of the five categories: open meshwork, wave, closed meshwork, colour fringe and amorphous.

##### I. A Computer Aided System to Support Dry Eye Diagnosis Based on Tear Film Maps (CASDES)

In [23], a computer aided system to support dry eye diagnosis based on tear film maps is proposed. It is an automatic system that takes input in the form of image. From the input image, the CASDES system produces output in the form of tear film map. This tear film map contains the region that indicates dry eye. The three steps to produce tear film map are as follows. First, the iris is located in the input image by removing sclera and eyelid portion of the eye. Second, the image is converted from RGB to CIE-LAB colour space. The texture features are then calculated by generating gray level co-occurrence matrix. The colour and texture features together are fed to Support Vector Machine (SVM) classifier. The SVM classifier is trained to produce output as one of the following five classes: open meshwork, wave, closed meshwork, colour fringe or amorphous. The region growing algorithm is then applied on the output of SVM to find the dry eye region. The output image of region growing algorithm is known as tear film map. This image is also annotated manually by ophthalmologist to locate dry eye region. Third, the dry eye



regions located by technique and ophthalmologist are compared to diagnose dry eye disease.

## II. *iDEAS: A Web Based System for Dry Eye Assessment*

In [24], authors have presented a web based system for dry eye disease assessment. As shown in Figure 11, the system consists of four main parts: remote user interface, web application server, image processing module and data storage. The input to this system is interference pattern obtained using tearscope device. Output is in the form of tear film map that contains dry eye areas.

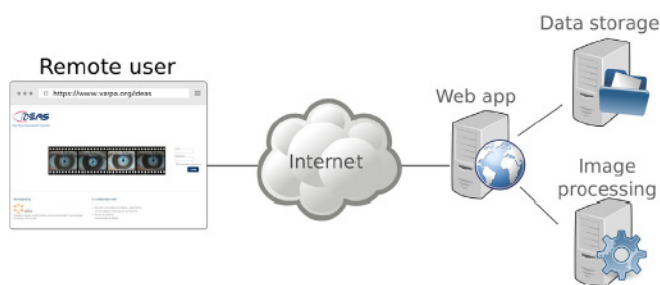


Figure 11: iDEAS system architecture [24]

The dry eye detection process is started by user via uploading patient's interference pattern. Once the interference pattern is uploaded, following steps are carried out by image processing module to detect dry eye. First, the iris is located in the interference pattern. Next, the low level colour and texture features such as mean, luminance of colour and gray levels are calculated. These features are then fed to SVM classifier. The SVM classifies the image into one of the five categories as mentioned in the previous technique. The region growing algorithm is then applied on the output of SVM to find the dry eye region. However, unlike previous technique, the dry eye region produced by system is not compared with any manually annotated dry eye region. Hence, dry eye related decision produced by the system is considered as the final decision. Data storage module of iDEAS system stores input patterns (tear film pattern of patients) as well as output patterns (labelled tear film pattern and classification results). iDEAS system is an easy to use system. Moreover, it can be used as a research tool as its data storage module has a large amount of patient's data. Additionally, it can be used over the internet with different underlying architectures.

### 3.1.3. *Techniques based on Thermal Infrared Images*

In literature, merely one technique is available that detects DED using thermal infrared images [25]. The input to this technique is an infrared image. The input image is converted from RGB to grayscale. Grayscale image is pre-processed using adaptive histogram method to enhance its contrast level. Next, the features are extracted from the image using radon transform method and High Order Spectra (HOS) method. The radon transform method converts 2D image into 1D data and the HOS method calculates the bispectral phase entropy function. The features extracted by both these method are then fed to different classifiers such as k-Nearest Neighbor (KNN), decision tree, Probabilistic Neural Network (PNN), SVM and Naive Bayes (NB). The result produced by this technique is binary that is either normal eye or dry eye. Authors observed that for left eye images,

PNN and KNN give better accuracy, whereas for right eye images, SVM gives better accuracy.

### 3.2. *DED Detection Technique Based on Blink Rate Detection*

Eye blink plays a major role in maintaining the moisture of eye. Use of electronic gadgets such as television, computer, mobile and laptop reduces eye blinks. Reduction in eye blinks indicates evaporation of moisture from eye. A DED detection technique based on blink rate has been proposed in literature for automatic measurement of blinks [26]. The monitoring system proposed by the authors detects blink rate using front camera of a tablet. The real time video having 30 to 35 frames per second is captured 18 using front camera. Then, the eye movements in video are digitized by extracting the pixels of pupil. Pixel variation in pupils of two consecutive video frames remains high if there is blink between two consecutive frames. Thus, high variation in pixels of pupils indicates blinks. If the detected blink rate is low, it alerts user about dry eye disease. The user reported with low blink rate is then checked manually through phenol red thread test to confirm dry eye disease. Based on this technique, authors also developed a mobile application which alerts users to take a break to give rest to eyes. This mobile application is based on Japan's guidelines for labor health management in a visual display terminal.

### 3.3. *DED Detection Techniques based on Amount of Tears Produced*

A technique named automatic dynamic tear meniscus measurement in optical coherence tomography has been proposed in literature [27]. It measures tear meniscus from optical coherence tomography images. Meniscus, also known as Tear Lake, is the collection of tears accumulated at the corner of eyelids. Meniscus's height and shape help to assess dry eye disease. B-scan image of OCT is considered as input to this technique. A tear meniscus parameter is evaluated from the image by extracting region of interest and generating a binary mask. The mask is then used to estimate the Eye-Eyelid Edge (EEE). A complement of binary mask is created for extracting the Tear Meniscus Profile (TMP). Information from both EEE and TMP are merged and is used to calculate area, depth and height of meniscus using edge based formula. If the values of area, depth and height fall under the predefined threshold values, the patient is identified with the presence of dry eye disease.

## 4. **Analysis and Discussion**

From our in-depth study of the existing computerized DED detection techniques, we have identified the following set of parameters to evaluate them rigorously: related clinical test, imaging modality, device used to capture image/video, image dimension, dataset, feature extraction method and classification approach. In this section, we first define these parameters and then present a comparative analysis of DED detection techniques based on identified parameters.

Related clinical test specifies the clinical test for which automation is done in the technique. Imaging modality specifies the type of input to the technique. It is either eye image or eye



video. Device used mentions the medical device used to capture input image/video. Image dimension specifies the image resolution in terms of pixels. Dataset represents the source of data and the number of images or videos used for the evaluation of the technique. There is no general dataset available for DED detection. The source of medical data is generally private or public hospitals. Feature extraction method specifies the method used to extract the features from image or video frames. Classification approach specifies the classification method used to detect the absence or presence of dry eye. In Table 1, we show the parametric evaluation of various DED detection techniques using these discovered parameters. Table 2 shows the summary of the existing DED detection techniques. Specifically, it summarizes key characteristics and limitations.

From a detailed comparison of various DED detection techniques in Table 1 and Table 2, it is observed that techniques differentiate in terms of image modality being used and tested with dissimilar database. Techniques based on fluorescein tear

film video [15-22] identify appearance of dark spots and its time. The neural network based approach [22] has provided good accuracy for detection of breakup compared to others. The DED detection techniques based on interference pattern of lipid layer [23-24] detect predefined patterns and have potential to be used in clinical practice, as they provide a complete system with Graphical User Interface (GUI). Among the discussed imaging modality, thermal imaging [25] is useful image modality as it is non-invasive and does not come into direct contact with patient's eye. However, the TBUT based image modality is currently widely acceptable in clinical practice and hence, more automatized techniques should be developed. Perhaps, the main difficulty in developing new automated DED detection techniques lies in lack of public dataset. The dataset used in the mentioned techniques are private and limited in number of images/videos. Hence, a public dataset for all the image modalities would help to develop new techniques and develop computer aided diagnosis tool which can be used in clinical practice.

Table 1: Parametric evaluation of DED detection techniques

Technique	Related clinical test	Imaging modality	Device used to capture image/video	Image dimension	Dataset	Image/Video processing method used to detect dry eye	Classification approach	Evaluation parameters
Automatic detection of DED [15]	Tear film breakup time test	Fluorescein tear film video	Eye scan	355 x 282 pixels	100 videos from Lions eye institute, Australia	RANSAC algorithm, Segmentation method	Threshold based	Accuracy, Standard Deviation
Automation of tear film breakup test [17]	Tear film breakup time test	Fluorescein tear film video	Topcon DV3	1024 x 768 pixels	20 videos from university of Santiago de compostela	Morphological operations for rupture pattern	Decision tree classifier	Accuracy, Breakup time Measurement
Automation and analysis of tear film break up test [19]	Tear film breakup time test	Fluorescein tear film video	Topcon DV3	1024 x 768 pixels	18 videos from university of Santiago de compostela	Histogram based	Threshold based	Accuracy, Breakup time Measurement
Convolutional neural network based screening of DED [22]	Tear film breakup time test	Fluorescein tear film video	-	1024 x 960 pixels	80 videos from Far Eastern Memorial Hospital	Deep convolutional neural network	Softmax Classifier	Accuracy, Specificity, Sensitivity, Receiver operating characteristics curve
A computer aided system to support Dry Eye diagnosis based on tear film maps [23]	Lipid Layer pattern Assessment	Lipid layer inference pattern images	Tearscope plus	1024 x 768 pixels	50 images from VOPTICAL_R dataset	Feature vector with image segmentation	SVM	Accuracy, Specificity, Sensitivity, Precision
iDEAS: A web based system for dry eye assessment [24]	Lipid Layer pattern Assessment	Lipid layer inference pattern images	Tearscope plus	-	128 images from VOPTICAL_I1-v2	Producing tear film map using seeded region growing	SVM	Accuracy, Specificity, Sensitivity, Precision, F score
Technique based on thermal infrared images [25]	Assessing thermal image	Thermal imaging	Variotherm head II	442 x 299 pixels	500 images from Singapore eye research institute	Radon transform for forming feature vector	SVM, KNN, PNN	Accuracy, Specificity, Sensitivity

DED technique based on blink rate detection [26]	-	Eye blinks	Tablet	Low resolution	30 subjects	Digitizing eyeball movements using image processing techniques	Based on number of blinks	Number of blinks
DED technique based on amount of tear produced [27]	Tear meniscus test	OCT B scan images	Spectral OCT instrument	900 x 1009 pixels	OCT B-Scan from private hospital	Binary Mask Generation	Statistical Analysis	Tear Meniscus Parameters

Table 2: Summary of DED Detection Techniques

Technique	Key characteristics	Scope of improvement
Automatic detection of DED [15]	<ul style="list-style-type: none"> <li>Used RANSAC algorithm to locate iris in each video frame</li> <li>Used least square optimization method to control movement of iris</li> <li>DED is detected by identifying breakup spots</li> </ul>	<ul style="list-style-type: none"> <li>Identification of BUT sequences can be automated</li> <li>Other features such as rupture pattern can be identified and considered to increase accuracy</li> </ul>
Automation of tear film breakup test [17]	<ul style="list-style-type: none"> <li>Measurement area is located from the video</li> <li>Identifies the region of interest and aligns the location of eye</li> <li>Classification based on rupture pattern</li> </ul>	<ul style="list-style-type: none"> <li>DED detection can be based on TBUT measurement</li> <li>Accuracy can be further improved</li> </ul>
Automation and analysis of tear film break up test [19]	<ul style="list-style-type: none"> <li>DED detection based on TBUT measurements</li> <li>Identifies location, shape and size of breakup to measure severity</li> </ul>	<ul style="list-style-type: none"> <li>Identification of evolution of breakup can be considered to precisely detect DED</li> <li>A larger dataset should be used</li> </ul>
Convolutional neural network based screening of DED [22]	<ul style="list-style-type: none"> <li>Automatic detection of break up time through Convolutional Neural Network (CNN)</li> <li>CNN Breakup time is proposed to detect time at which first break up occurs</li> <li>Classifies into normal or dry eye</li> </ul>	<ul style="list-style-type: none"> <li>Severity level of DED can be detected</li> <li>Processing time can be further reduced</li> <li>This technique can be further extended to automatically diagnose DED</li> </ul>
A computer aided system to support dry eye diagnosis based on tear film maps [23]	<ul style="list-style-type: none"> <li>Considers tear film lipid layer interference pattern to detect DED</li> <li>Framework for diagnosing dry eye by observing the tear film lipid layer interference patterns</li> <li>Also supports diagnosis of meibomian gland dysfunction disease.</li> </ul>	<ul style="list-style-type: none"> <li>Can be extended to other imaging modalities</li> <li>Accuracy can be further improved</li> <li>Time taken to produce tear film maps can be reduced</li> </ul>
iDEAS: A web based system for dry eye assessment [24]	<ul style="list-style-type: none"> <li>Detection of dry eye through tear film map and tear film classification</li> <li>Unbiased and repeatable results</li> <li>Easy to use system for clinicians</li> </ul>	<ul style="list-style-type: none"> <li>Can be extended to other imaging modalities</li> <li>Processing time can be further reduced</li> </ul>
Technique based on thermal infrared images [25]	<ul style="list-style-type: none"> <li>Considers thermogram image to detect DED</li> <li>Classifies into normal or dry eye</li> </ul>	<ul style="list-style-type: none"> <li>It can be further extended to diagnose different stages</li> <li>Adequate storage space should be allotted to store tear film maps</li> </ul>
DED Technique based on blink rate detection [26]	<ul style="list-style-type: none"> <li>Detection of DED through blink rate</li> <li>Alerts user on low blink rate</li> <li>Easy detection of blink through low resolution of camera</li> </ul>	<ul style="list-style-type: none"> <li>Accuracy can be further improved</li> <li>Can be extended to other imaging modalities</li> </ul>
DED Technique based on amount of tear produced [27]	<ul style="list-style-type: none"> <li>Considers OCT image to detect DED</li> <li>Detects tear meniscus using OCT images for quantitative assessment of tears</li> </ul>	<ul style="list-style-type: none"> <li>Different scenarios such as post blink measurement of tear meniscus should be considered</li> </ul>

## 5. Conclusion

Dry eye disease is caused due to lack of moisture in eye. It is a common disease today that affects a significant population in the world. The burden of DED is expected to rise in future due to increasing use of visual devices. Thus, DED detection is important for effective medical treatment. In this paper, firstly, we have provided a systematic review on DED, its types and clinical diagnosis methods corresponding to which computerized DED detection techniques have been proposed in literature. Secondly, we have presented a detailed survey of various computerized DED detection techniques available in literature. Moreover, we have presented a parametric comparison of the discussed techniques. It is observed that only a few clinical methods have been automated and are able to show a good accuracy in DED detection. Therefore, there is an enormous research scope in the domain of DED detection by automating the current clinical tests. Our in-depth survey will help researchers to have a proper understanding of the existing image modality based computerized DED detection techniques. The future opportunities in the domain of DED detection include complete computerization of different clinical tests, so that the ophthalmologist can take advantage of the system for screening of DED.

## Conflict of Interest

The authors declare no conflict of interest.

## References

- [1] J. N. Galveia, A. Travassos, F.A. Quadros, L.A. Cruz, "Computer Aided Diagnosis in Ophthalmology: Deep Learning Applications", *Lecture Notes in Computational Vision and Biomechanics Classification in BioApps*, vol. 26, 263–293, 2017. [https://doi.org/10.1007/978-3-319-65981-7\\_10](https://doi.org/10.1007/978-3-319-65981-7_10).
- [2] H. Lin, S.C. Yiu, "Dry eye disease: A review of diagnostic approaches and treatments", *Saudi Journal of Ophthalmology*, vol. 28, 173–181, 2014. <https://doi.org/10.1016/j.sjopt.2014.06.002>.
- [3] M.S. Zeev, D.D. Miller, R. Latkany, "Diagnosis of dry eye disease and emerging technologies", *Clinical Ophthalmology*, vol. 8, 581-590, 2014. <https://doi.org/10.2147/oph.s45444>.
- [4] G.T. Vanley, I.H. Leopold, T.H. Gregg, "Interpretation of Tear Film Breakup", *Archives of Ophthalmology*, vol. 95, 445–448, 1977. <https://doi.org/10.1001/archoph.1977.04450030087010>.
- [5] P.A. Rouen, M.L. White, "Dry Eye Disease", *Home Healthcare Now*. 36(2), 74–83, 2018. <https://doi.org/10.1097/nhh.0000000000000652>.
- [6] S.P. Phadatare, M. Momin, P. Nighojkar, S. Askarkar, K.K. Singh, "A Comprehensive Review on Dry Eye Disease: Diagnosis, Medical Management, Recent Developments, and Future Challenges", *Advances in Pharmaceutics*.
- [7] J.L. Gayton, "Etiology, prevalence, and treatment of dry eye disease", *Clinical Ophthalmology*, vol. 3, 405-412, 2009. <https://doi.org/10.2147/oph.s5555>.
- [8] "Methodologies to Diagnose and Monitor Dry Eye Disease: Report of the Diagnostic Methodology Subcommittee of the International Dry Eye Workshop", *The Ocular Surface*, vol. 5(2), 108–152, 2007. [https://doi.org/10.1016/S1542-0124\(12\)70083-6](https://doi.org/10.1016/S1542-0124(12)70083-6).
- [9] A.J. Bron, V.E. Evans, J.A. Smith, "Grading Of Corneal and Conjunctival Staining in the Context of Other Dry Eye Tests", *Cornea*, vol. 22, 640–650, 2003. <https://doi.org/10.1097/00003226-200310000-00008>.
- [10] S.E. Moss, "Prevalence of and Risk Factors for Dry Eye Syndrome", *Archives of Ophthalmology*, vol. 118, 1264, 2000. <https://doi.org/10.1001/archoph.118.9.1264>.
- [11] T.L. Simpson, P. Situ, L.W. Jones, D. Fonn, "Dry Eye Symptoms Assessed by Four Questionnaires", *Optometry and Vision Science*, vol. 85(8), 692–699, 2008. <https://doi.org/10.1097/oxp.0b013e318181ae36>.
- [12] F. Ozcura, S. Aydin, M.R. Helvacı, "Ocular Surface Disease Index for the Diagnosis of Dry Eye Syndrome", *Ocular Immunology and Inflammation*, vol. 15(5), 389–393, 2007. <https://doi.org/10.1080/09273940701486803>.
- [13] Y. Guo, R. Peng, K. Feng, J. Hong, "Diagnostic Performance of McMonnies Questionnaire as a Screening Survey for Dry Eye: A Multicenter Analysis", *Journal of Ophthalmology*, vol. 2016, 1-6, 2016. <https://doi.org/10.1155/2016/6210853>.
- [14] F. Amparo, D.A. Schaumberg, R. Dana, "Comparison of Two Questionnaires for Dry Eye Symptom Assessment", *Ophthalmology*, vol. 122, 1498–1503, 2015. <https://doi.org/10.1016/j.ophtha.2015.02.037>.
- [15] T. Yedidya, R. Hartley, J.P. Guillon, Y. Kanagasigam, "Automatic Dry Eye Detection", *Medical Image Computing and Computer-Assisted Intervention – MICCAI 2007 Lecture Notes in Computer Science*, 792–799, 2007. [https://doi.org/10.1007/978-3-540-75757-3\\_96](https://doi.org/10.1007/978-3-540-75757-3_96).
- [16] T. Yedidya, R. Hartley, J.P. Guillon, "Automatic Detection of Pre-ocular Tear Film Break-Up Sequence in Dry Eyes", *2008 Digital Image Computing: Techniques and Applications*, 442-448, 2008. <https://doi.org/10.1109/dicta.2008.70>.
- [17] L. Ramos, N. Barreira, A. Mosquera, M. Curras, H. Pena-Verdeal, M.J. Giraldez, M. Penedo, "Computational Approach for Measuring the Tear Film Break-Up Time in an Unsupervised Manner", *Advanced Techniques for Knowledge Engineering and Innovative Applications, Communications in Computer and Information Science*, vol 246, 254–267, 2013. [https://doi.org/10.1007/978-3-642-42017-7\\_18](https://doi.org/10.1007/978-3-642-42017-7_18).
- [18] E. Cebreiro, L. Ramos, A. Mosquera, N. Barreira, M.F.G. Penedo, "Automation of the tear film break-up time test", *Proceedings of the 4th International Symposium on Applied Sciences in Biomedical and Communication Technologies- Isabel11*, 123, 1-5, 2011. <https://doi.org/10.1145/2093698.2093821>.
- [19] B. Remeseiro, N. Barreira, L. Sanchez-Brea, L. Ramos, A. Mosquera, "Machine Learning Applied to Optometry Data", *Advances in Biomedical Informatics, Intelligent Systems Reference Library*, vol. 137, 123–160, 2017. [https://doi.org/10.1007/978-3-319-67513-8\\_7](https://doi.org/10.1007/978-3-319-67513-8_7).
- [20] L. Ramos, N. Barreira, H. Pena-Verdeal, M. Giraldez, E. Yebra-Pimentel, "Computational approach for tear film assessment based on break-up dynamics", *Biosystems Engineering*, vol. 138, 90–103, 2015. <https://doi.org/10.1016/j.biosystemseng.2015.04.009>.
- [21] L. Ramos, N. Barreira, A. Mosquera, H. Pena-Verdeal, E. Yebra-Pimentel, "Break-Up Analysis of the Tear Film Based on Time, Location, Size and Shape of the Rupture Area", *Image Analysis and Recognition in Lecture Notes in Computer Science*, vol. 7950, 695–702, 2013. [https://doi.org/10.1007/978-3-642-39094-4\\_79](https://doi.org/10.1007/978-3-642-39094-4_79).
- [22] T.-Y. Su, Z.-Y. Liu, D.-Y. Chen, "Tear Film Break-Up Time Measurement Using Deep Convolutional Neural Networks for Screening Dry Eye Disease", *IEEE Sensors Journal*, vol. 18, 6857–6862, 2018. <https://doi.org/10.1109/jsen.2018.2850940>.
- [23] B. Remeseiro, A. Mosquera, M.G. Penedo, "CASDES: A Computer-Aided System to Support Dry Eye Diagnosis Based on Tear Film Maps", *IEEE Journal of Biomedical and Health Informatics*, vol. 20, 936–943, 2016. <https://doi.org/10.1109/jbhi.2015.2419316>.
- [24] B. Remeseiro, N. Barreira, C. García-Resúa, M. Lira, M.J. Giraldez, E. Yebra-Pimentel, M. G. Penedo, "iDEAS: A web-based system for dry eye assessment", *Computer Methods and Programs in Biomedicine*, vol. 130, 186–197, 2016. <https://doi.org/10.1016/j.cmpb.2016.02.015>.
- [25] U.R. Acharya, J.H. Tan, J.E. Koh, V.K. Sudarshan, S. Yeo, C.L. Too, C.K. Chua, E.Y.K. Ng, L. Tong, "Automated diagnosis of dry eye using infrared thermography images", *Infrared Physics & Technology* vol. 71, 263–271, 2015. <https://doi.org/10.1016/j.infrared.2015.04.007>.
- [26] E. Aihara, I. Torii, N. Ishii, "Development of Monitor System for Dry Eye Symptom", *2016 4th Intl Conf on Applied Computing and Information Technology/3rd Intl Conf on Computational Science/Intelligence and Applied Informatics/1st Intl Conf on Big Data, Cloud Computing, Data Science & Engineering (ACIT-CSII-BCD)*, 241-246, 2016. <https://doi.org/10.1109/acit-esii-bcd.2016.054>.
- [27] M.M. Bartuzel, D.H. Szczesna-Iskander, D.R. Iskander, "Automatic dynamic tear meniscus measurement in optical coherence tomography", *Biomedical Optics Express*, vol. 5(8), 2759-2768, 2014. <https://doi.org/10.1364/boe.5.002759>.

## Actigraph Analysis of Elderly Dementia Patients During Phototherapy Using Non-Linear Analysis

Fumiya Kinoshita<sup>\*1</sup>, Yuki Mukumoto<sup>1</sup>, Keiko Teranishi<sup>2</sup>, Hideaki Touyama<sup>1</sup>

<sup>1</sup> Department of Electrical and Computer Engineering, Faculty of Engineering, Toyama Prefectural University, Toyama 939-0398 Japan

<sup>2</sup> School of Nursing, Kanazawa Medical University, 5-11-80 Kodatsuno, Kanazawa, Ishikawa, 920-0942, Japan

### ARTICLE INFO

Article history:

Received: 25 March, 2020

Accepted: 16 April, 2020

Online: 20 April, 2020

Keywords:

Dementia,  
circadian rhythm,  
Actigraph,  
translation error,  
Hurst exponent.

### ABSTRACT

Dementia is one of the three primary diseases that increases the level of nursing care required for the elderly. Dementia can lead to an increased burden not only on those who have contracted it, but also their families and the surrounding environment; initiatives for preventing dementia and slowing the decline of cognitive function are expected to reduce these burdens. This study focuses on phototherapy as an alternative non-pharmaceutical treatment for dementia. This study examined the activity of elderly dementia patients to determine the effect of phototherapy on their circadian rhythms. A total of 15 dementia patients within the age range of  $86.3 \pm 6.2$ , were selected as subjects, and the data were collected using a wristwatch data logger (Actiwatch2). The phototherapy consisted of 5,500 lux intensity light exposure from 7 a.m. to 9 a.m., and data measurements were taken for three 14-day periods, i.e., before, during, and after phototherapy. Frequency analysis using discrete Fourier transform and nonlinear analysis called Hurst exponential and translation error were used to analyze the activity data. Compared to before phototherapy, the Hurst exponent values during phototherapy showed a significant increase in value ( $p < 0.05$ ) and the translation error values showed a trend of decreasing. The increase in the Hurst exponent values seen in the present experiment suggests that phototherapy may have improved the cyclicity of the circadian rhythm. However, when the phototherapy ended, the subjects' Hurst exponent values returned to the previous levels observed prior to phototherapy, and no significant differences in data were found before or after phototherapy. Thus, phototherapy, a possible treatment of sleep disorders, is also effective in promoting regularity in circadian rhythms in elderly dementia patients to a certain extent.

## 1. Introduction

In recent years, advances in medical technology and an improved nutritional standing of individuals has increased life expectancies globally. As the population is aging, the number of elderly people who require nursing care is increasing. Additionally, the cost of care, including insurance premiums, is also increasing, which is problematic. Dementia is one of the three main diseases that leads to nursing care requirements for the elderly. Dementia is defined as "a condition in which cognitive functions that had previously reached normal levels continually decline as a result of an acquired brain disorder, inhibiting the sufferer's day-to-day activities and social life." However, the

method for diagnosing dementia is not defined, and current medical science does not consider complete recovery from dementia as a possibility [1]. Because dementia results in an increased physical, mental, and emotional burden not only on the patient who contracts it, but also on their families and surrounding communities, there are increasing expectations for initiatives to prevent the onset of dementia and delay the decline of cognitive function.

The symptoms of dementia can be broadly categorized into two groups: core symptoms and peripheral symptoms. Core symptoms are the main symptoms of dementia, and they include disorders of thinking, decision-making, and executive functions. Peripheral symptoms related to these include behavioral and psychological symptoms, such as hallucinations, delusions, wandering,

\* Fumiya Kinoshita, Email: [f.kinoshita@pu-toyama.ac.jp](mailto:f.kinoshita@pu-toyama.ac.jp)



aggressive language, and violence. These symptoms are also called behavioral and psychological symptoms of dementia (BPSD). While visual hallucinations are associated with Lewy body dementia, and roaming behavior is associated with frontotemporal dementia, BPSD and core symptoms of dementia are not clearly separated by disease type [2-4]. Currently, a complete recovery from dementia is considered impossible; the core symptoms of dementia cannot be completely cured. Depending on whether appropriate pharmaceutical therapy and care methods are implemented, BPSD can be reduced in some cases and exacerbated in others [5]. Accordingly, the goals of rehabilitation implemented for dementia patients include psychological stability and improvement of BPSD.

A variety of non-pharmaceutical treatments for dementia have been proposed. Some examples include therapeutic exercise, reminiscence therapy, phototherapy, and music therapy. However, therapeutic exercise is the only effective treatment with established evidence. This is not because there is a lack of evidence for other treatments, but because not enough qualitative research has been conducted to derive evidence; as a result, they cannot be properly evaluated [6]. This study focuses on accumulating evidence for phototherapy as an alternative non-pharmaceutical treatment.

Phototherapy is a treatment method used for sleep disorders. Having 1-2 hours of exposure to a bright light over 2,500 lux in intensity, the central nervous system's production of the sleep hormone melatonin is suppressed, which has the effect of restoring a biological circadian rhythm. Because the human biological clock consists of approximately a 25-hour cycle, if individuals live in an environment without a sense of time, the phases of the circadian rhythm of body temperature controlled by melatonin and other hormones fall behind as the days progress [7, 8]. When light is transmitted from the retina to the supraoptic nucleus via the optic nerve, this information is used to adjust the phases of the biological clock. High-intensity light is the most powerful factor contributing to the adjustment of the human biological clock to a 24-hour circadian rhythm [9,10]. Because elderly dementia patients have trouble maintaining their sleep patterns due to factors such as frequently waking from sleep, they are at a high risk for disrupted sleep-wake patterns [11]. This is due to age-related changes in the supraoptic nucleus and decreased secretion of melatonin. Prior research suggests that exposure to high-intensity light in the early morning hours, when the circadian fluctuation of the body temperature shifts from falling to rising, can sync the sleep-wake patterns of dementia patients to an afternoon-night rhythm [12, 13]. However, the majority of these existing studies used questionnaires and sleep journals for the evaluation of sleep patterns after phototherapy, and there are few examples of quantitative data analyzed using numerical methods.

This study evaluates the effects of phototherapy on the circadian rhythms of elderly dementia patients using a portable activity measurement device system called Actigraph. The Actigraph system is being used in many sleep studies in recent years [16, 17]. Determining whether subjects are awake or asleep based on the body movement measurement results of the Actigraph system has a high rate of correlation to a polysomnogram [14, 15]; the device is also easy to wear, reducing the burden on both, subjects and researchers, making it easier to take measurements for a prolonged time period. In this study, activity volume

measurements were taken for 14 days prior to, during, and after phototherapy, for a total of 42 days. This was then evaluated using frequency and non-linear analysis.

## 2. Materials and Methods

Study participants included a total of 15 elderly dementia patient residents at geriatric health service facilities within Toyama Prefecture, ages (mean ± SD) 86.3 ± 6.2. The study was thoroughly explained to the subjects in advance, and they gave their written consent to participate. In addition, in cases where it was uncertain whether this consent was truly based on the will of the subject, consent was received by proxy. This study was implemented after obtaining approval from the Toyama Prefectural University Research Ethics Committee (R1-2).

Actigraph measurements were taken using a wristwatch type data logger, an Actiwatch2 by Philips Respironics. The Actiwatch2 uses an accelerometer signal for the level and frequency of body movements, and can record body movement activity counts in intervals of 60 s. For each subject, the study protocol consisted of activity count measurements for a 42-day period. This was broken up into three 14-day blocks before, during, and after phototherapy. Measurements started at 3:00 p.m. for all subjects, and during the phototherapy block, they were exposed to a 5,500 lux intensity light from 7:00 a.m. to 9:00 a.m.

## 3. Data Analysis

The chronological data for activity counts (below: AC chronological data) was analyzed using discrete Fourier transform (DFT) for frequency analysis, and both Hurst exponent and translation error methods were used for nonlinear analysis.

The translation error values estimated using the Wayland algorithm were used as quantitative evaluation indicators for the smoothness of the embedded attractor trajectory in the phase space [18, 19]. Although there exists an alternative method for focusing on the smoothness of the embedded attractor trajectory in the phase space called the Grassberger-Procaccia algorithm, it has drawbacks including the requirement of a large volume of data, as well as being sensitive to noise and interference in stacked chronological data.

An outline of the Wayland algorithm is shown below. For a vector  $\mathbf{x}(t_0)$  at time  $t_0$ , the closest vector  $K$  may be determined, Followed by measuring the Euclidean distance between the two vectors. These vectors are written as:  $\mathbf{x}(t_i)$  ( $i = 0, 1, \dots, K$ ). When  $\tau$  time step has elapsed,  $\mathbf{x}(t_i)$  moves to  $\mathbf{x}(t_i + \tau T)$ . At this time, the change in trajectory over time is approximated as  $\mathbf{v}(t_i) = \mathbf{x}(t_i + \tau T) - \mathbf{x}(t_i)$ . If the direction dispersion of  $\mathbf{v}(t_i)$  is calculated, the degree to which the directions are in line and the time development appears deterministic, can be quantitatively evaluated. Equation (1) provides directional variance:

$$E_{trans} = \frac{1}{K + 1} \sum_{i=0}^K \frac{|\mathbf{v}(t_i) - \bar{\mathbf{v}}|}{|\bar{\mathbf{v}}|} \quad (1)$$

$$\bar{\mathbf{v}} = \frac{1}{K + 1} \sum_{i=0}^K \mathbf{v}(t_i) \quad (2)$$

where  $E_{trans}$  is the translation error. In order to determine the  $E_{trans}$  error arising from the selection of  $x(t_0)$ ,  $M$  randomly selected values of  $x(t_0)$  must be used to calculate the median value of  $E_{trans}$  a total of  $Q$  times, and the mean of these  $Q$  median values expresses the translation error. For this study, the coefficient conditions selected were  $(M, Q, K) = (51, 4, 10)$ . If the trajectory of the attractor reconstructed in the embedded space is smooth, this shows that the chronological data is deterministic. Translation error takes a positive value, and a value close to 0 indicates that the mathematical model for generation of the chronological data is deterministic, while a large value indicates a probabilistic model. Specifically when the target is the Brownian motion, the translation error value is expected to equal 1.

Next, the Hurst exponents are a scale for bias in non-linear Brownian motion; they indicate the extent to which data deviates from the Brownian motion, expressing the degree of bias in changing trends [20]-[21]. If the Hurst exponent value is 0.5, this indicates Brownian motion in chronological data. This is the base value, and values closer to 0 indicate a discontinuity while values closer to 1 indicate a continuity. R/S analysis is one of the analysis methods Hurst devised for calculating the Hurst exponent. Eq. (3) is provided as a rudimentary model for explaining the random walk process in Brownian motion:

$$R = T^{\frac{1}{2}} \quad (3)$$

where  $T$  is an arbitrary time period and  $R$  represents the fluctuation range during that time period. With respect to Eq. (3), Hurst divided the range of observed values by standard deviation intervals in order to standardize the applicable time scale. This allows for the creation of a dimensionless scale that can be used for comparisons. Hurst provided Eq. (4) as a generalized version:

$$\frac{R^*}{S} = aT^H \quad (4)$$

Here,  $R^*$  is the range of deviation within an arbitrary time period,  $S$  is the standard deviation,  $H$  expresses the Hurst exponent, and  $a$  is a constant. In this study,  $\log\left(\frac{R^*}{S}\right)$  values corresponding to  $\log(T)$  for both logarithmic graphs were plotted, and a straight line was applied to the scatter plots drawn using the least-squares method. The slope of this line was taken as an estimated value for  $H$ . In addition, intervals ranging from 400 to 600 units of 60 were used as the time period  $T$  values for R/S analysis.

Because the AC chronological data acquired in this study was sampled in 60-s increments, there were a total of 20,160 chronological data points for each 14-day block. For each of the 14-day blocks, before, during, and after phototherapy, a 720-point width moving average was calculated after the high frequency components were removed from the data.

#### 4. Results

Figure 1 depicts an example of a typical AC chronological data series recorded by the Actigram system for the 14-day block before phototherapy. Among the elderly dementia patients, although there were some subjects whose activity counts showed regular activity (Figure 1a, Figure 1c), data for others confirmed irregular activity

(Figure 1b, Figure 1d). Next, DFT was used to analyze the frequency of the waveforms for AC chronological data recorded by the Actigram system before, during, and after phototherapy time blocks. In addition, the power spectrum shown in Figure 2 is normalized so that the total equals 1. Among the elderly subjects with regular circadian rhythms, the peak frequency of the power spectrum was close to 1 cycle per day (cpd). For those with irregular circadian rhythms, however, no power spectrum peak frequency near 1 cpd could be confirmed by visual examination. Using this data, the power spectral density (PSD) range before, during, and after phototherapy was calculated as 0.8-1.2 cpd. The mean value of results for the 15 subjects are depicted in Figure 3 below. The mean values for PSD fluctuated by around 0.17, decreasing during the phototherapy time block. Next, a one-way analysis of variance was conducted for each of the three time blocks, and when a main effect was observed, multiple comparisons were performed using the Bonferroni method. Results showed significant lower mean values for PSD during phototherapy than those before the phototherapy time blocks ( $p < 0.05$ ).

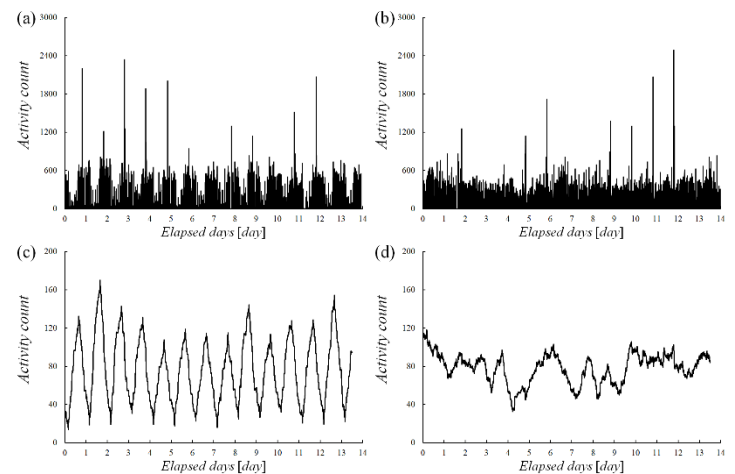


Figure 1: Typical example of AC chronological data recorded by the Actigram (during the 14-day period prior to phototherapy). Example of an elderly person with a regular (a) and irregular (b) circadian rhythm. After moving average for a regular (c) and irregular (d) circadian rhythm.

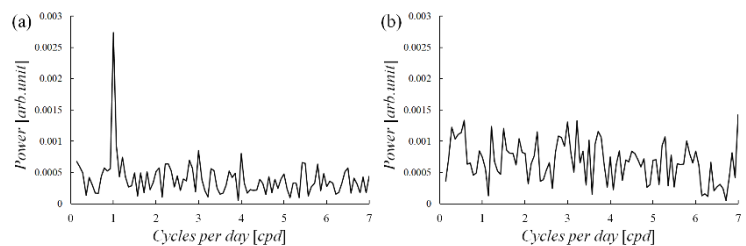


Figure 2: AC time series frequency analysis (14-day period prior to phototherapy). Example of an elderly person with a regular (a), and irregular (b) circadian rhythm.

Next, the translation error and Hurst exponent values for the AC chronological data for the three 14-day periods before, during, and after phototherapy were used for analysis. The mean results for the 15 subjects are depicted in Figure 4 and Figure 5. The translation error before the phototherapy block was around 0.32, with fluctuating values. However, the translation error decreased

to around 0.28 during the phototherapy block, then increased again to approximately 0.32 following the phototherapy block. This was followed by a one-way analysis of variance for the values before, during, and after phototherapy. The results indicated insignificant effects for translation error. The Hurst exponent value for the block before phototherapy was approximately 0.8, with fluctuating values. However, the exponent increased to approximately 0.89 during the phototherapy block, then finally decreased to approximately 0.82 in the after phototherapy block. Next, a one-way analysis of variance was conducted for each of the three time blocks, and when a significant effect was observed, multiple comparisons were performed using the Bonferroni method. The results indicated a significant increase in the Hurst exponent values during the phototherapy block compared to the before phototherapy block ( $p < 0.05$ ).

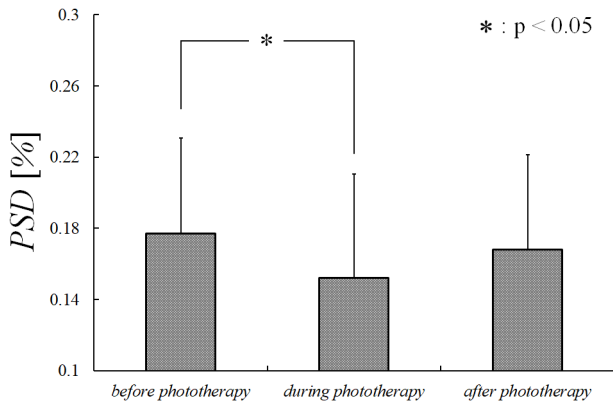


Figure 3: PSD mean values (mean ± SD)

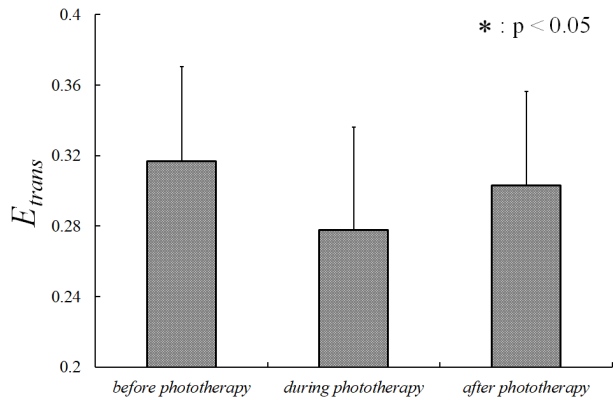


Figure 4: Translation error mean values (mean ± SD)

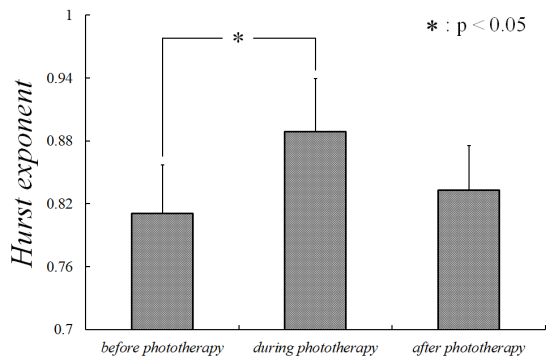


Figure 5: Hurst exponent mean values (mean ± SD)

## 5. Discussion

The effectiveness of high-intensity phototherapy for the treatment of seasonal affective disorder (SAD) was first reported in 1982 by Rosenthal et al. Since then, it has become the most popular treatment for SAD. High-intensity phototherapy modifies the phases of circadian rhythm, and it has been reported effective for sleep disorders related to old age, as well as dementia [22]. On the other hand, according to the "2017 Dementia Patient Treatment Guidelines" (Japan Society of Neurology), the only non-pharmaceutical therapy for dementia with established evidence for its effectiveness is therapeutic exercise. Although a variety of non-pharmaceutical treatment methods are being conducted at many facilities and day services, evidence for their effectiveness is currently weak across the board. However, this is not because the effectiveness of other non-pharmaceutical treatments is poor, but because there has been limited scientific evaluation of these treatments until now. Additionally, the majority of prior studies relative to phototherapy used questionnaires and sleep journals for the evaluation of sleep patterns after treatment, and there are few examples of quantitative data analyzed using numerical methods.

This study conducted an experiment focused on quantitative chronological activity data for before and after phototherapy as an initiative for accumulating evidence on these non-pharmaceutical treatments. Quantitative chronological activity data measurements were taken using a wristwatch type data logger, Actiwatch2 made by Philips Respironics, for a total of 15 subjects, all elderly dementia patient residents at geriatric health service facilities at Toyama Prefecture. Frequency analysis using discrete Fourier transform and nonlinear analysis called Hurst exponential and translation error were used to analyze the activity data. The periodicity and regularity of the time series can be quantitatively confirmed by using these analytical indicators. Data measurements were carried out for 14 days each before, during, and after phototherapy. The results indicated that both, PSD and Hurst exponent values for 0.8-1.2 cpd data either decreased or increased during phototherapy compared to before phototherapy ( $p < 0.05$ ). Hurst exponents express deviation from Brownian motion, and can be used to evaluate the continuity of chronological data. Continuity refers to the characteristic of rising trends continuing to rise, and falling trends continuing to fall in chronological data values. In the case of dementia, stronger symptoms are expected to cause more of an extreme failure of the circadian rhythm cycle, and the increased Hurst exponent values seen in this experiment suggest that phototherapy could have improved the circadian rhythm cycle in the subjects. However, when phototherapy ended, subjects' Hurst exponent values returned to the previous levels observed prior to phototherapy, and no significant differences were found when comparing data before and after phototherapy. This trend was also confirmed by the PSD values for 0.8-1.2 cpd data. The translation error values were approximately 0.3 with some fluctuation, and determinism in the patients' activity was confirmed. Although no significant differences were found in the measurement data from before and after phototherapy, translation error values tended to decrease during phototherapy. This indicates that the determinism of the chronological data increased, suggesting that the circadian rhythms of the elderly dementia patients became smoother.

Although the peak frequency of the power spectrum for elderly subjects with regular circadian rhythms was around 1 cpd, as in the healthy subjects, no power spectrum peak could be confirmed for the irregular rhythm subjects. Because the effects of phototherapy may differ between the regular and irregular circadian rhythm subjects, there should be an increased number of subjects for future studies to evaluate methods, such as circadian rhythm periodicity and MMSE scores, and further divide elderly dementia patients into groups for analysis.

## 6. Conclusions

This study collected quantitative chronological activity data for three 14-day periods before, during, and after phototherapy, for a total of 42 days of measurements. Frequency analysis and nonlinear analysis were then used for evaluation. The results confirmed that phototherapy, a treatment method used for sleep disorders, is also effective to a certain extent for promoting a regular circadian rhythm in elderly dementia patients. Additionally, the study confirmed that this effect was lost when phototherapy ended. Furthermore, the power spectrum data acquired from the frequency analysis confirmed that elderly dementia patients can be grouped with both, regular and irregular circadian rhythms. Further consideration is necessary to determine whether phototherapy is effective for both groups in light of control experiments. Future studies may use methods, such as circadian rhythm periodicity and Mini-Mental State Examination (MMSE) scores, to further divide the elderly dementia patients into groups. Moreover, the trends confirmed in this study must also be evaluated to determine whether they have the potential for preventing dementia and delaying cognitive decline.

## Conflict of Interest

The authors declare no conflict of interest.

## Acknowledgment

This work was supported by JSPS KAKENHI Grant Number 19K11232.

## References

- [1] Dementia Diagnosis and Treatment Guideline Planning Committee (supervised by the Japanese Society of Neurology): 2017 Dementia Diagnosis and Treatment Guidelines, Igaku Shoin, Tokyo, 2017.
- [2] International Psychogeriatric Association (translation supervised by the Japanese Psychogeriatric Society): Dementia behavioral and psychological BPSD (2nd Edition), ALTA Publishing, 2013.
- [3] SL. Finkel, Costa E Silva JA, G. Cohen, S. Miller, N. Sartorius, "Behavioral and Psychological Symptoms of Dementia: A Consensus Statement on Current Knowledge and Implications for Research and Treatment", International Psychogeriatric Association, 1998.
- [4] F. Matsushita, "Focusing on occupational therapy for improving daily activities and QOL as an approach for revalidation", Bulletin of Morinomiya University of Medical Sciences, 11, 25-32, 2017.
- [5] H. Yamaguchi, "Definition, clinical issues and etiology of BPSD", Tokyo Journal of Dementia Care Research, 2, 1-16, 2018.
- [6] M. Sato, "The present and future of non-pharmaceutical treatments for dementia", Cognitive Neuroscience, 15(3), 207-213, 2014.
- [7] D.J. Kennaway, C.F. Van Dorp, "Free-running rhythms of melatonin, cortisol, electrolytes, and sleep in humans in Antarctica.", Am. J. Physiol., 260(6), R1137-1144, 1991.
- [8] R.A. Wever: The Circadian System of Man -Results of Experiments Under Temporal Isolation-, Springer-Verlag, New-York, 1979.

- [9] S.S. Campbell, P.J. Murphy, C. J. van den Heuvel, et al., "Etiology and treatment of intrinsic circadian rhythm sleep disorders.", Sleep Med Rev., 3(3), 179-200, 1999.
- [10] S.S. Campbell, M. Terman, A.J. Lewy, et al. "Light treatment for sleep disorders: consensus report. V. Age-related disturbances.", J Biol Rhythms., 10(2), 151-154, 1995.
- [11] The Japan Foundation for Aging and Health: Sleep and its disorders in the elderly, 2016 essay collection, Aichi, 2017.
- [12] G.A. Dowling, E.M. Hubbard, J. Mastick, et al. "Effect of morning bright light treatment for rest-activity disruption in institutionalized patients with severe Alzheimer's disease.", International Psychogeriatric Association, 17(2), 221-236, 2005.
- [13] T. Ito, H. Yamadera, R. Ito, et al., "Effects of high intensity phototherapy on the cognitive impairment of patients with Alzheimer's type dementia", Journal of Nihon University Medical Association, 66(4), 229-238, 1999.
- [14] R.J. Cole, D.F. Kripke, W. Gruen, et al., "Automatic sleep/wake identification from wrist activity.", Sleep, 15(5), 461-469, 1992.
- [15] A. Sadeh, "The role and validity of actigraphy in sleep medicine: an update.", Sleep Med. Rev., 15(4), 259-267, 2011.
- [16] The Japanese Society of Sleep Research: Japanese Sleep Research Handbook, Asakura Shoten, Tokyo, 1994.
- [17] K. Yamanaka, A. Nakada, "Case study analysis of the effects of the implementation of day activities by student volunteers on the activity and sleep of elderly dementia patients using Actigram", Journal of Japanese Society for Dementia Care, 7(3), 535-545, 2008.
- [18] R. Wayland, D. Bromley, D. Pickett, "Recognizing determinism in a time series", Phys. Rev. Lett, 70, 580-582, 1993.
- [19] H. Takada, Y. Simizu, H. Hoshita, et al., "Wayland tests for differenced time series could evaluate degrees of visible determinism", Bulletin of Society for Science on Form, 17(3), 301-310, 2005.
- [20] H.E. Hurs, R.P. Black. Y.M. Simaika: Long-term storage: an experimental study Constable Press, London, 1965.
- [21] N. Oishi, M. Takubo, "Chronological data identification and R/S analysis, new perspectives on data analysis", Management Research, 10(3), 449-482, 1997.
- [22] Rosenthal NE, Sack DA, Gillin JC, Lewy FK, Goodwin FK, Davenport Y, Mueller PS, New-some DA, Wehr TA: Seasonal affective dis-orders: A description of the syndrome and preliminary findings with light therapy. Arch Gen Psychiat 41: 72-80, 1984.



## **Analysis of the Blockchain for Adoption in Electronic Commerce Management in Ecuador**

Segundo Moisés Toapanta Toapanta<sup>\*1</sup>, Daniela Monserrate Moreira Gamboa<sup>1</sup>, Luis Enrique Mafla Gallegos<sup>2</sup>

<sup>1</sup>*Department of Computer Science, Universidad Politécnica Salesiana (UPS), Guayaquil, Ecuador*

<sup>2</sup>*Faculty of System Engineering, Escuela Politécnica Nacional del Ecuador (EPN), Quito, Ecuador*

### **ARTICLE INFO**

*Article history:*

*Received: 09 December, 2019*

*Accepted: 10 April, 2020*

*Online: 24 April, 2020*

*Keywords:*

*Blockchain*

*E-commerce*

*Transactions*

*Security information*

*Cryptographic techniques*

### **ABSTRACT**

*The document describes the advancement of technology in commercial negotiations and functionality for various electronic transactions in Ecuador, with the aim of analyzing the blockchain and its adoption in managing e-commerce. The quantitative approach with a deductive and descriptive method has been used to identify the benefits in transactional activities and data security, both customers and businesses. The results indicated that it is effective use of cryptography, the algorithm EDCSA, together with the SHA algorithm to maintain greater security efforts. It was concluded that the use of these algorithms are effective for transactions of buying and selling and financial aspects, but it needs to maintain a permanent control and simulation processes to avoid flaws in procedures.*

## **1. Introduction**

The main problem of e-commerce in the country, is related to security transactions via the web, as ill-intentioned people, dabble systems, therefore, to improve business.

System implementation encrypted block databases to people who want to affect users or businesses use access keys and other mixed systems, may obtain better results, the answer to this is the use of the blockchain, which it consists of several blocks, where each block includes information specific addresses [1].

Also, the information security is one of the main characteristics to be achieved within organizations worldwide [2]. The object is to analyze the blockchain for adoption in managing e-commerce in Ecuador.

How to apply the blockchain management in e-commerce in Ecuador?

Commercial activities in medium and large companies are experiencing a revolution, involving the technological sphere and this requires the application of the blockchain, using cryptographic secure, especially the algorithm EDCSA, where the

chain applied blocks decentralized systems for distribution networks, whose properties allow transparency information.

Deductive and descriptive approach is used to analyze the information of reference articles and quantitative approach is applied, in order to present the result.

The results indicate that effective use of cryptography, the algorithm ECDSA, together with the SHA algorithm maintain greater security in trade negotiations.

It is concluded that the use of these algorithms are effective for transactions of buying and selling and financial aspects, but it needs to maintain a permanent control and simulation processes to avoid failures in future procedures.

## **2. Materials and Methods**

### *2.1 Materials*

They have been revised valuable resources that have allowed recognize the benefits of applying the technology blockchain in e-commerce. We have considered different bibliographic resources such as scientific articles and information regarding outstanding commercial activities carried out in the local context.

<sup>\*</sup>Segundo Moisés Toapanta Toapanta, Email: [stoapanta@ups.edu.ec](mailto:stoapanta@ups.edu.ec)

In Ecuador each year increase users who use payment methods online, but there are doubts security and protection of data and information, since people rely on the Internet for all types of transactions, whether banking, product purchases on -line, national or international, among other procedures. This maelstrom involves people of all ages and in all social contexts. Data were recorded and presented by means of figures, tables, formulas and algorithms were also used. It is undeniable that when technology is mentioned, is looking for ways to innovate in the market in terms of safety, as given in the use of blockchain [3].

2.2 Methods

To carry out this study the deductive and descriptive method is used to analyze the data and quantitative approach is applied, in order to present the result, point’s transverse, business and user views were also considered, as well as security, transactional processes and functionality of the blockchain.

2.2.1 The use of enterprise-level blockchain

The blockchain technology is being applied in different contexts, with important benefits, including those business, for which several aspects are analyzed:

- The use of mobile applications for web transactions
- Advantages and disadvantages of electronic commerce
- Solving problems of e-commerce through blockchain
- Blockchain implement successful national companies
- User benefits
- Cryptographic techniques, to provide security

In centralized models required a physical or electronic location on a network that allows transactions with securities centralized in one place, on the other hand, trade decentralized implementation of securities is facilitated since there is no single centralized server.

Industry 4.0 (I4.0) several emerging technologies, Internet of Things (IoT), artificial intelligence (AI), and cloud computing development is commonly known as the fourth revolution incorporating industry, including cyber physical systems open, secure and intelligent [4]. In addition, Tanwar adds Virtual Reality (VR) and Augmented Reality (AR), which have revolutionized engineering, and manufacturing industries including automotive, computer, electronics, defense and aerospace [5].

Thus, the introduction of disruptive technologies in any sector brings with it many challenges and complexities [6].

Figure 1 shows the process that electronic commerce has in recent years and the reception it has, translating into an increase in transactions where its application becomes relevant in the Ecuadorian electronic medium.

The figure shows the process with e-commerce in recent years and the welcome they have, resulting in an increase in transactions is observed.

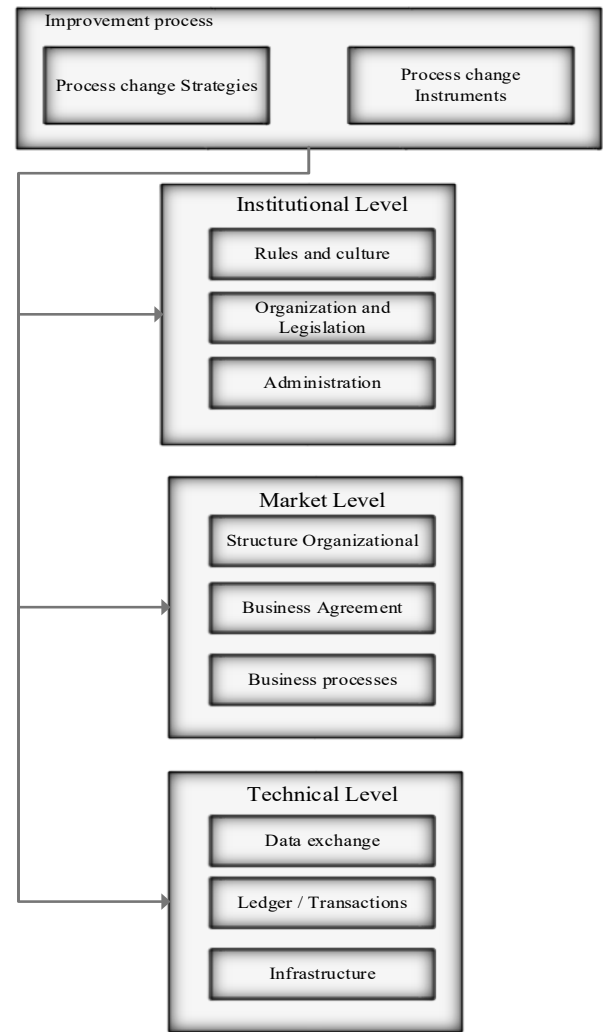


Figure 1: Analysis of the electronic commerce process.

2.2.2 Increased transactions

It is valuable to recognize the advantages of the use of technology blockchain:

- a) There are more people make purchases and payments services online
- b) The safety of this medium has increased
- c) The online procedures are more agile
- d) Are observed more transactions in financial areas, health, among others

About blockchain of technology, Khan states that it has brought a lot of attention with prominent applications in finance, health and the management system supply chain [7].

2.2.3 The decentralized model

In this system are presented, typically, nodes or miners collectively grouped validated and batch transaction blocks and then add these blocks to a chronological chain [8].

The development of new information technologies has allowed the world to move to the Industry 4.0, allowing

establishing new collaborative environments based on large-scale decentralized systems.

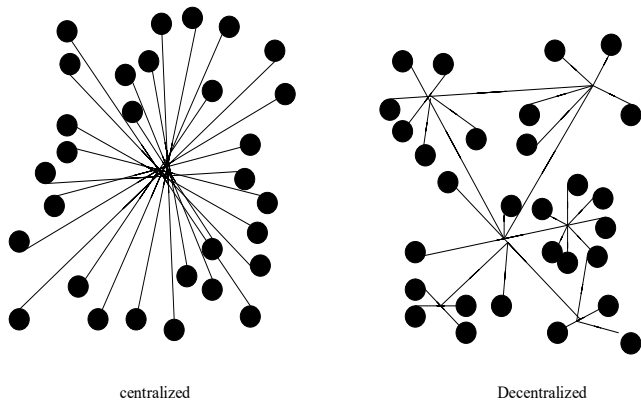


Figure 2: Centralized and decentralized model.

The figure 2 shows that the decentralized model sends information to all points, helping to decongest the means to send information and reduce the amount of work.

The decentralization of blockchain attribute facilitates the distribution of the same information across the network because no node can control the transaction [9].

Table 1: Advantages and disadvantages of the decentralized model.

DECENTRALIZED MODEL	
ADVANTAGES	DISADVANTAGES
It allows decision making is a way more efficient because no requires authorization from a central axis.	A poorly executed process can cause serious problems.
He did not receive commands from a single central authority or authorization of this, the decision-making process is accelerated.	If there isn't good communication between all points, it may be an unnecessary copy of tasks.
In the same increasing interaction channels also it increases accountability.	Lack of proper training can cause failure.

Table 1 an analysis of the strengths and limitations of the model is presented.

This information is stored not only on one site, but also on other computers at the same time, and this prevents a hacker can attack directly to the system.

The recent emergence of blockchain technology has been announced as the next revolution that will transform the shape and size of organizations and how business transactions are conducted [10].

The chain block is the next step in the evolution of the internet along with step resulting from technological advances in storage management and data encryption contribute the economy [11].

#### 2.2.4 Blockchain applied to electronic commerce

Applying blockchain is based on a set of problems presented by electronic commerce, in turn, born distrust the use of personal information.

The main problems emerged:

- Lack of confidence in payment systems
- Data security breaches
- Lack of control in the management of the supply chain
- Deficiencies in inventory and distribution systems

Blockchain implementation has the potential to solve problems with greater security and transparency through the implementation of smart payments and contracts.

This technology, in e-commerce, offers maintain a competitive market as well as reducing transaction costs through decentralized platforms. Today we live in a networked society [12] and use of mobile applications are taking more and more ground in the country and with them a number of benefits for the protection of personal data information through blockchain also promises secure transactions for users. Through the use of a cryptographic algorithm is able to demonstrate the operation and application of technology in e-commerce.

For a better analysis of e-commerce in the country has been divided into categories, as noted:

##### A. A store level.

E-commerce is a gateway for many companies in Ecuador, as there are countless online stores where you can find a variety of products, they especially target young people, but it requires:

- Reliability with respect to the delivery of data and personal information, credit cards, etc.
- Warranty, because nobody is exempt from buying a product that can be damaged in a short time
- Destination, the product may not reach its destination, because creating a possible fraud

Businesses and governments can use the chain blocks to make your work more efficient and reliable.

Table 2: Advantages and disadvantages of electronic commerce

Electronic commerce	ADVANTAGE	DISADVANTAGES
BUSINESS	Create new forms of marketing and sales.	Hackers.
	Reach many more users through advertising on social networks.	Problems sending the product to your destination.
	Variety of products in one place.	Do not ship the product on time.

	Catalog price list.	Web platform failures that cause waste of time and money.
USERS	Find products at good price.	No proximity between the seller and the buyer if the buyer does not agree with what has been received (product complaint).
	Offers	Display capability of the product (product quality) is lost.
	Delivery of the product to the comfort of home.	Ghost scam business.

The table 2 poses advantages and disadvantages for both the users make a purchase online, and companies that provide this service.

Blockchain is the new way of managing processes and sensitive information by much faster and reliable functional use of encryption where transactions would [13].

To the perform It online purchases using credit cards or other transaction is made by an application, what It facilitates users to transfer money on time without having to go to any institution financial or commercial.

B. At company level, the blockchain technology can lead to the emergence of new business models, which previously were not viable.

In different industries, food industry, textile, among others, are implementing systems for buying and selling online, but there are also problems with hackers, affecting markets or ill-intentioned people create fake companies.

The food industry also benefit con complex systems supply and the large number of products enter the market, your intermediaries often play key roles in reducing transaction costs and expanding the possibilities of transaction [14].

On the other hand, Blockchain promotes the demobilization of goods by offering deeper information for consumers [15].

### 2.2.5 Cryptography

Blockchain technology to make it functional requires use Cryptography, it born from the need to have a safe, private and understandable communication between two sides, this has led to increased security options online, which is in high demand in different parts of the world. Cryptographic considered two approaches, private cryptography or symmetric key, which establishes a key agreement between authorized users. It also has asymmetric public key cryptography in which a user has access only and only the user can decrypt the message.

This research was based on public key algorithms focused on solving issues of confidentiality, authenticity, integrity, unchanged.

To treat problems you can run two types of algorithms, which are of low complexity (easy), also called Polynomial Complexity and a second call difficult or not polynomial complexity. For this research we chose the difficult complexity without key is decrypted using Elliptic Curve Discrete Logarithm (PLDE).

With the PLDE is found the result where  $n \in \mathbb{N}$ , since  $P, Q \in (K)$  with  $Q = nP$ .

In addition, several algorithms using elliptic curves, including the Diffie -Hellman is used for the key exchange. Also, the Gamal algorithm used for sending encrypted messages, finally, Elliptic Curve Digital Signature Algorithm (ECDSA), which is based on the digital signature, being based in which this study option [13].

### 2.2.6 ECDSA algorithm

Elliptic Curve Digital Signature Algorithm (ECDSA) is a algorithm that makes use of operations on points of elliptic curves instead of exponentiation algorithm key short this creates a high level of security, being more complex so it is difficult to break.

Function footprint  $h$  must have certain characteristics that must be met for safety.

1. Existence of a message  $m$ , which should be quick and easy, is calculated  $h(m)$
2. With digital  $h_0$  footprint, very difficult characteristics (no existence in polynomial time algorithm) for calculating  $x_0$  so that  $h(x_0) = h_0$ . He is also known as resistance to find a pre image.
3. Calculate  $x_0$   $h(x_0) = h_0$ , where it is impossible to find  $x_1$ , such that  $h(x_0) = h(x_1)$ . He is also known as resistance to find a second pre-image.
4. Considered impossible to calculate  $x_0$  and  $x_1$ ,  $x_0 \neq x_1$  with such that  $h(x_0) = h(x_1)$ . He is also known as Crashworthiness.
5. The public key is the principal to decrypt the signature, thus ensuring data security.

For further understanding of the algorithm ECDSA the following occurs:

Where  $a$  uses  $E(K)$  and a base point  $P \in E(K)$ . To calculate  $Q = kP$  so that  $xQ$  differs from 0. Then is calculated  $k^{-1} \text{mod } n$   $Y \quad hm = h(m)$  and then  $s = k^{-1}(hm + nAxQ) \text{mod } n$ . With the condition if  $S = 0 \text{mod } n$  is chosen  $k$  again and proceeds to do all the calculations again, otherwise it  $(xQ, S)$ . To send the signature is inserted into the message  $(m)$  this is encrypted and sent to B. For signature verification proceeds to decrypt the file to get the message  $m$  and signature  $xQ, S$ .

6. For calculating  $h(m) = hm$  : (1)

$$V = hmS^{-1}P + xQS^{-1}RA \tag{2}$$

$$\text{Where: } xQ = Xv \text{mod } n \tag{3}$$

The signature is accepted, if otherwise is rejected.

7. The following formula was used for verification:



$$V = hmS^{-1}P + xQS^{-1}RA = (hm(hm + nAxQ)^{-1k})P + (xQ(hm + nAxQ)^{-1}knA)P = ((hm + nAxQ)(hm + nAxQ)^{-1k})P = kP = Q \tag{4}$$

Once the trace function (electronic signature) is in a document file, message, text, etc.), encryption is performed, which is attached to the document, which becomes a signed and encrypted document, which will be sent designated by the network to the recipient, who in turn passes the verification stage decrypting the message clearly and signature [16].

### 2.2.7 Algorithm SHA.

Secure Hash Algorithm (SHA) is an algorithm used to transform a lot of information in a single secure cryptographic chain. SHA is used to secure public addresses starting from a ECDSA key. The characteristic of blockchain storage technology involves distributed database [17].



Figure 3: Percentage of people who make purchases on the Internet in recent years.

In Figure 3, Ecuador observed in 65% of the population does not make purchases on the Internet, while the other 35% of the population itself, according to the SEO of Quito, but will increase over the years.

### 3. Results

The use of the blockchain is massing in the world, having a significant weight in financial activities.

To be effective the use is required of cryptography, for which the use of the algorithm ECDSA suggested.

#### 3.1 Process ECDSA signature algorithm.

By using a public key

Where:

d = it is the private key.

P = base point.

Q = public key.

The private key "d" can be an integer value to the random number in this case is used between 1 and n-1, where n is a prime number. The public key is Q that is obtained by multiplying the private key "d" base point "P".

The public key is obtained from the following equation.

$$Q = dP \tag{5}$$

Signing process:

1. Select a random number (k).
2. Select a base point (P).
3. Calculate kP

Where:

x1, y1 = are integers.

the following equation is obtained:

$$kP = (x1, y1) \tag{6}$$

For signing the message (m) are the numbers r and s, represented in the following equation (7).

4. Calculating r.

If r = 0, return to step 1.

$$r = x1 \text{ mod } n \tag{7}$$

5. Calculate S.

If S = 0, return to step 1.

H (m) is the hash of the message to be signed, calculated with the algorithm SHA-1. The equation is as follows:

$$k - 1(H(m) + dr) \text{ mod } n \tag{8}$$

Purchases and sales online transactional processes require valid, as evidenced in Figure 5.

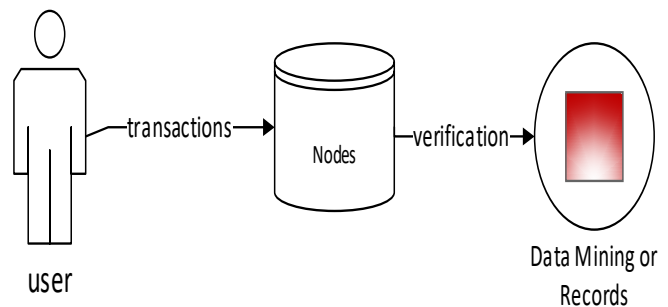


Figure 4: Model of transaction processing and validation.

Figure 4 evidences a transaction, requesting verification of data.

To work more safely is important la private key with a random number on which you can perform mathematical calculations.

Further, signature algorithm ECDSA, It contains:

Verification:

R and s are checked within the range [1, n-1].

1. Calculate w:

$$s - 1 \text{ mod } n \tag{9}$$

2. Calculate u1:

$$H(m)w \text{ mod } n \tag{10}$$

3. Calculate u2:

$$r - w \bmod n \tag{11}$$

Get u1 and u2 to perform the following equation:

$$u1P + u2Q = (x0, y0) \tag{12}$$

The signature verifies if and only if  $v = r$

$$v = x0 \bmod n \tag{13}$$

For the result of the firm, check the proof where r and s are first within the range [1, n-1] by v. If  $v = r$  mean r (process), v (verification) are well-executed.

$$A = \frac{n!}{(n-1)!} = x \tag{14}$$

Also, application of equation (14) based on transactions made by the blockchain. Where the variable "A" starts the transaction process and the verification takes place in the node to be validated or not accordingly you can determine whether or not the transaction was conducted successfully "B". Where:

- A: it is the uninitialized variable.
- N: it is passing through a process node.
- !: node N validated.
- x: it is the result of non-validated transaction.
- B: is the result of the validated transaction.

If node A is invalid, the calculation is done by adding the value of -1, which means that the transaction process has been invalidated.

$$A = \frac{n}{(n+1)} = B \tag{15}$$

Otherwise, the process of equation (15) is validated node n (n + 1) is reflected, resulting in B, a successful transaction.

Once transmitted, given the approval of the transaction, where the information block can be added to the rest of the chain as a successful registration and transparent. A successful transaction with B, ends the transaction.

To demonstrate how a transaction using chain block is performed is shown the diagram below where, flowchart shows how the block chain works, where A seeks to make a transaction to B via an electronic medium. This transaction is shown on the network as an information block, then this block of information is transmitted to all points of the entire network.

All transactions to go from point A to point B, pass through the safety chain, where the process requires authentications or comparative keys that can only be validated by the authorized person, this process is linked from the transmitter block to the receiver block.

In Figure 5 shows how a transaction can be performed from A to B using the validation of the equation (14) and equation (15).

The blockchain has helped to raise the security level transactional processes from different companies and this can be considered different algorithms.

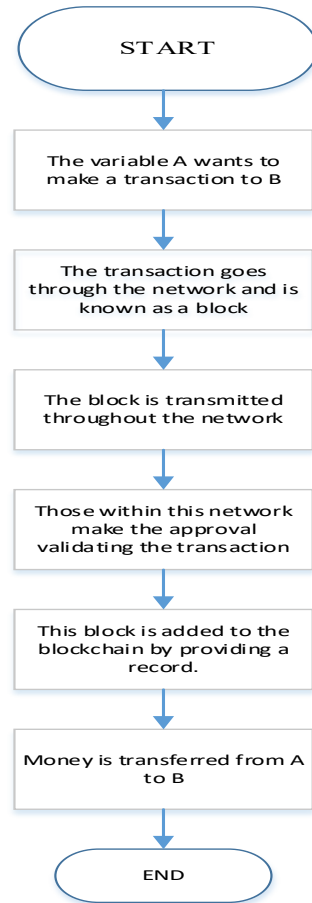


Figure 5: Analysis Diagram blockchain process.

#### 4. Discussion

A literature review focused on studies are in blockchain benefits of technology in business transactions of large companies, because their technology infrastructure is higher and cause a competitive advantage over companies with less capital.

The application of the chain blocks and security processes in e-commerce in Ecuador, can ensure effective, easy accessibility, greater acceptance of the market, but it requires superb manageability, better preparation of staff and management commitment high.

It is important that the country has policies that allow trade practices to exercise more smoothly and safety that benefits companies, workers and society in general.

But despite having a security system with the implementation of chain blocks in e-commerce, companies need to have several requirements to be effective:

- Security politics
- Detection system vulnerabilities that may arise in the system.
- Develop a contingency plan in case of breach in security measures.

Also, companies shall carry out the respective case study simulation and testing platform for observing management support and thus get better results.

## 5. Conclusions

Application of Blockchain technology in e-commerce for small businesses. Blockchain technology adoption in the financial and banking system.

Using blockchain allowed in increased electronic commerce in the world and himself in Ecuador, as companies are taking steps to adopt technologies, applying security measures to provide greater comfort and effectiveness in public and private transactions. Using EDCSA algorithm is effective for business transactions, by using the public key and chain blocks. Despite its effectiveness, should be performed simulations to identify the best options eligible companies, because some systems become ineffective in the course of time.

## Acknowledgment

The authors thank the Salesian Polytechnic University of Ecuador, the research group of the Guayaquil headquarters "Information Technology, Security and Information for a Globalized World" (CSITGW) created in accordance with the resolution 142-06-2017-07-19 and the Secretariat of Higher Education Science, Technology and Innovation (Senescyt).

## References

- [1] S. Singh, «Factores de éxito críticos de blockchain para una cadena de suministro sostenible,» web of science, vol. 152, n° 104505, p. 11, 2019.
- [2] S. M. Toapanta Toapanta, A. J. Bravo Jácome y M. G. Tandazo Espinoza, «An Immutable Algorithm Approach to Improve the Information Security of a Process for a Public,» Astes, vol. 4, n° 3, p. 6, 2019.
- [3] E. Gamme, «¿Pueden las cadenas de bloques revolucionar el comercio internacional,» 2018. [En línea].
- [4] Liu, X. L., Wang, W. M., Guo, H., Barenji, A. V., Li, Z., & Huang, G. Q. (2020). Industrial blockchain based framework for product lifecycle management in industry 4.0. *Robotics and Computer-Integrated Manufacturing*, 63, 101897.
- [5] Tanwar, S., Parekh, K., & Evans, R. (2020). Blockchain-based electronic healthcare record system for healthcare 4.0 applications. *Journal of Information Security and Applications*, 50, 102407.
- [6] Janssen, M., Weerakkody, V., Ismagilova, E., Sivarajah, U., & Irani, Z. (2020). A framework for analysing blockchain technology adoption: Integrating institutional, market and technical factors. *International Journal of Information Management*, 50, 302-309.
- [7] Khan, K. M., Arshad, J., & Khan, M. M. (2020). Investigating performance constraints for blockchain based secure e-voting system. *Future Generation Computer Systems*, 105, 13-26.
- [8] A. Islam, M. Mäntymäki y M. Turunen, «¿Por qué se dividen las cadenas de bloques? Una perspectiva de actor-red sobre las divisiones de Bitcoin,» Scopus - Technological Forecasting & Social Change, vol. 148, p. 10, 2019.
- [9] A. Zhang, «Arquitectura del sistema para la transparencia basada en blockchain de la sostenibilidad social de la cadena de suministro,» Scopus, vol. 63, n° 101896, p. 9, 2019.
- [10] K. Behnke, M. Janssen, «Condiciones límite para la trazabilidad en las cadenas de suministro de alimentos utilizando la tecnología blockchain,» Scopus, n° 0268-4012, p. 10, 2019.
- [11] Achargui, A. A., & Zaouia, A. (2016). Traditional, Web-based or Internet-enabled ERP systems adoption for SMEs in Developing Countries. In 2016 5th International Conference on Multimedia Computing and Systems (ICMCS) (pp. 676-680). IEEE.
- [12] Kanamori, S., Nojima, R., Sato, H., Tabata, N., Kawaguchi, K., Suwa, H., & Iwai, A. (2016). (pp. 418-422). IEEE.
- [13] Nosouhi, M. R., Yu, S., Zhou, W., Grobler, M., & Keshtiar, H. (2020). Blockchain for secure location verification. *Journal of Parallel and Distributed Computing*, 136, 40-51.
- [14] Y. Chen, C. Bellavitis, «Blockchain disruption and decentralized finance: The rise of decentralized business models,» Scopus, vol. 13, p. 8, 2019.
- [15] Allen, D. W., Berg, & Markey-Towler, B. (2019). Blockchain and Supply Chains: V-form Organisations, Value Redistributions, De-commodification and Quality Proxies. *The Journal of the British Blockchain Association*, 2(1), 1-8.
- [16] Castagna H., *Publicaciones Matemáticas del Uruguay*. Volumen 17, Julio 2019, Páginas 293–297 ISSN 0797-1443.
- [17] Lukmanova, O., Volkova, E., Zabolotnyi, A., & Gorelik, A. (2019, January). Blockchain Technology for Public Utilities. In 2019 IEEE Conference of Russian Young Researchers in Electrical and Electronic Engineering (EIconRus) (pp. 1790-1793). IEEE.

## Legal Regulation as Driver for Sustainable Development of Nigeria's Solid Mineral Sector

Isaac Onyeyirichukwu Chukwuma<sup>1</sup>, Benjamin Onoriode Mukoro<sup>1</sup>, Fidelis Odinakachukwu Alaefule<sup>1</sup>, Gertrude Chinelo Ugwuja<sup>1</sup>, Emmanuel Kalu Agbaeze<sup>\*1</sup>, Ifeanyi Leo Madu<sup>2</sup>

<sup>1</sup>University of Nigeria, Department of Management, Nigeria

<sup>2</sup>Gregory University, Department of Business Administration, Nigeria

---

### ARTICLE INFO

Article history:

Received: 01 January, 2020

Accepted: 22 February, 2020

Online: 24 April, 2020

---

Keywords:

Legal regulation

Sustainable development

Solid mineral

---

### ABSTRACT

*The need to optimally explore Nigeria's diverse mineral resource endowments via sustainable value chain practices has, in recent times, been the focus of the Nigerian government and relevant stakeholders. This development has amongst other things, been made a necessity since the decline in Nigeria's crude oil export and earnings, as well as the increased effort and commitment of the government to significantly diversify the economy from reliance on agriculture and the oil and gas sectors. This challenge has directed government efforts towards promoting the exploration of the solid mineral sector, to leverage its opportunities to attract investors and further sustainable development. The concept of sustainable development demands that economic ventures be both viable and environmentally sustainable. As a result of the self-seeking ethos of market economies, it is often necessary for the law to step in to moderate the profit-oriented tendencies of commercial interest. The paper aims to examine the sustainable development of Nigeria's solid mineral sector through legal intervention. The objectives are to: (i) determine the importance of law to the sustainable development of Nigeria's solid mineral sector; (ii) ascertain the current provisions of laws and policies in relation to the operation of the solid mineral sector and their impact on the sustainable development of the sector and (iii) make informed recommendations on how to use law as a tool to promote the sustainable development of Nigeria's solid mineral sector. This study employed a qualitative approach in examining how well the current legal framework governing the solid mineral sector in Nigeria is positioned to promote sustainable development. It was found that the major impediments to the sustainable development of the solid mineral sector in Nigeria are centralization of ownership and resultant alienation of communities, restiveness in alienated communities, poor administrative infrastructure and implementation of laws and policies, and corruption.*

---

## 1. Introduction

The need to optimally exploit Nigeria's diversified mineral resource endowments via sustainable value chain practices has, in recent times, been the focus of the Nigerian government and relevant stakeholders. This development has, amongst other things, been made a necessity since the decline in Nigeria's crude oil export and earnings, as well as the increased effort and commitment of the government to significantly diversify the

economy from reliance on agriculture and oil and gas sector [1]. This challenge or gap created has directed government efforts in promoting the exploration of the solid mineral sector, to leverage its opportunities to attract investors and further sustainable economic development.

The Nigerian government over time has built a framework that not only attracts but also secures and emboldens investors to explore the economic potentials embedded in the solid mineral sector; this was achieved via the diverse legal apparatus and reforms institutionalized by the government (i.e. Development

---

\*Corresponding Author: Emmanuel Kalu Agbaeze, University of Nigeria, emmanuel.agbaeze@unn.edu.ng



of the Nigerian Minerals and Mining Act, 2007; Development of the National Minerals and Metals Policy, 2008; Development of the Nigerian Minerals and Mining Regulations, 2011; Establishment of the Mining Cadastre Office (MCO) for mineral rights management; Establishment of the Nigerian Institute of Mining and Geosciences (NIMG); Enhanced geoscience data collection across Nigeria; Establishment of control departments for Mines Environmental Compliance and Artisanal and Small Scale Mining), and strategically tailored to stimulate best practices, as well as avoid the pitfalls that marred exploitation of mineral deposits in the past; nonetheless, the validity of this legal framework within the Nigerian context is yet to produce a concrete result within the scope of sustainable economic development.

There is extant literature on the concept of sustainable development and equivocalness in the definition of the concept; extrapolating the definition by the World Commission on Environment and Development [2], sustainable development is the development that meets the needs of the present without compromising the ability of future generations to meet their own needs. Within the Nigerian context, achieving a sustainable development connotes a real, positive and tangible development that is acknowledged by the diverse populace. The need for a viable, sustainable development in Nigeria is eminently required as it continues to face socio-economic challenges as well as domestic and foreign constraints [3], hence opportunities present within the solid mineral sector are projected for the world to see and exploit [4], as a tool to the furtherance of the Nigerian sustainable development agenda.

The paper aims to examine the sustainable development of Nigeria's solid mineral sector through legal intervention. Section 2 of the paper looks at the issues and challenges experienced in Nigeria's solid mineral sector. Section 3 discusses the role of law in the sustainable development of the sector. Section 4 evaluates how effective regulation of the solid mineral sector has been and the sustainable development potentials of effective legal regulation. Section 5 examines the construct within the dynamic capabilities theory. Section 6 proffers recommendations to promote sustainable development in the solid mineral sector.

## **2. The Mining Sector in Nigeria: Issues and Challenges**

The trajectory of the Nigerian mining sector was firmly pioneered by Britain's colonial economic exploration dating back to 1902; this exploration then moved to a private sector-focused model, and to an epoch of government-controlled operations at which Nigeria's earning from mining was a major revenue base, and mining was the leading employer of labour until the discovery of oil, at which point the mining sector was greatly neglected [5-7].

Notwithstanding the advantages in the oil sector, the keen focus on the sector by the government at the expense of other sectors (i.e. solid mineral sector) is blamed for the moribund state of these other sectors [7-8]. The long years of focus on hydrocarbon resources had neglected the overwhelming endowments Nigeria possesses in the solid minerals sector [5],

which is mostly under-developed notwithstanding its glorious past and its present potential to sustain the desired development.

Presently, the Nigerian government has shown a keen interest and commitment to the diversification agenda and actively plays a key role in ensuring the development of other sectors (i.e. solid mineral sector) as a driver for sustainable development. The minerals are classified as

- i. Industrial minerals (e.g. barite, kaolin, gypsum, feldspar, limestone).
- ii. Energy minerals (e.g. bitumen, lignite, uranium).
- iii. Metallic ore minerals (e.g. gold, cassiterite, columbite, iron ore, lead-zinc, copper).
- iv. Construction minerals (e.g. granite, gravel, laterite, sand).
- v. Precious stones (e.g. sapphire, tourmaline, emerald, topaz, amethyst, garnet, etc.).

Nigeria is known as a nation that is abundantly endowed with diverse solid mineral deposits that are valuable and explorable in the world [5]. The presence of these deposits has been the focus of economic attraction for both formal and informal mining activities; the solid minerals sector is capable of generating employment and creating wealth for over five million people [9]. The sector's contribution to GDP averaged 0.37 percent in 2011-2012 to over 12 percent in 2012-2013 [9], possessing a double-digit growth rate, evidence that the sector can sustain Nigeria from the intricacies of the oil saga and economic uncertainties.

Notwithstanding the projected potentials inherent in the exploration of solid minerals, and the legal leverages provided by the government in exploring it to achieve sustainable development, the following have been noted as constraints to this achievement [5, 10-11]:

- i. Insufficient geoscience data and information.
- ii. Inadequate infrastructure and support systems for investors' activities.
- iii. A decline in stakeholders' interest.
- iv. Weak Institutions and governance structure.
- v. Laxity in regulation enforcement.
- vi. Ecological mismanagement.
- vii. Activities of informal miners.

A common issue in this endowment of solid minerals across Nigeria is the ease of accessibility by any interested party, and this, the legal regulation seeks to formalize.

## **3. The Role of Law**

### *3.1. The Twin Imperatives of Economic Viability and Sustainability*

The concept of sustainable development demands that economic ventures be both viable and environmentally sustainable. As a result of the self-seeking ethos of market economies, it is often necessary for the law to step in to moderate the profit-oriented tendencies of commercial interests. In Nigeria, this has been done primarily by coordinating the powers of the Federal

Ministry of Mines and Steel Development and the Federal Ministry of Environment. The Federal Ministry of Mines and Steel Development administers the Minerals and Mining Act (MMA), 2007, the Minerals and Mining Regulations (MMR) 2011, and three policy documents: the National Minerals and Metals Policy 2008, the Vision 2020 Report of the National Technical Working Group on Minerals and Metals Development, and the Roadmap for the Development of the Solid Minerals and Metals Sector. The Federal Ministry of Environment, on its part, administers the National Environmental Standards and Regulations Enforcement Agency (NESREA) Act.

According to a UNDP Sourcebook [12], mining activities can contribute to sustainable development, particularly to its economic dimension. It can generate fiscal revenues to a nation, increase economic growth, create jobs, and contribute to building infrastructure. Thus, mining has both positive and negative implications for sustainable development goals (SDGs) with particularly strong impacts on goal 11 and 17. The question that arises from this double-edged nature of mining in the Nigerian context is; how properly-suited are Nigerian laws to creating a balance between economic and environmental interests? Can these laws ensure the optimal harnessing of the economic potentials of the mining sector while at the same time providing protection and incentives for the prosperity of the environment? Are there investment incentives in place to encourage investment in the solid mineral sector? How are problems such as illegal mining that lead to both revenue leakage and environmental degradation addressed?

### *3.2 The Legal Framework*

The Minerals and Mining Act 2007 is the primary statute governing mining activities in Nigeria. The Act contains some incentives for prospective investors in the mining sector. For example, a company granted a mineral title is entitled to tax relief for three years from the date of commencement of operation, which may extend for another two years subject to specified conditions. Operators in the mining sector are also granted exemption from the payment of customs and import duties in respect of plant, machinery, equipment, and accessories imported specifically and exclusively for mining operations [13]. The Industrial Development (Income Tax Relief) Act contains similar incentives. These incentives cover minerals such as lead, zinc, iron, barytes, bentonites, gold, coal, bitumen, and associated minerals [14].

The Companies' Income Tax Act (CITA) provides that a new company going into mining of solid minerals will be exempted from tax for the first three years of its operations. Additional incentives in CITA include a reduced tax rate of 20% for Nigerian companies which earn a total gross turnover of less than a million naira after commencement of business, accelerated capital allowances at 95% initial allowance, exemption of profits from corporate tax where minerals produced are exported from Nigeria, and the proceeds from such exports are repatriated to Nigeria and used exclusively for the purchase of raw materials, plants, equipment, and spare parts. There is also zero-rating for value-added tax (VAT) purposes for Nigerian mining companies [14].

As regards the protection of the environment, the Minerals and Mining Regulations mandate mineral title holders to carry out an environmental impact assessment and submit environmental impact assessment statement. They are also required to put in place environmental protection and rehabilitation programmes and have a community development agreement with host communities [15]. There are provisions targeted at particular aspects of the environment. For example, there are provisions relating to the protection of biodiversity, national parks, cultural heritage and sanctuaries, endangered species, etc. [15]. The Regulations also provide broad supervisory powers to the Mines Environmental Compliance Department including the power to inspect mines and the arrangements for disposal of different forms of waste including water and tailings [15].

Apart from the environmental protections contained in MMA, which relate specifically to the solid mineral sector, the NESREA Act, 2007, includes provisions relating to the protection of the environment in general. NESREA has also developed thirty-three Environmental Regulations. Among these are the National Environmental (Mining and Processing of Coal, Ores and Industrial Minerals) Regulations 2009, National Environmental (Base Metals, Iron and Steel Manufacturing/Recycling Industries) Regulations 2011, National Environmental (Non-Metallic Minerals Manufacturing Industries Sector) Regulations 2011, and the National Environmental (Quarrying and Blasting Operations) Regulations 2013. The NESREA Act and Regulations contain stipulations that are very relevant to the protection of the Nigerian environment.

## **4. Regulatory Challenges and the Potentials of Effective Regulation**

There are two common ways in which any regulatory framework may be deficient. Deficiency may exist in terms of the material provisions of legal documents or their implementation. In Nigeria, problems exist in both of these segments. As regards the letter of laws and policies, while a lot has been done to enact laws suitable to the advancement of the solid mineral sector, there is fundamental legal-structural incongruence that has to be rectified for super-structural legal changes to achieve their maximum effect. Concerning the legal/structural foundation of the solid mineral sector, two Nigerian Constitution statutes, the Land Use Act, 1978, and the MMA, 2007, come to mind. Section 44(3) of the 1999 Constitution vests title in all minerals found anywhere in the country on the Federal Government. The Land Use Act vests title in all the lands in a state in the Governor [16]. The Government may acquire lands with minimal compensation to the original owners for overriding public interest including for mineral exploitation by the Federal Government [16]. This practice alienates the host communities and leads to non-cooperativeness and instability that, in turn, affects the rate of investment in the sector.

Section 1 of MMA provides that the entire property in and control of all Mineral Resources in, under or upon any land in Nigeria, its contiguous continental shelf and all rivers, streams, and watercourses throughout Nigeria, any area covered by its

territorial waters or constituency and the exclusive economic zone is and shall be vested in the Federation for and on behalf of the people. Section 2 provides that the government of the federation shall from the commencement of this Act acquire all lands in which minerals have been found in commercial quantities under the provisions of the Land Use Act. As has been said concerning the Land Use Act, regulations like these lead to resentment among host communities who believe that is their right to the minerals found in their ancestral lands. This feeling of oppression and exclusion promotes non-cooperation and parallel exploitation of mineral resources by members of host communities, whether alone or in conjunction with outsiders. Parallel exploitation of mineral resources is illegal according to applicable laws, and very importantly, it leads to revenue leakage and environmental damage. While the government has tried to tackle the problem of illegal mining by providing for the grant of leases for artisanal and small-scale mining, it is not always easy for artisanal and small-scale miners to obtain these leases. Mineral titles may be granted to individual artisanal and small-scale miners as well as co-operatives. However, in reality, assistance to artisanal and small-scale miners has been through miners' co-operatives whose total membership does not embrace the greater majority of miners who remain unregistered and unregulated.

Apart from the legal-structural challenges mentioned above, there is the problem of poor implementation that generally plagues laws and policies in Nigeria, and this has also affected the solid mineral sector. Thus, environmental standards are routinely flouted and mostly without consequences for the offenders, and host communities do not get involved in the fight against environmental degradation as they should due to a combination of factors, for instance, the alienation mentioned above when combined with poverty and lack of awareness. Another reason for poor implementation of environmental standards is that relevant regulatory and enforcement institutions often do not have the capacity (technological and otherwise) to carry out enforcement.

The challenge of poor implementation is also sharply felt with regard to the administration of investment incentives. It is common to experience corrupt practices in the implementation of incentives as entities not qualified to enjoy incentives often access them fraudulently. At times, where a beneficiary's due period of enjoyment has elapsed for some reason, they find fraudulent ways to prolong their enjoyment of incentives. This means that those who need these incentives may not get them. It is also helpful to note that apart from the problems particularly associated with investment incentives in Nigeria, there are general questions related to the efficacy of tax incentives specifically, which are not peculiar to Nigeria. The positive theoretical effect of tax incentives has been questioned, and governments have used different models such as the Computable General Equilibrium (CGE) to conduct a cost-benefit analysis to ascertain their economic and revenue impact [17].

## **5. Dynamic Capabilities Theory (DCT) Perspective**

The DCT explores how sustainable advantage is achieved; [18] argues that successful nations in the global market place can

demonstrate timely responsiveness to market changes and speedy product innovation. Also, successful nations can optimally coordinate and reorganize internal and external resources; hence the increased effort and commitment of the Nigerian government to significantly diversify the economy from reliance on agriculture and the oil and gas sectors [1]. The ability to achieve a sustainable advantage in this context is referred to as the Dynamic Capabilities [18]. The term "dynamic" connotes the capacity to utilize resources to attain congruence with the changing business environment and national interest; this is relevant in a situation where values on resources (i.e. crude oil) are constantly evolving and unpredictable. Capabilities connote the crucial role of strategic management in suitably adapting, integrating and reconfiguring, internal and external national skills, resources, and functional competencies to fit the needs of a changing environment [18]. The theory postulates that the way nations develop sustainable development is to respond to changes in the global environment, and the optimality of this sustainable development is anchored on a nation's processes, market positions, and opportunities [18].

## **6. Recommendations and Conclusion**

There has been an overwhelming argument in support of the need to amend section 44(3) of the Nigerian Constitution and to repeal the Land Use Act, and this paper supports that argument. The Constitution and Act should be amended and repealed alongside the statutory and policy provisions that cascade from them; this would ensure inclusiveness and co-operation from all stakeholders at the host-community level. It must be admitted that there will be challenges in effecting the recommended constitutional and statutory challenges as they require the affirmative votes of a two-thirds majority of members in each House of the National Assembly. The case of the Constitution amendments requires an additional criterion, a resolution in two-third of all the state Houses of Assembly (Constitution of the Federal Republic of Nigeria, 1999, section 9). In a country like Nigeria that is divided along with ethnic interests; it would be a tough task to win broad legislative approval for the suggested amendments. Assuming that it is possible to make the constitutional and statutory amendments, contentions are likely to continue along ethnic lines, and this might negatively impact their effective implementation as well as the peaceful and smooth operation of the solid mineral sector generally. Concerning inclusiveness, it is necessary to enforce the tenets of the Extractive Industries Transparency Initiative (EITI). EITI is the global standard to promote open and accountable management of oil, gas, and mineral resources. EITI is predicated on the belief that a country's natural resources are the commonwealth of its citizens. The EITI Standard mandates disclosure of information along the extractive industry value chain from the point of extraction, to the flow of revenue, and how the public benefits [19]. Nigeria has already signed up to EITI and has put in place the Nigerian Extractive Industries Transparency Initiative (NEITI). In 2003, Nigeria voluntarily signed up to EITI. On May 28, 2007, a specific law, the NEITI Act, was enacted to enforce the implementation of the initiative.

It is also necessary to offer assistance to artisanal and small-scale miners with regard to the formalization of their operations.

While it has become much easier to register a company as a result of the improvements made by the Corporate Affairs Commission (CAC), a lot of artisanal and small-scale miners are either not well-informed about this opportunity or are too far removed from the capacities and facilities that are needed for registration of their businesses. To an extent, the legal and structural framework for assistance to artisanal and small-scale miners already exists as provided for under MMA 2007. However, there is a need to bring the bureaucracy and formal institutions closer to the grassroots to capture unregistered and unregulated activities. Any assistance may then be channeled through these bureaucracies and institutions. If the constitutional and statutory amendments recommended here are implemented, and administration of the solid minerals sector is decentralized, then States may adopt their structures with lessons from current practice.

More so, efforts should be made to build the capacity of regulatory and enforcement institutions to ensure effective implementation of environmental laws and policies.

Finally, investment incentives should not be adopted for their face value but considered pragmatically in terms of existing conditions and specific goals.

This study may be limited by the diverse reactions and evolving national realities, hence the need for ongoing evaluation and pragmatic response to operational challenges while implementing reforms in Nigeria's solid mineral sector. Further studies could examine these evolving national realities.

### **Conflict of Interest**

The authors declare no conflict of interest.

### **Reference**

[1] I. Aigbedion, S. Iyayi, "Diversifying Nigeria's petroleum industry" *International Journal of Physical Sciences*, 2(10), 263-270, 2007.

[2] World Commission on Environment and Development (WCED). "Our common future: The Brundtland report" Oxford: Oxford University Press, 1987.

[3] Nigeria Vision 20:2020. "Economic transformation blueprint. national planning commission" 2009. Retrieved from [http://www.nationalplanningcycles.org/sites/default/files/planning\\_cycle\\_repository/nigeria/nigeria-vision-20-20-20.pdf](http://www.nationalplanningcycles.org/sites/default/files/planning_cycle_repository/nigeria/nigeria-vision-20-20-20.pdf)

[4] UNDP; United Nations Development Programme. "Framework for harnessing the extractive industries for inclusive growth and development in Nigeria" United Nations Development Programme, 2014. Retrieved from <https://www.undp.org/content/dam/nigeria/docs/InclusiveGrwth/Framework%20for%20Harnessing%20the%20extractives%20in%20Nigeria.pdf>

[5] K. Fayemi, "Nigeria's solid minerals sector: alternative investment opportunities" Chatham House The Royal Institute of International Affairs. p 1-9, 2016.

[6] E. Sampson, "Oil resource dependency; emerging threats and concerns" *Zenith Economic Quarterly*, 9(4), 30-38, 2013.

[7] D. Fearon, "Primary commodities exports and civil war" *Journal of Conflict Resolution*, 49(4), 483-507, 2005.

[8] T. Karl, "The paradox of plenty; oil booms and petrol states" Berkeley: University of California Press, 1997.

[9] Transformation Agenda. "The mid-term report of the transformation agenda 2011- 2013" 2013. Retrieved from <https://www.slideshare.net/TransformNG/mid-term-report-of-the-transformation-agenda-complete>

[10] H. Adedeji, "Assessing the environmental impacts of inland sand mining in parts of Ogun State Nigeria" *Ethiopian Journal of Environmental Studies and Management*, 7(5), 478-487, 2014.

[11] D. Wapwera, "Abandoned mines, potential home for the people, a case study of Jos Plateau" *Journal of Civil Engineering and Architecture*, 9, 425-445, 2005.

[12] UNDP. "Managing Mining for Sustainable Development: A Sourcebook" Bangkok Regional Hub and Poverty-Environment Initiative Asia-Pacific of UNDP and UN Environment, 2018.

[13] Minerals and Mining Act 2007 s. 23 - 30

[14] B. Baba, "Are traditional tax incentives needed to stimulate the Nigerian mining industry?" *Tax Bites*, 2018. Accessed from [ww.pwc.com/ng](http://www.pwc.com/ng)

[15] Minerals and Mines Regulations (MMR) 2011 s. 154, 155, 156, 167 & 169

[16] Land Use Act 1978 s. 1 & 28(2)(c)

[17] UN. "Design and assessment of tax incentives in developing countries: selected issues and country experience" 2018. Accessed from [www.un.org/plods/2018/02](http://www.un.org/plods/2018/02)

[18] D. Teece, G. Pisano, A. Shuen, "Dynamic capabilities and strategic management" *Strategic Management Journal*, 18(7), 509-533.

[19] EITI, "Who We Are" (n.d). Accessed from [eiti.org/who-we-are](http://eiti.org/who-we-are)



## Mobile Based for Basic English Learning Assessment with Augmented Reality

Zuhri Syarifudin\*, Suharjito

Computer Science Department, BINUS Graduate Program - Master of Computer Science, Bina Nusantara University, Jakarta, Indonesia 11480

---

### ARTICLE INFO

*Article history:*

*Received: 21 February, 2020*

*Accepted: 31 March, 2020*

*Online: 24 April, 2020*

---

*Keywords:*

*Augmented Reality*

*Mobile Application*

*Formative Assessment*

*Basic English Learning*

---

---

### ABSTRACT

*Nowadays Augmented Reality (AR) is very popular in teaching and learning, especially in leading student to observe learning material targets which supported by online learning resources using mobile device and wireless technology. Because English is a foreign language, most students have problems in learning English. Generally, their problems were related to low motivation, bad study habit and attitude toward learning. Significantly, formative assessment is important in improving student learning achievement. furthermore, a formative assessment can help teachers to identified students' progress, modify instruction, provide immediately feedback and achieve learning goals. The aim of this study was to build Mobile Based Assessment with Augmented Reality based on formative assessment mechanism, examine student's learning achievement, student's acceptance and student's motivation in Basic English Learning. A total of 34 elementary students of Grade 4 were selected to participated in this study. The descriptive analysis was used to analyze and described the data obtained. The result indicated that using Mobile Based Assessment with Augmented Reality based on formative assessment mechanism improved not only student's learning achievement but also student's motivation in Basic English Learning.*

---

### 1. Introduction

Technology has greatly influenced our daily lives. Starting from the way we live, work, think, communicate, and interact with others continuously incessantly in all aspects of our lives [1]. In education section, information technology is one of the educational revolutions that has developed an education system to be more effective and efficient. According to [2] Mobile Based Assessment (MBA) is an alternative assessment model while complementing the Paper Based Test (PBT) or Computer Based Test (CBT) evaluation system. MBA has many advantages over PBA or CBT, such as ease of administration, saving time, not depending on location, adaptability, personalization and social interaction [3].

Augmented Reality (AR) is a technology which can translates or displays virtual data [4] and combine virtual objects into the real world [5]. AR can also be applied and connected with various technologies such as wearable computers, mobile devices and immersion technologies [6]. In education section, AR provides a great opportunity in online learning, especially in practical subjects [7]. AR technology can be applied in language learning too. Written, Vocabulary and oral comprehensive were important input

for students in language learning can be presented more interactive and more interesting. It can made student feeling interesting and spending more time to learn language learning [8]. Through AR-Based Mobile Learning material, also can help students to understand the lesson because students are directly involved in learning activities [9].

Using foreign languages in written communication is very difficult, because using foreign languages in written communication requires knowledge of linguistic and knowledge of meaning. English as Foreign Language (EFL) tends to make it difficult for students who have limited linguistic knowledge and background in understanding meaning [10]. English is a foreign language, most students spending more time for studying English composition and several students lost their motivation and their confidence in the learning process. This is caused when students practice in the writing skills, the students usually facing some problems (for example, inadequate vocabulary, less experience on the subject of composition and tough to describing their ideas) [11].

Several studies have investigated the formative assessment was significantly very important in improving student achievement, help teachers to understand student's progress

---

\*Corresponding Author Zuhri Syarifudin, Bina Nusantara-Jakarta, 534-5830, Indonesia, syarifudin.zuhri@binus.ac.id

[www.astesj.com](http://www.astesj.com)

<https://dx.doi.org/10.25046/aj050297>

during the learning process, modify learning methods and provide direct feedback [12, 13, 14, 15]. Direct feedback given to students is very important. Based on the researchers' statement on feedback, it can be concluded that during the feedback learning process it is very contributing, therefore feedback is part of formative assessment [16].

To enhance student's performance in the Basic English Learning, this study proposed a Mobile Based Assessment with Augmented Reality based on formative assessment mechanism, to examine student's learning achievement, student's motivation and student's acceptance in Basic English Learning. The following research questions are examined in this study:

- how to build Mobile-Based Assessment with Augmented Reality to measure student's achievement
- do the students who study with Mobile-Based Assessment with Augmented Reality have better motivation learning
- how student's acceptance who studied with Mobile-Based Assessment with Augmented Reality.

## 2. Related Work

Research on the use of Augmented Reality on 100 students grade 7 junior high school in learning "Solar System and Beyond" conducted by [17] has a positive impact on student's achievement and student's attitudes compared to traditional learning methods and textbooks. Based on the results of the study, several reasons for student's achievement and student's attitude who using AR are better than traditional learning methods in the learning process : (1) AR technology increases students' sense of interest and motivation in learning; (2) Objects transformation in AR draw student's attention; (3) 3D objects in AR enable students to observe learning material in more detail compared to 2D objects; (4) AR technology makes the learning process more interesting; (5) Students feel AR technology is a new and interesting technology, even some students think AR is like magic; (6) 3D objects in AR, attract the attention of students, allow students to be able to observe more thoroughly and make students feel the learning process of learning by doing; (7) AR technology makes learning in the classroom more enjoyable, attracting students' attention and interest in learning material.

The study has been done by [18] comparing academic achievement and student's motivation with 93 students at private school and public school in Mexico on Geometry learning using ARGeo and WebGeo as learning media. The results of the study revealed : (1) Based on the results of the Pre Test and Post Test that have been conducted on public school and private school, students who learn to use ARGeo have better academic achievements than students who learn to use WebGeo; (2) Students at Public School, learning Geometry using ARGeo are more effective than WebGeo, while students at Private School, learning Geometry using ARGeo and WebGeo are equally effective; (3) Students at Public School and Private School who learn to use ARGeo have good learning motivation compared to students who study with WebGeo.

The study conducted by [9] combines AR and Global Positioning technology in the learning process of English as a

Foreign Language (EFL), especially in writing. Students are asked to go around the campus area while activating the camera to aim at the learning target, then the system will display learning material information in English composition on the smartphone screen accordance with the target captured by the camera for observation. After making observation, students are asked to make an essay to test their writing skills using English. The results of this study reveal AR-Based Learning is very helpful for students in observing learning material, adding information and vocabulary, adding linguistic knowledge and meaning knowledge so that students can produce meaningful and good essays.

Using AR technology in interactive English language learning through the Phonics approached to Consonant-Vocal-Consonant material in kindergarten provides fun, interactive and effective learning. Through this method, students are enthusiastic and pro-active during the learning process and increase students' reading interest [19].

The study conducted by [20] presents an AR Book System based learning system to introduce Hakka Culture in Taiwan. The students read the book using the AR application using a mobile device and then the system will display virtual information in the form of 3D objects, audio and video narration. Researchers conducted experiments with 153 students and explained that learning using the AR Book system increases motivation, interest and attitude especially in reading context in the learning process.

Research by [21] compares learning strategy on u-learning using Augmented Reality based on formative assessment with conventional Augmented Reality. A total of 39 students majoring in architecture were divided into experimental groups of 19 students using Augmented Reality based on formative assessment and control groups of 20 students using conventional Augmented Reality. The learning scenario carried out by the two groups is observing the buildings in the Museum of World Religions to measure student's achievement, motivation learning and cognitive load (mental load and mental effort). The results of the study revealed: (1) Student's achievement in the experimental group was greater than in the control group. This is because formative assessment allows students to develop a sense of responsibility towards learning so that they actively build student understanding; (2) There is no significant difference Mental load between the two groups, because both groups studied the same content of learning material. But mental effort in the experimental group is greater than the control group, this reveals Augmented Reality (AR) based on formative assessment is a good learning strategy approach for students; (3) Motivation learning in the experimental group is greater than in the control group because feedback in formative assessment can be used by students to revise their learning activities to complete their assignments efficiently.

Previous research study demonstrated how AR technology can support the learning process and make effective learning. Therefore, in this study the researchers intend to make a Mobile Based Assessment with Augmented Reality in Basic English Language Learning based on formative assessment mechanism to examine student's learning achievement, student's motivation and student acceptance in Basic English Learning. Through this application, it is expected to be able provide information to the

teacher about what students have learned, show what difficulties students might find in the learning process, and help the teacher adjust the teaching to maximize the learning.

### 3. Research Methodology

Based on research conducted by [21], this study used a formative assessment strategy method based on the AR-based learning system in designing mobile applications for the assessment of basic English language learning using AR. During the learning process, the students will be learning the course using formative assessment mechanism. Through this mechanism, students will be guided to observe each learning material and then answer a series of questions that arise based on the guidelines displayed by the learning system. As shown in Figure 1, there are three main phases in this study as explained in more detail below.

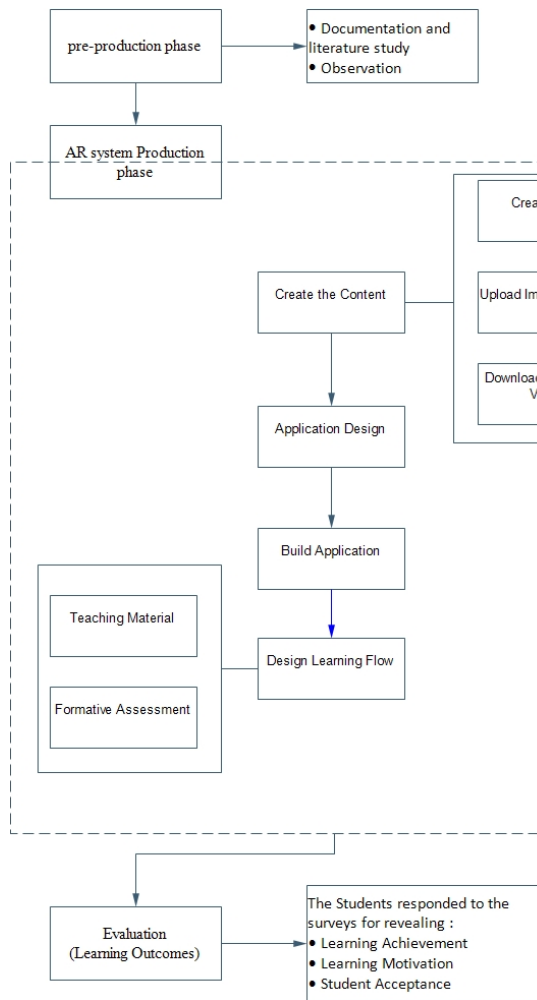


Figure 1 : Research Method

The pre-production phase: the stages of documentation and literature study related to research problems and preliminary surveys (observation) to obtain the data needed. In the literature study phase, researchers collect a number of books, archives, articles, journals and relevant documents about the use of AR technology in the learning process and learn how to implement AR in the learning process. While at the observation stage, researchers conduct observations or reviews carefully and directly at the research site to determine the conditions that occur.

AR system Production phase: the stage of making a mobile application for the assessment of basic English language learning using AR. Preparation started from finding information about learning material, determining 3D objects, designing book markers and integrating into the Vuforia library and making Augmented Reality in Unity until the application is ready for use by users as shown on Figure 2.

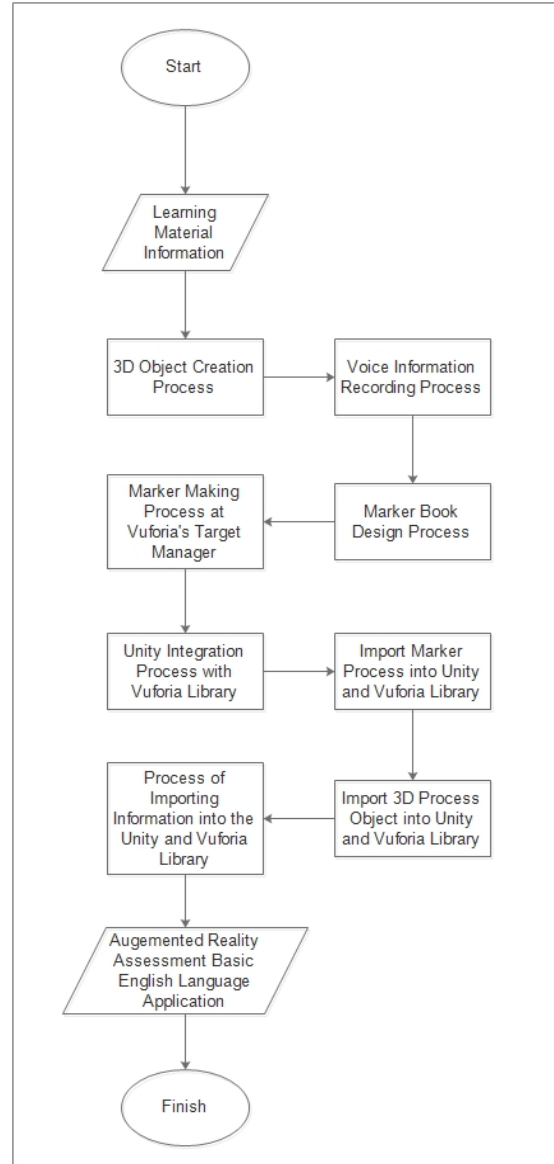


Figure 2: AR Application Design Flowchart

Hardware specifications that researchers use for making AR applications can be seen in Table 1 and software specifications used in Table 2.

Table 1 Hardware Specification

No	Component	Specification
1	RAM	4 GB
2	SSD	512 GB
3	VGA	1024 MB
4	Processor	Intel Core i3
5	Camera	Logitech 2 MP

Table 2 Software Specification

No	Component	Specification
1	OS	Win10
2	IDE	Visual Studio Code 1.38.1
3	Framework	Unity 3D Version 2018.3.11.fl (64bit)
4	AR Library	Vuforia 8.1.10
5	Android Emulator	Bluestack

While the minimum device target for user requirement can be seen in Table 3.

Table 3 Minimum Device Target

No	Component	Specification
1	Device	Android OS Based
2	Android OS Version	4.1
3	RAM	1 GB
4	API	14
5	Camera	8 MP

This AR application was built for Android-based devices, researchers chose the Vuforia Framework as a library for making AR on Android. This application was developed with Visual Studio Code as an IDE for making AR applications and using Unity 3D Version 2018.3.11.fl (64bit).

The AR application will display the views obtained from the camera on an android device. Then the camera will detect the presence of the marker where the marker is in the form of an ARBOOK book. When a marker is detected it will display virtual information in the form of 3D objects with audio narration and formative assessment.



Figure 3: AR Application

The evaluation (learning outcomes) structure used in this study are learning achievement, learning motivation and student's acceptance. The subjects were 34 students who studied in 4th grade at an elementary school.

Pre-Test and Post-Test were developed to evaluate students learning achievement. Pre-test aimed to evaluate the student's prior knowledge about the course content. Post-test aimed to evaluate student knowledge after using the system. Pre-Test and Post-Test both contained 10 multiple choice questions, with a perfect score is 100.

Motivation Strategies for Learning Question (MSLQ) developed by [22] was adopted to developed motivation questionnaire. The motivation questionnaire consisted of 5 items in a five-point Likert scale.

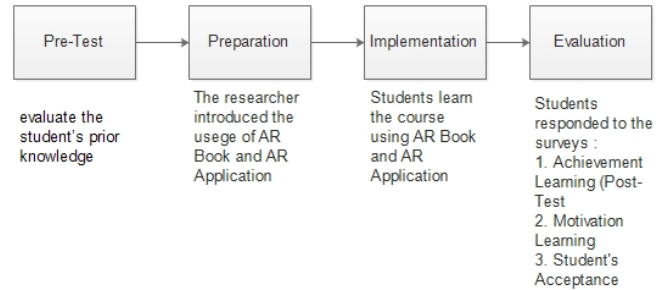


Figure 4: Evaluation Process

The student's acceptance questionnaire were developed with attitude questionnaire based on previous research [23] and [24] that has seven factors : perception of usefulness, perceived ease of use, teaching material, Interface Design, Multimedia Feature, Interactive Function, and Practicability. The student's acceptance questionnaire consisted of 20 items in a five-point Likert scale.

The overall Cronbach's alpha for the pre-post-test, motivation questionnaire, usefulness, perceived ease of use, teaching material, Interface Design, Multimedia Feature, Interactive Function, and Practicability were 0.753, 0.929, 0.774, 0.832, 0.881, 0.739, 0.703, 0.861 and 0.914 respectively, which are acceptable.

#### 4. Finding and Result

In this study, a material was designed supported with AR technology with an animation, 3D model object, and audio narration in order to help students better memorize the material. Assessment and immediately feedback helping student's for self-reflection in learning process. The implementation of learning basic English with Mobile Based Assessment with Augmented Reality in the classroom was presented in Figure 5.



Figure 5: The Implementation of AR in the classroom

A SPSS was used to perform a statistical data analysis based on the result of the pre-test, post-test, learning motivation and student acceptance. Descriptive analysis was adopted to analyze and describe the result of each test and the questionnaires of the participant in basic English classroom towards course materials designed with augmented reality technology.

Pre-test was conducted to evaluate the student's prior knowledge about the course content before experimental learning activity. After participating in the experimental learning activity, the student took the post-test. Results of the pre- post-test are shown in Table 4.



Table 4 Descriptive Analysis Results of pre- post-test

	N	Mean	Std. Deviation
Pre_Test	34	63.24	14.189
Post_Test	34	68.53	19.288
Valid N (listwise)	34		

Based on Table 1 was shown a brief summary of the descriptive analysis results. For the Pre-Test obtained the Mean value was 63.24. As for the Post-Test value, the Mean value was 68.53. Seeing the results of the calculation from mean value as shown in the table, there is an increase in learning outcomes (achievement learning) after learning to use the AR application as seen in Figure 6 Pre-Test and Post-Test Diagram.

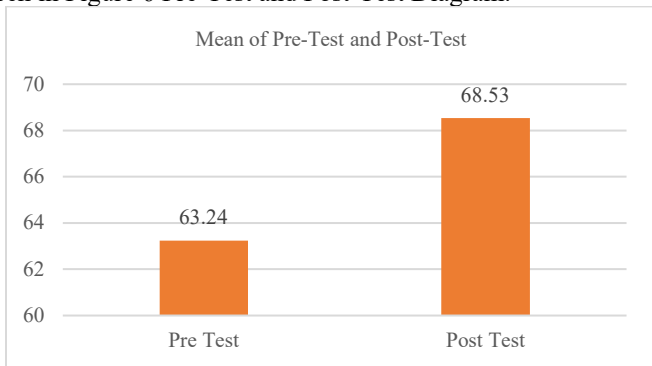


Figure 6: Pre-Test and Post-Test Diagram

The results of motivation learning related to this survey can be seen in Table 5.

Table 5 Descriptive Analysis Results Motivation Learning

Motivation	STS	TS	R	S	SS	Mean
	1	2	3	4	5	
Motiv1	2	0	1	10	21	4.41
	5,88%	0,00%	2,94%	29,41%	61,76%	
Motiv2	1	3	3	14	13	4.03
	2,94%	8,82%	8,82%	41,18%	38,24%	
Motiv3	2	0	2	10	20	4.35
	5,88%	0,00%	5,88%	29,41%	58,82%	
Motiv4	2	1	1	10	20	4.32
	5,88%	2,94%	2,94%	29,41%	58,82%	
Motiv5	2	0	2	10	20	4.35
	5,88%	0,00%	5,88%	29,41%	58,82%	
<b>Sum of Mean</b>						<b>4.29</b>

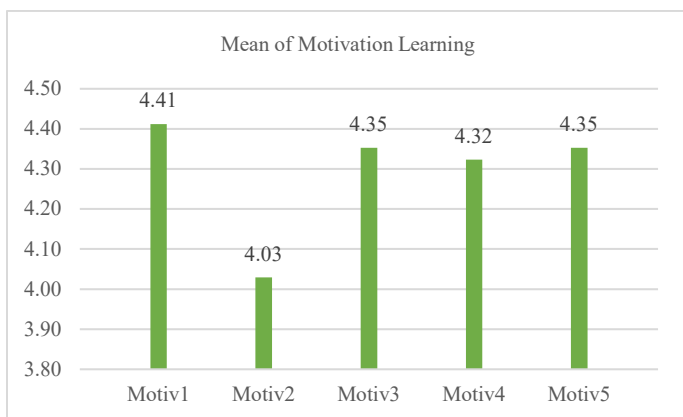
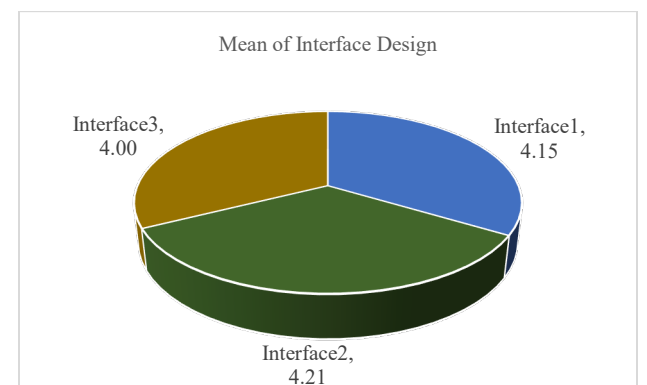
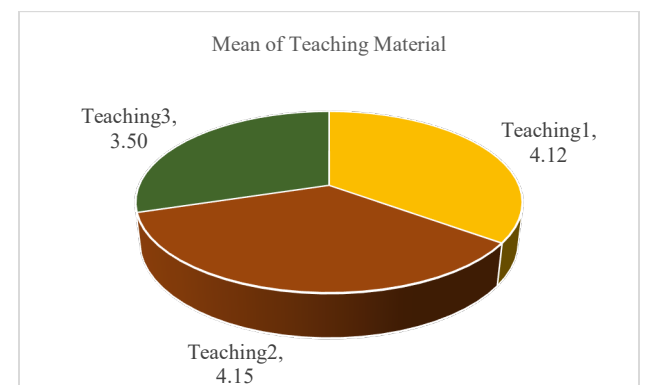
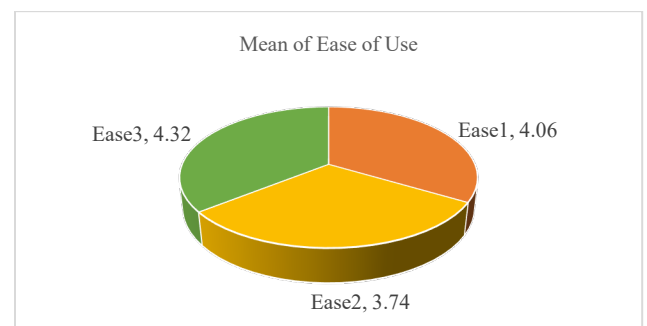
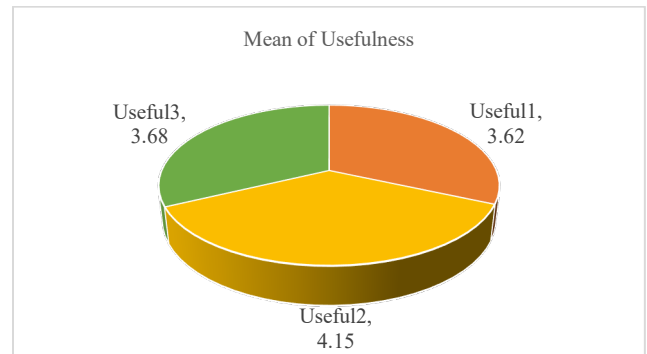


Figure 7: Motivation Learning Diagram

Based on Table 2 the students' answers to the questions asked for the Motivational Learning variable have an average of 4.03 to 4.35 with an average total value of 4.29. This shows that most

students agree with the questions in the questionnaire which means students assessed that learning Basic English with Mobile Based Assessment with Augmented Reality have good motivation learning.

Usefulness, perceived ease of use, teaching material, Interface Design, Multimedia Feature, Interactive Function, and Practicability are used to measure student acceptance in English learning activities using the AR application. Student acceptance results related to this variable in each category can be seen in Figure 8.



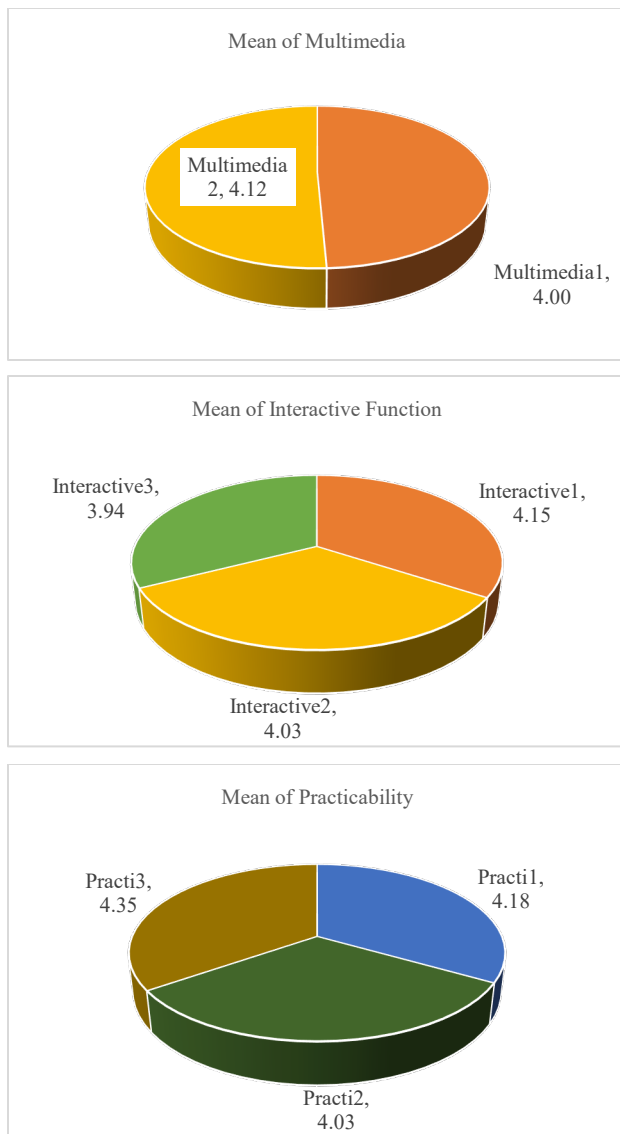


Figure 8: Descriptive Analysis Student's Acceptance Diagram

Information from Figure 8 is as follows:

- Based on the usefulness can be seen from the Figure 8 has mean value of 3.62, 4.15 and 3.68 which shows that students feel quite satisfied with the benefits felt from the AR application.
- Based on ease of use, has mean value of 4.06, 3.74, 4.32 which shows that students can easily use the AR application.
- Based on teaching material (teaching material) can be seen from the Figure 8 has mean value of 4.12, 4.15 and 5.50 which shows that students feel quite satisfied with the material displayed on the AR application.
- Based on the interface design (interface design) seen in the Figure 8 has mean value of 4.15, 4.21 and 4.00 which shows that students feel the design of the application is good.
- Based on multimedia features as shown in the Figure 8 has mean value of 4.06 and 4.12 which shows that

students feel the 3D model and the information displayed is good.

- Based on the interactive function in the Figure 8, it looks like it has mean value of 4.15, 4.05 and 3.94 which shows students feel the touch and assessment features are good enough.
- Based on practicability as seen in the Figure 8 has mean value of 4.18, 4.03 and 4.35 which shows students feel this application is quite useful

Based on Figure 8, most students choose the option above doubt (3) namely the choice of agree (4) or strongly agree (5). this shows that students have good student's acceptance in the process of learning basic English using the AR application as seen in Figure 9 Student Acceptance Diagram.

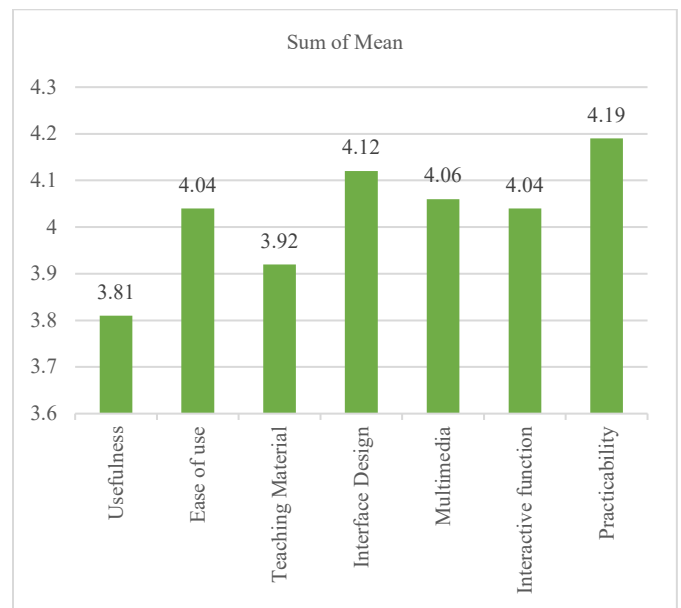


Figure 9: Student's Acceptance Diagram

Student's acceptance survey results that look like the picture 9. Student's Acceptance Diagram have similar result with research by [17] which revealing using AR technology in the learning process has a positive impact on student's acceptance. This is due to several reasons such as making students directly involved in learning so that learning is more fun, attracting students' attention and students' interest in learning. The features contained in AR technology allow students to observe learning objects in more detail so allowed students to feel the experience of learning by doing.

## 5. Conclusions

All Based on the results of the calculation of survey data and the results of the evaluation of AR applications can be seen a positive response from students. Applications designed in this study have the advantage of being able to display information in the form of 3D models, animation, text, sound, assessment and feedback so provided different nuances in presenting information on learning material that is more interesting and interactive to students. In addition, students are interested in the further development of this application and the desire to further using this application as a complement of the learning tools (media learning).

Based on the results obtained through this study, it can be concluded that the application of basic English learning using AR can help students in learning material and motivated students to learn English. There are some improvements and investigations that must be considered for future research, such as expanding the content of learning materials to meet the competency standards of learners, adding features of interaction between teacher and student or fellow students to support collaborative learning methods, conducting an statistical analysis involving teachers and students in learning process, and investigating student learning behavior to extend the explanation in this research.

## References

- [1] J. Challoner, 1001 Inventions that changed the world, Barron's, 2009.
- [2] L. Johnson, S. A. Becker, M. Cummins, V. Estrada, A. Freeman and C. Hall, NMC horizon report: 2016 higher education edition, The New Media Consortium, 2016.
- [3] S. A. Nikou and A. A. Economides, "A model for Mobile-based Assessment adoption based on Self-Determination Theory of Motivation," in Interactive Mobile Communication Technologies and Learning (IMCL), 2014 International Conference on, IEEE, 2014, pp. 86-90.
- [4] M. Akçayır and G. Akçayır, "Advantages and challenges associated with augmented reality for education: A systematic review of the literature," Educational Research Review, vol. 20, pp. 1-11, 2017.
- [5] T. C. Huang, M. Y. Chen and W. P. Hsu, "Do Learning Styles Matter? Motivating Learners in an Augmented Geopark," Journal of Educational Technology & Society, vol. 22, pp. 70-81, 2019.
- [6] X. Wei, D. Weng, Y. Liu and Y. Wang, "Teaching based on augmented reality for a technical creative design course," Computers & Education, vol. 81, pp. 221-234, 2015.
- [7] J. M. Andujar, A. Mejías and M. A. Márquez, "Augmented reality for the improvement of remote laboratories: an augmented remote laboratory," IEEE transactions on education, vol. 54(3), pp. 492-500, 2010.
- [8] E. Solak and R. Cakir, "Exploring the Effect of Materials Designed with Augmented Reality on Language Learners' Vocabulary Learning.," Journal of Educators Online, vol. 12(2), pp. 50-72, 2015.
- [9] P. H. E. Liu and M. K. Tsai, "Using augmented-reality-based mobile learning material in EFL English composition: An exploratory case study," British Journal of Educational Technology, vol. 44(1), pp. E1-E4, 2013.
- [10] M. Saville-Troike and K. Barto, Introducing second language acquisition, Cambridge University Press, 2016.
- [11] C. L. Shih, "The Relationship among Writing Self-efficacy, Apprehension, Motivation, Experience, and English Writing Performance of the Undergraduates and Graduate Students in Taiwan," Taiwan: National Kaohsiung Normal University, 2006.
- [12] B. Bell and B. Cowie, "The characteristics of formative assessment in science education," Science education, vol. 85(5), pp. 536-553, 2001.
- [13] P. Black and D. Wiliam, Inside the black box: Raising standards through classroom assessment, Granada Learning, 2005.
- [14] J. W. Gikandi, D. Morrow and N. E. Davis, "Online formative assessment in higher education: A review of the literature," Computers & education, vol. 57(4), pp. 2333-2351, 2011.
- [15] P. Perrenoud, "From formative evaluation to a controlled regulation of learning processes. Towards a wider conceptual field," Assessment in Education: Principles, Policy & Practice, vol. 5(1), pp. 85-102, 1998.
- [16] D. D. McMahon, D. F. Cihak, R. E. Wright and S. M. Bell, "Augmented reality for teaching science vocabulary to postsecondary education students with intellectual disabilities and autism," Journal of Research on Technology in Education, vol. 48(1), pp. 38-56, 2016.
- [17] D. Sahin and R. M. Yilmaz, "The effect of Augmented Reality Technology on middle school students' achievements and attitudes towards science education," Computers & Education, vol. 144, p. 103710, 2020.
- [18] M. B. Ibáñez, A. U. Portillo, R. Z. Cabada and M. L. Barrón, "Impact of augmented reality technology on academic achievement and motivation of students from public and private Mexican schools. A case study in a middle-school geometry course," Computers & Education, vol. 145, p. 103734, 2020.
- [19] J. Sidi, L. F. Yee and W. Y. Chai, "Interactive English Phonics Learning for Kindergarten Consonant-Vowel-Consonant (CVC) Word Using Augmented Reality," Journal of Telecommunication, Electronic and Computer Engineering (JTEC), Vols. 9(3-11), pp. 85-91, 2017.
- [20] K.-H. Cheng, "Reading an augmented reality book: An exploration of learners' cognitive load, motivation, and attitudes," Australasian Journal of Educational Technology, vol. 33, no. 4, 2017.
- [21] H. C. Chu, J. M. Chen, G. J. Hwang and T. W. Chen, "Effects of formative assessment in an augmented reality approach to conducting ubiquitous learning activities for architecture courses," Universal Access in the Information Society, pp. 1-10, 2017.
- [22] P. R. Pintrich and E. V. De Groot, "Motivational and self-regulated learning components of classroom academic performance.," Journal of educational psychology, vol. 82, no. 1, p. 33, 1990.
- [23] M. H. Kurniawan, Suhartjio, Diana and G. Witjaksono, "Human Anatomy Learning Systems Using Augmented Reality on Mobile Application," Procedia Computer Science, vol. 135, pp. 80-88, 2018.
- [24] C.-H. Chen, C.-Y. Huang and Y.-Y. Chou, "Effects of augmented reality-based multidimensional concept maps on students' learning achievement, motivation and acceptance," Universal Access in the Information Society, vol. 18, no. 2, pp. 257-268, 2017.

## A Novel Quantum No-Key Protocol for Many Bits Transfer with Error Correction Codes

Duc Manh Nguyen, Sunghwan Kim\*

School of Electrical engineering, University of Ulsan, 44610, Korea.

### ARTICLE INFO

Article history:

Received: 04 March, 2020

Accepted: 11 April, 2020

Online: 24 April, 2020

Keywords:

Quantum cryptography

Quantum three stage protocol

Quantum error correction code

### ABSTRACT

In this paper, a novel quantum transmission protocol which are based on the quantum no-key protocol is proposed. First, the quantum no-key protocol is discussed to show its important and its non-efficient on data transmission over quantum channel. Then, we improve it to carry many data bits via transmission. In addition, the error correction code is discussed and emerged into the proposed protocol to secure the transmission over quantum channel noise. Finally, the evaluation of transfer cost is discussed to show the effective of our proposed system.

### 1. Introduction

This paper is an extension of work originally presented in 2019 International Conference on Advanced Technologies for Communications (ATC) in Ha-Noi, Viet-Nam [1].

Quantum computation is problem solving and data computation using a system based on quantum mechanics, which is an effort to generalize classical computation. Quantum information systems could be able to transmit data fundamentally securely and solve complex problems better than classical information systems [2]. In 1994, Peter Shor invented a quantum algorithm for factoring integers into prime factors which runs on polynomial time [3]. In addition, in 1996 Lov Grover devised a quantum search algorithm for searching unstructured databases [4]. Hence, quantum algorithms promised big improvements on performance in comparison to classical computation; consequently, many problems have been considered in quantum computation [5]. However, the effects from imperfectly applied quantum gates, decoherence, and other quantum channel noise would affect the practical design of quantum computation. To overcome such problems, quantum error correction code (QECC) based on the theory of classical error correction code, was developed to protect quantum states from noise environment [6]. Since the first QECC was discovered by Shor [7], the method of containing redundancy to circumvent the no-cloning theorem has been popularly used. Therefore, the importance of QECC on practical building of quantum computer is no longer in doubt.

Cryptography is the research of secure communication techniques which allow only sender and intended receivers to view

the content of shared messages. With the advantages of quantum mechanism such as entanglement and no-cloning theory, quantum cryptography is an application of quantum mechanics to cryptography. The first quantum cryptography protocol is BB84 which is invented by Dr. C. H. Bennett [8], it is public-key cryptography. In 1980, a novel private key cryptography protocol named Shamir no-key protocol is invented where the sender and receiver do not exchange the key, however the protocol requires the sender and receiver to have their own private keys for encrypting and decrypting the messages with the hard and complex on computation. Since quantum mechanism with no-cloning theorem which can be used to improve no-key protocol; then, in 2002 a quantum cryptography protocol based on Shamir's no-key protocol is considered [9]. In [10], in combination with Hill-cipher algorithm, the quantum no-key protocol was proven to be a scheme for secure direct quantum communications wherein the information is encrypted into a binary string and each bit is exchange between sender and receiver.

The main result of this research is to propose a new quantum no-key protocol which a single quantum state to establish the transfer of many information bits. In addition, the qubit needs to be protected from noise for the correct quantum state exchanged between Sender and Receiver. Hence, we emerge the proposed protocol with quantum error correction codes to establish the secure communication channel which can against the quantum noise, decoherence, and unwanted environments. The organization of this paper is as follows. In Section 2, the basic of quantum computation and quantum error correction codes are reviewed. In Section 3, we first propose the quantum no-key protocol; then, the

\*Corresponding Author: Sunghwan Kim, [sungkim@ulsan.ac.kr](mailto:sungkim@ulsan.ac.kr)



emerging quantum no-key protocol with error correction code is discussed. Then, the conclusion is presented.

2. Preliminaries

2.1. Basic of Quantum Computations

Quantum theory uses qubit to represent information, the quantum systems with two levels such as: two polarization states of photons, two energy levels of atoms, etc. A qubit  $|\psi\rangle = a|0\rangle + b|1\rangle$  is considered to be found in the both basis states  $|0\rangle$  and  $|1\rangle$  where the probability value we saw that qubit at state  $|0\rangle$  is  $|a|^2$  and at state  $|1\rangle$  is  $|b|^2$ . It is superposition concept of a qubit, which is one of a main property of quantum information since the amount of information which presented in qubits are no limitation [11,12]. A qubit can be displayed in matrix form as,

$$|\Psi\rangle = \begin{bmatrix} a \\ b \end{bmatrix} = a \begin{bmatrix} 1 \\ 0 \end{bmatrix} + b \begin{bmatrix} 0 \\ 1 \end{bmatrix} = a|0\rangle + b|1\rangle. \tag{1}$$

According to norm condition for a qubit on the Bloch sphere space, the complex numbers  $a$  and  $b$  satisfy the equation  $|a|^2 + |b|^2 = 1$ . A  $n$  qubits system is constructed by multiple tensor products of some other qubits, it is given as follows,

$$|\Phi\rangle = \sum_{i=0}^{2^n-1} a_i|i\rangle = \sum_{i_k=\{0,1\}} a_{i_1 i_2 \dots i_n} |i_1\rangle |i_2\rangle \dots |i_n\rangle. \tag{2}$$

where  $i = \sum_{j=0}^{n-1} 2^j i_j$ .

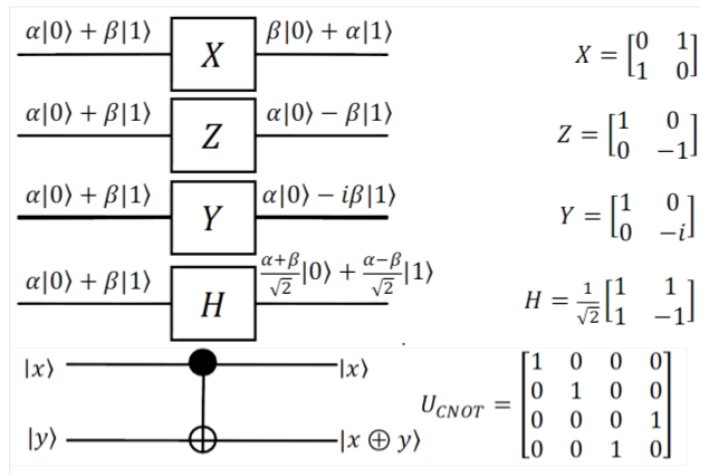


Figure 1: Basic quantum gates with matrices presentation

$$E = e_1 \otimes e_2 \otimes \dots \otimes e_n \text{ where}$$

$$e_i \in \{I, X, Y, Z\}.$$

2.2. Basic of Quantum Error Correction Codes

The simplest QECC is three qubits repetition code that can correct only one type error, namely bit flip or phase flip [13]. The QECC can be simulated by quantum circuit model; they are showing in the Figure 2, 3 for three qubits repetition code. The difference between them are on the Clifford gate has been used:  $X=HZH$  and  $Z=HXH$ .

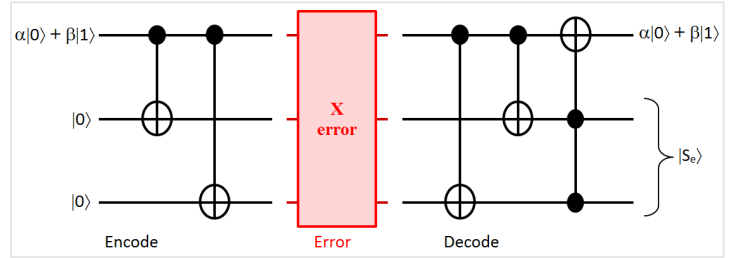


Figure 2: Quantum circuit for X-error 3- repetition code

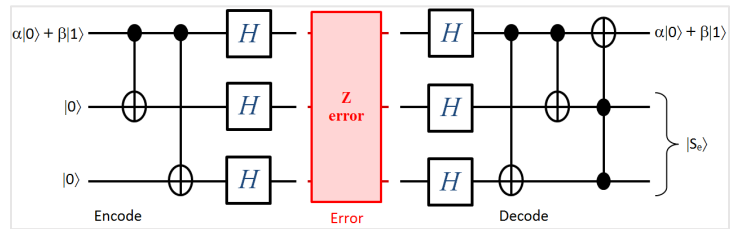


Figure 3: Quantum circuit for Z-error 3- repetition code

$$|0_L\rangle = |000\rangle, |1_L\rangle = |111\rangle. \tag{3}$$

Then, the quantum gates as previous mentioned must to be declared. Here, the quantum gates  $X$ ,  $Z$ , and two new types of  $CNOT$  gates are used. The tensor product was used to extend one qubit to many qubits system.

To extend the first full quantum code, Shor code for 9 qubits is created by Shor, which use both bit-flip correction and phase-flip correction and can correct bit-flip, phase-flip, and their combination [14]. To do so, for one qubit is protected against phase-flip we need extend it to codeword of three qubits. Then, each qubits of that three-qubits need to extend to three-qubits to protect against bit-flip error. Hence, the quantum circuit starts with the initial information, we extend it to the 9-qubits via helps of ancilla 8 qubits of zeros, after transformation by encode step, the logical states or encoded qubits are created. Here, two basis states of codewords 9-qubits repetition as well as

$$|0_L\rangle = \frac{1}{\sqrt{8}}(|000\rangle + |111\rangle) \otimes (|000\rangle + |111\rangle) \otimes (|000\rangle + |111\rangle), \tag{4}$$

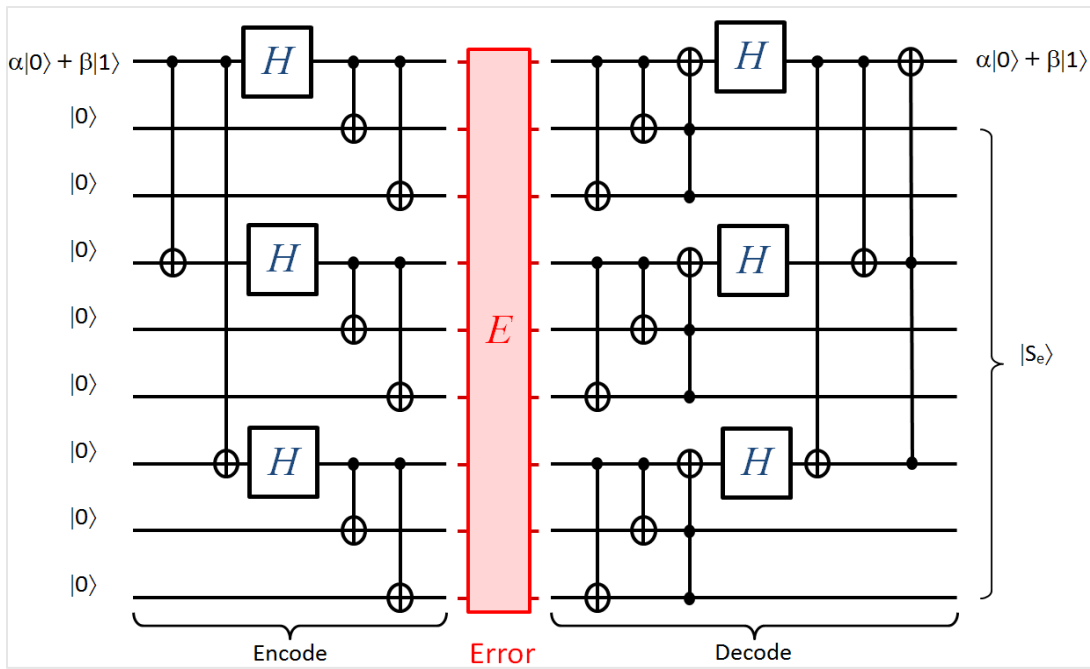


Figure 4: Quantum circuit for Shor code

$$|1_L\rangle = \frac{1}{\sqrt{8}} (|000\rangle - |111\rangle) \otimes (|000\rangle - |111\rangle) \otimes (|000\rangle - |111\rangle). \tag{5}$$

Using matrices transformation, the states after applying error and decoding can be found. The final states show us the correction state can be recovered the syndrome  $|S_e\rangle$  tell us which error has applied to logical states. The full quantum circuit for Shor code is given in Figure 4.

Generally, the quantum error correction code can be denoted as  $[[n,k,d]]$  where  $n$  is length of codeword,  $k$  is length of information bits, and  $d$  is minimum distance which corresponds to number of error the code can be detected and corrected. The parameter for Shor code at Figure 4 is  $[[9,1,3]]$ , and it is the first quantum error correction code. Since the first proposed of Shor code, many novel quantum codes with diverse parameters have been proposed [15,16], they are called quantum stabilizer codes. The most important of quantum stabilizer codes are that they could be constructed by binary formalism, then the quantum circuit model are easy created which points are discussed detailly in [12].

### 3.1. Quantum no-key protocol

Quantum no-key protocol was invented by S. Kak [9], which is an emerging of classical no-key protocol with quantum mechanism. In this system, Sender and Receiver do not share the public key, they have their own private keys. The private key on quantum no-key protocol is an unitary transformation which has following form:

$$U(\varphi) = \begin{bmatrix} \cos(\varphi) & \sin(\varphi) \\ -\sin(\varphi) & \cos(\varphi) \end{bmatrix}. \tag{6}$$

The private keys in (6) are commutative to each other, it means  $U(\varphi_1)U(\varphi_2) = U(\varphi_2)U(\varphi_1)$ . If Sender or Receiver choose  $U(\varphi_3)$  for its private encryption key, the corresponding decryption key will be  $U(-\varphi_3)$  since  $U(\varphi_3)^{-1} = U(-\varphi_3)$ .

We assume that Sender and Receiver want to share the quantum state  $|\varphi\rangle$ , the protocol is proceeded as Figure 5. The detail of each steps are as follows,

1. Sender randomly choice private encryption key,  $U(\theta_S)$ , apply it to quantum state to get  $U(\theta_S)|\varphi\rangle$ . Then, transfer that encrypted state to Receiver.
2. Assume that there is no noise on the channel, Receiver gets the correct recipient from Sender,  $U(\theta_S)|\varphi\rangle$ . Receiver also randomly choice its private encryption key,  $U(\theta_R)$ , apply it to current quantum state to get  $U(\theta_R)U(\theta_S)|\varphi\rangle$ . Then, transfer back encrypted quantum state to Sender.
3. Assume that there is no noise on the channel, Sender gets correct recipient from Receiver,  $U(\theta_R)U(\theta_S)|\varphi\rangle$ . Sender applies the decryption private key according to step 1,  $U(-\theta_S)$ , then current quantum state is  $U(\theta_R)|\varphi\rangle$ . Sender transfers its state to Receiver.
4. Assume that there is no noise on the channel, Receiver gets the correct recipient,  $U(\theta_R)|\varphi\rangle$ . Then, Receiver can get the original message by applying decryption private key according to step 3,  $U(-\theta_R)$ . Finally, Receiver gets  $|\varphi\rangle$ . Sender and Receiver successfully exchange original quantum state.

The original quantum no-key protocol just mentions the exchange one bit, 0 or 1, for each round by attached it to quantum state,  $|0\rangle$  or  $|1\rangle$ . In next subsection, we consider the proposed system for multi-bits transfer for each round. Then, it reduces the time of transferring long message.

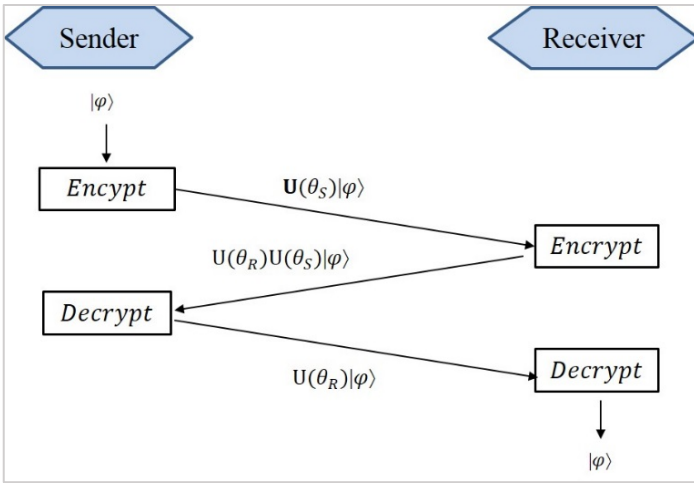


Figure 5: Quantum no-key protocol

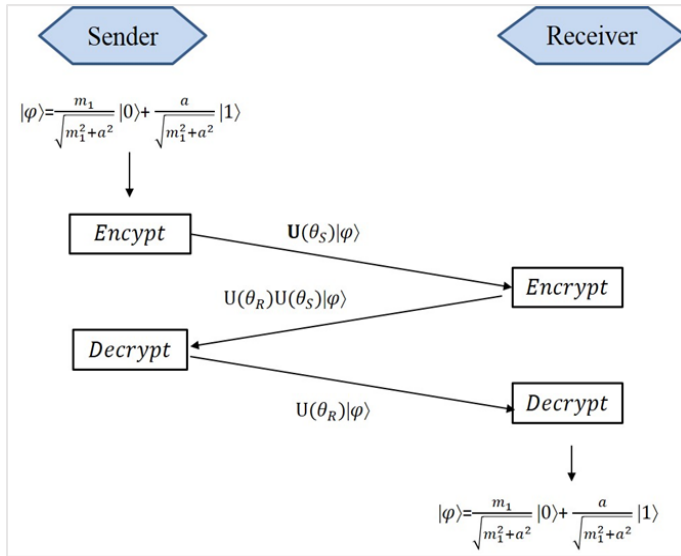


Figure 6: Quantum no-key protocol for many bits

### 3.2. Proposed quantum no-key protocol for many bits' transfers

We assume that Sender and Receiver wish to exchange the binary string  $\mathbf{m}_1\mathbf{m}_2 \dots \mathbf{m}_k$ , where each  $\mathbf{m}_i$  is binary string of length  $l$ , that means the total length of binary string Sender and Receiver want to exchange is  $k \times l$ . We denote that binary string  $\mathbf{m}_i$  has the decimal value  $m_i$ . The proposed protocol is as follows.

1. Sender and Receiver first exchange the binary string  $\mathbf{m}_0$  by using the quantum no-key protocol. As analysis on Section 3.1, since  $\mathbf{m}_0$  has length  $l$ , the cost of using quantum no-key protocol for successfully recipient is  $l$ . We denote  $a$  is the decimal value corresponding to binary string  $\mathbf{m}_0$ .
2. For binary string  $\mathbf{m}_1$ , Sender first encodes to the quantum state:  $|\varphi\rangle = \frac{m_1}{\sqrt{m_1^2+a^2}}|0\rangle + \frac{a}{\sqrt{m_1^2+a^2}}|1\rangle$ , where  $m_1$  is the decimal value of binary string  $\mathbf{m}_1$ . The detail of using quantum no-key protocol is shown in Figure 6. We assume that there is no error from quantum channel. Then, Receiver gets correct quantum state  $|\varphi\rangle = \frac{m_1}{\sqrt{m_1^2+a^2}}|0\rangle + \frac{a}{\sqrt{m_1^2+a^2}}|1\rangle$ . Since the value of  $a$  is known before, Receiver will know exactly  $m_1$  via measurement. Finally, Receiver will get binary string  $\mathbf{m}_1$ .

The cost for exchange binary string  $\mathbf{m}_1$  between Sender and Receiver is one time using quantum no-key protocol.

3. For remaining binary string  $\mathbf{m}_2, \mathbf{m}_3, \dots, \mathbf{m}_k$ , the same procedure as Step 2 is taken. The cost for successfully recipient is  $k - 1$ .

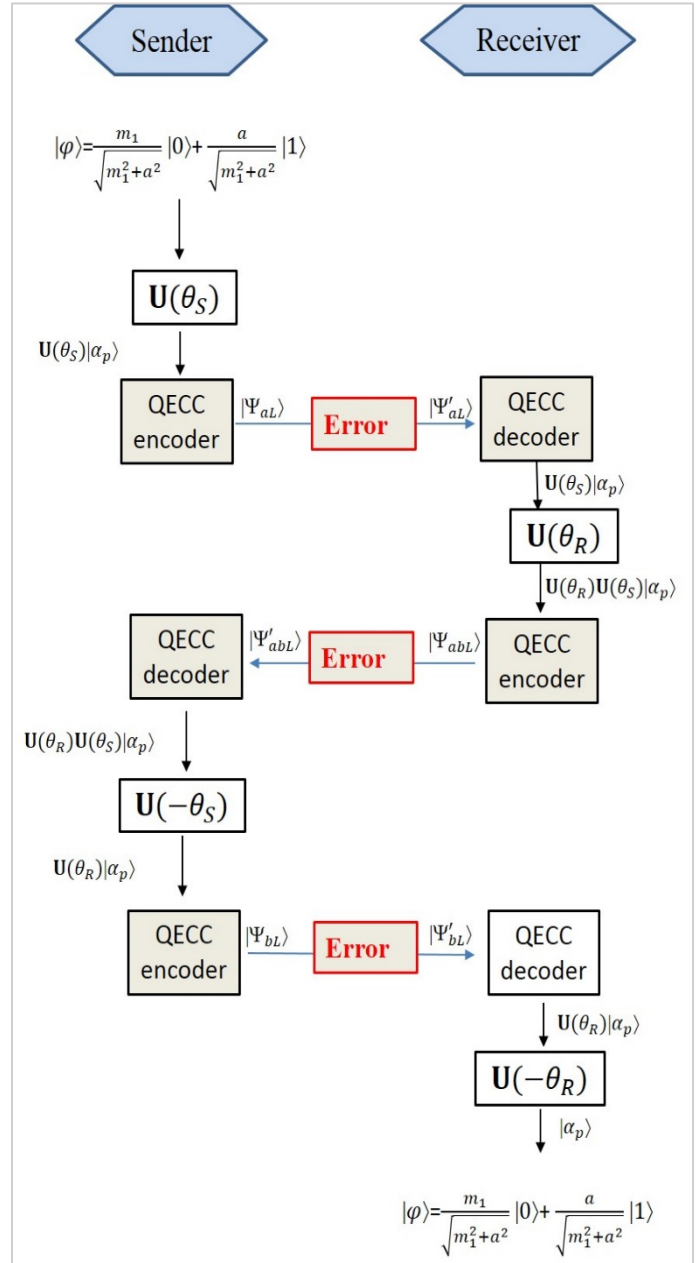


Figure 7: Quantum no-key protocol with error correction code

### 3.3. Analysis the cost of proposed protocol

For whole binary string  $\mathbf{m}_1\mathbf{m}_2 \dots \mathbf{m}_k$ , if we use original quantum no-key protocol, it is mentioned in [10], we need to use that protocol  $k \times l$  times, since the length of this binary string is  $cost = k \times l$ . In contrast, if we use proposed protocol, we need the cost is  $cost = k - 1 + 1 + l = k + l$ . This shows that our propose system is suitable to transfer a long binary string.

In this subsection, we still assume that the quantum channel is perfectly. Hence, Sender and Receiver will transfer quantum state

successfully to each other. In next Section, we will consider the channel have error and we propose the using of quantum error correction code to reduce that problem.

### 3.4. Proposed quantum no-key protocol with error correction codes

It is proved that in quantum channel quantum state can interact with unwanted environment, which can make bit-flip, phase-flip, or both of them, bit-phase flip. In quantum no-key protocol, we need to transmit quantum state three times, if the error or environment is bad, the result of our system will be go down. Quantum error correction code (QECC) is the solution to solve that problem. The key ideas of QECC is that the quantum state, length  $k$ , is extended to have large length, length  $n > k$ , where  $n - k$  redundant qubits we called them parity-check part. The novel QECC is discussed in Section 2.2 where we mention repetition codes for bit-flip and phase flip error, Shor codes for any error, bit-flip, phase-flip, or their combination.

Figure 7 shows the detail step of using QECC on quantum no-key protocol. The difference between Figure 7 and Figure 6 is that the QECC encoder and QECC decoder are inserted three times, since we have three times of transmission between Sender and Receiver.

## 4. Conclusion

In this research, we have proposed the quantum no-key protocol for many bits transfer which is suitable for long binary string transmission. The cost analysis is given in detail to show the effective of proposed system. In addition, the emerging of QECC on that proposed system is promised the way for secure transmission against the unwanted quantum channel.

## Conflict of Interest

The authors declare no conflict of interest.

## Acknowledgment

This work was supported by the Research Program through the National Research Foundation of Korea (NRF-2019R1A2C1005920).

## References

- [1] D. M. Nguyen, S. Kim, "A quantum three pass protocol with phase estimation for many bits transfer", in 2019 International Conference on Advanced Technologies for Communications (ATC), Viet Nam. <https://doi.org/10.1109/ATC.2019.8924514>
- [2] D. M. Nguyen, S. Kim, "Multi-Bits Transfer Based on the Quantum Three-Stage Protocol with Quantum Error Correction Codes", International Journal of Theoretical Physics 58 (6), 2043-2053, 2019. <https://doi.org/10.1007/s10773-019-04098-4>
- [3] P.W. Shor, "Algorithms for quantum computation discrete logarithms and factoring", IEEE Computer Society Press. 124-134, 1994. 10.1109/SFCS.1994.365700
- [4] L. Grover, "Quantum mechanics helps in searching for a needle in a haystack", Phys. Rev. Lett. 79, 325, 1997. <https://doi.org/10.1103/PhysRevLett.79.325>
- [5] A. M. Zidan et.al, "A Quantum Algorithm Based on Entanglement Measure for Classifying Boolean Multivariate function into Novel Hidden Classes", Results in Physics, 15, 102549, 2019. <https://doi.org/10.1016/j.rinp.2019.102549>
- [6] D. M. Nguyen, S. Kim, "Quantum stabilizer codes construction from Hermitian self-orthogonal codes over GF(4)", Journal of Communications and Networks 20 (3), 309-315, 2018. <https://doi.org/10.1109/JCN.2018.000043>

- [7] P.W. Shor, "Scheme for reducing decoherence in quantum computer memory", Physical Review A, 52, 2493, 1995. 10.1103/physreva.52.r2493
- [8] C. H Bennett, G Brassard, "Quantum cryptography: Public key distribution and coin tossing", International Conference on Computers, Systems & Signal Processing, Bangalore, India, Dec 9-12, 1984. <http://researcher.watson.ibm.com/researcher/files/us-bennetc/BB84highest.pdf>
- [9] S. Kak, "A three-stage quantum cryptography protocol". Found Phys Lett 19, 293, 2006. <https://doi.org/10.1007/s10702-006-0520-9>
- [10] A.A. Abdullah et.al, "A realizable quantum Three-Pass protocol authentication based on Hill-Cipher algorithm". Math. Probl. Eng., 2015, 481824, 2015. <https://doi.org/10.1155/2015/481824>
- [11] D. M. Nguyen, S. Kim, "New Constructions of Quantum Stabilizer Codes Based on Difference Sets", Symmetry 10 (11), 655, 2018. <https://doi.org/10.3390/sym10110655>
- [12] D. M. Nguyen, S. Kim, "Construction and complement circuit of a quantum stabilizer code with length 7", in 2016 Eighth International Conference on Ubiquitous and Future Networks (ICUFN), 2016. <https://doi.org/10.1109/ICUFN.2016.7537043>
- [13] D. M. Nguyen, S. Kim, "The fog on Generalized teleportation by means of discrete-time quantum walks on N-lines and N-cycles", Modern Physics Letters B 33 (23), 1950270, 2019. <https://doi.org/10.1142/S0217984919502701>
- [14] D. M. Nguyen, S. Kim, "A novel construction for quantum stabilizer codes based on binary formalism", International Journal of Modern Physics B, 03/2020. <https://doi.org/10.1142/S0217979220500599>
- [15] D. M. Nguyen, S. Kim, Quantum stabilizer codes based on a new construction of self-orthogonal trace-inner product codes over GF(4), International Journal of Modern Physics B, 34(5), 2050017, 02/2020. <https://doi.org/10.1142/S0217979220500174>
- [16] D. M. Nguyen, S. Kim, New construction of binary and nonbinary quantum stabilizer codes based on symmetric matrices, International Journal of Modern Physics B, 33(24), 1950274, 2019. <https://doi.org/10.1142/S0217979219502746>



## Low Carbon Sustainable Building Material: Maximizing Slag Potentials for Improved Lime Mortar Mechanical Properties

Sule Adeniyi Olaniyan\*

*Department of Architecture, Ladoko Akintola University of Technology, Ogbomosho, Nigeria*

---

### ARTICLE INFO

*Article history:*

*Received: 04 August, 2018*

*Accepted: 16 September, 2018*

*Online: 24 April, 2020*

---

*Keywords:*

*Carbon Emissions*

*Climate Change*

*E-value*

*Flexibility*

*Lime*

*Mortars*

---

### ABSTRACT

*Prior to the 19th century discovery of Portland Cement (PC), Lime Based Mortar remained popular due to its flexibility, permeability and more importantly, associated low carbon emissions. However, lime's characteristic delayed setting/hardening time, low mechanical strength, poor internal cohesion and some volumetric changes have overshadowed significance of its outstanding features particularly, flexibility, and consequently put its overall use into decline. This study therefore aims at integrating an industrial by-product, Ground Granulated Blast Furnace Slag (slag) with lime, in form of lime-slag mortar, with a view to addressing lime shortcomings for improved performance. The methodology involved mortars with the same Binder/Aggregate (B/A) mix ratio (1:3) using five separate volumetric compositions of 'lime-slag' binders (i.e. 1:1, 1:2, 1:3, 2:1 and 3:1). Physical properties of the mortars involving their Water/Binder (W/B) ratios, Air Contents and Bulk Densities were recorded. Comparative evaluations of the compositions in hardened state, involving mechanical characteristics, were carried out at specific intervals through a twelve-month curing period. These were partly monitored through assessments of the composites' microstructural behaviours over a six-month period. Results of the investigation show that addition of slag to mortars facilitate slightly larger pores with increased porosity. These effects are however minimal (i.e. from 23.42% to 25.37% porosity) when slag content is at equal volumetric content with lime. Also, at this same volumetric composition, the results show beneficial effects of slag on the composite's mechanical properties; while the flexural strength is increased by 50%, the compressive strength is improved by about 250%. Despite the improved mechanical characteristics, the composite exhibits comparable (with lime only) capacity for deformation absorptions, thus, preserving lime's known fundamental flexibility property. This is important for material's durability, and overall sustainable constructions.*

---

### 1. Introduction

Climate change, growing energy costs and the impacts of human activities on the environment have become key concerns for future developments. While construction processes facilitate infrastructure developments, they equally constitute major sources of carbon dioxide production and energy consumption [1, 2] as studies show that buildings account for 30-40% of the world's energy consumption [3, 4]. While a considerable part of this energy is commonly used to control internal microclimate conditions, other part is used to extract raw materials, transport them, make building components and, finally, to dispose of them. Therefore, interventions in this important productive sector through

promotion of low-impact building materials should be encouraged [5, 6]. Thus, efforts must be directed at exploring new technical approach, capable of evolving sustainable materials for improving environmental performances of buildings [7, 8]. One such approach is renewal of interests in a partially abandoned age-long environmentally sustainable building material, lime mortar.

Lime mortar refers to a proportional mixture of lime, sand and water. It is an age-long building material [9-11]. It is a plastic material that is slow to harden but allows movements within the mortar joints, without compromising its structural stability. Lime mortar has also been shown to exhibit great permeability, which enables it to reduce moisture entrapment, a phenomenon known as "breathability" [12-15]. Greater environmental awareness of its

---

\*Corresponding Author: Sule Adeniyi Olaniyan, [saolaniyan@lautech.edu.ng](mailto:saolaniyan@lautech.edu.ng)

advantages in terms of carbon dioxide emissions during manufacture (20% less than that of cement) and subsequent adsorption during carbonation promotes its use [13, 16, 17]. However, Lime Mortars are associated with exaggeratedly long setting and hardening periods, low internal cohesion, relatively low mechanical strengths and some volumetric changes, among others [18-23]. These, coupled with the absence of rigorous studies about their characteristics and properties (among others) resulted in its relative disuse. The study therefore sought to revive this age-long building material through integration of an industrial by-product, ‘Ground Granulated Blast Furnace Slag’ (slag), in form of a composite material, by formulating lime based blended mortars with varying proportions of slag.

Slag is a granular glassy amorphous waste material, formed as a by-product from production of steel and iron. It is obtained when the liquid slag, created at 1350–1500°C is cooled quickly using water, to produce granules or pellets which have hydraulic cementing properties when finely ground [24-28]. It is whitish, essentially of silicates and aluminosilicates of calcium and other oxides with main inorganic constituents such as silica (30–35%), calcium oxide (28–35%), magnesium oxide (1–6%), and Al<sub>2</sub>O<sub>3</sub>/Fe<sub>2</sub>O<sub>3</sub> (18–25%). The specific gravity of the slag is approximately 2.90 with its bulk density varying in the range of 1200–1300 kg/m<sup>3</sup> [27, 29-31]. Slag is widely used as a construction material due to its latent cementitious property when mixing with lime, alkali-hydroxides or Portland cement [32-36]. In some cases, it has been used as a successful replacement material for Portland cement, improving some properties [37, 38] and bringing environmental and economic benefits (such as low heat of hydration, long term strength, resistance to acid, better durability and general cost saving measure), to the cement industries [39-42]. It has also been used as a supplementary cementitious material for production of blended cement and slag cement. Recent advancements in Slag utilisation, as an alternative binding material in concrete production indicate its possible blend with lime, for improved lime mortar performance. Utilisation of slag in this area has significant environmental benefits (with least CO<sub>2</sub> emission to the atmosphere during this process) [43, 44]. Its production requires less energy than the production of Portland cement as slag generation is about 10% of the total steel production. Also, the requirement to recycle industrial wastes and by-products, rather than landfilling this potentially valuable material makes its integration acceptable [45-47]. Its potential re-use as a constituent in blended lime mortar would add to solve the associated problem related to its disposal [44, 48, 49]. Thus, this study aims at integrating this important industrial by-product,

Ground Granulated Blast Furnace Slag (slag) with lime, in form of lime-slag mortar, with a view to addressing lime shortcomings for improved performance. In effect, using the binders’ varying compositions, effects of lime partial substitution by slag in the evolving lime-slag mortars would be useful. This would attempt to synergise individual qualities of the constituents as the resulting composite would be characterized by faster setting and hardening, than lime, with overall improvements on their applications [50-52]. Through this attempt, growing interests in reviving sustainable lime based materials particularly mortar, would be enhanced.

**2. Experimental Procedure**

*2.1. Materials and mortar Preparation*

Commercially available Natural Hydraulic Lime of the class NHL-5.0 (St Astiers, UK), characterised with the lime’s highest compressive strength, based on the 28-day test (BSI, 2010a) [53] was adopted for this research. The selection of lime class was based on its relatively short setting time for optimal strength yield, its availability, ease of handling, as well as the need to maximise lime performance behaviour [2, 54]. Lime’s average Particle Size Distribution shown in Table 1 indicates particles with main equivalent diameter of 33.99 µm (by volume) and 10.19 µm (by Surface Area). 90% of these particles have sizes below 91.88 µm (by volume). Lime’s chemical compositions (by elements) determined by Energy Dispersive Spectrometry are given in Table 2. Ground granulated blast furnace slag (slag) for this investigation was obtained from ‘Hanson Cement’, United Kingdom. Its average Particle Size Distribution shown in Table 1 indicates particles with main equivalent diameter of 25.50µm (by volume) and 11.20µm (by Surface Area). 90% of these particles have sizes below 49.78µm (by volume). Slag’s chemical compositions (by elements) are given in Table 2. Commercially available siliceous fine kiln dried sand, obtained from Fife Silica Sands (a division of Patersons of Greenoackhill Ltd, United Kingdom) constituted the aggregates. The aggregate was passed through a sieve analysis in accordance with the requirements of (BSI, 2013) [55], and the particle size distributions in compliance with ASTM C 136 (ASTM, 2014) [56] are shown in Figure 1. The sand had Particle Size Distribution of 0-2 mm (i.e. 0.05 mm < Ø < 2 mm). The suitability of the gradation of the tested aggregates as mortar aggregates was evaluated by comparing the obtained gradation curve with the suggested particle size ranges of ASTM C 33 (ASTM, 2016) [57]. The results indicate that the sand has a suitable grading but with slightly lower particle sizes.

Table 1. Particle Size Diameters of the tested materials

Parameters		d(v,0.5)	d(v,0.1)	Mode	d(v,0.9)	D[4,3] (main equivalent diameter by volume)	D[3,2] (main equivalent diameter by Surface Area)
Specified Particle Diameter (µm)	Lime	10.78	5.28	6.50	91.88	33.99	10.19
	Slag	19.60	5.54	15.17	49.78	25.50	11.20

Table 2. Chemical Composition of the materials

Material	Elemental Chemical Composition of the materials (by % weight of the dry specimen)											
	Ca	O	Si	C	Sb	Al	Fe	Mg	S	K	Na	Ti
Lime	47.6	37.6	5.2	4.4	3.3	0.7	0.5	0.5	0.2	-	-	-
Slag	26.5	39.6	13.0	9.3	-	5.5	-	4.4	1.0	0.4	0.3	-
Sand	0.2	53.5	43.0	-	-	1.6	0.4	-	-	1.1		0.2

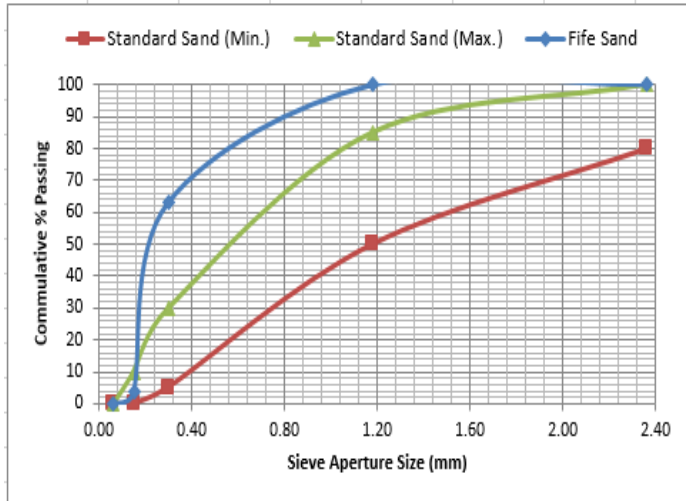


Figure 1: Grain size distribution of the aggregate

The mortars were prepared in accordance with the required standard (BSI, 2000). The binder-aggregate (B/A) ratio was maintained at 1:3 by volume, chosen from the commonest dosage reported in the literature [23, 58-60]. Volume proportions of components were converted to weights, to avoid measurement imprecision during batching processes (Hanley and Pavia, 2008). Mortar mixtures were prepared using the correct amount of water required to obtain adopted workability of  $145 \pm 5$  mm (measured by the flow table test – BS EN 1015-3 (BSI, 2000) [61] as BS EN 1015-6 (BSI, 1999a) [62] specifies a flow value of ‘140-200 mm’ for ‘plastic mortar’. Arising from visual and physical assessments of the mixes during the trial experimentation however, a flow value of 140 – 150mm (i.e.  $145 \pm 5$ mm) was adopted. As observed, either higher or lower value tends towards stiffness or fluidity respectively. This was determined in accordance with (BSI, 2005) [63]

Using the stated B/A ratio (i.e. 1:3), each mortar formulation was prepared with progressively increasing/decreasing slag contents as indicated in Table 3. Mixing was done in the laboratory mixer of 30 litres maximum capacity. The mixing procedure was performed in a number of stages: Aggregates were placed first, followed by other dry materials (i.e. lime and slag, pre-mixed earlier, where applicable) and these were blended consistently for 60 seconds as best practice dictates that the NHL powder should be thoroughly mixed through the dry sand, ensuring batch colour consistency prior to gradually adding water. Water was added slowly during 30 seconds and mixing continued for another 30 seconds. Mixing was stopped for 90 seconds as mortar adhering to the wall and bottom of the mixer bowl was scraped off. Mixing then resumed to obtain consistent mixture. The entire mixing period lasted about 5minutes. For every mortar mix, minimum of three prismatic specimens of  $40 \times 40 \times 160$  mm were prepared, the

average value of which represented the ‘actual value’ for consideration during the specimen evaluations afterwards (i.e. for microstructural analysis, and mechanical characteristics evaluations: Flexural and Compressive tests; Moduli of Elasticity determination). The specimens were compacted with a vibration table after mould filling in prismatic casts (BSI, 2010b) [64], removed from the moulds 2 days later and left to cure at the laboratory ambient conditions of  $21 \pm 4^\circ\text{C}$  (temperature) and  $40 \pm 5\%$  (relative humidity), until the test dates of 1, 3, 6, 9 and 12 months.

## 2.2. Analytical methodology

### 2.2.1. Microstructural Characteristics

Microstructural characteristics of the mortar samples were evaluated in terms of the total porosity (in %), median pore diameter (by volume in nm), bulk density and pore size distribution, using Mercury Intrusion Porosimetry (MIP) technique. This was achieved with AutoPore IV 9500 by Micrometrics (with pressure range up to 60000 psi). The test was carried out with samples of approximately 1.5g that were extracted from the core of the crushed prisms. Under short term loading and at a relatively low rate of load application (approximately 2mm/min), the chance of micro crack propagation is minimum [60, 65]. These samples were obtained at the test ages of one and six months, and dried in an oven at temperature of  $75 \pm 1^\circ\text{C}$  for 24 hours before the test, to ensure that the sample is devoid of moisture contents (which may otherwise affect its microstructural properties, thereby affecting the results).

### 2.2.2. Mechanical properties

The mechanical properties were evaluated with regard to the three-point flexural tests, and compressive strength. While the flexural strength tests were performed on the ELE AutoTest 2000 apparatus with a load application pace of 50 N/s, compressive strength tests were conducted on the two fragments of each specimen (resulting from the preceding flexural test) using INSTRON 3367 with 30kN load capacity, moving at a loading rate of 2mm/min. The results reported in this work were all taken as an average value of six similar specimen fragments. Additionally, INSTRON 3367 plots stress/strain graph on the screen, with the value for Modulus of Elasticity generated automatically. In generating the modulus output, the system algorithm determines the slope of the stress/strain curve in the initial linear portion of the curve. It calculates the slopes using least-squares fit on test data for a specified number of regions between the lower and upper bounds, and reports the steepest slope as the modulus. The algorithm will not calculate a result if the data does not contain either the specified upper or lower bound, and the data contains the same number or fewer points than the specified number of regions.

Table 3. Lime-Slag Mortars' Compositions by materials

Slag Contents	Mortar Reference I.D. (Slag Contents)	Volumetric Ratio (L-Sl-Sd)	Lime (L): Volume (Volume in 'ml'/ mass in 'g')	Slag (Sl): Volume (Volume in 'ml'/ mass in 'g')	Sand (Sd): Volume (Volume in 'ml'/ mass in 'g')
0%	L13 (0%)	1-0-3	1 (1700/ 1172)	0 (0/ 0)	3 (4350/ 6444)
25%	LS31 (25%)	3-1-12	3 (770/ 528)	1 (420/ 363)	12 (4350/ 6444)
33%	LS21 (33%)	2-1-9	2 (665/ 458)	1 (550/ 472)	9 (4240/ 6283)
50%	LS11 (50%)	1-1-6	1 (850/ 586)	1 (850/ 725)	6 (4350/ 6444)
66%	LS12 (66%)	1-2-9	1 (510/ 352)	2 (1000/ 870)	9 (3920/ 5800)
75%	LS13 (75%)	1-3-12	1 (260/ 176)	3 (1260/ 1088)	12 (4350/ 6444)

### 2.2.3. Other Preliminary Material Testing

Some preliminary material testing were also carried out as follows:

- Application of Scanning Electron Microscopy/Energy Dispersive X-ray Spectrometry using 'Carl Zeiss EVO 50' Scanning Electron Microscope was employed for examination and analysis of the microstructure, morphology and chemical composition characterizations of the experimental materials (Lime and slag);
- Application of Laser Diffractometry Xmastersize with air dispersion was adopted for determination of the Pore Size Distribution of the tested materials (Lime and slag);
- Consistency of fresh mortars was examined using the flow table test in accordance with (BSI, 2000) [61];
- Bulk Density of Fresh Mortar was determined accordance with (BSI, 1999a) [62], and;
- Air content of fresh mortars was determined by the pressure method using Air Entrainment Meter in accordance with (BSI, 1999b) [66].

## 3. Results and Discussion

### 3.1. Physical Characteristics

Table 4 shows the results of the W/B ratios, Air Contents and Bulk Densities obtained for lime, and lime-slag mortars using varying binders' contents. For lime only (0% slag content, i.e. L13), Table 4 indicates a W/B ratio of 1.53, Air Contents of 6.4 and Bulk Density of 1.93g/ml. Addition of slag content below 50%

of the binders resulted in higher water demand. This may be attributed to the higher lime content and its high water demand. However, at equal lime-slag content (LS11), a reduction in W/B ratio was observed, due to reduced lime content. Further slag addition (above 50%) resulted in subsequent rising water demand relative to LS11. This may be a consequence of higher slag content and hence higher degree of hydration relative to hydraulic lime hydration and carbonation [67, 68]. With progressive addition of slag to the mortar, there is a general increase in the air contents for the composites. This may be related to slag's higher degree of hydration and subsequent formation of air spaces arising from consumption of initial kneading water. Progressive addition of slag to the mortar increased the bulk densities, though not in a linear trend. These increments may be related to the rising water demand to obtain pastes of same consistency and subsequent deposition of the hydration products. Hence, the higher the slag content, the higher the resulting bulk density.

### 3.2. Microstructural features

Figs. 2(a) and (b) show the Pore Size Distribution (PSD) curves obtained by Mercury Intrusion Porosimetry (MIP) for the six different composites at 1 and 6 months of curing.

For lime only, at 1 month of curing, the graph indicates a bimodal PSD with predominant sizes between (0.5  $\mu\text{m}$  - 5  $\mu\text{m}$ ) and (5  $\mu\text{m}$  - 20  $\mu\text{m}$ ), as shown in Fig. 2(a). In this case, the mortar exhibits both gel pore (i.e. 1 nm - 3  $\mu\text{m}$ ) and substantial proportion of capillary pores (i.e. 3 - 30  $\mu\text{m}$ ). These large pores result from loss of excess unbound kneading water due to strong water-retaining characteristic of lime and its associated slow carbonation process. After 6 months, in spite of the continuous hydration and



carbonation processes, the median pore diameter increased (from 2.16  $\mu\text{m}$  to 3.96  $\mu\text{m}$ ) (Table 5), indicating more presence of larger pores (i.e. between 0.5  $\mu\text{m}$  and 40  $\mu\text{m}$ ) with the shift of the PSD curves to the left (Fig. 2(b)).

Table 4: Lime-Cement Mortars' Compositions by materials and Water/Binder ratios.

Slag Contents	Mortar Reference I.D.	Water/Binder Ratio	Air Content (%)	Bulk Density (g/ml)
0%	L13	1.53	6.4	1.93
25%	LS31	2.05	6.1	1.98
33%	LS21	1.91	6.5	2.01
50%	LS11	1.29	9.2	2.05
66%	LS12	1.35	8.4	2.05
75%	LS13	1.42	8.3	2.06

However, a reduction is observed in the total pore volume (i.e. from 27.77% to 23.42%), which indicates filling of some of the capillary voids due to deposition of the hydration and carbonation products (from hydraulic lime). The bulk density was reduced (from 1.75 g/ml to 1.72 g/ml) due to evaporation of excess kneading water and subsequent associated drying shrinkage.

Progressive addition of slag to the mortar resulted in similar patterns of PSD relative to lime mortar (i.e. bimodal distributions, between 0.6  $\mu\text{m}$  – 6.5  $\mu\text{m}$ , and 5  $\mu\text{m}$  – 10.5  $\mu\text{m}$  pore ranges) at 1 month curing. The only exception is LS13 with a wide distribution across, having additional identifiable pore sizes at both 13 nm and 40  $\mu\text{m}$  pore diameters (Figure 2(a)). Porosities of the composites also reduced with LS13 recording the highest value of 11% reduction (compared with lime only). At 6 months, the bimodal patterns of the curves still remained, with distinctive two pore size ranges at 1  $\mu\text{m}$  - 4  $\mu\text{m}$  and 4.5  $\mu\text{m}$  - 10.5  $\mu\text{m}$  (Fig. 2(b)). Progressive hydrations in the composites were also noticed with higher bulk densities (Table 5). However, all mortars had their individual median pore diameters increased. This could be a consequence of fine cracks formation due to autogenous deformation [32, 69]. Composite with the highest slag content (LS13) had a dominance of large pores with 6  $\mu\text{m}$  pore size diameter which may have a negative impact on compressive strength. Compared to lime mortar, porosities of the composites are higher at 6 months. This probably accounts for more CO<sub>2</sub> penetration for carbonation reactions. The above results indicate progressive addition of slag to mortars could facilitate slightly larger pores with increased porosity. These effects are however minimal (i.e. from 23.42% to 25.37% porosity) when slag content is at equal volumetric content with lime.

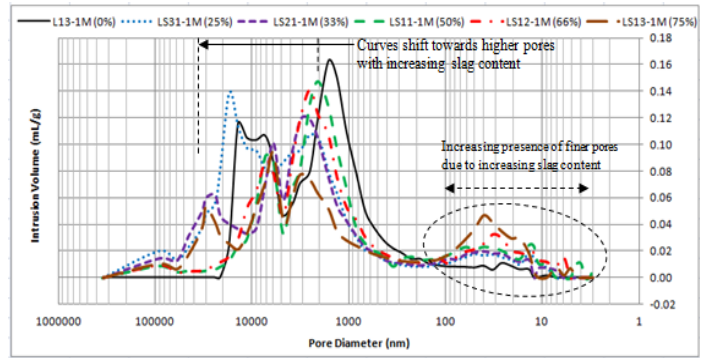


Figure 2 (a): At 1 month

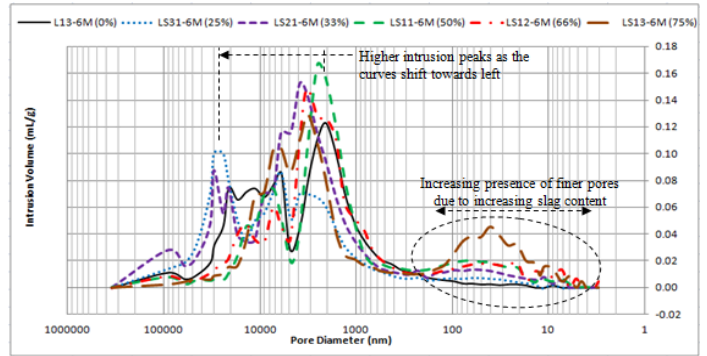


Figure 2 (b): At 6 months

Figure 2: Pore size distribution of lime mortars with increasing slag contents

### 3.3. Mechanical Properties

The results obtained for three mechanical parameters – flexural strength, compressive strength and modulus of elasticity, over a 12-month curing period are as summarised in Figures 3 - 5. Each result was taken as an average value of three similar specimens for flexural strength and five similar specimens for both compressive strength and modulus of elasticity. The coefficients of variation (COV) fall substantially within the lower range (0 – 15%). This suggests consistent results. However, there were also few cases of higher COV, which indicate some degree of scatter in those cases. Appropriate error bars are also displayed on the respective graphs. Fig. 3 illustrates the results of the Flexural Strengths obtained for lime and lime-slag mortars using varying binders' contents.

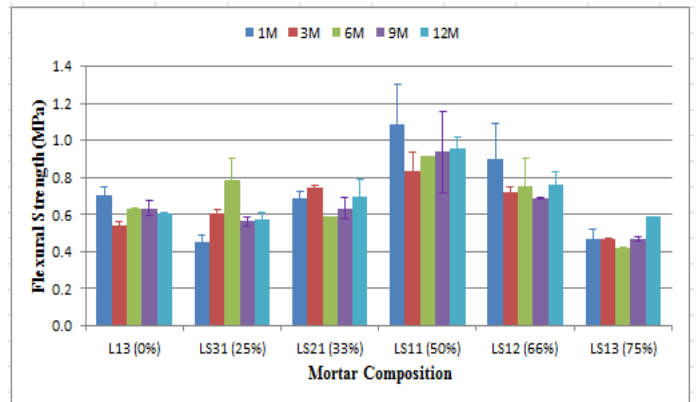


Figure 3. Flexural Strength developments for Lime Mortars with increasing slag contents

Table 5. Extracted Mercury Intrusion Porosimetry data for Lime-Slag mortars containing increasing slag contents

Specimen Reference I.D.	Curing Period	Median Pore Diameter (Volume) [nm]	Bulk Density at 0.52 psia [g/mL]	Porosity [%]
L13 (0%)	1 Month	2163.6	1.75	27.77
	6 Months	3955.0	1.72	23.42
LS31 (25%)	1 Month	5762.2	1.74	31.57
	6 Months	8599.5	1.79	23.71
LS21 (33%)	1 Month	4358.6	1.73	29.12
	6 Months	4840.3	1.75	29.87
LS11 (50%)	1 Month	2183.6	1.83	27.17
	6 Months	2495.2	1.85	25.37
LS12 (66%)	1 Month	2522.0	1.81	27.64
	6 Months	2678.9	1.88	27.15
LS13 (75%)	1 Month	3027.1	1.86	24.85
	6 Months	3576.8	1.82	28.84

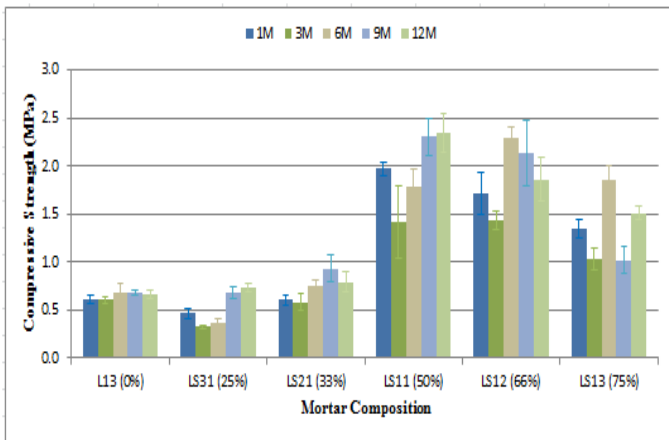


Figure 4. Compressive Strength developments for Lime Mortars with increasing slag contents

For lime only, Fig. 3 shows a flexural strength value of 0.70 MPa in the first month of curing which decreased to 0.61 MPa at the end of 12 months. This may be due to formation of different pore sizes (bimodal PSD between (0.5 – 5 μm) and (5 – 20 μm)) resulting from loss of excess unbound kneading water as explained earlier. Progressive addition of slag (up to 50% of binders’ content, i.e. LS11) to the mortar translates to the corresponding increase in the flexural strength (about 50%), though not in a linear trend. This may be related to high degree of slag hydration as evidenced by an increase in the composite bulk density (i.e. 1.85 g/mL for LS11, compared with 1.72 g/mL for L13) as well as decrease in the median pore diameter (i.e. 2.5 μm for LS11, compared with 4.0 μm for L13) over the same curing period. However, further slag addition (beyond 50%) resulted in subsequent reduction in the

flexural strength. In this case, slag exhibited higher hydration as the mortar exhibited more self-desiccation. This agrees with the results of the microstructural analysis which show increasing median pore diameters and higher porosities. This may be connected with the formation of fine cracks arising from autogenous deformation usually associated with slag hydration [70, 71]. These results therefore show beneficial effect of slag on composite’s flexural strength at equal lime-slag content as further addition may impact negatively on the flexural strength.

Results of compressive strength followed a similar pattern to flexural strength. Figure 4 shows a marginal increase in the strength of the mix containing lime only from 0.61 MPa to 0.66 MPa at 1 month and 12-month curing respectively. This may be a consequence of high W/B ratio and slow carbonation rate of lime.

Progressive addition of slag up to 50% to the mortar content results in about 250% increase in the compressive strength, (though not in a linear trend as slag content increased). This may be due to higher slag hydration relative to hydraulic lime. However, further increment of slag content induces an increased desiccation of slag, which in turn leads to formation of matrixes with higher median pore diameters and higher porosities. This possibly culminated in the formation of fine cracks and subsequent lower compressive strengths recorded. Thus, the results show beneficial effect of slag on composite’s compressive strength at equal lime-slag content as further addition may impact negatively on the strength.

Compressive strengths recorded above are related to the mortars’ practical performances. These are reflected in their moduli of elasticity (E) as shown in Figure 5.

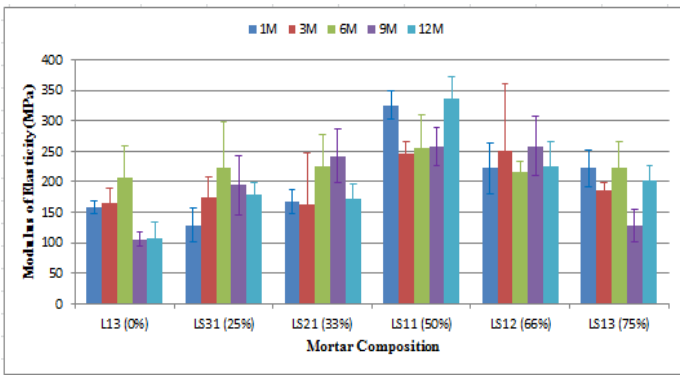
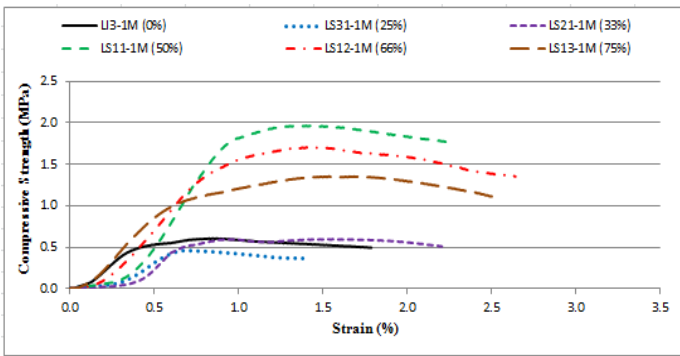


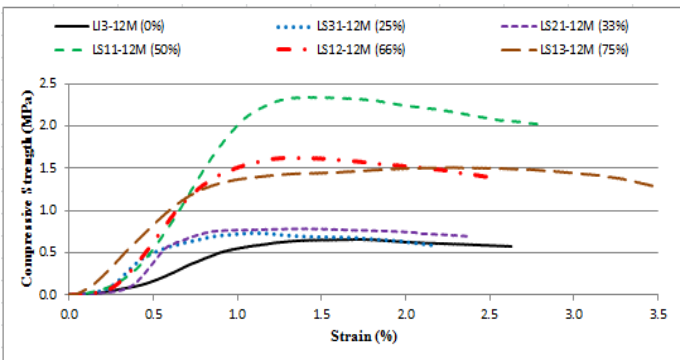
Figure 5. Moduli of Elasticity (E) values for Lime Mortars with increasing slag contents

From Figure 5, LS11 with highest compressive strength had the highest ‘E’ value at the 12th month of curing. This is against L13 which had the lowest compressive strength at the same time. Both L13 and LS11 have tendencies to exhibit interesting elastic behaviours as demonstrated in their stress-strain relationships at 1 and 12-month curing (Figures 6(a) and (b)), with varying capacities to absorb deformations. However, L13 with low compressive strength (low E-value) has higher capacity for deformation absorption relative to LS11.

From Figures 6(a) and (b), despite increased mechanical strengths of LS11, it is still able to exhibit capacities for deformation absorptions (compared with lime only). This characteristic feature therefore illustrates beneficial effect of slag on composite’s compressive strength at equal lime-slag volumetric content.



(a) At 1-month curing



(b) At 12-month curing

Figure 6: Compressive Strength versus Strain relationships for lime and lime-slag mortars

#### 4. Conclusions

The study reflects performance assessments of lime-slag composites with progressive addition of slag. It can be inferred therefrom, that addition of slag has significant impacts on lime mortar performance particularly, with regard to mechanical strength developments. At equal lime-slag volumetric composition, beneficial impact of slag on the mechanical behaviour of the composite could be obtained. This impact is a reflection of the microstructural behaviour of the composites, which in turn defines the mortar performance. Thus, performance of low-impact sustainable building materials such as lime may be enhanced, and its revival may be encouraged in form of lime-slag composites, for improved energy consumption and environmental performances of buildings, as demonstrated in this study.

#### Conflict of Interest

The author declares no conflict of interest.

#### Acknowledgment

The authors gratefully acknowledge the financial supports from ‘TETFUND AST&D’ Scheme, an educational development organ of The Federal Government of Nigeria. Thanks are also due to Hanson Cement, United Kingdom, for the provision of the slag used for this work.

#### References

- [1] Ciancio, D., Beckett, C. T. S., and Carraro, J. A. H. (2014). Optimum lime content identification for lime-stabilised rammed earth. *Construction and Building Materials*, 53, 59-65.
- [2] Olaniyan, S.A. (2017). Sustainable Lime Based Mortars: Performance Assessment of Composites for Building Construction. PhD Thesis, Glasgow Caledonian University, Glasgow, Scotland (UK).
- [3] Roberto De Lieto Vollaro, Calvesi, M., Battista, G., Evangelisti, L., Gori, P., and Guattari, C. (2013). A new method of technical analysis to optimise the design of low impact energy systems for buildings. *International Journal of Engineering and Technology Innovation*, 3(4), 241-250.
- [4] Fumo, N. (2014). A review on the basics of building energy estimation. *Renewable and Sustainable Energy Reviews*, 31, 53-60.
- [5] Olaniyan, S.A., and Klemm, A. J. (2015). Current trends in development of lime based composites. *Building Physics in Theory and Practice*, VII (3), 49-54.
- [6] Harish, V. S. K. V., and Kumar, A. (2016). A review on modeling and simulation of building energy systems. *Renewable and Sustainable Energy Reviews*, 56, 1272-1292.
- [7] Klemm, A. J., and Sikora, K. S. (2013). The effect of superabsorbent polymers (SAP) on microstructure and mechanical properties of fly ash cementitious mortars, *Construction and Building Materials*, 49, 134-143.
- [8] Goldstein, D. B., and Eley, C. (2014). A classification of building energy performance indices. *Energy Efficiency*, 7(2), 353-375.
- [9] Lanas, J., Pérez Bernal, J. L., Bello, M. a., and Alvarez Galindo, J. I. (2004). Mechanical properties of natural hydraulic lime-based mortars. *Cement and Concrete Research*, 34(12), 2191–2201.
- [10] Arandigoyen, M., and Alvarez, J. I. (2007). Pore structure and mechanical properties of cement–lime mortars, *Cement and Concrete Research*, 37(5), 767-775.
- [11] Hughes, J., Lindqvist, J. E., CBI Betonginstitutet AB, SP – Sveriges Tekniska Forskningsinstitut, and RISE. (2012). RILEM TC 203-RHM: Repair mortars for historic masonry: The role of mortar in masonry: An introduction to requirements for the design of repair mortars, *Materials and Structures*, 45(9), 1287-1294.
- [12] Banfill, P. F. G. (1994). Rheological methods for assessing the flow properties of mortar and related materials. *Construction and Building Materials*, 8(1), 43-50.

- [13] McDonald, L. (2000). Hydraulic lime mortar for the house of the future, *The Structural Engineer*, 78 (7).
- [14] Forster, A.M., (2002). An assessment of the relationship between the water vapour permeability and hydraulicity of lime based mortars with particular reference to building conservation materials science. PhD Thesis, Heriot-Watt University, Edinburgh.
- [15] Solak, A. (2016). Experimental investigation of lime mortar used in historical buildings in becin, turkey. *Materials Science*, 22(1), 105-112.
- [16] Edwards A.J. (2005) Properties of Hydraulic and Non-hydraulic Limes for Use in Construction. PhD Thesis, Napier University, Edinburgh.
- [17] Ball, R. J., El-Turki, A., Allen, W. J., Nicholson, J. A., and Allen, G. C. (2009). Deformation of NHL3.5 and CL90/PC hybrid mortars. *Proceedings of the Institution of Civil Engineers - Construction Materials*, 162(1), 29-35.
- [18] Hughes, J. J. and Valek, J. (2003). Mortars in Historic Buildings: A Review of the Conservation, Technical and Scientific Literature. Historic Scotland, & Historic Scotland, Technical Conservation, Research and Education Division. Edinburgh: Historic Scotland.
- [19] Olaniyan, S.A., Klemm, A.J. and Almeida, F.C. (2016). Evolving Low Carbon Sustainable Building Material: Making Case for Cement-Lime Composites. 9th International Concrete Conference on Environment, Efficiency and Economic Challenges for Concrete, Dundee.
- [20] Pacheco-Torgal, F., Castro-Gomes, J., and Jalali, S. (2008). Alkali-activated binders: A review: Part 1. Historical background, terminology, reaction mechanisms and hydration products. *Construction and Building Materials*, 22(7), 1305.
- [21] Izaguirre, A., Lanas, J., and Alvarez, J. I. (2011). Effect of a polypropylene fibre on the behaviour of aerial lime-based mortars. *Construction and Building Materials*, 25(2), 992-1000.
- [22] Forster, A. M., and Carter, K. (2011). A framework for specifying natural hydraulic lime mortars for masonry construction. *Structural Survey*, 29(5), 373-396.
- [23] Ventola, L., Vendrell, M., and Giraldez, P. (2013). Newly-designed traditional lime mortar with a phase change material as an additive. *Construction and Building Materials*, 47, 1210-1216.
- [24] Taylor G.D. (1983) *Materials of Construction*. New York: Longman Inc.
- [25] Song, S., Sohn, D., Jennings, H. M., and Mason, T. O. (2000). Hydration of alkali-activated ground granulated blast furnace slag. *Journal of Materials Science*, 35(1), 249-257.
- [26] Richardson, J. M., Biernacki, J. J., Stutzman, P. E., and Bentz, D. P. (2002). Stoichiometry of slag hydration with calcium hydroxide. *Journal of the American Ceramic Society*, 85(4), 947-953.
- [27] Kumar, R., Kumar, S., Badjena, S., and Mehrotra, S. P. (2005). Hydration of mechanically activated granulated blast furnace slag. *Metallurgical and Materials Transactions B*, 36(6), 873-883.
- [28] Juenger, M. C. G., Monteiro, P. J. M., and Gartner, E. M. (2006). In situ imaging of ground granulated blast furnace slag hydration. *Journal of Materials Science*, 41(21), 7074-7081.
- [29] Das, B., Prakash, S., Reddy, P.S.R. and Misra, V.N. (2007). An overview of utilization of slag and sludge from steel industries. *Resources Conservation and Recycling*, 50, 40–57.
- [30] Bellmann, F. and Stark, J. (2009) Activation of Blast Furnace Slag by a New Method. *Cement and Concrete Research* 39, 644–650
- [31] Chi, M., Liu, Y., and Huang, R. (2015). Mechanical and microstructural characterization of alkali-activated materials based on fly ash and slag. *International Journal of Engineering and Technology*, 7(1), 59-64.
- [32] Chen, W., and Brouwers, H. J. (2007). The hydration of slag, part 1: reaction models for alkali-activated slag. *Journal of Materials Science*, 42(2), 428-443. Doi: 10.1007/s10853-006-0873-2.
- [33] Haha, M. B., Lothenbach, B., Le Saout, G., and Winnefeld, F. (2011). Influence of slag chemistry on the hydration of alkali-activated blast-furnace slag — part I: Effect of MgO. *Cement and Concrete Research*, 41(9), 955-963.
- [34] Wang, Q., Yan, P., and Han, S. (2011). The influence of steel slag on the hydration of cement during the hydration process of complex binder. *Science China Technological Sciences*, 54(2), 388-394.
- [35] Provis, J. L., Myers, R. J., White, C. E., Rose, V., and van Deventer, J. S. J. (2012). X-ray microtomography shows pore structure and tortuosity in alkali-activated binders. *Cement and Concrete Research*, 42(6), 855-864.
- [36] Tan, Z., De Schutter, G., Ye, G., Gao, Y., and Machiels, L. (2014). Influence of particle size on the early hydration of slag particle activated by ca solution. *Construction and Building Materials*, 52, 488.
- [37] Escalantea, J.I., Gomez, L.Y., Johal, K.K., Mendozaa, G., Manchaa, H., and Mendez, J. (2001) Reactivity of Blast-Furnace Slag in Portland cement Blends Hydrated under Different Conditions. *Cement and Concrete Research* 31, 1403–1409.
- [38] Rashad, A. M., and Khalil, M. H. (2013). A preliminary study of alkali-activated slag blended with silica fume under the effect of thermal loads and thermal shock cycles. *Construction and Building Materials*, 40, 522-532;
- [39] Hooton, R. D. (2000). Canadian use of ground granulated blast-furnace slag as a supplementary cementing material for enhanced performance of concrete. *Canadian Journal of Civil Engineering*, 27(4), 754-760.
- [40] Gruskovnjak, A., Lothenbach, B., Winnefeld, F., Figi, R., Ko, S.-C., Adler, M., and Mäder, U. (2008) Hydration Mechanisms of Super Sulphated Slag Cement. *Cement and Concrete Research* 38, 983–992.
- [41] Bernal, S. A., Provis, J. L., and Green, D. J. (2014). Durability of Alkali-Activated materials: Progress and perspectives. *Journal of the American Ceramic Society*, 97(4), 997-1008.
- [42] Yao, X., Yang, T., and Zhang, Z. (2016). Compressive strength development and shrinkage of alkali-activated fly ash–slag blends associated with efflorescence. *Materials and Structures*, 49(7), 2907-2918.
- [43] Dubrawski, J.V. (1997) Thermal Characteristics of Aged Granulated Blast Furnace Slags. *Journal of Thermal Analysis*, 48, 63-72.
- [44] Aydin, S., & Baradan, B. (2014). Effect of activator type and content on properties of alkali-activated slag mortars. *Composites Part B: Engineering*, 57, 166-172.
- [45] Wu, X., Roy, D.M., and Langton, C.A. (1983). Early stage hydration of slag-cement. *Cement and Concrete Research*, 13, 277-286.
- [46] Shi, C., and Qian, J. (2000). High performance cementing materials from industrial slags — a review. *Resources Conservation and Recycling*, 29(3), 195-207.
- [47] Provis, J. L. (2014). Geopolymers and other alkali activated materials: Why, how, and what? *Materials and Structures*, 47(1), 11-25.
- [48] Nicolas, R. e., and Provis, J. L. (2015). The interfacial transition zone in alkali-activated slag mortars. *Frontiers in Materials*, 2.
- [49] Ye, H., and Radlińska, A. (2016). Shrinkage mechanisms of alkali-activated slag. *Cement and Concrete Research*, 88, 126-135.
- [50] Lanas, J., Pérez Bernal, J. L., Bello, M. a., and Alvarez Galindo, J. I. (2004). Mechanical properties of natural hydraulic lime-based mortars. *Cement and Concrete Research*, 34(12), 2191–2201.
- [51] Sébaïbi, Y., Dheilily, R. M., and Quéneudec, M. (2004). A study of the viscosity of lime–cement paste: Influence of the physico-chemical characteristics of lime. *Construction and Building Materials*, 18(9), 653-660.
- [52] Hossain, M. M., Karim, M. R., Hossain, M. K., Islam, M. N., and Zain, M. F. M. (2015). Durability of mortar and concrete containing alkali-activated binder with pozzolans: A review. *Construction and Building Materials*, 93, 95-109.
- [53] British Standards Institution (BSI) (2010a) BS EN 998: Masonry Mortar – Part 2: Specification for Mortar for Masonry.
- [54] Moropoulou, A. (2005) Reverse engineering: a proper methodology for compatible restoration mortars. RILEM Conference Proceedings on Historic Mortars, Delft.
- [55] British Standards Institution (BSI) (2013) BS EN 13139: Aggregates for mortar - Part 3 (PD 6682): Guidance on the use of BS EN 13139.
- [56] ASTM C136 (2014) Standard Test Method for particle size distributions
- [57] ASTM C 33 (ASTM, 2016) Standard Specification for mortar Aggregates
- [58] Moropoulou, A., Cakmak, A. S., Biscontin, G., Bakolas, A., and Zendri, E. (2002). Advanced byzantine cement based composites resisting earthquake stresses: The crushed brick/lime mortars of justinian's hagia Sophia. *Construction and Building Materials*, 16(8), 543-552.
- [59] Lanas, J., and Alvarez-Galindo, J. I. (2003). Masonry repair lime-based mortars: Factors affecting the mechanical behaviour. *Cement and Concrete Research*, 33(11), 1867-1876.
- [60] Mosquera, M.J., Silva, B., Prieto, B., and Ruiz-Herrera, E. (2006) Addition of cement to lime-based mortars: effect on pore structure and vapor transport. *Cement and Concrete Research* 36, 1635– 1642.
- [61] British Standards Institution (BSI) (2000) BS EN 1015: Methods of Test for Mortar for Masonry – Part 3: Determination of Consistence of Fresh Mortar (by Flow Table).
- [62] British Standards Institution (BSI) (1999a) BS EN 1015: Methods of Test for Mortar for Masonry – Part 6: Determination of Bulk Density of Fresh Mortar.
- [63] British Standards Institution (BSI) (2005) PD 6678: Published Document - Guide to the Specification of the Masonry Mortar.
- [64] British Standards Institution (BSI) (2010b). BS EN 459: Building Lime – Part 2: Test Method.
- [65] Pozo-Antonio, J. S. (2015). Evolution of mechanical properties and drying shrinkage in lime-based and lime cement-based mortars with pure limestone aggregate. *Construction and Building Materials*, 77, 472-478.



- [66] British Standards Institution (BSI) (1999b) BS EN 1015: Methods of Test for Mortar for Masonry – Part 7: Determination of Air content of Fresh Mortar.
- [67] Chi, M., and Huang, R. (2013). Binding mechanism and properties of alkali-activated fly ash/slag mortars. *Construction and Building Materials*, 40, 291-298.
- [68] Geng, H., and Li, Q. (2014). Development of microstructure and chemical composition of hydration products of slag activated by ordinary portland cement. *Materials Characterization*, 87, 149.
- [69] Bernal, S.A., Provis, J.L, Rose, V, Mejía de Gutiérrez, R. (2013). High-resolution X-ray diffraction and fluorescence microscopy characterization of alkali-activated slag-metakaolin binders. *Journal of the American Ceramic Society*, 96, 1951–57.
- [70] Burciaga-Díaz, O., Díaz-Guillén, M.R., Fuentes, A.F. and Escalante-García, J.I. (2013) Mortars of alkali-activated blast furnace slag with high aggregate: binder ratios. *Construction and Building Materials*, 44, 607–614.
- [71] Biernacki, J. J., Richardson, J. M., Stutzman, P. E., and Bentz, D. P. (2002). Kinetics of slag hydration in the presence of calcium hydroxide. *Journal of the American Ceramic Society*, 85(9), 2261-2267.